ACTA UNIVERSITATIS SZEGEDIENSIS

Search

ACTA
MINERALOGICA-PETROGRAPHICA
ABSTRACT SERIES

Volume 6 2010

IMA2010

20th General Meeting of the
International Mineralogical Association
21–27 August, 2010

Budapest, Hungary

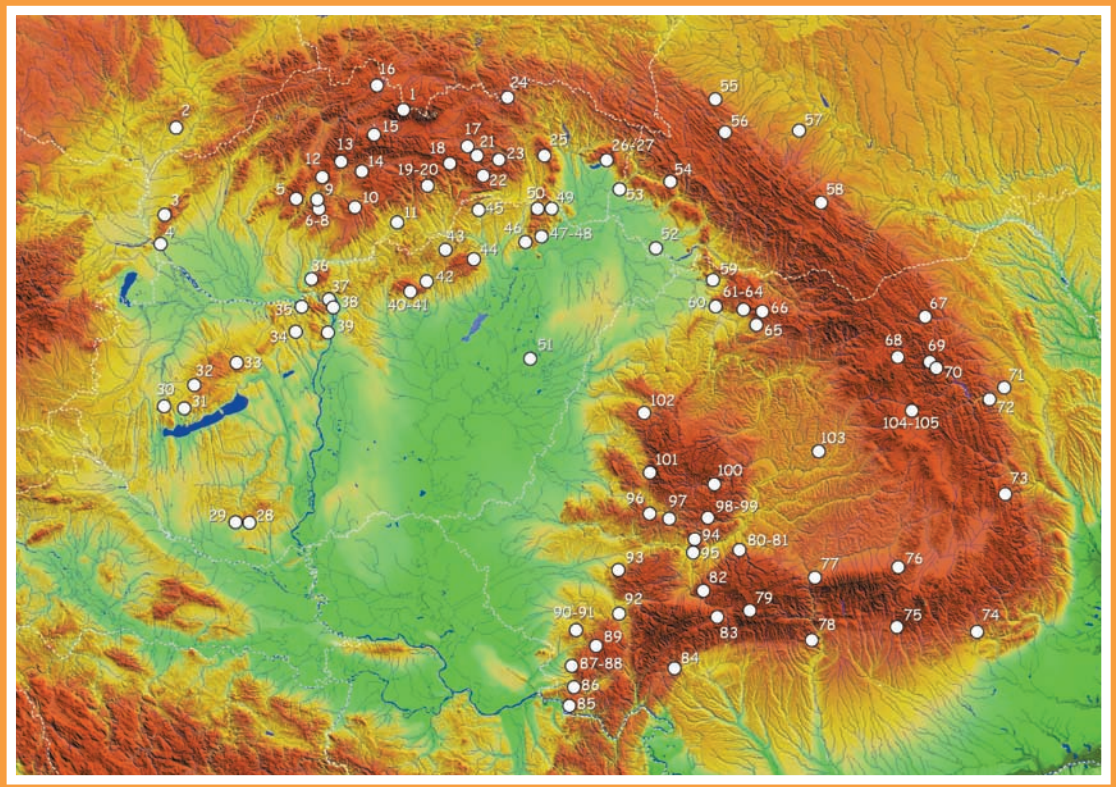

Published by the Department of Mineralogy, Geochemistry and Petrology, University of Szeged

ACTA MINERALOGICA-PETROGRAPHICA
established in 1922

ABSTRACT SERIES

HU ISSN 0324-6523
HU ISSN 1589-4835

Abbreviated title:
Acta Mineral. Petrogr. Abstr. Ser., Szeged

This volume was published for the 375th anniversary of the Eötvös Loránd University, Budapest.

The publication was co-sponsored by the National Office for Research and Technology, Budapest.

IMA2010 (www.ima2010.hu) is organised in the frame of the ELTE375 scientific celebration activities.

Editorial Office Manager
Anikó Batki
University of Szeged, Szeged, Hungary
E-mail: batki@geo.u-szeged.hu

Editorial Address
H-6701 Szeged, Hungary
P.O. Box 651
E-mail: asviroda@geo.u-szeged.hu

The Acta Mineralogica-Petrographica is published by the Department of Mineralogy, Geochemistry and Petrology, University of Szeged, Szeged, Hungary

---

On the cover: Map of the Carpathian region with type localities of new mineral species, rocks, fossil resins and hydrocarbons discovered in (first described from) the area, including both valid and discredited species. See the last page for the locality names corresponding to numbers. Map plotted by Ferenc Mádai from the data of Gábor Papp for the exhibition of the Hungarian Natural History Museum, entitled "There is something new under the earth", organised on the occasion of IMA2010.

IMA2010

20th General Meeting of the
International Mineralogical Association
21–27 August, 2010

Budapest, Hungary

ABSTRACTS

Edited by

Luminița Zaharia
Annamária Kis
Boglárka Topa
Gábor Papp
Tamás G. Weiszburg

MAIN SCIENTIFIC SPONSORS

International Mineralogical Association

Eötvös Loránd University, Budapest

MAIN FINANCIAL SPONSOR

National Office for Research and Technology (NKTH), Budapest

Organising societies

Mineralogical Society of Austria

Croatian Geological Society

Czech Geological Society

Hungarian Geological Society,
Mineralogical-Geochemical Branch

Mineralogical Society of Poland

Mineralogical Society of Romania

Geological Society of Slovakia,
Mineralogical-Geochemical Branch

Supporting societies

Bulgarian Mineralogical Society

Serbian Geological Society,
Mineralogical-Petrological Section

Slovenian Geological Society,
Mineralogical Branch

IMA2010 abstracts were revised by the session convenors, formatted by the editors with the help of Ramona Bălc, Evelyn Dömötör, Rodica Filipescu, Anamaria Mihăilă

Abstract index was prepared by the editors, with the help of Evelyn Dömötör, Melinda Jánosi, Ferenc Kristály, Erzsébet Tóth

---

Further scientific sponsors

National scientific academies and their research institutes in the organising countries
Universities from the organising countries
Museums of the organising countries
European Mineralogical Union and several mineralogical societies of Europe
Sister societies of IMA
IUGS Hungarian National Committee

International Organising Committee

Tamás G. Weiszburg, Chairman	(Hungary)
Dana Pop, Secretary General	(Romania)
Luminiţa Zaharia, Abstract Co-ordinator	(Romania)
Ekkehart Tillmanns (ex officio)	(Austria)
Vladimir Bermanec	(Croatia)
Károly Brezsnyánszky	(Hungary)
Igor Broska	(Slovakia)
Georgios Christofides	(Greece)
Attila Demény	(Hungary)
Mickey Gunter	(USA)
Szabolcs Harangi	(Hungary)
Imbarak S. Hassen	(Egypt)
Volker Höck	(Austria)
Corina Ionescu	(Romania)
Gabriella Kiss	(Hungary)
Friedrich Koller	(Austria)
Veselin Kovachev	(Bulgaria)
István Kovács	(Hungary)
György A. Lovas	(Hungary)
Ferenc Mádai	(Hungary)
István Márton	(Romania)
Ferenc Molnár	(Hungary)
Daniel R. Neuville	(France)
Milan Novák	(Czech Republic)
Ladislav Palinkaš	(Croatia)
Gábor Papp	(Hungary)
Zbigniew Sawłowicz	(Poland)
Simona Skobe	(Slovenia)
Tsveta Stanimirova	(Bulgaria)
Csaba Szabó	(Hungary)
Sándor Szakáll	(Hungary)
Géza Szendrei	(Hungary)
Veronika Szilágyi	(Hungary)
Darko Tibljaš	(Croatia)
Erzsébet Tóth	(Hungary)
Pavel Uher	(Slovakia)
Nada Vasković	(Serbia)
Sabine Verryn	(South Africa)

Scientific Programme Committee

Ekkehart Tillmanns, Chairman	(Austria)
Georges Calas, Vice-Chairman	(France)
István Kovács, Executive Scientific Secretary	(Hungary)
Tamás G. Weiszburg (ex officio)	(Hungary)
Péter Árkai	(Hungary)
Vladimir Bermanec	(Croatia)
Michael A. Carpenter	(UK)
Martin Chovan	(Slovakia)
Anne M. Hofmeister	(USA)
Georg Hoinkes	(Austria)
Gheorghe Ilinca	(Romania)
Peter Komadel	(Slovakia)
Anhuai Lu	(China)
Juraj Majzlan	(Germany)
Marek Michalik	(Poland)
Annibale Mottana	(Italy)
Milan Novák	(Czech Republic)
Bogdan P. Onac	(Romania/USA)
Herbert Palme	(Germany)
Mihály Pósfai	(Hungary)
Dmitry Yu. Pushcharovsky	(Russia)
Milan Rieder	(Czech Republic)
Tsutomu Sato	(Japan)
Bjoern Winkler	(Germany)

Publication Subcommittee

Gábor Papp, Chairman (Hungary)
(see the inside of the front cover for members)

Field trip Subcommittee

Friedrich Koller, Co-Chairman (Austria)
Ferenc Molnár, Co-Chairman (Hungary
(see the inside of the front cover of the field trip guides, *Acta Mineralogica-Petrographica*, *Field Guide Series*, Vol. 1–29, for members)

CONTENTS

PLENARY TALKS
Hazen, R.M.: Mineralogical co-evolution of the geosphere and biosphere v
Buseck, P.R.: 40 years of nanomineralogy v
Griffin, W.L. & O'Reilly, S.Y.: Composition and evolution of the SCLM, and the origin of its diamonds vi
Sigmarsson, O.: Mineralogical and glass compositional variations during the 2010 eruption of Eyjafjallajökull, Iceland vi
Lloyd, J.R.: The mineral-microbe interface and its defining role in controlling contaminant mobility in the subsurface vii
Hawthorne, F.C.: Toward theoretical mineralogy: the bond-topological basis of structure stability and mineral energetics .. vii
Wilke, M.: X-ray spectroscopy on geomaterials using synchrotron radiation viii

ELEMENTS 5 TALKS
Valsami-Jones, E., Oelkers, E.H., Skartsila, K. & Klasa, J.: Phosphate mineral reactivity: from nano to global scales ix
Ewing, R.C.: The nuclear fuel cycle: role of mineralogy and geochemistry in the safe management of nuclear waste ix
Kelly, N.M.: Zircon – more than just a chronometer x
Pósfai, M., Kasama, T., Simpson, E.T., Faivre, D., Schüler, D. & Dunin-Borkowski, R.E.: Biomineral attractions: magnets in organisms x
Sahai, N., Zhang, N., Murphy, W.L., Molenda, J., Yang Y. & Cui Q.: Mechanisms of cellular and biomacromolecular interactions with minerals in humans xi
Waychunas, G.A.: Mineralogy and geochemistry at lower dimensionality: mineral-water interfaces and nanoparticles xi

1. APPLIED MINERALOGY, MATERIALS SCIENCE
AM10G Applied mineralogy, Materials science (general session) 1
AM11 Gem materials: Origins, properties, and new analytical challenges 21
AM12 Structure and properties of silicate glasses and melts: From laboratory to volcanic activities 35
AM14 Zeolites and porous materials 47
AM15 Gas storage in minerals: Experimental and field studies 57
AM16 Chemical degradation kinetics of cementitious materials: Application to the durability of hydrated cement and concrete 65
AM17 Corrosion: From biofouling to mineral weathering 71
AM18C2 Colloidal properties and surface chemistry of clays 75
AM19C5 Interfacial phenomena of clay minerals: Adsorption, intercalation and nanohybrid materials 87

2. CLAY SCIENCE (co-sponsored by the Mid-European Clay Conference)
C20G Clay Science (general session) 97

3. CULTURAL HERITAGE
CH30G Archaeometry (general session): Composition, technology and provenance of archaeological artifacts 103
CH31 Mineralogical aspects of monument preservation 127

4. DEEP EARTH
DE41 Mineralogy of the Deep Earth 141
DE42 Planetary cores 161
DE43 "Water" in nominally anhydrous minerals: Analytical and experimental contributions 169
DE44 Diamond crystallization under natural and experimental conditions 177
DE45 Fluids in the Earth 189
DE46 Frontiers of ultrahigh-pressure metamorphism and deep subduction: From atomic scales to mountain building 207

5. ECONOMIC GEOLOGY/MINERALOGY
EG50G Economic geology (metallic and non-metallic ore deposits) (general session) 221
EG51 Crustal fluids and gold 245
EG52 Platinum-group minerals in the new millennium 263
EG53 Geo-metallurgy and Process mineralogy 275
EG54 Mineral deposits in terrestrial volcanic-hydrothermal systems 285
EG55 Mineral deposits of Africa 301
EG56C4 Industrial clay deposits: From the field to the industry 307
EG57C14 Clays in oil and gas industry 313

6. ENVIRONMENTAL MINERALOGY AND GEOCHEMISTRY, BIOMINERALOGY, HEALTH
EM60G Environmental mineralogy and geochemistry, Biomineralogy, Health (general session) 319
EM61 Mineralogy of mine wastes and contaminated soil 335
EM62 Contaminated land and sustainable remediation 353
EM63 Mineralogy and geochemistry of the nuclear fuel cycle 361
EM64 Biominerals and biomaterials: The interface between geosciences and life sciences 367
EM65 Interactions between microorganisms and minerals: From cell to environmental systems 379

EM66C6 Clays related to environment and health....393
EM67C13 Clay minerals and bio-molecules: From the origin of life to advanced biomedical applications....409

7. GENERAL AND SPECIFIC MINERALOGY
GM70G General and specific mineralogy (general session)....415
GM71 From the protoplanetary disc to lower mantle: Celebrating 170 years of perovskite research (session dedicated to Roger H. Mitchell)....441
GM72 Accessory minerals: Tracers of magmatic and metamorphic evolution....447
GM73 Cave minerals....465
GM74 Boron minerals, geochemistry and isotopes: What do they tell us about geologic processes?....473
GM75 New minerals, nomenclature and classification....487
GM76C9 Non-phyllosilicate clays....503

8. GEOCHEMISTRY AND PETROLOGY
GP80G Geochemistry and Petrology (general session)....505
GP81 Volcanoes: The mineral factory....537
GP82 Alkaline rocks/kimberlites/carbonatites....551
GP83 Ophiolites: From spreading to emplacement....581
GP84 Decoding P-T-t-d evolution in mountain belts: Significance for geodynamics....591
GP85 Jadeitites and their record of subduction zone processes....597
GP86 From gemstones to cell phones: The importance of pegmatites to society....603
GP87C3 Geology of clays....621
GP88C8 Weathering, soils and paleosol clays....639

9. METHODS AND APPLICATIONS
MA91 Advanced transmission electron microscopy methods....649
MA92 Mineral spectroscopy: Advanced spectroscopic methods applied to minerals and related inorganic materials....655
MA93 Application of synchrotron radiation in earth and planetary sciences....669
MA94 Advances in neutron techniques in earth and environmental sciences....679
MA95 Breakthroughs in geochronology and thermochronology and applications to tectonic problems....683
MA96 Advances in imaging techniques, and their application in the Earth sciences....687
MA97C10 Advanced instrumental techniques in clay science....695

10. MINERALOGICAL CRYSTALLOGRAPHY
MC100G Mineralogical crystallography (general session)....705
MC101 Bond topology in complex structures....731
MC102 Modularity and modulation in minerals....737
MC103C1 Crystal chemistry and structure of clay minerals and layered minerals....747

11. MINERAL MUSEUMS AND HISTORICAL MINERALOGY
MH110G Mineral museums and Historical mineralogy (general session)....761
MH111 History of mineralogy: The role of the Carpathian region in the 18th century....771
MH112 The scientific value of mineral beauty....775

12. PLANETARY MINERALOGY
PL121 Planetary mineralogy: Meteorites, shock metamorphism, and more....777
PL122/124 Minerals in meteorites / First solids in the solar system....787
PL123 Cometary and stellar mineralogy....791
PL125 Terrestrial and extra-terrestrial nanodiamonds: Recent progress in the occurrences, structures and uses....797

13. THERMODYNAMICS, KINETICS AND MINERAL PHYSICS
TH131 Influence of reaction kinetics on rock microstructure, texture and micro-chemistry: Assessing the petrogenetic record....799
TH132 Thermodynamic behaviour of Earth materials....807
TH134 Structure-property relations of minerals from atomistic models....815
TH135 Interactions between solids and aqueous solutions from theory and experiment....821
TH136 Mineral growth and interface processes....831
TH137 Nanoparticles: Structure, properties, reactivity....843
TH138C11 Physical properties of clays at non-ambient conditions....849
TH139C12 Fabric anisotropy and its influence on physical properties of clay-rich rocks....855

14. TEACHING AND OPEN SESSION
TM141G Teaching of mineral sciences....859
XO150G Open session: Mineral sciences-related other subjects....867

Addendum to GP87C3 – Geology of clays....872

Authors' index....873

Mineralogical co-evolution of the geosphere and biosphere

Hazen, R.M.
Geophysical Laboratory, Carnegie Institution, Washington DC, USA (rhazen@ciw.edu)

The mineralogy of terrestrial planets evolves as a consequence of varied physical, chemical and biological processes [1]. Initial evolutionary stages include the transition from ~12 nano-scale mineral phases in pre-stellar dense molecular clouds, to ~60 primary chondrite minerals, to ~250 different minerals in altered chondrites, achondrites and differentiated asteroids. Earth's subsequent prebiotic mineral evolution depended on a sequence of geochemical and petrologic processes, including volcanism and degassing, fractional crystallization, crystal settling, assimilation reactions, regional and contact metamorphism, plate tectonics and associated large-scale fluid-rock interactions. These processes resulted in perhaps 1500 different mineral species.

Biological processes began to affect Earth's surface mineralogy by the Eoarchean, when large-scale surface mineral deposits, including carbonates and banded iron formations, were precipitated under the influences of changing atmospheric and ocean chemistry. The Paleoproterozoic "Great Oxidation Event" and Neoproterozoic increases in atmospheric O_2 transformed Earth's surface mineralogy and are responsible, directly or indirectly, for most of Earth's 4300 known mineral species.

Mineral evolution arises from three primary mechanisms: (1) progressive separation and concentration of elements from their original relatively uniform distribution; (2) an increase in range of intensive variables such as pressure, temperature, and the activities of H_2O, CO_2 and O_2; and (3) generation of far-from-equilibrium conditions by living systems. The sequential evolution of Earth's mineralogy from chondritic simplicity to Phanerozoic complexity introduces the dimension of geologic time to mineralogy and thus provides a dynamic alternate approach to framing the mineral sciences.

[1] Hazen, R.M. et al. (2008) *Am. Mineral.*, **93**, 1693-1720.

40 years of nanomineralogy

Buseck, P.R.
School of Earth & Space Exploration and Dept. of Chemistry/Biochemistry, Arizona State University, Tempe, AZ, USA (pbuseck@asu.edu)

The warm feelings conveyed by Figure 1 reflect the substantial progress that has occurred in the study of crystalline materials, including minerals, during the last four decades. That figure, lacking the Valentine Day embellishments, appeared 30 years ago. It followed developments that transformed transmission electron microscopy from a technique used primarily by biologists to one routinely utilized by solid-state scientists, including mineralogists. The changes became possible through the availability of new, highly stable microscopes for producing high-resolution images and new theory for interpreting the results. This combination facilitated the study of defects and other irregularities in crystalline and, eventually, non-crystalline solids. Additional developments continue to this day.

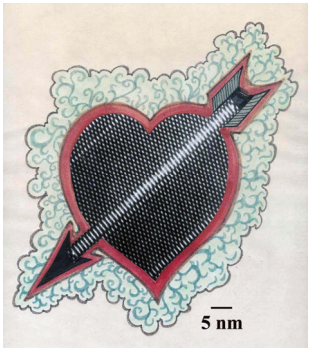

Fig. 1: Slightly edited HRTEM image of defects in biopyriboles; modified (by Sue Selkirk) from Fig. 1c in Veblen and Buseck [1].

High-resolution images of solids allowed the first direct visualization of structural irregularities in crystals. One no longer had to infer the crystal defects that permitted solid-state reactions to occur. Instead, it became possible to actually observe the reaction pathways through transitions and reactions "frozen" before completion. Such new information helped reconstruct processes that previously could only be inferred.

Transmission electron microscopes (TEMs) can be used to measure the crystalline structures and compositions of minerals at the micrometer to sub-nanometer scale. For particles, such as occur in the atmosphere and comprise an area of increasing interest for mineralogists, they can also be used to determine their sizes, 2D and 3D shapes, intergrowths, and coatings, all of which are of interest for atmospheric and climate studies.

The various nanoscale modes of modern TEMs include high-resolution imaging (HRTEM); energy-dispersive X-ray spectrometry (EDS) to determine compositions of inorganic species; electron energy-loss spectrometry (EELS) to measure the abundances of elements heavier than Li, their oxidation states, and chemical speciation; energy-filtered TEM (EFTEM) to show the distributions of elements within substances; selected-area electron diffraction (SAED) to determine crystallographic structures; environmental-TEM (ETEM) to measure hygroscopic properties, volatilities, and reactions at high temperature; electron holography (EH) for magnetic studies; and electron tomography (ET) to determine 3D shapes.

Mineral studies at elevated temperatures are almost routine, and we are currently trying to develop the use of TEMs to study minerals at high pressure. Examples will be provided of a range of problems addressed by studying minerals on a level ranging down to the nanoscale.

[1] Veblen, D.R. & Buseck, P.R. (1980) *Am. Mineral.*, **65**, 599-623.

Composition and evolution of the SCLM, and the origin of its diamonds

Griffin, W.L.* & O'Reilly, S.Y.
GEMOC, Earth and Planetary Sciences, Macquarie University, Sydney, NSW, Australia (*bill.griffin@mq.edu.au)

Recent developments in seismic tomography and the integrated modeling of geophysical and petrological data have stimulated a major re-evaluation of the original composition and present extent of Archean subcontinental lithospheric mantle (A-SCLM). Analyses of seismic and gravity data, and consideration of relationships in exposed Archean peridotite massifs, suggest that the primitive A-SCLM probably was a highly depleted, moderately oxidised dunite-harzburgite, formed by high-degree melting at high T and P. Seismic tomography of cratons at regional and local scales shows "knobs" of high-Vs material that can be modeled as primitive A-SCLM, surrounded by zones of lower Vs. Kimberlites preferentially intrude these low-Vs belts, bringing up xenolith suites dominated by garnet lherzolites. By analogy with Archean peridotite massifs, these less-depleted rocks are interpreted as the result of metasomatic refertilisation, with progressive addition of cpx and garnet, and lowering of Mg#, in the peridotites. Within individual kimberlite fields, there is a direct correlation between this refertilisation process and the presence of diamonds of the peridotitic paragenesis [1]. A strong correlation between subcalcic garnets and diamonds suggests a model in which diamonds are deposited as CH_4-rich fluids are oxidized by the SCLM, producing carbonate-rich, hydrous fluids.

EMP and FTIR analyses of µm-sized fluid inclusions in "fibrous" diamonds have identified a more complex suite of high-density fluids (HDF), ranging from carbonatitic melts to "hydrosilicic" fluids and super-saline brines. LAM-ICPMS analysis of such diamonds [2] yields trace-element patterns similar to kimberlites and carbonatites, with high LREE/HREE, and high contents of alkali elements (Na, K, Rb, Cs, Ba) and HFSE (Ti, Zr, Nb…). Within single localities, carbonatitic, hydro-silicic and saline fluids have broadly similar trace-element patterns. The different types of HDF may reflect complex interactions between low-volume (mostly carbonatitic) melts, saline brines and different wall rocks (peridotitic vs eclogitic, refractory vs metasomatised).

In contrast to the fibrous diamonds, most monocrystalline diamonds have REE patterns that are either are essentially flat, or are depleted in LREE relative to HREE. They also are depleted in the alkali elements relative to the LREE, and many show strong negative anomalies in Y and Sr. These fluids and those that form fibrous diamonds may be related through carbonate/silicate melt immiscibility; the transition between them has been observed in single stones. In the Diavik mines, some monocrystalline diamonds and their fibrous/granular coats appear to have grown from the same type(s) of fluid.

If most peridotitic diamonds are related to the metasomatic modification of the dunitic Archean SCLM, then progressive metasomatism of the SCLM through time should decrease its overall prospectivity for diamonds. However, in tectonothermally younger terrains, diamonds are commonly hosted primarily in eclogites. In the absence of oxidized dunites, these mafic rocks may provide the redox environment required to deposit diamonds. Metasomatism is an ongoing process, and it is not obvious that diamonds necessarily are ancient; some may be quite „modern."

[1] Malkovets, V. et al. (2007) *Geology*, **35**, 339-342. [2] Rege, S. et al. (2005) *J. Anal. Atom. Spectrom.*, **20**, 601-611.

Mineralogical and glass compositional variations during the 2010 eruption of Eyjafjallajökull, Iceland

Sigmarsson, O.
Inst. of Earth Sciences, University of Iceland, Reykjavik, Iceland (olgeir@raunvis.hi.is) and
Laboratoire Magmas et Volcans, CNRS - Université Blaise Pascal, Clermont-Ferrand, France

After three months of magma injection beneath Eyjafjallajökull volcano, and corresponding inflation of the volcano, a lateral eruption started March 20 at the Fimmvörðuháls pass. Relatively primitive olivine and plagioclase bearing basalt was produced from ca. 500 m long fissure. After the first two days, the activity was concentrated in a single strombolian crater until March 31 when a new eruption fissure opened orthogonal to the first one. Last lava-forming activity was observed March 12. The basalt composition has a restricted whole-rock compositional range (8-9% MgO) from 3% Hy-normative at the beginning to 3% Ne-normative composition at the end. The euhedral phenocrysts assemblage is composed of Cr-rich spinel (picotite), olivine in the range Fo79-71 (with four crystals of Fo86), and a bytownite plagioclase (An81-76). Abundant vesicules and microlites characterize the groundmass, suggesting degassing-related crystallization. The interstitial glass composition is similar to the evolved FeTi-basalts of the neighbouring Katla volcano (MgO: 4.5-5.0%). During the historical period Katla has erupted twice per century; it last erupted in 1918.

On April 14 an explosive summit eruption started beneath an ice-cap with an eruption column occasionally rising as high as 8-10 km. Very fine-grained tephra of trachy-andesitic composition was produced and dispersed to the east and later to the south covering the neighbouring area with a few cm thick tephra layer. Finest part of this tephra was ejected to significant heights in the atmosphere where it sojourned for several days, and was brought over continental Europe by prevailing northeast wind directions. The fine grain-size of the tephra is not only due to rapid quenching caused by ice-magma interaction but also by fragmentation caused by rapid strain of a relatively viscous melt. The trachy-andesite produced during the first five days result from a binary mixing between fractionated basalt (similar in composition to those of Katla volcano) and a dacitic melt, possibly left-over from the penultimate eruption at Eyjafjallajökull (the 1821 dacite), and a consequent rapid magma ascent. The magma mixing is reflected by linear correlations on element-element plots between major- and trace-element concentrations obtained on whole-rock samples and in-situ by EMPA and LA-ICP-MS methods applied to primitive melt-inclusions, groundmass glasses and tephra fragments from the 1821 eruption. Three glass types are observed in the early tephra with SiO_2 concentrations of 49-51%, 60-61% and 69-70% that illustrates a mechanical magma mingling without enough time for homogenization before eruption. This results in complex mineralogical zonation with Fo64-50, An69-9 and Mg-number of clinopyroxene in the range 72-26. On May 4 a deep seismic swarm (over 20 km deep) occurred with consequent higher magma output as measured from the height of the May 5 eruption column. The tephra produced that day is comprised of well-mixed glass with SiO_2 of 62-63% but has 50µm zoned-olivines with 10 µm tick rim of Fo_{48-50}. The core has Fo_{80}, a composition similar to the olivines of the Fimmvörðuháls basalts. These results indicate a direct link between the arrival of primitive basalts, deep seismicity, increased magma pressure in the plumbing system, and higher magma output rate. Taken together, the explosive phase of the 2010 Eyjafjallajökull eruption was caused by dynamic magma mixing of mantle-derived basalt with older silicic intrusion remobilized by the crystallizing primitive basalt.

The mineral-microbe interface and its defining role in controlling contaminant mobility in the subsurface

Lloyd, J.R.
School of Earth, Atmospheric and Environmental Sciences, The University of Manchester, UK (jon.lloyd@manchester.ac.uk)

Recent advances in mineralogy and microbiology have led to a molecular-scale understanding of the critical role of the mineral-microbe interface in controlling contaminant mobility in the subsurface. Of particular note are respiratory processes, mediated by specialist bacteria and archaea, and coupled directly to the redox transformations of minerals. These effectively control the mobility of both inorganic and organic species in a wide range of environments and, if harnessed, may offer the basis of a wide range of innovative biotechnological processes. These applications include the bioremediation of metal contaminated land and water, the oxidation of xenobiotics under anaerobic conditions, metal recovery in combination with the formation of novel functional bionanominerals, and even the generation of electricity from anoxic sediments. Under certain conditions, however, microbial redox transformations of minerals can also mobilise toxic metals and metalloids with potentially calamitous effects on human health.

Focusing on "dissimilatory" mineral reduction processes, I will discuss recent advances in the understanding of the mechanisms of anoxic Fe redox cycling in the subsurface, and the impact of Fe mineral biotransformations on sediment biogeochemistry and the mobility of trace metals, metalloids and radionuclides. The biotechnological application of mineral-transforming metal-reducing bacteria for the generation of commercially useful bionanominerals will also be discussed, alongside their use in a range of innovative *ex situ* applications. The dramatic impact of advanced imaging, synchrotron spectroscopy and genomics-enabled techniques in dissecting the mineral-microbe interface will be highlighted alongside current challenges in this rapidly developing area of multidisciplinary science.

Toward theoretical mineralogy: the bond-topological basis of structure stability and mineral energetics

Hawthorne, F.C.
Dept. of Geological Sciences, University of Manitoba, Winnipeg, Canada (frank_hawthorne@umanitoba.ca)

The electronic properties of the constituent atoms of a structure may be represented as the diagonal elements of a square matrix, and the interactions between these atoms may be represented by the off-diagonal terms of this matrix. The form of this matrix is identical to that of the adjacency matrix of the weighted chromatic digraph of the bond network. The electronic energy density-of-states can be derived using the method of moments [1], where the trace of the diagonalized Hamiltonian matrix (of the usual secular determinant equation) has a topological interpretation in terms of closed paths in the graph of the constituent orbitals. The energy difference between two structures depends primarily on the first few disparate moments of their respective energy density-of-states [2]. Consider what this means: (1) zero-order moments are >walks in place= and define chemical composition; (2) second-order moments define coordination number; (3) fourth- and sixth-order moments define local connectivity of coordination polyhedra; energy differences between structures are dependent on these features. Open-system behaviour changes zero-order moments, closed system behaviour does not change zero-order moments. Within this framework, we may divide mineral reactions into two types: (1) those where bond topology is conserved; (2) those where bond topology is not conserved. *Conservation of Bond Topology:* The edge set of the digraph is conserved but the weights may vary depending on local changes in the vertex set. Thus the energetically most important changes involve variation in patterns of Short-Range Order (SRO). In order to conserve bond topology with varying T and P, thermal expansion and elastic compression must be accompanied by element substitutions that accord with the short-range version [3] of the valence-sum rule of bond-valence theory [4]. Thus variation in SRO is an integral part of continuous mineral reactions and drives compositional change. *Non-conservation of Bond Topology*: In a closed system, zero moments are fixed and the lowest-order changes involve second-order moments, *i.e.*, changes in coordination number. Many reactions of geological interest involve conservation of cation-coordination number, and such reactions are driven primarily by changes in anion-coordination number. The correspondence principle of Lewis acidity – Lewis basicity [5] may be used to explain the structural and chemical complexity of many surficial minerals. Where data are available, species in aqueous solution follow the valence-sum rule, and their Lewis basicities scale with the pH values of the solution at maximum abundance of the species in solution. The complex species in aqueous solution actually form the building blocks of the crystallizing minerals, and in principle, the structures thus retain a record of the pH of the nascent solutions from which they crystallized. This general approach has an atomistic basis and yet is sufficiently simple that complex problems can be addressed in a transparent yet quantitative manner.

[1] Burdett, J.K. et al. (1984) *Croatia Chem. Acta*, **57**, 1193-1216. [2] Burdett, J.K. & Lee, S. (1985) *J. Am. Chem. Soc.*, **107**, 3063-3082. [3] Hawthorne, F.C. (1997) *Can. Mineral.*, **35**, 201-216. [4] Brown, I.D. (2002) *The Chemical Bond in Inorganic Chemistry. The Bond Valence Model.* Oxford University Press. [5] Hawthorne, F.C. & Schindler, M. (2008) *Z. Kristallogr.*, **223**, 41-68.

X-ray spectroscopy on geomaterials using synchrotron radiation

Wilke, M.
Helmholtzzentrum Potsdam Deutsches GeoForschungsZentrum, GFZ, Potsdam, Germany (max@gfz-potsdam.de)

In the last two decades, synchrotron radiation (SR) has become an indispensable tool for studying geomaterials using X-ray spectroscopic techniques. The continuous spectrum and the high brilliance produced by a SR source not only enable the acquisition of high quality data in short time, but also provide the possibility to focus the SR beam into small spots with very high photon flux. Particularly the latter feature is a prerequisite for many applications in Earth sciences. In this lecture, a sequence of examples using X-ray spectroscopic techniques is discussed, which highlight the versatile applicability to many materials of geological interest at the relevant geological conditions.

One very important application using the fine structure observed at the X-ray absorption edge (XANES) represents the investigation of redox processes. For Fe, the pre-edge region provides an almost direct way of quantifying the oxidation state in many crystalline and non-crystalline compounds [1], even with microscopic spatial resolution, e.g. [2]. XANES at the S K-edge may be used to study S-redox equilibria in melts, e.g. [3]. E.g., new XANES derived data show a much narrower transition from sulfide to sulfate with oxygen fugacity than previously determined with the electron microprobe. This may have considerable implications for the sulfur behaviour in subduction-related magmas [4]. Time-resolved XANES may even be used to determine the progress and mechanism of redox reactions. E.g., this was nicely shown for the case of oxidation of Mn(II) by bacteria [5].

Due to the rather low absorption of hard X-rays by matter, SR opens up the possibility to perform measurements in high-pressure or reaction cells. SR micro-XRF is used for obtaining trace element concentrations in aqueous fluids in-situ at high P and T using an XRF-optimized diamond anvil cell, with detection limits in the lower ppm range [6,7], even for low Z elements such as Ti [8]. A particular advantage over any quench technique is the possibility to study directly the kinetics of equilibration [9]. Furthermore, the high-pressure setup is used to investigate the element complexation in aqueous fluids by acquiring X-ray absorption spectra at conditions of the Earth's crust, e.g. REE in model fluid compositions [10]. XANES on Fe in hydrous melt at P & T provides evidence for non-quenchable structural re-organizations in the Fe environment during the cooling to a hydrous glass [11]. These valuable insights cannot be achieved on quenched samples at all and show the importance of these studies particularly for the understanding of processes at high P and T.

The soon dedication of new and upgraded SR sources for hard X-rays, will make sure that the conditions for such studies will improve and will certainly open up possibilities for new experiments to provide access to parameters not accessible so far.

[1] Wilke, M. et al. (2001) *Am. Mineral.*, **86**, 714-730. [2] Schmid, R. et al. (2003) *Lithos*, **70**, 381-392. [3] Wilke, M. et al. (2008) *Am. Mineral.*, **93**, 235-240. [4] Jugo, P.J. et al. (2010) *Geophys. Res. Abstr.*, **12**, EGU2010-7075. [5] Bargar, J.R. et al. (2000) *Geochim. Cosmochim. Ac.*, **64**, 2775-2778. [6] Schmidt, C. & Rickers, K. (2003) *Am. Mineral.*, **88**, 288-292 [7] Schmidt, C. et al. (2007) Lithos, **95**, 87-102, [8] Manning, C.E. et al. (2008) *Earth Planet. Sci. Lett.*, **272**, 730-737. [9] Borchert, M. et al. (2009) *Chem. Geol.*, **259**, 39-47. [10] Mayanovic, R.A. et al. (2009) *Chem. Geol.*, **259**, 30-38. [11] Wilke, M. et al. (2006) *Chem. Geol.*, **229**, 144-161.

Phosphate mineral reactivity: from nano to global scales

Valsami-Jones, E.[1*], Oelkers, E.H.[2], Skartsila, K.[1] & Klasa, J.[1]
[1]Dept. of Mineralogy, Natural History Museum, London, UK ([*]evj@nhm.ac.uk)
[2]Biogéochimie et Géochimie Expérimentale, LMTG-Université de Toulouse-CNRS-IRD-OMP, Toulouse, France

Life as we know it on Earth needs phosphate for its many biological roles, for example as the backbone of DNA. As a result, phosphorus availability often regulates biological productivity in many terrestrial and marine environments, but when in excess, leads to uncontrollable biological growth linked to water quality problems (eutrophication).

Phosphate minerals have a central role in this process, as they are the "gatekeepers", sources and sinks, of phosphorus in environmental and biological systems. Phosphate mineral solubility is particularly relevant, but exceptionally complex, notably in the case of apatite, the most common and perhaps most important of all phosphate minerals.

An important aspect of the phosphorus global cycle is that its only primary source is phosphate ore, which is a finite resource, with some predictions suggesting there remain as little as 125 years worth of global reserves. If phosphorus is no longer available or becomes too expensive, major consequences on global food production can be expected. It is therefore essential that the use of phosphorus be reviewed and potentially regulated.

Apatite in its various forms as a biological or chemical precipitate will form the focus of this paper. Its dissolution and precipitation kinetics and the influence of organic species in these processes will be reviewed and our efforts to understand its reactivity within environmental and biological matrices will be discussed. These processes, happening at the nano scale, could potentially have global consequences.

The nuclear fuel cycle: role of mineralogy and geochemistry in the safe management of nuclear waste

Ewing, R.C.
Dept. of Geological Sciences, University of Michigan, Ann Arbor, MI, USA (rodewing@umich.edu)

During the past five years, there has been a renewed interest in nuclear power as a source of energy that does not emit green house gases. An important consideration remains the environmental impacts of mining uranium and the final disposition of nuclear wastes. In addition, advanced nuclear fuel cycles, which involve new reactor types and reprocessing of used fuel, will require the development of new materials and create new waste streams.

In parallel with this renewed interest in nuclear power, the Office of Science of the U.S. Department of Energy has conducted a series of *Research Needs* workshops that have outlined cutting-edge research areas that will be required in order to support the nuclear "renaissance". Two of the reports, *Basic Research Needs for Advanced Nuclear Energy Systems* and *Basic Research Needs for Geosciences: Facilitating 21st Century Energy Systems* outline a research agenda for mineralogists and geochemists involved in both the "front-end" and "back-end" of the nuclear fuel cycle. A third report, *Basic Research Needs for Materials Under Extreme Environments* outlines a research agenda that has important overlaps with the research of the mineral physics community. The research agenda are organized according to:

- immediate research needs,
- "use-inspired" basic research,
- cross-cutting fundamental research,
- grand challenges

Typical of the scientific Grand Challenges are: *i.*) physics and chemistry of actinide-bearing materials; *ii.*) first principles, multi-scale modeling of complex materials under extreme conditions; *iii.*) the design of molecular systems for chemical selectivity during processing.

I will identify the relevant areas of research for mineralogists and geochemists with examples from:

- the design and properties of nuclear waste forms;
- corrosion of spent nuclear fuel;
- radiation effects under extreme conditions.

Zircon – more than just a chronometer

Kelly, N.M.
Dept. of Geology & Geological Engineering, Colorado School of Mines, Golden, CO, USA (nkelly@mines.edu)

Zircon ($ZrSiO_4$) is a mineral of singular importance in Earth Science. Based on its robust retention of formation ages and its ability to substitute a wide variety of trace elements that record the conditions of its formation or alteration, zircon has become the foremost among our geochronometers. No other mineral has the capability to help us unravel so much about how our Earth has evolved chemically and structurally through time. In addition, zircon is continually revealing how broad its capacity is to record the timing of events that have occurred across a vast range of geologic environments from the upper mantle through to the near surface environment. The rock types and environments in which we find zircon seems only limited by our curiosity to look.

The use of zircon for U-Pb dating by isotope dilution or microbeam methods has become almost routine, supported by continued advances in our ability to analyse smaller and smaller sample volumes at higher and higher analytical precision. However, it is the ability to directly link geochemical signatures with absolute time constraints that makes zircon such a powerful tool to be brought to bear on any number of geologic problems. For example it is now commonplace to integrate U-Pb zircon ages with Hf isotopes to fingerprint the sources of magmatic rocks; O isotopes to evaluate the contribution of mantle melts to crustal magmas as well as the role of high- vs low-temperature processes in the environment of zircon growth or alteration. The rare earth and other trace elements are commonly used to trace the environments of zircon growth be they high-temperature and in the presence of melts or during hydrothermal fluid events. The addition of Ti to this arsenal of geochemical tracers has now given us the ability to place direct temperature estimates on zircon growth. Moreover, U-Pb dating is now being integrated with U-Th/He methods thereby providing us with valuable information about exhumation in mountain belts and the coupled depositional histories of the detritus eroded from these mountains.

In the coming years research will address our incomplete understanding of the true complexity recorded at the micro-scale in zircon and what part of a geologic history fragments of a single zircon may represent. This work will hopefully enhance our ability to interpret the mechanisms that lead to zircon growth and modification, not only improving the meaning of zircon ages but also giving us robust means with which to use such fine-scale features to describe the intricacies in geologic processes that individual zircon grains bore witness. Such advances will continue to emphasise the importance of this tiny, but timely, mineral.

Biomineral attractions: magnets in organisms

Pósfai, M.[1*], Kasama, T.[2], Simpson, E.T.[3], Faivre, D.[4], Schüler, D.[5] & Dunin-Borkowski, R.E.[2]
[1]Dept. of Earth and Environmental Sciences, University of Pannonia, Veszprém, Hungary ([*]mihaly.posfai@gmail.com)
[2]Center for Electron Nanoscopy, Technical University of Denmark, Kongens Lyngby, Denmark
[3]Dept. of Materials Science and Metallurgy, University of Cambridge, Cambridge, United Kingdom
[4]Dept. of Biomaterials, Max Planck Institute of Colloids and Interfaces, Potsdam, Germany
[5]Dept. of Microbiology, Ludwig Maximilians-Universität, München, Germany

Many organisms contain ferrimagnetic nanocrystals. Bacteria, pigeons and fish are known to use magnets for navigating in the Earth's magnetic field, whereas some animals use the iron minerals for hardening or protection. However, in most cases the biological functions of magnetic crystals remain unknown.

Magnetotactic bacteria are the best known examples of organisms that contain nanoscale magnets. Specific strains of bacteria form magnetite (Fe_3O_4) or greigite (Fe_3S_4) crystals, or both, in their cells. The membrane-bound, ferrimagnetic nanocrystals (magnetosomes) have species-specific sizes and morphologies and various arrangements, most often in linear chains. Cells of magnetotactic bacteria provide a natural laboratory, in which the magnetic properties of nanometer-sized particles can be studied.

We have used a combination of advanced transmission electron microscopy techniques, including off-axis electron holography, to study the structural, magnetic and chemical properties of magnetic nanocrystals inside magnetotactic bacteria. The samples studied included uncultured magnetotactic cells collected from both marine and freshwater environments, and cultures of the strain *Magnetospirillum gryphiswaldense* and its genetically-modified mutants.

We studied the fine details of magnetic induction maps determined from electron holograms obtained from magnetosomes with a range of sizes and spacings. Based on these results, an experimental "magnetic-state phase diagram" was constructed that highlights the delicate balance between the magnetic state of a crystal, its size, shape and orientation, and the chain configuration, and illustrates graphically whether cells are able to respond effectively to the geomagnetic field. In general, the shape anisotropy of each crystal is the most important factor in controlling the magnetic microstructures of ferrimagnetic crystals in bacteria, followed by interparticle interactions and, least important, magnetocrystalline anisotropy. Despite significant variations in the magnetic properties of magnetosome chains, all of the wild-type cells had permanent magnetic dipole moments that were sufficient for magnetotaxis.

Biogenic magnets exhibit fascinating combinations of magnetic properties and biological functions. However, except for ferrimagnetic particles in magnetotactic bacteria, relatively little is known about them. Further work is needed to understand magnetic sensing in animals and the functions of magnetite particles in humans. A key challenge is the localization and preparation of tissues that contain ferrimagnetic particles. Once such samples are available, advanced analytical techniques, including off-axis electron holography, can be used to provide detailed characterization of the structures, compositions, arrangements and magnetic properties of biogenic nanomagnets.

Mechanisms of cellular and biomacromolecular interactions with minerals in humans

Sahai, N.[1,2*], Zhang, N.[2], Murphy, W.L.[3], Molenda, J.[3], Yang Y.[1] & Cui Q.[4]
[1]Dept. of Geoscience, University of Wisconsin-Madison, USA
[2]Materials Science Program, University of Wisconsin-Madison, USA ([*]sahai@geology.wisc.edu)
[3]Dept. of Biomedical Engineering, University of Wisconsin-Madison, USA
[4]Dept. of Chemistry, University of Wisconsin-Madison, USA

Medical Mineralogy involves the mechanistic study of interactions between of cells and biomacromolecules with minerals and aqueous solutions that are of relevance to biomedical applications and human health. The unique contribution of mineralogists to the health-related fields can be to emphasize the critical contributions of structure, composition, particle size, bulk and surface chemistry of the mineral or amorphous solid phase to the thermodynamics or kinetics of the relevant reactions of interest.

I will illustrate these ideas with two example studies. The first study deals with the potential for using bioactive silicate glasses and ceramics (wollastonite, pseudowollastonite) in orthopaedic implants for bone-tissue engineering. Porous silicate implants can be seeded with human mesenchymal stem cell (hMSCs). As the implant dissolves in the body, the silicon released from silicate hydrolysis may promote the differentiation of hMSCs down the osteoblastic lineage, promoting rapid bone growth and, eventually, complete replacement of the implant by newly-formed bone. However, Si released may also be potentially cytotoxic to and reduce adhesion of the hMSCs. Additional soluble factors such as Ca and P in the ambient fluid environment may also work cooperatively or as antagonists to Si, and physical factors such as surface rougness, porosity, etc., also affect hMSC adhesion, viability, and differentiation. Thus, numerous factors must be optimized simultaneously.

In the second example, I will discuss the potential role of acidic, non-collagenous proteins (ANCPs) in controlling the nucleation and growth of hydroxyapatite in bone biomineralization. Bone is a nano-composite material of collagen matrix fibrils in strict hierarchical arrangement with nancrystals of highly non-stoichiometric, highly substituted hydroxyapatite and associated ANCPs. I report the potential role of a NCP called Bone Sialoprotein (BSP) in nucleating a calcium phosphate phase. Using Molecular Dynamics simulations, we have studied the effects of both structure (alpha-helix versus random coil) and primary amino-acid sequence (wild-type versus *in silico* mutations) of a highly-conserved acidic peptide from BSP interacting with dissolved Ca^{2+} and HPO_4^{2-} ions to form an initial calcium phosphate nucleus, and to interact with (100) and (001) faces of hydroxyapatite in modulating crystal growth.

Mineralogy and geochemistry at lower dimensionality: mineral-water interfaces and nanoparticles

Waychunas, G.A.
The Berkeley Nanogeoscience Center, Earth Sciences Division, Lawrence Berkeley National Laboratory, Berkeley CA, USA
(gawaychunas@lbl.gov)

Over the last ten years experimental methods using synchrotron radiation have been developed to determine and refine the *in situ* molecular structure at mineral surfaces in analogy to that historically accomplished for bulk solids many years ago. We can thus begin to apply the rules of crystal chemistry, appropriately upgraded to include modern simulation tools, to surfaces, interfaces and grain boundaries. As surfaces are rarely precisely like the terminated bulk structure in terms of reactivity, chemistry and stoichiometry, we are thus gathering new insights into interface reactions like sorption, precipitation and acid-base equilibria [1]. These developments are timely inasmuch as nanomineralogical studies benefit markedly from an improved ability to understand the chemical characteristics of surfaces, edges and other "low coordination" surface topologies. Additionally, studies on both surfaces and nanoparticles yield information on local water structuring and hydrogen-bonding, with both being needed to completely define a nanoparticle surface and its properties [2].

Current studies include various surface-sensitive scattering and spectroscopic techniques, supported by both classical and ab initio calculations, but with almost all efforts aimed at characterizing near equilibrium or steady state interface structure. In the future, dynamic studies will be possible, with processes such as crystal growth, dissolution and even electron transfer reactions accessible on a true molecular level for the first time.

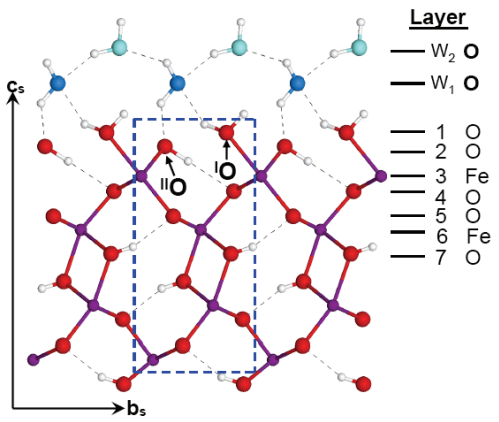

Fig. 1: Structure of the (100) cleavage face of goethite obtained from surface x-ray scattering showing surface bound functional groups ($FeOH$, $FeOH_2$) and two layers of ordered water [3]. The surface oxygens in Layer 1 and 2 are relaxed from their positions in the bulk structure. Dashed lines indicate likely hydrogen bonds.

[1] Barnett, M.O. & Kent, D.B. (2008) (eds.) *Adsorption of metals by geomedia II: Variables, mechanisms, and model applications*. Elsevier. [2] Spagnoli, D. et al. (2009) *Geochim. Cosmochim. Ac.,* **73**, 4023-4033. [3] Ghose, S.K. et al. (2010) *Geochim. Cosmochim. Ac.,* **74**, 1943-1953.

A new model of kink site reaction kinetics unifies crystal dissolution and growth theory

Luttge, A.[1,2*] & Arvidson, R.S.[1]
[1]Dept. of Earth Science, Rice University, Houston, TX, USA
[2]Dept. of Chemistry, Rice University, Houston, TX, USA
([*]aluttge@rice.edu)

It has been long recognized that kink site reaction kinetics govern crystal growth and dissolution at the molecular scale. It has also been uncritically assumed that equilibrium at kink sites is achieved if arrival and departure rates of lattice-building molecules are equal. Lastly, we have accepted that inhibition and catalysis of crystal growth and dissolution are controlled at kink sites.

New considerations, however, raise significant doubt that this simple model is correct. A detailed analysis of the elementary processes that imperatively occur at kink sites during the overall dissolution reaction leads to initially surprising results: the probability is always in favor of lattice destruction – this result is in agreement with the thermodynamic rule of increasing entropy. The destructive processes are eventually countered by the arrival of molecules at the kink sites. This modified model of kink site kinetics can explain several experimental observations that were unexplained or at odds with the existing theory. Importantly, the new model predicts that the reaction rate as a function of the distance from equilibrium (ΔG) must be continuous at equilibrium. Ultimately, our model allows us to unify crystal dissolution and growth theories.

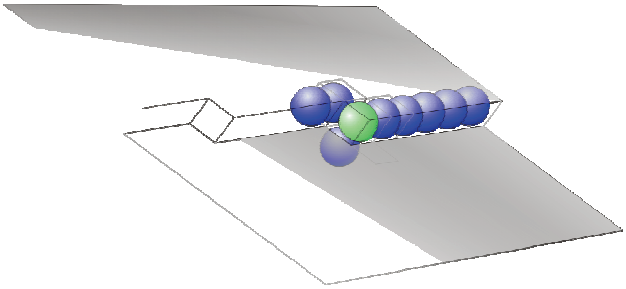

Fig. 1: Schematic view of kink site and nearest neighbours.

Dissolution of dolomite in HCl

Järvinen, L.J.[1-4*], Leiro, J.A.[1], Bjondahl, F.[5], Jäsberg, J.[2], Kara, J.[2], Carletti, C.[5,6], Sierra, S.[5,7] & Eklund, O.[2]
[1]Dept. of Physics and Astronomy, University of Turku, Finland
([*]ljjarv@utu.fi)
[2]Dept. of Geology, University of Turku, Finland
[3]Finnish Graduate School in Geology, Finland
[4]Graduate School of Materials Research, Turku, Finland
[5]Dept. of Chemical Engineering, Åbo Akademi University, Turku, Finland
[6]Universidad Simón Bolívar, Caracas, Venezuela
[7]Universidad Complutense, Madrid, Spain

Limestones are widely used as absorbents in various processes for removal of SO_2 from power plant flue gases. The most common method is called Wet Flue Gas Desulphurisation (WFGD) process, where the dissolution rate of limestone is essential for sizing and operation of the process. The presence of magnesium in limestones has been reported to reduce the dissolution rate [1], thus deteriorating the potentiality of the use of the rock in WFGD. The main limestone constituting mineral is calcite ($CaCO_3$), which can easily contain Mg^{2+} cations in its lattice. Another common mineral in limestones is dolomite ($(Ca, Mg)CO_3$), which has a bulk structure similar to calcite with the exception of every other cation layer in the c direction being composed of Mg atoms instead of Ca atoms. Obviously magnesium content in a limestone can vary greatly, and more profound knowledge of the influence of magnesium on the dissolution rate is needed.

The reactivity, calculated from the rate of dissolution and particle size distribution, of several dolomitic rocks has been tested using stepwise titration with hydrochloric acid (HCl) [2]. The specimens were crushed and ground into three size fractions of 63-106, 106-150 and 150-250 μm. The experimental setup consists of a stirred beaker containing sample particles in water, a pH electrode and a laser diffractometer for measurement of the particle size distribution. HCl has been used in the experiment, because the use of sulphur dioxide or sulphuric acid would result in the precipitation of calcium sulphate particles, which would influence the measurement of the particle size distribution.

The samples were characterised with X-ray Photoelectron Spectroscopy (XPS), Scanning Electron Microscopy (SEM), X-Ray Diffraction (XRD) and X-Ray Fluorescence (XRF). The rate determining steps of a dissolution reaction are generally considered to be surface kinetics and/or diffusion of reaction stimulating components through a barrier layer (that is surrounding the particle) to the immediate vicinity of the surface. Therefore the focus was kept on the surfaces of the dolomitic rocks with surface sensitive XPS and SEM.

The results show clear differences (an order of magnitude) in the reactivities of the dolomitic samples. Atomic concentrations were obtained with XPS and XRF, the former concentrating on surface composition and the latter on bulk composition. Mineral phases present in the rocks were identified from XRD spectra and polarizing microscope studies of polished thin sections. SEM micrographs obtained before and after the reactivity experiments gave information about the dissolution process on the surfaces of the samples. Relations between the reactivity and characterisation results are discussed.

[1] Siagi, Z.O. et al. (2009) *J. Hazard. Mater.*, **163**, 678-682. [2] Ahlbeck, J. et al. (1995) *Chem. Eng. Sci.*, **50**, 1081-1089.

Transformation of illite to K-feldspar on brick clay firing

Kristály, F.[1*] & Papp, I.[2]
[1]Inst. of Mineralogy and Petrology, University of Miskolc, Hungary ([*]askkf@uni-miskolc.hu)
[2]Inst. of Earth Sciences, University of Debrecen, Hungary

Two varieties of brick clay with chlorite – illite – muscovite dominated phyllosilicate fraction were applied in laboratory experiments. Before test body preparation, the raw clay was investigated for mineralogical and chemical composition. X-ray Powder Diffraction (XPD) was applied on whole-rock, random powder specimens, >106µm, >45µm and >2µm fraction random powder specimens. Oriented specimens were applied for clay mineral species investigation. Oriented specimens were analyzed in air-dried, ethylene-glycol saturated, 350°C and 560°C heated state. Thermal Analysis (TA) was performed to determine the temperature values at which transformation reactions occur. Simultaneous Differential Thermal Analysis (DTA), Thermogravimetry (TG) and Derivative Thermogravimetry (DTG) were run on a MOM-C Derivatograph. A second set of TA was performed with coupled Evolved Gas Analysis (EGA) by Quadrupole Mass Spectrometry (QMS). Both series of TA were run under similar conditions. Chemical composition of clay samples was analyzed by Atomic Absorption Spectrometry (AAS).

Prior to test body firing, powdered clay samples were undertaken for sequential firing experiment. The same specimen of clay was heated and subsequently analyzed by XPD. The experiment was repeated at temperatures of 560°C, 740°C, 780°C and 950°C, temperatures at which reactions were detected in TA. Fired test body samples were subjected to XPD and Scanning Electron Microscopy (SEM) with Energy Dispersive Spectrometry (EDS) and Wavelength Dispersive X-ray Mapping (WXRM).

The chemical investigations (both AAS and EDS) confirmed the existence of K-dominant mica in the clay samples. As shown by XPD analysis, the mica is present as a continuous series from muscovite to illite. Results are supported by the broadening of the 10Å and 5Å peaks by the lowering of grain size domain and oriented specimen investigations. Chlorite is Fe dominant, negligible amount of interstratified illite-smectite was detected. Plagioclase, Ca-dominant, was detected in the raw samples. Calcite contents are >3% in weight fractions.

TA and EGA indicated dehydration by H_2O and ^-OH loss up to ~240°C. From ~350°C a continuously increasing H_2O and ^-OH loss is registered up to ~960°C. CO_2 liberation is low, spiking at 733°C, corresponding to the low organic matter content and the low crystallinity calcite. After continuous base-line rising, an endothermic reaction was registered at ~780°C on DTA, with weight loss on DTG. This corresponds to the H_2O and ^-OH loss maxima.

On the XPD patterns registered during sequential firing experiment, besides the continuous decrease in illite – muscovite content the inversion of feldspar composition is observed. After ~900°C the K-feldspar (microcline – orthoclase mixtures) becomes dominant. A spinel-like phase is formed starting from ~850°C.

The chemical investigations, together with XPD and TA-EGA analysis confirmed the transformation of illite to K-feldspar by firing.

To our knowledge, this is the first experiment with this set of instrumentation demonstrating the transformation of illite to K-feldspar in dominantly illitic brick clay materials. Besides industrial applications, this type of reaction also has an important role in investigations on archaeological ceramics.

Evidence for the inability of periclase-calcite based monolithic refractories to absorb alumina inclusions in Al-killed steel liquids

Lee Yu-Chen[1,2*] & Jiang Wei-Teh[1]
[1]Dept. of Earth Sciences, National Cheng Kung University, Tainan, Taiwan ([*]t621@mail.csc.com.tw)
[2]New Materials R&D Dept., China Steel Corporation, Kaohsiung, Taiwan

Removal of alumina inclusions and retention of Al content in Al-killed steel liquids are of great importance to the control of the final properties of steel products. Periclase-calcite monolithic gunning refractories have been widely used for tundish materials in many steel plants and suggested to possess a subtle function to absorb alumina inclusions by some factories. Test samples obtained from laboratory experiments using periclase-based gunning refractories containing calcite up to 30 wt.% in Al-killed molten steel at 1600°C for 20 minutes were examined by cathodoluminescence microscope, XRD, and SEM-EDS in this study. All calcite grains in the refractories in a 1200°C preheating process transformed into porous lime grains of micrometer sizes. The refractories subsequently tested at 1600°C exhibited three distinct zones including (1) the outermost lime-free zone which was porous and contained Mg-bearing wüstite, (2) the transition zone consisting principally of lime and relatively Mg-rich wüstite, and (3) the inner unreacted zone composed of primitive periclase and lime clusters. Dissolution of lime grains, formation of magnesian wüstite phases, and slight surface splitting were recorded with no evidence of reactions between alumina inclusions and lime or periclase. Removal of alumina from Al-killed steel liquids by reactions with periclase-calcite gunning refractories was previously proposed on the basis of the reduced Al content in bulk steels. The aforementioned result suggests that such an absorption process is unlikely and the true mechanism for reduction of the bulk Al concentration in Al-killed steel melts needs further investigations.

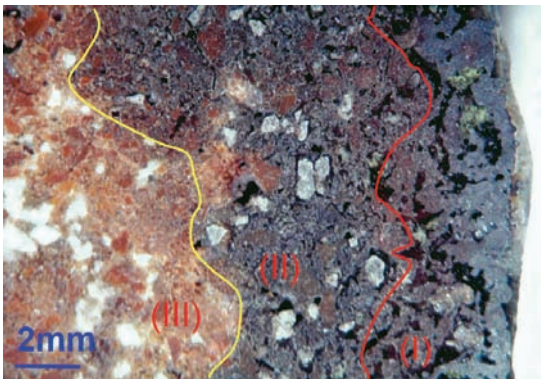

Fig. 1: Optical micrograph showing occurrence of the outermost lime-free zone (I), the transition zone (II), and the unreacted zone (III) on a periclase-based refractory with 18 wt.% CaO after being heated at 1600°C in a Al-killed steel melt for 20 minutes. White = lime particles; brown = periclase (detailed description given in the text).

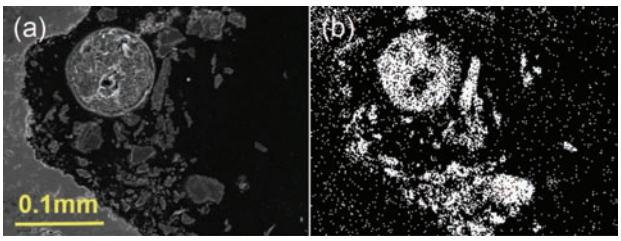

Fig. 2: SEM image of a spherical alumina inclusion in a steel melt at the edge of a periclase-lime refractory (a) and its Al X-ray elemental map (b).

Deciphering elemental substitutions in clinker minerals: a way to greener cements

Sulovský, P.[1,2*] & Staněk, T.[2]
[1]Dept. of Geology, Palacky University, Olomouc, Czech Republic ([*]petr@sulovsky.com)
[2]Research Inst. of Building Materials, Brno, Czech Republic

Among inorganic man-synthesized materials, clinker is the one that is produced in the greatest quantities. Clinker production consumes a lot of natural resources – fossil fuels as well as natural raw materials, what contributes to a great extent to the world CO_2 emissions. Substitution of both the fossil fuels and natural raw materials by waste materials represents a possibility to not only decrease the costs, but also to spare the natural reserves as well as to decrease CO_2 emissions. In the clinker burning process, any deviation from the customary fuel and raw meal chemistry can cause problems with the phase composition of clinker as well as with the reactivity of individual clinker minerals and devaluate thus the final product. Study of clinkers by mineralogical methods and application of mineralogical knowledge can help to solve such problems. Using electron microprobe to analyze individual clinker minerals can indicate the modes of occurrence of elements commonly absent in usual fuels or raw materials, but present in substantial quantities in the waste materials substituting them. Thus revealed substitution mechanisms can be utilized both to change the phase composition by accommodating higher amounts of foreign ions in the main clinker minerals, and/or to stabilize the more hydraulically active polymorphs of clinker minerals. An example of both benefits provided our study of clinkers burned with meal-and bone-meal (MBM) as alternative fuel [1]. Phosphorus from MBM normally hinders the formation of tricalcium silicate (alite) and causes excess formation of free lime and dicalcium silicate (belite). Earlier, phosphorus was assumed to enter the structure of both belite and alite via the $Ca_3(PO_4)_2 \leftrightarrow Ca_2SiO_4$ substitution. EMPA analysis of clinkers burned from raw meals enriched with P has revealed that phosphorus is also incorporated into the di- and tri-calcium silicate lattices by two other coupled substitutions: $Al^{3+} + P^{5+} \leftrightarrow 2Si^{4+}$ (berlinite substitution) and $Fe^{3+} + P^{5+} \leftrightarrow 2Si^{4+}$ (rodolicoite substitution). If the raw meal contains equivalent amounts of Al and Fe, the prevalent substitution mechanism of P incorporation into alite and belite structure is the berlinite one. Of these two, berlinite substitution proved to be more effective in incorporating P atoms in both Ca silicates and at the same time stabilizing the α´polymorph of belite as well as M1 form of alite – in both cases the most reactive forms of these clinker minerals. Design of raw meal compositions utilizing these findings enabled to produce white (Fe-free) clinker with P_2O_5 content exceeding 3.5 wt.% and „normal" Portland clinker with more than 2 wt.% P_2O_5 with standard phase composition. Another benefit of production of P-enriched clinkers is the possibility of using them as toxic elements immobilizing binder, as phosphate released from Ca silicates upon their hydration forms Ca phosphate fixing both cationic heavy metals as well as oxyanions-forming elements like As, Cr, V.

[1] Stanek, T. & Sulovsky, P. (2009) *Mater. Charact.*, **60(7)**, 749-755.

Combustion synthesis of ZnO powders and nitrogen analysis with Prompt Gamma Activation Analysis

Söllradl, S.[1], Canella, L.[2], Kudejova, P.[3*], Türler, A.[1] & Niewa, R.[4]
[1]Paul Scherrer Inst., Villigen, Switzerland
[2]RCM, Technische Universität München, Garching, Germany
[3]FRM II, Technische Universität München, Garching, Germany
([*]petra.kudejova@frm2.tum.de)
[4]IAC, Universität Stuttgart, Germany

Zinc oxide experienced a research boom within the last few years as cheap and less toxic alternative to GaN derivates in optoelectronics. ZnO is a direct, wide band gap semiconductor with a band gap of 3.37 eV [1] at ambient temperature.

Prompt gamma activation analysis (PGAA) is a radioanalytical, non destructive and bulk sensitive method, where samples are irradiated with a cold neutron beam. The $^{A}Z(n,\gamma)^{A+1}Z$ reaction is then utilised to measure the emitted prompt gamma spectra and analyse the chemical composition of the sample. Especially for light elements as H, Li, Be, B, C, N, P, S it is more effective than neutron activation analysis.

In this study a recently reported solution combustion method was utilised to synthesise nitrogen doped zinc oxide (ZnO:N) as described in [1] to estimate the detection limits for nitrogen within a ZnO matrix for PGAA measurements. The solution combustion method was chosen as it offers a simple sample preparation and promising results are reported.

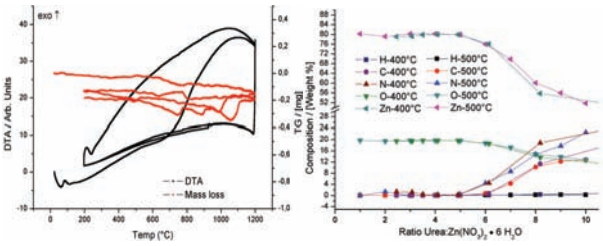

Fig. 1: DTA/TG diagram of sample prepared from a molar ratio of urea:zinc nitrate of 1:1 (left); Results of PGAA measurements for different treated samples (right).

In order to obtain similar data with the results from [1] differential thermal analysis with coupled thermo gravimetric measurements (DTA/TG), scanning electron microscopy with electron dispersive x-ray spectroscopy, Raman spectroscopy and powder x-ray diffraction are applied to the samples. Further PGAA measurements are applied and verified by elementary analysis (CHN).

After synthesis deep orange powders are obtained. After one DTA/TG cycle with a heating rate of 5 K/min up to 1200°C the product of the measurement is white ZnO powder. A measurement of two heating cycles (Fig. 1 left) shows a clear difference in the DTA curves and no significant change in weight (Fig. 1 left).

When evaluating the PGAA measurements (Fig. 1 right) it is clearly shown, that no nitrogen is found in deep orange samples (indicated with ratios 1-4, Fig. 1 right) at all. Only accompanied with an increasing presence of carbon, nitrogen is detected in PGAA and CHN measurements. These results show clearly, that the measurement of nitrogen in presence of a ZnO material is possible. On the other hand, nitrogen incorporated in ZnO can not be the source for the orange colour. A possible conclusion may be the introduction of defects under the harsh combustion conditions. The increasing carbon and nitrogen content are probably due to organic polymers, resulting from the decomposition of excess urea.

[1] Mapa, M. & Gopinath, C.S. (2009) *Chem. Mater.*, **21(2)**, 351-359.

The mineralogy and crystallography of pyrrhotite from selected nickel and PGE ore deposits

Becker, M.[1*], de Villiers, J.P.R.[2] & Bradshaw, D.J.[3]
[1]Centre for Minerals Research, University of Cape Town, South Africa ([*]megan.becker@uct.ac.z)
[2]Dept. of Materials Science and Metallurgical Engineering, University of Pretoria, South Africa
[3]Julius Krutschnitt Mineral Research Centre, University of Queensland, Australia

The non-stoichiometric sulfide pyrrhotite ($Fe_{(1-x)}S$), common to many ore deposits, occurs in a variety of crystallographic forms and compositions and occasionally is also inter grown with stoichiometric troilite (FeS). In this study, the mineralogy of pyrrhotite derived from several different nickel and PGE ore deposits in South Africa, Botswana and Canada, were examined in detail in terms of pyrrhotite association, crystallography and mineral chemistry. Pyrrhotite samples were subdivided into two phase 6C $Fe_{11}S_{12}$ pyrrhotite intergrown with 2C FeS troilite, two phase 4C Fe_7S_8 pyrrhotite intergrown with 5C Fe_9S_{10} pyrrhotite, single phase 5C Fe_9S_{10} pyrrhotite and single phase 4C Fe_7S_8 pyrrhotite. None of the pyrrhotite samples analysed was classified as two phase 4C pyrrhotite intergrown with pyrite due to the scarcity of pyrite in these samples. Average solid solution Ni contents of NC pyrrhotite (0.75 ± 0.10 wt% Ni) in this study were found to be greater than in 4C pyrrhotite (0.43 ± 0.10 wt% Ni), but only when the pyrrhotite occurred as two phase 4C pyrrhotite intergrown with NC pyrrhotite. For single phase pyrrhotite occurrences in this study, 4C pyrrhotite was more Ni-rich (up to 2 wt% Ni) than NC pyrrhotite (0.75 ± 0.19 wt% Ni). The average atomic metal/S ratios obtained for 4C Fe_7S_8 pyrrhotite was 0.869 ± 0.013 (n=699), for 5C Fe_9S_{10} pyrrhotite was 0.895 ± 0.013 (n=316) and for 6C $Fe_{11}S_{12}$ pyrrhotite was 0.918 ± 0.017 (n=101). The histogram comparing metal/S ratios of all the pyrrhotite samples analysed showed a continuum of metal/S ratios, although with frequency maxima corresponding to the ideal compositions of 4C, 5C and 6C pyrrhotite. The presence of the continuum however, was interpreted to be representative of non-stoichiometry in the pyrrhotite structure.

Grain size determination in the micrometer range from 2D X-ray diffraction patterns of polycrystalline samples

Rodriguez-Navarro, A.B.[*] & Alvarez-Lloret, P.
Dpto. de Mineralogía y Petrología, Universidad de Granada, Spain ([*]anava@ugr.es)

Crystal sizes can be calculated from peak intensities of spotty diffraction rings produced by a polycrystalline sample. Such patterns are collected using a small X-ray beam and an area detector. Peak intensities can be automatically measured using specially designed software. This technique is independent of the aggregation state of the material and can be applied to power and fully compact ceramics. Also, crystal sizes of different mineral phases present in a sample can be analyzed independently. This methodology has been applied to the characterization of different polycrystalline materials (i.e., quartz, SiC and α-Al2O3). The crystal sizes determined ranges from 3 to 100 micron, a much larger range than that obtained by conventional X-ray line-broadening analyses.

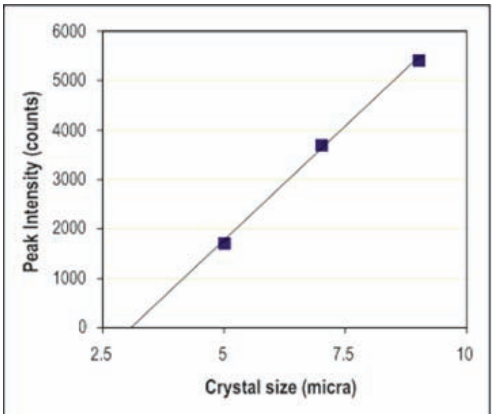

Fig. 1: Average intensity of peaks along the corundum 116 ring as a function of grain size of abrasive.

[1] Rodríguez-Navarro, A.B. (2006) *J. Appl. Crystallogr*., **39**, 905-909. [2] Rodriguez-Navarro, A.B. et al. (2006) *J. Am. Ceram. Soc.*, **89**, 2232-2238.

$Mg_xCu_{1-x}Cr_2O_4$ spinel solid solution: Jahn-Teller distortion and phase transitions

Tarantino, S.C.[1,2], Zema, M.[1,2*] & Giannini, M.[1,3]
[1]Dipt. di Scienze della Terra, Università di Pavia, Italy
([*]michele.zema@unipv.it)
[2]CNR-IGG, Pavia, Italy
[3]Bayerisches Geoinstitut, Bayreuth, Germany

Spinels are one of the most extensive series of related chemical compounds known and have a remarkable record of applicability, being used in numerous areas, including magnetic devices, electronics, catalysis, and batteries [1]. Chromium-rich spinels MCr_2O_4 are part of a group of exciting and challenging materials that have attracted much research interest in recent years due to complex magnetic ground states resulting from high geometrical frustration [2]. $MgCr_2O_4$ crystallises with the archetype cubic spinel structure (*Fd*-3*m*), while $CuCr_2O_4$ is a tetragonally distorted spinel with $c/a < 1$. The distortion is due to a cooperative Jahn-Teller (cJT) effect which is also associated, as recently proposed, with orbital ordering [3]. $CuCr_2O_4$ undergoes a first-order structural transition from $I4_1/amd$ to *Fd*-3*m* at 853 K [4].

The temperature- and composition-dependence of the $I4_1/amd$ – *Fd*-3*m* phase transition in $Mg_xCu_{1-x}Cr_2O_4$ solid solution, due to the melting of the cJT distortion, has been studied by means of single-crystal X-ray diffraction. Black octahedral crystals of $Mg_xCu_{1-x}Cr_2O_4$ (with x = 0, 0.10, 0.12, 0.18, 0.44, 0.50, 1), typically twinned and with a maximum size of 1×1×1 mm^3, have been prepared by flux decomposition method. All synthesised crystals but the Mg end-member have the $I4_1/amd$ symmetry. In situ high-temperature single-crystal diffraction data have been collected up to 900°C. The progressive substitution of the Jahn-Teller and d^9 Cu(II) cation with the spherical and closed-shell Mg(II) cation has a dramatic effect on the crystal structure. The tetragonal distortion, as measured by the c/a unit-cell parameters ratio and by the flattening of the tetrahedra, decreases with increasing Mg content. The substitution of Cu for Mg causes a shift of the transition temperature towards lower temperatures and a reduction of the discontinuity at the transition. Structure refinements of diffraction data collected at different temperatures reveal that heating induces a gradual reduction in the CuO_4 tetrahedron compression, which however remains significant until near the transition temperature. The variation with temperature of the tetrahedral O-Cu–O angles mimics the change in the lattice parameters.

The Mg ions, distributed over the tetrahedral sites, dilute the nearest neighbour interactions of the Cu ions, thus reducing the efficiency of the cooperative distortion. Indeed, the strength of the Cu-Cu interaction can be modulated by varying the Cu/Mg ratio.

[1] Grimes, N.W. (1975) *Phys. Technol*., **6**, 22-27. [2] Radaelli, P.G. (2005) *New J. Phys*., **7,** 53. [3] Kennedy, B.J. & Zhou, Q. (2008) *J. Solid State Chem.*, **181(9)**, 2227-2230. [4] Yé, Z.G. et al. (1994) *Ferroelectrics*, **162**, 103-118.

Utilization of perlite and waste slag from the South African steel and copper industry as cement extenders

Mogoru, T.J.[1], Verryn, S.M.C.[1*] & Kruger, R.A.[2]
[1]Dept. of Geology, University of Pretoria, South Africa
([*]sabine.verryn@xrd.co.za)
[2]Richonne Consulting, Pretoria, South Africa

The manufacturing of Portland cement is an energy-intensive process consuming substantial amounts of natural resources (limestone, shale and iron bearing mineral) and generating copious volumes of CO_2. The Portland cement can however be extended by the addition of alternative suitable material, which reduces the requirement from natural resources. This study discusses results from an investigation into the use of waste slag from copper- and steel industries and natural glass (perlite) as supplementary materials to Portland cement. The slags and perlite are blended in various ratios with ordinary Portland cement. The two South African cements used for this study are both of class Cem I (42.5). These are commercially available, ordinary Portland cement from PPC (Pretoria Portland Cement) and from AfriSam (South Africa) (Pty) Ltd.

The properties of the mixtures depend on the phase composition, chemistry, grain size and the sources of the materials. Compressive strength test results (Table 1), as well as heat flow curves showing the hydration behaviour, indicate that addition of the slag and perlite to ordinary Portland cement is viable. There is a large potential to use these materials in blended cements. The results of this study can be used to develop binder formulations that will reduce CO_2 emission, energy required in the production of cementitious binders and help to reduce large slag stockpiles.

Table 1: 28 day Compressive Strength of blends [1]

	Strength class	*Compressive 28 day Strength (MPa)*
AfriSam-blends		
AfriSam+30%ScawMetalsSlag	32.5R	41.5
AfriSam+20%ScawMetalsSlag	32.5R	46.3
AfriSam+10%ScawMetalsSlag	42.5N	50
AfriSam+30% Cu Slag	32.5R	36.2
AfriSam+20% Cu Slag	32.5R	37.1
AfriSam+10% Cu Slag		45.7
AfriSam+30% Perlite	32.5N	36.9
AfriSam+20% Perlite	32.5N	44.1
AfriSam+10% Perlite	32.5N	50.5
PPC-blends		
PPC+30%ScawMetal Slag	32.5R	32.5
PPC+20%ScawMetalsSlag	32.5R	35
PPC+10%ScawMetalsSlag	42.5R	43.7
PPC+30% Cu Slag		31.2
PPC+20% Cu Slag	32.5R	33.8
PPC+10% Cu Slag	32.5R	38
PPC+30% Perlite	32.5R	38.6
PPC+20% Perlite	32.5R	40
PPC+10% Perlite	42.5N	43.5

[1] SANS 5019 (2006) *Cement Part 1: Composition, specifications and conformity criteria for common cements*, South African Bureau of Standards, Pretoria.

Study of interaction of colorants with natural and modified clays for an environmental application

del Hoyo Martínez, C.[1*], Sánchez Escribano, V.[1], Queiruga Dios, A.[2] & Valero Juan, M.[3]
[1]Dept. of Inorganic Chemistry, University of Salamanca, Spain ([*]hoyo@usal.es)
[2]Dept. of Applied Mathematics, University of Salamanca, Spain
[3]Dept. of Physical Chemistry, University of Salamanca, Spain

Different materials are used in the adsorption and immobilization of chemical contaminants, most of whom remain under patent, therefore the procedures and products used are not known for the public. But in all cases, the safety and/or biodegradability of materials used are important issues in selecting them for environmental applications. Some biodegradable materials used for environmental purposes are lignins [1], alginate gel [2] and some derivatives cellulose [3].

In regard to materials, safe and low costs, clays and clay minerals must be mentioned, whose colloidal properties, ease of generating structural changes, abundance in nature, and low cost make them very suitable for chemical contaminants adsorption. The clay materials have led to numerous applications in the field of public health [6,7] having been demonstrated its effectiveness as adsorbents of all contaminants. The most used are organo-montmorillonites and hydrotalcite [4,5].

We have studied the adsorption of several colorants by natural or thermally modified clays, searching their interaction mechanisms and the possible recycling of these materials for environmental purposes and prevention of the public health.

[1] Valderrábano, M. et al. (2006) *4th Int. Workshop "Bioavailability of pollutants and soil remediation"*, **1**, 5-6. [2] Pepperman, A.B. & Kuan, J.C.W. (1995). *J. Control. Release*, 34, 17-23. [3] Sopeña, F. et al. (2005) *J. Agr. Food Chem.*, **53**, 3540-3547. [4] del Hoyo, C. et al. (2007) *Euroclay Conf.*, **1**, 77-79. [5] Undabeytia, T. et al. (2008) *Water Res.*, **42**, 1211-1219. [6] del Hoyo, C. (2007) *Appl. Clay Sci.*, **36**, 103-121. [7] Volzone, C. (2007). *Appl. Clay Sci.*, **36**, 191-196.

Mineralogy meets pharmacy - polymorphism of drug compounds

Kahlenberg, V.[1*] & Griesser, U.J.[2]
[1]Inst. of Mineralogy and Petrography, University of Innsbruck, Austria ([*]volker.kahlenberg@uibk.ac.at)
[2]Inst. of Pharmacy, University of Innsbruck, Austria

Polymorphism, i.e. the ability of a compound to form different crystal structures is frequently encountered among minerals. Since almost every important rock forming mineral undergoes at least one structural phase transition as a function of temperature and/or pressure, mineralogists are quite aware of this phenomenon and have gathered a considerable knowledge to deal with this solid state problem.

However, polymorphism is not a feature that exclusively concerns natural or synthetic inorganic materials, but occurs in organic compounds as well. Apart from being an intellectual challenge related to basic research, the importance of identifying and characterizing different crystal forms of a drug has been well documented in the literature. Differences in solubility, dissolution rate, morphology, mechanical properties and physicochemical stability of different modifications demand a detailed study of polymorphism of any new drug molecule. This has been recognized by the public authorities in the mid 90th why such studies are nowadays an integral part in drug development. Moreover, patenting of new solid state forms became an important part of modern life-cycle management of innovative pharmaceutical compounds.

The solid state characterization of the different polymorphs of a drug substance requires many analytical tools that are well established in mineralogy, including polarized light and hot stage microscopy, thermal analysis (DTA-DSC-TG), spectroscopic techniques (IR, Raman, solid state NMR) or X-ray diffraction (single crystal, powder).

In this contribution we will present some results from an industrial funded project where two groups from pharmacy and mineralogy work jointly in a research program and share their expertise for the benefit of a comprehensive understanding of the materials under investigation.

Optical microscopic observation of natural zeolite gravel after water purification treatment

Minato, H.[1*], Morimoto, T.[2] & Ogushi, N.[2]
[1]The University of Tokyo, Tokyo, Japan
([*]ogushi@mx3.alpha-web.ne.jp)
[2]ASTEC Corporation, Japan

The book entitled "Natural Zeolite, Quantification Guides and Data for Application, JSPS. Tokyo, Sept. 2006" [1] has been published to establish a common standard to evaluate the quality of natural zeolite commodities available in the market for the use of industries and/or agriculture fields. This book covers comprehensive technical procedures to evaluate natural zeolite commodities using physical, chemical, and mineralogical characteristics, together with various practical examples.

We present here an additional example of application of "natural zeolite" for pond water purification at famous Japanese garden named "Koko-En" that locates at Himeji Castle, Hyogo Prefecture, west of central Japan [2] (Fig. 1). The pond in the garden cultivates various kinds of decorative carp. The water quality to prevent an arising of algae is required to be kept pH between 6.8-8.6, SS below 5.0 mg/l, BOD below 3.0 mg/l, DO over 7.5mg/l, total N below 0.5mg/l, and total P below 0.02mg/l.

To maintain this condition, the water of the pond is provided from the pump station, and then flows out to the shallow stream that imitates a natural rivulet as a part of the scenery, before returning to the original pump station. The floor of the rivulet is covered by gravel of "natural zeolite" that comes from Futatsui, Akita Prefecture, north of central Japan, is an altered dacitic tuff of Miocene, and consists mainly of clinoptilolite. The returned water is filtered by matt with an aid of coagulant of natural inorganic materials to remove out solid suspensions at the pump station before providing the pond again.

After running the system for a year, recovered "natural zeolite" gravel shows dark coloured surface of manganese and iron oxides and significant adsorption of heavy metals such as Pb, As, Mn, and Fe, and loss of alkali and alkali earth metals, by X-ray fluorescence analysis, both on the surface and the core.

High magnification optical microscopic observation confirms the adsorption of manganese and iron oxides/oxy-hydroxides and the arising of some new phases of silicate minerals along the surface of the block and the surface of internal fissures and cavities of the altered tuff. Details of the arising new mineral species are under the investigation.

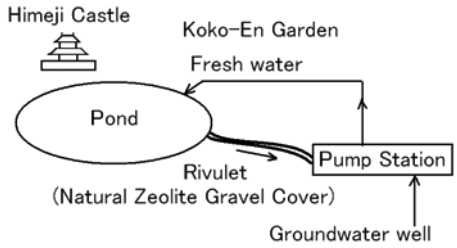

Fig. 1: Sketch of pond water purification system.

[1] Minato, H. (ed.) (2006) *Natural Zeolite, Quantification Guides and Data for Application*, **111**, Committee, JSPS. [2] Minato, H. et al. (2009) *Proceedings of 2009 Meeting of Japan Assoc. Mineral. Sci.*, R3-09.

Carbonation of iron metallurgy slags as a method of CO_2 sequestration

Kasina, M.[*] & Michalik, M.
Inst. of Geological Sciences, Jagiellonian University, Krakow, Poland ([*]monika.kasina@uj.edu.pl)

Mineral carbonation is one of the CO_2 capture and storage (CCS) methods. It is based on the crystallization of stable carbonates (calcite, magnesite, siderite) by the reaction of minerals rich in divalent cations (Ca^{2+}, Mg^{2+}, Fe^{2+}) with CO_2.

The aim of this research was to determine the potential application of industrial wastes in CO_2 capture from ambient air. Blast furnace and steel slag samples after different ageing periods were used in experiments. Powdered samples and crushed fragments (ca. 1 cm) were subjected to 21 wetting and drying cycles (50 g of a sample + 400 ml of deionised water in every cycle; dried under IR radiator).

Studied samples of blast furnace slag are composed mostly of calcium silicates: akermanite, gehlenite, rankinite, and wollastonite. Steel slags are composed of larnite and oxides (srebrodolskite and wüstite).

Blast furnace slag composition was not changed during experiments. Calcite crystallization and partial dissolution of larnite and srebrodolskite (relative decrease of XRD peaks intensity) were noted in steel slag samples.

Chemical analysis indicates the increase of LOI and C_{Tot} content in slag samples after experiments.

SEM-EDS analysis of slag fragments shows that both kinds of slag were subjected to mineral carbonation process. In case of blast furnace slag this process was not very advanced. Calcite crystalize as rims (~25 μm) of small crystals around some of slag fragments. In steel slag this process seems to be more advanced. Calcite appears not only as rims of small crystals around slag fragments but also as infillings in pore spaces. Rims around steel slag fragments composed mostly of SiO_2 (~50 wt%), CaO (~30 wt%), P_2O_5 (up to 20 wt%) and C (carbonate anion?) were also noted. Some of larnite crystals (especially those close to the border of slag fragments) are partly or fully replaced by material of composition similar to rims described above.

Results suggest that silicate minerals in blast furnace slag are less reactive, what is connected with lower dissolution rate of components. In case of steel slags divalent cations (mostly Ca^{2+}) required for calcite crystallisation come from the dissolution of silicate minerals (larnite), and oxide phases as well. Results indicate that slags, especially from steel production is an useful material in CCS procedures.

The influence of Fe content in Fe-Mg tourmalines on their intrinsic dipole moments and pyroelectric properties

Zhao Changchun & Liao Libing*
School of Materials Science and Technology, China University of Geosciences, Beijing, China (*lbliao@cugb.edu.cn)

Single-crystal X-ray diffraction data of four Fe-Mg tourmalines with different iron contents from Xinjiang, Sichuan and Yunnan (China) have been collected at room temperature and liquid nitrogen temperature. Polyhedras' intrinsic dipole moments and the total intrinsic dipole moment of the crystal unit cell have been calculated. The pyroelectric coefficients of the four Fe-Mg tourmalines have been determined and the influence of the intrinsic dipole moments in Fe-Mg tourmalines on their pyroelectric properties has been investigated. The results show that for tourmalines with different iron content, the intrinsic dipole moments decrease with the increasing of Fe content at room temperature and increase with the increasing of Fe content at liquid nitrogen temperature. It is inferred that in the temperature interval between room temperature and 80°C, the electric dipole moment of Fe-Mg tourmaline decreases with the increase of Fe content.

By calculating and comparing the intrinsic electric dipole moments of X, Y, Z, T and B polyhedron, we find that T polyhedron makes the most contribution to the total intrinsic dipole moment. X polyhedron takes the second place. However, the electric dipole moments generated by the two polyhedrons of the same crystal are in the opposite directions. The electric dipole moment of T polyhedron decreases with the increase of iron content, while the electric dipole moment of X polyhedron increases with the increase of iron content. From fluid nitrogen temperature to room temperature, the reversal of the electric dipole moment of Y polyhedron occurs. Iron affects T, X and other polyhedra's electric dipole moment through the distortion of its occupied Y and Z polyhedron and the electric dipole moment reversal of Y polyhedron, thus the total intrinsic electric dipole moment of Fe-Mg tourmaline.

The pyroelectric coefficient of tourmaline decreases with the increasing of Fe content in the temperature range of room temperature to 80°C. It is inferred that the pyroelectric coefficient of tourmaline also decreases with the increasing of Fe content in the temperature range of liquid nitrogen temperature to room temperature.

Characterization of reaction products from reductive decomposition of a natural garnet

Aparicio, C.[1*], Filip, J.[1], Mashlan, M.[1] & Všianský, D.[2]
[1]Centre for Nanomaterial Research and Dept. of Experimental Physics, Palacký University, Olomouc, Czech Republic
([*]claudia.aparicio01@upol.cz)
[2]Research Inst. of Building Materials, JSC, Brno, Czech Republic

The thermal decomposition of garnets from pyrope-almandine series occurs between 750°C and 1200°C, the decomposition products depends on the experimental conditions, i.e. temperature and duration of heating, heating and cooling rate, pressure and type of atmosphere. The present work is devoted to study the characteristics of the reaction products from decomposition of pyrope-almandine garnet in reducing atmosphere.

Natural garnets of near end-member composition pyrope – $(Mg_{2.22}Fe_{0.47}Ca_{0.33})(Cr_{0.11}Fe_{0.06}Al_{1.81})Si_{2.98}O_{12}$ – and almandine – $(Fe_{2.85}Mg_{0.15})(Al_{1.99})Si_{2.99}O_{12}$ – were dynamically heated from 35°C to 1200°C in a simultaneous thermal analyzer, including thermogravimetric analysis and differential scanning calorimetry, with a heating rate of 10°C/min. The decomposition products were identified by X-ray powder diffraction (XRD) and Mössbauer spectroscopy. Scanning electron microscopy (SEM), transmission electron microscopy (TEM), and energy-dispersive X-ray spectroscopy (EDX) were used to observe the morphology of the reaction products. Subsequently, in-situ monitoring of reductive decomposition was done by high-temperature XRD.

Pyrope decomposition started at 1105°C; the identified decomposition products are metallic iron (alpha and gamma), enstatite (ortho- and clino- polymorphs), spinel phase, and anorthite. Enstatite and spinel phase have been reported in previous works as decomposition products of pyrope in air [1,2], the difference here is the presence of metallic iron instead of iron oxides formed in oxidizing atmosphere. On the other hand, almandine decomposes at 1055°C, with the following decomposition products: hercynite, fayalite, cristobalite, Fe-cordierite and metallic α-iron. Metallic iron forms rounded-shape particles with sizes between 60 nm and 600 nm, they are randomly distributed over the surface of above mentioned reaction products (Fig. 1). The observed decomposition mechanism and structure could have an analogy in historical pottery [3].

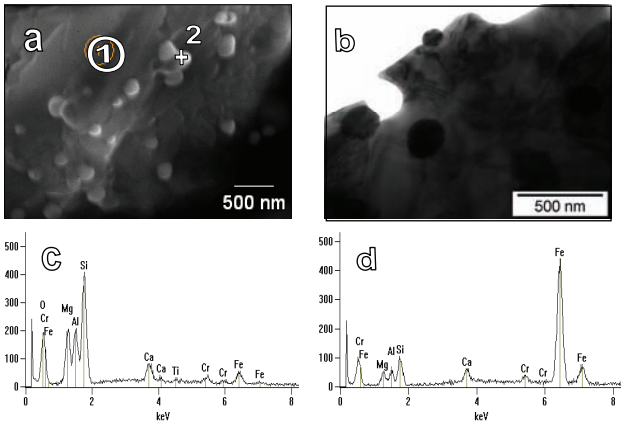

Fig. 1: SEM (a) and TEM (b) image of the decomposition products of pyrope showing the metallic iron particles. EDX analysis (c) and (d) from regions labelled 1 and 2 on figure 1a, respectively.

[1] Zboril, R. et al. (2003) *Phys Chem Miner*, **30**, 620-627. [2] Zboril, R. et al. (2004) *Hyperfine Interact*, **156/157**, 403-410. [3] Gregerová, M. et al. (2008) *Chem Listy*, **102**, 859-863.

High-temperature borate crystal chemistry and self-assembly of boron-oxygen fundamental building blocks (FBB)

Bubnova, R.S.[1*] & Filatov, S.K.[1,2]
[1]Inst. of Silicate Chemistry RAS, St. Petersburg, Russia
([*]rimma_bubnova@mail.ru)
[2]Dept. of Crystallography, St. Petersburg State University, St. Petersburg, Russia

Nowadays borates are well known as advanced materials due to their non-linear and linear optical, luminescent, piezoelectric, refractive and other useful properties. The functional, thermal, mechanical and chemical properties of material are caused by its crystal structure. One of distinguishing characteristics of unique borate crystal chemistry is occurrence of rigid groups consisting of the BO_3 and the BO_4 polyhedra. These groups constitute fundamental building blocks (FBB).

Coefficients of thermal expansion tensor have been investigated for more than 50 borates by powder X-ray diffraction. About 3/4 of them demonstrate highly anisotropic expansion; moreover, about half of them show negative linear expansion.

The structural temperature-dependent behavior has been investigated by single-crystal high-temperature X-ray diffraction for several borates as well. As a main result, thermal stability of size and configuration of BO_3 and BO_4 polyhedra and the rigid B–O groups have emerged from the studies [e.g. 1,2]. Here we present fundamental rules of high-temperature borate crystal chemistry [1,3,4 and refs therein] in contrast to those of high-temperature silicate crystal chemistry [5,6 and refs therein]. Finally from these principles it emerges self-assembly in borates at level of rigid boron-oxygen groups as a result of thermal vibrations of boron and oxygen atoms and the groups. Self-assembly of rigid groups in borates is explained in terms of exampling thermal vibrations anisotropy of isolated groups consisting of 3 and 5 B–O polyhedra.

Acknowledgements: This work is supported by the Russian Foundation for Basic Research (08-03-00232).

[1] Filatov, S.K & Bubnova, R.S. (2000) *Phys. Chem. Glasses*, **41**, 216-224. [2] Bubnova, R.S. et al. (2002) *Z. Kristallogr.*, **217,** 444-450. [3] Bubnova, R.S. & Filatov, S.K. (2008) *Phys. Stat. Sol.*, **245(b)**, 2469-2476. [4] Bubnova, R.S. & Filatov, S.K. (2008) *High-Temperature Crystal Chemistry of Borates and Borosilicates*. Nauka, St. Petersburg (in Russ.). [5] Hazen, R.M. & Finger, L.W. (1982) *Comparative crystal chemistry: temperature, pressure, composition and variation of the crystal structure*. John Willey & Sons, New York. [6] Hazen, R.M. (2000) (ed.) *Rev. Miner. Geochem.*, **41**, Mineral. Soc. Am., Washington, USA.

A study on shapes of hollow glass microspheres by glass composition

Choo KoYeon, Jeong HeonDo & Kim TaeHwan*
Reaction and Separation Materials Research Center, Korea Inst. of Energy Research, Daejeon, Republic of Korea
(*thkim@kier.re.kr)

Research on hydrogen to prepare for hydrogen economy is an urgent task which should be promoted constantly as a means of resolving skyrocketing energy issues. But regarding its application, hydrogen storage technology is a precedent study in energy storage. Many researchers are in the midst of development on hydrogen storage technology. In our country, hydrogen storage researches have been conducted according to the national R&D plan since hydrogen frontier R&D center was launched.

Our center is carrying out research on hydrogen storage using hollow glass microspheres among solid hydrogen storage materials. They were studied by J.E. Shelby's research group in Alfred University, New York, USA, according to the US DOE hydrogen project and can now store hydrogen up to 2.2 wt.% [1].

Hollow glass microspheres are non-toxic and lightweight as a solid hydrogen storage material and can be prepared from low-cost starting materials. They have a reversible hydrogen storage property, as well. Although they are sufficiently competitive with conventional organic and inorganic materials, their hydrogen storage capacity per unit weight is not even close to the target value of the US DOE (by 2010, on-board hydrogen storage systems achieving 2 kWh/kg or 6 wt.%) [2].

We investigated shape change of glass microspheres after heat treatment by controlling composition of sodium borosilicate gel as a starting material. The products were characterized by XRD and SEM, and the BET surface area was measured.

Although various processing methods can be applied to produce hollow spheres, for examples, the sol-gel/emulsion method, the sacrificial-core method, layer-by-layer deposition on colloidal templates, spray drying and the coaxial-nozzle method [3], we applied flame forming method containing a blowing agent as a feed.

[1] US DOE Hydrogen Program (2008) *Annual Progress Report, IV. Hydrogen Storage, D. New Materials* – Independent Project. [2] US DOE Technical Plan (2009) *Hydrogen Storage*. [3] Singh, R.K. et al. (2007) *Colloid. Surface. A*, **310**, 39-45.

The vitrification kinetics and phases composition of flotation waste of Bor mine (Serbia)

Cocić, M.[1], Matović, B.[2] & Logar, M.[3*]
[1]Technical Faculty, University of Belgrade, Bor, Serbia
[2]Vinča Institute, Belgrade, Serbia
[3]Faculty Mining and Geology, University of Belgrade, Serbia
(*milogar@eunet.rs)

The manufacturing processes of non-ferrous metals and their alloys, particularly the flotation enrichment and metallurgical processing of waste materials, cause major environmental pollution problems. Flotation waste dumps and slag from smelters represent large areas of degraded land and the permanent pollution of soil, water and air. This study is dedicated to examining the possibility of using flotation waste from RTB Bor (Serbia) in the production of silicon-ceramic materials.

Mineral composition of flotation waste consists of fayalite and magnetite with minimal amounts of copper and iron sulfide. By changing the conditions of heat treatment and cooling modes microstructure and properties of products can be controlled and desirable glass-ceramic materials can be produced [1].

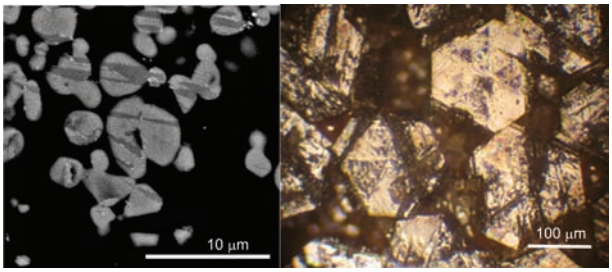

Fig. 1: Glass ceramics 1150°C/4h (left); 1480°C/6h (OM) (right)

Fig. 1 presents the two glass-ceramics microstructures build of glass and hematite crystals made at different temperature. At t = 1150°C the content of hematite is 32%. The crystals are anhedral, rarely subhedral, with diameter generally below 10 microns. At 1480°C viscosity decreases and the glass starts to flow. Therefore the glass surface is exposed to oxidation in the highest degree and growing rate of hematite becomes faster which leads to the formation of larger euhedral crystals, whose content reaches 44%. Between these two obtained microstructures, a series of glass-ceramic materials were synthesized under different time and temperature level by adding of basalt and tuff. The purpose is to find the optimal composition and crystallization conditions to obtain the applicable glass-ceramic materials.

[1] Karamanov, A., Aloisi, M. & Pelino, M. (2007) *J. Hazard. Mater.*, **140**, 333-339.

Relationships in the kesterite-stannite-kuramite pseudoternary system: from fundamentals to photovoltaic applications

Di Benedetto, F.[1*], Amthauer, G.[2], Borrini D.[3], Dittrich, H.[2], Foresti, M.L.[1], Fornaciai, G.[1], Innocenti, M.[1], Pardi, L.[4], Romanelli, M.[1] & Schorr, S.[5]

[1]Dept. of Chemistry, University of Florence, Italy ([*]dibenefr@geo.unifi.it)

[2]Inst. for Materials Science and Physics, University of Salzburg, Austria

[3]Dept. of Earth Sciences, University of Florence, Italy

[4]Inst. for Physico-Chemical Processes, CNR, Italy

[5]Inst. of Geological Sciences, Free University Berlin, Germany

The task for renewable energy resources is stimulating the research for new materials allowing setting up low cost and high conversion efficiency solar cells. Lowering the costs of raw materials, as well as increasing attention paid to the environmental consequences of the industrial production, both drive the development and the choice of materials on the basis of their chemical composition. The kesterite-like quaternary chalcogenides (Cu_2ZnSnS_4, or CZTS) attracted a relevant interest from worldwide researchers, due to their good performances with a simple chemistry and to the absence of relevant economic or environmental concerns associated to their use in the solar cells production.

The crystal chemical features of both natural and synthetic phases belonging to the pseudoternary system Cu_2FeSnS_4-Cu_2ZnSnS_4-Cu_3SnS_4, to which the CTZS materials belong, still await a definitive assessment. Major points of debate include the isostructurality between stannite and kesterite, the assessment of the structural model for kuramite, the possible occurrence of Cu and Fe in oxidised valence states, the mixed occupancy of structural metal sites. The last points in particular are related to two relevant topics of chalcogenide studies, i.e. the extent of cation disorder and the occurrence of partial intervalence charge transfer in Cu-, Fe-bearing chalcogenides. Moreover, both aspects can dramatically affect the physical properties of the host phase, and ultimately its eventual exploitation in photovoltaic materials. We approached the growth of these materials by solid-state reactions, hydrothermal syntheses and electrochemical deposition under morphological and compositional control to obtain ternary chalcogenide compounds (at the Cu end-member) with different physical properties. Moreover, this study reviews the state of the art of the literature on the knowledge about the pseudoternary system, and it sets up perspectives for photovoltaic applications.

Mullite-type Al_5BO_9 and $Al_{18}B_4O_{33}$, a crystal-chemical puzzle?

Fisch, M.[1*], Armbruster, T.[1] & Rentsch, D.[2]

[1]Mineralogie-Kristallographie, Institut für Geologie der Universität Bern, Switzerland ([*]fisch@krist.unibe.ch)

[2]EMPA Swiss Federal Laboratories for Materials Testing and Research, Dübendorf, Switzerland

Ceramic materials in the system Al_2O_3-B_2O_3-SiO_2 are of particular interest for industrial applications. Among these, whiskers of the most common aluminum borate, often cited as $Al_{18}B_4O_{33}$, are used to reinforce aluminum alloys and refractory linings [1]. This mullite-type compound is reported with two slightly different stoichiometries, Al_5BO_9 ($5Al_2O_3$:$1B_2O_3$) [2] and $Al_{18}B_4O_{33}$ ($9Al_2O_3$:$2B_2O_3$) [3-7]. Available crystal structure refinements are essentially identical, comprising $Al^{(IV)}$, $Al^{(V)}$, $Al^{(VI)}$ and $B^{(III)}$ [2-7]. However, to comply with the boron-richer formula of $Al_{18}B_4O_{33}=Al_{4.91}B_{1.09}O_9$, 9% of $Al^{(IV)}$ must be replaced by $B^{(IV)}$. In this study, samples from different starting mixtures representing both stoichiometries (Table 1) were investigated by single-crystal and powder XRD, as well as by ^{11}B and ^{27}Al solid state MAS-NMR.

Table 1: Sample description

Sample	Starting materials	Al_2O_3:B_2O_3
1[a]	Al_2O_3, B_2O_3	9:2
2[b]	Al_2O_3, B_2O_3	9:2
3[b]	Al_2O_3, B_2O_3	5:1
4[c]	$Al(NO_3)_3 \cdot 9H_2O$, H_3BO_3	1:2
5[b]	Al_2O_3, H_3BO_3	1.1:1

[a]flux grown single-crystals, [b]heat-treated for 10h at 1200°C [c]according to [7] but heat-treated for 10h at 1100°C.

Our single-crystal structure refinement is consistent with previous results [2,5,6]. Cell parameters are a=5.6686(2)Å, b=15.0060(9)Å, c=7.6892(4)Å and V=654.07(6)Å^3 in $Cmc2_1$; Z=4. Single-crystal X-ray data indicated a fully occupied $B^{(III)}$ site ($<d_{B-O}>$=1.3769(17)Å) and a "pure" $Al^{(IV)}$ tetrahedron ($<d_{Al4-O}>$=1.7464(12)Å). Refinements including a constrained 9% B $\rightarrow$ Al substitution at $Al^{(IV)}$ converged to significantly higher agreement factors.

Powder XRD was used to determine precise lattice parameters of all samples and to identify corundum as excess phase in samples 1-3 and boric acid in sample 5. Refined cell dimensions are identical for all samples within a few standard deviations.

^{11}B MAS-NMR spectroscopy indicated a single $B^{(III)}$ site and no sign for any $B^{(IV)}$, which is agreement with previous findings [8]. Judging from simulations, $B^{(IV)}$ amounts lower than 2% can be detected. ^{27}Al MAS-NMR spectra were consistent with Al-coordinations derived from our single-crystal structure refinement and previous NMR investigations [9].

Excess corundum in samples 1-3 could suggest B_2O_3 as limiting factor for $Al_{18}B_4O_{33}$ formation. However, results were the same for sample 5 having excess boron: Crystallographic and NMR data of all samples are consistent and no indication of $B^{(IV)}$ was found as expected for $Al_{18}B_4O_{33}$. We assume that all aluminum borate samples investigated in this study represent Al_5BO_9, casting doubt on the existence of $Al_{18}B_4O_{33}$.

[1] Fischer, R.X. & Schneider, H. (2008) *Eur. J. Mineral.*, **20**, 917-933. [2] Sokolova, Ye.V. et al. (1978) *Dokl. Akad. Nauk SSSR*, **243**, 655-658. [3] Baumann, H.N. & Moore, C.H. (1942) *J. Am. Ceram. Soc.*, **25**, 391-394. [4] Scholze, H. (1956) *Z. Anorg. Allg. Ch.* **248**, 272-277. [5] Ihara, M. et al. (1980) *J. Ceram. Soc. Jpn.*, **88**, 77-84. [6] Garsche, M. et al. (1991) *Eur. J. Mineral.*, **3**, 793-808. [7] Mazza, D. et al. (1992) *Am. Ceram. Soc.*, **75**, 1929-1934. [8] McKenzie, K.J.D. et al. (2007) *Appl. Magn. Reson.*, **32**, 647-662. [9] Hung, I. et al. (2006) *Chem. Phys. Lett.*, **432,** 152-156.

Impact of zeolitic material in improving sandy soil fertility features (Albania)

Goga Beqiraj, E.[1*] & Gjoka, F.[2]
[1]Faculty of Geology and Mines, Polytechnic University of Tirana, Albania ([*]ea_beqiraj@yahoo.com)
[2]Agricultural University of Tirana, Albania

This work presents an attempt for studying the effects of zeolitic material from Munella region (Albania) in improving the fertility features of a sandy soil from Divjaka region (Albania) [1].

On the basis of their petrographic and geochemical characteristics (Table 1) the following zeolitic rocks can be distinguished: basalts and basaltic andesites, dacites and rhyolites [2]. The zeolitic phase composes up to 60-80 % of these rocks.

Table 1: Geochemical data of zeolitic rocks

	SiO_2	Al_2O_3	Fe_2O_3	MnO	MgO	CaO	Na_2O	K_2O	TiO_2	P_2O_5	LOI	TOT
Mu1	60.95	11.97	5.84	0.056	2.07	5.18	0.27	0.09	0.378	0.1	13.01	99.92
Mu2/3	72.7	10.08	4.13	0.053	0.82	2.9	1.82	1.01	0.308	0.08	6.48	100.4
Mu3/5	60.2	12.44	5.69	0/072	1.16	6.15	0.39	0.14	0.411	0.16	13.27	100.1
Mu4/1	65.26	11.63	4.27	0.083	0.97	4.72	0.98	0.54	0.362	0.09	11	99.89
Mu5	64.77	11.4	5.48	0.092	0.9	4.71	0.58	0.8	0.364	0.09	11.11	100.3
Mu6	69.97	10.1	3.21	0.08	0.37	4.72	0.28	0.27	0.305	0.07	10.84	100.2

The sandy soils of Divjaka are characterized by small thickness of the active layer, low content of humus and other essential nutriments of plants. These soils have homogeneous mechanical and mineralogical composition because of their uniform parental material, mainly composed of quartz from sea-sediment formations (Tables 2 & 3).

Table 2: Chemical properties of the soil

pH		Humus %	N-total (%)	$CaCO_3$ %	P	K	KKK	Microelement-total				
H_2O	KCl				Available mg/kg			Cu	Zn	Mn	Fe	Ca
								mg/kg		%		
8.5	7.8	0.8	0.066	7.14	13.2	75	11.5	44	78.4	0.07	4.57	8.8

Table 3: Physical properties of the soil

Hygroscopic Moisture (%)	Water Capacity (%)	Clay (%)	Silt (%)	Sand (%)
3.08	30.21	2.6	8.0	89.4

Zeolites of Munella were tested as fertilizers for the sandy soils of Divjaka region (Central-western Albania). The experiment was realized in a greenhouse, in a randomized block with four repetitions of 7 fertilizer types obtained from zeolitic material alone or mixed in various proportions with NPK (nitrogen, phosphorous, potassium). Lolium multiflorium (ryegrass) was used as experimental plant.

Application of both zeolites and mixtures with NPK resulted in a significant increase in the shoot and roots yield of ryegrass compared to the control sample in the experiment (no NPK and zeolitic material added).

The buffer role of zeolites in improving the water capacity of soils was observed especially during the driest period of the year (July-August).

[1] Goga Beqiraj, E**.** **(**2005) *PhD thesis*. [2] Shallo, M. et al. (1987) *Ofioliti*, **12**, 125-136.

Chemical and mineral composition of steel slag – reasons of slag instability

Kasina, M.[*] & Michalik, M.
Inst. of Geological Sciences, Jagiellonian University, Krakow, Poland ([*]monika.kasina@uj.edu.pl)

Slags from iron metallurgy (steel slags) are considered as important co-products used in many fields of industry and civil-engineering. Slag is usually composed of high-temperature phases which are very reactive for a long period of time. The most unwanted result of slag reactivity is its swelling, which is caused by chemical reactions of slag components.

The aim of this study was to characterise chemical and mineral composition of two steel slag samples after different ageing periods (sample A – less than 1 year; sample B - after 4 years) to indicate which of slag component is responsible for its instability. Chemical and mineral composition of slag samples were studied using XRD, SEM-EDS, ICP-ES, and ICP-MS.

Chemical composition of studied slag is typical for this material. The main components are: CaO – 47.41 wt% and, 39.62 wt%; SiO_2 – 16.51 wt%, and 11.33 wt%; Fe_2O_3 – 28.29 wt%, and 42.79 wt%; MgO – 5.16 wt% and 3.35 wt% for sample A and B respectively. BI (basicity index) is 3.5 (sample A) and 3.0 (sample B). Chemical composition and BI values indicate that the risk of hydratation and slag dissolution is high.

The main slag components determined using XRD are: dicalcium silicate – larnite (Ca_2SiO_4), dicalcium ferrite – srebrodolskite ($Ca_2Fe_2O_5$), and iron oxide – wüstite (FeO). Using SEM-EDS minor components were determined: metallic iron and lime (CaO).

Previous studies (e.g. [1]) indicate that slag stabilization is related to: 1) larnite $\beta \rightarrow \gamma$ transition; 2) magnesia and lime hydratation and carbonation.

In studied samples MgO phase was not detected. Most of magnesia is combined with iron oxides (up to 15 %wt MgO in oxide phase). The presence of P_2O_5 in larnite (up to 5 wt%) may suggest that it is fully stabilized form [2] because phosphorus can be present in larnite in low temperature. However, taking into consideration lamellar texture of larnite, a complete stabilization is not so obvious, and it may suggest that stabilization processes has not been completed. Lime hydratation was not noted in studied samples, whereas carbonation of slags is a common reaction.

Lack of larnite-γ peaks in XRD patterns suggests that larnite $\beta \rightarrow \gamma$ transition is in initial stage or absent. Lime is the only oxide phase subjected to carbonation. Results indicate that slag is not stabilized.

[1] Waligora, J. et al. (2010) *Mater. Charact.*, **61**, 39-48. [2] Halicz, L. et al. (1983) *Cement Concrete Res.*, **14**, 8-11.

The role of liquid inclusions in the interface-mediated polymorph transition

Kulkov, A.[1,2*], Glikin, A.E.[1] & Putnis, A.[3]
[1]St-Petersburg State University, St. Petersburg, Russia ([*]aguacrystals@narod.ru)
[2]NITIOM "Vavilov State Optical Institute", St. Petersburg, Russia
[3]Institut für Mineralogie, University of Münster, Germany

The natural and synthetics crystals contain bubbles of liquid inclusions. Studying the composition and form of these inclusions allows drawing a conclusion about PT – conditions of crystal foundation and composition of mother solution. In this work we carried out the in-situ observation of behavior of bubbles of liquid inclusions during the interface-mediated (metasomatics) polymorphic transition of nickelhexahydrite to retgersite (β-$NiSO_4$*6 H_2O –> α-$NiSO_4$*6 H_2O). Crystals of nickelhexahydrite were grown by slow evaporation at 60°C. The study of bubbles was carried out with the help of optical microscope with digital camera at 20-25°C.

The bubbles had partly faced form. The bubble faces were paralleled to the parent crystal faces. Isolated inclusions were not the centers of beginning of phase transition but the transition began from the surface of parent. When the front of transition runs up to the liquid inclusion, rapid increasing of transition velocity takes place (from first μm / hour up to tens μm / min) (Fig. 1). The form of transition boundary changes from feather-like to flat. It is known that bubbles of liquid inclusions can faced through both the dissolution and the precipitation. In our case, the form of bubbles demonstrates the precipitation of salt from the inclusion solution. Thus, bubbles of inclusions facing during the temperature decreasing until temperature stabilize.

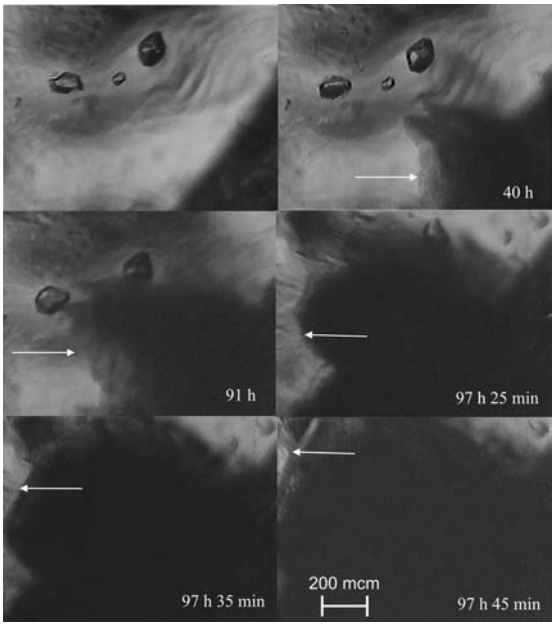

Fig. 1: Type changing of Nh-Rt transition boundary (boundary marked by arrow) and increasing of transition velocity after the capture the liquid inclusions by transition front.

Consequently, behavior investigation of bubbles of liquid inclusions during the interface-mediated polymorphic transition from nickelhexahydrite to retgersite demonstrated that isolated liquid inclusions: a) partly facing after the extraction the parent crystal from solution; b) cannot be the centers of transition beginning; c) have the influence on the velocity and boundary type of polymorph transition as the source of solution.

Efficient conversion and high stability: performance of Ni/NFS catalyst in CH_4-CO_2 reforming

Li Xuejun[1*], Wang Lijuan[1,2], Lang Bao[3], Ma Junhong[1,2] & Chen Jiawei[4]
[1]National Laboratory of Mineral Materials, China University of Geosciences, Beijing, China ([*]lixuejunwang@163.com)
[2]State Key Laboratory of Geological Processes and Mineral Resources, China University of Geosciences, Beijing, China
[3]State Key Laboratory of Chemical Resource Engineering, Beijing University of Chemical Technology, Beijing, China
[4]School of Earth Sciences and Resources, China University of Geosciences, Beijing, China

Nano-fibriform silica (NFS) (SiO_2 content is 90.5%) extracted from chrysotile by acid-leaching is a kind of mesoporous material with a high specific surface area, high adsorptive capacity and a large pore volume. A series of Ni/NFS catalysts was prepared by soaking NFS into 5, 7.5, 10, 12.5, 15, 20 wt% $Ni(NO_3)_2$ solutions for 24 hours and baking the filtered and washed residues at 550°C for 5 hours under air atmosphere. The catalytic performances of the Ni/NFS catalysts in CH_4-CO_2 reforming (CH_4/CO_2=2, O_2 as a gas feedstock) were investigated in a fixed-bed quartz micro-reactor. The results indicate that when $Ni(NO_3)_2$ concentration is ≥ 10 wt%, the CH_4 and CO_2 conversion by the corresponding Ni/NFS catalyst can respectively rise to 97.7% and 93.8% at 850°C. Stability evaluation of the Ni/NFS catalyst from 10 wt% $Ni(NO_3)_2$ solution shows that during 100 hours no catalyst deactivation occurs under the test condition of 850°C, 1atm, and GHSV=28200 $mL \cdot g^{-1} \cdot h^{-1}$, and the CH_4 and CO_2 conversion keeps 95% and 90% respectively with a H_2/CO ratio of ca. 1.25. The Ni/NFS catalysts were characterized using X-ray diffraction, transmission electron microscopy, physical N_2 adsorption techniques, and H_2 temperature-programmed reduction (H_2-TPR). It was found that the Ni/NFS catalyst is also a mesoporous material and the size of NiO particles is 5.3-6.3 nm. The NiO particles accrete on the surface of NFS fibers and fill in a single NFS tube or in other pores in NFS to exhibit a well distribution and a higher anti-aggregation ability. The H_2-TPR result shows that the Ni/NFS catalysts from ≥ 10 wt% $Ni(NO_3)_2$ solutions can be completely deoxidized at rather low temperature and effectively decrease the energy consumption in reaction. These properties ensure Ni/NFS catalysts, especially the Ni/NFS catalyst from ≥ 10 wt% $Ni(NO_3)_2$ solution, to have high activity and excellent performance in CH_4-CO_2 reforming.

Diatomite as both the template and the catalyst to produce hierarchically porous carbon

Liu Dong[1,2], Yuan Peng[1*], Tan Daoyong[1,2], Liu Hongmei[1,2], Zhu Jianxi[1] & He Hongping[1]
[1]Guangzhou Institute of Geochemistry, Chinese Academy of Sciences, Guangzhou, China ([*]yuanpeng@gig.ac.cn)
[2]Graduate School of Chinese Academy of Sciences, Beijing, China

Porous carbon-based materials with high specific surface area are currently attracting significant interest because of their increasing applications in various industrial fields, such as adsorption and purification. Templating method has been widely reported as a well-established route for the preparation of porous carbon in which various synthetic porous materials are used as templates. Some natural mineral materials are also chosen as templates due to their special porous structures and economical viability, such as zeolite and diatomite. Diatomite, the mineralised exo-skeletons of diatoms, has highly developed porous structure which is mainly macroporous with small amount of mesopores. In the few reports about the preparation of diatomite-based porous carbon, sulfuric acid was often used as the catalyst to catalyze the carbon precursor. However, the addition of liquid acid is potentially harmful to the environment, as well as increases the cost of the preparation. In our previous study, we have found that the diatomite itself contains solid acid sites. In this sense, it should be very interesting to utilize these inherent acid sites of diatomite instead of the additive acid to catalyze the carbon precursor, and to investigate the key effects of the solid acidity on the final structure of porous carbon.

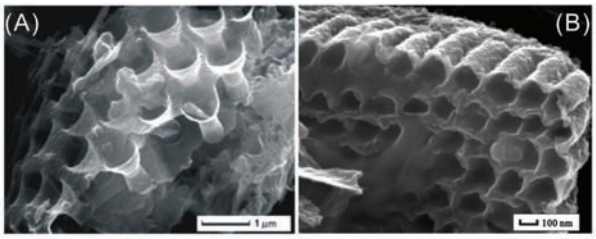

Fig. 1: SEM images of the differently macroporous structures: (A) disordered and (B) ordered macroporous structures.

In this study, we have successfully prepared hierarchically porous carbons by using intentionally selected diatomite and their thermally and acid activated derivatives as both the templates and the catalysts. The combined study by SEM, TEM, and N_2 adsorption indicates that there exists a highly morphological dependency between all of templates and their carbon counterparts which contain macropores, mesopores and micropores. The macroporous structures derive from two different types of pores of templates, one is replicated from the disordered central pores of the diatom shell, and the other from the smaller ordered edge-pores (Fig. 1). The micropores are generated mainly by the breaking of the carbon film, occurred universally in the process of the removal of the templates. The surface areas and pore volumes of the carbon products are higher than those of previously reported diatomite-based carbon prepared by using additional liquid acid as the catalyst, and there is a dramatically positive correlation between the concentratation of acid sites in the diatomite templates and the resulting values of surface area and pore volume of the crabon products. The obtained diatomite-based porous carbon products also exhibit desirable petrol absorption and H_2 storage performance, enabling potential applications in the fields of environment and energy.

Use of perlite in combination with clays for the production of low environmental impact filter for heavy metals polluted aqueous solution

Marchetto, P., Brigatti, M.F., Laurora, A. & Malferrari, D.[*]
Dipto. di Scienze della Terra, Università di Modena e Reggio Emilia, Modena, Italy ([*]dmalf@unimore.it)

The aim of this work is to prepare a relatively cheap mixture of perlite (a volcanic rock with intermediate composition between rhyolite and dacite) and clays, effective in the retention of heavy metals even after treatments at relatively high temperatures. The obtained product could be possibly reused and therefore not disposed of as toxic waste. The perlite used in this study comes from Greek quarries and is provided by the company "Perlite Italiana". Three different types of clay materials were used: 1) a clay material coming from the Argille Varicolori formation; 2) a commercial bentonite (supplied by Laviosa, Italy; 3) a standard montmorillonite (STx-1, from the County of Gonzales, Texas, USA), to be used as reference materials.

Column and batch tests were carried out on several different mixtures of the previously described materials in order to evaluate the effective adsorption of Cd, Pb, and Zn from aqueous solution. Pb, Zn, and Cd contents of the "polluted" mixtures were thus measured via inductively coupled plasma optical emission spectroscopy (ICP-OES) after acid digestion.

The obtained results indicate that the mixture consisting of Varicolori clay and perlite can be profitably used as adsorbent of metals in solution. Adsorption data are consistent with those expected from theoretical calculations.

The method chosen for the permanent inertization of polluted samples is thermal treatment, which, as evidenced by numerous literature data, can lead to a chemically inert product, eventually suitable for reuse in construction. Before being fired, each mixture was added from opportune amount of kaolinite and feldspar. Release tests were, thus, carried out on fired products using weakly acid solution (pH values between 5.5. and 6) as leaching media. Results, which are very encouraging, are reported in the Table 1.

Table 1: Heavy metals (Pb, Cd and Zn) contents in prepared mixtures, after applied tests

	Perlite + Bentonite Laviosa	Perlite + Argilla Varicolori	Perlite + STx-1
Pb, Cd, Zn concentration in the different adsorbants			
Pb (mg/100g)	719,53	157,20	286,30
Zn (mg/100g)	360,33	43,938	175,82
Cd (mg/100g)	2,1461	0,3675	1,6596
Pb, Cd, Zn release in weakly acid leaching solution			
Pb (μg/g)	n.d.	n.d.	n.d.
Zn (μg/g)	n.d.	n.d.	n.d.
Cd (μg/g)	n.d.	n.d.	5.45×10^{-6}

Sintering behavior of calcium silicate ceramics

Meiszterics, A.[1], Rosta, L.[2], Vainio, U.[3] & Sinkó, K.[1*]
[1]Inst. of Chemistry, L. Eötvös University, Budapest, Hungary (*sinko@chem.elte.hu)
[2]Neutron Spectroscopy Dept., RISP of the Hungarian Academy of Science, Budapest, Hungary
[3]Hamburger Synchrotronstrahlungslabor at DESY, Hamburg, Germany

A new preparation method based on solution technique was developed for synthesis of bioactive ceramic samples. The first step is the synthesis of calcium silicate gel samples by sol-gel technique. The hydrogel samples must be dried and heat treated to obtain the final ceramic product. One of the most important advantages of the sol-gel technique is the low energy requirement, much lower than that of conventional powder or melting technologies: 600-700°C in contrast to 1200-1300°C. In addition, the sol–gel processing allows one to produce gel glasses with compositions lying within the liquid–liquid immiscibility dome of several silicate systems. According to some published results, the bioactivity of the sol-gel derived glass-ceramics is unambiguously better than that of ceramics prepared by quenching of melts. The increase in bioactivity can be explained by the great differences in the textural properties of the materials synthesized by different techniques. The structure of a higher porosity obtained by sol-gel method can more fit the porous bone tissues than the compact one.

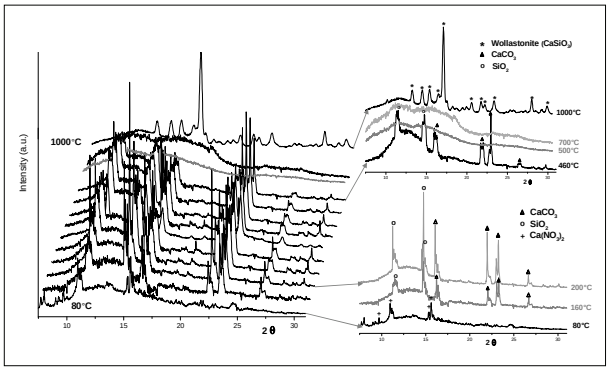

Fig. 1: WAXS curves for calcium silicate samples heat treated at various temperatures.

The present research work focused on the investigation of correlations in the *particle size – sintering temperature – Vickers-hardness* triangle. The synthesis route is: 1. preparation of hydrogel; 2. drying the wet gels (powders); 3. sintering (bulk). Ammonia catalyzed samples can be described with compact structure and good mechanical strength, however they keep some porosity. The structures of sol-gel derived calcium silicate ceramic products differ from that of fused product, which has crystalline wollastonite structure. The new structure can be characterized mainly with amorphous feature; it contains only a small volume of crystalline ordering (Fig. 1). The crystalline phase may be mono- or dicalcium silicate depending on the temperature of heat treatment. The Vickers-hardness, the water solubility, and the particle size of dried gels change together. The larger the particle, the better the strength is.

X-ray difraction study of opal-CT in siliceous rocks

Naumkina, N.I., Ilicheva, O.M.*, Vasserman, D.V. & Lygina, T.Z.
Central Research Institute for Geology of Industrial Minerals, Kazan, Russia (*atsic@geolnerud.net)

Siliceous sedimentary rocks are composed by silica (quartz and opal-CT), aluminium silicates (clay minerals, feldspars, zeolites), and, sometimes, carbonates. The originality and specificity of the opal-CT (the amount and structure) are determining the usage of siliceous raw materials: for the manufacture of liquid glass, ceramics, abrasives, rubber, refractories, concrete products, etc. We present the results of the opal-CT study with a phase-structural (mineralogical) term of a large number of samples of siliceous sedimentary rocks of Russia: flasks, tripoli, and diatomite, but not precious opals.

XRD patterns of natural opal-CT are showing complex profiles in a narrow range of 18-25° 2Θ CuK(α)(4.40-3.80 Å) and the reflex of 2.50 Å. The correct choice of standards is very important for the quantitative calculation of opal-CT by XRD method. Therefore as the majority of constituent phases is dispersed state, it's almost impossible to prepare the pure-phase substance. This difficulty is to be resolved by Rietveld method. Opal-CT profile is described by the reflection superposition of opal (low broad diffuse halo with a peak at 4.10 Å), cristobalite (clearly defined peak with a value of interplanar distance d = 4.05 Å) and tridymite (triplet reflections with values d =4.31-4.07-3.81 Å). At studying and quantifying the opal-CT in natural objects should be considered as a possible overlap the reflexes of zeolite, clay minerals, calcite, etc. The contribution of such "interfering phases" is clearly visible on the diffraction pattern of samples before and after hydrothermal leaching. Comparison of quantifying the content of opal-CT by XRD and of SiO_2 by hydrothermal leaching (5% KOH) gives a high value of the pair correlation R = 97%. XRD analysis of different Russian's deposit samples showed that the intensities ratio of the opal-CT diagnostic reflections with d = 4.3; 4.1; 2.5 Å to their sum is constant: 31.50% for d ~ 4.30 Å, 53.48% - 4.10 Å and 15.02% - 2.50 Å. [1]. In the presence of calcite in the sample use reflection d = 2.50 Å is not correct because of the superposition of calcite and opal-CT reflexes. Therefore, it was considered the ratio of two reflections 4.30 and 4.10 Å, given the contribution of the amplitude of their sum close to 37% and 63% respectively. It is seen that all points on the diagram lie close to the line with a high degree of correlation (R^2=0.92), such as for pare of quartz reflection with d=3.34 and 1.82 Å. The similar dependence of the reflex opal 4.1 Å – quartz 3.34 Å is shown in the figure for comparison.

XRD study of burned sample of opal-CT showed that the diffraction pattern does not change to 900-1000°C. At higher temperatures, it has been detected a sharp increasing of the intensity of the reflex of 4.10 Å, and reduction of 4.30 Å. The crystallite size has increased to 400 Å at 1300°C, whereas up to 1000°C it was 160 Å. TA-studies showed only the effects associated with the loss of water up to 220°C, decomposition of carbonates and destruction of zeolites at 500-800°C. No other effects in the temperature range up to 1000°C were detected.

Thus, the results of XRD and TA studies on opal-CT leads to the following conclusions: 1) Opal-CT is a stable mineral formation, solid-phase reaction of β-cristobalite formation begin after 1000 ºC. 2) Diagnostic reflexes of this phase are 4.30 Å (60 % from a maximum), 4.10 Å (maximum intensity), and 2.50 Å (30 % from a maximum). 3) The structure of opal-CT should be considered as alternating layers of α - cristobalite and tridymite with a deterministic quantitative ratio between them.

[1] Naumkina, N.I. et al. (2009) *RMS Annual Session*, 239-241.

Selective exchange process limit for dioctahedral smectite: case of solution saturated by Cu^{2+} and Co^{2+} cation

Oueslati, W.*, Meftah, M., Ben Rhaiem, H. & Ben Haj Amara, A.
Laboratoire de Physique des Matériaux Lamellaires et Nanomatériaux Hybrides, Faculté des Sciences de Bizerte, Tunisia (*walidoueslati@ymail.com)

Wyoming Montmorillonite (i.e SWy) is a clay mineral with ''T-O-T" layer consisting of an octahedral sheet sandwiched by two tetrahedral sheets. Isomorphic substitutions in octahedral and/ or tetrahedral sheets commonly make the clay platelets negatively charged, which are compensated by exchangeable cation. Water and other polar solvents can enter interlayer regions and cause clay-swelling. In addition, clays are able to retain inorganic and organic pollutants, and to stop the circulation of contaminated fluids in both aquatic and soil environments. Several works studied exchange process realized when clays mineral is in contact with solutions containing only one metallic cation [1-4] and shows a different hydration behavior related to the nature of exchangeable cation. The selective exchange problem was imposed when several metallic cation are present in solution, which is the most realistic case if we wants to apply clay properties in the context of industrial waste storage [5]. This paper aims at characterizing the structural bond between selectivity and exchangeable cations abundance in the case of Na-dioctahedral smectite. This goal was determined by equilibration of the clay with a mixed equinormal solution containing two competing heavy metal cations (i.e Cu^{2+}, Co^{2+}) with various concentrations. The quantitative XRD analysis is achieved using an indirect method based on the comparison of experimental XRD patterns to calculated ones.

XRD investigation showed that exchange process are stopped for a limit concentration values (i.e.10^{-3}N) characterized by a weak ions population and which does not saturate the intrinsic cation exchange capacity (i.e. CEC) of the host materiel. For high ions solutions abundance (i.e 1N), the clay CEC was saturated by Co^{2+} species characterized by d_{001}=15.17Å basal spacing value related to two water layer hydration state (2W). All structural parameter are reported in (Table 1).

Table 2: Optimum structural parameters used for the simulation of XRD profile in the case of mixture containing ($0.5Cu^{2+}$, $0.5Co^{2+}$) with variable concentration

conce	d_{001} (Å)	exch/cati	Z_n (Å)	W_A W_B	M
10^{-1}N	15,2 (2W) 12.4 (1W)	Co^{2+} Cu^{2+}	11.6 9.95	0.87 0.13	6
10^{-2}N	12,4 (1W) 15.2 (2W)	Cu^{2+} Co^{2+}	9.95 11.4	0.35 0.65	7
10^{-3}N	12.4 (1W) 15.2 (2W)	Na^{+} Cu^{2+}	9.8 9.9	0.95 0.05	7
10^{-4}N	12.3 (1W)	Na^{+}	9.8	1	7

[1] Bérend, I. et al. (1995) *Clay Clay Miner.*, **43**, 324-336. [2] Ferrage, E. et al. (2005a) *Am. Mineral.*, **90**, 1358-1374. [3] Laird, D.A. (1996) *Clay Clay Miner*, **44**, 553-559. [4] Oueslati, W. et al. (2007) *Z. Krist. Suppl.*, **26**, 417-422. [5] Oueslati, W. et al. (2009) *Appl. Clay. Sci.*, **43**, 224-227.

Physico-chemical constraints of apatite and crandallite formation in phosphorites from Ervenik, Croatia

Posilović, H.[1], Kniewald, G.[2*], Žigovečki-Gobac, Ž.[1] & Bermanec, V.[1]
[1]Dept. of Geology, Faculty of Science, University of Zagreb, Croatia
[2]Dept of Marine and Environmental Research, Rudjer Bošković Institute, Zagreb, Croatia (*kniewald@irb.hr)

Apatite group minerals and their secondary alteration phases were studied of Upper Cretaceous phosphorite-bearing deposits. Outcrops of these deposits are situated at the foot of the SE part of Mt. Velebit near Ervenik, Croatia. Phosphorite deposits can be found in fossil caves, caverns and other karstic phenomena in limestone, generally of Cretaceous age. The exact age of the deposits is not known but is assumed to be Pleistocene. The source of phosphorus could be the phosphate-rich guano material originating from bats and birds [1].

Collected sediment samples were disintegrated, or cut–and polished and analyzed by optical microscopy, SEM, EDS, and XRD. Phase stability diagrams were constructed on the basis of mineral phases identified in the samples. The aluminium, calcium and phosphate concentrations chosen for stability field calculations are considered normal for pore fluids in contact with soil and sediments [2]. The phosphate minerals occur as white to greyish spherulitic aggregates or single crystals up to 2 mm in size. Cave sediments are usually compact and reddish or greyish in colour, with a high Al_2O_3 and FeO content, but low in carbonate. Optical microscopy and SEM of spherulitic aggregates showed at least two different phosphate phases identified by EDS and XRD as hydroxylapatite and crandallite. In the inner core of the spherulites, apatite is precipitated in the form of sprays up to 1.5 mm in length; outer parts of the spherulites volume contain very fine grained radial to fibrous crandallite. Some spherulites are banded and composed of alternating apatite and crandallite layers.

Apatite and crandallite spherulites were formed during early diagenesis of the cave sediment; each single spherulite was precipitated in partially closed microenvironment of the sediment voids and pores. Apatite occupying the central portions of the spherulits centre formed prior to crandallite in the outer spherulite sector. The calculated stability fields for apatite and crandallite may be used to explain the bi-phase precipitation in the spherulites. Higher phosphate and lower aluminum concentrations with higher pH will favour apatite precipitation; such conditions prevailed during precipitation of the spherulite core. As a consequence of apatite precipitation, phosphate concentration is decreased and aluminum is increased, the stability field of crandallite prevails and crandallite becomes stable phase precipitating in the spherulite outer volume.

[1] Marković, S. (2002) *Mineral deposits of Croatia*. Institut za geološka istraživanja, Zagreb (in Croatian). [2] Nriagu, O.J. (1976) *Can. J. Earth Sci.*, **13**, 717-736.

Entry of SO_3 into the structure of dicalcium silicate

Staněk, T.[1*], Leichmann, J.[2] & Sulovský, P.[1]
[1]Research Inst. of Building Materials, Brno, Czech Republic
([*]stanek@vustah.cz)
[2]Faculty of Science, Masaryk University, Brno, Czech Republic

Dicalcium silicate containing foreign ions (Ca_2SiO_4 – C_2S) occurs as a component of Portland cement clinker and is called belite. Belite has lower hydraulic activity than alite (contaminated tricalcium silicate), which is the main component of Portland cement clinker. Belite can be prepared with lower expenditures and its hydraulic activation can have important impact on the economy and sustainability of cement industry.

Our research is focused on the activation of C_2S by incorporation of SO_3 into its crystal structure. Experiments with pure chemicals have shown that S substitutes Si, stabilizing thus monoclinic β-belite. Such stabilization was already described [1]. Analyzing a set of samples burned at 1450°C we found that the SiO_2 content decreases with increasing SO_3 content in C_2S with very high correlation coefficient R = -0,91 (see Fig. 1).

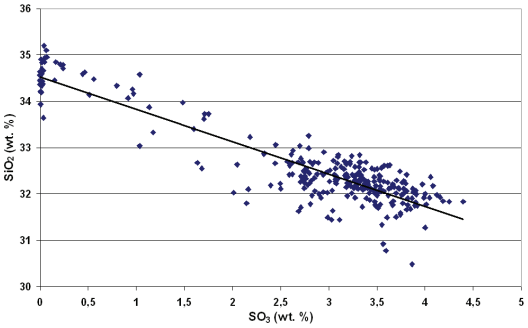

Fig. 1: The correlation of SiO_2 and SO_3 contents in C_2S.

Sulfur enters the structure of C_2S in the form of sulfate anion. The substitution of SiO_4 tetrahedra by sulfate is known e.g. in tobermorite structure, where the charge compensation compensation is by heterovalent substitution of SiO_4^{4-} with SO_4^{2-} and $2OH^-$. This is not possible in case of C_2S.

Results of belite microanalyses from belite clinkers doped with SO_3 in further experiments indicate that incorporation of S into the belite structure is connected with incorporation of increased amounts of Al. The charge compensation is probably similar to that known in the nagelschmidtite group or as berlinite substitution in silicates. The determination of the charge compensation by incorporation of other elements into the C_2S structure will be the subject of further study.

Maximum content of SO_3 in C_2S was observed in our sandwich experiments; it amounts (under normal burning conditions) to 4.4 wt.%. The empirical formula of this C_2S is $Ca_{1,929\pm0,004}Mg_{0,014\pm0,002}\square_{0,055}[(SiO_4)_{0,902\pm0,002}(SO_4)_{0,082\pm0,002}]$ (95%-confidence interval from 30 analyses, □ - vacancy). Taylor 1999 [2] found by analysis of industrial clinkers that at bulk content of SO_3 up to 3 wt.% belite contains more than 2 wt.% SO_3 only exceptionally; bulk SO_3 exceeds 3 wt.% are rare in industrial clinkers.

The incorporation of SO_3 into the C_2S structure leads to the decrease of CaO content (from 65.6 wt.% to about 63.7 wt.%), but the Ca:Si ratio rises from 2.03 ± 0.01 at 0 wt.% SO_3 in belite up to 2.16 ± 0.01 at 4.4 wt.% SO_3 in belite. The correlation between the Ca:Si atomic ratio and the number of S atoms per formula unit is 0.78, what at high number of analyses is statistically very significant value.

[1] Morsli, K. et. al. (2007) *Cement Concrete Res.*, **37**, 639-646. [2] Taylor, H.F.W. (1999) *Cement Concrete Res.*, **29**, 1173-1179.

Crystallization properties of Nb containing bioactive phosphate glass-ceramics

Stunda, A.[1*], Mironova-Ulmane, N.[2], Borodajenko, N.[1], Vempere, D.[1] & Berzina-Cimdina, L.[1]
[1]RTU Riga Biomaterials Innovation and Development Center, Riga Technical University, Riga, Latvia
([*]agnese.stunda@rtu.lv)
[2]Institute of Solid State Physics, University of Latvia, Riga, Latvia

Glass-ceramics are relatively new material. Glass-ceramics have higher solubility than ceramics and higher mechanical strength than glass. Both properties are important for using material as implant material and depend on crystallinity properties.

In this research glass-ceramics were obtained by crystallization of previously produced glass powder. The aim of research was to compare crystallization data given by differential thermal analysis (DTA), X-ray powder diffraction (XRD), infrared spectroscopy (FT-IR) and RAMAN spectroscopy. Samples contain transition element niobium which can replace either cation, either P in anion. Hence scrupulous investigation of processes is requested.

Materials investigated in this research were niobium and sodium containing calcium phosphates. Glass powders were melted from batch of analogous composition but using different techniques. FT-IR results indicate that glass structures differ a lot.

Crystallization temperatures were detected by DTA. 8 of samples crystallize above ~800°C, only 3 samples around 720°C. Glass transition temperatures for all samples are close to 650 degrees. In literature it is shown that glasses in pure P_2O_5-CaO-Na_2O system or with TiO_2 [1] or with ZnO [2] additives start to crystallize at 650°C. It can be concluded that Nb_2O_5 additives increase crystallization temperature, although crystallizing phases mainly are the same: $Ca_3(PO_4)_2$, $Ca_{10}Na(PO_4)_7$, $Ca_2P_2O_7$ and also $Na_4(Nb_8P_4O_{32})$, $NaNbO_3$.

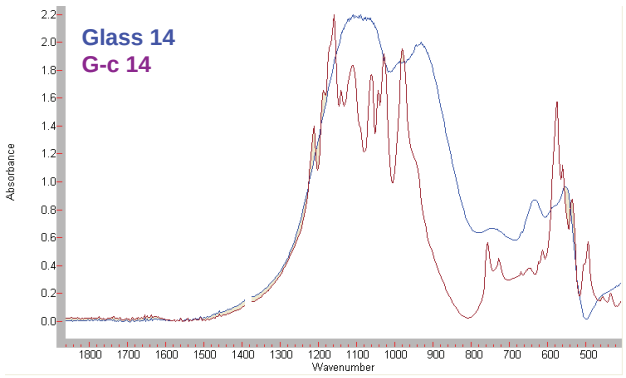

Fig. 1: Comparison of IR spectra of phosphate glass and glass ceramics.

Crystallization starts at lower temperature than temperature when first exothermal peak in DTA occurs. There are different intensities and temperatures of exothermal peaks but structures detected by XRD are almost similar. For more detailed investigation FTIR (Fig. 1) and RAMAN spectroscopy are used.

It was found that crystallization of every single phase does not have a corresponding DTA peak. In XRD pattern and IR spectra it can be seen that crystallization starts at lower temperatures than are exothermal DTA peaks. The DTA peaks can be explained by changing oxidation state of niobia. For all samples and all temperatures multiple crystalline phases are forming.

[1] Kasuga, T. (2005) *Acta Biomater.*, **1,** 55-64. [2] Cai, S. et al. (2009) *J. Non-Cryst. Solids*, **355,** 273-279.

Recycling BOF-slag: experimental constraints

Su Tung Hsin[1*], Yang Huai Jen[1], Lee Yu Chen[2], Shau Yen Hong[3] & Lin Ming Fong[2]
[1]Dept. of Earth Science, National Cheng-Kung University, Tainan, Taiwan ([*]l4897101@mail.ncku.edu.tw)
[2]China Steel Corporation, Kaohsiung, Taiwan
[3]Dept. of Marine Biotechnology and Resources, National Sun Yat-sen University, Kaohsiung, Taiwan

In the basic-oxygen furnace (BOF) process for steel-making, excess carbon in molten iron is reduced to carbon dioxide by oxygen inflow, meanwhile the phosphorus, silica, and other impurities in molten iron are also partitioned into the added stony material, usually lime (CaO). The resulting stony material is known as "BOF-slag". It mainly consists of dicalcium silicate (Ca_2SiO_4; C_2S), calcium ferrite ($Ca_2Fe_2O_5$), free-lime (CaO), wustite (FeO) and periclase (MgO). Because of a high production rate of 100 kg slag /ton steel, recycling of these "solid wastes" is an important issue for the operation of a steel-making plant. Theoretically, BOF-slag can be recycled as flux in blast furnace (BF) process for steel-making or as aggregate or as cement, after proper treatments. Being used as BF-flux, the BOF-slag must has P content < 0.1%. On the other hand, relatively higher volume stability from free-lime removal is required for utilization as aggregate or cement. In this study, experiments were carried out to develop proper treatments for recycling BOF-slag.

A series of high temperature experiments were designed following the concepts for phosphorus and free-lime removal; specifically, converting free-lime to stable silicates with the addition of SiO_2 and releasing phosphorus as a gas phase under high-T and reducing conditions. Mixtures of BOF-slag (< 0.5 mm) and coke were heated to 1600°C for 5 hours. Si-sand was added to react out free-lime and to suppress crystallization of C_2S, which is a major host of phosphorus in the BOF-slag. Detailed examination on experimental products using XRD and EDS confirmed that the free-lime in starting materials was completely reacted out, forming volumetrically stable Ca-Al-Mg silicates, although bulk phosphorus contents remained unchanged. However, it was found that the experimental products were segregated into two phase domains; metal and stony domains. The former is a Fe-Mn-Si-P alloy composed of three phases, Fe-Mn-Si, Fe-Mn-P and Fe-Mn alloys. The stony domain consists of akermanite (a major constituent phase of blast-furnace slag) and merwinite with low phosphorus content of < 0.1% and absence of C_2S. Magnetic separation effectively split the metal alloy from the stony matrix. The major oxides of the resulting stony domain (46-48% CaO, 36-38% SiO_2, 8–10% MgO, 3–4 % Al_2O_3, < 3% total iron, and < 0.3% P_2O_5) is similar to that of BF-slag, a major raw material of slag-cement. This low phosphorus and free lime stony matrix is not only suitable for recycling to steel-making processes but also of high quality aggregate. Compared to common dark BOF-slag, the stony matrix from our treatment is in light colors of white-grey with marble-like appearance that can be dyed to colorful glass ceramics. After these treatments, BOF-slag can be converted into 80 wt% high quality slag and 20 wt% high phosphorus metal alloy possibly for further refinement. Although scaling our experimental methods up to a practical level remains as a challenge, these experimental results provide a reference for commercializing BOF-slag.

Modification of copper phthalocyanine blue by nano-fibriform silica

Wang Lijuan[*], Li Yuanyuan, Chen Jiawei, Ma Junhong & Li Jinhong
State Key Laboratory of Geological Processes and Mineral Resources; National Laboratory of Mineral Materials, China University of Geosciences, Beijing, China
([*]lijuanwang@cugb.edu.cn)

The modification of copper phthalocyanine blue (CuPc) by nano-fibriform silica (NFS) with an in-situ polymerization method was studied by transmission electron microscopy, infrared spectroscopy, physical N_2 adsorption techniques, color difference analysis, and durability experiment. The results show that the best modified product (NFS-CuPc) is composed of $CuCl_2$, CuPc, gelatin and NFS at a mass ratio of 4:28:3:40, with a specific surface area of 98.4 m^2/g, adsorptive capacity of 485 cm^3/g, pore volume of 0.76 cm^3/g and average pore diameter of 30.9 nm, and is of the lowest value (0.20) of color difference in a lightfastness experiment. Compared to CuPc and PS-CuPc (CuPc modified by precipitated silica), NFS-CuPc is of the best durability, owing to the nano-tube form and anti-aggregation ability of NFS that make CuPc particles hard to be taken off. So NFS-CuPc is a better pigment and NFS is a good additive in pigments.

Shell–core morphology of injection molded polyamide–6 and polyamide–6/montmorillonite nanocomposites

Yebra-Rodríguez, Á.[1*], Álvarez-Lloret, P.[2], Cardell, C.[2], López-Galindo, A.[3] & Rodríguez-Navarro, A.B.[2]
[1]Dept. of Geology, IACT Associated Unit (CSIC-UGR), University of Jaén, Spain ([*]ayebra@ujaen.es)
[2]Dept. of Mineralogy and Petrology, University of Granada, Spain
[3]Andalusian Inst. of Earth Sciences (IACT, CSIC-UGR), Granada, Spain

Polymer/clay nanocomposites display an array of properties thus far not achievable from the neat polymer. The enhancement of mechanical, thermal, barrier and other properties ([1] and references therein) has been related to the close interaction between the polymer matrix and the organically modified clay minerals. Processing conditions during injection molding do affect the crystal structure and the crystallinity of the samples [2]. Moreover, the crystal structure of polyamide–6 (α, β and/or γ) depends strongly on the sample thickness [3].

This paper presents a study of the microstructure of injection molded samples of polyamide–6 (PA6) and polyamide–6/montmorillonite nanocomposites (PA6MMT) cooled to different temperatures (40, 60, 80 and 100 ºC) after the molding to 2 mm thickness tool. The samples were manufactured as described elsewhere [3] and examined by X-ray Diffraction (XRD, (Siemens D5005), Differential Scanning Calorimetry (DSC, DSC 2920; TA Instruments), and Transmission Electron Microscopy (TEM, Zeiss EM 902).

Results show that samples are organized in a shell-core structure across the sample thickness. Polyamide-6 crystals are better oriented in the nanocomposites (PA6 MMT) than in the pure polyamide (PA6 samples), and better in the shell than in the core for both sets of samples. The same trend is observed in the crystallinity values. The lamellae stacks of the shell slices are more highly oriented than in the core. In the PA6MMT samples, the montmorillonite platelets also present higher orientation in the shell than in the core. These observed characteristics may help to establish the most appropriate cooling temperature in the fabrication of thick pieces where these kinds of materials are involved.

Acknowledgements: This research was supported by Research Groups RNM–325 and RNM–179 (CICE, JA, Spain). The authors thank "Centro de Instrumentación Científico Técnica" (University of Jaén, Spain), "Centro de Instrumentación Científica" (University of Granada, Spain) and the technicians for data collection. We wish to thank Dr. A. Kowalski for English revision.

[1] Okada, A. & Usuki, A. (2006) *Macromol. Mater. Eng.*, **291**, 1449-1476. [2] Kamal, M.R., Borse, N.K. & García–Rejón, A. (2002) *Polym. Eng. Sci.*, **42**, 1883-1896. [3] Yebra–Rodríguez A. et al. (2009) *Appl. Clay Sci.*, **43**, 91-97.

Pyrite generations and ankerite in the deepest sediments of the Makó trench (Pannonian basin)

Zajzon, N.[1*], Vető, I.[2], Demény, A.[3], Pintér, F.[4] & Földvári, M.[5]
[1]Inst. of Mineralogy and Geology, University of Miskolc, Hungary ([*]nzajzon@uni-miskolc.hu)
[2]Consultant, Balogh Á. street 18/c, 1026, Budapest, Hungary
[3]Inst. for Geochemical Research, Hungarian Academy of Sciences, Budapest, Hungary
[4]Scientific Laboratory, Federal Office for Protection of Monuments, Vienna, Austria
[5]Geological Institute of Hungary, Budapest, Hungary

Chemical, mineralogical and isotopic records of the thermochemical sulphate reduction (TSR) active below 5 km in the Makó trench have been described briefly by [1]. Here its mineralogical aspects will be discussed in more details.

The most interesting core sample is studied by BSE, where four pyrite types are visible (Fig. 1): Type 1 consists of framboids of early diagenetic, obviously microbial origin forming balls and mat layers with the size of up to 100 µm. Types 2–4 are products of TSR. Type 2 infiltrates particular grains with uncertain organic origin, while type 3 consists of 100 µm sized aggregates of smaller crystals of pyrite and pyrite matrix, with somewhat spongeous texture. Type 4 is represented by hexagonal forms of 50–100 µm size. Types 2 and 3 are considered as transitional forms leading to formation of the final variant of the late diagenetic pyrite, represented by hexagonal crystals. TSR is likely a process active even today.

DTA curves show two pyrite peaks at around 405 and 465°C. According to micro XRF (attached to SEM) measurements, types 1–3 contain only Fe and S above the detection limit. Type 4 can be divided to two subtypes: the first is also free of other elements, till the second contains Zn and Mn, probably homogenously distributed in the pyrite, because no inclusion could be observed. The Zn enrichment could explain the higher thermal stability of the pyrite, reflected in the second DTA peak.

Ankerite was also observed in the samples, where TSR pyrite appears. The C and O isotope compositions show subtle variations. Ankerite (+dolomite): $\delta^{13}C$ = –0.6 to 2.8‰, $\delta^{18}O$ = –10.0 to –7.4‰; calcite: $\delta^{13}C$ = 2.1 to 3.4‰, $\delta^{18}O$ = –9.9 to –9.0‰ (V-PDB). A combined evaluation of mineral contents and isotopic compositions lead us to suggest that the TSR process may have happened at deeper positions, and the migrating H_2S+CO_2 fluid underwent significant isotopic exchange with the surrounding carbonate rocks. The pyrite+ankerite(+dolomite) formation was induced by mixing of this TSR-related fluid with a local one containing dissolved Fe and Mg.

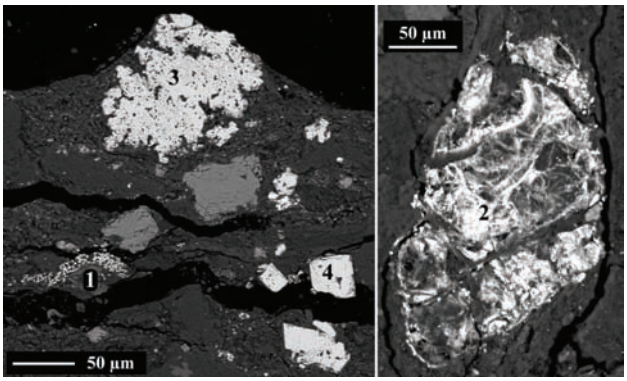

Fig. 1: BSE images of the different pyrite generations of the sample. The numbers are marking the different types (see in text).

[1] Vető, I. et al. (2009) *Mitt. Ost. Min. G.*, **155**, 171.

Formation of diamond in the lithospheric mantle

Stachel, T.[1*] & Harris, J.W.[2]
[1]Dept. of Earth and Atmospheric Sciences, University of Alberta, Edmonton, Canada ([*]tstachel@ualberta.ca)
[2]Dept. of Geographical and Earth Sciences, University of Glasgow, UK

With the exception of rare "super-deep" diamonds, gem diamonds derive from peridotitic, eclogitic and minor websteritic sources in the subcratonic lithospheric mantle. Geothermometry, based on silicate inclusions and the aggregation state of nitrogen in diamonds, shows that irrespective of source paragenesis, crystallization and storage of diamonds in the lithospheric mantle commonly occurs in a narrow temperature interval of ~1150 ±100°C. Geobarometry, based on garnet-orthopyroxene inclusion pairs, indicates diamond formation at depths of generally less than 200 km along 38-42 mW/m^2 model geotherms. Lower geothermal gradients observed for some diamonds likely represent re-equilibration of touching inclusion pairs during cooling ambient conditions, suggesting that diamond formation is associated with transient heating events.

Direct conversion from graphite is not considered relevant for the formation of gem diamonds since the high activation energy and associated overstepping will likely cause the graphite-diamond conversion to occur catastrophically resulting in very fine grained polycrystalline aggregates [1]. Precipitation of lithospheric diamonds is interpreted to occur during redox reactions associated with the infiltration of melts (super-solidus conditions) or CHO-fluids (sub-solidus), involving either carbonate reduction or methane oxidation. Both of these diamond growth modes are documented in nature [2,3].

Studies of mantle xenoliths from Phanerozoic kimberlites indicate a decrease of oxygen fugacity with depth that is presumed to reflect crystallochemical effects. Along the resulting depth-fO_2 trend, at pressure exceeding ~3 GPa elemental carbon (graphite/diamond) rather than carbonate is stable in "normal" subcratonic peridotitic mantle [4]. This implies that reduction to diamond can only occur for carbonate dissolved in upward migrating fluids/melts. Such comparatively oxidized melts/fluids cannot derive from the reduced deep upper mantle and, therefore, likely relate to recycling of oceanic lithosphere. Carbonate reduction appears to be the dominant mode of diamond formation during the Proterozoic and Phanerozoic [5].

For generally Paleoarchean harzburgitic diamonds (3.5-3.2 Ga) co-variations of $\delta^{13}C$–N suggest methane reduction as the principal mode of precipitation, relating their formation to upward percolation of reduced asthenospheric fluids. The apparent transition to carbonate reduction as the dominant mode of diamond formation after the Archean coincides with increasing recycling of biogenic carbonates into the mantle since the Paleoproterozoic.

[1] Sung, J. (2000) *J. Mat. Sci.*, **35**, 6041-6054. [2] Navon, O. et al. (1988) *Nature*, **335**, 784-789. [3] Thomassot, E. et al. (2007) *Earth Planet. Sci. Lett.*, **257**, 362-371. [4] Frost, D.J. & McCammon, C.A. (2008) *Annu. Rev. Earth Planet. Sci.*, **36**, 389-420. [5] Stachel, T. & Harris, J.W. (2009) *J. Phys.: Condens. Matter*, **21**, 364206.

Trace element substitution in gem feldspars using XAFS and XEOL

Taylor, R.P.[1,2*], Finch, A.[1] & Mosselmans, J.F.W.[2]
[1]Division of Earth Sciences, University of St Andrews, UK ([*]rpt5@st-andrews.ac.uk)
[2]Diamond Light Source, Didcot Oxford, UK

X-ray Absorption Spectroscopy (XAS) is used extensively in the study of local atomic coordination in materials. Here we apply this methodology in the investigation of minor and trace elements within feldspar. We compare and contrast the XAS information encoded in X-ray fluorescence (standard fluorescence XRF-XAS) with that expressed in the X-ray Excited Optical Luminescence (XEOL).

We have analysed Fe substitution in a suite of gem-quality material. For many samples, we obtain XAS spectra consistent with tetrahedral Fe^{3+} substituting for Al. Average bond distances around Fe have been determined. However Fe in many feldspars is present dominantly as nanoparticles of Fe oxides such as magnetite. The XRF-XAS data here provide a composite of the oxide and Fe substituted into feldspar.

To deconvolute the responses of the two phases, we have explored the XAS information expressed by the XEOL. Such methods have been applied successfully in other systems [1] although the interpretation is sometimes far from trivial. In principle, XEOL comes solely from the feldspar component of intergrowths and can provide a route to determine Fe coordination in feldspar independently of the nanoinclusions. These experiments require further development of the i18 beamline at Diamond but our preliminary experiments show no XAS information in the XEOL response. We hypothesise that the long (ms) lifetimes of luminescence in Fe-bearing feldspars divorces the XAS information from the XEOL response. Future experiments will isolate the fast (ns) component of the luminescence in the time domain and explore that for XAS information.

We will present data on Cu coordination in gem-quality red plagioclases (Plush feldspars) [2] that have recently been the subject of great controversy. Our results will include a comparison of XEOL and XRF-XAS data.

[1] Soderholm, L. et al. (1998) *J. Chem. Phys.*, **109**, 6745-6752. [2] Hofmeister, A.M. & Rossman, G.R. (1985) *Geology*, **13**, 644-647.

Emeralds from the Piteiras mine, Minas Gerais State, Brazil: genetic implications from fluid inclusion studies

Costanzo, A.[1*], Blamey, N.J.F.[2], Feely, M.[1], Lynch, E.P.[1], Pironon, T.[3] & Lavin, P.[1]
[1]School of Natural Sciences, Earth and Ocean Science, National University of Ireland, Galway, Ireland
([*]alessandra.costanzo@nuigalway.ie)
[2]Dept. of Earth and Environmental Science, New Mexico Tech, Socorro, USA
[3]UMR G2R, CREGU, Universite´ Nancy I, Vandoeuvre-le`s-Nancy, France

The Piteiras mine in Itabira is located in the Minas Gerais State, Brazil and produces gem quality emeralds. Ultramafic rocks in contact with granites are the preferred mineralised zones with amphibolite-phlogopite schists acting as the host rock for emeralds. The emerald crystals (~0.5-50mm in length) are spatially related to quartz boudins within the schists. Samples of emerald and boudined quartz were subjected to fluid inclusion (FI) studies, i.e., petrography, microthermometry, laser-Raman microprobe and gas analysis using mass spectrometry. The results presented below highlight significant differences between the chemistry of fluids trapped in FIs in emerald and in the boudined quartz. The geological constraints on emerald formation resulting from these differences will be discussed.

In quartz aqueous-rich FIs are trapped as secondary inclusions distributed along planar arrays in healed fractures. FIs consist of two-phase (L_{H2O}+V_{H2O}) aqueous inclusions Type 1 and monophase aqueous (L) Type 2. In Type 1 T_{Htot} to the liquid phase is between 182 and 381°C and to the vapour phase between 339 and 420°C; salinity ranges from 0.88 to 14.77 eq.wt.% NaCl. Primary fluid inclusions in emeralds are very abundant and occur as isolated individuals, in groups of FIs or distributed in trails parallel to the crystal growth zones. FIs consist of four FI types: Type 1 are two-phase (L_{H2O}+V_{H2O}) aqueous inclusions; type 2 are solid-rich aqueous inclusions (L_{H2O}+V_{H2O}+S); type 3 are three-phase (L_{H2O}+L_{CO2}+V_{CO2}) aqueous-carbonic inclusions (CO_2 ranging from 30 to 80 vol.%); type 4 are solid-rich aqueous-carbonic inclusions (L_{H2O}+L_{CO2}+V_{CO2}+S) with CO_2 occupying ca. 40–80 vol% of the inclusions. In emerald hosted aqueous-rich FIs type 1 and 2 T_{Htot} occurs to the liquid phase between 260 and 400 °C and salinity range from 4 to 7 eq.wt.% NaCl. Dissolution of the solids occurs from 220 to 255 °C. In aqueous-carbonic FIs type 3 and 4 CO_2 homogenises to the liquid state between 28.7 and 31 °C, and to the vapour between 27.7 and 31.8 °C indicating CO_2 densities between 0.31 and 0.64 g/cm^{-3}. CO_2 melting temperatures range from -56.6 to -58.8 °C. Clathrate melting takes place between +2.2 and +9.5 °C, indicating salinity for the aqueous phase between ~13 and 1 eq.wt.% NaCl. T_{Htot} to the vapour occurred between 330 and 440 °C.

The Raman microprobe analyses reveal a heterogeneous assemblage of solid phases trapped in Type 4 FIs. Carbonates are the dominant species (solid solutions of Ca-, Mn- and Fe-rich carbonates) but quartz, muscovite and sulphur phases are also present. Quantitative FI gas analysis by mass spectrometry showed that quartz analyses have <1% gas with very high argon and N_2/Ar ratios of ~2. The most probable source of argon is from K-bearing minerals above the closure temperature for argon systematics, thus implying a metamorphic origin. In contrast, the emeralds have about 17 mole% gas, dominated by CO_2 attributed to a metamorphic devolatilisation reaction. The emerald data indicates two potential end-member fluid sources, one that is metamorphic and the other where the N_2/Ar ratio is about 60. Fluid gases are attributed either to deep basinal brines or were sourced directly from basaltic rocks during metamorphism. Genetic models for Brazilian emeralds will be discussed in light of the data presented above.

Crystal chemistry and crystal growth of pezzottaite from Myanmar

Devouard, B.[1*], Labat, F.[1], Fritsch, E.[2] & Devidal, J.-L.[1]
[1]LMV, Univ. Blaise Pascal - CNRS, Clermont-Ferrand, France
([*]devouard@opgc.univ-bpclermont.fr)
[2]IMN, Univ. Nantes - CNRS, Nantes, France

Pezzottaite was described in 2003 as a new mineral species from Ambatovita, Madagascar [1,2]. It is the Cs-Li end-member of the beryl group, and an attractive gem with deep purplish pink color. Pezzottaite has subsequently been recognized from two other localities, in Afghanistan [3] and in Momeik, Myanmar [4]. Studying the crystal chemistry of pezzottaite is challenging, since it contains Li, Be and H_2O. It can be done, however, by combining EPMA, LA-ICP-MS, micro-FTIR, and SC-XRD analyses.

Pezzottaite crystals from Myanmar are slightly tabular hexagonal {10.0}+{00.1} prisms up to ca. 1 cm. We cut two crystals and prepared thick (90-400 µm) sections perpendicular to the **a** and **c** crystallographic directions. Both crystals displayed similar features.

The crystals show a complex hourglass sector zoning with a late-stage overgrowth on the basal faces (Fig. 1). Color is concentrated in the sectors bounded by the {10.0} faces (zone A), and in the overgrowths (zone C). The sectors outside the hourglass (zone B) are near colorless. SEM-BSE imaging further revealed small sectors (zone D) at the limit of zones B and C, corresponding to the development and resorption of {*h0l*} faces, and minute sectors parallel to **c**, in the C zone. Rare inclusions of elbaite, pollucite and calciotantite were identified by EDS.

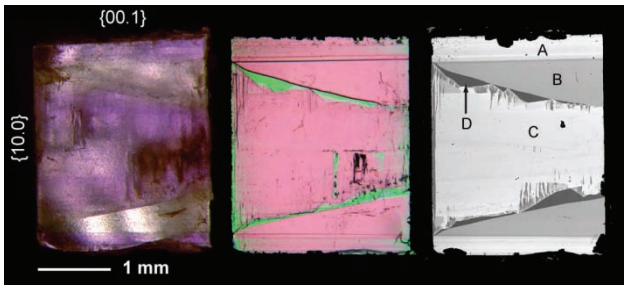

Fig. 1: Pezzottaite crystal cut parallel to the **a** axis (**c** vertical), showing half of the hourglass sector zoning (center of the stone to the right of the images); [left] polarized transmitted light, [middle] under crossed polarizers (section ca. 180 µm thick), and [right] SEM-BSE image.

Zones A and C have the highest Cs contents, averaging 12.8 wt% Cs_2O (0.56 apfu) and 12.1 wt% Cs_20 (0.53 apfu), respectively, and locally up to 14.3 wt% Cs_2O (0.63 apfu). Zone B has lower Cs contents, 8.8 wt% Cs_2O (0.37 apfu), and zone D is Cs-poor, 2.77 wt% Cs_2O (0.11 apfu). These crystals thus appear to be mixed pezzottaite-beryl crystals. Cs and Na show a negative correlation, except in zones D which are Cs-poor but contain Na up to 0.2 apfu. Although Na and Cs occupy distinct sites in the channels, these sites appear to be mutually exclusive because of electrostatic repulsion. Water content was determined using micro-FTIR spectrometry, using extinction coefficients estimated according to [5]. H_2O ranges from 1.1 to 2.0 wt%, and is anti-correlated with the Cs content. IR spectra show only type I water molecules in the Cs-rich zones, but a mixture of type I and type II water in the Cs-poor zone D.

[1] Laurs, B.M. (2003) *Gems Gemol.*, **39**, 284-301. [2] Hawthorne, F.C. (2004) *Mineral. Rec.*, **35**, 369-378. [3] Hänni, H.A. & Krzemnicki, M.S. (2004) *J. Gemmol.*, **29**, 75-75. [4] Devouard, B. et al. (2007) *Gems Gemol.*, **43(1)**, 70-72. [5] Libowitzky, E. & Rossman, G.R. (1997) *Am. Mineral.*, **82**, 1111-1115.

See through pearls using X-rays: micro-radiography vs. micro-computed tomography

Karampelas, S.[1*], Michel, J.[2], Zheng-Cui, M.[1], Schwarz, J.-O.[2] & Enzmann F.[2]
[1]Gübelin Gem Lab Ltd., Lucerne, Switzerland
([*]s.karampelas@gubelingemlab.ch)
[2]Inst. of Geosciences, Johannes Gutenberg University, Mainz, Germany

Understanding the internal textures of pearls can help to the separation natural vs. cultured pearls. The vast majority of the pearls' internal textures studies up-to-date were done using X-ray μ-radiography; e.g. in [1]. Recently, high resolution X-ray computed tomography (μCT), a method originally developed by the medical field and the last decade used in geosciences [2], is applied on some cultured pearls [3,4]. The originality of this study is that μCT and radiography in different directions were applied on the same cultured and natural pearls in order to better reveal and understand the internal structures observed by the latter method.

This study comprises samples which are covering the different major categories of both natural and cultured pearls presented in the market; i.e., saltwater natural (SWNPs), freshwater natural (FWNPs), saltwater with cultured solid nucleus -bead- (SWBCP), saltwater cultured and freshwater cultured without bead (SWNBCPs -a.k.a. "keshi" cultured pearls- and FWNBCPs respectively). Some of the studied samples were drilled and one was mounted in a white metal pendant. As expected, when using μCT, growth textures and cracks (when present) of all pearls, as well as the tissue related textures of cultured pearls are better revealed compared to those observed in X-ray film μ-radiography. This is, because results of μCT analyses give 3-dimensional information of sample related features.

Moreover, some textures are barely visible using X-ray film μ-radiography, thus the identification of their natural or cultured origin could be an issue (see also [1,5]). With μCT some of these textures are better revealed, and easier to interpret. Additionally, complicated internal textures, observed sometimes in X-ray film μ-radiography of FWNBCPs, are better revealed with μCT. Some of them seem to be related to more than one tissue. However, in the case of pearls mounted on metal it is difficult to get more details than with X-ray film μ-radiography. This is because the metal sometimes masks the internal textures of samples.

Despite the disadvantages of the method (e.g., measurement time and data reduction last more than 5 hours) the μCT seems to be a promising method for investigating the internal textures of natural and cultured pearls. Studies of a large number of samples using this method could help the better interpretation of internal textures of pearls as observed with X-ray μ-radiography. This will also lead toward a better understanding of pearl biomineralization.

[1] Akamatsu, S. et al. (2001) *Gems Gemol.*, **37**, 96-113. [2] Ketcham, R.A. & Carlson, W.D. (2001) *Comput. Geosci.*, **27**, 381-400. [3] Strack, E. (2006) *Pearls.* Rühle-Diebener Verlag. [4] Wehrmeister, U. et al. (2008) *J. Gemmol. Proc. Gemmol. GB*, **31**, 15-21. [5] Sturman, N. & Al-Attawi, A. (2006) *Gems Gemol.*, **42**, 142.

The blue-green-yellow sapphires from Nam Khun-Nam Yuen, Thailand, and Garba Tula, Kenya

Wathanakul, P.[1,2*], Atichat, W.[2], Satitkune, S.[1], Somboon, C.[2] & Leelawattanasuk, T.[2]
[1]Gem & Mineral Sciences SRU, Dept. of Earth Sciences, Faculty of Science, Kasetsart University, Bangkok, Thailand
([*]fscipww@ku.ac.th)
[2]The Gem and Jewelry Institute of Thailand, Bangkok, Thailand

The blue-green-yellow (BGY) sapphires have been reported related to various basaltic gem fields, e.g., Antsiranana, Northern Madagascar, Tumbarumba, NSW Australia, and Nam Khun-Nam Yuen, NE Thailand (e.g., [1-3]). The BGY sapphires of similar appearances have also occurred in other different geological terrane, i.e., the Pan-African monzonite dyke of the mantle origin, such as the Garba Tula BGY sapphires, Kenya [4].

Two groups of the similar looking BGY sapphire samples from Nam Khun-Nam Yuen and from Garba Tula (Fig. 1) have been analysed for their physical and optical characteristics, and trace element chemistry. BGY sapphires from both localities are commonly clear and contain rare inclusions, possibly only some fingerprints.

Fig. 1: Basaltic BGY sapphire samples from Nam Khun-Nam Yuen gem field, NE Thailand (top) compared to BGY sapphires from Garba Tula, central Kenya (bottom).

The results revealed the overlapping of their physical characteristics as well as chemistry. Nonetheless, the BGY sapphire samples from each locality did show their differences in the UV-Vis-NIR absorption spectra. Though having similar content of iron, and their colour is attributed to Fe^{3+}, Fe^{2+}/Fe^{3+}, and Fe^{2+}/Ti^{4+}, the basaltic BGY sapphire samples from Thailand tend to have Fe^{2+}/Fe^{3+} component more than the Garba Tula ones, and the latter tend to contain more Fe^{2+}/Ti^{4+}. Thus, differences in Fe^{2+}, Fe^{3+} as well as Ti^{4+} species can be used to distinguish the BGY sapphires of different geological gem fields.

[1] Schwarz, D. et al (2000) *Gems Gemol.*, **36(3)**, 216-233. [2] Sutherland, L. et al (2002) *Records of the Australian Museum*, **24**, 215-248. [3] Wathanakul, P. et al (2008) *Gemmologie* (75-years of DGemG. Special issue), 67-70. [4] Simonet, C. et al (2004) *J. Afr. Earth Sci.*, **38(4)**, 401-410.

The role of spectroscopy for the distinction of natural color and color treated diamonds in the 21st century

Hainschwang, T.
GEMLAB Laboratory, Balzers, Liechtenstein
(thomas.hainschwang@gemlab.net)

While the vast majority of diamond researchers work on the growth and defect characterization of synthetic diamonds for industrial applications there is a second important market which demands for in-depth diamond research: the gem diamond market. The high value of untreated natural diamonds versus the distinctly lower value of treated natural diamonds has driven the demand for the analytical capacities to distinguish untreated natural diamond specimens from treated ones.

Until the end of the 20th century the only important diamond treatments were irradiation with high energy particles, and annealing after irradiation when needed. The behavior of diamonds upon irradiation is rather uniform and consists of the formations of vacancies and interstitials. Annealing after irradiation of nitrogen-containing diamonds results mainly in nitrogen-vacancy type defects. In the gemological field such stones used to be mainly identified by UV luminescence and the use of direct vision spectroscopes; only from about 1977 spectrometers started to replace the spectroscopes in gemological labs ([1]; first published spectra: [2]).

With the appearance of the HPHT treatment in the 1990's the issue of diamond color treatments changed dramatically and became a highly complex matter (see e.g. [3]).

In the HPHT treatment brown type I and type II diamonds with deformation-related color are usually treated at temperatures of 1900 to near 2500°C and 55 to 85 kbar. The type I material generally turns yellow to yellow-green while the type II material turns either colorless or blue depending on the presence or absence of boron.

The HPHT treatment forced all laboratories that wanted to identify this treatment to work extensively with spectroscopic equipment; the technique of photoluminescence spectroscopy spread throughout the labs mainly because of this treatment.

After the introduction of HPHT in the 1990's the first decade of the 21st century brought many modifications of the HPHT process and today any type and color of diamond may be HPHT treated at temperatures up to nearly 3000°C; stones can be irradiated before or after HPHT, or treated by multiple steps involving HPHT, irradiation and annealing. The extreme variability of treatment conditions and diamonds that can potentially be treated makes a proper identification of colored diamonds a real challenge.

Today origin of color determination requires the characterization all types of naturally colored diamonds by a variety of methods including low temperature UV-Vis-NIR spectroscopy, FTIR spectroscopy and low temperature photoluminescence spectroscopy with various excitation wavelengths. Thus a complete picture of the defects occurring naturally in colored diamonds needs to be obtained and exactly the same needs to be done for the different groups of diamonds after the treatments.

This presentation gives an overview of all treatments, and important defects produced or destroyed by them; and it aims at demonstrating the importance of spectroscopy for origin of color determination of diamond in the 21st century. Furthermore a short tour through the properties of the different types of treated diamond is provided, and it is shown how treated diamond samples are commonly distinguished from their naturally colored counterparts.

[1] Bosshart, G. (2010) pers. comm. [2] Bosshart, G. (1977) *Lapidary J.*, **31(9)**, 1954-1964. [3] Collins, A.T., Kanda, H. & Kitawaki, H. (2000) *Diam. Relat. Mater.*, **9**, 113-122

The role of evaporites in the formation of high value coloured gemstones

Giuliani, G.[1,2*], Ohnenstetter, D.[2], Fallick, A.E.[3], Banks, D.[4] & Feneyrol, J.[2]
[1]IRD, Toulouse, France
[2]CRPG/CNRS, Vandœuvre-lès-Nancy, France
([*]giuliani@crpg.cnrs-nancy.fr)
[3]SUERC, East Kilbride, Glasgow, Scotland, UK
[4]School of Earth & Environment, University of Leeds, UK

The combination of field and geochemical studies on high value coloured gemstone deposits in meta-sedimentary platform carbonates has elucidated the role of evaporites and organic matter in their genesis. Emerald and ruby localities, from several areas worldwide, have in common, moderate to high temperatures of origin, saline fluids, high $\delta^{18}O$, and a lack of associated igneous rocks.

Colombian emeralds are hosted by Cretaceous carbonaceous black shales, and occur in veins, breccia and pockets with carbonates, quartz, albite and pyrite. Intense albitisation by hydrothermal fluids mobilized the Be necessary for emerald formation from the black shales. Stable isotopic studies of emerald and gangue minerals indicate a basinal brine source at ~300°C with high $\delta^{18}O$ and sulphate reduction by organic matter from evaporitic sulphur to form pyrite. δD ratio, cation and anion content indicate that two fluids were involved, a basinal brine (40 wt% eq. NaCl), and a surface-derived fluid.

Afghani emeralds are associated with a strong Na-K metasomatism of the host medium-grade metamorphic schists. The hydrothermal fluids derived their high salinity (40 wt% eq. NaCl) and halogen characteristics from leaching of meta-evaporite sequence.

Rubies in marbles from Central and South-east Asia were formed in a closed fluid system, at P ~3 kbar and $620<T<670$°C. The fluids were rich in CO_2 released, during metamorphic devolatilization of the carbonates, and in F-B-Cl-SO_4 released by melting of salts derived from evaporites. The presence of salts and sulphates in rubies and the unusual composition of the CO_2-H_2S-COS-S_8-AlO(OH)-bearing fluid inclusions confirms the thermal reduction of sulphate by organic matter, during the high temperature-medium pressure metamorphism of the Tertiary India-Asia collision. The carbonates were enriched in Al- and Cr-V-bearing detrital minerals, such as clays that were deposited on the platform, and in organic matter. Molten salts mobilized in situ Al and metallic transition elements contained in marble, leading to crystallization of rubies.

'Tsavorite' (vanadian grossular) in quartz veins deposits from the Lemshuku and Namalulu areas in Tanzania, are hosted by vanadian-graphitic schist i.e. amphibolite facies black shales. The association of anhydrite (and gypsum) with 'tsavorite' in quartz veins in Lemshuku, the presence of gypsum-anhydrite intercalations and lenses of graphite-scapolite-diopside-pyrite in carbonates at the bottom of the Namalulu marbles that overlay the graphitic schists, indicate the deposition of evaporites in a euxinic platform environment. H_2S-rich fluid inclusions, the high $\delta^{18}O$ of 'tsavorite', the presence of pyrite and graphite in the metasomatic zones indicate that sulphate reduction by graphite probably played a key role in gem formation.

The formation of evaporite-related gemstones can therefore be linked with meta-sedimentary platform carbonates. The association of evaporite-organic matter and black-shale-carbonates, plays a key role, as does the formation of highly saline fluids in open hydrothermal systems, and molten salts in high temperature closed metamorphic systems for mobilisation of the chemical elements necessary to produce the gemstones.

Mineral chemistry and structural relationships of inclusions in diamond crystals

Satitkune, S.[1*], Zubko, M.[2], Häger, T.[3], Kusz, J.[2] & Hofmeister, W.[3]
[1]Dept. of Earth Sciences, Faculty of Science, Kasetsart University, Bangkok, Thailand ([*]ton_toey@hotmail.com)
[2]Institute of Physics, University of Silesia, Katowice, Poland
[3]Inst. of Gemstone Research, Johannes Gutenberg University, Mainz, Germany

Co-existing inclusions occurring in individual diamonds are the special keys for determining the equilibrium of mantle mineral assemblages as well as the physical conditions prevailing in the mantle during diamond growth. The partitioning of Fe and Mg between two coexisting mineral phases has been recognized as potentially useful geothermometer [1]. The last equilibrium temperatures between the mineral assemblage diamond – chromium pyrope – enstatite, were calculated at a fixed pressure of 5.0 GPa, within the diamond stability field. The pressure evaluations were also estimated from alumina contents of orthopyroxenes coexisting with pyrope garnet [2]; average temperatures and pressures for diamond samples were calculated as shown in Table 1.

Table 1: Average temperature and pressure

Diamond localities	Temperature (^{o}C)	Pressure (GPa)
Koffiefontein mine	1087 (±15)	5.2 (±0.1)
Finsch mine	1041 (±5)	5.0 (±0.1)

The structural relationships of the host diamond crystals and their inclusions were studied by calculating the angle correlation between the [111] face of the diamond and specifically selected directions of their distinct mineral inclusions. Chromium pyrope or chromite inclusions, which are representing more than one trapped crystal in the individual diamond hosts, showed the angle correlation with small degrees of different orientations. The angle correlations between diamond [111] and chromium pyrope [111] or chromite [111] showed relatively small misalignments up to 2.2° and up to 3.4° between diamond and chromium pyrope, or chromite inclusions. The chromium diopside and olivine inclusions, however, showed a degree of miss-orientation up to 10.2° between diamond [111] and chromium diposide [010], and up to 12.9° between diamond [111] and olivine [100].

All inclusions of cubic phases (i.e., chromium pyrope and chromite) exhibit a relatively similar orientation to their diamond hosts, when the inclusions grew together in individual diamond. The crystal inclusions show the typical small misalignment angle among each other. Furthermore, all inclusions of the same cubic phase captured in diamond crystals from the same mine show nearly the same angle orientation to their host diamond. In contrast, inclusions of non-cubic phases (i.e., monoclinic chromium diopside and orthorhombic olivine) always show more extensive, variable orientations between the inclusions and their respective diamond host.

[1] Harley, S.L. (1984) *Contrib. Mineral. Petrol.*, **86**, 359-373. [2] Harley, S.L. & Green, D.H. (1982) *Nature*, **300**, 697-701.

Structure and provenance of freshwater cultured pearls

Jacob, D.E.[1*], Soldati, A.L.[1,2], Wehrmeister, U.[3] & Brügmann, G.[4]
[1]Dept. of Geosciences and Earth System Science Research Centre, Johannes Gutenberg-Universität, Mainz, Germany ([*]jacobd@uni-mainz.de)
[2]CONICET, Grupo Caracterización de Materiales, Centro Atómico, S.C. de Bariloche, Argentina
[3]Dept. of Gemstone Research, Johannes Gutenberg- Universität, Mainz, Germany
[4]Max-Planck Institut für Chemie, Mainz, Germany

Freshwater pearls, cultured in bivalves of the genus *Hyriopsis* have been increasing constantly in quality and size over the last years. Main producing countries are China and Japan, but other countries, e.g. Thailand, are also known to culture freshwater pearls. We review here the micro- and nanostructure of pearls that lead to their extra-ordinary material properties including the occurrence of vaterite which can cause considerable loss of quality and value [1,2].

Vaterite in freshwater cultured pearls has higher concentrations of organic material and higher manganese contents than aragonite. Most extreme values of ca. 3 wt% Mn are found in so-called lacklustre pearls [3] which consist entirely of vaterite. Freshwater bivalve shells incorporate Mn seasonally connected with algal blooms and it can therefore be suspected that water quality plays a significant role in the formation of vaterite in pearls.

Environments for pearl culturing are very different in China, where pearl farms of different sizes are located along the Yangtse Rivers, and in Japan, where freshwater are cultured traditionally in Lake Biwa and Lake Kasumigaura. These differences are mirrored by the trace element chemical composition of the pearls.

Trace element concentrations in the pearls were measured in situ by LA-ICP-MS. This method allows simultaneous measurement of ca. up to forty minor and trace elements with sub-ppm detection limits [4]. Laser craters of 100 µm or less are created on the surfaces of the samples and are hardly visible by eye. Additionally, Sr isotopic compositions were measured in situ in the pearls by LA-MC-ICP-MS to explore the potential of this geochemical tool for provenance determination.

Best discrimination between the different sample localities was achieved with Ba/Sr ratios vs B concentrations [5]. While Chinese freshwater pearls have higher and more variable Ba/Sr ratios, those from the Japanese lakes each occupy rather confined fields at lower Ba/Sr ratios. The field for pearls from Lake Biwa (Japan) overlaps with the Chinese sample population but Biwa pearls trend to lower boron concentrations than Chinese samples. Sr isotopic ratios range between 0.70759 and 0.71237. Lake Biwa samples show the most radiogenic compositions, while those from Lake Kasumigaura have the lowest $^{87}Sr/^{86}Sr$ ratios.

[1] Jacob, D.E. et al. (2008) *Geochim. Cosmochim. Ac.*, **72(22)**, 5401-5415. [2] Wehrmeister, U. et al. (2007) *J. Gemmol.*, **31**, 399-416. [3] Qiao, L. et al. (2006) *Cryst. Growth Des.*, **7**, 275-279. [4] Jacob, D.E. (2006) *Geostand. Geoanal. Res.*, **30(3)**, 221-235. [5] Jacob, D.E. et al. (2006) *Austral. Gemmol.*, **22**, 539-541.

Origin of the Revelstoke carbonate-hosted gem corundum occurrence, British Columbia, Canada

Dzikowski, T.J.[1*], Groat, L.A.[1], Dipple, G.M.[1] & Marshall, D.[2]
[1]Dept. of Earth and Ocean Sciences, University of British Columbia, Vancouver, Canada ([*]tdzikowski@eos.ubc.ca)
[2]Dept. of Earth Sciences, Simon Fraser University, Burnaby, British Columbia, Canada

The Revelstoke sapphire and ruby occurrence in southeastern British Columbia occurs in micaceous laminations within marble that is surrounded by calcareous schist within the Paleozoic Monashee cover sequence northwest of the Frenchman Cap dome. These laminations were once calc-schist lenses that were incorporated into the marble either during deposition or tectonism and were subsequently stretched by intense deformation. The thin, micaceous corundum-bearing laminations have metamorphic assemblages of corundum + calcite + muscovite + plagioclase + K-feldspar ± diopside.

The composition of fluid inclusions within corundum was determined by microthermometry to be composed of CO_2 with minor amounts of CH_4 and/or N_2. The intersection of fluid inclusion isochores with temperatures estimated from $\Delta^{18}O_{cal\text{-}cor}$ RAM thermometry indicate that corundum crystallized at pressures of 1.7-2.1 kbar and temperatures of 575-600 °C. Corundum formed during retrograde metamorphic conditions on the high temperature side of the muscovite → corundum + K-feldspar + H_2O reaction. In relation to the regional P-T-t path, corundum formed after rapid exhumation and cooling as a result of uplift along the Okanagan-Eagle River and Columbia River Faults between 52 and 47 Ma [1].

Exploration strategies for this type of corundum occurrence may be based on the genesis of corundum, but also on the preservation of corundum. When corundum is in association with K-feldspar and hydrous fluids are introduced, corundum will be altered to muscovite. This has implications for developing exploration strategies that include not only how corundum is formed, but also how it is preserved.

[1] Crowley, J.L. et al. (2001) *J. Struct. Geol.*, **23**, 1103-1121.

Provenance determination of alexandrite

Malsy, A.K.[1,2*] & Armbruster, T.[2]
[1]Gübelin Gem Lab Ltd, Lucerne, Switzerland
([*]a.malsy@gubelingemlab.ch)
[2]Mineralogical Crystallography, Institute of Geological Sciences, University of Bern, Switzerland

Alexandrite is the Cr-bearing variety of chrysoberyl ($BeAl_2O_4$) and renowned for its colour change property. "Gem-quality" alexandrite specimens from Brazil, India, Madagascar, Russia, Sri Lanka, and Tanzania have been investigated for their microscopic features and chemistry. Over 170 samples were tested for trace elements by laser ablation inductively coupled plasma mass spectrometry (LA-ICP-MS). With spot analysis of 100 µm in diameter and by adding small amounts of hydrogen (13 ml min^{-1}) to the carrier gas [1], the sensitivity could be improved for most elements. A set of 4 individual spot analyses was performed on each samples girdle or polished face.

In addition to the chromophore (Cr, ± Fe) elements, B, Mg, V, Ga, Ge, Nb, Sn, and Ta were found to be most indicative for the recognition of alexandrite sources. The distribution pattern of the latter trace elements is specific for most alexandrite sources. Alexandrite samples from the Hematita mines (Brazil) have typically high Sn (up to 2294 ppm) concentrations, whereas samples from Orissa (India) show distinctly high V concentrations (up to 0.15 wt% V_2O_3) and low Sn contents (Fig. 1). Germanium was found to be the key element in identification of alexandrite from the Ural Mountains (Russia). For samples from Sri Lanka and Ilakaka (Madagascar), trace element pattern overlaps for all elements and a proper distinction by chemistry is not feasible.

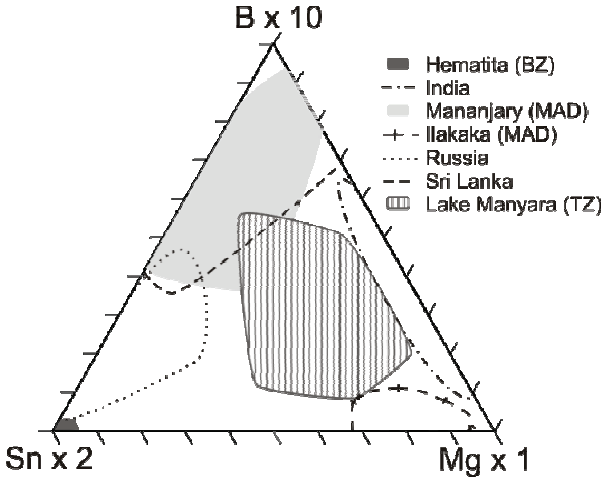

Fig. 1: Ternary B-Mg-Sn-diagram, showing LA-ICP-MS data [ppm] for alexandrites from Brazil (BZ), Madagascar (MAD), Russia, Sri Lanka, and Tanzania (TZ). Source fields are defined by the outline of individual plotting points.

Microscopic features generally yield only limited information on the provenance of alexandrite, as "diagnostic" inclusions (features that are unique for a specific mine or mining area) are mostly absent.

Thus, LA-ICP-MS provides new solutions for provenance analyses of alexandrite, where "standard" gemmological testing is facing its limitations.

[1] Guillong, M. & Heinrich, C.A. (2007) *J. Anal. Atom. Spectrom.*, **22**, 1488-1494.

Ruby and sapphire rimmed by spinel from the Luc Yen - Yen Bai gem mining area, Vietnam

Häger, T.[1*], Nguyen Ngoc Khoi[2,4], Duong Anh Tuan[3,4], Le Thi-Thu Huong[2] & Hofmeister, W.[1]
[1]Centre for Gemstone Research, University of Mainz, Germany ([*]haeger@uni-mainz.de)
[2]Faculty of Geology, Hanoi University of Science, Hanoi, Vietnam
[3]Inst. of Material Sciences Hanoi, Vietnam
[4]Doji Gold and Gems Group, Hanoi, Vietnam

Since the first ruby was found in February 1987 in Luc Yen (a small city in Yen Bai province, N- Vietnam), this country is an important source for gemstones in Southeast Asia. The quality and colour of rubies are comparable to the famous rubies from Burma.

On the way from the capital of the province, which is also named Yen Bai, to Luc Yen, a new star-ruby, red spinel and garnet mine has recently been opened by the Vietnamese company Doji. Beside idiomorphic ruby and corundum crystals, also rubies and corundum were found surrounded by a second phase. The second phase follows the morphology of the corundum crystals. The rim of the corundum crystal is spinel (determined using Raman spectroscopy and X-ray powder diffraction). The spinel formation can be explained by an overgrowth of spinel on the corundum or with the corundum consuming reaction:

corundum + dolomite = spinel + calcite + CO_2

The edges of the internal corundum and the second phase are slightly rounded, suggesting some disequilibrium between the two phases and favouring therefore the latter explanation.

A cross section of such a ruby crystal with spinel rim has been analysed with SEM. Fig. 1 shows the border between ruby and the spinel rim.

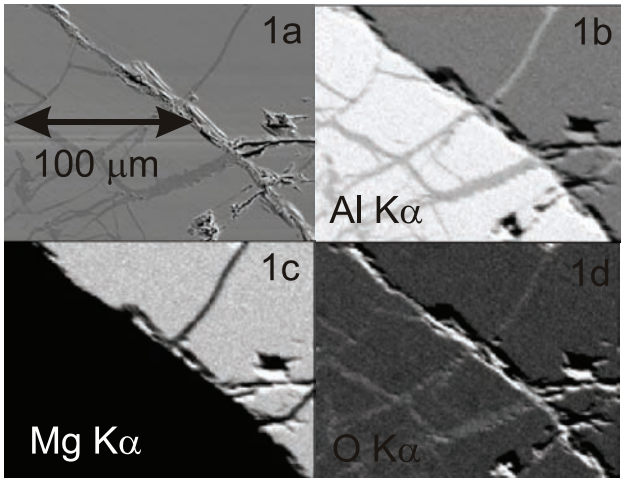

Fig. 1: BSE image of a typical corundum spinel border (1a). The cracks between corundum and spinel are filled with diaspore. Fig. 1b-d show element distribution maps of Al (1b), Mg (1c) and O (1d). High brightness displays high element content.

In the element-distribution maps shown in Fig. 1 it can bee seen clearly that the spinel is in the upper right corner and the corundum in the lower left corner. Both phases are cracked and the resulting fractures are healed and filled with a third phase. This third phase has lower Al content than corundum but a higher Al content than spinel. This observation suggests that the facture filling might consist of AlOOH. Using Raman spectroscopy, this third phase (which was obviously formed during retrograde metamorphism in the third stage) was identified as diaspore.

Emerald mineralization at the Glinka occurrence, Middle Urals, Russia

Bidny, A.S.[1*], Koshenskaya, T.O.[1], Baksheev, I.A.[1] & Popov, M.P.[2]
[1]Dept. of Mineralogy, Lomonosov Moscow State University, Moscow, Russia ([*]alexei.bidny@gmail.com)
[2]Dept. of Mineralogy, Petrography and Geochemistry, Ural State Mining University, Ekaterinburg, Russia

The Ural emerald mines are the only top quality emerald deposits in Russia [1]. It has been assumed that these deposits could extend further toward the north and south. To verify this assumption we have studied a new occurrence of green beryl (i.e., emerald) from Glinka, located 80 km north of the well-known Emerald mines.

The beryl from the Glinka occurrence is hosted by glimmerite occurring among talc schists, located close to the Murzinka pluton. The emerald-bearing rocks are composed of phlogopite and variable amounts of talc, plagioclase, tremolite-actinolite, and chlorite. Accessory minerals include beryl, chrysoberyl, tourmaline, corundum, apatite, fluorite, relict chromium spinel, and zircon. The 248 Ma Rb/Sr age of the Glinka pegmatite is consistent with that of the Murzinka pluton but differs appreciably from the 207 Ma age of the emerald mines [2].

Phlogopite occurs as brown or black flakes up to a few mm in size. Its fluorine content ranges from 2 to 5 wt.%. The Fe/(Fe+Mg) value varies from 0.05 to 0.36, with a clear increase toward the pegmatite body. Phlogopite associated with talc is lowest in Fe whereas that associated with muscovite adjacent to pegmatite contains much more Fe. The Be content in phlogopite varies from 5.8 to 16.8 ppm and reaches 23.2 ppm in muscovite. Transparent and colourless or light green beryl crystals are prismatic and vary from 13 to 200 mm in size.

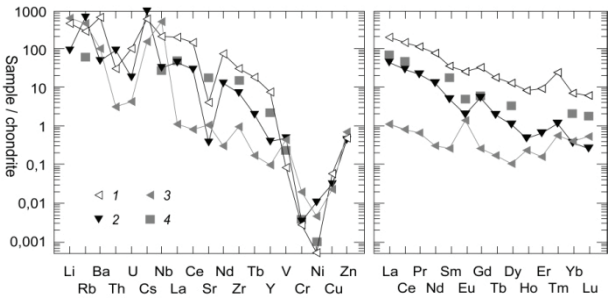

Fig. 1: Spider diagram of trace elements and REE distribution in (***1***) phlogopite-rich rock with high Be, (***2***) phlogopite-rich rock with low Be, and (***3***) muscovite of pegmatite from the Glinka occurrence, and (***4***) granite of the Murzinka pluton [3].

The geochemistry of the glimmerite from Glinka is shown in spider diagrams of trace elements and REE distribution (Fig. 1). The general distribution trends are similar to that of the Murzinka pluton granites. Notable differences include the enrichment of alkali elements (Li, Rb, Cs) and the depletion of Sr in glimmerite.

The results of our work show that mineralogical and geochemical features of the Glinka occurrence are similar to that of the Emerald mines. However, the ages of the two sources differ appreciably. The two occurrences therefore cannot belong to one extended deposit, even though their formation processes are widely similar.

[1] Laskovenkov, A.F. & Zhernakov, V.I. (1995) *Gems Gemol.*, **31(2)**, 106-113. [2] Popov, V.S. et al. (2003) *Litosphera*, **4**, 3-18. [3] Fershtater, G.B. et al. (1994) *Orogenic granitoid magmatism of the Urals*. Miass (in Russian).

Spectroscopy study of milky and rose quartz from the Borborema Pegmatitic Province (Brazil) irradiated with high gamma doses

Barreto, S.B.[1*], Guzzo, P.L.[2], Gonzaga, R.S.G.[2], Miranda, M.R.[2] & Khoury, H.J.[3]
[1]Dept. of Geology, Federal University of Pernambuco, Recife, PE, Brazil ([*]bsandra@ufpe.br)
[2]Dept. of Mining Engineering, Federal University of Pernambuco, Recife, PE, Brazil
[3]Dept. of Nuclear Energy, Federal University of Pernambuco, Recife, PE, Brazil

The origin of rose colour in polycrystalline quartz from granitic pegmatites was considered in numerous studies but no ultimate consensus was established until now [1]. In granitic pegmatities located in Borborema Pegmatite Province (BPP, Brazil), it is common to find areas of rose and milk quartzes randomly distributed inside the pegmatite cores. The rules defining the colour pattern into these quartz cores are unknown but we believe that proper characterization of samples taken from different areas can be useful to further discuss the origin of the rose colour. Thus, the aim of this work is to characterize the colour changing by gamma irradiation in milky and rose quartzes taken from the same core by means of electron paramagnetic resonance (EPR), optical, and infrared (IR) absorption spectroscopies. For this, milky and rose blocks of quartz samples collected from the Taboa pegmatite from the BPP were cut into small pieces and optically polished. The samples were irradiated with gamma rays (^{60}Co) with doses ranging from 0.5 to 96 kGy. The colour change was accessed by optical spectroscopy and the OH-related defects were analysed by mid-IR spectroscopy. Each irradiated sample was sectioned into two parts and 60 mg of powder in 75-150 µm size fraction was used to obtain the EPR signals using an spectrometer operating in the X-band. As a result, gamma radiation above 2 kGy induced smoky colour in both quartzes and optical bands near 230 nm and 460 nm, related to E' and $[AlO_4]^0$ centres, respectively, were observed. EPR spectra revealed several lines from 3500 to 3530 G at room temperature. Two sets of lines were assigned to $[GeO_4/Li]^0$ centre and E_1' centre perturbed by a substitutional Ge. It was observed that $[GeO_4/Li]^0$ signal increased with the increasing of gamma dose up to 4 kGy and then decreased. On the other hand, the signal related to E_1' appeared for doses higher than 16 and 32 kGy for milky and rose quartz, respectively. The onset of optical and EPR signals related to E' centers appeared at a higher dose for rose quartz. These results are summarized in Figure 1. In case of IR spectra, the rose quartz showed sharp bands assigned to $[H_40_4]^0$, Li-dependent OH and $[AlO_4/H]^0$ centers whereas the milky quartz only showed the typical broad OH band in the range of 3800 to 3000 cm^{-1}.

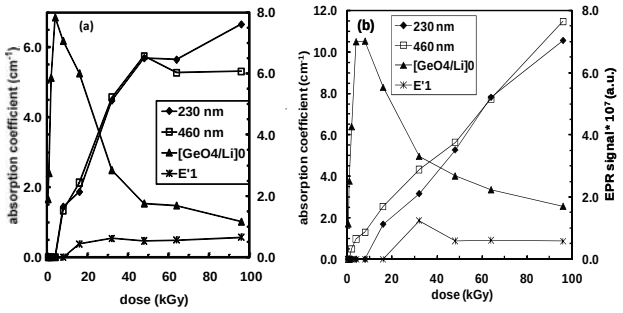

Fig. 1: Intensity of optical and EPR signals related to point defects induced by gamma rays in milky (a) and rose (b) quartz from BPP.

[1] Kibar, R. et al. (2007) *Radiat. Meas.*, **42**, 1610-1617.

Incorporation of iron and chromium in pegmatitic tourmaline

Bordage, A.[1*], Rossano, S.[1], Fuchs, Y.[1] & Horn, A.H.[2]
[1]Laboratoire des Géomatériaux et Environnement, Université Paris-Est Marne-la-Vallée, France ([*]amelie.bordage@impmc.jussieu.fr)
[2]Universidade Federal Minas Gerais (UFMG), Belo Horizonte, MG, Brazil

The mechanisms of trace elements incorporation in minerals are a crucial problem in gemmology, since it has an impact on the physical and chemical properties of the mineral. For instance, the presence of an impurity modifies the colour of the mineral. The colouring impurity content of a gem and the incorporation process are also related to the geological history of the host-rocks where it was found. A detailed study of the electronic structure, crystallographic environment and optical properties can help to understand the physical and chemical properties of the gem and the history of its host-rock.

We present here a detailed study on tourmalines from the Minas Gerais region (Brazil). These pegmatitic minerals contain Cr and Fe as impurities. The partitioning of these two elements between co-genetic minerals (tourmaline and emerald) may provide information on the geological processes involved in the ore deposit formation and the general chemistry of pegmatites. Green and blue tourmalines, as well as tourmaline set in emerald, are studied by optical spectroscopy to characterize the general property of the mineral. Microprobe analyses have been performed to understand the elements partitioning of Cr and Fe between the tourmaline and emerald, to get insight on the ore formation.

X-ray Absorption Spectroscopy measurements have also been performed at the Cr and Fe *K*-edge of tourmaline on SuperXAS@SLS (Switzerland). The features in *K*-edge X-ray absorption spectra of transition metal cations provide indeed useful information about their crystallographic environment and electronic structure in minerals. In particular, the energy and relative intensities of the pre-edge features depend on the valence state and site symmetry of the absorbing atom. The Extended X-ray Absorption Fine Structure (EXAFS) measurements enable the neighbours of the absorbing atom to be characterized. To get a more complete knowledge of the site incorporation of Fe and Cr in tourmaline, the experimental XAS study has been coupled to a theoretical study: the X-ray Absorption Near-Edge Structure (XANES) spectra have been theoretically determined by *ab initio* calculations, based on Density Functional Theory (DFT). The comparison between the calculated and experimental spectra makes it possible to obtain accurate information about the crystallographic and electronic structures of Cr and Fe in tourmaline. These DFT calculations therefore substantially complete the information obtained by EXAFS on the Cr and Fe site incorporation. In particular, the XAS study provides quantitative information about the relaxation of the crystal structure around the impurity, a key parameter for understanding the mechanisms controlling the incorporation of colouring trace elements in minerals.

Unusual twinned diamond crystals

Hurlbut, J.F.
Denver Museum of Nature and Science, Denver, USA
(jfhu@earthlink.net)

Unusual diamond twin crystals from the micromount collection donated to the Denver Museum of Nature and Science by Paul Seel were studied. Paul Seel was an invited speaker to the first Kimberlite conference held here.

Paul Seel (1904–1982) was a prominent mineral collector and micromounter; he was born in Silesia, Germany, but in 1925, with a degree in engineering, he immigrated to the United States. In Brooklyn, New York he acquired his first micromounts and then he became an avid micromounter for the rest of his life. Paul Seel was received into the Micromounters' Hall of Fame in 1981.

His interest in diamond crystals started in the late 1940's, when he also built a substantial collection for study purposes. Each specimen "illustrated some morphological fact" and the collection as a whole was considered to be the finest and largest one then in existence [1]. Besides the collection itself, valuable are also his drawings of crystals viewed under the microscope, which are remarkably accurate. According to his will, his excellent diamond collection was donated to the Denver Museum of Natural Science. This collection gathers 1240 mounted specimens, 1 to 3 mm in diameter, and 278 of them are twins. Many of the twins have drawings made of them by Paul Seel.

Several drawings and pictures showing details of the growth features of some of the most unusual crystals from the Seel collection (Figs. 1,2) will be presented.

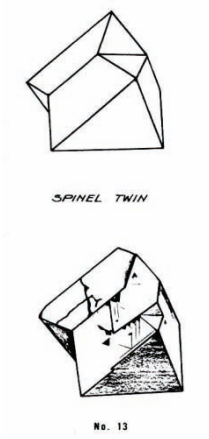

Fig. 1: Paul Seel, Multiple spinel twins (1954).

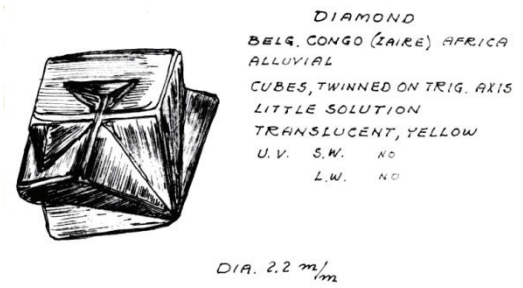

Fig. 2: Paul Seel, cubes twinned on trigonal axis (1959).

Such diamonds collections remain rare today, not only because of the high unit cost of good specimens, but also because the international diamonds market is not set up for providing collector-quality uncut diamond crystals.

[1] Desautels, P.E. (1970) *Mineral. Rec.*, **1(11)**, 31.

Hydrothermal synthesis of quartz

Lenart, A.[1*], Šturm, S.[1] & Mirtič, B.[2]
[1]Dept. for Nanostructured Materials, Jožef Stefan Institute, Ljubljana, Slovenia ([*]alenka.lenart@ijs.si)
[2]Dept. of Geology, Faculty for Natural Sciences and Engineering, Ljubljana, Slovenia

Quartz was one of the first minerals to be synthesised with the hydrothermal method in a high-pressure reactor [1]. Due to its melting point of 1720°C and high chemical resistance, synthetic quartz crystals can only be produced in this way. Normally, the temperature-gradient method is used, which enables the growth of crystals on seeds [1]. Our experimental work aims at the controlled growth of micro- to nano-sized low-temperature quartz.

We used the isothermal method, which is suitable for powder synthesis, where in the whole volume of an autoclave a constant temperature is applied. Colloidal silica was used as the starting material, distilled water as the solvent and NaOH as the mineralizer. The morphology of the crystals was controlled by varying the pressure-temperature conditions and the composition of the solution. In the framework of our research we have shown that morphologically well-developed micron-sized quartz crystals can be obtained under p-T conditions, which are significantly lower than the generally accepted p-T regime for the synthesis of low-temperature quartz [1]. These experiments were performed in a basic medium, at 250°C, 40 bar and 55 % autoclave fill. The XRD pattern shows that the obtained products are pure α-quartz, with no other phases being present (Fig. 1). With the extension of the synthesis time, from 8 hours to 6 days, crystals with a different morphology and a large size range were obtained (Fig. 2). When a longer reaction time was applied, the solid product consisted of double-terminated, long-prismatic crystals of α-quartz. If the synthesis is sufficiently long, the crystals develop prismatic m $\{10\bar{1}0\}$ and rhombohedral r $\{10\bar{1}1\}$ faces, which are typical of the trigonal trapezohedral class, to which quartz belongs. Some crystals have a pseudohexagonal shape, which means that all the rhombohedral faces are nearly equally well developed.

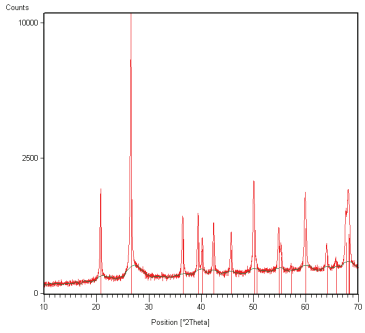

Fig. 1: The XRD analysis shows pure low-temperature quartz, with no other phases being present.

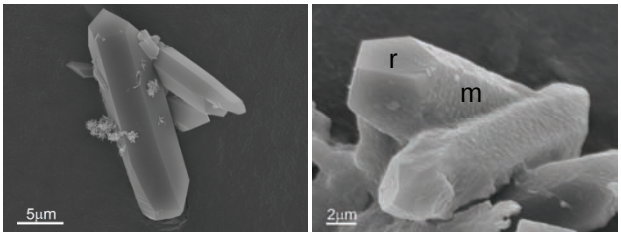

Fig. 2: SEM images of micron-sized quartz crystals obtained with hydrothermal synthesis at 250°C and 40 bar. The crystals have well-developed prismatic m $\{10\bar{1}0\}$ and rhombohedral r $\{10\bar{1}1\}$ faces.

[1] Byrappa, K. & Yoshimura, M. (2001) *Handbook of Hydrothermal Technology.* Noyes Publications/William Andrew Publishing, LLC, U.S.A.

Libyan glass gem formed at sea-water impact

Miura, Y.
Inst. of Earth and Planetary Material Sciences, Yamaguchi University,
Yamaguchi, Japan (dfb30@yamaguchi-u.ac.jp)

The Libyan Desert Silica Glass (LDSG) is a tektite composed of quenched silica glass with meteoritic inclusions that are assigned to an impact reaction [1,2], though other related impact data and its related impact crater are not reported so far. The purpose of the present paper is to elucidate impact material indicators on sea-water by using detailed features of carbon (C) and chlorine (Cl) of the LDSG determined by XRF and ASEM analyses.

The XRF bulk data (determined with EDX analysis) show significant amounts of C (ca. 4 wt% CO_2) in the LDSG samples. Carbon contents were checked also by IR bulk analysis. To avoid any contamination during thin section sampling, the analytical scanning electron microscopy (ASEM) was applied to obtain differences in composition and texture as follows [3,4]: Bulk XRF data indicate a high silica content with minor amounts of C, Na, K, Cl, Mg, Fe and Ca. The LDSG data of impact formation are different from that of volcanic obsidian samples, which have insignificant C and Cl contents. Bulk FE-ASEM data with elemental mapping method indicate high silica with minor amounts of Na, K, Cl and Ca, together with in-situ FE-ASEM analyses of inclusions C, Na, Cl, K, Cr and Fe (Fig. 1).

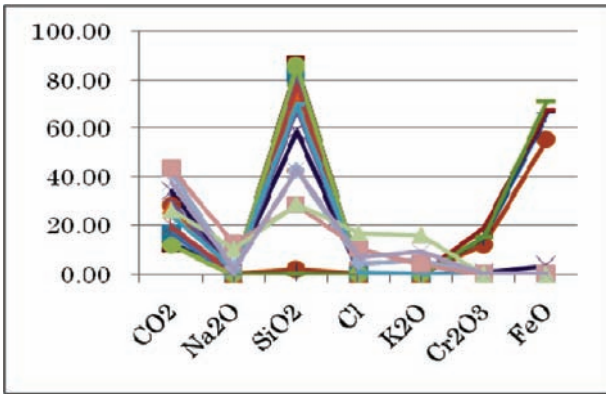

Fig. 1: The ASEM in-situ data of inclusions of the LDSG tektite sample with C, Mg, Al, K, Cr and Fe [4].

The highest C contents (ca. 43 wt% CO_2) with high silica (Fig. 1) are found in inclusions and radiated silica textures with minor contents of Na, Cl and K. The highest Cl contents (ca. 11 wt% Cl; Fig. 1) are mainly obtained in dendritic textures with high contents of Na, Si and O, and minor amounts of K. They are assigned to remnants of halite originating from the contact with sea water after impact. There are fine inclusions of Fe oxides in radiated textures.

The present analytical data can be explained as follows [3,4]. The LDSG tektite shows quenched textures with significant carbon (from limestone) and chlorine (from sea-water) contents which are new evidences of impact reaction on ocean (seawater) impact of the LDG sample. The XRF bulk data of the LDSG tektite and volcanic obsidian samples are different contents with major Si and minor C and Cl-Na elements.

[1] de Michele, V. (1997) (ed.) *Silica '96*. Bologna. [2] Clayton P. & Spencer, L. (1933) *Geograph. J.*, **82**, 375-377. [3] Miura, Y. (2009) *Lunar Planet. Sci.*, **XL**, #1090, #1468. [4] Miura, Y. (2009) *NIPR (Japan)*, 39-40.

Application of XANES analysis on blue sapphire samples from various geological environments

Monarumit, N.[1], Klysubun, W.[2] & Wathanakul, P.[1,3*]
[1]Dept. of Earth Sciences, Faculty of Science, Kasetsart University, Bangkok, Thailand
[2]Synchrotron Light Research Institute (Public Organization), Nakhonratchasima, Thailand
[3]The Gem and Jewelry Institute of Thailand
([*]fscipww@ku.ac.th)

Blue sapphire is a variety of gem corundum. This mineral has a chemical formula of Al_2O_3 and crystallises in the hexagonal system. Pure corundum is colourless; however colour of corundum can be generated by the introduction of trace elements into the structure. The blue colour of sapphire caused by iron (Fe^{2+}) and titanium (Ti^{4+}) is due to Fe^{2+}–O–Ti^{4+} charge transfer [1]. Even though blue sapphire can form in various geological environments, this corundum variety is mainly found in metamorphic (e.g., Sri Lanka, Madagascar) and basaltic deposits (e.g., Thailand, Australia, Laos) [2].

X-ray absorption near edge structure (XANES) spectroscopy is a powerful technique to study the electronic structure around the absorbing atom. The positions and shapes of lines in XANES spectra are highly sensitive to the valence state and symmetry of the surrounding, neighboring atoms [3].

XANES measurements were performed at the Synchrotron Light Research Institute, Thailand, using the X-ray absorption spectroscopy (XAS) beamline, BL-8, with synchrotron radiation from a bending magnet. Fe K-edge XANES spectra of blue sapphire samples were collected in fluorescence mode with a 13-element Ge detector. The Athena program was employed for the data reduction.

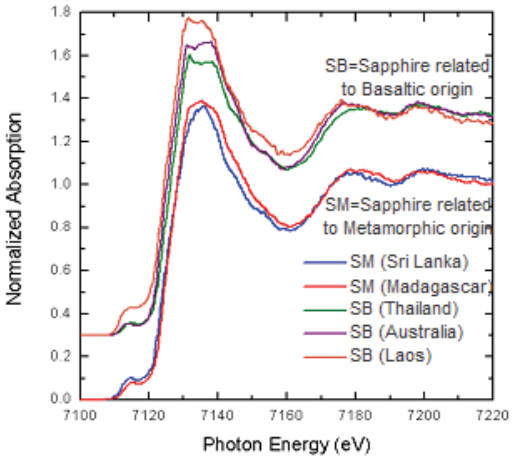

Fig. 1: Fe K-edge XANES spectra of blue sapphire samples from various geological environments.

The basaltic blue sapphire samples exhibit two convoluted absorption peaks followed by a broad shoulder feature overlaying on the high-energy side, which distinguish them from the metamorphic ones (see Fig. 1). This is possibly due to high Fe contents in basaltic hosted sapphires, i.e., Fe having a different atomic environment compared to those in metamorphic sapphire samples. Thus, this initial examination implies that the XANES technique may enable one to identify the geological origin of blue sapphire samples.

[1] Nassau, K. (1994) *Gemstone Enhancement Science and State of the Art*. Redwood Books, Wiltshire. [2] Kievlenko, E.Y. (2003) *Geology of Gems*. Ocean Pictures Ltd, Russia. [3] Koningsberger, D.C. & Prins, R. (1988) *X-ray Absorption*. John Wiley & Sons, New York.

Crystal chemistry of a sarcolite gemstone

Pandolfo, F.[1*], Guastoni, A.[2], Nestola, F.[2] & Cámara, F.[2]
[1]Dept. of Scienze della Terra, University of Pavia, Italy
([*]francesco.pandolfo@dst.unipv.com)
[2]Dept. of Geoscience, University of Padova, Italy
[3]CNR-Istituto di Geoscienze e Georisorse, Unità di Pavia, Italy

An outstanding gem sarcolite gemstone, orange in color and weighing 2.55 carats, has been cut from a large fragment of a crystal hosted in xenolitic rock from the type locality of Monte Somma (Vesuvius, Italy) [1]. This sample was found in a metamorphosed volcanic ejecta in association with augite, gehlenite and nepheline. It represents the largest cut gemstone of sarcolite known so far. Sarcolite has an ideal chemical formula of $NaCa_6Al_4Si_6O_{24}F$ and is tetragonal with space group *I*4/*m*. Gemmological properties give refraction indices of ω = 1.604(1) and ε = 1.613(2) and a density of 2.91 g/cm^3 [2]. The crystal structure of sarcolite was solved using single crystal X-ray diffraction (SCXRD) by [3] who obtained an R value of 0.054. Chemical investigations of sarcolite were performed by [4] and [5].

We have performed a crystal-chemistry study using SCXRD and WDS electron microprobe analysis. The CHNS elemental analysis technique was also used for the determination of volatile elements. Crystallographic results give lattice parameters of a = 12.3678(5), b = 12.3678(5), c = 15.4777(10) Å, V = 2367.51 Å^3, and an R value of 0.0414.

CO_3 and PO_4 groups and Na(K) polyhedrons are situated along the 4-fold axis. C is 3-fold coordinated in planar CO_3 groups showing four alternative positions, thus having the CO_3 plane parallel to {110}. There are P tetrahedra with two alternative configurations, i.e., with two opposed edges parallel to (001), thus showing a local violation of the space group. Na is 5-fold coordinated and is locally split. Al is 5-fold coordinated; two polyhedra are connected through a common apex being F (or minor OH). Silicon is present as one disilicate group and four isolated tetrahedra per unit cell. There are three alkali sites: two Ca sites and a Na site, which can have half occupancy at maximum.

Electron microprobe analysis revealed an average composition of SiO_2 35.45 wt%, CaO 32.93 wt%, Al_2O_3 18.79 wt%, Na_2O 3.98 wt%, P_2O_5 3.23 wt%, F 2.86 wt%, Fe_2O_3 0.50 wt%, MgO 0.28 wt%, MnO 0.03 wt%, K_2O 0.85 wt%, TiO_2 0.04 wt%, Cl^- 0.02 wt%, and SrO 0.83 wt%. The CHNS yielded CO_2 1.99 wt%, SO_3 0.07 wt%, and OH^- 0.22 wt%. The chemical formula (a.p.f.u.) calculated for the sarcolite specimen by combining single crystal XRD, EMPA, and CHNS is $[(CO_3)_{0.46}(PO_4)_{0.47}\ (Na_{0.82}K_{0.18})]\ Na_{0.47}\ (Ca_{6.01}Sr_{0.08})_{\Sigma=6.09}\ (Al_{3.79}Fe^{2+}_{0.07}Mg_{0.07}Ti^{4+}_{0.01}Mn^{2+}_{0.01})_{\Sigma=3.94}\ (Si_2O_7)\ (Si_{1.02}O_4)_4\ [F_{1.52}(OH)_{0.21}Cl_{0.01}]_{\Sigma=1.74}$.

[1] Fleischer, M. et al. (1979) *Am. Mineral.*, **64**, 241-245. [2] Anthony, J.W. (2003) *Handbook of mineralogy: Silicates.* Mineral data publishing. [3] Giuseppetti, G. et al. (1977) *TMPM Tschermaks Min. Petr. Mitt.*, **24**, 1-21. [4] Livingstone, A. (1984) *Mineral. Mag.*, **48**, 107-112. [5] Maras, A. & Paris, E. (1987) *Can. Mineral.*, **25**, 731-737.

Effects of heat treatment on synthetic gem corundum: an AFM approach

Pongkrapan, S.[1], Wongkokua, W.[2] & Wathanakul, P.[1,3*]
[1]Dept. of Earth Sciences, Faculty of Science, Kasetsart University, Bangkok, Thailand ([*]fscipww@ku.ac.th)
[2]Dept. of Physics, Faculty of Science, Kasetsart University, Bangkok, Thailand
[3]The Gem and Jewelry Institute of Thailand (GIT), Bangkok, Thailand

Untreated gemstones with high-quality colours and clarity are hard to find. These naturally born beauties are therefore very expensive when compared to artificially enhanced ones. Heat treatment is the most popular technique to improve the quality of gemstones [1]. While traditional heat treatment on gem corundum (α-Al_2O_3) is still practiced, a technique developed by Thai gem burners, called beryllium (Be) diffusion [2], has become increasingly popular during the past decade. Gem testing laboratories have oftentimes faced difficulties in non-destructively differentiating heat-treated gemstones from untreated ones, especially for those that experienced either low-temperature heat treatment or Be diffusion.

The still on-going research presented here aims at developing an AFM innovation to identify the heat treatment of gem corundum that is not clearly determinable by other spectroscopic techniques employed in standard gem testing laboratories. Tapping-mode AFM observation in ambient condition showed that the surface perpendicular to the *c* axis of a synthetic gem corundum sample has developed a significantly faceted terrace-and-step morphology after treatment at 1650 °C. Mechanisms of such sharp-edged formation are thoroughly discussed.

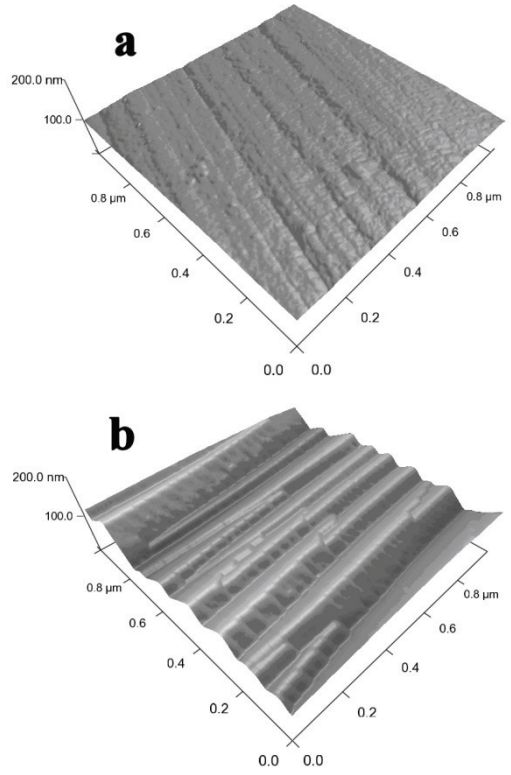

Fig. 1: AFM topographic images (1 µm × 1 µm) on the surface roughly perpendicular to the *c* axis of a synthetic gem corundum (a) before heat treatment, and (b) after heat treatment at 1650°C. The z-axis scale is 100 nm/division for both images.

[1] Nassau, K. (1981) *Gems Gemol.*, **17(3)**, 121-131. [2] Emmett, J.L. et al. (2003) *Gems Gemol.*, **39(2)**, 84-135.

Influence of geological formation on the quality of ruby from Myanmar, Sri-Lanka, and Thailand

Sorokina, E.S.[*] & Ozhogina, E.G.
Fedorovsky All-Russian Research Institute of Mineral Resources, Moscow, Russia ([*]elensorokina@mail.ru)

The most beautiful chrome-coloured gem corundum (ruby) is mined in alluvial deposits that originate from the weathering of primary rocks, in particular marbles and basalts. In this study, more than 300 samples of natural, non heat-treated and heat-treated rubies were investigated. These samples originate from deposits in Myanmar, Sri Lanka (both related to metamorphic origin), and Thailand (basaltic origin). Samples came from the collections of the A.E. Fersman Mineralogical Museum (Russian Academy of Sciences) and the Gemmology Chair of the Russian State Geological Prospecting University (RSGPU).

The quality of the raw material seems to depend strongly on the type of formation. The metamorphic ruby samples from in Myanmar and Sri Lanka often show the bright red colour (commonly referred to as "pigeon blood" red; more often found in Myanmar than in Sri Lankan stones) with slightly purple shade and are hence more expensive. In contrast, basaltic ruby from Thailand is often characterized by dark red and more often purplish red colours, which require additional heat treatment.

Stones belonging to the two types of formation can be distinguished based on their chemical composition, luminescence peculiarities, and the presence/absence of certain mineral inclusions (investigated earlier by [1,2] and many others). We report the discovery of Fe–Ti inclusions (probably ilmenite) in ruby from Myanmar, which, to the best of our knowledge, has not been reported thus far.

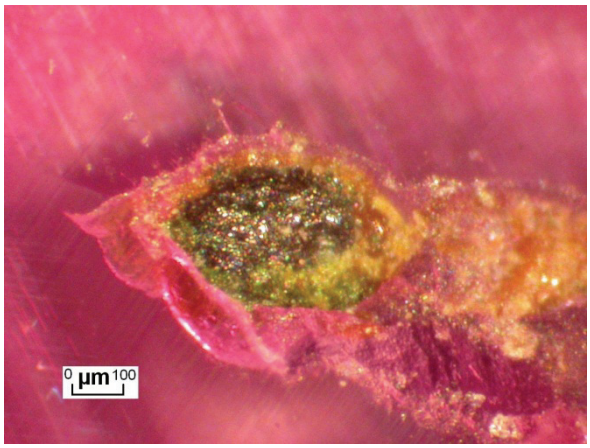

Fig. 1: Inclusion (probably ilmenite) in ruby from Myanmar, surrounded by rutile needles (sample №7734; Fersman Mineralogical Museum, RAS).

All investigated ruby samples from Thailand are presumably heat-treated. They show negative crystals within whitish cavities that are filled with a Si-rich material (all values in wt%: SiO_2 (78.0), Al_2O_3 (5.10), Cr_2O_3 (3.55), CaO (1.68), FeO (1.14), K_2O (0.91)), whereas there are virtually no inclusions in these stones (excluding, probably, well-shaped boehmite needles). Stones from Myanmar and Sri Lanka, in contrast, did not show any heat treatment. Our results allow us to contribute to a provenance assignment for unknown stones, and to assist in the prediction of the quality of raw materials depending on formation type.

Acknowledgements: We are indebted to Dr. O.V. Balitskaya, colleagues from the Fersman Mineralogical Museum, RAS, and the Gemmology Chair of the RSGPU.

[1] Gübelin, E.J. & Koivula, J. (1992) *Photoatlas of inclusions in gemstones.* ABC, Zürich. [2] Hughes, R.W. (1997) *Ruby & Sapphire.* RWH Publishing, Boulder, CO.

Crystal chemistry of pyralspite garnets from Shavaryn Tsaram, Mongolia

Soumar, J.[1*], Skála, R.[1,2] & Matějka, D.[1]
[1]Inst. of Geochemistry, Mineralogy and Natural Resources, Charles University, Prague, Czech Republic ([*]jansoumar@centrum.cz)
[2]Inst. of Geology, Academy of Sciences of the Czech Republic, Prague, Czech Republic

Garnets from the classic localities in Northern Bohemia (Czech Republic) and Shavaryn Tsaram (Mongolia, 48° 12´ N, 100° E), of mostly dark red (in some cases dark orange) colour, were studied by means of electron microprobe and X-ray powder diffraction analysis, with the aim to compare the mineralogical compositions of the two sample sets. BSE images were taken to check for potential zoning of the samples.

Table 1: Chemical composition of a pyrope-almandine from Mongolia (Cameca SX 100, National Museum, Prague, Czech Republic)

Pt.	SiO_2	TiO_2	Al_2O_3	FeO	MnO	MgO	CaO	BaO	Total
1	40.15	0.57	22.15	15.51	0.41	13.91	5.2	1.11	99.25
2	40.78	0.6	22.14	15.81	0.37	14.05	5.65	1.17	99.96
3	40.48	0.63	22.18	15.71	0.32	14.09	5.78	1.14	99.97
4	40.69	0.6	22.3	15.91	0.38	14.14	5.93	1.19	100.73
5	39.91	0.66	22.07	16.04	0.37	14.33	5.96	1.28	100.14
6	39.63	0.64	22.27	16.31	0.4	14.31	5.83	1.32	100.13
7	39.1	0.64	22.2	15.29	0.41	13.99	5.94	1.32	98.51
Av.	40.11	0.62	22.19	15.80	0.38	14.12	5.83	1.22	100.26

No obvious zoning was observed in the BSE images of polished grains; this is also consistent with the relatively uniform chemical compositions measured (Table 1). Other elements were below the detection limit of the electron probe micro-analyser used. The average empirical formula (based on 12 oxygens per formula unit, full occupancy of all sites, and maintaining charge balance) is

$$(Mg_{1.56}Fe^{2+}_{0.92}Ca_{0.46}Ba_{0.04}Mn_{0.02})_{\Sigma 3.00}(Al_{1.91}Fe^{3+}_{0.08}Ti_{0.03})_{\Sigma 2.00}(Si_{2.97}Al_{0.04})_{\Sigma 3.00}O_{12}$$

This corresponds to the simplified end-member composition $Pyr_{53}Alm_{31}Gr_{12}And_4$. X-ray powder diffraction confirmed the identity of the studied material to the pyrope–almandine garnet series.

Comparing the data with results of a previous study [1] shows the possibility of the Mongolian garnets to have a similar use as the Czech ones.

Acknowledgements: Support through the project FR-TI1/543 of the Ministry of Industry and Trade of the Czech Republic is acknowledged. This study is a part of the institution research plans MSM0021620855 and AV0Z30130516.

[1] Seifert, A.V. & Vrána, S. (2005) *Bull. Geosci.*, **80**, 113-124.

Spectroscopic features due to Ni- and Co related defects in gem-quality natural diamonds

Tretiakova, L.
Diamond Research Ltd, Fort Lee, NJ, USA
(Ltretiakova@yahoo.com)

Ni- and Co-related defects observed in some nitrogen-containing synthetic diamonds grown from a Ni- or Co-containing catalysts have been studied well enough [1-3], but a little known of Ni- and Co-related defects in natural diamonds.

Natural gem-quality faceted diamonds (ND) were analyzed of non-destructive techniques including Infrared (IR) and laser-induced photoluminescence (PL) spectroscopy.

Detailed study of spectroscopic features (IR and PL) of ND has made possible to detect various kinds of impurities (N, H, Ni, Co, Si, CO2, lonsdaleite) containing in these diamonds.

The behavior of Ni and Co impurities in ND containing various levels of nitrogen aggregation and different concentration of IR-active hydrogen has been studied and temperatures, which Ni- and Co-related systems create, exist and vanish in ND, have been determined.

At the first time Co-N and Co-C defects (weak lines at 519.3, 523.6, 542.5, 544.1, 561.6, 669.4 nm) have been observed in PL spectra (PLS) of ND. These systems exist at temperatures around 1750-2050 K.

Prominent 694, 535.2, 700.6 nm Ni-related systems and a lot of low intensity Ni-related defects are observed in PL spectra (PLS) of studied ND. Low intensity defects were attributed to Ni-N complexes that exist at temperature range around 1600-2200 K and, displaying a transitory behavior, giving rise to other Ni-N complexes such as the 694, 535.2, and 603.5, 640.5, 700.6 nm.

Spectroscopic features of the 694 nm PL system in mixed (IaAB irregular + Ib) type ND, containing nitrogen in the A (dominant), B, C, N+ forms and high concentration of IR-active hydrogen, have been described and this defect tentatively attributed to Ni-N-H complex that exists at temperatures around 1600 - 2350 K.

At the first time the 535.2 nm defect has been observed in PLS of mixed (IaAB regular + Ib) type ND where nitrogen presented in the A, B, B', C, N+, N3 forms, B' defect is shown strong peaks at the range 1370 - 1360 cm-ą and in some stones splitted up to six components. The 535.2 nm defect is tentatively ascribed to Ni-N complex that exists at temperatures around 1950-2500 K and determined as additional feature for the identification of the treatment of greenish-yellow diamonds.

The origin of the 603.6, 640.5, 700.6 nm PL defects are some complicated interstitial type defects (Ni-N-V complexes) [4] possibly comprised hydrogen atom(s) [5] and associated in the type Ia ND of mixed cubo-octahedral shape [4]. These systems exist at wide temperature range around 1950 - 2500 K.

Any knowledge of the origin and behavior of defects in ND help in the reconstruction of diamond growth conditions and origin, as well as the identification of diamond treatment.

[1] Yelisseyev, A. et al. (2003) *Diam. Relat. Mater*., **12**, 2147-2168. [2] Yelisseyev, A. & Kanda, H. (2007) *New Diam. Front. C. Tec.*, **17(3)**, 127-178. [3] Lawson, S.C. & Kanda, H. (1993) *J. Appl. Phys.*, **73(8)**, 3967-3973. [4] Lang, A.R. et al. (2004) *J. Cryst. Growth*, **263**, 575-589. [5] Tretiakova, L. (2009) *Eur. J. Mineral*., **21(1)**, 43-50.

Annealing of metamict zircon from Ratanapura, Sri Lanka

Wanthanachaisaeng, B.[1*], Bunnag, N.[1], Pattarawarin, P.[1], Ounorn, P.[3], Sutthirat, C.[2,3] & Pisutha-Arnond, V.[2,3]
[1]Faculty of Gems, Burapha University, Chanthaburi, Thailand
([*]bhuwadol@yahoo.com)
[2]Dept. of Geology, Chulalongkorn University, Bangkok, Thailand
[3]The Gem and Jewelry Institute of Thailand, Bangkok, Thailand

A green metamict zircon sample (no. GRAT 21) from Ratanapura, Sri Lanka, was investigated in this study. The sample was annealed in air at 600, 700, 800, 900 and 1000°C in an electric furnace with around 3 hours of dwelling at each target temperature. The specific gravity (SG) value and the Raman spectroscopic technique were used to monitor the decrease of the degree of metamictization of the zircon sample (compare [1]).

As shown in Fig. 1, the SG values of the sample show a continuous increase from 3.8 g/cm^3 recorded before treatment to 4.24 g/cm^3 after annealing at 1000°C, which however is well below the SG of 4.68 g/cm^3 for well-crystallised zircon [2].

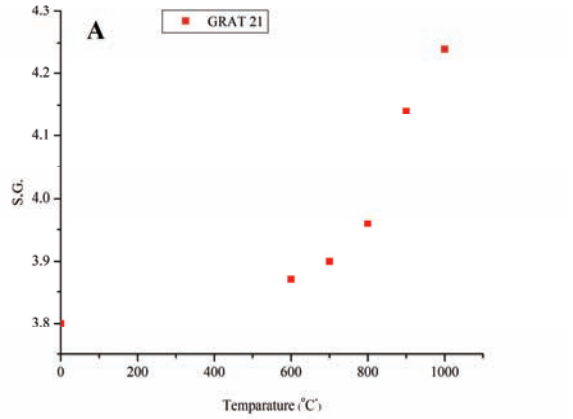

Fig. 1: Plot showing the continuous increase of SG values of a zircon sample (GRAT 21) from Ratanapura, measured before treatment and after annealing at 600, 700, 800, 900, and 1000°C.

The Raman spectrum of the sample before heating shows dramatically broadened Raman bands. This indicates a very high degree of metamictization of the original sample, which is perhaps close to the amorphous state. The sample's structure, however, started to improve after annealing at 700°C, as indicated by the appearance of some recovery bands and a general decrease of the band broadening. At higher annealing temperature, the structural recovery proceeds significantly. After annealing at 1000°C, the main υ_3 (anti-symmetric SiO_4 stretching) band lies at ca. 1006 cm^{-1} and has a full width at half maximum (FWHM) of ca. 15 cm^{-1}, indicating significant but still incomplete structural reconstitution. Based on the above SG and Raman spectroscopic results it is therefore concluded that the zircon structure was significantly recovered from a nearly amorphous state to almost crystalline state after dry annealing in air at 1000°C.

[1] Nasdala, L. et al. (2002) *Chem. Geol.*, **191**, 121-140. [2] Holland, H.D. & Gottfried, D.G. (1955) *Acta Cryst.*, **8**, 291-300.

Characterization of beryl samples from a novel deposit in the Erongo massif, Namibia

Wildner, M.[1*], Giester, G.[1], Hammer, V.M.F.[2], Niemetz, W.[3] & Lehrl, M.[4]

[1]Institut für Mineralogie und Kristallographie, Universität Wien, Vienna, Austria ([*]manfred.wildner@univie.ac.at)

[2]Staatliches Edelsteininstitut, Naturhistorisches Museum Wien, Vienna, Austria

[3]Österreichische Gemmologische Gesellschaft, Vienna, Austria

[4]Esme Fine Gemstones, Omaruru, Namibia

The described beryl claim belongs to the Erongo massif of the Damara orogen, Namibia, which is part of the Pan-African orogenic belt. This area is famous for spectacular findings (in 2000 and 2002) of aquamarine, associated with schorl, feldspar and fluorite. In 2009, the new deposit at Davib-Ost farm, Karibib District, was discovered. Miarolitic cavities within granite house loose beryl crystals of light blue to yellowish-green color, often intergrown with feldspar and colorless topaz. The pipes sometimes extend up to 100 m in length. Further associated minerals are e.g. quartz, apatite, fluorite, schorl, jeremejevite, bertrandite, siderite, goethite, and muscovite.

A faceted light blue aquamarine (~44 ct) with yellow-green hue shows overlapping healing fissures. Their boarders are very sharp and sometimes show "folds". The fissures consist of two- and three-phase inclusions. Along the *c*-axis fine needle-like growth tubes with milky appearance are observed. Single muscovite flakes may prove a granitic or pegmatitic origin. Such clear aquamarine crystals have not been known from other deposits of the Erongo massif so far.

Two further beryl samples, a pale blue and a more greenish-blue one, were characterized by single crystal X-ray diffraction and optical absorption spectroscopy. Lattice parameters are in the range a = 9.219–9.220 and c = 9.195–9.196 Å, as commonly observed for "normal" beryl. Structure refinements in space group *P6*/*mcc* yielded R_1-values of 2.8 %; residual electron densities within the channels are 1.7 and 1.3 $e^{-}Å^{-3}$, respectively. The optical spectra (Fig. 1) are dominated by a band centered at ~810 nm, which is strongly polarized perpendicular to the *c*-axis and assigned to the spin-allowed $^5E(D)$ crystal field state of Fe^{2+} in octahedral coordination. Minor features at 425 and ~370 nm are related to spin-forbidden levels of octahedral Fe^{3+}. In the NIR range, several overtone and combination modes of channel H_2O-molecules type I and II are observed. In the greenish blue sample the aforementioned band at 810 nm is broadened in polarization parallel to the *c*-axis due to additional components around 620 and 1000 nm, probably caused by Fe^{2+}–Fe^{3+} charge transfer (however, the detailed origin of these features is still a matter of controversial debate in the literature). The shift of the UV absorption edge towards the visible range has a further color-modifying effect as compared to the pale blue sample.

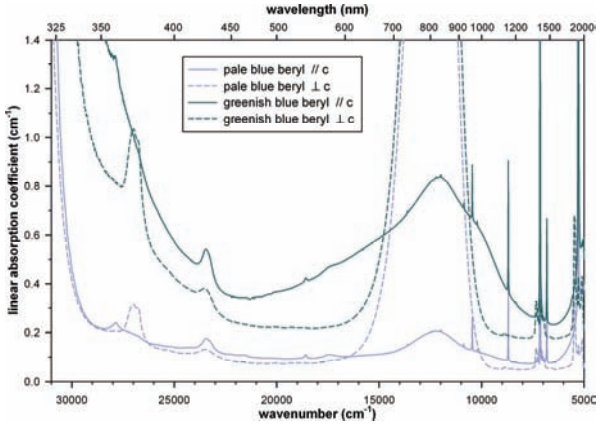

Fig. 1: Polarized optical absorption spectra of two beryl samples from the new deposit at Davib-Ost farm, Karibib District, Namibia.

The vibrational behavior of SiO_2 at the glass transition: some *ab-initio* vibrational calculations and their thermodynamic implications

Ottonello, G.*, Vetuschi Zuccolini, M. & Belmonte, D.
DIPTERIS, Università di Genova, Genoa, Italy
(*giotto@dipteris.unige.it)

We investigated with *ab-initio* procedures the structure-energy and vibrational properties of silica clusters incorporated in a continuum with appropriate permittivity (dielectric constant ε=3.8) through DFT/B3LYP gas phase calculations coupled with a Polarized Continuum Model approach, and, in the framework of the Block theorem [1], those of the periodical structure D_{6h} which leads to the α-cristobalite polymorph of silica when subjected to symmetry operations. The obtained energy properties and vibrational features indicate that none of the investigated moiety, when taken alone, justifies the observed energy and vibrational properties of the silica glass while, based on the computed energies and vibrational features, an aggregate of the D_{6h} network and the monomer locally ordered in the short-medium range present in the glass in a mutual arrangement lacking of spatial continuity reproduces satisfactorily both the experimentally observed low T heat capacity and the deviation from the Debye T^3 law, which, contrarily to what previously assumed, is largely due to low frequency internal modes, and only partly to coherent low frequency acoustic motions. The heat capacity of the glass at all temperatures below T_g is consistent with the (84) internal modes of 2 D_{6h} units variably linked with a $[SiO_4]^{4-}$ monomer plus the 3 (experimentally observed) acoustic modes [2,3] and an excess acoustic-like (i.e. coherent) mode of low frequency [4]. At T_g, the observed sharp increase in the isochoric heat capacity [5] is due to the onset of rotational and translational motions which replace the coherent (acoustic-like) motions of all atoms in the ensemble. The process is kinetically mediated by the number of bonds which are effectively broken at the various T above T_g and ceases out at the mode-coupling temperature T_{MC} where hybridization of acoustic-like and internal modes occur [6]. The hybridization process involves a substantial decrease of the force constant of the bond ϕ and an increase on the reduced mass m. The coupled effects would result in an overall increase of the ϕ/m ratio at T_{MC} of a factor $\sim 5\times10^2$, which suggests the onset of RUM-like stretching motions between rigid D_{6h} units intermingled with $[SiO_4]^{4-}$ bridging units. Our calculations indicate that, although for simple computational purposes one may eventually treat the glass transition as a (reversible) thermodynamic process occurring at T_g without incurring in substantial errors, it cannot be considered of high order because it involves discrete, though limited, transition entropy ΔS_{Tg} = 1.304 J/(mol×K) and transition enthalpy ΔH_{Tg} = 1.930 kJ/mol contributions.

[1] Pisani, C. (1996) *Lecture notes in Chemistry*, **67**, Springer, Berlin. [2] Flubacher, P. et al. (1959) *J. Phys. Chem. Solids*, **12**, 53-65. [3] McSkimin, H.J. (1953) *J. Appl. Phys.*, **24**, 988. [4] Masciovecchio, C. et al. (1997) *Phys. Rev. B.*, **55**, 8049-8051. [5] Richet, P. et al. (1982) *Geochim. Cosmochim. Ac.*, **46**, 2639-2658. [6] Sette, F. et al. (1998) *Science*, **280**, 1550-1555

The fate of CO_2 in silicate melts: a computer simulation study

Guillot, B.* & Sator, N.
Laboratoire de Physique Théorique de la Matière Condensée (UMR 7600), Université Pierre et Marie Curie, Paris, France
(*guillot@lptmc.jussieu.fr)

The distribution, recycling and storage of carbon in the Earth are of fundamental importance to understand the global carbon cycle between the deep Earth and near surface reservoirs. Degassing of CO_2 at mid-ocean ridges may give information on the source region but the very low solubility of CO_2 in tholeïtic basalts (~0.5 ppmw/bar) has for consequence that near all MORB glasses exsolve their CO_2 rich vapor at shallow depth as they approach the ocean floor. Hence their CO_2 contents mostly represent the pressure at eruption and not the source region. Recent petrological investigations [1] have shown that the presence of carbonates at depth in the upper mantle has a large effect on the solidus of carbonated silicates (e.g. peridotite) by inducing incipient melting at much lower temperature. So the role of carbon-rich melts at great depth is now becoming a credible scenario to explain the extraction of CO_2 from the source region to the surface. During the last three decades many studies have been devoted to measure the solubility of CO_2 in silicate melts of various compositions. But due to experimental difficulties these studies were generally restricted to low and moderate pressures (below ~20 kbar). IR spectroscopy has emphasized the importance of CO_2 speciation which may exist either as molecular CO_2 or as carbonate ion (CO_3^{2-}), the molecular form being favored in polymerized (silicic) melts while the carbonate ion is dominant in depolymerized (basic and ultrabasic) melts. However it has been demonstrated recently [2] that the CO_2 speciation observed in quenched glasses by IR spectroscopy may not be representative of that in silicate melts equilibrated at high temperature: in particular, the abundance of molecular CO_2 is underestimated in the liquid at magmatic temperatures.

By performing a series of molecular dynamics simulation where a supercritical CO_2 phase is in contact with a silicate melt of various composition (from felsic to ultrabasic) at different temperatures (1473-2273K) and pressures (20-150kbar), we have been able to evaluate the solubility of CO_2, the population of molecular and carbonate species, their diffusivity through the melt and the local structure. We will show that this kind of molecular simulation is a useful theoretical guide to better understand the behavior of CO_2 in magmas at depth.

[1] Dasgupta, R. & Hirschmann, M.M. (2006) *Nature*, **440**, 659-662. [2] Morizet, Y. et al. (2007) *Eur. J. Mineral.*, **19**, 657-669.

.

Evolution of microstructure and composition of refractories at their interaction with metallurgical melts

Shchekina, T.I.*, Gramenitskiy, E.N. & Batanova, A.M.
Dept. of Petrology, Moscow State University, Moscow, Russia
(*t-shchekina@mail.ru)

This work is a study of the deterioration mechanism of Martin furnaces hearth, which are used for stuffing the magnesia-dolomite ramming mixture of various marks: Ankerharth (Austria), Jehearth (Slovakia) and PPM 85 (Satka, Russia). Our purpose is to reveal the factors affecting the stability of the refractory materials during their service. Chemical corrosion during the service is the main reason of lowering fire-resistant materials stability.

Chemistry, phase composition and structure of samples from various hearth sites of Martin furnaces pre- and after service in zones at interaction of fire-resistant materials with metallurgical melts, were studied. The comparative analysis of the changes and parameters depending on refractory mark was carried out. The main result of this study is detection of diffusive zoning at the contact between metallurgical melts and a fire-resistant material, similar to natural metasomatic processes. [1]. Due to diffusive interaction of fire-resistant material with melts of steel and slag, new phases with technogenic origins are formed as unusual isomorphic replacement in minerals of calcium ferrites, aluminates, perovskite groups [2].

Chemical corrosion during the service is the main reason of lowering fire-resistant materials stability. Phase composition and the microstructure of samples change significantly in zones arising at interaction between fire-resistant materials and metallurgical melts. The composition of all fire-resistant materials used in Martin manufacture bear similarities, although the ratios vary: periclase MgO (80-90%), lime CaO (8-20%), impurities of the phases containing SiO_2, Fe_2O_3, Al_2O_3 (3-5%).

In the reactionary columns about 5 zones can be separated, from moderately changed zone 1 (closed to initial refractory material on phase composition) to most cardinal changed zone 5 (almost completely combined by new-formed phases). General thickness of reactionary columns reaches tens centimeters, while thickness of its most changed parts is about 5-7 mm.

The main change of material chemistry consist of carrying out Mg and introducing Fe and Si, thus the role of Fe^{3+} in relation to Fe^{2+} increases, as approaching the contact of the refractory - the melt. Mineral composition changes also. Periclase registers an increasing of ferruginosity up to 30% until its full replacement by magnesioferrite, magnetite and wustite. The aluminates form in moderately changed zones, while silicates of calcium, merwinite and ferrite of calcium – in more changed zones. The phase composition becomes similar for all refractory material closest to the contact with metallurgical melts. Periclase remains only as relict grains with high ferruginosity up to 30 %. Magnesioferrite, forming large crystals, becomes the main mineral in Ankerharth material. Smaller amounts of magnetite, ferrite of calcium and dicalcium silicate fill the space between high ferrrous phases. The main feature of structure of 5th zone on Jehearth material is occurrence of ferrous oxide melt. Ti-containing brounmillerite in accretions with calcium aluminates form the final zone in Satka material. About 30 % of iron position in brounmillerite is occupied with titan. Microstructure of this material is assumed to formation of appropriate melt at conditions of metallurgical process. Formation of such melts promotes a softening of the refractory material surface and its erosion.

[1] Korzhinskiy D.S. (1982) *The theory of metasomatic zoning*. Nauka, Moscow. [2] Shchekina T.I. et al. (2006) *Refrac. Ind. Ceram.*, **47**, 25-32.

In-situ structural investigation of hydrous and anhydrous $NaAlSi_3O_8$ melt at high pressure

Yamada, A.[1*], Inoue, T.[1] & Kikegawa, T.[2]
[1]Geodynamics Research Center, Ehime University, Matsuyama, Japan (*a-yamada@sci.ehime-u.ac.jp)
[2]Photon Factory, High Energy Accelerator Research Organization, Tsukuba, Japan

Microscopic structure of molten silicate at high pressure gives important insights into the fundamental understanding of the physicochemical properties of magma in the Earth's interior. In particular, *in-situ* observations of liquid are necessary for the realistic response of the structure to pressure because the information through the glass is always under-estimated due to the kinetic effect and the reversible property of the structure during decompression. A local structural change in AlO_4 tetrahedra is thought to happen at much lower pressures than in the SiO_4 tetrahedra, which influent to various properties of aluminous silicate melt. In addition, it is widely known that water changes the structure and properties of silicate melt dramatically. Here, we investigate the difference in local structure between hydrous and anhydrous albite ($NaAlSi_3O_8$) melt with high-pressure X-ray diffraction.

A sample of anhydrous albite was prepared with a mixture of $NaCO_3$, Al_2O_3, and SiO_2. The mixture was decarbonized at 1000°C for 9 hours, then melted at 1200°C, and finally quenched at room temperature to make a glass. Hydrous albite was made from sodium silicate glass ($Na_2Si_6O_{13}$) plus $Al(OH)_3$ gibbsite, which has 9.3-wt% water content. High-pressure X-ray diffraction experiments have been conducted at NE5C beamline in PF-AR, Tsukuba, Japan. A DIA-type press was used for the high-pressure and temperature experiments. A hydrous sample was encapsulated in single-crystal diamond tubing with platinum lids (e.g., [1]). Anhydrous melt was put in graphite or boron nitride containers. Diffractometry of the molten sample for the structural analysis was performed with polychromatic X-rays with the energy-dispersive method. Diffraction patterns of the sample were collected from $2\theta = 3°$ to 30° to cover a wider range of Q ($Q = 4\pi E \sin\theta/12.398$ [Å^{-1}], where E and θ are the energy of the X-rays and the Bragg angle, respectively). To obtain S(Q), software developed by Funakoshi (1997)[2] was exploited.

S(Q) and G(r) for hydrous albite melt are shown in Fig. 1.

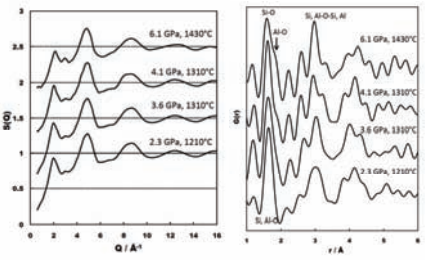

Fig. 1: Structure factor, S(Q), (left) and radial distribution function, G(r), (right) for hydrous $NaAlSi_3O_8$ melt.

The pressure dependence of the peak-shift of the first peak in S(Q) for the hydrous melt is much smaller than for the anhydrous melt although the position of the peak is located on the higher-Q side. The shoulder peak on the right side of the Si-O peak in G(r) appears from 4.1 GPa in the hydrous melt (allow in right figure), which becomes intense with pressure. This shoulder peak can be assigned to a highly coordinated Al-O atomic pair. This striking peak, which reflects the appearance of AlO_n polyhedra, was not seen in the anhydrous melt up to 6.2 GPa. Further discussion will be presented in the presentation.

[1] Yamada, A. et al. (2007) *Geophys. Res. Lett.*, **34**, L10303. [2] Funakoshi, K. (1997) *PhD thesis*, Tokyo Inst. Technol.

Effect of alkali content and Fe oxidation state on the S oxidation state and solubility in silicate glasses

Giuli, G.[1*], Paris, E.[1], Alonso Mori, R.[2], Glatzel, P.[2], Cicconi, M.R.[1], Scaillet, B.[3] & Eeckhout, S.G.[2]
[1]Dip. di Scienze della Terra, Universita' di Camerino, Italy ([*]gabriele.giuli@unicam.it)
[2]European Synchrotron Radiation Facility (ESRF), Grenoble, France
[3]Inst. de Sciences de la Terre D'Orleans, UMR, CNRS-UO, Orleans, France

The Fe oxidation state, coordination geometry and <Fe-O> distances have been determined by Fe K-edge XANES and EXAFS for a set of sulphur bearing silicate glasses of rhyolite composition in the aim of determining:

1) the effect of bulk composition on the iron oxidation state and local structural environment;

2) the effect of Fe oxidation state on sulphur behaviour in the corresponding magmas/melts.

Glass compositions have been chosen so as to represent S-Cl-F bearing rhyolitic magmas with low to high alkali content. These glasses have been equilibrated at a range of different oxygen fugacity conditions typical of magmatic conditions and ranging from –15.4 to –10.75 log units (at 800 ° C, 1.5 kbar).

Comparison of the pre-edge peak data with those of Fe model compounds with known oxidation state and coordination number allowed to determine the Fe oxidation state and coordination number for all the glasses analysed. The $Fe^{3+}/(Fe^{3+} + Fe^{2+})$ ratio varies from 0.25 to 0.80 (±0.05) in the glasses studied. Moreover, pre-edge peak data clearly indicate that Fe^{3+} can be present in [4] and/or [5] coordination according to the alkali content of the glass, whereas Fe^{2+} is present in [5] coordination units for these compositions. The presence of minor amounts of [6] coordinated Fe cannot be ruled out by XANES data alone. EXAFS derived Fe-O distance in the most oxidised sample (Fe-O=1.85 Å) indicates that Fe^{3+} is in tetrahedral coordination.

For these glass compositions, going from reducing to oxidising condition results in higher fraction of network forming $^{[4]}Fe^{3+}$, thus increasing the polymerisation of the tetrahedral network.

Alkali content has been found to have a very strongly effect on the Fe oxidation state: at a given oxygen fugacity, Fe oxidation state increase noticeably with increasing alkali content.

A direct proportionality has been found between the S^{2-}/Fe^{2+} molar fractions.

As Fe oxidation state is known to affect the solubility of S^{2-} species in silicate melts, Alkali content is expected to play a major role together with oxygen fugacity in the S geochemical behaviour in silicate magmas.

[1] Giuli, G. et al. (2002) *Geochim. Cosmochim. Ac.*, **66**, 4347-4353. [2] Giuli, G. et al. (in press) *Geol. Soc. Am. Sp. P.* [3] Giuli, G. et al. (in press) *Geol. Soc. Am. Sp. P.*. [4] Giuli, G. et al. (in prep).

Investigation of boron coordination in borate and borosilicate glasses and minerals using high resolution O *K*-edge XANES

Dong, D.[1], Henderson, G.S.[1*], Blyth, R.[2] & Regier, T.[2]
[1]Dept. of Geology, University of Toronto, Toronto, Canada ([*]henders@geology.utoronto.ca)
[2]Canadian Light Source Inc., University of Saskatchewan, Saskatoon, Canada

Oxygen *K*-edge XANES is sensitive to the coordination of the cations bound to the oxygen atoms. O *K*-edge XANES spectra 1have been collected for a number of crystalline reference compounds (B_2O_3, H_3BO_3, HBO_2-II, HBO_2-III, $Na_2B_4O_7$, CaB_2O_4, BPO_4), as well as, for a series of borosilicate and sodium borosilicate glasses. Crystalline phases (B_2O_3, H_3BO_3, HBO_2-II, and HBO_2-III) in which B bonds to 3 oxygens ($^{[3]}B$), exhibit a relatively narrow peak at around 537 eV, with a broad weak shoulder at around ~542 eV and a strong broad shoulder at ~545 eV. In crystalline phases containing only 4-fold B ($^{[4]}B$) (BPO_4) the spectra are characterised by 4 distinct features: a relatively sharp peak around ~539.5eV with 3 further peaks at ~538, ~541.5 and ~542.5 eV. A pre-edge feature is found around 533 eV in the spectra of both the $^{[3]}B$ and $^{[4]}B$ phases. Introduction of H as H_3BO_3, HBO_2-II, and HBO_2-III affects the intensity of the pre-edge feature but does not influence strongly the main XANES features. The spectra of calcium metaborate (CaB_2O_4) with nominal 100% $^{[3]}B$ suggest that there is a substantial amount of 4-fold B present similar to other studies. We suspect that the $^{[4]}B$ forms during sample preparation. The O *K*-edge spectra are clearly distinct for phases containing only $^{[3]}B$ and only $^{[4]}B$ and have the potential to be used to quantify the relative proportions of the different B coordination environments. Currently, we are analyzing the results for a series of borosilicate and alkali borosilicate glasses which will be reported upon.

Structure of glasses and melts in the Ca-Mg pyroxene join

Cormier, L.
Inst. de Mineralogie et Physique des Milieux Condensés, CNRS, Université Pierre et Marie Curie, Université Paris Diderot, IPGP, France (cormier@impmc.upmc.fr)

The structure of silicate melts determines their macroscopic properties such as viscosity, density, diffusivity, entropy, etc. Their understanding is still limited by the technical difficulties to obtain measurements at elevated temperatures in the liquid state. Glasses are thus often considered to describe melt structure but the structural variations with temperature are often poorly understood.

In this study, we have investigated the structure of glasses and melts on the Ca-Mg pyroxene join ($Ca_{2x}Mg_{2-2x}Si_2O_6$) using X-ray and neutron diffraction. Data were obtained from room temperature up to the liquid state. The experimental data have been coupled with numerical simulations (Molecular Dynamics and Reverse Monte Carlo). We report a detailed investigation focussing to understand the evolution of important structural parameter (Mg and Ca coordination, Mg-Ca mixing and silicate topology) with the composition and the temperature.

A molecular scale approach of the structure and properties of glasses: the role of "chameleon" elements

Calas, G.*, Cormier, L., Dargaud, O., Ferlat, G., Galoisy, L. & Lelong, G.
Inst. de Minéralogie et Physique des Milieux Condensés, Universités de Paris 6&7, IPGP and CNRS, Paris, France (*Georges.Calas@impmc.jussieu.fr)

More disordered than nanomaterials, amorphous solids such as glasses and gels have recently benefited from molecular scale approaches, which have provided at the same time a deeper knowledge of their structural organization as well as giving potential tools to predict their properties. Glass stability is required for environmental applications, including the development of insulating materials or nuclear waste matrices. On the other hand, nanophase crystallization is favored in glasses to form glass ceramics. It is interesting that the same glass components, such as Zr, B or Fe are used to develop such different properties.

The talk will summarize recent advances in rationalizing the sites of and the medium range structure around these key glass components. These data are obtained by an adequate combination of experimental approaches, mostly based on the determination of interatomic distances in glasses (EXAFS, neutron and X-ray diffraction), and of numerical modeling/simulation tools.

An extensive data set exists on Zr crystal chemistry in glasses and crystals. Zr is known to decrease the solubility of simulated nuclear glasses. In these glasses, Zr occurs in octahedral coordination and has a reticulating role. At the glass-water interface, Zr coordination may change or nor not depending on alteration conditions. Under SiO_2-saturated conditions, Zr retains its reticulating role in the alteration gel with a small nanoporosity, providing a protective role. By contrast, during alteration under open conditions, Zr coordination changes from 6 to 7, showing the formation of a mixed hydrous zirconia-silica gel at the glass surface, with a poor protective role. In glass ceramics, such as Mg- or Li-aluminosilicate glasses in which high cation field strength increases the disorder of the glassy network, Zr is used for enhancing the nucleation of nanocrystals. Zr occurs in a peculiar local surrounding, explaining its structural instability during thermal treatment. Molecular scale transformations occur about 30°C below the onset of crystalline nucleation and cause the appearance of peculiar nuclei in which surface stress effects provides these nanophases a peculiar structure.

Other structure-property relationships will be illustrated on the influence of Fe^{3+}-clustering on optical and magnetic properties of glasses, or of B-coordination on radiation- and thermal-dependent glass/melt properties. They show that bond valence rules and principles governing mineral crystal chemistry are also active in glasses, emphasizing the interdependence between the local surrounding and chemical state of the various glass components.

Fe and melt viscosity

Dingwell, D.[1*], Romano, C.[2] Giuli, G.[3], Potuzak, M.[4], Chevrel, O.[1] & Valenti, P.[5]
[1]LMU - University of Munich, Germany ([*]dingwell@lmu.de)
[2]Universita di Roma Tre, Rome, Italy
[3]Universita di Camerino, Italy
[4]Corning Glass, Corning, NY, USA
[5]GFZ, Potsdam, Germany

The rheology of magma and the viscosity of melts is a dominant control on the physical nature of magmatism and volcanism on Earth and other planets. Rheology is also a fundamental control on the efficiency of magmatic differentiation leading to the diversity of igneous rocks.

The physical description of melt rheology is well advanced and unexpected surprises in this field are likely able to be confined to extreme conditions of pressure, stress, and/or relaxation time.

The chemical description of melt rheology has also advanced rapidly in recent years. There are now a number of predictive models of varying power, both empirical and structure-based. General acceptance of a single, extrapolable, structure-based model of viscosity still lies however in the future.

Working towards a general model for melt viscosity, the influence of polyvalent elements in controlling melt viscosity is a special opportunity to understand structure-property relationships. Fe is the polyvalent element of major influence in terrestrial magmas. Its role in controlling melt viscosity is still unknown in detail.

Using a combination of viscometry, dilatometry, calorimetry and spectroscopy, the role of Fe and its redox state in controlling melt viscosity has been investigated. Compositions range from ferropicrite to pantellerite. The results reveal a (for us) surprising sensitivity of melt viscosity to Fe oxidation state. Scaling models for relating Fe-content to the magnitude of the redox effect are not yet clear. Based on these experimental determinations, we will speculate on the relationship between structure and viscosity in these systems and its implications.

Proton dynamics in hydrous silicates studied by high temperature high pressure quasielastic neutron scattering

Yang, F.[1*], Meyer, A.[1], Mamontov, E.[2] & Unruh, T.[3]
[1]Inst. of Material Physics in Space, German Aerospace Center (DLR), Cologne, Germany ([*]fan.yang@dlr.de)
[2]Spallation Neutron Source, Oak Ridge National Laboratory, Oak Ridge, Tennessee, USA
[3]Forschungsneutronenquelle Heinz Maier-Leibnitz (FRM II), TU München, Garching, Germany

Dissolved water in silicate melts plays an important role in many geological processes, especially in active volcanism. The knowledge of the dynamics of water species represents a key for the understanding of these processes and to predict melt properties like viscosity. We present results from quasielastic neutron scattering (QNS) on hydrous silicate melts, which provide informations about microscopic hydrogen dynamics in the sample on picosends to nanoseconds time scales.

Measurements were done at temperatures up to 1250 K. A constant pressure of 200 MPa was applied to prevent degassing of the sample. A Nb1Zr cell was built as sample environment for such study, which is transparent for cold neutron beams.

Experiments were carried out on several synthetic hydrous silicate systems, including pure silica, sodium trisilicate and albite compositions, all with 10 mol% water concentration. By combining experiments on different neutron spectrometers, we are able to study dynamics on the time scale from of about 0.2 picosecond up to 1 nanosecond, spanning over nearly 4 decades. Also, taking advantage of the large difference in neutron scattering cross-sections of H and D, a contrast variation via H_2O/D_2O substitution gives access to the pure incoherent proton dynamics.

The QNS signal reveals that the proton dynamics has a different nature as compared to the alkali ions in the Si-O matrix, although the addition of the water and alkali oxides both leads to a dramatic decrease of the silicate melt viscosity. In hydrous silica and albite, the relaxation time of the protons is larger than 60 picosends at 1250 K. Therefore, the proton dynamics is slower than *i.e.* the sodium dynamics in the sodium silicates under similar conditions [1]. Thus, in contrast to sodium silicates, no evidence of fast diffusion via channel structures in hydrous silica and albite has been observed. In the hydrous sodium silicate it has been found that the sodium dynamics is not significantly accelerated upon water addition. Note that although in both silica and sodium silicate cases, the macroscopic melt viscosity has dropped by orders of magnitudes, which is commonly understood as the depolymerization of the Si-O network. The slower proton dynamics may be attributed to the strong bondings between proton and Si-O matrix.

In addition, an unusual dynamics of the protons has been observed in sodium silicate melt. The proton relaxation consists of a fast process and a slow process. The later one only comes into the time window on the order of 1 nanosecond at the experimental temperature of 1150 K. This will give a transport coefficient on the order of 10^{-11} m^2s^{-1} at this temperature. However, within the neutron scattering study, decoupling of the relaxation time scale due to different proton environments can be excluded. The fast process exhibits extreme stretching of the intermediate scattering function S(q,t), which might be interpreted under a glass-glass transition scenario [2].

[1] Kargl, F. et al. (2006) *Phys. Rev. B*, **74**, 014304. [2] Voigtmann, Th. & Horbach, J. (2009) *Phys. Rev. Lett.*, **103**, 205901.

Compositional dependent compressibility of dissolved water in silicate glasses

Malfait, W.J.[1*], Sanchez-Valle, C.[1], Ardia, P.[1,2] & Médard, E.[3]
[1]Inst. for Geochemistry and Petrology, ETH Zurich, Switzerland ([*]wim.malfait@erdw.ethz.ch)
[2]Dept. of Geology and Geophysics, University of Minnesota, USA
[3]Lab. Magmas et Volcans, Universite Blaise-Pascal-CNRS, OPGC, Clermont-Ferrand, France

Because of the lack of available experimental density data, and motivated by the compositional independent partial molar volume of water in silicate glasses at atmospheric pressure [1], current density models for hydrous magmatic liquids [2] assume a composition independent from compressibility of the water component. In order to test this assumption, we have determined the acoustic velocities and elastic moduli of a series of hydrous rhyolite, andesite and basalt glasses at ambient conditions using Brillouin spectroscopy.

The measured velocities and bulk moduli are in good agreement with previous data on glasses with similar compositions, when available [1]. For all glass series, the addition of water leads to a decrease in the shear modulus (G). The increase in Poisson ratio with increasing water content for the rhyolite glasses provides indirect evidence for the depolymerization of the glasses [3]. For the rhyolite glasses, the bulk modulus (K_S) is essentially unaffected by the addition of water, but K_S decreases with increasing water content for the andesite and basalt glasses. The results show that the partial molar bulk modulus of water in depends on glass composition. The compositional dependence of the partial molar K_S, hence compressibility ($\beta_S=1/K_S$), limits the applicability of the current density models, in particular at higher pressures and/or for melt compositions that deviate strongly from liquid albite. The results of this study emphasize that the construction of more robust density models for hydrous magmatic liquids requires additional data on the density and compressibility at relevant temperature and pressure conditions.

[1] Richet, P. & Polian, A. (1998) *Science*, **281**, 396-398. [2] Ochs, P. & Lange, R.A. (1999) *Science*, **283**, 1314. [3] Rouxel, T. (2007) *J. Am. Ceram. Soc.*, **90**, 3019-3039.

Viscosity of basaltic magma at high pressure

Suzuki, A.[1*], Ohtani, E.[1], Ando, R.[1], Terasaki, H.[1], Sakamaki, T.[1] & Funakoshi, K.[2]
[1]Dept. of Earth and Planetary Materials Science, Faculty of Science, Tohoku University, Sendai, Japan
([*]a-suzuki@m.tains.tohoku.ac.jp)
[2]JASRI, SPring-8, Japan

The viscosity of magma (silicate melt) is one of the fundamental properties that control the generation, transportation, and eruption of magmas. Because magmas are formed in the Earth's interior and ascend to the surface, knowledge of the pressure dependence of viscosity is crucial in understanding the igneous processes. Therefore, the viscosities of various silicate melts have been investigated at high pressure. The viscosity of silicate melts at high pressure was measured with the falling-sphere method by a quenching experiment using a piston cylinder apparatus. In recent years, X-ray radiography has been applied to measuring viscosity for the purpose of improving uncertainty of the measurement and extending the experimental range at higher pressure and lower viscosity. Mid-ocean ridge basalt (MORB) is the most abundant basalt composing the oceanic crust. Furthermore, it is suggested that the recycling MORB would be molten again in a heterogeneous mantle plume in the deep upper mantle. The recycled MORB may be related to the activity of oceanic island basalts and continental flood basalts. Therefore, it is important to clarify the viscosity of the basaltic melt at high pressure to understand the behavior of the melts in the upper mantle. The viscosity was measured using the radiographic falling–sphere technique at the beamline BL04B1 of the SPring–8 synchrotron radiation facility. High–pressure and –temperature experiments were conducted using a Kawai–type multianvil apparatus driven by a 1500 ton uniaxial press, SPEED1500. The X-ray shadow image was observed using a CCD camera with a YAG:Ce fluorescence screen. The viscosity (η) of the melt was calculated by the Stokes' equation with the Faxén correction for the wall effect. The viscosity of the dry MORB melt decreased gradually up to a pressure of 4.5 GPa. At higher pressure, an increase in viscosity was observed to 6.5 GPa. At higher pressure the viscosity decreased up to 13 GPa. The present study revealed that the viscosity of dry MORB reached a minimum near 5 GPa. It has been suggested that the pressure dependence of viscosity changes because of modification of the structure of the melt such as the change in T–O–T bond angles in the melt and formation of the higher-coordinated aluminum and silicon. This study suggests that the structure of the MORB melt changes drastically near 5 GPa.

Structure, properties and implications for the formation of tektite glasses

Neuville, D.R.[1*], Bressel, L.[2], de Ligny, D.[2] & Cochain, B.[3]
[1]CNRS-IPGP, Géochimie et Cosmochimie, Paris, France
([*]neuville@ipgp.jussieu.fr)
[2]LPCML, UMR 5620, Université Lyon 1, Université de Lyon, Villeurbanne, France
[3]Institute for Study of the Earth's Interior, Okayama University at Misasa, Misasa, Tottori, Japan

Tektites are natural glasses corresponding to enigmatic glasses, which fascinate scientists in a number of diverse disciplines about their formation conditions. It is generally accepted that they must have formed in enormously energetic impact created by a gigantic hypervelocity object penetrating the atmosphere and striking the Earth with undiminished velocity.

First, to understand tektite glasses, we have decided to investigate viscosity measurements and glass transition temperature, which can link to the geometrical form of the tektite glasses.

The structure of the glasses investigated by Raman spectroscopy can provide also information about the quenching rate and their formation.

And finally, by using in situ XANES spectroscopy at the Fe K-edge at high temperature we can determine the redox state of tektite at high temperature. These variations of Fe^{3+}/Fe^{tot} ratio at high temperature can be compared at the Fe^{3+}/Fe^{tot} ratio at room temperature on the glass and assuming that the oxygen fugacity of the tektite formation is almost the same than during our XANES experiments, we can propose a temperature of formation of tektite glasses.

Volcanic glass textures from pyroclasts of the AD 1913 rift-edge phreatomagmatic eruption, Ambrym Island, Vanuatu

Németh, K.[*] & Stewart, R.B.
INR-CS, Volcanic Risk Solutions, Massey University, Palmerston North, New Zealand ([*]k.nemeth@massey.ac.nz)

Thermohydraulic explosions produce fine ash fragments as a result of brittle melt fragmentation and high kinetic energy release due to the interaction of magma and water. Fine ash particles (<2 Phi) formed during the explosive fragmentation represent the particles directly been involved in the thermal to kinetic energy transition, and their shape and texture can be directly linked to the processes generating them. These particles are commonly referred as active particles because they play an active role in the phreatomagmatic explosion. While the phreatomagmatic fragmentation quickly vaporizes the adjacent water, the suddenly generated vapour expansion can deform the melt immediately surrounding the explosion locus, causing ductile deformation and consequently spalling particles into the expanding pyroclast mixture. Textural features of pyroclasts such as shape parameters characteristic for brittle or ductile melt deformation are therefore able to provide information about the melt fragmentation. Here we tested the ability of morphological analysis of pyroclasts to identify brittle and ductile processes involved in fine ash generation in the AD 1913 phreatomagmatic, maar-forming rift-edge eruption in west Ambrym. It appears that the eruption was initiated off-shore and magma erupted through a shallow marine, fringe reef environment. Various image analysis methods were used on light microscopy (LM), SEM and BSE images to identify and quantitatively measure surface morphological parameters of ash particles of base surge beds. Morphological parameters were measured to calculate circularity (C), rectangularity (R), compactness (Co) and elongation (E) then a CXE versus RXCo discrimination diagram was prepared to define the deformation mode as either ductile or brittle for each particle. In the coarse ash (-1 - 2 Phi) the CXE values were dominantly around 1 indicating ductile deformation as the main deformation mode of these particles. While these particles are glassy, of low vesicularity and bulky in appearance, they have smooth surfaces and rounded vesicles suggestive being still molten during their fragmentation. Platy glass peels appeared to commonly form a mosaic-like surface. The shape of these mosaic-like zones indicate brittle deformation, and their shape compares well with platy particles in the fine (>4 Phi) ash, suggesting that they may have formed during transportation in the pyroclastic density current by spallation from the coarser particles. A gradual shift toward more brittle fragmentation shape characteristics has been recorded in the >2 Phi grain size fractions. It has also been recognized that shape parameters measured on BSE images tend to fall toward the brittle field of the discrimination diagram while parameters derived from SEM and LM images were less characteristically brittle. A same tendency has been observed using automatic-to-semi-automatic thresholding on images versus manual particle boundary retracing. These observations highlight the importance of sample preparation and technical methods applied to derive particle shape data from volcanic ash. FTIR data shows total water contents in the glassy particles range from 0.17% to 0.43% with CO_2 below detection. The low H_2O and CO_2 is consistent with degassing under the summit and in the rift and suggests that the eruption was almost entirely driven by thermohydraulic explosions. This study gives evidence of the thermohydraulic magma/water interaction triggering fragmentation of the melt and distinguishes active, passive and abrasion-produced juvenile particles in individual beds. It seems that the proportion of these types of particles strongly depends on the physical conditions in the vent and the location of the deposit sampled relative to the vent.

Europium geochemical behaviour in silicate glasses

Cicconi, M.R.[1*], Giuli, G.[1], Paris, E.[1], Ertel-Ingrisch, W.[2], Dingwell, D.B.[2] & Ulmer, P.[3]
[1]School of Science and Technology – Geology Division, University of Camerino, Italy ([*]mariarita.cicconi@unicam.it)
[2]Dept. of Earth and Environmental Sciences, LMU München, Germany
[3]Inst. fur Mineralogie und Petrographie, ETH Zürich, Switzerland

Rare Earth Elements (REE) have demonstrated to be important geochemical indicators; in fact, the distribution of REE in igneous rocks are frequently used to constrain the mineralogy of the source materials, the degree to which magma composition has been modified by crystal fractionation, and to identify the mineral phases removed from the magma during differentiation. Moreover, the variation of the $Eu^{+2}/(Eu^{+2} + Eu^{+3})$ ratio can be used as oxygen fugacity indicators. As the Eu^{+2}/Eu^{+3} buffer is located at very low oxygen fugacity, the $Eu^{+2}/(Eu^{+2} + Eu^{+3})$ ratio can be used to constrain the formation conditions within a very large range of oxygen fugacity down to few log units below the Fe/FeO buffer. The $Eu^{+2}/(Eu^{+2} + Eu^{+3})$ ratio is therefore very useful in the study of meteoritic material and in studying planetary evolution and many authors had used the Eu partition coefficient vs. fO_2 to extrapolate redox conditions under which magmas have crystallized A complete understanding of transition and REE elements is important for the geochemical and petrological interpretations of magmatic processes and partition properties between melt and crystals.

To this aim, synthetic silicate glasses corresponding to compositions relevant for the Earth sciences were used to study the dependence of the redox states of a Rare Earth Element (Eu) on the bulk melt composition and at different values of oxygen fugacity (from air to IW-2).

The samples have been analyzed via Eu L_{III}-edge X-ray Absorption Spectroscopy (XAS) to study the Eu oxidation states and local environments. Eu L_{III}-edge XANES peak analysis allowed the semi-quantitative assessment of Eu redox ratio; literature data report a difference of 7 – 8 eV between Eu^{+2} and Eu^{+3} in the experimental spectra and this energy shift is evident enough to well differentiate between the two oxidation states and to determine the Eu oxidation state in the glasses under investigation. XANES spectra vary systematically with composition and with fO_2 (log fO_2 from 0 to –11.6) indicating changes in the Eu oxidation state. The intensity of the 2 peaks of the absorption maximum were quantified and used to determine $Eu^{+2}/(Eu^{+2}+Eu^{+3})$ ratio. Moreover, the local structural environment of Eu was determined by EXAFS (Extended X-ray Absorption Fine Structure) analyses, highlighting the different Eu behaviour as function of the fO_2.

This work has clearly demonstrated that for a better interpretation of the Eu anomalies observed in rocks and minerals, which are often used to constrain magmatic evolutions of igneous regions, the melt composition and the redox condition must be taken into consideration.

TEM-analyses of nanocrystals in obsidian

Kirste, J.[*], Schulze, N., Wagner, G. & Kloess, G.
Inst. of Mineralogy, Crystallography and Materials Science, Leipzig University, Leipzig, Germany ([*]kirste@uni-leipzig.de)

TEM analyses of nanocrystals in obsidians lead to a number of unexpected results. Using a Philips CM 200 HRTEM we combined bright field (BF) and dark field (DF)-imaging, Nano-EDX, and SAED (Selected Area Electron Diffraction). We found that:

1. The average chemical compositions determined by TEM-EDX on the one hand and XRF on the other hand show a perfect match. However, on a nano-scale we found strong fluctuations from 70 up to 90 wt.% in SiO_2 content.

2. According to susceptibility the predominating mineral phases are hematite nanocrystals and magnetite microcrystals. But in some cases the measurements showed exceptional compositions like wuestite or Al-bearing hematite.

3. In contrast to the expected process of devitrification we observed evidences for decrystallisation, especially at albite-like feldspars and hematites. The process of decrystallisation is accompanied with a decolourization of the red-brown obsidian.

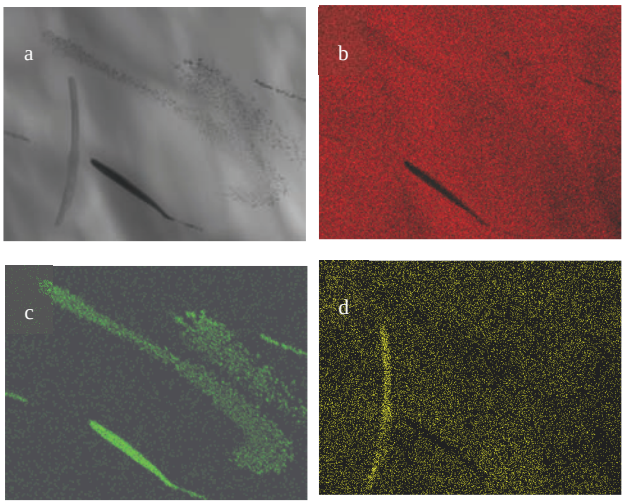

Fig. 1: STEM bright field image (a) and element distribution (b-d) in a section of Büyük Yayla obsidian; BF-image showing a dark hematite, vertical albite and cloudy nano-hematite crystals in the right; b – Si-distribution; c – Fe-distribution; d – Na-distribution.

The study deals with obsidians that stem from the Büyük Yayla Area, Eastern Pontides, Turkey. Showing unique layering structures in parts of the locality, the obsidian of Büyük Yayla is a rarely variety of obsidian.

[1] Heide, K. et al. (1996) *Chem. Erde–Geochem.*, **56**, 313-322.
[2] Yengingil, Z. et al. (2002) *Terra Nova*, **14**, 169-174.

Structure and properties of melts in the system Na_2O-K_2O-Al_2O_3-SiO_2

Le Losq, Ch.[1], Neuville, D.R.[1*], Florian, P.[2], Montouillout, V.[2] & Massiot, D.[2]
[1]CNRS-IPGP, Géochimie et Cosmochimie, Paris, France
([*]neuville@ipgp.jussieu.fr)
[2]CNRS-CEMHTI UPR3079 & Université d'Orléans, France

Rheological properties of silicate melts govern both magma ascension from the mantle to the surface of the earth and volcanological eruptions styles and behaviors. In this mind, it is very important to understand which parameters influence these properties. Up to now, we know for example that viscosity of silicate melts is dependent of temperature, pressure and chemical composition [1,2]. In this work, we will focus on the Na_2O-K_2O-Al_2O_3-SiO_2 system, which is of a prime importance because it deals with a non-negligible part of natural melts like silica rich alkali magmas. We will first present our viscosity measurements and some modelisation concepts based on the Adam and Gibbs theory. Also, while rheological properties are directly linked with structural properties of aluminosilicate melts, we will present our results obtained with Raman spectroscopy and NMR investigations at room and high temperature. These spectroscopies provide important structural informations on the polymerization of the glasses and melts and also on the environment of tetrahedral coordinated cations. It allows us to relate the rheological properties to the polymerization.

[1] Bottinga, Y. & Weill, D.F. (1972) *Am. J. Sci.*, **272**, 438-475.
[2] Urbain, G., Bottinga Y. & Richet P. (1982) *Geochim. Cosmochim. Ac.*, **46(6)**, 1061-1072.

Electroatmogenous apodolerite glasses (petrofulgurites from Norilsk area, Russia)

Lysyuk, A.
Institute of Geology, UB RAS, Syktyvkar, Russia
([*]andra227@yandex.ru)

Fulgurites are geologic bodies formed as a result of lightning strike to dry rocks; according with the target, they are classified into three types: clastofulgurites (aleuro- and psammito-), petrofulgurites and phytofulgurites.

Petrofulgurites are commonly found on small hills in the area of Norilsk copper-nickel deposit, Russia. They form fulgurite crusts covering the surface of small crystalline gabbro-dolerite bodies, or drop-like structures and black glass balls in shallow craters. In the highly porous glass the relic inclusions of target material (titaniferous magnetite, ilmenite) and newly formed mineral inclusions (magnetite, Fe-Ni alloys, high-silica glasses, silica) are observed.

The comparative analysis of chemical compositions shows that the content of elements in the initial gabbro-dolerite and products of its electroatmogenous transformation is only slightly different, but certain trends in the substance differentiation are observed. Thus, in fulgurite, in comparison to gabbrodolerite, the content of Al_2O_3, Fe_2O_3, CaO, P_2O_5 decreases, but SiO_2 increases. Among admixtures in fulgurites elements-hydrolyzates La, Ce, Nd, Zr and also Br are slightly accumulated. Ba, As, Sb, Cr, Ni are removed. Sr, Eu, Se, Th and U are characterized by various trends. Strontium and europium are accumulated in massive fulgurite, but brought in from glass drops. Selenium, thorium and uranium are also accumulated in fulgurite, but their contents in glass are practically unchanged. At last caesium is sharply accumulated in glass (which is known also for volcanic glasses).

The analysis showed that figures of cerium anomaly $A(Ce)=Ce_N/Ce_N*$ form sequence:

1.56 (initial rocks) ⇨ 0.55 (fulgurite) ⇨ 0.60 (glass),

that is, thermal impact alteration of the gabbro-dolerite transforms "positive" cerium anomaly into "negative" one.

The figures of europium anomaly $A(Eu)=Eu/Eu_N/Eu*_N$ form sequence:

0.78 (initial rocks) ⇨ 0.89 (fulgurite) ⇨ 0.32 (glass).

The behavior of europium anomaly repeats differentiated distribution of europium itself: its content increase in fulgurite is accompanied by the increase of the anomaly, and decrease of Eu content in glass – decrease of the anomaly, it becomes more "negative".

The determined changes trends of content of Norilsk gabbro-dolerite resulted from atmospheric electrical discharges on its surface are characterized by instantaneous local effect of superhigh temperatures and pressures, they are connected with passing of the target through gas stage and explained by degassing, successive-selective rock melting and somewhat different conditions of glass alloy solidification on the rock surface and in scattered drops. The processes of fulgurite formation are accompanied by reducing of all phases to the utmost reduced condition.

Acknowledgements: RFBR and RAS program 09-П-5-1026 support).

Study of complex silicate melts and glasses of geological interests by X-ray absorption spectroscopy, time resolved X-ray diffraction and molecular dynamics simulations

Madjer, K.[1], Rossano, S.[1*], Hennet, L.[2], Malavergne, V.[1], Reguer, S.[3], Wilke, M.[4], Harfouche, M.[5], Bytchkov, A.[6], Bordage, A.[1] & Leydier, M.[2]
[1]LGE, Université Paris-Est Marne-la-Vallée, Marne-la-Vallée, France ([*]rossano@univ-mlv.fr)
[2]CNRS-CEMHTI, Orléans, France
[3]Synchrotron Soleil, Gif sur Yvette, France
[4]Potsdam Deutches GeoForschungZentrum, Potsdam, Germany
[5]Paul Scherrer Institut, Swiss Light Source, Villigen, Switzerland
[6]ESRF, BP220, Grenoble, France

Mg-rich silicate materials are the major components of the Earth, from the very first stage of its formation to Archaean age. In this study, we focus on two different systems: CI and enstatite chondrites which, according to recent studies could be the building blocks of the Earth, and komatiites which are high-temperature, Mg-rich lavas typical of the Archaean age**.** The main aim of this study is to enlighten the relationship between the composition and structure of melts and the chemistry and mineralogy of the primitive and current mantle.

The samples consist of a simplified CI chondrite, a simplified composition of the silicate part of an enstatite chondrite, two simplified komatiites and, for future comparison purposes, a synthetic basaltic Martian glass EG. Their structure is investigated using Fe *K*-Edge EXAFS measurements, time resolved X-ray scattering and Molecular Dynamics (MD) simulations (DL_POLY code). The EXAFS measurements are performed on the Diffabs beam line at the Soleil Synchrotron facility and on the SuperXAS beam line at the SLS Synchrotron. The X-ray scattering experiments are conducted on the ID11 beam line at the ESRF. In order to achieve containerless melting, an elaborate installation is set up, including a confinement chamber, a heating laser and a gas operated levitation system. This allows the melting of the material under controlled atmosphere, using O_2, N_2 or Ar as the flowing gas. Time resolved X-ray scattering measurements are performed while controlling the cooling rate, giving access to the whole thermal history of the samples: in the liquid, during the glass transition and in the solid state. The experimental structure factors, radial distribution functions and local environments are compared to MD simulations results.

Aluminum coordination in hydrous rhyolite glasses: ^{27}Al NMR spectroscopy at 20 Tesla

Malfait, W.J.[1*], Verel, R.[2], Ardia, P.[1,3] & Sanchez-Valle, C.[1]
[1]Inst. for Geochemistry and Petrology, ETH Zurich, Switzerland ([*]wim.malfait@erdw.ethz.ch)
[2]Laboratory for Physical Chemistry, ETH Zurich, Switzerland
[3]Dept. of Geology and Geophysics, Univ. of Minnesota, USA

In this study, we investigate the Al environment in realistic analogs to natural granitic melts, *i.e.* glasses in the H_2O-Na_2O-K_2O-Al_2O_3-SiO_2 system quenched from pressures relevant to igneous crustal processes. More specifically, we investigate the effect of pressure (up to 2.5 GPa) and water content (up to 5.24 wt% H_2O) on the Al coordination. The ^{27}Al NMR measurements were performed at a high magnetic field of 20 Tesla to reduce broadening effects caused by the quadrupolar interaction, resulting in well resolved NMR bands for ^{IV}Al and ^{V}Al. For all measured glasses, the abundance of ^{V}Al was smaller than 0.5%, whilst no ^{VI}Al was detected. As expected, the amount of ^{V}Al increases with increasing pressure (Fig. 1a). However, the proportion of ^{V}Al seems to decrease with increasing water content (Fig. 1b). This is in contrast to what was observed for simplified basaltic glasses, where increasing the water content favored the formation of higher coordinated Al [1]. Taking into account the ^{V}Al-^{V}Si exchange reactions [2] and the temperature dependence of the ^{V}Al abundances [3], our results on the Al coordination in glasses constrain the ^{V}Al and ^{V}Si to a maximum of 1.5 and 0.015% respectively for granitic magmas at crustal pressure and temperature conditions.

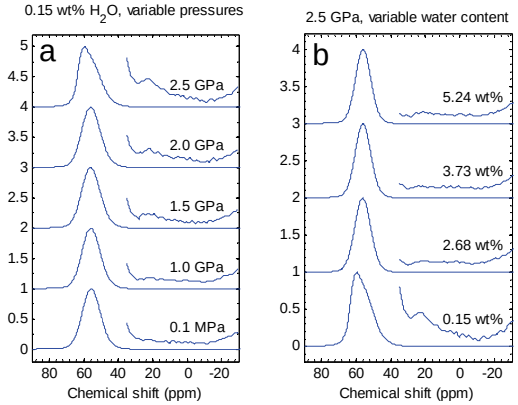

Fig. 1: ^{27}Al NMR spectra of hydrous rhyolite glasses; the intensities in the region between -25 and 35 ppm are magnified by a factor of 50 to visualize the contribution of ^{V}Al near 20 ppm. a) Spectra as a function of pressure for the nearly anhydrous glass. b) Spectra as a function of water content at a constant pressure of 2.5 GPa.

[1] Xue, X.Y. & Kanzaki, M. (2007) *Solid State Nucl. Magn. Res.*, **31(1)**, 10-27. [2] Kelsey, K.E. et al. (2009) *Am. Mineral.*, **94**, 1205-1215. [3] Stebbins, J.F. et al. (2008) *Geochim. Cosmochim. Ac.*, **72**, 910-925.

Quantifying Si-OH and Al-OH abundances in hydrous aluminosilicate glasses by ^{1}H, ^{27}Al-^{1}H and ^{29}Si-^{1}H NMR spectroscopy

Malfait, W.J.[1,2*] & Xue, X.Y.[1]
[1]Inst. for Study of the Earth's Interior, Okayama University, Okayama, Japan
[2]Inst. for Geochemistry and Petrology, ETH Zurich, Switzerland ([*]wim.malfait@erdw.ethz.ch)

The combined results of ^{27}Al-^{1}H and ^{1}H-^{29}Si-^{1}H cross polarization NMR experiments for hydrous glasses (containing 0.5 to 2 wt% water) along the SiO_2-$NaAlSiO_4$ join confirm that the dissolution mechanism of water in aluminosilicate glasses is fundamentally the same as for Al-free systems [1,2], i.e. the dissolved water ruptures oxygen bridges and creates Si-OH and Al-OH groups, in addition to forming molecular water (H_2O_{mol}).

The partial ^{1}H NMR spectra for Al-OH for the different glasses were derived from the ^{27}Al-^{1}H cross polarization spectra without any a priori assumptions about their lineshape [3]. The abundance of Al-OH was then determined from the fit of these partial spectra to the quantitative ^{1}H spectra.

The fraction of Al-OH increases non-linearly as the Al content increases with up to half of the OH groups as Al-OH for compositions close to $NaAlSiO_4$ (Fig. 1a). The relative abundances of the different species are controlled by the degree of Al-avoidance and the relative tendency of hydrolysis of the different types of oxygen bridges, Si-O-Si, Si-O-Al and Al-O-Al. A set of homogeneous reactions is derived to model the measured Al-OH/Si-OH speciation:

Si-O-Si + Al-O-Al = 2 Si-O-Al (1)

Si-O-Si + Al-OH = Si-O-Al + Si-OH (2)

The values of the corresponding equilibrium constants can be obtained by fitting reactions (1) and (2) to the experimentally derived Al-OH/OH_{tot} ratios (Fig. 1a). The result for K_1 is in agreement with literature data on the degree of Al-avoidance (Fig. 1b).

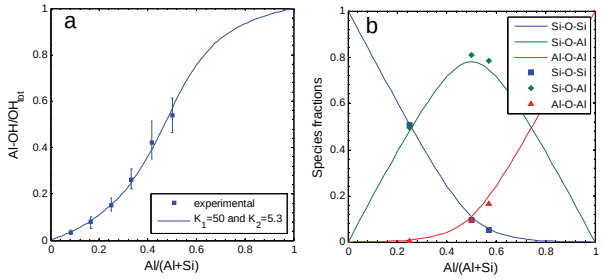

Fig. 1: a) Abundance of Al-OH as a function of the Al-content of the glass. Reactions (1) and (2) reproduce the experimental data well. b) Degree of Al-avoidance: symbols correspond to results from ^{17}O NMR [4]; the Al-avoidance corresponding to K_1=50 (lines), determined from the fit of reactions (1) and (2) to the experimentally determined Al-OH speciation (Fig. 1a), agrees with the ^{17}O NMR data.

With the values for K_1 and K_2, and literature data for the OH/H_2O_{mol} speciation in hydrous albite glasses [5], the abundance of the different oxygen species, i.e. Si-O-Si, Si-O-Al, Al-O-Al, Si-OH, Al-OH and H_2O_{mol}, can be predicted for the entire range of water and Al contents.

[1] Xue, X.Y. (2009) *Am. Mineral.*, **94**, 395-398. [2] Malfait, W.J. & Xue, X.Y. (2010) *Geochim. Cosmochim. Ac.*, **74**, 719-737. [3] Malfait, W.J. & Xue, X.Y. (subm.) *Solid State Nucl. Magn. Res.* [4] Lee, S.K. & Stebbins, J.F. (2000) *J. Non-Cryst. Solids*, **270**, 260-264. [5] Stolper, E. (1982) *Contrib. Miner. Petrol.*, **81**, 1-17.

High temperature topological transitions in the feldspar melts with composition $MAl_2Si_2O_8$ (M=Ba,Ca)

Simakin, A.[1], Salova, T.[1], Kucherinenko, Ja.[2], Eremyashev, V.[3] & Zakrevskaya, O.Ju[1*]
[1]IEM, RAS, Chernogolovka, Russia ([*]zakrev@iem.ac.ru)
[2]Moscow State University, Moscow, Russia
[3]Institute of Mineralogy, UB RAS, Miass, Russia

Proportion of the non-bridging oxygen (composition based NBO/T parameter) is usually considered as a measure of the polymerization degree. Recently conception of three coordinated oxygen introduces a factor independent of the composition [1]. At the same time layered polymorphs of the typical 3D connected feldspars give another mechanism of depolymerization. Indeed in respect viscosity there is no large difference is network locally interrupted along sheet of Q3 units ($Na_2Si_2O_5$) or along double sheet of $MAl_2Si_2O_8$ (M=Ca, Sr, Ba) composition.

Structural similarity of the hexagonal phylosilicate $BaAl_2Si_2O_8$ and its glass was probably first time suggested in [2]. We present IR spectra of $BaAl_2Si_2O_8$ glass and synthesized from the melt hexa-phase supporting this idea. Glass was prepared by the quenching on the metal plate. Due to the high affinity for Ba hexa-celcian crystallization pure glass was formed only on the outer drop rim. IR spectrum of the glass has bands set with maxima around 450, 670 and 967 cm^{-1} typical for known hexa-modifications of feldspars (Fig. 1).

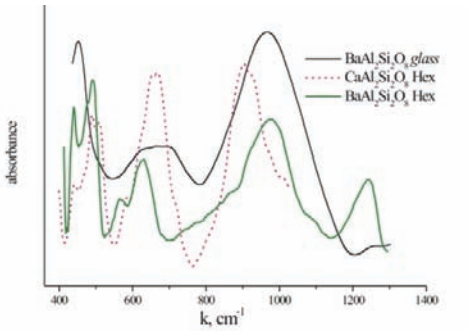

Fig. 1: IR spectra of the layered modifications of feldspars and glass.

Layered modification is stabilized with earth alkali ions radius (Ba>Sr>Ca) and temperature increase. We suggest that in anorthite ($CaAl_2Si_2O_8$) melt fraction of the layered type continuously increases with temperature while in the quenched glasses it returns practically to zero. Viscosity of anorthite melt can be described through the fraction of the layered type as a function of temperature [3]. Estimated energy of transformation $anorthite_L$ -> $hexa\text{-}anorthite_L$ is ca 50.6 kJ/mol that is substantially less than anorthite melting enthalpy of 133 kJ/mol.

[1] Stebbins. J.F., Oglesby. J.V. & Kroeker, S. (2001) *Am. Mineral.*, **86**, 1307-1311. [2] Djordjevic, J. et al. (2001) *Phys. Chem. Chem. Phys.*, **3**, 1560-1565. [3] Simakin, A. & Zharikov, V. (2008) *Dokl. Earth Sci.*, **423**, 1253-1256.

Iron redox and structural state in granitoidic melts according to experimental data

Volovetsky, M.V.[1*], Lukanin, O.A.[1], Rusakov, V.S.[2] & Kargaltsev, A.A.[1]
[1]Vernadsky Inst. of Geochemistry and Analytical Chemistry, Moscow, Russia (*volovetsky@gmail.com)
[2]Lomonosov Moscow State University, Moscow, Russia

Iron is widely distributed element with variable valence which is presented in natural acid melts of volcanic and impact origin. Redox state of iron in melts depends on a set of parameters: temperature, oxygen fugacity and melt composition. Knowledge of these parameters gives an opportunity to determine redox conditions during melt forming. Despite this problem were regarded in many previous experimental studies T-fO_2 influence on Fe^{2+}/Fe^{3+} ratio in acid melts is still poorly known.

Experiments were performed to study T-fO_2 influence on iron redox and structural state in acid melts (~70 % SiO_2). Two granitic compositions were chosen as initial glasses: 1) granite – I2; 2) pantellerite (alkaline granite) – P9. Glasses were obtained in a set of experiments under temperatures from 1120 to 1420°C and in a wide range of fO_2: from $10^{-0.7}$ (air) до 10^{-13} (buffer IW) bar using high-temperature furnace with controlled oxygen fugacity. Alumina crucibles were used as containers. Microprobe analysis has revealed that chemical composition of melts changes with increasing temperature (in particular Na volatilizes).

Valent and structural state of iron was investigated using Mössbauer spectroscopy. Mössbauer data analysis has shown that iron redox-ratio depends on oxygen fugacity in accordance to the equation $\lg(Fe^{3+}/Fe^{2+}) = a \cdot \lg(fO_2) + b(T)$ (Fig. 1). On the figure it is shown that $Fe^{3+}/\Sigma Fe$ ratio in pantelleritic melts is higher than in granitic on 10-20%. It is also noteworthy that redox-ratio decreases with increasing temperature.

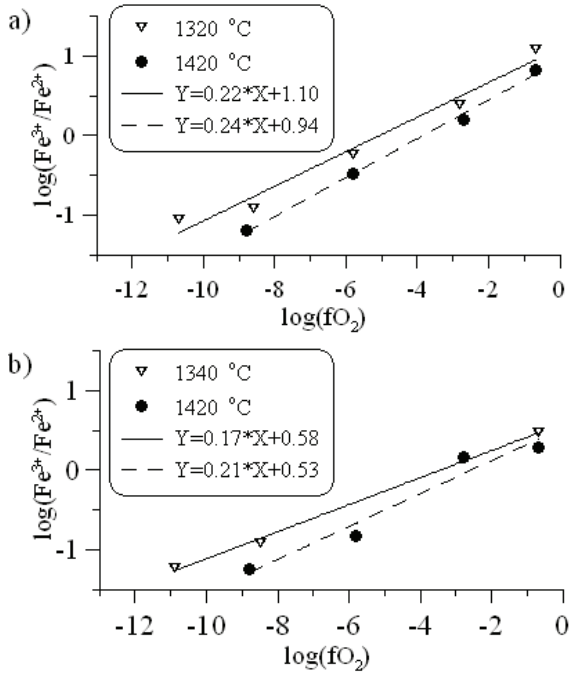

Fig. 1: Relationship between logarithms of Fe^{3+}/Fe^{2+} ratio and fO_2: a) pantelleritic composition (P9); b) granitic composition (I2).

Iron coordination state was determined from average Mössbauer line shifts of corresponding subspectra. Fe^{3+} ions were revealed to change coordination from octahedral to tetrahedral with increasing of iron redox ratio (beginning from $Fe^{3+}/\Sigma Fe>0.6$). At the same time a large amount of ions occupies five-fold positions. Fe^{2+} ions do not change coordination much and occupy five-fold and octahedral positions.

Elastic behaviour and HP-induced phase transitions in MFI-type zeolites

Quartieri, S.[1*], Montagna, G.[2], Arletti, R.[3] & Vezzalini, G.[1]
[1]Dept. of Earth Sciences, University of Messina, Italy
([*]squartieri@unime.it)
[2]Dept. of Earth Sciences, University of Modena and Reggio Emilia, Modena, Italy
[3]Dept. of Earth Sciences, University of Ferrara, Italy

High pressure applied to microporous materials can induce profound structural changes, which could give rise to modifications of the physical properties and of the accessibility to the zeolite catalytic sites by the molecular species entering the porous material.

The response to compression of different natural and synthetic zeolites with MFI topology, but with different framework and extraframework chemical composition (Mutinaite, H-ZSM5, silicalite), was explored by in-situ synchrotron X-ray powder diffraction (XRPD), using silicon oil as non-penetrating pressure transmitting medium. Two silicalite samples [s.g. $P2_1/n$] with different Si/Al ratios (1240 for silicalite1 and 1850 for silicalite2) and water content (8.9 and 2.3 molecules for silicalite1 and 2, respectively) were studied. Their pore system does not contain cations and their Si/Al ratios are much higher than in H-ZSM5 (10) and in mutinaite (7.6).

The main result of this study is the evidence of a *P*-induced phase transition in silicalite, from the monoclinic $P2_1/n$ (P_{amb}) to the orthorhombic Pnma (H*P*) (Fig. 1). In particular, silicalite1 becomes orthorhombic between P_{amb} and 0.3 GPa, while silicalite2 undergoes the same transition between 0.4 and 0.9 GPa. Otherwise, mutinaite and H-ZSM5 remain orthorhombic in all the studied *P*-range. Both the original s.g. and the unit cell parameters are recovered, for all the studied phases, upon decompression.

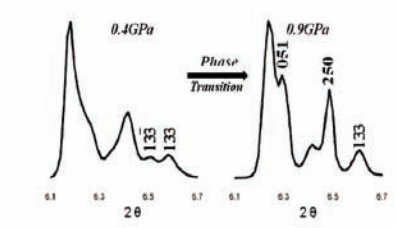

Fig. 1: XRPD patterns of silicalite2 as a function of pressure.

The cell volume decreases observed for the different phases in the P_{amb}–6 GPa range are reported in Fig. 2.

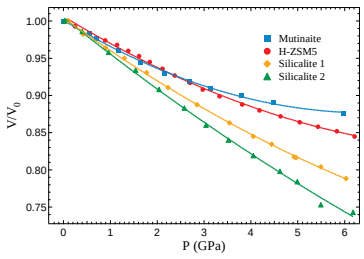

Fig. 2: Normalized unit cell volume vs. pressure behaviors for the studied phases.

Ion-exchange behavior of zeolite A

Lührs, H.[*], Derr, J., Gumbert, J. & Fischer, R.X.
Fachbereich Geowissenschaften, Universität Bremen, Germany
([*]hluehrs@uni-bremen.de)

Zeolites, especially Linde Type A zeolites ($Na_{12}Al_{12}Si_{12}O_{48} \cdot 27H_2O$, Na-A), have a high potential as cation exchangers with high selectivities. These properties are due to their uniform network of channels and pores, formed by the aluminosilicate framework, occupied by exchangeable cations and water molecules. Zeolite A represents one of the most extensively studied zeolites. We present here some additional information on its Ca, K, and Ba exchanged forms and its characterization by X-ray diffraction methods and thermal analyses.

Full cation exchanges of Ca, K and Ba were performed on Na-A using 0.1 and 1.0 molar solutions of the respective chloride salts. Experiments were carried out at room temperature and at 90°C, for periods between 30 minutes and seven days. For the Ca exchange, two different sources of Na-A materials were used. By static exchange methods a series with varying compositions between Na-A and Ca-A was synthesized.

The cation exchanged samples were characterized by X-ray powder diffraction (XRD) methods, including Rietveld refinements in space group $P\,m\,\bar{3}\,m$. In addition, scanning electron microscopy (SEM) and energy dispersive X-ray spectroscopy (EDX) techniques were performed on selected samples.

Na-A was completely Ca, K and Ba exchanged, all exchanges resulted in changes of lattice parameter *a*. For the Ca and Ba experiments these are clearly visible as peak shifts in the respective diffraction patterns. Rietveld refinements for the Ca exchanged samples revealed a linear dependence of lattice parameter *a* on the degree of exchange. For high Ca-contents, *a* is significantly smaller for Ca-A than for Na-A, which is in accordance with [1]. A trend towards larger values for *a* can be observed with decreasing degree of exchange. At very low Ca contents, *a* tends to become even larger than the corresponding value for Na-A. The K exchanged samples show a similar behavior. However, variation of *a* is distinctly smaller than for Ca-A which is in accordance with literature data [2]. Thermal analysis of the Ca-A series yielded a linear relationship between the degree of exchange and the water content.

The refined lattice parameters for Na-A and Ba-A are somewhat smaller than the ones reported in literature [3,4]. For the Ba exchanged samples, Rietveld refinements yielded significantly smaller lattice parameters *a* compared with the Na-form. The reduction of intensities in the X-ray diffraction data of the Ba-exchanged samples compared with the original Na-A zeolite is entirely due to the absorption effects introduced by Ba replacing Na, resulting in a reduction of the volume of the sample exposed to the X-ray beam. Thus, the loss of intensity does not indicate any destruction or amorphization of the crystalline zeolite.

Acknowledgements: We thank Wolfgang Schmidt (MPI, Mülheim a.d. Ruhr) for providing powdered samples of Na-A, Petra Witte (Bremen) for the EDX analyses.

[1] De Roy, G. & Vansant, E.F. (1980) in Rees, L.V.C (ed) *The Fifth International Conference on Zeolites*, Naples, Italy, 214-222. [2] Leung, P.C.W. et al. (1975) *J. Phys. Chem.*, **79**, 2157-2162. [3] Gramlich, V. & Meier, W.M. (1971) *Z. Kristallogr.*, **133**, 134-149. [4] Kim, et al. (1980) *A.C.S. Symp. Ser*, **135**, 137.

The (Al,Si)-ordered zeolites of the Bellerberg, Eifel area (Germany): the particular flörkeite case

Lengauer, C.L.[1*], Kolitsch, U.[2] & Tillmanns, E.[1]
[1]Inst. für Mineralogie und Kristallographie, Universität Wien, Vienna, Austria ([*]christian.lengauer@univie.ac.at)
[2]Mineralogisch-Petrographische Abteilung, Naturhistorisches Museum, Vienna, Austria

Flörkeite, $K_3Ca_2Na[Al_8Si_8O_{32}]\cdot 12H_2O$, is a new phillipsite-type zeolite, which was found in a Ca-rich xenolith from a quarry at the Bellerberg volcano near Ettringen, East Eifel volcanic area, Germany [1]. Prior to the finding of flörkeite, the Bellerberg volcano was also known as the type locality of the rare zeolites willhendersonite, bellbergite and tschörtnerite. Similar to flörkeite, all these zeolites exhibit (Al,Si) ordering [2]. Up to now no structurally related compound is known for tschörtnerite. Willhendersonite and bellbergite, however, represent the (Al,Si)-ordered analogues of chabazite and synthetic zeolite TMA-E [3], respectively.

The unit-cell parameters of flörkeite with space group *P*1 in the phillipsite-type cell setting are: a = 19.965(1), b = 14.274(1), c = 8.704(1) Å, α = 88.37(1), β = 125.08(1), γ = 89.57(1)°. In comparison to phillipsite with $P2_1/m$ symmetry (a ~ 9.9, b ~ 14.3, c ~ 8.7 Å, β ~ 124.5°), it is apparent that flörkeite exhibit a pseudomonoclinic, triclinically distorted unit-cell metric accompanied by a doubling of the *a*-parameter. The most significant change in the framework of flörkeite is the (Al,Si) ordering at the *T*-sites. As a consequence, *i.e.* the loss of the mirror planes and the pseudo-monoclinic distortion of the framework, the topochemical symmetry [5] of flörkeite is reduced to *B*2/*b*. The doubling of the *a*-parameter is induced by an ordering of the extra-framework constituents in the channel system along **a**. Basically responsible are alternating sequences of atom pairs with non-equivalent scattering factors and $\Delta \sim a/2$: Ca1–□–Ca1, Ca2–Na1–Ca2 and K3–OW2–K3. In contrast, K1 and K2 and their bonded ligands follow a phillipsite-type ordering with $a/2$.

Among the special extra-framework sites of zeolite-type compounds the centre of 8-rings is known to be a favoured site for the emplacement of large cations. As a further inference, one can state that a high K content in the crystallization environment is the predominant controlling variable during the formation of flörkeite and high-K batches will be required for possible syntheses routes of flörkeite-type tecto-aluminosilicates. Additionally, the observed (Al,Si) ordering can be attributed to the unusual, low-thermal conditions of formation within the Ca-rich xenolithic host, as it is also indicated by the co-occurrence of the already mentioned (Al,Si)-ordered zeolites.

[1] Lengauer, C.L. et al. (2009) *Eur. J. Mineral.*, **21**, 901-913. [2] Coombs, D.S. et al. (1998) *Eur. J. Mineral.*, **10**, 1037-1081. [3] Meier, W.M. & Groner, M. (1981) *J. Solid State Chem.*, **37**, 204-218. [4] Fischer, R.X. & Baur, W. (2006) *Zeolite-type crystal structures and their chemistry. Framework type code PHI*. Landolt Börnstein New Series IV/14/D, Springer, 412-425. [5] Gottardi, G. (1979) *Tschermaks Mineral. Petrogr. Mitt.*, **26**, 39-50.

From minerals to materials: tetrahedral sheets with $4^1 8^1$ and $4^1 5^1 6^1 8^2$ topologies as bricks to build heteropolyhedral microporous silicates

Cadoni, M. & Ferraris, G.[*]
Dipt. di Scienze Mineralogiche e Petrologiche & Nanostructured Interfaces and Surfaces (NIS), Centro di Eccellenza, Università di Torino, Italy
([*]giovanni.ferraris@unito.it)

A *ring symbol* is defined as a sequence $p_1^{r1}p_2^{r2}...p_n^{rn}$, where p_1, $p_2...p_n$ are numbers of nodes in a ring and r_1, $r_2...r_n$ are relative numbers of the corresponding rings in a graph [1]. If the nodes represent TO$_4$ tetrahedra, one obtains two-dimensional sheets that occur in (alumino)silicates and not necessarily are strictly planar. Some geometrical aspects of these sheets have been analysed [2, 3] emphasising the presence of wollastonite-type chains that condense to form xonotlite-like double chains containing eight-rings. The condensation of the double chains leads to $p_1^{r1}p_2^{r2}...p_n^{rn}$ sheets. A detailed nomenclature to classify the tetrahedral sheets, in particular naming tertiary, quaternary and non-tertiary those tetrahedra sharing three, four and less than three vertices, has been introduced [2]. The most common $p_1^{r1}p_2^{r2}...p_n^{rn}$ silicate sheet is 6^1 that occurs in layered silicates like micas, where all tetrahedra are pointing to one direction being generated by periodic repetition of a pyroxene-like chain. Mixed up- (*u*) and down-pointing (*d*) tetrahedra allow the formation of geometrical isomers. If only tertiary tetrahedra occur T/O = 2/5, as in micas and in the REE compounds described here [4]; the presence of non-tertiary tetrahedra implies T/O < 2/5; finally, quaternary tetrahedra require T/O > 2/5 and the sheet must be either branched or doubled to form microporous layers, as in the rhodesite series [5,6].

The sheets can act as building bricks (modules) either of *s.s.* layered structures, where the strong bonds are confined within layers that are interconnected by weak bonds (typically phyllosilicates), or of heteropolyhedral frameworks. The latter are obtained when the silicate sheets are interconnected by strong bonds *via* five-, six-, or seven-coordinated polyhedra and often are crossed by channels. Heteropolyhedral microporous structures are modular structures [7] and those occurring in the mineral realm [8] often were the incentive for the synthesis of compounds for technological applications. In heteropolyhedral structures the non-tetrahedral coordination polyhedra (typically octahedra) can host a variety of cations; thus, the frameworks offer a range of crystal-chemical opportunities far wider than in pure tetrahedral frameworks like zeolites.

The synthesis and structural characterisation of new heteropolyhedral microporous silicates [four with formula $A_3REESi_6O_{15}\cdot 2.25H_2O$, based on $4^1 5^1 6^1 8^2$ sheets (A = Na, K, H_3O; REE = Ce, La, Eu), and four members of the rhodesite mero-plesiotype series, based on $4^1 8^1$ sheets] will be presented. In the first group heteropolyhedral channels with an effective channel width (*e.c.w.*) ~ 4.5 x 2.8 Å occur; the second group shows tetrahedron-delimited channels with *e.c.w.* ~ 3.5 x 3.8 Å.

[1] Krivovichev, S.V. (2009) *Structural Crystallography of Inorganic Oxysalts.* Oxford Univ. Press. [2] Liebau, F. (1985) *Structural Chemistry of Silicates. Structure, Bonding and Classification.* Springer, Berlin. [3] Haile, S.M. & Wuensch, B.J. (1997). *Am. Mineral.*, **82**, 1141-1149. [4] Cadoni, M., Cheah, Y.L & Ferraris G. (2010) *Acta Crystallogr B.*, **66**, in press. [5] Cadoni, M. & Ferraris, G. (2009) *Eur. J. Mineral.*, **21**, 485-493. [6] Cadoni, M. & Ferraris, G. (2010) *Acta Crystallogr B.*, **66**, in press. [7] Ferraris, G., Makovicky, E. & Merlino, S. (2008) *Crystallography of Modular Materials*. Oxford Univ. Press. [8] Ferraris, G. & Merlino, S. (2005) (eds.) *Rev. Mineral. Geochem.*, **57**, Mineral. Soc. Am., Washington DC.

Analcime formation from alkaline hydrothermal alteration of bentonite

Fernández, R.*, Vigil de la Villa, R. & Cuevas, J.
Dept. of Geology and Geochemistry, Faculty of Science,
Autonomous University of Madrid, Spain
(*raul.fernandez@uam.es)

Analcime is one of the most common rock-forming zeolites. It forms in a wide range of geologic environments, from diagenesis of volcanoclastic sediments to precipitation in alkaline saline lakes at the surface of the earth. In all settings, the formation of analcime is very sensitive to chemical potential of SiO_2.

The interaction of cement pore fluids with bentonite is studied within the context of radioactive waste disposal due to the long term stability required for the materials used as engineered barriers. Calcium silicate hydrates and zeolites are the main secondary minerals produced by the alkaline alteration of bentonite.

Laboratory experiments in batch reactors were performed with bentonite and alkaline NaOH solutions at $Ca(OH)_2$ saturation (1:3 solid:liquid reactant mixture). Different geochemical conditions were used (NaOH concentrations of 0.1, 0.25 and 0.5 M, temperatures of 25, 75, 125 and 200 ºC, and reaction times of 1, 6, 12 and 18 months).

Analcime is observed to precipitate with changing morphology and composition as a function of the experimental conditions. Only minor precipitation of analcime is observed at 75 ºC with the highest NaOH concentration (0.5 M), but massive precipitation (20–35 % wt. in bulk reacted mixture) at higher temperatures (125 and 200 ºC), even with the NaOH 0.1 M solutions.

In general, Na is the dominant cation in the structural formula of the analcime formed, but also Ca becomes relevant in the composition at long time (12 and 18 months) with the lower concentrations of NaOH solutions (0.1 and 0.25 M) and could be related with the isostructural zeolite, wairakite. K and Mg are present but always remain in low concentration.

The Si/Al ratio in analcime is mainly controlled by the hydroxide concentration in solution. The decrease in pH observed in the reaction as a function of time produces a change in solubility of aluminosilicates, increasing thereby the Si/Al ratio.

The Si/Al ratio is related with the morphology of analcime observed by SEM (Scanning Electron Microscope). Hemihedral symmetry is observed in analcimes with lower Si/Al ratio and holohedral symmetry in analcimes with higher Si/Al ratio, being all values comprehended within a wide range (1.8–3.2).

In order to evaluate the chemical stability of the formed analcimes with different compositions and relate it with the potential geochemical conditions that will occur in a radioactive waste repository, a thermodynamic study has been applied, making use of the available thermodynamic data in literature (see [1]). The results of this study can be compared with the formation of other zeolites in similar experiments [2].

[1] Neuhoff, P.S. et al. (2004) *Am. J. Sci.*, **304(1)**, 21-66. [2] Fernández, R. et al. (2009) *Geochim. Cosmochim. Ac.*, **74(3)**, 890-906.

ZeoBase, a database for more than 5,000 standardized and corrected zeolite entries

Baur, W.H.[1] & Fischer, R.X.[2*]
[1]Dept. of Chemistry, Northwestern University, Evanston, USA
[2]Fachbereich Geowissenschaften, Universität Bremen, Germany
([*]rfischer@uni-bremen.de)

ZeoBase is a database for crystal structure data of zeolite-type compounds and minerals. Currently, it contains more than 5,000 entries with space groups, lattice parameters, atomic coordinates, chemical compositions and full references. Its unique characteristics are the standardized setting of all crystal structures and the individual examination of every data set for correctness, and internal and external consistency. The standardization procedure introduced in [1-3] allows the easy comparison of structural parameters and the unambiguous assignment of framework atoms to their sub- and supergroup counterparts, without being limited by space-group symmetry or settings. Thus, this set of crystal structure data provides information uniquely useful for the correlation of a host of structural and physico-chemical relationships. More than 40% of the data sets have been corrected or amended by additional information. Most of the entries contain additional information on synthesis and chemical composition.

The retrieval system of ZeoBase currently offers the following search options: zeolite name, framework type code, authors, year of publication, framework density, crystal system, T-O distances and their standard deviations, and chemical elements present in the zeolites as well as original and standardized space groups, unit-cell volumes, and lattice parameters. The possibility to select entries by their estimated standard deviations allows to list entries by the quality and accuracy of the structure determination. In addition, a number of keywords concerning method of sample preparation and treatment, and data collection is searchable.

The results can be displayed as tables, plots, or histograms. Data can be exported as cif files or they can be directly passed to the structure drawing program STRUPLO and the Rietveld program BRASS, where powder-diffraction diagrams can be calculated.

Since the names and labels of all individual atoms in each of the topologically identical crystal structures are standardized, one can follow particular bond lengths or bond angles in their symmetry-related changes from zeolite to zeolite. This can be visualized by plots that display various properties, such as framework density, mean bond lengths or angles, individual bond lengths or angles or chemical composition [4]. This is useful for studying the flexibility of zeolites as a function of their geometry, their topology or their chemistry. In addition one can see which zeolites can accommodate which cations within their frameworks or which frameworks can tolerate which exchangeable cations within their pores [4].

[1] Baur, W.H. & Fischer, R.X. (2000, 2002) *Zeolite-Type Crystal Structures and their Chemistry*. **14B** & **14C**, Landolt-Börnstein, Springer-Verlag, Berlin. [2] Fischer, R.X. & Baur, W.H. (2006, 2009) *Zeolite-Type Crystal Structures and their Chemistry*. **14D** & **14E**, Landolt-Börnstein, Springer-Verlag, Berlin. [3] Fischer, R.X & Baur, W.H. (2004) *Proc. 14th Intern. Zeolite Conf.*, 1246. [4] Baur, W.H. & Fischer, R.X (2004) *Proc. 14th Intern. Zeolite Conf.*, 1254.

Synthesis of zeolite X from fly ash at 25°C by using seawater. The role of cations in crystallization

Belviso, C.[1*], Cavalcante, F.[1], Huertas, J.[2] & Fiore, S.[1]
[1]IMAA – CNR, Tito Scalo, Potenza, Italy
[2]CSIC, Granada, Spain

In this study an Italian coal fly ash was converted into zeolite in laboratory experiments with crystallization temperatures of 25°C. Distilled water and natural seawaters with different salinity (W1 and W2) were used during the hydrothermal synthesis (Table 1).

Table 1: Artificial and natural seawater composition (Values in g/L – salinity g/kg)

	Salinity	Cl^-	Na^+	SO_4^{2-}	Mg^{2+}	Ca^{2+}	K^+	B^{3-}	Sr^{2+}
Artificial seawater	35.000	19.353	10.764	2.701	1.297	0.406	0.387	0.066	0.014
Seawater - W1	26.300	14.542	8.486	2.000	1.034	0.374	0.333	0.046	0.013
Seawater - W2	38.000	24.560	12.621	3.129	1.473	0.518	0.487	0.062	0.018

The results indicate that X-type and A-type zeolite crystallization takes place by using seawater with higher salinity (W2), whereas no new mineral forms in distilled water (Fig. 1).

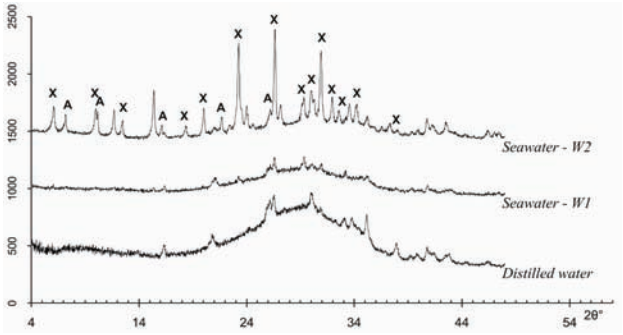

Fig. 1: XRD patterns of fly ashes incubated with: distilled water; W1 and W2 - seawater. X = zeolite X.

To minimize the biological effects and determine the role of different ions during the synthesis with seawater, experiments using artificial seawater and solutions with a salts concentration comparable with that of the single salts present in artificial seawater were carried out. In particular the effect of Na^+, Mg^{2+}, Ca^{2+} and Cl^- was studied and it was found that their availability in the solution accelerates the zeolite formation at a very low temperature (25°C) (Fig. 2)

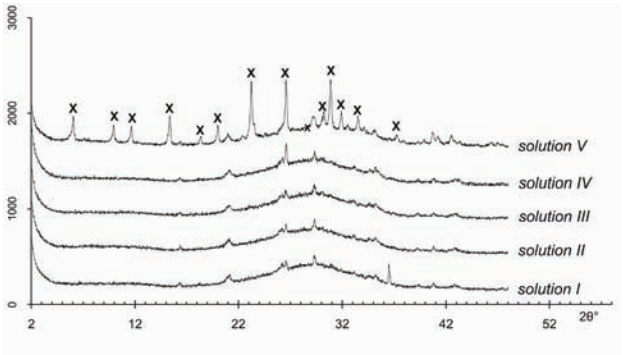

Fig. 2: XRD patterns by using different solutions corresponding to the total amount of NaCl (Solution I); MgCl (Solution II); CaCl (Solution III); C^- (Solution IV); NaCl plus MgCl (Solution V).

Mg^{2+} combined with Na^+ controls the process of synthesis. The dissolution process of alluminosilicate glass at higher incubation temperatures significantly reduces the effect of cations present in salt solution.

Melanophlogite: the only known natural molecule-containing SiO_2 clathrate

Geiger, C.A.* & Dachs, E.
Fachbereich Materialforschung und Physik, Universität Salzburg, Austria (*chg@min.uni-kiel.de)

Melanophlogite is the only known naturally occurring SiO_2 clathrate. It can occlude quasi-free N_2, CO_2, CH_4 and H_2S molecules but not H_2O in its micropores [1]. It has been reported from a number of localities worldwide in different low-temperature geologic environments. Melanophlogite's thermodynamic stability is not known. Low-temperature hydrothermal synthesis experiments indicate that structure-directing agents are needed for crystallization. The formation of silica-rich colloids/gels and crystal growth can be observed in glass-ampoule synthesis experiments. Other clathrasils/porosils have been synthesized in the laboratory but not found in nature.

In order to address the question of the thermodynamic stability of melanophlogite, the heat capacity of two different natural samples of approximate composition $46SiO_2 \cdot 1.80CH_4 \cdot 3.54N_2 \cdot 1.02CO_2$ from Mt. Hamilton, CA and $46SiO_2 \cdot 3.59CH_4 \cdot 3.10N_2 \cdot 1.31CO_2$ from Racalmuto, Sicily, along with a heated (molecule-free) sample of composition SiO_2, were studied between 5 and 300 K using relaxation microcalorimetry. The molecule-free sample was obtained by heating crystals from Racalmuto at 1173 K for 24 hr.

The standard third-law entropy of the molecule-free sample is S° = 2216.3 J/(mol·K) for 46 SiO_2 and the natural Mt. Hamilton and Racalmuto samples give S° = 2805.7 J/(mol·K) and S° = 2956.8 J/(mol·K), respectively. The entropy and the Gibbs free energy for molecule-free melanophlogite relative to quartz at 298 K are ΔS_{trans} = 6.7 J/(mol·K) and ΔG_{trans} = 7.5 kJ/mol, respectively. Thus, it does not have a thermodynamic field of stability in the SiO_2 system. The difference in C_p values between molecule-containing and molecule-free melanophlogite is characterized by an increase in C_p from 0 K to approximately 70 K and then reaches a roughly constant value at 70 K < T < 250 K. The ΔS_{rxn} at 298 K for $46SiO_2$(melan.) + xCH_4(gas) + yCO_2(gas) + zN_2(gas) = $46SiO_2 \cdot (xCH_4)_{12} \cdot (yCO_2,\ zN_2)_{14}$ is estimated to be about -642 J/(mol·K) and -802 J/(mol·K) for the Mt. Hamilton and Racalmuto samples, respectively.

The thermodynamic data, as well as published results on the occurrence of natural samples and associated phases such as cristobalite and chalcedony, suggest that melanophlogite can crystallize metastabily and possibly from a gel. The occurrence of melanophlogite and the lack of other SiO_2 clathrates/porosils in nature are probably due to the essential role of molecular structure-directing agents. For melanophlogite they can be CO_2, N_2 and CH_4, whereas the crystallization of other clathrate/porosils requires more chemically and structurally complex molecules that are not naturally abundant. Thus, many porosils that have been synthesized in the laboratory are not expected to be found in nature. Dodecasil 3C is an exception and an effort should be made to find natural specimens.

[1] Kolesov, B.A. & Geiger, C.A. (2003) Am. Mineral., **88**, 1364-1368.

New structural data on cation-exchanged forms of hilairite

Grigoryeva, A.A.*, Zubkova, N.V., Pekov, I.V., Turchkova, A.G. & Pushcharovsky, D.Yu.
Geology Dept., Moscow State University, Moscow, Russia (*arina1984@bk.ru)

Hilairite, $Na_2Zr[Si_3O_9] \cdot 3H_2O$, is a natural microporous zeolite-like zirconosilicate with the structure based on the heteropolyhedral framework. The framework consists of isolated $[ZrO_6]$ octahedra and infinite helical chains $[Si_3O_9]_\infty$. Zeolitic cavities of the framework are occupied by Na cations and H_2O molecules [1]. Among natural zirconosilicates hilairite and the representatives of hilairite group are characterized by the widest pores. This fact provoked the study of the cation-exchange properties of hilairite under different conditions and the study of crystal chemistry of the received forms [2,3, this work]. For the cation-exchange experiments we used hilairite from the Hilairitovoye pegmatite, Kirovskii apatite mine, Mt Kukisvumchorr, Khibiny alkaline complex, Kola Peninsula, Russia. Crystal structure investigation of the hilairite from Khibiny [4] (sp. gr. *R*3, *a* = 10.5530(5), *c* = 7.9541(4) Å; R_{hkl} = 0.0280) indicated the formula $Na_{1.64}H_{0.36}ZrSi_3O_9 \cdot 3H_2O$ (small amount of H^+ here and in cation-exchanged forms were assumed to charge-balance the formulae and can be considered as the result of the first stage of cation-exchange experiments or possibly as a part of H_3O^+ cations partially substituting H_2O). It should be noted that hilairite from Khibiny has identical symmetry and Zr,Si,O-framework with previously studied hilairite from Lovozero massif [1] but differs from the latter by the localization of Na and H_2O in the cavities of the framework. This leads to the halved *c*-parameter of the studied sample in comparison with the hilairite from Lovozero.

Cation-exchange experiments were carried out in 1*M* aqueous solutions of $RbNO_3$ and $Pb(NO_3)_2$ at 90°C and in 1*M* aqueous solutions of KCl and $CsNO_3$ at 150ºC. Crystal structure study of the four cation-exchanged forms allowed revealing the following structural formulas: $Rb_{1.48}Na_{0.45}H_{0.07}ZrSi_3O_9 \cdot 0.53H_2O$ (sp. gr. *R*3, *a* = 10.4743(4), *c* = 15.5433(7) Å; R_{hkl} = 0.0413) and $Pb_{0.60}Na_{0.40}H_{0.40}ZrSi_3O_9 \cdot 3H_2O$ (sp.gr. *R*3, *a* = 10.4718(3), *c* = 7.9392(2) Å; R_{hkl} = 0.0387) for Rb- and Pb-exchanged hilairites; $K_{1.81}Na_{0.09}H_{0.10}ZrSi_3O_9$ (sp.gr. *R*3, *a* = 10.3804(2), *c* = 14.9541(6) Å; R_{hkl} = 0.0526) and $Na_{1.14}Cs_{0.55}H_{0.31}ZrSi_3O_9 \cdot 0.90H_2O$ (sp.gr. *R*32, *a* = 10.5472(4), *c* = 15.8797(7) Å; R_{hkl} = 0.0423) for K- and Cs-exchanged hilairites.

All studied structures as well as the objects of previous investigations of cation-exchanged forms of hilairite [2,3] retain heteropolyhedral framework consisting of $[ZrO_6]$ octahedra and $[Si_3O_9]_\infty$ chains. At the same time strong deformation of the framework leads to the doubling of the *c*-parameter and the symmetry decrease from *R*32 to *R*3 in the structures of K- and Rb-exchanged forms of hilairite. In the structure of Pb-exchanged hilairite a slight distortion of the framework leads to the sp. gr. *R*3 but the value of *c*-parameter is close to those found for the initial sample. The heteropolyhedral framework in the structure of Cs-exchanged hilairite is not distorted. The doubling of the *c*-parameter is caused by the positions of extra-framework cations and H_2O molecules.

[1] Ilyushin, G.D. et al. (1981) *Sov. Phys. Dokl.*, **26**, 916-917.
[2] Zubkova, N.V. et al. (2007) *Crystallogr. Reports*, **52**, 65-70.
[3] Zubkova, N.V. et al. (2009) *Eur. J. Mineral.*, **21**, 495-506.
[4] Grigoryeva, A.A. et al. (2009) *Dokl. Earth Sci.*, **428**, 1051-1053.

Diagenetic zeolite formation / dissolution during burial diagenesis, and its influence on further cementation - examples from the Siri Canyon, Danish North Sea

Kazerouni, A.M.[1*], Weibel, R.[2], Friis, H.[1] & Svendsen, J.B.[3]
[1]Dept. of Earth Sciences, Aarhus University, Aarkus, Denmark
([*]afsoon.moatari@geo.au.dk)
[2]Geological Survey of Denmark and Greenland, Copenhagen, Denmark
[3]DONG Energy, Exploration and Production, Denmark

The Siri Canyon is a submarine canyon system eroded into the uppermost Chalk deposits and filled in with Palaeogene hemipelagic and turbiditic marls and mudstones interbedded with sandstones deposited from sandy mass-flows and turbidites. Core samples from 7 wells were studied. The reservoir sands in these wells all contain authigenic silica/quartz of various morphologies identified with a combination of traditional optical microscopy and scanning electron microscopy.

Late Paleocene–early Eocene volcanic ash layers are recognized throughout most of the North Sea and also recorded from the Siri Canyon wells. Volcanic lithoclasts are strongly altered and associated with diagenetic opal/ microquartz coatings and zeolite. Zeolite crystals formed simultaneously with opal and prior to microquartz but dissolved with increased burial depth. The dissolution of zeolite followed two steps; the core of the zeolite crystals appears to have been more unstable than the rim and dissolved first. Later the entire crystal dissolved and left an impression of the euhedral zeolite crystal in the microquartz coating. Such openings in the microquartz coating are nucleation points for macroquartz. Thus, the precipitation of zeolite may later facilitate further quartz cementation, which might otherwise be retarded by the presence of disordered microquartz.

The silica activity of pore fluids can influence zeolite precipitation. Although zeolite formation is clearly related to volcanic ash, zeolite has also formed in samples where no volcanic ash is demonstrated; it seems that a rapid supply of dissolved silica from dissolution of siliceous fossils was the main reason for the early co-precipitation of opal and zeolite.

There are two important sources for Si: 1) Biogenic opal from diatoms or radiolarians, which are abundant in some of associated shales; and 2) volcanic ash.

The dissolution of biogenic silica may result in a rapid release of silica thereby promoting the formation of diagenetic opal/microquartz, but there may be a limited release of Al. A limited release of Al may result in precipitation of Si-rich clinoptilolite, or zeolite may not precipitate at all. The dissolution of volcanic lithoclasts may also release a high rate of Al, resulting in abundant formation of Al-rich clinoptilolite. If both sources interact, a compositional variation may occur with time. The compositional variation may result in variable solubility and give rise to dissolution of the internal core prior to its rim. This dissolution behavior may have impact on the further quartz cementation.

The formation of various quartz morphologies influences the continued cementation by macroquartz. This effect may be counteracted by precipitation/dissolution of zeolite.

Occurrence and chemistry of natrolite group zeolites from Bakony–Balaton Highland Volcanic Field (West Hungary)

Kónya, P.[1*] & Szakáll, S.[2]
[1]Geological Inst. of Hungary, Budapest, Hungary
([*]kope@mafi.hu)
[2]Dept. of Mineralogy and Petrology, University of Miskolc, Hungary

Cavities of alkaline basalt of the Bakony–Balaton Highland Volcanic Field (BBHVF) contain miarolitic minerals, zeolites (phillipsite, chabazite, garronite, gmelinite, gobbinsite gismondine, analcime, leucite and natrolite group zeolites), carbonates (calcite and aragonite) and smectite (saponite and nontronite). Natrolite group minerals (natrolite, mesolite, scolecite, gonnardite, paranatrolite and thomsonite) of zeolites were investigated in detail. This assemblage was characterized by X-ray, DTA and WDS methods.

Natrolite usually occurs as colourless, translucent or transparent prismatic crystals up to 5 mm. It is frequently epitaxially intergrown with mesolite, scolecite and paranatrolite in radial aggregates. Gonnardite is a common zeolite mineral at BBHVF. It often occurs as epitaxial overgrowths with glassy, prismatic natrolite and thomsonite. It frequently appears as white centres (up to 1.5 cm in diameter) within hemispherical natrolite or thomsonite aggregates, but can also be observed as homogenous aggregates. Thomsonite commonly appears as white radial aggregates or epitaxially overgrown with gonnardite.

The natrolite has a significant CaO content, similar to a general character in many natrolites worldwide. Its R is between 0.59 and 0.61 Na/(Na+Ca) ratio of 0.94-0.99 close to the theoretical value (1.00). Chemical analyses show that gonnardites have a wide variation in CaO content (1.20 to 7.26). Si/Al ratio is between 1.21 and 1.45, the value of R ranges from 0.55 to 0.59. The Na/(Na+Ca) ratio (0.65-0.96) is also variable, reflecting, that all gonnardites are Na end-members. Scolecite has a significant Na_2O content, its Na/(Na+Ca) ratio is 0.28-0.34. Mesolite has a little higher concentration of Na than the ideal mesolite. The value of R is 0.58 to 0.59. It has a Na/(Na+Ca) ratio of 0.54-0.56. Si/Al ratio is 1.40. Paranatrolite has a higher CaO content than natrolite. Its lower Na/(Na+Ca) ratio (0.92) reflects more intensive $Ca \leftrightarrow Na_2$ substitution than in natrolite. Based on the WDS analysis the Na/(Na+Ca) ratio of thomsonite is 0.41-0.46, showing that it is a Ca end-member (Fig. 1).

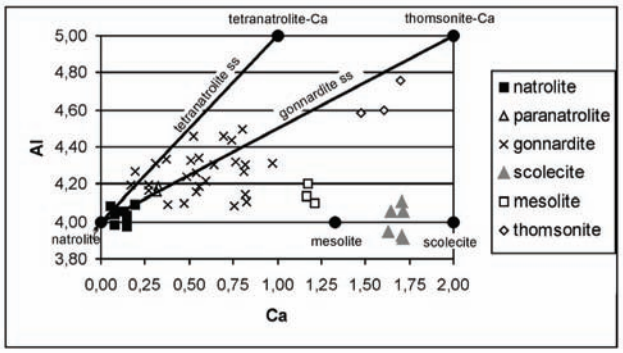

Fig. 1: Ca and Al contents per 20 framework O atoms per formula unit of samples (after Neuhoff et al. [1])

[1] Neuhoff, P.S. et al. (2002) *Am. Mineral.*, **87(10)**, 1307-1320.

Raman spectroscopic study of zeolite group minerals

Hong, H.T.[1], Huang, E.[2], Liu, T.C.[1*] & Iizuka, Y.[3]
[1]Dept. of Earth Science, National Taiwan Normal University, Taipei, Taiwan ([*]liutc@ntnu.edu.tw)
[2]Center for General Education, ChungChou Institute of Technology, Chang-Hwa, Taiwan
[3]Institute of Earth Sciences, Academia Sinica, Taipei, Taiwan

Twenty-one natural zeolite and ten synthetic zeolite samples were studied by Raman spectroscopy and analyzed by electron microprobe. The results showed that the zeolites with the same secondary building units have similar Raman spectroscopic pattern. However, the fine structure of the Raman spectrum varies with their chemical compositions. The most distinguished Raman peaks show up between 390 cm^{-1} and 530 cm^{-1} in zeolites. These peaks represent the vibration of T-O-T (T=Si, Al) in tetrahedron, the low frequency M-O vibration mode (M are cations: Ca, Na, K etc.), and the high frequency T-O vibration mode.

The main frame in the structure of zeolites is the interconnection of SiO_4 and AlO_4. The Raman spectrum may shift with the replacement of Si by Al. With the increase of Al content, the Raman peaks at 440 cm^{-1} and 530 cm^{-1} shift slightly to higher wavenumber. This may be attributed to the smaller angle in T-O-T as Si is replaced by Al. The most obvious Raman vibration modes in the single 4-ring chains and double 4-ring chains are at 400 cm^{-1}, 480 cm^{-1}, and 490 cm^{-1}, respectively. They shift toward lower wavenumber with an increase of Al content. In zeolite, the most predominant Raman vibration modes are at 495 cm^{-1}, 480 cm^{-1}, and 491 cm^{-1}. However, these vibraton modes do not change with the variation of Al content. The T-O-T Raman vibration modes of heulandite are at 405 cm^{-1} and 482 cm^{-1}; whereas, the T-O-T Raman vibration modes of stilbite are at 410 cm^{-1} and 497 cm^{-1}.

The role played by boron in ANA type structure: potential trap for radioactive waste

Montagna, G.[1], Arletti, R.[1,2], Vezzalini, G.[1*] & Di Renzo, F.[3]
[1]Dept. of Earth Sciences, University of Modena and Reggio Emilia, Italy ([*]mariagiovanna.vezzalini@unimore.it)
[2]Dept. of Earth Sciences, University of Ferrara, Italy
[3]Inst. Charles Gerhardt Montpellier, Ecole Nationale Supérieure de Chimie de Montpellier, France

Zeolites show a highly accessible micropore system, an asset for cation removal from radioactive waste solutions but a drawback for long-term stockage. The structure of pollucite $CsAlSi_2O_6$ [1] is such that, once Cs^+ cations have been encapsulated in the aluminosilicate network, their loss is negligible. Hence the direct formation of pollucite in a waste solution can represent a promising method to immobilize cesium cations [2].

Boro-aluminosilicates were synthesized to verify the effect of boron content on cesium incorporation and retention in ANA structure. It is important to find a correct B amount that can promote sintering process without increasing the leaching rate [3].

Cs-bearing B-Analcime samples were hydrothermally synthesized using B/(B+Al) and Cs/(Cs+Na) in different ratios. Chemical and crystallographic data indicate that: i) the yield of incorporation of B is lower than that of aluminum in the intermediate terms of the solid solution; ii) a lower incorporation of B is observed in the Na-bearing samples; iii) the presence of B in the framework favors the Cs incorporation; iv) the presence of B and Na in the synthesis batch favors the complete crystallization of the product.

All the samples crystallize in the cubic system, space group $Ia\bar{3}d$. This result is in agreement with a disordered Si, Al and B distribution in the tetrahedra. The framework atom positions of all samples are strictly comparable to those of the natural analcime. The variability of lattice parameters depends on B content.

[1] Barrer, R.M., Baynham, J.W. & McCallum, N. (1953) *J. Chem. Soc.*, **53**, 4035-4041. [2] Di Renzo, F. et al. (1996) *Microp. Mater.*, **6**, 151-157. [3] Ledieu, A. et al. (2004) *J. Non-Cryst. Solids*, **4**, 3-12.

N-doped mesoporous TiO_2 as photocatalyst in textile wastewater treatment. The effect of the synthesis procedure

Păstrăvanu, C.[1,2*], Seftel, E.M.[1], Alexa, I.F.[1], Creţescu, I.[2] & Popovici, E.[1]
[1]Dept. of Materials Chemistry, "Al. I. Cuza" University of Iaşi, Iaşi, Romania ([*]cristinapastravanu@yahoo.com)
[2]Dept. of Chemical Engineering and Environmental Protection, "Gh. Asachi" University of Iaşi, Iaşi, Romania

Titania is the most effective photocatalyst and widely applied in air and water purification, deodorization, antibacterial and self-cleaning coating and other environmental applications. However, as a photocatalyst, titania can only be activated by UV light [1] because of its large bandgap value. Nitrogen doped into substitutional sites of TiO_2 has shown a narrowed bandgap as well as photocatalytic activity in the visible light [2].

We synthesized N-doped and non-doped mesoporous titania via hydrothermal and ultrasound methods using blockcopolymers (Pluronic P123 and F127) as surfactants and organic sources of Ti. Different types of N-doped and non-doped mesoporous titania were synthetised by varying the composition of the surfactant and nitrogen precursor. Characteristics of the prepared photocatalysts were investigated using UV absorbtion spectroscopy and N_2 adsorbtion-desorbtion technique.

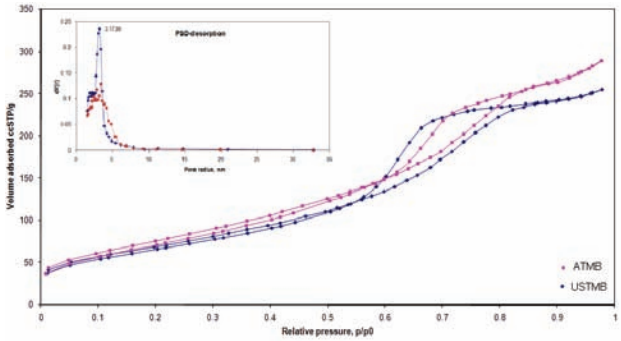

Fig. 1: Adsorbtion/desorbtion isotherms of the mesoporous titania (ATMB – via hydrothermal method; USTMB – via ultrasound method).

Mesoporous titania (N-doped and non-doped) were used as heterogeneous catalysts for the treatment of textile wastewater containing dyes. From the experimental results it was concluded that the N-doped mesoporous titania obtained by ultrasound method has higher photocatalytic activity as compared to N doped mesoporous titania prepared by hydrothermal method. Also, as expected, N-doped titania has proven to have higher photocatalytic activity than the undoped mesoporous TiO_2.

[1] Asiltürk, M., Sayılkan, F. & Arpac, E. (2009) *J. Photoch. Photobio. A*, **203(1)**, 64-71. [2] Liu, G. et al. (2010) *Mater. Chem.*, **20**, 831-843.

Mineralogy and properties of analcime-bearing rocks (Timan Region, Komi Republic, Russia)

Shushkov, D.
Inst. of Geology, Komi Scientific Center, Uralian Branch, Russian Academy of Sciences, Syktyvkar, Komi Republic, Russia (dashushkov@rambler.ru)

Analcime-bearing rocks from Carboniferous and Permian sediments occupy a vast area in the Timan – about 150,000 km^2. The Timan zeolite-bearing province dominated by analcime was discovered in the second half of the 20th century.

Analcime-bearing rocks are represented by siltstones and mudstones. Oligomictic and polymictic siltstones are characterized by spotty or irregularly bedded structures related to alternation of layers and nests of psammitic, silty, and pelitic material. The fine-grained material alternates with the coarse-grained material without any noticeable regularity in grain size. Silt-sized detrital particles are poorly rounded and sorted. Fragments of quartz, feldspar, volcanics and flakes of muscovite are cemented by the clayey and clayey–carbonate material. The cement has a spotty appearance owing to the presence of inclusions of reworked brown organic material of different tints. The cement has a basal and contact-basal pattern. Authigenic minerals are represented by sericite, chlorite, and pyrite.

Mudstones also have a spotty and irregularly bedded structure owing to the irregular development of ferrugination and different thicknesses of layers of inequigranular (psammitic and silty) material. Coarse-grained particles are represented by quartz, feldspars, carbonates, and volcanics. Pyrite and iron hydroxides are also present.

The analcime-bearing rocks have the following mineral composition (%): clay minerals (50–70), quartz (10–30), analcime (1–30), feldspars (2–10), carbonates (2–5), and pyroclastic material. The clay minerals are represented by disordered, mainly swelling, mixed-layer phases (illite-smectite, illite-chlorite), while kaolinite and chlorite are insignificant.

Analcime is found as isometric crystals, microoolite concretions, microgeode aggregates or cryptocrystallic cement. Analcime aggregates encrust roundish and oval cavities and also fill microfractures in rocks. Thin sections clearly reveal different stages of cavity filling by analcime – from insignificant encrustation to completely filling. Generally analcime aggregate has a different structure. Both thin-crystalline (size less than 0.01 mm) and medium-crystalline (crystal size of about 0.5 m) are observed. Intensively altered argillaceous-silica material is practically always present.

The mechanical, gravitational, magnetic, sorption and ion-exchange properties of analcime-bearing rocks have been studied. They are characterized by a high index of grindability and a low index of breakability and crush resistance, low values of the benzol-based pore volume and toluene-based specific surface area, and a medium porosity value.

Analcime-bearing rocks of the Timan region are characterized by low beneficiation potential. Preliminary ultrasonic treatment of the analcime-bearing rocks is efficient for the destruction of intergrowths along their boundaries and production of free analcime aggregates. The proposed beneficiation procedure yields 95 % analcime concentrate.

In the Komi Republic, analcime-bearing rocks are utilized in agriculture. They are also used for domestic needs (e.g. as biotoilets for domestic animals) and the solution of ecological problems (regeneration of soil polluted by oil). We have completed experiments on the purification of potable and industrial water using analcime-bearing rock subjected to thermal treatment. The experiments demonstrated that it was possible to decrease water coloration, turbidity, permanganate oxidation and total iron content.

Cation exchange properties of delhayelite (systems with Rb, Cs and Ba)

Turchkova, A.G.*, Pekov, I.V. & Yapaskurt, V.O.
Faculty of Geology, Moscow State University, Moscow, Russia
(*annaturchkova@rambler.ru)

The base of the crystal structure of delhayelite, ideally $K_4Na_2Ca_2[AlSi_7O_{19}]F_2Cl$ (Z=2), is a quasi-framework formed by two-layer tetrahedral blocks $[(Al,Si)_4Si_{12}O_{38}]$ and columns of CaO_5F octahedra linking them. K^+ and Cl^- ions are located in zeolite-like channels inside the tetrahedral block whereas Na^+ and F^- are between the blocks. Delhayelite is the only natural silicate with so strict ordering of both large cations and halogen anions. The mineral was formed in K-rich and H_2O-deficient, high-temperature peralkaline rocks. Under hydrothermal conditons, it alters to fivegite, $K_4Ca_2[AlSi_7O_{17}(O_{2-x}OH_x)][(H_2O)_{2-x}OH_x]Cl$ (x=0-2), and further to hydrodelhayelite, $KCa_2[AlSi_7O_{17}(OH)_2]\cdot(6-x)H_2O$, preserving the stable CaAlSiO fragment of the structure [1,2]. It caused our assumption that delhayelite can have ion-exchange properties.

Grains (0.5–3 mm) of delhayelite from the Khibiny alkaline complex (Kola Peninsula, Russia) were placed in 1N aqueous solutions of Na_2SO_4, K_2SO_4, $RbNO_3$, $CsNO_3$, $SrCl_2$, $BaCl_2$ and $CuSO_4$ for 3 hours at 80-90ºC and 1 atm and after that examined on polish sections using scanning electron microscopy and electron microprobe. In solutions of Na, K, Sr and Cu salts, the mineral shows no changes in its chemical composition while with cations Rb, Cs and Ba it demonstrates exchange. The distribution of cation-substituted areas in delhayelite crystals is very uneven: they are mainly concentrated around inner cracks and mineral inclusions. Ratios of Si, Al and Ca, forming the quasi-framework, remained without changes in these areas whereas contents of Rb_2O, Cs_2O and BaO increased from 0.0 wt.% in the initial delhayelite to 8.5–11.9, 10.1–27.0 and 8.5–11.3, respectively. In the Rb-exchanged form, content of Na_2O decreased from 6.4–6.7 wt.% to 1.2–2.5, K_2O from 19.2–19.8 to 3.5–7.2, F from 4.3–4.6 to 1.0–2.5, Cl from 3.8–4.1 to 1.0–1.8. In the Cs-exchanged form, their contents (wt.%) became: Na_2O 0.0–2.0, K_2O 0.9–8.8, F 0.0, Cl 0.0–1.8; in Ba-exchanged form: Na_2O 0.5–1.7, K_2O 3.3–9.8, F 0.0–2.4, Cl 0.6–1.8. Delhayelite shows the strongest affinity to Cs^+, and its most Cs-enriched form has the empirical formula: $Cs_{1.67}K_{0.16}Ca_{1.85}Al_{1.06}Si_{6.94}O_{17.47}(OH)_{1.53}(H_2O)_n$. It is most probable that large cations of Rb, Cs and Ba substitute K whereas Na and F are leached and the latter is partially replaced by H_2O.

Acknowledgements: This work was financially supported by the Russian Foundation for Basic Research (grants Nos. 08-07-00077-a, 09-05-00143-a, and 09-05-12001-ofi_m).

[1] Pekov, I.V. et al. (2009) *Dokl. Earth Sci.*, **428(7)**, 1216-1221. [2] Pekov, I.V. et al. (2010) *Zapiski RMO*, in press.

Stepwise dehydration of goosecreekite: a structural study

Wadoski, E.*, Armbruster, T., Lazic, B. & Fisch, M.
Mineralogical Crystallography, Inst. of Geological Sciences, University of Bern, Switzerland (*eva.wadoski@krist.unibe.ch)

Goosecreekite $CaAl_2Si_6O_{16}\cdot5H_2O$, monoclinic space group $P2_1$, is a rare natural zeolite that was first described by [1] and has been further characterized by crystal structure determination [2]. The framework consists of completely ordered Si and Al tetrahedra that form eight-membered rings which are highly deformed. These create channels that are parallel to the **a**-axis. The channels are intersected by two additional eight-membered ring-channels parallel to the **b**-axis and the **c***-axis. Ca is located at the intersection of the channels and is bound to two framework O and five H_2O molecules [2]. Samples were from the type locality in Loudon County, Virginia, USA and Jalgaon Quarries, Maharastra, India. Unit cell parameters measured under ambient conditions are a 7.2993(3), b 17.4164(7), c 7.4421(3) Å, β 105.584(2)°, V 911.32 Å^3 (Loudon sample). In contrast to the Loudon sample, crystals from Jalgaon were mostly twinned [001,010,100]. The structures of goosecreekite from both localities show identical frameworks and corresponding channel occupants. Methods for stepwise (Δ = 25°C) dehydration were temperature dependent single-crystal and powder XRD as well as TG/DTA analysis.

According to single-crystal structure refinement goosecreekite looses $1H_2O$ pfu below 100°C leaving the framework unaltered. The Ca coordination decreases from seven-fold to six-fold. TG/DTA indicates further loss of ca. 8 wt.% H_2O between 150 and 310°C accompanied by a strong endothermic DTA signal. Single-crystal X-ray data indicate collapse of the tetrahedral framework at 175°C with a doubling of the c-axis (quenched to -100°C: space group $P2_1$, a 7.2197(16), b 16.392(4), c 14.292(3) Å,β 101.716(4)°, V 1656.14 Å^3). In addition, the new structure exhibits complex twinning. Upon partial dehydration two T-O-T bonds break creating two structural varieties that occur in a 1:1 ratio. Variety I has the original framework connectivity. Variety II displays an interrupted framework with two tetrahedra "flipped" into the channels to bond with Ca. The flipped tetrahedra must be hydroxylated. A single crystal heated up to 230°C and left at ambient conditions for one month rehydrated, recovering the original cell parameters when re-measured. After one month a powdered sample previously heated to 325°C also rehydrated to its original structure. Up to ca. 600°C, the X-ray powder pattern characteristic of the collapsed structure persists. Upon further heating the pattern becomes increasingly X-ray amorphous until complete destruction at ca. 675°C.

An additional dehydration step occurring between 310° and 600°C which is associated with further loss of ca. one H_2O was identified by TG/DTA data. Variety II of the collapsed structure is predicted to become more prevalent relatively to variety I with increased heating.

Based on stepwise dehydration data of goosecreekite, it can be seen that if extraframework Ca has less than six ligands (two framework O and four H_2O), topologic structural changes occur, such as breaking of T-O-T bonds. These changes are reversible until the structure becomes amorphous. Similar "flipped" tetrahedra, which become hydroxylated in the new interrupted framework, have been described upon dehydration of stellerite, $CaAl_2Si_7O_{18}\cdot7.25H_2O$, B [3].

[1] Dunn, P.J. et al. (1980) *Can. Mineral.*, **18**, 323-327. [2] Rouse, R.C. & Peacor. D.R. (1986) *Am. Mineral.*, **71**, 1494-1501. [3] Alberti, A. et al. (1978). *Phys. Chem. Miner.*, **2**, 365-375.

Mineral reactions, development of porosity and their implications for CCS

Stanjek, H.
Clay and Interface Mineralogy, RWTH Aachen University, Aachen, Germany (helge.stanjek@cim.rwth-aachen.de)

Injection of CO_2 into (saline) reservoirs disturbs the thermodynamic equilibrium conditions because apart from temperature and pressure changes, the chemistry of the pore fluid changes, too. The induced reactions of the reservoir minerals towards new mineral assemblages will be associated with volume changes, which, in turn, will affect the long-term management and safety of reservoirs because of the development of porosity.

In a case study we investigated the possibility of combining CO_2 injection with the extraction of geothermal energy from deep saline reservoirs, which frequently contain anhydrite [1]. For modelling the redistribution of anhydrite and its potential conversion into calcite, near-equilibrium dissolution rates of anhydrite were measured and found to deviate significantly from transition-state-theory rates.

A safety-related aspect is the formation of porosity and permeability in cap rocks.

In laboratory experiments we could show that under certain hydrodynamic conditions the dissolution of Fe-bearing calcite led to the formation of preferential pathways, along which acid could percolate through long columns of calcite powder because of the formation of iron hydroxide coatings. These coatings shield the calcite from protonation.

In a current study, the impact of CO_2 on clay minerals is investigated. Apart from mineral transformations (e.g., dissolution of feldspars), it seems that supercritical CO_2 affects the amount of interlayer water in smectites. Changes of the interlayer composition, however, can lead to substantial volume changes, which in turn, will affect the porosity and permeability of cap rocks. There are also indications that clay minerals (especially smectites) can store some CO_2.

[1] Kühn, M. et al. (2009) in Grobe, M., Pashin, J.C. & Dodge, R.L. (eds.) *AAPG Studies in Geology*, **59**, 545-552.

CO_2/H_2O/clay system from molecular simulation

Botan, A.[1,2*], Rotenberg, B.[1], Marry, V.[1], Turq, P.[1] & Noetinger, B.[2]
[1]PECSA, Université Pierre & Marie Curie and CNRS, Paris, France ([*]alexandru.botan@upmc.fr)
[2]Inst. Français du Pétrole, Rueil Malmaison, France

The development and use of technologies to capture and subsequently store of carbon dioxide (CO_2) in deep geological formations offers significant opportunities to reduce greenhouse emissions. In this context, understanding the migration of stored CO_2 through the porous host formation and the clay-rich cap rock is of great importance. Up to now the main focus in the literature is placed on the two-phase flow in porous media on the macroscopic scale and as result there is a lack of studies on the molecular level. However, a microscopic description is necessary to study some processes (swelling, cation exchange) inaccessible to macroscopic scale methods. One such process is the possible clay dehydration due to the presence of CO_2 which can lead to a significant shrinkage of clay particles and affect the clay permeability. Furthermore, a molecular point of view can be also useful in study of two-phase flow in clay. The surface wettability, densities, viscosities obtained from molecular simulation can be basis for subsequent studies of transport properties by continuous methods. In this study, we first investigated the thermodynamical properties related to swelling and the structure of CO_2 in hydrated Na-montmorillonite for micropores using the grand canonical Monte Carlo method. The system is in equilibrium with a reservoir, which sets the chemical potentials of CO_2 and H_2O. We then used molecular dynamics to determine the diffusion coefficients for equilibrated configurations. Some important findings are: the presence of CO_2 leads to a slight increase in equilibrium interlayer distances and a considerable decrease in diffusion coefficients for all species; CO_2 adopts a nearly parallel arrangement to the clay surface.

We also considered large (interpaticle) pores. Similarly to the bulk reservoir, two states with different density and composition are generally observed for given experimental conditions (see Fig. 1). In this example, the system in "water-rich" phase (a) is characterized by the liquid density and a small number of CO_2, whereas in case (b) the "CO_2-rich" phase is heterogeneous with water remaining close to the clay surface and gas CO_2 in the middle. We then use nonequilibrium molecular dynamics to determine the viscosity of the confined fluids. This was achieved by applying a uniform force on the fluid and fitting the resulting velocity profile to a Poiseuille flow [1].

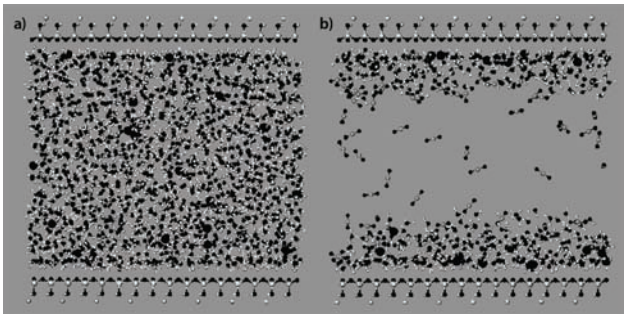

Fig. 1: Snapshots of phase transition of CO_2 in hydrated Na-montmorillonite: a)" H_2O-rich" phase, b)" CO_2 -rich" phase. The interlayer distance is 4.3 nm and the chemical potentials corresponds T=348.15 K and P = 25 bar in the bulk reservoir.

[1] Huang, D.M. et al. (2008) *Langmuir*, **24**, 1442-1450.

A high-pressure X-ray environmental chamber suitable for solid-liquid-gas studies

Guggenheim, S.* & Koster van Groos, A.F.
Dept. of Earth & Environmental Sciences, University of Illinois at Chicago, USA (*xtal@uic.edu)

An X-ray, high-pressure environmental chamber (HPEC) is described that is capable of pressures to 1000 bars and temperatures of -20 to 200°C. An integral, internal electromagnetic pump system was designed so that solid phases are maintained in suspension, thus allowing the sample to move freely in the aqueous liquid while being illuminated by the X-ray beam. In addition, the pump system allows the liquid to be readily saturated with gas (e.g., CH_4, CO_2, N_2). An external pump system is used to apply pressure, either using gas or liquid (e.g., CO_2 above the critical point). If gas is employed, this system controls the fugacity of the gas components by mixing with inert gases.

The HPEC is equipped with cooling jackets so that temperatures are varied by applying a cooling/heating fluid to the outside of the unit (using glycol or silicon liquid). This design readily accommodates experiments from -20 to 200°C. Window-to-window distances can be fixed from near 0.0 to ~4 mm, although a 2-mm spacing appears optimal. Most of our preliminary experiments have used this design. The unit uses 1-mm thick disks of vapour-deposited diamond as windows with O-ring seals, and employs a type-K thermocouple located at ~1 mm from the sample to measure temperature. The HPEC is mounted on an in-house, transmission-mode (Bruker) diffractometer equipped with Mo radiation, monochromator, MonoCap collimation, and area detector, although the design is compatible with transmission-mode diffractometers at the Advanced Photon Source (Argonne). The sample volume is ~10 mL, and catastrophic failure (of the O-rings) does not pose a significant hazard to either personnel or equipment.

Resultant diffraction frames consist of Debye rings from the solids and background effects (e.g., dispersion from the aqueous liquid, "hot" pixel effects). All background effects can be digitally removed by subtracting a diffraction frame from an experiment without solids present to produce a residual frame of Debye rings. A more traditional one-dimension pattern is obtained by integrating appropriately over chi to obtain a pattern that can be used as input into search-match or other data processing programs.

The chamber is well suited for experimental work that involves solids, liquids, and gases under high pressure over a wide range of temperatures.

Smectite–CO_2 interactions to 400 bars and 65°C

Giesting, P.[1*], Guggenheim, S.[1], Koster van Groos, A.F.[1] & Bertier, P.[2]
[1]Dept. of Earth & Environmental Sciences, University of Illinois at Chicago, USA (*giesting@alumni.nd.edu)
[2]Clay & Interface Mineralogy, RWTH Aachen University, Aachen, Germany

X-ray diffraction experiments were conducted on smectite in the presence of either CO_2 or He at high pressures and elevated temperatures using an environmental chamber. A Mg-exchanged smectite of approx. composition of $Mg_{0.17}(Al_{1.34}Fe_{0.44}Mg_{0.29})\ (Si_{3.75}\ Al_{0.25})\ O_{10}(OH)_2 \cdot nH_2O$ was dried for 42 hours at ~200°C and stored over desiccant until used. Experiments at 25°C and various CO_2 pressures (40, 80, 130, 200, 300, and 400 bars) show a 10-Å peak with a significant low-angle tail and, with increasing CO_2 pressure, this tail increases in height as the 10-Å peak diminishes in size. Experiments at 65°C and at CO_2 pressures of 1, 5, 10, 20, 40, 80, and 200 bars show similar X-ray patterns, except that the peak at 10 Å moved to 10.4 Å, and the peak did not diminish in height with increasing pressure. These results suggest that the 10.4-Å spacing is slightly more prevalent in the experiments at 65°C than at 25°C.

A series of experiments at 65°C with He (1, 40, and 130 bars) show similar behavior for the 10-Å peak as in the CO_2 experiments at 25°C. These results suggest that the change in peak and tail intensity is related to a partial dehydration and redistribution of H_2O within the interlayer of the smectite, rather than that a gas (e.g., He or CO_2) enters the interlayer of the clay. A near-second order, non-integral diffraction effect is observed at the 4.4-Å peak. This peak shows an intense tail at higher angles. Both effects indicate that two or more (001) spacings occur, further corroborating that the sample has undergone only partial dehydration. The similarity in patterns for both the CO_2 and He runs suggests that there is no evidence that CO_2 enters the interlayer of a nearly anhydrous clay at the conditions of these experiments. Additional experiments are being conducted to determine how changing the interlayer-cation population affects the interaction between smectite and CO_2.

Two sets of experiments were made under starting conditions of ambient humidity and with the clay suspended over a reservoir of H_2O. Under ambient humidity (~35 % RH) starting conditions, the environmental chamber was sealed and heated to 55°C. CO_2 was added and pressures were examined at 40, 80, 130, and 200 bars. A prominent peak occurs at 13.7 Å for all pressures and intensifies slightly as pressure is increased. Experiments with clay suspended over a reservoir of H_2O (at pressures of 1, 40, 80, 200, and 300 bars at 65°C) showed a peak at 16.3 Å, which intensified as pressure was increased. Additional experiments with He are underway.

Acknowledgements: Financial support from Shell Exploration and Production B.V. is gratefully acknowledged.

Fluid-rock interaction with impure CO_2 by combining geochemical and geomechanical investigations: first results from the COORAL project

Marbler, H.*, Lempp, Ch., Pöllmann, H., Erickson, K. & Schmidt, M.
Geo-sciences, Martin Luther University Halle Wittenberg, Halle/Saale, Germany (*herwig.marbler@geo.uni-halle.de)

The storage of CO_2 with inherent impurities, such as SO_X, NO_X, O_2, CO, etc., affects fluid-rock interactions in deep geological formations. These include alterations and mineralogical transformations within the reservoir formation. The injection pressure may decrease fracture strength of the reservoir rocks, which would impair the formation stability within a short time period.

To understand this interaction of CO_2 with the host rocks, laboratory experiments are carried out with samples of possible reservoir rocks and brine (formation waters). Geomechanical test series are conducted in triaxial cells under lithostatic pressure conditions with supercritical (sc)CO_2 acting as pore fluid. For mineralogical and geochemical investigations the experiments are executed in autoclave systems under simulated in-situ temperature conditions. In the autoclave system a set of rock samples of different silicate and carbonate bearing sandstones are allowed to react with fluids and well-defined compositions of impure scCO_2 to optimize the real-time alteration scenarios.

Geochemical modelling of CO_2/mineral interaction record various mineralogical and geochemical effects in the system i.e. changes of the major element and trace element composition as well as the initial formation of hydrocarbonate minerals. Laboratory experiments with scCO_2 in interaction with reservoir rocks will be carried out to verify such geochemical alterations and mineralogical transformations. Geomechanical tests show that increasing pore fluid pressure with scCO_2 as well as with water has strong effects on the rock strength. CO_2 in the supercritical state, acting as pore fluid, is able to displace formation water (brine) or dissolve into these waters as well as infiltrate smaller pore spaces in the reservoir rock in comparison to brines. This so called capillary trapping plays an important role for long term storage of CO_2 in deep geological formations. However, scCO_2 induces fine fractures in sandstones especially in inhomogeneities within the rocks which may result in decreasing fracture strength of the reservoir rocks, especially with enhanced injection pressure. Therefore, the evolution of the pore space and the formation of cracks and fractures as well as additional alteration effects by scCO_2 may influence the storage capacity and long-term safety of the storage formation. The knowledge of these dynamic processes both in geochemical/mineralogical and geomechanical terms is of great importance to allow for long-term safety predictions over timescales of up to thousands of years.

Acknowledgements: COORAL: "CO_2-Reinheit für Abscheidung und Lagerung" (CO_2 Purity for Capture and Storage); aided by the German Bundesministerium für Wirtschaft (grant ID: 0327790D).

Modelling of mineral alteration in a natural CO_2 reservoir

Montegrossi, G.[1], Ruggieri, G.[1], Bicocchi, G.[2], Vaselli, O.[1,2], Burgassi, P.[3], Tassi, F.[1,2], Jordi, B.[4] & Del Villar, L.P.[5]
[1]Inst. of Geosciences and Georesources, CNR, Florence, Italy (*fdibe@yahoo.com)
[2]Dept. of Earth Sciences, University of Florence, Italy
[3]Air Liquide Italia Service Srl, Ponte a Chiani, Arezzo, Italy
[4]Passeig de García i Faria, 49-51, Barcelona, Spain
[5]Centro de Investigaciones Energéticas, Medioambientales y Tecnológicas (CIEMAT), Madrid, Spain

The investigation of natural reservoirs as analogue of Carbon Capture and Sequestration (CCS) site has a considerable impact in the reaction path modeling. It is indeed the main information able to predict the mineral evolution during and after CO_2 injection in feasible CCS site.

In the 80's, during oil exploration in central Italy, a high pressure CO_2 reservoir was found while drilling the PSS1 well, located in the San Cassiano basin, Tuscany, Central Italy [1]. The CO_2 reservoir has pressure higher than 600 bar and a temperature of about 115°C. The reservoir rocks at depth of about 3,700 m consist of altered volcanic rocks. According to ENI report (1983) the original rocks had an andesitic composition.

The aim of this work is to assess a reaction path able to predict the reservoir rocks evolution from the pristine mineralogical composition to the present one. The mineralogical and mineral chemistry investigation was carried out on 6 drill core samples from the CO_2 reservoirs horizons. The examined samples are made of volcanic rocks almost completely replaced by hydrothermal minerals. The alteration mineralogical assemblage is mainly composed by silicates (quartz, albite, illite and chlorite) and carbonates (calcite and ankerite) and minor amount of Fe-oxides/hydroxides and Fe-Ti-oxides. The reaction path model here presented is performed by using the geochemical computer program PHREEQC (Version 2.15). The database is corrected to take into account the pressure by means of SUPCRT92.

The general idea is that a nearly iso-chemical evolution of the mineralogical assemblage has occurred, as a consequence of inflow of CO_2-rich aqueous fluid with a progressive dry-out of the reservoir fluid. Thus, the geochemical model strategy proceeds through a fully kinetic approach, because the carbonation is not expected to have reached the equilibrium. It seems reasonable to assume that CO_2 input has left a gross overpressure of about 230 bars. During such event the fluid present in the formation was displaced by CO_2, progressively drying the reservoir out. In this setting the chemical evolution of the system may have proceeded with a progressively lowering of the water/rock ratio.

[1] Anelli, L. et al. (1994) *Mem. Soc. Geol. Ital.*, **48**, 461-471.

Mineral traps for CO_2 in mine tailings

Wilson, S.A.[1,4*], Dipple, G.M.[1], Power, I.M.[2], Barker, S.L.L.[1], Fallon, S.J.[3], Raudsepp, M.[1] & Southam, G.[2]
[1]Mineral Deposit Research Unit, The University of British Columbia, Vancouver, BC, Canada ([*]siowilso@indiana.edu)
[2]Dept. of Earth Sciences, University of Western Ontario, London, ON, Canada
[3]Research School of Earth Sciences, Australian National University, Canberra, Australia
[4]Current address: Dept. of Geological Sciences, Indiana University, Bloomington, IN, U.S.A.

At some ultramafic-hosted mines, accelerated weathering of Mg-rich mineral waste (tailings) can produce significant amounts of hydrated Mg-carbonate minerals. In mine tailings, trapping and storage of atmospheric CO_2 within these minerals can occur on a kilotonne to megatonne scale and, in some instances, may represent a significant offsetting of a mine's greenhouse gas emissions [1,2].

We have investigated CO_2 mineralization within Mg-carbonate minerals (typically hydromagnesite, dypingite, nesquehonite, and lansfordite) in the tailings from four mine sites in Western Australia and Canada [1-3]. Among these ultramafic-hosted mines, the extent and rate of CO_2 trapping and the identities of the mineral hosts to CO_2 vary. Isotopic investigations suggest that the rate of carbon cycling between geological, industrial, and atmospheric reservoirs within ultramafic mine tailings is largely controlled by climate and tailings management practices.

Kinetic exchange of C isotopes, during fast precipitation of carbonate minerals in mine tailings, complicates interpretation of stable isotopic data. Therefore, we have used radiogenic ^{14}C to assess the extent to which modern, atmospheric CO_2 has been captured within hydrated Mg-carbonate minerals.

Quantitative mineralogical procedures that use X-ray powder diffraction data, including a combination of Rietveld refinement and reference intensity ratios, allow quantification of the mineral hosts to CO_2 from trace to readily detectable abundances. Quantitative mineralogical results can be used with ^{14}C data to assess the amount of CO_2 trapping within hydrated Mg-carbonate minerals. Furthermore, Rietveld refinement results can assist in determining which gangue minerals are the primary sources for Mg in these minerals.

Our results indicate that some large, ultramafic-hosted mining operations, like the Mount Keith Nickel Mine in Western Australia, are able to offset >15% of their annual greenhouse gas emissions by passive uptake of atmospheric CO_2 into carbonate minerals. Reaction of ~10% of the annual production of serpentine-rich tailings at Mount Keith has the potential to completely offset the mine's greenhouse gas emissions. Preliminary results suggest that this acceleration might be achievable through a combination of redesign for tailings storage facilities and microbially mediated processing of mineral waste [3-5].

[1] Wilson, S.A. et al. (2006) *Am. Mineral.*, **91**, 1331-1341. [2] Wilson, S.A. et al. (2009) *Econ. Geol.*, **104**, 95-112. [3] Wilson, S.A. et al. (2009) *Appl. Geochem.*, **24**, 2312-2331. [4] Power, I.M. et al. (2009) *Chem. Geol.*, **260**, 286-300. [5] Power, I.M. et al. (2010) *Environ. Sci. Technol.*, **44**, 456-462.

Long-term CO_2 storage in weathered peridotite due to replacement of low-T altered olivine (deweylite) by calcite

Beinlich, A.[1,2*], Plümper, O.[1], Hövelmann, J.[1] & Austrheim, H.[1,2]
[1]Physics of Geological Processes, University of Oslo, Norway (*andreas.beinlich@fys.uio.no)
[2]Dept. of Earth Sciences, University of Oslo, Norway

In contact with CO_2, peridotite is known to be reactive and eventually transforms into ophicarbonate and listwaenite. Here we present observations from serpentinized peridotite clasts from the Devonian Solund Basin, SW Norway. These clasts show evidence for a stepwise reaction history starting with initial serpentinization and resulting in the formation of carbonates and quartz. Thus, the clasts represent a natural analogue for CO_2 sequestration in ultramafic rocks, a strategy proposed by the Inter-Governmental Panel on Climate Change [1] for long-term CO_2 storage. In several layers of the basin, the carbonatized ultramafic clasts are important constituents and account for up to 20 vol.% of the basin infill.

The investigated clasts show a concentric build-up with green to grey olivine- and serpentine bearing cores surrounded by mm to 10 cm thick, carbonate-quartz-talc-zones of red to black shades. Textural observations indicate the following alteration sequence: An early stage is represented by ocean-floor serpentinization of peridotite resulting in a typical mesh texture, with veins of serpentine and Ni-rich hematite surrounding compartments of relict olivine (Fo_{90}). During subsequent low-T alteration under near-surface conditions, relict olivine breaks down to form an extremely fine grained alteration product. In the more advanced ophicarbonate stage, interaction with a Ca-bearing fluid within the basin caused calcite formation in cells surrounded by serpentine. The textural evolution is accompanied by a decrease in whole-rock MgO from 40 to 2 wt.% and a CaO increase from 1 to 35 wt.%. All clasts are characterized by high trace-element concentrations of Cr and Ni revealing their ultramafic origin.

Scanning transmission electron microscopy (STEM) enabling high-angle annular dark field (HAADF) imaging reveals that olivine breaks down to a fine grained intergrowth of amorphous serpentine and poorly crystalline talc (deweylite) and that subsequent carbonatization proceeds as dissolution of deweylite coupled with direct precipitation of calcite.

Hydrothermal batch experiments (130-160 bar PCO_2; 200°C; 1-3 weeks reaction time) show that the cells filled with deweylite are the favourable site of reaction presumably due to its large reactive surface area and high degree of disorder. In contrast, relict olivine and surrounding serpentine remain almost inert during the carbonatization stage.

Although the clasts are characterized by high initial Mg concentrations, calcite represents the dominant carbonate phase indicating that magnesite formation is thermodynamically not favoured as soon as Ca is introduced to the system which is further corroborated by geochemical modelling (PHREEQC). Mg removed from the clasts during alteration is partly consumed by replacement reactions in the vicinity of the clasts where Fe-minerals (almandine) are replaced by Mg-minerals (talc). For basins containing abundant peridotite clasts, the outlined process will influence the CO_2 and MgO budget.

[1] IPCC Special report (2005) *Carbon Dioxide Capture and Storage*. Summary for Policymakers.

Molecular species in microporous cordierite

Geiger, C.A.[1*], Rahmoun, N.S.[2] & Heide, K.[2]
[1]Fachbereich Materialforschung und Physik, Universität Salzburg, Austria (*chg@min.uni-kiel.de)
[2]Institut für Geowissenschaften, Universität Kiel, Germany

Cordierite, $(Mg,Fe)_2Al_4Si_5O_{18}\cdot x(H_2O,CO_2)$, is a microporous silicate having about 20 volume % void space. It is typically found in metamorphic and in certain igneous rocks. It can occlude a number of different molecular and atomic species that reflect the nature of the fluid phase during crystallization and/or equilibration.

We undertook a mass spectrometric study to investigate all occluded volatile species in a systematic manner for a series of cordierite samples. The method, DEGAS, requires only small milligram quantities of material, which are heated continuously at a controlled rate from 25°C to 1400°C. The mass-to-charge ratios of the degassed molecules and their related species are measured by a quadrupole mass spectrometer. Twenty cordierite samples from a wide range of petrologic environments and having different compositions were investigated.

The cordierites show H_2O and CO_2 as the most abundant primary occluded molecules. Their degassing temperatures lie between 750 and 1000°C and 750 and 1200°C, respectively. There is reasonable agreement in CO_2 and H_2O concentrations determined by the DEGAS method and those determined by the Karl Fischer titration method. H_2O contents range from approximately 0.0 wt% to 2.34 wt % and CO_2 from 0.0 wt% to 1.97 wt%. Ratios of X_{CO_2}/X_{H_2O} for samples containing measurable amounts of both molecules range from about 0.2 to 5.6 and there exists an inverse relationship between CO_2 and H_2O contents. Cordierites from pegmatites and medium-grade metamorphic rocks are relatively rich in H_2O and poor in CO_2, whereas cordierites from the granulite facies have more CO_2 than H_2O. Different isotopic compositions for both CO_2 and H_2O are observed. A number of other occluded molecular or atomic species were identified at minor and/or trace concentration levels. They include $^{40/36}Ar$, He, SO_2, N_2, H_2S, H_2 and Na and possibly CH_4 and HCl. The presence of primary CO could not be ascertained. The relative concentrations of primary occluded atoms and molecules in natural cordierite vary approximately as: $H_2O \sim CO_2 >> N_2 > Ar \sim H_2S > He > SO_2$ with possibly very minor H_2, CH_4 and HCl.

The types of molecules and atoms that are incorporated in cordierite and their concentrations depend on three factors: i) the temperature and pressure during crystal growth, ii) crystal-chemical and molecular properties and iii) the composition of the fluid under which the cordierite crystal crystallized or equilibrated.

The DEGAS profiles also sometimes show degassing peaks for Ar, H_2S, SO_2 and possibly a CH_3 species, for example, at low temperatures around 150°C. They are likely related to adsorbed surface species, whose exact physical and chemical state is not clear. Strong degassing "events" are also observed for some species at temperatures between about 300°C and 700°C and they are possibly related to very minute solid-phase inclusions such as those associated with pinite.

The DEGAS results give, for the first time, a broad picture of the various types of molecules and their relative concentrations in cordierites occurring over a wide range of geologic environments.

Changes in structure and cage occupancy of methane- and CO_2-hydrate under high pressure

Hirai, H.[1*], Machida, S.[1], Tanaka, T.[1], Honda, M.[1], Kawamura, T.[2], Yamamoto, Y.[2] & Yagi, T.[3]
[1]Geodynamics Research Center, Ehime University, Matsuyama, Japan ([*]hirai@sci.ehime-u.ac.jp)
[2]National Inst. of Advanced Industrial Science and Technology, Tsukuba, Japan
[3]Inst. for Solid State Physics, Tokyo University, Kashiwa, Japan

Gas hydrates are clathrate compounds composed of hydrogen-bonded water molecules forming cages and guest gas molecules contained in the cages. Methane hydrate, called fiery ice, is expected as a clean and fruitful energy resource, while methane is a greenhouse gas even more potent than carbon dioxide at causing global warming. In the solar system, methane hydrate is thought to be an important constituent of outer giant planets and their satellites, such as Uranus, Neptune, and Titan. CO_2-reduction in the Earth's atmosphere is one of the most urgent subjects of mankind. Some technical developments to seclude excess CO_2 at ocean floor as CO_2 hydrate or CO_2 fluid have been proceeded. In the solar system, a possible existence of CO_2 hydrate in and beneath Martian permafrost has been predicted from spacecraft probes and theoretical studies. Therefore, knowledge of the structural changes of both hydrates under wide pressure-temperature conditions is required from various standpoints for overcoming mankind's urgent problems of dwindling energy resources and global warming, as well as for answering fundamental questions about the internal structure of the neighbour planet and icy bodies.

High pressure experiments with methane hydrate and CO_2 hydrate were performed using diamond anvil cells. For the former one the pressure range was 0.2 GPa to 86 GPa at room temperature and for the latter one the pressure ranges was 0.2 to 3.0 GPa and temperature range was 300 K to 80 K using a helium-refrigeration cryostat system. Although, both hydrates have same structure, sI, at low pressure, they showed completely different behaviour under high pressure region.

X-ray diffractometry and Raman spectroscopy revealed phase changes of both hydrates as follows. For methane hydrate, sI transformed a hexagonal structure, sH, at about 1 GPa and further transformed to a filled ice Ih structure at 2 GPa, and it survived at least up to 86 GPa [1-3]. At about 15GPa, the guest methane molecules exhibited orientational ordering in the structure, although they rotated freely below the pressures. And, at about 40 GPa the host water molecules showed symmetrization of hydrogen bond. These properties might lead the outstanding stability under high pressure. For CO_2 hydrate, the phase boundary between the hydrate and CO_2 + water turned from positive slope to negative one at a inflection point (294 K, 328 MPa), thus CO_2 hydrate can survive only low temperature region at the higher pressures. The characteristic may come from some interaction between host water molecules and guest CO_2 ones, which is possibly induced by that CO_2 molecule has hydrophilic oxygen atoms at both sides.

[1] Hirai, H. et al. (2003) *Phys. Rev. B*, **68**, 172102. [2] Hirai, H. et al. (2006) *Am. Mineral.*, **91**, 826-830. [3] Hirai, H. et al. (2008) *J. Chem. Phys.*, **129**, 224503.

Experimental study of CO_2 capture and storage possibility on drilling core samples from Hungary

Király, Cs.[1*], Berta, M.[1], Falus, Gy.[2], Székely, E.[3] & Szabó, Cs.[1]
[1]Lithosphere Fluid Research Lab, Dept. of Petrology and Geochemistry, Eötvös University, Budapest, Hungary ([*]csilla.kiraly.hu@gmail.com)
[2]Eötvös Loránd Geophysical Institue (ELGI), Budapest, Hungary
[3]Budapest University of Technology and Economics (BME), Budapest, Hungary

The concentration of CO_2 in the atmosphere has increased significantly since the industrial revolution. To reduce the CO_2 level, a new area of research has been created, which has a clear goal to find geological formations below the surface where a long-term and safe storage of CO_2 can be guaranteed [1]. These reservoirs are found in salt domes, depleted hydrocarbon fields, non-economical coal beds, deep saline aquifers and mafic or ultramafic rocks [2].

The sedimentary system in the Pannonian Basin contains several sub-basins, which are potential storage places, namely porous sandstone bodies with regional coverage by low permeability pelitic rocks [3]. Our main aim is to carry out an experimental series on pairs of potential reservoir and cap rock from cores drilled for hydrocarbon exploration.

As the first step, rock samples have been selected from the Jászság Basin by using databases from hydrocarbon exploration because several deep wells had been drilled in the Pannonian Basin. Hence, we could choose the most promising area by evaluation of the well-logs~~,~~ containing the borehole-geophysical results, the carbonate~~-~~content and the petrologic description of the formations of the stratigraphic section.

In the studied area there are 4 major formations (2 storage and 2 cap rock formations) that are potentially available for future CO_2 storage. To decide what core sample to use in the experiments, we need to take into consideration all the~~se~~ data collected from the well-logs.

The second step of the presented work relates to preliminary petrophysical tests and geochemical analyses. These were made from thin section description for the original mineral composition and scanning electron microscope images taken from the natural surfaces of the rock to study directly the pores and surface morphology. Semi-quantitative analysis on mineral constituents in sandstone samples were also carried out. We were able to identify minerals such as plagioclase, orthoclase, albite, carbonate, clay minerals, micas, and pyrite.

As a third step we treated the samples with supercritical CO_2 at similar pressures and temperatures at the possible reservoir conditions to model the expected chemical processes.

In this way, we can make some restrictions about which geological formations would be reasonable for storage and which would be reasonable for the cap rock.

[1] Cole, D.R. (2008) *Elements*, **4**, 325-331. [2] Oelkers, E.H. & Cole, D.R. (2008) *Elements*, **4**, 305-310. [3] Juhász, Gy. (1998) in Bérczi, I. & Jámbor, Á. (eds.) *Magyarország Geológiai Képződményeinek Rétegtana. MOL Nyrt. & Magyar Állami Földtani Intézet*, 469-483.

Mineralogy and geochemistry of methane-bearing sediments of the Gulf of Cádiz (Atlantic Moroccan Margin)

Mata, M.P.[1*], Falagán, C.[2], Martos R.[2], González-López, N.[3], Casas, D.[1], Sánchez-Bellón, A.[2], Martínez, J.[2], López-Aguayo, F.[2], Narjisse, A.M.[4,2] & Somoza, L.[1]
[1]Instituto Geológico y Minero de España, Tres Cantos, Madrid, Spain ([*]p.mata@igme.es)
[2]Depto. Ciencias de la Tierra, Facultad de Ciencias del Mar y Ambientales, Universidad de Cádiz, Cádiz, Spain
[3]Instituto Español de Oceanografía, Fuengirola, Málaga, Spain
[4]Dept. Géologie et Océanologie, Faculté des Sciences et Techniques, Université Abdelmalek Essaâdi, Tétouan, Morocco

The Gulf of Cádiz has been extensively surveyed in recent years and several gas-related fluid escape seafloor structures have been identified as mud volcanoes, pockmarks and carbonate crusts. Methane-gas hydrates have been sampled at least from five mud volcanoes in the area. Sediments of mud volcanoes, named mud breccia, are made of mud and clasts and are carried up from deeper areas associated with the fluids. Diagenetic minerals, mainly carbonates and sulphides, resulting from the anaerobic oxidation of methane by microbial processes are frequent in the discharge areas

Gravity cores collected during the MVSEIS08 cruise on the Atlantic Moroccan Margin have been studied. The cores were taken on the summit and slopes of Moroccan mud volcanoes from 400 up to 1400 m depth. A detailed mineralogical analysis by XRD, chemical composition including XRF core-scanner ICP, and organic matter content (OM), C/N ratios, of 4 different mud volcanoes have been performed in order to determine whether there is a characteristic mineralogy in the gas-related sediments. A detailed clay mineralogy study is being carried out, as they can provide important information about the nature and depth of the fluids and the reactions of gas with clays, as smectite may interact at reticular scale with hydrates [1].

The results show that mud breccia of mud volcanoes show an enrichment in clay minerals compared with the adjacent sediments of the continental margin, being illite, smectite and minor chlorite and kaolinite the main clays present at the mud breccia. Anomalous contents of smectite have been detected in some mud breccia units. This enrichment has been previously reported in the Pacific, Mediterranean or the Iberian continental margin of the Gulf of Cádiz. Chemical composition as determined by XRF core-scanner and ICP, show a characteristic chemical composition for the mud breccia showing an increase in Al, Si, K, Ti, Fe and other clay-related elements. Low OM and carbonate contents have been observed in the mud breccia compared with the sediments of the area. C/N ratios show lower values for mud breccia than for the rest of the units.

The mineralogical and chemical analysis of the cores reflects different origins and diagenetic processes for each unit: hemipelagic sediments of the slope are carbonate-rich, and mineralogy reflects the terrigenous input and processes of the continental margin, while gas-related units have abundant clays and authigenic and diagenetic minerals. As a natural analogue of gas storage, this mineralogy reflects the origin, capture and storage of methane in the marine environment. Clays are related to the origin and transport of the fluids and sediments and the final storage of gas is made by bacterial carbonates. The clayey nature of the mud breccia, leads to considerations regarding new diagenetic processes in methane-seeping areas and also to the abundances and distribution of clay minerals on continental margins.

[1] Guggenheim, S. & van der Groos, A.F. (2003) *Geology*, **31**, 653-656.

Development of pressure cells for laboratory powder diffractometers

Whitfield, P.S.[1*], Mitchell, L.D.[1], Ross, J.[1] & Parise, J.B.[2]
[1]National Research Council Canada, Ottawa, Canada ([*]pamela.whitfield@nrc.gc.ca)
[2]Dept. of Geosciences, SUNY Stony Brook University, Stony Brook, NY, USA

Development of pressure cells for lab powder diffractometers at NRC began in 2006. The first cell (rated 125 bar, -40 to 200ºC) was based on the work of [1], but changes were made to make the design ASME pressure-code compliant. The cell was used successfully to collect in-situ MoKα XRD data on polymer crystallization under high pressure CO_2. On termination of the polymer project it was determined that such instrumentation could be useful for fundamental studies related to CO_2 sequestration. Given the sluggish nature of many sequestration-related reactions, long-term lab-based experiments can be more useful than the limited beamtime available at synchrotrons. Limited proof-of-concept studies were successfully undertaken on the carbonation of calcium silicate hydrate and wollastonite [2]. Unfortunately the design and materials (304SS) of the first generation stage were not capable of attaining and retaining the conditions required for serious sequestration studies.

A second generation stage has been designed for the physical and chemical conditions required for down-hole studies, including deep brine aquifers. Made from C-22 nickel superalloy for corrosion-resistance, it is designed for 300 bar and 300ºC (electrically heated) with concentrated chloride solutions at pH3. Use in lab systems requires the use of AgKα radiation with 0.635cm thick Ta-coated Be windows. The design allows use in both reflection and transmission geometry so is also suitable for synchrotron applications without modification. The design is undergoing pressure vessel certification in Ontario and a mock-up was constructed from C-22 (Fig. 1) to verify the FEA thermal modelling portion of the stress analysis.

Once commissioned, studies will be conducted under down-hole conditions on pure materials and core samples. The aim is to provide experimental kinetic data to improve geochemical models for long-term CO_2 storage. A second stage will be used at the NSLS for studies on more rapid reactions.

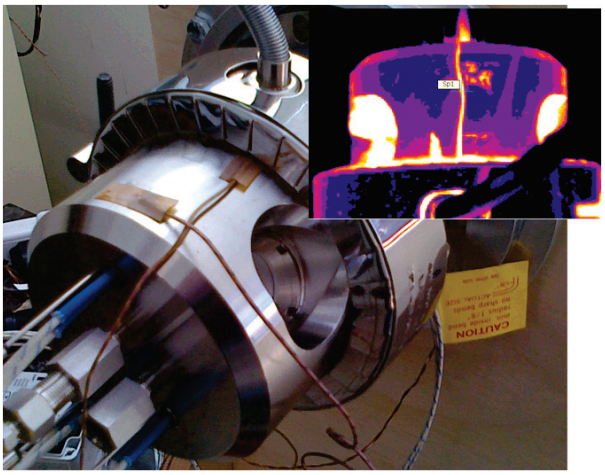

Fig. 1: Picture of 2nd generation stage mock-up instrumented for thermal tests. Inset is an infra-red image taken from above while holding at an internal temperature of 300ºC.

[1] Koster Van Groos, A.F. et al. (2003) *Rev. Sci. Instr.*, **74**, 273-275. [2] Whitfield, P.S. & Mitchell, L.D. (2009) *Appl. Geochem.*, **24**, 1635-1639.

Implications of sand-bentonite mixtures used for radioactive waste disposal

Rueedi, J.*, Marschall, P. & Schwyn, B.
National Cooperative for the Disposal of Radioactive Waste (Nagra), Wettingen, Switzerland (*joerg.rueedi@nagra.ch)

In the Swiss low- and intermediate level waste (L/ILW) disposal concept a design option (engineered gas transport system - EGTS) was studied in the past years aiming at increasing the gas transport capacity of the backfilled underground structures without compromising the radionuclide retention capacity of the engineered barrier system. It involves specially designed backfill and sealing materials such as high porosity mortars as backfill materials for the emplacement caverns and sand/bentonite (S/B) mixtures for backfilling other underground structures and for the repository seal.

Preliminary experimental studies confirmed the high gas transport capacity of the S/B mixtures. These experiments have shown the ability to design S/B mixtures with specific target permeabilities for water and gas flow. First experiences were gained through the Gas Migration Test (GMT) at Grimsel Test Site (GTS) for which a comprehensive laboratory programme on combined gas/water transport in S/B mixtures has been performed.

Numerical simulations were conducted which demonstrate the effective functioning of the EGTS concept for a range of repository configurations and parameter variants. The model calculations show clearly that the gas produced in emplacement caverns can be released efficiently along the engineered gas transport system to the backfilled access tunnel where it accumulates and eventually escapes into the adjacent rock formations. The model calculations show as well that both the length and the average gas/water permeability of the repository plugs and the seal are important design parameters to avoid excess gas pressures in the repository.

Two major scientific questions were raised in the previous studies. On the one hand, up-scaling of S/B material properties (e.g. water and gas permeability) gained from small scale laboratory samples to the behaviour of a repository plug or seal is seen as an important research topic. The impact of material heterogeneities induced during construction is important for the long-term prediction of gas pressure evolution in a repository. On the other hand, past research work has indicated that long-term interaction of cementitious materials with S/B mixtures may impair the gas transport capacity of S/B plugs and seals potentially leading to increased pressures in the system.

Building on experiences so far, a broad experimental program has started in 2009 as part of the EU 7th FP project FORGE. This laboratory program includes both small scale experiments to investigate in detail the material properties and small-scale gas and water transport behaviour and a larger scale demonstration (mock-up) experiment of the repository seal. An in-situ experiment at realistic scale is currently in the planning stage. This systematic approach will provide important insights into the up-scaling of S/B material properties and its potential impact on the overall system performance.

Parallel experiments are performed to investigate in detail the evolution of cement-S/B interfaces and their impact on the S/B material properties in general, and on gas permeability in particular. Recent developments in the analysis and visualisation of porous materials are applied and further developed to obtain detailed information on structural and hydrochemical changes at and near these material interfaces.

Crystallization of secondary sulfate and phosphate phases in cementitious conglomerates exposed to polluted environments

Secco, M.[1*], Maritan, L.[1], Lampronti, G.I.[2], Mazzoli, C.[1] & Artioli, G.[1]
[1]Dept. of Geosciences, University of Padova, Italy (*michele.secco@unipd.it)
[2]Dept. of Chemical Science "G. Ciamician", University of Bologna, Italy

A case study presenting considerable degradation of a reinforced concrete industrial building, constructed at Porto Marghera (Venice, North-Eastern Italy) in 1969, is described. The Porto Marghera area suffered from severe atmospheric pollution, with noteworthy industrial emissions of sulfate and nitrate pollutants. Moreover, the site was affected by intense phosphate soil pollution, related to the production of superphosphate-based fertilizers in the industrial plant.

The concrete of the structure is highly incoherent with intense superficial exfoliation, up to several centimetres thick. Superficial black crusts are uniformly distributed, whereas in the lower portions of the structure in close contact with the soil the cement matrix below the cortical layer shows an anomalous yellowish colour. Here the conglomerate is highly incoherent and the binder tends to pulverize.

A selection of altered concrete samples was analyzed through a profile multi-analytical approach consisting of a combination of optical microscopy, X-ray powder diffraction, and scanning electron microscopy coupled with EDS analysis, with the aim of characterizing the secondary phases formed and modelling the alteration processes. Furthermore, sequence of reactions, environmental conditions (ions concentration, temperature, pH, pe), and stability of secondary mineral phases were thermodynamically modelled using PHREEQC2 software.

The results of this combined approach suggest severe decalcification of the cement matrix and formation of secondary sulfates and phosphates according to a marked mineralogical and textural zoning: a) Gypsum in the superficial efflorescence; b) Gypsum-brushite solid solution in the superficial black crusts; c) Apatite in the inner altered portions.

The heterogeneous microstructural development of secondary phases was interpreted taking into account the different source of sulfate and phosphate pollutants, from atmospheric aerosols and through capillarity transport from the soil, respectively. Moreover, the presence of brushite – phosphate phase more stable at low pH – at the surface suggests that these portions were exposed to higher acidity conditions, related to sulfuric acid formation in the pore water after reaction with atmospheric sulfates (Fig. 1).

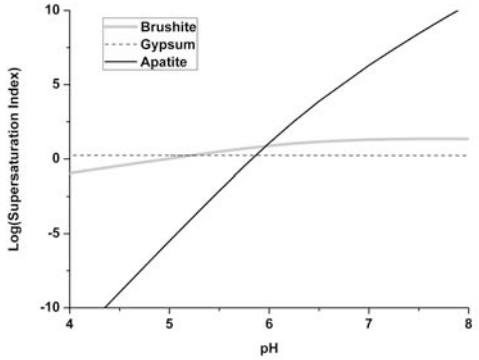

Fig. 1: Supersaturation index ($\log(a/a_{eq})$) of secondary phases as a function of pH: apatite and brushite precipitation and dissolution strongly depend on pH.

Reactive transport modeling of grout-rock interaction

Soler, J.M.[1*], Hautojärvi, A.[2] & Vuorio, M.[2]
[1]IDAEA-CSIC, Barcelona, Spain ([*]josep.soler@idaea.csic.es)
[2]POSIVA OY, Eurajoki, Finland

Grouting of water-conducting fractures with low-alkali cement is foreseen by Posiva (Finnish nuclear waste management agency) for the potential future repository for high-level nuclear waste in Finland. A possible consequence of the interaction between groundwater and grout is the formation of high-pH solutions which will be able to react with the host rock (gneisses) and alter its mineralogy and porosity.

A reactive transport modeling study of this possible alteration has been started following the recommendations from Posiva. First, the hydration of the low-alkali cement has been modeled, using results from the literature [1,2] as guide. The hydrated cement is characterized by the absence of portlandite and the presence of a C-S-H gel with a Ca/Si ratio about 0.8 after tens of years (Ca/Si is about 1.7 in Ordinary Portland Cement). Afterwards, a one-dimensional system simulating the contact between a grouted section of a fracture and the gneiss has been studied. The results from the simulations show a very fast (days to weeks) sealing of porosity at the rock-grout interface. The precipitation of C-S-H (tobermorite), and also ettringite in some cases, is responsible for this fast sealing of porosity. The mixing by diffusion of a Ca-rich solution from the grout and a Si-rich solution from the rock causes this precipitation.

New calculations have finally been started simulating the interaction between flowing water and grout and the alteration of the host rock as this water (high-pH plume) flows beyond the grouted section of a fracture.

[1] Lothenbach, B. & Wieland, E. (2009) *Chemical evolution of cementitious materials.* NEA Workshop, Brussels, Belgium. [2] Lothenbach, B. & Matschei, T. (2009) *Thermodynamic modelling: hydration modelling.* The Fred Glasser Cement Science Symp., Aberdeen, Scotland, UK.

C-S-H gel dissolution kinetics

Trapote, A., Cama, J.[*] & Soler, J.M.
Dept. of Geosciences, Institute of Environmental Assessment and Water Research, IDAEA, CSIC, Barcelona, Spain
([*]jordi.cama@idaea.csic.es)

C-S-H gel, which constitutes at least 60% of the fully hydrated Portland cement paste, is the main responsible of the durability and barrier properties of cement. Although C-S-H solubility has been studied by many authors, the dissolution kinetics is not known. In this communication we present kinetic data based on the results obtained from flow-through experiments.

The C-S-H gel used in the experiments was obtained by hydration of synthesized C_3S ($3CaO \cdot SiO_2$), which results in the formation of C-S-H and portlandite. C-S-H was ground to a size fraction of ~ 10 μm and the solid Ca/Si stoichiometric ratio was about 1.65 (electron microprobe analysis). The flow-through experiments were carried out at room temperature (22 ± 2°C) and under CO_2-free N_2 atmosphere to avoid carbonation. Ca and Si concentrations and pH were monitored during the experiments. The flow rate was kept constant either at 0.05 or 0.13 mL min^{-1}.

The evolution of pH and Ca and Si concentrations showed three distinct stages during the experiments: (1) Ca concentration was much larger than Si at the start of the experiments, indicating preferential dissolution of portlandite ($Ca(OH)_2$) and slow close-to-equilibrium dissolution of C-S-H. (2) As the portlandite content diminished a gradual decrease in Ca and increase in Si was observed, indicating an increase in C-S-H gel dissolution. The aqueous Ca/Si ratio decreased to values below 10. pH also decreased. (3) Concentrations of Ca and Si and pH (9.7 – 11.4) reached steady state. At this stage the aqueous Ca/Si ratio remained constant at about 0.9 indicating that (i) the C-S-H gel was the main dissolving phase and (ii) the dissolution reaction was stoichiometric with respect to a phase with a Ca/Si ratio similar to that of tobermorite. Steady-state dissolution rates of the C-S-H gel normalized to the final BET specific surface area ranged from 10^{-11} to 10^{-10} mol m^{-2} s^{-1}.

Based on these results two main conclusions can be drawn:

1) The dissolution of the C-S-H gel is initially incongruent (preferential release of Ca) and evolves to the congruent dissolution of a phase with tobermorite stoichiometry (Ca/Si = 0.83), which is consistent with the solubility model presented by Kulik and Kersten [1].

2) The dissolution rate of this end-member is not especially fast, similar for instance to that of feldspars. These values highlight the necessity of considering C-S-H dissolution kinetics in cases where water flows by advection through mortar or concrete (fast transport; dissolution rate is the limiting factor in C-S-H dissolution).

[1] Kulik, D.A. & Kersten, M. (2001) *J. Am.Ceram. Soc.*, **84**, 3017-3026.

Time- and space-resolved investigations of cementitious materials by X-Ray diffraction methods

Schlegel, M.*, Mueller, U., Panne, U. & Emmerling, F.
Federal Institute of Materials Research and Testing, Berlin, Germany (*moritz-caspar.schlegel@bam.de)

Cementitious building materials are present in our every day life almost everywhere. Due to the nature of the cementitious binder those materials can be described as multi component nano composite materials. However, analyzing their microstructure and the phase composition of the hydration products is a difficult task due to their nano size and poor crystallization. Furthermore, to study degradation mechanisms spatial data are needed linked to the microstructure of the cementitious paste. In recent years new possibilities have arisen in order to investigate these difficult materials by means of analysis with synchrotron radiation.

The objectives of this work are therefore the observation of the time resolved hydration of cement-phases and the analysis of spatial resolved phase assemblage of chemical attacked mortar and concrete including synchrotron methods.

The hydration processes were examined by diffraction with synchrotron radiation in transmission geometry with a wavelength of 1.0656 Å at the μ-spot beamline at BESSY II, Berlin. An ultrasonic trap provided the contact free analysis of a sample and ensures a constant water cement ratio. This is a tremendous improvement since former studies using capillaries coupled with water injection system could not guarantee a homogeneous dispersion of water within the cement suspension. The integration time for a single diffraction pattern was about 30 sec due to the high photon flux of the synchrotron facility and allowed a detailed view into the dynamics of the hydration processes at early stages. The results were completed by long-time studies over 28 days using the X-ray diffractometer D5000 from Bruker with $Cu_{K\alpha}$-X-Ray source and Bragg-Brentano geometry.

The space-resolved phase compositions were determined on sulphate and chloride attacked mortal and concrete. The reaction fronts were localised through micro XRF by determining the S and Cl concentrations at the interface of the sulphate and chloride solution and the bulk material. The synchrotron radiation source was used to identify the phase composition in-situ. The primary focussing optics allowed a spatial resolution down to 10 µm for samples with thicknesses of about 2 mm. This led to a comprehensive analysis of the reaction fronts induced by chemical attacks. In comparison to former investigations an in-situ characterisation of the phase composition within the dense microstructure of the cementitious materials was carried out. Additionally, it is not necessary to destroy the microstructure by e.g. grinding or milling as with common preparation techniques for standard powder diffraction methods.

Investigation of the decomposition mechanism of larnite (β-Ca_2SiO_4)

Apostolaki, Ch.*, Markopoulos, Th. & Perdikatsis, V.
Dept. of Mineral Resources Engineering, Technical University of Crete, Chania, Greece (*xapostol@mred.tuc.gr)

Natural Hydraulic Limes (NHL), produced by firing marly limestone, contain mainly portlandite $Ca(OH)_2$ and larnite (β-Ca_2SiO_4, e.g. β-C_2S). Mixing NHL with aggregates, a mortar is formed, appropriate for restoration and conservation purposes of monuments and historical buildings. Portlandite is transformed to calcite, while larnite in Ca-Si–Hydrates, such as $(CaO)_{2-n}SiO_2(H_2O)_{m-n}$ [1] or C_2SH [2].

Previous results of NHL samples, curred in an open atmosphere with a relative humidity of 50 to 65 % for six months, showed that the content of calcite was higher than of that expected due to the carbonation of portlandite, whereas the larnite content was reduced. The above observation indicates that the decomposition of larnite could also lead to the formation of calcite [3]. In order to study the decomposition of larnite by avoiding the presence and the carbonation of portlandite, experiments using pure synthetic larnite were carried out. The pure synthetic larnite was synthesised by mixing CaO and SiO_2, in 2:1 molar ratio and firing the mixture at 900°C for 12 hours. The produced larnite sample was pure and contains small amounts of SiO_2 less than 1%. Two different experiments have been done. In the first experiment 1 gr of larnite powder was exposed in continuous humidified airflow of 90% RH. In the second experiment 1gr of larnite powder was placed in distilled water. The water was boiled additionally in order to remove possible dissolved CO_2.

Mineralogical analysis was carried out by X-ray powder diffraction analysis (XRD) on a Bruker D8 Advance Diffractometer, using Ni-filtered Cu Kα radiation with a Lynx Eye strip silicon detector. Data were collected from 3° to 70° 2θ with a step size of 0.02° and a count time of 0.5 sec per strip step. The crystalline phases were identified using the Diffrac plus Software (Brucker AXS) and the PDF database. Corundum or silicon powder has been added as an internal standard for the quantification of the amorphous content. The quantitative analysis was performed by the Rietveld method using the TOPAS (BRUKER) software program. Using the Rietveld refinement Rwp and Rp were 9.15% and 6.87 % respectively while the relative error for the quantitative analysis was ~ 3%.

The XRD analyses of larnite in humidified airflow of 90% RH, after a curring period of three months, shows a content of 58.6 % larnite, 24.2 % calcite, 1% quartz and 16.2 % amorpous. In contrary, the XRD analysis of larnite in pure water, shows mainly portlandite and some weak reflexions, which could not be interpreted. Therefore the main quantity of portlandite has been removed from the sample. After removing, a small amount of portlandite was observed and the Ca-Si- Hydrates, Jennite $Ca_9H_2Si_6O_{18}(OH)_8.6H_2O$ and Oyelite $(CaO)_xSiO_2.zH_2O$ were identified proceedings.

In the first experiment portlandite is absent due to its conversion to calcite, while in the second one, calcite, was not detected due to the absence of CO_2. According to the above results the decomposition of larnite took place following the reactions:

$$Ca_2SiO_4 + 2H_2O \rightarrow 2Ca(OH)_2 + SiO_{2\ amorph} \quad (1)$$
$$Ca(OH)_2 + CO_2 \rightarrow CaCO_3 + H_2O \quad (2)$$
$$Ca(OH)_2 + SiO_{2\ amorph} \rightarrow \text{Ca-Si-Hydrates} \quad (3)$$

These results are in full accordance with previous research results on Natural Hydraulic Limes (NHL) [3].

[1] Ishida H., Sasaki K. & Mitsuda T. (1992) *J. Am. Ceram. Soc.*, **75**, 353-358. [2] Kim, Y.-M. & Hong, S.-H. (2004) *J. Am. Ceram. Soc.*, **87**, 900-905. [3] Apostolaki, Ch., Perdikatsis, V. & Markopoulos, Th. (2009) *DMG proceedings*, Halle.

Supercritically carbonation of calcium aluminate cements and silica fume. Application to a high level nuclear waste repository

Rozalén, M.[1], Hidalgo, A.[2] & Huertas, F.J.[1*]
[1]Instituto Andaluz Ciencias Tierra, CSIC-UGR, Granada, Spain (*javier.huertas@eez.csic.es)
[2]Estación Biológica de Doñana, CSIC, Isla de la Cartuja, Sevilla, Spain

Bentonite and concrete are essential components in building of a geological repository. Bentonite is used as an engineering barrier, due to its physico-chemical and mechanical properties, and cementitious materials are used for lining of tunnels for rock support, fix sealing cracks and many other purposes. In underground HLNW repositories, leachate of concrete elements will produce an alkaline plume. The alkaline solutions can react with the bentonite in the proximity of concrete, inducing dissolution and precipitation of a number of phases.

A strategy to reduce the potential damage of the alkaline plume over the bentonite barrier includes work with low pH concretes. The use of calcium aluminate cement (CAC) pastes, as an alternative for Portland cements, is tested in this work evaluating physical and chemical properties and the enhancement of these properties using supercritical carbonation methods.

High-pressure carbonation experiments were carried out using mixtures of CAC and silica fume (80%CAC+20%SF) in a high pressure apparatus with continuous CO_2 flow [1]. Additionally, cement pastes, raw and carbonated, were reacted with bentonite from Cabo de Gata (SE Spain) in natural granite solutions at 80°C until solution pH reached a stable value (approximately 9). The solutions were renewed periodically and analyzed for pH, Si, Al, Fe, Mg, Ca, Na and K. Solids were also analyzed by XRD, SEM and FTIR.

The results show that carbonation modifies the pH up to values below 8.5 in carbonated zones, which reduces the propagation of an alkaline plume towards other components of the barrier. Moreover, it causes changes in mineralogy reducing water permeability as a consequence and decreasing the chance of transport of aggressive fluids through pores.

Mineralogy obtained from bentonite/cement mixture experiments indicates partial dissolution of calcite and portlandite, as well as complete dissolution of hydrated and anhydrous Ca-Al-Si phases. No significance changes are observed in montmorillonite, whose exchange complex is saturated with calcium.

Partial dissolution of different phases yields pH decrease in non-treated cements. This effect is stronger in supercritically carbonated cements improving the durability of the system.

In conclusion, bentonite is able to buffer the alkalinity plume derived from concrete in the repository through dissolution of bentonite and precipitation of secondary products, as trioctahedral smectite (saponite like), zeolites and presumably Mg hydroxides and amorphous gels. The formation of these products contributes to maintain the properties of the barrier, preserving swelling and cationic exchange properties.

[1] García-González, C.A. et al. (2007) *Ind. Eng. Chem. Res.*, **45**, 4985-4992.

Characterization of the concrete alkali reactivity of granitoid and dolomitic aggregates

Sabino, N.[1,2], Santos Silva, A.[1], Menezes, P.[1], Moita, P.[2], Candeias, A.E.[3] & Mirao, J.[2*]
[1]Materials Dept., National Laboratory of Civil Engineering, Lisbon, Portugal
[2]HERCULES Laboratory and Geophysics Center of Evora, University of Évora, Portugal ([*]jmirao@uevora.pt)
[3]HERCULES Laboratory and Chemistry Center of Evora, University of Évora, Portugal

The general designation of "internal expansive reactions" includes the alkali-silica reaction (ASR) and the internal sulfate attack by delayed ettringite formation (DEF). These reactions are characterized by the formation of expansive compounds in hardened concrete and consequent cracking of the structure. In Portugal, the number of structures, mainly dams and bridges, affected by ASR is very significant and in some cases require considerable investment in rehabilitation interventions.

Moreover, previous research [1] has shown that the use of some aggregates, initially regarded as inert, can cause problems, proving the need for further insight on the role of aggregates and prevent the occurrence of ASR in constructions.

The economic value of various types of structures (e.g. dams, bridges, airfields) and the high costs related to structural degradation including losses of functionality and the permanent or temporary unavailability (for repair and rehabilitation) could be an important overthrow. Thus thorough understanding of the earth materials requirements for concrete manufacture are of vital economic importance in view of the prevention of deterioration and aging of structures whose longevity and functionality must be guaranteed. It is imperative to provide the concrete producers with the necessary knowledge in order to avoid this type of concrete degradation. Particularly important is the recently approved Lisbon-Madrid High Speed Train railway construction. This expensive operation will require large quantities of aggregates for the construction of bridges and other concrete infrastructures.

Three main sources of raw materials will be considered for the study: St. Eulalia, Montemor and Cano. These quarries are already major exploitation sites separated by 50 km and not far from the future High Speed Train railway. Two of them are granitoid rocks but the raw material from St. Eulalia is richer in quartz and poorer in ferromagnesian minerals than the Montemor aggregates (fig. 1 left). The enrichment in calcium of feldspar goes together with the iron and the magnesium. The Cano aggregates (fig. 1 right) are very different materials. The main lithology is a dolomite rock with local microscopic enrichments in phyllosilicates and very deformed quartz.

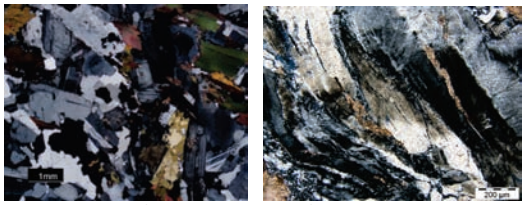

Fig. 1: Aggregates from Montemor (left) and Cano (right) quarries.

Mineralogical and textural characterization of the aggregates was done by optical microscopy. The crystallinity of quartz was also evaluated by XRD and FTIR. The aggregates were also studied by accelerated expansion mortar-bar and concrete-prism tests to evaluate their potentially alkali-reactivity. The relationship between aggregates characteristics and their behaviour in what concerns to alkali reactivity will be discussed.

[1] Santos Silva, A. (2005) *PhD thesis*, University of Minho, Guimaraes, Portugal.

Ettringite mapping by X-Ray diffraction computed micro-tomography and quantitative image analysis

Valentini, L.[1*], Dalconi, M.C.[1], Parisatto, M.[1], Cruciani, G.[2] & Artioli, G.[1]
[1]Dept. of Geosciences, University of Padua, Italy ([*]luca.valentini@nuigalway.ie)
[2]Dept. of Earth Sciences, University of Ferrara, Italy

The formation of ettringite plays a critical role in the process of hydration of cement pastes. During the early stages of hydration, reaction of the aluminate phase (C_3A) with calcium-sulfate, yielding ettringite, prevents the occurrence of the undesirable effect known as "flash-set". On the other hand, formation of ettringite during late stages of hydration, which commonly occurs in heat-cured pastes, induces the build-up of dilative stresses that may ultimately lead to severe cracking within the matrix and at the interface with aggregates. Therefore, investigating the rates and modes of ettringite formation, and its spatial location and local abundance within the paste, is crucial to understanding both early-stage kinetics and processes related to deterioration.

In this study, a 3D non-invasive technique based on computed micro-tomography, coupled with X-ray diffraction (XRD-CT) is developed with the aim of mapping the distribution of ettringite within a cement paste. The main advantage of this technique is that the spatial distribution of ettringite (or other phases) can be studied on a three-dimensional basis, and without perturbing the microstructure of the sample. The output of the tomographic reconstruction consists of a series of 2D slices in which the relative amount of ettringite is encoded as a grey intensity value. A strategy was devised in order to convert the grey intensity values into volume fractions of ettringite, by calibration with the overall weight fractions relative to the various phases, obtained by Rietveld refinement of the diffraction patterns acquired by XRD-CT. Moreover, analysis of the images by a multifractal technique provided a tool for quantitative comparison of the ettringite distribution patterns in different samples, e.g. collected at different hydration times, or in OPC pastes with and without admixtures. The results of the multifractal analysis may also provide information about the modes of ettringite growth and aggregation during hydration.

Quantification of surface topography alteration by converged roughness parameters

Fischer, C[1,2*] & Lüttge, A.[2]
[1]Georg-August-University, Göttingen, Germany
([*]cornelius@rice.edu)
[2]Rice University, Houston, TX, USA

Dissolution or corrosion at mineral or material surfaces results in rough surface topographies with amplitudes at the micron to submicron range. The quantification of the evolution of surface topography during dissolution or corrosion reactions is a prerequisite to understand surface reactivity and spatial reactivity anisotropies.

Characterization and quantification of spatial and amplitude variations of material surfaces by surface roughness parameters is limited by both the spatial frequency bandwidth of the sensor as well as the field of view. Superposition of several surface building blocks of a given surface leads to complex surface-roughness parameter results of surfaces modified by dissolution or corrosion processes.

Here we present an analytical approach to deconvolve results of roughness parameter measurements. We apply *converged* surface roughness parameters for the detection and quantification of surface building blocks responsible for the respective amount of roughness parameters as a function of the field-of-view of the dataset [1]. Subsections of varying size of a given surface topography dataset were analyzed. Surface data were collected using vertical scanning interferometry (VSI), a surface-sensitive method with sufficient lateral and remarkable high vertical resolution.

As an example, we apply root-mean-square (rms) roughness (*Rq*) to quantify amplitude variations and the interfacial area ratio (*F*) to quantify the evolution of the total surface area of reacted surfaces. This approach is helpful for several mineralogical and technical applications. As an example, the evolution of iron oxide encrustation topographies was investigated. Surface sections with a specific micron to submicron rms-roughness show preferred colloidal particle adsorption [2]. This example underlines the potential of the approach discussed here to understand environmental processes as well as to develop technical applications.

[1] Fischer, C. & Lüttge, A. (2007) *Am. J. Sci.*, **307**, 955-973.
[2] Fischer, C. et al. (2008) *Langmuir*, **24**, 3250-3266.

Iridescent surface layers on altered bottle glass: from the Outback into the nanoscale lab

Milke, R.[1*], Hammerschmidt, K.[1], Wirth, R.[2] & Ganzel, J.[3]
[1]Institut für Geologische Wissenschaften, Freie Universität Berlin, Germany ([*]milke@zedat.fu-berlin.de)
[2]Helmholtz-Zentrum Potsdam Deutsches GeoForschungszentrum GFZ, Potsdam, Germany
[3]Berlin-Zehlendorf, Germany

Iridescent glass is a familiar finding from archeological sites, when glass objects were buried in soil or sunk in the sea for several 100s or 1000s of years. The change in surface structure leading to this optical effect has been related to thin chipping-off alteration layers. Modern methods like FIB-FEG-SEM (focused ion beam – field-emission gun scanning electron microscopy) that provide high resolution in imaging as well as chemical and structural analysis allow new views on this phenomenologically long known type of glass corrosion.

We investigate surface layers on glass bottles dug up in Australian opal fields where they were thrown away by miners not longer than a few decades ago. According to the local people these colory bottles indicate recent opal precipitation. This is not confirmed by our analytical work. The surface layers are rich in SiO_2, and strongly depleted in Na_2O, K_2O and CaO compared to fresh bottle glass, but also Al_2O_3 is largely retained. From a bulk chemical point of view the glass surface alteration is similar to siallitic weathering of (sub)tropical soils.

Isotope analyses of fresh bottle glass *vs.* alteration layers indicate shifts both in the Sm-Nd and the Rb-Sr radiogenic systems that can only be explained by chemical exchange between a fluid and the glass surfaces. The surface layers contain about 1 wt% Cl that is absent in the fresh glass, thus indicating that the corrosion layers formed by interaction with salinar soil fluids.

Electron-transparent foils were produced and investigated by STEM and TEM methods. The surface layers are not comprised of regular spheres like precious opal, but of loosely connected and easily chipping-off regular layers. Their thickness is remarkably uniform in the 200–500 nm range, being in most cases constant for a specific sample over stacks of 20 or 30 alteration layers.

This constancy in layer thickness signals a close relation to either a material-specific or a site-specific quality of the altered glass that leads into a chemical-mechanical feedback. The most obvious driving force for this periodic effect is volume change (increase by hydration *vs.* decrease by leaching of alkali elements and others); nevertheless structural changes (devitrification) might also be important.

The iridescence at first place attracts notice because it produces bright colors in the narrow spectrum visible to the human eye; the significance of the corrosion processes behind this optical effect might be of much wider significance.

Impact of lichens on granite weathering in the High Tatra Mountains (South Poland)

Michalik, M.[1*], Maciejowska, A.[1] & Wilczyńska-Michalik, W.[2]
[1]Inst. of Geological Sciences, Jagiellonian University, Kraków, Poland ([*]marek.michalik@uj.edu.pl)
[2]Inst. of Geography, Pedagogical University, Kraków, Poland

Increase of weathering rate of aluminosilicate rocks caused by lichen encrustation is often suggested; however, a protective role of lichen is also postulated.

The aim of the study was to determine the transformation of the granite rock-forming minerals under lichen crust (*Rhizocarpon geographicum* and *R. alpicola*). Samples were collected in the northern part of the Tatra granite (from 1500 to 1860 m asl). Studied rocks are metaluminous to peraluminous, composed of quartz and plagioclase with lower amount of K-feldspar and biotite. Muscovite (both, primary and secondary) occurs as minor component. Granodiorite and tonalite dominate in the study area; granite is present mainly in pegmatite zones relatively rich in K-feldspar. Rocks are medium- to coarse-grained. Granites are hydrothermally altered (chloritization of biotite, albitization of feldspars, and development of epidote).

A yellowish, rusty or bleached zone (up to few mm thick) is present in the rock beneath lichen crusts. The outer layer of the rock is cracked, and the density of cracks is variable. Cracks are often filled by lichen hyphae but empty ones occur as well. Rock fragments are often detached and incorporated into the lichen crust. Fragmentation of the rock can be caused by mechanical action of lichen (swelling and contraction of hyphae inside rock related to changes of ambient humidity or freeze-thaw processes).

Contact between quartz and feldspar grains is usually sharp. Contact between lichen and biotite is complex especially in case of biotite crystals with cleavage plains oriented perpendicularly to the rock surface. In such case hyphae penetrate deeply into biotite (up to 1-2 mm). Deep penetration results in splitting of biotite fragments and formation of small lenses of biotite remains surrounded by hyphae.

Interaction between lichen and minerals results in chemical transformation of minerals. Feldspars in the vicinity of lichen hyphae exhibit lowering of alkali and increase of Al contents. Altered biotite exhibits relatively low content of K (often below 0.5 atom pfu based on 11 oxygen atoms) and high content of Al (and concentration of Ca in numerous spot analyses). This trend of chemical transformation can be connected with the formation of biotite/vermiculite interstratified minerals. However, biotite/vermiculite was not determined by using X-ray diffraction techniques. In the vicinity of altered biotite, accumulation of Fe (or Fe and Ti) is common.

The presence of Al, Si, K, Ca, Fe, S, Cl and P in the outer part of lichen encrustation suggests that these elements originate from decomposed minerals but probably partly also from adsorption of atmospheric pollution components.

Results indicate that biomechanical and biochemical processes are active during lichen-rock interaction. Chemical decomposition of feldspars is common; decomposition of biotite is often usually significantly advanced but depth of alterations is limited. Accumulation of different elements in the reaction zone was previously determined but newly formed minerals have not been recorded yet.

Improvement of engineering parameters of soil filling materials and their effect on the corrosion of steel

Ismail, A.I.M.[1*], Ghany, N.A.A.[2] & Ryden, N.[3]
[1]Geological Science Dept., National Research Centre, Dokki, Cairo, Egypt ([*]ali_ismail_2000@yahoo.com)
[2]Electrochemistry and Corrosion Lab, Dept. of Physical Chemistry, National Research Centre, Dokki, Cairo, Egypt
[3]Dept. of Engineering Geology, Lund Institute of Technology, Lund, Sweden

Structures such as natural gas, crude oil pipelines and water mains are only some of the many structures reported to have been affected by soil corrosion around the world. The fundamental cause of the deterioration of steel pipelines buried underground is soil corrosion. Before such a structure is put in place the risk of corrosion and the need for corrosion protection measures should be estimated. The position of the buried structure in relation to the groundwater table is of major importance for corrosion. Even in the soil above the groundwater table, there is water held by capillaries and pores. The finer the soil particles (e.g. clay) and pore size the more water is held.

In this study the effect of filling materials, comprising granular sand and gravel fill, on the corrosion rate was studied. The effects of curing time of soil blends were also investigated. Engineering properties including soil plasticity, compaction test, unconfined compression strength (UCS), swelling and shrinkage were measured using British Standards (BS) methods. The corrosion rates of steel in soil blends were determined by weight loss method and electrochemical technique. The soil blends were characterized using Scanning Electron Microscopy (SEM), X-ray Diffraction (XRD) and Energy Dispersive Spectroscopy (EDX). The results showed that addition of portland, iron and anti-sulphate cements as stabilizers reduces the corrosion rate of steel structures and increases the resistivity of soil blends.

Corrosion rates determined by Vertical Scanning Interferometry

Luttge, A.[1,2*], Salas E.C.[1] & Arvidson, R.S.[1]
[1]Dept. of Earth Science, Rice University, Houston, TX, USA
[2]Dept. of Chemistry, Rice University, Houston, TX, USA
([*]aluttge@rice.edu)

Corrosion is one of the critical challenges modern industrial societies are facing. Conservative estimates place an annual 276 billion dollar price tag on corrosion in the United States alone – and the tendency is quickly increasing. Challenges for our fight on corrosion include not only the repair of structures but a combination of assessment, prevention and process control. These tasks entail an interdisciplinary approach to the study of kinetics and corrosion mechanisms at the molecular level. As the repository of sophisticated analytical and experimental techniques, modern mineralogy is well suited to play a critical role in this interdisciplinary approach and our fight against corrosion.

We study surfaces of reflective materials such as crystalline materials, cements, glasses, metals, and living organisms, and their precipitation, dissolution, corrosion, and growth kinetics with Vertical Scanning Interferometry (VSI). Through coupling of experimental and modeling techniques (Fig. 1) and the complementary use of both Atomic Force Microscopy (AFM) and VSI we are able to directly observe the surface and its dynamic changes over a wide range of length and time scales. Although these methods do not typically permit the direct observation of molecular-scale sites, such as kink sites and their distribution, this information can be provided by parameterized kinetic Monte Carlo (MC) simulations and associated modeling techniques such as Molecular Dynamics calculations (MD).

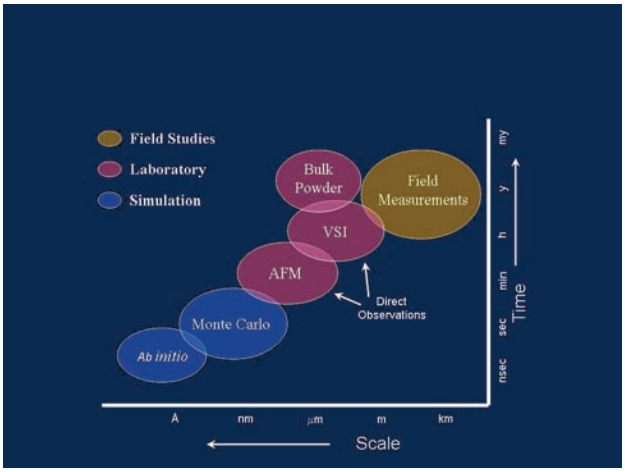

Fig. 1: Length and time scales relevant to corrosion processes.

The active surface of clays for healthy environments: dynamic of pesticides

Cornejo, J.
Instituto de Recursos Naturales y Agrobiología de Sevilla, CSIC, Seville, Spain (cornejo@irnase.csic.es)

Clays and "anionic clays" are layered natural and synthetic compounds, respectively, with very special surface properties. They are wonderful materials!

Clay minerals are composed by aluminosilicate layers negatively charged balanced with cations in the interlayer space. Smectites are a clay mineral group having swelling or expandable structure that makes the interlamellar structure accessible to cationic or polar organic molecules. On the contrary the "anionic clays" are layered double hydroxides (LDH) positively charged that is balanced by hydrated anions between the layers. Moreover, LDH has a very special property: when heated at 500ºC a mixed oxide is obtained and when put it in water rehydrates, recovering the original LDH structure. The sorption of anions from aqueous solutions by reconstruction of LDH structure is based on so-called "memory effect", which provides them with recycling possibilities. Several examples of interactions of these materials and organic molecules are shown.

The main characteristic of these materials is the high adsorption capacity and how easy they can be modified by changing the original surface properties into new ones almost "a la carte". The layer charge and the origin of the charge is a key parameter affecting sorption and chemical and phothochemical degradation reactions.

Clay minerals and LDHs are important sorbents when chemicals are ionic, ionizable or polar because their hydrophilic character. Replacement of inorganic interlayer exchangeable ions by organic ones has been shown to change the nature of the surface from hydrophilic to hydrophobic increasing mineral affinity for hydrophobic organic compounds. The selective modification of clay minerals with organic cations containing appropriate functional groups is a novel technique to maximize the affinity of the adsorbent for a given chemical.

These organoclays can be widely used as sorbents for diverse target molecules. These materials are of special interest for decontamination or contamination prevention purposes in soil and water environments e.g: in clay-pesticide formulations. Factors influencing the release rate and extent of pesticides from clays and organoclays are still issues which need to be addressed. The characteristics of the clay mineral, the amount and nature of exchangeable cations, the clay-pesticide ratio, and the procedure followed to prepare the formulation all affect the interaction of the pesticide with the sorbent and in turn its release from the formulation. Interactions mechanisms of original and modified clays with organic molecules are discussed.

Organoclays and organoLDHs based on large and small organic cations/anions are proposed not only as carriers in pesticide formulations to retard pesticide leaching after soil application and slow release of bioactive chemicals and photostabilizers but also as filters or barriers for water decontamination.

Uptake of uranium(VI) by clay minerals

Bachmaf, S.* & Merkel, B.J.
Dept. of Hydrogeology, Technische Universität Bergakademie Freiberg, Germany (*samerbachmaf@yahoo.de)

The transport of U(VI) in columns packed with different clay minerals was investigated. The major aim was to verify if the phenomena reported in previous batch experiments are true as well with flow through conditions.

Although smectites have higher cation exchange capacity than kaolinites, both kaolinite minerals (KGa-1b and KGa-2) showed much greater uranium sorption than smectites; requiring hundreds of pore volumes to achieve breakthrough. This can be considering as obvious evidence that surface complexation was the dominant mechanism for uranium retardation in all columns. The high uranium sorption capability for kaolinite is because it contains more exposed aluminol surface site which have greater binding affinity with respect to uranium than silanol sites.

The irreversible sorption of U(VI) observed in smectites packed columns can be attributed to the high content of iron oxide in the bentonite structure (e.g, 4.3% for SWy-2) comparing to that in the kaolinite structure (e.g., 0.2% for KGa-1b), which has a pronounced sorption affinity to uranium. In addition, the presence of the basal plane in (2:1) clay minerals can obviously delay the U(VI) desorption. Therefore, a slow diffusion of uranium from the surface into the interlayer forming stable surface complexes is delaying uranium extraction. The mineral composition and the degree of crystallinity plays an important role for sorption and desorption of U(VI).

Quantitative U(VI) recovery rates were obtained from the calculation of mass balance in all columns. U(VI) was totally recovered from kaolinite (although slowly), whereas 53 µg and 93µg of U(VI) remains in STx-1b and SWy-2 at the end of the experiments, which is an clear indication for irreversible adsorption (Table 1).

On the contrary, it is noticeable that the amount of U(VI) desorbed from IBECO was significantly higher than sorbed before. This can be attributed to an amount of uranium released from bentonite structure.

Table 1: Mass balance for sorbed and desorbed uranium

	Total U in µg/L	
Columns packed with	**sorbed**	**desorbed**
IBECO	474	542.1
STx-1b	566	513
SWy-2	724	631
KGa1b	877	877
KGa-2	939	928

A fast method to determine the cation exchange capacity of clays with guanidinium

Minder, P.* & Plötze, M.
Institute for Geotechnical Engineering, ClayLab, ETH Zurich, Switzerland (*pascal.minder@igt.baug.ethz.ch)

The common procedures of determining the cation exchange capacity (CEC) of clays with ammonium ions are often time-consuming and laborious [1]. Fast methods have been developed for a wide range of clay minerals using transition metal ions as exchanging index cations, e.g. copper triethylenetetramine $[Cu(trien)_3]^{2+}$ [2]. However, this method suffers from a significant underestimation of the CEC of vermiculite-bearing soils. The values depend from sample preparation. Excessive mechanical and chemical pretreatment and a longer exchange reaction time are needed to measure vermiculite CEC values effectively [3].

A new method was developed to measure the CEC of vermiculites in a simple way by exchanging the cations in one step by the highly adsorbing organic cation guainidinium $C(NH_2)_3^+$. Guanidinium (Gdn) concentrations were measured by fluorescence spectroscopy following a method proposed by Conn and Davis [4].

In our approach only some simple mechanical sample preparation is required before the exchange reaction. The sample material needs to be grinded down to a grain size less than 63 µm. Dispersion in water is achieved by ultrasonic treatment prior to the addition of the index ions. The exchange reaction then takes place within 4 hours in an aqueous solution of guanidine hydrochloride. Table 1 gives a comparison of the CEC obtained by different methods for a bentonite and a vermiculite.

Table 1: CEC (meq/100 g) from different methods

	(1)	(2)	(3)
Bentonite Calcigel	65	65	64
Vermiculite <63 µm	159	25	150

(1) Ammonium method [1], (2) Cu(II)trien method [2]. (3) Gdn method

First results show good agreement of the CEC measured with guanidinium and those measured with ammonium. Currently an experimental program is running, to apply the method to a larger range of clay minerals and to determine and improve the accuracy and the precision of the method.

[1] Mackenzie, R.C. (1951) *J. Coll. Sci.*, **6**, 219-222. [2] Meier, L.P. & Kahr, G. (1999) *Clay. Clay Miner.*, **47**, 386-388. [3] Steudel A. et al. (2009) *Clay. Clay Miner.*, **57**, 486-493. [4] Conn, R.B. & Davis, R.B. (1959) *Nature*, **183**, 1053-1055.

Investigation of adsorption properties of a kaolinite and nontronite containing clay from Dikozu region (Eskisehir-Turkey)

Orhun, O.*, Dikmen, Z. & Dikmen, S.
Dept. of Physics, Anadolu University, Eskisehir, Turkey
(*oorhun@anadolu.edu.tr)

Instrumental characterization of a clay sample from Dikozu region (Eskisehir-Turkey) was performed by various techniques such as XRD, XRF, TGA/DTA, SEM. XRD analysis was realized by XRD apparatus (Rigaku, Rint 2200). Weight percentages of the sample were calculated from XRD pattern via the method developed by Moore and Reynolds [1] (Table 1). Besides, IR spectrum of the sample was obtained from FTIR spectrometer (Bruker, IFS 66v/S). Chemical analyses of the sample were taken by means of an WDXRF apparatus (Rigaku, ZSX Primus) (Table 1). TGA/DTA analysis of the sample was obtained from Thermal Analysis System (Setaram Setys Evolution 1750) and SEM images were taken by SEM system (Zeiss, EVO 50 EP). The results of instrumental analyses were compared with each other and they show consistency [2,3].

Table 1: XRD and XRF results of the sample from Dikozu region (Eskisehir-Turkey)

Components of the clay sample: nontronite (20.1%), dolomite (35.1%), kaolinite (44.8%)
Chemical analysis of the clay sample: SiO_2(49.183%), Al_2O_3(29.35%), Fe_2O_3 (2.654%), K_2O(0.043%), MgO(8,571%), TiO_2(0.08%), other (0.814%), ignition loss (23.516%)

The clay sample, 90 µm in size, was prepared by grinding and sieving processes. After the preparation of the sample, the investigation of adsorption properties was realized by high speed volumetric sorption analyser (Quantachrome, Nova 2200). Before analysis of the adsorption properties, the sample was activated thermally in 110°C during 3 hours. Specific surface area and density of the sample were determined in the medium of liquid nitrogen (77K) by using B.E.T. method. Adsorption isotherms were consistent with B.E.T. model. After obtaining the B.E.T.isotherms, the values of the specific surface area and density of the sample were 53.043 m^2/g and 2.2 g/cc respectively.

Investigation of water vapour adsorption properties of the sample was realized by volumetric adsorption system (Quantachrome, Autosorp 1). Water vapour adsorption-desorption isotherms were consistent with B.E.T. model. Specific adsorbed water vapour, specific surface area and specific retention capacity of the sample were 30 cc/g 147.2 m^2/g and 32.630 cc/g respectively. The specific surface areas of the sample determined by using different adsorbates were found different. This difference comes from the molecular structures of nitrogen and water.

[1] Moore, D.S.M. & Reynolds, R.C. (1997) *X ray diffraction and identification and analysis of clay minerals*, Oxford University Press, Oxford. [2] Celik, K.M. (2006) *Kil Minerallerinin Ozellikleri ve Tanımlama Yontemleri*. BizimBuro, Ankara. [3] Orhun, O. et al. (2009) *Final report of research project 041061*. Anadolu University, Anadolu University, Eskisehir.

Stability and forms of Fe in natural and modified clays: connection to sorption properties

Dousova, B.[1*], Kolousek, D.[1], Grygar, T.[2], Herzogova, L.[1], Lhotka, M.[1], Machovic, V.[1], Krejcova, S.[1] & Jakubikova, B.[1]
[1]Institute of Chemical Technology in Prague, Prague, Czech Republic ([*]Barbora.Dousova@vscht.cz)
[2]Institute of Inorganic Chemistry ASCR, Rez, Czech Republic

The stability and forms of structural Fe in natural aluminosilicates have been usually based on the redox potential, predominantly in aqueous environment. The oxidation-reduction processes of Fe particles in soils and sediments strongly influenced not only physical chemical properties, but also surface properties of aluminosilicates (specific surface area, surface charge) [1], closely related to the adsorption behaviour of solid phase.

Recently Fe-modified aluminosilicates have opened new possibilities in adsorption technologies due to the change of surface charge (pH_{ZPC}) and thus a strong affinity to anionic contaminants. Four natural and two modified clays with a high content of Fe (Table 1) were investigated in term of Fe forms, their changes during adsorption processes and the stability under balanced and/or disturbed conditions in solid-aqueous system (redox potential, ionic strength, pH, microbial activity, competitive ions, etc.) [2,3].

Table 1: Relative content of Fe in natural and modified clays (% wt.)

	locality	characteristic	Fe (%wt)
Kaolinite	Király Hill, Hungary	natural	3.0
Illite clay	Illite pit in Tokai, Hungary	natural	1.7
Smectite clay	Lignite pit, Visonta, Hungary	natural	to 6.9
Calcined kaolin	West Bohemia, CR (pit)	modified Fe^{2+}/Fe^{3+}	4.1/27.2
Bentonite	West Bohemia, CR (pit)	natural	14.6
		modified Fe^{2+}/Fe^{3+}	17.8/28.6
Kaolinite clay	West Bohemia, CR (clay deposit)	natural	8.9

The detailed characterization of Fe chemistry in different types of aluminosilicates anabled to predict the stability and detention time of surface fixed particles forming complexes and/or covalent bonds via Fe ions. These properties particularly affected the adsorption quality of clay sorbent both in natural systems and in technological processes. The adsorption/ desorption of dissolved ions including toxic contaminants strongly depended on their initial concentration, and also on surface Fe phases (their amount and chemical forms). However, the stability of saturated sorbent also related to the type and purity of clay matrix, binding character, physical chemical properties and ageing time.

Acknowledgements: This work was the part of the project P210/10/0938 (Grant Agency of Czech Republic) and the research programme MSM 6046137302 (CR).

[1] Manceau, A. et al. (2000) *Am. Mineral.*, **85**, 153-172.
[2] Doušová, B. et al. (2009) *J. Hazard. Mater.*, **165**, 134-140.
[3] Burleson, D.J. & Penn, R.L. (2006) *Langmuir*, **22**, 402-409.

Synthesis and investigation of physicochemical properties of Zr,Al-pillared montmorillonites

Timofeeva, M.N.[1*], Panchenko, V.N.[1], Chesalov, Yu.A.[1], Tsybulya, S.V.[1] & Bolormaa, O.[2]
[1]Boreskov Institute of Catalysis, Novosibirsk, Russia ([*]timofeeva@catalysis.ru)
[2]Faculty of Chemistry, National University of Mongolia, Ulan Bator, Mongolia

Nowadays for direct elimination the pollutions considerable attention has been given to the development of new functionally active sorbents based on clay minerals due to their unique structural and physicochemical properties. Multicomponent systems containing two mixed ions, such as Al/Ga-, Al/Fe-, and etc., are of particular interest due to their unique textural and physicochemical properties.

A Na-containing naturally occurring montmorillonite was intercalated with solutions containing Al-, Zr-, and mixed Zr,Al-cations, with various Zr/Al ratios [1]. The Zr,Al-PILCs were obtained by calcination of the intercalated precursors at 450°C. Characterization studies were performed by use of XRD, FTIR, DR-UV-vis and N_2-adsorption/desorption analysis.

Effect of Zr/Al ratio of Zr,Al-containing pillaring solution on structural and physicochemical properties of Zr,Al-PILCs was examined. As can be seen from Table 1 all Zr,Al-PILCs showed ordered, layered structures with basal spacing between 18.3 -16.4 Å (14.7 Å for Na-clay). The increase in Zr content in Zr,Al-PILCs favours the increase in interlay distance (d001), although the specific surface area slightly changes.

Table 1: Textural data of Zr,Al-PILCs

	Al % wt	Zr % wt	S_{BET} $m^2 \cdot g^{-1}$	d_{001} Å
Al-CAC	8.80	0	216	18.3
Zr,Al-CAC(70/10)	8.76	1.89	271	17.6
Zr,Al-CAC(70/20)	8.72	3.58	240	17.0
Zr,Al-CAC(70/30)	8.15	3.00	205	16.4
Zr-CAC	5.55	11.6	206	10.7

The increase in Zr content makes alterations in nature and strength surface functional groups that were confirmed by IR spectra of adsorbed CO and $CDCl_3$. The increase in Zr content leads to the change in surface acidity. The Zr,Al-PILC in the aqueous suspensions became coloured after the adsorption of Congo red (CR). The following stainings were obtained, on Zr,Al-PILC(10/70) - red, on Zr,Al-PILC(20/70) - violet-red and on Zr-PILC - dark violet (Fig. 1). It appears that CR can serve as an indicator of the surface acidity of montmorillonite.

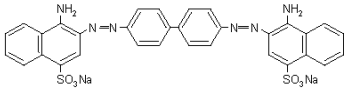

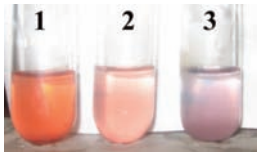

Fig. 1: Adsorption of Kongo red (0.035 $mg \cdot ml^{-1}$) on Zr,Al-PILC(10/70) (1), Zr,Al-PILC(20/70) (2) and Zr-PILC (3) at 25°C.

The effects of surface acidity of Zr,Al-PILCs, initial pH value of the Congo red dye solution and temperature on adsorption capacities of samples for CR dye have been investigated.

[1] Timofeeva, M.N. et al. (2009) *Appl. Catal. B Environ.*, **90**, 618-627.

Electric-field induced alignment of modified Na-fluorohectorite clay particles

Rozynek, Z.*, Wang, B. & Fossum, J.O.
Dept. of Physics, NTNU, Trondheim, Norway
(*zbigniew.rozynek@ntnu.no)

The electric field induced alignment of organically modified sodium-fluorohectorite (Na-Fh) clay particles suspended in silicone oil was studied by means of synchrotron wide angle X-ray scattering (WAXS).

This report focuses on the comparison between the anisotropic arrangement of organically modified clay particles and their previously studied non-modified counterparts [1].

Na-Fh particles suspended in oil undergo a fast and extended structuring when subjected to an electric field [2]. As a coarse approximation, the Na-Fh clay platelets forming the chain can be represented as disk-shaped aggregates, whose orientation is defined by a unit normal vector. Thus, the anisotropic arrangement of the system can be described by an orientation distribution that is a function of the normal vectors for all aggregates [3]. The classical Maier-Saupe function was used for the orientation distribution, since it was found to be suited to our data, as discussed previously by Méheust, et al. [4]

In fig. 1 the experimental set-up is presented whereas fig. 2 shows two-dimensional diffractograms.

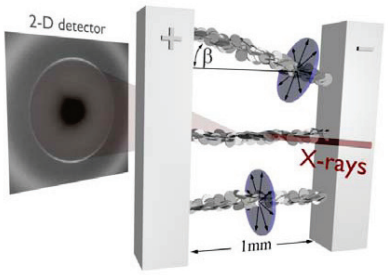

Fig. 1: Experimental geometry for the WAXS measurements. Particles are forming chains along the E-field.

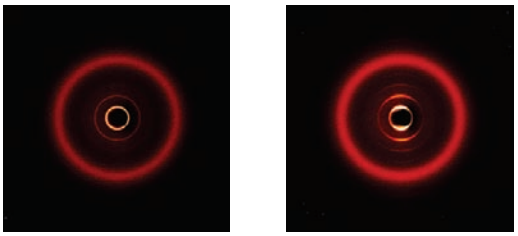

Fig. 2: WAXS patterns of modified clay particles without (left) and with (right) E-field applied (0.35 kV/mm).

The WAXS data showed that the degree of anisotropy was higher for the system with organically modified Na-Fh particles (S=0.71) than for unmodified clay particles (S=0.63). This can be explained by fact that the modified clay particles do not form large aggregates as it is the case with unmodified particles, leading to a better organization of the constituents of this electrorheological fluid.

[1] Rozynek, Z. et al. (2010) *J. Phys. Condens. Matter* (in press). [2] Fossum, J.O. et al. (2006) *Europhys. Lett.*, **74,** 438-444. [3] Rozynek, Z. et al. (2009) *J. Phys. Conf. Ser.*, **149,** 012026. [4] Méheust, Y. et al. (2006) *J. Appl. Crystallogr.*, **39,** 661-670.

Dissolution of the surfactants modified montmorillonite in HCl

Pálková, H.[1*], Jankovič, Ľ.[1], Zimowska, M.[2] & Madejová J.[1]
[1]Institute of Inorganic Chemistry SAS, Bratislava, Slovakia
(*helena.palkova@savba.sk)
[2]Institute of Catalysis and Surface Chemistry PAS, Krakow, Poland

Various concepts have been applied to modify the properties of clay minerals in order to widen their possible applications. For example, cationic organic surfactants are often used to change their surface properties. On the other hand, acid activation is an appropriate method for alteration of the clay minerals structure. In this work these two methods of modification are united and the stability of organo-modified montmorillonite in inorganic acid and the influence of the acid treatment on final textural and morphological properties of obtained products are examined.

Ca^{2+} cations in Ca-SAz-1 montmorillonite were exchanged with organic cations with different length of alkyl chains: tetramethylammonium (Me_4N^+), tetraethylammonium (Et_4N^+), tetrapropylammonium (Pr_4N^+), and tetrabutylammonium (Bu_4N^+). The results of the chemical analysis revealed very low Mg and/or Al content present in the solid reaction product after 8 hrs dissolution of Ca-SAz-1 in 6 M HCl, indicating almost completely decomposed sample. Me_4N-SAz sample was dissolved in similar extent. However, with increasing size of the organic cation higher resistance to acid attack in order Ca ≤ Me_4N^+ < Et_4N^+< Pr_4N^+< Bu_4N^+ was observed. About one half of the initial aluminium content still remained in the solid reaction product for Bu_4N-SAz dissolved even for 8 hrs. SEM analysis showed that destruction of the original layer composition upon acid treatment became evident also from the overall morphology of the particles, their size and aggregation. The exposed planes of large plate-like montmorillonite aggregates were disintegrated and smaller fine grains were created. Formation of protonated silica as a product of acid leaching led to the sharp increase in BET surface area of Ca-SAz-1 from 70 m^2/g to 467 m^2/g, after 4 hrs of treatment. The only sample reaching the similar maximal BET value was the 4 hrs treated Me_4N-SAz. The course of the BET values for all samples is given in Fig. 1. The gradual increase in the BET surface area was also observed for Bu_4N-SAz, but it did not reach the values found for other studied samples (Fig. 1), which confirmed only partial decomposition of this montmorillonite. Bulky organic cations cover larger surface area of montmorillonite, what decreases the accessibility of the interlayers to proton attack causing the increase in the resistance of the clay layers to the acid.

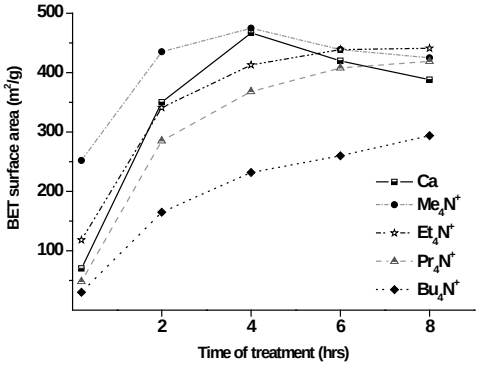

Fig. 1: BET surface areas of untreated samples and samples dissolved in 6M HCl at 80°C for various times.

Influence of clay's cation exchange capacities (CEC) on organoclay structure and locations on the loaded surfactants

He Hongping*, Ma Yuehong, Qing Yanhong, Zhu Jianxi & Yuan, Peng
Guangzhou Institute of Geochemistry, Chinese Academy of Sciences, Guangzhou, China (*hehp@gig.ac.cn)

During the last two decades, organoclays have attracted great interest due to their wide applications such as adsorbents for organic pollutants and clay-based nanocomposites [1]. However, some important aspects still have not received enough attentions, such as the influence of the characteristics of the used clays and configuration of the used surfactants on the microstructure and property of the resultant organoclays, the microstructural evolution of organoclays when heated. These are of high importance for the applications of organoclays.

In this study, three montmorillonites with different cation exchange capacities (CECs) and surfactants with different alkyl chain length and chain number were used to prepare organoclays at different surfactant concentrations. A combination of various characterization techniques was applied to investigate the microstructure of the obtained organoclays and their microstructural evolution when heated. The present study shows that the basal spacing of the organoclays increased with surfactant loading [2,3], while the maximum basal spacing increased as the alkyl chain length of the surfactant increased [2]. For the same surfactant, the maximum basal spacing of the organoclays was little influenced by the CEC of the montmorillonite component [4]. The level of surfactant loading required to reach the maximum basal spacing, however, strongly depended on the CEC. For a given surfactant, the maximum basal spacing increases with the increase of chain number.

When heating the organoclays, there is a slight increase of basal spacing before 340°C and after this temperature, there is an obvious decrease of the basal spacing, indicating the degradation the intercalated surfactants. The XRD patterns at different temperatures and TG curves of the organoclays indicate that there are two basic different locations of the loaded surfactants: 1) adsorbed on the clay external surfaces, including in the pores available between clay particles with a "house of cards" structure [5], 2) intercalated into clay interlayer spaces via two different ways, i.e., surfactant cations replacing the interlayer exchangeable metals and surfactant molecules being adsorbed into interlayer spaces [6,7].

[1] Bergaya, F. & Lagaly, G. (2001) *Appl. Clay Sci.*, **19**, 1-6. [2] Lagaly, G. (1981) *Clay Miner.*, **16**, 1-21. [3] Zhu, J.X. et al. (2003) *Chin. Sci. Bull.*, **48**, 368-372. [4] He, H.P. et al. (2010) *Appl. Clay Sci.*, **48**, 67-72. [5] He, H.P. et al. (2006) *Clay. Clay Miner.*, **54**, 691-698. [6] Yariv, S. (2004) *Appl. Clay Sci.*, **24**, 225-236. [7] Theng, B.K.G. et al. (2008) in Huang, Q.Y., Huang, P.M. & Violante, A. (eds.) *Soil Mineral-Microbe-Organic Interactions: Theories and Applications.* Springer-Verlag, Berlin, 145-174.

Effect of clay amendments on wettability of peat-based growing media – relation between capillary water uptake and EDX data on surface composition

Below, M.*, Walsch, J. & Dultz, S.
Institute of Soil Science, Leibniz University of Hannover, Germany (*m-below@web.de)

In Europe 200.000 tones of clays are used for growing-media annually. Peat, an important substrate component gets highly hydrophobic if it is getting dry. The addition of clay to peat induces a coated surface with hydrophylic properties on the organic matter which improves rewettability and reduces the risk of erroneous irrigation. At present there is only empirical knowledge about the amount of clay needed and the optimum mineral parameters for different horticultural purposes.

For the organic substrate component a blend of different sphagnum peats with a moderate degree of decomposition, obtained from Klasmann Deilmann GmbH (Geeste-Groß Hesepe, Germany) was used. Seven clay samples highly different in their mineral parameters from the Mesozoic-Tertiary weathering mantle, Rhenish Massif were obtained from Stephan Schmidt KG (Langendernbach, Germany). A saprolitic clay, two bentonites, and two translocated clays as well as two blends were included. Mixtures of 10, 20, and 30 kg clay with 1 m³ peat were prepared.

For the evaluation of the water uptake characteristics a capillary-rise method, developed for inhomogeneous, fibrous and swelling materials (Dutch RHP-foundation) was used. The coverage degree of the peat surfaces with clay minerals was described by the C/Si ratio determined by energy dispersive X-ray spectroscopy (Quanta 200, Fei) for sections of 6 mm².

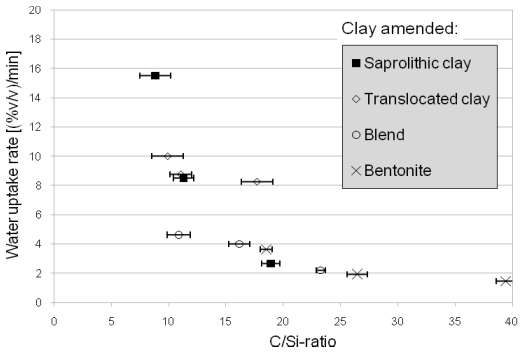

Fig. 1: Effect of four different clays amended in amounts of 10, 20, and 30 kg/m³ peat on the water uptake rate. The C/Si ratio (n=5) indicates the coverage degree of peats surfaces with clay.

At low C/Si ratios, where the surfaces of peat are most complete coated with clay minerals, all clay-peat systems show the highest water uptake rate (Fig. 1). Highest variability is observed for a saprolitic clay rich in illite and kaolinite, where the water uptake rate ranges from 2,6 to 15,5 %v/v/min. For the translocated clay and bentonite, the absolute amount of amended clay showed minor effects, but water uptake rate is quite higher than that of original peat (1,3 %v/v/min). Water uptake rate is not only affected by clay mineralogy where clays rich in illite and kaolinite show quite stronger effects than bentonites, but also by parameters such as particle size, content of secondary oxides and sorption capacity for dissolved organic matter.

Future work focuses on the stability of peat and clay aggregation during a vegetation period, which is determined at present in tests on flocculation considering electrolyte effects of fertilizers.

Spectral properties of Rhodamine 6G in smectite dispersions: effect of the monovalent cations

Czímerová, A.*, Bujdák, J. & Jankovič, Ľ.
Institute of Inorganic Chemistry, Slovak Academy of Sciences, Bratislava, Slovak Republic (*uachczim@savba.sk)

Montmorillonite monoionic forms with alkali metal and NH_4^+-cations were prepared by ion exchange. The hydration properties and binding of the ions to montmorillonite surface and the swelling properties of the mineral specimens were analyzed. Whereas Na^+- and Li^+-ions were fully hydrated over a large range of conditions, large size K^+, NH_4^+, and mainly Rb^+ and Cs^+ ions were apt to bind directly to the oxygen atoms on the mineral surface. The forms with large ions exhibited reduced hydration and swelling and the absence of macroscopic swelling of the respective aqueous colloids. The interaction of laser dye rhodamine 6G (R6G) in montmorillonite colloids was investigated by absorption and steady-state fluorescence spectroscopies. Significant effects of the properties of both the inorganic ions and swelling properties of colloidal dispersions on R6G molecular aggregation were observed. Large amounts of the molecular aggregates were formed in the colloids of Na^+- and Li^+-montmorillonites. The aggregates absorbed light at significantly lower wavelengths (~460 nm) with respect to the light absorption by non-aggregated dye (535 nm). Fluorescence spectroscopy provided a key evidence for the assignement of the type of the aggregates: The emission of the aggregates at relatively low energies proved these assemblies are rather a mixed *H*-/*J*-type than ideal *H*-aggregates. The presence of parent inorganic cations of larger size led to a significant lowering of the amount of the R6G aggregates in favor of the monomers. Investigations of the evolution of the dye aggregation with time indicated basic features of dye aggregation reaction: The size of parent inorganic ions did not affect the reaction mechanism, but rather limited the extent of the reaction. Probably the forms with large inorganic ions, such as Rb^+ and Cs^+, did not provide sufficient surface for the formation of the large size assemblies of the dye. This property can be explained in terms of strong association of the large alkali metal ions to clay mineral surface, as well as to reduced swelling in the colloidal systems of respective forms.

Characterization of Turkish kaolinite and its electrokinetic behavior in some aqueous solutions

Dikmen, S.*, Dikmen, Z. & Orhun, O.
Physiscs Dept., Science Faculty, Anadolu University, Eskisehir, Turkey (*sdikmen@anadolu.edu.tr)

The interaction of kaolinite [$Al_2Si_2O_5(OH)_4$] particles is of particular importance in widespread applications, e.g., in ceramics, in the manufacture of paper (as a coating, pigment, and filler), in inks and paints (as an extender), and as an additive in the production of rubber and polymers [1]. The behavior of kaolinite particles in suspensions, pastes, and composite materials is controlled by surface chemistry properties. Investigation of the electrokinetic behavior, characterization of the particle sizes, shapes and surface properties of the particles that compose the clay is essential [2].

In the first part of study, to determine some characterization of kaolinite sample obtained from Eskişehir (Mihalıççık) region various analysis techniques such as X-Ray Diffraction (XRD), X-Ray Flouresence (XRF), Fourier Transform Infrared- (FT-IR), Scanning Electron Microscope (SEM), specific surface area (BET), Thermal Analysis (DTA-TG), PSD (Particle Size Distribution) have been used. In the second part of the study, zeta potential (ZP) of the powdered kaolinite was investigated behavior in the presence of chloride-based metal salts (NaCl, $CaCl_2$ and $AlCl_3$) at a constant pH and also at different pHs, without metal salts.

Based on the result of semi-quantitative XRD analyses by Moore and Reynold's method [3], content of Ahirozu kaolinite is 92.2% kaolinite and 4.7% quartz and 1.1% calcite.

Investigating the variation of zeta potential of kaolinite, according to pH, it was found that it has point of zero charge (pzc) on about pH 3.5 and its zeta potential is negative above the pzc and positive under the pzc. Because of its pzc' value on about pH 2 and increasing the concentration of H^+ ions through the aqueous medium, electrical double layer is pressed and then the value of zeta potential increases to 3 mV.

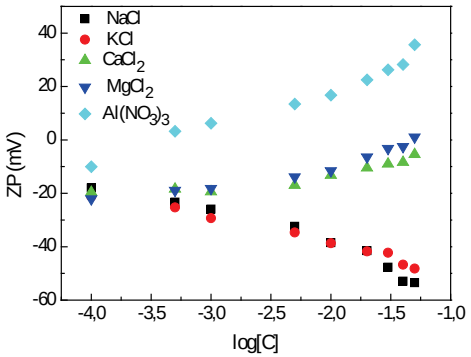

Fig. 1: Effect of the metal salts on the zeta potential of Turkish kaolinite.

[1] Kogel, J.E. et al (2006))eds.) *Industrial Minerals and Rocks*. Society for Mining, Metallurgy, and Exploration, Inc. [2] Alkan, M., Demirbaş, O. & Dogan, M. (2005) *Micropor. Mesopor. Mat.*, **83**, 51-59. [3] Moore, D.M. & Reynolds, R.C. Jr. (1989) *X-ray Diffraction and the Identification and Analysis of Clay Minerals*. Oxford Univ. Press, Oxford.

Complexation and interfacial behavior of possible environmental contaminants

Fazekas, P.[1], Fenyvesi, É.[2], Lovas, G.[3] & Csempesz, F.[1*]
[1]Inst. of Chemistry, Laboratory of Colloid and Supramolecular Systems, Eötvös University, Budapest, Hungary
(*csf@chem.elte.hu)
[2]Cyclolab Cyclodextrin Research & Development Laboratory Ltd., Budapest, Hungary
[3]Dept. of Mineralogy, Eötvös University, Budapest, Hungary

The removal of damaging chemicals has been a fundamental point in environmental research and technology, and in many related fields. For this reason, increasing attention has recently been directed to studies concerning the interfacial properties of possible environmental contaminants since they may underlie efficient technologies in treatments of soils and/or surface waters. supramolecular substances offer potential in controlling interfacial processes and represent unique models for the study of their non-covalent interactions with several chemicals.

In this paper, the relevance of inclusion complexation in improving the aqueous solubility of possible soil and water contaminants and also, the interfacial behavior of the formed supramolecular complexes are outlined. To this end, solubilization of a sparingly soluble polycyclic aromatic hydrocarbon (phenantrene, which may accumulate in soils) and a better soluble drug (carbamazepine, which may contaminate surface and ground waters) with native cyclodextrins (α-, β- and γ-cd), and with randomly methylated β-cd (rameb) or hydroxy-propyl β-cd (hpbcd), respectively, was studied in aqueous solutions. In addition, the surface properties of these chemicals and inclusion complexes at air/solution interfaces, and their adsorption from aqueous suspensions onto particles of a fractionated clay mineral (activated bentonite, particle size < 1 μm) were investigated.

The aqueous solubility of both the phenantrene and the carbamazepine could be considerably increased in solutions of suitable cyclodextrins. RAMEB and HPBCD proved to be the most efficient solubilizers for these substances. These results suggest that dissolved cyclodextrins may form inclusion complexes with each chemical. Association constants ($K_{1:1}$) for the complexes of 1:1 molar ratio have been; therefore, calculated from the experimentally determined solubility isotherms.

Certain supramolecular complexes exhibited surface activity. The complexes of both chemicals formed with the RAMEB of individually amphiphilic character and also, with the HPBCD resulted in definite reduction in the surface tension of their aqueous media.

In individual adsorption from aqueous media only slight amounts of each chemical accumulated on the Na-bentonite particles. However, the dissolved inclusion complexes adsorbed much better onto this mineral than either the individual host or the quest molecules. Especially, the carbamazepine-RAMEB and the carbamazepine-HPBCD complexes exhibited high affinity for the particle surfaces. Correlation was found between the extent of adsorption of the different inclusion complexes and their surface activity.

Preparation of modified sorbents from rehydrated clay materials

Lhotka, M.*, Machovič, V., Doušová, B. & Koloušek, D.
Institute of Chemical Technology in Prague, Prague, Czech Republic (*miloslav.lhotka@vscht.cz)

The use of clay materials as selective sorbents of different contaminants belongs to very efficient methods [1]. A natural kaolin was calcined to metakaolin and than rehydrated at different temperatures to a highly porous sorbent. The kinetics of this process was measured, with subsequent XRD and IR characterization of arised phases [2]. The specific surface and pore distribution of new phases were also assigned. In addition, the obtained kaolin was also pre-treated with Fe^{3+} ions to improve its sorption affinity to anionic particles. Fe-modified kaolin was then used for the adsorption of As/Se oxyanions, and the adsorption efficiency in dependence on the physical chemical properties (pH, As/Se concentration) of initial solution and the surface properties of sorbent (specific surface, modification method) were investigated. The adsorption properties of newly prepared sorbents were finally compared with calcined kaolins in both raw and modified forms. The theoretical and maximum adsorption capacities of rehydrated kaolins are summarized in Table 1.

Table 1: As(V)/Se(IV) adsorption on raw and Fe-modified rehydrated kaolin under the various rehydration time

Sorbent	S(BET) (m2/g)	As(V) sorption		
		$Q_{theor.}$ (mg/g)	q(max) (mg/g)	ε(max) (%)
1 day	31,75	0,49	0,35	0,5
4 days	98,57	**0,98**	**0,65**	**5,9**
7 days	103,1	0,04	0,27	1,1
1 day-Fe	27,06	6,12	6,43	96,2
4 days-Fe	**40,66**	**6,93**	**7,33**	**96,8**
7 days-Fe	38,71	6,30	6,45	96,8

Sorbent	Se(IV) sorption		
	$Q_{theor.}$ (mg/g)	q(max) (mg/g)	ε(max) (%)
1 day	1,92	1,36	8,5
4 days			
7 days			
1 day-Fe	-	5,64	59,4
4 days-Fe	-	**7,52**	**70,7**
7 days-Fe	-	6,36	62,1

As(V) adsorption on Fe-modified kaolin ran almost quantitatively by high sorption capacities, and the procedure according to Langmuir model should be considered. Se(IV) adsorption proved a different mechanism and lower sorption capacity probably resulted from the surface and binding properties of adsorbed anion. The 4-days rehydrated kaolin demonstrated the highest specific surface and the best adsorption properties for both As(V) and Se(IV) oxyanions.

[1] Doušová, B. et al. (2009) *J. Hazard. Mater.*, **165**, 135-140. [2] Rocha, J., Adams, J.M. & Klinowski, J. (1990) *J. Solid State Chem.*, **89**, 260-274.

Quantification of particle retention at natural rough black slate surfaces

Michler, A.[1*], Darbha, G.K.[1], Schäfer, T.[2], Lüttge, A.[3] & Fischer, C.[1,3]
[1]Georg-August-Universität, Göttingen, Germany (*amichle@gwdg.de)
[2]Inst. fur Nukleare Entsorgung, KIT, Karlsruhe, Germany
[3]Rice University, Houston, TX, USA

Adsorption of colloids at rock surfaces is an important environmental process. Quantitative predictions about immobilization of colloids are critical for colloid-aided contaminant transport. In the field of acid mine drainage (AMD) the retention of colloids is of particular interest because of their high potential to sorb and transport heavy metals, trace elements or radionuclides, often released during oxidative and acid rock weathering conditions [1]. Our recent studies showed that under unfavourable electrostatic conditions, the importance of surface roughness for deposition of colloids is increased [2].

Here we present a quantitative and experimental approach to investigate the relationship between micrometer to submicrometer roughness of black slates and the retention of polystyrene latex particles. Rock surface topography as well as particle retention were quantified using three-dimensional data, collected by vertical scanning interferometry (VSI). Roughness parameters (root mean square roughness, *Rq* and interfacial area ratio, *F*) were calculated based on previous studies about roughness quantification at irregular surfaces [3]. The adsorption experiments were performed as flow-through (fluid cell) and dipping experiments at pH = 6.5, where the rock surface is negatively charged according to streaming potential measurements. In a first experimental approach we used spherical particles with a diameter of 2 µm. They were negatively charged to assure conditions of electrostatic repulsion.

First results showed that micrometer-sized slopes at edges of clay mineral or organic matter aggregates are the preferred sites of adsorption of black slates (Fig. 1). Typical *Rq* and *F* values for these inclined planes of high particle density were around 0.3 µm respectively 2.8.

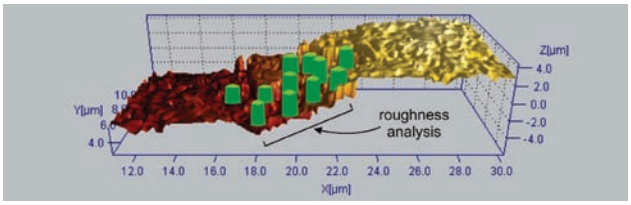

Fig. 1: High density of adsorbed particles (cylinders) at micrometer-sized slope.

Further experiments will be accomplished with smaller polystyrene particles of colloidal size. Additionally, iron and phosphate colloids will be used to resemble more AMD conditions.

[1] Fischer, C. et al. (2008) *Langmuir*, **24(7)**, 3250-3266. [2] Darbha, G.K. et al. (2010) *Langmuir*, **26(7)**, 4743-4752. [3] Fischer, C. & Lüttge, A. (2007) *Am. J. Sci.*, **307(7)**, 955-973.

Layer charge characterization of acid treated clay minerals by their interaction with methylene blue cations

Pentrák, M.*, Czímerová, A., Madejová, J. & Komadel, P.
Institute of Inorganic Chemistry, Slovak Academy of Sciences, Bratislava, Slovakia (*martin.pentrak@savba.sk)

Changes in layer charge of various clay minerals upon acid treatment were studied using their interactions with methylene blue (MB) cations. This fast method is frequently used for qualitative estimation of the layer charge of smectites; however, its utilization for other clay minerals is rare. Less than 2 μm fractions of bentonites SAz-1 (Cheto, Az, USA), SWy-2 (Wy, USA) and JP (Jelšový Potok, Slovakia) containing dominantly montmorillonite were studied together with illite/smectite DVS (Dolná Ves, Slovakia), IL (Ca-illite #36, Morris, Il, USA) and kaolinite GF (Gold Field, Pugu Hills, Tanzania). Dissolution in HCl was performed at 95°C for periods of 1–36 hours.

Dye cation agglomeration at the mineral surface depends on layer charge density and results in creation of different forms of MB absorbing visible light at different wavelengths. The spectrum of MB adsorbed on SAz-1 shows a single band at 568 nm attributed to H-aggregates which are preferentially formed on the high charge surface. Two bands of similar intensities at 568 nm and 668 nm assigned to H-aggregates and monomers, respectively, prove medium layer charge density in JP. Mainly monomers absorbing at 668 nm are detected on SWy-2 confirming the lowest charge of this montmorillonite. Absorption bands of both H-aggregates and monomers appear in the spectra with DVS and IL. The intensities of the 568 and 667 nm bands indicate medium layer charge density for IL and slightly higher for DVS. The spectrum of MB on GF kaolinite shows only a band at 667 nm attributed to the monomers and proving very low charge of this sample.

The extent of structural modification of clay minerals upon acid treatment depends on the mineral type and its chemical composition. Chemical analyses of the liquid reaction products show that the dissolution rate of the montmorillonites decreases in order SAz-1>JP>SWy-2. Non-expandable interlayers in DVS and IL increase their stability in HCl as compared to montmorillonites. Kaolinite with none or minor substitution in the layers dissolves most slowly. The spectra of MB on the acid-treated samples show that the degradation of the mineral structure is closely connected with the layer charge reduction. The negative charge sites in these materials are too far each other and MB cations cannot form H-aggregates with neighbouring cations. Therefore the intensity of the H-aggregates band at 570 nm gradually decreases in favour of monomers.

The fastest decrease of the layer charge occurs for high charged montmorillonite SAz-1. The intense band of monomers at 668 nm in the MB spectrum of SAz-1 treated for 8 h confirms that the reaction product is a material of low charge density. To get similar MB spectra for middle charged JP and low charged SWy-2, at least 18 and 24 hours dissolution time, respectively, is needed. The presence of some expandable interlayers in DVS and IL allows the interaction of MB not only on the surfaces but also in the interlayer space of these minerals. The intensities of the H-aggregates and monomers bands show only small effect of HCl on the layer charge of DVS and IL upon treatments up to 12 h. On the other hand, the changes of the spectral properties are significant after 36 h, while the charge on kaolinite has not changed. The layer charge density controls the extent of MB agglomeration on natural and acid-treated clay minerals.

Thermal behaviour of ground and unground leached vermiculite

Perez-Rodriguez, J.L.[1*], Maqueda, C.[2], Subrt, J.[3] & Balek, V.[3]
[1]Instituto de Ciencia de Materiales de Sevilla CSIC, Sevilla, Spain (*jlperez@icmse.csic.es)
[2]Instituto de Recursos Naturales & Agrobiologia de Sevilla, Sevilla, Spain
[3]Institute of Inorganic Chemistry, Řež, Czech Republic

The preparation of porous materials from clay minerals including vermiculite by selective leaching with acid has been study by several authors. The presence of iron in vermiculite plays an important role in the specific surface area obtained after acid treatment. Grinding of clay minerals significantly influences their leaching behaviour [1,2].

Ground and unground vermiculite from Santa Olalla (Huelva, Spain) was used as starting material. Vermiculite samples (<80 μm) left untreated and ground for three minutes were leached with HCl solution 1.0 M at a solid/acid mass ratio of 1:20. The suspensions were maintained at 80 ºC and stirred for 24 h.

The ground vermiculite from Santa Olalla treated with 1M HCl produced a residue constituted by silica and iron oxides.The porosity studies showed that the high surface area of this residue may be attributed to the presence of iron coming from structural iron. Using HRTEM it was found that the HCl treated ground vermiculite sample consists of amorphous silica and β-FeOOH (akaganeite) microcrystals containing a small amount of Ti and Cl^- as impurities.

The DTA-TG study showed an endothermic effect at 70ºC attributed to water mass loss and a small exothermic at 280ºC.The XRD diagrams of the residue heated in a high temperature chamber from 30 to 1200ºC at 10º min^{-1} were registered every 50ºC. The starting ground 1 M HCl leached vermiculite was partially crystalline on account of presence of the crystalline β-FeOOH. This phase is present untill150 ºC. Whereas the sample heated between 150 and 800ºC was practically amorphous. This is in agreement with the observations that β-FeOOH decomposes to amorphous or poorly crystalline phase β-Fe_2O_3 transforming only slowly to crystalline α-Fe_2O_3. At 850 °C the sample showed the first signs of crystallinity fully developed at 1050 °C. At this temperature the sample was crystalline, consisting of quartz, cristobalite, α-Fe_2O_3 and ε-Fe_2O_3. The shifting of the crystallization temperature toward higher temperature and the consequent stabilization of the amorphous Fe_2O_3 nanophase is attributed to what is called the preventive role of the silica matrix. This effect results in fact that well crystalline iron oxide nanoparticles embedded into the silica matrix are formed usually at relative high temperatures in range 600-1000 °C in contrast to silica free material.

[1] Maqueda, C. et al. (2008) *Clay. Clay Miner.*, **50**, 380-388.
[2] Maqueda, C. et al. (2009) *Appl. Clay Sci.*, **44**, 178-184.

Influence of thermal pre-treatment conditions on the reactivity of kaolinite and illite/smectite clays in alkaline and alkaline earth solutions

Seiffarth, T.*, Hohmann, M., Posern, K. & Kaps, Ch.
Chair of Building Chemistry, Bauhaus-University Weimar, Weimar, Germany (*torsten.seiffarth@uni-weimar.de)

Metakaolins, or alumosiliceous fly ashes are commonly used as starting materials for the generation of geopolymeric binders. Geopolymers are made by the means of reactive materials containing a certain amount of silicate and aluminate phases which can be dissolved by an alkaline medium. As a result of this, stable polymeric networks of alumosilicates will be formed [1]. The search for alternative low cost or high available resources as geopolymer raw materials is a matter of economic interest. This study focuses on the potential of kaolinite and illite/smectite clays in this regard.

The influence of the thermal pre-treatment conditions on the reactivity of the clays in alkaline and alkaline earth solutions has been investigated. Kaolinite and illite/smectite based clays were thermally activated between 550 and 950°C in oxidizing and reducing atmosphere, respectively. Changes were characterized by different methods (thermal analysis, XRD, dissolution tests). Isothermal calorimetric measurements were carried out to characterize the reaction process in alkaline media. The reached activity was followed by the degree of dehydroxylation and the amorphous content.

The potential of a raw material for the geopolymer reaction by alkaline activation can be derived from the molar ratio of soluble Si/Al in alkaline solutions. Therefore, dissolution tests in 10% NaOH solution (150 mg solid, 150 ml solution, 60°C) were carried out. Time of dissolution was varied (1d, 3d, 7d). Additionally, the standard Chapelle test was executed to determine the pozzolanic reactivity.

More Si than Al is dissolved from all samples after any dissolution time. That was already found for raw kaoline [4]. But on the one hand, the molar ratio of soluble Si/Al decreases with increasing dissolution time. On the other hand, this ratio increases with increasing pre-treatment temperature. This behaviour was remarkably influenced by the atmosphere of the thermal pre-treatment. The reactivity of the clays calcined in reducing atmosphere was higher than those calcined in oxidizing atmosphere at the same temperature.

It could be found that the influence of the thermal pre-treatment conditions on the reactivity of clays becomes more dominant in case of illite/smectite clay. The presence of 2:1 clay minerals results in a Si/Al ratio higher than 2. The dissolution of these minerals is slower than the dissolution of metakaolin. That was also demonstrated in former studies [3]. In addition to the type of clay minerals, the miner components (like calcite and dolomite) affect the molar ratio of soluble Si/Al [2].

Special attention should be paid to the determination of the optimal pre-treatment conditions when illite/smectite based clays are utilized as geopolymer raw materials.

[1] Davidovits, J. (2008) *Geopolymer Chemistry and Applications. Part I.* Institut Géopolymère, Saint-Quentin. [2] Buchwald, A. et al. (2007) *Proceedings of the 3rd Conference on alkali-activated Materials*, Prague, 137-148. [3] Buchwald, A. et al. (2009) *Appl. Clay Sci.*, **46**, 300-304. [4] Petrák, M. et al. (2009) *Clay Miner.*, **44**, 511-523.

Computational simulations of interactions of aflatoxin B1 with smectite

Szczerba, M.[1*] & Deng, Y.[2]
[1]Inst. of Geological Sciences, Polish Academy of Sciences, Kraków, Poland (*ndszczer@cyf-kr.edu.pl)
[2]Dept. of Soil and Crop Sciences, Texas A&M University, College Station, TX, USA

Adsorption isotherms, animal feed and human diet trials have demonstrated the effectiveness of smectite-rich bentonites in reducing or alleviating the toxicity of aflatoxin B1 (AfB1). More and more spectroscopic and mineralogy data have been accumulated to elucidate the molecular mechanisms of reactions between the mycotoxin and the minerals. Unambiguous explanations, however, have been hindered by the complexity of the spectra and lack of definite assignments on the vibrational bands. The objective of this study was to verify and refine the theories about the bonding of AfB1 to smectite. We conducted computational simulations to find the theoretical band positions in the hypothesized models and compared the simulated patterns with the experimental data to find the best match. Geometry optimization and theoretical IR spectra for aflatoxin and aflatoxin-smectite complexes were performed with density functional theory (DFT) at PCM/B3LYP/DGDZVP level of theory.

It was found that in the humid environment AfB1 forms complexes with smectite through water bridges between AfB1 and exchange ions in smectite. On the other hand, at 0% humidity AfB1 carbonyl groups were connected to the ions through ion-dipole interactions. The experimental spectra were in excellent agreement with theoretical calculations. The calculation allowed accurate assignments of the bands of experimental spectra.

Organoclay-herbicide interaction mechanism as affecting the bioavailability of organoclay-based formulations of atrazine in soil

Trigo, C.[1], Koskinen, W.C.[2], Celis, R.[1], Hermosín, M.C.[1] & Cornejo, J.[1*]
[1]Instituto de Recursos Naturales y Agrobiología de Sevilla, CSIC, Sevilla, Spain ([*]cornejo@irnase.csic.es)
[2]USDA-ARS-University of Minnesota, Minnesota, USA

Organoclays have been proposed as pesticide supports to prolong the efficacy and reduce the large runoff and leaching losses that usually suffer pesticides when they are applied in an immediately available form [1]. The bioavailability of several organoclay-based formulations of atrazine for bacterial degradation in soil was studied. Two different organic cations, L-carnitine (CAR) and hexadecyltrimethylammonium (HDTMA), were incorporated into Na-rich Wyoming montmorillonite (SW) and Ca-rich Arizona montmorillonite (SA) as a strategy to enhance the affinity of the clay minerals for atrazine (Table 1), and then organoclay-based formulations of atrazine were prepared by supporting the herbicide on the organoclays.

Table 1: Some characteristic of the organoclays used

Organoclay	OCTS[1]	d_{001} (Å)[2]
SW-CAR	61	14
SW-HDTMA	100	18
SA-HDTMA	101	24

[1]Percentage of the CEC of the clay compensated by organic cations, [2] Basal spacing value (Å)

Solvent extraction methods were used to correlate atrazine residue bioavailability in soil to atrazine mineralization using an atrazine degrading bacterium. A soil from Minnesota (USA) was treated with the organoclay-based formulations of ^{14}C-atrazine and with free ^{14}C-atrazine, and then inoculated with *Pseudomona* sp. strain ADP, a microorganism capable of rapidly mineralizing atrazine. Evolved-$^{14}CO_2$ was determined during a two-week incubation period. The amounts of ^{14}C-atrazine residues distributed between the aqueous-extractable, metanol-extractable, and bound fractions in the soil were determined at t=0 and after the two-week mineralization period, for the different formulations assayed.

Results indicated that non-extractable atrazine residues in soil increased with aging and that the mineralization rate of atrazine adsorbed on SW-HDTMA and SA-HDTMA decreased with the affinity of the organoclay for the herbicide. However, the formulation based on SW-CAR displayed a distinct behavior. Despite the very high affinity of SW-CAR for atrazine, mineralization occurred at a similar rate compared to that found for the free herbicide. Desorption experiments demonstrated that atrazine is readily released from SW-CAR at high pH levels, such as that provided by the soil tested, making the herbicide immediately available for degradation.

[1] Hermosín, M.C. et al. (2006) *Soil Biol. Biochem.*, **38**, 2117-2124.

Improving the wettability of peat based growing media by the amendment of clay

Walsch, J.[*] & Dultz, S.
Inst. of Soil Science, Leibniz Universität Hannover, Germany
([*]walsch@ifbk.uni-hannover.de)

Clays are widely used in horticulture for the amelioration of the chemical and physical properties of peat based growing media. A common problem of such substrates rich in organic matter arises from their poor wettability in the dry state. Up to now, less is known on how clay amendments differing in mineralogical composition and other mineral parameters affect the wettability behaviour of peat based growing media. In this study special emphasis was given on the adsorption of peat derived dissolved organic matter (DOM) onto the external surfaces of clay minerals in the substrate, as this process may render a clay surface from hydrophilic to hydrophobic.

Seven different clays varying in their mineral parameters (texture, mineralogical composition, cation exchange capacity (CEC), specific surface area (SSA) and oxalate and dithionite soluble Fe and Al) were used to investigate their effect on wettability and water uptake characteristics on a peat blend with a moderate degree of decomposition. The wettability was assessed in terms of contact angle (CA) measurements, calculation of surface free energies (SFE), and water uptake measurements using a capillary rise method (CRM). Differences in the affinity for peat derived DOM was determined in batch adsorption experiments and variations in the kind of adsorbed DOM fractions were traced by UV-Vis spectrometry before and after adsorption.

The wettability of peat based growing media was markedly influenced by the amount and kind of amended clay. Both, the substrate wettability as well as sorption of peat derived DOM onto clay surfaces showed strong relation to mineral parameters. Sorption of DOM increased with increasing CEC, SSA, Fe_d, and $\sum Fe_o+Al_o$ of the clays, while the substrate wettability was negatively correlated with the SSA ($r^2 = 0.66$), CEC ($r^2 = 0.69$), Fe_d ($r^2 = 0.68$) and $\sum Fe_o+Al_o$ ($r^2 = 0.61$). By considering the amount and kind of mineral bound DOM species, a non-linear regression explained 69% and 85% of the variations in substrate wettability. Overall, the results provide a useful basis for the selection of suitable clay amendments for improving the wettability of peat based growing media.

Nanocomposite clay minerals with fluorescence properties based on intercalation of kaolinite

Zacher, T.[1*] & Janek, M.[1,2]
[1]Dept. of Physical and Theoretical Chemistry, Faculty of Natural Sciences, Comenius University, Bratislava, Slovakia
([*]zacher@fns.uniba.sk)
[2]Institute of Technology, Slovak Academy of Sciences, Bratislava, Slovakia

The topic of this contribution is preparation of new organomineral derivatives, because they combine the structural, physical and chemical properties of both the inorganic host material and the organic guest species at a nanometer scale [1]. Kaolinite, despite its wide abundance in nature [2] and interesting intercalation properties [1,3] has been less studied as a precursor mineral for new organomineral materials, when compared to the smectite clays for example [4], presumably due to the difficulty in expanding the interlayers of kaolinite compared to other expandable layered materials. Methods based on the modification of preexisting inorganic structures offer considerable flexibility in the design of new hybrid materials [5].

This study has shown that the new inorganic - organic layered hybrid materials with fluorescent properties based on kaolinite can be prepared by intercalation of laser dye Coumarine 4 using guest – displacement reaction with ethylene glycol according to [6]. Prepared material was characterized using X - ray diffraction (XRD) and Fourier transform infrared spectroscopy (FTIR).

New type of inorganic – organic nanocomposite based on intercalation of kaolinite with fluorescent dye could be used to prepare antiseptic systems (e.g. painting colours, textile fibres etc.) because these systems have potential to produce singlet oxygen which has antiseptic and disinfecting effects.

Acknowledgements: This work was financially supported by grant from the Ministry of Education of the Slovak Republic No. VEGA 1/4457/07 and APVV-0491-07, as well as by student grant from Commenius University No. UK/144/2009.

[1] Rausell-Colom, J.A. & Serratosa, J.M. (1987) in Newman, A.C.D. (ed.) *Chemistry of Clays and Clay Minerals.* Mineral. Soc., London, 371-422. [2] Theng, B.K.G. (1974) *The chemistry of Clay – Organo Reactions.* Adam Hilger, London. [3] MacEwan, D.M.C. & Wilson, M.J. (1984) in G. W. Brindley, G.W. & Brown, G. (eds.) *Crystal Structures of Clay Minerals and Their X – Ray Identification.* Min. Soc., London, 197-248. [4] Okada, A. et al. (1995) in Mark, J.E., Lee, C.Y.-C. & Bianconi, A.P. (eds.) *Hybrid Organic – Inorganic Composites.* Am. Chem. Soc., Washington, DC, **55**. [5] Ozin, G.A. (1992) *Adv. Mater.*, **4,** 612-649. [6] Janek, M. et al. (2007) *Chem. Mater.*, **19**, 684-693.

Thermal treatment of organoclays enhances their sorptive potential: a weakened water-organic sorbate competition on mildly heated sorbents?

Borisover, M.[1*], Yariv, S.[2], Bukhanovsky, N.[1] & Lapides, I.[2]
[1]Institute of Soil, Water and Environmental Sciences, The Volcani Center, ARO, Bet Dagan, Israel
([*]vwmichel@volcani.agri.gov.il)
[2]Institute of Chemistry, The Hebrew University of Jerusalem, Jerusalem, Israel

Recently, we have observed that thermal treatment of organoclays (formed by exchange reactions between organic cations and inorganic cations of a clay mineral) can improve their ability to sorb organic compounds from water [1,2].The aim of the presented work is to examine how this thermal treatment effect is related to the structure of organic sorbates and exchanged organic cations. The organoclay sorbents were prepared from Wyoming bentonite through replacing exchangeable Na+ by n-hexadecyltrimethylammonium (HDTMA), tetraethylammonium (TEA) and benzyltrimethylammonium (BTMA). Then, the organoclays (and Na-bentonite itself) were heated at 150, 250, 360 and 420oC for 2 hours in air and subjected to aqueous sorption of a series of probe organic compounds (phenanthrene, nitrobenzene, atrazine, phenol, m-nitrophenol) capable of different types of molecular interactions. We have demonstrated that a mild heating (at 150 0C) of organoclays can result in a distinct increase of a sorptive efficacy of sorbents. As follows from XRD, FTIR, elemental composition and TG data, this mild thermal treatment of organoclays is associated with fairly small changes (if any) in the sorbent structure.

Heating of organoclays at higher temperatures results in a loss of organic carbon and significant changes in the organoclay structure. Further improvement of a sorptive efficacy as compared with treatment at 150 0C, if occurs, is minor. This was in contrast to our earlier expectations of a significant contribution of charcoal and oxidized organic matter formed in the clay interlayer space to the organic sorbates-organoclay interactions. It is suggested that a mild thermal treatment of clay-based sorbents results in a partial loss of a sorbent ability to rehydrate in aqueous solutions thus weakening water-sorbate competition for sorption sites on a mildly heated sorbent, and therefore, increasing a potential of organoclays to sorb organic compounds from water. In particular, organic sorbates capable of specific interactions with siloxane surfaces may demonstrate the increase of sorption on a pre-heated organoclay. In organoclays with long-chain organic cations (e.g. HDTMA) capable of additional blocking the clay surface, the enhancing effect of thermal pre-treatment on sorption of organic compounds may be mitigated as compared with organoclays formed by smaller-size organic cations (e.g. TEA and BTMA).

A parallel is hypothesized between a mechanism suppressing a hydration of a sorbent after its mild thermal pre-treatment and a recognized fixation of certain inorganic cations occurring during clay heating at higher temperatures. Important implications associated with the observed phenomena include a possibility of activating organoclays for environmental applications and a better understanding of relative role of natural organic and clay components in retention of organic pollutants by environmentally important sorbents influenced by elevated temperatures (e.g. soils affected by fire).

[1] Borisover, M. et al. (2009) *ISSHAC-7, Seventh International Symposium – Surface Heterogeneity Effects in Adsorption and Catalysis on Solids*, Extended Abstracts, 229-231. [2] Borisover, M. et al. (2010) *Appl. Surf. Sci*, **256**, 5539-5544

Simultaneous sorption of lead and phenol by bentonite and organobentonite

Honfi, K.[1], Klumpp, E.[2], Kilár, F.[1], Dékány, I.[3] & Pernyeszi, T.[1*]
[1]Dept. of Analytical and Environmental Chemistry, Faculty of Science, University of Pécs, Pécs, Hungary
([*]ptimea@ttk.pte.hu)
[2]Research Centre Jülich GmbH, Institute of Chemistry and Dynamics of the Geosphere IV, Agrosphere, Jülich, Germany
[3]Dept. of Physical Chemistry and Material Science, Faculty of Science, University of Szeged, Szeged, Hungary

Clays or organoclays have been used as barrier to prevent the transport of hazardous contaminants in landfills. However, clays are known to effectively sorb mostly inorganic contaminants, while organoclays are mainly used for organic contaminants. Since the organoclays are basically clay particles modified with cationic surfactants, there might be an optimal coverage of cationic surfactant on the clay particles to sorb both inorganic and organic contaminants. In order to determine the optimal mass of cationic surfactants on the bentonite, bentonites were treated with various ratios of dodecyltrimethylammonium bromide (DDTMA) and benzyldodecyldimethylammonium bromide (BDDDMA). The role of the benzyl group of surfactant molecules was also studied in the sorption processes.

Phenol and lead were selected as representative contaminants. Sorption kinetics and isotherms of contaminants by both organobentonites were selectively studied in the function of surface coverage. When either phenol or lead exists as a single contaminant, phenol sorption increased with increasing DDTMA and BDDDMA to bentonite ratios, and lead sorption decreased with increasing DDTMA and BDDDMA to bentonite ratios. Sorption of phenol was a function of DDTMA and BDDDMA coverage on the bentonites, while lead sorption was much more influenced by the initial lead concentration than the mass of surfactants added to the bentonites.

Hydrotalcite – like compounds as adsorbents of phenols and their environmental applications

Butenko, E.[*] & Kapustin, A.
Azov Sea State Technical University, Mariupol, Ukraine
([*]butenkoeo@rambler.ru)

This work is devoted to studies of processes of sorption of phenols by synthetic clay minerals of different composition.

To prevent dangerous contamination of the environment, industrial wastewaters should be cleaned from pollutants such as phenols [1]. The problem of pollution of natural waters, the growth in the amounts of waste waters and the search for effective methods of cleaning them are realy urgent.

The purpose of this work is the search for new anionic sorbents. Their application would help to effectively remove phenols from wastewaters.

The most promising sorbents are those based on double hydroxides of metals with the structure of hydrotalcite. They are cheap, accessible and effective, universal sorbents, with a high absorption capacity, resistance to environmental stress and can serve as excellent carriers for fixing on the surface various compounds including their modification.

The 2:1 clay minerals capable of changing the interlayer distances are very effective. Water molecules, as well as the cations and anions can be adsorbed also in the interlayer space of these minerals. Therefore it is possible to place large ions between the layers and form columns to create a system of pores where various small molecules can be placed. The pores size resulting in the intercalation process is about several tenths of nanometers. The samples were synthesized with the following ratios of cations in the matrix (Table 1).

Table 1: Samples of LDHs

MgO, mol/mol	k, мol/l·s
0,52	833,3
0,72	1290,3
0,81	1666,7
0,86	1739,1

The specific surface of LDHs was determined by low-temperature nitrogen adsorption chromatographic method with subsequent processing of the results obtained by BET method.

The change of interlayer distance in LDHs after the adsorption of phenol, were investigated.

[1] Kapustin, A. (2008) *Heterogeneous basic catalysis*. Renata, Mariupol.

Nanotubular particles derived from kaolin group minerals - structural and textural examination

Matusik, J.[1*], Wisła-Walsh, E.[2], Gaweł, A.[1], Bielańska, E.[3] & Bahranowski, K.[1]
[1]Dept. of Mineralogy, Petrography and Geochemistry,
AGH University of Science and Technology, Krakow, Poland
([*]jakub_matusik@wp.pl)
[2]Dept. of Power Engineering and Environmental Protection,
AGH University of Science and Technology, Krakow, Poland
[3]Institute of Catalysis and Surface Chemistry,
Polish Academy of Sciences, Krakow, Poland

Modified intercalation/deintercalation method was used to increase the efficiency of nanotubes formation from kaolin group minerals differing in degree of structural order [1]. At variance with our earlier work [2], methanol was used instead of 1,3-butanediol for the grafting reactions. The intercalation of hexylamine was followed by intercalation of octadecylamine [3]. Materials obtained by different procedures were subjected to detailed physico-chemical characterization (nitrogen adsorption/desorption, XRD, FTIR, DSC and TEM). The use of methanol instead of 1,3-butanediol led to a significantly different result. The content of nanotubes was much higher in the case of "Maria III" kaolinite samples containing minerals of high structural order. Poorly ordered samples ("Jaroszów kaolinite and "Dunino" halloysite) yielded less nanotubes than in the case of grafting with 1,3-butanediol. Enhanced formation of nanotubes in "Maria III" kaolinite was tentatively attributed to higher reactivity of well ordered kaolin minerals toward methanol rather than 1,3-butanediol, resulting in a more efficient amine intercalation. The additional intercalation of longer chain octadecylamine significantly increased the content of formed tubes.

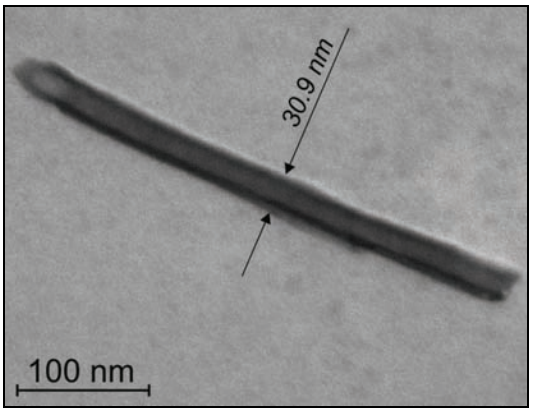

Fig. 1: TEM microphotograph of a kaolinite nanotube.

The diameters of rolled layers observed by TEM were ca. 30 nm (Fig. 1) and corresponded to diameters of newly formed group of pores detected by textural analysis. This confirmed that nanotubes contributed to a significant increase of surface area and total pore volume, observed for "Maria III" kaolinite. In the case of "Jaroszów" kaolinite and "Dunino" halloysite the changes of textural parameters were connected with the presence of macropores and mesopores with diameters different from these observed for nanotubes. These pores were assigned to interparticle and interaggregate spaces in stacks of platey particles and small amount of nanotubes.

Acknowledgements: The work was financed by Ministry of Science and Higher Education (project no. N N307 315 336, 2009-2012)

[1] Matusik, J. et al. (2010) *Micropor. Mesopor. Mater.* (in press). [2] Matusik, J. et al. (2009) *Clay. Clay Miner.*, **57**, 452-464. [3] Gardolinski, J.E.F.C. & Lagaly, G. (2005) *Clay Miner.*, **40**, 547-556.

Halloysite–TiO_2 and palygorskite–TiO_2 nanocomposites: synthesis and photocatalytic activity in decomposing air pollutants

Papoulis, D.[1,2], Komarneni, S.[2], Nikolopoulou, A.[1*], Tsolis-Katagas, P.[1], Panagiotaras, D.[3], Kacandes, H.G.[4], Zhang, P.[5], Yin, S.[5], Sato T.[5] & Katsuki, H.[6]

[1]Dept. of Geology, University of Patras, Greece
([*]athanasianikolopoulou@gmail.com)
[2]Dept.of Crop and Soil Science and Materials Research Laboratory, The Pennsylvania State University, University Park, USA
[3]Dept. of Mechanical Engineering, Technological Educational Institute of Patras, Greece
[4]Geohellas S.A., Athens, Greece
[5]Inst. of Multidisciplinary Research for Advanced Materials, Tohoku University, Sendai, Japan
[6]Saga Ceramics Research Laboratory, Arita-machi, Saga, Japan

In the present study TiO_2/clay nanocomposites were sythesized by dispersion of TiO_2 on the surfaces of two different natural clay minerals, palygorskite and halloysite, in order to increase the dispersion of TiO_2 and therefore its photocatalytic action. Deposition of TiO_2 on the clay minerals surfaces were conducted by using a sol-gel method with titatnium isopropoxide as a precursor under hydrothermal treatment at 180 ^oC. The phase composition, particle morphology and physical properties of the samples were characterized by several analytical techniques including XRD, SEM-EDS, TEM, ICP, ATR-FTIR, BET and porosimetry analysis. The synthetic procedure allows the homogeneous distribution of TiO_2 grains on the surfaces of the clay minerals leading to the improvement of the properties and potential uses of the nanocomposites. It was found that after treating with TiO_2, the halloysite and palygorskite samples showed mesopores of about 5.6 and 6.5 nm, respectively, while the macropores of halloysite (lumen) disappeared. The latter is attributed to the covering of the lumen of halloysite tubes by TiO_2 nanoparticles and for that reason the pore size of the TiO_2–treated halloysite was significantly smaller. The photocatalytic efficiency of clay-titania nanocomposites was measured in decomposing NOx, CO_2, and CH_3CHO gas. The supported catalysts showed higher activity in decomposing NO*x* gas and lower in CO_2 and CH_3CHO gas under visible-light irradiation (λ> 510 nm) and UV light irradiation (λ> 290 nm) compared to that of the standard commercial titania, P 25.

Effect of oligomerically modified montmorillonite on morphologies and properties of polycarbonate/montmorillonite nanocomposites

Huang Xiaoling, Wang Xiaoli, Su Haiquan[*] & Zhang Bingbing

School of Chemistry and Chemical Engineering, Inner Mongolia University, Hohhot, P.R. China
([*]haiquansu@yahoo.com)

Great efforts have been paid to polymer-clay nanocomposites in the past decades since those materials possess significantly improved physical [1] and other properties including thermal stability [2] and decreased flammability [3,4] over the virgin polymer.

In this work, two oligomeric surfactants (COPS-B and COPS-O) as shown in Fig. 1 were used to treat sodium montmorillonite via standard ion-exchange methods to give thermally stable oligomerically modified montmorillonites to prepare polycarbonate/montmorillonite nanocomposites (PC/MMT) by melt processing using a twin screw extruder.

Fig. 1: Structure of oligomeric surfactants used to treat sodium montmorillonite.

The results of TEM and XRD indicated that the PC/MMT nanocomposites had partially exfoliated and partially intercalated structures. Both clay loading and organic treatment structure of MMT influenced the morphologies and properties of the nanocomposites. The structure similarity, i.e., the strong interaction, between the polymer matrix and the organic treatments of the clay was a critical factor for controlling clay dispersion and exfoliation, and hence the mechanical and the heat insulation properties of the nanocomposites.

Analysis of all the composites indicated that once the clay mineral loading exceeded a critical value, it became a negative factor for forming high level dispersion to obtain better mechanical properties. Good mechanical properties of PC/MMT nanocomposites were obtained with a clay loading less than 2 wt%. A thermal-stable organic treatment was crucially important for an expected nanocomposite system with good thermal stability. It partly depended on the organic treatments of MMT used in the composites.

Great differences were observed between COPS-B and COPS-O composites. COPS-B showed visible advantage to COPS-O. Benzyl group of COPS-B in composites might play an important role in the process.

Acknowledgements: Project Supported by National Natural Science Foundation of China (grant no. 50763004, 50362002).

[1] Usuki, A. et al. (1993) *J. Mater. Res.*, **8(5)**, 1174-1178. [2] Lee, S.S. et al. (2005) *Polymer*, **46(7)**, 2201-2210. [3] Gilman, J.W. (1999) *Appl. Clay Sci.*, **15(1-2)**, 31-49. [4] Gilman, J.W. et al. (2000) *Chem. Mater.*, **12(7)**, 1866-1873.

Bentazone and phenanthrene adsorption on external montmorillonite surface - Monte Carlo modelling

Tunega, D.[1,2*] & Meleshyn, A.[3]
[1]Inst. of Soil Research, University of Natural Resources and Applied Life Sciences, Vienna, Austria
[2]Inst. for Theoretical Chemistry, University of Vienna, Austria
([*]daniel.tunega@univie.ac.at)
[3]Center for Radiation Protection and Radioecology, Leibniz University Hannover, Germany

Bentazone and phenanthrene are pesticides with different fate in soil. Bentazone can be rapidly transported by infiltrating water into ground water due to its high solubility, minimal sorption to soil particles, and low degradability. On the contrary, phenanthrene is retained by sediments and soil materials. The mechanism of the retention of nonionic hydrophobic organic compounds in soil is still debated and has been attributed to their partitioning either to organic matter or to soil clay minerals. A recent study has reported on strong phenanthrene sorption capacities of smectites, which are comparable to those of soil clays containing a considerable amount of organic matter [1].

In order to address open questions, the structural and energetic characteristics of bentazone and phenanthrene interaction with external surface of montmorillonite were studied using Monte Carlo simulations at ambient conditions. In the first part of this work, the adsorption of the studied molecules at the montmorillonite-air and montmorillonite-water interface is simulated in a constant *NVT* ensemble using the Metropolis algorithm for sampling structural properties. The simulations predict the most favourable alignments of adsorbed molecules in dependence on the varying coverage and on the thickness of the adsorbed water film. In the second part, an expanded ensemble density of states method [2] based on the Wang-Landau algorithm [3] is applied to the equilibrated systems for sampling potential of mean force profiles between the adsorbed molecule and the montmorillonite surface. Reaction path coordinate is defined as the distance between the centre of mass of the molecule and the montmorillonite surface. The following possible reaction paths are explored: (1) above a free octahedral substitution, (2) above a ditrigonal cavity centre near a tetrahedral substitution paired with Na+ ion, and (3) above a tetrahedral Si site near the octahedral substitution chosen in (1). The simulations predict the most favourable reaction path between bentazone/phenanthrene and the montmorillonite surface. A discussion on the detailed molecular-scale data on the preferred adsorption positions of the studied pesticides at the montmorillonite-water and montmorillonite-air interface based on the calculated free energy profiles will be given.

[1] Hundal, L.S. et al. (2001) *Environ. Sci. Technol*., **35**, 3456-3461. [2] Kim, E.B. et al. (2002) *J. Chem. Phys*., **117**, 7781-7787. [3] Wang, F. & Landau, D.P. (2001) *Phys. Rev. Lett*., **86**, 2050-2053.

Molecular dynamics simulation of TCDD adsorption on clay mineral

Zhu, R.[1,2], Parker, S.C.[2*] & Shapley, T.[2]
[1]Dept. of Environmental Science and Technology, Xiangtan University, Hunan, China
[2]Dept. of Chemistry, University of Bath, Bath, UK
([*]s.c.parker@bath.ac.uk)

Adsorption of organic toxicants on clay minerals is now receiving considerable attention, because contact with clays is thought to influence the transport, toxicity and bioavailability of the organic toxicants in the environment. Although experimental methods have been employed to investigate the adsorptive characteristics (e.g., batch equilibrium adsorption, spectroscopic characterization), molecular simulations represent a significant complementary approach because they can provide atomic-level insight into the adsorption process.

We report our recent research work about TCDD (2,3,7,8-Tetrachlorodibenzodioxin) adsorption on pyrophyllite and montmorillonite using molecular dynamics simulations. One of the central challenges is to develop and apply an effective force field between the pollutant and clay surfaces. We have considered a number of models. One of the most efficient is where the clay minerals were built using the ClayFF model from Cygan et al [1], and the CVFF force field was used to build TCDD and clay-TCDD potential.

Table 1 lists the adsorption energies of TCDD on the outer surface and interlayer of pyrophyllite and montmorillonite using these models within the NVT ensemble at 300K.

Table 1: Adsorption energy of TCDD on clay minerals (eV)

	Pyrophyllite	Montmorillonite
Surface	-0.44	-0.83
Interlayer	5.33	3.60
Interlayer[a]	-0.62	-1.51

The adsorption energy of TCDD on pyrophyllite was comparable with the results from DFT calculation [2], while on montmorillonite the adsorption energy was more negative. This indicates a stronger interaction between TCDD and montmorillonite. Examination of the structure shows that the interaction between K^+ and TCDD accounts for the larger adsorption energy at the montmorillonite surface.

The intercalation energies of TCDD for both pyrophyllite and montmorillonite are highly positive, because this contains the energy to separate the two layers and insert the TCDD molecule. This strong interaction between the layers of the clay minerals has also been shown by Heinz et al [3].

In another simulation, we inserted TCDD into the interlayer region but with the layers already separated. Thus, the energy for separating the layers is excluded. In this case, the adsorption energies were more negative than for the free surface (Table 1). This was because both the two layers could contribute to the adsorption of TCDD.

The above results show that although TCDD could interact strongly with clay minerals in the interlayer region, the large energy for separating the sheets could prevent the adsorption into the interlayer space of the clay minerals. However, once the layers were separated by other pillars (e.g., organic cations), the clay minerals are predicted to strongly adsorb the organic toxicants, and then influence their environmental behaviours.

Acknowledgements: This work was supported by the Royal Society-BP-Amoco Research Fellow project (RC-H1054).

[1] Cygan, R.T. et al (2004) *J. Phys. Chem. B*, **108**, 1255-1266. [2] Austen, K.F. et al (2008) *J. Phys.: Condens. Matter*, **20,** 035215. [3] Heinz, H. et al (2006) *J. Chem. Phys.*, **124**, 224713.

The influence of heteropolyacids on the textural properties of Fe-montmorillonite

Badmaeva, S.V.* & Khankhasaeva, S.Ts.
Baikal Institute of Nature Management SB RAS, Ulan-Ude, Russia (*badma77@binm.bscnet.ru)

Intercalated clays present great interest as supports for synthesis of new catalysts [1]. For synthesis of composite metal-oxide materials with high disperse uniform distribution of metals it is perspective the use polyoxometallates, containing several metals atoms in the structure of their complex ions [2].

Materials have been synthesised using two methods: I - adsorption of heteropolyacids $H_4SiW_{12}O_{40}$, $H_3PMo_{12}O_{40}$ on Fe-montmorillonite (Fe-MM-500°C) calcinated at 500°C; II - simultaneous introduction of pillaring solution (1M $FeCl_3$ + 1M NaOH) and a solution containing the heteropolyacids into suspension of clay previously dispersed by ultrasound (22 kHz, 3 min). The preparation Fe-MM method was described in our early work [3]. All the samples were calcinated at 500°C for two hours.

The samples obtained belong to mesoporous materials (Fig. 1), but the samples obtained by method II contain also micropores which surface area is equal to 5.0-17.7 m^2/g (Table 1). At that the treatment by heteropolyacids in both cases leads to a decrease in specific surface area and pore volume in comparison with Fe-MM, that may be caused by adsorption of polyoxometallates in their mesopores.

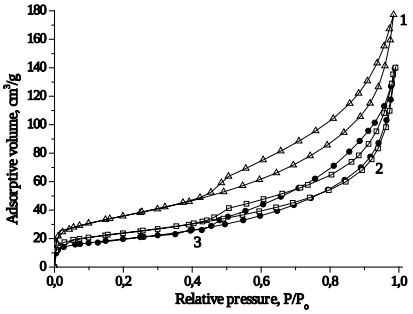

Fig. 1: N_2 adsorption/desorption of samples: 1- Fe-MM, 2- $SiMo_{12}$/Fe-MM (I) and 3- SiW_{12}/Fe-MM (I).

The Fe content in the samples is 4.0-4.6 wt.%. The quantity of introduced Mo and W depends on the method of synthesis of the material. The content of W in the samples SiW_{12}/Fe-MM obtained by method I and II is 1.82wt.% and 0.17 wt.% accordingly. The content of Mo in the samples $SiMo_{12}$/Fe-MM is 1.13wt.% (method I) and 0.53 wt.% (method II).

Table 1: Textural characteristics of composite materials

Materials (method)	Fe wt.%	W(Mo) wt.%	S_{BET} m^2/g	ΣV pore cm^3/g	D_{pore} Å	S_μ m^2/g	ΣV_μ cm^3/g
Fe-MM	4.6	0	128	0.274	85	-	-
SiW_{12}/Fe-MM (I)	4.5	1.82	84	0.217	103	-	<0.001
SiW_{12}/Fe-MM (II)	4.0	0.17	93	0.235	101	5.0	0.003
$SiMo_{12}$/Fe-MM (I)	4.4	1.13	70	0.216	123	-	<0.001
$SiMo_{12}$/Fe-MM (II)	4.6	0.53	92	0.183	80	17.7	0.009

S_{BET} – surface area, ΣV pore – total volume pore, D_{pore} – diameter pore, S_μ - surface area of micropore, ΣV_μ - volume pore of micropore.

The results of this work confirm the possibility of application of Fe-MM as supports for synthesis of catalysts.

[1] Marme, F. et al. (1998) *Micropor. Mesopor. Mat.*, **22**, 151-163. [2] Yadav, G.D. (2005) *Catal. Surv. Asia*, **9**, 117-137. [3] Shapova, M.A. et al. (2002) *Chem. Sustain. Development*, **10**, 347-353.

Dispersion influence on activation energy of kaolinite dehydratation

Bortnikov, N.S., Piloyan, G.O.*, Novikov, V.M. & Soboleva, S.V.
Institute of Geology of Ore Deposits, Petrography, Mineralogy and Geochemistry, Russian Academy of Science, Moscow, Russia (*piloyan@igem.ru)

Kinetics of kaolinite dehydratation has been studied for many decades revealing that, depending on the degree of structural perfection, concentration and extensive defects, the activation energy of dehydratation reaction changes within the range of 80-175 kJ/mol, significantly changing the reaction rate. According to the particle size, kaolinite belongs to so-called nanocrystalline materials, being characterized by size effects: dependence of material properties on its dispersivity**.** It was shown theoretically and experimentally in Piloyan & Bortnikov [1] that activation energy of reaction should decrease with dispersivity increasing. Using the approach developed in Piloyan & Bortnikov [1], in the present work the influence of dispersions on kaolinite activation energy has been investigated. As the object of study the alluvial kaolinite from Zhyravliny Log deposit (South Ural) has been chosen. The different technologically important kaolinite fractions (10-5, 5-1, 1-0.5, <0.5 μm) have been investigated by the method of transmission electron microscopy (including SAED and HRTM). Following the methodology of Piloyan & Bortnikov [1], the formula connecting the size of the coherent dispersion block with activation energy of dehydratation reaction and surface enthalpy has been received:

$$\ln(r) = A - \frac{E}{RT_m} + \frac{2H_F}{r\rho RT_m} - B\ln(I)$$

Where A and B are constants, r – the size of coherent dispersion block, E – energy of activation, R – gas constant, H_F–surface enthalpy, ρ – molar density of kaolinite, T_m – temperature of thermal effect peak on DTA curve, I – index of thermal effect form. Using experimental data the following regression equation was obtained

$$\ln(r) = 29.8887 - 21248.6 T_m^{-1} + 17.2323\, T_m^{-1} r^{-1} - 3.48522 \ln(I)$$

From this equation it has been found, that the activation energy of dehydratation reaction for kaolinite macrocrystals is 176,6 kJ/mole, that is characteristic for well crystallized kaolinites. Surface enthalpy is 0.73 J/m^2 coinciding (within the limits of experimental error) with the value of 0.62 J/m^2, obtained in Salles et al. [2]. The results obtained are shown in Table 1.

Table 1: Experimental data for the kaolinite studied

Fraction (μm)	Kaolinite content (%)	T_mK	I	r (нм)	E kJ/mole
10-5	86,4	823	1,56	27	171,3
5-1	89,3	833	1,85	23	170,4
1-5	89,24	848	2,4	17	168,2
<0,5	88,64	833	2,5	15	167,1

[1] Piloyan, G.O. & Bortnikov, N.S. (2010) *Dokl Akad Nauk*, **432**, N3. [2] Salles, F. et al. (2006) *J Colloid Interf Sc*, **303**, 617-626.

Role of clays in the preservation of organic matter

Drouin, S.[1], Boussafir, M.[1] & Robert, J.-L.[2*]
[1]ISTO, Orléans, France
[2]Institut de Minéralogie et de Physique des Milieux Condensés, Université Pierre et Marie Curie, Paris, France
([*]jean-louis.robert@impmc.upmc.fr)

It is commonly admitted that clay minerals can play a major role in the preservation of organic matter under aquatic environments and their transfer to sediments. The mechanisms of fixation of organic molecules by clays remain obscure. Series of *in vitro* and *in vivo* experiments have been performed, under marine and lacustrine environments, with synthetic saponites of variable charge and a natural low-charge montmorillonite.

This study shows the absence of intercalation of organic molecules in the interlayer space of clays. Only sorption on clay surfaces and edges occurs. *In vitro* experiments show that organo-clay interactions are mainly controlled by the type of organic molecules and particularly by the nature of their functional groups. *In vivo* experiments indicate that fresh organic matter is more easily adsorbed than diagenetically evolved one. The clay surface charge density also controls the nature and concentration of adsorbed organic species. Under lacustrine environments, a selective sorption of aromatic molecules is observed on low-charge clays.

Attempts to destabilize the obtained organo-clay compounds, by hard alkaline treatment, were unsuccessful and indicate the great stability of these associations, with strong and probably multiple bonds. Owing to this high stability of organo-clay assemblages, the organic matter becomes unavailable to benthic fauna and bacteria in natural environments.

Therefore, sorption on clays can be considered as one of the preservation mechanisms of organic matter and controls the incorporation of metabolisable molecules into sediments.

Ag- and Cu-vermiculite nanocomposites and their antibacterial effect

Hundáková, M.[1*], Valášková, M.[1] & Pazdziora, E.[2]
[1]Nanotechnology Centre, VŠB – Technical University of Ostrava, Czech Republic ([*]marianna.hundakova@vsb.cz)
[2]National Reference Laboratory, Institute of Public Health in Ostrava, Czech Republic

Clay minerals belong to the important materials which can serve as metal nanoparticles matrixes thanks to their structural properties. In this study, vermiculite from Brazil was used as starting material. Beside montmorillonite [1, 2], vermiculite is sometimes used as a matrix for silver and copper nanoparticles [3].

Vermiculite (V) was treated with different molar concentrations of aqueous solutions of $AgNO_3$ and $Cu(NO_3)_2$ and Ag-V, Cu-V, Ag,Cu-V materials were synthesized. Samples were evaluated for the effect of solutions concentrations on the quantity of Ag and Cu, structure changes of vermiculite and antibacterial activity.

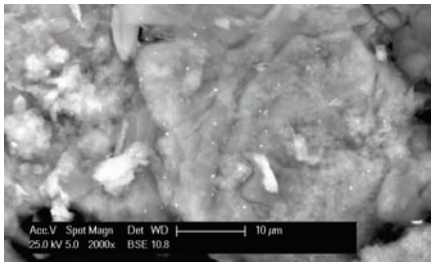

Fig. 1: The SEM micrograph of Ag-V (white dots represent Ag agglomerates on the vermiculite surface).

The morphology was studied using scanning electron microscopy (SEM). The SEM micrograph of Ag-V (Fig.1) showed agglomerates of silver nanoparticles anchored on the vermiculite substrate. Powder X-ray diffraction (XRD) was employed mainly to determine the interplanar spacings in the starting clay minerals and in the Ag- and/or Cu-V composites. The XRD patterns showed Ag (111) reflection of metallic silver. According to the basal reflection (001) intercalation of Ag and Cu into interlayer space of vermiculite was supposed.

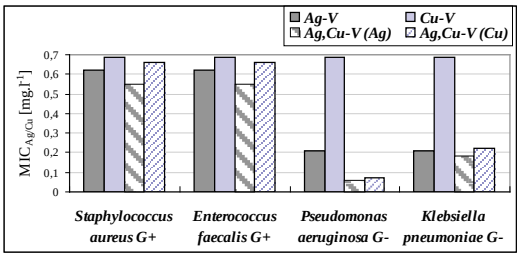

Fig. 2: The MIC Ag/Cu (Minimum Inhibitory Concentration of Ag and Cu) was determined by the lowest concentration that completely inhibits visible bacteria growth.

The antibacterial activity tests on the Gram positive (G^+) and Gram negative (G^-) bacteria strains showed dependence of antibacterial effect upon content of Ag and/or Cu with the result that the highest effect was observed against G^- bacteria (Fig. 2).

Acknowledgements: The work was supported by projects: Ministry of Education, Youth and Sport of Czech republic (SP/2010111) and Czech Grant Agency (GA ČR 205/08/0869).

[1] Valášková, M. et al. (2007) *J. Nanosci. Nanotechnol.*, **8**, 3050-3058. [2] Magaña, S. M. et al. (2008) *J. Mol. Catal. A-Chem.*, **281**, 192-199. [3] Li, B. et al. (2002) *J. Min. Mat. Char. & Eng.*, **1**, 61-68.

Preparation of oriented films of layered double hydroxides with photoactive properties

Kovanda, F.[1*], Jiřičková, M.[1] & Lang, K.[2]
[1]Dept. of Solid State Chemistry, Institute of Chemical Technology, Prague, Czech Republic
([*]Frantisek.Kovanda@vscht.cz)
[2]Institute of Inorganic Chemistry of the AS CR, v.v.i., Řež, Czech Republic

Layered double hydroxides (LDHs) represent suitable hosts for intercalation of various anionic species. The intercalated LDHs attract increasing attention in various medical applications as drug carriers, gene therapy, etc. [1]. Photoactive molecules such as porphyrins can be excited by visible light to the triplet states that rapidly interacts with molecular oxygen by energy transfer to form singlet oxygen, $^1O_2$, a highly reactive oxidation agent with cytotoxic effects enabling its application in photodynamic therapy. In our recent reports [2,3], the structural and photophysical properties of LDH powders and oriented films with intercalated porphyrin sensitizers were described and the formation of singlet oxygen followed by its diffusion to solid-liquid or solid-gas interfaces was proven.

The oriented LDH films were prepared on quartz substrates by deposition from a colloidal suspension of delaminated LDH particles. Two colloidal suspensions were prepared. The first one was obtained by delamination of coprecipitated Mg-Al-NO_3 LDH in formamide. Second, the acetate form of Mg-Al LDH was used for the preparation of a colloidal suspension in water: nitrate anions in Mg-Al-NO_3 LDH were exchanged in an aqueous solution in an excess of sodium acetate and the washed product was dispersed in distilled water [4]. Porphyrins 5,10,15,20-tetrakis(4-sulfonatophenyl)porphyrin or Pd(II)-5,10,15,20-tetrakis(4-carboxyphenyl)porphyrin were embedded in oriented LDH films prepared by the layer-by-layer technique. The absence of non-basal diffraction lines in powder XRD patterns confirmed a preferential arrangement of LDH particles parallel to the substrate surface. Transparent films were obtained, their absorbance in visible light increased gradually with the number of deposition steps (Fig. 1). The photophysical properties of the prepared LDH/porphyrin films including the formation of singlet oxygen are discussed.

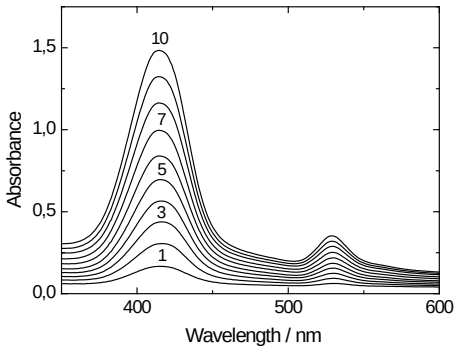

Fig. 1: Absorbance of the oriented LDH/porphyrin film increasing with the number of deposition steps (up to 10 deposition steps were applied).

Acknowledgements: This work was supported by the Czech Science Foundation (P207/10/1447) and by the Ministry of Education, Youth and Sports of the Czech Republic (MSM 6046137302).

[1] Del Hoyo, C. (2007) *Appl. Clay Sci.*, **36**, 103-121. [2] Lang, K. et al. (2007) *Chem. Mater.*, **19**, 3822-3829. [3] Lang, K. et al. (2008) *Chem. Phys. Phys. Chem.*, **10**, 4429-4434. [4] Iyi, N. et al. (2008) *Langmuir*, **24**, 5591-5598.

Potassium acetate-intercalated kaolinite obtained by mechanochemical and aqueous suspension techniques – a comparative study

Makó, É.[1*], Kovács, A.[1], Kristóf, J.[2] & Horváth, E.[2]
[1]Institute of Materials Engineering, University of Pannonia, Veszprém, Hungary ([*]makoe@almos.vein.hu)
[2]Institute for Environmental Engineering, University of Pannonia, Veszprém, Hungary

Intercalation complexes of a high-defect kaolinite have been prepared by direct reaction with potassium acetate solution as well as by co-grinding with potassium acetate in the absence of water (mechanochemical intercalation). Potassium acetate-intercalated high-defect kaolinite has been aged for up to 2 months. The aged and non-aged complexes were studied by X-ray diffraction, thermal analysis, DRIFT spectroscopy and electron microscopy. Ageing of the mechanochemically intercalated kaolinite increases the degree of intercalation [1] by almost 20 %, as well as decreases the structural deformation of the intercalation complex. At the same time, the aqueous suspension technique creates kaolinite–potassium acetate intercalation compound which shows practically no change after ageing.

[1] Wiewiora, A. & Brindley, G.W. (1969) *Proc. Int. Clay Conf.*, Tokyo, **1**, 723.

Time- and pH-dependent sorption of veterinary antimicrobial sulfamethoxazole to bentonite and organobentonite

Netzkár, A.[1], Kilár, A.[1], Páger, Cs.[1], Kilár, F.[1], Klumpp, E.[2] & Pernyeszi, T.[1*]
[1]Dept. of Analytical and Environmental Chemistry, Faculty of Science, University of Pécs, Hungary ([*]ptimea@ttk.pte.hu)
[2]Research Centre Jülich GmbH, Institute of Chemistry and Dynamics of the Geosphere IV, Agrosphere, Jülich, Germany

Sulfonamide antimicrobials comprise a class of synthetic sulfanilamide derivatives which are used in human therapy, livestock production and aquaculture. Substantial amounts of sulfonamides, ionizable, polar veterinary, may reach the environment through grazing livestock and spreading of manure on agricultural soils. Further pathway into the environment is direct use in aquaculture. Residues of sulfonamides have been found in soils and adjacent environmental compartments [1,2]. In soils, parts of added sulfonamides are retained over months [1]. Sorption to soils and sediments is a crucial but not sufficiently understood process influencing the environmental fate of sulfonamides.

The objective of this study was the influence of contact time and pH on sulfomethoxazole sorption to native bentonite (Rátkai Pettyes, Hungary) and surfactant-modified bentonite. The sulfamethoxazole (pK_a = 4.7) was analyzed by capillary electrophoresis using Tris (tris(hydroxy-methyl)aminomethane) at pH of 8.3. Organobentonites were prepared from bentonite by using benzyldodecyldimethylammonium (C_{12}) bromides. The degree of modification was 100 % (C_{12}-100-B) and 50 % (C_{12}-50-B) of the cation exchange capacity. Adsorption kinetics and isotherms determined in aqueous suspensions using batch technique were modelled.

The bentonite sorbent was expected to interact mainly with cationic sulfonamide at pH < 4.7, above this pH value little adsorbed amount could be measured (q_s = 1.5 - 2 mg/g at pH 6.4 in natural form without pH adjustment). Modification of bentonite surfaces by benzyldodecyldimethylammonium assisted the sulfamethoxazole adsorption (q_s = 4 - 5 mg/g at pH 6.4 in natural form without pH adjustment). Following the adsorption kinetics five days was needed to reach the adsorption equilibrium.

Our results imply that inorganic sorbents compared to organic substances can play a minor role for sulfonamide sorption in many soils and sediments. Especially the potential of organic sorbents for increased sorption with contact time would be important. On the other hand organobentonite (modified by benzyldodecyldimethylammonium bromide) could be used as biosorbent material in soil and sediment remediation.

[1] Thiele-Bruhn, S. et al. (2004*) J. Environ. Qual.*, **33**, 1331-1342. [2] Hamscher, G. et al. (2005) *Environ. Toxicol. Chem.*, **24** , 861-868.

Spectroscopic study of intercalated cationic dyes into montmorillonite with different layer charge

Pustková, P.[1*], Klika, Z.[1] & Malý, P.[2]
[1]Dept. of Analytical Chemistry and Material Testing, VŠB-Technical University of Ostrava, Czech Republic
([*]petra.pustkova@vsb.cz)
[2]Dept. of Chemical Physics and Optics, Charles University, Prague, Czech Republic

Modified montmorillonites with cationic dye exhibit unique optical properties. These novel materials enable many applications in photochemical and photophysical branch [1]. Generally, cationic dyes form the aggregates on surface and/or in the interlayer of montmorillonite. Dye loading and layer charge of montmorillonite are control elements of dye aggregation [2].

In this study a Ca^{2+}-montmorillonite with high (SAz) and reduced charge (RC-SAz(210)) were used for the preparation of cationic dye/montmorillonite complexes. The RC-SAz(210) was prepared from parent material (SAz) by Li^+ saturation and subsequent heating at 210°C. The exchanges in fluorescence and Vis electron spectra of the complexes were observed.

Vis absorption spectra of four cationic dyes (CD), i.e. methylene blue (MB), crystal violet (CV), nile blue (NB) and rhodamine B (RB) were measured. The percentage distribution of non aggregated and aggregated CD species in variously concentrated aqueous solution was calculated using equilibrium stepped aggregation constants K_n. The study showed that nile blue forms the higher aggregates in aqueous solution already at relatively low concentration compared with the other tested dyes.

Vis electronic spectroscopy and X-ray diffraction analysis revealed that cationic dye in fully intercalated CD/SAz complex is located in the interlayer of montmorillonite mainly in form of higher aggregates. The higher aggregates of dye are effective quenchers of fluorescence hence these complexes exhibit a very low fluorescence intensity. The reduction of montmorillonite layer charge and low dye loading in the CD/RC-SAz(210) complexes cause suppression of dye aggregation and huge increase of fluorescence (Fig. 1).

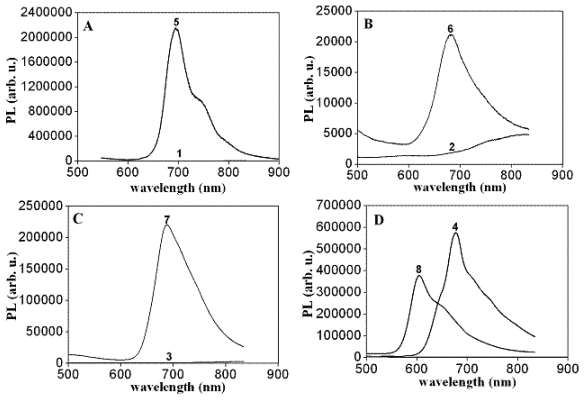

Fig. 1: Fluorescence spectra of fully intercalated CD/SAz complexes (spectra 1, 2, 3 and 4) and spectra of CD/RC-SAz(210) prepared by 10% dye loading (spectra 5, 6, 7 and 8). A- Methylene blue; B- Crystal violet; C- Nile blue; D- Rhodamine B.

[1] Bujdák, J. (2006) *Appl. Clay Sci.*, **34**, 58-73. [2] Klika, Z. et al. (2009) *J. Colloid Interf. Sci.*, **339**, 416-423.

Wettability of clay mineral surfaces – molecular dynamics study

Šolc, R.[1*], Tunega, D.[1,2], Pašalić, H.[2], Gerzabek, M.H.[1] & Lischka, H.[2]
[1]Inst. of Soil Research, University of Natural Resources and Applied Life Sciences, Vienna, Austria
([*]roland.solc@boku.ac.at)
[2]Inst. for Theoretical Chemistry, University of Vienna, Austria

Wetting properties of soil and soil components affect a wide variety of soil processes including infiltration, preferenti al flow and surface runoff [1]. The wetting ability of a solid surface is mainly determined by its chemical composition and structure and is directly related to the solid surface free energy [2]. The solid-liquid contact angle method is often used to characterize wettability of surfaces and to determine its surface energy. In soil chemistry, contact angle measurements are influenced by many factors because of the heterogeneous and complex nature of soil particles. Therefore, it is important to know how individual soil components behave with respect to polar liquids like water.

Clay minerals represent an important inorganic part of soil mineral phases and significantly affect overall properties of soils. Owing to compositional variability ad structural complexity various clay minerals behave considerably differently with respect to wetting.

In order to elucidate structural and compositional factors affecting hydrophilic/hydrophobic character of clay minerals we studied interactions of water nanodroplets with basal surfaces of selected clay minerals (particularly kaolinite and phlogopite) by means of classical molecular dynamics simulations at room temperature. From the behaviour and shape of the nanodroplet it was possible to characterize hydrophobic/hydrophilic character of studied surfaces. In case of the kaolinite octahedral surface formed from surface hydroxyl groups, the water droplet was completely spread and a monomolecular network of hydrogen-bonded water molecules was formed. In opposite, the tetrahedral surface, which is formed from basal oxygen atoms, is less interacting with the water nanodroplet and the shape of the droplet is partially preserving. The molecular simulations clearly showed a difference between both basal surfaces of kaolinite. While the octahedral surface is strongly hydrophilic, the tetrahedral surface has partially hydrophobic character. Structural and energetic aspects of both surfaces are obtained as well.

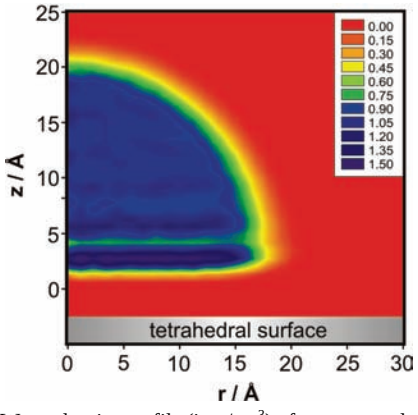

Fig. 1: Water density profile (in g/cm^3) of water nanodroplet on tetrehadral kaolinite surface. (500 water molecules, 2 ns MD, 300K).

[1] Anderson, M.A. et al. (1995) *Soil Sci.*, **160**, 111-116. [2] Bachmann, J. et al. (2000) *Soil Sci. Soc. Am. J.*, **64**, 564-567.

Organic modified montmorillonite supported cobalt catalyst for Fischer–Tropsch synthesis

Su Haiquan[1,2*], Zhang Bingbing[1], Ding Ning[2], Li Xuefen[1], Zhang Xiaohong[1,2] & Zeng Shanghong[2]
[1]College of Life Science, Inner Mongolia University, Hohhot, P.R. China
[2]Inner Mongolia Key Laboratory of Coal Chemistry, School of Chemistry and Chemical Engineering, Inner Mongolia University, Hohhot, P.R. China ([*]haiquansu@yahoo.com)

The Fischer-Tropsch synthesis (FTS) is a process that converts syngas into mixtures of higher molecular weight hydrocarbons. Supported cobalt catalysts are the preferred catalysts because of their high F-T activity, high selectivity for linear hydrocarbons, low activity for the water gas shift reaction, and relatively lower cost. In this paper, organically modified montmorillonite as a novel support is first applied to cobalt-based Fischer-Tropsch synthesis.

Normally, XRD is a good method for identification and characterization of the F-T active phases. However, only the in-situ XRD shows reliable data about the structure of cobalt active phases present in the reduced and working catalysts because of easy reoxidation of cobalt species in the air. Our results show that ex-situ XRD was also an effective method for the active phase identification of the Co/ OMMT catalysts after F-T synthesis (see Fig. 1), because there was no reoxidation on the catalysts after F-T reaction due to the formation of carbon protective layer outside the metallic cobalt, which was from decomposing of the organic component inside the layer of montmorillonite. This retains precious information about cobalt dispersion and reducibility under the FT reaction conditions.

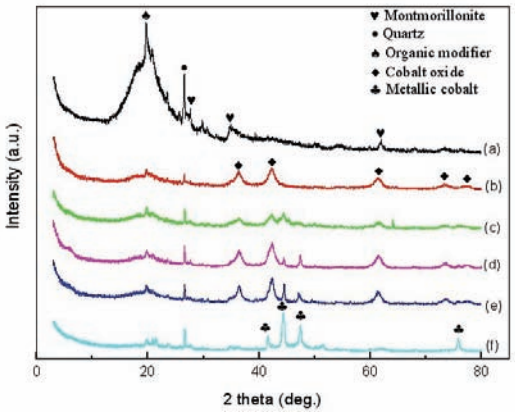

Fig. 1: XRD patterns of the samples (a: organically modified montmorillonite (OMMT); b: Co/ OMMT; c–e: Co/ OMMT catalysts after different Fischer-Tropsch reaction conditions).

Table 1: Catalytic performance of catalysts for F-T synthesis reaction

Sample	CO conversion (%)	CH_4 selectivity (%)	C_2-C_4 selectivity (%)	C_5^+ selectivity (%)
c	24.48	19.98	6.67	73.35
d	14.65	16.53	0.78	82.69
e	26.27	7.08	2.45	90.47
f	15.84	94.28	1.69	4.03

The data in table 1 show that the C_5^+ selectivity was improved with the increase of metallic cobalt content in catalysts c–e. The C_5^+ selectivity of the catalyst f was the worst on the highest metallic cobalt content, due to the catalyst producing more carbon under these conditions.

Acknowledgements: Project supported by National Natural Science Foundation of China (grant no.20661001).

A molecular dynamics simulation studies of ethylene glycol intercalated in smectites

Szczerba, M.[1*], Kłapyta, Z.[2] & Skiba, M.[3]
[1]Institute of Geological Sciences, Polish Academy of Sciences, Kraków, Poland (*ndszczer@cyf-kr.edu.pl)
[2]Faculty of Geology, Geophysics and Environmental Protection, University of Mining and Metallurgy, Kraków, Poland
[3]Institute of Geological Sciences, Jagiellonian University, Kraków, Poland

Intercalation of ethylene glycol in smectites is widelly used to discriminate smectites from other clays. This technique has been known since pionnering work of MacEvan [1], however still little is known about the structure of ethylene glycol between smectite sheets. The work by Reynolds [2] gave some insights into the structure, hovewer since that time no significant input into the understanding of this structure has been done.

Molecular dynamics simulations allow to find that the structure proposed by Reynolds [2] should be a bit different. Ethylene glycol forms two distinct layers between sheets, but ions forms inner and outer sphere complexes, not only the outer ones as it was described in [2]. Moreover water in this structure was found not to form distinct layers but is rather spread out and concentrated around ions. There is also no tendency to form water bridges between ions, water and ethylene glycol.

Molecular simulations were carried out using the DLPOLY computer program using CLAYFF and CVFF force fields to describe clay and ethylene glycol, respectively.

[1] MacEwan, D.M.C. (1946) *J. Soc. Chem. Ind.*, **65**, 298-304.
[2] Reynolds, R.C. (1965) *Am. Mineral.*, **50**, 990-1001.

Formation of a second-staged alkylammonium-sericite complex

Tamura, K.[1*], Hatta, T.[2], Morimoto, K.[1] & Yamada, H.[1]
[1]National Institute for Materials Science, Tsukuba, Japan
([*]TAMURA.Kenji@nims.go.jp)
[2]Japan International Research Center for Agricultural Sciences, Tsukuba, Japan

The intercalation dynamics of layered materials, such as graphite, clays, and transition-metal dichalcogenides, has been reported in detail, both experimentally and theoretically. In particular, the phenomenon of staging has generated a large amount of interest in these materials. Staging is a process by which layered host materials intercalate guest compounds. A staged layered compound has a regularly repeating series of interlayers, alternating periodically between an intercalated layer and non-intercalated layer. In the present study, the staging phenomenon was investigated for the organic/sericite complexes.

We have conducted ion exchange experiments using sericite (SE) and dehydrated sericite (dhSE) with dodecylammonium (DDA) solutions of various initial concentrations (7.3, 21.9, and 73.3 mM, corresponding to DDA^+/K^+ mole ratio = 1.0, 3.0 and 10.0, respectively), at 70°C. The dhSE sample was prepared by dehydration of a SE powder (medium particle diameter: 7.8 μm) at 800°C for one hour [1]. The staging phenomenon was studied by X-ray diffraction (XRD), X-ray photoelectron spectroscopy (XPS) and infrared absorption spectra. Typical XRD patterns of DDA-SE and DDA-dhSE prepared by ion exchange with a low DDA concentration (DDA^+/K^+ = 1.0), are shown in Figure 1. In the case of the SE complexes, two separated phases, 1.0 and 2.3 nm, were obtained, which were ascribed to the non-intercalated layers, and vertical (perpendicular to the layers) orientations of the incorporated DDA, respectively. On the other hand, in the case of the dhSE complexes, a large basal spacing of 3.3 nm was observed (Fig. 1b). The 3.3 nm basal spacing is close to the sum of the basal spacing for the vertical (perpendicular to the layers) orientations and that for the non-intercalated layers, so it can be interpreted as regular alternation of the 2.3 nm layer and the 1.0 nm layer, exhibiting *c* =3.3 nm supercell ("1:1 ordered interstratifications" or "second-staging").

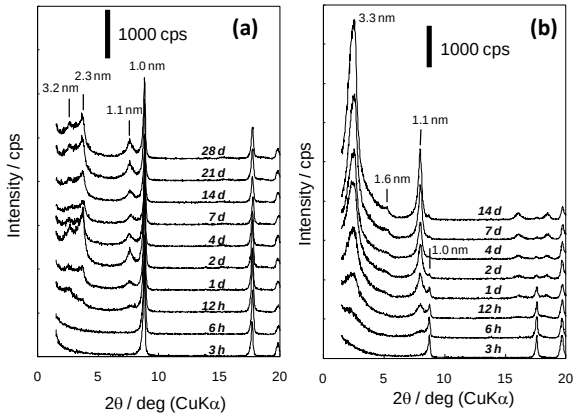

Fig. 1: XRD patterns of (a) DDA-SE and (b) DDA-dhSE complexes prepared by ion exchange with DDA^+ (DDA^+/K^+ mole ratio = 1.0) at 70°C for various duration times.

[1] Tomita, K. & Dozono, M. (1972) *Clay. Clay Miner.*, **20,** 225-231.

Alteration mineralogy, geochemistry and genesis of volcanic rocks of the Hasandağ area (Giresun), NE Turkey

Kadir, S.[1*], Acarlıoğlu, S.[1], Abdioğlu, E.[2] & Arslan, M.[2]
[1]Dept. of Geological Engineering, Eskişehir Osmangazi University, Eskişehir, Turkey ([*]skadir_esogu@yahoo.com)
[2]Dept. of Geological Engineering, Karadeniz Technical University, Trabzon, Turkey

The Eocene subvolcanic and volcanic rocks of the Hasandağ (Giresun) area in the eastern Pontides (NE Turkey) have undergone several stages of hydrothermal alteration. The rocks of the area comprise andesitic flows, andesitic pyroclastic rocks, phreatomagmatic breccia, andesite dykes and granodiorite-syenogranite intrusions. Development of phreatomagmatic breccias was related to penetration of silica-rich hydrothermal fluids along fractures. Consequently, silicification and scarce argillisation are widespread main types of hydrothermal alteration in the area. These units were studied via standard petrography, reflected-light polished-section microscopy, X-ray diffractometry (XRD), scanning electron microscopy (SEM-EDX), and geochemical analysis. Alteration of plagioclase and iron-oxidation in amphibole and biotite are widespread. Development of silicification, advanced argillisation (alunite±kaolinite), argillic (smectite±illite) and propyllitic zones (chlorite±sericite±calcite) – associated with decreasing alunite±kaolinite and some increase in chlorite±sericite±calcite from the central to the outer part of the study area – indicate acidic hydrothermal activity. The operation of these hydrothermal processes is also evidenced by geological and geochemical determinations. In the study area, pyrite, visible gold and native elements were all determined via ore microscopy. The pyrite is of three types; type 1 is coeval with the host rocks, the other two types of pyrite occurrence developed via epithermal activity. Pyrite crystals are 1-1000 microns, gold 2-15 microns, and native elements 1-20 microns in size. Hypogene minerals include goethite and lepidocrocite. Based on geochemical analyses, the trace- and rare-earth element patterns of the volcanic rocks (except the phreatomagmatic breccia) are similar to each other, and all resemble arc volcanic rocks. Thus, geological, petrographic, mineralogical and geochemical data on these Eocene volcanic rocks and their hydrothermally altered equivalents indicate an epithermal system.

Geology, mineralogy and depositional environment of the Pliocene Cappadocian Volcanic Province, Yeşilhisar (Kayseri, central Anatolia, Turkey)

Kadir, S.[1*], Gürel, A.[2], Göz, E.[1] & Külah, T.[1]
[1]Dept. of Geological Engineering, Eskişehir Osmangazi University, Eskişehir, Turkey ([*]skadir_esogu@yahoo.com)
[2]Dept. of Geological Engineering, Niğde University, Niğde, Turkey

Pliocene alluvial and lacustrine deposits characterize the so-called Kısladağ Formation of the Cappadocian Volcanic Province (central Anatolia). The Güzelöz Plateau (Yeşilhisar) in the central part of the Cappadocian Volcanic Province contains many ignimbrite levels, andesite, and basalt intercalated with paleosols, calcretes, lacustrine carbonates, fluvial sediments, diatomaceous clayey sediments and pyroclastic sedimentary levels. The presence of root traces and remnants, paleosols, and calcrete indicate fluvial and shallow-lake environments. These environments are dominated by feldspar, quartz, calcite, opal-CT, serpentine coexisting with smectite, illite and accessory palygorskite. Smectite predominates in paleosols and calcrete units. Development of microsparitic to sparitic calcite cement between irregular clay nodules in paleosol and calcrete samples, and dog-tooth-type sparitic calcite crystals in fractures and cracks, indicate alternating dry and wet periods, that resulted in the development of paleosols and calcretes. The $\delta^{18}O$ values of the calcretes range from –9.13 to –10.69 ‰ PDB, reflecting their formation under the influence of meteoric water. $\delta^{13}C$ values of the calcretes are between +4.97 and +3.00, and may have been related to drought conditions, increase in C_4 biomass, and decrease in atmospheric CO_2 concentrations below a threshold that favoured C_3 plants [1]. $\delta^{18}O$ and $\delta^{13}C$ isotope values from limestone samples vary between –9.81 to –10.71 and 1.85 to –4.84 ‰ PDB, respectively. Negative $\delta^{18}O$ values and low [MgO/(MgO+CaO)] ratios indicate low salinity and freshwater influx into the lake [2]. The negative calcite $\delta^{13}C$ values of the limestones clearly indicate a biogenic origin, lake expansion and increased through-flow conditions, whereas positive values indicate lake contraction, decreased through-flow conditions and biogenic activity. The Pliocene interval, represented by paleosols, calcretes and lacustrine carbonate rocks in Cappadocia region, is of special interest insofar as it included global changes in vegetation (C_3 to C_4 ecosystems) and drought-wet fluctuations.

[1] Cerling, T.E. et al. (1997) *Nature,* **389**, 153-158. [2] Dutkiewicz, A., Herczeg, A.L. & Dighton, J.C. (2000) *Chem. Geol.*, **165**, 309-329.

Investigation of magnetic and adsorption properties of natural and magnetic sepiolite

Dikmen, Z.* & Orhun, O.
Dept. of Physics, Anadolu University, Eskisehir, Turkey
(*zdikmen@anadolu.edu.tr)

In this study, we investigated a sepiolite sample obtained from Sivrihisar region (Eskisehir-Turkey). Firstly, instrumental characterization of the clay sample was performed by various techniques such as XRD, XRF, TG/DTA, SEM. Magnetic modified forms of clay minerals have been prepared and then adsorption and magnetic properties of unmodified and modified clays were compared with each other. The magnetic modified forms of clay samples have been prepared in the following way: The fractions of clay samples that have dimensions smaller than 63μm have been separated by sieving. They were mixed and intensively ground with powder forms of magnetite in a mortar. The resulting powder mixture was slowly heated up to 950°C at 1°C/min and maintained at this temperature for 6 hours. The solid sample was cooled and washed with de-ionized water until no Cl^- ions were detected in the eluted water, and then dried at 80°C during 16 hours [1].

The adsorption isotherms of nitrogen gas on natural and magnetic modified clays have been obtained by means of Quantachrome Nova 2200E model high speed gas analyzer. The magnetic properties of the samples have been determined by means of LakeShore 7307 model Vibrating Sample Magnetometer.

Table 1: Comparison of specific surface areas, average pore diameters for natural and magnetically modified clays

Forms of Clay	Specific Surface Area(m^2/g)	Average Pore Diameter (Å)
Sepiolite	293.52	84,38
Sepiolite-Fe	68.34	92,17

As shown Table 1, the specific surface areas of magnetically modified clays are smaller than the specific surface areas of natural clays. The average pore diameters of magnetically modified clays are greater than the average pore diameters of natural clays.

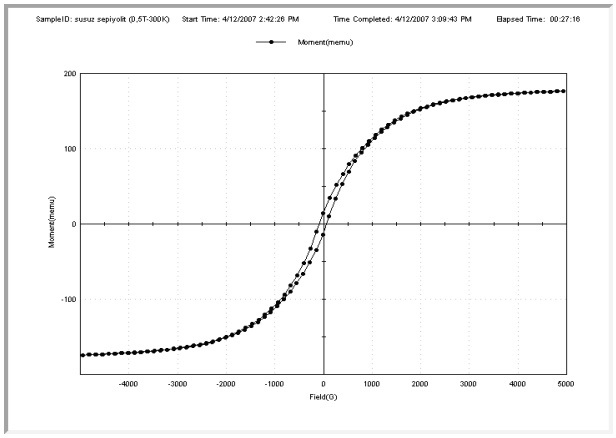

Fig. 1: Magnetization versus applied field curve at room temperature (max. magnetic field 0.5T) for the magnetic modified sepiolite.

The magnetic clay sepiolite is characterized by the maximum magnetization value of 176,4 memu (Fig. 1). Similar results could be obtained for other natural clays and porous materials.

[1] Čapek, L. et al. (2005) *Micropor. Mesopor. Mat.*, **80(1-3)**, 279-289.

Hungarian contribution to mineralogy and geology of clays

Viczián, I.
Hungarian Institute of Geology, Budapest, Hungary
(viczian@mafi.hu)

The Hungarian Clay Minerals Group was founded in 1960. On the occasion of the *50th anniversary* the main results of the Hungarian clay research in the field of earth sciences is reviewed.

A *general textbook* on clay minerals was published by the founder of the Clay Group, professor Nemecz. In a broader sense the fundamental books of Bárdossy on bauxites belong to the clay research. Soil clay minerals were discussed in the textbooks of Stefanovits, Szendrei and Nemecz, and recently by Nagy and Kónya.

Specific clay minerals. The famous illite mineral of Füzérradvány, the "second illite of the world" was described by Maegdefrau & Hofmann as early as 1937 and later reviewed by Nemecz & Varjú. Weiszburg and E. Tóth contributed much to the chemical systematics of celadonite, glauconite and "Fe-rich montmorillonite" series. Serpentine minerals were extensively studied by Erdélyi and in the last years by Dódony (structural analyses of antigorite and polygonal serpentine).

Determinative methods in clay mineralogy. A method of quantitative analysis by X-ray diffraction was introduced by Náray-Szabó. A special apparatus for thermal analysis called "Derivatograph" was developed by Paulik & Paulik. Atlas of thermal analysis was created first by Földvári-Vogl. The application of the method was later continued on a high level by M. Földvári.

Soils and rocks. Stefanovits and Dombóvári published the map of clay minerals in Hungarian soils. Red clays, mostly relict fossil soils were studied by Bidló. Fekete published book on recent tropical soils. *Fossil lake sediments* of basaltic craters were recognised by Solti and analysed by Földvári, Barna and others. Mostly rhyolite-related bentonite deposits of the Carpathian Basin were studied by Kovács-Pálffy.

Lithostratigraphic application. Clay minerals of Hungarian sedimentary formations were systematically characterised by Viczián. Today this line is continued by Raucsik, Varga and Szakmány. The *diagenetic transformation* of smectite to illite was widely applied for CH prospecting by Viczián, J. Mátyás and others. The *very low grade metamorphic stage* is studied by Árkai and his co-workers M. Tóth, Judik etc. He introduced the parameter "chlorite crystallinity" (Árkai index), studied index minerals, applied textural analysis etc. His studies extended to Hungary, the Swiss Alps, and to SE-Europe.

Zones of *hydrothermal alteration* in the Tokaj Mts. were first recognised by Széky-Fux, later intensively studied by Nemecz and Varjú and recently by Molnár. *Economic clay deposits* were studied for several decades by E. Mátyás and Zelenka, their colloidal properties by Juhász, Szántó and their students. Model experiments of *environmental pollution* by heavy metals are carried out by Németh. Clay liners for communal *waste depositories* were developed by Szabó. Pelitic host rocks for radioactive waste depositories are studied in Mecsek Mts.

Mineralogical and chemical composition of clayey deposits in caves

Klimova, E.V.* & Matrenichev, V.A.
Institute of Precambrian Geology and Geochronology, RAS, St. Petersburg, Russia (*katya_kli@list.ru)

Clay deposits in caves are quite specific in nature due to their origin and therefore are not well investigated.

For the purposes of this research samples from: Sumgan-Kutuk Cave (Bashkortostan, the Urals), Kapova Cave (Bashkortostan, the Urals), Canyon Cave (Krasnodar region, the Caucasus), Voronya Cave (Abkhazia, the Caucasus) and Cascade Cave (the Crimea, Ai Petri) have been considered.

Analysis of particle size distribution showed that in all the caves studied there are two types of deposits: sandy silt, where percentage of clay fraction (less than 0.002mm) is 3.7% with predominant silt fraction (0.002 to 0.01mm) of 50-75%; and clayey silt where the percentage of clay fraction is 12.6%, with silt (0.002 to 0.05mm) being dominant (70-80%).

The mineral composition of the clay fraction is dominated by illite-smectite interlayerings (35-50%) with predominant illite layers, kaolinite (4-10%), chlorite (approximately 6%), smectite (approximately 1%), calcite (approximately 1%), iron hydroxides (approximately 1%). The amount of detrital quartz reaches 40% in the <0.002 mm fraction.

Further chemical analysis of the alumo-silicates from the clay fraction, carried out using a Jeol JSM-5300 scanning electron microscope equipped with EDS, showed that: *Illite* has high potassium content and characterized by 52.27% SiO_2, 26.49% Al_2O_3, 3.92% Fe_2O_3, 4.90% MgO, 3.58% of CaO, 2.44% Na_2O and 6.40% of K_2O. *Chlorite* is represented by the magnesium type and contains 31.23% SiO_2, 27.43% Al_2O_3, 5.89% Fe_2O_3, 29.05% MgO, 0.51% CaO, 4.91% Na_2O and 0.99% K_2O. *Smectite* is defined by high iron content and has 32.35% SiO_2, 22.84% Al_2O_3, 32.13% Fe_2O_3, 5.81% MgO, 2.86% CaO, 2.09% Na_2O and 1.91% K_2O. The clay minerals from the studied deposits have similar chemical compositions, regardless of the sampling site.

The chemical composition of clay fraction of the main type deposits is presented by: SiO_2 55.81%, Al_2O_3 27.41%, Fe_2O_3 4.94%, MgO 3.44%, CaO 1.35%, Na_2O 2.27%, K_2O 4.78% for clayey silt; and SiO_2 54.19%, Al_2O_3 27.73%, Fe_2O_3 3.66%, MgO 5.38%, CaO 0.90%, Na_2O 2.36%, K_2O 5.77 for sandy silt.

As shown in Fig. 1, REE spectrum of clay fraction in sandy and clayey silt (average of all samples) is quite similar.

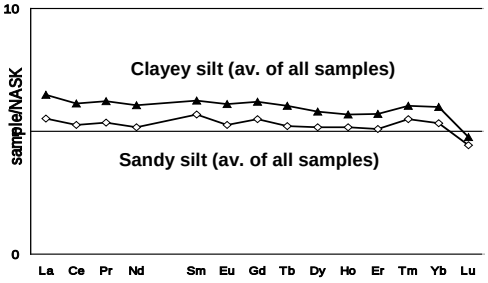

Fig. 1: REE spectrum of clay fraction in sandy and clayey silt (average of all samples).

Taking into account the results of mineralogical and chemical composition of clayey deposits from caves in Caucasus, Crimea, and the Urals, the following conclusion can be made. Clayey deposits from all considered caves are represented by two types of sediments (sandy silt or clayey silt) that show differences in the micro-facies of their deposition environment. Mineralogical composition of clay fraction is similar for all analyzed samples, with predominant illite-smectite mixtures with a percentage of smectite layers < 35%.

Montmorillonitic alteration of tourmaline from the Quintos de Baixo pegmatite, Borborema Pegmatite Province, NE Brazil

Strmić Palinkaš, S.[1], Bermanec, V.[1*], Žigovečki Gobac, Ž.[1], Palinkaš, L.A.[1], Kampić, Š.[1], Wegner, R.[2] & Odúlio, J.M.M.[3]
[1]Institute of Mineralogy and Petrography, Dept. of Geology, University of Zagreb, Croatia (*vberman@public.carnet.hr)
[2]Centro de Ciências e Tecnologia, Dept. de Min. e Geol., Universidade Federal de Campina Grande, Brazil
[3]HR Exportação e Importação de Minérios, Governador Valadares, MG, Brazil

Tourmaline is a common boron-rich mineral in granitic pegmatites [1]. It is resistant to weathering and typically occurs as a detrital mineral in sedimentary rocks and soils. However, tourmaline in pegmatites may be partially altered to various aluminous minerals. Alterations are mostly associated with late magmatic and hydrothermal fluids [2].

Tourmaline from the Quintos de Baixo pegmatite, Borborema Pegmatite Province, NE Brazil, displays zonal structure with Li-Al-rich core (elbaite) and Fe-rich rim (schorl). The core is frequently altered to clay minerals. The matrix between tourmaline crystals comprises clay minerals as well. According to X-ray powder diffraction (XRPD) analysis the principal clay mineral is montmorillonite with cation exchange capacity (CEC) of 75.5 ± 0.4 mEq/100g.

The following reaction illustrates the breakdown of tourmaline (elbaite) into Li-montmorillonite:

$$Na(Li,Al)_3Al_6(BO_3)_3Si_6O_{18}(OH)_4 + 5H_4SiO_4 + 3H^+ \leftrightarrow 3[Al_3(Si_{3.67}Al_{0.33})O_{10}(OH)_2]Li_{0.33} + 3H_3BO_3 + 2Li^+ + Na^+ + 6H_2O \quad (\Delta_rG^0 = -69.7 \text{ kcal/mol})$$

The reaction requires increased activity of H_4SiO_4 and points to the influence of late magmatic or hydrothermal fluids (Fig. 1). Alternatively, the weathering of spodumene can represent an important source of montmorillonite:

$$7LiAlSi_2O_6 + 6H^+ + 6H_2O \leftrightarrow 3[Al_3(Si_{3.67}Al_{0.33})O_{10}(OH)_2]Li_{0.33} + 3H_4SiO_4 + 6Li^+ \quad (\Delta_rG^0 = -2.6 \text{ kcal/mol})$$

Gibbs free energies for above mentioned reactions (Δ_rG^0) have been estimated according to the thermodynamic data published by Woods & Garrels [3], Tardy & Garrels [4] and Ogorodova et al. [5].

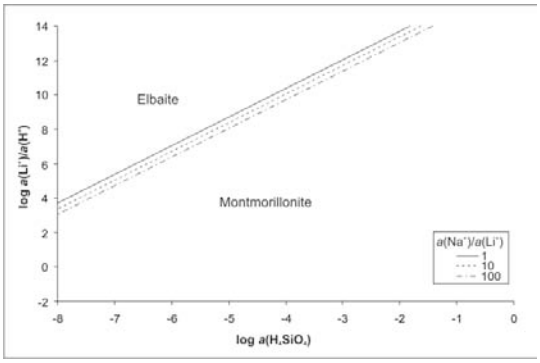

Fig. 1: Logarithmic activity diagram, constructed for standard conditions (1 bar, 25°C).

[1] London, D. et al. (1996) *Rev. Mineral.,* **33**, 299-330. [2] Ahn, J.H. & Buseck, P.R. (1998) *Am. Mineral.,* **83**, 535-541. [3] Woods, T.L. & Garrels, R.M. (1987) *Thermodynamic values at low temperature for natural inorganic materials.* Oxford University Press, New York. [4] Tardy, Y. & Garrels, R.M. (1974) *Geochim. Cosmochim. Ac.,* **37**, 1101-1116. [5] Ogorodova, L.P. et al. (2004) *Thermochim. Acta,* **419**, 211-214.

The mineralogical and petrographic study of zeolitic tuffs around Karamürsel, NW Turkey

Uz, B.[1], Bacak, G.[2*] & Özdamar, S.[1]
[1]Dept. of Geology, Istanbul Techical University, Istanbul,Turkey
[2]Dept of Geololgy, Karaelmas University, Zonguldak, Turkey
([*]bacakgur@karaelmas.edu.tr)

Paleocene pyroclastic rocks of the volcano-sedimentary sequence which disconformably overlie Triassic conglomerates and sandstones underwent locally a strong alteration in the area around Karamürsel, NW Turkey (Fig. 1).

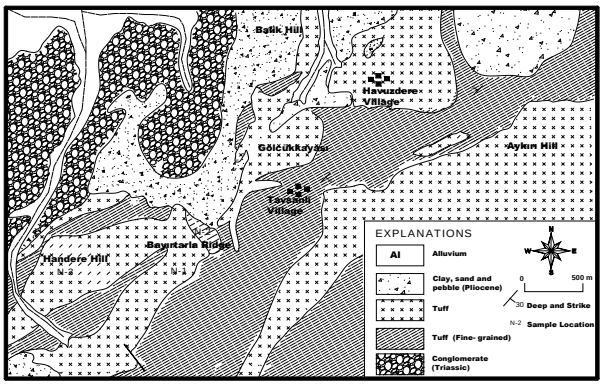

Fig. 1: Geological map of the study area [3].

Volcanic tuffs, which have the composition from andesite to rhyolite, underwent diagenetic alteration. Zeolites (clinoptilolite, heulandite), clay minerals and micas (smectite, illite, celadonite, glauconite and biotite), siliceus minerals (opal-CT, quartz), carbonate minerals (calcite) and feldspars are authigenetically formed. Thermal stability studies indicate that the zeolite types are clinoptilolite and heulandite-2 (Ca-clinoptilolite). Clinoptilolite is stable at 550°C. Si/Al ratios of selected 3 zeolite samples range from 4.70 to 5.84. Heulandites have been distinguished from iso-structural clinoptilolites on the basis of their Si/Al ratios, heulandites having Si/Al <4 and clinoptilolites having Si/Al>4 [1,2]. XRD studies indicate that Karamürsel samples contain typical heulandite with d(060) spacing higher than 1.51Å (Fig.2). Glauconite (Al-glouconite) identified with celadonite-glauconite distinguishing methods was found to be a mixed-layer mineral.

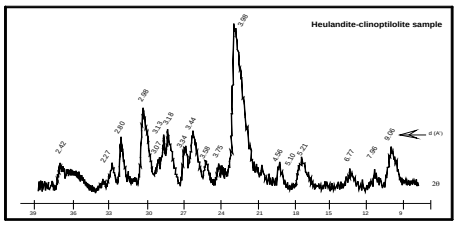

Fig. 2: XRD pattern of heulandite-clinoptilolite bearing tuff

Cationic values were recalculated on the basis of 72 oxygen atoms, providing the following average half unit cell composition of the glauconite: $K_{0.53}(Fe_{0.89}, Al_{0.53})$ $(Mg_{0.48}, Fe_{0.17})$ $(Si_{3.65}\ Al_{0.35})\ O_{10}\ (OH)_2$.

[1] Coombs, D.S. et al. (1997) *Can. Mineral.*, **35**, 1571-1606. [2] Esenli, F. et al. (2005) *Geol. Croatica*, **58/2**, 151-161. [3] Uz, B. et al. (1995) *Geosound*, **27**, 135-147.

Effects of dry grinding on kaolinite powders

Valášková, M.[1*], Barabaszová, K.[1] & Plevová, E.[2]
[1]Nanotechnology Centre, VŠB-TU of Ostrava, Czech Republic
([*]marta.valaskova@vsb.cz)
[2]Institute of Geonics AS CR, Ostrava-Poruba, Czech Republic

Particle size reduction in clays and clay minerals is produced by grinding, which plays an important role in the physicochemical properties of the resulting powders and in the further processing steps. Most papers report that short-time milling of kaolinite flakes causes fracturing along the basal planes coupled with an increase of the specific surface. Several author teams examined the mechanochemical effects of grinding of kaolinite on its structure and thermal behavior and subsequent thermal transformations. Physicochemical changes of the material were observed after applying grinding friction forces, such as present in vibratory, oscillating, and planetary mills [1]. The effects of different times of dry grinding using ball-milling on the structure of kaolinite powders KGa-1 and KGa-2 from Georgia showed that the peak temperatures of the endothermic DTA effects shifted slightly to lower temperatures as grinding time increased. The exothermic peaks were affected only after longer grinding periods [2].

Well-ordered (KGa-1) and low-ordered (KGa-2) kaolinite powders from Georgia were compared after 15 min jet- and ball –milling. The surface area increased, the particle size distribution and the weight loss on heating were different in dependence on the type of milling. he DTA effects did not change after milling.

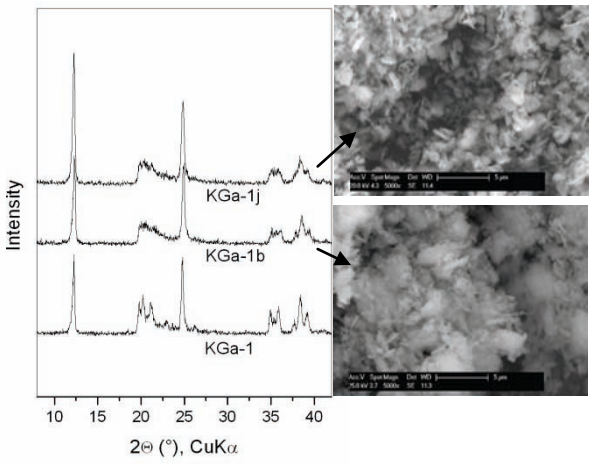

Fig. 1: XRD patterns of KGa-1, ball-milled KGa-1b, jet-milled KGa-1j and SEM micrographs of KGa-1b and KGa-1j.

The X-ray powder diffraction (XRD) patterns (Fig. 1) show the loss of resolution of the peaks near 21.5 °2Θ which is some evidence for a small disorder in the ordered phase [3].

Acknowledgements: This work was supported the Czech Grant Agency (projects GA ČR 105/08/1398 and 205/09/0352).

[1] Aglietti, E.F. et al. (1986) *Int. J. Miner. Process.*, **16**, 125-133. [2] Sánchez-Soto et al. (2000) *J. Am. Ceram. Soc.*, **83**, 1649-1657. [3] Reynolds, R.C.,Jr. & Bish, D.L. (2002) *Am. Mineral.*, **87**, 1626-1630.

Detailed clay mineralogy of a continuous, marine Tr/J boundary section at Kendlbachgraben, Austria

Zajzon, N.[1*], Kristály, F.[1], Pekker, P.[2] & Pálfy, J.[3]
[1]Institute of Mineralogy and Geology,University of Miskolc, Hungary (*nzajzon@uni-miskolc.hu)
[2]Institute for Nanotechnology, Bay Zoltán Foundation for Applied Research, Miskolc, Hungary
[3]Research Group for Paleontology, Hungarian Academy of Sciences–Hungarian Natural History Museum, Budapest, Hungary

A marine Triassic/Jurassic boundary section is exposed at Kendlbachgraben in the Northern Calcareous Alps. It is located in the Eiberg basin, similarly to the Kuhjoch section, which has been chosen as the Global Stratotype Section and Point for the base of Jurassic.

Selected samples of the Kendlbachgraben section were investigated for clay mineral species determination. Routine oriented specimen diagnostic procedures were followed. Cation exchange for Mg and K was performed. Peaks of X-ray diffraction patterns were resolved by deconvolution procedures. Observed species are ~15 Å smectite (Mg>Fe), together with vermiculite (K-bearing) and chlorite (Fe>Mg) (14,2–14,5Å), illite and kaolinite. The identified "14Å type" minerals are Mg-dominant, with varying Fe, K and Ca content. Chlorite is evident only after heating to 560°C and diminishes upwards in the section. Kaolinite shows a decrease in quantity and degree of crystallinity upwards in the section. Cation exchange and glycerol saturation indicates the mixing of high and low layer charge smectites, with the dominance of the high-charge type. Vermiculite is of the low layer charge, expanding type.

The lowermost sample of section (KB1) has a very different clay mineral content compared to the other samples. It contains dominantly high-charged smectite and also vermiculite. These clay minerals may be formed by the alteration of mafic and ultramafic rocks. Upwards in the section (KB8) smectites has a Ca–Na enrichment and vermiculite (chlorite) becomes dominant. In the boundary shale the clay mineral distribution is the following: kaolinite≥ illite + muscovite >> smectite. This suggests weathering under humid climate, and intensive terrigenous input. Above the boundary interval the clay mineral pattern changes to illite + muscovite >> kaolinite >> smectite, which corresponds to a less humid, mainly moderate climate.

Some pale-green, opaque or slightly transparent grains, 70–80 μm in size, are found in the topmost layer of the Triassic Kössen Formation (KB1). Their shapes vary from the perfectly spherical (Fig. 1) to the angular. They are identified as illite/aluminoceladonite, their average EDX composition is $K_{0.49}Na_{0.08}Ca_{0.07}Mg_{0.65}Fe^{2+}_{0.07}Al_1Fe^{3+}_{0.41}[Al_{0.4}Si_{3.6}O_{10}(OH)_2]$. They presumably represent alteration products of volcanic material, on the basis of their shape and size. Most probably the rounded grains were altered from volcanic glass spherules.

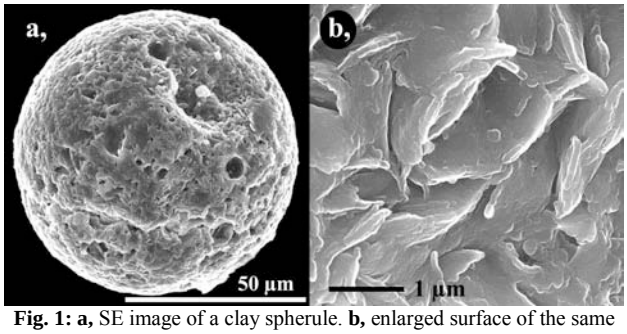

Fig. 1: a, SE image of a clay spherule. **b,** enlarged surface of the same spherule.

Archaeometrical investigation on glass beads coming from Villanovian excavations in Bologna (Italy)

Arletti, R.[1*], Bertoni, E.[2], Vezzalini, G.[2] & Mengoli, D.[3]
[1]Dipto. di Scienze della Terra, Università degli Studi di Ferrara, Italy ([*]rossella.arletti@unimore.it)
[2]Dipto. di Scienze della Terra, Università degli Studi di Modena e Reggio Emilia, Modena, Italy
[3]Lares s.n.c., Pisa, Italy

Excavations performed in seventies around the actual fair area of Bologna brought to light remains of VII-VIII century civilizations [1]. The archaeological work allowed the collection of a large number of objects which clearly indicate the presence of a large Villanovian village. The archaeological excavations on the annexed necropolis are still in progress and the study is unpublished. The necropolises of Bologna Fair are dated from 800 to 750 BC (Villanovian II) and from 750 to 680 BC (Villanovian II).

Several glass beads were recovered during the excavations. Twenty-seven blue, turquoise, black and dark green glass beads were selected and analysed. The chemical analyses of major and minor elements were obtained by WDS-EMPA, while the analyses of eventual opacifiers dispersed in the matrix were carried out with the combination of XRD and SEM-EDS observations.

The chemical data of the samples allow identifying a group of four beads characterized by a mixed alkalies composition, typical of the Final Bronze Age production found in [2,3]. All the other samples show low levels of K_2O (<2 wt%) and rather high Na_2O (>15 wt%). Some of these samples can be classified as natron-based glass, while for a number of beads the classification is not straightforward, since they contain, along with low K_2O, a high amount of MgO (about 3 wt%). These low potassium high magnesium glasses show, in addition, extremely high levels of Al_2O_3. These results indicate that the glass found in this site derive at least from three different melts. Regarding the opacity of the samples, in most of the cases the effect is due to the dark colour of the glass (i.e. in blue, dark green and black beads) which prevent obliterate the transmission of light. Only in the turquoise samples, crystalline particles of calcium antimonate were found.

[1] Tovoli, S. (1994) in Forte, M. & Von Eles Masi, P. (eds.) *La pianura Bolognese nel villanoviano. Insediamenti delle età del Ferro (catalogo della mostra)*. Firenze. [2] Biavati, A. & Verita`, M. (1989) *Rivista della stazione sperimentale del vetro*, **4**, 295-303. [3] Angelini, I. et al. (2004). *J. Archaeol. Sci.*, **31**, 1175-1184.

An advanced methodology for Remote Operation Vehicle magnetic survey to delineate buried targets and estimate medium magnetization

Eppelbaum, L.V.
Dept. of Geophysics and Planetary Sciences, Raymond and Beverly Sackler, Faculty of Exact Sciences, Tel Aviv University, Tel Aviv, Israel ([*]levap@post.tau.ac.il)

A role of iron in the Earth evolution and investigation of the present environment is extremely important (e.g., [1]). Magnetic survey is one of most applied geophysical method for searching and localization of any objects with contrast magnetic properties (for instance, in Israel detailed magneric survey has been succesfully applied at more than 40 archaeological sites [2]). However, land magnetic survey cannot be performed in swampy and karstic areas, districts with dense natural growth and in some other districts. Conventional airborne magnetic measurements are limited by a flight level, too high velocity of flight, heightened danger for the aircraft crew by low-altitude survey, and financial considerations. At the same time the new Remote Operation Vehicle (ROV) generation – small and maneuvering vehicles – can fly at levels of few (and even one) meters over the earth's surface (flowing the relief forms or straight) with simultaneous precise magnetic field measurements. Such geophysical investigations should have an extremely low exploitation cost. Finally, measurements of geophysical fields at different observation levels could provide new unique geological-geophysical information [2].

The developed interpretation methodology for magnetic anomalies advanced analysis [3] may be successfully applied for ROV magnetic observations. This methodology includes: (1) non-conventional procedure for elimination of secondary effect of magnetic temporary variations, (2) calculation of rugged relief influence by the use of a correlation method, (3) estimation of medium magnetization, (4) application of various logical-heuristic and informational algorithms for revealing small anomalies against noise background, (5) advanced procedures for magnetic anomalies quantitative analysis (they are applicable in conditions of rugged relief, inclined magnetization, and an unknown level of the total magnetic field for the models of thin bed, thick bed and horizontal circular cylinder; some of these procedures demand performing measurements at two levels over the earth's surface), (6) advanced 3D magnetic-gravity modeling for complex media, and (7) development of 3D physical-geological (or magnetic-geological) model of the studied area. ROV observations also permit to realize a multimodel approach to magnetic data analysis [4]. Results of performed 3D modeling confirm an effectiveness of the proposed ROV low-altitude survey.

Khesin's methodology [3] for estimation of upper geological section magnetization consists of land magnetic observations along a profile disposing under inclined relief with the consequent data processing (this method cannot be applied at flat topography). It was suggested that integrated ROV straight and inclined observations will help to obtain parameters of the medium magnetization even over the flat relief.

[1] Pilchin, A.N. & Eppelbaum, L.V. (2006) *Iron and its unique role in the Earth Evolution, Monogr.* Mexican Geoph. Soc., **9**. [2] Eppelbaum, L.V. (2010) *Advances Geosci.*, **24**, 45-68. [3] Khesin, B.E. et al. (1996). *Interpretation of Geophysical Fields in Complicated Environments.* Modern Approaches in Geophysics. Kluwer Academic Publishers. [4] Eppelbaum, L.V. (2005) *Proceed. of the 6th Conference of Archaeological Prospection*, Roma, Italy.

Mineralogy and archaeometry: fatal attraction

Artioli, G.
Dipto. di Geoscienze, Università di Padova, Italy
(gilberto.artioli@unipd.it)

The difficult and fascinating relationship between archaeometry and mineralogy continuously offers challenges and topics for research, though it is often troubled by the sectorial organization of academic structure, at present also severely limited by budgetary cuts [1,2]. The existing competition between traditional academic disciplines in the field of cultural heritage is often pernicious and poorly effective as far as information and knowledge transmission is concerned. The continuity in the employment of highly trained researchers and the poor strategy in the data publication are issues of great concern. Centralised research facilities could have a leading role in the management of multi-disciplinary research, though they have a limited practical effect in a shrinking budget world.

Within this frame, disciplines such as mineralogy and petrology, intrinsically used to deal with complex systems, found new natural areas of applications in cultural heritage materials. Archaeometry-oriented applications rose from the status of exotic studies to widely diffused areas of research within the last decade, partly because of the fascination of the involved problems, and partly because of the limited funding in the traditional fields of research. It is argued that mineralogy as a discipline at the crossroad between the core Earth Sciences, crystallography, materials science, and geochemistry might be a key area of innovation for cultural heritage studies.

A few case studies will be discussed to convey a personal view of mineralogical applications within the broader context of cultural heritage investigations [3]. Key issues are: the use of combined techniques for the characterization of complex systems, the optimization of non-invasive techniques, the appropriate use of data bases in archaeometry.

[1] Maggetti, M. (2006) *Geol. Soc. London, Spec. Publ.*, **257**, 1-8. [2] Artioli, G. (2007) *Riv. Archeol.*, **XXXI**, 207-209. [3] Artioli, G. (2010) *Scientific methods and the cultural heritage.* Oxford University Press.

On the origin of the green colour of archaeological bone artefacts of galloroman period

Ferrand, J.[1], Rossano, S.[1*], Rollet, Ph.[2], Farges, F.[3], Allard, T.[4], Pont, S.[3] & Catillon, G.[1]
[1]LGE, Université Paris-Est Marne-la-Vallée, France
([*]rossano@univ-mlv.fr)
[2]INRAP Reims, France
[3]LMCM, Museum National d'Histoire Naturelle, Paris, France
[4]IMPMC, Paris, France

Bone artefacts of the Gallo-Roman period have been discovered in the Reims city in 2004 in a place that was identified as a workshop dedicated to bone objects. Among the bone pieces, some of the finished objects are coloured in green by copper. However, the colouration cannot be due to a long contact with a metallic object made of bronze or copper. The understanding of the origin of this colour is very important to decipher if the colouration was made intentionally and to get knowledge about the processes developed by the craftsman.

In this work, two archaeological green objects from the site of Reims, one archaeological bone coloured by contact with a metallic object and fresh bones coloured in the laboratory are compared. Infra-red spectroscopy was used to get information on the organic part of the samples while X-ray diffraction allowed us to characterize the crystalline part. X-ray absorption spectroscopy at the Cu K-edge was used to obtain information about the environment of Cu in the artefacts. Finally, SEM-EDS experiments have been used to localize the copper in the bone structure.

Ancient metals provenancing: a geochemical database of Alpine copper mines

Giunti, I.[1*], Angelini, I.[1], Artioli, G.[1], Nimis, P.[1] & Villa, I.M.[2,3]
[1]Dipto. di Geoscienze, Università di Padova, Italy
([*]ilaria.giunti@unipd.it)
[2]Dipto. di Scienze Geologiche e Geotecnologie, Università di Milano Bicocca, Milan, Italy
[3]Institut für Geologie, Universität Bern, Switzerland

The provenance of ore minerals used in prehistoric and historic times for copper smelting and extraction is one of the basic questions that archaeologists pose to modern analytical archaeometry [1]. To aid metal provenancing studies, a database of fully characterized Alpine copper mineralisations is being developed as the fundamental reference frame for metal extraction and diffusion in the past.

The abundances of about 60 minor and trace elements, including most transition metals and chalcophile elements, and Rare Earths Elements were measured in all samples via ICP-Q-MS. Furthermore, the feasibility of the routine reliable measurement of the $^{65}Cu/^{63}Cu$ isotope ratio [2] and its eventual use as a possible ore tracer was tested. Multicollector ICP-Mass Spectrometry was used to determine precise Pb isotopic ratios ($^{206}Pb/^{204}Pb$, $^{207}Pb/^{204}Pb$, $^{208}Pb/^{204}Pb$).

Advanced strategies based on multivariate analysis were then used to discriminate the ore mineral provenance. Data were treated with the chemometric software "The Unscrambler Version 9.5" (CAMO AS, Trondheim, Norway). Data pre-treatment, PCA [3] and PLS-DA [4,5] models were performed as implemented in the software. Moreover, mines dataset was analyzed using inferential multivariate nonparametric methods [6,7].

Application of statistical analysis to the geochemical and isotopic database proved to be a very powerful tool to discriminate the ore source areas with very little ambiguity.

The applications to archaeometallurgical copper and slag specimens from the Agordo area (Veneto, Italy) and the recently found prehistoric slags from Millan (SüdTirol, Italy) indicate that the approach is successful in provenance and trade route investigations.

[1] Renfrew, C. & Bahn, P. (2000) *Archaeology: Theories, methods and practice*. Thames & Hudson, London. [2] Ciceri, E. et al. (2005) *Atti del XIX Congresso di Chimica Analitica*, 11-15 settembre 2005. Università degli Studi di Cagliari. [3] Wold, S. et al. (1987) *Chemometrics Intell. Lab. Syst.*, **2**, 37; [4] Esbensen, K. (2002) *Multivariate Data Analysis* - In Practice, CAMO Process AS, Oslo, 5th Edition. [5] Geladi, P. & Kowalski, B.R. (1986) *Anal. Chim. Acta*, **185**, 1-17. [6] Basso, D. et al. (2009) *Permutation Tests for Stochastic Ordering and ANOVA: Theory and Applications with R.* Springer, Heidelberg. [6] Pesarin, F. (2001) *Multivariate Permutation Tests With Applications in Biostatistics*. Wiley, Chichester.

Mineralogy of slags from South African prehistoric tin smelting activities

Heimann, R.B.[1*], Chirikure, S.[2] & Killick, D.[3]
[1]Am Stadtpark 2A, D-02826 Görlitz, Germany
([*]robert.heimann@ocean-gate.de)
[2]Dept. of Archaeology, University of Cape Town, South Africa
[3]Dept. of Anthropology, University of Arizona, Tucson, AZ, USA

A suite of vitreous slag remains from two prehistoric tin smelting sites at Rooiberg, Limpopo Province, South Africa were analyzed by wavelength-dispersive X-ray fluorescence spectrometry (WD-XRF), energy-dispersive X-ray spectroscopy (EDX), and electron microprobe analysis (EMPA). The cassiterite ore utilized at the Smelterskop site (ca. 1650-1850 cal CE) is associated with iron-rich tourmaline (schörl) and was mined from fracture fillings of rocks associated with the Precambrian granite intrusion of the Bushveld Magmatic Province. Evidence exists that the cassiterite feed was carefully beneficiated by panning of the crushed ore. Ore containing some zircon and rutile smelted at the Elandsberg Ledge site (15^{th}-17^{th} centuries cal CE) was presumably collected from alluvial placer deposits**.**

The mineralogical composition of the Smelterskop slags comprises skeletal cassiterite and complex spinels, as well as metallic tin prills ranging in size from a few to tens of micrometers. The spinels contain substantial amounts of tin, titanium and vanadium. The larger tin prills frequently contain Sn-Fe intermetallic compounds called 'hardhead' whereas the small, generally spherical blobs are essentially pure tin. Owing to the different composition of the ore feed processed at the Elandsberg Ledge site these slags contain in addition zirconium-rich minerals such as zirkelite, zirconolite and baddeleyite, and ilmenite.

In the presentation emphasis will be devoted to the role tin (II) and (IV) species appear to play during formation of the glassy slags as well as to the characterization of the complex spinels precipitated from the molten slag. From this study a consistent picture arises of the technology of prehistoric tin smelting in this part of the world.

Provenance determination of raw materials and production technology used in ancient mortars from Tournai (Belgium)

Mertens, G. & Elsen, J.*
Dept. of Earth and Environmental Sciences, Katholieke Universiteit, Leuven, Belgium (*jan.elsen@ees.kuleuven.be)

At the Cathedral of Tournai in Belgium, archaeological excavations are exposing structures from Roman to Medieval age. Samples from these excavations have been subjected to a detailed investigation as part of a broader study considering the transition of ancient cities and their rural territories from Roman to late Roman society and the transformation to the early middle ages. Masonry mortars and mortars used for flooring have been characterized from the Imperial Roman period, the Carolingian style period and the Romanesque style period (4^{th} -11^{th} century AD) to trace the origin of the raw materials and to study the traditional knowledge on mortar production technology.

Computer assisted image analysis techniques were applied on thin sections of the mortar samples to obtain the grain size distribution curve of the aggregate [1]. The results were compared as a fingerprint with the grain size distribution curves of locally available sands, obtained with the same methodology. Based on the resemblance of the curves, it appears that locally available, fine glauconitic quartz sand was used integrally as an aggregate in some mortars, whereas it could not be excluded that somewhat finer sand, present in some mortar samples was sieved before use. However, no clear correlation could be established between the nature of the aggregate and the age or function of the mortar in which it was used.

To identify the origin of the binder a great number of binder related particles were investigated in detail using SEM/EDX and microprobe methods to investigate their nature. Three types of binder-related particles could be distinguished; underburned fragments, overburned fragments and lime lumps (sensu stricto). Underburned fragments as relicts of incompletely burned limestone helped to retrace its source, both Cretaceous marls/chalk and Carboniferous limestone have a highly variable Si- and Al-content and can therefore both yield a hydraulic or air-hardening lime. The presence of characteristic fossils and glauconite helped to refine the provenance of the chalk/marls used for the lime production. Overburnt particles gave helpful information about the burning and slaking of the lime. Overburnt particles containing wollastonite and rankinite associated with a C-S-H phase have been identified in several of the post-Palaeo-Christian mortars. These cathodoluminescent particles are scarcer in Roman and Palaeo-Christian mortars. They could be indicative for the selectivity of the ancient builders towards source materials and/or processed products.

[1] Mertens, G. & Elsen, J. (2006) *Cement Concrete Res.*, **36**, 1453-1459.

Fingerprinting of Cornish gold for provenancing prehistoric gold artefacts from Central Europe

Ehser, A.[1*], Borg, G.[1] & Pernicka, E.[2]
[1]Inst. of Geosciences, Martin-Luther-University Halle-Wittenberg, Halle, Germany (*anja.ehser@geo.uni-halle.de)
[2]Curt-Engelhorn-Centre for Archaeometry, Mannheim, Germany

Previous studies of possible sources of gold used for the Bronze Age Sky Disc of Nebra initially pointed towards South Eastern Europe by indirect evidence, i.e. similar geochemical compositions of gold artefacts from this region [1]. The relatively high tin content in the gold of the Sky Disc, however, suggested a mineral association of gold and tin, similar to the one found in Cornwall. In this study, one lode and seven placer gold deposits from Cornwall have been analysed by LA-ICP-MS to determine the trace element signature of the natural gold for comparison with the gold inlays on the Sky Disc.

To characterise the locally heterogeneous composition of individual deposits as well as their nuggets, a minimum of ten nuggets per deposit as well as three points or lines per nugget were measured after pre-ablation had cleaned the surface. To compare the natural gold with the artefact gold, specific elements were selected, which, besides being useful for individual "fingerprinting", tend to show a low relative standard deviation (RSD) and a high stability during geological (fluvial transport) and metallurgical (smelting) processes. Mn, Co, Ni, Cu, Ru, Pd, Ag, Sn, Sb, Pt, Ir together with Au seem to be the most suitable elements, based upon the results of previous studies. The relatively strong natural variability of Au and Ag contents in natural gold, however, can result in a limited comparability with artefact gold. Artefact gold, on the other hand, can be alloyed with Cu, which is commonly geologically associated with elevated concentrations of Co, Ni, Ag, and Sb. The limited applicability of Ru and Ir for provenance studies is predominantly caused by their concentrations within natural gold being below the detection limits of the LA-ICP-MS instrument. The behaviour of elements that tend to partition into the slag during smelting, such as Mn, still needs further consideration. Since the geochemical signature of individual gold deposits gets homogenised during smelting, the mean value of each deposit has been calculated and used for correlation with the artefact gold.

For Cornwall, the trace element composition of the analysed natural gold strongly correlates with that of the gold inlays on the Sky Disk of Nebra. No similarly well matching "fingerprint" has been detected for previously studied gold deposits from Central and parts of South Eastern Europe. The best correlation is observed in the trace element pattern of the prehistorically important alluvial tin and (minor) gold deposit of the Carnon valley in South Cornwall, strongly suggesting this deposit as the source of the gold used for the Sky Disc. Recent studies of tin isotopes [2] suggest that the tin for the bronze of the Sky Disc also originates from Cornwall supporting the presumed concept of trade of metals from the Atlantic region towards central Germany during the Bronze Age. Further investigations, however, will need to be carried out based on the results of this study and the initial indications for a South Eastern European source of the gold as some important prehistoric gold mining districts have not been studied yet within this context.

[1] Pernicka, E. et al. (2003) *European Network of Competence at 1600 BC. BESSY, Scientific Highlights*, 8-9. [2] Haustein, M. et al. (in print) *Archaeometry*, **52**.

Archaeological gold provenance studies based on SR-XRF and micro-PIXE analyses

Constantinescu, B.[1*], Bugoi, R.[1], Vasilescu, A.[1], Radtke, M.[2], Calligaro, T.[3], Salomon, J.[3], Pichon, L.[3], Röhrs, S.[3], Ceccato, D.[4] & Pop, D.[5]
[1]National Institute of Nuclear Physics and Engineering, Bucharest, Romania (*bconst@nipne.ro)
[2]Federal Institute for Materials Research and Testing (BAM), Berlin, Germany
[3]Laboratoire de Recherche et de Restauration des Musées de France, CNRS UMR 171, Paris, France
[4] INFN, Laboratori Nazionali di Legnaro, Italy
[5]Babes-Bolyai University, Cluj-Napoca, Romania

The territory of today Romania was one of Europe main gold-producing areas since the Antiquity, mostly due to the deposits from the "Golden Quadrilateral" in the Apuseni Mountains, and less to the Eastern and Southern Carpathians deposits. The goal of the study is to find out if so-called "Transylvanian gold", originated either in the Apuseni Mts. or/and in the Southern Carpathians was used to manufacture some archaeological objects i.e. the twelve Dacian gold bracelets (Fig. 1). For gold artifacts, trace elements such as Te, Sb, Hg, Pb, Cu, as well as Platinum Group Elements (PGE), Sn, Ta and Nb are more significant for provenance than the main components i.e. Au, Ag. On the other hand, Sb, Te and Pb are specific for the Apuseni Mts. gold, whereas the presence of Sn might be characteristic for the alluvial gold from the Southern and Eastern Carpathians. Each bracelet weights around 1 kg and consists of a thick gold rod, 6 to 8 times coiled in the shape of a spiral. The rods range from 2.30 to 2.80 m in length and end with palm leaf-like ornaments. The SR-XRF analyses (Berlin BESSY synchrotron) show various Au (78.2 to 92.9 wt.%), Ag (6.3 to 20.3 wt.%) and Cu (0.3 to 2.1 wt.%) content [1]. Sn, up to 0.15 wt.%, and traces of Sb were also detected.

The data obtained for archaeological artifacts were compared with analyses of 22 native "Transylvanian gold" samples. The latter were studied by means of both SR-XRF (Berlin BESSY synchrotron) and micro-PIXE (Paris AGLAE accelerator and Legnaro micro-beam) techniques. The results show high Ag (8 to 30 wt.%) and low Cu (0.2 to 1 wt.%) amounts in all studied samples. In particular, gold from Southern Carpathians placer deposits contains Sn (150-300 ppm) whereas gold from the Apuseni Neogene hydrothermal deposits (veins) have a highly variable content of Te (200-2000 ppm) and Sb (150-300 ppm).

Fig. 1: One of the Dacian gold bracelets.

Due to the high possibility that the artifacts were manufactured from a mixture of native and previous gold object(s), it can be only presumed that at least partly, the metallic material used for the Dacian bracelets originated from the placer deposits from the Southern Carpathians and alluvial and Neogene veins from the Apuseni Mts. This is supported by the presence of Sn (for placers) and Sb (for veins).

Acknowledgements: Study supported by PN 91-020 project (Romanian Ministry of Education).

[1] Stan, D. et al. (2009) *Studia UBB, Geol., Sp. Is.*, 99-100.

Mineralogical and geochemical characterization of ceramic "sugar jars" ("formas de açúcar") from Aveiro town (Portugal)

Morgado, P.[1] & Rocha, F.[2*]
[1]Geobiotec Unit, University of Aveiro, Portugal
[2]Geosciences Dept., Geobiotec Unit, University of Aveiro, Portugal (*tavares.rocha@ua.pt)

During the 15th to 19th centuries, the old pottery centre from the Aveiro town produced one typical form of ceramic called "formas de açúcar" ("sugar forms") or "cerâmica do açúcar" (Fig. 1), used only in the cycle of sugar production, specifically for the stage of the purge of the sugar cake. These ceramics were exported to sugar production areas, such as Madeira Island and Brazil.

Fig. 1: Two ceramic "sugar jars" ("formas de açúcar") from Aveiro town (Portugal).

Such ceramics, including integrally preserved forms, were found at a sub aquatic archaeological site in a channel of Aveiro coastal lagoon. Same ceramics was found in the old urban areas, where mostly shards but also whole forms were used as construction materials for the walls.

In this work we present a synthesis of the main results obtained so far in the mineralogical and geochemical characterization of the ceramic "sugar forms" found in Aveiro (NW littoral region of Portugal).

Mineralogical analysis with X-ray diffraction was carried out on bulk samples, and on suspensions and oriented aggregates of <63 and <2 μm on air-dried, glycolated and heated samples. Scanning electron microscopy with elemental analyses was also done on selected samples. Chemical composition was assessed by X-Ray fluorescence and provided the major elements chemical data: SiO_2, Al_2O_3, Fe_2O_3, TiO_2, MnO, CaO, MgO, K_2O, Na_2O, P_2O_5 and Loss-on-Ignition. Some trace elements such as: As, Sb, Cd, Co, Cu, Pb, Ni, Zn, Se, Te, Tl, and Ba were also analysed.

Multivariate statistical methods were applied, in particular, Cluster, Principal Components and Discriminant Analysis, the later being a statistical method that assigns samples to one or more of previously/-defined groups. The application of Discriminant Analysis, by means of the *Statistica* Software Program, implies that only the variables that exhibit variance in each defined group are used, leading to the exclusion of all others. The acceptation of both, the discriminant function and the variables that define it, is based on the interpretation of the Wilk's Lambda associated to each variable, and on the Classification Matrix. After verification of the validity of the determined function the Classification Matrix of each sample based on the posterior probabilities determined was interpreted.

The obtained results of composition have given important information about the provenance of the studied materials, and also about their raw materials. Mineralogical and chemical data obtained so far point to local production, using local and regional Upper Cretaceous (Maastrichtian) clays and sandy clays as main ceramic raw materials.

Prospecting for archaeological pottery provenance: experiences on Middle Neolithic Bükk culture pottery from Hungary

Szilágyi, V.[1*], Csengeri, P.[2], Szakmány, Gy.[3], Taubald, H.[4], Tóth, M.[5], Leno, V.[4], Zöldföldi, J.[4] & Biró, T.K.[6]
[1]Inst. of Isotopes, HAS, Budapest, Hungary
([*]szilagyiv@iki.kfki.hu)
[2]Herman Ottó Museum, Miskolc, Hungary
[3]Dept. of Petrology and Geochemistry, Eötvös Loránd University, Budapest, Hungary
[4]Dept. of Geochemistry, University of Tübingen, Germany
[5]Inst. of Geochemical Research, HAS, Budapest, Hungary
[6]Hungarian National Museum, Budapest, Hungary

Provenance investigations of archaeological pottery mean the tracking a complex manufacturing process which can involve both natural (sediments) and artificial (tempering) mixture of components. In addition, significant changes can affect the mineralogical and chemical composition turning from the raw material to the fired pottery (e.g. levigation of clay, tempering, firing, using, burial in sediment/soil). A possible and reasonable way of observation is to sample the possible raw materials and to compare them to the pottery. Investigation of silt-sand sized components (aplastics, temper) is based on petrography, but fine-grained constituents (clayish paste) require instrumental mineralogical and geochemical analysis.

Taking these aspects into consideration, our research group investigated Middle Neolithic Bükk culture pottery and natural samples of fine-grained soil-sediment profiles from different archaeological sites in Hungary (Aggtelek-Baradla cave, Bodrogkeresztúr, Felsővadász, Garadna, Boldogkőváralja, Sajószentpéter) [1,2]. Local sediments, mapped as Quaternary and Neogene in age, and partly soils were sampled by ca. 2 m deep hand drillings close to the archaeological sites. The samples were investigated as possible raw materials for pottery-making, shaped and fired accordingly. From the little "bricks", thin sections and powdered samples were made, same as for the archaeological pottery samples. Results of petrographic (PM), mineralogical (XRD) and geochemical (XRF) analyses were compared.

Based on our results, it can be stated that

(1) the near surface sediments/soils (similar to raw materials exploitable from shallow clay pits) can differ very much from the pottery found at the same site;
(2) in the 2 m lithological columns, there is large variety concerning mineralogical and chemical composition, which means that any similarity with the pottery material suggests intentional selection of raw material from the available local sources;
(3) mineralogical and geochemical data of pottery from various sites seem to cluster more tightly than that of the sediment/soil samples; even from one borehole;
(4) fabric and grains size properties suggest a definite physical quality requirement for the pottery raw material or specific treatment of that to reach the appropriate properties;
(5) fineware is even more consistent than average household ware;
(6) coarse household pottery shows more petrographic and geochemical affinity to the local soil samples than fineware.

[1] Szilágyi, V. et al. (2010) *37th ISA Proceedings, Siena*. [2] Taubald, H. & T. Biró, K. (2007) *Archeometriai Műhely / Archaeometry Workshop*, **4(2)**, 1-4.

Written sources and archaeometric results: from fiction to truth

Maggetti, M.
Dept. of Geosciences, University of Fribourg, Switzerland
(marino.maggetti@unifr.ch)

Ancient and modern ceramic products can be studied from different perspectives. To the petrologist, they are artificial rocks which have been subjected to relatively high temperatures and have recrystallized to become thermometamorphic products, analogue to those naturally formed through metamorphism and anatexis. In contrast to natural rockforming processes, pressure is insignificant in the genesis of such objects, because the kiln can be considered as a technical system. In such open systems, neither pore solutions, present before firing, nor gaseous reaction products, which may have been produced during the high temperature process, have an influence on the transformation, because they can leave the system at any time. Similar to natural rocks, ceramic objects consist of an assemblage of crystalline and amorphic phases, which can be analysed with the same petrographic, mineralogical and chemical methods such as micaschists, which are formed from clay during metamorphism. Any ceramic fragment, how insignificant it may appear, can be compared to a potential 'book', because it contains, as if stored on pages, a wealth of information about its history. The lifespan of a piece of pottery can be divided into five steps: (1) extraction of the clay from the pit; (2) manufacture of the object (processing of the clay, firing); (3) use, with subsequent breakdown; (4) burial; (5) excavation, cleaning, treatment and analysis [1]. During all these steps, the sherd has stored information, and this 'memory' can be activated by a variety of chemical and physical methods [2,3]. Why study "young" ceramic objects, i.e. those from the 18th and 19th c. AD, when all aspects concerning the provenance and/or the specific technique are accessible in written, published or unpublished sources? Recent archaeometric projects showed contradicting results to the written convictions. Some of these studies of French and Swiss whiteware will illustrate the potential of mineralogical, petrographical and chemical methods in deciphering the real origin, the real recipe and the real technique of the studied objects. In all these cases, apparently firmly established written evidences are not reliable and must be revised.

[1] Maggetti, M. (1982) in Olin, J.S. & Franklin, A.D. (eds.) *Archaeological Ceramics*. Smithsonian Institution Press, 121-133. [2] Maggetti, M. (1994) in Burragato, F., Grubessi, O. & Lazzarini, L. (eds.) *1st European Workshop on archaeological ceramics*. Università degli Studi di Roma "La Sapienza", Roma, 23-35. [3] Maggetti, M. (2001) *Chimia*, **55**, 923-930.

Characterization of the Copper Age ceramics of the Cucuteni-Tripolye culture (Ruginoasa site, NE Romania) by ICP-MS and EMP

Ionescu, C.[1*], Hoeck, V.[2,1], Ghergari, L.[1], Simon, S.[1], Precup, C.[1], Lazarovici, M.[3] & Lazarovici, Gh.[4]
[1]Babeş-Bolyai University Cluj-Napoca, Romania
([*]corina.ionescu@ubbcluj.ro)
[2]Paris Lodron University, Salzburg, Austria
[3]Institute of Archaeology, Iaşi, Romania
[4] Eftimie Murgu University, Reşiţa, Romania

The Copper Age pottery exhumed at Ruginoasa, 60 km west of Iaşi (Romania) was assigned to the so-called Cucuteni-Tripolye cultural complex. It extended in the V-IV milenium BC from the central and north of today-Romania towards east, into Moldavia and Ukraine. Geologically, the region consists of Sarmatian clays, marls and sands, being part of the Eastern European Platform.

The elegant-shaped light red to orange pots, painted with white, red and brown-black geometric patterns are characteristic for this culture. Optical microscopy shows a red, porous ceramic body, with oriented texture. The matrix ranges from microcrystalline to amorphous. The non-plastic inclusions consist of quartz, plagioclase, K-feldspar, muscovite, biotite. Characteristic is the high number of fragments consisting of different clays and siltitic clays, partly calcareous. Other lithoclasts are scarce and consist of mainly metamorphics, some granite, grauwacke and silicastone. Granulometrically, the pottery classifies as fine ceramics, with maximum 3-4% arenitic grains.

The ceramics shows an intermediate to acidic chemistry, with 58.46-64.77 wt.% SiO_2, 12.78-16.64 wt.% Al_2O_3, 5.28-6.33 wt.% Fe_2O_3, 4.31-7.51 wt.% CaO and 2.73-3.48 wt.% K_2O. The content of Rb, Cs, Nb, Th, U and in particular Au (1.9 to 54.1 ppb) is relatively high.

The Backscattered Electron images revealed, besides the large non-plastic inclusions, a highly inhomogeneous matrix, consisting of a fine grained groundmass of clay minerals, amorphous phases and glass in which tiny, smaller than 0.02 mm non-plastic inclusions are embedded. The latter include quartz, feldspar, muscovite, some chlorite and calcite. Accessory minerals such as titanite, anatase, apatite, epidote and hematite occur as well.

Electron Microprobe analyses show that upon softening and possible partial melting the quartz grains, in particular along their rims, incorporate variable amounts of Al and K, with a trend in the direction of K-illite. The alkali-feldspar ranges from pure K-feldspar to anorthoclase and albite. Ca-bearing plagioclases are extremly rare. Muscovite varies from Al-rich compositions to phengitic micas with variable Fe and Mg content. They show a systematic decrease of Al and K and an increase of Mg, Fe and Ca. This transformation process of muscovite has a trend towards compounds with considerably less K and Al than usually measured in K-illite. The final firing products of clay minerals are crystalline, amorphous or glassy. Their composition resembles an intermediate compound between K-illite and a hypothetical Ca-illite with a wide range of composition. Such thermal transformations are obviously not unique in ceramics. They were also found in ceramics from Ilişua - a Bronze Age settlement in north Romania.

The non-stoichiometry of the newly-formed phases gives an insight into a fast firing, whereas their composition indicates a high temperature of firing, between 850 and 950°C.

Acknowledgements: The study was financially supported by ID-2241/2008 project funds (Romanian Ministry of Education).

Mineralogical and geochemical „fingerprints“ of historical bricks from Vienna

Ottner, F.[1*], Fröschl, H.[2], Mitterlehner, C.[1], Hartinger, S.[1] & Holawe, F.[3]
[1]Institute of Applied Geology, University of Natural Resources and Applied Live Sciences, Vienna, Austria
[2]Seibersdorf Labor GmbH, Seibersdorf, Austria
[3]Institute of Geography and Regional Research, University of Vienna, Austria

Vienna has an at least 2000 years old tradition in making and use of bricks. The first bricks were probably produced by Romans in order to have enough construction material to fortify the Petronell and Vindobona military camps. We assume that the first brick-kilns were situated at the banks of the Alserbach River, where excellent raw material for bricks was available. During medieval times huge amounts of building material were needed to build and preserve the town walls. In particular, the urban expansion in the 19th century is a highlight in historical brick use.

Mineralogical and petrographical parameters as well as technological properties were analysed on several 100 to 300 years old brick (samples) from the surroundings of Vienna. In addition, elemental analyses were performed on total digestions of the powdered materials using inductively coupled plasma mass spectrometry (ICP-MS) as powerful technique for the determination of the trace element composition of the samples.

In the present work we aim to characterise which parameters are the most significant for tracing the origin of historical bricks. In archeometry it is a big task to determine the provenance and get information about the production technology in historical times.

Like in forensic studies, we are using an interdisciplinary approach to detect markers like „fingerprints“ which are significant for the materials. The natural elemental distribution, characterised by the geochemical and geological environment and the technological process during the brick making, influences the chemical and mineralogical composition of the material. Additionally, different inclusions in the bricks like by-products or recycling material can be typical for different production places. Further to the variables measured, the signs – possibly the symbols of the producer – are available.

Several multivariate statistical methods like factor analysis, cluster analysis and discriminant analysis were performed on the data set. The available variables are manifold. There are more variables available than objects to be classified. It is therefore necessary to reduce the dimensionality and the multicolinearity. This is done with factor analysis. The factors are then used in the classification process. There are about 5 to 7 different sources and/or production sites for the 36 bricks. Discriminant analysis is used in two ways. One way takes the results of the cluster analysis as classes which are tested with the same variable set. Second the symbols on the upper side of the brick stones are used as different classes and the measured variables as explanatory variables to find out if the symbols could be used as hints about the different sources and production sites, which is obviously not the case.

Protohistoric amber in Europe: new data from Italy and state of the art

Angelini, I.* & Artioli, G.
Dipto. di Geoscienze, Università degli Studi di Padova, Italy
(*ivana.angelini@unipd.it)

The main European sources of amber are located in the Baltic region. Several Palaeolithic amber objects and the earliest workshop have been found in this area. In Southern Europe amber as workable material is employed much later, it appears in Italy in the Aeneolithic, and it is widely diffused in the Mediterranean word during the Bronze Age [1]. Amber deposits are also present elsewhere in Europe, but generally they supply a much smaller quantity of material with respect to the Baltic region, and the amber nodules are normally of limited size. The trade of Baltic amber is well documented during Roman times, whereas the hypothesis of Baltic amber diffusion throughout Europe since the Pre- and Proto-history has been long supported by archaeometric investigations [2,3].

The earlier archaeometric characterizations of the minor European amber deposits and of a few archaeological finds have not been followed by systematic investigations. Common knowledge that virtually all archaeological amber was imported from the Baltic regions has not been adequately supported or challenged by appropriate characterization of the materials, until very recent studies performed both on amber deposits and on archaeological objects. In some instances the use of local amber sources is proved since the Palaeolithic [4]. Our research is focused on the investigation of the amber sources of the earliest Italian materials, and on the change of sources and trade routes from the Aeneolithic to the beginning of the Iron Age [1,5].

The analyses have been carried out by infrared spectroscopy (FTIR), as a fast, inexpensive, poorly invasive and reliable technique for the characterization of amber [2,6,7]. The use of the Diffuse-Reflectance Infrared Fourier Transform Spectroscopy (DRIFT) mode allows non invasive characterization or the use of a minimal amount of sample. About 200 objects have been analysed by DRIFT. The data show that succinite is indeed the principal amber type present in Italy during protohistory, though in a few sites the contemporary use of different amber sources is observed, especially in sites dated to the earliest Iron Age. As a matter of fact the archaeological objects found in two important Italian sites show the substantial presence of non Baltic amber [1,8].

The recent results on protohistoric Italian ambers will be presented and discussed as a function of material's age and geographic distribution, and compared to the available data on coeval European finds.

[1] Angelini, I. & Bellintani, P. (2006) in *Atti XXXIX Riunione Scientifica IIPP, Firenze 2004*, **III**, 1477-1494. [2] Beck, C. W. (1970) *Archaeology*, **23**, 7-11. [3] Negroni Catacchio, N. & Guerreschi, G. (1970) *Studi Etruschi*, **XXXVIII(S.II)**, 165-183. [4] Peñalver, E. et al. (2007) *Arch. Sci.*, **34**, 843-849. [5] Angelini, I. & Bellintani, P. (2005) *Archaeometry*, **47(2)**, 441-454. [6] Beck, C.W. (1986) *App. Spect. Review*, **22**, 57-200. [7] Angelini, I. (2010) in Artioli, G. (ed.) *Scientific methods and the cultural heritage*. Oxford University Press. [8] Angelini, I. (in press) in *Atti XLIV Riunione Scientifica IIPP, Cagliari-Barumini-Sassari, 2009.*

Discrimination of prehistoric polished stone tools from Hungary by non-destructive chemical analyses

Szakmány, Gy.[1*], Kasztovszky, Zs.[2], Szilágyi, V.[2], Starnini, E.[3], Friedel, O.[4] & Biró, T.K.[4]
[1]Dept. of Petrology and Geochemistry, Eötvös L. University, Budapest, Hungary (*gyorgy.szakmany@geology.elte.hu)
[2]Dept. of Nuclear Research, Institute of Isotopes, Hungarian Academy of Sciences, Budapest, Hungary
[3]Dept. of Archaeology and Classical Philology, University of Genova, Genoa, Italy
[4]Hungarian National Museum, Budapest, Hungary

Prehistoric polished stone tools with fine to very fine grained texture may show striking similarities in their macroscopic appearance by texture and colour. Therefore, it is very difficult to distinguish the different rock types by the naked eye. Prompt Gamma Activation Analysis (PGAA) is one of the powerful, absolutely non-destructive chemical methods for the analysis of archaeological materials. Contrary to other non-invasive chemical methods this technique measures bulk composition. As regards polished stone tools, PGAA measures all major elements and few trace elements [1].

189 polished stone tools from different collections and localities of Hungary, and 25 geological samples from potential raw material sources were analyzed by PGAA. To interpret the results, bivariant and ternary diagrams, as well as statistical analyses were used. To control the method, several broken pieces were studied also by destructive methods, mainly thin section petrography. Our aims were:

1) to obtain chemical composition of the analyzed artefacts;

2) to create an initial database of PGAA results of the most important raw materials of polished stone tools occurring in Hungary;

3) to explore the potentials and limitations of PGAA in the determination of the raw materials used for the polished stone tools.

As a result, several different raw material groups, basalt – dolerite – metadolerite, greenschist – metabasite – amphibolite, blueschist, hornfels, "white stone" (siliceous magnesite, siliceous siltstone, micritic limestone, tuff, diatomic schist) [2,3], ultrabasic rocks, acidic-intermediate volcanics, could be distinguished. Moreover, different rock types and their compositional varieties were recognized within each group (e.g. greenschist-metabasite, basalt-dolerite). It turned out that weathering or alteration can essentially change the chemical composition beyond the limit of recognisability of the rock.

Macroscopic description combined with PGAA will help to determine raw material types of polished stone tools. However, in some cases other methods are also necessary to achieve precise determination.

[1] Szakmány, Gy. & Kasztovszky, Zs. (2004) *Eur. J. Min.*, **16**, 285-295. [2] Antonović, D. (1997) *Starinar*, **48**, 33-39. [3] Szakmány, Gy. et al. (2009) in Ilon, G. (ed.) *Raw materials and trade*. Szombathely, 369-384.

Copper Age polished stone shaft-hole axes in Caput Adriae: archaeological implications

Bernardini, F.[1*], De Min, A.[2], Velušček, A.[3], Eichert, D.[4], Montagnari Kokelj, E.[5] & Tuniz, C.[1]
[1]The 'Abdus Salam' International Centre for Theoretical Physics, Trieste, Italy ([*]fbernard@ictp.it)
[2]Dept. of Geosciences, University of Trieste, Italy
[3]Institute of Archaeology, ZRC SAZU, Ljubljana, Slovenia
[4]Elettra Sincrotrone Trieste, Basovizza, Trieste, Italy
[5]Dept. of Antiquity Sciences 'Leonardo Ferrero', University of Trieste, Italy

During the Neolithic-Copper Age transition, production of polished stone axes in the Caput Adriae (northeastern Italy, central and western Slovenia and northwestern Croatia) underwent a drastic change in terms of raw materials and typology of the artefacts. Shaft-hole axes, mainly produced from meta-dolerites (A), serpentinites (B) and meta-ultramafites (C), became increasingly important in the Copper Age, spreading all over the region. However, the above mentioned rock types do not show a homogeneous distribution. Group A is concentrated in the southern part of Caput Adriae, group B in the northern one, and group C, not yet completely investigated, was unearthed mainly in the Karst and in central Slovenia.

Chemical, mineralogical and textural analyses, by Inductively Coupled Plasma-Mass Spectrometry, X Ray Diffraction, Electron Microprobe Analysis, Synchrotron Radiation Fourier Transform Infrared Spectroscopy, Optical Microscopy, were carried out. The results give evidence of a strong connection between provenance areas of the raw material and main copper mineralizations close to Caput Adriae. In particular, meta-dolerites come from Banija Ophiolite Complex at the northernmost edge of the Central Dinaric Ophiolitic Belt [1], while serpentinites probably originate in the Hohe Tauern area [2].

On the basis of these results, the position of Ljubljansko Barje (central Slovenia) - between eastern Alpine and Balkan copper-rich deposits - could contribute to explaining the importance of this area as metallurgical district at least from IV millennium BC, and, consequently, its important bridging role between Eastern Europe and the Mediterranean.

Finally, a possible source of raw material for the meta-ultramafites has not yet been recognized, even if preliminary indications suggest they could originate in Eastern Austria or Czech Republic.

[1] Bernardini, F. et al. (2009) *Archaeometry*, **51(6)**, 894-912.
[2] Bernardini, F. et al. (accepted) *Archaeometry*.

Archaeometric analysis on limnic quartzite-limnic opalite raw materials and chipped stone tools (Tokaj Mountains, NE-Hungary)

Szekszárdi, A.[1*], Szakmány, Gy.[2] & Biró, T.K.[3]
[1]Dept. of Exploration and Production, MOL Ltd., Budapest, Hungary ([*]aszekszardi@mol.hu)
[2]Dept. of Petrology and Geochemistry, Eötvös Lóránd University of Budapest, Hungary
[3]Dept. of Archaeology, Hungarian National Museum, Budapest, Hungary

Late-Badenian-Sarmatian siliceous sedimentary rocks from limnic basins of the Tokaj Mountains were commonly used for chipped stone tools in prehistory. These rocks have perfect physical and mechanical properties for this purpose. Due to the richness of the raw materials in several outcrops, they were accessible to the inhabitants of the area. Studying these tools helps to understand the history of the culture in this region. These facts demand a basic work to describe the outcrops, identify and characterise the siliceous rock types (generally with petrographic analysis).

The main goals of this study are comparing the limnic-quartzite, limnoopalite raw materials to chipped stone tools made from similar rock types, identifying the sources of the artifacts, extending the range of the technical methods and working out the methodology to identify the outcrops and quarries of the stone tools made of limnic quartzite or limnoopalite. To approach these goals, petrological, geochemical, mineralogical analysis of the artifacts and the possible raw materials were used and the results were compared. Detailed macroscopic and microscopic petrographic descriptions were made. XRF, NAA, PGAA were used as geochemical analysis and XRD, FTIR as mineralogical methods.

There is a clear relationship between raw materials and artifacts studied, according to the results of this study. A quarry could be assigned for most of the artifacts. The knowledge about the sorting method of raw materials for the stone tools was extended. Evidence for the suggestion of sorting parameters (phase/rate of silification, chalcedony content, opaline content) were found.

Petrographic and mineralogical methods were useful to identify the source of the stone tools in the Tokaj Mountains and to extend the technological knowledge (f.e. well thought selection of the raw materials). The geochemical methods should be useful for further exploration comparing more rock samples from the surrounding mountains (Matra Mt., Bükk Foreland, Börzsöny Mt. and Cserhát Mt.).

Different classes of matt-painted pottery from the sanctuary of the archaeological site of "Timpone della Motta" in the Sibaritide area (CS) Calabria – Southern Italy

Andaloro, E.[1*], De Francesco, A.M.[1] & Jacobsen, J.K.[2]
[1]Dipto. di Scienze della Terra, Università della Calabria, Rende, Italy ([*]eliana.andaloro@unical.it)
[2]Groningen Institute of Archaeology, Groningen, Holland

This study presents the comparison between three different classes of Matt-Painted pottery attributed to the 8th century BC from the sanctuary on the Timpone della Motta in the Sibaritide (CS), Calabria – Southern Italy.

Matt-Painted pottery was widely produced in southern Italy during the early Iron Age and finds from many indigenous sites underline that it was one of the favored pottery types both for dining and storage purposes. The term Matt-Painted refers to handmade vessel of typical indigenous shape with applied decoration in a matt dark paint.

Traditional archaeological research divides Matt-painted pottery into a range of regional classes based on the decorative styles of each region. The thousands of fragments from the sanctuary on the Timpone della Motta, together with the finds of Matt-Painted vessels in indigenous graves and houses, show that two predominant styles were present in the Sibaritide. These two styles have been named the "Undulating Band Style" and the "Fringe Style" based on their many decorative elements. In addition, another range of stylistic groups may be observed in the local indigenous pottery production. Recent research has, however, documented a group of Matt-Painted pottery on the Timpone della Motta, which is notably different from all other Matt-Painted vessels on the site. These vessels display a high level of craftsmanship in being very thin-walled and decorated in a miniaturist and very elaborated style. The closest typological and stylistic ceramics are found among the Matt-Painted pottery productions in the southern Salento region, which naturally raises the question if the vessels from the Timpone della Motta were imported from the Salentine area. In that case the fragments from the Timpone della Motta constitute the only example of deliberated export of Salento Matt-Painted pottery.

Twenty nine fragments of Matt-Painted pottery (one sample was misfired) have been submitted to petrographical analysis applying optical microscopye, mineralogical XRD analysis and chemical analysis in XRF with the aim to investigate on different ceramic productions. The results show that the composition of the "Undulating Band Style" and "Fringe Style" fragments is analogous, while is different the composition of the six ceramic fragments with characteristics similar to the Matt-Painted potteries of the southern Salento region.

Another important aim is to clarify possible correspondence between the used raw material and local clay deposits. For this purpose the clay sediments collected around the archaeological site have been submitted to mineralogical analysis in XRD, chemical analysis in XRF and granulometric analysis. The SEM morphological study of the fragments is devoted to the distinction between different workshop techniques.

Analysis of bricks from Brazilian historic places

Asfora,V.K.[1], Barreto, S.B.[2*], Khoury, H.J.[1], Lavalle, H.[3] & Araujo, R.[4]
[1]Dept. of Nuclear Energy, Federal University of Pernambuco, Recife, PE, Brazil
[2]Dept. of Geology, Federal University of Pernambuco, Recife, PE, Brazil ([*]bsandra@ufpe.br)
[3]Dept. of Archeology, Federal University of Pernambuco, Recife, PE, Brazil
[4]Center of Advanced Studies on Integrated Environmental Protection, Olinda-PE, Brazil

This contribution presents results of the qualitative determination of the chemical elements in Brazilian and Dutch bricks found in historic places in the State of Pernambuco, located in the Northeastern Region of Brazil. Seven bricks, two dated in the 17th century (Dutch bricks), one from the 18th century, three from the 19th century, and one from the 20th century, were analyzed by means of energy dispersive X-ray fluorescence (EDXRF) and X-ray powder diffraction (XRD) in order to identify the mineral phases. The XRD results are displayed in Table 1.

Table 1: Mineral phases identified in the brick samples by XRD

Red-brick (Dutch)	Yellow-brick (Dutch)	Building "Convento de Santo Antônio"	Building "Casa de Câmara e Cadeia"	Building "Casa de Câmara e Cadeia" Nº 03
(17th century)	(17th century)	(18th century)	(19th century)	(20th century)
Quartz	Quartz	Quartz	Quartz	Quartz
Kaolinite	Kaolinite	Illite	*	Illite
	Anorthite	Anorthite		Rutile

*evidence of kaolinite with low crystallinity.

To identify possible patterns in the data, the Principal Component (PC) analysis was applied. For each brick, four points were measured by EDXRF. The results illustrate the differences in the composition among the samples, and allow a Fe and Ca based discrimination. Five distinct clusters resulted and they reflect the inter-correlation or covariance degree among few of the principal components, as shown in Fig. 1.

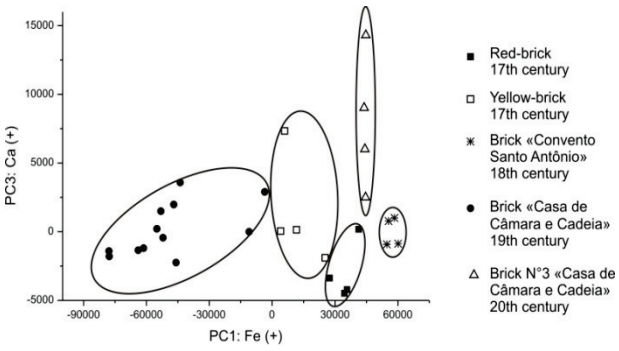

Fig. 1: Principal component analysis based on EDXRF data: PC1: Fe(+) (positive influence) versus PC3 Ca(+) (positive influence).

These results indicate that the bricks were manufactured from different raw materials, i.e. clays, in different times and places.

Microstructure and composition of glaze of Haban ceramics from Sárospatak (NE-Hungary)

Bajnóczi, B.*, Tóth, M. & Nagy, G.
Institute for Geochemical Research, Hungarian Academy of Sciences, Budapest, Hungary (*bajnoczi@geochem.hu)

Production of tin-glazed ceramics (faience) in Central Europe, thus in the historical Hungary as well, was established by Haban (Anabaptist) potters. In the 16th century Anabaptist ceramists had to emigrate from Switzerland, South Germany and Italy due to religious repression, and they moved to Austria, Moravia and Hungary and in the 17th century to Transylvania and further. They brought their skills and implanted a local pottery production under the influence of their new artistic language.

Notable settlement of Habans in Hungary occurred after 1620. In 1645 one of their groups moved from Moravia to Sárospatak (NE-Hungary) where they lived until 1680. One of the main activities of the settled Habans in Sárospatak was pottery, among others faience production.

Archaeological excavations in the last years revealed a 17th century cannon and bell casting workshop in the yard of the Sárospatak castle. During the excavations fragments of tin-glazed ceramics were found, which were most probably produced by the local Haban workshop.

There are no written sources from the 17th to 18th centuries about the production technology of Haban (tin-glazed) ceramics. Our archaeometric research focuses on the mineralogical, petrographic and geochemical investigation of the ceramic body, the white, tin-opacified glaze and the decorations of different colours, and aims to identify the used raw materials and to reconstruct the production technology.

Preliminary electron microprobe analyses indicate that white glaze of the Sárospatak faiences is lead-alkali type with ~38 wt% PbO, 2.2 to 4.4 wt% SnO_2 and 4.9 to 5.8 wt% K_2O+Na_2O content (according to EDS spot analyses). The opaque glaze layer contains tin oxide particles and aggregates (SnO_2 is present in orthorhombic and tetragonal forms according to X-ray diffraction analysis), and relict grains with Sn-Pb-Si composition. Rounded to subangular quartz and feldspar particles are also present.

Decorations were made by using coloured (yellow, blue, green and black) glazes. Blue decoration is associated with cobalt (0.7 to 1.4 wt% CoO) and contains significant amounts of arsenic, nickel and iron as well (1.6 to 2.1 wt% As_2O_3, up to 1.3 wt% NiO, 1.3 to 1.8 wt% FeO) suggesting use of impure cobalt ore (zaffre). Yellow decoration contains lead antimonite particles ($Pb_2Sb_2O_7$ according to X-ray diffraction analysis) and significant amount of dissolved iron (>3 wt% FeO) is also present in the matrix. Black decoration was prepared by using manganese colorant (>2.5 wt% MnO).

A metabasite shaft-hole axe from Grotta Azzurra di Samatorza (Trieste Karst): first evidence of connections between northeastern Italy and central Europe during Neolithic

Bernardini, F.[1*], De Min, A.[2], Šída, P.[3], Velušček, A.[4], Montagnari Kokelj, E.[5] & Tuniz, C.[1]
[1]The 'Abdus Salam' International Centre for Theoretical Physics, Trieste, Italy (*fbernard@ictp.it)
[2]Dept. of Geosciences, University of Trieste, Trieste, Italy
[3]Institute of Archaeology, Faculty of Arts, University in Hradec Králové and West Bohemian University in Plzeň, Czech Republic
[4]Institute of Archaeology, ZRC SAZU, Ljubljana, Slovenia
[5]Dept. of Antiquity Sciences 'Leonardo Ferrero', University of Trieste, Italy

A fragment of a shaft-hole axe, made from a metabasitic rock, was found in the second half of last century in the Grotta Azzurra di Samatorza in Trieste Karst (northeastern Italy). The artefact, without stratigraphic information, was previously attributed to a general Dinaric origin.

Recently, thanks to the systematic interdisciplinary study of polished stone axes from Caput Adriae (northeastern Italy, central and western Slovenia and northwestern Croatia) [1;2], it has been discovered that the artefact is texturally and mineralogically indistinguishable from the Jizera Mts. fine-grained amphibole-rich metabasites [3]. These rocks belong to Krkonoše-Jizera Crystalline Unit (Bohemian Massif).

This material has been largely employed for the production of polished stone axes during the Neolithic of central Europe [3]. The distribution of the Jizera Mts. raw material includes a wide area - Bohemia, Moravia, western Slovakia, southern Poland, Germany and probably northern Austria and Netherlands.

According to the available data the axe from Grotta Azzurra is the southernmost ever found. It is a rare archaeological proof of early connections between Caput Adriae and central Europe (whose directions still have to be fully understood). This is also testified by a few occurrences of Carpathian obsidians in the Danilo/Vlaška archaeological sites of Caput Adriae.

[1] Bernardini, et al. (2009) *Archaeometry*, **51(6)**, 894-912. [2] Bernardini, et al. (accepted) *Archaeometry*. [3] Šída, P. & Kachlík, V. (2009) *J. Geosci.*, **54**, 269-287.

Analysis of some ancient Roman mortars from Ulpia Traiana Sarmizegetusa (Romania)

Cherata, I.[1*], Mertens, G.[2], Benea, M.[1] & Alicu, D.[3]
[1]Dept. of Geology, Babeş-Bolyai University, Cluj-Napoca, Romania ([*]iulian_cherata@yahoo.com)
[2]Dept. of Earth and Environmental Sciences, Catholic University of Leuven, Belgium
[3]National History Museum of Transylvania, Cluj-Napoca, Romania

Ulpia Traiana Sarmizegetusa was the capital of the Roman province Dacia. The city was founded by the emperor Trajan in the early 2nd century AD, and deserted in 271-274 AD under the rule of emperor Aurelian. At its maximum development, it had over 20,000 inhabitants.

This study focuses on several samples of mortars from different walls and structures (probably a bone-processing workshop, the prison, the pedestal of Trajan's statue and the school of gladiators). In the case of the samples from the recently unearthed bone-processing workshop larger samples of mortar from the walls were collected (up to 7 cm in thickness), where we could observe different layers meant to level the surface of the walls, from the other locations smaller pieces from the outer parts of the walls were selected.

The collected samples were studied by optical microscopy (thin sections), XRD and thermogravimetry.

The mortars have a porphyroclastic texture and in general the aggregate includes 1 to 5 mm-sized lithoclasts, crystalloclasts and ceramoclasts. One notable exception is represented by the mortar from the thick walls of the workshop which additionally contains fragments of ceramics in the centimetric range (up to 3.5 cm in length). The crystalloclasts are mainly represented by calcite, quartz, plagioclase and K-feldspars, muscovite, epidote, magnesiohornblende and pyroxene. Quartz clasts fissured due to thermal shock were identified in some thin sections. Feldspars are frequently transformed into clay minerals and sericite. The whole matrix is carbonatic, with secondary calcite deposited in pores and fissures. The lithic fragments consist of quartzites, micaschists, gneisses and limestones. In one thin section fossil remains could be observed. Two samples contain visible straw and plant remnants.

The ratio between CO_2 and the structurally bound water from the thermogravimetric data suggests that some mortars were of hydraulic type. Others were probably of subhydraulic type: lime was obtained from a purer limestone and therefore the mortar did not yield a hydraulic binder.

According to the identified mineralogical composition we presume that the raw material which was used has a local provenience. The metamorphic material used as aggregate comes from the nearby Retezat Mountains (Southern Carpathians), and is common in the alluvia of small rivers. It was probably extracted from pits. Limestones were most likely quarried 5 km west of the city.

Mineralogical and chemical study of ceramic sherds and clay samples from Cameroon

Epossi Ntah, Z.L[*], Sobott, R. & Bente, K.
IMKM, University of Leipzig, Germany
([*]epossi@uni-leipzig.de)

This work is a contribution to the archaeometry of ceramics from Cameroon. Ceramic sample material together with regional clay material were collected in three regions of Cameroon: Mfomakap-(Central region), Mombal-(Eastern region), and Zamala-(Far North region). The purpose of this work is to find answers to the questions of the provenance of the ceramics (local production, imported ware?) and the production techniques (processing of raw material, moulding of vessels, firing temperature and conditions).

The polarized light microscopy, X-ray diffraction, X-ray fluorescence spectrometry, differential thermal analysis, thermogravimetry, and X-ray computer tomography were used as analytical methods.

The results of thin section analyses show that quartz is always the most abundant component (70-80%) of the temper. Additional minerals are micas, mainly biotite, scarce K-feldspars and very rare plagioclase in Mombal, plagioclase, some K-feldspars and rare biotite in Zamala, hornblende, K-feldspars, biotite and plagioclase in Mfomakap. These mineral combinations suggest that the potter's workshops were situated in a landscape with more or less acidic magmatic rocks.

The mica-flakes and the arrangement and shape of pores in the sherds from the three regions do not show any preferred orientation, as one would expect if the objects had been shaped by means of a potter's wheel. All the ceramic artefacts were probably hand moulded.

The X-ray diffraction analyses of sherds show the presence of quartz, K-feldspars and biotite in all three areas. Additionally, kaolinite is observed in Mombal, hornblende and plagioclase in Mfomakap, and plagioclase in Zamala.

According to the results of X-ray fluorescence analyses of ceramics and raw material, local clay as it comes from the pit was used for making the pottery in Mombal and Zamala. In the case of sherds from Mfomakap the chemical data suggests that the raw material was obtained by mixing two types of clay, one rich in Al_2O_3 and rather low in SiO_2 and the other rich in SiO_2 and rather low in Al_2O_3.

Firing experiments in conjunction with DTA/TG and X-ray diffraction analyses with clays from the three locations showed that kaolinite disappears through an endothermic reaction between 400 and 500°C (onset temperature 470°C), illite breaks down between 900 and 1000°C, and mullite forms in the range of 1000 – 1100°C. Comparing the phase assemblages of the sherds with the phase assemblages of fired clay samples, the firing temperatures were deduced.

In conclusion, the pottery of the three regions seems to be a local production. The firing temperature was always below 900°C. In Mombal the presence of kaolinite in the ceramics indicates a firing temperature below 500°C. In sherds from Mfomakap and Zamala micas are still present and this finding points out to firing temperatures below 900 - 950°C.

Archaeometric study of the Neolithic pottery from the "Le Grottelline" site (Spinazzola, Italy)

Fabbri, B.[*], Gualtieri, S. & Lorenzi, R.
CNR, Institute of Science and Technology for Ceramics, Faenza, Italy ([*]bruno.fabbri@istec.cnr.it)

The archaeological site of "Le Grottelline", in the territory of Spinazzola, province of Bari (Southern Italy), dates back to the ancient Neolithic Age. Abundant ceramic materials were recovered, which mainly belong to the Culture of "Archaic-Impressed Pottery" and appear similar to those found in other Neolithic sites of the area [1].

The archaeologists recognised four ceramic classes: coarse, semi-depurated, depurated and *figulina*, even though in many cases it was difficult to make a clear distinction between them. In fact, coarse and semi-depurated ceramics differ between them only for the dimensions of the inclusions, while depurated ceramics differ from *figulina* mainly due to its macro-porosity. Semi-depurated and coarse ceramics represent the main part of the recovered pottery (about 80%).

Three samples were selected for each of the four classes for the archaeometric investigation, which was carried out mainly by means of optical microscopy in thin section, WDS-X-ray fluorescence, and X-ray diffractometry.

The results individuate two ceramic classes: coarse pottery and fine pottery, and three isolated samples. Coarse pottery is constituted by large silicate inclusions in a fine carbonate-poor clay matrix and includes samples from the archaeological coarse and semi-depurated classes. Fine pottery includes the *figulina* ceramics, together with one 'depurated' sample and one semi-depurated sample, and is characterised by medium calcium contents (10-13% wt CaO). The three isolated samples differ from the previous ones both for the microstructure and the chemical composition. The crystalline phases allow to hypothesize a firing temperature <800°C for the coarse pottery and the isolated samples, and 800 to 900°C for the fine pottery.

Comparing our archaeometric results with those of other Apulian Neolithic sites, great similarities have been registered in particular with pottery from Pulo di Molfetta, considered as local production [2]. On this base, also the main part of the "Le Grottelline" pottery has to be considered as local. In addition, the raw materials show geological features typical of the Murge Plateau that is characterized by the presence of calcareous-arenaceous-argillaceous deposits with frequent fossiliferous levels and shaley marl horizons are present.

The variations in the microstructural and chemical characteristics could be attributed to different collecting areas and/or to the nearness to the Bradanic Hole, in which fine quartz-rich micaceous sands are present.

On the base of all the obtained results, the pottery of "Le Grottelline" site shows the technological characteristics of the Ancient Neolithic productions, that used raw materials not so far from the housing areas, often without purification. The firing process was carried out by means of systems with low-medium temperatures and prevalently oxidant firing atmosphere, even if fluctuations were possible, which are responsible of the chromatic variations of the pieces.

[1] Lorenzi, R. & Serradimigni, M. (2009) *Origini*, **XXXI**, Nuova Serie IV, 41-74. [2] Muntoni, I.M. ed. (2003) *Modellare l'argilla. Vasai del Neolitico antico e medio nelle Murge pugliesi*. Collana Origines, I.I.P.P., Firenze.

The browning phenomenon of medieval stained glass windows

Ferrand, J.[1], Rossano, S.[1*], Loisel, C.[2], van Hullebusch, E.[1], Orial, G.[2], Bousta, F.[2] & Munoz, M.[3]
[1]LGE, Université Paris-Est Marne-la-Vallée, France ([*]rossano@univ-mlv.fr)
[2]LRMH, Champs sur Marne, France
[3]LGCA, Grenoble, France

Manganese is a chemical element which has long been used as a colouring or a bleaching ingredient in the glass industry. Its existence at various oxidation states is at the origin of a large variety of colours. This latter can evolve according to environmental parameters such as radiations or the atmospheric pollution. In some ancient stained glass windows, the simultaneous presence of manganese and iron, coupled with the alteration by water and micro-organisms, can induce a browning and, consequently, a loss of transparency in stained glass windows.

To better understand this browning phenomenon, ancient stained glass windows displaying a browning are characterized using optical microscopy, SEM-EDS, microprobe analysis and XAS at the Fe *K*-edge. The ancient glasses that present the browning phenomena appear to be potassic glasses and more precisely calco-potassic samples that contain equivalent quantities of CaO and K_2O. In these potassic glasses, the brown zones are very rich in Mn as compared to the fresh glass but also to the altered glass. In parallel, the Mn-oxidizing bacteria (*Burkolderia Cepacia* [1]) present on the historical samples are isolated and cultivated. Finally, simplified model glasses of various compositions but containing the Fe/Mn couple will be altered in presence of these microorganisms.

[1] Orial, G. et al. (2007) *L'actualité chimique*, **312-313**, 34-39.

A petrographical study of lithic tools from Petreşti archaeological site (Romania)

Filipescu, R.* & Benea, M.
Dept. of Mineralogy, Babeş-Bolyai University, Cluj-Napoca, Romania (*roro_fili@yahoo.com)

The present study focuses on ten lithic tools recovered from Petreşti archaeological site, located 4 km south of Sebeş (Southern Carpathians), now in custody of Sebeş Town Museum. The objects belong to the Petreşti Neolithic culture, dated between 2400–2100 B.C. [1] and famous mainly for its painted ceramics. The objects were submitted for a mineralogical-petrographical study, in order to establish the rock types and, furthermore, to identify possible source areas for the raw materials.

Based on the definition of typical functional Neolithic tools (i.e. simple axes, truncheons, fighting axes and hammers [2]), nine samples classify as axe-hammers (according to the criteria defined by Iuliu [3]), and one is a truncheon with three bumps. For the truncheon-shaped one, a decorative purpose is presumed. In order to determine the shape, size and colour of the objects, macroscopical investigations with the naked eye or with a magnifier were carried out. The tools are made of rocks with relatively high hardness. They are very well polished and all but one have similar shape. Predominantly their colours are dark (grey, brown, black), but in three cases lighter hues were observed.

For the optical microscopy investigation, small fragments of the lithic objects were sampled by wet coring with an electrical drill (10 mm in diameter) to a maximum depth of 15 mm, and prepared as thin sections. Mineralogical and petrographical (structure and texture) features were observed by using a Nikon Eclipse E200 Pol microscope with an attached digital camera. A dominant microgranular massive texture was revealed, with local porphyric varieties. One sample has orientated texture. All the three main genetic rock types were used as raw materials (in brackets, number of tools within the group): igneous (diorite, andesite with hornblende and basaltic andesite) (3), metamorphic (sericite-chlorite schist, metapsammite, serpentinite, hornfels with quartz) (5), and sedimentary (chemical precipitation limestone, sandstone with quartz and feldspar) (2).

In order to identify possible sources of raw materials for the investigated lithic objects, the geological structure of the area was studied. According to the geological map, Orăştie sheet (1:200.000), not all the rock types identified as raw materials in this study can be found around Petreşti village. The area is mostly covered with Holocene sediments. Therefore, knowing the petrographic nature of the ten tools, it can only be concluded that most of the raw material (metamorphic and sedimentary rocks) was either transported by Sebeş River, which springs in the Southern Carpathians. Regarding the provenance of the igneous rocks, they could come from the Mureş River alluvia. This river collects similar rocks from the Apuseni Mts. The exact structural units delivering all raw materials have to be further investigated.

[1] Vlassa, N. (1976) *Neoliticul Transilvaniei* III. [s.n], Cluj Napoca. [2] Comşa, E. (1982) *Neoliticul din România*. Ed. Ştiinţifică şi Enciclopedică, Bucharest. [3] Iuliu, P. (1992) *Cultura Petreşti*. Ed. Museion, Bucharest.

Provenance of graphite in Celtic graphitic ceramics from North-west Romania

Havancsák, I.[1*], Bajnóczi, B.[1], Tóth, M.[1] & Németi, J.[2]
[1]Institute for Geochemical Research, Hungarian Academy of Sciences, Budapest, Hungary (*havancsaki@geochem.hu)
[2]Piata Eliberarii Bl. 33. Ap. 41, Carei (SM), Romania

The Celts settled in the Carpathian basin in the 4th century B.C. (Iron Age, La Tène period) from Western Europe. Their expansion took place in two main directions leading to two significant settlement areas: the Transdanubian region, along the Danube towards Serbia as well as the Hungarian Northern Mountains, the North-west Romania and the southern territories [1].

Peculiarity of the Celts was the production of graphitic (i.e. graphite-bearing) situla-type ceramics. Graphitic ceramics are found not only in the close vicinity of the geological occurrences of graphitic rocks, but also on archaeological sites scattered all around Europe, which suggests an extensive trade of graphitic ware or graphitic raw material. Former archaeometric studies [2,3], carried out on Celtic graphitic ceramics from the Transdanubian region, indicated that graphitic rock temper was probably originated from the South Bohemian Massif (from the Variegated unit in the Southern Czech Republic).

The present archaeometric study focuses on graphitic ceramics from several archaeological sites of North-west Romania [4,5] to determine the source (provenance) of the graphitic temper. Vessels investigated derive from 9 localities: Érendréd / Andrid (1), Kálmánd / Căminˇ (2), Börvely / Berveni (3), Piskolt-Kincsverem / Pişcolt-Lutărie (4), Mezőfény / Foieni (5), Bere-Nyúlvár / Berea-Nyúlvár (6), Piskolt-Gárdovány / Pişcolt-Gárdovány (7), Nagykároly-Bobáld / Carei-Bobald (8) and Lázári / Lazuri (9) (Fig. 1).

Fig. 1: Location of the archaeological sites of the studied graphitic ceramics in North-west Romania.

Graphitic rock fragments found in the studied north-west Romanian ceramics consist of graphite, quartz, K-feldspar, plagioclase, kyanite, sillimanite and altered mica. The graphitic rock used as temper for ceramics is medium to high grade metamorphic rock, graphitic paragneiss. Formerly studied graphitic ceramics from the Transdanubian region show similar mineralogical composition [2,3].

Based on metamorphic grade and mineralogical composition, the potential provenance of the graphitic rock fragments is the Variegated Unit in the Moldanubian zone of the Bohemian Massif. Celts in North-west Romania used the same trade network for importation of graphite (graphitic rock) or graphitic ceramics as the Transdanubian population.

[1] Szabó, M. (2005) L'Harmattan Kiadó, Budapest [2] Havancsák, I. et al. (2009) *Archeometriai Műhely*, **1**, 39-51. [3] Havancsák, I. et al. (2009) *Archeometriai Műhely*, **2009/4**, in press. [4] Rustoiu, A. (1993) *Thraco-Dacica*, **XIV(1-2)**, 131-142. [5] Németi, J. (2009) in Ilon, G. (ed.) *ΜΩΜΟΣ*, **VI**, 267-277.

Provenance and technology study on a collection of loose garnets from a late 5th century Gepidic grave in Northeast Hungary

Horváth, E.
Inst. of Archaeological Sciences, Dept. of Archaeometry and Archaeological Method, Eötvös Loránd University, Budapest, Hungary (sztr.horvath@gmail.com)

Red gemstones identified mostly as garnets generally occurred in the 5th-6th century Europe as decoration of fine metal works. They are known mainly in mounted form, the loose, unmounted pieces are very rarely found. Therefore, it is of great importance that seventeen such loose red gemstones were unearthed at a rescue excavation at Hajdúnánás-Fürj-Halom-dűlő (Hajdú-Bihar County) in a late 5th century cemetery of the Gepids, an East Germanic tribe settled on the eastern bank of the Tisza River from the late 4th century. The discussed pieces considered as remains in a robbed grave were investigated in order to identify the mineral species, its provenance and the technology of cutting. The lack of any related goldsmith's artefact and the visible different phases of the gem-cutting process allow us to regard them as independent pieces of a collection. The noticed inclusions and the measured refractive index revealed that the discussed gemstones are garnets. In addition to the gemmological observation, the analysis was focussed on the chemical composition. The resulting spectra were obtained by a scanning electron microscope (SEM) equipped with an energy dispersive spectrometer (EDS) and display characteristics of Fe-rich as well as Fe-Mg-rich garnets, i.e. *almandine* and *rhodolite*. The comparison of the concentration ratios of the major constituents with the literature data suggests that while the almandine garnets may have been imported from Rajasthan, North India, the rhodolite garnets may have been mined in Sri Lanka [1]. The image analysis based on optical and scanning electron microscopy clearly showed traces left by polishing and shaping. All of the six flat cabochons and seven of the flat plates look like semi-finished products where final steps of shaping were not carried out. Besides, the other four plates may be regarded as finished products with regular shapes. In some cases intentionally engraved outlines were noticed running along the edges. These straight shallow grooves were interpreted as an indirect proof for the use of a template or a sort of pointed marker. Based on our observations, the cutting process could be reconstructed, and the following steps were inferred: 1) cutting the raw surfaces to the desired steepness and thickness; 2) polishing these surfaces on the top and base; 3) designing the shape and size of the prepared pieces by a marker (occasionally) and finally 4) cutting off or breaking the unnecessary edges. Considering the semi-finished pieces characterized by irregular edges, the final steps of their shaping were apparently carried out in a satellite or local workshop. This observation contributes to the recurring debate about the character of imported garnets [2]. The discussed findings suggest that in the Early Middle Ages garnets for inlays were traded in the Carpathian Basin both in pre-cut and ready-to-set form. While mounts and cell walls usually make the accurate observation difficult, the loose character of these pieces permitted us to perform an extensive investigation focussing both on the raw material and the technology. Results may clarify or identify the geographical origin as well as the applied equipment and the organisational aspects of gem-cutting.

Acknowledgements: The study was carried out with the support of the Archaeological Research Laboratory, Stockholm University, Sweden. Help of Brigit Arrhenius and Maria Wojnar-Johansson related to this research is highly appreciated.

[1] Calligaro, T. et al. (2002) *Nucl. Instr. Method. B,* **189**, 320-327. [2] Arrhenius, B. (1985) *Merovingian Garnet Jewellery – Emergence and Social Implication.* Stockholm.

Mineralogy and geochemistry of Bronze Age potsherds: weathering influence of a Mediterranean climate (Cres Island, Croatia)

Ilijanić, N.[1*], Miko, S.[1], Hasan, O.[1] & Posilović, H.[2]
[1]Croatian Geological Survey, Zagreb, Croatia
([*]nikolina.ilijanic@hgi-cgs.hr)
[2]Geological Dept., Faculty of Science, University of Zagreb, Croatia

The aim of this study was to study the causes of well preserved status of potsherds in Bronze Age hill forts on Cres island (Northern Adriatic Sea) exposed to Mediterranean climate and their buried equivalents in colluvial deposits. The island of Cres has a long history of settlement and hosts some very important Mesolithic, Neolithic and Bronze Age sites. Due to erosion large areas are bare karst lacking soil cover and prehistoric potsherds can be found in stonewalls of hill forts or caves.

The potsherds were analyzed by microscopy methods as well as geochemistry to study the weathering process in both exposed and buried potsherds. The colluvial soil containing potsherds was dated and a calibrated ^{14}C AMS date ranging from 2030 to 1870 BC was obtained. Under the optical microscope, the potsherds are texturally homogeneous and display inclusions of similar type, abundance, and grain size. XRD analyses show that they contain quartz and calcite as dominant mineral phases, and fewer amounts of micas and feldspars (K-feldspar and plagioclase).

The enrichment of Ca in exposed potsherd rims is accompanied by depletion of light REE's and enrichment of heavy REE's. The results show that potsherds exposed to the Mediterranean climate for four thousand years have an improved durability due to calcite re-crystallization and notable change in the chemical composition of potsherd rims which have to be considered when using bulk geochemistry for provenance studies.

Mineralogical investigations of clay-bricks from Árpád-age (11th-14th century A.D.), southern Hungary

Kristály, F.[1*], Rózsa, P.[2] & Kelemen, É.[2]
[1]Institute of Mineralogy and Petrology, University of Miskolc Hungary ([*]askkf@uni-miskolc.hu)
[2]Dept. of Mineralogy and Geology, University of Debrecen, Hungary

During the so-called "Árpád age" (11th-14th century A.D.) clay-bricks were a common building material in the southern region of The Great Hungarian Plain (Szeged-Békéscsaba region). In the area, it was mainly the local production that provided bricks for churches and monasteries.

Brick samples from nine archaeological sites (churches and monasteries from the Great Hungarian Plain), now in the custody of "Munkácsy Mihály" Museum of Békéscsaba, were selected for the study. Representative specimens were obtained by sectioning and weight reduction of samples. Optical and Scanning Electron Microscopy, Electron Microprobe and X-Ray Powder Diffraction (XRPD) investigations were used to determine the mineralogical composition of samples, and to constrain the firing temperature.

Although the archaeological sites are closely located, for the purpose of comparison between different groups of sites, the samples were separated in four groups: I. Örménykút (Ö)-Décse (D), II. Kamuth (K)-Megyer (Me)-Gerla (Ge), III. Gyula (Gy) and IV. Bánkút (B).

The mineralogical composition of all brick samples is highly similar and points to illitic clays. The abundant use of vegetal tempering materials (wheat chaff) in most of the studied bricks is characteristic. The presence of dolomite is only observed in one of the Örménykút samples.

Several neoformation phases due to firing, such as K-feldspars (anorthoclase–sanidine), anorthite, gehlenite, diopside were detected (Fig. 1).

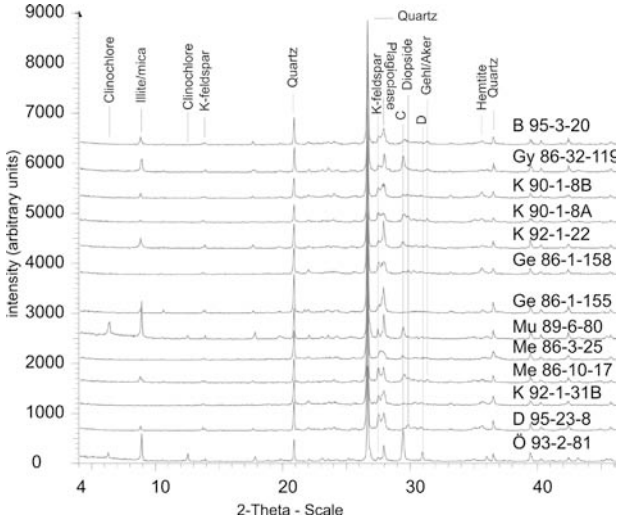

Fig. 1: XRPD diagrams of the investigated samples (Cu-Kα radiation).

The mineralogical composition of primary components, as well as the newly-formed phases upon firing, suggests the use of similar raw materials, i.e. Ca-rich illitic clays.

The type and amount of firing phases indicate temperatures in a range of 900-950°C. Only one sample from the group II shows a lower firing temperature, around 850°C.

The mechanism of thermal decomposition of dolomite and its implications in pyrotechnology: new insights from 2D-XRD and TEM analyses

Kudlacz, K, Ruiz-Agudo, E., Arizzi, A., Rodriguez-Navarro, A. & Rodriguez-Navarro, C.[*]
Dept. Mineralogía y Petrología, Universidad de Granada, Spain ([*]carlosrn@ugr.es)

Dolomite has been thoroughly used for ceramic and building purposes (e.g., dolomitic lime mortars) since ancient times. Pyrotechnology of dolomite ($CaMg(CO_3)_2$) involves its thermal decomposition into CaO and MgO. This process, called calcination, influences the physicochemical properties of dolomitic limes and affects the textural properties of dolomite-based ceramic materials. Although the thermal decomposition of dolomite has been studied for more than one century, the mechanisms of this reaction still remain obscure.

Here, single crystals of dolomite were calcined in air atmosphere at a *T* range of 500°C-1100°C, and analyzed by XRD, 2D-XRD, FESEM and TEM. Decomposition was also studied in-situ, by the TEM, by irradiating dolomite crystals with the electron beam. The decomposition is pseudomorphic and topotactic, and results in oriented CaO and MgO ((Ca,Mg)O) nanocrystals, which aggregate and grow as *T* increases. In-situ TEM shows that the first step of decomposition involves the formation of a face centred cubic (Mg,Ca)O mixed oxide, with the following orientation relationships: $[-441]_{dolomite}//[001]_{oxide}$ and $(110)_{dolomite}//(110)_{oxide}$ (Fig. 1). 2D-XRD results are consistent with in-situ TEM results, and show the presence of highly oriented oxides in the dolomite pseudomorph. Unlike the case of the in-situ TEM decomposition, the range of (Ca,Mg)O solid solution is very limited (up to 8%) and only occurs at low *T* (500°C – 750°C). A further *T* increase leads to the formation of oriented, pure CaO and MgO nanocrystals. In air, thermally activated ion diffusion favours de-mixing (spinodal decomposition) of the initial (Ca,Mg)O phase as *T* increases. Conversely, "cold" in-situ TEM decomposition prevents de-mixing of the initial (Ca,Mg)O.

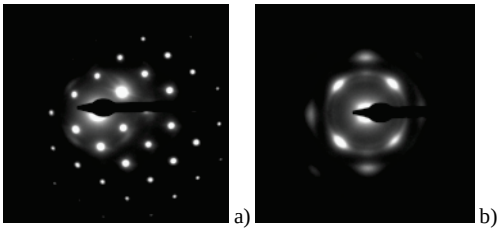

Fig 1: Selected area electron diffraction (SAED) images before decomposition of (a) dolomite ([-441] zone axis), and after its decomposition into (b) a mixed Ca-Mg oxide ([001] zone axis).

These results show that the thermal decomposition of dolomite involves its direct transformation into a mixed Ca and Mg oxide (at low *T*), and subsequent separation into two oxides (spinodal demixing) with increasing *T*. The reaction is topotactic and independent of pCO_2. Formation of $CaCO_3$ during the so called "half decomposition" of dolomite was observed in some runs. However, either calcite or vaterite formed. The fact that vaterite has no structural relationship with dolomite suggests that previous models based on the transformation of dolomite into $CaCO_3$ plus MgO (i.e., "half decomposition" of dolomite) are flawed. Apparently, $CaCO_3$ formed during re-carbonation of highly reactive CaO nanocrystals. This solves the problem of the so-called "two-stage" decomposition of dolomite. These results may help in constraining processing parameters (e.g., calcination *T*) in ancient dolomite-based ceramics, and may also help defining appropriate processing parameters during preparation of modern dolomitic lime-based conservation mortars.

The raw materials and manufacture of pottery during Bronze Age-Early Iron Age in the North-Western Russia

Kulkova, M.A.[1*], Yushkova, M.A.[2] & Subetto, D.A.[1]
[1]Herzen State Pedagogical University, St Petersburg, Russia
([*]kulkova@mail.ru)
[2]Institute for the History of Material Culture, Russian Academy of Sciences, St Petersburg, Russia

The ceramic artifacts are the main material which can be used for reconstruction of prehistoric people life and different cultural traditions. Numerous settlements of Bronze Age – Early Iron age (2000 cal. BC – 500 cal. AD) were excavated in the area of basin of Volkhov River basin (Shkurina Gorka, Porogi sites:800cal BC-400 cal.BC, Kholopii Gorodok site: 800cal.BC-500cal AD); Ilmen Lake (Prost' site: 800calBC-400 cal.AD, Gorodok na Lovati site: 10cal.AD-500cal.AD, Sel'tco site: 800calBC-400cal. AD); Ladoga Lake (Ust'-Ribezgna II site: 2000cal.BC-1500cal.BC), located in the North-Western Russia. It is one of the perspective regions of archaeological works on the North-Western of Russia in the present time. The main problem is the chronology and cultural attribute of different sites and their connection with sources of raw materials.

The investigation of pottery included a complex approach. To determine the cultural and historical belonging of ceramics the archaeological methods (typology and morphology) were applied. The mineralogical and geochemical methods (optical microscopy, XRD, thermal analysis, XRF) were used for the determination of the ceramic composition, the manufacturing technology and the sources of row material (more than 70 samples of ceramic sherds and 16 samples of clay raw material).

Based on both the mineralogical composition and geochemistry of ceramic material and the archaeological typology, a number of ceramic type groups were distinguished. The ceramics of Bronze Age (Ust'Ribegna II site) consist of montmorillonite clay and disintegrated plant remains; the estimated firing temperature was about 650°C. The ceramics of Volkhov type (Shkurina Gorka, Porogi, Prost', Kholopii Gorodok, Sel'tco sites) consist of kaolinite-illite clay, crushed gravel of granite-plagioclase composition and grog; the estimated firing temperature was around 500-700°C. The Iron Age ceramics (Kholopii Gorodok, Gorodok na Lovati sites) consist of illite clay and a temper made of crushed granite-plagiogranite gravel; a firing temperature around 800°C could be infered. These characteristics give possibilities for identification the ceramics from different settlements and chronological periods.

The changes of environmental conditions about 1500 cal. BC (Ladoga Lake transgression) most likely influenced the prehistoric people life. The flood on Ust'Ribegna II site was one of the reasons of that the population has left this place and changes the raw material sources for pottery produced in this and successive periods.

Characterization of earthen building materials from a Phoenician site, Malaga (Spain)

López–Arce, P.[*], Gómez-Villalba, L.S. & Fort, R.
Group of Applied Petrology to Heritage Conservation,
Instituto de Geología Económica (CSIC-UCM), Madrid, Spain
([*]plopezar@geo.ucm.es)

Earthen building materials, adobe walls and pavements, were characterized to determine the materials composition and constructive techniques from a Phoenician site. Clay samples from the surroundings were also studied, to identify the raw materials used in their manufacture. X-ray diffraction, polarized light optical and environmental scanning electron microscopy (ESEM) with energy dispersive X-ray spectroscopy was used to study the composition. Mercury intrusion porosimetry was performed to obtain the total porosity and pore size distribution.

Adobe samples display a calcareous clay composition, with different proportion of clay minerals (27-39 wt%), quartz (21-45 wt%) and Ca and Mg carbonates (calcite 17-47 wt% and dolomite 2-11 wt%). Filosilicates are mainly kaolinite (24-34 wt%), smectite (31-46 wt%) and illite (20-45 wt%). Barium sulphate, various phosphates, iron oxides and hydroxides, bioclasts, pyrite, zircon and lithic fragments (Fig. 1) are also present. Iron oxides and iron hydroxides provides red and yellow colours.

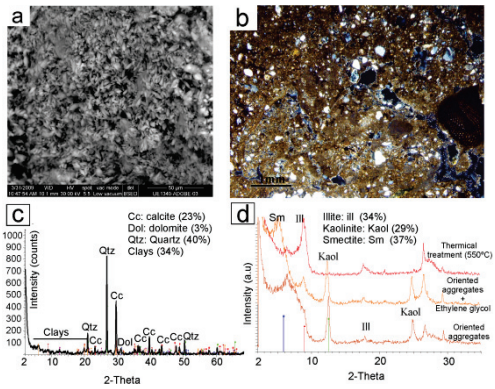

Fig. 1: Characterization of adobe. a) ESEM image; b) Polarized light microscopy image; crossed nicols; c) XRD of bulk sample; d) XRD of clay fraction.

Clay samples are very similar to the earthen materials and they could have been used as raw materials mixed with clays and sands from other geological sources (continental, fluvial and marine). The natural presence of roots and stems of plants, the cementation reactions of carbonates and silicates and intentional addition of grog (ceramic fragments) and organic materials in the clay paste could have improved the natural properties of the ceramic paste. Clays from the earthen pavement display white-yellow color (due to carbonate and hydrated iron hydroxides) being probably selected with aesthetic purposes. Difference in porosity between adobe and clay samples indicates compaction of the clays, with the consequent reduction in porosity and decrease in the pore sizes.

Understanding earthen construction methods and raw material selection has significant implications for understanding either the selection of settlement sites or the labour required to build in specific settings not directly adjacent to suitable raw materials [1]. These studies provide new insights to the knowledge of Phoenician construction techniques, since there are few or no other references available.

Acknowledgements: to ArqueoEstudioS. Coop. for providing the samples and collaboration. We are also grateful to the financial sources Geomateriales (S2009/MAT-1629) and Consolider (CSD2007-0058).

[1] Nodarou, E. (2008) *J. Archaeol. Sci.*, **35**, 2997-3015.

The building materials of Koule Castle, Heraklion, Crete (Greece)

Markopoulos, Th., Repouskou, E.* & Karampatsou, G.
Dept. of Mineral Resources Engineering, Technical University of Crete, Chania, Greece (*repusku@mred.tuc.gr)

This work is a primary study of the architectural elements and corresponding building materials of the Koule Castle in Heraklion, Crete (Greece). The characterization of the building materials of a historic structure is a necessary part of a conservation study.

Eighteen core samples of rocks and masonry mortars have been extracted by the 13th Municipality of Byzantine Antiquities from different parts of the monument, in order to determine their physical and technical characteristics as well as their deterioration state. Their morphological characteristics, granulometry, specific weight, water absorption index, compressive strength, as well as the mineralogical composition and the included fossils species have been determined.

The building stones of Koule Castle are sedimentary rocks, excavated nearby and in the island Dia. In their majority, they are biomicritic breccias and limestone conglomerates and bioclastic limestones with various marine fossils. In particular, the north monumental part is built of Triassic limestones, breccias and coarse conglomerates. Biomicritic breccia limestones show the highest strength values and lower water absorption index compared with the bioclastic limestones.

The old mortars have been studied by optical microscopy, X-ray diffraction (XRD) and scanning electron microscopy. Their examination revealed that beach sand has been used as inert material.

In some representative old mortars particle size analysis by wet sieving was carried out, in order to determine the nature of their constituents and evaluate the inert to binder material ratio. These data are necessary for simulation - reproduction of these materials used for restoration. The sum of the 2 mm - 0.125 mm fractions is regarded as inert material, whereas the material finer than 0.125 mm is regarded as the binder [1].

At least three types of mortars were identified and considered as the construction mortars during the different construction- reconstruction periods. Their basic mineralogical components are: calcite, portlandite, brucite, magnesite, dolomite, quartz and plagioclase. The presence of calcite in the binder of the studied mortars is a result of the carbonation of lime. The presence of portlandite and brucite is probably associated with the absence of adequate carbon dioxide in the interior parts and at the lower parts of the castle surrounded by sea, thus prohibiting the formation of calcite and magnesium carbonate correspondingly. Furthermore, the presence of both portlandite and brucite indicate the use of dolomites and Mg-rich limestones for the binder production.

[1] Markopoulos, Th., Maravelaki, P. & Repouskou, E. (1994) in Fassina, V., Ott, H. & Zezza, F. (eds.) *III Inter. Symp. on the conservation of Monuments in the Mediterranean Basin*. Venice, 22-25 June 1994, 687-692.

Production and distribution centers of Serra-d'Alto-style pottery (4th millennium BC) in southeastern Italy

Marrese, G.[1*], Tucci, P.[2], Coppola, D.[3] & Lezzerini, M.[4]
[1]Centro di Ricerca per le Scienze Applicate alla Protezione dell'Ambiente e dei Beni Culturali, Sapienza Università, Rome, Italy (*giovannamarrese@live.it)
[2]Dipto. di Scienze della Terra, Sapienza Università, Rome, Italy
[3]Dipto. di Storia dell'Antichità, Università degli Studi di Bari Aldo Moro, Bari, Italy
[4]Dipto. di Scienze della Terra, Università degli Studi di Pisa, Italy

The Serra d'Alto pottery is a pot production occurring in southern Italy during the 4th millennium BC [1]. The use of depurated clays and firing temperatures around 700-800°C [2] suggest the presence of advanced ceramic technology, where the thin solid walls and the medium-to-large size of the products offer pictorial support to complex painted decorations [2]. These are black, and characterized mainly by spiral to meandrous motives with symbolic meaning. The Serra d'Alto style ceramic production coincides with a period of significant changes overall southern Italy, especially Apulia. The change to a hot-arid climate developed during the 4th millennium brings with itself the collapse of village agricultural civilization and the development of mobile communities of shepherds invading internal areas to find new pastures. Pottery is found in both cultural areas, thus not only in the villages, where it was presumably produced (need of depurated clays and appropriate ovens etc.), but also in internal sites such as caves. This testifies changes in the economy that involve population mobility and distribution of artifacts to mobile communities [3].

The archeometric study of a series of samples allows to define the production centers of Serra d'Altro ceramics and to follow the commercial distribution along the transhumance ways used by the ancient shepherds [4]. Together with the distribution of marine shell, the Serra d'Alto ceramics represents the oldest testimony of an exchange economy in Neolithic Italy. During the study, we evaluated technological aspects such as firing temperature, production and preparation of clay support, decoration and refining, all data indicating the state of art reached by the Neolithic workers [5,6]. The ceramic objects have been analyzed by OM and XRD for the minero-petrographic characteristics and by XRF and EDS/WDS for the chemistry. Moreover, a sampling of clays located near the ceramic production centers has been undertaken to establish a relationships between occurrence of the artifacts and local geology. The locating of clay extraction areas bears importance in reconstruction of the economic evolution in the 4th millennium BC.

[1] Geniola, A. (2007) *ATTI della XXVI Riunione Scientifica "Il Neolitico in Italia"*. Firenze, 7-10 nov. 1985 [2] Cassano, S.M., Laviano, R. & Muntoni, I.M. (1995) in Fabbri, B. (ed.) *The Cultural Ceramic Heritage*. Eur. Ceramic Soc. 4th Conf., Gruppo Editoriale Faenza, **14**, 137-148. [3] Laviano, R. & Muntoni, I.M. (2003) in Di Pierro, S., Serneels, V. & Maggetti, M. (eds) *Ceramic in the Society*. Proceed.6th Eur. Meeting on Ancient Ceramics, University of Fribourg, 163-173. [4] Laviano, R. & Muntoni I.M. (2004) in Ingravallo, E. (ed.) *Il fare e il suo senso, Dai cacciatori paleo-mesolitici agli agricoltori neolitici*. Congedo, Galatina, 113-164. [5] Muntoni I.M. (2002a) *Atti del Convegno Internazionale, Rome, 29–30 Marzo 2001*, Accademia Nazionale dei Lincei, Roma, 203-213. a. [6] Muntoni I.M. (2002b) *Origini*, **XXIV**, 165-234.

Mineralogical and geochemical study of coloured and white marbles from Spain and Portugal in the provenancing of some marble artefacts from *Thamusida* (Kenitra, Morocco)

Origlia, F.[1], Turbanti Memmi, I.[1*], Spangenberg, J.[2], Gliozzo, E.[1] & Meccheri, M.[1]
[1]Dipto. Scienze della Terra, Università di Siena, Italy ([*]memmi@unisi.it)
[2]Institute of Mineralogy and Geochemistry, University of Lausanne, Switzerland

First results of an archaeometric study carried out in order to asses the provenance of marble artefacts from *Thamusida* (Kenitra, Morocco) have shown that local raw material exploitation was very rare. Most of the archaeological artefacts come from classical marble areas (Greece, Turkey, Italy), but not all the Mediterranean sources were successfully determined. Considering the possibility of a commercial exchange between Mauretania Tingitana and Betic and/or Lusitanian Roman Provinces, we focused our study on various types of marbles from those regions. Here, we present the results of a minero-petrographical and geochemical study on some of these marbles. The data obtained, combined with those already available from literature, represent a reliable basis for comparison with the undetermined artefacts. The marbles were collected from the Ossa Morena zone, including the Estremoz anticline (Spain-Portugal), and from Malaga and Almeria districts in the Betic chain (Spain). The specimens were investigated by XRD to detect the carbonate mineral type as well as by geochemical analyses to determine the carbon and oxygen stable isotope composition. OM observation and SEM-EDS analysis were carried out only on a representative selection of samples to find out the main textural features and the accessory mineral contents. We distinguished calcitic and dolomitic marble varieties. Dolomitic marbles mainly belong to Malaga district, but are sporadically present in other Spanish marble deposits.

The accessory minerals are quartz, plagioclase, muscovite/illite, phlogopite, Fe-Mg chlorite and tremolite (Viana do Alentejo, Almaden de la Plata), apatite, Fe and Ti oxides, titanite and Fe-sulphide. Dolomitic marbles usually have a scarce accessory mineral content, consisting of quartz and calcite. The geochemical data were reported in two different $\delta^{13}C$-$\delta^{18}O$ diagrams for Ossa Morena and Betic chain marbles. The isotopic values of Ossa Morena quarries overlap, mainly in the ranges $\delta^{18}O$: -9 and -5‰ VPDB and $\delta^{13}C$: 0.5 and 3‰ VPDB. The isotopic values of betic marbles fall in the range $\delta^{18}O$: -8.83 and 0.27‰ VPDB and δ^{13} C: 1.26 and 4.28‰ VPDB.

A preliminary comparison between the artefacts and the studied materials provided interesting results. The Malaga provenance seems highly probable; the Estremoz or Ossa Morena Almaden de la Plata quarry provenances are still uncertain. More analyses are needed to address the open questions and clarify the development of the commercial exchanges between Spain, Portugal and Morocco during Roman times.

Major element composition of Transylvanian gold: can it be used for archaeological provenance studies?

Pop, D.[1*], Ionescu, C.[2], Benea, M.[2], Tămaş, C.[2] & Forray, F.[2]
[1]Museum of Mineralogy, Babeş-Bolyai University, Cluj-Napoca, Romania ([*]dana.pop@ubbcluj.ro)
[2]Dept. of Mineralogy, Babeş-Bolyai University, Cluj-Napoca, Romania

Transylvanian gold is related to both epithermal ore deposits and their associated placer deposits in the Southern Apuseni Mountains (Romania). The primary deposits were formed during the Neogene volcanic event. Tens of economically-important ore deposits are concentrated in an area of about 900 km^2 known as the "Gold Quadrilateral" - a major source of gold for Europe throughout history. According to historical records, gold mining in Transylvania spans over more than 3,000 years. Between 1500–2000 t of gold were estimated to have been extracted in the Apuseni Mountains since prehistory [1].

Archaeological provenance studies are generally based on comparing the composition of the artefacts with that of the potential raw materials. No general consensus was reached yet concerning the most reliable correlation factors in the case of gold. As a first approach, we chose major elements chemistry and electron microprobe (EMP) measurements. Eight samples from the collection of the Museum of Mineralogy, Babeş-Bolyai University were selected: five samples from Roşia Montană (RM) (Fig. 1) and three from other historically-significant deposits: Trestia (T), Musariu (Mu), and Măgura (Ma). RM deposit is hosted by dacites, while the others by andesites [2].

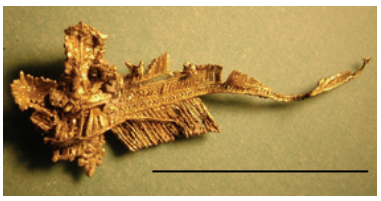

Fig. 1: Dendritic gold crystals from Roşia Montană, one of the IMA2010 logos (scale bar: 1 mm).

Au, Ag, Te and Cu contents have been measured. Based on 164 point EMP analyses, three compositional groups were outlined: a) low- (RM), b) medium- (RM, Mu, Ma), and c) high-Ag content (RM). Mineralogically, only the first group can be defined as gold, the other two are electrum (the full range of fineness is 577 to 875). For all groups, the same trend could be observed: whereas the Ag content is constant, Te (0.06–0.2 wt.%) and Cu (<0.02 wt.%) substitute Au. RM gold shows a remarkable compositional variability, ranging from $Au_{0.43}Ag_{0.57}$ to $Au_{0.79}Ag_{0.21}$. Thus, samples with the same origin plot into different groups, while those originating from different deposits plot in the same narrow compositional field (b).

Summarizing, the major elements in gold cannot be used for chemical fingerprinting, but EMP proved to be suitable for deciphering chemical mechanisms at micrometer scale. However, for gold provenance studies, hierarchical cluster analyses on larger sets of data for major, as well as trace elements and isotopes studies are required.

Acknowledgements: The study was supported by ID-2241 project funds (Romanian Ministry of Education).

[1] Cook, N.J. & Ciobanu, C.L. (2004) in Cook, N.J. & Ciobanu, C.L. (eds.) *IAGOD Guidebook Series*, **12**, 1-4. [2] Roşu, E. et al. (2004), *Schweitz. Miner. Petrogr.*, **84**, 153-172.

Mineralogical-geochemical characteristics of the mammal skeletal remains from the selected archaeological sites in Poland

Rogoz, A. & Sawlowicz, Z.*
Institute of Geological Sciences, Jagiellonian University, Krakow, Poland (*zbigniew.sawlowicz@uj.edu.pl)

We have studied bones and teeth of woolly mammoths (*Mammuthus primigenius*) from the site Spadzista Street (B) in Krakow and bones of cave bears (*Ursus spelaeus)* from two caves (Bisnik and Nietoperzowa) in Southern Poland. The materials were studied using SEM-BSE, XRD, and FTIR methods. Samples from Spadzista Street and Biśnik are quite well preserved, in contrast to Nietoperzowa cave where only fragments of bones few centimetres long were found. In scanning electron microscope their histological structures (osteons, bone trabeculae, enamel prisms, dentine canaliculi) are easily seen. The studied skeletal remains are built of carbonate-rich apatite-(CaOH). The crystallinity indexes (calculated after Person et al. [1]) are rather low: 0.03-1.14 in woolly mammoth samples, 0.1-0.21 and 0.02-0.15 in cave bear samples from Biśnik and Nietoperzowa caves, respectively. Only in enamel the crystallinity indexes were much higher: 0.67-0.78 in woolly mammoth and 0.95 in cave bear samples. The typical range of Ca/P mole ratios of fresh bones is 1.59-1.67 [2]. The average ratios, calculated from EDS analyses of the studied samples, are different: mammoth bones - 1.92, cave bear bones from Biśnik and Nietoperzowa caves - 1.73 and 1.23, respectively. The higher values can be caused by replacement of PO_4^{3-} groups by CO_3^{2} and/or enrichment in Ca^{2+} ions which is not surprising because of common presence of calcite in those bones. The lower values can result from a decrease of CO_3^{2-} in apatite, which is one of the common diagenetic processes [3]. There are some differences in secondary minerals infillings between cave bears and woolly mammoth remains. In the bear bones Haversian canals are usually not infilled with minerals, only occasionally calcite is present. Fe-Mn (hydroxy)oxides coat or infill both the osteocyte lacunae and the dentine canaliculi. In addition, in the bones from Nietoperzowa Cave manganese is sometimes present in a form of dendrites. In the woolly mammoth remains Haversian canals, bone trabeculae and cracks are commonly infilled with calcite or carbonate sediment. The dentine canaliculi are coated or infilled with secondary apatite. The Fe-Mn (hydroxy)oxides are present occasionally in osteocyte lacunae. It is worth to note that in woolly mammoth bones the bacterial alterations were found. In some samples they are very common, whereas in the cave bear bones we have not found any microbial changes. It seems that differences between studied bones are caused by different burial environment.

[1] Person, A. et al. (1995) *J. Archaeol. Sci.*, **22**, 211-221. [2] Elliott, J.C. (2002) *Rev. Mineral. Geochem.*, **48**, 427-453. [3] McClellan, G. (1980) *J. Geol. Soc. London*, **137**, 675-681.

Iron age pottery from Garvão votive site (SW Iberia) – an interdisciplinary study

Rosado, L.[1], Candeias, A.E.[1], Schiavon, N.[2*], Lopes, M.C.[3], Mayet, F.[3], Tavares, D.[4], Alfenin, R.[3,4] & Mirao, J.[2]
[1]HERCULES Laboratory and Chemistry Centre of Evora, University of Évora, Portugal
[2]HERCULES Laboratory and Geophysics Centre of Evora, University of Évora, Portugal (*schiavon@uevora.pt)
[3]University of Coimbra, CEAUCP, Coimbra, Portugal
[4]Alentejo Regional Directorate of Culture, Evora, Portugal

The Iberian Peninsula was a highly sought after area in ancient times due to its abundance in geological resources. Hence, the Iberian Iron Age was a period of successive social and political transformations, sometimes resulting in conflicts. These began with the earliest Celtic invasions (or migrations) that imposed a strong continental influence in Iberia against the oriental inspired societies like the Tartessos kingdom. The movement of these populations toward south is constant throughout the entire period. Simultaneously, the Semitic civilizations (i.e. Phoenician and Punic) control was maintained in south Iberia through the presence of autonomous cities with strong commercial and cultural connections to the Mediterranean. This political framework was broken in 218 AC by Romans disembark in the context of the second Punic war.

In this general context, at around 200 AC, Garvão probably belonged to the Conii territory corresponding to the current SW Portugal or "Baixo Alentejo" and the western Algarve. It is believed that this region, although inhabited by populations of Celtic origin, was characterized by a very strong Mediterranean cultural influence. It seems that Garvão was an important Iron Age II holy site where an impressive votive deposit was discovered. The materials recovered (mainly pottery) were intentionally deposited, carefully arranged in order to optimize the available space.

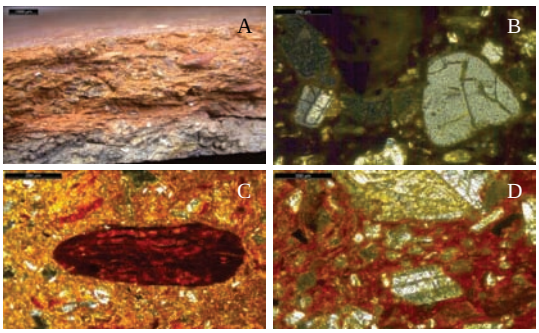

Fig. 1: Iron-age Garvão pottery. (A) Chromatic heterogeneity in cross section. (B) OM micrograph NX. Plagioclase and rounded quartz in black matrix, (C) OM Micrograph NX. Ceramic fragment. (D) OM Micrograph NX. plagioclase in red matrix.

A detailed study of the pottery based on stylistic analysis was carried out allowing the classification into different clusters. As the ceramics mineralogical and chemical composition depends also on technological know-how and social environmental parameters, a combined analytical approach was adopted to characterize the pottery samples by means of Optical (OM) and Electron microscopy (SEM + EDS), Fourier Transform Infrared Spectroscopy (FT-IR) and X-ray Diffraction (XRD). The combination of these techniques applied to selected Gãrvao pottery allowed the recognition of the ceramic phase composition, firing temperature, kiln atmosphere, ceramic manufacturing processes and origin of raw materials.

The chemical and mineralogical results suggest that the Gãrvao region was characterised by strong connections both with Mediterranean as well as with local production areas reflecting its role in ancient times as a rich and important multicultural centre.

On the use of Earth Materials in SW Iberia mortars – an historical perspective

Santos Silva, A.[1], Adriano, P.[1], Cruz, T.[2], Veiga, R.[1], Candeias, A.E.[3] & Mirao, J.[2*]
[1]National Laboratory of Civil Engineering, Lisbon, Portugal
[2]HERCULES Laboratory and Geophysics Center of Evora, University of Évora, Portugal ([*]jmirao@uevora.pt)
[3]HERCULES Laboratory and Chemistry Center of Evora University of Évora, Portugal

Traditional and historic mortars are composite materials consisting of a binder (usually lime or hydraulic lime), aggregates (quartz sand, calcite or dolomite) and some additives (e.g. brick dust, volcanic ash) in order to increase adherence, workability, strength and durability [1]. The characterization of mortars allows the identification of their phase and chemical compositions and the characteristic features related to the physical properties. Moreover, sometimes it is possible to identify the alteration products and, in some cases, establish the provenance of materials used in the manufacture of mortars [2].

Thus, the study of the ancient mortars composition, using techniques of chemical, mineralogical and microstructural characterization, plays a major role in the preservation of cultural heritage, guiding all actions for the conservation and restoration. On the other hand, it gives a very deep knowledge about the techniques of construction, previous repairs and their performance. This type of information is likely to be historically integrated, contributing to the knowledge of the societies that constructed the buildings.

The similarity between traditional mortars and sedimentary clastic rocks are evident (Fig. 1). In both, it is possible to figure out cement that sustains together the clasts (in sedimentary rocks) or the aggregates (in mortars). Nevertheless important differences are obvious. Additives are frequently present in order to get better mechanical properties and the very alkaline environments during the merging of the lime and the aggregates cause frequently the partial dissolution of quartz aggregates.

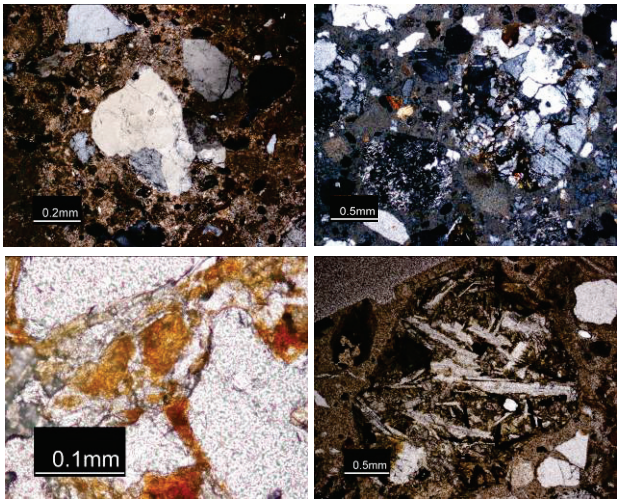

Fig. 1: Microphotos of Southwest Iberia ancient mortars. A-Concufate villa (Roman), B-Evora (Medieval), C- Elvas (16th century), D-Lisbon (18th century). A, B – crossed polarizers; C, D – one polarizer.

Methods like XRD, TGA, optical microscopy, SEM-EDS and chemical analyses techniques are currently employed. The results can be assigned to the society's capability to manage technology and to access and select raw materials. Over the past few years research applied to roman, Islamic and medieval mortars will be revisited and an evolutionary trend to the use of earth materials in SW Iberia mortars will be presented.

[1] Adriano, P. et al. (2010) *Mater. Charact.*, **60(7)**, 610-620.
[2] Guerreiro, T. et al. (2008) *Microsc. Microanal.*, **14(3)**, 77-80.

Rock crystal artefacts and determination of their provenance

Slobodník, M.[*] & Přichystal, A.
Institute of Geological sciences, Masaryk University, Brno, Czech Republic ([*]marek@sci.muni.cz)

In Central Europe, there are numerous archaeological sites from which chipped rock crystal artefacts are known. The raw material is commonly considered of Alpine region provenance. However other possible sources could be mentioned in other areas (Fig. 1). The most important places are located in the Bohemian Massif, especially in the Moravian Moldanubicum (Sklené – Rousměrov SE of Žďár nad Sázavou and the vicinity of Brtnice), and there are proofs of their prehistoric exploitation. Another source area becomes evident in the Silesicum (Jegłowa near Strzelin, Žulová). We record also rock crystal sources in the Austrian Moldanubicum or within Lower Carboniferous rocks in N Moravia (Bílovec) [1].

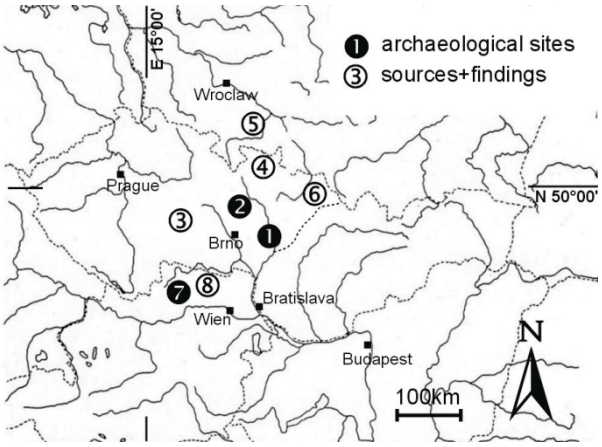

Fig. 1: The major occurrences of rock crystal sources and findings of artefacts. Sites: 1 – Nová Dědina, 2 – Žitného cave, 3 – Sklené, Brtnice (Moldanubicum area), 4 – Žulová area, 5 – Jeglowa, 6 – Bílovec, 7 – Gudenushöhle, 8 – Nödersdorf.

Microthermometry, Raman spectrometry and some other techniques have been applied on material from the Paleolithic (Aurignacian) site Nová Dědina (ND, no. 1 in Fig. 1) where several hundreds of rock crystal chips have been discovered and compared to the mentioned sources. The used methods, based on the investigation of fluid inclusions, can be considered as a model for progress in further research.

Fluid inclusions (FI) represent defects (cavities) in crystal lattice, being filled with liquids (L), gases (V), and solids (S). Trapped and sealed parental fluids in primary inclusions are regarded as isochoric systems telling story on genetic conditions at particular places. If we are able to decipher the genetic information from the fluid inclusions of the "lost" material (with unknown provenance) we have a chance to find the site of origin. The most important petrographic aspects have been revealed within FI assemblage from ND. Two types of 3-phase inclusions L+V+S1+S2 and L1+L2+V and their fluid properties enable to exclude the sources from the Alps, Silesicum and northern Moravia. Fluids nature coincides well with sources from Moldanubicum with pegmatite signature.

The used combination of genetic parameters, both from natural sources and archaeological sites, is a very sensitive methodological approach how to select and define the provenance of rock crystal raw material.

Acknowledgements: Our investigation has been supported by the research project MSM0021622427 and grant Kontakt 6-06-11.

[1] Přichystal, A. (2009) *Lithic raw materials in prehistoric times of the Eastern Central Europe*. MU, Brno (in Czech).

Pietra ollare artefacts from Červar Porat (Istria, Croatia): composition and possible origin

Tibljaš, D.[1*], Balen, D.[1], Šimić-Kanaet, Z.[2] & Girardi Jurkić, V.[3]
[1]Inst. for Mineralogy and Petrology, Dept. of Geology, Faculty of Science, Zagreb, Croatia ([*]dtibljas@geol.pmf.hr)
[2]Dept of Archaeology, Faculty of Philosophy, Zagreb, Croatia
[3]International Research Centre for Archaeology, Medulin, Croatia

During archaeological excavations performed between 1976 and 1980 at a Roman villa rustica in Červar-Porat located close to the town Poreč (Istria peninsula, Croatia), among other Late Antique period fragments (glass, metal, ceramics), fourteen peculiar stone vessel fragments were discovered. They show characteristic tracks of the manufacturing by means of lathe. Vessels made by analogous processes from similar materials have already been found at several localities at Croatian Adriatic coast, but no systematic mineralogical study on this kind of material was performed so far.

Two of these vessel fragments were recently investigated in more detail by mineralogical methods. The first one (inv. no. 7912) is greenish-grey in colour (Fig. 1). X-ray powder diffraction revealed that the only constituent of this fragment is a chlorite group mineral. The mineral composition together with visible schistosity indicates that source material was chlorite-schist, a low–grade metamorphic rock. Such material is one of different lithologies included by Italian term *pietra ollare* and German *Lavez*.

The other fragment (inv. no. 7907) is dark greenish-grey on the fresh broken surface and brownish on outer and inner vessel surfaces. Distinctive bronze coloured flakes can be seen in some parts. The fact that XRD pattern of the second fragment was similar to the XRD pattern recorded on the material from the first fragment after heating to 1100ºC indicate that the second vessel was most probably used for cooking, and during that process it was exposed to elevated temperatures.

Fig. 1: Vessel fragment (inv. no. 7912), 8 cm wide, showing tracks of manufacturing by means of lathe.

In order to determine possible origin of analysed fragments their mineral and chemical composition was compared with those recorded for samples collected in Valle d'Aosta and Valli di Lanzo (north-western Italy) and literature data for *pietra ollare* originating from other localities in Italian Alps.

Mineralogical and experimental study by FTIR of archaic ceramics from Amathous (Cyprus)

Ventalon, S.[1*], Daniel, F.[2], Fröhlich, F.[3], Fourrier, S.[4] & Dubois, M.[5]
[1]GEOSYSTEMES, FRE 3298, Université Lille 1, Lille, France ([*]sandra.ventalon@univ-lille1.fr)
[2]CRPAA, UMR 5060, Université de Bordeaux 3, Bordeaux, France
[3]Centre de spectroscopie infrarouge, Muséum national d'Histoire naturelle, Paris, France
[4]HISOMA, UMR 5189, Lyon, France
[5]LGCgE, EA4515, Université Lille 1, Lille, France

Many ceramics of the archaic period have been found in the archaeological Amathous site, southern Cyprus (Fig. 1). Previous studies on these ceramics indicated a good agreement between chemical analysis and the typo-chronological classification [1]. However a geological survey and an experimental study were required in order to complete these data. The aim was to localize sources of raw materials (clay and temper) and to understand the manufacturing methods, especially firing processes.

The infrared spectroscopy and X-ray diffraction have been used to characterize 44 materials sampled around Amathous, 10 ceramics fragments and the results of firing experiments.

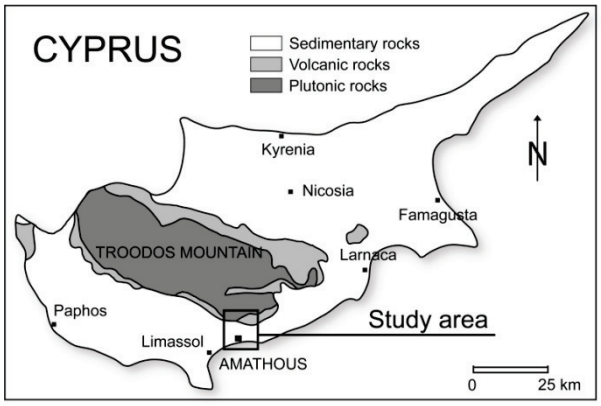

Fig. 1: Study area location within Cyprus territory

The Cretaceous marine clay ("Moni formation") and the black basaltic sand from the beach west of Amathous (used as temper) were identified as the source of raw materials. In addition, firing experiments show that ceramics were fired at 650°C (Fig. 2). The red-fabric pithoi ceramics were made from the same materials but firing temperatures are higher than 650°C.

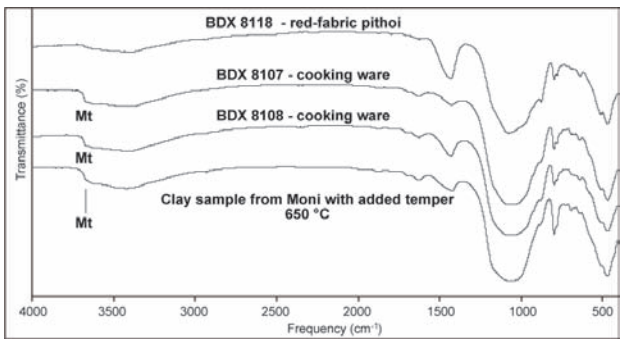

Fig. 2: Cooking ware and red-fabric pithoi spectra. Comparison with the spectra obtained through experimental firing of raw material samples.

[1] Fourrier, S. & Hermary, A. (2007) *EtChypr* XVII.

Characterization and provenance of building stone from Notre-Dame-de-Grâce, Sérignan (southern France)

Ventalon, S.[1*], De la Boisse, H.[2], Raynaud, S.[2], Mazeran, F.[3] & Dubois, M.[4]
[1]GEOSYSTEMES, FRE 3298, Université Lille 1, Lille, France ([*]sandra.ventalon@univ-lille1.fr)
[2]Equipe Pierres et Monuments, Université Montpellier 2, Montpellier, France ([*]boisse@gm.univ-montp2.fr)
[3]Service du Patrimoine, Conseil général de l'Hérault, France
[4]LGCgE, EA4515, Université Lille 1, Lille, France

The restoration project of Notre-Dame de Grâce church (Sérignan, southern France, Fig. 1) was accompanied by a detailed study of the building materials. The aim was to characterize the various lithologies, their repartition on the frontage (linked or not with reconstructions and restorations) and their origin. Some substitution materials were also sought.

Fig. 1: Notre-Dame de Grâce: photography and plan (© Cabinet D. Larpin).

The macroscopic and microscopic investigation of 25 samples from the edifice permitted to characterize 5 different stone types: 1) bioclastic limestone, 2) sandy limestone, 3) Ostrea-bearing limestone, 4) red-algae-bearing limestone and 5) fine-grained limestone. All these materials were formed in the carbonate shelf during Miocene.

The (1), (2) and (3) limestones correspond to the most voluminous monument blocks and have a local origin. They are found in old quarries around Sérignan and Béziers (Fig. 2). The (4) and (5) types were respectively used for mullions of the church windows and for the four pillars of the western frontage. This two rock types originate in the still exploited quarries of Beaulieu (4) and Fonvieille (5) (Fig. 2).

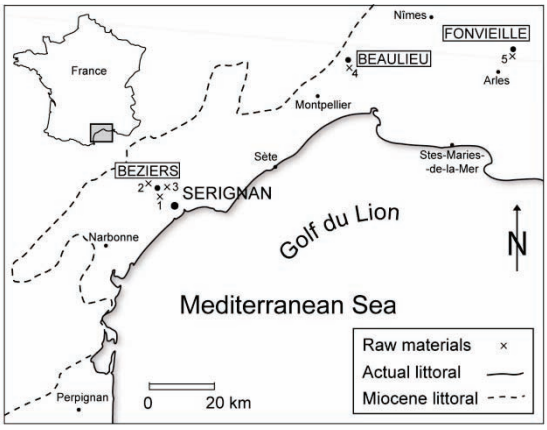

Fig. 2: Source of building materials used for Notre-Dame-de-Grâce, Sérignan. The insert in upper left shows the position of the map within France territory.

Traditional earthen building materials in the Western Himalayas

Wimmer-Frey, I.[1*], Peresson, M.[1], Gruber, M.[2] & Krist, G.[2]
[1]Geological Survey of Austria, Vienna, Austria ([*]i.wimmer-frey@geologie.ac.at)
[2]University of Applied Arts, Vienna, Austria

The Tibetan mountain village of Nako in the Indian Western Himalayas houses a Buddhist monastery temple complex dating from the 11th - 12th centuries, which reflects both significant aspects of Tibetan artistic and cultural history as well earthen building traditions. Within the "Nako Project" dedicated to saving the endangered temple buildings, the "Scientific study of the Artwork at Nako, India", funded by the Austrian Science Fund (FWF), addresses local clay raw materials used for the historic temple structures and in recent local building practice. The soils THAWA, TUA and SASSA make up the building materials, the adobe, joint mortars and plasters, as well as the supports of the sculptures in the four temples.

THAWA, meaning "earth" in local Bhoti language, consists mainly of poorly sorted, gravel- and sand-sized detritus derived from granitoids of the High Himalaya crystalline. THAWA has a yellowish brownish colour. The clay content, and thus its plastic component, is low. It is composed of quartz, K-feldspar, albite and abundant mica. The mineralogical composition suggests a granitic parent rock. The predominant clay minerals of the fraction < 2 µm are illite/muscovite and chlorite, both of detrital origin. Small amounts of kaolinite and traces of vermiculite occur. The plasticity index is low, the shear strength is rather high.

TUA is most likely a fine-grained deposit of a glacial lake. It is light grey in colour. The silt- and clay-content of TUA is high, which gives better plasticity properties, also expressed by a higher plasticity index. The bulk rock mineralogy consists of calcite, quartz, mica, chlorite and little feldspar. The clay mineral assemblage of illite/muscovite, chlorite and low amounts of kaolinite is very similar to THAWA.

SASSA is a greenish white, well-compacted, unstratified deposit, resembling a till. Similar portions of gravel, sand, silt and smaller amounts of clay produce extremely poorly sorted sediment. Varying amounts of dolomite, calcite, amphiboles and pyroxenes are the main constituents of the bulk mineralogy. Besides illite and kaolinite in traces, the predominant clay minerals are a mixed layered smectite/chlorite and/or a smectite. SASSA shows the highest plasticity index and the lowest shear strength of the three types.

Adobe, joint mortars, plasters, and sculpture supports show similar grain size distributions and similar mineralogical compositions. They consist of a mixture of THAWA and TUA and plot along a line indicating a mixing ratio of 4:1, which is still used as a recipe for plastering, passing on the tradition of the old building history of the temples. Additionally, fibres deriving from plants, animal hair and skin, ash, as well as proteinaceous binding materials were found admixed to the local soils in order to improve the strength and plastic qualities of the historic building and support materials. The use of organic additives correlates with Buddhist literature sources. SASSA, nowadays used as water resistant coating for indoor walls, was detected only in one case of a later sculpture repair.

Raman spectroscopic study of ancient potteries in Thailand: Wiangkalong pottery samples

Won-in, K.[1], Pongkrapan, S.[1], Dararutana, P.[1,2], Thawornmongkolkij, M.[3] & Wathanakul, P.[1,3*]
[1]Dept. of Earth Sciences, Faculty of Science, Kasetsart University, Bangkok, Thailand ([*]fscipww@ku.ac.th)
[2]The Royal Thai Army Chemical Dept., Bangkok, Thailand
[3]The Gem and Jewelry Institute of Thailand

The aim of this work is to explore the potential of Raman spectroscopy in assessing the chemistry and mineralogy of ancient potteries from Wiangkalong, a major ceramic-production city in northern Thailand, once colonized by the ancient Lanna Kingdom (1296 AD). Potteries from such locality were produced with shapes and designs resembled those of the Chinese Yuan and Ming Dynasties. Fragments of the pottery samples from Wiangkalong were analysed for the first time. Characterizations of clay minerals were also carried out using X-ray diffractometer and scanning electron microscope equipped with energy dispersive X-ray fluorescence spectrometer. These instruments in combination have been proved to be useful in archaeological science research.

The experiment results showed the peculiar components of ancient ceramic bodies. As for an example, the result of corresponding Raman spectra probed at specific areas on a fragment of an ancient bowl showed different absorption patterns (Fig. 1). This reflects the differences in matrix compositions, both chemically and mineralogically, of the areas measured. The research results based on instrumentations mentioned above showed that the body matrix mineralogy of the Wiangkalong potteries is highly heterogeneous, suggesting the presence of large variety of minerals and trace elements in the clay, as well as the variable conditions of firing control.

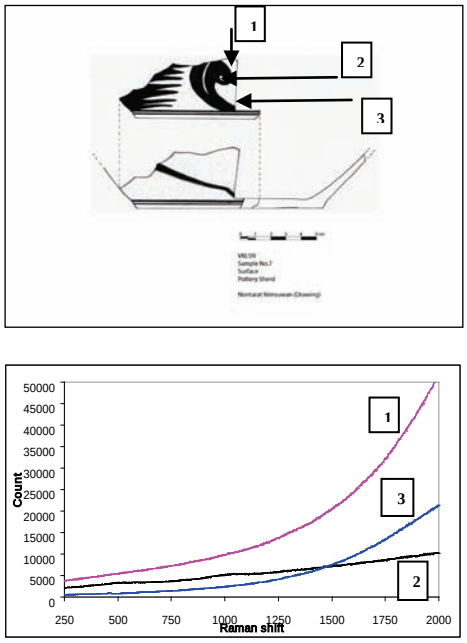

Fig. 1: Wiangkalong pottery fragment (upper image), and the Raman spectra corresponding to the specific areas pointed as 1, 2, and 3, which are the enamel, the flower muster, and the matrix respectively (lower image).

Implications of phase transitions on fire-generated decay of building granites

Gomez-Heras, M.[1,2*], Gomez-Villalba, L.S.[2] & Fort, R.[2]
[1]Depto Petrología y Geoquímica, Universidad Complutense de Madrid, Spain ([*]mgh@geo.ucm.es)
[2]Instituto de Geología Económica (CSIC-UCM), Madrid, Spain

Fire stands out among building stone decay agents because it generates irreversible disruptions, with long-lasting effects, in a very short period of time [1]. In the past few years, research on fire decay of building stone has drifted from mere observations of bulk changes after fires to focus mainly on mineralogical-scale processes as a key for understanding the larger scale decay effects of fire on stone.

This paper focuses on the effects of high temperature on building granites to show the key role of mineralogical phase transitions in the development of decay forms (such as cracking) during fires and in the long-term behaviour (through the modification of argilization patterns) of granites after a fire.

To achieve this, a series of experimental techniques with novel approaches, such as Environmental Scanning Electron Microscope (ESEM) with heating stage and X-Ray diffraction (also with heating stage) were used. These were combined to Transmission Electron Microscopy – Electron Diffractometry for mineral characterization before and after heating.

Additional studies were made to characterize changes in reactivity of feldspar after being heated and the relations between feldspar phase transitions and the increase of argilization observed in the burnt areas of building granites affected by historical fires [2].

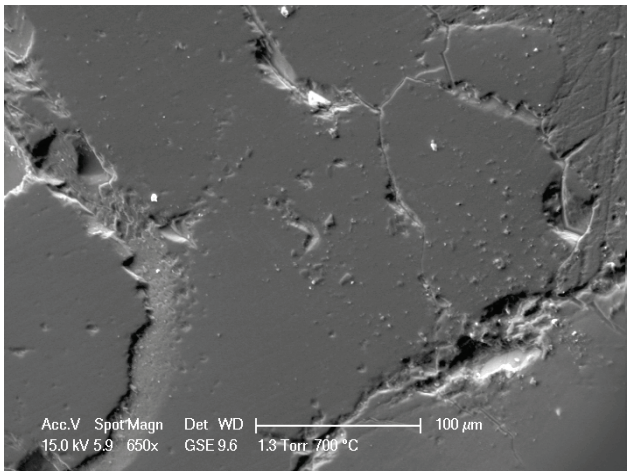

Fig. 1: ESEM image of quartz at 700ºC showing the cracking generated by the α–β quartz transition.

Results show that α–β quartz transition at 573ºC is the main process involved in the generation of cracking during both heating and cooling of granite. Together with this, the amount of defects in feldspar lattice changes during heating. The interaction of these deffects generate strains that contribute to exarcebate grain boundary disruptions, in addition to promoting textural changes in the feldspar that may be related to an increase of reactivity and contribute to the modification of argilization rates in the long term, as observed in samples of building granites undergoing historical fires.

[1] Gomez-Heras, M. et al. (2009) *J. Archit. Conserv.*, **15(2)**, 47-58. [2] Gomez-Heras, M. et al. (2006) in Kourkoulis, S.K. (ed.) *Fracture and failure of natural building stones.* Springer, Dordrecht, 427-437.

Mineralogical indicators of the magnitude of sandstone decay on Scottish buildings

Duthie, L.[1*], Lee, M.R.[1], Phoenix, V.[1], Kennedy, C.[2] & Hyslop, E.[3]
[1]Dept. of Geographical & Earth Sciences, University of Glasgow, UK ([*]duthie@ges.gla.ac.uk)
[2]Historic Scotland, Edinburgh, UK
[3]British Geological Survey, Edinburgh, UK

Here we have asked how decay mechanisms and rates can be evaluated using the mineralogy, chemical composition and molecular structure of detrital and diagenetic minerals present within Scottish sandstones. This is important because to treat and conserve stone-built historic monuments, we have to understand the full depth and range of mineralogical change within the material. At what stage is the decay, are all minerals present suffering, or has only one mineral been affected?

The buildings of south-west Scotland (in particular City of Glasgow) have suffered much weathering in the 150-200 years since construction due to the cold wet climate and past industrial pollution. The main rock forming minerals within these blond Carboniferous sandstones are detrital quartz, Or-rich alkali feldspar and mica, with diagenetic kaolinite, quartz, ankerite and iron oxides. One key indicator of the magnitude of weathering is dissolution of ankerite cement, which sometimes leaves a skeletal iron oxide pseudomorph. These effects have been detected to a depth of 10 mm in a variety of sandstone samples.

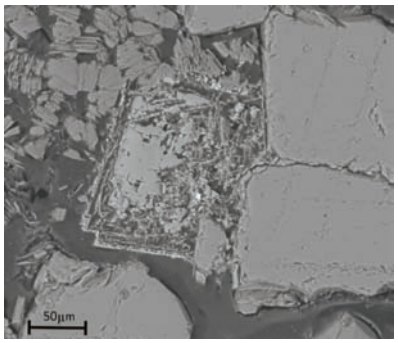

Fig. 1: SEM image of partially weathered ankerite.

Not all of the Glasgow sandstones have a carbonate cement, therefore other minerals have to be explored to help identify the full weathering profile. For example, the movement of iron oxides, mobilised from depth and reprecipitated close to the surface, has long been associated with Scottish stone decay [1], and we have explored whether Raman spectroscopy can be used to distinguish these different generations of oxides. Using Fourier transform infra-red spectroscopy, [2] concluded that during weathering of sandstones from Sydney, Australia, the original kaolinite had become unstable and polymorphs had formed within the weathered section. Using Raman spectroscopy we hope to identify these subtle alterations of the clay structure to pinpoint the depth to which weathering has penetrated. The sheet structure of mica means it may also be sensitive to weathering and may show different levels of alteration.

Our preliminary results confirm that these sandstones have been structurally weathered by decay and that different minerals have the potential to track these changes.

[1] Bluck, B.J. & Poter, J. (1991) *Stone Industries*, **26**, 21-27. [2] Ip, K.H. et al. (2008) *Spectrochim. Acta A*, **71**, 1032-1035.

Composition of limestone weathering crust and associated dust in samples from urban and rural areas of Germany and Hungary

Török, Á.[1*], Licha, T.[2], Simon, K.[3] & Siegesmund, S.[4]
[1]Dept. of Construction Materials and Engineering Geology, Budapest University of Technology and Economics, Budapest, Hungary ([*]torokakos@mail.bme.hu)
[2]Dept. of Applied Geology, Geoscience Center, Göttingen, Germany
[3]Dept. of Geochemistry, Geoscience Center, Göttingen, Germany
[4]Dept. of Structural Geology, Geoscience Center, Göttingen, Germany

The weathering mechanism of limestone monuments located in urban, industrial and rural areas were studied. Black weathering crusts, settling dust and host limestone samples were collected in Hungary and Germany at 13 sites. Micro-fabric (microscopy, SEM), mineralogical composition (XRD) and trace element distribution (LA-ICPMS) were analyzed to understand the contribution of dust to the formation of weathering crusts.

The morphology of weathering crusts are very similar in urban and rural areas, meanwhile the micro-fabric rather reflects the morphology than the location (urban or rural). Laminar and dendritic black crusts have been found in both countries in urban, in industrial and in rural areas. Gypsum is the primary reaction product at the limestone/air pollutant interaction surface with different concentrations at urban and rural sites. Both weathering crusts and the dust found at urban sites are enriched in gypsum.

In dust samples siliceous fly-ash particles are more common, than carbonaceous ones in both countries indicating the longer term stability of these particles. Mineral fragments in dust are abundant and their composition represents the geology of the background area. Gypsum crystal aggregates were also identified within dust samples indicating the rapid sulphation process. Lead mostly accumulates in dust, but also in the black crust. According to LA-ICPMS analyses the highest lead concentrations were found not on the surface of the black crust but close to the crust/limestone boundary especially in the samples, which were collected from urban areas of Budapest and Cologne. As expected, lower levels of lead were found in samples of rural areas, having higher concentrations in the black crusts and lower ones in the host rock

The present study suggests that both settling dust and black crust samples collected from limestone buildings could be used as environmental indicators of past and recent pollution levels.

The role of calcium phosphates in calcium oxalate patinas

Vazquez-Calvo, C.[1*], Alvarez de Buergo, M.[1], Fort, R.[1] & de los Ríos, A.[2]
[1]Instituto de Geología Económica (CSIC-UCM), Madrid, Spain ([*]carmenvazquez@geo.ucm.es)
[2]Instituto de Recursos Naturales (CCMA, CSIC), Madrid, Spain

The calcium oxalate patinas found on historical monuments have long been studied [1-3]. On occasion, they have been associated with calcium phosphates. While some authors attribute the compound substantial or relative importance, others fail to mention its presence, perhaps because the methods used are not the most suitable for its detection.

The present study introduces a re-assessment of the presence of calcium phosphate in calcium oxalate patinas, as well as of calcium phosphate patinas in which no calcium oxalate was detected [4]. A number of hypotheses and theories about the origin of these patinas are discussed. The most suitable methods for identifying calcium phosphate are described, along with their drawbacks and the drawbacks to other methods. Recent reports of calcium phosphates on Spanish monuments [5,6] are compared to earlier findings and the possible origin of this compound is discussed. A classification of patinas based on their phosphorous content and characteristics is also put forward. Finally, a new nomenclature is proposed.

Acknowledgements: This research was funded under the Consolider-Ingenio 2007 (CSD2007-0058) and Geomateriales (S2009/MAT-1629) programmes.

[1] Lazzarini, L. & Salvadori, O. (1989) *Stud. Conserv.*, **34**, 20-26. [2] Salvadori, O. & Realini, M., (1996) in Realini, M. & Toniolo, L. (eds.) *II Int. Symp. The Oxalate Films in the Conservation of Works of Art, Milán, Italia*. EDITEAM s.a.s. Gruppo Editoriale, 335-352. [3] Vazquez-Calvo, C., Alvarez de Buergo, M. & Fort, R. (2007) in Prikryl, R. & Smith, B. (eds.) Geo. Soc. London - Sp. Publ., **271**, 295-307. [4] Polikreti, K. & Maniatis, Y. (2003) *Sci. Total Environ.*, **308(1-3)**, 111-119. [5] Vazquez-Calvo, C., Alvarez de Buergo, M. & Fort, R. (2006) in Fort, R. et al. (eds.) *Proceed. Int. Conf. on Heritage, Weathering and Conservation, 21-24 June 2006, Madrid*. Taylor & Francis (Balkema) Leiden, Madrid, 969-974. [6] Vazquez-Calvo, C., Alvarez de Buergo, M. & Fort, R. (2008) in Lukaszewicz, J.W. & Niemcewicz, P. (eds.) *11th Int. Congr. Deterioration and Conservation of Stone (STONE 2008), 15-20 September, 2008. Torun, Poland*. Nicolas Copernicus University Press, Torun, Poland, 1153-1161.

SO_2 exposure effect in monumental granitic stones

Vázquez, P.* & Alonso, F.J.
Dept. Petrología y Geoquímica, Universidad de Oviedo, Spain
(*pvazquez@geol.uniovi.es)

Granites are very durable materials. When they are placed in a building, their surface is exposed to a wide range of weathering agents, among which, pollution must be remarked [1]. SO_2 exposure may affect Ca-minerals such as plagioclase, or produce Fe-minerals oxidations [2].

Four granites (two grey and two pink granites) commonly used as ornamental stone all along the world, were exposed to SO_2 action. This test was carried out following the standard UNE-EN 13919:2003 but with some modifications. The test was divided into two parts, one for macroscopic evaluation with slabs to measure surface properties (colour, gloss and roughness), and another with smaller specimens for microscopic evaluation and chemical analysis. Both tests were carried out with different temperatures (20º and 60ºC) and concentrations of the solutions (150 and 350 ml of H_2SO_3 for 500 ml of total solution).

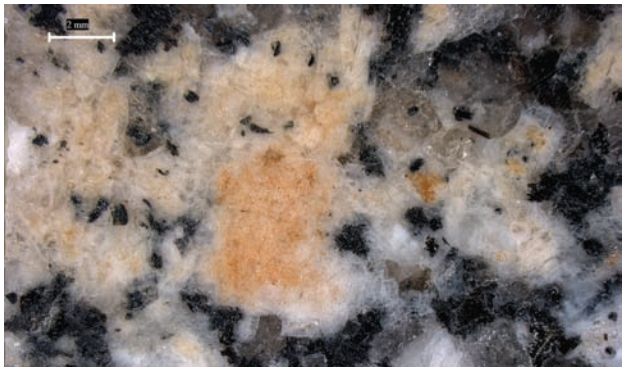

Fig. 1: Detail of plagioclase after SO2 exposure. The orange colour is due to Fe oxidation.

After three weeks of SO_2 exposure, changes in colour, gloss and roughness are measured. Colour changes are very remarkable in grey granites, showing a homogeneous yellowing, which is more intensive with higher temperature. Even orange spots may be observed on some slabs. Pink granites show and increase of red and yellow colours in the measurements, nevertheless with naked eye the variations are not very evident. Gloss exhibits a decrease in all the granites about 30% in relation to original values. Roughness shows an increase in peaks, due to the mica detachment. This effect is more evident in grey granites at low temperature, and in pink granites at high temperature.

The main characteristics found by microscopic evaluation are that there are a lot of crystal habits in all the tested specimens, but they are more developed in low temperature tests (at 20ºC gypsum crystals are rather prismatic and at 60ºC rather acicular). Crystals do not appear in all minerals equally, they tend to crystallise in Ca rich minerals or in those with higher relief. There are crystals with a lot of impurities not showing the typical gypsum habit.

[1] Simão, J., Ruiz-Agudo, E. & Rodriguez-Navarro, C. (2006) *Atmos. Environ.*, **40(36)**, 6905-6917. [2] Kovács, T. (2009) *Tesis de Doctorado*, Universidad de Oviedo.

Engineering properties and problems of rocks used in historical monuments: Tyana Aqueducts case, Nigde/Turkey

Korkanç, M.[1*] & Tuğrul, A.[2]
[1]Geological Engineering Dept., Nigde University, Nigde, Turkey (*mkorkanc@nigde.edu.tr)
[2]Geological Engineering Dept., Istanbul University, Avcılar-Istanbul, Turkey

There are many historical monuments constructed from past to present by different civilizations in Nigde region located in Central Anatolia. Tyana aqueducts as a continuation of the Roma Pool are one of these historical monuments. The aqueducts that carry the antique Roma Pool's water to Tynana thought to have been made by the Roman Emperors Trajan and Hadriyen. 1.5 km part of approximately 3 km long aqueducts is apparent, the rest of it is under ground and it is useless. In historical monuments determination of engineering properties of the rocks used is very important in terms of conservation of these historical monuments and transmitting these buildings to the next generations. In this study, the rock type, deterioration occured in the stone, the problems originated from the selection and use of stone was evaluated. In aqueducts travertines were used as a building block. Due to different textural properties five different block samples were complied. Laboratory studies were performed to determine the mineralogical, petrographic and geomechanical in the collected samples. To identify the mineralogical properties of travertines XRD analysis were performed. Petrographic properties of travertines were determined on thin sections using polarizing microscope. To determine the geomechanical properties of travertines dry and saturated unit weight, water absorption, effective porozity, stability index against dissolution in water, P- wave velocity and uniaxial compressive strength experiments were conducted. Moreover, Schmidt hammer hardness measurements were performed on site with the different levels and different textural characteristics of the belts on the travertines. The samples with fine-grained, massive-textured and low porous properties were found to show relatively higher strength values according to the experimental data obtained from these samples. In most of travertines used, the weathering effects are very low. In destruction of Tyana aqueducts, beside the human effects, selection of small sized stone dimensions (especially the sones used in belts as a keystone) and the stone usage from the same quarry but showing different and bad features are thought to be effective.

Stones for a monument: geological aspects of the rehabilitation of the Cuyahoga County Soldiers" and Sailors" Monument in Cleveland, Ohio, USA

Hannibal, J.[*] & Saja, D.B.
Cleveland Museum of Natural History, Cleveland, Ohio, U.S.A.
([*]hannibal@cmnh.org)

We have been involved with multiple geologically-related aspects of the rehabilitation of the interior of the Cuyahoga County Soldiers' and Sailors' Monument, a splendid 1894 Victorian Monument located in downtown Cleveland, Ohio. This has included identification of various stone types based on observations of in-situ stone, microscopic examination of broken pieces, and, in the case of marble, thin-section examination. We also conducted investigations of bowed slabs of marble inside the monument and we evaluated the latex product used in cleaning marble inside the monument. In addition, we researched archival and historical sources for information on the stone used for the monument, finding a key article that confirmed that most of the white marble had been colored and this led to its re-coloration. Our investigation of bowed marble and our observations related to the cleaning and coloring of the stone have been reported elsewhere. We here summarize these findings and provide additional observations and conclusions.

White marble used inside the monument is from Carrara or is a stone very similar to Carrara. Some of it was stained yellow, and before cleaning resembled Siena Marble. We identified a dark gray, crinoidal limestone used as trim inside the monument as one of the Belgian "marbles" or a stone very similar to the Belgian stone. Some of this had to be replaced, but an easily obtained black "granite" was used instead of limestone. The original gray trim had been stained black and was re-colored black, so the two stone types cannot be easily distinguished.

The latex product sprayed onto the stone as a cleaning agent did work effectively for the most part. Solidified latex pulled from the marble was analyzed using an environmental Scanning Electron Microscope. These samples showed grains of calcite attached to the latex as well as grains of Ca- and S-rich material, probably calcium sulfate. The sulfur-rich material was fuzzy-globular to bladed when seen with the microscope. It is likely that this material (probably gypsum) formed sometime in the history of the monument due to a chemical reaction of the calcium carbonate with acidic water or air. The sulfation of marble is well documented for the exteriors of buildings, but not interiors. Veining in the marble may have facilitated the movement of water through the stone.

The multiple facets of our work on the monument show that it is useful to have geologists involved with all stages of restoration projects that involve stone. Our work on the interior of this building also has broader implications as it shows that the same type of problems (bending of marble slabs; the formation of sulfur minerals) that are widely known to occur on the exterior of buildings may also occur within buildings.

Mineralogical and textural changes in historical lime mortars

López-Buendía, A.M.[1*], Rodriguez-Guanter, M.J.[1] & Urquiola, M.M.[2]
[1]AIDICO, Paterna, Valencia, Spain ([*]angel.lopez@aidico.es)
[2]Dept. Geologia, Universitat de València, Spain

Historical lime mortar suffers mineralogical and textural modifications since they are mixed and placed in the buildings. Carbonatation of lime produces calcite as stable mineral although other unstable carbonate mineral phases can also appear during the process of hardening to form a hard binder. In normal conditions, carbonatation is produced from external to internal section of the mortar. The transformation is not stable along the history of the building and the mortar suffers changes of dissolution and crystallization that are affected mainly by the water availability (humidity, capillarity, rain) and hydrodynamic in the mortar microstructure and environment.

Some studied core drill sections of mortars from historical buildings were selected and characterized with and X-ray diffraction and microscopy, having different concentration calcite and products of alteration along the section. Calcite from lime was identified also by X-ray diffraction with a high crystallinity and purity, compared with aggregates. The methodology can determine changes of the calcite binder along the mortar profile, indicating the dynamic of calcite dissolution and precipitation with internal dissolution domain to external precipitation. A sub-zone of dissolution also appears showing 2 cm of affected depth. The mechanical result is an external hard crust with high concentration of calcite and an internal part with a week wall mortar of a low content of a new precipitated generation of zoned calcite. This model is quite general and affect as much to the mortar of ashlars as the blocks masonry. This phenomenon affects mainly to the aerial lime mortar, but has been also detected in hydraulic lime and the stone.

Gypsum is generally assumed than is related with alteration of calcite in presence of pollution with high sulphur content. The results suggest that gypsum formation has been made from the calcium and bicarbonate rich water rather than the alteration of calcite directly.

A model of mineral mobilising in a masonry wall with lime-based mortar is proposed, as well as the degree of mechanical effect that this calcite dissolution and precipitation can produce into the building structure.

Removal of salts from clay rich and porous sandstones by sepiolite poultices

Herrero Fernández, H.[1,3], García-Talegón, J.[2,3*] & Iñigo, A.C.[1,3]
[1]Instituto de Recursos Naturales y Agrobiologia de Salamanca, CSIC, Salamanca, Spain
[2]Depto. de Geología, Universidad de Salamanca, Spain (*talegon@uasl.es)
[3]Unidad Asociada "Química del Estado Sólido" Universidad de Salamanca / IRNASA-CSIC, Spain

The effectiveness of the sepiolite poultices has been carried out for the extraction of salts (Cl^-, NO^-_3, $SO^=_4$) in clay rich and porous sandstones [1,2]. One of the most important decay processes in the monuments is salt crystallization. The aim in this study is to reproduce in the laboratory the situations usually found in practice in altered stones for which conservation desalting is recommended. Three varieties of Villamayor Sandstone, employed in the monuments of Salamanca (World Heritage City, NW of Spain) have been selected [3]. The Villamayor sandstone is an arkosic stone whose skeleton comprises grains of microcline, plagioclase and quartz, involved into palygorskite and illite/mica [4]. The varieties selected are: i) VAC: fine-grained, microporous, is partially cemented by dolomite, 27% (bulk porosity), ii) VF: ochre and fine-grained, microporous, with smectite, 30% (bulk porosity), iii) VHN: medium-grained, 38% (bulk porosity) [5].

Blocks 5x5x5 cm in size were studied and salts precipitated inside following the Vicente and Vicente-Tavera method [6]. The salt-extraction process is carried out by the consecutive application of three poultices of sepiolite. For every application, the samples were introduced in closed boxes of 7 cm of edge, completely submerged in the poultice during three days. The paste was removed and was performed following the Iñigo et al method [7].

The order of salt removal in the first extraction was according to the mineralogy of the phyllosilicates in each selected varieties, and porosity. Thus, the VHN variety (Fig. 1) was able to extract more anions (without smectite and highly porous), then the VF (smectite and medium porosity) and later on the VAC (contains dolomite and less porosity). The retention of the ions (Cl^-, NO^-_3, $SO^=_4$) for the phyllosilicates is higher than the poultice of sepiolite (agent to removal). This is explained because the skills of retention of anions are great in the dolomite than in the smectite.

Acknowledgements: Authors thank financial support from JCYL (SA024A07) and MCYT (CGL2007-62168).

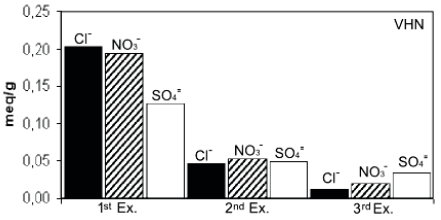

Fig. 1: Results of the analysis after the three extractions treatments on the Villamayor sandstone variety (VHN).

[1] Trujillano, R. et al. (1995) *Appl. Clay Sci.*, **9**, 459-463. [2] Carretero, M.I. et al. (2006) *Appl. Clay Sci.*, **33**, 43-51. [3] García-Talegón, J. et al. (1998) *Color Res. Appl.*, **23(1)**, 46-51. [4] Vicente, M.A. et al. (1993) in Thiel, M.J. (ed.) *Causes of Disorders and Diagnosis*, Chapman & Hall, London, England, **1**, 320-327. [5] Herrero, H. et al. (2007) in Perez-Rodríguez, J.L. et al. (eds.) *Jornada Científica de la SEA*, Sevilla, Spain, **6**. [6] Vicente, M.A. & Vicente-Tavera, S. (2001) *Clay. Clay Min.*, **49(3)**, 227-235. [7] Iñigo, A.C. et al. (2001) *Ultrason. Sonochem.*, **8(2)**, 127-130.

Mineralogy and micro-fabric of Hungarian building stones used in historic constructions at Székesfehérvár Ruin Garden (Hungary)

Theodoridou, M.[1,2*] & Török, Á.[3]
[1]Dept. of Petrology and Geochemistry, Eötvös Loránd University, Budapest, Hungary
[2]Dept. of Civil and Environmental Engineering, University of Cyprus, Nicosia, Cyprus (*mtheodo@ucy.ac.cy)
[3]Dept. of Construction Materials and Engineering Geology, Budapest University of Technology and Economics, Budapest, Hungary

Mineralogical characterization of the building materials provides valuable information on their use and provenance. Additionally, by analyzing mineralogical composition and micro-fabric alteration processes and possible changes related to former conservation actions are detected. Mineralogical studies are also crucial from the point of view of archaeology and art history since it gives us a picture of the construction methodologies followed in the past. At the same time, the achieved information is indispensable for the appropriate design of any intervention needed in the conservation of a monument.

The example of the Ruin Garden of Székesfehérvár in Hungary was selected for the demonstration of the importance of these methods. That assemblage of monuments in Székesfehérvár is of a great historic importance since it served as the coronation and burial church for most of the Hungarian kings in the Middle Ages. Moreover, its several reconstructions and expansions throughout history and the presence of several lithotypes found among the remained building and decorative stones makes the research related to the materials crucial not only for the conservation of that specific monument but also for a series of other historic structures in the Hungarian territory.

A total of 65 samples were collected both from left over pieces and the existing walls and went under mineralogical investigation. The microstructure and fabric of the samples were examined by polarizing microscopy, and Scanning Electron Microscopy (SEM). X-ray diffractometry (XRD) was applied for the identification of the main mineral phases. Limestone was found to be the prevailing stone type among the studied materials, including ooidal peloidal types of different grain sizes, red bio-micritic, shelly, foraminifera-bearing limestones and travertine. Polimict sandy calcarenite, marble, quartz-porphyre rhyolite and silica-cemented red sandstone were also found.

As a further step for understanding the behaviour of the three most relevant materials, additional samples were taken from local quarries with similar physical and mineralogical characteristics: a medium-grained and a coarse-grained oolitc limestone from Sóskút and a Red compact Limestone from Tardos, Hungary. When comparing the micro-fabric of the samples from the monuments and quarries under the SEM it is visible that the samples from the monuments show some alterations. The oolitic limestone is composed of micritic to micro-sparitic calcite crystals. The calcite crystals of the freshly quarried samples show clear crystal faces with no dissolution features, while the samples from the monuments display various forms of surfaced alterations. Besides micro-cracks small crystal aggregates and secondary calcite crystal growth was detected on weathered samples of the monument by using SEM.

Contact sponge method

Vandevoorde, D.[1*], Cnudde, V.[2], Dewanckele, J.[2] & Verhaeven, E.[1]
[1]Artesis Hogeschool, Antwerp, Belgium
([*]vandevoordedelphine@yahoo.co.uk)
[2]Geology and Soil Science – UGCT, Ghent University, Ghent, Belgium

French porous limestones are able to absorb large quantities of water. This phenomenon will accelerate the deterioration of the material. In such cases, the material might be treated with a hydrophobic product, which creates a superficial layer that hampers the penetration of water. In order to decide if such a treatment should be applied or not, the water absorbing behaviour of the material should be measured. With the same measuring technique the efficiency of the hydrophobic barrier can be evaluated. Moreover, it allows the monitoring of such barriers as a function of time. At the same time, the water absorption of porous stone material is an indication of the degree of deterioration and its sensitivity to future deterioration. Up to now, two different measuring techniques exist, the capillary rise method and the Karsten pipe. The latter can be operated in laboratory as well as *in situ*, but is not always reliable for *in situ* analysis. This research proposes an alternative method: the contact sponge method. The contact sponge method consists of a contact-plate, containing a humid sponge. The contact plate is pressed against the stone surface and is weighted before and after contact with the surface. The difference in weight corresponds with the water absorption by the stone. Results can be expressed by the mass difference as a function of area and time. This recently developed method was tested on non-treated and treated porous stone materials in a laboratory environment by traditional techniques and highly advanced imaging techniques such as X-ray CT, in order to evaluate its performance in comparison with the two existing methods.

Mineralogical and textural patterns for fluids migration and consolidation

López-Buendía, A.M.[1*], Guillem López, C.[2], Cuevas Castell, J.M.[2] & Baeza, N.[2]
[1]AIDICO - Materials Research Unit, Paterna, Valencia, Spain.
([*]angel.lopez@aidico.es)
[2]AIDICO - Marble Technical Unit, Novelda, Alicante, Spain

The pathways of the fluids of the natural stone are a very relevant parameter with a wide range of applications. In conservation and restoration, consolidation of stone can be used applying resin injection or, eventually, with other inorganic or organic components. In damage prevention, salt-rich water migration can trigger the apparition of diverse pathologies, such as eflorescences, and crypto-eflorescences, which are related to the precipitation of salts dissolved into the fluids, on the surfaces or inside the rocks. The pathologies could decrease dramatically the mechanical properties of the materials, as well as to produce a loss of the esthetical effect of the stones.

The dynamic of fluids through the stone depends on properties related with the liquid (surface tension, viscosity) and the mineral (surface energy) as well as their interaction in the pathway media (pore size distribution) and with the environment (pressure). Contac angle measurement was applied was applied as a direct and quick method for wettability determination of the parameters controlling the fluids circulation. Liquids with different polarity and known surface tension were used for the energy surface approach of the mineral. Porosity was evaluated by petrography analysis, Hg porosimetry and capillarity. The energy surface shows significant mineral variations, following the trends, as follows:

dolomite>sparry calcite>micrite calcite>quartz >micas

The methodology was applied for consolidation of stone using resin with different surface tensions. Results were evaluated using the penetration depth into the stone and the mechanical effect of the consolidation.

On the mineralogy of β-Dicalcium silicate of hydraulic lime binders in various calcination conditions

Triantafyllou, G.[1*], Markopoulos, Th.[1] & Přikryl, R.[2]
[1]Dept. of Mineral Resources Engineering, Technical University of Crete, Chania, Greece ([*]gtriant@mred.tuc.gr)
[2]Inst. of Geochemistry, Mineralogy and Mineral Resources, Charles University, Prague, Czech Republic

Neogene limestone resources from Crete/Greece were mineralogically and chemically characterized as potential raw materials for the production of hydraulic lime binders in order to be used in restoration and conservation applications. A series of calcination experiments was undertaken in the range 850 - 950 °C for 3, 6, 9 and 12 hours respectively, followed by rapid cooling. The calcination products are characterized as eminently natural hydraulic lime binders [1].

The evaluation of the X-ray powder diffraction patterns evidences the presence of dicalcium silicate, entirely of the β-Ca_2SiO_4 monoclinic polymorph phase, space group $P2_1/n$. The amount of β-Ca_2SiO_4, which is the major hydraulic phase, increases at higher temperatures and longer residence times. Lime, gehlenite, aluminate and ferrite phases, and quartz are present in minor amounts. The range of diffraction scans from 30° to 46° 2θ (CuKα) encompass the interval of strong diffraction peak intensities. The first and the second strongest reflection of β-Ca_2SiO_4 at 32.14° and 32.57° (2θ) (d=2.77 Å-2.74 Å), overlap certain peaks of other minerals present, thus influencing their height and width. However, the reflection at 2θ=41.19° (d=2.1898 Å) is appreciable, free of any overlapping and quite intense. An estimation of the average crystallite size, by the Scherrer equation, is proposed here in, taking into account the line broadening at half maximum intensity (FWHM), of this reflection which appears in each calcination condition. The cell parameters have been calculated from the X-ray powder patterns using the Diffrac plus software (Brucker AXS). Representative results are shown in Table 1.

Table 1: Crystallographic data of the β-Dicalcium silicate phase in various calcination conditions

Cell parameters	(1)	(2)	(3)
a (Å)	5.509(5)	5.512(5)	5.514(5)
b (Å)	6.755(5)	6.756(5)	6.758(5)
c (Å)	9.306(5)	9.310(5)	9.313(5)
Angle β	93.95°	94.12°	94.28°
Average crystallite size (Å)	260	295	325

(1) 850° C, (2) 900° C, (3) 950° C and 12 hours of firing respectively

The calcination conditions directly affect the crystallinity of the β-Ca_2SiO_4 phase, since a significant increase of the average crystallite size is observed, at higher temperatures and longer residence times. The crystal size of the β-Ca_2SiO_4 mineral phase present is considered to be sufficient small and it does not transform to the γ-Ca_2SiO_4 upon cooling [2]. The precence of other elements in the raw material, such as Al, Na, K, Mg, Fe, etc., may contribute to the stability of the β-phase. There is no significant change in the values of the cell parametres, except in the case of angle β, whose values increase under intense firing conditions. These lattice parametres are quite similar with those reported by [3].

Due to this investigation, the amount of β-Ca_2SiO_4 appears to be well crystallized and of a more stable structure at higher calcination conditions, which is important since the hydration process of this phase is slow.

[1] EN 459-1 (2001) *Building lime: Part 1. Definition, specification and conformity criteria*. [2] Chan, C.J. et al. (1988) *J. Am. Ceram. Soc.*, **75,** 1621-1627. [3] Udagawa, S. & Urabe, K. (1978) *Semento Gijutsu Nempo*, **32**.

Mineralogical, physicochemical and mechanical characterisation of historical lime mortars from Cyprus

Theodoridou, M.[1*], Ioannou, I.[1] & Philokyprou, M.[2]
[1]Dept. of Civil and Environmental Engineering, University of Cyprus, Nicosia, Cyprus ([*]mtheodo@ucy.ac.cy)
[2]Dept. of Architecture, University of Cyprus, Nicosia, Cyprus

The use of composite construction materials, such as mortars, is evident throughout the history of mankind. Mortars with various binding materials have been used across different pre-historic and historic periods to meet several construction applications, such as jointing masonry blocks, finishing walls and isolating water bearing structures.

In the framework of an ongoing research, more than 70 samples of mud, gypsum and lime mortars from different archaeological sites and historic buildings and monuments (i.e. cisterns, water mills, churches and fortifications) in Cyprus have been collected and studied following a systematic analytical approach. Here we present macroscopic observations and experimental results on selected lime-based mortar specimens, aiming to characterize these samples and to determine their composition and properties, in order to reproduce appropriate repair mortars by reverse engineering. We focus on petrographic observations of thin sections carried out by polarizing optical microscope. Scanning electron microscope equipped with energy dispersive X-ray microanalyser (SEM-EDX) is also used to examine the microstructure and texture of the mortar samples and to determine semi-quantitatively the chemical composition and interface of their binders. X-ray diffractometry (XRD) is performed to identify the main mineral crystalline phases of the specimens, while their physical properties (i.e. open porosity and bulk density) are also determined by vacuum saturation using water as the wetting liquid. The samples also undergo mercury intrusion porosimetry (MIP) analysis in an effort to collect further information about their pore structure and volume. Last but not least, a portable drilling resistance measurement system (DRMS) is used for a micro-destructive assessment of their mechanical state.

Our macroscopic observations and experimental results confirm that the studied mortars differ in terms of colour, texture, grain size and surface roughness. Petrographic observations provide evidence that the samples mostly consist of fine to medium bioclastic aggregates and aggregates of a reef limestone nature. Traces of feldspars are also observed in some cases.

SEM photos provide occasional evidence of boundary reactions at the interface between the (calcitic) binding matrix and some small (angular, sub-angular and rounded) reddish inclusions of size 1-3 mm. These inclusions are identified by EDX as regions of silica-alumina composition. XRD analyses confirm that calcite is the main mineralogical constituent of the studied historic mortars. These analyses also confirm the occasional presence of calcium aluminosilicate compounds in some of the specimens. We presume that these compounds originated from the addition of crushed brick or ceramic powder in the original mortar mix. The latter has probably been used in the absence of natural pozzolanas on the island to enhance the performance of mortars, increase their mechanical strength, adhesion and hydraulicity and prolong their longevity.

It is anticipated that the results of this study will prove to be useful in understanding the production technology of ancient lime-based mortars in Cyprus. It is also expected to contribute towards the design of new compatible mixtures that may be used in the conservation and restoration of monuments and historic structures.

Materials of decorative stuccoes on an historic theatre of the early XXth century in Bari (Southern Italy) and study of the fire effects

Calia, A.*, Lettieri, M., Masieri, M. & Quarta, G.
CNR- Institute for Archaeological and Monumental Heritage, Lecce, Italy (*a.calia@ibam.cnr.it)

This paper sets out the study of decorative stucco elements in the Petruzzelli Theatre in Bari (Southern Italy), consisting of mouldings and decorations in greater or lesser relief present on the ceilings and walls, and on statues. The Petruzzelli Theatre is an important example of a nineteenth century "Politeama" (i.e. a venue intended for various forms of live entertainment) which was inaugurated in 1903. The stuccoes were affected by the fire which struck the Theatre in 1991, causing serious damage to the main auditorium, whose furnishings and roof were almost completely destroyed; the foyer was less badly affected, and a large part of the decorations (stucco, papier-mâché and wood) on the walls and ceilings remained intact.

Examination by naked eye detected diverse forms of damage to the decorations (Fig. 1); both, extensive blackening due to the presence of combustion deposits, and superficial "roasting", crumbling, cracks and separation of the stuccoes from the wall were observed in the areas affected by the flames. In contrast, in the areas furthest from the heart of the fire the damage appears to be basically due to the effect of high temperature fumes, with the presence of combustion deposits, underneath which the material is apparently intact.

Fig. 1: a: Stuccoes of stage box affected by the fire; **b, c:** Stuccoes of Foyer covered by a layer of combustion deposits; **d:** Piece of stucco fallen from the stage box decorations; **e:** Golden stucco in area not affected by the fire.

The present study aims at the characterization of the constituent materials and the painted surface decorations, as well as ascertaining the effects of the fire.

It was carried out on the samples from the surviving parts of the stage-box decorations, directly affected by the fire, and on those present inside the foyer, affected by the fire to varying degrees. These stuccoes were compared with samples not affected by the fire, which were taken from rooms next to the Theatre.

The composition and structure of the stuccoes were investigated by Optical microscopy in transmitted and reflected light, DRX, FT-IR, DTA-TGA, ESEM with EDS microanalyses.

The combined analyses pointed out different kinds of stuccoes in terms of mineralogical-petrograhical composition. The effects of the fire action were identified in new mineralogical phases, coming from the de-hydration of the gypsum binder, as well as from the mineral pigments used in the painted layers. Microcracks in the stucco groundmass, detachments and melting phenomena of the superficial finishings were also observed, as well as micro-blisters likely due to the burning of the oil binder.

Deterioration of the Sasov castle (Slovakia) and replacement material for the weathered building stone

Adamcova, R.[1*], Petrinec, R.[1], Valter, M.[2] & Plötze, M.[2]
[1]Dept. of Engineering Geology, Faculty of Natural Sciences, Comenius University in Bratislava, Slovakia
([*]adamcova@fns.uniba.sk)
[2]Inst. for Geotechnical Engineering, ETH Zurich, Switzerland

The Sasov castle in Middle Slovakia belongs to the cultural heritage, being one of the national monuments. The ruins of the medieval castle on a volcanic hill above the Hron River are a characteristic landmark, 4 km SE from the town Ziar nad Hronom. In 1997 the condition of the buildings was documented. In a revision after 12 years, the comparison with the previous documentation revealed the fastest deteriorating parts. Searching for the reasons, an engineering geological map of the castle hill was created, showing the relation of tectonic faults and slow slope movements (tilting) with cracks in the masonry and some collapsed walls. Most of the cavities and overhangs in the remaining masonry are due to the weathered binder. Intensive weathering of the building stone, studied within the project VEGA 1/0413/09, caused other reasonable part of the damages.

The masonry is built mainly of Neogene andesite, which is common in this area, as part of the volcanic Stiavnicke Vrchy Mts. More altered highly macro-porous stones show some yellowish-brownish coatings on the surface and fissures. The comparison of some better preserved building stones with the rock in an old local quarry showed a very good match in the properties (mineral assemblage, colour, porosity, strength) with the most altered parts in the rock mass. The accessible but more weathered rock of the upper part of the quarry was exploited as first for the castle. Exposed to environment on the castle hill without any cover, it disintegrates faster than in the rock mass. Volume changes due to smectite swelling as well as freezing-thawing processes in the effective pores probably enhance the deterioration. The most altered building stones are almost white and disintegrate into sand. But there, the X-ray diffraction indicates the possibility of other source or an epiclastic origin.

The sound quarry stone is an andesite of dark grey colour, from medium-grained to aphanitic texture, micro-porous, and extremely strong. Results of the X-ray powder diffraction showed that the mineral assemblage is dominated by andesine (62 wt%) and amorphous phases/glass (27 wt%). As minor phases, augite (8 wt%) and magnetite (3 wt%) were identified. With increasing alteration, smectite content is increasing up to 22 wt%, while augite, magnetite and amorphous phases are decreasing. A considerable part of the macro-pores is the result of selective leaching of weathering products, even when some of the macro-pores are primary voids, caused by the rapid cooling of the melt near the surface. Comparison of the sound rock with the altered one shows an increase in total porosity (from 2.4% to 21.2%) and in effective porosity (from 2.2% to 15.0%). There is a clear relation between the porosity and smectite content on one side, and the uniaxial strength (tested by the Point Load Test) on the other side. The strength dropped from 270 MPa to 51 MPa for more weathered macro-porous stone. Enlin-Neff tests on rock powders proved higher water adsorption in the weathered rock mainly due to the smectite content.

For any castle reconstruction, sound stone from deeper parts of the quarry can be taken as replacement material. It promises better durability, good mechanical properties, as well as acceptability from a historical point of view.

Incorporation of fine and coarse sepiolite in lime-metakaolin mortars

Andrejkovičová, S.[1*], Ferraz, E.[2], Velosa, A.[2] & Rocha, F.[1]
[1]Geosciences Dept., Geobiotec Unit, University of Aveiro, Portugal ([*]slavka@ua.pt)
[2]Civil Engineering Dept., Geobiotec Unit, University of Aveiro, Portugal

The aim of this research was to assess the behaviour of fine and coarse sepiolite acting as water reservoir in lime-metakaolin mortars for applications in building rehabilitation. With this purpose three sets of mortars were prepared: a) mortars with 1:3 air lime (AL): sand volumetric ratio, in which lime binder was replaced by 10% and 20% of metakaolin (MK, commercial product, Portuguese origin); b) the same mortar compositions in which air lime was substituted by 5% of i) fine sepiolite (S, average particle size 2.4 μm, commercial product, Spanish origin), ii) coarse sepiolite (CS, particle size within the range 0.3-1.2 mm). Samples were cured for 28 days according the EN 1015-11 standard.

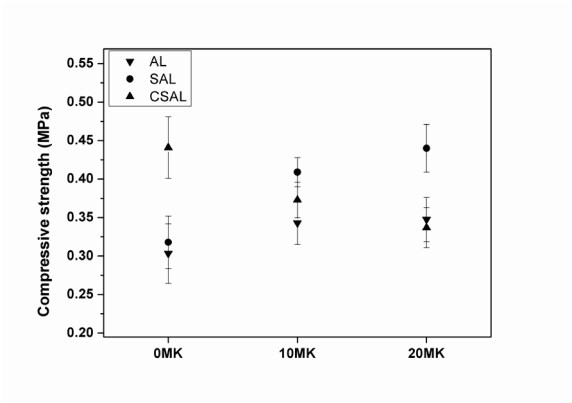

Fig. 1: Compressive strength (MPa) of mortars.

The obtained results showed the increase of mechanical properties in AL-metakaolin mortars when compared to AL-mortar, as well as the improvement of flexural and compressive strengths with the addition of metakaolin content (Fig. 1). Compared to AL mortar, flexural and compressive strengths increased 20% and 12% for AL-metakaolin mortars, respectively. New calcium-silicate and calcium-aluminium-silicate mineral phases were identified in mortars containing metakaolin, which result in higher mechanical strength in metakaolin-blended mortars.

As expected, the fibrous habit of sepiolite caused enhanced conjugation with the individual components and comprehensive compatibility in the mortar system. Considerable improvement is related to fine sepiolite-AL-metakaolin mortars, where compressive strength increased 24% in comparison with AL-metakaolin mortars, while 6% enhancement is associated with addition of sepiolite to AL mortar without metakaolin. It is a consequence of high specific surface area and absorbent properties of sepiolite. The incorporation of coarse sepiolite in AL mortar raises the compressive and flexural strength, by 47% and 52% respectively, compared to AL mortar. On the contrary, the presence of coarse sepiolite in AL-metakaolin mortars promotes a significant decrease of mechanical strengths. Phenolphthalein tests showed an improvement of carbonation rate with the addition of both fine and coarse sepiolite. In early ages, the addition of fines has a significant impact on mortar compressive strength. The fibrous structure of the fine sepiolite also has a possible positive outcome on mortar strength due to binding effect. The effect of chemical reactions, both carbonation and pozolanic reaction will be more evident at 90 days due to slow reaction rate.

Sandstones at the historical "Berlin City Palace"

Ehling, A.[1*] & Jörg Bowitz, J.[2]
[1]Federal Inst. for Geosciences and Natural Resources, Berlin, Germany ([*]angela.ehling@bgr.de)
[2]Berlin, Germany

The "Stadtschloss" or "*Berlin City Palace"* was a royal palace in the centre of Berlin, Germany, heavily damaged in WWII, its remnants being demolished by the East German (GDR) authorities in 1950. The palace bore features of the Baroque style, and its shape, finalized by the mid 18th century, is attributed to Andreas Schlüter, whose first design likely dates back to 1702, although the palace incorporated earlier parts, such as a foundation from 1443. It was the principal winter residence of the kings of Prussia from 1701-1918 (who were the German Emperors from 1871-1918), converted to a museum following the fall of the German Empire in 1918. Following the reunification of Germany, it was decided to rebuild the "Stadtschloss".

According to the present plans, there is an interesting constellation: a historical building has to be rebuilt with 3 historical facades, yet the original building is lost. There are no specific guidelines for the use of rock and plaster materials, but the architects want to restore the historical impression as best as possible, which requires the use of original materials.

The historical facades of the palace had been composed of plastered bricks with architectural elements made of sandstones. How do we know, which sandstones had been used? Around Berlin there are no outcropping sandstones. There is some literature about the use of sandstones since 1700, and some of the original sculptures were saved during the demolition. Provenance analyses have been carried out on about 40 samples of these materials by mobile, non-destructive IR-spectroscopy (Fig. 1).

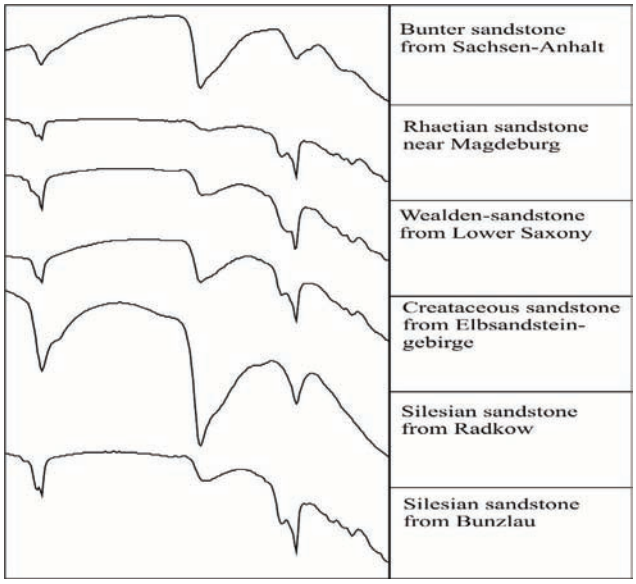

Fig. 1: IR spectra of some analyzed sandstone samples for provenance determination.

The data show that most of the sandstones came from the Elbsandsteingebirge in Saxony, south of Dresden, quarried prior to 1870. In addition, Buntsandstein from Sachsen-Anhalt (near Halle), Rhaetian sandstone from the Magdeburg region, and Wealden sandstones from Lower Saxony were used later on. From the 1870's onward the only rock material used was Cretaceous sandstones from Lower Silesia.

Historic quarries in Hungary

Gherdán, K.[1*], Biró, T.K.[2], Péterdi, B.[3],Markó, A.[2], Schaller, K.[4] & Uhlir, C.[4]
[1]Eötvös Loránd University, Budapest, Hungary ([*]gherdankata@hotmail.com)
[2]Hungarian National Museum, Budapest, Hungary
[3]Geological Institute of Hungary, Budapest, Hungary
[4]CHC-University of Salzburg, Austria

Historic Quarries is a Culture 2007-2013 project of the European Union coordinated by Salzburg University. The most important aim of the project is to present historic quarries as significant parts of European cultural heritage and to provide open access to the historic quarry heritage of Central Europe (Austria, Czech Republic, Hungary, Poland, Slovakia, Romania) through an online information system, aimed at providing geographical, historical, petrographic and touristic information. This paper summarizes the results of the research carried out on quarries situated in Hungary.

The starting point of our work was Ferenc Shafarzik's catalogue and rock collection established in the beginning of the 20th century. This important scientific and industrial enterprise was created in order to collect information on active coeval quarries and their rock types in the Kingdom of Hungary, now extending to the territory of eight countries. The catalogue lists 3162 quarries, from which 1058 are in the territory of present day Hungary: 153 gravel and 13 sand pits, and 892 quarries of other (42) rock types. Together with previously visited quarries (in the framework of previous projects by OTKA (National Science Foundation Project T-25086, Prehistoric raw material atlas...) and the Erosion and Humidity, Culture 2000 program of the European Union) this makes up 143 Schafarzik quarries in 97 villages/towns. Since the beginning of the current project 24 Schafarzik quarries have been visited, where scientific data and samples have been collected, photographs taken, geographical coordinates recorded. Besides, 10 other quarries, which do not appear in the Schafarzik catalogue, but have geological, archaeological or historical importance, have also been visited.

A sample collection of ten quarries has already been published on the internet (http://www.historic-quarries.org/quarries/showlist/46) and five entries about five quarries for quarrypedia have also been presented.

The collected information will help us to better understand lithic raw material utilisation over thousands of years and preserve and spread the knowledge of historic quarry sites and landscapes both among professionals and non-professionals.

Calcite dilatation potential and its influence in marble thermal expansion

Luque, A.*, Álvarez-Lloret, P., Cardell, C., Cultrone, G. & Sebastián, E.
Dept. of Mineralogy and Petrology, Faculty of Sciences
University of Granada, Spain (*analuque@ugr.es)

In the last decades, much research has focused on the physic decay that some marbles show when exposed to environmental thermal change (e.g. The Finland Hall in Helsinki, the Grande Arche de la Defense in Paris, the Courtyard of the Lions in the Alhambra, Spain). It has been demonstrated that this effect is a direct consequence of the anisotropy of thermal dilatation of marble rock-forming minerals (calcite and dolomite), mainly calcite [1]. According to [2,3] preferential mineralogical orientation, fabric and texture of the marble are, among others, the main parameters that influence the physical behaviour of these rocks under thermal oscillation [4].

White Macael marble is a typical ornamental stone used in the Architectural Heritage of Spain. It has been used in numerous ornamental elements as Roman inscriptions, fountains, columns, etc., including the Lions Fountain and the columns of the Lions Courtyard in the Alhambra of Granada (Spain), which are among the most valuated ornamental pieces in Spain. As reported by [5], White Macael is a marble with great thermal susceptibility. Indeed, the results obtained by [6] showed that this marble has a marked preferential crystallographic orientation, simple grain boundaries and large anisotropic thermal dilatation coefficient, all of which directly favour its decay under thermal changes.

The present research documents other two fundamental factors to be taken into account when assessing the effect of thermal dilatation of this marble: i) the dilatation degree that calcite crystals display when are confined in a compact rock and ii) the dilatation degree they show when are in powder state and, therefore, free from confinement pressures. To perform this investigation, an on site thermal experiment has been carried out by applying X-ray thermo-diffraction (XRTD) [7] in both White Macael marble slabs (2000x1000x400 μm) and on powder samples obtained after grinding the above. The preliminary results revealed that the White Macael marble has a greater dilatation coefficient when is analysed in powder state than in marble samples. We suggest that this yield to confinement pressures (strains) at the boundary grains which could triggers physical decay in the marble. Further analyses currently under way are aimed at correlating thermal differences with degree of marble decay after thermal changes by using different types of marbles.

[1] Kessler, D.W. (1919) *Technologic Papers of the Bureau of Standards*, **123**, Government Printing Office, Washington D.C. [2] Siegesmund, S. et al. (1999) *Thermenheft Marmorkonservierung. Z dt geol Ges*, **150/2**, 237-506. [3] Siegesmund, S. et al. (2000) *Int. J. Earth Sci.*, **89**, 170-182. [4] Koch, A. & Siegesmund, S. (2004) *Environ. Geol.*, **46**, 350-363. [5] Rodríguez-Gordillo, J. & Saez-Páez, M.P. (2005) *Const. Build. Mater.*, **20**, 355-365. [6] Luque, A. et al. (in press) *Eng. Geol.* [7] Cardell, C. et al. (2007) *Anal. Chem.*, **79**, 4455-4462.

Anisotropic behaviour of calcitic and dolomitic Spanish marbles

Luque, A.[1*], Leiss, B.[2], Cultrone, G.[1], Sebastián, E.[1] & Siegesmund, S.[2]
[1]Dept. of Mineralogy and Petrology, Faculty of Sciences, University of Granada, Spain (*analuque@ugr.es)
[2]Geowissenschaftliches Zentrum der Universität Göttingen, Germany

Marbles used as construction material have shown a great susceptibility to temperature changes and several researches have pointed at the anisotropic thermal behaviour of its constituent minerals, calcite and dolomite, as one of the main factor influencing the thermal decay of marbles [1]. These two minerals, mainly calcite, show a marked anisotropy of their physical properties with respect to the crystallographic c- and a-axes of the single crystal [2]. The anisotropy of physical properties is conditioned by the lattice preferred orientation (texture) of these minerals [3]. Numerous studies already show how the microstructural and textural characteristics influence physical parameters, clearly demonstrate that these parameters can help predicting stone durability [4-7].

Six marbles are described in our study: four calcitic and two dolomitic, showing marked differences with respect to grain sizes, grain boundaries and twinning, indicating different degrees for deformation and post-deformative recrystallisation.

Texture measurements were carried out on an X-ray texture goniometer (PANalytical X'pert System X-ray diffractometer). On the basis of at least five experimental pole-figures of each sample, a quantitative texture analysis was carried out by calculating the orientation distribution function by means of the WIMV-algorithm [8] and the iterative series-expansion method [9]. The bulk rock anisotropy of the thermal dilatation coefficient and ultrasound waves velocity were calculated by applying the VOIGT averaging method [10].

The velocity of compressional pulses was measured to define a first visual reference - coordinate system (X-, Y- and Z-). Thermal expansions were measured parallel to these directions and the thermal expansion coefficients were calculated. To relate direct and experimental measurements, the fabrics of all marbles were studied by an environmental scanning electron microscopy equipped with a heating stage in three steps of one thermal cycle (in 20º, 90º and 20º C). Different degrees of microcrack-developments were identified in all marbles depending on orientation. The results show that texture type and intensity also influence the behaviour of marbles exposed to thermal changes. We suggest that even in marbles with a strong anisotropy, i.e. a large thermal dilatation, grain size and grain boundary configuration can influence the development of preferred oriented microcracks of marbles and, as a consequence, their thermally controlled decay.

[1] Kessler, D.W. (1919) *Nat. Bur. Stds. Tech. Paper* **123**. [2] Kleber, W. (1959) *Einführung in die Kristallographie*. VEB Verlag Technik, Berlin, Germany. [4] Siegesmund, S. et al. (1999) *Z. d. Deut. Geol. Ges.*, **150(2)**, 237-258. [5] Siegesmund, S. & Dahms, M. (1994) in H.J. Bunge et al. (eds.) *Textures of Geological Materials.* DGM Informationsgesellschaft, Oberursel. 353-379 [6] Siegesmund, S. et al. (2000) *J. Earth Sci.*, **89**, 170-182. [7] Leiss, B. & Weiss, T. (2000) *J. Struct Geol*, **22**, 1737-1745. [8] Matthies, S. & Vinel, G.W. (1982) *Phys. Stat. Solid. (b)*, **112**, K111-114 [9] Dahms, M. & Bunge, H.-J. (1989) *J Appl Crystallog*, **22**, 439-447. [10] Bunge, H. J. (1985) in Wenk, H.-R. (ed.) *Preferred Orientation in Deformed Metals and Rocks: An Introduction to Modern Texture Analysis*. Academic Press, 507-525.

Sulphatation process in calcitic and dolomitic marbles altered by SO_2

Luque, A.[1*], Martínez de Yuso, M.V.[2], Cultrone, G.[1] & Sebastián, E.[1]
[1]Dept. Mineralogy and Petrology, University of Granada, Spain
([*]analuque@ugr.es)
[2]Central Research Services, University of Malaga, Spain

Atmospheric pollution is one of the main decay agents of monumental pieces located in industrialized urban centres. SO_2 is a permanent and abundant component of air pollution and, although it does not have an immediate visual effect, after a continuous exposition, it can end up damaging irreversibly the construction material.

Marble is an ornamental stone commonly used in monuments and it is very susceptible to deteriorate by SO_2 attack because of its mineralogical composition (calcitic and dolomitic) which favours the development of gypsum on the surface [1]. This reaction is known and the final gypsum development is via an initial formation of $CaSO_3$ which is subsequently oxidized to $CaSO_4$ by atmospheric oxygen [2]. However, if many researches described the epsomite growth ($MgSO_4$+$7H_2O$) on dolostone surfaces, this reaction seems to not show the existence of previous sulphite stage formation ($MgSO_3$) in this types of rocks, even if this salt is know as a component employed in wood pulping process and paper production processes [3].

To measure how easily marble suffers atmospheres rich in SO_2, selected calcitic and dolomitic samples were exposed during 24 h to sulphur dioxide in a climatic chamber under controlled thermohygrometric conditions (20ºC and > 90% HR). The superficial damage produced by SO_2 on marbles was studied using two non-destructive techniques: chromatic change by means colorimetry and chemical analysis using X-ray photoelectron spectroscopy (XPS). Moreover, the development of new reaction phases was observed by variable pressure scanning electron microscopy (VPSEM).

Colorimetric analysis evidenced a decrease in lightness (L*) and chromatic parameters (a* b*) showing that these changes are due to the formation of new minerals phases. XPS, generally used in the analysis of metallic pieces, is somehow novel in the field of stone deterioration. The use of this technique has allowed to demonstrate the development of sulphites and sulphates in marbles with high precision, after just 24 hours of their exposure to SO_2 and to distinguish a different decay path between calcitic and dolomitic marbles. Salts crystals show different morphologies and concentrations depending on the type of salt and the compositions of substrate where they grow.

[1] Buginia, R., Laurenzi-Tabasso, M. & Realini, M. (2000) *J. Cult. Herit.*, **1**, 111-116. [2] Böke, H. et al. (1999) *Appl. Surf. Sci.*, **140**, 70-82. [3] Steindl, M. et al. (2005) *Chem. Eng. Process.*, **44**, 471-475.

Mapping, weathering forms and petrographic features – the western portal of Cârţa Cistercian Monastery (Sibiu County, Romania)

Mihăilă, A.
Dept. of Geology, Faculty of Biology and Geology, "Babeş-Bolyai" University, Cluj-Napoca, Romania
([*]anamaria.mihaila@ubbcluj.ro)

At the end of the XIII[th] century, one of the most imposing monastic architectural assemblies from south-eastern Europe was built in Cârţa (Sibiu County, Romania). The abbey played an important role in medieval Transylvania, as it was located at the interference of Byzantine and Occidental cultural-religious influences [1]. The style of the monastery is early gothic, but the western façade and portal must have been finalized later on (probably still before 1300), as the portal shows mature gothic features [2].

The research focuses on the western portal of the abbey, which was chosen for its architectural importance and the use of dimensional building stones. Three types of mapping were performed: a standard mapping of the sandstone blocks and of mortar types including the numbering of each block, the sound velocity mapping after clash-test and the relative humidity mapping after more than 650 measurements by using Hydromette Compact B Gann equipment.

Based on Fitzner's classification [3], the most frequent weathering forms identified after *in situ* investigations of the portal were: granular disintegration, breakout, discoloration and biological colonization prevails in the lower part; the middle part is highly affected by winds and thus typical weathering forms appear (alveolar weathering, rounding and notching), especially on the northern side; the upper part, frequently exposed to atmospheric factors, is dominated by intense biological colonization and the formation of crusts. The different weathering patterns of the portal's parts correlate with the relative humidity and sound velocity mappings, pointing to a more intense alteration of the northern side, because of its exposure and the action of the winds from the Făgăraş Mountains.

The identified source area of the raw material is located 12 km away, near Colun village. The Sarmatian sandstones from Colun were analyzed both macroscopically and microscopically in order to compare them with the sandstones used at the construction of the abbey. The optical microscopy study shows that both rocks are litharenites with carbonatic cement and bioclasts, metamorphic quartz with undulatory extinction, and altered feldspars.

Acknowledgements: I wish to thank for the financial support provided from programs co-financed by The SECTORAL OPERATIONAL PROGRAMME HUMAN RESOURCES DEVELOPMENT, Contract **POSDRU 6/1.5/S/3 – „**Doctoral studies: through science towards society**".**

[1] Busuioc-von Hasselbach, D.N. (2000) *Ţara Făgăraşului în secolul al XIII-lea; Mănăstirea Cisterciană Cârţa.* Fundaţia Culturală Română, Cluj-Napoca, **I**, 32-170. [2] Vătăşianu, V. (2001) *Istoria artei feudale în Ţările Române.* Fundaţia Culturală Română, Cluj-Napoca, 98-126. [3] Fitzner, B. & Heinrichs, K. (2002) in Prikryl, R. & Viles, H. A. (eds.) *Proceed. Intern. Conf. "Stone weathering and atmospheric pollution network (SWAPNET 2001)"*, 11-56, Charles University in Prague, The Karolinum Press.

Sulfation of carbonate rocks as an important factor of cultural heritage monuments deterioration in different climatic regions

Mosyagin, A.V.[*], Frank-Kamenetskaya, O.V., Vlasov, D.Yu. & Zelenskaya, M.St.
Saint Petersburg State University, Saint Petersburg, Russia
([*]al.mosyagin@gmail.com)

The paper presents the results of study and comparison of the sulphate deterioration processes of carbonate rocks (marble and limestone) that were used as building materials for cultural heritage monuments in urban environment of several cities: Saint Petersburg (Russia), Sevastopol (Crimea, Ukraine), Oslo (Norway), Orebru (Sweden). It is shown that formation of gypsum-rich patina plays one of the leading roles in deterioration (Fig. 1a) [1,2].

During the study carbonate rocks (limestone and marble) used for the construction were examined and the condition of their surface (presence of cracks, chipping etc.) were described, black crusts of gypsum-rich patina were sampled. Collected samples were studied by optical microscopy, powder X-Ray diffraction, scanning electron microscopy. Microbial species were determined by the use of different microbiotical techniques.

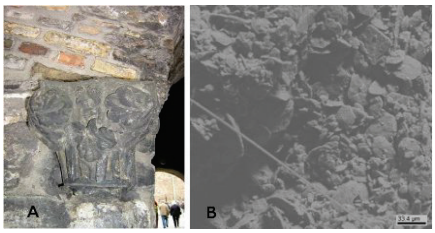

Fig. 1: a. Limestone column volute totally covered with black crust of gypsum-rich patina, Akershus caslte,Oslo (Norway).**b.** SEM image of flattened gypsum crystals from the black crust, Akershus caslte,Oslo (Norway).

Our study shows that sulfation processes take place in all studied climatic regions due to the presence of SO_2 in atmosphere. The gypsum crystals morphology is quite similar and the most often habit is lamellar, strongly flattened after the second pinacoid (Fig. 1b). Prismatic elongated crystals were observed much more rarely. It was shown that the range of deterioration was closely connected with the shape and the material of the monument. The largest diversity of crystal habits was investigated in Saint Petersburg due to the wide diversity of substrate rocks. The largest gypsum crystal was found in Tauric Chersonesos on the porous limestone wall and reached 240 μm. Three stages of the gypsum-rich patina formation were noticed: the initial, when tiny gypsum crystalls occur beneath the biofilm; the intermediate stage, with multiple large gypsum crystals and microorganisms among them; the intensive stage with microbial community under the gypsum layer [2].

The presence of microorganism communities was shown in every investigated specimen by microbiological studies. Six species of micromicetes from genera Cladosporium, Alternaria, Epicoccum, Scytalidium, common for all specimens were picked out. It seems that they take part in the gypsum-rich patina formation, while the way of this process is not clear yet. The simulation experiments are still in progress.

Acknowledgements: The work was supported by Russian Foundation of Basic Research (Projects 09-05-01062,09-06-90406). Authors thank Irina Knauf and Maria Timasheva for their valuable assistance during the study.

[1] Mosyagin, A.V. et al. (2009) *Stud. Univ. Babes-Bolyai, Geol.*, **54(2)**, 13-16. [2] Timasheva, M.A. et al. (2007) *Russ. Mineral. Soc. Notes*, **5**, 98-104 (in Russian).

Enhanced weathering of stone by salts: physical, chemical and remediation strategies

Schiro, M.[1*], Ruiz-Agudo, E.[2] & Rodriguez-Navarro, C.[1]
[1]Dept. of Mineralogy and Petrology, University of Granada, Spain ([*]mschiro@gmail.com)
[2]Dept. of Mineralogy, University of Münster, Germany

In the presence of salt and water, stone monuments suffer from both physical and chemical weathering. An effective remediation strategy should inhibit both weathering processes [1[. In order to develop this type of conservation treatment, a full understanding of salt-enhanced physical and chemical weathering must first be achieved. For this we have chosen to study sodium sulphate, as one of the most damaging salts known [2]. As model substrates we have selected a non-porous glass slide and a sintered porous glass of controlled porosity.

Using these salt and model substrates, we have started examining physical weathering due to crystallization pressure generation. First we have studied the crystallization of a single drop of saturated sodium sulfate solution evaporating on the surface of a non-porous glass slide. Evaporation at 21°C and 35% relative humidity resulted in precipitation of the single phase thenardite (anhydrous $NaSO_4$), as determined by polarized optical microscopy, environmental scanning electron microscopy (ESEM) and X-ray diffraction (XRD).

Next, we used the porous glass to understand crystallization in a porous system. The evaporation rate was recorded using thermal gravimetry (TG) and results were used to calculate the concentration of sodium sulfate in solution at every point during evaporation. The heat of crystallization was measured in parallel by differential scanning calorimetry (DSC), which determined crystallization events and the timing of phase transitions [3]. Results from DSC in combination with TG enabled calculation of supersaturation with respect to each phase. However, it is not possible to determine which phases precipitate using these methods. In order to overcome this limitation, we needed a tool that allowed us to probe below the surface. Two-dimensional X-ray diffraction (2D-XRD) is an innovative and powerful tool which performs synchrotron-like experiments in a normal lab, by using a Molybdenum X-ray source (more than 5 times more penetrative than conventional Copper source). The first phase to form is the metastable heptahydrate ($NaSO_4 \cdot 7H_2O$) [4], followed by a phase transition to mirabilite ($NaSO_4 \cdot 10H_2O$), with the final phase transition forming thenardite (anhydrous $NaSO_4$). In combination with the results from TG/DSC, critical supersaturation at the onset of crystallization within the porous system was calculated, as well as the associated crystallization pressure.

The combination of instruments used in this work provides the basis for understanding the process by which crystallization of salt phases occurs by evaporation (i.e., the most common situation leading to salt damage in building stones and natural environments). By examining different salts and different substrates, we will have a clear background against which we can measure how effective a specific remediation treatment is at reducing crystallization pressure and inhibiting damage.

[1] Ruiz-Agudo, E. et al. (2006) *Cryst. Growth Des.*, **6**, 1575-1583. [2] Rodriguez-Navarro, C. et al. (2000) *Cement Concrete Res.*, **30**, 1527-1534. [3] Espinosa, R. & Scherer, G. (2008) *Environ. Geol.*, **56**, 605-621. [4] Hamilton, A. & Hall, C. (2008) *J. Anal. Atom. Spectrom.*, **23**, 840-844.

Provenance study of marbles based on qualitative and quantitative petrography (Moldanubian Zone, Czech Republic)

Šťastná, A. & Přikryl, R.*
Inst. of Geochemistry, Mineralogy and Mineral Resources, Faculty of Science, Charles University in Prague, Czech Republic (*prikryl@natur.cuni.cz)

The present provenance study was carried out on calcite and dolomite marbles of the Moldanubian Zone (south part of the Bohemian Massif, Czech Republic). Local marbles have been quarried and used as dimension stones in the 19th and 20th centuries [1].

The complex geological situation here is reflected partly in the petrographic variability of marble properties (e.g. presence of non-carbonate phases and various fabric). The mineralogical composition of petrographic types varies significantly, marbles verge into calc-silicate rocks in some localities. The fact that Czech marbles differ from white Mediterranean marbles also means that there are special requirements on the selection of provenancing techniques. Previously successfully used conventional analytical procedures such as X-ray powder diffractometry or stable isotope geochemistry may not usually provide a stringent criterion for a provenance determination [2,3].

Provenance methodology was based on detailed optical microscopy (OM) of the whole rock in combination with cathodoluminescence (CL) of microfacies, petrographic image analysis (PIA) of carbonate grains and electron backscatter diffraction (EBSD) of carbonate grains. The studied marbles were distinguished on the basis of the mineral assemblage, the colour type of cathodomicrofacies and fabric parameters (carbonate grain size and grain shapes, index of grain size homogeneity, presence of shape or crystallographic preferred orientation).

[1] Rybařík, V. (1994) *Dimension stones from the Czech Republic*. Nadace Střední průmyslové školy kamenické a sochařské v Hořicích v Podkrkonoší (In Czech). [2] Šťastná, A. & Přikryl, R. (2009) *Int. J. Earth Sci*, **98**, 357-366. [3] Šťastná, A. & Přikryl, R. (2010) in Bostenaru, D.M. et al. (eds.) *Materials, Technologies and Practice in Historic Heritage Structures*. Springer, 157-175.

Substrate effects on stone bioconsolidation by bacterial carbonatogenesis

Jroundi, F.[1], Rodríguez-Navarro, C.[2], Vicente Navarro, J.[3] & Gonzalez-Muñoz, M.T.[1*]
[1]Dept. of Microbiology; Sciences Faculty, University of Granada, Spain (*mgonzale@ugr.es)
[2]Dept. of Mineralogy and Petrology; Sciences Faculty, University of Granada, Spain
[3]Instituto del Patrimonio Histórico Español, Madrid, Spain

Carbonate and silicate stones (e.g., limestones and sandstones) have been widely used as sculptural and construction materials since ancient times, thus constituting a significant part of mankind's Cultural Heritage [1]. They are, however, highly sensitive to weathering. Consequently, the study of stone decay and conservation has become an important research field. Among the newly developed conservation treatments, those based on the use of bacterial carbonatogenesis are gaining interest. In this context, we developed an efficient consolidation method based on the activation of the carbonatogenic microbial community that inhabits building stone (calcarenite) by the application of a suitable nutritional solution [2]. For the effective use of this novel conservation treatment, it is pivotal to shed light on how deep the new bacterial carbonate precipitates within porous stones. However, we have found some difficulties in identifying the newly formed carbonate cement because these treatments were carried out on calcarenite stone [1,3], and the bacterial carbonate was typically calcite (i.e., the same mineral existing in the original stone). In order to by pass this problem, a treatment was applied on a sandstone sample (from Prague, Czech Republic) which typically shows extensive damage (e.g., Prague´s Charles Bridge [4]) and presents similar porosity and pore size distribution than the previously treated calcarenite [1,3;5]. The treatment was applied by spraying a nutritional solution M-3P [5] on one of the larger surface of sandstone slabs (150x30x15 mm). XRD analyses of depth profiles in the treated sandstone show that calcium carbonate precipitated as vaterite down to a depth of 8-9 mm. SEM observations revealed that quartz grains in the sandstone were fully covered with mineralized bacterial EPS and numerous micrometer-sized espherulites of vaterite in contact with mineralised bacterial cell down to a depth of 15 mm (that is, the full thickness of the treated stone slabs).

These results indicate that: (i) the activation of carbonatogenic bacteria inhabiting the sandstone results in the production of consolidating $CaCO_3$ cement, and (ii) the nature of the substrate (carbonate or silicate) strongly influences polymorph selection of the carbonate biomineral phase (stable calcite or metaestable vaterite). These results may have important implications in bacterial conservation of ornamental stones others than carbonate stones, and demonstrate that the crystallographic affinity between the substrate and the bacterial biomineral (i.e., possible existence of epitaxy or its absence) controls which calcium carbonate phase is formed.

Acknowledgements: Project RNM 3943 (Junta de Andalucía), and C. Jiménez-López for her help.

[1] Rodriguez-Navarro, C. et al. (2003) *Appl. Environ. Microbiol.*, **69**, 2182-2193. [2] Gonzalez-Muñoz, M.T. et al. (2008). *Method and product for protecting and reinforcing construction and ornamental materials*. Spanish Patent nº 2008/009771. [3] Jimenez-Lopez, C. et al. (2008) *Int. Biodeter. Biodeg.*, **62**, 352-363. [4] Přikryl, R. et al. (2004) *Eur. J. Mineral.*, **16**, 609-618. [5] Jroundi, F. et al. (in press) *Microb. Ecol.*

Reasons of variations of the mineral compositions of the mantle rocks beneath the Yakutian kimberlite province

Ashchepkov, I.[1*], Afanasiev, V.[1], Vladykin, N.[2], Pokhienko, L.[1], Ntaflos, T.[3], Travin, S.[2], Ionov, D.[4], Palessky, V.[1], Logvinova, A.[1], Kuligin, S.[1] & Mityukhin, S.[5]
[1]Institute of Geology and Mineralogy SB RAS, Novosibirsk, Russia ([*]Igor.Ashchepkov@uiggm.nsc.ru)
[2]Institute of Geochemistry SB RAS, Irkutsk, Russia
[3]University of Vienna, Austria
[4]Université J. Monnet, Saint-Etienne, France
[5]ALROSA Company, Russia

Minerals from the deep seated xenoliths concentrates (>20000 EPMA and >9000 LAM ICP MS) form seven regions of Yakutian kimberlite conference reveal a significant difference in the major and trace elements [1,2] which is mostly seen on the clinopyroxene compositions [2]. It result in the difference of the mantle layering in separate tectonic units [3-5] and due to the reactions with the plum (PM) and subducted related melts (SRM) during [6,7] the evolution of the SCLM beneath each part of Yakutia. Cpx from Central (M.Botuobinsky) reveal relatively fertile mantle source due to high scale hybridization and fertilization with carbonatitic and protokimberlitic melts. Alakite mantle subjected to SRM essentially K-(Na) metasomatism (800-600 ma) with richterites and K-Cpx in deep SCLM reveal more La/Yb_n rations for Cpx increasing with the pressure in opposite to those from M.Botuobinsky field. Daldyn field SCLM reveal more depleted SCLM with the silica enrichment due to SRM reactions [6,7]. In Kuoyka and Anabar regions dunites dominte, SRM fertilization starts <40kbar [2,3,8] due to shallow subduction producing Cr- pargasite metasomatism. The most upper levels on SCLM mantle show the high scale Na- metasomatism probably fluid related. Mantle sections beneath the periphery of Siberian SCLM in Mesozoic show the enrichment due to basaltic PM reactions detected in Cpx TRE spidergrams. Layering determined by monomineral thermobarometry [3] for Gar, Opx, Cpx, Chr and Ilm is in a good agreement with OPx –Gar barometry showing the 10-12 contrast units. Pervasive metasomatism passed through the general layering. Monomineral thermobarometry allows to construct the mantle transects through the fields and kimberlite regions. The thermobarometry for the ilmenites allow to reconstruct the layers subjected to the metasomatuism by the protokimberlites. Precise data for the Ol obtained using 20 min measurements at 20KV on CAMECA 50 SX allow to obtain preliminary Ol geotherms using methods [9-10] are coinciding in general with those produced by pyroxene methods.

Acknowledgements: RBRF 05-05-64718, ALROSA 77-2 65-3; 2-05.

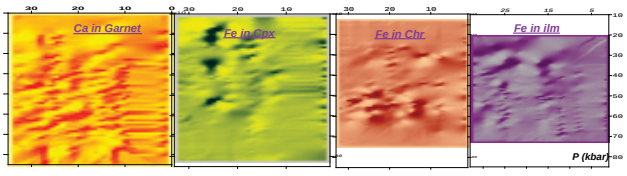

Fig. 1: Transect from Zarnitsa to Udachnaya with thermobarometry [3].

[1] Sobolev, N.V. (1977), [2] Taylor, L.A. et al. (2003) *Contrib. Mineral. Petrol.*, **145**, 424-443. [3] Ashchepkov, I. et al. (2010) *Tectonophysics*, **485**, 17-41. [4] Ashchepkov, I. et al. (2008) *9IKC Abst.*, 386. [5] Griffin, W.L. et al. (1999) *Tectonophysics*, **310**, 1-35. [6] Boyd, F.R. et al. (1997) *Contrib. Mineral. Petrol.*, **128**, 228-246. [7] Ionov, D. et al. (2010) *J. Petrol.*, (submitted). [8] Brey, G.P. & Kohler, T. (1990) *J. Petrol.*, **31**, 1353-1378. [9] De Hoog, J.C.M. et al. (2010) *Chem. Geol.*, **270.** 96-215. [10] Köhler, T. & Brey, G. (1990) *Geochim. Cosmochim Ac.*, **54**, 2375-2388.

Detectability of the post-perovskite transition in mantle-related multi-phase systems

Grocholski, B.[1*], Shim, S.-H.[1] & Prakapenka, V.[2]
[1]Massachusetts Institute of Technology, Cambridge, Massachusetts, USA ([*]brent_g@mit.edu)
[2]University of Chicago, Illinois, USA

Seismic observations of the D" discontinuity, especially in regions of high velocity where it is more readily observed [1], have been attributed to the thermal response of the perovskite to post-perovskite (PPv) transition. This interpretation is dependent on the assumption of a narrow depth interval for the transition combined with a large and positive Clapeyron slope. However, our recent study on binary and ternary systems [2] showed that 10% Fe and 10% Al increase the thickness of the two-phase region to 400-600 km, making seismic detection of the PPv transition difficult.

We have made new measurements on pyrolitic and San Carlos olivine compositions up to 170 GPa and 3000 K in laser-heated diamond cell at the GSECARS sector of Advanced Photon Source. Gold was used as the internal pressure standard and argon was used as a pressure medium. Both compositions include ferropericlase (Fp), for which the effect on the transition has only been modelled in our previous study [2]. Pyrolite contains 10% Al, while San Carlos olivine is aluminium-free.

The effect of aluminium on the Pv to PPv transition is profound even in the multi-phase systems, with our measurements on a pyrolitic composition indicating a PPv transition begins at a depths 100±100 km below the core-mantle boundary (CMB) and has a wide two-phase region of 800±200 km. In contrast, the PPv transition in a San Carlos olivine composition occurs at a depth 100±100 km above the CMB with a two-phase region thinner than 100±100 km.

These are in good agreement with our predictions in [2] in that Al increases both depth and thickness of the PPv transition (as measured in pyrolite) while Fp (or high Mg/Si) decreases the thickness through buffering effect (as measured in San Carlos olivine). Harzburgite, existing in the subducting lithosphere, has much smaller amount of Al and higher Mg/Si ratio, making an ideal candidate rock for a sharp PPv transition. Therefore, the PPv transition may exist in harzburgite subducted into the deep mantle, while it does not exist in pyrolitic mantle.

[1] Wysession, M.E. et al. (1998) in Gurnis, M. et al (eds.) *The Core-Mantle Boundary Region*. AGU, Washington, DC, 273-297. [2] Catalli, K. et al. (2009) *Nature*, **462**, 782-785.

Phase transitions, densities, and sound velocities of mantle and slab materials down to the upper part of the lower mantle

Irifune, T.[1*], Nishiyama, N.[1], Tange, Y.[1], Kono, Y.[1], Shinmei, T.[1], Kinoshita, Y.[1], Negishi, R.[1], Kato, T.[1], Higo, Y.[2] & Funakoshi, K.[2]
[1]Geodynamic Research Center, Ehime University, Matsuyama, Japan ([*]irifune@dpc.ehime-u.ac.jp)
[2]Japan Synchrotron Radiation Research Institute, Hyogo, Japan

Phase transitions, densities, and elastic wave velocities have been accurately measured on mantle and subducting slab lithologies by a combination of multianvil and ultrasonic techniques, coupled with synchrotron in situ X-ray observations, under the P, T conditions of the whole mantle transition region. Moreover, use of sintered diamond as the second-stage anvils has dramatically extended the P, T conditions for in situ X-ray diffraction studies toward those of the middle part of the lower mantle.

We have performed such experiments on rocks such as pyrolite, MORB, and harzburgite, which are supposed to be the major consituents in the mantle and the slabs, at pressures to the upper part of the lower mantle. The resultant density and elastic wave velocity data are compared with those obtained seismologically, and we found that pyrolite is a reasonable model composition for the mantle transition region and the upper part of the lower mantle, except for the bottom part of the mantle transition region, where the sound velocities, particularlly Vs, are significantly higher than those of the typical seismologica models.

One possible senerio for this discrepancy is the presence of a layer of harzburgite, the main body of the subducted slabs, which may globally exist near the 660km seismic discontinuity. The feasibility of this idea will be discussed on the basis of our recent experimental data on phase relations, densities, and sound velocities of pyrolite and harzburgite under the P, T conditions of this region of the mantle.

Pressure-induced phase transitions in transition-metal sesquioxides: effect of d electrons

Umemoto, K.
Dept. of Geology and Geophysics, University of Minnesota, Minneapolis, USA (umemoto@cems.umn.edu)

After discoveries of the $CaIrO_3$-type post-perovskite (PPV) phase in $MgSiO_3$ and Al_2O_3, sesquioxides (M_2O_3) have been investigated in search of low-pressure analogs of these minerals. Here we investigate three 4d-transition-metal sesquioxides: Y_2O_3, Rh_2O_3, and In_2O_3. Y_2O_3 and In_2O_3 undergo pressure-induced transitions accompanied by increase in cation coordination number from 6 to 7. However, in Rh_2O_3, such transition does not occur up to ~350 GPa. This cannot be explained by simple arguments based on ionic radii ratio. By calculating electronic density of states and spatial distributions of the 4d states, it is clarified that effects of 4d electrons are crucial for stability of crystal structures. Extraordinary stability of Rh_2O_3(II)-type Rh_2O_3 against other phases is naturally explained. This study indicates that the complexity of phase sequences in 3d/4d-transition-metal sesquioxides is caused not only by the ionic radii ratio but also by electronic occupancy and spatial distribution of the d states.

Acknowledgements: Research was supported by NSF grants EAR-0135533, EAR-0230319, and ITR-0426757 (Vlab).

The post-spinel transition in Si- and Cr-bearing Fe_3O_4 solid solutions

Schollenbruch, K.[1], Woodland, A.B.[1*], Frost, D.J.[2], Langenhorst, F.[2] & Boffa Ballaran, T.[2]
[1]Institut für Geowissenschaften, Universität Frankfurt, Germany
([*]woodland@em.uni-frankfurt.de)
[2]Bayerisches Geoinstitut, Universität Bayreuth, Germany

Spinel-structured phases occur in many different geological environments and play an important role in the Earth´s upper mantle and transition zone. At high P, some spinels like magnetite (Fe_3O_4) and chromite ($FeCr_2O_4$) transform to denser post-spinel phases (magnetite at ~10 GPa, [1]; chromite at ≥12.5 GPa, [2]), while others break down into their constituent oxides (e.g. $FeAl_2O_4$, [3]). The high-P phase, h-Fe_3O_4, is not quenchable, hampering study of this transition. On the other hand, two high-P polymorphs of chromite were found in a meteorite [2] indicating a stabilizing effect of Cr for the post-spinel structures. Following on our results for Fe_3O_4 [4] we are experimentally studying Si and Cr-bearing Fe_3O_4 solid solutions in an attempt to 1) recover the post-spinel phase for structural investigation, and 2) determine the effects of these cations on phase stabilities at transition zone pressures.

Multi-anvil experiments were performed between 8 and 13 GPa and 1000-1300°C using pre-synthesized spinels with Si-bearing compositions 0.85 Fe_3O_4 – 0.15 Fe_2SiO_4 and 0.7 Fe_3O_4 – 0.3 Fe_2SiO_4 and Cr-bearing solid solutions $Fe(Cr_{0.2},Fe_{0.8})_2O_4$ and $Fe(Cr_{0.5},Fe_{0.5})_2O_4$. In the Si-bearing experiments, a new phase appears at 8 GPa that coexists with a spinel-structured phase. This phase is Si-poor and drives the spinel to higher Si contents than the original bulk composition. At ≥ 10 GPa, the new Si-poor phase becomes dominant and coexists with stishovite. Observed reflections in X-ray and electron diffraction patterns are inconsistent with magnetite or either structure reported for h-Fe_3O_4 (e.g. $CaMn_2O_4$-type, [5], $CaTi_2O_4$-type [6,7]). The new phase is magnetic under ambient conditions and its Mössbauer spectrum is distinct from magnetite. Interestingly, the diffraction peaks are essentially the same as those reported by [8] for an unknown phase found in the system Fe_3O_4-Fe_2SiO_4-Mg_2SiO_4, which they referred to as a "mystery phase". The same structure also occurs in Cr-bearing samples at ≥10 GPa along with either a spinel or an eskolaite - hematite solid solution. In this case, significant amounts of Cr can apparently be incorporated in this new phase.

Structural determination of the "mystery phase" is in progress, but made difficult by its apparent rather low symmetry. Our study points to the stability of another type of high-P post-spinel phase in addition to the reported $CaTi_2O_4$- or $CaMn_2O_4$-type structures found at yet higher pressures.

[1] Schollenbruch, K. et al. (2009a) *High Press. Res.*, **29**, 520-524. [2] Chen, M. et al. (2003) *P. Natl. Acad. Sci. USA*, **100(25)** 14651-14654. [3] Schollenbruch, K. et al. (2009b) *Phys Chem Minerals*, DOI 10.1007/s00269-009-0317-z. [4] Schollenbruch, K. et al. (2009c) *AGU abstract*, MR31B-1649, Fall meeting. [5] Fei, Y. et al. (1999) *Am. Mineral.*, **84**, 203-206. [6] Dubrovinsky, L.S. et al. (2003) *J. Phys. Condens. Matter.*, **15**, 7697-7706. [7] Haavik, C. et al. (2000) *Am. Mineral.*, **85**, 514-523. [8] Koch, M. et al. (2004) *Phys. Earth Planet. Int.*, **143**, 171-183.

Ab initio calculation of seismic velocities of phase AnhB ($Mg_{14}Si_5O_{24}$) and implication for the 300 km discontinuity in the Earth's mantle

Belmonte, D.[1*], Civalleri, B.[2], Ganguly, J.[3], Ottonello, G.[1] & Vetuschi Zuccolini, M.[1]
[1]DIPTERIS, Università di Genova, Genoa, Italy
([*]donato.belmonte@unige.it)
[2]Dipto. di Chimica IFM and NIS Centre of Excellence, Università di Torino, Turin, Italy
[3]Dept. of Geosciences, University of Arizona, Tucson, USA

We have carried out *ab-initio* calculations of the longitudinal and transverse seismic velocities, along with the effect of pressure, of the phase Anhydrous B ($Mg_{14}Si_5O_{24}$) (AnhB), using a developed version of the CRYSTAL06 code [1] and the hybrid B3LYP density functional method [2].

The unit cell previously invetigated by us at zero pressure [3] was brought at several compressional states corresponding to different static pressures, carrying out a full optimization of internal coordinates. The calculated second-order elastic constants (*stiffnesses*) were corrected for P through the general equation of Barron & Klein [4,5] expressed in terms of eulerian strain. Fig. 1 shows the single crystal seismic anisotropy obtained at P = 3 GPa using the program CAREWARE [6].

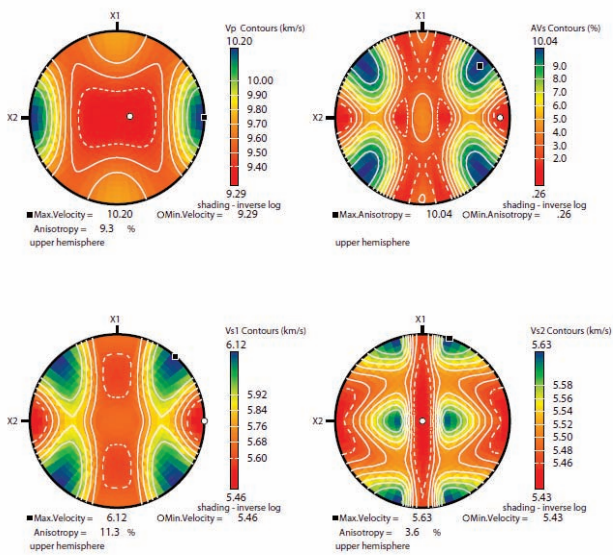

Fig. 1: Single-crystal seismic anisotropy of phase AnhB at P = 3 GPa. Projections are upper hemisphere. X1, X2, X3 are the reference axes for the elastic constants, X1≡[100], X2≡[010], X3≡[001]. Contours in Km/s for Vp, Vs1, Vs2, and in % anisotropy for dVs (top right of the figure).

Single crystal values were then adopted to determine the aggregate seismic velocities using a Voigt-Reuss-Hill averaging procedure. The shear wave impedance change associated with the reaction 5 Forsterite + 4 Periclase = AnhB, which takes place at P-T condition corresponding to the 300 km discontinuity in the Earth's mantle [7], seems to be compatible with that observed for this discontinuity [8].

[1] Dovesi, R. et al. (2006) *CRYSTAL06 User's Manual*, University of Torino, Torino. [2] Becke, A.D. (1993) *J. Chem. Phys.*, **98**, 5648-5652. [3] Ottonello, G. et al. (2010) *Am. Mineral.*, **95(4)**, 563-573. [4] Barron, T.H.K. & Klein, M.L. (1965) *Proc. Phys. Soc.*, **85**, 523-532. [5] Wallace, D.C. (1972) *Thermodynamics of Crystals*. Wiley, New York. [6] Mainprice, D. (1990) *Comput. Geosci.*, **16**, 385-393. [7] Ganguly, J. & Frost, D. (2006) *J. Geophys. Res.*, **111**, B06203. [8] Bagley, B. & Revenaugh, J. (2008) *J. Geophys. Res.*, **113**, B12301.

Elasticity of antigorite and seismic anisotropy of subduction zone

Bezacier, L.[1], Reynard, B.[1], Bass, J.D.[2*], Sanchez-Valle, C.[3] & Van de Moortèle, B.[1]
[1]ENS Lyon, CNRS, Lyon, France
[2]Dept. of Geology, University of Illinois, Urbana, USA
([*]jaybass@illinois.edu)
[3]Institute for Mineralogy and Petrology, ETH, Zürich, Switzerland

Serpentinization of the mantle wedge is an important process that influences the seismic and mechanical properties in subduction zones. Seismic detection of serpentines relies on the knowledge of elastic properties of serpentinites, which thus far has not been possible in the absence of single-crystal elastic properties of antigorite. The elastic constants of antigorite, the dominant serpentine at high pressure in subduction zones, were measured using Brillouin spectroscopy under ambient conditions. In addition, antigorite lattice preferred orientations (LPO) were determined using an electron back-scattering diffraction (EBSD) technique. Isotropic aggregate velocities are significantly lower than those of peridotites to allow seismic detection of serpentinites from tomography. The isotropic V_P/V_S is 1.76 in the Voigt-Reuss-Hill average, not very different from that of 1.73 of peridotite, but may vary between 1.70 and 1.86 between the Voigt and Reuss bonds. Antigorite and deformed serpentinites have a very high seismic anisotropy and remarkably low velocities along particular directions. V_P varies between 8.9 and 5.6 (46% anisotropy), and 8.3 and 5.8 (37%), and V_S between 5.1 and 2.5 (66%), and 4.7 and 2.9 $km.s^{-1}$ (50%) for the single-crystal and aggregate, respectively. The V_P/V_S ratio and shear-wave splitting also vary with orientation between 1.2 and 3.4, and 1.3 and 2.8 for the single-crystal and aggregate, respectively. Thus deformed serpentinites can present seismic velocities similar to peridotites for wave propagation parallel to the foliation or lower than crustal rocks for wave propagation perpendicular to the foliation. These properties can be used to detect serpentinite, quantify the amount of serpentinization, and to discuss relationships between seismic anisotropy and deformation in the mantle wedge. Regions of high V_P/V_S ratios and extremely low velocities in the mantle wedge of subduction zones (down to about 6 and 3 $km.s^{-1}$ for V_P and V_S in pure serpentinite, respectively) are difficult to explain without strong preferred orientation of serpentine. Local variations of anisotropy may result from kilometer-scale folding of serpentinites. Shear wave splittings up to 1-1.5s can be explained with moderately thick (10-20 km) serpentinite bodies.

Metallic alloys and zoned spinels in interstitial glasses from mantle lherzolites

Ryabchikov, I.D.[1*], Ntaflos, Th.[2], Kogarko, L.N.[3] & Kurat, G.[2]
[1]Institute for Geology of Ore Deposits, Russian Academy of Sciences, Moscow, Russia ([*]iryab@igem.ru)
[2]Dept. of Geological Sciences, University of Vienna, Austria
[3]V.I. Vernadsky Institute of Geochemistry, Russian Academy of Sciences, Moscow, Russia

We report evidence that suboceanic lithospheric mantle under island of Sal, Cape Verde archipelago was infiltrated by the highly reduced magma at some time prior to the eruption of host melanephelenites, which brought fragments of these mantle material to the surface. These melts are now represented by interstitial glasses in peridotites which contain sulphide grains, among them troilite, with the inclusions of Fe-Ni alloys and separate metallic phases [1]. Outer part of zoned spinel grains which have grown from such melts show abrupt drop in Fe^{3+} contents, which indicates drastic decrease in f_{O_2} values (Fig. 1). On the other hand, $Fe^{3+}/\Sigma Fe$ values for inner zones are close to 0.27 which is normal for spinels from mantle lherzolites.

In order to assess oxidation state of iron in spinels we performed analyses on electron microprope with separate determination of metals and oxygen. This permitted to calculate Fe^{2+} and Fe^{3+} contents using balance of charges principle.

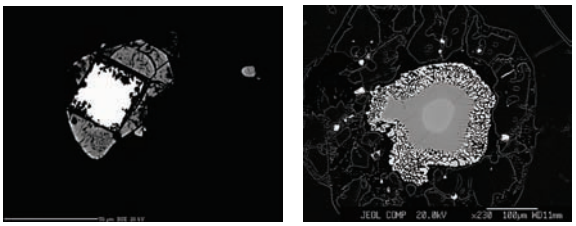

Fig. 1: Ni-Fe alloy surrounded by pentlandite in glass (left) and zoned spinel with Fe^{3+}-free rim surrounded by glass with small grains of Cr-rich spinel (right).

Analysed spinels are very close to ideal stoichiometry: number of cations per 4 oxygens does not differ from 3 by more than 0.002. Therefore, ferric and ferrous iron contents in spinels from spinel lherzolites may be calculated from usual microprobe analyses under the assumption of ideal stoichiometry.

Oxygen fugacity calculated for the equilibrium of intergranular melt and microphenocrysts of olivine and clinopyroxene with Fe-Ni alloys present in Sal mantle xenoliths using equilibrium constants of the following reactions

$Fe_2SiO_4 + CaMgSi_2O_6 = 2Fe + CaMgSiO_4 + O_2$ and

$Ni_2SiO_4 + CaMgSi_2O_6 = 2Ni + CaMgSiO_4 + O_2$, is approximately 4÷5 log units below QMF buffer. At such low f_{O_2} values spinels should contain almost no ferric iron, which is observed in the rims of zoned spinels surrounded by glass.

Very narrow widths of transitional zones between Fe^{3+}-bearing cores and Fe^{3+}-free rims of spinels imply that parts of Cape Verde mantle were invaded shortly before the eruption by highly reduced melt carrying sulphur deficient sulphides and Fe-Ni alloys. Extreme redox differentiation in the mantle may be caused by the disproportionation of Fe^{2+} into Fe^{3+} and Fe^0, which may occur in the lower part of subcontinental lithosphere, in transition zone, in lower mantle or in D" layer near the core-mantle boundary. Fe^0 will be dissolved in interstitial sulphide melts present in the mantle. Migration of such S-deficient sulphide melts would create relatively oxidised and reduced domains in the mantle.

[1] Ryabchikov, I.D. et al. (1995) *Mineral. Petrol.*, **55**, 217-237.

Thermal expansivity and dehydrogenation process in gedrite

Oberti, R.[1*], Welch, M.D.[2] & Zema, M.[3]
[1]CNR-IGG, UOS Pavia, Italy ([*]oberti@crystal.unipv.it)
[2]Dept. Mineralogy, The Natural History Museum, London, UK
[3]Dept. Earth Sciences, University of Pavia, Italy

The crystal chemistry of gedrite-group amphiboles has been recently discussed by [1,2], who also clarified relations among bond topology, bond valence and site preference and identified similarities and differences between monoclinic and orthorhombic amphiboles. The present work is aimed at providing information on the behaviour of gedrite at high-T conditions, in terms of thermal expansivity and cation order and dehydrogenation processes. The only data available on thermal expansivity of orthorhombic amphiboles concern anthophyllite [3], and no dehydrogenation occurs due to the lack of Fe^{2+}. Sample A(26) in [1] (code AMNH136484), with reported composition $^{A}Na_{0.46}$ $^{B}(Mg_{1.11}Fe^{2+}_{0.83}Mn_{0.02}Ca_{0.04})$ $^{C}(Mg_{3.44}$ $Fe^{2+}_{0.33}$ $Al_{1.18}Ti_{0.05})$ $^{T}(Si_{6.26}$ $Al_{1.74})$ $O_{22}OH_2$, was annealed up to 1273 K at intervals of 25 K using a micro furnace. Unit-cell parameters were measured *in situ* at each step, and structure refinement was done from single-crystal diffraction data collected at 533, 723 and 973 K during both annealing and reversal (thus on the partially dehydrogenated phase).

The almost linear increase in the unit-cell parameters (α_V = 3.15 $\times 10^{-5}$ K^{-1}, α_a = 1.10 $\times 10^{-5}$ K^{-1}, α_b = 0.94 $\times 10^{-5}$ K^{-1}, α_c = 1.19 $\times 10^{-5}$ K^{-1}) ends around 973 K, where an abrupt contraction in all the edges (much stronger in *a*) indicates the start of the dehydrogenation process, which proceeds by migration and oxidation of all Fe from the *M*4 to the *M*1 and *M*3 sites and significant changes in site geometry. When dehydrogenation stops (as monitored through unit-cell variations), reversal experiments down to R*T* allowed calculation of thermal expansion coefficients of the partially dehydrogenated phase: α_V = 3.51 $\times 10^{-5}$ K^{-1}, α_a = 1.15 $\times 10^{-5}$ K^{-1}, α_b = 1.09 $\times 10^{-5}$ K^{-1}, α_c = 1.26 $\times 10^{-5}$ K^{-1}. The crystal was then heated at 1273 K and finally cooled to room *T* to check for the completeness (as far as allowed by the Fe^{2+} content) of the dehydrogenation process.

A significant difference in thermal expansivity with respect to anthophyllite is observed only for the much greater stiffness of the *a* edge (α_a = 1.49 $\times 10^{-5}$ K^{-1} in [3]), and is related to the presence of a half-filled A site in gedrite. Na disorders into two different positions within the A cavity in the dehydrogenated sample, the second of which is closer to the A chain and particularly to the O3A oxygen atom. Hence, the dehydrogenated samples have a different bond valence arrangement. The behaviour of the different cation polyhedra and structure moduli during annealing and dehydrogenation, and differences with respect to anthophyllite and monoclinic amphiboles will be discussed.

[1] Schindler, M. et al. (2008) *Mineral. Mag.*, **72**, 703-730. [2] Hawthorne, F.C. et al. (2008) *Mineral. Mag.*, **72**, 731-745. [3] Cámara F. et al. (2010), this meeting.

Single-crystal elasticity of superhydrous phase B, $Mg_{10}Si_3O_{18}H_4$, by Brillouin scattering spectroscopy

Rosa, A.D.[*], Sanchez-Valle, C., Wang, J. & Saikia, A.
Inst. for Geochemistry and Petrology, ETH Zurich, Switzerland
([*]angelika.rosa@erdw.ethz.ch)

Superhydrous phase B, $Mg_{10}Si_3O_{18}H_4$ (here referred to ShyB), belongs to the group of dense hydrous magnesium silicate phases (DHMS) that have been identified as the major water reservoirs in deep subducted slabs. Experimental studies in peridotitic compositions have shown that ShyB can be stable up to 30 GPa and 850°C and thus play an important role in the recycling of water at depth. In order to formulate accurate mineralogical and compositional models of subducted slabs and to interpret seismic observations in these areas, precise elasticity data at relevant P-T conditions are needed for this phase. The bulk modulus of ShyB has been measured by X-ray diffraction in both multi-anvil apparatus and diamond anvil cells in single-crystals and polycrystalline samples [1-3] as well as by Brillouin scattering spectroscopy [4]. However, existing results show large discrepancies.

In this contribution we present results of Brillouin scattering measurements of sound velocities and single-crystal elastic properties of ShyB at ambient conditions. Single-crystals used in this study were synthesised in a multi-anvil press at ETH Zurich at 20 GPa and 1200°C. The samples were confirmed to be ShyB by single-crystal x-ray diffraction and chemical composition determined by EMPA is $Mg_{10.4}Si_{3.1}O_{18}H_{2.7}$. Brillouin scattering measurements were conducted in platelet scattering geometry in three different samples at ambient conditions. A total of 82 mode velocities were used to invert the 9 independent components of the C_{ij} elastic tensor.

The Voigt-Reuss-Hill averages of the adiabatic bulk and shear moduli are K_S = 150(3) GPa and μ = 98(2) GPa, respectively. These results are in good agreement with the previous Brillouin scattering study by [4]. The results show that the aggregate compressional and shear wave velocities, V_P = 9.17(9) and V_S = 5.43(4) km/s, are the lowest among coexisting phases in subducted peridotites, including Mg-Perovskite, hydrous Ringwoodite or Ferropericlase. The velocity distribution calculated from the best-fit elastic model of ShyB reveals nearly isotropic seismic behaviour of ShyB at room conditions. The compressional anisotropy (A_P) amounts only 6.6% whereas the shear anisotropy (A_S) has a slightly higher value of 1.6%. If the moderate anisotropy of ShyB is maintained at high P-T, the strong seismic anisotropy observed in subducted slabs below the transition zone may be difficult to explain without strong preferential orientation (LPO) in this phase. In view of the structure of ShyB we will further discuss the effects of various possible LPO types on the single-crystal anisotropy of ShyB in the slab.

[1] Kudoh, Y. et al. (1994) in Schmidt, S.C. et al. (eds.) *High-Pressure Science and Technology*. Am. Ins. Phys. Conf. Proc., **309**, 469-472. [2] Inoue, T. et al. (2006) in Jacobsen, S.D. & Van der Lee, S. (eds.) *Earth Deep Water Cycle*. AGU, Washington DC, 147-157. [3] Litasov, K.D. et al. (2007) *Phys. Earth Planet. Int.*, **164**, 142-160. [4] Pacalo, R.E.G. & Weidner, D.J. (1996) *Phys. Chem. Min.*, **23**, 520-525.

Geoelectric abnormity in earthquake and thermoelectricity of magnetite

Shen, Junfeng[1*], Shen, Xuhui[2] & Liu, Qian[1]
[1]State Key Laboratory of Geological Processes and Mineral Resources, China University of Geosciences, Beijing, China ([*]shenjf@cugb.edu.cn)
[2]Institute of Earthquake Science, China Earthquake Administration, Beijing, China

Geothermal and geoelectric fields are often changed in the course of the earthquake's gestating and occurring periods. According to the theory on thermo-electricity conversion, geoelectricity can be impacted by gradient thermal field which formed on the room around the earthquake focus. By understanding accurately on the discipline of geoelectric variety, some important information which related with earthquake occurrence in deep crust can be obtained.

Because the magnetite is existed far and wide in crust, and also often form a large aggregate. So that magnetite is maybe better medium for thermoelectric conversion.

BHTE-06 thermoelectric instrument was used for the thermoelectricity test on magnetite by under 10-80°C. temperature difference (also called active-temperature). The results showed that approximative 0.3mm magnetite grain can generate -2.175mv voltage in average, and max. value is -4.5mv. Which means natural magnetite belongs to N type semiconductor minerals. Thermoelectric coefficient (thermal voltage increment above temperature difference) was computed, and showed it is a constant nearly, and is approximatively -0.05mv/°C. Also, it is a remarkable linear between thermal voltage and temperature difference, and its correlation coefficient is 0.985. Other more, the thermoelectricity is independent of the genesis and crystal direction of magnetite.

Based on the results mentioned above, authors consider that thermoelectric mode in earthquake is a possible mechanism on geoelectric abnormity. So, a new idea on geoelectric abnormity in earthquake was proposed, that is thermoelectric mode.

The following viewpoints were emphasized in the thermoelectric mode. Namely, more magnetite mineral aggregates are existed in the crust, and once excitated by pulsed gradient thermal field caused by earthquake, it will be turned into dipole voltaic source in underground due to dipole effect, and the dipole voltaic source will produce an accessional dipole pulsed electric field. Moreover, this electric field leads to a pulsed electric field abnormity while it was added to telluric electricity field and natural electric field. Therefore, based on related physical geography theory, a calculation formula on intensity for additional thermoelectric field caused by thermoelectricity can be written as:

$$E = -0.159\frac{\sigma \times \Delta T \times \Phi \times \rho_c \times [(h^2 - 2x^2)Cos\alpha + 3hxSin\alpha]}{\rho_m (h^2 + x^2)^{5/2}}$$

The formula showed that thermoelectric fields E are impacted by several factors, such as thermoelectric coefficient of semi-conductive mineral σ, resistivity ρ_m, embedded depth h, vertical section area to thermo current Φ and angle of connective line to two pole with horizontal plane α, also temperature difference ΔT, crust resistivity ρ_c, and the distance from observation point to semi-conductive mineral aggregate projective point on earth face x. In terms of simulated calculation followed the formula, the additional thermoelectric field E may reach to n mV/km to $n\times10^2$ mV/km, and the max. value is more than $n\times10^3$ mV/km. Such electric field intensity is strong enough to cause geoelectric abnormity on earth face, so that thermoelectricity is one of criterions for deep crust information in earthquake.

High-pressure behavior of $FeTiO_3$: decomposition into $(Fe_{1-x},Ti_{0.5x})O$ and $FeTi_3O_7$

Yagi, T.[1*], Nishio-Hamane, D.[1], Ohshiro, M.[1], Niwa, K.[2], Okada, T.[1] & Seto, Y.[3]
[1]Inst. for Solid State Physics, University of Tokyo, Kashiwa, Japan ([*]yagi@issp.u-tokyo.ac.jp)
[2]Dept. of Materials Science and Engineering, Nagoya University, Nagoya, Japan
[3] Dept. of Earth and Planetary Science, Kobe University, Kobe, Japan

Divalent transition metals do not favor perovskite structure and most of the ABO_3-type compounds with divalent transition metal decompose into simple oxides under pressure. Among them, $FeTiO_3$ is a unique compound which crystallizes into a single phase of perovskite above about 16 GPa. In order to clarify the stability of this perovskite phase, we have studied the phase relation of $FeTiO_3$ up to a pressure of about 67 GPa by synchrotron X-ray diffraction and analytical transmission electron microscopy.

We have found that $FeTiO_3$ perovskite decomposes into $(Fe_{1-x},Ti_{0.5x})O$ wüstite and $FeTi_3O_7$ phase, at above 40 GPa and 2000 K. The $FeTi_3O_7$ phase has the orthorhombic unite cell, although the detail of the crystal structure is still unclear. Figure 1 shows the representative X-ray diffraction patterns and TRP is the $FeTi_3O_7$ phase while WP is the wüstite phase. Although the recent study on $FeTiO_3$ [1] reported almost the identical X-ray diffraction pattern, their explanation on decomposed products was clearly in error, because they did not do any direct chemical analysis.

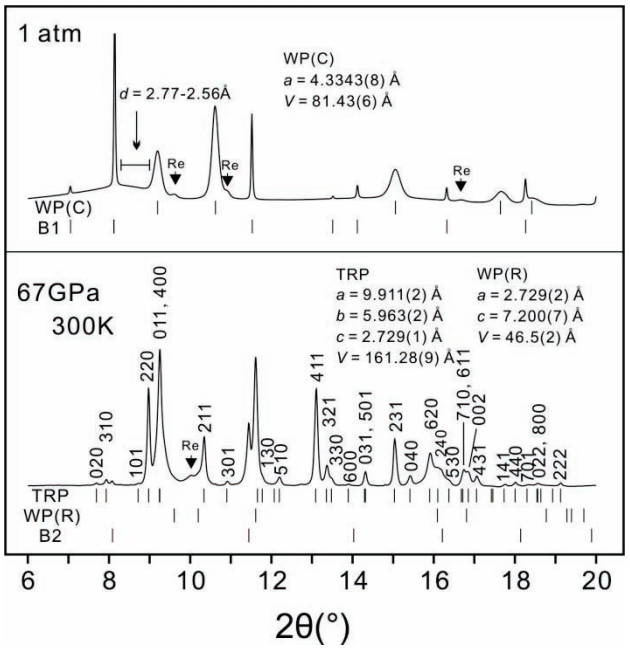

Fig. 1: Representative X-ray diffraction pattern of $FeTiO_3$ after heating at 67GPa (bottom) and after recovering to ambient condition (top).

Our study also demonstrates that the phase assemblage of $(Fe_{1-x}, Ti_{0.5x})O$ and $FeTi_3O_7$ is the densest in the $FeTiO_3$ system, implicating a new fate for ABO_3-type compounds under high pressure condition such as the deep interior of the terrestrial planets.

[1] Wu, X. et al. (2009) *Phys. Rev. Lett.*, **103**, 065503.

Effect of hydrogen and aluminum on the elastic properties of orthopyroxene: implications for mantle discontinuities

Wang, J.Y.[1*], Sanchez-Valle, C.[1] & Stalder, R.[2]
[1]Institute for Geochemistry and Petrology, ETH Zurich, Switzerland ([*]jingyun.wang@erdw.ethz.ch)
[2]Inst. für Mineralogie und Petrographie, Universität Innsbruck, Austria

Olivine, orthopyroxenes, garnets, and clinopyroxenes are major minerals in the upper mantle. Studies on the elastic properties of the minerals have provided essential understanding of geochemical and seismic observations for the upper mantle. While the elastic properties of Mg- and Fe-end-members have been relatively well-studied, there is still a lack of knowledge for the effect of minor element on the elastic properties of opx.

Aluminum and hydrogen are two important minor elements observed in natural opx. Here we investigate the effect of these elements on the single-crystal elastic properties of orthopyroxees using Brillouin scattering spectroscopy. Hydrous aluminum-free opx (HyOpx) and hydrous aluminum-bearing opx (AlOpx) samples were synthesized at 2.5 GPa and 1150°C in piston-cylinder apparatus. HyOpx contains 280 ppm H_2O, while AlOpx has Al_2O_3 content of 6.3 wt% similar to natural opx with 1500 ppm H_2O and 0.26 wt% FeO. The aggregate bulk (K_S) and shear (μ) elastic moduli of HyOpx, K_S = 108.5(9) GPa and μ = 77.0(4) GPa, are indistinguishable from those of anhydrous opx. This comparison suggests that incorporation of H_2O up to 280 ppm does not significantly affect the elastic properties of $MgSiO_3$-orthoenstatite. The aggregate elastic moduli of AlOpx, K_S = 126.2(1.2) GPa and μ = 81.3(8) GPa, are however higher than those of pure $MgSiO_3$-orthoenstatite by 14.7 and 6%, respectively. These results indicate that substitution of Al^{3+} for smaller Si^{4+} in tetrahedral sites in natural opx increases the bulk modulus relative to Mg-end-members. This conclusion is supported by the strong increase in the C_{33} elastic constant upon Al substitution showing the stiffening of the tetrahedral chains along c-axis. Consequently, the aggregate velocities of AlOpx, V_P = 8.50(9) km/s and V_S = 5.01(6) km/s, are 7% and 4% higher than those of the magnesian end-member. Aluminum has thus the strongest effect on the seismic velocities of opx among all minor elements.

Results of elasticity of AlOpx at high pressure conditions will be presented to explore the influence of Al^{3+} on the phase transition from orthopyroxene to clinopyroxene and discuss its relation to the seismic X discontinuity (~300 km depth) observed in the upper mantle. We will also discuss the effect of Al^{3+} on the aggregate velocities and elastic anisotropy of opx at high pressures to provide better constrains on the composition and mineralogy of the upper mantle.

High-pressure behaviour of $SrAl_2Si_2O_8$ feldspar

Pandolfo, F.[1*], Boffa Ballaran, T.[2], Nestola, F.[3], Koch-Müller, M.[4], Mrosko, M.[4] & Bruno, E.[5]
[1]Dept. Scienze della Terra, University of Pavia, Italy ([*]fra.pandolfo@gmail.com)
[2]Bayerisches Geoinstitut, Universität Bayreuth, Germany
[3]Dept. of Geoscience, University of Padova, Italy
[4]Dept. Chem. Earth, GeoForschungsZentrum, Potsdam, Germany
[5]Dept. Scienze Mineralogiche e Petrologiche, University of Torino, Turin, Italy

A single crystal of Sr-feldspar with end-member composition $SrAl_2Si_2O_8$ (space group *I*2/*c* at room pressure) and 1100 ppm of structural OH was investigated by X-ray diffraction at high-pressure *in situ* using a diamond anvil cell up to 7.8 GPa and compared with a sample of the same composition totally anhydrous investigated up to 5 GPa. Between 6.57 and 6.61 GPa the hydrous sample shows a thermodynamically first order phase transition from *I*2/c to $P2_1/c$ (a previous phase transformation reported from *I*2/c to a triclinic phase is not confirmed here for the same end-member composition [1]). The compressibility of the *I*2/*c* phase is clearly lower than that of $P2_1/c$ one. Moreover, the *I*2/*c* phase showed an anomalous unit-cell volume behaviour between 3.67 and 6.57 GPa, which cannot be ascribed to a further symmetry change (based on the systematic absence analysis) and neither an isosymmetric phase transformation can be evoked (e.g. no discontinuous change in the volume typical of a isosymmetric transition is found). Due to such anomaly (volume softening) it was impossible to fit the pressure – volume data using a single equation of state. Comparing these data up to 5 GPa with those of anhydrous sample we did not find any observable difference indicating that an amount of only 1100 ppm of water does not influence the compressional behaviour of $SrAl_2Si_2O_8$ feldspar. With respect to a previous work on a composition $(Ca_{0.20}Sr_{0.80})Al_2Si_2O_8$ (showing a sequence of transitions from $I\bar{1}$ to *I*2/*c* to $P2_1/c$ with pressure [2]) our data show that the same *I*2/*c* to $P2_1/c$ transformation occurs at a pressure 0.6 GPa higher due to entrance of Ca.

Our new results supply further information on the stability field diagram along the $CaAl_2Si_2O_8$ - $SrAl_2Si_2O_8$ join as function of pressure and provide new insights relative to the high-pressure behaviour of anorthite, which remains still to be investigated for pressures above 7-8 GPa and that could show the same transformation sequence showed in the Sr-richer side of the diagram.

[1] McGuinn, M.D. & Redfern, S.A.T. (1994) *Am. Mineral.*, **70**, 24-30. [2] Nestola, F. et al. (2004) *Am. Mineral.*, **89**, 1474-1479.

Formation of a perovskite solid solution between $MgSiO_3$ and $MnSiO_3$ at the lower mantle condition

Nagai, T.[1*], Ishido, T.[1] & Fujino, K.[2]
[1]Dept. of Natural History Sciences, Hokkaido University, Sapporo, Japan ([*]nagai@mail.sci.hokudai.ac.jp)
[2]Geodynamics Research Center, Ehime University, Matsuyama, Ehime, Japan

Silicate perovskites are important constituent minerals in the lower mantle. We recently found that $MnSiO_3$ perovskite with orthorhombic symmetry is stable at the lower mantle condition [1]. Now it is greatly interesting how much $MnSiO_3$ component can incorporate into $MgSiO_3$ perovskite.

We prepared gel compounds with chemical compositions of $MgSiO_3$:$MnSiO_3$ = 9:1, 3:1, 1:1 and 1:3 (mol ratios) as the starting materials. High pressure and high temperature experiments were performed using a laser-heated diamond anvil cell combined with synchrotron X-ray diffraction (PF-AR and Spring8, Japan) at the pressures between 30 and 60 GPa, and at the temperatures between 1300 and 2000 K.

From the diffraction patterns obtained at high pressure, we confirmed the existence of $(Mg,Mn)SiO_3$ perovskites with all the compositions prepared. All the perovskites have orthorhombic symmetry and variations of lattice parameters at about 50 GPa shows almost linear correlation with the chemical composition. Only $(Mg_{0.9},Mn_{0.1})SiO_3$ perovskite is quenchable at an atmospheric pressure, but the others become amorphous during decompression. We conclude that the system of $MgSiO_3$-$MnSiO_3$ forms a complete perovskite solid solution at the lower mantle condition.

[1] Fujino, K. et al. (2008) *Am. Mineral.*, **93**, 653-657.

Sodium-bearing majoritic garnet: natural and experimental aspects

Bobrov, A.[1*], Dymshits, A.[1], Litvin, Yu.[2], Litasov, K.[3], Shatskiy, A.[3] & Ohtani, E.[3]
[1]Geological Faculty, Moscow State University, Moscow, Russia ([*]archi673@yandex.ru)
[2]Institute of Experimental Mineralogy, Chernogolovka, Russia
[3]Tohoku University, Sendai, Japan

Majoritic garnets were found as inclusions in diamonds from several localities worldwide, including South Africa, Guinea, Canada, Brazil, Russia, and China (see [1] for review). They belong to both the peridotitic and eclogitic suites. However majoritic garnets with Si atoms pfu >3.07 are almost exclusively eclogitic. These majorites show high Na with Na_2O wt% ranging up to ~1.4. Recently Harte and Cayzer [2] have documented evidence of exsolution textures involving clinopyroxene and majoritic garnet which indicate original majoritic garnets with up to 2.16 wt% Na_2O. Most of the Na present in majoritic garnet is accommodated via the pressure dependent exchange reaction $Na^+ + Si^{4+} = Mg^{2+} + Al^{3+}$ (Na for Mg in the X site and Si for Al in the Y site). Such mechanism of sodium incorporation in majoritic garnet supports the idea of a presence of the $Na_2MgSi_5O_{12}$ end-member in garnet solid solution [3].

As is evident from the experimental study of the model systems pyrope ($Mg_3Al_2Si_3O_{12}$)-Na-majorite ($Na_2MgSi_5O_{12}$), pyrope-jadeite ($NaAlSi_2O_6$), and pyrope-Na_2CO_3 at P = 7.0 and 8.5 GPa and T = 1100-1900°C [4], magmatic crystallization of Na-bearing majoritic garnet and its composition are controlled by several factors, among which are melt composition, pressure, and temperature. Experiments confirmed the compatibility of Na-bearing majoritic garnet with sodium-rich silicate and carbonate-silicate melts. In all systems, an increase of pressure leads to the growth of sodium content in garnet. In addition, in all studied systems, a decrease of temperature relatively to liquidus values resulted in the successive increase of sodium content, so that the highest sodium concentrations were observed at the solidus of the systems.

Multianvil experimental study of the pyrope-$Na_2MgSi_5O_{12}$ system at 11–20 GPa and 1900–2300°C demonstrated further increase of both Na and Si in liquidus garnet. Maximal concentration of $Na_2MgSi_5O_{12}$ end-member (3.785 pfu Si and 0.739 pfu Na or 5.7 wt% Na_2O) was obtained at 20 GPa. Our experiments provide evidence for complete miscibility in this system at least up to 40 mol% of Na-component. We synthesized pure $Na_2MgSi_5O_{12}$ garnet and established P-T conditions of the pyroxene/garnet transition for the first time. The results obtained allow us to assume that Na-majorite is a possible concentrator of sodium under the conditions of deep upper mantle and transition zone, where the stability of pyroxene phase is limited.

Acknowledgements: Financial support: RFBR grant no. 09-05-00027.

[1] Stachel, T. (2001) *Eur. J. Mineral.*, **13**, 883-892. [2] Harte, B. & Cayzer, N. (2007) *Phys. Chem. Minerals*, **34**, 647-656. [3] Bobrov, A.V et al. (2008) *Contrib. Mineral. Petrol.*, **156**, 243-257. [4] Bobrov, A.V. et al. (2009) *Geochem. Int.*, **47**, 951-965.

A new hydrated high pressure phase in the MASH system

Gemmi, M.[1], Merlini, M.[1*], Fischer, J.[1], Poli, S.[1], Mugnaioli, E.[2] & Kolb, U.[2]
[1]Dipto. di Scienze della Terra, Università degli Studi di Milano, Italy ([*]marco.merlini@unimi.it)
[2]Institute of Physical Chemistry, Johannes Gutenberg-University, Mainz, Germany

The MgO-Al_2O_3-SiO_2-H_2O (MASH) system is well known to be a simplified model system for the study of water transport and recycling into Earth's mantle via subduction processes. Therefore any new water bearing phase arising in P, T conditions compatible with the subducted slab is highly interesting for the comprehension of the complex geological processes determining the dynamical evolution of subducting zones. A new phase with these characteristic have been discovered in experimental runs having clinochlore bulk composition, in the P,T range of 5.2-5.5 GPa and 680-720 °C. It is monoclinic with space group C2/c and unit cell parameters a=9.882(1), b=11.623(1), c=5.081(1), β=111.1(1)°. The new phase has been identified with conventional electron diffraction. Its structure has been solved using the automated electron diffraction technique (ADT) [1-3]. This new technique allows a single crystal electron diffraction experiment on crystals of less than 1μm. The obtained intensities are quasi kinematical and therefore suitable for a conventional direct methods structure solution attempt. To our knowledge this is the first high pressure phase solved in this way. It has chemical composition of $Mg_{2.1}Al_{1.8}Si_{1.1}O_6(OH)_2$, and has a pyroxene like structure with 3 cations instead of 2 in the octahedral layer, which force the tetrahedral chains to be more separate. The two anion sites of the extra octahedral cation, that are not shared with any tetrahedra are occupied by an hydroxyl. Thanks to the structure solution obtained by ADT it has been possible to synthesise an almost pure sample suitable for powder x-ray diffraction analysis. Rietveld refinement on this data and image simulation of high resolution electron microscopy images further confirm this structural model.

[1] Kolb, U. et al. (2007) *Ultramicroscopy*, **107**, 507-513. [2] Kolb, U. et al. (2008) *Ultramicroscopy*, **108**, 763-772. [3] Mugnaioli, E. et al. (2009) *Ultramicroscopy*, **109**, 758-765.

First crystal-structure determination of an olivine inclusion still trapped in a diamond: composition and implications for diamond source pressure

Nestola, F.[1*], Nimis, P.[1], Ziberna, P.[1], Longo, M.[1], Marzoli, A.[1], Harris, J.W.[2], Manghnani, M.H.[3] & Fedortchouk, Y.[4]
[1]Dipt.o di Geoscienze, Università di Padova, Italy ([*]fabrizio.nestola@unipd.it)
[2]Dept. of Geographical and Earth Sciences, University of Glasgow, UK
[3]Hawaii Institute of Geophysics and Planetology, University of Hawaii, Honolulu, USA
[4]Dept. of Earth Sciences, Dalhousie University, Halifax NS, Canada

A novel experimental approach using single-crystal X-ray diffraction has been applied to the study of an olivine inclusion still trapped in a Siberian diamond. The experimental procedure, typically used for in situ high-pressure studies (i.e. diamond-anvil cell), allowed us (i) to determine with high precision the internal pressure at the inclusion, and (ii) to refine for the first time the crystal structure of the olivine without extracting it from the host diamond. The crystallographic data allowed us to refine the mean number of electrons on the M2 and M1 crystallographic sites of the olivine and to obtain a composition Fo93Fa7. Knowing the P-V equation of state for such composition, we determined an internal pressure of 0.40(2) GPa. This pressure value is used to estimate the pressure of formation of the host diamond, taking into account elastic relaxation and using the most up-to-date compressibility and thermal expansion parameters for olivine and diamond.

High-pressure phase relations in $FeCr_2O_4$ and in the system $NaAl_3Si_3O_{11}$-$CaAl_4Si_2O_{11}$ with implications to post-spinel phases and Na-rich CAS phase in shocked meteorites

Akaogi, M.*, Tsukamoto, S., Kojitani, H. & Haraguchi, M.
Dept. of Chemistry, Gakushuin University, Tokyo, Japan
(*masaki.akaogi@gakushuin.ac.jp)

Studies on natural high-pressure minerals in shocked meteorites provide valuable information on mineralogy and properties of the Earth's deep mantle, as well as the shock processes. Recently, two high-pressure polymorphs of $FeCr_2O_4$-rich chromite were found in a shocked meteorite by [1,2]. The two phases have calcium-ferrite ($CaFe_2O_4$) type and calcium-titanate ($CaTi_2O_4$) type structures. These were the first report on natural occurrences of post-spinel polymorphs of $A^{2+}B^{3+}{}_2O_4$. Although high-pressure stability relations in $FeCr_2O_4$ can be used to constrain the P,T conditions of the shock events, they have not yet been fully examined. In several shocked Martian meteorites, [3] found a high-pressure calcium aluminosilicate (CAS) phase with 75mol% $NaAl_3Si_3O_{11}$-25mol%$CaAl_4Si_2O_{11}$ composition. Although $CaAl_4Si_2O_{11}$-rich CAS phase with the hexagonal Ba-ferrite structure has been synthesized in HP phase assemblages of continental crust, sediments and basalt, no stability relations in the system $NaAl_3Si_3O_{11}$-$CaAl_4Si_2O_{11}$ have been examined.

In this study, we have determined the phase relations in $FeCr_2O_4$ and in the $NaAl_3Si_3O_{11}$-$CaAl_4Si_2O_{11}$ system, in order to apply the results to evaluate P,T conditions of the formation processes of the natural high-pressure minerals in the shocked meteorites. The high-pressure experiments were carried out up to 27 GPa and 1900°C, using a multianvil apparatus. The quenched samples were analyzed by means of microfocus and powder X-ray diffractometers and a scanning electron microscope with an energy-dispersive detector. Above about 14 GPa, $FeCr_2O_4$ chromite with spinel structure first dissociates into a new $Fe_2Cr_2O_5$ phase and Cr_2O_3 with corundum structure. The new $Fe_2Cr_2O_5$ phase has the same structure as a high-pressure form of $Mg_2Al_2O_5$ found by our recent high-pressure experiments in $MgAl_2O_4$ [4]. At 16-19 GPa, the two phases further combine into $FeCr_2O_4$ polymorph with calcium-ferrite structure below about 1300°C, while the other polymorph with calcium-titanate structure becomes stable above about 1300°C. Both of the calcium-ferrite and calcium-titanate phases are stable up to at least 27 GPa. These results suggest that the natural $FeCr_2O_4$-rich calcium-ferrite and calcium-titanate were formed at pressure above 19 GPa at temperature below and above 1300°C, respectively, during the shock event.

The CAS phase with $CaAl_4Si_2O_{11}$ composition is stable above about 13 GPa at 1600°C [5]. In the system $NaAl_3Si_3O_{11}$-$CaAl_4Si_2O_{11}$, the CAS phase dissolving $NaAl_3Si_3O_{11}$ component coexists with jadeite, corundum and stishovite below 22 GPa, above which the CAS phase coexists with Na-rich calcium ferrite, corundum and stishovite. At 1600°C, the maximum solubility of $NaAl_3Si_3O_{11}$ component in the CAS solid solution is about 50 mol% at 22 GPa, and it increases to about 70 mol % at 1900°C. The dissociation of $NaAlSi_2O_6$ jadeite to $NaAlSiO_4$ calcium ferrite plus stishovite occurs at about 22 GPa at 800-2000°C. When we adopt the Na:Ca ratio of 75:25 of the natural Na-rich CAS-phase in the shocked Martian meteorite [3], our results suggest that the natural CAS-phase crystallized at pressure around 22 GPa and temperature of about 2000-2200°C. The inferred P,T conditions are consistent with those estimated using other high-pressure minerals in the shocked meteorite.

[1] Chen, M. et al. (2003a) *GCA*, **67**, 3937-3942. [2] Chen, M. et al. (2003b) *Proc. Nat. Acad. Sci*., **100**, 14651-14654. [3] Beck, P. et al. (2004) *EPSL*, **219**, 1-12. [4] Enomoto, A. et al., (2009) *J. Solid State Chem*., **182**, 389-395. [5] Akaogi, M. et al. (2009) *Phys. Earth Planet. Int*., **173**, 1-6.

Sound velocities of Earth's deep materials

Murakami, M.
Tohoku Univesity, Aramaki Aoba-ku, Sendai, Japan
(motohiko@m.tains.tohoku.ac.jp)

Average composition and structure of the Earth's deep interior can be approached by comparing observed seismic velocities to appropriate laboratory data collected for candidate materials under relevant conditions. Precise knowledge of the elastic properties of Earth's deep materials under high-pressure condition is crucial for constructing the accurate mineralogical model of the Earth's deep interior. However, only few experimental acoustic measurements exist under relevant high-pressure conditions. Recent technical advances in high-pressure Brillouin spectroscopic measurements combined with diamond anvil cell apparatus extended significantly the upper pressure limit for acoustic measurements [1,2] and also enable us to explore the sound velocities under high-pressure and high-temperature conditions using infrared laser heating technique [3]. Here we present the recent progress of elastic wave velocity measurements on Earth's deep materials by Brillouin spectroscopy in a diamond anvil cell (DAC) in conjunction with synchrotron X-ray diffraction technique under ultrahigh-pressures. Based on the results we have recently obtained on mantle minerals [4] and glass materials [5] (Fig. 1), the mineralogy of deep mantle and the structure of the silicate melt in the deep magma ocean will be discussed.

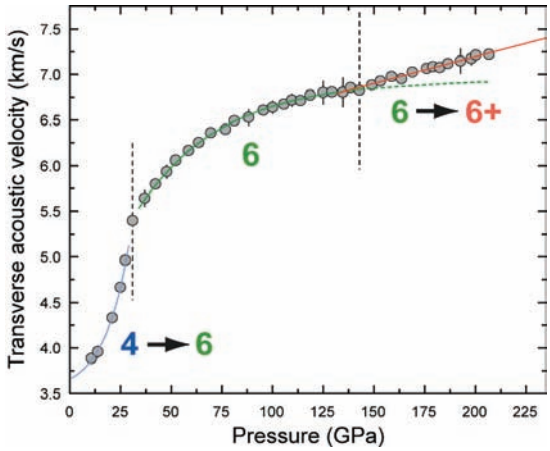

Fig. 1: Transverse acoustic wave velocities of SiO_2 glass as a function of pressure up to 207 GPa [5]. The velocity trajectories for three distinct high-pressure regimes are shown as blue, green and orange lines, respectively. Numbers indicate the potential Si-O coordination number within each pressure regime. Approximate pressure boundaries for each Si-O coordinated structure are shown as the vertical dotted lines.

[1] Murakami, M. et al. (2007) *Earth Planet. Sci. Lett*., **256**, 47-54. [2] Murakami, M. et al. (2007) *Earth Planet. Sci. Lett*., **259**, 18-23. [3] Murakami, M. et al. (2009) *Phys. Earth Planet. Int.*, **174**, 282-291. [4] Murakami, M. et al. (2009) *Earth Planet. Sci. Lett*., **277**, 123-129. [5] Murakami, M. & Bass, J. (2010) *Phys. Rev. Lett*., **282**, 124-128.

Spin transition of ferric iron in Mg-perovskite up to 200 GPa and its implication to the lower mantle

Fujino, K.[1,5*], Hamane, D.[2], Seto, Y.[3], Sata, N.[4], Nagai, T.[5], Shinmei, T.[1], Irifune, T.[1], Ishii, H.[6], Hiraoka, N.[6], Cai, Y.Q.[6] & Tsuei, K.D.[6]

[1]Geodynamics Research Center, Ehime University, Matsuyama, Japan (*fujino@sci.ehime-u.ac.jp)

[2]Institute for Solid State Physics, University of Tokyo, Kashiwa, Japan

[3]Dept. of Earth and Planetary Sciences, Kobe University, Kobe, Japan

[4]Institute for Research on Earth Evolution, Jamstec, Yokosuka, Japan

[5]Dept. of Natural History Sciences, Hokkaido University, Sapporo, Japan

[6]National Synchrotron Radiation Research Center, Hsinchu, Taiwan

Pressure-induced high spin - low spin transitions of iron in the lower mantle minerals are very important to understand the mineral behaviours such as structural change and iron partitioning, and to understand the dynamics of the lower mantle. However, the spin transition of iron in Mg-perovskite, the most abundant lower mantle mineral, has been the issue of a great deal of controversy. There have been large discrepancies among previous experimental studies and also between the results of theoretical and experimental studies. We think that these discrepancies largely originate from the poor quality and/or poor characterization of the experimental samples. This time, we could obtain the data on the spin state of Fe^{3+} in Mg-perovskite up to 200 GPa (the highest pressure ever reported) by the X-ray emission spectroscopy (XES) using well qualified samples. These results are fairly consistent with the theoretical reports and explain the diversity among the experimental reports to a certain extent.

We measured the XES data of Fe^{3+} in Mg-perovskite of the composition $Mg_{0.85}Fe^{3+}_{0.15}Al_{0.15}Si_{0.85}O_3$ loaded in a diamond anvil cell at BL-12 of SPring-8. The obtained XES patterns show high spin at pressures up to around 120 GPa and then the k_β' peaks gradually decrease at higher pressures. However, even at 200 GPa, the XES pattern is still intermediate between the high spin and low spin patterns. These XES patterns at various pressures are well fitted by the linear combination of the high spin and low spin patterns of the reference material Fe_2O_3, and the fitted ratio of the low spin pattern increases gradually, not stepwise, with pressure. These results indicate that Fe^{3+} at the A-site of Mg-perovskite is high spin up to 200 GPa, while Fe^{3+} at the B-site becomes low spin at relatively low pressure. In addition, the gradual increase of the fitted ratio of the low spin pattern suggests that Fe^{3+} at the A-site replaces Al at the B-site by the cation exchange reaction caused by the annealing (around 1000 K - 1400 K) of the samples during the XES measurements. This means that the spin state of iron in the experimental samples is not only a function of pressure and temperature during measurement but also affected by the heat treatment of the samples during the experiments. From the present results, most Fe^{3+} in $FeAlO_3$-bearing Mg-perovskite in the deep lower mantle is expected to be in the low spin state at the B-site.

Garnet of the pyrope-majorite series

Bryanchaninova, N.I. & Makeev, A.B.*
Dept. of Petrography, Institute of Geology of Ore Deposits, Petrography, Mineralogy and Geochemistry RAS, Moscow, Russia (*abmakeev@mail.ru)

Majorite discovered in Coorara meteorite is very rare in the terrestrial rocks. The pyrope with high content majorite component $Mg_3Fe_2[SiO_4]_3$ (26–42%), similar that described only from meteorites and as small inclusions in superdeep diamonds and was found in the kersantite-spessartite dikes in the Middle Timan. Majorite pyrope to variable degree is associated with diamond. On the one hand, it occurs as inclusions in diamond crystals, on the other hand, in rocks, where such garnet is found, microcrystalline diamond is established. According to modern systematics of garnets, ideal formula of majorite is expressed as $Mg_3Fe_2[SiO_4]_3$. Majorite end-member is not found in nature. Recalculated microprobe data of majorite grains found in Australian meteorite, give 66% of of majorite component and the remainder of pyrope. Pyropes with 26–42% of majorite component from the Middle Timan lamprophyre and pyrope inclusions with 24–26% of majorite in diamonds from the Juin Field, Brazil are the closest to majorite from the the Coorara meteorite. These garnets and majorite from the Coorara meteorite are Cr- and Ca-free.

Inclusions of pyrope-majorite in diamonds associated with ferripericlase, perovskite and manganese ilmenite indicate ultrahigh pressure of formation of the garnet. Mantle xenoliths with the pyrope-majorite garnet in volcanic rocks can be served as indicator of deep origin of such rocks. Formation conditions of mineral assemblage *Ca,Mg-perovskite+"majorite"+diamond* were estimated by through empiric barometer using formula coefficient of Si in garnet formula, which is resulted in very high pressure of 22 GPa and consequently, depth of crystallization of this mineral assemblage of 400–670 km. These calculated data are consistent with experiments for Al-free iron-magnesium garnets. According to [1], majorite is stable at 2000±200°C and 20 GPa. The notion «majorite» in scientific literature has double meaning. In some papers, majorite is considered as garnet, in which according to microprobe data SiO_2 is in excess, i.e., there are non-stoichiometry between cations and Si excess at tetrahedral site. No special X-ray structural study was carried out to support incorporation of Si at octahedral sites of trivalent cations in garnets. Non-stoichiometry and excess of silica in composition of real garnets of minute inclusions (which size rarely exceeds 1–20 microns), most likely could be caused by technical problems of electron microprobe measurements or inhomogeneous sample resulted from microingrowths of pyroxene in garnet. Currently, the latter is received fact. In natural pyrope from garnet-bearing xenoliths of diamond-bearing kimberlites, [2,3] described omphacite, diopside-jadeite solid solution, and showed, that with the clinopyroxene content in garnet of 20 and 30%, SiO_2 was 44–45.5 wt.% and crystallo-chemical coefficients of Si^{4+} calculated on the basis of 12 O, were 3.14–3.24. Oriented inclusions of pyroxenes in garnets, which in turn are enclosed in diamond crystals from Brazil and South Africa, are described by many researchers. Experimental study suggests that oriented pyroxene inclusions found in natural garnets are resulted from exsolution of hypothetical mantle Fe-Mg-silicate. However, it does not follow that homogeneous phase enriched in pyroxene component should be mineral with the cubic garnet structure. Findings of tetragonal almandine-pyrope phase (TAPP) included in diamonds from the San-Luis placers, Juin district, Brazil support this conclusion.

[1] Kato, T. (1986) *Earth Planet. Sci. Lett.*, **77**, 399-408. [2] Haggerty, S.E. & Sautter, V. (1990) *Science*, **248**, 993-996. [3] Sautter, V. et al. (1991) *Science*, **252**, 827-830.

Synchrotron spectroscopy of Fe-bearing $MgSiO_3$ perovskite and post-perovskite to over 1 Mbar

Catalli, K.[1*], Shim, S.-H.[1] & Sturhahn, W.[2]
[1]Massachusetts Institute of Technology, Cambridge, MA, USA (*krystle@mit.edu)
[2]Argonne National Laboratory, Argonne, IL, USA

Iron- and aluminium-bearing Mg-silicates are the dominant minerals in the lower mantle of the Earth. Iron may exist in multiple valence (2+ and 3+) and spin states (high, low, and intermediate), which may change with pressure and profoundly affect the properties of minerals in the Earth. We have investigated the electronic state of ferric iron in $MgSiO_3$ perovskite and post-perovskite using synchrotron Mössbauer spectroscopy (SMS) and X-ray emission spectroscopy (XES).

Fe^{3+} and Al^{3+} are thought to enter perovskite and post-perovskite by charge-coupled substitution. Previous studies of perovskite with Fe^{2+} starting materials reveal the charge disproportionation of iron at high pressure, transforming up to 60% of Fe^{2+} to Fe^{3+}, and the amount of Fe^{3+} in the sample is further increased by the presence of Al [1,2].

Perovskite was synthesized in the diamond anvil cell above 45 GPa with all iron as Fe^{3+}. Two Fe^{3+}-bearing compositions were investigated, 18% Fe^{3+} (Fe^{3+}-Pv) and 10% Fe^{3+} + 10% Al (Fe^{3+},Al-Pv). Fe^{3+}-bearing post-perovskite (Fe^{3+}-PPv) was synthesized at 120 GPa.

Both the $K\beta_{1,3}$ line position and the $K\beta'$ line intensity of Fe^{3+}-Pv in XES suggest a decrease in average spin to ~50 GPa. SMS data reveal that there are two distinct iron environments in the sample. One is low quadrupole splitting and suggestive of high spin Fe^{3+} which we assign to the dodecahedral site. The second site has very high quadrupole splitting, which is consistent with low spin Fe^{3+} in the octahedral site. The SMS results also support the XES results of a gradual spin transition, but reveal that it only occurs in one cation site (likely octahedral site) in the structure [3].

XES data of Fe^{3+},Al-Pv also reveal a gradual reduction in spin with pressure, however between 63 and 84 GPa there is discontinuous drop in the intensity of $K\beta'$ and shift in the $K\beta_{1,3}$ line. SMS reveals that low spin Fe^{3+} exists in the octahedral site from 26 GPa, but above 70 GPa a third iron site appears in the spectra, that we also assign to low spin Fe^{3+}. This third site has a quadrupole splitting value consistent with low spin Fe^{3+}. The different behaviour observed for Fe^{3+},Al-Pv relative to Fe^{3+}-Pv suggests Al is likely the cause. The sharp increase in the low spin component at high pressure may be due to an increased amount of Fe^{3+} entering the octahedral site at the expense of Al, a consequence of the combined substitution of Fe^{3+} and Al in perovskite.

SMS of Fe^{3+}-PPv at 120 GPa reveal that approximately half of the Fe^{3+} exists in the octahedral site in low spin and half exists in the 8-fold coordinated site as high spin, revealing that Fe^{3+} does not change spin states across the Pv-PPv phase transition.

Our study suggests that Fe^{3+} in the octahedral sites of mantle silicates likely undergoes a spin transition in the lower mantle and Al has greatly affects the spin transition.

[1] Frost, D. et al. (2004) *Nature*, **428**, 409-412. [2] McCammon, C. (1997) *Nature*, **387**, 694-696. [3] Catalli, K. et al. (2010) *Earth Planet. Sci. Lett.*, **289**, 68-85.

Equation-of-state of Fe^{3+}-bearing phase-X

Comodi, P.[1*], Nazzareni, S.[1], Bindi, L.[2] & Bobrov, A.[3]
[1]Dipt.o di Scienze della Terra, University of Perugia, Italy
([*]comodip@unipg.it)
[2]Museo di Storia Naturale, University of Florence, Italy
[3]Geological Faculty, Moscow State University, Moscow, Russia

Phase X is a synthetic phase with general formula $A_{2-x}M_2Si_2O_7H_x$ where A= K, Na, Ca, [], and M= Mg, Fe, Al, Cr^{3+} (with H_2O contents from 1.8 to 4.2 wt.%) [1]. Experimental petrology showed that it coexists with a typical mantle assemblage (olivine/wadsleyite, clinopyroxene and garnet) in a pressure range of 14 - 20 GPa and temperature up to 1600°C. Besides, phase X represents a potential host for incompatible and large elements (Na, K, Rb, Cs, Ba) in metasomatized upper mantle and transition zone. In subduction slabs settings, it was found from the breakdown of phlogopite and K-rich amphibole ([2] and the reference therein), thus it might be one of the possible candidates for carrying water and K deep into the Earth's mantle.

The structure of phase X, sp.gr. $P6_3cm$, consists of di-octahedral sheets of MO_6 octahedron stacked along the *c* axis and linked together by Si_2O_7 group, which form pillars between the layer where A atoms are contained. Two different OH environments were found by Raman spectroscopy.

The H*P* behaviour of hydrous and anhydrous end-members $K_2Mg_2Si_2O_7$ were studied by synchrotron X-ray diffraction and IR spectroscopy [3]. Only limited variation on the EoS of the two compositions was found with a K_0 ~ 74 GPa for both, and the structures remain stable up to 30 GPa. The hydrous sample showed a softening and broadening of the OH stretching modes by increasing pressure up to 20 GPa when they become very weak. However, density functional based computations [4] showed bulk moduli about twice than that measured by Liu et al. [3] for the Na (K_0 = 128 GPa, K' = 4.0) and K (K_0 = 132 GPa, K' = 4.4) anhydrous end-members. So up to now the baric behaviour of phase-X it not well constrained. To better define the EoS of phase-X, and how the Fe^{3+} -> Mg substitution may influence the elastic constants, we investigate the sample studied by Bindi et al. [5] with chemical composition $(K_{1.307}Na_{0.015})(Mg_{1.504}Fe^{3+}_{0.373}Al_{0.053}Ti^{4+}_{0.004})Si_2O_7H_{0.36}$, [sp. gr. $P6_3cm$, lattice constants a = 5.005(1) Å, c = 13.148(2) Å; V = 285.23(9)Å^3]. The sample was synthesized with the high-pressure toroidal "anvil-with-hole" apparatus at 7 GPa and 1650°C in the model peridotite system with 70 wt% of chemical K_2CO_3. Peridotite was prepared from a mixture of stoichiometric gels (60 wt% olivine, 16 wt% orthopyroxene, 12 wt% clinopyroxene, and 12 wt% garnet), and had the composition of garnet lherzolite (wt%) similar to pyrolite. H*P* single-crystal X-ray diffraction data from in house apparatus (Perugia University) and synchrotron source (ID-27 beamline ESRF, Grenoble) were collected by using diamond anvil cell loaded with different pressure media (methanol-ethanol-water mixture, neon) and pressure calibrant (ruby, quartz, Sm^{2+}:BaFCl).

Preliminary compressibility data at low pressure (<5 GPa) give a bulk modulus K_0 = 135(10) GPa with K' fixed to 4, more similar to the calculated than measured values for the potassium end-member. Details on the compressibility pattern and the stability over a large pressure range will be presented.

[1] Inoue, T. et al. (1998) *Phys. Earth Planet. Int.*, **107**, 221-231. [2] Frost, D.J. (2006) in Keppler, H. & Smyth, J.R. (eds.) *Rev. Mineral. Geochem.*, **62**, 243-271. [3] Liu, Z. et al. (2002*) J. Phys. Condens. Matter*, **14**, 10641-10646. [4] Mookherjee, M. & Steinle-Neumann, G. (2008) *Bayerisches Forsch. fur Exp. Geoch. Geophys. Annual Rep.*, 98-100. [5] Bindi, L. et al. (2007) *Min. Mag.*, **71**, 265-272.

Experimental HP-HT study of the incorporation of Pb in two important Ca-bearing silicates of the Earth's mantle

Dubrail, J.[1,2*], Gautron, L.[2], Gréaux, S.[3] & Wilke, M.[1]
[1]GFZ German Research Centre for Geosciences, Potsdam, Germany ([*]julien@gfz-potsdam.de)
[2]Laboratoire Géomatériaux et Environnement, Université Paris-Est, Paris, France
[3]Geodynamics Research Center, Ehime University, Matsuyama Japan

Pb isotopes are geochemical tracers of primary importance. Three isotopes of Pb are the ultimate radioactive decays products of the actinides ^{238}U, ^{235}U and ^{232}Th (respectively ^{206}Pb, ^{207}Pb and ^{208}Pb – ^{204}Pb being the stable non-radiogenic form). The U-Th-Pb decay system constitutes the richest families of radionuclides in geochemistry (43 isotopes from 12 different elements). The three half-lives of this system span the age of the Earth, and make it the most used for dating the early Earth processes. Moreover, Pb presents an anomalous geochemical behaviour, called the Pb paradox, observed in almost all oceanic basalts: MORB and OIB basalts have more radiogenic Pb than expected for the primordial mantle [1]. To explain this isotopic imbalance, one of the solutions is the existence of non-radiogenic reservoirs in the deep Earth. The core and the lower continental crust have been proposed as reservoirs but neither of them contains sufficient non-radiogenic Pb to resolve the paradox [2-4]. Therefore, complementary reservoirs in the mantle need to be considered [4].

We explored here the possible existence of hidden Pb reservoirs in the mantle by studying the incorporation of Pb in two Ca-rich silicates of the Earth's mantle: the $CaSiO_3$ perovskite (Ca-pv) and the CAS phase. The Ca-pv is the third major mineral phase of the Earth's lower mantle, host of U and Th [5] and proposed source of radiogenic Pb for HIMU basalts [6,7]. The second phase explored is the CAS phase of composition $CaAl_4Si_2O_{11}$, which is formed in the mantle transition zone from subducted slabs [8], and is expected to be present as a solid residue in partially molten slabs subducted to the deep mantle [9].

High-pressure and high-temperature reactions between grossular garnet $Ca_3Al_2Si_3O_{12}$ (which gives Ca-pv and CAS at HP-HT) and PbO_2 along with parent actinides oxides UO_2 and ThO_2 have been performed up to 18 GPa and 2200 K using a multi-anvil press apparatus. The chemical compositions were characterized by electron probe microanalysis and analytical scanning microscopy. X-ray micro-diffraction analyses were also carried out to study the effects of the incorporation of heavy elements on the host structures. The principal results show significant Pb incorporation without major structural changes in both Ca-pv and CAS with up to 2 wt% of PbO in Ca-pv and 12 wt% of PbO in CAS. The results also show that the Ca-pv incorporates together U, Th and Pb. While the CAS phase does not incorporate U and Th alongside Pb. This suggests that the CAS phase could constitute a major host of non-radiogenic Pb in a long-lived garnetite mantle reservoir that is proposed in the portion of the transition zone that harbours subducted slabs [4].

[1] Allègre, C.J. (1969) *Earth Planet Sci Lett.*, **5**, 261-269 [2] Kramers, J.D. & Tolstikhin, I.N. (1997) *Chem. Geol.*, **139**, 75-110. [3] Malavergne, V. et al. (2007) *Geochim. Cosmochim. Ac.*, **71**, 2637-2655. [4] Murphy, D.T. et al. (2002) *J. Petrol.*, **44**, 39-52. [5] Gréaux, S. et al. (2009) *Phys. Earth Planet. Int.*, **174**, 254-263. [6] Taura, H. et al. (2001) *Phys. Earth Planet. Int.*, **124**, 25-32. [7] Yurimoto, H. et al. (2004) *Phys. Earth Planet. Int.*, **146**, 231-242. [8] Gautron, L. et al. (1997) *Phys. Earth Planet. Int.*, **102,** 223-229. [9] Hirose, K. & Fei, Y. (2002) *Geochim. Cosmochim. Ac.*, **66**, 2099-2108.

The deep carbon observatory: unanswered questions in deep carbon science

Hazen, R.M.*, Hemley, R.J. & Bertka, C.M.
Geophysical Laboratory, Carnegie Institution, Washington DC, USA (*rhazen@ciw.edu)

In spite of carbon's importance, many unanswered questions remain regarding the physical, chemical, and biological behavior of carbon-bearing systems at depths greater than a few hundred meters. Recent results from field, experimental and theoretical studies point to the need for a new broadly interdisciplinary effort to understand deep carbon reservoirs and fluxes, the extent of possible deep abiotic organic synthesis, and the nature and extent of the deep biosphere. The Deep Carbon Observatory is a new international organization devoted to the study of these unanswered questions [1].

Recent findings underscore the need for a focus on deep carbon science. In particular, experimental discoveries of high-P-T organic synthesis from inorganic precursors [2], observations of complex interactions between organic molecules and minerals [3], field evidence for significant outgassing of C-O-H-N volatiles [4], recognition of extensive deep microbial ecosystems [5], and new experimental measurements and theoretical models of carbon sources and sinks [6] demand a careful reappraisal of deep carbon.

[1] http://dco.ciw.edu [2] Kuterov, V.A. et al. (2002) *Proc. Russ. Acad. Sci.*, **387**, 789-792. [3] Scott, et al. (2004) *Proc. Natl. Acad. Sci.*, **101**, 14023-14026. [4] Hazen, R.M. (2006) *Am. Mineral.*, **91**, 1715-1729. [5] Sohn, R.A. et al. (2008) *Nature*, 453, 1236-1238. [6] Roussel, E.G. et al. (2008) *Science*, **320**, 1046. [7] Oganov, A. et al. (2008) *Earth Planet. Sci. Lett.*, **273**, 38-47. [8] Nakajima,Y. et al. (2009) *Phys. Earth Planet. Int.*, **174**, 202-211. [9] Zhang, C. & Duan, Z. (2009) *Geochim. Cosmochim. Ac.*, **73**, 2089-2102.

Postspinel transition boundaries in pyrolite and Mg_2SiO_4: comparison by high-pressure experiments with multicell technique

Ishii, T.*, Kojitani, H. & Akaogi, M.
Dept. of Chemistry, Gakushuin University, Tokyo, Japan
(*puchan_cat@yahoo.co.jp)

The 660 km discontinuity which separates mantle transition zone and lower mantle is considered to be due to decomposition from spinel phase to the assemblage of perovskite phase and rocksalt phase (postspinel transition). Precise postspinel phase relations in Mg_2SiO_4 and pyrolite have been frequently examined with quench and in situ X-ray diffraction experiments in previous studies. But it is still discussed whether this transition really corresponds to the 660 km discontinuity, based on uncertainty of pressure in various pressure scales, and so on. To compare precisely the postspinel transition in pyrolite and Mg_2SiO_4, we examined the transition at P, T conditions of the 660 km discontinuity with a multicell sample chamber technique. We also compared phase boundaries of formation of perovskite in Mg_2SiO_4 and $MgSiO_3$.

Mg_2SiO_4 forsterite was synthesized from a mixture of MgO and SiO_2 with a 2:1 mole ratio by heating for 75 hours at 1500°C. $MgSiO_3$ enstatite was synthesized as follows. A mixture of MgO and SiO_2 with a 1:1 mole ratio was heated for 1 hour at 1670°C and quenched to form $MgSiO_3$ glass. The glass was crystallized into enstatite by heating for 63 hour at 1300°C. Pyrolite was prepared by mixing SiO_2(44.98), TiO_2(0.20), Al_2O_3(4.45), Cr_2O_3(0.38), FeO(8.05), NiO(0.25), MgO(37.78), CaO(3.55) and Na_2O(0.36), where numbers in parentheses are contents in wt%. High-pressure experiments were made at 21-25 GPa and 1400-1800°C with a 6-8 type multianvil apparatus. Three samples (pyrolite, Mg_2SiO_4, and $MgSiO_3$) were packed in three holes in a single Re capsule, kept simultaneously at desired pressure-temperature conditions for 2-6 hours, quenched and recovered after the run. Phase identification of each sample was made with a microfocus X-ray diffraction apparatus, and compositional analyses of them were made with a SEM-EDS (scanning electron microscope with energy dispersive X-ray spectrometer).

The postspinel transition boundaries in Mg_2SiO_4 and pyrolite are placed at about 22.5-23.5 GPa and 1400-1800°C. The postspinel transition in pyrolite occurs at lower pressure than that of Mg_2SiO_4 by about 0.5 GPa. The reason why pyrolite and Mg_2SiO_4 have the different phase relations and different transition pressures is that pyrolite contains minor components such as Fe, Al, and Ca. The postspinel transition boundary in pyrolite has a less negative slope than that in Mg_2SiO_4. The experimental results indicate that a part of garnet in pyrolite first transforms to ilmenite, and subsequently spinel and ilmenite transform to the perovskite assemblage at temperatures lower than 1500°C. A part of spinel in pyrolite is dissociated into garnet and magnesiowustite, and then the rest of spinel transforms to perovskite and magnesiowustite at temperatures higher than 1700°C. When we also compare phase boundaries of formation of perovskite in Mg_2SiO_4 and $MgSiO_3$, the two boundaries have almost the same slopes, and the former boundary is placed at higher pressure by about 0.7 GPa than the latter.

Thermal expansion of $CaIrO_3$

Katerinopoulou, A.[1*], Balic-Zunic, T.[1], Krüger, H.[2], Kahlenberg, V.[2] & Trønnes, R.G.[3]
[1]Dept. of Geography and Geology, University of Copenhagen, Denmark ([*]aka@geo.ku.dk)
[2]Inst. of Mineralogy and Petrography, University of Innsbruck, Austria
[3]Dept. of Geology and Mineral Reseources Engineering, NTNU, Trondheim, Norway

Deep Earth dynamics are greatly affected by the $MgSiO_3$ perovskite (pv) to post-perovskite (ppv) transition. The transition conditions correspond to the D"-zone, which has long been an enigmatic region in the boundary between the Earth's mantle and core. The thermodynamic properties of the transition would give important constraints on the phase stability relations. However, such a study can only be performed on an analogue material, because the post-perovskite phase of $MgSiO_3$ is not stable at ambient conditions. $CaIrO_3$ is the only known material where both pv and ppv phases are quenchable at 1 atm. It is stable at 1 atm as ppv (*Cmcm*) and also crystallizes as metastable orthorhombic pv phase (*Pbnm*) [1].

The thermal expansion of $CaIrO_3$ in both *Cmcm* and *Pbnm* phases has been determined by single crystal X-Ray diffraction (SXRD). In the case of the post-perovskite structure, an anisotropic linear expansion is observed. The *b*-axis, which is normal to the edge-linked octahedra, shows the largest expansion. Data can be fitted with a second-order Grüneisen approximation [2]. The *Pbnm* perovskite is a more open and flexible crystal structure, where the octahedra are corner linked. An even larger anisotropy is observed in this case, the expansion curve of the *b*-axis has a negative slope. The *a*-axis expands with temperature while the *b*-axis contracts. This suggests that the [IrO_6] octahedra in the structure rotate in the sense that diminishes the discrepancy to the ideal cubic archetype. The results shed new light on the thermodynamic processes in the D´´ region of the lower mantle.

[1] Stølen, S. & Trønnes, R.G. (2007) *Phys. Earth Planet. Int.*, **164**, 50-62. [2] Lindsay-Scott, A et al. (2007) *Phys. Earth Planet. Int.*, **162**, 140-148.

An unusual mantle mineral grouping in the Luobusha ophiolite chromitites, Tibet, China

Li Guowu[1*], Shi Nicheng[1], Xiong Ming[1], Bai Wenji[2], Fang Qingsong[2] & Ma Zhesheng[1]
[1]China University of Geosciences, Beijing, China ([*]liguowu@126.com)
[2]Institute of Geology, Chinese Academy of Geological Sciences, Beijing, China

After the discovery in 1980 of diamonds in ophiolite rocks from Luobusha and Dongqiao, Tibet, China, a mineralogical study of the Luobusha area was proposed. Within the Luobusha ophiolite chromitites, an unusual mineralogical grouping was discovered as inclusions in chromite. This includes silicates, oxides, sulphides and very large variety of metallic and intermetallic compounds. Apart from the natural occurrence of diamond, moissanite, wüstite, coesite, *etc*., the presence of UHP minerals was confirmed. Together with this discovery, native metallic elements (Si, Fe, Zn, Pb, Al, Cr, Ni, Os, Ir, Ru, Rh, Pd, Au, Ag, W, Cu and Ti), alloy minerals (Fe-Si, Fe-Ti-Si, Ni-Fe-Cr, Ni-C, Fe-C, Cr-C, Ti-C, W-C, SiC, Fe-Co, Al-Fe-La, W-C, Fe-Mn, Au-Ag, Ag-Sn Ti-W, Cu-Zn, Si-Ca, Ti-N, Fe-Si Si-Ca-Cu as well as PGE minerals (Ni-Fe-Ir, Rt-Fe, Pt-Fe-Pd, Fe-Ru) were found. Although most crystal sizes of the inclusions are very small (about 15-60 μm for the most grains), XRD work was carried out on a diffractometer equipped with a CCD detector (SMART APEX, Bruker AXS Inc.) In every particular element group a certain amount of mineral species have been discovered, for example in Fe-Ni-Cr and Fe-Co, taenite, awaruite, iron and wairauite were have been identified by XRD. In the Fe-Si, Fe-C and W-C systems, luobusaite, qusongite, yarlongite and zangboite were discovered as new mineral species. Of these, single crystals of yarlongite and zangboite were obtained for the crystal structure determination. However, for most crystal samples, including luobusaite and qusongite, only a powder XRD pattern could be obtained and therefore the crystal structures were refined using the Reitveld method. In the above-mentioned metal and alloy minerals, XRD data was successfully obtained for only 30% of the minerals.

Metal and intermetallic compounds were presumably formed under reducing conditions. Therefore, they cannot coexist with chromites. An SEM image showed the PGE minerals were enclosed in the chromites. Interestingly, other native metals and alloys were also discovered as inclusions in the PGE minerals. The species enclosed in the PGE minerals are diamond and coesite. Native silicon can also be found as an inclusion in moissanite. "Ferdisilicite", "fersilicite" and native silicon were observed as inclusions in luobusaite. This kind of complex enclosed relationship indicates that the minerals had to undergo a long process of migration.

These metal and intermetallic compounds are believed to have been transported from deep within the mantle by a plume and incorporated in the ophiolite during seafloor spreading. Blocks of the mantle containing the minerals were presumably picked up by later boninitic melts from which the chromitites precipitated, transported to shallow depth and incorporated into the chromitite.

Acknowledgements: This study was supported by the National Natural Science Foundation of China (40872043).

Morphogenetic evidence of the mantle fluid activity

Posukhova, T.V.
Dept. of Mineralogy, Moscow State University, Moscow, Russia (tposukhova@mail.ru)

Diamonds and accompanying minerals from the Arkhangelsk kimberlites and different placers (Ural, Timan, North Yakutiya, Sierra-Leone, Chikapa) were investigated. Morphology, physical properties, and interior structure of the diamonds have been examined by different methods: SEM, IR-spectroscopy, X-ray tomography, Raman-spectroscopy, cathodoluminesence. Chemical composition of the accompanying minerals has been examined with EDS and WDS- micro-beam spectroscopy.

It was established that diamonds in all objects have a specific peculiarities. The round dodecahedron forms prevail, among colored polyhedra grey crystals are the most abundant, crystals have a lot of black inclusions. Usually the degree of resorption is high. Knob-like asperities, ribbing, frosting corrosion sculptures, fetch channels and lamination lines are well developed on the surface of diamond crystals from these sources. Comparison with experimental data shows that such morphological peculiarities were formed during the solution of the octahedron crystal in carbonate-silicate systems in presence of H_20-CH_4 fluids with C=O, -OH, -HOH, CO_3, CH_2, CH_3 groups at T=1300-1450^{o}C and P=0,1-2,5 GPa. The presence of H_2O in diamonds was established previously and was confirmed with our IR-spectroscopic data. In addition, spectroscopic data show that in diamonds from Arkhangelsk province and investigated placers on average slightly higher nitrogen, CO_2 and H_2O contents are present. Results of IR-spectroscopy and Raman-spectroscopy permitted us to propose a presence of carbon-hydrogen inclusions. Such inclusions in diamonds were investigated in North Yakutian placers. CH_4, C_3H_8, C_4H_{10}, and C_5H_{12} were established by Raman-spectroscopy and gas-chromatography methods. We investigated such inclusions in garnets from the Mir pipe.

Another evidence of the fluid activity gives us peculiarities of the minerals which accompany diamonds in these objects. We found flogopite and millerite as inclusions in investigated diamonds. Specific coronary structure of garnets and clinopyroxenes (keliphitic rims, higher Mg and lower Fe in outer zone) and wide extent of garnet-pyroxene-flogopite association in the Grib pipe were established. All mineral grains of garnets, pyroxenes and ilmenites in Arkhangelsk kimberlites have round form. A higher proportion of them are heavily frosted and contain etch channels. Such mineralogical peculiarities are typical for the potassium metasomatic processes.

Thus, our data permit us to propose an important role of potassium carbonatic melts and mantle fluid in the origin of the investigated diamonds and accompanying minerals.

Phase and melting relations of a residual eclogite within an upwelling heterogeneous upper mantle

Rosenthal, A[1*], Yaxley, G.M.[1], Green, D.H.[1,2], Hermann, J.[1], Spandler, C.S.[1,3], Kovács, I.[1,4] & Mernagh, T.P.[5]
[1]Research School of Earth Sciences, The Australian National University, Canberra, Australia ([*]anja.rosenthal@anu.edu.au)
[2]School of Earth Sciences and Centre for Ore Deposit Studies, University of Tasmania, Hobart, Australia
[3]School of Earth and Environmental Sciences, James Cook University, Townsville, Queensland, Australia
[4]Department of Data Management, Eötvös Loránd Geophysical Institute of Hungary, Budapest, Hungary
[5]Geoscience of Australia, Canberra, Australia

The existence, creation and modification of compositional heterogeneities within the Earth's upper mantle and their influences on the petrogenesis of primitive magmas have been highly debated for decades. The possible origins of mantle heterogeneities within the Earth's peridotite-dominated mantle are numerous and complex.

One major mechanism invokes an important role for recycling of oceanic crust at subduction zones, and the storage of these recycled mafic (and sedimentary) materials in the deep mantle, before it is thought to be incorporated in the adiabatically upwelling upper mantle sources of some primitive magmas.

To assess the influence of recycled oceanic crust on the creation of mantle heterogeneities and on the petrogenesis of primitive magmas in homogeneous, buoyant, upwelling peridotite-dominated mantle, high pressure experimental investigations of the melting behaviour of subducted oceanic crust and its residues will be presented.

We track a sequential process in which melts are redistributed from the (initially) low temperature melting of average oceanic crust [1], and then from the residue (nominally anhydrous eclogitic compositions) of such subducted oceanic crust (Res2, this study). This study establishes the phase and melting relations of a reasonable melting residue, which is itself derived directly from subducted oceanic crust at high pressures and temperatures (GA2; [1]). In particular, this study has systematically determined the solidus temperatures, phase relations, and partial melt compositions during upwelling of a residual rutile-bearing quartz/coesite eclogite (Res2) from 5 to 3 GPa and 1500-1200°C.

This data is then combined with the results of earlier experimental investigations to constrain the complex melting behaviours of (residual) eclogite bodies in upwelling mantle, the nature of the interactions of their partial melts with ambient peridotitic mantle, and the nature of re-melting of such metasomatised mantle assemblages, with a brief evaluation of the contributions of these processes to the genesis of some primitive magmas.

[1] Spandler, C. et al. (2008) *J. Petrol.*, **49(4)**, 771-795.

Characterization of the pressure induced Ringwoodite → Mg-perovskite + Mg-wüstite phase transition by Catastrophe Theory

Sciascia, L.[1*], Parisi, F.[2], Princivalle, F.[2] & Merli, M.[1]
[1]Dipto. di Chimica e Fisica della Terra e Applicazione alle Georisorse ed ai Rischi Naturali, Università degli Studi di Palermo, Italy ([*]lucianasciascia@gmail.com)
[2]Dipto. di Geoscienze, Università di Trieste, Italy

Seismic discontinuities in the terrestrial mantle have significant impact on geodynamics and several experimental and theoretical works aimed at understanding their physical and chemical origin have been performed in the last decades. It had long been accepted that seismic discontinuities at about 520, and 660 km depth are related to phase changes involving olivine and its polymorphs. In particular, the less pronounced 520-km discontinuity [1] has been attributed to a phase change from wadsleyite (β-olivine) to ringwoodite (γ-olivine) [2], while the origin of discontinuity in the lower mantle is still not fully understood [2,3]. According to recent phase equilibria studies, it seems that it is mainly due to the breakdown of ringwoodite to Mg-perovskite + Mg-wüstite [4,5].

In order to shed light on this issue, the evolution of the electron arrangement in the crystal-structure across the pressure induced phase transition has been investigated in terms of topology of the electron density.

Calculations of the electron densities have been performed by means of the ab initio CRYSTAL computer program [7] at the HF/DFT level, using an Hamiltonian based on the B3LYP scheme [8]. The local functions to construct the crystalline orbitals were chosen as a Gaussian-type. The topological characteristics of the electron density have been obtained following the Bader's 'Atoms In Molecules' approach. All the calculation have been performed for pressures ranging from a nominally negative pressure of ~-10 GPa (corresponding to a virtual expanded state) to ~60 GPa. To address the compression mechanism, calculations have been performed at different unit cell volumes and the energies obtained as function of the volumes have been fitted by means of the Murnaghan equation.

Aiming at explaining the observed breaking of some chemical bonds with increasing the pressure, a topological mechanism based on the Catastrophe Theory [6] applied to the framework of the Bader's theory [7] has been proposed for the first time.

One of the most interesting results observed was the progressive approach of a bond critical point (BCP) and a ring critical point (RCP) near the transition point, until the coalescence is reached at the transition point. It has been also found that the angle between the stable manifold of the BCP and the unstable manifold associated to the RCP approximate 0° at the transition point, which means that the couple of coalescent critical point are candidates to represent a catastrophe scene in the theory of catastrophes [6,7].

The present analysis, characterizing the electron arrangement in the polymorphs, allowed us to determine the real coordination environments as a function of pressure and therefore its relationship with the high-pressure transition.

[1] Shearer, P.M. & Flanagan, M.P. (1999) *Science*, **285**, 1545-1548. [2] Helffrich, G.R. & Wood, B.J. (2001) *Nature*, **412**, 501-507. [3] Kaneshima, S. & Helffrich, G. (1999) *Science*, **283**, 1888-1891. [4] Vinnik, L., Kato, M. & Kawakatsu, H. (2001) *Geophys. J. Int.*, **147**, 41-56. [5] Deuss, A. & Woodhouse, J. (2001) *Science*, **294**, 354-357. [6] Thom R. (1969) *Topology*, **8**, 313-335. [7] Bader R.F.W. (1990) *Atoms in Molecules - A Quantum Theory*. Oxford University Press, Oxford. [7] Saunders, V.R. et al. (2003) *CRYSTAL2003, User's Manual*. University of Torino. [8] Becke, A.D. (1993) *J. Chem. Phys*, **98,** 5648-5652.

Crystal chemistry and mineralogy in Earth's interior and a special mineralogical grouping from Luobusha ophiolite

Shi Niheng[1*], Li Guowu[1], Bai Wenji[2], Xiong Ming[1], Fang Qingsong[2] & Ma Zhesheng[1]
[1]China University of Geosciences, Beijing, China ([*]shinicheng@vip.sina.com)
[2]Institute of Geology, Chinese Academy of Geological Sciences, Beijing, China

Under the conditions in mantle oxides and silicate minerals occur a series of phase transitions as the pressure increases. They lead to a unit volume decrease, a density increase which in turn leads to decrease of the oxygen ion radius. However, for the cation radius of silicon, it not only failed to decrease, on the contrary, an trend to increasing was found. For example, the radius of oxygen in stishovite is smaller than the radius of oxygen in quartz, but Si-O bond length is 1.75 Å in stishovite, and Si-O bond length is 1.60 Å in quratz. Obviously, the cation radius of silicon in stishovite is larger than the cation radius of silicon in quartz. Along with pressure increases and the occurrence of the phase transition, the cationic radii of silicon continue to increase. For corresponding polymorphs, every cationic radius for silicon has been calculated from crystal structure data as follows (Table1):

Table 1: The cation radius of silicon (Å) in SiO_2 polymorphs

phase	quartz	coesite	stishovite	SiO_2 as α PbO_2 type	SiO_2 as pyrite type
$R_{(Si)}$ (Å)	0.296	0.293	0.512	0.533	0.530
Pressure (GPa)	normal	4-8	8-50	90-200	200-260

The Earth's core material phase and its crystal structure have been clarified by experimental mineralogy. Their crystal chemistry features can be concluded as following: 1. A simple metallic substance or intermetallic compounds (Fe-Ni metallic compounds); 2. The crystal structure displays an equal-sphere closest packing model; 3. Strong reducing environment; 4. High melting point and a high chemical stability.

This kind of crystal structure will preserve invariableness in different layers of the earth. In this case the phase transition and crystal structure can not be used to indicate pressure and depth. In fact, the four crystal chemistry characteristics mentioned above are important indicators for mineral species formation.

A mass of inclusion minerals has been discovered in the Luobusha ophiolite chromitites, Tibet, China. They include silicates, oxides, sulphides and very abundant metal and intermetallic compounds. The occurrence of diamond and coesite indicated that the formation depth of the minerals must be below 120 km and the pressure must be at 4-8 GPa. Spinel with silicon-oxygen octahedra coordination and high silicon rutile may be from the transition zone. In the metallic and intermetallic compounds luobusaite, qusongite, yarlongite and zangboite have been discovered as new minerals. These species of metallic carbides and silicides may be derived from the core-mantle boundary region. In this area, taenite, awaruite, iron and wairauite were discovered as Fe-group elements. According to chemical composition, crystal structure, reducing environment, it is possible that this four mineral species may be derived from the Earth's core.

Acknowledgements: This study was supported by the National Natural Science Foundation of China (40872043).

Stability field and thermodynamic properties of $Mg_{14}Si_5O_{24}$ anhydrous phase B determined by high-pressure experiments and calorimetry

Terata, S.*, Kojitani, H. & Akaogi, M.
Dept. of Chemistry, Gakushuin University, Tokyo, Japan
(*sakilily@ca3.so-net.ne.jp)

Anhydrous phase B (Anh-B:$Mg_{14}Si_5O_{24}$) is a high-pressure magnesium silicate possibly stable in magnesium-rich regions in the upper mantle [1]. Finger et al. (1991) [2] analysed the crystal structure of Anh-B. Ganguly and Frost (2006) [3] examined the equilibrium boundary of the reaction, 5forsterite (Fo) + 4periclase(Per) = Anh-B, at 9.0-12.5 GPa and 1173-1873 K. However, the upper stability limit of Anh-B has not yet been examined. In this study, we determined stability relations of Anh-B by high pressure experiments and calorimetry, and inferred possible stability of Anh-B in the deep mantle.

High-pressure high-temperature experiments to determine the phase relations on Anh-B were performed with a Kawai-type 6-8 multianvil high pressure apparatus. The starting material was a mixture of Per and Fo with 4:5 molor ratio. The experimental conditions were 12-23GPa and 1673 -2073 K for 3 hour. Samples recovered after quenching were analyzed with powder X-ray diffraction method and SEM-EDS. Calorimetry was performed with a Calvet-type calorimeter which was kept at temperature of 978 K. Drop-solution enthalpy of Anh-B was measured with Ar bubbling technique, using lead borate as the solvent. For calorimetric measurements, Anh-B was synthesized from 14:5 mixture of Per and quartz by keeping at 15 GPa and 1723 K for 3 hours, and was recovered after quenching.

Results by the high-pressure and high-temperature phase equilibrium experiments indicated that the equilibrium boundaries of 5 Fo + 4 Per = Anh-B and of Anh-B = 5 Wadsleyite(Wads)+ 4 Per are located at 12-13.5 GPa and at 18-21 GPa, respectively at 1673-2073 K. From these boundaries, enthalpies and entropies for the two relations were constrained. The measured drop-solution enthalpy of Anh-B was 867.5(233) kJ/mol. The drop-solution enthalpy of Fo was 168.2(9) kJ/mol, and that of Per was 33.7(10) kJ/mol (H. Kojitani, unpublished data), and that of Wads was 142.2(27) kJ/mol [3]. Therefore, the enthalpy for the reaction 5 Fo+ 4 Per = Anh-B was obtained as 108.5(241) kJ/mol, and Anh-B = 5 Wads + 4 Per as 21.7(235) kJ/mol by calorimetry. From both of the results of high-pressure high-temperature experiments and calorimetry, best values of enthalpy and entropy for the two reactions were determined. For the reaction of 5Fo+4Per=Anh-B, enthalpy was 110.9 kJ/mol, and entropy was -17 J/(mol·K). For the reaction of Anh-B= 5Wads+4Per, and enthalpy was 37.8 kJ/mol, entropy was -24 J/(mol·K). The two equilibrium boundaries were calculated with these values. The boundary of 5 Fo + 4 Per = Anh-B is expressed as P(GPa)=0.0015 T(K)+9.87, and that of Anh-B= 5 Wads + 4Per as P(GPa)=0.0056 T(K)+9.00. This study shows that Anh-B decomposes into Wads and Per, and Anh-B is stable in magnesium-rich upper mantle and transition zone in the depth range of about 370 - 550 km.

[1] Ganguly, J. & Frost, D.J. (2006) *J. Geophys. Res.*, **111**, B06203. [2] Finger, L. et al. (1991) *Am. Mineral*., **76**, 1-7. [3] Akaogi, M. et al. (2007) *Phys Chem. Minerals*, **34**, 169-183.

Single-crystal diffractometer with an ultrahigh intensity rotating anode X-ray source

Trots, D.M.*, Kurnosov, A., Boffa Ballaran, T. & Frost, D.J.
Bavarian Research Institute of Experimental Geochemistry and Geophysics, University of Bayreuth, Germany
(*dmytro.trots@uni-bayreuth.de)

The layout and first test measurements of single crystal diffractometer with an ultrahigh intensity rotating anode source is described. We intend to employ this diffractometer system in combination with Brillouin spectroscopy for simultaneous acquisition of precise lattice parameters and acoustic velocities in minerals under extreme conditions.

The diffractometer is installed within an interlocked experimental hutch. A rotating anode FR-E+ SuperBright X-ray source from Rigaku is implemented. MoKα radiation is selected from the rotating anode spectrum using VaryMax^{TM} focusing optics. The optics employs two focusing parabolic-curved mirrors in a "side-by-side" Kirkpatrick-Baez scheme. The beam intensity is monitored by PIN diode. The flux at the detector position (~1400 mm from optics) at an operating power of 2.475 kW is approximately 10^8 photons/sec^{-1}. The beamsize at the sample position is approximately 200 microns. The diffractometer itself is an Eulerian four-circle diffractometer from Huber. It controlled via the code Single [1], which allows 8-position centring for accurate determination of lattice parameters. An X-ray counting system is based on a YAP:Ce scintillator and placed onto a counter arm. The layout of diffractometer leaves sufficient space for the focusing and collecting lenses of a Brillouin spectrometer to access the sample.

Initial test measurements in air on ruby, quartz, phase-D, periclase, diomignite as well as test measurements of quartz (~35 microns maximal dimension) and diomignite at high pressures in a diamond anvil cell have been performed. Performance of the diffractometer system is well demonstrated by diagnostic $(d_{obs}-d_{calc})/d_{calc}$-plots in figure 1. Δd/d values show a maximum scatter of ~0.00014 (low-angle reflections are ignored because $K\alpha_1$ and $K\alpha_2$ doublets are not resolved). Comparison between the intensity of weak (424) reflections measured with a diffractometer system based on a conventional X-ray tube and the rotating anode combined with multilayer optics, shows a significant increase in intensity and signal-to-noise ratio (see figure 1), while preserving the line width.

Acknowledgements: Support from European research Council Advanced Grant "Deep Earth Elastic Properties and a Universal Pressure Scale".

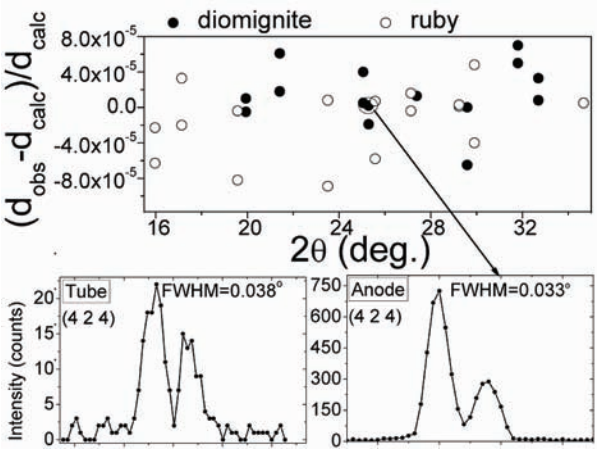

Fig. 1: Δd/d-plots and comparison between reflections measured with X-ray tube and rotating anode/multilayer optics tandem.

[1] Angel, R.J. (2000) in Hazen, R.M. & Downs, R.T. (eds.) *Rev. Mineral. Geochem.*, **41**.

Elastic properties of natural orthoenstatite to 12 GPa: implications for mantle velocity structure

Zhang, J.[1] & Bass, J.D.[1,2*]
[1]Dept. of Geology, University of Illinois, Urbana, USA
[2]COMPRES (Consortium for Materials Properties Research in Earth Sciences), Urbana, USA ([*]jaybass@illinois.edu)

Orthopyroxene, $(Mg,Fe)SiO_3$, is one of the primary minerals in Earth's upper mantle. Knowledge of the elastic properties of pyroxene is essential for understanding the seismic properties of the upper mantle, including the nature of seismic anisotropy and the origin of the low velocity zone. However, previous single crystal measurements are limited up to 3Gpa while polycrystal measurements could not give us enough information about anisotropy. In this study, we have measured the sound velocities of a natural single crystal of orthoenstatite up to 12 GPa by Brillouin spectroscopy with a diamond anvil cell. The orthoenstatite samples were extracted from a peridotite from San Carlos, Arizona. The chemical composition determined by EPMA analysis is $(Mg_{1.77}Fe_{0.17}Ca_{0.04}Cr_{0.02})(Si_{1.95}Al_{0.05})O_6$. Measurements have been made on three different crystal planes, including (100) (010) and (0-11), allowing us to constrain all of the elastic moduli for this phase. Density at ambient conditions is calculated to be 3.200 g/cc based on X-Ray Diffraction average on both three samples, bulk and shear modulus are determined as 109.581 GPa and 73.882 GPa. High pressure density profiles as well as bulk and shear modulus are determined by both fourth order and third order finite strain equation of state. For third order finite strain EOS, pressure derivative are calculated as Ks'= 7.832 G'=1.947, while for fourth order finite strain EOS, Ks'= 7.832 G'=1.947 Ks''= -0.889 GPa-1 G''=-0.324GPa-1 .These results are generally in good agreement with previous studies, orthoenstatite maintain the very unusual high value of the pressure derivative [comparing with all the other mantle minerals] of the elastic modulus through the whole pressure range of its existence. Besides, a significant change in the velocities and acoustic anisotropy has been observed between 10.5-12 Gpa, which we infer to be caused by a phase transition from a low-pressure orthorhombic structure, to a high-pressure monoclinic structure (OEN-HPCEN transition). The transition pressure is higher than previously reported number for pure $MgSiO_3$. This discrepancy may be due to the presence of some other elements in our natural samples. So in a word, both the unusual value of the pressure derivatives of elastic modulus of orthoenstatite and the significant change of sound velocities as well as elastic anisotropy across the OEN-HPCEN transition has to be accounted for in interpretations of discontinuities in the upper mantle, and the cause of seismic anisotropy in this region.

HCP iron at the center of the Earth: a diamond-anvil cell study

Tateno, S.[1*], Hirose, K.[1,2], Sata, N.[2] & Ohishi, Y.[3]
[1]Dept. of Earth and Planetary Sciences, Tokyo Institute of Technology, Tokyo, Japan ([*]tateno.s.aa@m.titech.ac.jp)
[2]Institute for Research on Earth Evolution, Japan Agency for Marine-Earth Science, Yokosuka, Kanagawa, Japan
[3]Japan Synchrotron Radiation Research Institute, Sayo-cho, Hyogo, Japan

The Earth's core is mainly composed of iron. Thus the crystal structure of iron is of prime importance for understanding the nature of solid inner core. Despite many efforts on the phase relations of iron have been extensively studied by shock wave, static compression, and theoretical calculation, consensus on the stable phase at the inner core condition has never been achieved. Ab initio calculation repeatedly suggests the body-centered-cubic (bcc) iron is stable at very high temperature to the inner core pressure above the stability field of hexagonal close-packed (hcp) phase, thus being the strong candidate for inner core material [1]. On the other hand, because accessible pressure and temperature (PT) range in static experiment by a diamond-anvil cell (DAC) is limited particularly on high temperature, high PT generation simultaneously inside the inner core has never been achieved. So far, it is confirmed that hcp structure is stable up to 300 GPa and 2000 K by DAC experiment [2].

Here we examined the phase relations of iron at the extreme conditions on the basis of synchrotron X-ray diffraction measurement in situ at high P-T in a laser-heated DAC. Pure iron powder was used as a starting material, which was embedded between SiO_2 for thermal insulation. The sample was heated by the newly developed flat top double-sided laser heating system using fiber lasers installed at BL10XU of SPring-8. With this technique, the accessible PT conditions in a DAC were significantly extended, reaching 350 GPa and 5700 K. The results show that iron is stable with hcp structure in the entire experimental PT range of 130-350 GPa and 2500-5700 K. We observed no evidence for phase transition in these conditions. We also found that very small temperature dependence of c/a ratio above 300 GPa, contrary to the theoretical studies, which report rapid increase of c/a with temperature [3]. The elastic property of hcp iron at the inner core should be reconsidered to explain seismic anisotropy observed in the inner core.

[1] Belonoshko, A.B. et al. (2003) *Nature*, **424**, 1032-1034. [2] Kuwayama, Y. et al. (2008) *Earth Planet. Sci. Lett.*, **273**, 379-385. [3] Steinle-Neumann, G. et al. (2001) *Nature*, **413**, 57-60.

Melting of iron-rich alloys at high pressures and implications for planetary cores

Campbell, A.J.[*], Fischer, R.A. & Miller, N.A.
Dept of Geology, University of Maryland, USA
([*]ajc@umd.edu)

Many planetary bodies are thought to have metallic, iron rich cores, with a significant component of some 'light' alloying element(s). The identity of this light alloying component has a profound effect on the chemical properties of the core, including its melting/crystallization behavior, partitioning of minor and trace elements during core/mantle segregation and core crystallization, and other phase relations. Despite this importance, the light element component(s) of planetary bodies generally remain unknown, apart from those of a few iron meteorite parent bodies. Experimentally determined physical and chemical properties of iron-rich systems can be compared to observations and models of planetary interiors to constrain compositions of planetary cores. Here we summarize our recent high pressure, high temperature experiments on the phase diagrams of iron+light element (Fe-X) binaries. We focus mostly on melting curves in the iron-silicide and iron-oxide systems, because Si and O are leading candidates for the light element component in Earth's core.

Melting curves for FeO and Fe-Si alloys were determined in the laser heated diamond anvil cell. Temperature distributions were measured by imaging radiometry [1]. Melting transitions were identified using multiple methods: discontinuities in the temperature-emissivity relationships across the laser heated spot; discontinuities in laser power-temperature curves; and visual observation combined with the 2D temperature measurement. All three methods gave consistent results. In addition, synchrotron X-ray diffraction was used to establish the solidus and subsolidus phase relations in these Fe-alloy systems. Synchrotron methods provide more complete structural information, but optical methods can establish the phase boundaries with finer precision.

We find that both Fe-9Si and Fe-16Si alloys produce only a small (~100 K) melting point depression relative to pure Fe. X-ray diffraction reveals that at high pressures (>40-50 GPa), the solidus phase for these compositions is in the B2 structure, implying a eutectic between these alloy compositions and hcp-iron. Our melting curve of FeO, combined with recent work on the eutectic melting of Fe-FeO [2], likewise indicates a modest (300-400 K) eutectic melting depression relative to Fe. Therefore, both silicon and oxygen produce lower melting point depressions then sulfur [3] at high pressures, and the minimum temperature of an oxygen and/or silicon bearing core is necessarily greater than an iron-sulfide core.

Despite important gaps and discrepancies that remain in the available data, these and other experimental results can be compared to thermal and chemical models of terrestrial planet interiors (including Earth's). Because of the differences in melting point depressions, an iron-silicon or iron-oxygen core will crystallize more rapidly during cooling than an iron-sulfur core under equivalent conditions. This is especially so in smaller planets such as Mercury, because the pressure range spanned in a smaller planet's core is smaller, hence the eutectic depression plays a more important role in the phase relations.

[1] Campbell, A.J. (2008) *Rev. Sci. Instrum.*, **79**, 015108. [2] Seagle, C.B. et al. (2008) *Earth Planet. Sci. Lett.*, **265**, 655-665. [3] Campbell, A.J. et al. (2007) *Phys. Earth Planet. Lett.*, **162**, 119-128.

Effect of carbon and hydrogen on phase relations in Fe-Ni system at high pressures and temperatures

Dubrovinsky, L.*, Narygina, O., McCammon, C. & Dubrovinskaia, N.
Bayerisches Geoinstitut, University of Bayreuth, Germany
(*Leonid.Dubrovinsky@uni-bayreuth.de)

The phase diagram of iron-enriched Fe-Ni alloy at elevated pressures and temperatures comparable to those in the Earth's core as well as the effect of the potential light element in the core (H, C, Si, S, O, etc.) on the system remains under debate. The reason is very simple: the necessary pressure-temperature range (300-350 GPa and 5,000-7,000 K) is hardly achieved in the laboratory. Conditions close to those in the core can be created in LH-DAC experiments; however the main disadvantage of the technique is a lack of control on the system under study. In contrast, the large-volume press (LVP) provides rather equilibrated and controllable experimental conditions, although at significantly lower pressures. Therefore we carried out a "cross-checking" study of phase relations in $Fe_{1-x}Ni_x$ ($0.10 < x < 0.22$) and $Fe_{0.90}Ni_{(0.10-x)}C_x$ ($0.01 < x < 0.05$) systems at pressures to 100 GPa and temperatures to 3000 K, using LH-DAC and LVP high pressure techniques. *In situ* and *ex situ* sample analyses were done by means of XRD, Mössbauer spectroscopy, and scanning and transmission electron microscopies.

We showed that laser heating in the DAC can promote undesired reactions between the sample (Fe-Ni alloy in our case) and carbon, which upon laser heating diffuses from the diamond anvils through the pressure-transmitting layers. Therefore we suggest that results obtained in LH-DAC experiments should be interpreted very carefully in general.

We investigated the mechanism of carbon and hydrogen incorporation into the structure of Fe-Ni alloy at high pressures and temperatures. We found, particularly, that rapid cooling of *fcc*-structured carbon-bearing Fe-Ni alloy to room temperature (either in the case of LH-DAC or LVP quenched experiments) results in the formation of the metastable solid solution of *bcc*-FeNi, *bct*-Fe-Ni-C (known in metallurgy as martensite) and a certain amount of preserved *fcc* Fe-Ni-C. We also showed that carbon solubility in the Fe-Ni system at high temperatures decreases with pressure.

Experimental investigation of the Fe-Si-O system at high pressures

Seagle, C.T.[1,2*], Cottrell, E.[1] & Fei, Y.[2]
[1]Dept. of Mineral Sciences, National Museum of Natural History, Smithsonian Institution, Washington, DC, USA
[2]Geophysical Laboratory, Carnegie Institution of Washington, Washington, DC, USA (*seaglec@si.edu)

Our only direct information regarding Earth's core results from seismological observations. Acoustic waves propagate through Earth at velocities dependent on the density and elastic properties of the medium. Interpretations of these measurements are dependent on our understanding of the material properties at the environmental conditions that exist within Earth's deep interior. It is believed that Earth's outer core is composed of an iron rich alloy plus ~10 wt. % light elements while the inner core consists of ~3-6 wt. % light elements; possible light elements are O, S, Si, and others [1].

We have investigated the iron rich portion of the Fe-Si-O system at pressures between 40 and 90 GPa using the laser heated diamond anvil cell in conjunction with synchrotron x-ray diffraction (XRD) at the Advanced Photon Source, Argonne National Laboratory. The XRD data indicates that at sub-solidus temperatures, solid iron coexists with wüstite and stishovite, in general agreement with previous data obtained at lower pressures [2]. However, as temperature is further increased (or decreased in reversal experiments) Bragg reflections associated with stishovite disappear (appear) around 1800 K at 40 GPa. This temperature is too low to be associated with melting and implies two phase coexistence at high temperatures (Fe-Si alloy and wüstite). This may suggest oxygen exclusion from the solid during inner core crystallization.

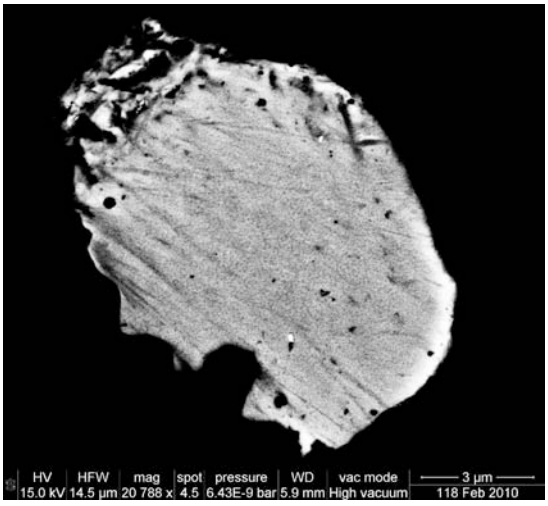

Fig. 1: Backscattered electron image of a laser heated spot in an Fe-Si-O sample recovered from 40 GPa and 3500 K. Small chemical variations are apparent in the wispy texture. X-ray diffraction data indicates that at these conditions the sample was completely molten.

The samples were recovered after the XRD experiments and polished for analysis using a scanning electron microscope and electron microprobe. Very small (~50 nm) circular features in the heated areas quenched from liquid are thought to indicate the exsolution of wüstite during rapid quenching. The bulk compositions of the quenched liquids were determined at several pressures and temperatures. The in-situ XRD measurements and ex-situ characterization will help us to better understand the melting relations in the system at high pressure.

[1] Poirier, J.P. (1994) *Phys. Earth Planet. Int.*, **85**, 319-337. [2] Ohtani, E. (1979) *J. Phys. Earth*, **27**, 189-208.

Iron-silicate reaction and silicon in the core

Ohtani, E.[1*], Sakai, T.[1], Kamada, S.[1], Terasaki, H.[1], Sata, N.[2], Hirao, N.[3] & Ohishi, Y.[3]
[1]Dept. of Earth Science, Tohoku University, Sendai, Japan
([*]ohtani@mail.tains.tohoku.ac.jp)
[2]IFREE, JAMSTEC, Yokosuka, Japan
[3]SPring8, JASRI, Hyogo, Japan

It has been suggested that the core has a density lower than that of pure iron (Fe). Si is a major candidate for the light element in the core because it is one of the most abundant elements in the Earth. The solubility of Si in metallic iron increases with increasing pressure [1,2]. Here, we will discuss the possible existence of Si in the core based on our recent results on phase and melting relations and the equation of state of the Fe-Si and Fe-Ni-Si systems at high pressure.

The melting temperature of $Fe_{0.7}Si_{0.3}$ （Fe-18 wt.% Si）alloy was determined up to 119 GPa based on a change of laser heating efficiency and the texture of the recovered samples in the laser heated diamond anvil cell experiments. The melting curve of the alloy was fitted by the Simon's equation as $P(GPa)/3.5=(T_m(K)/1473)^{4.5}$. The measured melting curve is slightly lower than that of pure Fe in the pressure range of the present experiment. The melting temperature of $Fe_{0.7}Si_{0.3}$ alloy is estimated to be 3300-3500 K at 135 GPa, and 4000-4200 K at around 330 GPa, which may provide the lower bound of the temperatures at the core-mantle boundary and the inner core-outer core boundary if the light element in the core is silicon.

We studied the melting and phase relations of the Fe-Si system under the conditions of the Earth's core [3] by using in situ X-ray diffraction study at BL10XU of Spring-8. We confirmed that a single hcp phase is stable up to 3600 K at 242 GPa and to 2400 K at 257 GPa in $Fe_{0.93}Si_{0.07}$ (Fe 3.4 wt. % Si) alloy. These results suggest that the inner core is likely to be composed of the hcp-phase of FeSi alloy. We made static compression of the $Fe_{0.93}Si_{0.07}$ alloy up to 252 GPa and the $Fe_{0.83}Ni_{0.09}Si_{0.08}$ (Fe-9.8 wt% Ni-4.0 wt% Si) alloy up to 374 GPa at 300 K, applying the NaCl-B2 pressure scale [4] with a correction at above 100 GPa made by a pressure scale based on the pressure shift of the Raman mode of diamond [5] calibrated by the Pt pressure scale [6].

We compared the densities of the present FeSi and FeNiSi hcp-alloys with the pure hcp iron and hcp iron-nickel ($Fe_{0.8}Ni_{0.2}$) alloys [7] at 330 GPa and 300 K by extrapolation of the previous data, and found that the density difference among these alloys is comparable with the uncertainty of the density of the alloys due to the uncertainty of the pressure scales. It is essential to establish the pressure scale at high pressure and temperature in order to make quantitative assessments of the Ni and Si contents in the core.

[1] Sakai, T. et al. (2006) *Geophys. Res. Lett.*, **33**, L15317. [2] Takafuji, N. & Hirose, K. (2005) *Geophys. Res. Lett.*, **32**, L06313. [3] Asanuma, H. et al., (2008) *Geophys. Res. Lett.*, **35**, L12307. [4] Fei, Y. et al. (2007) *P. Natl. Acad. Sci. USA*, **104(22)**, 9182-9186. [5] Akahama, Y. & Kawamura, H. (2004) *J. Appl. Phys*., **96**, 3748-3751. [6] Holmes, N.C.et al. (1989) *J. Appl. Phys*., **66**, 2962-2967. [7] Mao, H.K. et al. (1990) *J. Geophys. Res*., **95**, 21737-21742.

Compression of Fe-Ni-S alloy up to the pressure of the center of the Earth

Sakai, T.[1,2*], Ohtani, E.[2], Terasaki, H.[2], Kamada, S.[2], Hirao, N.[3], Sata, N.[4] & Ohishi, Y.[3]
[1]Institute for International Advanced Research and Education, Tohoku University, Sendai, Japan
([*]t-sakai@m.tains.tohoku.ac.jp)
[2]Institute of Mineralogy, Petrology, and Economic Geology, Faculty of Science, Tohoku University, Sendai, Japan
[3]Japan Synchrotron Radiation Research Institute, Hyogo, Japan
[4]Institute for Research on Earth Evolution, Japan Agency for Marine-Earth Science and Technology, Yokosuka, Kanagawa, Japan

It is considered that the Earth's core is composed of Fe-Ni alloy with small amounts of light elements based on comparison between the density of Fe-Ni alloy and that of the Earth's core [1,2]. Sulfur is one of the major candidates of the light element due to its high solar abundance, formation of iron-sulfur compounds easily, and existence in iron meteorites as troilite, FeS. Metallic iron can contain small amount of sulfur at high pressure conditions. Kamada et al. [3] reported that the sulfur content in metallic iron was 7.6 at.% (4.5 wt.%) at 85.6 GPa and 2200 K. Theoretical studies on the electronic band structure [4,5] predicted that Fe-FeS system becomes solid solution at the core pressure. Therefore, it is important to clarify the compressibility of Fe-Ni-S alloy in order to discuss the density of the inner core. Here we report the result of compression study of Fe-Ni-S alloy up to 360 GPa.

Fe-Ni-S alloy was synthesized at 21 GPa and 1173 K using a multi-anvil apparatus. The composition of Fe-Ni-S alloy was $Fe_{0.881}Ni_{0.091}S_{0.0028}$ (Fe-9.6wt.%Ni-1.6wt.%S) determined by an electron probe microanalyzer. Diamond anvil cell was used for high pressure experiments. Samples were placed in the sample chamber with sodium chloride pressure medium. We calibrated the NaCl-B2 scale against the diamond Raman scale [6,7] up to 272 GPa in the additional experiment. The pressure was determined by the calibrated NaCl-B2 scale. We performed *in situ* powder X-ray diffraction experiments at BL10XU in SPring-8. $Fe_{0.881}Ni_{0.091}S_{0.0028}$ alloy has a bcc structure at ambient pressure and the unit cell parameters were a=2.951 Å and V=25.71 $Å^3$. The bcc phase transforms to the hcp structure at above 19 GPa. $Fe_{0.881}Ni_{0.091}S_{0.0028}$ alloy has been compressed up to 360 GPa successfully, and the hcp structure was stable at the maximum pressure. The fit yielded a bulk modulus K_0 = 153(30) GPa and its pressure derivative K_0' = 5.2(4) and V_0 = 22.8(6) $Å^3$. The density of $Fe_{0.881}Ni_{0.091}S_{0.0028}$ alloy at the inner core boundary (ICB) pressure (330 GPa) and 300 K is 13.75 g/cm^3. The density of the inner core material at 330 GPa and 300 K was calculated to be 13.35 g/cm^3 using the thermal expansion at 330 GPa and 5000K reported by Stacey and Davis [8]. 9 at.% of nickel and 5.3-12.0 at.% (3.1-7.2 wt.%) of sulfur can account for the density of the inner core using the present results together with the previous results [2]. The uncertainty of the sulfur content is derived from the uncertainty of the pressure scale [7]. Since metallic iron contains 7.6 at.% (4.5 wt.%) of sulfur at 85.6 GPa and 2200 K [3], hcp Fe-Ni alloy is likely to contain 5.3-12.0 at.% (3.1-7.2 wt.%) of sulfur at the ICB pressure and temperature conditions.

[1] Birch, F. (1952) *J. Geophys. Res*., **57**, 227-286. [2] Mao, et al. (1990) *J. Geophys. Res*., **95**, 21737-21742. [3] Kamada et al. (2010) *Earth Planet. Sci. Lett*. (in press). [4] Boness, D.A. & Brown, J.M. (1990) *J. Geophys. Res*., **95**, 21721-21730. [5]Sherman, D.M. (1991) *J. Geophys. Res*., **96**, 18029-18036. [6] Akahama, Y. & Kawamura, H. (2004) *J. Appl. Phys*., **96**, 3748-3751. [7] Akahama, Y. & Kawamura, H. (2007) *High Pressure Research*, **27**, 473-482. [8] Stacey, F.D. & Davis, P.M. (2004) *Phys. Earth Planet. Int*., **142**, 137-184.

Equation of state and B1/B8 phase transition in FeO

Fischer, R.A.* & Campbell, A.J.
Dept. of Geology, University of Maryland, College Park, Maryland, USA (*raf815@umd.edu)

Wüstite, $Fe_{1-x}O$, is an important endmember of (Mg,Fe)O in the Earth's lower mantle. The Earth's core contains several weight percent of an unknown light element; if this element is oxygen, then wüstite may also be a significant component of the core. Therefore the high pressure, high temperature behavior of FeO, including its phase diagram and equation of state, is essential knowledge for understanding the properties and evolution of Earth's deep interior.

We performed X-ray diffraction measurements on wüstite+iron mixtures at beamline 13-ID-D of the GSECARS sector of the Advanced Photon Source, using a laser-heated diamond anvil cell to achieve simultaneous high pressures and temperatures (90 to 155 GPa and up to 3100 K). Pressures were determined from the lattice parameters of hcp iron and of NaCl, the insulator and pressure medium. Temperatures were determined by spectroradiometry. To confirm the accuracy of our temperature measurements, we verified the location of the hcp-fcc transition in Fe [1]. The wüstite in our experiments was mixed with metallic iron to produce stoichiometric FeO at high pressures and temperatures [2].

We have determined the thermal equation of state of FeO to 155 GPa, combining our new P-V-T data with earlier data [2, 3]. We find a bulk modulus K_0 = 147 GPa, and whereas prior studies assumed a value of four for the pressure derivative of the bulk modulus, K_0' [2], our higher pressure data require a lower value, K_0' = 3.72. The updated equation of state produces a high pressure Fe-FeO oxygen fugacity buffer curve that is only slightly different than that previously reported [2], over the range of overlapping conditions (<0.2 log units at 100 GPa), but with more significant differences at higher pressures such as those achieved in the present study.

The location and slope of the subsolidus phase boundary between the B1 and B8 structures in FeO at high pressures has been controversial. Our data are broadly consistent with a recent study performed above 180 GPa [3], showing a similar positive slope for the transition but temperatures that are systematically ~300 K lower.

Our results for the equation of state for FeO can be compared to the equation of state of hcp-Fe [4] to match the seismologically determined density of the outer core. Assuming a core-mantle boundary temperature of 4000 ± 500 K and a 1-2% density decrease upon melting, the amount of oxygen in the outer core required to match PREM at the core-mantle boundary is 8.0 ± 1.1 weight percent, under the simplifying assumption of a purely Fe-O outer core.

[1] Komabayashi, T. & Fei, Y. (2010) *J. Geophys. Res.*, **115**, B03202. [2] Campbell, A.J. et al. (2009) *Earth Planet. Sci. Lett.*, **286**, 556-564. [3] Ozawa, H. et al. (2010) *Phys. Earth Planet. Int.*, **179**, 157-163. [4] Dewaele, A. et al. (2006) *Phys. Rev. Lett.*, **97**, 215504.

Electrical conductivity measurement of iron at high static pressure

Gomi, H.*, Ohta, K. & Hirose, K.
Dept. of Earth and Planetary Sciences, Tokyo Institute of Technology, Tokyo, Japan (*gomi.h.aa@m.titech.ac.jp)

The knowledge of the thermal conductivity of the core constrains the heat flow and the amount of radiogenic elements in the core [1]. The electrical conductivity of iron has been measured by shock compression experiments. The thermal conductivity can be then calculated using the Wiedemann-Franz law. Stacey and Loper [2] estimated the thermal conductivity of outer core liquid and suggested the absence of radiogenic heat source. However, no conductivity measurement has been carried out under core pressures by static experiments. In this study, we have conducted the electrical conductivity measurements of pure iron under high static pressure at room temperature in a diamond-anvil cell. The sample resistance was obtained by the four-terminal method. The results demonstrated that the conductivity increased with increasing pressure and dropped at ~15 GPa across phase transition from bcc to hcp structure. It then increased again with pressure up to 65 GPa. The electrical conductivity was determined to be about 1×10^7 S/m at 65 GPa. We estimated the electrical conductivity of iron under the CMB pressure and temperature condition to be ~ 1×10^6 S/m, which is comparable to the previous estimate by Stacey and Anderson [3]. The details of the experiments will be reported at the presentation.

[1] Stevenson, D.J. (2003) *Earth Planet. Sci. Lett.*, **208**, 1-11. [2] Stacey, F.D. & Loper, D.E. (2007) *Phys. Earth Planet. Int.*, **161**, 13-18. [3] Stacey, F.D. & Anderson, O.L. (2001) *Phys. Earth Planet. Int.*, **124**, 153-162.

Prediction of turbostratic iron from first-principles

Ishikawa, T.[1*], Tsuchiya, T.[1] & Tsuchiya, J.[2]
[1]Geodynamics Research Center, Ehime University, Matsuyama, Ehime, Japan ([*]ishikawa@sci.ehime-u.ac.jp)
[2]Senior Research Fellow Center, Ehime University, Matsuyama, Ehime, Japan

Determining the crystal structure of iron in the Earth's inner core has been a long standing challenge for mineral physics. The hexagonal close-packed (hcp) structure has been predicted to be a dominant candidate structure [1,2]. However, the double hcp structure [3], the face-centered cubic (fcc) structure [4], the body-centered cubic structure [5] have also been suggested and it is still controversial.

Here we propose another model for the structure of iron at the extreme conditions. The model was predicted by structural exploration methods based on first-principles calculations, which are free energy surface trekking (FEST) and multiple-configuration sampling method (MCS) [6]. Exploring the metastable structures at 400 GPa by FEST, we found that the hcp iron transforms to a structure with complex stacking sequence by shear deformation and it is much more easily obtained from hcp than fcc. Based on the results of FEST, we inferred a stacking disorder structure stabilizing with a temperature-dependent stacking fault concentration, which we call turbostratic iron. Then, we determined the thermally-equilibrated stacking fault concentration at each temperature by the MCS method. We found that iron has the stacking fault concentration of about 6% at around 1000 K but it increases to about 38% at the inner core conditions. Then, we analyzed elastic properties of turbostratic iron and found that the stacking fault enhances elastic anisotropy. We anticipate that the model of the turbostratic iron gives some new aspects for the inner core structure.

[1] Ma, Y.Z. et al. (2004) *Phys. Earth Planet. Int.*, **143**, 455-467. [2] Steinle-Neumann, G. et al. (2001) *Nature*, **413**, 57-60. [3] Saxena S.K. et al. (1995) *Science*, **269**, 1703-1704. [4] Mikhaylushkin, A.S. et al. (2007) *Phys. Rev. Lett.*, **99**, 165505. [5] Vočadlo, L. et al. (2008) *Phys. Earth Planet. Int.*, **170**, 52-59. [6] Tsuchiya, J. & Tsuchiya, T. (2008) *Proc. Natl. Acad. Sci. USA*, **105**, 19160.

Stability of body-centred-cubic and hexagonal closed-packed iron-magnesium alloys in the Earth's inner core

Kádas, K.[1,2*], Vitos, L.[1,2,3], Johansson, B.[1,3] & Ahuja, R.[1,3]
[1]Dept. of Materials Science and Engineering, Royal Institute of Technology, Stockholm, Sweden
([*]Krisztina.Kadas@fysik.uu.se)
[2]Research Institute for Solid State Physics and Optics, Budapest, Hungary
[3]Dept. of Physics and Astronomy, Uppsala University, Uppsala, Sweden

The composition and the structure of the Earth's solid inner core are still unknown. Iron is accepted to be the main component of the core. Lately, the body-centred cubic (bcc) phase of iron was suggested to be present in the inner core, although its stability at core conditions is still in discussion. The higher density of pure iron compared to that of the Earth's core indicates the presence of light element(s) in this region, which could be responsible for the stability of the bcc phase. However, so far none of the proposed composition models were in full agreement with seismic observations. The solubility of magnesium in hexagonal Fe has been found to increase significantly with increasing pressure, suggesting that Mg can also be an important element in the core. Here, we report a first principles density functional study of bcc and hcp Fe-Mg alloys at core pressures and temperatures [1,2]. We show that at core conditions 5-10 atomic percent Mg stabilizes the bcc Fe both dynamically and thermodynamically. Our calculated density, elastic moduli and sound velocities of bcc Fe-Mg alloys are consistent with those obtained from seismology, indicating that the bcc-structured Fe-Mg alloy is a possible model for the Earth's inner core.

[1] Kádas, K. et al. (2009) *Proc. Natl. Acad. Sci. USA*, **106**, 15560-15562. [2] Kádas, et al. (2008) *Earth Planet. Sci. Lett.*, **271**, 221-225.

Phase relations of iron-sulphur alloys above 2 Mbar

Ozawa, H.[1*], Hirose, K.[1,2], Tateno, S.[1], Sata, N.[2] & Ohishi, Y.[3]
[1]Dept. of Earth and Planetary Sciences, Tokyo Institute of Technology, Tokyo, Japan ([*]ozawa.h.aa@m.titech.ac.jp)
[2]Japan Agency for Marine-Earth Science and Technology, Institute for Research on Earth Evolution, Kanagawa, Japan
[3]Japan Synchrotron Radiation Research Institute, Hyogo, Japan

In 1952, Birch first proposed that the Earth's core is made of alloys of iron and lighter elements. The core is thought to contain considerable amount of light element(s) such as S, O, Si, C, and/or H. The identification of light element(s) in the core, however, still remains uncertain, although the density and seismic velocity profiles and the physical properties of iron and iron-alloys have been much more precisely determined in these fifty years. Since the solid inner core has been growing by crystallization of the liquid outer core with Earth's cooling, the phase diagram of iron-light element system at inner-core/outer-core boundary (ICB) pressure should be known to identify the light elements in the core. Sulphur is thought to be a plausible light element because of its high solar abundance and the easy alloying with iron. Ab initio calculations predict the formation of Fe-FeS solid solution at least in iron-rich part at the ICB condition (e.g., [1]). On the other hand, experimental studies suggest that the Fe-Fe_3S system exhibits a eutectic to 65 GPa (e.g., [2]).

Here we have determined the phase relationships of iron-sulphur alloys up to 250 GPa and 3000 K on the basis of synchrotron X-ray diffraction (XRD) measurements *in situ* at high pressure and temperature using a laser-heated diamond-anvil cell. Starting material was mixed fine powder of Fe and FeS with 20 at.% S composition. We observed coexistence of hexagonal close-packed iron and Fe_3S as subsolidus phases over the entire present experimental conditions. In addition to the XRD measurements, chemical analyses were carried out on the sample recovered from 198 GPa and 3500 K with the field-emission-type electron probe microanalyzer. The direct analyses of the recovered sample demonstrated that solid iron coexisting with Fe_3S contained small amount of sulphur (about 2 at.%) which is less than required to account for the density deficit of the solid inner core. The present results imply that the system Fe-Fe_3S exhibits a eutectic system at least to 250 GPa. Because the solubility of sulphur in the solid iron is still quite limited at such high pressure, other light elements might be necessary to account for the core density deficit.

[1] Alfè, D. et al. (2002) *Earth Planet. Sci. Lett*, **195**, 91-98. [2] Morard, G. et al. (2008) *Earth Planet. Sci. Lett*, **263**, 128-139.

Thermodynamics of iron melting up to 100 GPa

Steinle-Neumann, G.[1*] & Dolejš, D.[2]
[1]Bayerisches Geoinstitut, University of Bayreuth, Germany ([*]g.steinle-neumann@uni-bayreuth.de)
[2]Institute of Petrology & Structural Geology, Charles University, Prague, Czech Republic

The division of the Earth's core into a solid interior and its liquid envelope has been established by seismological constraints decades ago. The crystallization of the inner core from the outer liquid plays an essential role in the generation of the Earth's magnetic field. In addition, the exclusion of the light elements during freezing contributes buoyancy to convection in the outer core, and the latent heat released contributes to the energy budget of the planetary interior. While experiments are difficult to perform at conditions of the inner core boundary (~330 GPa, 5000-7000 K) ab-initio computations considering both the hcp and liquid iron phases have placed important constraints on these values (e.g. [1,2]).

While the division of the core for other terrestrial planets is not established, models for origin of their magnetic fields can only be advanced if thermodynamic parameters of the liquid and relevant solid phases of iron are well characterized, especially along the melting curve.

Here we have adopted recently published internally consistent equations of state for solid and liquid iron [3] in order to explore its relevant thermodynamic properties up to 100 GPa. The model closely reproduces the experimentally determined phase equilibria. We further explore the thermodynamics by investigating the density contrast and the latent heat difference between the solid and liquid phase during transformations from the bcc (δ) to the fcc (γ) at ~6 GPa and from the fcc to the hcp (ε) phase at ~55 GPa along the melting curve. Along the univariant solid-liquid curve, the density difference between the two states decreases with pressure, and the latent heat released by cooling shows significant differences, increasing from bcc (~14 kJ/mol) through fcc (~17 kJ/mol) to the hcp phase (~25 kJ/mol).

With central pressures of ~10 GPa for the Moon, ~45 GPa for Mercury, and ~60 GPa for Mars and lower pressures for their respective core-mantle boundary different amounts of heat will have been released in the solidification of their respective inner cores.

[1] Alfe, D. et al. (2002) *Phys. Rev. B.*, **65**, 165118. [2] Alfe, D. et al. (2002) *Earth Planet. Sci. Lett.*, **195**, 91-98. [3] Lu, X.G. et al. (2005) *Calphad*, **29**, 68-89.

Structural and elastic properties of Fe_4P at high pressure

Wu Xiang[1*], Qin Shan[1] & Steinle-Neumann, G.[2]
[1]School of Earth and Space Sciences, Peking University, Beijing, China ([*]xiang.wu@pku.edu.cn)
[2]Bayerisches Geoinstitut, Universität Bayreuth, Germany

The earth's core is composed mainly of iron, nickel and several light elements. Recently many Fe-Ni-P meteorites have been discovered, which implies that phosphorus is a candidate light elements in the Earth's core. Melliniite (Fe_4P) with 12.2 wt% phosphor is the most iron-rich Fe-phosphide. It provides a basis for exploring the effect of phosphorus in the Earth's core. However, natural Melliniite grains are very small (<100 μm)[1], and it has not been synthesized in the laboratory, which puts considerable limits on its structural and elastic characterization at high pressure. Here our study aims to answer this issue using *ab initio* calculations based on the density function theory with LSDA+U, implemented in VASP code.

At ambient condition, Melliniite is cubic with space group $P2_13$ and Z=4. Phosphorus atoms occupy the 4a site and iron atoms are at the 4a (labeled Fe1) and 12b sites (Fe2) [1]. From the computations the equation of state of Melliniite is deterimned with V_0 = 214.2 $Å^3$, K_0 = 203 GPa and K_0' = 3.6. The zero pressure volume is 2% smaller than that obtained in experiments (218.76 $Å^3$) [1]. The magnetic moment of Fe1 is larger than that of Fe2. A magnetic collapse occurs for Fe1 at ~80 GPa and completely loses at ~110 GPa. Magnetic moment of Fe2 gradually decreases on compression and disappears at ~110 Gpa. The elastic constants C_{11} and C_{22} show softening at high pressure, associated with the loss of magnetization. The static *P*-wave and *S*-wave velocities also show the same softening behavior in the corresponding pressure range. At 0 K the density of Fe_4P is 3% smaller than that of pure Fe at outer core condition [2]. The temperature effect is estimated, and the results show that phosphorus can play a modest role in reducing the density of an iron-nickel alloy at conditions of the Earth's core.

[1] Pratesi, G. et al. (2006) *Am. Mineral.*, **91**, 451-454. [2] Anderson, O.L. & Isaak, D.G. (2002) *Phys. Earth Planet. Int.*, **131**, 19-27.

Combined SIMS and FTIR studies of "water" in nominally anhydrous minerals

Mosenfelder, J.L.*, Rossman, G.R. & Guan, Y.
Geological and Planetary Sciences, California Institute of Technology, Pasadena, CA, USA (*jed@gps.caltech.edu)

The accurate analysis of trace concentrations in nominally anhydrous minerals (NAMs) is a long-standing problem [1], with implications for a wide variety of geophysical and petrologic problems in the Earth and other planetary bodies. SIMS and IR are powerful, complementary analytical tools capable of measuring concentrations down to levels of less than 1 ppm H_2O. Each technique has its advantages and disadvantages. Importantly, however, neither is an absolute method, relying on other techniques such as manometry or nuclear reaction analysis (NRA) for full quantification.

We have conducted calibrations comparing FTIR and SIMS data for a wide variety of NAMs: olivine, orthopyroxene, clinopyroxene, pyrope and grossular garnet, rutile, zircon, kyanite, andalusite, and sillimanite. We employ both primary standards, whose H concentrations were determined independently using manometry or NRA, and "secondary standards", whose H concentrations were determined using polarized IR spectroscopy (or unpolarized, for garnets) referenced back to calibrations developed using primary standards. Our most extensive work has been on olivine, for which we collected repeated calibration data in order to bracket measurements of H diffusion profiles in experimentally annealed crystals at levels of ~25-100 ppm H_2O. A representative calibration is shown in Figure 1.

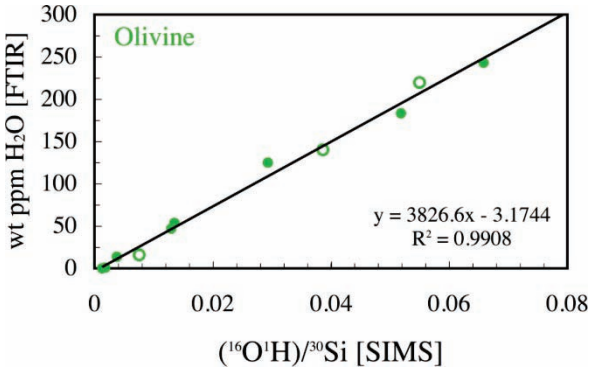

Fig. 1: $^{16}O^{1}H/^{30}Si$ (SIMS) vs. H_2O (FTIR) for 11 olivines. Primary and secondary standards shown with open and closed symbols, respectively. "Near blank" standards include synthetic forsterite (0 ppm H_2O) and San Carlos olivine (0.5 ppm H_2O).

Some of the issues to which we paid careful attention and will address in this presentation include: 1) sample cleaning and assessment of contaminated surfaces, as reflected by relative C, F, Cl, and S counts; 2) "contamination" of measurements by nm-scale hydrous inclusions (e.g. titano-clinohumite in olivine; amphibole in orthopyroxene; muscovite in kyanite), reflected by sudden and extreme changes in $^{16}O^{1}H$ (and/or ^{19}F) counts during crater sputtering; 3) assessment of reproducibility through multiple measurements on each sample (typically ≥5); 4) measurement of matrix effects both for minerals of different composition, and polymorphs (in the case of Al_2SiO_5); and 5) assessment of the potential of SIMS for determining site-specific IR absorption coefficients in minerals [2].

[1] Rossman, G.R. (2006) in Keppler, H. & Smyth, J.R. (eds) *Rev. Mineral. Geochem*, **62**, 1-28. [2] Kovács, I. et al. (2010), *Am. Mineral*., **95**, 292-299.

Towards a protocol for quantitative micro-FTIR measurements of water in the nominally anhydrous minerals of the upper mantle

Kovács, I.[1*], Hidas, K.[1,2], Dégi, J.[3], Ingrin, J.[4], Hermann, J.[5] & Falus, Gy.[1]
[1]Eötvös Loránd Geophysical Institute of Hungary, Budapest, Hungary (*kovacsij@elgi.hu)
[2]Lithosphere Fluid Research Lab, Eötvös University, Budapest, Hungary
[3]Research Institute for Solid State Physics and Optics, Budapest, Hungary
[4]LMTG, Université de Toulouse, CNRS, IRD, OMP, Toulouse, France
[5]Research School of Earth Sciences, The Australian National University, Canberra, Australia

"Water" in the nominally anhydrous minerals (NAMs) of the upper mantle is considered to play a significant role in determining the rheological, seismic, electrical conductivity and melting properties. Both the concentration and the way how water is incorporated is important to understand and formulate the effect of water on these properties. There are several different analytical techniques (i.e., SIMS, NRA, ERDA, manometry and proton-proton scattering) which are able to give accurate quantitative information, but only Fourier-transform infrared (FTIR) spectroscopy is capable of providing qualitative and quantitative information simultaneously. The qualitative information appears to be better constrained than the quantitative as the assignment of infrared bands to particular substitution mechanisms is relatively well constrained for olivine [1] and also has some preliminary results on pyroxenes [2]. The quantitative aspects of micro-FTIR seem to be less determined because there are several different ways for undertaking quantitative analysis and data processing. Our goal is two-fold: 1) To give an overview of analytical setups and data evaluation routines that have been used so far and demonstrate that the non-uniform analytical conditions and data evaluation prevent any direct quantitative comparison among different studies; 2) To outline a protocol for future studies. The most problematic part of quantitative infrared spectroscopy is the use of both polarized [3] and unpolarized [4] radiations, and the application of mineral- [5], substitution mechanism-[6] and wavenumber-dependant calibrations [7] for determining absolute concentrations. It has been demonstrated that there is a systematic relationship over a wide range of absorption properties between polarized and unpolarized light [4] which would make it possible to re-evaluate and, thus, make comparable previous results. It was also shown that wavenumber-dependant calibrations give only a rough first-order approximation on water concentrations, but for more accurate results mineral- and substitution mechanism calibration should be used [6]. The protocol would give instructions on both the analytical setup (i.e., sample preparation, microscope settings) and data evaluation (i.e., background substraction, integration and calibration factors) which may facilitate the achievement of more accurate quantitative measurements and direct comparison of quantitative FTIR results in the future.

[1] Berry, A.J. et al. (2005) *Geology*, **33**, 869-872. [2] Skogby, H. (2006) *Rev. Min. Geochem.*, **62**, 155-167. [3] Libowitzky, E. & Rossman, G.R. (1996) *Phys. Chem. Min.*, **23**, 319-327. [4] Kovács, I. et al. (2008) *Am. Mineral.*, **93**, 765-778. [5] Bell, D.R. et al. (2004) *J. Petrol.*, **45**, 1539-1564. [6] Kovács, I. et al. (2010) *Am. Mineral.*, **95**, 292-299. [7] Libowitzky, E. & Rossman, G.R. (1997) *Am. Mineral.*, **82**, 1111-1115.

"Water" in nominally anhydrous minerals and its influence on some physical properties

Koch-Müller, M.
Deutsches GeoForschungsZentrum, Potsdam, Germany
(mkoch@gfz-potsdam.de)

Hydroxyl incorporation in nominally anhydrous minerals called NAMs is an important research field in geosciences with many implications in analytics, geochemistry, mineral physics and thermodynamics. Since the first studies on NAMs of the Earth's crust in the early 60ties our knowledge and understanding in this field has grown exponential. In this contribution I will summarize the latest developments. The paper is divided in three part: in part one recent analytical developments and/or improvements for "water" quantification in NAMs will be presented, compared and discussed; part two deals with important incorporation mechanisms of hydrogen and how to access it, e.g. for wadsleyite; in part three some data on the influence of "water" incorporation in NAMs on physical properties such as kinetics of phase transitions, phase stabilities and mineral reactions will be presented.

Spatial OH-defect distribution in single crystals of synthetic enstatite

Prechtel, F.* & Stalder, R.
Institute of Mineralogy and Petrography, University of Innsbruck, Austria (*felix.prechtel@uibk.ac.at)

Single crystals of pure enstatite ($Mg_2Si_2O_6$) up to 800x600 µm were synthesized under water-saturated conditions at 6 GPa and 1250°C with variable silica activity. Run products were investigated using a novel technology, a FT-IR-spectrometer equipped with a focal plane array detector enabling IR-imaging with a spatial pixel resolution of 2.7 µm.

IR spectra within the OH-absorption region show strong pleochroic behaviour: absorption bands (1) at 3687 cm^{-1} and 3592 cm^{-1} show strongest absorptions for $E||n_\beta$, whereas absorption bands (2) at 3362 cm^{-1} and 3067 cm^{-1} show strongest absorptions for $E||n_\gamma$. The intensity ratio of the bands within one group is always constant within a narrow range but absorption bands are sensitive to the silica activity (Fig. 1). The most probable interpretation is an assignment of the high-energy absorption bands (1) to tetrahedral (T-site) defects (i.e., V_T) caused by a lower availability of Si and the low-energy absorption bands (2) to octahedral (M-site) defects (i.e., V_M) caused by a lower availability of Mg.

All crystals show an internal zonation pattern with an increasing T-site to M-site defect ratio from core to rim which is interpreted to be caused by changing silica-activity during the experiments. The defect ratio and the zonation pattern are applied as monitor for crystal growth conditions. Furthermore, our observations can be used for the estimation of high-pressure diffusivities of metal cations and metal vacancies. Diffusion models have been developed to strengthen this theory (Fig. 2).

Continuative experiments at 4 GPa and 8 GPa are currently object of investigation.

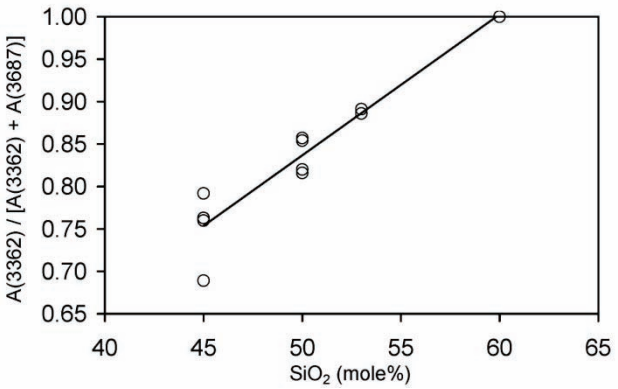

Fig. 1: Influence of silica activity on the dominance of the band around 3362 cm^{-1} expressed as A(3362)/[A(3362) + A(3687)].

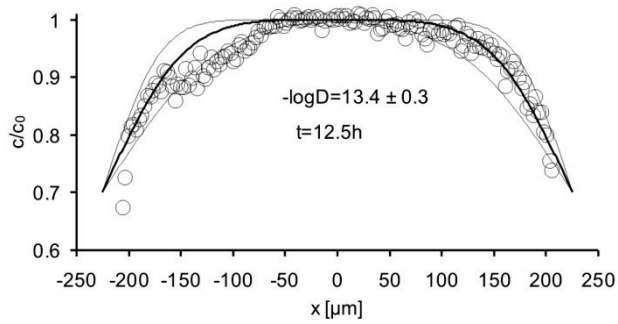

Fig. 2: Concentration profile of Mg-vacancies charge balanced by protons derived from the absorption band at 3362 cm^{-1} with apparent diffusion coefficients of $D_{Mg(M)}$ for a realistic defect equilibration time.

Water content of pyroxenes from Italian volcanoes: implications for the hazard of Etna and Aeolian volcanoes

Nazzareni, S.[1*], Skogby, H.[2], Pompilio, M.[3] & Zanazzi, P.F.[1]
[1]Dept. of Earth Sciences, University of Perugia, Italy ([*]sabrina.nazzareni@unipg.it)
[2]Dept. of Mineralogy, Natural History Museum, Stockholm, Sweden
[3]Istituto Nazionale di Geofisica e Vulcanologia, Sezione di Pisa, Italy

Volcanic clinopyroxenes NAMs may be used to evaluate volatiles evolution during magma crystallization and ascent, especially when glass and melt inclusions are not available or appear totally crystallized. Southern Italy (Aeolian arc and Etna) is one of the most active volcanic areas of Europe and being densely populated has a high level of volcanic hazard.

We performed polarized FTIR, SC-XRD, LA-ICP-MS and EPM analysis on the same clinopyroxene (Cpx) phenocrystals from Etna (3930 BP picritic eruption, Cono del piano - 2001 and 2002 eruptions) and from different volcanic stages of Vulcano, Salina and Alicudi (Aeolian arc), and Mössbauer on selected samples to account for possible H loss by Fe oxidation. We calculated the water contents of Cpxs from the FTIR spectra using the Libowitzky & Rossman [1] calibration.

The H_2O contents of Cpx:s from the Aeolian volcanoes reach up to 390 ppm H_2O by weight in Salina, up to 345 ppm H_2O by weight in Vulcano and up to 270 ppm H_2O by weight in Alicudi. Vulcano cpxs showed a large variation in water content, within the same volcanic stage: primordial Vulcano 23-236 ppm H_2O; Lentia complex 22-345 ppm H_2O; Vulcanello 40-101 ppm H_2O. To evaluate if this variation might be ascribed to H loss during the late stage of eruption or due to variation in the reservoir, we carried out which Mössbauer analyses and re-hydrogenation experiments on 5 selected samples. Two heat treatments were performed under hydrogen gas flow at 700°C for 6 hours each, and after each experiment the IR spectra were collected again. The most "dry" samples take up H (i.e. Pl7 from 23 to 136 ppm H_2O, Lt2 from 36 to 187 ppm H_2O), while the most H_2O rich remains almost unchanged suggesting H loss for the former while the latter may be representative of original crystallisation conditions.

The water content of the Etna cpx:s is quite high suggesting a water rich magmatic system and showed only minor variations from the different eruptions: 254 ppm H_2O for 3930 BP picritic eruption; 214 ppm H_2O for 2001 eruption; 161-254 ppm H_2O for 2002 eruption. Zoned Cpx's from 2001 and 2002 eruptions showed, in general, a more water and trace elements (Y, Zr, Yb, Ce, La) rich core and a more "dry" and trace elements depleted rim possibly grown during a late volcanic stage. In general we found that the H_2O contents of our Cpx's correlate inversely with Ce, La between REE and Y, Yb between HREE, while no correlation is found with elements like Sr. Although Fe oxidation could have been responsible for partial water loss, different physico-chemical magma conditions during the rim growth is a more likely explanation. Wade et al [2] proposed a partition coefficient $D_{H2O}^{cpx/liq}$ as function of Al^{IV}. For the present samples we observe a partition coefficient slightly higher than 0.005, as based on the water contents measured in cpx and olivine-hosted melt inclusions. The above data are the first measured on etnean minerals and since pyroxene is one of the early phases on the liquidus, they are useful, together with melt inclusions, for estimate the total budget of volatiles in the ascending magma.

[1] Libowitzky, E. & Rossman, G. (1997) *Amer. Mineral.*, **82**, 111-121. [2] Wade, B. et al. (2008) *Geology*, **36**, 799-802.

Water contents of majorite garnet, Al-bearing perovskite and Al-bearing stishovite generated in pyrolite-H_2O systems

Inoue, T.[1*], Katsuda, M.[1] & Yurimoto, H.[2]
[1]Geodynamics Research Center, Ehime University, Matsuyama, Japan ([*]inoue@sci.ehime-u.ac.jp)
[2]Dept. of Earth Sciences, Hokkaido University, Sapporo, Japan

Water is the most abundant volatile component in the Earth, and the presence of H_2O in mantle minerals affects elastic and rheological properties. It is well known that wadsleyite and ringwoodite, which are the most abundant minerals in the mantle transition zone, can accommodate a significant amount (up to ~3 wt %) of H_2O in their crystal structures (e.g. [1,2]). Recently, we have reported the partitioning of H_2O between high pressure polymorphs of olivine (wadsleyite, ringwoodite, and perovskite) [3] in the system $(Mg,Fe)_2SiO_4$-H_2O, and knowledge of the water content in these minerals has been clarified well. On the other hand, majorite garnet is the second abundant mineral in the mantle transition zone, but there are few reports for the H_2O content except for [4]. In addition, there are few reports for the H_2O content of Al-bearing perovskite and Al-bearing stishovite, except for [5-7]. We have conducted high pressure experiments to determine the water content of majorite garnet, Al-bearing perovskite, and Albearing stishovite.

High-pressure experiments were conducted by an MA-8 type (Kawai-type) high-pressure apparatus at Ehime University. We used a pyrolite composition which was approximated with respect to five major components, CaO, MgO, FeO, Al_2O_3, and SiO_2. Two starting H_2O contents, 2.9 and 8.3 wt% were selected. The experimental P-T conditions were 22-23 GPa and 1300-1700°C. The recovered samples were polished and then the chemical compositions were determined by EPMA at Ehime University and the H_2O contents of the minerals were measured by SIMS at Hokkaido University.

The recovered run products at 22 GPa and in the H_2O 2.9 wt% system were basically majorite garnet + ringwoodite + liquid, and ringwoodite was transformed to perovskite at 23 GPa. On the other hand, those at 22 GPa and in the H_2O 8.3 wt% system were basically majorite garnet + stishovite + liquid, because the extra MgO-rich liquids were generated under hydrous and highpressure conditions and stishovite became liquidus under those conditions. The H_2O content of ringwoodite decreased with increasing temperature from ~1.8 wt% at 1400°C to ~0.5 wt% at 1700°C, which is consistent with Ohtani et al. (2000). However, the H_2O content of majorite did not change so much with increasing temperature from ~0.3 wt% at 1400°C to ~0.2 wt% at 1700°C. In addition, the coupling phenomena between H^+ and Al^{3+} were observed in both Al-bearing perovskite and Al-bearing stishovite. Further details will be presented.

[1] Inoue, T. et al. (1995) *Geophys. Res. Lett.*, **22**, 117-120. [2] Kohlstedt, D.L. et al (1996) *Contrib. Mineral. Petrol.*, **123**, 345-357. [3] Inoue, T. et al. (2010) *Phys. Earth Planet. Int.*, in press. [4] Katayama, I. et al. (2003) *Geophys. Res. Lett.*, **30**, SDE5-1 - SDE5-4. [5] Murakami, H. et al. (2002) *Science*, **295**, 1885-1887. [6] Litasov, K.D. et al. (2003) *Earth Planet. Sci. Lett.*, **211**, 189-203. [7] Litasov, K.D. et al. (2007) *Earth Planet. Sci. Lett.*, **262**, 620-634.

Hydrogen defects and diffusion in alkali feldspars

Behrens, H.
Institut für Mineralogie, Leibniz Universität Hannover, Germany (h.behrens@mineralogie.uni-hannvoer.de)

Hydrogen defects in Eifel sanidines and an adularia from unknown locality were studied combining IR spectroscopy with heating and diffusion experiments under well controlled conditions. Near infrared spectra show that OH groups are predominant hydrous species in Eifel sanidine but presence of minor amounts of molecular H_2O cannot be excluded. Short term annealing at 400°C produces a small but significant irreversible change in the OH stretching vibration band. The portion of hydrous species with low H-bonding (adsorbing at wavenumbers around 3450 cm^{-1}) is increased on expense of species with low hydrogen bonding (adsorbing at 3200 cm^{-1}).

Polarized mid-infrared spectra of sanidine and adularia plagioclase recorded *in situ* at temperatures up to 600°C show shifts of maxima towards higher wavenumber and an overall decrease in integrated intensities. However, no evidence was found for further rearrangement in local environment of hydrogen upon heating. The dichroic scheme of OH vibration bands remains basically unchanged with predominant orientation of OH dipoles along the crystallographic *a*-axis. In Eifel sanidine a second type of OH dipoles oriented parallel to *b** is observed also in the high temperature spectra.

At 900 – 1000°C Eifel sanidines rapidly lost about one third of hydrogen which is very mobile in the feldspar structure. The remaining hydrogen is more strongly bonded and can be removed only by long term annealing at high temperatures under extremely dry conditions (i.e. in air dried by phosphorus pentoxide). Annealing experiments under controlled water pressures show constant hydrogen contents in the sanidine below 1 bar (except for extremely low water fugacity) and a continuous increase in hydrogen concentration with water fugacity above 1 bar. These findings support that the Eifel sanidines contain two OH species, a mobile one and a strongly localized one.

Diffusion of hydrogen in sanidine and adularia was investigated by D/H isotope exchange in the T range 600 – 1050°C at ambient pressure and at elevated pressures up to 400 MPa. Runs at 1 atm were performed in a fused silica tube connected to a liquid D_2O reservoir at room temperature. In the high pressure experiments samples were sealed with D_2O in gold capsules and processed in externally heated pressure vessels using Ar/D_2O as the pressure medium. Diffusion coefficients were determined either by measuring concentration-distance profiles of OH and OD with an IR microscope or by measuring the total exchange of oriented plates after various run durations using a macroscopic IR technique. Both methods gave consistent data. D/H interdiffusion in sanidine is independent on the crystallographic orientation and can be described at ambient pressure by

$$D = 9.6^{+4.6}_{-2.8} \cdot 10^{6} \frac{m^2}{s} \exp\left(\frac{-162 \pm 3\, kJ / mol}{RT}\right).$$

Diffusion rates are almost identical for adularia and sanidine implying that the chemical composition and the degree of Al/Si disorder have minor influence on D/H interdiffusion in alkali feldspars. On the other hand, the hydrogen diffusivity is strongly enhanced by water pressures, i.e. D is 0.7 log units faster at 200 MPa than at ambient pressure. When using mixed D_2O/CO_2 fluids for isotope exchange, the diffusion coefficients are systematically lower than for a pure D_2O fluid, which demonstrates that the enhancement of hydrogen diffusivity is due to water fugacity and not to pressure.

Diffusion of water through quartz: the use of synthetic fluid inclusions

Bakker, R.J.
Dept. of Applied Geosciences and Geophysics, Mineralogy and Petrology, University of Leoben, Austria (bakker@unileoben.ac.at)

Diffusion of water and water-related species, such as D_2O, $H_2{}^{18}O$, H_2, O_2 through anhydrous quartz were experimentally investigated in this study by analyzing the properties of fluid inclusions. Fluid inclusions with known fluid composition and density were synthesized in anhydrous natural quartz. The fluid inclusions are synthesized in cylindrical cores that were drilled in specific crystallographic orientations from the starting material. Micro-cracks are formed in those cores by rapid cooling after heating up to about 400°C. The fluid inclusions are synthesized by crack-healing at high experimental temperature and pressure in autoclaves with a confining hydrostatic pressure (argon). The experimental conditions were selected within the α-quartz or β-quartz stability field (max. 700°C and 1 GPa). The inclusions were characterized by a detailed petrographical study (distribution and morphology), microthermometry and Raman spectroscopy. Subsequently, those inclusions were re-equilibrated at high temperature and pressures in a fluid environment that differs from the included fluid. Re-equilibration conditions are selected at similar temperature-pressure conditions to minimize the effect of pressure gradients that could induce additional mechanisms of fluid inclusion alteration. The imposed gradients in chemical potential (or concentration) between fluid inclusions and the outside of the crystal provoke diffusion of the specific fluid components. Any change in the properties of the original fluid inclusions were detected and quantified mainly by microthermometry and Raman spectroscopy. A relationship between the length of the diffusion path (depth of inclusion below the crystal surface) and fluid inclusion properties were expressed in a "concentration" profile along the crystal, that was used to determine a three dimensional diffusion model and corresponding diffusion coefficients.

The available mathematical diffusion models and temperature dependent diffusion constants for water-related species through quartz are not consistent with the obtained results, which is mainly caused by the difficulty by which those parameters were determined. Therefore, a new mathematical diffusion model was developed according to the boundary conditions of the experiments as a specific solution of the Fick's laws.

The new diffusion model is applied to the study in re-equilibration of natural fluid inclusions, and results in extremely fast re-equilibration rates. Diffusion according to this model may be restricted and partly inhibited by several important boundary factors, such as the low porosity in metamorphic rock and relative low temperatures in sedimentary and diagenetic rocks. The imprecision of estimated diffusion coefficients and the undetermined accuracy do not allow reliable diffusion calculations. A computer-program has been developed to perform mathematical experiments on the re-equilibration-rate of randomly located fluid inclusions in spherical quartz grains. The diffusion of H_2O, CO_2, CH_4 and NaCl can be taken into account in this computer model, which is freely downloadable from the web site http://fluids.unileoben.ac.at.

Isotopic diffusion of hydrogen in apatite

Ingrin, J.*, Calvot, G., Condamine, P. & Sicard, D.
LMTG, Université de Toulouse, CNRS, IRD, OMP, Toulouse, France (*ingrin@lmtg.obs-mip.fr)

Kinetics of hydrogen - deuterium exchange were investigated by FTIR spectroscopy on two gem quality single crystals from Durango (Mexico) and Madagascar. Annealing experiments were performed at ambient pressure, between 973-1273 K under a flux of argon enriched in D_2 and D_2O. During exchange all the OH absorption bands have the same behaviour, but the kinetics are different with the direction of diffusion:

$$D_{\perp C} = D_0 \exp\left[\frac{-(150 \pm 22)\,\mathrm{kJ/mol}}{RT}\right], \log D_0\,(\mathrm{m^2/s}) = -7.7 \pm 1.0$$

$$D_{//C} = D_0 \exp\left[\frac{-(124 \pm 21)\,kJ/mol}{RT}\right], \log D_0\,(m^2/s) = -9.9 \pm 0.9$$

The diffusion in the basal plane of the crystal is faster than the diffusion perpendicular to it in the direction [001], with almost one order of magnitude difference. The diffusion rates are faster than the diffusion rates measured by Brenan [1] for the exchange of H, Cl and F at room pressure. However, our rates of diffusion are closer to the average result exchange rates found by Brenan [1] at high pressure. This suggests that the exchange of H, Cl and F in apatite could be controlled at high pressure by the mobility of hydrogen.

The knowledge of hydrogen diffusion in apatite can be used to measure fast event in volcanic processes.

[1] Brenan, J. (1994) *Chem. Geol.*, **110**, 195-210.

Water concentrations in the lithosphere from three different tectonic settings of the Carpathian-Pannonian region

Kovács, I.[1*], Falus, Gy.[1], Hidas, K.[1,2], Szabó, Cs.[2] & Ingrin, J.[3]
[1]Eötvös Loránd Geophysical Institute of Hungary, Budapest, Hungary ([*]kovacsij@elgi.hu)
[2]Lithosphere Fluid Research Lab, Eötvös University, Budapest, Hungary
[3]LMTG, Université de Toulouse, CNRS, IRD, OMP, Toulouse, France

The identification of "water" (i.e., OH^-, H_2O) as a trace element at defect sites in nominally anhydrous minerals (NAMs for short) has drastically changed the concept of "water" storage in the upper mantle and crust. In the past decades our knowledge on the lithosphere and astenosphere beneath the Carpathian-Pannonian region (CPR) has been greatly improved by the studies of xenoliths hosted in the Plio-Pleistocene alkaline basalts [1]. Studying "water" in xenoliths of the CPR improves considerably our understanding on its concentrations and on its possible effect on rheological properties in a well-known geological setting. A new infrared technique [2] utilizing unpolarized light enables accurate determination of water concentrations in NAMs even from fine-grained mantle xenoliths. Peridotite xenoliths from three Plio-Pleistocene alkaline basaltic localities were studied in different tectonic settings (BBH, NG, ETB). The Bakony-Balaton Highland (BBH) is in the center of the CPR and the lithosphere beneath the area suffered considerable extension in the Miocene, therefore the lithosphere is considerably thinned (~60 km) and characterized by high heat flow. The Nógrád-Gömör area (NG) is in a transitional tectonic setting as its southern part is characterized by a thinned lithosphere similar to BBH, but the lithosphere thickens gradually towards the north and at its northernmost part it shows a thickness similar to the ambient (100-120 km) lithospheric thickness in the CPR. The East Transylvanian Basin (ETB) is in a different tectonic setting as it was not affected by the Miocene extension. The ETB area has normal lithospheric thickness, but it is close to the youngest subduction system in the CPR. Our preliminary results indicate that the concentration of "water" in NAMs of the shallow lithosphere (<60km) close to the young subduction along the Eastern Carpathians (ETB) and in the transitional setting (NG) are higher than in the shallow lithosphere of the BBH situated in the central CPR. These results may imply that the lithospheric mantle in the ETB [3] and NG areas has higher water concentrations due to the Miocene subduction in the ETB and the smaller or transitional extension in the NG. This is an indication that water concentration in the lithosphere may be used as an additional „tool" to put constraints on the geodynamic history of a particular lithospheric column.

[1] Szabó, Cs. et al. (2004) *Tectonophys.*, **393**, 119-137. [2] Kovács, I. et al. (2008) *Am. Mineral.*, **93**, 765-778. [3] Falus, G. et al. (2008) *Earth Planet. Sci. Lett.*, **272**, 50-64.

IR-imaging of synthetic crystals and natural rocks

Stalder, R.
Institut für Mineralogie und Petrographie, Universität Innsbruck, Austria (roland.stalder@uibk.ac.at)

During the last decades IR spectroscopy has been the major technique to characterise the water incorporation in nominally anhydrous minerals in terms of structural environment, orientation of the OH dipole and quantification of water content. When using single element detectors the spatial resolution is limited to about 20µm, because of significant diffraction of the IR radiation at the rim of the aperture masking the analysed spot.

By the application of a focal plane array detector (FPA) no aperture is needed and a pixel resolution of <3 µm (i.e. in the order of the wavelength of the IR radiation) can be reached.

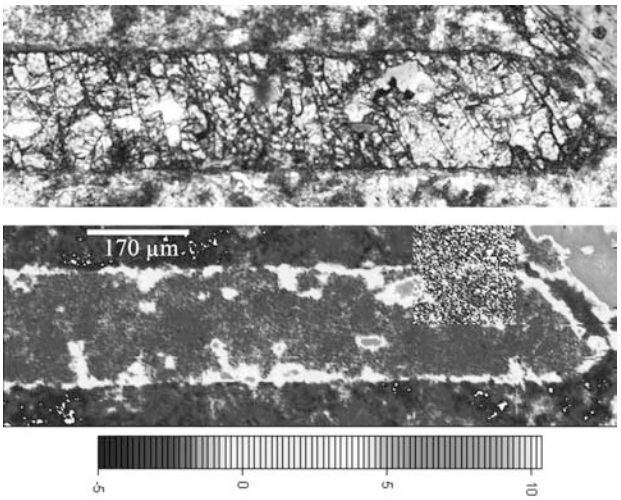

Fig. 1: Cpx from a carbonatite from Alnö/Sweden in transmitted light (above) and as IR-absorption image of the integral absorbance of the band between 3630 and 3740 cm^{-1} (below), characteristic for OH in mica and amphibole.

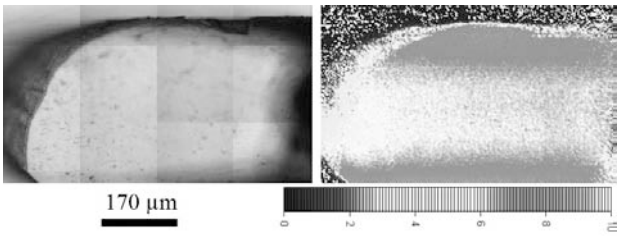

Fig. 2: Synthetic enstatite doped with Cr and Al synthesized at 25 kbar and 1150°C in transmitted light (left) and as IR-absorption image of the integral absorbance of the band between 3490 and 3590 cm^{-1} (right), which is characteristic for tetrahedral OH-defects in Opx.

In this study an IR-microscope equipped with a focal plane array detector consisting of 64 x 64 MCT-pixel is applied to image IR absorption bands of a broad variety of natural and synthetic samples, ranging from oriented single crystals from high-pressure experiments to thick sections of igneous and metamorphic rocks. The work is focussed on the detection of nominally OH-bearing micro-inclusions in nominally anhydrous minerals (Fig. 1) and the distribution and zonation of OH-defects in single crystals (Fig. 2).

Experimental rehydration of mantle pyroxenes

Sundvall, R.* & Skogby, H.
Dept. of Mineralogy, Swedish Museum of Natural History, Stockholm, Sweden (*rickard.sundvall@nrm.se)

The role of low water contents occurring in the nominally anhydrous minerals (NAMs) of the upper mantle has received a strong interest during recent years, since these phases are capable of storing water in the upper mantle. However, one crucial question that has not yet received a satisfying answer is: To what extent has hydrogen been lost in mantle xenoliths during ascent process, and how representative are the water concentrations reported from these xenoliths for the original conditions of the upper mantle?

From a considerable amount of studies of dehydration kinetics of pyroxenes and other mantle NAMs it is clear that dehydration may occur relatively fast following the redox reaction:

$$OH^- + Fe^{2+} = O^{2-} + Fe^{3+} + \tfrac{1}{2}H_2 \qquad (1)$$

This reaction proceeds by the diffusion of protons and electron holes (polarons) and appears fast enough to allow substantial changes in H concentrations during the time and temperature regimes of most magma ascent processes. However, the reactions controlling the host defects associated with H incorporation (i.e. vacancies and charge-deficient substitutions) involve cation diffusion, with kinetics typically two orders of magnitude slower than that for redox exchange [1]. This means that the host defects have a much higher likelihood to be preserved than the hydrogen itself. Hence, it appears possible to experimentally restore lost hydrogen into the structure by driving reaction (1) backwards, as long as the temperature and time of such experiments are limited to leave the defect state of the structure largely unchanged.

We have performed a systematic study on a range of ortho- and clinopyroxene samples from different mantle occurrences to investigate their re-hydration capacity. The experiments were performed as step-wise heat treatments in 1 atm. H_2 of crystallographically oriented crystal sections. FTIR spectroscopy was used to monitor the change in OH concentration after each heating step. The results show that most natural samples do not respond significantly to thermal annealing in H_2 under these conditions. However, two of twelve studied samples show a strong stepwise increase in water contents that level off to a saturation value. Prolonged heat treatments in H_2 cause a slight decrease of the water contents. The results indicate that most mantle samples have not lost substantial amounts of water during late stages of the ascent process, and that it is possible to experimentally restore water contents in samples which do have lost water by the redox reaction (1).

[1] Ingrin, J. & Blanchard, M. (2006) *Rev. Mineral. Geochem.*, **62**, 291-320.

Evidence of structural OH groups in xenotime

Talla, D.[1,2*], Beran, A.[2], Losos, Z.[1] & Skoda, R.[1]
[1]Institute of Geological Sciences, Masaryk University, Brno, Czech Republic (*sutrar@volny.cz)
[2]Institut für Mineralogie und Kristallographie, Universität Wien, Vienna, Austria

Xenotime, YPO_4, a well-known accessory mineral in the Earth's crust, has been subject to FTIR-spectroscopic investigations. A series of absorption bands, of which the most prominent peak occurs at 3519 cm^{-1}, has been determined in xenotime samples from different localities. The occurrence of these bands indicates the presence of traces of structurally bound hydrogen atoms in the xenotime structure.

Based on their pleochroic behaviour, determined by polarized IR measurements, the studied absorption bands can generally be divided into three groups. Whereas those centered at lower wavenumbers up to 3550 cm^{-1} have their absorption maxima parallel to the crystallographical *c*-axis, absorption phenomena at higher energies are generally most pronounced with the polarization direction of the IR beam perpendicular to the main crystal axis. Finally, a weak band doublet with a different degree of orientation in respect to the crystallographical axes occurs at wavenumbers exceeding 3600 cm^{-1}. The high wavenumber of these bands, along with the poor degree of their pleochroism, is indicative of submicroscopic inclusions of phyllosilicates, such as sericite [1,2].

A more detailed investigation of the band pleochroism within both 'intrinsic' OH absorption bandgroups, supported by spectral measurements at LN_2 temperature, confirms further variations of the pleochroic behaviour with respect to the crystal structure. The IR spectra recorded at low temperature are characteristic with enhanced band resolution, also aiding in the determination of hidden peaks.

Based on the O_D-O_A distance correlation diagrams [3] and with regard to the crystal structure of xenotime [4], several possible OH defect incorporation sites have been determined. Bands displaying absorption maxima parallel to the *c*-axis are indicative of a hydrogen atom bound to the corner oxygen of either a vacant PO_4 polyhedron, or an occupied one, associated with a vacancy on the Y site. OH dipoles oriented nearly perpendicular to the *c*-axis may also be associated with the mentioned Y-site vacancy. In general, the role of the replacement of Y by $REEs^{3+}$ as well as P^{5+} by Si^{4+} has to be taken into account to explain minor differences in the OH dipole orientation as well as band splitting.

The results of heating experiments confirm the presence of several types of structural OH groups in xenotime, but also cause new OH absorption phenomena at lower wavenumbers.

The results of sample deuteration at 900°C prove a different response of the various OH defect types to this procedure, as maximum absorption of prominent O-D bands occurs solely perpendicular to the *c*-axis.

Xenotime is isostructural with zircon, where the presence of hydrous defects is now well established. The results of the current study can be used among other for a valuable comparison of both mentioned phases.

Acknowledgements: The support of the current work by grants (MSM0021622412-10, KJB301630801) is gratefully acknowledged.

[1] Farmer, V.C. (1974) in Farmer, V.C. (ed.) *The infrared spectra of minerals*. Mineral Soc., London, 331-363. [2] Wieczorek, A. et al. (2004) *Schweiz. Mineral. Petrogr. Mitt.*, **84**, 333-343. [3] Libowitzky, E. (1999) *Mh. Chemie*, **130**, 1047-1059. [4] Ni, Y. et al. (1995) *Am. Mineral.*, **80**, 21-26.

Water in tektites by proton-proton scattering, IR- and Raman spectroscopy

Thomas, S.-M.[1*], Thomas, R.[2], Reichar, P.[3], Bina, C.R.[1] & Jacobsen, S.D.[1]
[1]Dept. of Earth and Planetary Sciences, Northwestern University, Evanston, IL, USA
([*]smthomas@earth.northwestern.edu)
[2]Helmholtz Centre Potsdam, GFZ German Research Centre for Geosciences, Potsdam, Germany
[3]Universität der Bundeswehr München, Neubiberg, Germany

Raman spectroscopy and proton-proton (pp) scattering routines have been developed to determine water contents ranging from a few wt ppm to wt% in glasses and nominally anhydrous minerals [1,2]

Those routines are promising examples of quantification tools to determine material specific molar absorption coefficients for infrared (IR) spectroscopy. Material specific absorption coefficients are required because general IR calibrations do not necessarily apply to minerals and silicate glasses with water incorporated in the form of OH groups.

Absorption coefficients and water contents for a set of tektite glasses were independently determined with pp-scattering, IR and Raman spectroscopy. First precise measurements of water content in this material were only reported in the 70s using IR spectroscopy. Accordingly, the water content in tektite glasses is very low, ranging from 2 to 300 wt ppm H_2O [3] and has been used for debating their origin, terrestrial or lunar. However, independent studies using advanced techniques are not available.

In this study we will present new measurements and test, discuss and review available data, the feasibility of existing IR calibrations and implications for tektite glass origin.

[1] Thomas, S.-M. et al. (2008) *Am.. Mineral.*, **93**, 1550-1557. [2] Thomas, S.-M. et al. (2009) *Phys. Chem. Minerals*, **36**, 489-509. [3] Beran, A. & Koeberl, C. (1997) *Meteor. Planet. Sci.*, **32**, 211-216.

Environment of diamonds in eclogites from kimberlites (Yakutia): application to their genesis

Spetsius, Z.V.[1*] & Kamenetsky, V.S.[2]
[1]Scientific Investigation Geology Enterprise, ALROSA Co Ltd, Mirny, Russia ([*]spetsius@cnigri.alrosa-mir.ru)
[2]ARC Centre of Excellence in Ore Deposits, University of Tasmania, Hobart, Tasmania, Australia

Eclogite xenoliths from kimberlites worldwide display evidence of partial melting and metasomatism, caused by introduction of K-Na–rich fluids. There is compelling evidence for a late and multistage formation of diamonds in eclogites that is connected with partial melting and metasomatism [1,2]. The primary eclogite minerals and various secondary phases around diamonds in eclogites from the Udachnaya pipe were investigated by ESM with EDS in order to elucidate the relationships between diamonds and metasomatic processes.

Diamonds in eclogites are distributed between rock-forming garnet and clinopyroxene, and in most cases surrounded by metasomatic minerals. These minerals represent different stages of metasomatic events that start as a partial melting of primary garnet and clinopyroxene. The crystallization products of this reaction, typically represented by a "spongy" cpx around primary omphacite, include secondary clinopyroxene (with lesser Na_2O and Al_2O_3), feldspar and glass. Primary garnet also shows evidence for partial melting with typical development of kelyphitic rims. Intragranular veins of crystallized partial melt are represented by spinel, plagioclase, amphibole and phlogopite. Metasomatic assemblages around diamonds are rich in carbonate, apatite and sulfide blebs.

The compositions of secondary phases suggest that these metasomatic and partial melting events took place at decreasing P and varying T, usually tlower than the equilibration T of the rock-forming garnets and clinopyroxenes. The compositions of newly-formed minerals indicate that melting was not isochemical, but involved the introduction of metasomatic fluids rich in alkalis, mainly K, and probably volatile elements, such as carbon. Fluids play an important role in initiating partial melting of eclogites and metasomatic growth of diamonds.

The diamonds in xenoliths can have unusual forms of growth such as hopper crystals, which include partially melted clinopyroxenes. Some diamonds show skeletal growth and have captured secondary pyroxene as inclusions. There are also crystals that look like "coated" diamonds. These observations suggest that some of the diamonds in eclogites grew simultaneously with the metasomatic minerals in non-equilibrium, metastable conditions. Diamonds crystallized in a volatile-rich melt or formed from a fluid. Metasomatic processes occurred over a broad spectrum of PT-conditions, as well as compositions of both original rocks and mantle fluids that are now recorded in the secondary mineral assemblages.

The partial melting of primary eclogitic minerals was initiated by metasomatic fluids upon entrapment of xenoliths by the kimberlite magma, and continued during upward movement of the kimberlite to depths of ~30 km. Metasomatic growth of diamonds in eclogite xenoliths could be repeated and may have been closely associated with metasomatic influx that resulted in partial melting. Spatial correlations exist between the presence of some diamonds and the partial-melt products, as well as metasomatic zones. We propose that the growth of some diamonds was associated with partial melting and metasomatism that further promoted formation of second generation of diamonds, as well as last-stage fibrous diamond coatings, some microdiamonds, and cubes.

[1] Spetsius, Z.V. (1998) *Proceed. 7th IKC, Cape Town*, **2**, 823-828. [2] Spetsius, Z.V. & Taylor, L.A. (2002) *Int. Geol. Rev.*, **44**, 973-987.

"Maltese-cross" diamonds: a spectroscopic approach to understanding formation conditions and element partitioning

Howell, D.[*], Griffin, W.L., O'Reilly, S.Y., O'Neill, C., Pearson, N. & Grant, K.
GEMOC, ARC National Key Centre, Macquarie University, Sydney, Australia ([*]dhowell@science.mq.edu.au)

An interesting set of diamond samples (locality unknown) shows a variety of 'maltese-cross' sectorial growth features (Fig. 1). The samples are all in the form of plates cut from the centre of the original diamonds. They are characterised by high nitrogen concentrations (>1800 ppm) and 10–20% IaB nitrogen aggregation.

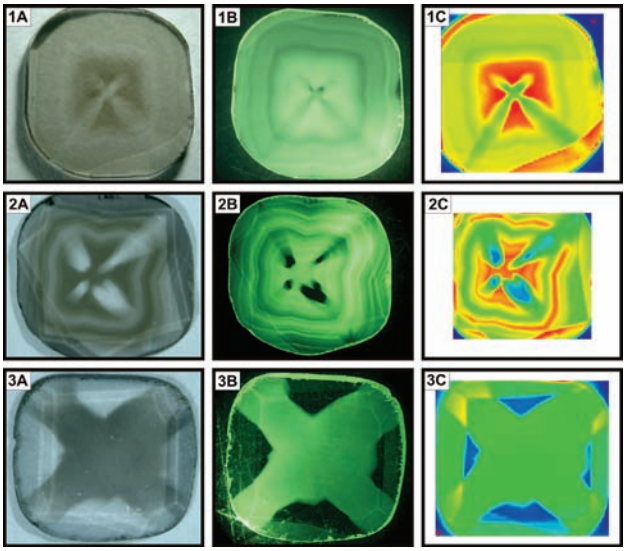

Fig. 1: Images of 3 diamonds from the collection of 13. Images A are taken under visible light, B are taken under UV & C are false colour IR maps showing the relative intensity of the 3107 cm^{-1} (hydrogen) band (blue shows lowest absorption and red the highest).

A new method of IR mapping that can deconvolute several thousand spectra from an individual stone is being applied to these samples. This novel technique can produce false-colour maps showing the distribution of nitrogen content and aggregation states, as well as hydrogen and platelet defects. These maps should allow for easier characterization of samples based upon their concentration and distribution parameters of these various defects [1]. They may also provide data regarding the preferential incorporation of nitrogen on the octahedral faces compared to the cube faces [2,3].

Nitrogen incorporation in diamond has been interpreted as being both compatible [4] and incompatible [5]. The incompatible-behaviour model suggests that high nitrogen concentrations occur due to rapid disequilibrium growth, while slow equilibrium growth would produce nitrogen-free (Type II) diamonds. How the interpreted growth histories of these samples fit into this argument will be of great interest.

[1] Kaminsky, F.V. & Khachatryan, G.K. (2004) *Lithos*, **77**, 255-271. [2] Boyd, S.R. et al. (1988) *Nature*, **331**, 604-607. [3] Boyd, S.R. et al., (1994) *Chem. Geol.*, **116**, 29-42. [4] Stachel, T. & Harris, J.W. (2009) *J. Phys. Condens. Matter.*, **21**, 364206. [5] Cartigny, P. et al. (2001) *Earth Planet. Sci. Lett.*, **185**, 85-98.

Combined FIB/TEM and micro computer-tomography of polycrystalline diamond (framesite) from Orapa, Botswana

Jacob, D.E.[1*], Wirth, R.[2], Enzmann, F.[1] & Kronz, A.[3]
[1]Dept. of Geosciences and Earth System, Science Research Centre, Johannes Gutenberg-Universität, Mainz, Germany
([*]jacobd@uni-mainz.de)
[2]GFZ Potsdam, Germany
[3]Geowissenschaftliches Zentrum der Universität, Göttingen, Germany

Micro- and nano-inclusions in polycrystalline diamonds provide a unique source of information on the nature and timing of small scale processes that lead to diamond formation [1,2] and complement research on fibrous diamonds as well as more "traditional" inclusion suites in gem diamonds.

A single specimen from the Orapa kimberlite was studied in detail by SEM, EPMA, FIB-assisted TEM and µCT. It is the first time that these methods were applied in combination to a single framesite specimen. The beauty of this approach lies in the resulting dataset that combines 3D-structual data by µCT with a resolution of ca. 1.3µm per voxel (see Fig. 1) with a "seamless" extension into nanometre-scale resolution achieved by FIB/TEM [3].

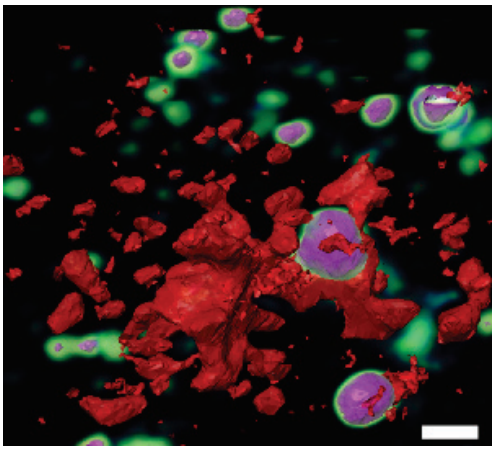

Fig. 1: High-resolution µCT showing magnetite (purple) surrounded by hematite (green) and open pore space (red) in polycrystalline diamond. The diamond is rendered invisible in this view. Scale bar is 100µm.

Macro-inclusions, larger than 5µm, in the specimen are magnetite, FeS, low Cr garnet ($Py_{50}Alm_{39}Grs_{11}$) and omphacite as discrete grains in the interstices. TEM analyses of 25 FIB foils yielded a micro-inclusion assemblage of magnetite, hematite, FeS, rutile, omphacite and C-H-O fluid [4].

Hematite was always found to surround magnetite (Fig. 1), often in paragenesis with a sheet silicate. Diamond in the vicinity of these minerals is always corroded, implying that this paragenesis is of late (possibly surface) origin. In contrast, one FeS micro-inclusion was found to be rimmed with magnetite and a layer of amorphous carbon towards the inclusion-diamond interface. This clearly attests to formation of this paragenesis in the diamond stability field.

Importantly, the micro-inclusion suite described here is distinct from that found in fibrous and in microdiamonds. Instead of carbonates and halides, the micro-inclusion suite here consists of the typical eclogitic minerals (rutile, garnet, omphacite, sulphide) plus a C-H-O fluid.

[1] Jacob, D.E. et al. (2004) *Contrib. Mineral. Petrol.*, 146, 566-576. [2] Jacob, D.E. et al. (2000) *Science*, 289, 1182-1185. [3] Wirth, R. et al. (2004) Eur. J. Mineral., 16, 863-876. [4] Jacob, D.E. (2008) *Extended Abstr. 9th Intern. Kimberlite Conf.*, A0015

Finding primary fluid inclusions in carbonado diamond and its implication to the origin

Kagi, H.[1*], Sakurai, H.[1], Ishibashi, H.[1] & Ohfuji, H.[2]
[1]Geochemical Research Center, University of Tokyo, Japan
([*]kagi@eqchem.s.u-tokyo.ac.jp)
[2]Geodynamic Research Center, Ehime University, Matsuyama, Japan

Carbonado is a group of natural polycrystalline diamonds whose origin is still controversial. Our recent study on infrared absorption spectra and Raman spectra of Central African carbonado reported the presence of fluid inclusions and high residual pressure in the diamond [1]. These results suggested that C-O-H mantle fluid was trapped in the carbonado sample and carbonado had grown in the volatile-rich environment in the mantle. However, it was still unclear that the fluid inclusions in carbonado existed inside of diamond grains or in the grain boundaries. In this study, we precisely investigated location of the fluid inclusions from spectroscopic measurements and TEM observations.

A carbonado grain with hundreds of micrometer in diameter was heated incrementally at temperatures from 700 to 1100°C under vacuum. After heating at each temperature condition, infrared absorption spectra were measured. Absorption bands assignable to liquid water were observed up to 950°C right before graphitization occurred. This observation strongly suggests that the fluid was trapped inside of diamond grains.

For obtaining direct evidence of fluid inclusion existing inside of a diamond grain, we conducted TEM observations on an FIB-fabricated thin foil of carbonado. Fig. 1 shows a void found in the carbonado sample. The void was surrounded by (111) equivalent crystal faces. The octahedral void controlled by crystal habit of host diamond strongly suggests that the void is the negative crystal of diamond. The existence of negative crystal of diamond indicates that the fluid equilibrated with diamond crystals. The present study supports that the growth environment of carbonado was in the mantle being rich in C-O-H fluid.

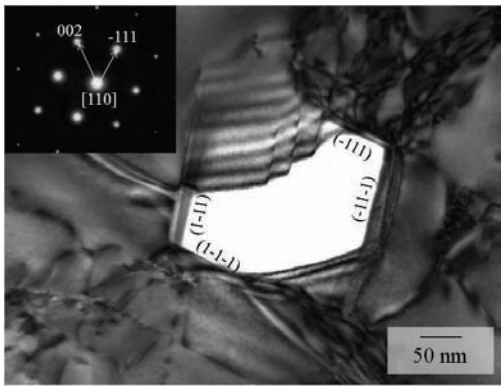

Fig. 1: TEM image of a void in FIB film of carbonado obtained using the [110] convergent beam.

[1] Kagi, H. & Fukura, S. (2008) *Eur.J. Mineral.*, **20,** 387-393.

Experimental study of syngenetic relations of diamond and its inclusions in the heterogeneous system eclogite-carbonatite-sulfide-diamond at 7.0 GPa

Vasiliev, P.[1*], Okoemova, V.[1], Litvin Y.[2] & Bobrov, A.[1]
[1]Geological Faculty, Moscow State University, Moscow, Russia
([*]prokvsailiev@gmail.com)
[2]Institute of Experimental Mineralogy, Chernogolovka, Russia

The role of physicochemical experiment is decisive for understanding of chemical and phase state of mantle diamond-forming media [1]. Application of the criterion of syngenesis of diamonds and primary inclusions is special importance for investigation of the systems with compositions similar to natural multi-component diamond-forming media. We studied melting relations for syngenesis of diamond and inclusions in the system eclogite (garnet +clinopyroxene) – K-Mg-Ca-carbonatite – sulfide (mixture of pyrrhotite, pentlandite, and chalcopyrite) – diamond at 7.0 GPa by the analysis of a fragment of the syngenesis diagram within the pseudo-binary section eclogite50-carbonatite50-diamond. The main element of this diagram is the curve of diamond solubility in completely miscible carbonate-silicate melts depending on temperature. The diagram shows melting relations in carbon-saturated diamond-forming carbonate-silicate melts with silicate (garnet and clinopyroxene) and carbonate (magnesite, aragonite, and K-carbonate) mineral phases.

The syngenesis diagram for the sulfide-diamond system contains the curve of diamond solubility in sulfide melts depending on temperature and demonstrates the areas where diamond growing in carbon-sulfide melts captures inclusions of sulfide melts and minerals. The general diagram of the multi-component eclogite-carbonatite-sulfide-diamond systems is a combination of two discussed diagrams. It demonstrates two curves of diamond solubility in sulfide and carbonate-silicate melts. The results obtained provide evidence for complete immiscibility of carbonate-silicate and sulfide components of parental melts and predominant crystallization of diamond in carbonate-silicate media. This is consistent with the carbonatite (carbonate-silicate) model of diamond genesis [1].

[1] Litvin, Y.A. (2007) in Ohtani, E. (ed.) *Geol. S. Am. S.*, **421**, 83-103.

Mantle-carbonatite genesis of diamond by mineralogical and experimental evidence

Litvin, Yu.A.
Inst. of Experimental Mineralogy, Russian Academy of Science, Chernogolovka, Moscow Region, Russia
(litvin@iem.ac.ru)

The physicochemical characteristics of the growth medium for most mantle-derived diamond can be only disclosed by combined use of mineralogical and experimental data. Diamond-hosted primary inclusions under residual pressure are representatives of the parent media. The parental compositions are multi-component and heterogeneous: major and minor components include oxides of Mg, Ca, Fe, Ti, Zr, Al, Si; silicates of Mg, Fe, Ca; alumino-silicates of Na, K, Mg, Ca, Fe; Fe, Ni, Cu sulfides; Ca phosphate; carbonates of Mg, Ca, Fe, K, Na, K; Na chloride; Si, Fe carbides; H_2O, CO_2, CH_4 fluids, native Fe, etc. The syngenesis of diamond and its primary inclusions is well-grounded. The importance of any of these heterogeneous materials in the crystallization of diamond cannot be evaluated by mineralogical data alone. Attempts to determine the most efficient medium in high-pressure experiments (by diamond "synthesis") fail because not one but a series of primary included materials (silicate-carbonate, carbonate, silicate, sulfide, chloride, metal, C-O-N-fluid…) were recognized. The only way out of the situation is the use of experimental criteria demanding that the growth medium should be equally efficient for the formation of diamond and its syngenetic phases. Experimental studies on diamond-forming multi-component heterogeneous systems peridotite-carbonatite-carbon, eclogite-carbonatite-carbon, grospydite-carbonatite-carbon, sulfide-diamond, eclogite-carbonatite-sulfide-diamond were carried out at 7.0 – 8.5 GPa and 1200 – 2000°C. It was found that (1) completely miscible carbonate-silicate melts saturated with dissolved carbon satisfy the syngenesis criterion because diamond forms together with silicate and carbonate minerals of peridotite and eclogite parageneses; (2) sulfide melts are completely immiscible with the carbonate-silicate ones and inconsistent with the syngenesis criterion, (3) diamond formation in peridotite-carbonatite-carbon and eclogite-carbonatite-carbon melts of variable composition is controlled by carbonatitic compositions (< 30 – 35 wt % silicate constituent). This is compatible with the mantle-carbonatite version of diamond genesis [1]: the growth medium for diamond and inclusions consists of the major carbonate and silicate components and phases ("paragenic"), contains minor admixed soluble ones ("paragenic") and coexists with insoluble immiscible components and phases ("xenogenic"). On the basis of the mantle-carbonatite model, a genetic classification of primary inclusions of minerals, melts and fluids in mantle-derived diamond has been developed [2].

Acknowledgements: Support: RFBR 08-05-00110.

[1] Litvin, Yu.A. (2007) in Ohtani, E. (ed.) *Geol. S. Am. S.*, **421**, 83-103. [2] Litvin, Yu.A. (2009) *Russ. Geol. Geophys.*, **50(12)**, 1188-1200.

Major and trace element composition of diamond-forming fluids: what do they tell us?

Weiss, Y.[1*], Griffin, W.L.[2] & Navon, O.[1]
[1]The Fredy and Nadine Herrmann Institute of Earth Sciences, the Hebrew University of Jerusalem, Israel
([*]yakov.weiss@mail.huji.ac.il)
[2]ARC National Key Centre for Geochemical Evolution and Metallogeny of Continents (GEMOC), Macquarie University, Sydney, Australia

The metasomatic medium in which fibrous diamonds grew is usually preserved in the form of high-density fluids (HDFs) trapped in sub-micrometer inclusions. Major and trace elements, and the volatile content of these fluids sheds light on the mantle sources and processes which promote diamond genesis. The major-element compositions of the HDFs span two arrays: (a) between a high-Mg carbonatitic end-member and a saline one and (b) between a low-Mg carbonatitic and a hydrous silicic end-member [1]. All four end-members are rich in K. In line with this enrichment, all are highly enriched in incompatible elements compared to primitive mantle. Their REEs are fractionated with $La/Dy_{(PM\ normalized)}$ varying from 6 in the silicic HDFs to 430 in the saline compositions; Sr, Ti, Zr, Hf and Y show variable negative anomalies relative to the REEs. The highly incompatible elements, Cs – La, exhibit two patterns. One is mostly flat and has moderate decrease of concentrations with decreasing ionic radius (this pattern is designated "Bench"); the other (designated "Table") has elevated Ba, U, Th and LREE, depleted Nb and Ta and in most cases, highly depleted alkalis (K, Rb and Cs). Both patterns were found in HDFs of either major element arrays.

The appearance of similar trace elements patterns in fluids of such diverse major element compositions suggest that major and trace elements are decoupled and that they are controlled by different sources or processes. Based on the similarity of the major-element composition of the HDFs to experimental near-solidus melts of carbonated/hydrous peridotites and eclogites, we suggest that the source-rock for the high-Mg carbonatitic HDFs is peridotitic, while the one for the low-Mg carbonatitic to hydrous-silicic compositions is eclogitic. The clear array between the saline and the high-Mg carbonatitic compositions suggests the involvement of saline fluids in the generation of the high-Mg carbonatitic HDFs. Saline fluids may be the metasomatic agent that triggers the formation of the silicic to carbonatitic fluids in the eclogitic case. However, melting of carbonates or K-bearing phases in the source-rock or interaction of such sources with carbonatitic and potassic melts/fluids may also generate similar compositions. Either way, potassium and carbonate should be available during HDF generation.

The trace element abundance patterns of the high-Mg carbonatitic HDFs resemble those of kimberlites. The huge variation in Th/Nb and La/Nb in carbonatitic-silicic and carbonatitic-saline HDFs suggests the involvement of rutile or a similar phase during HDF evolution. Similar arguments, based on major and trace element patterns, may be made for the involvement of other phases, such as zircon, apatite, mica and carbonates. Rocks rich in the above phases are known from xenoliths in kimberlites (e.g., MARID, PIC and glimmerites) and in many cases show the complementary anomalies to the "Table" pattern. On a K/Rb vs Cs/Rb diagram, HDFs with "Table" patterns fall on or very close to an array forms by Rayleigh fractionation of phlogopite from a MARID-like melt. These features indicate the importance of phlogopite in the formation and evolution of diamond forming fluids.

[1] Weiss, Y. et al. (2009) *Lithos*, **112**, 660-674.

Iron carbide inclusions within lower-mantle diamond: a result of oxidation of carbide to magnetite or the reduction of magnetite to native iron?

Kaminsky, F.[1*] & Wirth, R.[2]
[1]KM Diamond Exploration Ltd., West Vancouver, Canada
([*]felixvkaminsky@cs.com)
[2]Dept. Chemistry of the Earth, GeoForschungsZentrum Potsdam, Germany

A series of iron carbides have been identified in diamond from the Juina area, Brazil; this diamond crystal has also been shown to contain a set of carbonatitic-type inclusions. The iron carbides present are associated with magnetite, native iron and graphite, and form polymineralic inclusions of up to 7 μm in size (Fig. 1).

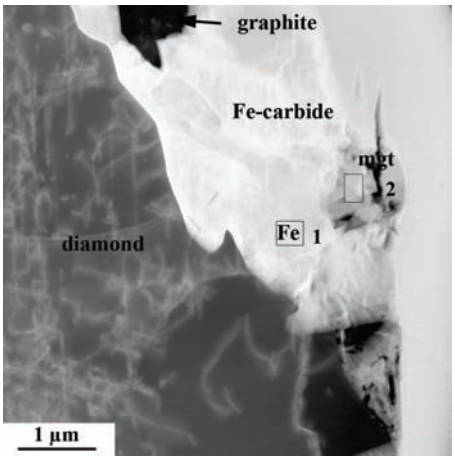

Fig. 1: HAADF image of an inclusion in diamond composed of magnetite, iron carbides, native iron, and graphite.

The studied iron carbides, by their chemical compositions, vary widely from grain to grain ($Fe_{3.98}C$ to $Fe_{1.25}C$). Chemical variations within grains are smaller, with Fe/C ratios varying within a range of 0.02 to 0.31. Minor amounts of Cr (0.03-1.30 at.%) and Ni (0.08-0.50 at.%) were identified in some iron carbide grains. Of particular interest is a nitrogen admixture in native iron.

The iron carbides form a compositional range with the following approximate formulas: Fe_4C – Fe_7C_2 – Fe_3C – Fe_2C – Fe_7C_4 – Fe_4C_3 – Fe_5C_4; as such, they are analogous to chromium carbides known from industry and are, most likely, interstitial compounds. From the six iron carbide varieties identified only one is known from a terrestrial environment, cohenite (Fe_3C). Cohenite has previously been identified in both monocrystalline diamond and polymineralic diamond aggregate. Another variety, chalypite (Fe_2C) is known only from meteorites; it predominates among the analysed grains (comprising around one third of them). The other iron carbide varieties are not known to occur in nature at this time.

There are two mechanisms which could explain the existence of this iron carbide series in a single diamond grain. The first related to the oxidation of an initial iron carbide: i.e., $FeC + O_2 \rightarrow Fe_3O_4 + C$ (graphite). This reaction occurs as the result of a change in oxygen fugacity under low pressure conditions (outside of the diamond stability field). Another scenario is that magnetite (or perhaps another iron oxide) is reduced during ascent of the host diamond to the surface, close to the boundary between the diamond/graphite stability fields, when it experienced local deviatoric stress conditions that resulted in the local recrystallisation of diamond carbon as graphite carbon. Simultaneously iron-containing phases were reduced and recrystallized to form of iron carbide(s) and native iron.

Natural silicon carbide from kimberlites: polytypes, trace elements, inclusions and speculations on its origin

Shiryaev, A.A.[1*], Griffin, W.L.[2], Tomshin, M.D.[3] & Okrugin A.[3]
[1]Institute of Physical Chemistry and Electrochemistry RAS, Moscow, Russia (*a_shiryaev@mail.ru)
[2]GEMOC, Macquarie University, Sydney, Australia
[3]Institute of Geology, Yakutsk, Russia

The origin of natural SiC (moissanite) found in carbonates, granitoids, kimberlites and other oxidised rocks is poorly understood, and it has often been assumed that the SiC is introduced during processing. However, in many cases contamination with synthetic SiC is implausible; it is clear that natural SiC (moissanite) does exist, but at present there is no consistent model for its formation. An extensive collection of moissanite grains from the Mir, Aikhal and Udachnaya kimberlite pipes, Yakutia, has been characterized in terms of structural perfection, defects, inclusions, and major- and trace-element chemistry and compared with synthetic SiC produced by various methods (Acheson, Lely).

Most natural SiC grains are 6H and 15R polytypes; some are 4H, 8H and 21R. No 3C grains were observed. Some grains (<10%) show extremely complex Raman spectra indicating strongly disordered structures, e.g., long-period polytypes. The shape of the LO band in the Raman spectra suggests the presence of significant amounts of non-compensated impurities. The spectra of some grains show vibrations related to OH groups or H in the SiC lattice. On average, the 15R grains are more enriched in impurities than the 6H grains. Cathodoluminescence maps and in-situ isotopic measurements indicate the existence of growth-related zoning on ~10-micron scale. Surprisingly, the density of dislocations and stacking faults is very low.

Our work has revealed considerable similarity between the geochemical properties (abundances of major and trace elements) of moissanites from geologically contrasting environments and stark differences with synthetic SiC. Trace-element chemistry provides a reliable method for distinguishing natural SiC from synthetics. Moissanite is virtually stoichiometric SiC with low O contents (0.1-0.3 wt%). Concentrations of some impurities (Al, B, Ti, V, Sc) are similar in natural and synthetic samples. However, the composition of natural SiC is much richer, due to the different degrees of perfection and amount/type of inclusions in natural and synthetic crystals. Inclusions are heterogeneously distributed in the host SiC and their size varies from few nanometers to hundreds of microns. They typically have rounded to negative-crystal shapes suggesting trapping of melt phases. Silicon is the most abundant inclusion phase. Less abundant are iron silicides ($FeSi_2$, $FeSi_3$) and not fully identified Si(C,O) phase(s) which could be silicon oxycarbide(s). Most chemical impurities are concentrated in the $FeSi_2$ and Si(C,O) phases. Trace-element patterns of $FeSi_2$ from different kimberlites are generally similar but also show locality-specific differences. The $FeSi_2$ is strongly enriched in LREE/HREE; extreme negative anomalies in Eu and Sm are consistent with highly reducing conditions. The overall pattern is similar to those of fibrous diamonds, suggesting formation from similar fluids. Textural and chemical features, the residual pressure on Si inclusions, and intergrowth with oxidation products (Si(C,O) phases and SiO_2) suggest that moissanite grew at high temperatures and elevated pressures and was subsequently partly oxidised, also at high T.

Black diamonds: the crustal origin for carbonado

Sautter, V.[1*], Lorand, J.P.[1], Cordier, P.[2], Rondeau, B.[3], Leroux, H.[2] & Meibom, A.[1]
[1]Laboratoire de Minéralogie et Cosmochimie du Muséum, UMR 7202, Paris, France (*vsautter@mnhn.fr)
[2]Laboratoire de Structure et Propriétés de l'Etat Solide, UMR CNRS-Université Lille, Villeneuve d'Ascq, France
[3]Laboratoire de Planétologie et de Géodynamique, UFR des Sciences et des Techniques, Nantes, France

Carbonado is a polycrystalline variety of black diamond that occurs as pebbles in mid-Proterozoic (~1.4 Gy) sedimentary deposit and is geographicxally restricted to Brazil and Central Africa. Its genesis remains one of the most controversial questions in diamond geology [1]. Crustal and mantle [2] formation processes have been debated and even an extraterrestrial origin [3] has been proposed. We present a carbonado from Bahia (Brazil) with a texture resulting from a three-stage growth process: black diamond clasts (up to 500 µm: stage-1) embedded in a grayish fine-grained matrix (stage -2) are associated with columnar transparent diamond (stage-3). Pyroxenitic assemblages of augite, ilmenite and phlogopite (all Fe-rich minerals) are shielded in primary diamond clasts, providing direct evidence for carbonado formation on crustal seeds under oxidizing conditions. Metallic phases (Fe, Ti, Cr, Cu, Al, and alloys of Fe-Cr, Fe-Mn and SiC), that require extremely reducing formation conditions, occur exclusively in the fine-grained carbonado matrix (stage-2). The $\delta^{13}C$ composition of the diamond clasts and fine grained matrix falls within the range -27‰ to -32‰. This points toward sedimentary organic materials as the source of carbon for the carbonado agregate. Then carbonado crystallized in a dynamic subduction zone environment. A later shearing event granulated the clasts and coincided with a dramatic drop in fO_2, due to the infiltration of reduced fluids generated by the serpentinization of mafic minerals. This later event led to the reduction of silicates into metallic phases.

[1] Heaney, P.J., Vicenzi, E.P. & De, S. (2005) *Elements*, **1**, 85-89, [2] Cartigny, P. (2010) *Earth Planet. Sci. Lett.*, in press. [3] Garai, J. et al. (2006) *Astrophys. J.*, **653**, 153-156.

Synthesis of ultrahard nano-polycrystalline diamond at high pressure and temperature using a large-volume multianvil apparatus

Irifune, T.[1*], Isobe, F.[1], Shinmei, T.[1], Sanehira, T.[1], Ohfuji, H.[1], Kurio, A.[1] & Sumiya, H.[2]
[1]Geodynamic Research Center, Ehime University, Matsuyama, Japan ([*]irifune@dpc.ehime-u.ac.jp)
[2]Electronics and Materials R&D Laboratories, Sumitomo Electric Industries, Ltd., Itami, Hyogo, Japan

Since the first report of synthesis of ultrahard nano-polycrystalline diamond (NPD) by direct conversion from graphite using multianvil apparatus [1], we have been trying to synthesize larger volumes of NPD for scientific and industrial applications. For this purpose, we have recently constructed a large-volume multianvil apparatus (BOTCHAN-6000) operated in a 6000-ton hydraulic ram at GRC, Ehime Univ., which enabled us to synthesize flawless NPD rods with dimensions as large as 8 mm in both diameter and length.

We use second-stage tungsten carbide cubic anvils with edge lengths of either 52 mm or 65 mm, with the largest truncation edge length (TEL) and the edge length of the octahedrral pressure medium (OEL) being TEL=18 mm and OEL=30 mm, respectively. Using the largest cell assembly, we are able to produce pressures of ~15 GPa (at a press load of ~4000 tons) and temperatures up to ~2700K, where a starting graphite rod of about 1 cm in diameter and length can be accommodated. Attempts to synthesize further larger NPD rods are currently planned with a larger anvil of 75 mm edge length, which should yield rods with dimensions even exceeding 1 cm.

These synthesized NPD rods were found to be easily processed with a pulse laser, followed by chemical etching and/or polishing with diamond powders, to form various shapes. We have been applying our NPD anvils to some high-pressure apparatus, such as diamond-anvil cell, multi-anvil apparatus, and Drickamer-type apparatus. Some of the early results on the performance of NPD anvils will also be reported in the talk.

[1] Irifune, T. et al. (2003) *Nature*, **421,** 599-600.

Influence of graphite crystallinity on the microtexture of polycrystalline diamond obtained by direct conversion

Ohfuji, H.[*], Okimoto, S., Kunimoto, T. & Irifune, T.
Geodynamics Research Center, Ehime University, Matsuyama, Japan ([*]ohfuji@sci.ehime-u.ac.jp)

The influence of crystallinity of polycrystalline graphite rods on the resulting textures of nano-polycrystalline diamond (NPD) synthesized by high pressure and high temperature experiments [1,2] was investigated through comprehensive analysis using Raman spectroscopy, X-ray diffractometry and electron microscopy. High pressure and temperature experiments were conducted at 16 GPa and at 2200 K using a 3000 ton multianvil press. Four types of high-purity graphite rods (G1, G2, G3 and G4) purchased from different companies were used as starting materials and were pressurized and heated all together in a high-pressure cell assembly.

Raman spectroscopy measurements of the four graphite starting materials showed various ratios of D band (1350 cm^{-1}) and G band (1580 cm^{-1}) intensities ranging from (D/G =) 0 to 0.34. Since the D/G intensity ratio reflects the crystalline state of graphite such as lattice defect density within each analyzed area (ca. 1 μm), the observed Raman data suggests that graphite crystals with a variety of crystallinity coexist in a rod sample. This is probably related to its manufacturing process, in which relatively large graphite flakes (coke) are mixed with binder pitch, which will transform to fine graphite particles after baking treatment to make a rod shape. The graphite crystallite sizes estimated using the Tuinstra-Koenig equation [3] range from 10 nm to 1 μm, which is in a good agreement with direct observation by TEM. G1 and G2 samples consist of graphite particles with relatively larger crystallite sizes than G3 and G4. It is also noted that G4 sample is unlikely to have large crystals more than 400 nm.

TEM observations of the recovered samples showed that grain size distribution of diamond nanocrystals is apparently different. NPDs synthesized from G1 and G2 starting materials have a grain size range of 40-100+ nm, whereas those obtained from G3 and G4 show smaller grain size distributions (mostly, 30-60 nm). The formation of lamella structure was observed commonly in the recovered samples except in that synthesized from G4.

Our results show that smaller the crystallite size of the starting graphite samples used, smaller the individual grain size of the synthesized NPD. This is probably due to increase in relative number of dangling bonds (sp3-like bonds) at crystal edges and lattice defects, which provide preferential sites for diamond nucleation, in smaller graphite crystals. In addition, the volume fraction of the lamella structure likely correlate positively with the relative frequency of well-crystallized large graphite flakes in the starting material, as suggested our earlier work [4]. Therefore, the microtexture of NPD can potentially be controlled by choosing the crystalline states of the starting graphite sources.

[1] Irifune, T. et al. (2003) *Nature*, **421**, 599-600. [2] Sumiya, H. et al. (2004) *J. Mater. Sci.*, **39**, 445-450. [3] Tuinstra, F. & Koenig, J.L. (1970) *J. Chem. Phys.*, **53**, 1126-1130. [4] Ohfuji, H. & Kuroki, K. (2009) *J. Miner. Petrol. Sci.*, **104**, 307-312.

Transformation mechanism of graphite to diamonds in ureilites revealed by TEM observation

Nakamuta, Y.[1*], Toh, S.[2] & Aoki, T.[1]
[1]University Museum, Kyushu University, Fukuoka, Japan
[2]HVEM Laboratory, Kyushu University, Fukuoka, Japan
([*]nakamuta@museum.kyushu-u.ac.jp)

Diamond in ureilites was first reported in 1888 [1]. The genesis of diamond in meteorites has been a problem of many years. The existence of compressed graphite associated with diamond reveals that diamonds in ureilites formed as a result of shock conversion of graphite [2]. The mechanism of conversion from graphite to diamond has also been discussed based on high-pressure experiments (e.g., [3]) and molecular dynamics (e.g. [4]). However, direct observation of diamond in ureilites suggesting a conversion mechanism has not been done until now. In this study, we observed diamonds associated with graphite by high resolution transmission electron microscopy (HRTEM).

A carbon-rich grain about 50 microns in size which pseudomorphs graphite was taken out of a polished thin section (PTS) of the Goalpara ureilite. X-ray powder diffraction analysis using a Gandolfi camera shows the grain is a mixture of hexagonal and cubic diamonds and graphite. Thin films for TEM observations were prepared by the focussed ion beam (FIB) technique. The graphite pseudomorph was observed by TEM in the three unique directions of graphite, i.e. with an electron beam parallel to [001], [010] and [210] of the original graphite. Fig. 1 shows a selected-area electron diffraction pattern taken with the electron beam parallel to the [001] of the original graphite. The diffraction pattern is composed of those from three-layered rhombohedral and two-layered orthorhombic polymorphs of carbon. The rhombohedral one is suggested to be similar to n-diamond [5] and the orthorhombic one to the intermediate phase proposed by [4], from the observations from the directions parallel to [010] and [210] of original graphite, respectively. These results reveal that a sliding of graphite layers is the initial dominant process in the conversion of graphite at high P and T, and then hexagonal and cubic diamonds form through a buckling of atoms in graphite layers.

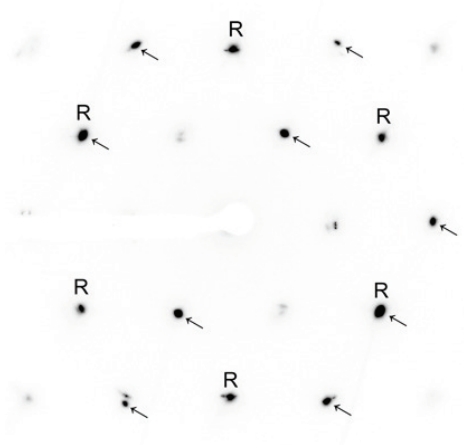

Fig. 1: Selected area electron diffraction pattern taken with an electron beam parallel to the [001] of original graphite. R: reflections from a three-layered rhombohedral polymorph of carbon; arrow: reflections from a two-layered orthorhombic polymorph of carbon.

[1] Kunz, F.K. (1888) *Science*, **11**, 118-119. [2] Nakamuta, Y. & Aoki, Y. (2000) *Meteorit. Planet. Sci.*, 35, 487-493. [3] Bundy, F.P. & Kasper, J.S. (1967) *J. Chem. Phys.*, 46, 3437-3446. [4] Scandolo, S. et al. (1995) *Phys. Rev. Lett.*, 74, 4015-4018. [5] Hirai, H. & Kondo, K. (1991) *Science*, 253, 772-774.

Monomineral thermobarometry for the diamond inclusions from Siberia: genetic links

Ashchepkov, I.[1*], Pokhienko, N.[1], Afanasiev, V.[1], Logvinova, A.[1], Pokhienko, L.1, Ntaflos, T.[3], Ionov, D.[4], Kuligin, S.[1] & Mityukhin, S.[5]
[1]IGM SB RAS, Novosibirsk, Russia ([*]garnet@uiggm.nsc.ru)
[2]IGC SB RAS, Irkutsk, Russia
[3]University of Vienna, Austria
[4]Université J. Monnet, Saint-Etienne, France
[5]ALROSA Company, Russia

The methods of the monomineral thermobarometry used for the reconstruction of the mantle sections beneath the kimberlite pipes [1] allow to determined PT range for the diamond inclusions (DI) and diamond bearing associations. They show various conditions for the crystallization of diamond for in mantle lithosphere beneath the Yakutia. Most of DI [2-6 and ref their in] (Cr-pyropes, Mg -opx) form Mir and Udachnaya pipes are referred to the cold geotherms 35 (partly 33 mvm-2) at the pressure range from 35 to 80 kbar. Cr- pyropes (Ti-bearing) partly drops the on the heated area near convective branches 40-45 mvm-2 convective geotherms. Most Cr- rich pyroxenes refer to the coldest or heated (metasomatic type) at the deeper parts of the mantle columns while mildly Cr-rich varieties refer to the conditions of the crystallization from the melts related to the protokimberlites and associated carbonatites near the Graphite-Diamond boundary (G-D). They are more widely distributed in mantle beneath the Mir pipe where the essential part of mantle column from 50 to 35kbar was subjected to the refertilization. But chromite PT estimates mostly refer the heated conditions of the convective branch at the lithosphere base (~70-60kbar). They are most typical for the Alakite pipes. Diamond bearing eclogites show the some separate levels of crystallization with the high T-range reflecting conditions 35 to 45 mvm-2 mostly in the 60-50 kbar interval. They coincide with the levels of the intensive heating in the mantle columns. Thus the mantle inclusion in different part of the Earth mantle in general repeats the conditions of the whole mantle column. They reflect higher PT gradients in ancient time. In Africa they are hotter in general and often trace advective branches. While in the thicker and colder lithosphere beneath the Slave craton DI reveal colder and deeper in general conditions. In Siberia many of DI especially Chr as well as Diam- eclogites reflect the heating by protokimberlite RBRF05-05-64718, ALROSA 77-2;65-3; 2-05.

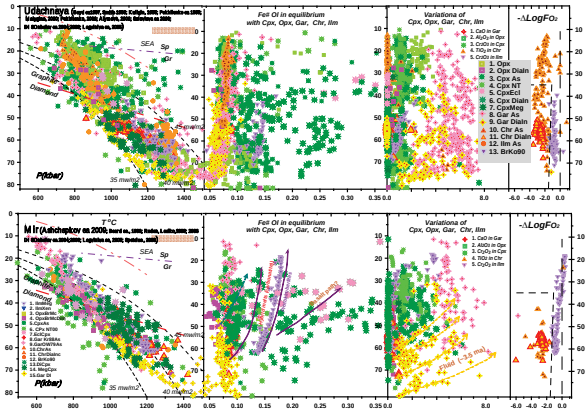

Fig. 1: PT diagram for the SCLM beneath Udachnaya & Mir pipes [2,7].

[1] Ashchepkov, I. et al. (2010) *Tectonophysics*, **485**, 17-41. [2] Sobolev, N.V. et al., (2004) *Lithos*, **77**, 225-242. [3] Boyd, F.R. et al. (1997) *Contrib. Miner. Petrol.*, **128**, 228-246. [4] Logvinova, A.M. et al. (2005) *Int. Geol. Rev.*, **47**, 1223-1233. [5] Jacob, D. et al. (1994) *Geochim. Cosmochim. Ac.*, **58**, 5191-5207. [6] Pokhilenko, N.P. et al. (1999) *VII IKC P.H. Nixon v.*, 690-707. [7]. Brey, G.P. & Kohler, T. (1990) *J. Petrol.*, **31**, 1353-1378.

A theoretical examination of diamond precipitation from fluids in the Earth's mantle

Crossingham, A.[1*], Huizenga, J.M.[2], & Viljoen, K.S.[1]
[1]Dept. of Geology, University of Johannesburg, South Africa
([*]alexandrac@postgrad.uj.ac.za)
[2]Dept. of Geology, North-West University, Potchefstroom, South Africa

Diamond precipitation may occur as a result of the infiltration and mixing of oxidised and/or reduced mantle fluids with surrounding mantle peridotite [1]. If so, important aspects that should be considered include fluid speciation, carbon speciation (CH_4, CO_2, or carbonate), as well as the oxidation state of the surrounding lithosphere (Fig. 1).

Mantle xenoliths from the Kaapvaal Craton have been widely studied, in order to determine e.g. the relationship between pressure, temperature, and oxygen fugacity in the Earth's mantle [2]. These studies have shown that (1) the sub-lithospheric mantle beneath the Kaapvaal Craton is relatively reduced i.e. oxygen fugacity varies between 1 and 3 log units below the FMQ buffer, and (2) oxygen fugacity is strongly correlated with depth in that the mantle becomes increasingly reduced with increasing depth. The observed correlation between pressure, temperature and oxygen fugacity allows for the modelling of fluid composition in the mantle within the C-O-H system [3].

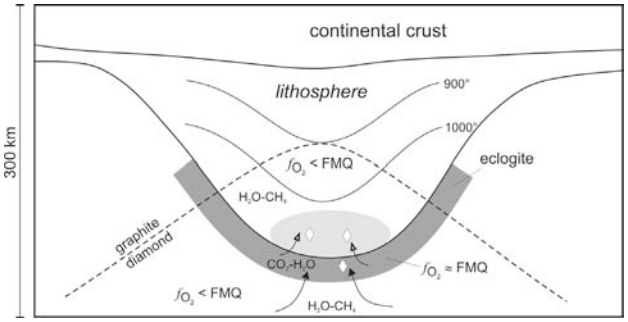

Fig. 1: Vertical section through the continental crust and underlying mantle. Diamonds are typically formed in relatively cold, deeper parts of the mantle (shaded area), probably along the the contact of oxidized and reduced lithologies [1]).

Aspects of the current study include the theoretical analysis of fluid infiltration and mixing, in the Kaapvaal Craton, in relation to the crystallisation of diamond. This involves the theoretical examination, using thermodynamic data and related calculations, of the effect of variations in oxygen fugacity of the host mantle on the composition of possible 'ambient' (equilibrium) fluids in the mantle, and the effect of various introduced fluids (e.g. methane, CO_2) and combinations of fluids, on the degree of carbon oversaturation in the mantle, and consequent diamond crystallization. These calculations suggest that the most ideal conditions for diamond precipitation are low fluid-rock ratio systems of which the oxygen fugacity is controlled by the rock system.

[1] Haggerty, S.E. (1999) *Science*, **285**, 851-860. [2] McCammon, C.A. et al. (2001) *Contrib. Mineral. Petrol.*, **141**, 287-296. [3] Huizenga, J.M. (2001) *Lithos*, **55**, 101-114.

Informative value of the diamonds' minerals-indicators study

Makeyev, A.B.
Dept. of Petrography, Institute of Geology of Ore Deposits, Petrography, Mineralogy and Geochemistry RAS, Moscow, Russia (abmakeev@mail.ru)

The brief historic note on the discovery of diamond fields in Russia emphasizes the leading role of the mineralogical methods of search, giving also the overview of the recent achievements in the studies of minerals-indicators. One of the most valuable discoveries in this field is that of the syngenetic metal films on the surface of diamonds (Fig.1). The metal films were found on the diamonds of all the diamond-bearing provinces of Timan, Perm and Arkhangelsk regions, Yakutiya, as well as on diamonds from deposits of China, Angola, and Brazil [1–3]. Noteworthy, 40 to 100 per cent of the examined crystals were covered with thin (0.1–1.0 mcm) metal films of various chemical compounds (Au, Ag, Cu, Au_7Ag, Au_2Pd_3, Au–Cu–Ag, Au–Cu–Hg–Pd, Cu_5Au_3Ag, Au_4Cu_3Ag, Al, Pb, Sn, Bi, Zn, Cu–Zn, Cu_2Zn, Cu–Zn–Pb, Cu_3Zn_2, Cu_3Sn, Zn–Cd(S), Pb–Sn, Pb–Sn–Cu(Au), Fe, Ni, Cr, Ti, W, Ta, Fe_7Cr, Fe_7Cr_2Ni, Ni–Fe, Ti–Fe, W–Mo, W–Ni–Mo, Fe–Cd, Fe–Cr–Mo, Fe–Zn, Cr–Zn, Cr–Zn–Mg, Fe–Zn–Mg, Sn–Fe, Fe–Ni–Cu, Sn–Fe–Cu, Fe–Ni–Pt, Fe–Cu, $(Ce,Nd,La,Y)_2O_3$ Zr–Yb), which were preserved only in negative forms of relief (in prints, twin seams, holes, and between vicinal forms of growth). At the fresh split of one carbonado next to the center there was discovered a diamond crystal covered by the buried titan dioxide film (former metallic titan film) [4]. We believe that the presence of metal films on diamonds discloses the mechanism of diamonds' growth in nature, namely their growth from solution in metal melt.

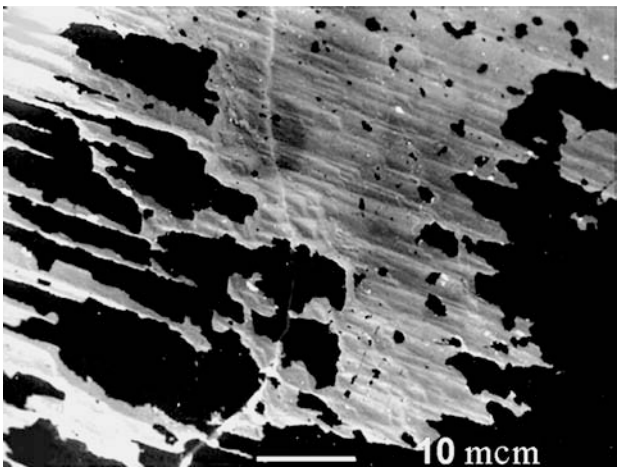

Fig. 1: The fragment of thin half-effaced metal gold-palladium (Au_2Pd_3) films on the surface of curvishaped diamond of Ichetju deposit (Middle Timan, Russia).

The compounds of metal films on diamonds can serve a source for preparation of new charge receipts for growing artificial diamond crystals. In addition, the article contains the results of the research of curvishaped diamonds by cathodoluminescent which show that curvishaped habits of diamond crystals of urals-brazilian type can be admitted a form of growth or solution only after individual study.

[1] Makeev, A.B. & Filippov, V.N. (1999) Dokl. Earth Sci., **369(8)**, 1161-1165. [2] Makeyev, A.B. & Braynchaninova, N.I. (2001) *Geosciences*, **15(2)**, 124-130. [3] Iwanuch, W., Makeev, A.B. & Kondo, M.M. (2005) *Materials of II South Am. Symp. on diam. Geol. Diamantina. Boletin*, **4**, 73-75. [4] Makeev, A.B. et al. (2002) *Geol. Ore Deposits*, **44(2)**, 87-102.

Organic-looking carbon and nitrogen isotope compositions in mantle derived diamondites: mantle fractionation vs. reworked crustal organics?

Mikhail, S.[1,2*], Dobosi, G.[3], Verchovsky, S.[2], Jones, A.[1] & Kurat, G.[4]
[1]Dept. of Earth Sciences, University College of London, UK (*s.mikhail@ucl.ac.uk)
[2]PSSRI, The Open University, Milton Keynes, UK
[3]Inst. for Geochemical Research, Hungarian Academy of Sciences, Budapest, Hungary
[4]Naturhistorisches Museum, Vienna, Austria

Diamondites (polycrystalline diamonds, framesites) are fine to coarse-grained (from 50 μm to >1 mm) rocks consisting almost entirely of diamonds with abundant pores and cavities [1]. Most of them contain silicates (mainly garnets, and less frequently clinopyroxenes) which are mostly interstitial or occupy the space in cavities and often contain inclusions of euhedral diamonds, giving evidence for a cogenetic origin of these phases. However, olivine, which is the most common mineral of the upper mantle, is not present in diamondites.

Carbon and nitrogen isotope ratios and nitrogen contents have been studied in diamonds from diamondites of unknown origin (presumably from southern Africa) that have previously been studied in detail for garnet geochemistry and carbon isotope composition [2,3]. Nitrogen aggregation states have also been determined in a subset of samples. Both carbon and nitrogen isotope ratios show wide range of variation within the sample set (mean values for $\delta^{13}C$ and $\delta^{15}N$ are -16.9 ± 7.2 ‰ and +11.9 ± 8 ‰, respectively), which suggest an "organic-looking" signature. The nitrogen content of the diamonds from the diamondites is generally high (above 500 ppm on the average), and the aggregation states of the nitrogen vary between 16 to 100 % 1aB with a mean value of 78 %. There is no relationship between the isotope ratios of the diamonds and the compositional characteristics of the associated silicate phases (mainly garnets) in the diamondites.

The coupled carbon and nitrogen isotope composition of the diamondites can be interpreted in two ways: (1) Reworking (either recycling via remobilisation of the lower lithosphere or subduction) could have provided the C and N which have preserved their 'organic-like' signatures; or (2) the loss of ^{13}C rich oxidised C from the system by carbonisation of olivine (explaining the lack of olivine inclusions in diamondites) during diamondite crystallisation would result in increasing of the N/C ratio and decreasing of the $\delta^{13}C$ value, the small variation in $\delta^{15}N$ to higher values (at this early stage) is thought to be a function of the removal of a small fraction of N from the substrate. This is followed by continuous diamond formation where oxidised carbon is lost via silicate carbonisation and the formation of carbonates (decreasing $\delta^{13}C$ in the source) and N is removed from the source by being partitioned into the crystallising diamonds (increasing $\delta^{15}N$ in the source). During such progressive crystallisation of diamondites the C and N isotope compositions can be fractionated to extremely 'organic-like' values. We find that both models warrant sufficient discussion for this data set.

[1] Kurat, G. & Dobosi, G. (2000) *Mineral. Petrol.,* **69**, 143-159. [2] Dobosi, G. & Kurat, G. (2010) *Mineral. Petrol.,* **99**, 29-42. [3] Maruoka, T. et al. (2004) *Geochim. Cosmochim. Ac.,* **68**, 1635-1644.

XANES spectroscopy at the potassium K-edge of inclusions in kimberlitic diamonds

Shiryaev, A.A.[1*], Safonov, O.G.[2] & Ragozin, A.L.[3]
[1]Insitute of Crystallography, Moscow, Russia
([*]a_shiryaev@mail.ru)
[2]Institute of Experimental Mineralogy, Chernogolovka, Russia
[3]Institute of Geology and Mineralogy, Novosibirsk, Russia

High potassium activity in fluids and melts producing kimberlitic diamonds worldwide is recorded in fluid/melt and mineral inclusions in them (cf. [1]). In order to characterize a structural position of K in diamonds, we have firstly examined XANES spectra at the K K-edge of two types of K-bearing inclusions in kimberlitic diamonds: (1) fluid/melt microinclusions in fibrous diamonds from Brazil [2], (2) individual macroinclusion of K-bearing clinopyroxene (0.73 wt.% of K_2O), KCpx, in a gem stone from Yakutia. Spectra were collected at the LUCIA beamline at SLS.

The "bulk" spectra for the fluid/melt inclusions were obtained from numerous submicron inclusions covered by the beam of FWHM ~10 μm. Despite noisiness of the spectra (Fig. 1) they could be described as superposition of contributions from KCl and K-silicate glass. Spectra are similar to those of synthetic glasses produced from the chloride-carbonate-silicate melts immiscible with the chloride-carbonate liquids [3].

The spectrum of the KCpx macroinclusion (Fig. 1) is consistent with the theoretical spectra (full multiple scattering approximation using feff8.2 code) of KCpx structures simulated via lattice dynamics [5] and produced experimentally [6], suggesting a disordered distribution of K in the Cpx structure. The spectrum of another inclusion resembles mica. However, K environment in various micas is rather similar and unique identification of the mineral requires additional information.

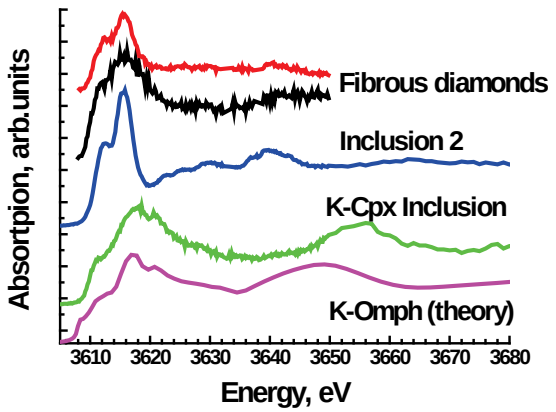

Fig. 1: K K-edge XANES spectra of fluid/melt and macroinclusions in diamonds.

Acknowledgements: The study is supported by RFBR grants 10-05-00040 to OGS and 09-05-00985 to ALR, RF President's Grant MD-380.2010.5, the Russian Science Support Foundation and the Ministry of education and science of RF (02.740.11.0328).

[1] Perchuk, L.L. et al. (2002) *Lithos*, **60**, 89-111. [2] Shiryaev, A.A. et al. (2005) *Russ. Geol. Geophys.*, **46**, 1185-1201. [4] Safonov, O.G. et al. (2007) *Earth Planet. Sci. Lett.*, **253**, 112-128; [5] Vinograd, V.L. et al. (2010) *Petrology*, in press; [6] Safonov, O.G. et al. (2003) *Contrib. Mineral. Petrol.*, **146**, 120-133.

Solid inclusions in carbonados

Sukharev, A.E.[1*], Petrovsky, V.A.[1], Silaev, V.I.[1] & Martins, M.[2]
[1]Institute of Geology, Komi Scientific Center, Ural Division, Russian Academy of Sciences, Syktyvkar, Russia
([*]sukharev@geo.komisc.ru)
[2]Federal University of Minas Gerais, Belo Horizonte, Brazil

The urgency of researches of micropolycrystalline diamonds is defined by that, as now not only the opposite opinions on genesis carbonados are kept in all acuteness, but sometimes in general filogenetic identity and genetic affinity with monocrystalline diamonds calls into question. The object of our researches is carbonados from recent and neogene-quaternary alluvial placers of basic diamond territories of Brazil. Gas-fluid phase of carbonado and associated minerals were studied with pyrochromatograph technique using chromatograph, equipped by pyrolytic add-on device. Gas composition was determined in the mode of two-stage (20-500 and 500-1000°C) and multi-step (20-300 and further at 100°C) heating. In pyrolyzate carbonados obtained as a result of multistage heating, are found out (in sequence of reduction of the contents) H_2O, CO, CO_2, N_2, H_2, CH_4, C_4, C_3, C_2. During heating the structure allocated from carbonados of gases changes from CO_2-water up to NO_2-H_2O-wastegaseous. In carbonados we established more than 100 kinds of mineral inclusions. We attributed the most part of xenomineral impurities attributed to epigenetic inclusion type, among those we distinguish products of condensation of mantle-magmatic fluids (epigenetic inclusions of the first type) and exogenic mineralization, which developed during diagenesis of the diamond object on the terrestrial surface (epigenetic inclusions of the second type). We attributed syngenetic inclusions of phase-homogeneous solid solutions to those based on zircon, which prototype is possible to consider inclusion Ti-Fe-Si-Zr-Al oxides solid solutions we established earlier in the Uralian monocrystalline diamonds. Besides in carbonados us have been revealed micro-nanoscale mineral and fluid inclusions in individuals of actually diamond phase: cerianite, rutile, zircon, α-Fe (Cr), quartz, apatite, mica, Pb-Zn, communities of liquid and gas phases of not established structure, KCl, Al_2O_3, S, Ca-K-Fe-Ti-aluminosilicate. The data received allow refusing from rough genetic opposition between polycrystalline and monocrystalline diamonds. It is possible, that these minerals represent only variations of products of uniform process mantle diamonformation. Researches were carried out with use SEM, TEM, spectral semiquantitative and instrumental neutron-activated analyses, photoroentgenostructure, Raman spectroscopy and photo-FIB-methods (Focus ion Beam, GeoForschungsZentrum, Potsdam, Germany), gas mass-spectrometry, ESP, photo-, roentgenoluminescence and gas pirochromotography.

Acknowledgements: This work was supported by the Program's Presidium RAS №27 (09-P-5-1028) and Department of Science Earth SB (09-S-5-1022).

Trace element geochemistry and Ni thermometry of garnet inclusions in peridotitic diamonds from Premier and Finsch, South Africa: implications for diamond formation

Viljoen, K.S.[1,6*], Harris, J.W.[2], Ivanic, T.[3,4], Richardson, S.H.[5] & Whitehead, K.[5,6]
[1]Dept. of Geology, University of Johannesburg, South Africa
([*]fanusv@uj.ac.za)
[2]Earth Sciences, University of Glasgow, UK
[3]Geology and Geophysics, University of Edinburgh, UK
[4]Geological Survey of Western Australia, Australia
[5]Geological Sciences, University of Cape Town, South Africa
[6]Previously: Geoscience Centre, De Beers, South Africa

It is apparent that highly depleted harzburgite in the sub-cratonic lithosphere may be subject to refertilisation [1], which might also result in the crystallisation of diamond [2]. This could, for instance, explain the presence of a lherzolitic diamond population in the worldwide diamond inclusion database (in addition to commonly observed harzburgitic diamonds).

Some kimberlites, e.g. Premier and Orapa, are characterised by a higher eclogite+lherzolite:harzburgite diamond paragenesis relative to e.g. Venetia, Finsch and De Beers Pool [3], suggesting that these diamonds crystallised in refertilised mantle. The purpose of this study is therefore to investigate the contrasting conditions of formation of peridotitic diamonds from Premier and Finsch.

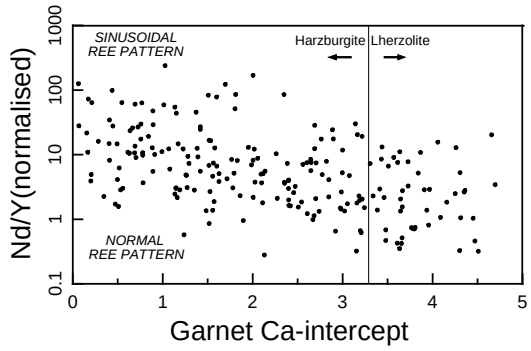

Fig. 1: Chondrite normalised Nd/Y plotted as a function of the Ca-intercept [4] for peridotitic garnets occurring as inclusions in diamonds.

Peridotitic garnets in diamonds from Premier provide evidence for refertilisation of subcalcic harzburgite through infiltration of a metasomatic medium characterised by relatively elevated Y, Zr, and Ti. During re-enrichment highly depleted subcalcic harzburgite with sinusoidal rare earth element patterns in the garnets were converted to more calcic harzburgite, and lherzolite, with a progressive change in rare earth element patterns in the garnets from sinusoidal to 'normal' REE patterns (LREE depleted, flat HREE; Fig. 1). Ni-thermometry on garnet inclusions provide evidence for increasing temperature during this process, a likely consequence of the infiltration of basaltic magma into, and mixing with, highly depleted harzburgite [5].

In contrast, peridotitic garnets in diamonds from Finsch are characterised by comparatively low inclusion encapsulation temperatures, dominantly sinusoidal REE patterns, and low Ti and Y but variably elevated Zr – a likely signature of low-temperature, fluid-dominated metasomatism accompanying diamond crystallisation [1].

[1] Stachel, T. & Harris, J.W. (2008) *Ore Geol. Rev.*, **34**, 5-32. [2] Malkovets, V.G. et al. (2007) *Geology*, **35**, 339-342. [3] Shirey, S.B. et al. (2004) *Lithos*, **77,** 923-944. [4] Grütter, H. et al. (2004) *Lithos*, **77,** 841-857. [5] Richardson, S.H. et al. (2009) *Lithos*, **112S**, 785-792.

Granulite lower crust: dry, but full of fluids

Touret, J.L.R.
Musée de Minéralogie, Mines-Paristech, Paris, France
(jacques.touret@ensmp.fr)

About 40 years ago, the discovery of CO_2-rich inclusions in granulites has initiated a debate which is still an important issue in metamorphic petrology. Experimental and stable isotope data have led to the conception of a "fluid-absent" model, opposed to the "fluid-assisted" hypothesis, derived from fluid inclusion evidence. Besides CO_2, other fluids have been found to be of importance in these rocks, notably concentrated aqueous solutions (brines), also able to coexist with granulite mineral assemblages at high *P* and *T*. Brines also occur in inclusions, but they are much smaller and less spectacular than the CO_2-bearing ones («collapsed» inclusions). This is easily explained by the slope difference between aqueous and CO_2-isochores, respectively, compared to the isobaric-cooling post–peak P-T path commonly encountered in granulites [1].

But brines have left their trace in an impressive array of metasomatic effects, systematically found in granulite terranes, notably in high-temperature (UT, UHT) types: intergranular K-feldspar veining and quartz exsolution (myrmekites) at quartz-feldspar of feldspar-feldspar grain boundaries, carbonate metasomatism along km-scale shear zones (Norway, India), "incipient charnockites" cross-cutting a variety of metamorphic protoliths (India, Sri Lanka, Scandinavia), high oxygen fugacity in many granulites (India), prohibiting graphite deposition during CO_2-streaming (Archean granulites), etc. All together, this impressive amount of evidence suggests that the amount of fluids in the lower crust, under peak metamorphic conditions, was very large indeed, far too important to be only locally derived. Then, except for remnants contained in inclusions, these fluids have left the rock system during postmetamorphic uplift.

Fluid remnants identical to those occurring in deep crustal granulites are also found in mantle minerals, including diamonds. Major mantle fluid source is related to the final stages of melting processes: late magmatic emanations from alkalic basaltic melts, carbonate-metasomatizing aqueous fluids issued from igneous carbonatites. Even if a local derivation of some fluids by crustal melting cannot be excluded, most lower-crustal granulite fluids seem to have the same origin [2]. They are transferred from the mantle into the crust by synmetamorphic intrusives, also responsible for the high thermal gradient typical of granulites, notably HT- and UHT-types.

These are mostly found in Precambrian times, generated during a small number of time intervals: e.g., around 500, 1000, 1800, 2500 Ma. HT-granulites forming events occur at world-scale in supercontinents or supercratons, either at the end of amalgamation, or shortly before breaking-off [3,4]. They provide a mechanism for a vertical accretion of the continental slab, which complement the more classical way of lateral accretion above subduction zones at convergent boundaries.

[1] Touret, J.L.R. (2009) *Russ. Geol Geophys.*, **50**, 1052-1062. [2] Touret, J.L.R. (2010) *Symposium GP 82*, this meeting. [3] Brown, M. (2007) *Earth Sci. Frontiers*, **14**, 1-18. [4] Santosh, M. & Omori, S. (2008) *Gondwana Res.*, **14**, 82-96.

Using different methods to determine the composition of upper mantle fluid inclusions from the Central Pannonian Basin

Berkesi, M.[1*], Dubessy, J.[2], Kovács, I.[3], Szabó, Cs.[1], Perucchi, A.[4] & Vaccari, L.[4]
[1]Lithosphere Fluid Research Lab, Eötvös University, Budapest, Hungary ([*]marta.berkesi@gmail.com)
[2]Nancy University, Vandœuvre-les Nancy Cedex, Nancy, France
[3]Eötvös Loránd Geophysical Institute, Budapest, Hungary
[4]ELETTRA Synchrotron Light Laboratory, Trieste, Italy

Individual fluid inclusions in upper mantle xenoliths from the Central Pannonian Basin (western Hungary) are hosted either in rock-forming silicates (olivine and pyroxenes) or in interstitial glasses. To determine their composition, microthermometry coupled with Raman microspectroscopy was applied on silicate hosted fluid inclusions. Based on microthermometry, the fluid phase in the inclusions is dominantly CO_2, whereas the room temperature Raman analyses also confirmed the presence of H_2S as additional volatile and magnesite as a solid phase. At the wall of fluid inclusions, the band of liquid water was also found rarely. Moreover, high temperature Raman microspectroscopy (120-150°C) revealed the presence of H_2O in each fluid inclusion as a band corresponding to the dissolved H_2O in the CO_2-rich phase. Even though the complete homogenization of the fluid inclusion cannot be recognized, at high temperature the distribution of dissolved H_2O in CO_2 is presumably uniform, which allows (semi-) quantification of spectra of the CO_2-rich phase. At 150°C, the calculated H_2O content in silicate-hosted fluid inclusions from the studied series ranges from 0.1 to 7 mol% (with one exception at 11.7 mol %) and shows an average value of 3.6 mol%. To calibrate the molar percentages of CO_2 and H_2O in natural fluid inclusions, calculated using the Raman spectra, silica fused synthetic capillary fluid inclusions were also prepared and applied subsequently. Because of optical reasons and a problem caused by fluorescence, the above mentioned techniques could not be used for the glass and its bubble inside. However, infrared spectroscopy allowed to determine the H_2O content of the wall-rock pyroxenes (orthopyoxene: 91.7±27.5 ppm, clinopyroxene: 395.8±98.9 ppm) and the glass (0.55±0.2 wt.%), using the calibration method developed by Kovács et al. [1]. In addition, the infrared spectroscopy confirmed the dominance of CO_2 in the glass-hosted bubbles. Our present study provided direct evidence for the presence of H_2O within deep lithospheric fluid inclusions, which has been rarely reported (e.g., [2,3]) so far. Our results imply that fluid inclusions trapped at conditions of the lithospheric mantle generally contain small amount of H_2O which may hold important implications for the geochemical and geodynamic evolution of the Earth's deep lithosphere and upper mantle.

[1] Kovács, I.J. et al. (2008) *Am. Mineral.*, **93**, 765-778. [2] Roedder, E. (1965) *Am. Mineral.*, **50**, 1746-1782. [3] Frezzotti, M.-L. & Peccerillo, A. (2007) *Earth Planet. Sc. Lett.*, **262**, 273-283.

Fluid migration process beneath a volcanic front: H_2O-rich inclusions in mantle peridotites from Avacha volcano, the Kamchatka arc

Ishimaru, S.[1*], Arai, S.[1], Tamura, A.[2], Mizukami, T.[1], Kawamoto, T.[3], Yamamoto, J.[3] & Morishita, T.[2]
[1]School of Natural System, College of Science and Engineering, Kanazawa University, Kanazawa, Japan
([*]jaja@earth.s.kanazawa-u.ac.jp)
[2]Frontier Science Organization, Kanazawa University, Kanazawa, Japan
[3]Institute for Geothermal Science, Kyoto University, Kyoto, Japan

We characterized petrographic and geochemical features of peridotite xenoliths from Avacha volcano in detail: high depletion in melt components, refractory mineralogy (e.g., high-Fo olivine (Fo_{90-92}) and high-Cr# spinel [= Cr/(Cr + Al) atomic ratio] (0.5-0.7)), and multi-stage metasomatism. The metasomatism gave rise to enrichment of SiO_2, and/or transitional elements (e.g., Ni, and Fe) and rarely sulfur and arsenic in peridotites. The addition of SiO_2 is observed as formation of secondary orthopyroxenes with a minor amount of clinopyroxene at an expense of olivine. The secondary orthopyroxene frequently accompanies amphiboles (edenite and pargacite). In addition, we found some peculiar peridotite xenoliths mainly composed of extremely fine-grained minerals (= F-type peridotite). The F-type peridotites are almost the same as ordinary coarse-grained peridotites in terms of metasomatism, although the protolith of the former is dunite. In addition, some F-type peridotites have been metasomatized by a high-Mg, high-SiO_2 agent, being converted to clinopyroxenite, websterite or wehrlite with extremely high-Mg# [= Mg/(Mg + total Fe) atomic ratio] mineralogy (the highest Mg# of clinopyroxene is 0.99!).

Silicate minerals of Avacha peridotites frequently contain minute inclusions, e.g., chromian spinel, sulfides and fluids. The fluid inclusions are especially abundant in highly metasomatized samples, and are possibly relics of the metasomatic agent. We checked phases of the fluid inclusions in both coarse-grained (6 samples) and F-type (2 samples) peridotites to recognize only H_2O rarely with carbonate. This is one of the rare cases where the mantle wedge H_2O fluids have been detected (cf. Iraya volcano, Iwanaidake massif and Higashi-akaishi massif). We try to discuss the fluid species in the inclusions, the geochemical features and the relationships between the host peridotite features and fluid phases.

[1] Ishimaru, S. et al. (2007) *J. Petrol.*, **48**, 395-433. [2] Schiano, P. et al. (1995) *Nature*, **377**, 595-600. [3] Arai, S. & Hirai, H. (1985) *Nature*, **318**, 276-277. [4] Mizukami, T., Simon, W.R. & Yamamoto, J. (2004) *Nature*, **427**, 432-436.

Immiscibility in a peralkaline nephelinite melt: the Oldoinyo Lengai case (Tanzania)

Sharygin, V.V.[1*], Kamenetsky, V.S.[2], Zaitsev, A.N.[3], Kamenetsky, M.B.[2] & Yemel'yanov, M.V.[1]
[1]V.S.Sobolev Institute of Geology and Mineralogy SB RAS, Novosibirsk, Russia ([*]sharygin@uiggm.nsc.ru)
[2]School of Earth Sciences, University of Tasmania, Hobart, Australia
[3]Saint Petersburg State University, Saint Petersburg, Russia

Melt inclusions with silicate-carbonate immiscibility are found together with microlites (diopside, etc.) along growth zones in nepheline phenocrysts from peralkaline nephelinite lavas of the 1917 eruption of the Oldoinyo Lengai volcano, Tanzania. Coexisting fluid, carbonate-salt and sulfide inclusions are scarce. Melt inclusions with immiscible phases (10-100 μm) are represented by green glass ± gas-carbonate globules ± daughter or trapped crystals. The most typical inclusions contain glass and one gas-carbonate globule in variable proportion. In some inclusions gas and carbonate components are separated into individual phases, and gas bubble always contains some salt crystals. Trapped crystals in silicate glass are diopside, apatite, Ti-andradite and titanite, whereas daughter phases are aegirine, fluorite, Na-Mg-Ti-rich tetraferriannite, Fe-rich delhayelite and Fe-rich leucite, rarely K-feldspar and wollastonite. Carbonate globule is commonly fine-devitrified and texturally zoned, and individual phases (calcite, nyerereite, chlorides, fluorite) are rare. Same immiscible inclusions were previously described in nepheline of the 2007-2008 eruptions of Oldoinyo Lengai [1].

Heating experiments with the Oldoinyo nepheline-hosted inclusions (silicate glass + gas-carbonate globule) have shown that first changes are observed in a gas-carbonate globule at 470-510°C and assigned to recrystallization of phases. The carbonate-rich component of gas-carbonate globules melts instantaneously at 550-570°C. Silicate glass fuses at 600-670°C. The appearance and then disappearance of blebs of different salt liquids (fluoride, chloride or sulfate) occur in both silicate and carbonate melts at 670-810°C. The salt and carbonate blebs then amalgamate into one large globule, which gradually decreases in size and gas bubble in it also decreased in size at 800-900°C. The gas-carbonate melt globule homogenizes at 900-940°C. At this temperature phase composition of the melt inclusions is silicate melt + carbonate-rich melt. Quenching of inclusions led to the initial phase composition.

The silicate glass is peralkaline and strongly varies in SiO_2 (43.6-53.0), FeO_t (7.5-18.6), CaO (1.0-7.2), alkalis (16.5-24.5) and SO_3+F+Cl (1.0-4.3 wt.%). This glass is poor in H_2O (0.1-0.6 wt.%), Cr and Ta (<10 ppm) and rich in Ba (1720-6490), Sr (1880-6700), Zr (1440-2200), REE (520-1040), Nb (450-980), Rb (250-460) and Li (240-390 ppm). The EDS and EMPA data have show that the carbonate globules are natrocarbonatite in composition and Na, Ca, K, C, Cl, F, S and P are major components, like in the Oldoinyo natrocarbonatites.

Our study of nepheline-hosted inclusions in nephelinite lavas advocates very complicated history during cooling of initial silicate melt as suggested by [2]. The silicate-natrocarbonatite immiscibility took place at temperature above 900°C and nepheline phenocrysts crystallized from immiscible liquids in an intermediate chamber. After trapping of inclusions by nepheline (closed system) the gas phase and different salt liquids may be separated from natrocarbonatite melt in the 900-600°C range. In nephelinite lavas (open system) the silicate-natrocarbonatite immiscibility phenomenon is commonly hidden, owing to degassing of silicate melt, separation of carbonate melt from silicate melt and/or reaction of carbonate melt with primary silicate minerals.

[1] Mitchell, R.H. (2009) *Contrib. Mineral. Petrol.*, **158**, 589-598. [2] Dawson, J.B. (1998) *J. Petrol.*, **39**, 2077-2094.

Carbonate melts in the Earth's mantle

Caracas, R.[1*], Cohen, R.E.[2] & Gygi, F.[3]
[1]Laboratoire de Sciences de la Terre, ENS de Lyon, CNRS, Lyon, France ([*]razvan.caracas@ens-lyon.fr)
[2]Geophysical Laboratory, Carnegie Institution of Washington, USA
[3]Dept. of Applied Science, University of California, Davis, USA

We perform a molecular dynamics study of the properties of the carbonated silicate melts at realistic thermodynamic conditions of the Earth's mantle. We employ the Qbox package based on a highly efficient plane wave and pseudopotentials implementation of the density-functional theory.

We work on three distinct compositions: Mg_2SiO_4, $16Mg_2SiO_4+CO_2$ and $16Mg_2SiO_4+MgCO_3$ and study the effect of the carbonization on the melt properties as well as the difference in effects between the CO_2 molecule and the CO_3^{2-} anionic group. We focus on the Earth-relevant isotherm at 3000K.

At ambient pressure the silicon is in tetrahedral coordination as SiO_4 with little or non-existent. The O atoms are the most mobile in the system. The diffusion of the CO_2 molecule takes place through intermediate unstable CO_3^{2-} states. In agreement with previous studies on pure magnesium silicate melts the polymerization of the tetrahedra is enhanced by pressure; the onset of the five-fold coordination of the silicon atoms occurs above 40 GPa. The formation of the CO_3^{2-} states out of the CO_2 molecule is equally enhanced by pressure; the effect of the temperature is minimal. The thermal dilatation of the CO_2-bearing fluid is about 1GPa/1000K at ambient pressures. The density differences due to the addition of CO_2 and of $MgCO_3$ to the Mg_2SiO_4 melts are minimal at ambient pressures and 3000K, and can be related only to the mass addition. At higher pressures CO_2 decreases the density of the Mg_2SiO_4 melts.

Nanogranite and melt inclusions: new tools in crustal anatexis

Cesare, B.[1*], Ferrero, S.[1], Bartoli, O.[2], Braga, R.[3], Salvioli-Mariani, E.[2], Acosta-Vigil, A.[4], Meli, S.[2] & Groppo, C.[5]
[1]Dipt. di Geoscienze, Università di Padova, Italy ([*]bernardo.cesare@unipd.it)
[2]Dipt. di Scienze della Terra, Università di Parma, Italy
[3]Dipt. di Scienze della Terra e Geologico-Ambientali, Università di Bologna, Italy
[4]Inst. Andaluz de Ciencias de la Tierra, CSIC, Granada, Spain
[5]Dipt. di Scienze Mineralogiche e Petrologiche, Università di Torino, Italy

The growth of peritectic minerals during incongruent melting reactions represents an ideal situation for the entrapment of inclusions of anatectic melt. Although this is a straightforward theoretical consideration, melt inclusions in anatectic rocks, and in particular in metapelitic migmatites, have received very little consideration in the past, with just a few exceptions [1,2].

Based on the experience acquired with glassy inclusions in enclaves, we started a systematic research looking for inclusions of anatectic melt in garnet and other peritectic phases in crustal anatectic migmatites from various localities worldwide, until we found them in the granulites from the Kerala Khondalite Belt, India [3]. Here, tiny inclusions are hosted within garnet: those between 15-25 μm are fully crystallized to a Qtz-Ab-Kfs-Bt cryptocrystalline aggregate, whereas those <15 μm are completely glassy. Both re-melted cryptocrystalline and glassy inclusions have a peraluminous, ultrapotassic granitic composition which does not correspond to a "minimum melt" and points to melting temperatures well above minimum or eutectic temperatures, in agreement with the UHT origin of the rock. Given the microstructural and chemical features, we named "*nanogranite*" the cryptocrystalline aggregate within these inclusions, and concluded that nanogranite is the crystallized melt that was trapped by peritectic minerals growing during anatexis.

Since then, nanogranite inclusions have been found also in migmatites from other geological settings of various P-T conditions, such as the Ulten Zone (Italy), Ronda (Spain) and the Barun Gneiss (Nepal). Inclusions are hosted in garnet at all these localities, and also in ilmenite at Ronda.

The study of nanogranites is analytically challenging, as inclusions are very often <10 μm in diameter, and mineral grains in them <1 μm. Therefore we combine field emission gun-based SEM and EMP techniques with synchrotron-based micro-XRD and micro-XRF. Being particularly interested in the bulk composition of the trapped anatectic melt, nanogranites are experimentally re-melted both in the high-temperature stage and in a piston cylinder apparatus.

We present and discuss the textural and microanalytical data recently obtained from nanogranites and their melting products. Comparison of results from the different occurrences allows making important petrological inferences, such as differences in the P-T conditions of anatexis and fluid activity among the various cases, and confirms the importance of these inclusions as a new tool for the study of crustal anatexis. In fact, the composition of anatectic melts in migmatitic terranes can now be directly analyzed rather than assumed.

After entrapment, the preservation of inclusions depends on the extent of chemical interaction with the host mineral, and on the mechanical behaviour of the host during the subsequent history. Therefore, melt inclusions should be targeted in strong and refractory minerals from the least deformed rock domains.

[1] Cesare, B. (2008) in Saywer, E.W. & Brown, M. (eds.) *Working with migmatites*. Mineral. Assoc. Canada Short Course, **38**, 37-55. [2] Acosta-Vigil, A. et al. (2010) *J. Petrol.*, in press. [3] Cesare, B. et al. (2009) *Geology*, **37**, 627-630.

Hydrosilicate liquids as a medium for metal transport in experiments and nature

Smirnov, S.Z.[1,2*], Thomas, V.G.[1] & Kamenetsky, V.S.[3]
[1]Institute of Geology and Mineralogy SB RAS, Novosibirsk, Russia (*ssmr@uiggm.nsc.ru)
[2]Novosibirsk State University, Novosibirsk, Russia
[3]CODES, University of Tasmania, Hobart, Australia

The latest stages of evolution of felsic magmas play important role in formation of ore-forming media. At these stages the magmatic system divides into variety of fluids that coexist immiscibly with parental melt. Some of them are crucial for postmagmatic ore and mineral formation. Aqueous fluids and hydrosaline melts (brines) are capable for transporting metals from magmas to ore deposits. Hydrosilicate liquids (HSL) with molar SiO_2/H_2O~1 are suggested to be another alternative, explaining joint metal and silica transport in late magmatic and post magmatic hydrothermal systems.

This study is focused on the HSL, which appear when alkali or salt of weak acids are added to the system SiO_2-H_2O. Polymerization of dissolved silica in those systems results in formation of viscous liquid, which is supposed to have colloidal nature. We have studied the effect of addition of Al_2O_3, NaF, NaCl on the formation of the HSL in the system Na_2O-SiO_2-H_2O and their ability to concentrate rare litophile elements at 600°C and 1.5 kbar.

Experiments show that addition of Al_2O_3 promotes the formation of HSL with lower SiO_2 and H_2O content as compared to the system Na_2O-SiO_2-H_2O. Addition of NaF or NaCl has no effect on the process of HSL formation. However NaF is concentrated predominantly in the HSL, while NaCl – in the aqueous fluid. Rb, Cs, Ta, Sn, Mo, W and Zn are concentrated in various degrees by the HSL. Concentrations of Cs and Mo in HSL are about 3.6 times higher than in aqueous fluid. Rb and W contents in HSL exceed those of the aqueous fluid by 5.1 times. The highest degrees of concentrations were recorded for Sn, Zn (C_{HSL}/C_{aq}=19.9 and 50.7 respectively) and Ta. The latter is completely accumulated by HSL. It is expected that the metals should fractionate between HSL and coexisting aqueous fluid according to theirs affinities to Cl or F.

Based on the data from experiments we conclude that HSL may form in nature when alkaline aqueous fluid reacts with felsic magma or granitic rock. With time and decreasing temperature HSL can easily exchange elements with coexisting fluids. This leads to change their chemistry and physical properties. Further evolution of HSL can result in mineral assemblages that are dominated by clay minerals or zeolites. Thus we can find evidence of natural HSL with unchanged compositions only if they are isolated as inclusions in minerals. Inclusions of melts from the roots of miarolitic quartz from granitic pegmatites can be regarded as examples of natural HSL [1,2]. They are composed of crystalline micaceous aggregate and aqueous solution of orthoboric acid. These inclusions were re-melted or homogenized in autoclaves under 2 – 3 kbar external pressure of H_2O at 600-650ºC. The quench glasses of these inclusions after re-melting or homogenization have molar SiO_2/H_2O~1 and contain unusually high concentrations of B, F and metals (Ta, Nb, Be, Rb and Cs).

The natural and experimental data suggest that hydrosilicate liquids should be considered as a medium for metal transport in late magmatic and postmagmatic mineralization, which is related to evolution of felsic magmas.

[1] Smirnov, S.Z. et al. (2003) *Dokl. Earth Sci.*, **392(7)**, 999-1003. [2] Peretyazhko, I.S. et al. (2004) *Chem. Geol.*, **210**, 91-111.

Constraining asthenosphere-lithosphere interactions from fluid/melt inclusion study of Qiaoshan xenoliths, Linqu, Shandong Province, E. China

Ni, P.[1*], Liu, J.Q.[1,2] & Chen, L.H.[1]
[1]State Key Laboratory for Mineral Deposit Research, Institute of Geo-Fluid, School of Earth Sciences and Engineering, Nanjing University, Nanjing, China (*peini@njut.edu.cn)
[2]Earthquake Administration of Jiangsu Province, Nanjing, China

Earth's mantle fluids influence not only phase transformation of mantle minerals and rheology of mantle, but also melting behaviour of mantle peridotites. Fluid inclusions in mantle xenoliths provide the most direct mean to improve our understanding of the nature and the physicochemical condition of mantle fluids.

We conduct a case study of fluid/melt inclusions from Qiaoshan xenoliths, Linqu (Fig. 1) which represent fertile mantle of the North China craton (NCC). In order to determine the chemical compositions of the trapped mantle fluids, explore the origin of different fluid/melt inclusions, and their potential inter-relationships, and discuss the possible relationships between the geochemical characteristics of mantle fluids and the evolution of the NCC, detailed petrographic observation, microthermometry and laser Raman microspectroscopy were carried out.

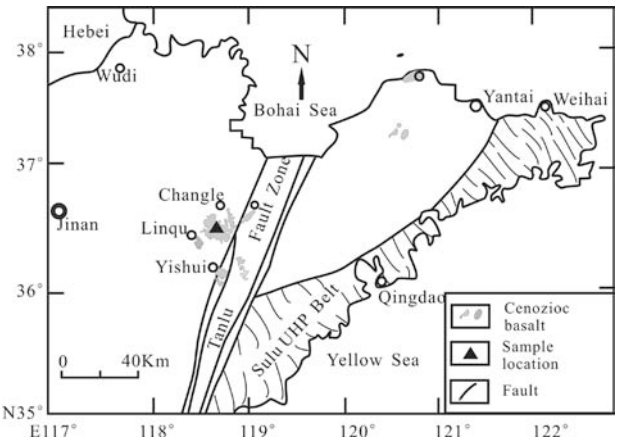

Fig. 1: The sketch map of sample location.

Two generations (four types) of fluid inclusions were identified in Qiaoshan xenoliths: (1) early CO_2 fluid inclusions, (2) early carbonatite melt inclusions, (3) late CO_2 fluid inclusions, and (4) late silicate melt inclusions. Among the early CO_2 fluid inclusions, most consist of high-density pure CO_2, while others have small amounts of other components besides of CO_2, including graphite, magnesite, Mg-calcite, CO and N_2.

Based on microthermometric works on fluid/melt inclusions, this work reveals that the entrapment temperatures of two generations fluid inclusions are about 1200°C, and their minimum entrapment pressure are 1.42 GPa and 0.80 GPa, respectively. The genetic link of early carbonatite melt inclusions with orthopyroxene suggests that they may be produced via interactions of CO_2 fluids with other mantle silicate minerals (such as olivine, clinopyroxene). Moreover, complex components in early CO_2 fluid inclusions also support that the origin of host mineral may be related to the reaction with CO_2-rich fluids. In conclusion, the compositional signatures observed in the fluid/melt inclusions of Qiaoshan xenoliths reflect recent asthenosphere-lithosphere interactions in this area.

Crack-seal cementation of natural fractures recording pore fluid evolution in tight gas sandstone reservoirs

Fall, A.[1*], Eichhubl, P.[1], Bodnar, R.J.[2] & Laubach, S.E.[1]
[1]Bureau of Economic Geology, The University of Texas at Austin, Texas, USA ([*]andras.fall@beg.utexas.edu)
[2]Dept. of Geosciences, Virginia Tech, Blacksburg, Virginia, USA

Natural opening-mode fractures in tight gas sandstone reservoirs are partially cemented with crack-seal quartz cement bridges that precipitated synkinematically with fracture opening. Fluid inclusions trapped in the crack-seal cement increments record pressure, temperature, and fluid composition (PTX) during subsequent fracture opening and cementation. High-resolution SEM-CL imaging of quartz cements combined with fluid inclusion microthermometry and Raman spectroscopy constrain fluid evolution during fracture generation in tight gas sandstone reservoirs. Homogenization temperatures (T_h) indicate a thermal history from ~140 to 185°C in sandstones of the southern Piceance Basin and ~135-155°C in the East Texas Basin, respectively [1]. Fluid salinities range from 1 to 2.5, and 14 to 15 wt% NaCl equivalents, respectively. Coexisting hydrocarbon-saturated aqueous inclusions and hydrocarbon gas inclusions indicate that T_h represent formation temperatures. The CH_4 Raman peak position of the vapor bubble was used to determine the pressure of the aqueous inclusions at room temperature [2]. Based on microthermometry, Raman spectroscopy, and equation of state modeling, the pressures at trapping were calculated for the observed inclusions [1]. Trapping pressures range from ~60 MPa to ~100 MPa (Fig. 1) in the southern Piceance Basin, and ~30 to 60 MPa in the East Texas Basin, respectively, suggesting that fracture opening occurred under significant pore fluid overpressures.

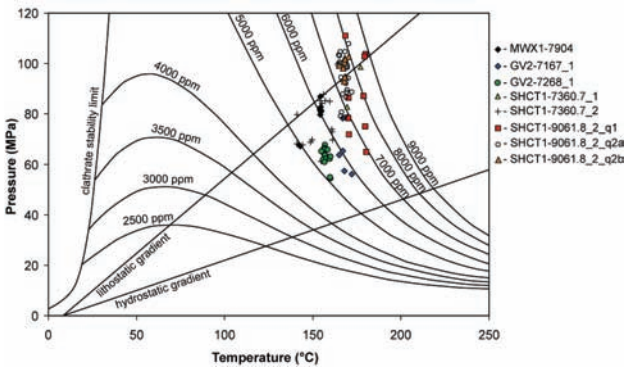

Fig. 1: P-T diagram showing isopleths in the H_2O-NaCl-CH_4 system for the 2 wt% NaCl-CH_4 pseudobinary and fluid inclusion trapping conditions in wells from the southern Piceance Basin, Colorado.

The subsequent pore fluid overpressure and fracturing is a result of hydrocarbon generations in shales and coal beds that surround the sandstones. The fractures significantly increase the permeability of the sandstones and permit vertical migration of the hydrocarbons [3].

[1] Becker, S.P. et al. (2010) *Geol. Soc. Am. Bull.*, **122**, 1081-1093. [2] Lin, F., Bodnar, R.J. & Becker, S.P. (2007) *Geochim. Cosmochim. Ac.*, **71**, 3746-3756. [3] Cumella, S.P. & Scheevel, J. (2008) *AAPG Hedberg Series*, **3**, 137-155.

H_2O-NaCl-KCl fluid system: purely empirical and thermodynamic modelling

Bakker, R.J.
Dept. of Applied Geosciences and Geophysics, Mineralogy and Petrology, University of Leoben, Austria
(bakker@unileoben.ac.at)

H_2O-NaCl-KCl-rich fluids occur occasionally in fluid inclusions in a variety of geological environments. The properties of this fluid provide information about the conditions of entrapment, and thereby, conditions that have affected the rock. This fluid system has already been studied extensively and modelled according to thermodynamic principles and purely empirical "best-fit" analyses. However, the provided models are internally inconsistent and are partly not reproducing the available experimental data. Therefore, new models are developed to reproduce the properties of the H_2O-NaCl-KCl fluid system, especially the liquidus at variable pressures (the solid+liquid+vapour surface, i.e. HLV), and at constant pressures (the solid+liquid surface, i.e. HL). The HLV surface reaches pressures up to 39 MPa (NaCl-H_2O-rich fluids), and the behaviour of fluid inclusions during microthermometric experiments, i.e. the dissolution of a halite crystal and a sylvite crystal in the presence of a vapour bubble, is defined according to the thermodynamic properties at this surface. The HLV surface is modelled in this study according to purely empirical "best-fit" polynomial equations, which relate temperature, pressure and composition. The HL surfaces, at constants pressures, are modelled according to thermodynamic principles, i.e., the equality of chemical potentials of components (NaCl and KCl) in each phase at equilibrium The HL-equations can be applied in the range of 300 to 1000°C, and pressures from 30 to 250 MPa, which is defined by the experimental data that is used to develop this model.

The new models are included in the software package FLUIDS [1], to be able to apply directly the mathematical functions in fluid inclusion studies and in general fluid properties investigations. The computer program AqSoWNK has been developed in REALBasic (© Real Software, Inc.) with a graphical user interface. The program is composed of two main applications: 1. salinity determination from known dissolution temperatures, at variable pressures (HLV) and constant pressures (HL); 2. dissolution temperature determination from known salinities at variable pressures (HLV) and constant pressures (HL). In addition, the program reveals thermodynamic properties, including the excess Gibbs energy and chemical potentials at selected conditions.

[1] Bakker, R.J. (2003) *Chem. Geol.*, **194**, 3-23.

New equation of state for aqueous species to high temperatures and pressures

Dolejš, D.
Institute of Petrology and Structural Geology, Charles University, Prague, Czech Republic (ddolejs@natur.cuni.cz)

Aqueous fluids play a fundamental role in mass transfer in the Earth's interior. Reactive fluid flow exerts major control on mass transfer in subduction zones and during metamorphism in the crust as well as is responsible for various element enrichment and depletion patterns in magmatic, hydrothermal ore-forming and geothermal systems. Aqueous solutes include neutral and charged nonelectrolytes and electrolytes, and their thermodynamic properties are frequently described by the Helgeson-Kirkham-Flowers model [1,2]. This equation of state is, however, applicable at liquid-like water densities and below 5 kbar, and it incorporates the dielelectric constant of water, which has been experimentally measured to 600°C only.

We propose a new equation of state for aqueous species, which combines intrinsic properties with caloric and volumetric effects of species hydration. It consists of two thermodynamic contributions: (i) caloric part, which includes enthalpy, entropy and heat capacity of the species, representing intrinsic properties of the solute species and energetics of its hydration, and (ii) volumetric part, which combines hardcore volume with a contribution from volume work due to electrostriction and spatial rearrangement during the formation of a hydration sphere. The approach based on the solvent density is more accurate in the vicinity of the critical point [3,4] and it is not limited by the availability of dielectric properties of the solvent.

Accuracy of the new equation of state has been tested by evaluating solubility and speciation of representative rock-forming minerals in aqueous fluid at 25-1100°C and up to 20 kbar. Experimental solubilities for quartz, corundum, rutile, calcite, apatite, fluorite and portlandite are reproduced to better than 5 % or 0.1 log molality units. The solubility increases for a given phase by 4-5 orders of magnitudes as temperature rises from 200 to 1100°C along typical geotherms. At constant pressure, however, mineral solubilities initially increase with rising temperature, but subsequently drop. This effect is caused by a reversal in isobaric expansivity of the aqueous solvent, which propagates into the enthalpy of dissolution. The onset of retrograde solubility typically occurs at 300-400°C and it is a characteristic of all minerals.

Thermodynamic properties of aqueous species reveal systematic relationships between charge and volumetric properties. Neutral species such as $Si(OH)_4$, $Ti(OH)_4$ or $Al(OH)_3$ exhibit very small dependence on the solvent properties. In contrast, variably charged ions cause much stronger electrostriction effects and their isobaric properties are profoundly affected by the isothermal expansivity of the solvent. In both cases, only a small number of parameters (four to five) are sufficient to represent partial molal properties to very high temperatures and pressures. This also permits retrieval of the model parameters from the standard thermodynamic properties at arbitrary reference conditions (e.g., 25°C and 1 bar), which are readily available. The new thermodynamic formulation thus alleviates several drawbacks of the Helgeson-Kirkham-Flowers model and provides a promising tool for modelling reactive fluid and mass transfer in magmatic, metamorphic, hydrothermal and groundwater systems.

[1] Helgeson, H.C. et al. (1981) *Am. J. Sci.*, **281**, 1249-1516. [2] Tanger, J.C. IV & Helgeson, H.C. (1988) *Am. J. Sci.*, **288**, 19-98. [3] Manning, C.E. (1994) *Geochim. Cosmochim. Ac.*, **58**, 4831-4839. [4] Dolejš, D. & Manning, C.E. (2010) *Geofluids*, **10**, 20-40.

Modelling quartz solubility in miscible and immiscible H_2O-NaCl-CO_2 fluids

Steele-MacInnis, M.J.*, Bodnar, R.J., Rimstidt, J.D. & Lowell, R.P.
Dept. of Geosciences, Virginia Polytechnic and State University, USA (*mjmaci@vt.edu)

A fluid density-based approach (e.g., [1]) was used to develop a predictive model for quartz solubility in aqueous fluids at crustal P-T conditions. While the origins of the density model are empirical, we propose a theoretical explanation of the model. An advantage of this model is that it appears to be solute independent. For example, the model predicts quartz solubility for H_2O-NaCl as well as H_2O-CO_2 fluids, without adjusting the parameters in the model. This suggests that the model may be used to predict quartz solubility in aqueous fluids of *any* composition, including non-idealized geologic fluids with many dissolved components.

An additional advantage of the predictive capability of this model is the ability to extrapolate quartz solubility estimates to immiscible fluid systems, for which experimental quartz solubility measurements in coexisting liquid and vapor are less abundant compared to the single-phase region. Partitioning of dissolved silica between liquid and vapor has been investigated for the system H_2O-NaCl using the model developed in this study (Fig. 1). Fluid phase equilibria control the dissolution and precipitation of quartz in hydrothermal systems, where bulk quartz solubility is a function of quartz solubility in the liquid and vapor phases and the proportions of those phases present. In addition, quartz may exhibit prograde solubility with respect to temperature in the liquid phase and retrograde solubility in the vapor (or vice-versa), within the same P-T range, indicating the possibility of quartz dissolution into one fluid phase concurrent with quartz precipitation from the other.

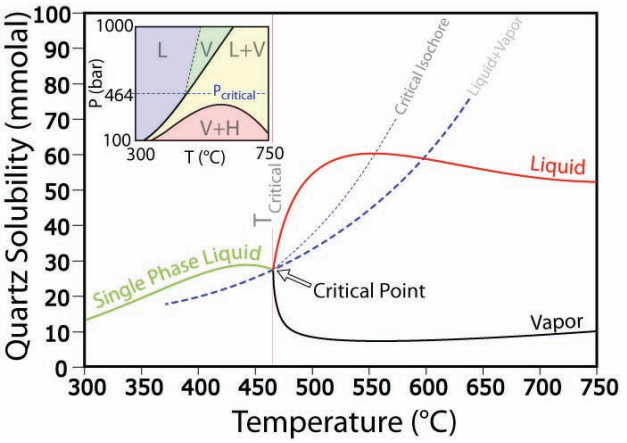

Fig. 1: Quartz solubility on the isobar of the critical pressure for a fluid of 10 wt.% NaCl. In the two-phase region, quartz solubility in the liquid is shown in red and that in the vapour is shown in black.

The model developed in this study can be used to predict the spatial and temporal evolution of quartz mineralization in hydrothermal systems, including those in which immiscibility occurs. The model can be applied to studies involving vein paragenesis, fluid inclusions, permeability evolution and reactive transport modelling. Furthermore, the density based predictive approach may be extended to other fluid-mineral systems.

[1] Fournier, R.O. (1983) *Geochim. Cosmochim. Ac.*, **47**, 579-586.

Tungsten mobility in subduction zones – a high P-T synthetic fluid inclusion study

Bali, E.*, Audetat, A. & Keppler, H.
Bayerisches Geoinstitute, University of Bayreuth, Germany
(*eniko.bali@uni-bayreuth.de)

The behaviour of tungsten varies in different geochemical environments. In the presence of metallic iron it behaves siderophile, thus, $^{182}W/^{184}W$ isotopic ratios have been successfully used for timing of differentiation of planetary bodies (e.g., [1]). During mantle melting however, it behaves highly incompatible (e.g., [2]), leaving a depleted mantle behind and producing a relatively tungsten-rich crust (13 ppb vs. 1 ppm; [3,4]). Moreover, the existence of hydrothermal tungsten-ore deposits indicates that it should be mobile in aqueous fluid.

Recently, König, S. et al. [5,6] have carried out high precision W-analyses on different sets of subduction related lavas. They confirmed that tungsten, and also molybdenum, can be mobilized by subduction zone fluids, although their enrichment can be decoupled. They suggested that the reason of decoupling might be the variable redox-sensitivity of W and Mo mobility in aqueous fluids.

Currently there are no available experimental data on relevant pressure, temperature and fO_2-conditions to test this hypothesis. We carried out W-solubility experiments at 26.1 kilobars, 600 to 800°C, at fO_2 conditions -5.09 to +1.94 logarithmic units relative to the FMQ buffer, and fluid salinities between 2 and 20 wt% $NaCl_{equiv}$. The fluid was trapped as synthetic fluid inclusions in quartz and subsequently analyzed by LA-ICPMS. In order to establish realistic fluid compositions for the mantle, the maximum solubility of W in the major mantle phases in equilibrium with a W-saturated fluid should also be determined. From this one can then estimate solid-fluid partition coefficients and determine their sensitivity on the previously described variables.

Our current dataset shows that W solubility is high and nearly independent on fluid salinity at 800°C and fO_2 conditions buffered by NiNiO, suggesting that tungsten did not dissolve in form of chloride complexes. On the other hand, tungsten solubility strongly depends on oxygen fugacity, increasing from 0.30 wt% W to 3.62 wt% W as fO_2 increases from the IW to the ReReO buffer. Thus, W is more efficiently mobilized at oxidizing conditions.

Our preliminary dataset suggests that W-incorporation into clinopyroxenes decreases with increasing Al_2O_3-content, thus $D^W_{fluid/cpx}$ increases with the same parameter. Similar relationship was established by Hill, E. et al. [7] and Righter, K. & Shearer, C.K [8] for clinopyroxene-melt partitioning data. At conditions buffered by CoCoO (-1.67 log units relative to FMQ) $D^W_{fluid/cpx}$ reaches up to 240 in diopside containing 3.8 wt% Al_2O_3. This suggests that subduction-derived fluids will not lose their W content when they percolate through the mantle wedge.

[1] Lee, D.-C. & Halliday, A.N. (1995) *Nature*, **378**, 771-774. [2] Adam, J. & Green, T. (2006) *Contrib. Mineral. Petrol.*, **152**, 1-17. [3] Arevalo, R. & McDonough, W.F. (2008) *Earth Planet. Sci. Lett.*, **272**, 656-665. [4] Rudnick, R.L. & Gao, S. (2004) in Holland, H.D. & Turekian, K.K. (eds.) *Treatise on Geochemistry*. Elsevier, Amsterdam, **3**, 1-64. [5] König, S. et al. (2008) *Earth Planet. Sci. Lett.*, **274**, 82-92. [6] König, S. et al. (2010) *Geochim. Cosmochim. Ac.*, **74**, 684-704. [7] Hill, E. et al. (2000) *Lithos*, **53**, 203-215. [8] Righter, K. & Shearer, C.K. (2003) *Geochim. Cosmochim. Ac.*, **67**, 2497-2507.

Ammonium in subduction zone fluids

Watenphul, A.* & Schmidt, C.
GFZ German Research Centre for Geosciences, Potsdam, Germany (*watenphul@gfz-potsdam.de)

Ammonium, NH_4^+, can be an important constituent in many crustal and subduction zone fluids, but is usually overlooked because of analytical difficulties. Large amounts of NH_4^+ are generated by the decomposition of organic material during diagenesis. Ammonium is readily mobilized by hydrothermal processes. Geothermal brines can contain more than 1000 ppm NH_4^+. Hydrothermal deposits often display substantial ammonium halos with up to 25000 ppm NH_4^+ in the host rocks [1]. In minerals, ammonium is mainly incorporated into potassium silicates, some of which can transport NH_4^+ to eclogite facies conditions [2], or even into the mantle [3]. Usually, a large fraction of the incorporated ammonium is released upon progressive metamorphism [4] because NH_4^+ strongly fractionates into the fluid relative to mica and feldspar [5].

The behaviour of ammonium in aqueous fluids was experimentally studied to 600°C and about 1.3 GPa using a hydrothermal diamond-anvil cell. The observed Raman spectroscopic detection limit for NH_4^+ in aqueous solutions is about 0.2 molal, which explains that it is rarely reported in fluid inclusion analyses. The Raman spectra reveal that addition of ammonium chloride causes a strong reduction of the dynamic three-dimensional network of water. This points to a substantial decrease in the water activity even if only quite small amounts of NH_4Cl (<1 molal) are present. Experiments on the assemblages NH_4Cl solutions plus quartz or quartz + kyanite + K-feldspar ± muscovite show that the silica solubility is significantly lower than that in equimolal NaCl solutions. This indicates that ammonium causes an even stronger decrease in the activity of water in chloridic solutions than sodium.

At temperatures above 300°C, a significant fraction of NH_4^+ is converted to ammonia, NH_3, indicating a large shift towards acidic conditions. The NH_3/NH_4^+ ratio increases with temperature and decreases with pressure. This implies that more ammonium should be retained in K-bearing minerals coexisting with chloridic fluids upon high-pressure low-temperature metamorphism.

The kinetics of the reaction K-feldspar + kyanite + water = muscovite + quartz was much faster with NH_4Cl solutions than in comparable experiments with water. This is attributed to the enhancement of the rate-limiting alumina solubility. The nucleation and growth of mica on the expense of K-feldspar and NH_4^+/K exchange between fluid and K-feldspar occurs simultaneously. However, Raman and IR spectroscopy indicate that the incorporation of NH_4^+ into K-feldspar is even faster than the consumption of the K-feldspar during the reaction, which is already a very rapid reaction.

Ammonium has strong effects on fluid properties, element solubilities, and reaction kinetics. It is not only the determinant for the recycling of nitrogen, but also has considerable effects on the composition of crustal and subduction zone fluids and the reactions occurring during the subduction process.

[1] Ridgway, J. et al. (1990) *Appl. Geochem.*, **5**, 475-489. [2] Busigny, V. et al. (2003) *Earth Planet. Sci. Lett.*, **215**, 27-42. [3] Watenphul, A. et al. (2009) *Am. Mineral.*, **94**, 283-292. [4] Mingram, B. & Bräuer, K. (2001) *Geochim Cosmochim. Ac.*, **65**, 273-287. [5] Pöter, B. et al. (2004) *Lithos*, **74**, 67-90.

Trapped high density fluids in superdeep diamonds

Brenker, F.E.[1*], Vincze, L.[2], Vekemans, B.[2], Schmitz, S.[1], De Nolf, W.[3], Janssens, K.[3], Stachel, T.[4] & Harris, J.[1,5]
[1]Geosciences Institute, Goethe University, Frankfurt/M., Germany ([*]f.brenker@em.uni-frankfurt.de)
[2]Dept. of Analytical chemistry, Ghent University, Belgium
[3]Centre for Micro- and Trace Analysis, Dept. of Chemistry, Antwerp University, Belgium
[4]Dept. of Earth and Atmospheric Sciences, University of Alberta, Edmonton, Canada
[5]Division of Earth Sciences, University of Glasgow, Scotland, UK

Synchrotron based confocal X-ray fluorescence analyses were performed at the ESRF (European Synchroton Radiation Facility, Grenoble) on a set of Kankan diamonds [1,2]. Of special interest was a large Kankan diamond containing many Ca-Si-O rich inclusions (KK200). Investigations applying Raman spectroscopy yield $CaSiO_3$ walstromite, $CaSi_2O_5$ titanite and larnite (beta-Ca_2SiO_4) as inclusion paragenesis. The varying proportions of the respected phases indicate a depth of origin within the two phase field of larnite + $CaSi_2O_5$ titanite between 300 and 360 km [3].

Detailed trace element tomography of several cubo-octahedral inclusions indicate a Ca,Si-rich source, in the absence of several common mantle minerals, like olivine, garnet and Ca-poor pyroxene. This reservoir may represent metasomatized oceanic lithosphere (rodingites, ophicarbonates), metamorphosed carbonaceous sediments or a trapped carbonatitic melt. In addition investigations on the surrounding narrow fractures around the inclusions show that contrary to our expectation the fractures are actually filled with material. The fracture filling shows close similarities in trace element composition to the mineral inclusions, in addition to being generally enriched in REE. The former existence of a fluid or melt is required to transport material into these elongated fractures. This interpretation is further confirmed by X-ray diffraction measurements which indicate the presence of florencite and La-cerite crystals within the fracture fills.

The most likely interpretation is the entrapment of a volatile component during diamond growth, probably dissolved at high pressure within the solid inclusion phases. During uplift of the diamonds and associated pressure release this volatile content is expelled from the solid inclusion as a fluid and penetrates into the newly forming fractures.

[1] Brenker, F.E. et al. (2005) *Earth Planet. Sc. Lett.*, **236**, 579-587. [2] Vekemans, B. et al. (2004) *J. Anal. Atom. Spectrom.*, **19**, 1302-1308. [3] Vincze, L. et al. (2004) *Anal. Chem.*, **76**, 6786-6791.

Sulfide minerals in mantle xenoliths from Cretaceous lamprophyres of the Carpathian-Pannonian region

Azbej, T.*, Nédli, Zs. & Szabó, Cs.
Lithosphere Fluid Research Lab, Eötvös University, Budapest, Hungary (*tristan@elergeo.hu)

Alkaline basalts, lamprophyres and kimberlites hosted mantle xenoliths are significant sources of information on the composition and physical and chemical processes of the upper mantle. Sulfide minerals are common, but minor phases in upper mantle peridotite and pyroxenite xenoliths. Several papers have reported the textural and compositional features and Os-Re characteristics of sulfides occurring in alkaline basalt and kimberlite hosted xenoliths. However, less attention has been paid for sulfides in mantle xenoliths derived from lamprophyres. It is widely accepted that sulfide minerals in the mantle peridotite xenoliths can provide information on mantle depletion (i.e., melting) and enrichment events (i.e., metasomatism). Sulfide inclusions in the pyroxenite xenoliths, however, can contribute to our knowledge on crystallization processes and related metasomatism in the deep lithospheric mantle.

14 sulfide mineral bearing peridotite mantle xenoliths have been selected for detailed petrographic and geochemical study from two Cretaceous lamprophyre occurrences in the Carpathian-Pannonian Basin: NE Transdanubian Central Range (TCR, Hungary) [1] and Poiana Rusca Mts. (PRM, Transylvania, Romania) [2]. Based on textural and geochemical features of the lamprophyre hosted xenoliths, they represent highly depleted mantle portions, however, the TCR xenoliths went through previously significant mantle metasomatism as their minor phlogopite modes, with high mg-number, clearly indicate.

According to mineral petrography, two kinds of sulfide assemblages can be distinguished: 1) sulfide blebs enclosed in mantle silicates and 2) interstitial sulfides at the grain boundaries of the rock-forming minerals. In the TCR xenoliths the interstitial sulfides are predominated, whereas they can be observed very rarely in the PRM xenoliths. The single sulfide blebs consist of pentlandite, pyrrhonite, chalcopyrite, and rarely millerite and violarite in the TCR xenoliths, however millerite and violarite never have been observed in the PRM xenoliths. The TCR xenoliths are characterized by high variation of the sulfide minerals in modes, and pentlandite is always present with wide compositional range (Ni content up to 39.4 m/m%) and moderate Co content (up to 1,47 m/m%). The PRM xenoliths show much less variation in modes and no significant compositional variation of pentlandite (Ni up to 34.0 m/m%, Co up to 0.46 m/m%).

Bulk sulfide compositions, calculated by mass balance calculation, in the TCR xenoliths show extremely high variance and overlap with the compositional field of monosulfide solid solution (MSS) at 900 °C [3]. On the other hand, bulk sulfide compositions in the PRM xenoliths overlap the narrower MSS composition at 1000 °C [3]. It is highly interesting that both sulfide compositions indicate enrichment in Cu corresponding to increase in Ni content (or decrease of Fe content) which may be related to ancient fertilization process in the mantle during pre-Cretaceous times.

[1] Szabó, Cs. (1985) *Acta Miner. Petrogr.*, **XXVII**, 39-50. [2] Downes, H. et al. (1995) *Acta Vulcanol.*, **7**, 209-218. [3] Kullerud et al. (1969) in Wilson, H.D.B. (ed.) *Econ. Geol. Monogr.*, **4**, 323-343.

Genesis of the Hanle Rhyolite in comparison to the Ladakh granitoid batholith based on petrographic, geochemical and fluid inclusion studies (Ladakh Himalayas, India)

Bodor, B.[1*], Sachan, H.K.[2] & Szabó, Cs.[1]
[1]Lithosphere Fluid Research Lab, Eötvös University, Budapest, Hungary (*szurkevolvo@gmail.com)
[2]Wadia Institute of Himalayan Geology, Dehra Dun, India

Previously unknown rhyolite occurrences were found in the southern part of the Ladakh batholith near Hanle (Ladakh Himalayas, India). The Ladakh batholith is built up by intrusive bodies of granodiorite and granite. These are parts of the Trans-Himalayan batholith range which is the product of Andean-type calc-alkaline igneous activity resulting from the northward subduction of the Neo-Tethyan oceanic crust. There is only little direct evidence for the existence of extrusive rocks along the Ladakh batholith. However, rhyolite occurrences near Hanle can be one of these remnants along with the Teah and Deskhit volcanics NW of Leh.

The Hanle Rhyolite has spherulitic texture with phenocrysts of quartz, plagioclase and alteration products after mafic minerals like biotite and probably amphibole. Quartz grains contain significant amount of multiple generation fluid inclusions. Plagioclase is largely altered into clay minerals, sericite and calcite. Relics of biotite exist but they are highly altered to chlorite. The groundmass is entirely devitrified, thin laths of quartz, K-feldspar and plagioclase form the characteristic spherulitic texture.

Major element geochemistry and, principally, distribution of rare earth elements were used to describe the relation between the Hanle Rhyolite and surrounding granitoid rocks. Harker variation diagrams show that the Hanle Rhyolite fits in the evolution trend of plutonic rocks of the Ladakh batholith. It is also very close in composition to the older Dras volcanics. Rare earth element patterns also show a very close connection between plutonic rocks and the Hanle Rhyolite.

Fluid inclusion studies identified at least three different types of inclusions: 1) primary CO_2 inclusions, 2) primary, two-phase H_2O-NaCl inclusions with low salinity (max. 5 NaCl eq. wt%), and 3) secondary, two-phase H_2O-NaCl inclusions with lower salinity (1-3 NaCl eq. wt%). Secondary inclusions were also found in the granite and these may be interpreted as a common feature in the late evolution of the two rocks. Primary inclusions were found in quartz grains of the rhyolite. Co-exiting CO_2 and H_2O-NaCl inclusions suggest that the crystallization of quartz in the rhyolite took place under immiscible CO_2-H_2O conditions.

Results from geochemical data suggest that the Hanle Rhyolite was probably cogenetic with the major phases of the granodiorite intrusions and it is less likely to represent later remelting of the underlying intrusive bodies.

Zoning of copper mineralization away from an igneous heat source at Allihies, Co. Cork, Ireland: mineral and fluid inclusion evidence

Costanzo, A.*, Moore, K.R. & Feely, M.
School of Natural Sciences, Earth and Ocean Sciences, National University of Ireland Galway, Ireland
(*alessandra.costanzo@nuigalway.ie)

Lower Palaeozoic sedimentary rocks in the southwest of Ireland are cut by copper-rich vein mineralization at Allihies, an old mining village located on the western tip of the Béara Peninsula in County Cork, Ireland. Samples from metal-bearing veins at two 19th century mines (the northerly Mountain Mine and the southerly Caminches Mine) were studied in order to investigate whether there is any relationship between igneous activity elsewhere on the Beara Peninsula and the Allihies mineralization.

The primary ore mineral assemblage comprises copper, iron and molybdenum sulphides and oxides including chalcopyrite, pyrite, bornite, tetrahedrite, hematite (var. specularite), molybdenite, and chalcocite. The oxide minerals are more common at the southern Caminches Mine than the northerly Mountain Mine. The secondary mineral assemblage comprises copper, iron and molybdenum carbonates and oxides such as malachite, covelline, goethite and limonite. The main gangue mineral is quartz, which is accompanied by carbonate minerals: typically rhodochrosite in the northerly mineralization and calcite in the southerly mineralization. Thus it appears that mineralization to the north may have formed in a higher temperature, more reduced system than that to the south.

In quartz veins containing ore minerals, a large number of fluid inclusions (FI) are hosted within quartz crystals, particularly those crystals in proximity to sulphide minerals. Large (up to 80 μm in length), primary, two-phase fluid inclusions are the most abundant and are most commonly distributed along linear planes within the crystals or along crystal rims. Solid-rich fluid inclusions generally contain only one solid phase and are also considered to be primary. Microthermometric studies of primary FIs show that the temperature of homogenization (T_H) is significantly higher (mean T_H = 256°C; maximum T_H = 398°C) for the northerly mineralization than for the southerly mineralization (mean T_H = 187°C). Likewise, fluid salinity is higher for the northerly mineralization (mean = 17.28 eq.wt.% NaCl; maximum = 22.2 eq.wt.%NaCl) than for the southerly mineralization (mean salinity = 14.8 eq.wt.%NaCl). Microthermometric data also reveal a compositional difference in the fluid species between the mines: Na^+ and K+ are the dominant phases, and Fe^{2+} and Mg^{2+} are minor phases at both mines, but Ca^{2+} is present only in the southerly mineralizing fluids.

The fluids that formed the Allihies mineralization reach significantly higher homogenization temperatures and salinities, particularly in the north, than fluids that formed the regional Irish-type mineralization trend (homogenization temperature = 150-200°C, salinity = 13-20 eq.wt.% NaCl; [1]). Thus an additional local energy source is required to drive the mineralization at Allihies (with decreasing temperature and increasing oxidation from north to south), with potentially more saline fluids. Field investigations have identified an area of large mafic igneous intrusions (with some evidence of hydrothermal alteration) 3.5 km to the northwest of the Allihies Area, with smaller related intrusions close to the northern mine. This area is now a target for ongoing investigations as a potential source of heat and fluid.

[1] Wilkinson, J. & Earls, G. (2000) *Mineral. Mag.*, **64**, 1077-1096.

Fracture filling minerals in the Baksa Gneiss Complex (Hungary): indicators of paleofluid migration

Fintor, K.*, Tóth, T.M. & Schubert, F.
Dept. of Mineralogy, Geochemistry and Petrology, University of Szeged, Hungary (*efkrisz@gmail.com)

Ca-Al silicate dominant veins with characteristic paragenetic mineral sequence (di→ep→sph→ab+kfp→chl1→prh±adu→ chl2→chl3→pyr→cal1→cal2→cal3) can be found frequently in the Baksa Gneiss Complex, which forms a part of the crystalline basement of SW Pannonian Basin. Detailed petrographical, mineral chemical and fluid inclusion analysis of the vein filling minerals can reveal traces of ancient fluid migrations along fracture network of the Baksa Complex. The high calcic vein filling diopside contains numerous primary fluid inclusions exhibiting T_h: 276-362°C, and 0.7 - 2.9 *w*NaCl eq. % salinity. Subsequent epidote phase often shows growth zonation pattern with Al-rich cores and Fe-rich rims (Fig. 1a), but irregular patchy zonation also frequently occurs (Fig. 1b), which refers to retrograde dissolution-precipitation processes.

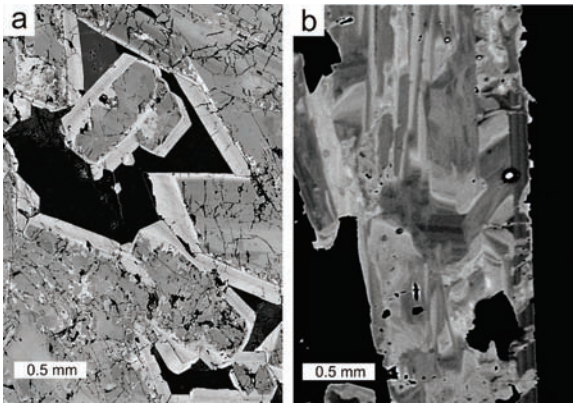

Fig. 1: a) epidote crystals with Fe-rich rims; b) irregularly zoned epidote single crystal.

Primary fluid inclusions of epidote show similar salinity (0.2-1.6 *w*NaCl eq. %) to the case in diopside but a broader range in T_h (181-359°C) values is observable. Textural patterns of albite+kfeldspar vein filling assemblage indicate cogenetic crystallization of these phases. Precipitation temperatures of the alkali feldspars (~$Or_{1.0}$ $Ab_{99.0}An_{0.0}$ and ~$Or_{99.0}Ab_{1.0}An_{0.0}$, respectively) are ~260±40°C by two feldspar thermometers [1]. Both feldspar phases show reddish-brown turbidity and contain several sub-micrometer size cavities. This special habit denotes infiltration of fluid subsequently the precipitation of feldspar. Three different chlorites can be distinguished in the veins, based on morphology and chemical composition. Decreasing Al^{IV} content of the chlorites is detectable in individual grains from core to rim, which refers to temperature decrease during chlorite crystallization. Values of chlorite thermometry [2] (T_{chl1}: 260±32°C→T_{chl2}: 222±20°C→T_{chl3}: 156±10°C) support this assumption. Sporadic pyrite crystals occur after chlorite and its composition indicate considerable amount of As, Co, Ni, Cu, Zn, and Mn in the pyrite grains. Co/Ni ratio (Co/Ni~1-5) of the pyrite grains refers to post-magmatic hydrothermal origin of this ore phase. In case of calcites, the calculated stable $\delta^{18}O$ isotope signature of water from which cal1 precipitated (-4 to -12.9‰ $\delta^{18}O$ V-SMOW) together with microthermometric results of primary fluid inclusion of cal1 indicate that this carbonate phase had to precipitated from downward-penetrating high salinity fluid.

[1] Whitney, A.J. & Stormer, C.J. Jr. (1977) *Am. Mineral.*, **62**, 687-691. [2] Zhang, W. & Fyfe, W.S. (1995) *Miner. Deposita*, **30**, 30-38.

Silicate melt and fluid inclusions in olivine phenocryst from the Gătaia lamproite (Banat, Romania)

Káldos, R.[1*], Seghedi, I.[2] & Szabó, Cs.[1]
[1]Lithosphere Fluid Research Lab, Eötvös University, Budapest, Hungary ([*]rekakaldos@gmail.com)
[2]Institute of Geodynamics, Bucharest, Romania

Study of the approximately 1.3 Ma old Gătaia lamproite (Banat, Romania) [1] revealed that olivine phenocrysts contain large number of silicate melt, fluid and spinel inclusions in different textural positions. Presence of silicate melt inclusions and fluid inclusions in olivine phenocryst provide a unique opportunity to reconstruct stages in evolution of magma during crystallization.

Based on a detailed optical microscopic study on olivine phenocrysts, apart from the spinel, inclusions can be divided into two groups: 1) primary silicate melt inclusions and 2) coeval and coexistence secondary silicate melt and fluid inclusions based on Roedder's classification [2].

Considering that the first crystallized phase in the lamproite is olivine, therefore the primary silicate melt inclusions in the olivine phenocrysts reflect the early evolution stage of the lamproite magma. The primary silicate melt inclusions are 10 to 25 μm in size, rounded or oval in shapes, and contain clinopyroxene daughter phase, glass and one-phase bubble. The secondary silicate melt inclusions are 5 to 10 μm in size, spherical, multi-phased (daughter mineral, glass, two-phase bubble) and occur together with the secondary one- or two-phased fluid inclusions along healed fractures running across the host olivine phenocrysts.

According to the high-temperature homogenization experiments, apart from homogenization of the bubble, we observed the homogenization temperature of the primary silicate melt inclusions between 1140 and 1150 °C, which could be a minimum crystallization temperature of the olivine phenocryst and spinel inclusions. By low-temperature microthermometry measurements we recognized CO_2 as the dominant component in the bubble of the secondary silicate melt inclusions, as well as in the secondary fluid inclusions. In contrast, bubbles in the primary silicate inclusions were empty or consisted of extremely low density gas. Raman microspectroscopic analysis of the bubbles in the secondary silicate melt inclusions and the fluid inclusions detected the presence of CO, N_2 and CH_4 next to CO_2 at room temperature.

The homogenization temperatures of the bubbles of the secondary silicate melt inclusions and the secondary fluid inclusions are corresponding to the fluid densities. Applying the determined densities and the widely accepted Duan-equation [3], a minimum trapping pressure of 5-6 kbar of the coexistence secondary silicate melt inclusions and fluid inclusions can be estimated at the time of entrapment. This pressure value may represent the conditions of a magma chamber (or conduit) in the middle crust. The emplacement and the composition of the secondary silicate melt inclusions and fluid inclusions in olivine phenocrysts indicate that, besides the crystallized minerals (i.e., olivine and spinel), two different fluid phases were present, a silicate melt and a CO_2 rich volatile that formed by a melt-volatile immiscibility at the time of entrapment of the secondary inclusions in the olivine phenocrysts.

[1] Seghedi, I. et al. (2008) *Geol. Soc. London, Sp. Publ.*, **293**, 83-100. [2] Roedder, E. (1984) *Rev. Mineral.*, **12**, 1-640. [3] Duan, Z. et al. (1992) *Geochim. Cosmochim. Ac.*, **56**, 2605-2617.

The immiscibility of water-salt fluids determined by synthetic fluid inclusions study

Kotelnikova, Z.[1*] & Kotelnikov, A.[2]
[1]Institute of Geology of Ore Deposits, Petrography, Mineralogy and Geochemistry of RAS, Moscow, Russia ([*]kotelnik@igem.ru)
[2]Institute of Experimental Mineralogy of RAS, Chernogolovka, Russia

Salt of the P-Q type (NaF, Na_2SO_4, Na_2CO_3) have inverse solubility dependence on temperature: it is about zero under 374°C. In such systems critical phenomena are observed in saturated solutions.

In order to obtain experimental evidence on salt-containing fluids, inclusions of solutions containing NaF, Na_2SO_4, Na_2CO_3 were synthesised at 300–800°C and P=0.5–3 kb by craks healing method.

The obtained results show that under t>500°C and P≥1 kbar the active interaction of fluid with quartz began, leading to formation of hydrosilicates. The interaction leads to increasing of quartz imaginary solubility.

An investigation of fluid inclusions showed that two liquids (contrary to vapor + liquid) coexist within the upper two-phase field of the phase diagramme.

In H_2O–salt (P-Q type)–SiO_2 ternary system, equilibria $V+L_1+L_2+S_1$ or $V+L_1+L_2+S_2$ are possible, absent in binary systems. In critical points of ternary system minimum temperature and pressure for critical equilibria correspond to $L_{1=}L_2+V+S_1$ and $L_{1=}L_2+V+S_2$, and not to the Q point with $L_{1=}L_2+S_{salt}+S_{SiO2}$ equilibrium.

During some fluid inclusion's heating at temperature 250ºC the liquid immiscibility took place.

The second liquid phase has appeared in saturated and unsaturated solutions and in "heavy fluid". Two salt solutions and vapor were coexistent in one inclusion at the temperature interval 250–400ºC. In multi component fluid-silica systems the possibility of equilibrium of not only two, but three, four and even more immiscible phases may occur.

At the intersection of two critical curves with vapor-liquid and liquid1-liquid2 equilibria non-variant equilibrium does not appear and transition of one critical equilibrium into another occur gradually. Therefore one can not talk about phase boundaries in this case. Apparently, this is a peculiarity of the studied system's phase diagram.

The interaction of fluid with quartz can be even more clearly seen in experiments at higher pressures and temperatures. In an experiment at 800ºC and 3 kbar, glass was observed in some inclusions together with vapor, liquid, and crystals. During heating of this inclusion, unmixing was observed in the glass phase. The ternary system water-salt-quartz includes a field of stable liquid immiscibility.

The obtained results suggest, first and foremost, that modeling of silicate-fluid systems on the basis of phase diagrams of simple binary water-salt systems may be misleading, because such a simplification implies that the sequence of phase transformations occurring in binary systems must be identical to that in the case of multicomponent equilibria.

Comparison in melt composition of two volcanoes (Hegyestű and Haláp) from the Bakony-Balaton Highland Volcanic Field (Hungary) based on primary silicate melt inclusion study

Kóthay, K.[1*], Szabó, Cs.[1] & Sharygin, V.V.[2]
[1]Lithosphere Fluid Research Lab, Dept. of Petrology and Geochemistry, Eötvös L. University, Budapest, Hungary ([*]klara.kothay@t-online.hu)
[2]Institute of Mineralogy and Petrology, UIGGM, Novosibirsk, Russia

Two volcanoes were selected in the Bakony-Balaton Highland Volcanic Field (Hungary) with different ages and slightly different modal and major and trace element features to compare original chemical composition of their magmas, based on bulk composition of olivine phenocryst hosted primary silicate melt inclusions (SMI).

The bulk compositions of the primary multiphase SMIs and crystallization sequences of the melt in the SMIs determined by homogenization experiments, furnace technique and microthermometry and Raman microspectroscopy of the fluid phases show characteristic differences, besides the similarities, between melts of the two volcanoes (Fig. 1).

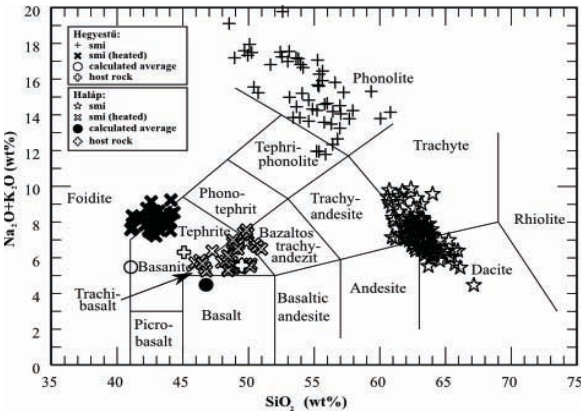

Fig. 1: TAS diagram comparing the calculated and measured bulk chemical compositions of silicate melt inclusions (SMI) and glass compositions of unheated SMI's in olivine phenocrysts of Hegyestű and Haláp volcanoes.

Bulk composition of SMIs from Hegyestű derived from a more alkaline mafic melt than that of Haláp (Fig. 1). Furthermore, with lower FeO and MgO and higher TiO_2, Al_2O_3 and CaO contents the Hegyestű melt clearly differs from the bulk composition of SMIs from the Haláp volcano. However, both melts are relatively volatile-rich, the CO_2 content of the Hegyestű melt is 2 m/m% and that of Haláp is ~1.5 m/m%.

The evolution of the magma droplets entrapped in olivine phenocrysts can be characterized at both localities by sulfide-silicate immiscibility as well as partially crystallization of daughter minerals at magma chamber level. The solidification continued and CO_2 separation from the silicate melt happened particularly at conduit level. This process in the Hegyestű SMIs follows a definite trend: sulfide bleb→ Al -spinel → rhönite → Ti-augite → apatite±rutile±ilmenite → CO_2 + glass. In contrast, the Haláp SMIs show a more variable chemical composition (Fig. 1) suggesting a more heterogeneous melt system. During their solidification they formed the following crystallization sequence: Al-rich spinel + sulfide bleb→ rhönite + amphibole + clinopyroxene → apatite + ilmenite → CO_2 + glass. The non-crystallized, highly silicic melt quenched as glass with high Na and/or K content, whereas the considerable CO_2 content occur separated as bubbles among the daughter minerals in both magmas.

Characterization of alteration, mineralization and fluid properties associated with the porphyry copper - high sulfidation epithermal transition at Red Mountain, AZ, USA

Lecumberri Sanchez, P.[1*], Bodnar, R.J. [1] & Kamilli, R.[2]
[1]Dept. of Geosciences, Virginia Polytechnic Institute and State University, Blacksburg, USA ([*]pilar@vt.edu)
[2]Western Mineral and Environmental Resources Science Center, US Geological Survey, USA

The porphyry copper deposits (PCD) in the southwestern US show variable degrees of erosion due to the complex structural evolution of the region. Frequently, the upper part of the systems is no longer present, which has limited the study of the geochemical evolution of the lithocap region of PCDs. The objective of this study is to characterize the relationships between mineralization, alteration and physicochemical properties of fluids in time and space in the lithocap, and Red Mountain has an exceptionally well-preserved lithocap, making it an ideal system to study.

The Red Mountain PCD constitutes a caldera-type subsidence structure where the dominant lithologies are andesite evolving in time toward trachyte-latite and later quartz-monzonite [1]. Three distinct mineralized regions are identified. The two primary mineralization zones are an upper, low Cu grade enargite zone associated with phyllic and pyritic-argillic alteration and a relatively higher Cu grade chalcopyrite mineralized zone associated with potassic and weak potassic alteration. The secondary mineralization is a chalcocite enrichment blanket. The enargite zone is characterized by an inner region with quartz-pyrite veins that shows sericitic halos and an outer region where quartz veins are less frequent and disseminated pyrite is abundant. The chalcopyrite zone shows abundant quartz and anhydrite veins with secondary biotite and orthoclase as well as disseminated magnetite around the veins. Small amounts of bornite are typically found in the chalcopyrite zone. The secondary chalcocite blanket is located within the enargite zone and it has been proposed that the source of copper for this enrichment zone is likely the enargite. Some of the common minerals within this region are chalcocite, covellite, pyrite, enargite and less abundant bornite and chalcopyrite.

Deposits with similar characteristics have been described at El Salvador, Chile; Sunnyside, Colorado; Lepanto-Far Southeast, The Phillipines; Recsk, Hungary. It is considered that the low grade enargite zone constitutes a high sulfidation epithermal system that is genetically related to a deeper PCD system. The presence of the deeper porphyritic part of the system related to the shallower high sulfidation epithermal system provides information about the genetic relationship between them. In this context, it is observed that the fluid inclusions (FI) in the deeper parts of the system (related to the potassic and weak potassic alteration zones) are mainly vapor-rich at room temperature (B35-B60) [2] and contain chalcopyrite daughter minerals, and halite-bearing FI with lower vapor-liquid ratio at room temperature (B15H) that frequently contain sylvite, chalcopyrite and anhydrite daughter minerals. These FI indicate that the deeper fluids are high-salinity, high-Cu. It is also observed that in the shallower parts of the system the abundance of FI with halite and chalcopyrite daughter minerals decreases, which indicates a decrease in salinity and Cu content in the fluids toward the shallower parts of the system. This change in fluid composition, mineralization and alteration characterizes the transition from a deep PCD system to a high sulfidation epithermal system

[1] Corn, R.M. (1975) *Econ. Geol.*, **70**, 1437-1447. [2] Rusk, B.G. et al. (2008) *Econ. Geol.*, **103**, 307-334

Fluid inclusion study on the barite-calcite veins of the Boda Aleurolite Formation (Mecsek Mts., Hungary)

Lenti, F.[*], Azbej, T., Németh, B. & Szabó, Cs.
Lithosphere Fluid Research Lab, Eötvös University, Budapest, Hungary ([*]lentifruzsi@gmail.com)

The main aim of our study was to constrain the formation conditions of barite-calcite hydrothermal veins in the Boda Aleurolite Formation (Mecsek Mts., Hungary). Based on preliminary studies, the Boda Aleurolite, deposited under arid climate in a Permian lake [1], is thought to be the best candidate in Hungary for high level nuclear waste disposal [2]. The studied rock samples originate from the so-called ALPHA-1 prospect tunnel from depth of 1050 m, which was made to carry out in situ physical and chemical experiments and measurements on the aleurolite rocks.

To our study we collected the mostly veined aleurolite samples to better understand the mechanism of fracture filling, as well as to study fluid inclusions in the veins. Based on petrographic observations, an older and a younger fracture filling event can be distinguished. The earlier phase resulted in formation of barite, whereas during the later event crystallization of carbonate (calcite and dolomite) took place in the vein.

Primary fluid inclusions can be recognized in both barite and carbonates minerals. Barites contain tiny (<3 μm), two-phase, negative crystal-shaped fluid inclusions, whereas primary fluid inclusions in calcites also have two phases in room temperature and irregular shapes in sizes of 7-8 μm. We have also observed secondary fluid inclusions in calcites along healed fractures, however their small size (<3 μm) did not permit additional study on them.

Results of microthermometric measurements indicate that the fluid inclusions entrapped a low-salinity (3.2 to 4.3 m/m% NaCl) aqueous solution. This compositional range is characteristic of all identified fluid inclusion assemblages in the calcite veins of the studied sample. The similarity of trapped fluids may suggest that the hydrothermal parent fluid did not evolve significantly during the crystallization of the carbonates. The homogenization temperatures (minimum temperature of entrapment) measured in the inclusions fall between 105 and 107 °C. Based on microthermometric data and geobarometric assumptions, we have estimated the maximum of the formation temperature range at 177 °C.

The presence of the secondary fluid inclusions in calcite suggests past fracture renewal events in the veins. Considering that the fractures have had completely healed and that the volumetric portion and size (3-8 μm) of the fluid inclusions is insignificant compared to the solid hydrothermal phases, it can be suggested that the studied veins do not represent weakness zones or impose threat on safe radioactive waste storage.

[1] Árkai, P. et al. (2000) *Ac. Geol. Hung.*, **43**, 351-378. [2] Bárdossy, Gy. (1995) *Magy. Tudomány*, **8**, 935-942.

Traces of primary hydrocarbon migration in the outcrop of the fractured Jurassic Hosszúhetény Calcareous Marl Formation (SW Hungary)

Lukoczki, G.[1,2*] & Schubert, F.[2]
[1]Dept. of Geology, University of Pécs, Hungary ([*]lukoczki@gamma.ttk.pte.hu)
[2]Dept. of Mineralogy, Geochemistry and Petrology, University of Szeged, Hungary

Latest researches revealed that certain part of the Hosszúhetény Calcareous Marl Formation (HCMF) contains mature organic matter [1]. Numerous calcite veins have been discovered in an outcrop of the HCMF near Pécsvárad (SW Hungary), which have an odour of bitumen, caused by petroleum inclusions. It proves that in the past the fracture system acted as a migration pathway for petroleum-bearing fluids.

The aims of the study were to determine the type of the organic matter in the marl and its maturation stage to verify whether the HCMF could serve as a source rock of the oil, which was trapped in fluid inclusions (FIs) of the vein filling calcite, as well as to study the inclusion fluids.

The relative ratio of the three main maceral types (liptinite, vitrinite, inertinite) was determined by visual kerogen analysis. The organic matter in the HCMF is composed mainly of liptinite of marine origin, but there are also vitrinite and ineritinite of terrestrial origin, therefore it can be established that the accumulation of the HCMF took place in a marine environment, which was relatively proximal to land.

The results obtained by vitrinite reflectance measurements (Ro%=0.688 and 0.791) and Rock-Eval Pyrolysis (RE) [1] show that the maturation state of the organic matter in the marl reached the oil window and oil has been generated. The studied part of HCMF was heated to a temperature of 106-117 °C at its deepest buried state, which was evaluated by the Vitrinite Reflectance Geothermometry (VRG) method [2].

Six pure calcite veins with different textural habits were distinguished in the studied outcrop. Two basic fluid inclusion assemblages (FIAs) were found in the calcites, which were suitable for microthermometry. Under UV-excitation numerous secondary FIs show an intense fluorescence referring to a hydrocarbon-bearing fluid infill. Visually three different fluorescence colours could be determined (yellowish blue, light blue and vivid blue). Nevertheless, the UV-fluorescence microspectroscopy does not show any difference between FIAs of yellowish blue and light blue fluorescence colours.

The temperature of the hydrocarbon-bearing fluid migration falls between 65 and 110 °C, which was evaluated using the homogenisation temperature (T_h) of the co-genetic aqueous fluid inclusions [3]. There are no significant differences in the T_h of the FIAs with different fluorescence colour. Thus microscale fractionation of the original hydrocarbon fluid during trapping could be responsible for the different fluorescence colours [4], therefore we suppose that they originate from the same hydrocarbon fluid.

Since the marl contains type II-III kerogen in sufficient amount for oil generation and it reached the oil window during the subsidence, it is likely that the HCMF has been the source rock of the hydrocarbon fluid trapped in petroleum inclusions. Biological marker analysis of the organic matter extract of the marl and the petroleum inclusion fluid would be necessary to make exact oil-source rock correlation.

[1] Raucsik, B. et al. (2002) *Geol. Carpath.*, Sp. Iss., **53**. [2] Barker, C.E. & Pawlewicz, M.J. (1994) *ACS Symp. Series*, **570**, 216-229. [3] Hanor, J.S. (1980) *Econ. Geol.*, **75**, 603-617. [4] Pironon, J. & Bourdet, J. (2008) *Geochim. Cosmochim. Ac.*, **72**, 4916-4928.

Study of felsic granulite xenoliths from the Pannonian Basin

Németh, B.[1*], Koller, F.[2], Török, K.[3], Dégi, J.[1,4] & Szabó, Cs.[1]
[1]Lithosphere Fluid Research Lab, Dept. of Petrology and Geochemistry, Institute of Geography and Earth Sciences, Eötvös University, Budapest, Hungary ([*]bianca.nemeth@gmail.com)
[2]Dept. for Lithospheric Research, University of Vienna, Austria
[3]Eötvös Loránd Geophysical Institute of Hungary, Budapest, Hungary
[4]Metals Research Dept., Research Institute for Solid State Physics and Optics, Hungarian Academy of Sciences, Budapest, Hungary

The Pannonian Basin is well known due to its ultramafic mafic and felsic xenoliths hosted in late Tertiary alkaline basalts, where rock fragments from different depths of the lithosphere were studied. In this work we present petrography, mineral chemistry, geothermobarometry and fluid inclusion study of mid-crustal felsic granulite xenoliths from Beistein (Styrian Basin, SBVF) and compare the results to other xenoliths of similar origin from the Bakony-Balaton Highland Volcanic Field (BBHVF). Based on our studies, the felsic granulite xenoliths went through at least three evolutional stages. The characteristic mineral assemblage of the felsic granulites consists of Pl + Opx + Qtz ± Cpx ± Bt ± Grt ± Ksp. The accessories are: Zrn + Ilm + Mag + Ttn + Gr + Rt. The samples have granoblastic texture, but in several cases relic poikilitic microtexture was also observed. These textural features refer to a silicic magmatic precursor rock, which intruded into the middle crust. The cooling of the igneous body resulted in antiperthitic exsolution of former high temperature ternary feldspars. Another cooling and crystallization gave rise to formation of a felsic granulite. According to the data of mineral equilibrium and geothermobarometry, the studied xenoliths from Beistein were in equilibrium in the middle crust, in depth of about 20-28km similarly to those from the BBHVF. The first fluid invasion and entrapment was coeval with the emplacement and crystallization of the magmatic body at middle crustal level as it is witnessed by primary pure CO_2 inclusions in the relic magmatic minerals, like apatite and zircon. The second evolutionary stage of the magmatic body was connected to partial melting of biotite-bearing assemblages occurred in association with the trapping of CO_2 rich fluid. Biotite is found either in the rock matrix partially molten and surrounded with melt or as remnants in orthopyroxene. This second fluid event also resulted in primary fluid inclusions in the main rock-forming minerals such as Pl, Qtz and pyroxenes. The majority of the fluid is CO_2 and the presence of additional N_2, H_2S and CO was identified by Raman spectroscopy. This event happened in the lower crust and could be connected to partial melting of biotite-bearing assemblages in the granulite facies. The third step was the sampling the magmatic body by the basaltic melt, and then uplift of the xenoliths to the surface, which caused a temperature increase and a pressure decrease, thus, limited melting of the xenoliths. All xenoliths contain different amounts of melt patches with associated secondary fluid inclusions. This later generation of secondary fluid inclusions was mostly observed in the felsic minerals and the fluids could be associated with the host basalt, with the compound of mostly CO_2, but there are also presented N_2, H_2S and CO, as well.

Fluid inclusion study of upper mantle xenoliths from the Cameroon Volcanic Line

Pintér, Zs.[1*], Tene Djoukam, J.F.[2], Tchouankoue, J.P.[2] & Szabó, Cs.[1]
[1]Lithosphere Fluid Research Lab, Eötvös University, Budapest, Hungary ([*]zsanett.pinter.hu@gmail.com)
[2]Dept. of Earth Sciences, University of Yaoundé I., Yaounde, Cameroon

We have studied upper mantle xenoliths from alkali basalts outcropped at Nyos and Barombi Lakes, which are situated along the Cameroon Volcanic Line. The main aim of this study is to find out whether upper mantle, containing plenty fluid inclusions, can be a potential source of the CO_2 that erupted from the Nyos Lake and killed about 2000 people and animals in 1986. Based on the results of previous study [1], the CO_2 gasses in the crater lake waters can be derived from the a degassing mantle. The studied peridotite xenoliths are spinel lherzolites (with protogranular and porphyroclastic texture) show similar lithology and mineral chemistry to the other xenoliths from the continental sector along the Cameroon Volcanic Line, and also to the average subcontinental lithospheric mantle.

Two generation of fluid inclusions can be distinguished in the Cameroon peridotitic xenoliths studied: an older and a younger one. The older generation fluid inclusions occur randomly in olivine and orthopyroxene in the Nyos peridotites. Fluid inclusions in this population have negative crystal shape with 50-80 μm average size and they are partly or completely decrepitated. The younger generations of fluid inclusions occur in all mantle silicates from both Barombi and Nyos xenoliths. They are trapped along healed fractures; however, they can also be seen in the neighborhood of the older decrepitated inclusions, in case of Nyos peridotites with size of 8-15 μm. Microthermometric measurements were carried out on this population of fluid inclusions. In these fluid inclusions for both Barombi and Nyos peridotites similar last melting temperatures were observed. In the Barombi xenoliths melting temperature is in the range of -57.9 and -56.6 °C, and in the Nyos samples it shows a very close range between -58.1 and -56.6 °C. The negative shift from the triple point of CO_2 (-56.6 °C) suggests presence of minor amount of other apolar component(s), for instance CH_4 and N_2 or H_2S [2] besides the common and major CO_2. Based on the density of CO_2 inclusions in pyroxenes, the estimated minimum trapping pressure conditions are between 8.4-9.8 kbar.

Raman microspectroscopy at room temperature indicates that beside the CO_2 a small amount of H_2S also occurs in some younger generation inclusions. This is in good accordance with the results of the observed low melting temperatures. Raman spectroscopy also reveals the presence of liquid H_2O as dissolved component in the CO_2-rich phase. Solid phases, namely carbonates, in the fluid inclusions were identified under polarized microscope.

Our results suggest that the CO_2 rich fluid inclusions, occurring both in the Barombi and Nyos upper mantle xenoliths, were trapped at lithospheric mantle conditions in the mantle silicates. Our study provides additional information on the composition of mantle fluids that can be indeed a potential source of volcanic hazards along CVL, especially in maar lakes such as Nyos.

[1] Tanyileke, G.Z. et al. (1996) *J. Afr. Earth Sci.*, **22**, 433-441.
[2] van Kerkhof, A.M. (1990) *Geochim. Cosmochim. Ac.*, **54**, 621-629.

Alkalic silica-undersaturated melts formed via interaction of peridotite with chloride-carbonate liquids: an experimental study

Safonov, O.
Institute of Experimental Mineralogy, Chernogolovka, Russia (oleg@iem.ac.ru)

Kamafugitic (SiO_2-undersaturated potassic) melts are believed to originate from peridotite source mixed with phlogopite-pyroxene-carbonate veins produced from the influx of alkalic fluids at 4-6 GPa [1]. Association of kamafugites with carbonatites [2] and fluid/melt inclusions in minerals of these rocks [3,4] suggest that evolution of such melts was accompanied by complex salt liquids enriched in K-Na carbonates and halides, S, P, etc., which are able to provoke liquid immiscibility [4].

In order to demonstrate the role of immiscibility [5] in generation of the kamafugite-like melts, experiments on interaction of a model peridotite $Fo_{63}En_{30}Prp_5Di_2$ with the $CaCO_3$+Na_2CO_3+KCl melt were performed at 1, 2 and 7 GPa. At 7 GPa, chloride-carbonate melt (L_{CC}) coexists with Fo, Grt, and KNCM-phase $(Na,K)_2Ca_4Mg_2Si_4O_{15}$ below 1460°C. Alkalic melt containing 32-34 wt. % of SiO_2, up to 28 wt. % of Na_2O+K_2O and 2-3 wt. % of Cl, immiscible with L_{CC}, appears at 1460°C. At 1-2 GPa such melt forms at 1100-1200°C via melting of the assemblage Fo+Cpx+Kls, generated from reaction of enstatite and pyrope constituents of the starting peridotite with the chloride-carbonate liquid: Prp+2En+[KCl+ Na_2CO_3+$CaCO_3$]=2Kls+7/3Fo+1/3Di+[2NaCl+4/3CO_2]. SiO_2 content of the melt increases (up to 45 wt. %), Cl and K_2O+Na_2O contents decrease (1.2 and ~16 wt. %, respectively) with decreasing pressure. De-carbonation (which is more active at low pressures) of the chloride-carbonate liquid produces CO_2-rich fluid.

Thus, immiscible KCl-rich liquid assists to a strong enrichment of the SiO_2-understurated melts in K_2O. Being formed within metasomatised peridotite in equilibrium with chloride-carbonate liquids, the melts loose Cl [6] during assent through the mantle preserving high K_2O content.

Acknowledgements: The study is supported by the RFBR (10-05-00040), Russian President Grant (MD-380.2010.5) and Russian Science Support Foundation.

[1] Rosenthal, A. et al. (2009) *Earth Planet. Sci. Lett.*, **284**, 236-248. [2] Stoppa, F. et al. (2003) *Per. Mineral.*, **72**, 1-18. [3] Stoppa, F. et al. (1997) *Mineral. Petrol.*, **61**, 27-45. [4] Panina, L. & Motorina, I. (2008) *Geochem. Int.*, **46**, 448-464. [5] Safonov, O. et al. (2009) *Lithos*, **112S**, 260-273. [6] Kamenetsky, V.S. et al. (1995) *Contrib. Mineral. Petrol.*, **120**, 186-196.

Carbonic and highly saline fluids in Precambrian deep-crustal metamorphism, southern peninsular India

Srikantappa, C.
DOS in Geology, University of Mysore, Manasagangotri, Mysore, India (srikantappa@googlemail.com)

Orthopyroxene bearing granitic - granodioritic - tonalitic, ortho-gneiss and para-gneiss of Precambrian age (3.3 to 2.5 Ga), termed as charnockitic-enderbitic granulites are well exposed in southern Peninsular India. Based on field relationship, petrography, mineral assemblage and geochemistry two major types of granulites are recorded in south India [1]: 1) Massive/banded charnockites (MBC) and 2) Incipient charnockite (IC). The MBC show regional granulite facies metamorphism with P-T (M1): 700 – 730 °C, 6 - 11 kbar. They show ITD and IBC P-T-t trajectories. In contrast, IC localities occur on a local scale, occupying low-land areas, confined to shear zones with mineral P-T (M2): ~ 650 - 700°C, ~ 6 kbar.

Deep-crustal fluids like CO_2, CO_2-H_2O and CO_2-CH_4-N_2 have been recorded in granulites from south India [2,3]. In this paper occurrence of halite bearing, highly saline fluids (up to 35 wt.% NaCl eqv.) coeval with carbonic fluids have been identified in granulites from the Dharwar craton (Fig. 1).

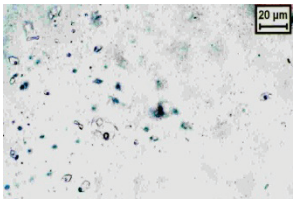

Fig. 1: Halite bearing fluids in south Indian granulites.

Different types of fluids in granulites is dependent on factors like lithology, mineral assemblage, protolith characters (ortho or para) and type of deformation. CO_2 and CO_2-H_2O fluids and, in some instances, hypersaline fluids appears to be the dominant fluids characteristic of massive granulites, derived from igneous precursors in contrast to CO_2, CO_2-CH_4-N_2 and N_2 bearing fluids which are common in granulites derived from sedimentary protoliths. High density CO_2 (1.10 to 1.14 g/cm^3) and CO_2-H_2O inclusions are common in minerals like garnet, plagioclase and quartz in MBC, indicating to their entrapment conditions at deeper crustal levels. High density carbonic inclusions (1.00 to 1.12 g/cc) have been found in many syn-metamorphic basic granulites. Lower density CO_2-fluids (0.90 to 0.95 g/cc) are common in IC. A combined micro-textural, mineral P-T, fluid evolution and the chronology of entrapment of fluids in MBC show synmetamorphic nature of CO_2 fluids [2], which exhibit an initial IBC path, followed by ITD path, suggesting an early collisional event followed by extensional tectonic regime for the evolution of most of these granulites.

The present study has shown occurrence of both high density carbonic and highly saline fluids in granulites from south India. This study brings into light importance of highly saline fluids in Precambrian deep-crustal metamorphism in south India in contrast to the earlier hypothesis of "Carbonic metamorphism" [2,3]. The source for these fluids appears to be the underplated basaltic/alkali basaltic magmas, suggesting addition of mantle derived fluids into lower crust, implying growth of the continental crust vertically. For the formation of incipient charnockites, "fluid release" model [4] has been proposed.

[1] Srikantappa, C. (2008) *Mem. Geol. Soc. India*, **58,** 156-168. [2] Srikantappa, C. et al. (1992) *J. Petrol.*, **33**, 733-760. [3] Newton, R.C. (1992) *J. Metamorph. Geol.*, **10**, 383-400. [4] Raith, M. et al. (1993) *J. Metamorph. Geol.*, **11**, 815-832.

Significance of silicate melt inclusions in olivine and spinel phenocrysts in alkaline basalt from Pohang (South Korea)

Vetlényi, E.[1], Bartucz, D.[1], Németh, B.[1], Yang, K.[2] & Szabó, Cs.[1*]
[1]Lithosphere Fluid Research Lab, Eötvös University, Budapest, Hungary ([*]cszabo@elte.hu)
[2]Dept. of Geological Sciences, Pusan National University, Busan, South Korea

Silicate melt inclusions generally represent melt composition from at the time of entrapment. Therefore, silicate melt inclusions entrapped in minerals that crystallized at different stages of igneous evolution can preserve the composition of a continuously changing melt. In the approx. 2 million years old alkaline basalt at Pohang (South Korea) large amounts of silicate melt inclusions have been found enclosed in olivine and spinel phenocrysts. These inclusions provide unique opportunity to reconstruct the evolution path of the crystallizing mafic magma.

The studied alkaline basalt has porphyritic texture and contains phenocrysts of olivine (0.3-5.0 mm in size) with forsteritic (mg#=0.85-0.89) composition, Cr-bearing spinel (cr#=0.18-0.25) and anorthite-rich plagioclase. The groundmass also consists of microphenocrysts of olivine, clinopyroxene, spinel, plagioclase and glass.

Silicate melt inclusions as isolated inclusions are enclosed in the core of olivine and spinel phenocrysts. These inclusions usually have rounded or elongate shape with sizes ranging up to 150 microns in diameter. Both olivine-hosted and spinel-hosted silicate melt inclusions contain daughter minerals such as Ni-Fe-rich sulfide blebs, Al-Mg rich spinel, zoned clinopyroxene, and addition Na-K-rich residual glass, and empty bubble (Fig. 1). The composition of clinopyroxene daughter phases shows differences in function of the host minerals: clinopyroxenes of melt inclusions hosted in olivine have higher Ca content than those of spinel host. Hence, a somewhat different evolution of the silicate melt inclusions can be suggested in the different host minerals. Based on the preliminary results obtained from petrographic observations and geochemical analyses on phases of SMI, we assume that the SMI of olivine and spinel phenocrysts were entrapped at the very early stages of the crystallization process and their bulk compositions can be representative for the primary mafic magma.

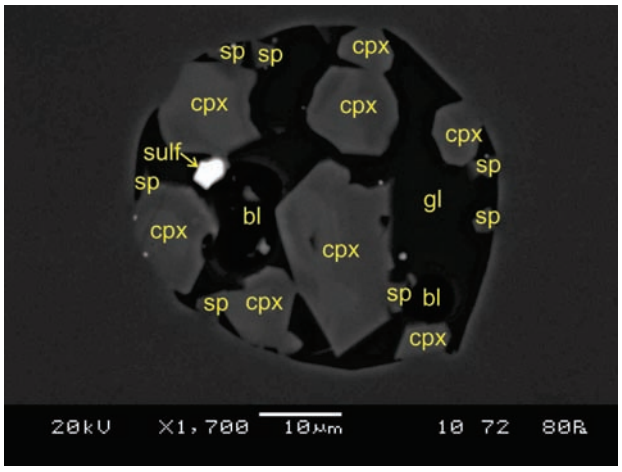

Fig. 1: BSE image of olivine-hosted silicate melt inclusion containing sulfide (sulf), spinel (sp), zoned clinopyroxene (cpx), glass (gl) and bubble (bl).

Deformation and metamorphism in the Mengku iron deposit, Southern Altaides, China: ore textures and fluid inclusions

Xu, J.H.[*], Lin, L.H., Wei, X.F., Shan, L.H., & Chu, H.X.
Resource Engineering Dept., University of Science and Technology, Beijing, China ([*]jiuhuaxu@ces.ustb.edu.cn)

The Mengku iron deposit, located at the south margin of Altaides, occurs in metamorphic volcanic-sedimentary rocks of the lower Devonian Kangbutiebao group. There has been a controversy on genesis of the deposit, such as volcanic-sedimentary, metamorphic and skarn [1-3]. Our research shows that the deposit has experienced a volcanic sedimentary, a metamorphic and a hydrothermal metasomatic mineralizing periods, based on field geology and ore textures (Fig. 1). The regional metamorphic mineralizing period consists of a disseminated-banded magnetite stage and a massive magnetite stage, which is important for iron mineralization. The hydrothermal metasomatic mineralizing period includes a calc-silicate metasomatic stage, a sulfide stage and a calcite-quartz vein stage. The vein copper mineralization is related to hydrothermal metasomatic mineralizing period.

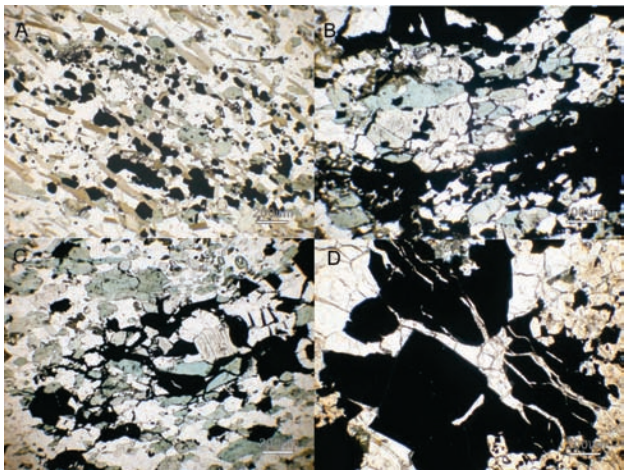

Fig. 1: Microphotos of ore textures of the Mengku iron deposit, Altay:
A- Dissemination magnetite cut by biotite, MK31A; B-Pressure solution and enrichment of magnetite in amphibolic leptynite, MK38;
C- Pressure solution of magnetite in amphibolic leptynite, MK38B;
D- Abnormal heterogeneous garnet interpenetrating magnetite, MK43.

Fluid inclusion study shows that homogenization temperatures of fluid inclusions hosted in metamorphic vein quartz are 133-250°C and 265-337°C respectively, and the salinities are 3.87-10.61 % NaCl eq. The homogenization temperatures of fluid inclusions hosted in hydrothermal metasomatic quartz are 122-207°C and 222-337°C respectively, and the salinities are 22-23.6 % NaCl eq. The $\delta^{18}O$ values of magnetite are -2 ‰~1.28 ‰, which are similar to that of volcanic sedimentary – metamorphic deposits. It could be believed that the Mengku iron deposit was finally enriched during regional metamorphism and hydrothermal metasomatism from Late Devonian to Early Permian.

*Acknowledgements***:** Funded by National Nature Science Foundation of China (40972066 and 40672060) and National Project (2007BAB25B01) (Xinjiang 305).

[1] Li, J.X. et al. (2003) *Xinjiang Geology*, **21**, 307-311. [2] Guo, Z.L. et al. (2007) *Miner. Deposits*, **26**, 128-138. [3] Yang, F.Q. et al. (2008) *Miner. Deposits*, **27**, 659-680.

Group II ultramafic xenoliths from Jeju Island, South Korea: evidence for melt migration and secondary orthopyroxene formation

Yang, K.[1*], Szabó, Cs.[2] & Arai, S.[3]
[1]Dept. of Geological Sciences, Pusan National University, Busan, South Korea ([*]yangkyhe@pusan.ac.kr)
[2]Lithosphere Fluid Research Lab, Eötvös University, Budapest, Hungary
[3]Dept. of Earth Sciences, Kanazawa University, Kanazawa, Japan

Group II xenoliths, corresponding to lithology of wehrlite, olivine clinopyroxenite, olivine websterite and websterite in Pleisto-Holocene basalts from Jeju Island, South Korea, are reported in this study. Jeju Island (75×32 km) is located at the eastern margin of the Eurasian plate surrounded by the SW Japan arc to the east and Okinawa through of the Jeju-Taiwan back-arc system to the south, which is similar to the East Sea back-arc on the eastern part of the Korean peninsula. This area is particular for two distinct magmatism sites such as convergent plate margins where Pacific and Philippine plates are being subducted beneath the Eurasian Plate and divergent tectonic settings where intraplate magmatism is active [1]. The large grain sizes (1–5 mm), moderate mg# of olivines (79-82) and pyroxenes (77-83), and absence of metamorphic textural features indicate that the studied Group II xenoliths have igneous origin. Strikingly similar major element and trace element variations of constituent minerals between the studied in Group II xenoliths and the host basalt suggest that the xenoliths formed as magmatic cumulates crystallized from the host basaltic magma-related system emplaced at the Moho beneath Jeju Island prior to the onset of Pleisto-Holocene volcanic activity. Secondary orthopyroxenes with moderate mg# (77-83) and Cr contents (0.15-0.34 wt%), free of exsolution, are pervasive in the studied Type II xenoliths, having formed by reactions between cumulate olivine and evolved basaltic melt that migrated through solidified crystalline assemblages [2] (Fig. 1). The evolved basaltic melts producing secondary orthopyroxenes resulted from the underplating and fractionation of mafic magma.

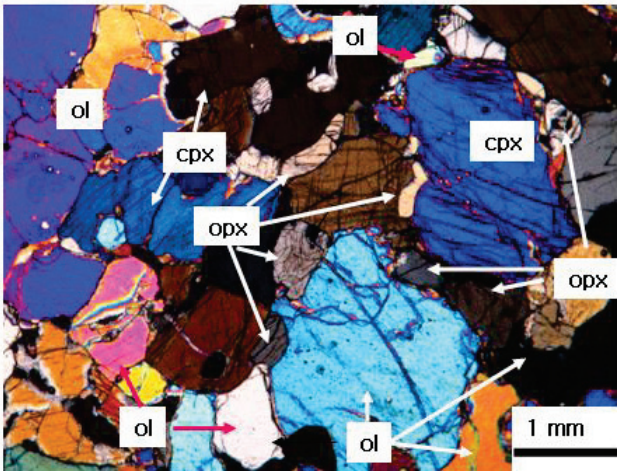

Fig. 1: Photomicrographs of Type II xenoliths from the Jeju Island showing secondary orthopyroxenes associated with olivines. ol=olivine, opx=orthopyroxene, cpx=clinopyroxene.

[1] Park, J.B. & Kwon, S.T. (1993) *J. Geol. Soc. Korea*, **29**, 39-60 (in Korean with English abstract). [2] Arai, S. et al. (2006) *Contrib. Mineral. Petrol.*, **152**, 387-398.

Fate of subducted continental margins

Cuthbert, S.J.
School of Science, University of the West of Scotland, Paisley, United Kingdom (simon.cuthbert@uws.ac.uk)

Substantial parts of ultra-high pressure (UHP) terrains probably represent subducted passive continental margins (PCM). This contribution reviews and synthesises research on processes operating in such systems and their implication for the wider Earth system. PCM sediments are large repositories of volatiles including hydrates, nitrogen species, carbonates and hydrocarbons. Sediments and upper/ mid-crustal basement are rich in incompatible elements and are fertile for melting. Lower crust may be more mafic and refractory. Juvenile rift-related mafic rocks also have the potential to generate substantial volumes of granitoid melts, especially if they have been hydrated. Exposed UHP terrains demonstrate the return of continental crust from mantle depths, show evidence for substantial fluxes of aqueous fluid, anatexis and, in entrained orogenic peridotites, metasomatism of mantle rocks by crust-derived C-O-H fluids. However, substantial bodies of continental material may never return to the surface as coherent masses of rock, but remain sequestered in the mantle where they melt or become entrained in the deeper mantle circulation. Hence during subduction, PCM's become partitioned by a range of mechanisms. Mechanical partitioning strips away weaker sediment and middle/upper crust, which circulate back up the subduction channel, while denser, stronger transitional pro-crust and lower crust may "stall" near the base of the lithosphere or be irreversibly subducted to join the global mantle circulation. Under certain conditions sediment and upper crustal basement may reach depths for UHPM. Further partitioning takes place by anatexis, which either aids stripping and exhumation of the more melt-prone rock-masses through mechanical softening, or separates melt from residuum so that melt escapes and is accreted to the upper plate leading to "undercrusting", late-orogenic magmatism and further refinement of the crust. Melt that traverses sections of mantle will interact with it causing metasomatism and refertilisation. Partitioning also takes place by solid-fluid and melt-fluid partitioning. Dehydration may take place both during subduction and exhumation, and fluxes between dehydrating and hydrating rock masses influence the internal fluid budget of the orogen (essential for eclogitisation and densification of mafic lithologies). Ascending granitic melts advect dissolved water to shallow levels, or even the atmosphere. Irreversible subduction of PCM sediment carries water plus nitrogen species to the deeper mantle. Decarbonation of voluminous PCM carbonates depends on thermal regime and may release a pulse of CO_2 to the atmosphere, but is limited in colder subduction zones hence transferring large volumes of CO_2 to the deep mantle. This may ultimately be mobilised by melting or dissolution to form fluid media for diamond formation.

Origin and metamorphic evolution of Grt-clinopyroxenite from the Sulu UHP terrane, China: evidence from microstructure and composition of mineral

Zhang, R.Y.[1,3*], Liou, J.G.[1], Xu, H.F.[2], Huberty, J.M.[2], Maki, K.[3] & Jahn, B.-M.[3]
[1]Dept. of Geological & Environmental Sciences, Stanford University, Stanford, CA, USA
[2]Dept. of Geosciences, University of Wisconsin – Madison, Madison, WI, USA
[3]Institute of Earth Sciences, Academia Sinica, Taipei, Taiwan
([*]ryzhang@earth.sinica.edu.tw)

The studied Grt-clinopyroxenite is unusual in widespread exsolution textures and transformation of initially coarse-grained mantle-derived rock to a fine-grained ultrahigh-pressure (UHP) metamorphic rock. The Grt-clinopyroxenites (Cpx + Grt + Ilm ± Ol) occur as lenses in a dunite body in the Sulu UHP terrane, eastern China. Two types of clinopyroxenite, Grt-poor (Grt < 5-10vol%) and Grt-rich (10-35vol%), are identified, and both contain rare, nearly initial coarse-grained (1-6 mm) and later recrystallized fine-grained (< 0.4 mm) clinopyroxenites. Some layers show porphyroblastic texture, and a few others contain megacrystic garnet of 2-12 cm in size. Coarse-grained Cpx and Cpx inclusions in megacrystic garnets contain numerous of oriented lamellae of Grt + Ilm/Mag ± Spl ± Amp. AEM and EBSD studies indicate that Ilm, Spl, and Amp lamellae have epitaxial relationship with host Cpx, and $[001]_{Grt}//[001]_{Cpx}$. This suggests that the lamellar phases were produced by solid-state exsolution. Fracture, kink band and wave extinction resulting from deformation are observed in the coarse-grained Cpx. The coarse-grained garnets and garnet inclusions in lamellae-bearing Cpx show that pyrope decrease with increasing grossular components from core ($alm_{16-20}sps_{0-2}prp_{36-54}grs_{22-44}$) to rim ($alm_{12-24}sps_{0-2}prp_{17-38}grs_{39-70}$). Fine-grained Grt in the matrix and Grt lamellae in Cpx are rich in grossular component (44-70%). This is similar to the rims of coarse-grained garnets. The lamellae-bearing Cpx contains Al_2O_3 (1.45-4.20 wt%) higher than matrix Cpx (0.59.6-1.20 wt%). Matrix Grt-Cpx yields P-T estimates of 5.2-6.6 at 850 ± 30 ^oC that lie in a high P/T regime. All the available data indicate that the Grt clinopyroxenite was derived from mantle, and the formation of UHP garnet clinopyroxenite with fine-grained granoblastic texture is attributed to multiple processes including exsolution and recrystallization of primary high-Al Cpx, deformation, and subduction-zone UHP metamorphism.

Polyphase oriented solid inclusions in Ti-rich pyropes from the Bohemian Massif peridotites: possible role of fluids in their origin

Bakun-Czubarow, N.[1*], Dobrzhinetskaya, L.[2], Jung, H.[3] & Kusy, D.[1]
[1]Institute of Geological Sciences, Polish Academy of Sciences, Warszawa, Poland ([*]nbakun@twarda.pan.pl)
[2]Institute of Geophysics and Planetary Physics, University of California at Riverside, CA, USA
[3]School of Earth and Environmental Sciences, Seoul National University, Seoul, Korea

Within the Bohemian Massif there can be found garnet-bearing peridotites which preserved microtextural memory of ultradeep origin – UDO. The peridotites are Mg–Cr pyrope lherzolites, associated with garnet pyroxenite and/or eclogite layers. The rocks under consideration occur either as small boudins within felsic granulites in the Sowie Mountains Block (SMB) of Saxothuringian zone in the Polish West Sudetes, or within migmatitic gneisses of Kutna Hora (KH) complex of Moldanubian zone in Czech Republic. The peridotites in question display inequigranular texture with large (up to 12 mm in diameter) garnet porphyroblasts set in a fine-grained groundmass of olivine, pyroxenes, garnet, clinoamphibole and spinel. Some of the large garnet porhyroblasts have in the cores abundant oriented solid inclusions of rutile, ilmenite-geikielite solid solutions, orthopyroxene, ±clinopyroxene, ±olivine, ±spinel. Among solid inclusions found in cores of garnet porphyroblasts there can be distinguished mono- or two-phase topotaxial exsolutions of Rt, Ilm_{ss}, Opx, Ol precipitated during decompression and located mainly along {111} planes of the host garnets; metasomatic solid inclusions with crichtonite, phlogopite, magnesite, pentlandite as well as mysterious oriented polyphase inclusions with Rt, Ilm, Ol, Sp (Fig. 1). The precursor garnet for rich in topotaxial exsolutions garnet cores was not supersilicic but contained Ti-rich and Al-deficient molecules: $Ca_2Na(AlTi)Si_3O_{12}$ and $M_3(MgTi)Si_3O_{12}$ being indicators of UDO for garnets. On the basis of the results of EBSD studies of rutile needles in garnets from the SMB peridotites [1] the hypothesis can be put forward that decompressional exsolution of rutile needles from Ti-rich majoritic-like garnets was accompanied by simultaneous deformation of the host peridotites.

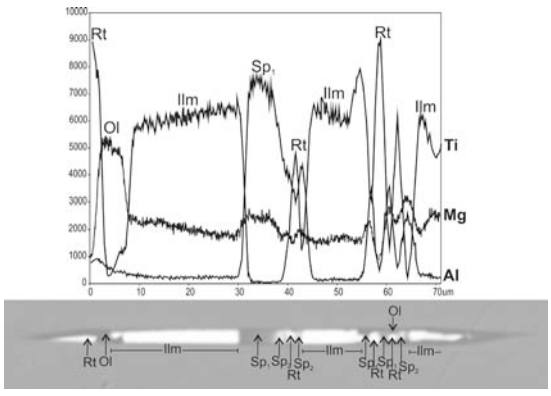

Fig. 1: Polyphase oriented inclusion in garnet core from Kutna Hora peridotite. The inclusion consists of Rt, Ilm, Ol, Sp_1 and Sp_2.

The oriented polyphase inclusions in UDO garnets are most likely the results of fluid interaction with solid phases at the grain boundaries of the previously exsolved inclusion. Further study is being carried to address fluid interaction with solids in nanoscale.

[1] Jung, H. et al. (2009) *Prog. & Abst., 8th Int. Eclogite Conf.* Xining, China.

Ultramafic cumulates of oceanic mantle affinity in a continental subduction zone: UHP garnet peridotites from Pohorje (Eastern Alps, Slovenia)

De Hoog, J.C.M.[1,*], Janák, M.[2], Vrabec, M.[3] & Hattori, K.H.[4]
[1]School of Geosciences, The University of Edinburgh, United Kingdom ([*]ceesjan.dehoog@ed.ac.uk)
[2]Geological Institute, Slovak Academy of Sciences, Bratislava, Slovak Republic
[3]Dept. of Geology, University of Ljubljana, Slovenia
[4]Dept. of Earth Sciences, University of Ottawa, Canada

Rare UHP garnet peridotites have been reported from the Slovenska Bistrica Ultramafic Complex (SBUC) in the Pohorje Mts., NE Slovenia, Eastern Alps [1]. The SBUC is a strongly serpentinised remnant of oceanic mantle entrained within lower Central Austroalpine basement units during Eo-alpine intracontinental subduction in the Cretaceous [1,2]. Peak *P-T* conditions of the garnet peridotites reached up to 4 GPa and 900°C [1].

The UHP metamorphic assemblage of the garnet peridotites consists of olivine (Fo 87-90), Mg-rich (Py 65-67) and low-Cr (Cr_2O_3 <0.2 wt.%) garnet and low-Al orthopyroxene and diopside. Remnants of magmatic minerals include Al and Cr-rich Opx and Cpx, Ti-rich chromian spinel, ilmenite and apatite, but their primary compositions are seldom preserved. Low-TiO_2 (<0.3 wt.%) spinel with Cr# 0.1-0.5 is replaced or rimmed by metamorphic garnet, whereas TiO_2-rich spinel with higher Cr# is not. Two types of magmatic clinopyroxene can be recognised: (a) low-Ti (0.5±0.1 wt.% TiO_2) Cpx with LREE-depleted trace-element patterns that strongly resembles Cpx in primitive olivine-rich gabbros from an oceanic spreading ridge [3], and (b) high-Ti cpx (1.4±0.4 wt.% TiO_2) with strongly negative Eu anomalies and less depleted LREE, which indicates crystallisation from more fractionated melts than low-Ti Cpx. Both types of Cpx show strong HREE depletions towards the crystal rims probably due to partial re-equilibration with garnet during meta-morphism. Fine-grained metamorphic Cpx shows the strongest depletions in HREE (Lu_N<0.3) and has very low TiO_2 (<0.1 wt.%) which indicates equilibrium with TiO_2-poor (<0.1 wt.%) metamorphic garnet.

Bulk rock compositions comprise 28-33 wt.% MgO, 7-10 wt.% Al_2O_3, 3-8 wt.% CaO and 0.3-0.8 wt% Na_2O. They show nearly flat and subparallel REE patterns over a range of HREE contents (Lu_N=0.5-3) and commonly have positive Eu anomalies (Eu*/Eu 1.0-2.3). This suggests that the protoliths were olivine-rich gabbros with ca. 60% olivine, 25% An-rich plagioclase and 10% Cpx, and not refertilised mantle, which is supported by their low but fractionated PGE contents (0.1-0.2 ppb Ir, Pd/Ir=5-15). Trace-element patterns are very similar to those of Pohorje zoisite and kyanite eclogites of predominantly MORB affinity.

The geochemistry of the garnet peridotites and their association with the SBUC and eclogites indicates their oceanic lithosphere origin. This implies that ultramafic plagioclase-bearing cumulates, the protoliths of garnet peridotites, were incorporated into the continental crust during subduction and subsequently experienced UHP metamorphism.

[1] Janak, M. et al. (2006) *J. Metamorph. Geol,*. **24**, 19-31. [2] De Hoog, J.C.M. et al. (2009) *Lithos*, **109**, 209-222. [3] Drouin, M. et al. (2009) *Chem. Geol*., **264**, 71-88.

Using garnet peridotite as tools to reconstruct paleo-geodynamic settings of fossil continental collision zones

Zhang, Cong[1,2*], Van Roermund, H.[2] & Zhang, Lifei[1]
[1]School of Earth and Space Sciences, Peking University, Beijing, China ([*]zhc@pku.edu.cn)
[2]Dept. of Earth Sciences, Structural Geology and Tectonics, Utrecht University, Utrecht, The Netherlands

Orogenic garnet peridotites (metamorphic rocks containing the characteristic HP garnet-olivine mineral assemblage) exposed in ancient orogenic belts may contain quantitative data regarding formation of subcontinental/subcratonic lithosphere, evolution of a lithospheric mantle wedge, incorporation of garnet peridotite into subducted continental crust, subsequent (ultra)high pressure metamorphism during ongoing continental subduction and final exhumation back to subcrustal levels. Allowing a more systematic way to investigate such variables in nature we propose here a simplified conceptual model that can be used to classify orogenic garnet peridotites. In addition to the "classic" mantle wedge- versus subduction zone garnet peridotites, the model subdivides mantle wedge garnet peridotites into four subtypes, called type A, B, C and D, equivalent to young/hot/dynamic- versus cold/old/static mantle in thick or thin garnet-olivine bearing mantle wedges.

We have chosen three well studied orogenic belts in Scandinavia (Scandinavian Caledonides) and China (Sulu-Dabie and North Qaidam orogen) to illustrate the applicability of the model. For garnet peridotites of the Scandinavian Caledonides, our conceptual model seems to fit well with geological observations and petrological, mineral-chemical and isotope characteristics of the orogenic garnet peridotites. Different types of mantle wedge garnet peridotite can be recognized when garnet peridotites of the WGR (type A =old, cold, thick, depleted mantle wedge- and/or subduction zone garnet peridotite) are compared to those in the Seve-, Lindås- and Tromsø Nappes (type C=old, cold, thin, depleted mantle overprinted by subduction zone garnet peridotite). Similar investigations on Chinese orogenic garnet peridotites appear to be more complicated except for the crustal origin of the Bixiling and Maowu subduction zone garnet peridotites in Dabieshan. Published models concerning the origin and evolution of the Zhimafang garnet peridotite in the Sulu terrane have two contrasting interpretations, 1) Type A=Old, cold, depleted (subcratonic) lithospheric mantle and 2) type B or D= hot, fertile, young upwelling asthenosphere. Recent evidence points towards the idea that the Xugou garnet peridotite also originates from the subcratonic lithospheric mantle underneath the Sino-Korean Craton (type A). There are also three contrasting interpretations for the origin of the Lüliangshan garnet peridotite in the North Qaidam orogenic belt: 1) type D = thin, hot, young & dynamic (Alaska type magmatic cumulate), 2) subduction zone type = serpentinised cumulates formed by dehydration of serpentinites during the subduction process and 3) type A = Archean fragments underneath a subcratonic lithosphere. It is clear from the results presented that our model is able to classify all garnet peridotites but in the case of the Chinese occurrences more detailed work is still needed before the final subtype of the model can be identified.

Assuming universal applicability of our model we conclude that the most important discriminative parameters in our model are: 1) The mean bulk temperature (T) that is operative in the mantle wedge at the onset of continental collision/subduction and 2) the thickness (P) of the lithosphere underneath the overriding plate during collisional. Finally it needs to be emphasized that also the age of melting, as well as the depth at which melting takes place (LP versus HP) are important parameters to be determined in garnet peridotites.

Garnet growth and dissolution in high-pressure metamorphic rocks; implication for multi-phase/multi-stage metamorphism in the Bohemian Massif

Faryad, S.W.[1*], Klápová, H.[1] & Jelínek, E.[2]
[1]Institute of Petrology and Structural Geology, Charles University, Prague, Czech Republic ([*]Faryad@natur.cuni.cz)
[2]Institute of Mineralogy, Geochemistry and Natural Resources, Charles University, Prague, Czech Republic

Garnet crystals with multi-stage growths in eclogites from two different units in Krušné Hory (Erzgebirge) and Mariánské Lázně Complex (western part of the Bohemian Massif) were studied to analyse chemical zoning in relation to a change of PT conditions during metamorphism and reactions with coexisting phases. In the Krušné Hory, garnet core was formed during blueschist facies stage and during the passage to eclogite facies stage it became unstable and formed atoll garnet structure which was interpreted as resulting from fluid infiltration and element exchange between the garnet core and matrix of the rock. The outstanding feature of the atoll garnet is its homogeneous central islands or peninsulas, which show composition similar to the rim-ring, implying growth under similar conditions. In addition, due to fluid access, the primary textures, mainly grain size, were also effective for the atoll garnet formation. Small grain fractions with thin rims were easily infiltrated by fluid, which used the short distance for element exchange between core and matrix. Both core and rim contain micro-veins that were used for compositional change due to fluid infiltration through the vein-channels. The core garnet was gradually dissolved and new garnet formed first island or peninsula and finally completely replaced the old core. Electron backscatter diffraction analyses show that the new garnet (II), including the outermost ring and islands or peninsulas in the core, have crystallographic orientations identical to that of the old garnet (I).

In the Mariánské Lázně Complex, core and rim of garnet were formed during different metamorphic events; the older core (garnet I) during amphibolite and younger rim (garnet II) during eclogite facies conditions. Garnet (II) may contain inclusions of Na-Ca amphibole and of omphacite. These two garnets have highly different composition: the core is rich in Mg and has lower Ca comparing with the surrounding garnet crystal. Both core and rim show different crystallographic orientation supporting their formation during different metamorphic events. Growth zoning is preserved in both core and surrounding crystals. Full multicomponent diffusion modelling of compositional zoning at the interface of amphibolite - eclogite facies garnets in conjunction with the retrieved P-T paths were used to evaluate average subduction / exhumation as well as heating / cooling rates during eclogite facies event. In addition to conventional geothermobarometry, pseudosection and garnet isopleths were used to estimate PT conditions for the early amphibolite facies and subsequent eclogite facies metamorphic events.

Tubular Mg-ferrite in magnesiowüstite inclusions in diamond from superdeep origin: control of Fe-valence by dislocation core structure

Wirth, R.[1], Dobrzhinetskaya, L.[2], Harte, B.[3] & Green, H.W.[2]
[1]German Research Centre for Geosciences GFZ, Potsdam, Germany ([*]wirth@gfz-potsdam.de)
[2]Dept. of Earth Sciences, University California at Riverside, USA
[3]University of Edinburgh, UK

Inclusions of ferropericlase and Mg-wüstite frequently occur as inclusions in diamond from the lower mantle. Under mantle conditions, diamond plus inclusion are regarded as a closed system. Therefore, the original oxygen activity f_o inside inclusions in diamond should have remained unchanged. Here, we report on TEM investigations on FIB-cut foils from Mg-wüstite inclusions in diamond enclosed in superdeep diamonds (Sao Luiz, Brazil) [1]. Along the inhomogeneously distributed dislocation lines in Mg-wüstite tubular structures of Mg-ferrite are observed. The tube-like structures are usually 70 - 150 nm in diameter and associated with "negative crystals" (50 nm in size) that are arranged along the original dislocation lines. Additionally, HREM imaging of the tube-like Mg-ferrite reveals nanometer-sized magnetite crystals 20 – 50 nm in size. The different phases have been identified by their chemical composition and electron diffraction or fast Fourier transforms from HREM images. Mg-wustite, Mg-ferrite and magnetite have identical crystallographic orientation. It is suggested that Mg-ferrite has formed under constant oxygen fugacity solid stateconditions by a solid state reaction:

$$(Mg, Fe)O \Rightarrow MgFe_2O_4 + \rho Mg_{vacancies} + Fe_3O_4$$
$$3Mg^{2+} \Rightarrow 2Fe^{3+} + 1\ Mg_{vacancy}$$

The atomic structure of a dislocation reveals that around the dislocation core the atomic positions are shifted. In the upper part of the dislocation (inserted half plane) above the dislocation line, the ions are compressed whereas below the dislocation line the atomic distances are slightly expanded. The effective ionic radius of Fe^{2+} in octahedral coordination is 0.078 nm and that of Mg^{2+} in octahedral coordination is 0.072 nm. Shifting the ions towards each other, then, at a certain distance, repulsive electrostatic forces will hinder further compression. In the compressed region of the dislocation core neighboring Fe^{2+} or Mg^{2+} ions would come to close to each other and repulsive forces are acting. These repulsive forces can be minimized by replacing Mg^{2+} by Fe^{3+}, which has a significantly smaller ionic radius (0.0645 nm). Replacing 3 Mg-ions by 2 Fe^{3+} plus 1 Mg vacancy makes the inter-atomic distances in the compressed part of the dislocation core more favorable because the ionic radius of Fe^{3+} (0.0645 nm) is smaller than that of $(Fe^{2+})^{VI}$ (0.078 nm) and $(Mg^{2+})^{VI}$ (0.072 nm). 3 Mg ions diffuse out of the core region into the bulk lattice and simultaneously 2 Fe ions diffuse into the dislocation core region leaving one Mg-position unoccupied thus creating one Mg-vacancy. The Mg-vacancies condense along the dislocation core forming negative nanocrystals. The observation that the tubes have approximately the same thickness of 70 nm can be explained by the size of the stress field around the dislocation core. The stress field around the dislocation core determines the width of the tubes.

[1] Harte, et al. (1999) in Fei, Y., Bertka, C.M & Mysen B. (eds.) *Mantle petrology: Field observation and high pressure experimentation: A Tribute to Francis R. (Joe) Boyd*. The Chemical Society, Sp. Publ., **6**, 125-153.

Synthesis of clinopyroxene from CNMAS system at P = 6-12 GPa and T = 900-1200°C

Dobrzhinetskaya, L.[1*], Zhao, S.T.[1,2], Nee, P.[1] & Green, H.[1]
[1]Dept. of Earth Sciences, University of California at Riverside, USA ([*]larissa@ucr.edu)
[2]China University of Geosciences, Wuhan, China

The publications of 1960-70s report that many eclogitic pyroxenes are characterized by non-stoichiometry, when sum of cations calculated per 6 oxygen atoms is <4, caused by the reaction: $CaAl(AlSi)O_6 + 3SiO_2\square \rightarrow \square\ Ca\square Al_2Si_4O_{12}$, where □ is a vacancy.

The reaction runs to the right by substitution of Si for Al in tetrahedral sites, displacing Al to M1 octahedral sites, where it is electrically balanced by a vacancy. The right side of the reaction has a smaller volume than the left, hence increasing pressure drives the reaction to the right. Day & Mulcahy [1] showed three possible ways of SiO_2-exsolution: (1) vacancy consumption in non-stoichiometric pyroxene; (2) dissolution of Ti-phases in pyroxene or garnet; (3) reactions between accessory phases and either pyroxene or garnet. We have conducted a series of anhydrous experiments in a Walker-style multianvil apparatus at P = 6, 8, 10, 12 GPa, and T = 900, 1000, 1100 and 1200 °C using powdered glass of the composition (wt%): SiO_2 = 58.29, Al_2O3 = 24.12, MgO = 5.44, CaO = 11.37, Na_2O = 0.78.

Our experiments demonstrate that at given bulk chemistry the Px with the largest CaEsk value is crystallized at P = 6 to 8 GPa at all temperature ranges; with increasing P up to 12 GPa and T up to 1200 °C the CaEsk component tends to decrease. Our data are in a good agreement with experiments by [2] because CaEsk component exhibits similar tendency, though the values of the CaEsk components are significantly different due to differences in the bulk chemistry chosen as starting materials. For example, Px synthesized from the starting material A toleiite at 10 GPa, 1200 °C contains CaEsk = 0.10 [2], whereas at similar conditions we have synthesized Px with CaEsk = 0.19. Our experiments showed that the nonstoichiometry of omphacite reaches a maximum between 5 and 8 GPa, followed by rapid decrease in CaEsk component when stishovite becomes stable in the assemblage and the pyroxene progressively dissolves into garnet, culminating in a garnetite at ca. 15 GPa. We conclude, that the CaEsk component can be responsible for SiO_2 lamellae exsolution formation in pyroxenes uplifted from depth not more than 180 km, and therefore decompressed from P = 6 – 8 GPa to ambient pressures.

[1] Day & Mulcahy (2007) *J. Metamorph. Geol.*, **25**, 35-70. [2] Irifune, T. et al. (1986) *Earth Planet. Sci. Lett.*, **77**, 245-256.

Lattice preferred orientation, water content, and seismic anisotropy of orthopyroxene

Jung Haemyeong*, Park Munjae, Jung Sejin & Lee Jaeseok
School of Earth and Environmental Sciences, Seoul National University, Seoul, Korea (*hjung@snu.ac.kr)

Lattice preferred orientation (LPO) and seismic anisotropy of orthopyroxene (enstatite) in mantle xenoliths from Spitsbergen, Svalbard, near the Arctic, are studied. LPOs of enstatite were determined using electron backscattered diffraction (EBSD). We found five types of LPOs of orthopyroxene and defined them as type-AC, -AB, -BA, -BC, and -ABC. Type-AC LPO of orthopyroxene is defined as (100) plane aligned sub-parallel to foliation and [001] axis aligned sub-parallel to lineation. Type-AB LPO is defined as (100) plane aligned sub-parallel to foliation and [010] axis aligned sub-parallel to lineation. Type-BA LPO is defined as (010) plane aligned sub-parallel to foliation and [100] axis aligned sub-parallel to lineation. Type-BC LPO is defined as (010) plane aligned sub-parallel to foliation and [001] axis aligned sub-parallel to lineation. Type-ABC LPO is defined as both (100) and (010) planes aligned sub-parallel to foliation and [001] axis aligned sub-parallel to lineation.

We report for the first time the type-AB and -BA LPO of orthopyroxene. LPO pattern has a correlation with the content of orthopyroxene in the specimen. FTIR study showed that type-AC LPO was observed mostly in the samples of enstatite with low water content. It is found that the strength of the LPO of enstatite decreases with increasing water content and has a correlation with the strength of the LPO of olivine: the stronger the LPO of enstatite, the stronger the LPO of olivine. Seismic anisotropy of enstatite was smaller than that of olivine in the same specimen.

Open system precipitation – a new way to explain crystallographically oriented precipitates/exsolutions in minerals from high-T/high-P rocks

Proyer, A.*, Krenn, K. & Hoinkes, G.
Institute of Earth Sciences, University of Graz, Austria
(*alexander.proyer@uni-graz.at)

The deep earth is where pressure and temperature have increased to an extent that substitutions considered rather exotic for "normal" crustal conditions become significant. The preservation of such exotic mineral compositions, directly or indirectly as precipitates/exsolutions, is an important criterion to derive prior extreme conditions of formation in ultrahigh-pressure and – to a lesser extent – ultrahigh-temperature rocks or regions.

The presence of crystallographically oriented inclusions in garnet (mainly rutile), in clinopyroxene (amphibole, quartz, Ti-minerals) and in titanite (mainly amphibole) from a high-grade metamorphic complex in the Rhodope mountains, where the presence of microdiamond indicates prior UHP conditions, cannot be explained by exsolution in a closed (intracrystalline) system. Hence we postulate that these precipitates form by an exsolution process at relatively high temperatures, where those components of an exotic high-P/T endmember with the slowest diffusion rates (Ti, Si, Al) can form precipitate minerals only because ions are to some extent exchanged with the rock matrix or a melt-phase in intergranular pore space. In other words, the host mineral is to some extent an open system where the exchange rates of ions with the matrix are a function of chemical potential gradients and diffusion rates. Example reactions would be:

For garnet: 2 $M_{2,5}TiAlSi_3O_{12}$ (grt) + 4 $M_3TiAl[AlSi_2]O_{12}$ (grt) + Si^{4+}= 5 $M_3Al_2Si_3O_{12}$ (grt) + 2 M^{2+} + 6 TiO_2 (ru);

For clinopyroxene: 6 $CaMgSi_2O_6$ (cpx) + 2 $CaAl_2SiO_6$ (cpx) + 1 $NaAlSi_2O_6$ (cpx) + 4 H^+ + 2 Mg^{2+} = 2 $Na_{0.5}Ca_2Mg_4Al[Al_{1.5}Si_{6.5}]O_{22}(OH)_2$ (amph) + 3 SiO_2 (qtz) + 4 Ca^{2+};

For titanite: 24 $CaAlSiO_4OH$ (tit) + 6 Si^{4+} + 20 Mg^{2+} + 5 Na^+ = 5 $NaCa_2Mg_4Al[Al_2Si_6]O_{22}(OH)_2$ (amph) + 14 H^+ + 9 Al^{3+} + 14 Ca^{2+}.

This apparently exotic exsolution mechanism is in fact to be expected in rocks where temperatures are high enough to reset bell shaped composition profiles – even in elements like Al – towards plateaus and where the absence or strongly reduced grain size of oriented inclusions near grain boundaries indicates (diffusional) material transport even of highly charged (slowly diffusing) ions out of the host crystals.

If this mechanism can be confirmed as valid and significant for high grade rocks in the future, the practice of calculating the composition of a precursor high grade mineral by broad-beam analysis or simple adding of exsolution and host mineral compositions must be considered imprecise and should be used with caution. It may also significantly affect the derivation of exchange vectors from metamorphic mineral compositions because any open system process "falsifies" the compositional record. More experimental work, including diffusion experiments, will clarify the significance and importance of open system behaviour in general and open system precipitation in particular.

Metamorphism and devolatalization in subduction zones

Perchuk, A.L.[1,2]
[1]Petrology Dept., Geological Faculty, Moscow State University, Moscow, Russia (alp@geol.msu.ru)
[2]Institute of Experimental Mineralogy, Chernogolovka, Russia

High pressure experiments, thermodynamic modeling and studies on (U)HP metamorphic rocks provide important knowledge on composition of fluid and net transfer reactions operated within the subducting slabs. Metamorphic fluids liberated from downgoing slabs are essential for metasomatic and magmatic processes in the overriding mantle as well as for the global element cycling in subduction zones. The contribution aims to overview the most poorly understood aspects of subduction zone process such as devolatalization, fluid escape from subducting slabs and its transfer to the mantle wedge, and to discuss a novel experimental method which allows studying these processes simultaneously in the high-gradient zone of piston-cylinder apparatus.

Experimental runs with glaucophane schist and olivine as analogs of crust and mantle, respectively, were carried at pressure up to 2.7 GPa. The temperature up to 1050°C at the top of the capsules was measured by the thermocouple whereas temperature up to ~700°C at the bottom of the capsules was quantified from the numerical modeling. The experiments demonstrate glaucophane and chlorite breakdown reactions in the schist and behavior of liberated liquid (supercritical fluid?). The liquid often migrates either through the grains or along the grain boundaries towards the high temperature olivine zone. Si-rich liquid reacts with the olivine and produce an orthopyroxene layer at the boundary between the olivine and the glaucophane schist. Pathways of liquid escape from the glaucophane schist are not identified in some domains, however presence of the orthopyroxene layer provides strong evidence that fluid can migrate in the schist without visible traces. Liquid migration above the orthopyroxene layer causes neither no changes in olivine composition nor its partial melting.

Acknowledgements: Financial support by RFBR grants N 09-05-01217 and 09-05-00991.

Subduction-related fluid activity in the Austroalpine Polinik complex: constraints from tourmaline-bearing eclogites

Hoinkes, G.[1*]**, Krenn, K.**[1]**, Konzett, J.**[2] **& Hauzenberger, C.A.**[1]
[1]Inst.of Earth Sciences, University of Graz, Austria (*georg.hoinkes@uni-graz.at)
[2]Inst. of Mineralogy and Petrography, University of Innsbruck, Austria

Tourmaline is a rare constituent in eclogites since boron contents are usually too low in mafic protoliths to stabilize tourmaline during metamorphism. Hence the occurrence of tourmaline in an eclogite of eo-Alpine age in the Austroalpine unit is an exceptional feature indicating metasomatic activity. These eclogites occur as boudins of a few tens of metres in diameter interlayered in pelitic gneisses and schists from the Texel area in the W to the Koralpe area in the E and mark an eo-Alpine collision zone appearing as Southern Limit of Alpine Metamorphism (SAM) within the Eastern Alps. The eclogite investigated belongs to the Polinik Complex, the northern part of the Kreuzeck Mountains between the Möll valley in the N and the Drau valley in the S in Upper-Carinthia. Textures imply that tourmaline occurs as mm-sized idiomorphic grains as part of the HP-assemblage comprising garnet, omphacite (Jd_{33-48}), Ca-amphibole, clinozoisite and quartz as major constituents. Additional minor or accessory constituents are phengite, rutile, titanite, apatite, zircon and K-feldspar. The calculation of a pseudosection for a phengite-bearing sample yields *P-T*-conditions of 1.6 GPa and 650°C. Tourmaline contains inclusions of omphacite, rutile, apatite and rarely K-feldspar and is typically intergrown with abundant small zircons of up to 100 μm in size. Chemically the tourmalines are schoerl-dravit solid solutions with unusually high TiO_2-contents of up to 3.4 wt%. Their trace element content is high in Sr (1288 – 3948 ppm), Pb (32 – 71 ppm) and Li (16 – 30 ppm) and low in Be (< 1 ppm). The zircons contain omphacite and rutile inclusions and have high U (264 – 419 ppm), Th (1.2 – 2.5 ppm) and Li (5.0 – 8.3 ppm) contents compared to a single very large zircon grain of 300x500 μm in size. Both zircon generations give similar U-Pb – SIMS ages of 86+1 and 109+2 Ma for the small generation and 90+9 Ma for the larger one. These ages are consistent with well documented ages of the eo-Alpine HP-metamorphism of the Austroalpine unit. Two main chemical systems of fluids are included in tourmaline: System 1 consists of H_2O-CH_4-N_2-NaCl-CO_2 with salinities of ca. 6 mass% NaCl, is restricted to tourmaline and occurs as single inclusions. System 2 comprising saline aqueous fluids of NaCl-$CaCl_2$-H_2O chemistry, are arranged along cracks in tourmaline and dominate in apatite and quartz with a wide range in salinities between 8 and 30 wt%. Independent of salinity, the fluids occur either as single, primary inclusions or along planes. Aqueous inclusions in quartz rarely contain calcite daughter crystals which may coexist with halite. Trace element contents of the aqueous fluids determined by SIMS result in high Sr-, Pb- and B-contents of up to 1081 ppm Sr, 16 ppm Pb and 372 ppm B and resemble the tourmaline composition. Calculated isochors of primary inclusions in tourmaline, apatite and quartz combined with petrologic thermobarometric estimates yield minimum pressures of 10 – 12 kbar. Since postentrapment leakage of fluid inclusions is common minimum *P-T* estimates point to formation of tourmaline, zircon, apatite and quartz at eclogite facies metamorphic conditions. Enrichment of HFSE-LILE – elements in zircon of eo-Alpine age are in agreement with a continental-derived fluid in course of a Cretaceous collision/subduction event within the Austroalpine lithosphere.

Tourmaline – an ideal geochemical recorder in UHP metamorphic rocks?

Marschall, H.R.
Dept. of Earth Sciences, University of Bristol, UK
(Horst.Marschall@bristol.ac.uk)

The extensive *P-T* stability and the high chemical variability of tourmaline (Tur) together with its common occurrence in metasediments proves its high potential for petrologic and (isotope) geochemical studies on fluid-rock interaction in subduction and collision-related rocks. Its occurrence in natural rocks combined with experimental data demonstrates that at least some members of the Tur group are stable in subducting slabs to a depth of at least 150 km, possibly even 250 km. Tur of the schorl-dravite solid-solution series with coesite inclusions has been discovered from the Erzgebirge and from the Western Alps, and is taken as unambiguous evidence for the crystallisation of Tur under UHP conditions.

(U)HPM rocks are the products of complex histories, and the occurrence of Tur in any given sample may be related to one or several of a number of different processes. The first aim in a petrologic or geochemical study involving Tur, therefore, has to be the identification of the Tur-forming process by petrographic or petrologic means. In general, Tur may be (1) a relic from the pre-metamorphic protolith (e.g., detrital grains), or (2) may have formed from B released from surrounding minerals during prograde metamorphism, or (3) may have formed during metasomatism at any stage of the *P-T* history. Metasomatic formation of Tur is a common mechanism and has been documented for (U)HP metamorphic rocks in a number of fossil subduction zones. These metasomatic Tur porphyroblasts form by reaction of silicates with incoming B-rich fluids or melts, in most cases during the decompression history of the rocks.

Inclusions of Tur in (U)HP phases, or of (U)HP phases in Tur are probably the best indicators for (U)HP stability and/or formation of Tur. Coesite found as inclusions in Tur can be recognised by Raman spectroscopy, which allows for rapid analyses of a large number of inclusions down to micrometer size.

Tourmaline is chemically highly variable, confronting us with the difficulty to decipher a highly relatively complex mineral system. On the other hand, it presents us with a geochemical recorder of unparalleled broad representation across half of the periodic table. Tur records the magmatic or metamorphic *P-T-X* evolution of its host rock by changing major element compositions, such as Mg/Fe and Ca/Na ratios. Recently, advancements have been made in the investigation of the thermodynamic properties of Tur towards a quantification of the metamorphic *P-T* history during its crystallisation. A wide range of isotope systems has been applied to Tur, including major (O, B, Si, H), minor and trace elements (Sr, Pb, Nd, Li) and both radiogenic and stable isotope systems. Fluid-rock interaction processes, magmatic-hydrothermal systems and ore-forming processes have been reconstructed this way.

Dating of tourmaline has been achieved using the K-Ar and Ar-Ar techniques, which show blocking temperatures in Tur in the same range as in amphibole. Pb-Pb and Sm-Nd dating has also been successfully applied to Proterozoic and Archean tourmaline. Therefore, it is in some cases even possible to directly link the wide range of geochemical signals documented in tourmaline to the ages of their formation.

Metasomatic hide and seek: origins of the Roberts Victor eclogites, South Africa

Huang, J-x[1,2*], Greau, Y.[1], Griffin, W.L.[1] & O'Reilly, S.Y.[1]
[1]GEMOC, Macquarie University, Sydney, Australia
([*]jhuang@els.mq.edu.au)
[2]School of Earth Sciences and Resources, China University of Geosciences, Beijing, China

Eclogite is an important minor constituent of subcontinental lithospheric mantle (SCLM) (1-3 vol%) and a clear picture of its origin will help us to understand the origin of the ancient SCLM. Extensive studies of these rocks have generated two contradictory hypotheses about their origin; one regards the eclogites as deep-seated magmatic rocks, while the other regards them as components of subducted oceanic slabs. Xenolithic eclogites from Roberts Victor kimberlite (South Africa) have been studied to constrain their origin.

The Roberts Victor eclogites can be divided into two types based on differences in microstructure and mineral composition. Type II eclogites have low Na in gnt and low K in cpx, while Type I has high values. Type II eclogites are generally fresh and show equilibrated microstructures. Rutile exsolution in gnt and cpx, and gnt exsolution in cpx, are only found in Type II. Type I eclogites, in contrast, are texturally not in equilibrium, and have many fluid inclusions. Only Type I eclogites contain diamond, graphite, sulfides and apparently-primary phlogopite.

All the minerals are homogeneous within each sample. Reconstructed whole-rock compositions show that Type I eclogites are richer in Mg, K, Rb, Sr, LREE and LILE than Type II. P-T estimates indicate Type II eclogites are distributed from 170-200 km depth, but Type I are strongly concentrated in a layer at 180-190 km depth, just beneath lithosphere-asthenosphere boundary. However the abundance of Type II is low, about 6-8% of Type I.

Sr, Nd and Hf isotopes of gnt and cpx were analyzed in clean small grains after acid-leaching. The Nd-Hf data for Type I eclogites define two-point isochron ages (Sm-Nd 100±21 Ma; Lu-Hf 133±17 Ma) that are identical to the kimberlite eruption age (128 Ma). Lu-Hf isochron ages for Type II eclogites (1354±9 Ma) may suggest a connection to the Namaqua-Natal Orogenic Belt to the south of Kaapvaal Craton. These differences suggest that Type II eclogites have retained their initial isotopic compositions whereas the isotopic systems of Type I eclogites were actively re-equilibrating at the time of kimberlite eruption. This is also consistent with the petrographic and mineralogical evidence of fluid metasomatism in Type I eclogites. Sr, Nd and Hf isotopic ratios at the time of kimberlite eruption also show marked differences between Type II and Type I; $^{87}Sr/^{86}Sr$ is 0.7060-0.7064 in Type I and 0.7013-0.7030 in Type II. O- isotope ratios are also different. Type II eclogites have $\delta^{18}O < 4.3‰$ and those of Type I have mantle values (ca 5.4) or higher.

These data and observations suggest that Type I eclogites were being actively metasomatized slightly prior the kimberlite eruption. Inter-element correlations suggest that the metasomatism was adding Mg, K, S, Rb, Sr, C (diamonds), LREE and LILE. Some samples (the present Type II eclogites) from the same depth range appear to have escaped this process and preserved their original characteristics.

The calculated fluid in equilibrium with Type I eclogitic gnt and cpx is LREE-enriched and shows trace-element patterns similar to those of fibrous diamonds and carbonatitic/kimberlitic melts. The Sr- and Nd-isotope values are also consistent with reaction between Type II eclogites and diamond forming fluid to form Type I eclogites. Type II eclogites therefore are the key samples for studying the origin of this eclogite suite, since they may represent the protoliths. Type I, in contrast, are heavily metasomatised rocks, and retain little evidence of their primary origin.

Chromian kyanite, chromian magnesiostaurolite and ruby in UHP eclogites from Pohorje (Eastern Alps) and Tromsø Nappe (Northern Scandinavian Caledonides)

Janák, M.[1*], Vrabec, M.[2], Krogh Ravna, E.[3], Kullerud, K.[3] & Hurai, V.[1]
[1]Geological Institute, Slovak Academy of Sciences, Bratislava, Slovakia ([*]marian.janak@savba.sk)
[2]Dept. of Geology, University of Ljubljana, Slovenia
[3]Dept. of Geology, University of Tromso, Norway

Chromian kyanite, magnesiostaurolite and ruby were found in eclogite associated with metaultramafic rocks (garnet peridotite, serpentinite) from Pohorje Mountains (Eastern Alps) and the Tromso Nappe (Northern Scandinavian Caledonides). At both localities eclogite is composed of primary Mg-rich garnet (X_{Mg} = 0.75-0.81), omphacite (Jd = 16-29 mol%) and kyanite with secondary amphibole (pargasite, magnesiohornblende) and zoisite, which are abundant in strongly retrogressed rocks. Chromian kyanite (Cr_2O_3 up to 14.2 wt%) of turquoise-blue colour contains inclusions of chromite (Cr* = 0.74-0.78), Cr-rich garnet (Cr_2O_3 = 2.0 wt%), omphacite (Cr_2O_3 = 0.5 wt%) and Cr-rich amphibole (Cr_2O_3 = 3.5 wt%). Chromian kyanite shows the highest Cr content near chromite. Rarely, a very Cr-rich chromian magnesiostaurolite (Cr_2O_3 = 8.8-15.0 wt%, X_{Mg} = 0.7-0.81) occurs as inclusions in Cr-rich domains of kyanite. Texturally different staurolite occurs in the retrogressed rocks with abundant amphibole and zoisite. This staurolite forms subhedral, up to 500 μm large crystals of blue-green colour, the composition is magnesian (X_{Mg} = 0.76-0.82) and Cr-rich (Cr_2O_3 = 5.4-8.5 wt %). Blue-green staurolite is associated with blue Cr-kyanite, brown Cr-spinel and pink Cr-corundum (ruby) which are surrounded by pargasitic amphibole. The ruby from Pohorje shows the highest chromium content (Cr_2O_3 = 12.4 wt%). Some kyanites are surrounded by coronas composed of sapphirine + corundum + Al-spinel + plagioclase assemblage. Sapphirine corresponds to 3:5:1 end-member with 1.7 wt% Cr_2O_3. Mg-chlorite, margarite and plagioclase are present in the most retrogressed domains. Chromium enrichment in kyanite, staurolite and corundum was controlled by substitution for Al in the octahedral sites. The highest Si content and almost absence of tetrahedrally coordinated Al was observed in the most Cr-enriched staurolite in primary assemblages of the Pohorje eclogite. Metamorphic peak-pressure conditions of the Pohorje eclogites reached >3 GPa at 800-850°C. Experimental studies demonstrate that magnesiostaurolite can be stable at such UHP conditions and chromium content in kyanite tends to increase with pressure. Formation of Cr-kyanite and chromian magnesiostaurolite is inferred by reactions involving Cr-spinel, during subduction and UHP metamorphism of the mantle-derived, Cr-rich magmatic protolith of eclogite. Formation of blue-green magnesiostaurolite, ruby and less chromian, Mg-rich spinel seems to be related to partial breakdown of Cr-kyanite, involving garnet and omphacite during decompression and exhumation of the eclogite. Lower *P-T* limits can be constrained by the stability of magnesiostaurolite at >1.2 GPa and 750°C in the system MgO-Al_2O_3-SiO_2-H_2O, however, chromium may shift the magnesiostaurolite stability field. The Cr-kyanite, chromian magnesiostaurolite and ruby reported here show chromium contents which are among the highest recorded in natural samples.

Mantle wedge convection and metasomatism: evidences from the Maowu mafic-ultramafic rocks in Dabieshan UHP terrane, eastern China

Chen Yi[*], Ye Kai, Guo Shun & Liu Jingbo
State Key Laboratory of Lithospheric Evolution, Institute of Geology and Geophysics, Chinese Academy of Sciences, Beijing, China ([*]chenyi@mail.iggcas.ac.cn)

The Maowu mafic–ultramafic body occurs in paragneisses in the Dabieshan ultrahigh-pressure (UHP) metamorphic terrane, eastern China. It is a lens (50x250 m^2) composed of millimeter- to centimeter-thick compositional layers, dominated by garnet orthopyroxenite and orthopyroxenite with minor dunite, harzburgite, garnet websterite and garnet clinopyroxenite. Previous researchers assumed that the protolith of the Maowu mafic-ultramafic body was a cumulate complex, fromed by fractional crystallization of a basaltic magma in the Yangtze Craton, which suffered by deep subduction and UHP metamorphism in the Triassic [1-5]. However, these rocks exhibit a sequence of symmetric layering ranging from Mg-rich to Mg-poor, Fe-, Al- and Ca-rich composition, and no rhythmic bandings have been found in the outcrops. The matrix orthopyroxene from the garnet websterite, garnet orthopyroxenite and orthopyroxenite have high NiO content and high Ni/Mg and Fe/Mn ratios, which is similar to that in olivine from dunite. The same is true for the relicts of fine-grained olivine and orthopyroxene in the core of matrix orthopyroxene in pyroxenites, which have composition similar to the matrix olivine and orthopyroxene in the dunite, respectively. These features indicate that the Maowu pyroxenites were derived by metasomatic interactions between refractory mantle wedge dunite and slab-derived silica-saturated fluid or hydrous melt.

The Maowu garnet orthopyroxenite preserves mineralogical and mineral chemical evidence for multistage metamorphism related to progressive mantle wedge convection during the Triassic subduction of oceanic and continental plates. Six stages of metamorphism are distinguished, based on detailed mineralogical and petrological studies: (I) High-T low-P metamorphism (~1.4 GPa, ~900 ^oC); (II) Low-T low-P metamorphism (1.3-1.7 GPa, 700-750 ^oC); (III) Low-T low-P metamorphism (2.1-2.5 GPa, 740-760 ^oC); (IV) UHP metamorphism (5.3-6.3 GPa, ~800 ^oC); (V) Early stage retrogression (< 3 GPa, > 750 ^oC); (VI) Late stage retrogression (< 2.3 GPa, < 670 ^oC). Mineral textures and compositions indicate that the Maowu garnet orthopyroxenite was derived by metasomatic interactions between precursor refractory dunite in the mantle wedge and slab-derived fluid. M1-M2 defines an isobaric cooling P-T path, implying that the protolith dunite convected from a hot depleted mantle wedge to the cold and wet mantle wedge corner and was metasomatized by oceanic slab-derived fluid rich in SiO_2, Al_2O_3, TiO_2, CaO, Na_2O, K_2O, FeO, P_2O_5, SO_2, BaO and Cl. M2-M4 defines an isothermal compression P-T path, suggesting that the rock subsequently convected from the shallow, cold and wet mantle wedge corner to deep mantle up to ~ 200 km depth and suffered HP-UHP metamorphism. Dehydration during subduction might have released fluid that migrated into the above hotter mantle wedge and resulted in partial melting and formation of arc magmatism. M4-M6 defines a retrograde P-T path during exhumation to the crustal level together with the UHP terrane and was continuously metasomatized by fluid derived from the country UHP crustal rocks.

[1] Okay, A.I. (1994) *Contrib. Mineral. Petr.*, **116**, 145-155. [2] Zhang, R.Y. et al. (1998) *Chem. Geol.*, **150**, 161-170. [3] Liou, J.G. & Zhang, R.Y. (1998) *Isl. Arc*, **7**, 115-134. [4] Jahn, B.M. et al. (2003) *Lithos*, **70**, 243-267. [5] Liu, D.Y. et al. (2006) *Earth Planet. Sci. Lett.*, **250**, 650-666.

The Triassic age of oceanic eclogites in the Dabie orogen: entrainment of oceanic fragments in the continental subduction

Cheng, H.[1*], DuFrane, S.A.[2], Vervoort, J.D.[2], Nakamura, E.[3], Li, Q.L.[4] & Zhou, Z.Y.[1]
[1]State Key Laboratory of Marine Geology, Tongji University, Shanghai, China ([*]oahgnehc@gmail.com)
[2]School of Earth and Environmental Sciences, Washington State University, Pullman, Washington, USA
[3]Institute for Study of the Earth's Interior, Okayama University, Tottori, Japan
[4]State Key Laboratory of Lithospheric Evolution, Institute of Geology and Geophysics, Chinese Academy of Sciences, Beijing, China

Low-temperature and high-pressure eclogites with an oceanic affinity in the western part of the Dabie orogen have been investigated with combined Lu–Hf and U–Pb geochronology. These eclogites formed over a range of temperatures of 482–565°C at 1.9–2.2 GPa. Three eclogites, which were sampled from the Gaoqiao country, yield Lu–Hf ages of 240.7 ± 1.2 Ma, 243.3 ± 4.1 Ma and 238.3 ± 1.2 Ma, with a corresponding lower-intercept U–Pb zircon age of 232 ± 26 Ma. Despite the well-preserved prograde major- and trace-element zoning in garnets, these Lu–Hf ages mostly reflect the high-pressure eclogite-facies metamorphism instead of representing the early phase of garnet growth due to the occurrence of omphacite inclusions from core to rim and the shell effect. An upper-intercept zircon U–Pb age of 765 ± 24 Ma is defined for the Gaoqiao eclogite, which is consistent with the weighted mean age of 768 ± 21 Ma for the country gneiss. However, the gneiss has not been subjected to successive high-pressure metamorphism. The new Triassic ages are likely an estimate of the involvement of oceanic fragments in the continental subduction (Fig. 1).

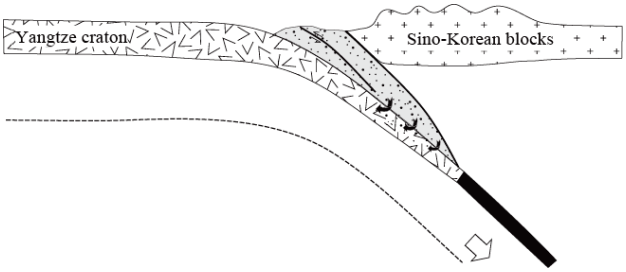

Fig. 1: Continental subduction started and oceanic subduction terminated. Some early oceanic fragments were probably entrained by the subducted continental crust.

Fluid-rock interaction and element mobilization in deep subduction zone: evidence from mass transfer calculation of UHP eclogite

Guo Shun*, Ye Kai, Chen Yi & Liu Jingbo
State Key Laboratory of Lithospheric Evolution, Institute of Geology and Geophysics, Chinese Academy of Sciences, Beijing, China (*guoshun@mail.iggcas.ac.cn)

In order to study the complex UHP fluid-rock interaction and element mobility involved in deep subduction zone, we calculated the mass transfers of eclogite profile towards the HP vein in Dabie UHP metamorphic belt, eastern China. The normalized Isocon diagram (Fig. 1) indicates various degrees of trace elements mass transfers which reflect their mobilities during the formation and precipitation of the fluid released from the host UHP eclogites. (1) The less mobile LILEs (U, Th, Pb and Sr) are dramatically scavenging from the elcogites towards the vein, indicating that they were released from the host eclogites during the vein formation and largely deposited in the vein during the fluid precipitation. (2) The REEs are also gradually scavenged towards the vein, however, they exhibit remarkably different mobility behaviors. The HREEs (from Gd to Yb) decrease gradually with the increase of their atomic number. In contrast the LREEs (from Ce to Gd) show gradual increase with increasing atomic number. This tendency is significantly inconsistent with the results of laboratory experiments [1], thus reveal the residual fluid after the precipitation of the HP vein carries significant LREEs back into the host eclogites. (3) The HFSEs (Nb, Ta, Zr and Hf) show low degree of reductions towards the vein in the host eclogites, indicating the HFSEs are also mobile, but their mobility is limited. (4) The water soluble LILEs (Cs, Rb, K and Ba) that are assumed to be most mobile, are however low in the vein and are gained in the eclogites a little away from the vein. This indicates that they were mainly dissolved in the residual fluid after the precipitation of the vein and were carried back into the host eclogites. The mobility of LREEs and water soluble LILEs in the residual fluid and their depositions in the host eclogites is assumed by the formation of later stage hydrous minerals such as epidote, barroisite, phengite and apatite in the host eclogites.

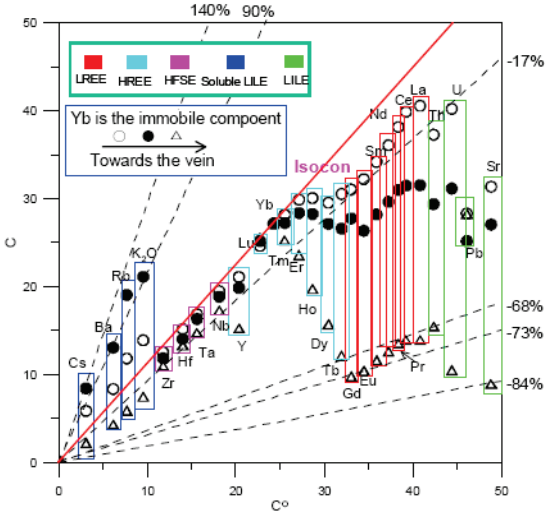

Fig. 1: A normalization Isocon diagram for mass transfer along profile from the vein towards the host eclogite in Dabieshan. The results of calculation using the method by [2] suggest that Yb is the immobile component due to its very low mobility in the fluid-rock interaction [1]. $\mathbf{c^o}$ is composition of eclogite far away from the vein and **c** is near to the vein. Ecolgite samples gradually closer to the vein are indicated by open circle, solid circle and triangle.

[1] Kessel, R.M. et al. (2005) *Nature*, **437**, 724-727. [2] Guo, S. et al. (2009) *Econ. Geol.*, **104**, 881-886.

Lattice preferred orientation of olivine in garnet peridotites from Finsch, South Africa

Lee Jaeseok* & Jung Haemyeong
School of Earth and Environmental Sciences, Seoul National University, Seoul, South Korea (*shoo3680@snu.ac.kr)

Olivine is a major mineral in the upper mantle and plays an important role in deformation processes and seismic anisotropy. It has been known that water and stress influence lattice preferred orientation (LPO) of olivine [1,2]. In addition, recent experimental study at high pressure & high temperature showed that LPO of olivine can be changed due to pressure [3]. To understand the deformation processes in the deep upper mantle, garnet peridotites from Finsch, South Africa were studied. Lattice-preferred orientation (LPO) of olivine was determined by the electron back-scattered diffraction (EBSD) with CHANNEL 5 software. Water content of olivine was measured using the Nicolet 6700 FTIR with Continuum FTIR Microscope. Thermo Scientific DXR Raman Microscope was used to check the high pressure mineral phases.

Three samples showed that [001] axes of olivine are aligned subparallel to the lineation and [010] axes are aligned normal to the foliation, which is known as B-type LPO of olivine. The B-type LPO of olivine could be formed at the high stress condition with large amount of water [1,2]. However, there was no water observed inside of the olivine. Samples were dry. Study of Raman spectroscopy of specimens showed that some diamonds exist in garnet. We found peaks at the Raman shift wavenumbers of 1320cm^{-1} and 1322cm^{-1} which are known to be diamond peaks. These result suggest that the peridotite from Finsch, south Africa, orignated from a depth greater than ~120km (P ~ 4GPa), and the LPO of olivine was formed by high pressure. This is the first report of natural samples showing the type-B LPO of olivine most-likely induced by high pressure.

[1] Jung, H. & Karato, S.-i. (2001) *Science*, **293**, 1460-1463. [2] Jung, H. et al. (2006) *Tectonophysics*, **421**, 1-22. [3] Jung, H., Mo, W. & Green, H.W. (2009) *Nat. Geosci.*, **2**, 73-77.

Tectonic exhumation rates of eclogite bodies from a Neoproterozoic subduction zone; Zambezi belt, Zambia

Mapani, B.S.[1*], Johnson, S.[2] & Tembo, F.[3]
[1]Geology Dept., University of Namibia, Windhoek, Namibia ([*]bmapani@unam.na)
[2]Tectonics Special Research Centre, Dept. of Earth and Geographical Sciences, University of Western Australia, Perth, Australia
[3]School of Mines, Dept. of Geology, The University of Zambia, Lusaka, Zambia

The Neoproterozoic to early Palaeozoic Gondwana supercontinent formed by the amalgamation of numerous cratonic blocks over an extended period of ca. 150 M.y. Although the post-collision configuration of Gondwana is relatively well constrained, the timing, order and nature of collisions leading to amalgamation are, in part, poorly understood. The African cratonic blocks form the core of the Gondwana supercontinent and thus determining the precise location and number of sutures and blocks, and the timing of their collisions are critical for understanding the supercontinents amalgamation. Neoproterozoic to Cambrian, i.e., Pan-African, tectono-magmatic activity in southern and eastern Africa formed the Damara-Lufilian-Zambezi (DLZ) and East African orogens, respectively. Evidence from the Lusaka eclogites and the Chongwe area of Zambia suggest a more complicated and perturbed exhumation history [1]. *PT* conditions in the Chongwe River area were based mainly on the whiteschist lithologies (10kbar at 700°C) [2]. Mafic eclogites that rest tectonically on the Congo Craton margin in southern Zambia, record maximum pressures of 26-28 kbar and have MORB-like geochemistries [2]. Isotopic mineral isochron ages between 659-595 Ma [3, 4] are interpreted as the time of eclogite-facies metamorphism and record the subduction and hence closure of the Zambezi Ocean. The very-high pressure-metamorphism and metasomatism recorded at ca. 570 Ma in the Chongwe River area and the various whiteschists marks the first contact between the Congo and Kalahari Cratons, or at least a promontory of one or other craton [1]. The formation of whiteschists and very-high-pressure rocks that comprise the Congo Craton margin indicate that it was subducted to at least 50km [1]. In this paper we outline the mineralogical, chemical and structural evidence that point to a staggered exhumation history during exhumation of the the subducted eclogitised gabbroic rocks.

[1] Johnson, S., Rivers, T. & DeWaele, B. (2005) *J. Geol. Soc. London*, **162**, 433-450. [2]. John, T. & Schenck, V. (2003) *Contrib. Mineral. Petrol.*, **146**, 174-191. [3] John, T. et al. (2003) *Geology*, **31(3)**, 243-246. [4] John, T. et al. (2004) *J. Geol.*, **112**, 71-90.

Decompression and partial melting of subducted continental crust rocks: example from felsic high-*PT* granulites in the Bohemian Massif

Nahodilová, R.[1,2], Faryad, S.W.[1*] & Dolejš, D.[1]
[1]Inst. of Petrology and Structural Geology, Charles University, Prague, Czech Republic ([*]faryad@natur.cuni.cz)
[2]Czech Geological Survey, Prague, Czech Republic

Felsic granulites are closely associated in space and time with high-temperature eclogites and garnet peridotites in the Moldanubian and Saxothuringian zones of the Variscan orogen. Ultra-high pressure conditions for some mafic and ultramafic precursors were documented by the presence of coesite and microdiamonds (Saxothuringian) or were derived from phase equilibria and geothermobarometry (Moldanubian). Felsic granulites from the Kutná Hora complex in the Moldanubian zone consist of quartz, ternary feldspar, garnet, biotite, kyanite and rutile, and exhibit modal layering and discordant leucocratic veining. The layering is interpreted as evidence for partial melting along the exhumation path from the eclogite to granulite facies. Garnet grains show relatively high and constant Ca in their cores but in the rim, pyrope concentrations increase whereas those of grossular and almandine drop. In contrast, garnets from the leucocratic layers have comparably low Ca contents that further decrease towards the rim. Mineral assemblage and garnet chemical zoning constrain a prograde metamorphic path from 530 °C and 3.0-3.1 GPa through muscovite dehydration melting at 900 °C and 2.0-2.2 GPa to 850 °C and 1.4 GPa where the partial melt has crystallized. Phase formation and melt productivity were independently estimated by experiments in the piston-cylinder apparatus at 850-1100 °C and 1.7-2.1 GPa. The partial melt was produced by the dehydration melting: muscovite + omphacite + quartz = melt + K-feldspar + kyanite. The melt fraction was controlled by the whole-rock H_2O budget present throughout the eclogite facies, estimated to be 0.21 wt. % H_2O and accommodated by shifting the equilibrium: phengite + quartz = K-feldspar + kyanite + H_2O. Minimum water solubilities in silicic melts predict the bulk fertility to 2.8-4.2 wt. % melt during decompression but the actual melt fraction varied by as much as 28 wt. % on centimeter scale due to deformation-enhanced melt redistribution. The melt accumulation was probably controlled by shear instabilities and strain accommodation within foliation-parallel sites, eventually leading to the formation of modal layering. The presence of partial melt was responsible for attaining equilibrium during decompression at 850-900 °C, thus eliminating any potential relics of precursor high-pressure phases such as phengite or omphacite. In contrast, adjacent mafic granulites and eclogites, which apparently share the same metamorphic path but have not undergone partial melting, often preserve relics or inclusions of eclogite-facies mineral assemblages. The presence of partially molten domains of felsic granulites in the Variscan orogenic continental root probably exerts major rheological control on the incorporation and immersion of lenses and boudins of mafic granulites, eclogites and garnet-bearing ultramafics and their common extrusion *via* an exhumation channel to the middle continental crust.

Mössbauer spectroscopy studies of valence state of iron in a Tibetan chromite containing high-pressure mineral inclusions

Ruskov, T.[1*], Spirov, I.[1], Georgieva, M.[2], Yamamoto, S.[3], Green, H.[4], McCammon, C.[5] & Dobrzhinetskaya, L.[4]
[1]Institute for Nuclear Research and Nuclear Energy, Sofia, Bulgaria ([*]ruskov@inrne.bas.bg)
[2]University of Sofia, Bulgaria
[3]Tokyo Institute of Technology, Tokyo, Japan
[4]University of California, Riverside CA, USA

The Mössbauer spectroscopy studies show that chromites from massive ore are characterized by $Fe^{3+}/\Sigma Fe = 0.42$, and chromites from nodular and disseminated ores contain $Fe^{3+}/\Sigma Fe = 0.22$, all are from a Tibetan ophiolite. The massive ores record traces of ultrahigh pressure minerals: diamond, exsolution lamellae of coesite and diopside in chromite, inclusions of metal-nitrides, SiC and Fe^0 [1,2], the latter indicate a strongly reducing environment [3]. In contrast, chromites from nodular and disseminated ores contain abundant low-pressure OH-bearing mineral inclusions whose formation requires a more oxidizing environment. The high value of $Fe^{3+}/\Sigma Fe$ in the "reduced" massive ores is explained by stabilization of Fe^{3+} in a high-pressure polymorph of spinel deep in the upper mantle through a mechanism such as charge coupled substitution, or creation of oxygen vacancies, accompanied by Fe disproportionation to balance charge.

We suggest that the massive chromitite and their host peridotite were transported in the solid state from a highly reduced deep mantle (>300km) to an ocean spreading center. In this shallow environment they partially reacted with their host peridotite in the presence of hydrous melt, yielding the nodular and disseminated chromitite ores as proposed previously. Given that the high pressure highly-reduced mineral assemblage within the Tibetan massive chromitite is not unique, similar examinations of chromitites worldwide and high-pressure experiments on reduced Cr-rich systems should help to decipher further the missing history of the deep mantle processes that are involved in their formation.

[1] Yang, J.S. et al. (2007) Geology, **35**, 875-878. [2] Yamamoto, S. et al. (2009) *Lithos*, **109**, 314-322. [3] Dobrzhinetskaya, L. et al. (2009) *P. Natl. Acad. Sci.*, **106**, 19233-19238.

Preservation of prograde high-pressure assemblages and textures in granulites from the Rychleby Mts., Bohemian Massif

Schlöglová, K.[*], Faryad, S.W., Dolejš, D. & Klápová, H.
Institute of Petrology and Structural Geology, Charles University, Prague, Czech Republic ([*]schloglo@gmail.com)

Mafic and felsic granulites in the Rychleby Mts. (Czech Republic and Poland) represent an high- to ultrahigh- pressure crustal segment exhumed along the eastern margin of the Bohemian Massif. These occurrences are related to the granulites and eclogites of the Sówie Góry Mts. which contain pseudomorphs after coesite [1]. Their metamorphic history can provide valuable insight into burial mechanisms of pre-Variscan crust and its exhumation during the Variscan orogeny. Mafic granulite varieties are composed of omphacite, garnet, kyanite and rutile. Garnet grains are zoned with composition ranging from Py18Gr36 in the core to Py30Gr24 in the rim, and host inclusions of omphacite and phengite; kyanite was found in the matrix only. Omphacite with 23-25 mol. % jadeite component is frequently replaced by symplectitic overgrowths of diopside, amphibole and plagioclase whereas biotite and ilmenite are secondary phases. Felsic granulites contain ternary feldspar, garnet, kyanite and quartz, with minor amounts of biotite and plagioclase formed during decompression and retrogression. Large garnet grains preserve compositional zoning, which spans Py01Gr31 in the core to Py18Gr25 in the rim. Inclusions of phengite in garnet contain up to 5.4 wt. % TiO_2 and were partially replaced by biotite. The phase assemblages of granulites and eclogites in this area reveal decompression path from high- to ultra-high pressure and high-temperature conditions - 1.8-3.0 GPa and 850-950 °C [1-4]. In addition to information gained from garnet compositional zoning and mineral inclusions, the presence of titaniferous phengite documents maximum temperatures that were reached at the transition from eclogite to granulite facies, and were accompanied by high-pressure partial melting. This scenario provides new insights into exhumation mechanisms of mafic and felsic high-pressure precursors from the continental root to the orogenic middle crust

[1] Klemd, R. & Bröcker, M.(1999) *Contrib. Mineral. Petrol.*, **136**, 358-373. [2] Pouba, Z., Paděra, K. & Fiala, J. (1985) *Neues Jb. Miner. Abh.*, **151**, 29-52. [3] Kryza, R., Pin, C. & Vielzeuf, D. (1996) *J. Metamorphic Geol.*, **14**, 531-546. [4] Štípská, P., Schulmann, K. & Kröner, A. (2004) *J. Metamorphic Geol.*, **22**, 179-198.

Elasticity of serpentine: first principles investigation

Tsuchiya Jun[1*], Tsuchiya Taku[2], Usui Yusuke[2] & Katayama Ikuo[3]
[1]Senior Research Fellow Center, Ehime University, Ehime, Japan ([*]junt@sci.ehime-u.ac.jp)
[2]Geodynamics Research Center, Ehime University, Ehime, Japan
[3]Dept. of Earth and Planetary Science Systems, Hiroshima University, Hiroshima, Japan

Serpentine is formed by reaction between peridotite and water which is released from hydrous mineral in subducting slab under pressure. Partially serpentinized peridotite may be a significant reservoir for water in the subducted cold slab and is considered to play an important role in subduction zone processes such as generation of arc magmatism. Precise determination of elastic properties of serpentine is essential for estimating the degree of serpentinization, and is important for investigating the transporting processes of water into deep Earth interior. Several studies on the degree of serpentinization have been reported so far based on limited experimental data on elasticity of serpentine. Here we investigate by first principles calculation, the detailed structures and elastic properties of lizardite and antigorite which are lower and higher temperature polymorphs of serpentine up to 10 GPa at 2 GPa interval, and discuss the difference of compression mechanism and elasticity between these polymorphs.

Our calculations are based on density functional theory within generalized gradient approximation for exchange correlation functional. We calculated the crystal structure and elasticity of antigorite m=16 polysome which contains 273 atoms in primitive cell. We found the bulk modulus of antigorite and lizardite are almost same at ambient pressure, but they show significant difference at high pressure conditions. On the other hand, antigorite always has a few % larger shear modulus than lizardite presumably because of corrugated layer structure of antigorite. Combining the data from the present ab initio calculations, latest high-pressure deformation experiments with the lattice preferred orientation of serpentine and seismological observations for the velocity and anisotropy structures of subduction zones, we analyzed the degree of serpentinization and possible water content in subducting slabs.

The "Chessboard" classification scheme of mineral deposits-geology and mineralogy from aluminium to zirconium

Dill, H.G.
Bundesanstalt für Geowissenschaften und Rohstoffe, Hannover, Germany (dill@bgr.de)

Economic geology is a "*mixtum compositum*" of all geoscientific disciplines focused on one goal, finding new mineral deposits and enhancing their exploitation. The keystones of this "*mixtum compositum*" are geology and mineralogy whose studies are focused around the emplacement of the ore body and the development of its minerals and rocks. In the present study, mineralogy and geology act as x- and y-coordinates of a classification chart of mineral resources called the "chessboard" ("spreadsheet") classification scheme. Magmatic and sedimentary lithologies together with tectonic structures (1-D / pipes, 2-D/ veins) are plotted along the x-axis in the header of the diagram representing the columns in this chart diagram. 63 commodity groups, encompassing minerals and elements are plotted along the y-axis, forming the lines of the spreadsheet. These commodities are subjected to a tripartite subdivision into ore minerals, industrial minerals and gemstones/ ornamental stones.

Further information on the various types of mineral deposits, as to the major ore and gangue minerals, current models and mode of formation or when and in which geodynamic setting these deposits mainly formed throughout the geological past may be obtained from the text by simply using the code of each deposit in the chart. This code can be created by combining the commodity (lines) shown by numbers plus lower caps with the host rocks or structure (columns) given by capital letters.

Each commodity has a small preface on the mineralogy and chemistry and ends up with an outlook into its final use and the supply situation of the raw material on a global basis, which may be updated by the user through a direct link to databases available on the internet, e.g., the database of the US Geological Survey. The internal subdivision of each commodity section corresponds to the common host rock lithologies (magmatic, sedimentary, metamorphic) and structures. Cross sections and images illustrate the common ore types of each commodity. Ore is given priority over the minerals. The minerals are listed by their chemical composition and may be viewed by the reader by clicking on-line the pertinent databases, where the "showroom" varieties, seldom found in a mine, are on display.

A metallogenetic-geodynamic overview is given at the bottom of each column in the spreadsheet describing the geodynamic models put forward by the various researchers for all the deposits pertaining to a certain clan of lithology or structure. This classical or conservative view of metallotects related to the common plate tectonic settings is supplemented by an approach taken for the first time for such a number of deposits, using the concepts of sequence stratigraphy. The relationship supergene-hypogene and syngenetic-epigenetic has been the topic of many studies for ages but to keep them as separate entities is often unworkable in practice, especially in so-called epithermal or near-surface/shallow deposits. Vein-type and stratiform ore bodies are generally handled also very differently. To get these different structural elements (space) and various mineralizing processes (time) together and to allow for a forward modeling in exploration, architectural elements of sequence stratigraphy are adapted to mineral resources. Deposits are geological bodies which need accommodation space created by the environment of formation and the tectonic/geodynamic setting through time. They are controlled by horizontal to subhorizontal reference planes and/or vertical structures. Prerequisites for the deposits to evolve are thermal and/or mechanical gradients.

Major metallogenic provinces and epochs of Mexico: a review and new perspectives

Camprubí, A.
Instituto de Geología, Universidad Nacional Autónoma de México, México D.F., Mexico (camprubitaga@gmail.com)

Epithermal, porphyry, skarn, MVT, VMS, SEDEX, and IOCG deposits are the most outstanding types in Mexico. Such deposits are distributed in various metallogenic provinces that grossly mimic the distribution of major geological provinces and events. Most ore deposits in Mexico are associated with two major metallogenic domains: (1) the Pacific convergent margin and the resulting magmatism since the Jurassic, or (2) the evolution and migration of basinal brines, and diagenesis in the Gulf of Mexico basin, that formed after the breakup of Pangea. Other events like the opening of the Gulf of California have also associated other types of ore deposits. This paper is based on the typological analysis and the compilation of geochronological data of over 200 deposits.

Prejurassic deposits are relatively scarce: Ti-bearing anortosites, rare-element pegmatites (Proterozoic) and chromitites (obducted during the Ordovician) in S Mexico, barite SEDEX deposits in Sonora (Devonian), and several metalliferous mafic-ultramafic complexes in W Mexico (Paleozoic to middle Jurassic). Since the Jurassic epithermal, porphyry, skarn, VMS, IOCG "clan", rhyolite-hosted Sn and U-Au deposits, as well as other minor types formed along the Pacific margin. The metallogenic epochs associated with Pacific magmatism can be sketched as follows:

1. Middle Jurassic to Early Cretaceous in SW Mexico: mostly VMS in volcanosedimentary series;
2. Cretaceous in SW Mexico and the Pacific margin: mostly deposits in oceanic-crust or island-arc ultramafic-mafic complexes;
3. Paleocene to Early Eocene in NW Mexico and the Pacific margin: porphyry, deposits; also skarn and IOCG deposits;
4. Early Eocene to Late Eocene in NW and central Mexico: skarn and epithermal deposits;
5. Oligocene, elsewhere: mostly epithermal; several Sn and skarn deposits;
6. Final Oligocene to Early Miocene in SW and central Mexico: epithermal;
7. Middle Miocene to Present: several hypogenic and supergenic types.

The Eastern Mexican Alkaline Province deserves to be mentioned as a special case in the Pacific domain: it formed southeastwards and contains IOCG, carbonatite, agpaitic complex, porphyry, skarn and epithermal deposits, usually telescoped or overprinted.

The evolution of the Gulf of Mexico since the Late Jurassic, besides the vast majority of oil and gas fields in the country, generated important and world-class MVT, SEDEX, and red-bed Cu-U deposits all along the basin. Also, the opening of the Gulf of California since the Miocene generated several shallow SEDEX deposits during the early stages of crustal spreading, and recent VMS deposits.

See details at https://www.e-sga.org/index.php?id=1284.

Yanshanian (J-K) magmatism and metallogenesis in Taihang Mt region (China)

Dong Guochen[1,2*], Mo Xuanxue[1,2], Li Shengrong[1,2] & Qu Kai[1]
[1]China University of Geosciences, Beijing, China
([*]donggc@cugb.edu.cn)
[2]State Key Laboratory of Geological Processes and Mineral Resources, CUGB, Beijing, China;

Taihang Mt area as a part of Yanshanian orogenic belt lies in the middle part of North China Craton. It is characterized that Mesozoic intensive magmatism and related mineral deposits such as copper, molybdenum, gold, sliver, iron, lead, zinc etc. so it was named as a Yanshanian Au-Mo-Pb-Zn-Ag-Cu-Fe metallogenic belt in East China. Since Mesozoic, the orogenic belt is controlled by an intra-continental orogenic process, and Mesozoic granitic magmatism, related mineralization are the result of the processes. It was found that the middle Jurassic to early Cretaceous granitic intrusion and related mineralization widely distributed in the area and the ore deposits mainly formed during late Jurassic to early Cretaceous. The Cretaceous deposits distribute along a few NE trending fault belts. Geochemical and isotopic data proved that the ore deposits are controlled by Mesozoic granitic magmatism, and Mesozoic orogenic process. All ore-forming are related to the origin and evolution of granites.

Based on detail field investigation and former works, the authors marked clearly the location of granitic intrusion and its mineralization, established a series of Mesozoic granitic magmatism and related mineral deposits. Then geochemical and isotopic ages data were dealt with for both intrusive rocks and related ore deposits. The evidences show that magma differentiation and related metallization were formed as one continuous process. The magmatism in the process consists of temporal series from diorite → granodiorite → monzonite →granite→ lueco-granite, while the metallization is from Pb-Zn, Fe-Cu, Fe-Au, → Fe, Cu-Ag→Mo, Au, Ag → Pb-Zn, Cu. The geochemical signatures of the magma intrusions were characterized by a high K and $Mg^{\#}$ (locally), highly fractionated REE patterns (with minor Eu anomalies), high Sr-Ba abundances, and enriched Sr-Nd isotopic compositions, which were probably related to originate from both enriched mantle-derived mass and crustal materials. On the basis of the available data, magmatism and related mineralization during the early, peak and late orogenic episodes (J_2-K_1) were studied. The magma source, the division for metallogenic systems, and origin of the mineralization also discussed as a focal point in this paper.

[1] Jinfu, D. et al. (2007) *Geoscience*, **21(2)**, 232-240. [2] Feng, Z.Y, Chen, T.L. & Zhao, Y.C. (1999) *Earth Sci. Frontiers*, **6(2)**, 343-349. [3] Chen, B., Zhai, M.G. & Shao, J. (2003) *Science in China, Series D*, **46**, 941-953.

Mineralogical mapping and its significance in Jinqingding gold-quartz lode of Jiaodong peninsula, east margin of North China Craton

Li Shengrong[*], Zhang Xiubao & Chen Haiyan
State Key laboratory of Geological Processes and Mineral Resources, China University of Geosciences, Beijing, China
([*]lisr@cugb.edu.cn)

Jinqingding gold-quartz lode is located in the center of Muping-Rushan gold belt within the Kunyushan monzonitic granite, the eastern margin of the North China Craton in Jiaodong peninsula, Shandong Province. The gold-quartz lode extends and plunges northeastly for > 900m along the Jiangjunshi fault, and dips steeply with angle of 75-85° for > 1100m towards southeast. The lode is pyrite-rich with gold reserves greater than 50 tonnes. Although more than 10 tunnels and 40 exploring holes had been completed, the gold enrichment regularity was not revealed and margin of the orebody had not been clearly delineated before 1991. Having conducted numerical processing, 10 mineralogical parameters were adopted for mapping the pyrite-rich gold-quartz lode. For the case of quartz, the parameters include integral intensity (R) of natural thermoluminescence, distribution density (Nf) of fluid inclusions, homogenization temperature (T) of fluid inclusions, infrared optical density of CO_2 (DCO_2), infrared optical density of H_2O (DH_2O), DCO_2/ DH_2O, and the number of structural zones (Nz). For pyrite, the parameters include crystallomorphological ballotage score (Y), percentage of thermoelectric conduction P-type of pyrite (P%), and average thermoelectric coefficient value (α). Beside the first author's work, Yang L.X. (1993) selected another 2 parameters for pyrite, namely the a0 value of the cell and the infrared spectral peak value (υs-s). The maps with T and Nz as parameters show mainly the flowing tracks of the ore-forming fluid, namely one major stream and 2 branches flowing upwards from northeast down to southwest upper. The frontier of the flowing fluid found at around –200m level have pulsated many times. The areas with small variation gradient at about –300m and –500m levels were stable metallogenic domains and suitable for gold to precipitate forming thick and rich gold ore sectors (pay sectors). This conclusion matches with the known high value areas of the gold grade contours. Other maps, in different precision, indicate the controlling of NE and SW plunged fracture systems to the major orebody and the pay sectors respectively. It is interesting that the pay sectors tend to 'float' in the major orebody and plunged southwest. It means that the ore-forming fluid not only flowed towards southwest upper in the main stream and 2 branches, but also flowed towards northeast upper in the southwest plunged fracture system. Based on these considerations, combined with other geological studies, the authors concluded that the area between exploration lines 17 and 19, and at the levels of –200m and –500m, should be payable for further exploration by tunnels, although previous drilling (more than 5 holes) had 'proved' to be hopeless. It is also revealed that the pay sectors tend to occur repeatedly along the lode plunge and the gold mineralization intensity decreases from the level of –200m to –700m. Later tunnel and drilling exploration had given abundant return and more evidences for the above mentioned regularity of gold enrichment.

Acknowledgements: This work is supported by National Natural Science Foundation of China (No. 90914002) and the "111" Project of the Ministry of Education of China.

Identification of bauxite deposits with the aid of remote sensing techniques (case studies)

Komlóssy, G.
Geo-Kom Geological Exploration Ltd., Budapest, Hungary
(geokom@mail.datanet.hu)

In recent years companies interested in developing their bauxite–alumina industries are in competition to find new bauxite sources. Although, in the past decade, huge deposits have already been explored and developed, there is now greater pressure to operate even more efficiently and a continuing need for additional ore reserves.

During the past decade the author, with co-operation of his GIS, has applied remote sensing techniques in identification of laterite bauxite deposits. The method elaborated with co-operation of the Remote Sensing Division of the Ministry of Agriculture (Budapest – Hungary) has been proven to be useful in delineation of prospect areas to serve different targets:

(1) establishing of further prospects in the vicinity of formerly discovered occurrences, deposits;

(2) identification of new deposits in promising bauxite districts.

The methods applied are basically Shuttle Radar (SRTM) and Thematic Mapping (TM) techniques with different channel combinations and also complex terrain model analysis for a special case. The method is fitted to the given bauxite geological conditions (geology, geomorphology, altitude, relative elevation, etc.) which vary at different places. Since no standardisation can be introduced, the technical process should be elaborated for each target area. The basis of the procedure, (where possible) is the investigation of the already discovered deposits (explored bauxite contours - actual data) from which the prognostic chart (forecast) can be made. Reliability of the Land-Sat maps needs checking at site, and calibration and modification of the procedure to be done accordingly.

The author in his contribution gives an overview on his experiences (both successes and failures) achieved in India (East Coast), Indochina (Laos, Cambodia and Vietnam) Indonesia (West Kalimantan), West Africa (Guinea Bissau, Guinea, Ghana), Guiana Shield (Venezuela, Guyana and Suriname) and Brazil. The interpretation, in some cases, has proved to be fairly exact, so that even a resource estimate in hypothetical category is possible. In other cases their reliability is much less, and no more than delineation of prospect areas can be indicated with acceptable probabilities. Investigation of the hydrogeological (leaching) condition of the parent rock is essential. Field checking, measuring the bias with GPS, is important.

Mineralizations of Tantalum and Niobium in Vichada and Guainía, eastern part of Colombia

Cramer, T.[*], Bonilla Pérez, A., Amaya Perea, Z., Franco Victoria, J.A. & Iregui Ramírez, I.
Dept. of Geosciences, Universidad Nacional de Colombia, Bogotá, Colombia ([*]thcramer@unal.edu.co)

At the end of 2009, the Colombian public opinion was surprised by news about the presence of "Coltán", mineralizations of Tantalum and Niobium in the Amazonas and Orinoco region of Colombia, in spite of an informal exploitation during years. Our group has been working with samples, which we had recollected in the last two years in Matraca and other places in the Colombian rainforest [1].

The main Ta-Nb-occurrences are alluvial concentrations of "black sands" produced by tropical weathering, transport and depositation in old and recent riverbeds. The placer grains (Fig. 1) are accompanied by normally smaller magnetite, hematite and titanite grains. The chemical element composition of the heavier minerals (D > 4,5g/cm^3), determined by means of a recently acquired Bruker Tracer V-III XRF instrument, is highly variable and sometimes exceeds 50% Ta, 20% Nb, the rest being mainly Fe and Ti. Mn is nearly never present, indicating that the minerals are not tantalite/columbite sensu strictu. In some cases, cassiterite with tantalium (Sn 90-99%, Ta 0-9%) predominates in the black sands.

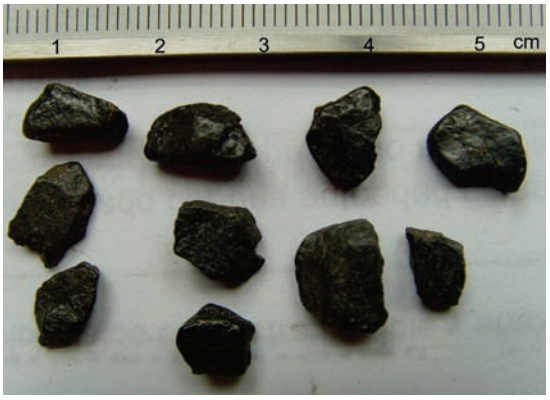

Fig. 1: Grains of alluvial Ta- and Nb-minerals.

Table 1: Average mineral composition of the pegmatitic dykes

Normalized minerals	*%*
Quartz	37
Albite	35
Microcline	28
Biotite, Fe-poor	2
Sericite	1

In some parts of the difficult-to-access area, pegmatitic dykes and lenses are present, which are assumed to be the primary enrichment sources of the Ta-, Nb- and Sn- mineralizations, although we did not find them in the samples. The visible unweathered micas are Fe-poor biotites, and microscopically in the feldspars quartz and altered sericite inclusions can be observed.

The results are preliminar, but indicate the presence of larger economically exploitable Ta-, Nb- (Sn-, Ti?) mineralizations in the Colombian area of the ancient South American Guayana-Shield, which until now is poorly understood. Hopefully, they will contribute to estimulate more detailed mineralogical, geochemical, isotopic and geological research activities, which do not exclude social and environmental aspects.

[1] http://historico.agenciadenoticias.unal.edu.co/matices/.

REE and their relevance to the development of the Kupferschiefer copper deposit in Poland

Sawlowicz, Z.
Institute of Geological Sciences, Jagiellonian University, Krakow, Poland (zbigniew.sawlowicz@uj.edu.pl)

Over hundred samples, representing different ore sections which contain carbonate-rich shales (Kupferschiefer) and hanging-wall dolomites (Z1 Werra) have been collected in different mines of the Lubin-Glogow mining district, mainly near the contact (transitional zone) between the copper-mineralized zone and secondarily oxidized (Rote Fäule-RF) zone. In general, the Polish Kupferschiefer shales are enriched in MREE in comparison to NASC. In a typical copper-rich section the REE amounts and patterns depend on lithologies, being generally similar in shales and dolomite. ΣREE vary among sandstones, shales and dolomites (average 73, 143 and 85 ppm, respectively), probably reflecting their clay contents.

The REE patterns of shales from the mineralized Cu-zone are generally convex (MREE enriched) and have negative Eu anomalies. However, in a section with Cu-, Zn- and Pb- shales the REE pattern of Pb-bearing shales shows a positive Eu anomaly, in contrast to other shales and overlying dolomite. More oxidizing conditions of deposition can be assumed for Pb-shales, as was also suggested by a study of Ph/Pr ratios of organic matter [1].

No significant differences between REE distributions in transitional and oxidized zones have been observed. Their REE patterns are more convex and are much higher (av. 247ppm) than those in the mineralized zone and they do not show Eu anomalies. The strongly convex pattern may suggest either enrichment in MREE or relative depletion in LREE due to localized precipitation of light REE minerals, both in shales and in the uppermost part of the sandstones**.** Sandstones have strongly convex REE patterns with positive Eu and negative Gd anomalies and depletion in LREE and enrichment in MREE relative to HREE. The REE patterns of shale and dolomite are similar and rather flat, with strong negative Eu anomalies, and a small positive Gd anomaly in the case of shales.

Two unusual sections, one Cu-rich and one Cu-lean (partly oxidized), comprising three shale beds interbedded with dolomites have been compared. Generally ΣREE contents are similar in these two sections. Also similar are contents of REE between beds in both sections, which decrease significantly upwards (from 157-171 ppm to 54-60 ppm). The REE patterns of the lowermost beds (directly overlying sandstones) are ramp-like, with LREE enrichments. The upper beds have concave REE patterns. Comparison between sections shows generally stronger negative Eu and positive Gd anomalies in the highly-mineralized section.

There is a highly significant positive relationship between Cu and∑REE contents in Cu -rich shales and slightly less significant for their concentration in oxidized and transitional shales.

The observed differences in REE contents cannot be provenance dependent but have been caused by diagenetic processes, possibly related to the ore mineralization and the oxidation. Europium anomalies, generally reflecting different Eh conditions in the deposit, can be eliminated by the prolonged oxidation. Strong enrichment of the RF zones in REE may result from their desorption from large volumes of oxidizing, including mineralizing, solutions which probably emerged from the underlying molasse lithologies into the Rote Fäule areas. Higher contents of REE in the lowermost shales suggest upward movement of solutions from the underlying sandstones also far away from the RF areas.

[1] Large, D.J. & Gize, A.P. (1996) *Ore Geol. Rev.*, **11**, 89-103.

Genetic and age relationship of base metal mineralization along the Periadriatic-Balaton Lineament system on the basis of radiogenic isotope studies

Benko, Zs.[1*], Molnar, F.[1], Billström, K.[2], Pecskay, Z.[3] & Lespinasse, M.[4]
[1]Dept. of Mineralogy, Eötvös Lorand University, Budapest, Hungary ([*]benko.zsolt@ttmk.nyme.hu)
[2]Laboratory of Isotope Geology, Natural History Museum, Stockholm, Sweden
[3]Institute of Nuclear Research, Hungarian Academy of Sciences (ATOMKI), Debrecen, Hungary
[4]UMR CNRS 7566 G2R; University HP-Nancy 1, Nancy, France

The Late-Palaeozoic granite intrusion of the Velence Mts. (W-Hungary) and the Early-Palaeozoic metasedimentary block of the Koszar-hegy are located along the Periadriatic-Balaton Lineament System which is a major fault between the Southern and Eastern Alps as well as between the ALCAPA and Tisa Megaunits of the Pannonian basin. Both Palaeozoic blocks are hosts of quartz-galena±sphalerite±fluorite vein type mineralization. According to the most accepted theory, formation of the base metal sulphide veins of the Velence Mts. can be related to a hydrothermal system developed by the cooling host granite. However, several fluid inclusion data and radiometric age dates suggest that the formation of the veins cannot be simply derived from the granite. In case of the Koszár-hegy mineralization, Carboniferous, Triassic and Palaeogene ages were also put forward but no direct evidences confirmed these theories.

In order to determine the source rocks, and indirectly the age of mineralization, detailed radiogenic isotope analysis (Pb-Sr-Nd) have been carried out on galena, sphalerite, fluorite, calcite and on the potential source rocks (Early-Palaeozoic schist, Carboniferous granite, Permian sandstone, Oligocene andesite).

Results have proven that the mineralization hosted by the granite cannot be derived from a single source rock (e.g. from the granite) and the Oligocene andesite certainly couldn't be the source rock of lead for the ore minerals. The remaining potential source rocks are the Carboniferous granite and different Early-Palaeozoic metamorphic-metasedimentary rock types. Isotope data of the two localities show a limited variation indicating a similar source rock and age for the two occurrences. Comparing the new isotope data with data of the Triassic Alpean-type carbonate-hosted stratiform-stratabound Pb-Zn mineralizations and their source rocks located along the Periadriatic Lineament system in the Eastern and Southern Alps, the similarities are obvious. Fluid inclusion properties and ore paragenesis are also similar, and therefore a common origin of these ore mineralization is suggested. This conclusion, however, isn't surprising in light of the Alp-Carpathian geodynamics: by the time of the Triassic both investigated localities were located in their original position, e.g. in the region of the Alpean deposits. Their displacement took place by the time of the Late-Palaeogene - Early Neogene. According to our model, veins in the Velence Mts. granite and in the Early-Paleozoic carbonate at the Koszar-hegy represent deeper zones of the shallow level Alpean type carbonate hosted Pb-Zn deposits. The shallow, carbonate hosted stratiform level of the studied mineralization, however, had been eroded or sheared down from its base due to the Alpean orogenesis.

Styles and stages of the Rudabánya base metal mineralizations, Hungary

Földessy, J.[1*], Németh, N.[1], Kristály, F.[1], Zajzon, N.[1], Kupi, L.[1], Majoros, P.[2] & Gerges, A.[2]
[1]Institute of Mineralogy and Geology, University of Miskolc, Hungary ([*]foldfj uni-miskolc.hu)
[2]Rotaqua KFT, Hungary

Rudabánya, an iron ore mine closed in 1986, lies in NE-Hungary, in a region which was traditional host of mining (ores, lignite, brown coal, non-metallics.

Its annual iron ore production reached a pick of around 1 million tonne/year in the 1970s. In the last active years copper ore was found in small orebodies and mined.

Its new exploration has started in 2007 after careful geological remodelling of the deposit, and verifying its potential for base metals. The deposit is hosted in a major shear zone, formed in Triassic dolomites and siltstones, the NNE-SSW Darnó zone. A major porphyry and skarn copper mineralization, Recsk, lies along the same zone, some 80 km SSW from Rudabánya. The iron ore is dominantly siderite origined from the metasomatic alteration of dolomites, with extensive limonites in the oxidized cap. The base metal ores are partly stratiform in sediments, partly superimposed and younger than the siderite mineralization.

In the 2600 previous drillhole logs there are numerous indications of base metal ores. Copper mineralization was also known from the surface as supergene enrichment. The existence of low grade Pb mineralization was also known, but the Zn mineralization has been discovered recently and considered to be widespread through different lithologies and alteration zones. At least four major stages of ore mineralization have affected the host lithologies, from the Triassic until the Paleogene.

The new geological model has been tested on the field by detailed re-mapping of surface outcrops, partial revision of acccessible underground workings, surface geochemistry, trenching and shallow drillholes. All these methods have supported the geological model and allowed to discover a major multi-stage ore occurence, yet to be explored in detail.

Fig. 1: Position of the Rudabanya mineralization in the Carpathian belt.

Mineral assemblages of Cu-Sn-sulfides as indicators of HS-IS transition in epithermal environments

Kovalenker, V.A.[*] & Plotinskaya, O.Yu.
Institute of Ore Geology, Petrography, Mineralogy, and Geochemistry RAS Moscow, Russia ([*]kva@igem.ru)

Ores of numerous epithermal deposits referred to HS type, e.g., Akturpak, Kairagach, Kochbulak (Kurama Mountains, Middle Tien Shan), Bereznyakovskoe (South Urals), Lahoca, Chelopech, Elshica, Radka (Carpathian-Balkan region), El-Indio (Ands), Ozernovskoe (Kamchatka) etc., contain large group of minerals, with Cu, Sn and S as major components, and with variable amounts of Fe, As, Sb, Mo, V, Ge. This group includes both well known (e.g. stannite, këserite, stannoidite, mawsonite, colusite, hemusite), and recently discovered minerals (mohite, kuramite, nekrasovite, vinciennite, chatkalite), as well as several unnamed phases.

The Kochbulak gold deposit (Middle Tien Shan) was chosen as a key example to reveal spatial and temporal peculiarities of Cu-Sn sulfides distribution within an HS epithermal system. The earliest mineralization of the Kochbulak deposit is represented by pipe-like ore bodies. At shallow levels of these bodies kuramite Cu_3SnS_4 and mohite Cu_2SnS_3 occur in assemblage with goldfieldite, enargite, famatinite, alunite, diaspore, pyrophyllite (typical minerals for HS environment), and with native gold (~ 900‰) and Au ditellurides. At deeper levels as well as at neighboring Akturpak and Kairagach deposits Cu-Sn-sulphides are represented by mawsonite $Cu_6Fe_2SnS_8$, chatkalite $Cu_6FeSn_2S_8$, stannoidite $Cu_8Fe_3Sn_2S_{12}$, nekrasovite $Cu_{26}V_2Sn_6S_{32}$, and by few unnamed phases ($Cu_{10}Fe_3Sn_3S_{12}$, $Cu_{10}Fe_2Sn_4S_{12}$, $Cu_{11}Fe_2Sn_3S_{16}$). They coexist with tetrahedrite-tennantite, chalcopyrite, electrum (~ 800-860‰), Au-Ag-tellurides and sericite. Vein bodies of the Kochbulak deposit represent later mineralizing stage. Hemusite Cu_6MoSnS_8 and stannite-këserite $Cu_2(Zn,Fe)SnS_4$ associate here with electrum (500-650‰), petzite, and hessite.

Mineral assemblages listed above evidence an evolution from high to low oxidized environment and from high to low sulfidation state of the fluids: from the formation of enargite (famatinite) (As^{5+}, Sb^{5+}), goldfieldite (Te^{4+}) and high Cu minerals of the Cu-Fe-Sn-S system to stability of tetrahedrite-tennantite (Sb^{3+}, As^{3+}) and chalcopyrite. The transition to lower sulfidation state is accompanied by pH increase: from alunite, diaspore, and pyrophyllite to sericite.

Thus, the data obtained allow considering Cu-Sn-sulphides as indicators of HS to IS transitional zones.

Acknowledgements: This study is supported by Russian Foundation for Basic Research, Project 10-05-00354.

Geochemistry of indium-bearing sphalerite from Toyoha polymetallic deposit, Japan

Shimizu, T.* & Morishita, Y.
Geological Survey of Japan, AIST, Tsukuba, Japan
(*t.shimizu@aist.go.jp)

Sphalerite (ZnS) is an economically important indium-bearing mineral, as indium is mainly produced from zinc concentrates for high technology applications (e.g., Liquid Crystal Display). Our study presents electron microprobe analyses and fluid inclusion study of indium-bearing sphalerite to decipher the chemical environment of indium mineralization. Toyoha was one of the largest xenothermal Zn-Pb-Ag-Cu-Sn-In deposits in Japan. Indium mineralization occurs southeast of the deposit. The ore veins locally contained more than 1000g/t In. Indium-bearing minerals are typically indium-bearing sphalerite and unnamed Zn-In mineral ($CuZn_2InS_4$) with lesser stannite, kesterite, roquesite, sakuraiite and chalcopyrite [1].

The inspection of X-ray and optical microscopes shows that indium-bearing sphalerite occurs as crustiform bands with the maximum thickness of 2mm. Its color varies from black (opaque) to dark-red (translucent) in thin sections. The crustiform bands show invisible oscillatory variation in In, Sn, Cu, Ag and Fe contents. The metal concentrations in sphalerite vary: 0.06-3.63 atom.% In, 0.00-1.67 atom.% Sn, 0.22-3.55 atom.% Cu, 0.00-1.21 atom.% Ag and 2.98-6.22 atom.% Fe. These data show that Cu+Ag and In+Sn are close to 1:1 in atomic proportions; the compositions of indium-bearing sphalerite can be expressed as $(Cu, Ag)_x(Zn, Fe)_{(4-2x)}(In, Sn)_xS_4$, where x is between 0 and 0.29. Near-infrared and visible light microthermometry was applied to fluid inclusions in indium-bearing sphalerite with U.S.G.S gas flow heating/freezing stage. Primary liquid-rich fluid inclusions occur along growth bands of which indium and iron contents are 0.17-0.70 and 3.00-3.96 atom.%, respectively. Homogenization temperatures (Th) range between 281 and 288°C. Assuming that pressure correction can be neglected, the obtained Th represents formation temperature of indium-bearing sphalerite. The consistent Th are lower than mineral equilibrium temperature (350-400°C) among polymetallic sulfides [2], but they are close to the highest value of Th range (150-300°C) from quartz and transparent sphalerite that were not contemporaneous with the indium mineralization [2]. Our obtained Th (281-288°C) are within a range of calculated closure temperatures (290±30°C) of indium-bearing sphalerite from Grandchamp polymetallic vein deposit, Loire, France [3] and measured precipitation temperatures of In, Cu and Zn (280-350°C) of an active hydrothermal vent in the Southern Lau Basin, SW-Pacific [4]. These temperature comparisons suggest that the range of our obtained Th (281-288°C) represents a minimum indium-precipitation temperature at Toyoha. The similarity of the minimum indium-precipitation temperatures between 260 and 290°C among different ore deposits suggests that a careful comparison of Th combined with chemical analyses of sphalerite enables us to distinguish between indium-enriched and barren zones of the deposits. This attempt of distinction may be useful for indium exploration.

Considering the pyrite-sphalerite assemblage, FeS (6.0-8.0 mol%) in sphalerite, sulfur fugacities of indium mineralization were calculated as a range between $10^{-11.4}$ and $10^{-10.8}$ atm using Th from the indium-bearing sphalerite (281-288°C). This sulfur fugacities-temperatures relationship corresponds to an intermediate sulfidation state [5].

[1] Ohta, E. (1989) *Mining Geol.*, **39**, 355-372. [2] Ohta, E. (1995) *Resour. Geol.*, **18**, 187-195. [3] Bente, K. (1993) *Proc. 8th Quad IAGOD Symp.*, Ottawa, 141-147. [4] Schwartz-Schampera, U. & Herzig, P.M. (1997) *Proc. 4th Biennial SGA Meeting, Turku/Finland*, 379-382. [5] Einaudi, M. et al. (2003) *Soc. Eco. Geo. Sp. Publ.*, **10**, 285-313.

Micro- and nanomineral assemblages are indicators of typification and searching for gold

Koneev, R.I.
Dept. of Mineralogy and Geochemistry, Faculty of Geology, National University of Uzbekistan, Tashkent, Uzbekistan
(rkoneev@yahoo.com)

The appearance of new directions – nanomineralogy and nanogeochemistry created conditions for new approaches to research, classification, exploration, evaluation of gold ore deposits. It is available now the systematization of the deposits on the basis of direct signs – peculiarities of gold and elements, defining its metallogeny (Au, Ag, Te, Se, Bi, Sb, As, Hg) and not on indirect indicators – quartz, carbonate, sericite, adularia, kaolin.

Long-term research on gold and gold-silver deposits of Uzbekistan (Muruntau, Daugyztau, Charmitan, Kochbulak, Kyzylalmasay and others) determined that independently from host rocks they all were formed by standard row of geochemical paragenesis: /Au-W/Au-As/Au-Te/Au-Ag/Au-Sb/Au-Hg/. Certain nanoassemblages of minerals, micro- and nanominerals are appropriate for each parageneses:

Au-W – nanogold, scheelite, wolframite, tungstenite, molybdenite, cassiterite;

Au-As – nanogold, arsenopyrite, pyrite, loellingite, gersdorffite, cobaltite;

Au-Te – maldonite, calaverite, hedleyite, tsumoite, petzite, hessite, tetradymite, kawazulite, altaite, tellurantimony, golfieldite, annivite;

Au-Ag – electrum, custelite, freibergite, stephanite, polybasite, pyrargyrite, prustite, acantite, naumannite, aguilarite, servellite;

Au-Sb – aurostibite, antimonite, boulangerite, zinkenite, jamesonite, gudmundite, meneghinite, andorite, owyheeite, eucairite;

Au-Hg – Au amalgam, kongsbergite, cinnabar, realgar, schwatzite, tiemannite, crookesite.

Depending on geodynamical position, depth of formation, vertical and lateral zoning, erosion cut the industrial resource of the deposit is determined by 2-4 paragenesis. For instance, Muruntau – /Au-W/Au-As/Au-Te/, Charmitan – /Au-W/Au-As/Au-Te/Au-Sb/, Kochbulak – /Au-As/Au-Te/. Au-As arsenopyrite-pyrite mineralization is developed on all deposits and all subsequent ones are combined with it. /Au-As/+/Au-Hg/ form the Karlyn-type. The form of elements changes with the depth. Bi tellurides form on hypoabyssal levels (Muruntau), on epithermal – Au, Ag, Pb, Sb, Hg (Kochbulak). The presence or absence of separate parageneses determines type, erosion cut, perspectives and scales of the object. The more and various the composition of micro- and nanoassemblages of gold is, the more the deposit is.

Mass loss in chromite and ferritchromite formation during metamorphism of chromite ores in the Golyamo Kamenyane serpentinite massif (Eastern Rhodopes, Bulgaria)

Gervilla, F.[1*], Kerestedjian, T.[2], González-Jiménez, J.M.[1], Sergeeva, I.[2] & Hadjiev, A.[2]
[1]Dept. of Mineralogy & Petrology, University of Granada, Spain ([*]gervilla@ugr.es)
[2]Geological Institute, Bulgarian Academy of Sciences, Sofia, Bulgaria

The Golyamo Kamenyane massif is a portion of a metaophiolite, located in the Upper high-grade unit of the metamorphic basement of Eastern Rhodopes [1]. The regional-scale tectonic setting is dominated by two late Alpine metamorphic core complexes, (Kesebir-Kardamos and the Biala Reka-Kechros) domes [2], flanking the considered metaophiolite. The massif mainly consists of serpentinized dunites and harzburgites, containing several chromitite pods and asbestos veins. Serpentinites also contain rodingite layers in their upper part and are topped by metagabbros.

Chromite from chromitites can be classified into three textural groups: i) zoned chromite; ii) porous chromite, and iii) homogeneous chromite. Zoned chromite shows unaltered, Al-rich cores with unit cell size (according to Guinier powder diffraction data) of 8.26(3) Å and Cr#[Cr/(Cr+Al)]=0.50-0.60, Mg#[Mg/(Mg+Fe^{2+})]=0.60-0.70 and $Fe^{3+}/(Fe^{3+}+Fe^{2+})$=0.20-0.30, surrounded by porous chromite, having cell size of 8.33(2) Å, $Fe^{3+}/(Fe^{3+}+Fe^{2+})$<0.20 and values of the Cr# and Mg# evolving from 0.60 to 0.90 and 0.60 to 0.47 from core to rim, respectively. Porous chromite has a relatively homogeneous composition varying within the following ranges: $Fe^{3+}/(Fe^{3+}+Fe^{2+})$=0.20-0.52, Cr#=0.92-0.97 and Mg#=0.35-0.48. Its unit cell sizes also vary in the range 8.35(1)-8.36(1) Å. Most pores are filled with clinochlore. Homogeneous chromite has $Fe^{3+}/(Fe^{3+}+Fe^{2+})$=0.55-0.65, Cr#>0.96, Mg#=0.32-0.20 and cell size of 8.38(1) Å.

Zoned chromite is the most abundant and can be interpreted as the result of reaction between the primitive, Al-rich chromite (+H_2O) and either olivine or antigorite, during an early metamorphic stage. This reaction forms Cr-rich chromite (and clinochlore) by progressive loss of Al_2O_3 and, at lesser extent MgO and Fe_2O_3, with no addition of FeO. Change in chromite takes place with less than 1% increase of specific volume, insufficient to compensate the mass loss. The reaction can progress until the primitive core is completely consumed, giving rise to the porous chromite.

During a later stage, oxidizing metamorphic fluids percolated through the pores of chromite, supplying Fe_2O_3 and FeO to form ferritchromite, dissolving clinochlore, eliminating the porous texture and promoting chromite recrystallization. In fact, the Fe-richest ferritchromite tends to exhibit euhedral habit or polygonal texture.

[1] Bonev, N. (2006) *Geol. S. Am. S.*, **409**, 211-235. [2] Marchev, P. et al. (2008) *IOP Conf. Ser.: Earth Environ. Sci.*, **2**, 012015.

Modification of chromite to ferritchromit in the Archaean Nuggihalli Schist belt, Western Dharwar Craton (southern India)

Mukherjee, R.[1] & Mondal, S.K.[1,2*]
[1]Dept. of Geological Sciences, Jadavpur University, Kolkata, India
[2]NordCEE, Geological Museum, Natural History Museum of Denmark, University of Copenhagen, Denmark
([*]skmondal@snm.ku.dk)

Reflected light and scanning electron microscopic (SEM) study of chromites in the Archaean Nuggihalli Schist belt, Western Dharwar Craton, southern India, reveals a compositionally zoned character of the grains. In the Nuggihalli chromitite deposits ferritchromit is identified as relatively higher reflectant rims around the chromite, vestiges of which occur as dark rounded islands at the centre. Sometimes, ferritchromit occurs along fractures and as patches within the grain. Detailed electron probe micro-analysis (EPMA) shows a compositional change in the chromite where cations like Cr (core 9.32%; rim 8.68%) Al (core 4.81%; rim 0.81%) and Mg (core 2.12%; rim 0.93 %) are lost from the core and consequently substituted by cations like Fe^{3+} (core 1.6%; rim 5.85%), Ti (core 0.05%; rim 0.15%), Mn (core 0.16%; rim 0.24%) and Ni (core 0.004%; rim 0.03%) towards the ferritchromit rim. This type of zoning is attributed to differences in cation mobility during diffusion. Among the cations that diffuse out of the grain Al has the highest mobility relative to Cr and Mg, while for the cations that enter the grain Fe^{3+} has the greatest mobility relative to Ti, Mn and Ni.

Formation of ferritchromit is most intense in accessory chromite within serpentinite and in chromite within silicate-rich chromitite such that some of the chromite grains are completely replaced by ferritchromit composition. Zoning is no longer optically discernible in these grains, which appear homogeneous. Compositional profiling of these grains show substitution of only Cr by Fe^{3+} with progressive alteration. The cores of completely altered grains are reset as understood from their much lower Cr (9.29%), Al (4.80%) and Mg (2.11%) values compared to the unaltered chromites (Cr 12.74%; Al 3.27%; Mg 4.66%) in massive chromitite.

In the chromite compositional space ferritchromit formation is represented by a trend of extreme Al loss ((Cr/(Cr+Al) cation ratio ~ 0.98) and strong enrichment of Fe^{3+} in the chromite grains. The former is explained by the formation of secondary chlorites and the latter is explained by the prevalence of oxidation conditions during alteration. Low temperature hydrothermal alteration during serpentinization was responsible for the formation of ferritchromit in Nuggihalli. This is understood from the specific occurrence of ferritchromit around grain boundaries and fractures, as these are the usual pathways for fluid interactions. Although the chemistry of ferritchromit remains largely uniform in different types of occurrences, the intensity of alteration varies greatly between them and also between different deposits, indicating a heterogeneous nature of alteration and probable involvement of fluids. Complete alteration of the grains to ferritchromit and modification of the chromite core is explained by later metamorphism of the rocks because of consequent increase in the capacity for cation diffusion.

Sulfur isotope constraints for a dynamic magmatic sulfide ore deposition model in the sill-like South Kawishiwi Intrusion of the Duluth Complex, Minnesota, USA

Molnár, F.[1*], Peterson, D.[2], Arehart, G.B.[3], Poulson, S.[3] & Hauck, S.A.[4]
[1]Eötvös Loránd University, Budapest, Hungary
([*]molnar@abyss.elte.hu)
[2]Duluth Metals Ltd., Minnesota, USA
[3]University of Nevada, Reno, Nevada, USA
[4]Natural Resources Research Institute, University of Minnesota, USA

The 1.1 Ga old Duluth Complex (DC) is the second largest mafic intrusion on Earth and probably contains the largest undeveloped magmatic Cu-Ni-(Co)-PGE ore resource [1]. The troctolitic sill-like South Kawishiwi Intrusion (SKI) of the DC currently hosts three major magmatic sulfide deposits: the Spruce Road deposit (529 Mt, 0.43% Cu, 0.15% Ni); the Nokomis deposit (449 Mt, 0.63% Cu, 0.2% Ni, 0.6 g/t Pt+Pd+Au); and the Birch Lake deposit (195 Mt, 0.53% Cu, 0.16% Ni, 0.93 g/t Pt+Pd+Au). These deposits are located along the contact of the SKI and the monzonitic Giant Range Batholith (GRB) of Archean age in the footwall. The basal mineralized zone (BMZ) of the SKI is highly heterogeneous: rock compositions range from norite to melatroctolite-troctolite-anorthosite-olivine gabbro with fine- to coarse-grained ortho- and adcumulate and pegmatitic textures. The BMZ contains assimilated inclusions of GRB, BIF and metapelite. Charnokitisation of GRB is espe-cially strong along the major conduits of the parent melts of SKI. The BMZ hosts fractionated ore in the forms of inter-cumulus patches of chalcopyrite, cubanite, pentlandite and pyrr-hotite with local semi-massive, replacive, less-fractionated ore with pyrrhotite, pentlandite and chalcopyrite along the immedi-ate contact. Disseminated ores in the footwall have replacive-infiltration texture with enrichment of chalcopyrite and bornite away from the contact. The highest sulfur isotope compositions (from +5 to +12‰ $\delta^{34}S$) of sulfides and whole rock samples occur along the contact, with a systematic gradual decrease in $\delta^{34}S$ to around 0‰ upward within the BMZ. Ore in the footwall and in association with footwall inclusions is also characterized by the heavy sulfur isotope signature. Another aspect of spatial distribution in the $\delta^{34}S$ values in footwall ores is that more positive values occur under the northern and southern parts of SKI (Spruce Road and Birch Lake deposits) in comparison to the central part (Nokomis Deposit). This distribution is largely coincident with occurrences of 'confined' (metal enrichment at the top of BMZ) and 'open' (metal enrichment at the bottom of BMZ) style of distribution of metals in the SKI and thus confirms that the footwall/SKI interaction had an important role in defining styles of mineralization. Observations support a dynamic model for ore deposition consisting of early accumulation of magmatic sulfides from the mantle-derived and metal-laden mafic melts along the contact and in the footwall due to custal sulfur assimilation and assimilation of some parts of the more SiO_2 and alkali rich footwall rocks, followed by superimposed sulfur isotope exchange between the early stage ores and later pulses of sulfur-undersaturated melts moving above the early stage sulfide mineralisation. This model offers keys for understanding the Cu- and PGE-enriched nature of ores in the BMZ, and suggests that re-mobilized volatile sulfur was included in the ore-forming processes.

Acknowledgements: This work has been supported by the HAESF Senior Fellowship grant to F. Molnár.

[1] Peterson, D.M. (2001) *Report of Investigations, NRRI-2001-02*. University of Minnesota Duluth, Natural Resources.

Mineralization in the Kamsdorf ore field, Thuringian Basin, Germany

Brey, M.[*] & Majzlan, J.
Institut für Geowissenschaften, Friedrich-Schiller-Universität, Jena, Germany ([*]Maria.Brey@uni-jena.de)

The Thuringian sedimentary basin is a series of Upper Permian and Triassic strata (Zechstein, followed by Buntsandstein, Muschelkalk, and Keuper). The Tertiary tectonic activity uplifted the marginal portions of the today's basin where the pre-Permian rock complexes are exposed [1].

In our work, we concentrate on the mineralization of fissures in and around the Thuringian Basin. For this purpose, samples were taken in Kamsdorf, situated at the SE-Zechstein fringe at the interface between the basin and the uplifted horst (*Thüringer Schiefergebirge*). Hydrothermal veins and lenses pervade the Rotliegendes up to the Zechstein [2] (Lower to Upper Permian) and are either vertical or horizontal. The mineralization consists mostly of barite, calcite, and dolomite (Ca/(Ca+Mg)~0.52 to 0.59), and locally quartz. The primary fluid inclusions in barite are biphasic (liquid > vapour).

The ores were analysed by means of reflected-light microscopy, X-ray diffraction, and the electron microprobe. The principal ore mineral is tetrahedrite, with 2.1 to 4.0 Sb apfu. In some analyses, the arsenic component dominates (Sb/(Sb+As)<0.5 to 0.39). The fahlores are zinc-rich and silver-poor, with these concentrations: Cu 33.4 to 39.5 at%, Fe 0.32 to 3.2 at%, Ag 0.4 to 0.7 at%, Hg 1.3 to 1.5 at%, and Zn 3.4 to 8.5 at%). Furthermore, we found siderite, chalcopyrite, pyrite, arsenopyrite, Co sulfarsenides, subordinate sphalerite, galena, and secondary minerals such as malachite, covellite, goethite, and cerussite.

The paragenesis of the ore minerals and the fluid inclusions are used here as indicators of the chemical composition and the physical properties of the hydraulic fluid system that circulated in the Thuringian Basin during the Mesozoic.

Acknowledgements: This work is a part of INFLUINS, a high performance research project granted by the German Federal Ministry of Education and Research (BMBF). BMBF financial assistance is gratefully acknowledged.

[1] Ziegler, P.A. (1990) *Geological atlas of Western and Central Europe*. Shell Internationale Petroleum Maatschappij B. V. & Geological Society of London, 39 S. (2. Auflage). [2] Rüger, F. et al (1992) *Bergbaugeschichte, Geologie und Mineralien des Saalfeld- Kamsdorfer Bergreviers*. Bd. 19 Naturwissenschaftliche Reihe, Museum für Naturkunde, Gera, Germany.

Metamanganolites of Ural (Russia): mineralogy and genesis

Brusnitsyn, A.I.[1] & Zhukov, I.G.[2*]
[1]Faculty of Geology, St. Petersburg State University, St. Petersburg, Russia
[2]Institute of Mineralogy, Ural Division, Russian Academy of Sciences, Miass, Russia ([*]igorzhukov2009@yandex.ru)

We use "metamanganolite" term to describe metamorphic rocks of sedimentary or hydrothermal-sedimentary genesis, with different mineral composition. The study on these rocks, using as example the Ural manganese deposits (Kyzyl-Tash, Faizulino, Bikkulovo, Kozhaevo, Urazovo, Malosedelnikovo, Kurganovo, Borodulino, Parnok, etc.) has shown that:

1. More than 60 mineral species are known in manganese ores. They form three types of mineral assemblages: (a) assemblage of the main volume of orebodies formed during low-grade regional metamorphism, (b) assemblage of segregated and metasomatic veinlets that fill the systems of late tectonic fractures, and (c) assemblage of near-surface supergene minerals. The most part of minerals are metamorphic silicates.

2. During regional metamorphism of Mn-bearing sediments, the character of metamorphic assemblages and chemical composition of minerals were controlled by petrogenic elements (Mn, Fe, Ca, Mg, Al, and Si) ratio and organic matter (OM) distribution therein, dissolution of which regulated carbon dioxide and oxygen balance in pore solution. OM-bearing sediments were replaced by oxide-carbonate-silicate rocks mostly composed of Mn^{2+} silicates and carbonates (tephroite, pyroxmangite, rhodonite, rodochrosite, etc.), andradite, quartz, hematite, and hausmannite; and OM-free sediments were transformed into oxide-silicate rocks with predominant braunite (silicate of Mn^{3+}) and quartz.

3. Crystallization of Mn silicates is possible at the early stages of metamorphism at T≈ 200 –260 °C and P= 2–3 kbar. Caryopilite and hydrosilicates (friedelite, bementite, parsettensite, etc.) are typical minerals of low-temperature metamorphic Mn rocks. Presence of Mn-Si gel in primary sediments is a favorable condition of low-temperature crystallization of silicates (rhodonite, pyroxmangite, tephroite, etc.). Transformation of Mn-Si gel during increase in temperature occurs as follows: gel→ neotocite → caryopilite + quartz → caryopilite + pyroxmangite (±rhodonite) + tephroite → pyroxmangite (±rhodonite) + tephroite. Replacement of caryopilite by pyroxmangite (±rhodonite) with tephroite takes place at a temperature interval of the prehnite-pumpellyite facies. Thus, there are low-temperature caryopilite and high-temperature tephroite-pyroxmangite (±rhodonite) facies, PT-boundaries between which correspond to zeolite (prehnite-pumpellyite and greenstone) and deeper facies, respectively.

4. Assemblages of Mn silicates are stable at low concentration of carbon dioxide in pore solution. Insignificant increase in its molar share leads to replacement of silicates by assemblage of rhodochrosite+quartz, which is stable in the whole PT-interval of regional metamorphism.

Acknowledgements: This study was supported by Russian Foundation for Basic Researches (project no. 08-05-00415).

Ti-rich Cr-spinel and Ni-Fe-Cu sulphides from the Hamutenha basic-ultrabasic intrusion (Cunene anorthosite complex, Angola)

Campeny, M.[1*], Proenza, J.[1], Torró, L.[1], Villanova, C.[1], Castillo, M.[1], Gonçalves, O.A.[2] & Melgarejo, J.C.[1]
[1]Dept. Cristal·lografia, Mineralogia i Dipòsits Minerals, Universitat de Barcelona, Catalunya, Spain ([*]markcamp100@hotmail.com)
[2]Depto. de Geologia, Universidade Agostinho Neto, Luanda, Angola

The Cunene complex is a large group of gabbro-anorthosite intrusions that covers an area of 15.000 km^2 between southern part of Angola and northern Namibia. Although ultrabasic rocks have not been found to data in the main anorthositic intrusion of the Cunene complex, a great number of small basic-ultrabasic bodies appear close to the west margin of the main intrusion.

This work is based in one of these Cunene associated basic-ultrabasic-intrusions outcropping close to the Hamutenha village, and especially on the study of its Ti-rich Cr-spinel and Ni-Fe-Cu sulphides associated mineralization. Both appear as a disseminated mineralization included in the olivine and clinopyroxene grains from the dunites and olivinic gabbros situated at the centre part of the intrusion.

The Ti contents of the Cr-spinel of Hamutenha are very high, even up to 15.66 % of TiO_2, with an average value of 5.17%. On the other hand, the Cr-spinel contains abundant exsolutions of ilmenite lamellae. The ratio Cr_2O_3/Al_2O_3 in Cr-spinel presents a positive correlation. This is an atypical behaviour, because the typical tholeiitic magmas that generate this kind of intrusions use to display a negative correlation.

These aspects suggest that the parental magma of Hamutenha was relatively rich in Ti, and had a similar composition as the estimated magma for Mount Ayliff intrusion (Karoo Igneous Province, South Africa [1]; and Jinbaoshan (SW China [2]) and Xinjie (SW China [3]) intrusions in which appear associated mineralizations of Fe-Ti-Cr and Pt-Pd sulphides.

Although Ni-Cu ore deposits are currently explored in the Cunene complex, in the Hamutenha intrusion Ni-Fe-Cu sulphides have been found only as accessory minerals disseminated in dunites and olivine gabbros. The sulphides occur as interstitial grains, in inframillimetric size. Primary sulphides are pentlandite, chalcopyrite and pyrrhotite. The secondary association is complex, and consists of thiospinels, heazlewoodite (Ni_3S_2), godlevskite ($(Ni,Fe)_7S_6$) and putoranite ($Cu_{16-18}(Fe,Ni)_{18-19}S_{32}$).

[1] Cawthorn, R.G. et al. (1991) *Am. Mineral.*, **76**, 561-573. [2] Wang, C.Y. et al. (2005) *Lithos*, **83**, 47-66. [3] Wang, C.Y. (2008) *Lithos*, **102**, 198-217.

Cu-U-V stratabound deposits in red beds in the Catalan Pyrenees: structure and mineralogy

Castillo, M.[*], Torró, L., Campeny, M., Villanova, C., Tauler, E. & Melgarejo, J.C.
Dept. of Cristallography, Mineralogy and Ore Deposits, University of Barcelona, Spain ([*]montgarricastillo@gmail.com)

The Eureka mining group (La Plana de Mont-Ros, Pyrenees, Catalonia) has one of the best outcrops of Cu-U-V stratabound deposits in red-beds of Western Europe. The deposit was mined in surface trenches and underground galleries. This has allowed an accurate mineralogical and textural study of this deposit, which can be used as a model to explain the relationships between Cu-U-V minerals during precipitation of primary mineralization and supergenic stages.

The deposit is hosted by Lower Triassic detritic series, which are arranged approximately in an E-W direction, and were deformed during the Alpine Orogeny.

Field mapping and a study of the mineral assemblages, with the petrographic microscope, SEM-BSE-EDS and EMPA, have enabled to distinguish three mineralization stages:

1. Stratabound mineralization: this concentrates the main part of the stock. It is directly related to centimetric coal levels interbedded with greenish greywackes and conglomerates. This reducing trap caused the precipitation of redox sensitive elements (U, V, Cu, Sb, Bi, Ag, As, Se, Ni and Co) from a fluid with low S activity. Ores comprise native metals (silver, bismuth), pyrite, sphalerite, galena, Cu sulphides (djurleite, digenite, anilite), Ni-Co sulphoarsenides (gersdorffite, cobaltite), sulphosalts (wittichenite, tetraedrite, tennantite), selenides (chlausthalite and aguilarite) and uraninite. These ore minerals are found as a late cement of the detritic rocks, and replace an early calcitic cement. The general sequence starts with pyrite, which is replaced by copper sulphides, Ni-Co sulphoarsenides and sulphosalts. The matrix of the greywackes is made up of roscoelite and V-rich illite.

2. Vein mineralization: during the alpine compression, Cu remobilization took place and generated mm-sized veins filling small joints with chalcopyrite and bornite, along with quartz and ankerite.

3. Supergenic mineralization: oxidized minerals associated with supergenic alteration, like sulphates (brochantite), arsenates (zeunerite, erythrite, chenevixite), vanadates (carnotite, tyuyamunite, sengierite), carbonates (malachite, azurite), selenites (demesmaekerite and haynesite), and phosphates (torbernite) appear as crusts and efflorescences on the surface of the outcrop, as pseudomorphs or filling small cracks. On the other hand, leaching of the ores by ground waters produces the precipitation of a suite of recently-formed carbonates (cejkaite, andersonite) and sulphates (zippeite, uranopilite) in the galleries. Hence, these minerals fix the uranium again.

This study shows that acid fluids generated by alteration of sulphides can produce the leaching of U and RSE. Vanadates, arsenates and phosphates fix U in the supergene zone; the remaining U can be remobilized and reprecipitated, forming crusts of U carbonates on the mine walls. These observations could be considered in the management of radioactive waste products.

Formation and mineral chemistry of a Zn-Pb skarn from the Gageok mine, South Korea

Choi Bu Kap[1,2], Choi Seon-Gyu[2*], Seo Jieun[2], Kim Tae Hyung[1], Kang Heung Seok[1], Lee Sangbong[2], Koo Minho[2], Yoo In Kol[3] & Jung Yeon Ho[1]
[1]Korea Resources Corporation, Seoul, Republic of Korea
[2]Dept. of Earth and Environmental Sciences, Korea University, Seoul, Republic of Korea ([*]seongyu@korea.ac.kr)
[3]Korea Alumina Co., Ltd., Mokpo, Republic of Korea

The Gageok skarn deposit, located at the eastern edge of the Taebaeksan Basin, South Korea, is the result of the intrusion of the Cretaceous granitic pluton into the Paleozoic calcareous rocks. The subvolcanic intrusion ranges in composition from quartz monzonite to granite porphyry with numerous dikes having I-type, calc-alkaline and weakly peraluminous characteristics. Both endoskarn and exoskarn are developed at the Gageok Zn–(Pb) deposit, with more exoskarn than endoskarn. The alteration of the subvolcanic rocks began with very weak disseminated diopsidic pyroxene, epidote, actinolite, and titanite. Epidote skarn zones were formed as endoskarn during the intrusive phase. The clinopyroxene skarn, clinopyroxene- garnet skarn and garnet skarn developed as exoskarn from the calcareous wall rocks and the pluton, respectively, prior to mineralization. Garnets and pyroxenes show a wide range of variation in composition. Early pyroxene is diopsidic whereas pyroxene in distal/late veinlets is hedenbergitic containing varying amounts of johannesenitic. Similarly, garnet and pyroxene become more Mn-rich with paragenetic sequence. Some zoned garnets from a vein skarn display a prominent increase in Mn content (22.9 wt. % MnO). Sphalerite precipitated after pyroxene and garnet in exoskarn. Zn sulfide precipitated together with pyrrhotite in proximal locations, associated with prograde garnet+pyroxene+rhodonite and retrograde quartz+amphibole+calcite+chlorite. Based on the geological, mineralogical, petrological and fluid inclusiondata, an integrated fluid evolution model (involving magmatic and meteoric fluids) is developed to explain the geological and fluid controls on Zn-Pb-skarn mineralization associated with granite porphyry.

Origin of stibnite-bearing hydrothermal veins in the Tatric superunit, Western Carpathians

Chovan, M.[1*], Hurai, V.[2], Lüders, V.[3], Prochaska, W.[4] & Balogh, K.[5]
[1]Dept of Mineralogy and Petrology, Comenius University, Bratislava, Slovakia ([*]chovan@fns.uniba.sk)
[2]Geological Institute, Slovak Academy of Sciences, Bratislava, Slovakia
[3]Helmholtz Centre GFZ, Potsdam, Germany
[4]Dept. of Geosciences, Montanuniversität Leoben, Austria
[5]Institute of Nuclear Research, Hungarian Academy of Sciences, Debrecen, Hungary

Variscan basement of Western Carpathians contains most important resources of antimony in Europe. Magurka and Dúbrava in the Nízke Tatry Mts. and Pezinok in the Malé Karpaty Mts. were the largest Sb deposits within Tatric tectonic unit. Stibnite-bearing hydrothermal veins crosscut the Tatric basement, which consists predominantly of medium-to-high grade metasedimentary and metavolcanic rocks intruded by large Variscan granitoid plutons. Variscan brittle and ductile deformation structures are generally well-preserved. $^{40}Ar/^{39}Ar$ data on muscovite from mylonitised orthogneisses point to a Late Palaeozoic tectonothermal activity at 330 Ma (about 300 Ma using K/Ar method), and an Alpine overprint at 80-100 Ma.

The sulphidic vein mineralizations can be subdivided into three stages: 1. quartz – pyrite/arsenopyrite (sometimes Au-bearing) – gold. 2. quartz – Fe-dolomite – stibnite – pyrite accompanied by minor berthierite, native antimony, and Sb-oxides. Later but in places also earlier is the sphalerite – Pb-Sb sulphosalt sub-stage. 3. quartz – carbonate – barite – tetrahedrite. Chlorite, muscovite and carbonate-illite alteration zones have been distinguished around the Sb-bearing veins. Crystallization of high temperature arsenopyrite - pyrite - gold assemblage was triggered by influx of low-salinity CO_2-rich aqueous fluids of magmatic or metamorphic origin. Mesothermal quartz-sulphidic (stibnite, berthierite, zinkenite, sphalerite, tetrahedrite) assemblages have precipitated from NaCl–KCl aqueous solutions, representing mostly deep-circulating heated meteoric waters.

Stibnite from quartz-carbonate veins of the Nízke Tatry Mts. precipitated from medium temperature (~150-200°C) and moderately saline fluids (12-16 wt. % NaCl eq.). Recrystallisation of the early stibnite and crystallisation of the superimposed, fine-grained stibnite occurred at similar temperatures in the presence of low salinity (1-5 wt. % NaCl eq.) aqueous solutions. Significant compositional and density differences exist between the ore- and gangue-precipitating fluids. Crush-leach and microthermometry data corroborate combined sources of water in the stibnite-precipitating fluid. Increased concentrations of bromine, $CaCl_2$ and sulphate and oxygen isotope ratios in Fe-dolomite are diagnostic of a basinal fluid component derived primarily from seawater, whereas carbon isotopes suggest a ^{13}C-depleted CO_2 derived from organic matter in low-grade sediments. The $^{207}Pb/^{204}Pb$ and $^{206}Pb/^{204}Pb$ ratios indicate a crustal origin of lead in stibnite and the associated sulphosalts. The high temperature pyrite – arsenopyrite - gold assemblage may be genetically linked to the evolution of the late Variscan granitoids and retrograde metamorphism within ~300 Ma old shear zones. Crystallization of stibnite, sfalerite and Pb-Sb sulfosalts was probably connected with Jurassic continental rifting dated at 210-170 Ma using K/Ar method applied to illite from alteration zones. Sulphide mineralization was recrystallized during the Alpine (Cretaceous) orogenic cycle.

Acknowledgements: This work was supported by the APVV project VVCE -0033-07.

Provenance analysis of gold and associated heavy minerals in the Black Reef Formation, South Africa, using geochemical fingerprints

Fuchs, S.[1,2*] & Gauert, C.D.K.[1]
[1]Dept. of Geology, University of the Free State, Bloemfontein, South Africa
[2]Institute of Mineralogy, Crystallography and Materials Science, University of Leipzig, Germany
([*]sfuchs@uni-leipzig.de)

The Black Reef Formation (BR), a thin, but laterally extensive unit of primarily conglomerates and quarzites at the base of the Transvaal Supergroup contains erratical gold at economic grade confined to regional areas. Highest gold grades are exploited in the West and East Rand area on top of underlying Witwatersrand Reefs. BR gold however occurs also outside of the Witwatersrand Basin in the eastern Mpumalanga and Limpopo Provinces, e.g. Kaapsehoop, in close contact to greenstone units. Platinum, Osmium and Iridium as well as Uranium-bearing minerals have been reported in association with gold in the BR mainly from BR exposures east of Klerksdorp [1]. Although most economic BR Au mineralization occurs at localities within the Witwatersrand Basin, a large number of Au occurrences are found in RR overlying Ventersdorp and Swaziland Supergroup strata; therefore, the reworking of Au placers of the prominent Wits Reefs such as the Ventersdorp Contact Reef the BR cannot be regarded as the only one source of gold within the BR.

Current geochemical fingerprinting attempts of BR Au and associated heavy minerals using Electron Microprobe, LA-ICP-MS, and NanoSims give an indication about a genetic relationship between the several Au deposits and their different underlying rocks. Constantinescu et. al [2] and McCandless et. al [3] successfully used indicator trace elements as such as Sb, Sn, As, Ru, Rh, Pd, Te, Ta, Os, Ir, (+Au, Ag, Cu) to characterize different gold deposits.

Average Ag contents in free gold from the East Rand determined by EMPA are high (14.8wt%, n=20), Hg contents low (on average 0.51 wt%); trace concentrations of S, Fe, Ni, Cu, As, Th, U and Cd in decreasing order were detected possibly because of micro-inclusions. The pyrite mineral chemistry shows minor As, Pb and traces of Ni and Cu, cobaltite contains minor Pb, gersdorffite Sb, and sphalerite shows minor Cu, Cd, and traces of Au and Pb. U-bearing phases such as Uraninite show minor Pb and Th and detectable trace amounts of S, Fe, Bi, As, Cd, Ag, Sb and In. The value of these trace elements for genetic and provenance interpretations still has to be assessed.

Investigation of detrital gold, gold in hydrocarbons and invisible gold in sulphides by LA-ICP-MS trace element of various BR sections is ongoing. In combination with NanoSims analyses for the visualization of invisible gold in pyrites, Ag-Au zoning in detrital gold grains the information could be relevant to determine possible gold sources, transport mechanisms, and depositional conditions. Finally it may allow to develop a holistic genetic model of the Au mineralization in the Black Reef Formation.

[1] Henry, G. & Master, S. (2008) *Black Reef Project - Internal report*. CSIR, 31 March 2008. [2] Constantinescu, B. et al. (2008) *9th Int. Conf. on NDT of Art*, Jerusalem Israel, 1-9 [3] McCandless, T, Baker, M.E. & Ruiz, J. (1997) *Geostandard Newslett.*, **21(2)**, 271-278.

Composition and stability of garnierites: Caribbean examples

Galí, S.[1*], Soler, J.M.[2], Proenza, J.A.[1], Lewis, J.F.[3], Cama, J.[2] & Tauler, E.[1]
[1]Dept. de Cristal·lografia, Mineralogia i Dipòsits Minerals, Universitat de Barcelona, Catalonia, Spain
([*]gali@ub.edu)
[2]Institute of Environmental Assessment and Water Research, IDAEA, CSIC, Barcelona, Catalonia, Spain
[3]Dept. of Earth and Environmental Sciences, The George Washington University, Washington, DC, USA

The chemical and structural characterization of garnierite minerals from several Caribbean lateritic mineralizations shows that this group of minerals is formed by intimate intermixings of three main Mg-Ni phyllosilicate solid solutions: serpentine-népouite, kerolite-pimelite and sepiolite-falcondoite [1-5]

The published experimental solubility constants for Mg end-members and the calculated constants for pure Ni end – members are used to calculate Lippmann diagrams for the three solid solutions, on the assumption that they are ideal. With the help of these diagrams, it is proposed that congruent dissolution of Ni-poor primary serpentine followed by equilibrium precipitation of Ni richer secondary phyllosilicates is an efficient mechanism of Ni supergene enrichment along the lateritic profile. The stability fields of the solid solutions are represented using [log $a_{SiO2(aq)}$, log (a_{Mg2+} + a_{Ni2+})/a_{H+}^2)] diagrams (Fig. 1). These, combined with Lippmann diagrams [6] give an almost complete chemical characterization of the solution and the precipitating phase(s) in equilibrium. The temporal and spatial succession of hydrous Mg-Ni phyllosilicates often encountered in Ni lateritic deposits is explained by the low mobility of silica [7] and the increase in its activity.

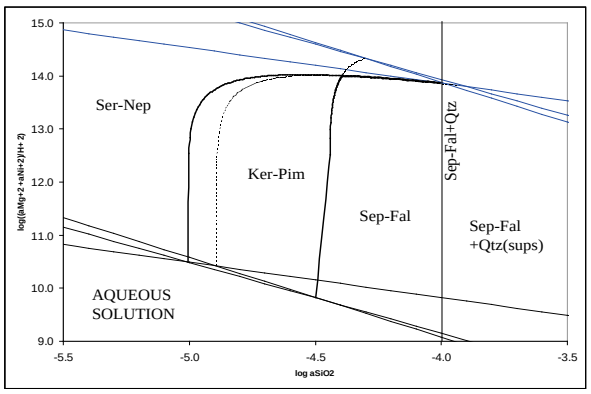

Fig. 1: Fields corresponding to the three solid solutions and boundaries: Ser-Nep+Ker-Pim; Ker-Pim+Sep-Fal and Ser-Nep+Sep-Fal. Dashed lines are metaestable extensions of these equilibria. Vertical line at log($a_{SiO2(aq)}$) = -4 gives equilibrium between quartz+Sep-Fal.

[1] Springer, G. (1974) *Can. Mineral.*, **12**, 381-388. [2] Brindley, G.W. & Maksimovic, Z. (1974) *Clay Minerals*, **10**, 271-277. [3] Manceau, A., Calas, G. & Decarreau, A. (1985) *Clay Minerals*, **20**, 367-387. [4] Golightly, J.P. (1981) *Econ. Geol.*, 75th Anniv. Vol., 710-735. [5] Tauler, E. et al. (2009) *Clay Minerals*, **44**, 435-454. [6] Lippman, F. (1980) *Neues Jb. Miner. Abh.*, **139(1)**, 1-25. [7] Soler, J.M. et al. (2008) *Chem. Geol.*, **249**, 191-202.

Mineralogical and geochemical characteristics of W>Sn quartz veins from Murçós (Northeastern Portugal)

Gomes, M.E.P[1,4*], Antunes, I.M.R.H.[2,4], Neiva, A.M.R.[3,4] & Teixeira, R.J.S.[1,4]
[1]Dept of Geology, UTAD, Vila Real, Portugal
([*]mgomes@utad.pt)
[2]Polytechnic Institute of Castelo Branco, Castelo Branco, Portugal
[3]Dept. of Earth Sciences, University of Coimbra, Portugal
[4]Geoscience Centre, University of Coimbra, Portugal

The Murçós mining area is located at the Galiza-Trás-os-Montes Zone, northeastern Portugal. The hydrothermal W>Sn quartz veins from Murçós cut Silurian schists and a Variscan biotite granite. The mineralization is of stockwork type and the veins fill mainly N40-50 ºW fractures that are probably related to the dextral shear zone which deformed the biotite granite. The exploitation of scheelite and cassiterite took mainly place at the surface in four open pit areas between 1948 and 1976 and 335 tons of W and 150 tons of Sn were produced [1].

The W>Sn quartz veins contain quartz, muscovite, tourmaline, scheelite, cassiterite, wolframite, arsenopyrite, pyrite, sphalerite, chalcopyrite, galena, native bismuth, rare pyrrhotite and stannite. Late minerals such as marcasite, bismuthinite, joseite, matildite, anglesite, zavaritskite, scorodite and roosveltite also occur. Tourmaline is subhedral and chemically zoned. There is an increase in Fe/(Fe+Mg) and Ti content and a decrease in Al content from core to rim. Scheelite is anhedral, light coloured with a typical blue fluorescence and irregularly zoned. Cassiterite is subhedral and usually zoned, with slightly pleochroic darker zones alternating with lighter zones. The darker and lighter zones have a similar chemical composition and contain inclusions of rutile and rare ilmenite. However, the darker zones of some crystals are richer in Ti than the lighter zones. Wolframite has a homogeneous composition and is enriched in the hubnerite component. Arsenopyrite is the most common sulphide. The richest euhedral arsenopyrite is in equilibrium with pyrrhotite and the subhedral arsenopyrite contains inclusions of bismuth, bismuthinite and matildite. Arsenopyrite is replaced by pyrite, scorodite and roosveltite. In general, pyrite occurs as fracturated euhedral to subhedral crystals. The sphalerite is anhedral associated with arsenopyrite and quartz. Chalcopyrite has an homogeneous composition and occurs included in subhedral arsenopyrite and as blebs aligned in sphalerite. Galena is homogeneous with Ag and Bi up to 1.5 wt% and 3.5 wt%, respectively. Galena has many exsolutions of bismuthinite and matildite which show ortogonal alignments. The coexisting suhbedral arsenopyrite and sphalerite have 31,9 wt% As and 18 mole% FeS, respectively, and give estimated temperature above 425ºC [3]. Pyrrhotite is monoclinic and probably resulted from the inversion of hexagonal pyrrhotite at about 248ºC [2]. Veinlets of quartz containing anhedral stannite and individual grains consisting of 75% Au + 20 % Pd + 5 % Ag fill fractures in arsenopyrite.

Aggregates of secondary phases of bismuthinite, joseite, zavaritskite and roosveltite occur around bismuth and fill fractures in subhedral arsenopyrite. Scorodite occurs as an alteration product of arsenopyrite. Anglesite is the alteration product of galena crystals.

[1] SIORMINP (2009) http://e-geo.ineti.pt/bds/ocorrencias/.[2] Scott, S.D. & Kissin, S.A. (1973) *Econ. Geol.*, **68**, 475-479. [3] Scott, S.D. (1983) *Mineral. Mag.*, **47**, 427-435.

Textural and mineralogical constraints in chromite sand enrichment by shaking tables at Brieville plant (Madagascar)

Grieco, G., Pedrotti, M.[*], Merlini, A. & Pileri, D.
Dipto. di Scienze della Terra "A. Desio", Università degli Studi di Milano, Milan, Italy ([*]maria.pedrotti@unimi.it)

Textural and mineralogical characters of ore together with technical parameters of enrichment plants strongly affect efficiency of chromite sand concentration with shaking tables. Such parameters were studied at Brieville gravity enrichment plant that works chromite ore from different mines within Andriamena district (Madagascar).

Ore is a massive to densely disseminated chromitite hosted by a peridotitic and pyroxenitic rock. Gangue mineralogy is very rich, comprising ortho and clinopyroxene, tremolitic to edenitic amphibole, phlogopite, chlorite, talc and minor pentlandite, pyrrhotite, ilmenite, rutile and dolomite.

Ore is firstly crushed and sieved to a grain size below 2.5 mm, and then it is hydroclassified and sent to shaking tables. As a result of hydroclassification different tables receive sand of decreasing grain size.

Mineralogy, chemistry and granulometry show that hydroclassification operates a pre-selection of chromite sand and as a consequence tables are fed with sands different not only for grain size but also for mineralogy and chemistry.

Separation of grains in a shaking table occurs due to contrasts in specific weight, grain size and, to a minor extent, grain shape. Specific weight contrast between grains for a given grain size distribution of sand depends on density and degree of liberation of phases [1]. At Brieville the degree of liberation of chromite was assessed for each table and for each grain size. Results show that the degree of liberation depends on the relation between crystal size distribution of chromite in the rock and grain size of sand. For grain size above 300 μm, the degree of liberation is low enough to considerably reduce enrichment efficiency of tables working at such grain sizes.

Increase of sorting from feeding sand to concentrate confirms that shaking tables separate grains also according to grain size and low sorting of feeding sand suggests sieving as a more efficient technique to select sand to be sent to shaking tables rather than hydroclassification.

Results of mineralogical distribution suggest that gangue minerals behave in different ways according to their density and habit, showing differential enrichments due to pre-selection operated by hydroclassification and to selection operated by gravity separation through shaking tables.

At Brieville the main parameter affecting efficiency of shaking tables is the degree of liberation of chromite. As a result the table working the coarsest grain size is able to enrich Cr_2O_3 content of feeding sand by only 5.14 wt%, against an enrichment of 20.26 wt% for the table working the finest grain size. This result is disguised by the Cr_2O_3 pre-enrichment of the coarser sand operated by hydroclassification as the combination of the two processes gives a concentrate sand similar in Cr_2O_3 content for all the tables.

In general results show that a detailed mineralogical and textural study of the ore can provide useful information to get the highest efficiency of the plant through an appropriate choice of crushing degree and shaking table settings and by substitution of hydroclassfiers with sieves.

[1] Wills, B.A. & Napier-Munn, T.J. (2006) *Mineral processing technology*. Elsevier.

Two genetic types of secondary native gold in epithermal gold-telluride deposits of the Far East of Russia

Ivanov, V.V.
FIGI FEB RAS, Vladivostok, Russia (dom101@mail.ru)

Native gold in ores of hydrothermal deposits of precious metals is frequently rated as typically hydrothermal mineral. It is known at the same time that a part of native gold in some deposits is secondary, i.e. a product of decomposition of the primary minerals of gold, specifically of gold tellurides. There are recognized two types of such secondary (newly formed) native gold: hypergenic and hypogenic gold, which have been found in the epithermal deposits located in various volcanic belts of the Russian Far East.

Hypergenic native gold - Secondary gold as a product of oxidation and full decomposition of various gold tellurides during hypergenic processes has long been known for a number of the world deposits. Brownish-earthy gold of lacy structure has a name of "mustard" gold in some countries. Such high-fineness gold cannot always be unambiguously considered the end product of the gold-rich tellurides minerals decomposition. In our case, a characteristic is given for the hypergenic newly formed gold presented in the partly oxidized samples of gold telluride ores from the Svetloye and Amy high-sulphidation epithermal gold deposits of the Alalindinskoye ore field (Priokhotye region). The gold is represented by very fine grains within the ortho-paragenetic assemblage of primary and secondary minerals of tellurium and other chemical elements. The author revealed in these ores also rare oxycompounds of gold and other metals concerning to Au – (Ag) – Cu − (As) – Fe – Te − O system.

Hypogenic native gold - It is a poorly-known type of newly formed native gold which was formed through the solid-phase thermal decomposition of Au-Ag tellurides. The author has proved the existence of such genetic (metamorphogenic) type of gold when carrying out the geological-mineralogical investigations of locally thermally metamorphosed adular-quartz ores in Priamurye and Kamchatka regions. The experimental modelling of hupogenic secondary gold growth through petzite thermal decomposition has been done (Fig. 1).

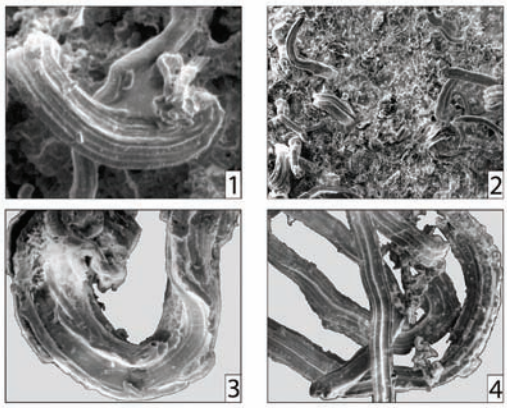

Fig. 1: Secondary high-fineness gold: 1, 2 – native-grown crystals; 3, 4 – crystals on secondary hessite surface experimentally grown throug petzite thermal decomposition.

Such authigenic gold formed "in situ" is characterized: in the case of the crystallization strained conditions by a specific root-limbate type of separations in hessite, and in the case of free growth conditions – by thread -like forms of individuals (whiskers of a pressure) with ribbed-grooved surface and different degree of twisting (for example, helical type).

REE distribution and mineralogy in a Palaeoproterozoic apatite-iron oxide deposit: Grängesberg, Bergslagen, Sweden

Jonsson, E.[1*], Persson Nilsson, K.[1], Högdahl, K.[2], Troll, V.R.[2] & Hallberg, A.[1]
[1]Geological Survey of Sweden, Uppsala, Sweden
([*]erik.jonsson@sgu.se)
[2]Dept. of Geosciences, Uppsala University, Uppsala, Sweden

The apatite-iron oxide deposits of the Grängesberg District (GD; past production 152 Mt of ore @ 58% Fe and 0.81% P) are situated in the Palaeoproterozoic Bergslagen ore province in central Sweden. The deposits have historically been compared to those of the Kiruna type, and were more recently suggested to be related to the IOCG-clan of deposits [1].

The GD Fe oxide ores range from magnetite to hematite-dominated, variably rich in apatite-(CaF). This mostly occurs as banded, fine-grained aggregates, and was recrystallised together with ores and metavolcanic host rocks during c. 1.85-1.80 Ga regional lower amphibolite facies metamorphism.

In the ores, REEs are mainly hosted as trace contents in the granular apatite, which is typically high in Y, Ce, La and Nd, but are also present in monazite, allanite and epidote, as well as in REE-fluorocarbonate(s). The host rocks exhibit REE patterns similar to the apatites, the major GD ore types and alteration assemblages (Fig. 1), linking the apatite-iron oxide ore to the (formation of the) host rocks.

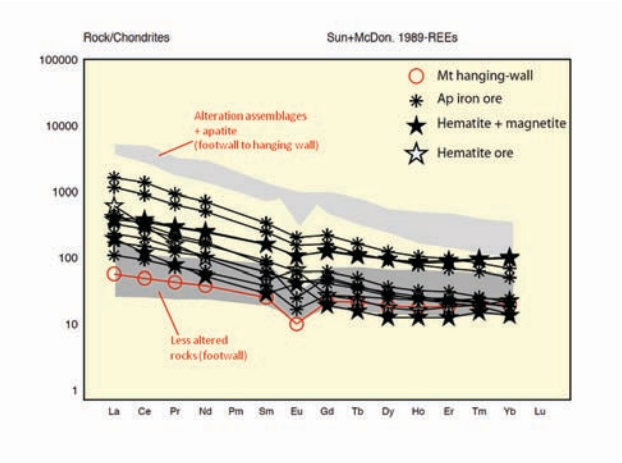

Fig. 1: Chondrite-normalised REE patterns för apatite (Ap), Fe oxide ores (Mt = magnetite) and host rocks at Grängesberg.

In relation to Kiruna ore apatites [2], the Grängesberg samples lack both the very abundant monazite inclusions and the patchy REE distribution. Instead, the recrystallised apatite often exhibits strong intra-grain REE zoning, with slightly depleted outer rims, intermediate REE-rich (Y>Ce≥La,Nd) rims, and REE-poor cores. Monazite occurring along apatite grain boundaries exhibits Ce≥La>Nd, in part mimicking the apatite LREE distribution. The last REE-phase to form, synchysite-(Ce), exhibits Ce≥La>Nd, and occurs in pockets in apatite and calcite. This assemblage indicates the presence of a late-stage carbonaceous fluid.

The systematic relation between zoned REE patterns and granoblastic grain shape in apatite indicates that this is a consequence of regional metamorphism, driving an REE mobilisation process which was variably arrested in different grains. Mobilisation of REEs from the apatite led to formation of intergranular monazite ± allanite, and finally, REE-fluorocarbonates.

[1] Hitzman, M. et al. (1992) *Econ. Geol.*, **100**, 1657-1661. [2] Harlov, D. et al. (2002) *Chem. Geol.*, **191**, 47-72.

Identification of uranium and vanadium minerals in black shale, South Korea

Kang, S.A.[1], Kim, Y.J.[1], Jung, S.Y.[2], Shin, J.K.[2] & Lee, Y.J.[1*]
[1]Dept. of Earth and Environmental Science, Korea University, Seoul, Korea ([*]youngjlee@korea.ac.kr)
[2]Uranium Exploration Team, Korea Resources Corporation, Seoul, Korea

Uranium, which is rich in metalliferous black slates of Okcheon Metamorphic Belt in South Korea, has been the subject of interest in mineral resources because of its potential roles in energy industries. Identification of mineral species has been played an important role in controlling mineral processing and extraction of metals such as uranium and vanadium in mine exploration and development. Despite the importance of uranium and vanadium minerals in the black slates, the identification of these minerals is still not clearly understood and verified. Moreover, no direct observation and confirmation of these minerals in the slates have been provided.

Systematic studies, combined conventional experiments with electron probe micro-analyzer (EPMA) methods have been used to evaluate uranium and vanadium minerals in the black slate. Results show that concentrations of these minerals increase with increasing total organic carbon contents. However, the relation between the concentration of uranium and that of vanadium is inversely proportional; the concentration of uranium increases with decreasing that of vanadium whereas the concentration of vanadium increases with decreasing that of uranium. EPMA results show that the primary minerals for uranium are uraninite ($(U^{4+}_{1-x-z}U^{6+}_{x}M^{2+}_{z})O_{2+x-z}$) and brannerite ($(U,Ca,Y,Ce)(Ti,Fe)_2O_6$). These minerals are aggregated with round shape. EPMA also shows that vanadium-bearing minerals contain high concentrations of Al, Si, Ca, Ti, suggesting that the main mineral is muscovite. This result is good agreement with microscopic observation, showing that greenish muscovite is frequently observed. No differences for vanadium concentrations on muscovite are observed by a point or an area microanalysis in EPMA, indicating that vanadium is in the structure of muscovite rather than found as a single mineral. In addition, Ba is also detected in K-feldspar where Ba is substituted for K of the feldspar in samples showing high concentrations of uranium. Our results suggest that the primary minerals of uranium in the black slate would be formed by the reduction of uranium due to reducing agents such as H_2S, CH_4, and Fe^{2+} or organic matters.

Micromineral composition of deposits of Zarmitan gold ore zone

Koneev, R.I. & Khalmatov, E.A.[*]
Dept. of Mineralogy and Geochemistry, Faculty of Geology, National University of Uzbekistan, Tashkent, Uzbekistan
([*]e_khalmatov@yahoo.com)

The Zarmitan gold ore zone is located on the South side of the Northern Nuratau range. It bowingly stretches from the south-east exocontact to the south-west side of the Koshrabad intrusion and relates to junction of the sub-latitudinal Karaulkhana-Zarmitan fault zone with hidden, abyssal, sub-meridional Zirabulak-Koshrabad fault. The Zarmitan gold ore zone consists of (from the south to the west) the Charmitan, the Urtalik and the Guzhumsay deposits. The Charmitan is located within the slates, sandstones and aleurolites (siltstone) of the Djazbulak suite (S_1) and endocontact of granosyenites of the Koshrabad intrusion (C_3-P_1); the Guzhumsai is nearly entirely located in the granosyenites.

Researche of ores from the Charmitan and the Guzhumsay deposits showed that the compositions of ores are practically identical, in spite of different host rocks. Geochemical numbers of elements accumulation intensity calculated concerning clarkes in the Earth crust coincided:

Charmitan – As-Te-Bi-Au-Sb-Ag-Se-Pb-W-Hg-Mo-Pd-Sn-Co-Zn; Guzhumsay – As-Te-Bi-Au-Se-Sb-Ag-Pb-W-Hg-Sn-Pd-Mo-Cu-Zn.

The ores from both deposits were formed by standard set of mineral associations, typical for gold ore deposits of Uzbekistan: 1. Scheelite – molybdenite (Au-W); 2. Gold-arsenopyrite – pyrite (Au-As); 3. Gold – telluride – selenide – polymetallic (Au-Te); 4. Electrum – selenide – polysulfidic (Au-Ag); 5. Gold – silver – antimonite – sulfoantimonite. Au-Hg association with cinnabar is not established. Au-As, Au-Te, Au-Ag and Au-Sb associations determine industrial productivity. In macromineral composition presence, development of the certain productive associations is clearly registered by micromineral composition.

Au-As association is characterized by presence of thin gold, loellingite, pyrrhotite, gersdorffite inclusions and mineral microparagenesises of consequent associations in arsenopyrite, pyrite and quartz.

Au-Te differs by development of bismuthic compounds – maldonite, bismuthinite, chorobetsuite, kobellite and tellurides – hedleyite, tsumoite, pilsenite, sulfotsumoite, joseite, calaverite, petzite and others. This association is the most typical for the Charmitan deposit.

Au-Ag mineralization is represented by electrum, kustelite, acanthite, freibergite, pyrargyrite, stephanite and other Ag sulfo-salts.

Au-Sb association is widely presented, especially on the Guzhumsayi deposit – aurostibite, boulangerite, jamesonite, zinkenite, gudmundtite, owyheeite, andorite and others.

Very original microparagenesises (nanoassemblages) are formed by combination of associations. Micromineralogical analysis allows completer determination of specific associations'development, estimation of the level of erosional cut and conditions of formation. Longer and more diverse list of minerals is, larger the scale of mineralization. The Guzhumsay deposit had being formed in less deep conditions than the Charmitan deposit, and both of them compose extensive ore-bearing zone pitching to the east.

Banded Iron Formation deposits from the Tiris region (Western Sahara): structure, mineralogy and textures

Lehbib, S.[1*], Arribas, A.[2] & Melgarejo, J.C.[1]
[1]Dept. Cristal·lografia, Mineralogia i Dipòsits Minerals, Universitat de Barcelona, Catalunya, Spain
([*]slehbib@yahoo.es)
[2]Escuela Técnica Superior de Ingenieros de Minas, Madrid, Spain

Many important showings of iron oxide deposits have been reported since the 1950's in the Tiris region, SE of Western Sahara. These deposits are located in the same Precambrian belt which hosts the world-class iron deposits of Quidiat Iyil in Mauritania, which are close to the border with Western Sahara. Unfortunately, the iron deposits of Western Sahara have not been characterized until the present, mainly because of the political conflicts in the area. Hence, the occurrence of these outcrops in Western Sahara defines new and interesting metallogenetic targets. Therefore, the aim of this work is to provide new data on the mineralogy of the main deposits, as well as their textures, paragenesis and origin.

Most of these deposits have been intensively deformed, in particular, by folds at macro, meso and micro-scale. On the other hand, most of these deposits have been affected by medium to high-grade regional metamorphism, and coarse-grained textures have been widely developed. This aspect could favour the benefit of the ores.

According to the age of the deposits, three main groups can be established:

1) Southern group. It is found in the Jneifisat zone, and it is hosted by the migmatitic units of the Lower Archaean. They are affected by high grade regional metamorphism, and all display a lepidoblastic texture. Magnetite can reach up to 35% modal of the rock. The rest is made up of quartz, which occurs in small bands or metamorphic rods.

2) Central group. These deposits are hosted in the highest part of the Archaean series, comprising paragneiss, metabasites and some marble beds, metamorphosed in amphibolite facies. The most important deposit of this type is found at El Farfarat, NW of Miyec, although there are many other mineralized units in different levels of the series. Some noticeable outcrops can be distinguished in Galb Leazib, Galb Fula and several outcrops in the vicinity of Miyec. The thickness of these BIF can vary a lot, being less than 3 m in all cases. These deposits have a modal content of magnetite which is slightly higher than the above mentioned, up to 50%; the content in quartz ranges from 30 to 50%. However, some outcrops can consist of massive magnetite, as in Galb Fula (more than 75 %), accompanied by small amounts of quartz and siderite. Other minerals, as siderite and grunerite, may appear in small amounts, as in Galb Leazib or Galb Laana. All these minerals have been formed by medium-grade regional metamorphism.

3) Northern group. These deposits are interbedded with Eburnean volcanosedimentary series. These BIF are the thickest in Western Sahara (more than 10 m in some points). In addition, they are massive, as in the Bu Daira Ranges, and the content in magnetite may reach 75% in volume. However, although the texture is also lepidoblastic, the fine grained textures (in the range 500 μm-1 mm) are not as suitable for the benefit of the ore as in the above-mentioned cases. Quartz is the only gangue mineral found there up to date.

In all these deposits, magnetite has been partially replaced on surface by fine-grained supergenic hematite.

The potential for magmatic metal sources in the Iberian Pyrite Belt

Marques, A.F.A.[1,2*], Scott, S.D.[1], Relvas, J.M.R.S.[2], Rosa, C.[3] & Guillong, M.[4]
[1]Dept. of Geology, University of Toronto, Toronto, Canada
([*]marques@geology.utoronto.ca)
[2]CREMINER (LA-ISR), University of Lisbon, Portugal
[3]LNEG, Alfragide, Portugal
[4]ETH, Zürich, Switzerland (present address CODES, Australia)

The Iberian Pyrite Belt (IPB), located in southern Portugal and Spain, hosts several giant volcanic-hosted massive sulfide (VHMS) deposits within a bimodal - siliciclastic volcanic-sedimentary succession of Late Devonian to Lower Carboniferous age [1]. Felsic volcanic centres display a complex architecture of lava domes, pyroclastic units and intrusions defining lava cryptodome pumice cone volcanoes [2]. Although current knowledge indicates that the direct contribution of metals of magmatic origin may have not been predominant in typical IPB deposits [3], the exceptional nature of the ores in some giant VMS deposits are best explained by a magmatic – hydrothermal model [3,4]. Volcanic successions in the Neves Corvo and Serra Branca areas are mineralized and Neves Corvo is a world-class giant high Cu and Sn grade VHMS deposit [1,3]. Conversely, Albernoa quartz-feldspar-phyric volcanics have no known sulfide mineralization or ore-related hydrothermal activity. Exposed melt inclusions hosted in quartz phenocrysts in felsic rocks from these three distinct volcanic centres were analysed by SEM/EDX [5] and LA-ICP-MS. EDX showed that melt inclusions present in Albernoa samples contained metallic precipitates with Sn, Cu, Cl and S suggesting that the magmatic source beneath the volcanic centre had high contents in these elements. LA-ICP-MS analyses on the unexposed melt inclusions determined the bulk composition. Quantification of element concentrations followed Halter et al's [6] methodology in which mass ratio was determined using whole rock differentiation trends. In clear contrast with their host rock compositions, melt inclusions from Serra Branca and one Albernoa sample showed higher concentrations of mafic-related elements (e.g. FeO, MgO, Co, Ni, Cu and Zn) and low Na_2O. The remaining rhyolite and rhyodacite rocks from Albernoa have melt inclusions with a composition similar to those of their hosts. The high-silica melt inclusions found in the Neves Corvo samples are depleted in Cu and have low Sn (12 ppm Sn). Sn concentrations are higher in the melt inclusions than in their host rocks. Serra Branca and Albernoa melt inclusions can contain up to 35 ppm Sn, much higher than in melt inclusions from Neves Corvo. Preliminary results of contrasting concentrations in particular elements observed in the melt inclusions and their host rocks suggest mixing of magmas. On the other hand, it is puzzling to observe that higher concentrations of ore-metals (e.g. Cu, Sn) are found in melt inclusions hosted in volcanic rocks from volcanic centres without known mineralization and not in the Neves Corvo volcanic rocks. On-going research should provide additional arguments for this discussion. Nevertheless, these observations have strong implications for the understanding of the pre-eruptive processes that occurred beneath the IPB volcanic centres and the on the evaluation of the role of magmatic-hydrothermal processes in the formation of high-grade Cu (±Sn) mineralization in this remarkable province.

[1] Relvas, J. et al. (2006) *Econ. Geol.*, **101-104**, 791-804. [2] Rosa, C.J.P. et al. (2007) *Proc. 9th Bien. SGA meeting Dublin, Ireland.* [3] Relvas, J. et al. (2009) *Proc. 10th Bien. SGA meeting, Townsville, Australia.* [4] Yang, K. & Scott, S.D. (2006) in Christie, M.R et al. (eds.) *Geoph. Mono.*, **166**, 163-184. [5] Marques, A.F.A. et al. (2008) *Geoph. Res. Abs.*, **10**, A-07082. [6] Halter, W.E. et al. (2002) *Chem. Geol.*, **183**, 63-86.

Vent chimneys of Devonian black smokers in Rudniy Altay

Maslennikov, V.V.[1], Zhukov, I.G.[1*], Maslennikova, S.P.[1] & Simonov, V.A.[2]
[1]Institute of Mineralogy, Ural Division, Russian Academy of Sciences, Miass, Russia ([*]igorzhukov2009@yandex.ru)
[2]Institute of Geology and Mineralogy, Siberian Division, Russian Academy of Science, Novosibirsk, Russia

The occurrences of well-preserved ancient black smoker chimneys in VHMS deposits are rare [1-3]. Last years the Devonian massive sulphide deposits at Rudniy Altay (Nikolayevskoe, Artemyevskoe, Zarechenskoe) have yielded a number of very well-preserved sulfide vent chimneys. The VHMS deposits were formed in ensialic island arc basin in to anoxic to suboxic environments. This district comprises bimodal felsic (Altay subtype Kuroko type) classes of VHMS deposits hosted by black shales in dacites and rhiolites.

Three main chimney types are classified by the principal chemistry: 1) Cu-Fe-Zn-rich (in Nikolayevskoe deposits); 2) Zn-Cu-Ba-rich (in all mentioned deposits); 3) Ba-Fe-rich (Artemyevskoe); 4) Ba-rich (Zarechenskoe).

In general, the mineralogical zonation shown by various ancient chimneys is broadly comparable with those studied in modern black or gray smoker chimneys, with the exception of the lack of evidence for the former initial chimney shell of anhydrite or silica. In the Cu-Fe-Zn-rich chimneys, the pyrite in the outer walls (zone A) is represented by primary colloform, and fine varieties as well as pseudomorphs, probably after hexagonal pyrrhotite. In the inner parts of outer walls of the chimneys, the colloform and fine pyrite were partly replaced by marcasite and euhedral pyrite in association with sphalerite and chalcopyrite. The chimneys with sphalerite and barite outer wall were found, too. The inner walls (zone B) of the chimneys were always formed of coarse subhedral chalcopyrite, which sometimes demonstrates textures of relict intermediate solid solution copper-iron or copper-zinc sulfide phases (ISS). The enargite and fahlores are wide spread. The axial conduit zones (zone C) of some chimneys were consequently filled with sphalerite, pyrite, marcasite quartz and/or barite. In the Zn-Cu-Ba-rich, the outer wall is, commonly, sphalerite of barite sphalerite with minor euhedral pyrite. In Ba-Fe-rich chimneys, the outer wall is composed of framboidal or collloform pyrite. The pyrite-arsenipyrite-fahlore-galena-gold and bismuth assemblages have been revealed in the chimneys. The axial conduits were filled with barite and minor sphalerite and galena. In fragments of Ba-rich chimneys, concentric barite zones contain dissemenated galena, sphalerite, fahlores and native gold. The all chimneys canbe ranged from black smokere to gray and white smokers with increasing of sphalerite and barite. The significants of gold-galena-fahlore assemblage increase in the range. The mineralogical zonation may be interpreted in terms of zoned formation temperatures and redox conditions across the chimney wall during formation.

Acknowledgements: This work was supported by the Integration project with Siberian Branch of RAS (no. N 09-I-5-2004)

[1] Maslennikov, V.V. et al. (2009) *Econ. Geol.*, **104(8)**, 1111-1141. [2] Oudin, E. & Constantinou, G. (1984) *Nature*, **308**, 349-353. [3] Scott, S.D. (1981) in Goldie, R. & Botrill, T.J. (eds.) *Seminars on Seafloor Hydrothermal Systems*. Geosci. Can., **8**, 103-104.

Genetic study of the primary hydrothermal mineralization in Špania Dolina and Ľubietová ore districts (Slovakia, Western Carpathians)

Michňová, J.[*] & Ozdín, D.
Dept. of Mineralogy and Petrology, Comenius University, Bratislava, Slovakia ([*]michnova@fns.uniba.sk)

Sulphidic and carbonate veins were from the Middle Ages the main sources of metals in the area of today`s Slovakia.

Older works dealing with the topic of hydrothermal carbonate-quartz-sulphide mineralization were focused mainly on mineralogical study, while from the half of 20th century more complex investigations including detailed geochemistry and genetic study of these systems were done.

These work was focused on two Cu abandoned deposits; first of them of known origin - hydrothermal Cu mineralization at Ľubietová deposit, which occurs in metamorphic crystalline rocks of Veporic Unit and originated during Alpine tectono-metamorphic events as many others siderite-sulphidic veins in Tatric and Veporic units. The second one Špania Dolina deposit is situated in sedimentary rocks of Permian age and some features indicated (according to older works) affinity to sedimentary copper deposits (e.g. Novoveská Huta deposit).

New results from our investigation show, that on both localites studied, mineralization has been developed in three stages:

1. siderite (carbonate) stage, 2. stage of Alpine mineralization and 3. – sulphidic stage. The 4. stage represented by Ca-carbonates was identified only at Špania Dolina.

Fluid inclusion study indicates, that minerals from siderite and sulphidic stage of mineralization in Špania Dolina precipitated from medium temperature (~120 – 314 °C) and moderately saline (~ 10 – 23 wt. % NaCl eq.) H_2O - NaCl fluids, which contain small amount of $FeCl_2$ and $MgCl_2$.

Minerals from stage of Alpine paragenesis and sulphidic stage of mineralization in Ľubietová precipitated from medium temperature (156 – 330 °C) and low to moderately saline (~ 3 – 20 wt. % NaCl eq.) H_2O - NaCl and H_2O - CO_2 0 NaCl fluids with small amount of $MgCl_2$ and $FeCl_2$. That means that fluids were influenced by metamorphic source.

Average temperature of the origin of Alpine paragenesis calculated using chlorite thermometry is 320°C and age of mineralization according to monazite dating is 92 ± 11 Ma (Upper Cretaceous tectono-metamorphic origin).

Isotopic study of secondary barite and primary sulphates of barite-celestine group shows different composition of isotopes S and O. Isotopic study in case of primary sulphates suggest, that their origin was influenced by Permian evaporates and in case of secondary barite juvenile fluids were most important.

C and O isotope data of carbonates from the siderite stage indicate mixing of fluids from various sources, but the most important were crustal fluid solutions.

All obtained results suggest, that mineralization at both studied localities have the same character of hydrothermal deposit, that „Cu – sulphidic mineralization“ in permian sedimentary rocks is analogue of sulphidic stage at siderite-sulphidic veins in crystalline rocks and differences in structures were caused just by different character of host rocks.

Acknowledgements: This work was supported by Slovak Research and Development Agency under the contract No. APVV-VVCE -0033-07.

Giant quartz orebodies: structural, mineralogical and geochemical evolution

Moroni, M.*, Zucali, M., Tiboni, Ch. & Leoni, F.
Dipto. di Scienze della Terra "A. Desio", Università degli Studi di Milano, Milan, Italy (*marilena.moroni@unimi.it)

Quartz veins are frequent but giant quartz-only orebodies, mostly mined for metallurgy and ceramic industry, are not so common and their origin and mechanisms of emplacemen are not completely understood (e.g., see [1] for a geological-structural model). At the location of Sondalo, in the Central Alpine Belt (Northern Italy), a huge orebody of pure quartz is emplaced in high-grade continental basement of the Austroalpine Languard-Campo Nappe. The orebody, currently extensively mined and in development, is open ended at depth. It has never been studied. The orebody is irregularly tubular-shaped, and is in direct, brecciated to faulted contact with basement migmatites, garnet-biotite-sillimanite gneisses and amphibolites as well as with a Permian gabbro intrusion (Sondalo Gabbro) emplaced in the basement. The orebody consists of extremely hard, highly deformed, varicoloured (white, light pink, grey, black) quartz. Muscovite and tourmaline are the rare but coarser accessory minerals near the margins of the body, although sub-micrometric accessory phases variably disseminated throughout the body were observed. Fluid inclusions are locally abundant.

3D meso- and micro-structural relationships between orebody and basement and thermo-barometric estimates suggest emplacement of the quartz intrusion later than Permian but before Alpine convergence, at T >750°C and P ≈ 0.7 Gpa. However unusual, coarse skeletal biotite and orthopyroxene intergrowths in reaction rims of breccia fragments also suggest a remarkably high thermal regime of the quartz emplacement, at T > 670°C (biotite-opx thermometer). During the emplacement widespread brittle deformation occurred likely associated with hydrofracturing mechanisms. Quartz also bears evidences of intense plastic deformation with localized annealing, in addition to widespread mm- to cm-spaced late-stage fracturing. At the mesoscale highly strained portions of the orebody may show impressive colour variations from pure white to black.

Selected trace elements, Al, B, Ba, Fe, Ge, P, Ti were analyzed for evaluating colour variations and provenance of quartz based on mechanisms of Si replacement in the quartz lattice in pegmatite-like contexts (see [2,3]). The trace element composition of the Sondalo quartz revealed unusually high values of Si-substituting Ge, P Ti and Al contents and related ratios relative to pegmatite-related quartz, as well as high contents in Ba. Trace elements show roughly zoned, coherent distribution patterns and show some relationships with colour variations. Coupled Ba and Ti enrichments may also cope the occurrence of phases like benitoite (revealed only in XRD patterns) among the submicrometric accessory phases. Coupling of structural and geochemical mineralogical investigations of orebody and wall rock may give additional clues on the still poorly understood nature, mechanisms of formation and emplacement of huge quartz-only bodies in orogens.

[1] Bons, P.D. (2001) *Tectonophysics*, **336**, 1-17. [2] Larsen, R.B. et al. (2004) *Contrib. Miner. Petrol.*, **147**, 615-628. [3] Götze, J. et al. (2004) *Geochim. Cosmochim. Ac.*, **68**, 3741-3759.

Au-Bi-Te mineralization of the Myutenbay deposit (the Muruntau ore field, Uzbekistan)

Mun, Yu.S.
Dept. of Mineralogy and Geochemistry, Faculty of Geology, National University of Uzbekistan, Tashkent, Uzbekistan (ju.moon@yahoo.com)

The Myutenbay deposit is located in the Kyzylkumsky region. It is a south-eastern flank of the Muruntau deposit. It is localized in the block of Besapan suite schists (O_2-S_1*bs*) dropped relatively the Muruntau deposit and it is separated from it by sublatitudinal South Fault. The main productive mineralization is a gold-pyrite-arsenopyrite with fine dispersed nanogold and Ni-Co minerals – gersdorffite, pentlandite, ulmanite, Ni-loellingite, gold-tellurium-selenide-polymetallic with bismuth sulfides (bismuthinite, ikunilite), sulpho-salts (gustavite, kobellite, sakharovaite, pavonite, treasurite, galenobismutite), tellirides (hedleyite, tsumoite, pilsenite, tellurobismuthite), sulpho-tellurides (sulphotsumoite, joseite A, B, tetradymite, ingodite), seleno-tellurides (kawazulite), as well as maldonite, Ag-maldonite, native bismuth. On composition bismuth compounds are nonstoichiometric and they form transitional compounds of different homologous series and very often enriched in selenium, from 1 to 8 %.

Previous research (as it was on the Muruntau) determined the high indicated role of Bi, but it was marked that tellurides and selenides in the ores of the Myutenbay were not found. However, our research showed that tellurides and other Bi compounds have very wide abundance and are mainly segrerated in micro- and even nanoforms within arsenopyrite, pyrite and quartz forming close intergrowths (nanoassemblages or microparageneses) with gold, probably with maldonite, native Bi.

Mineral-geochemical research of gold ore deposits of Uzbekistan showed that on gold deposits proper (Au:Ag – 10:1-1:10) Au-As and Au-Te mineral associations of geochemical parageneses are constantly present. But Au-Te mineralization in the deposits of Kyzylkumsky and Nuratinsky ore districts is mainly represented by bismuth tellurides, sulphotellurides, selenides and sulpho-salts, and in Kuraminsky region by various tellurides of Au, Ag, Pb, Sb, Hg and Bi selenides. It is connected with that fact that the deposits of the Kyzylkumsky and Nuratinsky regions were formed in hypabyssal hypomesothermal conditions and in the Kuramninsky region in epithermal ones.

Geochemical rows of the elements accumulation intensity within the ores calculated on the basis of concentration coefficients that were calculated relatively clarks of elements in the Earth crust show that on the Myutenbay and Murunatau deposits following elements are accumulated with gold:

Muruntau – Bi-As-Te-Au-Se-Pd-W-Ag-Sb-Mo-Hg-Pb-Cu-Pt-Sn; Myutenbay – As-Te-Bi-Au-Se-Sb-W-Ag-Hg-Pd-Mo-Cu-Pb-Sn-Ni.

It should be also mentioned that Au, Bi, Te, As concentrations are thousands of units, and the rest elements are hundreds-tens units.

Thereby, Au-Bi-Te mineralization, together with Au-As one is the most important during formation of gold deposits in hypabyssal conditions.

Mineralogy of Sn-Nb-Ta-W(-Au) mineralizations in the Musha-Ntunga, Bugarura-Kuluti and Rwinkwavu mineral districts, south-eastern Rwanda

Ngaruye, J.C.[1,2*] & Gauert, C.D.K.[2]
[1]Rwanda Geology and Mines Authority (OGMR), Kigali, Rwanda ([*]jclaudengar@yahoo.fr)
[2]Dept. of Geology, University of the Free State, RSA

The cassiterite – wolframite - columbite/tantalite and gold mineralisation in Rwanda belong to the Kibaran metallogenic province which extends over an area of 1500*400 km from Katanga in southern DRC to south-western Uganda in the north-east. An approximate age of 1380 Ma were determined by several workers for the G1-3 granites, an age of 980+/-10 Ma for the G4 granites, the columbite mineralisation at 965+/-5 Ma, and cassiterite in mineralized quartz veins of Burundi at 951+/-18 Ma [1]. Intrusive orogenic S-type granites are supposed to function as the heat source for the mineralizing fluids [2].

Motivation for the study is a renewed economic interest in those commodities and the intention to strengthen the mining industry and exploration in Rwanda. Eastern Rwandan deposits in particular require modern mineralogical and geochemical investigations which are lacking to date.

Both primary and secondary mineralizations do exist: a) Cassiterite-ferberite-quartz veins and b) mineralization in pegmatite represent the first type of mineralization while the second consists of alluvial and/or eluvial cassiterite, wolframite, 'coltan' and gold placers.

Fig. 1: W-Sn-Nb-Ta-Au deposit map of Rwanda (OGMR, 2006).

SEM-W/EDX analyses of ore minerals reveal Mn-Ta-Fe-bearing ferberite, Mn-Sn-W-Fe-bearing columbite-tantalite, Fe-Ti-W-bearing cassiterite, and F-rich biotite; therefore, in combination with the co-occurrence of tourmaline we infer pegmatitic to pneumatolytic conditions during mineral deposition.

[1] Dewaele, S. et al. (2007) in Colin, J. (ed.) *Biennial Meeting of the Society for Geology applied to mineral deposits Proceeding 2*. Dublin, Ireland, 1489-1492) [2] Pohl, W. (1988) *IGCP n 255 Newsletter/Bulletin*, **1**, 47-50.

Copper potential resources in ophiolites of Albania and new possibilities of their development

Onuzi, K.[*], Bakallbash, J., Deda, T. & Kaza, Gj.
Geosciences Institute, IGJEO, Tirana, Albania
([*]onuzikujtim@yahoo.com)

This contribution presents a brief description of Albanian copper mining and processing industry, in the past and the trends of its future development.

In the four main minerals of Albania, chromites, copper, iron-nickel and coal, the copper seizes the second important place. The copper ores started to be mined and processed before the Second World War in Mirdita Region (central north of Albania). Later on, this region became the most important centre of copper mining and processing industry. Through an extensive programmer of exploration carried out in the past, new copper-bearing areas were found and were put into operation, but some of them had been ineffective.

After the year of 1990, under the conditions of Free Market Economy, the reevaluations for every mine and deposit were carried out, trending so to put into operation only the effective mines and deposits. By this way, there already started closing the ineffective mines, restructuring the effective ones and planning to open new deposits, applying new technologies in drifting, mining and processing.

Besides others, this contribution aims to show to the domestic and particularly to the foreign investors the real copper potential of Albania and new possibilities to attract their investments.

Copper deposits are localized in the ophiolites of Albanides, mainly in the upper and middle part of their sequence. From the regional aspect, the most important region of their occurrence is that of Central Mirdita. Based on the the geological conditions of position in the sequence of ophiolites, morphology, mineral and substantial composition, genesis, etc., four types of copper deposits are distinguished: 1. Hydrothermal - metasomatic and volcano - sedimentary deposits (Munella, Qafe-Bari, Gurth, Rruga e Rinise); 2. Volcanogene - hydrothermal - metasomatic vein deposits (Tuc, Spac, Derven, Paluce); 3. Volcano - sedimentary deposits (Gjegjan, Palaj, Karme, Rubik); 4. Vein-massive metasomatic sulphide deposits (Kurbnesh, Golaj, Thirre, Nikoliq). The geological reserves of all Albanian copper deposits are about 53 million tones and mine able reserves are about 27 million tones.

The activity of mining in all regions of Albania is carried out through 6 enterprises, with about 20 mines, which are included in the Copper Corporation-Albbaker. Before 1990 in the copper industry, about 7000 employees have been employed, most of them in the mining sector. Annual production of the copper ore has been, for a period more than 10 years, about 1 to 1.2 million tones of a grade averagely 1,3 to 1,4% Cu Together with the copper was produced a small amount of pyrite ore. Mining methods used in the copper mines are generally those of sublevel caving, as high-productivity methods, but with losses about 20 % and dilution 18 %.

Based on existing situation of copper industry, the development of this branch is foreseen to be supported from reconstruction of the existing objects, in order to improve the technology, as well as the construction of new mines, beneficiation plants and smelters. It is indispensable, that the development of such industry must be orientated through the production of cathodes copper and the production of wire and cables of high quality, as well as their export in the world market. To realize such objective, it will be planned a general invested program which consists on the implementation of a technical-economical study based on the actual situation and foreseen investments.

Mineralogical and genetical study of primary hydrothermal siderite-quartz-sulphidic veins hosted by Tatric and Veporic unit (Western Carpathians, Slovakia)

Ozdín, D.
Dept. of Mineralogy and Petrology, Faculty of Natural Sciences, Comenius University, Bratislava, Slovak Republic
(ozdin@fns.uniba.sk)

Fe-carbonate-quartz-sulphidic mineralizations are the most abundant ones in Slovakian Carpathians, where occur in cca thousand localities. These veins occurs in the Tatric and Veporic Unit mainly in high metamorphic Palaeozoic rocks (gneisses) or in Permian sedimentary rocks (greywacke, arcose, conglomerate), in the Vysoké Tatry Mts. and Slovenské rudohorie Mts. are more frequently also in Palaeozoic granitoides. Hydrothermal veins form mainly carbonate lenses on mylonitized (cataclased) vein zones in crystalline basement. Their length is from some meters to 2.5 km (e. g. Vyšná Boca deposit), thickeness up to 6 m, mostly SW-NE to W-E direction and very steep slope toward S. Mineralizations form in sedimentary rock usually thin veinlets of sulphides with quartz or it is disseminated in rocks. More abundant are brecciated and cockarded (siderite, quartz), banded (barite), disseminated (sulphides) and drusy (minerals of Alpine-type veins) textures. Alteration processes represented only silicification and pyritization. Characteristic succession scheme for this type mineralization has 3 stages: 1. Fe-carbonates → 2. alpine paragenese → 3. quartz-sulphides. Predominant carbonates first stage are siderite/magnesite and carbonates dolomite-ankerite series. We can to observe space zonality in Slovakian occurrences from SE to NW: Mg-carbonates (almost chemical pure magnesite)→ Fe -Mg carbonates (transition members between magnesite and siderite and dolomite/ankerite)→ Fe -carbonates (predominantly siderite)→ Ca -carbonates (calcite, dolomite with low isomorphism Mg→Fe). On base leached of fluid inclusions formation temperature of siderite were 298 °C (Vyšná Boca) and 310 °C (Jedľové Kostoľany). An isotope study of siderite has provided the following data: ~$\delta^{18}O_{SMOW}$ +13-17‰ and $\delta^{13}C_{PDB}$ -3 to -5‰. Ankerite contains two-phased fluid inclusions (FI) (water solution of NaCl and vapour) with homogenization temperature (Th) from ~170 to 250°C and salinity 17-27 wt% $NaCl_{eq}$. Second stage is abundant mainly in Veporic Unit and at Pezinok in Malé Karpaty Mts. and Vysoké Tatry Mts. in Tatric unit. In this stage are following mineral assemblages: Aa. quartz-tourmaline-albite (two-phase FI in tourmaline: Th ~120-230°C, ice-melting temperature (Tm) -2 to -11°C, salinity 3-14 wt% $NaCl_{eq}$) with younger mineral assemblages Ab. chlorite (crystallization temperature on the base chlorite thermometry is 315-375°C) and Ac. muscovite (Ar/Ar ages of hydrothermal muscovite in J. Kostoľany gave 75.1 ± 1 and 75.4 ± 2 Ma); B. axinite-actinolite-calcite (FI in ferroaxinite: Th ~120-235°C, Tm -3 to -26°C, average of salinity (2 localities) ~18 wt% $NaCl_{eq}$); C. Apatite-REE phosphate (EMPA monazite dating: J. Kostoľany 83±9 Ma, Ľubietová 93±11 Ma); D. epidote-calcite; E. zeolites-calcite. Third stage have a few substages: Ni-Co-Fe-As → quartz → Cu-Fe sulphides→ Bi -sulfosalts. Ni-Co sulfoarsenides probably crystallized at the two different conditions – higher (300-550°C (?) and lower temperature (< 300°C). Two-phase fluid inclusions are very characteristic for quartz this stage (Th ~ 100-220°C, salinity 11-25 wt% $NaCl_{eq}$). On base presence of exsolutions in Bi sulphosalts (bismuthinite, pekoite, gladite etc.) these one crystallized at ~300°C. According to mineralogy, studies of fluid inclusions as well as stable isotopes is mineralization of Alpine age, minerals crystallized probably at prograde pT conditions (temperature mainly ~150-350°C) and fluids was formed various fluids at low ratio of fluid/rocks.

Mineralogical composition and mineral chemistry of supergene cobalt ores from eastern Cuba and Dominican Republic Ni-laterite deposits

Proenza, J.A.[1*], Roque, J.[2], Labrador, M.[1], Galí, S.[1], Tauler, E.[1], Gallardo, T.[1], Lewis, J.F.[3] & Longo, F.[4]
[1]Dept. de Cristal·lografia, Mineralogia i Dipòsits Minerals, Universitat de Barcelona, Barcelona, Spain
([*]japroenza@ub.edu)
[2]CEMES, Toulouse, France
[3]Dept. of Earth and Environmental Sciences, George Washington University, Washington, USA
[4]Falcondo XStrata Nickel, Santo Domingo, Dominican Republic

Cobalt is a strategic and critical metal used in many diverse industrial applications. The vast majority of identified world cobalt resources are in Ni-laterite deposits. In this contribution, new data on the mineralogical composition and mineral chemistry of cobalt ores from eastern Cuba (Moa Bay) and Dominican Republic (Falcondo) Ni-laterite deposits are reported. The samples were investigated using XRD, μXRD, μRAMAN, SEM, μXRF and EMPA.

In eastern Cuba Ni-laterites (oxide-type), the cobalt mineralization occurs in the limonite horizon, mainly in the lower part, as veins and coatings or concretions along fractures. At the hand sample scale the picture is a matrix of Fe-oxyhydroxides in which scattered bluish black aggregates corresponding to Co-Ni-Mn-oxyhydroxides are present. The cobalt ore consists mainly of lithiophorite [$(Al,Li)MnO_2(OH)_2$, with up to 13 wt.% Co], Al-rich asbolane [$(Co,Ni)_{1-y}(MnO_2)_{2-x}(OH)_{2-2y+2x}\cdot n(H_2O)$, with up to 7 wt.% Co, 14 wt.% Ni], lithiophorite-asbolane intermediate minerals (up to 10 wt.% Co), cryptomelane (< 2 wt.% Co), and minor heterogenite [CoO(OH)]. Our results suggest the existence of a continuous series between lithiophorite and asbolane.

In Dominican Republic Ni-laterites (hydrous silicate-type), the cobalt mineralization occurs at the upper part of the saprolite horizon, as veinlets, coatings along joints, and cracks developed by spheroidal weathering. At the microscopic scale, Co-bearing minerals replace pyroxene, olivine and serpentine along grain boundaries and fractures. The cobalt ore consists of heterogenite, Ni-rich asbolane (up to 5 wt. % Co, and 18 wt% Ni) and minor, lithiophorite-asbolane intermediate minerals (up to 4 wt.% Co) and cryptomelane. However, lithiophorite, a characteristic mineral in eastern Cuban Ni-laterite deposits, has not been detected. This absence of Al-rich phases is consistent with the Al-depleted composition of parent rocks in Dominican Republic deposits. In contrast, the abundant presence of lithiophorite in the Cuban deposits implies the availability of Al, consistent with the presence of plagioclase-bearing peridotites, and sills of gabbros, in the parent rocks from which the lateritic profiles were developed. In summary, the mineralogy of the Co-bearing ores depends on the composition of the parent rocks, and their depth within the laterite profile is probably related to the variation in Eh-pH.

Paleogeodynamic criteria of the presence of diamonds in the northern part of the European craton

Pystin, A.* & Pystina, Y.
Institute of Geology, Komi Science Centre, Ural Branch of RAS, Syktyvkar, Russia-Republic of Komi
(*pystin@geo.komisc.ru)

It is well known that, as a rule, diamondiferous kimberlites coexist with Early Precambrian cratones (Clifford's principle). However, these are non-uniformly distributed within the cratones. The lateral heterogeneous distribution of alkaline-ultrabasic magmatism and associated diamondiferousity over the cratones is stipulated by different causes. An assumption on connection of the heterogeneity with the location of Early Proterozoic junction zones of lithospheric plates has been made in the last few years.

According to O. G. Sorokhtin's opinion, the distance from an ancient subduction zone to the areas of productive magmatic manifestations to be expected is estimated as 390-660 km. It is taken into account that the speed of lithospheric plates movement in the Early Proterozoic was 5-6 times as large as a contemporary one, the maximum thickness of continental lithosphere reached 220 km, and the minimum depth of diamondiferous melts formation was at least 130 km.

On the ground of the above hypothesis, O. G. Sorokhtin and other researchers have explained the spatial distribution of alkaline-ultrabasic magmatism within the Archangelsk diamondiferous province.

Another Early Proterozoic paleosubduction zone has been established on the basis of investigations of the structural-material complexes in the Urals, Timan, and South-East Pritimanie. The zone is of the south-east orientation and south-west dip. The south-east fragment of the zone is exposed in the Subpolar Urals.

The territory including the Polyudov uplift in the Northern Urals (a region of diamonds present extraction from placers), the Timan, the Kanin Peninsula, and the South-western Pritimanie is prospective in respect to exploration of the diamondiferous alkaline-ultrabasic rocks connected with the zone mentioned. The territory can be treated as the Timan-Ural diamondiferous province.

Concentration technology for Devonian bauxites of Timan, Russia

Vakhrushev, A.V. & Kotova, O.B.*
Institute of Geology, Komi Scientific Center, Uralian Branch, RAS, Syktyvkar, Russia (*kotova@geo.komisc.ru)

Aluminum is the most widespread metal in the nature: its content in earth's crust reaches 8.8%. Due to its chemical activity it is not found free practically. It is widely used as constructional material, as reducer, for alloys etc.

The most important mineral of aluminum is bauxite, a mixture of basic oxide AlO(OH) and hydroxide $Al(OH)_3$. The largest bauxite deposits are located in Australia, Brazil, Guinea and Jamaica.

The probable reserves of Russian bauxites are assessed as more than 404 mln. tons (2% of the world reserves); they are related to P1 and P2 categories and distributed practically equally. The biggest part of the probable reserves (66%) is determined within Middle Timan and South Timan bauxite-bearing areas in Komi Republic.

The major reserves of Middle Timan bauxites are concentrated at the Vezhayu-Vorykva deposit. These bauxites are characterized by a high quality. About 80% of the ores suitable for Bayer processing, 20% are sintering ores.

At the deposit three types of ores are determined, which differ by their lithologic-mineralogic characteristics. The first type (77.7%) is hematite-boehmite, red bauxites. The Bayer ores make 85-90%. The second type (19%) is gematite-chamosite-boehmite, variegated bauxites. This type consists of sintering ores at 60%. The third type (3.3%) kaolinite-chamosite-boehmite, pelitomorphic bauxites (white and red). These are high-grade Bayer ores, low-developed.

The bauxites, recommended for concentration, form stony varieties. The soiled bauxites are generally high-modulus Bayer ores.

On the basis of the concentration, mineralogical and physical researches of Timan bauxites it is determined that the basic ore-forming minerals for Middle Timan bauxites are the following: boehmite, hematite, kaolinite and chamosite.

Various concentration methods are tested on the Middle Timan bauxites: dispersion, classification, annealing, magnetic separation, flotation. The results of these researches will be expressed in the report.

Ti-V oxide deposits in the Kunene anorthositic complex (SW Angola)

Villanova, C.[1*], Galí, S.[1], Torró, L.[1], Castillo, M.[1], Campeny, M.[1], Gonçalves, A.O.[2] & Melgarejo, J.C.[1]
[1]Dept. de Cristallografia, Mineralogia i Dipòsits Minerals, Universitat de Barcelona, Catalonia, Spain
([*]cvillanovadb@hotmail.com)
[2]Dpto. de Geologia, Universidade Agostinho Neto, Luanda, Angola

The Kunene Complex, outcropping between SW Angola and NW Namibia, is one of the biggest Proterozoic anorthositic complexes in the world [1]. It is cut by a set of Ti-Fe oxide dykes or lenticular bodies, which are hectometric to kilometric in length and metric to decametric in width.

The mineral associations of four oxide bodies have been studied: Dongue Sul, which presents a concentric structure with a nelsonitic core; the massive decametric ore bodies of Tchimbueio and Tchingunguanganda; and Chiange Velho, a kilometric dike, which may show millimetric foliations due to shear deformation.

The main mineral assemblage is composed by ulvöspinel, ilmenite and spinel (s.s.), in order of abundance (Fig. 1). These minerals coexist with apatite and minor graphite, phlogopite, and olivine. Most grains exhibit evidences of orthomagmatic textural equilibria in grain borders. The proportions of these minerals in the ore have been obtained by quantitative X-ray diffraction using the Rietveld fitting profile method. In average, they are: 60% Usp, 25% Ilm, 5% Spl, and 10% (Ap+Hem+Gt).

Ulvöspinel is rich in V (up to 0,15 wt%) and presents characteristic laminar or patchy micrometric double exsolutions of a Ti and Fe-richer phase and spinel (s.s.) lamellae. In ilmenite the geikielite component is 14-21 wt%, and does not contain exsolutions. Spinel is rich in the hercynite component (14-35 wt% Fe).

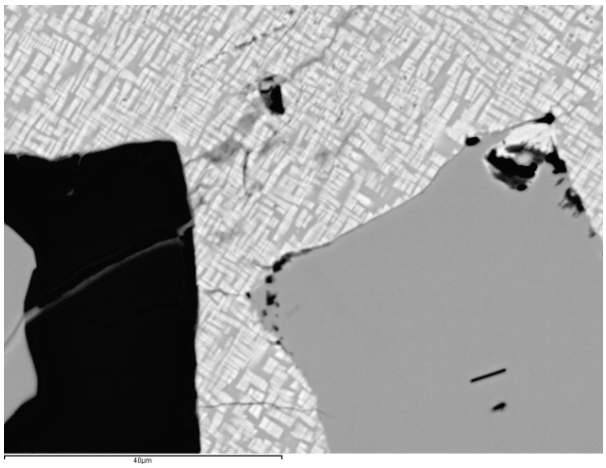

Fig. 1: Equilibrium texture between ulvöspinel (patchy texture), ilmenite (light grey), spinel (dark grey); exsolutions in ulvöspinel are clearly distinguishable. SEM-BSE Image. Field width: 100 µm.

Furthermore, when equilibrium can be assumed on the basis of textural and compositional evidences, the temperature of crystallization and the oxygen fugacity can be estimated using reported geothermobarometers [2,3]. For instance, in the case of Tchimbueio deposit, the temperatures obtained range from 973 to 1026 ºC, and the fO_2 from 10^{-12} to 10^{-10}.

[1] Ashwal, L.D. & Twist, D. (1994) *Geol. Mag*., **131(5)**, 579-591. [2] Spencer, K.J. & Lindsley, D.H. (1981) *Am. Mineral*., **66**, 1189-1201. [3] Andersen, D.J. & Lindsley, D.H. (1985) *Am. Geoph. Union*, **66(18)**, 416.

Geology and geochronology of magmatic centers in the Urumieh-Dokhtar Arc, Iran

Zarasvandi, A.
Dept. of Geology, Faculty of Sciences, Shahid Chamran University, Ahvaz, Iran (zarasvandi_a@scu.ac.ir)

The relationship among of basement lineaments, volcano-plutonic suites have been studied in three parts of the Urumieh-Dokhtar magmatic arc, using by satellite images, geological and geochronological data. This magmatic arc is result of closure of the Neo-Tethys Ocean and the collision of the Iranian and Afro-Arabian plates. Almost all of the Eocene to Miocene granitoids subduction-related is located in the north western and central-south eastern parts of the Urumieh-Dokhtar belt. Volcanic and plutonic domains in several parts of the Urumieh-Dokhtar belt are separated by N-S and NW-SE trending reactivated faults and lineaments. These features are very important for distribution of granitoid magmatism. In this study, three areas selected for detailed investigation: Shahr-e-Babak, Sungun and Khezr-Abad area (Fig. 1). These areas have semi-arid type of climate with many outcrops that makes them suitable for application of remote sensing technique.

Geological, structural and location of magmatism centers were extracted from Landsat TM and IRS images and geological information. Based on these images and maps, location of volcanoes and magmatic centers can be related to structural framework of these areas, and are shown to occur near the intersections of strike-slip faults and pull apart structures. K/Ar whole rock geochronology of felsic to intermediate igneous rocks suggested that the granites are Oligocene (~28 Ma) in age, whereas the intermediate plutons are Miocene. This periods and situations are the best developed in the Urumieh-Dokhtar magmatic arc for pooling of large volumes of granitoid magmatism and several important mineralization provinces.

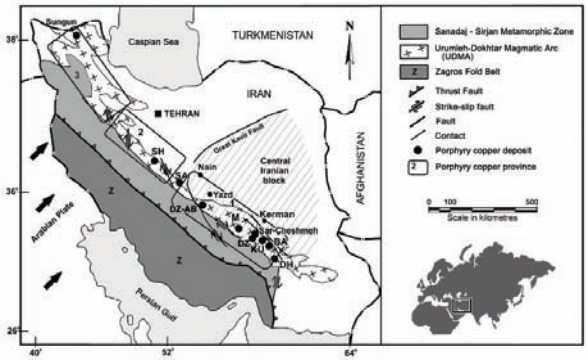

Fig. 1: Main tectonic zones of Iran and geographical position of selected studied areas.

[1] Zarasvandi, A. et al. (2005) *Int. Geol. Rev.*, **47**, 620-646.

Gold-bearing ore occurrence of Karasay, Uzbekistan: mineral-geochemical characteristics of ores

Zavarzina, M.S.[*] & Jukov, A.V.
Dept. of Mineralogy and Geochemistry, Faculty of Geology,
National University of Uzbekistan, Tashkent, Uzbekistan
([*]mzavarzina@yahoo.com)

The Karasay gold-bearing ore occurrence is located in the eastern Uzbekistan, in the north-western part of Kuraminsky mountain ridge, in Apantepa-Karatagatinsky area.

The Karasay gold-bearing occurrence is hosted by lower Devonian (D_1) quartz porphyries, which are intruded by Carboniferous to Permian sub-volcanic granodiorite-porphyries (C_3-P_1) as well as dykes of diabase porphyries. Faults in the ore occurrence have trends of differing orientation including north-eastern and north-western strike.

To study the mineral-geochemical characteristics of Karasay gold-bearing ore occurrences, samples were selected from adit and open pit.

Analysis of ore mineral composition (Jeol Superprobe 8800R) identified three main gold-bearing associations. A wall rock ore quartz-carbonate-sericite-pyrite association, was not analysed.

The first association is quartz-gold-pyrite, mainly low sulfide, with disseminations of pyrite and fine-dispersed gold.

Dark grey quartz has increased concentrations of Mo due to the presence of amorphous of molybdenite – jordisite. A $PbMoS_2$ phase is also present. Arsenopyrite was also found.

The second productive association is quartz-gold-polymetallic. It is developed as massive nests of sulfide ores or as dispersion in the first association. Main minerals are galena, sphalerite, pyrite, chalcopyrite, tetrahedrite and tennantite. Native gold has a fineness ranging from 600 to 850. The following tellurides were found: hessite, petzite and altaite.

The third hypergene association contains secondary minerals of Fe, Pb, Zn and sulfides of copper. Of note it is a secondary mineral form of molybdenum – wulfenite ($PbMoO_4$). Gold in this association has very high fineness from 900 up to almost 1000. Its variance from pure Au is due to a rare admixture of copper.

In 13 whole-rock ore samples analyzed by ICP-MS, gold content varies from 0.21 to 35.6 ppm, and silver content varies from 1.17 to 223.58 ppm.

The ratio of Au:Ag varies from 1:21.7 up to 3.2:1, though ratio of more than 1 is peculiar to high gold-bearing ores.

In the cases of sulphide-rich ores, increased concentration of Pb, Zn, Cu, As, Sb is usual. A distinctive feature of ores in the Karasay ore occurrence is a high concentration of molybdenum (0.01-0.1%). Among other noticeable admixtures Se, Te, Re, Tl, Hg, Cd, as well as Pd and Rh are noted.

Ores are distinguished by the content of non-ore oxides. Silica varies from 60 to 80%, Al_2O_3 from 6 to 19%. MgO and CaO content do not exceed 1% in average. Increased concentration of K_2O from 1.5 to 7%, Na_2O is not more than 0.5%. According to technological tests ores can be used as fluxstones

Main gold-bearing associations in the Karasay ore occurrence are hypergene and quartz-gold-polymetallic types.

After the examination of geochemical characteristics of Karasay ore occurrence, it is possible to conclude that they are complex, significantly multimetallic with high concentration of Mo, Re, As, Sb, Se, Te, Pb, Zn, Cu. Ore occurrences is an upper part of gold mineralization.

Genesis of sediment-hosted Au-As deposits: a two-stage process of early syngenetic gold followed by later epigenetic upgrading

Large, R.R.
CODES, School of Earth Sciences, University of Tasmania, Hobart, Australia (ross.large@utas.edu.au)

Currently accepted ore genesis models for orogenic and Carlin-style deposits assume that gold is sourced from deep below the deposits, in the lower crust or mantle, and transported upwards, along major crustal fractures or shear zones, during metamorphism and deformation, to become concentrated in second order structures during the peak, or post-peak, of metamorphism. Recent evidence, based on the textural and chemical association of both gold and arsenic in pyrite in certain sedimentary rock facies, supports a two-stage process of gold ore genesis for some gold provinces, with the gold sourced from organic-bearing shales in the basin.

The first gold stage involves pre-concentration of gold and arsenic in black mudstone facies of continental margin sedimentary basins. In the sediments, the gold is present as either invisible gold trapped in diagenetic arsenian pyrite or micro-nuggets (< 5 microns) of free gold associated with fine-grained clays and organic matter. These gold-bearing sediments are also enriched in a characteristic suite of elements, particularly V, As, Mo, Se (Te), Ni, Ag and Zn, giving rise to the term VAMSNAZ sediments. Gold contents of the VAMSNAZ sediments commonly range from 5 to 100 ppb, arsenic from 10 to 100 ppm, and organic carbon from 0.2 to 2 wt %.

The second stage, of the two-stage process, occurs during late diagenesis and metamorphism of the sediments, associated with deformation, basin inversion and/or granite intrusion. Gold and arsenic are released from the arsenian pyrite and from clay-organic matter intergrowths, associated with diagenetic and low grade metamorphic reactions in the VAMSNAZ sediments. Conversion of gold-bearing diagenetic arsenian pyrite to pyrrhotite at higher grades of metamorphism (lower-greenschist to upper-greenschist facies) is a particularly effective way of releasing gold to the metamorphic fluid. The H_2S-CO_2-CH_4-bearing metamorphic fluid (probably a mixture of seawater, meteoric water and diagenetic fluid trapped in the sediments), transports the gold and arsenic, through the permeable silt and sand facies sedimentary rocks, to become concentrated in zones of intense fluid flow and related pressure release, such as anticlinal fold axes, shear zones or dilatant quartz-vein reefs or stock-work zones.

This two-stage model is the first to account for the ubiquitous association of gold and arsenic in sediment-hosted orogenic and Carlin style deposits.

Geochemistry and genesis of Guqiong Ag-Au polymetallic deposit in Southern Tibet, China

Wei Huixiao[1], Sun XiaoMing[2,1,3*], Zhai Wei[2,3], Yi Jianzhou[4] & Zhou Feng[1]
[1]Dept. of Earth Sciences, Sun Yat-sen University, Guangzhou, China
[2]School of Marine Sciences, Sun Yat-sen University, Guangzhou, China ([*]eessxm@mail.sysu.edu.cn)
[3]Guangdong Provincial Key Laboratory of Marine Resources and Coastal Engineering, Guangzhou, China
[4]Geological Survey of Tibet Bureau of Geology and Mineral Exploration and Development, Lhasa, China

The Himalayan orogen is increasingly considered a remarkable orogenic gold metallogenic province [1]. The Guqiong Ag-Au polymetallic deposit (altitude ~5200 to 5500 m; total resource ~Ag 173t @ 272.2g/t, Au 4t @ 6.07 g/t, Pb 9938t @ 1.98% & Zn 8212t @ 1.39%) is a significant discovery which was found recently to the south of the east section of the Yarlung Zangbo tectonic suture zone in southern Tibet. A preliminary study on the genesis of the Guqiong deposit further indicates great prospecting potential in the southern Tibetan detachment system (STDS).

Rocks in the area are mostly made up of Triassic to Cretaceous low-grade metamorphic, intensely folded clastic sedimentary rocks. Magmatic activities in this district comprise few Jurassic andesite bodies and voluminous Cretaceous intrusive rocks. The main host rock for the mineralization at Guqiong is altered Cretaceous diabase. Ag-Au-Pb-Zn occurs principally within quartz-sulphide veins developed in the tectonic fracture zone. Ore minerals include electrum, silver-bearing tetrahedrite, pyrite, galena, sphalerite and arsenopyrite, etc. The main alterations include sulfidation, sericitization, and carbonatization.

Analysis of ore stage fluid inclusions from the Guqiong deposit indicate high content of CO_2, low to moderate temperatures (184.3~338.1°C), low salinities (4.2~6.2 wt% NaCl *eq.*) and shallow depth (0.1~1.6 km) for ore deposition. Measured $\delta^{18}O$ values for the ore-bearing quartz from Guqiong deposit range between 19.0 and 20.7 per mil; the estimated $\delta^{18}O$ fluid values range from 8.6 to 12.5 per mil, suggesting a mainly crust-derived fluid, which is similar to the typical orogenic gold deposits [2] and two proved orogenic gold deposits in southern Tibet (Mayum [1] & Bangbu [3]). A broad range of measured δD fluid values, between –172.3 and –113.9 per mil, is suggestive of a contribution from devolatilization of organic matter from the sedimentary rocks and/or minor amounts of mixing with geothermal fluids, which accord with the rock types in the area and the shallow formation depth of the Guqiong deposit.

From the above, general features of Guqiong deposit are basically consistent with orogenic gold deposits [1-3]. The ore-forming elements were deposited in the shallow part of the tectonic fracture zone, which was dominated by orogenic system. Further study on geological characteristics and genesis of Guqiong deposit would enrich the metallogenesis theory of the Himalayan orogen.

Acknowledgements: This study was financially supported by the National Basic Research Program (No.2009CB421006, 2002CB412610) from the Ministry of Science and Technology, China, and the National Natural Science Foundation of China (No. 40830425, 40873034, 40673045).

[1] Jiang, S.H. et al. (2009) *Ore Geol. Rev.*, **36**, 160-173. [2] Goldfarb, R.J. et al. (2004) *Econ. Geol.*, **99(4)**, 643-671. [3] Wei, H.X. et al. (2010) *Acta Petrol. Sinica* (in press).

The gold-silver-tellurium mineralogy of the polymetallic Shahumyan deposit, Armenia: gold scavenged by tellurium-rich melts?

Mederer, J.* & Moritz, R.
Dept. of Mineralogy, Section of Earth and Environmental Sciences, University of Geneva, Switzerland
(*johannes.mederer@unige.ch)

The polymetallic Cu-Au-Ag-Zn±Pb Shahumyan deposit in the Lesser Caucasus of southeastern Armenia is hosted within Middle Jurassic subvolcanic quartz-dacite with a calc-alkaline signature. Pyrite, chalcopyrite, sphalerite, tennantite and galena are the main ore minerals of the more than 100 east-west striking and steeply dipping veins. Pyrite rarely contains up to 40 µm-sized inclusions of digenite, bornite, chalcocite and enargite. Quartz, carbonates (including kutnohorite) and sporadic hydrothermal apatite are the main gangue minerals.

Gold and silver distribution in Shahumyan is controlled by different Au-Ag-tellurides, including krennerite ($AuTe_2$), sylvanite ($AuAgTe_4$), petzite (Ag_3AuTe_2) and hessite (Ag_2Te). Native gold is a minor phase, altaite (PbTe) and native Tellurium are subsidiary phases. The telluride assemblages occur as droplet-shaped inclusions in pyrite, along grain boundaries between sulfide minerals, as elongated aggregates along healed microcracks in sulfides or associated with the carbonate and quartz gangue, as in Fig. 1, in which droplet-shaped tellurides are hosted by hydrothermal quartz in close proximity to an assemblage of krennerite and altaite. Most of the observed telluride occurrences consist of at least 2 different phases (e.g. petzite-hessite-altaite).

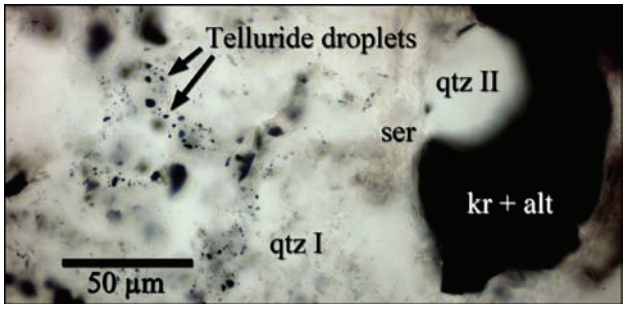

Fig. 1: Droplet-shaped tellurides within quartz (qtz) and sericite (ser) in the vicinity of a composite krennerite (kr) and altaite (alt) association.

The crystallization of tellurides from precipitates extracted from fluids as a liquid (melt) was proposed in earlier studies for the genesis of some telluride deposits, such as at Săcărîmb, Romania [1]. Thermodynamic modelling of Au-Te melt segregation from hydrothermal fluids [2] shows the potential for Au scavenging of such a melt, even from Au-undersaturated fluids. Textural relationships in the Shahumyan deposit, like droplet-shaped inclusions of tellurides in pyrite or quartz and the observation of composites commonly constituted by at least two main phases are interpreted as separation of a complex Au-Te rich melt from hydrothermal fluids at temperatures above the solvus curve/melting point of the composite, poly-component precipitate as a whole, but below the melting point of individual phases.

[1] Ciobanu, C.L. et al. (2004) in Cook, N.J. & Ciobanu, C.L. (eds.) *Au-Ag-telluride Deposits of the Golden Quadrilateral, Apuseni Mts., Romania.* IAGOD Guidebook Series, **12,** 145-186. [2] Wagner, T. (2007) in Andrew C.J. et al. (eds.) *Mineral exploration and research: Digging deeper*, Proc. 9th biennial SGA meeting, Dublin, 769-772.

Geochemical characteristics and evolution of the mineralizing fluids within the Eastern Rhodopian sedimentary rock-hosted low-sulphidation epithermal gold systems, Bulgaria

Márton, I.* & Moritz, R.
Dept. of Mineralogy, Section of the Earth and Environmental Sciences, University of Geneva, Switzerland
(*Istvan.Marton@unige.ch)

A useful understanding of the origin of epithermal gold mineralization requires accurate knowledge about the source and interaction of four important components: heat, fluids, ligands and metals. The geochemical investigation and modelling is an important tool for understanding ore genesis and the interaction of these components. The ore fluids that formed fossil hydrothermal systems are difficult to study due to a number of assumptions about the ore fluid(s) that must be made, but which can be characterized by fluid inclusion analysis, by ore mineral assemblages and by alteration minerals. However, these do not necessarily define the original ore fluid but rather one, which had already interacted to an unknown extent with the host rocks.

The main purpose of this contribution is to characterize the mechanism of transport and deposition of associated gold and sulphides, which are the main ore components in sedimentary rock-hosted gold deposits from the Tertiary Eastern Rhodopes, Bulgaria. This contribution presents new major and trace element compositions, stable isotope and fluid inclusion data on these gold deposits. Emphasis is placed on comparison of ore textures, mineralogy and geochemical data from different occurrences. The likely source of the mineralizing fluids and their evolution during the gold depositional processes is discussed and modelled based on new geochemical data.

The geochemical results show, that a single ore fluid from different sources and various precipitation processes might be responsible for the range of ore types identified in the sedimentary rock-hosted gold deposits from the Eastern Rhodopes.

Abundant bladed quartz pseudomorphs replacing platy calcite suggest boiling in several prospects (Ada Tepe, Kuklitsa and Kupel), a process which is typical in case of low-sulphidation epithermal deposits. The chemical changes of the fluid during boiling included a raise in pH caused by preferential partitioning of volatiles into the steam phase, and an increase in concentration of non-volatile constituents in the liquid phase as the result of steam separation. These factors promoted super saturation, which resulted in sudden silica, adularia, sulphides and electrum precipitation.

By contrast, at other prospects, such as Rosino, Surnak, Kremenitz and Skalak, boiling textures are scarce to absent, and intense fluid-rock interaction may be responsible for gold mineralization. In such a case, gold deposition was controlled by cooling of a sulphide-rich fluid, change in oxidation state and mass transfer accompanied by sulphidation of iron present in the host rocks, as modelled for the Carlin-type gold deposits. The geochemical characteristics of the ore assemblages and the mass transfer studies show that gold might have been transported and deposited with other elements, and the thermodynamic conditions during ore precipitation can be modelled by phase relationships of the Fe-Au-As-Sb-Hg-Ag-S-O-H-Cl system. It is concluded that decline in temperature (at constant oxygen fugacity) lead to a reduction in solubility of all elements. Changes in oxidation state, accompanied by H_2S-loss during sulphidation of host rock iron, had the greatest effect on gold and arsenic solubility. As changes in arsenic mineral stability and solubility are so sensitive to the oxidation state of the system, arsenic minerals are likely an important indicator of redox conditions during the formation of sedimentary rock-hosted gold deposits in the Eastern Rhodopes.

Gold deposits along the Tethys belt: products of diverse tectonic and magmatic settings

Moritz, R.
Dept. of Mineralogy, Section of the Earth and Environmental Sciences, University of Geneva, Switzerland (robert.moritz@unige.ch)

The Tethyan orogenic belt is the result of a complex evolution, with several successive and locally overprinting subduction, collision, magmatic, and extensional events, as a consequence of convergence between the African, Arabian and Eurasian plates. Favourable conditions for gold ore deposit formation were generated in the different magmatic and tectonic settings throughout the evolution of the Tethys belt.

Tethyan gold deposits were mostly formed during three major tectonic and magmatic stages, including: (1) Jurassic-Late Cretaceous subduction extending from Romania to Iran; (2) Paleogene, calc-alkaline to shoshonitic magmatism, related to post-collisional (southeastern Europe, Armenia) and to subduction/collisional settings (northeastern Turkey-western Georgia, Iran); and (3) discontinuous Neogene magmatism, mostly related to extensional tectonics (Carpathians, Aegean Sea, Lesser Caucasus, Iran). The economically most important types of gold deposits include: epithermal, porphyry copper, and volcanogenic massive sulphide (VMS) deposits.

The metallogenic picture is still fragmentary, however several distinct patterns start to be recognized along the belt. Typically, gold deposits were formed during discrete or relatively short durations within a given tectono-magmatic zone. For instance, in the Andean-type, Late Cretaceous Timok-Srednegorie belt, major and economically important world-class high-sulphidation systems, such as Chelopech, Bulgaria, and Bor, Serbia, and associated porphyry copper deposits were emplaced within a short time span, during the early geological evolution of each tectonic zone, whereas the subsequent, younger magmatic activity produced economically less significant deposits. In the Eastern Rhodopes, characterized by Late Eocene-Oligocene post-collisional magmatism and extension, argon dating reveals that formation of the ~32 Ma old volcanic rock-hosted (e.g. Madjarovo, Sappes) and ~37.5-34.5 Ma old detachment-related sedimentary rock-hosted epithermal systems (e.g. Ada tepe) coincided with the onset of major tectonic plate reorganization in the Aegean Sea, as a consequence of African and Eurasian plate collision along the Caucasus and the Rif-Betic belts at about 35 Ma.

The Cenozoic evolution of the Tethys belt is dominated by post-collisional, orogenic collapse tectonics, in which slab detachment is interpreted as one of the key players during the geologic evolution in several gold deposit localities (e.g. Carpathians, Lesser Caucasus, Iranian Sanandaj-Sirjan zone). Slab break-off resulted in astenospheric upwelling, extension, exhumation of deep crustal rocks and a compressed geothermal gradient providing favourable settings for extensive fluid circulation, magma ascent and gold ore deposit formation.

Fluids and metals are of predominantly magmatic origin in many of the gold deposits, with variable meteoric contributions, in particular in the younger Cenozoic extensional settings. Seawater associated with gold-rich VMS deposits in the Turkish Eastern Pontides and the Bolnisi district, Georgia, is also recognized in some high-sulphidation systems, such as Chelopech, possibly recording emerging island arc-type environments during the Late Cretaceous. A magmatic-metamorphic fluid controversy exists for some gold deposits, like the ones hosted by metamorphic rock complexes in the Iranian Sanandaj-Sirjan zone interpreted by some authors as orogenic deposits, although argon dating indicates that gold ore formation coincided with Eocene extension, magmatism and basement metamorphic rock exhumation.

New Lu-Hf and U-Pb data for detrital zircon from the Eldorado Reef (upper Central Rand Group, South Africa)

Koglin, N.[1*], Zeh, A.[1,2] & Frimmel, H.E.[1]
[1]Geodynamics and Geomaterials Research Division, University of Würzburg, Germany ([*]nikola.koglin@uni-wuerzburg.de)
[2]Division of Geochemistry, Hydrogeology and Mineralogy, Freie Universität, Berlin, Germany

In order to constrain the source of the detrital components in the gold-rich conglomerates („reefs") of the Mesoarchaean Witwatersrand Supergroup, we analysed zircon grains from the approximately 2.8 Ga Eldorado Reef in the upper Central Rand Group. That reef represents alluvial fans that developed when syn-depositional folding and thrusting affected the western margin of the Central Rand foreland basin and led to intense re-working of older Witwatersrand strata.

The analysed zircon grains are of magmatic origin and mostly yielded Mesoarchaean U-Pb ages clustering at about 2940 and 3060 Ma, and minor Palaeoarchaean ages at 3285 and 3440 Ma. The initial εHf of the Mesoarchaean zircon populations is mostly super-chondritic and varies from -1.6 to +5.6, whereas the Paleoarcheaen zircons are roughly chondritic with εHf(t) ranging from -1.3 to +2.0. These data, in particular the abundant zircon grains with super-chondritic εHf(t) values, provide evidence for magmatic rocks from a depleted mantle source in the direct hinterland of the Central Rand Basin at 3060 and 2940 Ma. In agreement with geochemical and isotopic studies on calc-alkaline intrusive rocks of the same age in the immediate vicinity of the Central Rand Basin [1], a magmatic arc along the northern margin of the Witwatersrand Block is suggested as provenance at 3060 Ma. The 2940 Ma detrital zircon fraction was derived more likely from juvenile magmatic rocks in a volcanic arc setting related to subduction processes immediately prior to collision between the Witwatersrand Block and the Kimberley Block to the west. A possible source is the Kraaipan greenstone belt that occurs to the west of the Central Rand Basin. The lack of zircon grains younger than 2860 Ma in the Eldorado Reef can be explained by the development of a foreland fold-and-thrust belt that acted as a barrier between the upper Central Rand Basin and the internal zone of the Kraaipan greenstone orogenic belt, which contains abundant granite bodies with ages as young as 2.7 Ga. The Palaeoarchaean zircon grains (~3285 and ~3440 Ma) were derived from felsic intrusive rocks that formed by partial melting of even older continental crust. Sources for these zircons may be the Barberton greenstone belt and/or the Limpopo Belt.

Our data are in good agreement with the results of some previous U-Pb zircon studies across the Witwatersrand basin [2,3], which show a good correlation between detrital zircon age spectra and the grain size fraction of the sediment detritus, and thus a systematic difference between proximal and distal sources. Zircon grains from the arenitic fraction, thus reflecting a more distal source, in both the footwall and hangingwall of individual reefs show a wide range of ages. In contrast, zircon grains in the gold-bearing conglomerates, coming from more proximal sources, show a more restricted age distribution with a dominance of ages at around 3060 and 2940 Ma.

[1] Frimmel, H.E. et al. (2009) *J. Petrol.*, **50**, 2187-2220. [2] Kositcin, N. & Krapez, B. (2004). *Precambrian Res.*, **129**, 141-168. [3] Ruiz, J. et al. (2006) *Geochim. Cosmochim. Ac*, **70**, A543.

Constraining the source of the Witwatersrand gold

Frimmel, H.E.[1,2*], Depiné, M.[1], Koglin, N.[1], Emsbo, P.[3], Koenig, A.E.[3] & Minter, W.E.L.[2]
[1]Geodynamics & Geomaterials Research Division, University of Würzburg, Germany ([*]hartwig.frimmel@uni-wuerzburg.de)
[2]Dept. of Geological Sciences, University of Cape Town, Rondebosch, South Africa
[3]US Geol. Survey, Denver, CO, USA

The Witwatersrand "Basin" in the Archaean Kaapvaal Craton, South Africa, is the world's largest known gold anomaly, constituting c. 40 % of all gold that has ever been mined or is known as reserves and resources. A hydrothermally modified palaeoplacer model has been favoured by most workers over the past years to explain the high Au grades in the auriferous conglomerates most of which were deposited between 2.90 and 2.78 Ga in the Central Rand foreland basin. The source for this exceptional amount of detrital gold (in total >90,000 t) remains enigmatic. Previous studies revealed unusually high Os concentrations in the Witwatersand gold [1], which led to the suggestion that the gold was derived from a magmatic-hydrothermal source without constraining this source any further [2].

In this study we present lithogeochemical data on Witwatersrand shale units to describe the overall lithology of the source area(s) as well as data on rock fragments from Au-rich polymictic conglomerate beds, summarize important characteristics of the immediate basement rocks next to the margin of the former Central Rand Basin, and present trace element data on critical minerals of the ore assemblage, i.e. pyrite and uraninite. The results obtained, in combination with a geochronological provenance study based on detrital zircon grains, make it possible to characterize the likely setting of the primary magmatic-hydrothermal gold mineralization in the source area.

Even the fine-grained sediments now present in metapelitic units that can be correlated across the entire Witwatersrand "Basin" show distinct chemical differences depending on their position within the basin, i.e. they reflect regionally different provenances. The provenance as derived from shale geochemistry and heavy mineral populations conforms to that of a granite-greenstone terrane as presently exposed in a number of belts all over the Kaapvaal Craton. The detrital zircon age spectra in the non-mineralized arenitic fraction are complex and conform to the wide variety of Palaeo- to Neoarchaean zircon ages from the surrounding granite-greenstone belts, whereas those in mineralized conglomerates, reflecting more proximal sources, show a distinct peak at around 3060 Ma – in agreement with the available Re-Os age for the gold and associated detrital pyrite grains [1]. Basement rocks of equivalent age in the proximal hinterland are granite/granodiorite and gabbro as well as their volcanic equivalents. They have calc-alkaline composition and isotopically reflect a combination of juvenile and re-cycled older crust. The style of late- to post-magmatic alteration in these rocks is comparable to that around IOCG deposits. Equivalent rocks are found as volcanic clasts in the auriferous conglomerates. Unexpected high Au contents in detrital uraninite point to a relationship between Au-enrichment and U-mineralization in the source region for which a magmatic arc setting is suggested.

[1] Kirk, J. et al. (2002) *Science*, **297,** 1856-1858. [2] Frimmel, H.E. et al. (2005) in Hedenquist, J.W. et al. (eds.) *Economic Geology One Hundredth Anniversary Volume*. Soc. Econ. Geol., Littleton, 769-797.

Crustal fluids formed world class gold deposits in different metallogenic provinces of Russia

Bortnikov, N.S. & Prokofyev, V.Yu.[*]
IGEM RAS, Moscow, Russian Federation
([*]vpr2004@rambler.ru)

Composition of mineral-forming fluids is a critical parameter for an identification of genesis of a mineral deposit. One may be expected that gold deposits within the same metallogenic province were formed from a similar fluid at similar physical and chemical conditions. Fluid inclusions were studied in quartz from 10 world class (productions+reserves more 100 t Au) and several ordinary gold deposits located in Lena (PR), Sayan-Yenisei (PR), Urals (Pz), Verkhoyansk (Mz), Kolyma (Mz), Okhotsk-Chukotka volcano-plutonic belt (Mz) and Eastern Transbaikalian (Mz). Deposits under consideration are Sukhoi Log, Olimpiada, Sarylakh, Sentachan, Nezhdaninskoye, Maiskoye, Natalkinskoye, Berezovskoye, Kochkarskoye, Darasun. Some of them are located in the metasedimentary sequence, while others are intrusion-hosted deposits. Four main types of fluid inclusions are recognized in quartz at room temperature in orogenic (mesothermal) deposits from Lena (PR), Sayan-Yenisei (PR), Urals (Pz), Verkhoyansk (Mz), Kolyma province: (1) two-phase aqueous inclusions, containing liquid and vapor; (2) type II, two- or three-phase, $(H_2O)L + (CO_2)V$ or $L + (CH_4)V$ or L fluid inclusions, including IIa, H_2O-CO_2-inclusions; (3) type III, vapour-rich inclusions, rarely with small liquid rims or meniscus, including IIIa, $(CO_2)V + (CO_2)L$, and IIIb $(CO_2)V + N_2 + NH_4$; and (4) type IV, multi-phase inclusions containing $(H_2O)L$-$(H_2O)V$, and solid-daughter mineral identifying as halite on the basis of habit and optical characteristics. The data obtained indicate that the commercial ore bodies in orogenic (mesothermal) deposits studied were deposited from the $H_2O+CO+NaCl\pm CH_4\pm N_2$ fluid with low- to moderate salinity. A mineral formation occurred at 100 to 450°C and 1 to 3 kbars. Dilute aqueous fluids recorded in the late gold-sulphosalts-bearing veins. Such a fluid regime is typical for orogenic gold deposits.

Compositionally contrasting fluids are responsiple for a formation of gold deposits in the the Darasun district (Transbaikalian). Brines with salinity 56.3–29.9 wt% NaCl-equiv. formed early metasomatites. Auriferous quartz -base metal-sulphosalt veins crystallized from aqueous fluids with salinity 22.2–0.4 wt% NaCl-equiv. Such fluids are characteristic for porphyry or "intrusion related" deposits.

Dilute aqueous fluids with salinity of 9.2–0.4 wt% NaCl-equiv. formed epithermal gold deposits within Okhotsk–Chukotka volcanic belt and Transbaykalia.

Acknowledgements: This work was carried out within the framework of the UNESCO-IGCP project 540 "Gold-bearing hydrothermal fluids of orogenic deposits" and the Russian RFBR (projects № 09-05-00697a and 09-05-12037ofi_m).

Gold in sedimentary basins: role of reduced basinal brines and hydrocarbons

Emsbo, P.[*] & Johnson, C.A.
U.S. Geologic Survey, Denver, CO, USA ([*]pemsbo@usgs.gov)

Epicontinental sedimentary rift basins host some of the world's largest gold deposits. It is increasingly clear that many of these basins contain synsedimentary gold enrichments that, in some cases, reach ore grade. While the metallogenic relationship between enrichments and subsequent epigenetic gold mineralization is an important question, the objective of this presentation is to explore processes resulting in primary gold enrichments. Our ongoing studies of synsedimentary gold occurrences, combined with chemical modelling and new laboratory experiments, have identified several pathways for gold transport in basinal environments.

Gold-rich sedex mineralization in Nevada, with Au as high as 70 g/t, and the occurrence of significant amounts of gold in classic sedex deposits like Rammelsberg (30 mt at 1 g/t) and Anvil (120 mt at 0.7 g/t) demonstrate that basin brines can form gold ore. Studies of ore deposits, modern brines, and chemical modelling indicates that variation in gold content is controlled by the concentration and redox state of sulfur in brine. For example, Au and Ba solubilities are highest in H_2S-rich, SO_4-poor fluids, whereas base metal solubilities are highest when H_2S is absent. The varying solubility of base metals, barite, and gold may explain a range of sedex deposits from very large Pb-Zn-Ag, intermediate size Pb-Zn-Ag-Ba±Au, to low base metal-high barite and/or Au deposits. This spectrum is believed to reflect the concentration and redox state of sulfur in the ore forming brine, which is ultimately controlled by the lithology and redox buffering capacity of basin fill sediments in the metal source regions. The lithology of basin fill is an important component of our model and has significant implications for deposit formation, metal endowment, and prospectivity of sedimentary basins.

A variety of basin hosted gold deposits are characterized by a distinct metal signature that includes V-Ni-Mo-PGE-U-Hg-Se-As. Vastly different, and sometimes contrasting, solubilities of these metals are incompatible with their transport in reducing H_2S-rich brines. Our work suggests that petroleum may transport these metals. Our analyses of bitumen in ore deposits, analyses of metals in modern petroleum, and experimental work demonstrate that petroleum uniquely explains this geochemical signature. Our experiments demonstrate that Au and other metals are significantly more soluble in petroleum then in traditional aqueous fluids and that the metals can be incorporated into oils through several pathways. As demonstrated in locally derived bitumen within the Rodeo deposit and through our hydrous pyrolysis experiments, metals are efficiently stripped from source rocks and partitioned into organometallic complexes in oils during primary catagenesis. We have also demonstrated that petroleum is remarkably efficient at scavenging metals from rocks and aqueous fluids that are encountered during secondary migration. Our interpretations are supported by analyses of petroleum by us and others, which document high concentrations of metals. In fact, mass balance estimates show that the metal content of some large petroleum systems far exceeds the metal content of conventional ore deposits. Our observations demonstrate a new environment and mechanism of metal transport with significant implications for the metallogenic evolution of sedimentary basins. Incorporation of the well-understood processes of petroleum generation and migration may enhance gold exploration efforts and provide new potential exploration targets in sedimentary basins.

The physical-chemical properties of Au-bearing hydrothermal fluids from orogenic and intrusion-related deposits based on a record of multi-technique, fluid inclusion analytical data

Garofalo, P.S.[1*], Fricker, M.[2], Günther, D.[2], Bersani, D.[3], Ridley, J.R.[4], Gibson, J.L.[4] & Prokofiev, V.Y.[5]
[1]Dept. of Earth and Environmental Sciences, University of Bologna, Italy ([*]paolo.garofalo@unibo.it)
[2]Dept. of Chemistry and Applied Biosciences, ETH Zurich, Switzerland
[3]Dept. of Physics, University of Parma, Italy
[4]Dept. of Geosciences, Colorado State Univ., Fort Collins, USA
[5]Institute of Geology of Ore deposits, Russian Academy of Sciences, Moscow, Russia

From our work towards constructing a database on the properties of Au-transporting hydrothermal fluids in the Earth's crust, we present preliminary microthermometric determinations, Raman spectra, volume fraction determinations of fluid phases via spindle stage measurements, and Laser Ablation-ICP-Mass Spectrometric analyses for a set of 25 fluid inclusion assemblages. This record has been collected for a number of well-documented orogenic (Sigma and Beaufor, Canada; Wattle Gully, Australia; Berezovskoe, Russia; and Pestarena, Italy) and intrusion-related (Fairbanks district, Alaska; Teremkin and Talatui, Transbaykalia, Russia) Au deposits from various tectonic settings and age. Where possible, data have been collected for assemblages petrographically associated with Au nuggets, in order to better constrain stages of ore fluid entrapment.

Data show that the ore fluid of orogenic deposits can be represented by a two- to three-phase (aqueous liquid, carbonic liquid, vapour) H_2O-CO_2-NaCl model fluid, with a relatively low bulk salinity (< 7.1 eq. wt% NaCl), a φ=13-50 vol% vapour fraction, and a relatively uniform vapour composition (CO_2±CH_4-N_2). A subordinate H_2O-NaCl fluid is also present. *T*h(total) range from values as low as 200°C (Wattle Gully) to 400°C (Sigma), and homogenisation occurs by bubble and liquid disappearance. LA-ICP-MS data show that the most abundant analyte in this fluid is Na (4000-28000 μg/g), with subordinate K (300-4500 μg/g) and B (200-2800 μg/g), and minor to trace amounts of (in the most commonly recognised order of decreasing abundance) As, Cu, Sr, Rb, Mg, Mn, Li, Ba, Cs, Sb, and Pb (range: 1-450 μg/g). These trace components are not systematically determined in all the studied deposits or samples. Au has been determined only in few assemblages from the Sigma deposits to be in the 0.5-5 μg/g range.

Intrusion-related deposits contain two-phase aqueous (liquid, vapour) fluid inclusions, but multi-phase aqueous inclusions containing one or more solids (halite and opaque phases), and an aqueous-carbonic fluid, are also common in some deposits, corresponding to a much broader range of bulk salinities (0.4-56 eq. wt% NaCl). The volume fraction of the vapour phase is similar to that of orogenic deposits, and its composition is dominated by CO_2 (±CH_4). The *T*h(total) documented in quartz associated with early- and main-stage Au range from about 300°C to 600°C, and homogenisation occurs by bubble and liquid disappearance. LA-ICP-MS data show that the most abundant analyte in this fluid is Na (3500-55000 μg/g), with subordinate K (850-9000 μg/g) and B (400-1500 μg/g). With the exception of Fe, Zn, Pb, and Mn, which have a high bulk concentration in the halite-saturated fluid (*e.g.* 28000 μg/g of Fe), the components As, Cu, Sr, Rb, Mn, Li, Ba, Cs, and Pb have been determined in the liquid-vapour and vapour-rich inclusions to be in the 2-300 μg/g concentration range. All these data show remarkable compositional similarities between the fluid types, which will be discussed in light of possible ore fluid source and evolution

Tourmaline Sr-O isotopes: evidence for fluid mixing in the Val-d'Or orogenic gold vein field

Beaudoin, G.[1,2]
[1]Université Laval, Québec, Canada (Beaudoin@ggl.ulaval.ca)
[2]Université de Genève, Genève, Switzerland

The Val-d'Or (Québec, Canada) vein field is a classical example of orogenic gold deposits in Archean rocks. The Val-d'Or vein field contains a large number of early quartz-carbonate and later quartz-tourmaline-carbonate (QTC) gold-bearing veins within a consistent structural setting and formed during two successive hydrothermal events.

The oxygen isotope composition of 24 coexisting quartz and tourmaline samples from 18 QTC veins representing the regional distribution in the vein field shows that quartz and tourmaline are in oxygen isotope equilibrium at temperatures ranging from 250 to 500°C (Fig. 1).

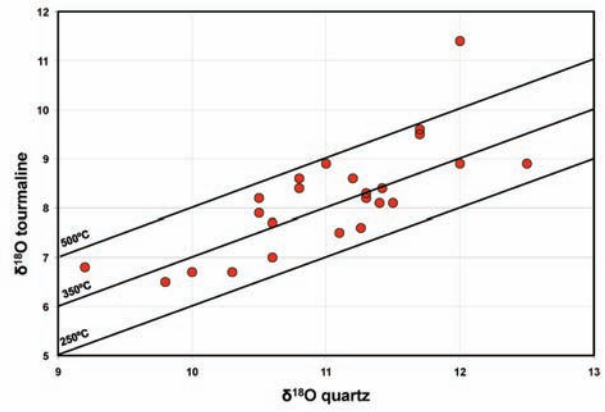

Fig. 1: Tourmaline vs quartz $\delta^{18}O$ values with 250, 350 and 500 °C isotherms. One sample with a tourmaline $\delta^{18}O$ value of 11.4 ‰ contains quartz impurities as shown by XRD analysis.

Age-corrected (2.7 Ga) initial strontium isotope composition ($^{87}Sr/^{86}Sr_{(i)}$) of 24 tourmaline samples range from 0.7007 to 0.7023. The tourmaline $^{87}Sr/^{86}Sr_{(i)}$ and $\delta^{18}O$ values show a broad inverse covariation (Fig. 2) interpreted to indicate mixing between two fluids: 1) a high $^{87}Sr/^{86}Sr_i$ (≥0.7023) and low $\delta^{18}O$ value (<3.9 ‰) fluid considered to represent evolved Archean seawater that reacted at shallow crustal levels with radiogenic felsic intrusions and, perhaps, sedimentary rocks; and 2) a low $^{87}Sr/^{86}Sr_i$ (≤0.7007) and high $\delta^{18}O$ value (>8.5 ‰) fluid, most likely derived from deep-seated metamorphism of more primitive strontium-bearing Archean volcanic-plutonic host-rocks.

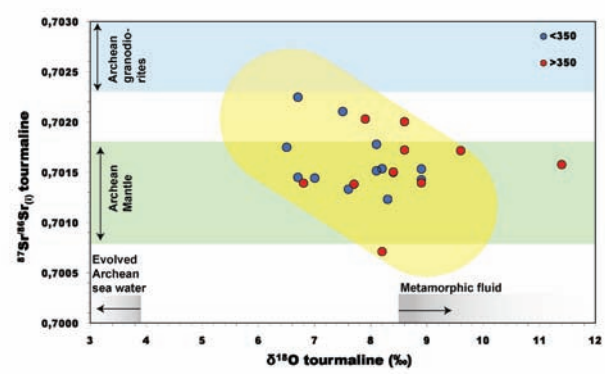

Fig. 2: Tourmaline $^{87}Sr/^{86}Sr_i$ vs $\delta^{18}O$ values with fields for Archean Mantle and granodiorite plutons, and range of values for evolved Archean sea water and metamorphic fluids. Samples with quartz-tourmaline O-isotope equilibrium temperatures below or above 350 °C shows no temperature effect on tourmaline $\delta^{18}O$ values.

Crustal scale mineralogical zonation in active orogenic gold deposits, Taiwan and New Zealand

Craw, D.[1*]**, Upton, P.**[2] **& MacKenzie, D.J.**[1]
[1]Geology Dept., University of Otago, Dunedin, New Zealand
([*]dave.craw@stonebow.otago.ac.nz)
[2]GNS Science, Dunedin, New Zealand

Gold-bearing vein systems with orogenic style form beneath active collisional mountain belts, and these are analogues for similar deposits in ancient belts. The vein systems form in a complex array of structures between the brittle-ductile transition and the near-surface. A characteristic set of mineral assemblages accompanies these veins, with mineralogy governed by the depth and temperature of formation of the veins.

Deepest formed veins (ca 10 km) have a greenschist facies mineral assemblage: quartz, albite, muscovite, chlorite, calcite, and some biotite locally. These alteration minerals formed in geochemical equilibrium with the greenschist facies host rocks. Fluid flow occurred along grain boundaries and in microfractures, and alteration is locally extensive (metres to tens of metres) adjacent to veins. This style grades up into, or is overprinted by, extensive disequilibrium alteration zones in which chlorite has altered to ankerite and pyrite. Ankeritic alteration grades up to shallow-formed vein systems with little alteration in which chlorite is a common vein mineral with quartz, calcite and, locally, adularia.

This alteration sequence is displayed in the active mountains of Taiwan. Gold-bearing vein systems in the high mountains of Taiwan are part of the youngest tectonic-hydrothermal system on Earth. Tectonic collision initiated in the Pliocene has stacked Eocene-Miocene marine sedimentary rocks to form steep mountains nearly 4 km high. Thinner portions of the sedimentary pile (ca 5 km) are currently producing hydrocarbons on the western side of the island. Orogenic gold occurs in quartz veins in thicker parts of the pile (ca 10 km) beneath the mountains in the central part of the island. Veins were formed by a mix of meteoric and metamorphic waters in localized fault/fracture zones. Deep formation of greenschist facies veins, some with gold, have caused embrittlement of the host rocks, and facilitated focusing of shallower fluid flow through the same rock packets, with auriferous ankeritic veins overprinted by late quartz-calcite veins with rare adularia.

The active Southern Alps of New Zealand also display the same sequence of mineral alteration assemblages. High mountains (4 km) and abundant rainfall cause deep circulation of meteoric water. Mesozoic basement is being reworked in this transpressive collisional orogen, releasing metamorphic fluids in the greenschist facies near the brittle-ductile transition. Localised gold deposition occurs at this level. More extensive auriferous ankeritic alteration is widespread in a fracture system that carries fluids from depth to shallow levels beneath the highest mountains. Shallow level quartz veins with calcite, chlorite, and adularia fill fractures throughout the mountains. The Southern Alps fluid flow system is more diffuse than that in Taiwan, but the mineralogical zonation is essentially identical.

Gold deposits in the central part of the Bohemian Massif: controversies and overview of genetic models

Zachariáš, J.
Inst. of Geochemistry, Mineralogy and Mineral Resources, Faculty of Science, Charles University in Prague (zachar@natur.cuni.cz)

The Bohemian Massif, a part of European Variscan Belt, hosts numerous economic and non-economic accumulations of Au, Ag-Pb-Zn and U ores. To classify gold deposits, mineral association and gold fineness represent the most practical criteria: (1) deposits with gold of high fineness (>900) where gold is accompanied by scheelite, minor molybdenite and numerous accessory Bi-Te-S phases; (2) deposits with high gold fineness (> 900) but accompanied by largely abundant Sb-mineralization (stibnite, aurostibite, Pb-Sb-sulphosalts); (3) deposits with gold of lower fineness (< 700, i.e., electrum) and lacking W-Mo-Bi-Te-S phases. A common feature of all these deposits is a variable, but generally low, sulfide content (<5 vol. % of pyrite, arsenopyrite, pyrrhotite) and quartz-dominated gangue. In the literature, these principal Au-deposit groups are referred to as high-fineness (HFAu), high-fineness Sb (HFSb) and low-fineness deposits (LFAu), respectively. They all were traditionally classified as mesothermal gold deposits (orogenic gold). Recently, for some of them a magmatic fluid phase contribution was demonstrated, and some authors used the term "intrusion-related gold deposits" [1-3]. In this paper, recent development in understanding of processes of deposit formation, based on fluid inclusion and stable isotope mineralogy studies, are summarized.

Early mineralization stages of HFAu were dated by the Re-Os method on molybdenite flakes [4]. The ages (349-339 Ma) are statistically indistinguishable from ages of individual intrusive phases of CBPC (355-336 Ma). Dominant fluid is usually represented by low-salinity aqueous-carbonic fluid. At some localities, presence of discrete pulses of CO_2-free, high-salinity aqueous fluid of likely magmatic origin was also found. Geological evidence for "continuous" transition from magmatic into hydrothermal phase is, however, missing. There is textural evidence both for early and late incorporation of gold in the ores. CH_4-rich fluids seem to be locally important and shortly precede gold precipitation. At many localities, however, gold was introduced exclusively by late aqueous fluids. Another yet unsolved observation represent spherical solid inclusions composed of Bi, Bi-Te-S, and Au and Pb-Sb-Bi-Te-S phases, sporadically also with remnants of a fluid phase. They might represent an immiscible low-temperature metallic alloy. Isotope data (S, O, C, Sr) suggest not uniform source of dissolved elements [5] and presence of fluids with both metamorphic and meteoric signatures.

The LFAu deposits are younger (ca. 300 Ma) and formed in response to a late metamorphic phase in the Moldanubian Unit. Deep seated fluids were focussed trough regional tectonic zone and mixed at subsurface levels (<2 km) with meteoric fluids [6].

[1] Thompson, J.F.H. et al. (1999) *Miner. Deposita*, **34**, 323-334. [2] Boiron, M.C. et al. (2001) *Chem. Geol.*, **173**, 207-225 [3] Zachariáš J. et al. (2001) *Miner. Deposita*, **36**, 517-541 [4] Zachariáš, J. & Stein, H. (2001) in Piestrzyński, A. et al. (eds.) *Mineral Deposits at the Beginning of the 21st Century*. Swets & Zeitlinger Publishers Lisse, 851-854. [5] Zachariáš, J. et al. (2001) in Piestrzyński, A. et al. (eds.) *Mineral Deposits at the Beginning of the 21st Century*. Swets & Zeitlinger Publishers Lisse, 855-859. [6] Zachariáš, J. et al. (2009) *Econ. Geol.*, **104**, 53-72.

Transport and deposition of gold in the Greywacke Zone, Eastern Alps

Kucha, H.[1] & Raith, J.G.[2*]
[1]University of Mining & Metallurgy, Krakow, Poland
[2]Dept. of Applied Earth Sciences and Geophysics, University of Leoben, Austria ([*]johann.raith@unileoben.ac.at)

Native gold and unusual gold-oxysulphides occur in low-grade Palaeozoic rocks of the Upper Austroalpine Greywacke Zone (GWZ). Gold is associated with tetrahedrite and can be traced in the GWZ (~250 km E-W extension) between Veitsch (Styria) and Schwaz (N Tyrol); further to the W where arseniferous tetrahedrite and tennantite are more common Au is lacking. Gold occurs as electrum, as gold of high fineness, and as refractory gold. Refractory gold shows two valence states: Au^0 in submicron native gold inclusions, and Au^{+1} where Au is bound to the host lattice of tetrahedrite or As-bearing pyrite.

In several historic stratabound to vein-type polymetallic Cu deposits (e.g., Mitterberg, Larzenbach/Hüttau, St. Veit im Pongau) gold-oxysulphides are associated with native gold in non-weathered primary ores and remobilized Cu-rich gold in weathered ores [1]. Solid inclusions of gold-oxysulphides, chalcopyrite, minor arsenopyrite and gold rich in gold-oxysulphide microinclusions occur along re-healed microfractures within tetrahedrite together with fluid inclusions.

Fluid inclusions within tetrahedrite (isolated inclusions, clusters, trails) were studied by infrared (IR) microthermometry. They are aqueous two-phase liquid (L)+vapour (V) inclusions of low to moderate salinity (Tm −3 to −14°C). Homogenisation temperatures (Th V→L) range between 85 and 200°C. The composition of these tetrahedrite-hosted fluid inclusions corresponds to one type of fluid inclusion in quartz showing a similar range in salinity (Tm −3 to −12°C) and total homogenisation temperatures (Th→V, 71.5 to 250°C). Another type of higher saline aqueous two-phase (L+V) inclusions in quartz is apparently unrelated to gold mineralization.

Tetrahedrite is replaced by arseniferous tetrahedrite/tennantite along the same microfractures hosting solid and fluid inclusions. It is therefore suggested that in addition to cooling the exchange of As for Sb on tetrahedrite surfaces was one of the factors controlling precipitation of gold.

From structural and textural considerations and the few available age data [2] we suggest that gold mineralization in the GWZ is late to post-orogenic with respect to Eoalpine metamorphism (~90 Ma). However, the association of gold with gold-oxysulphides, which are mixed S valence compounds containing sulphur and oxygen, and the T-X conditions of ore forming fluids (<250-300°C, no CO_2) are atypical for orogenic gold deposits. Hence, we suggest that S-As oxocomplexes (gold thiosulphate, possibly thioarsenite complexes) transported the gold in the hydrothermal fluid. Gold thiosulphate complexes were also involved in the supergene remobilization of gold.

Gold-bearing tetrahedrite-rich polymetallic ores in the GWZ are a neglected potential exploration target for gold in the Eastern Alps, which is distinct to the well established orogenic Au deposit type.

[1] Kucha, H. & Raith, J.G. (2009) *Ore Geol. Rev.*, **35**, 87-100. [2] Petraschek, W.E. (1978) *Mitt. Österr. Geol. Ges.*, **68**, 79-87.

Submarine hydrothermal activity and gold-rich mineralization at Brothers volcano, Kermadec arc, New Zealand

de Ronde, C.E.J.[1*], Massoth, G.J.[2], Butterfield, D.A.[3], Christenson, B.W.[1], Ishibashi, J.[4], Ditchburn, R.G.[1], Hannington, M.D.[5], Brathwaite, R.L.[1], Lupton, J.E.[6], Dziak, R.P.[6], Kamenetsky, V.S.[7], Graham, I.J.[1] & Zellmer, G.F.[8]

[1]Ocean Exploration, GNS Science, Lower Hutt, New Zealand ([*]cornel.deronde@gns.cri.nz)
[2]Mass-Ex3 Consulting, Renton, USA
[3]Pacific Marine Environmental Lab, NOAA, Seattle, USA
[4]Dept. of Earth and Planetary Sciences, Kyushu University, Fukuoka, Japan
[5]Dept. of Earth Sciences, University of Ottawa, Canada
[6] Pacific Marine Environmental Lab, NOAA, Newport, USA
[7]CODES, University of Tasmania, Hobart, Australia
[8]Institute of Earth Sciences, Academia Sinica, Nankang, Taiwan

The Brothers hydrothermal system is unique among seafloor hydrothermal systems along the Kermadec arc, and elsewhere around the world, as it is host to two very different vent fields. The NW caldera field is perched on the caldera walls and is an older (up to 1,200 yrs), more mature system that has high temperature (~300°C), focused venting of metal-rich fluids. Large Cu- and Zn-rich sulfide chimneys occur at this site. The cone vent field is much younger and sits atop the summits of a main cone and a satellite cone inside the caldera, near the southern caldera walls. This field is dominated by S-rich vents with vent fluids more diffuse, lower in temperature (<120°C), very gassy and acidic (pH 1.9), and relatively metal-poor. Vent fluids of the NW caldera site show evidence for sub-seafloor phase separation. Concentrations of SiO_2 suggest these vent fluids are supersaturated and/or kinetic effects are occurring, with evidence for higher than hydrostatic fluid pressures at shallow depths. Vent fluids at the cone site have Mg and SO_4 concentrations higher than seawater, indicating these ions have been *added* to the hydrothermal fluid and are not being depleted via normal water/rock interactions.

Isotopic compositions of the NW caldera and cone vent fluids show evidence for magmatic water with negative δD and $\delta^{18}O$ values, consistent with $^3He/^4He$ values showing that the Brothers hydrothermal system has shifted towards more magmatic conditions over the past several years. Similarly, $\delta^{34}S$ values for vent fluid sulfides and for sulfide minerals from NE caldera chimneys indicate disproportionation reactions involving magmatic SO_2.

Minerals such as chalcopyrite, bornite, chalcocite, covelllite and euhedral grains of hematite occurring in high temperature chimneys from the NW caldera site are consistent with a more oxidizing, magmatic fluid, and bulk sulfide geochemical data show evidence for a higher temperature suite of elements (e,g., Mo, Co, Se) associated with Cu-rich chimneys. Gold mineralization occurs in these high temperature chimneys and is associated with the most recent deposition of high concentrations of Cu, where $\delta^{34}S$ values are most negative.

Geophysical evidence suggests that the top of a magma chamber occurs ~2.5 km below the caldera floor, beneath the cone site in the SSE quadrant of the volcano. Very low velocities of < 1 km^{-2} are seen in the seismic data and occur between the magma and the seafloor. They are interpreted to represent gas release. Harmonic tremor data provide evidence for a vertical pipe-like 'conduit' at least 500 m in length being located above the magma chamber (and beneath the cone), linking it with the overlying hydrothermal system and thus providing a mechanism for magma-derived metals to enter the hydrothermal system under the cone site.

Gold- bearing tellurides in a black smoker chimney, Brothers submarine volcano, Kermadec arc

Berkenbosch, H.A.[1*], de Ronde, C.E.J.[2], McNeill, A.W.[1] & Gemmell, J.B.[1]

[1]ARC Centre of Excellence in Ore Deposits, University of Tasmania, Hobart, Australia ([*]heidib1@utas.edu.au)
[2]Ocean Exploration, GNS Science, Lower Hutt, New Zealand

A distinct, but relatively poorly understood magmatic component contributes to hydrothermal vent fluids and their associated mineral deposits at hydrothermal systems hosted by submarine arc volcanoes. The dacitic Brothers caldera volcano of the Kermadec intraoceanic arc is such an example, and is host to two chemically distinct hydrothermal systems. One is the cone site, a relatively recent magmatic fluid-dominated system, while the other is the NW caldera site, dominated by modified seawater but with evidence for earlier magmatic 'pulses' [1]. Here, we focus on various petrographic techniques combined with detailed geochemical analysis of the mineralogy of the Lena black smoker chimney that was recovered from the NW caldera vent field at Brothers.

In 2004 the manned submersible *Shinkai 6500* collected Lena chimney from a depth of 1,670 m. Lena is the top ~66 cm of a black smoker chimney that was venting 274°C fluids at the time of sampling. The chimney is dominated by distinct, narrow bands of Cu-rich mineralization juxtaposed against broader, more porous zones of Zn-rich mineralization towards the chimney margins. Anhydrite and barite form the initial substrate upon which later sulfides are deposited. Pyrite and marcasite are commonly deposited first, followed by chalcopyrite from hotter fluids and sphalerite from relatively cooler fluids. Finely laminated bands of chalcopyrite, separated by bands of more disseminated chalcopyrite, typically line vent orifices. Trace minerals in Lena chimney include tellurides, galena, covellite, tennantite, hematite, goethite, and Pb-As sulfosalts (Fig. 1).

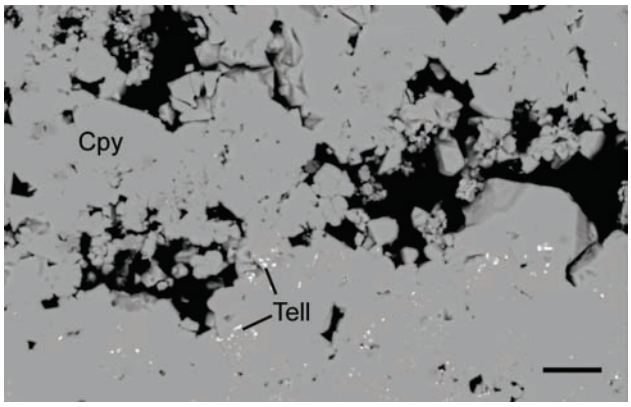

Fig. 1: Band of fine gold-rich tellurides (tell) within band of massive chalcopyrite (cpy). Black is void space, scale bar is 20 μm.

Analytical work using a SEM with EDS capability revealed both Bi- and/or Au-rich tellurides occur in some parts of the chimney. For example, they occur as inclusions throughout the major phases in anhydrite-rich areas, commonly along previous grain boundaries, and as 'trails' within some massive chalcopyrite bands. Together with the chalcocite, enargite and alunite previously described by de Ronde et al. [1] in other NW caldera chimneys, the occurrence and distribution of gold-rich tellurides are consistent with pulsed magmatic input into the Brothers hydrothermal system.

[1] de Ronde, C.E.J. et al. (2005) *Econ. Geol.*, **100**, 1097-1133.

Au-Ag minerals in volcanogenic massive sulphide deposits of the Urals

Vikentev, I.V.
Inst. of Geology of Ore Deposits, Petrography, Mineralogy and Geochemistry (IGEM), Russian Academy of Science, Moscow, Russia (viken@igem.ru)

Most gold in the Urals is extracted from sulfide ores from volcanogenic massive sulfide (VMS) Cu-Zn-Au-Ag deposits [1,2] but with very poor gold recoveries (20-45%). Such poor recoveries are due to the relative scarcity of Au as large, readily extractable grains in most of the Uralian VMS deposits. This study is based on mapping and sampling of the giant Gai, the large Uchaly and Uzelginsk as well as minor and medium-sized VMS deposits. In the VMS deposits of the Urals, gold occurs mainly as "invisible" gold in pyrite, chalcopyrite and sphalerite at abundances between 1 and 20 ppm. Silver occurs mainly in fahlore (0.1-6 wt % Ag) and Ag sulfosalts. Discrete Au-bearing minerals (Au-Ag alloys, tellurides and sulfides) are rare and occur as extremely fine-grained inclusions within common sulfides in the ores. They are associated mainly with pyrite, chalcopyrite, galena, bornite, fahlore.

The Au-Ag mineral assemblages are mainly argentiferous tetrahedrite, Ag sulfosalts (freibergite, kolusite, pearceite), Ag-bearing galena and bornite, various tellurides (altaite, hessite, petzite, stuetzite, krennerite, kalaverite, sylvanite), some sulfides (petrovskaite, uytenbogaardtite), native gold and native silver. Native gold and gold minerals occur in ores grading >5 ppm Au (rarely ~3 ppm). Native gold forms grains and aggregates from 2 to 50 μm (with rare larger grains up to 150 μm). The largest grains of native gold (100–1000 μm, or larger) are in deposits that have been highly metamorphosed (Gai, Degtyarsk, Karabash, San Donato, and contact metamorphosed, Tarnjer). In slightly to moderately metamorphosed deposits (Uzelginsk, Uchaly, Molodezhny, Aleksandrinsk, Valentorsk and Safjanovsk), native gold grains are rare and small (commonly <25 μm). The fineness of native gold ranges from 500 to 975 in the metamorphosed deposits, and is much lower in the non- or slightly-deformed deposits (440 to 860).

The native gold from massive sulfide deposits may be regarded as a series of continuous Au–Ag solid solutions from $Au_{0.98}Ag_{0.02}$ to $Au_{0.60}Ag_{0.40}$. Compositions of native gold of VMS deposits of the Urals cluster close to the formulae Au_3Ag, Au_2Ag and Au_3Ag_2.

Most gold contained in VMS ores (47-87%) occurs at low abundances (Au 0.2-3 g/t) and is incorporated in the sulfides as "invisible" gold; this Au is therefore unrecovered and lost to tailings, mostly along with pyrite. The proportion of visible gold minerals (chiefly native gold) as gold carriers is accordingly much higher in those massive sulfide ores which have been metamorphosed.

[1] Prokin, V.A. & Buslaev, F.P. (1999) *Ore Geol. Rev.*, **14,** 1-69. [2] Vikentyev, I.V. (2006) *Mineral. Petrol.*, **87**, 305-326.

Variable ore mineralogy in the world-class epithermal Waihi vein system, New Zealand

Mauk, J.F.
School of Environment, University of Auckland, New Zealand (J.Mauk@auckland.ac.nz)

The world-class adularia-sericite epithermal vein system at Waihi in the North Island of New Zealand has an estimated total Au endowment that exceeds 12 Moz, including 7.5 Moz mined to December 2008. Much of the past production has come from the Martha mine, and recent production has included contributions from underground operations at the Favona and Moonlight deposits. Available geological, geophysical, and geochronology data suggest that the veins in the Waihi vein system formed as part of a single hydrothermal system at 6.1 Ma, but significant variability in the ore mineralogy of the veins indicates a more complex history.

Most veins in the Waihi vein system have some minerals in common, including pyrite, sphalerite, galena, chalcopyrite, and electrum, although the absolute and relative abundance of these minerals vary significantly. Pyrite and marcasite from altered host rocks are stoichiometric FeS_2 with no significant trace elements. In contrast, pyrite in veins commonly contains appreciable As (up to 3.2 wt%), and locally several tenths of a percent of Cu, Zn, Co, Ag and Sb. Electrum is the only source of Au in the deposits; its composition typically ranges from $Ag_{0.47}Au_{0.53}$ to $Ag_{0.39}Au_{0.61}$. Chalcopyrite is stoichiometric $CuFeS_2$. Most galena is PbS, although it commonly contains ca. 0.22% Se. Sphalerite averages 4 mol% FeS, though ranges up to 15 mol%.

Tetrahedrite $[(Cu,Ag)_{10}(Zn,Fe)_2(As,Sb)_4S_{13}]$, acanthite ($Ag_2S$), aguilarite ($Ag_4SeS$), stromeyerite (CuAgS), naumannite (Ag_2Se), and mckinstryite $[(Ag,Cu)_2S]$ have more localised distributions in the Waihi vein system. For example, the Favona deposit in the eastern portion of the Waihi vein system contains tetrahedrite, aguilarite, naumannite, rare mckinstryite and stromeyerite, but lacks significant acanthite. By contrast, at the nearby Moonlight deposit, limited petrographic and microprobe results suggest that tetrahedrite is the dominant Ag containing mineral; acanthite, aguilarite, stromeyerite, naumannite, and mckinstryite appear to be largely absent, although some samples contain either minute grains of acanthite or native Ag as <0.5 micron inclusions in pyrite.

The Martha deposit contains several veins that were mined underground over a vertical interval of 500 m, and the area is currently mined as an open pit. Ore mineralogy in the veins varies significantly. Some veins are dominated by the base metal sulphide mineral assemblage, some veins have significant acanthite, and other veins have significant concentrations of aguilarite and naumannite. The Reptile vein, which lies between the Favona and Martha deposits, contains an assemblage with base metal sulphides and electrum. The most abundant sulphide minerals are pyrite, sphalerite, galena, and chalcopyrite; the vein lacks acanthite, aguilarite, and naumannite.

Significant variability in the ore mineralogy of the veins in the Waihi vein system reflects, in part, variability with depth. At Martha and Favona, depth exerts a strong control on mineralogy as base metal sulphide minerals increase with depth at the expense of the silver sulphides and sulfosalt minerals. However, some deposits contain significant concentrations of Se-bearing minerals, some deposits lack Se-bearing minerals, and others have variable concentrations of Se-bearing minerals in different portions of their orebodies. The ultimate controls on the Se:S ratios in the Waihi vein system remain poorly understood, but these may include variations in the Se:S ratios of the fluid, different fluid sources, and/or the redox state of the fluid.

Zoning in pyrite as a source of physicochemical information

King, J.J.[*], van Hinsberg, V.J. & Williams-Jones, A.E.
Dept. of Earth & Planetary Sciences, McGill University, Montreal, Canada ([*]julia.king2@mail.mcgill.ca)

Pyrite is a common mineral in many types of metallic mineral deposits, formed over a wide range of physicochemical conditions. In a large number of these deposits, the pyrite is compositionally zoned, and thus changes in trace element concentrations between zones can be used to reconstruct the chemical evolution of the ore fluid, and potentially determine its temperature. Gold-bearing pyrite in the Bowone and Binebase high-sulphidation epithermal Au prospects on Sangihe Island, Indonesia, display evidence of both growth and sector zoning. Here we report the results of a study of pyrite from these deposits, and document the distribution of trace elements among growth and sector zones in this mineral with the goal of understanding how the deposit formed.

Compositional variations among growth zones in pyrite are controlled by changes in fluid composition, pressure and temperature. We have mapped trace element compositions for elements that show zonation (Cu, Se, Te, Ni, Zn, As, Au, Ag) in the Bowone and Binebase pyrite using EMPA and SIMS techniques as a means to quantify chemical changes parallel to the growth direction and investigate substitutions in the pyrite structure. Copper in particular shows strong zonation with an average concentration of 0.83 wt% and up to a maximum of 5.2 wt%. A similar observation was made for the Pascua high-sulphidation deposit [1].

In addition to growth zoning, the pyrite of the Bowone and Binebase deposits displays intense sector zoning. The sector zoning developed as trace elements were preferentially and systematically incorporated onto different crystallographic surfaces. The partitioning of trace elements between crystallographic faces is independent of fluid composition because the same fluid is in contact with each crystal face. However, this partitioning is very sensitive to temperature. Sector zonation can be calibrated for geothermometry, as was done for sector zoning in tourmaline [2]. Sector zoning at Bowone and Binebase is most evident for copper. For example, a late pyrite breccia vein shows, yet un-calibrated, temperature variations over time, with copper partitioning coefficients ranging from 0.32 to 0.94. Element partitioning is more pronounced at lower temperatures, thus the increased partitioning corresponds to a decrease in temperature. In the case of the above breccia vein, temperature initially increased, then decreased, increased again and finally decreased. We are currently calibrating the pyrite geothermometer using measured inter-sector partition coefficients for well-constrained natural and synthetic samples.

Although quantitative geothermometry is an eventual goal of this study, changes in the inter-sector partition coefficients provide important qualitative information on the temporal evolution of temperature and the corresponding changes in fluid chemistry. Studies of this type are useful, not only for ore depositing systems, but also for all the other environments in which pyrite forms (i.e., metamorphic, diagenetic and even sedimentary environments).

[1] Chouinard, A. et al. (2005) *Can. Mineral.*, **43**, 951-963. [2] van Hinsberg, V. & Schumacher, J. (2007) *Contrib. Mineral. Petrol.*, **153**, 280-301.

Gold deposits in the northern Fennoscandian Shield

Eilu, P.[1*], Billström, K.[2], Martinsson, O.[3], Niiranen, T.[4], Broman, C.[5], Weihed, P.[3], Wanhainen, C.[3] & Ojala, V.J.[6]
[1]Geological Survey of Finland, Espoo, Finland ([*]pasi.eilu@gtk.fi)
[2]Laboratory for Isotope Geology, Museum of Natural History, Stockholm, Sweden
[3]Dept. of Chemical Engineering and Geosciences, Luleå University of Technology, Luleå, Sweden
[4]Geological Survey of Finland, Rovaniemi, Finland
[5]Dept. of Geology and Geochemistry, Stockholm University Stockholm, Sweden
[6]Store Norske Gull AS, Rovaniemi, Finland

The Palaeoproterozoic evolution of the northern part of the Fennoscandian Shield includes a stage of repeated rifting with sedimentation and igneous activity during 2.5–1.95 Ga and the multistage Svecofennian orogeny with accretion and continent-continent collision from 1.95 to 1.77 Ga. All stages of geological evolution included hydrothermal activity some of which also produced, or were possibly indirectly related to, gold mineralisation. During the rifting stages, shallow level intrusion-related and basinal hydrothermal systems produced stratiform-stratabound (VMS-like) Cu-Zn (±Ag, Au) sulphide mineralisation throughout the region, but locally possibly also VMS(?) gold-baryte and sediment-hosted Au-Co-Cu±U occurrences. During the Svecofennian orogeny, compressional stages at 1.92–1.87 and 1.85–1.79 Ga produced structurally-controlled gold-only and gold-copper orogenic deposits. Accretional stages at ca. 1.89 Ga also produced porphyry-type copper-gold mineralisation. Iron oxide-copper-gold deposits were intermittently formed during the orogeny until ca. 1.77 Ga. The orogenic processes may also have remobilised parts of the early deposits, and even overprinted them by later alteration ± mineralisation. Much of the sulphide mineralisation is related to saline fluids potentially deriving both from originally evaporate-bearing rift sediments and from intrusions, but gold shows a good correlation with low-salinity H_2O–CO_2 fluids. There also are many potential metal sources available for the deposits: the extensive sedimentary and volcanic sequences formed during rifting, and the many types of intrusive and extrusive rocks of the Svecofennian orogeny. Also, the pre-orogenic deposits may have released metals into orogenic fluids. This 600–700 myr geological evolution, with a multitude of potentially mineralising processes, explains the large variation between gold deposits and the complexity of individual occurrences in the northern Fennoscandian shield, and also is the ultimate reason why it has been, and still is, difficult to agree on all the genetic types of the deposits in the region.

Gold exploration using baro-acoustic decrepitation

Burlinson, K.
Burlinson Geochemical Services P/L, Darwin, Australia
(kgb@synix.com.au)

Early attempts to use fluid inclusion decrepitation methods for mineral exploration were compromised by a failure to understand the importance of the presence of gas rich inclusions and their thermodynamic behaviour when heated, leading to misinterpretation and the premature demise of the technique.

We know that many gold deposits form from CO_2 rich fluids and these fluids can be readily detected using baro-acoustic decrepitation. Consequently we can use decrepitation as a mineral exploration method to locate CO_2 rich, potentially auriferous hydrothermal quartz. Using a computerised decrepitation instrument provides quick, cheap, reproducible and objective measurements of CO_2 in contrast to the slow, subjective and labour intensive microthermometric techniques. Although the method is best applied to mesothermal deposits formed at high pressures, it does also work with many epithermal deposits. Gas-rich fluid inclusions give a distinctive low temperature decrepitation peak because these inclusions have high internal pressures at room temperature and when heated, the pressure increases linearly with temperature in accordance with the gas law. In contrast, aqueous fluid inclusions have a condensed liquid phase and do not generate high internal pressures until temperatures above their homogenisation temperatures.

Samples from the Waihi epithermal gold deposit, NZ, have been analysed and they show low overall decrepitation intensities, as expected from epithermally formed fluid inclusions, but they clearly show low temperature decrepitation indicating the presence of CO_2 rich fluid inclusions. Samples from or near the active workings show low temperature decrepitation caused by CO_2 rich inclusions whereas distal samples either from the same vein or from other veins nearby lack this CO_2 caused decrepitation peak. This provides a means of evaluating potentially auriferous quartz veins based on their CO_2 fluid contents.

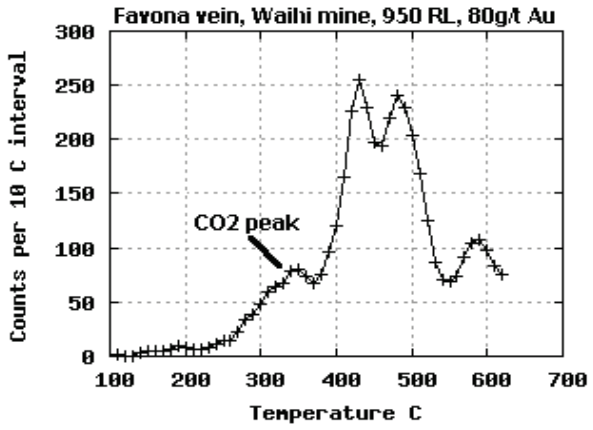

At the Brusson mine in northern Italy, alpine quartz veins were mined for their gold content. These mesothermal veins give intense decrepitation with large and prominent low temperature peaks caused by CO_2 rich inclusions. The decrepitation patterns can be used to distinguish between quartz samples which otherwise appear to be identical.

Baro-acoustic decrepitation can give valuable fluid inclusion data to use in mineral exploration. Many mineral deposits are “fossilized” fluid systems and we can surely benefit by using fluid inclusion information when exploring for them, not merely for forensic analysis of the deposits we have already found.

Geochemistry of Sb-Au quartz veins from Valongo, northern Portugal

Carvalho, P.C.S[*], Neiva, A.M.R. & Silva, M.M.V.G.
Dept. of Earth Sciences, Geosciences Centre, University of Coimbra, Coimbra, Portugal ([*]paulacscarvalho@gmail.com)

The Valongo area is located about 18 km from Porto, in the Dúrico-Beirão region, northern Portugal. The Valongo anticline formed during the Variscan Orogeny, comprises Cambrian to Carboniferous metasedimentary rocks and is limited to the northeast by late- to post-D3 granitic rocks and to the southwest by the Porto-Tomar-Cordoba shear zone. Several Sb-Au quartz veins crop out mainly at the western limb and rarely in the core of the anticline, filling N-S, N10-75ºE, N30-50ºW and E-W faults and are hosted by Cambrian and Carboniferous metasedimentary rocks. They were mostly exploited in the late 19th century. The Sb-Au quartz veins consist of quartz, arsenopyrite, pyrite, pyrrhotite, marcasite, sphalerite, chalcopyrite, galena, boulangerite, jamesonite, electrum, tetrahedrite, fuloppite, zinkenite, berthierite, stibnite, gold, native antimony, ankerite, siderite, calcite, dolomite and also schafarzikite, apuanite, valentinite and cervantite.

Minerals precipitated during a polyphase process due to drastic fluid cooling. Arsenopyrite and pyrite are the earliest sulfides to have formed. Arsenopyrite is rarely zoned with a Sb-rich core. The Au content is up to 0.28 wt% at Tapada and is due to minute inclusions of native gold. First and second generation of arsenopyrite formed at 390ºC and 300ºC, respectively [2]. Sphalerite and chalcopyrite are homogenous in composition and the former shows diffusion-induced segregations of the chalcopyrite. The ranges of mol % FeS in sphalerite are 0 to 5 at Medas, 9 to 11 at Alto do Sobrido and 3 to 4 at Montalto, reflecting variation in the activity of FeS in the fluid and in physico-chemical conditions during precipitation. Berthierite and stibnite are the most abundant Sb-bearing minerals and precipitated between 225ºC and 128ºC [2]. Gold occurs in different generations, in quartz, arsenopyrite, fuloppite, stibnite, carbonates and valentinite. Fineness ranges from 998 to 1000 in gold included in quartz and from 993 to 998 in gold included in stibnite.

The Sb and As mean content of granites is up to 0.43 ± 0.27 ppm and 17 ± 4 ppm, respectively. However, Cambrian metasedimentary rocks have Sb contents of as much as 56 ppm and 13 ± 5 ppm of As, whereas Sb content is 13 ppm in Carboniferous metasedimentary rocks, suggesting that ore-forming fluids were derived from Cambrian and Carboniferous metasedimentary rocks. The metamorphic fluids have low salinity with constant 2 wt % NaCl equiv. and the CO_2 content decreased during precipitation changing to aqueous fluids [1]. Variscan folding, deformation and regional metamorphism would have provided the anomalous crustal heat flow that triggered the hydrothermal activity [2]. Sb-Au deposits from Valongo would have formed during the last phases of Variscan orogeny, similarly as the Sb-Au deposits from French Massif Central and Central Iberian Zone.

[1] Couto, H. et al. (1990) *Miner. Deposita*, **25** (Suppl.), 569-581. [2] Neiva, A.M.R., Andráš, P. & Ramos, J.M.F. (2008) *Ore Geol. Rev.*, 34(4), 533-546.

Pre-Witwatersrand LREE and potassic high-T alteration of mafic hinterland to the Central Rand Basin, South Africa

Depiné, M.[1*], Frimmel H.E.[1,2], von Seckendorff, V.[1] & Harris, C.[2]
[1]Geodynamics & Geomaterial Research Division, University of Würzburg, Würzburg, Germany
([*]marco.depine@uni-wuerzburg.de)
[2]Dept. of Geological Sciences, University of Cape Town, Rondebosch, South Africa

Assuming a palaeoplacer model for the Witwatersrand gold, this study concerns the immediate hinterland to the highly auriferous Central Rand Basin (2.90-2.78 Ga), in the search for a possible source of the detrital gold. Pre-Witwatersrand granitoid bodies have been known from limited surface outcrops all around the basin. The following report is on calc-alkaline granite and hornblende metagabbro that were intersected in a drill core at the northwestern margin of the former Central Rand Basin. Both rock types are of indistinguishable age (3063 ± 5 Ma) [1], which corresponds to that of the Witwatersrand gold particles [2].

Two types of alteration can be distinguished in the intersected rock types: (i) post-Witwatersrand, low-T alteration that is comparable to that previously described from the Witwatersrand Basin fill and surrounding granitoids in the wider region; and (ii) LREE and potassic high-T alteration in the mafic rock. The contact between granite and hornblende metagabbro is marked by a distinct, meter-thick, biotite-rich zone, also containing a discrete layer rich in ferriallanite-(Ce). Breakdown of magmatic plagioclase during allanite growth is supported by a positive Eu-anomaly and high Sr-concentrations in allanite, which is in textural equilibrium with fluorapatite and microcline. The presence of hornblende and microcline (Or95) in the metagabbro are indicative of temperatures above 550 °C. The oxygen isotope ratio of hydrothermal quartz (11.3 ‰) corresponds to a δ18O of at least 9 ‰ for the precipitating fluid assuming a crystallization temperature of at least 550 °C, a value that would be in agreement with a magmatic derivation of that fluid. Thus the high-T alteration explains the formation of allanite and the high amounts of fluorapatite in the biotite-zone as well as microcline in the biotite-zone and throughout the metagabbro. The concentration of allanite in a distinct layer is interpreted as reaction front between the emplacing granite and the cooling gabbro. The infiltration zone was characterized by increasing pH with increasing distance from the granite due to progressive reaction with the hornblende metagabbro. This is reflected by decreasing and increasing amounts of biotite and microcline from the biotite-zone to the metagabbro, respectively.

The inferred magmatic character of the infiltrating fluid and Ar-Ar hornblende ages that are identical within error with the U-Pb zircon ages of the granite and the metagabbro [1], leads to the conclusion that the described high temperature alteration is due to a late-magmatic infiltration of a granite-derived fluid. In summary, this study shows that the *c*. 3060 Ma pre-Witwatersrand basement in close proximity to the Central Rand Basin experienced a late-magmatic alteration that was marked by enrichment in LREE, P, F, Th as well as U and thus compares favourably with alteration that can lead to Au-enrichment.

Fluid inclusions and gold ore genesis in the Jiaodong Peninsula, Eastern China

Fan Hong-Rui*, Hu Fang-Fang & Yang Kui-Feng
Key Laboratory of Mineral Resources, Institute of Geology and Geophysics, Chinese Academy of Sciences, Beijing, China
(*fanhr@mail.igcas.ac.cn)

The Jiaodong gold province in the Jiaodong Peninsula of eastern China is currently the most important gold producer in China. Seven world-class gold deposits (>100 t gold), eight large gold deposits (20 to 100 t gold) and more than one hundred medium to small gold deposits (<20 t gold) have been discovered in the Peninsula during the past three decades, accounting for about 25% of Chinese gold reserves. The gold deposits of the peninsula can be divided into two types based on vein styles: 1) quartz vein-style (Linglong style) and 2) fault-zone hosted disseminated/stockwork-style (Jiaojia style).

Fluid inclusion studies have been carried out on major gold deposits and prospects in the Tanami region to determine the compositions of the associated fluids and the processes responsible for gold mineralization. The pre-gold H_2O-CO_2 fluid inclusions occur isolated in samples of the early milk-white quartz and are assumed to have been trapped during deposition of the earliest quartz. Fluid inclusions associated with gold mineralization at both deposit types contain mostly CO_2-H_2O-NaCl±CH_4 fluids and have variable CO_2 and CH_4 contents. The molar volumes of H_2O-CO_2 and CO_2-H_2O±CH_4 inclusions calculated for the Sanshandao (stockwork) and Denggezhuang (lode/vein) deposits are 50 - 60 cm^3/mole and 55 - 70 cm^3/mol, respectively. There are similar changes of molar volumes of H_2O-CO_2 and CO_2-H_2O±CH_4 inclusions from the other deposits in the Jiaodong Peninsula. Estimated fluid trapping pressures of pre-gold and gold-stage are 1.0 - 3.5 kbar and 0.7 - 2.5 kbar, respectively. The pressure decreased during the evolution of the fluid.

Age determinations by the different techniques show that the deposits in the Jiaodong Peninsula formed at similar times within 120 ± 10 Ma. Fluid inclusion measurements and previous isotope data have determined that ore-forming fluids of Linglong style and Jiaojia style gold deposits are identical and that all deposits of the Jiaodong Peninsula have essentially formed from the same fluids under similar temperature and pressure conditions. Differences among the deposits are related to structure. As the first-order regional faults formed at an earlier time and suffered recurrent deformation, rocks in the faults show cata-clastic deformation. Mineralization by replacement and infiltration by ore-forming fluids took place in the faults and formed disseminated and stockwork-style gold deposits. In the second- or third-order faults, deformation intensities were relatively weak, and rocks in the faults have been weakly cracked. In the regional-scale faults, the degree of deformation decreased from the centre to the outside. Disseminated-style gold mineralization occurred in the fault centre. Towards the outside, fine vein or stockwork-style gold mineralization was formed, and then quartz-sulphide vein-style gold mineralization was produced. In the margin of the Jurassic basin, as deformation caused separation of the basement and volcanic rocks, interstratified shears and fractures took place. Ore-forming fluids ascended along these channels to form the special example of Jiaojia style mineralization along the interstratified shear zone.

Acknowledgements: The present study was supported by The National Natural Science Foundation of China (Project No. 40625010).

Gold ore-forming fluids in the Denggezhuang gold deposit, Jiaodong Peninsula, Eastern China

Hu Fang-Fang*, Fan Hong-Rui & Yang Kui-Feng
Key Laboratory of Mineral Resources, Institute of Geology and Geophysics, Chinese Academy of Sciences, Beijing, China
(*huff@mail.igcas.ac.cn)

The Degezhuang gold deposit is currently the second largest lode gold deposit in the Muping-Rushan gold belt of Jiaodong Peninsula, eastern China. Gold occurs mainly in pyrite- and polymetallic sulfide-quartz vein/veinlet stockworks. Fluid inclusions in the altered wallrocks and gold ores show C-O-H fluids of three main types, namely H_2O-CO_2, CO_2-H_2O±CH_4 and aqueous inclusion. Early milk white quartz contains original H_2O-CO_2 inclusions and secondary CO_2-H_2O±CH_4 inclusions. In the pyrite quartz vein and polymetallic-sulphide quartz vein, CO_2-H_2O±CH_4 inclusions occur in isolation with a large range of H_2O/CO_2, whereas the aqueous inclusions occur as secondary trails in microfractures, cutting earlier quartz grains. In places CO_2-H_2O±CH_4 inclusions with variable aqueous phase proportions occur together within the same clusters, and mostly homogenize to liquid or vapor at the same temperatures, indicating immiscibility did occur at the deposit. Quartz and calcite in the late ore-forming stage developed original aqueous inclusion. Microthermometric data show homogenization temperatures (to liquid) of the CO_2-H_2O inclusions in the early ore-stage between 254 and 365°C. Homogenization temperatures, obtained mainly from inclusions with relatively small CO_2±CH_4 bubbles in the main ore-stages, range from 195 to 317°C. Homogenization temperatures (to liquid) of the aqueous inclusions in the late stage range from 156 to 219°C. The initial auriferous fluids were CO_2-dominant, and were gradually evolved into the increased amount of CH_4 in the main ore-stages and into H_2O-riched fluids with low temperature in the late stage. Fluid-wallrock interaction and fluid immiscibility possibly led to the gold precipitation.

Acknowledgements: The present study was supported by The National Natural Science Foundation of China (Project No. 40625010).

Mineralogy, mineral chemistry and isotope geochemistry of gold mineralization at San Martin de Loba, San Lucas Range, Colombia

Leal-Mejía, H.[*] & Melgarejo, J.C.
Dept. de Cristal·lografia, Mineralogia i Dipòsits Minerals, Facultat de Geologia, Universitat de Barcelona, Spain
([*]hildebrandolealm@yahoo.co.uk)

Gold mineralization in the San Martín de Loba mining district, Colombia (including the La Puja, La Chiva, La Puerta, El Cano and Juana Sanchez sectors), is hosted by the 180-190Ma San Martin-Norosi Batholith, which forms one segment of an extensive Jurassic calc-alkaline magmatic arc extending from northern-most Colombia through Ecuador and northern Peru.

At La Puja, 60-70ºSW-dipping mineralized veins are hosted within anastomosing, broadly WNW-striking left-lateral shears. Veins are composed of at least two generations of quartz, +Cc+Ser+Tourm+Py+Cpy+Aspy+Sph+Gn+Au, with related strong to pervasive Qtz-Ser+\-Py alteration extending for tens of centimentres into the intrusive wallrocks. Quartz and tourmaline grow against asperities on left-lateral shears indicating vein emplacement was synchronous with movement along the faults.

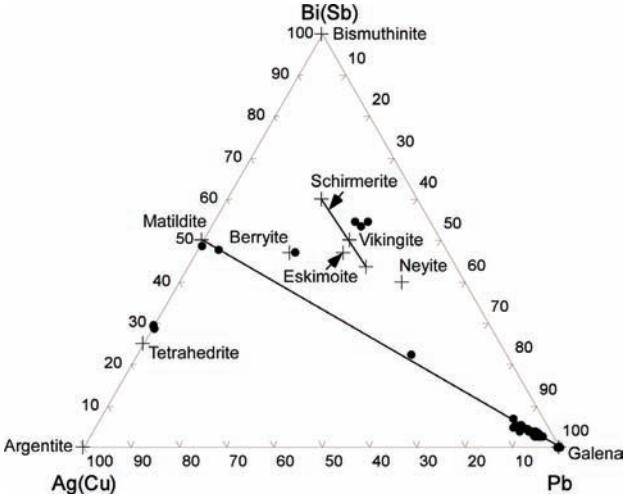

Fig. 1: Compositions of sulfides and sulfosalts analyzed in terms of the Pb-Bi(Sb)-Ag(Cu) system (dots) and of Ag-Bi-Cu sulphides and sulfosalts (crosses).

Pb isotope analyses of galena and pyrite return the following isotope ratios: $^{206}Pb/^{204}Pb$=18.097-18.147, $^{207}Pb/^{204}Pb$=15.569-15.633 and $^{208}Pb/^{204}Pb$=37.482-37.649. High Th/Pb ratios imply a lower crustal influence. The steep array in both thorogenic and uranogenic Pb-Pb diagrams indicates mixing between mantle and crustal sources [1]. Tightly constrained $\delta^{34}S$ analyses (+0.7 to +3.8‰) in pyrite and sphalerite indicate sulphur affinity with a magmatic source.

The presence of galena with intergrowths of Pb_{ss}, matildite and Bi-Ag-Cu sulfosalts, and coarse-grained alteration sericite indicates gold mineralization at La Puja is related to a multi-stage, chemically complex paragenesis at temperatures of +280 to *ca.* 400ºC [2]. Radiogenic Pb and stable S isotope geochemistry suggests mantle sourced magmatic fluids mixed with lower crustal fluids prior to the deposition of hydrothermal mineralisation/alteration in/along brittle-ductile shear zones at higher crustal levels under broadly mesothermal conditions.

[1] Leal-Mejía, H. et al. (2009) *Cardiff Caribbean Workshop* 2-4th September 2009. [2] Foord, E.E. & Shawe, D.R. (1989) *Can. Mineral.*, **27**, 363-382.

Anomalous Pd values in ores of the Kalmakyr Cu-Au(Mo) porphyry type deposit, Uzbekistan

Pašava, J.[1*], Vymazalová, A.[1], Košler, J.[2], Koneev, R.I.[3], Jukov, A.V.[3] & Khalmatov, R.A.[3]
[1]Czech Geological Survey, Prague, Czech Republic
([*]jan.pasava@geology.cz)
[2]Dept. of Earth Science and Centre for Geobiology, University of Bergen, Norway
[3]National University of Uzbekistan, Tashkent, Uzbekistan

Ores and host rocks from different types of gold deposits and the Cu-Au porphyry type deposit Kalmakyr have been studied for their Platinum group elements (PGE) and Au contents. Palladium is recovered as a by-product during the processing and refining of gold ores at a number of gold and Cu-Au porphyry types deposits in Uzbekistan [1].

No anomalous PGE concentrations were detected in the studied ore samples from various types of gold deposits (Kyzylalma, Kochbulak, Charmitan, Guzhumsai, Daugystau, Amantaytau, Vysokovoltnoye, and Myutenbai) in Uzbekistan. Prosperous Pd concentrations have been found from the porphyry Cu-Au(Mo) deposit Kalmakyr in Uzbekistan. High Pd concentrations have been reported from a number of porphyry copper deposits worldwide [2,3]. However, the PGE data on porphyry systems from Uzbekistan are very limited [1,3].

The Kalmakyr deposit belongs to the Almalyk ore field and is a part of the Chatkal–Kurama ore district, in the eastern Uzbekistan, where the main host rocks are Middle Carboniferous monzonite and locally preserved remnants of Devonian volcanic and carbonate rocks [4].

The study of primary ores (disseminated and stockwork type of mineralization) at the Kalmakyr deposit showed that our average Cu-Au(Mo) ore (Cu = 2.4 wt.%, Mo = 0.18 wt.%, Au = 4.1 ppm) contains 55.2 ppb Pd, 0.95 ppb Rh, 0.49 ppb Ir and 5.5 ppb Pt. Similar Pd values were reported in flotation concentrates from the Assarel porphyry deposit, Bulgaria (54 ppb), Grasberg deposit, Indonesia (58 ppb) and Sora porphyry deposit in Russia (50 ppb) [2]. At Kalmakyr, the peak Pd content of 291 ppb was determined in a Pb-Zn-Cu-rich sample hosted in quartz veinlets in granodiorite porphyrite, characterized mainly by the presence of galena, sphalerite, chalcopyrite, tetrahedrite and gold.

Geochemical study showed an important relationship between Pd and a group of metals (Cu, Ag, Se, S). Subsequent mineralogical and laser ablation ICP-MS study of base metal sulfides confirmed that anomalous Pd concentrations are likely bound to the crystal lattice of chalcopyrite and tetrahedrite or, alternatively, homogeneously distributed as sub-micron inclusions of PGE minerals. Chalcopyrite contains up to 110 ppm Pd and tetrahedrite up to 20 ppm Pd.

[1] Turesebekov, A.H. et al. (2005) in Tormanen, T.O. & Alapieti, T.T. (eds.) *Platinum-group elements – from genesis to beneficiation and environmental impact*, 10th Platinum Symp., Oulu, Finland, 596-598. [2] Economu-Eliopoulos, M. (2005) in Mungal, J.E. (ed.) *Exploration for Deposits of Platinum Group Elements*, Short Course Series, **25**, 203-246, MAC [3] Tarkian, M. & Stribrny, B. (1999) *Mineral. Petrol.*, **65**, 161-183. [4] Shayakubov, T. et al. (1999) in Shayakubov, T. et al. (eds.) *Au, Ag, and Cu Deposits of Uzbekistan*. Excursion Guidebook, IGCP 373, **11**, GeoForschungsZentrum Potsdam, 75-90.

In-situ trace element and ID-TIMS Sm-Nd analysis of scheelite and Re-Os dating of molybdenite at Schellgaden, a Au-(W) deposit in the Eastern Alps, Austria

Raith, J.G.[1*], Wieser, B.[1], Thöni, M.[2], Cornell, D.[3], Stein, H.[4] & Paar, W.H.[5]
[1]Dept. of Applied Earth Sciences and Geophysics, University of Leoben, Austria ([*]johann.raith@unileoben.ac.at)
[2]Dept. of Lithospheric Research, University of Vienna, Austria
[3]Dept. of Earth Sciences, University of Gothenburg, Sweden
[4]AIRIE Program, Colorado State University, Fort Collins, USA
[5]Dept. Materials Engineering and Physics, University of Salzburg, Austria

Scheelite-bearing gold occurrences ("Schellgaden type") are located along the eastern margin of the Penninic Tauern Window in the upper parts of the pre-Alpine sequences of the Storz-Kareck complex. The volcano-sedimentary and calc-alkaline plutonic rocks of this complex, interpreted as an island arc sequence, were intruded by Variscan granitoids (Central Gneiss). Subeconomic molybdenite mineralization, which is spatially distal and presumably unrelated to the Au-(W) occurrences, is associated with an aplitic granite gneiss. Both host rocks and the ore deposits were affected by polyphase deformation and metamorphism during the Alpine orogeny. Three types of sulfide-bearing Au-quartz veins are known: concordant mylonitic (Type 1), remobilized sub-concordant (Type 2), and discordant (Type 3)[1]. Scheelite is restricted to Type 1 veins. It shows bluish fluorescence under UV light and is associated with galena, pyrite, minor other sulfides and native gold. Large scheelite crystals (Scheelite 1) are deformed and show metamorphic re-crystallization (Scheelite 2).

Molybdenite from the aplitic granite gneiss was dated with the Re-Os chronometer. Two runs of one molybdenite sample yielded ages of 362 +/-3 and 366 +/- 1 Ma, the first run less than optimally spiked. Trace element concentrations in scheelite were obtained using EMS and LA-ICPMS techniques [2]. Both scheelite generations are Mo-poor, do not show pronounced zonation in cathodoluminescence images and have similar trace element concentrations. Total REE concentrations in scheelite are high (454-2378 ppm). Chondrite normalized REE patterns of both scheelite generations show enrichment in MREE and a relative depletion of LREE and HREE, resulting in convex (bell-shaped) patterns. Similar REE patterns are known from orogenic (mesozonal) gold deposits.

Sm-Nd isotope systematics of scheelite 1 obtained by micro-drilling from polished sections was analyzed by ID-TIMS [2]. Concentrations of Sm (65-171 ppm) and Nd (111-365 ppm) are remarkably high. However, $^{147}Sm/^{144}Nd$ ratios vary only within a very narrow range from 0.1836 to 0.2623. Thus, the calculated regression ages have very large uncertainties. An age of 322+/-140 Ma can be calculated from all (n=12) analyzed samples. Initial ε_{Nd} values for all scheelites are slightly positive (+1.9 to +2.9). Hence, an old crustal source, strongly enriched in LILE, can be ruled out and an Alpine age for Type 1 mineralization is excluded. An epigenetic hydrothermal formation for the Au-(W) deposits during the Variscan orogenic cycle is favored, although the large age uncertainty does not preclude a pre-Variscan, syngenetic origin.

Acknowledgements: Financial support for this project was provided by the Austrian Academy of Sciences (ÖAW, Kommission für Rohstoffforschung), the AIRIE Program, Colorado State University kindly provided the Re-Os dating.

[1] Amann, G et al. (1997) *Zentralbl. Geol. Paläont.*, Teil I, 1996, 215-228. [2] Wieser, B. (2010) *Unpubl. Master Thesis*, University of Leoben, Austria.

Multistage gold mineralization at Lapa mine, Abitibi greenstone belt (Canada)

Simard, M.[*], Daigneault, R. & Gaboury, D.
Centres d'Études sur les Ressources Minérales, Université du Québec à Chicoutimi, Chicoutimi, Quebec, Canada
([*]marjorie.simard@uqac.ca)

The Lapa gold deposit (1.1 Moz of Au @ 8.8 g/t Au) is one of the few deposits located directly within the Cadillac Larder-Lake Fault Zone (CLLFZ), a first order crustal fault that separates two Archean terranes, the Abitibi Greenstone Belt to the north and the Pontiac Subprovince to the south. This deposit is characterized by a number of features that are compatible with orogenic gold deposits including: (1) deformed and metamorphosed host rocks, (2) low sulfide content, (3) abundant quartz veinlets, and (4) spatial association with transpressional or compressional structures (e.g. CLLFZ). However, this deposit differs by being hosted directly within the CLLFZ and by showing well-developed mineralogical and metallic vertical zoning.

Mineralization defines vertically continuous ore zone from 400 to 1400 m depth hosted in strongly altered and foliated mafic to ultramafic units, metamorphosed at upper greenschists to lower amphibolite facies. Metamorphic grade transition defines a subhorizontal isograd, at depth of about 1 km, coincident with a well-developed wallrock alteration assemblage of biotite-dominated above 1 km depth and amphibole-dominated below. The metallic zoning is defined by an Au-Sb association developed mostly in the upper half of the deposit (depth≤ 1 km) whereas an Au -As association is relatively evenly distributed along main ore zones. Gold mineralization occurs mostly as disseminated sulfides (arsenopyrite-pyrrhotite ± pyrite) and as native gold in deformed quartz ± carbonates veins and veinlets and their alteration selvages.

Textural and mineralogical relationships show evidence of peak prograde metamorphism followed by a retrograde metamorphic event in the ore zones, including: (1) hornblende porphyroblasts partially replaced by actinolite; (2) biotite plages replaced by chlorite, and (3) occurrence of actinolite-albite assemblage whereas hornblende-orthoclase assemblage occurs in distal zone. Furthermore, backscattered electron images and electron microprobe analysis on disseminated arsenopyrite reveal primary crystallographic zoning with rims that are enriched in As over S. LA-ICP-MS analysis show that gold are homogeneously distributed in arsenopyrite crystals as solid solution. Theses results reflect that arsenopyrite are affected by an overall increase in temperature at the deposit-scale, caused by the prograde metamorphic event. This event has permitted liberation of invisible gold promoted by recristallisation and As enrichment of arsenopyrite.

Conversely, native gold is common in transposed quartz veinlets, and as free grains in altered wallrocks. This style is clearly associated with Sb-bearing phases at shallower depth in the deposit, is interpreted as indicative of a later decrease in temperature. Precipitation of native gold and Sb-minerals may results from the vertical cooling path of hydrothermal fluid, during retrograde metamorphic event.

These complex relationships between ore, alteration and metamorphic mineralogical and chemical assemblages indicate that gold mineralization has a protracted history of precipitation and remobilization, a feature not typical of most orogenic gold deposits. However, this can be explained by the complex deformation and metamorphism recorded by the CLLFZ induced by the successive variations of tectonic regime and strain, crustal level, heat flow and fluid flow.

Fluid inclusion investigation and Re-Os dating of the Pataz-Parcoy intrusion-hosted gold deposits, Eastern Cordillera, Peru

Szappanosné-Vágó E.[1*], Moritz, R.[1] & Barra, F.[2]
[1]Dept. of Mineralogy, Section of the Earth and Environmental Sciences, University of Geneva, Switzerland
([*]edina.vago@unige.ch)
[2]Dept. of Geosciences, University of Arizona, Tucson, USA

The major Carboniferous continental arc, intrusive belt of the Eastern Peruvian Cordillera is hosting auriferous quartz-sulphide veins. Subvertical to subhorizontal veins striking approximately to north-northwest, with a typical width of one to two meters, were emplaced along several km in two main districts located about 40 km from each other, within granodioritic to monzogranitic bodies. The genetic classification of gold deposits of the Pataz and Parcoy districts has been the subject of controversy in the last twenty years. On the one hand, they are considered as hydrothermal ore deposits related to deeper intrusive bodies associated to the Carboniferous magmatic activity. On the other hand, they are classified as orogenic, shear zone-hosted gold deposits emplaced along the western margin of the South-American continent. The present study addresses the issue of the controversial genetic classification of the Pataz-Parcoy gold belt, and presents new geochronological data on the magmatic and mineralising system and fluid chemical characteristics of the vein forming hydrothermal systems.

New Re-Os geochronological data on molybdenite from an early quartz-arsenopyrite-molybdenite vein from the Parcoy deposit constrains the early stage of the mineralisation to 331.9±1.7Ma. The host Pataz Batholith was dated by previous authors with ages ranging between 336 and 329 Ma (zircon TIMS U-Pb and Ar-Ar plateau biotite and hornblende ages) and between 314 and 301 Ma (zircon LA-ICP-MS U-Pb dating). In previous studies, hydrothermal muscovite associated with the gold veins yielded Ar-Ar plateau ages of 312-314 Ma at Pataz.

Our new results from fluid inclusion microthermometry allow us to define three different fluid stages responsible for the hydrothermal vein formation. Euhedral early stage-quartz contains primary low salinity (1-5wt% NaCl equiv.) aqueous-carbonic fluid inclusions with moderate to high homogenisation temperatures (170-300°C). Pseudosecondary fluid inclusions in quartz of the intermediate sphalerite-galena-chalcopyrite-bismuthinite-gold stage show entrapment of a medium to high salinity (5-25 wt% NaCl equiv.) $CaCl_2$-NaCl-H_2O($\pm CO_2$) fluid with low homogenisation temperatures (100-160°C). Low temperature and low salinity NaCl-H_2O fluids (100-120°C; ~5 wt% NaCl equiv.) have been trapped in secondary fluid inclusion trails, and represent the late stage of the mineralising system. This study is the first report of bismuthinite in the Pataz-Parcoy belt.

The strongly banded texture of the whole vein system reflects recurrent, incremental vein opening during hydrothermal fluid circulation. The new Re-Os age reveals a close temporal and spatial association of early vein formation with respect to its host intrusion. The approximately 15 m.y. difference between the Re-Os molybdenite age at Parcoy and the Ar-Ar plateau age of gold mineralisation at Pataz raises the questions whether there were distinct pulsating magmatic hydrothermal systems continuously over a duration of 15 m.y. or discrete overlapping mineralizing fluid events from different sources (magmatic vs metamorphic?), at time interval of several m.y.

Chemical variations in tetrahedrite-tennantite minerals from the Berezovsk mesothermal Au deposit, Ural, Russia: mineralogical zoning and ore fluid evolution

Vikenteva, O.V.[*] & Bortnikov, N.S.
Inst. of Geology of Ore Deposits, Petrography, Mineralogy, and Geochemistry (IGEM), Russian Acad. Sci., Moscow, Russia
([*]ovikenteva@rambler.ru)

The large Berezovsk gold deposit is located in metamorphosed volcanosedimentary rocks (S_1ln-v) with subconformable bodies of serpentinized ultrabasic rocks. The rocks are crosscut by numerous granitoid dykes and are located above the gently dipping roof of the Shartash granite massif. Mineralization is represented by sulfide-quartz veins in the granitoid dykes and host rock and by disseminated gold-sulfide mineralization in the wall-rock metasomatites. Ore minerals in the gangue mass account for no more than 10 vol%. Quartz, calcite, ankerite, pyrite, galena, fahlore, chalcopyrite, aikinite, sphalerite, and native gold are the most abundant minerals.

Fahlore may be a sensitive indicator of physicochemical conditions during ore deposition and therefore can be used as a tool for fluid evolution with respect to time and space. Fahlore is enriched in the tennantite component with As/(As+Sb) ratio ranges from 0.50 to 0.98. Zink predominates over iron (Fe/(Fe+Zn) = 0.15 - 0.67). Contents of silver is very low (0-0.9 wt %) and there is a correlation between the Sb and Ag contents in fahlore (r = 0.8) (Fig. 1).

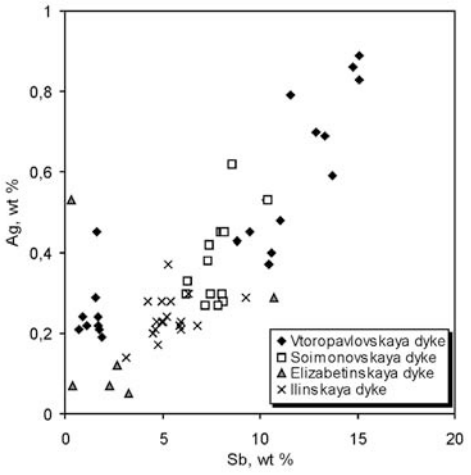

Fig. 1: Relationship between Ag and Sb in tennantite-tetrahedrite from Berezovsk deposit.

The model of fractional crystallization of fahlore from hydrothermal solution [1] is discussed for explanation of the variations of the Sb/As and Cu/Ag ratios in minerals of tennantite-tetrahedrite series.

Ag content in native gold decreases (and accordingly fineness of gold becomes higher) along with increase of Ag and Sb contents in coexisting fahlore. There is the direct correlation between Fe in coexisting fahlore and sphalerite related with the temperature of mineral formation. The chemical composition of tennantite-tetrahedrite can record some of the chemical variables of the hydrothermal fluids at the time of mineralization.

[1] Hackbarth, C.J. & Petersen, U. (1984) *Econ. Geol.*, **79**, 448-460.

The formation mechanism of shear zone-related gold deposits as exemplified by the Tianger gold deposit (Xinjiang, NW China)

Zhu Yongfeng
School of Earth and Space Sciences, Peking University, Beijing, China (yfzhu@pku.edu.cn)

Orogenic gold deposits typically formed in the later part of the deformational - metamorphic - magmatic history of the evolving orogen. The nature of gold-bearing fluids and the mechanism of gold deposition in shear zones in orogenic gold deposits are still largely unknown. Some studies have demonstrated that gold has been introduced syn-deformationally during a period of brittle-ductile shear development of the shear zone, with the gold-bearing sulfides subsequently deformed in the brittle field [1-3]. Others have shown that gold introduction is post-deformational and related to a brittle fracture event [4].

In this contribution, we attempt to address these problems in our study of the Tianger gold deposit in the west Tianshan mountains (NW China), a typical shear zone hosted gold lode deposit. We provide a detailed petrographic description of Au-bearing rocks and report, in detail, on the trace element, S, H, O, Ar, and Rb-Sr isotope geochemistry of the deposit.

The Tianger (also called Bingdaban in China) shear zone strikes roughly E-W, varies between 500 and 2,000 m in width and extends >100 km. This shear zone cuts a Silurian gneissic granite, dated at 442 Ma by zircon SHRIMP [5]. The shear zone is comprised of mylonitized granite with a strong mylonitic fabric and yellowish alteration. Disseminated sulfides are abundant in sheared rocks and rare in weakly deformed rocks.

Three gold deposits have been found in the Tianger shear zone: Wangfeng, Tianger, and Saridala. The orebodies and their wall rocks in these deposits are heterogeneously mylonitized. The degree of mylonitization of the wall rocks increases gradually towards the orebodies. Sub-horizontal fractures are filled with syntaxial quartz-fibres and antitaxial fibrous muscovite, which was dated to be 220Ma by Ar-Ar technique [4]. Pyrite is mainly disseminated in mylonite consisting of quartz subgrains, albite, muscovite and calcite. The pyrite-bearing mylonite is cut by a late-stage sulfide-quartz vein, which generally is 1-2 mm wide and consists of pyrite and quartz showing undulose distinction. Such pyrite-quartz veins formed after the major ductile deformation stage of the Tianger shear zone. They are, in turn, crosscut by micro-scale veins carrying pyrite, mica and quartz.

Based on stable isotope characteristics and high initial 87Sr/86Sr ratio, ore-forming materials are interpreted to have been sourced in gold-bearing rocks of the continental crust.

[1] Allibone, A. (1998) *Miner. Deposita*, **33**, 495-512. [2] Klemm, D.D. & Krautner, H.G. (2000) *Miner. Deposita* **35**, 90-108. [4] Zhu, Y.F. et al. (2007) *Ore Geol. Rev.*, **32**, 337-365. [3] Voicu, G. et al. (1999) *Econ. Geol*, **94**, 1277-1304. [5] Zhu, Y.F. & Song, B. (2006) *Acta Petrol. Sinica*, **22**, 135-144.

The Ag-Pd-Se system – experimental study and mineralogy

Vymazalová, A.[1*], Drábek, M.[1], Laufek, F.[1], Chareev, D.A.[2], Kristavchuk, A.V.[2], Voronin, M.V.[2] & Osadchi, E.G.[2]
[1]Czech Geological Survey, Prague, Czech Republic
([*]anna.vymazalova@geology.cz)
[2]Institute of Experimental Mineralogy RAS, Chernogolovka, Russia

The Ag-Pd-Se system comprises Platinum-group minerals like chrisstanleyite $Ag_2Pd_3Se_4$, verbeekite $PdSe_2$ and palladseite $Pd_{17}Se_{15}$ and silver selenide naumannite Ag_2Se. Furthermore nine binary phases are known from the system Pd-Se [2,3] and these phases could be found as new minerals in nature. Nevertheless only phase relations within the binary sub-systems are known. Therefore we carried out experiments in the Ag-Pd-Se system.

The isothermal sections 350, 427 and 527°C were studied using the evacuated silica glass tube technique [1]. Our first results are presented herein.

The experimental study revealed the existence of two new ternary phases in the system: Ag_2Pd_2Se and $AgPd_3Se$. The crystal structure of the phases was solved and refined from the powder X-ray diffraction data. The $AgPd_3Se$ phase is cubic ("cubic approximant of quasicrystals") with space group *Pa*3 and *a*=8.6288(1) Å. The first results of the X-ray data evaluation of the Ag_2Pd_2Se phase have shown that the phase is most likely tetragonal. The new Ag_2Pd_2Se and $AgPd_3Se$ phases are stable at temperature interval 350 – 527°C. The Ag_2Pd_2Se forms an extensive solid solution, chemical composition at 350°C varies between 38.3-46.3 at.% of Ag, 31.9-41.2 at.% of Pd, and 20.5-22.0 at.% of Se.

Our experiments confirmed the following binary phases to be stable in the temperature interval 350-527°C: Pd_4Se, Pd_7Se_2, $Pd_{34}Se_{11}$ (stable up to 430°C), Pd_7Se_4 (stable up to 415°C), Pd_5Se_4, $Pd_{17}Se_{15}$, PdSe, $PdSe_2$, and Ag_2Se. PdSe forms a narrow solid solution and dissolves up to 5 at.% of Ag at 350°C. At 427°C the ternary melt appears in the Ag_2Pd_2Se – Pd_4Se – Pd_7Se_4 field.

At 350°C the ternary $Ag_2Pd_3Se_4$ phase, an analogue to mineral chrisstanleyite, forms stable associations with naumannite (Ag_2Se) and verbeekite ($PdSe_2$) and coexists with PdSe and the new ternary phase Ag_2Pd_2Se. At 527°C the phase $Ag_2Pd_3Se_4$ is not stable.

The new recognised ternary phases Ag_2Pd_2Se and $AgPd_3Se$ and binary phases Pd_9Se_4, Pd_4Se, Pd_7Se_2, $Pd_{34}Se_{11}$, Pd_7Se_4, Pd_5Se_4, and PdSe, so far unknown as minerals could be found in nature in close association with other PGM, particularly with known minerals of the Ag-Pd-Se system.

[1] Kullerud, G. (1971) in Ulmer, G.C. (ed.) *Research Techniques for High Pressure and High Temperature*. Spinger-Verlag, New York, 288-315. [2] Massalski, T.B. (1990) *Binary alloy phase diagrams*. ASM International, Materials Park, Ohio, **3**, 3041-3045. [3] Okamoto, H. (1992) *J. Phase Equilib. Diff.*, **13(1)**, 69-72.

X-ray absorption spectroscopic study of oxygen-bearing platinum-iron grains from New Caledonia

Hattori, K.H.[1*], Takahashi, T.[2] & Auge, T.[3]
[1]Dept. of Earth Sciences, University of Ottawa, Ontario, Canada
([*]khattori@uOttawa.ca)
[2]Dept. of Earth and Planetary Systems Science, Hiroshima University, Higashi-Hiroshima, Japan
[3]BRGM, Orléans, France

Oxygen-bearing platinum group minerals have been reported in weathered rocks and placers from many locations, but their mineralogy has been debated. We obtained X-ray absorption spectra of Pt and Fe from oxygen-bearing Pt-Fe grains collected from a stream in southern New Caledonia. The use of a micro X-ray beam allowed us to obtain spectra from target grains in polished sections. The absorption spectra of Pt-L_{III} edge show that Pt is mostly in the metallic state, not combined with oxygen or OH^-. The calculated bond length between Pt and the neighbouring atoms is much longer than that of Pt-O bond, indicating that Pt is not bonded with oxygen or OH^-. A quantitative simulation of the atomic structure around Pt in the oxygen-bearing Pt-Fe indicates that Pt has lower coordination numbers than that of isoferroplatinum. The results suggest that the oxygen-bearing Pt-Fe has a similar, but disturbed crystal structure around Pt compared to isoferroplatinum.

The absorption spectra of Fe *K*-edge show prominent two peaks at 7122 eV and 7128 eV. Isoferroplatinum has also two peaks at these positions with a larger peak at 7122 eV. On the other hand, oxygen-bearing Pt-Fe has a larger peak at 7128 eV and a smaller peak at 7122 eV, suggesting the presence of a different phase in the sample. Considering the electron probe data of these Pt-Fe grains, possible phases are Fe^{3+}-bearing phases. A 10:90 mixture of ferrihydrite (Fe^{III}-O-OH) and isoferroplatinum yields the observed absorption spectra. The data suggest that the oxygen-bearing Pt-Fe is a physical mixture of relict isoferroplatinum and newly precipitated Fe^{III}-O-OH. We suggest that oxygen-bearing Pt-Fe grains formed from isoferroplatinum by the dissolution of metallic Fe from isoferroplatinum in reduced alkaline waters within weathering ultramafic rocks, followed by the dissolution of Pt and precipitation of Fe^{3+} after the host ultramafic rocks are exposed to the atmosphere.

Application of laser micro-Raman spectroscopy: an efficient tool to identify platinum group minerals

Zaccarini, F.[*], Bakker, R.J., Garuti, G. & Thalhammer, O.A.R.
Dept. of Applied Geosciences and Geophysics, University of Leoben, Austria ([*]federica.zaccarini@unileoben.ac.at)

The identification of nanometer-scale minerals, such as most of Platinum group minerals (PGM) is a challenging target. The main reason for that resides in their size and mode of occurrence (i.e. polyphasic aggregates) that prevent any XRD structural study. Although with some limitations, optical and electron microscopy and determination of micro-hardness are the most used techniques for mineralogical identification of PGM. Even the most precise technique, the electron microprobe, requires accurate calibration of the instrument in order to reduce analytical uncertainties. In this contribution we present the results obtained using laser-Raman microprobe on different PGM, such as sulphides, arsenides, sulpharsenides and alloys. All the analyzed PGM, with the exception of alloys, show a very well-defined and characteristic spectrum, suggesting the presence of covalent bonding. On the contrary, the Raman spectra of alloys are flat suggesting that the possible bonds present in these PGM are metallic or ionic. Our data indicate that Raman is also sensitive on the compositional variation, particularly in the PGM characterized by a solid solution substitution such as laurite-erlichmanite series. These results, although preliminary, demonstrate that Raman spectroscopy is a fast and cost-efficient technique that can be considered innovative and complementary method with a huge potential to identify and to better characterize the nanometer-scale PGM. However, this technique does not provide a chemical composition of the investigated minerals. Therefore, it is intended to apply the Raman spectroscopy to a great number of different PGM, already characterized by electron microprobe, with the aim of assembling a future data base of Raman spectra of PGM.

Mineral chemistry of Pt-Fe-Cu-(Ni) nuggets from the Yubdo placer deposit (Ethiopia)

Mogessie, A.[1*], Zaccarini, F.[2], Garuti, G.[2], Belete, K.H.[3] & Mali, H.[2]
[1]Dept. of Earth Sciences, Karl Franzes University, Graz, Austria ([*]aberra.mogessie@uni-graz.at)
[2]Dept. of Applied Geosciences and Geophysics, University of Leoben, Austria
[3]Golden Prospect Mining, Addis Ababa, Ethiopia

The system Pt-Fe-Cu-Ni consists of the following phases accepted by IMA: platinum (Pt), isoferroplatinum (Pt_3Fe), iron (Fe) all of which are cubic in symmetry have a cubic structure, and tetraferroplatinum (PtFe), tulameenite Pt_2CuFe and ferronickelplatinum, which are tetragonal. On the basis of chemical composition, a phase with ideal formula Pt_2Fe has been recognized in Russian samples, and in particular in nuggets from Nizhny Tagil and Guli massifs and in the chromitites of Kytlim and Uktus complexes. Tetraferroplatinum and tulameenite crystallized in the same system and have a similar cell size. Therefore, a possible solid solution between these two phases is postulated. In this contribution we report on the chemical composition of about 100 Pt-Fe-Cu-(Ni) nuggets collected in the Yubdo placer deposit (Ethiopia). The nuggets have a size variable from 100 µm up to 3 mm. According to their mineral chemistry (about 800 analyses), the following alloys in the Pt-Fe-Cu-Ni system have been identified: 1) Pt_3Fe, possibly isoferroplatinum, 2) tetraferroplatinum that always contains appreciable amounts of Cu and minor Ni, 3) tulameenite and 4) an unknown phase that approaches the Pt_2Fe composition. Based on the chemical composition of the investigated Pt-Fe-Cu-Ni nuggets, we can conclude that: 1) the continuous substitution Cu-Fe at constant Pt found in the Yubdo alloys clearly indicates a complete solid solution between tetraferroplatinum and tulameenite, as previously postulated on the basis of their structural parameters and 2) a Pt_2Fe phase, previously described in Russian localities, has been also found in the Yubdo nuggets. Data available suggest that this alloy possibly represents a new mineral in the Pt-Fe-Cu-Ni system. However, it is not possible to support this conclusion because of the absence of X-ray data (work in progress).

Mineral chemistry of apatite and its relationship to enrichment of platinum-group elements in the South Kawishiwi Intrusion (Duluth Complex)

Gál, B.[1*], Molnár, F.[1], Mogessie, A.[2] & Peterson, D.[3]
[1]Dept. of Mineralogy, Eötvös Loránd University, Budapest, Hungary ([*]galbenedek@yahoo.com)
[2]Institute of Mineralogy and Petrology, Karl-Franzens University, Graz, Austria
[3]Duluth Metals Ltd., Minnesota, Duluth, USA

The South Kawishiwi Intrusion is one of the intrusions that constitute the 1.1 Ga old Duluth Complex, one of the largest unexploited reserves of magmatic Cu-Ni-PGE of the Earth. Involvement of hydrothermal fluids in the partial remobilization and enrichment of platinum-group elements has been reported by several authors in the Duluth Complex [1-3], which is further supported by the results of our current research.

The connection of the late-stage sulfide segregation and fractionation processes with hydrothermal fluid segregation is traced by the halogen chemistry of various minerals phases, primarily apatite. Halogen content of apatite is variable as a function of type and texture of the host troctolitic rocks and stratigraphic height above the footwall contact (Table 1). The Cl-content of apatite is generally the lowest in medium-grained, homogeneous and unmineralized troctolitic units. The presence of a fluid phase enriched in Cl is indicated by the elevated Cl-content of apatite in pegmatitic patches from the same depths. Segregation of a magmatic fluid during crystallization is moreover implied by the increase of F-content (and coeval Cl-depletion) in apatite within single grains and also in late-stage differentiates.

Table 1: Proportions of F, Cl and OH (%) in apatite from selected samples

Drillhole & height above footwall (feet)	Description	X^F	X^{OH}	X^{Cl}
Dh-1 – 178 ft	homogeneous troctolite	73.0	5.5	21.5
Dh-1 – 178 ft	pegmatite	55.4	4.2	40.4
Dh-1 – 73 ft	apatite core[1]	48.9	34.1	17.0
Dh-1 – 73 ft	apatite rim[1]	52.1	36.5	11.4
Dh-2 – 207 ft	average value of sample	51.5	39.3	9.3
Dh-2 – 270 ft	average value of sample	37.8	48.8	13.4

[1] apatite is from a late-stage, differentiated felsic dyke

Platinum-group minerals (e.g. Platinum-Arsenides, Platinum-Palladium-Bismuth-Tellurides, and Rhodium-Arsenides) have been found in association with magmatic sulfides, fractionated sulfide stringers as products of late-stage sulfide melt differentiation, felsic differentiates and hydrothermal alteration (serpentine, Ca-enriched plagioclase). It is clear that distribution of PGEs is not only a function of simple intrusion and crystallization of a silicate melt but interaction with the felsic footwall and later segregation of a volatile-rich phase had its role in later redistribution of these metals.

[1] Mogessie, A. et al. (1991) *Econ. Geol.*, **86**, 1506-1518. [2] Mogessie, A. & Stumpfl, E.F. (1992) *Aust. J. Earth Sci.*, **39**, 315-325. [3] Pasteris, J.D. et al. (1995) *Am. J. Sci.*, **295**, 125-172.

Pt- and Pd- sulfides in ores from Noril'sk region (Russia)

Sluzhenikin, S.F. & Evstigneeva, T.L.[*]
IGEM RAS, Moscow, Russia ([*]evst@igem.ru)

Pt- and Pd- sulfides occur in ores of Noril'sk deposits as cooperate, braggite and vysotskite. As in other deposits these minerals contain Ni less pyrite-chalcopyrite exocontact ores where there is no Ni (Fig. 1).The field of Noril'sk cooperite is quite narrow ranging from $(Pt_{0.96}Pd_{0.02}Ni_{0.02})_{1.00}S_{1.00}$ to $(Ptt_{0.84}Pd_{0.09}Ni_{0.07})_{1.00}S_{01.00}$. Grains of cooperite are always homogeneous in composition. In contrast to those of the braggite – vysotskite series, these are heterogeneous and often zoned.

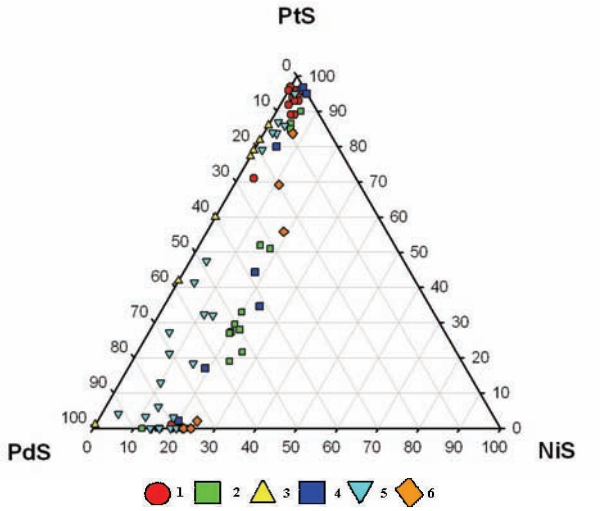

Fig. 1: Composition of Pt-Pd sulfides from Noril'sk region (1 and 6 – Noril'sk 1, 2-5 – Talnakh): 1. Disseminated ores (Noril'sk 1); 2. Dissem.-veinlet exocontact Mil-Bor-Cp and Mil-Pyr-Cp ores; 3. Veinlet-dissem. exocontact Pyr-Cp ores; 4. Breccia ores; 5. Low-sulfide platinum ores; 6. Vertical Cp veins, Morozov mine.

The cores of these zoned aggregates are enriched in Pt, and the rims in Pd e.g., cores with compositions $(Pt_{0.83}Pd_{0.14}Ni_{0.03})_{1.00}S_{1.00}$, middle zones with compositions $(Pd_{0.56}Pt_{0.31}Ni_{0.13})_{1.00}S_{1.00}$, and rims with compositions $(Pd_{0.89}Ni_{0.11})_{1.00}S_{1.00}$. The clearly defined boundary is observed between zones of Pd- and Pt braggites. Grains of Pt- and Pd- braggites are often heterogeneous too. Zoned overgrowths are also typical for Ni-poor Pt- and Pd monosulfides: cores are characterized by "Σ_{metals}:S" varying up to $(Pd,Pt)_{16}S$; intermediate zones are braggite; and the rims are vysotskite. By contrast, monomineral vysotskite grains are homogeneous with compositions that lie within narrow limits, $(Pd_{0.76}\ Ni_{0.24})_{1.00}S_{1.00}$ - $(Pd_{0.86}Ni_{0.14})_{1.00}S_{1.00}$.

The compositions of (Pt,Pd,Ni)S minerals can often be represented using integral numbers of atoms in their formulae, i.e. $Pt_1Pd_1S_2$, $Pd_4Pt_3Ni_1S_8$, $Pt_3Pd_1S_4$ etc. This is in good agreement with composition of phases synthesized in the system Pt-Pd-Ni-S, and characterized by ordered metal atom distribution among 2d, 2e and 4j positions in the tetragonal structure derivative from PdS structure type [1]. Based on this data the minerals relationships in the series PdS-PtS-NiS are discussed.

Acknowledgements: This study was carried out thanks to the financial support of Fundamental Research Programme n.5, Dept.Dci.Earth RAS.

[1] Evstigneeva, T.L. et al. (2004) *Abstracts of EMPG- X, CD-version*. Frankfurt am Main.

Jamestownite: a new PGE-rich rock type from the Barberton greenstone belt, South Africa

Tredoux, M.[1*], Chabangu, N.[1], Wildau, A.[1], Miller, D.E.[2], Zaccarini, F.[3], Garuti, G.[3] & Madala, F.[1]
[1]Geology Dept, University of the Free State, Bloemfontein, South Africa ([*]mtredoux@ufs.ac.za)
[2]Centre for Materials Engineering, University of Cape Town, Rondebosch, South Africa
[3]Dept. of Applied Geosciences and Geophysics, University of Leoben, Austria

It has been demonstrated [1] that the mafic and ultramafic rocks of the Barberton greenstone belt can be interpreted as the remnant of an Archean ophiolite, which was named the Jamestown complex [1]. Part of the lowermost stratigraphic unit of this ophiolite is exposed in the northwestern flank of the belt on the farm Bon Accord (BA); it is an ultramafic rock which has been intensely altered to talc and serpentine. All the contacts are sheared, indicating that it is allochthonous. The geochemistry shows a severe depletion in the LILEs, and dating (Sm-Nd and Pb-Pb) [1,2] points to ~3.5 Ga as the most likely time for the depletion. This rock is therefore interpreted [1,2] as the depleted upper mantle restite from which the overlying volcanic rocks were extracted at an Archean ridge system.

In 1920, a very Ni-rich body was discovered embedded in the BA ultramafite [3] — see Table 1 for its major element chemistry, and Table 2 for some of the unusual Ni minerals it contains. Initially the body was described as an oxidized meteorite [3], but this was rejected on geological and geochemical grounds by Tredoux et al. [2], who postulated a deep mantle origin of a metal-rich silicate, potentially from the D" layer, which got progressively oxidized as it moved through the various redox boundaries in the mantle in a plume.

Table 1: Major element chemistry of the BA body; all values in wt %; analyses obtained by WDXRF

SiO_2	Fe_2O_3	NiO	MgO	Al_2O_3	CoO	Cr_2O_3	Total
15.51	32.57	47.27	2.39	0.88	0.68	0.23	99.52

Table 2: Some of the major minerals in the BA body

Mineral	Composition	Group
Liebenbergite	Ni_2SiO_4	Olivine
Nepouite	$Ni_3Si_2O_5(OH)_4$	Serpentine
Trevorite	$NiFe_2O_4$	Spinel

Investigation of sub-mm sized phases and mineral inclusions in the trevorite has indicated the presence of Fe-Ni alloy, and metallic Si and Ag. Although the body is highly enriched in the PGE (PGE_{tot} > 5000 ppb), only occasional small (<1μm) grains of Ru have been identified as yet.

A metal-rich (FeNi alloy) rock type, found in rivers which drain the Josephine ophiolite in Oregon, USA, was first described and named 'josephinite' in 1892 [4]. In 1975, Bird and Weathers [5] suggested that josephinite may have a deep mantle origin, a suggestion that received support from a study of its $^{186}Os/^{187}Os$ in the 1990s [6].

In light of the fact that BA and josephinite may have a similar origin, we suggest, in line with the naming convention created by Melville [4], that BA be recognised as a new rock type, called jamestownite.

[1] De Wit, M.J. et al. (1987) *J. Afr. Earth Sci.*, **6**, 681-730. [2] Tredoux, M. et al. (1989) *J. Geophys. Res.*, **94**, 795-813. [3] De Waal (1978) in Verwoerd W.J. (ed.) *Mineralisation in metamorphic terranes, Spec. Publ. Geol. Soc. S. Afr.*, 87-98. [4] Melville, W.H. (1892) *Am. J. Sci.*, **43**, 509-515. [5] Bird, J.M. and Weathers, M.S. (1975) *Earth Planet. Sci. Lett.*, **28**, 51-64. [6] Bird, J.M. et al. (1999) *Earth Planet. Sci. Lett.*, **170**, 83-92.

Garutiite, (Ni,Fe,Ir), a new PGE-bearing, hexagonal polymorph of native Ni from Loma Peguera, Dominican Republic

McDonald, A.M.[1*], Proenza, J.A.[2], Zaccarini, F.[3], Rudashevsky, N.S.[4], Cabri, L.J.[5] & Stanley, C.J.[6]
[1]Dept. of Earth Sciences, Laurentian University, Sudbury, Canada ([*]amcdonald@laurentian.ca)
[2]Dept. de Cristal·lografia, Mineralogia i Dipòsits Minerals, Universitat de Barcelona, Spain
[3]Dept. of Applied Geological Sciences and Geophysics, The University of Leoben, Austria
[4]Center for New Technologies, St. Petersburg, Russia
[5]Cabri Consulting Inc., Ottawa, Ontario, Canada
[6]Mineralogy Dept., Natural History Museum, London, United Kingdom

Garutiite (Ni,Fe,Ir) is a new hexagonal polymorph of native Ni discovered in chromitite from Loma Peguera, Dominican Republic. The mineral was identified in heavy mineral concentrates obtained through the use of electric pulse disaggregation (EPD) and hydroseparation (HS) techniques. It forms as anhedral, botryoidal grains typically 10 to 60 μm in size (maximum of 110 μm). Grains are single or composite, frequently porous and zoned, and occasionally display an unusual lamellar internal texture. Associated minerals include hexaferrum, ferrian chromite, chlorite-group minerals, serpentine-group minerals, awaruite, irarsite, laurite, native Ru and unidentified species including Ru-Os-Ir-Fe and Pt-Ni-Fe-Ir compounds, $Pt(Ni,Fe)_3$, $(Fe,Ru,Ni,Os,Ir,Co)_2S$ and RhNiAs. The mineral is megascopically grey to grey-black with a metallic luster. In plane-polarized light, garutiite is white in color, exhibits a very weak anisotropy and no pleochroism, bireflectance or internal reflections were observed. No cleavage was noted and the hardness could not be determined owing to the porous nature of the mineral. The calculated density is 11.33 (1) g/cm^3. Reflectance values (%) in air are: 63.8 at 470, 65.9 at 546, 67.0 at 589 and 68.0 at 650 nm. The average result of electron microprobe analyses (n = 42 from 27 grains) is: Ni 27.91, Fe 19.94, Ir 43.78, Pt 6.98, Co 0.55, Cu 0.43, Ru, 0.50, Rh 0.74, Os 0.67, total 101.51 wt. %, corresponding to $(Ni_{0.421}Fe_{0.316}Ir_{0.202}Pt_{0.032}Co_{0.008}Cu_{0.006}Rh_{0.006}Ru_{0.004}Os_{0.003})_{\Sigma 1}$ or the simplified formula, (Ni,Fe,Ir). Garutiite is the Ni analogue of hexaferrum, osmium and ruthenium and is classified as belonging to the osmium group. As such, the mineral is considered to be hexagonal, crystallizing in space group $P6_3/mmc$ with a 2.6941(4) and c 4.2731(6) Å, V = 26.86(1) Å^3, Z = 2. The strongest lines of the X-ray powder diffraction pattern [d(in Å)(I)(hkl)] are: 2.330(50)(100), 2.136(30)(002), 2.046(100)(101), 1.576(30)(102), 1.3470(40)(110), 1.2155(40)(103). Based on its morphology, internal texture, and the associated minerals, garutiite is interpreted to be secondary in origin, *i.e.*, having formed at low temperatures during post magmatic processes, such as serpentinization and/or lateritization. The mineral may have developed as a highly strained *hcp* polymorph of Ni that was stabilized through heteroepitaxial growth on a precursor phase (native Ru?).

Clay minerals as PGE precursor

Evstigneeva, T.L.* & Trubkin, N.V.
IGEM RASS, Moscow, Russia (*evst@igen.ru)

Some PGM assemblages are closely associated with secondary minerals or their alteration products. Such observations lead to the conclusion that PGM formation could be happened under large temperature scale, possibly up to low-temperatures. There is no question that there are minerals making possible PGM crystallization under different conditions. In such processes clay minerals play a role as natural buffers and PGE precursor.

The formation of PGE-phases under low-temperature conditions with the clay mineral participation was studied experimentally earlier [1]. Results of these experiments showed that the phenomenon of clay saturation in PGE by metal adsorption by clay minerals remains not clear, as well as the position of "adsorbed" metal atoms in clay minerals. These atoms could: a) occupy the structural positions of clay minerals; b) be distributed within the interlayer space; c) form "germs" of proper phases etc. For study the mechanism of PGE-concentration in clay minerals, and check if there is any dependence between PGE content and clay mineral crystal structure the "clay minerals – PGE precursors" a reinvestigation of clay mineral pre-saturated in PGE-bearing solutions at T~60°C was carried out using SEM+EDD and XRDA.

The following results are obtained:

1. Despite the low temperature of "saturation", ~60°C, this process may result in PGE phase formation;
2. After treatment in PGE-bearing solutions near all clay minerals contain different Pt- and Pd- phases with grain dimension ~ 0.0n-0.n microns;
3. In spite of different adsorption capacity of clay minerals used as precursors, kaolinite/halloisite and montmorillonite/smectite there is no remarkable difference in PGE content in clay minerals after saturation;
4. PGE phase composition depends on the solution used for saturation. High acidity favours the formation of Pt/Pd-phases. When the starting solution is Cl-bearing the crystallization of Pt/Pd phases is "blocked" because of Cl-bearing Pt and Pd complex stability.

The presence of tiny PGE particles shows that there is any PGE adsorption by clay minerals. According to XRDA Pt and Pd are not included in clay mineral structures. Based on data obtained the reason PGE concentration in clay minerals is not the surface charge, as was proposed [2], but the precipitation of PGE nanoparticles or their aggregates on the clay mineral surface. The similar fine-grained PGM (i.e. Pt, PtS and Pd-sulphides) were found in coals and black shales (i.e. [3,4]).

Acknowledgements: The reinvestigation of PGE-precursors was carried out thanks to the financial support of RFBR, Grant n. 08-05-01016a, and Fundamental Research Programme n.5, Dept.Dci.Earth RAS.

[1] Evstigneeva, T. & Tarkian, M. (1995) in Pašava, J., Kribek, B. & Žak, K. (eds.) *Mineral Deposits: from their origin to their environmental impacts*. A.A.Balkema, Rotterdam, 731-734. [2] Fuks, W.A. & Rose, A.W. (1974) *Econ. Geol*., **69**, 332-346. [3] Seredin, V.V. et al. (1994) *Abstracts of 7th Platinum Symposium*. Moscow, IGEM, 110. [4] Negrutsa, V.S. & Polekhovsky, Y.S. (1994) *Abstracts of 7th Platinum Symposium*. Moscow, IGEM, 85.

Gold-platinum mineralization in the laminated pluton, the Polar Urals

Pystin, A.M.*, Pystina, Yu.I. & Potapov, I.L.
Institute of Geology, Komi Science Centre Ural Branch of RAS, Syktyvkar, Russia, Republic of Komi (*pystin@geo.komisc.ru)

Endogenic platinoid manifestations in chromite-bearing ultrabasites of the Paleozoic ophiolite association have been well known in the Polar Urals for a long time. The platinum group minerals are represented by relatively infusible Ru-Os-Ir–content varieties with secondary Pt, Pd, and Rh. During the additional geological study (scale 1:200000) of the territory, in 2002, a low-sulphide copper appearance has been discovered in the Kharamatalou river drainage system. Au and Ag minerals in association with Pd, Bi, and Te ones were established for the first time in the above mentioned region's copper ores; Pt minerals were revealed later.

According to a modern point of view, the Ozernoe manifestation is confined to the Kershor intrusive complex being a gabbroid part of the Voikar ophiolite complex chiefly. As a result of our investigations, the Dzelyatysher ore-bearing wherlite-clinopyroxene massif (1.0 x 4.0 km in area) was established to be sharply different from surrounding it basic-ultrabasic formations in rhythmic sheeting, orientation of primary structures (transversal in relation to the Uralian ones), and peculiar chemical composition of rocks and rock-forming minerals. On the basis of these characteristic features, the massif is considered as similar to laminated plutons and is construed as a fragment of the ancient (Precambrian) sheeted pluton combined with the Paleozoic ophiolite association rocks tectonically [1].

The precious metal mineralization in the Dzelyatysher massif is confined to the olivine pyroxenites taking middle to upper positions in the observed section.

Precious metal minerals are represented by Au, Ag, and Pt native formations; Au, Ag, Pt, and Pd intermetallids; arsenides, tellurides, antimonides, and Pt-Pd bismuthides. The natural formations and intermetallids of precious metals, as well as Pt and Pd sulphides, compose little inclusions in initial silicates and ore minerals. The arsenides, tellurides, antimonides, and bismuthides constitute two genetic groups. One of them consists of the substitutional products after native platinoids, intermetallids, and sulphides. The other is characterized by the independent neogeneses in association with secondary silicates and ore minerals.

The following model of ore elements formation and accumulation is proposed:

- Precious metals and copper were stored in magnesial rocks (high-olivine content clinopyroxenites) during the massif formation.

- Hydrothermal-metasomatic processes, which were connected with intruding and cooling of gabbro intrusions, led to the formation and accumulation of Au-Cu sulphide mineralization along the borders on the gabbro intrusions and in zones parallel to them. The same processes resulted in transformation of platinoids into the sulphide type.

- Low-temperature alterations of rocks, majorly appearing in their serpentinization, brought to Au and Cu sulphides redistribution. The processes contributed to crystallization of platinoids as arsenides, antimonides, and bismuthides.

[1] Pystin A.M. et al. (2007) in *Geodynamics, magmatism, sedimentogenesis and mineralogeny of the North-western Russia*. Petrozavodsk, 329-331.

Primary and secondary platinum group minerals (PGM): an example from the chromitites of Bursa ophiolite (NW Turkey)

Uysal, I.[1*], Zaccarini, F.[2], Garuti, G.[2], Koprubasi, N.[3], Demir, Y.[4] & Thalhammer, O.A.R.[2]
[1]Dept. of Geological Engineering, Karadeniz Technical University, Trabzon, Turkey ([*]iuysal@ktu.edu.tr)
[2]Dept. of Applied Geosciences and Geophysics, University of Leoben, Austria
[3]Dept. of Geological Engineering, University of Kocaeli, Turkey
[4]Dept. of Geological Engineering, University of Gumushane, Turkey

Based on their textural position, shape and morphology, the PGM associated with ophiolitic chromitites have been grouped in: (1) primary magmatic and (2) secondary hydrothermal or weathering-related. Primary PGM form polygonal grains and generally occur enclosed in fresh chromite. They crystallized at magmatic T, above 1000°C, under the appropriate condition of $f(S_2)$. Secondary PGM have an irregular shape and zoning and are associated with altered minerals. Their origin is still not totally understood. They may have formed in situ, after a pre-existing unstable PGM or precipitate from a solution at low T. We report on the presence of primary and secondary PGM discovered in the Bursa ophiolitic chromitites, (NW Turkey). The PGM have a size between 1 and 10 μm and according to their chemical composition, PGE sulphides (laurite, erlichmanite, cuproiridsite and unknown Ir-Ni-Fe-S), sulpharsenides (irarsite and hollingworthite) and alloys (iridium) have been found. Considering their morphology and textural position, the PGE sulphides are primary. Irarsite, hollingworthite and iridium are secondary. The absence of magmatic Os-Ir-Ru alloys and the presence of abundant Os-rich laurite, erlichmanite and other Ir sulphides as primary PGM indicate that they crystallized at T of about 1000°C, under relatively high $f(S_2)$. Few PGM (iridum, irarsite and hollingworthite) were altered and it was possible to establish that iridium represents a low-temperature exsolution product, whereas the presence of secondary sulpharsenides suggest an increase in the As activity, probably related with hydrothermal solutions, capable to remobilize PGE at small scale.

Platinum group minerals in Brazilian chromitites from Serro, Alvorada de Minas and Pedra Branca: evidence for a stratiform origin

Angeli, N.[1*], Zaccarini, F.[2], Garuti, G.[2], Thalhammer, O.[2], Proenza, J.A.[3] & Walsh, L.[1]
[1]Sao Paulo State University, Rio Claro, Brazil ([*]nangeli@rc.unesp.br)
[2]Dept. of Applied Geosciences and Geophysics, University of Leoben, Austria
[3]Dept. of Crystallography, Mineralogy and Ore Deposits, University of Barcelona, Spain

Chromitites from Serro and Alvorada de Minas (Minas Gerais) and Pedra Branca (Ceara) have been studied for Platinum-Group Minerals (PGM), using the traditional *in situ* investigation. Therefore, the PGM were previously located on polished section using reflected-light and electron microscopy, and subsequently they have been identified by electron microprobe analyses. PGM are less than 10 μm in sizye and they have been found in the altered silicate matrix, mainly composed of chlorite, or in contact with ferrian chromite. They occur either as single-phase grains or associated with secondary Co-Ni sulfarsenides. The mineralogy includes laurite (RuS_2), irarsite (IrAsS), hollingworthite (RhAsS), native osmium, sperrylite ($PtAs_2$), cooperite (PtS), and unnamed Pd-Te-Bi-(Sb) compounds, possibly referable to one of the following species: merenskyite ($PdTe_2$), kotulskyite $Pd(Te,Bi)_2$, michenerite (PdBiTe). Besides the Co-Ni sulfarsenides, the assemblage comprises pentlandite, millerite, pyrite, pyrrhotite, chalcopyrite, galena and a number of secondary sulfides formed at low temperature (siegenite, heazlewoodite, polydimite). Texture and paragenesis of the PGM indicate that the minerals were reworked or re-deposited under hydrothermal conditions, possibly by alteration-dissolution of primary PGM originally occurring in the rim of chromite grains or in the interstitial silicates. The most abundant PGM contains PPGE, whereas IPGE phases are rare. Although the PGE mineralogy has been modified by hydrothermal alteration, it strongly suggests a stratiform origin of the chromitite layers and their ultramafic host. This assumption is also supported by the composition and texture of the host chromite (well preserved cumulate texture).

PGE concentrations in spinel-group minerals from Guli massif, Polar Siberia

Zaitsev, V.A.
V.I. Vernadsky Institute for Geochemistry and Analytical Chemistry (GEOKHI), RAS, Moscow, Russia (va_zaitsev@inbox.ru)

Guli massif (Polar Siberia, Russia) is the word-largest alkaline-ultramafic massif. Among the alkaline-ultramafic massifs with native-metal mineralization, Guli massif is unique by the Os-specific. If was shown that ultramafic rocks of Guli massif strongly vary in concentrations of PGE [1].

Our studies, as well as studies ones, show that ultramafites of Guli massif vary in spinel-group minerals composition from ferrichromite to titanomagnetite and magnetite [2-4].

We studied samples of dunite with chromite and magnetite idiomorphic crystals, dunite with xenomorphic chrommagnetite and olivenite with titanomagnetite. We have obtained the native-metal concentrations in monomineral concentrates of spinel-group minerals using neutron-activation analyses.

Wall-rock concentrations of PGE do not correlate with spinel composition. But Os, Ir and Ru content in monomineral fractions decrease from chromite (161 ppb Os+Ir+Ru) to chrome-magnetite (78 ppb Os+Ir+Ru), titano-magnetite (47 ppb Os+Ir+Ru) and magnetite (0.5 ppb Os+Ir+Ru). In the same time, all spinel concentrates are close in Pt-content (115-250 ppb).

We believe that difference in PGE behaviour can be explained if spinel minerals concentrate the Os-group metals during magmatic stage, while Pt – in postmagmatic process.

[1] Kogarko, L.N., Ukhanov, A.V. & Nikolskaja, N.E. (1994) *Int. Geochemia*, **11**. [2] Egorov, L.S. (1991) *Ijolite-carbonatite plutonism (on the sample of Maymecha-Kotuy complex, Polar Siberia)*. Nedra, Leningrad. [3] Malich, K.N. (1999) *Platinoides of clinopyroxenite-dunite massifs of East Siberia*. VSEGEI, St. Peterburg. [4] Zaitsev, V.A. & Senin, V.G. (2009) *Abstr. XXVI Int. Conf. "Geochemistry of magmatic rocks"*. Moscow, 173-175.

Platinum-group elements (PGE) – mineralization from ophiolitic complex of Albania

Çina, A.
Institute of Geosciences, Polytechnic University of Tirana, Albania (al_cina@yahoo.com)

The Jurassic ophiolitic complex of Albania, situated between the Dinarides and Helenides, is constituted by two well distinguished belts: the Eastern belt is of IAT-type, composed of low-Ti basaltic pillow-lavas, and is considered to be formed in a SSZ. The Western belt is of MORB-type, composed of high-Ti basaltic volcanites. The Eastern belt is characterised by high partial melting of upper mantle and is remarkable for its metallageny, particularly important are Cr-deposits of metallurgical type. Four types of PGE mineralizations were identified, on the basis of the geological setting, the mineral assemblages, the chemical composition, and the PGE contents [1,4].

The first PGE-mineralization is related to the deepest mantle chromitites. It is composed of Ru-Os-Ir alloys and their sulphides, occurring as minute inclusions within host chromite grains. The (Pt + Pd)/(Ru + Os + Ir) ratios are very low, less than 0,1, but Pt/ (Pt + Pd) ratios are very high, from 0,65 to 0,75. The PGE concentration is very limited, ranging from 200 to 350 ppb.

The second type is related to upper mantle chromitites. It is represented by PGE-BM sulphides and arsenides, forming interstitial grains between the chromite. The Pt/(Pt + Pd) ratios are high (i.e. 0,65 to 0,75). The PGE concentrations are relatively higher, ranging from 580 to 2050 ppb [1,2].

The third type of PGE mineralization is represented by PGE-hosting pentlandite disseminations related to super MOHO dunites. The Pt+Pd concentrations dominate compared to Ru+Os+Ir expressed by Pt+Pd/(Ru+Os+Ir) ratios from 50 to 80. Pd predominates over Pt, the Pt/(Pt +Pd) ratios are 0,26 - 0,32. This PGE mineralization-type is similar to those in stratiform complexes; the total PGE concentrations range from 2200 to 8820 ppb.

The fourth type is related to cumulate Fe–rich chromitites, of a brecciated dunite-pyroxenite sequence. The mineral composition comprises of dominant PGE + BM alloys and PGE-BM sulphides and arsenides. The abundant minerals are Pt+Fe alloys, tetraferroplatinum and isoferroplatinum. Pt+Pd concentrations predominate over Ru+Os+Ir, the Pt+Pd/(Ru+Os+Ir) ratios range from 14 to 16. The Pt/(Pt + Pd) ratios are 0,8 to 0,9, mirroing the predominance of Pt. The total PGE concentrations lie between 1950 and 9750 ppb. The PGM usually form euhedral inclusions within chromite grains, but some of them are situated as interstitial grains [3,4].

The mineralogical and geochemical characteristics of these PGE mineralizations, are strongly related to the geological settings and the evolution of mineral-forming processes, starting from the lower mantle upwards to cumulate sequences. A primary magmatic genesis is suggested for PGM, followed by latter hydrothermal-serpentinization processes, which had partly transformed early minerals, into new PGM and BMS [1,4].

[1] Cina, A. et al. (1995) *Documents du BRGM*, **244**, 47-60. [2] Karaj, N. (1992) *PhD Thesis*, Univ. D'Orleans. [3] Neziraj, A. (1992) *PhD Thesis*, Univ. D'Orleans. [4] Ohnenstetter, et al. (1991) *C.R. Acad. Sci. Paris*, **313(II)**, 201-208.

Platinum group minerals in podiform chromitites from Khoy and Neyriz ophiolites (Iran): genetic implications

Azim Zadeh, A.M.[1*], Zaccarini, F.[1], Garuti, G.[1], Moayyed, M.[2], Uysal, I.[3] & Mirmohammadi, M.[4]
[1]Dept. of Applied Geosciences and Geophysics, University of Leoben, Austria ([*]amir.azimzadeh@unileoben.ac.at)
[2]Faculty of Natural Sciences, University of Tabriz, Tabriz, Iran
[3]Dept. of Geological Engineering, Karadeniz Technical University, Trabzon, Turkey
[4]School of Geology, University College of Science, University of Tehran, Tehran, Iran

We report on the presence of platinum group minerals (PGM) in podiform chromitites from the Khoy and Neyriz ophiolites (Iran), with the aim of better understanding the mechanism of PGM precipitation in ophiolitic chromitites. The Khoy massif is Upper Cretaceous in age, originated in a slow-spreading oceanic ridge. The Neyriz complex is considered a supra subduction zone (SSZ) ophiolite of Cretaceous age. The investigated chromitites are hosted in serpentinized mantle tectonites. The Khoy chromitites are Al-rich, whereas those of Neyriz are Cr-rich. Both the chromitites proved to contain PGM less than 10 microns in size. The PGM generally occur included in fresh chromite, suggesting their magmatic origin. With the exception of one unnamed Ir-Cu sulfide, possibly cuproiridsite, laurite is the only magmatic PGM found in the Khoy chromitites. Most of the laurite occur as single phase grains. The Neyriz chromitites contain laurite, erlichmanite, osmium and iridium. Most of these PGM occur associated with amphibole and chlorite. The Khoy PGM crystallized in a narrow range of T around 1000°C, at relatively low $f(S_2)$ and in absence of fluids. PGM in the Neyriz precipitated at higher T, up to 1200°C, at very low $f(S_2)$, as testified by the prsence of PGE alloys, and continued up to reach the erlichmanite stability field at lower T and higher $f(S_2)$. The common paragenesis of PGM + hydrous silicates found in the Neyriz chromitite suggests that they precipitated in the presence of fluids, in a similar way proposed for PGM associated with other SSZ chromitites. The PGM of Iranian chromitites, coupled with chromite composition, can be successfully used to model the mechanism of their precipitation as well as to provide information on the geodynamic setting in which their host chromitites formed.

PGM types and trends from Novoseltsi placers, Bourgas district, Bulgaria

Bogdanov, K.B.[1*] & Tsintsov, Z.L.[2]
[1]Dept. of Mineralogy, Petrology and Economic Geology, Sofia Universiy "St. Kl. Ohridski", Sofia, Bulgaria ([*]kamen@gea.uni-sofia.bg)
[2]Central Laboratory of Mineralogy and Crystallography, Bulgarian Academy of Sciences, Sofia, Bulgaria

Wide variety of PGM [1,2,6] including the type locality of vasilite $(Pd,Cu)_{16}(S,Se)_7$ [1] occur amongst the Middle Eocene gravels, sands and clays around the Novosetsi (Konstantinovo) village in the Eastern Srednogorie of Bulgaria. The PGM obtained from the heavy mineral concentrates include: 1) Fe-bearing platinum and isoferoplatinum Pt_3Fe; 2) Os-rich (Os-Ir-Pt) alloys and Cu-Sn-Zn alloys; 3) Sulphides: PtS, (Pt,Pd)S, (Pd,Ni)S, RhAsS, RuS_2, OsS_2, $(Cu,Pt.Ir)S_2$, $(Rh,Ir,Pt)_{1.77}S_3$ and $(Pd,Cu)_{16}(S,Se)_7$[1,2,6]; 4) Tellurides: Pd_9Te_4. Other minerals found in the polished sections are Cu-Sn-Zn alloys ($Cu_{0.83-0.88}Sn_{0.03-0.12}Zn_{0.05-0.10}$) and gold displaying zoned pattern of electrum rich core ($Au_{0.61}Ag_{0.39}$) and rim almost devoid of Ag ($Au_{0.99}Ag_{0.01}$) as a result of leaching during the transport.

The individual grains of the studied PGM are subhedral to anhedral and from about 10μm to 2-3mm in size. Os-dominant minerals are most abundant varieties associated with Fe-bearing platinum which also occur as homogeneous and separate grains. Some grains have euhedral shapes and others have round shapes, suggestive of melt droplets. Most of these grains consist mainly of Pt (62.33-81.85 at%) and Fe (11.96-24.73 at%) accompanied by varying amounts of other PGE such as Pd (0.30-19.49 at%), Rh (1.44-4.38 at%), Ir (0.27-6.18 at%) and Os (0.10-2.19at%). Os-rich (Os-Ir-Pt) alloys (56.65-87.18 at% Os) are intergrown with Fe-bearing platinum and contain Ir (13.37-27.69 at%), Pt (2.36-20.04 at%), Ru (1.64-2.84 at%) and Rh (0.39-1.12at%). Os:Ir ratios are most commonly approximately between 5:1 and 2:1 with two compositions with empirical formulas $Os_{0.57}Ir_{0.16}Pt_{0.20}Fe_{0.03}Ru_{0.02}Rh_{0.01}$ and $Os_{0.62}Ir_{0.17}Pt_{0.15}Fe_{0.03}Ru_{0.02}Rh_{0.01}$ plotted in the field of the given immiscibility gap [3,5].

Os and Pt dominant alloys represent the main magmatic trend. The close association of the Pt-Fe alloys and Os-dominant alloys suggests a common origin. Next, abundant and characteristic for Novosetsi placers is the sulphide trend with exsolution of laurite, erlichmanite, braggite, vysotskite, hollingworthite, vasilite, indicating for rise of fS_2 with increasing role of Pd, Ni, Cu and As in addition to Se and Te with decreasing temperature. The Pt x 100/(Pt+Ir+Os) ratio [4] seems to be extremely high (>98) supporting the conclusion that possible source for the PGM are relics of non-ophiolitic pyroxene bearing hidden, or eroded mafic intrusions affected by post magmatic alterations.

[1] Atanasov, A.V. (1990) *Can. Mineral*., **28**, 687-689. [2] Bonev, I. & Jordanov, J. (1986) *Geol. Zbornik*, **37(6)**, 709-713. [3] Daltry, V.D.C. & Wilson, A.H. (1997) *Mineral. Petrol*., **60(3-4)**, 185-229. [4] Cabri, L.J. & Harris, D.C. (1975) *Can. Mineral*., **13**, 266-274. [5] Harris, D.C. & Cabri, L.J. (1991) *Can. Mineral*., **29**, 231-237. [6] Tsintsov, Z.L. & Petrov, O.E (1993) *Compt. Rend. Acad. Bulg. Sci*., **47(2)**, 65-68.

First report of Platinum Group Minerals in garnet peridotites from the Central Vosges, France

Delangle, C.[1], Ohnenstetter, M.[1,2*], Ohnenstetter, D.[1,2] & Grémillet, J.P.[1]
[1]Centre de Géologie Terrae Genesis, Saint Amé, France
[2]C.R.P.G.-C.N.R.S. Nancy-Université, Vandoeuvre-lès-Nancy, France ([*]mohnen@crpg.cnrs-nancy.fr)

Platinum Group Minerals (PGM) are described for the first time in garnet peridotites from the Moldanubian zone of the Central Vosges. Garnet peridotites occur as lenses of variable size (length up to 1 km) in the uppermost leptynitic granulite unit [1,2]. During their rapid ascent towards the upper crust, garnet peridotites evolved from high pressure >4.9 GPa and T >1100°C, towards lower pressure conditions 1.6-2 GPa and 700-800°C [3], bedore final emplacement against crustal granulites [4]. PGM have been found in garnet dunite and garnet pyroxene-poor lherzolite samples from the Blanchefontaine and Malpoirier bodies, respectively. PGM are of very small size, less than µm. Some of them were analyzed using an EDS coupled with a Hitachi SEM.

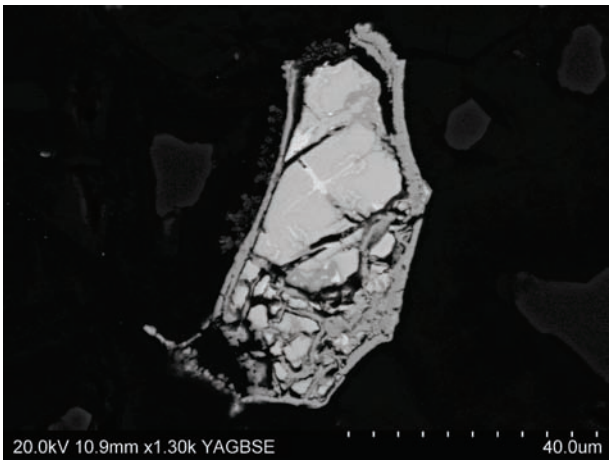

Fig. 1: Sperrylite (inside the circle) within a Co-rich pentlandite partly transformed into hematite (scale bar 40 µm).

Sperrylite ($PtAs_2$), genkinite $(Pt,Pd)_4Sb_3$, kotulskite $Pd(Te,Bi)_2$, zvyagintsevite Pd_3Pb, and pasavaite $Pd_3Pb_2Te_2$ have been found as well as a Pt-bearing aurostibite $AuSb_2$. PGM are often associated with Co-bearing pentlandite (see Fig. 1) and less commonly with pyrrhotite and millerite.

The presence of tellurides, antimonides and intermetallic compounds reflects hydrothermal low temperature formation conditions [5] possibly related to late-stage serpentinization. It is suggested that high temperature sulphide solid solutions and some PGM such as sperrylite, would have been deposited during melt percolation in an ascending garnet peridotite sub-continental mantle slice. This process is comparable to what is recorded in some oceanic and ophiolitic mantle diapirs [6] and documents a new case of platinum-group element resetting.

[1] Mougeot, A. (1880) *Not. Sci. Ann. Vosges*, **2**, 9-12. [2] Hameurt, J. (1967) *Mém. Serv. Carte Géol. Als. Lorr.*, **26**. [3] Altherr, R. & Kalt, A. (1996) *Chem. Geol.*, **134**, 27-47. [4] Gayk, T & Kleinschrodt, R. (2000) *J. Metamorph. Geol.*, **18**, 293-305. [5] Watkinson, D. & Ohnenstetter, D. (1992) *Can. Mineral.*, **30**, 121-136. [6] Ohnenstetter, M. (1992) *Mineral. Petrol.*, **46**, 85-107.

A self-aggregation of platinum group minerals from clusters

Distler, V.V.[*] & Yudovskaya, M.A.
IGEM RAS, Moscow, Russia ([*]distler@igem.ru)

The surfaces of crystals of isoferroplatinum, Os-Ir-Ru alloy and other noble-metal bearing minerals recovered from active volcanic fumaroles have been analyzed and found to contain distinctive, nano-sized features. The nano-block “parquet”-type structure was first observed using atomic force microscopy (AFM) on the facet surface of crystals of isoferroplatinum (Fig.1). The surface is characterised by a structure that is based on the regular combination of square-shaped (for isoferroplatinum) or rhomb-shaped blocks (for Os-Ir-Ru alloy) The different scales and self-similar character of the nano-block integration were estimated using conventional Fourier- and wavelet transforms. This specific type of scalable structure, comprising a regular combination of nano-blocks (or parquets) of different sizes, can be considered as a quasi-crystalline structure. The smallest elements of the structure were estimated to be a few tens of nm.

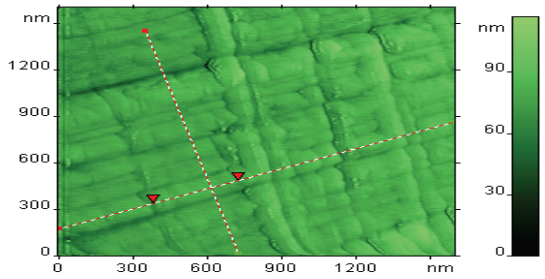

Fig. 1: AFM-image of the surface of isoferroplatinum which reveals parquet-type pattern.

A possibility of the nano-phase self-aggregation was also observed in the sublimates of gaseous fluids in the fumarole fields of the Kudryavy volcano, the Iturup Island, Kuril islands. Nano-sized particles of native Pt, $Pt(OH)_2$ and platinum-chloro-phosphoro-hydrocarbon compound $PtCl_2[P(C_4H_9)_3]_2$ in an assemblage of various rare- and noble-metal phases were identified using an XPS.

New additional evidence of a naturally occurring periodic structure was recently obtained for natural alloy Khatyrskite $(Cu,Zn)Al_2$ that confirm that quasicrystals can form and remain stable under geologic conditions [1]. It was also experimentally shown using in situ transmission electron microscopy that a growth of platinum nanocrystals can occur not only by monomer attachment but also by particle coalescence or self-aggregation [2].

The given data confirm the existence of such periodic structures as quasicrystals in nature. Their structure is characterised by rotational symmetry and fractal ordering although the absence of a translation mechanism. The formation of similar fractal structures in nature appears to relate to specific disequilibrium conditions involving steep temperature or chemical gradients that lead to formation of great number of compounds with various structures. Such processes can be a result of heterogeneous gas-transport reactions of gas - solid and gas - liquid - solid under disequilibrium conditions. One of the most important features of the gas-transport reactions is that they provide formation of zero-valent metal state without achieving high-reduced conditions of mineralisation.

[1] Bindi, L. et al. (2009) *Science*, **324**, 1306-1309. [2] Zheng, H. et al. (2009) *Science*, **324**, 1309-1312.

Platinum Group Minerals of Ranomena chromitite, Tamatave district, Madagascar

Grieco, G., Merlini, A.*, Cazzaniga, A. & Moroni, M.
Dept. of Earth Science, University of Milan, Milan, Italy
(*anna.merlini@unimi.it)

Madagascar is rich in chromite deposits scattered through the Archean terranes. The main ore districts are, from North to South, Befandriana, Andriamena and Tamatave. Platinum Group Minerals (PGMs) were detected as inclusions in chromite grains as well as in the chromitite matrix in the Ranomena deposit, belonging to the Tamatave chromite district. The Ranomena deposit is characterised by a series of highly deformed and metamorphosed, subparallel metric chromitite lenses, hosted within basic-ultrabasic rocks. Chromitite is characterized by variable textures from disseminated to massive.

The chromitite mineral assemblage is mainly composed of low Cr_2O_3 chromite (with compositional variation up to ferritchromite and magnetite), orthopyroxene, olivine and secondary phases like chlorite, amphibole, talc and serpentine. Rutile and ilmenite as well as minor sulphides, like chalcopyrite, pentlandite and hazlewoodite, occur in the matrix.

Several small (10-30 µm) PGM grains were observed in almost all samples, regardless of the chromitite texture.

The most abundant phase is euhedral laurite (RuS_2) included in chromite grains. X-ray atomic maps confirmed the polyphase nature of very fine-grained PGM aggregates, in which at least the occurrence of irarsite ((Ir, Ru, Rh, Pt,)AsS) and stillwaterite (Pd_8As_3) was ascertained by micro-analysis. Some alloys containing Pt, Ru, Fe and traces of As were also detected within the matrix.

Platinum Group Elements (PGEs) were analysed on whole rock samples by Nickel Suphide Fire Assay- Instrumental Neutron Activation Analysis (INAA). All analysed samples show similar trends characterized by a general depletion in Pt, Pd and a high Os/Ir ratio. The general PGE trends are in accordance with the occurrence and the composition of PGMs detected, therefore suggesting that they are representative of the chromitite PGM assemblage.

According to the model proposed by Maier and Barnes [1] for the UG1-UG2 Bushveld chromitites, the PGE geochemical signatures (except for Pd) suggest a Bushveld-type genesis for the Ranomena Cr-PGE ores. The low abundance of Pd in Ranomena ores might be related to post-ore metasomatic processes.

The relationships between the Ranomena chromitite and the other main chromitite ores of Madagascar are still unclear. Chromitite ores display significant compositional differences, in spite of their similar geological settings. These differences might be related either to different depositional processes that influenced also the distribution of PGMs (less abundant in the Andriamena and Befandriana chromitites than in Ranomena), or to different post-ore processes (e.g., metamorphic imprints).

[1] Maier, W.D. & Barnes, S.J. (2008) *South Afr. J. Geol.*, **111**, 159-176.

In-situ, MLA-based mineralogical assessment of Platinum Group Minerals associated with chromitite stringers in the Merensky Reef of the Eastern Bushveld Complex, South Africa

Rose, D.H.*, Knoper, M.K, Rajesh, H.M. & Viljoen, K.S.
Dept. of Geology, University of Johannesburg, South Africa
(*derekr@postgrad.uj.ac.za)

Although primarily optimised for the examination of mineral concentrates (e.g. platinum group minerals, PGM), modern, automated electron microscope-based image analysers such as FEI's Mineral Liberation Analyser (MLA) has proven to be useful in mineralogical studies at the thin section scale [1]. In view of this, a study to assess the nature and abundances of PGM's occurring within the Merensky Reef was undertaken at the Two Rivers Platinum Mine on the Eastern Limb of the Bushveld Complex in South Africa. The application of the Field Emission MLA at the University of Johannesburg allows for rapid data acquisition, while the examination of thin sections ensures that mineral association information is preserved. A primary aim of the study is to identify the PGM phases present in chromitite stringers within the Merensky Reef at Two Rivers, and also to determine the nature of associated phases, in a statistically representative manner. As is typical for the Merensky [2], three primary mineral associations are observed, being (i) PGM-base metal sulphide (BMS), (ii) PGM-silicate, and (iii) PGM-chromite.

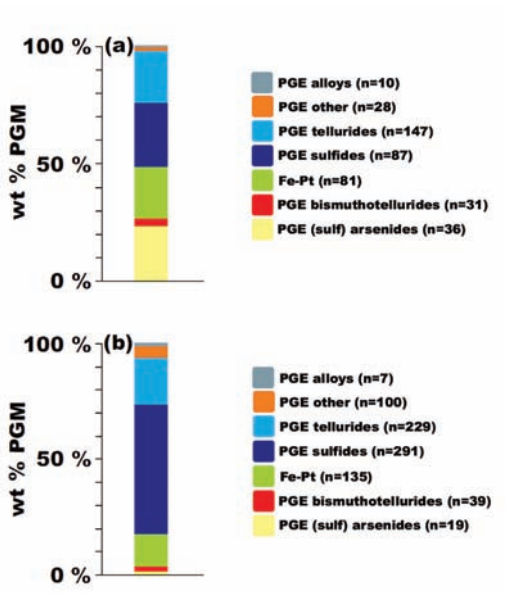

Fig. 1: Histograms illustrating the variation in PGM abundance (wt%) for samples from (a) Upper and (b) Lower chromitite stringers in the Merensky Reef at Two Rivers. n = grain counts of the PGM.

Zonation of the PGM assemblages associated with the chromitite stringers is observed (Fig. 1). Chromitite stringers that occur in the uppermost reaches of the Merensky Reef are associated predominantly with ferroplatinum, PGE sulfarsenides, sulfides and tellurides, all of which occur in similar proportions. These PGM assemblages are also observed in samples of basal chromitites The PGE sulfarsenides however now form a negligible group relative to that of the same group in the chromitites of the uppermost reaches. PGE sulfides are also dominant in the basal chromitite stringers

[1] Voordouw, R.J., Gutzmer, J. & Beukes, N.J. (2010) *Miner. Deposita*, **45(2)**, 147-59. [2] Vermaak, C.F. & Hendriks, L.P. (1976) *Econ. Geol.*, **71**, 1244-1269.

Associations and genesis of Pd, Pt, Au, Ag, Co, Cu, Ni, Fe in magmatic sulphide ores in Pay-Khoy (Russia, Nenets Autonomous District)

Shaybekov, R.
Institute of Geology, Komi Scientific Center, Uralian Branch, Russian Academy of Sciences, Syktyvkar, Russia, Republic of Komi (shaybekov@geo.komisc.ru)

The work presents new data on the composition, associations and genesis of sulphide minerals and minerals of platinum group (MPG) in copper-nickel shows in the Central Pay-Khoy (370±2.0 – 381.4±2.0 Ma). By now a wide areal distribution of differentiated intrusions of basic composition is determined in the Central Pay-Khoy, where sulphide copper-nickel ores are found. The sulphide mineralization is spatially and genetically related to subintrusive bodies of dolerites, having a distinct stratigraphic distribution and being confined to the horizons of the most differentiated coarse-crystalline dolerites. In ore occurrences the primary Co, Cu, Ni, Fe associations and later are determined, which are formed by substitution of earlier ore associations. Fe – Ni – Co – Cu – sulphides are developed in intergranular space of plagioclase and pyroxene; less frequently they form accretions with late- and postmagmatic minerals.

As a rule, the sulphides are dominated by pyrrhotine, chalcopyrite, pentlandite, cobaltite. *Pyrrhotine*, predominating mineral of the given object, forms small buildups in rock forming minerals and shliers of different sizes. *Chalcopyrite*, the second sulphide by the level of distribution is found as separate xenomorphic grains of irregular form in distal parts of pyrrhotine shliers and inclusions or forming independent inclusions. One of the most important ore minerals and rather widely developed, *pentlandite* is observed as xenomorphic grains in distal parts of pyrrhotine shliers and inclusions, often at the boundaries of pyrrhotine and chalcopyrite. *Nickel cobaltite* is mineralogically the most interesting mineral, and found as independent angular and irregular white or grey grains. Often cobaltite formed along distal pyrrhotine, chalcopyrite, pentlandite grains.

The sulphide minerals are associated with native gold, silver, lead, cobalt, melonite, nagyagite, altaite-clausthalite minerals, tellurides, selenides. *Isomorphic altaite(PbTe)-clausthalite (PbSe)* is rather common, formed generally in edges and as small inclusions in pyrrhotine and nickel cobaltite, and represented by foliated scaly plates, rarer isometric grains. Among inclusions there is gold, silver, iron and sulphur. *Melonite* appears as impregnations and inclusions in interstitials and fractures of cobaltite. Among admixtures only iron is found. *Nagyagite* is formed in distal parts and fractures in pyrrhotine and represented by nano-size elongated and irregular white-grey grains. Light irregular nano-size grains of *native gold* are observed as impregnations and inclusions in the main bulk of nickel cobaltite. Admixtures are represented by silver (11,4–13,6%). *Native cobalt* is concentrated in fractures and main bulk of julukulite, as nano-size white filling forms. As cobald, *native lead* is concentrated in fractures and between crystals of nickel cobaltite as stannic white nano-size irregular grains, but it is relatively abundantly and product of later generation.

Pt-Pd minerals are found in association with magmatic sulphides and represented by kotulskite, sperrylite and vavrinite. Apart from intrinsic minerals, Pd and Pt are found as admixture in nickel cobaltite, pentlandite, chalcopyrite and arsenopyrite. The substitution of primary sulhide minerals and formation of complex submicron and nano-size accretions and substitutions of the sulphides by platinoids, silver and gold are resulted from several mineral-forming processes and definitely connected to fluid-hydrothermal processes and redistribution of minerals from primary sulphide to later associations. This resulted in a complex character of platinum element distribution and consequently their mineral associations.

An in-situ, MLA-based mineralogical investigation of the Akanani Platinum Group Metal Project, Bushveld Complex, South Africa

Van der Merwe, F.*, Viljoen, K.S. & Knoper, M.W.
Dept. of Geology, University of Johannesburg, South Africa (*fritsvdm@postgrad.uj.ac.za)

Modern mineral processing operations require detailed characterization of the ore for beneficiation purposes. In the past, mineralogical aspects of ore characterization (e.g. mineral liberation, particle size distributions, and mineral associations), critical to recovery grade, were typically performed utilising optical microscopy. With the more recent introduction of automated electron microscope-based instruments such as the Mineral Liberation Analyser, the speed and accuracy of these measurements have advanced to such a degree, that fully quantitative and statistically relevant data can now be acquired with ease [1]. The metallurgical extraction of platinum group elements (PGE) from the Platreef on the Northern Limb of the Bushveld Complex is complicated by the mineralogical variability of the ore. In spite of this, and, in comparison to the more established PGE sources of the Bushveld Complex (Merensky and UG2), the Platreef has recently experienced a phase of increased expansion of exploration and mining activity e.g. the establishment of a mining operation by Anglo Platinum [2]. To date, very little data on platinum group mineral (PGM) assemblages, size frequency distributions and associated mineral phases are available for the Platreef [2,3]. Two drill cores through the main mineralized zone of the Platreef at Lonmin's Akanani project (adjacent to, and down-dip from, Anglo Platinum's Sandsloot and Zwartfontein mines) were selected for detailed mineralogical study of PGM's, utilising a FEI 600F Mineral Liberation Analyser at the University of Johannesburg. A variety of PGM's were encountered (Table 1).

Table 1: List of Major PGM's and associated phases present

Mineral Name	General Formula	Area%
Maslovite	PtBiTe	27.63
Michenerite,	PdBiTe,	14.17
Kotulskite	Pd(Te,Bi)	
Isoferroplatinum	Pt_3Fe	10.84
Hessite, Empressite	Ag_2Te, AgTe	8.23
Sperrylite	$PtAs_2$	7.99
Altaite	PbTe	6.27
Cooperite	PtS	5.28
Plumbopalladinite	Pd_3Pb_2	4.60
Electrum	AuAg	4.26
Platarsite	(Pt,Rh,Ru)AsS	2.71
Maslovite	(Pt,Pd)(Bi,Te)	1.49
Hollingworthite	(Rh,Pt)AsS	1.11
Other PGM's (<1%)	-	5.38

Mineral phases co-existing with these PGM's comprise predominantly of pentlandite, chalcopyrite, pyrrhotite, magnetite, and pyroxene. Mineral association data obtained prove the existence of both primary and secondary PGE mineralization within the Platreef. Hydrous silicate phases and their association with PGM's correspond to the degree of alteration present, being variable.

The samples that the information was derived from are at this stage not considered representative of the entire Akanani Mineral Resource. However, the data may be used to derive some preliminary qualitative conclusions. The ultimate aim of the project is to better understand the mineralogy, mineralogical associations, and genesis of the various PGM's at Akanani. This will eventually assist in optimising recovery of PGE's from the Platreef.

[1] Fandrich, R. et al. (2007) *Int. J. Min. Process*, **84**, 310-320. [2] Holwell, D.A. et al. (2006) *Mineral. Mag.*, **70**, 83-101. [3] Kinloch, E.D. (1982) *Econ. Geol.*, **77**, 1328-1347.

Synthetic analogue of naturally occurring 'Pt_2HgSe_3'

Vymazalová, A.[1], Cabral, A.R.[2,3*], Drábek, M.[1] & Lehmann, B.[3]

[1]Czech Geological Survey, Prague, Czech Republic

[2]Exploration Geology, Rhodes University, Grahamstown, South Africa ([*]a.cabral@ru.ac.za)

[3]Lagerstätten und Rohstoffe, Technische Universität Clausthal, Germany

A naturally occurring selenide of platinum and mercury was recently described from auriferous, specular haematite-rich veins that truncate the host itabirite rock at Itabira, Minas Gerais, Brazil [1]. The selenide is about 50 μm across and coexists with haematite, auriferous potarite and atheneite. Its empirical composition, determined by electron-microprobe analysis, corresponds to Pt_2HgSe_3. A selenide mineral with such a stoichiometry is unknown in both natural and synthetic systems.

In an attempt to properly characterise the selenide phase, experimental work was carried out at the Experimental Laboratory of the Czech Geological Survey. The synthetic Pt_2HgSe_3 phase was prepared following the Kullerud's evacuated silica-glass tube method [2]. The phase was synthesised using pure elements (Pt, Hg and Se) as starting material. The silica tube with the charge was heated at 800°C for 840 hours and at 400°C for 1704 hours. The experimental result of the quench at both temperatures, 800 and 400°C, is identical. The strongest lines in the X-ray powder diffraction pattern of synthetic Pt_2HgSe_3 are [*d* in Å (I)]: 6.1416(57), 5.2885(100), 5.0779(13), 4.0625(14), 2.7241(67), 2.6452(15), 2.4416(37), 2.0326(73), 1.8357(29), 1.7631(90), 1.6993(23), 1.5901(19), 1.5424(35), 1.5224(16), 1.3632(19), 1.3235(51), 1.2964(16.7), 1.2729(26). This diffraction pattern is unique, suggesting that the natural phase is a potential new mineral species.

Further investigation to resolve the crystal structure, as well as other physical and chemical characteristics of the synthetic phase is currently underway. The experimental study has hitherto confirmed the existence of the phase Pt_2HgSe_3 at 400 and 800°C.

[1] Cabral, A.R. et al. (2008) *Terra Nova*, **20**, 32-37. [2] Kullerud, G. (1971) in Ulmer, G.C. (ed.) *Research Techniques for High Pressure and High Temperature*, Springer-Verlag, New York, 288-315.

A tale of two elements - the Gamsberg Zn study illustrating the importance of a geometallurgical approach

Schouwstra, R.P.[1*] & De Vaux, D.[2]
[1]Mineralogical Research, Anglo Research, Johannesburg, South Africa ([*]rschouwstra@angloresearch.com)
[2]Metallurgical Services, Anglo Research, Johannesburg, South Africa

The study of exploration samples and process feeds and products using metallurgical test work is practised by many mining companies. This happens either in-house, or is outsourced to service providers. Although, historically, mineralogical information has been used to supplement metallurgical test work on an infrequent basis, the growth in automated mineralogical techniques over the last 10 to 15 years has contributed to increased utilisation of mineralogical data in this important area of research.

The combination and interaction of the disciplines of geology and metallurgy (geometallurgy) leans heavily on mineralogy, but few mining houses have access to in-house mineralogical facilities. Therefore, with the work being outsourced, the necessary integration of metallurgical and mineralogical data can become quite problematic.

Without a thorough understanding of the metallurgical processes and final product requirements, it will be difficult for the mineralogist to establish data needs. For this reason the mineralogist might provide irrelevant or inappropriate information, or worse, withhold relevant information without realising its importance. Similarly, if the project metallurgist is not aware of the type of information that mineralogy can provide, the interpretation of test work could be flawed. Information such as the variation in mineral compositions (including penalty element deportment), the impact of grind size on liberation, and the reason for the deportment of minerals to certain streams can be decisive. In the worst case scenario incorrect interpretation could lead to incorrect decisions being made.

It is only by utilising a variety of techniques and integrating the knowledge of the various disciplines that geometallurgy becomes a powerful instrument. To demonstrate this, the presentation will focus on a study of a Zn-ore. A team consisting of mineralogists and metallurgists made use of in-house mineralogical as well as metallurgical techniques to study the relationship between the mineralogy and the floatability of the ore from various reef intersections.

Quantitative mineralogy of the nonsulphide zinc ores at Jabali (Yemen) using the Rietveld method

Mondillo, N.[1*], Boni, M.[1], Balassone, G.[1], Grist, B.[2] & Woollett, A.[2]
[1]Dipto. di Scienze della Terra, Università di Napoli, Naples, Italy ([*]aktort@tin.it)
[2]ZincOx Resources plc, Surrey, UK

The Jabali deposit (ZincOx Resources - Jabal Salab Ltd), which is located 110 km northeast of Sana'a, the capital city of Yemen (http://www.zincox.com/projects/jabali.asp), contains a resource of 12.6 million tonnes of oxide ore grading 8.9% zinc, 1.2% lead and 68g/t silver, with potential to further increases.

The zinc-lead ores are hosted in dolomitized limestones of Jurassic age, which were later partly de-dolomitized [1]. They occur as massive and disseminated orebodies, characterized by vuggy to highly porous, brown to orange and white Zn-"oxide" minerals with variable reddish-black Fe-Mn staining. The ore will be treated by means of a proprietary hydrometallurgical process (LTC), test work on which has indicated an 80 % zinc recovery so far. A complete mineralogical study of a number of mineralized core samples, selected as representative of the Jabali ore, coupled with a quantitative evaluation of the different mineralogical phases, has been carried out recently.

Through petrographic characterization, X-ray diffractometry and SEM-EDS analysis, it was possible to identify at Jabali the most important nonsulphide ore and gangue minerals. Quantitative phase analysis (QPA) was performed using the Rietveld method [2]; X-ray powder diffraction data were analyzed using the GSAS package (General Structure Analysis System) [3] and its graphical interface EXPGUI [4].

The most abundant Zn-mineral in the Jabali cores is the Zn carbonate smithsonite ($ZnCO_3$), which is generally ranging from few units to 20 wt. % in average, with a maximum abundance of about 80 wt. %. No hydrozincite was detected in the core samples; Zn-smectite is rare. Cerussite, anglesite and pyromorphite have been recorded locally. A resource evaluation based on the overall mineralogical composition of the drill cores, inferred by quantitative X-ray diffraction of the key economic minerals in the Jabali deposit, shows that the results are only partly consistent with the metal grades derived from the chemical assays. In respect to the latter, both lower and higher Zn wt.% have been calculated. This difference between the assayed and calculated zinc amounts in the drill cores can be related to the presence of several dolomite phases with variable Zn content (up to 20% Zn in the lattice), as well as to the local occurrence of Mg-smithsonite (up to 12% Mg in the lattice), as detected from the SEM-EDS analyses.

It is still extremely difficult to define with quantitative diffractometric methods, the zinc contained in several dolomite phases with variable contents of this metal; nevertheless, the occurrence of this "concealed", hardly recoverable zinc should be taken into account when evaluating the assay data. The work carried out has successfully confirmed why the projected recovery for the Jabali deposit, based on earlier metallurgical testwork, is constrained to around 80%.

[1] Al Ganad, I. et al. (1994). *Miner. Deposita*, **29**, 44-56. [2] Rietveld, H.M. (1969). *J. Appl. Crystallogr.*, **2**, 65-71. [3] Larson, A.C. & Von Dreele, R.B. (1994) *General Structure Analysis System (GSAS)*. Los Alamos National Laboratory Report, LAUR, 86-748. [4] Toby, B.H. (2001). *J. Appl. Crystallogr.*, **34**, 210-213.

Novel mineralogical quantitative phase analysis methodology applied to Canadian oil sands for ore characterization, processability prediction, and optimization of froth treatment technologies

Mercier, P.H.J.[1*], Patarachao, B.[1], Kung, J.[1], Dongbao, F.[1], Kingston, D.M.[1], Le Page, Y.[1], Sparks, B.D.[2], Kotlyar, L.S.[1], Woods, J.R.[1], Toll, F.[1], McCracken, T.[1], Ng, S.[3] & Kresta,J.[3]
[1]National Research Council of Canada, Ottawa, Ontario, Canada ([*]patrick.mercier@nrc-cnrc.gc.ca)
[2]V. Bede Technical Associates, Ottawa, Ontario, Canada
[3]Syncrude Canada Ltd., Edmonton, Alberta, Canada

Recent papers [1,2] underscore the key role played by relatively minor amounts of clay minerals and clay-organic complexes in the hydrocarbon recovery and environmental problems associated with the exploitation of the Alberta oil sands of Canada [3,4]. This bitumen deposit is the largest in the world and is second only to Saudi Arabia in proven oil reserves. In a talk abundantly illustrated with examples, we detail here a novel methodology merging weighted experimental results from X-ray fluorescence (XRF) spectrometry, carbon and sulphur analyses, and X-ray diffraction (XRD) powder profiles in a single least-squares refinement, leading to a complete phase analysis of solid fractions in the soils, including crystalline, amorphous and organic phases. Particular attention is given to standard uncertainties (*s.u.*) through use of singular-value decomposition (SVD) of the normal matrix. This allows objective identification of the source of singularities and quasi singularities [5] that cause large *s.u.* values unless properly accounted for in the statement of the solution.

To determine precisely the mineralogical composition of oil sands ore and input/output streams from bitumen extraction processes, a novel quantitative phase analysis methodology parameterized with SVD-based least-squares refinement was developed. An over-determined linear system of weighted observations $\mathbf{A} \cdot \mathbf{x} = \mathbf{b}$ is first built by combining experimental results from (i) metal concentrations by XRF, (ii) carbon and sulphur contents by standard elemental analysis techniques, and (iii) mineral mass ratios determined by Rietveld analysis of XRD powder patterns. The mineralogical composition of the analyzed sample is then obtained directly as the least-squares solution $\mathbf{x} = \mathbf{C}^{-1} \cdot \mathbf{A}^{\mathbf{T}} \cdot \mathbf{b}$, where $\mathbf{C} = \mathbf{A}^{\mathbf{T}} \cdot \mathbf{A}$ is the matrix of normal equations and the elements of $\mathbf{x}$ (x_i) are the mass fractions of each individual mineral phase comprised in the sample. Non-uniqueness problems associated with linear combinations of variables x_i giving rise to identical overall sample composition are unambiguously identified as described elsewhere [5] by performing the SVD of matrix **C**.

The practical examples detailed in the presentation involve the application of this novel methodology to characterize two different sets of oil sands materials. First, key correlations are identified between bitumen recovery and mineralogical compositions for a set of ten oil sands in which currently used processability markers such as bitumen and fines (<44μm solids) contents show no correspondence with recovery rates. Second, it is shown how the evolution of mineralogical compositions, precisely determined with our novel methodology, can be useful in process design and optimization of bituminous froth treatment technologies to analyze the effect that different processing conditions can have on bitumen product quality.

[1] Dongbao, F. et al. (2010) *Energ. Fuel.*, **24**, 2249-2256. [2] Mercier, P.H.J. et al. (2008) *Energ. Fuel.*, **22**, 3174-3193. [3] Kotlyar, L.S. et al. (1998) *Rev. Proc. Chem. Eng.*, **1**, 81-110. [4] Sparks, B.D. et al. (2003) *J. Petrol. Sci. Eng.*, **39**, 417-430. [5] Mercier, P.H.J. et al. (2006) *J. Appl. Cryst.*, **39**, 458-465.

A comparative study of quantitative methods in ore microscopy: digital image analysis *vs.* point counter device

Pérez-Barnuevo, L.[*], Castroviejo, R. & Espí, J.A.
School of Mines, Universidad Politécnica de Madrid, Spain ([*]laura.perez.barnuevo@upm.es)

Quantitative mineralogical analyses of metallic concentrates from an ore-processing plant with reflected light microscopy have been carried out independently, on the same samples, by an expert mineralogist using a point counter device (**PCD**), and by digital image analysis (**DIA**) operated by a post-graduate student in order to compare the performance and results obtained with both methods [1].

The results obtained by both methods (Table 1) are broadly similar [2] and differences do not exceed the expected margin of error inherent to the statistical significance of the samples studied [3]. But there are major differences when comparing the performance of both methods. While at best some 3000 particles per hour can be registered with PCD, it is possible with DIA to process 100000 particles per hour, extracting data not only about volumetric fractions, but also about morphological parameters of every mineral grain. This difference is enhanced if the work conditions are considered. While a human operator may work with PCD some 6 h a day, if risk factors as fatigue are to be avoided, DIA systems can work 24 h a day. Moreover, PCD should be handled by an expert ore microscopist, but there is at present a trend to reduce this training at universities, thus leading to a gradual disappearance of this type of experts. DIA does not need such a high grade of expertise, even if some sort of supervision is needed [4].

Table 1: Modal analysis by PCD vs. DIA

	Mo	SFsCu	Py	Ccp
PCD (%)	69	13	8	10
DIA (%)	62	14	11	13

Pay-back for both methods has been calculated based on data shown on Table 2 and considering the number of samples that it is possible to analyze by means of each method. Although initial investment for DIA is more than twice the investment for PCD, pay-back is just one year for DIA, while the return of investment increases to three years for PCD.

Table 2: Pay-back comparison for PCD vs. DIA

	Equipment Cost	Labour (annual)	Income/ sample	Pay-back
PCD	30 000 $	50 000 $	150 $	**3 years**
DIA	70 000 $	30 000 $	150 $	**1 year**

To conclude, DIA coupled to reflected light microscopy is a powerful and cost-efficient tool to support ore-processing with varied quantitative mineralogical data, as modal analysis, morphological characterization of mineral particles, and mineral liberation analysis. DIA can provide more complete, reliable and efficient mineral characterizations than the traditional methods as PCD, which are less performing and do not preclude human error, e.g. by fatigue. It is also by far more economical than the methods based on SEM images, while providing comparable results. DIA can satisfy the demands of geometallurgy with low investment and maintenance costs.

[1] Project *Ore characterization by computer vision* (CAMEVA CGL2006-13688-C02, MEC, Spain). [2] Pérez-Barnuevo, L. et al. (2008). *Proc. Symp. Mineralogía Apl. Geometalurgia*, abs. R5. XIII Congr. Latinoamericano de Geología, Lima. [3] Castroviejo, R. et al. (1999) *Geovision. Int. Symp. Imaging Appl. Geology*, Liège, Belgium, 37-40. [4] Castroviejo, R. et al. (2009) *Queensland. Proc. 10th Biennial SGA Meet*, Townsville, Australia, 692-684.

Minor element distribution and partitioning in bornite and associated Cu-sulphides

Cook, N.J.[1,2*], Ciobanu, C.L.[1,2], Danyushevsky, L.V.[3] & Gilbert, S.[3]
[1]University of Adelaide, Australia
([*]nigel.cook@adelaide.edu.au)
[2]South Australian Museum, Adelaide, Australia
[3]CODES, University of Tasmania, Australia

Bornite (Cu_5FeS_4) is a major Cu-mineral in high-sulphidation epithermal deposits, sedimentary-hosted Cu-deposits, Cu- and polymetallic skarns, parts of porphyry-Cu and VMS deposits, and in iron oxide-copper-gold (IOCG) systems. The Cu-rich corner of the system Cu-Fe-S is complex, featuring many low-T phases. This complexity is reflected by the presence of fine intergrowths and varying textures.

We provide a baseline dataset on minor element contents in bornite and accompanying Cu-sulphides using *in situ* LA-ICP-MS methods; 22 samples from 12 deposits were analysed. 122 spot analyses of bornite, and 42 of chalcocite/digenite (40-80 μm diameter) were made using an Agilent 7700 Quadripole ICPMS instrument; 28 elements were monitored. Samples are (i) from 5 vein-type deposits in the Late Proterozoic Sveconorwegian province of Scandinavia and (ii) bornite-bearing samples from skarns, porphyry and epithermal deposits from the Late Cretaceous Banatitic Magmatic and Metallogenetic Belt, SE Europe. One bornite sample from the Olympic Dam IOCG deposit, Australia, was analysed for comparison.

Although the samples are from different deposit types and provinces, the resulting dataset shows common trends:

(1) Silver and Bi have the highest measured values among analysed elements; all bornites contain hundreds or thousands ppm Bi (up to 1 wt.%) and mean Ag concentrations from 71 to ~8000 ppm. Both elements mimic the behaviour of Cu in the time-resolved downhole profiles, regardless of whether Ag- or Bi-minerals are present in the sample, suggesting both elements reside in solid solution. Data for samples where both bornite and Cu-sulphides coexist shows partitioning between bornite and Cu-sulphides: Ag is preferentially partitioned into Cu-sulphides whereas Bi is partitioned into bornite. Highest Ag concentrations in bornite are from a sample in which chalcocite is conspicuously absent.

(2) Bornite from deposits characterized by an abundance of selenides and tellurides show enrichment in Se (up to >2,000 ppm) and Te (up to >400 ppm). These elements also mimic Cu in the profiles, suggesting residence in a solid solution.

(3) Concentrations of Co, Ni, Ga, Ge and Cd in bornite are low; Zn, Mo, Sb and U are at or below minimum detection limits (<1 ppm). Considering large signal variations in the time-resolved LA-ICPMS downhole profiles, a few anomalous concentrations of Co, Ni, Pb, Sn and As relate to μm- and sub-μm-scale inclusions rather than solid solution.

(4) Measured Au values in bornite are low (rarely >0.1 ppm). Although individual spots from some samples gave values up to 6 ppm, large signal variations in the time-resolved profiles suggest these concentrations relate to sub-μm inclusions. The aforementioned partitioning trend extends to Au: values in digenite may be an order of magnitude higher than coexisting bornite and when the proportion of digenite to bornite is low, values can go up to 24 ppm. We believe that Au is partitioned preferentially into the Cu-sulphide(s) during cooling.

The Elura Pb – Zn – Ag deposit, central NSW, Australia: ore characterisation and geo-metallurgy, preliminary results

Loidl, G.C[1*], Plimer, I.R.[1] & Thalhammer, O.A.R[1,2]
[1]School of Earth and Environmental Sciences, Dept. of Geology and Geophysics, University of Adelaide, Australia
([*]gernot.loidl@adelaide.edu.au)
[2]Dept. of Applied Geosciences and Geophysics, University of Leoben, Austria

The Elura lead-zinc-silver deposit, with an estimated total pre-mined resource of 45Mt at 8.5% Zn, 5.3% Pb and 69g/t Ag, is located in central NSW, approximately 800km west of Sydney, Australia. The orebody is of epigenetic nature, sediment-hosted and strongly structural controlled. Sulphides comprise sphalerite, galena, pyrrhotite, pyrite, chalcopyrite, arsenopyrite and argentian tetrahedrite, quartz, siderite, subordinate calcite and ankerite, with varying quantities of sericite and chlorite as the major gangue minerals. The host rock is a turbiditic sequence, characterised by interbedded sand-, mud- and siltstone layers. The first mining activities commenced in 1983. The deposit, now known as Endeavor, is currently exploited by CBH Resources Ltd. Despite (a) the long and continues mining history, (b) the frequent and significant fluctuations of Zn and Pb ore to concentrate metal recovery rates, and (c) elevated Bi concentration in the lead concentrate, no comprehensive ore characterisation study has been undertaken in the past. In order to increase the knowledge and the understanding about geo-metallurgical characteristics, a detailed multi-disciplinary study covering mineralogy, mineral chemistry, ore textures and trace element distributions, in particular those of smelter penalty elements e.g. Bi, has been undertaken as part of a PhD project.

Trace elements were analysed by ALS (Australia), electron microprobe analyses (EMP) were conducted on a JEOL Superprobe JXA 8200 at the University of Leoben, particle mineral analyses (PMA) and field scans were conducted on a QEMSCAN® E430 by AMDEL (Adelaide).

Trace elements on whole rock samples revealed several significant concentration trends as a function of depth within the orebody. Bi and Se have rather low concentrations in the uppermost parts and significantly increasing with depth and reaching a maximum of 714ppm and 45ppm, respectively. A converse trend has been observed for Hg and Sb, which reach maxima in the uppermost zones of the ore body. The observed maximum values are over 2000ppm for Sb and 66ppm for Hg. As concentrations are highly variable, ranging between 10ppm and 1.5wt%. EMP analyses of galena showed elevated Bi concentrations with maximum values between 0.1 and 0.7wt%. Element mapping suggests that Bi is occurring in solid-solution rather than as discrete Bi mineral phases intergrown with galena. Elevated Hg concentrations are observed in pyrite, pyrrhotite, sphalerite and chalcopyrite. The increase of Sb corresponds with the occurrence of argentian tetrahedrite in the uppermost zones of the orebody.

QEMSCAN® analyses are being processed by the author; preliminary results will be presented at the conference. Particle mineral analysis on particle separates mounted on polished blocks were undertaken in order to investigate mineral liberation, mineral associations and mineral specific surface exposure for all major sulphide phases. Field scans on polished thin-sections were used to study textural ore characteristics such as grain size distributions, intergrowths, inclusions and exsolutions. Both data sets will help to identify host mineral phases for smelter penalty elements not identified in the course of microscopic and EMP investigations.

Acknowledgements: The authors acknowledge the support of AMDEL laboratories, FEI Company and CBH Resources Ltd.

The geometallurgical characterization of different Merensky Reef facies in the western limb of the Bushveld Complex, South Africa

Smith, A.J.B.[1*], Viljoen, K.S.[1], Schouwstra, R.[2], Roberts, J.[2], Schalkwyk, C.[2] & Gutzmer, J.[1,3]
[1]Dept. of Geology, University of Johannesburg, South Africa ([*]bertuss@uj.ac.za)
[2]Mineralogical Services, AngloResearch, Johannesburg, South Africa
[3]Dept. of Mineralogy, Technische Universität Bergakademie Freiberg, Germany

The Merensky Reef is a major platinum group element (PGE) bearing unit in the Bushveld Complex of South Africa [1] and is laterally continuous throughout most of the western and eastern limbs [2]. Variations in platinum group mineral (PGM) content [2] and lithostratigraphy [3] of the reef do however occur across the complex. Lithostratigraphic variations include the width of the pegmatoidal feldspathic pyroxenite (PFP) which constitutes the reef, development of chromitite stringers and incidence of potholing which results in reef development at several different stratigraphic positions. These lithostratigraphic variations have been used by mining houses to classify the Merensky Reef into many different geological reef facies types [3].

The genetic impact of the lithostratigraphic controls on the mineralogical characteristics of the PGM is poorly understood and can have an important bearing on the milling, liberation and flotation response of the reef. Geometallurgical characterization of the different Merensky Reef facies in a mining area provides valuable insight into these potential problems. This approach aims to 1) quantify the lateral and vertical distribution of PGMs in each facies type; 2) establish the flotation behaviour of each facies type in relation to the mineralogical characteristics of the milled flotation feed and 3) perform detailed petrographic and geochemical studies on each reef facies type to establish trends and correlations with the mineralogical and metallurgical data. Apart from some traditional optical microscopy, this approach makes liberal and extensive use of recent advances in automated scanning electron microscope technologies [4] to quantify the mineralogy of coarsely crushed as well as milled fractions.

Preliminary results from a study of potholed Merensky Reef from the western limb of the Bushveld Complex show that the top of the mineralised envelope is rich in PGE-sulphide whereas the bottom portion has a high PGE-telluride, iron-platinum-alloy and olivine content. The PGMs show a strong association with base metal sulphides. Most of the olivine is altered to serpentine.

[1] Cawthorn, R.G. et al. (2006) in Johnson et al. (eds.) *The Geology of South Africa*. Geol. Soc. of SA, Johannesburg, 261-282. [2] Cawthorn, R.G. et al. (2002) *Can. Mineral.*, **40**, 311-328. [3] Lionnet, M.D. & Lomberg, K.G. (2007) *J. S. Afr. I. Min. Metall.*, **107**, 1-6. [4] Fandrich, R. et al. (2007) *Int. J. Miner. Process.*, **84**, 310-320.

Geometallurgy of the northern Kalahari manganese deposit, with respect to smelting operations

Chetty, D.[1,2*] & Gutzmer, J.[2,3]
[1]Mineralogy Division, Mintek, Randburg, South Africa ([*]deshc@mintek.co.za)
[2]Paleoproterozoic Mineralisation Research Group, Dept. of Geology, University of Johannesburg, South Africa
[3]Dept. of Mineralogy, TU Bergakademie Freiberg, Germany

The Kalahari Manganese Field is situated in the northern Cape Province of South Africa, and accounts for 80% of the world's Mn reserves. South Africa is the second largest producer of manganese alloys, with virtually all the feedstock derived from the KMF.

A study into mineral distribution in the northern part of the main deposit (Fig. 1) has revealed not only that mineralogy varies as a function of distance from faults that abound in the area [1], but that overall, mineralogical changes are evident from W to E across the deposit.

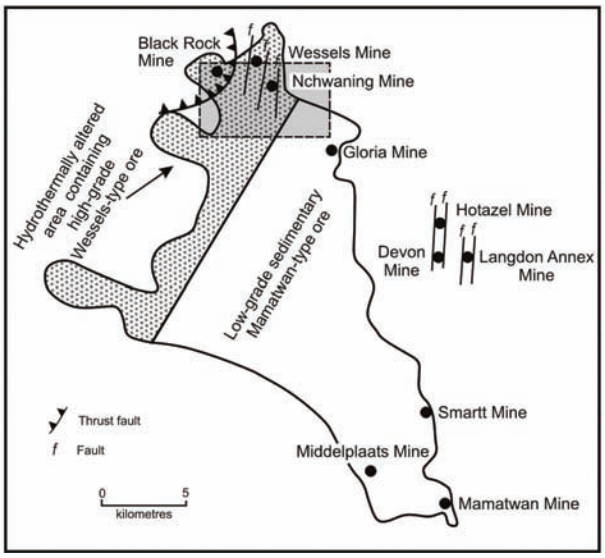

Fig. 1: Map of the KMF, showing the faults in the study area (rectangular block).

Changes in mineralogy as function of distance from the faults may be ascribed to non-redox reactions and the degree of fluid-rock interaction, such that high-grade alteration represents the highest influx of fluid, whereas lower degrees of fluid-rock interaction result in less pronounced alteration.

Modelling physico-chemical and structural controls allows prediction of mineral assemblage distribution. This is useful for selective mining, ore blending or changes to the smelting plant parameters, since mineral distribution is predicted to affect 1. energy input, 2. reductant input and 3. boron content in the smelter feed.

High alteration hausmannite-rich assemblages dominate the eastern part of the deposit, and should require increased energy input, result in lower reductant consumption and have low B levels. Lower alteration braunite-group-rich assemblages dominate the western part of the deposit, and should require lower energy input, result in higher reductant consumption, and contribute more B to the system, a concern in silicomanganese production.

[1] Gutzmer, J. & Beukes, N.J. (1995) *Econ. Geol.*, **90**, 823-844.

Evaluation of nonsulphide zinc ores of Accha (Peru) using QEMSCAN automated mineralogy and Rietveld analysis

Stickland, R.J.[1], Rollinson, G.K.[1], Andersen, J.C.[1*], Balassone, G.[2] & Boni, M.[2]
[1]Camborne School of Mines, University of Exeter, Cornwall Campus, Penryn, UK ([*]J.C.Andersen@exeter.ac.uk)
[2]Dipto Scienze della Terra Università di Napoli, Naples, Italy

The mineralogy of supergene nonsulphide zinc ores from the Accha deposit (Peru) [1] was investigated using QEMSCAN analysis and quantitative X-ray diffraction (XRD) by the Rietveld method. The methodology was developed to gain a detailed insight into the mineralogical relationships of different lithotypes in the deposit. The QEMSCAN instrument is a Scanning Electron Microscope with automated energy dispersive X-ray spectrum collection, recognition and classification that allows for the rapid determination and quantification of mineral species and their spatial relationships.

The QEMSCAN study included the development of a Species Identification Protocol (SIP) to facilitate the automatic recognition of mineral species. The resulting SIP facilitates the detailed mapping of mineral distributions in the individual lithotypes within the Accha deposit. The method provides detailed mineralogical information, visualization and quantitative information on mineral abundances and associations. This information is essential to evaluate how the ore would respond to different mineral processing techniques. The mineralogical data obtained by QEMSCAN are in agreement with previous mineralogical studies, but provide increased knowledge of mineral quantities, associations, and accessory phases. The main limitation of the method is that minerals with closely matching X-ray spectra cannot be discriminated (for nonsulphide zinc ores this includes the mineral pairs hydrozincite/smithsonite and hemimorphite/willemite). These minerals need to be verified independently by XRD and/or optical microscopy.

The Rietveld methodology allows for calculated XRD profiles of individual minerals to be fitted to the measured profiles of multi-mineral mixtures by least-squares analysis. This allows for quantification of the mineral percentages in rock samples based on their crystal structure. XRD was used at Accha as a tool to evaluate the proportions of ore and gangue minerals. The quantitative evaluation was carried out with the Rietveld-based processing system (GSAS-EXPGUI) on the same samples analyzed by QEMSCAN. The Rietveld analysis confirmed smithsonite and hemimorphite at Accha rather than hydrozincite and willemite.

The spatial information collected by the QEMSCAN method provides valuable insight into the nature of the Accha ore. Although the bulk quantification of minerals is largely in agreement between the QEMSCAN and the quantitative XRD, there are variations between the results. These can be explained by short-range sampling variations. Where the QEMSCAN in this case measured a thin slice through the sample, the XRD collected information from a larger homogenized bulk. Disaggregation and homogenization of the sample for QEMSCAN would give a better compositional match but at the expense of the valuable mineral association information.

[1] Boni, M. et al. (2009) *Econ. Geol.*, **104**, 267-289.

Characteristics, recovery and provenance of rutile from the Namakwa Sands heavy mineral deposit, South Africa

Rozendaal, A.[*], Philander, C. & Carelse, C.
Dept. of Earth Sciences, Stellenbosch University, Stellenbosch, South Africa ([*]ar@sun.ac.za)

The Namakwa Sands heavy mineral deposit is located along the West Coast of South Africa and the mine is a world class producer of high quality zircon ($ZrSiO_4$), ilmenite ($FeTiO_3$) and rutile (TiO_2) concentrates from essentially unconsolidated marine and aeolian sands of Cenozoic age. Resources are in excess of 650 million tons at a grade of approximately 10 per cent total heavy minerals with a life-of-mine of 30 years.

The objective of this study was to characterize rutile with respect to distribution, grain size, textures, colour and mineral chemistry within the Namakwa Sands Orebody with the aim to explain its overall poor recovery. A representative suite of heavy mineral concentrates from various sections of the ore body and stages in the recovery circuit has been investigated microscopically and by means of SEM-EDS and LA-ICP-MS. This allowed the study to establish the relationship between grain size distribution, mineral chemistry, density and sediment maturity for the Namakwa Sands placer deposit. The rutile grain size distribution displays a wide range and is directly related to its variable chemistry and consequently density. In placer deposits such as Namakwa Sands, mineral sorting is a function of hydraulic equivalence and high density grains are smaller than the lighter grains when deposited under similar conditions. Grain size is also a function of sediment maturity and the highly mature red aeolian sand (RAS) component of the deposit has a finer grain size than the less mature orange feldspathic marine sands (OFMS). The above primary characteristics of rutile are responsible for the loss of the fine-grained fraction during screening and given the empirically determined relationship that increased substitution elements reduce conductivity, also during electrostatic separation.

Provenans studies using geothermometry have shown that the heavy mineral suite has been mainly sourced by the proximal medium-to high-grade Namaqualand Metamorphic Complex. The positive relationship between substitution elements and temperature of formation explains their high concentration in rutile of this deposit.

The heterogeneity of rutile, produced by the combination of a high temperature primary source and the typical marine-aeolian placer genesis is deposit-specific and unfortunately not conducive to high recovery levels in the Namakwa Sands beneficiation circuit.

Mineralogical variability in a New Zealand ironsand deposit and its impact on ironmaking

Cocker, H.A.[1*], Mauk, J.L.[1], Rogers, H.[2] & Padya, A.B.[3]
[1]University of Auckland, Australia ([*]h.cocker@auckland.ac.nz)
[2]BlueScope Steel Ltd, Australia
[3]Waikato North Head Mine Site, New Zealand Steel Ltd, New Zealand

The Waikato North Head ironsand mine on the west coast of the North Island of New Zealand contains sub-horizontal stratigraphic layers of ironsand with an inferred resource of 620 Mt at 21 percent magnetic minerals. The ironsand was sourced from Neogene to Quaternary volcanoes, and transported by longshore drift, and then aeolian processes to form titanomagnetite-rich Quaternary sands. Ironsand is dry mined by bucket wheel excavators and wet processed by the mine-site concentrator using magnetic and gravity methods. The ironsand is not crushed at any stage. Ironsand concentrate is conveyed 18 km by slurry pipe–line to New Zealand Steel's integrated steel mill at Glenbrook

Titanomagnetite is the most abundant oxide in the ironsands. It predominantly occurs as homogeneous grains, but some grains contain exsolution lamellae of titanium bearing hematite-ilmenite and spinel. Inclusions of pyrite, apatite and other gangue minerals, occur locally. Gangue minerals consist of pyroxenes (diopside and hypersthenes), feldspars, hornblendes, quartz, and minor biotite. Gangue grains commonly occur with inclusions of titanomagnetite through to, composite titanomagnetite / gangue grains. The average concentration of gangue in the magnetic fraction of samples from the ironsand mine varies among the stratigraphic units (Table 1). The base of the most ore-rich unit, the Waiuku Black Sands, is the lower limit of open pit mining. Samples from mine faces show that there is significant vertical and lateral variability in the abundance of gangue in the magnetic fraction within individual stratigraphic units.

Table 1: Stratigraphy at the Waikato North Head deposit showing the average % gangue in the magnetic fraction; %Fe (mags) is the % Fe in the magnetic fraction, % Mags is the % magnetic minerals in a sample

Formation		Description	% Fe (mags)	% Mags	% Clay minerals	Average % gangue in the magnetic fraction samples	
10 ka to recent	Mitiwai Sands	Alder Sand	50.6	8.0	2.6	26.2	↑
		Entrican Sand	54.8	13.4	2.7	8.7	mined
200 ka to 10 ka	Hood Sands	Ash	58.4	16.6	16.2		
		Bothwell Sand Upper Hood Sand	58.8	19.7	8.7	4.0	
		Waiuku Black Sand	60.4	47.1	6.7	1.8	
		Lower Hood	56.6	12.7	9.2	8.4	
1.2 Ma to 200 ka	Awhitu Sands	River Sand					
		Awhitu Clay	57.9	7.7	18.4	16.6	not mined
		Awhitu Sand	58.2	4.6	11.5	29.0	
		Sandstone					↓

The New Zealand Steel ironmaking process involves the sequential processing of the ironsand concentrate through multi-hearth furnaces (mixing with sub-bituminous coal, drying and partial coal devolatilisation), SL/RN rotary reduction kilns (solid state ironsand reduction) and submerged arc melters (final reduction and melting). Formation of accretions in the multi-hearth furnaces and kilns occurs from time-to-time. Understanding the mineralogical and geochemical variability in the mined resource, the incorporation of gangue into the ironsand concentrate, and the transformations in the concentrate on high temperature processing are key elements in developing an understanding of accretion formation.

Green liquids - acid leaching of Ni-laterites

Hunter, H.M.A.[1*], Herrington, R.J.[1] & Oxley, A.[2]
[1]Mineralogy Dept., Natural History Museum, London, UK
([*]h.hunter@nhm.ac.uk)
[2]European Nickel, London, UK

European Nickel, a mid-tier mining company, has pioneered a low temperature acid leach extraction method for Ni-laterites which is being heralded as a breakthrough in environmentally conscious mining.

Our Industry-Academia collaborative research, based at the NHM in London, has been using EPMA and XRD techniques, coupled with mass balance calculations, to examine the leaching characteristics of various Ni-laterite ores, with a view to predicting their process efficiency using this extraction method. XRD confirms that the ore is dominated by nickeliferous goethite with quartz, relic serpentinite and minor calcite also present.

Small-scale experiments on the Turkish Çaldağ ore were carried out with material examined over various lengths of time. Typically 45ml of a 75gpl sulphuric acid solution was used to leach 1.0g of ore fragments, for between 2-72 days. These tubes were capped and placed on a rotating/shaking table at room temperature before being removed periodically and tested. The supernatant liquor was analysed by ICPAES, whilst the residual ore material was prepared as polished blocks for SEM and a powdered sample was examined by XRD and analysed by whole rock chemical methods.

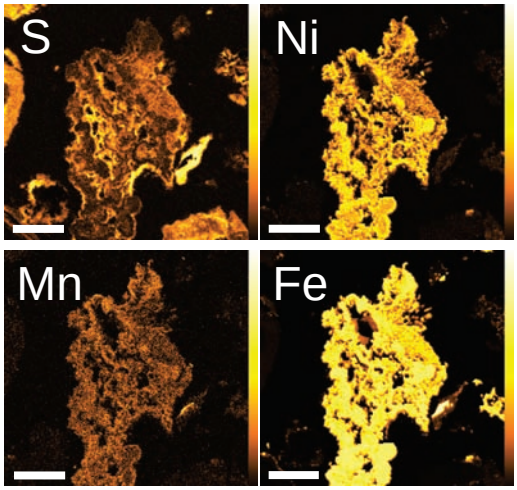

Fig. 1: X-ray element maps for a nickeliferous goethite grain exposed to 35 days of acid leaching (scale bar = 100μm).

The data have been analysed to investigate the chemical and mineralogical changes that occur during leaching. Figure 1 shows a sample of Çaldağ goethitic ore that was subjected to 35 days of acid leaching. Of note is the developed porosity and clear indication of sulphur penetration (Fig. 1, top left) into the ore fragment. Further experiments indicate that there is a staged dissolution of relic silicate and goethitic phases. These results have implications for the design of larger scale leach testing. The full results will be discussed in the presentation.

A fully automated system for multispectral ore microscopy

Castroviejo, R.[1*], Catalina, J.C.[2], Bernhardt, H.J.[3], Pirard, E.[4], Segundo, F.[2], Brea, C.[1] & Pérez-Barnuevo, L.[1]
[1]School of Mines, Universidad Politécnica de Madrid, Spain
([*]ricardo.castroviejo@upm.es)
[2]AITEMÍN, Madrid, Spain
[3]Ruhr-Universitaet Bochum, Germany
[4]Université de Liège, Belgium

A joint research to develop an efficient method for automated identification and quantification of ores [1], based on Reflected Light Microscopy (**RLM**) in the *VNIR* realm (Fig. 1), provides an alternative to modern SEM based equipments used by geometallurgists, but for ~ $1/10^{th}$ of the price.

Fig 1: Equipment used on automated Leica DM6000M scope.

Quantitative measurements as reflectance and hardness, mainly *VHN*, are traditionally used to support RLM ore identification. Still, this relies mostly on qualitative observations, which can not be applied directly for automated reconnaissance. Today, accurate colour measurements [2] and systematic spectral reflectance data from QDF3 [3] provide a sound base for automation [4] and for multispectral imaging [5,6]. Once automated identification is achieved [7,8], processing the digital images can provide results similar or superior in discrimination compared to the SEM methods. The method is also more performant than the classical point-counter [9].

The automated ore identification procedure now presented is based on direct classification of individual pixels. Training of the identification system has been carried out by using actual pixel multispectral reflectance values of a subset of the mineral regions selected for the database. Tests of the system have provided very good recognition rates, well in excess of 99% of the pixels for mineral regions selected for the database. To further enhance the efficiency of the process, additional mineralogical criteria [10] may be applied.

[1] Project *Ore characterization by computer vision (CAMEVA* CGL2006-13688-C02, MEC, Spain). [2] Piller, H. (1966) *Min. Deposita*, **1**, 175-192. [3] Criddle, A. & Stanley, C. (1993) *Quantitative Data File for Ore Minerals (3rd ed.)*. Chapman & Hall, London. [4] Bernhardt, H.J. (1987) *Miner. Petrol.*, **36**, 241-245. [5] Pirard, E. (2004) *Mineral. Mag.*, **68(2)**, 323-333. [6] Pirard, E. et al. (2008) *9th Int. Congr. Appl. Miner.*, Brisbane, 1-6. [7] Castroviejo, R. et al. (2009) *10th Biennial SGA Meet*, Townsville, NQLD, 692-684. [8] Brea, C. et al. (2010) *this vol*. [9] Pérez-Barnuevo, L. et al. (2010) *this vol*. [10] Castroviejo R. et al. (2009) *Rev. Metal.*, Madrid, **45**, 277-286.

New data on the specular reflectance of ores (VNIR: 400 - 1000nm) and their significance for ore microscopy

Brea, C., Castroviejo, R.[*] & Samper, J.
ETSI de Minas, Universidad Politécnica de Madrid, Spain
([*]ricardo.castroviejo@upm.es)

This work is part of the project *CAMEVA* for the development of an expert system aimed at the automatic identification of ores [1,2]. It relies on the measure of their reflectance values, **R**, on digital images. Software for calibration, acquisition and analysis of the multispectral data was designed by *AITEMIN* [3]; the research was also assessed by H.J. Bernhardt and E. Pirard [1].

The work deals with the first stage in the development of the system: the creation of a reference data base, **DB**, including multispectral reflectance values of the most important ore minerals in the *VNIR* realm [4,5]. A most delicate step is the selection of the ores and fields to be measured, implying a previous and very careful study of the samples. A poor quality of the polished surface or an ill-defined mineralogy would invalidate the results. The samples studied belong essentially to the collections of the Madrid School of Mines, and to the well-known Rehwald / Ramdohr collection of ores.

The DB, still to be completed, allows some insights [6] into the behaviour of the common ore minerals beyond the visible spectrum (Fig.1). The change in the slope of some spectral curves entering the IR realm is very remarkable, as is the case with pentlandite and niccolite, whose R exceeds that of pyrite, marcasite and arsenopyrite in IR. The same contrast is seen in the *VNIR* behaviour of couples like pyrrhotite – chalcopyrite, pyrrhotite – galena and cubanite – galena. On the other hand, the spectral curves of pyrrhotite and cubanite, very close in the visible realm, are diverging in IR.

Furthermore, it is important to note that on entering the IR realm some minerals, as tetrahedrite, hematite, and magnetite, show a sensible decrease in their reflectance values, while others like covellite and bornite undergo a dramatic increase.

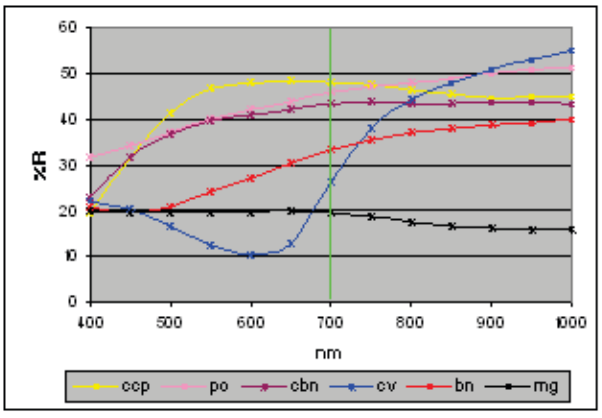

Fig. 1: Reflectance curves of chalcopyrite (ccp), pyrrhotite (po), cubanite (cbn), covellite (cv), bornite (bn) and magnetite (mg).

The DB is consistent with published values in the visible realm [7: values 400 – 700 nm], and shows that the new information in the near IR (700-1000 nm) may be of high diagnostic value.

[1] Castroviejo, R. et al (2010) *This vol*. [2] Castroviejo, R. et al (2009) *10th Biennial Meet. SGA*, Townsville, QLD. [3] Catalina, J. et al (2008) *Proc. Symp. Min. Apl. Geomet*, abs. R3, XIII Congr. Lat. Geol., Lima [4] Pirard, E. (2004) *Mineral. Mag.*, **68(2)**, 323-333. [5] Pirard, E. et al. (2008) *9th Int. Congr. Appl. Mineralogy*, Brisbane, 1-6. [6] Brea, C. (2009) *MSc Thesis*, UPM, Madrid [7] Criddle, A. & Stanley, C. (1993) *Quantitative Data File for Ore Minerals (3rd ed.)*. Chapman & Hall, London.

Pulsed power methods for hydrocarbon raw

Kotova, O. & Tropnikov, E.*
Institute of Geology, Komi Scientific Center, Uralian Branch,
Russian Academy of Sciences, Syktyvkar, Russia
(*tropnikov.83@mail.ru)

Surface of minerals represents a nice field for studying natural processes. The knowledge of dependencies of surface kinetics and organic matter transformation on physical parameters with the use of achievements un the field of mineral surface physics allows generating the organics-mineral surface model for revealing mechanisms of formation of hydrocarbon raw, synthesis of new carbon-containing materials and to create new technologies.

Within the framework of our studies on the convergence of hydrocarbon raw, experiments on modeling of controlled growth of diamond from Yarega oil raw under influence of pulse laser radiation (impulse duration 0.5 ms) have been conducted.

The structure of the initial and irradiated crystal were studied by means of four-circle X-ray diffractometer P4.The study of parameters of lattice, distribution of electron density, and also tension and sizes of blocks, coherently disseminating X-rays, specify that the pulse laser irradiation renders essential influence on monocrystals, namely, it creates a high pressure in oil disperse systems resulting in change of size of complex structural units even beyond the area of irradiation. The received results can be treated as buildup of layers and individual formations on the surface of monocrystals with lattice parameters slightly exceeding the parameters of initial crystal.

Parameters were determined by angular position of reflection from 30 atomic planes alternately taken in vertical position. The distribution of electronic density was made on the basis of Fourier transformation. Tensions and sizes of the blocks were determined by the width of reflexes.

Thus, as a result of the experiments, build up of monocrystal layers of diamond on the surface is observed. The experiments specify the opportunity of crystallization of molecules of diamond and (or) classes of compounds known as diamondoids in Yarega oils.

Fluid evolution in Cordilleran polymetallic veins – insights from microthermometry and LA-ICP-MS of fluid inclusions

Catchpole, H.[1*], Kouzmanov, K.[1], Fontboté, L.[1], Guillong, M.[2] & Heinrich, C.A.[2]
[1]Ore Deposits Group, Dept. of Mineralogy, University of Geneva, Switzerland ([*]Honza.Catchpole@unige.ch)
[2]Isotope Geochemistry and Mineral Resources, Dept. of Earth Sciences, ETH Zurich, Switzerland

Cordilleran polymetallic veins, massive manto- and chimney-type carbonate replacement bodies are important Zn-Pb-Ag-Cu resources. Although post-dating mineralised porphyry systems, the meso- to epithermal polymetallic ore bodies are considered to be genetically related to porphyry intrusions. However, it is not yet well understood where the mineralising fluids that produce polymetallic mineralisation originate from, nor how they evolve in time and space.

In this contribution we present microthermometric and LA-ICP-MS data of fluid inclusions throughout the paragenesis of polymetallic veins cutting barren and mineralised Cu-Mo porphyries in the Morococha district, Central Peru. Fluids related to early precipitation in the veins are moderately-low saline (~ 4-5 wt% NaCl eq), have homogenisation temperatures (T_h) of up to 380°C, up to 5 mol% CO_2 and high metal contents of over 1000 ppm Cu and Fe, 100 ppm Pb, 10 ppm Ag, and several 100 ppm Zn. Several thousand ppm S are recorded in inclusion fluids, mostly precipitating as pyrite in early vein formation stages, but enough S is present in the fluid to later precipitate all of the economically interesting minerals such as sphalerite, galena and fahlore. Metal contents decrease with T_h, showing different precipitation trends corresponding to the paragenetic position of the ore minerals. Copper content decreases several orders of magnitude. Coinciding with abundant carbonate precipitation in late stages of vein formation, the latest fluids have T_h ranging from 260 to 240°C, low metal values, no measurable CO_2 and salinities of about 2 wt% NaCl eq.

Secondary fluid inclusions in porphyry-related quartz stockwork veins predate polymetallic vein formation and show typical characteristics of a single-phase magmatic fluid with vapour-liquid ratios of 50 - 60%, ~8 mol% CO_2, very high Cu values of around 1 wt%, T_h of 420 - 440°C and salinities of 3 – 4 wt% NaCl eq. These results, together with preliminary O and H isotope data, support the hypothesis that the fluids producing the Cordilleran polymetallic veins developed from similar low to moderately saline and metal rich fluids, rather than evolving from strong dilution of porphyry brines with meteoric water, as previously assumed.

Au-Ag deposits along the Cauca River canyon, northwestern margin of the Central Cordillera, Colombia

Gallego, A.N.[*], Akasaka, M. & Roser, B.P.
Dept. of Geosciences, Shimane University, Matsue, Japan
([*]albanurygh@yahoo.com)

The Buritica, Titiribi and Marmato gold mines are major deposits located at the northwestern margin of the Central Cordillera in Colombia. The occurrence and chemical compositions of ore minerals in each were investigated to determine the genetic processes of the ore minerals and the genesis of the deposits overall.

These three deposits are related to small but prominent Neogene hypabyssal porphyry geoforms of andesitic to dacitic composition. The Neogene age of the porphyry body in the Burica area is still controversial. However, its form and chemistry are similar to the porphyry bodies in the other two mining areas. Sulfides in the Buritca veins comprise sphalerite, pyrite, chalcopyrite, Ag-rich tetrahedrite, hessite, electrum, and bornite. Gangue minerals are K-feldspar, sericite, apatite, quartz, and carbonates. Argillic alteration is predominant. Crystallization temperatures have been measured in fluid inclusions from both quartz and calcite grains, revealing a minimum crystallization temperature between 220°C and 300°C. Tellurium and sulfur fugacities are estimated to be between $10^{-12.96}$ to $10^{-9.55}$ and $10^{-6.3}$ to 10^{-10} atm, respectively.

The Titiribi mining district contains two different styles of mineralization. The first is represented by the El Zancudo deposit, which has a long history of production. The ore veins are emplaced in schist, and contain differing Ag-Cu-Pb-Sb-bearing sulfosalts along with sphalerite, pyrite, arsenopyrite, galena, chalcopyrite, and electrum. At least two main crystallization stages have been defined; the second stage is accounted for the crystallization of most of the ores, and is divided into two sub-stages with minimum crystallization temperature ranging from 264 to 350°C and 134 to 262°C, respectively. Sulfur fugacity varies from 10^{-3} to 10^{-7} atm. for temperatures higher than 300°C. Gangue minerals accompanying the ore veins are quartz, carbonates, sericite and K-feldspar. Argillic and advanced argillic alteration is observed in the host rocks. The second style of mineralization comprises magnetite-hematite rich veins hosted in a porphyry body. These veins also contain sphalerite, chalcopyrite, and bornite. Hydrothermal titanite, chlorite, K-feldspar and sericite occur as gangue minerals. Propylitic and argillic alteration are predominant, and homogenization temperatures measured in quartz fluid inclusions range from 306 to 420°C.

The Marmato mine is one of the historically most significant mining districts in this area. The constituent sulfide minerals are sphalerite, pyrite, chalcopyrite, galena, argentite and electrum. Gangue minerals are carbonates, sericite, K-feldspar, and quartz. Homogenization temperatures in both quartz and carbonates reveal temperatures between 259 to 292°C. Argillic and propylitic alteration is commonly observed.

The chemistry of the hydrothermally altered host rocks of these deposits was compared with that of unaltered porphyries from the Titiribi district. The common geomorphologic features among these prominent porphyry bodies are also well correlated with Nb/Y and Zr/Ti immobile element ratios, which indicate andesite to rhyodacite magmatism. Although the time gap between each crystallization stage in these deposits remains unclear, some evidence suggests the main mineralizing stages are linked to late Miocene magmatic activity. Extensive Middle-Miocene to Early-Pliocene magmatism is well documented along the north Andes. These three hydrothermal-related deposits are classified as intermediate sulfidation mesothermal to epithermal type (Cordilleran polymetallic vein deposits).

Hydrothermal gold mineralization in island arc environment: case study in Western Java, Indonesia

Rosana, M.F.
Faculty of Geology, Padjadjaran University, Bandung, Indonesia (mega_fr@unpad.ac.id)

Western Java area occupies a part of Sunda Banda magmatic belt, and is well known for the prevailed hydrothermal gold mineralizations where active gold mines of the Gunung Pongkor, and Cibaliung and formerly produced mines of the Cikidang the Cirotan and the Cikotok are located. And several other areas are under exploration such as Arinem, Cineam, Cipunagara, Ciemas and Gunung Subang.

Hydrothermal gold ore deposits of western Java are mainly distributed along the NNE-SSW strike-slip faults cutting Miocene to Pliocene volcanic and plutonic formations. The ore veins are hosted mainly in calc-alkaline andesitic and dacitic volcanic breccia and tuff, less commonly in limestone, sandstone, claystone and microdiorite intrusive. Pervasive hydrothermal wall rock alterations are well developed in the mineralized area. An intensive silicic, propylitic and argillic alterations are generally observed in the most of deposits, indicated by chlorite/smectite and/or illite/smectite, epidote, sericite, kaolinite and locally montmorillonite.

The mineralization ages are ranging from 1.7 to 11 Ma based on the K-Ar dating among the deposits. The deposits are extensively in the form of gold bearing quartz veins of epithermal low sulfidation type characterized by the occurrence of sericite, adularia and manganese oxide, and also in the quartz-carbonate-polymetallic gold bearing veins of epithermal to shallow mesothermal and/or transition to porphyry tin type environment.

In the former low sulfidation type deposits, the ore is composed mainly of gold and silver minerals. This type deposits are estimated to be formed under the shallow (180-350m in depth) epithermal conditions from low salinity (<4 wt% NaCl eq.) fluids in the temperature from 170 to 250°. Gold might be transported as $Au(HS)^{2-}$ under nearly neutral pH and relatively high fS_2 (10^{-14} to 10^{-11}) and fO_2 (10^{-30} to 10^{-45}) in conditions. On the other hands, the latter mesothermal and/or transition to porphyry type ore is characterized by the occurrence of not only gold and silver minerals, but also the presence of tin minerals such as canfieldite and cassiterite, wolframite, and bismuth and tellurium minerals. This type deposits are estimated to be formed at the depth below 400m from slightly higher salinity (1.5 to 7.5 wt% NaCl eq.) fluids in the temperature at 260 to 350°. Gold might be transported under neutral to slightly acidic and relatively high fS_2 (10^{-20} to 10^{-10}) and fO_2 (10^{-30} to 10^{-40}) in conditions.

The Pb, S, and C isotope ratios indicate the magmatic source for associated metals, while the association of tin-minerals, wolframite and bismuth minerals suggest the recycling of older continental crust underlying the Malaysia-Sumatra porphyry tin belt as the source of the metals. The oxygen stable isotope ratio suggests a mixing of hydrothermal fluids with meteoric water in the ore depositions.

The mineralization ages (Pongkor: 2.7 to 8.6Ma, Cikidang: 2.4Ma, Cipanglengseran: 2.1Ma, Cirotan: 1.7Ma, Cibaliung: 11 Ma, and Arinem 8.8 Ma) indicate a lateral shift of volcanic front, where they are getting young toward south of Java island. The time-spatial change of hydrothermal activity with gold mineralizations corresponds to magmatic activity in the Sunda-Banda magmatic arc, which was caused by subduction of the oceanic plate under the continental crust. The crust is relatively thin and young with mostly intermediate composition accompanying a few ignimbrite deposits, such as in the Bayah dome where most of gold mineralizations are localized in western Java.

Magmatic control of volcanic hosted mineralization in the Carpatho-Pannonian region

Lexa, J.[1*], Molnár, F.[2] & Szakács, A.[3]
[1]Geological Institute, Slovak Academy of Sciences, Bratislava, Slovakia ([*]geoljalx@savba.sk)
[2]Dept. of Mineralogy, Eötvös University, Budapest, Hungary
[3]Dept. of Environmental Sciences, Sapientia University, Cluj-Napoca, Romania

Paleogene and Neogene volcanic-hosted mineralizations of the Carpathian-Pannonian region show a great variety of styles and geological settings. Simple andesite stratovolcanoes either show no mineralization or they host unmineralized advanced argillic alteration. Mature andesite stratovolcanoes involving differentiated rocks and shallow subvolcanic intrusions host either this kind of alteration and/or productive HS (high sulphidation) and IS/LS (intermediate/low-sulphidation) epithermal systems. Multiple-stage complex andesite stratovolcanoes with some felsic rocks host early intrusion-related porphyry-style mineralization and usually late-stage IS/LS hydrothermal systems. Areas of the bimodal andesite/rhyolite volcanism host intrusion-related advanced argillic alteration and/or IS/LS as well as hot-spring/LS hydrothermal systems related to rhyolite dome/flow complexes and regional extension. In volcanic centers eroded down to the level of subvolcanic intrusions, we distinguish counterparts of the above-mentioned mineralization styles - unmineralized andesite/diorite porphyry intrusions, intrusion-related IS/LS base metal stockworks ± IS/LS epithermal veins, skarn type magnetite and base metal mineralizations, skarn/porphyry or porphyry Cu ± Mo, Au mineralizations, and porphyry Au mineralizations, with a related suite of HS and/or LS epithermal veins.

The observed variability of mineralization styles reflects differences in magmatic evolution and structural control. Ore-productive systems associates only with those intrusive-volcanic systems that have reached the maturity stage including evolution of magmas in the high level crustal magma chambers. Favourable systems show long-lasting volcanic activity associated with evolution of volcano-tectonic grabens in back-arc tectonic settings. High-level magmatic chambers/ systems are principally of two types: those associated with andesite stratovolcanoes and those associated with rhyolitic magmatism.

Intrusive systems of andesite stratovolcanoes are of diorite composition and evolve towards granodiorite composition due to AFC processes. If they give rise to a shallower subvolcanic stock magmatic fluid partitioning into vapour and brine creates conditions for the development of advanced argillic alteration in the volcanic edifice which may evolve into a HS type ore, as well as for the complementary Cu-porphyry and intrusion-related IS/LS systems. Due to gradual crystallisation of the stock and decrease in temperature, the early stage marked by the vapour-brine partitioning and related advanced argillic alteration in the shallow volcanic zones is followed by the stage of deeper fluid separation giving rise to mineralization only if a larger magma chamber is involved. A deeper subvolcanic stock will not experience processes related to magmatic fluid partitioning and thus the diluted magmatic fluids will generate LS hydrothermal systems without contemporaneous HS and Cu-porphyry systems. Longer-living shallow crustal magma chambers evolve via AFC processes towards more felsic compositions with or without a prior stage of andesitic volcanism at surface. This type of shallow magma chambers supply fluids to the deeply-rooted IS/LS systems associated with rhyolite magmatism and horst/graben tectonic structures. Structural control by normal faults played an important role in their localization.

Acknowledgements: A supports of VEGA 1/0311/08 and 2/0171/08 (Slovakia) and Hungary-Slovakia S&T SK 27/06 grants are acknowledged.

Mineral zoning, cross-cutting relationships, and radiometric dating: keys to trace fluid evolution during polymetallic stages of porphyry intrusion-related systems

Fontboté, L.
Ore Deposits Group, Earth and Environmental Sciences, University of Geneva, Switzerland (lluis.fontbote@unige.ch)

Epithermal and sub-epithermal polymetallic Cordilleran ores occur frequently in porphyry intrusion-related systems [1]. High Zn, Pb, Ag and Mn contents are traced in hypersaline fluid inclusions formed during potassic alteration [2], and it it could be perhaps followed that the polymetallic mineralization just represents distal low temperature precipitation of these metal rich fluids. However, detail study of several Cordilleran polymetallic deposits, suggests that the history is more complex. Cross-cutting relationships and radiometric dating indicate that Cordilleran or Butte Type polymetallic veins and replacements bodies cut early potassic and, in places, phyllic alteration assemblages and that they postpone by several hundred of thousands of years the early stages of deposit life span [3] a temporal evolution that is comparable to that of many porphyry deposits [4].

The sulfidation state and fluid acidity in Cordilleran ore deposits depends on several factors, including the involvement or not of acidic gas phases [5], the formation depth, and in general the temperature and spatial path followed by the ore forming fluids. Thus, the zoned character is a frequent, but not compulsory characteristic of the class. Strongly zoned deposits are characterized by the presence of cores with high sulfidation and/or advanced argillic mineral assemblages. In such cases, cores dominated by enargite or famatinite, pyrite, quartz±(tennantite, wolframite, chalcopyrite, covellite, chalcocite, alunite, dickite, kaolinite) grade to external parts with Fe-poor sphalerite, galena±(sericite, kaolinite, dickite, hematite, Fe-Mn carboantes). In contrast, weakly zoned deposits may display internal parts bearing pyrrhotite, pyrite, quartz±(chalcopyrite, arsenopyrite, tetrahedrite, carbonates, sericite, chlorite, quartz) and external parts of Fe-rich sphalerite, galena, pyrrhotite±(rhodocrosite, siderite, and other carbonates, sericite, chlorite, quartz). In extreme cases, both end-member styles may be present in the same deposit.

Available information [6,7] suggests that Cordilleran polymetallic deposits may be formed by low to moderately saline fluids of magmatic isotopic signature. Therefore, it is more likely that these fluids represent single-phase magmatic fluids than diluted magmatic brines.

[1] Fontboté, L. & Bendezú, R. (2009) *10th Biennial SGA Meeting, Townsville*, 521-523. [2] Heinrich et al. (1999) *Geology*, **27**, 755-758. [3] Baumgartner, R. et al. (2008) *Econ. Geol.*, **104**, 479-504. [4] Sillitoe, R. (2010) *Econ. Geol.*, **105**, 3-41. [5] Fontboté, L. & Bendezú, R. (2009) *Econ. Geol.*, **104**, 905-944. [6] Baumgartner, R. et al. (2008) *Econ. Geol.*, **103**, 493-537. [7] Catchpole, H. et al. (2010) *Session EG54, this volume.*

Formation of advanced argillic lithocaps over porphyry systems by increasingly acidic fluid

Hedenquist, J.W.[1*] & Taran, Yu.[2]
[1]Earth Sciences, University of Ottawa, Canada
([*]hedenquist@aol.com)
[2]Instituto de Geofisica, UNAM, Mexico D.F., Mexico

Hypogene advanced argillic alteration, typically quartz-alunite with halos of kaolinite ± dickite and roots of pyrophyllite-diaspore, forms in the epithermal environment from condensates of magmatic vapor that contain SO_2 and HCl, derived from an underlying intrusive source. The most aggressive, nearly isochemical leaching of the host rock by the most acidic condensate, commonly pH~1, leaves a residual silica that recrystallizes to quartz closest to the flow channel, in the core of alteration; the alteration flares upward along feeder structures, and if a lithologic unit is intersected, the alteration forms a sub-horizontal blanket, termed a lithocap. Where subsequently mineralized, the residual quartz, commonly with a vuggy texture, has higher Au (and Cu) grades than the halo of quartz-alunite. Tonnage in these high-sulfidation systems may develop within the sub-horizontal lithocap, although the highest grades are in the structurally controlled feeders.

Our modelling of the condensation of a typical volcanic vapor and its cooling and reaction with a felsic rock reproduces the alteration pattern observed along structures and in lithocaps that may host high-sulfidation deposits. The modelling indicates alumino-silicates (pyrophyllite, diaspore, locally andalusite) are stable only at higher temperatures at depth; at lower temperatures and more shallow depth, Na- and K-alunite become stable, eventually followed by residual quartz at higher condensate:rock ratios (>10:1). The reason for this transition, and the upward flare (widening) of the zone of alteration along structures, is related to the increased reactivity of HCl and H_2SO_4 acids as the temperature decreases; only quartz, pyrite, anhydrite and native S are stable below ~200°C, hence the abundance of quartz residue. As a further check on the modelling, the calculated composition of the condensate after reaction with fresh rhyolite and the alteration minerals to 100°C is similar to acidic springs, with pH~1, that discharge around active volcanoes, e.g., Satsuma Iwojima, Japan.

It is observed that the most extensive lithocap alteration, residual quartz and/or quartz-alunite, is commonly offset from the surface projection of the causative intrusion, the latter associated with porphyry deposits. This is caused by a combination of two factors. There is typically lateral flow of acidic condensate away from the high-temperature vapor plume that forms directly over the intrusion, caused by hydraulic gradients at shallow depths if there is a volcanic edifice at the surface. As a result of this lateral flow, the most intense and abundant advanced argillic alteration that forms at lower temperatures may occur away from the near-surface projection of the intrusion. The potential for lithocap alteration to be offset from the intrusion must be determined when exploring for high-sulfidation ore, since the highest grades are commonly related to structures that are proximal to the underlying intrusion. In addition, defining the likely location of the source intrusion will help the explorer to efficiently assess any potential for deeper porphyry-style mineralization.

The porphyry to epithermal transition in atypical late Neoproterozoic REE-Au-Ag-Te occurrences

Tuduri, J.[1*], Dubois, M.[2], Try, E.[2], Chauvet, A.[3], Barbanson, L.[4] & Ennaciri, A.[5]
[1]ENAG – BRGM School, Orléans, France ([*]j.tuduri@brgm.fr)
[2]LGCgE and Université Lille1, France
[3]UMR 5573, Université de Montpellier II, France
[4]ISTO, Université d'Orléans, France
[5]Reminex, Marrakech, Maroc

The Neoproterozoic terranes of the Eastern Anti-Atlas ranges (Morocco) host numerous precious and base metal deposits. The Kelâa M'Gouna showings are found at the interface between i) a basement made of Cryogenian detrital sediments intruded by early Ediacaran granodiorite plutons and ii) a late Ediacaran upper unit composed of lava flows and caldera-related ash-flow tuffs associated with cogenetic granites.

We proposed a two-stage formation model: **Stage I** is related to high-temperature hydrothermal system. Alteration structures are different if hosted by the basement or the volcano-plutonic unit, but supposed to occur during the same time with respect to fluid inclusions studies and mineral geochemistry. Within basement rocks, intense silicification produces the formation of a quartz-rich stockwork with F-Cl-rich amphibole, Cl-F-rich biotite, muscovite, scarce F-rich tourmaline and sulfides. Within the volcanic rocks a strong pervasive silicification is related to development of quartz, pyrite, F-rich tourmaline, F-rich phlogopite, Cl-F-rich apatite, andalusite, rutile, hematite, monazite, xenotime, thorite and uranothorite. Sulfides appear in both types and mainly consist of pyrite. Inclusions of chalcopyrite, pyrrhotite, electrum, galena, tetradymite and brannerite are observed in the stockwork, whereas inclusions of galena, coloradoite, hessite and altaite characterize pyrite of the pervasive alteration area. Fluid inclusions were used to constrain palaeohydrothermal conditions during **stage I**. Primary multiphase inclusions are composed of liquid, vapour and halite cube, as well as solids such as sylvite, calcite, $CaCl_2$. In addition, uncommon mineral inclusions that remain abundant have been identified such as titanite, hematite, magnetite, a refringent solid phase identified as andradite. Chalcopyrite and gold were observed in a multiphase inclusion. Multiphase inclusions have a high but very variable salinity (30 to 45 wt% eq. NaCl) and are characterized by homogenization by halite-disappearance. The large range of temperatures (150-400°C) related to an advanced argillic alteration is herein characteristic of alteration zones located in the upper part of Cu-Au porphyries and transition to high-sulfidation environments. **Stage II** is related to a low-temperature system characterized by epithermal structures such as veins and breccias. It begins by pervasive tourmaline-rich fractures and chlorite-rich breccias, then emplacement of adularia-, quartz- and chlorite-rich veins. Sulfides occur late in the core of previously formed quartz-adularia-chlorite veins by deposition of As- and Co-rich pyrite, minor chalcopyrite and precious metal (Au-Ag tellurides, electrum, Ag-telluride and Bi-telluride). Paragenetic study reveals that sulfides could coexist with iron oxides (hematite and magnetite). Microthermometric study shows lower salinity inclusions probably belonging to the H_2O-NaCl-$CaCl_2$ and the absence of multiphase inclusions. Homogenisation temperatures are ranging between 120 and 300°C. Thus, stage II appears as a transition from stage I and corresponds to a low sulfidation epithermal style deposit.

The study of the Kelâa M'Gouna showings reveals that late-Neoproterozoic hydrothermal activity may provide atypical ore systems: a REE-Au deposit related to an advanced argillic alteration telescoped by an iron oxide, Au-Ag-Te low sulfidation epithermal deposit.

Re-examination of sulfidation state of the Victoria gold deposit, Northern Luzon, Philippines

Tanaka, T.[*], Imai, A. & Watanabe, K.
Dept. of Earth Resources Engineering, Kyushu University, Fukuoka, Japan ([*]takahiro-tanaka@mine.kyushu-u.ac.jp)

The Victoria epithermal gold deposit is located in the Mankayan mineral district, northern Luzon, Philippines. The Mankayan mineral district is known as a porphyry copper-type hydrothermal system. In the Mankayan mineral district, the Victoria gold deposit is adjacent to the FSE porphyry copper-gold deposit and the Lepanto enargite deposit. Although, it is considered that the Victoria gold deposit has no relationship to FSE porphyry copper-gold deposit and the Lepanto enargite deposit [1]. Sphalerite, galena, chalcopyrite, tetrahedrite and native gold/electrum occur as the principal ore minerals in the Victoria deposit [2]. Thus, it has been recognized as a low-sulfidation epithermal deposit by geologists of Lepanto Consolidated Mining Company [3]. Additionally, Sajona et al. (2002) classified it as a carbonate-base metal low-sulfidation epithermal deposit [1].

However, mineralogical and fluid inclusion studies in this study indicate that some veins at the Victoria deposit consist of high-sulfidation veins and intermediate-sulfidation assemblage. Especially, colusite, enargite and luzonite often occur in quartz veins and pyritic sulfide veins at the southern portion of the Victoria deposit. Bismuth and Tellurium minerals are also observed in quartz veins at the southern potion of the Victoria deposit. Further, the assemblage of bornite-chalcopyrite-pyrite is often observed at the deeper levels. Homogenization temperatures of fluid inclusions in the quartz veins, which have the assemblage of bornite-chalcopyrite-pyrite, range from 230 to 280°C. These results indicate that (1) part of the Victoria veins are formed in a high-sulfidation condition (Fig. 1); (2) Bismuth, Tellurium and Selenium bearing ore fluid might be derived from a magmatic source located at the southwest and deeper portion of the Victoria deposit.

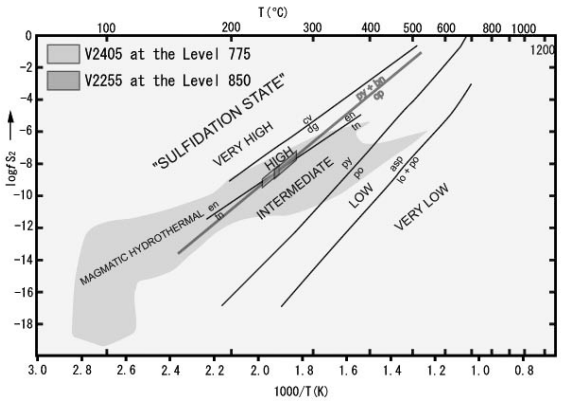

Fig. 1: LogS_2 - 1000/T diagram, showing sulfidation state of the Victoria deposit (modified after Einaudi et al. [4]).

Furthermore, melting temperatures of fluid inclusions in the quartz veins, which have the assemblage of bornite-chalcopyrite-pyrite, show two trends. This result may indicate that the Victoria veins formed by two different hydrothermal fluids.

[1] Sajonam, F.G. et al. (2002) *Resour. Geol.*, **52**, 315-328. [2] Claveria, R.J. (2001) *Resour. Geol.*, **51**, 97-106. [3] Cuison, A.-L.G. et al. (1998) *Proc. 1998 Ann. Philippine Geol. Convention* (GEOCON '98), 211-219. [4] Einaudi, M.T. et al. (2003) *Soc. Eco. Geo. Spc. Pub.*, **10**, 285-313.

Hydrothermal alteration, fluid inclusions and stable isotopes (O, H) in a porphyry and related epithermal system of the Palaeogene volcanic belt of the Alp-Carpathian Orogen (Velence Mts., W-Hungary)

Molnár, F.[1*], Bajnóczi, B.[2], Pécskay, Z.[3], Prohászka, A.[1] & Benkó, Zs.[1]
[1]Dept. of Mineralogy, Eötvös Lorand University, Budapest, Hungary ([*]molnar@abyss.elte.hu)
[2]Institute for Geochemical Research, Hungarian Academy of Sciences, Budapest, Hungary
[3]Institute of Nuclear Research, Hungarian Academy of Sciences, Debrecen, Hungary

The calk-alkaline andesitic intrusive-volcanic complex of the Velence Mts. is located within the Palaeogene Volcanic Belt of the Alp-Carpathian system. This belt is situated on a displaced fragment of African Plate origin which has escaped into the Carpathian realm from the highly compressive Alpine collision zone during the Late Oligocene-Miocene. This belt is the host of the world class Cu-porphyry-Cu-Zn-skarn-epithermal Cu-Au ore complex at Recsk (Ne-Hungary). The underexplored mineralization of the intrusive-volcanic complex in the Velence Mts. bears several similarities with Recsk.

The outcrops of volcanic rocks in the Velence Mts. are strongly altered lava and pyroclastic units in an erosional remnant of a stratovolcano with about 10 km diameter. The topographic high areas form an E-W trending zone in the volcanic structure and consist of vuggy silica bodies. Geophysical surveying and drillings found a diorite intrusion at about 600 m depth under the central part of the volcanic structure. The diorite intrusion shows K-metasomatic (K-feldspar and biotite) and superimposing propylitic (actinolite-epidote-chlorite) alteration. Stockwork mineralization in the intrusion consists of early brittle-ductile K-feldspar-quartz-biotite and magnetite-chlorite and late brittle quartz-calcite-pyrite-chalcopyrite-bornite-Pb-Zn-sulphide, as well as the latest barren calcite-zeolite veins. The transitional zone between the porphyry and epithermal mineralization is characterised by illite alteration with increasing amount of kaolinite towards the epithermal zones. In the high temperature (300 to 400°C) advanced argillic alteration zones around brecciated vuggy silica bodies topaz and zunyite occurs together with pyrophyllite, diaspore and kaolinite. These zones probably indicate major upflow zones of magmatic volatiles with high fluorine contents causing formation of topaz and zunyite instead of andalusite. Vuggy silica bodies with more peripheral position have pyrophyllite/diaspore-kaolinite alteration halo. Na-enriched alunite containing APS mineral inclusions is ubiquitous in late infillings of vuggy silica. Marginal zones of the epithermal system lack of vuggy silica and silicified zones show illite, illite-kaolinite or illite-dickite alteration along major fault and breccia zones. Strong pyritization (oxidised to ochre in most areas) is characteristic to vuggy silica and occurrences of enargite is also detected. K-Ar ages for K-feldspar, illite and biotite+amphibole from the porphyry intrusion (29-32 Ma) are essentially identical with those for illite and alunite in the epithermal zones (31-33 Ma).

Fluid inclusion data indicate high temperature boiling producing high salinity-high density magmatic brine and low density vapour during the variation of pressure between hydro-lithostatic conditions at the level of intrusion. Mixing of both types of magmatic fluids with meteoric water is supported by variation of fluid inclusion salinity and stable isotope (O, H) data for biotite, amphibole, chlorite, illite, kaolinite, pyrophyllite and alunite from the subvolcanic to the volcanic level and to the peripherial zones.

Tracing low sulfidation systems from their roots down to foothills - example from the Kremnica ore and industrial minerals fields (Slovakia)

Koděra, P.[1*], Lexa, J.[2], Fallick, A.E.[3], Biroň, A.[2], Gregor, M.[1], Uhlík, P.[1] & Kraus, I.[1]
[1]Dept. of Geology of Mineral Deposits, Comenius University, Bratislava, Slovakia ([*]kodera@fns.uniba.sk)
[2]Geological Inst., Slovak Acad. of Sci., Bratislava, Slovakia
[3]Scottish Universities Environmental Research Centre, UK

Deciphering paleohydrology of epithermal systems is critical for determining the location of boiling, precipitation of metals and distribution of zones of alteration that may represent economic ore and industrial mineral deposits. Neogene Kremnica system is an excellent example of a classical low-sulfidation Au deposit, accompanied by several economic accumulations of K-bentonite, bentonite and zeolite.

The ore deposit is hosted by andesitic rocks, situated on marginal faults of a resurgent horst in central part of a volcanotectonic graben. Mineralization is contemporaneous with uplift of the horst and emplacement of rhyolitic rocks S of the horst in the graben. Wallrock alteration includes adularia, illite or I/S and kaolinite. Mineralogical and fluid inclusion data indicate multistage filling of veins with at least two episodes of boiling at different temperatures and paleodepths. Boiling was responsible for Au deposition and adularia-illite alteration. Kaolinite represents a later overprint on mineralised structures, resulting from penetration of subsurface water acidified by condensation of H_2S and CO_2-bearing vapour released by boiling. Individual parts of the vein system originated from low-salinity (<2 wt% NaCl eq.) fluids showing decrease in temperature from 270 to 150°C in the N-S direction due to decreasing erosion level (~350 to 50 m). Fluids were isotopically homogenous (~ -3.5 ‰ $\delta^{18}O$) mostly of meteoric origin affected by isotopic reequilibration with country rocks.

Less mineralised S section of the vein system was emplaced in rhyolite domes and volcanoclastic rocks, filling the graben. This area also hosts the industrial mineral deposits. Regional I/S alteration (incl. K-bentonite deposits) next to veins probably result from lateral outflow of hydrothermal fluids into permeable pumiceous/glassy volcanoclastic rocks as indicated by their similar $\delta^{18}O_{fluid}$ compositions and paleotemperatures (135-190°C – concordance of fluid inclusion data, oxygen isotope and I-S geothermometers). A local elevation with blocks of silicites resting on breccias cemented by quartz and kaolinite is interpreted as an ancient hot-spring system. S and SE parts of the area host numerous bentonite (smectite) deposits, representing altered tuffs and glassy marginal breccias of rhyolite domes. There is not a continuous decrease of expandability and paleo-temperatures between areas with I/S and smectite alterations (I/S has rarely >45% of smectite layers), which is probably a consequence of a hidden fault, dividing relatively subsided and uplifted parts of the area. Bentonite is often interlayered with limnic/lacustrine silicites representing the former paleosurface. Silicites result from episodical inflow of groundwater enriched in silica due to decomposition of volcanic glass. Oxygen isotope values of both smectite and silicites show decreasing temperature from N to S-SE as the result of paleoflow of heated groundwaters and/or recrystallisation during shallow burial. Smectite crystallinity (crystal size distribution) well correlates with their $\delta^{18}O$ values as the result of decreasing temperature (70 to 15°C based on isotopic equilibrium with meteoric water). Silicites give slightly higher temperatures (80 to 30°C), while some correlation between crystallinity and $\delta^{18}O$ also exists. Smectite alteration changes into zeolite alteration with clinoptilolite and mordenite towards depth probably due to diagenesis and thermal effect of rhyolite extrusives.

Acknowledgements: Support by VEGA grant 2/0171/08.

Phreatomagmatic breccia at the Pb-Zn-Ag Trepča deposit, Kosovo

Strmić Palinkaš, S.[1*], Palinkaš, L.A.[1] & Molnar, F.[2]
[1]Institute of Mineralogy and Petrography, Dept. of Geology, University of Zagreb, Croatia ([*]sabina.strmic@inet.hr)
[2]Dept. of Mineralogy, Eötvös Loránd University, Budapest, Hungary

The Trepča Pb–Zn–Ag deposit (42.9°N, 20.9°E) is located in the Kopaonik block of Western Vardar Zone, Kosovo. The mineralization is represented by skarn and hydrothermal parageneses. Skarn paragenesis comprises prograde (hedenbergite) and retrograde mineral assemblages (ilvaite, magnetite, pyrrhotite, arsenopyrite, pyrite, quartz and carbonates). The economically important sulfides, such as galena and sphalerite, are associated with hydrothermal stage superimposed onto the skarn mineralization [1].

The mineralization is spatially and temporary related to Tertiary postcollisional magmatism. Recrystallized Triassic limestone with paleokarst features represents the principal host rock. The limestone is placed within the core of an anticline and covered by Triassic schist. A nearly circular volcanic pipe transects the limestone-schist contact along the crest of the anticline. The volcanic pipe consists of trachytic core and breccia mantle. The core, with the form of steeply dipping inverted cone, is intensely hydrothermally altered into the mixture of K-feldspar, quartz and muscovite. Sanidine phenocrysts comprise sanidine relics accompanied with various micas and quartz. Breccia mantle is composed of angular to subround fragments of country rocks (limestone, schist), fragments with magnetite core and pyrite rim, and round clasts of trachyte. The contact between breccia and the wall rocks is sharp and sporadically branches into lateral fractures, filled with rock flour ("milled matrix, fluidized breccia") or with angular fragments ("jigsaw-fit breccia"). The breccia pipe is exposed at all horizons of the deposit, from the surface (+860 m above sea level) downwards to Horizon XI (+ 15 m above sea level) and its downward termination is not observed. An intimate relation of breccia with trachytic dyke suggests that phreatomagmatic explosions were controlled by direct contact of magma with an external source of water.

The contact between the breccia and host limestone is marked by presence of low saline (~ 4 wt.% NaCl equ.) and moderate temperature fluids (T_H = 275-290°C). Stable isotopes of carbonates point to the influence of magmatic fluids ($\delta^{13}C$ = -2.8 ‰; $\delta^{18}O$ = 12.5 ‰). Fluid inclusions preserved within recrystallized limestone fragments display moderate salinity (13-14 wt.% NaCl equ.) and T_H up to 340°C. Decreased $\delta^{13}C$ (-4.3 ± 0.1 ‰) and $\delta^{18}O$ values (13.0 ± 0.4‰) suggest recrystallization under influence of magmatic CO_2. Fragments composed from magnetite core and pyrite rim occur mostly in the upper part of the breccia pipe. Textural features suggest that fibroradial magnetite, accompanied by mixture of quartz and carbonates, was formed as retrograde alteration of hedenbergite under increased oxygen fugacity:

$$3CaFe^{2+}Si_2O_6 + 3CO_2 + ½O_2 \rightarrow Fe^{2+}Fe^{3+}{}_2O_4 + 3CaCO_3 + 6SiO_2$$

Increased oxygen fugacity is attributed to the opening of the system during the phreatomagmatic explosion. Once formed breccia pipe had served as a sink for invasion of groundwater into the system and initiated the retrograde stage. Furthermore, opening of the system decreased the pressure and amplified the sulfur release. The occurrences of pyritic rims point to the sulfur fugacity increase:

$$Fe^{2+}Fe^{3+}{}_2O_4 + 3\ S_2 + 8\ H^+ + 8\ e^- \rightarrow 3\ FeS_2 + 4\ H_2O$$

Isotopic composition of pyrite ($\delta^{34}S$ = 3.1± 0.7 ‰) supports a magmatic source of sulfur.

[1] Strmić Palinkaš, S. (2009) *Unpublished PhD thesis*. University of Zagreb, Croatia.

Te and Se mineralogy of Paleozoic epithermal Au deposits of the Ural - Mongolian belt

Plotinskaya, O.Yu.[1*], Kovalenker, V.A.[1] & Seltmann, R.[2]
[1]Institute of Ore Geology, Petrology, Mineralogy, and Geochemistry, Russian Academy of Sciences, Moscow, Russia ([*]plotin@igem.ru)
[2]Natural History Museum, CERCAMS, London, UK

Although most of the known epithermal deposits were formed during Mesozoic or Cenozoic eras, there are numerous sites of Paleozoic age. Among these, the best examples are in the epithermal-porphyry province of the Kurama ridge (Middle Tien Shan) and the recently discovered Birgildinsk-Tominsk ore district in the South Urals. The first area is a part of C_3-P_1 Andean-type continental margin while the second one is supposed to be located within D_3-C_1 island arc. In the present study two epithermal orefields, Kochbulak-Kairagach (Kurama) and Bereznyakovskoe (Urals), are considered as most remarkable due to their variable telluride-selenide mineralogy.

The Kochbulak and Kairagach deposits (estimated reserves 120 and 40 t of Au, respectively) are located in the same volcanic structure and have been formed within the same ore-forming system [1,2]. Au-Ag-Cu-Bi-Te-Se mineralization is confined to veins and dissemination zones accompanied by quartz-sericite wall-rock alteration. The deposits are characterized by similar mineralogy. Among tellurides, calaverite, altaite, hessite, and tetradymite are most widespread in both deposits; at Kairagach selenides and sulfoselenides of Bi and Pb are common, while at Kochbulak only various Bi and Pb telluroselenides and sulfotelluroselenides are typical. At both deposits the native gold assemblages change from Au+calaverite+altaite to Au+petzite±hessite and, finally, to Au+hessite±petzite, accompanied by increase of Ag contents in native gold and correlating with temperature decrease, pH increase and fO_2 drop during each ore stage [3].

The Bereznyakovskoe orefield includes several small deposits with a total Au potential of 50–100 t [4]. Mineralization is hosted by dacite-andesite tuffs interlayered with limestones. Wall rock alteration is represented by pyrophyllite-quartz alteration followed by argillic alteration [5]. Three ore stages were identified: pyrite, polymetallic (with enargite, fahlore-telluride, and gold-telluride sub-stages) and galena-sphalerite stages. The generalized sequence of gold-telluride bearing assemblages is as follows: native Te+sylvanite via krennerite+petzite and altaite+calaverite via Au+calaverite+altaite+coloradoite+tellurantimony to native Au+galena+antimonite and hessite+galena. The observed evolution was controlled by temperature decrease accompanied by drop in fS_2 and fTe_2. Selenides are absent except for galena-clausthalite [6].

Fluid inclusion data supported by mineral thermobarometry suggest Kairagach to represent shallower parts of the epithermal system than Kochbulak, while Bereznyakovskoe belongs to deeper parts of such system. At the same time, on a High to Low sulfidation line the Central Bereznyakovskoe establishes the highest degree of sulfidation, whereas its SE and North periphery, as well as Kochbulak and Kairagach, belong to high-to-intermediate sulfidation types.

Acknowledgements: This study was supported by NHM (CERCAMS), and RFBR 09-05-00697 and 10-05-00354.

[1] Kovalenker, V.A. et al. (1997) *Geol. Ore Deposit.*, **39**, 107-128. [2] Kovalenker, V.A. et al. (2003) *Geol. Ore Deposit.*, **45**, 171-200. [3] Plotinskaya, O.Yu. et al. (2006) *Mineral. Petrol.*, **87**, 187-207. [4] Lehmann, B. et al. (1999) *Miner. Deposita*, **34**, 241-249. [5] Grabezhev, A.I. et al. (2000) *Geol. Ore Deposit.*, **42**, 33-46. [6] Plotinskaya, O.Yu. et al. (2009) *Geol. Ore Deposit.*, **51**, 371-397.

Trace elements and cathodoluminescence of quartz in stockwork veins of Mongolian porphyry-style deposits

Müller, A.[1*], Herrington, R.[2], Armstrong, R.[2], Seltmann, R.[2], Kirwin, D.J.[3], Stenina, N.G.[4] & Kronz, A.[5]
[1]Geological Survey of Norway, Trondheim, Norway
([*]Axel.Muller@ngu.no)
[2]Natural History Museum, London, UK
[3]Ivanhoe Mines, Bangkok, Thailand
[4]Institute of Geology SB RAS, Novosibirsk, Russia
[5]Geowissenschaftliches Zentrum Göttingen, Germany

In this study, results are presented from a comprehensive study of quartz from mineralised A-type and other associated veins of the late Devonian Central Oyu Tolgoi and early Carboniferous Zesen Uul porphyry copper-gold deposits in the south Gobi region of Mongolia. The investigated A-type veins, which are considered to have formed during the early stage of stockwork formation, show complex growth structures with multiple overprinting and replacement revealed by cathodoluminescence (CL) imaging. Electron probe microanalysis (EPMA) was then used to determine quartz trace element chemistry (specifically Al, K, Ti, and Fe). The use of backscattered electron imaging helped to establish the paragenetic relationships between ore mineral assemblages and different quartz generations. Finally fluid inclusion microthermometry was carried out on recognized quartz generations.

The study of the Central Oyu Tolgoi and Zesen Uul Cu-Au porphyry systems shows that despite differences in the alteration and mineralisation styles, the CL features of the different quartz generations are generally similar. Four major quartz crystallisation stages Q1 to Q4 were identified in the central mineralised stockworks of both deposits namely:

Q1 occurs in barren A-type veins and as massive silicification of the host rocks. Q1 is brightly luminescent with high Ti contents, indicative of crystallisation temperatures greater than 600°C. This quartz stage forms more than 90 vol.% of the quartz mass of the stockworks in each deposit.

Q2 is mineralised, occurring as dull luminescent quartz with high and variable Al contents together with high K values in places. Q2 quartz precipitated from a fluid with a low but fluctuating pH. This onset of high and variable Al and K in quartz is indicative of the onset of sulfide mineralisation.

Q3 is largely barren of mineralisation and forms dull to non-luminescent quartz with low Ti, Al, K, and Fe contents. Q3 stage fluids had moderate salinities.

Q4 formed dull luminescent quartz with high and variable Al and Fe contents hosted in calcite vein breccias which in places have associated sulfides.

The distinct trace element signature of each of the individual quartz generation reflects the variability of fluid temperature and acidity at different stages of the evolution of the magmatic-hydrothermal system. CL patterns and related trace element variations seen in this study of the Mongolian porphyries appear identical to those described recently from other porphyry systems, despite major difference in formation time and geological setting. Just as paragenetic studies have long revealed consistent sequences of overprinting vein assemblages, trace element and textural studies of quartz, revealed by EPMA and CL, appear to support the idea that a common sequence of quartz crystallisation exists at least for the earliest vein stages (Q1-Q3). Detailed understanding of the strongly heterogeneous distribution of trace elements within a paragenetically complex series of quartz generations assists in understanding the processes involved in the early evolution and mineralisation in porphyry copper systems.

The discovery history of epithermal gold-silver deposits in the Haenam District, South Korea

Kirwin, D.J.[1*], Spadafora, M.J.[2], Sennit, C.M.[2], Kim, W.J.[2], Panther, C.[1], Forbes, M.[2], Rovillos, P.[2], Lograsso, J.[2] & Morales, N.[1]
[1]Ivanhoe Mines Ltd., Phathumthanee, Bangkok, Thailand
([*]douglaskirwin@mail.com)
[2]Independent Consultants

Gold mining in Korea dates back more than 3,000 years and most primary production has been from mesothermal quartz vein deposits associated with Jurassic or Cretaceous granites. Initial interest in the prospectivity for epithermal precious metal deposits in South Korea commenced with the release of the Atlas of Mineral Resources by the United Nations ESCAP division in 1987. Detailed metallogenetic maps included in the Atlas showed both widespread, numerous gold occurrences and many hydrothermal clay deposits. While the clay deposits did not feature as gold occurrences, the alteration assemblages were described as being composed of silica, alunite, dickite and pyrophyllite. Furthermore many were hosted in Cretaceous to Early Tertiary volcanic rocks. A field evaluation of all the known clay deposits commenced in 1988 and this demonstrated that some of the clay deposits were indeed related to both high and low sulphidation epithermal systems, especially in the Haenam district in the south west part of the country. A field inspection of the Tongyeong gold-silver deposit which was still operational in 1988 also clearly confirmed the presence of an epithermal deposit in South Korea. Prospecting continued intermittently from 1988 to 1993 resulting in gold discoveries at the Seongsan and Gasado Island clay. The main vein at Gasado Island, called the Lighthouse vein was actually first recognized in 1988 from offshore while traversing the southern part of the island by boat. A very large prominent hill on the mainland, known as Ogmaesan comprises alunite-pyrophyllite-dickite-pyrite altered volcanics, however despite the intense high sulphidation alteration it appears to be unmineralised.

The epithermal potential of South Korea was followed up in earnest by Ivanhoe Mines (formerly Indochina Goldfields) from 1994 to 2000 and this lead to additional gold discoveries at Kohung, Dogcheon, Moisan, Eunsan and Chunsan; all in the Haenam district where there was no previous knowledge of precious metal mineralisation. Bonanza complex Au, Ag, Te, Se mineralization encountered at Eunsan was mined by Ivanhoe from 2001 to 2003 and subsequently by a Korean company who are currently mining at Eunsan and Moisan. The discovery of the epithermal gold-silver deposits in southwestern South Korea may be attributed to conceptual geological thinking, subsequent field validation, persistent and systematic prospecting by a team of dedicated field orientated geologists. It is concluded that additional epithermal gold-silver deposits will be found in the southern part of South Korea.

Native minerals found in the Baogutu gold deposit, west Junggar (Xinjiang, NW China)

An Fang & Zhu Yongfeng*
School of Earth and Space Sciences, Peking University, Beijing, China (*yfzhu@pku.edu.cn)

The Sb-bearing minerals, usually coexisting with native gold, are common in Sb-Au or Au-Sb hydrothermal deposit. Most of the Au-Sb hydrothermal deposits are mesothermal or epithermal, hosted in black shale or in limestone, as these rocks could contribute enough sulfur [1,2]. Relatively alkaline and slightly reducing hydrothermal conditions provided by limestone favor transportation of Au and Sb are essential for the formation of Au-Sb deposits, while decrease of pH is the major controlling factor for co-precipitation of stibnite and native gold [3]. Sulfur activity might play an important role in the co-precipitation of native gold and antimony minerals (stibnite, berthierite) in the intrusion-related gold system [4]. Native antimony generally coexists with native gold or aurostibite in gold deposit [4]. It is scarce to find native antimony coexisting with stibnite, because their stable fields are separated by berthierite field. Here we describe antimony minerals (stibnite, ullmannite, native antimony, tetraedrite) coexisiting with native gold, found in the Baogutu hydrothermal gold deposit (west Junggar, NW China).

The west Junggar is an important constituent of the central Asian metallogenic region [5], which is characterized with occurrence of several ophiolite belts, contacting with the Lower Carboniferous volcanic-sedimentary strata (LCVS) via faults. The LCVS is mainly composed of coarse tuff sandstone with alternating layers of tuff, tuff siltstone with basalt and siliceous locally. Post-collisional granitic plutons with ages of 295-310 Ma [6] intruded into the LCVS.

One medium-sized copper deposit formed in the porphyry body. Molybdenite separated from this porphyry copper deposit was dated to be 310Ma by Re-Os method [7]. The Baogutu gold mine, occurring 15km SW from the porphyry copper deposit, is a typical hydrothermal gold deposit hosted in the LCVS. The tuff and tuff siltstone are the wall-rocks of most gold-bearing quartz-sulfide veins. Most of the gold-bearing quartz-sulfide veins are lensoid or ribbon-like. Some veins reach 400 m in depth with length of 10m to 150 m and thickness of 0.5m to 3m in plane. More than twenty gold-bearing veins are exposed on the surface, while the buried lodges are the major ore-bodies mined presently. The NNE-trending faults (F_4) controlled the distribution of the gold-bearing quartz-sulfide veins and diorite dykes, while the F_5-F_6 faults cut through most of these veins and dykes.

The ore-forming process of the Baogutu gold deposit can be divided into three paragenetic stages based on the cross-cutting relationships and mineral assemblages. Gold-bearing fine-grained quartz-sulfide veins, formed at stage II, cross-cut the coarse-grained quartz-sulfide veins formed at stage I. Native antimony-bearing calcite veins, formed at stage III, always cut through the mineral assemblages formed at stages I and II.

[1] Arias, D. et al. (1997) *J. Geoch. Explor,* **59**, 1-10. [2] Wagner, T. & Boyce, A.J. (2003) *J. Geol. Soc. London*, **160**, 299-308. [3] Williams-Jones, A.E. & Normand, C. (1997) *Econ. Geol,* **92**, 308-324. [4] Thorne, K.G. et al. (2008) *Explor. Mining Geol*, **17**, 13-49. [5] Zhu, Y.F. et al. (2007) *Geol. Bull. China*, **26**, 1167-1177. [6] Han, B. F. et al. (2006) *Acta Petrol. Sinica*, **22**, 1077-1086. [7] Song, H.X. et al. (2007). *Acta Petrol. Sinica*, **23**, 1981-1988.

Hydothermal alteration related to the formation of the Pb-Zn-Ag deposit Crnac, Mts. Rogozna

Borojević Šoštarić, S.[1*], Palinkaš, L.A.[1] & Neubauer, F.[2]
[1]Dept. of Mineralogy and Petrography, University of Zagreb, Croatioa (*sborojsost@geol.pmf.hr)
[2]Dept. of Geography and Geology, University of Salzburg, Austria

Pb-Zn-Ag deposit Crnac, Western Vardar zone is a structurally controlled deposit, composed of vein type mineralization hosted by Jurassic amphibolites terminating into overlying serpentinites of the same age, and listwaenite type of mineralization developed along serpentinite-amphibolite interface (Fig. 1).

Ore is deposited subsequent to injection of the quartz porphyry dykes into the Jurassic amphibolites and serpentinites at 28.9±0.3 Ma within several stages: *(i) porphyry stage* commencement with the pervasive propylitic alteration within amphibolites and quartz porphyry dykes, causing break down of amphibole and formation of a chlorite-epidote-actinolite-magnetite mixture, whereas some of the plagioclase are altered to albite-oligoclase. *(ii)* Priori and synchronous with the deposition of the *pre-ore stage*, composed of pyrite, arsenopyrite, pyrhottite, quartz and kaolinite, pervasive sericitization (sericite-quartz-pyrite assemblage) affected host amphibolites and quartz porphyry dykes, and is dated at 28.6±0.5 Ma. Pervasive and veinelets type silification is also widespread within amphibolite hosts, whereas kaolinitization predominantly occur as veins banding or breccia clasts within veins and listwaenite type of mineralization. Kaolinite is also found within the matrix of the quartz porphyry dykes. Magnetite-pyrite intergrowth occurs at the closing stages of the pre-ore deposition. *(iii) Syn-ore stage* deposited massive galena and sphalerite together with tetrahedrite, chalcopyrite and stefanite, as massive veins bending or listwaenite breccia matrix. *(iv) Post-ore stage* deposited predominantly carbonates banded with negligible amount of pyrite, arsenopyrite or galena. Open space filling in vugs, cavities and geodes, colloform and comb textures are often found. Within host amphibolites and quartz porphyry dykes carbonatization is recognized as vinelets and matrix infill.

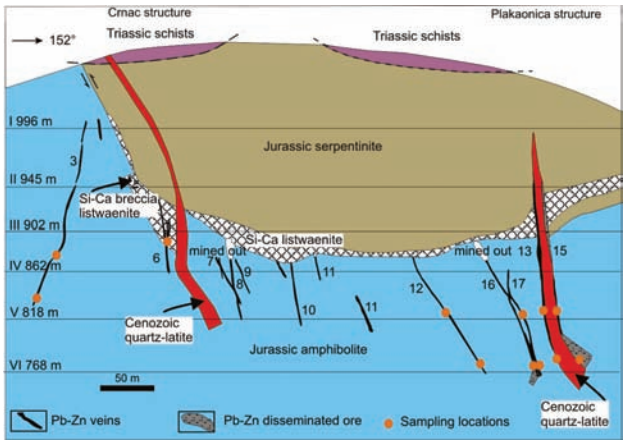

Fig. 1: Geological cross-section of the Crnac Pb-Zn-Ag deposit (modified after [1]).

[1] Miletić, I. (1995) *Annal. Géol. Péninsule Balkanique*, 299-304 (in Serbian).

The origin of hydrothermal fluids in the Kumarlar Pb-Zn veins, Çanakkale, NW Turkey

Bozkaya, G.[1*] & Celik, S.[2]
[1]Dept. of Geological Engineering, Cumhuriyet University, Sivas, Turkey ([*]gbozkaya@cumhuriyet.edu.tr)
[2]Dedeman Mining Group, İstanbul, Turkey

Kumarlar (Çanakkale) lead-zinc mineralization is the typical example of lead-zinc deposits occurred in the Tertiary volcanic rocks, outcropped in the Biga Peninsula [1]. Ore veins along the fault zones in the tuffs contain mainly galena and sphalerite, and minor amounts of pyrite, chalcopyrite, fahlerz (tennantite), marcasite, chalcosine, covelline, bornite, tenorite and quartz. Fluid inclusion and stable isotope (O, S) studies were investigated on the sulfur and quartz minerals, to determine of the origin of hydrothermal fluids.

T_{FM}, Tm_{ICE} and T_H values, measured during fluid inclusions within the quartz, indicate the presence of $CaCl_2$ and $MgCl_2$ types of salts in the mineralizing hydrothermal solutions. The salinity of the hydrothermal solutions is 15.8 (% NaCl *eqv.*) during sphalerite crystallization in the early episode of mineralization, while % 18.5 (% NaCl *eqv.*) during the quartz crystallization of the later episode of mineralization. T_H values, obtained from the fluid inclusions within the sphalerite and quartz crystals, show that the sphalerite and quartz were formed in the temperature ranges of 238.6-263.5 and 247.2-281.4 °C.

$\delta^{18}O$ values of water in equilibrium with quartz are in the range of -6.14 – 8.36 ‰ SMOW, and suggest that the ore fluids were originated from both meteoric and magmatic waters (Fig. 1a). Relatively higher temperature values are found in quartz with probably magmatic origin, collected from deeper parts of the veins. In contrary, the lowest values are detected in quartz with meteoric origin, collected from shallow parts of the veins. In other words, $\delta^{18}O$ values increase with the increasing temperatures (Fig. 1b).

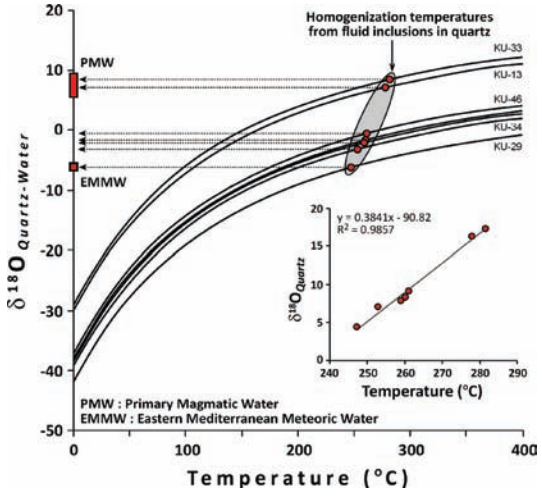

Fig. 1: (a) Oxygen isotope vs. temperature curves of the quartz samples, calculated from quartz-water fractionation [2]. **(b)** Regular variations of oxygen isotope and temperature values in quartz.

$\delta^{34}S$ values of galena (-10.41 to -6.28, mean -7.6 ‰) suggest that the sulfur was reduced from sulfate (SO_4^{2-}) from the sea water or sulfate minerals in the sedimentary rocks by bacterial or inorganic processes. According to sulfur isotopic fractionation during the reduction sulfate in closed systems and age curves of sulfur isotope in marine sulfates [3], sulfur could be leached from the Triassic sedimentary basement rocks.

[1] Bozkaya, G. (2009) *Turkish J. Earth Sci.*, **18**, 127-137. [2] Sharp, Z.D. & Kirschner, D.L. (1994) *Geochim. Cosmochim. Ac.*, **58**, 4491-4501. [3] Claypool, G.E. et al. (1980) *Chem. Geol.*, **28**, 199-260.

A statistics-based method for the short-wave infrared (SWIR) spectral analysis of altered rocks: an example from the Acoculco caldera, eastern Trans-Mexican Volcanic Belt

Canet, C.[1], Arana, L.[2], González-Partida, E.[3], Pi, T.[4], Prol-Ledesma, R.M.[1], Franco, S.I.[1], Villanueva-Estrada, R.E.[1], Camprubí, A.[4] & López-Hernández, A.[5]
[1]Instituto de Geofísica, Universidad Nacional Autónoma de México, Ciudad Universitaria, Delegación Coyoacán, México D.F., Mexico
[2]Posgrado en Ciencias de la Tierra, Universidad Nacional Autónoma de México, Ciudad Universitaria, Delegación Coyoacán, México D.F., Mexico
[3]Centro de Geociencias, Universidad Nacional Autónoma de México, Campus Juriquilla, Santiago de Querétaro, Qro., Mexico
[4]Instituto de Geología, Universidad Nacional Autónoma de México, Ciudad Universitaria, Delegación Coyoacán, México D.F., Mexico ([*]camprubitaga@gmail.com)
[5]Gerencia de Proyectos Geotermoeléctricos, Comisión Federal de Electricidad, Morelia, Michoacán, Mexico

We propose a simple graphic and statistical method for processing of SWIR reflectivity spectra of alteration minerals. It generates a classification of the spectra according to its shape and absorption features, thus obtaining groups of spectra equivalent to mineral assemblages. It also permits to select a reduced number of samples for further mineralogical verification. This method uses the SWIR spectra without hull subtraction. The first step is to normalize the spectra reflectivity to 100 % at maximum. In order to reduce the reflectance dataset, a decimation filter is used, obtaining one value each 10 nm. Subsequently, a cluster analysis, using as input data the decimated reflectance values for each sample, results in a dendrogram that allows deducing assemblages of SWIR active minerals.

The effectiveness of this methodology is illustrated with a study of the Acoculco Caldera, which is a geothermal prospective area. Two major zones of alteration have been recognized: an upper of ammonium illite, and a lower with epidote-chlorite-calcite. Four additional assemblages have been deduced: (a) buddingtonite and (b) smectite, in the recent volcanic sequence, and (c) calcite marble and (d) granitic rocks, in the Mesozoic basement. The upper alteration zone reaches a depth of 500-600 m, affecting most of the caldera sequence. It consists in a pervasive ammonium-argillic alteration of ignimbrites and dacitic lavas. Although ammonium illite is the main alteration mineral, kaolinite, buddingtonite and smectite locally occur at depths up to 300 m. The occurrence of ammonium silicates suggests temperatures above 200ºC. There is a correspondence between the abundance of ammonium minerals and the total nitrogen content of the rocks. The highest value (0.653 N wt.%) corresponds to a sample rich in buddingtonite. Ammonia probably derived from the organic matter-rich Mesozoic sedimentary series underlying the caldera.

The Zn-Pb-Ag skarns of Zacatepec, Northeastern Oaxaca (Mexico): a study of mineral assemblages and ore-forming fluids

Canet, C.[1], Romero-Guadarrama, J.A.[2], Sánchez-Vargas, L.I.[2], Camprubí, A.[3*], Castro-Mora, J.[4,5], González-Partida, E.[6], Martín Romero, F.[3], Prol-Ledesma, R.M.[1] & Linares-López, C.[1]

[1]Instituto de Geofísica, Universidad Nacional Autónoma de México, Ciudad Universitaria, Delegación Coyoacán, México D.F., Mexico

[2]Centro Interdisciplinario de Ciencias Marinas, Instituto Politécnico Nacional, La Paz, Baja California Sur, Mexico

[3]Instituto de Geología, Universidad Nacional Autónoma de México, Ciudad Universitaria, Delegación Coyoacán, México D.F., Mexico ([*]camprubitaga@gmail.com)

[4]Posgrado en Ciencias de la Tierra, Universidad Nacional Autónoma de México, Ciudad Universitaria, Delegación Coyoacán, México D.F., Mexico

[5]Facultad de Ingeniería, Universidad Nacional Autónoma de México, Ciudad Universitaria, Delegación Coyoacán, México D.F., Mexico

[6]Centro de Geociencias, Universidad Nacional Autónoma de México, Campus Juriquilla, Santiago de Querétaro, Qro., Mexico

The Zn-Pb-Ag skarns of Zacatepec are located in the eastern Sierra Madre del Sur, southern Mexico. They are hosted by the Cuicateco Terrane, which is composed of deformed Jurassic and Cretaceous volcanic and sedimentary rocks deposited in an arc environment, which also hosts several precious- and base-metal epithermal deposits and Cu-Mo occurrences. The mineralization occurs as irregular masses along the contact between Cretaceous limestones and Tertiary porphyritic dacites. Over widths of few decimeters, an epidote-rich ($Ep_{44–97}Czo_{01–55}Pie_{00–03}$) endoskarn is developed. For the most part, the mineralization consists in skarns of calcic garnet ($Adr_{62–22}Grs_{78–38}$) with disseminated hematite. Calcic garnets show chemical oscillatory zonation. Skarns rich in calcic clinopyroxenes ($Di_{28–54}Hd_{22–55}Jh_{07–32}$) locally occur, farther from the porphyry contact. As a result of a retrograde mineralizing event, the above assemblages are locally silicified, and chamosite and ore minerals (sphalerite, galena and chalcopyrite with subordinate amounts of scheelite) deposited. The iron contents in sphalerite range between 5.0 and 9.4 mol % FeS. A later association of bismuth sulfosalts consists of vikingite and an Ag-Bi-S phase akin to the aikinite group. Locally, magnesian skarns develop and are composed of almost pure diopside ($Di_{98–100}Hd_{00–01}Jh_{00}$), clinochlore, chrysotile, and vesuvianite that is extremely rich in Ti (6.48 to 7.93 wt. % TiO_2). The magnesian skarns have the highest metal grades, up to 595 g/t of Ag in an ore-rich sample. After weathering of the ores, botryoidal crusts of supergene minerals as smithsonite, rosasite and hemimorphite developed. Microthermometric studies of fluid inclusions were carried out in calcite, calcic garnet, quartz and sphalerite. Homogenization to the liquid phase occurred between 335º and 470ºC. Salinities were calculated assuming a H_2O-NaCl system and range from 11.7 to 16.0 wt % NaCl eq. The temperature of formation of the prograde skarn, calculated from microthermometric data, for an assumed pressure of 500 bar, ranges between 470º and 510ºC. A slight increase in fO_2 caused the formation of garnet form after clinopyroxene. The formation of the retrograde assemblage implies a temperature drop down to 350º to 405ºC coupled with a great increase in fO_2. These changes can be explained by boiling followed by mixing with cooler and dilute meteoric water.

Occurrence of the colusites-(Sn) at the ore-body „T“ of the Bor copper deposit (Serbia)

Cvetković, L.[*], Pačevski, A. & Tončić, T.

Faculty of Mining and Geology, University of Belgrade; Serbia

RBB – Cooper Mines Bor, Serbia

([*]cvetkovicljub@yahoo.com)

The ore body „T“ is the newly discovered one which is located in the central part of the Bor copper mine, in the vicinity of the ore bodies F1, F2 and famous Tilva Roš. It belongs to the massive-pyrite ore bodies group, passing gradually into the stockwork and porphyry-copper types, at the outer parts. The most abundant copper minerals are chalcocite-digenite and some less covellite, followed by lesser amounts of enargite, bornite and chalcopyrite. Galena and sphalerite appear in very small amounts, in thin veinlets which intersect all previously formed mineral aggregates. The gangue minerals are silicifying quartz, veinlets of anhydrite, gypsum and calcite, as well as the traces of fluorite

Common microscopic investigation of the samples of the drilling-cores from this ore-body revealed the frequent presence of the minerals of the colusite group, which occur in single grains, or in rare aggregates, up to 0.5 mm approximately. They appear in irregularly shaped and oval grains, or rare in deformated crystals, displaying moderate reflectivity and creamy-yellowish colour of the reflected light. Sometimes, a weak anomal anisotropy of these grains could be observed. The grains-aggregates of colusite usually overgrowth the covellite grains, or are embeded in the chalcocite-digenite aggregates. These minerals are accompained by the single grains-crystals of a mawsonite-like mineral, occurring in traces

The minerals of the colusite group in this ore-body were analysed by SEM-EDS by using JEOL JSM-6610LV instrument located at the Belgrade University, Faculty of Mining and Geology. The analyses yielded the compositions of investigated minerals, whose calculated formulae ranged from

$$Cu_{24.93}V_{1.72}As_{4.63}Sb_{0.20}Sn_{0.84}S_{31.86}$$ to

$$Cu_{23.74}V_{2.03}As_{3.85}Sn_{2.16}S_{32.21},$$

what confirmed that the most of the present colusites belong to the stannocolusite variety. Also, the analyse of the single-grain occurring mineral gave the formula $Cu_{15.99}Zn_{1.87}Fe_{3.87}Sn_{3.90}S_{24.39}$, what verify the presence of the mineral stannoidite. This is the first appearance of this mineral in the Bor copper mine and in Serbia, generally.

Illite and kaolinite in the Coranda low sulphidation type epithermal deposit, Apuseni Mts., Romania

Gál, Á.[1*], Kristály, F.[2], Szakács, A.[3], Molnár, F.[4] & Weiszburg, T.G.[4]
[1]Dept. of Mineralogy, Babeş-Bolyai University, Cluj-Napoca Romania ([*]agi.gal@ubbcluj.ro)
[2]Inst. of Mineralogy and Geology, University of Miskolc, Hungary
[3]Dept. of Environmental Science, EMTE-Sapientia University, Cluj-Napoca, Romania
[4]Dept. of Mineralogy, ELTE University, Budapest, Hungary

The Coranda (Certej deposit) low sulphidation type epithermal ore deposit is located at the southeastern part of the Neogene Brad-Săcărâmb inter-mountain basin, NW from the more famous Săcărâmb ore deposit, in the Apuseni Mts., Romania.

Polarizing optical microscopy observations and X-ray Powder Diffraction investigations were performed on whole-rock specimens. Interstratified smectite content was tested by powder specimen ethylene-glycol saturation. Most of the samples with >10 Å basal spacing values did not show any interstratified smectite content. Samples showing high degree of sericite – quartz phyllic alteration were selected for Scanning Electron Microscopy (SEM) and Energy Dispersive Spectrometry (EDS) investigations. Kaolinite group minerals are associated to these types of phyllic alteration products, with degree of crystallinity varying on a large scale. Peak broadening is directly proportional with the value of basal spacing. Mica-type, dioctahedral clay mineral ($d_{(060)}$~1,500 Å) was detected with ~10.040 Å basal spacing during random powder specimen diffraction. This phase is intrinsically associated to ~7,400 Å halloysite with poor degree of crystallinity. Characteristic paragenesis is given by sanidine (adularia), pyrite, anatase and jarosite (Fig. 1). Aluminium-phosphate-sulphate minerals occasionally occur, with cationic and anionic substitution between large limits and micrometric scale.

Thermal Analysis with simultaneous Differential Thermal Analysis (DTA), Thermogravimetry (TG) and Derivative Thermogravimetry (DTG) revealed the devolatilization of clay minerals in more small reactions. DTA at 126°C and 185°C is with two-stepped DTG, and at 595°C and 713°C with continuous weight loss and no DTG peak.

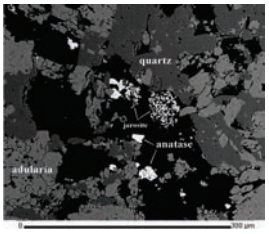

Fig. 1: General composition of phyllic alteration paragenesys (Back-scattered electron image, 40kv, 15nA).

K-deficiency and absence of other cations and smectite layers suggests the presence of NH_4 in the interlayer space. Higashi [1] gives a correlation of 0.1 – 0.15 NH_4 ratio in the interlayer for 10.040 Å spacing. EDS investigation proved the absence of Fe, Mg, Ca and Na from the illite. The intrinsic intergrowth of halloysite – illite, and K-deficiency of the mica structure is supported by the double Si+Al/K ratio of analyzed spots compared to the theoretic value.

Anatase is mostly present in euhedral or anhedral grains, no shift in composition towards Fe-Ti oxides is observed. Pyrite shows strong alteration, and the presence of a secondary, micrometric unaltered generation is characteristic.

[1] Higashi, S. (2000) *Appl. Clay Sci.*, **16**, 171-184.

Low-sulfidation Eusan (Se-type) and Moisan (Te-type) epithermal gold-silver deposits, Korea

Kim Chang Seong, Choi Chang Seong[*] & Koo Minho
Dept. of Earth and Environmental Sciences, Korea University, Seoul, Republic of Korea ([*]seongyu@korea.ac.kr)

The epithermal gold–silver deposits of the Haenam-Jindo Basin, located on the south-western margin of the Korean Peninsula, occur within the Cretaceous calc-alkaline volcano-tectonic depressions and calderas, confined to rifts within magmatic arc environment. Veins of the Eunsan and Moisan deposits are mostly hosted by felsic pyroclastic rocks. The ore mineralogy of these veins is characterized by the dominance of silver-arsenic-antimony sulfosalts with silver selenides and tellurides over argentite. However, mineralogical differences between the Eunsan (e.g., naumanite and aguilarite) and Moisan deposits (e.g., petzite, sylvanite, frohbergite, goldfieldite, native tellurium, altaite, tellurobismuthite and mackayite) appear to reflect their intrinsic geochemical characteristics.

The K–Ar ages of adularia from the Eunsan deposit and adularia and sericite from the Moisan deposit are 75.0 ± 1.6, 74.7 ± 1.6 and 75.1 ± 1.6 Ma, respectively [1]. The similarity of these ages, combined with the close proximity and similar geochemical characteristics of the deposits, indicates that the mineralization occurred as part of a single hydrothermal system. Based on their ore and gangue mineralogy, geochemical signatures and stable isotope data, the Eunsan (Se-type) and Moisan (Te-type) veins might have resulted from different parts of the same geothermal system. The Eunsan and Moisan deposits were formed at shallower crustal levels (<0.5 kbar) and relatively lower temperature (<300°C) conditions from the hydrothermal fluids containing large components of less-evolved meteoric waters.

The systematic mineralogical and geochemical differences can be explained by variations of the physicochemical conditions existed during the gold-silver deposition. The alteration, ore and gangue mineralogies of the Au-Ag deposits are typical of the adularia-carbonate-sericite (low-sulfidation) class of volcanic-hosted epithermal deposits. This implies that the physicochemical conditions of the Moisan deposit exhibit mineral assemblages deposited closer to the heat source than those of the Eunsan deposit.

[1] Kim, C.S. & Choi, S.-G. (2009) *Resour. Geol.*, **59**, 415-421.

Biely vrch Au-porphyry deposit, Slovakia: a new economic mineralization type in the Carpathian volcanic arc

Koděra, P.[1*], Lexa, J.[2], Bakos, F.[3], Biroň, A.[2], Fallick, A.E.[4], Fuchs, P.[3], Hanes, R.[3] & Žitňan, P.[3]
[1]Dept. of Geology of Mineral Deposits, Comenius University, Bratislava, Slovakia ([*]kodera@fns.uniba.sk)
[2]Geological Inst., Slovak Acad. of Sciences, Bratislava, Slovakia
[3]EMED - Slovakia, s. r. o., Banská Štiavnica, Slovakia
[4]Scottish Universities Environmental Research Centre, UK

Biely Vrch deposit represents a new economic Au-porphyry type of mineralisation discovered recently in Slovakia by EMED Mining company. The deposit is located in the central zone of the Neogene Javorie stratovolcano and shares many properties typical for Au-porphyry deposits. Mineralization extends to a depth of at least 450 m. Resource estimation stands at 140.2 Mt geological resources (JORC inferred category) with average grade 0.57 g/t Au using 0.3 g/t cut-off [1].

Parental diorite to andesite porphyry stock 300x400 m in diameter and surrounding andesite are affected by extensive alteration. Intermediate argillic (IA) alteration (Ill-Sme, Ill, Chl, Ep, Py) variably overprints earlier high-T K-silicate (Kfs, Bt, Mag) and Ca-Na silicate (An-rich Pl, Act) alteration in deeper levels of the system. Propylitic alteration represents outer zone of the system (Ill-Sme, Chl-Sme, Chl, Qtz, Py). Ledges of advanced argillic (AA) alteration (Kln, Dic, Prl, Alu, Dsp, vuggy Qtz) are the youngest stage of alteration, probably related to a younger intrusion at depth. Alterations are accompanied by several generations of hydrothermal-explosive breccias and veinlets. They involve the oldest Bt-Mag veinlets (EB-type) associated with K-silicate alteration and several generations of widespread Qtz veinlets including A-type (Qtz ± Bt-Mag) and later banded veinlets. Younger Py veinlets (± rare Ccc, Mrc, Gn, Sp, Mo) and coeval IA veinlets (Chl, Ill-Sme, Py) are affiliated to IA alteration. Carbonate-zeolite and AA veinlets are the youngest veinlets types. Gold grains are of high fineness (875-994) and occur next to Qtz veinlets in altered rock with Ill, Ill-Sme, Chl and Kfs, sometimes attached to sulphides or Mag [2].

Vapor-rich fluid inclusions (FIs) dominate in vein quartz, locally accompanied by Fe-rich brine inclusions (>70 wt% total salts, Th > 600°C). They are interpreted to result from fluid immiscibility of hot magmatic fluids associated with shallow emplacement of dioritic magma. Vapor FIs also dominate in later quartz veinlets with banded texture, derived from former silica colloid due to rapid fluid decompression. Rare associated liquid-rich FIs (mostly 0-5 wt% NaCl eq., Th 230–260°C) represent a later fluid, likely resulting from condensation of the low density fluid and associated with IA alteration [3].

Oxygen isotope data from vein quartz (7.6-12.4 ‰ $\delta^{18}O$) indicate a strong magmatic signature of associated fluids. Ill-Sme equilibrium fluids (-0.5 to -0.1 ‰ $\delta^{18}O_{fluid}$, -76 to -87 ‰ δD_{fluid}) were rich in meteoric component. Fluids in equilibrium with Kln and Prl (2.1 to 5.2 ‰ $\delta^{18}O_{fluid}$, -55 to -84 ‰ δD_{fluid}) and S isotope data of Alu ($\delta^{34}S$ 10.6-15.6) are consistent with magmatic-hydrothermal source of these latest fluids and S [3].

Gold was introduced into the system probably in bisulfide complexes in vapor during the emplacement of quartz veinlets and precipitated due to reaction of fluid with Kfs (effective H^+ sink) and Fe-oxides (effective for de-sulfidation) in the regime of rapid fluid decompression. Several Au generations with different fineness point to multiphase introduction of Au and its remobilisation mainly during the stage of AA alteration.

Acknowledgements: Support by EMED Mining, Ltd. and VEGA grant 1/0311/08 is acknowledged.

[1] Hanes, R. et al. (2010) *Mineralia Slovaca*, **42**, 15-32. [2] Koděra, P. et al. (2010) *Mineralia Slovaca*, **42**, 33-56. [3] Koděra, P. et al. (2009) *ECROFI XX 2009*, Granada.

Mineralogical, petrological and fluid inclusion study of the Brehov ore deposit (Eastern Slovakia)

Molnár, F.[1], Molnár, L.[1*] & Bačo, P.[2]
[1]Dept. of Mineralogy, Eötvös Loránd University, Budapest, Hungary ([*]luismoloar@gmail.com)
[2]Štátny geologický ústav D. Štúra, Košice, Slovakia

We have analyzed drillcore (VSB-2 and VSB-2a) and surface samples from the buried base metal ore deposit near Brehov. The samples were divided into four lithological groups: rhyodacite, hydrothermal breccias, pyroclastics, diorite. The rhyodacitic samples are heavily altered to illite-sericite, while kaolinite is the product of steam heated acid-sulfate alteration in pyroclasics. The ore forming minerals occur in stockwork and veins (sphalerite, galena, pyrite, hematite). The gangue minerals are quartz together with barite in pyroclastics and rhyodacite and with calcite in diorite. Results of fluid inclusion study which was carried out on quartz samples show that boiling occurred at different depths of the same palaeohydrological system, and thus the 10 wt% NaCl boiling curve can be fitted to the location of samples from various depths. This data shows that we can count about 200 meters of erosion in relation to the paleogroundwater table. Compared to the Tokaj Mts., the age of the volcanic rocks and mineralization fits into the trend observed in the Tokaj Mts., where hydrothermal centres exposed on the surface are progressively younger towards south. Fluid inclusion data for the Brehov deposit show similar salinity as fluids in the transitional zone between the porphyry and epithermal mineralization in the Zlatá Baňa stratovolcano. According to these results, a base metal sulfide rich low sulphidation type epithermal mineralisation is present near Brehov and the hydrothermal system can be connected to the subvolcanic diorite intrusions of the area.

Variety in texture and chemical composition of pyrite from the Čoka Marin polymetallic deposit, Serbia

Pačevski, A.* & Šarić, K.
Faculty of Mining and Geology, University of Belgrade, Serbia
(*aleksandar.pacevski@gmail.com)

The Čoka Marin polymetallic (Cu-Au-Ag-Zn-Pb) deposit belongs to the world-class Bor ore district which is situated in eastern Serbia. This ore district is one of the major ore deposit clusters along the Late Cretaceous Banat-Timok-Srednogorie belt with abundant porphyry-copper and associated high-sulfidation epithermal deposits [1]. The Čoka Marin deposit consists of three volcanic-hosted orebodies which are composed predominantly of pyrite and barite. Other common minerals in the deposit are enargite, luzonite, chalcopyrite, bornite, sphalerite, galena and marcasite. The deposit contains relatively high contents of Au and Ag, however, native gold (enriched in silver) is the only mineral of these precious metals and it rarely occurs. This deposit shows many features typical for high-sulfidation epithermal deposits.

Pyrite from the Čoka Marin deposit displays great variety in texture and minor and trace element contents of Cu, Pb, As, Ag, Sb. It occurs mainly as fine- to coarse-grained, with a grain size from 50 μm to 5 mm and variable crystal shapes from irregular to idiomorphic. Irregular pyrite masses often admixed with minor amounts of other minerals are also common. Then, pyrite partly occurs as spongy pyrite, generally showing a yellow brown color (due to minor contents of Cu), framboidal pyrite and colloform pyrite. Pyrite replacement of phenocrysts in the volcanic rock and some ore minerals (luzonite and enargite) was also noticed. Pyrite oolits and the distinct shapes of pyrite which could be interpreted as pyritized microfossils, suggest that the mineralization was partly hosted by the sediment rocks. Chemical zoning and variable contents of Cu, As, Pb, Ag, and Sb, measured by Electron Microprobe Analysis (EMPA), are generally present in all textural varieties. Copper is almost always present in pyrite in concentrations up to 8 wt.% Cu. Solid solution of Cu in pyrite was proved by EMPA, micro-Raman spectroscopy and X-ray diffraction [2]. Pb-bearing zones (up to 7 wt.% Pb) in pyrite frequently occurs (Pačevski et al., in prep). These zones often contain minor amounts of As (up to 2.5 wt.%), sometimes Cu and Ag, and rarely Sb. Arsenian pyrite (3-4 wt.% As) occurs in colloform forms and replacement textures. Silver is occasionally present in the studied pyrites, with concentrations up to 1 wt.% Ag. Sector zoning in some pyrite grains is caused by silver distribution.

Regarding that pyrite is generally the most abundant sulfide in the ore deposits and that this mineral represents a waste component during a mine processing, incorporation of Cu, Pb, Ag and As as trace and minor elements in pyrite could have implications for utilization of the ores and for environmental questions. Further, as the Čoka Marin deposit shows general features of the high-sulfidation epithermal deposits, this study emphasizes the question about variety of pyrite texture and minor and trace elements contents in pyrites from this important type of the deposits.

[1] Ciobanu et al. (2002) *Miner. Deposita*, **37**, 541-567. [2] Pačevski et al. (2008) *Can. Mineral.*, **46**, 249-261.

Relationships of rhyolite magmatism and epithermal systems in the Central Slovakia and Tokaj Mts. regions of the Western Carpathians: K/Ar dating of volcanic and hydrothermal processes

Pécskay, Z.[1], Lexa, J.[2*] & Molnár, F.[3]
[1]Institute of Nuclear Research, Hungarian Academy of Science, Debrecen, Hungary
[2]Geological Inst., Slovak Academy of Sciences, Bratislava, Slovakia (*geoljalx@savba.sk)
[3]Dept. of Mineralogy, Eötvös L. University, Budapest, Hungary

Middle-Upper Miocene (Sarmatian-Pannonian) low to intermediate sulfidation epithermal systems of Central Slovakia (Banská Štiavnica, Kremnica, Pukanec, Nová Baňa, Banská Belá) and the Tokaj Mts. region (Telkibánya, Füzérradvány, Mád) are variably hosted by andesitic and rhyolitic volcanic complexes. While in Central Slovakia rhyolitic volcanism concludes evolution of major andesitic stratovolcanoes, in the Tokaj Mts. rhyolitic and andesitic volcanic formations alternate in the bimodal type of suite, often with well defined rhyolitic eruption centers of the dome/flow type.

In Central Slovakia, epithermal systems evolved at horst-related fault systems that post-date andesitic volcanism, rhyolite dykes are emplaced along the same faults and such dykes are affected by adularization and/or argillization. K/Ar ages of rhyolites (whole rock, groundmass, biotite) and early epithermal mineralization (adularization) overlap in a narrow interval of time and are coeval at all mentioned districts (Table 1).

In the Tokaj Mts., there are several stages of andesitic-rhyolitic volcanic activity and related hydrothermal mineralization (Table 2). Hydrothermal activity occurred in three major periods between 12.5 – 12.2 Ma, 11.9-11.5 Ma and around 10.9 Ma. In studied areas andesites are altered and pre-date rhyolite volcanic activity that appears to be coeval with epithermal systems.

Apparently, high-level rhyolite magma chambers, rather than andesitic ones, play an essential role in evolution of epithermal systems of the Western Carpathians. K/Ar ages of hydrothermal activity in the Central Slovakia Volcanic Field and in the Tokaj Mts. overlap, implying interval 12.5 – 11.0 Ma as a peak period of hydrothermal activity in the Western Carpathians. This suggests that large scale regional processes have also been involved in development of hydrothermal systems in addition to the local volcanic/magmatic control. Considering that faults controlling hydrothermal fluid flow are equivocally N-S oriented in both districts, this regional factor appears to be the extension that developed due to the coeval westward subduction in the Eastern Carpathians.

Acknowledgements: Work supported by the Hungary-Slovakia S&T SK 27/06 grant (APVV grant SK-MAD-01106), VEGA grant 2/0171/08, grant 1506 of the Slovak Ministry of Environment and OTKA grant K68153.

Table 1: K/Ar ages of rhyolites and mineralization in Central Slovakia (Km – K-metasomatised rock, ill – illite)

	rhyolites (Ma)	*mineralization (Ma)*
Nová Baňa	12.31±0.44 – 12.03±0.38	12.12±0.37 – 11.79±0.37 (Km)
B. Štiavnica	11.60±0.30	11.4±0.20 (ill.)
Kremnica	12.29±0.42 – 11.52±0.36	12.09±0.37 – 11.58±0.34 (Km) 11.03±0.20 (ill.)

Table 2: K/Ar ages of volcanic rocks and mineralization in the Tokaj Mts. (an – andesite, rh – rhyolite, at – acidic tuff, ad – adularia, ill – illite, al – alunite)

	Volcanic rocks (Ma)	*mineralization (Ma)*
Telkibánya	13.1±1.2 – 11.6±0.5 (an)	12.2±0.7 – 12.4±0.5 (ad)
	12.6±0.6 – 11.2±0.7 (rh)	12.49±0.51 – 12.27±0.57 (al)
Mád	11.5±1.2 (an)	10.85±0.26 (al)
Füzérradvány	12.2±0.7 – 10.8±0.8 (rh)	11.73±0.54 – 11.71±0.29 (al) 11.89±0.3 – 11.53±0.4 (ill)

Native copper ore-bearing formation

Rudenko, K.V.[1*], Derevska, K.I.[2] & Shumlyanskyy, V.O.[3]
[1]Institute of Geological Sciences of National Academy of Sciences of Ukraine, Kyiv, Ukraine ([*]rena-li@ukr.net)
[2]National Museum of Natural History of National Academy of Sciences of Ukraine, Kyiv, Ukraine
[3]Institute of Fundamental Studies of National Academy of Sciences of Ukraine, Kyiv, Ukraine

Native copper ore-bearing formation in basic volcanic rocks and sedimentary rocks, which associated with them, is well known. The oldest occurrences of it are deposits in Western Australia with age near 3000 Ma. Native copper occurrences of Kola Peninsula are associated with basalts, trachybasalts, tuffolavas, tuffs and tuffites of Proterozoic [1]. There are two Riphean examples of this formation in North America: the Michigan ore district (1640-880 Ma) [2], which is the most well known representative of this formation, and area of native copper mineralization in North Western part of Canada (1200 Ma). Native copper deposits and occurrences were discovered in basalts and tuffs, which are referred to Vendian continental flood basalts, of the Volyn region in Ukraine (550 Ma). Paleozoic native copper ore-bearing formation occurrences were reported in basic volcanic rocks of the Kuznetst Alatau (Russia), the Novaya Zemlya, in basic mandelstones in Europe and in upper part of Yunnan flood basalts (China). Mesozoic native copper occurrences known in trap of Western Siberia and in basic volcanic rocks of the Novaya Zemlya, the Korean Peninsula and in other regions. There are some examples of Cenozoic representative of native copper ore-bearing formation, which are situated in Peru, Azerbaijan, the Solomon Islands. The modern native copper-bearing lavas, which erupted from Kilauea (Hawaii), was reported in 1963 [1,3,4].

In addition, native copper ore-bearing formation of Volyn region is considered in detail below. Within the Volyn region, sedimentary rocks of the Riphean polesie are altereted to medium catagenesis substage while Vendian continental flood basalts of the Volynian series that overlie Polesie sediments have experienced chlorite-zeolite alternation that corresponds to an early catagenesis. Alterations of basalts, which related to impact of meteoric water on the hot lava flows, are presented by development of palagonite, opal, and oxidation of magnetite. These processes led to initial phases of copper release and to formation of copper aggregates and of palagonite. Further alteration of the Volynian flood basalt is replacement of low-temperature mineral associations by moderate-temperature ones. This might be caused by the heating due to magma intrusion at the end of flood basalt sequence formation. Underground waters resided in the Riphean sedimentary series are considered as ore-forming solutions. After these alterations, almost all areas were subjected to the hydrothermal stage. The richest native copper mineralization localized in the chloride-analcime-quartz zone.

[1] Shumlyans'kyy V.O. et al. (2006) in *Naukovi pratsi Instituti fundamental'nikh doslidzhen'*. Kyiv, Logos, 179-197. [2] White, U.S. (1972) in *Mestorozhdeniya samorodnoy medi v severnoy chasti shtata Michigan* (Vol. 1). Mir, Moscow, 457-481. [3] Domarev, V.S. (1984) *Formatsii rudnikh mestorozhdeniy v istorii zemnoy kory*. Nedra, Leningrad. [4] Zhu B.Q. et al. (2003) *Sci. Chin. Ser D (Earth Sci).* **46**, S2, 60-72.

Progressive oxidation of magma in gabbro-granodiorite intrusives in the Cretaceous-Paleogene Inner Zone batholith of southwest Japan - very pure magnetite formation

Yamaguchi, Y.[1*] & Kawakatsu, K.[2]
[1]Dept. of Geology, Shinshu University, Matsumoto, Japan ([*]yoshia_ygutti@d4.dion.ne.jp)
[2]Kakogawahigashi High School, Kakogawa, Japan

Cretaceous-Paleogene granitoids (62-75Ma) [1] of the central San-in district are exposed in large batholiths, composed of various rock-types ranging from gabbro through granodiorite to granite. Small masses of gabbro-granodiorites (0.5-10 km), from which samples were collected for this study, are early-stage intrusives exposed in the Mizawa-Nita area. Field observation shows that, in the intrusives, gabbroic magmas multiply injected into granodiorite magmas and mixed with it and partially mingled to form numerous mafic microgranular enclaves. The intrusive rocks typically contain magnetite (Magnetite-series granitoids) [2], and magnetite is mined from the weathered parts of some intrusives. Very pure magnetite (< 0.02 Wt% TiO_2) commonly occurs coexisting with titanite and quartz under a highly oxidized condition [3].

Pyrrhotite, an early Fe-bearing phase, is found in various occurrences: 1) sulfide inclusions in amphibole; 2) discrete sulfide grains among amphibole and plagioclase; 3) corroded sulfides included in magnetite. On the other hand, magnetite is not early phase.

Initially, just after the mafic magma injection, amphibole began to crystallize together with plagioclase and sulfide, and continually crystallized to form strongly patchy zoning from brownish green pargasitic core to pale green actinolitic-hornblende rim, with a systematic decreasing in $Fe^{2+}/(Fe^{2+}+Mg)$ [4]. Correspondingly, the progressive increase in Fe^{3+}/Fe^{2+} induced the precipitation of magnetite around amphibole. Although this initial magnetite phase (> 1.0 Wt% TiO_2) coexisted with ilmenite, the further continuing Fe^{3+}/Fe^{2+} increasing of the residual magma led to depletion of ilmenite to develop magnetite-titanite-quartz assemblage. Magnetite decreased here in TiO_2 (< 0.02 Wt% TiO_2).

Crystallization trends of these sulfide, amphibole, and oxide indicate that this hydrous mafic magma was progressively oxidized during crystallization on cooling. Some possible mechanisms have been previously proposed for the progressive oxidation of magma during crystallization: 1) hydrogen evolution hypothesis, involving oxygen liberation from the evolved high H_2O/FeO felsic magma at shallow place near the chamber roof; 2) assimilation of oxidized country rocks; 3) oxygen liberation in response to transformation of sulfur species from SO_2 to H_2S on cooling of originally SO_2-rich hydrous magma [5, 6].

The late-stage magnetite formation corresponding to the simultaneous decreasing in Fe^{2+} during amphibole crystallization were likely related to progressive oxidation of iron in magma by sulfur species conversion. Transformation of sulfur species from SO_2 to H_2S probably causes oxidation of iron in the minerals in this hydrous magma on cooling, as suggested in previous models for large sulfur supplies and magma oxidation in subduction related magmatisms [5, 7, 8].

[1] K. Nishida et al. (2005) *J. Geol. Soc. Jpn*., **111**, 123-140. [2] Ishihara, S. (1977) *Mining Geol.*, **27**, 293-305. [3] Wones, D.R. (1989) *Am. Mineral*., **74**, 744-749. [4] Kawakatsu, K. & Yamaguchi, Y. (1987) *Geochim. Cosmochim. Ac.*, **51**, 535-540. [5] Hattori, K. (1993) *Geology*, **21**, 1083-1086. [6] Takagi, T. & Tsukimura, K. (1997) *Econ. Geol*., **92**, 81-86. [7] Yamaguchi, Y. et al. (2003) *J.. Mineral. Petrol. Sci*., **98**, 151-155. [8] Yamaguchi, Y. et al. (2008) *IAVCEI 2008 Conf. Progr.* **6**, 3.

Metal sulfide minerals from deep-seated granitic geothermal reservoir

Yanagisawa, N.
Institute for Geo-Resources and Environment, AIST, Tsukuba, Japan (n-yanagisawa@aist.go.jp)

At Kakkonda geothermal area, Iwate prefecture, north-eastern of Japan, there is a 80MW geothermal power plant using high temperature fluid from the reservoir at the boundary between Quaternary Kakkonda granite and Pre-Tertiary formations about 3km depth. Metal sulfide minerals deposited at production wellhead and pipeline from fluid. These sulfide minerals were collected and analyzed [1].

The scales are classified into two types based on sulfide mineralogy, which are Pb-Zn rich type and Cu rich type. Pb-Zn rich scale is found in Well-19 located at the marginal part of the Kakkonda granite as shown in figure 1. It is mainly composed of amorphous silica, galena (PbS), Sphalerite (ZnS) and Pyrite (FeS_2). Cu-rich scale is found in Well-13, located at the central part of the Kakkonda granite. It is mainly composed of amorphous silica, chalcocite (Cu_2S), bornite (Cu_5FeS_4), loellingite ($FeAs_2$) and native antimony (Sb). It is also rich in Au, Ag, As, Cr, Ni and Mo compared to Pb-rich scale. On progress of production the fluids from deep reservoir suffered by the fluid of shallow reservoir and meteoritic water. And mineral assemblage of scales of Well-13 changed to tetrahedrite ($Cu_{10}[Fe,Zn]_2[As,Sb]_4S_3$). But the ratio of metal composition is almost constant. The metal contents of the scale in Well-22 show intermediate features between the two types of scales.

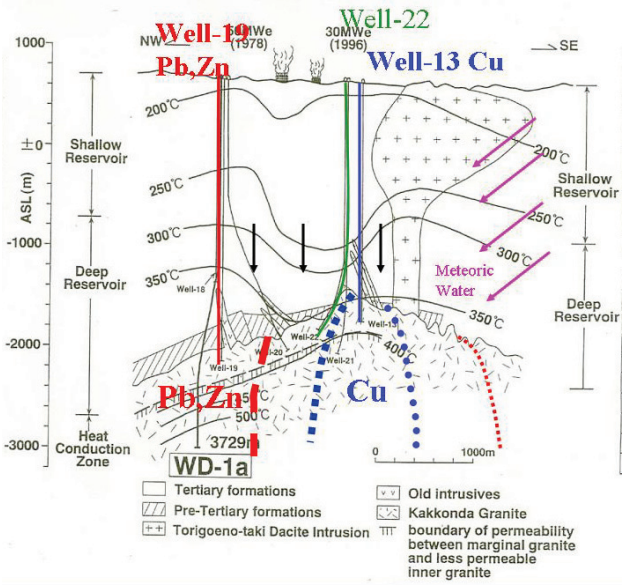

Fig. 1: Schematic geothermal cross-section of the Kakkonda geothermal system including well name and metal in precipitated sulphide and brine in granite.

The brine of WD-1a at 3.7km depth, into Quaternary Kakkonda granite rock underlied Well-19 is rich in Pb and Zn and similar composition as the Well-19 scale [2]. Therefore, deep reservoir of Kakkonda field evolves with mixing the fluid of shallow reservoir and the brine of occurred in the Quaternary Kakkonda granite. Then, the existence of both Pb-Zn rich scale and Cu rich scale is a characteristic feature of Kakkonda geothermal and this fact suggest to have similar zoning as found in Porphyry Copper Zoning.

[1] Yanagisawa, N. et al. (2000) *Proc. WGC2000*, 1969-1974.
[2] Kasai, K. et al. (2000) *Proc. WGC2000*, 1325-1330.

Te-bearing gold-silver-basemetal mineral deposit of Arinem, Western Java, Indonesia

Yuningsih, E.T.[1*], Matsueda, H.[2] & Rosana, M.F.[3]
[1]Graduate School of Science, Hokkaido University, Sapporo, Japan ([*]etintiny@yahoo.com)
[2]Hokkaido University Museum, Hokkaido University, Sapporo, Japan
[3]Faculty of Geology, Padjadjaran University, Bandung, Indonesia

The Arinem area is located in a part of the Sunda-Banda magmatic arc (well known as gold copper belt) within the Indonesia archipelago at the southern margin of the Sundaland and the Eurasian plate (Fig. 1). The mineralized body is in form of quartz vein trending N140-160ºE for about 5,900m long and 3-5m width, exposed at elevation 365-530m above sea level. The ore body is hosted in andesitic lava, breccias and tuff of the Oligocene-Middle Miocene Jampang Formation. The pyroclastic host rocks mainly suffered of propylitic and argillic alterations and are characterized by the occurrence of chlorite, sericite, kaolinite, and in place by carbonate. Outcrop and drill core samples containing gold-silver are intimately associated with basemetal minerals of copper, lead and zinc. K-Ar dating of sericite associated with the quartz vein indicates a Late Miocene age (8.8±0.3 Ma) for the ore mineralization.

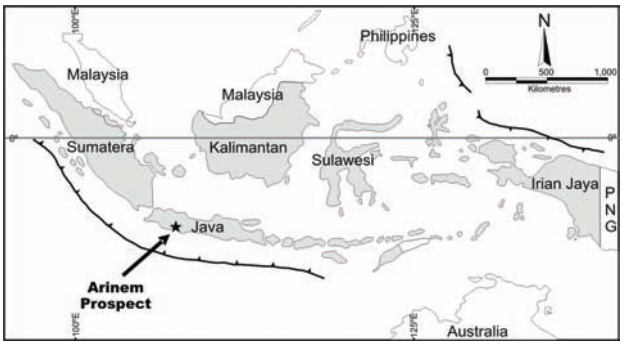

Fig. 1: Map of the Indonesia region, where the location of the Arinem prospect is also indicated by the star with black arrow.

The ore mineral deposition could be categorized into three stages, where stages I and II are Au-Ag bearing, and stage III is barren. The ore mineral assemblages of the deposit consist of sphalerite, galena, chalcopyrite, pyrite, marcasite, arsenopyrite with a little amount of pyrrhotite, bornite, calcocite, covellite, hematite, argentite, electrum and sulfosalt minerals of enargite and tennantite. Some of Te-bearing minerals such as hessite, tetradymite, stutzite, petzite and altaite are observed in the mineralization stage II. The deposit is characterized by low iron content in sphalerite, ranging from 0.25-4.71 wt%. Gold is detected in petzite with the ranges of 14.32-18.32 wt%, while in some hessite and altaite grains up to 1.77 and 0.55 wt%, respectively. Otherwise, up to 1.31 wt% selenium element is detected in tetradymite.

Fluid inclusion studies for quartz of the stages I and II reveal the homogenization temperatures with the ranges of 176.6-325.1ºC and 156.9-311.8ºC, and with the low salinity of less than 4.3 wt% NaCl equiv. in both. Based on the microscopic observation of the occurrences of inclusions there are some boiling phenomena observed. They also tend to show a slight cooling of ore-forming fluids through stages I to II. In the decrease of temperature, it might be followed by both decrease of sulphur fugacity and increase of tellurium one.

Considering the preliminary stable isotopic studies of sulphide and quartz minerals from the deposit, it might be suggested that the mixing of magmatic ore fluids with meteoric water caused the ore precipitation in underground beside of boiling.

Franklin-type mineralization in the Zambesi Metamorphic Belt (Zambia): the Star Zinc and Excelsior willemite prospects

Boni, M.[1*], Terracciano, R.[1] & Gleeson, S.A.[2]
[1]Dipto. di Scienze della Terra, Università di Napoli, Naples, Italy ([*]boni@unina.it)
[2]Dept. of Earth & Atmospheric Sciences, University of Alberta, Edmonton, AB, Canada

The Zambian willemite (Zn_2SiO_4) deposits occur in Proterozoic metasedimentary carbonate rocks (Kabwe and Lusaka areas). The Star Zinc and Excelsior prospects (Lusaka area), discovered in the early twenties and since then subjected to sporadic exploration [1], are hosted in the highly metamorphic lithotypes of the late Proterozoic Zambezi Supracrustal sequence, deposited in a transtensional basin formed during the oblique collision of the Kalahari and Congo cratons. In these prospects willemite occurs epigenetically along joints and fissures in the Cheta and Lusaka Fms, consisting mainly of limestone and dolomite marbles, with minor quartz-muscovite schists and feldspathic quartzite. On a local scale, the willemite ore displays open-space filling, colloform and vuggy textures. Structural analysis suggests that mineralization is hosted by two main sets of fractures trending E-W and N-S, the latter being compatible with the Riedel shears related to the pan-African Mwembeshi dislocation zone (a major geotectonic boundary between the Lufilian Arc and the Zambezi Belt).

Willemite is associated with specular hematite and replaces the Zn-spinels franklinite and gahnite. Calcite commonly replaces willemite. The Zn-Be bearing sulfosilicate genthelvite [$Zn_4Be_3(SiO_4)_3S$] occurs as a minor mineral in irregular aggregates and may contain micrometric inclusions of Fe-Sr-Ba-Fe sulfates. Fluorapatite is also recurrent in the mineral association. Thermometric analyses of willemite inclusions from both prospects result in the following homogenization temperatures: Th: 160-250 °C, and salinities: 8 to 16 wt% $NaCl_{equiv}$. Even if these temperatures are still well below those reached during the regional metamorphism of the Zambezi belt, they point to a hypogene-hydrothermal origin for the willemite concentrations. A preliminary crush leach fluid inclusion study was carried out on two calcite and one willemite sample from Star Zinc and one willemite sample from Excelsior. The samples were analysed for F^-, Cl^-, Br^-, SO_4^{2-}, Na^+, K^+ and Li^+. Two samples (one calcite, one willemite) contained Br above the detection limit. These samples have Cl/Br (molar) ratios of 54 and 230 respectively; this suggesting that the fluids that formed these samples may have ultimately derived their salinity from evaporated seawater.

The origin of this peculiar type of willemite-franklinite-gahnite mineralization in the Lusaka area is still unclear. However, the existing concentrations could represent a metamorphosed occurrence derived from primary sulfide ores (now completely disappeared), as those occurring in the Nampundwe massive sulfide deposit SW of Lusaka. If this is the case, the seawater signature has not been lost during metamorphism. The zinc spinels franklinite and gahnite are commonly associated with willemite in several other hypogene nonsulfide zinc deposits. The typical occurrences are in the Franklin Marbles of the Middle Proterozoic Grenvillian basement in North America, with the best example represented by the Franklin-Sterling Hill deposit. In the latter, the franklinite-gahnite-willemite ore association is considered as having been originated by amphibolite-granulite facies metamorphism from a previous zinc sulfide/nonsulfide mineralization.

[1] Sweeney, M.A. et al. (1991) in Pagel, M. & Leroy, J. (eds.) *First Biennial SGA Meeting, Nancy*, Rotterdam, Balkema, 139-142.

Genesis of supergene Co and Cu deposits in the Katanga Copperbelt (DR Congo)

Decrée, S.[*], Dewaele, S., Mees, F. & De Putter, Th.
Royal Museum for Central Africa, Tervuren, Belgium & GECO project, Belgium ([*]sophie.decree@africamuseum.be)

The Katanga Province (DR Congo) hosts world-class cobalt and copper deposits, accounting for 49% and 5% of the world reserves, respectively [1].

Heterogenite (CoOOH) and malachite ($Cu_3(OH)_2(CO_3)$), the most ubiquitous oxidized ores, ultimately derived from the oxidation of primary sulfides, which occur as stratabound deposits within fine-grained Neoproterozoic metasediments.

The oxidation and weathering processes are economically significant since they strongly concentrate Co and Cu in the oxidized part of the mineralization.

In the Katanga deposits, heterogenite is concentrated as "cobalt caps" along the top of silicified dolomite inselbergs (Fig. 1) [2]. Malachite is mostly present under the cobalt cap (Fig. 1), as thick nodular precipitates filling voids and cavities [3]. Geochemical data suggest that heterogenite forms in (sub)surface oxidizing conditions, whereas Cu tends to migrate downward and to precipitate as malachite in slightly deeper conditions, probably at or near the fluctuating water table.

Heterogenite caps can therefore be considered as residual deposits, similar to lateritic iron deposits and Mn-ore occurring in the southern part of Katanga [4,5].

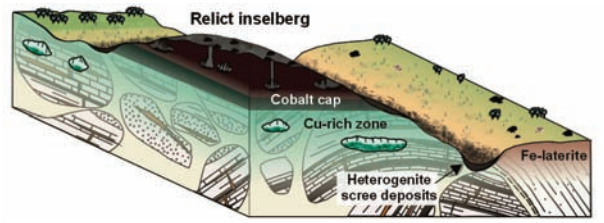

Fig. 1: Sketch diagram illustrating the settings of the Co, Cu and Fe supergene ores in the Katanga Copperbelt [2].

These residual deposits have been dated to the Pliocene (based on field observations, Ar-Ar dating and U-Pb dating) and resulted from: (i) regional Mio-Pliocene uplift, creating conditions favorable for massive erosion and for oxidation of the sulfide ores; and (ii) humid climate conditions, favoring element mobilization. This process results in a vertical gradient of the oxidized ores (Co on top of Cu) that all form in shallow supergene settings: residual surface caps, weathered rock impregnation and infilling of voids and cavities.

Eventually, part of these deposits were dismantled and accumulated in valleys and along foot slopes (as scree, Fig. 1), because of erosion and valley incision during the Quaternary.

[1] USGS (2009) *Mineral Commodity Summaries 2009*. [2] Decrée, S. et al. (submitted) *Geology*. [3] De Putter, Th. et al. (submitted) *Ore Geol. Rev.* [4] Alexandre, J. (2002) *Annales du Musée Royal de l'Afrique Centrale, Sciences Géologiques*, **107**. [5] Doyen, L. (1973) in Amstutz, G.C. & Bernard, A.J. (eds.) *Ores in Sediments*. Springer-Verlag, Heidelberg, 93-100.

The syngenetic-epigenetic baryte-phosphate-bearing Pb-Zn deposit Sekarna (Tunisia), in the stratotype area of the K/P boundary

Dill, H.G.[1*], Botz, R.[2], Dohrmann, R.[1] & Weiss, W.[1]
[1]Bundesanstalt für Geowissenschaften und Rohstoffe, Hannover, Germany ([*]dill@bgr.de)
[2]University Kiel, Germany

The El Kef area (official stratotype of the K/P boundary), Tunisia, is host of complex metallic and non-metallic mineralization at Djebel Sekarna, encompassing syn(dia)genetic shale- and carbonate-hosted Zn-P and epigenetic Pb-Zn-Ba ores in Cretaceous and Paleogene rocks. Geological, mineralogical, and chemical studies including C- and O isotopes analyses resulted in a subdivision of this mineralization into 8 distinct stages.

Stages 1 and 2 (late Cretaceous to early Paleogene) are representative of syn(diagenetic) shale- and carbonate-hosted sulfidic and siliceous (Fe)-Zn-P mineralization deposited in shallow marine to slightly brackish sediments. The presence of zinc and iron-bearing calcite is indicative of poorly-aerated conditions. Kaolin-group minerals prevailing over smectite may be taken as proximity indicators relative to the Kasserine Island. The El Haria Formation, a regressional facies, is interpreted as a large inner ramplike shelf deposit. Limited water circulation during deposition of this Formation resulted in anoxic conditions and the formation of ZnS and FeS_2. The REE patterns of apatite of the Métlaoui Formation leave little doubt that the phosphorites in the district are of lower Eocene age, similar to other phosphorites in the Mediterranean region. Stages 3 to 5 (early Eocene) are represented by epigenetic sulfidic and sulfatic (Fe)-Zn-Pb-Ba mineralization that formed at temperatures as high as 170°C/200°C. Stage-5 barite-bearing Pb-Zn mineralization differs from the predecessor stages by elevated Sr contents accommodated in the barite lattice to form celestobaryte. The epithermal (to mesothermal) carbonate-hosted hydrothermal celestobaryte Zn-Pb mineralization evolved from seawater that underwent evaporation and precipitated from brines circulating down to a considerable depth into the carbonate platform. Stages 6 and 7 (late early Eocene) include non-sulfidic Zn-(Pb) mineralization that formed at temperatures as high as 60°C, transitional from hypogene into supergene conditions ("epithermal calamine deposits"). Stage 8 represents alteration of the pre-existing mineral assemblages in the course of the Holocene weathering.

The distribution of the syn(dia)genetic shale- and carbonate-hosted mineralization in the Late Cretaceous and Paleogene rocks is controlled by planar structural elements of sequence stratigraphic relevance distribution of the mineralization. The Similar planar structural elements delimit the epigenetic vein- and replacement-type ore mineralization in their vertical extension to the lower Eocene. The Cretaceous through Paleogene aquatic system is characterized by a poisoning of the sea with base metals, mainly Zn, and the atmosphere was choked with clouds of fine-grained volcanic ejecta. Both processes contributed to the build-up of Zn-(Pb) deposits and uneconomic bentonitic clay deposits around the K/P boundary. Ore mineralization in the El Kef area is a multiple-phase process which reached its climax during the early Eocene. These inorganic concentration processes resulting in the formation of mineral deposits had obviously also a negative effect on the long-term course of regional Earth's biological history during the late Cretaceous to early Eocene period with lethal consequences for some species. The inorganic and organic data reveal that such extraordinary metallogenetic processes close to the K/P boundary in its stratotype area in Tunisia were "strictly terrestrial".

Mineralogy and geochemistry of the Black Reef Au mineralization at Consolidated Modderfontein, East Rand, South Africa

Gauert, C.D.K.[1*], Deacon, J.[1] & Fuchs, S.[1,2]
[1]Dept. of Geology, University of the Free State, Bloemfontein, RSA ([*]Gauertcdk@ufs.ac.za)
[2]Inst. für Kristallogr. und Materialwiss., Leipzig University, Leipzig, Germany

The Proterozoic Black Reef Formation (BR) is a widespread, thin, small pebble unit at the base of the Transvaal Supergroup, locally occurring in well–defined, deeply scoured channels and gullies deeply eroded into the footwall. In the East Rand, Randfontein and Klerksdorp areas the unit contains considerable gold, minor uranium as well as associated platinum group element (PGE) mineralization, being exploited extensively since the 1930s and renewed since 2002. Its economic importance is indicated by Gold One Ltd. quoting a probable reserve of 5.4 Mt of ore at an average grade of 6.1 g/t for its Modder East Mine (2009) and Pamodzi Gold's total measured and indicated resources of 13.22 Mt at a grade of 4.23 g/t for 2007 [1].

Deposition of the BR was characterized by previous workers as having occurred under fluvial to shallow marine conditions. Of the three BR facies types at Consolidated Modderfontein on the East Rand, the pyrite-rich 'blanket facies' and the 'basal channel facies' [2] contain most of the gold and have the highest amount of heavy minerals (Fig. 1).

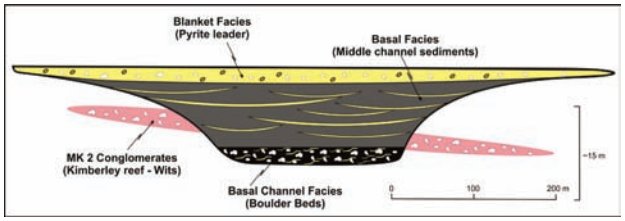

Fig. 1: Schematic section through an incised Black Reef Channel at the Consolidated Modderfontein Mine (Modified after Barton & Hallbauer [2])

Gold occurs in the form of free gold and as inclusions in pyrite, as well as refractory, 'invisible' gold in (arseno-) pyrite and submicroscopic gold particles with carbon. Detrital and heavy minerals comprise compact, concretionary rounded and porous rounded pseudomorphic pyrite [2], zircon, chromite, Ni-Co-Fe-sulpharsenides, cobaltite, gersdorffite, rutile, arsenopyrite, uraninite, and rare galena and sphalerite.

Electron microprobe analyses (EMPA) reveal true fineness values of free gold between 793 and 851, and its Hg content between 0.20 and 0.85 wt%; the pyrite mineral chemistry reveals minor As and Pb, as well as traces of Ni and Cu. Ongoing EMPA, nano-SIMS, and PIXE investigations try to fingerprint the gold chemistry in order to distinguish its provenance as derived from reworked upper Wits Reefs or from different gold deposit types in the 'hinterland'.

Mechanisms contributing to the gold mineralization in the BR are probably a combination of a) detrital processes as evidenced by sediment structures and rounded grains, b) hydrothermal processes as illustrated by several later stages of epigenetically formed pyrite, and c) low-grade metamorphic processes indicated by the paragenetic sequence.

[1] Gold One Ltd.: http://www.gold1.co.za/index.php?option=com_content&view=article&id=52&Itemid=41; Pamodzi Gold Ltd.: http://www. Pamodzi gold.co.za /operations_east.php. [2] Barton, E.S. & Hallbauer, D.K. (1996) *Chem. Geol.*, **113**, 173-199.

Uranium mineralogy – a critical parameter for successful mining

Kinnaird, J.A.*, Nex, P.A.M., Freemantle, G.G. & Youlton, B.J.
EGRI, University of the Witwatersrand, Johannesburg, South Africa (*Judith.Kinnaird@wits.ac.za)

Southern Africa is a world-class uranium province, with an age span of deposits from Archaean to Recent. The current demand for uranium, together with a rising commodity price and a projected increase in world requirements, has rejuvenated project development. The potential to mine lower U grades makes it imperative to understand uranium deportment and the mineralogist is vital in providing relevant information.

Primary deposits include Cambrian uraniferous leucogranite sheets in Namibia that are typified by the Rössing deposit. Other similar deposits are being developed nearby. The typical cut-off grade was >350 ppm U but has been reduced as price for the commodity has increased. The main U-bearing mineral is uraninite, although refractory betafite occurs locally, while whole-rock values of < 40 ppm may be accounted for by zircon, monazite or xenotime.

In the Witwatersrand Basin, detrital uraninite was transported into the Basin together with detrital gold and other heavy minerals and preserved in quartz-pebble conglomerates. Fluvial transport of detrital uraninite was possible because of the anoxic atmosphere in the Archaean. Uranium was subsequently remobilized and concentrated during circulation of hydrothermal fluids. Where uraninite is produced as a by-product of gold mining the grade may be as low as 0.01%. From ~2200 Ma, when an oxidising atmosphere formed, uranium could dissolve in surface waters, be transported in solution, and subsequently precipitated. In South Africa, Karoo-age sandstones formed in river channels where oxidising surface water interacted with local reducing conditions and uraninite was deposited in sandstone layers. Surficial U has been deposited in the last 5 Ma in near-surface valley-fill sands and gravels in arid areas of Namibia. Carnotite was precipitated in association with calcite and halite in early Tertiary sediments, while near-surface gypsum is sourced from sea-mist, rather than from the fluids that formed the carnotite. The gypsum may prevent the efficient processing of surface material because gypsum reacts with sodium compounds during alkaline leaching and forms calcium carbonate and sodium sulphate in solution, which inhibits U leaching.

For all types of deposits, it is imperative to know the size and association of the uranium-bearing minerals as a guide to milling and liberation. In primary deposits, very small uraninite grains hosted by magnetite or biotite would be difficult to process, whilst minerals such as brannerite, davidite and betafite do not yield their uranium during conventional processing. For secondary deposits, it is vital to understand the relationship between carnotite and clay minerals so as to develop successful metallurgical processing, whilst the accessory minerals dictate whether an acid or alkaline leach is appropriate. Automated scanning electron microscopy has provided valuable information on the mineralogy of uranium deposits towards efficient and cost effective processing.

Archean chromitites and PGM from the Northern West African Craton (Amsaga, Mauritania)

Berger, J.[1*], Diot, H.[2], Féménias, O.[3] & Lo, K.[4]
[1]Université Libre de Bruxelles, Brussels, Belgium (*juberger@ulb.ac.be)
[2]Université de Nantes, France
[3]IAMGOLD corporation, Mali
[4]Université de Nouakchott, Nouakchott, Mauritania

The Amsaga area in the Northern West African Craton consists of Archean TTG series and greenstones belts with ages ranging from 3.5 to 2.7 Ga [1,2] and almost no thermal or magmatic overprint since the end of the Neoarchean era. Chromitites are hosted within ultramafic-mafic complexes that are mainly composed of serpentinised and carbonated spinel-peridotites, werhlites, pyroxenites, leuco-/mela-metagabbros and metabasalts, which show evidence of a peak granulite facies metamorphism with subsequent retrogression into amphibolite and greenschist facies conditions. These complexes occur as tectonic slices in the greenstone belts and might consequently be interpreted either as pretectonic continental intrusion or relics of the Archean oceanic lithosphere. Three deformation phases can be distinguished on the field. D1 is evidenced by low-angle foliation planes and down-dip mineral lineations, probably formed during an early thrusting event. Foliation planes were subsequently verticalised during formation of straight folds with subvertical axial planes (D2) and steeply plunging mineral lineations. Late strike-slip shear zones (D3) have generated folds with vertical axis and subhorizontal lineations that are clearly evidenced in the surrounding BIFs.

Chromitites are either present as pods enclosed in serpentinites or as distinct layers in serpentinised peridotites. Chromites usually form more than 90 vol.% of the samples; the remaining silicate matrix being composed of serpentine, Cr-chlorite, talc or Cr-pargasite. Late hydrothermal events have led to the formation of a (Fe-Cr)-enriched rim around primary spinel grain. This rim also contains chlorite and sulphides inclusions. Preliminary SEM investigations have shown that pargasite-chromitites are rich in base metal sulphide inclusions (mainly pentlandite and chalcopyrite) and contain sperrylite ($PtAs_2$) with sub-micrometric inclusions of Pd, Rh, Ir arsenides and Bi-bearing phases within Ni sulphide grains. The external position of PGE-hosting minerals within chromite grains suggests that the crystallisation of PGM is not synchronous with the early magmatic formation of the chromites but rather results of the PGE remobilisation, either during the granulitic metamorphism or during the late-stage hydrothermal events.

[1] Potrel, A. et al. (1998) *J. Soc. Geol. London*, **153**, 507-510.
[2] Potrel, A. (1998) *Precambrian Res.*, **90**, 107-117.

A structural, metallogenic and lithological analysis for gold exploration in the Manica - Mutare - Odzi greenstone belt, West Mozambique and East Zimbabwe: field evidences from Fair Bride mine

Mondlane, S.* Jr., dos Muchangos, A. & Fumo, S.M.
Geology Department, Eduardo Mondlane University, Maputo, Mozambique (*salmond@zebra.uem.mz)

The Manica - Mutare - Odzi (MMO) greenstone belt of West Mozambique and East Zimbabwe is a late Archaean linear structure (anastomosing, transcrustal, first order shear zone [1]) that formed around 2,74 Ga. The ENE - trending belt is roughly synformal, with ultramafic metavolcanic rocks along the margins and coarse clastic metasedimentary rocks in the core. Volcanism was associated with emplacement of early granites. Shear zones commonly separate individual lithological packages. Lithological units are intensely folded and a regional penetrative foliation has developed. Fold axes generally plunge shallowly either to the east or to the west and parallel the regional mineral lineation. To the east, the belt is bound by N-S trending Proterozoic gneisses of the Bárue Complex and quartzites and pelites of the Frontier Formation.

The MMO greenstone belt has produced c. 84 tonnes of Au [1]. Historically Au has been produced mainly from shear zone hosted deposits (ave. grade 12.36 g/t), faults hosted deposits (ave. grade 23.51 g/t) and quartz vein deposits (ave. grade 10.07 g/t). Most of these deposits are steep and strike E-W to NE-SW.

Recently, old deposits have received special attention by mining companies. This is the case of Fair Bride, a deposit located on the southern limb of the MMO greenstone belt, in highly sheared and vertically folded metavolcanic mafic and ultramafic rocks in contact with metassediments of Shamvaian age. This sheared contact is reportedly associated with significant mineralization of gold in late quartz-sulphide veins. The Fair Bride gold deposit is an epigenetic quartz vein associated with sulphides in a hydrothermal system that generated different types of alteration, namely, carbonitization, silicification, chloritization, sulphidation and alkaline metassomatism that precipitated gold in BIFs and quartzites. This deposit is a result of reactivation of the shear zones and remobilization of ancient deposits by thermo-tectonic and magmatic events during late Archaean.

Our study established the metallogenetic and lithological setting of gold deposits in the MMO greenstone belt. The main mineralogical paragenesis at Fair Bride consists of arsenopyrite + chalcopyrite + pyrite + pyrrhotite ± gold ± galena ± magnetite. Gold is disseminated within idiomorphic arsenopyrite, suggesting a single source of the mineralizing fluids.

[1] Forster, H., Koenemann, F.H. & Knittel, U. (1996) *Trans. Inst. Min. Metall. B*, **105**, 60-73.

Microscopic and spectroscopic studies of Pb-Zn deposits along Red Sea coast, Egypt

Hassan, M.S.
Central Metallurgical R & D Institute, Helwan, Egypt
(hassan_mervat@yahoo.com)

Recently, due to new extraction technologies, there has been a marked revival of interest in the geology and exploration for non-ferrous deposits in the world. Along Red Sea Coast of Egypt, there are a number of the oldest mining districts in the world. Significant occurrences of non-ferrous Zn-Pb-Cu ores were exploited from the Um Ghieg, Zug El-Bohar and El Russa mines. Lead and zinc mineralization in the Miocene sedimentary sequences is the most promising locality for production of these minerals in Egypt. Non-ferrous zinc-Pb minerals (carbonates, silicates, and oxide) found at these historical mining areas was characterized. Mineral abundance has been evaluated on the basis of petrographic studies using optical microscope (thin polished sections), scanning electron microscope (SEM+EDX), backscattering and secondary electron modes, as well as Infrared spectroscopy.

Nonsulfide zinc phases are fine-grained and dominated by hemimorphite ($Zn_4Si_2O_7(OH)_2 \cdot H_2O$), hydrozincite ($Zn_5(CO_3)_2(OH)_6$) and smithsonite ($ZnCO_3$). Lead phases occur as cerussite ($PbCO_3$) and rare anglesite ($PbSO_4$), whereas iron oxyhydroxides and oxides (mainly goethite and hematite) derived from the oxidation of pyrite are commonly present in "limonitic" boxworks and in small concretions with amorphous manganese minerals. Remnants of the primary ore, mainly sulfides (sphalerite, galena and pyrite/marcasite) and barite were detected. Infrared spectra of lead-zinc minerals were discussed from the structural point of view. The paper is a part of systematic studies of vibrational spectra of minerals of secondary origin in the oxide supergene zone.

Pan African sinistral transpression regime in southern Eastern Desert of Egypt: structural control on gold mineralization

El Amawy, M. & Zoheir, B.*
Dept of Geology, Faculty of Science, Benha University, Benha, Egypt (*basem.zoheir@gmail.com)

The Neoproterozoic (720-750Ma) Allaqi-Heiani ophiolitic belt in the extreme southern Eastern Desert of Egypt is a major ductile shear zone that comprises anastomosing WNW- trending sinistral transpression zones against older shelf metasediments (Pre-Pan African?). These zones are delineated by discontinuous mylonites, subhorizontal stretching lineations, steep and high strained slices of ophiolites. Along the belt, ophiolitic slices are progressively curved southeastward and merged into the N-S sinistral Hamisana shear zone, suggesting structural continuity of a major transpression corridor. Field studies revealed four episodes of deformation, namely: an early pure-wrenching along the WNW-trending Allaqi-Heiani belt and formation of tight and intrafolial folds. In the course of a second deformation episode, transpression preceded and N- to NNE-dipping anastomosing shear planes and SW-vergent folds developed. These two events represent a single progressive phase of shortening due to a major E-W sinistral simple shear. Consistently, the E-W shortening was accelerated during the third deformation expisode, particularly in the eastern part of belt, in response to deflection into the N-S Hamisana shear zone and exhumation (re-emplacement) of ultramafic rocks under oblique convergence in a generally NNW- trending pop-up structure. During the last (fourth) deformation episode, the entire pattern was re-oriented in a north-trending flower structure. The exhumed belt was then fragile and brittle deformation prevailed during the emplacement of syn- to late orogenic granitoids.

Along the Allaqi-Heiani belt, distribution of gold mineralization is controlled by the WNW-transpression between the highly sheared ultramafic derivatives and related pelagic sediments and wherever syn-orogenic granitoids are tapered along the transpressive planes. Gold occurrence is also markedly traced along the NNW-SSE transpressive planes either developed between the highly sheared ultramafics and ophiolitic metagabbro or as sigmoidal lenses of ultramafics re-emplaced within the highly sheared mélange matrix in a pop up structure. These two settings refer to formation of mineralized shear zones in the frontal, low displacement parts of the transpression system. Finally, a third occurrence is confined to brittle shear zones, developed later in the deformation history contemporaneous with the intrusions of acidic dykes and granitic offshoots, commonly along the ENE-WSW trend.

Geochemical trends within Madagascar chromite ores

Merlini, A.* & Grieco, G.
Dept. of Earth Sciences, University of Milan, Italy
(*anna.merlini@unimi.it)

The most important chromitite deposits of Africa are mainly located in South Africa, in the well known Bushveld complex, nevertheless Madagascar hosts some important chromitite deposits making Madagascar the world's 10th largest chromite producer.

Kraomita Malagasy, the state-owned mining company, produces a chromite concentrate grading between 48 and 50 wt% Cr_2O_3 with 0.002 to 0.003 wt% P_2O_5 and lumpy chrome ore grading from 42 to 44 wt% Cr_2O_3.

Since strong quality parameters are required for the commercialization of both concentrate and lumpy products, a detailed chemical and textural analysis of such mineralization was focused on understanding quality profile of these ores in ordrer to maximize future exploitation that strongly depends on chemical and textural features of the ore itself.

Mineralized regions present different geochemical and textural features that strongly influence explotaition and developing of chromite mining industry of Madagascar.

The main chromitite ores are located in Andriamena, Befandriana and Tamatave regions and are related to Archean basic-ultrabasic intrusions set in the central zone of the island.

The Andriamena complex, located in the southern end of the Tsaratanana Mineral Field, has been the leading chrome producing region for the last decades. In Andriamena complex most of chromite production comes from three mines: Ankazotaolana, Bemanevika and Telomita.

Ankazotaolana mine is characterized by a series of ultramafic lenses hosted by a gneissic rock of Archean age. Chromitite shows values of Cr_2O_3 wt% between 35 and 40 with a Cr/Fe ratio up to 2.7. Bemanevika mine, characterized by a series of parallel lenses at different depth, shows Cr_2O_3 content close to 40 wt% and a Cr/Fe ratio of 2.3. Recent estimates predict 2.6 Mt of reserves for this area. Telomita mine, recently reopened to increase the production of Kraomita Malagasy, is characterized by Cr_2O_3 content similar to that of Ankazotaolana and a Cr/Fe ratio of 2.2.

Befandriana district represents another strategic zone where chromitite lenses, ranging from few meters up to 10 meters in thickness, are highly massive, with Cr_2O_3 close to 53 wt% and Cr/Fe ratio close to 2.6.

Tamatave district was the first to be exploited in the ’60 of last century and is characterized by highly deformed and metamorphosed chromitite lenses located in two main sites: Ambodiriana and Ranomena. Tamatave chromitites show a low Cr_2O_3 content, close to 30 wt% and a Cr/Fe ratio lower than 1.5.

Comparison of geochemical and textural chromitites features of all analysed regions highlighted, some important differences among the ores that need to be considered for the future developing of chromite mining industry in Madagascar

In general chromite ores of Madagascar show a trend of decreasing Cr_2O_3 content from north to south, related to differences in ore genesis, which strongly affects ore quality for exploitation. Andriamena chromitites show an average good quality, but with differences between mines. Befandriana ores show the best quality due to their massive texture together with high Cr_2O_3 content of chromite. Chromitites from Tamatave are absolutely unsuitable due to the low Cr_2O_3 content of chromite. On the other hand a surplus value of Tamatave chromitite is the presence of Platinum Group Minerals (PGM) mainly laurite or complex solutions observed both included in chromite grains as well as in the matrix.

Carbonate mineral-chemistry in Late Archean to Early Proterozoic banded iron formations: a proxy for the evolution of ocean chemistry and implication for metal concentrations

Morgan, R.[1*], Orberger, B.[1], François, P.[1], Hofmann, A.[2] & Rosière, C.A.[3]
[1]Université Paris Sud 11, Paris, France
([*]rachael.morgan@u-psud.fr)
[2]University of KwaZulu-Natal, South Africa
[3]UFMG, Minas Gerais, Brazil

The geochemistry of sedimentary carbonates provides important clues about the evolution of the ocean, atmosphere and biological conditions during Archean and Early Proterozoic times. The geochemistry of carbonates associated with mineral deposits may also be of importance for tracing the origin of economic metal (e.g. U, As, Au etc) bearing fluids i.e. marine, diagenetic, hydrothermal or metamorphic, since pH and the HCO_3^- content of the mineralizing fluids can significantly influence metal concentrations. We investigated carbonate mineralogy and chemistry in carbonate facies BIFs and associated cherts from two well preserved shallow-marine successions: the 2.7 Ga old Spring Valley Member (SVM), Manjeri Formation (Belingwe Greenstone Belt, Zimbabwe), and the 2.4 Ga old Gandarela Formation (Minas Supergroup, Brazil).

The SVM is an oxidised (Fe-oxides) and a reduced (Fe-sulphides) chert facies, representing respectively, distal and proximal, marine-hydrothermal chemical precipitates [1]. Both facies contain early diagenetic ankerite, siderite and as a late precipitate, calcite and secondary euhedral ankerites. Au and U mineral inclusions were observed in these carbonates. SVM carbonates are significantly richer in FeO (~20 wt.%) and poorer in MgO (~8 wt%) than the Gandarela carbonates (~8 and 20 wt.%, respectively). The latter consists of primary massive bedded Fe-dolomites alternating with beds of banded chert Fe-oxide and Fe-dolomite and secondary euhedral Mg-siderite [2]. Our samples show that the late Archean (2.7 Ga) shallow environment may have been richer in dissolved Fe2+, reflecting acidic and reducing conditions in agreement with the general model for the evolution of the Archean ocean. However, in the Early Proterozoic (2.4 Ga) the ocean evolved to conditions more favourable (kinetics?) for Mg-carbonate precipitation. In the (Late) Archean, primary carbonates may have acted as a trap for Au, Ag (and possibly U) and further studies are currently being undertaken in order to provide more evidence for this model. In both formations, calcite replaces in part the primary carbonates, resulting in the liberation of noble trace metals, which may allow for their transport and economic concentration.

[1] Bah, M.S.I. et al. (2009) *Geochim. Cosmochim. Ac.*, **73(13)**, A71. [2] da Mota Carvalho, C., Rosière, C.A. & Orberger, B. (2008) *Geochim. Cosmochim. Ac.*, **72(12)**, A196.

U-mineralization in Tranomaro, Madagascar

Ramdohr, R.[1*] & Evstigneeva, T.[2]
[1]Consultant Geologist, Bonn, Germany
([*]reinramdohr@yahoo.com)
[2]IGEM RAS, Moscow, Russia

The Tranomaro U-Th is located in the SE of Madagascar, ca. 80 km from Fort Dauphin. In this region there is a sequence of ~ NS striking, steeply dipping highly metamorphosed rocks (granulite facies, i.e. ca. 750 degrees C and 5 kbar pressure) consisting of granite-gneiss, leptinites (migmatites), marble, and magnesium skarn . High grade mineralized zones contain 4,329 ppm U or 11.25 lbs/metric ton U_3O_8.

Magnesium skarns formed at the contact “granite – dolomitic marble”. The metasomatic zoning from magmatic rock to dolomitic marble is determined by Fe- and Al- mobility decreasing: granite (pegmatite) → spinel-pargasite-anorthite-fassaite skarn → pargasite-anorthite-fassaite skarn → pargasite-fassaite and pargasite-diopside skarn→ spinel -pargasite-fassaite skarn→ pargasite -diopside and diopside-pargasite skarn → spinel -calcite-forsterite skarn. The spinel-anorthite-fassaite, spinel-fassaite, diopside and spinel-calcite-forsterite skarns were formed during the magmatic progressive stage. The postmagmatic regressive stage is represented by calcite-bearing skarns with pargasite that replaces clinopyroxene.

The possible source of Th and U could be the granitic magma. Geochemical mobility of these elements determines their concentration in pargasite-fassaite and pargasite-diopside skarns with moderate alumina and ferrous monoclinic pyroxenes. It is necessary to note that the largest thorianite crystals of South Madagascar were found in phlogopite magnesium skarns.

Uranium generally occurs as uranothorianite, hosted in North-South trending pyroxene-rich skarn units. Uranothoriante, $(Th,U)O_2$, the main U-bearing mineral, is characterized by Th:U ratio varying from 0.5 to more than 30. The most typical value Th:U in uranothorianite from Tranomaro is close to 3:1. The central part of some grains is richer in Th in comparison with the border. There are two types of (Th,U)-oxide: a) separate $(Th,U)O_2$ grains with Th:U ~ 3:1, and b) very tiny grains $(U,Th)O_2$ with Th:U ~ 1:2 or 1:3. Uranothorianite of first type seems to be the primary mineral of magmatic origin (source - granites). Th-Uraninite is the product of secondary processes (hydrothermal, metasomatic etc.). It is associated with other Th-bearing minerals (monazite, thorite etc.) generally enriched in Ce and La.

Th- and Th-bearing minerals are monazite, Ce-Nd-Th phosphate (often with Si); Th-bearing apatite; $ThSiO_4$ (very rare). These minerals form small grains, 0.n – n microns in tiny fractures or jointly zones, and are common in many samples.

Th content in rocks is determined as sum “Th in Th-oxide” + “Th in other minerals (monazite, apatite etc.). This is responsible for Th:U ratio variations, often noted in probe analyses Tranomaro.

Acknowledgements: The work was carried out thanks to the financial support of RFBR, Grant n. 08-05-01016a, and Fundamental Research Programme n.5, Dept.Dci.Earth RAS.

Spanish sepiolite deposits

García-Romero, E.[1*] & Suárez, M.[2]
[1]Dpto. Cristalografía y Mineralogía, Fac. C.C. Geológicas, Universidad Complutense de Madrid, Spain ([*]mromero@geo.ucm.es)
[2]Area de Cristalografía y Mineralogía, Dpto. de Geología, Universidad de Salamanca, Spain

Spain is the world leader in sepiolite production. Madrid hosts the world's largest sepiolite deposit with reserves estimated over 15 Mt of high quality material. The main Spanish producer is TOLSA (300 kt of sepiolite in 2008), which mines the main deposits, located in the Madrid basin (Vicalvaro, Madrid, and Cabañas de la Sagra, Toledo). SEPIOLSA produced 164 kt in 2002, from the deposits of Paracuellos del Jarama and Barajas (Madrid) and BENESA 70000 tpa in Valdemoro (Madrid). Another important deposit currently under exploitation is located in Orera, in the Calatayud basin (Zaragoza). MYTA produced 131 500 t from this deposit.

The Madrid Basin is a Tertiary basin developed during the Alpine orogeny. The Miocene sediments of the Madrid basin display a concentric facies distribution pattern. Close to the margins of the basin there are detrital sediments corresponding to alluvial fan systems. These sediments are predominantly arkosic to the NW and S, and litharenitic to the NE and E. Transitional facies correspond to mud flat environments between the detrital and lacustrine sediments. The lacustrine sediments are mostly evaporites. In the northern and southern margins of the basin, arkose sands dominate gradually passing to carbonatic paleosols and clays in the distal facies of the alluvial fans and in the lacustrine systems. These clayey facies include the important Mg-rich clay deposits.

At least seven layers (≥ 1 m thick) of lacustrine sedimentary rocks containing sepiolite can be recognized in the Vicálvaro-Barajas area east of Madrid [1]. The layers are up to 7 m thick in places, with a virtual pure sepiolite composition. The Vicálvaro sepiolite deposit covers a 7.5 km^2 area elongated in NW-SE direction (5 km long and 1.5 km wide), with maximum thickness 12-15 m in the center and progressively decreasing towards the borders of the deposit. Clay layers with variable colors dominate in this unit, intercalated with carbonates (marly mudstones, marls, dolostones, and limestones). In the southern area of the Madrid basin (Cabañas de la Sagra, Toledo) the sepiolite is located in an arkosic unit, (distal parts of alluvial fans). Clayey levels consist almost exclusively of sepiolite and trioctahedral smectites, with variable ratios between pure end members. At the top of the unit sepiolite is associated with dolomite and chert.

The deposit in Orera in the Calatayud basin (Zaragoza) currently exploited by MYTA develops in the marly-carbonate transitional facies of the Calatayud Tertiary lacustrine basin. It corresponds to an alluvial fan marginal deposit which during late Miocene closed a valley producing a lake in which sepiolite was formed. Sepiolite clays and sepiolite-palygorskite clays also occur in the Cuesta facies of the Duero Tertiary basin, and in Lebrija (Sevilla).

The sepiolite from Madrid basin has specific surface area ~270 – 330 m^2g^{-1}, and fibres longer than 10 μm in places Sepiolite from Calatayud has also high specific surface area (~270 m^2g^{-1}) and the size of the fibres is medium, generally smaller than 11 μm in lengh. The contribution of external and microporous surface area is similar in both cases.

[1] Leguey, S. et al. (1995) in Churchman, G.J., Fitzpatrick, R.W. & Eggleton, R.A. (eds.) *Clays: Controlling the Enviornment*. Proc. 10th Clay Conf., Adelaide, Australia, 1993, CSIRO Publishing, Melbourne, Australia, 383-392.

Distribution of layer charge of smectites in the Miloan bentonites, Aegean Greece

Christidis, G.E.[*], Makri, P., Pogaridou, E., Theodoridou, G. & Kantsou, P
Dept. of Mineral Resources Engineering, Technical University of Crete, Chania, Greece ([*]christid@mred.tuc.gr)

Layer charge is a fundamental property of smectites which controls cation exchange capacity, ion exchange selectivity swelling and rheological properties. Within this context, determination of layer charge and charge distribution within a bentonite deposit is of particular importance because a) it can shed light on the formation mechanism of the bentonite and any possible subsequent modifications, and b) it controls the variability of bentonites in various industrial applications. This knowledge, in turn, can assist in an understanding why production of Na-activated smectites from Ca-Mg smectites usually yields unpredictable results.

Layer charge and charge distribution of smectites was studied in three bentonite profiles in Eastern Milos. The two profiles were 120 x 30 m long, whereas the third one was 200 x 45 m long and has been affected by contemporary solfatara spring activity along a NE-SW trending fault. The bentonites formed by submarine alteration of Lower Pleistocene pyroclastic flows. The deposits consist of Ca-smectite (60-95%) with subordinate quartz and/or traces of opal-CT. Minor calcite, kaolinite and K-feldspar are present in places. Determination of layer charge was carried out according to [1]. Briefly, the less than 2 μm fractions were separated by settling, saturated with K and dried on glass slides to make oriented clay mounts, which were subsequently saturated in ethylene glycol vapour at 60°C for 16 hours. The layer charge and charge distribution of smectites was determined by means of the LayerCharge program [1]

Although mineralogy is similar in the three profiles, the layer charge distribution follows different patterns. The first profile is characterized by a high charge anomaly (layer charge > 0.50 eq/phuc) in the lower WNW sector whereas the remaining profile is characterized by smectites with intermediate layer charge (layer charge 0.43-0.47 eq/phuc). The second profile is dominated by gradual increase of the layer charge towards the top of the profile, from 0.41 eq/phuc at the bottom, to 0.48 eq/phuc at the top. Moreover tetrahedral charge tends to increase towards the top of the profile. The third larger profile is dominated by a high charge bentonite layer ~ 12 m thick at the bottom (layer charge > 0.5 eq/phuc), followed by a thick layer > 30 m thick with layer charge 0.44-0.47 eq/phuc, which does not display certain trends. In the area affected by the solfatara spring activity the layer charge decreases (0.41-0.42 eq/phuc).

The different distribution patterns of layer charge in the three profiles reflect different evolution of the bentonites. In the first profile the high charge smectites are attributed to hydrothermal alteration which postdated the formation of bentonite and are associated with fine-grained K-feldspar and kaolinite. The distribution of layer charge in the remaining profiles reflects the geological environment during bentonite formation. The formation of low charge smectites in the vicinity of the solfatara spring is also attributed to contemporary hydrothermal alteration and intensive leaching of the original smectites

Acknowledgements: We thank S&B Industrial Minerals S.A. for their permission to sample their quarries.

[1] Christidis, G.E. & Eberl, D.D. (2003) *Clays Clay Miner*., **51**, 644-655.

Sustainable use of fines from the sand and gravel industry

Schmitz, M.*, Röhling, S. & Dohrmann, R.
Federal Institute for Geosciences and Natural Resources, Hannover, Germany (*martin.schmitz@bgr.de)

In 2008, some 260 million tons of sand and gravel were produced in Germany [1]. During processing sand and gravel are split into different grain size fractions. Fines are separated by washing and screening and usually dumped as water-sediment suspensions in tailing ponds close to the quarries. Up to now fines are rarely used in industry, e. g. as aggregates to produce bricks and tiles [2]. Pflug (2001) estimates that about 50 million tons of fines are produced in Central Europe every year [3]. The aim of the study is to determine the qualitative potential of fines from the processing of sand and gravel in Germany for applications in the brick and tile industry.

Fines were sampled in 28 sand and gravel pits all over Germany. After the particle size analysis the mineralogical and chemical composition of the fines were determined in the laboratories of the German Federal Institute for Geosciences and Natural Resources. As a result, 12 samples with an average grain size >200 µm, low clay mineral content or high concentrations of carbonates were rejected due to the fact that they cannot be used in the brick and tile industry.

The mineralogical composition of the remaining 16 samples is presented in Table 1. Four samples are dominated by kaolinite (samples 1, 7, 11, 16) and one by illite/muscovite and an expandable mixed-layer mineral (sample 4). In general, the selected samples consist of different mixtures of quartz, feldspar and a wide variety of clay minerals, carbonates, and oxides (Table 1).

Table 1: Simplified mineralogical composition of selected samples (I/Sm/M-L=illite/muscovite, smectite and mixed-layer minerals, K/Ch=kaolinite and chlorite; Q=quartz; F=feldspars; C=calcite and dolomite; Ox=Fe-oxihydroxides and Ti-oxides; O=others)

	I/Sm/ M-L	K/Ch	Q	F	C	Ox	**O**
1	15	35-40	35	10	-	<5	<1
2	15	5	45	15-20	10	6	<5
3	20-30	10-20	10-20	10-20	10-20	<1	<1
4	40-50	5-10	20-30	20-30	-	<1	<1
5	15	-	50	15-20	10-15	5	<1
6	15	5	40	30-35	5	<5	<1
7	15	30-35	40	10	-	<5	<1
8	25-30	20	15-20	25-30	<1	5	<1
9	20-25	5-15	25-30	15-25	-	<5	<1
10	10-15	5-10	70-75	5	-	<5	<1
11	-	55	40	-	-	5	<1
12	15	-	45	35	-	<5	<1
13	15	5	55	10-15	<10	5	<1
14	20	10	20-25	10-15	25-30	<5	<5
15	15-20	5-10	30-35	25-35	<5	<5	<5
16	25	45	20	10	-	<5	<1

The chemistry and the mineralogy of the fines reflect the composition of the source rocks the sediments derived from. A regional distribution of different qualities within Germany was not identified.

The ceramic properties of the samples will be discussed and the potential uses of fines in the brick and tile industry estimated.

[1] Bundesanstalt für Geowissenschaften und Rohstoffe (2009) *Rohstoffwirtschaftliche Länderstudien*, **XXXVIII**. [2] Krakow, L. (2003) *ZI*, **7**, 34-40. [3] Pflug, R. (2001) *Steinbruch und Sandgrube*, **6**, 6-7.

Bentonite deposits of Hungary – a review of their mineralogy and geology

Kovács-Pálffy, P.[1*], Földessy, J.[2], Kónya, P.[1] & Bertalan, É.[1]
[1]Geological Institute of Hungary, Budapest, Hungary (*kovacs@mafi.hu)
[2]Dept. of Geology and Mineral Resources, University of Miskolc, Hungary

In the Hungarian part of the Pannonian Basin several bentonite deposits of some recent or historic economic importance are known (Mád-Sima, Mád-Újhegy, Istenmezeje, Komlóska, Pétervására, Salgótarján-Kazár, Budatétény, Sóskút, Egyházaskesző, Gérce). Some of these are being exploited in our present days. This summary gives details of their mineralogy, geochemistry and geology.

Most of these deposits are related to Neogene volcanic areas. These activities are marked partly by submarine pyroclastic accumulations and coeval andesitic lavas of Carpathian age (~17.5–16.2 My), followed by Badenian (~16.2–13 My) pyroclastics and associated basaltic, andesitic, rhyodacitic and rhyolitic flows. In the Late Miocene to Pliocene/Pleistocene period (~12–2 My in the western Pannonian Basin) alkali basalts have been produced, associated by lacustrine sediments.

The bentonites derive from different alteration styles of volcanic rocks:

- Primary, syn-volcanic bentonitisation: halmyrolitic and hydro-diagenetic (Tokaj Mountains), maar lake bentonites in W-Hungary (Egyházaskesző, Gérce).
- Secondary processes: these secondary bentonites are the results of intense argillization around hydrothermal centres in several parts of the Tokaj Mountains (Komlóska).
- Tertiary processes: are characterized by erosion and re-deposition in isolated marine gulfs and lagoons (e.g. Istenmezeje, Budatétény) or re-worked deposits in post-volcanic warm-water geyser lakes (e.g. Mád-Sima and Mád-Újhegy).

In general these bentonites are characterised by the dominance of the montmorillonite (Ca, Ca/Na, Fe), with small amounts of quartz, cristobalite, feldspars and biotite. Also in few cases are presents beidelite (Fe), kaolinite and mixed-layer clay minerals (rectorite) at Mád-Újhegy, and vermiculite/smectite at Egyházaskesző-Gérce.

Their swelling capacities vary in wide range, few bentonites are not activated (e.g. Kazár). Chemically these bentonites are resulted from argillization of rhyolitic-rhyodacitic, and basaltic pyroclastic rocks (Fig. 1).

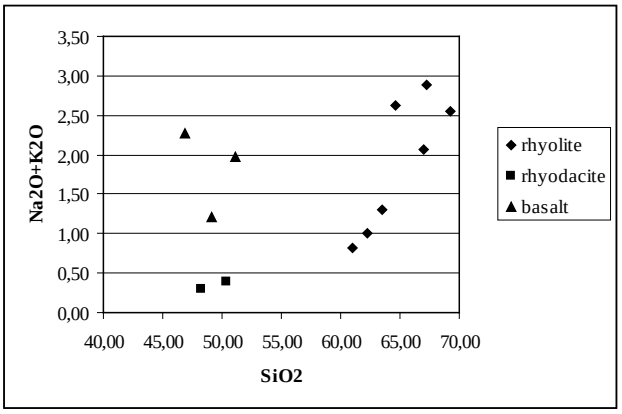

Fig. 1: Na_2O+K_2O vs SiO_2 diagram of bentonites from different pyroclastic rocks.

Natural pigments in clayey sediments of Kuprava pit in Latvia

Randers, M.[1*], Lūse, I.[2], Stunda, A.[3] & Karpovičs, A.[1]
[1]Dept. of Geography and Earth Sciences, University of Latvia, Riga, Latvia ([*]martins.randers@inbox.lv)
[2]Institute of Soil and Plant Sciences, Faculty of Agriculture, Jelgava, Latvia
[3]Riga Biomaterials Innovation and Development Centre, Riga Technical University, Latvia

Clayey pigments are relatively easy to obtain, therefore they have been used since prehistoric times for painting and decorating of bodies, ceramics, cave walls and temples. Despite utilization and research of natural pigments not much is known about their origin, chemical, physical and mineralogical properties.

There is a close link between colour of clay pigments and their mineralogical composition. Therefore aim of this study is to clarify which of the minerals represent clay colour in Upper Devonian clays of Latvia and possible new applications aspects. Study site is Kuprava clay pit in north-eastern part of Latvia where Devonian clays are exposed.

To determine mineral composition, X-ray powder diffraction method was used. Diffractometer X-ray tube operated at 40kV and 30mA, CuKα radiation, diffraction angle range 2° to 70° 2θ and step size 0.050° 2θ. For quantitative analyse data was processed using Quanto software. For granular composition of samples pipette method was used. Colour of all 70 samples was determined using Munsell colour scale, and 26 of them were chosen for detailed study.

Overall there were separated 19 different colour tones, ranging from purple and red tones to greyish. Reddish and gray clays have different mineral composition. Dominating minerals in all samples are illite (30–60%) and quartz (25–40%), in some samples amount of dolomite also is high (till 20%). Elevated amount of hematite and goethite were detected in red coloured samples. Grey and light coloured samples are sandier and there is higher amount of quartz, dolomite and kaolinite than in red samples. Red colouring minerals, like goethite or hematite, are present in all fractions, though amount of hematite, which gives intense red or purple colour tone to the sediments, is much higher in sand fraction, and amount of goethite is higher in clay fraction. Amount of goethite and hematite in red coloured samples is small, approximately 1–5% but such small amounts still is enough to colour clays red.

Results of this study show that colour of clays is mostly dependent on content of iron compounds, and role of other minerals is smaller. Grey clays do not contain ferric compounds, but have high amounts of quartz (35–40%) and dolomite (15–20%).

Results of this study further could be used for research on natural dyestuffs and cosmetics as well as other possible applications.

Acknowledgements: This work has been supported by the European Social Fund within the project „Support for the implementation of doctoral studies at University of Latvia”.

Palygorskite clays from Borshhovskoe deposit (Kaluga region, Russia): composition, crystal chemical particularities of clay minerals and colloidal properties

Bogrash, A.[1], Matskova, N.[1*], Zakusin, S.[1], Krupskaya, V.[1,2], Pokidko, B.[3], Voloshin, V.[4] & Krupnov, I.[4]

[1]Lomonosov Moscow State University, MSU, Moscow, Russian Federation ([*]nataliamatskova@hotmail.com)

[2]Institute of Geology of Ore Deposits, Petrography, Mineralogy and Geochemistry, Russian Academy of Science, IGEM RAS, Moscow, Russian Federation

[3]M.V. Lomonosov Moscow State Academy of Fine Chemical Technology, MITHT, Moscow, Russian Federation

[4]Lafarge Cement, Moscow, Russia

Palygorskite clays are used in various branches of industry, such as pharmaceutics, constructing, drilling, wine-making etc. Palygorskite clays as a component of drilling fluid are the main application. Clays can form a stable suspension with surplus water. Main technological characteristics of the raw clays are cation-exchange capacity, slurry yield with fixed viscosity etc.

Clays from production horizon of Borshhovskoe clay deposit (Kaluga region, Russia) were used as a test subject. Detailed research which includes study of relation between mineral composition, crystal chemical particularities and colloidal properties of clays should provide better exploitation of deposit and their proper use as a raw material.

The following methods have been used during this study: x-ray diffraction analysis, differential thermal analysis, near-infrared spectroscopy, middle-infrared spectroscopy, grain-size analysis, viscosity measurement (according to API requirements), and measurement of cation-exchange capacity. Characteristics of mineral composition and quantitative mineral analysis were carried out using the data received from XRD-analysis conducted in MSU. Thermal analysis was performed in MSU, infrared spectroscopy was carried out in MSU and Theoretical and Physical Chemistry Institute (Athens, Greece). Technological testing took place in MITHT.

Clays from different areas of upcoming quarry were studied during the research. It was found that clay composition varies from primary palygorskite to montmorillonite clays within the limits of deposit. Montmorillonite has quite stable composition while palygorskite has the complex one. NIR examination results clarified that palygorskite represents mechanical mixture of Al- and Al-Fe-varieties in different proportion with overall prevalence of Al-variety.

Testing the colloidal properties of clay suspensions has demonstrated generally good properties. The application range of these clays is determined chiefly by the quantitative ratio of clay and non-clay minerals, the suspension viscosity and the cation-exchange capacity. Standard technological tests require considerable amounts of time and sample volume. This work will underlie in development of express methods which could be used as fast and precise evaluation of the main characteristics of colloidal properties (used in grade of clay powder analysis) based on mineral composition and particularities of clay minerals structure.

Acknowledgements: Authors are grateful to Dr. G. Chryssikos and Dr. V. Gionis from Theoretical and Physical Chemistry Institute, National Hellenic Research Foundation, Athens, Greece for their kind help in NIR measurements. Authors wish to acknowledge “Lafarge Cement” company for providing samples from Borshovskoe deposit. The work was partially supported by the Russian Foundation for Basic Research, grant #09-05-00302 a and the National Hellenic Research Foundation.

Mineralogical characterization of talc from the Western Carpathians (preliminary results)

Čavajda, V.[1*], Uhlík, P.[1], Madejová, J.[2], Smolárik, M.[1] & Čaplovičová, M.[1]

[1]Dept. of Geology of Mineral Deposits, Comenius University, Bratislava, Slovakia ([*]cavajda@fns.uniba.sk)

[2]Institute of Inorganic Chemistry, Slovak Academy of Sciences, Bratislava, Slovakia

Several talc deposit are located in Slovak part of the Western Carpathians. The main deposits are evolved in Veporic unit (Early Paleozoic Sinec belt) and in Gemeric unit (Early Paleozoic Gelnica group). Most of talc occurrences in Slovakia belong to the deposits in association with Mg-carbonates [1]. Nowadays, a big talc deposit is opened in Gemerská Poloma. The objective of the study is mineralogical characterization of talc from Gemerská Poloma deposit and his comparison with talc from others areas (e.g. Hnúšta-Mútnik) and also investigation of structural order and crystal size. Research was performed on bulk rock and clay fraction (< 2 μm). Samples were studied by XRD, electron microscopy and IR spectroscopy.

Results from XRD quantitative mineral analysis by RockJock software [2], showed that amounts of talc from Hnúšťa-Mútnik samples vary from 85% to 1%. Samples from Gemerská Poloma contain 90-25% of talc. Other minerals are chlorite, quartz, magnesite, dolomite, biotite, muscovite (illite), and pyrite. The mean thickness of talc crystals from fraction < 2 μm was analysed by BWA technique (MudMaster software, [3]). It was indicated differences in mean thickness of talc crystals. Samples from Gemerská Poloma have bigger mean thickness (23,4 nm) than samples from Hnúšťa-Mútnik (15,6 nm). IR spectroscopy was used for partial crystallochemical characterization of the samples. The specific talc bands were significant in the samples with dominant amount of talc (e.g. OH-stretching band (Mg_3OH) at 3676 cm^{-1} and bending band at 669 cm^{-1}). Presence of small amount of Fe in the talc structure is probably determined by weak stretching band (Mg_2FeOH) at 3660 cm^{-1}. Stretching bands at 3571 and 3428 cm^{-1} were significant in samples with high amount of chlorite. Position of these stretching bands points out the presence of trioctahedral chlorite, probably clinochlore.

Talc samples are composed with platy crystals. Planar surface is almost isometric with dominant dimensions from 3 to 10 μm. The shapes of crystals are anhedral and subhedral according to SEM study.

Acknowledgements: The authors are grateful to Slovak grant agency (VEGA) for providing research funding by project 1/0219/10

[1] Grecula, P., Radvanec, M. & Németh Z. (2000) *Miner. Slovaca*, **32**, 533-542. [2] Eberl, D.D. (2003) *User’s guide to RockJock - a program for determining quantitative mineralogy from powder X – ray diffraction data*. U.S. Geol. Survey, Open – File Report: OF 03 – 78. [3] Eberl, D.D. et al. (1996) *MudMaster: A program for calculating crystallite size distributions and strain from the shapes of X-ray diffraction peaks*. U.S. Geol. Survey, Open-File Report 96-171.

Mineralogy of Devonian Timan bauxites

Vakhrushev, A.V.[1*], Kotova, O.B.[1] & Ozhogina, E.G.[2]
[1]Institute of Geology, Komi Science Centre, Ural branch of The Russian Academy of Sciences, Syktyvkar, Russia
([*]vahal@yandex.ru)
[2]Federal State Unitary Enterprise "N.M.Fedorovsky" All-Russian Scientific-Research Institute of Mineral Resources, Moscow, Russia

The mineralogical analysis of fine bauxite ores is recently considered as mandatory component of geological prospects because its results considerably supplement (including nanolevel of mineral formations) concentration techniques and volumes of separated effective mineral and its satellites, quality of mineral raw for further processing of the concentrate.

To evaluate technological characteristics of ore-bearing rocks it is first of all necessary to study in detail various lithotypes of ore-bearing rocks. Therefore we paid special attention to the technique of their material study.

Bauxites are rocks, which components are represented by fine minerals; the study of their mineralogical and physical-technical characteristics allow new look at problems of bauxite concentration.

The most promising new source of this raw in Russia is the Middle Timan group of deposits at the north-east of Komi Republic (reserves up to 200 m depth – more than 200 mln tons). The explored reserves of the Middle Timan are concentrated in the Vezhayu-Vorykva deposit (150 mln. tons).

The deposit includes three types of ores that are different by their lithologic and mineralogic features: hematite-boehmite, hematite-chamosite-boehmite, kaolin-chamosite-boehmite.

The content of boehmite (to 55-65%) often tends to the medium part of the bauxite member. The quantity of silica minerals (kaolin, chamosite and others) increases in top and bottom parts of the section (to 35-45%), but sometimes higher contents of kaolin are determined throughout the whole section.

The features of the mineral composition, as well as the degree of bauxite cementation, affect the degree of substance differentiation, which determines possible ways of concentration. Therefore both, discovery of distribution regularities (in the section or area) of bauxite lithological varieties, and determination of areas of bauxite development with predominance of various minerals, present interest for mapping of areas of concentrated ores development.

During the investigation of the Vezhayu-Vorykva bauxites the characteristic features of mineral composition and physical properties were determined. The high dispersity of the main bulk of composing minerals (mechanical mixtures with micron and sub-micron particle sizes) is characteristic for all the lithologic-mineralogic varieties. For example fine-crystalline boehmite with sizes <5-10 mcm is widely distributed; and also the considerable part of hematite and goethite is concentrated in the thinnest classes (<0.5 mcm). Often isomorphous substitution of iron oxide by aluminum is determined in goethite and hematite with formation of alumohematite and alumogoethite. The main silica minerals are kaolin and chamosite. The major part of chamosite is represented by a fine form; content of iron oxide reaches 10-15%. The X-ray amorhous phase is widely distributed, which is determined at comparison of various diagnostic methods (X-ray structural analysis, chemical analysis, IR spectrometry, Moessbauer spectroscopy).

Characteristics of smectite and palygorskite clays from the Dashkovskoe Industrial Deposit (Serpuchov Region, Russia)

Zakusin, S.V.[1*], Matskova, N.V.[1], Krupskaya, V.V.[1,2], Chryssikos, G.D.[3], Gionis V.[3] & Pokidko, B.V.[4]
[1]Lomonosov Moscow State University (MSU), Moscow, Russia
([*]zakusinsergey@gmail.com)
[2]Institute of Geology of Ore Deposits, Petrography, Mineralogy and Geochemistry RAS (IGEM RAS), Moscow, Russia
[3]Theoretical and Physical Chemistry Institute, TPCI, National Hellenic Research Foundation (NHRF), Athens, Greece
[4]M.V. Lomonosov Moscow State Academy of Fine Chemical Technology, (MITHT), Moscow, Russia

Palygorskite and bentonite clays are used in many industrial applications. The subject of this research was Dashkovskoe clay deposit (Moscow region, Serpukhov).

XRD analysis showed that samples contain palygorskite, montmorillonite, calcite, dolomite and quartz at various ratios (Fig. 1). Palygorskite is dioctahedral and Al-rich, with very minor FeIII substitution in M2 sites. The chemical composition of palygorskite in the different horizons of the Dashkovskoe deposit is found to be remarkably constant, despite the fact that this mineral is capable to exhibit large variations in the speciation of its octahedral sheet. This indicates that palygorskite was crystallized under the same chemical condition and deposited in sedimentary basin without transportation. Area of Dashkovskoe deposit is represented by a source of palygorskite for Moscow region.

The Dashkovskoe clay suspensions possess quite good structural-mechanical properties. All samples demonstrated pseudoplastic behaviour with Bingham yield value ranging between 1.9 and 9.5 MPa•s (Fig. 1). The best apparent viscosity (AV) and yield point (YP) have been found in the case of nearly 50/50 palygorskite and smectite mixture. This fact can be explained by the presence of optimal quantities of particles with different shapes in dispersion media. It is well known that palygorskite displays good stability in saline solutions and under high temperatures. This is especially important when using drilling mud with rotatory drilling of rocks bearing soluble salts. Thus combining smectite and palygorskite at a certain ratio not only allows acquirement of salt- and thermal-resistant mud but also significantly improves their rheological characteristics.

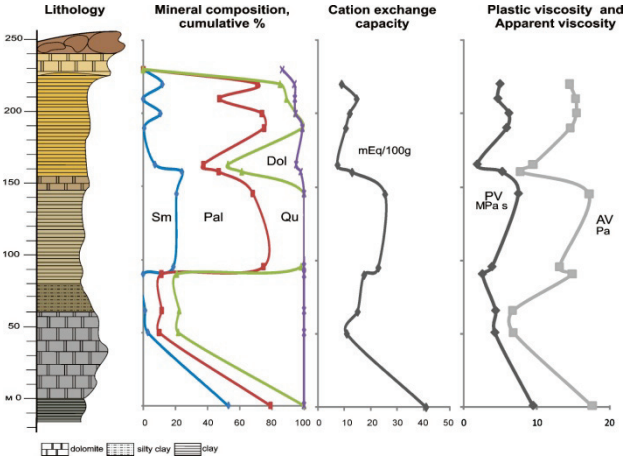

Fig. 1: Relations between lithology, mineral composition, cation exchange capacity and viscosity.

Acknowledgements: The work was partially supported by the Russian Foundation for Basic Research, grant #09-05-00302 a and the National Hellenic Research Foundation. Authors wish to acknowledge "Keramzit" company for providing industrial samples from Dashkovskoe deposit.

Identification and stabilization of clays for productivity/injectivity optimization in the hydrocarbon industry

Dormán, J.
New Technologies and R&D, MOL Hungarian Oil and Gas Plc, Hungary (jdorman@mol.hu)

Most of the sandstone type hydrocarbon bearing formations are severely contaminated by detrital clay minerals, which can cause severe formation damage and productivity impairment. Maximization of productivity of hydrocarbon producing wells or optimization of productivity/injectivity of underground gas storage wells require efficient preferably proactive formation damage control. The most common source of permeability damage in such wells is the destabilization and mobilization of fine particles with fluid flow (fines migration). Clay minerals are mostly prone to disintegration, mobilization and entrapment within the pore structure, causing permanent loss of permeability in case of improper drilling/completion fluid chemistry. In drilling/completion technology design and fluid chemistry optimization the need for characterization and determination of types and concentrations of mineral constituents of formation rocks, especially clay minerals (XRD, FTIR, CEC, etc.) are essential and inevitable and are routinely used to support advanced field practice.

Fluid flow in the porous formation is controlled at pore scale, while fines migration at micron-to-submicron scale, therefore extensive studies of pore structure/morphology and visualization, identification of potentially mobilizable particles and their typical position in the pore structure (SEM, ESEM) are also key issues in combating permeability reduction. Clay minerals commonly appear in a very complex coexistence with different detrital minerals.

Core flow studies (using representative core plugs) can efficiently support to evaluate the potential fluid chemistry/flow effects at semi-macro scale, but can't give direct answer for the effect of formation heterogeneity.

Potassium salts and selected cationic (organic) polymers of different molecular weight and other specialty additives are the key components of the new "fit-to-purpose" drill-in and completion fluids, which were formulated by complex engineering approaches. The main tasks in Hungary are to maintain formation integrity and to control formation damage in mostly under-consolidated, water-sensitive sandstone reservoirs.

The paper gives an overview of clay identification and stabilization techniques, results and illustrates their aspects in drilling/completion fluid design and successful field applications.

Evolution of boron and nitrogen content during illitization of bentonites

Środoń, J.
Institute of Geological Sciences, Polish Academy of Sciences, Kraków, Poland (ndsrodon@cyf-kr.edu.pl)

The contents of boron and nitrogen in illite-smectite clays from pyroclastic horizons of sedimentary rocks (bentonites) were studied using samples from different sedimentary basins, representing a complete range of diagenetic alteration. Bentonites were chosen to deal only with the authigenic clay, avoiding complications related to the recycled (detrital) clay material. The bulk rock chemical measurements, performed on raw rock samples in order to avoid any loss of exchangeable B and N, were referred to the contents of illite-smectite clays and to the content of illite alone, both measured by a combination of XRD and chemistry-based techniques [1].

The results indicate that the smectite illitization reaction in the studied range between 100 and <20 %S is not so much redistributing B and N present in the original smectite, but it is a net consumer of both boron and nitrogen from the pore waters.

Both B and N (as NH_4^+) are contained mainly in illite, so their contents in illite-smectite clay increase in more or less linear manner with progressing illitization. The content of N in illite layer is decreasing during diagenesis and the content of B is either decreasing or remains stable. In one diagenetic cycle bentonitic illite fixes up to 800-1000 ppm B and up to over 1% $(NH_4)_2O$, corresponding to over 20% of the fixed cation sites.

The studied rocks are different from regular sedimentary clays, because smectite in bentonitic horizons is not detrital but it crystallizes *in situ* during early diagenesis at the expense of volcanic glass. The conclusions drawn above refer only to this particular case. Similarities in diagenetic evolution of boron and nitrogen contents of illite, documented in this study, argue in favor of the kerogen as the dominant common source of both elements in sedimentary basins.

[1] Środoń J. (2009) *Clay Minerals*, **44**, 417-430.

Reservoir properties dependence upon the compositional features of clay minerals

Kulyapin, P.S.[1*], Moiseenko, A.S.[2] & Strelchenko, V.V.[1]
[1]Well Logging Systems Dept., Gubkin Russian State University of Oil and Gas, Moscow, Russia ([*]pavel.kulyapin@gmail.com)
[2]Information and Measuring Systems Dept., Gubkin Russian State University of Oil and Gas, Moscow, Russia

Present-day core laboratories widely use the following method of clay content evaluation. The term “shaliness” is considered as an ability of rocks to contain particles with diameters d<0,01 mm, in the US laboratory practice d<0,001 mm. Hence, clay content is estimated by means of sieve analysis procedure.

Nevertheless, described approach eliminates the probability of fine-grained oxides and hydroxides of silicon and aluminum which aren’t related to clay minerals. Besides, clay fraction can be underestimated as the diameter of large kaolinite crystals exceeds 0,01 mm. Providing clay content is calculated thus-and-so, mistakes in formation evaluation are expectable.

Presence of certain clay minerals can indicate particular sedimentation conditions. Analyzing the alteration of clay minerals composition, it is possible to define depositional environments more exactly.

There is close correlation between depositional environments and natural radionuclide distribution. This fact is a basis for applying spectral gamma ray in order to determine clay mineral composition. Also, it is very helpful to estimate clay minerals content quantitatively using X-ray analysis, infrared spectroscopy or thermal gravimetric analysis.

Clay minerals impact on properties of oil and gas reservoir in a significant way. The study of clay minerals composition and estimation of their influence on physical and fluid-flow properties of rocks is a vital and high-demand task.

Clay minerals belonging to various groups affect reservoir properties differently. The estimation of a pore space filled by a clay material and the influence of certain clay minerals on filtration properties is applicable to drilling technology, formation evaluation and oilfield development. The information about clay minerals composition is used for adjustment of log-derived evaluation algorithms.

In the research the in-depth analysis of clay minerals is presented in scope of their effect on petrophysical properties of rocks. Also, the application of infrared spectroscopy for a qualitative and semi-quantitative estimation of clay minerals content is addressed.

Multi-constituent modeling of gasoline contamination in laboratory – sorption of light hydrocarbons by clay

Tóth, J.
New Technologies and R&D, MOL Group Exploration and Production Division, Budapest, Hungary (judittoth@mol.hu)

Petroleum hydrocarbons are common site contaminants, but little is known about their natural attenuation processes. Due to the diversity of hydrocarbon compounds a range of remediation technologies may be applicable. Volatilization and gas transport of VOCs are the bases for some remediation technologies (for example soil venting, air sparging, and soil vapor extraction), consequently knowledge of the volatility of hydrocarbon compounds is important for understanding their fate in subsurface media. In order to investigate volatility and sorption of light hydrocarbon compounds, a special column experiment was conducted in laboratory.

The volatile components of the used hydrocarbon could be transported only in one direction (upward through fillings), therefore the investigation of their sorption on natural clay and sand was possible. At the end of the experiment more than half of the initial fluid volatilized, due to the volatility of the individual constituents. The volatilization was very effective in the first year.

The sorbed HCs are mainly paraffins and aromatics, while napthenes rarely occur. After half a year, n-C_7 was found to be the lightest and C_{11} the heaviest constituent. The range enlarged continuously, it was possible to measure n-C_6 and C_{12} after one year, while at the end of the modeling n-C_5 and C_{15} were already measurable in clays. It was possible to detect sorbed HCs after half a year only in clay layers and in every sample at the end of modeling. Quantity of sorbed compounds decreased with growing carbon numbers. Models with clay-caps contained larger amounts of HCs also in deeper layers compared to their sandy pairs (totally three to six times more quantities). The reason for this is presumably the good sealing property of the clay, therefore volatilized components remained in the pores among sand particles or sorbed onto the individual constituents. Quantity of sorbed HCs is the greatest in the vicinity of the fluid phase. Fine tendencies, dependent on depth, can be seen mostly in case of cyclohexane, benzene, as well components with slightly larger carbon number (e.g. C_{10}, C_{11}, C_{12} and C_{13}). These clearly show the effect of less volatility.

By comparing the results of detailed analyses (GC, Rock-Eval, XRD), adsorption was the main sorption process.

On the basis of comparative assessment of the results derived from the analyses of samples from different phases (fluid, gas and solid), the best practice for identifying the source of a gasoline type contamination is a joint analysis of sorbed and free hydrocarbons of the soil samples, while the best way to monitor a contamination is to analyze free gas components. It is worth applying the analyses together, because a different range of the initial fluid phase can be measured from the free gas and the sorbed phase. The ratio of the lightest hydrocarbons in the total amount of hydrocarbons may indicate the time when the contamination occurred.

Laboratory methods in evaluation of shale interaction with drilling fluids: effect of clay content and shale characterization

Gomez, S.
M-I SWACO, Houston, TX, USA (sgomez@miswaco.com)

The behavior of shale samples exposed to drilling fluids may differ significantly due to the rock characteristics. Type and amount of clay minerals, rock structure, distribution of minerals, and other geologic features are important elements that need to be integrated in the execution of successful testing programs. This paper includes the descriptions of different test methods used to evaluate the interaction between shale and drilling fluids and how the characteristics of the shale samples are used to select the experimental methods. Understanding and comprehending clay content and distribution in the shale samples is one of the most valuable steps before the testing. The response of clays with fluids can be manifested in swelling process, dispersion, propagation of fractures and other mechanisms. The type of response can be closely related to the type of clay. The rock structure and mineral distribution also play important roles. Presence of laminations, lenses, and just bulk structure may control, restrict or direct the areas where the fluids can interact with the clays in the rock. Compositional and structural variations in shale samples can be obtained from shale samples and constitute the base information for the selection of the laboratory tests for the drilling fluid design.

Clay minerals features application for reservoir pressure estimation

Deshenenkov, I.S.* & **Gorodnov, A.V.**
Gubkin Russian State University of Oil and Gas, Moscow, Russia
(*isd@post.com)

This research is devoted to the development of the abnormally high formation pressure (AHFP) zones determining innovative technique on well logging data. The method is based on changes in dependences of clays physical properties in AHFP zones. It takes into account the nonsteady thermal field in the borehole.

Normal pressure is formation pressure is due to the presence of fluids in pore spaces of the rock matrix. Abnormal pressure is any geopressure that is different from the established normal trend for the given area and depth.

AHFP represent a serious threat for the well and its staff maintenance while deep wells drilling and development. High technological and economic performance in drilling and deep wells development can be achieved in case of correct prediction and estimation of AHFP zones.

Abnormal pressure predicting methods in the thickness of sedimentary rocks are based on the pattern of rocks properties changes as a result of compaction in the process of sediments accumulation. Physical properties of pure clays, used as an indicator of pore pressure, are determined by its compaction degree. Clayed rocks containing deposits with AHFP are less sealed and have higher porosity in comparison with similar rocks with normal pore pressure [1].

Physical parameters depend on rocks density and as result porosity. This dependence of clayey rocks is the basis of various identifying and estimation by abnormal pressures methods.

There are following methods for AHFP zones predicting: equivalent depths method, «normally clay compacted curves» technique, compression curve method.

Factors determining changes in physical properties of pure clay rocks are changes of clay mineral composition and temperature. However, the impact of changes in clay mineral composition at depths of more than 2000-2500 m (in AHFP zones) is nonessential fact. A significant contribution to the calculation of reservoir pressure makes temperature [2].

Temperature correction is traditionally calculated on the geothermal gradient. Nevertheless, the real thermal field in the borehole can differ greatly from stationary geothermic data. Therefore, thermal field in the borehole was simulated. Also the distribution of the temperature over time after flushing out of well was surveyed within the radius of well logging methods study.

Authors investigate the thermal field formation in the vicinity of the borehole. Dynamics of the thermal field during drilling, well cleanout and well shutdown are studied. Temperature factor effects on the accuracy of abnormal pressure on well logging data calculation are determined. A modified «normally clay compacted curves» technique is developed. It involves the introduction of the correct temperature adjustment to electrologging curves before the line of normal clay compaction tracing.

Formation of thermal field in the vicinity of the borehole was investigated. Innovative method AHFP calculation, based on changes in dependences of clay physical properties in AHFP zones and taking into account nonsteady thermal field in the vicinity of the borehole, was developed. Maps of abnormal pressures and anomaly pressure coefficients in sediments of Bazhenov formation were charted.

[1] Dobrinin, V.M. & Serebryakov, VA (1978) *Abnormally high formation pressure prediction methods.* Oil and gas, Moscow. [2] Ipatov, A.I. & Kremenetsky, M.I. (2006) *Geophysical and hydrodynamic control of oil and gas fields*. Oil and gas, Moscow.

Possibilities of gamma-ray log quantitative interpretation

Ezhov, A.K.* **& Lazutkina, E.N.**
Well-logging Systems Dept., Gubkin Russian State University of Oil and Gas, Moscow, Russia (*ejcyril@mail.ru)

Current work is devoted to studying of influence of separate clay minerals on collector properties and to definition of their maintenances according to gamma-ray log in complex of well-logging data.

On the basis of the revealed laws, petrophysical modeling of collectors and adaptive techniques of well-logging data interpretation [1] the algorithm of an estimation of kaolinite and hydromicas maintenances in structure of clay cement was developed (Fig. 1). In this work results of interpretation of Jurassic deposits of Tevlinsko-Russkinskoe field (West Siberia, Russia) are presented.

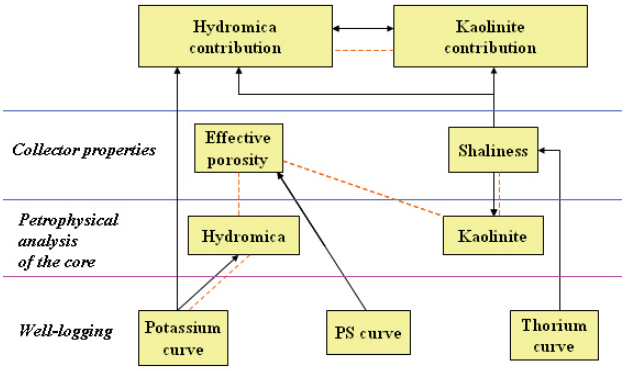

Fig. 1: The scheme of estimation of kaolinite and hydromica maintenances in cement of terrigenic collectors.

The ways of an estimation of kaolinite and hydromica maintenances in clay cement of collectors according to gamma spectrometry in complex of borehole surveys are offered. It's based on their interrelation in clay cement of terrigenic collectors.

It is revealed that character of ratio between contributions of hydromica and kaolinite in clay cement of terrigenic collectors is maintained for different adjournment of various deposits.

[1] Kozhevnikov, D.A. (2005) *Geofizika*, **2**, 42-49.

The specificity of clay minerals influence on the residual water layer formation

Petrov, A.N.
Gubkin Russian State University of Oil and Gas, Moscow, Russia (*al.n.petrov@gmail.com)

Clay minerals have specific features. A distinctive feature of all clay minerals is their high dispersity. High dispersion creates a well-developed specific surface area of rock (up to 800 m2/g for montmorillonite), which causes a high margin of free surface energy and the manifestation of molecular interaction forces in the surface layers. The most important physical-chemical characteristics of clay minerals is their ability to surface dissociation (formation of a water shell), the ability to anomalous high ion exchange (cation exchange capacity) [1]. Patterns of distribution of residual water saturation for the multimineral reservoirs are complex and nonlinear. Dispersion of clay material greatly affects the quantitative assessment, and even small admixture of chlorite or hydromica will make significant changes.

Appearance of reservoir nonuniformity on the dependence of residual water saturation from the total porosity due to clay minerals variation is discussed. The set of factors contributing to the heterogeneity of the matrix and cement composition and properties, defines the dynamic range of cement and matrix properties, which is why scatter points on the plane residual water saturation – total porosity appear. This means that, although the dependence between residual water saturation and total porosity, as well as other petrophysical relations, the "statistical" comparisons is not functional, but it is not in the full sense of statistics. The scatter of points in the field of correlation is due not only to measurement errors, but to the differences in petrophysical properties of clay minerals comprising the matrix and cement. Petrophysical informative field configuration have the degree of correlation and the scatter of points in the field of correlation. The most general definition of a complex manifold, regardless of the nature of the latter, will be the following: complex reservoirs are reservoirs, which are meaningless concepts conditioned values of petrophysical characteristics, or relevant testimony well logging techniques.

Filtration, capacity, and structure, water storage capacity and other petrophysical characteristics depend primarily on the content of clay minerals, their composition and morphology in terrigenous reservoirs. If no or little content in the carbonate rocks, silicate and iron cement quantity and composition of the clay material is a decisive factor in the separation of rocks on the reservoirs and non-reservoirs.

In conclusion, for reservoirs with multimineral composition, the dependence of residual water saturation from total porosity cannot be unambiguously determined. For each part of the reservoir, this dependence can vary, due to the heterogeneity of the mineral composition.

All types of reservoirs and their filtration-capacitive properties manifested in different kinds of dependencies residual water saturation – total porosity. With a fixed capacitance matrix of the diversity of these relationships is due to a variation of the properties of clay cement.

This heterogeneity of polymineral clay and other reservoirs can formulate, the most common definition of "complex" reservoirs, as such, which make no sense notion of fixed values conditioned volumetric or appropriate evidence of well logging techniques.

[1] Gudok N. et al. (2007) *Physical properties determination of rocks containing hydrocarbons and water*. Nedra, Moscow.

Burial diagenetic processes of clay mineral and non-clay mineral, and their relation to quartz cementation in sandstones of the Siri Canyon, Danish North Sea

Kazerouni, A.M.[1*], Friis, H.[1] & Svendsen, J.B.[2]
[1]Dept. of Earth Sciences, Aarhus University, Aarhus, Denmark
([*]afsoon.moatari@geo.au.dk)
[2]DONG Energy, Exploration and Production, Denmark

The deep marine sandstones in the Siri Canyon, Danish North Sea, have been reported to import significant amounts of dissolve silica from adjacent Palaeocene shales during early diagenesis, and the authigenesis of silica developed several morphologies in the studied sandstones. We have studied the diagenesis of one of these shales, the Sele Formation shale, to document the diagenetic steps which release silica and to evaluate the possible capacity and timing of silica export from the shale into the interbedded sandstones. Initially, the shales were rich in smectite and had variable admixtures of silicious fossils (diatoms, radiolarian and sponge spicules) and volcanic ash.

Depth dependant alteration of the various components in the shale, results in successive stages of silica-release. In shallow samples (<1700 m), the alteration of volcanic ash has already been completed. Released silica was partly consumed for the precipitation of smectite and zeolite. Opal-CT is not systematically related to volcanic ash, and some silica may have been mobilized and migrated into the interbeded sandstones. In addition, a major part of the biogenic silica has been transformed into opal-CT and partly to microcrystalline quartz. The microcrystalline quartz is an internal sink for dissolved silica, but the shale may also have been an active silica exporter during this transition.

With deeper burial (2000-2900m), opal-CT is fully transformed to microcrystalline quartz. During this phase, silica has been partly mobile and depending on the rate of dissolution compared to the rate of precipitation, silica may have been lost to sandstone cementation. Zeolite is also dissolved and mobilized silica may also have activated the shale as silica exporter.

At deep burial, iron-rich chlorite has replaced a minor part of smectite. The smectite to chlorite transformation released silica at the expense of iron. Therefore, a third phase of silica mobility was active. Microcrystalline quartz may have been an internal sink, but the shale would also be a potential silica supplier at this stage. At maximum burial depth (2900 m), the major part of the smectite is still not transformed, and the smectite to illite transformation has not yet been activated as a potential silica source. Early cementation by opal and microquartz depends on the supply of dissolved silica from a readily dissolvable source. The process starts with biogenic silica dissolution and supersaturation of pore fluids with respect to opal-CT and quartz. Relative rates of opal-A dissolution and opal-CT nucleation govern the extent to which silica activity is buffered and hence the possible silica flux into adjacent sandstones. With progressively less remaining opal-A, silica activity starts to decline and opal-CT nucleation becomes subordinate to growth. Precipitation of cryptocrystalline quartz began once the thermodynamic drive for the opal-CT became insignificant. Relative rates of opal-CT dissolution with respect to quartz nucleation and growth buffer the silica activity and the possible silica flux into adjacent sandstones. The early stages of the sandstone diagenesis are dominated by massive precipitation of opal cement and microquartz. This indicates a large flux of silica at the time of opal-A to opal-CT transformation and possibly at the time opal-CT to microquartz transformation. Therefore, the dissolution rate of precursor phases (biogenic silica, opal-A and/-CT) was fast enough to create a sufficient silica gradient to exports silica from shale to sandstone.

Molecular simulation of the hydration of methane confined in the clay interlayer or in nanopores between clay basal surfaces

Lu Xiancai[*], Zhang Lihu, Zhou Qing & Liu Xiandong
State Key Laboratory for Mineral Deposits Reseach, School of Earth Sciences and Engineering, Nanjing University, Nanjing, P. R. China ([*]xcljun@nju.edu.cn)

Methane hydrate is not only a potential energy resource, but also would be an ideal crystalline solid for gas storage. In general, the rate of nucleation and growth of the clathrate can be increased by operating at either higher pressure or lower temperatures, but such conditions may be undesirable for many applications. One of the alternative strategies to increase the kinetics of clathrate formation is to increase the interfacial contact between liquid water and the gas by inducing solid supports such as silica [1] to generate a thin, confined water layer in contact with the gas. The promotion mechanism of the clathrate nucleation and growth by mineral surface should be disclosed in order to understand the formation of methane hydrate in muddy sediments and in artifical conditions. In this study, molecular dynamic simulations have been carried out to investigate the formation and stability of methane hydrate in Na-smectite interlayer with different layer-charge distribution and water content, as well as in the nanopores with clay walls in various P-T conditions. In the simulation, the MD program Dlpoly and Clayff forece field [2] was employed.

The simulation results indicate that the methane clathrate can be formed in the interlay spaces under much higher temperature and lower pressure than that of the bulk hydrate. As methane molecules confined in the interlayer of clay minerals, most of the methane molecules are solvated by nearly 12-13 water molecules and coordinated with six oxygen atoms from the clay surface simultaneously. The methane molecules are generally trapped in the six-member rings through the strong H-bonds, which is exactly similar to the behaviors of K^+ or Cs^+ in montmorillonite interlayers [3]. The self-diffusion coefficients of the methanes in the newly-formed cages remarkably decrease from 0.452×10^{-9} m^2/s to 0.060×10^{-9} m^2/s at 277 K and 50 atm.

The layer-charge distribution displays remarkable effects on the stability of interlays hydrated methane complexes. A clay surface with negative charge sites is hydrophilic and present lowers surface affinity for methane moleculars. As the net layer charge is similar, the distance between negative charge sites and methane moleculars play important roles. It is disclosed that the tetrahedral negative charge site near the surface is hydrophilic and reduces the clay surface affinity for methane, which leads to less stability of hydrated methane complex in the smectite with tetrahedral substitutions. As Arizona-type montmorillonite has no tetrahedral negative charge site, the hydrated methane complex in it is more stable than other clays with tetrahedral charges.

The stability of the methane hydrates confined in nanopores with talc basal surface also shift to the higher pressure region depending on pore size when compared with those of bulk hydrates. The surface of the clay walls act as templates for the cystallization of methane hydrate, and a layer of methane hydrates are firstly formed, which is tightly contacting to the clay surface.

Acknowledgements: Authors acknowledge National Science Foundation of China (No. 40973029).

[1] Anderson, R., Chapoy, A. & Tohidi, B. (2007) *Langmuir*, **23**, 3440-3444. [2] Cygan, R.T., Liang, J.-J. & Kalinichev, A.G. (2004) *J. Phys. Chem. B*, **108**, 1255-1266. [3] Liu, X.D. & Lu, X.C. (2006) *Angew. Chem. Int. Ed.*, **45**, 6300-6303.

Increase of porosity in turbiditic sandstones by late-stage diagenetic formation of chlorite and kaolinite

Marchel, C.
Wietze E & P Laboratory - RWE Dea, Wietze, Germany
(christian.marchel@rwe.com)

Core material of miocene aged turbiditic sandstones, located in the Nile Delta area (Egypt), have been analyzed by means of thin-section petrography, scanning electron microscopy/ energy dispersive X-ray, petrophysical measurements, X-ray diffraction and IR-spectroscopy.

The sandstones vary from fine grained- to conglomeratic sandstones, representing ancient channel fill deposits. Values of porosity range from 2-32 % and permeability vary between 0.005 and 1100 mD. Eodiagenetic alterations are represented by moderate mechanical compaction and grain reorientation, calcite replacement of former aragonitic clasts and formation of anatase, siderite and pyrite. Early quartz precipitation occurs as quartz overgrowth. Mesodiagenetic alterations are mainly represented by illitization of smectites, quartz overgrowth, formation of chlorite and kaolinite and late-stage pore filling calcite.

Evolution of the reservoir quality has been controlled by both, eodiagenetic and mesodiagenetic processes, and shows that formation of secondary porosity plays an important role. Whereas primary porosity occurs mainly as intercrystalline macroporosity and takes 30 Vol.-% of total amount of porosity, secondary porosity comprises around 70 Vol.-% of total amount. The main part of secondary porosity belongs to intercrystalline micropores between chlorite and kaolinite. Investigations indicate that the formation of chlorite and also kaolinite proceeded at a late stage of diagenetic history, later than generally expected. It occurred via transformation of Fe-Mg rich detrital grains, fragments and clayey compound as well as precipitation within open pore space. This “late-stage formation” might be the result of rapid burial to greater depths and therefore decelerated mineral reactions. Thereby the detrital components stabilized the framework to a certain degree and prevented the sediment for strong mechanical compaction prior to the formation of chlorite and kaolinite. Thus, the new formed intercrystalline micropores increase the total porosity and also permeability of the reservoir section.

Structure of nanocrystalline phyllomanganates produced by freshwater fungi

Grangeon, S.[1], Lanson, B.[1*], Miyata, N.[2,3], Tani, Y.[2] & Manceau, A.[1]
[1]Mineralogy & Environments Group, Laboratoire de Géodynamique des Chaines Alpines, Université J. Fourier – CNRS, Grenoble, France ([*]bruno.lanson@obs.ujf-grenoble.fr)
[2]Institute for Environmental Sciences, University of Shizuoka, Japan
[3]Dept. of Biological Environment, Akita Prefectural University, Shimoshinjo-Nakano, Akita, Japan

Chemically reactive nanosized manganese dioxides are produced by a variety of living organisms including bacteria, fungi, and plants. The biotic oxidation of Mn^{2+} to Mn^{4+} is approximately two orders of magnitude faster than the heterogeneous oxidation catalyzed by mineral surfaces, thus supporting the currently held view that the biogenic route to Mn oxide formation prevails in nature. Vernadite, a nanosized phyllomanganate consisting of randomly-stacked layers of edge-sharing $(Mn^{4+}O_6)^{8-}$ octahedra [1], is the main biogenic Mn oxide, possibly with tectomanganates, such as todorokite. Phyllomanganates such as birnessite owe their surface reactivity to the presence of vacant layer sites and/or to Mn^{3+} for Mn^{4+} substitutions that confer to the layer a charge deficit up to three times higher than that of smectite. Vernadite has in addition high amounts of border sites because of its very small particle size. The ratio of external to internal Mn sites increases indeed when the crystal size decreases, and biogenic vernadite with a layer dimension of 60-70 Å [2] has approximately 20% of its Mn atoms exposed at the crystal border compared to ~0.4% for a birnessite layer ~300 Å [3]. Thus, organic pollutants can be degraded and trace metals taken up by vernadite in natural systems.

The production and sorption capacity of fungal vernadite are well documented, but progress in the interpretation and modeling of sorption data is limited by the lack of a comprehensive structure model. In the present study, chemical analyses, XANES (X-ray absorption near edge structure) and EXAFS (extended X-ray absorption fine structure) spectroscopy, and powder X-ray diffraction (XRD) were combined to determine the nature and amounts of structural defects in vernadite produced by three fungal strains. The fungi-mediated oxidation of aqueous Mn^{2+} produces layered Mn oxides analog to vernadite, a natural nanostructured and turbostratic variety of birnessite. The crystallites have domain dimensions of ~10 nm in the layer plane (equivalent to ~35 MnO_6 octahedra), and ~1.5-2.2 nm perpendicularly (equivalent to ~2-3 layers), on average. The layers have hexagonal symmetry and from 20 to 30% vacant octahedral sites. This proportion likely includes border sites, given the extremely small lateral size of the layers. The layer charge deficit, resulting from the missing layer Mn^{4+} cations, is balanced mainly by interlayer Mn^{3+} cations in triple-corner sharing position above and/or below vacant layer octahedra. The high surface area, defective crystal structure, and mixed Mn valence confer to these bio-minerals an extremely high chemical reactivity. They serve in the environment as sorption substrate for trace elements and possess catalytic redox properties

[1] Giovanoli, R. (1980) *Miner. Deposita*, **15**, 251-253. [2] Lanson, B. et al. (2008) *Geochim. Cosmochim. Ac.*, **72**, 2478-2490. [3] Lanson, B. et al. (2000) *Am. Mineral.*, **85**, 826-838.

Oxidation of As(III) by β-MnO_2 in the presence of Fe(II) under acidic conditions

Gu, J.-D.[1*], Han, X.[1] & Li, Y.L.[2]
[1]School of Biological Sciences, The University of Hong Kong, SAR, China ([*]jdgu@hkucc.hku.hk)
[2]Dept. of Earth Science, The University of Hong Kong, SAR, China

Arsenite [As(III)] is a highly toxic inorganic pollutant and is mobile in sediments and aquifers because of its neutral, uncharged molecular state (H_3AsO_3) below pH 9.1 in soil-water environments. Oxidation of As(III) to the less toxic As(V) is always observed in aqueous environment containing Mn-oxides. Fe(II), which often co-exists with As(III) in groundwater, can also be oxidized by Mn-oxides; however, the contribution to As(III) oxidation by Mn-oxides has not been reported.

Effects of Fe(II) on As(III) oxidation at MnO_2-water interface under acidic conditions were investigated in this study and kinetic experimental results showed that oxidation of As(III) could be described by a pseudo-first order kinetic model and oxidation rate of As(III)/Fe(II) decreased with the increase of pH (2.0-5.0) in mono system. Competitive oxidation between Fe(II) and As(III) occurred on MnO_2 surface in the binary system, and the inhibitory effects of Fe(II) on As(III) oxidation decreased with the increase of Fe(II)/As(III) ratios. The inhibition could be attributed to the formation of Fe(III) compounds on the surface of MnO_2 and thus preventing the MnO_2 surface being accessible to As(III), and the produced Fe(III) compounds sequestered more oxidized As(V) with the increase of Fe(II)/As(III) ratios (Fig. 1).

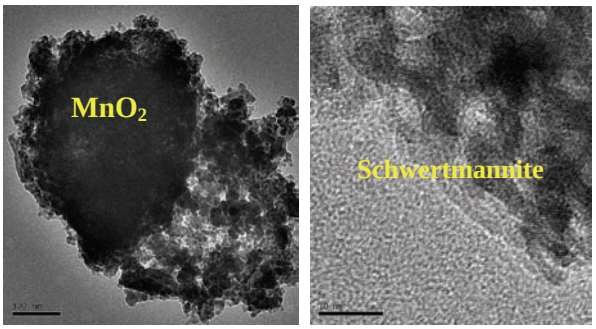

Fig. 1: Surface characterization of MnO_2 after the treatment with 15 mg L^{-1} Fe(II) at pH 3.0 and Precipitates formed around MnO_2 after the treatment of 20 mg L^{-1} As(III) at pH 3.0 with Fe(II):As(III)=1:1.

TEM results confirmed the formation of Fe compounds around or away from MnO_2 particles in both mono and binary systems, and schwertmannite particles were detected (Fig. 1) in the mono-oxidation of Fe(II) by MnO_2, while a new phase, most likely ferric arsenate ($FeAsO_4$) as confirmed by EDX was detected in the Fe(II)-As(III) binary system.

On the basis of the above results, mechanism involved in the process was proposed that competitive oxidation occurred between Fe(II) and As(III) on MnO_2 first and followed by the formation of Fe compounds around MnO_2, which inhibited oxidation rate of As(III) and Fe(II) in solution. Then, As(III), but not Fe(II) in the bulk solution, could slowly diffuse through the layer of the Fe(III) compounds and access the surface of MnO_2 for further oxidation, and some of the produced As(V) was released back into solution.

The present study suggested that the presence of Fe(II) played an important role in the oxidation of As(III) by MnO_2 on surface of minerals under acidic conditions.

Detailed crystal chemistry and iron topochemistry of naturally occurring asbestos (NOA): a first step to understanding their chemical reactivity

Pacella, A.[1], Andreozzi, G.B.[1*] & Fournier, J.[2]
[1]Dipto. di Scienze della Terra, Sapienza Università di Roma, Rome, Italy ([*]gianni.andreozzi@uniroma1.it)
[2]Laboratoire de Réactivité de Surface, Université Paris 6, 4, Paris, France

Five samples of naturally occurring tremolite asbestos (NOA) from Italy and USA were fully characterized by means of a well tested multi-analytical approach (ICP-MS, SEM, EMPA, FT-IR, MS, XRPD), with the aim to correlate crystal chemistry with chemical reactivity. Iron topochemistry was investigated in detail, due to Fe recognized contribution to aetiology of respiratory inflammatory diseases. The Italian tremolite samples have different Fe content (San Mango > Ala di Stura > Rufeno > Castelluccio Superiore), and the North American sample from Maryland shows a value almost double than the Italian ones. The bulk Fe^{3+}/Fe_{tot} ratio was quantified by Mössbauer spectroscopy, and the values obtained ranged from 6% Fe_{tot} (San Mango tremolite) to 24% Fe_{tot} (Mt. Rufeno tremolite). A possible site distribution of Fe was retrieved from combining chemical, spectroscopic and structural (Rietveld refinement) data. For all samples a substantial Fe^{2+} equidistribution was observed over M(1), M(2) and M(3) octahedral sites, whereas Fe^{3+} was only allocated at M(2). Results of EPR measurements on the Italian samples evidenced chemical reactivity (that is, HO° radical production) for all of them, with the highest value observed for San Mango sample and the lowest for Castelluccio Superiore sample. Notably, the HO° radical production resulted to be related to the Fe_{tot} content and, in particular, linearly related to the Fe population at [M(1) + M(2)] octahedra. Considering that Fe_{tot} population at M(2) > M(1) > M(3), that M(1) and M(2) have site multiplicity twice that of M(3) and are more exposed than M(3) on the external surface of the fibrils, the Fe at M(1) and M(2) sites has the highest probability to be involved in surface reactions.

Chemical composition of voltaite formed from flue gas of a coal-fired power plant

Gieré, R.[1*] & Williams, C.T.[2]
[1]Institut für Geowissenschaften, Universität Freiburg, Germany ([*]giere@uni-freiburg.de)
[2]Dept. of Mineralogy, The Natural History Museum, London, UK

Coal combustion facilities represent a major source of fine particulate matter (PM) in the atmosphere. We report results from analytical scanning electron microscope investigations on PM emitted from a commercial coal-fired power plant equipped with a stoker boiler. In an experiment designed to test the viability of co-combustion of coal and waste tires, two types of fuel were combusted: pure coal (a high-volatile *C* bituminous coal); and a mixture consisting of 95 wt% of the same coal and 5 wt% of shredded tires.

The samples were collected on borosilicate glass filters placed in the smokestack above all air pollution control devices. The filters remained overnight (12 h) in the stack (gas temperature: 183-195 °C; flow rate: 108±2 ML/h) and trapped the PM that would normally have escaped into the atmosphere.

As shown in a previous study [1], these fugitive particles are typically small (<2.5 µm) and consist of amorphous material and a variety of crystalline phases, including: lime [CaO]; mullite [$Al_6Si_2O_{13}$]; anglesite [$PbSO_4$]; anhydrite [$CaSO_4$]; gunningite [$ZnSO_4{\cdot}H_2O$]; and yavapaiite [$KFe(SO_4)_2$]. The filters, however, also contain crystals that are larger than 2.5 µm. These larger crystals comprise: millosevichite [$Al_2(SO_4)_3$]; meta-aluminite [$Al_2(SO_4)(OH)_4{\cdot}5H_2O$]; tamarugite [$NaAl(SO_4)_2{\cdot}6H_2O$]; and members of the voltaite group [$K_2Me^{2+}{}_5Fe^{3+}{}_3Al(SO_4)_{12}{\cdot}18H_2O$, where Me^{2+} = Fe^{2+}, Mg, or Zn].

The voltaite-group phases are present on the filters as euhedral, mostly twinned crystals, ranging in size from a few µm to ~100 µm across. The chemical composition of the voltaite phases was found to depend on the type of fuel used: combustion of the coal+tire mixture led to the formation of homogeneous voltaite, which contains almost equal molar amounts of ZnO and FeO and only small amounts of MgO. Combustion of pure coal, however, led to formation of strongly zoned voltaite, characterized by a Mg-poor core rich in FeO and ZnO and two surrounding growth zones. The outer growth zone is nearly devoid of Zn, but contains similar molar amounts of FeO and MgO. It is concluded that the voltaite phases, like all other sulfate phases, crystallized from the flue gas upon cooling.

[1] Gieré, R., Blackford, M. & Smith, K. (2006) *Environ. Sci. Technol.*, **40**, 6235-6240.

Speciation of arsenic in brown-coal fly ashes from central Slovakia

Bolanz, R.M.[1*], Majzlan, J.[1], Jurkovič, L.[2] & Göttlicher, J.[3]
[1]Inst. of Geoscience, Friedrich-Schiller-University, Jena, Germany ([*]ralph.bolanz@uni-jena.de)
[2]Dept. of Geochemistry, Comenius University, Bratislava, Slovakia
[3]Inst. for Synchrotron Radiation, Karlsruhe Institute of Technology, Eggentein-Leopoldshafen, Germany

Neogeone brown coal seams in central Slovakia were contaminated by arsenic from volcanic-related hydrothermal fluids [1]. This coal is mined and burned for electric power generation until today. It contains on average 518 ppm As [2]. Fly ashes are disposed as waste products in uncovered ash impoundments where they interact with their surrounding environment. In 1965, an impoundment failure released approximately 1.5 million m^3 of As-rich fly ash into the Nitra river flood plain, thus contaminating 19,000 ha of mostly agricultural land. In our work, we investigated the speciation of arsenic in the fresh ash and in the 1965 ash mixed with soil. We combined graphite-furnace atomic absorption spectrometry (GF-AAS), electron microprobe analysis (EMPA) and synchrotron techniques (µXRD, µXRF, and µXANES) to identify the arsenic carriers. The completely digested samples revealed high As concentrations in the fresh ashes (1,411 ppm) and in the ashy soils (1,381 ppm). Sequential extractions after TESSIER et al. (1979) [3] hint at the affinity of As to Fe-Mn oxides and carbonates in the fresh ashes but only the affinity to Fe-Mn oxides in the ashy soils. In the fresh ashes, five constituents could be identified by EMPA and µXRD with the following average As_2O_5 concentrations: (i) Mineral fragments, mainly quartz and plagioclase, showed no As at all. (ii) Vesicular glasses are the main component of the fly ashes with 0.13 wt% As_2O_5. These particles hold presumably a considerable amount of the total As. The same counts for the unburned coal particles (iii) with 0.10 wt% As_2O_5. (iv) Spheroidal glasses are only accessory but reveal the highest As_2O_5 concentrations, on average 1.35 wt%. (v) Calcite veins occur sporadically in the unburned coal particles and contain 1.60 wt% As_2O_5. Within the ashy soils, the spheroidal glasses (0.44 wt% As_2O_5), unburned coal particles (0.46 wt% As_2O_5) and their calcite veins (0.33 wt% As_2O_5) reveal the highest As concentrations. Considering that the abundance of those ash-derived components is rather low in comparison to the fresh fly ashes, these components might have a subordinate role as As carriers in the soils. However, three additional constituents were identified in the ashy soils. Calcite grains and decomposing organic fragments show no As at all. Much more interesting is the matrix cementing the mineral grains. Although the As concentrations are rather low (0.05 wt% As_2O_5), the cement is ubiquitous and therefore carries the bulk of the arsenic in the ashy soils. The µXRF results show a strong spatial correlation between As and Ca in the fly ashes as well as As and Fe in the ashy soils. The µXANES-spectra reveal that most arsenic within the fly ash and ashy soils is bound as As^{5+}.

[1] Čech, F. & Petrík, F. (1972) *Miner. Slovaca*, **4**, 257-265. (in Slovak). [2] Keegan, T.J. et al. (2006) *Sci. Total Environ.*, **358**, 61-71. [3] Tessier, A., Campbell, P.G.C. & Bisson, M. (1979) *Anal. Chem.*, **51**, 844-851.

Composition and source of aerosols in Kraków (S Poland)

Wilczyńska-Michalik, W.[1*], Tyrała, L.[2], Borowiec, W.[3], Damrat, M.[2] & Michalik, M.[2]
[1]Inst. of Geography, Pedagogical University, Kraków, Poland ([*]wmichali@up.krakow.pl)
[2]Inst. of Geological Sciences, Jagiellonian University, Kraków, Poland
[3]Inst. of Geography and Spatial Management, Jagiellonian University, Kraków, Poland

High concentration of particulate matter (PM) in atmosphere in Kraków has always been a great concern of local and state authorities. Concentration of PM10 and PM2.5 in air often exceeds permissible values.

The study is based on single particles analysis. Morphology, chemical composition and size were determined using SEM-EDS method. Aerosols samples were collected on the Petrianov filters and transferred onto polycarbonate filters for SEM observations.

Quartz, feldspars and mica-like particles are abundant but irregular aluminosilicate particles of non-stoichiometric composition dominate. Spherical aluminosilicate particles are present in all samples. Carbonate particles (calcite, dolomite or non-stoichiometric Ca, Mg, Fe carbonates) are also common. Fe oxides, metallic iron, other metal-rich particles are present in numerous samples. Cr and Ni rich particles were noted only occasionally. Fe-rich particles are spherical or irregular. Na and Ca sulphates are common in numerous samples. Barite particles and Fe sulphate occur sporadically. Particles of mixed composition (sulphates and chlorides of Ca, Na, Mg, Fe) are abundant. Carbonaceous particles are relatively common in aerosol samples. Soot in form of fine-grained aggregates is a dominant type of the carbonaceous aerosol. Soot particles usually contain S and Cl. Biological particles (spores, pollen) are present in numerous samples. Seasonal variation in relative abundance of several types of particles is also determined. Soot and spherical aluminosilicate particles are very common in winter period (heating period) whereas biological particles occur in spring and summer. Composition and seasonal variation of aerosols is similar to those determined in earlier period [1].

It is difficult to distinguish anthropogenic and natural particles in the studied samples. A dominant part of aluminosilicate particles are devoid of characteristic features of their origin. Only in several cases morphology or composition of particles can be considered to be clear signature of their industrial origin (spherical aluminosilicate from coal fired power plants, spherical metallic Fe or Fe-oxide from power plants or iron metallurgy, Cr and Ni rich particles from metallurgical plants, soot from domestic furnaces).

The study of particles from local industrial sources (e.g. power plants, steel plant, cement production) indicates that local sources can be considered as very important. Transport and heating installations in private houses are an additional source.

Distant sources of aerosols are also significant but their role is difficult to recognize based on the obtained results.

[1] Kozak, K. et al. (1998) in Suchecki, T.T. & Zwoździak, J. (eds.) *Proceedings of II Intern. Scientific Conf. „Air protection in theory and applications”*. Polska Akademia Nauk, Instytut Podstaw Inżynierii Środowiska, Komitet Inżynierii Środowiska, *Prace i Studia*, **48**, 207-225.

Environmental study at a former military camp, Kiskunhalas (Hungary)

Baricza, Á., Pataki, A.*, Szabó, K.Zs. & Csaba, Sz.
Lithosphere Fluid Research Lab, Eötvös University, Budapest, Hungary (*bouboux@freemail.hu)

In our contribution we studied a former military barrack and yard in Kiskunhalas (Hungary) for a request to determine the local radiation and the level of radon because the owner wanted to reconstruct the building into a dormitory. Our goal was to make an assessment and ensure the probable radiation load.

During our in situ measurements we determined the gamma radiation with a gamma dozimeter in the three-storey building and in nine types of tiles used in the building. The results show the gamma radiation between 70-90±20 nSv/h in each floor and 123±32 nSv/h in the most active tile. We collected a gas silicate building material because indoor radon partially stems from the building [1] for measurements of HPGe gamma spectroscopy and defined the radium equivalent index (0.32) and Finnish activities (100 Bq/kg). We conducted relatively short-term indoor monitoring in building on 12 points by RAD7 and AlphaGUARD active detectors where the highest value was 111±42 Bq/m^3. The building isolation was unsatisfying; therefore, we took 2 drilling cores in the yard about 20 m from the building.

In course of labor measurements, we studied the collected soil samples in radon chambers and screened 4 samples in each drilling core for mineral separate to identify the potential radon sources. By the result of radon chambers, the highest radon activities concentration was 401±187 Bq/m^3 in a soil sample of one of the drilling cores derived from depth of 100-135 cm. The grain size distribution also indicates an anomaly here, being dominated by the courser grain size fractions. This layer also shows the highest U content (4.41 ppm) determined by gamma spectroscopy measurements. Scanning electronmicroscopy was applied to identify those grains which can be potential sources of radon. We have found grains of charcoal, coke and coal in all size ranges, which means that the examined particular layer contains allogenic materials, behind natural soil minerals, related to human activity. These organic substances easily include the Ra^{220} because this element can constitute strong complex with organic ligands [2]. To ensure that this soil sample has not any risk, we made a measurement in the soil with soil-gas probe. The result was 15500±1350 Bq/m^3 what corresponds to a medium risk [3]. The indoor radon and gamma concentration results show no any risk, neither the building material nor the drilling samples, except one soil sample. However, the risk is minimal because it is located deeply enough and has not a really high concentration of radon therefore the building studied is suitable for living.

[1] Németh, Cs. et. al. (2000) *J. Environ. Radioactv.*, **51**, 371-378. [2] International Atomic Energy Agency (1990) *The environmental behaviour of radium*, 1-446. [3] Kemski, J. et al. (2001) *Sci. Total Environ.*, **14**, 217-230.

Distribution of calcite and dolomite in alkaline lake sediments

Bozsó, G.* & Pál-Molnár, E.
Dept. of Mineralogy, Geochemistry and Petrology, University of Szeged, Hungary (*bozso.gabor@geo.u-szeged.hu)

The major aim of the present study is to investigate the processes which determine the vertical distribution of calcite and dolomite in anthropogenic alkaline lakes of different hydrology. The distribution of dolomite and carbonate among hypersaline conditions is usually affected by evaporation, CO_2 concentration generated by root respiration and the chemical properties of rain and groundwater [1].

In harmony with our aims, samples were collected from the territory of the Fehér Lake (Hungary) at two sites during the spring of 2007. The profile K is situated on a saline meadow (temporarily inundated, desiccated during the summer), while the profile S1 was deepened at a fish breeding lake with a permanent water cover (drained only for a month in April). In case of both sites, a 4 m deep and 10 cm wide (diameter) undisturbed coring was made. The mineralogical analysis of calcite and dolomite was made with a DRON UM-1 type X-ray diffractometer equipped with a Cu tube, using 35 kV excitation voltage and 20 mA anode current.

The calcite and dolomite distribution in the two studied profile is very different (Table 1). Concerning the profile K, calcite appears below a depth of 55 cm; underneath, its quantity can be considered more or less constant (20-25 %) and its concentration decreases back to 0 only at a depth of 195 cm. The vertical distribution of dolomite in the profile K is not in a close relation with calcite, as it appears only below 145 cm and its maximum (42 %) is right at 195 cm. The vertical gradient of calcite and dolomite in the profile S1 is very different when compared to the profile K. The highest concentrations of calcite can be found between 0 and 40 cm (43-50 %), underneath its quantity continuously decreases but from 65 cm it settles at a fairly constant 15 % ratio. In case of the profile S1, the distribution of dolomite and calcite is very similar. In the upper 100 cm, the quantity of dolomite is around 18-20 %, and by increasing depth its ratio decreases gradually.

Table 1: The amounts of calcite and dolomite in the profiles

Depth (cm)	Profile "K"		Profile "S1"	
	Calcite (%)	Dolomite (%)	Calcite (%)	Dolomite (%)
0	0	0	50	18
40	0	0	43	18
55	16	0	20	18
65	24	0	15	22
95	25	0	0	20
145	15	27	18	15
195	0	42	15	15
295	28	25	15	0
345	25	10	15	0

Consequently, the distribution of calcite and dolomite in the profile K is affected by a strong leaching process, as both minerals appear only in the deeper-lying strata. The permanent water cover at the profile S1 inhibits leaching, thus dolomite formation can be observed also close to the surface layers. Based on our results, we claim that the distribution of dolomite formed in a lacustrine environment is primarily determined by the distribution of calcite and the prevailing hydrological conditions.

[1] Molnár, B. et al. (1980) *Acta Miner. Petr. Szeged*, **24**, 315-337.

Geochemical atlas of soils and stream sediments of Santiago island, Cape Verde

Cabral Pinto, M.M.S.[1,2*], Hernandez, R.[1], Silva, E.A.F.[1], Silva, M.M.V.[2], Reis, P.A.[1], Rocha, F.[1], Dinis, P.A.[2], Inácio, M.[1], Prudêncio, M.I.[3], Marques, R.[3] & Patinha, C.A.[1],

[1]Geobiotec Center, University of Aveiro, Portugal
[2]Geociences Center, University of Coimbra, Portugal
([*]marinacp@ci.uc.pt)
[3]Nuclear and Technological Institute, Lisbon, Portugal

Climatic conditions and erosion are some of the natural problems of the Cape Verde archipelago. Furthermore, human influence on the surface environment has often proven to be inappropriate and pollutant. There is construction on soil fit for agriculture or forestry, dumping of solid or liquid materials in an inadequate manner, incorrect and intensive farming practices, the abuse of pesticides and fertilizers, watering with contaminated water, over-exploitation of aquifers in a manner that often leads to salinization. These factors cause innumerable consequences in terms of contamination of soil and both surface and subterranean water. Knowledge of the natural geochemical variability is essential for the proper resolution of economic, environmental, planning, medical and legal issues.

The need for building a database of georeferenced geochemical information that comprises the surface environment of the island of Santiago was the prime motivation for carrying out this study. A geochemical survey of 337 of stream sediment samples and 249 soil samples from the island of Santiago was conducted, following the guidelines of the International Project IGCP 259 not only at the sampling stage, but also in the subsequent stages of preparation, analysis, data treatment and mapping. Levels were determined, in the fraction < 2mm, of 36 elements: 9 major elements (Al, Ca, Fe, K, Mg, Mn, Na, P, Ti) and 27 trace elements (Ag, As, Au, B, Ba, Bi, Cd, Co, Cr, Cu, Ga, Hg, La, Mo, Ni, Pb, S, Sb, Sc, Se, Sr, Th, Tl, U, V, W, Zn), and total contents of REE.

Granulometric analyses were also carried out, and the mineralogical composition of about 25% of the soil and stream sediments samples was studied. 83 rock samples taken from various formations on the island of Santiago were also analysed, the levels of K_2O, Na_2O, $Fe_2O_{3(T)}$, MnO, Sc, Cr, Co, Zn, Ga, As, Br, Rb, Zr, Sb, Cs, Ba, Hf, Ta, W, Th and U and REE having been determined. The geochemical patterns obtained from spatial distribution maps were correlated with the nature of the parent rock, the soil type and also some sources of contamination. The interpretation of the results was carried out not only by observation of the geochemical maps, but also after statistical analysis of the data gathered, and supported by a wide range of available information. The use of Principal Component Analysis allowed associations between chemical elements to be perceived, whether geogenic or anthropogenic in origin. Spatial distribution maps of various multi-element indices of environmental importance were also drawn up, such as the Al/(Ca+Mg+K) Acidification Index, the Combi Index , the Environmental Risk Assessment Index, and the Enrichment/Contamination Indices for several groups of elements considered primary pollutant metals.

Control of pyrite oxidation for AMD by treatment agents

Choi, J.[1*], Ji, W.H.[2], Yang, J.S.[1], Lee, J.Y.[1] & Park, Y.T.[1]
[1]KIST Gangneung Institute, Gangneung, South Korea
([*]jchoi@kist.re.kr)
[2]MIRECO, Seoul, South Korea

In this study, several treatment agents have been applied to control acid mine drainage (AMD) from an abandoned coal mine in South Korea. Five natural minerals (calcite, dolomite, apatite, birnessite, smectite) and 3 chemicals (KH_2PO_4, MgO, $KMnO_4$) were selected as treatment agents for reducing the oxidation of the iron sulfide (pyrite) minerals which occur in the coal mine. For measuring the acid neutralizing capacity (ANC), net acid generation (NCG), and maximum potential acidity (MPA), ASTM D 5744-07 method was used. Among the treatment agents, both MgO and $KMnO_4$ showed a higher ability of reacting with the surface of pyrite.

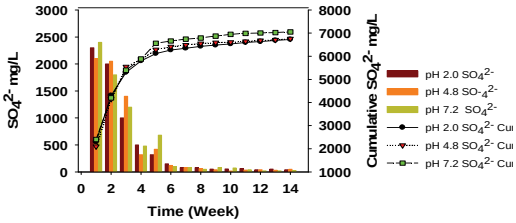

Fig. 1: The cumulative concentration of SO_4^{2-} at the coal mine.

The optimal conditions of coating with chemicals are 0.01 M $MgO+H_2O_2+NaOAc$ and $KMnO_4+H_2O_2+NaOAc$ at the initial pH of 6.0, respectively. Hydrogen peroxide and NaOAc were required to generate surface oxidation of pyrite and pH maintaining around 6.0, respectively.

Contamination level of arsenic and heavy metals, their bioaccessibility and risk assessment in the vicinity of the Songcheon and the Dongjung gold mines in Korea

Chon, H.T.[1*], Chung, E.H.[1], Lim, H.S.[1], Lee, J.S.[2] & Sager, M.[3]
[1]Dept. of Energy Resources Engineering, Seoul National University, Seoul, Korea ([*]chon@snu.ac.kr)
[2]Institute of Mine Reclamation Technology, Mine Reclamation Corporation, Seoul, Korea
[3]Austrian Agency for Health and Food Safety, Vienna, Austria

Gold mining industry in Korea was most extensive during the early and middle 20th century, and most of gold mines have been closed during 1970s – 1990s without any environmental treatment of the mine sites. In this paper, two gold-silver mines, the Songcheon (SC) and the Dongjung (DJ) mines, were selected in order 1) to investigate the contamination levels and dispersion patterns of arsenic and heavy metals (Cd, Cu, Pb, Zn and Hg) in soils, crop plants and water in the vicinity of the mine sites, 2) to estimate the bioaccessible fractions of arsenic and metals in soils and plants by using the SBET (Simple Bioavailability Extraction Test), and the EHS (Extraction of Heavy metals in Stomach and small intestine) test, and 3) to assess human health risk for the residents around the mine areas.

Contamination levels of As and heavy metals in tailings, soils, sediment, water and crop plants were determined and plotted around the mine sites, and the pollution index (PI) of multi-elements in soil was proposed in this study. Arsenate was more predominant than arsenite in water collected near the SC mine sites and the concentration level of arsenate was higher than 50 μg/L. Arsenic concentration in the fingernails of the residents around the DJ mine was 12 mg/kg. The main contamination sources of As, Cd, Cu, Pb, and Zn are from tailings and their effluents according to ore and gangue mineralogy. The contamination level of Hg is almost negligible except for some mine tailings. The pathways of metals from tailings – agricultural soils - surface and ground water – annual crops - to finally human were suggested.

From the EHS test, bioaccessible contents of metals in soils and crop plants were determined and risk characterization was estimated. The hazard index (HI) value of the SC and the DJ mines was 16 and 46, respectively, and particularly hazard quotient (HQ) value of As of each mine was 15 and 23, respectively. The cancer risk for As of each mine was estimated as 2.7 E-03 and 4.0 E-03, respectively, which exceed the acceptable risk (1 in 100,000) for regulatory purposes. But the SBET results showed some different HI and cancer risk values of each mine.

Mineral composition of PM_{10} particles from the atmosphere near the coal mine power plant: Veliki Crljeni (Serbia)

Cvetković, Ž.[1], Logar, M.[2*] & Erić, S.[2]
[1]Geological Institute of Serbia, Belgrade, Serbia
[2]Faculty of Mining and Geology, University of Belgrade, Serbia
([*]milogar@eunet.yu)

This research contribution is a part of a one-year project to collect particles from the atmosphere in the vicinity of power plants and the surface coal mine in the Kolubara basin and to analyze their mineral composition. Air samples for PM10 (particles of the matter with aerodynamic diameter smaller than 10 microns) particles were collected on filter paper using an appropriate instrument during February and March 2007. Measured concentrations of PM10 are gravimetrically certain. Even though the average monthly concentration is 89.6 μg/m, 30.8% of measurements are above recommended daily limits of 120 μg/m3 for PM10.

SEM examination showed that the collected samples of dust from the surrounding coal mines and power plants consist largely of the association of minerals and waste particles from vehicle exhaust (Fig. 1). Mineral composition of PM10 particles is complex, heterogeneous and constantly changing. However, the association shown in the picture is characteristic and similar as those reported in the literature [1]. In addition to the minerals shown, almost always present are quartz and feldspars as confirmed by X-ray powder diffraction.

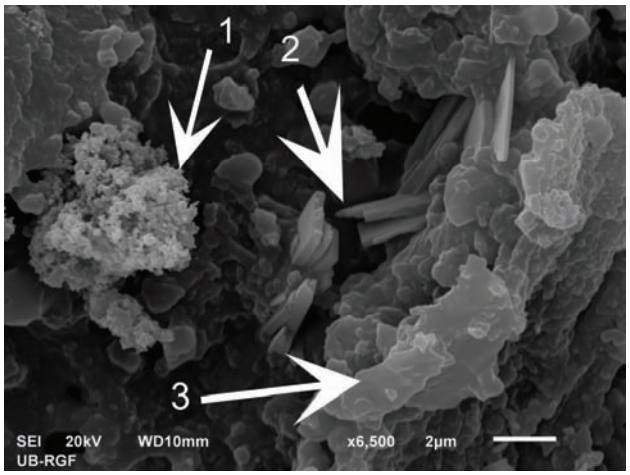

Fig. 1: Atmospheric particles (SEM): 1- particles from vehicle exhaust, 2- gypsum, 3- clay particles.

This paper shows that the concentration and mineral composition of atmospheric particles from the mine and the power plant is crucial for the fractions that are inhaled and for the identification of potentially hazardous components within the PM10.

[1] Tasic, M. et al. (2007) *J. Phys.: Conf. Series*, **71**, 11-13.

Authigenic Fe-minerals as indicators of the Late Permian and Early Triassic depositional conditions (Velebit Mt., Croatia)

Fio, K.[1*], Posilović, H.[1], Sremac, J.[1], Vlahović, I.[2], Bermanec, V.[1] & Velić, I.[3]
[1]Faculty of Science, University of Zagreb, Croatia
([*]karmen.fio@geol.pmf.hr)
[2]Faculty of Mining, Geology and Petroleum Engineering, University of Zagreb, Croatia
[3]Croatian Geological Survey, Zagreb, Croatia

The uppermost Permian deposits in the Velebit Mt. area (Croatia) are characterized by the stratigraphic break caused by emergence and subsequent transgression which continued through the Permian–Triassic Boundary (PTB) into the Early Triassic. Two informal lithologic units can be distinguished – Transitional Dolomite (TD), relatively rich in fossils, and Sandy Dolomite (SD), characterized by recrystallized grains, scarce fossils, and enhanced input of terrigenous siliciclastic material [1,2].

Selected TD and SD samples were disintegrated, or cut and polished and analyzed by optical microscopy, SEM, EDS, and XRD. Preliminary studies of the authigenic Fe-minerals found in the TD and SD units have shown characteristic mineral associations connected to the changes in the depositional environment. Fossiliferous TD deposits contain randomly dispersed red hematite grains. Highly recrystallized SD deposits above the lithologic change only occasionally contain hematite. Further up in the SD unit, due to the increased siliciclastic input and scarce fossils after the PTB, iron oxides form hematite, identical as in the TD unit, and magnetite. Magnetite, in framboidal form, in places accompanied with larger cubic crystals, is confined to recrystallized calcite and do not appear in the dolomite. The interstices between framboid microcrystals are filled with calcite; some magnetite hexahedra intergrow with calcite rhombohedra or contain calcite crystals.

Fine granulation, random dispersion, and association with fossil remains imply early diagenetic origin of hematite, when pore waters were more oxygenated and iron migrated by diffusion and not by pore water flow. Magnetite was formed during late diagenesis when more oxygen depleted waters penetrated into the sediment and mobilized iron from hematite. Locally concentrated magnetite suggests ion migration with pore water flow. Mineral stability fields of hematite and magnetite in an iron–carbonate–water system display magnetite as dominant mineral at high pH and low Eh conditions. In the absence of oxygen and at the high pH, precipitation was driven through OH^- addition. As precipitation reduces OH^- concentration and lowers pH, a small amount of carbonates was dissolved and restored equilibrium conditions within a solution.

[1] Salopek, M. (1948) *Nat. Sci. Yug. Acad. Sci. Art*, 101-143.
[2] Fio, K. et al. (submitted)

Ferromagnetic mineralogy of dust accumulated on *Nerium oleander* leaves in the cities of Praia, Cape Verde, and Coimbra, central Portugal

Gomes, C.R.[1,5*], Rocha, A.F.[2], Gomes, E.C.[3,5] & Pereira, A.[4,5]
[1]Centre for Geophysics (CG), University of Coimbra, Portugal
[2]Lousã Secondary School, Lousã, Portugal
[3]Geosciences Centre (GC), University of Coimbra, Portugal
[4]IMAR, University of Coimbra, Portugal
[5]Earth Sciences Dept., University of Coimbra, Portugal
([*]romualdo@dct.uc.pt)

Atmospheric dust particles are a mixture of organic and inorganic materials, components of natural and antropic origin. Some of the inorganic particles are ferromagnetic *s.l.* and easily identified by their magnetic properties. In the last decade, some studies have been done in order to characterize airborne dust particles and especially those accumulated on plant leaves, particularly *Nerium oleander* leaves, of the urban area of Coimbra. Magnetic parameters of leaves have been interpreted to characterize ferromagnetic structures, their composition, size and sources. In Coimbra these ferromagnetic particles have been attributed to the vehicular traffic. The main goal of the present study is to compare ferromagnetic mineralogy of urban dust accumulated on the *Nerium oleander* leaves samples from the cities of Praia and Coimbra. Sampling of *Nerium oleander* was done on the 10th and 11th of April 2009. The samples which were taken in Coimbra are from 12 of the most polluted sites, identified in previous studies. Magnetic parameters (isothermal remanent magnetization (IRM), at 1 T, -25 mT, -100 mT and S-ratios) of sampled plant leaves were measured and determined using a pulse magnetizer and a Minispin magnetometer (Molspin). The mineralogical characterization was performed by S-ratios and SEM with an integrated EDS microanalysis system. The size of particles on the surface of plant leaves is between 50 μm and less than 1μm. The IRM_{1T} values measured were normalized for leaf surface area and were in the range $125.00x10^{-6}$ - $844.00x10^{-6}$ A, for samples of Praia, and $24.00x10^{-6}$ - $310.00x10^{-6}$ A, for samples of Coimbra. Mean values are $342.00x10^{-6}$ and $85.80x10^{-6}$ A, respectively. Praia's mean value is 4 times higher than Coimbra's value. These different mean values can be interpreted considering that the SEM images show that the density of particles distribution is higher for samples from Praia, probably due to the drier climate in Cape Verde. These samples show essentially irregular and angular particles and rare spherical structures. The latter are relatively abundant in Coimbra. Some of these ferromagnetic particles from Praia samples (Fig. 1a) have a natural origin in Santiago Island substrate rocks, mainly in basalts. Irregular ferromagnetic particles are also present in Coimbra's samples (Fig. 1b) and they could be either anthropogenic or geogenic. These particles were identified as magnetite-like particles considering the S_{-300} values (0.98 from Praia and Coimbra's samples). Elemental mapping shows that Si, Ca, Fe, and Al are the most abundant elements on dust particles, reflecting the bedrock mineralogy and also the contribution of foreign dust, mainly from Sahara.

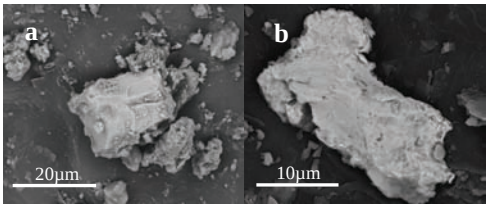

Fig. 1: SEM images of iron oxides from Praia a) (EDS: Fe, Ti, Si, Al, Mg, Ca) and Coimbra dust b) (EDS: Fe, C, Si, Ca).

Mineralogy and magnetic parameters of dust accumulated on *Nerium oleander* leaves in the city of Coimbra, central Portugal

Gomes, E.M.C.[1,2*], Saragoça, C.S.[2] & Gomes, C.S.R.[2,3]
[1]Geosciences Centre (GC), University of Coimbra, Portugal ([*]egomes@dct.uc.pt)
[2]Earth Sciences Dept., University of Coimbra, Portugal
[3]Centre for Geophysics (CG), University of Coimbra, Portugal

The purpose of this study is to characterize the mineralogy of urban dust accumulated on *Nerium oleander* leaves and to relate the mineralogical composition to magnetic parameters of leaves in order to recognize source origins.

Sampling of *Nerium oleander* leaves was done on the 4th of July 2007 in 122 sites in the urban area of Coimbra. Magnetic parameters (isothermal remanent magnetization (IRM), at 1 T, -25 mT, -100 mT and S-ratios) of sampled plant leaves were measured and determined. The IRM_{1T} values obtained were in the range $10.1x10^{-6}$-$172.2x10^{-6}$ $A.m^2$. Considering that IRM_{1T} values are proxies of pollution levels and allow the identification of pollution hot spots, plant leaves with higher values of IRM were used to study particles morphology, size, and chemical composition.

The mineralogical characterization was performed by S-ratios values and SEM with an EDS microanalysis system. Particle size on the leaves surface is between 50 µm and less than 1 µm. The major mineral components are quartz and phyllosilicates (mostly illite). Magnetite-like particles are also a major component. The S-ratios, S_{-25}, S_{-100}, and S_{-300} confirm the presence of these ferromagnetic structures. Less abundant mineral phases are calcite, calcium sulphate, and halite. Quartz particles are angular to subangular and range from 30 µm to less than 5 µm. Illite may appear covering spherical particles (Fig. 1a) or as aggregates exhibiting a vesicular texture. These aggregates reach 50 µm as maximum size. Individual grains are usually platy. The chemical composition of these clay particles includes Si, Al, K, Fe, Mg, and Na. Ferromagnetic particles are spherical to irregular. The mean size of these spherical particles is about 10 µm but the irregular ones can reach 30 µm. However, S-ratios indicate particles with diameter less than 10 µm. Some show cortical texture (Fig. 1b), with contours. Others seem to be built by stacking of tetrahedral and half-octahedral units. The X-ray analysis showed that these particles are composed of Fe, as a major element, with minor Ca, Cr, and Mn concentrations. Some particles, mainly aggregates, contain a group of elements in such proportions that cannot be attributed to a known mineral. These particles may show major concentrations of Fe, Cu, Ti, and Pt and minor Mg. Biological particles consist of pollen grains, sometimes covered by fine and ultra-fine mineral particles. Elemental mapping shows that Si, Ca, Fe, and Al are the most abundant elements on dust particles.

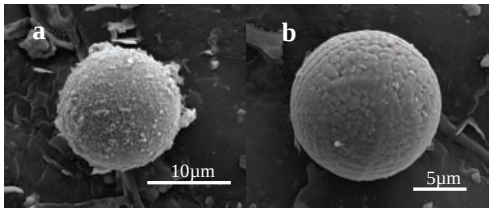

Fig. 1: SEM image of: **a)** illite covering a spherical particle (EDS: Si,Al,K,Fe,Na,Mg) and **b)** ferromagnetic dust particle (EDS: Fe,Cr,Mn).

Considering that Coimbra is a non-industrial city, located at about 40 km from the Atlantic coast, the main source of dust particulates found on *Nerium oleander* leaves surface may be substrate rocks, soil, and vehicular emissions. Quartz and phyllosilicates are terrigenous minerals. Most of the ferromagnetic particles are ascribed to the traffic pollution.

Environmental geochemical study at vicinity of a thorium anomaly in the Buda Mts. (Hungary)

Grosch, M.[1*], Müller, M.[1], Szabó, Zs.[1], Boros, Á.[1,2] & Szabó, Cs.[1]
[1]Lithosphere Fluid Research Lab, Eötvös University, Budapest, Hungary ([*]hun.grosch@gmail.com)
[2]BGT Hungaria Environmental Technology Ltd., Budapest, Hungary

The thorium anomaly of Nagy Kopasz hill (Buda Mts., Hungary) has been studied since the 1950s. The former Mecsek Ore-mining Company heightened test trenches, prospect pits and drillings on the area. Study of the drilling cores and air borne gamma mapping showed a significant thorium anomaly, as well as rare earth element and Y indication [1,2]. Our major goals were to perform a pilot study by use of physical and geochemical methods on one of the prospect pits and its damp to assess the environmental impact of this portion of the thorium anomaly.

Based on in-situ gamma dose rate measurements, the dump showed maximum 2730 nSv/h, which is ten times higher than the average background value (70-90 nSv/h). Two soil samples were collected from the dump for additional laboratory investigations. Gamma-spectroscopy analysis was carried out, and thorium and uranium activity concentrations were determined, which show high content of thorium (max. 143±8 ppm), and low content of uranium (max. 0.26±0.02 ppm). Another part of the soil samples was sieved and divided into seven grain size fractions. Two grain size fractions were selected and grains were separated on the basis of morphology and color for scanning electron microscopy (SEM-EDS) study to define the content of thorium in the selected grains and identify minerals.

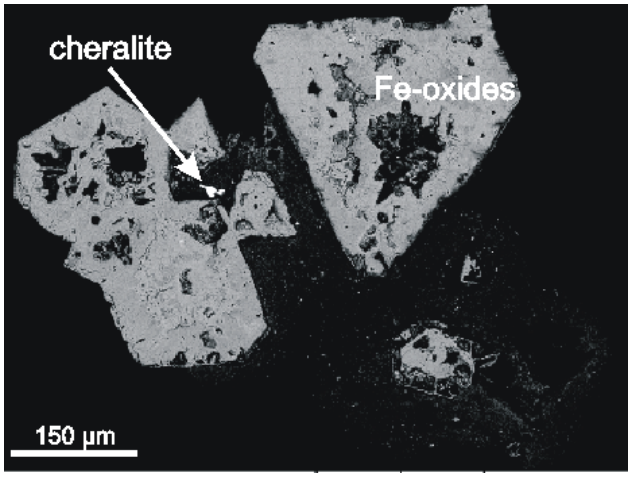

Fig. 1: SEM image with cheralite and Fe rich oxide minerals.

The high Th-bearing grains have been identified as mineral of cheralite (Fig. 1), which is always connected to the presence of Fe-oxide minerals and clay minerals. Due to the fact that the dump is rich in clay minerals, the local thorium anomaly does not mean a potential risk as it cannot be mobilized.

[1] Wéber, B. (1962) *Magyar Állami Földtani Intézet* **XCII**, 455-457. [2] Wéber, B. (2002) *Közlemények a magyarországi ásványi nyersanyagok történetéből* **XIII**, 103-121.

Environmental mineral formation in a Medieval (1664) bomb from Zrínyi-Újvár, Őrtilos, Hungary

Jánosi, M.[1*], Weiszburg, T.G.[1], Márialigeti, K.[2], Vajna, B.[2] & Négyesi, L.[3]
[1]Dept. of Mineralogy, Eötvös L. University, Budapest, Hungary
([*]janosim@vipmail.hu)
[2]Dept. of Microbiology, Eötvös L. University, Budapest, Hungary
[3]Museum of Military History, Budapest, Hungary

The Hungarian Museum of Military History (Budapest) owns unexploded cast iron bombs, collected during the 2006 year excavations near Belezna and Őrtilos villages, on the banks of river Mura, at the scarcely surviving remnants of an adobe fortress (Zrínyi-Újvár, Novi Zrin). The castle was built in 1661 and was then demolished in 1664 during a Turkish siege.

The bombs were found fully intact, their internal parts communicated with the neighbouring soil/sediments only via a wooden plug, serving originally as fuse. Such bombs contained originally KNO_3, sulphur and charcoal. Recently two bombs were halved in order to perform combined mineralogical and microbiological studies for understanding the alteration processes of the original gunpowder filling.

In the larger bomb's half (external diameter 265 mm, Fig. 1 left) more or less concentric yellow, white and brown colour zones are visible, starting from the fuse. 6 subsamples were separated and studied by X-ray powder diffraction (XRD) and SEM+EDX. The yellow part proved to be jarosite. Both the c_0 unit cell parameter, 17.224(5) Å, sensitive for the large cation substitution, and the a_0 parameter 7.2998(6) Å, sensitive for the Fe-Al substitution indicate no Na, H_3O or Al in jarosite. SEM+EDX confirmed that observation, thus jarosite in the bomb is practically pure end-member jarosite.

The main mass of the bomb infilling is goethite. Other identified minerals are: rozenite, mohrite, siderite and sulphur, as relic of the gunpowder.

Fig. 1: Cut surface of the bombs, 265 mm diameter (left), 171 mm diameter (right).

In the smaller bomb's half (external diameter 171 mm, Fig. 1 right) goethite, jarosite and rozenite minerals and sulphur were identified. The bombs were exposed to oxygen, water and most probably, certain colonies of bacteria (utilising N and S), leading to the formation of the identified sulphates.

Secondary Sb mineral phases from abandoned Sb deposit Dúbrava (Slovakia)

Klimko, T.[*], Lalinská, B. & Chovan, M.
Dept. of Mineralogy & Petrology, Faculty of Natural Sciences, Comenius University, Bratislava, Slovakia
([*]klimko@fns.uniba.sk)

Secondary Sb mineral phases were studied as the products of oxidation of the sulphide minerals in the environment of mine tailings, dumps and soils at the abandoned Sb deposit Dúbrava in the eastern part of the Low Tatra Mts. in Slovakia. The mine tailings contain a high amount of toxic elements (up to 3.46 g/kg of Sb and up to 0.38 g/kg of As). The extent of the old dumps is also significant and contamination of the soils at the deposit is high (up to 9.62 g/kg of Sb and up to 0.93 g/kg of As). Therefore, these sites are significant sources of toxic elements (mainly Sb and As) that may migrate into the surrounding environment.

Pyrite, arsenopyrite and stibnite are the dominant primary sulphide minerals in the tailings and the soils. As a result of their oxidation, a high amount of secondary mineral phases with a variable content of Fe, Sb and As is created. From the mineralogical point of view, these phases are mostly Fe oxides/oxyhydroxides (ox./oxyh.), Fe(Sb) ox./oxyh. (Fe>Sb) and Sb(Fe) ox./oxyh. (Sb>Fe). Probably due to observed rapid decomposition of stibnite, these minerals often contain a high amount of Sb incorporated in their structures.

Besides, the main secondary products of sulphide oxidation in the environment of the tailings and the soils are weathering rims on the pyrite and the arsenopyrite crystals that are formed by Fe ox./oxyh.. The rims on pyrite have high content of Fe (up to 63.93 wt. %) and often significant content of Sb (up to 7.75 wt. %) and As (up to 3.63 wt. %). The rims on arsenopyrite contain up to 60.06 wt. % of Fe, up to 7.01 wt. % of Sb and up to 19.87 wt. % of As. Additionally, Sb as well as As binds in the oxidation rims with a concentration gradient from the edge of the rim to its contact with the primary sulphide.

However, the more important secondary min. phases in the process of distribution of toxic elements are the Fe(Sb) and Sb(Fe) ox./oxyh. with high content of Sb. These minerals are mostly created by crystallization from pore solutions in the environment of the tailings and the soils *in situ*. The crystals of Fe(Sb) and also Sb(Fe) ox./oxyh. are often chemically zoned, cracked and have sinter character. The WDS analyses proved increased concentration of Sb in the light zones, on the other hand decreased concentration of Fe in these zones. The content of Fe in Fe(Sb) ox./oxyh. is up to 62.82 wt. %, the content of Sb is up to 27.95 wt. % and As is up to 4.29 wt. %. Sb(Fe) ox./oxyh. have high content of Sb (up to 61.34 wt. %) and lower content of Fe (up to 27.22 wt. %). Content of As in these phases is usually low (up to 1.26 wt. %). In some cases, phases with significant content of Ca (up to 9.88 wt. %) were identified. In the environment of the old dumps the secondary Sb mineral phases are created by oxidation of the primary stibnite in the forms of thin films and crusts. The chemical composition of these phases correspondents to the minerals stibiconite (up to 69.50 wt. % of Sb) and romeite (up to 52.17 wt. % of Sb and up to 7.77 wt. % of Ca). This was also confirmed by XRD diffraction.

Observed results show the high affinity of As to Fe ox./oxyh. and a different behaviour of Sb, as it precipitates in the form of Sb(Fe) ox./oxyh. from pore solutions. Similar differences in As and Sb mobility were shown by sequence analyses of tailing material and stream sediments at the Dúbrava locality.

Acknowledgements: This work was supported by Slovak Research and Development Agency under the contract No. APVV-0268-06.

Unusual green Cr-rich smectite from Suweileh area, Jordan

Khoury, H.N.* & Al-Zoubi, A.S.Cr.
Dept. of Geology, University of Jordan, Amman, Jordan
(*khouryhn@ju.edu.jo)

In Jordan the green soft earthy volkonskoite is mainly associated with travertine of Pleistocene age. The chromium content in volkonskoite is responsible for the green color of the travertine. Volkonskoite exists as a filling material in cavities, voids, fractures and replacing pre-existing smectite.

A new green earthy clay locality is found in Suweileh Area, near Amman, Jordan. The green clay crops out at the surface and is found along bedding planes and filling voids and fractures in the limestone and phosphorite beds of Upper Cretaceous. The petrographic and mineralogical investigations have revealed that the green clay from Suweileh area is Cr-smectite with the structural formula: $(Ca_{0.30}\,Na_{0.23})\,(Al_{0.47}\,Cr_{0.63}\,Fe_{0.13}\,Mg_{0.66}\,Zn_{0.06}\,Ti_{0.03})\,(Si_{3.88}\,Al_{0.12})\,O_{10}\,(OH)_2$.

The infiltration of highly alkaline water through the combusted bituminous zone had led to leaching of Cr^{3+} and the precipitation of Cr-rich smectite in the Phosphorite Unit.

Suweileh volkonskoite is similar in structure and origin to that found in central Jordan [1].

[1] Khoury, H. et al. (1984) *Clay Mineral.*, **19**, 43-57.

Texture of calcium oxalates in human urinary stones

Kořistková, T.[1] & Leichmann, J.[2]
[1]Laboratory Specializing in Urinary Stones Analyses, Calculi®, Brno, Czech Republic (*calculi@calculi.cz)
[2]Dept. of Geological Sciences, Faculty of Science, Masaryk University, Brno, Czech Republic

We investigated the textures of urinary stones formed by calcium oxalate monohydrate (whewellite), calcium oxalate dihydrate (weddellite) and apatite. We selected two typical stones with different ratio of weddellite, whewellite and apatite. We focused on the role of apatite in forming these textures. The methods employed in our study were scanning electron microscopy (SEM, JEOL electron microscope), electron microprobe (EMP, CAMECA SX100) and polarised-light microscopy.

The first observed stone consisted approximately from 50% apatite, 50% whewellite, and traces of weddellite. The apatite fills up the pores and caverns or it is arranged in continuous layers. There is no sharp boundary between the oxalates and the apatite at some contact of those phases. Apatite infiltrates into oxalates locally. There are also the relics of oxalates in apatite.

The other stone consisted from 90% whewellite, and 10% weddellite, with traces of apatite. In this case, we have also observed similar dissolution texture of oxalates, but without apatite infiltration.

Dissolution textures in oxalates are caused by dehydration and transformation of weddellite into whewellite. The layers of apatite correspond to the change in the crystallization conditions, probably with a higher activity of phosphate. Apatite fills hollows in the aggregates of the oxalates.

Metal sorption on coal mine drainage sludge

Lee, H.E.[1], Choi, S.Y.[1], Doan, D.H.[1], Oh, S.G.[2,3], Lee, J.Y.[3], Sung, Y.H.[2] & Lee, Y.J.[1*]
[1]Dept. of Earth and Environmental Sciences, Korea University, Seoul, Korea (*youngjlee@korea.ac.kr)
[2]Development and Environment Team, Korea Resources Corporation, Seoul, Korea
[3]Dept. of Environmental Engineering, University of Seoul, Seoul, Korea

Coal mine drainage sludge (CMDS), with special interest as recycling products with rich mineral resources, has been tested as an effective sorbent for sorption of different metals. Development and understanding of mechanism(s) of metal uptake by effective sorbents like CMDS is essential for predicting the fate and transport of toxic metals in environments.

Zn sorption on CMDS have been investigated systematically to determine the mechanism(s) of Zn uptake by CMDS collected from Ham-Baek mine site and Ham-Tae mine site, South Korea over a wide range of pH and Zn concentration. These mine sludges were characterized by various techniques, and schwertmannite was also synthesized to compare with these sludges. XRF results show that both Ham-Baek (HB) and Ham-Tae (HT) sludges have an iron oxide as one of the major components. However, XRD indicates that HT sludge is mainly composed of iron (oxy)hydroxides such as goethite whereas HB sludge is composed of an iron sulfate mineral like schwertmannite.

Sorption of Zn on the HB and HT sludges, and the synthesized schwertmannite increases with increasing concentration of zinc at pH 4.0. At pH 7.0, however, the sorption rapidly increases, levels off, and then followed by little changes showing Langmuir sorption behavior. Results also show that Zn sorption on the two sludges and the synthesized schwertmannite increases with increasing concentration of the background electrolyte, suggesting that physicochemical properties of these minerals are likely changed by increasing the ionic strength at the mineral-water interface.

Forming mechanism and geological significance of glauconite in the Cretaceous Xiala section from Zanda, southwestern Tibet of China

Li, X.*, Cai, Y., Hu, X. & Huang, Z.
State Key Laboratory of Mineral Deposits Research, School of Earth Sciences and Engineering, Nanjing University, Nanjing, China (*lixiang_503@163.com)

Glaucony as a typical facies mineral formed at the water-sediment interface with a low sedimentation rate. Glaucony, especially evolved potassium-rich, is the only mineral facies that can give the age of a stratum without volcanic intrusion or well-preserved fossils. Up to date, previous researches were mainly focused on the origin and geological significance extracted from its host rock. None or less attention was brought to its forming mechanism.

A suite of glauconitic sandstone and limestone was outcropped in Xiala section from Zanda, southwestern Tibet of China. Three glauconitic samples, XL33, 34 and 35 were collected at this section. To determine the habit, mineralogy and chemistry of this glauconitic mineral, we carried out the observation under both petrographical microscope and Scanning Electron Microscope (SEM), and the analysis by X-ray diffractometry (XRD) and electron microprobe (EMP) on glauconite in the thin section and hand-picked sample, respectively. Furthermore, we also investigated the samples from the underlying strata which contain no or a few glauconite grains.

XRD pattern of purified glauconitic mineral shows that the basal lattice spacing (d_{001}, ~1nm) is sharp and symmetrical, indicating low content of swelling layer (<10%). The present of other peaks at 0.435($11\bar{1}$), 0.364 ($11\bar{2}$), 0.310 (112) shows that this glauconite has an ordered 1*M* mica-like structure. The EPMA result demonstrates that the content of K_2O is in the range of 6.93-8.30 %, with an average 7.86%. This suggests that the glauconite is highly evolved. Furthermore, there is no correlation between K_2O and Fe_2O_3 in three samples but both XL34 and XL35 show a negative correlation between Al and Fe^{3+} in octahedron.

According to the observation carried under both petrographical and SEM, the glauconite grains were constructed by microslabs of glauconite with the size of several microns. The occurrence of sparry calcite as rims on the periphery of glauconite grains and irregular contour of glauconite grains in glauconitic sandstone suggest their autogenic origin. Petrographical observation shows that glauconite gains closely coexist with detrital quartz in sample XL35. Furthermore, the chemical variation of sample XL35 is similar to XL34 with respect to the correlation between Al and Fe^{3+} in glaunocite grains. These suggest that the glauconite grains in limestone may come from the underlying glauconic sandstone.

As it illustrated in the SEM images, the glauconite grains in the sandstone were well-preserved the shape of debris and plenty of pore among the microslabs. These may suggest that the forming of glauconite was in an open but very quiet environment, and controlled by the dissolution-coprecipitation mechanism. The iron incorporated in the structure of glauconitic mineral come from the iron-bearing minerals while the potassium is supplied by the dissolution of potassium-bearing mineral. The open and quiet environment may be associated with transgression. This may relate to the last break-up of the Indian continent from the Australian-Antarctic continent during the Early Cretaceous.

Utilization of electrochemical methods for monitoring pyrite oxidation by *Thiobacillus ferrooxidans*

Liu Yun[1*], Dang Zhi[1,2] & Shu Xiaohua[1]
[1]School of Environmental Science and Engineering, South China University of Technology, Higher Education Mega Center, Guangzhou, China (*liuyunscut@163.com)
[2]The Key Lab of Pollution Control and Ecosystem Restoration in Industry Clusters, Ministry of Education, Guangzhou, China

In this work, the monitoring of the bacterial and chemical dissolution of pyrite was evaluated using Tafel polarization curves and electrochemical impedance spectroscopy (EIS). A pyrite-carbon paste electrode was utilized in an electrochemical cell in 9K culture medium with a 1% w/v pyrite concentrate as the sole energy source by replacing Fe^{2+} ions for different immersion times in the presence or absence of bacterium. The concentrations of Fe^{2+}, Fe^{3+} and total Fe had also been measured in the different systems during the leaching process. The results of Tafel polarization curves and the concentration of Fe^{3+} in leaching solutions indicated that the presence of bacteria enhances the corrosion process due to their ability to maintain an oxidizing environment rich in Fe^{3+} ion which increases the dissolution rate of pyrite comparing to the chemical attack. The total impedance of pyrite electrode measured in the presence of bacteria was much lower than in their absence, due to the acceleration of the mineral dissolution, because an oxidizing environment was maintained. The results also showed that the corrosion current density and impedance had been changed with leaching time, and these changes were in correspondence with the change of the concentration of Fe^{3+} in leaching solution. This proved that electrochemical methods could be used in a kinetic study of pyrite oxidation.

"Bacterioform" gold in placers and oxidation zones of Northern Uralian deposits (Russia)

Mayorova, T.P.*, Arteeva, T.A. & Filippov, V.N.
Institute of Geology, Komi Scientific Center, Uralian Branch, Russian Academy of Sciences, Syktyvkar, Russia
(*mayorova@geo.komisc.ru)

The problem of participation of microorganisms in dissolving, fining, reprecipitation and mineralization of primary gold and formation of secondary gold has been being discussed so far. However recent works [1] and others showed that "bacteriomorphous" structures on the grains of secondary gold from placers really resulted from the vital activity of bacteria; the attributes of such "bacteriomorphous" structures have been revealed. The direct evidences of biogenic nature of "bacteriomorphous" structures favored revision of previously obtained material on placer gold of the Northern Urals and drew special attention to determination of such structures in other gold-bearing objects of the territory.

In the Northern Urals the "bacteriomorphous" structures of various types were determined on detrital grains of gold from modern alluvial placers, detrital and secondary gold grains of Devonian paleoplacers, in oxidation zones of gold-quartz-sulphide deposits.

The placer gold of modern alluvial placers is characterized by the development of reniform bacteriomorphous structures, which were previously considered as a result of electrochemical dissolution of silver. In the oxidation zone of the gold-quartz-sulphide (arseno-pyrite) deposits the aggregates of filiform crystals were determined for the first time, in the intergranular space the bacterium-like pseudomorphs were found (Fig.1a). On the surface of crystalline grains the areas with reniform bacteriomorphous structures are often observed, where gold is purer (96–98 wt %), than in the bulk volume (58–76 wt %). Bacteriomorphous structures of various types – reniform, bacterium-like pseudomorphous (Fig.1b) and others – are determined both in detrital, and in authigenic sponge gold from Devonian paleoplacers widespread in the north of the Urals and in Timan.

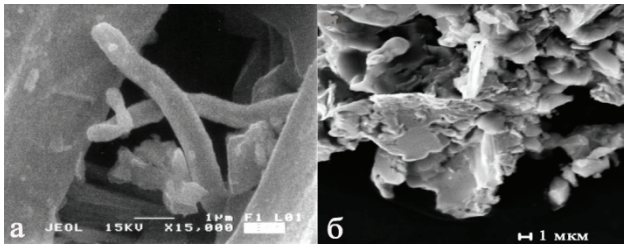

Fig. 1: Bacterium-like pseudomorphs of gold on filiform aggregates from oxidation zone (a) and on authigenic gold from paleoplacer (b).

The wide development of "bacteriomorphous" structures of gold, determined only by morphological characters, is just an indirect evidence of participation of bacteria in the transformation of primary gold in genetically different gold deposits of the Northern Urals; it requires direct evidences [1] and further investigations.

[1] Southam, G.et al. (2009) *Elements*, **5**, 303-307.

A study of cave sediments as a potential source of radon in Pál-völgyi show cave (Budapest, Hungary)

Nagy, H.É.[1,2*], Szabó, Cs.[1] & Horváth, Á.[2]
[1]Lithosphere Fluid Research Lab, Eötvös University, Budapest, Hungary (*jadzsa@gmail.com)
[2]Dept. of Atomic Physics, Eötvös University, Budapest, Hungary

Several radon measurements in the Pál-völgyi show cave (Budapest, Hungary) indicate high annual average radon concentration (1800 Bq/m^3) [1]. However, the source of this remarkable radon concentration is not understood, therefore the cave sediments as a potential radon source were studied.

Pál-völgy cave is situated in the Buda Hills, which is the NE part of the Transdanubian Central Range. The wall rock of the cave is Eocene Szépvölgy Limestone Formation. Above the limestone, the Eocene Buda marl and Oligocene Tard clay were deposited. A huge multiphase hydrothermal cave system developed in the Szépvölgy limestone resulted in a long-term composite palaeokarstic evolution lasting from the Late Eocene to the Quaternary [2].

The radon concentration in the cave air has been measured continuously by AlphaGUARD radon monitor and meteorological parameters (i.e., temperature, relative humidity, air pressure, wind speed and wind direction) are being measured simultaneously since November 2009 inside and outside the cave. The data show that the radon concentration in the cave air varies in a wide range and depends on the temperature difference between the indoor and outdoor air.

Clayish cave sediments were collected and their radon exhalation rate and radium content was defined in laboratory. Four clay samples derive from section the cave located in the Szépvölgy Limestone, and one sample derives from the cave developed in the Buda Marl.

Based on the results, the radon exhalation rate of the sediment from the Buda Marl is higher (12 Bq/kg) than the sediments located in the Szépvölgy Limestone (1.5-5 Bq/kg). This result is supported by simultaneous in situ radon measurement in three chambers of the cave performed by RAD 7 radon detector in the Buda Marl and in the Szépvölgy Limestone. Average radon concentration during the same period in the Buda Marl is 1096 Bq/m^3, and in the Szépvölgy Limestone in two different chambers 478 and 546, respectively.

However, thoron concentration of the soil gas is close to 0 in the clay sediments on the Buda Marl, and the radon/thoron exhalation rate in this sample is the highest one (E_{Rn-222}/E_{Rn-220}=7). Thus, it is possible that the clay sediment which covers the Buda Marl contains higher amount of uranium and less thorium than the cave clay sediment deposited on the Szépvölgy Limestone.

[1] Somlai, J. et al. (2009) *V. Magyar Radon Fórum Környezetvédelmi konferencia*, Pannon Egyetemi Kiadó **5**, 47-53. [2] Korpás, L. et al. (1999) *Sediment. Geol.*, **123**, 9-29.

The occurrence and speciation of arsenic in serpentinites in northern Vermont, USA

Niu, L.[1], Hattori, K.[1*], Takahashi, Y.[2] & Ryan, P.C.[3]
[1]Dept. of Earth Sciences, University of Ottawa, Ottawa, Ontario, Canada ([*]khattori@uottawa.ca)
[2]Dept. of Earth and Planetary Systems Science, Hiroshima University, Higashi-Hiroshima, Japan
[3]Geology Dept., Middlebury College, Middlebury, Vermont, USA

High concentrations of As are reported in ground waters and bedrocks in many parts of New England [1]. Ryan et al. [2] reported that hydrated ultramafic rocks contain high concentrations of As (up to 449 ppm in serpentinites and 1,100 ppm in talc-magnesite rocks) in northern Vermont. Altered ultramafic rocks are common in the Appalachians in New England. We investigated the occurrence of As in representative serpentinites from northern Vermont (103-450 ppm As in bulk rocks). The study includes the examination of polished-thin sections, electron microprobe analysis of minerals, mechanical separation of mineral fractions (ferrihydrite films, antigorite-rich fraction, magnetite-rich fraction), acid leaching and digestion of these fractions, and X-ray absorption spectroscopic study of As. Magnetite-rich fractions yielded high concentrations of As in hot HNO_3 digestion at 90 ºC. Brown films of ferrihydrite along cracks and on surfaces contain very low concentrations of As. Antigorite-rich fractions contain minor As (<50 ppm). X-ray absorption spectra of these fractions show that the As is predominantly +3 in magnetite- and antigorite- fractions.

Magnetite commonly forms a fine dusting in serpentine since the hydration of olivine releases Fe(II). Magnetite also forms rims of chromite grains during serpentinization. Our data suggest that As(III) in water was fixed in magnetite and minor amounts in serpentine during the hydration of ultramafic rocks. Our earlier study of serpentinites in northwestern Himalayas show that As (V) is fixed in serpentinites by replacing Si(IV) in antigorite [3]. The results of these studies suggest that hydrating ultramafic rocks are capable of fixing both As (III) and As(V) and that the speciation of As in serpentinites is controlled by the oxidation state of As in the hydrating fluids.

[1] Ayotte, J.D. et al. (2003) *Environ. Sci. Technol.*, **37,** 2075-2083. [2] Ryan, P.C. et al. (2009) *Abst. GSA Mtg*., **77**-**3**. [3] Hattori, K. et al. (2005) *Geochim. Cosmochim. Ac.*, **69**, 5585-5596.

Mineralogy and genesis of Mn carbonate ores of the Úrkút deposit, Hungary

Polgári, M.[1*], Hein, J.R.[2], Gutzmer, J.[3], Németh, T.[1], Hahn, T.[3], Müller, A.[1] & Vigh, T.[4]
[1]Inst. for Geochemical Research, Hungarian Academy of Sciences, Budapest, Hungary ([*]rodokrozit@gmail.com)
[2]USGS, Menlo Park, USA
[3]Dept. of Mineralogy, TU Bergakademie Freiberg, Germany
[4]Mangan Ltd, Úrkút, Hungary

An almost continuous stratigraphic section of the Jurassic (Lias) Úrkút black shale-hosted manganese ore body was subjected to careful mineralogical (X-ray powder diffractometry) and petrographic (light microscopy and SEM) studies, with the aim to determine the abundance and distribution of minerals in the microcrystalline ore and to document micro-textural evidence that may hold clues as to the origin of the finely laminated carbonate-rich manganese ore. A total of 112 oriented samples were collected through the extent of the ore-bearing succession for this purpose. These samples represent all macroscopically different ore types, distinguished mainly by their coloration in black, brown and green laminated carbonate-rich ore types. Light cream to pink coloured laminae composed mainly of rhodochrosite occur in all ore types; carbonate concretions up to dm in size, are formed of very similar carbonate-rich material.

Bulk ore samples and subsamples representing individual laminae can be categorized not only by colour, but by their mesoscopic appearance, including attributes such as lamina thickness and abundance of detrital grains.

Black, brown and green laminae are very dense, microcrystalline and rather uniform in mineralogical composition. The most abundant mineral is Ca-rhodochrosite in all ore types. Slight variations in abundance of celadonite (10Å phyllosilicate, green ore), goethite (brown ore), and manganite (black ore) cause the obvious color variations.

Light coloured carbonate-rich laminae are more compact and appear coarser grained than the enclosing darker (including green) laminae. The mineralogical composition of these carbonate-rich laminae is rather variable, with 5 distinct compositional groups, including (i) almost monomineralic Ca-rhodochrosite layers (ii) apatite-rich laminae (mainly fish remnants, and rarely secondary accumulations), (iii) Mn-bearing calcite-rich laminae (often coarse grained, biodetritus accumulation), (iv) barite-bearing laminae (often associated with Mn-bearing calcite, quartz, or apatite), (v) laminae rich in siliciclastic detritus, mainly quartz and K-feldspar.

Mineralogical and petrographic observations are used to suggest that the different laminated ore types owe their origin to a single genetic process. All the formations took place under neutrophylic, mildly alkaline pH. Obvious variations in color are thought to reflect slight changes in Eh during deposition and/or early diagenesis.

Acknowledgements: The study was supported by Hungarian Science Foundation (OTKA-NKTH No. K 68992).

Interaction of mineral dust with pollution and clouds: an individual-particle study of atmospheric aerosol from Saudi Arabia

Pósfai, M.[1*], Axisa, D.[2], Tompa, É.[1], Freney, E.[3], Bruintjes, R.[2] & Buseck, P.R.[3]
[1]Dept. of Earth and Environmental Sciences, University of Pannonia, Veszprém, Hungary ([*]mihaly.posfai@gmail.com)
[2]National Center for Atmospheric Research, Boulder, CO, USA
[3]School of Earth and Space Exploration, Arizona State University, AZ, USA

Aerosol particles from desert dust interact with cloud drops and influence climate on both regional and global scales. The Riyadh aerosol campaign was initiated to study the effects of dust particles on cloud-droplet nucleation and cloud properties. Here, we report the results of individual-particle studies of samples that were collected from an aircraft in April 2007. We used analytical transmission electron microscopy, including energy-dispersive X-ray spectrometry, electron diffraction, and imaging techniques for the morphological, chemical, and structural characterization of the particles.

During five days of sampling both dust storms and polluted background conditions were encountered. Under dusty conditions, the coarse (supermicrometer) fraction resembles freshly crushed rock. The particles consist almost exclusively of mineral dust and include common rock-forming minerals, among which clay minerals, particularly smectites are most abundant. Unaltered calcite grains also occur, indicating no significant atmospheric processing. The particles have no visible coatings and may contain only traces of sulfur. The fine (submicrometer) fraction is dominated by particles of anthropogenic origin, primarily ammonium sulfate (with variable organic coatings and with or without soot inclusions) and combustion-derived particles (mostly soot). In addition, submicrometer, iron-bearing clay particles also occur, many of which are internally mixed with ammonium sulfate, soot, or both.

Concerning the cloud nucleating ability of the observed particles, almost any type is likely to be effective as cloud condensation nuclei (CCN). Giant mineral aggregates, particularly those that include clay minerals, are wettable and large enough to be CCN. In the fine fraction, minerals partly reacted and coagulated with ammonium sulfate and pollution particles, forming mixtures that are hygroscopic in nature. We studied the relationships between the properties of the aerosol particles and the microphysics of cumulus clouds that formed above the aerosol layer. Under dusty conditions, when a large concentration of coarse-fraction mineral particles was present in the aerosol, cloud drop concentrations were lower and droplet diameters larger than under background conditions, when the aerosol was dominated by submicrometer sulfate particles.

Prevention of the oxidation of mining tailings by etraethylenepentamine

Shu Xiao-Hua[*], Dang Zhi, Yi Xiao-Yun & Yang Chen
Dept. of Environmental Sciences and Engineering, South China University of Technology, Guang Zhou, China
(sxh-9911@163.com)

The ability of etraethylenepentamine (TEPA) to inhibit the oxidation of metal-sulfide tailings was investigated. Samples uncoated and coated by TEPA were both exposed to hydrogen peroxide for one day. This study demonstrates that the extent of tailings oxidation can be reduced by as much as 97% by treating the wastes with TEPA. A passivating layer forms on the tailings surface after exposure to the TEPA as shown by SEM images. This layer presumably suppresses mining tailing oxidation by limiting the advection of aqueous oxidants between oxidants and the tailings because of its nucleophilic functional group. The results presented here show that TEPA is an effective coating agent which can prevent surface oxidation of mine wastes.

A study of wind-polished rock surfaces in the Transdanubian Range (Hungary)

Thamó-Bozsó, E.*, Csillag, G., Kákay-Szabó, O., Kónya, P. & Müller, P.
Geological Institute of Hungary, Budapest, Hungary
(*bozso@mafi.hu)

Wind-polished gravel and rock surfaces are relatively abundant in the hilly area of Transdanubia. They were recognised more than a century ago and mapped later [1-2]. Their polished shiny surfaces are sometimes mentioned as desert varnish which formed under arid climate of Pleistocene [3]. Rock varnish or desert varnish is about 1-600 micrometers thick smooth, high sheen, dark brown to black coating usually with a high clay, iron and manganese oxide content. It is a microlayered mixture of clays and metal oxides [4]. Formation of varnish is not clear yet; beside the chemical processes (weathering, precipitation), microbial action plays probably also an important role [5]. Varnish microlamination can be also used as a correlative dating method [6].

To study the wind-polished rock surfaces, we collected samples from the forelands of the Vértes and Gerecse Hills and from the Keszthely Mountains. The samples are quartzite, metasediments, chert, and dolomite, and were all studied in the Geological Institute of Hungary by optical microscopy, scanning electron microscopy (JEOL JSM-35), electron dispersive spectroscopy (Kevex), and X-ray diffraction (Philips PW 1730).

The studied shiny wind-polished surfaces show different micro-forms under scanning electron microscope according to the composition and texture of the rocks (Fig. 1). On the surfaces of the different rocks, we detected high Si and Mg, and sometimes Fe concentration. They contain illite, kaolinite, chlorite, and goethite.

Acknowledgments: The research was supported by the Hungarian National Research Fund (OTKA K-62478).

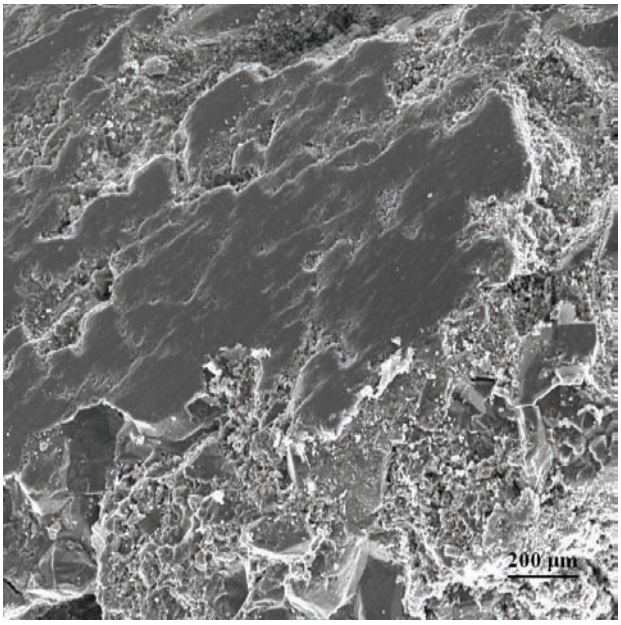

Fig. 1: SEM image of wind polished rock surface from Transdanubia.

[1] Jámbor, Á. (1992) *Acta Geol. Hung.*, **35(4)**, 407-436. [2] Csillag, G. et al. (2008) in Budai, T. & Fodor, L. (eds.) *Geology of the Vértes Hill*. MÁFI, 110-133. [3] Schweitzer, F. (1997) *Z. Geomorph.* N.F. Suppl., **110**, 37-43. [4] Perry, R.S. & Adams, J. (1978) *Nature*, **276**, 489-491. [5] Dorn, R.I. & Oberlander, T.M. (1981) *Science*, **213**, 1245-1247. [6] Dorn, R.I. (1988) *Nat. Geogr. Res.*, **4**, 56-73.

Radiological and chemical investigation of coal slag and fly ash bearing building materials in the central part of Hungary

Völgyesi, P.*, Nagy, H.É. & Szabó, Cs.
Lithosphere Fluid Research Lab, Eötvös University, Budapest, Hungary (*petervolgyesi11@gmail.com)

By-products of industrial production processes are often used in national and international construction technologies as building materials on their own or as additives to building materials. In Hungary, from a radiological point of view, one of the most important issues is the utilization of the different types of coal slags and fly ashes. However, such building materials can contain relatively high levels of natural radionuclides [1,2]. Therefore, the main aim of this study is to analyze gas silicate, containing fly ash, and coal slag concrete samples from ten different locations from the central part of Hungary, using a wide range of radiometric and chemical methods. Gamma dose rate in all rooms of the studied houses at the ground floor and at one meter height was measured. To determine the radon concentration, short-term measurements by use of RAD7 and AlphaGUARD radon detectors were carried out. In the course of laboratory analysis, the ^{226}Ra-, ^{232}Th- and ^{40}K content of the samples was determined by HPGe Gamma-spectrometry. These results were use to classify the building materials studied. The radon exhalation of the building materials was measured by Rad7 continuous radon monitor. On the thin sections, made from the coal slag and gas silicate samples, microscopic description and observation, mineralogical/phase estimation ratios were carried out. To identify the chemical composition of phases in the building materials, scanning electron microscope measurement was performed, and they indicate that there are several 2-3 µm uranium-bearing grains in the coal slag sample (Fig. 1), which occur separately in the grain size fraction of the smallest fraction. Around the uranium bearing phases there are phases which contain Mg-Al-Ca-Ti-Fe silicates (Fig. 1).

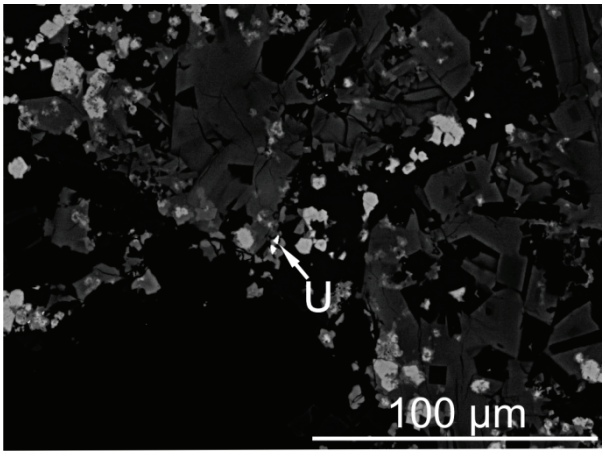

Fig. 1: BSE image of two 2.5-3 µm sized uranium bearing phases (marked with U) in a coal slag sample.

Our study draws the attention to the need of complex radiometric survey which should include the determination of gamma dose rates beside the commonly used radon measurements in case of building materials. The results show that we are facing the radiation-exposure problems not only in geologically exposed sites but also in the fifth floor apartments of a block of flats.

[1] Kovler, K. et al. (2002) *Build. Environ.*, **37**, 531-537. [2] Somlai, J. et al. (2006) *Radiat. Prot. Dosim.*, **1**, 82-87.

Experiment and a mechanism of utilization of apatite in phosphorus removal under alkaline condition

Xu Hong*, Zhang Jing & Deng Yanxi
State Key Laboratory of Geological Processes and Mineral Resources, China University of Geosciences, Beijing, China (*hongxu88@126.com)

At room temperature, we analyzed the phosphate concentration of K_2HPO_4 solution when apatite, $CaCl_2$ and NaF are added into the different solution respectively with an identical initial phosphate concentration.

The results showed that the phosphate concentration declined significantly when apatite and calcite were added. When apatite along with fluorite was added, phosphate concentration dropped considerably, from the initial 5 mg/L to 0.02 mg/L, indicating that increasing F and Ca with apatite is helpful to P removal. Comparative experiments suggested that a Ca:P:F ratio of 11:3:2.2 is the ideal one for the removal of phosphate. The pH value influenced the efficiency of phosphate removal. At pH=10, apatite can reduce the phosphate concentration to the level below the eutrophic critical line (Fig. 1) and there is no significant pH value change in the solution after P removal.

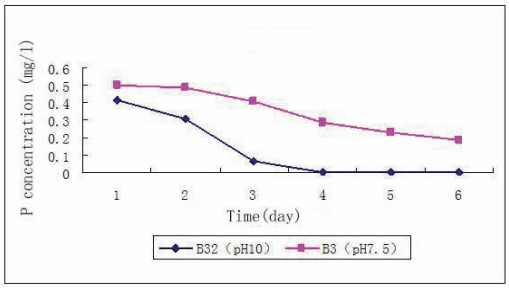

Fig. 1: The results of dephosphorization by apatite under different pH.

Infrared and FT-Raman spectroscopy and electron microscopy (SEM and TEM) analysis of the dried precipitate at room temperature suggests that the precipitate is compositionally and structurally similar to poorly crystalline apatite. Apatite can remove more phosphate from the solution at higher pH condition, and phosphate in the solution might precipitate as apatite-like compound. Other experiments were carried out with sewage and at pH=9 or above, the phosphate concentration of 0.02 mg/L to the level below the eutrophic critical line after P removal. Ca and phosphate crystallize under alkaline condition [1]. In previous P removal experiments with sewage, the product was thought to be calcium phosphate [2]. We carried out the dephosphorization experiments with calcite, and the concentration of the residual phosphate in the solution was higher than that with apatite after P removal. Therefore, apatite likely acts as the seed for P-Ca crystal growth while calcite does not play such a role.

[1] Stumm, W. et al. (1970) *Aquatic Chemistry, An Introduction Emphasizing Chemical Equilibria In Nature Water*. Wiley-Interscience, New York. [2] Donnert, D. & Saleker, M. (1999) *Wat. Sci. Tech.*, **40(4-5)**, 195-202.

Mineralogical, magnetic and geochemical investigation of the seasonal PM 10 dust fraction from Miskolc, Hungary

Zajzon, N.[1*], Márton, E.[2], Pethe, M.[2,3], Sipos, P.[4], Németh, T.[4], Kovács Kis, V.[5] & Uram, J.[6]
[1]Institute of Mineralogy and Geology, University of Miskolc, Hungary (*nzajzon@uni-miskolc.hu)
[2]Palaeomagnetic Laboratory, Eötvös Loránd Geophysical Institute of Hungary, Budapest, Hungary
[3]Geophysics Dept., Eötvös Loránd University, Budapest, Hungary
[4]Institute for Geochemical Research, Hungarian Academy of Sciences, Budapest, Hungary
[5]Research Institute of Technical Physics and Materials Sciences, Hungarian Academy of Sciences, Budapest, Hungary
[6]North Hungarian Environmental, Nature Conservancy and Water Policy Inspectorate, Miskolc, Hungary

Air monitoring station was installed for collecting PM 10 at a point where vehicular traffic is heavy in the centre of Miskolc. Four times a year the station is ran for two weeks to collect PM 10 fractions. The filters were collected between the period of February of 2009 and February of 2010.

PM 10 from Feb. and Aug. of '09 were investigated with analytical TEM. In the winter sample, shapeless or angular K-Ca sulfates dominate. Large number of black carbon and clay minerals are also present. Only one amorphous Fe-oxide particle was found in this sample with Co content. In the summer sample, the sulfate salts are low, while black carbon and clay particles dominate. There were large amount of Fe-rich particles occasionally with high Zn content. According to the magnetic information and previous studies of the authors on dust fractions from steel factories and coal using power plants (SEM-XRD-ATEM) this phase is magnetite–franklinite.

The PM 10 collecting instrument has a pre-trap for the larger particles of the dust. The XRD mineral composition of the crystalline part of the trapped dust is: quartz > calcite > albite > muscovite >> dolomite > magnetite > amphibole.

Magnetic data, toxic metals (Pb, Ni, As, Cd) and organic compounds were measured on the PM 10 daily filters. The observed minimum values of the mass specific susceptibilities on Sundays suggested that, the magnetic pollutants originate from vehicles. At the same time, no correlation was found between mass specific susceptibilities and the concentrations of the toxic metals. The latter seem to originate from distant industrial sources and although their concentrations is far from constant, the weekend days are by no means less polluted than the work days. The Pb and Cd are in good correlation; they can have the same source. Their amounts increase with the N–NW–W wind, and decrease if the wind direction is opposite (Fig. 1).

The total amount of PM 10 fraction is usually decrease with increasing wind. The lighter samples have higher mass specific susceptibilities, till the absolute values are similar. It means that the magnetic component of the sample, which is coming from the vehicular traffic, is in the same range, but in windy days is less diluted on the filter with non-magnetic components.

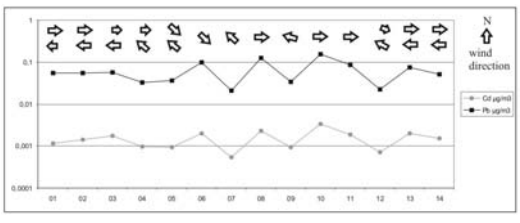

Fig. 1: Pb, Cd and wind data from November of 2009. The Pb and Cd are good correlation with the wind direction.

Mine waste: the good, the bad and the mineralogy

Hudson-Edwards, K.A.
Dept. of Earth and Planetary Sciences, Birkbeck, University of London, UK (k.hudson-edwards@bbk.ac.uk)

Since the dawn of civilization, humankind has been extracting metals and minerals for the production of goods, energy and buildings. These activities have created great wealth, but they have also produced huge quantities of solid and liquid waste, known collectively as 'mine waste'. Mine waste may be considered 'good' in that it contains potentially valuable metal and thus may be a future resource, and because it hosts unique metallophyte communities. However, the often high amounts of metals and metalloids in mine wastes are potentially toxic to other ecosystems and humans if ingested or inhaled, and weathering of mine wastes can lead to problems such as acid mine drainage. As the retention and release of potentially toxic metals and metalloids is controlled by the behavior of their mineral hosts, a full understanding of the ways that these minerals form and incorporate and release these elements in mine waste can help to predict and mitigate related potential risks. Mine waste minerals are characterised using standard (e.g., X-ray diffraction, electron microprobe micro-analysis) and advanced techniques (e.g., XANES, EXAFS), and their behavior is determine using field, laboratory (e.g., column experiments, microcosms) and computer simulation methods. These techniques, which are often used in combination with one another, give insights into the molecular-scale processes affecting metal and metalloid cycling from mine waste. This presentation will describe the complex world of mine waste mineralogy, using case studies to give an overview of the techniques of characterisation, processes of formation and transformation and avenues for future research.

Weathering products in mine wastes at several abandoned ore deposits in Slovakia

Lalinská, B.[1*], Majzlan, J.[2], Chovan, M.[1], Klimko, T.[1], Göttlicher, J.[3] & Steininger, R.[3]
[1]Dept. of Mineralogy & Petrology, Faculty of Natural Sciences, Comenius University, Bratislava, Slovakia
([*]lalinska@fns.uniba.sk)
[2]Institute of Geosciences, Friedrich-Schiller University, Jena, Germany
[3]Institute for Synchrotron Radiation, Karlsruhe Institute of Technology, Karlsruhe, Germany

Mineralogical composition of weathering products in mine wastes is an important factor that controls migration of pollutants. Results from 6 abandoned Sb-Au deposits show differences in As and Sb behavior in the mine wastes. The average content of Fe, Sb, and As present in the studied tailing impoundments is high; Fe average content is in the range from 15.3 g/kg (Dúbrava deposit) to 106.7 g/kg (Medzibrod deposit); Sb from 1.2 g/kg (Dúbrava) to 6.6 g/kg (Pezinok deposit) and As from 0.4 g/kg (Čučma deposit) to 6.0 g/kg (Pezinok). In most of studied localities, pH values of the tailing material are near-neutral, because the acidity produced by sulfides decomposition is neutralized by abundant carbonates. Carbonates are scarce only at the Poproč deposit and the tailings here are acidic.

The most common sulfides in flotation wastes are pyrite and arsenopyrite, stibnite is rare probably due to its rapid oxidation.

At all studied mine sites, oxidation rims on pyrite and arsenopyrite grains are developed and act as effective scavengers of As and Sb. Oxidation rims on pyrite contain up to 10.12 wt.% of As (Pezinok) and up to 7.5 wt. % of Sb (Pezinok); As content in rims on arsenopyrite is generally lower compared to the unaltered arsenopyrite grains, conversely Sb content is up to 14.3 wt.% (Čučma) and in one extreme case even 50 wt.% (Pezinok). The most rapid decomposition of pyrite and arsenopyrite was observed under acidic conditions (Poproč).

In general, As is sorbed onto Fe oxides. According to our μ-XRD data, Fe oxides with the low As content are made of goethite and poorly crystalline As-rich phases are probably made of ferrihydrite. When Pb is present in the pore solutions, Pb/As oxides with chemical composition close to paulmooreite, $Pb_2As_2O_5$, are formed (Medzibrod).

Sb is most often present in form of Sb, Sb/Fe and Fe/Sb oxides (valentinite, stibiconite) and these may be the products of complete replacement of Sb ores or they may have precipitated from solutions which circulate through the impoundments. Sb/Fe oxides were identified as tripuhyite, $FeSbO_4$. Sb oxides with various content of Ca similar to romeite, $Ca_2Sb_2O_6(O,OH)$, are also common (Čučma) and if Pb is present in the tailings, a mineral chemically close to bindheimite, $Pb_2Sb_2O_7$, is formed (Medzibrod).

Fe ochres associated with tailing impoundments and adit discharges are composed mainly of ferrihydrite which transforms slowly into the more stable goethite. Concentration of As in the ochres is high and varies from hundreds mg/kg (Pernek) up to 205.9 g/kg (Medzibrod). Comparison of As and Sb concentrations in the ochres and coexisting waste waters indicates lower sorption affinity of Sb to Fe oxyhydroxides as compared to As.

Acknowledgements: This work was supported by Slovak Research and Development Agency under the contract No. APVV-VMSP-P-0115-09.

Preferential oxidation of euhedral pyrite containing relict framboidal morphologies

Weisener, C.G.[1*], Gagnon, J.[1] & Weber, P.A.[2]
[1]Great Lakes Institute for Environmental Science, University of Windsor, Windsor, Canada ([*]weisener@uwindsor.ca)
[2]Environmental Division, Solid Energy New Zealand Ltd, Christchurch, New Zealand

Environmental damage produced from acid generating mines currently represents one of the largest problems facing the mining industry. The aim of this research is to investigate possible mineralogical controls on acid rock drainage (ARD) and metal release associated with pyritic mudstone collected from, the Brunner Coal Measures (BCM), Stockton Mine NZ. Laboratory-based kinetic tests were performed on the potentially-acid forming material by measuring, over time, the changes in mineralogical compositions and acid generating potential along with changing effluent chemistries from the columns. The rate of pyrite oxidation in the BCM is strongly dependent on the reactivity of two morphological types (euhedral and framboids) of pyrite in this region.

After a 4 month period between 70 to 100% of all framboidal pyrite had undergone complete oxidation, despite this acid generation (1730 (mgL-1 CaCO3) after 390 days) continued during the column experiments. SEM micrographs show the persistence of larger euhedral pyrite grains as a contributing factor with evidence of preferential oxidation associated with relict framboidal morphology (figure 1).

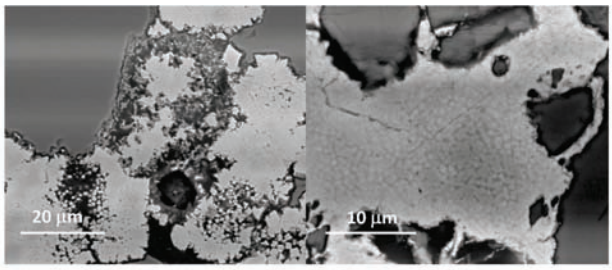

Fig. 1: After 13 months within a humidity cell euhedral pyrite shows preferential oxidation confined to pyritic overgrowth textures.

Samples collected from laboratory humidity cells after 13, 16 and 24 months show preferential dissolution features associated with large pyritic overgrowth textures. From a kinetic perspective the oxidation of pyrite in these samples tend to target the more recent crystallographic overgrowths. Results of the 24 month study will be presented detailing the mineralogical alteration, acidity generation and their controls on trace metals specifically thallium deportment.

Characterization of arsenical compounds and minerals in refractory gold processing residues: implications for arsenic control

Paktunc, D.
CANMET, Mining and Mineral Sciences Laboratories, Ottawa, Canada (dpaktunc@nrcan.gc.ca)

A range of ferric arsenate-sulphate minerals and synthetic compounds representing residues from the processing of refractory gold ores were characterized by XRD, XAFS and microanalysis techniques. Compounds synthesized under hydrothermal conditions in the temperature range of 150 to 225ºC include $Fe(AsO_4)_{0.8\text{-}1}(SO_4)_{0\text{-}0.2}\cdot 2H_2O$ (scorodite), $FeAsO_4(OH)_{0.2\text{-}0.6}$ (phase 4), $Fe(AsO_4)_{0.3\text{-}0.5}(SO_4)_{0.7\text{-}0.5}(OH)_{0.5\text{-}1.5}$ (phase 3) and $Fe(SO_4)_{0.9\text{-}1}(AsO_4)_{0\text{-}0.1}(OH)$ (phase 5), all of which are characterized by a 1:1 molar $Fe/(AsO_4+SO_4)$ ratio (Fig.1). Synthetic scorodite accommodates up to 20 mole % SO_4. Substitution of AsO_4 is limited to between 30 and 50 mole % in phase 3 and 10 mole % in phase 5. In comparison, synthetic jarosite can incorporate up to 17 mole % $AsO_4/(AsO_4+SO_4)$. These compounds represent those formed in the autoclaves during pressure oxidation of refractory gold ores where gold is locked in arsenopyrite and pyrite.

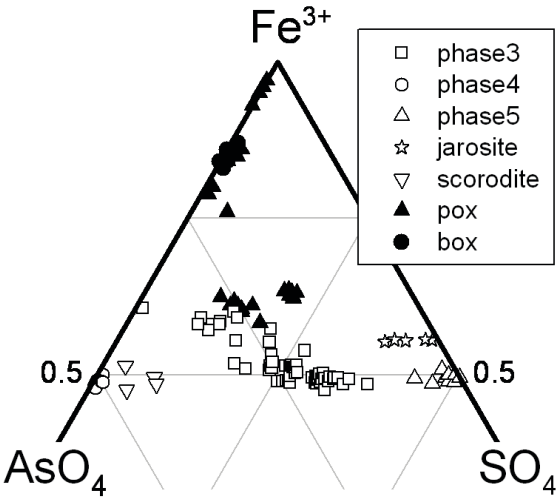

Fig. 1: Compositions of synthetic compounds and residues (pox: pressure oxidation; box: bacterial oxidation) resulted from processing of refractory gold ores.

Natural analogs in this system include hydrated ferric arsenate and sulphate minerals such as bukovskyite, sarmientite, zykaite, scorodite, parascorodite, kankite, ferric arsenate, kaatialaite and ferrisymplesite. Such occurrences, along with arsenate-adsorbed goethite, ferrihydrite, schwertmannite and hematite, were reported in mine tailings, oxidized portions of gold and base metal mineral deposits and acid mine drainage settings. Long- and short-range structures of these compounds and their hydrated natural analogs will be presented along with the experimental data, and their implications on arsenic control practices at mine sites will be discussed.

Crystal-chemistry of Ni and Cr within phyllosilicates and Fe/Mn oxyhydroxydes along a lateritic regolith in New Caledonia

Fandeur, D.[1], Juillot, F.[1*], Fritsch, E.[1], Morin, G.[1], Ambrosi, J.P.[2] & Brown, G.E., Jr.[3]
[1]Institut de Mineralogie et de Physique des Milieux Condenses (IMPMC), UMR CNRS, Université Pierre et Marie Curie; Université Paris Diderot; IPGP; Paris, France ([*]juillot@impmc.jussieu.fr)
[2]Centre Europeen de Recherche et d'Enseignement en Geosciences de l'Environnement (CEREGE), UMR CNRS, Université Paul Cezanne, Aix-en-Provence, France
[3]Surface & Aqueous Geochemistry Group, Dept. of Geological and Environmental Sciences, Stanford University, Stanford, CA, USA

Ultramafic rocks cover about 1% of the continental surfaces and are related to ophiolitic bodies formed near convergent plate boundaries [1]. The most typical ultramafic rocks are dunite and harzburgite, which are composed of easily weatherable ferromagnesian mineral species (olivines and pyroxenes), but also of more resistant spinels (chromite and magnetite). Oceanic serpentinization of these ultramafic rocks usually leads to partial transformation of these initial mineral assemblages by forming hydrous layer silicates such as serpentine (lizardite, chrysotile and antigorite) talc, chlorite and actinolite [2]. However, these ultramafic rocks can lead to different mineral assemblages when they are exposed to meteoritic weathering. Such a situation is encountered in New Caledonia, where tropical meteoritic weathering of ultramafic rocks (peridotites) obducted about 35 millions years ago [3] has lead to the development of very thick regoliths, which contain large amounts of trace elements (Ni, Co, Mn, Cr). Although interesting from an economical point of view, such an occurrence of large amounts of potentially toxic elements can be hazardous for the environment. Characterizing the crystal-chemistry of these elements is then very important to identify the processes driving their transport and/or immobilization upon weathering of ultramafic rocks.

Results of a study performed along a 64 m depth lateritic regolith in the Mt Koniambo (West Coast of New Caledonia) emphasize the major control of phyllosilicates (talc and serpentine) and Fe and Mn oxyhydroxides on the crystal-chemistry of Ni and Cr. When going from the bedrock to the lateritic part of the regolith, Ni moves from Ni/Mg-phyllosilicates to secondary Fe oxyhydroxides, whereas Cr moves from primary silicates and chromite to Cr(III) bearing Fe oxyhydroxides [4,5]. In addition, the occurrences of Ni/Co asbolane and of Cr(VI) after oxidation of Cr(III) by Mn oxyhydroxides emphasize the importance of this mineral species in the intermediate part of the regolith [4,5].

These results bring interesting insights on the importance of phyllosilicates and Fe/Mn-oxyhydroxides on the crystal-chemistry of trace elements upon weathering of ultramafic rocks under tropical conditions.

[1] Coleman, R.G. (1977) *Ophiolites: Ancient oceanic lithosphere?*. Berlin, Germany, Springer-Verlag. [2] Malpas, J. (1992) in Roberts, B.A. & Proctor, J. (eds.) *The ecology of areas with serpentinized rocks: A world view*. Kluwer Academic Publishers, Netherland, 7-30. [3] Cluzel, D. et al. (2001) *Tectonophysics*, **340**, 23-59. [4] Fandeur, D. et al. (2009) *Am. Mineral.*, **94**, 710-719. [5] Fandeur, D. et al. (2009) *Environ. Sci. Technol.*, **43**, 7384-7390.

Jarosites as indicator minerals for acidic conditions in Bányabérc waste dump (Mátra Mts., Hungary)

Farkas, I.M.[*] & Weiszburg, T.G.
Dept. of Mineralogy, Eötvös L. University, Budapest, Hungary ([*]farkasizabella@yahoo.com)

Weathering of Fe-sulphides in mine wastes produces acidity and elevated levels of heavy metals. Common secondary minerals formed on these sites are hydrated metal oxides and sulphates. One of these secondary sulphate phases is jarosite. The presence of jarosites in mining wastes refers to a low pH, high sulphate content and highly oxidative media. In our work natural jarosite samples from the Bányabérc sulphidic waste dump (Mátra Mts., Hungary) were characterized mineralogically and chemically. X-ray powder diffraction, chemical analyses (SEM-EDX, ICP-AES), Mössbauer and Raman spectroscopy were used to characterize the jarosites. Analyses suggest a solid solution series between jarosite and hydroniumjarosite. The c_0 unit-cell dimension in our samples has lower values (17.082(1), 17.087(2), 17.104(3), 17.124(4), 17.136(1), 17.125(4), 17.091(1) Å) than pure jarosite (17.2043 Å; [1]), supporting H_3O^+ substitution. Beside X-ray powder diffraction, chemical data also reveal deficiency in the alkali site. In some of the jarosites, As, P and Al were measured. In the SO_4 anion position in the structure, substitution of AsO_4 and PO_4 is possible.. The lattice constant a_0, which is sensitive to substitution in the Fe site, is very close to that reported for pure end-member K-jarosite (7.3346(4), 7.3325(5), 7.3238(5), 7.3117(4), 7.3241(4), 7.3143(7), 7.3317(5) Å). Although Al was measured in some of the samples, it is not ubiquitous and may reflect other included minerals. In some cases, the Raman measurements demonstrated also a mixing between jarosite and goethite, especially around weathered pyrite, increasing the Fe/S atomic ratio from 1.5, characteristic for ideal jarosite, to higher values. The Mössbauer spectrum of jarosite is characterized by a doublet, revealing six-coordinated Fe^{3+} (*IS* = 0.31–0.38 mm/s; *QS* = 1.00–1.23 mm/s).

Well-crystalline plumbojarosite forms an outer ring around anglesite, the latter enclosing an unaltered core of galena. These textural relationships suggest that galena was the Pb source for the two secondary minerals. Anglesite, Pb-bearing jarosite and plumbojarosite are stable phases under acidic conditions, but as pH increases above 6, their dissolution is favoured. In the pH window between jarosite breakdown and iron oxide/oxyhydroxide uptake, Pb may remain in solution and fully bioavailable. The Raman spectra of jarosite-group minerals slightly differ from each other. Plumbojarosite shows some special spectral features. The 451 and 472 cm^{-1} doublet (splitting) are believed to originate from the doubly degenerate ν_2 bending mode of the sulphate ion that appears at 450 cm^{-1} in aqueous solution. There are three broad bands at 990–1030 cm^{-1} $\nu_1(SO_4)$, around 1180–1120 cm^{-1} $\nu_3(SO_4)$ and around 1160–1180 cm^{-1} $\nu_3(SO_4)$ which are due to overlapping of multiple peaks.

As an oxidation product of pyrite, jarosite is ubiquitous in the Bányabérc waste dump, indicating an acidic environment. Hydronium-bearing jarosite is thought to contribute to acid generation in mine wastes because the H_3O^+ ion accelerates jarosite dissolution. This means that the As in the jarosite is stored only temporary because of the limited pH and redox conditions of jarosite stability.

[1] Basciano, L.C. & Peterson, R.C. (2007) *Am. Mineral.*, **92,** 1464-1473.

Mineralogical evolution in arsenic and lead contaminated soils-water systems. Portuguese mine soils laboratory assays

Magalhães, M.C.F.[1*], Anjos, C.[1] & Abreu, M.M.[2]
[1]Dept. of Chemistry & CICECO, University of Aveiro, Portugal ([*]mclara@ua.pt)
[2]UIQA, Instituto Superior de Agronomia, Universidade Técnica de Lisboa (TULisbon), Lisboa, Portugal

Hazardous elements mobilization from mine tailings is a potential contamination process of the surrounding soils and waters. The environmental impact from those elements is not quite related to their presence in anomalous amounts in soils and sediments but is related to their availability (several media available fraction and chemical speciation) to the biota.

The presence of: i) high concentrations of total lead (1.48 – 13.4 g/kg) in the soils of the abandoned Braçal lead mine area together with high percentage of the lead available fraction (12 – 68 % of total Pb) determined by the calcium nitrate method [1]; ii) high concentrations of total arsenic (0.15 - 34 g/kg) in the soils of the abandoned Penedono arsenic and gold mine area also with moderately high percentage of the arsenic available fraction (dl – 6 % of total As) determined by the dtpa method [2]; and iii) high concentrations of total arsenic (0.5 – 3.0 g/kg) and lead (1.9 – 9.2 g/kg) in the soils of the abandoned São Domingos copper mine area where very low concentrations of the arsenic (0.001 – 0.02 % of total As) and lead (0.001 – 0.9 % of total Pb) available fractions were determined as above, induced a search for the identification of possible secondary solid phases that could control arsenic and lead availability. The X-ray diffraction analyses of the soil samples show the presence of langite ($Cu_4(SO_4)(OH)_6 \bullet 2H_2O$), cerussite ($PbCO_3$), and cotunnite ($PbCl_2$) in Braçal, scorodite ($FeAsO_4 \bullet 2H_2O$) in Penedono, and beudantite ($Fe_3Pb(AsO_4)(SO_4)(OH)_6$), carminite ($Fe_2Pb(AsO_4)_2(OH)_2$), kankite ($FeAsO_4 \bullet 3.5H_2O$), mimetite ($Pb_5(AsO_4)_3Cl$), and segnitite ($Fe_3PbH(AsO_4)_2(OH)_6$) in São Domingos [3].

Laboratory experiments were conducted with soils of the above referred mine sites to study the secondary minerals possible changes, mainly, containing arsenic and lead, when in contact with water with characteristics of normal rainwater. Soils were left in contact with distilled water, at room pressure and temperature, for periods ranging from 2 to 393 days in closed vessels shaken and aerated frequently. Aqueous solutions were analysed for elemental composition, and soils were analysed by X-ray diffraction for mineral composition.

The X-ray diffraction analyses of the samples, resulting from the soil-water experiments, evidence different behaviours. The soils from Braçal didn't appear to have noticeable changes with water contact time. In the samples from Penedono the amount of scorodite decreased with water contact time, but intermingled changes evolving with time were perceived in the São Domingos soils.

This study shows that, in the soils, can be found mineral phases considered metastable under those conditions of pressure and temperature, *e.g.* kankite and langite. Once all the aqueous solutions had similar values for the pH and Eh, the diverse behaviour of the studied soils seems to lie in their chemical elemental composition. The São Domingos mine soils are richer than those from the other two mines. Under the experimental conditions the Braçal cerussite and cotunnite only undergo congruent dissolution, but several reactions can occur in São Domingos soils where many chemical elements are in presence of heterogeneous nucleating agents and organic precursors.

[1] Berti, W. et al. (1997) in Prost, R. (ed.) *Contaminated Soils.* Les Colloques 85, INRA, Paris, 121-131. [2] Lindsay, W.L. & Norvell, W.A. (1978) *Soil Sci.*, **42**, 421-428. [3] Abreu, M.M. et al. (2009) *Revista de Ciências Agrárias*, **31**, 155-169.

Mineralogical and geochemical survey of Lisbon (Portugal) urban soils

Rocha, F.[*], Reis, A.P., Terroso, D., Patinha, C., Dias, A.C. & Ferreira da Silva, E.F.
Geosciences Dept., Geobiotec Unit, University of Aveiro, Portugal ([*]tavares.rocha@ua.pt)

This study is a part of the working program of a research project titled "PTDC/CTE-GEX/68523/2006: URBSOIL-LISBON_ Geochemical survey of Lisbon urban soils: a baseline for future human health studies". The aim of this research is to assess the contribution of soil mineralogy to the geochemistry of the urban soils of Lisbon city. A total of 51 soil samples were collected over Lisbon city. According to the location and land-use, the samples were classified as air side: airport (AE), public garden (GD), public park (PA), road-side (RS: small flower beds along the road-side), playground (PG) and schoolyard (SC). Among the 51 soil samples, 3 were collected in AA land, 7 in GD land, 11 in PA land, 2 in RS land, 22 in PG land and 6 in SC land. Figure 1 shows the sample locations and land-use. Each sample site is labelled from 1 to 51.

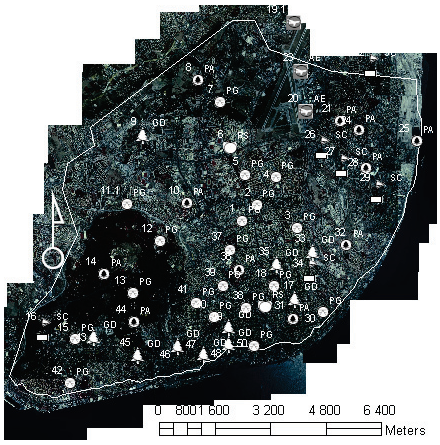

Fig. 1: Soil sampling sites and local land-use.

Of the 51 samples, 11 were selected for the mineralogical study. Table 1 shows the major geochemical outliers in the urban soil at each of those 11 sites.

Table 1: Anomalous elements in the selected soil sampling sites

urban site	land-use	geochemical outliers in the urban soil
11.1	PG	Be, Nb, B, **Y**, Co, **Sc**, **Zr**, Sr, **Ga**, Ni, Fe, Mn, Ti, Cr, V, K, Al, Mg, Na, **HREE**, LREE
15	PG	**Li**, **Y**, Be, **Co**, Ba, Sc, Zr, **Sr**, **Ga**, Ni, **Fe**, **Mn**, **Ti**, Cr, **V**, **Al**, **Mg**, Na, **REE**
20	AE	**Nb**, S, Bi, Pb, Ba, Sb, Cd, Mo, Zn, Cu, Ca
29	SC	very low concentration in all elements
31	PA	**Au**, P, Ag
33	GD	**Pb**, Ba, **Sb**, **Sn**, **Cd**, **Zn**, **Cu**
37	PG	very low concentration in all elements
39	PG	**Au**, **P**, B, **Bi**, **Pb**, Sb, **Sn**, **Cd**, **Ag**, Cu, Ca
43	GD	**Y**, Au, Co, Ba, Sn, **Sc**, Sr, **Ga**, **Ni**, **Fe**, **Mn**, **Ti**, **Cr**, V, Al, Mg, Na, REE
47	GD	S, **P**, B, Bi, **Pb**, Ba, Sb, Sn, Cd, **Ag**, **Sr**, Zn, **Cu**, **Ca**, **Mg**
48	GD	**Bi**, **Pb**, Ba, **Sb**, Sn, **Cd**, **Ag**, **Mo**, **As**, Zn, **Cu**, Na

In general, the samples are siliceous (quartz, feldspars and phyllosilicates) but some show relevant presence of carbonates; iron oxides/hydroxides, sulphates and sulphides are common accessory minerals. Illite is the predominant mineral of the clay fractions, smectite and kaolinite showing dicothomic behaviour.

Characterization and mitigation of the Sn-Ag San Jose mining district, Oruro, Bolivia

Walder, I.F.[1*], Victoria, J.[2], Boon, R.G.J.[2] & Walder, P.[1]
[1]Kjeøy Research & Education Center, Kjeøy, Vestbygd, Norway ([*]ifwalder@kjeoy.no)
[2]Environmental Dept., COMIBOL, La Paz, Bolivia

The San Jose mining district is a typical Bolivian tin-silver province with numerous mines producing silver and tin from a volcanic hosted poly-metallic epithermal, alunite-kaolinite breccia deposit. Silver production started back in the mid sixteen hundreds by the Spaniards. Mining continued, via private companies and was nationalized in 1954. The state mining company COMIBOL, which operated the mines, closed the mines in 1992. Small cooperatives were allowed to continue mining, however, in very small scale by primitive methods.

Mine adits, mine excavations, mine tunnels, tailings and waste rocks are scattered throughout the Oruro Mountains, where these mines are located. The largest operations were San Jose and Itos mines, with smaller, but environmentally important, San Miguel, Del Norte, and Jallpha operations. Most of the tailings and waste rocks have been characterized: the smaller ones primarily with paste pH and on-site mineralogical identification, the larger waste material with ABA, microscopy, leach tests, whole rock chemistry, and kinetic testing.

The upper part of the mineralization has gone through strong weathering. The tailings and waste rocks from the deeper part (below the weathering zone) are very acidic with soil pH 1-3. The pyrite-pyrrhotite content, however, is not very high in most of the analyzed samples. Some of the tailings material has arsenic content of 1-2 wt.%. The leach tests indicate very high TDS loaded with metals. The strong alteration during the ore forming process left little or no neutralizing capacity in the wall rocks and gangue minerals.

Mitigation is complicated due to families living on top of the waste material and interest groups wanting access to the waste material for reprocessing. COMIBOL has suggested several different mitigation options depending upon the location of the waste material and the severity of the contaminant loading on the receiving environment.

Study of hydrodynamic behaviour, fluid conductivity and composition analysis in granite fines

Falcon, I.[1], Rammlmair, D.[2*], Delgado, J.[1] & Juncosa, R.[1]
[1]Civil Engineering School, University of A Coruña, Spain
[2]Federal Institute for Geosciences and Natural Resources (BGR), Hannover, Germany ([*]rammlmair@bgr.de)

'Granite fines' is the silty-clay material generated by the granite dimension stone industry during rock sawing and polishing operations. Such materials have been physico-chemically, mineralogically and geotechnically characterized during the last decade in order to recognize their suitability for various applications of civil engineering such as landfill sealing and waterproofing. This material consists of fine mineral and granite particles of the primary rock and some components added during the process such as a fraction of lime and variable steel grit introduced into the system during the sawing process mixed with water (~38 wt.%).

This study is focused on fluid conductivity and composition analysis, and the hydrodynamic behaviour of a column of granite fines under wetting and drying cycles. Non-destructive methods were used to not disturb the free dynamics of the fluid along the capillary fringes. To achieve it, the material was filled homogeneously into PVC (polyvinyl chloride pipe 7 cm x 50 cm) equipped with a foil having embedded wires for conductivity measurement at 20 different levels of four electrodes each fixed at the inner wall of the tube. Electrical conductivity of the fines was measured at each level for each step of saturation Simultaneously X-ray radiography measurements were carried out through opposing windows with 50 μm thin PVC-foils for the whole length of tube, in order to recognize the kinetics of water movement in the column. It was progressively saturated by adding water from the bottom of the pipe in different steps, while the evolution of the system was monitored.

Once the saturation was completely achieved, the extraction of the interstitial solution was carried out by inserting metal free Rhizon until the suction of the soil was in absolute terms higher than the Rhizon limit, representing around 30% of the total water allocated in the soil. The water was extracted in different steps distinguishing different types of water in relation to the rising difficulty in the extraction: fast water to slow water. In addition, dissolved ions measured by ICP-MS and ICP-OES from the extracted water show different trends in relation to the soil saturation degree and the position in the column where Rhizons are located. Results show a normal fast kinetic behaviour during saturation steps that can be explained by the strong effect of capillary fringes. On the other hand, an exponential increment from the bottom to the top of the column was measured in the conductivity of soil water, which also decreases from the first extraction (fast water) to the last one (slow water). The strong increase in electrical as well as fluid conductivity from bottom to top shows a fast rising capillary head fluid enriched in ions, but with reduced vertical equilibration. The high amount of dissolved ions in the rising head is eventually responsible for cementation processes taking place during the alteration of the fines. The characterization of secondary mineral phases such as green rust helps to understand the alteration processes.

The spatial and temporal evolution of conductivity, fluid composition during saturation and drainage and the amount of water extracted from the granite saw dust, allows understanding the influence of wetting-drying cycles in the granite fines.

Thermal activity of the coal waste dump in Katowice-Wełnowiec, Poland

Ciesielczuk, J.[1*], Bzowska, G.[2] & Cebulak, S.[2]
[1]Dept. of Fundamental Geology, University of Silesia, Sosnowiec, Poland ([*]justyna.ciesielczuk@us.edu.pl)
[2]Dept. of Mineralogy, Geochemistry & Petrology, University of Silesia, Sosnowiec, Poland

The coal waste dump in Katowice-Wełnowiec, Upper Silesia Coal Basin, Poland, which superstructures the former rubbish dump is located in the center of the capital town of Silesian voyewodship. The processes of selfheating of the organic matter still present within the waste rocks, as dispersed or as tiny laminas, has caused the selfignition of the dump on its northern, eastern and south-eastern slopes. As effects of burning, bad smell and toxic fumes emanate from the overburned places. The aim of our study is to recognize the main factors which influence the acceleration or delaying of the selfignition process in the coal waste rocks deposited on the dump, as it has been observed only in some selected places.

The following methods were used: mineral phases were determined by XRD, chemical composition and mineral habits and association by SEM-EDS, and the kind of coal and its percentage in the waste rock as well as temperatures of OH and H_2O loses from clay minerals by DTA.

All the samples were collected from different parts of the dump which have been thermally affected. The measured temperatures in sampling places range from 12^o to 460°C. They were collected from the surface, and up to a depth of 4 m. We have separately investigated samples of: (1) different mass, (2) with high and low oxygen access, (3) fine and semi-grinded, (4) with high amounts of coal (e.g. 53% of C)) and up to almost no coal (0.6% of C), (5) samples were heated up to 600-700°C and 1000°C, (6) different sorts of coal, (7) different degrees of weathering, (8) different locations of coal laminas inside the waste rock piece or on its surface, (9) presence of iron minerals, (10) mineral composition of the waste rock (the amount of quartz and feldspars, kinds of clay minerals and micas, presence and amount of carbonates), and (11) geographical and climatological factors: the location of the slopes, wind direction, intensity of the rainfall and snowfall. The only factor which is important, but impossible to be taken into consideration, was the time of the processes duration.

The best example exemplifying the difficulty of the investigated problem is the sample collected from the place where measured temperature was 350°C. Mineralogically mullite was the main phase present there. According to literature data, mullite can form as a result of kaolinite heating at 1150-1250°C. The ceramic experiments show that the presence of iron minerals and feldspars can lower the temperature of mullite formation to 850°C, suggesting that in hydrothermal environment mullite can crystallize at 500-575°C, but not at 350°C as it has been measured so far!

As the results show, all factors which have been taken into account are important and have the effects on the sample behaviour. This is why the problem of selfheating and selfignition of the coal dumps requires a precise and detailed research.

CO_2 binding by alkaline waste materials: reduction of greenhouse gas emissions and benefit for waste deposition?

Bauer, M.[*], Gassen, N. & Peiffer, S.
Dept. of Hydrology, University of Bayreuth, Germany
([*]markus.bauer1@uni-bayreuth.de)

Alkaline waste materials were shown to be capable of CO_2 binding through fast carbonation reactions [1]. While natural minerals feasible for such a process normally have to be mined, transported or pretreated before use, alkaline wastes (such as combustion fly ashes) are often already available on site at CO_2 sources, like power plants, and readily react on short time scales [2]. During carbonation the mineralogy of the material changes [3]. The ALCATRAP project therefore determines the CO_2 binding potential of different alkaline wastes in laboratory and pilot scale experiments and estimates the effect of carbonation on leaching of metals or anions.

Alkaline wastes, such as fly/bed ashes from lignite, coal, biomass, wood and municipal solid waste incinerators and steel slags, were therefore tested in CO_2 uptake experiments under different conditions (temperature, mixing, pCO_2, CO_2 flow). Two different mixing systems, one for aqueous (Solid/Liquid ratio < 0,2 w/w) and one for semidry (Solid/Liquid ratio > 2 w/w) conditions, were compared. Furthermore, these laboratory findings were used for construction and experimental design of an ALCATRAP pilot plant, operating since September 2009, which enables us to elucidate the applicability of the method on a larger scale.

All waste materials from the sources listed above were able to sequester considerable amounts of CO_2. CO_2 gas phase concentrations decreased while the dissolved inorganic carbon concentration of the aqueous phase and the carbonate content of the solid phase increased. The process was controlled by the initially fast dissolution of CaO/MgO minerals, providing alkaline earth metal cations and increasing the pH. Dissolution of CO_2 induces the $CaCO_3$ precipitation.

The CO_2 uptake varied for different alkaline waste samples, with highest binding capacities (up to 0,1 g kg^{-1}) with lignite fly ashes and steel slags. Increasing temperature accelerated the reaction rate but also increased the overall CO_2 binding capacity (up to between 0,15 and 0,23 g kg^{-1}). This suggests that at high temperatures other mineral phases, e.g. Ca/Mg silicates or sulfates, become involved in the process. Currently source materials and reaction products are tested for the changes in the material properties due to carbonation. This includes grain size, pH as well as the leaching of heavy metals, sulphate and chloride.

Acknowledgements: The project is financed by the GEOTECHNOLOGIEN program of the German Federal Ministry of Education and Research.

[1] Costa, G. et al. (2007) *Environ. Monit. Assess.*, **135**, 55-75. [2] Back, M. et al. (2008) *Environ. Sci. Technol.*, **42**, 4520-4526. [3] Meima, J. et al. (2002) *Appl. Geochem.*, **17**, 1503-1513.

Heavy metal speciation on iron oxides precipitates in south Portugal abandoned mines

Antunes, R.[1], Candeias, A.E.[1], Goettlicher, J.[2], Steininger, R.[2] & Mirao, J.[3*]
[1]University of Évora, Chemistry Center of Evora and HERCULES Laboratory, Evora, Portugal
[2]Karlsruhe Institute of Technology, Institut für Synchrotronstrahlung, Eggenstein-Leopoldshafen, Germany
[3]University of Évora, Geophysics Center of Evora and HERCULES Laboratory, Evora, Portugal ([*]jmirao@uevora.pt)

In south Portugal, ores are composed mainly of pyrite with Cu, Zn, Pb and As sulphides and sulfosalts. Furthermore, ores include several minor elements like Mn, Co, Ni, Cd, Sb, Hg and Bi. Sulphides are quickly weathered, leading to water acidification and release of heavy metals. Some of these are hazardous and the drainage basins of the pollutant source areas often induce health concerns in resident populations. Consequently, mining and mineral-processing activities in south Portugal contribute with high amounts of metals to the environment and affect surrounding land and water quality, due to their cytotoxic, carcinogenic and mutagenic potential.

The geochemistry of pollutant elements is controlled by iron that precipitates by chemical bonding with oxygen. The stability of these iron oxides is controlled by climatic factors, imposing a parageneses that is geographically dependent and seasonal. It was hypothesised that these phases could uptake pollutant metals from contaminated waters either by coprecipitation, surface precipitation or a combination of the two.

The iron oxides were collected as chemical sediments in streams and ponds. Selected samples were mounted in epoxy resins preserving the original stratigraphy. The spatial characterization by micro-XRF mapping and XAFS spectroscopy was conducted at the SUL beamline, ANKA synchrotron.

The X-ray fluorescence mapping shows that the chemical elements associations are complex. For example, a large cross-section roughly at the base of the sequence is very enriched in iron and copper and depleted in zinc whereas, at the top of the sequence, the three elements coexist in a same enriched cross-section. This means that the cooper is associated with iron but the zinc has a more complex behaviour. Furthermore arsenic and lead are both associated to sulphate compounds.

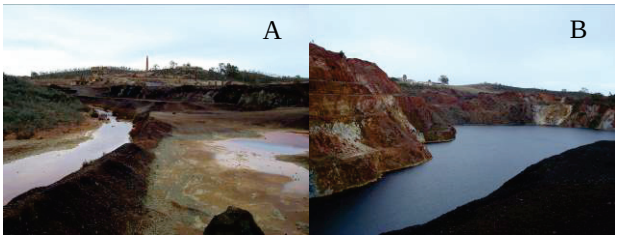

Fig. 1: St. Domingos abandoned mine, south Portugal, image from the open pit (A) and from drainage basin (B).

Preliminary XANES and EXAFS data show that iron is in several different phases. This kind of behaviour is well known from pH/Eh stability diagrams applied to iron compounds in these environments. In addition, copper, arsenic and zinc change their speciation when the iron phases change.

It is expected that the experiments can enlighten the electronic state of each metal and crystalline state of iron oxides. We hope to contribute to a better understanding of the general processes of heavy metal dispersive phenomena in sulphides from abandoned mines.

[1] Morais, C. et al. (2008) *Mineral. Mag.*, **72(1)**, 467-472 [2] Rosado, L. et al (2008) *Mineral. Mag.*, **72(1)**, 489-494

Mineralogical and geochemical spatial analyses of the Hop waste-rock dump at the Roşia Montană gold mine, Romania

Azzali, E.[1], Dal Santo, M.[2], De Capitani, L.[2], Forray, F.L.[3] Gál, Á.[3], Grieco, G.[2], Marescotti, P.[1*], Pareschi, R.[2], Porro, S.[2] & Szakács, A.[4]
[1]DIP.TE.RIS., Università di Genova, Genoa, Italy ([*]marescot@dipteris.unige.it)
[2]Dip. Scienze della Terra, Università di Milano, Milan, Italy
[3]Dept. of Geology, Babeş-Bolyai University, Cluj Napoca, Romania
[4]Dept. of Environmental Sciences, Sapientia University, Cluj Napoca, Romania

In this work, the 2.5 ha Hop waste-rock dump from the Roşia Montană gold mine (Romania) was investigated using mineralogical, geochemical, and geostatistical analyses.

The Roşia Montană hydrothermal ore deposit is hosted in andesites and dacites of Neogene age piercing the prevolcanic sedimentary basement as breccia pipes [1]. The volcanic and subvolcanic rocks show pervasive adularia alteration with a phyllic overprint, as well as local silicification and argillic alteration. They host polymetallic sulphides and Au-Ag-Te mineralisations; they are present in epithermal veins, mineralized phreatomagmatic breccias, and stockworks [2]. The ore deposit was mined both underground and in open pit for more than 2000 years. Intensive supergenic alteration due to AMD processes is testified by acid sulphate waters and by the precipitation of large amounts of secondary minerals.

The waste dump shows heterogeneities even at the field scale mainly evidenced by differences in colour. Twenty-two samples were collected following a square cells grid. The particle size distribution was obtained by dry sieving. The mineralogy, petrography and geochemistry were studied by means of optical microscopy, SEM-EDS, XRPD, XRF and ICP-AES analyses.

Samples were poorly sorted and could be classified as sandy gravel sediments. Their paste pH values show a wide variability (3-8) strictly related to sulphur and carbonate contents. Lithology is heterogeneous, comprising the following lithotypes: metasomatized porphyritic dacites, andesites, s flyschoid rocks and polygenic breccias. According to Acid Mine Drainage (AMD) potential these lithotypes contains the following mineral species: 1) AMD-producing sulphides (pyrite ± sphalerite ± chalcopyrite ± marcasite) varying from << 1% up to 5%; 2) AMD-neutral silicates (quartz, alkaline feldspar and micas with variable amounts of cryptocrystalline aphanitic groundmass of the volcanic rocks; 3) AMD-reducing carbonates (calcite + dolomite ± siderite ± rodochrosite) that are generally trace to minor constituents, with the exception of few samples where they represent about 5% of the total constituents. Amphiboles, apatite, rutile and zircon are the main accessory minerals. Secondary minerals that formed as a consequence of AMD processes vary from 5 to 15 %; they are mainly represented by Fe-oxyhydroxides and -oxides and occur as pseudomorphic replacement after primary sulphides, or as voids and fractures filling. They are also present as oxidation halos within the groundmass and as tiny coatings that rim sulphide and silicate grains. Ephemeral sulphates recognized on field were not preserved in the samples. Metallic paragenesis is rich comprising both heavy metals derived from the mineralisation (Cu, Zn, Ag, Pb) and metals from host rock (Rb, Sr, Zr). Further investigation on heavy metal geochemistry and mineral chemistry is ongoing to define the relationships between metals distribution and AMD processes also in order to evaluate the pollution potential of the dump.

[1] Roşu, E. et al. (2004) *Schweiz.Mineral.Petrogr.Mitt.*, **84/1-2**, 153-172. [2] Wallier, S. et al. (2006) *Econ.Geol.*, **101**, 923-954.

The effect of Sb(V) on the transformation of ferrihydrite to goethite

Bolanz, R.M.[1*], Majzlan, J.[1], Ackermann, S.[2], Reich, T.Y.[3] & Kersten, M.[3]
[1]Inst. of Geoscience, Friedrich-Schiller-University, Jena, Germany ([*]ralph.bolanz@uni-jena.de)
[2]SGS INSTITUT FRESENIUS GmbH, Kölliken, Switzerland
[3]Inst. of Geoscience, Johannes-Gutenberg-University, Mainz, Germany

Many aspects of the environmental chemistry of antimony, from its global cycling to its local speciation, are still poorly understood [1]. Antimony can become a pollutant of soils and sediments, especially in acid mine drainage systems and shooting ranges, where it can become adsorbed by iron oxides. The most common Fe oxide in these settings is the poorly crystalline 2-line ferrihydrite, which can be transformed upon ageing to goethite or hematite [2]. The rate and products of the transformation depend on temperature, pH, and the presence of adsorbing ions or molecules [3]. The focus of this study was the formation rate of goethite from synthetic ferrihydrite in the presence of Sb(V).

To verify the association of Sb(V) with ferrihydrite, EXAFS spectra were collected at the Super-XAS beamline at the Swiss Light Source (SLS). In addition to the first coordination sphere (6 O atoms at 1.98 Å), two Fe atoms at the distance ~3.11 Å and four Fe atoms at the distance ~3.57 Å were detected. This result can be interpreted as a strong inner-sphere edge- and corner-sharing complexation on the ferrihydrite surface and agrees well with the conclusions of related studies of antimony adsorption onto Fe oxides [4,5].

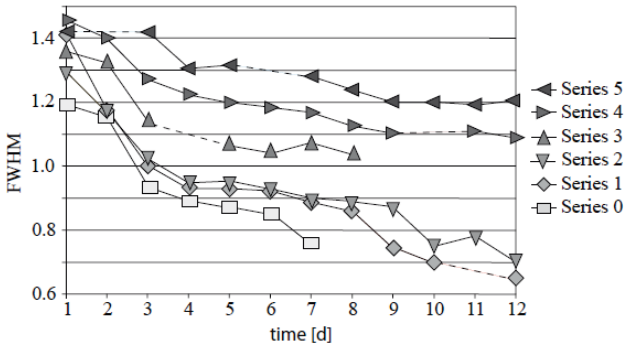

Fig. 1: Full width at half maximum (FWHM) of the (101) peak of goethite (Pnma setting) as a function of ageing time. Series 0 shows the formation of goethite without Sb(V), whereby the Sb(V) concentration increases from series 1 to series 5.

Two-line ferrihydrite was doped with different concentrations of Sb(V) by $KSb(OH)_6$. During aging of the doped ferrihydrite at 60 °C, twelve samples were taken, washed, dried and measured by X-ray diffraction (XRD). An increase of the FWHM with increasing Sb(V) indicates retardation of the transformation of ferrihydrite to well-crystalline goethite, similarly as already known for silicate [3].

[1] Filella, M., Williams, P.A. & Belzile, N. (2009) *Environ. Chem.*, **6**, 95-105. [2] Cudennec, Y. & Lecerf, A. (2006) *J. Solid State Chem.*, **179**, 716-722. [3] Cornell, R.M. (1987) *Z. Planzenern. Bodenk.*, **150**, 304-307. [4] Mitsunobu, S., Harada, T. & Takashi, Y. (2006) *Environ. Sci. Tech.*, **40**, 7270-7276. [5] Ackerman, S. et al. (2009) *J. Sci. Total Environ.*, **407**, 1669-1682.

Mineralogy and geochemistry of ferruginous AMD precipitates in the Łęknica region (the Muskau Arch, western Poland)

Bożęcki, P.[*] & Rzepa, G.
Dept. of Mineralogy, Petrography and Geochemistry, Faculty of Geology, Geophysics and Environmental Protection, AGH - University of Science and Technology, Krakow, Poland
([*]pbozecki@geol.agh.edu.pl)

The Muskau Arc is a large horseshoe-shaped glaciotectonic belt formed mainly during the Mid Polish Glaciation. Intense disturbances caused uplifting of the Neogene lignite beds (as well as co-occurring sands and clays). These deposits were excavated in numerous quarries and mines, from the late 18th to the late 20th century. The last active lignite mine pit “Babina” (located on the south east of Łęknica) was closed during the early seventies. The abandoned mining areas were filled with water, forming so-called "anthropogenic lakeland". Oxidation of sulphide minerals caused the formation of highly acidic waters. Released iron and sulphates precipitated by forming ochreous Fe-rich accumulations. The aim of this study was to determine the mineralogical and geochemical characteristics of these sediments. For this purpose, over 65 water and precipitate samples were collected.

The waters in the studied area are highly mineralised (electrolytic conductivity ranges from 600 up to 2900 μS/cm), acidic (pH 2,3-7,4) and characterised by very high Fe and sulphate concentrations, reaching ca. 525 and 3000 mg/dm^3, respectively. Ca^{2+} and Mg^{2+} contents are also high and reach about 380 mg/dm^3 and 58 mg/dm^3, respectively, while concentrations of Na^+, K^+ and Cl^- are relatively low (usually few mg/dm^3).

The precipitates are reddish-brown and orange, highly porous and contain numerous organic remnants. In many cases, especially during dry periods, white, yellowish or transparent crystals of gypsum (up to 2 mm in size) cover the sediment’s surface.

Apart from gypsum, the main constituents of the precipitates are goethite α-FeOOH, schwertmannite $Fe_{16}O_{16}(OH)_{12}(SO_4)_2 \cdot nH_2O$ and jarosite $KFe_3(OH)_6(SO_4)_2$. Goethite can be either well or poorly crystalline, depending probably on the formation conditions and water chemistry. Schwertmannite is always poorly ordered and usually forms, typical for this hydroxysulphate, hedgehog-like aggregates of small needle-shaped crystallites (< 2 μm long). Jarosite, on the other hand is much better crystalline, forming a few micrometers in size, pyramidal or platy crystals. Such mineral associations are typical of the AMD environments, although; the concentrations of trace elements in the sediment are lower than these of the other AMD areas. This is probably due to relatively simple composition of the weathering sulphides.

Oxidation of Fe^{2+} is relatively slow, while the rate of sediment formation in the Łęknica region is more rapid. This implies that formation of the precipitates is catalyzed by microorganisms. Seasonal variability in the rate of sediments formation and in the number of specific groups of microorganisms supports this conclusion.

Acknowledgements: This work was supported by MNiSW: (project No. 0700/B/P01/2009/37) and AGH-UST (research project no. 11.11.140.158).

Mineralogy of silicoclastic rocks deposited on an overburned coal waste dump in Wojkowice, Upper Silesia, Poland

Ciesielczuk, J.[1*] & Bzowska, G.[2]
[1]Dept of Fundamental Geology, University of Silesia, Sosnowiec, Poland ([*]justyna.ciesielczuk@us.edu.pl)
[2]Dept. of Mineralogy, Geochemistry & Petrology, University of Silesia, Sosnowiec, Poland

For the purpose of investigating the mineral transformations which have occurred on coal waste dumps due to self-heating and self-ignition, the dump at the Coal Mine Jowisz in Wojkowice, Upper Silesia, Poland, was chosen as an example. The Jowisz Coal Mine was active from November 1912 to April 2000. Coal wastes were deposited there from the sixties to the eighties of the XX century. The coal dump in Wojkowice covers an area of approximately 7 ha, reaching to 21.5 m at its highest point and containing about 1,200,000 tons of waste. The dump had been affected by self-ignition. High temperatures have caused changes to the mineral compositions of the waste rocks. For the last few years, the dump has been cool and the wastes have been exploited.

Areas of dumps affected by fire are divided into three zones: (1) the central fire core, where strongly overburned rocks are welded together by slag, (2) the external aureole where rocks have the colour of hematite, but no slag is present, and (3) the part unaffected by fire in which the rocks are black in colour with small laminae of coal. Three types of rock with different grain sizes were collected from each zone: sandstones, mudstones and siltstones. In addition, slag from the core of fire was studied. For precise identification of the mineral phases present, and for chemical identification, the following methods were used: XRD, SEM-EDS and microprobe analysis.

The intensity of the thermal influence on the waste rocks deposited on the dump can be estimated based on the presence of amorphous material of silica- or feldspathic composition, and of mullite and indialite – the products of high temperature transformation of clay minerals. The presence of spinels or hematite is also indicative.

Among the silicoclastic samples from within the first zone, the most highly thermally altered is a siltstone joined to slag. It consists of amorphous material (~30%), indialite and mullite (~55%), hercynite and hematite (~10%), quartz (~5%) and traces of anorthite and pyroxene. Mudstone also contains amorphous material (~48%) but no indialite and only ~6% of mullite. This rock also contains mica, the structure of which is thermally changed, quartz (~20%) and K-feldspar (~12%). Very fine-grained sandstone is mainly composed of kaolinite and chlorite (clinochlore) (~30%), thermally-affected dioctahedral mica (~20%), quartz (~30%), K-feldspar (~12%), hematite (~3%) and an amorphous substance. The least thermally affected is feldspathic sandstone which consists of quartz (~50%), the clay minerals kaolinite and chlorite (~16%), illite or thermally affected mica (~8%), K-feldspar (~18%) and hematite (~5%). Neither of the last two rocks contains mullite or indialite. The mineralogical composition of the slag differs significantly from the other rocks. It is composed of cristobalite and tridymite (~40%), magnetite, hercynite and hematite (~25%), anorthite (~20%), augite (~8%), indialite (~6 %), and traces of quartz. There is no mullite.

The mineral transformations in the silicoclastic rocks depend on not only the temperature, but also rock type, grain size, and the local conditions generated by the penetration of heat and the lack of oxygen. Minerals crystallized from the melt that formed the slag represent the mineral assemblage of a magmatic rock.

Seasonal variations of Zn, Cu, As and Mo in an As-rich stream at the Mokrsko, Czech Republic

Drahota, P.[1,2*], Mihaljevič, M.[1], Grygar, T.[3] & Filippi, M.[2]
[1]Inst. of Geochemistry, Mineralogy and Mineral Resources, Faculty of Science, Charles University, Prague, Czech Republic ([*]drahota@natur.cuni.cz)
[2]Inst. of Geology, Academy of Science, v.v.i., Prague, Czech Republic
[3]Inst. of Inorganic Chemistry, Academy of Science, v.v.i., Prague, Czech Republic

The Mokrsko gold deposit (Czech Republic) is probably the largest gold deposit in Central Europe unaffected by mining. Monthly sampling of slightly alkaline stream draining the natural As geochemical anomaly of the gold deposit revealed seasonal variations in dissolved Zn (maximum concentration 7.2 μg/l), Cu (≤2.7 μg/l), As (≤316.1 μg/l) and Mo (≤1.9 μg/l). The contents of dissolved trace metal cations increased by 330% (Zn) and 178% (Cu), with minimum and maximum mean concentrations in the autumn and spring, respectively. The lowest concentrations were associated with the highest pH values (Zn: $r=-0.51$, $p<0.01$; Cu: $r=-0.41$, $p<0.05$) during the autumn. The seasonal variations of the oxyanions were slightly smaller (As: 189%; Mo: 123%) and displayed almost opposite patterns to those of the metal cations. Inconsistent timing of seasonal streamflow and trace element cycling suggested that one or more in-stream biogeochemical processes rather than mere hydrologic changes are the primary control mechanism for seasonal trace element cycles in the stream.

The seasonal Zn and Cu cycles are believed to be caused by cyclic sorption and desorption onto oxyhydroxide substrates in response to the seasonal cycle of the stream pH. In contrast, the As and Mo seasonal variations are more consistent with Mn redox reactions. This hypothesis is supported by the very significant correlation of these oxyanions with Mn (As: $r=0.72$, $p<0.001$; Mo: $r=0.69$, $p<0.001$). The opposite concentration effect for trace metal cations relative to trace element oxyanions and Mn could be attributed to consistent timing among seasonal changes in the pH and oxic/anoxic conditions within the stream sediment. Both processes are controlled by the balance between photosynthesis and respiration.

Some part of the As in the stream sediment is bonded in crystalline arsenates (pharmacosiderite and arseniosiderite), jarosite and coprecipitated Ca-As arsenate in Fe oxyhydroxides, indicating a relevant thermodynamic and/or kinetic barrier in their dissolution after their erosion from the soil and saprolite [1]. Under fluvial conditions, As as well as other trace elements were mainly scavenged by low crystalline Mn oxides and ferrihydrite. The results of mineralogical study and single extractions indicated the abundance and reactivity of oxyhydroxide substrates that could undoubtedly play an important role in the assumed sorption and redox processes.

[1] Drahota, P. et al. (2009) *Sci Total Environ*, **407**, 3372-3384.

Arsenic mineralogy and mobility in a medieval mine dump

Filippi, M.[1*], Drahota, P.[1,2], Machovič, V.[3,4] & Böhmová, V.[1]
[1]Inst. of Geology, Academy of Science, v.v.i., Prague, Czech Republic ([*]filippi@gli.cas.cz)
[2]Inst. of Geochemistry, Mineralogy and Mineral Resources, Faculty of Science, Charles University, Prague, Czech Republic
[3]Inst. of Chemical Technology, Prague, Czech Republic
[4]Inst. of Rock Structure and Mechanics, Academy of Science, v.v.i., Prague, Czech Republic

Environmental samples collected from an arsenic-rich medieval waste dump and the surrounding soils near the arsenopyrite Giftkies mine (Jachymov ore district, Czech Republic) have been studied to understand the fate of arsenic (As) in such an environment.

Successive application of XRD, SEM, EMPA, Raman micro-spectroscopy and a set of chemical extractions and solubility measurements helped to distinguish and characterize the As-bearing minerals and evaluate their environmental stability. Abundant ferric arsenate minerals kaňkite, scorodite and pitticite, locally associated with arsenian jarosite, sulphur and ferric oxyhydroxides (goethite, hematite and lepidocrocite), were determined as the major oxidation products of arsenopyrite. Field observations together with an SEM investigation pointed toward the following succession of arsenates: scorodite – pitticite – kaňkite. Scorodite originated directly on the weathered arsenopyrite; kaňkite and especially pitticite (often present in the form of stalactites) precipitated from As-rich solutions migrating downwards for a very short distance. Chemical analyses of the whole samples showed very high As contents in the dump material (up to 13 wt. %) but relatively low contents in the underlying and surrounding soils (up to 0.6 and 0.4 wt. %, respectively). Goethite and hematite are the only detected As-bearing minerals in the soils.

Selective chemical extractions (sulphate and phosphate sorbed fractions and oxalate reducible fraction [1]) were performed (i) on the dump and soil bulk samples as well as (ii) on the pure ferric arsenates to interpret the chemical extractions in the bulk samples. According to these observations, As was mainly released during reducible extraction in the dump (up to 85% of the total As content - TAC) which corresponded to the total dissolution of pitticite and kaňkite and traces of scorodite (~5%). The reducible fraction of As is lower in the soil (up to 62% TAC) and is especially related to the dissolution of goethite. In contrast, the content of phosphate-exchangeable As is much higher in the soil (up to 28% TAC) compared to the dump samples (< 8% TAC). This points towards a significant amount of specifically-sorbed As that may be potentially mobilized due to changes in the pH or addition of P.

The dissolved arsenic concentrations in the dump (1.4-2.8 mg/l at pH 3.3-4.1) are controlled by the scorodite solubility, which is approximately an order of magnitude lower than the kaňkite solubility and at least two orders of magnitudes lower than the pitticite solubility. The content of pore-water As in the surrounding and underlying soil is very low (<20 µg/l As at pH 4.5-6.1), suggesting efficient As adsorption by Fe oxyhydroxides.

[1] Wenzel, W.W. et al. (2001) *Anal Chim Acta*, **436**, 309-323.

Bukovskýite from medieval dumps at Kutná Hora, Czech Republic; An example of crystallization from Si-Al gel-like medium

Loun, J.[1*], Novák, M.[2] & Kocourková, E.[3]
[1]Dept. of Mineralogy and Petrology, National Museum, Praha, Czech Republic ([*]loun.jan@seznam.cz)
[2]Dept. of Geological Sciences, Masaryk University, Brno, Czech Republic
[3]Dept. of Mineralogy and Petrography, Moravian Museum, Brno, Czech Republic

Bukovskýite (Fe^{3+}_2 $(AsO_4)(SO_4)(OH)$. $7H_2O$) was described as a new mineral from this locality [1,2]. It occurs in medieval dumps at Kaňk village near Kutná Hora along with common Fe^{3+}-arsenates and sulphoarsenates (scorodite, parascorodite, kaňkite, zýkaite) and less common sulphates (gypsum, melanterite, jarosite, aluminite, alunogen, rozenite) as pale yellowish-white to grayish-yellow microcrystalline aggregates forming nodules commonly several cm across but locally up to ~1 m in size.

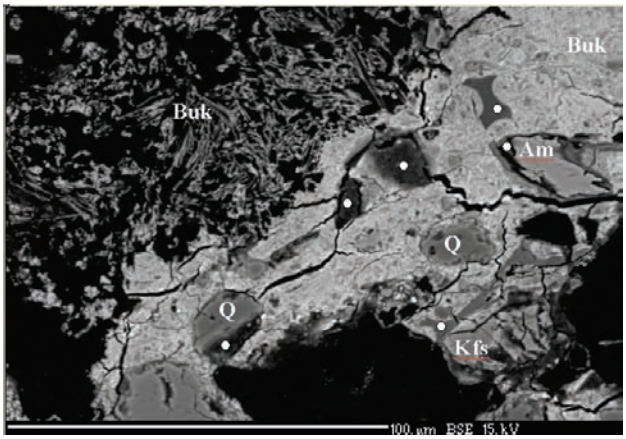

Fig. 1: BSE image showing dissolution of various minerals and crystallization of bukovskýite from Si-Al gel-like medium. The light substance consists of partly crystallized bukovskýite (Buk), relics of various minerals: Q = quartz, Kfs = K-feldspar, Am = Amphibole, and Si-Al gel-like medium (white dots).

Bukovskýite is a product of recent weathering of common sulphides arsenopyrite and pyrite. Field survey revealed two distinct As-rich mineral assemblages on the dumps: 1) scorodite+kaňkite+zýkaite aggregates (with no bukovskýite) in clastic gangue waste material, and 2) abundant bukovskýite with small nodules of parascorodite in clayish parts of the dumps. The almost monomineralic bukovskýite-rich zone commonly occurs ~ 1-2 m under the dump surface. The nodules studied primarily by EMPA revealed the crystallization of bukovskýite needle-like crystals from Fe,As,S-bearing Si-Al gel-like medium (10-82 wt.% SiO_2; 0.7-7 wt.% Al_2O_3; 1.7-24 wt.% Fe_2O_3; 2.2-19 wt.% As_2O_3, 1.2-4.6 wt.% SO_3; ∑oxides 37-89 wt.%; Fig. 1). It is a product of dissolution of various minerals of the dump (Fig. 1) at strongly acidic conditions (pH = 2.4-3.9). This process may be related to the clays used during processing in medieval times.

[1] Novák, F. et al. (1967) *Acta U. Carol. Geol.*, **4**, 297-325. [2] Johan, Z. (1986) *Neues Jb. Miner. Monat.*, **H.10**, 445-451.

Significance of bacterial adhesion in the microbiologically mediated dissolution of metal sulfides: an experimental approach

Lu Xiancai[1*], Lu Jianjun[1], Tu Bowen[2], Zhao Xingqing[1], Li Juan[1], Zhou Yuefei[1] & Han Xiaodong[2]
[1]State Key Lab for Mineral Deposits Research, School of Earth Sciences and Engineering, Nanjing University, Jiangsu, China ([*]xcljun@nju.edu.cn)
[2]Medical school, Nanjing University, Jiangsu, China

The dissolution of the metal sulfides in polymetallic mines not only produces acid mine drainage (AMD), but also releases abundant heavy metals into the surroundings, which generally results in serious environmental contamination. Extensive studies indicate that various microorganisms play important roles in the dissolution of minerals. In recent years, the adhesion of bacteria on mineral surfaces has attracted a lot of attention [1]. In general, the contact between the bacterial external structure and the mineral surface can ehance the dissolution of minerals. This study experimentally investigated the effects of adhesion of *Acidithiobacillus ferrooxidans* on the dissolution of pryite, chalcopyrite and arsenopyrite. Furthermore, key proteins of this bacterium closely related to adhesion behaviors were studied by using two-dimensional electrophoresis, MALDI-TOF MS and checkage of amino acid sequence and peptide mass fingerprint between local and NCBI database. *Acidithiobacillus ferrooxidans* was separated and purified from acid mine drainage (AMD) in eastern China and identified by 16S rDNA. In order to disclose the contribution of adhesion of bacteria, comparative experiments with/without direct contact between cells and minerals were carried out by the employment of dialysis bags.

Remarkable differences were observed between the experimental minerals with and without dialysis bags. The dissolution rates of the sulfides with bacterial adhesion are clearly higher than those in comparative cases. The mineral surface with bacterial adhesion displays many erosion pits, whereas the encased mineral particles are covered by secondary sulfate precipitation and no pit was found. The shape and size of the pits are similar to that of bacteria cells despite of the mineral types. It is deduced that adhered bacteria and their metabolites can promote the dissolution of sulfides via surface corrosion.

In proteomic analysis, more than 30 types of proteins up-regulated had been identified in the two-dimensional electrophoresis of the total protein fraction from different phases of the experimental bacteria cells. Several proteins possibly control bacterial adhesion and quorum sensing during the dissolution of sulfides. Based on the correlation between their functions and expression levels of these proteins in different experimental stages, it is concluded that some of these proteins can help bacteria adhere to mineral surfaces, and that overtop density of cells will result in expression levels of the other proteins down-regulated, and then it greatly influences the bacterial adhesion and even to the formation of biofilms on mineral surfaces. However, more detailed studies about the roles of specific proteins related to oxidation of sulfides are still not resolved for the high complexity of the interfacial components and interactions.

Acknowledgements: This research was supported by National Priority Development Project Fundamental Research ("973" program) (No. 2007CB815603) and National Natural Science Foundation of China (No. 40930742).

[1] Harineit, K. et al. (2006) *Hydrometallurgy*, **83**, 245-254.

EXAFS analysis of As speciation in poorly ordered Iron(III) (oxyhydr)oxides and oxyhydroxysulfates from Acid Mine Drainage deposits

Maillot, F.[1*], Morin, G.[1], Wang, Y.[2], Juillot, F.[1], Cassiot, C.[3], Bruneel, O.[3], Egal, M.[3] & Calas, G.[1]
[1]Institut de Minéralogie et de Physique des Milieux Condensés, Universités Paris 6 et 7, et IPGP, Paris, France ([*]fabien.maillot@impmc.upmc.fr)
[2]Laboratoire de Chimie de la Matière Condensée de Paris, Université Paris 6, Paris, France
[3]Laboratoire Hydrosciences Montpellier, Université Montpellier 2, Montpellier, France

Acid Mine Drainage (AMD) is generated by the microbially catalyzed oxidization of sulfide minerals (usually pyrite and arsenopyrite) exposed to the atmosphere and meteoric waters in metal sulfide mines and associated mine wastes. The resulting waters are highly acidic and enriched in sulfates and in ferrous iron. The concentrations of arsenic in AMD can reach hundreds of mg/l, as a result of the oxidation of As-rich sulfides [1]. Such As concentrations are potentially harmful for the aquatic ecosystem located downstream from mining sites and compromise a significant part of freshwater resources. In AMD, aqueous arsenic occurs either as As(III) or As(V) [1], with As(III) being more toxic for humans and animals and more mobile than As(V)

The investigation of acid mine drainages, using synchrotron-based techniques, has shown the importance of As adsorption on, or coprecipitation with, hydrous ferric oxides in delaying the long-term impact of As on the biosphere. Although in rare cases the precipitation of tooeleite, an As(III)–Fe(III) mineral, has been observed [2], the As(III) form is rather stable in solution, especially at low pH. On the contrary, As(V) presents a strong affinity for Fe(III). In AMD from the former Carnoule`s mine (France), the formation of an amorphous As(V)–Fe(III)-oxyhydroxysulfate precipitate has been reported [2] [3]. More frequently, As(V) forms scorodite or adsorbs on schwertmannite and ferrihydrite as a function of pH [4] [5]

In the present communication, we will present further EXAFS results on the speciation of arsenic in biogenic various iron(III) oxyhydroxide and oxyhydroxysulfate sampled in Acid Mine Drainage systems. Spectroscopic data indicate arsenic can be adsorbed or coprecipitated with Fe(III) depending on the As/Fe ratio and As oxidation state. This work bring further information on the mechanism of the As scavenging by iron minerals at the atomic scale, in impacted natural context.

[1] Williams, M. (2001) *Environ.Geol.,* **40**, 267-78. [2] Morin, G. et al. (2003) *Environ.Sci.Technol.,* **37**, 1705-1712. [3] Leblanc, M. et al. (1996) *Appl.Geochem.,* **11**, 541-54. [4] Carlson, L. et al. (2002) *Environ.Sci.Technol.* **36**, 1712-9. [5] Morin, G. & Calas, G. (2006) *Elements,* **2,** 97-101

Effect of mineralogy and chemistry of metal polluted soils on biodiversity and metal bioaccumulation (Libiola Mine, Italy)

Marescotti, P.*, Carbone, C., Azzali, E., Roccotiello, E., Zotti, M. & Mariotti, M.G.
DIP.TE.RIS., University of Genova, Genoa, Italy
(*marescot@dipteris.unige.it)

The research was carried out in the contaminated soils of the abandoned Libiola sulphide mine (NW Italy) in order to study the relationships between soil composition and biodiversity and to assess the possible accumulation of specific ecotoxic metals in plants and fungi. Nowadays, the entire mining site is characterized by active Acid Mine Drainage process, which determines acidification and heavy metals pollution of soils and waters. As a consequence, the soil related to the waste-rocks deposits and the open pit excavations exceeds residential and industrial limits for a number ecotoxic metals, such as Cr, Co, Ni, Cu, Zn, and Cd.

Ten sampling sites have been chosen in the mining area; seven of these sites (V-sites) correspond to an area of open pit mining, whereas the remaining three sites (F-sites) are located at the base of a 2 ha sulphide-rich waste-rock dump. The V-sites are composed by minor amount (5%) of pyrite showing various degree of oxidation. Clasts of serpentinite, basalts, and ophiolitic breccias are the main components ranging from 50 to 80 wt%. As a consequence the mineralogy of the V-sites is dominated by serpentine-group minerals, chlorite, plagioclase, magnetite and other spinels. Secondary minerals (5-10 wt%) are mainly represented by Fe-rich smectites with very minor amount of goethite and hematite. Serpentinite and basalts mineral assemblages are the main constituents (40-60 wt%) also of the F-sites. Nevertheless, with respect to V-sites, they are significantly enriched (10-30 wt%) in sulphide minerals (pyrite ± chalcopyrite ± sphalerite). The remaining fraction (10-30 wt%) is mainly represented by goethite and hematite with minor Fe-smectites. V-site and F-site samples are significantly different also in their chemical composition: V-sites are enriched in Ca, Mg, Mn, Ni and Cr. Conversely, the F-sites samples are enriched in Fe, Cu, Zn, S, Ag and Au due to the high amounts of Fe-Cu sulphides and Fe-bearing secondary minerals. Specifically for the F-sites, it is worth noting that most of the heavy metals released during sulphide oxidations are efficiently scavenged by the new forming Fe-oxides and oxyhydroxides.

As regards fungi, the study has considered both the micro and macro fungal flora. Most isolated microfungi species are tolerant to a wide range of pH and the biodiversity is remarkable in spite of heavy metals concentrations in native soils (F-sites) as high as 2400 mg kg^{-1} Cu and 1500 mg kg^{-1} Cr.

As concerns macrofungi, *Scleroderma polyrrhizum* (J.F. Gmel.) Pers. and *Thelephora terrestris* Ehrh. sporomata from F-sites have highlighted the capability to accumulate Ag (>50000 µg kg^{-1}) and Cu (>1000 mg kg^{-1}), respectively.

The V- and F-sites are characterised by different successional plant communities ranging from herbaceous to arboreal stages. Among several species *Alyssoides utriculata* has showed more than 1000 mg kg^{-1} Ni in leaves, suggesting a preferential metal allocation. The plant grows on V-sites and is almost absent on F-sites where-Cu sulphides and Fe-bearing secondary minerals are abundant.

The contaminated environment largely affected the biodiversity of the area and exerted a strong selective pressure on the local flora and mycoflora. The study has revealed peculiar plants, which could be fruitfully employed for future phytoremediation, while fungi could help the natural recolonisation of the surrounding vegetation.

Mineralogical and chemical evolution of ochreous precipitates from the Libiola Fe-Cu-sulphides mine (Eastern Liguria, Italy)

Marescotti, P.[1*], Carbone, C.[1], Comodi, P.[2], Frondini F.[2] & Lucchetti, G.[1]
[1]DIP.TE.RIS., University of Genova, Genoa, Italy
(*marescot@dipteris.unige.it)
[2]Dip. Scienze della Terra, University of Perugia, Italy

The Libiola mining area is characterized by active and intense AMD processes involving both the sulphide-rich waste rock deposits and the remaining outcropping and underground ore bodies. Due to these processes, most of the circulating surface and underground waters are strongly acidic (pH ≤ 3) and contain very high levels of ecotoxic elements derived from not only the sulphide mineralizations (such as Cu, Zn, As) but also the host rocks and gangue minerals (such as Cr, V, Ni). At the confluence of the mine-water discharge and unpolluted streams or runoff channels, extensive precipitation of Fe-rich authigenic minerals takes place. Significant mineralogical and chemical differences of the authigenic precipitates occur as a function of pH-Eh variations.

To better quantify the processes as well to monitor the changes in mineralogy and toxic elements distribution, we sampled water and ochreous precipitates (OP) at four mine adits (that continuously discharge acid mine waters) and downstreams from the emergence points where mixing with uncontaminated streams and runoff channels took place during raining periods. Electrical conductivity, pH, Eh, and T of the streaming waters were measured *in situ*, whereas the chemistry of waters and precipitates was determined by ICP-AES and -MS analyses. The mineralogy of the samples was analysed by means of XRPD and TEM.

Two groups of waters were distinguished on the basis of pH, Eh, SO_4, and dissolved metals contents. The first group corresponds to unmixed mine water and it is characterized by the lowest pH (2.37-2.72) and the highest Eh (562-624mV), SO_4 (4903-9450 mg/kg), and metal contents. The second group, sampled after the mixing with unpolluted waters, is characterized by a general reduction of metal load as well as by significant variations of pH (3.67- 4.40), Eh (336-496 mV), and SO_4 (492-1049 mg/kg).

The mineralogy of the OP were controlled by the pH, Eh, and SO_4 content of the corresponding waters; five groups have been distinguished on the basis of main mineral species (for each water, in parenthesis are reported pH, Eh (mV), and SO_4 (mg/kg), respectively): 1) jarosite-rich OP (2.37-2.42; 622-624; 7473-9450); 2) schwertmannite-rich OP (2.55-2.72; 562-588; 4903-5224); 3) goethite-rich OP (3.66-3.67; 465-497; 769-1049); 4) amorphous Fe-oxides rich OP (4.08; 356; 668); 5) ferrihydrite-rich OP (4.4; 490; 492). HR-TEM analyses revealed that most of mineral species within OP are nanominerals (ferrihydrite) or mineral nanoparticles (schwertmannite) that rapidly evolve toward more stable species (mostly goethite) as a consequence of ageing and/or variations of physico-chemical parameters of the circulating waters, as indicated by aqueous speciation and mineral stability calculations.

The bulk chemistry of the OP varies significantly among the different 5 groups. In particular, schwertmannite- and ferryhydrite- and amorphous-OP efficiently scavenge many metals of environmental concern (Cu, Pb, Zn, Ni, As, Cd, and Ag) due to their high surface area and adsorption capacity. Nevertheless, these elements are mainly scavenged through absorption and co-precipitation mechanisms and can be easily released during seasonal transformation and dissolution processes. Therefore, these ephemeral secondary minerals not only represent a short-lasting storage of contaminants but can also act as instantaneous sources of contaminants and/or acidity.

Kinetic testing and mineralogical characterization of sulphide mine wastes from the Oruro deposit (Bolivia)

Móricz, F.[1], Mádai, F.[1*] & Walder, I.F.[2]
[1]Institute of Mineralogy and Geology, University of Miskolc, Hungary ([*]askmf@uni-miskolc.hu)
[2]Kjeøy Research & Education Centre, Kjeøy, Vestbygd Norway

The Itos mine is located in the San Jose Mining District, Oruro, Bolivia. It is a worldwide-known polymetallic vein deposit that had been mined in the 20th century for silver in the early decades and later for tin. The deposit was formed by the superposition of two hydrothermal phases: a high-temperature one defined by cassiterite, pyrite and quartz; and a later one which deposited mostly silver-bearing sulfosalts such as jamesonite, freibergite, andorite, boulangerite, zinckenite and franckeite, accompanied by galena, chalcopyrite and pyrite.

Recently enormous heaps of mining wastes with strong ARD activity surround the town Oruro. Paste pH of the seepage water ranges between 1 and 2. The remediation strategy needed the detailed investigation of kinetics of mine waste minerals decomposition.

Three set of samples were collected from different mining wastes of the Itos mine: reprocessed flotation tailings, oxidized jig processing tailings (Itos jig tailing 01 and 02) and waste rocks (Itos Granza 01 and 02). The samples have been analysed using the column test as a kinetic test method, sequential extraction, EPMA and XRPD. The column test results were interpreted in terms of mineralogical data.

The kinetic test on waste rock samples were run for 101 days at the Kjeøy Research and Education Center (KREC) in Norway. The sequential extraction was made in a specialized Canadian geochemical laboratory and the mineralogical analyses were performed at the University of Miskolc.

The results from the kinetic tests (column test) show that these mine wastes have already been intensively oxidized; furthermore, the pyrite is partly replaced by different sulphates. The kinetic parameters and their change in time depend on average grain size, pyrite content and soluble sulphate content.

The analysis of the sequential extraction indicated that most of sulphur-bearing phases have been decomposed at step 5, that points to the secondary sulphate release potential of the wastes. Sequential extraction proved that there are also easily soluble heavy metal ions in the samples with high or toxic concentration.

The mineralogical analyses show that there are still large amount of those minerals which can oxidise and catalyse the ARD impact. The acid production have two sources: the main is the pyrite and the second one is the soluble secondary sulphate minerals, as jarosite, coquimbite, römerite, copiapite and melanterite.

Table 1: Calculated time for total pyrite degradation

Sample	Pyrite content (1)	Pyrite oxidation rate (2)	Estimated time (3)
Itos jig tailing-01	60	1.56	38
Itos jig tailing-02	50	5.95	8
Itos Granza-01	20	1.35	15
Itos Granza-02	20	5.72	4

(1) [g pyrite/kg sample] , (2) [g pyrite/kg sample/year], (3) years, if the speed of oxidation will not decrease in the future.

The geochemical model calculated from the kinetic test results and mineralogical analyses shows that the waste dumps need several decades to increase the pH to a normal level and decrease the concentration of the dissolved heavy metal ions.

Geological and biological characteristics of the environmental pollution in the Nistru-Băiţa mining area (Eastern Carpathians, Romania)

Nagy-Korodi, I.[1*], Fodorpataki, L.[1], Forray, F.L.[1], Ionescu, C.[1] & Tippelt, G.[2]
[1]Babeş-Bolyai University, Cluj-Napoca, Romania
([*]nagy-korodi.istvan@ubbcluj.ro)
[2]Paris Lodron University, Salzburg, Austria

The Nistru-Băiţa base metal and gold deposit is located in the Oaş-Gutâi Mountains. and belongs to the north-western part of the Neogene volcanic chain in the Eastern Carpathians. In the area the volcanic activity took place in Badenian-Pannonian, 15.4–7.0 M.a. ago [1] and produced calco-alkaline rocks ranging from basalts and basaltic andesites to dacites and rhyolites. The deposit was exploited mostly for Au, Pb, Zn and Cu, by underground and surface mining for a long period of time. Nowadays, the only active open pit still contaminates the Nistru-Băiţa river catchments system.

The samples taken from the Nistru-Băiţa waste dumps and alluvial sediments were investigated by X-Ray Diffraction (XRD) and Electron Microprobe (EMP) in order to outline the speciation of the main cations (Fe^{2+}, Fe^{3+}) and anions (SO_4^{2-}) and to identify the secondary minerals. The biological studies focused on experiments regarding the response of some terrestrial and aquatic plants to the Nistru-Băiţa waters.

The results show a significant pollution with high amounts of Fe, Al, Zn, Cu, Pb, as well as SO_4^{2-} in the mining effluents, and Nistru-Băiţa waters.

The Nistru waste dump material consists mostly of quartz, hydronium- and K-jarosites, goethite and gypsum. Kaolinite and akaganéite [β-$Fe^{3+}_8(OH,O,Cl)_{17}$] are subordinate.

The presence of light yellow to dark yellowish-reddish-brown precipitate forming rhythmic thin layers in the alluvia of the Băiţa creek indicates the mine influence. These deposits consist of Fe-SO_4-O-OH minerals, with metal scavenger properties. The light yellow layers are composed of K-jarosite, goethite, ferrihydrite, akaganéite and gypsum. The dark yellowish-brown and reddish-brown layers consist mainly of poorly crystallised akaganéite and schwertmannite [$Fe^{3+}_{16}(OH)_{12}(SO_4)_2$] mixed with goethite and quartz. In overall, the relative element concentration as revealed by EMP is the following: Fe >> S > Si > Al > P > Zn > As > Ca > Cu > Na > Mg >K > Mn. The presence of Zn, As and Cu is due to the alteration of sphalerite, arsenopyrite and chalcopyrite mineralization.

The experiments of growing various terrestrial and aquatic plants using the Nistru-Băiţa waters show reduced germination energy for seeds and inhibition of growth and reproduction. The ubiquitous presence of *Euglena mutabilis* Schmitz, a good microalgal indicator for acidic waters, demonstrates the intensity of the pollution in the area. The specific parameters of *Euglena mutabilis*, *i.e.* low pH, high concentration of total dissolved solids, and specific conductivity, reduce the biodiversity of periphyton in the environment area.

[1] Pécskay, Z. et al. (2006) *Geol. Carpathica*, **57(6)**, 511-530.

Removal of lead from wastewater by modified Venezuelian Red Mud

Omana Sanz, B., Gauthier, A.* & Dubois, M.
Laboratoire Génie Civil et géoEnvironnement, Université Lille, Villeneuve d'Ascq, France (*arnaud.gauthier@univ-lille1.fr)

Venezuela produces more than two millions tons of alumina per year. This production generates wastes (such as red mud) which are dumped in old lagoons near the Orinoco river. Actually, the quantity of stored mud is more than 15 million cubic meters [1]. Due to a high alkalinity (pH between 10 and 13) and its mineralogical and chemical composition, this waste becomes a real environmental problem. In order to reduce environmental impact, studies were performed on the adsorption capacity of this kind of wastes. In fact, textural and mineralogical properties of mud provide an important reactive surface with potential adsorption capacity for elements such as cadmium, lead or zinc [2,3]. The aim of this work is to evaluate the remediation potential of Venezuelan red muds. With this aim, we have studied the sorption capacity using lead (Pb) artificially contaminated solutions with varying pH and the lead concentration. The results are interpreted using the Langmuir's Isotherm (Fig. 1). The results show that the simple adsorption is not the only responsible for the lead retention in the system. Other mechanisms like absorption and precipitation can take place.

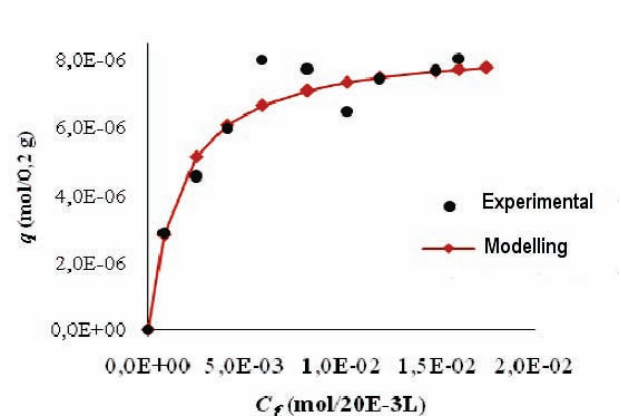

Fig. 1: Lead adsoption isotherm on red muds (pH 4, 25°C).

The Venezuelan red mud has a great potential as a sorbant of pollutant lead and possibly of other heavy metals, which gives it a remediation importance for the treatment of contaminated soils and waters.

[1] Lisen, M. et al. (2006) *Estudio Exploratorio de la Siembra del Vetiver en un Área Degradada por el LR.* The Fourth Internacional Conference on Vetiver – ICV4. [2] Apak, R. et al. (1998) *Water Research*, **32**, 430-440. [3] Brunori, C. et al. (2005) *J. Hazard. Mater.*, **117**, 55-63

Rapid mineralogical transformation of schwertmannite in presence of dissolved Fe^{2+}: mobility and effect of adsorbed arsenic

Paikaray, S* & Peiffer, S.
Dept. of Hydrology, University of Bayreuth, Bayreuth, Germany (*susanta@uni-bayreuth.de)

Poor structural stability of schwertmannite often leads to mineralogical transformation to thermodynamically stable iron oxides, i.e., goethite or hematite through extremely slow processes that completes in months to years [1]. Fe3+ reductive processes widely occur along schwertmannite-rich mine drainage localities catalyzing the reaction kinetics [2] where the phenomena is poorly understood. Excellent sorptive efficiency causes enriched arsenic levels in schwrtmannite, the fate and effect of which on transformation kinetics are unclear.

We investigated schwertmannite (SHM) metastability as a function of varied dissolved Fe^{2+} (0.4, 0.7 and 1.0 mmol L^{-1}) in a glove box for ~ 8 days at pH 7. The pH was maintained using PIPES buffer (pKa=6.8). Schwertmannites sorbed with 0.92 wt % As(III) (SHM-As) was investigated to study the fate and effect of sorbed arsenic. Solid phase was characterized by X-ray diffraction (XRD) and microscopic techniques (SEM), while aqueous phase was analysed for residual Fe^{2+}, As and desorbed SO_4^{2-}.

SO_4^{2-} was released rapidly releasing >45 wt % during 202 h and rate of desorption was relatively higher for SHM and also as dissolved Fe^{2+} concentrations increased. Complete adsorption of Fe^{2+} was observed in case of SHM, whereas minor amounts (~20 umol L^{-1}) was detected in case of SHM-As for initial 1.0 mmol L^{-1} dissolved Fe^{2+}. Schwertmannite was found as the predominant phase together with ferrihydrite (Fh) at lower dissolved Fe^{2+} (≤0.7 mmol L^{-1}), while lepidocrocite (Li) formed after 10 h with traces of goethite (Gt) that eventually transformed to Li and Gt after 202 h in presence of 1 mmol L^{-1} Fe^{2+} (Fig 1). Contrarily, sorbed As inhibits the reaction kinetics resulting Li formation after 34 h at 1 mmol L^{-1} dissolved Fe^{2+}. As was partially mobilized in course of transformation (< 1.0 %) and triggered by increased Fe^{2+} suggesting strong binding of As within SHM and the ageing products.

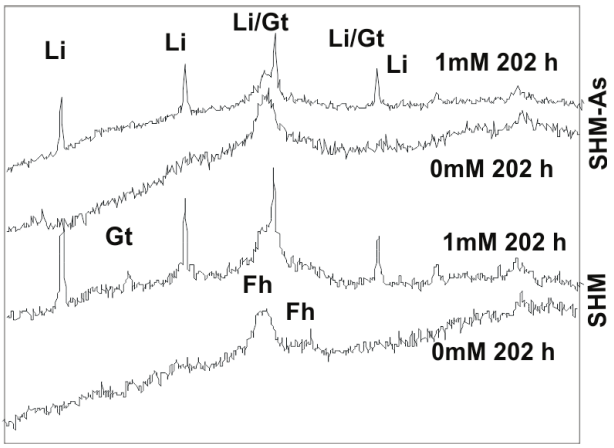

Fig. 1: Diffractograms of transformation products after 202 h.

This study demonstrates that presence of dissolved Fe^{2+} in schwertmannite rich natural streams significantly influence its metastability leading to high SO_4^{2-} loading into the stream. As-rich schwertmannites, which are commonly reported from mine effluents, stabilize the structure towards its sensitivity for Fe^{2+} catalytic transformation and hinders As mobility.

[1] Jönsson, J. et al. (2005) *Appl. Geochem.*, **20**, 179-191. [2] Burton, E.D. et al. (2008) *Geochim. Cosmochim. Ac.*, **72**, 4551-4564.

Uranyl sulphate minerals from the vein Červená, Jáchymov (St. Joachimsthal), Czech Republic

Plášil, J.[1*], Čejka, J.[1], Sejkora, J.[1], Novák, M.[2], Škoda, R.[2] & Dušek, M.[3]
[1]Dept. of Mineralogy and Petrology, National Museum, Prague, Czech Republic ([*]jakub_plasil@nm.cz)
[2]Institute of Geological Sciences, Masaryk University, Brno, Czech Republic
[3]Dept. of Structure Analysis, Institute of Physics, Academy of Sciences of the Czech Republic, Prague, Czech Republic

An interesting association of uranyl sulphate minerals was found in an abandoned adit at Červená vein (Rovnost shaft), Jáchymov, Czech Republic. Uranyl minerals are of supergene origin; their formation is related to the precipitation from acid mine drainage in the environment of the open mine-adit. The mineral association includes zippeite, pseudojohannite, Cu–Ca rich marécottite, rabejacite, uranopilite, unnamed Cu^{2+}–$(UO_2)^{2+}$–SO_4^{2-} phase and the new mineral sejkoraite-(Y)[1]. Minerals were studied by X-ray diffraction, EMPA, TG analysis and spectroscopic methods. A short description giving important physico–chemical properties of studied phases follows.

Zippeite occurs often as yellow to yellow-orange crystalline aggregates up to 1 mm. Refined unit-cell (Spgr. *C*2) is a=8.785(1)Å, b=14.025(1)Å, c=17.699(2)Å and β =104.196(7)°. According to EMPA main cation present in studied sample is potassium (0.91 K *apfu*).

Pseudojohannite occurs as yellow-green to green fine crystalline aggregates up to few mm in size. According to single crystal diffraction is triclinic of space group *P*-1, refined unit-cell is a=10.15(1)Å, b=11.52(8)Å, c=13.39(7)Å, α=95.5(5)°, β=108.1(4)°, γ=93.3(5)°. EMPA showed that at least two chemically different types of pseudojohannite exist, differing mainly in their Cu contents.

Cu-Ca rich marécottite forms sulphuric yellow to light green yellow aggregates up to few mm in diameter. Its powder diffraction pattern is similar to that of marécottite [2] even if slightly shifted. EMPA showed the presence of high Cu (up to 0.68 Cu *pfu*) and Ca (up to 0.40 *pfu*) in the cationic site.

Rabejacite occurs as yellow to orange yellow crystalline aggregates consisting of fine bipolar crystals (up to 10 μm in size). X-ray powder diffraction pattern is consistent with the published data [3]. By visual inspection, two types of rabejacite can be distinguished. Aggregates of orange colour represent altered ones with the surface enriched by Fe^{3+} and depleted in $(UO_2)^{2+}$ contents.

Uranopilite forms rich crystalline aggregates consisting of elongated prismatic crystals of sulphuric yellow colour. Its refined unit-cell is (Spgr. *P*-1) a=8.874(1)Å, b=13.985(2)Å, c=14.363(2)Å, α=96.71(1)°, β=98.75(1)°, γ=99.76(1)°.

Sejkoraite-(Y) forms orange to yellow-orange plate crystals up to 0.5 mm. According to single-crystal diffraction sejkoraite-(Y) is triclinic of the space group *P*-1 with the unit-cell of , a=14.0734(4),□b=14.3172(4),□c=15.0446(5)Å,□α=107.289(3) ,□β=95.716(2),□γ=102.826(2)°, V=2777.2(1)Å^3, Z=2. The chemical composition corresponds to the ideal formula $Y_3[(UO_2)_8O_8(SO_4)_4(OH)](H_2O)_{25}$; its crystal structure consists of zippeite-type sheets and yttrium/*REE* based polyhedra and water molecules in the interlayer space. The interlayer spacing 9.28 Å is similar to that found in pseudojohannite [4].

[1] Plášil, J. et al. (in prep.) [2] Brugger, J. et al. (2003) *Am. Mineral.*, **88**, 676-685. [3] Sejkora, J. et al. (2000) *Neues Jb. Miner. Mh.*, **H.7**, 289-301. [4] Brugger, J. et al. (2006) *Am. Mineral.*, **91**, 929-936.

Mineralogy of the wastes from diamond-bearing mines

Posukhova, T.V.[1*], Dorofeev, S.A.[2] & Gao Xiaoying[3]
[1]Dept. of Mineralogy, Moscow State University, Moscow, Russia ([*]tposukhova@mail.ru)
[2]TsNIGRI Institute, Moscow, Russia
[3]Scientific & Technical University of China, Hefei, China

Extraction of diamonds is accompanied by huge amount of wastes. New technological classification of kimberlites, based on features of their mineral composition, will help to develop rational ways of recycling of these waste products. The samples from 18 kimberlitic bodies of Russia (Arkhangelsk & Yakutian provinces) and China (Liaonin & Shandong provinces) were investigated for this purpose. The kimberlites were studied by X-ray diffraction, thermal and electron-beam analysis, IR-spectroscopy and Ca-measurements (fig. 1).

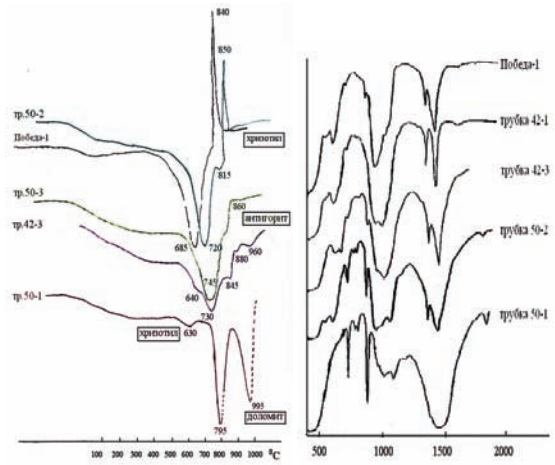

Fig. 1: Results of thermal analyses and IR – spectres of kimberlites from China.

The investigated kimberlites differ by individual ratio of the mineral phases: serpentine, carbonates, phlogopites and saponite where established kimberlites in which dolomite is prevailing (Chernyshevskaya, Botuobinskaya, Morkoka and pipe 50). The prevailing type of serpentine is also different. Basic mineral is close to pure chrysotile in pipes Victory 1 and 50, and in pipe 42 – and to antigorite. Differences in the chemical composition of the minerals were also established. Phlogopites from Liaoning have increased TiO_2. High-Al and low-Ti phlogopites are absent in kimberlites of China, and they are present in the Arkhangelsk provinces. Phlogopites with increased FeO were established in kimberlites of China

Proceedings from the received data, all investigated kimberlites were divided into four mineral-technological types: 1 - with prevalence of saponite (Chidviya and Lomonosov); 2 - with high contents of serpentine (Snegopadnaya, Aikhal, Dalnyaya, Udachnaya); 3 - with increased contents of carbonate and phlogopite (Chernyshevskaya and Botuobinskaya); 4 - with a complex mixed structure (Morkoka, 23 s'ezd KPSS, Nurbinskaya, Mir and pipes of China). The circuit of recycling is offered for each of the allocated types of kimberlites.

Mineralogical speciation of Pb-bearing secondary phases from a former lead-silver district (Pontgibaud, France)

Rakotoarisoa, O.*, Courtin-Nomade, A. & Bril, H.
GRESE, University of Limoges, France
(*ony.rakotoarisoa@etu.unilim.fr)

Because of its abundance and toxicity in mining environments as reported in previous studies (e.g. [1,2]), Pb was studied in the former mine of Roure (Pontgibaud district, France) where Ag and Pb were extracted from the middle to the late 19th century. Lead was present in the primary mineralization as galena (PbS) always associated with silver in quartz veins [3].

Studied residues from these activities are slags or tailings deposited on a 0.25 km^2 area. Tailings show various textures and structures (e.g. with a sandy texture or as hardpan) and Pb concentrations vary from a few mg/kg to 6.6%. Slags show a vesicular texture and Pb concentrations ranging from 850 mg/kg to 2.5%. Whatever the material, primary gangue minerals prevail on the mineralogical assemblages (e.g. quartz or muscovite) but the most important Pb-bearing phase is anglesite ($PbSO_4$). Anglesite results from the oxidative dissolution of galena and is observed in various forms as massive minerals (anhedral to euhedral up to 100 µm), associated to barite or embedded in a silicated matrix. The presence of anglesite as the main Pb-mineral species is in agreement with the oxidizing conditions and the pH values measured for the collected samples (3.5<pH<6.5), which explain that this species is stable according to the Pourbaix diagram. In mine tailings, however, the mineralogical assemblages show numerous other secondary Pb phases, even if more widely distributed in the residues, such as sulphates and phosphates mainly as: plumbojarosite ($PbFe^{3+}{}_6(SO_4)_4(OH)_{12}$), beudantite ($PbFe_3(AsO_4,SO_4)_2(OH)_6$), plumbogummite ($PbAl_3(PO_4)_2(OH)_5(H_2O)$), kintoreite ($PbFe^{3+}{}_3(PO_4)_2(OH,H_2O)_6$) or phosphohedyphane ($Ca_2Pb_3(PO_4)_3Cl$). The identification of these secondary phases is only supported by spatially resolved and more sensitive techniques such as SEM, micro-Raman spectrometry and EPMA.

In slags from smelter residues, galena or Pb metallic droplets are usually reported [4, 5]. In our case, none of these two phases have been observed which may be explained by the specific metallurgical process used at Pontgibaud due to the low Pb ore content (c.a. 12,6 kg/t) [6]. It may also be due to the fact that part of the tailings has been treated during the exploitation by crushing and flotation in order to collect the residual sulphides. Thus, it is expected that no galena and/or very little amounts of Pb should be detected [7,8]. However, even if galena was present in small quantities in the residues from this second treatment, the lack of galena in every residue as observed nowadays could also be explained by the in situ geochemical conditions which may have favoured its complete oxidative dissolution. Therefore, as the secondary Pb-bearing phases in the on-site conditions represent the main source of Pb towards the environment, their stability should be determined and would be achieved by leaching experiments, currently carried out at different pH.

[1] Sileo, L. et al. (2001) *Arch. Environ. Contam. Toxicol.*, **41**, 364-368. [2] Paulson, A. (1997) *Appl .Geochem.*, **12**, 447-464. [3] Boulandon, J. et al. (1964) *Bulletin BRGM*, **1**, 1-41. [4] Kucha, H. et al. (1996) *Environ. Geol.*, **27**, 1-15. [5] Ettler, V. et al. (2003) *C.R. Geosci.*, **335**, 1005-1012. [6] Rivot, M. & Zeppenfeld, M. (1851), in Dunod (ed.) *Description des gîtes métallifères, de la préparation mécanique et du traitement métallurgiques des minerais de plomb argentifères de Pontgibaud*, 133. [7] Rodriguez, L. et al. (2009) *J. Environ. Management*, **90**, 1106-1116. [8] Schuwirth, N. et al. (2007) *J. Environ. Qual.*, **36**, 61-69.

Understanding micro-environment development in mine tailings using MLA and Image Analysis

Redwan, M. & Rammlmair, D.*
[1]BGR - Federal Institute for Geosciences and Natural Resources, Hannover, Germany (*rammlmair@bgr.de)

Discharge of mine tailings by spilling generates vertical and lateral grading in grain size, and subsequently chemical and mineralogical patterns different from the bulk spilled material along the spilling path. After deposition, these finely laminated mine tailings are exposed to alteration. Due to the depositional premises, the level of water saturation and the degree of alteration are variable. But even at the relatively coarse grained dam intercalated fine grained lamina change the hydraulic properties, creating capillary barriers, and lamina with enhanced water retention capacity. Alteration occurs in microenvironments at the interface of lamina contrasting in grain size, porosity, saturation, mineralogy, redox, pH and chemistry. The oxidation/dissolution and hydration of minerals cause a loss and gain of volume, respectively by generating new micro porosity and clogging pores at different positions. The aim of the investigation was to obtain quantitative information on the distribution of primary minerals, porosity as well as secondary crystalline and amorphous phases, for individual layers of the tailings, and for grain size distribution of all primary minerals, related to the mineral processing. This will help to reconstruct the primary porosity and to understand the role of the newly formed phases in clogging pores and in the development of cemented horizons, elucidating processes at individual positions in the heap.

The quantitative mineralogical analysis was carried out by using the MLA (Mineral Liberation Analyzer) software package from JKTech. The MLA method is based on the grey value evaluation of back-scattered electron (BSE) signals in conjunction to the EDX spectra collected from each individual grain in the image by means of SEM. [1,2]. A database was created for all phases based on BSE-images, EDX spectra and identification of phases by optical microscopy (Fig. 1).

The MLA results were further evaluated by using image analysis. Regions of interest (ROI) were chosen to evaluate the mineral distribution, and changes in porosity in individual layers, and to elucidate the progress in alteration due to dissolution and precipitation processes in microenvironments.

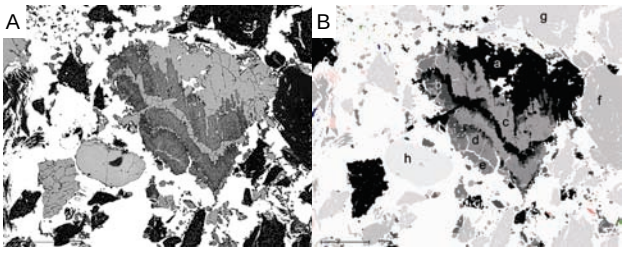

Fig. 1: Back-scattered electron image (A) and classified image (B) using MLA for an altered pyrite crystal (**a** Pyrite; **b** Fe Arsenate; **c** As-gel with high Fe, S and mod. Si; **d** As-gel with high Fe, mod. S and low Si; **e** As-gel with low Fe, S and high Si; **f** Alkali feldspar; **g** Quartz).

[1] Gu, Y. (2003) *J. Miner. Mat. Charact. Eng.*, **2**, 33-41. [2] Fandrich, R. et al. (2007) *Int. J. Miner. Process.*, **84**, 310-320.

Unusual fibrous mimetite from the Rovnost mine, Jáchymov (St. Joachimsthal), Czech Republic

Sejkora, J.[1*], Plášil, J.[1], Císařová, I.[2] & Hloušek, J.[3]
[1]Dept. of Mineralogy and Petrology, National Museum, Prague, Czech Republic (*jiri_sejkora@nm.cz)
[2]Dept. of Inorganic Chemistry, Faculty of Science, Charles University in Prague, Prague, Czech Republic
[3]U Roháčových kasáren 24, Prague, Czech Republic

An interesting mineral association of morphologically anomalous mimetite and other supergene Pb minerals was found in the Rovnost mine, Jáchymov (St. Joachimsthal) ore district, Czech Republic. Mimetite forms greyish white fine-crystalline aggregates (up to 1 cm in the area) growing on the surface of strongly supergene altered gangue. Individual mimetite crystals are represented by colourless transparent flexible fibers of up to 1 mm in lenght and up to 10 μm in diameter. Mimetite was studied by X-ray powder diffraction but obtained pattern is significantly different from the published data of mimetite. According to EPMA (WD mode), its chemical composition is: PbO 75.92, SiO_2 0.45, As_2O_5 20.13, P_2O_5 1.05, SO_3 0.07, Cl 2.19, F 0.10, O=Cl+F -0.53, total 99.38 wt. % and its empical formula is $Pb_{5.15}[(AsO_4)_{2.65}(PO_4)_{0.23}(SiO_4)_{0.11}(SO_3)_{0.01}]_{\Sigma 3.00}(Cl_{0.93}F_{0.08})_{\Sigma 1.01}$ which are consistent with known members of mimetite - pyromorphite series; only contents of (SiO_4) in range 0.08 - 0.16 *apfu* were observed. A possible presence of clinomimetite or other structurally close mineral phase was checked by single crystal diffraction. The crystal structure of studied mineral has been solved by direct method and refined to an R_F index of 3.96 % based on 305 observed reflections (F_o>4sig(F_o)) collected on a four-circle diffractometer with Mo$K\alpha$ X-radiation. The obtained results - hexagonal space group $P6_3/m$, unit-cell parameters a=10.2373(6) Å, c=7.4257(4) Å and V=673.97(7) Å^3 (from 9868 reflections) and atom positions agree very well with published data for mimetite [1]. Differences between the experimental and calculated X-ray powder diffraction patterns of the studied mimetite are probably caused by its fibrous nature. There is a preferred orientation of the sample usual only for minerals with perfect cleavage.

Studied mimetite and associated minerals are of (sub)recent supergene origin; their formation is connected with very specific conditions in the supergene zone of the ore-vein *in-situ*. This type of supergene alteration has not been previously observed in the Jáchymov ore district and the research has not been completed yet.

[1] Dai, Y. et al. (1991) *Can. Mineral.*, **29**, 369-376.

Mineralogy and bio-weathering of fallen dusts at ferrosilicon production factory. Example from Si-Fe foundries in the Pirapora-Várzea da Palma region, Minas Gerais, Brazil

van Hullebusch, E.[1*], Fuchs, Y.[1], Horn, A.H.[2], Baggio, H.[3], Trindade, W.M.[2], Ribeiro, E.[2] & Rossano, S.[1]
[1]Laboratoire Géomatériaux et Environnement, Université Paris-Est, Marne la Vallée, France (*Eric.vanHullebusch@univ-mlv.fr)
[2]Laboratório de Geoquímica Ambiental Universidade Federal Minas Gerais, Belo Horizonte, MG, Brasil
[3]Laboratório de Ggeologia e Geomorfologia, Universidade Estadual de Montes Claros, Pirapora, MG, Brasil

Industrial activities that use processes of high temperature to produce ferrosilicon alloys (FeSi) and silicon metal (Si-metal), starting from diversified raw materials cause, among other problems, the release of fine dusts in the atmosphere. These particles are quite heterogeneous in term of shape and size features and elemental composition. In addition, they may have adverse impacts on the quality and quantity of agricultural products in the surrounding areas and drastic changes in the aquatic and irrigation systems. This influence can happen following two different ways: (i) deposition on plants, causing a direct chemical interaction, and (ii) through the deposition on soil and entrance into the bio-cycles.

Samples studied in this work come from two foundries located in the Varzéa da Palma region in Central to Northern Minas Gerais State, Brazil that generate air emissions from Fe-Si and Si furnaces. The raw materials used in these processes are barite, crushed quartz from, argillite, charcoal and wood for the Si production together with scrap materials for the Fe-Si alloys production.

Particulate matter in smoke display spherical C- compounds (μ), chromium - spinel balls (μ), irregular amorphous and crystalline SiO_2-agglomerates and rare well formed magnetite and Si crystals. The particle shapes are irregular to spherical. Grain size varies from tenths of a micrometer to one millimetre.

The plumes show transport distances of up to 50 km with changing flux conditions due to temperature and wind direction changes. The preferential transport directions are (NE to SSW 50%, NW - SW 15% and N - S 35%). The depositional factors were studied by field observations, optical microscope, grain-size measurements, XRD, environmental SEM and microprobe. ICP-OES and ICP-MS analyzes of the primary dust composition may show the direct impact over plants and soils in the selected area and the specific problems. Investigation performed in the laboratory about the bio/leaching of the particulate matter in smoke and leaching tests point out direct and chronic dangers by direct plant-dust and dust-soil-plant contacts.

Mineralogical and geochemical characterization of mine tailings from central Mexico, environmental implications

Villasenor-Cabral, M.G.[1*], Romero Martín, F.[1], Luna, L.[2] & Morales, I.[2]
[1]Instituto de Geología, Universidad Nacional Autonoma de México (UNAM), Ciudad de México, México
([*]mgvc@servidor.unam.mx)
[2]Postgrado en Ciencias de la Tierra, UNAM, Ciudad de México, México

Mining activity in Mexico has been very intense since Colonial times up to the present. This fact has been reflected as well in a great quantity of mining-waste. Here we present the mineral and chemical characterization of tailings from two different mines in central Mexico: one in the state of San Luis Potosi and the other one in the state of Guerrero. The purpose of this study is to establish the mobility of arsenic and lead as the main possible contaminants.

Total content of arsenic (140-3627 $mg.kg^{-1}$), lead (148-10900 $mg.kg^{-1}$), zinc (0.021–3.86 %) and iron (2.4–35.7 %) has been done with ICP-AES and mineralogical determinations with optical microscopy, XRD and SEM-EDS. In both sites, oxidized tailings (brown color) and reduced tailings (gray color) were identified. The oxidized samples from Guerrero presented acid pH values from 2.4 to 3.7, indicating the formation of acidic drainage as a consequence of extensive sulfide mineral oxidation. However, the pH values found in the oxidized tailings San Luis Potosi varied between 6.5 and 8.2.

Minerals of the reduced tailings from both areas included quartz (SiO2), calcite ($CaCO_3$), plagioclase, orthoclase, pyrite (FeS_2), and sphalerite (ZnS). Reduced tailings from San Luis Potosi additionally contained wollastonite and more calcite. Relative abundances of the sulfide minerals, determined by point-counting in polished sections, indicate that the unoxidized tailings from the Guerrero contain approximately 10% pyrite, 4% sphalerite and traces of chalcopyrite and galena. However, unoxidized tailings from San Luis Potosi contain approximately 5% pyrite, 7% sphalerite and trace galena. Oxidized samples of both areas have gypsum, Fe-oxyhydroxides, kaolinite, jarosite and anglesite. Oxidized tailings from the Guerrero also contain beudantite.

The results of the mineralogical characterization and acid-base accounting tests allow to predict that unoxidized gray tailings from Guerrero will be acid generating when they oxidize.

The highest concentrations of dissolved Zn (55 $mg.L^{-1}$) and Fe (28 $mg.L^{-1}$) were found in the acidic tailings from Guerrero, while low concentrations of As (0.4 $mg.L^{-1}$) and Pb (0.2 $mg.L^{-1}$) were found in these acidic oxidized tailings showing low mobility of these potentially toxic elements (PTE). Because the reported solubility for beudantite is very low under acidic conditions, this minerals may serve as the most important control in the mobility of As and Pb from the oxidized tailings at Guerrero. In contrast, Fe-oxyhydroxides are relatively soluble under acidic conditions; therefore, they may have a less significant role in PTE on-site immobilization. The dissolved concentrations of PTE in oxidized tailings from San Luis Potosi were below the detection limits. Our results may indicate that the sorption on Fe-precipitates play an important role in the mobilization and attenuation of PTE within the oxidized circum neutral tailings from San Luis Potosi.

The mineralogical determinations are very useful for interpretation of mobility.

Preferential oxidation of euhedral pyrite containing relict framboidal morphologies

Weisener, C.G.[1*], Gagnon, J.[1] & Weber, P.A.[2]
[1]Great Lakes Institute for Environmental Science, University of Windsor, Windsor, Canada ([*]weisener@uwindsor.ca)
[2]Environmental Division, Solid Energy New Zealand Ltd, Christchurch, New Zealand

Environmental damage produced from acid generating mines currently represents one of the largest problems facing the mining industry. The aim of this research is to investigate possible mineralogical controls on acid rock drainage (ARD) and metal release associated with pyritic mudstone collected from, the Brunner Coal Measures (BCM), Stockton Mine NZ. Laboratory-based kinetic tests were performed on the potentially-acid forming material by measuring, over time, the changes in mineralogical compositions and acid generating potential along with changing effluent chemistries from the columns. The rate of pyrite oxidation in the BCM is strongly dependent on the reactivity of two morphological types (euhedral and framboids) of pyrite in this region.

After a 4 month period between 70 to 100% of all framboidal pyrite had undergone complete oxidation, despite this acid generation (1730 (mgL-1 CaCO3) after 390 days) continued during the column experiments. SEM micrographs show the persistence of larger euhedral pyrite grains as a contributing factor with evidence of preferential oxidation associated with relict framboidal morphology (figure 1).

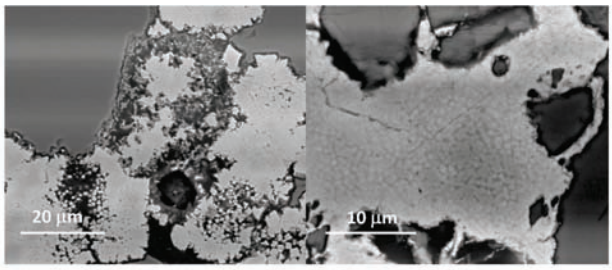

Fig. 1: After 13 months within a humidity cell euhedral pyrite shows preferential oxidation confined to pyritic overgrowth textures.

Samples collected from laboratory humidity cells after 13, 16 and 24 months show preferential dissolution features associated with large pyritic overgrowth textures. From a kinetic perspective the oxidation of pyrite in these samples tend to target the more recent crystallographic overgrowths. Results of the 24 month study will be presented detailing the mineralogical alteration, acidity generation and their controls on trace metals specifically thallium deportment.

Mechanisms of contaminant metal and metalloid sequestration using reactive amendments for soil and sediment remediation

O'Day, P.A.[1*] & Vlassopoulos, D.[2]
[1]School of Natural Sciences, University of California, Merced, California, USA ([*]poday@ucmerced.edu)
[2]S.S. Papadopulos & Associates, Inc., Portland, Oregon, USA

Reactive amendments optimized for specific (bio)geochemical site conditions offer a promising remediation technology for high-priority metal and metalloid contaminants in soils and sediments. The overall aim of *in situ* amendment technologies, whether added directly to geomedia or emplaced within barriers or caps, is to sequester and stabilize contaminants in place in order to reduce their ability to partition to water or biota, their toxicity, and their potential for transport. Metal and metalloid elements are especially problematic because many are considered hazardous at low bulk solid concentrations (i.e., ~1-10's ppm). They are often widespread in the surface and shallow subsurface at these low concentrations, making removal and disposal of a large volume of material impractical or prohibitively expensive. Many soil amendment studies have focused on performance as measured by standardized leaching or bioavailability tests. Less research has been aimed at understanding the basic chemistry, molecular mechanisms, reaction rates, or detailed mineralogy associated with amending contaminated soils or sediments with different types of treatment.

Sequestration mechanisms fall into two broad categories, surface adsorption and structural incorporation, which may each have several molecular-scale variations. In complex mixtures of amendments and soil, both mechanisms may occur and change with time. Adsorption using media such as clays, zeolites, or iron oxides can be an effective immobilization mechanism for metal contaminants, which may change speciation but do not degrade. However, there is an inherent risk that future changes in soil water pH or ionic strength, or in other environmental factors, will shift surface equilibria and lead to desorption. Treatments that react with soil water and minerals, leading to dissolution and precipitation reactions, can structurally incorporate contaminant species into new phases that form as a result of altering the composition and pH of the system. This class of sequestration mechanisms has the potential for more permanent immobilization since mineral dissolution is required to partition the bound contaminant to water, rather than simple desorption or exchange. A variety of mineral-based solids or mixtures of materials are used in reactive amendment treatments, including phosphates, carbonates, sulfates, iron-based solids, silica, lime, and Portland-type cements, as well as industrial residual and by-product materials such as coal fly ash, furnace slags, mining residuals, and scrap iron. In addition to coprecipitation or solid solution formation, amendments may also encapsulate contaminants in nano-to-microscale inclusions, or encapsulate contaminant-bearing nanoparticles within other resistant phases. Once molecular-scale mechanisms have been identified, reactive transport models incorporating thermodynamic and kinetic data can be used effectively to constrain biogeochemical outcomes of sediment-amendment reactions, which can then be tested in laboratory and field experiments. Better understanding of chemical and physical controls on contaminant immobilization, together with a framework for site assessment, would aid in both extending the use of mineral and other amendments for soil and sediment remediation, but also in selecting materials that are compatible with, and optimized for, a specific site.

Iodine uptake by Layered Double Hydroxides

Aimoz, L.[1,5*], Taviot-Guého, C.[2,3], Vespa, M.[4], Dähn, R.[1], Leroux, F.[2,3], Mäder, U.[5] & Curti, E.[1]
[1]Laboratory for Waste Management, Paul Scherrer Institute, Villigen, Switzerland ([*]laure.aimoz@psi.ch)
[2]Clermont Université, Université Blaise Pascal, LMI, Clermont-Ferrand, France
[3]CNRS, UMR 6002, Laboratoire des Matériaux Inorganiques, Aubière, France
[4]Dept. of Chemistry, Division of Molecular and Nanomaterials, Catholic University of Leuven (K.U. Leuven), Heverlee, Belgium & DUBBLE CRG, ESRF, Grenoble, France
[5]Institut für Geologie, University of Bern, Bern, Switzerland

Spent nuclear fuel from nuclear power plants contains ^{129}I which is dose-determining in repository safety analyses due to its long half life, anionic form and weak retention by common minerals. Often, safety analyses do not include the uptake of anionic radionuclides by secondary minerals such as Layered Double Hydroxides (LDHs). The most common naturally occurring LDH phase is hydrotalcite (Mg-Al LDH). LDHs have a brucite-like structure of edge-sharing hydroxide octahedra forming layers of positive charge, balanced with anions in the interlayer space surrounded by water molecules. The retention mechanisms of anions in LDH phases are poorly understood, particularly at the atomic-scale. The structural configuration of iodine-bearing LDH phases was elucidated by the Rietveld refinement of the average structure from powder X-ray diffraction data, together with Extended X-ray Absorption Fine Structure (EXAFS) spectroscopy.

Zn-Al LDHs were selected as an analogue to hydrotalcite since they usually display a higher crystallinity compared to the Mg-Al phases, allowing better access to further structural investigation by means of XRD. LDHs were synthesized by co-precipitation of I (as I^- or IO_3^-) with Zn^{II} and Al^{III} salts at Zn/Al ratios = 2, 3 and 4. XRD analysis confirmed the formation of pure LDHs, with a layered hexagonal structure (R-3m), and I sitting in the interlayer space. A Rietveld structural refinement was attempted on the most crystalline sample (I-LDH, Zn/Al=4). This structural refinement revealed the occurrence of stacking faults, a common feature in LDH phases. Such disorders prevent the resolution of structural features using XRD alone and require methods such as EXAFS which can probe the short-range order.

Fourier transformed EXAFS spectra at the zinc K-edge showed a local order within the octahedral layer for all samples. An oxygen shell was found at ~2.10 Å. Wavelet transforms of the EXAFS spectra confirmed the presence of both Zn and Al in the three subsequent shells found between 3 and 6 Å, as already observed by Funke et al. [1]. In addition, the wavelet transform analysis did not reveal the presence of any heavy backscattering atoms such as iodine, suggesting a lack of short-range ordering between Zn in the octahedral layer and I in the interlayer. This interpretation was further confirmed by data measured at the iodine K-edge on the same samples, which did not reveal any preferred distance for I-Zn pairs.

The results unambiguously show that iodine can be incorporated in the interlayer space of LDH phases via co-precipitation, confirming their potential as a sink for ^{129}I. A short-range ordering within the octahedral layer was confirmed, whereas no local preferential arrangement was found between the interlayer anions and the octahedral sheets.

[1] Funke, H. Scheinost, A.C. & Chukalina, M. (2005) *Phys. Rev. B*, **71**, 094110.

Mineral formation and anion sorption at naturally-occurring hyperalkaline springs in Oman

Anraku, S.[1*], Morimoto, K.[2], Sato, T.[3] & Yoneda, T.[3]
[1]Graduate School of Engineering, Hokkaido University, Sapporo, Japan ([*]anraku@eng.hokudai.ac.jp)
[2]National Institute for Materials Science, Japan
[3]Facluty of Engineering, Hokkaido University, Sapporo, Japan

In Japanese transuranic (TRU) waste disposal facilities, ^{129}I is the most important key nuclide for the long-term safety assessment. Thus, the distribution coefficients (Kd values) of I to natural minerals are important factor in the safety assessment. However, the degradation of cement materials in the repositories can produce high pH pore fluid which can affect the anion transport behaviour. Therefore, it should be necessary to understand the behaviour of anions such as I- under the hyperalkaline conditions.

This study examined the naturally-occurring hyperalkaline conditions near the springs in Oman as natural analogue for the interaction between cement pore fluid and natural Mg-HCO_3^- river water. The generated natural hyperalkaline spring water (pH>11) from the partly serpentinized peridotite in the Oman ophiolite is characterized as hyperalkaline, reducing, low-Mg, Si and HCO_3^-, and high-Ca while the river water where the alkaline spring , is moderately alkaline, oxidizing, high-Mg and HCO_3^-. The mixing of these spring and river water resulted in the formation of secondary minerals, forming river terrace with height of more than 10 meters. The present aim of this paper is to examine the conditions of secondary mineral formation and the anion uptake capacity of these mineral phases generated. The long-term satiability of this sorption behaviour in this system was also investigated.

Water and precipitate samples were collected at various distances from the spring vent to identify the effect of mixing ratios between spring and river water on mineral composition and water-mineral distribution coefficient of various anions. On-site synthesis was also carried out to support these data quantitatively. Furthermore, samples of deposits were collected from the river terrace at different height which corresponds approximately to the the depositional age in order to find out the alteration of minerals and possible anion desorption.

The results of the mineralogical and chemical characterization of the collected samples confirmed that the formation of secondary mineral was dominated by aragonite at the mixing points of the spring and surface water, due to high Mg content of the latter. Hydrotalcite like compound (Mg-Al hydroxides) was also detected as accessory minerals since the hyperalkaline springs contain relatively rich in Al.

During the formation of the minerals at the mixing points, HCO_3^- in the river water was fixed as carbonate minerals in aragonite and calcite phases while $H_3SiO_4^-$ in the river water was dominantly fixed into the interlayers and surfaces of HTlc. Iodine in spring and river water was mainly fixed in aragonite. XRD quantitative analysis by Rietveld method indicated Kd values of iodine increase proportionally to the aragonite content in the precipitate samples. Consequently, in terms of short-term assessment, particularly for I^-, uptake by secondary minerals can be expected at hyperalkaline conditions as observed at Oman hyperalkaline springs.

Synthesis, characterisation and environmental application of bentonite organoclays

Sarkar, B.[*], Xi, Y., Megharaj, M., Krishnamurti, G.S.R. & Naidu, R.
Centre for Environmental Risk Assessment and Remediation (CERAR) & Cooperative Research Centre for Contamination Assessment and Remediation of the Environment (CRC CARE), University of South Australia, Mawson Lakes, Australia ([*]Binoy.Sarkar@postgrads.unisa.edu.au)

Organoclays are generally synthesised by incorporating alkyl ammonium surfactant cations into clay structure. Such modification imparts hydrophobic properties to the clay products and enhances their affinity towards hydrophobic organic contaminants in the environment [1]. Moreover, some organoclays can also adsorb inorganic anionic contaminants [2]. However, one of the main hindrances that discourages widespread uptake of this remediation technology is the high cost involved with the synthesis of these materials. Therefore, attempts are necessary to synthesise organoclays from comparatively cheaper surfactants to reduce the cost of production to some extent.

In the present study, organoclays were synthesised from natural bentonite in hydrothermal cation exchange reaction using a commercially available cheap surfactant known as Arquad 2HT. Organoclay products having various surfactant loadings were obtained and characterised by XRD and FTIR. As the surfactant loadings increased, the XRD results showed incremental basal spacing (d 001) in the organoclays due to incorporation of the surfactant molecules in the interlayer space of the bentonite (Table 1). The IR peaks generated by symmetric and asymmetric stretching of the $–CH_2$ groups at 3000-2800 cm^{-1} wave number further proved successful organic modification of the natural bentonite.

Table 1: Basal spacing of the natural bentonite and its organoclays

Clay/organoclays	Clay-surfactant ratio (w/w)	d (Å)
QB	Natural bentonite	15.03
QB-Aq1	0.60:1	15.15
QB-Aq2	1.19:1	15.36
QB-Aq3	1.79:1	27.93
QB-Aq4	2.38:1	30.00
QB-Aq5	3.57:1	34.73

The synthesised organoclays were tested for their environmental application in batch adsorption experiments using phenol and *p*-nitrophenol as the model contaminants in water. The adsorption data fitted reasonably well into Langmuir isothermal models and the adsorption maxima for these two contaminants were calculated (Table 2). Results showed that removal efficiency of phenol and *p*-nitrophenol improved with incremental surfactant loadings in the organoclays.

Table 2: Langmuir maxima (mg g^{-1}) for adsorption of phenol and *p*-nitrophenol by natural bentonite and its organoclays

Clay/organoclays	Langmuir adsorption maxima (mg g^{-1})	
	Phenol	*p*-nitrophenol
QB	No adsorption	23.1
QB-Aq1	13.7	45.2
QB-Aq2	34.8	59.1
QB-Aq3	47.6	63.3
QB-Aq4	61.0	79.4
QB-Aq5	82.6	87.7

This study demonstrates the potential of Arquad 2HT modified bentonite in remediation of polar organic contaminants similar to phenol and *p*-nitrophenol from contaminated waters and soils.

[1] Xi, Y. et al. (2005) *Langmuir*, **21**, 8675-8680. [2] Krishna, B.S. et al. (2001) *Appl. Clay Sci.*, **20**, 65-71.

Groundwater chemistry of Kandal province, Cambodia and arsenic removal from tube well water

Pich, B.[1*], Yoneda, T.[1], & Sato, T.[1]
Laboratory of Environmental Geology, Hokkaido University, Sapporo, Japan ([*]pichoeun@eng.hokudai.ac.jp)

A comparative study of arsenic-rich groundwater in alluvial aquifer of the Cambodian Mekong delta between rainy and dry season was conducted in Prek Tameng and Prek Thom villages of Kandal province, Cambodia. As a result, Kandal groundwater was characterized by low to high concentration of dissolved As, moderate to high concentrations of dissolved Fe, Mn, HCO_3^-, NH_4^+ and DOC, and low concentrations of SO_4^{2-} and NO_3^-, circum-neutral pH and slightly reducing condition. Comparatively, the groundwater chemistry of Prek Tameng slightly varies due to chemical dilution caused by surface water infiltration during rainy season, while that of Prek Thom remain almost the same throughout the year.

Positively stronger correlations of high As with DOC, NH_4^+, and SO_4^{2-} but negative correlation with low Fe and PO_4^{3-}, in Prek Thom in dry and rain season, indicated that arsenic mobilization was more probably in association with microbial activities and organic matter degradation. This process could be mostly found in less reducing condition of the near-surface wetland site of the Kandal province in the Cambodian Mekong delta. However, dissolved Fe(II) was thought to be still retained in the sediment to form Fe(II) or mixed Fe minerals.

On the contrary, low As in Prek Tameng was well-correlated with high Fe, Mn, HCO_3^-, and low PO_4^{3-} and inversely-related with low SO_4^{2-} and NO_3^-. This suggests that arsenic in Prek Tameng is mobilized to the groundwater due to reductive dissolution of Fe and/or Mn(hydr)oxide minerals rather than oxidative desorption/decomposition of organic matter. This mechanism was mostly found in more reducing condition of deeper aquifer of the Cambodian Mekong delta. Last but not least, competitive adsorption to the same surface site between As and PO_4^{3-} due to their similar affinities may also contribute to arsenic release.

This research provided some significant information on how to deal with the arsenic problem in Kandal province, Cambodia since nearly 1 million residents in this province have been threaten and at risk by the presence of arsenic in groundwater. Therefore, it is definitely necessary to remove arsenic from tube well water by utilizing locally available low-cost adsorbents. In the presentation, applicability on usage of the laterite from Kampong Cham province, Cambodia as arsenic adsorbent will be also discussed based on the groundwater chemistry.

Utilization of schwertmannite for sustainable remediation of contaminated land and water

Sato, T.[1*], Fukushi, K.[2], Ito, K.[3], Takada, M.[4] & Yoneda, T.[1]
[1]Faculty of Engineering, Hokkaido University, Sapporo, Japan ([*]tomsato@eng.hokudai.ac.jp)
[2]Institutes of Nature and Environmental Technology, Kanazawa University, Kanazawa, Japan
[3]Cooperative Research Center, Miyazaki University, Miyazaki, Japan
[4]Graduate school of Engineering, Hokkaido University, Sapporo, Japan

Schwertmannite, poorly crystalline Fe (III)-oxyhydroxysulfate with the composition $Fe_8O_8(OH)_{8-2x}(SO_4)_x$ (where ideally x=1), is more commonly reported as an orange or ocherous precipitate in streams and lakes affected by acid mine drainage. Schwertmannite has a large reactive surface and is capable of scavenging significant quantities of trace elements. Therefore, there are many reports describing sorption properties and mechanisms of hazardous element. According to the high affinity with arsenate, phosphate and chromate anions, schwertmannite has been expected as geochemical sink and candidate material of adsorbents for hazardous oxyanions. However, there is hardly able to find reports on practical utilization of schwertmannite for remediation of contaminated land and water.

In Japan, we intensively introduced schwertmannite for practical utilization to prevent an arsenic release from contaminated soils and to remediate contaminated water such as acid mine drainage in passive treatment systems. In remediation of contaminated land, the stabilized schwertmannite has directly been mixed with the contaminated soils and used with fibrous materials in adsorptive bed installed between contaminated soils and aquifer. In passive treatment facility of acid mine drainage including arsenic, schwertmannite was successfully synthesized from acid mine drainage by pH adjustment to pH 3.5 and almost completely removed arsenic from the drainage. From the synthesis, it has been achieved economical use of the reagent for the neutralization process, reduction of the sludge produced from the neutralization, and safety encapsulation of arsenic into the solid material.

For performance and safety assessments in utilization of schwertmannite for sustainable remediation of contaminated land and water, sorption capacity of arsenic, kinetics of schwertmannite transformation to goethite and solid-solution relationship between sulphate and arsenate schwertmannite have been investigated by our research group. Therefore, performance and long-term safety assessment for the utilization of schwertmannite are available in reactive transport modelling for sustainable remediation of contaminated land and water. In the presentation, the authors would like to introduce some of examples in utilization of schwertmannite for sustainable remediation of contaminated land and water, and their performance and long-term safety assessment.

Clustering of impurities in natural calcite: theoretical and spectroscopic study of As-As and As-Eu relationships

Bardelli, F.[1], Benvenuti, M.[2], Charlet, L.[3], Costagliola, P.[2], Di Benedetto, F.[4*], Fernandez Martinez, A.[5], Valenzano L.[1], Lattanzi, P.F.[6], Meneghini, C.[7] & Romanelli, M.[4]
[1]NIS - Nanostructured Interfaces and Surfaces, Dipto. di Chimica IFM, Università di Torino, Turin, Italy
[2]Dipto. di Scienze della Terra, Università di Firenze, Florence, Italy
[3]LGIT – Université Joseph Fourier, Grenoble, France
[4]Dipto. di Chimica, Università di Firenze, Sesto Fiorentino, Italy ([*]dibenefr@geo.unifi.it)
[5]Lawrence Berkeley National Laboratory, Berkeley, USA
[6]Dipto. di Scienze della Terra, Università di Cagliari, Cagliari, Italy
[7]Dipto. di Fisica, Università di Roma Tre, Rome, Italy

An experimental and theoretical study was undertaken on crystal chemical features of the $CO_3^{2-} \leftrightarrow AsO_3^{3-}$ substitution in calcite lattice, which is suggested to occur in As-bearing travertine rocks from Tuscany (Italy). This study has been carried out by means of As K-edge XAFS (X-ray Absorption Fine Structure), Electron Paramagnetic Resonance, Electron Spin Echo spectroscopy and Density Functional Theory (DFT) calculation.

In particular, the possible self-clustering of As impurities or the hetero-clustering of As with other trace elements were investigated. The former was studied by means of XAS and DFT in natural As-bearing travertines, whereas the latter was pursued through EPR and ESE on opportunely synthesized As-, Eu- co-doped calcites, chosen on the basis of ionic radius of Eu (>Ca).

The experimental confirmation of the As clustering was provided by the presence of strong signal (i.e. with coordination number close to the maximum allowed for the calcite cell) from an As-As coordination shell to the EXAFS signal of a travertine sample.

Although involved in a relatively rare replacement process, the uptake of As(III) by calcite feasibly occurs via self-clustering in local domains of calcite.

Conversely, scarce evidence of As-Eu clustering in calcite was observed in the EPR-ESE characterisation of synthetic calcite samples, suggesting that general clustering of impurities (independent of their nature) can occur only under specific boundary physico-chemical conditions, and that the steric effect in this case can be imputed to prevent the clustering of impurities in calcite.

A new approach for remediation of polluted soils: interaction between vitreous matrix and metallophyte plants

Gauthier, A.[*] & Dubois, M.
Laboratoire Génie Civil et géoEnvironnement EA 4515, Université Lille 1, Villeneuve d'Ascq, France
([*]arnaud.gauthier@univ-lille1.fr)

The contamination of soils by heavy metals has become a really important problem, especially in some highly industrialized areas such as North of France. One solution is to treat soils by remediation using metallophyte plants able to trap pollutants from soils. The aim of this work is to follow the evolution of a plot of polluted land in the presence of metallophyte plants (*Arabidopsis halleri*) and of a phosphated amendment. This amendment consists of a glassy matrix (Ca-Si-P) in order to increase the phosphorus concentration into the soil. In addition the alteration of this glass results in the formation of crystallized secondary phases (hydroxyapatite) which can trap heavy metals.

The metal content in metals after culture is about 2 % for cadmium and 4 % for lead. Moreover, the metal content of the superior parts is much more important than in the absence of amendment (5 and 8 % respectively for Cd and Pb). Samplings of ground were besides realized and prepared in order to observe root / soils contacts by ESEM. To investigate the impact of amendment on the behaviour of metals contained in the sediment, element mappings were made on polished sections (Fig 1).

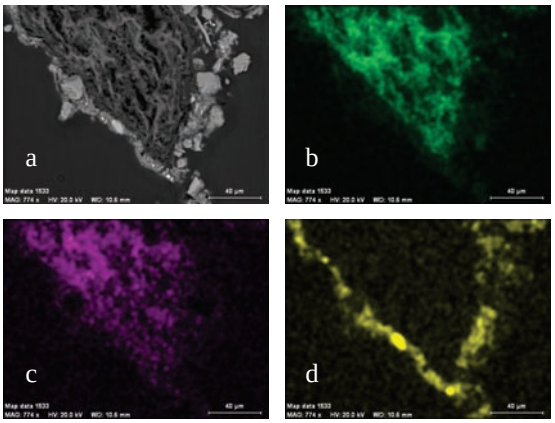

Fig. 1: SEM-BSE observation (a) and elementary mapping (b: Ca, c: Zn, d: Pb) of an A. halleri root

Observations tend to prove that the zinc diffuses and was preferencially integrated within the root. When using a stake in absence of amendment, we observe a gradient of rather weak concentration with only the presence of a zone more concentrated in periphery (pas compris). In presence of amendment, the mapping brings to light a more important concentration, with a gradual increase towards the heart of the root. A very clear enrichment in lead is set up in the outer border, whereas this element is absent in the heart of the root. Besides, the lead distribution on the edge of the root seems to be correlated to the type of substratum of culture. So in presence of amendment this border appears more continuous and thicker.

This study has permitted to show a great capacity of *A. halleri* to mobilize specifically zinc from solid phases of soil. A complementary approach will be performed in order to quantify the distribution of metal in the plant and in the neo-formed minerals.

Formation of ettringite in steel slag recycled as roadbed materials

Mikami, M.[1*], Oota, S.[1], Sato, T.[2] & Yoneda, T.[2]
[1]Graduate School of Engineering, Hokkaido University, Sapporo, Japan ([*]m.masato@eng.hokudai.ac.jp)
[2]Faculty of Engineering, Hokkaido University, Sapporo, Japan

Steel slag is a by-product of the steel manufacturing process and is currently reused as roadbed materials in Japan. From the results of previous experimental researches, some of steel slag could be altered and form secondary minerals such as hydrotalcite, hydrocalumite, and ettringite ($[Ca_6Al_2(OH)_{12}](SO_4)_3 \cdot 26H_2O$) by interaction with water. Among the secondary mineral phases, hydrotalcite and hydrocalumite have a much amount of anion exchangeable capacity due to the isomorphic substitution of Mg for Al and Ca for Al, respectively. However, the selectivity of anion sorption depends on the chemistry of solution, especially the concentration of competitive anions. On the other hand, ettringite can incorporate some oxyanions such as sulphate anion into the structure, even though ettringite also have anion sorption capacity on the surface. Once some oxyanions incorporated into the structure, the oxyanions can stably retain in the structure until the dissolution. Thus, ettringite is important phase determining chemistry of the pore water in the roadbed steel slag.

In this context, this study investigated the formation of secondary minerals in the mixed steel slags with different mixing ratios, especially ettringite. The three different kinds of slag used in this study were air cooled blast furnace slag (ACBFS), granulated blast furnace slag (GBFS) and basic oxygen furnace slag (BOFS). Flow-through experiments were conducted to calculate the dissolution rates of different ions and the formation of various secondary minerals were evaluated.

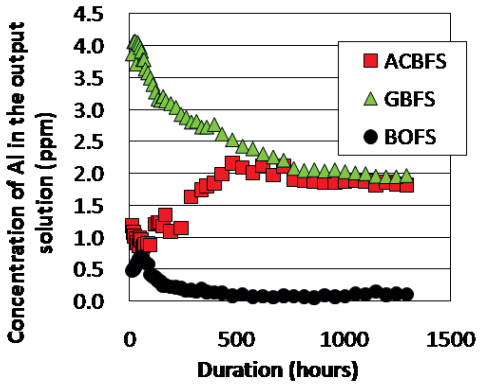

Fig. 1: Al concentration of the output solution obtained from flow-through experiments for the three different kinds of slag.

The results of the flow-through experiments showed that the concentration of Al and SO_4^{2-} at initial state in GBFS and ACBFS were significantly higher compred to other type of slag. Batch experiments were also conducted in relation to particle size, temperature, liquid/solid ratio and blend ratio. The results from batch experiments indicated that ettringite was detected only in coarse samples and large blend ratio of ACBFS samples. Additionally, ettringite was not observed when GBFS blend ratio was 0%. In the case of coarse samples, it is expected that soluble parts (dissolution at initial state) were concentrated on the surface of particle. The overall results of this study confirmed that the formation of ettringite is mainly controlled by the concentration of Al and SO_4^{2-} from GBFS and ACBFS at initial state, respectively. Thus, formation of the secondary minerals can be controlled by mixing ratio of the slag for release control of the anions, although the mixing ratio should be selected with consideration of physical behaviour of the slag used as roadbed materials.

Alteration and hazardous anions behavior of steel slag used as roadbed materials

Oota, S.[1*], Mikami, M.[1], Anraku, S.[1], Sato, T.[2] & Yoneda, T.[2]
[1]Graduate school of Engineering, Hokkaido University, Sapporo, Japan ([*]shunsuke.oota@gmail.com)
[2]Faculty of Engineering, Hokkaido University, Sapporo, Japan

The steel slag which is a by-product from iron manufacturing processes has been utilized as recycle materials since it has low impact on the environment. In Japan, the fluorine emission standard recently gives rise to regulations at 0.8 mg/L. Therefore, the use of fluorite (CaF_2) as a fusion agent in the refining process causes a great environmental concern. In the previous research, however, the results showed that some of steel slag could easily generate anion absorbents such as hydrotalcite and CSH by interaction with water in the laboratory experiments. Therefore, the fluorine in the steel slag which is currently used as roadbed materials and cement admixture would be expected to retain in the secondary mineral phases.

In this context, the aim of the study is to confirm the alteration and hazardous anions behavior (especially fluorine) of the steel slag which was used as roadbed materials. Moreover, this study aims to propose a construction method of steel slag based on the data obtained from the analyses of field site. To understand alteration and hazardous anions behavior, different combination ratios of Air-cooled blast furnace slag (ACBFS), Granulated blast furnace slag (GBFS), Basic oxygen furnace slag (BOFS) and durations were examined and the samples were analysed by using XRD, XRF, SEM-EDX and X-ray CT analyses. Leaching test of fluorine was also conducted. To evaluate the alteration behavior of each three types slag, flow-through and batch experiments were also carried out with the same types of steel slag used as roadbed materials. The results of flow-through and batch experiment as well as the behavior of hazardous anions were modeled to duplicate the dissolution and alteration process in slag by using REACT program in The Geochemist's Workbench-professional software.

Ten samples of roadbed materials using a combination of three kinds of steel slag (ACBFS, GBFS and BOFS) were collected from six different sites in order to compare the difference of combination ratios and durations. Samples of three types of slag used before as roadbed materials (ACBFS, GBFS, BOFS) were also collected.

The results of XRD analyses showed that the secondary minerals such as ettringite, hydrotalcite and hydrocalumite which have anion adsorption properties were actually generated in the slag samples. The differentiation of these minerals phases could be dependent on the various initial combination ratios of slag. SEM-EDX analyses showed the high concentration of fluorine was observed at the same point where magnesium content was rich. This result suggests that fluorine could be associated with the secondary minerals generated during the alteration of GBFS. The results of the leaching test also revealed that the highest concentration of fluorine was observed in GBFS (100% after construction sample) in which hydrotalcite, hydrocalumite and CSH were observed. Moreover, the results of flow-through experiment showed that the behavior in the dissolution of different elements were dependent on each type of slag. The difference in the generation of secondary minerals in these experiments may be attributed to the different of reactions in each slag.

Lastly, the geochemical modeling was able to simulate generally the result of batch experiment. However, there is a need to consider more several thermodynamic data to improve the fit and further determine the better combination ratio of steel slag to provide better results in fluorine leaching inhibition.

Acknowledgements: This study is partially supported by steel industry foundation for the advancement of environmental protection technology.

Persistence and bioaccumulation of heavy metals around an ancient mine site at Gromo-Gandellino (Valseriana, Northern Italy)

Porro, S.*, De Capitani, L. & Grieco, G.
Dipto. di Scienze della Terra "Ardito Desio", Milano University, Milan, Italy (*Silvia.Porro@unimi.it)

The land surface is altered by mining activities and mine dumps often become sources of pollution. Near Gromo and Gandellino villages, on both sides of the Valseriana in the Central Orobic Alps (Bergamo, Italy), several signs of historical mining activities are present. Since XIth century these mines, exploited specifically for Fe and Ag, played an important role for the economic development of the valley. The deposits, whose ore mineralogy is dominated by sulphides, sulphosalts and carbonates were intensely exploited in the Middle Ages and abandoned in the early decades of XXth century. The ore mineralization, represented by a complex and polyphase association of sulphides and sulphosalts containing Cu, Fe, Zn, Pb, Co, Ni, Ag, Sb, As with dominant chalcopyrite and tetrahedrite, is hosted in quartz breccia bodies that crop out along contacts between South Alpine basement and Permo-Triassic cover rocks.

Mining activities generated a large amount of waste rock dumps located close to villages. Three dumps (Coren del Cucì, Pradel and Vedriol) were investigated in details: an amount of 75 earth samples were collected from 15 to 40 cm depth and the fraction < 2 cm was separated for subsequent pH and geochemical analyses. Representative quantities of aerial parts and roots of two plant species that grow over the dumps, *Calluna vulgaris* (15 samples) and *Dryopteris filix-mas* (20 samples), were collected in the same soil sampling places. Trace-element concentrations (Pb, Zn, Co, Ni, Ag, Cu, Cd and As) in both earth and plant samples were determined by ICP-AES. Bioaccumulation Factor (BF) and Traslocation Factor (TF) were calculated for plants data set.

In earth materials all elements reach high level concentrations: if only averages are considered, Zn and Pb exceed 3500 and 3000 mg kg^{-1} respectively, while As reaches 860 mg kg^{-1}. The three sites show different element associations. High metal concentration values were founded also in soils far from dumps, upholding the presence of an anomalous area that must be carefully controlled and monitored for its potential geochemical risk. Data set elaboration led to establish that elements are in conditions of geochemical immobility and several accumulations are mainly related to morphological factors.

C. vulgaris shows several BF values >1 displaying an evident tendency to accumulate metals, especially in roots. In aerial parts BF value for Cd reaches 2.90. Ranges of TF values uphold the behaviour of this species as a metal bio-accumulator, when present around mine sites [1]. In *D. filix-mas* metal concentrations are like to baseline values for plants that grow over not contaminated soils and slightly exceed toxic levels [2] only for As and Pb. BF values are low and < 1 for all elements. Evaluation of trace-element concentrations shows that these two species are not hyperaccumulators; however they are interesting for soil stabilization and could be used to re-establish a vegetative cover at sites where natural vegetation is scarce due to high metal concentrations, such as contaminated habitats. Especially *C. vulgaris* is able to grow on acid, ore-characterized and nutrients-poor substrates by employing a metal exclusion-strategy and could be used for contaminated land phytostabilization.

[1] Wilson, B. & Pyatt, F.B. (2007) *Ecotox. Environ. Safety*, **66**, 224-231. [2] Kabata-Pendias, A. (2001) *Trace Elements in Soils and Plants.* CRC Press, Florida.

Ab initio investigation of actinide incorporation in Ti, Zr, Hf, and Sn-containing garnet crystals

Rak, Zs.*, Ewing, R.C. & Becker, U.
Dept. of Geological Sciences, University of Michigan, Ann Arbor, MI, USA (*rakzsolt@umich.edu)

Garnets, with general formula $A_3B_2X_3O_{12}$, have recently been investigated as a potential candidate for actinide-bearing host matrices [1-3]. Due to the presence of the three different cation sites (A, B, and X) various elements can be incorporated into the structure. This not only gives rise to a significant range of elemental compositions, but also opens up the possibility of synthesizing artificial actinide-bearing phases with garnet structure. Present efforts are focused on structures that are derivatives of the fluorite structure, e.g., pyrochlore [1-4]. Garnet crystals with high level of Zr and Ti have been found in nature, and their synthetic analogues have been investigated experimentally as nuclear waste form materials [4]. In order to understand the capability of garnet crystals to incorporate actinides, it is crucial to obtain a basic theoretical understanding of the bonding and electronic structure of the materials.

We have investigated the crystal structure, nature of interatomic bonding, and electronic structure of $Ca_3(Ti, Zr, Hf, Sn)_2Fe_2SiO_{12}$ garnet, using first-principles calculations within the density functional theory (DFT). The calculated equilibrium lattice parameters and the interatomic distances are close to the available experimental values, with a slight overestimation of bond lengths due to the generalized gradient approximation (GGA) used in our calculations. The incorporation of actinides has been simulated by substituting different cation sites with uranium. The theoretical total density of states (DOS) and its projections onto the atomic orbitals are presented and analyzed for different values of the on-site Coulomb interaction (Hubbard *U*) within the Fe *d* states. In order to quantify the strength of the interatomic bonds, we have performed Bader analysis of the charge density. The results of this analysis provide insight into the relative radiation resistance of the garnet crystals as a function of composition.

[1] Omel'yananko et al. (2007) *Geol. Ore Dep.*, **49**, 137-193. [2] Livshits (2008) *Geol. Ore Dep.*, **50**, 470-480. [3] Laverov et al. (2010) *Geochem. Int.*, **48**, 1-14. [4] Whittle et al. (2006) *J. Solid State Chem.*, **180**, 758-791.

Comparison of kinetic models for the adsorption of *p*-nitrophenol by organopalygorskites

Sarkar, B.[*], Xi, Y., Megharaj, M., Krishnamurti, G.S.R. & Naidu, R.
Centre for Environmental Risk Assessment and Remediation (CERAR) & Cooperative Research Centre for Contamination Assessment and Remediation of the Environment (CRC CARE), University of South Australia, Mawson Lakes, SA, Australia ([*]Binoy.Sarkar@postgrads.unisa.edu.au)

The potential of palygorskite to synthesise organoclays is less explored as compared to bentonite and montmorillonite. As palygorskite is a 2:1 type clay mineral having moderately high negative structural charge, it can be modified with cationic organic surfactant [1]. Palygorskite has high surface area and it is non-swelling in nature. Also, organopalygorskites supposed to be more permeable than bentonite based organoclays when used to remediate environmental contaminants through a permeable barrier.

We synthesised organoclays from palygorskite using cetylpyridinium chloride. The cation exchange capacity (CEC) of the palygorskite was 17.0 cmol (p+) kg-1. For organic modification, we used surfactant doses equivalent to 100% (CP1) and 200% (CP2) CEC of the palygorskite. We conducted FTIR studies to prove successful organic modification of the palygorskite.

We studied the kinetics of *p*-nitrophenol (PNP) adsorption on to the synthesised organopalygorskites (adsorbent dose 10 g L^{-1}; PNP concentration 3.59 mM L^{-1}; agitation time 2 h; pH = 4.8; temperature 23^0C) and compared various kinetic models by fitting the kinetic data into them. Table 1 shows the goodness of fit of various kinetic models for PNP adsorption onto CP1 and CP2.

Table 1: Kinetic models fitting parameters for PNP adsorption on to the organopalygorskites

Kinetic model	CP1			CP2		
	R^2	F	p	R^2	F	p
Pseudo second	1.0	302049	<0.0001	0.9998	47298	<0.0001
Pseudo first	0.9443	119	<0.0001	0.9246	86	<0.0001
Elovich equation	0.9098	81	<0.0001	0.948	146	<0.0001
Power function	0.9094	80	<0.0001	0.9456	139	<0.0001
Parabolic diffusion	0.7593	25	0.001	0.8185	36	0.0003
Second order	0.5566	10	0.0132	0.6565	15	0.0045
First order	0.5544	10	0.0135	0.6440	14	0.0052
Zero order	0.5521	10	0.0138	0.6309	14	0.0061

We demonstrate in this study that the adsorption of PNP on to the organopalygorskites is best explained by the pseudo second order kinetic model. The best fitness of pseudo second order kinetic model confirms that chemical adsorption, rather than physical adsorption, controls the adsorption rate over the whole range of PNP concentrations [2]. The maximum amounts of PNP adsorption calculated from the pseudo second order model are 0.12 and 0.18 mM g^{-1}, respectively for CP1 and CP2. Therefore, the adsorption process and adsorption rate of PNP on organopalygorskites depend on the surfactant concentration at their surface. This study will be helpful to design palygorskite based organoclay adsorbents for remediating ionisable organic contaminants in the environment.

[1] Chang, Y. et al. (2009) *J. Hazard. Mater.*, **168**, 826-831. [2] Ho, Y.S. & McKay, G. (1999) *Process. Biochem.*, **34**, 451-465

Use of silico-manganese slag for the production of industrial aggregate

Žigovečki Gobac, Ž.[1*], Oršulić, D.[2], Mladenovič, A.[3], Jadrijević, A.[2], Kampić, Š.[1] & Bermanec, V.[1]
[1]Inst. of Mineralogy and Petrology, Faculty of Science, University of Zagreb, Croatia ([*]zeljkaz@geol.pmf.hr)
[2]CSS d.o.o., Zagreb, Croatia
[3]Slovenian National Building and Civil Engineering Institute, Ljubljana, Slovenia

Silico-manganese slag is an industrial by-product of manganese production in the former TEF factory, Šibenik, Croatia. The crushing and separation facility has been used to produce industrial aggregate fractions. Test samples were taken from stockpiles of the slag and crushed aggregate fractions deposited in the Crnica area, near Šibenik.

Analyses of the mineralogical, chemical, radiological, physical and mechanical properties of the manufactured aggregate were performed in order to determine the composition, possible use in civil engineering, and potentially hazardous effect on the environment.

The samples of silico-manganese slag were investigated using X-ray powder diffraction, scanning electron microscopy (associated with an energy dispersive spectrometer), gamma spectrometry and leaching tests.

Silico-manganese slag contains a silicate glassy phase with various micro- to nano-crystalline phases, which originated in the reaction with the melt or in subsequent crystallization. These crystalline artificial/synthetic phases include akermanite, pyroxene, cristobalite and ramsdellite, which are the equivalents of minerals originating in high-temperature contact metamorphic areas or in basic volcanic rocks. Nodules or grains of silico-manganese alloy are also identified in the glassy matrix (Fig. 1).

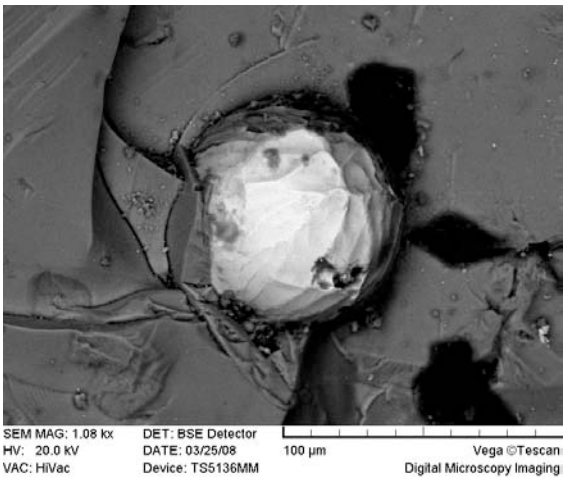

Fig. 1: A ferro-silico-manganese nodule (cca. 60 µm in diameter) in a glassy matrix.

The potentially hazardous properties of slag may be due to radioactivity or from the release of heavy metals. Tests of radioactivity showed that aggregate is not, globally, dangerous, and tests on the leaching of heavy metals gave values lower than the maximum permitted values.

The results of all the tests performed show that the aggregate can be used for the production of asphalt and concrete, according to the EU standards. This provides a good example of converting waste material from the ferroalloy industry into secondary raw material, as has been described earlier [1].

[1] Frías, M. et al. (2006) *Cement Concrete Res.*, **36**, 487-491.

Isotopes and predicting the long-term behaviour of high-level nuclear waste

Fayek, M.
Dept. of Geological Sciences, University of Manitoba, Winnipeg, MB, Canada (fayek@cc.umanitoba.ca)

A main criterion for performance assessment of a potential high-level nuclear waste (HLNW) repository is predicting the fate of HLNW. For example, most geologic disposal concepts require that the spent nuclear fuel (SNF) remain isolated from the accessible environment for more than 100 000 years (i.e., the time required for the fission and actinide products to reach safe levels [1]). Therefore, one of the most challenging aspects of nuclear waste management is the extrapolation of laboratory data, collected over short periods of time (hours to years) to longer periods required in performance assessment calculations [2]. Most studies that attempt to predict the behavior of HLNW under repository conditions are based on models which, when unconstrained by data, often produce ambiguous results. Therefore, researchers have studied natural analogues and characterized the fluid history of potential repository sites to provide data on the long-term performance of radioactive waste forms and assess a potential repository site.

Geochronology and stable isotope geochemistry are techniques well suited for investigating potential sites and the study of natural analogues. Hydrogen and oxygen isotopes can provide information on the origin of water that has interacted with minerals along fractures and analogous material to SNF such as uraninite. Variations in stable isotope contents can be related to palaeohydrological and palaeoclimatic conditions [3]. Carbon isotopic composition of dissolved carbon in pore fluids and carbonates can be used to determine the source of the carbon. Strontium and sulfur isotopes can be used to discriminate between several generations of fracture-filling minerals. Studies have shown that multiple mineralizing events represent migration of fluids ranging from high-temperature hydrothermal systems to present-day groundwater circulation [4].

U-Pb and U-series geochronology can be used to constrain the chronology of minerals that form along fast diffusion pathways (e.g., fractures [5]), and provide a record of geologically significant fluid or thermal events that may have affected the repository site. Geochronology of uraninite from several deposits that are considered natural analogues for SNF (e.g., Cigar L., Nopal I, Oklo) has shown that fluid events related to large-scale tectonic and paleoclimatic events can cause radionuclide migration in near surface environments [6]. *In situ* isotopic micro-analysis of zoned minerals with a spatial resolution on the scale of a few μm can provide information at the forefront of scientific research. For example, U-Th-Pb isotope studies of Quaternary opal occurring in calcite–silica fracture and cavity coatings within Tertiary tuffs at Yucca Mountain preserve a record of paleohydrologic conditions [5].

The age of groundwater is also a key factor for performance assessment of HLNW disposal in deep geological formations. Radiogenic noble gases (He, Ar, Xe) and Cl isotopes can in some circumstances provide age information due to their inertness, their well-known sources and their increase in concentration with time [7]. The age of the water table can be used to assess the rate of recharge and whether the water table may someday engulf the repository.

[1] Ewing, R.C. (1999) *Science*, **286**, 415-416. [2] Janeczek, J. et al. (1996) *J. Nucl. Mater*., **238**, 121-130. [3] Fontes, J.C. (1994) *Terra Nova*, **6,** 20-36. [4] Sandström, B. & Tullborg, E-L (2009) *Chem. Geol*., **266**, 126-142. [5] Neymark, L.A. et al. (2000) *Geochim. Cosmochim. Ac.*, **64**, 2913-2928. [6] Fayek, M. et al. (2003) *Am. Mineral*., **88**, 1583-1590. [7] Osenbrück et al. (1998) *Geochim. Cosmochim. Ac.*, **62**, 3041-3045.

Potential of radiation-induced defects in clay minerals to trace past uranium transfers in the Athabasca Basin (Canada)

Morichon, E.[1,2], Allard, T.[1*], Beaufort, D.[2] & Quirt, D.[3]
[1]IMPMC, UMR, Paris, France
([*]thierry.allard@impmc.jussieu.fr)
[2]Hydrasa, University of Poitiers, France
[3]AREVA Resources Canada Inc., Saskatoon, Canada

Defects produced by radiations in the structure of clay minerals such as kaolinite have been used to reconstruct past migrations of uranium in the geosphere [1]. They may also be helpful for prospection. This study presents the first unequivocal identification of radiation-induced defects in proterozoic kaolinite, illite and sudoite (di-trioctahedral Al-Mg chlorite) from the alteration halo surrounding the unconformity-type uranium deposits in the Athabasca basin (Canada), using Electron Paramagnetic Resonance spectroscopy. In all samples originating from 25 drill holes, defects of the clay minerals are similar and consist in electron holes on oxygen atoms of the structure. Defects in illite and sudoite are thus new potential tracers of ancient radioactivity. The concentrations of defects can widely vary from the regional background to several orders of magnitude. The maximum of fluctuations of defects concentrations is observed at the level of the unconformity between upper sandstones and underlying basement rocks and associated crosscutting brittle structures, which appears as the main vector of U-bearing fluids transfer in the basin. A somewhat scattered pattern of defect concentrations decreasing from unconfomity levels towards the barren rock is observed without correlation with the present dose rate produced by the radioelements (U, Th decay chains and ^{40}K). More specifically, concentrations of defects can vary significantly for a same dose rate. These observations are strong indications of past migrations of radioelements in the studied system that occurred after the clay mineral formation. Moreover, the proximity of mineralization can be revealed through defects that recorded past presence of radioelements in the altered rocks at significant distance from the mineralized bodies, an interesting perspective for prospection.

[1] Allard, T. & Calas, G. (2009) *Appl. Clay Sci.*, **43**, 143-149.

Coupled substitution of neptunium (V) and iodate into a uranyl phosphate: implications for mitigating the release of ^{237}Np and ^{129}I in repositories

Wu, Shijun[1,2], Chen, Fanrong[1], Simonetti, A.[2] & Albrecht-Schmitt, T.E.[2*]
[1]Guangzhou Institute of Geochemistry, Chinese Academy of Sciences, Guangzhou, Guangdong, China
[2]Dept. of Civil Engineering and Geological Sciences, University of Notre Dame, Notre Dame, Indiana, USA ([*]talbrec1@nd.edu)

The simultaneous incorporation of IO_3^- and NpO_2^+ into $Ba_3(UO_2)_2(HPO_4)_2(PO_4)_2$ (BaUP), which serves as a model for uranyl alteration phases, was investigated. LA-ICP-MS data demonstrate that the incorporation of both of these species is significantly enhanced when they are present together. The most probable explanation is that charge balance is obtained by the coupled substitutions of $NpO_2^+ \leftrightarrow UO_2^{2+}$ and $IO_3^- \leftrightarrow HPO_4^{2-}$. In the absence of iodate as much as 2.91±0.14% to 3.44±0.25% of the uranium in BaUP can be replaced by neptunium. When iodate is present in the reaction, the uranium substituted by neptunium was as high as 6.05±0.65% to 7.93±0.83%. The net increase for neptunium is 116±0.30% to 225±0.25%. Similarly, in the absence of NpO_2^+, iodate incorporation into BaUP reaches an I/U level of 0.0021±0.0004 to 0.0038±0.0005; whereas in its presence there is a as much as 100±0.11% increase to 0.0042±0.00100. Some H_2O should be substituted for HPO_4^{2-} to get charge balance because of the high Np level (Fig. 1).

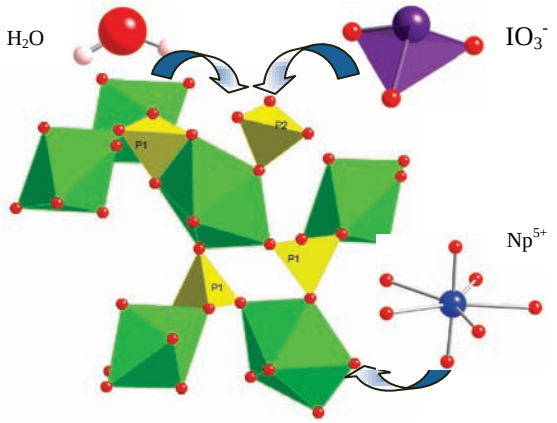

Fig. 1: An illustration of the substitution of IO_3^-, NpO_2^+ and H_2O in BaUP.

The radionuclides within the waste form, such as ^{137}Cs, ^{235}U, ^{237}Np, ^{239}Pu, ^{79}Se, ^{99}Tc, ^{129}I, can be divided into cations and anions. In the previous studies, the retardation of cationic and anionic radionuclides was investigated separately though they exist together in the waste form [1-3]. Since coupled substitution of $NpO_2^+ \leftrightarrow UO_2^{2+}$ and $IO_3^- \leftrightarrow HPO_4^{2-}$ is observed in BaUP, it provides an enhanced mechanism for mitigating the release of ^{129}I and ^{237}Np from a nuclear waste repository. Similar phenomena for coupled substitution are expected to occur in other uranyl phases, such as uranyl silicates and carbonates. Furthermore, coupled substitution of other cationic and anionic radionuclides is also expected.

[1] Burns, P.C. et al. (2004) *Radiochim. Acta*, **92(3)**, 151-159. [2] Douglas, M. et al. (2005) *Environ. Sci. Technol.*, **39(11)**, 4117-4124. [3] Wu, S. et al. (2009) *Radiochim. Acta*, **97(8)**, 459-465.

Structural investigations of minor actinide-bearing fuels

Vespa, M.[*], Rini, M. & Somers, J.
Institute for Transuranium Elements, European Commission, Joint Research Centre, Karlsruhe, Germany
([*]Marika.VESPA@ec.europa.eu)

Fast reactors (e.g. as outlined in the Gen IV initiative and in the Sustainable Nuclear Energy Technology Platform (SNETP)) provide a means by which nuclear energy sustainability is ensured. Furthermore, they make a positive step forward in the destruction of the minor actinide (MA) waste that they produce. Novel nuclear fuels will be needed and, in a likely first step, they should be based on actinides-U mixed oxides. Fuel development is a lengthy process, and little is known about MA-bearing fuels, which needs to be treated through experimental and theoretical approaches at the molecular level.

The Strategic Research Agenda (SRA) of the SNETP (www.snetp.eu) clearly indicates the need to establish fundamental properties and irradiation behaviour of these new and largely untested materials. Nuclear fuel research is facing a paradigm shift from "Observe and Validate" towards "Design and Control" and is being driven by advances in multiscale modelling, and in particular ab initio calculations and molecular dynamics. Though tremendous advances have been made in these areas, there is a clear need for validation by experiments. Local structure investigation, by means of X-ray absorption spectroscopy (EXAFS and XANES), is one method poised to make important contribution towards the validation of such codes. An important fuel parameter, which has to be taken into consideration, is the oxygen potential and the corresponding O/M (oxygen to metal) ratio of the Am containing-mixed oxides. Since the O/M will increase during the irradiation time, an increase in the oxygen potential may limit the fuel burn-up due to possible fuel-cladding interactions. During this process Am is expected to be reduced to its trivalent state, a requirement to limit cladding oxidation. Consequently, the thermal conductivity should decrease due to the defects and distortion in the cubic structure [1-4].

In this study (U, Am)O_2 samples with different O/M, have been prepared and investigated at the beamline for radioactive materials (INE-beamline) at the ANKA-synchrotron light source. EXAFS measurements were performed on the U- and Am-L_{III} edges. These first measurements demonstrated the feasibility of analysing highly radioactive materials (7.93×10^8 Bq/g), and will aid in developing and improving future nuclear fuels.

In the next steps, it is planned to complement the EXAFS investigations with magic angle spinning nuclear magnetic resonance (MAS NMR) measurements. The combination of these spectroscopic methods will lead to an accurate determination of the coordination number and bond length change within the structure, and the evolution thereof as the sample undergoes self irradiation damage.

[1] Walter, M. et al. (2007) *J. Solid State Chem.*, **180**, 3130-3135. [2] Walter, M. et al. (2009) *J. Solid State Chem.*, **182**, 3305-3311. [3] Walter, M. et al (2008) *J. Nucl. Mater.*, **373**, 90-93. [4] Walter, M. et al. (2007) *J. Nucl. Mater.*, **362**, 343-349.

Mineral matrix material development for immobilization of REE radionuclides and actinoids

Kovalskii, A.M[*], Suvorova, V.A., Kotelnikov, A.R. & Akhmedshanova, G.M.
Institute of Experimental Mineralogy of Russian Academy of Sciences, Chernogolovka, Russia ([*]kovalsky@iem.ac.ru)

For synthesis of ceramics on the basis of titanates, zirconates and complex phosphates with the purpose immobilization of REE radionuclides and actinoids techniques of hot pressing and pirosynthesis [1] are used. These methods allow obtaining high-leaching stability matrix materials, however technology of that maintain are complex enough. In this work the method of synthesis of matrix materials is based on metasomatic replacement reactions under the scheme of "wet process" [2]. The method allows spending process of radionuclides sorption on phosphate-containing mineral compositions at room temperature and atmospheric pressure in wet conditions

Synthesis of phosphates of strontium and cerium were carried out, as well as synthesis of mineral matrixes on the basis of (Sr, Na) - and (Ce, Na) – phosphates. Products of experiments were investigated by an X-ray method; for an estimation of compositions of the synthesized solid phases on the elements maintenance, the method local X-ray microanalysis was applied. The analysis of a filtrate on the strontium maintenance carried out by a method AAS spectroscopy on devices AAS-1N, cerium – by a method photocolorimetry on the device "Spekol 11".

Deficiency of solutions of nitrate Sr or Ce leads to formation in a column of the minerals allied substances to natural minerals olgite $NaSrPO_4$ or vitusite $Na_3Ce(PO_4)_2$. These minerals are met in hydrothermal changed rocks of Lovozero and Khibina alkaline massifs, Kola Peninsula and have shown high stability to leaching as the age of these massif formations exceeds 360 million years. So those minerals can serve as matrix materials in spite of the fact that the maintenance of strontium and cerium in them is essential less, than in simple orthophosphates.

Simple orthophosphates of Sr and Ce were synthesized at use of super quantities of nitrates solutions. For decrease in temperature of sintering of matrixes with the purpose of their density increase, instead of separate grains feldspar and quartz, as initial has been used leucocratic granite of Spokojninskoe deposit. As a result of experiences on metasomatic replacement, the subsequent drying and calcinations, the polymineral ceramic compositions consisting of feldspar, quartz and phosphates of strontium in two experiences and cerium in one experience have been received.

Strontium ortophosphate is analogue of apatite, and phosphate of cerium – of monazite, enough widespread accessory mineral of granites, its high stability to processes leaching is shown in work [1]. The granite matrix serves as an additional barrier to leaching elements processes by hydrothermal solutions.

Acknowledgements: This work is executed with support of Russian Federation President grant № MK-4888.2009.5 and BES RAS.

[1] Ringwood, A.E. et al. (1988) in Lutze, W. & Ewing, R.C. (eds.) *Radioactive waste forms for the future.* Elsevier, 233-334.
[2] Kotelnikov, A.R. et al. (2005) *Materials of XV Russ. Meeting Experim. Mineral.* Syktyvkar. Inst. Geol. Komi., 468-470.

Local and medium range order around fission products: implication for structural control of the stability of nuclear waste glasses

Galoisy, L.[1*], Calas, G.[1], Cormier, L.[1], Jollivet, P.[2], Delaye, J.-M.[2], Gin, S.[2] & Ghaleb, D.[2]
[1]Institut de Minéralogie et de Physique des Milieux Condensés, Universités de Paris 6&7, IPGP and CNRS, Paris, France ([*]Laurence.galoisy@impmc.upmc.fr)
[2]CEA, Laboratoire du Comportement à Long Terme, Centre de Valrho, Marcoule, France

Vitrification of liquid high-level radioactive waste in borosilicate glasses has received a great attention in several countries. As for other waste forms, their fundamental properties are their chemical and mechanical durability.

In a first part, we will present an overview of the local structure around some elements such as Zn, Mo, Fe or Zr, in a borosilicate glass (SON68) taken as an inactive analogue of the French nuclear glass (R7T7). Due to the complex composition of these glasses (up to 30 oxides), chemically selective methods are required to understand the environment of these elements. Structural information was obtained by a combination of X-ray Absorption Spectroscopy (XAS) and Wide Angle X-ray Scattering (WAXS) to probe local and medium range order, respectively. Eventually, XAS was used to study the interaction between noble metals (Pd and Ru) and the glassy matrix. These elements are at the origin of small precipitates that induce changes in melt viscosity. These structural data were compared with MD calculations on simplified glass compositions.

Assessing the long-term behavior of nuclear glasses implies the prediction of their long-term performance during interaction with water or under irradiation. In the second part, we will present some structural features of the evolution of the glass under these forcing conditions. The protective character of the gel, observed during alteration in near- or under-saturated conditions will be rationalized by its structural properties.

These structural modifications may explain the chemical dependence of the initial alteration rate and the transition to the residual regime. They also illustrate the molecular-scale origin of the processes at the origin of the glass-to-gel transformation. During external irradiation, there is direct evidence of a coordination change of B at the glass surface. In addition, for a better understanding of the modification of glass structure under irradiation by heavy ions, complementary information is provided by molecular dynamics simulations, showing a combination of elastic and inelastic effects. These two processes are suspected to produce a modification of different physical properties of nuclear glasses during irradiation.

Uranium speciation in opals from the Nopal I deposit (Sierra Peña Blanca, Mexico): a SEM, TEM and TRLFS study

Othmane, G.[1*], Allard, T.[1], Menguy, N.[1], Vercouter, T.[2], Morin, G.[1], Galoisy, L.[1], Calas, G.[1] & Fayek, M.[3]
[1]Institut de Minéralogie et de Physique des Milieux Condensés, CNRS UMR 7590, UPMC, Paris, France
([*]Guillaume.Othmane@impmc.upmc.fr)
[2]LSRM, CEA Saclay, Gif-sur-Yvette, France
[3]University of Manitoba, Winnipeg, Manitoba, Canada

The study of uranium migration and trapping in the environment is relevant to estimate the safety of high-level nuclear waste repositories (HLNWR). With this aim in view, the analysis of speciation in natural analogues of HLNWR can be used to determine the conditions of uranium sequestration.

The Nopal I uranium deposit (Sierra Peña Blanca, Mexico) is a natural analogue located in volcanic tuff. The primary uranium mineralisation occurred in a breccia zone and consisted in uraninite, subsequently altered in secondary uranium minerals. During a last episod, opal was formed and coated uranyl silicates such as uranophane and weeksite [1,2].

The aim of this study is to determine the uranium speciation in these opals from the millimeter-micrometer scale of electron microscopies to the atomic or molecular scale provided by spectroscopy. Three samples of green or yellow opals have been analysed by scanning electron microscopy (SEM) on cross-section embedded in resin and by transmission electron microscopy (TEM) on a focused ion beam (FIB) section.

The first results mainly show:

1) uraniferous opal with a Ca:U atomic ratio of 1:1 showing spherical growth-features (Fig.1).

2) the complex association of uranium-bearing species like uranophane and calcium phosphates.

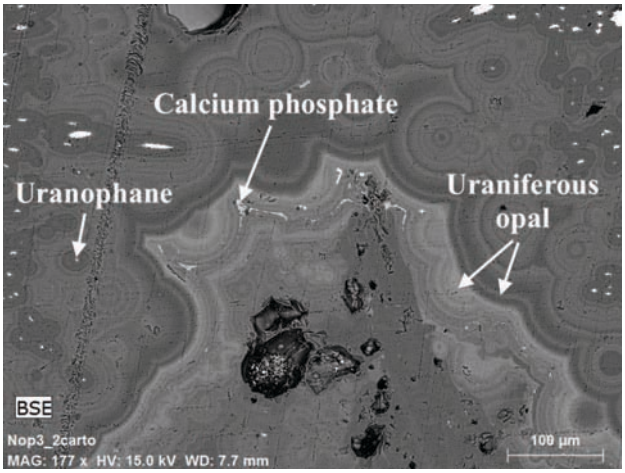

Fig. 1: SEM back-scattered electron picture of a yellow opal cross-section from the Nopal I uranium deposit, Mexico.

In addition, a combination of TEM observations in the uraniferous opal and time-resolved laser fluorescence spectroscopy (TRLFS), a well-suited technique to coordination chemistry of uranyl complexes [3], will be shown. These observations will help revealing the speciation of uranium occurring either as embedded complexes or uranium-bearing nanophases in the opal.

[1] Calas, G. et al. (2008) *Terra Nova*, **20**, 206-212. [2] Schindler, M. et al. (2010) *Geochim. Cosmochim. Ac*, **74**, 187-202. [3] Wang, Z. et al. (2008) *Radiochim. Acta*, **96**, 591-598

Uranium nanoparticles: synthesis, structures, compositions and aggregation

Burns, P.C.[*], Ling, J., Sigmon, G.E., Unruh, D.K. & Forbes, T.Z.
Dept of Civil Engineering and Geological Sciences, University of Notre Dame, Notre Dame, IN, USA ([*]pburns@nd.edu)

The structural and compositional details of approximately thirty nano-scale clusters containing uranium will be examined. All of these clusters are built from uranyl peroxide polyhedra and some also include pyrophosphate or oxalate units. Their topologies are highly varied, incorporating combinations of squares, pentagons and hexagons. Many of these clusters are highly soluble in water, and small-angle X-ray scattering (SAXS) data has demonstrated that these clusters persist when dissolved in ultrapure water. Aggregation of such clusters into colloidal materials is readily triggered by addition of cations, as demonstrated by SAXS data. The ramifications of such cluster formation on the performance of nuclear waste forms will be examined.

Selenite reduction by green rust

Nedel, S.*, Skovbjerg, L.L., Christiansen, B.C., Bovet, N. & Stipp, S.L.S
Nano-Science Center, Dept. of Chemistry, University of Copenhagen, Denmark (*sorin@nano.ku.dk)

Relying more on nuclear energy for production of electricity will inevitably result in an increase of spent nuclear fuel that countries need to store. As a consequence, ensuring the safety of radioactive waste repositories and improving performance assessment models of storage facilities is crucial. Se^{79}, a long-lived fission product (half-life~10^6 years), may dominate the radiation dose from high level radioactive waste and is therefore of concern when considering a radionuclide leakage scenario. Se can be rather mobile, if present as the soluble species Se(VI) and Se(IV), but is less mobile as the sparingly soluble Se(0) and Se(–II). The prevalence of one form or another can be related to the interaction with dissolved ions and minerals in the near and far field. Se(VI) and Se(IV) are known to sorb to iron oxides and to be reduced by Fe(II)-bearing minerals. GR, an Fe(II)-Fe(III) layered double hydroxide, is a redox active compound with high surface area that forms where iron concentrations are high such as during Fe(0) corrosion. The purpose of this study was to examine the interaction of Se(IV) with sodium sulphate green rust ($GR_{Na,SO4}$) and propose a mechanism for the observed processes.

$GR_{Na,SO4}$ was synthesised using typical methods such as oxidation of an Fe(II) solution. Selenium was then added to the $GR_{Na,SO4}$ suspension as selenite, $Se(IV)O_3^{2-}$ and its concentration was followed with time. In less than 12 hours, all Se was removed from solution. Transmission electron microscopy (TEM) and X-ray diffraction revealed that Se(IV) was reduced to elemental selenium while iron oxides replaced $GR_{Na,SO4}$ (Fig. 1).

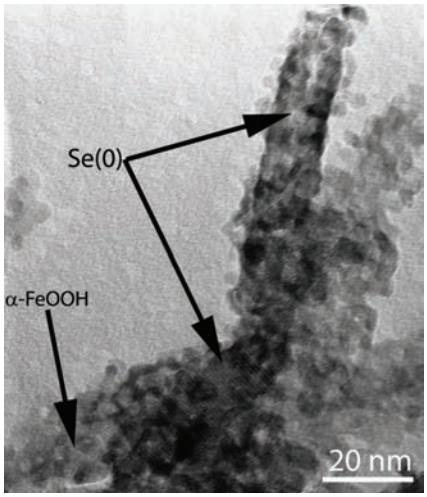

Fig. 1: TEM showing the formation of Se(0) (plates) and α-FeOOH (spheres) after $GR_{Na,SO4}$ interaction with Se(IV).

These results demonstrate that $GR_{Na,SO4}$ can decrease the mobility of Se^{79} by transforming the aqueous species into solids. The iron oxides formed during the reduction process could potentially limit even more Se migration in the soil through sorption of the remaining Se(VI) and Se(IV) .

Preliminary studies of bioreduction and biooxidation of biotite and chlorite and implications for radionuclide mobility

Kountcheva, D.R.*, Lloyd, J.R., Pattrick, R.A.D.P. & Vaughan, D.J.
School of Earth, Atmospheric and Environmental Sciences, University of Manchester, United Kingdom
(*diana.kountcheva@postgrad.manchester.ac.uk)

As part of a larger study of radionuclide mobility in the subsurface, interactions between pure cultures of the model Fe(III) reducing bacterium *Shewanella oneidensis* MR1 and the iron-containing phases biotite and chlorite have been investigated in the presence (and absence) of Cs and Sr as proxies for their radioactive equivalents. Biotite and chlorite are recognised as key mineral phases in subsurface environments [1] with the potential to control the mobility of radionuclides. Biologically promoted redox reactions involving iron are important for the stability of these mineral phases and their interactions with radionuclides.

Time course anaerobic batch experiments have been conducted where both dissolution of the mineral and uptake of either Cs or Sr have been compared in biotic and abiotic experiments Microbial reduction of structural iron was stimulated by the addition of lactate as an electron donor, while microbial oxidation of structural iron was stimulated by addition of nitrate to act as an electron acceptor. The minerals were characterised by XRD, ESEM, Microprobe and Mössbauer spectroscopy before and after the batch experiments. Analysis of dissolved species was carried out by ICP-MS.

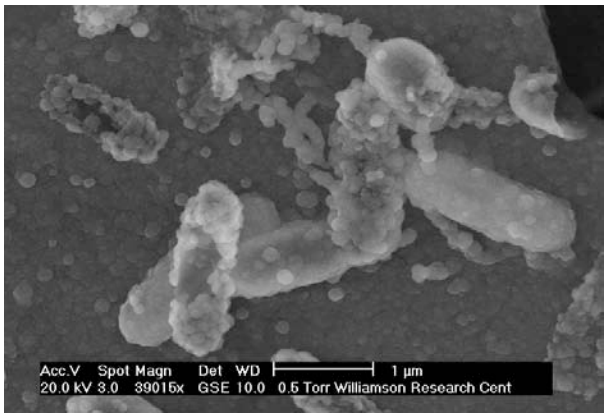

Fig. 1: ESEM image of *S. oneidensis* encrusted with secondary Fe phases formed from released Fe(II).

Bioreduction results show that microbial reduction of structural iron in biotite and chlorite is achieved and promotes mineral dissolution (releasing Si and Fe(II)) resulting in a change of reactive sites. In the presence of trace oxygen, a thin film of secondary Fe(III) oxide minerals formed at the redox interface on the liquid surface and was reduced by bacteria to form Fe-nanophases (Fig 1). The relationship between the microbes and iron minerals suggests that cell surface functional groups may act as nucleating sites. Microbially mediated mineral dissolution was not accompanied by a reduction of Cs sorption despite the likely loss of sorption sites. With the precipitation of secondary phases of iron oxy/hydroxides the sorption capacity of the system increased.

[1] McKinley, J.P. et al (2004) *Environ. Sci. Technol*., **38,** 1017-1023.

Synthesis and structural characterization of four new U^{6+} germanate compounds

Morrison, J.M., Moore-Shay, L.J. & Burns, P.C.*
Dept of Civil Engineering and Geological Sciences, University of Notre Dame, Notre Dame, United States (*pburns@nd.edu)

As the United States moves into a new era of nuclear energy development, interest is growing in the basic science associated with the nuclear fuel cycle. Uranium, the key element in the nuclear fuel cycle, has a storied history and a host of dynamic properties that must continue to be rigorously explored. Specifically, there is value in the study of U^{6+} crystal chemistry as the nearly linear uranyl ion, (UO_2^{2+}), complexes readily in a variety of inorganic systems within oxidizing environments [1].

Here we present the syntheses and structural characterizations of four new uranium germanate framework compounds. The crystal structure determinations of these isotypic compounds reveal three symmetrically distinct U^{6+} sites—two that are coordinated by five equatorial oxygen atoms each to form pentagonal bipyramids and one that is coordinated by six oxygen atoms to form a distorted octahedron with U-O bond lengths that do not indicate the presence of the uranyl ion.

These complex framework structures also include cation-cation interactions (CCIs), which occur when an oxygen atom of the uranyl ion acts as an equatorial oxygen atom in a neighboring U^{6+} polyhedron. As CCIs are present in fewer than 2% of U^{6+} compounds, and it is uncommon for a U^{6+} compound to occur without the uranyl ion, these compounds exhibit unusual structural connectivities and are expected to have interesting properties, while also providing direction for future studies.

[1] Burns, P.C. (2005) *Can. Mineral.*, **43**, 1839-1894.

Development of novel bioactive materials based on nucleation and crystal growth concept

Kokubo, T.
Dept. of Biomedical Sciences, Chubu University, Kasugai, Japan (kokubo@isc.chubu.ac.jp)

Various kinds of bone-bonding bioactive calcium phosphate ceramics have been developed and clinically used as important bone substitutes. However, they have poor mechanical strengths, and hence cannot be used under load-bearing conditions.

We attempted to prepare a composite of apatite with wollastonite which occurs in a fibrous form in nature by a process of crystallization of a glass. A glass in the system $3CaO_3{\cdot}P_2O_5$-$CaO{\cdot}SiO_2$-$MgO{\cdot}CaO_2{\cdot}SiO_2$ was crashed into fine powders, pressed into desired form and heat-treated up to 1050°C for sintering and crystallization. A glass-ceramic containing nano-sized apatite and wollastonite in a glassy matrix was obtained. It showed a higher mechanical strength than human cortical bone and high bioactivity. It was named glass-ceramic A-W and clinically used as bone substitutes in various shapes. However, its fracture toughness was lower than that of the human cortical bone [1].

During a study of the bone-bonding mechanism of glass-ceramic A-W, we found that it bonds to living bone through an apatite layer formed on its surface, and that this apatite can be reproduced even in an acellular simulated body fluid (SBF) with ion concentrations nearly equal to those of the human blood plasma. Based on these findings, it was assumed that a material able to form bonelike apatite on its surface, in SBF also forms apatite in the living body and bonds to living bone through this apatite layer.

Later it was found that even a pure titania gel forms apatite on its surface in SBF. This indicated that even Ti metal would induce apatite formation in the living body and bond to living bone through the apatite layer, if a functional group effective for apatite nucleation could be formed on its surface. Actually, Ti metal that formed a sodium titanate surface film by reaction with NaOH and subsequent heat treatments was confirmed to induce apatite formation in the living body and tightly bonded to living bone. Bioactive Ti metal prepared in this way was applied to artificial hip joints and has been clinically used in Japan since 2007. Although this treatment is not effective for inducing apatite formation on new types of Ti-Zr-Nb-Ta alloy free of cytotoxic elements, a slightly modified treatment with $CaCl_2$ solution and water applied before and after the heat treatment, respectively, is suitable for these alloys. The apatite formation on chemically treated Ti metal and its alloys was attributed to electrostatic interaction of the negatively charged metal surface with the positively charged calcium ions in the body fluid.

On the other hand, it was also shown that if acid treatment is applied to Ti metal after the NaOH treatment or without the NaOH treatment, Ti metal forms a titanium oxide film on its surface after subsequent heat treatment, and induces apatite formation on its surface in the living body to bond to bone. This apatite formation was also attributed to electrostatic interaction of the positively charged metal surface with negatively charged phosphate ions in the body fluid. Porous Ti metal with titanium oxide formed on its surface by the present method showed bone formation not only at bone defect sites but also ectopically in muscle tissue. Most recently this bioactive porous Ti metal was successfully subjected to clinical trials as a spinal fusion device [2].

[1] Kokubo, T. (2008) in Kokubo, T. (ed.) *Bioceramics and their clinical application*. Woodhead Pub. Cambridge, 284-301. [2] Kokubo, T. et al. (2010) *Materials*, **3**, 48-63.

New insights into acid-induced structural changes of enamel apatite the effect of sodium fluoride and artificial saliva

Mihailova, B.[1*], Wang, X.[1], Klocke, A.[2], Fittschen, U.E.A.[3], Broekaert, J.A.C.[3] & Bismayer, U.[1]
[1]Dept. of Earth Sciences, University of Hamburg, Germany ([*]boriana.mihailova@uni-hamburg.de)
[2]Dept. of Orofacial Sciences, University of California San Francisco, San Francisco, USA
[3] Dept. of Chemistry, University of Hamburg, Germany

Changes in the chemistry and structure of tooth enamel due to a non-peroxide-based home bleaching product were studied in vitro using attenuated total reflectance infrared (ATR IR) spectroscopy, Raman spectroscopy, electron probe microanalysis, flame atomic absorption spectroscopy and total reflection X-ray fluorescence [1]. The results revealed that the citric-acid-containing gel-like component of the bleaching system substantially impacts on the dental hard tissue. Within a layer at least several microns thick, the organic component of enamel is removed and remnants of the bleaching gel are embedded in the ensuing voids. Cracks and severe chemical inhomogeneities occur on the enamel surface. Within a submicron layer of enamel, the Ca--O bond strength in apatite decreases, thus enhancing calcium leakage from the bleached enamel hard tissue.

Citric acid-induced changes in the local atomic structure of enamel stored in distilled water and in artificial saliva were further studied by ATR-IR spectroscopy as well as electron-induced X-ray emission spectroscopy and scanning electron microscopy [2,3]. The protective potential of fluorine-containing reagents against citric acid-induced erosion was investigated on enamel and geological apatite treated with aqueous solutions of citric acid and sodium fluoride of different concentrations. The two solutions were applied either simultaneously or consecutively. The application of basic fluoride-containing solutions did not demonstrate a protective effect on the enamel apatite structure per se. However, the addition of NaF to citric-acid solutions leads to formation of surface CaF_2 and considerably reduces the changes in the apatite P-O-Ca framework. The CaF_2 globules deposited on the enamel surface appears to be insufficient to prevent the alteration of the apatite structure upon further exposure to acidic agents. No evidence for fluorine-induced structure recovery of enamel apatite stored in water was found, whereas the application of artificial saliva for several hours leads to partial recovering of the local structure of eroded enamel apatite. However, artificial saliva surrounding cannot stop the process of loosening and breaking of P-O--Ca atomic linkages in enamel subjected to multiple citric acid treatments.

[1] Wang, X et al. (2009) *J. Biomed. Mater. Res. A*, **88A**, 195-204. [2] Wang, X. et al. (2008) *J. Phys. Chem. B*, **112**, 8840-8848. [3] Wang, X. et al. submitted to *Caries Research*.

Biocompatibility of inorganic materials utilizable for mimetic bone substitution

Šesták, J.[1*], Strnad, J.[2], Strnad, Z.[2] & Holeček, M.[1]
[1]New Technology-Research Center in the Westbohemian Region, West Bohemian University, Pilsen, Czech Republic ([*]sestak@fzu.cz)
[2]LASAK-Laboratory for Glass and Ceramics, Prague, Czech Republic

Since 1970 two material groups have been identified capable to form a mechanically stable and functional interface with bone. One group consisted of certain soda-lime-silica glasses [1-4], which are exhibiting the bone bonding ability (defined as "*the bioactivity is the characteristics of an implant material which allows it to form a bond with living tissues*"). Another material found to exhibit the bone–bonding ability [5,6] was machined titanium [7,8]. The phenomenon of attachment to bone was named osseointegration (defined as "*osseointegration represents the formation of a direct contact of a material with bone without intermediate fibrous tissue layer, when observed using light microscope*"). Apparently, surface quality [4-6] determines tissue reactions to an oral implant and its assets can be classified regarding (i) mechanical (j) topographic (roughness, porosity, fractality) and (v) chemical properties. Bio-chemical bonding is related to bioactivity, which existence, however, has often been questioned because there is not a clear evidence of separated effects of surface roughness and interfacial chemical reactions. In modern dental and spinal implantology, advanced treatment protocols (e.g. early or immediate loading) are frequently used to enable reduction of the treatment time. A shorter healing period and shorter time of unloading, entails new demands on both the primary and secondary stability of the implant. The bioactivated surface, which is rich in hydroxyl groups, in contrast to machined surface, rapidly induces adsorption of calcium and phosphate ions on contact with the ions of the blood plasma. The calcium phosphate-rich layer promotes adsorption and concentration of proteins and constitutes a suitable substrate for the first apatite structures of the bone matrix, which are synthesized by the osteogenic cells at the beginning of the formation of the new bone tissue. The clinical study on dental implants was designed as a comparative study of two commonly used surfaces: classical machined titanium surface and bioactivated titanium surface (LASAK©). The bio-surface is created by sand-blasting, acid etching and a final treatment in an alkaline solution andexhibits more favorable values of the major surface characteristics compared to the machined surface and other commercially available implant surfaces studied so far studied, such as the resonance frequency analysis method used to measure the implant stability quotient. A more easily wettable hydrophilic bio-surface allowed the contact formation between the body environment (blood) and the complicated rough and porous structure of the implant surface, and thus contributes to cell and bio-molecule migration and adhesion.

[1] Strnad, Z. (1992) *Biomaterials*, **13**, 317-321. [2] Šesták, J. (ed) (1996) *Thermochim. Acta (Sp. Iss.)*, **280/281**. [3] Strnad, Z. & Šesták, J. (2001) in Meel, J. (ed.) Proceeding of 3rd IPMM (*Intelligent Processing and Manufacturing of Materials*). Vancouver University, Canada [4] Koga, N. et al. (2003) *J. Thermal Anal. Calor.*, **71**, 927-937. [5] Strnad, J., Urban, K. & Strnad, Z. (2005) *Clin. Oral. Impl. Res.*, **16** 4-8. [6] Strnad, J., Strnad , Z. & Šesták, J. (2007) *J. Thermal Anal. Calor.*, **88**, 775-779. [7] Strnad, J. et al. (2004) *J. Thermal Anal. Cal.*, **76**, 17-31 [8] Strnad, J. et al. (2007) *J. Phys. Chem. Solids*, **68,** 841/844 [9] Holeček, M. & Moravec, F. (2006) *Int. J. Solids Struct.*, **43** 7393-7397. [10] Šesták, J. et al. (2008) *Adv. Mat. Res.*, **39/40**, 329-733.

Polarized FTIR of B type carbonate in fluorapatite

Tacker, R.C.[1*], Lawver, D.R.[1], Vance, Z.R.[2] & Douglas, N.K.[3]
[1]North Carolina Museum of Natural Sciences, Raleigh, North Carolina, USA ([*]christopher.tacker@ncdenr.gov)
[2]Dept. of Geological Sciences, University of North Carolina, Chapel Hill, North Carolina, USA
[3]Division of Earth and Ocean Sciences, Duke University, Durham, North Carolina, USA

Several substitution mechanisms have been proposed for carbonate in apatite, the details of which have importance for petrology, biomaterials and biomimetic materials. Recent FTIR research documented two B type substitutions within large natural fluorapatite crystals [1] and synthetic carbonate apatites [2]. Three hypotheses can be advanced: (A) The substitutions take place on different faces of the phosphate tetrahedron; (B) The differences in peak positions result from differing charge balance mechanisms; or (C) The differences result from a combination of hypotheses (A) and (B).

Polarized infrared spectra have been taken of oriented sections of fluorapatite with the objective of elucidating the orientation of the carbonate group within the structure. Spectra and polarization are very similar to that of francolite investigated in earlier studies [3], but with additional features resolved (Fig. 1). Hence the earlier francolite spectra likely reflect two substitutional types and not one alone.

Orientation of the two different B type absorbers is very similar, which supports hypothesis (B), that the differences in dipole transition moment are due to differences in local structure and charge balance. These substitutions would be near the O1-O2-O3 face of the substituted phosphate tetrahedron. Polarized spectra rule out the possibility that the carbonate group lies on the mirror plane [4], or near the O1-O3-O3 or O2-O3-O3 faces of the tetrahedron.

In addition, some spectra display a weak OH stretching vibration polarized parallel to the *a*-axis at about 3550 cm^{-1}. First principles calculations predict a Ca(2) vacancy charge balancing a B type substitution, leading to an OH group rotating perpendicular to its usual position [5].

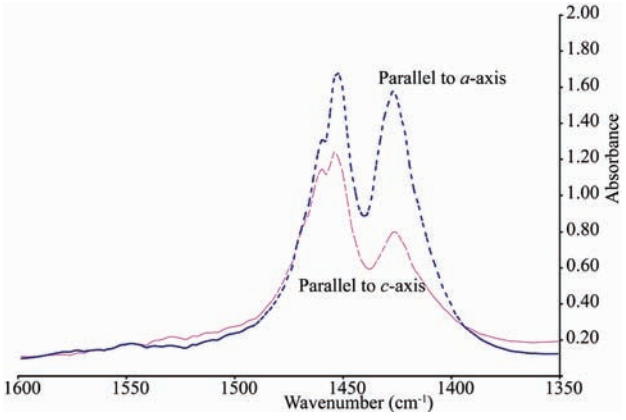

Fig. 1: Polarized infrared spectra of carbonate υ_3 region in naturally occurring fluorapatite.

[1] Tacker, R.C. (2008) *Am. Mineral.*, **93**, 168-176. [2] Fleet, M.A. (2009) *Biomaterials*, **30**, 1473-1481. [3] Elliott, J.C. (1994) *Structure and Chemistry of the Apatites and Other Calcium Phosphates*. Elsevier, Amsterdam. [4] Leventouri, Th. (2006) *Biomaterials*, **27**, 3339–3342. [5] Astala, R. & Stott, M.J. (2005) *Chem. Mater.*, **17**, 4125-4133.

Understanding biological control and environmental influence – unlocking the secrets of biomineralisation

Cusack, M.[1*], Ji, B.[1,2,3], Freer, A.[2], Yin, H.[3], Gadegaard, N.[3], Dobson, P.[3], Pérez-Huerta, A.[1] & Dalbeck, P.[1]
[1]Dept. of Geographical & Earth Sciences, University of Glasgow, UK ([*]Maggie.Cusack@ges.gla.ac.uk)
[2]Dept. of Chemistry, University of Glasgow, UK
[3]Dept. of Electronics & Electrical Engineering, University of Glasgow, UK

In the natural world of biominerals, elegant functional structures are produced from the most basic of resources. Vertebrates have skeletons made from calcium phosphate (apatite) while invertebrates tend to assemble mineral structures from silica or calcium carbonate. Although the ingredients are simple, the control of how these fundamental building blocks are put together is very much under the control of biological processes. Understanding this biological control and its rôle in the formation of biominerals has implications in a number of diverse areas and offers the possibility to exploit this high level of control to produce novel materials of pre-determined material and physical properties. We are currently exploring these processes using lab-on-a-chip (microfluidics) (Fig. 1) to investigate the complexities of the diffusion processes involved in these complex reactions [1].

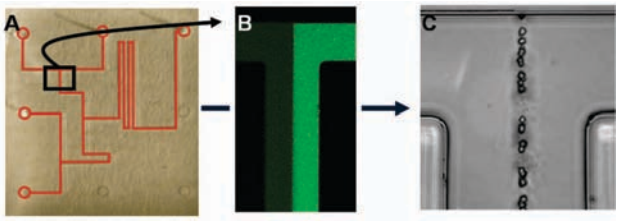

Fig. 1: Lab-on-a-chip microfluidics to screen activity of biomineral proteins. A. Channels in chip highlighted in red. B. Interface between two solutions indicated with fluorescent dye on right side to indicate lack of turbulence. C. Calcite crystals formed at interface between calcium chloride and sodium carbonate solutions. Channel width = 50 µm throughout.

From a climate proxy standpoint, understanding the biomineralisation process [2-4] will also provide a much more accurate interpretation of climate data stored within marine biominerals, e.g. brachiopods [5-7] and corals [8]. Exploring the biological control exerted in biomineral formation across several phyla provides an essential context to unravelling this environmental information.

[1] Yin, H. et al. (2009) *Anal. Chem.*, **81**, 473-478. [2] Cusack, M. et al. (2008) *J. Struct. Biol.*, **164**, 96-100. [3] Cusack, M & Freer, A. (2008) *Chem. Rev.*, **108**, 4433-4454. [4] Pérez-Huerta, A. et al. (2009) *J. Struct. Biol.*, **167**, 62-67. [5] Cusack, M. et al. (2008) *Chem. Geol.*, **253**, 172-179. [6] Cusack, M. et al. (2008) *Chem. Geol.*, **257**, 59-64. [7] Parkinson, D. et al. (2005) *Chem. Geol.*, **219**, 193-235. [8] Cusack, M. et al. (2008) *Coral Reefs*, **27**, 905-911.

On the way to understanding surface processes that drive biomineralisation

Bovet, N.[*], Yang, M., Javadi, M.S., Sand, K.K., Pasarín, I.S. & Stipp, S.L.S.
Nano-Science Center, Dept. of Chemistry, University of Copenhagen, Denmark ([*]bovet@nano.ku.dk)

Calcium carbonate minerals account for almost 50% of known biogenic material. Among them is chalk, which hosts oil in reservoirs and water in aquifers. Work in our group is showing that the biogenic nature of chalk plays an important role in the behaviour of both water and oil in chalk. Despite calcite having been widely studied, a better understanding of the processes that control the calcite interface with fluids is still needed to truly understand the mechanisms of biomineralisation.

Surface sensitive techniques such as X-ray photoelectron spectroscopy (XPS), X-ray reflectivity and atomic force microscopy (AFM), together with theoretical simulation, have provided new insight into the interaction between organic molecules (such as alcohols, carboxylic acids, saccharides) and the calcite surface. We used this fundamental information for simple organic compounds to interpret interaction of more complex organic molecules (as polysaccharides and proteins) produced by organisms to control biomineral formation.

It is possible to observe direct interaction between clean surfaces and these organic molecules, as shown in Fig. 1 for ethanol sorbed on calcite, in-situ, in the XPS chamber.

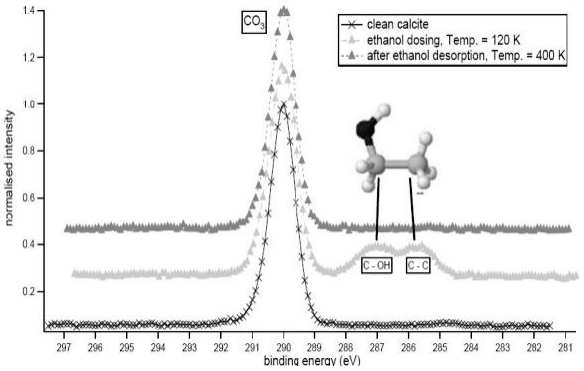

Fig. 1: X-ray photoelectron spectra of the carbon region during ethanol dosing on freshly cleaved calcite. The ethanol is present at low temperature and it desorbs at 270 K, returning the surface to its initial, unreacted state. Ethanol links through the OH end of the molecule and the CH_3 group extends into the solution. T-butanol behaves differently.

The fundamental knowledge we have gained in these studies shows that mineral surfaces structure organic molecules into distinct patterns and through them, the fluids in contact, so dissolution and precipitation are inhibited, except at specific locations.

Self-organized tubular honeycombs near weathered feldspar surfaces: perfect reactors for prebiotic chemistry

Parsons, I.[1*] & Lee, M.[2]
[1]Grant Institute of Earth Science, University of Edinburgh, UK ([*]ian.parsons@ed.ac.uk)
[2]Dept. of Geographical and Earth Sciences, University of Glasgow, UK

Parsons et al. (1998) [1] proposed that orthogonal networks of μm-diameter tunnels near the surface of weathered alkali feldspars would provide ideal protected reactors for the assembly of prebiotic molecules, and Smith et al. (1999) [2] suggested that coatings of zeolite minerals on tunnel walls, particularly organophilic zeolites related to the synthetic molecular sieve silicalite, would have catalytic properties. Branciamore et al. (2009) [3] have carried out cellular automaton simulations of how replicator communities might evolve in such a reactor.

We here review how understanding of both tunnels and of atomic structure close to weathered feldspar surfaces has developed since 1998. Tunnels develop by dissolution of strained structure around misfit dislocations on semicoherent perthite lamellae. Studies of alkali feldspars from a wide range of geological environments and ages show that the potential to develop honeycombs is a near-universal feature of plutonic alkali feldspars, from both igneous and metamorphic rocks, limited only by the relationship between bulk composition and the feldspar solvus. The existence of honeycombs in detrital feldspars in ancient sedimentary rocks has been demonstrated. Large feldspar crystals from surfaces exposed by the last glaciation show much deeper development of weathering features (>10 mm) than predicted by experimental dissolution rates. Tunnels with diameters of a few nm (nanotunnels) have developed in many feldspars by reaction with deuteric fluids during their initial cooling, and have been enlarged by weathering. The tunnels therefore taper from ~1 μm at the crystal surface to <10 nm in the interior, itself a feature favouring the assembly of long-chain organic molecules. Fluids in such tunnels will be buffered by two-feldspar–aqueous fluid phase relationships to have Na:K ratios close to sea-water (and modern extracellular fluids in mammals), suggesting that compatibility of emerging pre-biotic molecules with fluids of such compositions could have been a restriction imposed within the honeycomb without the threat of dispersion in the open ocean.

Understanding of the structure, at atomic level, of weathered feldspar surfaces has been considerably advanced by application of Focussed Ion Beam sample preparation techniques to TEM work, and of X-ray Photoemission Spectroscopy to obtain the composition of near-surface layers. Great care must be taken to avoid amorphization during sample preparation. Neither crystalline 'leached layers', preserving feldspar structure, nor amorphous layers, have been found on feldspars weathered in acid soils, although the latter have been found in material treated at pH 1 in the laboratory. Clay mineral surfaces are common. Zeolitic surface layers have not yet been found.

[1] Parsons, I., Lee, M.R. & Smith, J.V. (1998) *P. Natl. Acad. Sci. USA*, **95**, 15173-15176. [2] Smith, J.V. et al. (1999) *P. Natl. Acad. Sci. USA*, **96**, 3479-3485. [3] Branciamore, S. et al. (2009) *J. Mol. Evol.*, **69**, 458-469.

Attachment of biomolecules to mineral surfaces: surface speciation as a function of environmental conditions

Hazen, R.M.[1], Sverjensky, D.A.[1,2*], Klochko, K.[1], Lee, N.[1,2], Cleaves, H.J.[1], Cody, G.D.[1] & Ohara, S.[1]
[1]Geophysical Laboratory, Carnegie Institution, Washington DC, USA
[2]Dept. of Earth & Planetary Sciences, Johns Hopkins University, Baltimore MD, USA ([*]sver@jhu.edu)

Biomolecule attachment to mineral surfaces is of fundamental importance in a wide range of topics including biomineralization, adhesives, medical implants and the role of mineral-molecule interactions in the origin of life. Our studies have focussed initially on the adsorption of amino acid and nucleic acid fragments on rutile because it is a model colloidal substance that is highly insoluble and well-characterized. We have studied the adsorption of these molecules under wide ranges of environmental conditions including pH, ionic strength, and surface loading using batch adsorption and potentiometric titration methods. Modeling of the data using the extended triple-layer model indicates the importance of different modes of attachment of the molecules to the rutile surface. For example, glutamate and aspartate adsorb at low pH and low surface coverages with four points of attachment, i.e. lying down on the surface. However, at pH values of 5 to 7 they adsorb with only two points of attachment through the oxygens of the carboxylate on the side-chain, i.e. standing up. These different modes of attachment and their dependence on environmental conditions are important for understanding the potential reactivity of the adsorbed molecules in geochemical and industrial processes.

Quantification analysis of mineral content and crystallinity in bone using FTIR spectra deconvolution

Álvarez-Lloret, P.[1*], Yebra-Rodríguez, A.[2] & Rodríguez-Navarro, A.B.[1]
[1]Dept. of Mineralogy and Petrology, Faculty of Sciences, University of Granada, Spain ([*]pedalv@ugr.es)
[2]Dept. Geology, IACT Associated Unit (CSIC-UGR), University of Jaén, Jaén, Spain

Bone tissue is one of the most important biological structures in the field of biomineralization [1]. Bone is composed of an organic matrix (mainly collagen type I) and a mineral component (nanocrystalline carbonate hydroxylapatite) in proportions varying with age and location within the skeleton [2]. Mineral bone features such as crystallinity, phosphate content, carbonate content, and mineral environment may be substantially altered as a function of different remodelling/turnover mechanisms. FTIR is a well suited technique for the quantitative investigation of bone mineral content and composition providing insights into the chemistry of bone mineral deposition and organic matrix components [3].

Bones from different species were analysed (rats, chickens, partridges). The amounts of phosphate, carbonate and collagen in bone tissue were determined from the peak area absorption bands associated with phosphate, carbonate and amide groups in the FTIR spectra. Overlapping peaks were resolved using a second derivative methodology, allowing for a detailed and quantitative analysis of different molecular constituents of bone. This methodology provides the most information about the underlying peak by determining width, area, amplitude and position of each absorption band/peak. Different parameters were used to characterise bone chemical composition and crystallinity from FTIR spectra. Integrated areas of the v_1, v_3 stretching phosphate and amide I regions were calculated to determine the relative quantity of mineral present in bone tissue (degree of mineralization). The quantity of carbonate present in the apatite phase was calculated by taking the integrated areas under v_2 carbonates and v_2, v_3 stretching bands (carbonate/phosphate ratio). Crystallinity Index was also determined as the ratio of the area corresponding to one of the peaks related to highly crystallinity phosphate divided by another peak related to lower crystalline phosphate. Samples were also analyzed by X-ray diffraction to develop FTIR spectra-structure correlations (Crystallinity Index from FTIR vs. FWHM diffraction from different apatite diffraction peaks). Thermogravimetric analyses were also performed to compare the values obtained from different FTIR parameters related to carbonate and mineral content.

This study demonstrates the capabilities of combining second-derivative spectroscopy and curve-fitting of FTIR spectra in the analysis of mineral content and crystallinity in bone. In addition, FTIR spectra allow quantifying the amount of different components (mineral and organic matrix) of such a complex material as is bone.

[1] Dove, P.M., De Yoreo, J.J. & Weiner, S. (2003) (eds.) *Rev. Mineral. Geochem.*, **54**. [2] Mann, S. (2001) *Biomineralization: Principles and concepts in bioinorganic materials chemistry*. Oxford University Press, Oxford. [3] Boskey, A.L. & Mendelsohn, R. (2005) *Vib. Spectrosc.*, **38**, 107-114.

Crystal growth patterns in foliated aragonite of monoplacophorans (Mollusca)

Checa, A.G.[1], Sanchez-Navas, A.[2] & Rodriguez-Navarro, A.B.[2*]
[1]Dpto. Estratigrafía y Paleontología, Universidad de Granada, Granada, Spain
[2]Dpto. Mineralogía y Petrología, Universidad de Granada, Granada, Spain ([*]anava@ugr.es)

Crystal growth features of the foliated aragonite from two species (Micropilina arntzi and Rokopella euglypta) of the rare monoplacophoran mollusks have been analyzed in detail by SEM and EBSD. These analyses show the occurrence of a discrete number of constant angular relationships between the aragonite crystals which is explained by twin laws and different epitaxial relations. Additionally, the morphology of the crystals of the foliated aragonite is unique and very different to that found in inorganic aragonite, which usually precipitates as prisms or fibres elongated along the ***c*** axis. In contrast, in foliated aragonite, growth along the ***c*** axis is restricted and lath-like crystals elongated along the ***a***-axis form. The occurrence of these unusual morphologies is explained by different structural factors and the action of specific organic matrix components [1].

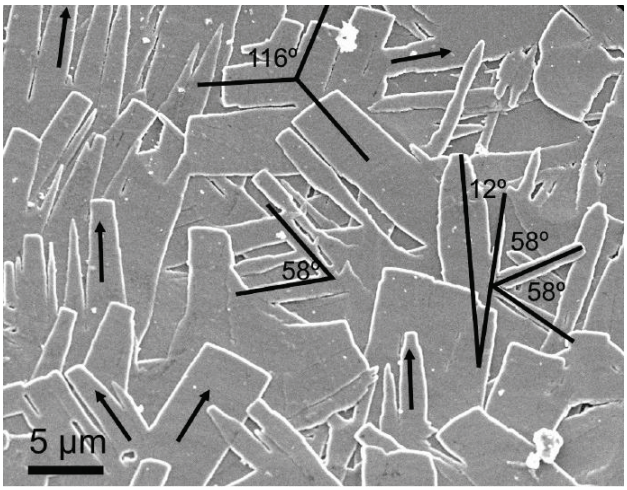

Fig. 1: Secondary electron images of the shell interiors of Micropilina arntzi.

[1] Checa, A.G. et al. (2009) *Cryst. Growth Des.*, **9,** 4574-4580.

Stone analysis: mineralogy and morphology of pathological biominerals in humans

Giannossi, M.L. & Summa, V.*
Laboratory of Environmental and Medical Geology, IMAA-CNR, Tito Scalo (PZ), Italy (*summa@imaa.cnr.it)

Stone analysis is rarely carried out in clinical centres even if the identification of the components of kidney stones is essential for deciding on future prophylaxis. Furthermore, very few studies on this issue have been published in Italy up to now [1]. All this encouraged a study on a regional scale in order to analyze the type of kidney stones affecting the Basilicata (southern Italy) inhabitants so as to classify them in accordance with new classifications which take into account the relations between the components and the packing arrangements of the stone crystals.

A total of 80 kidney stones of different compositions were collected, photographed, observed under an optical and scanning electron microscope, and analysed by X-ray powder diffraction.

The results show that 65% of the kidney stones studied are composed of calcium oxalates (38% calcium oxalate monohydrate - whewellite; 27% calcium oxalate dihydrate - weddellite). Trace quantities of other organic and inorganic components are still present. Calcium oxalates are absent or negligible in the remaining 35%, these being composed mainly of uric acid (15%), hydroxyapatite (13%), struvite (6%) or cystine (1%). 32% of stones are multi-composed (eg. weddellite plus hydroxyapatite or whewellite plus uric acid).

The internal structure and the relations between the major and minor components provide information to classify the 80 kidney stones in 8 distinctive types and 13 subtypes in accordance with the scheme proposed by Grases et al. [2], but improved considering a new type of kidney stone composed of weddellite mixed-struvite.

Among stones with predominant calcium oxalate, there is also a high percentage of papillary kidney stones consisting of whewellite developed on kidney walls. The core of this stone type can form exclusively on sites with altered (damaged or just slightly injured) epithelium [3]. Cells of damaged epithelium tend to accumulate calcium thus creating favourable conditions for the formation of kidney stones containing crystals which, under urinary conditions suitable for the crystallization, produce an important deposit of material on the damaged epithelium which serves as a substrate for ulterior nucleation of whewellite stones.

The results of the study of some thin petrographic sections, obtained from a representative number of bigger kidney stones, show that there are usually more cores within whewellite kidney stones which are the result of several simultaneous nucleation and growth processes. Cores appear as spherulitic aggregates, the form best adapted to non-equilibrium conditions. Simultaneous crystallization and oscillation between growth and dissolution events contribute to stone formation.

[1] Ramello, A. et al. (2000) *J. Nephrology*, **13**, S45-S50. [2] Grases, F. et al. (1998) *Adv. Colloid. Interface. Sci.*, **74**, 169-194. [3] Giannossi, M.L. et al. (2009) *NDT plus*, **2**, 418-419.

Magnetic biomimetic scaffolds: peculiarities of cell development

Goranov, V.A.[1,2*], Russo, A.[1,3], Panseri, S.[1,3], Sandri, M.[4], Tampieri, A.[4], Landi, E.[4], Valentini, F.[4] , Makhaniok, A.A.[5], Haranava, Y.A.[5], Dediu, V.A.[6] & Marcacci, M.[1,3]
[1]University of Bologna, Bologna, Italy
[2]Belarussian State Medical University, Minsk, Belarussia (*lbmi@tut.by)
[3]Rizzoli Orthopaedic Institute, Bologna, Italy
[4]Institute of Science and Technology for Ceramics, Faenza, Italy
[5]Biodevice Systems s.r.o. Prague, Czech Republic
[6]Institute of Nanostructured Materials, Bologna, Italy

Magnetic scaffolds (MagS) can provide an additional advantage to manipulations of magnetic nanoparticles (MNPs) and cells with MNPs in magnetic field and creation of tissue-engineered constructions. The cell development inside MagSs strongly depends on both biocompatibility and microarchitecture of the scaffold material that defines nutrient and oxygen distribution. Therefore it is extremely important to optimize the scaffold size and microarchitecture for optimum growth of cells in static conditions using mathematic modelling. In its turn, the analysis of experimental parameters allows to create an adequate mathematic model for cell proliferation evaluation in different layers of the scaffolds.

Two kinds of porous magnetic scaffold [1] were used for loading with human Bone Marrow Mesenchymal Stem Cells (BMSCs). The first was a hydroxyapatite/collagen (HA/C) scaffold obtained through a biomimetic mineralization process, whereby the apatitic and the magnetic phases were co-precipitated over and inside the collagen fibers. The second was a hydroxyapatite (HA) ceramic scaffold produced by foaming technique and magnetized using vacuum-assisted infiltration with magnetite nanoparticles (diameter <50 nm). Nonmagnetized HA and HA/C scaffolds were used as a control.

Scaffolds were saturated with cells and incubated in osteogenic medium according to a standard protocol [2]. Proliferation and distribution of BMSCs were assessed using standard tests (MTT-test, acridine orange/ethidium bromide, hematoxylin/eosin staining, etc). Mathematic modeling to predict cell proliferation/distribution in the scaffold space was carried out based on the dynamic nutrient distribution model according to Dunn [3] using the Comsol 3.5a.program.

It was found in vitro that MagSs provide suitable microenvironments for supporting BMSCs proliferation. However, no differences in the ability of MagSs to support proliferation of BMSCs were observed in comparison with non-magnetized scaffolds ($p<0,05$; $n=6$). At the same time the distribution of cells in the scaffold space was different in HA and HA/C MagSs. Intensive proliferation was observed basically in superficial layers of HA/C MagS especially during the first 5 days after saturation with cells. In HA-scaffolds we observed much more homogenous cell distribution during all period of incubation (20 days), but the proliferation rate was lower by a factor of two at least. The computerized model of cell proliferation and distribution used agrees reasonably well only with experimental data for periods between 7 and 12 day of cell cultivation in scaffolds and hence should be further developed in future researches. Thus, it can be concluded that MagSs showed similar dynamic of proliferation processes as the non-magnetic scaffolds.

Acknowledgement: The work has been suported by the EU project “MAGISTER” FP7-NMP-2007-4.2.3.-1

[1] Bock, N. et al. (2010) *Acta Biomater.*, **6**, 786-796. [2] Costa-Pinto, A.R. et al. (2009) *Biomacromolec.*, **10(8)**, 2067-2073. [3] Dunn, J.C.Y. et al. (2006) *Tissue Eng.*, **12,** 705-715.

Calcium oxalates in renal stones

Izatulina, A.R.[*], Punin, Yu.O., Shtukenberg, A.G., Frank-Kamenetskaya, O.V. & Gurzhiy, V.V.
Dept. of Crystallography, Saint-Petersburg State University, Saint-Petersburg, Russia ([*]alina.izulina@mail.ru)

Urolithiasis is a rather widespread disease. However till now there are no reliable methods of preventive maintenance of this illness, despite of significant efforts made in the past. Moreover, it is not completely clear, how renal stones are forming.

The majority of renal stones consist of the calcium oxalate hydrates whewellite $CaC_2O_4 \cdot H_2O$ and weddelite $CaC_2O_4 \cdot (2+x)H_2O$. Origin and growth kinetics, area of stability and the phase transitions of calcium oxalate crystals were studied in details for a long time. However, the comparison of experimental data shows strong differences suggesting that some additional factors may influence formation and stability of calcium oxalate phases.

The main purpose of this work is to research the factors that raise the weddellite stability: temperature, pH, proportion of calcium and oxalate ions, organic and inorganic components of physiological solution, amount of micromycets and bacterial-viral associates, and time of crystallization. Special attention has been devoted to study the variability of the water content in the structure of weddellite and its influence on the dehydration and phase transitions in renal stones. Besides, another purpose of the work was to reveal correlations between *x* and weddellite unit cell parameters and to offer on this basis an express way to estimate the amount of zeolitic water present.

The influence of crystallization conditions on the formation of calcium oxalates was investigated by simulation experiments according to a physiological medium. To estimate the variation of the amount of zeolitic water in the structure of weddellite and to reveal the ratio of *x* and unit cell parameters the crystal structures were refined by single crystal x-ray diffraction of nine weddellite crystals from different renal stones.

The results showed that the factors increasing the weddellite stability are supersaturation, pH, concentration of stabilizing impurities (for example CO_3^{2-} or Mg^{2+}), and the amount of protein substance. Since it was found that weddellite transforms into whewellite with time, the stability of the former presumably depends on the amount of structural water.

In the weddellite crystal structure (S.G. *I*4/*m*) [1] Ca atoms are coordinated in slightly distorted square antiprisms linked by a common edge to two adjacent ones to form chains along the *c* axis. These chains are connected to each other by common oxalate groups and hydrogen bonding of water molecules. Ca-polyhedra chains form channels occupied by "zeolitic" water molecules.

Our investigation showed that the amount of "zeolitic" water indeed causes a variation of the unit cell parameters, especially the *a* parameter (12.336 – 12.371 Å) as well as the interatomic spacing. For example, the distance between W1 water molecules, adjacent to the "zeolitic" water of one layer parallel to (001) varies from 3.211 – 3.287 Å.

According to the limiting values of the *a* unit cell parameter our result allows to estimate the variation of the *x* values (0.13 – 0.37 at. u.) in the weddellite crystals of renal stones. Thus in most cases *x* is close to the upper limit.

Acknowledgements: This work was supported by the Russian Foundation for Basic Research (grant #10-05-00881-a).

[1] Tazzoli, V. & Domeneghetti, C. (1980) *Am. Mineral.*, **65**, 327-334.

Quaternary mammalian bones and teeth diagenesis in karst cavities of Middle and Northern Urals, Russia: implications of thermal, elemental and spectroscopy data

Kiseleva, D.V.[1*], Votyakov, S.L.[1], Smirnov, N.G.[2], Shchapova, Yu.V.[1] & Sadykova, N.O.[2]
[1]Institute of Geology and Geochemistry, UB RAS, Ekaterinburg, Russia ([*]kiseleva@igg.uran.ru)
[2]Institute of Plant and Animal Ecology, UB RAS, Ekaterinburg, Russia

Chemical composition and microstructure of Quaternary mammalian bones and teeth remains have been investigated by means of scanning electron and atomic force microscopy, electron probe microanalysis, trace element inductively coupled plasma mass-spectrometry, thermal and thermokinetic analysis, infrared, Raman and electron spin resonance spectroscopy.

Samples of bones and teeth remains represented 11 various sites of Middle and Northern Urals, Russia. They included Holocene and Pleistocene ornithogenic and zoogenic rodent remains from the earth surface, rock-shelters, grottoes and karst cavities [1].

The hydrolytic degradation of the organic component of bone tissue and the conversion of the inorganic constituents of bone have been registered on SEM images, *e.g.* porosity increase, peeling, bacterial attack, rotting, initial structure decomposition and secondary mineral formation [2].

The dynamics of elemental composition of bone have been investigated and geochemical indices were calculated. The rare earth elements (La-Lu) and high field strength elements (Y, Zr, Hf, Ta, Th, U) appear to be promising indicators of relative age estimation by tissue accumulation degree.

After thermal analysis (20-800°C) estimates of organic content determined as mass loss at 200-650°C in bone remains series have been used to reveal different age admixtures and chronological ranging.

Ion-radicals induced by thermo-chemical transformations of organic constituent in the temperature range of 200-650°C have been observed in bone (tooth) tissues. The line shape and width parameters of ion radicals have been analyzed and their age variations examined.

Phase transformation during fossilization has been examined by infrared and Raman spectroscopy in four spectrum ranges attributed to inorganic phase structural fragment vibrations (PO_4^{3-}, H_2O and OH^-, CO_3^{2-} in A and B-positions). From this, bone apatite crystallinity, degree of apatite P-O bond ionicity-covalency, carbonate-ion relative concentration and its inter-positional distribution, and alterations in bone surface micro- and nanostructure were deduced.

Several types of fossilization distinguished by correlations of organic components of bone and trace elements content have been assigned. The results obtained were used to evaluate the relative age of bone. Some questions about the degree of synchronism were discussed for the investigated series of fossil and sub-fossil rodent bone remains representing various sites in the Urals.

[1] Smirnov, N. et al. (2009) *Physical and chemical characteristics of mammal fossil bone remains and the problem of their relative age estimation. Part I. Thermal analysis and trace element mass-spectrometry.* Goshchitzky, Ekaterinburg (in Russian). [2] Votyakov, S. et al. (2009) *Physical and chemical characteristics of mammal fossil bone remains and the problem of their relative age estimation. Part II. Infrared and radio-spectroscopy, microscopy.* Goshchitzky, Ekaterinburg (in Russian).

Nucleation and growth of hydroxylapatite as proxy for bone apatite

Klasa, J.[*] & Valsami-Jones, E.
Dept. of Mineralogy, Natural History Museum, London, UK
([*]jolk@nhm.ac.uk)

Bone and teeth are biomineralised materials with a unique organic/inorganic composite structure. The main inorganic component is nanocrystalline bioapatite which is embedded in collagen matrix. During the lifetime of the organism bones are continuously remodeled by dissolution/reprecipitation processes although the details of the mechanisms are still poorly understood. For example nanosized crystals in bone have been shown to be insensitive to demineralisation in experiments using constant composition method [1].

Bioapatite is a complex solid solution [2] and understanding its interaction with body fluids requires a fundamental study of the solid solution – aqueous solution system. Furthermore nucleation of nanoapatite from multicomponent solutions is also likely to involve the formation of compositionally inhomogeneous phases. For example a solution supersaturated with respect to hydroxylapatite may also be supersaturated with respect to other apatite solid solutions as well as other calcium phosphate phases.

We have carried out nucleation and growth experiments under constant composition conditions (in which supersaturation is kept constant throughout the experiment) at physiological pH (7.4) and in a solution resembling blood plasma. The aim is to investigate the effect of solution composition and saturation on apatite properties, particularly size and shape and rate of formation. Scanning Electron Microscopy (SEM), Atomic Force Microscopy (AFM) and Fourier Transform Spectroscopy (FTIR) were used to characterise and understand fundamental properties of the precipitates formed.

[1] Wang, L. et al. (2006) *Biointerphases*, **1(3)**, 106-111. [2] Skinner, H.C.W. (2005) *Mineral. Mag.*, **69(5)**, 621-641.

Pathological biomineralization from human aortic and mitral valve stenosis

Maras, A.[1*], Cottignoli, V.[1], Cavarretta, E.[2,3], Salvador, L.[2,4] & Valfrè, C.[2]
[1]Dept. of Earth Sciences, *La Sapienza* University of Rome, Italia ([*]adriana.maras@uniroma1.it)
[2]Div. of Cardiac Surgery, Treviso Regional Hospital, Italy
[3]*La Sapienza* University of Rome, Italy
[4]Div. of Cardiac Surgery, San Bortolo Hospital, Vicenza, Italy

Samples were collected as surgical waste from patients (demographic characteristics are shown in Table 1) undergoing valvular replacement caused by severe aortic (n=6) and mitral (n=2) stenosis. Pathological mineral formations have been investigated with XRPD and SEM-EDS, both in high and in low vacuum conditions. Samples were not coated because of metallic coating artifacts.

Table 1: Cell parameters of pathologic bioapatite ($P6_3/m$)

Samples	*a*(Å)	*c*(Å)	Sex/Age
2a	9.4172(5)	6.8954(4)	M 73
3m	9.4161(8)	6.8948(6)	F 75
6a	9.4153(8)	6.8952(7)	M 75
9a	9.4165(7)	6.8957(6)	M 71
12a	9.4165(8)	6.8951(7)	M 68
14a	9.4161(9)	6.8958(7)	M 69
15m	9.4161(9)	6.8961(7)	M 64
18a	9.4158(5)	6.8958(4)	M 41

a = aortic valve, m = mitral valve
a = 9.441(2)Å; *c* = 6.878(1)Å dental enamel apatite [1]

The *a* cell parameters were found to be smaller than the *a* parameter of human dental enamel apatite, while the *c* parameters were greater.

High resolution images show a complex relationship between inorganic component and organic matrix as well as particular morphologies of the pathogenic biomineralization. Bioapatite appears as lamellar crystals, globular aggregated and massive; at high magnification it appears to be constituted of spherical particles of variable size (Fig. 1).

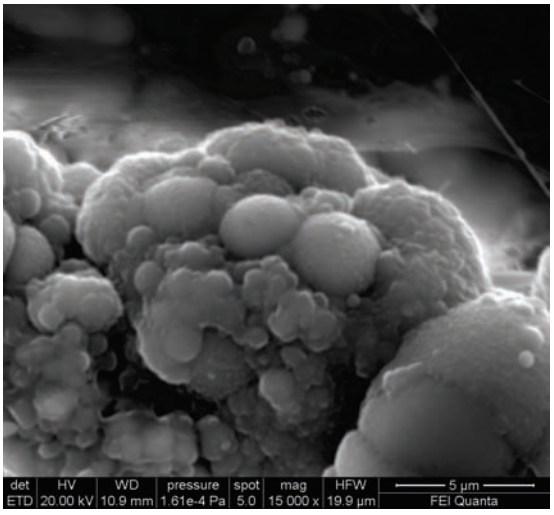

Fig. 1: SEM micrograph of pathologic bioapatite.

Bioapatite morphology observed in this study appears to be different from biogenic calcium phosphate crystals and from inorganically produced counterparts. The small spheres could be considered as nanobacterial-like [2,3] structures (?) This attractive hypothesis has not been confirmed yet.

[1] Wilson, R.M. et al. (1999) *Am. Mineral.*, **84**, 1406-1414. [2] Gilinskaya, L.G. et al. (2007) *Lithol. Miner. Resour.*, **42**, 56-67. [3] Miller, J.A. et al. (2004) *Am. J. Physiol. Heart Circ. Physiol.*, **287**, 1115-1124.

Cathodomicrofacies analysis of a petrified wood

Ninagawa, K.[1*], Yamaguchi, Y.[1], Tabara, T.[1], Nishido, H.[1], Kawano, S.[2], Nomura, R.[3], Gucsik, A.[4,5] & Bérczi, Sz.[6]
[1]Okayama University of Science, Okayama, Japan
([*]kninagawa@dap.ous.ac.jp)
[2]The Shimane Nature Museum of Mt. Sanbe, Oda, Japan
[3]Shimane University, Shimane, Japan
[4]Max Planck Institute for Chemistry, Mainz, Germany
[5]Savaria University Center, Szombathely, Hungary
[6]Eötvös Loránd University, Budapest, Hungary

Cathodoluminescence (CL) imaging and spectroscopy have been used to clarify growth fabric textures observed in authigenic and biogenic minerals during diagenetic process. A cathodomicrofacies analysis has been developed in the field of environmental geology and archaeology, especially for the study of biogenic carbonates. Few investigations of silicified fossils have been conducted so far. In this study a microfacies analysis of petrified wood has been carried out by CL imaging and spectroscopy combined with Raman spectroscopy.

A unique sample of petrified wood with bright CL emission was obtained from the conglomerate in the Omori Formation (middle Miocene), Kurihara, Izumo City, southwest Japan. It has a diameter of around 5 cm in section, which shows concentric rings of clear silicified layers filling the cracks among a black layer including carbonaceous materials. The polished sections were examined by CL method. CL color images were recorded using the Luminoscope (ELM-3R). CL scanning images at high magnification were obtained by a Mini-CL detector (Gatan) installed in a SEM (JEOL: JSM-5410). CL spectroscopy was made by a SEM-CL systemcomprising an SEM combined with a grating monochromator (OXFORD: Mono CL2).

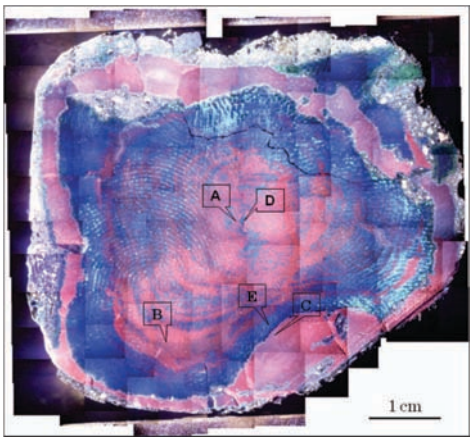

Fig. 1: CL image of petrified wood with analytical positions.

The black layer contains remnants of a carbon phase exhibiting many radial clear lines, which should be divided into two areas: (1) red CL and blue CL parts as shown in Figure 1. Compared to the reflected optical microscope image, the CL image shows two rings. Raman spectra and CL spectra at A (center red CL), B (fringe, red CL), C (outside of silicified wood, red CL), D (center, blue CL), and E (fringe, blue CL) points were obtained in this silicified wood. As a result, we recognized quartz signal at all red CL points (A, B, C). We also recognize D and G bands of amorphous carbon at A, B, D, and E inside of silicified wood. The red CL has a peak at 650 nm, and the blue CL exhibits a peak at 450 nm. These CL spectral features are related to agate [1].

[1] Götze, J. et al. (2009) *Mineral. Mag.*, **73**, 673-690.

Investigation of bone apatites by thermoanalytical methods

Papp, I.[1*], Buday, T.[1] & Pap, L.[2]
[1]Dept. of Mineralogy and Geology, University of Debrecen, Hungary ([*]asvanypista@citromail.hu)
[2]Dept. of Inorganic and Analytical Chemistry, University of Debrecen, Hungary

There is much controversy on the crystal structure of bone apatites, especially regarding the carbonate substitutions. In this study, swine and poultry bone samples were examined by thermoanalytical methods (thermogravimetry, differential thermal analysis and evolving gas analysis, EGA), in order to determine the amount of carbonate ions and their position in the crystal lattice. Although calcite is a common mineral in fossil bones, it may be present in living bones as well. The role of these phases is unclear, probably related to degenerative effects. Carbonate ions may play a significant role in the biocompatibility of bone prostheses as well.

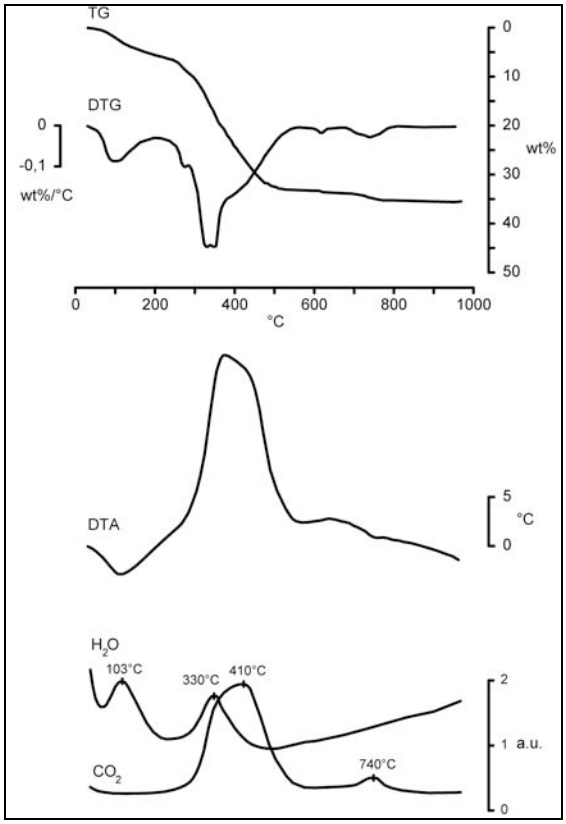

Fig. 1: Thermoanalytical curves of the bone sample Sk4.

The EGA results show CO_2 elimination above the temperature of burning of organic material. The shapes of the thermoanalytical curves imply that CO_2 derives from the dissociation of the carbonate ions. In some samples the high carbonate content and the temperature of the dissociation may imply the presence both of carbonate apatite and calcite phases (Fig. 1) in the inorganic bone material.

The calcium phosphate binding properties of the serum protein fetuin-A explored with SANS contrast variation technique

Schwahn, D.[1*], Heiss, A.[2], Pipich, V.[3] &Jahnen-Dechent, W.[2]
[1]Institute of Solid State Research of the Helmholtz Research Center Jülich GmbH, Jülich, Germany ([*]d.schwahn@fz-juelich.de)
[2]Biomedical Engineering, Biointerface Group, RWTH University, Aachen, Germany
[3]JCNS – Jülich Centre for Neutron Research at the FRM II, Garching, Germany

The patho-physiologic relevance of the serum protein fetuin-A/alpha$_2$ HS-glycoprotein as a systemic inhibitor of uncontrolled mineral deposition in the soft tissue has been demonstrated in fetuin-A knockout mice [1]. Moreover, clinical studies showed that patients with a low fetuin-A serum level are exposed to an increased calcification risk [2]. To elucidate the inhibition mechanism of calcification by the protein fetuin-A, we explored several *in vitro* model systems with SANS contrast variation technique [3]. The principle outcome was a two stage formation process of transiently stable nanometer sized colloidal composites of fetuin-A and calcium phosphate, which we denoted as calciprotein particles (CPPs); the initial form is spherical with a diameter in the 500Å range which, after several hours at room temperature, transform to elongated particles of about twice the initial size. The CPPs consist of fetuin of about 25% volume fraction and of the octacalcium phosphate (OCP) polymorph representing the mineral phase [3]. The secondary CPPs are stable for at least 24 hours, which can be explained by a dense fetuin monolayer covering the mineral as determined from SANS contrast variation experiments [3].

However, a detailed analysis suggested that the buffering of calcium and phosphate ion super saturation by the CPPs is not the whole story of the inhibition mechanism. The analysis of the SANS scattering patterns revealed that 3-5% of the total fetuin-A and about half of the total mineral can only be attributed to the CPPs. As SANS reflects the presence of fetuin monomers at large momentum transfer, we speculated that the other half of the mineral is attached to the monomers. Recent contrast variation experiments indeed identified these particles as calciprotein monomers (CPM) with varying amount of the mineral when changing the fetuin concentration. So, the inhibition mechanism of mineralization in the presence of the protein fetuin-A proceeds on two pathways, namely by CPP and CPM formation.

[1] Schäfer, C. et al. (2003) *J. Clin. Invest*., **112**, 357-366. [2] Ketteler, M. et al. (2003) *Lancet*, **361**, 827-833. [3] Heiss, A. et al. (2007) *Biointerphases*, **2**, 16-20.

Biomimetic synthesis and characterization of Zn-substituted calcium phosphates

Titorenkova, R.[1*], Rabadjieva, D.[2], Petrov, O.[1], Gergulova, R.[2], Tepavitcharova, St.[2], Dyulgerova, E.[3] & Konstantinov, L.[1]
[1]Central Laboratory of Mineralogy and Crystallography, BAS, Sofia, Bulgaria ([*]rosititorenkova@dir.bg)
[2]Institute of General and Inorganic Chemistry, BAS, Sofia, Bulgaria
[3]Dental Medicine Faculty, University of Medicine, Sofia, Bulgaria

Biomimetic methods are often applied instead of conventional ones to synthesize calcium phosphates resembling the composition and structure of biological apatite.

A biomimetic approach was applied to synthesize Zn-substituted amorphous calcium phosphates (ACP) with Zn/Ca ratios of 0, 0.03, 0.05, 0.07, 0.10 and 0.13. The method includes quick mixing of calcium chloride, zinc chloride and potassium hydrogen phosphate solutions prepared by dissolution of the salts in a simulated body fluid (SBF). The initial molar ratio (Ca+Zn)/P was 1.67. The reaction pH was kept at about 11 by the addition of 25% NH_4OH. The precipitates were filtered, washed with water and with acetone (solid-to-liquid ratio 1:1) and then dried for a week at a temperature of -18°C in the presence of silica gel. The applied method allows obtaining apatite precursor containing impurities of Mg, Na, K and Cl in concentrations similar to those in the mineral part of the hard bone tissues. The addition of Zn was chosen in order to improve the specific bioactivity of calcium phosphate, as zinc activates bone formation and has inhibitory effect on the osteoclast differentiation.

The initial precipitates were calcified for 2 h at 600 and at 800°C under atmospheric pressure. The effect of Zn-concentration on the phase composition and structural characteristics of the obtained ceramics was investigated. After calcification at 600°C, amorphous calcium phosphate with a ratio Zn/Ca = 0 transforms into hydroxyapatite, samples with Zn/Ca = 0.03 and 0.05 into mixture of hydroxyapatite and Zn-substituted β-TCP while those with Zn/Ca = 0.07, 0.1 and 0.13 into Zn-substituted β-TCP. After calcification at 800°C all the samples with various Zn/Ca ratios transformed into Zn-substituted β-TCP.

The results obtained indicate that the addition of Zn promotes the formation of single-phase β-TCP ceramics. XRD and IR absorption data reveal that the isomorphic substitution of Zn^{2+} for Ca^{2+} in the β-TCP structure proceeded in a stepwise manner. The increase of the concentration of Zn is followed by a decrease in the unit cell parameters and volume.

Applying this method of synthesis leads to ion (Zn, Mg, Na, K and Cl) modified single- and bi-phase calcium-phosphate materials with potential to be used as biomaterial.

Acknowledgements: This work is financially supported by the Bulgarian Ministry of Education, Youth and Science under Projects DO-02-82/2008 and DTK 02/70/2009.

A study on psammoma body mineralization in meningioma

Wang Changqiu[1*], Yang Ruochen[1], Lu Anhuai[1], Zhao Wenwen[1], Li Yan[1], Liu Jianying[2] & Zhang Bo[2]
[1]School of Earth and Space Sciences, Key Laboratory of Orogenic Belts and Crustal Evolution, MOE, Peking University, Beijing, China ([*]cqwang@pku.edu.cn)
[2]Pathology Dept. in School of Basic Medical Science, Peking University Health Science Center, Beijing, China

The psammoma body mineralization is a common type of pathological mineralization in human meningioma (Fig.1 upper left). The mineralogical studies of the psammoma body mineralization may provide some supporting information in finding the reason of the origin and development of the disease. In this paper, mineralogical characteristics of psammoma bodies in the mineralized focus from a meniningioma patient are investigated in terms of their composition, structure and morphology, using HRSEM, ESEM, EDAX, EPMA, HRTEM, XRD and FTIR. The formation mechanism of the psammoma bodies is also discussed.

The results show that in the early stage of psammoma body mineralization in meningiomas, many small mineralized balls composed of octacalcium phosphate were precipitated on the collagen fibers (Fig.1 upper right). These balls continued to grow and aggregate, and were gradually hydrolyzed to become dahllite nano-crystals. The continuing mineralization resulted also in mineralization of the collagen fibers (Fig.1 lower). The study reveals that the concentric layered structure of the psammoma bodies in meningiomas is formed by a spiral arrangement of the mineralized collagen fibers on which the mineralized grains precipitated.

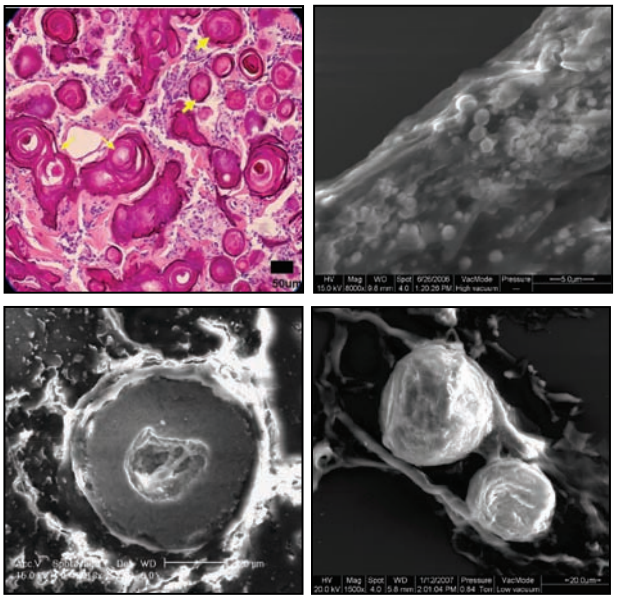

Fig. 1: The photomicrograph (upper left) and ESEM morphology (lower left, and right) of the meningiomas organizations with psammoma bodies.

Thermal stability of bio-aragonite and the textural characteristics of cuttlefish shell

Wang Hejing[1*] & Zhou Jian[2]
[1]School of Earth and Space Sciences, Peking University, Beijing, P.R. China ([*]hjwang@pku.edu.cn)
[2]Chinese Academy of Geological Sciences, Beijing, P.R. China

The internal shell of cuttlefish is composed of aragonite and plays two important roles in the life of the animal: providing it with buoyancy and withstanding the external hydrostatic pressure e.g. a maximum pressure of 2.1 - 6.2 MPa at 200 to 600 meter depths, respectively [1].

The *in-situ* XRD technique was used to investigate the thermal stability and phase transition of bio-aragonite from cuttlefish bone under both vacuum and air non-ambient conditions. From room-temperature to 900ºC bio-aragonite changes via calcite to lime in both vacuum and air conditions (Table 1). The coexisting range of aragonite-calcite in vacuum condition is 365-475ºC and that of calcite-lime is 475-625ºC respectively, whilst the coexisting range of aragonite-calcite in air condition is 385-435ºC and that of calcite-lime as 625-750ºC respectively.

Table 1: Phase transitions of bio-aragonite and corresponding temperatures under non-ambient vacuum and air conditions

		25 100 200 300 400 500 600 700 800 900 ºC
Vac	CaO	475----------
	Cc	365----------625
	Arg	----------475
Air	CaO	625----------
	Cc	385----------750
	Arg	----------435

Vac: vacuum, Cc: calcite, Arg: aragonite

SEM analysis demonstrates that the cuttlefish bone possesses the characteristic of a floor-pillar-like architecture. XRD textural analysis reveals that the aragonite crystallites of cuttlefish bone prefer growing in a comb-like habit between layers (orientation distribution function (ODF) parallel to psi-phi plane) and in a 45º crossing angle within both the comb-like pillars and the layers (Fig. 1), producing a strong interlace texture of the internal shell.

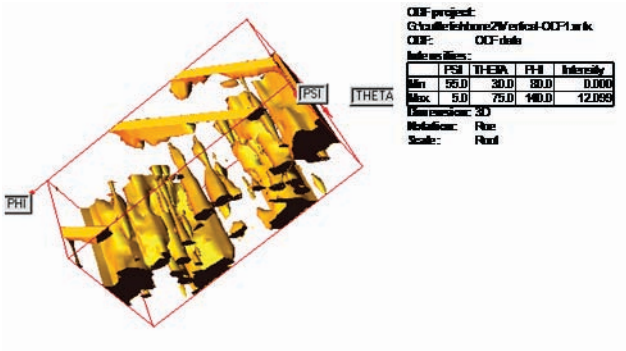

Fig. 1: ODF of bio-aragonite calculated from pole data of reflections (020), (111), (122) and (220).

It is concluded that the bio-aragonite of cuttlefish bone possesses high temperature stability up to 365ºC and a crossgrowth habit both in layers and in vertical pillars which well supports the cuttlefish to withstand high pressure condition up to 6 MPa.

[1] Birchall, J.D. et al. (1983) *J. Mater. Sci.*, **18**, 2081-2086.

Determination of amorphous and nano-crystalline calcium carbonate polymorphs in pearls by Raman spectroscopy

Wehrmeister, U.[1,3], Jacob, D.E.[1*], Soldati, A.L.[1,2], Loges, N.[1], Häger, T.[3] & Hofmeister, W.[3]

[1]Dept. of Geosciences and Earth System Science Research Centre, Johannes Gutenberg- Universität, Mainz, Germany ([*]jacobd@uni-mainz.de)

[2]CONICET, Grupo Caracterización de Materiales, Centro Atómico Bariloche, S.C. de Bariloche, Argentina

[3]Dept. of Gemstone Research, Johannes Gutenberg-Universität, Mainz, Germany

The nacre of pearls and mussels is well known to display a "brick and mortar" – structure which is a challenging composite organic-inorganic model system for research in nanotechnology. FIB/TEM and AFM methods show that nacre presents a nanostructure with the smallest structures in the range of 50 – 100 nm [1]. The $CaCO_3$ vesicles, extruded by the mantle epithelial tissue cells of the bivalve are primarily composed of amorphous calcium carbonate (ACC) before being transformed into the crystalline phase [2].

Micro Raman spectroscopy is a powerful tool in identifying the different calcium carbonate polymorphs [3, 4]. Analyses were carried out on cultured pearls from freshwater (genus *Hyriopsis*) and marine bivalve species (*Pinctada maxima*). Raman spectra for vaterite and ACC are discussed. Results for ACC are compared to synthetically produced ACC and to Raman spectroscopic features of stable biogenic ACC from the crustacean *Porcellio scaber*.

ACC in the pearls is confined to areas close to the centre of the pearls [1]. Decomposition of the most intense signal of the calcium carbonate polymorphs – the ν_1 symmetric stretching mode of the carbonate ion, leads to the identification of two polymorphs within the ACC areas: a mix of an amorphous and a nanocrystalline fraction.

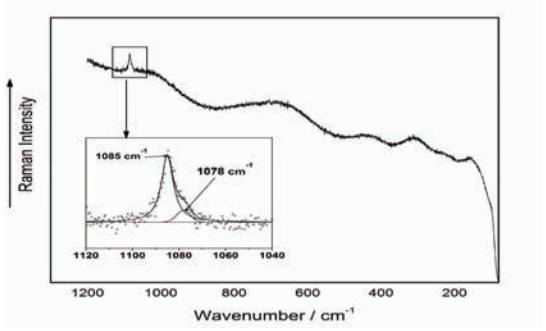

Fig. 1: Raw Raman spectrum of ACC in a South Sea cultured pearl (*Pinctada maxima*). Inset: The ν_1-mode is clearly to decompose into an amorphous (Gaussian line profile, centred at 1078cm^{-1}) and a nanocrystalline fraction (Lorentzian line profile, centred at 1085 cm^{-1}).

As a rule, the degree of mineral crystallinity is mirrored by the FWHM, the broader the spectral bandwidth, the lower the degree of the mineral crystallinity. The amorphous phase in the samples is characterised by a broad peak (FWHM of ca. 120 cm^{-1}) in the region of the lattice modes. While for monocrystalline and biogenic aragonite typically FWHMs of 1.3 cm^{-1} and 2.2 cm^{-1} are measured, nanocrystalline aragonite in paragenesis with ACC shows an FWHM between 5 cm^{-1} and 10 cm^{-1} of the ν_1 – Raman band. A shift to lower wavenumbers is clearly related to the peak broadening.

[1] Jacob, D.E. et al. (2008) *Geochim. Cosmochim. Ac.*, **72(22)**, 5401-5415. [2] Addadi, L. et al. (2003) *Adv. Mater.*, **15(12)**, 959-969. [3] Urmos, J. et al. (1991) *Am. Mineral.*, **76**, 641-646. [3] Wehrmeister, U. et al. (2010) *J. Raman Spectrosc.*, **41**, 193-201.

EPS composition and calcification potential of filamentous cyanobacteria

Zippel, B.[1*], Dynes, J.J.[2], Obst, M.[3], Lawrence, J.R.[4] & Neu, T.R.[1]
[1]Dept. of River Ecology, Helmholtz Centre for Environmental Research – UFZ, Magdeburg, Germany
([*]barbara.zippel@ufz.de)
[2]Dept. of Soil Science, University of Saskatchewan, Saskatoon, Canada
[3]Center for Applied Geoscience, Tuebingen University, Tuebingen, Germany
[4]Environment Canada, Saskatoon, Canada

Tufa deposits in freshwater habitats are often the result of calcium carbonate precipitation within interfacial microbial ecosystems. Calcite precipitation is influenced by the saturation index and the occurrence of extracellular polymeric substances (EPS), which are produced by a variety of microorganisms [1]. STXM has been used at the C K-edge to map the major biomolecules (proteins, lipids, and polysaccharides) in complex microbial biofilms [2]. Furthermore, by means of STXM it is possible to differentiate between different species and calcium carbonate phases at the Ca L-edge [3]. The purpose of this study is to determine if there are differences in calcium adsorption dependent on the specific composition of the EPS produced by filamentous cyanobacteria isolated from a hard water creek (Westerhöfer Bach, Harz Mountains, Germany).

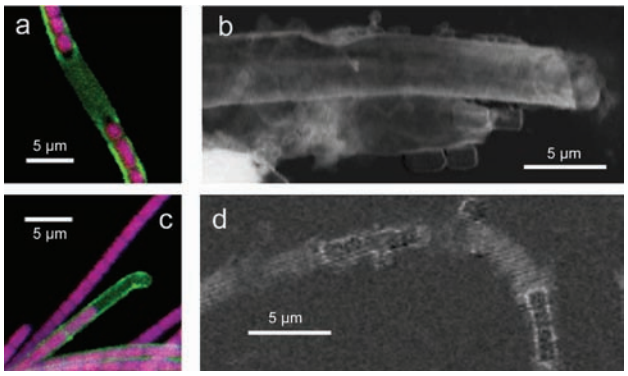

Fig. 1: (a, c) Maximum Intensity Projection of Laser Scanning Microscopy images represent lectin-specific EPS glycoconjugates (green) associated with the investigated cyanobacteria (pink). (b, d) STXM Ca maps $OD_{352,3eV} - OD_{350,3eV}$ showing the presence of extracellular Ca accumulations in close association with cells or in cyanobacterial sheaths.

The sheaths of the cyanobacteria contained mainly polysaccharides and proteins, and a small amount of lipids (Fig. 1). Both cyanobacterial sheaths contained spectral signatures of Ca^{2+} adsorbed to EPS. In *Pseudanabaena* sp. sheaths, the adsorbed Ca was distributed more homogeneously. Aragonite-like $CaCO_3$ in close association with the cyanobacterial cell surface was detected in *Leptolyngbya* sp. only. In the same region, polysaccharides were detectable. In the case of *Pseudanabaena* sp., only very small aragonite-like spots were recorded in association with accompaning cells of heterotrophic bacteria.

EPS produced by cyanobacteria were shown to be a component for calcium adsorption. Depending on the spatial composition of EPS, different components potentially participate to various extents in nucleation processes of calcium carbonate in close association with the cells.

[1] Dupraz, C. & Visscher, P.T. (2005) *Trends Microbiol.*, **13**, 429-438. [2] Lawrence, J.R. et al. (2003). *Appl. Environ. Microb.*, **69**, 5543-5554. [3] Benzerara, K. et al. (2004) *Geobiology*, **2**, 249-259.

Microbial induced calcite precipitation and its application in remediation technologies

Phoenix, V.R.[*] & Tobler, D.J.
Dept. of Geographical and Earth Sciences, University of Glasgow, UK ([*]Vernon.Phoenix@ges.gla.ac.uk)

The precipitation of calcite by ureolytic bacteria has potential in a wide range of environmental applications. The strength of this approach lies within its ability to precipitate considerable quantities of calcite. This approach has been shown to, for example, efficiently scavenge radionuclides (^{90}Sr) [1], seal fractures and permeable zones in concrete and rock [2,3] and protect and repair building materials [4].

Here we explore its potential to (a) seal fractures in rock around nuclear waste repositories and (b) immobilize nanoparticles.

Thus far, most studies on ureolysis and its impact on calcite precipitation have been perfomed in artificial groundwater using single species of urease positive bacteria, such as *Sporosarcina pasteurii*. While *S. pasteurii* may be used as an innoculum to seal fractures around nuclear waste repositories, indigenous communities also have potential to drive ureolytic calcite precipitation. Here we compare (in laboratory microcosms) urea hydrolysis and calcite recipitation rates by *S. pasteurii* with those of indigenous groundwater communities. In this particular groundwater, ureolytic activity of indigenous groundwater communities was almost zero. However, stimulation with dilute nutrients such as BHI or molasses promoted a notable increase in rates of urea hydrolysis. However, these rates were significantly lower than those obtained from aerobic experiments with *S. pasteurii* and may thus well be too low to plug soils and fractured rocks. However, when an innolculum of aerobically grown *S. pasteurii* was added to the anaerobic groundwaters, the ureolysis rates by *S. pasteurii* were significantly higher than those produced by stimulated groundwater communites. Significantly, this suggests *S. pasteurii* can be grown in large densities aerobically, and then injected into anaerobic groundwaters where the sudden change in fO_2 does not inhibnit the ureolytic activity of this facultative anaerobe.

We also examined the potential of microbial calcite precipitation to remediate nanoparticulate pollution, by trapping nanoparticles into the mineral precipitate. Batch microcosms were built containing articifial groundwater, urea, *S. pasteurii* and Fe_2O_3 nanoparticles as a model nanoparticle. Although some loss of nanoparticles from solution did occur due to floculation and settling, calcite precipitation showed much faster immobilization of the nanoparticles compared to controls, immobilizing 100% in just 1 day.

[1] Mitchell, A.C. & Ferris, F.G. (2006) *Environ. Sci. Technol*, **40**, 1008-1014. [2] Ferris, F.G., & Stehmeier L.G. (1992) *Bacteriogenic mineral plugging*. USA Patent US5143155. [3] Ramachandran, S.K. et al. (2001) *ACI Mater. J.*, **98**, 3-9. [4] De Muynck, W. et al. (2008) *Cement Concrete Res.*, **38**, 1005-1014.

Marine Mn nodules as stromatolites with fractal signature: examination by X-ray, TEM, SEM and mathematical simulation

Akai, J.
Dept. of Geology, Faculty of Science, Niigata University, Niigata, Japan (akai@sc.niigata-u.ac.jp)

Mn nodules are very problematic materials since the first finding: Why are the shapes nodular? Why are they not buried? Is the origin fundamentally biogenic or abiogenic? Many bio signatures containing bacteria have been found on the surface and within nodules. Although many suggestions are present, the genesis has not been fully confirmed.

Mn nodule samples from Clarion-Clipperton Fracture zone in other 4 localities in Pacific Ocean were mineralogically examined. Two types of constituent Mn oxide minerals were identified: 10A buserite-like phase and 2.5A vernadite-like phase. Mineralized bacteria and their possible traces were observed by SEM and TEM (Fig. 1a-d). The mineralized bacteria with Mn oxides (Fig. 1a) and Fe hydroxides (Fig. 1b) may be Mn-oxidizing bacteria and Fe-oxidizing bacteria, respectively. HRTEM images of constituent Mn minerals showed low crystalline layer structures (Fig. 1e).

Under the optical microscope, cross sections of the nodules were studied and characteristic columnar stromatolite structures were found. These thin rhythmic bands have often been described as stromatolitic. However, here, we refer to this structure as the stromatolite structure itself. The term 'stromatolite' has a genetic meaning, i.e., biogenesis. The rhythmic band structure found in the manganese stromatolite may be induced biomineralization products. Surface morphology of botryoidal characteristics was described. The characteristics bear fractal-like nature. Forms of four different orders are recognizable (Fig. 2a-d). The 1st order is the nodule forms themselves (several up to 10 cm in size), the 2nd order represents aggregated dome-like forms (several cm); the 3rd order dome-like forms are very clearly found (5mm to 1cm) i.e. the main morphological parts of botryoidal textures; 4th order (~0.2~ 1mm) dome forms correspond to stromatolite top form. X-ray CT images also resulted in confirmation of inner dome-like textures in Mn nodules. Mathematical simulation based on fractal models using basic sphere unit (Fig. 3a) reproduced similar morphological characteristics (Fig. 3b,c) to the natural samples.

So, we arrive at the concluding hypothesis that Mn nodules are aggregated stromatolite with fractal-like characteristics.

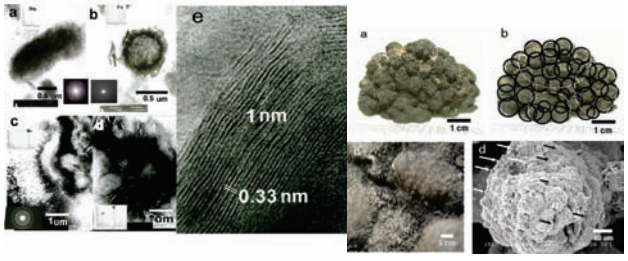

Fig. 1: (left) TEM image of Mn nodules.
Fig. 2: (right) Fractal-like features.

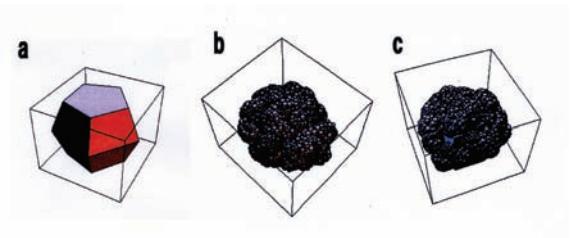

Fig. 3: Simulation of fractal pattern based on spherical units (represented in (a))

Biominerals of greigites (Fe_3S_4) in sediments – formation, stability and reaction in sea water

Preisinger, A.*, Aslanian, S. & Wernisch, J.
Vienna University of Technology, Vienna, Austria
(*anton.preisinger@tuwien.ac.at)

The widespread occurrence of a stable ferrimagnetic spinel structure of Fe_3S_4 (greigite) in sulfate reducing bacteria is well-established [1]. We analyzed nanocrystals of greigites in gravity cores of the Black Sea (BS), the Marmara Sea (MS) and the Caspian Sea (CS), as well as in the K/T-fallout in the former Tethys by utilizing X-ray diffraction, ore microscopy, transmission electron microscopy, and scanning electron microscopy. Two types of clusters of ferrimagnetic nanocrystalline structures were found [2]. They can be categorized as magnetotactic and framboidal greigites (Fig. 1 and 2).

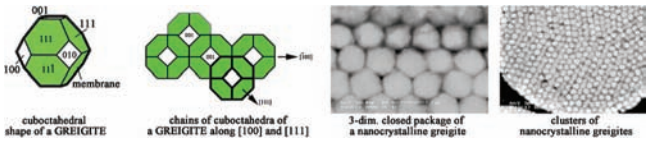

Fig. 1: Closed packed chains of greigite nanocrystals called "magnetotactic greigites".

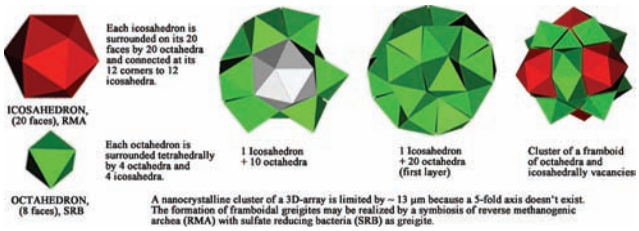

Fig. 2: Regular three dimensional array of greigite nanocrystals called "framboidal greigites".

From the MS over the sill in strait of Bosporus, clusters of magnetotactic greigites entering the BS since 9.300 yrs BP, which was at this time in an oxic state. The greigites are only stable under anoxic conditions. Under oxic conditions, the greigite reacts to non-magnetic pyrite (FeS_2) and FeOOH (Fig. 3).

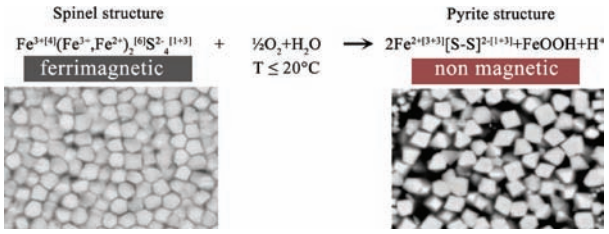

Fig. 3: Change of ferrimagnetic greigites (Fe_3S_4) + Oxygen → nonmagnetic Pyrite (FeS_2) + FeOOH.

In comparison to the climatic time scale, the quantitative counting of the greigites in gravity cores shows that water kept entering the BS from the MS stepwise between 9.300-8.500 yrs BP. The change of ferrimagnetic greigites to non-magnetic pyrites under oxic conditions in the BS reveals this clearly. Besides the more recently formed clusters of framboidal greigites under the chemocline of the BS, we also found such clusters in the former Tethis, which were built after the Cretaceous/Paleogene (K/T)-impact of Chicxulub (Mexico) as a consequence of the sulfuric acid rain in the worldwide K/T-fallout [3].

[1] Kasama, T. et al. (2006) *Am. Mineral.*, **91**, 1216-1229. [2] Preisinger, A. et al. (2005) *Acta Cryst.*, **A61**, C312. [3] Preisinger, A. et al. (2002) *Geol. S. Am. S.*, **356**, 213-229.

Bacterially induced micro- and nano-textures of massive sulphides, Silvermines Zn-Pb deposit, Ireland

Kucha, H.[1*], Raith, J.G.[2] & Southam, G.[3]
[1]University of Mining & Metallurgy, Krakow, Poland
([*]kucha@geol.agh.edu.pl)
[2]Dept. of Applied Earth Sciences & Geophysics, University of Leoben, Austria
[3]Dept. of Earth Sciences, The University of Western Ontario, London, Ontario, Canada

At Silvermines Zn-Pb ores occur in two forms: 1) Epigenetic ores (zones G, K) present within or close to the Silvermines fault with 4.74 Mt ore at 2.4wt.% Pb and 5.9wt.% Zn [1]. Sulphur isotopes of sulfides from these ores are typically in the range $\delta^{34}S$= +4 to –5‰, while barite values are between $\delta^{34}S$= +18 to +23‰. 2) Stratiform ores are developed within the pyrite, siderite and barite facies. Ore reserves amounted to 12.94 Mt with 2.6wt.% Pb, 6.8wt.% Zn and 5.0 Mt of barite [1]. These sulphides have $\delta^{34}S$= –4 to –43‰. Barite falls in the range of $\delta^{34}S$= +12 to +23‰. Stratiform ores contain ubiquitous bacterially induced micro- and nano-textures (Figs. 1 & 2), as well as compounds with intermediate and mixed sulphur valences. Bacterially induced textures occur in up to a few cm thick patchy to layered ZnS accumulations. Sulphur isotope data and biogenic textures suggest a massive involvement of sulphate reducing bacteria in the accumulation of the stratiform massive sulphide ores at Silvermines [2].

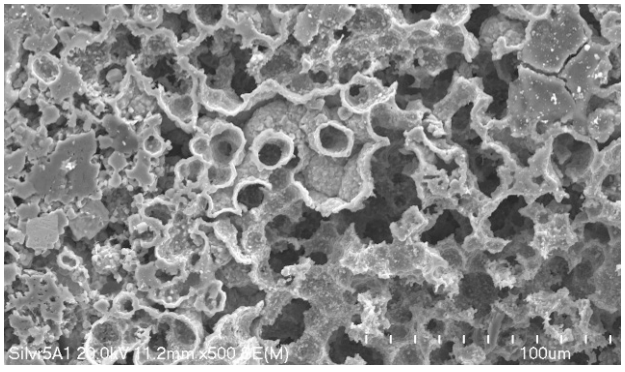

Fig. 1: FESEM image of etched biogenic ZnS aggregate with tubiform to sub-circular micro-texture.

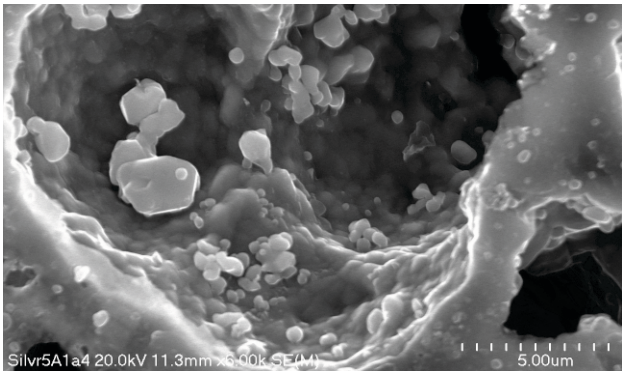

Fig. 2: FESEM image showing detail of biogenic micro-texture in Fig.1. The ZnS aggregate is composed of small mostly circular nanoforms. The smallest globules are ~100nm in size.

[**1**] Andrew, C.J. (1986) in Andrew, C.J. et al. (eds.) *Geology and genesis of mineral deposits in Ireland*. Ir. Assoc. Econ. Geol., 377-417. **[2**] Kucha, H. et al. (1990). *Miner. Deposita*, **25**, 132-139.

Microbially enhanced dissolution of pyrrhotite polytypes: surface roughness, reactivity and rates

Pollok, K.[1*], Hopf, J.[1], Harries, D.[1], Chust, T.[1], Hochella, M.F.[2] & Langenhorst, F.[1]
[1]Bayerisches Geoinstitut, Universität Bayreuth, Germany
([*]kilian.pollok@uni-bayreuth.de)
[2]Center for NanoBioEarth, Dept. of Geosciences, Virginia Polytechnic Institute and State University, Blacksburg, Virginia, USA

Chemical and biological dissolution and oxidation of pyrrhotite ($Fe_{1-x}S$) can significantly contribute to acid mine drainage (AMD) from sulphidic mine heaps and tailings [1] which is an environmental concern to the water quality of ground and surface waters worldwide. Dissolution rates for this mineral are less constrained especially for biologically enhanced dissolution but they are always considerably faster compared to pyrite. An important complication for studies on pyrrhotite dissolution is the variable iron deficiency that results in various polytypes and superstructures which in turn affect surface reactivity. Furthermore, almost all natural pyrrhotites are intergrowths of different polytypes down to a submicroscopic scale which limits the ease of use of powders in bulk dissolution studies, but allows a direct comparison of surface reactivity in abiotic/biotic experiments.

Here, we show results adapted from completed dissolution experiments on natural pyrrhotite (Tysfjord, Norway) in presence of *Acidithiobacillus ferrooxidans* at pH 2 over 40 days which were conducted together with an abiotic control. The polished samples show an intergrowth of 1-3 µm wide lamellae of the ordered 2C type in a matrix of NC type. The lamellae are close to stoichiometric FeS (troilite) while the matrix contains about 2 wt% less iron. Abiotic pyrrhotite dissolution yielded almost no morphological changes on the mineral surface. In contrast, *Acidithiobacillus ferrooxidans* developed a thick whitish biofilm on the samples. The underlying mineral surface showed deep and extremely long trenches with a width of ca. 3.5 µm and a depth of several µm. Obviously, bacterial activity preferentially dissolved the more iron-rich lamellae of the 2C type pyrrhotite. However, whether this effect indicates a preference of the microorganisms to the higher iron content or an enhanced kinetic effect due to lower mineral stability is arguable.

To quantify the evolution of the altered surface area we used confocal microscopy which allows to collect 3D topographic data from a large field of view (160 x 160 µm) with a submicrometer resolution in x, y, and z. The approach of converged surface roughness parameters [2] was used to explore how different surface components impact roughness parameters over a range of lateral scales. The calculation of the surface roughness in relation to the size of the sampling area has been automated in order to minimize the bias of choosing 'representative' areas and to visualize the roughness distribution. Furthermore, the topographic data allow us to evaluate the difference in dissolution rates of the 2C and NC polytype which may offer a way to predict overall dissolution rates of complex pyrrhotite intergrowths.

[1] Schippers, A. et al. (2007) *J. Geochem. Explor.*, **92**, 151-158. [2] Fischer, C. & Lüttge, A. (2007) *Am. J. Sci.*, **307**, 955-973.

Biomineralization of magnetite: implications in the search for life in Mars

Jiménez-Lopez, C.[1*], Perez-Gonzalez, T.[1], Valverde Tercedor, C.[1], Romanek, C.S.[2] & Bazylinski, D.A.[3]
[1]Dpto. Microbiología, Facultad de Ciencias, Universidad de Granada, Spain ([*]cjl@ugr.es)
[2]Dept. of Earth & Environmental Sciences, University of Kentucky, Lexington, Kentucky, USA
[3]School of Life Science, University of Nevada-Las Vegas, USA

Nanometer-sized magnetite (Fe_3O_4) crystals have been recovered from many modern and ancient environments and even meteorites. In some cases these crystals have been used as magnetofossils for evidence of the past presence of specific microbes. The rationale behind that is that magnetite nanocrystals can be formed by biological and inorganic mechanisms. Prokaryotes (bacteria) biomineralize magnetite through a biologically-induced mineralization (BIM) and biologically-controlled mineralization (BCM) [1]. Magnetite nanocrystals produced by BIM synthesized by the dissimilatory iron-reducing bacteria, are deposited external to the cell and generally are though to be indistinguishable from magnetite particles formed inorganically. BCM magnetites, in contrast, synthesized by the magnetotactic bacteria, are precipitated intracellularly as membrane-bounded structures called magnetosomes. These magnetites have unique properties, leading to their use as magnetofossils. Because of the discovery of nanometer-sized crystals of magnetite in the Martian meteorite ALH84001, the use of these criteria for the determination of whether magnetite crystals could constitute a prokaryotic biomarker was questioned. In this study we have formed BIM magnetite induced by *Shewanella oneidensis* and we have observed that organic material incorporates into the crystal structure, altering such a structure. This alteration could be used as a biosignature. Moreover, and regarding the inorganic pathway proposed by [2] for the formation of ALH84001 magnetites, based on the thermal decomposition of the carbonate matrix in which those magnetites are embedded, we have also demonstrated that: (1) the thermal decomposition of $(Fe,Ca,Mg)CO_3$ yields magnetites that incorporate Ca and Mg into their crystalline structure, and (2) such a decomposition is topotactic, conferring a specific structural relationship between the precursor ankerites and the newly formed magnetites as well as between the magnetite crystals (Fig. 1). Such a relationship differs substantially from that observed in the magnetosomes of the magnetotactic bacteria and from that of the ALH84001 magnetites. Therefore, the decomposition of the carbonate matrix does not explain ALH84001 magnetites.

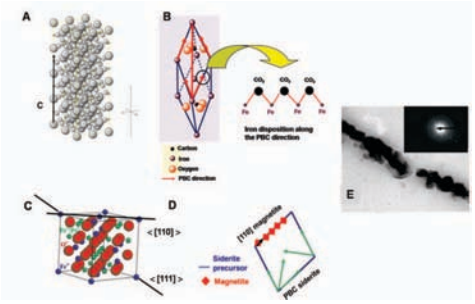

Fig. 1: A) Siderite cell unit; B) PBC directions and atomic distribution along those directions; C) Magnetite cell unit; D) Structural relationship between the precursor (siderite, in blue) and the product (magnetite, in red), and within the newly formed magnetite crystals; E) HRTEM image showing magnetite crystal formed by the thermal decomposition of an ankerite, aligned by facing their corners.

[1] Bazylinski, D.A. & Frankel, R.B. (2003) *Rev. Mineral. Geochem*, **54**, 95-114. [2] Golden D.C. et al. (2004) *Am. Mineral.*, **89**, 681-695.

Characterization of ferric iron oxyhydrosulfate compounds precipitated in different cultivations of *Acidithiobacillus ferrooxidans*

Wang Xin, Li Yan, Lu Anhuai[*] & Wang Changqiu
School of Earth and Space Sciences, Peking University, Beijing, China ([*]ahlu@pku.edu.cn)

This study focused on the ferric iron oxyhydrosulfate compounds precipitated during the culture of *Acidithiobacillus ferrooxidans* in a modified 9K medium by applying a potential control on the electrode. X-ray diffraction (XRD), environmental scanning electron microscope (ESEM), Raman spectroscopy (Raman) and Fourier Transform Infrared spectroscopy (FTIR) were performed to characterize and identify the ferric iron oxyhydrosulfate precipitates formed, respectively, in the electrolysis cultivation using a fixed cathode potential (bias-experiment) and in the conventional batch cultivation without cathode potential control (no-bias-experiment).

The results showed that K-jarosite appeared in both experiments while NH_4-jarosite and schwertmannite were only turned up in the no-bias-experiment (Fig. 1). The formation of different precipitates was supposed to be attributed to the different growth status and rates of *A. ferrooxidans* and the different concentrations of Fe^{3+} (Fig. 2). In the bias-experiment, external electrons recycled Fe^{2+} promoting the growth of *A. ferrooxidans*, thus resulting in the low Fe^{3+} concentration and rapid depletion of NH_4^+ as the nitrogen source, in which K-jarosite was preferential to be formed. In the no-bias-experiment, the lower concentration of *A. ferrooxidans* was observed, which was due to the rapid consumption of Fe^{2+} by *A. ferrooxidans*, thus resulting in the relatively higher Fe^{3+} and NH_4^+ concentrations in culture. The high concentration of Fe^{3+} favored the precipitation of the solid solution of K-NH_4-H_3O jarosite and led to schwertmannite precipitation after K^+ and NH_4^+ were depleted.

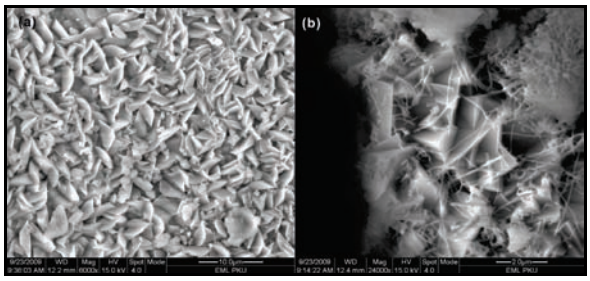

Fig. 1: ESEM images of the precipitates obtained in bias- (a) and no-bias- (b) experiments.

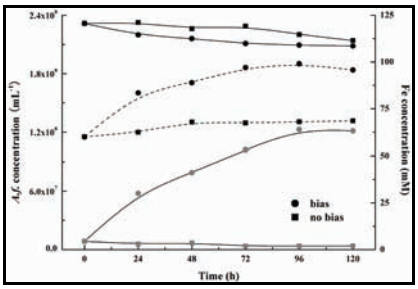

Fig. 2: *A. ferrooxidans* growth curves and ferrous/total ferric concentrations in the bias and no-bias experiments (black solid dots - ferric, gray solid dots - ferrous, solid lines - Fe concentration, dash lines - *A.f.* concentration).

Iron biomineralization by neutrophilic iron-oxidizing bacteria

Miot, J.[1], Benzerara, K.[1*], Morin, G.[1], Kappler, A.[2], Obst, M.[2] & Brown, G.E. Jr.[3]
[1]IMPMC, IPGP, Paris, France
([*]karim.benzerara@impmc.jussieu.fr)
[2]Geomicrobiology Center for Applied Geoscience, ZAG, University of Tuebingen, Germany
[3]Surface & Aqueous Geochemistry Group - Stanford University, Stanford & SSRL, Menlo Park, CA, USA

The processes of Fe biomineralization induced by Fe(II) bio-oxidation at neutral pH under anoxic conditions remain poorly understood. We present here a spectro-microscopic study of the biominerals produced by the nitrate-reducing iron-oxidizing bacteria Acidovorax sp. strain BoFeN1 cultured in the presence of dissolved [1] or solid Fe(II) [2]. We present also for comparison a spectromicroscopy study of the biominerals produced by the phototrophic iron-oxidizing Rhodobacter sp. strain SW2 [3]. As characterized by bulk X-ray Absorption Spectroscopy (EXAFS), the final products of Fe(II) oxidation consisted of amorphous Fe(III)-phosphate in the presence of BoFeN1 and goethite in the presence of SW2. Transmission Electron Microscopy (TEM) and Scanning Transmission X-ray Microscopy (STXM) highlighted the progressive periplasmic encrustation of BoFeN1 cells by iron minerals, accompanied by an accumulation of protein moieties while precipitates form outside SW2 cells. For both SW2 and BoFeN1 cells, extracellular iron precipitated in association with exo-polysaccharides. For BoFeN1, solid Fe(II) (composing extracellular abiotic vivianite precipitates formed during medium preparation) was partly oxidized with a few day delay compared to dissolved Fe(II). For SW2 Fe redox gradients were observed around the cells. This led to strong redox heterogeneities at the nano-scale within the sample. Direct or indirect mechanisms can be proposed to account for these observations. All these findings provide new information to further the understanding of molecular processes involved in iron biomineralization by anaerobic iron-oxidizing bacteria.

[1] Miot, J. et al. (2009) *Geochim. Cosmochim. Ac.*, **73**, 696-711. [2] Miot, J. et al. (2009) *Appl. Env. Microbiol.*, **75**, 5586-5591. [3] Miot, J. et al. (2009) *Geobiol.*, **7**, 373-384.

Microbially-mediated uranium reduction: role of solutes and biomolecules in product formation

Bernier-Latmani, R.[*], Alessi, D.S., Uster, B., Dalla Vecchia, E., Suvorova, E.I., Lezama-Pacheco, J.S., Bargar, J.R. & Persson, P.
Environmental Microbiology Laboratory, Ecole Polytechnique Federale de Lausanne, Switzerland
([*]rizlan.bernier-latmani@epfl.ch)

Uranium is a contaminant of concern at a number of sites around the world as a result of mining, milling and processing of the radionuclide for nuclear weapons and fuel production. Uranium is typically encountered in the hexavalent valence state in these contaminated sites. This is particularly problematic because U(VI) is very soluble and can thus be quickly transported off site via groundwater flow. Microbially-mediated U(VI) reduction is considered as a potential strategy for the immobilization of uranium *in situ*. It relies on the natural activity of a variety of metal- and sulfate-reducing bacteria and the formation of U(IV) species that are less mobile than U(VI) species. Previous work [1] has shown that the product of microbially-mediated U(VI) reduction varies as a function of the chemical composition of the reduction medium. The products identified to date include the mineral uraninite (UO_2), the mineral ningyoite ($CaU(PO_4)_2$) and sorbed U(IV) species referred to as molecular U(IV).

This work explores the role of inorganic solutes such as Ca^{2+}, Mg^{2+}, NH_4^+ and PO_4^{3-} as well as biomolecules such as extracellular polymeric substances (EPS), phospholipids and lipoteichoic acids in the formation of reduced uranium products as a result of microbial U(VI) reduction. In particular, we tackle the question of whether nucleation and precipitation of U(IV) minerals is controlled directly by the chemical composition of the medium or by biological effects induced/caused by the chemical composition of the medium.

We use a variety of techniques to characterize the product of U(VI) reduction under the conditions considered including a selective chemical extraction method that we developed [2], electron microscopy, x-ray absorption spectroscopy and Fourier transform infrared spectroscopy to interrogate the role of solutes and biomolecules in UO_2 formation or inhibition.

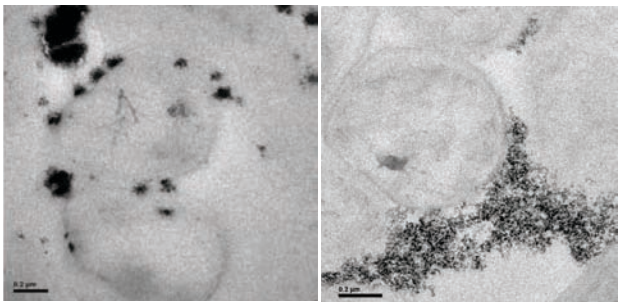

Fig. 1: Transmission electron micrographs of *Shewanella oneidensis* MR-1 cells after U(VI) reduction under variable chemical conditions. In the right panel, the product is a sorbed species molecular U(IV) species and in the left panel is the mineral UO_2. Morphological differences between the sorbed species and the mineral are readily observable.

[1] Bernier-Latmani, R. et al. (2010) *Environ. Sci. Technol.*, submitted. [2] Alessi, D.S. et al. (2010) *Geochim. Cosmochim. Ac.*, **74(12)**, A11.

Mycomineralization: fungal deterioration and transformation of metal and mineral-based substrates

Gadd, G.M.* & Fomina, M.
Division of Molecular Microbiology, College of Life Sciences, University of Dundee, Dundee, Scotland, UK
(*g.m.gadd@dundee.ac.uk)

"Geomycology" can be considered a subset of "geomicrobiology" and simply defined as the impact of fungi on geological processes, including the alteration and weathering of rocks and minerals, the accumulation of metals, and their roles in element and nutrient cycling. Although the main focus of geomicrobiology is on prokaryotes, it is clear that epi- and endolithic fungi comprise a significant component of the microbiota in a range of rocks and mineral-based substrata. Our research seeks to understand the mechanisms of metal and mineral biotransformations, and their environmental and applied significance in bioremediation and biodeterioration. This presentation will include examples of our research on fungi inhabiting certain rock types, soil, including the mycorrhizosphere, particularly regarding mineral dissolution and transformation, and the formation of secondary mycogenic minerals. An important mechanism of metal mobilization from minerals is a combination of acidification and ligand-promoted dissolution: if oxalic acid is produced, the production of metal oxalate biominerals may result. In other cases, mobilized metal species may interact with phosphate. Examples outlined in this presentation will include fungal communities and roles in degradation and transformations of rocks and metal-containing minerals, depleted uranium and uranium oxides, and fungal biodeterioration of concrete, the latter being of general biodeteriorative significance regarding built concrete structures.

Assessing the contribution of acidolysis and complexolysis in the microbial dissolution of colloidal size silicates particles

Grybos, M.[1,3*], Billard, P.[1], Desobry, S.[1], Michot, L.[2] & Mustin, C.[1]
[1]LIMOS (Lab. des Interactions Microorganismes-Minéraux-Matière Organique dans les Sols), UMR 7137 CNRS, Vandoeuvre-lès-Nancy, France
[2]LEM (Lab. Environnement et Minéralurgie), UMR 7569 INPL & CNRS, ENSG, Vandoeuvre-lès-Nancy, France
[3]GRESE (Groupement de Recherche Eau Sol Environement), Université de Limoges, France (*malgorzata.grybos@unilim.fr)

In soils and near subsurface environments, heterotrophic bacteria play an important role in the dissolution of colloidal-size mineral particles. They accelerate mineral dissolution directly through the acquisition of limiting nutrients from mineral surfaces or indirectly through the release of metabolic by-products that can lower pH, thereby enhancing proton-promoted dissolution and/or withdraw cationic constituents from the mineral lattice through the complexation (1). To assess the respective role of acidolysis and complexolysis processes in the microbial dissolution of colloidal-size mineral particles, we performed controlled incubations of 600 nm length and 60 nm width particles of Fe-rich phyllosilicate (nontronite, NAu2) in the presence of a set of phylogenetically diverse heterotrophic soil bacteria. To prevent any uncontrolled particle aggregation and adsorption onto bacterial cells, the colloids were homogeneously dispersed in a biologically friendly, porous TEOS-derived silica gel by a sol-gel procedure (2).

The results showed that NAu2 incubation in presence of bacteria released from 0.1 to 2% of the total Fe and was accompanied by a pH decrease. Higher Nau2 dissolution rates were observed for highly acidifying bacteria. For a given pH value, the amount of released Fe varied between the strains and was two to ten fold greater than under abiotic conditions (i.e. HNO_3) indicating that complexing metabolites play an important role in the overall dissolution process. We conclude that the dominant mechanisms by which Nau2 was dissolved was complexolysis accounting from 50 to 90% of the total Fe released in the solution.

[1] Kalinowski, B.E. et al. (2000) *Chem. Geology*, **169**, 357-370. [2] Grybos, M. et al. (2010) *J. Colloid Interf. Sci.*, **343**, 433-438.

A novel solar-powered device for studying the synergistic effects of natural semiconducting minerals and microorganisms

Lu Anhuai*, Li Yan & Wang Changqiu
School of Earth and Space Sciences, Peking University, Beijing, China (*ahlu@pku.edu.cn)

Microbial fuel cell (MFC) is a popular bio-electrochemical device in which microorganisms catalyze electrons transport from avaible substrates towards terminal electron acceptors through a circuit containing a solid-state anode, an external load and a cathode. Photofuel cell (PFC), which consists of a semiconductor photoanode and a species-reducing cathode, is the similar electrochemical device as the operation of MFC. Enlightened by both MFC and PFC, we reported here a novel solar energy-powered device (Fig. 1), which realized the biocatalytic oxidation (anode) and photocatalytic reduction (cathode) of pollutants while producing electrical energy.

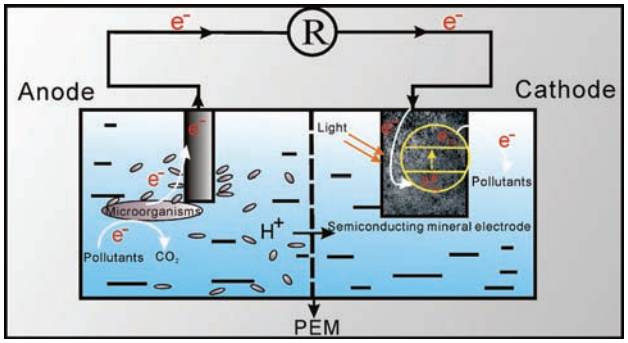

Fig. 1: The configuration of the solar-powered device by using natural semiconducting minerals as cathodic catalysts for wastewater treatment and electricity generation.

In this device, a class of semiconducting mineral-based catalysts (rutile, sphalerite, pyrrhotite) were used as the cathodes. The open circuit voltage (V_{OCV}), maximum power density (P_{max}), fill factor (FF), incident monochromatic photon to current conversion efficiency (IPCE) and coulombic efficiency (CE) was calculated to characterize and compare the performance of the device by using different minerals. Then, the influences of mineral species, cathode fabrication methods, terminal electron acceptors, pH and equipment configuration on the power output were discussed. Further experiments were conducted to evaluate its prospects in environmental application. The results showed that a solar photocatalytic treatment of a broad range of pollutants (e.g., hexavalent chromium, chlorinated ethenes, azo dyes and landfill leachate) was achieved.

This kind of solar-powered device offered a potential strategy for strengthening pollutant treatment and simultaneously harvesting electricity. In order to distinguish this novel system from the conventional MFC and PFC, we refer to this system as the bioelectrochemical-photoelectrochemical cell (BPC). BPC is driven by solar energy and believed to be effectively applied in environmental fields, because it succeeds in arranging energy flow between two different pollutants via two different catalytic mechanisms.

Quantification of plant-driven fungal alteration at the surface of biotite

Bonneville, S.[1*], Morgan, D.[1], Bray, A.W.[1], Duran, A.[2], Brown, A.[3], Schmalenberger, A.[4], Gonzales-Romero, M.[4] & Benning, L.G.[1]
[1]School of Earth and Environment, University of Leeds, UK (*earscb@leeds.ac.uk)
[2]Institute for Materials Research, University of Leeds, UK
[3]Dept. for Animal and Plant Sciences, Univ. of Sheffield, UK
[4]Kroto Research Institute, University of Sheffield, UK

Initially thought mainly in term of abiotic dissolution reactions, weathering science now integrate the role of plant and their root associated micro-organisms. In particular, mycorrhiza (fungi in mutualistic symbiosis with roots) are the object of intense research because of their position at the interface between the lithosphere and biosphere. Fuelled by a significant fraction of energy from plant photosynthesis, fungi expand into soils via a vast network of microscopic filaments (5 µm in width and up to 1 mm in length). The mycelium developed around the roots is responsible for extracting and transfering a large spectrum of elements and nutrient to the plant. In doing so, mycorrhiza alter rock-forming minerals and help form our soils. Here, we present the results of a liquid-free culture in which a freshly-cleaved biotite flake was exposed for three months to a fungus (*Paxillus involutus*) grown in symbiosis with a tree (*Pinus sylvestris*) under controlled but close-to-natural conditions. Fungal hypha, similar to the majority of soil microbes, strongly adhere to and interact with the mineral surface (Fig. 1).

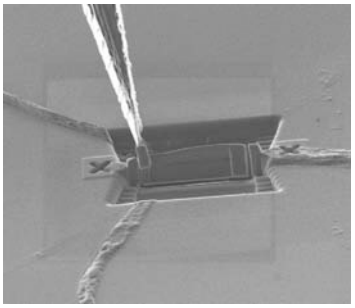

Fig. 1: Lift-off of the hypha-biotite ultrathin Focused Ion Beam (FIB) section from a biotite where the fungal strands were firmly attached. Scale bar is 20 µm.

Along a single hyphae, we sampled the interface between the mycorrhiza and the biotite using FIB (Fig 1) in order to capture the temporal evolution of the weathering process. The FIB sections were analyzed for mineralogical and chemical changes by TEM (SAED and STEM-EDS) and synchrotron-based STXM. Additionally, on a parallel incubation, the spatial distribution of functional groups along single hyphae was quantified using synchrotron µ-FTIR. Finally, confocal microscopy was used to determine the pH variations in the microenvironment near the hyphae.

Our results show that a mechanical constraint operates in the first stage of contact between hypha and biotite causing a mis-orientation of the most superficial 500 nm to 1µm of the mineral in contact with the hypha. In a later stage, significant export of elements from the mineral (namely K, Al, Mg and Fe) occurs concomitantly with a mineralogical transformation of the interfacial biotite into vermiculite and Fe oxide [1]. The pH measurement around the hypha revealed values between 4-5 and the µ-FTIR showed marked differences in functional group distribution along the hyphae. Using this dataset, a model based upon solid state diffusion in biotite was established which permit the first quantification of chemical alteration in relation to mycorrhizal and plant growth.

[1] Bonneville, S. et al. (2009) *Geology*, **37**, 615-618.

Bioweathering of a reduced chondritic material: implications for enstatite chondrites

Avril, C.[1], Malavergne, V.[1], van Hullebusch, E.[1], Guyot, F.[2], Brunet, F.[3], Borensztajn, S.[4], Labanowski, J.[5] & Rossano, S.[1*]

[1]Laboratoire Géomatériaux et Environnement, Université Paris Est, Paris, France ([*]rossano@univ-mlv.fr)
[2]IMPMC/IPGP, 75015 Paris, France
[3]Laboratoire de Géologie, ENS-CNRS, 75005 Paris, France
[4]Laboratoire Interface et Systèmes Electrochimiques , UPR 15 CNRS, Ivry sur Seine, France
[5] Laboratoire de Chimie et Microbiologie de l'Eau, UMR CNRS 6008, Poitiers, France

Enstatite chondrites (E chondrites) are the most reduced existing natural materials. Studying their aqueous alteration could provide useful data about the low temperature evolution of these potentially important Earth forming chondritic blocks. Moreover, finding specific signatures of their bio-alteration could be important for the astrobiological issue of detecting traces of life in such reduced materials. The aim of this study was thus to investigate the mineralogical and chemical processes which take place during the aqueous oxidative and acidic weathering of an E chondrite without or in presence of bacteria. Synthetic E chondrites were made in laboratory in order to begin this complex study with simplified and well-defined materials. Synthesis conditions of 0.8 GPa and 1473 K (4 to 7 days in a piston-cylinder apparatus) were suitable to achieve well-equilibrated E chondrite analogs. A simplified CI chondritic glass mixed with FeS and metallic Si was used as starting material. These analogs were shown to contain the major phases of E chondrites: enstatite, Si-rich kamacite, troilite, SiO_2 and unusual sulfides such as oldhamite or niningerite. In order to better understand the global E chondrite alteration, each major phase (also synthesized in a piston-cylinder apparatus) was separately submitted to aqueous alteration with or without bacteria.

Pure cultures of an iron oxidizing bacterium (*Acidithiobacillus ferrooxidans DSM 14882- DSMZ Germany*) and of a sulfur oxidizing bacterium (*Acidithiobacillus thioooxidans*), were used for the bioweathering experiments (42 to 48 days of weathering). Abiotic alteration was also systematically studied. All the experiments were buffered at pH of ≈2. The culture media were initially Fe and S-deficient in order to maximize the bacterial extraction of these elements from the starting solid material. All experiments were characterized before and after alteration using scanning electron microscopy (SEM), transmission electron microscopy (TEM), electron microprobe analysis, Raman spectroscopy and X-Ray diffraction. Compositions in major and trace elements were analyzed by inductively coupled plasma optical emission spectrometry (ICP-OES) in filtered leachates recovered from different bioweathering experiments.

Bacterial activity leads to the formation of P and S–rich biofilms on the minerals. The presence of the bacteria also modifies the chemical composition of the medium: ICP-OES data show that, in the leachates, the concentration of Si is lower in the biotic experiments than in the abiotic ones. The bacteria indeed restrict the dissolution of silicon from the minerals probably as a consequence of a protective effect of the biolfilms against the acidic solution. After weathering, monosulfides are no longer present in the samples showing their dissolution in the aqueous medium in both the bioweathering experiments and the abiotic controls. Important phosphate and sulfate precipitations from the interaction of the culture medium with ions dissolved from the minerals also occur. A thermodynamic and kinetic model rationalizing these observations will be discussed.

Synergistic effect of natural rutile and electricigens on azo dye decolourization

Ding Hongrui, Li Yan, Lu Anhuai[*] & Wang Changqiu
School of Earth and Space Sciences, Peking University, Beijing, China ([*]ahlu@pku.edu.cn)

Photocatalytically reductive decolorization of azo dye in wastewater was investigated in a dual-chambered electrochemical setup equipped with a rutile-coated cathode and a microorganism anode. When the visible light irradiated on the rutile-coated cathode, a rapid decolourization of a model azo dye, methyl orange (MO), was achieved, coupled by electrical energy generation. The electrochemical impedance spectra (EIS) showed the polarization resistance (R_p) of the rutile-coated cathode decreased by 67.8 % from dark to light (Table 1), indicating the photocatalysis of rutile-cathode can enhance the electron transfer process and promote the cathodic reduction.

Table 1: Fit parameters for EIS of the graphite and rutile-coated cathode under different light controls.

Parameter	Rutile-coated cathode		Graphite cathode	
	Light	Dark	Light	Dark
R_p (Ω)	443.4	1378	1429	1844
R_s (Ω)	2.706	1.336	6.063	6.922

As compared with the sole biocatalysis by microorganisms or photocatalysis by rutile, the co-catalysis of electrons transfer by microorganisms in the anode and natural rutile in the cathode resulted in higher MO degradation efficiency and more power generation. By analyzing the decolorization products with UV-Vis spectra, the azo bond of MO was fully cleaved due to the photocatalytic reduction of natural rutile (Fig. 1).

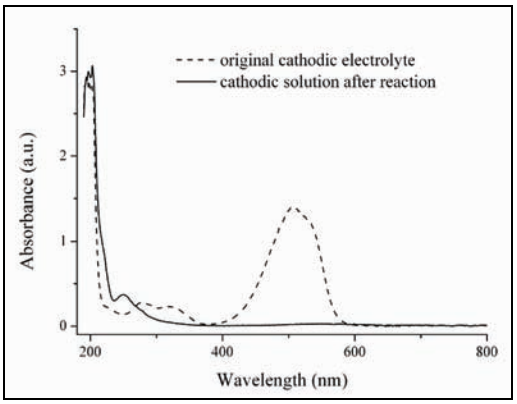

Fig. 1: UV-Vis spectra of cathodic electrolytes when using an irradiated rutile-coated cathode.

This research provided insightful viewpoint of integrating a bioelectrochemical process with a photoelectrochemical process, which offered a novel and cost-effective remedy for treating azo dye wastewater with simultaneous electrical power generation.

Minerals dissolution: from ions to eukaryotes

Gazze, A.S.[1*], Saccone, L.[1], Ragnarsdottir, K.V.[2] & McMaster, T.J.[1]
[1]H.H. Wills Physics Laboratory, University of Bristol, UK ([*]andrea.gazze@bristol.ac.uk)
[2]Institute of Earth Sciences, School of Engineering and Natural Sciences, University of Iceland, Reykjavik, Iceland

Atomic Force Microscopy (AFM) was used to visualize the effects of a wide range of weathering agents, from protons to filamentous fungi, on phyllosilicates. The effects of protons and oxalate on the basal and {hk0} surfaces of these minerals have been followed in *real-time*. On biotite, weathering process consisted in the retreat of {hk0} surfaces and in the formation of etch-pits on basal surface. For the first time, we have been able to follow the dynamics of the formation of etch-pits which consisted in a progressive removal of the first tetrahedral layer, followed by the octahedral and then the second tetrahedral sheet. The removal of the first tetrahedral layer takes place through the detachments of building blocks, suggesting that some Si-O-Si bonds are not broken. The presence of the underlying octahedral layers also implies that even if some cations could have been removed, this layer is still present before the removal of the first tetrahedral sheet.

AFM have been also used to extensively characterize an ectomycorrhizal fungus, *Paxillus involutus*, colonizing mineral surfaces. Basal surfaces of both biotite and chlorite present channels created by the fungus. High-resolution imaging allowed us to detect channels that are only one basal layer deep (1.5 nm) and to identify non-mineral material, probably of fungal origin, associated with the channels. The latter often presented lateral, smaller channels. While the central part of hypha could be involved in the formation of the main channels, the lateral channels could participate to their enlargment.

Here we show how the direct visualization of mineral surfaces during weathering processes is fundamental in order to interpret the possible mechanisms involved in the process, both at the atomic (protons on surface) and multicellular (fungi on surface) levels.

Photocatalytic reduction of carbon dioxide by natural sphalerite in a bioelectrochemically assisted reactor

Li Yan, Lu Anhuai[*] & Wang Changqiu
School of Earth and Space Sciences, Peking University, Beijing, China ([*]ahlu@pku.edu.cn)

Mineral-microbial interactions and their role in energy transformation play an important role in the earth surface. This paper presents a novel viewpoint of interactions between semiconductor minerals and microorganisms. Electron transfer pathways were hypothesized for such interactions. During the electron transfer, photogenerated electron-hole pairs can be well separated by accepting/donating electrons from/to microorganisms. On one hand, microorganisms could gain energy from oxidation of organic/inorganic compounds and use visible light-excited semiconductor minerals as electron acceptor for the electron transport chain. The separated photoelectrons of semiconductor minerals could be used to photo-reduce carbon dioxide.

Experiments were conducted to demonstrate the proposed viewpoint. In a dural-chambered electrochemical equipment, natural sphalerite was employed as a photocatalyst in the cathode to reduce carbon dioxide, while electrochemically active bacteria was involved in the anode to provide driving force to separate photogenerated electron-hole pairs. With the addition of a small voltage between the anode and the cathode, carbon dioxide was photoreduced at the sphalerite cathode. The effects of various experimental paraments, e.g., amount of sphlaerite, additional voltage, catholyte species, pH, light intensity and reaction time were investigated. Further, the mechanism of carbon dioxide reduction was proposed basing on the analysis of intermediates and products.

Cyanobacterial calcite cementation in a tidal channel of the Bay of Cádiz Natural Park: a field experimental study

Mata, M.P.[1*], García Robledo, E.[2], Corzo, A.[2], Jimenez Arias, J.L.[2] & Perez-Outeiral, F.J.[2]
[1]Dept. Investigación y prospectiva geocientífica, Instituto Geológico y Minero de España, Tres Cantos, Madrid, Spain
([*]p.mata@igme.es)
[2]Dept. Biología, Fac. Ciencias del Mar y Ambientales, Universidad de Cádiz, Puerto Real (Cádiz), Spain

Beachrocks are formed in the intertidal zone by a rapid cementation of sandy beach sediments. The proposed origins are: physico-chemical or biological processes being the last one related to micro-environments created by microbial metabolisms. Carbonate crusts located along a tidal channel close to a hypersaline tidal lagoon in the Bay of Cádiz Natural Park (Spain) have been studied to determine their formation mechanism. In order to differentiate between the effects of physico-chemical or microbial processes that give rise to beachrock-like concretions, an experimental field study has been performed.

Carbonate crust is found at the bottom of a tidal channel and occurs making up to centimetric-thick consolidated fragments. The petrographic and mineralogic study has been done by means of XRD and SEM study of fragments and polished thin sections, and show that the crust is made of coarse calcite crystals cementing sandy sediments and biogenic debris with minor authigenic pyrite and clay crystals.

The field experimental study has been conducted during a period of a month and a tidal cycle in four different locations along the channel. A series of glass slides, where a carbonate-free sandy substrate was added, were located on the surface of the tidal channel and a posterior mineralogical and textural study was done. SEM images of the slides showed a fast growing (in the order of days) of calcium carbonate crystals, as indicated by EDS and XRD analyses. The precipitates are composed of uniform micron-size calcite crystals and are clearly related to cyanobacterial and exopolymer remains.

The results of the microelectrodes study, made on the marginal sediments of the channel, reveal also an incipient calcification process and show how the photosynthetic activity of biofilms dominated by cyanobacteria and diatoms growing in the sediment surface seems to control the calcite precipitation on the intertidal sediments.

Well cemented older fragments from the inner part of the channel, may have the same origin and therefore have undergone several diagenetic phases, each one producing calcite cements exhibiting evolved textures and where biological remains and smaller calcite crystals are absent. Active currents of a tidal channel can erode, broke and move the calcified marginal sediments and place them in a different chemical environment leading to an evolution in a diagenetic context different of which they were formed. From this experiment, biological processes such as bacterial mat developments may control calcification processes and can be more important in beachrock formation on marsh areas than previously considered as proposed by several previous studies in other coastal environments.

Hematite formation catalyzed by organic matter in banded iron formations

Orberger, B.[1*], Wagner, C.[2], Wirth, R.[3], Derré, C.[2], Quirico, E.[4], Montagnac, G.[5], Noret, A.[1], Jayananda, M.[6], Massault, M.[1] & Rouchon, V[7]
[1]Dept. des Sciences de la Terre, Université Paris Sud XI, CNRS-UMR IDES 8148, Paris, France
([*]beate.orberger@u-psud.fr)
[2]Laboratoire MMM, Université Pierre et Marie Curie-Paris 6, ISTEP, CNRS-UMR 7193, Paris, France
[3]GeoForschungs Zentrum Potsdam (GFZ), Potsdam, Germany
[4]Laboratoire de Planétologie de Grenoble, CNRS-UMR 5109, Université Joseph Fourier, OSUG, Grenoble, France
[5]Laboratoire de Sciences de la Terre, CNRS-UMR 5570, ENS-Lyon, France
[6]Dept. of Geology, Bangalore University, Bangalore, India
[7]IFP, Rueil Malmaison, France

Carbonaceous matter is rarely detected intergrown in Fe-(Mn) oxides and its origin and role in the formation and subsequent transformation of BIFs is little discussed and/or understood. For the first time, carbonaceous matter was detected in hematite spherules hosted in one of the thickest (~ 500 m) mid-Archean (2.9 Ga) banded iron formation from the Dharwar craton in Southern India. The BIF is composed of millimetric to centimetric alternating quartz and iron oxide bands. The mineral paragenesis at the time of deposition is still present as relicts and consisted of quartz, magnetite, Fe-sulphides and Ca-Mg or Fe-Mg-carbonates. The iron oxides evolved from magnetite into martite (hematite), but occur also as hematite spherules in microquartz cavities. Carbonaceous matter of semi-anthracitic maturity and low N/C ratios occurs encapsuled in the quartz grains and hematite spherules, and of lower maturity degree (higher N/C ratios), as wall fillings of the cavities. The carbone isotopic composition ($\delta^{13}C$) of the total CM ranges from -19.98 to -26.15 ‰ and indicates an organic origin, although no distinction is possible between mature and immature organic matter. The fertilizing conditions during the BIF formation were favorable for plankton production, which was later mainly remineralized in the water column. Relict organic matter was incorporated within the magnetite layers and in the adjacent quartz grain, and it was transformed into semi- anthracite during the greenschist facies metamorphism at ~2.5 - 2.6 Ga. Post-metamorphic oxidizing hydrothermal fluids of about 150°C, circulated preferential along permeable zones, martitized most of the magnetite, and dissolved interstitial carbonates and sulphides leaving cavities behind. These isolated or connected cavities compartmentalized the Fe-rich fluids, which supersaturated, precipitated abiotically hematite spherules around the semi-anthracite. Organic matter served as a catalyzer and hematite as a protector against organic matter complete oxidation. Immature organic matter was introduced after the hematite spherule formation either during paleo-or modern weathering.

Biomineralization of iron and calcium: their role in biogeochemical processes of sedimentary sequences in the coastal sector of the Argentine Pampean Plains

Osterrieth, M.
Instituto de Geología de Costas y del Cuaternario, FCEyN – UNMdP, CC 722, Mar del Plata, Argentina
(mosterri@yahoo.com.ar)

The biomineralizations present in every level of the biosphere are the result of the metabolic function of the biota. The goal of this paper is the mineral-chemical characterization of the biomineraizations of iron and calcium in pedosedimentary sequences in the south east sector of the Pampean Plains of the province of Buenos Aires. Work was completed on meso-, micro- and sub-microscopic scales on disturbed and undisturbed samples. Biomineralizations of iron we found in the form of framboidal and polyframboidal pyrite, greigite, mackinawite and iron oxyhydroxides associated with gypsum, barite, calcite and halite, which permit us to define the redoxymorphic conditions in paleoestuary pedosedimentary sequences [1,2]. The biofilms are recurrent, which is a product of the intense microbiological and multifunctional activity. Besides the development of the ability to precipitate minerals, these organisms have also acquired the ability to dissolve or erode minerals; the bioerosion occurs on the surface, in the cracks and through the direct perforation in the interior of the minerals and/or biominerals. This is how the biomineralizations of calcium we found in the bioclastic and calcretized levels, associated with the processes of dissolution and reprecipitation of calcium carbonates and oxalates via biogenic action. The genetic sequence of the calcite was defined via weddellite and whewellite associated with biomineralizing hyphas and bacteria in the soil. The morphology and mineral chemistry would indicate different origins, within the fungi biomineralization of the process, coexisting in the same pedosedimentary levels. Also present were calcified bacteria in the micro and mesopores and the matrix of the peds of calcium and petrocalcium horizons of the alluvial paleosoils. These biomineralizations demonstrate the complex biogeochemistry that occurs in the temperate-wet paleoesturaries of the Pampean Plains. Furthermore they contribute to a greater comprehension of the significant effects of microorganisms on the mineral texture, microstructure and on the biogeochemistry of the surrounding microenvironment and they transfer to present-day and past environments.

[1] Osterrieth, M. (1992) *Actas IV Reunión Arg. de Sedimentología,* **2,** 73-80. [2] Oyarbide, F, Osterrieth, M. & Cabello, M. (2001) *Microbiol. Res.*, **156**, 113-119.

Use of hybrid silica gels containing natural clay colloidal particles for bioweathering kinetic study versus abiotic process

Oulkadi, D., Billard, P., Grybos, M., Mustin, C. & Desobry, S.*
LIMOS (Laboratoire des Interactions Microorganismes-Minéraux-Matière Organique dans les Sols), UMR 7137 CNRS, Université Henri Poincaré, Vandoeuvre-lès-Nancy, France
(*sylvie.desobry@limos.uhp-nancy.fr)

It is well known that silicates dissolution by microorganisms is related to proton, organic acids and other metabolites production [1-4].

In order to precise role of bacteria in dissolution by comparison with the abiotic process and to characterize the mechanisms involved, artificial materials were used in this study. They consisted in natural colloidal clays particles homogeneously dispersed in TEOS-derived silica gels [5].

Montmorillonite and nontronite size-selected particles were the species chosen for bioweathering kinetics by soil bacteria. Cultures of pure strain were performed in batch or in Petri dishes with clays-gels in minimum salt medium and with glucose as sole carbon source.

The interactions of microorganisms with minerals were analyzed by comparison with cultures minerals-deprived and abiotic conditions (HNO_3). For these Fe-rich phyllosilicates, iron dissolution was used as bioweathering indicator. Organic acids profile was analyzed by ionic chromatography and an O-CAS method was performed for siderophore detection.

The results showed a larger iron dissolution under biological conditions than in abiotic conditions for a moderate pH variation down to pH 4,0. The organic acids mainly produced in these conditions were lactate, acetate, citrate, pyruvate, oxalate, and gluconate. They were proposed to play a major role in the bio-dissolution process by complexolyse.

[1] Hiebert, F.K. & Bennett, P.C. (1992) *Science*, **258**, 278-281. [2] Barker, W.W, Welch, S.A. & Banfield, J.F. (1997) in Banfield & Nealson, K.H (eds.) *Rev. Mineral.*, **35**, Mineral. Soc. Am., Washington. 391-428. [3] Bennett, P.C., Rogers, J.R. & Choi, W.J. (2001) *Geomicrobiol. J.*, **18**, 3-19. [3] Rogers, JR. & Bennett, P.C. (2004) *Chem. Geol*., **203**, 91-108. [4] Grybos, M. et al. (2010) *J. Colloid Interf. Sci.*, **343**, 433-438.

Bioweathering of Mg-bearing silicate glasses in presence of heterotrophic bacteria

Rossano, S.[1*], Jean-Soro, L.[1,2], Trcera, N.[3], Combes, R.[1], Tarrida, M.[1], Labanowski, J.[4], Razafitianamaharavo, A.[5] & van Hullebusch, E.[1]

[1]LGE, Université Paris-Est Marne-la-Vallée, Marne-la-Vallée, France ([*]rossano@univ-mlv.fr)

[2]Laboratoire Central des Ponts et Chaussées, Bouguenais, France

[3]Synchrotron Soleil, Gif-sur-Yvette, France

[4]Université de Poitiers, Poitiers, France

[5]Nancy Université-INPL, Vandoeuvre-les-Nancy, France

Although relatively abundant in Earth materials, the effect of Mg in bioalteration processes is not well known. In this study, we investigated the biotic vs abiotic alteration processes of glasses of variable polymerization degree and Mg coordinance [1] (Na_2O-MgO-$2SiO_2$, Na_2O-0.9MgO-0.1FeO-$2SiO_2$, Na_2O-MgO-$3SiO_2$, Na_2O-0.9MgO-0.1FeO-$3SiO_2$, K_2O-MgO-$2SiO_2$, K_2O-MgO-$3SiO_2$).

The synthesis of the silicate glasses were performed in a vertical furnace allowing a fast and reproducible quenching rate and the use of a variable atmosphere (H_2, air or O_2). Glasses were prepared either as sections polished down to 3□m (SEM observations) or as powders of controlled granulometry (kinetic experiments). The specific area of powders was characterized by BET experiment using Kr gas. The samples have been bioweathered by *Pseudomonas aeruginosa* (Psa) under conditions similar to the natural environment (pH 7.8 and 20 °C). Psa was chosen because it is widespread in nature and because of its ability to form biofilm on solid surfaces [2]. Two kinds of experiments were performed. (i) Short term experiments were performed during 14 days without renewal of the growth medium aiming at the monitoring of the kinetic of glasses element leaching (ii) Long term experiments have been performed in order to study the rates of dissolution of these glasses in batch mode in presence and absence of microbial activity. In both cases, Inductively Coupled Plasma Optical Emission Spectroscopy (ICP-OES) has been used to determine aqueous concentrations for the calculation of dissolution rates normalized to the initial specific surface of the studied materials.

As expected the alteration was more intense for disilicate glasses than for trisilicates in biotic and abiotic conditions. Concerning microbial activity, it strongly modified the leaching kinetic and the solubility of the leached elements expected to precipitate with the medium compounds. The leached surface was analysed by Scanning Electron Microscopy-Energy Dispersive Spectrometry, μ-Raman and μ-XANES measurements at the Mg *K*-edge.

[1] Trcera, N. et al. (2009) *Phys. Chem. Miner*., **36**, 241-257.
[2] Aouad, G. et al. (2008) *Sci. Total Environ*., **393**, 385-393.

X-ray powder diffraction analysis of biogenic manganese and iron oxides

Seyama, H.[1*], Watanabe, J.[2], Miyata, N.[3], Tani, Y.[2] & Iwahori, K.[2]

[1]National Institute for Environmental Studies, Ibaraki, Japan ([*]seyamah@nies.go.jp)

[2] University of Shizuoka, Shizuoka, Japan

[3] Akita Prefectural University, Akita, Japan

Various microorganisms such as bacteria and fungi in aquatic environments have the ability to produce minerals (micro-biomineralization). Biomineralization is an important geochemical process to control deposition of elements composing the biominerals. In addition, a number of biominerals produced by microorganisms are fine particles having large reactive surface areas and highly effective scavengers of a variety of metals and molecular species in natural systems. Therefore naturally occurring biominerals play important roles in the geochemical cycling of elements on the earth's surface. In this study, we will report characterization of biogenic manganese and iron oxides by X-ray diffraction (XRD) analysis. X-Ray diffraction patterns of powder samples, deposited on a low background quartz plate, were recorded using a Rigaku ultima+ diffractometer with a Cu X-ray source.

Biogenic manganese nodules (5 - 20 mm) collected from the ground water in the Oppu mine, Aomori, Japan were preserved in water. The wet manganese nodule sample was powdered and examined by XRD. Its XRD pattern showed characteristic diffraction lines (d = 0.98 and 0.49 nm) of phyllomanganate with a 1 nm d-spacing (buserite). After air-drying for 10 days, these two lines of the wet sample disappeared and new diffraction lines (d = 0.72 and 0.36 nm) were observed, suggesting the formation of phyllomanganate with a 0.7 nm d-spacing (birnessite) due to the loss of interlayer water. This transformation of buserite into birnessite was irreversible dehydration.

Biogenic manganese oxides were produced by repeated-batch cultures of Mn(II)-oxidizing microorganisms with dissolved Mn(II). Fresh water epilithic biofilms were collected in the Kikukawa river system, Shizuoka, Japan and used as the initial inocula. Suspended manganese oxide deposits containing biomass, which were accumulated in the reactor for a few hundred days, were analyzed by XRD after separation and drying. Weak broad diffraction lines (d = ~1, ~0.5, 0.25 and 0.14 nm) were recorded in XRD patterns of the manganese oxide samples, indicating the formation of poorly crystallized phyllomanganate (buserite) by the Mn(II)-oxidizing microorganisms.

Biogenic iron oxides were produced by enrichment cultures of Fe(III)-reducing microorganisms with ferrihydrite under anaerobic condition. Sediment containing Fe(III)-reducing microorganisms was taken from Lake Sanaru, Shizuoka, Japan and used as the initial inocula. After cultivation for 3 - 14 days, ferrihydrite was reduced, resulting in the formation of magnetic iron oxides. The detected XRD lines of the biogenic iron oxide samples were broad, but characteristic of spinel group. Their interplanar spacings (d-values) were somewhat smaller than those of magnetite and comparable to those of maghemite (gamma-Fe_2O_3) suggesting the reduction of ferrihydrite to magnetite through maghemite by the Fe(III)-reducing microorganisms.

Role of heterotrophic bacteria on enhanced weathering of metallurgical slags: a chemical and mineralogical study

van Hullebusch, E.[1], Avril, C.[1], Romero Sanchez, S.[1], Combes, R.[1], Borensztajn, S.[3], Gauthier, A.[2], Labanowski, J.[4] & Rossano, S.[1*]

[1]Laboratoire Géomatériaux et Environnement, Université Paris Est, France ([*]Rossano@univ-mlv.fr)

[2]Laboratoire Génie-Civil et géoEnvironnement, Université Lille 1, France

[3]Laboratoire Interface et Systèmes Electrochimiques , UPR 15 CNRS, France

[4]Laboratoire de Chimie et Microbiologie de l'Eau, Université de Poitiers, France

Metallurgical activities generate high amount of industrial wastes bearing heavy metals. In most cases these wastes, partially vitrified during the metallurgical process, are landfilled or recycled. However, in the vicinity of former metallurgical plants sprawling abandoned slag heaps are prone to weathering. The tow studied slags come from a former metallurgical factory (Noyelles-Godault, Northern France) and were generated by the processing of lead and zinc ores, were studied. As lead and zinc ores are often mixed, the production of primary lead leads to the production of some primary zinc and vice versa. Therefore, the slags contain both lead and zinc but in different amounts. Our research uses a slag produced in the smelting of zinc using an imperial smelting furnace, termed the ISF slag, and a slag produced in the smelting of lead using a lead blast furnace, termed the LBF slag. Despite being the by-product of a lead production system, LBF slags (11 wt% ZnO and 3.5 wt% PbO) contain twice the amount of zinc of the ISF slags (7 wt% ZnO and 1 wt% PbO). LBF and ISF slags are granulated heterogeneous wastes. They are mostly composed of an iron–silica–lime glass matrix (80 vol.%), which still contains high quantities of lead and zinc. In order to mimic soil weathering conditions, LBF and ISF slags were submitted to a 6 months batch leaching procedure in bacterial growth medium solutions, in presence of a pure heterotrophic bacterial strain (*Pseudomonas aeruginosa*). This study presents a detailed description of the slag leaching kinetics up to reach equilibrium conditions. ICP-AES and SEM-EDS measurements have been used to monitor the evolution of the water chemistry and the slags (compositions and textures) during the experiments.

The leaching in both sterile and inoculated growth media showed that the microbial activity strongly increases the leaching of the dissolved Fe, Si, Ca, Mg concentrations. This higher release is ascribed to the presence of microbial complexing molecules. In contrast, the dissolved Pb concentration was much lower in the cultivated medium compared to the sterile medium. However, it was shown that most of lead release in the liquid phase was scavenged by the bacterial cell membrane which finally displays higher total lead content in the liquid phase compared to the sterile medium.

The ISF and LBF bioweathered slags samples were microscopically characterized and displayed that microscale mineral structure influences the weathering of specific area. In addition, the leaching experiments were coupled with the Visual-Minteq speciation-solubility modelling and mineralogical study of newly formed products (SEM/EDS and XRD).

Microbial community associated with Late Cenozoic desert varnish in Hungary

Varga, G.[1], Kovács, J.[2]* & Fábián, S.Á.[1]

[1]Dept. of Physical Geography, University of Pécs, Hungary

[2]Dept. of Geology, University of Pécs, Hungary

([*]jones@gamma.ttk.pte.hu)

Desert or rock varnish is a dark patina on stable rock surfaces in arid to semi-arid regions of the world [1]. Such coatings represent a fine mixture of clay minerals and Fe–Mn oxyhydroxides, which form micrometer-thick laminations that parallel the topography of the rock substrate [2]. The microbial diversity associated with desert varnish collected from Lower–Middle-Pleistocene sand in Hungary was investigated using SEM method.

It has often been suggested that the process of varnish formation may be microbially mediated. In the biogenic model, it has been shown that some adventitious Gram-negative bacteria, Gram-positive bacteria, and microcolonial fungi (MCF) that live on the surfaces of rocks can take manganese particles from atmospheric dust and oxidize them.

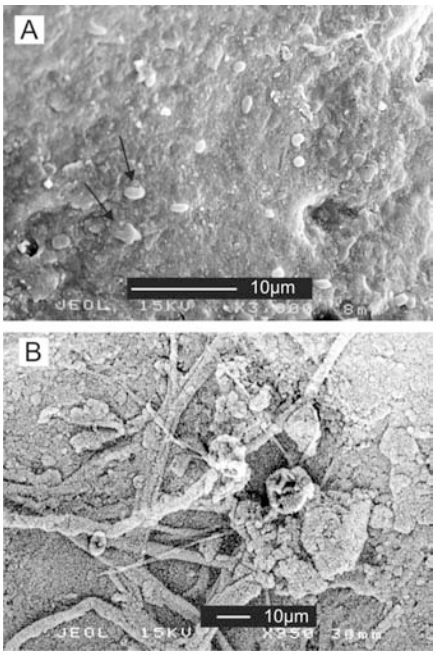

Fig. 1: SEM micrographs showing various morphologies of Mn-enhanced bacterial forms. The cocci "bacteria" in (A), and the hyphae "fungi or MCF" in (B).

Scanning electron micrographs of rock varnishes from Hungary show the surface of varnish to be inhabited by fungi and bacteria (Fig. 1). Perry et al. [3] have shown that MCF mineralize over time and as they degrade their appearance and chemistry becomes indistinguishable from varnish coatings. Large amounts of exopolymeric substances (EPS) are produced by the colonies. MCF become coated with detritus over time. Small wind-blown clay platelets can be oriented by EPSs (polysaccharides) and perhaps the encrustation of these grains and mineral plates provides additional protection from light and heat.

Our investigations have shown that MCF and various bacteria still play an important role in further development of relict desert varnish.

[1] Dorn, R.I. (1998) *Rock Coatings*. Elsevier, Amsterdam. [2] Potter, R.M. & Rossman, G.R. (1977) *Science*, **196**, 1446-1448. [3] Perry, R.S. et al. (2004) *ESA Publications*, **SP-545**, 55-58.

Growth of *Acidithiobacillus ferrooxidans* in the presence of natural limonite

Yan Yunhua, Li Yan, Lu Anhuai* & Wang Changqiu
School of Earth and Space Sciences, Peking University, Beijing, China (*ahlu@pku.edu.cn)

The growth of *Acidithiobacillus ferrooxidans* (*A.f.*) by indirectly accepting photoelectrons from the photocatalysis of natural limonite was studied in a dual-chambered system. X-ray diffraction analysis (XRD) showed the natural limonite sample was mainly composed of goethite and hematite. Both the UV-Vis diffuse reflectance spectra and time-current curve indicated the limonite sample had a good photoelectrochemical response. For evaluating the effects of limonite photocatalysis on *A.f.* growth, three sets of control experiments were conducted, depending on whether the light source was supplied or not and the circuit was open or closed.

The variation of Fe^{2+} concentration was consistent with the growth curve of *A.f.* in different controls (Fig. 1). It was obvious that *A.f.* grew better when external electrons were supplied by the photocatalysis of limonite, which revealed the natural limonite indirectly promoted the growth of *A.f.* The mechanism could be interpreted as follows: natural limonite produced photo-generated electron-hole pairs under visible light, then the photo-generated holes were captured by the electron donor (ascorbic acid in this study), while the separated photo-generated electrons transferred into the cathode chamber to reduce Fe^{3+} to Fe^{2+}. The process achieved the photoelectrochemical regeneration of Fe^{2+}, which provided adequate electron energy for the growth of *A.f.*

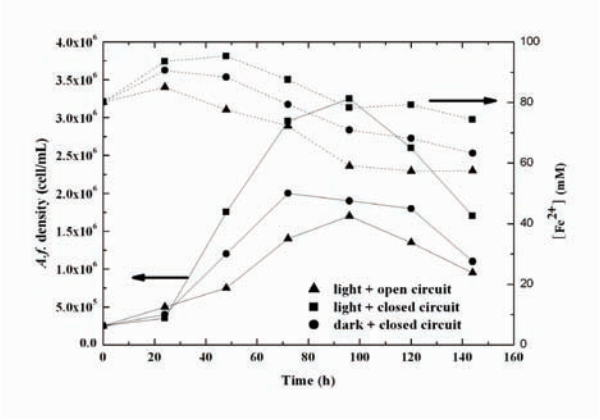

Fig. 1: The growth curves of *A.f.* and variation of ferrous concentration under different conditions (solid dots – ferrous concentration, lines - *A.f.* concentration).

The influence of the photocurrent on the growth of *Alcaligenes faecalis*

Zeng Cuiping, Li Yan, Lu Anhuai* & Wang Changqiu
School of Earth and Space Sciences, Peking University, Beijing, China (*ahlu@pku.edu.cn)

This study focused on the synergistic interaction between a natural semiconducting mineral, rutile and a heterotrophic bacteria, *Alcaligenes faecalis* by applying a potential control on the cathode to simulate the photocurrent of rutile photocatalysis. Scanning electron microscope (SEM), cyclic voltammetry (CV) and electrochemical impedance spectroscopy (EIS) were carried out to characterize the morphology, electrochemical activity and interfacial charge transfer resistance of the bacteria, which adhered to the electrode. The influence of the photocurrent on the growth of *Alcaligenes faecalis* was further identified and analyzed.

The results indicated that both the bacteria and the corresponding metabolites on the electrode were involved in the interfacial electron transport when external electrons were supplied. As influenced by the photocurrent, a significant increase in the biomass on the electrode was observed and the bacterial morphology changed from short rod to long slender rod (Fig. 1). The new redox peaks appearing in the cyclic voltammetry demonstrated that the photocurrent stimulated the electrochemical activity of *Alcaligenes faecalis* and the metabolites on the electrode. This study offered evidence for that the growth of the heterotrophic bacteria might be affected by the photoelectrons generated from the photocatalysis of natural semiconducting minerals.

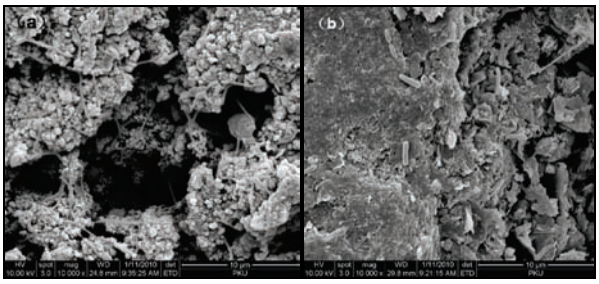

Fig. 1: SEM images of the *Alcaligenes faecalis* on the surface of the electrode with photocurrent(a) and without photocurrent (b).

Mineral stability of bentonites as potential barriers

Šucha, V.[1*], Osacký, M.[2], Striček, I.[3], Madejová, J.[4], Uhlík, P.[1] & Czímerová, A.[4]
[1]Faculty of Sciences, Comenius University, Bratislava, Slovakia ([*]sucha@fns.uniba.sk)
[2]Building Testing and Research Institute, Bratislava, Slovakia
[3]Slovak University of Technology, Bratislava, Slovakia
[4]Inst. of Inorganic Chemistry, Slovak Academy of Sciences, Bratislava, Slovakia

Bentonites are widely tested and used as a barrier material, due to their exceptional properties like plasticity, very low hydraulic conductivity, expandability and cation retardation capacity. All these parameters are directly related to the smectite - bentonite's the most important mineral component. That is why its properties are so important, particularly if a very long-term stability is required (e.g. radioactive waste repositories).

In this study a variety of possible impacts on the smectite structure were tested focusing mostly on the material from two large Slovak bentonite deposits (Jelsovy Potok, Lieskovec). The Jelsovy Potok represents Al-Mg bentonite and the Lieskovec belongs to Fe-bentonite. Several additional well known bentonites were used for some specific comparative tests. Particular attention was focused on the effect of temperature, impact of the acid and the alkaline solutions, and the gamma radiation. A special attention was focused on the bentonite-iron interactions. Iron used in the study was in the form of a 99 % pure Fe^0 powder metal, as well as in the form of pyrite and Fe oxyhydroxide. Pure metal should represent the possible iron construction elements of the repository. The pyrite and the Fe-oxyhydroxide should represent the iron sources from the geological environment of the repository. The batch laboratory experiments, as well as the long-term mock-up test, on the compacted bentonite blocks, were used.

Several laboratory techniques were used to test the reaction products including the XRD, FTIR, UV-VIS, AAS, electron microscopy of the ultrathin sections etc. Basically a large stability of bentonites towards the acidity and the alkalinity at the moderate conditions was confirmed. The smectites lost their original properties only if the extensive treatments in the batch experiments were applied.

No effect of heavy doses (up to 1,5 MGy) of gamma-radiation on the structural and mineralogical parameters (crystal size distribution, specific surface area, cation exchange capacity, layer charge, etc.) of the smectites was identified. Equally no effect was observed during the interactions with the iron in the form of pyrite an/or Fe-oxyhydroxide. Neither batch nor the mock-up tests revealed the changes of the smectites.

Different situation was observed during the interactions of bentonites with a pure iron. The batch experiments showed the significant changes – formation of the magnetite and 7 Å phyllosilicate (berthierine-like), dissolution of the silica phases and deterioration of the smectite structure. Fe-rich smectites were affected more than the others. Mock-up tests with the iron did not show any impact on the bentonites.

Overall we can confirm a long term stability of the bentonites from both deposits at the moderate pH conditions (pH 4-8), resistance towards gamma radiation, and no interaction with the iron. Only potential risk could be linked to the Lieskovec Fe-bentonite extreme exposure to the interactions with pure Fe.

Seeking relations between metal fractions and clay mineralogy in the urban soils of Lisbon city (Portugal)

Patinha, C.[*], Reis, P., Dias, A.C., Terroso, D., Rocha, F. & Ferreira da Silva, E.
Geosciences Dept., Geobiotec Research Unit, University of Aveiro, Portugal ([*]cpatinha@ua.pt)

This study is a part of the working program of a research project untitled "PTDC/CTE-GEX/68523/2006: URBSOIL-LISBON_ Geochemical survey of Lisbon urban soils: a baseline for future human health studies". The aim of this research is to assess the control exert by soil clay mineralogy in the fixation of contaminants in the urban soils of Lisbon city, Portugal. To achieve this aim, the specific bonding forms of heavy metals (Cu, Zn, Pb, Ni and Co) to the clay minerals of several soil phases of Lisbon urban soils will be determined. A total of 51 soil samples were collected over Lisbon city. Figure 1 shows the sample sites and classed post map of the % of clay. Each sample site is labelled from 1 to 51. Thirteen samples were selected based on the percentage of the clay fraction in each sample.

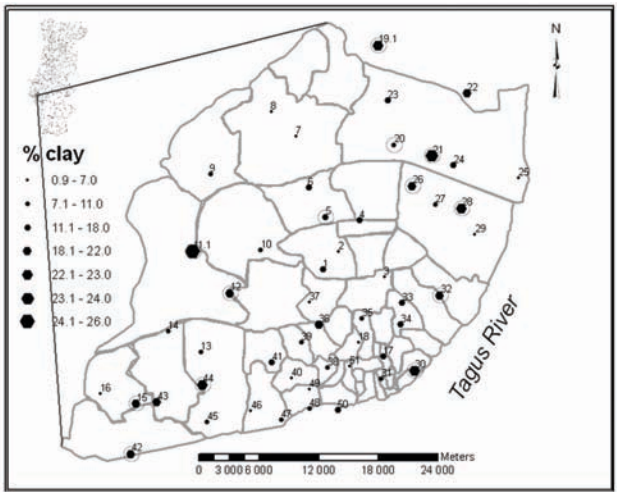

Fig. 1: Soil sampling sites and classed post map of the % of clay fraction; the circles identify the samples used in this study.

The results show that the clay minerals play different roles for the different metals in the soils. High concentrations of Co and Ni occur in samples with high contents in esmectite and low or null contents of illite. The role played by clay minerals in the fixation of Pb, Cu and Zn in the studied soils is still not clear, needing more research. Most of the Pb in these urban soils has an anthropogenic origin being present essentially in the extractable cation soil phase. Like Pb, Cu and Zn have also essentially an anthropogenic origin. The results suggest that organic matter plays an important role in the fixation of Cu while carbonates seem to be effective restraining the mobility of Zn.

Photosensitizer/clay mineral colloids as potential disinfection materials

Bujdák, J.[1,2*], Jurečeková, J.[2] & Bujdáková, H.[2]
[1]Inst. of Inorganic Chemistry, Slovak Academy of Sciences, Bratislava, Slovakia ([*]uachjuro@savba.sk)
[2]Faculty of Natural Sciences, Comenius University in Bratislava, Slovakia

Methylene blue (MB) adsorbed on clay mineral surface forms molecular aggregates [1] and looses its photochemical (photosensitizer) activity [2]. Whereby MB dilute aqueous solutions produce large amounts of singlet oxygen ($^1O_2$), its production was significantly reduced in MB-clay colloids. The photoactivity of MB solution and hybrid MB/clay colloids was measured directly by luminescence measurements at near infrared region and by electron spin resonance spectroscopy (spin-trapping method).

Surprisingly, enhanced antimicrobial effects of MB were achieved in the colloids of montmorillonite. Under visible light irradiation, MB/montmorillonite dispersions prevented the sporulation of *Aspergillus niger* and *Penicillium* sp.

Fig. 1: Reduction of *Aspergilus* sporulation in methylene blue/montmorillonite colloid. No spurulation was observed in the dye/montmorillonite colloid. Sporulation was influenced neither in clay colloid without the dye (middle) nor in MB solution (right).

Moreover, the presence of clay mineral colloidal particles inhibited the growth of yeasts *Candida albicans* and bacteria *Escherichia coli*. *Staphylococcus aureus* proved to be the most susceptible to the MB/clay effects and its growth was significantly reduced even at the lowest dye concentrations ($1.1 \cdot 10^{-6}$ mol dm^{-3}).

The contradiction between enhanced antimicrobial properties and reduced $^1O_2$ formation in MB/clay colloids can be explained in terms of the mechanism of antimicrobial effect. The role of clay particles is most likely to promote the contact between the surface of microorganism cells and MB cations. Clay particles mediate the delivery of dye molecules on the surface or inside the cells. Dye solutions, although producing large amounts of $^1O_2$, were inefficient against microbes, because of a short lifetime of activated oxygen species. The enhanced activity of photosensitizers in clay colloids indicates new perspectives of the implementation of clay minerals in environmental industries for microbial disinfection [2].

[1] Bujdák, J. (2006) *Appl. Clay Sci.*, **34**, 58-73. [2] Bujdák, J. et al. (2009) *Environ. Sci. Technol.*, **43**, 6202-6207.

Effect of particle preparation on intercalation of vermiculite using HDTMA cations

Plachá, D.[*], Barabaszová, K., Valášková, M. & Simha Martynková, G.
Nanotechnology Centre, VSB – Technical University of Ostrava, Czech Republic ([*]daniela.placha@vsb.cz)

Vermiculite has a significant commercial and technological importance. It is 2:1 planar hydrous phyllosilicate that can be modified using intercalation by various organic cations in the interlayer space similarly as smectites. This modification makes possible among others to use an organovermiculite as sorbent for nonpolar organic compounds from polluted water or gas in the environmental technologies. Organophylic vermiculites were prepared by using hexadecyltrimethylammonium and hexadecylpyridinium cations with various organic cation loadings and their effective sorption ability for non polar organic compounds from water and gas phase was studied [1,2].

Vermiculite particles were prepared for intercalation using two procedures: 1) Conventional sedimentation. Particle size fractions < 5 and < 2 μm were obtained (according to Stoke's law) and 2) Jet milling. Three different fractions under different conditions characterized with particle size < 5 μm. Particle size distribution and specific surface area were measured. Morphology of vermiculite particles was studied using SEM and AFM. It was found that morphology of particles after sedimentation did not change. Particles after jet milling had corrugated edges. This characteristic can contribute to the effective accessibility for organic cations between layers. The effectivity and intercalation rate of the synthesized vermiculite/hexadecyltrimethylammonium intercalates were determined based on the content of organic carbon and characteristics from IR spectrometry and XRD analysis. The results confirmed that intercalation rate of vermiculite size fraction prepared using sedimentation procedure was distinct from intercalation rate of those size fraction obtained using sedimentated and jet milling.

Acknowledgements: This work is supported with the Czech Grant Agency, GA ČR 205/09/0352 and GA ČR 205/08/0869.

[1] Plachá, D. et al. (2008) *J. Colloid Inter. Sci.*, **327**, 341-347.
[2] Plachá, D. et al. (2010) *J. Sci. Con. Proceed.*, **2**, 36-41.

Effect of wetting and drying on metal-adsorbed montmorilonites

Németh, T.[1,2*], Dódony, I.[2] & Pekker, P.[3]
[1]Institute for Geochemical Research, Hungarian Academy of Sciences, Budapest, Hungary ([*]ntibi@geochem.hu)
[2]Dept. of Mineralogy, Eötvös Lorand University, Budapest, Hungary
[3]BAY-NANO Institute for Nanotechnology, Miskolc, Hungary

It is well known that several subsequent wetting and drying (WD) causes the "illitization" of potassium saturated montmorillonite, and thus the loss of expansion and adsorption capacity of the original clay mineral. In this work heavy metal adsorbed (Cu, Pb, Zn, Cd, Co) montmorillonites with different layer charge were submitted to WD cycles. The aim of this study is to reveal the effect of WD on the mineralogical properties of montmorillonites by means of X-ray powder diffraction (XRD) and transmission electron microscopy (TEM).

Decrease of the intensity and broadening of 001 peak are general features on the XRD patterns for all metal-adsorbed montmorillonites indicating the decrease of the crystallite thickness with WD cycles (Fig. 1).

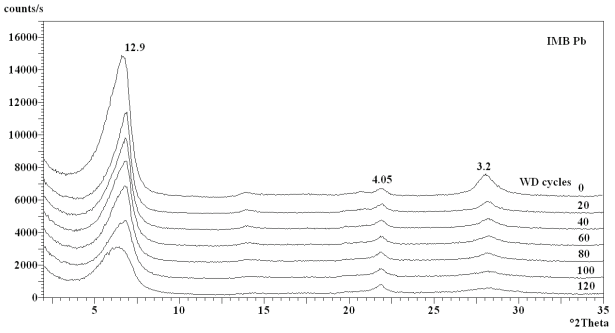

Fig. 1: X-ray patterns of Pb-adsorbed montmorillonite submitted to WD cycles.

TEM analyses revealed the significant decrease of the particle size and the thickness of montmorillonite grains. After 120 WD cycles one or two layer thick crystallites are not rare, and the lateral dimension does not exceed 20 nm. This decomposition due to WD is influenced by the number of WD cycles and by the nature of the metal ion. Pb-montmorillonites are the best affected, because Pb is fixed in the montmorillonite structure and becomes partially non-exchangeable. Chemical composition of montmorillonites also changes with the number of WD cycles, the heavy metal and Si content increase. A possible way of Contrary to K-montmorillonites, metal adsorbed montmorillonites do not lose their expansion capacity during WD. Mineralogical and physico-chemical changes due to WD have relevant application importance, for example in the characterization of the clay liners of waste deposits.

Acknowledgements: The financial support of this study is acknowledged to the Hungarian Research Found (OTKA) in the frame of the project F62760.

Photocatalytic degradation of anionic dye by Zn-substituting layered double hydroxide in water

Morimoto, K.[*], Tamura, K. & Yamada, H.
Photocatalytic Materials Center, National Institute for Materials Science, Tsukuba, Japan ([*]MORIMOTO.Kazuya@nims.go.jp)

Photocatalytic reactions are currently attracting a lot of attention as an efficient and sustainable purification procedure in water contamination. In photocatalytic reactions, degradations of some chemical substances are induced after an approaching or adsorption on the surfaces of photoactive materials. However, major photocatalysts such as TiO_2, ZnO and CdS show little adsorption performance for ions. On the other hand, layered double hydroxide (LDH) has extremely high anion adsorption capacities, and these are well known as anionic clays. Recently LDH has received considerable attention as environmentally-friendly materials because of its harmless composition. It is also noted that LDH has catalytic and photocatalytic properties associated with its solid basicity or modifications with various polyacids. However, the photocatalytic properties of LDH itself have not yet been fully elucidated. There are a few studies [1, 2] of photocatalytic behaviors of LDH for organic substances, but the actual photocatalytic function of raw LDH was not clearly marked in these previous studies. To examine the photocatalytic activity of non-treated LDH itself, this study focused on the photodegradation of anionic dye by synthetic Zn-Al LDH in aqueous solution under light irradiation. It is particularly expected that Zn-substituting LDH has a potentially photocatalytic activity since ZnO exhibits a remarkable photocatalytic ability.

Photocatalytic degradation of anionic dye, sulforhodamine B (SRB), was determined along the following method. SRB aqueous solution of 0.01 mmol/L was mixed with synthesized Zn-Al LDH in polypropylene centrifuge tube. The solid concentration was adjusted at 50 mg/L. The suspension was dispersed in an ultrasonic bath, and then placed in a shaker for 24 hours at room temperature. It was conducted under light shielding. The suspension was added in a quartz cell, and served to light irradiation experiments using a super-high pressure mercury lamp (250 W) or a xenon short-arc lamp (500 W). The absorbance of SRB was monitored with an UV-Vis spectrometer during light irradiation.

The absorption band of SRB was appeared from 450 to 620 nm, and SRB presented absorption peak at 565 nm. The absorbance of SRB with Zn-Al LDH was unchanged after leaving in a dark condition. The result suggests that Zn-Al LDH itself didn't have just a catalytic activity. On the other hand, it was observed that the absorbance of SRB with Zn-Al LDH gradually decreased during light irradiation. The degradation rate of SRB with Zn-Al LDH was reached approximately 50 % in 300 minutes of mercury lamp irradiation. After xenon lamp irradiation, more than 50 % of the initial SRB with Zn-Al LDH was decomposed within 60 minutes. And degradation rate of SRB with Zn-Al LDH was faster than in SRB without LDH during both lamps irradiation. Therefore, Zn-Al LDH certainly has the photocatalytic activity for SRB, and the degradation and decolorization reactions are accelerated without being stabilized under UV irradiation. It was expected that Zn-Al LDH could be utilized as an efficient photocatalyst for harmful organic anions.

[1] Seftel, E.M. et al. (2008) *Micropor. Mesopor. Mater.*, **113**, 296-304. [2] Valente, J.S. et al. (2009) *Appl. Catal. B*, **90**, 330-38.

Clay biopolymers matrix (montmorillonite modified by biofilms) to improve uranium uptake: adsorption isotherms models

Olivelli, M.[1,2], Curutchet, G.[2] & Torres Sanchez, R.M.[1*]
[1]Mineral Resources and Ceramic Technological Center (CETMIC), M.B.Gonnet, Argentina
([*]rosats@cetmic.unlp.edu.ar)
[2]Science and Technology School, The National University of General San Martín, S. Martín, Argentina and CONICET

Uranium is heavy metal, with noticeable toxicity associated with nuclear energy processes and acidic mine drainage. Conventional sorption techniques for heavy metals removal from wastewaters are not useful due to the great volumes treated and the low concentration of pollutants.

Biosorption is an alternative process where different types of biomass allow concentrating heavy metals from diluted solutions. Among the biomass described until now bacteria, algae and fungi were the most used.

Fungal biomass had the advantage of being easily and low cost generated. The main technological drawback in biosorption processes is getting a suitable immobilisation of the biomass to obtain efficient biofilters. A methodology to increase biosorption surface and retain biomass is to generate clay biopolymers matrix. Montmorillonite (MMT) clays have optimal characteristics to be used as innocuous sorbents, with the advantage to be able also to complex all kind of organic as well as inorganic compounds on its surface.

In this study, two fungi: *Aphanocladium* sp., *Acremonium* sp., and the acidophilic bacteria *Acidithiobacillus ferrooxidans* were used as microorganisms growth supported on MMT matrix (in P5 and K9 saline media, respectively). The Uranium adsorption isotherms on all MMT/biofilm studied were fitted to Langmuir, Freundlich, Tempkin, Redlich-Peterson, and Toth models, in order to determine monolayer coverage of adsorbate over homogeneous adsorbent surface; heterogeneous system; indirect adsorbate/adsorbate interactions; homogeneous/heterogeneous system and systems with submonolayer coverage, respectively.

MMT/microorganisms systems were characterized by specific surface area determined by water vapour adsorption (Sw). Also, XRD (analysis of the reflection peak d(001)) was applied on MMT/microorganisms systems and Uranium adsorbed on MMT/microorganisms systems.

Specific surface area (Sw) indicates differences from -5% to +50% for MMT in P5 and K9 saline media, respectively. While the different microorganisms growth on MMT evidenced only around 5-10% difference respect to the Sw value of MMT.

All MMT/microorganisms systems showed higher maximum Uranium adsorption that those obtained from microorganisms or MMT alone.

Adsorption isotherms for MMT+ *Aphanocladium* sp fitted with Freundlich model while MMT+ *Acremonium* sp. and MMT+ *Acidithiobacillus ferrooxidans* fitted with Toth adsorption model, indicating the presence of heterogenous and submonolayer coverage, respectively.

The XRD analysis of the reflection peak d(001) performed on MMT and MMT/micro organisms indicated: intensity decrease and interlayer space collapse with the microorganisms presence respect of that of raw MMT. This behaviour was mainly produced by the different saline growth media or an interlayer water displacement by the microorganism entrance in the interlayer space.

Uranium adsorption shift the MMT reflection peak d(001) around 3.5Å, indicating an Uranium entrance in the interlayer clay space.

Comparison of the physicochemical and catalytic properties of micro- and mesoporous Fe-containing materials in phenol oxidation

Timofeeva, M.N.[*], Mel'gunov, M.S., Malyshev, M.E., Panchenko, V.N. , Chesalov, Yu.A. & Shmakov, A.N.
Boreskov Institute of Catalysis, Novosibirsk, Russia
([*]timofeeva@catalysis.ru)

Nowadays, the increasing water utilization in industrial and agricultural activities leads to the expansion of wastewater containing pollutants, such as phenol, which is of the main chemical pollutants. Fenton type homogeneous catalytic systems ($Fe^{2+}/Fe^{3+}/H_2O_2$) are known active catalysts of PhOH complete oxidation with H_2O_2. Iron-containing solid materials have attracted considerable attention as heterogeneous replacement of homogeneous systems due to their Fenton like behaviour. We review herein major aspects of our research in this field for iron-containing high-surface-area pillared clays (Fe-PILC and Fe,Al-PILC) and iron-containing mesoporous molecular sieves (Fe-MMM and Fe,Al-MMM). Fe-PILCs and Fe,Al-PILCs were prepared from naturally occurring montmorillonites by exchanging interlayer ions to Fe^{3+} and Keggin type cation $[FeAl_{12}O_4(OH)_{24}(H_2O)_{12}]^{7+}$ ($FeAl_{12}^{7+}$), correspondingly [1]. Fe-MMM and Fe,Al-MMM were synthesized via sol-mesophase rout under weak acidic conditions using Fe^{3+} and $FeAl_{12}^{7+}$ as Fe and Al source, correspondingly [2]. XRD, low-temperature N_2 adsorption, IR, DR-UV-vis and DRIFT spectroscopic techniques, were used for characterization of these materials.

Catalyst design principles are summarized and discussed to illustrate the effective development of catalysts that would meet the requirements of the catalytic application (Table 1).

Iron-containing materials have been tested as catalysts for wet phenol oxidation with H_2O_2 at pH = 6.2. The following parameters influencing catalytic properties of these materials and stability to leaching of metal from the solid are considered: *a)* Fe and Al content in the samples; *b)* agglomeration and isolation of iron ions; *c)* pH of the synthesis mixture. It was shown that the increase in Al/Fe ratio, which depends on pH of the synthesis mixture, reduces to the decrease in the formation of oligomeric iron species and favours the increase in reaction rate. The catalytic activity of Fe,Al-containing samples is higher than that of Fe-containing samples. The increase in Al content favours the increase of the strength of basic sites of Fe-containing samples detected with $CDCl_3$ adsorption. The insertion of Al leads to the changes in type and content of OH-groups which facilitate the sorption-desorption processes of reagents. Activity of Fe,Al-MMM(4.4) is higher than that of Fe,Al-PILC(4.4) at 40-50^{0}C due to the decrease of diffusion limitation.

Table 1: Phenol oxidation with H_2O_2 in the presence of Fe-containing samples

	S_{BET}	d_{001}	Fe/Al	Time[A]	Fe leaching
	$m^2 \cdot g^{-1}$		wt/wt	h	wt %
Na-clay	113	15	0.8/5.6	30	-
Fe-PILC	136	16	1.1/5.6	2.0	5.4
Fe,Al-PILC(4.4)	215	18	1.5/9.8	1.5	<0.1
				0[B]	-
Fe-MMM(2.4)	930	38	1.7/0	10.0[C]	0.2
Fe,Al-MMM(2.4)	1518	39	1.1/3.1	3.5[C]	6.7
Fe,Al-MMM(4.4)	1315	38	1.1/6.4	1.0	<0.1
				2.5[B]	<0.1

The reaction condition: PhOH 1 mM, H_2O_2 14 mM, Fe,Al-PILC 1 g·L^{-1}, pH 6.2, 60^{o}C; [A] Time of 100% conversion of PhOH; [B] 40^{0}C; [C] 60^{0}C (pH of the synthesis mixture is shown in parentheses)

[1] Timofeeva, M.N. et al. (2010) *Appl. Catal. B-Environ.*, **95**, 110-119. [2] Timofeeva, M.N. et al. (2009) *Appl. Catal. B-Environ.*, **88**, 127-134.

Technological characterization of peloids maturated with montmorillonite and sepiolite

Aguzzi, C.[1], Cerezo, P.[1], Sanchez, R.[1], Salcedo, I.[1], Machado, J.[2], Alba, M.D.[3] & Viseras, C.[1,4*]
[1]Depto. de Farmacia y Tecnología Farmacéutica, Universidad de Granada, Granada, Spain
[2]Aguas Termales de Graena, Cortes y Graena, Granada, Spain
[3]Instituto de Ciencia de los Materiales, CSIC, Sevilla, Spain
[4]Instituto Andaluz de Ciencias de la Tierra, CSIC-Universidad de Granada, Granada, Spain ([*]cviseras@ugr.es).

Dermatological semisolid preparations such as thermal muds (peloids) require a suitable rheological profile in view of their manipulation and therapeutic efficacy. Indeed, the rheological properties of such preparations affect the entire life of the formulation, since the mixing, filling and packaging until use and "in vivo" behaviour [1]. From a broad point of view, these formulations must be consistent at rest and easily to pour and spread when applied. However, the rheological behaviour of a clay/water system may change over time, leading to unstable and inadequate formulations [2]. These semisolid systems must therefore be considered as complex materials whose stability must be evaluated on the basis of rheological analysis as complete as possible. With these premises, aim of this work was to study the rheological behaviour of thermal muds matured under different conditions as part of a wider research whose focus is on standardizing the development of therapeutic muds.

Peloids of montmorillonite or sepiolite in mineral water from Graena Spa (25 % w/w) were prepared by using a mechanical shaker (Ultraturrax T25, Janke and Kunkel GMBH & Co., G) at 10,000 rpm for 5 minutes. Peloids were maturated in static conditions (without agitation) and with manual agitation every seven days, for a maximum period of three months. At specific times (time zero, one, two and three months), complete rheological analysis of aliquots of the peloids were taken by means of a rotational rheometer (Bohlin ® CS, Bohlin Instrument Division, Metrics Group Ltd., UK). The analysis was conducted using a cone/plate (CP 4 / 20) measurement system at 25°C, applying increasing and decreasing shear rate in the range 70 - 800 s^{-1}.

Flow curves of standardized systems prepared with montmorillonite or sepiolite showed typical profiles of viscoplastic fluids, with yield values depending on the type of clay mineral and conditions of maturation. The samples also showed rheological time-dependent properties, with hysteresis areas. In particular, montmorillonite samples showed thixotropic behaviours, whereas sepiolite systems were anti-thixotropic when prepared, changing to thixotropic as a result of dynamic maturation. It can be concluded that dynamic maturation is preferable to static conditions, in view of the rheological behaviour (thixotropy) of peloids formulated with laminar and fibrous clays.

[1] Lee, CH., Moturi, V. & Lee, Y. (2009) *J. Control. Rel.*, **136**, 88-98. [2] Martin, A. (1993) *Physical pharmacy: physical chemical principles in the pharmaceutical sciences* (4th ed.). Lea & Fedinger, Philadelphia (USA).

Removal of Cu^{2+} from aqueous solutions by using bentonites as adsorbents

Brtáňová, A.[1,2*], Melichová, Z.[3] & Komadel, P.[1]
[1]Institute of Inorganic Chemistry, SAS, Bratislava, Slovakia ([*]anna.brtanova@savba.sk)
[2]Dept. of Inorganic Chemistry, Faculty of Natural Sciences, Comenius University, Bratislava, Slovakia
[3]Dept. of Chemistry, Faculty of Natural Sciences, Matej Bel University, Banská Bystrica, Slovakia

Adsorption of heavy metal cations on clays is of great scientific interest due to their toxicity and harmfulness. Numerous papers on the use of bentonites as adsorbents have been published, e.g. [1]. This work is focused on various effects on the sorption of Cu^{2+} on two commercial bentonite products prepared from two Slovak bentonites Lieskovec (S011) and Jelšový potok (S110).

They were characterized by powder X-ray diffraction (XRD) and infrared spectroscopy (FTIR). XRD analysis revealed smectite to be the major component present in both samples, while the accessory minerals were quartz, mica and feldspar in both samples and kaolinite in S011. FTIR spectra helped to identify montmorillonite compositions (Fig. 1).

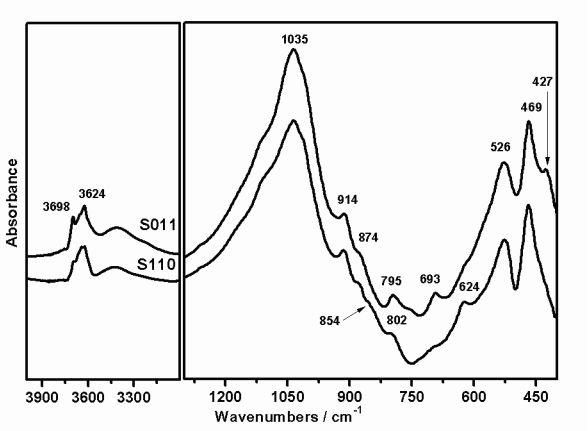

Fig. 1: The IR spectra of S011 and S110.

AlAlOH bending vibrations at 915 cm^{-1} show montmorillonite and the band at 854cm^{-1} (AlMgOH) confirm higher Mg for Al substitution in S110 while the AlFeOH component at 874 cm^{-1} and the absence of an AlMgOH band reflect higher Fe and lower Mg contents in S011, thus causing the lower cation exchange capacity (CEC) of S011. CEC as determined by the Cu-triethylenetetraamine method was 40 mmol/100 g for S011 and 79 mmol/100 g for S110. Specific surface area determined by EGME (Ethylene Glycol Monoethyl Ether) adsorption was 386 m^2/g for S011 and 459 m^2/g for S110.

The adsorption experiments were carried out using the batch technique. The effects of pH, contact time and initial Cu^{2+} concentration were tested. The adsorption was strongly dependent on pH of the medium; the uptake of Cu^{2+} was increasing from pH 2.0 to 7.0. At higher pH values, formation of copper hydroxyl compounds affected the sorption results. The uptake of Cu^{2+} was rapid and it increased with increasing metal concentrations. The sorption percentage decreased with increasing concentration of Cu^{2+}. Langmuir adsorption isotherms were found to fit best the obtained experimental data for both bentonites.

[1] Bhattacharyya, K.G. & Gupta, S.S. (2008) *Adv. Colloid Interface Sci.*, **140,** 114-131.

X-ray diffraction and desorption study of the phases formed upon calcinations synthetic layered double hydroxides

Butenko, E.* & Kapustin, A.
Chemical Technology and Engineering, Azov Sea State Technical University, Mariupol, Ukraine
(*butenkoeo@rambler.ru)

The thermal and kinetic parameters of heating processing of LDHs, providing a complete lack of transfer of sorbed substances into the liquid phase due to the formation spinel structures were determined.

Traditional sorbents can undergo the reverse process of desorption and ion exchange, resulting in a possible penetration of pollutants into the environment. Prevention of this process can be achieved by turning hydroxide sorbent in spinel. The purpose of this work is to define the area of formation spinels, ensuring the absence of pollutants desorption:

$$Mg_xAl_yCr_z(OH)_m \rightarrow xMgO \cdot y/2Al_2O_3 \cdot 2/zCr_2O_3$$

The thermogravimetric analysis allows to trace the processes occurring during heating of hydroxide materials. These experimental curves show the temperature of the beginning of thermal decomposition of the original samples and a deep restructuring of compounds. Thermogravimetric curves represent the mass loss of the sample during heating. These results allow to characterize the thermal stability of the hydroxide ion - exchangers. LDHs were saturated by solution containing of chromate ions. Then LDHs were dried. Samples of the sorbent with adsorbed chromate ions were selected and placed in a muffle at regular intervals, at certain temperatures.

The temperatures above 500°C the irreversible dehydration with the formation of spinel structure take place. This feature of LDHs, are essential for their use as adsorbents of toxic anions. Heat treatment can bond the layers to form insoluble compounds and burying without fear of the reverse process of desorption under the influence of external conditions. That may take place traditional for adsorbents such as activated, but not heat treatment LDHs take place. There is a formation of new oxides phases at the heat treatment.

Table 1: The concentration of chromate ions after desorption

τ\t	150°C	250°C	400°C	600°C	800°C	1000°C
5	$1{,}51\cdot10^{-5}$	$0{,}88\cdot10^{-5}$	$0{,}51\cdot10^{-5}$	$0{,}25\cdot10^{-5}$	$0{,}19\cdot10^{-5}$	**0**
15	$1{,}28\cdot10^{-5}$	$0{,}86\cdot10^{-5}$	$0{,}49\cdot10^{-5}$	$0{,}25\cdot10^{-5}$	$0{,}18\cdot10^{-5}$	**0**
30	$1{,}09\cdot10^{-5}$	$0{,}81\cdot10^{-5}$	$0{,}42\cdot10^{-5}$	$0{,}24\cdot10^{-5}$	$0{,}18\cdot10^{-5}$	**0**
60	$1{,}05\cdot10^{-5}$	$0{,}76\cdot10^{-5}$	$0{,}39\cdot10^{-5}$	$0{,}23\cdot10^{-5}$	**0**	**0**

In the table are shown the area of spinels formation. Analyzing the obtained data, we may say that with increasing of temperature and time of heat treatment the process of desorption is minimized. After 800°C the spinel structures formed and the process of desorption becomes impossible. We may assume that the used anionic sorbent can be subjected to heat treatment at 800°C, and after that the processes of burial of the sorbent is not risky. It was shown that at temperatures above 1000°C and the residence time more than 2 hours the shpinel structures will be disintegrate. The thermal and kinetic parameters of heating processing of LDHs, providing a complete lack of transfer of sorbed substances into the liquid phase due to the formation spinel structures were determined.

New insights on the humic acid uptake by homoionized montmorillonite and CTMA-montmorillonite

Fernández, M. & Torres Sánchez, R.M.*
Mineral Resources and Ceramic Technological Center (CETMIC), M.B.Gonnet, Argentina
(*rosats@cetmic.unlp.edu.ar)

Contaminated water is one of the biggest problems in the world, not just the low percentage (2.5%) of fresh water available, but also the unequal distribution in the world is still worrying. To improve the drinking water quality various procedures can be applied according to the characteristics of water contamination.

Particularly, the organic matter (OM) in water is responsible, among others, of the water turbidity and enables to the formation of stable aggregates with metals, commonly associated with high levels of microorganisms. The OM consists mainly of humic and fulvic acids, difficult to remove with conventional techniques used in flocculation water treatment processes. As an alternative to conventional drinking water treatment and to reduce the humic acid content, this paper presents the use of homoionic montmorillonites and a cetyl trimethyl ammoniun-montmorillonite (CTMA-MMT) to uptake humic acid of water.

The raw montmorillonite used (Rio Negro Province, denoted MMT), contains 84% montmorillonite and 4% quartz and 12% feldspar as impurities. Fractions of MMT sample were homoionized with Na, Ca, K and exchanged with CTMA (1 CEC). Zeta potential determinations of MMT, HA, CTMA-MMT and CTMA-MMT+HA were realized, to identifie their surface charge. The HA adsorption isotherms were determined on all samples in absence and presence of ionic strength (10^{-2}M of the respective chloride cation solutions). The samples without and with HA were characterized by XRD, specific surface determined by water and N_2 adsorption and apparent diameter (Dapp).

The Sw values showed an increase order related to the cations exchanged: CTMA-MMT <K-MMT <MMT <Na-MMT <Ca-MMT. The presence of HA causes a decrease in these values showing the hydrophobic character of the new surface with the HA complex. While the SN_2 values showed almost inverse correlation, confirming the non-polar status of N_2 and its difficulty to enter in the montmorillonite interlayer. The Dapp values follow inverse correlation to that found for Sw on all samples.

Negatives surface charge values were found for both HA and MMT in all pH range studied (from pH 3 to 10). The CTMA exchange originated in the CTMA-MMT sample shifted the surface charge to positive values and the HA adsorption decreases the positive surface charge values found in CTMA-MMT sample.

The XRD spectra showed a shift of the reflection peak d (001) respect to the MMT dependent of the water layer related to the interlayer cation in the following order: Na-MMT < K-MMT< MMT< Ca-MMT< CTMA-MMT. The presence of HA, in all samples causes a slight decrease in the interlayer spacing, possibly originated by the complex formed between the AH with the interlayer cation.

The HA adsorption, in the absence of ionic strength, for all homoionized samples showed a Langmuir type behavior, while the HA adsorption on CTMA-MMT showed a high adsorption at low HA concentrations and max adsorption kept constant with HA concentration increase.

In ionic strength presence (10^{-2} M) only the Ca-MMT sample showed a different behavior than that of Langmuir adsorption.

Formation of brom-pyromorphite as the effect of lead and phosphates sorption on surfactant-modified smectite

Figuła, A. & Bajda, T.*
Dept. of Geology, Geophysics and Environment Protection,
AGH University of Science and Technology, Krakow, Poland
(*bajda@geol.agh.edu.pl)

Sorption on organo-modified clays (e.g. smectites) is one of the methods used for the removal of toxic compounds (inorganic anions and cations, neutral organics) from solutions [1]. The objective of this study was to evaluate potential application of surfactant-modified smectite for sorption of PO_4^{3-} and Pb^{2+}. Precipitation of brom-pyromorphite $Pb_5(PO_4)_3Br$ is observed when Br-surfactant is used for modification.

Sample of smectite was modified with the use of amine hexadecyltrimethylammonium bromide (HDTMA-Br) in the amounts of 2.0 Cation Exchange Capacity (CEC) of the clay. HDTMA is a large organic cation, that in this experiment was used in bilayers form (surfactant concentration was higher than a critical micelle concentration). It changes the charge on natural smectite from negative to positive, but it does not use up all negative sites. Therefore, it is possible to use surfactant-modified smectite as a sorbent for various classes of aqueous solutes.

Modified smectite was reacted with solutions containing 5 to 20 mM/L of Pb or PO_4 ions at initial pH from 2 to 5. In the first step, surfactant-modified smectite was reacted with PO_4 or Pb ions. In the second step, Pb-sorbed samples from the first step were reacted with solution containing PO_4 while PO_4-sorbed samples from the first step were reacted with Pb ions.

Sorption of PO_4 was highest on Pb–surfactant-modified smectite, while sorption of Pb was highest on surfactant-modified smectite with no PO_4 pretreatment. In both cases sorption was highest at pH = 5. Also, formation of brom-pyromorphite $Pb_5(PO_4)_3Br$ was noted in the reaction products, which was identified with the use of X-ray diffraction and SEM. Pyromorphite forms crystals either in the volume of solution (homogeneous crystallization: reaction of aqueous PO_4 with Pb desorbed from ion-exchange positions) or on the surface of a surfactant-modified smectite (heterogeneous crystallization: Pb ions from solution react with PO_4 absorbed and still present on the organic HDTMA bilayers) (Fig. 1).

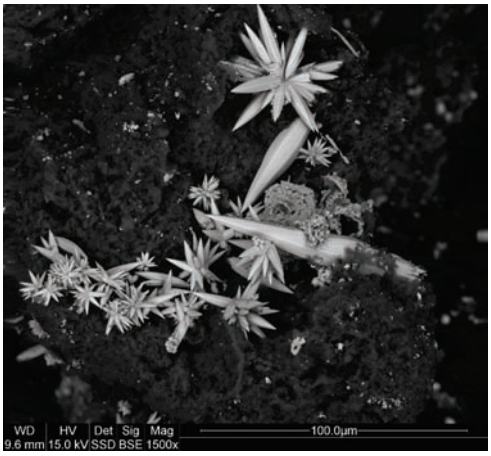

Fig. 1: SEM microphotographs of brom-pyromorphite formed in the reaction of aqueous Pb^{2+} and PO_4–surfactant-modified smectite (heterogeneous crystallization).

Acknowledgements: We gratefully acknowledge support of the MNiSW through grant N N525 461236.

[1] Bowman, R.S. (2003) *Micropor. Mesopor. Mat.*, **61**, 43-56.

Clay characterization in sediment cores from Novigrad sea area, Croatia

Fiket, Ž.[1*], Bermanec, V.[2] & Kniewald, G.[1]
[1]Division for Marine and Environmental Research, Ruđer Bošković Institute, Zagreb, Croatia (*zeljka.fiket@irb.hr)
[2]Institute of Mineralogy and Petrology, Faculty of Science, University of Zagreb, Croatia

The Novigrad sea is a small, semi-closed bay located in the central part of the eastern Adriatic coast, about 20 km north of Zadar (Fig. 1). It is connected to the Adriatic sea in the northwest by Velebit channel and the Karin sea in the southeast. In the surrounding area several bauxite deposits have been exploited for many years with the transshipment port situated in the Novigrad sea. Assessment of the influence of dispersion of bauxite dust by wind and water from dozens of open bauxite pits and waste disposal site of an abandoned alumina plant in the vicinity of the Novigrad sea on the environment is necessary.

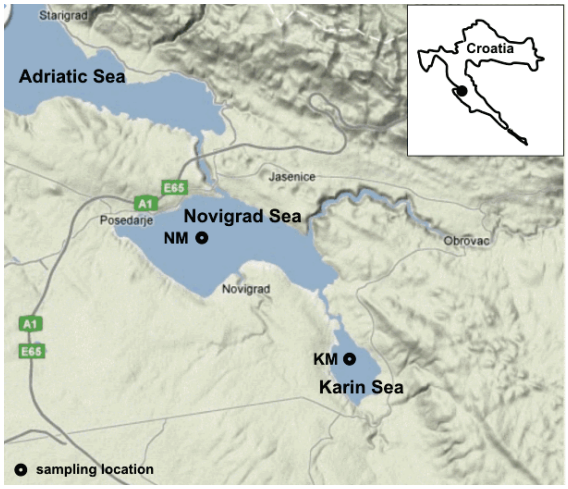

Fig 1: Map of the Novigrad sea area.

Clay minerals have an important role in aquatic systems, as both a carrier and source of pollutants. Therefore, detailed characterization of clay content in recent marine sediments is a prerequisite for an assessment of source and distribution pathways of contaminants. In case of high carbonate content of studied sediments, removal of carbonate phases prior to detailed clay analysis is necessary.

Removal of carbonate minerals from sediments at room temperature was investigated by three different acids, hydrochloric acid (0.5M HCl), acetic acid (4M CH_3COOH) and formic acid (4M HCOOH). Our aim was to evaluate the effects of different chemicals on the properties and structures of present clay minerals in order to develop the optimal procedure for further detailed characterization of clay minerals in marine sediments of the Novigrad sea area.

The analysis was performed on two sediment cores of different carbonate content, one from Novigrad sea **NM** (~19% $CaCO_3$) and one from Karin sea **KM** (~31% $CaCO_3$) (see Figure 1). X-ray diffraction was used to obtain mineralogical composition of the bulk, carbonate free, as well as glycolated and heat-treated (at 450°C and 550°C) samples.

Results indicate that the bulk samples are dominantly made up of carbonates (calcite – Ca and dolomite – D), quartz (Q) and halite (H), while clay minerals (chlorite – Cl, illite/mica – I/M) occur as minor phases. Detailed characterization of clay content of samples after the carbonate removal by different acids will be discussed.

The surface modification of clays for removal of toxic Se-oxyanions

Herzogová, L.[1*], Doušová, B.[1], Lhotka, M.[2], Koloušek, D.[1], Krejčová, S.[1], Jakubíková, B.[1] & Grygar, T.[3]
[1]Dept. of Solid State Chemistry, Institute of Chemical Technology, Prague, Czech Republic
([*]lenka.herzogova@vscht.cz)
[2]Dept. of Inorganic Technology, Institute of Chemical Technology, Prague, Czech Republic
[3]Dept. of Inorganic Chemistry, Academy of Sciences, Řež, Czech Republic

Selenium compounds represent serious threat for environment and human health. They arise mostly anthropogenically and occur in organic or inorganic forms (predominantly as SeO_3^{2-}, SeO_4^{2-}) in natural systems [1]. The adsorption is one of the applicable methods of these toxic substances removal. Clays (kaolines, bentonites) can be classed as technologically important adsorbents. They are characterized by the low value of pH_{ZPC} (zero point of charge) and attract mostly cations. It is possible to increase their anionic affinity for obtaining the efficient and inexpensive adsorbents by a simple chemical Fe, Al, Mn-modification [2-4]. The aims of this work is the preparation of new low-cost adsorbents, their qualitative and quantitative description, the adsorption of toxic SeO_3^{2-}, SeO_4^{2-} oxyanions and the verification of their stability on prepared adsorbents.

Mineralogically pure clays were used for surface changes study – two kaolines from West Bohemia with higher content of kaolinite (> 60 %), bentonite (Riedel de Haën, Germany) containing mostly montmorillonite and standard Ca-rich montmorillonite SAz-2 (Arizona, USA).

The initial concentration of Se in model aqueous solutions was 10 - 40 mg/L and the amount of solid samples ranged from 1 - 10 g/L. Sorption processes ran 72 h. Kinetic experiments were carried out as well.

The sorption capacities of clays increased markedly after the modification (from 0 to 20 mg/g). The kinetic study revealed that 8 h was needed for Se removal. The stability of Se on the solid surface was checked by leaching tests which confirmed the release of it in the range of 0.1 – 2 %.

XRD, XRF, S_{BET}, IR and pH_{ZPC} measurements were used for the characterization of the surface changes during the treatment and next adsorption. The surface of newly prepared adsorbents was amorphous and porous. Specific surfaces (BET) did not change notably after the treatment. The pH_{ZPC} of treated clays moved from 6 to 10.

Acknowledgements: This work was supported by research program MŠMT č. 21/2010 (ČR).

[1] Plant, J.A. et al. (2005) in Holland, H.D. & Turekian, K.K. (eds.) *Treatise Geochem*, **9**, 17-66. [2] Doušová, B. et al. (2006) *J. Colloid Interf. Sci.*, **302**, 424-431. [3] Kuan, W.H. et al. (1998) *Water Res.*, **32**, 915-923. [4] Doušová, B. et al. (2008) *J. Hazard. Mater.*, **165**, 130-140.

Bioleaching effects and binding of Zn on clay, iron and manganese minerals

Jablonovska, K.[*] & Styriakova, I.
Institute of Geotechnics SAS, Kosice, Slovakia
([*]jablonov@saske.sk)

Water reservoir Ruzin I in the region of Eastern Slovakia is a long – therm problem of sediments contaminated with heavy metals (Zn, Cd, Ni, Cu, Hg, As) as a result of mining and metallurgical activities in the basin. The focus of this work is to assess the mobility of Zn in sediment samples in the presence of clay minerals and iron oxides. X-ray diffraction analysis of sediment confirmed presence of quartz, illite, kaolinite and montmorillonite (Philips XPERT, Germany).

Table 1: The amount of Zn, Fe and Mn in the sediment (AAS, Varian AA-30, Australia), BL –bioleaching with Bacillus megaterium

Elements	Before BL (mg/kg)	After BL (mg/kg)	TV (mg/kg)
Zn	427	192	140
Fe	44 600	24 500	-
Mn	1315	1210	-

TV – Target value by MP MŽP SR No. 549/98-2

Sequential extraction method by Tessier was applied to obtain information about chemical binding Zn in the sediment matrix. Adsorption of Zn on Fe and Mn oxides was confirmed in 55% (wt) and in the structure of clay minerals of the so-called residual fraction of Zn was found in 28 % (wt). Heterotrophic bacterial species *Bacillus cereus* and *Bacillus megaterium* presented in the sediments were identified by biochemical BBL identification system. They control mobility of Zn in Fe – Mn oxides and clay minerals. Figure 1 presents kinetics of Zn dissolution in bioleaching medium (containing glucose as carbon source for active heterotrophic bacterial species) and comparing the effect of inoculation of *Bacillus megaterium* and *Bacillus cereus.*

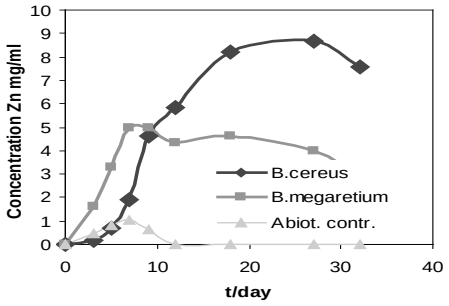

Fig. 1: Kinetics of bioleaching Zn from sediment inoculated with Bacillus cereus and Bacillus megaterium bacterial strains.

Efficiency of discontinous bioleaching Zn from contaminated sediments lasting 6 months with use selected bacterial species were as follows: *Bacillus cereus* 71 % > *Bacillus megaterium* 64 %. These bacterial strains use for their metabolism Fe/Mn oxides and clay minerals therefore they increase the mobility of Zn in aquatic sediments. This principle is usable in prospective *in-situ* remediation of contaminated bottom sediments.

Acknowledgements: This work was supported by the Science and Technology Assistance Agency under the contract No. APVV-0472-07 and No. APVT-51-006304.

Decontamination processes for removal of some pharmaceuticals from aqueous systems

Jakubikova, B.*, Dousova, B., Herzogova, L. & Krejcova, S.
Dept. of Solid State Chemistry, Institute of Chemical Technology in Prague, Czech Republic
(*bohumila.jakubikova@vscht.cz)

Pharmaceuticals have become the inherent part of current modern society. Several pharmaceutical substances have been annually used in amounts up to hundreds of tons in some countries [1]. Therefore the big attention has been paid to the influence of these compounds on the environment. After their application, pharmaceutical substances are excreted in an unchanged form or eventually in the form of water-soluble metabolites [2].

The pharmaceutical industry, hospital facilities, private households and landfills are the next inconsiderable sources of these contaminants [3]. That´s how the pharmaceutical substances reaches the sewage water and regarding they are not completely eliminated in sewage treatment plant [4]. Therefore, they infiltrate into the ground water, surface water and drinking water. They also settle in river sediments and water reservoir sediments.

The aim of this work is to find suitable decontamination processes for the removal of mass-used pharmaceutical substances from aqueous systems. For this purpose, the sorption properties of natural inorganic materials (especially clay minerals) have been used. Sorptions have been carried out from the model solutions of analgetics representatives (e.g. paracetamol, salicylic acid). The sorption capacities of clay minerals have been determined. In the next part of this work, the influence of reaction conditions on the sorption process has been studied.

Acknowledgements: This work was the part of the project P210/10/0938 (Grant Agency of Czech Republic).

[1] Loffler, D. et. al. (2005) *Environ. Sci. Technol*., **39**, 5209-5218. [2] Mutschler, E. & Derendorf, H. (1994) *Drug Action Basic Principles and Therapeutic Aspects*. Medpharm Scinetific Publisher, Stuttgart (Germany). [3] Kummerer, K. (2009) *J. Environ. Manag.*, **90**, 2354-2366. [4] Ternes, T.A. (1998) *Water Res*., **32**, 3245-3260.

Modification of the montmorillonite with the cationic and non-ionic surfactants

Jankovic, L.
Institute of Inorganic Chemistry SAS, Bratislava, Slovakia
(Lubos.Jankovic@savba.sk)

Many industries give rise to dye-bearing effluents in their production processes. Textile industries, particularly, are major consumers of water and release a fair amount of color in their effluents. It follows that dyes need to be removed before the effluents are discharged into rivers. However, this has always been a major problem because of the difficulty of treating such wastewaters by conventional methods. Biological procedures, although widely utilized in the removal of color, are very inefficient because of the low biodegradability of dyes. A variety of other methods, including coagulation, chemical oxidation, photocatalysis, and electrochemical and adsorption techniques [1], has been examined.

Adsorption techniques have been widely applied to the treatment of industrial wastewater containing dyes, heavy metals, and other inorganic and organic impurities. In some cases, it is possible to recover the adsorbed dye through desorption and to reuse the large amounts of water employed by textile industries. The adsorption phenomenon has been known since the 17th century when it was discovered that porous materials have the property of adsorbing gases and, subsequently, the same phenomenon was observed for solutions. Adsorption has been found to be one of the most efficient physicochemical processes, superior to many other techniques for water reuse in terms of the simplicity of operation. If the adsorption system is designed correctly, it will produce a treated effluent of high quality. Activated carbon has been widely used for this purpose because of its high adsorption capacity. However, its high cost sometimes tends to limit its use. Several nonconventional, low-cost adsorbents have also been tried for dye removal.

The present work is aimed to study the adsorption capacity and mechanism of removal of industrial anionic textile dye Acid Red 88 by organobentonite. The organoclay adsorbent used was prepared by modification of commercial Nanocore montmorillonite with octadecyl ammonium bromide (ODTMA) and compared with materials prepared with the non-ionic surfactants [2] containing the same hydrophobic C_{18}- end-chain and various repetitive units of hydrophilic poly(ethylene oxide) (PEO) segments.

The layer spacing of the ODTMA- and $C_{18}PEO_n$ - smectite composite was well preserved during water washings, indicating stability of cationic organoclay and higher molecular weight non-ionic surfactant molecules in the interlayer galleries. The non-ionic surfactant treatment preserved >90% of the CEC of the smectite while ODTMA-clay lost almost all cation exchange capacity. The surfactant-montmorillonite composites effectively removed aromatic textile azo dye from water solution while untreated smectite did not adsorb these molecules. The enhanced adsorption of the aromatic compounds is attributed to the aliphatic segments (C_{18}) of the five surfactants, however ODTMA-montmorillonite showed highest sorption capacity for naphthalene based textile dye AR88.

[1] Deng, Y. et al. (2006) *Coll. Polym. Sci.*, **284**, 347-356. [2] Guegan, R. et al. (2010) *Clays Clay Miner.*, **57**, 502-509.

Geopolymers: new products for sustainability of the environment

Khoury, H.[1*], Aldabsheh, I.[1], Slaty, F.[1], Esaifan, M.[2], Rahier, H.[3], Wastiels, J.[2] & Hourani, M.K.[4]
[1]Dept. of Geology, University of Jordan, Amman, Jordan ([*]khouryhn@ju.edu.jo)
[2]Dept. of Mechanics of Materials and Constructions, Vrije Universiteit Brussel, Brussels, Belgium
[3]Dept. of Physical Chemistry and Polymer Science, Vrije Universiteit Brussels, Brussels, Belgium
[4]Dept. of Chemistry, University of Jordan, Amman, Jordan

Geopolymerization is the process of polymerizing minerals with high silica and alumina at low temperature by the use of alkali solutions. Geopolymers could be a substitute for Portland cement and for advanced composite and ceramic applications. The geopolymer technology would eliminate the need for energy requirement as they may be cured at ambient temperature.

Current research at the University of Jordan concentrates on developing building products (geopolymers) through geopolymerization. The goal is to produce low cost construction materials for green housing. The produced construction materials are characterized by high strength, high heat resistance, low production cost, low energy consumption, and low CO_2 emissions.

The results have confirmed that natural kaolinite satisfy the criteria to be used as a precursor for the production of high quality inexpensive, stable materials. Geopolymeric products gave a high unconfined compressive strength values up to 52 N/ mm^2 for dry test. This value has been increased to 57 N/ mm^2 by the immersion of the geopolymerzed products in 10% solution of triethylene glycol.

The addition of rock wool gave the maximum unconfined compressive strength up to 90 N/ mm^2 after heating to 500°C for one day. The addition of zeolitic tuff as a filler has increased the adsorption capacity of the polymerized products towards heavy metals. This result enables the use of geopolymers in waste water treatment plants.

Acknowledgements: This research is supported by the University of Jordan and the Flemish (Belgium) Vlaamse Interuniversitaire Raad (VLIR).

Environmental impacts associated with a landfill in the municipality of Zakynthos, Greece

Koutsopoulou, E.[*], Tsolis-Katagas, P. & Papoulis, D.
Dept. of Geology, Section of Earth Materials, University of Patras, Greece ([*]ekoutsop@upatras.gr)

Landfills are widely used as a disposal method for municipal solid waste in most European countries. However, landfills if not properly managed, may pose a serious threat to the environment due to leachate run-off and contaminant transport in the surrounding environment. Landfill leachates can contaminate groundwater and surface water [1]. The mineralogy of the clay material used in the landfill liners controls the mobility of contaminants therefore, clay mineralogy is important in order to minimize migration of pollutants in the environment.

To evaluate the environmental risks associated with a landfill in the municipality of Zakynthos, Western Greece, samples were collected from the material used in the landfill and from sediments from a stream system, in the vicinity of the waste disposal site. Surface and groundwater samples were collected and analysed to determine some geochemical parameters usually considered to be indicators of pollution from solid waste disposal. The mineralogical composition of all samples was determined by XRD and revealed the presence of calcite, quartz, albite, smectite, chlorite, illite and mixed-layer chlorite-smectite. Trace element analyses showed that the abundance in Cu and Zn is higher in the stream sediments compared to the uncontaminated samples and since stream sediments are in contact with run-off waters from the landfill this could be an indication of contamination from the landfill. According to drinking water standards, the concentrations of all trace elements in the studied waters were below the maximum contaminant level values given by European Council Directive [2] and WHO [3]. Finally, the concentrations of Cl^-, SO_4^{2-}, NO_3^- and NO_2^- in the water samples exceeded the average permissible concentrations and are considered as human induced contamination from the landfill.

Acknowledgements: This research was funded by the University of Patras through the K. Karatheodoris basic research funding scheme.

[1] Kjeldsen, P. et al. (1993) in Cossu, R., Christensen, H.T. & Stegmann, R. (eds) *Proceedings Sardinia 93, Fourth International Landfill Symposium*. Sardinia, Italy, 1519-1531. [2] European Council Directive 80/778/EEC concerning Drinking Water Quality of 15/7/1980. [3] WHO, World Health Organization (2003) Guidelines for drinking-water quality, 2nd ed., **2**, *Health criteria and other supporting information*, WHO/SDE/WSH/03, 04/03, Geneva.

ZnS particles deposited on montmorillonite and their photocatalytic efficiency for CO_2 reduction

Kozák, O.* & Praus, P.
Dept. of Analytical Chemistry and Material Testing, VŠB-Technical University of Ostrava, Ostrava, Czech Republic
(*ondrej.kozak@vsb.cz)

Semiconductors such as metal sulphides and metal oxides appear to be very promising materials for photocatalysis due to rapid generation of electron–hole pairs by photoexcitation and highly negative reduction potentials of the excited electrons. CO_2 is a well know greenhouse gas. To convert it by force, a severe condition of high pressure and high temperature is required. The reduction of CO_2 using photocatalysts is one of the most promising methods because CO_2 can be reduced to utilizable compounds (e.g., methanol, ethanol, methane, hydrogen) by irradiating with UV light at room temperatures and low pressure [1,2].

The ZnS nanoparticles were deposited on montmorillonite (MMT) in the presence of cetyltrimethylammonium (CTA). UV spectrometry and transmission electron microscopy proved the formation of nanoparticles with the diameter ranging from 3 nm to 5 nm. Selected area electron diffraction confirmed the existence of romboedric ZnS. Photoluminiscence spectra exhibited a strong emission band between 300 nm and 600 nm, which was assigned to transitions due to sulphur vacancies in ZnS. The prepared ZnS-montmorillonite (ZnS-MMT) nanocomposite was used for the photocatalytic reduction of CO_2 providing considerably high efficiency which exceeded the results of commercial TiO_2 Degussa P25 5-6 times. Methane, methanol, carbon monoxide and hydrogen were the main reduction products of the reduction. The stability of ZnS against oxidation was proved by the determination of sulphate by capillary isotachophoresis.

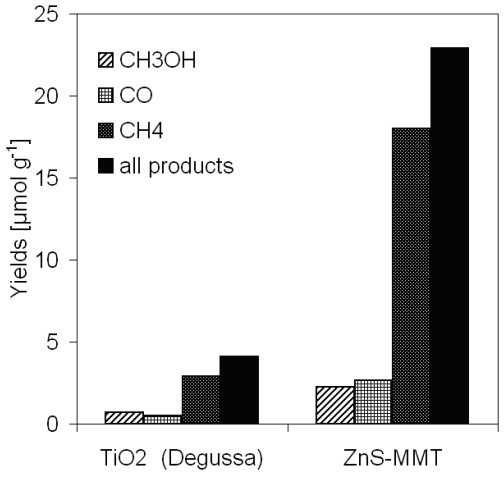

Fig. 1: The comparison of product yields per gram of the photocatalyst.

[1] Yoneyama, H. (1997) *Catal. Today*, **39**, 169-175. [2] Inoue, H. et al. (1995) *J. Photoch. Photobio. A*, **86**, 191-196.

Effect of clay content on As, Se-adsorption in soils

Krejcova, S.*, Dousova, B., Herzogova, L. & Jakubikova, B.
Institute of Chemical Technology, Prague, Czech Republic
(*krejcova.s@quick.cz)

The aim of this work is the study of soil adsorption properties depending on the portion and characteristics of clay fraction. Soil samples from protected area Cesky Kras and Labe river basin (Middle Bohemia, Czech Republic) used in this research, where the elevated concentration of As and Se have been observed. The samples were dried at laboratory temperature, grinded, fractioned and digested in the microwave mineralization device MWS-2 Berghoff. The amount of As and Se in mineralised samples was assessed by HG AAS. The content and type of clay mineral presented in the soil samples were determined by X-ray diffraction and subsequently, the sorption capacity of soils and the stability of adsorbed As and Se under different conditions (pH, Eh) were investigated [1]. pH_{H2O}, pH_{KCl} [2] and pH_{ZPC} [3] were also measured.

Table 1: Concentration of arsenic and selenium in investigated soil samples; A1-A3 – Cesky Kras protected area, B1-B3 – Labe river basin

	c [mg/kg]		pH	
	As	Se	pH(H_2O)	pH(KCl)
A1		2.7	6.5	6.7
A2		2.1	7.2	6.9
A3		14.4	7.0	6.7
B1	25.1		7.5	7.1
B2	35.3		7.5	7.4
B3	26.5		7.2	7.1

The results in Table 1 show elevated As/Se concentration in all investigated samples. The presence of clay and hydrated oxides and/or Fe-oxyhydroxides influenced sorption properties of soils.

Acknowledgements: This work was the part of the project P210/10/0938 (Grant Agency of Czech Republic).

[1] Goldberg, S. et al. (2009) *Vadose Zone J.*, **7**, 1231-1238. [2] Thunjai, T. et al. (2001) *J. World Aquacult. Soc.*, **32,** 142-152. [3] Fiol, N. & Villaescua, I. (2009) *Environ. Chem. Lett.*, **7,** 79-84.

Clay minerals and landslides on the slopes of Medvednica Mt. in Zagreb city area (Croatia)

Miklin, Ž.[1], Hećimović, I.[1], Tibljaš, D.[2] & Grizelj, A.[1*]
[1]Croatian Geological Survey, Zagreb, Croatia
([*]anita.grizelj@hgi-cgs.hr)
[2]Faculty of Science, University of Zagreb, Croatia

The landslides problem is pronounced on the slopes of Medvednica Mt. in Zagreb city area. Therefore, in 2005-2007, Zagreb city government engaged Croatian Geological Survey to make detailed engineering geological map M 1:5.000 of this area.

The landslides problem occurrs in the Miocene and the Pleistocene deposits, so those sediments were the main object of investigation. Litological composition of the Miocene deposits varies from marls, limestones, silts, sands and sandstone to rarely represented coarser-grained sediments such as conglomerates and breccias. The Pleistocene sediments which discontinuously cover the older deposits consist of poorly sorted clays, silts, sands and gravels.

The aim of this study was to determine relationship between clay mineralogy and occurence of landslides. Apart from standard engineering-geological investigations (SPP tests, pocket penetrometar, wane shire tests, liquid limit and shrinkage limit, grain size distribution, uniaxial compressive strength test), mineralogical investigations of sediments (XRD, DTA, SEM and chemical analysis) were included.

It was found that the largest number of landslides is related with Pontian silty-marl deposits (7.1-5.6 Ma) and Pleistocene silty-clay deposits (1.8 Ma – 10.000 years). These deposits contain continuous layers with clay minerals having high to very high and extremely high plasticity. In the Pontian sediments the most common clay minerals are smectite and illite / muscovite, and in some samples small quantities kaolinite and chlorite appear [1] [2]. Vermiculite and illite / muscovite are the most common clay minerals in the Pleistocene deposits. Kaolinite is present in almost all Pleistocene samples [1]. Smectite occurs in very small quantities only in certain samples, while chlorite is present mainly in the sandy and the silty fraction of these deposits.

In the wider Zagreb city area landslides are activated mainly during the first spring months, which is associated with content of water in soil, high groundwater levels and increased yield sources. It is known that increasing the amount of water in soil leads to swelling of clay minerals such as vermiculite and smectite. The presence of swelling clay minerals in the Pontian and the Pleistocene depositescausee cause the instability of slopes in the wider Zagreb city area. Differences in levels of slope instability are related to the different amount of expandable clay minerals in sediments and differences in water content in soil that directly influence the behavior of expandable clay minerals. Other factors which have important influence on instability of slopes are tectonics, shear strength, increase of the incline slope and antropogenic influence.

[1] Tibljaš, D. & Prohić, E. (2007) unpublished data. [2] Grizelj, A. (2008) *PhD thesis*, University of Zagreb, Croatia.

Sorption of cadmium (II) by the natural bentonite and magnetic clay composite

Orolínová, Z.[*] & Mockovčiaková, A.
Institute of Geotechnics SAS, Kosice, Slovakia
([*]orolinova@saske.sk)

The objective of this work is to compare the removal of cadmium (II) by the natural bentonite and composite, prepared by magnetic modification of the clay. The composite material was prepared by the method of precipitation from the solution of ferrous and ferric salts (Fe^{2+}/Fe^{3+} = 0.5), where the bentonite was added prior to the reaction. The weight ratio of bentonite to iron oxides was 5 to 1. The structural and surface study realized by XRD method, FE-TEM and low nitrogen adsorption method showed that the surface properties of the composite (Table 1) were affected by the precipitation of maghemite and goethite in agglomerated form.

Table 1: Surface parameters of the investigated samples obtained from the low temperature nitrogen adsorption method (S_{BET} – specific surface area, V_a – total pore volume, V_{micro} – volume of micropores, S_t – external surface area)

Sample	S_{BET} [$m^2 g^{-1}$]	V_a [$cm^3 g^{-1}$] STP	V_{micro} [$cm^3 g^{-1}$] STP	S_t [$m^2 g^{-1}$]
bentonite	39.44	0.096	0.006	25.43
composite	90.68	0.187	0.002	84.23

The sorption properties were examined under different conditions such as pH of the model solutions, contact time and initial metal ion concentration. The adsorption of cadmium (II) was dependent on the pH of the solution as well as the concentration of ions. The optimal pH for removal of cadmium (II) was found equal 5. The batch type experiments with the natural bentonite and composite material were first conducting using metal ion solutions ranging from 10 to 700 mg L^{-1}. Maximum adsorption capacities (61.35 and 63.29 mg g^{-1} for the bentonite and composite, respectively) were calculated using linearized Langmuir isotherm. Different adsorption rates observed in the low initial metal ion concentrations indicated the further study of adsorption at lower ranges. The highest efficiency of the composite material (more than 98 %) was observed in the range from 1 to 10 mg L^{-1}, Fig. 1.

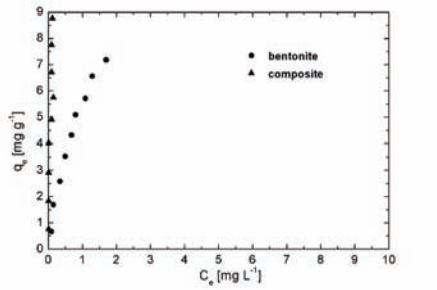

Fig. 1: Sorption of Cd(II) ions on the natural bentonite and composite material in the low initial metal ion concentration range 1 – 10 mg L^{-1}, sorbents dose 1 g L^{-1}, initial pH 5, contact time 24 hours.

Removal of heavy metals at low concentrations from aqueous environment is generally difficult, but the studied composite material showed very good sorption ability especially in these conditions. Therefore it seems to be convenient to use it in desposal of metals from aqueous solution, where their concentration is very low, but still harmful, as well as for the final purification of pre-treated waste waters.

Acknowledgements: The authors are thankful for financial support of VEGA grant No. 0119/09 and APVV project No. 0728-07.

Aquocomplex structure in the interlayer space of swelling high-charged micas

Pavón, E.[1*], Alba, M.D.[1], Castro, M.A.[1], Cota, A.[2], Naranjo, M.[1], Orta, M.M.[1] & Pazos, M.C.[1]
[1]Instituto Ciencia de los Materiales de Sevilla, CSIC-Universidad de Sevilla, Spain ([*]epavon@us.es)
[2]Laboratorio de Rayos-X. CITIUS, Universidad de Sevilla, Seville, Spain

The structure of the interlayer region of swelling high-charged micas is one of the fundamental problems of clay science. The mobility of the cations is important for describing chemical reactions in the environment as well as for estimating the environmental behaviour of metal ions. However, the chemical species of metal cations at solid-water interface in the interlayer space of swelling high-charged micas is still not clearly understood.

It is known that cation sorption is governed by cation size and charge, but the location of structural charge within a clay layer and the existence of hydrophobic patches on its surface provide important modulations. On one hand, larger the interlayer cation, greater the influence of clay mineral structure and hydrophobicity on the configurations of adsorbed water molecules. On the other hand, larger hydrated radius means that the cationic center of charge is farther from the clay surface so the clay-cation electrostatic interaction is weaker.

The aim of this research was the systematic study of hydrated swelling high-charged M-Mica-n,-where n represents the layer charge equal to n=2, 3, 4 and M is the interlayer cation, ($M=Na^{+}$, Li^{+}, Mg^{+2}, Al^{+3})- using Thermal Analysis (ATD/TG), X-ray Diffraction and Solid State NMR.

Na-Micas-n (n=2,3,4) prepared as reported by our research group were used as starting materials.[1] M-Micas-n were prepared by cation-exchange reaction, in accordance with the method described by Powell et al. [2]

The results obtained with TG measurements revealed that the cation hydration state did not only depend on the cation nature, as expected in solutions, but did on the Mica layer charge. Hence, an interaction between interlayer cation and the basal plane of the tetrahedral sheet of Mica could be infered. It was confirmed by ^{29}Si MAS NMR and the variation of the 060 reflection. Therefore, it can be concluded that the nature of the cations and Mica determine the equilibrium between inner-sphere and outer-sphere complex formation.

[1] Alba, M.D. et al. (2006) *Chem. Mater*., **18**, 2867-2872. [2] Powell, H.D. et al. (1998) *J.Phys.Chem.B*, **102**, 10899-10905.

Vertical and horizontal distribution of ^{137}Cs in Pest County, Hungary

Szabó, K.Zs.[1*], Udvardi, B.[1], Horváth, Á.[2], Bakacsi, Zs.[3], Szabó, J.[3], Pásztor, L.[3] & Szabó, Cs.[1]
[1]Litosphere Fluid Research Lab, Eötvös University, Budapest, Hungary ([*]sz_k_zs@yahoo.de)
[2]Dept. of Atomic Physics, Eötvös University, Budapest, Hungary
[3]GIS Lab, Research Institute for Soil Science and Agricultural Chemistry of the Hungarian Academy of Sciences, Budapest, Hungary

This paper presents the results of measurements of ^{137}Cs in soils which were sampled in Pest County, Hungary. The studied soil samples of 45 soil monoliths from TIM (Soil Information and Monitoring System) were collected in 1992. The ^{137}Cs content has been determined for all locations by gamma spectroscopy and found that only the upper layer of soil (0-30 cm) contains ^{137}Cs from the all layers (0-30, 30-60, 60-90, 90-120, 120-150 cm). Cesium-137 concentration in these layers ranged 0.7 ± 0.5 Bq/kg to 41.3 ±1.5 Bq/kg. These activity values were illustrated on a map that can be consider as the first detailed cesium map in Hungary. We found salient value (31.7 Bq/kg and 41.3 Bq/kg) compared to the average activity (5.8 Bq/kg) at two points of the sampling sites. One of them is at Gödöllő Hills and the other is at the western foot of Buda Mountain. It is known that there is a strong relationship between ^{137}Cs concentration and clay, as well as organic matter content of the soils [1,2]. This relationship was studied in details in soil samples from drilling in brown forest soil from the same location as the highest activity concentration (41 Bq/kg) occurred. Aggregate size fractions were separated using dry sieving technique and their clay mineral contents were determined by differential thermal analysis and XRD techniques. According to the results of these analyses, an amount of organic matter less than 40% and prevailing illite and kaolinite were determined in the sample. The amount of clay minerals was found closely proportional to cesium-137 activity in the aggregate fractions, which indicates the cesium fixation to these clay minerals. For analyzing the vertical distribution and migration of cesium, a soil profile at the same locality was studied. It was found that it is present in the upper 20 cm of the soil, indicating that penetration of cesium into the soil is very slow process here. 23 years after the Chernobyl accident most of the cesium activity is still in the top 16 cm, and the 78% is located in the top 3 cm. This corresponds to results of other studies [3,4] and suggests slower cesium migration than predicted earlier [5]. This prediction was applied in the framework of convective-diffusional model using time independent diffusion coefficient and convection velocity. Our results demonstrated for this site that either the migration speed is very low, or it is time dependent and slowed down during the last 10 years.

[1] Tamura, T. & Jacobs, D.G. (1960) *Health Phys.*, **2**, 391-398. [2] Valcke, E. & Cremers, A. (1994) *Sci. Total Environ.*, **157**, 275-283. [3] Almgren, S. & Isaksson, M. (2006) *J. Environ. Radioactv.*, **91**, 90-102. [4] Persson, H. (2008) *Examensarbete I Markvetenskap*, Uppsala. [5] Szerbin, P. et al. (1999) *Sci. Total Environ.*, **227**, 215-227.

Hungarian adobe as source of thoron

Szabó, Zs.[1*], Szabó, Cs.[1] & Horváth, Á.[2]
[1]Lithosphere Fluid Research Lab, Dept. of Petrology and Geochemistry, Eötvös University, Budapest, Hungary ([*]zsszabo86@gmail.com)
[2]Dept. of Atomic Physics, Eötvös University, Budapest, Hungary

Thorium (^{232}Th) is a naturally occurring radioactive element and thoron (^{220}Rn) isotope is the only one gaseous daughter of its decay chain. Thorium is estimated to be about three times higher abundance than uranium (^{235}U, ^{238}U) in natural environment including soils [1]. Thorium can also be quantifiable trace element like thoron source in clayey soils, which are the major raw materials of adobe houses beside straw.

Thoron, similar to radon (^{222}Rn) [2] in uranium (^{238}U) decay chain, has a high capability to enter the air of rooms from the walls of adobe houses, which makes possible to accumulate in indoor air, as well as its solid decay products as aerosols. Thoron has an effect in dose increasing which is underestimated in many cases. This is the reason why has not been done extended survey on it yet in Hungary.

The average of total annual effective dose from thoron is only 0.1 mSv [1], however, several studies [3-7] showed much higher values in dwellings made mostly by soil or soil bricks. Among these examples, annual effective dose goes up to about 5 mSv average [4]. It indicates that adobe houses in Hungary can be endangered by thoron more than other type of buildings, although they have several propitious features in many respects.

The main aim of this work is to obtain knowledge on possible risk from thoron and its source. Therefore, three distinct areas of Hungary have been selected to study. All of them have local soils suitable, experience and tradition for building adobe houses and a probability to be endangered by thoron. These areas are Sajó and Hernád Rivers' Valleys (NE-Hungary), where redeposited loess is typical, E-Mecsek Mts. (S-Hungary) and Békés County (SE-Hungary), where loess and alluvial sediments of Körös and Maros Rivers are prevailing, respectively [8].

Present work is focusing on Békés County where six settlements (Gyomaendrőd, Gyula, Kondoros, Sarkad, Újiráz, Vésztő) have been selected for detailed investigation based on geological and geographical differences and previous surveys, too. Experimental one-day indoor radon and thoron concentration measurement by RAD7 radon detector refers that fairly high thoron concentrations (even more than 400 Bq/m^3) can be detected in adobe houses of this area.

Soil samples of sought out adobe making places at selected six settlements have been collected, as well as abode samples at least from one dwelling of each sites. The origins of raw materials of adobe samples presumably are the mentioned adobe making places. Detailed study of the samples was done in laboratory, which refers that adobe can actually be a potential source of thoron.

[1] UNSCEAR (United Nations Scientific Committee on the Effects of Atomic Radiation) (2000) *Report*. New York, NY: United Nations. [2] Minda, M. et al. (2009) *Environ. Geol.*, **57**, 601-609. [3] Németh, C. et al. (2005) *Int. Congr. Series*, **1276**, 283-284. [4] Sciocchetti, G. et al. (1992) *Radiat. Prot. Dosim.*, **45**, 509-514. [5] Shang, B. et al. (2005) *Radiat. Environ. Biophys.*, **44**, 193-199. [6] Yamada, Y. et al. (2005) *Int. Congr. Series*, **1276**, 76-80. [7] Yonehara, H. et al. (2005) *Int. Congr. Series*, **1276**, 58-61. [8] Gyalog, L. (2005) *Magyar Állami Föld. Intézet, Magyarország fedett földtani térképe*, ISBN 963 671 251 4.

Reduced leaching of the herbicide metribuzin by using clay-gel-based formulations

Undabeytia, T.[1*], Maqueda, C.[1], Morillo, E.[1], Villaverde, J.[1], Pérez-Sayago, M.[1] & Partal, P.[2]
[1]Institute of Natural Resources & Agrobiology, CSIC, Seville, Spain ([*]undabeyt@irnase.csic.es)
[2]Dept. of Chemical Engineering, University of Huelva, Huelva, Spain

Herbicide mobility in soils has long been of concern for many reasons, including the following: (i) contamination of groundwater; (ii) reduction in efficacy due to herbicide leaching below the weed seed zone, which can reduce herbicidal activity and crop yield; and (iii) surface migration of the herbicide which harms neighboring crops.

To reduce herbicide leaching and increase weed control, new slow release formulations were developed by entrapping metribuzin within a sepiolite-gel-based matrix using two clay/herbicide proportions (0.5/0.2 and 1/0.2) (loaded at 28.6 and 16.7% active ingredient) as a gel (G28, G16) or as powder after freeze-drying (LF28, LF16).

A rheological characterization of the formulated products showed a viscoelastic behaviour as noted in the higher storage modulus G' than the loss modulus G'', within the experimental frequency range employed. A more detailed analysis of the rheological properties such as the apparent yield stress and plateau modulus indicated that samples containing metribuzin up to 2% of sepiolite form a microstructure, which is independent of sepiolite concentration. Addition of metribuzin seemed to weaken the microstructure, and its release behaviour seemed to be related to the microstructure.

The release of metribuzin from the prepared formulations into water was retarded, when compared with the commercial formulation, except in the case of G28. These results were in accordance with those from soil column experiments where the G28 and the commercial formulation eluted almost completely after 4 pore volumes. On the contrary, the total leaching percentages of the other gel-clay based formulations were about half of the total applied amount. An extraction of the active ingredient along these soil columns showed a larger amount in the upper part of the soil column which is of prime interest for weed control (Fig. 1). Bioassays performed at different soil depths paralleled those of the extracted amounts showing a high herbicidal activity in the 0-8 cm depth.

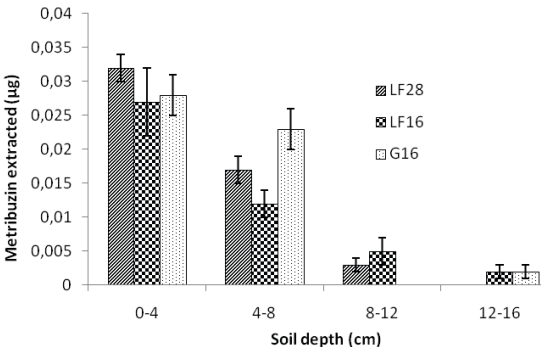

Fig. 1: Metribuzin residues extracted at different depths of the soil columns.

Hydration thermodynamics of SWy-1 montmorillonite saturated with alkali and alkaline-earth cations

Vieillard, P.[1*], Blanc, P.[2], Gailhanou, H.[2], Gaboreau, S.[2] & Fialips, Cl.[3]
[1]INSU-UMR6269, Hydrasa, Poitiers, France
([*]philippe.vieillard@univ-poitiers.fr)
[2]BRGM, BP 6009, Orléans, France
[3]ANDRA, Chatenay Malabry cedex, France

In the context of using clayey barriers, such as in the disposal of radioactive waste within clayey formations, the assessment of the long-term behavior of the clay materials by geochemical modeling requires a perfect knowledge of their thermodynamic properties. The "Thermochimie" database, created by ANDRA in 1996, provides coherent thermodynamic data sets for many minerals of interests, including clay minerals. However, the thermodynamic properties of clay minerals, which govern their stability in solution, are still poorly understood and few experimental data of hydration are available for smectites. A set of consistent data of hydration is proposed from numerous measurements of enthalpy of immersion, and isotherms of adsorption – desorption for SWy-1 montmorillonite saturated with alkali and alkaline-earth cations. To retrieve standard state thermodynamic properties for smectite hydration and dehydration from such data, the amount of H_2O in excess of that located in the interlayer space must be assessed and subtracted from the total amount taken up by the clay sample. Careful measurements of water uptake and release during the hydration and dehydration of the SWy-1 montmorillonite have therefore been taken into account [1,2].

Considering the following reaction: Smectite n_m H_2O = Smectite (0 H_2O) + n_m H_2O (l), the hydration of smectite is calculated by assuming a regular solid solution involving anhydrous and hydrous components in which n_m is the maximal number of moles of water in the fully hydrated end-member [3]. Paired hydration and dehydration isotherms in the one hand and enthalpy of immersion in the other hand, which characterize the equilibrium between water and smectite, can be regressed to assess standard state thermodynamic parameters (enthalpy and entropy) for the hydration - dehydration process.

Validation of standard state thermodynamic properties of hydration of the end members has been achieved by (1) comparing the behavior of hydration-dehydration with experimental measurements done on hetero-ionic SWy-1 and homo-ionic SWy-1 samples at different temperatures; (2) comparing experimental integral enthalpy and entropy of hydration of SWy1 samples with calculated values; and (3) comparing results with those obtained for various smectites with different layer charges (Upton, MX80).

The developed and validated model can predict the standard state thermodynamic properties of hydration and the number of moles of interlayer water in smectites for a given temperature and relative humidity. It may help solving many questions like: the mechanism of exchange between two cations, the number of moles of water transferred during exchange for a given temperature, and the cation selectivity at a given relative humidity. When a limited number of measurements are available, the predictive model can be applied to different compositions to provide theoretical thermodynamic values of formation for hydrated smectites and calibrated with measured data from the literature or acquired within the framework of the project.

[1] Bérend, I. et al. (1995) *Clays Clay Miner.*, **43(3)**, 324-336. [2] Cases, J.M. et al. (1997) *Clays Clay Miner.*, **45(1)**, 8-22. [3] Ransom, B. & Helgeson, H.C. (1994) *Am. J. Sci.*, **294(4)**, 449-484.

Photocatalytic degradation of Rhodamine B in water by synthetic Zn-substituted phyllosilicates

Yamada, H.[1*], Morimoto, K.[1], Tamura, K.[1], Pascua, C.S.[2] & Hatta, T.[3]
[1]National Institute for Materials Science, Tsukuba, Japan
([*]YAMADA.Hirohisa@nims.go.jp)
[2]National Institute of Geological Sciences, UP-Diliman, Quezon City, Philippine
[3]Japan International Research Center for Agricultural Sciences, Tsukuba, Japan

Nanolayer has been paid attentions as building block for novel photonic, electronic, environmental, and energy-related materials. Phyllosilicates are abundant in nature, and are layered materials that contain two-dimensional metal octahedral sheet and silica tetrahedral sheet. In another point of view, phyllosilicates are considered to be the self-assembled silicate nanolayers of octahedral and tetrahedral sheets. Phyllosilicates containing transition metal ions can be used for specific catalytic applications. In the present work, we have demonstrated the photocatalytic activity of Zn-substituted phyllosilicates (smectite, vermiculite and mica) which synthesized by "adaptation of processes in the formation of natural geologic analogues"; a new concept called Geonics [1].

The decomposition of organic dye, Rhodamine B (RhB) in aqueous suspensions of the synthetic Zn-substituted phyllosilicates, Zn-saponite and Zn-hectorite, Zn-vermiculite, Zn-mica and rutile under ultraviolet light illumination were monitored with a UV-visible absorption spectroscopy. In aqueous solution with Zn-smectites, the reduction of peak absorbance for RhB was observed in the adsorption spectra, although the shape and the width of their absorption bands were similar to that in aqueous solution. This adsorption behavior indicated that RhB molecules adsorbed onto the surface of Zn-smectites particles without discernible aggregation and the adsorbed RhB molecules were well dispersed. It was confirmed that the hybridization of RhB with the exfoliated Zn-smectites particles enhanced a photodegradation exponentially. On the other hand, Zn-vermiculite and Zn-mica in aqueous solution showed little photodegradation of RhB. The results indicated clearly that the high photocatalytic activity of smectites is attributed to the exfoliation behavior, that is, the nanosheet structure of the synthesized Zn-smectites. Furthermore, the characteristic stability of smectites in aqueous systems in a wide range of pH and redox conditions would make it an ideal nanomaterial in environmental purification.

[1] Yamada, H. et al. (2009) *Trans. Mater. Res. Soc. Jpn.*, **34**, 363-366.

Removal of silica impurities from bentonite by NaOH dissolution

Zhang Bingbing[1], Su Haiquan[1,2*], Li Jia[2], Pan Hui[2] & Huang Xiaoling[2]

[1]College of Life Science, Inner Mongolia University, Hohhot, P.R. China

[2]School of Chemistry and Chemical Engineering, Inner Mongolia University, Hohhot, P.R. China

([*]haiquansu@yahoo.com)

Bentonites usually contain quartz, α-cristobalite, opal-C, opal-CT, and opal-A as associated silica impurities, which must be removed from bentonites due to the designation of respirable quartz and cristobalite as 'type 1' human carcinogens. These silica impurities could hardly be separated from montmorillonite by conventional wet sedimentation.

In this paper, bentonite was sampled from Xinhe County, Inner Mongolia, China; the mineral composition is as follows: montmorillonite (65.1%), cristobalite (33.0%), and quartz (1.9%). The removal of cristobalite and quartz from bentonite by NaOH dissolution was explored in detail. The result (see Fig. 1 and Fig. 2) shows that the quartz had very different reactivity compared with the cristobalite, only the cristobalite could be separated from montmorillonite by this method.

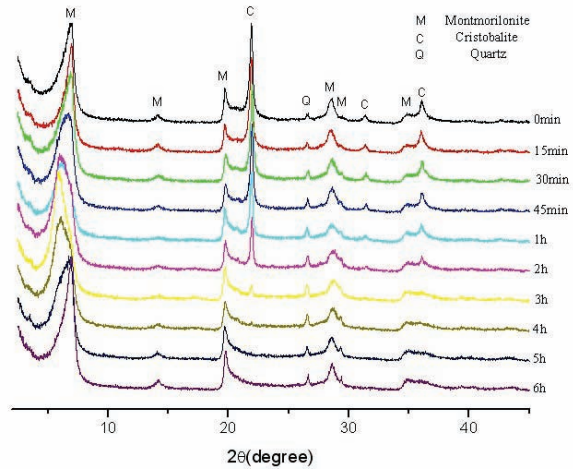

Fig. 1: XRD patterns of the bentonite samples reacted with 0.5 M NaOH at 90 °C with different reaction time.

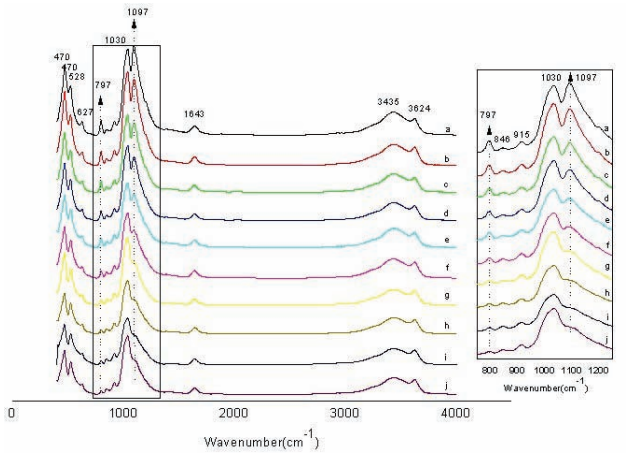

Fig. 2: FTIR spectra of the bentonite samples reacted with 0.5 M NaOH at 90 °C with different reaction time (a-j corresponding 0min-6h).

Acknowledgements: Project Supported by National Natural Science Foundation of China (grant no. 50763004).

Layered minerals nanotopography and surface potential: biomedical and bioengineering applications

Valdrè, G.
Dept. of Earth And Geo-Environmental Sciences, University of Bologna, Italy (giovanni.valdre@unibo.it)

The knowledge of the surface properties of layered minerals is of great importance to understand basic and applied technology, such as, for example liquid/surface interactions, microfluidity, friction or tribology and biomolecules self-assembly and adhesion. Recent developments of Scanning Probe Microscopy (SPM) have widened the spectrum of possible investigations that can be performed at a nanometer-scale level on the surface of minerals. Investigations involve physical properties, such as surface potential and electric-field topological determinations, and chemical and spectroscopic analysis in air, in liquid or in a gaseous environment.

After a brief introduction of new technological developments relating to SPM, recent achievements are presented in characterization and application of nanomorphology and surface potential properties of minerals, in particular the behaviour of some layer silicates. Two general research directions are presented: application of bio/organic surface interactions of layer silicates, and mineral hydrophilicity/phobicity and friction/adhesion issues.

(1) The ability to control the binding of biological and organic molecules to a crystal surface is central in biotechnology, catalysis, molecular microarrays, biosensors and environmental sciences. For instance, recent achievements showed that DNA molecules have different binding affinities and assume different conformations when adsorbed to various layer silicate surfaces. On certain crystals, the electrostatic surface potential anisotropy can order and stretch the DNA filament, thus inducing a natural change in its conformation. The experimental results are in good agreement with simulations and mathematical modeling. The active stretching of DNA on extensive layer silicate surfaces is a clear indication of the potential in understanding basic behavior and developing technological uses of these minerals when used as substrates for biomolecules. Examples involving nucleotides, RNA and cells are presented also.

(2) Investigations of nano-confined adhesive and shear forces of water (and other liquids) onto layer silicate and other mineral surfaces are presented. The study of water in confined geometries is very important because it can provide simple models for nano-bio-tribology and fluid/mineral interactions. Nano-confinement is obtained between a resonating (oscillating) probe and layer mineral surfaces. When the liquid-film thickness is less then a critical value, the oscillation amplitude curve follows a step-like trend, suggesting that the liquid molecules are organized in layers. By using a harmonic oscillator model it is possible to calculate the variation in the elastic and viscous stress response of the confined liquid and to characterise its state respect to the mineral surface.

Montmorillonite as efficient carrier of Gentamicin used for antibiotic treatment: comparison of MD simulations with experiments

Ori, G.[1*], Montorsi, M.[1], Bellini, A.[2], Iannuccelli, V.[2] & Siligardi, C.[1]
[1]Dept. of Materials and Environmental Engineering, University of Modena and Reggio Emilia, Modena, Italy
([*]guido.ori@unimore.it)
[2]Dept. of Pharmaceutical Sciences, University of Modena and Reggio Emilia, Modena, Italy

There is a strong demand to identify new strategies in order to set optimal drug delivery systems for antibiotic treatments. Intercalation of organic molecules into layered inorganic solids provides a useful and convenient route to prepare hybrids that show properties of both the inorganic host and organic guest in a single material [1,2]. Both natural and synthetic clays have been already used with success for this purpose. One of the main system widely investigated to modulate drug release, consider smectite clay particles, especially montmorillonite (Fig. 1).

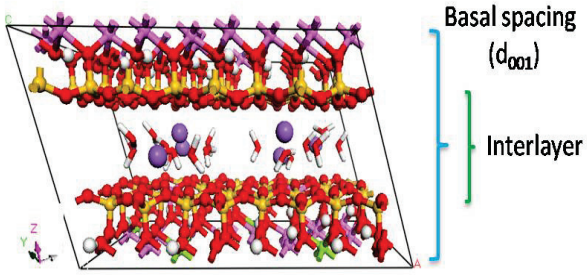

Fig. 1: Ideal model of a Wyoming-type montmorillonite.

High specific surface, adsorptive capacity, rheological properties, chemical inertness and low or null toxicity make clay minerals futuristic drug delivery vehicles [3].The presented work shows the potential of a montmorillonite-based clay mineral (bentonite) to contribute to the development of novel antibiotic materials. In our knowledge, it is the first time the have been tested the intercalation of gentamicin molecules in montmorillonite as a drug delivery carriers for antibiotic treatment (Fig.2).

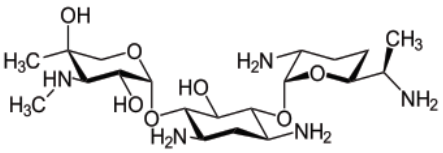

Fig. 2: Gentamicin.

Comparison of experimental measurements (XRD, TGA, DTA) with simulations (MD modelling) have provided a more detailed understanding of the geometry, organization of gentamicin molecules confined in the cationic clay. By MD simulations it has been possible obtain a further insight into the interactions between the organic guest and the clay framework in view to optimize the cationic exchange process.

[1] Mohanambe, L. et al. (2005) *J. Phys. Chem. B*, **109**, 1561-1568. [2] Ghanshyam, V.J. et al. (2009) *Int. J. of Pharm.*, **374**, 53-57. [3] Lin, F.H. et al. (2002) *Biomaterials*, **23**, 1981-1987. [4] Bujdàk, J. et al. (2009) *Envir. Sci. Technol.*, **43**, 6202-6207.

Adsorptive properties of Fe-, Al-, Fe/Al-montmorillonites

Khankhasaeva, S.Ts.[1,2*] & Dashinamzhilova, E.Ts.[1]
[1]Baikal Institute of Nature Management SB RAS,Ulan-Ude, Russia ([*]shan@binm.bscnet.ru)
[2]Chemical Dept., Buryat State University, Ulan-Ude, Russia

The use of natural sorbents can increase economic efficiency of sorption technologies due to their availability, relative cheapness and the possibility of recycling. Natural montmorillonite (MM) clays are effective cation exchangers. At present, an urgent task remains the development of anion-exchange sorbents, based on montmorillonite. Layer-pillar structured materials synthesized by intercalating metallic polyoxocomplexes between silicate layers of swelling clays, such as montmorillonites attract the interest as sorbents. Fe-, Al- and Fe/Al-montmorillonites were prepared from naturally occurring montmorillonite (clay deposit Mukhortala, Russia) by exchanging interlayer cations (Mg^{2+}, Na^{+}, K^{+}) with polyoxocations containing a) iron (Fe-MM), b) iron and aluminium within the complex with Fe/Al = 1:1 (Fe/Al-MM), c) $[Al_{13}O_4(OH)_{24}(H_2O)_{12}]^{7+}$ (Al-MM). The synthesized solids were calcined for 2 h at 400°C, 500°C and characterized by IR-spectroscopy, XRD, chemical analysis and BET surface area measurements.

The cation and anion exchanging properties of solids were studied in aqueous solutions using as adsorbates cationic (Methylene blue (MB)) and anionic (Acid chrome blue-black (ACBB), Congo red (CR)) organic dyes, NH4+, phosphate, chloride ions and anionic surfactants (Sodium dodecylsulphate and Sulphonole). An intercalation MM by Al, Fe and Fe / Al-polyoxocations reduces the cation exchange capacity (CEC) of ammonium cations and adsorption capacity (AC) of the cationic dye MB in comparison with natural MM. Adsorption of dye MB on studied sorbents depends not only on the number of cation-exchange centers, but also on the size of their accessible surface. Value of adsorption on the sorbents decreases in the series: Fe-MM> Fe/Al-MM> Al-MM, which corresponds to the decrease of the total surface area of meso- and macropores. Introduction of Al, Fe and Fe/Al-polyoxocations to the structure of MM leads to a significant increase in the adsorption properties with respect to anions (chloride, phosphate), due to an increase in the number of anion-exchange centers. Results on the adsorption of anionic surfactants also confirm the increase in anion-exchange capacity of MM for intercalation. Adsorption capacity of phosphate decreases in the series: Al-MM> Fe-MM> Fe/Al-MM> Natural MM, which corresponds to a change in the total specific surface of these sorbents, indicating the accessibility of micropores for adsorption of phosphates. Adsorption capacity for anions of organic dyes for sorbents were subjected to heat treatment at temperatures $\leq$ 300 °C, correlates with the number of anion-exchange centers and the total surface area. Calcining at temperatures$\geq$ 400 °C leads to a decrease in accessible pores surface for microporous adsorbent Al-MM and reduction of AC for large organic anions, whereas the adsorption of inorganic anions remains high and 3-6 times higher than AC for natural MM. Increasing the size of sorbed anions and their degree of association in aqueous solutions leads to a decrease in AC by steric factors, as was observed for the large anions of dyes ACBB and CR. Microporous sorbent Al-MM is effective for removal from aqueous solutions of inorganic anions, and for the removal of large organic anions are effective Fe-MM, Fe/Al-MM having mesoporous structure.

Acknowledgements: The work was supported by the Russian Foundation for Basic Research.

ACE anionic inhibitors-clay nanocomposites: synthesis and characterization

Alexa, I.F.*, Seftel, E.M., Păstrăvanu, C. & Popovici, E.
Dept. of Materials Chemistry, "Al. I. Cuza" University, Iaşi, Romania (*alexaiulianaflorentina@yahoo.com)

ACE inhibitors are used for controlling blood pressure, treating heart failure, preventing strokes, and preventing kidney damage to people with hypertension or diabetes. In the present study, the selected drug for loading onto the layered matrix was captopril (Fig. 1).

Layered double hydroxides (LDHs), also called hydrotalcite-type anionic clays, consist of cationic brucite-like layers and exchangeable interlayer anions [1]. Due to their biocompatibility, some LDHs having different cationic pairs, such as Mg/Al, Zn/Al, Fe/Al or Li/Al-LDH, can be used as host materials for drugs in order to obtain LDH host–guest supramolecular structures [2, 3].

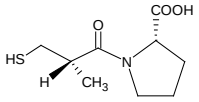

Fig. 1: The chemical structure of captopril, (*2S*)-1-[(*2S*)-2-methyl-3-sulfanylpropanoyl]pyrrolidine-2-carboxylic acid.

Calcined layered double oxide precursor (MgAl–LDO) used for intercalation was obtained by calcination of the layered double hydroxide containing Mg and Al (MgAl–LDH) at 500°C for 2h. Then, the calcined product was re-hydrated in the presence of a captopril solution under a N_2 atmosphere. The obtained material was analyzed by N_2 sorption, UV-vis DR and FTIR Spectroscopy methods.

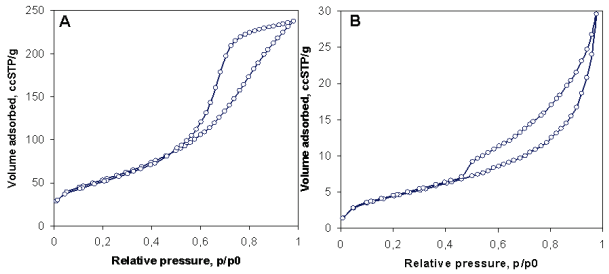

Fig. 2. The N_2 adsorption/desorption of (A) MgAl-LDO and (B) Captopril-MgAl-LDH.

The N_2 adsorption isotherms (Fig. 2) showed that the captopril molecules are successfully loaded into the layered matrix. The specific surface area and the pore volume decrease significantly after the drug loading (Table 1).

Table 1: Textural properties of the studied samples

Sample	S_{BET} (m^2/g)	V_p (cm^3/g)
MgAl-LDO	195.5	0.3571
Captopril-MgAl-LDH	16.2	0.0371

The FTIR and UV-vis DR spectra show the presence of the absorption bands characteristic to the organic captopril molecules. The present study may offer broad perspectives in utilizing MgAl-layered double hydroxides as an alternative biocompatible inorganic matrix for a feasible drug reservoir or a drug delivery carrier.

[1] Costantino, U. & Nocchetti, M. (2001) in Rives, V. (ed.) *Layered Double Hydroxides: Present and Future*. Nova Science Publishers, New York, 383-411. [2] Yang, J.H. et al. (2007) *Chem. Mater*., **19**, 2679-2685. [3] Xu, Z.P et al. (2006) *Chem. Eng. Sci.*, **61**, 1027-1040.

Effect of microbiological activity on the flow/rheologic properties of aqueous kaolin mineral suspensions

Papp, I.P.[1*], Babcsán, N.B.[1] & Tombácz, E.T.[2]
[1]Bay Zoltán Foundation for Applied Research Institute for Logistics and Production Systems, Miskolc, Hungary (*papp.ildiko@bay-logi.hu)
[2]Dept. of Colloid Chemistry, University of Szeged, Hungary

The aim of the present study was to investigate the rheologic properties of different type of kaolin infected by microorganisms.

Microorganisms are widespread in the different environmental systems, such as air, water and soil. However, interactions between industrial raw materials and microorganisms are not investigated in details [1]. It was found that these industrial raw materials (different type of kaolin) provide appropriate conditions for microorganisms especially sulfate reducing bacteria. Organic and inorganic compounds of kaolin can serve as nutrition source for microorganisms, accordingly of lignite for fungi and metals for specific bacteria. The organic additives (e.g. regulator substances, hydraulic oil, machine oil) that facilitate the processing serve as additional nutrition sources. Temperature, moisture and nutrition play a key role in the reproduction of microorganisms. Each long-term process involves the danger of proliferation of microorganisms, which phenomenon has an effect on the rheologic properties of kaolin suspensions. 30-40°C temperature for a long time had been creating ideal conditions for proliferation of microorganism, which caused drastic changes in the rheologic properties of kaolin samples. We investigated the rheologic changes of infected and uninfected kaolin samples depended on temperature. According to our results, sulfate reducing bacteria influenced significantly the rheologic properties of kaolin.

[1] Heimstädt, K.H & Mörtel, H.M. (1995*) Ceramic Forum Int.*, **72(9)**, 546-550.

Water uptake and mucoadhesion of chitosan/montmorillonite composite

Salcedo, I.[1], Aguzzi, C.[1], Bonferoni, C.[2], Sandri, G.[2], Sanchez, R.[1], Cerezo, P.[1], Alba, M.D.[3] &Viseras, C.[1,4*]
[1]Depto. de Farmacia y Tecnología Farmacéutica, Universidad de Granada, Spain
[2]Dipto. di Chimica Farmaceutica, Universitá di Pavia, Italy
[3]Insituto de Ciencia de los Materiales, CSIC, Sevilla, Spain
[4]Instituto Andaluz de Ciencias de la Tierra, CSIC-Universidad de Granada, Spain ([*]cviseras@ugr.es)

Naturally occurring clays and clay minerals may be suitable to effectively modulate drug release. However, sometimes it is necessary to use modified or synthetic clay minerals and/or polymeric additives [1]. Clays and biopolymers have been proposed as interesting materials for new drug delivery systems [2]. Chitosan, a polymer derived from chitin used as a pharmaceutical excipient [3], have been added to montmorillonite dispersions to modify rheological properties related to flocculation state of the resultant dispersions [4]. Chitosan has been also proposed to be used in colon-specific drug delivery systems as regards of its degradation by colonic bacteria [5]. However, due to its high solubility and swelling properties in acidic media, chitosan alone is unable to prevent drug release in the stomach and small intestine, being desirable to get some strategies to avoid such problems. In particular, synthesis of composites with clay minerals may be a novel approach to modify swelling and water uptake of polysaccharides [6]

With these premises, biocomposites between chitosan base (CS) and a commercial montmorillonite (Veegum HS©, VHS) have been prepared by solid-liquid interaction and the water uptake profiles in acidic environment and mucoadhesive properties evaluated, in comparison with the single components. Water uptake measures were done by using a modified Enslin apparatus [7]. Mucoadhesive properties were investigated with a TA-XT2 Plus Texture Analyser (Stable Micro Systems, Enco, Italy) using porcine gastric mucin as biological substrate.

The CS/VHS composites showed lower solubility than pure chitosan in acidic environment and mucoadhesión followed the trend CS > CS/VHS > VHS. It can be concluded that the interaction between the clay particles and polymer chains results in a composite with good mucoadhesive properties, and promising solubility pattern to be used as colonic delivery excipient.

[1] Aguzzi, C. et al. (2007) *Appl. Clay Sci.*, **36**, 22-36. [2] Viseras, C. et al. (2008) *Mat. Sci. Technol.*, **24(9)**, 1020-1026. [3] Baldrick, P. (2009) *Regul. Toxicol. Pharmacol.*, 56, 290-299. [4] Günister, E. et al. (2007) *Carbohyd. Polym.*, **67**, 358-365. [5] Zhang, H.S. & Neau, H. (2002) *Biomaterials*, **23**, 2761-2766. [6] Pongjanyakul, T., Priprem, A. & Puttipipatkhachorn, S. (2005) *J. Control. Release*, **107**, 343-356. [7] Ferrari, F. et al. (1991) *STP Pharma Sci.*, **1(2)**, 137-144.

Iron-clay-bacteria interactions in quartz sands purification

Štyriaková, I.[1*], Kraus, I.[2], Mockovčiaková, A.[1], Orolínová, Z.[1] & Štyriak, I.[1]
[1]Institute of Geotechnics SAS, Kosice, Slovakia
([*]bacil@saske.sk)
[2]Comenius University, Bratislava, Slovakia

Several natural sands are brown for the presence of iron and clay minerals that coat or which are impregnated on quartz grain surfaces. *In-situ* washing and bioleaching processes can remove iron and clay minerals.

The following mineral composition (wt %) of the different grain sizes was obtained using Rock Jock software: 31 % quartz, 11 % K-feldspar, 15 % plagioclase, 20 % mica, 11 % kaolinite and 12 % chlorite in the fraction 0.002-0.063 mm and 15 % quartz, 8 % K-feldspar, 4 % plagioclase, 28 % mica, 19 % kaolinite and 26 % chlorite in the grain size fraction < 0.002 mm. Iron-clay-bacteria interaction was found during a laboratory bioleaching of separated iron-clay fraction. The impoverishment by fine-grained fraction is a result of bacterial destruction of silicate minerals. After bioleaching the amount of the fraction 0.9 - 25 μm μm decreased, on the other hand the distribution of the coarse-grained fraction with particle size from 25 to 87 μm increased in the clay sample.

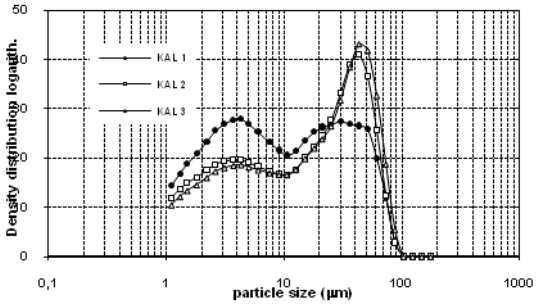

Fig. 1: Granulometric analysis of the clay fraction before (KAL 1) and after bioleaching (KAL2 – *Bacillus* spp., KAL3 – indigenous bacteria).

Dissolved Fe amount under pH ranging between 4 and 7 and in a nutrient-rich environment simulating the conditions of an *in-situ* quartz sands purification, was periodically monitored for 30 days. Mössbauer spectroscopy was used to detect the present iron cations in the natural sample (KAL 1); experimental data indicated that Fe^{3+} cations in KAL 1 can be ascribed to a ferrihydrite-like phase. In *Bacillus* spp., and indigenous bacteria treated samples (KAL 2 and KAL 3, respectively) Fe^{3+} was prior removed always from the same position and, in addition, higher Fe^{3+} decrease was obtained for sample KAL 2.

Table 1: Chemical composition of the clay fraction before (KAL 1) and after bioleaching (KAL2 – *Bacillus* spp., KAL3 – indigenous bacteria)

Elements (%)	KAL 1	KAL 2	KAL 3
SiO_2	56.9	57.5	57.3
Al_2O_3	18.5	18.1	18.5
Fe_2O_3	7.04	4.42	4.65
TiO_2	0.44	0.44	0.45
CaO	1.27	0.90	0.85
MgO	0.92	0.80	0.79
Na_2O	1.19	1.34	1.35
K_2O	2.01	2.33	2.38

The effect of iron-bacteria complexation by exudates caused the clay dissolution with the release of silica. Bacterial clay dissolution liberated iron to promote quartz sands purification.

Acknowledgements: This work was supported by the Science and Technology Assistance Agency under the contract No. APVV-0472-07 and No. APVT-51-006304.

Selection of protein amino acids in natural montmorillonite gel

Yushkin, N.P.
Institute of Geology, UB RAS, Syktyvkar, Russia
(yushkin@geo.komisc.ru)

At the studies of biomineral interactions the natural montmorillonite gels from mineral deposits provide the most versatile information on the real environments and processes of synthesis of nucleotides and other biomolecules.

We studied gel accumulations from hydrothermal fluorite deposit Palat in Bulgaria, where in 1983 the gel samples were selected and hermetically packed. The material of preserved and fresh samples is completely identical by their composition and properties.

The gel represents homogeneous jelly-like snow-white mass. The dispersed phase are two-dimensional (length 15 mcm, width 0.4-0.8 mcm) thin-banded individuals of Ca, Mg-montmorillonite, the dispersion medium-strongly mineralized water of chloride-sulphate-bicarbonate calcium-natrium composition.

The electronic microscopy studies of fresh or not long preserved (one-two years) samples of gel-montmorillonite showed numerous rod-like bacteria. In the long preserved gel living bacteria were not observed, however SEM studies showed bacterium-like forms of Cu-Fe-Zn composition without sulphur, which probable represent brass pseudomorphoses on fossilized bacteria.

The gel-montmorillonite contains 0.28% $C_{org.}$ Chromato-mass-spectrometry of organic matter extract from the montmorillonite testifies to its peculiar composition. The group of acyclic alkans and alkens are the most interesting, which are distinguished by the isomerism of carbon framework and position of multiple bonds. There is also a number of aromatic and heterocompounds. Such a composition of organic compounds is not characteristic for hydrocarbons (of geological nature), and seems to be consequence of montmorillonite selection. At the end of the chromatogram there are C_{26}-C_{35} n-alkans, which are typical components of petroleum series.

In the natural gel-montmorillonite the presence of a wide spectrum of amino acids (Glu, Gly, Ala, Val, Leu, Tyr, Phe, His, Lys, Arg) has been determined, which considerably differs from the corresponding spectra of sedimentary montmorillonite clays and is closer to the amino acid composition of abiogenous hydrocarbon ordered structures. It is not excluded that the formation of the amino acids results from catalytic action of montmorillonite to the structural transformation of the organic matter of mineral-forming solutions. In 12 years the total content of amino acids decreased by 5 times (from 8.9 to 1.72 mg/100 g of matter). The qualitative composition of the amino acids is practically the same, excluding tyrosine, which is not determined in the primary preservative even in trace quantities. All the amino acids, identified after 12 year-preservation, are represented exclusively by L-enantiomers; D-amino acids were not determined. It is quite reasonable that for the period between two studies the montmorillonite continued to directly select protein amino acids, and the complete chiral selection of left enantiomers passed.

Thus, the peculiarities of structural evolution of montmorillonite gel and its interaction with organic matter allow using the natural gel-montmorillonite both for simulation of possible environments of biomolecular formation and more complex protobiological structures, and as simulations of some biological processes responsible for transfer and transformation of information and feedback

Acknowledgements: RFBR and RAS program 09-П-5-1013support.

Oxidation state of Fe and precipitates in olivine from scoria and lava of Kasayama volcano, Yamaguchi, Japan

Ejima, T.[1*], Akasaka, M.[2] & Nagao, T.[2]
[1]Dept. of Geosciences, Shimane University, Matsue, Japan
([*]olivinefe3@yahoo.co.jp)
[2]Dept. of Geosphere Sciences, Yamaguchi University, Japan

Oxidation states of Fe and precipitates in olivine from andesitic scoria and orthopyroxene-olivine-clinopyroxene andesite (Opx-Ol-Cpx andesite) lava of Kasayama volcano, Hagi, Yamaguchi Prefecture, Japan, were investigated in order to formulate the oxidation process in olivine by high temperature oxidation of the scoria and lava.

Kasayama volcano consists of Opx-Ol-Cpx andesite lava (L1), olivine-clinopyroxene basaltic andesite (Ol-Cpx-andesite) lava (L2, L3-l, L3-u), Opx-Ol-Cpx-andesite lava (L4), and scoria cone composed of Opx-Cpx-Ol andesitic scoria (S1) and Cpx-Ol andesitic scoria (S2) in the ascending order.

The inside of the Kasayama scoria cone is welded and red in color, whereas, on the outer surface of the cone, black or reddish black scorias are deposited. In olivine phenocrysts of the reddish black scoria, only a small amount of precipitates occur on the rim. However, olivine phenocrysts in the red scoria include a lot of precipitates, such as hematite, enstatite and magnesioferrite, which form simplectite zone on the rim, simplectite domain in the core, and fillings in fractures. Hematite occurs as vermicular rods or flame-like form. The Fo contents of olivine in the black scoria were 81-90, whereas those in the red scoria attaind 99 to 91 mol%. The ^{57}Fe Mössbauer spectrum of olivine in the reddish black scoria consists of three doublets assigned to Fe^{2+}(M1, M2) and Fe^{3+}(M2) in olivine, and Fe^{3+}(M2) in laihunite, and the Fe^{2+}(M1, M2):Fe^{3+}(M2)-ratio is 69:31. The resulted chemical formula of the olivine is $[^{M2}(Mg^{2+}_{0.83}\ Fe^{2+}_{0.06}Fe^{3+}_{0.11})\ ^{M1}(Mg_{0.84}Fe^{2+}_{0.17})]_{\sum 2.01}\ SiO_4$.

Although the Opx-Ol-Cpx andesite lava is generally black in color, there are some areas with red surface and reddish black subsurface. Olivine in the reddish black and red lavas includes precipitates consisting of titanohematite, magnesioferrite and enstatite, and tends to be Mg-rich. The stronger the red colors of the lavas, the more the amounts of the precipitates in olivine, which results in increase of Mg content in olivine: in olivine from the black lava, the cores and rims are $Fo_{68.54\text{-}74.89}$ and $Fo_{64.90\text{-}72.90}$, respectively, whereas olivine compositions of the red lava are $Fo_{91.01\text{-}95.43}$. Fe in olivine from the black lava is commonly ferrous, but, in some cases, Fe^{3+} was detected in the rim. Small amounts of Fe^{3+} (< 0.05 apfu) were inevitably detected in olivine from the reddish black and red lavas. The textures and chemical composition of the precipitates in olivine suggest that titanohematite and magnesioferrite may have been grown on primary titanomagnetite and chromian spinal, respectively.

High temperature oxidation process in olivine from the Kasayama scorias and lavas is as follows: 1. Primary olivine with normal zoning was crystallized from magma. Oxidation state of Fe was essentially ferrous. Primary titanomagnetite and chromian spinel were included; 2. By high temperature oxidation, a part of Fe^{2+} was changed to Fe^{3+}, hematite and magnesioferrite were crystallized on the margin of olivine, and Fo-contents became higher than those of the primary olivine; 3. With an advance of the high temperature oxidation, significant amounts of vermicular shaped hematite and cubic magnesio-ferrite were crystallized on the rim and around fractures in olivine, Fo-value on the mantle became higher than that in the core and a small amount of Fe changed from ferrous to ferric; 4. Fe^{3+}-rich precipitates consisting of hematite and magnesioferrite developed widely in olivine phenocrysts, and olivine became extremely Fo-rich.

Oscillatory zoned liddicoatite from central Madagascar: crystal chemistry, structure, and compositional variation

Lussier, A.J.[1*], Hawthorne, F.C.[1], Aguiar, P.M.[2], Michaelis, V.K.[2], Abdu, Y.[1] & Kroeker, S.[2]
[1]Dept. of Geological Sciences, University of Manitoba, Winnipeg, Canada ([*]aaron.j.lussier@gmail.com)
[2]Dept.of Chemistry, University of Manitoba, Winnipeg, Canada

The variation in composition, crystal structure, and crystal chemistry of Madagascar liddicoatite with complex oscillatory zoning in both pyramidal and prismatic crystal sectors is examined. The crystal structures of 23 samples are refined with $\langle R_1 \rangle$ = 1.78%, and cell parameters are: *a* 15.83-15.87 and *c* 7.10-7.12 Å. The crystal shows anomalous biaxiality, and spindle-stage measurement of 2*V* gave values of 0.0° for a fragment from the (001) zone and 8(3) and 18.9(5)° for fragments from the pyramidal zone of the crystal. ^{57}Fe Mössbauer spectroscopy gives $Fe^{3+}/\Sigma Fe$ = 5-10 %. Structure data gave <*T*-O> = 1.6175(7) and <*Z*-O> = 1.905(3) Å, and ^{27}Al and ^{11}B Magic Angle-Spinning Nuclear Magnetic Resonance (MAS NMR) shows all Al and B to be [6]- and [3]-coordinated, respectively. Hence, Si = 6.00 *apfu* and ^{Z}Al = 6.00 *apfu* throughout this complexly zoned crystal and all comp-ositional variation involves only *X*- and *Y*-site constituents.

In the crystal, four colours of zones are observed from core-to-rim: purple, light green, dark green and greenish-black, owing to an overall decrease in Mn and increase in Fe, respectively. The variation in bulk composition from core to edge of the crystal corresponds to the substitutions $^{X}Na + {}^{Y}Fe^* \rightarrow {}^{X}Ca + {}^{Y}Li$ and $^{Y}Fe^* + {}^{Y}Fe^* \rightarrow {}^{Y}Li + {}^{Y}Al$, ($Fe^* = Fe^{2+} + Mg + Mn^{2+}$). Oscillatory zoning is superimposed on a smooth monotonic variation in principal constituents: Fe and Mg show prominent oscillatory behaviour superimposed on background values of ~0 *apfu*, whereas Mn^{2+} decreases monotonically from 0.60 to < 0.05 *apfu* at the crystal centre, remaining ~0 to the edge (Fig 1).

The zoning pattern differs completely between the {201} and {110} sectors. The pyramidal sector shows zones of <1 to ~8 mm in thickness, each marked by a sharp, dark discontinuity, fading in colour toward the start of the next zone. Compositionally, this corresponds to a sharp increase in Fe and Mg which monotonically decreases to ~0 *apfu* across the zone. The prismatic sector shows only zones of <1 mm in thickness. Here, Fe and Mg are 0 *apfu* at the beginning of each zone and gradually increase to reach maximum values at the end of the zone, followed by a sharp drop back to ~0 *apfu*. The element-selective zoning pattern observed in Madagascar liddicoatite is consistent with the operation of a coupled-feedback mechanism at the crystal surface as opposed to rhythmic variation in melt properties. This requires a more complex model than those previously suggested for oscillatory zoning in crystals.

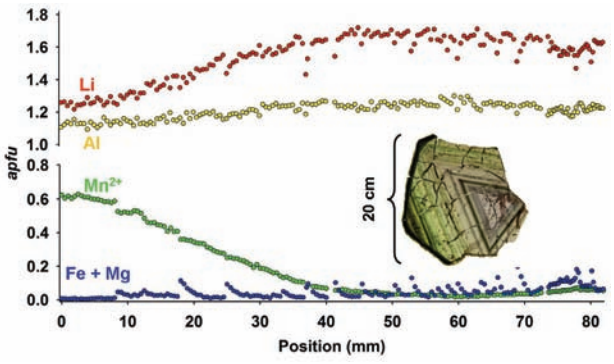

Fig. 1: *Y*-site cation variation from core to rim in Madagascar liddicoatite.

Relationship between optical anomalies, growth topography, and zoning in vesuvianite from Asbestos, Quebec, Canada

Smith, V.C.[*] & Paquette, J.
Dept. of Earth and Planetary Sciences, McGill University, Montreal, Canada ([*]varina.smith@mail.mcgill.ca)

Optical anomalies observed in vesuvianite have piqued mineralogists' interest for decades. The principal optical anomaly observed is the biaxial character, deviant from the uniaxial optical symmetry expected from a morphologically tetragonal crystal like vesuvianite. Such dissymmetrization has been explained in other minerals by different degrees of cation ordering during growth on faces bearing steps that are unrelated by (or oblique to) symmetry elements found in the bulk structure. However, to our knowledge, no studies have documented the relationship between growth step orientation, element partitioning, and optical properties in vesuvianite.

This was done in natural vesuvianite crystals from Jeffrey Mine, Asbestos, Quebec, by using optical microscopy, atomic force microscopy, electron microprobe analysis, and single-crystal X-ray diffraction. This study documents for the first time the selective uptake of the minor elements Fe and Al by non-equivalent growth steps on three forms of vesuvianite, {100}, {110}, and {121}, in addition to the sector-specific zoning of extinction angles and 2V angles in crystals that show a range of growth habits and step orientations. Electron microprobe analysis performed across vicinal faces of growth hillocks show step-specific incorporation of Al and Fe. On hillocks of {100} and {110} prisms, the vicinal faces grown on [001] steps consistently take up more Fe and less Al than those grown on [010] and <1 $\bar{1}$ 1> steps, and concentric (oscillatory?) zoning is detected only on the latter steps.

Unit cell parameters obtained from fragments of |100| and |110| sectors also suggest a symmetry lower than tetragonal. When the prisms {100} and {110} grew by non-equivalent steps, their cell parameters show sector-specific differences. These sector-specific differences diminish in crystals where both prisms grew dominantly by [001] steps.

A visual inspection of (100) and (110) slices suggests that the alternating orientation of Y1 sites at the edge of steps could be a factor in the kinetic disequilibrium of Al and Fe incorporation.

Extremely rich iodide mineralization at the Rubtsovskoe base metal deposit (North West Altay, Russia) and its genesis

Pekov, I.V.[1*], Lykova, I.S.[1], Bryzgalov, I.A.[1], Ksenofontov, D.A.[1], Zyryanova, L.A.[2] & Litvinov, N.D.[3]
[1]Faculty of Geology, Moscow State University, Moscow, Russia ([*]igorpekov@mail.ru)
[2]Faculty of Geography and Geology, Tomsk State University, Tomsk, Russia
[3]JSC "Sibir'-Polimetally", Altayskiy Kray, Russia

Unusual, extremely rich iodide mineralization was found in 2009 in the oxidation zone of the Rubtsovskoe VMS deposit (NW Altay, Russia) that is in operation by underground mine. Primary ores contain >50%, typically 80-90%, sulfides. The stratiform orebody is surrounded by wide aureole of the argillized rocks and covered by sedimentary clays of 80-100 m thick. The oxidation zone, formed in Miocene, occurs in head of the orebody (300 m long, 3-17 m thick; hypsometric interval from +144 to +163 m). Its upper part is a typical iron cap, while lower part contains very rich secondary ores with native copper, cuprite, chalcocite, cerussite, etc.

Iodide mineralization shows a clear zoning. Iodargyrite is distributed in the iron cap, from +156 to +163 m; length of the iodargyrite-rich zone is >150 m. Cu-rich iodides of the marshite-miersite series occur lower, in rich secondary Cu ores (mainly from +146 to +151 m; length of the marshite-richest zone is 50 m). Iodargyrite and Ag-poor marshite are "antagonistic", while miersite is assosiated with marshite or iodargyrite in different areas. Ag-bearing iodides only occur within the oxidized orebody while Ag-free marshite is also abundant in argillized zone near ore. Concentration of iodides in some areas is up to 5% (!) of a rock; 1% is their typical content.

Iodargyrite is a stoichiometric AgI represented by 2*H* polytype ($P6_3mc$, *a* 4.574, *c* 7.519 Å). Isostructural cubic marshite, CuI, and miersite, (Ag,Cu)I, form an isomorphous series in the compositional limits of $Mar_{100}Mie_0$ – Mar_9Mie_{91}, with main break at $Mar_{82.5}Mie_{17.5}$ – $Mar_{57}Mie_{43}$; the *a* parameter of the unit cell varies from 6.050 to 6.424 Å. Well-shaped crystals of marshite are up to 3 cm, iodargyrite – up to 1 cm in size. Iodides are ones of the latest minerals at Rubtsovskoe. Iodargyrite only occurs in cracks or cavities; marshite crystallizes in clay pockets, fulfills cavities or replaces azurite, cuprite, native copper, malachite and osarizawaite. Marshite formed under reducing conditions and does not occur in parageneses with O-bearing Cu minerals unlike Ag-rich iodides. Iodargyrite formed later than miersite that shows an increase of the I:Ag ratio. Distinctive feature of the oxidation zone of Rubtsovskoe is very low concentrations of Cl and Br and almost complete absence of their minerals, unlike other iodide-rich ore deposits (Australia, Chile, Kazakhstan, etc.).

In our genetic model, exhalations of ore-forming "seafloor fumaroles" are the most probable source of iodine. Furthermore, it was captured by clays of argillized aureole near ore and concentrated in absorbed forms and as I^0 and I^- in pore solutions. Surface waters do not seem as a probable source of iodine, because, in this case, it is a geochemical satellite of strongly prevailing Cl. Very important factor for iodine concentration at Rubtsovskoe is a high content of sulfides in primary ores. During first stages of oxidation, such ores produced much sulfuric acid that altered illite of argillized rocks to kaolinite, dickite and alunite. It also oxidized I^0 and I^- to $(I^{5+}O_3)^-$. Sulfate solutions containing much Cu^{2+} (and very mobile iodate ions) infiltrated down and formed, as a result of reactions with sulfides, extremely rich ores with native copper and cuprite. In this process, I^{5+} was reduced to I^0 and further to I^- that was fixed in hardly soluble iodides of Ag^+ and Cu^+.

Application of Fe oxidation kinetics to Precambrian paleosols for the estimation of atmospheric oxygen levels

Murakami, T.[1*] & Sreenivas, B.[2]
[1]Dept. of Earth and Planetary Science, University of Tokyo, Japan ([*]murakami@eps.s.u-tokyo.ac.jp)
[2]National Geophysical Research Inst., Hyderabad, India

Atmospheric oxygen increased irreversibly, first time in Earth's history, from $\leq \sim 10^{-6}$ atm at 2.5 Ga to $\geq \sim 10^{-3}$ atm at 2.0 Ga during the Paleoproterozoic [1,2]. Although the evolution of atmospheric oxygen during the Precambrian is a key to understand the co-evolution of life and environment, the precise nature of quantitative evolution of atmospheric oxygen during the Paleoproterozoic has remained elusive. Paleosols, ancient soils formed by weathering, can be a powerful tool to determine a quantitative pattern of oxygen evolution because they formed at the Earth's surface, in direct contact with the atmosphere at the time of their formation and redox sensitive elements such as Fe retained in weathering profiles should reflect the atmospheric oxygen levels. Applying Fe(II) oxidation kinetics to 2.8 - 1.8 Ga paleosols, we here report our quantitative estimation of atmospheric oxygen levels during the Paleoproterozoic.

Fe(II)-bearing primary minerals release Fe(II) in solution by weathering. Because of the solubilities of Fe(II) and Fe(III), some part of dissolved Fe(II) is oxidized to Fe(III) that forms Fe(III) (hydr)oxides and remains in a weathering profile while the other part is not oxidized and flows out of the profile. The oxidation rate of Fe(II) to Fe(III) is given by [3]:

$$\frac{-d[Fe^{2+}]}{dt} = k[Fe^{2+}](P_{O_2})^x[OH^-]^2$$

where k is the rate constant (temperature dependent) and x the variable (0 to 1). This equation becomes:

$$\frac{\psi}{\psi_A} = \frac{k_A[OH^-]_A^{\,2}(P_{O_2})_A^{\,x_A}}{k[OH^-]^2(P_{O_2})^x}$$

where ψ is the ratio of [flowing-out Fe(II)]/[dissolved Fe(II)] and the parameters with subscript A are values for reference paleosol A. Variations in P_{O_2} with time can be calculated using above equation if differences in the parameters between a given paleosol and reference paleosol A are known. Values of ψ can be obtained from the data set of Fe(II) and Fe(III) concentrations in paleosols in literature. We used the ψ_A and $(P_{O_2})_A$ values at 2.32 Ga [4]. The constraints of the atmospheric oxygen concentrations ($\leq 10^{-5.7}$ atm at 2.45 Ga, $\geq 10^{-5.7}$ atm at 2.32 Ga and $\geq 10^{-2.7}$ atm at 2.0 Ga) were obtained from references [2,4,5].

We assumed four cases for the calculations of P_{O_2} variations between 2.5 and 2.0 Ga: no change in either temperature or P_{CO_2} (affecting pH or OH^-), long-term change in only P_{CO_2}, long-term changes in both temperature and P_{CO_2}, and short-term fluctuations of both temperature and P_{CO_2} during the possible, multiple global-scale glaciations. The calculations indicated that P_{O_2} increased gradually, linearly on the logarithmic scale, from $< \sim 10^{-6}$ to $> \sim 10^{-3}$ atm between 2.5 and 2.0 Ga. Our model also rules out the possibility of a drastic rise at around 2.3 Ga. Our calculations imply, if intense, global glaciation(s) followed by greenhouse conditions are characteristic of the Paleoproterozoic, then P_{O_2} levels would have fluctuated significantly.

[1] Rye, R. & Holland, H.D. (1998) *Am. J. Sci*., **298**, 621-672. [2] Farquhar, J. & Wing, B.A. (2003) *Earth Planet. Sci. Lett*., **213**, 1-13. [3] Stumm, W. & Lee, G.F. (1961) *Ind. Eng. Chem*., **53**, 143-146. [4] Bekker, A. et al. (2004) *Nature*, **427**, 117-120. [5] Pavlov, A.A. & Kasting, J.F. (2002) *Astrobiol*., **2**, 27-41.

Smithsonite from sphalerite replacement fabric types in the Rudabánya base metal ore deposit (N-E Hungary)

Kristály, F[*], Németh, N., Földessy, J., Szakáll, S. & Zajzon, N.
Inst. of Mineralogy and Petrology, University of Miskolc, Hungary ([*]askkf@uni-miskolc.hu)

The Rudabánya base metal ore deposit has a long history of research and exploitation. First, it was an important copper (Bronze Age), then iron (20th c.) source. Native copper and Cu-carbonates, as well as Fe-bearing carbonates were extracted. Among these major components, sulphides and carbonates of Zn and Pb, along barite are abundant. Detailed investigation of their compositions and textures has never been performed.

Sphalerite and galena are common in the whole volume of the dolomite–ankerite–siderite-bound mineralization. Two types of textures are found: a massive, banded sulphide–carbonate, and a fragmented marl-like texture. The two types have very similar chemistries and mineralogies.

The direct replacement of sphalerite to smithsonite can be studied on samples from the massive ore type. Colour, texture and structure are diagnostic for the sulphide to carbonate transformations. Transitions from partly altered sulphide to totally carbonatized zones are detected on the level of centimeters. However, there are zones of the deposit where this process is more dominant and others where Zn and Pb are absent.

We applied analytical techniques including X-ray powder diffraction (XPD), scanning electron microscopy through back-scattered electron imaging (SEM-BSE), chemical analysis by energy dispersive spectrometry (EDS) and wavelength dispersive X-ray mapping (WXRM). Optical microscopy was applied for general fabric characterization. Slices of 3-4 cm in diameter and 0.5 cm in height were cut from the blocks, a pair for each sample. For XPD, color and texture-based manual separation was applied on one of the slices. A proper identification of minerals was possible for each fraction of the sample. On the other slice, SEM-BSE, EDS and WDXM were performed. Then, results of the different methods were easy to correlate.

Several regularities were detected for the carbonatization process of the investigated material. Both Zn and Pb are strongly bound to barite, regardless of their forms. Smithsonite with a cerussite corona, enclosed in barite, suggests selective diffusion during carbonatization. Direct replacement fabric is observed for both sphalerite and galena. For galena, the formation of a cerussite reaction corona is characteristic. On the contrary, sphalerite remnants can display a large variety of replacement patterns. Euhedral quartz, as inclusions, is characteristic for all samples, in all phases. K-dominant mica in ~10 μm-long flakes is frequent. Smithsonite has <1 wt.% Fe and Ca content, irregularly distributed (WDXM). Accidentally, micrometric zones of minrecordite – with $CaZn(CO_3)_2$ composition – are encountered.

The carbonatization process also affected the Fe sulphides, as reflected by the Fe-dominant coronas on dolomite, calcite and the presence of siderite. The detrital fabric of carbonaceous material, overprinted by chemical transformations suggests the combination of tectonic and chemical processes in the carbonatization process.

The fabric produced by replacement reactions shows that the main driving force was the presence of CO_2. Moderate contribution of fluids explains the lack of Mg and trace amounts of Fe and Ca in the carbonate phases of Zn and Pb. The volume of affected materials raises the question whether the carbonatization was driven by oxidation-zone or hydrothermal-related processes.

New hardness scale

Bezerra, U.T.[1*], Vasconcelos, K.K.F.[1] & Wegner, R.R.[2]
[1]Civil Construction, IFPB, João Pessoa-PB, Brasil
([*]dartarios@yahoo.com.br)
[2]Academic Unit of Mining and Geology, UFCG, Campina Grande-PB, Brasil

The most common hardness scale of minerals is the Mohs scale, created by Friedrich Mohs in the nineteenth century. Although it is useful for evaluating the hardness by a simple scratch, this scale has the disadvantage of irregular hardness (jumps) from one hardness to the next. When Mohs chose ten minerals to make up the scale, he probably had in mind the availability with respect to their common occurrence. The problem is, that the differences of the chosen minerals are neither linear nor logarithmic. The proposed new hardness scale comes closer to a more regular difference between its members. Typical examples of the Mohs scale are the significant differences in hardness between gypsum-calcite and calcite-fluorite in the Mohs scale - see Table 1. If the Mohs scale would be linear, these differences should be equal or nearly equal. However, the idea of Mohs remains ingenious and his scale is still used around the world. Looking for a scale that has more regularity, this paper presents the results of tests of Vickers microhardness of different minerals, with talc and diamond still at the extremes and choosing other eight minerals in order to create a more homogeneous scale (Table 1).

Table 1: Minerals of the new hardness scale compared with the Mohs scale, using Vickers microhardness results

New hardness scale	Hardness	Mohs scale	Hardness
Talc	0	Talc	0
Fluorite	196	Gypsum	82
Wollastonite	609	Calcite	180
Hematite	902	Fluorite	196
Tourmaline	1 408	Feldspar	320
Beryl	1 635	Quartz	520
Topaz	1 851	Apatite	564
Chalcopyrite	2 031	Corundum	685
Chrysoberyl	2 328	Topaz	1 851
Diamond	2 650	Diamond	2 650

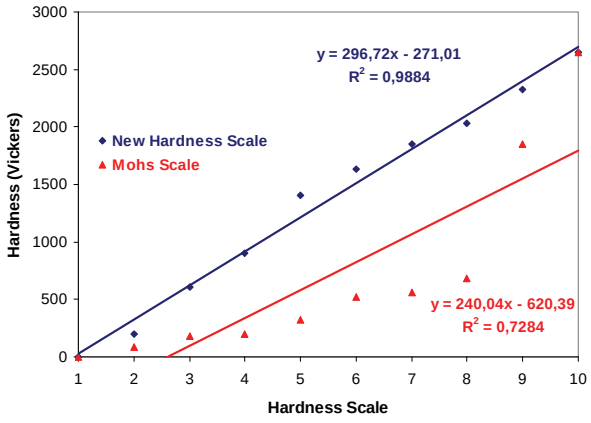

Fig. 1: Graphic of the differences of Vickers hardness between Mohs and the New Scale - see Table 1.

Using the numbers of Table 1, a better homogeneity between the hardness-steps is obvious (the correlation coefficient comes closer to unity). Between the minerals topaz and corundum, the Mohs scale shows a large difference; from topaz down these distances are much smaller, making it more difficult to differentiate minerals with inferior hardness. The main purpose, therefore, is to offer a scale of common minerals of easier application because of more similar differences among the chosen members.

Comparison of jarosite-group minerals formed on surface and subsurface environment of the abandoned base metal mine, Mátraszentimre – Gyöngyösoroszi (Mátra Mts., Hungary)

Jánosi, M. [*], Farkas, I.M. & Weiszburg, T.G.
Dept. of Mineralogy, Eötvös L. University, Budapest, Hungary
([*]janosim@vipmail.hu)

The low-sulfidation epithermal type base metal deposit at Gyöngyösoroszi-Mátraszentimre was mined between the 1950s and 1986, and closed without any remediation. The mine and waste dumps were exposed to oxygen, water and certain colonies of bacteria, and the oxidation of sulphides (predominantly pyrite) resulted in extremely acidic mine drainage (AMD), also containing large amounts of Pb, Zn, Cd, Cu, As. Within the frame of current complex remediation measures, waste rock piles/dumps, underground shafts and adits of the mine have been opened up.

The mine opening contains huge stalagmite-stalactite structures that span from floor to ceiling. These are mostly composed of efflorescencent iron sulfate minerals (melanterite, halotrichite, copiapite etc.), while in the lower level of the mine and in the intensely fractured zones the stalagmite-stalactite structures are composed of jarosite and/or amorphous/fine-grained, poorly crystalline iron oxyhydroxides, sometimes covered with gypsum.

In this work, we have focused on the mineralogy and geochemistry of natural jarosite samples collected from the re-opened underground mine adits, and compared them with samples of excavated high-sulphide mine waste piles. X-ray powder diffraction and chemical (SEM-EDX, ICP-AES) methods were applied. Most of the samples consist of a mixture of phases. Jarosites are not pure end-member phases, as shown also by cell parameters (Fig. 1).

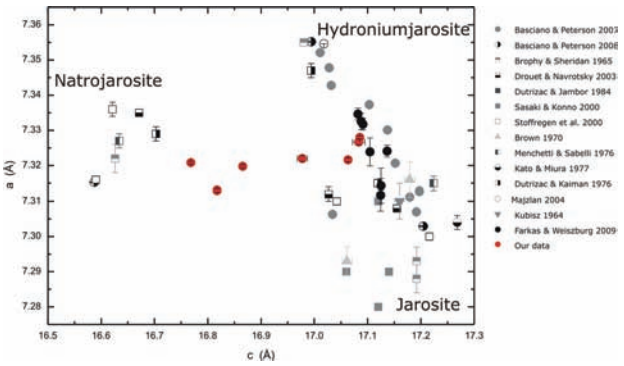

Fig. 1: Cell parameters of jarosites, red symbols indicating the underground samples of this study, black symbols representing the comparative surface samples of [1].

Analyses suggest complete solid solution between K-H_3O-Na-jarosites in the underground samples. The main difference between the surface and the underground jarosites is that the natrojarosite component occurs only in underground conditions.

[1] Farkas, I.M. et al. (2009) *Can. Mineral.*, **47,** 509-524.

Wolframite and cassiterite: age of forming and isotope characteristics Sr and Nd

Abushkevich, V.S.[1*], Badanina, E.V.[2] & Syritso, L.F.[2]
[1]Institute of Precambrian Geology, St-Petersburg, Russia
([*]v.s.abushkevich@ipgg.ru)
[2]State Universty of St.-Petersburg, Russia

Modern methods of isotope geochemistry and geochronology allow to bring to minerals research methodology a new quantitive parameter - estimation of age of its crystallisation - and to solve a problem of source of ore material and degree of mantle-core interaction during its forming. Such researches was performed on the basis of study of different genetic types of tin-tungsten mineralization, connected with Li-F granites (Orlovka), albitized greisenized granites (Spokoynoye) and quartz-topaz greisens with Li-micas (Sherlovaya Gora) (Eastern Transbaikalia).

Methodological basis of this research is a studying of isotope-geochemical (Rb-Sr, Sm-Nd, Pb-Pb) characteristics of wolframite (Wt) and cassiterite (Kas) and mineral-forming environment in quartz. Main results are coming to this: (1). It is ascertained, that on studied deposits a different age ratios between tin-tungsten mineralization and granites containing it are observed. Thus, age of crystallization of wolframite from Spokoinoye is 139,8±1,3Ma, on the same time forming of the massive is 144,5±1,4Ma [1]. It allows to consider the interval, at least, 2.5Ma, as a time necessary to form of hydrothermal solution. The age of ore mineralization (Wt, Kas) of Sherlovaya Gora (Wt (142,4±1,5Ma), Kas (141,1±1,5Ma)) and Orlovka (Wt (139,5±2,1Ma), Kas (138,5±1,6Ma)) is almost identical to the age of forming of mother granites (141,4±1,8Ma and 139,9±1,9Ma respectively). It is noteworthy, that age of cassiterite mineralization is conditionally younger than the age of wolframite one (in bounds of 1Ma error). (2). Ascertained differences in isotope characteristics Sr and Nd between mother granites of Spokoinoye (εNd(144) = -3,4), Orlovka (εNd(140) = -1,7), Sherlovaya Gora (εNd(141) = -0,3) massifs and associated mineralization (wolframite, cassiterite) (wt: εNd(T) от -1,9 до +2,1; kas εNd(T) от +0,9 до +3,2) are points out to participation of juvenile part during ore-material forming. At the same time, in the bounds of universal system, isotope composition of wolframite is characterized by more depleteness than cassiterite one. Thus, there is reason to believe, that possible mechanism of mineralization is remobilization of ore material from crystallized magma chamber(?) influenced by fluid with significantly mantle characteristics. (3). Estimation of W concentration in the melt of Spokoinoye massive on the basis of study of melt inclusions in quartz showed extremely low solubility of wolframite: log K_{sp} varying from -6,5 to -6,7 $mole^2/kg^2$ (from 8,78 up to 3,67 ppm W in melt).

Discovery of reasons of age ratios difference between ore mineralization and mother granites of different genetic types of deposits, also problems of ore material sources is an object of further research.

Acknowledgements: This study was supported by the Russian Foundation for Basic Research (grants 09-05-01222-a, 08-05-00766-a, 08-05-00771-a).

[1] Abushkevich, V.S. & Syritso, L.F. (2007) *Isotope-geochemical model of forming of Li-F granites of Khangilaisky ore node in Eastern Transbaikali.* Nauka. SPb.

The Ashadze ultramafic hosted sea-floor sulfide deposits (Mid-Atlantic Ridge, 12°58'N): mineralogy and fluid inclusion study

Amplieva, E.E.[1*], Bortnikov, N.S.[1], Stavrova, O.O.[1], Simonov, V.A.[2] & Fouquet, Y.[3]
[1]IGEM RAS, Moscow, Russia ([*]Amplieva@igem.ru)
[2]Institute of Geology and Mineralogy, SB RAS, Novosibirsk, Russia
[3]FREMER, Centre de Brest, Plouzané, France

A mineral composition of sulfide edifices and fluid inclusions in anhydrite from the Ashadze fields were studied. Samples were collected in 2007 during the French-Russian *"Serpentine"* cruise of French R/V "*Pourquoi Pas?*" with the ROV *Victor 6000*. The Ashadze field is a deepest active hydrothermal area, which occurs at 3300 – 4530 m below the sea level. During the Serpentine cruise, two active "black smoker" sites were discovered, which consist of active discrete chimneys on sea-floor or small sulfide mounds, clusters of several dozens of active and inactive chimneys from several centimeters up to 2 m in height. Few chimneys vent fluids as "black smokes" and are shimmering warm water. Holes in the sea floor and "embryos" of chimneys venting "black smokes" occur in this area as well. Two morphological and mineral types are identified among the sulfide edifices.

Type I is represented by sulfide chimneys and diffusors. In general, they consist of pyrrhotite, isocubanite, sphalerite, and chalcopyrite with small amount of copper-glance, covellite, Fe-oxyhydroxides, hematite. Active chimneys are composed mainly of pyrrhotite, Cu-Fe sulfides, and rare sphalerite. Zn sulfides prevail in inactive or diffuse chimneys. Chimney spires all show radial changes in composition. Outer zones consist of porous sphalerite aggregates with minor hematite, marcasite, covellite, and bornite. Sphalerite occurs as euhedral and anhedral grains. Reniform, colloform and dendritic aggregates of sphalerite and marcasite were found. Anhydrite was found in outer zones of active chimneys. Intermediate zone contains pyrrhotite (occuring as tabular grains or radiate-fibrous aggregates) with minor isocubanite and chalcopyrite. The intimate lamellar intergrowths of chalcopyrite and isocubanite are typical. Chalcopyrite and isocubanite with sphalerite occur in inner zones. Relics of tabular pyrrhotite were found. Chalcopyrite and isocubanie form aggregates of isometric grains, colloform and concentrically-zoned aggregates. Two types of Fe-Zn sulfides and sphalerite intergrowths were identified: (1) sphalerite core rimmed with isocubanite and chalcopyrite aggregates overgrown by idiomorphic grains of sphalerite; (2) isometric chalcopyrite and isocubanite aggregates are overgrown with idiomorphic grains of sphalerite which are rimmed with isocubanite and chalcopyrite aggregates.

Type II is represented by sulfide mounds composed mainly of isocubanite and chalcopyrite, sphalerite, pyrite, pyrrhotite, and marcasite. Fine-grained texture is typical for massive sulfide ores. Isocubanite with chalcopyrite lamellae occur as aggregates of isometric grains and colloform segregations. Colloform, radial aggregates of marcasite, isometric grains of sphalerite, and relics of tabular pyrrhotite were found. Chalcosine develops as pseudomorphs after separate growth zones in colloform aggregates of isocubanite.

Primary three-phase (liquid + vapor + solid) fluid inclusions 5-40 μm in size and tabular in shape were found in anhydrite. Non-transparent solid phases are presumed to be sulfide minerals. Freezing of primary two-phase (liquid + vapor) fluid inclusions in anhydrite at the Ashadze field indicate that NaCl is a major dissolved constituent in the trapped fluid and its concentration is 4.7 to 7.8 wt. % NaCl-equiv. Homogenization temperatures of fluid inclusions vary from 265 to 324°C ("Long Chimney") and from 210 to 320°C ("Embrio" chimney).

Deformation mechanism of antigorite considered from microstructures of naturally deformed serpentinite

Ando, J.[1*], Urata, Y.[1], Soda, Y.[2] & Ohfuji, H.[3]
[1]Dept. of Earth and Planetary Systems Science, Hiroshima University, Hiroshima, Japan (*jando@hiroshima-u.ac.jp)
[2]Dept. of Earth Sciences, Waseda University, Tokyo, Japan
[3]Geodynamic Research Center, Ehime University, Matsuyama, Japan

Antigorite serpentinite is an important rock in order to understand the dynamics of subducting oceanic plates. However, the plasticity of antigorite serpentinite under mantle/crust conditions has not been fully understood so far. Naturally deformed rocks preserve probably any information about deformation process including its mechanism. Here we observed microstructures of naturally deformed serpentinite with optical and transmission microscopes (TEM) to study its deformation mechanism.

The sample is antigorite grains composed of serpentinite which exposes along the Sashu Fault in the Saganoseki Peninsula of Oita Prefecture, Japan. This serpentinite contains minor magnetite and Cr-spinel in addition to antigorite grains. The grain size of most antigorite is ca. 10 to 50 μm. These antigorite grains show the undulose extinction and shape preferred orientation defining the foliation and lineation. The "S" and "S-C" fabrics are observed on an optical microscopic scale. Moreover, these antigorite grains show the lattice preferred orientation (LPO) characterized by [010] and [001] density maximums subparallel to lineation and normal to foliation, respectively. All of these microstructures suggest that the sample antigorite grains were deformed by dislocation creep with [010](001) slip system.

TEM observation indicates that several types of lattice defects are developed in the antigorite grains. The most typical microstructures are (001) twins and damaged layers parallel to (001) planes. The mirror plane of the (001) twin is always parallel to (001) plane. The (001) twins make twin lamella throughout samples. The serious damage of (001) planes leads to amorphization of the layers. Moreover, subgrain rotation is observed accompanied with amorphization of (001) planes. All of these defects such as (001) twins, damage and amorphization of (001) planes, and subgrain rotation can be created by slip of (001) planes.

We can also observe “modulation dislocation”, but its density is much smaller than those of the other defects described above. Therefore, these facts on TEM scale microstructures suggest that (001) slip, not dislocation glide is important mechanism for deformation of antigorite serpentinite.

The microstructures on an optical microscopic scale suggest that the sample antigorite grains were deformed by dislocation creep, because the antigorite grains show LPO. However, the microstructures on TEM scale do not support this suggestion and intend that (001) slip is an important for deformation. Here we consider that (001) slip of antigorite creates LPO of antigorite grains in serpentinite.

Chemical composition of sphalerite from Mangazeyskoe deposit (Sakha, Russia)

Anikina, E.* & Bortnikov, N.S.
Institute of Geology of Ore deposits, Petrography, Mineralogy and Geochemistry RAS (IGEM RAS), Moscow, Russia
(*anikina@igem.ru)

Investigations of chemical composition of sphalerite are important for understanding mineral-forming processes. In this work, we have studied distributions of Fe, Mn, and Cd in sphalerites from the Mangazeyskoe deposit located in the Kolyma-Verkhoyansk fold belt. Ore bodies of this deposit occur in Carboniferous and Permian siltstones and sandstones, which are intruded by Endybal stocks and dykes of various compositions. Three mineral-forming stages have been recognized there: 1) gold-rare-metal quartz veins (GRM); 2) cassiterite-sulphide-quartz veins (CS); and 3) silver-polymetallic mineralization (SP).

Four generations of sphalerite were found in ores of the deposit. Sphalerite-1 occurs in mineral aggregates of the GRM stage, sphalerite-2 is associated with the CS, and sphalerite-3,4 was found in the SP.

Electron microprobe analyses revealed the following variation of chemical composition of sphalerite (Fig. 1):

Sphalerite-1: from 1.0 to 4.4 wt.% Fe; from 0.2 to 0.4 wt.% Cd; from 1.0 to 4.4 wt.% Mn.

Sphalerite-2: from 1,0 to 4.4 wt.% Fe; from 0.0 to 1.4 wt.% Cu; from 0.1 to 1.2 wt.% Cd; from 0.0 to 0.4 wt.% Mn.

Sphalerite-3: from 0.0 to 9.73 wt.% Fe; from 0.0 to 4.6 wt.% Cu; from 0.0 to 1.1 wt.% Cd; from 0.0 to 0.1 wt.% In; from 0.0 to 0.1 wt.% Mn.

Sphalerite-4: from 0.0 to 3.4 wt.% Fe; from 0.0 to 2.3 wt.% Cu; from 0.1 to 1.3 wt.% Cd; from 0.0 to 0.1 wt.% In.

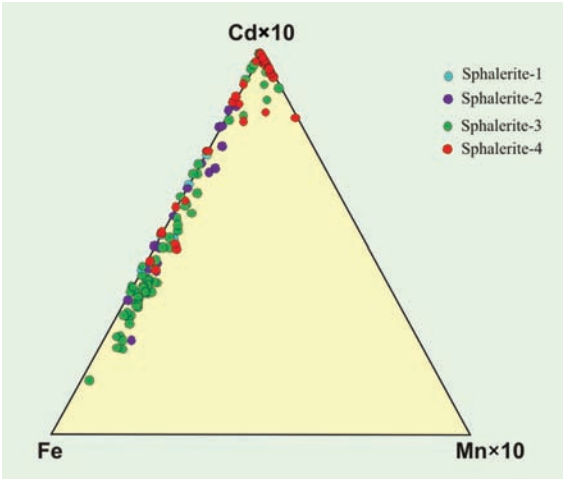

Fig. 1: Fe-Cd-Mn diagram of sphalerite from the Mangazeyskoe deposit.

Groups of points corresponding to sphalerites of different generations overlie one onto another (Fig. 1). It may be explained by the uniform source of fluids. It is probable the change of chemical composition occurs as a result of evolution of mineral system. These data are in disagreement with studies of trace element distributions in sphalerite from typical Pb-Zn deposits [1] that pointed out that sphalerite of different origins can be distinguished in the Fe-(Mn×10)-(Cd×10) diagram.

Acknowledgements: This study was supported by the Russian Foundation for Basic Research project 09-05-12037-ofi_m.

[1] Qian, Zh. (1987) *Geochem.*, **6(2)**, 177-190.

Isomorphism of Bi-Sb-Pb and Te-Se-S in Bi-bearing minerals in deposits of North-East Asia (Russia)

Anikina, E.[1*], Goryachev, N.A.[2] & Gamyanin, G.N.[1]
[1]IGEM RAS, Moscow, Russia ([*]anikina@igen.ru)
[2] NEISRI FEB RAS, Magadan, Russia

Bi mineralization is widely present in Sn, Ag-Pb and Ag-rare-metal deposits of the North-East Asia (NEA). The NEA regional geochemistry is characterized by a high geochemical background of Sb. Owing to this fact, Bi-bearing minerals of these deposits always contain admixtures of Sb, with the Sb concentration increasing from early to late paragenetic associations. Influence of Sb in Pb-Bi parageneses increases at overlay of Ag-Pb mineralization on cassiterite-sulphide (Prognoz deposit) or cassiterite-silicate (Alyaskitovoe) mineralizations. In these deposits, some Ag-Pb-Sb-Bi minerals have been identified: Sb-gustavite (13-17 % Sb), Bi-owyheeite and teremkovite (2-5 % Bi), Bi-ramdohrite (up to 8 % Bi). A nearly complete solid solution between andorite and its Bi-analogue was revealed (Fig. 1). A considerable admixture of Bi in miargyrite (up to 22 wt.%) was detected as well (Fig. 2).

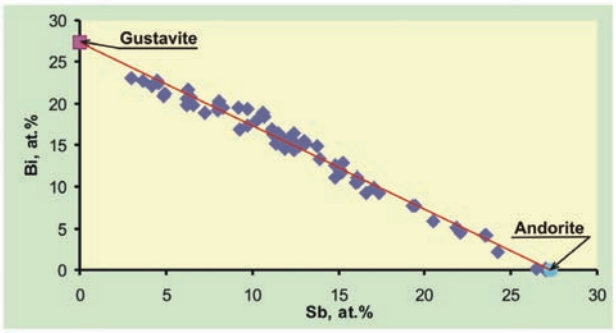

Fig. 1: Plot of andorite-gustavite series microprobe analyses showing relationships between Bi and Sb.

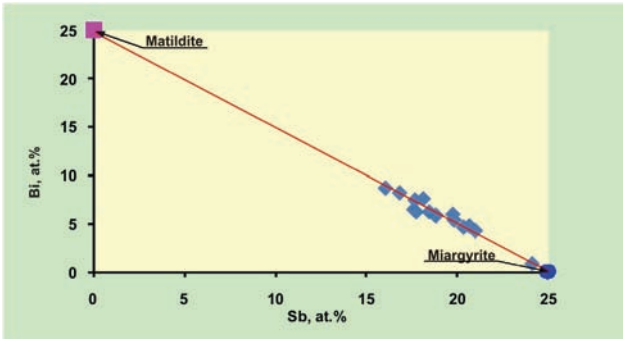

Fig. 2: Plot of miargyrite (with high Bi content) microprobe analyses showing relationships between Sb and Bi.

In Ag-rare-metal deposit, native Bi, sulphides, selenides and sulphotellurides of Bi were identified. One of the interesting features of these minerals is their wide Te-Se-S isomorphic substitutions. In some grains of joseite, Se content varies from 0.9 to 7.6 %. Wide isomorphic substitutions between Se, Se and Te were observed in the bismuthinite-ikunolite-laitakarite series. Silver minerals can be subdivided into sulphide-selenide-telluride and sulphide-bismuth associations.

The wide S-Se-Te and Pb-Sb-Bi isomorphism of studied Bi-bearing minerals is caused by the specificity of ore-forming processes in different Sn, Ag and Ag-Pb deposits of the North-East of Asia.

Acknowledgements: This study was supported by the Russian Foundation for Basic Research project 09-05-00819.

Sulfide minerals of nickel and platinum in the Abdasht Ultramafic Massive (Esfandaghieh region, Iran)

Bagheryan, S.
Islamic Azad University - Aligudarz Branch, Aligudarz, I.R.Iran (syamak.bagheryan@gmail.com)

The Abdasht peridotitic massive is part of the Esphandaghieh ophiolite complex. Constituents of the Abdasht rocks are mostly dunite harzburgite which occasionally convert to lherzolite and wherlite. Chromite deposits occur in 15 mineralized horizons. As constituents of one of the world's ophiolite complexes, Abdasht rocks might be worthwhile sources of PGM, Ni and Co, in addition to Cr. Therefore, various geochemical and ore microscopic studies were conducted to identify sulfide minerals.

The studies reveal the presence of nickel sulfide minerals (especially pentlandite) in the region. These are found in two different parts: (1) in the host rocks of the chromite deposits and (2) in chromite lenses.

PGM occur in very low concentrations (at most 83 ppb in Kamalabad mine), often as inclusions and fine grains in chromite and silicate gangue. Other sulfide minerals such as pyrrhotite, pyrite, millerite, chalcopyrite, chalcocite, nickelpyrite, chalcopentlandite, valleriite etc. were also found. These sulfide minerals (Ni, Co and PGM) do not represent worthwhile resources, and are therefore economically negligible.

Minerals of Jas-Roux (France): an update

Boulliard, J.C.[1*], Morin, G.[1], Bourgoin, V.[2] & Favreau, G.[2]
[1]IMPMC, UPMC, Paris, France
([*]jean-claude.boulliard@impmc.upmc.fr)
[2]Assoc. Jean Wyart (IMPMC) and AFM, ENSMP, Paris, France

Jas-Roux is located in the Parc des Ecrins, Hautes-Alpes, France. It is a hydrothermal stratiform deposit in dolomitc limestones. It appears as several lenses embedded in the Pigeonnier anatexites. These lenses protrude and form small cliffs parallel to the valley. The mineralisation mainly consists of barite, quartz and pyrite. Other minerals reported so far are Zn, Sb, As, Tl, Ag, Hg, Pb sulfides and sulfosalts. Jas-Roux is the type locality of chabourneite, laffitite, routhierite and pierrotite discovered after field researches performed at the end of the 1960's. More recently this deposit has appeared as a good candidate for the study and modelisation of As, Sb, Pb, Tl, Hg diffusion in the soil. Our recent prospects have given rise to the discovery of a dozen of minerals which were not known in this locality so far. Five of them are new in France: dorallcharite, klebelsbergite, millosevichite, szomolnokite and voltaite.

Origin of red colouring in Turonian pelagic limestones from the Vispi Quarry in the Cretaceous of central Italy

Cai Yuanfeng[*], Li Xiang, Hu Xiumian, Chen Xiaoming & Pan Yuguan
State Key Laboratory of Mineral Deposits Research, Dept. of Earth Sciences, Nanjing University, Nanjing, China
([*]caiyf@nju.edu.cn)

Hematite pigmentation has been considered to be the most common and important factor in the formation of the red colour in sediments. Two hypotheses were usually put forward for the origin of the red colour [1]: the first involves the derivation of detrital hematite from lateritic soils while the second involves authigenic precipitation from the weathering of iron-bearing (detrital) minerals such as pyrite, chlorite, biotite, amphibole, pyroxene and olivine. Similar explanations have been suggested for the red pigmentation in limestones but there are some red limestones, such as the Upper Cretaceous Scaglia Rossa limestone from Gubbio in central Italy, in which no hematite is detectable by X-ray diffractometry (XRD). Interpretation of the source of this red colour has been much disputed: the most important and frequently mentioned one is "fine particle size and random distribution".

Mn^{2+}-doped materials have been widely used as optical material to produce different wavelengths of visible light, causing yellow to orange-red, red, dull orange and violet cathodoluminescence in Mn^{2+}-doped calcite. Thermoluminescence occurred at 620 nm, when the Mn^{2+} returned from the excited state back to the ground state. Hence, manganese may be considered another origin of red colour in Mn^{2+}-bearing calcite.

Samples of Turonian red limestones from the Vispi Quarry in central Italy have been examined by XRD, EPMA, ESR, DRS and HRTEM. The ESR, EPMA and XRD results suggested that Mn^{2+} was incorporated into the structure of calcite during the precipitation of the limestones. DRS results suggested the presence of hematite. Under both SEM and EPMA, we use EDS to check the iron signal in the whole section. The observation shows that hematite coexisted with detrital qurtz or layer minerals. However, this type of hematite is very rare and difficult to be found. We selected an area without detrital hematite for futher observation with HRTEM and found that nanometer-size hematite grains were present in red limestones. Grains have neither perfect crystal shapes nor regular or straight boundaries. However, it is most important that they have a typical 0.271 nm diffraction line in selected-area electron diffraction (SAED) patterns and weak iron but no sulphur signal in energy-dispersive X-ray spectra. The hematite grains were present in two forms: one type is present in the interstices of calcite grains, and another is a film-like wrapping substance in which the calcite crystals are buried. Hence, these observations suggest that amorphous nanosize hematite grains and the Mn^{2+}-bearing calcite endowed the limestone with a red colour as the major pigmentation, and the Mn^{2+}-bearing calcite gave it a pink tinge. This study may suggest that the nanosize hematite grain and the Mn^{2+}-bearing calcite granted the red colour of CORBs. Two forms of hematite grains play major roles in the development of colour. These results may suggest that the bottom sea water was oxidized when red limestone precipitated.

Acknowledgements: This study was financially supported by the Chinese MOST 973 Project (2006CB701402). This abstract is a contribution to the international Geosciences Project 555.

[1] Yilmaz, I.Ö (2008) *Turkish J. Earth Sci.*, **17**, 263-296.

Sulfate mineralization at the geyser near Pinchollo, South Peru

Ciesielczuk, J.[1*], Żaba, J.[1], Bzowska, G.[1], Gaidzik, K.[1], Głogowska, M.[2] & Rygał, J.[3]
[1]University of Silesia, Sosnowiec, Poland
([*]justyna.ciesielczuk@us.edu.pl)
[2]Central Mining Institute, Katowice, Poland
[3]The University of Science and Technology, Kraków, Poland

Surface, sulfate mineralization precipitated from thermal water in the vicinity of a geyser located above village Pinchollo, at the foot of Hualca Hualca volcano (6025 m a.s.l.) in the Western Cordillera of Southern Peru were studied. Recent volcanism and thermal activity in Southern Peru is connected with subduction zone as a result of underthrusting of Nazca Plate under the Southamerican Plate. The geyser is one of many thermal activity manifestations in Arequipa department, where a belt of recent stratovolcanoes of Central Volcanic Zone of the Andes coincides with lava fields and small scoria cones of Andahua volcanics. The area is built of crystalline Arequipa Massif, overlain by thick suite of folded Mesozoic sedimentary formations, intruded by Late Mesozoic-Paleogene granitoids and then by Oligocene-Miocene volcanics of Tacaza Group, Plio-Pleistocene Barroso stratovolcanoes (some of them still active), and Pleistocene-Holocene Andahua Group. Seismic activity and fault tectonics is very strong. The area abounds in thermal springs, contains few geysers, and several Neogene epithermal gold-silver deposits are present. Therefore long established Cenozoic geothermal system exists there.

Thermal water present in the Chivay area is mainly chloride. It has a neutral pH and is enriched in Li, Sr, and B. Water erupted in geyser was boiling, but as it is located at the altitude of 4353 m a.s.l. its temperature could be 70-80°C. Temperature of the reservoir is 110-120°C. In the vicinity of Pinchollo three geysers are known, but presently only one of them appears active. Two others situated lower turned to be hot springs, one ceased during an earthquake in 2001.

Minerals of different habits and yellow, orange and white colours have precipitated on the soil and dry plants close to the geyser (location 1) and in a distance of ca 100 m east of the geyser (location 2). Collected samples were dried for one week. Chemical composition and habit of the minerals were investigated using scanning microscope coupled with EDS and phase composition was checked by XRD. All are sulphates.

The chemical composition of all sulfate minerals is simple, consisting only of Al, Fe, S, O and K, Mg, Ca, N. But phase composition is strongly complicated proving with no doubts the presence of the following minerals: alunogene, copiapite, coquimbite, tschermigite, jarosite - ammoniojarosite, gypsum, alunite, apjohnite - pickeringite - halotrichite , boussingaultite, mohrite, rozenite, voltaite - voltaite-(Mg) and mascagnite, picromerite.

Quartz and clay minerals as kaolinite or illite/mica are residual belonging to the soil composition.

Above mentioned set of minerals is very similar to these formed on the burning coal dumps in Poland, where the host rocks are silicoclastic suite of clays, mudstones, sandstones and subordinate carbonatic rocks as siderites, dolomites and limestones.

Fluorine-rich vesuvianite from Borborema province, Brazil

Čobić, A.[1*], Mikulčić Pavlaković, S.[2], Zebec, V.[2], Wegner, R.[3] & Bermanec, V.[1]
[1]Institute of Mineralogy and Petrology, Faculty of Science, University of Zagreb, Croatia ([*]ancobic@geol.pmf.hr)
[2]Croatian Natural History Museum, Zagreb, Croatia
[3]Dept. de Min. e Geol, Centro de Ciências e Tecnologia, Universidade Federal de Campina Grande, Brazil

Investigated crystals were collected from a skarn deposit with molybdenite and F-apophyllite in paragenesis in Sítio São Gonçalo, Santa Luzia, Borborema Province, state of Paraiba, Brazil (coordinates: S 06º54.916´ W 036º50.478´). During this investigation, calcite, pyrite, zircon and molybdenite were noticed. Crushing of samples releases H_2S. There is a record of vesuvianite crystals from this province in literature [1].

Crystals are well developed, but occur as fragments in breccia and are often zoned. Several habits can be distinguished: shorter prismatic where {001} is the dominant form and are lavender-grey in colour; elongated with smaller {001} which are ipe yellow. The habits of purple–orange crystals are between the shorter prismatic and elongated habits. Colourless or almost colourless crystals are minute and covered with calcite crystals. They are probably the latest.

Goniometric measurements on 8 samples exhibit following 30 forms: {001} and {110} as dominant forms, {100}, {450}, {320}, {210}, {310}, {410}, {510}, {102}, {203}, {101}, {201}, {1.1.10}, {113}, {111}, {443}, {221}, {331}, {10.10.3}, {551}, {313}, {414}, {312}, {211}, {311}, {511}, {223}, {421} and {955} which appears very rarely on vesuvianite crystals. Axis ratio calculations yield a:c = 1:0.5373 which is very similar to ratio given by Goldschmidt (a:c=1:0.5376; [2]).

X-ray powder diffraction data of investigated samples show following unit cell parameters: for lavender-grey - a = 15.512(2) Å, c = 11.786(3) Å, V = 2835.8(7) $Å^3$; for ipe yellow - a = 15.598(1) Å, c = 11.784(2) Å, V = 2833.9(5) $Å^3$. Annealing at 1025°C results in decomposition to gehlenite and wollastonite type structures with the remnants of vesuvianite structure. Due to annealing the following loss of water occurs: for lavender-grey 2.39 wt. %; for ipe yellow 3.09 wt. %;

Microprobe analysis performed on a lavender-grey sample, calculated on the basis of Ca+Na = 19.00 apfu, yield following formula:

$(Ca_{18.86}Na_{0.14})_{\Sigma 19.00}(Al_{10.30}Mg_{1.23}Fe_{1.34}Ti_{0.16}Mn_{0.04})_{\Sigma 13.08}[SiO_4]_{10}[Si_2O_7]_4(OH_{4.75}F_{3.38}O_{3.10})_{\Sigma 11.23}$.

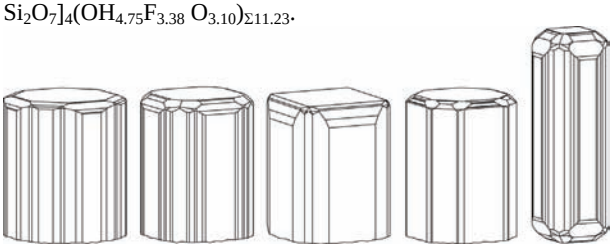

Fig. 1: Morphology of measured vesuvianite crystals.

According to Britvin et al. [3], a mineral can be classified as a fluorvesuvianite if containing F> 4.5 apfu. Thus, this sample is a fluorine-rich vesuvianite.

[1] Souza Neto, J.A. et al. (2008) *Miner. Deposita*, **43**, 185-205.
[2] Goldschmidt, V. (1918) *Atlas der Krystallformen, Text, band IV*. Carl Winters Universitätsbuchhandlung, Heidelberg.
[3] Britvin, S.N. et al. (2003) *Can. Mineral.*, **41**, 1371-1380.

Morphology investigation of brazilianite from different localities

Čobić, A.[1*], Zebec, V.[2], Scholz, R.[3] & Bermanec, V.[1]
[1]Faculty of Science, Institute of Mineralogy and Petrology, Zagreb, Croatia ([*]ancobic@geol.pmf.hr)
[2]Croatian Natural History Museum, Zagreb, Croatia
[3] Universidade do Estado de Minas Gerais - Faculdade de Engenharia, João Monlevade – MG, Brazil

On the morphology of brazilianite there hasn't been published many papers since its discovery [1]. From the importance of crystallogenetic study and possible differences between material from different localities arises need for a study of brazilianite crystals.

Two circle goniometric measurements were performed on 34 single crystals of brazilianite from different localities in Brazil. 26 measured crystals originate from Telírio claim, Linopolis, Divino das Laranjeiras, one from Divino das Laranjerias province (exact mine not determined), three from São Geraldo do Baixio district and four from Araçuai region.

All brazilianite crystals are well developed, but were probably attached to matrix on one end of [100] so in almost all crystals that side is missing. Crystals colour ranges from yellow, through yellowish-greenish to green, while some crystals are colourless. All forms in [001] zone are striated parallel to [001]. Forms that occur on every measured brazilianite crystal are {010} and {110} and they are striated. Other forms that are very common are: {011}, {$\bar{1}$11}, {211} and {$\bar{1}$01}. Four forms, not measured before, appear on investigated crystals. These are: {143}, {520}, {322} and a form with {hkl} indices. Indices for the {hkl} form could not be exactly determined due to restrictions in precision of stereographic/gnomic projection. The face is very gently inclined and close to {001}.

There is a record of several habits of brazilianite crystals in literature [1, 2]. Several new habits can be distinguished after these measurements (fig. 1).

Two new habits, together with four new forms are recognized during this morphological investigation of brazilianite crystals.

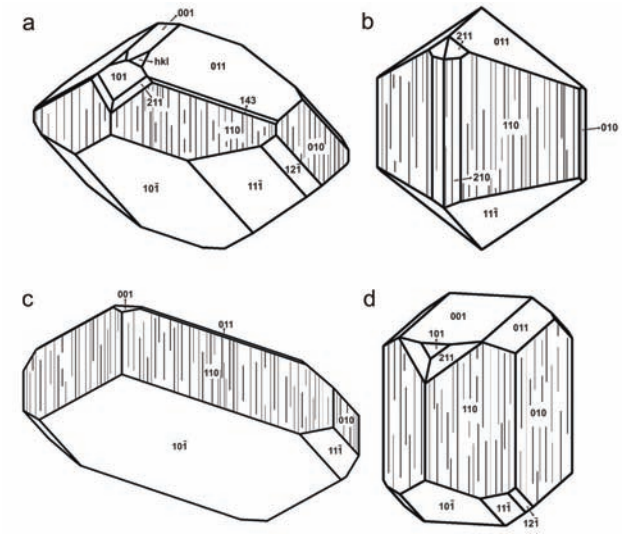

Fig. 1: Different habits of brazilianite crystals.

[1] Frondel, C. & Lindberg, M.L. (1948) *Am. Mineral.*, **33**, 135-141. [2] Pough, F.P. & Henderson, E.P. (1945) *Am. Mineral.*, **30**, 572-582.

Unusual minerals of tin in explosive breccias of the Churpunn'ya deposit (East Yakutia, Russia)

Gamyanin, G.[1*], Anikina, E.[1], Kholmogorov, A.[2] & Popova, S.[2]
[1]IGEM RAS, Moscow, Russia ([*]ggn@igem.ru)
[2]IDPMG SB RAS, Yakutsk, Russia

Churpunn'ya deposit is located in the northern part of Eastern Yakutia. It belongs to cassiterite-silica-sulphidic deposits and is related to complex vulcano-plutonic area. Crater facies (J_3) of paleovolcano is intruded by dacite dykes (K_2). Vein bodies and mineralized zones cross dacites and are composed of two stages: cassiterite-quartz-tourmaline and quartz-pyrrhotite-chalcopyrite-sphalerite with admixture of Sn-Pb-Sb sulphosalts. One of the most remarkable features of the deposit is a wide spread of explosive breccias at the early stage and intra-ore explosions at the late stage of its formation. Intra-ore explosions are interesting by its wide variety of Sn minerals. There are small fragments of minerals of an early stage and new-formed mineral in the cementing black ultrafine-grained porous mass of Sn-Fe-oxide-silicate composition (Fig. 1, points 6, 7; table 1). Fragments consist of rhomb-like crystals of ilmenite (Fig. 1, point 4; table 1), Sn-titanomagnetite (Fig. 1, point 5), TiO_2 - the zone lamellar isolations forming polygonal structures. The central part of lamellae correspond to ilmenite composition with admixture of Cr and Sn (up to 2-3 %), whereas their external part contains Sn-bearing (to 8 %) titanomagnetite with admixture of Si (to 5 %). Dendrites of Sn-Fe-Ti-Si-oxide composition and numerous microspheroids (from <1 to 20 μm) are irregularly distributed in the cementing mass. Microspheroids consist of Sn-Sb (Sn–40-56 wt.%; Sb–41-56 wt.%), Sn-Sb-Pb (Sn–44-58 wt.%; Sb–26-48 wt.%; Pb–6-16 wt.%), Sn-Cu-Sb-Ni (Sn–24-56 wt.%; Cu–23-32 wt.%; Sb–8-42 wt.%; Ni–5-10 wt.%) intermetallides and sulphostannates (Sn–56-65 wt.%; Pb–18-25 wt.%; S–18-20 wt.%). The composition of microspheroids is generally similar to that of sulphostannates and intermetallides of sulphide ores, but with prevalence of metals.

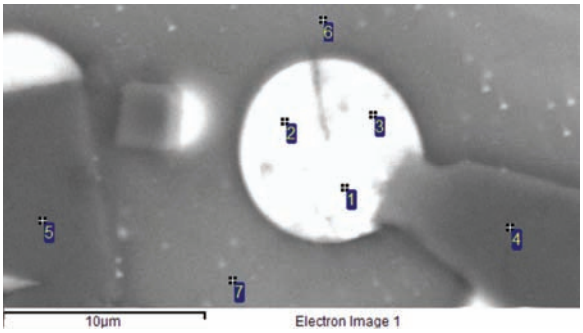

Fig 1: Mineral intergrowths of explosive ores.

Table 1: Microprobe analyses of minerals of explosive ore (№ analyses correspond to those in fig.1)

№	O	Si	Ti	Mn	Fe	Pb	Sb	Sn	S	Sum
1						16,7		63,2	19,6	99,5
2						7,1	48,6	43,9		99,6
3						16,4	26,1	58,4		100,9
4	39,2		36,5	1,9	18,8			1,9		98,3
5	26,5		11,6	1,4	56,2			4,3		100,0
6	34,9	16,3			16,7			31,6		99,5
7	32,8	15,8	1,5		12,6			36,0		98,7

The observed specificity of ore textures and variety of Sn minerals are the result by deposit formation in near-surface conditions under thick effusive cover and the enrichment of fluid by gaseous components.

Composition of arsenopyrite from giant ore deposits of Northeastern Asia

Gamyanin, G.N.[1*] & Goryachev, N.A.[2]
[1]Institute of Geology of Ore Deposits, Petrography, Mineralogy, and Geochemistry, Russian Academy of Sciences, Moscow, Russia ([*]ggn@igem.ru)
[2]Northeastern Interdisciplinary Scientific Research Institute, Far East Branch of Russian Academy of Sciences, Magadan, Russia

Arsenopyrite is the main ore mineral for all giant ore deposits of the North East Asia (Au – Mayskoye, Natalka, Nezhdaninskoye; Sn – Deputatskoye and Ag – Prognoz). The comparison of compositions of arsenopyrite from these deposits indicated that the mineral is formed as three common generations: Ars-1 forms meta crystals in altered rocks; Ars-2 is represented by coarse grains in quartz veins; small grains and crystals of Ars-3 are formed by latest (Sb or Ag-Pb) regeneration-type mineralization. Microprobe and atom-absorbtion analyses provide chemical differences between these generations of arsenopyrite (Table 1).

Table 1: Composition of arsenopyrite generations

Deposit type	Ars 1	Ars 2	Ars 3
Au	S/As-1,095-1,064 Au-20-10000ppm Sb= 50-150 ppm	S/As-1,0611,044 Au - <<200 ppm Sb - 40-300 ppm	S/As-1,020-1,009 Au-<< 50 ppm Sb-200-1500 ppm
Sn	S/As-0,925-0.961 Sb-20-70 ppm Bi-30-400 ppm Ag-100-300ppm Au-5-50 ppm	S/As-0,970-1,030 Sb-100-500 ppm Bi-1-100 ppm Ag- 200-700ppm Au-0.5-5 ppm	S/As=1,040-1,080 Sb-0,3-2,8% Bi-1-20 ppm Ag->1000ppm Au-5-10 ppm
Ag	S/As-0,890-0,930 Sb-0-2% Co-0,1-1,6% Ni-0,1-2% Ag-60-200 ppm Au-0,1-0,3 ppm	S/As-0,975-1,028 Sb-0,5-3% Co-up to 2% Ni-up to 3% Ag-300-600 ppm Au-0.5-1 ppm	S/As-1,025-1,050 Sb- 2-8% Co-0.8-2.9% Ni-2-9% Ag-500-4000 ppm Au-1,5-5 ppm

For composition of arsenopyrite from gold deposits, the data given in Table 1 show a decrease in the S/As ratio and the Au content from Ars-1 to Ars-3 accompanied by the increase of the Sb content. Prismatic crystals of Ars-1 are strongly enriched by Au. The composition of arsenopyrites from tin deposit Deputatskoye shows an opposite trend. Here tendency is to increase S/As ratio and Sb and Ag content from Ars-1 (from tin-bearing greisens) via Ars-2 (from cassiterite-sulphide ores) to Ars-3 (from latest Ag stage) accompanied by the decrease of the Bi content. The Au content in these arsenopyrites is variable. Ars-1 from this deposit has a high content of Co (up to 1%) and Ni (up to 0.3%). The S/As ratio in Ars-2 is very low. For the Ag deposit of Prognoz, we investigated three stages of ore formation: (1) Au-Bi, (2) Sn-sulphide, and (3) Ag-Pb ores. The data of Table 1 demonstrate a tendency of increasing the S/As ratio and Co, Ni, Sb, Au, and Ag contents from Ars-1 to Ars-3. Ars-1 associates with nickeline and gersdorffite. Small prismatic crystals of Ars-3 have zones enriched in Co (up to 8%), Ni (up to 11%), and Sb (up to 15%).

In general, composition of arsenopyrite from different giant ore deposits depends upon mineralogy and geochemistry of ores as well as upon the ore genesis.

Acknowledgements: This study was supported by the Russian Foundation for Basic Research project – 09-05-98593r_vostok_a.

Rhönite and associate minerals in a basaltic pillow lava from the Basque-Cantabrian Basin (Vizcaya, Spain)

Gil-Crespo, P.P.[1*], Pesquera, A.[1] & Torres-Ruiz, J.[2]
[1]Depto. de Mineralogía y Petrología, Universidad del País Vasco, Bilbao, Spain ([*]pedro.gil@ehu.es).
[2]Depto. de Mineralogía y Petrología, Universidad de Granada, Spain

Rhönite is a relatively rare mineral that is isostructural with aenigmanite. It occurs in a basaltic pillow lava from the Basque-Cantabrian Basin (Vizcaya, Spain), with kaersutite, Ti-augite, plagioclase and ilmenite as main components. The rhönite-bearing basaltic pillow lava is a laminar body of variable thickness (2 to 20 m thick), which appears interbedded between upper Albian-lower Cenomanian "flysch" sediments. It shows a porphyritic texture in which centimetric phenocrysts (up to 7 cm) of ferromagnesian minerals can be observed.

Plagioclase phenocrysts are coarse grained (<1,5 cm), frequently displaying a normal, oscillatory to patchy zoning with a composition that ranges from ~70 to 90%An. Resorbed plagioclase phenocrysts with sieve and dusty textures are common. Ti-augite phenocrysts have a variable grain size and the largest phenocrysts may reach up to 5 cm in length. They show a prismatic euhedral to subhedral habit, purplish brown, pale brown to yellowish green coloured in thin section, and a complex optical zoning (oscillatory, continuous to patchy zoning). Kaersutite phenocrysts (up to 7 cm in length) show a prismatic subhedral habit to rounded shapes with a strong pleochroism, from reddish brown to yellow brown colour. Ilmenite occurs as (i) subhedral to rounded crystals (<5mm) associated to ferromagnesian minerals, (ii) acicular ilmenite; and (iii) small rounded grains that form part of the groundmass. Subhedral to subrounded apatite is a common accessory mineral. Pyrite and amigdales up to 1 cm filled by chlorite and calcite can be also observed.

Rhönite has been observed in some samples from the central part of the lava, typically associated to the amphibol. It constitutes an accessory mineral, very fine grained (<300 μm), with a prismatic subhedral to skeletal habit, and a dark-reddish brown to black colour. The microprobe analysis of 17 rhönite grains reveals the following compositional variations: SiO_2, 22.30-24.10; TiO_2, 11.56-12.94; Al_2O_3, 15.84-17.01; FeO_t, 19.49-22.07; MnO, 0.11-0.28; MgO, 12.68-14.09; CaO, 11.13-12.28; Na_2O, 0.73-0.89; K_2O, 0.0-0.27. Based on textural relationships, it is believed to be formed as a reaction product after kaersutite, probably under P-T conditions of < 0.5 Kbar, 1090-1120ºC, and an oxygen fugacity lower than the FMQ buffer.

New mineralogical data and genesis of limnosilicites from the Kremnica graben, Central Slovakia

Gregor, M.[1*], Koděra, P.[2], Lexa, J.[3] & Fallick, A.E.[4]
[1]Geological Inst., Comenius University, Bratislava, Slovakia ([*]geolgregor@yahoo.com)
[2]Dept. of Geology of Mineral Deposits, Comenius University, Bratislava, Slovakia
[3]Geological Inst., Slovak Academy of Sciences, Bratislava, Slovakia
[4]Scottish Universities Environmental Research Centre, East Kilbride, UK

Kremnica volcanotectonic graben in the Central Slovakia Volcanic Field hosts several localities with silica-rich rocks, deposited mainly in limnic/lacustrine environment hosted by altered rhyolite tuffs. This area is located S of the Kremnica low-sulfidation Au-Ag deposit, situated at the E side of a local horst. Silicites are often interlayered with bentonite (smectite) deposits and result from episodical inflow of groundwater enriched in silica due to decomposition of volcanic glass.

Limnosilicites are massive, laminated or occasionally brecciated rocks of variable colour, changing from white or reddish-brown to black. Colour variations depend on the content of organic matter and Fe-oxides/hydroxides. XRD and IR analyses showed that *white limnosicilites* are composed exclusively of quartz with index of crystallinity [1,3] ranging from 1 to 8. Their etched surface revealed the presence of quartz pseudomorphs after opal-CT lepispheres. White silicites originated in environment with flowing water as indicated by alignment of sillicified fossil flora. XRD data of dark limnosilicites exhibit diffraction peaks of quartz and peaks corresponding to opal-C or cristobalite (4.11 and 2.50 Å). Diminishing of the 4.11 Å peak after orthophosphoric digestion [2] and increase in FWHM values after refiring at 1050°C [3] confirmed the presence of opal-C. IR spectra showed vibration bands characteristic for amorphous silica, while quartz bands were absent. Crystallinity index of quartz from *dark silicites* is low (<<1), and is interpreted to depend on the content of carbon and Fe oxides/hydroxides that retard recrystallization of amorphous silica to quartz. The presence of organic matter probably results from origin in boggy anoxic environment with standing water. Infrequent *brecciated limnosilicites* have opal-AG matrix. Rarely, limnosilicites are overlain by layers of pure opal-CT.

Oxygen isotope composition of opal-AG and opal-CT bearing samples showed lower $\delta^{18}O$ values (22-29 ‰) compared to opal-C bearing and quartz only samples (14-24 ‰). Systematic increase in $\delta^{18}O$ values of silicites from N to S was observed, while individual localities showed just a limited variation of data. Clear correlation of $\delta^{18}O$ values of silicites and smectites indicates the influence of a similar factor responsible for change in $\delta^{18}O$ composition, which was most likely the change in temperature. This is also supported by correlation of smectite $\delta^{18}O$ composition with smectite crystal size [4]. Temperatures of crystallisation of silicites 80°C in N part to 30°C in S and SE parts were calculated based on equilibrium isotope fractionation between silicites and water [5]. Changes in temperature resulted from paleoflow of heated groundwaters and/or recrystallisation during subsequent shallow burial.

Acknowledgements: Support by VEGA grant 2/0171/08 is appreciated.

[1] Murratta, K.J. & Normann, B.M. (1976) *Am. J. Sci.*, **276**, 1120-1130. [2] Kahram, S. et al. (2005) *Anal. Chim. Acta*, **525**, 201-206. [3] Herdianita, N.R. et al. (2000) *Geothermics*, **29**, 65-81. [4] Koděra, P. et al. (2010) this volume. [5] Kita, I. et al. (1985) *Nature*, **314**, 83-84.

Alluvial minerals from Crişul Negru hydrographic basin (Bihor, Romania)

Hadnagy, A.
Romanian Geological Institute, Cluj-Napoca Mineralogical Branch, Cluj Napoca, Romania (hadnagyarpad@clicknet.ro)

Alluvial deposits are potential sources for recovering certain deficient mineral resources. They could be cheaply mined and easily separated. Thus the complex study of recent alluvia, done on aleatory basis so far, especially the re-evaluation of heavy mineral contents is a must for modern economic geology.

Crişul Negru River hydrographic basin is almost completely located in Bihor County, Apuseni Mts., Romania. The basin basement was intensely studied by previous authors; it shows very different petrographic features resembling a geological mosaic, mainly consisting of acid and neutral igneous rocks (granites, granodiorites, pegmatites, rhyolites, andesites etc.) commonly bearing Ti- and Zr- accessory minerals. These premises justify a re-evaluation for some rare alluvial heavy minerals not used so far.

In order to investigate the qualitative and quantitative (percentage and areal distribution) characteristics of all the possible alluvial mineral resources, the sediment discharge by recent alluvia has been thoroughly separated and studied by using modern equipment: automatic sieving machine, electromagnetic sorting device, electron scanning microscope (SEM), three-stimulus colorimeter, high precision analytical balance; satellite infra-red photographs complemented the study. Special attention has been paid to the structural and textural environment of these heavy minerals in order to present useful metallogenetic data for future investigations. The study has also concerned the mechanic aureoles boundaries of the already-known various lithostratigraphic formations and metallogenetic areas, as well as the delimitation of subordinate heavy mineral areas resulting from hydro-gravitational sorting. The morpho- and hydrodynamic relations inferred from the structural and textural features of the studied alluvia informed on several novel sedimentogenetic characteristics.

The mineralogical study of the 20,000 grain classes and subclasses led to the identification of several rich mineral parageneses which connected well to the known accessory mineral assemblages in the basement rocks. The morphologic study proved different morphoscopic features and very fine crystal shapes, which together with the graphic representations and the photographs provide scientific reference material to be used for future micromineralogic studies of similar minerals. The most relevant heavy mineral concentrate (sample nr. 812) yield 9 kg/m³ ilmenite, 1 g/m³ "leucoxene", 6 kg/m³ hematite, 0.2 kg/m³ rutile, and 0.01 kg/m³ zircon.

The theoretical value of this work consists in the indirect definition of accessory mineral parageneses related to the different rock types of the basement, by the micromineralogic study of monolithic alluvia. By using light reflection capacity of sands resulting from very diverse genetic processes, the role of colour parameters has been stated. The study aimed discriminating between magnetic and non-magnetic metallic spherules according to their origin (cosmic, volcanic and industrial) based on their chemical composition and morphoscopic features (by SEM). About 100 mineral species and varieties were added to the mineralogical topography of Romania, and some minerals were described for the first time in alluvia (nontronite, clinochlore, scheelite, bismuthinite, molybdenite, magnetite replacing fossils etc.). The "leucoxenisation" grade marks the relative age of the rocks. The major distribution source areas are presented. A new scientific view on the bauxite genesis in the Pădurea Craiului (Apuseni Mts.) is offered.

Tasmanian crocoite occurrence and water chemistry – implications for environmental metal contamination

Ii, Hiroyuki[1*], Taniguchi, Masanobu[1] & Sherwood, J.[2]
[1]Faculty of Systems Engineering, Wakayama University, Wakayama, Japan ([*]hiro@sys.wakayama-u.ac.jp)
[2]School of Life and Environmental Sciences, Deakin University, Australia

Crocoite ($PbCrO_4$) is a very rare mineral but abundant in the Dundas area of western Tasmania, Australia. Cr^{3+} is stable in most natural environments and so in most of minerals containing Cr it exists in this form. However, Cr in crocoite exists as Cr^{6+}. Pb and Cr are relatively common metals in the natural environment. However, compounds containing both Pb and Cr are very rare in natural environments. Artificially, Cr^{6+} is easily produced by oxidizing Cr^{3+} under high temperature conditions and it is useful as an oxidizing agent. Therefore, Cr^{6+} is very often used in chemical factories or chemical laboratories. And also, Pb is widely used for battery and historically as pipes for drinking water, in petrol and in paints. Because of this, artificial Cr and Pb contamination for soil and water can be an environmental problem. Therefore it is useful to trace the origins of the Cr and Pb of crocoite under natural conditions in order to better understand migration of Cr and Pb under artificial metal contamination. For this reason, the occurrence condition of crocoite and its associated water chemistry in the Dundas area was studied. Ultrabasic rock contains Cr minerals and sometimes Cr^{6+} is found in groundwater and spring water in the ultrabasic rock. In the Dundas area, Cr ion concentrations were low ranging from 0.004 to 0.01 ppm. However, Cr ion concentration of spring water in serpentinite containing stichtite $Mg_6Cr_2(CO_3)(OH)_{16}\cdot 4(H_2O)$ is 0.13 ppm. Under high pH condition, Cr^{6+} is produced from Cr_2O_3 or Cr^{3+} and Cr^{6+} does not need high Eh conditions. Serpentinite contains Mg hydroxide minerals and so spring water shows high pH. Pb, Zn and Ni ion concentrations of spring, river and crocoite mine adit water were 0.001 to 0.07 ppm, 0.006 to 4 ppm and 0.1 to 0.8 ppm respectively. Crocoite was observed at three old silver mines - the Adelaide, Red Lead and Dundas extended mines. Silver was produced from hydrothermal galena veins in serpentinite. At the Adelaide mine, a 100m deep shaft remains but is filled with water to the river level. Crocoite occurred at the old adit wall and in porous highly weathered rock along the vein above the river level. Because of the strongly weathered zone, original Pb minerals were not observed around the adit. On the other hand, compact silicified rock sometimes contains the Pb carbonate mineral, cerussite. At the Red Lead mine, the ore area was open cut. Crocoite occurred along highly weathered silicified rock or clay veins in the highly weathered rock. Again the original Pb mineral was not observed. In both mines crocoite was observed along weathered veins. At the Dundas extended mine, original and secondary Pb minerals were observed. Crocoite was observed at the adit wall however most crocoite was accompanied by Pb minerals along the galena vein. The original Pb mineral, galena, remains in the vein. Anglesite ($PbSO_4$) occurs around galena. White normal cerussite was observed beside anglesite and galena. Yellow Cr bearing cerussite was observed outside of anglesite and white cerussite. Crocoite was observed outside of galena, anglesite, and white and yellow cerussites. From these observations and the water chemistry, Cr^{6+} of crocoite is thought to be derived from serpentinite containing Cr^{3+} minerals such as stichtite by weathering. Under high pH condition, Cr^{3+} is oxidized to Cr^{6+}. Cr^{6+} is thought to migrate into galena veins via groundwater. Crocoite forms where and Pb and Cr ions co-occur through weathering processes. Therefore, the Cr ion is thought to migrate more easily in groundwater than the Pb ion.

Occurrence of crandallite series minerals in Variscan granitoid rocks in Poland

Kajdas, B.[*], Jerzykowska, I. & Michalik, M.
Institute of Geological Sciences, Jagiellonian University, Krakow, Poland ([*]bartlomiej.kajdas@uj.edu.pl)

Crandallite series minerals belong to APS minerals (aluminium phosphates and sulphates from the alunite supergroup). The general formula of the series is $AB_3(XO_4)_2(OH)_6$ (A – Ca, Sr, REE, Pb, Ba; B – Al, Fe^{3+}; X - P, As, S, Si).

Crandallite series minerals were noted during studies of samples from two Variscan granite massifs in Poland. Samples of the Karkonosze granite (Kowary Średnie) represent highly grusified rock. Samples of the High Tatra granite (Waksmundzki Wierch Mt) were collected as small rock fragments from soil profile. Minerals identification is based on chemical composition determined using SEM-EDS method.

At both localities crandallite series minerals were found in almost completely sericitized K-feldspars as 5-10µm skeletal crystals. In the Karkonosze granite examined minerals are square-shaped in cross-sections. They occur in clusters along fractures and cleavage planes of feldspar. Single pseudohexagonal in cross-section crystals of crandallite series minerals are present in the High Tatra granite. In some feldspars these crystals are replaced by iron oxides containing REE.

SEM-EDS results indicate that chemical composition of crandallite series minerals is close to florencite-(Ce) and goyazite (Table 1).

Table 1: Average chemical composition of crandallite series minerals obtained from EDS analysis (wt%)

	(1)	(2)	(3)
P_2O_5	26.15	30.29	22.37
SO_3	0.10	3.97	9.51
SiO_2	9.97	2.19	9.33
As_2O_5	4.25	n.d.	n.d.
Al_2O_3	32.98	35.47	34.54
Fe_2O_3	0.36	3.17	2.54
La_2O_3	7.20	4.70	1.75
Ce_2O_3	14.27	12.78	3.98
Pr_2O_3	0.27	n.d.	n.d.
Nd_2O_3	2.30	n.d.	0.11
Sm_2O_3	n.d.	1.15	1.37
Gd_2O_3	0.09	n.d.	n.d.
MgO	0.76	0.30	0.49
CaO	0.07	0.36	1.01
SrO	n.d.	4.09	12.11
Na_2O	n.d.	n.d.	0.25
K_2O	1.06	0.18	0.70

Florencite-(Ce) from the Karkonosze granite is characterized by the presence of small amount of arsenic in X position (about 4 wt% of As_2O_5). Florencite-(Ce) crystals from the Tatra Mts. contain Sr in A position (about 4 wt% of SrO) and S in X position (about 4 wt% of SO_3). Goyazite is REE bearing. Presence of SiO_2 in all minerals can be related partly to small crystal size and mixed X-ray signal.

Origin of the crandallite group minerals can be related to weathering or low-temperature hydrothermal processes. Taking to account that crandallite series minerals have not been described in hydrothermally altered or weathered rock samples from both granitic massifs we can assume that specific chemical environment is needed for their formation.

Indium mineralization in the Au-Mo(W)-porphyry Bugdaya deposit, Eastern Transbaikalia, Russia

Kiseleva, G.D.*, Kovalenker, V.A. & Mokhov, A.V.
Institute of Ore Geology, Petrography, Mineralogy, and Geochemistry, RAS, Moscow, Russia (*kis60@rambler.ru)

Indium mineralization consisting of rather exotic mineral species dzhalindite, $In(OH)_3$, was found in Au metal veins cross-cutting Mo(W)-porphyry stockwork at the 50 m depth below earth surface [1]. It occurs only in chalcedony, which cements Fe-rich and In-Cd-bearing sphalerite fragments. Most of the sphalerite fragments are rimmed by CuS-Cu_2S minerals, sometimes with greeenockite, and late galena forming the rims on covellite and greeenockite. Dzhalindite forms euhedral cubic or cubo-octahedral crystals in the zoned chalcedony. Some of the crystals have a spheroidal center and outer parts of rather complicated structure (Fig. 1). In many cases, external zones of crystals are inclined by 45° relative to the internal parts. Some crystals bear evidence of intermediate partial dissolution. Size of the crystals varies from 30 to 94 μm with the most frequent size of 60-70 μm.

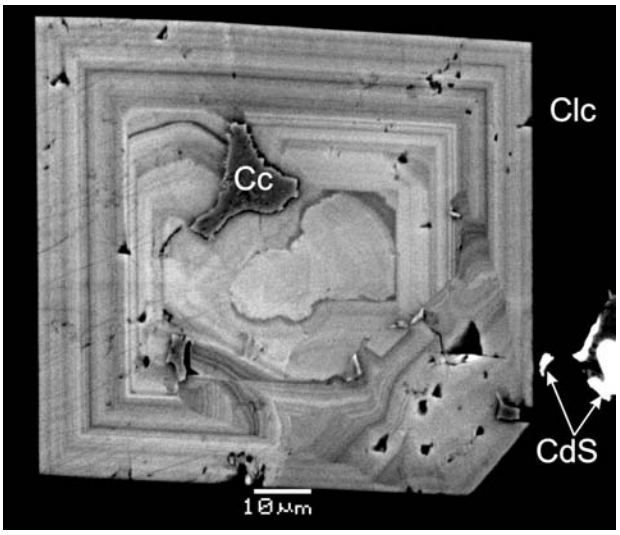

Fig. 1: BSE image of dzhalindite crystal with complicated internal structure. Cc – chalcocite, Clc – chalcedony, CdS – greenockite.

Dzhalindite is transparent or semitransparent, colorless, yellowish, pinkish-yellowish to light brown. All crystals of dzhalindite have oscillatory zoning clearly seen in the BSE images (Fig. 1). The zoning (and color intensity) is caused by the variations of Fe (0.61 – 3.6 wt.%) and In (63.27-78.5 wt.%) content. The lighter internal parts of crystals are most pure $In(OH)_3$ with a higher In-content. Some analyses also show additional components as follows (wt.%): W (1.29-1.5), Sn (4.77), Te (0.67-1.22), Cd (0.83-1.03). Dzhalindite contains inclusions of covellite-chalcocite relics and, very rarely, microspheroidal inclusions of low fineness electrum. Dzhalindite-bearing chalcedony contains native Ag (sometimes with stromeyerite relics), Ag-amalgams, stolzite, Pb oxide, goethite, greenockite, and covellite-chalcocite relics. This assemblage can indicate supergene origin of dzhalindite as the result of dissolution of In-bearing sphalerite and precipitation $In(OH)_3$ from Si-colloidal solution.

Acknowledgements: This work was supported by RFBR (10-05-00345).

[1] Kiseleva, G.D. et al. (2008) *New Data on Minerals*, **43**, 13-22.

Anisotropic garnet from the Yamansu deposit, Xinjiang, China

Kobayashi, S.[1*], Fujisawa, A.[1], Miyawaki, R.[2] & Kaneda, H.[3]
[1]Dept. of Applied Science, Okayama University of Science, Okayama, Japan (*kobayashi@das.ous.ac.jp)
[2]Dept. of Geology and Paleontology, National Museum of Nature and Science, Tokyo, Japan
[3]Dept. of Environmental Science, Toho University, Funabashi, Japan

Anisotropic garnet was found in skarn ores occurring in the Yamansu orthomagmatic deposit, located along a fault in the back arc basin of the Carboniferous, east part of Xinjiang, China. Constituent ore minerals in the skarn ores are chalcocite, chalcopyrite, bornite, magnetite, and pyrite. Gangue minerals are composed mainly of garnet, diopside, actinolite, and calcite. The anisotropic garnet sample was polished to be examined by a petrographic microscope. The garnet has been analyzed for major elements using EPMA, and checked for water content by infrared (IR) absorption spectra. Lattice parameters of the garnet were examined using a micro beam X-ray diffractometer (PSPC-MDG) with a total diffraction collimator of 30 μm in diameter and a single crystal diffractometer.

Optical birefringence of one of the anisotropic garnets (Fig. 1) was 0.002, which was calculated from optical retardation and the thickness. The chemical composition of the garnet showed that the garnet belongs to the grossular-andradite series regardless of the presence of a small amount of Cr, Fe^{2+}, Mn, Ti, Mg shown as chemically ($Gro_{32}An_{61}Uv_1Alm_5Sp_1$ - $Gro_{43}And_{51}$ $Uv_0Alm_5Sp_1$). No chemical zoning observed in a single garnet. IR spectrum of the garnet showed no absorption band by OH stretching vibration. The d_{420}, d_{444} and d_{400} values of the garnet were determined by PSPC-MDG and compared with these of the grossular – andradite series garnets hydrothermally synthesized at temperatures between 536 and 652°C under a pressure of 100 MPa for 5 to 23 days. The d_{400}, d_{420} and d_{444} values of the anisotropic garnets have been plotted on a curved line joining each d value of the synthesized grossular and andradite, respectively. Some of the values were not plotted along the estimated curved line. Moreover, we'd like to discuss the crystal structure of anisotropic garnet with the comparison of other natural optically anisotropic garnets.

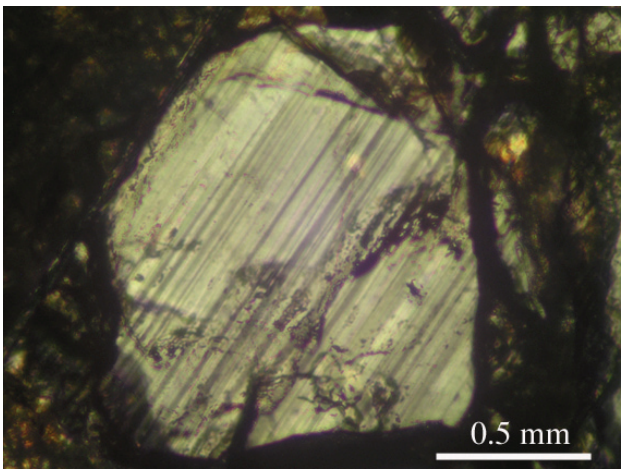

Fig. 1: Photomicrograph of anisotropic garnet from the Yamansu deposit, Xinjiang, China. Crossed-polarized light.

REE arsenates in rare-metal greisens from the Sn-W deposit Verkhnee (Priamyrie, Far East, Russia)

Korostelev, P.G.[1], Gorelikova, N.V.[2*], Semenyak, B.I.[1], Karabtzov, A.A.[1], Orekhov, A.A.[1] & Safronov, P.P.[1]
[1]Far East Geological Institute, RAS, Vladivostok, Russia
[2]Institute of Geology of Ore Deposits (IGEM), RAS, Moscow, Russia ([*]ngor@igem.ru)

REE arsenates and phosphoarsenates of variable composition have been found at the chimney body of Sn-W quartz-fluorite-topaz greisens from the Verkhnee deposit embedded in K_2 rhyolites. REE arsenates are associated with brown zones of zoned green fluorite crystals as replacement products of monazite and xenotime. They form small grains and grain agreggates of 0.1-0.3 mm in size. The mineral replacing monazite has a composition of gasparite-Ce [1], whereas one replacing xenotime is similar to chernovite [2].

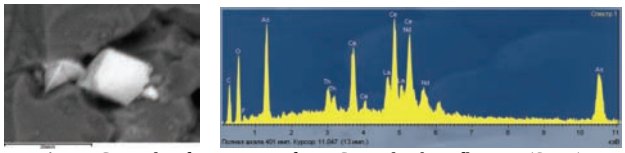

Fig. 1: Crystals of arsenates of La, Ce, Nd, Th in fluorite (SEM).

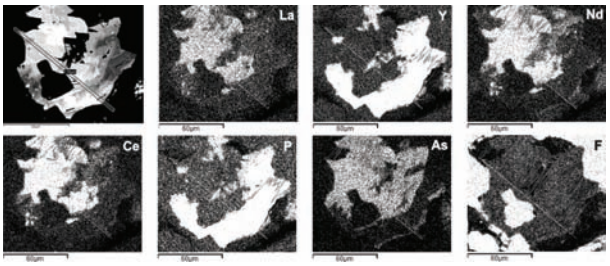

Fig. 2: The replacement of monazite and xenotime by REE arsenates (EMPA).

Electron-microprobe analyses in different points of monazite and xenotime grains provided the following composition (in wt.%): Y 9.58-15.09, Ce 3.17-22.82, La 8.53, Nd 1.19-6.95, Sm 0.95-3.88, Gd 1.25-4.85, Dy 3.33-4.99, Yb 0.92-1.76, Th 0.57-37.87, As 9.87-23.15, P 0.55-3.52, Ca 1.09-2.41, O 16.05-19.09, F 0.98-6.39.

In addition to REE arsenates, phosphoarsenates of Y, REE, Th and a britholite-like mineral have been observed in marginal zones of monazite.

REE arsenates and phosphoarsenates formed at the high redox-potential under conditions of the S deficiency and a higher alkalinity. At these conditions, As exists as As^{4+} and shows more covalent properties than in sulphides and sulphosalts, which promotes replacement of P by As in REE minerals. Owing to its variable valence, As reflects redox conditions of the mineral formation [3].

[1] Graeser, S. & Scwander, H. (1987) *Schweiz. Mineral. Petrogr. Mitt.*, **67**, 103-113. [2] Goldin, B.A., Yushkin, N.P. & Fishman, M.V. (1967) *Zap. VMO*, 1967, 699-704. [3] Grigoriev, D.P. (1965) in *Geochemical Processes*. Moscow, Nauka.

Rare Mg-hydrocarbonates in mineral assemblage of fissures in serpentinite at Hrubšice, Moldanubian zone, western Moravia

Kovář, O.[1], Losos, Z.[1*], Houzar, S.[2] & Zeman, J.[1]
[1]Institute of Geological Sciences, Masaryk University, Brno, Czech Republic ([*]losos@sci.muni.cz)
[2]Dept. of Mineralogy and Petrography, Moravian Museum, Brno, Czech Republic

The unique low-temperature Mg- (Mg-Fe) hydrocarbonate mineralization was found in the Hrubšice serpentinite, Moravian Moldanubicum. It is linked to the fissure system in serpentinite in the active quarry „U Pustého mlýna“ and it consists of rare minerals (hydromagnesite, artinite, brugnatellite, coalingite), followed by aragonite, brucite, dolomite and calcite. Artinite [1], brugnatellite and coalingite are mineral phases found for the first time in Czech Republic.

Hydrocarbonate mineralization occurs as small veins few mm thick or druses in the fissures in serpentinite. Thicker small veins provided outstanding examples of artinite and partly also magnesite. Remaining described minerals were found only locally in microscopic size. From geochemical viewpoint the minerals belong to the Mg-CO_2-H_2O system, locally with Ca-, Fe- a Mn-, and two latter elements are present only in the oldest mineralization stage. In the system, Al is completely missing.

Based on the carbonate assemblage study, three temporal crystallization stages have been recognized: (1) the oldest stage comprising higher Fe- (Mn-) activity: brugnatellite, coalingite and Fe-bearing brucite, i.e. minerals with high Fe content and locally also with slightly increased Mn content occur. (2) Younger stage is represented by hydromagnesite. Simultaneously, there are separate occurrences of chemically pure artinite in fissures, rarely present with hydromagnesite. There is a rare common occurrence of artinite with hydromagnesite, when younger hydromagnesite grows on artinite. Similarly hydromagnesite is surrounding older Mg-Fe-hydrocarbonates (brugnatellite, coalingite). (3) The youngest fill of fissures is formed by calcite and druses of prismatic aragonite crystals. Even younger, but only with respect to hydromagnesite, is huntite, which probably forms pseudomorphoses after hydromagnesite [2].

The mineralization of described Mg-hydrocarbonates probably precipitated from low temperature solutions rich in Mg^{2+}, at pH ~ 9, low activity of CO_2 and at temperatures less than 44°C. The presence of brugnatellite and coalingite with associated Fe-hydrooxide (i.e. phase comprising Fe^{3+}) indicates at least locally oxidizing conditions during the precipitation of the phases. Source of Mg and of Fe were the processes of serpentinite alteration by aqueous solutions of local circulation.

From genetic viewpoint, the spatial distribution of Mg-carbonates in the Hrubšice serpentinite body is remarkable. Described Mg-, Mg-Fe-hydrocarbonates and huntite represent a typomorph association in fissures only in the southern part of the body. Their genesis may be related to the manifestation of young or even sub-recent re-activation of faults, which was documented at Biskoupky close to the study site [3].

Acknowedgements: The work was supported by grant projects MSM 0021622412 and MK 00009486201.

[1] Kovář, O. & Losos, Z. (2005) *Bull. mineral.-petrolog. Odd. Nár. Muz. (Praha)*, **13,** 137-139. [2] Jirásek, J. (2007) *Ac. Mus. Moraviae (Brno), Sci. geol.*, **92**, 103-109. [3] Leichmann, J. & Hejl, E. (1996) *Geol. Mag.*, **133**(1),103-105.

Dissolution of NaCl crystals studied by X-ray diffraction, reflection and absorption methods

Kryazhev, A.A.[1*] & Petrakov, A.P.[2]
[1]Institute of Geology Komi SC UD of RAS, Syktyvkar, Russia (*reflect@rambler.ru)
[2]Syktyvkar State University, Syktyvkar, Russia

Single-crystal X-ray diffraction method (Bragg-Brentano geometry) was used to study NaCl crystals after splitting and dissolution in distilled water. The (100) reflection was accompanied by several additional peaks arising due to disoriented block microstructure of the crystal studied.

X-ray reflectometry is a useful tool to study physical and geometrical properties of the near-surface region of a crystal in solution with a high accuracy. Using this method, quality of NaCl crystal faces after splitting, as well as short and long time processes of their changes in solution have been estimated. Dynamics of roughness changes of fresh NaCl surface during dissolution in the distilled water was characterized.

NaCl aqueous solution was investigated by X-ray absorption and phase contrast methods. The absorption calibration curve for NaCl solution was obtained. The X-ray phase contrast method [1] provides high resolution visualization of the internal structure of low absorbing substances with a flat density gradient. This method can also be used for the study of processes that induce changes in refraction indices. As a result, changes in density and concentration of NaCl solution near the dissolving crystal were obtained (Fig. 1).

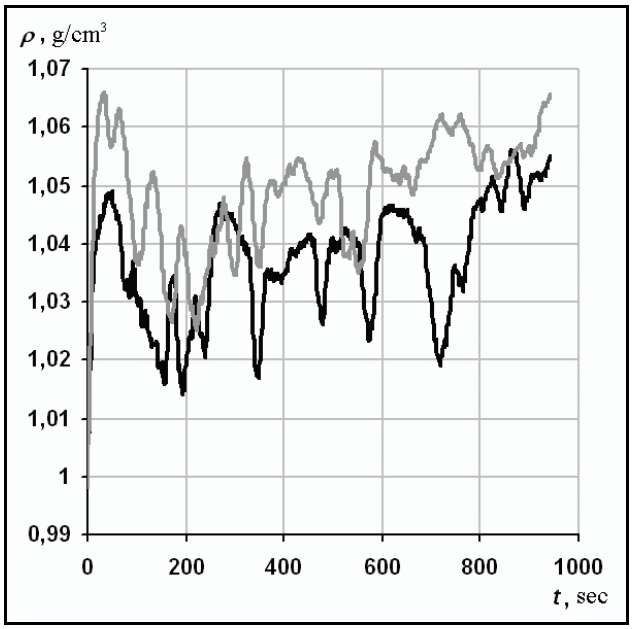

Fig. 1: Solution density change near the crystals NaCl. ▬ – for the crystal with weight m1 = 0.105g, ▬ – m2 = 0.160g.

Acknowledgements: The work has been completed with the partial support of RFBR (grant № 08-05-00346a) and Program of BES RAS SB (09-C-5-1022).

Copper-amalgams from the Rudabánya base metal mineralization, NE Hungary

Kupi, L.[1*], Szakáll, S.[1], Zajzon, N.[1], Kristály, F.[1] & Fehér, B.[2]
[1]Institute of Mineralogy and Geology, University of Miskolc, Hungary (*laszlokupi@gmail.com)
[2]Herman Ottó Museum, Miskolc, Hungary

The Rudabánya metasomatic iron ore formation lies in a 25 km long, NNE-SSW trending range of uplifted and sheared Mesozoic sediments. This regional strike-slip fault zone worked as an upleading zone for fluids. The main mass of the mineralization is composed by siderite with two phases of base metal enrichment (copper and zinc-lead, which differ both in time and space) with barite in the edges of the carbonate bodies. The extensive secondary enrichment zone has been formed after the uplift of the area.

The oxidized zone was overprinted by a low-temperature, epithermal system in the SW parts, with weak silicification. This Sb-As-Hg-enriched fluid saturated the silicified gossan, forming a multi-origin association of elements. In this environment a unique paragenesis has been formed [1].

Copper-amalgams were observed by X-ray diffraction and electron microprobe, supported by reflection optical microscopy. The presence of belendorffite is proven by using a Gandolfi X-ray camera. The Gandolfi-camera results show a good match with the belendorfitte structure of Bernhardt & Schmetzer [2]. Bragg-Brentano geometry measurements indicate the combination of multiple polytypes, with strong preferred orientation, but deconvolution of peaks was possible. The X-ray diffraction data from Bernhardt & Schmetzer [2] and Cipriani & Mazzetti [3] was used to identify single peaks.

The results suggest a belendorffite-dominated composition, with varying kolymite contribution. The Cu-Hg alloy with ~ 1:1 atomic ratio is a combination of the hexagonal or pseudocubic and cubic polymorphs. It forms isometric crystals up to 1 mm in cavities of cuprite and native copper, or coats irregular aggregates of copper (Fig. 1)

Fig. 1: Native copper is margined by belendorffite in cuprite 1N 250x (Andrássy I. mine district, Rudabánya)

[1] Hadobás, S. & Szakáll, S. (2001) *Minerals of Rudabánya. New life of an old mine.* Kőország kiadó, Budapest (in Hungarian). [2] Bernhardt, H.-J. & Schmetzer, K. (1992) *Neues Jb. Miner. Monat.*, 21-28. [3] Cipriani, C. & Mazzetti, G. (1989) *Eur. J. Mineral.*, **1(5)**, 719-720.

The structural behaviour of Cr-spinels from the Rum Layered Suite, NW Scotland

Lenaz, D.[1*], O'Driscoll, B.[2] & Princivalle, F.[1]
[1]Dept. of Geosciences, University of Trieste, Trieste, Italy
([*]lenaz@units.it)
[2]School of Physical and Geographical Sciences, Keele University, Keele, United Kingdom

The Rum Layered Suite, NW Scotland, intruded at 60.53 ± 0.08 Ma during Paleogene opening of the North Atlantic and is widely considered to be a classic example of a layered mafic intrusion formed by open-system magmatic differentiation. The Eastern Layered Intrusion of the Rum Layered Suite comprises 16 coupled feldspathic peridotite-troctolite (± olivine gabbro) cyclic units and outcrops over ca. 25 km^2. Cr-spinel seams occur at the junctions of some of the major cyclic units. At certain unit boundaries, so-called "subsidiary" Cr-spinel seams also occur. The here studied Cr-spinels, analysed by means of X-ray single crystal diffraction and electron microprobe, are from the anorthosite, the subsidiary and main seams, the troctolite and the peridotite.

According to [1], Cr-spinel compositions in the Eastern Layered Intrusion can be divided into two distinct groups: one comprised Fe- and Cr-rich spinels occurring in the anorthosite and troctolite, the other Mg- and Al-rich Cr-spinels from the subsidiary and main seams. This fact is clearly reflected also in the structural data of the analysed spinels. Both cell edges (a_0) and the oxygen positional parameter (*u)* are related to the chemistry of the spinels, so that a_0 values for spinels in anorthosites and troctolites range between 8.3215 (5) and 8.3582 (4) Å, while those from the seams are in the range 8.2126 (1) – 8.2569 (2) Å. The most important feature is that, as far as the *u* values are concerned, three, instead of two, groups have been recognised here. In fact, the Cr-spinel in the anorthosite ranges from 0.2584 to 0.2607, those in the troctolite are between 0.2618 and 0.2625, those in the seam from 0.2629 to 0.2632. The cell edge and *u* values calculated for Cr-spinel in anorthosites are very important; they reflect a high Fe^{3+} composition quite similar to those of synthetic spinels belonging to the series $MgCr_2O_4$ - $MgFe_2O_4$ [2]. Due to the impossibility of performing Mössbauer analyses on these disseminated spinels, it is noteworthy that single-crystal X-ray diffraction, coupled with the electron microprobe analyses can provide a clear indication of an high Fe^{3+} content.

[1] O'Driscoll, B. et al. (2009) *Lithos*, **111**, 6-20.[2] Lenaz, D. et al. (2006) *Phys. Chem. Mineral.*, **33**, 465-474.

Fe^{3+}/Fe_{tot} ratio in the mantle: a micro-Mössbauer study of chromites included in diamond and kimberlites

Lenaz, D.[1*], Skogby, H.[2], Logvinova, A.M.[3], Princivalle, F.[1] & Sobolev, N.V.[3]
[1]Dept. of Geosciences, University of Trieste, Italy
([*]lenaz@units.it)
[2]Dept. of Mineralogy, Swedish Museum of Natural History, Stochkolm, Sweden
[3]Inst. of Geology and Mineralogy, Russian Academy of Sciences, Siberian Branch, Novosibirsk, Russian Federation

Oxides with the spinel structure AB_2O_4 occur as main or accessory minerals in many different rocks of the Earth, from the upper mantle to the crust. The wide ranges of composition and mineral assemblages of spinels allow them to be employed as petrogenetic indicators. Being sensitive to temperature, pressure, oxygen fugacity, bulk rock and fluid composition, intra- and inter-crystalline equilibria in spinel are extremely useful for constructing mineral geothermometers and geobarometers. In such a context, problems with the correct evaluation of Fe^{2+}/Fe_{tot} ratio can lead to important mistakes in calculated temperatures, pressures and oxygen fugacities.

The oxidation state of the upper mantle and its evolution with time are among the most important problems facing geologists. Oxygen fugacity (f_{O_2}) is a fundamental but little known intensive variable in mantle processes. It influences the P/T position of a mantle solidus and the composition of mantle-derived melts and fluids, and constrains mantle-core equilibria and a number of geophysical properties of the mantle. An important source of information on oxidation states is the ferric/ferrous iron ratio in mantle spinels. Since the magnetite component is low in mantle spinels, normal analytical errors translate into considerable f_{O_2} uncertainties. Recently, the most accurate evaluation of ferric/ferrous ratio have been achieved by using different spectroscopic methodologies (single crystal X-ray diffraction, electron microprobe analyses, Mössbauer spectroscopy) and comparing their results. Because spinel usually occurs as small grains, Mössbauer cannot be widely applied because it requires a relatively large sample size. Given that, in the same sample analysed by conventional Mössbauer there could be a large number of spinels with different degrees of oxidation/alteration leading to possible errors in the interpretation of the results.

The diamond deposits of Siberia (Russia) compose the Yakutian kimberlite province, located in the northwestern region of the Siberian craton. About 1000 kimberlite bodies of a wide range of emplacement ages from Early Paleozoic to Late Mesozoic are known within several kimberlite fields. In this study single crystals of chromites previously analysed by means of single crystal X-ray diffraction and electron microprobe [1] occurring in the kimberlites of the Mir and Internatsionalnaya mines, in the Obnazhennaya barren pipe and included in a diamond from the Udachnaya mine have been analysed by Micro-Mössbauer in order to avoid possible errors deriving from different oxidation/alteration degrees of multiple grains.

The Fe^{3+}/Fe_{tot} ratios obtained from the Mössbauer spectra are in fair agreement with X-ray diffraction data for some samples, but show higher Fe^{3+} values for other samples, which may indicate a minor deviation from stoichiometry.

[1] Lenaz, D. et al (2009) *Am. Mineral*., **94**, 1067-1070.

Probing the geological environments and occurrences of quartz crystals in south-west Central Mountain Range, Taiwan

Li Yu-Ho[1], Chen Huei-Fen[1*] & Fang Jian-Neng[2]
[1]Institute of Applied Geosciences, National Taiwan Ocean University, Keelung, Taiwan ([*]diopside0412@yahoo.com.tw)
[2]Dept. of Collection Management, National Taiwan Museum, Taipei, Taiwan

This study investigates the regional geological environments in which well-developed quartz crystals can be found and the formation mechanisms of quartz in the Central Mountain Range (CMR), Pingtung, Southern Taiwan. We discovered three morphological types of quartz crystals: (a) prismatic quartz (Fig. 1a), (b) faden quartz (Fig. 1b), and (c) doubly terminated quartz (Fig. 1c). We listed observed occurrences, crystal morphology, micro-observation of inclusions, and micro-Raman spectroscopy of intergrowth minerals to probe formation mechanisms and thermobaric ranges of this quartz.

According to the geological survey and locations data faden quartz occurs in the older anchizone to low epithermal environments (Lushan Formation), doubly terminated quartz is mainly found in the high diagenetic zone (Mudan Formation), while prismatic quartz grows in this whole region and often intergrows with the other two types. The faden quartz grows from near-plastic deformation cracks under higher temperature and higher pressure conditions at 2 to 5 km depth. Its preferred-orientation crystals bear thread-like inclusions, which indicate the direction of the extension crack. Moreover, it can intergrow with rutile and chlorite. The doubly terminated quartz grows in brittle fractures from sandstone joints. Its host rocks proceeded from an uplift history to the shallow tectonic region. An obvious character is that the doubly terminated quartz has large fluid inclusions of variable sizes. Its crystals did not attach to host rocks, because they grew from autonucleation under fluid oversaturation passing through decreasing temperature/pressure. The two types of quartz can show fissure development due to the host rock uplifting at different depths in the region.

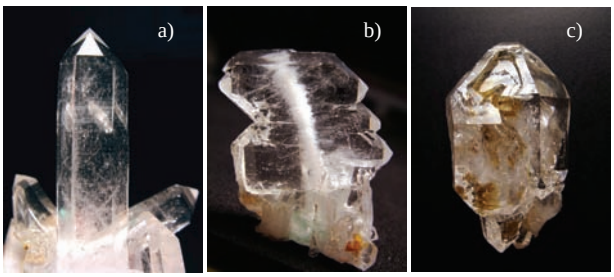

Fig. 1: a) Prismatic quartz; b) faden quartz; c) doubly terminated quartz.

Nanostructures of manganese oxides in ferromanganese nodules

Lysyuk, G.
Institute of Geology, UB RAS, Syktyvkar, Russia
(glysiuk@geo.komisc.ru)

Manganese oxides, widespread and of great practical importance, are formed and transformed in natural environments due to the active role of microorganisms.

In our study, all of the previous observations of the biogenic origin of ferromanganese nodules (FMNs) were confirmed by scanning electron microscopy (SEM). Numerous relics of planktonic organisms often replaced by Mn oxide as coating films were identified in the inner zones of FMNs. X-ray amorphous Mn oxides are widespread in FMNs. As follows from the SEM examination, these phases are mineralized glycocalyx. Experiments on high-temperature transformations allowed identifying this phase as todorokite, and SEM images indicate that todorokite was formed under the influence of bacterial activity. A cyanobacterial mat detected in the interlayer space of nodules is an additional evidence for the participation of bacteria in nodule growth and the formation of finely dispersed Mn minerals. The chemical composition of this cyanobacterial mat is as follows (wt.%): 48.35 MnO, 6.23 Fe_2O_3, 8.67 MgO, 5.05 Al_2O_3, 4.45 SiO_2, 3.63 NiO, 2.30 Na_2O, 2.19 CuO, 1.31 CaO and 0.68 K_2O.

The SEM examination of the inner zones of FMNs allowed detection of numerous biofilms in the interlayer space of nodules. These biofilms are composed of fusiform, rod-shaped, and coccoid bacteria and their filamentary cover. The bacterial mass is composed of (wt.%) 28.34 MnO, 17.14 Fe_2O_3, 7.11 SiO_2, 2.41 CaO, 7.90 TiO_2, 1.74 Na_2O, 1.73 Al_2O_3, 1.30 MgO, 1.25 P_2O_5, 1.25 SO_3, 0.68 CoO, 0.54 CuO, 0.53 NiO and 0.50 K_2O. Thus, the chemical composition of cyanobacteria and bacterial mass of biofilms corresponds to Mn oxides. A great variety of bacterial forms were found on the nodule surface, testifying to their participation in the mineral formation on the ocean bottom.

Numerous findings of finely dispersed native metals confirm the great contribution of the biogenic factor to the formation of FMNs. Sulfide minerals in nodules (pyrite, chalcopyrite, pyrrhotite, troilite, covellite, and bornite) are usually associated with organic remains and were formed in the reducing environment created by bacterial activity. The occurrence of Ni minerals (taenite, bunsenite, niccolite, and violarite) in FMNs is related to biochemical processes as well.

Inclusions of native metals were found in FMNs and Mn-bearing zones of weathering. Numerous copper red and brass yellow metal lamellae, flakes, and dendrites in FMNs were identified by a microprobe as native copper and intermetallic compounds of Cu and Zn (brass yellow grains). Fe-Cu compounds and pure Fe are less abundant. In addition, sporadic grains of native Al and Zn were found. The occurrence of native metals can be explained by segregations of organic matter that served as microscopic domains with highly reducing conditions.

The association spurrite – perovskite in the inner exoskarn zone from Cornet Hill (Metaliferi Mountains, Romania)

Marincea, Ş.[1*], Dumitraş, D.G.[1] & Fransolet, A.M.[2]
[1]Geological Institute of Romania, Bucharest, Romania
([*]marincea@igr.ro)
[2]Laboratoire de Minéralogie, Université de Liège, Belgium

The high-temperature skarn occurrence from Cornet Hill (Metaliferi Mountains, Romania), located approximately 20 km west of Brad, and 40 km northwest of Deva, is known as one of the rare occurrences of spurrite and tilleyite worldwide. The skarn contains essentially spurrite, tilleyite and gehlenite and develops at the contact of a monzodiorite - quartz monzonite body, of Upper Cretaceous age, with Tithonic - Kimmeridgian reef limestones of the Căpâlnaş-Techereu unit. The skarn from Cornet Hill is clearly zoned, the zoning being, from the outer to the inner part of the metasomatic area: calcite (marble) / tilleyite / spurrite / wollastonite + gehlenite + vesuvianite / wollastonite + grossular / quartz monzonite.

Spurrite from Cornet Hill concentrates in the outer endoskarn zone, and practically defines a monomineralic zone where it forms 90-95% of the rock volume. A minute study shows, however, that the typical assemblage is spurrite + perovskite, with minor proportions of tilleyite, wollastonite, gehlenite, titanian andradite and hydroylellestadite. The spurrite-bearing skarn is characterized by a massive appearance with medium-grained crystals of grayish blue to pale gray spurrite that exceed generally 5 mm in their largest dimension, without preferred orientation. Some of the larger patches of spurrite are, however, cross cut by microveins containing scawtite, plombièrite, tobermorite, calcite and secondary aragonite. The optical constants of a representative sample are α = 1.637(2), β(calc.) = 1.675(2), γ = 1.680(3) and 2V = 39°. The measured density of the same sample [D = 3.02(2) g/cm^3] agrees perfectly with the calculated density (D_x = 3.022 g/cm^3). The cell parameters, obtained as mean of 6 different sets of individual values obtained by least-squares refinement of X-ray powder data are: a = 10.493(15) Å, b = 6.716(9) Å, c = 14.179(16) Å and β = 101.36(4)°. The chemical composition, obtained as average of 23 electron-microprobe spot analyses on different samples is (in wt% oxides): SiO_2 = 26.84, TiO_2 = 0.03, Al_2O_3 = 0.01, FeO = 0.03, MgO = 0.05, CaO = 63.11, Na_2O = 0.07, K_2O = 0.01, CO_2 (calculated) = 9.83. The chemical-structural formula, calculated on the basis of 11 oxygen atoms, is: $Ca_{5.010}Mg_{0.002}Mn_{0.003}Fe^{2+}_{0.002}Ti_{0.002}Na_{0.011}K_{0.001}(Si_{1.990}Al_{0.001})O_{8.015}(CO_3)_{0.995}$.

Granular inclusions of perovskite in the spurrite mass are common in most of the samples, and are particularly abundant in the close vicinity of the gehlenite-bearing endoskarn. The grain sizes commonly vary between 0.01 and 0.05 mm. The physical constants of a selected sample are α = 2.302(2), β(calc.) = 2.341(2), γ = 2.383(2), D_x = 4.049 g/cm^3, D = 4.04(1) g/cm^3. The average composition taken as mean of 15 point analyses on various crystals is (in wt.% oxides): SiO_2 = 0.36, TiO_2 = 57.25, Al_2O_3 = 0.28, FeO = 1.19, MnO = 0.02, CaO = 40.23, Na_2O = 0.02, K_2O = 0.01 and leads to the chemical-structural formula: $(Ca_{0.983}Fe^{2+}_{0.023}Mg_{0.002}Na_{0.001})(Ti_{0.982}Si_{0.008}Al_{0.008})O_3$, approaching the stoichiometry.

The unit-cell parameters, obtained by least-squares refinement of the X-ray powder dataset obtained for a spurrite-included perovskite separate are: a = 5.382(3) Å, b = 5.437(3) Å, c 7.634(4) Å. The refinement was carried out accepting the orthorhombic symmetry of the mineral, space group Pbnm.

Trace elements in anorthite megacrysts from West Japan volcanic belt

Matsui, T.[1*], Arakawa, Y.[2] & Kimata, M.[2]
[1]Faculty of Education, Kagoshima University, Kagoshima, Japan ([*]matsui@edu.kagoshima-u.ac.jp)
[2]Graduate School of Life and Environmental Sciences, University of Tsukuba, Tsukuba, Japan

Anorthite megacrysts from eight volcanic regions (Aso, Aira, Kaimon-dake, Satsuma-Iou-jima, Kuchierabu-jima, Kuchino-shima, Suwanose-jima, Akuseki-jima) of the West Japan volcanic belt were analyzed by inductively coupled plasma analysis (ICPA) for concentrations of Mg, K, P, Ba, Be, Co, Cr, Cu, Dy, Eu, La, Li, Mn, Mo, Ni, Pb, Sc, Sn, Sr, Ti, V, W, Y, Zn, and Zr. The anorthite megacrysts, reaching a maximum size of approximately 2 cm in diameter, are mainly found as phenocrysts in the andesitic lava series, but are also present in basalts and as crystal bombs in basaltic scorias from a number of these volcanic regions. These megacrysts show no or only slight optical zoning, and electron microprobe studies show that these megacrysts are chemically homogeneous and unzoned [1]. Anorthite content of the megacrysts is approximately 90-94 mol %, although the content varies slightly in each volcanic region [1]. Similar anorthite megacrysts are found in the East Japan volcanic belt [2] and have been mineralogically and geochemically characterized, with a focus on their genesis and migration of subduction components (e.g., [3]; [4]; [5]; [6]).

The anorthite megacrysts from the East Japan volcanic belt occur in Neogene and Quaternary basaltic rocks, and their host rocks are grouped into two types: tholeiite and high-Al basalt [2]. In contrast, most Quaternary volcanism in Kyushu and Ryukyu Islands is classified into calc-alkaline rock series [7]. The $^{87}Sr/^{86}Sr$ ratio of the anorthite megacrysts is somewhat lower than that of their host rocks which suggests that the anorthite megacrysts did not crystallized from the surrounding host magmas [8].

Trace element partition coefficients between the anorthite megacrysts and their host rocks differ slightly in several specimens. The measured large-ion lithophile element content exhibits a gradual increase in concentration toward the rear arc and appears to be related to the $^{87}Sr/^{86}Sr$ ratio of the anorthite megacrysts, which shows a systematic decrease from south to north in accordance with the Trench Volcano Gap. Since the megacrysts have virtually constant anorthite content, and accordingly, megacryst/melt partitioning is expected to be identical, the observed variation in the megacryst/host-rock partition coefficients indicates that some of the anorthite megacrysts are xenocrysts

It follows from the present data that the environment was favorable for anorthite megacrystallization within the magmatism under the island arc, regardless of differences in the host magma. After megacrystallization, these anorthites were incorporated as xenocrysts into a different magma in which strontium was not isotopically equilibrated. It seems reasonable to conclude that regional variations in tectonic settings of subduction zones resulted in differences in host magma between the anorthite megacrysts.

[1] Matsui, T. et al. (2002) *Abstr. 18th General Meeting of the IMA*, 223. [2] Ishikawa (1951) *J. Fac. Sci., Hokkaido Univ.*, Ser. IV, Vol. VII, No.**4**, 339-354. [3] Murakami, H. et al. (1991) *J. Min. Pet. Econ. Geol.*, **86**, 364-374. [4] Arakawa, Y. et al. (1992) *J. Min. Pet. Econ. Geol.*, **87**, 226-239. [5] Nishida, N. et al. (1994) *Naturwissenschaften*, **81**, 498-502. [6] Kimata, M. et al. (1995) *Mineral. Mag.*, **59**, 1-13. [7] Matsumoto, Y. (1983) *Mem. Geol. Soc. Japan*, **22**, 81-91 (in Japanese with English abstract). [8] Matsui, T. et al. (2007) *Abstr. Frontiers in Mineral Sciences 2007*, 118.

Gartrellite and other arsenates from Likas-kő, Velence Hills (Hungary)

Menyhárt, A.* & Szakáll, S.
Dept. of Mineralogy and Petrology, University of Miskolc, Hungary (*adrienn711@gmail.com)

At Likas-kő, Meleg Hill, Velence Hills, at the tectonic contact of the granite and contact schist a siliceous zone was formed. This siliceous zone contains enargite mineralization, which produced secondary arsenate minerals, like beudantite, cornubite, cornwallite, conichalcite. A greenish-yellow earthy aggregate is assumed to be gartrellite. Its ideal formula can be expressed as $PbCuFe(AsO_4)_2(OH,H_2O)_2$.

We performed electron microprobe spot analyses on several samples (greenish-yellow globular aggregates and greenish-yellow aggregates of small plates) which gave Pb, Cu, Fe, (Al)-arsenate compositions. The chemistry of 2 samples (seen on the pictures) in normalized weight percentage – average of 4 (sample 1) and 2 (sample 2) spot analyses – is shown in Table 1.

Table 1: Average composition of samples 1 and 2

	(1) wt%	(2) wt%
As_2O_5	44.42	41.84
PbO	28.99	26.94
CuO	16.85	20.52
Fe_2O_3	6.65	8.79
Al_2O_3	2.92	1.91

These analyses show more As_2O_5 and less PbO than the type material [1]. The total amount of cations thus does not correspond to the amount of As_2O_5.

Inside the aggregate of small plates (Fig. 1a) there is a Cu-arsenate mineral (cornubite; darker phase on Fig. 1a), which formed earlier than gartrellite. In contrast, on Fig. 1b gartrellite is surrounded by a Cu-arsenate (cornubite), and this is connected to malachite (the dark grey phase on the right side of Fig. 1b). Ba-pharmacosiderite also surrounds gartrellite. On another sample gartrellite is intergrown with a (Ca,Cu)-arsenate (probably conichalcite).

The X-ray powder diffraction pattern shows the reflections (d_{meas} and intensity) of gartrellite at 2.948 (100), 3.299 (83), 2.899 (81), 3.202 (73), 3.177 (61), 2.509 (66), 4.461 (37).

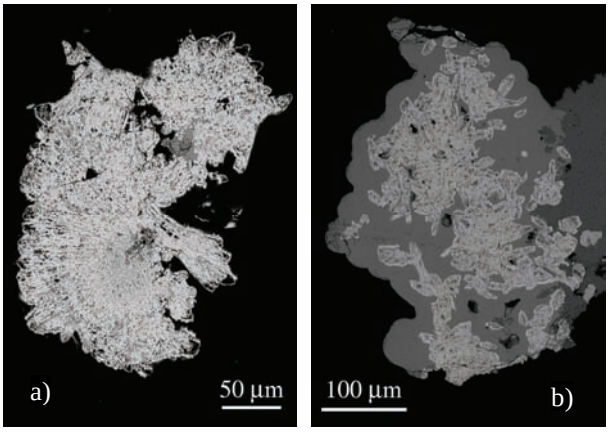

Fig. 1: a) SEM BSE image of sample (1); b) SEM BSE image of sample (2).

[1] Nickel, E.H. et al. (1989) *Austral. Mineral*., **4**, 83-89.

Mineralogical research of opals in Slovakia

Mesiarkinová, M.[1*]& Ozdín, D.[2]
[1]SOLIPHA – Laboratory of X-Ray Diffraction, Dept. of Mineralogy and Petrology, Faculty of Natural Sciences, Comenius University, Bratislava, Slovak Republic (*mesiarkinova@fns.uniba.sk)
[2]Dept. of Mineralogy and Petrology, Faculty of Natural Sciences, Comenius University, Bratislava, Slovak Republic

A lot of historical occurrences of opal exist in Slovakia. We identified samples from some of them, determined their structural ordering, chemical composition as well as the role of Fe in the structure of SiO_2 phases with several analytical methods (EMPA, Powder XRD, Mössbauer methods and DTA). Most of opals occur in volcanic tuffs mainly of andesitic composition. A part of opals, especially silicified woods, occurs in Neogene (Baden-Sarmat) sedimentary rocks. Opals on the localities Ľubietová-Jamešná and Tri Vody are formed on the contact of Triassic carbonates and Neogene andesites. As suggested by the study of opals on the locality Ľubietová – Jamešná and Tri Vody, samples originally regarded as opals are formed of grey to brown quartz with content of iron up to 0.25 at% and Fe oxides with content of Si up to 19.91 at% [1]. On the base of XRD and Mössbauer spectroscopy, Fe is trivalent and may be incorporated in minerals goethite and probably hisingerite. Textures of silicites/opalites are very complicated. Brecciated textures are composed of several types of matrix and veinlets (Fig. 1). We observed two distinct sequences of SiO_2 phases formed from fluids filling the voids in goethitic quartz,: 1 – forming of higher-temperature void fillings begin with the crystallization of jasper-like SiO_2 phase with banded texture and crystallization process finished with crystallic quartz; 2 – lower-temperature void fillings comprise following SiO_2 phases (from outer zone to inner zone): chalcedony (microcrystalline) → opal-CT (with banded texture) → opal-AN (collomorph hyalite).

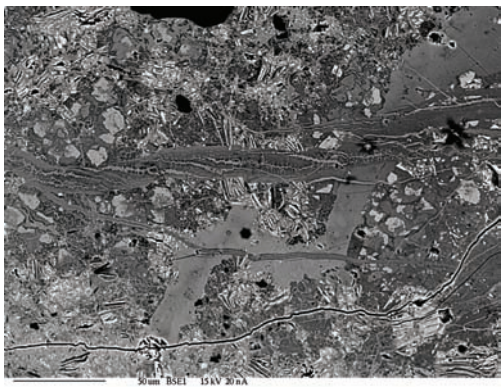

Fig. 1: Complicated brecciate texture of Fe-rich silicate (loc. Ľubietová).

Our XRD and EMPA research on silicified woods from several localities in Slovakia, previously described as wood opals, indicates that they are represented by: 1 - silicified or petrified trunks formed by α-quartz [2]; 2 - wood opals composed mostly of opal-CT and rarely of opal-AN (hyalite). Fossilized residues of plants and microbes in SiO_2 phases contain quartz and opal-CT according to XRD study.

Acknowledgements: Financial support was provided by the Grant VEGA No. 1/0287/08 and Grant VVCE-0033-07 SOLIPHA.

[1] Mesiarkinová, M. & Ozdín, D. (2009) *Mitt. Österr. Miner. Ges.*, **155**, 101. [2] Mesiarkinová, M. et al. (2009) *Mineralia Slov.*, **41(4)**, 503-510.

Reinvestigation of "dognácskaite"

Papp, G.[1*] & Stanley, C.J.[2]
[1]Dept. of Mineralogy & Petrology, Hungarian Natural History Museum, Budapest, Hungary ([*]pappmin@ludens.elte.hu)
[2]Dept. of Mineralogy, The Natural History Museum, London, United Kingdom

"Dognácskaite" (hereinafter we omit parentheses for simplicity) is an invalid mineral species described originally in 1884 by Krenner [1], for a detailed research history see [2]. It is usually regarded as "a mixture of various sulfides" [3] but major reference works disagree about its exact mineral composition. This research was aimed at clarifying this open question.

Five specimens labelled dognácskaite from Dognecea (Caraş-Severin County, Banat, Romania) were studied by ore microscopy, SEM, EPMA, and XRPD methods during a systematic reinvestigation project of inadequately known minerals first described from the Carpathian region. One of the studied specimens is probably that used for the original description by József Krenner. Every specimen proved to be a mixture with a similar mineral composition and texture. The main component of dognácskaite is bismuthinite rimmed by wittichenite (containing strings of native bismuth), the latter is again rimmed by copper sulfides (mainly djurleite with some covellite). Emplectite can also be found occasionally in the larger voids of bismuthinite. Magnetite (sometimes martitized), chalcopyrite, bornite (replacing chalcopyrite), rare sphalerite and tetradymite form inclusions in bismuthinite or in the rims surrounding it. Goethite, calcite, bismuth ochre and other unspecified fine-grained alteration products are abundant in the voids. Data from earlier studies can easily be explained on the basis of this mineral assemblage, suggesting that every dognácskaite specimen is a mixture of this kind. The samples may correspond to a (pyrite-)magnetite-chalcopyrite skarn ore replaced by a post-skarn hydrothermal bismuthinite ore, later affected by supergene copper enrichment then by oxidation processes.

The exact locality of dognácskaite within the Ocna de Fier–Dognecea ore field cannot be determined but, based on an old museum label, one of the specimens studied was collected in the mine "Petri-Pauli" (or "Péter-Pál"), now "Petru şi Pavel" on Mt. Danilii. This fact implies that at least some of the specimens came from an area that is now included in the Ocna de Fier ore field (at the time of description it belonged to the Dognecea [in Hungarian Dognácska] ore field)

Acknowledgements: This research received support from the SYNTHESYS Project http://www.synthesys.info/ whic h is financed by European Community Research Infrastructure Action under the FP6 "Structuring the European Research Area" Programme.

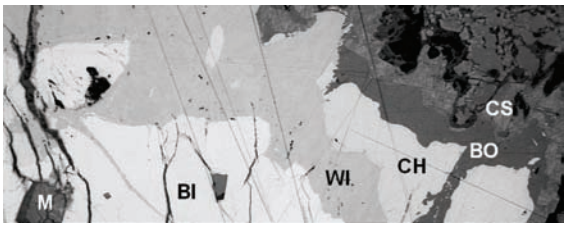

Fig. 1: Typical textural pattern of the rim of a dognácskaite specimen in reflected light. Minerals from left to right: martitised magnetite (M), bismuthinite (BI), wittichenite (WI), chalcopyrite (CH), bornite (BO), copper sulfides (CS). Real width 0.5 mm.

[1] Krenner, J. (1884) *Földt. Közl.*, **14**, 519-521, 564-566. [2] Papp, G. (2004) *History of minerals, rocks and fossil resins discovered in the Carpathian region.* Magyar Természettudományi Múzeum, Budapest. [3] Strunz, H. & Nickel, E.H. (2001): *Strunz mineralogical tables*. Schweitzerbat'sche, Stuttgart.

Preliminary data of oxidation kinetics of $Fe^{2+}Cr_2O_4$ synthetic spinel

Parisi, F., Lenaz, D.[*] & Princivalle, F.
Dept. of Geosciences, University of Trieste, Italy
([*]lenaz@units.it)

The spinel structure is based on a nearly ideal cubic close-packed array of oxygen atoms with tetrahedral (T) and octahedral (M) cavities. In common 2-3 spinels, one eighth of the T sites and one half of the M sites are occupied by heterovalent cations A and B in the ratio AB_2O_4. In general, spinels do not show this idealized configuration, with A cations in T sites and B cations in M sites. Commonly there exists octahedral-tetrahedral disorder of A and B cations depending on thermal history. Consequently, the crystal-chemistry of spinels is described by the general formula $^{IV}(A_{1-i}B_i)^{VI}(A_iB_{2-i})O_4$, where "i" refers to the inversion parameter. With increasing temperature, disorder takes place, i.e. A and B cations undergo increasing intersite exchange over the three cation sites per formula unit. Modifications of T-O and M-O bond distances to accommodate various chemical compositions and/or cation distributions determine variations in the oxygen positional parameter u and the cell edge a_0.

The aim of this study is the investigation of oxidation mechanism in $Fe^{2+}Cr_2O_4$ spinels previously synthesized using a flux-growth method and analyzed by single-crystal X-ray diffraction, electron microprobe, and optical absorption-, infrared-, and Mössbauer spectroscopies [1]. These analyses showed that iron occurs almost exclusively as $^{IV}Fe^{2+}$ while Cr is present as a trivalent cation in the octahedral site. It is to notice that the large excess octahedral crystal field stabilisation energy of Cr^{3+} should ensure that Cr-bearing spinels have an almost completely normal cation distribution [2]. Given that the M site is completely filled by Cr, and that Cr should not be oxidized in spinels, we would expect that heating affects only the iron cation present in the T site. Consequently, the only possible effect is the oxidation of Fe^{2+} to Fe^{3+} and the formation of vacancies following the mechanism proposed by [3].For our purposes the crystals were put in a thin-walled quartz tube and heated in a vertical tube furnace at 600, 700 and 800°C. Heating runs were performed at room pressure in air. Run temperatures were accurately measured and controlled by means of a calibrated Pt/Pt-Rh thermocouple located near the sample; the uncertainty is estimated to be about ± 5°C.

Preliminary results showed that after 30 days, the heatings at 600°C show very few changes with cell edge moving from 8.3754 (1) to 8.3745 (3) Å. Spinel heated at 700°C, after 13 days, show cell edge moving from 8.3761 (1) to 8.3737 (1) Å, and that heated at 800°C (2 days) from 8.3759 (1) to 8.3641 (2). It is to notice that $Fe^{2+}Cr_2O_4$ spinel heated at 600°C, where an exchange between the two sites was observed, showed after the same heating time a change in the cell edge from 8.1396 (1) to 8.0989 (6) Å [4], so that the presence of Cr, fully occupying the M site, may prevent large variations in the cell parameter.

[1] Lenaz, D. et al. (2004) *Phys. Chem. Miner.*, **31,** 633-642.
[2] Urusov, V.S. (1983) *Phys. Chem. Miner.*, **9,** 1-5.
[3] Menegazzo, G. et al. (1997) *Mineral. Mag.*, **61**, 411-421.
[4] Lavina, B. et al. (2005) *Phys. Chem. Miner.*, **32,** 83-88.

Antiphase boundaries found in sillimanite phenocrysts in Tosu rhyolite (Japan)

Shimobayashi, N.
Dept. of Geology and Mineralogy, Graduate School of Science, Kyoto University, Kyoto, Japan (shimo@kueps.kyoto-u.ac.jp)

Al_2SiO_5 polymorphs (andalusite, sillimanite and kyanite) are of a great significance for mineralogists and petrologists because of their value as indicators of the pressures and temperatures of the rocks containing them. Of these three, sillimanite has Al-Si disorder because it contains both Al and Si in tetrahedral coordination. [1] suggested that the *dP*/*dT* slope of the kyanite-sillimanite equilibrium is affected by Al-Si disorder in the sillimanite. [2] implied the Al-Si disordering transformation in sillimanite at high temperature. The Al-Si disorder would result in a space group change from *Pbnm* to *Pbam*. However, the high-temerature form of sillimanite has not been established because the breakdown reaction sillimanite → mullite + SiO_2 and incongruent melting occur at high temperatures.

TEM investigation of sillimanite in Tosu rhyolite was carried out in the present study. Tosu rhyolite, characterized by containing a plenty of sillimanite phenocrysts (over 10% in modal per cent), is distributed only at a small hill (relative height: 5 m) in the western part of Tosu City, Kyushu, Japan. The sillimanite phenocrysts are perfectly euhedral and show a long prismatic shape (0.5 to 1.5 mm in length). No chemical zoning can be seen although their chemical compositions, $(Al_{2.01}Fe^{3+}_{0.02})_{\sum 2.03}Si_{0.98}O_5$ in average, are slightly Si-deficient from the ideal stoichiometric composition. Neither reaction rims surrounding them nor erosion texture can be observed. The sillimanite phenocrysts are assumed to crystallize directly from the magma at high temperature [3].

The present sillimanite specimens gave sharp *l*=odd reflections in electron diffraction patterns, the fact of which indicates that they have the Al-Si ordered *Pbnm* structure. However, features resembling APB's can be found in dark-field images only used with *l*=odd reflections (Fig. 1). The fact that these features cannot be seen in dark-field images with *l*=even reflections suggests that the displacement vector should be ***R***=1/2[001]. APB's in the natural sillimanite in absence of mullite are first found in the present study although [4] observed APB's in sillimanite porphyroblast of the Bergell tonalite, which coexists minute domains of mullite. As pointed out by [6], APDs with stacking vector of 1/2[001] would be expected to appear during an ordering transformation from *Pbam* to *Pbnm* in sillimanite. Therefore, the present observation of the APB's may suggest the natural occurrence of the high-temperature disordered sillimanite (*Pbam*).

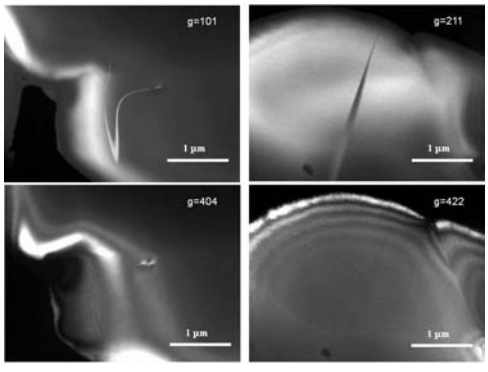

Fig. 1: Dark-field TEM images of sillimanite in Tosu rhyolite.

[1] Anderson, P.A.M. & Kleppa, O.J. (1969) *Am. J. Sci.*, **267**, 285-290. [2] Greenwood, H.G. (1972) *Geol. Soc. Am. Mem.*, **132**, 553-571. [3] Sawamura, M. et al. (1986) *J. Geol. Soc. Jap.*, **92**, 65-68. [4] Wenk, H.-R. (1983) *N. Jb. Miner. Abh.*, **146**, 1-14. [5] Holland, T.J.B. & Carpenter, M.A. (1986) *Nature*, **320**, 151-153.

Morphological varieties of cannonite from Nagybörzsöny (Hungary)

Szakáll, S.[1*], Fehér, B.[2], Kristály, F.[1] & Bigi, S.[3]
[1]Dept. of Mineralogy and Petrology, University of Miskolc, Hungary ([*]askszs@uni-miskolc.hu)
[2]Dept. of Mineralogy, Herman Ottó Museum, Miskolc, Hungary
[3]Dept. of Earth Sciences, University of Modena and Reggio Emilia, Modena, Italy

Nagybörzsöny is a Bi-Cu-As-(Au-Ag) meso-epithermal ore deposit in the Börzsöny Mts. (Hungary). The characteristic Bi minerals are bismuthinite, native bismuth and the members of cosalite-lillianite series. There are some secondary minerals in the cavities of bismuth ores. Among them the most widespread is cannonite – a rare monoclinic $Bi_2O(OH)_2(SO_4)$ phase. In close association with cannonite, native sulphur, gypsum, an unknown Bi-bearing mineral, and a non-crystalline Fe-Bi arsenate were identified.

In Nagybörzsöny four morphological types of cannonite were observed: 1) thick tabular crystals up to 20-30 μm in diameter; 2) lath-like crystals up to 50-60 μm in length (Fig. 1); 3) short prismatic crystals up to 100-120 μm in length; 4) globular aggregates consisting of lamellae up to 250-300 μm in diameter (Fig. 2).

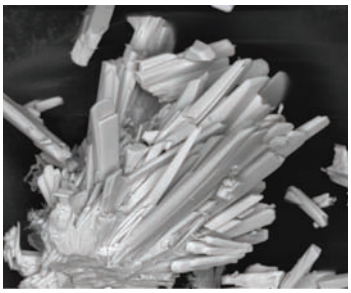

Fig. 1: Lath-like cannonite crystals (type 2) (width of the picture 120 μm).

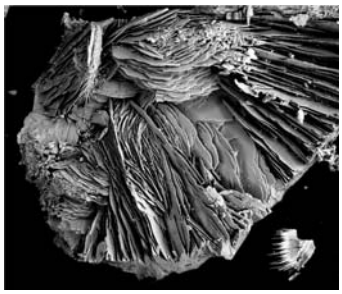

Fig. 2: Globular aggregate consisting of lamellae (type 4) (width of the picture 150 μm).

All the studied materials have been identified by X-ray powder diffraction. Cannonite is monoclinic with space group $P2_1/c$. The refined unit-cell parameters for type 2: a = 7.731(4) Å, b = 13.890(8) Å, c = 5.702(3) Å, β = 109.20(5)° are based on 32 reflections in the X-ray powder pattern obtained using a 114.6-mm Gandolfi camera. It has a cell volume of 578.2(4) $Å^3$ with Z = 4. Calculated density is 6.213 g/cm^3.

We performed some spot analyses on these materials by electron microprobe:

Average of 9 spot analyses for type 2: Bi_2O_3 78.97, Fe_2O_3 0.03, SO_3 15,42, H_2O (calc.) 3.26, Total 97.68 wt%. It corresponds to $Bi_{1.88}O(S_{1,06}O_4)(OH)_2$.

Average of 7 spot analyses for type 4: Bi_2O_3 78.96, Fe_2O_3 0.05, SO_3 15,36, H_2O (calc.) 3.25, Total 97.62 wt%. It corresponds to $Bi_{1.88}O(S_{1,06}O_4)(OH)_2$.

Low-temperature samarskite modification: structural relationship between pre-metamict and recrystallised structure

Tomašić, N.[1*], Bermanec, V.[1], Gajović, A.[2] & Čobić, A.[1]
[1]Institute of Mineralogy and Petrology, Faculty of Science, University of Zagreb, Croatia ([*]ntomasic@geol.pmf.hr)
[2]Ruđer Bošković Institute, Zagreb, Croatia

Previous investigations on samarskite proposed two structural modifications: low-temperature samarskite, being observed at temperatures up to 550°C, and high-temperature samarskite, which occurs at temperatures above 950°C [1]. A sample of samarskite-(Y) from Ampangabe, Madagascar, was investigated to trace relics of the original structure in metamict matrix and to relate them to the sample recrystallised in air at temperatures around 500°C.

Investigations performed by high-resolution electron microscopy (HRTEM) revealed occurrence of regions containing relics of pre-metamict structure. These relics were surrounded by amorphised mineral matrix (Fig. 1). Selected area electron diffraction (SAED) of these regions reveals an orthorhombic unit cell having following unit cell parameters: a = 5.66 (4) Å, b = 4.97 (2) Å, c = 5.28 (6) Å, V = 149 (2) Å^3.

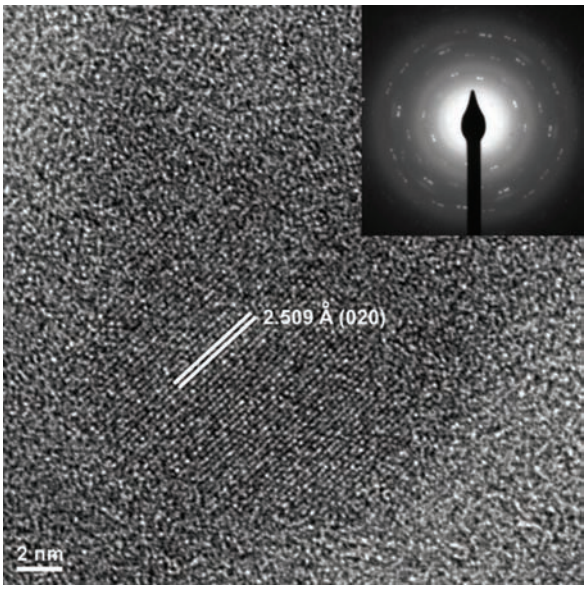

Fig. 1: HRTEM and SAED image (inset) of the thermally untreated samarskite-(Y) from Ampangabe, Madagascar.

X-ray diffraction (XRD) pattern of the thermally untreated sample is typical for heavily metamictised minerals. Four low-intensity diffraction maxima were observed that could be attributed to the low-temperature samarskite modification. X-ray diffraction pattern of the sample annealed at 500°C revealed mostly recrystallised low-temperature samarskite with an orthorhombic unit cell: a = 5.58 (2) Å, b = 4.92 (2) Å, c = 5.19 (2) Å, V = 142.3 (7) Å^3.

A comparison of HRTEM and XRD data indicates a structural relation of the preserved pre-metamict structure and the recrystallised mineral at 500 °C. This can be used as a prerequisite in a structure solution for samarskite samples.

[1] Sugitani Y. et al. (1985) *Am. Mineral.*, **70**, 856-866.

Tennantite-tetrahedrite minerals from the Madan Pb-Zn deposits, Bulgaria

Vassileva, R. D.[*] & Atanassova, R.
Geological Institute, Bulgarian Academy of Sciences, Sofia Bulgaria ([*]rosivas@geology.bas.bg)

The minerals from the tennantite-tetrahedrite series are characteristic, though in subordinate quantities in the veins of the Madan Pb-Zn deposits, Central Rhodopes. Fahlore minerals are indicative for increased Sb and As in the late ore precipitating fluids. The behavior of these minerals in the hydrothermal deposits and mining sites could help in resolving some environmental issues.

Tennantite-tetrahedrites are formed in the late phases of the main quartz-sulphide stage with galena, sphalerite, pyrite and chalcopyrite. Representative samples are studied from the deposits of Petrovitsa, Gradishte and Strashimir. These minerals occur: 1) as single crystals and their aggregates overgrowing galena, pyrite and chalcopyrite. The tetrahedral crystals (1-3 mm) are shaped by *o* {111}, *d* {110}, *a* {100} and *n* {211}; 2) in close association with chalcopyrite and sphalerite, presented mainly as crusts, resembling the polyhedral sulphide crystals (Fig. 1). Oriented overgrowth of tetrahedrite on chalcopyrite (due to the similar structural motifs) and on galena with parallel mutual orientation (Gal (100) [100] // Td (001) [110]) occurs.

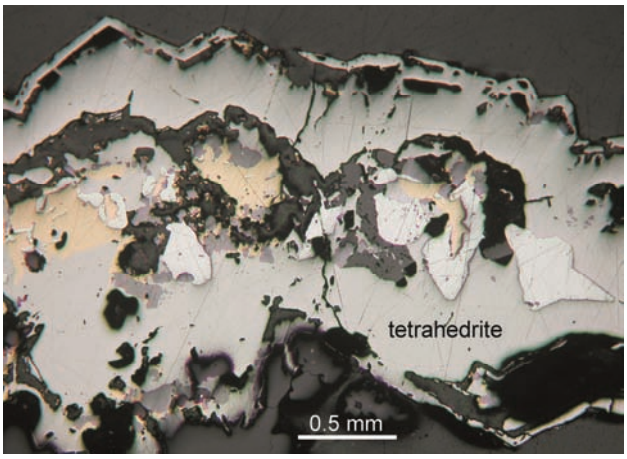

Fig. 1: Mineral relationships of tetrahedrite with main sulphides from the Petrovitsa deposit, reflected light.

The well-known variations in the chemical composition of tennantite-tetrahedrites (Cu-Ag, Zn-Fe and Sb-As) and trace-element distribution are determined by EPMA, ICP-AES, LA-ICP-MS. A considerable increase in the Zn-content in most samples is registered (up to 7.08 wt. %), and insignificant Fe-content (always less than 0.80 wt. %). Silver reaches 1.40 wt. % in several tetrahedrites. Some amount of Mn, Hg, Bi, Se, and Cd traces are revealed as well. The mean crystallochemical formulae calculated on the basis of 29 apfu are:

Petrovitsa $(Cu_{9.72}Zn_{1.73}Ag_{0.18}Fe_{0.15})_{11.78}(Sb_{3.69}As_{0.99})_{4.68}S_{12.54}$
Gradishte $(Cu_{9.58}Zn_{1.57}Fe_{0.19})_{11.34}(Sb_{0.90}As_{3.74})_{4.64}S_{13.02}$
Strashimir $(Cu_{10.35}Zn_{1.46}Fe_{0.59})_{12.40}(Sb_{2.33}As_{1.72})_{4.05}S_{12.55}$.

All studied minerals belong to the zincian members of the tennantite-tertrahedrite group.

The increased Zn-content reflects in the unit cell parameter *a* 10.37(8) Å of Petrovitsa tetrahedrite, determined by data from XRD. The chemical variations in tennantite-tetrahedrite minerals correspond to the geochemical specialization of the Madan Pb-Zn deposits.

Acknowledgements: This study is part of the 2009-2010 Scholarship of the World Federation of Scientists. Financial support (SCOPES IZ73Z0-128089, DO1-904/MON projects) is greatly acknowledged.

Johannsenite-rhodonite replacement in the base metal deposits, Central Rhodopes, Bulgaria

Vassileva, R.D.
Geological Institute, Bulgarian Academy of Sciences, Sofia, Bulgaria (rosivas@geology.bas.bg)

Pyroxenoids are major constituent of the retrograde stage of alteration of manganoan skarns [1] in the replacement ore bodies in the Central Rhodopean Pb-Zn deposits (Madan, Laki districts and Enyovche deposit), South Bulgaria. The radiate and sperulitic aggregates of the primary skarn clinopyroxenes belong to the Mn-enriched members of hedenbergite-johannsenite series.

Extensively distributed, though subordinate, rhodonite is among the wide spread alteration products after johannsenite. In Madan deposits it occurs as: 1) oriented epitactic and topotactic overgrowths and replacements after the pyroxene crystals; or 2) massive, 1-2 cm narrow zone along the pyroxene-marble replacement front, without any orientation to the primary pyroxene, and considered as reprecipitated after partial natural dissolution of the earlier pyroxene.

The complete reaction of alteration from johannsenite to rhodonite according to [2] occurs stepwise. The intermediate products are found to have increased Ca content in their structure, in studied case 9-10, reaching up to 12 wt.% CaO, corresponding to ~1/5 of octahedral sites in rhodonite structure. The pyroxenoids show structural orientation to the direction of pyroxene chains $[110]_{px}$// $[100]_{rdn}$ at 52°. Products of johannsenite-rhodonite reaction are observed as: i) small crystals epitaxically overgrowing the pyroxene prismatic faces or forming nests together with calcite (Fig. 1a); ii) as interstitial radial grains in the pyroxene aggregates; iii) as fine-lamellar intergrowths, observed also by [3], replacing topotaxically the johannsenite prismatic crystals (Fig. 1b). The replacement takes place initially along the grain boundaries, and later - thoroughly, forming radiating rhodonite pseudomorphs after johannsenite. The reaction mechanisms include: 1) topotactic solid-state replacement with cation re-arrangement and inheritance of the O-stacking; 2) epitactic overgrowth of rhodonite crystals with reconstructive reprecipitation of material on preliminary oriented nuclei. The mutual orientation in both cases is equal. Substantial transfer and reprecipitation of material in second case is connected with more liberated open space after dissolution.

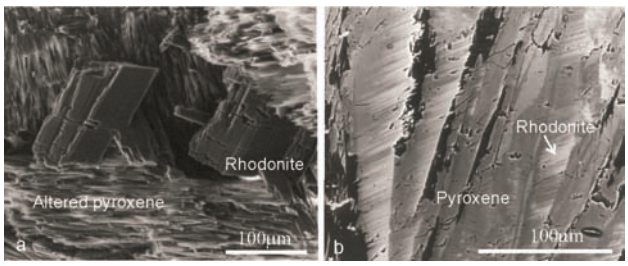

Fig. 1: Epitactic (a) and topotactic (b) replacement of johanssenite from rhodonite.

Acknowledgements: The study is supported by 2009-2010 Scholarship by World Federation of Scientists and SCOPES IZ73Z0-128089 project of the Swiss Science Fund.

[1] Vassileva, R.D. & Bonev, I.K. (2003) in Eliopoulos et al. (eds.) *Mineral Exploration and Sustainable Development*, Millpress, Rotherdam, 403-406. [2] Livi, K.J.T & Veblen, D.R. (1992) *Am. Mineral.*, **77**, 380-390. [3] Veblen, D. (1985) *Am. Mineral.*, **70**, 885-901.

Zirconolite family minerals in the alumina-rich fenites of the Khibiny alkaline complex (Kola Peninsula, Russia)

Yakovleva, O.S.* & Pekov, I.V.
Geological Faculty, Moscow State University, Moscow, Russia (*ya_olik@mail.ru)

Zirconolite, ideally $CaZrTi_2O_7$, known in several natural modifications (2*M*, 3*O*, 3*T*), is common accessory mineral in the fenites formed after xenoliths of alumina-rich rocks in the Khibiny alkaliny complex, Kola Peninsula, Russia. Zirconolite occurs there in the rocks mainly composed by alkali feldspars, typically with nepheline. Other common associated minerals are hercynite, ilmenite and zircon. Corundum, sodalite, rutile, biotite, crichtonite, sekaninaite, Ti-rich magnetite, freudenbergite, dawsonite, fayalite, baddeleyite, srilankite, *etc*. are also found there. Zirconolite forms equant or elongate crystals (up to 0.5 mm) and rims around zircon and baddeleyite grains. Zirconolite-like minerals with prevalence of *REE* (with Ce-, Nd- or Y-maximum) or Na over Ca in the large-cation site are also typical in the alumina-rich fenites at Khibiny. These minerals and zirconolite form continuous solid-solution system and can be united in the zirconolite family. The major schemes of substitutions in this family are: $2Ti^{4+} \rightarrow Nb^{5+} + Fe^{3+}$; $2Ca^{2+} \rightarrow REE^{3+} + Na^{+}$; $Ca^{2+} + (Th,U)^{4+} \rightarrow 2REE^{3+}$; $Ca^{2+} + Ti^{4+} \rightarrow REE^{3+} + Fe^{3+}$. Other possible schemes are: $Ca^{2+} + O^{2-} \rightarrow Na^{+} + (OH)^{-}$; $Zr^{4+} + Ti^{4+} \rightarrow Nb^{5+} + Fe^{3+}$; $2Ca^{2+} \rightarrow (Th,U)^{4+} + {}^{0}$. Typical feature of all zirconolite-like minerals is strong affinity to Nd (all analyses show Nd > La). Having also significant affinity to Ca, they are typically the only concentrators of this element in some kinds of the alumina-rich fenites at Khibiny. Thus, appearance of zirconolite analogues with prevalence of *REE* or Na over Ca indicates strong deficiency of Ca in the mineral-forming systems. In some rocks, zirconolite replaces zircon. Such evolution of mineral form of Zr, from silicate to oxide, shows decrease of silica activity during the formation of the Khibiny alumina-rich fenites. Generally, presence of *REE*- or Na-analogues of zirconolite can be considered as an indicator of both low silica activity and deficiency of Ca in natural alkaline systems.

Is the study of crystal morphology really old-fashioned?

Zebec, V.[1], Bermanec, V.[2*] & Čobić, A.[2]
[1]Croatian Natural History Museum, Zagreb, Croatia
[2]Faculty of Science, Institute of Mineralogy and Petrology, University of Zagreb, Croatia ([*]vberman@public.carnet.hr)

In 1998, at the 17th General Meeting of IMA in Toronto, one of the goals was to encourage further studies of crystal morphology and its relation to growth conditions, as a part of mineralogical investigations in the 21st century.

What is the purpose of these morphological studies?

This kind of investigation has irreplaceable value for a better understanding of crystals and crystal growth. The explanation of this is presented by some examples.

1. By investigating morphology, one can study morphogenesis. For example, studies of barite and calcite from Krapinske toplice thermal spring in Hrvatsko Zagorje, Croatia, where six generations of barite (Fig. 1) were investigated in order to determine crystal genesis [1].

2. Oriented coalescence is practically impossible to study in any other way but via morphological studies. Several oriented coalescences are described on minerals from Stari Trg - Trepča mine, Kosovo [2-4].

3. Parallel-perspective drawings of crystals in addition with growth prints on crystal faces make possible the orientation of crystals. Very good examples of this are measurements of epidote crystals from Smilevski dol near Dunje in Macedonia [5].

4. Using morphological measurements one should be in a position to acquire axis ratio which is the basic information about a crystal [5].

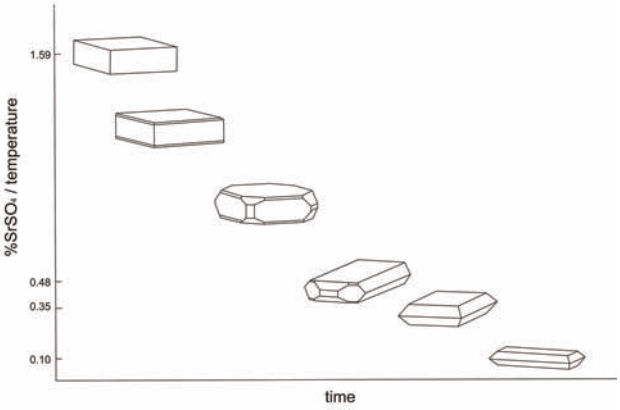

Fig. 1: Six generations of barite (from Zebec [1]).

[1] Zebec, V. (1976) *Geol. Vjesnik*, **29**, 323-345. [2] Zebec, V. (1977) *Bull. Mus. d'Histoire Naturelle*, **32/a**, 5-8. [3] Zebec, V. (1978) *Bull. Mus. d'Histoire Naturelle*, **33/a**, 95-100. [4] Zebec, V. (1981) *Geol. Vjesnik*, **33**, 227-234. [5] Zebec, V. (1984) *Geol. Macedonica*, **1**, 63-103.

Rhodonite group mineral from Morro da Mina mine, Conselheiro Lafaiete, Minas Gerais, Brazil

Žigovečki Gobac, Ž.[1*], Scholz, R.[2] & Bermanec, V.[1]
[1]Inst. of Mineralogy and Petrology, Faculty of Science, University of Zagreb, Croatia ([*]zeljkaz@geol.pmf.hr)
[2]Faculty of Engineering, University of Minas Gerais State, João Monlevade, Brazil

Deep pink to red, transparent tabular crystals of gem quality were collected at Morro da Mina mine, located in the city of Conselheiro Lafaiete, 115 km south from Belo Horizonte, the capital city of Minas Gerais state, Brazil.

The manganese deposits of Morro da Mina are hosted in a metavolcanosedimentary sequence of Archean age, cutted by granodioritic bodies. The regional and contact metamorphism and a sequence of hydrothermal events produced a complex mineralogy, including Mn-bearing minerals rhodonite, pyroxmangite, spessartite and others [4].

According to similar physical properties, the sample was erroneously assumed to be rhodonite. Subsequent X-ray powder diffraction analysis (using CuKα radiation) identified the sample as a mineral belonging to the p-p (pectolite-pyroxene) isostructural series of pyroxenoides, most probably natronambulite.

Crystal structure of investigated minerals belonging to p-p isostructural series of pyroxenoides [5], including nambulite, natronambulite, marsturite and lithiomarsturite, although similar, differs from those of rhodonite [3], which belongs to the w-p (wollastonite-pyroxene) isostructural series. The differences in their structures are reflected in X-ray diffraction pattern (Fig. 1), helping their identification.

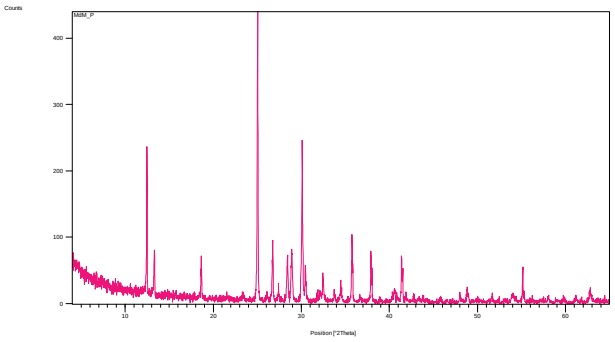

Fig. 1: XRD pattern of the sample from Morro da Mina mine.

Further investigation of chemical composition, particularly possible Na, Li, Ca and Mg presence, will help to distinguish mineral member of p-p isostructural series of pyroxenoides [1].

This is the first report of a mineral belonging to this isostructural series from this locality. So far nambulite and natronambulite have been recorded in various localities, including Japan [1,7], Namibia [6] and India [2], all in the metamorphosed manganese ore deposits.

[1] Matsubara, S. et al. (1985) *Mineral. J.*, **12**, 332-340. [2] Mukhopadhyay et al. (2005) *J. Miner. Petrol. Sci.*, **100**, 26-30. [3] Narita, H. et al. (1975) *Ac. Crystalogr.*, **B31**, 2422-2426. [4] Pires, F.R.M. (1983) *Anais da Acad. Brasileira de Ciências*, **55**, 271-285. [5] Takéuchi, Y. & Koto, K. (1977) *Mineral. J.*, **8**, 272-285. [6] von Knorring et al. (1978) *Neues Jb. Monat.*, **8**, 346-348. [7] Yoshii, M. et al. (1972) *Mineral. J.*, **7**, 29-44.

Structural complexities of natural and synthetic perovskites

Mitchell, R.H.
Dept. of Geology, Lakehead University, Thunder Bay, Ontario, Canada (rmitchel@lakeheadu.ca)

The structural hierachy of perovskite group compounds as derived from group theory and experimental data is briefly described together with the classification of naturally occurring perovskite-structured oxide, fluoride, hydroxide, and silicate minerals. Aspects of the structure and compositional variation of the quaternary solid solution series perovskite-loparite-lueshite-tausonite are described.

The crystal structures $(CaTiO_3)_{50}(SrTiO_3)_{50}$ and Sr_2CrTaO_6 are described to illustrate some of the experimental problems in the determination of simple perovskite structures by X-ray and neutron diffraction.

Neutron and X-ray diffraction data are presented for the system $CaTiO_3$ - $Ca_4Nb_4O_{14}$ to illustrate how Nb is incorporated into latrappite [(Ca,Na)(Nb,Fe,Ti)O_3]. These data show the limit of solubility of Nb in $CaTiO_3$ is 16 wt.% Nb_2O_5 and that increasing amounts of Nb result in the formation of layered perovskites belonging to the $A_nB_nO_{3n+2}$ series with the general formula $Ca_n(Ti_{n-x}Nb_x)O_{3n+0.5x}$. These adopt the space groups $Cmc2_1$, $Pnn2$, and $Pbn2_1$ for the n = 6, 5, and 4 compounds, respectively.

The structure of lueshite [(Na,Ca)(Nb, Ti)O_3] is shown not to be identical to that of synthetic $NaNbO_3$. Single crystal XRD data suggests that lueshite adopts the space group *Pbmn* at room temperature. However, these data are not corroborated by powder XRD (Rietveld) or high resolution time-of-flight neutron diffraction (GSAS). Lueshite, in common with synthetic $NaNbO_3$ undergoes a series of structural phase transtions from *Pm*3*m* through I4/*mcm* to *Cmcm* from high to low termperature. However, the room temperature structure of lueshite remains ambiguous, due to pinning of the higher temperature *Cmcm* structure and/or failure of even high resolution neutron diffraction to resolve possible orthorhombic or monoclinic structures.

Perovskite and post-perovskite in Earth's lower mantle

Hirose, K.*, Sinmyo, R. & Ohta, K.
Dept. of Earth and Planetary Sciences, Tokyo Institute of Technology, Tokyo, Japan (*kei@geo.titch.ac.jp)

A phase transition from $MgSiO_3$ perovskite to post-perovskite occurs above ~120 GPa at 2500 K corresponding to about 2600 km depth from the surface, which has significant implications for the nature and dynamics in the lowermost mantle. Post-perovskite has a layer stacking crystal structure with density higher than that of perovskite by about 1%. The changes in elastic properties and the large Clapeyron slope, about four times larger than those of upper mantle phase changes, explains the abrupt shear wave velocity jump at the D" seismic discontinuity and its rich topography. In addition, thermal and electrical conductivities, viscosity, and diffusivity can all vary greatly across the perovskite to post-perovskite phase transition. We report our recent measurements of such transport properties at high pressure in a diamond-anvil cell. These lower mantle transport properties are fundamental to heat transport and thermal evolution, electromagnetic core-mantle coupling, chemical heterogeneity and dynamical properties of the deep mantle.

The valence state and spin state of iron can be also different between perovskite and post-perovskite. Al-bearing (Mg,Fe)SiO_3 perovskite is known to include substantial amount of Fe^{3+}. Our recent electron energy-loss near-edge structure (ELNES) spectroscopy measurements demonstrate that the $Fe^{3+}/\Sigma Fe$ ratio in Al-bearing post-perovskite depends on the oxygen fugacity but does not increase with increasing Al content, which is in remarkable contrast to the case of perovskite. This suggests that upon perovskite to post-perovskite phase transition, Fe^{3+} in perovskite and coexisting metallic iron recombine to form Fe^{2+}. Since Fe^{2+} partitions preferentially into (Mg,Fe)O ferropericlase, post-perovskite should be depleted in iron compared to perovskite. This is consistent with our previous report on crystal chemistry change in a pyrolitic mantle across the post-perovskite phase transition [1]. Such a marked change in the valence state of iron and resultant redistribution of iron has broad implications for the seismic and transport properties in the lowermost mantle. The phase transition from perovskite to Fe-depleted post-perovskite can occur in relatively narrow pressure range of about 5 GPa [2], although seismology suggests even sharper seismic discontinuity.

[1] Murakami, M. et al. (2005) *Geophys. Res. Lett.*, **32**, L03304.
[2] Ohta, K. et al. (2008) *Earth Planet. Sci. Lett.*, **267**, 107-117.

Iron in mantle silicate perovskite

Shim, S.-H.[1*], Grocholski, B.[1], Catalli, K.[1], Sturhahn, W.[2] & Prakapenka, V.[3]
[1]Massachusetts Institute of Technology, Cambridge, USA
([*]sangshim@mit.edu)
[2]Argonne National Laboratory, Argonne, IL, USA
[3]University of Chicago, USA

Magnesium silicate in the perovskite structure may be the most abundant mineral in the Earth as it represents 70% of the most voluminous layer, the lower mantle. Therefore, its properties are fundamental to understand the physical and chemical processes in the lower mantle.

Iron is the most dominant transition metal cation in mantle silicate perovskite (Pv) and undergoes changes in the spin and valence states at the pressure-temperature conditions relevant to the lower mantle [1,2]. However, the effects of its different spin and valence states on the properties of Pv have not been well understood.

We have synthesized Pv samples with iron dominantly in Fe^{2+}, all iron in Fe^{3+}, and iron in Fe^{3+} combined with Al^{3+} in the diamond-anvil cell at 50 GPa and 2000 K, in order to isolate the effects of different valence states [3-7]. We also synthesized Pv with realistic amounts of Fe and Al for the lower mantle under the appropriate redox condition for the region, in order to measure the content of Fe^{3+} [4,7]. The valence and spin states were measured using Mössbauer spectroscopy (Sector 3 of Advanced Photon Source, USA) and their effects on the crystal structure of Pv were measured using X-ray diffraction (GSECARS of Advanced Photon Source) up to 100 GPa. The measurements were conducted under quasi-hydrostatic stress conditions.

We found that Fe^{2+} remains high spin to at least 70 GPa. We observed the high quadrupole-splitting site that was previously assigned to the intermediate spin state [8,9]. Because a similar value was also found in garnet at 1 bar, we favor an interpretation of the high quadrupole-splitting site as high spin Fe^{2+}. Fe^{2+} decreases the distortion in the unit cell of Pv and expands the unit cell throughout the lower mantle. However, Fe^{2+} does not change the compressibility of Pv.

We found that Fe^{3+} undergoes a high-spin to low-spin transition at 0-55 GPa in an Al-free system [5] and 70-80 GPa in an Al-bearing system [6]. The spin transition is likely limited to Fe^{3+} in the octahedral site of Pv. In both Al-free and Al-bearing systems, Fe^{3+} increases the compressibility of Pv. In the Al-free system, Fe^{3+} expands the unit cell of Pv throughout the lower mantle. In the Al-bearing system, Fe^{3+} collapses the volume to that of Mg-end member Pv. The Al dependence is likely due to Al-Fe^{3+} site mixing.

Under reducing oxygen fugacity and quasi-hydrostatic stress conditions, we found that iron is dominantly in Fe^{2+} in aluminous Pv at pressures of the deep lower mantle. This is in sharp contrast with an earlier low-pressure study that reported as much as 60% of iron is Fe^{3+} [2]. Our new results may have important implications for the oxygen fugacity and transport properties of the lower mantle.

[1] Badro, J. et al. (2004) *Science*, **305**, 383-386. [2] McCammon, C. et al. (1997) *Nature*, **387**, 694-696. [3] Lundin, S. et al. (2008) *Phys. Earth Planet. In.*, **168**, 97-102. [4] Grocholski, B. et al. (2009) *Geophys. Res. Lett.*, **35**, L05312. [5] Catalli, K. et al. (2010) *Earth Planet Sc. Lett.*, **289**, 68-75. [6] Catalli, K. et al. (2010), in prep. [7] Grocholski, B. et al. (2010) in prep. [8] McCammon, C. et al. (2008) *Nat. Geosci.*, **1**, 684-687. [9] Lin, J.F. et al., 2008, *Nat. Geosci.*, **1**, 688-691.

Nuclear resonance studies of lower mantle perovskite: spin state and elastic properties

McCammon, C.[1*], Dubrovinsky, L.[1], Glazyrin, K.[1], Narygina, O.[1,2], Wu, X.[1,3], Kantor, I.[4], Sergueev, I.[5] & Chumakov, A.[5]
[1]Bayerisches Geoinstitut, Universität Bayreuth, Germany
([*]catherine.mccammon@uni-bayreuth.de)
[2]now at: School of Physics and Astronomy, University of Edinburgh, UK
[3]now at: School of Earth and Space Sciences, Peking University, Beijing, China
[4]GSECARS, University of Chicago, Argonne, USA
[5]European Synchrotron Radiation Facility, Grenoble, France

The remarkable ability of the perovskite structure to accommodate widely varying sizes of cations and anions through angular distortions and a strong tolerance for non-stoichiometry leads to a wealth of interesting and useful properties, as well as the capability to incorporate more than half of the elements of the periodic table. In the dominant chemical system of the Earth's mantle, MgO-SiO_2-Al_2O_3-FeO-Fe_2O_3, the perovskite structure is the most stable host over a wide range of pressure and temperature conditions, constituting up to 80% of the lower mantle. The ability of iron to adopt multiple valences and spin states can drastically change the physical and chemical properties of lower mantle perovskite from those of the endmember composition $MgSiO_3$, which can have significant implications for the modelling of lower mantle properties and dynamics. Iron occurs as both Fe^{2+} and Fe^{3+}, where the latter is expected to predominate in lower mantle perovskite compositions due to the stabilising influence of Al^{3+} on Fe^{3+} [1], even under reducing conditions. Spin transitions are possible in both Fe^{2+} and Fe^{3+}, and a number of controversial results have been reported, including the discovery of the unusual intermediate spin state of Fe^{2+} (four paired and two unpaired 3*d* electrons), which appears to be stable over pressure and temperature conditions covering the bulk of the lower mantle [2,3].

In order to resolve existing controversies and to assess the implications of different valence states and spin transitions in silicate perovskite on the properties of the lower mantle, it is necessary to conduct *in situ* studies on relevant perovskite compositions at high pressure and high temperature conditions. Nuclear resonance methods offer a unique opportunity for studying both the electronic and dynamic properties of iron compounds, and include laboratory-based methods such as Mössbauer spectroscopy, and synchrotron-based methods such as nuclear forward scattering (NFS) which allows the measurement of hyperfine parameters complementary to Mössbauer spectroscopy, and nuclear inelastic scattering (NIS) which allows the determination of elastic wave velocities for direct comparison with bulk geophysical data.

We will report recent results using a new approach to conduct nuclear resonance experiments in the diamond anvil cell with a portable laser heating system. These results include the measurement of elastic wave velocities in iron-bearing silicate perovskite using NIS, coupled with NFS to determine spin populations. We will discuss our results in the context of other studies on iron-bearing silicate perovskite using complementary methods, and explore their implications for the structure and properties of the lower mantle.

[1] McCammon, C. (1997) *Nature*, **387**, 694-696. [2] McCammon, C. et al. (2008) *Nat. Geosci.*, **1**, 684-687. [3] Lin, J.-F. et al. (2008) *Nat. Geosci.*, **1**, 688-691.

Stability of mantle silicate in Super-earths: insights from a high-pressure study of neighborite

Grocholski, B.[1*], Shim, S.-H.[1] & Prakapenka, V.[2]
[1]Massachusetts Institute of Technology, Cambridge, USA
([*]brent_g@mit.edu)
[2]University of Chicago, USA

The Clapeyron slope of a phase transition has important implications on the thermal evolution of planets. For instance, in the Earth a negative Clapeyron slope of the ringwoodite to perovskite + ferropericlase boundary at 660-km depth behaves as a permeable barrier for thermal mantle flow [1]. Newly discovered Super-earth type extrasolar planets have brought up questions about their mantle structure and the stability of magnesium silicates at the extreme high pressures in these objects.

Computer simulations by [2] indicate a breakdown of $MgSiO_3$ into MgO + SiO_2 at a pressure achieved in the interior of 10 earth-mass Super-earths (~1000 GPa). They predict a strongly negative Clapeyron slope that would make the boundary impermeable for thermal mantle flow, allowing for an oxide-rich stratified deep mantle.

Our current static compression techniques are not capable of reaching the relevant pressure conditions of Super-earth to assess the stability of the silicate phase. However, we can investigate analog materials, which undergo the same sequence of phase transitions as mantle silicates but at much lower pressures. Umemoto et al. (2006) [3] predicted that mineral neighborite $NaMgF_3$ ($MgSiO_3$ analog) dissociates into NaF (MgO analog) and MgF_2 (SiO_2 analog) at 40 GPa which is readily obtained using the diamond cell. Neighborite has orthorhombic perovskite structure and undergoes a transition to post-perovskite (at 15-20 GPa), similar to mantle silicate perovskite.

We have conducted in situ X-ray diffraction measurements on neighborite and MgF_2 in the laser-heated diamond-anvil cell at the GSECARS sector of Advanced Photon Source. The samples were loaded with an Ar medium, which provides thermal insulation and quasi-hydrostatic stress conditions. We do not observe the breakdown of $NaMgF_3$ up to 70 GPa and 2500 K, much higher than the predicted breakdown pressure. Diffraction patterns can be indexed as a combination of the perovskite and post-perovskite structures with some residual NaF from the starting material. Notably, we did not observe any diffraction intensity at the angle where the most intense diffraction line from MgF_2 would appear. The absence of the 100% line of MgF_2 is unambiguous evidence for the stability of $NaMgF_3$ against decomposition at pressures at least up to 70 GPa.

In the computational simulations, the primary driving force for the breakdown is a large decrease in volume at a phase transition in SiO_2 and MgF_2 from the pyrite-type to cotunnite-type. We find a new phase of MgF_2 whose stability field exists between these two structures. This new phase appears to be one (or more) of the several possible distorted pyrite types with seven-fold coordination. SiO_2 likely has a similar high pressure phase, expanding the stability field of $MgSiO_3$ to pressures in excess of those found in the rocky mantle fraction of Super-earths.

Our experimental results suggest that mantle silicates are stable to the highest pressures found in rocky planets of all sizes. The implication of this finding is that the mantles of Super-earths may not have phase boundary which would behave as a barrier for the mantle convection.

[1] Tackley, P.J. et al. (1993) *Nature*, **361**, 699-704. [2] Umemoto, K. et al. (2006) *Science*, **311**, 983-986. [3] Umemoto, K. (2006) *Geophys. Res. Lett.*, **33**, L15304.

New empirical constraints on the capability of perovskite to sequester and fractionate trace elements

Chakhmouradian, A.R.[1*], Kamenetsky, V.[2], Reguir, E.P.[1], Zaitsev, A.N.[3], Golovin, A.V.[4] & Sharygin, V.V.[4]
[1]Dept. of Geological Sciences, University of Manitoba, Winnipeg, Canada ([*]chakhmou@cc.umanitoba.ca)
[2]School of Earth Sciences, University of Tasmania, Hobart, Australia
[3]Dept. of Mineralogy, St. Petersburg State University, St. Petersburg, Russia
[4]V.S. Sobolev Inst. of Geology and Mineralogy, Russian Academy of Sciences (Siberian Branch), Novosibirsk, Russia

Although perovskite sensu stricto ($CaTiO_3$) is universally recognized as one of the principal repositories for a variety of incompatible elements in undersaturated rocks and is widely used in isotopic chronological and provenance studies, we still know very little about the partitioning of trace elements between this mineral and magmas, or even about the extent of substitution of Ca and Ti by cations of different valence [1,2]. The well-characterized structural parameters of perovskite and zoning patterns observed in natural samples are not consistent with some of the partitioning data available for this mineral in the literature. In this work, we examined the extent of compositional variation in perovskite from several different types of igneous rock (including kimberlites, carbonatites, ijolites, clinopyroxenites, olivinite, melilitolite and katungite) using electron-microprobe analysis and laser-ablation ICP-MS. In contrast to the published work, our data show that the Rb and Ba contents in this mineral do not exceed 1.5 and 120 ppm, respectively, whereas Cs was not detected in any of the samples (i.e. << 1 ppm). With respect to their calculated partition coefficients, the examined trace elements can be grouped into four categories: strongly incompatible with $^{Prv/L}D$ << 0.1 (Zn, Ba, Rb, Cs); moderately incompatible with $^{Prv/L}D$ = 0.1-0.5 (Mn, Al, Cr); moderately compatible (Sr, Sc, V, Fe) and strongly compatible with $^{Prv/L}D$ > 10 (Y, REE, Th, U, Zr, Hf, Nb, Ta). In agreement with the published data [1,2], light lanthanides (with a peak at Nd) are much more compatible than heavy REE or Y. There is surprisingly little variation in Y/Ho ratio, which is consistently subchondritic (11.5-18.5) in both primary perovskite and that equilibrated with subsolidus fluids. These data indicate that the so-called non-CHARAC partitioning of Y and Ho is not restricted to fluid-rich systems [3] and may result from fractionation of perovskite (and possibly other minerals) in magmatic systems. The composition of perovskite from primitive mantle-derived rocks also indicates that it is a very effective vehicle of Zr-Hf, Th-U and Nb-Ta decoupling. However, some samples from carbonatites and ijolites show anomalously low Th/U ratios (< 3), possibly resulting from preferential partitioning of Th into an as yet unidentified phase or phases.

[1] Corgne, A. & Wood, B.J. (2005) *Contrib. Mineral. Petrol.*, **149**, 85-97; [2] Melluso, L. et al. (2008) *Can. Mineral.*, **46**, 19-40; [3] Bau, M. (1996) *Contrib. Mineral. Petrol.*, **123**, 323-333.

Megawite $CaSnO_3$ – a new mineral of the perovskite group

Galuskin, E.V.[1*], Galuskina, I.O.[1], Gazeev, V.M.[2], Dzierżanowski, P.[3], Prusik, K.[4], Pertsev, N.N.[2], Zadov, A.E.[5] & Gurbanov, A.G.[2]

[1]Faculty of Earth Sciences, University of Silesia, Sosnowiec Poland (*evgeny.galuskin@us.edu.pl)

[2]Inst. of Geology of Ore Deposits, Petrography, Mineralogy and Geochemistry (IGEM), Russian Academy of Sciences, Moscow, Russia

[3]Inst. of Geochemistry, Mineralogy and Petrology, University of Warsaw, Poland

[4]Inst. of Materials Science, University of Silesia, Katowice Poland

[5]OOO Science-Research Center NEOCHEM, Moscow, Russia

Megawite [a = 5.56, b = 5.71, c = 7.94 Å, *Pbnm*) with end-member formula $CaSnO_3$ was discovered in an altered carbonate xenolith in the Upper Chegem caldera, Kabardino-Balkaria, Northern Caucasus, Russia [1]. Associated minerals are spurrite, reinhardbraunsite, rondorfite, wadalite, srebrodolskite, lakargiite, perovskite, kimzeyite, periclase, fluor- and hydroxylellestadite, while secondary minerals are brucite, ettringite-group minerals, afwillite, hydrocalumite and hydrogrossular. The formation of megawite is connected to high-temperature contact metamorphism of carbonate xenoliths within diatreme-facies ignimbrites of Pliocene age (2.8 Ma) under larnite-facies conditions (temperatures > 800ºC and low pressures). Megawite is usually represented by a Zr-bearing variety and commonly occurs together with lakargiite, $CaZrO_3$ [2] (Fig. 1). Investigation of the megawite-lakargiite natural solid solution suggests the existence of a continuous series from pure lakargiite to megawite with 60 mol.% $CaSnO_3$ end-member. High contents of Ti (up to 17 wt.% TiO_2) and U (up to 10 wt.% UO_3), characteristic of lakargiite, are not noted for megawite. Raman spectra of lakargiite and megawite are similar, so for identification of these minerals it is necessary to measure their composition (Fig. 1).

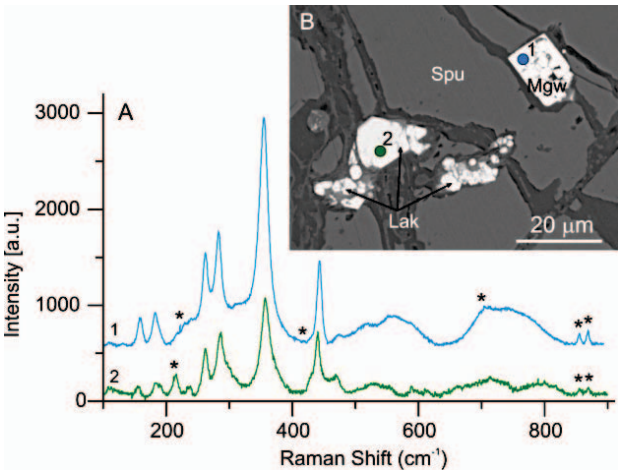

Fig. 1: A: Raman spectra of Zr-rich megawite (1) and Sn-rich lakargiite (2); B: Sn-rich lakargiite (Lak) and Zr-rich megawite (Mgw) in spurrite (Spu). Points of microprobe analyses are shown [1- $Ca(Sn_{0.58}Zr_{0.34}Ti_{0.07}Fe^{3+}_{0.01})_{\Sigma1}O_3$; 2 - $Ca(Zr_{0.68}Sn_{0.28}Ti_{0.02}Fe^{3+}_{0.02})_{\Sigma1}O_{2.99}$] and the Raman spectra were obtained at the same points (* - impurity of spurrite).

The name megawite honors the crystallographer Dr. Helen Dick Megaw (1907–2002), who pioneered the structural studies of perovskites [3].

[1] Gazeev, V.M. et al. (2006) *Vestnik Vladikavkazskogo Nauchnogo Centra*, **6**, 18-27. [2] Galuskin, E.V. et al. (2008) *Am. Mineral.*, **93**, 1903-1910. [3] Megaw, H.D. (1946) *Proc. Phys. Soc.*, **58**, 133-152.

The perovskite-brownmillerite series: perspectives for temperature estimation in Ca-rich pyrometamorphic rocks

Sharygin, V.V.

V.S.Sobolev Institute of Geology and Mineralogy SB RAS, Novosibirsk, Russia (sharygin@uiggm.nsc.ru)

Synthetic compounds from the $CaTiO_3$-$Ca(Fe,Al)_2O_5$ series have been extensively studied since 1960-70s, and several polymorphs of perovskite $CaTi_{1-x}Fe_xO_{3-x/2}$ ($0 \le x \le 0.5$), two polymorphs of $Ca_2(Fe_{1-x}Al_x)_2O_5$ ($0 \le x \le 0.67$), $Ca_4Ti_2Fe_2O_{11}$, $Ca_3TiFe_2O_8$ and $Ca_5TiFe_2Al_2O_{13}$ have been recognized [1-4]. Natural analogues of all these phases, sometimes enriched in Al and Si, have already been discovered. If pure perovskite is a common mineral in diverse rocks from skarns to kimberlites, the occurrence of other Fe-Ti-phases is limited to Ca-rich pyrometamorhic rocks (larnite rocks, melilite-bearing paralavas and hornfels in combustion metamorphic complexes; metacarbonate xenoliths in alkali basalts; skarn-like rocks in siliceous volcanics) [5-8]. It is not always possible to reliably constrain the crystallization temperature of these rocks on the basis of their mineralogy. For example, larnite rocks of the Hatrurim Formation (Dead Sea region) are considered as high-temperature products of solid-state reactions during combustion metamorphism, and their mineral associations are stable in a wide temperature range (900-1200°C).

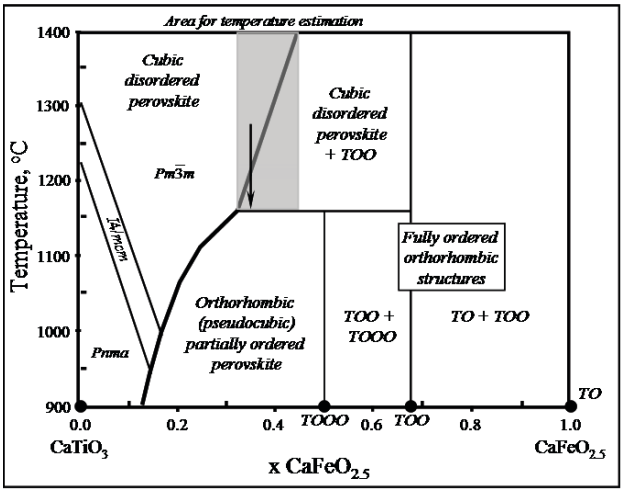

Fig. 1: Phase diagram for the system $CaTiO_3$–$CaFeO_{2.5}$ after [4-5]. TO - $Ca_2Fe_2O_5$; TOO - $Ca_3TiFe_2O_8$; TOOO - $Ca_4Ti_2Fe_2O_{11}$. Arrow shows a possible cooling trend for the Fe-perovskite + $Ca_3Ti(Fe,Al)_2O_8$ association in the Hatrurim Basin larnite rocks.

Analysis of the phase diagram $CaTiO_3$–$CaFe_2O_5$ shows that the coexistence of Fe-perovskite and $Ca_3TiFe_2O_8$ may be used for temperature estimation, whereas the brownmillerite - $Ca_3TiFe_2O_8$ pair is non-informative for temperature evaluation (Fig. 1). According to this phase diagram, the Fe-perovskite - $Ca_3Ti(Fe,Al)_2O_8$ association implies the minimum formation temperature for some Hatrurim larnite rocks as 1170-1200°C [5]. This paragenesis can serve as a new thermometer for metacarbonate rocks of the high-temperature region of the spurrite-merwinite facies.

[1] Grenier, J.-C. et al. (1976) *Mat. Res. Bull.*, **11**, 1219-1226. [2] Marinho, M.B. & Glasser, F.P. (1984) *Cem. Concr. Res.*, **14**, 360-368. [3] Gonzáles-Calbet, J.M. & Valet-Regí, M. (1987) *J. Solid State Chem.*, **68**, 266-272. [4] Becerro, A.I. et al. (2002) *J. Solid State Chem.*, **167**, 459-471. [5] Sharygin, V.V. et al. (2008) *Russ. Geol. Geophys.*, **49**, 709-726. [6] Žáček, V. et al. (2005) *Eur. J. Mineral.*, **17**, 623-633. [7] Galuskin, E.V. et al. (2008) *Am. Mineral.*, **93**, 1903-1910. [8] Zateeva, S.N. (2009) *PhD dissertation*, IGM, Novosibirsk.

Non-stoichiometry in perovskites: the role of "surplus" oxygen

Chakhmouradian, A.R.[1*] & Mitchell, R.H.[2]
[1]Dept. of Geological Sciences, University of Manitoba, Winnipeg, Canada ([*]chakhmou@cc.umanitoba.ca)
[2]Dept. of Geology, Lakehead University, Thunder Bay, Ontario, Canada

Oxide minerals commonly contain an excess amount of high-charged cations that is not compensated by any coupled substitutions in the cation sites and can only be explained by the uptake of additional oxygen [1,2]. Among minerals, one of the most extreme cases of this type of substitution is Nb-rich perovskite and latrappite (Ca,Na)(Nb,Ti,Fe)O_3, where "surplus" Nb cannot be accounted for by the substitutions $NaNb(CaTi)_{-1}$ or $NbFe^{3+}(Ti)_{-2}$ and is conventionally assigned to the hypothetical end-member $Ca_4Nb_4O_{14}$ (CN). Unlike perovskite, this compound has a layered structure, which can be interpreted as a stacking of perovskite-like slabs four NbO_6 octahedra thick and related to one another by ½[011] crystallographic shears [3,4]. The inter-slab spacings allow for the accommodation of more oxygen atoms in $Ca_4Nb_4O_{14}$ relative to perovskite ($4 \times CaTiO_3 = Ca_4Ti_4O_{12}$). We investigated limits of solubility between the $CaTiO_3$ (CT) and $Ca_4Nb_4O_{14}$ (CN) end-members using synthetic samples obtained by sintering of bulk compositions containing 20, 40, 60, 80 and 100 mol% CN (CN-20...100), i.e. fitting the general formula $Ca_n(Ti^{4+}_{n-x}Nb^{5+}_x)O_{3n+0.5x}$. The synthesis products were characterized by scanning and transmission electron microscopy, electron-microprobe analysis and X-ray powder diffraction combined with full-profile structure refinements. The limit of Nb uptake by perovskite is ca. 16 wt.% Nb_2O_5 (or 17% of the total occupancy of the B site). Charge neutrality of the Nb-doped compositions is maintained through the accommodation of "surplus" oxygen along non-periodic shear planes, and formation of minor vacancies in the Ca site. $Ca_{0.99}(Ti_{0.87}Nb_{0.13})O_{3.06}$ is isostructural with, but has a larger cell than, CT: *Pbnm*, *a* 5.3922(4), *b* 5.4552(4), *c* 7.6619(5) Å. In addition to the Nb-doped perovskite, samples CN-20-60 contain an increasing proportion of $Ca_6Ti_2Nb_4O_{20}$ (n = 6, x = 4). This phase is orthorhombic, *Cmcm* or *Cmc*2_1, *a* 3.844(1), *b* 37.573(8), *c* 5.478(2) Å; its structure is similar to that of $Ca_4Nb_4O_{14}$, but consists of perovskite-like slabs six $(Nb,Ti)O_6$ octahedra thick. Sample CN-80 consists entirely of $Ca_5TiNb_4O_{17}$ (n = 5, x = 4). This phase is orthorhombic, *Pmnn* or *P*2*nn*, *a* 3.843(2), *b* 32.020(11), *c* 5.485(2) Å, and consists of slabs five octahedra thick. Sample CN-100 corresponds to $Ca_4Nb_4O_{14}$ (n = 4, x = 4) well characterized in the literature [3,4]. In summary, a subsolidus assemblage of Nb-doped perovskite with $Ca_6Ti_2Nb_4O_{20}$ is stable over a wide compositional range, and is replaced at high Nb contents by layered perovskite-like structures with x = 4 and progressively decreasing n. Our data show that the incorporation of limited amounts of high-charged cations in oxide minerals can be effectively compensated by anionic non-stoichiometry.

[1] Eror, N.G. (1981) *J. Solid State Chem.*, **38**, 281-287. [2] Balachandran, U. & Eror, N.G. (1982) *J. Mater. Sci.*, **17**, 1207-1212. [3] Brandon, J.K. & Megaw, H.D. (1970) *Philos. Mag.*, **21**, 189-194. [4] Nanot, M., Queyroux, F. & Gilles, J.-C. (1977) *J. Phys. Colloq.*, **38**, C791–C794.

Perovskite from the Proterozoic Tiksheozero carbonatite (Russia): age and genesis

Lepekhina, E.N.[1*], Antonov, A.V.[1], Belyatsky, B.V.[2] & Sergeev, S.A.[1]
[1]Centre of Isotopic Research, VSEGEI, St.-Petersburg, Russia ([*]Elena_Lepekhina@vsegei.ru)
[2]VNIIOkeangeologia, St.-Petersburg, Russia

The Tiksheozero carbonatite complex located near the NE continental margin of the Karelian Craton within Archean TTG gneisses is a typical ring complex where carbonatites are associated with intrusions of ultramafic and alkaline rocks: olivinites, pyroxenites, theralites, jacupirangites, ijolites and nepheline syenites. Carbonatites occur as large bodies more than several hundred meters wide and up to 3 km long. The main carbonatite associations are: calcite, apatite, tetraferriphlogopite, magnetite and amphibole (high-T association); ankerite, dolomite, amphibole and apatite (low-T association) [1].

There were many attempts to determine the age of the complex by various radiometric techniques, but the results were not satisfactory [1]. We have also attempted to constrain the time of carbonatite intrusion by U-Pb dating of zircon and baddeleyite. The obtained data confirm the Proterozoic age of the carbonatites, but the internal structure of the zircon crystals unequivocally demonstrates metasomatic recrystallization of metamict areas of the crystals, which probably took place much later during the Caledonian orogeny.

It is well known that perovskite is a ubiquitous mineral in alkaline-ultramafic rocks and carbonatites [2]. This mineral is used as a geochronometer, which in contrast to zircon cannot be xenogenous and, hence, allows the time of emplacement to be determined precisely. Perovskite separated from a drill-core sample of Tiksheozero carbonatite is represented by anhedral crystals typically 100-500 μm in size with composition close to $CaTiO_3$ and limited variations in Fe, Na, Sr, Ce and Nd (0.6-1.7 and ≤ 1.2, 0.9, 3.7 and 1.6 wt.% respective oxides). Most of the grains contain inclusions of rock-forming and accessory minerals (calcite, dolomite, mica, diopside, apatite, ilmenite, pyrrhotite), as well as plucked inclusions. Sixteen perovskite grains were analyzed with a SIMS SHRIMP-II for U-Pb isotope abundances using Tazheran perovskite as a standard (465 ± 15 Ma). The obtained spread in isotope compositions was sufficient for regression best-fitting of the analytical data with a common-lead $^{207}Pb/^{206}Pb$ ratio of 0.836. The calculated age of the Tiksheozero perovskite is 381 ± 10 Ma (MSWD = 0.63).

The obtained age contradicts the generally accepted Proterozoic age for the Tiksheozero complex, but agrees well with the age of zircon recrystallization during a hypothetical metasomatic overprint event [1]. We speculate that the studied perovskite is not a primary magmatic phase and that its formation is related to the processes of recrystallization and metasomatic reworking of the carbonatites. A similar origin has been proposed for some of the perovskite from the Devonian alkaline-ultramafic/carbonatite complexes in the Karelia-Kola region [3]. Moreover, there are well-known examples of metasomatic perovskite in skarns at the contact with alkaline and mafic intrusions such as the Shishim Mountains in the Urals and Tazheran complex in Siberia [2]. We propose that the metasomatic event responsible for the perovskite formation in the Tiksheozero carbonatites is connected with the widespread alkaline magmatism in the region, which was triggered by mantle-plume activity at 360-380 Ma [4].

[1] Tichomirowa, M. et al. (2006) *Lithos*, **91**, 229-249. [2] Mitchell, R.H. (2002) *Perovskites. Modern and ancient*. Almaz Press, Canada. [3] Kukharenko, A.A. et al. (1965) *The Caledonian Complex*. Nedra, Moscow. [4] Kramm, U. et al. (1993) *Lithos*, **30**, 33-44.

Major and trace elements in perovskite from a micaceous kimberlite nodule, Udachnaya-East pipe, Siberia

Sharygin, V.V.[1*] & Kamenetsky, V.S.[2]
[1]V.S.Sobolev Inst. of Geology and Mineralogy SB RAS, Novosibirsk, Russia ([*]sharygin@uiggm.nsc.ru)
[2]School of Earth Sciences, University of Tasmania, Hobart, Australia

A unique nodule of micaceous kimberlite (6 cm in size) has been found in unaltered kimberlite of the Udachnaya-East pipe. This cognate nodule contains large olivine xenocrysts (3-7 mm) in a medium-grained matrix consisting of olivine, phlogopite, zoned spinel and perovskite. Mg-rich ilmenite, monticellite, djerfisherite, sodalite, calcite, shortite, chlorides, apatite and Mg-silicate (humite or serpentine) occur as minor or accessory phases. The contact between the nodule and its host kimberlite is sharp and does not show any reaction relations. The micaceous kimberlite differs from the host rock in containing higher modal abundances of phlogopite, spinel and perovskite and in the scarcity of carbonates, sulfides and chlorides.

Perovskite forms euhedral crystals (up to 150 μm), some of which show normal zoning (bright core, dark rim) in reflected light and BSE images. The zoning is more common in perovskite near the contact with the host kimberlite. The core-to-rim variations in discrete crystals with simple zoning involve a decrease in $LREE_2O_3$ (from 4-5 to 2-2.5), ThO_2 (from 0.5-1.6 to 0) and sometimes Nb_2O_5 (from 1.5-2 to 0.7-1 wt.%). Perovskite from the central part of the nodule exhibits fine oscillatory zoning and does not contain a Th-rich interior. Oscillatory-zoned crystals show only subtle variations in Ca, Ti, LREE and Nb, although there is general tendency in a slightly decreasing LREE and Nb levels from the core rimward. Perovskite from the micaceous kimberlite does not differ in major- and trace-element contents from perovskite in the host kimberlite. In both cases, perovskite approaches the ideal composition ($CaTiO_3$), and the total contribution from all other end-members ($Na_{0.5}Ce_{0.5}TiO_3$, $NaNbO_3$, $CeFeO_3$, $Th_{0.5}TiO_3$) does not exceed 8 mole %. Such composition is typical of perovskite from kimberlites worldwide [1]. LA-ICP-MS data for perovskite from the nodule and host kimberlites confirm EMPA data with regard to the distribution of REE, Th and Nb, and indicate a decrease in Ta (from 2700 to 700), Cr (from 300-400 to 30-50), Pb (from 200 to 10 ppm) toward the rim at approximately constant values of Zr (450-1100), U (200-300), Y (200-300) and Hf (20-40 ppm).

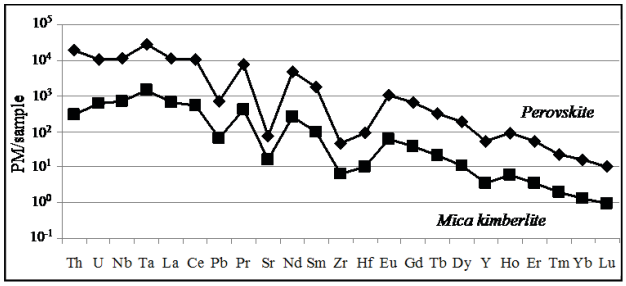

Fig. 1: Spider diagram for perovskite and mica kimberlite nodule from the Udachnaya-East pipe, LA-ICP-MS and ICP-MS average data.

Comparison of the ICP-MS data for perovskite and host micaceous kimberlite shows that perovskite is the principal carrier of the incompatible trace elements in the nodule (Fig. 1). The same pattern of perovskite-rock element distribution is observed in the host kimberlite.

[1] Chakhmouradian, A.R. & Mitchell, R.H. (2000) *Can. Mineral.*, **38**, 975-994.

Pyrophanite after perovskite from serpentinite at Perkupa, northern Hungary

Zajzon, N.[1*], Kristály, F.[1], Szakáll, S.[1], Fehér, B.[2], Váczi, T.[3] & Pekker, P.[3]
[1]Inst. of Mineralogy and Geology, University of Miskolc, Hungary ([*]nzajzon@uni-miskolc.hu)
[2]Herman Ottó Museum, Miskolc, Hungary
[3]Inst. for Nanotechnology, Bay Zoltán Foundation for Applied Research, Miskolc, Hungary

The Perkupa serpentinite, a member of the Bódva Valley Ophiolite Formation, was formed from dunite or pyroxenite under regional metamorphism. The first occurrence of pyrophanite in serpentinite in the Carpathian region is documented here.

Pyrophanite occurs as brownish-maroon-coloured euhedral crystals 10–200 μm in size in the serpentinite. Pleochroism is not visible. Internal reflections are common and strong. Commonly, a well-defined, semi-transparent, dark central zone and a pinkish, more opaque rim can be recognized (Fig. 1A). These zones are visible in BSE images as well. The chemical composition is $Mn_{0.96}Fe_{0.04}TiO_3$ (WDX analysis). Some crystals contain perovskite inclusions (Fig. 1B). The perovskite cores are close to the ideal formula and contain only 0.01 apfu Fe. The identity of this mineral as pyrophanite was confirmed by Gandolfi X-ray diffraction and Raman spectroscopy (Fig. 2).

Occasionally, large white inclusions were found in the pyrophanite. On the basis of optical, Raman and electron–microscopic examination, they are interpreted to consist of two phases: anatase and calcite. Dolomite (Ca, Mg > Mn) inclusions were also found.

Perovskite is a common constituent of this type of ultrabasites, but it becomes instable under CO_2-rich secondary processes, and gives way to TiO_2 polymorphs, calcite and titanite. Pyrophanite can form by reaction of the perovskite with Mn-bearing hydrothermal fluids. Manganese is an important component of fluids involved in ocean- floor metamorphism. Pyrophanite crystals described here are pseudomorphs after perovskite, sometimes retaining a remnant perovskite core (Fig. 1B). Chemical alteration of some of these remnants explains the formation of the white calcite-anatase inclusions.

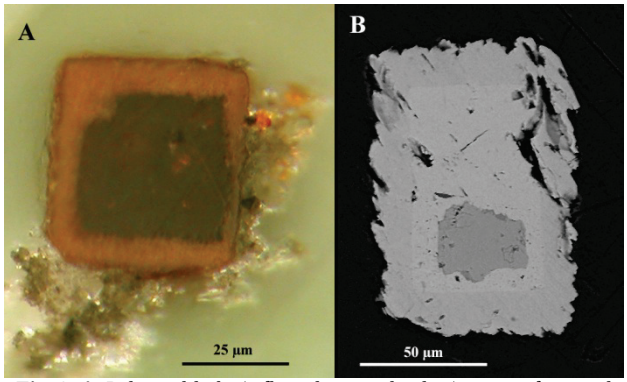

Fig. 1: A: Polarized-light (reflected, crossed polars) image of a zoned pyrophanite crystal. B: BSE image of a pyrophanite crystal with a perovskite core (dark grey).

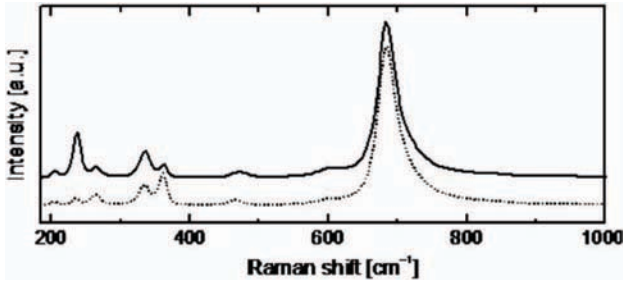

Fig. 2: Raman spectra of pyrophanite in two perpendicular orientations.

Partial alteration of monazite and xenotime during mineral-fluid interaction: implications for geochronology

Harlov, D.E.[1*], Williams, M.[2], Jercinovic, M.[2], Budzyn, B.[3] & Hetherington, C.[2]
[1]GeoForschungsZentrum Potsdam, Germany ([*]dharlov@gfz-potsdam.de)
[2]Dept. of Geosciences, University of Massachusetts, Amherst, Massachusetts, USA
[3]Inst. of Geological Sciences, Polish Academy of Sciences, Kraków Research Centre, Kraków, Poland

Monazite and xenotime can give significant information about a rock during its initial formation and subsequent geological evolution. This information takes the form of both geochronology (e.g. crystallization age and/or the age of various metamorphic events) and geochemistry (P-T-X constraints, fluid monitors, etc.). In metamorphic rocks, monazite and xenotime may either grow as the net product of a series of mineral reactions or be inherited from igneous and/or sedimentary precursors. Any Th in the system normally is strongly partitioned into the monazite as the monoclinic huttonite [$ThSiO_4$] and/or cheralite [$CaTh(PO_4)_2$] components via the coupled substitution reactions $Th^{4+} + Si^{4+} = REE^{3+} + P^{5+}$ and $Th^{4+} + Ca^{2+} = 2\ REE^{3+}$, respectively. To a lesser extent, Th can also be partitioned into xenotime as the tetragonal thorite [$ThSiO_4$] component via the coupled substitution $Th^{4+} + Si^{4+} = REE^{3+} + P^{5+}$. In contrast, xenotime commonly takes more U than monazite via the coupled substitution $U^{4+} + Si^{4+} = REE^{3+} + P^{5+}$. Once formed, monazite and xenotime can be partially or totally altered with respect to the Th, U, and (Y+REE) distribution and content. During alteration, Th or U is gained or lost in variable amounts such that irregular patches, extending from the rim into the grain interior, with sharp compositional boundaries, either depleted or enriched in Th and/or U are developed in the body of the original monazite or xenotime grain due to the presence of locally mobile Th, U, Si, Ca, P, and (Y+REE) in a grain boundary/pore fluid that is reactive with regard to monazite or xenotime.

A series of experiments have been performed in sealed Au capsules at amphibolite-facies to granulite-facies temperatures and pressures (600–900°C and 500–1000 MPa) in the piston-cylinder (CaF_2 setup, cylindrical graphite oven) and hydrothermal autoclave utilizing a natural monazite (20 mg) relatively homogeneous with respect to Th (7–8 wt% ThO_2) and a natural xenotime (20 mg) with a Th and U content below the EMP detection limit. Fluids (20–25 mg) used included 2N NaOH, 2N KOH, and $Na_2Si_2O_5 + H_2O$. Silicon was added as quartz (5 mg) or $Na_2Si_2O_5$. In the monazite experiments the source of Th was the monazite itself whereas in the xenotime experiments UO_2 or ThO_2 were added. In each experiment, the monazite or xenotime reacted with the fluid via a coupled dissolution-reprecipitation process [1] such that patches of variable enrichment or depletion in the Th or U with sharp compositional boundaries occurred, resulting in textures similar to that seen in nature. The metasomatised regions represent a pseudomorphic, partial replacement of the original monazite or xenotime with new Th- or U-enriched or -depleted monazite or xenotime. In a subset of the experiments Pb was totally removed. These experiments support the hypothesis that similar patches observed in natural monazite or xenotime could be the result of fluid-induced alteration via coupled dissolution-reprecipitation. If so, such altered regions would yield information concerning the nature of the fluid responsible for their formation as well as allow for the dating of single or multiple metasomatic events assuming that all pre-existing radiogenic Pb is removed during alteration.

[1] Putnis, A. (2009) *Rev. Mineral. Geochem.*, **70**, 87-124.

Multiple phases of monazite growth in the South Bohemian HP-HT granulites: a chance to constrain the entire timing of metamorphic evolution from subduction to exhumation by Th-U-Pb geochronometry?

Finger, F.[1*], Dunkley, D.[2] & Knop, E.[1]
[1]Dept. of Materials Engineering and Physics, University of Salzburg, Austria ([*]friedrich.finger@sbg.ac.at)
[2]National Inst. of Polar Research, Tokyo, Japan

High-pressure, high-temperature felsic granulites are important tectonic elements in the Variscan Bohemian Massif. Formed from Early Palaeozoic granitic protoliths [1], the rocks were initially metamorphosed in a Variscan subduction setting, probably passing through an eclogite-facies stage (peak pressure around 3 GPa at 800-900°C)[2] into a HP-HT granulite facies stage (1.6 GPa at ~900-1000°C)[3]. Subsequently, the rocks were rapidly exhumed (near isothermal decompression to ~0.8 GPa), then retrogressed to varying degrees under decreasing temperatures and pressures.

There is a long-standing debate as to whether zircon and monazite U-Pb ages of ~340 Ma, which have been consistently obtained in several studies, record the timing of subduction *versus* exhumation-stage metamorphism (*e.g.*, [4]). It has been suggested that subduction and eclogite-grade metamorphism took place considerably earlier, in the late Devonian (*e.g.*, [5]; see [6] for review and tectonic model).

High-spatial resolution U-Th-Pb dating of monazite may provide more information regarding the timing of multistage metamorphism. A microstructural and crystallochemical study carried out by electron microprobe indicates that several generations of monazite are preserved in the granulites. The youngest monazite (M3) formed during the decompression stage by reaction from REE enriched high-pressure apatite. Granulite-facies monazite (M2) is generally characterized by low yttrium content, due to Y-partitioning into garnet. Garnet occasionally contains inclusions of monazite, some of which preserve yttrium-rich cores. It is possible that this monazite type (M1) formed during prograde metamorphism, and could be used to directly date the subduction stage of orogenesis. In examples studied so far, electron microprobe-based Th-U-Pb dating provided no evidence for a large time gap between the formation of relict monazite and 340 Ma peak *P-T* monazite. This may indicate that the subduction stage immediately preceeded granulite-facies metamorphism. Since a time difference smaller than 10 Ma cannot be reliably resolved by the electron microprobe, further dating is planned on zoned monazite grains by SIMS.

[1] Janoušek, V. et al. (2004) *T. Roy. Soc. Edin. Earth*, **95**, 141-159. [2] Faryad, S.W. et al. (2010) *Lithos*, **114**, 54-69. [3] O´Brien, P.J. (2000) *Geol. Soc. London Spec. Publ.*, **179**, 369-386. [4] Roberts, M. & Finger, F. (1997) *Geology*, **25**, 319-322. [5] Anczkiewicz, R. et al. (2007) *Lithos*, **95**, 363-380. [6] Schulmann, K. et al. (2009) *C. R. Geosci.*, **341**, 266-286.

Unusually yttrium rich monazite with 6-14 wt.% Y_2O_3 in a granulite from the Bohemian Massif: implications for monazite-xenotime miscibility gap thermometry

Krenn, E.* & Finger, F.
Dept. of Materials Engineering and Physics, University of Salzburg, Austria (*erwin.krenn@sbg.ac.at)

Accessory monazite with an unusually high xenotime solid solution component of 21-42 mol.% (6.5-14 wt.% Y_2O_3, 6-11 wt.% $HREE_2O_3$) was discovered in a retrogressed Variscan HP-HT granulite from the Dunkelsteiner Granulite Massif (Gföhl unit), Lower Austria. These granulites experienced peak-PT conditions of ~16 kbar/1000°C and a subsequent rapid, near-isothermal uplift, which was followed by a stage of near isobaric cooling at around 5-7 kbar [1,2].

The sample consists of a fine grained (0.1-0.5 mm), statically recrystallized quartz-feldspar-biotite matrix with several up to 3 mm garnet crystals, a few 0.2-1 mm kyanite crystals and accessory sillimanite, rutile, apatite, zircon, monazite and opaques. Garnet often displays marginal alteration to biotite, quartz, some plagioclase, and occasionally sillimanite. Clusters (~1 mm) of fine grained biotite-quartz intergrowths probably represent pseudomorphoses after orthopyroxene.

The Y-rich monazite occurs as small (3-15 µm) crystals at grain boundaries. Apart from their high xenotime component, they contain minor amounts of cheralite (2-10 mol.%) and huttonite (0.4-3 mol %). A chemical Th-U- total Pb age of 340 ± 13 Ma (weighted average) is consistent with the Variscan age of the HP-HT granulite series.

Projection of xenotime values into published monazite-xenotime miscibility gap thermometers [3, 4, 5] give temperatures between 800 and 1200°C. Taking the highest measured X(Y+HREE) value of 0.41, the empirical thermometers of [3] and [4] give temperatures of 1050°C and 1100°C, which are close to previously published temperature estimates for the granulite-facies stage [1,2]. The experimental thermometer of [4] that was calibrated in the pure YPO_4-$CePO_4$ system yields ca. 50-100°C higher temperatures.

The results are geologically important because the Y-rich monazite provides a new and independent argument for the high-T nature of this granulite series.

The Y-rich monazite grew either at HT/HP conditions or during isothermal decompression. The yttrium source could have been probably free xenotime, which reacted out at peak temperatures. During decompression Y+HREEs could have become available from garnet breakdown. The extremely high xenotime component in monazite was attained because only little monazite-substance precipitated during the high-T stage. At this stage, significant proportions of REEs were trapped in apatite as is evidenced by abundant secondary monazite at apatite rims.

[1] Cooke, R.A. (2000) *Int. J. Earth. Sci.*, **89**, 631-651. [2] O´Brien, P.J. & Carswell, D.A. (1993) *Geol. Rundsch.*, **82**, 531-555. [3] Pyle, J.M. et al. (2001) *J. Petrol.*, **42**, 2083-2107. [4] Heinrich, W. et al. (1997) *J. Metamorph. Geol.*, **15**, 3-16. [5] Gratz, R. & Heinrich, W. (1997) *Am. Mineral.*, **82**, 772-780.

Gadolinite and crichtonite group minerals: breakdown products of primary monazite and xenotime in granitic and metamorphic rocks

Uher, P.[1*], Dianiška, I.[2], Bačík, P.[1], Ondrejka, M.[1], Pršek, J.[3] & Zubaj, R.[1]
[1]Dept. of Mineralogy and Petrology, Comenius University, Bratislava, Slovakia (*puher@fns.uniba.sk)
[2]Geo, s.r.o., Rožňava, Slovakia
[3]AGH University of Science and Technology, Kraków, Poland

Monazite and xenotime represent the principal REE-bearing phosphate minerals of common granitic and metamorphic rocks. They usually precipitate as primary accessory phases. Younger post-magmatic, hydrothermal or metamorphic, fluid-rich processes caused their partial to complete breakdown and formation of secondary assemblage usually including apatite (REE-rich), epidote-allanite s.s. and thorite [1,2]. However, recent detailed EMP study reveals more complex and diverse breakdown products after monazite and xenotime in selected Hercynian granitic and metamorphic rocks of the Western Carpathians (Slovakia), including the members of gadolinite and crichtonite group.

Secondary minerals form corona-like overgrowths around primary monazite-(Ce) + xenotime-(Y) assemblage in the S-type granites of the Gemeric Unit. The breakdown products located of the monazite-(Ce) comprise apatite, LREE-rich epidote to allanite-(Ce), thorite and titanite, whereas xenotime-(Y) is overrimed by apatite, epidote, thorite and gadolinite-(Y) to hingganite-(Y) s.s. In addition, late synchysite-(Y), synchysite-(Ce), calcite and rutile occur in outer rim zone around the both primary REE phosphate minerals.

Hingganite-(Y) to Nd-dominant hingganite (members of the gadolinite group) in association with S,Sr-rich secondary monazite-(Ce) (up to 0.3 S and 0.2 Sr apfu) originated after primary metamorphic, Nd-depleted monazite-(Ce) and xenotime-(Y) in banded, magnetite-rich metaquartzitic rocks near Bacúch, Veporic Unit. The secondary hingganite + S,Sr-rich monazite form tiny anhedral grains or overgrowths on the primary monazite-(Ce) crystals along the fracture fillings of the parental rocks.

The members of the crichtonite-group minerals [generally $(Sr,Ca,Ba,Pb,Na,K,La,Ce)(Mn,Fe,Y,U,Zr)(Fe,Mg,Zn)_2(Ti,Fe,V,Nb,Cr)_{18}(O,OH)_{38}$] were described in mylonitized granodiorites to granites of the Western Tatra Mountains. Crichtonite, dessauite-(Y) and loveringite-like phase, in association with rutile, allanite-(Ce) to REE-rich epidote, rarely hydroxylapatite-britholite-(Ce) s.s., calcite, titanite, pseudorutile and yttrocrasite-(Y), form secondary lensoid cleavage-fillings of chlorite pseudomorphs after biotite or irregular veinlets and overgrowths on monazite or apatite. Textural relationships indicate a dissolution and breakdown of primary magmatic monazite-(Ce), apatite, biotite and plagioclase, and reprecipitation of the secondary REE- and Ti-rich minerals.

All the above mentioned examples indicate a partial dissolution and/or breakdown of primary magmatic or metamorphic REE-phosphate phases (monazite, xenotime), and precipitation of complex secondary assemblage, including the REE-bearing minerals of gadolinite and crichtonite group. The process was driven by hydrothermal-metamorphic fluids probably during Alpine overprint of the parental rocks.

[1] Finger, F. et al. (1998) *Am. Mineral.*, **83**, 248-258. [2] Broska, I. et al. (2005) *Lithos*, **82**, 71-83.

U-Pb SHRIMP dating, Hf isotope and trace element investigations on multiple zoned zircons from a South-Bohemian granulite

Friedl, G.[1], Cooke, R.[2], Finger, F.[2*], Gerdes, A.[3], McNaughton, N.J.[4] & Fletcher, I.[4]
[1]Dept. of Geography and Geology, University of Salzburg, Austria ([*]friedrich.finger@sbg.ac.at)
[2]Dept. of Materials Engineering and Physics, University of Salzburg, Austria
[3]Dept. of Geosciences, University of Frankfurt, Germany
[4]Centre for Global Metallogeny, University of Western Australia, Crawley, Australia

High-pressure-temperature granulites are a conspicuous feature of the Variscan Bohemian Massif. Formed from Early Palaeozoic granitic protoliths [1], the rocks were initially metamorphosed in a Variscan subduction setting, probably passing through an eclogite-facies stage (peak pressure around 3 GPa at 800-900°C)[2] into a HP-HT granulite facies stage (1.6 GPa at ~900-1000°C)[3,4]. Subsequently, the rocks were rapidly exhumed (near isothermal decompression to ~0.8 GPa), then retrogressed to varying degrees under decreasing tem-peratures and pressures [4]. Resolving the exact time-frames of the individual evolution stages preserved in the granulites is a great challenge for geochronologists and a pre-requisite for understanding the tectonic evolution of the Central European Variscides.

Zircons from the south Bohemian granulites have a complex multi-phase internal growth zoning. Apart from abundant remnant cores, considered to be derived from the granitoid protoliths, two chemical distinct outer growth shells have been recognised using BSE imaging. An U-rich shell around the inherited cores with bright BSE-signal is followed by a distal U-poor shell which is dark in BSE. Conventional zircon dating techniques which utilise whole grains, may not resolve potentially small, but distinct age differences between such growth shells. Therefore, the SHRIMP method was applied in an attempt to individually date single stages of zircon growth. The sample used is a typical leucocratic, medium grained and weakly foliated Moldanubian granulite from the Dunkelsteiner Wald granulite massif, S of Krems (Gföhl unit). The peak metamorphic assemblage of garnet + kyanite + ternary feldspar + quartz is remarkably preserved in this sample.

SHRIMP analyses carried out in the protolithic zircon cores produced strongly scattering, although concordant ages. Most fall in the time range between 450 und 400 Ma. We assume that the granitic protolith formed at that time. A concordant Cadomian age of c. 580 Ma has been measured in one core. A further generation of inherited cores records an age of ca. 480-500 Ma. In one case a discordant $^{207}Pb/^{206}Pb$ age of ca. 2.3 Ga was detected.

Analyses in the U-rich growth shells around the cores yielded concordant to subconcordant ages of around 340 Ma. Analyses from the U-poor outermost growth zones give slightly younger ages with a mean average $^{206}Pb/^{238}U$-age of 333 ± 6 Ma (2σ). The results are tentatively interpreted as dating two distinct stages in the metamorphic evolution of the rock. The age of 333 ± 6 Ma (zircon rims) probably dates the exhumation of the granulite to mid crustal levels. The older age may represent granulite facies zircon growth at higher PT-conditions.

Hf isotope data suggest that dissolved zircon material from the granitic protolith functioned as the main source for the Variscan zircons.

[1] Janoušek, V. et al. (2004) *T. Roy. Soc. Edin. Earth*, **95**, 141-159. [2] Faryad, S.W. et al. (2010) *Lithos*, **114**, 54-69. [3] O´Brien, P.J. & Carswell, D.A. (1993) *Geol. Rundsch*., **82**, 531-555. [4] Cooke, R.A. et al. (2000) *J. Met. Geol.*, **18(5)**, 551-569.

Pre-Variscan evolution of the Western Tatra Mts., Poland: new insights from U-Pb zircon dating

Burda, J.[1*] & Klötzli, U.[2]
[1]Faculty of Earth Sciences, University of Silesia, Sosnowiec, Poland ([*]jolanta.burda@.us.edu.pl)
[2]Dept. of Lithospheric Research, University of Vienna, Austria

The crystalline basement of the Tatra Mts. comprises a polygenetic Variscan granitoid intrusion dated at 360–340 Ma [1] and its metamorphic envelope. In the metamorphic complex, mainly represented by paragneisses, orthogneisses and amphibolites (metabasalts), two superimposed units (Upper and Lower) have been distinguished. In the Lower Unit peak metamorphic conditions were estimated at T=550-580°C and P=5-8 kbar, while in the Upper Unit T=690-780°C and P=7.5-10 kbar [2].

The protolith ages and geochemical characteristics of selected orthogneiss samples from these two units were determined, providing new constraints for reconstructing of the Palaeozoic geodynamic evolution of this sector of the Variscan chain.

Orthogneisses from the Lower Unit are mostly banded, fine- to medium-grained rocks while in the Upper Unit varieties with augen structures predominate. They consist of aligned dynamically recrystallised qtz+pl+bio±grt with zircon and apatite as accessory phases. Muscovite is a late post-kinematic. Some primary feldspar relics with recrystallised mantles are preserved within a strongly oriented granoblastic matrix. They are peraluminous (ASI=1.2–1.27) and belong to high-K calc-alkaline suites within a VAG–type tectonic setting.

LA-MC-ICP-MS U-Pb zircon ages from both samples from crystals with oscillatory zoning yield a similar ages of ca. 534 Ma. The Th/U ratios of all analyses range from 0.19 to 0.67 and have values typical of magmatic zircons. This is interpreted to reflect the magmatic crystallization age of similar igneous precursors, in agreement with the geochemical characteristics of these rocks. In zircons from a gneiss from the Upper Unit, a luminescent internal part with well-developed oscillatory zoning is surrounded by weakly luminescent, low contrast rims (Th/U ratios of 0.02-0.08). These yield a well defined weighted mean U-Pb age of 387±14.

In summary, two distinct Early Cambrian and Middle/Upper Devonian tectonothermal events are recognized. The first event represented by the oldest meta-magmatics so far dated in the Western Carpathians could be an expression of rifting and crustal thinning at the northern Gondwana margin. The granodiorites from the Upper Unit experienced a subsequent high-grade metamorphic event, constrained by partial recrystallisation of primary magmatic zircon and growth of new zircon rims at ca. 387 Ma. These could be connected with the formation of crustal-scale nappe structures and generation of collision-related magmatism.

[1] Poller, U. et al. (2000) *Int. J. Earth Sci.*, **89**, 336-349. [2] Gawęda, A., Kozłowski, K. & Piotrowska, K. (2000) *Acta U. Carol. Geol.*, **42(2)**, 252-253.

Xenotime–zircon solid solutions in topaz granites of the Saxothuringian Zone

René, M.
Institute of Rock Structure and Mechanics, Academy of Sciences of the Czech Republic, Prague, Czech Republic
(rene@irsm.cas.cz)

Topaz granites form two distinct magmatic suites in the Saxothuringian Zone in the Bohemian Massif. The first suite is formed by high-P (>0.4 wt% P_2O_5), highly evolved S-type granites. High-P topaz granites occur in granite stocks of the western part of the Saxothuringian Zone (Horní Slavkov–Krásno and Ehrenfriedersdorf ore districts). The second topaz granite suite is formed by low-P (<0.4 wt% P_2O_5), aluminous A-type granites. These granites include small granite bodies and stocks with important Sn-W ore deposits (Altenberg and Zinnwald/Cínovec).

Both types of topaz granites are alkali feldspar granites with variable contents of quartz, albite, K-feldspar, Li-mica and topaz. Zircon, Nb-Ta-Ti oxides and uraninite are common accessory minerals. High-P granites host large amounts of apatite, together with monazite and relative scarce xenotime. Apatite is absent in low-P granites, and the low contents of whole-rock phosphorus are reflected by variable amounts of monazite and xenotime and by low phosphorus contents in zircon. However, the distinctly high phosphorus contents in high-P granites are reflected also in feldspar, topaz and zircon. The P_2O_5 concentrations in zircon reach 8.3 wt% (Krásno) and max. 20.2 wt% (Podlesí, [1]).

Both types of topaz granites are characterized by zircon–xenotime intergrowths. Zircon grains very often show strong hydration and fluorination. The highest concentration of H_2O and F are displayed by zircon crystals from the apical part of the low-P granites Cínovec cupola (max. 18.5 wt% H_2O and 1.2–2.4 wt% F). However, the hydration and fluorination of zircon from high-P granites is likewise high. Fluorine reaches max. 2.1 wt.% in zircons from topaz-albite granites of the Horní Slavkov–Krásno ore district and even 3.5 wt.% in zircons from Li-mica dyke granite of the Podlesí granite stock [1]. All these zircons contain moderate Hf concentrations (1.2–9.8 wt% HfO_2) with no considerable differences between the two types of topaz granites. However, zircons from low-P and high-P granites show significant differences in the contents of Y. Zircon from low-P granites displays high concentrations of Y. Zircons from the Cínovec granite cupola contain max. 9.2 wt.% Y_2O_3 [2], whereas Y contents in high-P granites from the Horní Slavkov-Krásno ore district reach only 4 wt.% Y_2O_3.

Xenotime occurs also in both granite types, but highly intimate zircon–xenotime intergrowths are present in low-P granites from the Cínovec cupola. Epitaxial overgrowths of xenotime in zircon were frequently observed in these granites. Xenotime from the low-P granite of the Cínovec cupola displays a considerable enrichment in Th and HREE compared to xenotime from high-P granites of the Horní Slavkov–Krásno ore district. The contents of Zr in xenotime are relatively low, commonly in the range of 0.4 to 1.0 wt% ZrO_2, with no significant difference between xenotimes from low-P and high-P granites. However, xenotimes from low-P granite of the Altenberg and Markersbach granite stocks display a considerable enrichment in Zr (13.0–14.5 wt% ZrO_2, [3]).

Acknowledgements: This study was supported by the Czech Science Foundation (project No. 205/09/0540).

[1] Breiter, K. et al. (2006) *Lithos*, **88**, 15-34. [2] Johan, Z. & Johan, V. (2004) *Mineral. Petrol.*, **83**, 113-150. [3] Förster, H.J. (2006) *Lithos*, **88**, 35-55.

Crystal chemistry of zircon from granitic rocks (Japan): genetic implications of HREE, U and Th enrichment

Hoshino, M.[1*], Kimata, M.[2], Nishida, N.[3], Shimizu, M.[2] & Akasaka, T.[4]
[1]Mineral Resources Research Group, Inst. for Geo-Resources and Environment, AIST, Tsukuba, Japan
([*]hoshino-m@aist.go.jp)
[2]Earth Evolution Sciences, Graduate School of Life and Environmental Sciences, University of Tsukuba, Japan
[3]Chemical Analysis Div., Research Facility, Center for Science and Technology, University of Tsukuba, Japan
[4]Center for Tsukuba Advance Research Alliance, University of Tsukuba, Japan

Zircon from granitic rocks from Japan is classified into two major types; based on the minor element content determined by electron microprobe, a heavy rare earth element (HREE)-U-Th-poor (Type I) and a HREE-U-Th-rich (Type 2). Zircons characteristically occurring in common granites of type-1 are relatively poor in HREE including Y and Sc, up to 2.72 wt% $HREE_2O_3$; up to 0.44 wt% ThO_2; up to 2.10 wt% UO_2, while zircons characteristically occurring in granitic pegmatites of type-2 are much richer in HREE including Y and Sc, up to 18.99 wt% $HREE_2O_3$; up to 11.09 wt% UO_2; and up to 6.58 wt% ThO_2.

However, analyses showing a significantly high amount of REE+Y almost certainly represent altered zircon and/or accidental analysis of inclusions [1]. Only crystal structure of zircon free of inclusions and zoning (type-2; Takenouchi granitic pegmatite) was refined to R = 4.3 % and for the first time has been confirmed that zircons of type-2 exist as a single-crystal phase in nature.

High enrichment of HREE, Y, and Sc are preferentially incorporated by xenotime substitution $HREE^{3+} + P^{5+} \leftrightarrow Zr^{4+}+Si^{4+}$ (Fig. 1). Furthermore, incorporation of U and Th into zircon is primarily governed by coupling the thorite substitution with the coffinite one $U^{4+} + Th^{4+} \leftrightarrow 2Zr^{4+}$. Zircon crystals from granites and granite pegmatites, extraordinarily enriched in HREE, U, and Th, are generally anhydrous, which strongly suggested that they were formed at the magmatic stage of granitic rock formation. Enrichments of HREE, U and Th are generally observed in both the zircons from granitic pegmatites and the rims of zircons from granites, and originate in fractionation processes in the last stage of crystallization of granitic magma. The discovery of both type-1 and type-2 zircons occurring in granitic rocks from the magmatic arc in Japan means that the former were formed from the granitic magmas at high temperature while the latter were from the magmas intimately related to the formation of granitic pegmatites at low temperature.

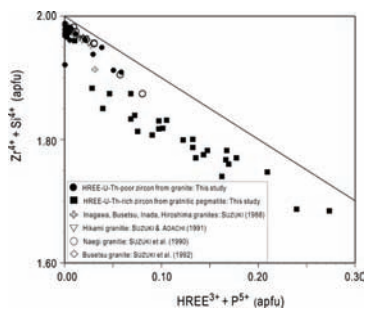

Fig. 1: Compositional correlation between the two types of zircon from granitic pegmatites and granites, in terms of cations per formula unit. There is a negative correlation between $Zr^{4+} + Si^{4+}$ and $HREE^{3+} + P^{5+}$, which deviates from the 1:1 line due to other substitutions.

[1] Hoskin, P. & Schaltegger, U. (2003) in Hanchar, J. & Hoskin, P. (eds.) *Rev. Mineral. Geochem.*, **53**, 27-62.

Titanite as a prospecting tool in the tin granite belt, Nanling Range, South China: a comparison study

Wang RuCheng[*], Xie Lei, Chen Jun, Lu JianJun & Wu JinWei
School of Earth Sciences and Engineering, Nanjing University, Nanjing, China ([*]rcwang@nju.edu.cn)

Titanite is a common accessory silicate in metaluminous granites (I-type or A-type). It was studied in order to assess its potential role for determining the ore potential of tin of granites. The targets include three tin granites (Qitianling, Huashan, Guposhan) related with large Sn deposits and two barren granites (Lianyang, Dadongshan) in the Nanling tin belt, South China. These granites, whatever their tin contents, are metaluminous with ACNK of about 1.1, lithologically (amphibole)-biotite granites and are classified as A-type granites.

In three tin granites, titanite includes at least two distinctive types: one is euhedral, closely associated with perthitic feldspar, quartz and biotite, and is primary and magmatic phase, while the other is anhedral, always associated with chlorite, thus as secondary product of biotite chloritization. Electron-microprobe results reveal subordinate but distinctive contents of Sn, Al and Fe in two types of titanite, suggesting alternative substitutions: $Ti^{4+} = Sn^{4+}$ and $Ti^{4+} + O^{2-} = (Al, Fe)^{3+} + F^{-}$. The primary titanite contains 0.2 to 1.2 wt% SnO_2 (on average about 0.4 to 0.5 wt%), 3.46 to 4.60 wt% Al_2O_3 and 1.79 to 3.75 wt% Fe_2O_3. However, chemical composition of the secondary titanite is simply characterized by elevated concentrations of Al_2O_3 and F up to 9.56 and 2.14 wt% respectively, but lower concentrations of Fe_2O_3, similar to hydrothermal titanite after biotite reported in literature [1,2]. The average content of SnO_2 is 1.49 wt%.

As a comparison, titanite from the barren granites of Dadongshan and Lianyang in the same district was also studied. Primary and secondary categories were identified for titanite according to the morphology and Al-Fe-F concentrations. Very interestingly, the Sn contents of both primary and secondary titanite are clearly lower than those from the tin granites.

Therefore, titanite can be used as an indicator mineral to distinguish tin granites from barren systems, although the whole-rock features are not distinguishable between them.

[1] Eggleton, R.A. & Banfield, J.F. (1985) *Am. Mineral.*, **70**, 902-910. [2] Broska, I. et al. (2007) *Lithos*, **95**, 58-71

Tracing evolution of peraluminous granitoids through contrasting tourmaline types

Balen, D.[1*], Broska, I.[2] & Petrinec, Z.[1]
[1]Faculty of Science, University of Zagreb, Croatia ([*]drbalen@geol.pmf.hr)
[2]Geological Inst., Slovak Academy of Sciences, Bratislava, Slovakia

The peripheral parts of the Cretaceous Moslavačka Gora (Croatia) peraluminous granites host two contrasting tourmaline types (Fig. 1) having separated origin: slightly alkali-deficient nodular schorl to dravite (Fe# 0.43-0.58) and disseminated schorl (Fe# 0.75-0.85). Origin of the nodular tourmaline has been attributed to the interaction of a fluid phase from the residual granitic melt with a fluid derived from the wall rock environment [1], which resulted in increasing the MgO content in the nodular tourmaline compared to the disseminated one. Observed textures suggest that nodular tourmaline crystallized as the last mineral in a quasi-closed system inside host granite.

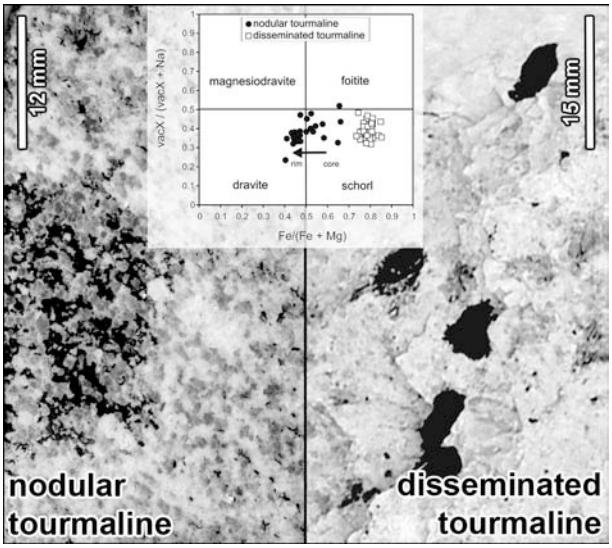

Fig. 1: Anhedral to subhedral nodular (left) and disseminated tourmaline (right); inset show compositional variations for two tourmaline types occurring in the Moslavačka Gora granites.

The peculiar texture and distribution of tourmaline nodules can be most suitably explained through an emplacement setting of the studied granite intrusion. In a situation when magma rapidly reached shallow crustal levels, resulting decompression and cooling lead to the separation of a boron-rich melt in form of distinct volatile-rich bubbles [2] ± crystals. If these bubbles were unable to escape the system owing to impermeable host and wall rock, they cause the formation of tourmaline nodules in almost completely solidified granite. The Moslavačka Gora two-mica granite that hosts tourmaline nodules can thus be regarded as an occurrence of magma that escaped from the plutonic levels and stalled in a low pressure crustal setting (ca. 720 °C, 70 – 270 MPa, H_2O_{melt} up to 4.2 wt. %). Decreasing pressure and related cooling were major factors controlling the melt differentiation, liquid immiscibility, fluid behaviour, partitioning of elements and crystallization path of the two-mica granite.

Disseminated tourmaline from leucogranite host, on the other hand, can be considered as a typical magmatic product and common accessory phase.

[1] Balen, D. & Broska, I. (2010) *Geol. Soc. London Spec. Publ.*, in press. [2] Balen, D. & Petrinec, Z. (2010). *IMA 2010 Abstracts, GM 74 session*.

The Shilu iron–polymetallic ore deposit on Hainan Island, South China: origin of andradite and chemical dating of metallogenic processes

Bakun-Czubarow, N.[1*], Kusiak, M.A.[1], Xu, D.[2], Wang, Zh.[2], Konecny, P.[3] & Kusy, D.[1]
[1]Inst. of Geological Sciences, Polish Academy of Sciences, Warszawa, Poland ([*]nbajun@twarda.pan.pl)
[2]Guangzhou Inst. of Geochemistry, Chinese Academy of Sciences, Guangzhou, China
[3]Geological Inst. of Dionyz Stur, Bratislava, Slovakia

The Shilu iron-polymetallic ore deposit located in western Hainan Island, South China, occurs within the Meso-Neoproterozoic complex of low-grade metamorphosed volcanoclastic sediments and carbonates. The amphibole itabirites (banded diopside–tremolite rocks), dolomite itabirites and dolostones are the main hosts for iron ores. At the present state of knowledge, the Shilu ore deposit is considered to be a structurally re-worked as well as hydrothermally altered and enriched ore deposit of Banded Iron Formation (BIF) type [1,2].

The aim of the project is dating of the skarnization process caused by hydrothermal activity in this region to understand metallogenic processes in the Shilu ore deposit. We applied *in situ* dating of monazite (using the Th–U–Pb_{tot} isochron method), combined with the study of mineral chemistry of coexisting minerals, characteristic for skarn, hydrothermal stage of metallogeny. For the present research we selected 3 rock samples from the close vicinity of the Beiyi iron mine – one gangue rock: F8–7 – amphibole itabirite and the two garnet–bearing itabirites belonging to iron–poor ores: 0907 and ZSL6–14. In the sample 0907, andradite (Adr) garnet megacryst of 5 mm in diameter recorded distinct zoning (Fig. 1). In this grain the Adr content decreases from the plateau-like core (99.7 mol.% Adr) to rim (71.2 mol.% Adr), while the content of grossular (Grs) increases. Moreover, the garnet grain, almost devoid of solid inclusions in core, contains numerous tiny quartz inclusions in middle zone, and small inclusions of iron oxides are abundant in rim zone. Thus, most likely, the andradite megacryst recorded during crystallization the temperature decrease and distinct changes in composition of fluids.

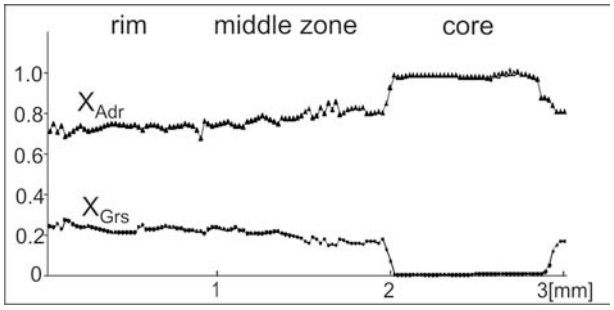

Fig. 1: Zoning profile for the andradite megacryst from the iron-poor ore, sample no 0907.

Monazite grains from the gangue amphibole itabirite yield 564±7 Ma and 442±14 Ma isochron ages, while monazites from garnet–bearing iron–poor ore gave much younger result of 258±7 Ma. In this sample, monazite often occurs as inclusion in garnets. Obtained Permian age could be considered then as the age of skarnization process. Further study is being carried to address metallogenic processes in this complex ore deposit.

[1] Xu, D. et al. (2010) *Ore Geol. Rev.*, in press. [2] Klein, C. (2005) *Am. Mineral.*, **90,** 1473-1499.

Origin of Palaeoproterozoic high-metamorphic metacarbonate rocks (calciphyres) of the Irkut block (Sharyzhylgai Uplift, Siberian Craton)

Urmantseva, L.N.[*] & Turkina, O.M.
Institute of Geology and Mineralogy SB RAS, Novosibirsk, Russia ([*]urmantseva@gmail.com)

The Sharyzhalgai Uplift of basement is the southern termination of the Tungusska Province of the Siberian Craton [1]. The Irkut Block metamorphic complex is subdivided into two associations. The metavolcanic association includes the hypersthene-bearing biotite and amphibole-biotite gneisses and two-pyroxene and amphibole-pyroxene basic schists. The second, metasedimentary one, is dominated by garnet-biotite, hypersthene-biotite and cordierite-bearing gneisses. Also this association contains marbles and calciphyres. Archean magmatic protolith of metavolcanic rocks underwent at least two stages of metamorphism during Neoarchean (2.55-2.57 Ga) and Palaeoproterozoic (1.85-1.87 Ga) [2-4]. Metasedimentary rocks are from Palaeoproterozoic stage (1.85-1.97 Ga) [5]. The aim of this study was to define conditions of metacarbonate rocks formation and time of carbonate rock metamorphism.

Garnet-bearing and cordierite-garnet-biotite gneisses of the Irkut block have been formed during granulite metamorphism of sedimentary rocks. Paragneisses' protoliths correspond to terrigenous sediments, ranging from greywacke to shale. Full characteristic is given in [6]. The REE distribution indicates that the terrigenous material of the paragneisses was derived from felsic and mafic provenance. Increase in contents of Fe, Ti, Cr, Ni, Sc and decrease in La/Sc from the garnet-biotite to the cordierite-bearing gneisses reflect growth of the abundance of mafic rocks in the provenance.

Metacarbonate rocks are represented by calciphyres. Using the programm MINLITH [7] the averaged normative mineral composition was determined. The protolithes of calciphyres are represented by three main parts: carbonate (70-90%), clay (3-20%), and debris (5-10%). Calciphyres are presented of dolomite varieties. They have fractionated REE spectra, characterized by $(La/Yb)_n$=59-71 and show strong Eu minimum (Eu/Eu*=0.4-0.5). It can be concluded that such characteristics are due to clay component in carbonate sediments.

Zircons from calciphyres have irregular form without traces of zoning. The analyses of zircons yield an upper intersect of discordia and concordia at 1873±6 Ma (MSWD=1.6). This age corresponds to the time of Palaeoproterozoic granulitic metamorphism within the Irkut block. Metamorphic origin of these zircons is confirmed by REE distribution. Zircons are characterized by low $(La/Yb)_n$=8.5-14.6 and $(Sm/La)_n$=0.4-4.6. They have strong Ce (Ce/Ce*=1.4-1.7) and Eu anomalies (Eu/Eu*=0.4-0.6).

Results of this study indicate that the formation of calciphyres relates with metamorphism of terrigenous-carbonate rocks. Accumulation of carbonates was accompanied by supply of clay material.

[1] Rosen, O.M. et al. (1994) in Condie, K.C. (ed.) *Archean Crustal Evolution*. Elsevier, Amsterdam, 411-459. [2] Sal'nikova, E.B. et al. (2007) *Strat. Geol. Correl.*, **15(4)**, 343-358. [3] Turkina, O.M. et al. (2009) *Dokl. Earth Sci.*, **429(9)**, 1505-1510. [4] Poller, U. et al. (2005) *Precam. Res.*, **136**, 353-368. [5] Urmantseva, L. & Turkina, O. (2009) *Acta Geol. Sin. (Eng. Ed.)*, **83(5)**, 875-883. [6] Turkina, O.M. & Urmantseva, L.N. (2009) *Lithol. Miner. Resour.*, **44(1)**, 43-57. [7] Abbyasov, A.A. (2006) in Rosen, O.M. et al. (eds.) *Early Precambrian sedimentation: rock types, high metamorphosed sedimentary basins, clastic deposits evolution.* Moscow, Scientific World, 108-132 (in Russian).

Iron oxide minerals in Western Carpathian granitoids in relation to the assimilation processes and granite mapping

Broska, I.[1*], Ondrejka, M.[2], Bónová, K.[3], Petrík, P.[1] & Konečný, P.[4]
[1]Geological Inst., Slovak Academy of Sciences, Bratislava, Slovakia ([*]igor.broska@savba.sk)
[2]Dept. of Mineralogy and Petrology, Faculty of Natural Sciences, Comenius University, Bratislava, Slovakia
[3]Inst. of Geography, Faculty of Sciences, Pavol Jozef Šafárik University, Košice, Slovakia
[4]Dionýz Štúr Inst. of Geology, Bratislava, Slovakia

Fe-oxides, mainly magnetite, belong to the most important mineral phases for the recognition of I-type granitoid suites in the Western Carpathians. Magnetite is generally present as individual grains or clusters, as well as inclusions in accessory and rock-forming minerals. The host granitoids of the Fe-oxides showing the I-type affinity are coarse to medium grained, metaluminous to slightly peraluminous biotite (leuco)tonalites to granodiorites, with minor proportion of muscovite-biotite granites. The bulk rock concentration of magnetite is variable, but usually reaches ca hundreds g/t but can increase to several thousands g/t in some parts of the granitoid body, especially in the areas with occurrences of microgranular mafic enclaves. The increase of magnetite concentration was observed also in the late magmatic differentiates, in leucocratic dikes.

Fe oxides in the Western Carpathian I-type granitoids occur as (1) early-orthomagmatic, pre-mixing titanomagnetite, which breaks down upon cooling, (2) late-magmatic, post-mixing, stochiometrically pure magnetite, which crystallizes from mixed tonalite magma, and (3) low-temperature hydrothermal hematite replacing both earlier magnetite types. The orthomagmatic titanomagnetite is volumetricaly much smaller, pure magnetite dominates. The primary magnetite and Ti-hematite during cooling release titanium by inter-oxide re-equilibration and form ilmenite exsolutions, followed by rutile precipitation. The second late-magmatic stage of Fe-oxide formation, results in the assemblage of pure magnetite, titanite and apatite the magnetite itself having originated from reaction of early titanomagnetite, annite and anortite. The magnetite may be locally transformed to hematite or Ti-hematite.

The mafic enclaves in the West-Carpathians I-type granites have always a high precentage of Fe oxides. They are tonalitic to dioritic in composition, the rock-forming plagioclase having a similar composition to those one in host tonalite. The elevated values of magnetic susceptibility observed in the I-type granitoids in places with abundant mafic microgranular enclaves may be explained by more extensive precipitation of the Fe-Ti oxides or titanomagnetites after mixing with a hotter mafic melt, rich in siderophile elements, or by partial assimilation of trapped and mingled blobs of the basic melts, i.e. enclaves. The increased content of Fe-oxides in aureolas around microgranular mafic enclaves in host I-type granitoids may indicate a higher degree of mixing of Fe components from mafic magma to a crustal acid silicate melt and inheritance of titanomagnetite from the mafic magma. The abundance of magnetite in I-type granites causes the increase of whole rock magnetic susceptibility in host granitoids. The enclaves show natural remanent magnetisation commonly around 16 x 10^{-3},SI units. A typical value discriminating I/S-type Western Carpathian granitoids is 2 x 10^{-4} SI units. The measurement of rock magnetic susceptibility index in the field appears as a useful tool for regional geological mapping of I-type granites and searching of enclave rich regions.

Uranium and thorium distribution in the Double S Zone of the uraniferous Lac Turgeon Intrusive Complex, Quebec, Canada

Beal, K.*, Lentz, D.R. & McFarlane, C.
Dept. of Geology, University of New Brunswick, Fredericton, New Brunswick, Canada (*k.beal@unb.ca)

The Double S Zone is located along the North Shore of the St. Lawrence Seaway, in the Grenville Province of Canada. The zone (along with the neighboring Middle and TJ zones) contain 40.7 million pounds U_3O_8, averaging 0.012% U_3O_8 [1]. The Double S Zone is a sequence of granitic pegmatites with adjacent, coeval, coarse-grained granites-alaskites. Granitic gneiss and quartzite xenoliths are also present. SEM-BSE and SEM-CL imaging followed by EMPA were completed on U- and Th-bearing accessory minerals from the uraniferous Double S zone. Preliminary geochronology on the Double S pegmatite yielded approximately 944 Ma (U-Th-Pb monazite; see [2] for method), approximately 150 Ma younger than the age of peak Grenvillian metamorphism commonly reported. This date is slightly younger than dating by [3] (962 ± 9 Ma by U-Th-Pb in monazite for the pegmatite) and dates reported for the host granite include >980 (U-Pb monazite and uraninite [4]), 961 ± 7 Ma (U-Th-Pb monazite; [3]) and 948 ± 23 Ma (Rb-Sr whole rock isochron; [5]).

The distribution of uraninite and uranothorite are relatively heterogeneous in the pegmatite and granite, but each suite of minerals contains similar average elemental content (compiled with [3]). Uraninite in the granite shows a greater distribution in U/Th, ThO_2, PbO, and CaO impurities (7.5-14.3%, 3.7-9.9%, 5.5-12.0%, and 0.6-6.0%, respectively) than the pegmatite suite. Uranothorite in the pegmatite shows a greater distribution in U/Th, UO_2, and PbO (0.1-0.6%, 4.5-27.8%, and 0.0-2.5%, respectively) than the host granite. Zircon displays xenocrystic cores, oscillatory zonation, and recrystallization along the rims. Zircon in pegmatite samples associated with uraninite and thorite contain higher average REE content and U/Th (3457 ppm and 36.3) compared to 1979 ppm and 8.6 in unmineralized pegmatite. Pegmatite zircons also contain the highest U/Th ratio (average 12.2) compared to the less fractionated leucogranite (average 11.1). Apatite displays blocky, equant crystals and common simple zonation that is indicative of a slow-cooling magma [6]. The apatite contains erratic actinide content, but averaged 0.6% REE in the granite and 0.2% in the pegmatite reflecting the greater distribution of REE-rich phases in the pegmatite. A fergusonite analysis from the pegmatite contained 6.5% REE, 16.5% UO_2, and 2.5% ThO_2 and xenotime crystals contained up to 13.4% REE, 0.5% UO_2, and 0.4% ThO_2. Monazite, compiled with data from [3], contains up to 20.2% ThO_2 and 0.9% UO_2 in the pegmatite with a lower distribution of ThO_2 and UO_2 (up to 16.2% and 0.8%, respectively) in the granite.

Overall, uraninite and uranothorite in the pegmatite and host granite explain the high levels of radioactivity in the Double S zone. Additional radioactivity produced by other actinide-bearing phases contributes to the high background levels.

[1] Lafleur, J. (2006) *UFM Ventures Ltd. NI 43-101 Technical Report, The North Shore Property: Turgeon, Weegee, Highway, Pontbriand and NE Costebelle Claim Blocks.* Province of Quebec, Canada. [2] Montel, J.M. et al. (1996) *Chem. Geol.*, **131**, 37-53. [3] Brodie, S. (2008) *BSc thesis*, UNB, Fredericton, NB Canada. [4] Rimsaite, J. (1982) *Geol. Survey Can.*, Paper **81-23**, 19-23. [5] Fowler, A.D. & Doig, R. (1982) *Can. J. Earth Sci.*, **20**, 92-104. [6] Piccoli, P.M. & Candela, P.A. (2002) *Rev. Mineral. Geochem.*, **48**, 255-292.

PGE compositions of magnetite from porphyry Cu-Mo deposits of Siberia and Mongolia

Berzina, A.N.
Institute of Geology and Mineralogy, Novosibirsk, Russia
(anitansk@gmail.com)

This study provides the first platinum group elements (PGE) data in magnetites from some porphyry Cu-Mo deposits in the Central Asian Orogenic Belt (Siberia and Mongolia). Primary magnetites were analyzed for all PGE (Os, Ir, Ru, Rh, Pt and Pd), and Au, as well as Cu and Ni, using ICP-MS. Magnetites show low to intermediate PGE contents ranging from 5 to 60 ppb. For most samples Os and Ir concentrations are less than limits of detection. Ruthenium concentrations range from <1 to 14 ppb, Rh from <1 to 12 ppb, Pt from <1 to 7 ppb, and Pd from <1 to 56 ppb. Palladium concentrations are typically higher than Pt. Positive anomalies of Rh are consistent with the experiments of Capobianco et al. [1] showing high Rh compatibility in magnetite. There is a wide range of Ni, Cu and Au contents in magnetites. The Au content varies from below detection levels (1 ppb) to 240 ppb. Ni content ranges from 1 to 221 ppm, while Cu content ranges from 3 ppb to 384 ppm. Au shows no correlation with other PGEs, indicating that Au was probably redistributed during later hydrothermal activity.

Overall shape of the average magnetite PGE patterns of the deposits studied are relatively similar with variations toward Rh maximum, a Pt drop and a Pd rise (Fig.1). Within each deposit the metals show relatively similar behaviour, except Au. The magnetite mantle-normalized metal distribution between Os and Pd display patterns similar in shape to basalt rocks in other areas (e.g. basaltic rocks from Jiding ophiolite [2]). This suggests that PGE in magnetites are of magmatic origin.

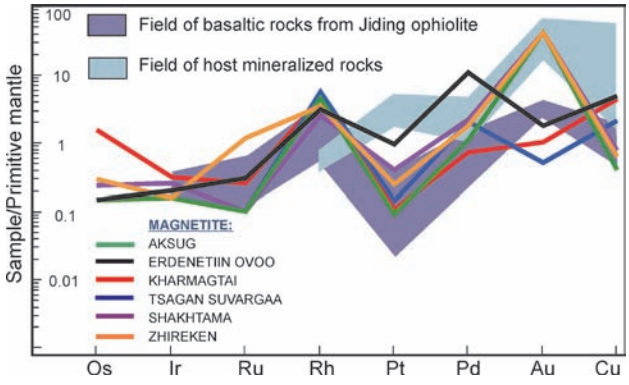

Fig. 1: Mantle-normalized PGE patterns of magnetites and host mineralized rocks from porphyry Cu-Mo deposits of Siberia and Mongolia in comparison with basaltic rocks from Jiding ophiolite [2].

The mineralized rocks hosting magnetite show intermediate PPGE (Rh+Pt+Pd) contents. IPGE (Os+Ir+Ru) concentrations were not determined in mineralized samples. The Cu and Mo content in analyzed samples vary from 45 ppb to 1.7 ppm and from 3 ppb to 550 ppb, respectively. The PGE distribution patterns in the mineralized samples are steep, positively sloped, and different from the irregular distribution patterns in magnetites. Mineralized rocks don't appear to be enriched of Pd over Pt. With the exception of Erdenetiin Ovoo deposit, Pd contents are typically higher in host rocks than in magnetites. It is suggested that PGE distribution in magnetite is inherited from the parent magmatic source. The PGE patterns of sulfide-mineralized samples imply that PGE were redistributed and concentrated during the late stage hydrothermal activity with preferential mobilization of more soluble Pt, Pd and Au.

[1] Capobianco, C.J. et al. (1994) *Chem. Geol.*, **113**, 23-43. [2] Xia, B. et al. (2001) *Sci. China*, **44**, 1019-1028.

Zircon U-Pb and Hf isotope constraints from Gandese Paleogene granitoids on the collisional magmatism and tectonic evolution in Tibet

Dong Guochen[*], Mo Xuanxue, Zhao Zhidan & Zhu Dicheng
State Key Laboratory of Geological Processes and Mineral Resources & School of Earth Science and Mineral Resources, China University of Geosciences, Beijing, China
([*]donggc@cugb.edu.cn)

The collision between India-Asia continents preceding the north subduction consumed the Neotethyan Ocean in Cenozoic period and gave rise to the extensive magmatism in southern Tibet, forming a giant magmatic belt in Gangdese and causing of crustal uplift along the collision zone. Based on the research of the Natural Science Foundation (NSFC) project (No.40672044), in this contribution, we selected Hf and U-Pb isotope analyses of in situ zircon from 4 separate cross sections of Cenozoic granites in southern Tibet in order to identify the significant magmatism and magma evolution of whole Gangdese. Igneous zircons from the 4 Gangdese granite sections gave out a discrete magmatic event of 65-40Ma and systemic $\varepsilon_{Hf}(t)$ values between +13.4 and -23, in which the $\varepsilon_{Hf}(t)$ values tended to be increased gradually southwards. The positive $\varepsilon_{Hf}(t)$ values with young Hf model ages of 1200-500Ma are accepted that they were derivate from juvenile crust. The zircons with minus $\varepsilon_{Hf}(t)$ values up to 23 with crustal Hf model ages from ca.1.4 to 2.1 Ga is knowing as an old crust remelting in Cenozoic time. It is likely concluded that the predominantly Early Paleogene intrusive activity was contributed with both juvenile mantle and India Continent, which induced that more mantle masses southwards to Yalo Tsangbo suture zone were introduced to the crust and mixed with the partial melted older crust. Combining these with literature data [1,2], we interpret the Gangdese Paleogene magmatism as an early product of the India-Asia continental collision that started up the mass exchange both mantle and crust and played a long-lasting role in the tectonic evolution of southern Tibet.

[1] Dong, G.C. et al. (2005) *Acta Geol. Sinica*, **79**, 787-794. [2] Mo, X. et al. (2005) *Geol. J. China Univ.*, 11, 281-290.

Fluid-mediated re-equilibration and self-irradiation of euxenite-zircon assemblage in pegmatites, South Norway

Duran, C.[1], Seydoux-Guillaume, AM.[1], Bingen, B.[1,2], de Parseval, Ph.[1*] & Ingrin, J.[1]
[1]LMTG-UMR 5563 CNRS-Université de Toulouse-OMP-UPS, Toulouse, France ([*]parseval@lmtg.obs-mip.fr)
[2]Geological Survey of Norway,Trondheim, Norway

The Sveconorwegian belt hosts abundant pegmatites in South Norway. Pegmatites are well known for their rare mineral assemblages. They are distributed in several fields, notably the Evje-Iveland field in the Telemarkia terrane and the Froland and Arendal-Kragerø fields in the Bamble terrane. Pegmatites spatially unrelated to granite plutons, intruded during the waning stage of Sveconorwegian high-grade metamorphism as crosscutting dykes to sills, at ca. 1094-1060 Ma in Arendal-Kragerø and ca. 911 Ma in Evje-Iveland.

We sampled several localities to evaluate the respective effect of self-irradiation damage and fluid mediated alteration on the crystal chemical properties of radioactive minerals and their U-Th-Pb geochronological systematics. Particular attention was given to (Y, REE, U, Th)-(Nb, Ta, Ti) oxide minerals. The statistical classification of Ercit [1] allows sorting these minerals in four groups: samarskite, pyrochlore, fergusonite and euxenite-aeschynite. Here we report SEM images and chemical data on euxenite, with special focus on a locality in Iveland, showing a cogenetic assemblage of euxenite, zircon, xenotime and monazite. Euxenite crystals always show altered (A) and unaltered (B) zones (Fig. 1). The first ones appear dark in BSE, highly porous, have a poor resistance to the e-beam during microprobe analyses with low wt% total, and contain 9% UO_2 and 1% ThO_2. FTIR analyses show the presence of O-H stretching (at 3600 cm^{-1}) within these altered zones, in agreement with an alteration by hydrothermal fluids. Sometimes galena crystallized within these altered zones (white crystals in figure 1). In the unaltered domains (bright in BSE - B in Fig. 1), Euxenite contains 11.5% UO_2 and 1.5% ThO_2. Plotting analyses in the Ercit statistical diagram allows denoting alteration paths from euxenite into pyrochlore group; moreover, analyses done within altered rim of euxenite and within healed cracks (dark grey in BSE) correspond to pyrochlore. Finally, self-irradiation (and irradiation coming from neighbored radioactive minerals, e.g. zircon), caused volume increase, and therefore is responsible for cracks formation that allow fluid circulation within fractures, and led to chemical reactions with elements remobilization.

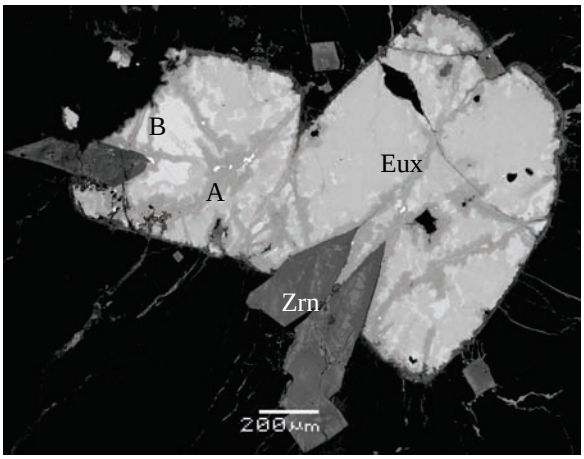

Fig 1: Back Scattered Electron image of an euxenite (Eux) –zircon (Zrn) assemblage in a pegmatite from Iveland, Norway, showing intense alteration coupled with irradiation effects.

[1] Ercit, T.S. (2005) *Can. Mineral.*, **43**, 1291-1303.

Partitioning of As and Sn among among apatite, vesuvianite, Ca-garnet and malayaite in calc-silicate rocks

Houzar, S.[1*], Hrazdil, V.[1], Škoda, R.[2] & Cempírek, J.[1,2]
[1]Dept. of Mineralogy & Petrography, Moravian Museum, Brno, Czech Republic ([*]shouzar@mzm.cz)
[2]Dept. of Geological Sciences, Faculty of Science, Masaryk University, Brno, Czech Republic

Geochemically significant As,Sn-rich mineralization was found in a skarn-like rock enclosed in a marble close to Kozlov near Nedvědice, Svratka Unit, eastern Bohemian Massif. The mineral assemblage consists of predominant Sn-bearing andradite (with relics of grossularite), As-rich vesuvianite, malayaite and rare As-bearing fluorapatite, nordenskiöldine and cassiterite.

Three stages of skarn evolution were distinguished from textural and geochemical features. The first, high-temperature stage features low Fe-content in the system. It is represented by diopside, clinozoisite and grossularite (< 0.300 apfu Fe^{3+}). The second stage, characterized by introduction of Fe, Sn and As in the system, produced malayaite, tin-bearing andradite (85-90 % Adr; 10-13% Grs), As-bearing fluorapatite and arsenic-rich vesuvianite. The third, retrograde stage caused alteration of the primary assemblages and produced secondary cassiterite (*"hydrocassiterite"* or *"varlamoffite"*), stokesite and unidentified Ca,Fe-arsenates [1].

The green Sn-bearing andradite overgrows the grossularite; vesuvianite intergrows with fluorapatite and malayaite. Uncommon relics of diopside and clinozoisite were observed. Rare accessory phases represent nordenskiöldine and löllingite in calcite [2]. The characteristic features of the assemblage are high contents of tin, arsenic and boron, and lack of sulfur.

Distribution of As and Sn among the individual minerals is uneven. Highest contents of tin are present especially in malayaite and nordenskiöldine, but the most important tin carrier in the system is andradite (1.2-2.4 wt.% SnO_2; 0.038-0.081 apfu Sn), replacing grossularite with low Sn-contents (≤ 0.17 wt.% SnO_2; ≤ 0.005 apfu Sn). Grossularite and andradite exhibit very low content of As (< 0.05 wt. % As).

Arsenic is preferentially accommodated in fluorapatite (up to 12.24 wt.% As_2O_5; ≤ 0.56 apfu As) due to AsP_{-1} substitution. It also is an important component in vesuvianite (up to 1.97 wt.% As_2O_5; ≤ 0.597 apfu As), the observed As -contents are the highest recorded worldwide. Similar As-bearing vesuvianite was found at Hemlo, Canada [3]. The LA-ICP-MS data show elevated contents of boron (~8000 ppm). On the other hand, tin contents in vesuvianite are rather low (≤ 0.30 wt.% SnO_2; ≤ 0.060 apfu Sn).

The assemblage originated in relatively oxidizing conditions, in environment with elevated $a(F)$ and $a(H_2O)$, locally also $a(B)$. The equilibrium textures of the prograde second stage (Sn-, As-, Fe-rich) of skarn evolution implies that the distribution of As and Sn among mineral phases was constrained rather by structures of individual phases than by the P-T-X conditions (T_{min} > 300°C, elevated activity of fluids) alone.

[1] Hrazdil, V., Houzar, S. & Škoda, R. (2009) *Geol. Výzk. Mor. Slez.*, **16**, 109-113. [2] Houzar, S. & Hrazdil, V. (2009) *Acta Mus. Morav., Sci. geol.*, **94**, 61-66. [3] Pan, Y. & Fleet, M.E. (1992) *Contrib. Mineral. Petrol.*, **109**, 511-525.

Progressive alteration of spinel phases in listvenitization

Huang Ko-Chun[*] & Jiang Wei-Teh
Dept. of Earth Sciences, National Cheng Kung University, Tainan, Taiwan ([*]chinkuahshih@yahoo.com.tw)

Listvenitic rocks from the Miocene Kenting Mélange in southern Taiwan are possibly among the youngest of the rock type found in the world, without overprinting by regional metamorphism. The rocks were highly fractured, sheared, serpentinized, and subsequently carbonatized and silicified, which provided an excellent opportunity to understand evolution of spinel phases under changing hydrothermal conditions typical of listvenitic rocks. Initial transformation of primary chromium spinel $[(Mg_{0.45}Fe^{2+}_{0.55})(Fe^{3+}_{0.12}Al^{3+}_{0.78}\text{-}Cr^{3+}_{1.10})O_4]$ to thin ferritchromite rims during the serpentinization was followed by formation of thick ferritchromite $[(Mg_{0.15}Fe^{2+}_{0.85})(Fe^{3+}_{0.59}Al^{3+}_{0.16}Cr^{3+}_{1.25})O_4]$ skirts and a reaction with serpentine to form Cr-bearing Mg-rich chlorite in a carbonatization event. The process led to pervasive crystallization of magnesite and dolomite and subsequently gave rise to rapid diminishment of Cr-bearing chlorite and serpentine, locally in association with the formation of disseminated sphalerite and galena and Cr magnetite arcs surrounding ferritchromite relics. In the final stage of listvenitization, ferritchromite was completely replaced by Cr magnetite having hollow cores filled by quartz, apparently coeval with precipitation of euhedral Cr magnetite, intensive replacement of carbonates by silica, and local massive crystallization of pyrite. The first stage of listvenitization (carbonatization) was associated with increased fCO_2 and possibly enhanced fO_2 as well, leading to the extensive formation of Fe^{3+}-increased ferritchromite and the second stage (silicification) involved a relatively acidic fluid with a raised total activity of dissolved sulfur and fO_2, producing a magnetite-quartz-pyrite assemblage. The progressive changes of spinel phases in listvenitization appear to be different from those occurring in simple serpentinitization of ultramafic rocks in which nearly no increase of the Fe^{3+} content in spinels was recorded and occasional occurrence of magnetite was commonly attributed to a later regional metamorphic event.

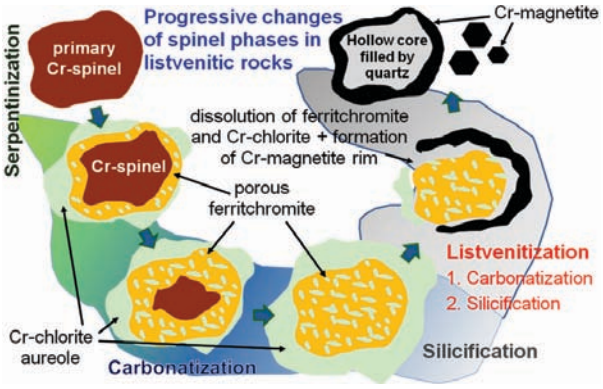

Fig. 1: Evolutionary model of progressive mineralogical and microtextural changes of spinel species observed in the listvenitic rocks from southern Taiwan.

Cathodoluminescence spectra of zircons from some eruptive and endogenous rocks located in Romanian Western and Southern Carpathians

Iancu, O.G.[1*], Robu, I.N.[2] & Brandtstaetter, F.[3]
[1]Dept. of Geology, University „Al. I. Cuza", Iaşi, Romania
([*]ogiancu@uaic.ro)
[2]Geological Institute of Romania, Bucharest, Romania
[3]Naturhistorisches Museum, Vienna, Austria

The main purpose of this study is to investigate the SEM-CL signature of zircons from some volcanic rocks located in the Apuseni Mountains (andesites of Băiţa, Faţa Băii, Roşia, Barza, Cetraş and Săcărâmb types), plutonic rocks from Southern Carpahians (Tismana granitoids, Albeşti granites and Bârsa Fierului granitoids) and metamorphic rocks (metagranites and metapelites from Semenic, Făgăraş, Sebeş and Iezer-Păpuşa Mountains). Cathodoluminescence measurements were made at the Museum of Natural History from Vienna in a JEOL JSM-6400 SEM with an Oxford Instruments CF302 CL system (Room Temperature), a computer-controlled SPEX 340S spectrometer, and a Hamamamtsu-R928 GaAs photomultiplier tube detector. Cathodoluminescence spectral measurements of all zircons analyzed in this study revealed peaks located both in the blue and the yellow parts of the electromagnetic spectrum. The most important spectral features of the zircons from plutonic rocks (9 samples from Tismana granitoids – T3, T6, T8, Albeşti granites – 1154, 1156, 1157 and Bârsa Fierului diorites – 5001, 5002 and 5006) are the peaks located at: 315 nm, 405 nm, 485 nm and 580 nm. The peak with the highest intensity is the 485 nm one, in the blue area of the spectrum, similar with the kimberlitic zircons [1] (Fig. 1).

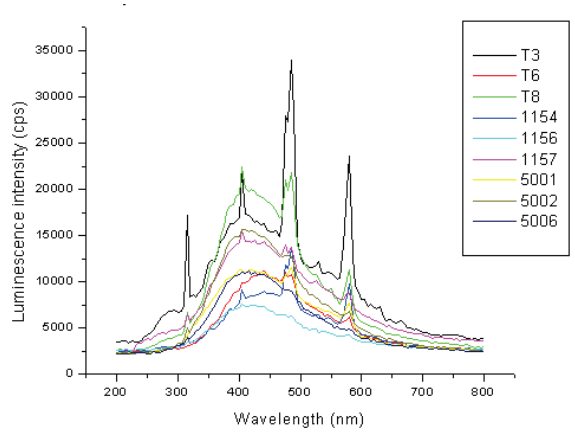

Fig. 1: CL spectra of zircons from plutonic rocks (Southern Carpathians)

The most important spectral features of the zircons from volcanic rocks (7 samples) are the peaks located at: 282 nm (which has the highest intensity) and 352 nm. The most important spectral features of the zircons from metamorphic rocks (5 samples) are the peaks located at: 280 nm (which has the highest intensity), 486 nm, 354 nm and 580 nm. Dy^{3+} is probably the dominant activator element in the zircons analyzed in this study [2]. CL spectra of zircons from the rocks investigated in this study indicate a genesis from fluid or melts with mixed character (crust + mantle). In the case of zircons from plutonic rocks the mantle signature prevails whereas the volcanic and metamorphic zircons formed at the boundary between upper mantle and lower crust [3].

[1] Belousova, E.A. et al. (1998) *Mineral. Mag.*, **62(3)**, 355-366. [2] Gorobets, B.S. & Rogojine, A.A. (2003) *Luminescence spectra of minerals: Reference Book*. All-Russia Institute of Mineral Resources (VIMS). Moscow. [3] Pupin, J.P. (1992) *Bull. Soc. Geol. France*, **163(4)**, 495-507.

Recrystallisation of monazite as a potential monitor of cryptic fluid events

Kelly, N.M.[1*] & Möller, A.[2]
[1]Dept. of Geology & Geological Engineering, Colorado School of Mines, Golden, CO, USA ([*]nkelly@mines.edu)
[2]Dept. of Geology, University of Kansas, Lawrence, KS, USA

Monazite has proven to be a remarkably versatile mineral for providing absolute time constraints on event histories and the rates of geological processes across a range of crustal conditions. However, robust interpretation of age data requires that we not only understand the mechanisms of monazite growth, but also its ability to recrystallise either in the solid state or in the presence of fluids. This requires that textural *and* geochemical indicators for the origin of the monazite grain or zone being dated are recognised. An integrated micro-analytical study has revealed age and chemical complexity in monazite that was altered during a medium-T fluid event subsequent to its initial formation at high-temperature conditions.

Monazite grains targeted in this study occur in orthopyroxene-sapphirine granulites from the Oygarden Islands, East Antarctica, deformed and metamorphosed to peak temperatures in excess of 900°C and at pressures of 9-10 kbars, during the Rayner Structural Episode at ~930-900 Ma. The textural context of monazite suggests that initial growth or recrystallisation at, or near peak conditions, with dominant EMP chemical ages for formation (or closure) falling between ~910-890 Ma. Backscattered Electron (BSE) imaging of monazite grains exposed zoning patterns that are typically characterized by BSE-bright rims developed on either near-homogeneous or more complex patchy, lobate cores. BSE-bright rims commonly form irregular and lobate boundaries with cores reminiscent of chemical fronts penetrating into the monazite grains. In addition, narrow BSE-bright veins that may envelope pores or inclusions within the monazites cut some grains. Critically, grain boundaries of most monazite grains are in textural equilibrium with peak (~900°C) major minerals such as sapphirine. Electron microprobe (EMP) data indicate that bright zones are depleted in Y, HREE, U and Ca, and enriched in Th, Si and LREE. EMP chemical ages reveal partial to complete resetting of ~910-890 Ma monazite core ages to ~500 Ma with resetting clearly correlated with BSE zoning where core-rim geometries are preserved.

Vein-like zoning patterns in monazite indicate that fluid may have been a driver of composition and age alteration. However, the preservation of high-T Rayner mineral textures and compositions in the host rocks and absence of retrogression, suggests that resetting of monazite must have occurred during a relatively low-T event and by low water-activity fluids. In addition, the presence of altered boundaries between monazite and its orthopyroxene host supports the notion of fluid-driven alteration to a radiation-damaged host mineral.

Preliminary data from Focused-Ion-Beam thin-foils extracted from across rim-core boundaries in age and chemically altered monazites suggests that the mechanism of resetting did not involve complete destruction of the monazite rim prior to regrowth, but likely occurred as a result of either a diffusion-related process, or more likely due to coupled dissolution-reprecipitation along a chemical front moving inwards into the grains. Importantly this process did not alter the textural context of grain margins initially formed during a previous high-grade event, but chemically records an event that did not have a major impact on major minerals in the rocks. Monazite has therefore acted as a sensitive monitor of a fluid-mediated event not otherwise recorded by rocks in the terrane.

First report of apatite with pyrrhotite exsolution lamellae in retrogressed Ky-eclogites from the Rhodope UHP metamorphic province (Greece)

Kostopoulos, D.K.[1], Moulas, E.[2*] & Burg, J.-P.[2]
[1]Dept. of Mineralogy and Petrology, National and Kapodistrian University of Athens, Greece
[2]Geological Institute, Dept. of Earth Sciences, ETH-Zürich, Switzerland ([*]evangelos.moulas@erdw.ethz.ch)

Apatite crystals with pyrrhotite exsolution lamellae have been found in kyanite (ky)-eclogites from the Rhodope metamorphic province (RMP), northeastern Greece. RMP is a synmetamorphic nappe stack that was formed during Jurassic-Cretaceous times and underwent extension during the early Cenozoic. Kyanite eclogites occur as boudins in orthogneisses located in the lower parts of the structurally upper unit of the RMP in Greece. These rocks have recorded an early (U)HP event followed by a metamorphic overprint at granulite-facies conditions. The (U)HP mineral assemblage is omphacite, garnet, kyanite and phengite, while rutile, apatite and zircon occur as accessories. Diopside, amphibole and biotite symplectites with plagioclase were formed upon decompression during which corundum, spinel and plagioclase symplectites were formed at the expense of kyanite at granulite-facies conditions (T~800°C, P≈1.0GPa).

The apatite grains often reach 0.5 mm in size and contain a dense network of crystallographically-oriented, needle-like pyrrhotite exsolution lamellae (Fig.1a). The exact composition of the lamellae could not be determined directly, due to their very fine nature. Careful energy-dispersive (EDS) microprobe analyses have nonetheless revealed the existence of a sulphide phase composed of Fe and S (Fig.1b) in atomic proportions of 1:1, thus allowing us to deduce the presence of pyrrhotite.

The occurrence of apatite with pyrrhotite exsolution lamellae is pivotal in the reconstruction of the metamorphic evolution of the RMP since similar occurrences have been reported from eclogites of the Sulu UHP province, China [1,2] as well as from non-HP metamorphosed rocks such as granites [3]. The exsolution of Fe and S from the apatite lattice bears witness to high-temperature conditions since the initial incorporation of Fe in the apatite lattice is restricted because of its limited solubility. An alternative scenario [3] suggests the simultaneous crystallisation of apatite and pyrrhotite from a melt. Although there is no constraint for the pressure at which this process occurred, two scenarios seem possible at present. Either the exsolution lamellae formed during decompression and cooling from UHP/HT conditions or they formed during cooling following the granulite facies overprint. Partial melting may have occurred in both cases.

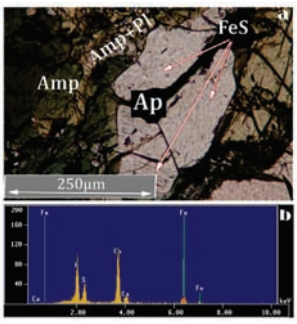

Fig. 1: (a) Photomicrograph of matrix apatite where the lamellar FeS is indicated. (Amp: amphibole, Pl: plagioclase, Ap: apatite); (b) EDS spectrum of FeS in apatite.

[1] Zeng, L. et al. (2006) *Geochim. Cosmochim. Ac.*, **70**, 18, 1, A733. [2] Zhu, Y.F. & Massonne, H.J., (2005) *Acta Petrol. Sin.*, **21**, 405-410. [3] Gottesmann, B. & Wirth, R., (1997) *Eur. J. Mineral.*, **9**, 491-500.

Yttrium mineralization in the north-west of Russia (Pre-Polar Urals)

Kozyreva, I.V.[*] & Shvetsova, I.V.
Institute of Geology UB RAS, Syktyvkar, Russia
([*]kozyreva@geo.komisc.ru)

The aluminium- and iron-rich metamorphic rocks are developed in the Pre-Polar Urals. The nature of these metamorphites is convergent: partly they are metamorphized Precambrian crusts of weathering and their resedimentation products; on the other hand they are products of Late Paleozoic fault metasomatism. These rocks are geochemically special: they are anomalous by Sn, Be, Ge, Zr, As and especially TR. Their study has revealed a wide complex of accessory minerals both widespread, and exclusively rare. The present report shows results of study of yttrium-containing minerals. At present about 150 carriers and concentrators of yttrium are known; more than 10 of them are determined in the studied rocks (minerals are given according to decrease of Y content). *Thalenite-(Y)* ($Y_2[Si_2O_7]$) is found as accretions of brown-red thick tabular crystals. *Xenotime-(Y)* (YPO_4) has three morphotypes: xenomorphic xenotime-1, idimorphic xenotime-2 (prismatic) and xenotime-3 (dipyramidic). *Churchite-(Y)* ($YPO_4 \times 2H_2O$) forms grains and radial yellow and milk-white nodules. *Chernovite-(Y)* ($YAsO_4$) is represented by two varieties: xenomorphic cryptocrystalline structures and idiomorphic yellow crystals. *Kainosite-(Y)* ($Ca_2(Y, Ce)_2Si_4O_{12}(CO_3) \times H_2O$) is represented by pink-yellow short prismatic crystals. *Yttrocrasite-(Y)* ($(Y,Th,Ca,U)(Ti,Fe^{3+})_2(O,OH)_6$) is observed as red-brown isometric grains. *Paraniite-(Y)* ($Ca_2Y(AsO_4)(WO_4)_2$) forms yellow dipyramidal crystals. *Allanite-(Ce)* ($(Ce, Ca, Y)_2(Al, Fe)_3(SiO_4)_3(OH)$) shows four varieties: rare separate grains of allanite-1, allanite-2 has thin and cryptocrystalline structure, radial aggregates of allanite-3 columnar crystals and reticulate undulate structures of allanite-4. *Davidite-(La)* ((La, Ce, Ca)(Y, U)$(Ti, Fe)_{20}O_{38}$ is represented by black grains with metal shine and tabular crystals with side faces of phombohedron. *Gramaccioliite-(Y)* $(Pb, Sr)(Y, Mn)Fe_2(Ti, Fe)_{18}O_{38}$ is found as well formed tabular crystals of trigonal shape with black side faces of rhombohedron with metal shine. *Keilhauite* $Ca_3YFeTi_3Si_4O_{20}$ is of sealing wax and red-brown color and forms roundish, almond-shaped structures. Metamict *zyrtolite* $Zr_{0.9}Hf_{0.05}REE_{0.05}SiO_4$ is represented by idiomorphic, prismatic, dipyramidal, tabular, pancake-shaped crystals and grains of brown, grey and orange colors. The studied minerals are characterized by complex variable composition, unusual look, microcrystallinity or poor crystallinity and apparently connected with authigenic mineral formation in old crust of weathering. In the process of green shale metamorphism they formed more perfect crystalline generations. The variability of mineral forming solutions at various stages of metamorphism conditioned formation of crystals of various habits and various chemistry.

Experimental constraints on the partitioning of REE between fluorapatite and monazite at high pressures and temperatures

Krenn, E.[1*], Harlov, D.E.[2], Heinrich, W.[2], Wunder, B.[2] & Finger, F.[1]
[1]Dept. of Materials Engineering and Physics, University of Salzburg, Austria ([*]erwin.krenn@sbg.ac.at)
[2]GeoForschungsZentrum, Potsdam, Germany

Natural observation implies that high-pressure rocks often bear REE (Nd-MREE) enriched fluorapatite that reacts during decompression to REE-poor fluorapatite plus secondary Nd-rich monazite [1,2]. Due to the presence of Nd- and MREE-rich fluorapatite, high pressure monazite is often particularly rich in La and poor in Nd and MREEs.

We have studied REE partitioning between fluorapatite and coexisting monazite in a series of piston cylinder experiments at 800°C and 1.5, 3 and 4 GPa. Experimental runs utilized synthetic REE-free Ca-fluorapatite, allanite (as REE source), albite and a 1 molar NaF solution as reactants.

As predicted [3], monazite crystals formed in all experiments from the reaction between fluorapatite and allanite. At the same time REE-rich fluorapatite formed through partial replacement of REE-free Ca-fluorapatite via dissolution and repricipitation (Fig. 1). These newly formed apatite rims yield up to 20 wt.% ∑REE. While fluoarapatite rims show a strong enrichment in Nd relative to the bulk, the experimentally produced monazite crystals are enriched in La.

The results from this study confirm the existence of a strong fractionation of La and Nd between monazite and apatite in high pressure rocks, similar to what has been observed in nature. They also demonstrate that fluorapatite at high pressures can contain considerable amounts of REEs and thus serve as a major storehouse of REE as well as source of secondary monazite during decompression.

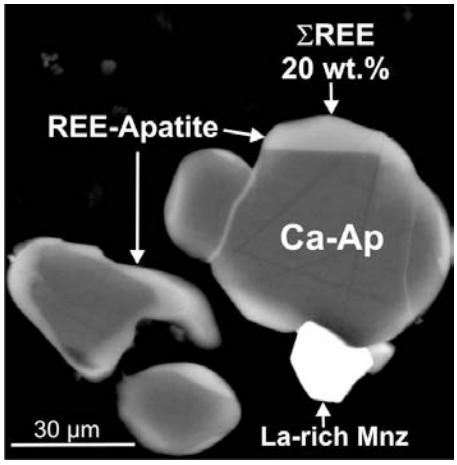

Fig. 1: BSE image showing La-rich monazite (La/Nd 2.5) and newly formed REE-rich apatite at the margin of REE-free, Ca-fluorapatite. Starting materials and run conditions: allanite + Ca-fluorapatite + 1M NaF-H_2O; 800°C, 30 kbar, 5 days).

[1] Krenn, E. et al. (2009) *Am Mineral*, **94**, 801-815. [2] Finger, F. & Krenn, E. (2008) *Lithos*, **95,** 115-125. [3] Janots, E. et al. (2007) *Contrib Mineral Petrol*, **154**, 1-14.

Textural features and geochemistry of titanite in granitic rocks from Ciborro – Aldeia da Serra area, Ossa-Morena Zone (southern Portugal)

Lima, S.S.M[1*], Neiva, A.M.R.[1] & Ramos, J.M.F.[2]
[1]Dept. of Earth Sciences and Geoscience Centre, University of Coimbra, Portugal ([*]selmalima252@gmail.com)
[2]LNEG, S. Mamede de Infesta, Portugal

Titanite, $CaTiSiO_4(O,OH,F)$, occurs in rocks from a wide range of geological environments. In Ciborro – Aldeia da Serra area, Ossa-Morena Zone (southern Portugal), titanite is the dominant titanium-bearing mineral in biotite>amphibole tonalite, biotite trondhjemite and biotite>amphibole granodiorite.

In tonalite and granodiorite, titanite is euhedral to subhedral, wegde-shaped and light-brown in colour. It occurs mainly as individual matrix grains and rarely as inclusions in biotite and amphibole. In backscattered imaging, the grains present sectorial zoning, which is indicative of magmatic origin [1]. In general, the lighter zones present higher values of $Al+Fe^{3+}$than the darker zones. Titanite from tonalite has slightly lower Ca and Ti concentrations than titanite from granodiorite.

In trondhjemite, titanite occurs as rims around ilmenite in close association with biotite (Fig. 1A, B). Although this titanite is optically unzoned, it presents a higher chemical variation, mainly in Ca, Ti and $Al+Fe^{3+}$ contents than titanite from the other lithologies. On the other hand, backscattered images show that this ilmenite is chemically zoned (darker zone is richer in Mn than lighter zones) and presents exsolved lamellae (Fig. 1B). A similar texture to that presented in Fig. 1 was reported by [2] for titanite from metamorphic rocks and interpreted that titanite was formed due to hydratation and oxidation reactions.

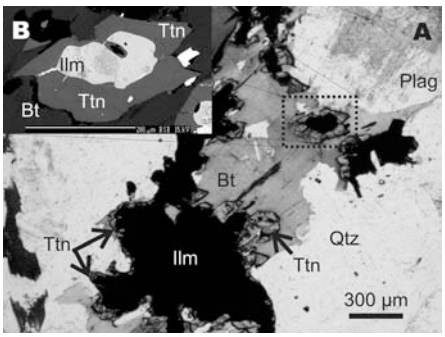

Fig. 1: Titanite from the biotite trondhjemite: A) titanite rimming ilmenite showing that both minerals are closely associated with biotite (plain polarized light); B) backscattered image showing ilmenite zonation and the exsolved lamellae. Abbreviations to biotite (Bt), ilmenite (Ilm), plagioclase (Plag), titanite (Ttn) and quartz (Qtz).

In general, in titanite from the three granitic rocks the $(Al+Fe^{3+})$-OH component exceeds the $(Al+Fe^{3+})$-F component. The parameters used to distinguish between primary and secondary titanite are the contents in $Al+Fe^{3+}$ and F, $X_{Fe}{}^{3+}=Fe^{3+}/(Al+Fe^{3+})$, $Al+Fe^{3+}$ vs F diagram [3] and the $Al\text{-}Fe^{3+}$-Ti ternary plot [4]. Titanite from all lithologies falls within the accepted ranges for a primary origin, including titanite rimming ilmenite that presents values from 0.075-0.124 for $Al+Fe^{3+}$, 0.005-0.031 for F and 0.263-0.387 a.p.f.u. for $X_{Fe}{}^{3+}$. Tonalite and granodiorite present the following values for the same parameters of titanite: $Al+Fe^{3+}$=0.070-0.101 and 0.078-0.096; F=0.000-0.058 and 0.005-0.041 and $X_{Fe}{}^{3+}$=0.315-0.440 and 0.304-0.370 a.p.f.u., respectively.

Acknowledgements: This study was supported by the first author PhD fellowship from FCT-MCTES.

[1] Broska, I. et al. (2007) *Lithos*, **95**, 58-71. [2] Harlov, D. et al. (2006) *Lithos*, **88**, 72-84. [3] Enami, M. et al. (1993) *Eur. J. Mineral.*, **5**, 219-231. [4] Morad, S. et al. (2009) *Can. Mineral.*, **47**, 801-811.

Alkali-rich beryl from Fe-deposit Skály near Rýmařov, Czech Republic; an example of coupled substitutions in CH-, O- and T_2-site

Novák, M.[1*], Filip, J.[2], Gadas, P.[1] & Přikryl, J.[1]
[1]Dept. of Geological Sciences, Masaryk University, Brno, Czech Republic ([*]mnovak@sci.muni.cz)
[2]Centre for Nanomaterial Research, Palacký University, Olomouc, Czech Republic

Beryl-group minerals feature the following principal substitutions including O-site e.g.: (1) Al = Fe^{3+}; CH-site + T_2-site: (2) $^{CH}\square$ $^{T}Be^{2+}$ = $^{CH}R^{+}$ $^{O}Li^{+}$ and CH-site + O-site: (3) $^{CH}\square$ $^{O}R^{3+}$ = $^{CH}R^{+}$ $^{O}R^{2+}$, where R^{+} = Na, Cs, Rb, K; R^{2+} = Mg, Fe^{2+} and R^{3+} = Al, Sc, Fe^{3+}. Subhedral to euhedral columnar crystals of deep blue beryl, up to 2 cm long, occur in quartz>calcite>Fe-chlorite veins, up to ~10 cm thick, cutting hematite-rich ore. They were mobilized from host rocks of the Lahn-Dill type deposit where one of the rock types - magnetite-chlorite rock - yielded up to 60 ppm of Be [1]. Accessory hematite, albite, dravite, bornite, digenite, chalcopyrite, monazite-(Ce), REE-epidote, and fluorapatite were also identified in the veins. Beryl is locally cut by late veins of calcite, quartz and chlorite and occasionally shows corrosive contacts chiefly to calcite. Crystals of beryl contain small subhedral inclusions of euclase, up to ~200 μm in size, partly replaced by calcite. The fluid inclusion study of quartz yielded temperatures of homogenization of aqueous inclusions 110 - 180 °C, low fluid salinity (2.2-4.3 wt.% of NaCl equiv.) and Na-Mg-Cl salt composition [1]. Zoned beryl crystals are built of volumetrically dominant homogeneous core of beryl I and homogeneous narrow rims and minor euhedral inclusions of beryl II, up to ~200 μm in size, located chiefly around rims. Beryl exhibits a unique chemical composition (based on the EMPA, room- and low-temperature Mössbauer spectroscopy and LA-ICP-MS data): Li_2O = 0.20 and 0.43; Na_2O = 2.43 and 2.46; MgO = 2.41 and 2.36; FeO_{tot} = 4.07 and 0.90 (Fe^{3+} = 39 at.% from total Fe for beryl I) and Al_2O_3 = 11.69 and 14.34 for beryl I and beryl II, respectively (all in wt.%) with the empirical formulas: $^{CH}Na_{0.45}$ $^{T}(Be_{2.92}Li_{0.08})_{3.00}$ $^{O}(Al_{1.31}Fe^{3+}_{0.13}Mg_{0.34}Fe^{2+}_{0.19})_{1.97}$ $Si_{6.06}$ O_{18} and $^{CH}Na_{0.45}$ $^{T}(Be_{2.84}Li_{0.16})_{3.00}$ $^{O}(Al_{1.59}Mg_{0.33}Fe^{2+}_{tot0.07})_{1.99}$ $Si_{6.04}$ O_{18}, respectively. The LA-ICP-MS study revealed concentrations of the trace elements similar in beryl I and beryl II (all in ppm): Sc ≤ 38; Mn ≤ 45; Co ≤ 18; Cu ≤ 84; Ga ≤ 46; As ≤ 94; Rb ≤ 39; except for Ti≤ 91; V ≤ 38; Cs ≤ 242 (all higher in beryl I) and Zn ≤ 373 (higher in beryl II). Beryl I exhibits two dominant substitutions (1) up to 0.13 apfu of Fe^{3+} and (3) up to $\sum R^{2+}$ = 0.53 apfu (Mg > Fe^{2+}); whereas the substitution (2) is only minor up to 0.08 apfu of Li. In beryl II, where Mössbauer data are not available, the substitution (1) is likely less important due to low amount of Fe_{tot}. The substitution (2) is more significant, up to 0.16 apfu of Li, and the substitution (3) is dominant with $\sum R^{2+}$ = 0.40 apfu (Mg >> Fe^{2+}). Participations of the substitutions (1), (2) and (3) within single crystal of beryl are remarkable, because usually substitutions affiliated to O-site or T-site are dominated [2,3]. The textural relations of both compositional types of beryl characterized by coupled substitutions in CH-site, O-site and/or T_2-site, respectively, indicate their immiscibility.

[1] Fojt, B. et al. (2007) *Čas. Slez. Muz. Opava (A)*, **56**, 1-22. [2] Franz, G. & Morteani, G. (2002) *Rev. Mineral.*, **50**, 551-589. [3] Aurisicchio, C. et al. (1988) *Am. Mineral.*, **73**, 826-837.

Two types of monazite and the REE tetrad effect in the Surovec Li-F-P micro- and leucogranite (Gemeric Unit, Western Carpathians, Slovakia)

Petrík, I.[1*], Broska, I.[1] & Konečný, P.[2]
[1]Geological Institute, Slovak Academy of Sciences, Bratislava, Slovakia ([*]igor.petrik@savba.sk)
[2]D. Štúr State Geological Institute, Bratislava, Slovakia

Two varieties of specialised S_s-type granite occur in the area of Surovec in western part of the Gemeric unit. A small body of the Li-F-P microgranite contains topaz, Li-mica (zinnwaldite), and a variety of rare phosphates (lacroixite, arrojadite, viitaniemiite). Accompanying ordinary leucogranite contains phengitic mica, but topaz and rare phosphates are absent. Both types are characteristically poor in REE contents which results in virtual absence of REE accessories. Only couple of monazites was found and their analyses showed that while leucogranite monazite is Th-poor, Li-F-P microgranite contains extremely Th-rich monazite (25 % ThO_2). The latter was convenient for chemical dating which yielded a well defined age of 263 ± 3 Ma, identical with Re-Os dating of molybdenite from the nearby Hnilec body [1].

Whole rock REE contents of both granite types are very low (14REE=5-10 ppm) showing characteristic pronounced tetrad patterns: positive curvature La-Nd, Gd-Ho and Er-Lu segments. The tetrad effect originates in fluid environment where chemical properties of the REE are controlled by filling 4f orbitals (e.g. [2]). The positive pattern, called M-type, is conventionally explained by removal of a phase with reciprocal tetrads (W-type)[3]. Such a phase is however not commonly found, on the contrary, the analysed late minerals (fluorite) show also the M-type pattern [4]. This means that late fluids were equilibrated with already M-type bearing residual melt. The Th-rich monazite from microgranite with the distinct M-type tetrad pattern is interpreted in such a way. However, a single monazite found in leucogranite shows a distinct W-type pattern (Fig. 1). Because whole rock patterns of both rock types are almost identical it is suggested that fractionation of W-type monazite (possibly accompanied by some apatite) could explain the tetrad effect in both rocks. While the fractionation may have removed early monazite from microgranite some has been preserved in leucogranite. A local enrichment of Th in the late melt may have promoted the M-type monazite formation in microgranite.

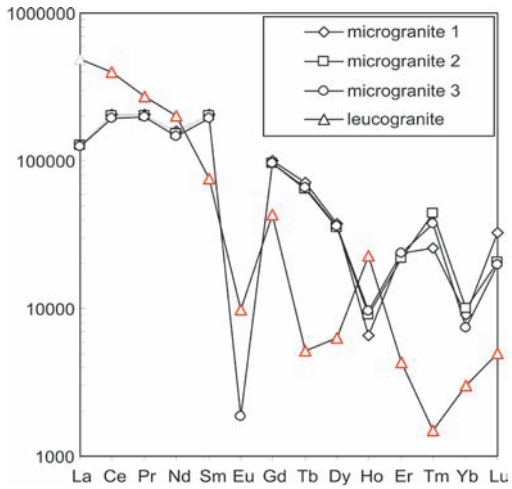

Fig. 1: Two types of tetrad REE patterns in monazites from Surovec leuco- and microgranite.

[1] Kohút, M. & Stein, H. (2005) *Mineral. Petrol.*, **85**, 117-127 [2] Irber, W. (1999) *Geochim. Cosmochim. Ac.*, **63**, 489-508. [3] Masuda, A. et al.(1987) *Geochem. J.*, **21**, 119-124. [4] Monecke, T. (2002) *Geochim. Cosmochim. Ac.*, **66**, 1185-1196.

Allanite–monazite–xenotime–zircon–apatite assemblage in two-mica granites of the Moldanubian (South Bohemian) batholith

René, M.
Institute of Rock Structure and Mechanics, Academy of Sciences of the Czech Republic, Prague, Czech Republic (rene@irsm.cas.cz)

Two-mica Variscan granites of the Moldanubian (South Bohemian) batholith represent the most significant rock type of this magmatic body. Three main geochemical two-mica granite types can be distinguished in the SBB: the low-Th Deštná granite, the intermediate-Th Eisgarn granite and the high-Th Lipnice and Steinberg granites. All these granites were emplaced at shallow levels (equivalent to 100–200 MPa) and at relatively reducing fO_2 conditions (presence of ilmenite). The two-mica granites are peraluminous (A/CNK = 1.02–1.34) with low CaO concentrations. Th concentrations and REE element patterns are quite distinct class marks for the above mentioned three geochemical types of two-mica granites. The highest bulk content of REE is significant for the Lipnice and Steinberg granites, whereas the lowest bulk of REE was observed in the Deštná granites. These granites are also characterized by the smallest amounts of accessory minerals. The Eisgarn granites typically show highly variable bulk contents of REE, controlled by variable amount of biotite and accessories (allanite, monazite, zircon, apatite). In the Lipnice, Steinberg and Eisgarn granite types, apatite is the most common accessory mineral. Large (100–600 μm), anhedral to subhedral grains of apatite often contain inclusions of zircon and monazite. In the Deštná granite apatite, zircon and monazite are usually included in K-feldspar and/or biotite grains.

The Deštná granites are leucocratic biotite-muscovite granites with predominance of muscovite. They contain very common schlieren or small nodular aggregates of restitic biotite. Their accessory minerals assemblage consists of monazite, zircon, apatite, and a significant occurrence of xenotime. The Eisgarn granites are texturally highly variable granites (porphyritic and/or equigranular, fine- to medium-grained), with a variable ratio of muscovite and biotite. The accessory minerals assemblage is formed by allanite, monazite, zircon and apatite. The Lipnice granite is a medium-grained monzogranite usually containing high amounts of restite enclaves. The Steinberg granite is a hiatalporphyritic, medium-grained monzogranite with a strong dimensional fabric of K-feldspar phenocrysts. The accessory minerals assemblage of monazite, zircon and apatite is significant for both granite types.

Whole-rock geochemistry is notably controlled by chemical composition of the accessory minerals assemblage. The highest Th contents in monazite and high Th/U ratios are significant for monazites from the Lipnice and Steinberg granites. On the other hand, monazites from the Deštná granites show higher values of U and Y. The relatively high contents of Y in the Deštná granites are also expressed by the presence of xenotime. Considerable differences in the Mn/Fe ratio were observed for apatites from different two-mica granite types. The highest values of this ratio are characteristic for the Deštná granite. Zircon compositions in all three granite types are quite variable, with the occurrence of zircon grains enriched in P, Y and Sc. In the Lipnice and Steinberg granites, the zircon composition is closest to a stoichiometric zircon.

Acknowledgements: This study was supported by the Ministry of Education, Youth and Sports of the Czech Republic (project No. ME10083).

Zirconium-bearing minerals in phonolites of northern Bohemia

Skála, R., Ulrych, J., Böhmová, V.*, Korbelová, Z. & Novák, J.K.
Institute of Geology, Academy of Sciences of the Czech Republic, Praha, Czech Republic (*bohmova@gli.cas.cz)

The Tertiary nepheline phonolites of the České Středohoří and the Lužické hory volcanic mountain ranges are characteristic by extremely high Zr contents ranging from 950 to 2650 ppm. Zirconium is concentrated mainly in otherwise rare zirconium silicates as hainite and fluorian eudialyte [1]. Hainite is a mineral occurring exclusively in northern Bohemia within the region of the Central European Volcanic Province (CEVP).

Hainite was first described from the phonolite of the Chlum (or Hradiště) Hill near Raspenava in the Lužické hory Mts. [2]. It occurs as either (i) acicular crystals in amygdales vugs and bands enriched in aegirine-augite, in places also in the phonolite matrix reaching up to 1 mm length (called here hainite I) or (ii) thin lobate lamellae in matrix (called here hainite II). Crystal structure of the hainite I was published in [3]. The microprobe analyses of original hainite I were published in [4]. Corresponding empirical formula recalculated considering 18 (O,F) per formula unit is:

$(Ca_{1.356}Zr_{0.400}Mn_{0.166}REE_{0.077})_{\Sigma 2.000}(Ca_{0.880}Na_{0.762}Al_{0.006}\square_{0.353})_{\Sigma 2.000}Ca_2Na(Ti_{0.759}Fe_{0.125}Mn_{0.061}Nb_{0.045}Ta_{0.010})_{\Sigma 1.000}[(Si_{1.951}\square_{0.049})O_{6.918}F_{0.082}]_2F_4$

The analyses of hainite II from the matrix of phonolite of the same locality are first presented in this abstract recast to empirical formula based on 18 (O,F) per formula unit:

$(Ca_{1.002}Zr_{0.802}Mn_{0.139}Si_{0.047}REE_{0.010})_{\Sigma 2.000}(Ca_{1.070}Na_{0.833}K_{0.010}Al_{0.006}U_{0.001}\square_{0.080})_{\Sigma 2.000}Ca_2Na(Nb_{0.534}Ti_{0.224}Fe_{0.142}Mn_{0.096}Ta_{0.004})_{\Sigma 1.000}[Si_2O_7]_2(F_{2.224}O_{1.776})_{\Sigma 4.000}$

The hainite II occurs also at many other phonolite localities of the region, e.g., the Klíč Hill or the Rýdečský vrch Hill in the České Středohoří Mts.

Next to hainite, another zirconium-bearing mineral was found in the phonolite of the Sokol Hill in the Lužické hory Mts. This rock is extremely enriched in Zr (2650 ppm) and other incompatible elements (Rb, REE, Hf, U, Th, Nb, Ta). The mineral forms irregular lamellae that are similar to hainite II but their colour is deeper brown. The phase was identified as fluorian eudialyte.

The appearance of hainite and fluorian eudialyte in phonolites as well as the accompanying mineral association comprising aegirine-augite, apatite, titanite, carbonates, analcime and zeolites imply that these zirconium-bearing minerals represent products of the late-stage hydrothermal or metasomatic processes.

Acknowledgments: This study has been supported through the project of the Grant Agency of the Academy of Sciences of the Czech Republic No. IAA300130902.

[1] Ulrych, J. et al. (1992) *Geol. Carpath.*, **43**, 91-95. [2] Blumrich, J. (1883) *Tscher. Miner. Petrogr.*, **13**, 465-595. [3] Giester, G., Pertlik, F. &. Ulrych, J. (2005) *Mitt. Österr. Miner. Ges.*, 151. [4] Johan, Z. & Čech, F. (1989) *C.R. Acad. Sci.*, **308**, 1237-1242.

2.90 to 2.40 b.y. old monazites from the Archaean Sargur Group and the Biligirirangan and Male Mahadeshwara Hill granulites, Dharwar craton, south India

Srikantappa,C.[*] & Gobi, R.
DOS in Geology, University of Mysore, Mysore, India
([*]srikantappa@googlemail.com)

Along the southern margin of the Archaean Dharwar craton, the two crustal blocks, the Sargur Group (SG) and the Biligirirangan and Male Mahadeshwara Hill (BRH-MMH) granulites, are juxtaposed along a narrow, sub-vertical to steeply dipping, ductile-brittle Kollegal shear zone (KSZ).

Sargur Group consists of meta-sediments like quartzites, BMQ's, meta-pelites and carbonates, intruded by layered ultramafic-mafic igneous complex. All these rocks occur within the Peninsular gneiss, forming part of the Western Dharwar craton. In BRH-MMH, enderbitic granulites are predominant rock types, with garnet-cordierite bearing gneiss, forming part of the Eastern Dharwar craton.

The rocks of SG show upper amphibolites facies metamorphism (T=643 - 741°C; P=7.2 - 9.0 Kbar) in contrast to granulites exposed in the BRH-MMH (T= 645 - 722°C; P= 6.8 – 7.2 kbar)[1]. The rocks show IBC cooling P-T path with reaction of CPx+Plag → Grt+qtz. Crustal melting results in the formation of garnet and cordierite according with the reaction Bio+Sill+qtz → Grt+K-felds+Melt and Bio+Sill+qtz (+Plag) → Cord+K-fedls+Melt (+Ilm). U-Pb ages for zircon in meta-sediments vary from 3.58 to 2.96 Ma [2]. The timing of regional high grade metamorphism is not well constrained in these two crustal blocks, which is essential to unravel tectanometamorphic process in the Dharwar craton.

Monazite occurs predominantly in metapelitic rocks in both the SG and BRH-MMH granulites. They occur as euhedral crystals, either as inclusions in biotite and garnet or as intergranular crystals within the quartz matrix and few grains occur along the grain boundary of apatite crystal. Some of monazite show zoning. EPMA, in-situ U-Pb dating carried out for monazite in different textural relations in both SG and BRG rocks, show varying isotopic ages from 2.90 to 2.40 Ma. The older ages are obtained for the BRH and the younger ages for SG. The older ages (2.90 and 2.63 Ma) are recorded mainly in monazite bordering apatite grains and as inclusion in porphyroblastic garnet, suggesting a closed system behavior of isotopes. Younger ages of 2.4 Ma are obtained for monazites associated with biotite in the matrix, suggesting an open system behavior. U-Pb isotopic study on monazite, combined with micro-textural and mineral P-T data reveal that the two crustal blocks, show contrasting geological set up and metamorphic history. Deeper part of the crust is exposed in the WDC when compared to relatively shallower crustal levels in the EDC.

The present data suggest an early metamorphic event around 2.9 Ma followed by the regional high-grade metamorphism around 2.63 Ma, suggesting a collissional and crustal melting event in the Dharwar craton.

[1] Srikantappa, C. et al. (1985) *Precam. Res.*, **30**, 189-219. [2] Nutman, A.P. et al.(1992) *J. Geol. Soc. India*, **39**, 367-374.

Zircons in Variscan granites from the Slavonian Mountains, Croatia

Starijaš, B.[1*], Gerdes, A.[2], Balen, D.[3], Tibljaš, D.[3] & Finger, F.[1]
[1]Dept. of Materials Engineering and Physics, University of Salzburg, Austria ([*]biljana.starijas2@sbg.ac.at)
[2]Geozentrum, Dept. of Mineralogy, Goethe University, Frankfurt am Main, Germany
[3]Institute of Mineralogy and Petrology, University of Zagreb, Croatia

The Slavonian Mountains in Croatia expose Variscan crystalline basement of the Tisia terrane. Apart from different metamorphic units, this basement comprises large bodies of Variscan granites [1]. In the course of current attempts to constrain the formation ages of these granitic rocks by means of LA-SF-ICP-MS-based U-Pb zircon dating, a detailed study of the accessory zircon crystals was undertaken with reference to morphology, internal growth textures and crystal chemistry. Eight samples of granites from Papuk and two granite samples from Psunj were prepared for the study. The work was carried out using a combination of methods, including optical microscopy, cathodoluminescence (CL) and backscattered-electron imaging (BSE), electron microprobe and laser ICP-MS analysis.

The granite samples from Psunj carry a distinctive zircon population characterized by relatively large, stubby to normal prismatic zircons with prominent {100} and {101} crystal faces. {211} and {110} faces are small or missing, as is often the case in high-temperature I-type and A-type granites [2]. Characteristic are numerous inclusions of tiny apatite needles (Fig. 1a) and uranium rich inner zones, which are sometimes metamict (Fig. 1b).

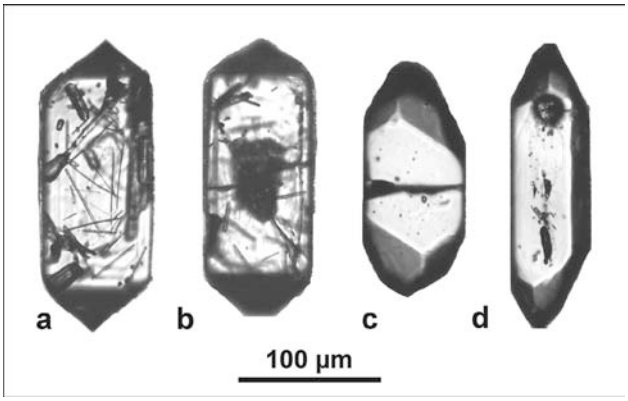

Fig. 1: Typical zircons from Psunj granite (a, b) and Papuk S-type granites (c, d).

Zircons in the Papuk granites are short prismatic to normal prismatic, with prominent steep pyramids {211} and a dominance of the {110} prism (Fig. 1c, d). Short prismatic crystals often contain a large inherited core with bright CL signal, mantled by an oscillatory zoned outer growth shell. Zircon types are consistent with the interpretation of [1], according to which the granites from Papuk have an S-type origin.

[1] Pamić, J. et al. (1996) *Neues Jb. Miner. Abh.*, **171,** 143-162.
[2] Pupin, J.P. (1980) *Contrib. Mineral. Petrol.*, **73**, 207-220.

Zircon growth in granulites: relationship to metamorphic mineral formation (Irkut block of Sharyzhalgai Uplift)

Sukhorukov, V.P.* & Urmantseva, L.N.
Institute of Geology and Mineralogy SB RAS, Novosibirsk, Russia (*svp@uiggm.nsc.ru)

The Irkut block is the SW part of the Sharyzhylgai Uplift of the Siberian Craton. Metamorphic complex of the Irkut block is composed of metasedimentary and metavolcanic rocks. The available data indicate that the magmatic protoliths were undergone at least two stages of metamorphism during Neoarchean (2.55-2.57 Ga) and Palaeoproterozoic (1.85-1.87 Ga) [1-3]. In turn, in metasedimentary gneisses detrital zircon cores with ages of 2.7, 2.3 and 1.95-2.0 Ga were found. Metamorphic rims of these cores yield the age interval between 1.85 and 1.95 Ga [4]. Therefore it can be concluded that the sediments deposition occurred 1.95-1.85 Ga. For better understanding of relationship between the zircon growth and metamorphic conditions is necessary to study the mineral paragenesis and zircon's REE composition as well.

Metasedimentary rocks are represented by migmatites with mineral assemblage Grt+Crd+Sil+Bt+Kfs+Pl+Qtz. Leucosome composed of Kfs+Qtz+Pl+Grt+Bt is characterized by magmatic structure. Melanosome is represented by mineral association Grt+Crd+Sil+And+Bt+Sp+Crn+Kfs+Pl+Qtz+Ilm+Mt with accessory Rt, Zrn, Mnz. Several types of reaction structures are developed in rocks: 1) Spl is surrounded with Sil rim and located into Crd grains. 2) Bt within Crd grains is replaced by Sil and Ilm with formation of pseudomorphoses. 3) Crd grains are surrounded with Grt rims with inclusions of Sil. 4) Crn grains always contact with Mt and Spl located within Bt. We suggest mineral reactions Crd→Grt+Sil+Qtz; Bt+Crd+Spl→ Grt+Sil+Ksp+Ilm; Sp→Mt+Crn on the base of observed reaction structures. Therefore reaction structures observed in the rock have been formed at progressive stage of metamorphism [5]. PT – parameters of metamorphism was obtained using mineralogical geothermobarometers and TWQ and THERMOCALC programmes. Compositions of contacting Crd and Grt grains were used for PT – estimations. The F value (Fe/(Fe+Mg)) of Grt increases from 0.68 in the center to 0.73 on the rim of grain, the F of Grt decreases from 0.23 to 0.17 in direction to the contact with Grt. PT – parameters of regressive stage of metamophism was 600°C at 5.8-6 kbar. It has been obtained using contacting rims of cordierite and garnet. Values about 700°C at 6.5 kbar was obtained using inner parts of grains are close to the peak of metamorphism.

Zircon detrital cores are characterized by HREE enrichment ($(Lu/Gd)_n$=9-24). They have positive Ce (Ce/Ce*=2.4-5.3) and negative Eu (Eu/Eu*=0.1-0.3) anomalies and high Y concentrations (551-999 ppm) typical in magmatic zircons. Metamorphic rims show lower HREE concentrations ($(Lu/Gd)_n$=0.9-2.6), Y contents (131-290 ppm). Also there is LREE concentrations similar to the cores but differ by weaker Ce anomaly (Ce/Ce*=1.2-3.9). The sharp decreasing of HREE contents in metamorphic rims is typical for zircons formed during high grade metamorphism. It can be considered as a result of the concurrent Grt crystallization at PT-conditions close to peak of metamorphism.

[1] Sal'nikova, E.B. et al. (2007) *Strat. Geol. Correl*., **15(4)**, 343-358. [2] Turkina, O.M. et al. (2009) *Dokl. Earth Sci*., **429(9)**, 1505-1510. [3] Poller, U. et al. (2005) *Precam. Res*., **136**, 353-368. [4] Urmantseva, L. & Turkina, O. (2009) *Acta Geol. Sin. (Eng. Ed.)*, **83(5)**, 875-883. [5] Lonker, S.W. (1981) *Amer. J. Sci*., **281(8)**, 1056–1090.

Mixing of karstic and basinal fluids affecting hypogene cave formation and mineralization in the Buda Thermal Karst, Hungary

Poros, Zs.[1,2*], Erőss, A.[1], Mádl-Szőnyi, J.[1], Mindszenty, A.[1], Molnár, F.[2], Ronchi, P.[3] & Csoma, A. É.[4]
[1]Dept. of Physical and Applied Geology, Eötvös L. University, Budapest, Hungary ([*]poroszsofi@gmail.com)
[2]Dept. of Mineralogy, Eötvös L. University, Budapest, Hungary
[3]ENI S.p.A. Exploration & Production Division, S. Donato Milanese, Italy
[4]Shell International E&P, The Netherlands, currently ConocoPhillips Upstream Technologies

The Buda Thermal Karst (BTK) is located at the boundary of uplifted Mesozoic-Tertiary carbonates and the adjacent sedimentary basin with carbonatic basement. Being a "marginal" area, the BTK serves as the discharge zone of regional fluid flow. This implies that it may receive fluid components from several sources, resulting in a wide range of discharge features, including springs, caves and mineral precipitates.

Recent- and palaeo-hydrogeology were studied in parallel, to understand the effects of palaeo-fluid migration on the recent hydrogeological setting and the distribution and development of the extensive hypogene cave-systems in the BTK. On the basis of geochemical analyses of recent waters, petrography and fluid inclusion analyses of palaeo-precipitates (calcite and barite), three types of fluids from different sources were distinguished: (i) regional karst water, (ii) local karst water and (iii) basinal fluid. The basinal contribution to the BTK from the East was suggested first by Alföldi [1], whose hypothesis was confirmed by the present study. Moreover, based on the HC indications detected in both palaeo- and recent waters it is proposed that the basinal contribution had been continuous from the late Middle Miocene. The age of initiation of basinal fluid migration to the Buda Hills was estimated by structural geological considerations and fluid inclusion data. Compressional tectonics (inversion of the Pannonian Basin) has been maintaining flow from the basin side up to now.

Changes in mineral assemblages and paragenesis, as well as an increase in dissolution at the expense of precipitation from the Miocene to present suggest an evolving groundwater system in which the proportion of karst waters increased at the expense of the basinal component. The increase likely has been the result of accelerating Neogene uplift and gradual exposure of the Mesozoic-Tertiary carbonates.

Along with the omnipresent calcite, in the Miocene, barite was the only sulphate mineral in the paragenesis, while recently gypsum is the predominant sulphate phase with minor amounts of barite. This change may indicate that originally there were equal amounts of Ba and S in the fluid, however, later on S of different origin must have been added to the system, resulting in the precipitation of gypsum following the barite. This assumption was confirmed by $\delta^{34}S$ values measured in the sulphate minerals. Barite showed positive values restricted to a rather narrow interval (22.7–27.6‰), while gypsum precipitates of various morphologies are characterised by negative values with a much wider range (-32.3 – -1‰). Microbial activity was detected in the case of the recent precipitates that may explain the occasional extreme negative $\delta^{34}S$ values.

Cave formation in the BTK has been most likely influenced by the complex hydrogeological system and the various fluid components. In addition to the frequently mentioned mixing corrosion, other processes might have been effective in dissolution, e.g. aggressive gases (H_2S, CO_2) from the basin fluids, the presence of microbial activity, or the cooling of upwelling waters.

[1] Alföldi, L. (1979) *VITUKI Közl.*, **20**, 1-102.

The present day genesis and evolution of cave minerals inside the Ojo de la Reina cave (Naica Mine, Mexico)

Badino, G.[1], Calaforra, J.M.[2], Forti, P.[3*], Garofalo, P.[4] & Sanna, L.[3]
[1]Dept. of Physics, University of Torino, Italy
[2]Dept. of Geological Sciences, University of Almeria, Spain
[3]Italian Institute of Speleology, University of Bologna, Italy ([*]paolo.forti@unibo.it)
[4]Dept. of Earth and Geological-Environmental Sciences, University of Bologna, Italy

The Naica caves and their amazing gypsum crystals were discovered almost a century ago inside a silver mine in the state of Chihuahua (Mexico). From 2000 to 2008 mining activities at -290 met 4 small caves hosting the largest gypsum crystal of the world. Ojo de la Reina is one of the smallest caves, therefore it was the first cavity in which the lowering of temperature induced by ventilation caused condensation since 2006. The consequent dissolution of the gypsum crystals and subsequent evaporation lead to the deposition of several new diagenetic minerals, among which some highly soluble Mg/Na compounds (Blödite, Halite, Epsomite, Hexahydrite, Kieserite, Starkeyite), the presence of which in a extremely moist environment was completely unexpected. Moreover no evident source for Mg and Na ions is available within the cave because its entire walls are completely covered by the giant gypsum crystals. The study proved that their existence is the consequence of several boundary conditions, the most important of which may be summarized as follow. During the process of cooling down thermal stresses induced the slight opening of the main exfoliation planes (010) within the giant crystals. When the dew point was reached, the strong uplift of hot moist air was forced to condensate over the cold crystal surfaces, the preferential place where this phenomenon occurs being just inside the widened exfoliation planes. Here the capillary flow brings the unsaturated water to dissolve gypsum deep inside the crystals, until some of the giant fluid inclusions (the only possible source for Mg and Na ions) just along these planes are reached. Thus the Mg/Na rich fluids stored inside them have the possibility to drip outside the crystals, giving rise to small pools in the depression between two or more crystals on the cave floor. Finally the strong air current flowing within the cave causes the total evaporation of these pools, thus the very soluble salts are deposited as whitish powder.

Peculiar minerogenetic mechanisms occurring in the cavern environment

Forti, P.
Italian Institute of Speleology, University of Bologna, Italy
(paolo.forti@unibo.it)

Caves are among the longest-lasting components of the environment and throughout their complete lifespan they act as accumulation traps for physical, biological and chemical deposits. Perhaps man's first motivation to explore caves was the search for substances that were not available elsewhere: most of them were minerals. Anyway the genesis of many of the minerals found in caves is unrelated to the existence of the cavern itself: in fact often they were brought inside by flowing water or exposed by corrosion on the cave walls. By definition a cave mineral is a secondary mineral developed within a natural cave due to the peculiar environmental conditions existing there. For a long time it was believed that the cavern environment was scarcely interesting from the mineralogical point of view. This was because most cave deposits are normally made of a single compound: calcium carbonate. Therefore the systematic study of cave mineralogy started only recently, but although only a limited number of natural cavities have been analysed in detail, more than 350 cave minerals have already been observed, some of which are new to science. Each year some new cave minerals are found somewhere. The presence of such unexpected richness is obviously the direct consequence of the variety of the different formations crossed by water before entering a cave, but there is much more. The different cavern environments allow the development of several minerogenetic mechanisms, the most important of which are: sublimation, deposition from aerosols and vapours, evaporation, diffusion, oxidation, hydration-dehydration, double exchange, digestion, self-combustion, segregation. Most of them are strictly controlled by the cavern temperature, while some are driven by micro-organisms. Each of them gives rise to different cave minerals and/or different forms of the same chemical deposit. Sometimes the cavern environment, due its stability lasting over long time periods, allows for the development of huge euhedral crystals like those found in the Naica caves (Chihuahua, Mexico), but the presence of extremely small complex aggregates of different minerals is by far more common. Future development in the field of cave mineralogy will be focused mainly on hydrothermal caves and on the role played by micro-organisms in controlling some of the most important cave minerogenetic processes. In conclusion, the recent studies proved that the cavern environment is surely one of the most complex and interesting minerogenetic environments on our planet.

Secondary minerals inside the Argentiera mine galleries (Nurra region, NW Sardinia, Italy)

Ara, D.[1], De Waele, J.[2*], Galli, E.[3], Rossi, A.[3] & Sanna, L.[1]
[1]Gruppo Speleo Ambientale Sassari, Sassari, Italy
[2] University of Bologna, Italy ([*]jo.dewaele@unibo.it)
[3]Dept of Earth Sciences, University of Modena and Reggio Emilia, Modena, Italy

The Pb-Zn-Ag-Sb deposit of the Argentiera mine has been known since the Roman times. Furthermore, this one of the most important silver mines of Sardinia, Italy hosted within late-Hercynian veins that cut into a Palaeozoic basement (Silurian graphite-siderite rich finely laminated phyllites of black shale facies and pinkish metasandstones). During the last century, the extensive mining activities dug deep shafts and several kilometres of galleries at different levels. In 1963, the mineral exploitation was not economical and production at the mine ceased. This study focuses on the secondary minerals (crusts or coatings) and speleothems (stalactites, flowstones, and gours) formed in a strongly oxidizing environment in the ancient mine galleries in atmospheric conditions similar to those found inside caves. Mineral samples were collected on wooden supports, on abandoned equipment, and on the rock wall inside the main mine galleries: Pozzo Alda (PA), Fornello Centrale di Ripiena (GA), and Miniera Vecchia (MV). In addition, mineral samples were collected in small exploration galleries along the coast (SAG). A detailed analysis of all the samples under stereoscopic microscope was performed to distinguish and to separate the different mineralogical phases present. Then the single phases were analyzed by an X-ray diffractometer (Philips PW 1050/25) when the material was sufficient enough and homogeneous. A Gandolfi camera (Ø: 114.6 mm, exposition: 24/48 hrs) was used for analyses when the material was scarce or inhomogeneous. In all mineral analysis, the experimental conditions used in the Philips PW were a 40Kv and 20 mA tube and CuKα Ni filtered radiation (λ = 1.5418 Å). The analyses of the clay minerals were done before and after glycerine treatment. Most of the samples analyzed by Gandolfi camera were later used to obtain images and chemical qualitative analyses through an electron scanning microscope (ESEM Philips XL40) with an electronic microprobe (EDS-EDAX 9900) at the C.I.G.S. (Centro Interdipartimentale Grandi Strumenti) of the Modena and Reggio Emilia University. This research has revealed a diversity of minerals for this abandoned mine environment: about 20 crystalline phases have been observed, 11 of which are rare for the artificial caves (akaganeite, copiapite, dypingite, giorgiosite, hydromagnesite, hydrozincite, jarosite, melanterite, metavoltine, sideronatrite, and todorokite), and 2 were previously cited, but inadequately described, in the literature (giorgiosite and todorokite). Most of the detected mineral deposits are sulphates (barite, copiapite, epsomite, gypsum, jarosite, melanterite, metavoltine, and sideronatrite) and carbonates (aragonite, calcite, dypingite, giorgiosite, hydromagnesite, and hydrozincite). Also present are oxides (hematite and akaganeite), hydroxides (goethite and todorokite) and silicates (quartz, illite, feldspar). Few metallic amorphous compounds have been found. Quartz is ubiquitous as well as illite. The most uncommon mineral association (akaganeite, dypingite, giorgiosite, and hydromagnesite) grew on a derelict nail that was the source for iron and magnesium. The development of some metallic sulphates on the mine wall is the direct consequence of the oxidation of the polysulphides dispersed in the host rock. The minerogenetic processes are driven by small volumes of water flowing, dripping, or condensing over the mine equipment/wall and are strictly related to the evaporation induced by the ventilation of the mine tunnel network. All the minerals developed in a short interval of time (in a few tens of years) while others are seasonal (i.e., epsomite).

Speleothems in the Gamslöcher-Kolowrat Cave System, Untersberg (Austria)

Bieniok, A.[1*], Zagler, G.[2] & Brendel, U.[2]
[1]Dept. of Materials Research & Physics, University of Salzburg, Austria ([*]anna.bieniok@sbg.ac.at)
[2]Landesverein für Höhlenkunde, Salzburg, Austria

The Untersberg is a 70 km^2 large karst massif southwest of Salzburg in Austria. It belongs to the upper Juvavikum of the Northern Calcareous Alps and consists mainly out of dolomite (Ramsaudolomite) and limestone (Dachstein-, Hierlatz-, Plassenkalk). The karst plateau (1500 m to 1970 m) is characterized by dolines, shafts and pits. More than 300 caves are described from the Untersberg massif, some of them with remarkable depths [1,2].

One famous Untersberg cave is the Kolowrat Cave, known since 1842 for adventurously ice skating. In 1979 a connection to the Gamslöcher Cave and in 2004 to the Salzburgerschacht have been found [3], comprising a large cave system of 34 km length. Dripstone formations are rare in the Gamslöcher-Kolowrat Cave system; their occurrences are rather locally limited.

Recent speleological research [4] has been carried out in the Kolowrat Cave at ca. 1000 m, discovering unexpectedly dry parts, which hardly resemble the other parts of the cave. Low passages alternate with large halls of 10 to 40 m in height over a total length of 4 km. The inner part of the labyrinth does not show any indications of flowing water. The area is characterized by a stronger air current, compared to any other part of the cave, and it is rich in speleothems. Samples of white coloured minerals with different morphologies were collected and later analyzed by X-ray diffraction.

Needle-like minerals (e.g. gypsum) are dominating the transition zone of the dry section. Within the dry zone gypsum also occurs as white crusts composed of skeletal crystals. In the windy corridors calcite is the main speleothem, but it occurs in a snowflake-like form with a remarkably low density of 75 kg/m^3. The rock walls are covered by this white dusty coatings and the air is filled with calcite flakes. In the 'White Hall' near the central part of the dry zone, thenardite Na_2SO_4 was found. Thenardite in association with its hydrated form mirabilite was described earlier from the Salzburgerschacht (Untersberg) but in a quite different environment and with different morphology [2]. Another cave mineral, which was described earlier from the Salzburgerschacht is hydromagnesite $Mg_5(CO_3)_4(OH)_2 \cdot 4H_2O$. It occurs here as hard, white, cauliflower-like crusts, associated with aragonite.

The cause for the development of the dry parts in the Gamslöcher-Kolowrat Cave system is not yet clear. Further explorations are planned to get better insight into this part of the cave system.

[1] Klappacher, W. & Mais, K. (ed.) (1975) *Salzburger Höhlenbuch*. LVHK, Salzburg. [2] Haseke-Knapczyk, H. (1989) *Der Untersberg bei Salzburg*, Ö.MaB-Programm (15), Wagner, Innsbruck. [3] Zehentner, G. et al. (2006) *Die Höhle*, **57,** 90-102. [4] Zagler, G. (2010) *Atlantis*, 1/2 (in press)

High-resolution trace-element data from a Sardinian flowstone as evidence of environmental change

Caddeo, G.A.[1], Railsback, L.B.[2], Frau, F.[1] & De Waele, J.[3*]
[1]Dipto. di Scienze della Terra, Università degli Studi di Cagliari, Italy
[2]Dept. of Geology, University of Georgia, Athens (GA), USA
[3]Dipto. di Scienze della Terra e Geologico-Ambientali, Università di Bologna, Italy ([*]jo.dewaele@unibo.it)

In a study of many speleothems from southern Sardinia (Italy), a highly variable flowstone has been analysed by X-ray diffraction, Scanning Electron Microscopy / Energy Dispersive X-ray Spectroscopy and Laser Ablation-ICP-MS. This flowstone is from a natural cave intercepted by San Giovanni mine (Iglesias), which exploited Pb and Zn sulfides. Most of the sample is composed of alternating layers of blue-green and light aragonite. Beneath the aragonite, at the base of the sample, primary brown calcite is found. In the upper part of the sample, an irregular section of secondary light calcite has partially replaced some blue and light aragonite.

Mg concentration in the primary calcite increases strongly toward the lowest aragonite, reaching its maximum value of 5 mol% $MgCO_3$ just below the latter. Concentrations of Zn, Cu, Sr, and Ba also increase upward in the calcite, reaching about 1 mol% $ZnCO_3$. Increasing concentration of Mg in a speleothem is commonly attributed to upstream precipitation of calcite and resultant increase of the solution's Mg/Ca ratio [1,2]. That may be the case here, but a residual solution should be depleted of Zn and Cu, rather than enriched, because their partition coefficients in calcite are more than 1, opposite those of Mg, Sr and Ba. We hypothesize that the increase in Zn and Cu was driven by more extensive oxidation of sulfides in the overlying ore deposit during a change to drier conditions that favoured higher saturation states and more thorough precipitation of $CaCO_3$.

Concentrations of many elements change abruptly at the transition from calcite to aragonite. Mg, Zn and Cu concentrations decrease, and Ba and Sr increase, because of the difference in distribution coefficients for these elements in calcite and aragonite. The aragonite layer can be divided in two sublayers on the basis of Pb content, with the higher sublayer much richer in Pb. The transition from the first to second sublayer of aragonite is very evident in backscatter-SEM images because of a sharp increase of brightness. In some minor horizons of the second aragonite sublayer, small crystals of cerussite ($PbCO_3$) were observed. We attribute this increase in Pb content to oxidation of Pb sulfides and mobilization in descending waters, and thus as a continuation of the trend noted with regard to Zn and Cu in calcite.

Secondary calcite shows much lower Mg concentration with respect to primary one. Instead, Sr is greater in secondary calcite probably because Sr was inherited from the precursor aragonite.

[1] Bar-Matthews, M. et al. (1991) *J. Geol.*, **99**, 189-207. [2] Fairchild, I.J. et al. (2000) *Chem. Geol.*, **166**, 255-269.

Morphology and genesis of halite cave deposits in the Iranian salt karst

Filippi, M.[1*], Bruthans, J.[2] & Palatinus, L.[3]
[1]Inst. of Geology, Academy of Science, v.v.i., Prague, Czech Republic ([*]filippi@gli.cas.cz)
[2]Charles University in Prague, Faculty of Science, Czech Republic
[3]Inst. of Physics, Academy of Science, v.v.i., Prague, Czech Republic

South-western Iran represents area with the highest number of piercing salt diapirs in the world. Tens of diapirs offer variability of well developed karst phenomena, including countless salt caves. Various types of halite cave deposits were observed in these caves. This contribution characterizes them from the morphological and genetic point of view.

Among the numerous forms of halite cave deposits found in the Iranian salt karst the following types were observed as most abundant: a) euhedral crystals and their clusters, b) macrocrystalline speleothems, c) microcrystalline (fine grained) speleothems, d) straw (tubular) stalactites, and e) filamentary speleothems (helictites). A new and unusual subtype of macrocrystalline halite formations (form b) was recognized – the „skeletal" speleothems with more or less regularly developed shape. They consist of a central column composed of adjacent cubes stacked along their body diagonal. Other stair-step organized cubes grow away down-dip from the cube surfaces (Fig. 1).

Fig. 1: Macrocrystalline skeletal stalactite.

The occurrence of particular forms depends strongly on the environment, especially on the type of the water (brine) flow (capillary water, gravity driven flow, splashing water), flow-rate intensity and oscillation, evaporation rate and in some cases on air direction. Therefore, combined or transitional speleothem formations may be observed, if the conditions change during the deposition. Euhedral halite crystals and clusters originate solely below the water table of supersaturated streams and lakes. Macrocrystalline and skeletal speleothems occur at places with rich irregular dripping and splashing (i.e., waterfalls, places with strong dripping from the cave ceilings, etc.). Microcrystalline (fine grained) speleothems are generated by evaporation of capillary water at places where water is not present in a macroscopically visible form. These forms with laminated internal structure are the most widespread secondary halite deposits in all caves. Straw stalactites form at places where dripping is concentrated into small spots and is frequent enough to assure that the tip of stalactite will not overgrow by halite precipitates. In case the tip is blocked by halite precipitates, brine remaining in the straw will seep through the walls and helictites start to grow in some places.

The macrocrystalline and skeletal forms and straw stalactites usually grow after the rains when dripping is strong, while the microcrystalline speleothems are formed continuously during much longer periods and ultimately, (usually) overgrow the other types of speleothems during dry periods.

Mineralogical investigation of cave rims and vents in Cova des Pas de Vallgornera (Mallorca Island, Spain)

Hunt, G.A.[1*], Merino, A.[2], Fornós, J.J.[3], Onac, B.P.[1,4], Ginés, J.[2,3] & Ginés, A.[2,3]
[1]Dept. of Geology, University of South Florida, Tampa, Florida, USA ([*]gahunt2@mail.usf.edu)
[2]Federació Balear d'Espeleologia, Palma de Mallorca, Spain
[3]Dept. de Ciències de la Terra, Universitat de les Illes Balears, Palma de Mallorca, Spain
[4]"Babeş-Bolyai" University Cluj/"Emil Racoviţă" Institute of Speleology, Cluj, Romania

Recent exploration of Cova des Pas de Vallgornera, a coastal cave located in the southern region of the island of Mallorca, has revealed rim features surrounding vents and cracks which connect upper and lower levels of the cave [1]. The mineral assemblage of the rims consists not only of minerals common to limestone/dolostone caves (e.g., calcite, aragonite, gypsum, huntite, dolomite, and goethite), but also of unexpected hydrothermal-related minerals (e.g., strontianite, celestine, barite, and nordstrandite) [2,3].

Fig. 1: Typical vertical vent and mineral rim (view is from above).

The vents in this cave allow air movement that results in condensation corrosion and mineral precipitation as described by Audra [4]. Two vent morphologies exist in Cova des Pas de Vallgornera: simple vertical cracks or dissolution pipes and complex horizontal dissolution features. Vertical vents (Fig. 1) are small, internally smooth, lined with weathered limestone and mineral deposits and connect an upper air-filled chamber with a lower chamber at the level of the water table [3]. Horizontal vents may be large enough for human entry, are lined with precipitated minerals and may contain secondary vertical vents with mineral rims [3].

When considered alongside discrete dissolution features distributed throughout the cave's galleries and passages, the unexpected suite of hydrothermal minerals supports a partial hypogenic origin in addition to the initially deduced mixing zone dissolution typical of coastal caves such as Cova des Pas de Vallgornera [3,5].

[1] Merino, A. (2006) *Endins*, **30**, 49-70. [2] Onac, B.P. et al. (2005) *Endins*, **27**, 131-140. [3] Merino, A. et al. (2009) *Proc. 15th Int. Speleol. Congr.*, **1**, 309-311, Kerrville, TX. [4] Audra, P. et al. (2007) *Acta Carsologica*, **2**, 185-194. [5] Ginés, J. et al. (2008) *Endins*, **32**, 49-79.

Allophane-like deposits in Izvor Cave (NW Romania)

Onac, B.P.[1,2*], Provencio, P.[3] & Polyak, V.J.[4]
[1]Dept. of Geology, University of South Florida, Tampa, USA ([*]bonac@usf.edu)
[2]Dept. of Geology, Babeş-Bolyai University/Emil Racoviţă Institute of Speleology, Cluj Napoca, Romania
[3]Sandia National Laboratories, Albuquerque, New Mexico, USA
[4]Dept. of Earth & Planetary Sciences, University of New Mexico, Albuquerque, New Mexico, USA

Izvor (Spring) Cave, located in the Padurea Craiului Mountains (NW Romania), is formed in middle Triassic limestone that is overlain by early Jurassic micro-conglomerates and sandstones rich in biogenic sulfides. The length of the cave is approximately 230 m with a shallow water underground stream that is present throughout most of the cave [1]. In the main chamber, the stream forms several large, shallow pools. The stream bed (including the breakdown blocks) is covered along its entire length by a thick, white to slightly yellowish gel-like material. The thickness of the deposit varies from a few millimeters up to 5-6 cm on the sides of the pools. The pH of the water is acidic (4.3 to 5.2) and its mean electric conductivity value is 1127 µS/cm. The chemical composition of the gel-like material is dominated by Al_2O_3 (> 45%), SiO_2 (7-9.2%), SO_3 (12.9-14.0%), K_2O (~1.5%), and Fe_2O_3 (~1.25%). The mean $\delta^{34}S$ value of this compound is -20.1‰.

A sample of this white deposit, amorphous to x-ray diffraction, consists of submicron-sized particles, ranging from 0.05 to 0.2 µm. High resolution transmission electron microscopy (HRTEM) imaging shows an amorphous-like nature with some short-range crystalline structure. Small nm-sized domains of lattice fringes, ranging from 5 to 10 nm, yielded electron diffraction spots (Fig. 1). Generally, broad electron diffraction rings were observed.

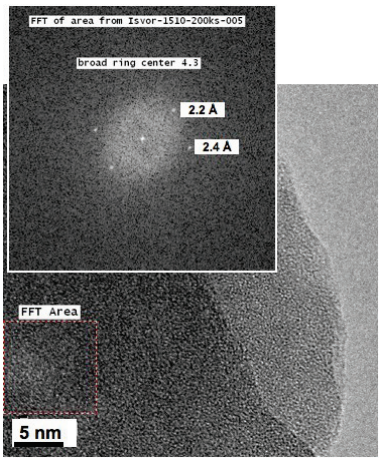

Fig. 1: Short-range crystalline structure in the white deposit from Izvor Cave.

This white deposit from Izvor Cave is similar in occurrence and composition to an allophane-like compound earlier described in a nearby cave [2]. The negative δ34S values suggest oxidation of biogenic sulfides (mainly pyrite) as the main source of sulphate in this material. Al, Si, Fe, and K are probably leached by acidic waters from the fireclay mines located in the vicinity of the cave. While this material seems amorphous, HRTEM shows some crystalline structure indicating that it might be a not yet identified or new mineral.

[1] Valenas, L. & Iurkiewicz, A. (1981) *Nymphaea*, **8-9**, 311-378. [2] Ghergari, L. & Onac, P.B. (1993) *Bull. Soc. Géogr. Liège*, **29**, 97-104.

Rapidcreekite, $Ca_2(SO_4)(CO_3)•4H_2O$, in the H_2S-rich environment of Diana Cave (Romania)

Onac, B.P.[1,2*] & Effenberger, H.S.[3]
[1]Dept. of Geology, University of South Florida, Tampa, USA
([*]bonac@usf.edu)
[2]Dept. of Geology, Babeş-Bolyai University/Emil Racoviţă Institute of Speleology, Cluj, Romania
[3]Institute of Mineralogy and Crystallography, University of Vienna, Austria

Diana Cave, located in SW Romania, is developed along a fault line at the contact between upper Jurassic limestones and lower Cretaceous marls. The cave gives access to a hot spring (T = 42-53°C) with near-neutral pH water containing 44 mg/l SO_4^{2-}, 37 mg/l S^{2-}, 76 mg/l HCO_3^-, 107 mg/l Ca^{2+}, and 58.5 mg/l K^+, from which H_2S rises into the cave atmosphere [1-3]. The $\delta^{34}S$ values of the sulfate and sulfide in the thermal water as well as in the mineral association from Diana Cave range from 18 to 19.5‰ [3].

Rapidcreekite, ideally $Ca_2(SO_4)(CO_3)•4H_2O$, is one of a suite of secondary, hydrated sulfate minerals reportedly formed by oxidation of hydrogen sulfide degassing from the thermal water in Diana Cave. To date, this mineral was documented in only two other locations worldwide [4,5]. In Diana Cave, rapidcreekite commonly occurs as radiating sprays of white to colorless acicular crystals, closely associated with minerals of the halotrichite group. Precise single crystal X-ray diffraction analysis combined with micro-chemical and scanning electron microscope investigations enabled us to characterize this rare mineral species. This is the first time rapidcreekite is documented in a cave environment. Stable sulfur isotopic results reported in this presentation will shed light on the redox processes, the source of dissolved sulfur in the hot water of Diana Cave, and the precipitation of rapidcreekite in this unique thermo-mineral cave.

[1] Povara, I. et al. (1972) *Trav. Inst. Spéol. "Emile Racovitza"*, **11**, 355-365. [2] Povara, I. et al. (2008) *Studia Univ. Babes-Bolyai, Geol.*, **53(2)**, 41-45. [3] Onac, B.P. et al. (2009) *Acta Carsologica*, **38(1)**, 27-39. [4] Roberts, A.C. et al. (1986) *Can. Mineral.*, **24**, 51-54. [5] Rüger, F. et al. (1995) *Lapis*, **20(1)**, 15-26.

Revisiting three minerals from Cioclovina Cave (Romania)

Onac, B.P.[1,2*], Kearns, B.J.[3], Effenberger, H.S.[4] & Collins, N.C.[1]
[1]Dept. of Geology, University of South Florida, Tampa, USA
([*]bonac@usf.edu)
[2]Dept. of Geology, Babes-Bolyai University/Emil Racovita Institute of Speleology, Cluj, Romania
[3]Materials Research Institute, Pennsylvania State University, USA
[4]Institute of Mineralogy and Crystallography, University of Vienna, Austria

Cioclovina Cave, in Romania's Southern Carpathians, is a world renowned cave site for its paleontological, anthropological, and mineraological (type locality of *ardealite*) findings [1,2]. During the cave evolution, large amounts of allogenic sediments were deposited along the main cave passage. At times of low flow conditions, thick guano layers accumulated on top of the siliciclastic deposits. Subsequently, washed-in sediments buried each of these organic layers. Due to the presence of interbedded guano material, the sandy-silty sediments were highly phosphatized (~35% P_2O_5) generating within them and at the contact with the limestone bedrock a suite of interesting minerals. To date, over 20 mineral species have been documented, some of these rather unusual for the cave environment [3-6].

This paper presents details on the occurrence of collinsite [$Ca_2(Mg,Fe^{2+})(PO_4)_2·2H_2O$], atacamite [$Cu_2^{2+}Cl(OH)_3$], and kröhnkite [$Na_2Cu^{2+}(SO_4)_2·2H_2O$] based on single crystal X-ray diffraction, electron microprobe analyses, and scanning electron microscope imaging. Collinsite occurs near the entrance in the *Bivouac Room* and is closely associated with apatite-(CaOH)-rich crusts in the upper part of the sedimentary sequence. The collinsite crystals line millimeter-sized dissolution cavities developed within the apatite-(CaOH) crusts. Atacamite and kröhnkite were collected just outside the *Bivouac Room* at its southern edge. Both minerals were identified within a thick layer of white-yellowish brushite. Atacamite (mismatched with paratacamite in our previous powder diffraction) forms delicate and crumbly greenish nodules (millimeter size in diameter) and represents the weathering product (in the presence of chlorine from meteoric water) of copper minerals washed into the cave from nearby ore deposit. Kröhnkite forms sky blue platy crusts (sub-millimeter thick) in the vicinity of atacamite and around minute crystals of gypsum. It was found at a depth of 25 to 35 cm below the sediment surface and is highly soluble when it comes in contact with dripping water. As the case of atacamite, in kröhnkite copper comes from the outside ore deposit, whereas the sodium originated from clay minerals.

[1] Breban, R. et al. (2003) *The history of guano-phosphate exploration and discovery of human fossils in Ciclovina Uscata Cave*. Proteus, Hunedoara. [2] Schadler, J. (1932) *Centralbl. Miner.*, **A**, 40-41. [3] Marincea, S. et al. (2002) *Eur. J. Mineral.*, **14**, 157-164. [4] Onac, B.P. et al. (2002) *Theor. Appl. Karstol.*, **15**, 27-34. [5] Onac, B.P. et al. (2006) *Am.. Mineral.*, **91**, 1927-1931. [6] Onac, B.P. & Effenberger, H. (2007) *Am.. Mineral.*, **92**, 1998-2001.

Peculiarities of gypsum in the Great Cave from Şălitrari Mountain (SW Romania)

Puşcaş, C.M.[1,2*], Onac, B.P.[1,2,3], Tămaş, T.[2,3] & Kearns, B.J.[4]
[1]Dept. of Geology, University of South Florida, Tampa, USA ([*]cpuscas@mail.usf.edu)
[2]Dept. of Geology, Babeş-Bolyai University, Cluj-Napoca, Romania
[3]Emil Racoviţă Institute of Speleology, Cluj-Napoca, Romania
[4]Materials Research Institute, Pennsylvania State University, USA

Several caves situated along the Cerna Valley (SW Romania) have formed under complex settings involving epigene, phreatic, and hypogene speleogenetic phases. Only a few of these caves, in particular the Great Cave from the Şălitrari Mountain (GCSM), host a rich variety of mineral associations. Detailed presentations of the mineral species discovered in this cave have been presented in [1,2]. This paper reports unusual patterns of gypsum occurrences throughout the GCSM and how these features shed light on the cave's speleogenesis.

The Main Passage (MP) and Nitrate Passage (NP) in GCSM display the highest mineralogical variety. The MP exhibits a transition from surface climate (near the cave entrance) to an anomalously warm and dry (11.7°C and 75% RH) climate in the NP. Except for these two sectors, the cave atmosphere throughout the Final Passage (FP) and Speo-Timiş Passage (SP) is cooler (~10ºC) with a constant relative humidity of ~99%. Gypsum in the MP occurs predominantly as thin crusts on the walls and in the alluvial sediment sequence as nodules or micro-crystals. In the FP, where clastic sediments are absent, gypsum forms crusts on the walls and aggregates on the floor, whilst in the SP it is completely absent.

Based on $\delta^{34}S$ ratios of gypsum, darapskite, and alunite from the NP [1] and stable isotope mass balance calculations, the origin of sulfate in solution can be traced back to a marine sedimentary source [4]. Redox reactions in the presence of ascending thermo-mineral waters, mediated by bacterial activity led to the precipitation of SO_4-bearing minerals with $\delta^{34}S$ values between -2.6‰ and 6.5‰ (NP) [1, 3], similar to the sulfur isotope ratios of modern sulfates from the present-day H_2S-rich caves in the region [1]. The $\delta^{34}S$ value of gypsum from the MP is -19.8‰, leading us to conclude that it originated from the oxidation of biogenic pyrite nodules disseminated either within the limestone bedrock or from the alluvial sediments. The lack of sulfate minerals in the SP can be explained by considering it the youngest section of the cave, unaffected by hypogene fluids.

Hypogene speleogenesis has certainly played an important role in the evolution of GCSM [1-3], but the three main passages were either affected in different ways by hypogene fluids or developed within different time intervals. Thus, evidence for thermo-mineral fluids affecting these parts of the cave has now been documented.

[1] Onac, B.P. et al. (2009) *Acta Carsologica*, **38**, 67-79. [2] Puşcaş C.M. et al. (2010) *Carbonate. Evaporite.*, **25**, 107-115. [3] Sumrall, J. (2009) *Unpubl. MS Thesis*. Univ. South Florida. [4] Wynn, J. et al. (2010) *Chem. Geol.*, **271**, 31-43.

A Late Holocene cave ice geochemical record of atmospheric metal deposition in the Apuseni Mountains, Romania

Vereş, D.[1*], Onac, B.P.[2,3,1], Perşoiu, A.[2] & Atlas, Z.D.[2]
[1]"Emil Racovita" Institute of Speleology, Cluj-Napoca, Romania ([*]danveres@hasdeu.ubbcluj.ro)
[2]Dept. of Geology, University of South Florida, Tampa, USA
[3]Dept. of Geology, Babes-Bolyai University, Cluj Napoca, Romania

Independent sedimentary records of air-borne metals may provide a strong basis for investigating the development of mining and metallurgy through time. Here we report the initial results of a geochemical investigation of approximately two thousand year old ice-core section recovered from Scărişoara Cave, Apuseni Mountains, Romania. Trace metals in melted ice relevant to historical mining techniques (Cu, Pb, As, Sb, Sn, Au, Pd, Pt, Rh, etc.) were determined at high resolution by ICP-MS. The ~26 m thick ice deposit from Scărişoara Cave, archives a detailed atmospheric deposition record of volatized metals, fly ashes and other particulates related to mining and smelting activities in the nearby mining fields. It could provide one of the first long records of anthropogenic pollution in Romania; the trends in most metals seem to reflect various pollution events related to historical episodes of mining and smelting of the region's widespread polymetallic ores. The new data could have immediate implications in better constraining the magnitude and extent of mining activities and anthropogenic impact in the well-known mining districts of Transylvania. This work is part of on-going efforts by the authors to explicitly document the anthropogenic impact and the long-term mining and metallurgical history of this region in a securely-dated, multi-proxy approach. Lead isotope studies are on-going and the new data are expected to provide an accurate evaluation of metal sources and clear insights into the developments of metallurgy in one of the oldest mining regions of Europe.

The crystal chemistry of the dumortierite group

Groat, L.A.[1*], Grew, E.S.[2], Evans, R.J.[1], Pieczka, A.[3] & Ercit, T.S.[4]
[1]Dept. of Earth and Ocean Sciences, University of British Columbia, Vancouver, Canada ([*]lgroat@eos.ubc.ca)
[2]Dept. of Earth Sciences, University of Maine, Orono, Maine, USA
[3]Dept. of Mineralogy, Petrography, and Geochemistry, AGH-University of Science and Technology, Krakow, Poland
[4]Canadian Museum of Nature, Research Division, Ottawa, Ontario, Canada

The dumortierite group comprises dumortierite [c. $(Al,\square)Al_6(BO_3)Si_3O_{13}(O,OH)_2$], magnesiodumortierite [c. $(Mg,\square)(Mg,Al)_6(BO_3)Si_3O_{13}(O,OH)_2$], and holtite [c. $(Al,Ta,\square,)Al_6(BO_3)(Si,Sb,As)_3O_{12}(O,OH,\square)_3$]. Dumortierite may contain up to several wt% of TiO_2, Fe_2O_3, MgO, Bi_2O_3, Sb_2O_3, As_2O_3, Ta_2O_5, Nb_2O_5. In holtite the last four constituents taken together exceed 30 wt.%, although none dominate their crystallographic site. Single-crystal X-ray refinements and FTIR results suggest[1] a general formula for holtite, $Al_{7-[5x+y+z]/3}(Ta,Nb)_x\square_{[2x+y+z]/3}BSi_{3-y}(Sb,As)_yO_{18-y-z}(OH)_z$, where x is the total number of pentavalent cations, y is the total amount of Sb + As, and $z \leq y$ is the total amount of OH. Holtite compositions tend to cluster into Sb-poor and Sb-rich varieties having the approximate general formulae, respectively, $Al_{5.83}(Ta,Nb)_{0.50}\square_{0.67}BSi_{2.50}(Sb,As)_{0.50}O_{17.00}(OH)_{0.50}$, and $Al_{5.92}(Ta,Nb)_{0.25}\square_{0.83}BSi_{2.00}(Sb,As)_{1.00}O_{16.00}(OH)_{1.00}$, with Ta + Nb content not correlated with Sb + As content, which is also true of dumortierite. The crystal structure refinements do not indicate a fundamental difference in cation ordering or anion composition that might serve as a criterion for recognizing the two holtite compositions as distinct species, or for that matter, for recognizing holtite as a distinct species from dumortierite. Moreover, new analyses of dumortierite showing up to 4.30 wt.% As_2O_3, 1.51 wt.% Sb_2O_3, and 3.94 wt.% Ta_2O_5 have blurred the compositional distinctions between dumortierite, Sb-poor holtite and Sb-rich holtite, although dumortierite tends to have As > Sb. Crystal structure refinements of dumortierite samples with moderate Sb, As and/or Ta contents show very high disorder at the channel Al1 and (As,Sb) sites, much more than is seen in holtite.

A more precise definition of holtite and its distinction from dumortierite awaits detailed study of both minerals, including experiments to determine the maximum amount of As and Sb that can be accommodated in the dumortierite-holtite structure. Such a definition will have to consider differences in diffraction behaviour (i.e. presence or absence of superstructure maxima), not just changes in bulk chemistry.

[1] Groat, L.A. et al. (2001) *Geol. Soc. Am. Abstracts with Programs*, **33(6)**, A-383. [2] Groat, L.A. et al. (2009) *Mineral. Mag.*, **73**, 1033-1050.

Boron-bearing magnesium minerals of the humite group: chemical, IR-spectroscopic and structural data

Gerasimova, E.I.[1,2*], Kononkova, N.N.[2], Pekov, E.I.[1,2] & Zubkova, N.V.[1]
[1]Dept. of Mineralogy, Lomonosov Moscow State University, Moscow, Russia ([*]ekgera@gmail.com)
[2]Vernadsky Inst. of Geochemistry and Analytical Chemistry of Russian Academy of Sciences, Moscow, Russia

Boron is a typical impurity in the magnesium minerals of the humite group. This fact is confirmed by IR-spectroscopy and electron microprobe data. We have studied 376 samples from 108 localities and in 63 of them the boron was found in quantities which are detected by this method (> 0.1 - 0.2 wt.%). The maximum content is 4.9 wt.% B_2O_3.

We found boron in each of the five magnesium members of the humite group but it is the most common for chondrodite. Distribution of boron in crystals of humite-group minerals is typically quite irregular, frequently spotted. Two bands in the IR-spectrum of humite from Vesuvius, Italy, are assigned as corresponding to B-O stretching vibrations. Their wavenumbers are 1271 and 1323 cm^{-1} (Fig. 1); the band near 1410 cm^{-1} in some spectra of different samples is also corresponding to B-O.

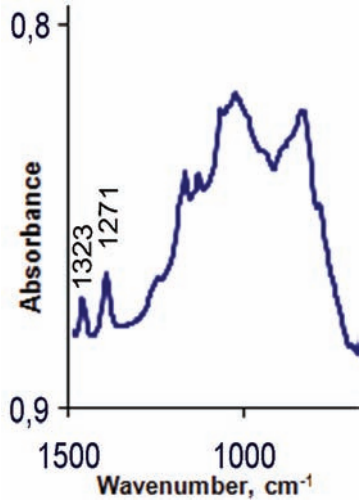

Fig. 1: IR spectrum of B-bearing humite from Vesuvius; wavenumbers of bands corresponding to B-O stretching vibrations are marked.

We assume that B occupies tetrahedral positions in humite-group minerals, together with Si. This assumption is based not only on stoichiometry (there is a Si deficiency in B-bearing samples), but also on the structural data. Refinement of the crystal structures of B-bearing humite and clinohumite showed that the tetrahedral positions are characterized by lower number of electrons than if they would be occupied only by Si. It allows to consider that B substitutes Si, according to the following scheme: Si + O <=> B + (F,OH), like in pertsevite, $Mg_2(B,Si)O_3(F,OH,O)$, a natural silicate with olivine-related structure [1].

Acknowledgements: This work was supported by Russian Foundation for Basic Research, grant No. 09-05-00143-a.

[1] Schreyer, W. et al. (2003) *Eur. J. Mineral.*, **15**, 1007-1018.

The hard-rock isotope geochemistry of boron: obstacles and future potential

Marschall. H.R.
Dept. of Earth Sciences, University of Bristol, UK
(*Horst.Marschall@bristol.ac.uk)

Boron is a moderately volatile, lithophile non-metal with a low atomic mass and two stable isotopes (^{10}B and ^{11}B). The $^{11}B/^{10}B$ ratio in terrestrial materials is ~4, but the high relative mass difference (~10 %) of the two isotopes has produced a variation of ~100 permil in nature. The large B isotopic fractionation at low temperatures has encouraged the use of the B stable isotope system for studies of processes acting on the Earth's surface and for the detection of material altered at low-*T* in the source of fluids, and in metamorphic and magmatic rocks.

More than 25 % of the Earth's B budget is stored in the continental crust. Upper crustal rocks are typically enriched in B, while B concentrations in the mantle are very low. Boron is highly mobile in hydrous fluids and in silicate melts. Hence, the great potential of B is as an isotopic tracer for subducted material in fluids, mud volcanoes, serpentinite diapirs and mantle-derived volcanic rocks sampled in volcanic arcs, ocean islands or mid-ocean ridges.

However, the very low abundance of B in mantle rocks and primitive volcanics confronts us with a major analytical problem. B isotope analyses of silicate materials at the trace abundance level are highly challenging with fractionation and contamination being the major obstacles. The B isotopic compositions of the Earth's major reservoirs (i.e., continental crust, primitive and depleted mantle, MORB) are still poorly constrained, despite a decade-long history of B isotope geochemistry. Inter-laboratory calibration studies in the past have demonstrated that B isotope work is still a long way from routine and discrepancies between various mass spectrometric and sample-preparation methods are still significant.

First-order B isotope fractionation is governed by the coordination of B to O in minerals, melts and fluids. Boron is either trigonally or tetrahedrally coordinated to oxygen, with a strongly covalent character of B-O bonds. Experimental studies have determined the temperature dependence of B isotopic fractionation between phases of different B coordination (e.g. silicate melt, hydrous fluid, minerals), and have quantified the systematic decrease of isotopic fractionation from ambient to magmatic temperatures. Fractionation between phases containing B in identical coordination to O has also been identified. The underlying mechanisms, however, are a matter of speculation and require further investigation.

Recently, the isotope geochemistry of lithium underwent a major reinterpretation, after experimental and natural evidence had demonstrated that Li isotopes are kinetically fractionated during diffusion, outstripping the effects of equilibrium fractionation. In the case of boron, kinetic fractionation by diffusion through melts and fluids is unlikely, as B forms large complexes with O that are expected to marginalise the mass difference effect of the two B isotopes during diffusion. Experiments on B diffusion have shown that diffusive B isotope fractionation is insignificant in silicate melts, but experiments and natural studies are required to quantify potential kinetic fractionation in melt-fluid-rock systems.

In addition to studies on modern subduction systems, the strong enrichment of B in the crust and the significant difference in B isotopic compositions between continental crust, modern seawater and the depleted mantle make B a potentially powerful tracer for the *secular* evolution of the ocean-crust-mantle system, once the analytical hurdles have been cleared.

Three- and four-coordinated boron minerals in pegmatites hosted in dolomitic marble in Central Madagascar; paragenesis and boron isotopes

Pezzotta, F.[1*], Dini, A.[2] & Tonarini, S.[2]
[1]Mineralogy Section, Natural History Museum, Milan, Italy
(*fpezzotta@yahoo.com)
[2]C.N.R., Istituto di Geoscienze e Georisorse, Pisa, Italy

A number of gem-bearing granitic pegmatites of Neo Proterozoic age, hosted in the dolomitic marbles of the Itremo Formation, in central Madagascar, are characterized by exceptionally abundant boron minerals. Minerals with B in 3-fold coordination with O (3BM), dumortierite and tourmaline group minerals (dravite-elbaite-liddicoatite), and danburite with B in 4-fold coordination (4BM), formed during all stages of crystallization of the pegmatitic veins. Dravite and dumortierite are confined to the most primitive rock units; elbaite-liddicoatite and danburite formed up until the latest stages of crystallization (miarolitic zone) of the veins. The central, most evolved zone of numerous pegmatites is characterized by a suite of borates that include the 4BM rhodizite-londonite solid solution, with local strong Rb enrichments, the 4BM behierite-schiavinatoite solid solution (Ta borate and Nb borate, respectively), and, occasionally, the 3BM hambergite.

The most typical of such B-enriched pegmatites are quartzofeldspathic in composition, with significant quantities of the above listed B-minerals and spodumene. Pollucite and numerous other rare accessory phases can occur in the core zone. The narrowest veins (mostly sub-vertical fissure-like veins, only a few centimetres in width) are occasionally composed only of tourmaline-group minerals and danburite, with or without quartz, and with rare accessory rhodizite and Ta-Nb oxides. The largest veins, occasionally up to several meters in width and of sub-horizontal attitude, can contain geochemically highly evolved core zones characterized by the occurrence of abundant Li-bearing micas. Such mica-bearing units can host giant cavities containing large crystals of numerous minerals including multicoloured liddicoatite and, occasionally, danburite and rare hambergite. Rhodizite, londonite, behierite, and schiavinatoite are totally absent in such mica-bearing units.

B isotopic studies were conducted on: (1) "tourmaline", danburite, and hambergite sampled from the border zone to the mica-rich, highly evolved, core zone of the famous and large Anjanabonoina pegmatite (AJB); (2) "tourmaline", danburite, rhodizite-londonite, and behierite-schiavinatoite sampled in the border zone and in the highly evolved core zone (mica free) of two representative pegmatites, in the Tetezantsio area (TTZ).

For primitive rock units, the results indicate for AJB: $\delta^{11}B_{dravite}$ 4.70‰ and $\delta^{11}B_{danburite}$ -0.83‰; and for TTZ: $\delta^{11}B_{dravite\text{-}elbaite}$ -2.33‰ and $\delta^{11}B_{danburite}$ -8.45‰.

For zoned crystals of "tourmaline" from AJB formed in pegmatitic units of intermediate geochemical evolution, $\delta^{11}B$ is homogeneous with values between 6.21 and 7.38‰. Cogenetic hambergite crystals have similar values ($\delta^{11}B$ 7.02‰).

For the most evolved rocks from AJB: $\delta^{11}B_{elbaite\text{-}schorl\ core}$ 6.94‰ and $\delta^{11}B_{liddicoatite\ rim}$ 14.72‰ and $\delta^{11}B_{danburite}$ from -0.26‰ to 8.03‰ $_{(rim)}$; and for TTZ: $\delta^{11}B_{elbaite\text{-}liddicoatite}$ 0.60‰, $\delta^{11}B_{danburite}$ -6.72‰, $\delta^{11}B_{rhodizite}$ -6.93‰, $\delta^{11}B_{behierite}$ -10.70‰.

These data indicate that cogenetic 3BM ("tourmaline", hambergite) and cogenetic 4BM (danburite, rhodizite, behierite) represent two distinct B isotopic populations, characterized by rather homogeneous values, with $\delta^{11}B$ of 4BM systematically shifted to lower values with respect to the cogenetic 3BM. Whatever was the nature of the crystallizing medium, the data reported above indicate that an isotopic fractionation process occurred in response of the distinct boron coordination in the two major minerals, "tourmaline" and danburite.

Boron isotopes in tourmaline of dravite–schorl series from granitic pegmatites of the Moldanubian Zone, Czech Republic

Míková, J.[1], Novák, M.[2*] & Janoušek, V.[1]
[1]Czech Geolological Survey, Prague, Czech Republic
[2]Dept. of Geological Sciences, Masaryk University, Brno, Czech Republic ([*]mnovak@sci.muni.cz)

Prismatic tourmaline sections cut perpendicular to c axis from three groups of granitic pegmatites distinct in mineralogy, geological setting and origin were examined using EMPA and SIMS. (i) Homogeneous Tur occurs in the simple mineral assemblage Kfs+Qtz+Ab±Bt of metaluminous, intragranitic, NYF pegmatites derived from the ultrapotassic, quartz syenitic–melagranitic Třebíč Pluton [1]. (ii) Tourmaline associated with the assemblage Kfs+Qtz+Ab+Ms±Crd, And, Bt was obtained from peraluminous, LCT pegmatites cutting the HT felsic granulites of the Bory Massif [2]. (iii) Heterogeneous Tur from the assemblage Kfs+Qtz+Ab+Ms±Crd, And is typical of peraluminous, anatectic pegmatites enclosed in migmatites surrounding the Bory Granulite Massif, where this mineral, in contrast to the other pegmatite occurrences, typically crystallized in pockets [2]. The δ^{11}B signatures of the individual pegmatite groups and crystals (Fig. 1) vary from highly homogeneous (most of the analyses from Třebíč Pluton, 2DB) to highly variable, even within single grains (8LAV, 1DB, 3HB). Isotopic zoning is commonly independent of the compositional variations in major and minor elements except for slightly heavier δ^{11}B in Ca, Ti-enriched domains [3] of the sample 3HB. The concentric zoning developed in some crystals (1DB, 8LAV, 3HB) is characterized by isotopically heavy rims (Fig. 1).

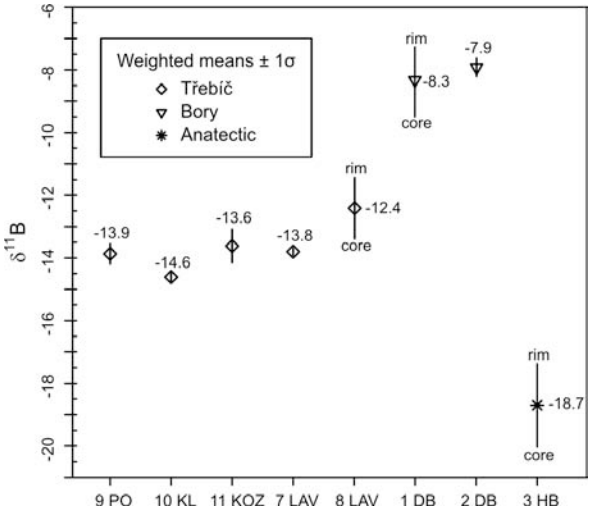

Fig. 1: Isotopic composition of tourmaline.

The homogeneous δ^{11}B signature of Tur from pegmatites of the Třebíč Pluton implies a closed-system evolution, perhaps as it is the only mineral incorporating B both in the pegmatites and the host syenite except for the sample 8LAV associated with rare Ms from pegmatite enclosed in leucocratic granite related to Třebíč Pluton. The heavier δ^{11}B signature of the Bory Tur requires a different source compared to the Třebíč pegmatites. The tourmaline from the anatectic pegmatite (3HB) differs strikingly from the other groups by its crystallization from fluid phase. Thus its δ^{11}B signature could have been controlled by abundant Ms, affecting the isotopic ratio of the co-existing fluid phase.

[1] Novák, M. et al. *Can. Mineral.*, submitted. [2] Novák, M. (2005) *Acta Mus. Moraviae, Sci. Geol.*, 3-72. [3] van Hinsberg, V.J. & Marschall, H.R. (2007) *Chem. Geol.*, **238**, 141-148.

Incorporation of fluorine in tourmaline: internal crystallographic vs. external environmental influences

Henry, D.J.[*] & Dutrow, B.L.
Dept. of Geology and Geophysics, Louisiana State University, Baton Rouge, Louisiana, USA ([*]glhenr@lsu.edu)

Tourmaline is a common mineral in a wide variety of rock types largely because it is the primary mineral host for boron in rocks, it can accommodate a large array of chemical constituents and it has an extreme stability range. The manner in which chemical constituents are incorporated into the tourmaline structure depends on external influences such as temperature, pressure, local mineral assemblage and fluid composition. It also depends on internal influences such as crystallographic and surface energy constraints. The general systematics of F contents in natural tourmaline are particularly intriguing and the relative importance of the crystallographic constraints and the petrologic environment in which the tourmaline forms make an interesting case study of these dynamics.

A general formula for tourmaline is $XY_3Z_6(T6O_{18})(BO_3)_3V_3W$; with the most common site occupancies being: X = Ca, Na, K, $^{X}\square$ (vacancy); Y = Li, Mg, Fe^{2+}, Mn^{2+}, Al, Cr^{3+}, Fe^{3+}; Z = Al, Mg, Fe^{3+}, Cr^{3+}; T = Si, Al; B = B; V = OH, O; W = OH, F, O. Of particular importance is that F occurs at a single anion site, the W site. Incorporation of F in this site is influenced by the occupancy (total charge) of the X and the Y sites. The X-site is generally occupied by cations of variable charge (Na^{1+} or Ca^{2+}) and/or is vacant (zero charge). There are three Y-site cations that can have charges of +1, +2, +3 and +4. However, the local bond valence arrangements are most commonly +6 (e.g. Mg_3) or +7 (e.g. Mg_2Al). Because of local bonding of the W site anion to three neighboring Y-site cations and an X-site cation, the charge of the X-site and the Y site cationic affects the F occupancy in the W site. Natural tourmaline data verifies the threshold charge level at the X-site at which significant amounts of F are supported. A summary of >900 tourmaline analyses from different tourmaline environments illustrates that if the X-site charge is <0.5 little F is present, but at higher X-site charge F ranges from 0-1.0 apfu (Fig. 1).

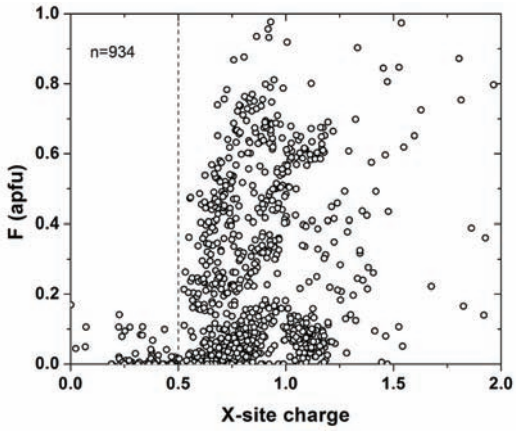

Fig. 1: Tourmaline data from multiple rock types.

Petrologic factors superimpose local environmental influences on F concentrations. Features such as F-saturating phases (e.g. fluorite), local mineral assemblages and fractionating fluids control the amount of F that can be made available to and incorporate in tourmaline.

Tourmaline: from short-range to long-range arrangements

Bosi, F.
Dept. of Earth Sciences, Sapienza University of Rome, Italy
(ferdinando.bosi@uniroma1.it)

Tourmaline is a complex borocyclosilicate that occurs in a wide variety of igneous, metamorphic and sedimentary environments. The general formula is $XY_3Z_6(T_6O_{18})(BO_3)_3V_3W$. The stability of tourmaline has been investigated to understand the effect of long-range disordered distributions of Al, Mg, Fe^{3+} and Fe^{2+} over the *Y* and *Z* non-equivalent octahedral sites, coupled with Mg and Fe^{2+} occurring at *Z* [1], as well as to the short-range occupancies around the *V* and *W* anion-sites. In this regard, only local arrangements involving Mg and Al were examined in Li-free tourmaline [2].

Extension of the local bond-valence approach from Mg-Al to Fe^{2+}-Fe^{3+} short-range arrangements has been explored. Stable local configurations involving R^{3+} cations (Al, Fe^{3+}) and R^{2+} cations (Mg, Fe^{2+}) around *W* and *V* have been determined as a result of short-range bond-valence requirements. The coupling of these stable local arrangements determines the formation of larger clusters of octahedra of general form $[WY_3VZ_2]$, Fig. 1, which can have either ordered or disordered distributions of R^{3+} and R^{2+} cations.

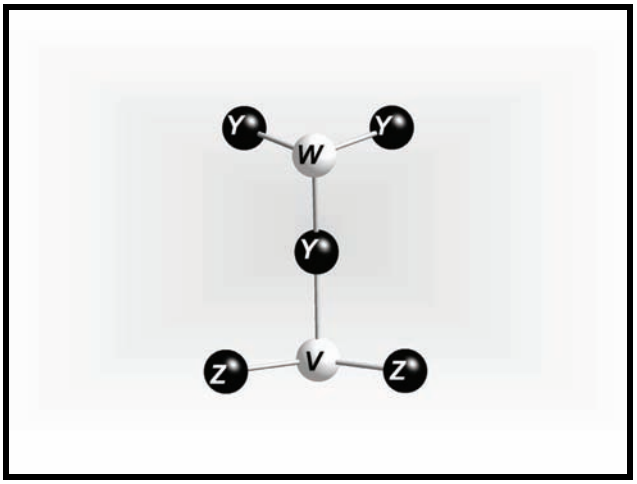

Fig. 1: Schematic view of part of the tourmaline structure around the *W* and *V* anions. Cations are shown as black circles, anions are shown as white circles.

These clusters are related through four different relations:

$$2\ {}^{Y}R^{2+} + {}^{Z}R^{3+} + {}^{W}(OH,F)^{1-} \rightleftarrows 2\ {}^{Y}R^{3+} + {}^{Z}R^{2+} + {}^{W}O^{2-}$$

$$2\ {}^{Y}R^{2+} + 2\ {}^{Z}R^{3+} + {}^{W}(OH,F)^{1-} \rightleftarrows 2\ {}^{Y}R^{3+} + 2\ {}^{Z}R^{2+} + {}^{W}O^{2-}$$

$$^{Y}R^{2+} + 2\ {}^{Z}R^{3+} \rightleftarrows {}^{Y}R^{3+} + 2\ {}^{Z}R^{2+}$$

$$^{Y}R^{2+} + {}^{Z}R^{3+} \rightleftarrows {}^{Y}R^{3+} + {}^{Z}R^{2+}$$

Such relations describe the occurrence of both R^{3+} cations at the octahedrally coordinated *Y* site and R^{2+} cations at the octahedrally coordinated *Z* site of tourmaline, and lead to long-range ordered or disordered arrangements.

In nature disordered configurations are the rule owing to long-range requirements of geometrical fit and minimization of strain.

[1] Bosi, F. & Lucchesi, S. (2007) *Am. Mineral.*, **92**, 1050-1063.
[2] Hawthorne, F.C. (2002) *Can. Mineral.*, **40**, 789-797.

The correct formula for Mg- and Fe^{3+}-bearing tourmaline: the influence of the <*T*-O> distance on the <*Z*-O> bond length

Ertl, A.[1*], Hughes, J.M.[2] & Tillmanns, E.[1]
[1]Institut für Mineralogie und Kristallographie, Universität Wien, Vienna, Austria ([*]andreas.ertl@a1.net)
[2]Dept. of Geology, University of Vermont, Burlington, Vermont, USA

The general chemical formula of the tourmaline-group minerals is $XY_3Z_6(BO_3)_3[T_6O_{18}]V_3W$. Several efforts have been made in the past to address the Mg-Al disordering between the *Y* and *Z* sites in the tourmaline atomic arrangement (e.g., [1]). It has been demonstrated that Mg and Fe^{3+} not only occupy the *Y* site, but also the *Z* site in tourmaline. However, in many cases it is not possible to assign the cations in a way that the average ionic radius of the *Y*-site occupants fits the <*Y*-O> bond length, while simultaneously the average ionic radius of the *Z*-site occupants fits the <*Z*-O> bond length. However, with Mg-rich tourmaline samples from the Austroalpine basements units, Styria, Austria, we were very successful in developing accurate formulae [2]. We attribute the difference to the varying *T*-site occupancy in many tourmalines compared to the samples from the Austroalpine basement units and suggest a relationship between *T*-site occupancy and the <*Z*-O> bond length. Whereas all tourmalines from the Austroalpine basement units show a <*T*-O> distance of 1.620 Å, the recently investigated tourmalines from the Moldanubicum have <*T*-O> distances varying from 1.614 to 1.623 Å. This results from mixed occupancy among Si, Al and B at the *T* site in these tourmalines, whereas in the samples from the Austroalpine basements unit the *T* site is exclusively occupied by Si [2]. Hence, we checked the possibility of an influence of the <*T*-O> bond length on the <*Z*-O> bond length. To be sure that the *Z* site is exclusively occupied by Al we used only samples of the elbaite-olenite-rossmanite series, without Mg and Fe^{3+} (e.g., [3,4]). Indeed, we found a positive correlation between the <*T*-O> bond length and the <*Z*-O> bond length in tourmalines where the *Z* site is only occupied by Al (R^2 = 0.778). This is not unexpected because the TO_4 tetrahedron is connected through two oxygens (O6 and O7) to the ZO_6 octahedron. The influence of the <*T*-O> bond length on the <*Z*-O> distance (for a *Z* site which is only occupied by Al) can now be calculated by using the following formula (1): $\langle Z\text{-O}\rangle_{Al} = (\langle T\text{-O}\rangle_{meas.} + 2.3651\ Å)/2.0885$. Then the <*Z*-O> bond length (corrected for the inductive effect of the varying <*T*-O> bond length) can be calculated. The <*Z*-O> bond length was calculated for a *T* site only occupied with Si by using the following formula (2): $\langle Z\text{-O}\rangle_{calc.} = \langle Z\text{-O}\rangle_{meas.} + 1.9079\ Å - \langle Z\text{-O}\rangle_{Al}$. The value of 1.9079 Å was calculated for a <*Z*-O> distance for a Z site which is only occupied by Al while the *T* site is only occupied by Si by using the average value of the <*T*-O> bond lengths of tourmalines from the Austroalpine basement units [2], because of the high-quality structure refinements ($R1$ = 0.013-0.015). Finally the *Z*-site occupants can be assigned by optimising the relation between the <*Y*-O> bond length and the average ionic radius of the *Y*-site occupants and also the relation between the $\langle Z\text{-O}\rangle_{calc.}$ bond length and the average ionic radius of the *Z*-site occupants.

Acknowledgements: This work was supported by Österreichischer Fonds zur Förderung der wissenschaftlichen Forschung (FWF) project no. P20509.

[1] Ertl, A. et al. (2003) *Can. Mineral.*, **41**, 1363-1370. [2] Ertl, A. et al. (2010) *Mineral. Petrol.*, **99**, 89-104. [3] Ertl, A. et al. (2005) *Am. Mineral.*, **90**, 481-487. [4] Ertl, A. et al. (2010) *Am. Mineral.*, **95**, 24-40.

Crystal chemistry of Al-rich tourmalines from metamorphic and hydrothermal systems (Western Carpathians, Slovakia)

Bačík, P.*, Uher, P. & Ozdín, D.
Dept. of Mineralogy and Petrology, Comenius University, Bratislava, Slovak Republic (*bacikp@fns.uniba.sk)

Aluminium-rich tourmalines were found in several distinctive occurrences in Slovakia. A pebble of tourmalinite from Orlové has two generations of tourmaline – Al-rich prismatic tourmaline and Al-poor tourmaline matrix. The origin and genetic environment of the tourmalinite are unclear, but the influence of the hydrothermal processes is possible. Prismatic tourmaline contains 0.54-0.77 Na *pfu*, 0.65-1.27 Fe *pfu*, 0.75-1.63 Mg *pfu*, and 6.53-7.07 Al *pfu* [1]. Al-rich tourmaline occurs also in hydrothermally altered andesite near Detva. It contains up to 8.23 Al *pfu*, 0.52-0.57 *X*-site vacancies, 0.30-0.35 Ca *pfu*, but only up to 0.81 Mg *pfu* and 0.51 Fe *pfu*. Tourmaline in an Alpine-type vein from Limbach contains up to 6.69 Al *pfu*, 0.90 Fe *pfu*, 1.31 Mg *pfu*, and has moderate *X*-site vacancy (0.55-0.59). The degree of Al-Mg disorder was calculated from the lattice parameters of tourmaline [a = 15.9387(5) Å, c = 7.1636(4) Å] determined by powder XRD; 0.95-1.21 Al *pfu* and 0.46 Mg *pfu* might occupy the *Y* site and *Z* site, respectively [2]. Metamorphic Al-, Mg- and V-enriched (up to 3.3 wt. % V_2O_3, 0.40 V *pfu*) tourmaline with strong chemical zonality occurs in metachert from Chvojnica. The Al content attains 6.50 *apfu* in two Al-rich zones and it is lower than 6.25 *apfu* in other two zones (intermediate and rim2). Central Al-rich zone has more vacancies (0.42-0.46), Al-rich rim1 has dominant Na (0.45-0.52 *apfu*) in the *X* site. The content of Mg is quite uniform in all zones (2.15-1.38 *apfu*), V is concentrated in Al-poorer zones (up to 0.40 *apfu*) but it is also high in Al richer zones (0.21-0.29 *apfu*). The content of Fe is very low (up to 0.01 *apfu*). Mineral classification of Al-rich tourmalines is complicated by the Al-Mg disorder between the octahedral sites. If the Fe/(Fe+Mg) ratio in the *Y* site dividing schorl and dravite (or foitite and magnesiofoitite) varies between 0.4-0.6, there is no possibility to exactly determine the mineral species without structural refinement. Moreover, in Al-enriched disordered tourmalines, Al may be a major cation in the *Y* site; tourmaline that seems to be dravite as suggested by the total Al content may be olenite [2]. Another complication results from unknown valence of Fe and proportion of $(OH)^-$ vs. O^{2-} in *V* and *W* anion sites determined by EMPA. Tourmaline from Orlové may be classified as schorl as well as dravite or olenite, but there is a possibility that it belongs to a new mineral species ("*oxyschorl*" or "*oxydravite*"). The Al content of tourmaline from Detva suggests the composition of olenite, but the proportion of *X*-site vacancy and the Fe and Mg content may be closer to the composition of a new *X*-vacant oxytourmaline. Tourmaline from Limbach belongs to magnesiofoitite. *X*-site vacant tourmaline from Chvojnica is likely magnesiofoitite, but Na-dominant Al-rich tourmaline may belong to dravite as well as olenite if there were more Al-Mg disorder. The Al increase is likely controlled by the several distinct substitution mechanisms. Alkali-deficient substitution $^{X}\square AlNa_{-1}(Fe,Mg)_{-1}$ may explain the Al enrichment in *X*-site vacant tourmalines from Detva, Limbach and Chvojnica. However, there must be an influence of proton-deficient substitution $AlO(Fe,Mg)_{-1}(OH)_{-1}$ not only in alkali tourmalines from Orlové and Chvojnica, but also in *X*-site vacant tourmalines with Al content over 7.0 *apfu*.

Acknowledgement: This work was supported by the Slovak Research and Development Agency under the contract No. VVCE-0033-07.

[1] Bačík, P. et al. (2008) *Can. Mineral.*, **46**, 1117-1129. [2] Ertl, A. et al. (2008) *N. Jb. Miner. Abh.*, **184(3)**, 243-253.

Magnesiofoitite in the "*Equador Quartzites*", Borborema Pegmatite Province, Northeast Brazil

Beurlen, H.[1*], DaSilva, M.R.R.[1] & Soares, D.R.[2]
[1]Dept.of Geology, Univ. Federal de Pernambuco, Recife-PE, Brazil (*beurlen@terra.com.br)
[2]Federal Inst. Of Education,Science and Technology-IFPB, Campina Grande-PB, Brazil

Color banded gray, light green to pink quartzites of the Neoproterozoic Equador Formation in northeast Brazil are widely explored as dimension stones under the fashion name *"Zinwalita"* or *"Equador Quartzite"*. They present an easy cleavage along foliation planes with concentration of light green or pink micas. The quartzites host over hundred Li-Ta-Be bearing pegmatites and are the exclusive host rock of five granitic lithium rich pegmatites of the Borborema Pegmatite Province mined for the prized gem-quality elbaite known as "Paraíba Tourmaline". Within the foliation planes, the pink quartzites sporadically contain up to 10cm sized acicular to long prismatic pink to reddish brown tourmaline, occurring as isolated crystals or as radial arrangements of late metamorphic porphyroblastic origin. Tourmaline with the same color and habit is also observed with quartz in fractures perpendicular to the foliation, interpreted as late to post metamorphic metasomatic lateral segregations. Electron microprobe analyses allowed identify the pink micas as phlogopite. The tourmaline composition spreads around the center of the triangular classification diagram [1] according to the dominance of (Na+K), Ca or vacancy in the X-site of the tourmaline formula (Fig 1).

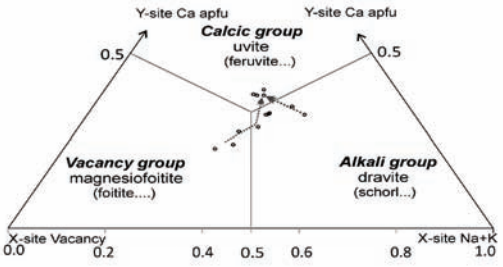

Fig. 1: Compositional variation in the X-site of zoned magnesiofoitite-dravite-uvite tourmaline in quartzites of the Equador Formation.

Taking into account the dominance of Mg in the Y-site [Mg/(Mg+Al+Fe) > 2.0/3.0 apfu)], the tourmaline plots either in the magnesiofoitite [2], uvite or dravite field of this diagram. In two zoned crystals the core had respectively magnesiofoitite or dravite compositions, both with uvite rims as indicated by the arrows in Fig. 1. This tourmaline seems unusual due to the fact that even small compositional variations in the X-site would lead to classify the mineral in three different tourmaline sub-groups and due to the composition very far from any of the corresponding end-member compositions (Table 1).

Table 1: Variation of X- and Y-site compositions of studied tourmaline

Magnesiofoitite	$^{X}[vac_{0.46}, Na_{0.31}, Ca_{0.22}]$ $^{Y}[Mg_{2.1}, Al_{0.4}, Fe_{0.3}, Li_{0.2}]$
Dravite	$^{X}[vac_{0.29,}\ Na_{0.44}, Ca_{0.34}]$ $^{Y}[Mg_{2.2}, Al_{0.3}, Fe_{0.4}, Li_{0.1}]$
Uvite	$^{X}[vac_{0.30}, Na_{0.30}, Ca_{0.40}]$ $^{Y}[Mg_{2.3}, Al_{0.1}, Fe_{0.4}, Li_{0.2}]$

The also uncommon Mg- and B-enrichment in quartzites is ascribed to volcano-exhalative syn-sedimentary activity.

[1] Hawthorne, F.C. & Henry, D.J. (1999) *Eur. J. Mineral.*, **11**, 201-215. [2] Hawthorne, F.C. et al. (1999) *Can. Mineral.*, **37,** 1439-1444.

Tourmalines in the Naipa Li-Cs-Ta granitic pegmatite group and adjacent host rock, Mozambique

Neiva, A.M.R.[1*] & Leal Gomes, C.A.A.[2]
[1]Dept. of Earth Sciences, University of Coimbra, Portugal (*neiva@dct.uc.pt)
[2]Dept. of Earth Sciences, University of Minho, Braga, Portugal

The Naipa granitic pegmatite group has been mined for tourmaline and beryl gems. The Naipa blue tourmaline gem crystals are significant for their sizes and quality. Electron-microprobe compositions of magmatic tourmalines from the Naipa Li-Cs-Ta pegmatite group, such as schorl and 'fluor-elbaite' from the inner intermediate zone and pockets (concentrations) in this zone, and 'fluor-elbaite' from core zones record a differentiation sequence. Progressively zoned magmatic tourmaline crystals from the inner intermediate zone contain green Fe-rich 'fluor-elbaite' outer and inner cores and a blue 'fluor-elbaite' rim, showing increases in Al_Y+Li content, Al/(Al+Fe) at the Y site, and X site vacancy together with decreases in Fe^{2+} and Na contents from core to rim. In pockets from the inner intermediate zone, the progressively zoned magmatic crystals have: a) a black schorl core and a black Fe-rich 'fluor-elbaite' rim; b) a bluish grey Fe-rich 'fluor-elbaite' core and a blue Fe-bearing 'fluor-elbaite' rim. Reversely zoned magmatic crystals also occur with a Naipa blue Fe-bearing 'fluor-elbaite' core and a bluish grey Fe-rich 'fluor-elbaite' rim showing increase in Fe^{2+} content and decrease in Al/(Al+Fe) at the Y site from core to rim.

The magmatic tourmaline crystals from the pegmatite core zones are up to 70x5 cm, reversely zoned and consist of a red 'fluor-elbaite' inner core, a colourless to light pink 'fluor-elbaite' outer core and a green or blue Fe-rich 'fluor-elbaite' rim, showing decreases in Al_Y+Li content, Al/(Al+Fe) at the Y site, and X site vacancy, together with increases in Fe^{2+} and Na contents from inner core to rim. Progressive zoning is attributed to fractional crystallization and reverse zoning is due to nucleation and growth of evolved cores and back-reaction of them with the more primitive bulk magma. In pockets of the pegmatite core zones, 'fluor-liddicoatite' is either mainly blue with blue or pink tips or is only pink, which is the richest in Ca. The magmatic tourmalines result from strong fractionation of an uncontaminated (Na, Al, Li, B)-rich pegmatite melt and 'fluor-liddicoatite' formed due to added Ca by late interaction with fluids derived from the wall rocks. The main substitution $3Fe^{2+} \leftrightarrows 1.5Al+1.5Li$ at the Y site corresponds to the fractionation schorl-elbaite trend. The substitution Na⇆□ at the X site also takes place in 'fluor-elbaite' and the substitution Ca for Na at the X site occurs in 'fluor-liddicoatite'.

In replacement units of the inner intermediate zone, individual zoned hydrothermal crystals consist of a green core and a pink rim, both of 'fluor-elbaite', showing increases in Al_Y+Li content and Al/(Al+Fe) at the Y site, together with decreases in Fe^{2+} and Mn contents from core to rim. The main substitutions are $3Fe^{2+} \leftrightarrows 1.5Al+1.5Li$ at the Y site and $(\square Al)(NaR)_{-1}$. Hydrothermal 'fluor-elbaite' has higher Al, Li contents and lower Fe^{2+} and Na contents than magmatic 'fluor-elbaite' from the inner intermediate zone and pockets.

Hydrothermal 'fluor-dravite' from metasomatized chlorite phyllite adjacent to the granitic pegmatite group resulted from mixing of magmatic-hydrothermal fluids carrying Na, Al, Li, F and B with a meteoric fluid that interacted with this Fe-Mg-bearing pelitic country rock. Fe⇆Mg is the main substitution in this tourmaline.

Reexamination of Mg-Li tourmalines from the elbaite pegmatite Bližná I, Czech Republic

Cempírek, J.[1*] & Novák, M.[2]
[1]Dept. of Mineralogy and Petrography, Moravian Museum, Brno, Czech Republic (*jcempirek@mzm.cz)
[2]Dept. of Geological Sciences, Masaryk University, Brno, Czech Republic

Tourmaline of elbaite-dravite solid solution is extremely rare due to the strong fractionation of Li from Mg in geological environments. To date, it has only been reported from elbaite-subtype pegmatite Bližná I, which intrudes dolomite-calcite marble [1]. Part of the pegmatite exhibits in-situ fluid exchange with the surrounding marble, resulting in an Ca,Mg-contaminated pegmatite border zone and a B-enriched exocontact of the pegmatite. The tourmaline composition in the pegmatite varies in a range typical for elbaite-subtype pegmatites [2], i.e. from Ca-rich schorl-elbaite to Mn-rich elbaite and Mn-rich elbaite-liddicoatite. The tourmaline from contaminated pegmatite ranges from Na-rich uvite and Ca-rich schorl-elbaite-dravite to Mg-bearing Ca-rich elbaite and Mn-rich liddicoatite-elbaite. The tourmaline from the exocontact ranges from Na-rich uvite to dravite-elbaite and liddicoatite-elbaite [1,3].

Preliminary study of the crystal structure of the various types of tourmaline started with a sample from the contaminated zone. The dark brown core of a zoned tourmaline with composition $^{X}(Na_{0.52}Ca_{0.34}\square_{0.13})$ $^{Y,Z}(Li_{0.32}Mg_{2.39}Fe_{0.32}Mn_{0.06}Al_{5.83}Ti_{0.02})$ Si_6 $(BO_3)_3$ $(OH_{3.8}F_{0.2})$ has a = 15.946(2) Å, and c = 7.1977(14) Å. Its average <T-O> is 1.620 Å and the T-site is fully occupied by Si. The refined occupancy of the Z-site and the average <Z-O> = 1.927 Å shows that it is partially occupied by Mg (~ 0.6 *apfu*) and that Mg and Al are significantly disordered between Z and Y sites. The refined formula of the tourmaline is $^{X}(Na_{0.52}Ca_{0.34}\square_{0.13})$ $^{Y}(Li_{0.32}Mg_{1.83}Fe_{0.32}Mn_{0.06}Al_{0.43})$ $(Mg_{0.60}$ $Al_{5.40})$ Si_6 $(BO_3)_3$ $(OH_{3.8}F_{0.2})$ and it represents a solid solution dominated by dravite, liddicoatite and feruvite.

The light brown crystal rim shows significantly different composition $^{X}(Na_{0.44}Ca_{0.43}\square_{0.12})$ $^{Y,Z}(Li_{1.72}Mg_{0.28}Fe_{0.08}Mn_{0.11}$ $Al_{6.71}Ti_{0.11})$ Si_6 $(BO_3)_3$ $(OH_{3.8}F_{0.68})$ and has a = 15.872(2) Å, c = 7.1203(14) Å. Its average <T-O> is 1.619 Å, which implies that the T-site is fully occupied by Si or contains only a very small amount of tetrahedral B. The refined occupancy of the Z-site and the average <Z-O> = 1.907 Å suggest that Al is dominant in the site, with only minor Mg (~ 0.01 *apfu*). The refined formula of the tourmaline is $^{X}(Na_{0.44}Ca_{0.43}\square_{0.12})$ $^{Y}(Li_{1.72}Mg_{0.18}Fe_{0.08}Mn_{0.11}$ $Al_{0.81}Ti_{0.11})$ $(Al_{5.98}$ $Mg_{0.02})$ Si_6 $(BO_3)_3$ $(OH_{3.8}F_{0.68})$; it represents a solid solution of elbaite, liddicoatite and dravite.

The crystal chemistry of tourmalines from the Bližná I pegmatite reflect the processes of fractionation/contamination in a system enriched in Li, Mn, Ca and Mg. Magnesium played a significantly greater role during crystallization of the Bližná I pegmatite than during crystallization of other highly fractionated complex pegmatites. Further data will provide valuable information on solid solutions and range of possible immiscibility among the tourmaline-group minerals in this unusual system.

[1] Novák, M. et al. (1999) *Eur. J. Mineral.*, **11,** 557-568. [2] Novák, M. & Povondra, P. (1995) *Mineral. Petrol.*, **55,** 159-176. [3] Novák, M. (1998) *J. Czech Geol. Soc.*, **43,** 24-30.

Werdingite from SW Norway: the role of iron in a borosilicate with a mullite-type structure

Grew, E.S.[1*], Armbruster, T.[2], Lazic, B.[2], Yates, M.G.[1], Medenbach, O.[3] & Huijsmans, J.P.P.[4]
[1]Dept. of Earth Sciences, University of Maine, Orono, Maine, USA ([*]esgrew@maine.edu)
[2]Mineralogical Crystallography Institute of Geological Sciences, University of Bern, Switzerland
[3]Institut für Geologie, Mineralogie und Geophysik – Mineralogie, Ruhr-Universität Bochum, Germany
[4]Shell Global Solutions International B.V., Amsterdam, The Netherlands

Werdingite from a pegmatite on Almgjotheii in the aureole of the Rogaland anorthosite complex, Norway was reported as the "Fe-dominant analogue" because of its high total Fe (to 8.00 wt% as FeO) and atomic Fe/(Mg + Fe) ratio (X_{Fe} to 0.75) [1,2]. A crystal of composition $Fe_{1.27}Mg_{0.48}Al_{14.44}Be_{0.10}B_{4.18}Si_{3.61}O_{37}$ (Be from [2], B by EMPA) from sample HE138B has α = 1.619(2), β = 1.652(2), γ = 1.658(2), $2V_x$ = 43(2)°, space group *P*-1, *a* = 7.9696(2) Å, *b* = 8.1559(3) Å, *c* = 11.3607(3) Å, α = 110.364(1)°, β = 110.881(1)°, γ = 84.670(2)°, *V* = 646.41 Å^3, calc. ρ = 3.12 g/cm^3, *Z* = 1. Comparison with literature data [2-5] shows refractive indices increase with increasing X_{Fe}, but cell *V* does not. A crystal structure refinement (R_1 = 0.057) gave 1.21 Fe occupying the one tetrahedral and two 5-coordinated sites present in type werdingite [4-5] plus a new, largely vacant tetrahedral site, FeX (Table 1).

Table 1: Iron site occupancies in HE138B and type werdingite

Site	Fe(1)	Fe (2)	Al(1)	Al (2)	Mg(1)	Mg (2)
Al(4)1	0.12	0.21	0.75	0.79	0.00	0.00
Al(5)1	0.04	0.00	0.96	1.00	0.00	0.00
Mg(5)1	0.35	0.16	0.41	0.00	0.24*	0.84
FeX	0.09	羊	0.00	羊	0.00	羊

(1) HE138B [this study], (2) Type [5]. *Fixed in refinement

Fe is not dominant at any site. As we have no data on Fe valence, we cannot determine whether divalent cations are dominant at Mg(5)1, i.e., we cannot show that HE138B werdingite is a Fe-dominant analogue of type werdingite.

Werdingite in HE138B is intergrown with boralsilite, ideally $Al_{16}B_6Si_2O_{37}$, also related to mullite. B varies inversely with Si in a single trend for both minerals (per 37 O): 5.91-5.11 B and 1.95-2.56 Si in boralsilite [6] and 4.76-4.02 B and 3.05-3.74 Si in werdingite, whereas Al and (Mg + Fe) show no trend with Si in werdingite. Charge balance for B → Si substitution could be achieved by oxidation of Fe rather than loss of O in werdingite. Subparallel prisms of werdingite and boralsilite have a ladder-like appearance due to plates of one mineral oriented perpendicular to prism length of the other [2,7], i.e., perpendicular to the mullite-type chains of Al octahedra. Matching the two structures in this plane is possible: the pseudo-tetragonal cell perpendicular to the mullite-type chains is 7.65 x 7.42 Å in werdingite vs. 7.54 x 7.38 Å in boralsilite [8]. Moreover, the two structures have in common Si_2O_7 dimers and 5-coordinated sites. Thus, our data are consistent with the suggestion [7] of limited solid solution between the two minerals with subsequent exsolution of one from the other.

[1] Huijsmans, J.P.P. et al. (1982) *N. Jahrb. Miner. Abh.*, **143**, 249-261. [2] Grew, E.S. et al. (1998*) Can. Mineral.*, **36**, 399-414. [3] Werding, G. & Schreyer, W. (1992) *Eur. J. Mineral.*, **4**, 193-207. [4] Moore, J.M. et al. (1990) *Am. Mineral.*, **75**, 415-420. [5] Niven, M.L. et al. (1991) *Am. Mineral.*, **76**, 246-256. [6] Grew, E.S. et al. (2008) *Am. Mineral.*, **93**, 283-299. [7] Grew, E.S. et al. (1998) *Am. Mineral.*, **83**, 638-651. [8] Peacor, D.R. et al. (1999) *Am. Mineral.*, **84**, 1152-1161.

A new boron feldspar, $KBSi_3O_8$: synthesis, crystal structure and thermal behaviour

Krzhizhanovskaya, M.G.[1*], Bubnova, R.S.[2], Depmeier, W.[3], Smirnova, D.A.[2], Rahmoun, N.S.[3] & Filatov, S.K.[1]
[1]Dept. of Crystallography, St. Petersburg State University, St. Petersburg, Russia ([*]krzhizhanovskaya@mail.ru)
[2]Institute of Silicate Chemistry RAS, St. Petersburg, Russia
[3]Dept. of Earth Sciences, University of Kiel, Germany

Up to now in the $K_2O–B_2O_3–SiO_2$ system two synthetic compounds were known: boroleucite $KBSi_2O_6$ [1] and borodanburite $KBSi_3O_8$ [2], prepared by cooling of stoichiometric melt and hydrothermal synthesis, respectively. Also there are the structural data on naturally occurring lisitsynite, $KBSi_2O_6$ [3], considered as a polymorph of boroleucite. In present work the results of hydrothermal synthesis experiments in $K_2O–B_2O_3–SiO_2$ system are discussed. Single crystals as well as powder sample of $KBSi_3O_8$ feldspar-type phase were obtained at 180 and 550°C. Both single crystals and powder were obtained always mixed with quartz.

Crystal structure of $KBSi_3O_8$ was determined by direct methods: it is monoclinic *C*2/*m*, *a*=8.4377(8), *b*=12.4152(11), *c*=6.8769(7) Å, *β*=116.133(7)°, *V*=646.75(11) Å^3, d_{calc}=2.693 g/cm^3. The structure is identical to that of monoclinic feldspar with a difference only in size and density of tetrahedral framework due to the presence of boron instead of alumina. The distribution of Si and B over tetrahedra is partially ordered with one Si-rich tetrahedra (<T–O>=1.60 Å) and 2nd one occupied by Si and B almost in equal proportion (<T–O>=1.55 Å).

According to the high temperature X-ray diffraction study the expansion of structure is highly anisotropical: α_1=19, α_2=2, α_3=5×10^{-6} °C^{-1}, ∠(α_3c)=9°. The direction of maximal expansion approximately coincides with the short diagonal of *ac* parallelogram. The expansion is similar to that of intermediate monoclinic member of Na-K feldspar series (Or_{38}) described in [4] with the mean linear expansion coefficient 24 and 26×10^{-6} °C^{-1} for alumino- and borosilicate correspondingly.

$KBSi_3O_8$ obtained by hydrothermal synthesis is stable up to 600°C. Above it decomposes by solid state reaction with the boroleucite $KBSi_2O_6$ phase formation.

Acknowledgements: The work was supported by Russian Foundation for Basic Research (10-03-00732-a).

[1] Ihara, M. & Kamei, F. (1980) *Yogyo-Kyokai-Shi*, **88**, 32-35. [2] Kimata, M. (1993) *Mineral. Mag.*, **57**, 157-164. [3] Sokolova, E.V. et al. (2001) *Can. Mineral.*, **39**, 159-169. [4] Henderson, C.M.B. (1979) *Contrib. Mineral. Petrol.*, **70**, 71-79.

Multi-disciplinary investigation of datolite from basalts in the Northern Apennines ophiolites (Italy): genetic implications

Zaccarini, F.[1,2*], Garuti, G.[1,2], Scacchetti, M.[2], Bartoli, O.[2] & Bakker, R.J.[1]
[1]Dept. of Applied Geosciences and Geophysics, University of Leoben, Austria ([*]federica.zaccarini@unileoben.ac.at)
[2]Society of Natural Sciences of Reggio Emilia, Italy

A multi-disciplinary investigation based on fluid inclusion petrography and microthermometry, X-ray diffraction, electron microprobe and inductively coupled plasma mass spectrometry (ICP-MS) and Raman spectroscopy, was carried out on datolite, ideally $CaBSiO_4(OH)$, from hydrothermal veins crosscutting pillow basalt in ten different localities of the Northern Apennine ophiolites (Italy). Two-phase (L + V) fluid inclusions texturally identifiable as primary and secondary were observed, yielding average homogenization-temperatures of 236°C and 173°C respectively. Fluid-inclusion cooling data yield calculated salinity in the range of 10-16 wt% NaCl equivalents, thus relatively higher compared with seawater. Results of electron microprobe analysis indicate that probably B-OH is the predominant substitution and not B-Si. Chlorine and fluorine were also analyzed but their concentration was below detection limit. Bulk analyses of datolite crystals show REE contents below chondritic, except for La and Ce. With respect to host rock, datolite is occasionally enriched in La, Rb, Cs, Be, and shows relatively high contents of chalcophile elements (Cu, Zn, Pb, Ni) when occurring in contact with sulfide mineralized basalt. Fluid inclusion results are compatible with those reported for fluids formed under diagenetic conditions rather than in the seafloor hydrothermal systems and/or emanating from magmas. Compositional data of datolite indicate that the mineral is able to concentrate only a few elements such as La, Rb, Cs, Be, Ni, Cu, Zn and Pb. The lithophile elements can be hosted in the datolite lattice, whereas the chalcophile metals and Ni are probably carried in sub-microscopic inclusions

Tourmaline nodules – 3D insight into late-stage boron separation from granite melt

Balen, D.* & Petrinec, Z.
Faculty of Science, University of Zagreb, Croatia
(*drbalen@geol.pmf.hr)

Spatial distribution, shape and internal structure of tourmaline nodules found in the peripheral parts of the Cretaceous Moslavačka Gora (Croatia) peraluminous granite pluton [1] have been visualized and reconstructed using BLOB3D software [2]. Data acquisition included serial cutting and lapping i.e. serial sectioning tomography. The "data brick" obtained from investigated granite consisted of a series of grayscale images with physical resolution of 3.5 mm (cutting) or 0.35 mm (lapping) between individual slices.

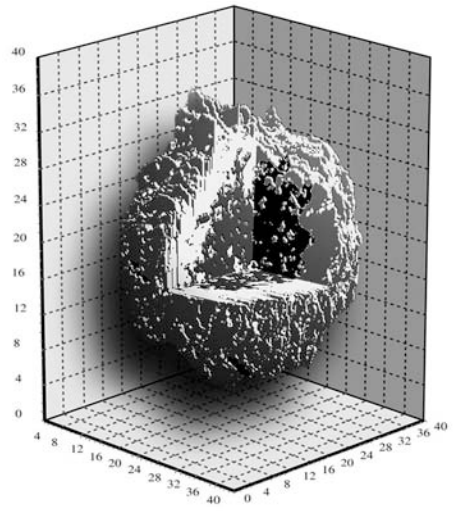

Fig. 1: 3D reconstruction of tourmaline nodule displaying a complex internal structure with separated volumes pertaining to the nodule's core and envelope (halo). Data obtained by serial lapping. Scale in mm.

The origin of tourmaline nodules and their peculiar textures has been related to the separation of a late-stage boron-rich volatile fluid phase from the granite magma [1]. Based on the field, mineralogical and textural observations, it is evident that tourmaline nodules formed during the final stage of granite evolution, when an undersaturated granite magma intruded shallow crustal horizons, becoming saturated and exsolving the fluid phase from the residual melt in the form of buoyant bubbles or pockets. Immiscibility of aluminosilicate and water-rich melts seems like a plausible mechanism which could have produced such spherical segregations. It also produced adequate concentrations of elements essential for the formation of the tourmaline nodules, especially boron, a crucial component enabling the physical formation of bubbles or pockets, followed by tourmaline crystallisation. Tourmaline nodules (usually 1 to 10 cm in diameter) that formed from these bubbles show a complex texture (Fig. 1) comprising two clearly distinct units: tourmaline-bearing core and leucocratic envelope (halo). The core, a spherical aggregate of tourmaline crystals, consists of dravite-enriched (Fe# 0.43-0.58) and slightly Na-deficient tourmaline, together with quartz + albite + K-feldspar ± muscovite. The nodule's halo, consisting of quartz + feldspar + muscovite, represents an integral part of the nodule and envelopes the tourmaline-bearing core.

[1] Balen, D. & Broska, I. (in press) *Geol. Soc. London Spec. Publ.* [2] Ketcham, R.A. (2005) *Geosphere*, **1**, 32-41.

MAS NMR measurements and *ab initio* calculations of the ^{29}Si chemical shifts in dumortierite

Evans, R.J.[1*], Fyfe, C.A.[2], Groat, L.A.[1], Lam, A.E.[2] & Grew, E.S.[3]
[1]Dept. of Earth and Ocean Sciences, University of British Columbia, Vancouver, British Columbia, Canada
(*rjamesevans@gmail.com)
[2]Dept. of Chemistry, University of British Columbia, Vancouver, British Columbia, Canada
[3]Dept. of Earth Sciences, University of Maine, Orono, Maine, USA

Dumortierite, $(Al,\square)Al_6Si_3BO_{16}(O,OH,\square)_2$, is the second most abundant aluminum borosilicate after tourmaline, with a complex structure featuring a face-sharing chain of Al octahedra connected to a pseudo-hexagonal framework of edge-sharing Al octahedra via isolated Si tetrahedra. A sample of dark blue dumortierite from Madagascar, D34, was characterized by single crystal X-ray diffraction (XRD), electron microprobe analysis (EMPA), and magic angle spinning (MAS) nuclear magnetic resonance (NMR). The structure was refined to R = 1.69% in space group *Pnma* with unit cell dimensions a = 4.6882(1) Å, b = 11.7924(2) Å, c = 20.1856(3) Å. Structure refinements indicate 0.26 vacancies per formula unit (pfu) at the face-sharing octahedral M1 site, with 0.42 octahedral vacancies pfu total. EMPA indicates approximately 0.07 Mg, 0.03 Fe^{3+} and 0.03 Ti pfu, and high Al and low Si total concentrations suggest that some ^{IV}Al is present at the Si sites. Fourier transform infrared spectroscopy confirmed the presence of structural OH groups, which are believed to coordinate the Si sites when the M1 site is vacant.

Although there are only two crystallographically distinct Si sites, Si1 and Si2, in 1:2 ratio, the ^{29}Si MAS NMR spectrum of D34 contains five major peaks at –96.0, –94.2, –92.8, –90.6 and –88.2 ppm, with the most intense peaks at –96.0 and –94.2 ppm. The NMR chemical shift is highly sensitive to the local environment of the ^{29}Si nucleus, and so the various chemical substitutions and vacancies at the M1 site give rise to different chemical shifts at the nearby Si sites. Ab initio electronic structure calculations were performed on model clusters using density functional theory (DFT) with the B3LYP functional to identify the structural environments responsible for those peaks seen in the spectrum. Model clusters were constructed using the refined structure as a starting point, consisting of first and second shell of atoms around Si, with the third shell replaced by H atoms. NMR chemical shifts were calculated relative to tetramethylsilane using the gauge-including atomic orbital method (GIAO) with the 6-311++g(2d,p) basis set. Positions of the Si and M1 cations and their coordinating O and H atoms were optimized with the 6-31g* basis set when substituting at the M1 site.

Azoproite crystals with nanorod inclusions of baddeleyite

Galuskin, E.V.[1*], Kusz, J.[2], Starikova, A.E.[3] & Pertsev, N.N.[4]
[1]Faculty of Earth Sciences, University of Silesia, Katowice Poland (*evgeny.galuskin@us.edu.pl)
[2]August Chełkowski Institute of Physics, University of Silesia, Katowice, Poland
[3]Institute of Geology and Mineralogy SB RAS, Novosibirsk, Russia
[4]Institute of Geology of Ore Deposits, Petrography, Mineralogy and Geochemistry (IGEM) RAS, Moscow, Russia

Azoproite $Mg_2(Mg_{0.5}Ti^{4+}_{0.5})BO_5$, which is isostructural with ludwigite, occurs with Zr-oxides (baddeleyite, calzirtite, tazheranite), spinel, geikielite, forsterite, and diopside in periclase (brucite) calciphyre in the aureole of the Tazheran Massif (Baikal area, Russia) [1]. Association with Zr-oxides and the similar ionic radii of Zr (0.72 Å) and Sn (0.69 Å), which is a characteristic impurity in orthorhombic borates of the ludwigite-vonsenite series $(Mg^{2+},Fe^{2+})_2Fe^{3+}BO_5$ [2], suggest that Zr could be incorporated in azoproite, but none yet has been reported [2]. Only the structure of Ti-ludwigite from Tazheran has been refined [3]. Based on systematic studies of crystals collected at the type locality [1] during 2006-2009, we selected the following compositions for single-crystal investigations: (1) crystals with the highest contents (= 65-67%) of the azoproite end member $(Mg,Fe^{2+})_2(Mg_{0.5}Ti^{4+}_{0.5})BO_5$, (2) aluminian azoproite with ca. 34% of the $(Mg,Fe^{2+})_2AlBO_5$ end member, 3) titanian ludwigite with ca. 37% of the azoproite end-member. Structure refinement of one crystal gave the following formula (×2) $^{M1}Mg_{0.99}{}^{M2}(Mg_{0.77}Fe^{3+}_{0.23})^{M3}Mg_{1.99}{}^{M4}(Mg_{0.58}Ti^{4+}_{0.65}Fe^{2+}_{0.32}Al_{0.28}Fe^{3+}_{0.15}Zr_{0.02})(BO_{4.99})_2$ in which site occupancies were determined in light of inter-atomic distance data for end-member borates [4]. Azoproite from Tazheran contains ca. 1 wt.% ZrO_2 and abundant monocrystal nanorod inclusions of baddeleyite less than 1 μm thick and up to 1-2 mm long (Fig. 1).

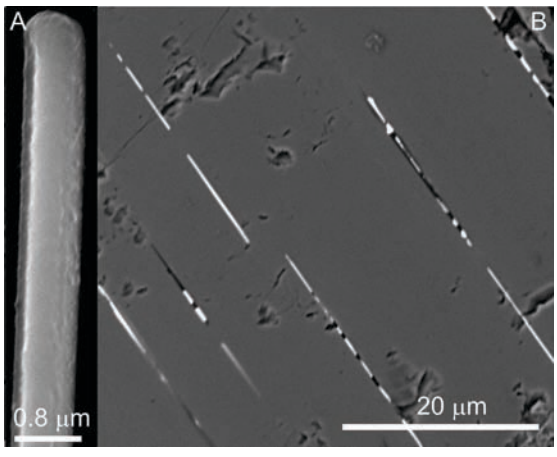

Fig. 1: Nanorod baddeleyite crystals are elongated along the Y axis (A), which in turn is sub-parallel to the Z axis of azoproite host crystals (B).

Growth of nanorod baddeleyite crystals results from the exsolution of the high-temperature compound $(Mg,Fe^{2+},Fe^{3+},)_2(Mg,Ti^{4+},Fe^{2+},Fe^{3+},Al,Zr)BO_5$. The primary solid solution is calculated to have contained up to 10-12 wt.% ZrO_2.

[1] Konev, A.A. et al. (1970) *Zapiski VMO*, **99**, 225-231. [2] Aleksandrov, C.M. & Troneva, M.A. (2008) *Geokhimia*, **8**, 862-876. [3] Brovkin, A.A. et al. (2002) *Kristallografiya*, **47**, 457-459. [4] Appel, P.W.U. & Brigatti, M.F. (1999) *Mineral. Mag.*, **63**, 511-518.

Rutile and tourmaline as indicators of the magmatic origin of tourmalinite levels in the São José do Barreiro area, NE Ribeira Belt, Southern Brazil

Garda, G.M.[1*], Beljavskis, P.[1], D'Agostino, L.Z.[2], Trumbull, R.B.[3] & Wiedenbeck, M.[3]
[1]Instituto de Geociências, São Paulo University, Sao Paulo/SP, Brazil (*giagarda@usp.br)
[2]Laboratório de Caracterização Tecnológica, Escola Politécnica, São Paulo University, Sao Paulo/SP, Brazil
[3]Helmholtz Centre Potsdam, GFZ German Research Centre for Geosciences, Potsdam, Germany

Coarse-grained tourmalinite layers associated with quartzitic lenses occur in the highly weathered, hilly area of São José do Barreiro-Formoso of the Central Ribeira Belt (São Paulo State, Brazil). Country rocks belonging to the Embu Complex include tourmaline-bearing schists (sample BM2) and gneisses of the Rio Una Unit and migmatites and gneisses of the Redenção da Serra Unit.

Tourmaline from a quartzitic lens (sample 3A) and a massive, rutile-bearing tourmalinite (sample 3B) were analyzed by microprobe (major elements and F), ICP-MS (REE, Y, Zr, Hf, Th) and SIMS (B isotopes). Mg# values for 3A and 3B fall respectively in the 0.62-0.67 and 0.69-0.76 intervals. Al_2O_3 (Fig. 1A), FeO and Na_2O contents are higher and CaO (Fig. 1B) and F contents are lower for 3A than 3B.

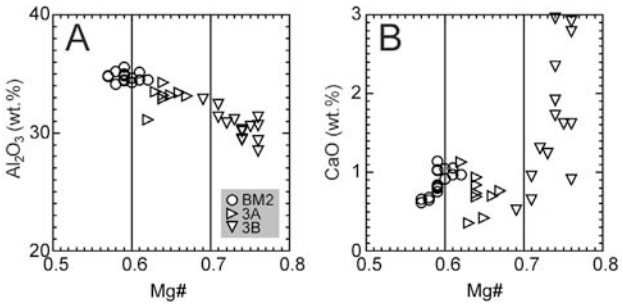

Fig. 1: Al_2O_3 (A) and CaO (B) *vs*. Mg# in tourmaline from samples BM2 (schist), 3A (quartzitic lens) and 3B (rutile-bearing tourmalinite).

The LREE pattern for 3B is approximately 70 times enriched compared to that for 3A. Eu anomalies are positive for 3A and negative for 3B. Relatively high Y (50.5 μg/g), Zr (778 μg/g), Hf (20 μg/g), Th (6.36 μg/g) contents are also observed in 3B.

$\delta^{11}B$ values fall in the –12.3 and –13.9 ‰ interval for 3A and –13.9 and –15.8 ‰ interval for 3B, typical for tourmalines occurring in metasediments and S-type granites [1].

Microprobe analyses of green and red rutile crystals from are shown in Table 1.

Table 1: Microprobe analyses of green and red rutile from sample 3B

	Ti (%)	Cr (μg/g)	Fe (μg/g)	Nb (μg/g)	Sn (μg/g)
green	56.5-58.5	433-1007	1871-10000	2000-7500	3985-28000
red	58.1-58.6	2392-6497	1393-3208	3918-5203	4578-7959

Applying the geothermometer proposed by [2], temperatures from 570°C to 700°C are obtained (112 μg/g < Zr < 454 μg/g), compatible with the observed regional metamorphic grade [3]. Our tourmaline and rutile chemical data indicate that the syn-collisional, S-type São José do Barreiro Granite [3] is a possible fluid source for tourmalinite (3B) of this study area.

[1] Palmer, M.R. & Swihart, G.H. (1996) in Grew, E.S. & Anovitz, L.M. (eds.) *Rev. Mineral.*, **33**, 709-744. [2] Zack, T. et al. (2004) *Sedim. Geol.*, **171**, 37-58. [3] Pereira, R.M. et al. (2003) *Geociências*, **22**, 107-109.

Significance of compositional and boron isotope variations in tourmaline of Passagem de Mariana gold mine, Quadrilátero Ferrífero, Minas Gerais, Brazil

Garda, G.M.[1*], Xavier, R.P.[2], Cavalcanti, J.A.D.[3], Trumbull, R.B.[4] & Wiedenbeck, M.[4]
[1]Instituto de Geociências, São Paulo University, Sao Paulo/SP, Brazil ([*]giagarda@usp.br)
[2]Instituto de Geociências, Campinas Statal University, Campina, Brazil
[3]CPRM -REFO, Serviço Geológico do Brasil, Fortaleza, Brazil
[4]GFZ German Research Centre for Geosciences, Potsdam, Germany

The association of tourmaline and gold mineralization is conspicuous in the Passagem de Mariana Mine (Minas Gerais, Brazil) [1]. Tourmaline occurs as: very fine-grained foliation-parallel crystals in massive to banded tourmalinite (type 1); coarser-grained, color-zoned crystals forming massive (type 2) or comb-texture (type 3) aggregates within tourmalinite; and in associated quartz-carbonate-sulfide veins and breccias (type 4). Compositional variations in the four types of tourmaline can be expressed in terms of TiO_2 contents, which in turn reflect the color or color zones of tourmaline crystals. Generally the TiO_2 contents correlate negatively with SiO_2 and Al_2O_3, and positively with CaO and MgO. Na_2O and F contents increase from types 1 to 3. The most pronounced changes in composition can be observed in the very dark zones of type-4 tourmaline, *e.g.* related to a decrease in MgO (trend a, Fig. 1A) and the increase in FeO (trend b, Fig. 1B).

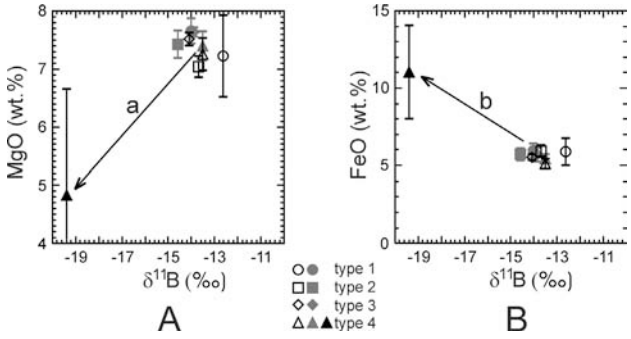

Fig. 1: MgO (A) and FeO (B) *vs.* $\delta^{11}B$ in tourmalines from the Passagem de Mariana Mine. Empty symbols: TiO_2 < 0.5 wt.%, gray symbols: 0.5 wt.% < TiO_2 < 1.0 wt.%, black: TiO_2 > 1.0 wt.%. Vertical bars on each symbol show compositional variations within the samples. The total uncertainty in $\delta^{11}B$ values (1 s) is less than 2 ‰.

$\delta^{11}B$ values obtained by SIMS for the four types of tourmaline range from –19 to –12 ‰, indicating non-marine evaporites, metasedimentary rocks and S-type granites as possible crustal B sources [2]. Considering the geological setting, the probable B source for tourmaline of types 1 to 3 (–15 to –12 ‰) would be the carbonaceous phyllites of the Batatal Formation, though a contribution of boron derived from non-marine evaporites cannot be excluded. In contrast, the much more negative $\delta^{11}B$ values of –19 ‰ from dark zones of type-4 tourmalines (Fig. 1) cannot be explained by fractionation effects during metamorphism, but instead require an external source. External B sources may be related to thermal events of the Paleoproterozoic Transamazonian Orogeny [3] or to veining and brecciation induced by the overthrusting of the Minas Group, accompanied by gold mineralization [1].

[1] Vial, D.S. et al. (2007) *Ore Geol. Rev.*, **32**, 596-613. [2] Palmer, M.R. & Swihart, G.H. (1996) in Grew, E.S. and Anovitz, L.M. (eds.) *Rev. Mineral.*, **33**, 709-744. [3] Alkmim, F.F. & Marshak, S. (1998) *Precambrian Res.*, **90**, 29–58.

Boron variation in the calc alkaline volcanic arc of the Western Carpathians, Central Europe

Gméling, K.[1*], Pécskay, Z.[2], Harangi, Sz.[3] & Birkenmajer, K.[4]
[1]Institute of Isotopes, Hungarian Academy of Sciences, Budapest, Hungary ([*]gmeling@iki.kfki.hu)
[2]Institute of Nuclear Research of the Hungarian Academy of Sciences, Debrecen, Hungary
[3]Eötvös University, Budapest, Hungary
[4]Institute of Geological Sciences, Polish Academy of Sciences, Krakow, Poland

Boron (B) is rarely found in the solar system, while on the Earth B is concentrated in the continental crust (~10 µg/g) [1]. The most suitable analytical technique for B concentration measurements in whole rocks is prompt gamma activation analysis (there is a PGAA instrument connected to the Budapest Research Reactor). Boron is an important tracer of the recycled materials in subduction zones as it is an incompatible and fluid-mobile element, with various abundances in different reservoirs. In the slab B is concentrated in the oceanic crust and sediments, but most of it leaves at the beginning of subduction close to the suture zone. Some minerals can retain B and carry it further down into the mantle. Thus, arc volcanic rocks have relatively high B content (~35 µg/g) [2].

The Western Carpathian calc alkaline volcanic arc serves a special case, as these volcanic rocks show subduction related trace element pattern and B content, although there is no seismic sign of a subducted slab under the studied area [3]. We focused on the B geochemistry of different type of Western Carpathian volcanic rocks originating from different volcanic eruptions of various ages (9.4-16.7 Ma; B 2-90 µg/g). The variation in the B content is the highest in the Central Slovak Volcanic Field (4-76 µg/g), as is the case for the variation in the age of the measured rocks. The range of B content is also similar in the Tokaj Mts. (7-68 µg/g). Smaller the changes in the B content in the other volcanic areas: Börzsöny Mts. (11-43 µg/g); Visegrádi Mts. (7-43); Mátra Mts. (8-30 µg/g). For comparison B content of connected andesite intrusions from the Pieniny and Moravia (3-30 µg/g), flysch sediments from the Pieniny region (60-154 µg/g), lower and upper crustal xenoliths (0.1-2.5 and 50-60 µg/g) and mantle xenolith (0.1-0.26 µg/g) samples were measured from the Carpathian Pannonian region. The higher B content of volcanic rocks generally originates 1) from the subducted slab: the altered oceanic crust and sediments; 2) form the metasomatic effect of an earlier subduction; or 3) from melting the more B enriched upper crust. In active subduction zones the slab derived B content of volcanic arcs is decreasing toward the back arc region [4]. However, the age and the spatial distribution of the Western Carpathian volcanics do not show any correlations with their B content or other trace elements. The relatively high K_2O/Sm vs B/Sm ratio refers to fluid enrichment mainly originating from a crustal material rather then from subducted sediment (represented by the flysch samples). All these support the assumption [5,6] of the decompression melting of a previously metasomatised lithospheric mantle and lower crustal materials, rather then a direct fluid induced melting under the Western Carpathians.

Acknowledgements: Supported by: Hungarian Science Fundation OTKA 68153 and NAP VENEUS05 OMFB 00184/2006.

[1] Taylor, S.R. & McLennan, S.M. (1995) *Rev. Geophys.*, **33**, 241-265. [2] Leeman, W.P. et al. (1994) *Geochim. Cosmochim Ac.*, **58**, 149-168. [3] Grad, M. et al. (2006) *J. Geophys. Res. Sol. Ea.*, **111**, B3, B03301. [4] Ryan et al. (1995) *Science*, **270**, 625-628. [5] Lexa, J. & Konečný, V. (1998) *Geol Surv. Slovak Rep.*, 219-240. [6] Harangi, Sz. (2001) *A. Geol. Hung.*, **44**, 223-258.

Evidence for BO_3-groups in nominally boron-free minerals (NBFM) of mantle affinity

Hålenius, U.[1*], Skogby, H.[1] & Kristiansson, P.[2]
[1]Dept. of Mineralogy, Swedish Museum of Natural History, Stockholm, Sweden ([*]Ulf.Halenius@nrm.se)
[2]Dept. of Nuclear Physics, Lund Institute of Technology, Lund University, Lund, Sweden

The fact that boron may substitute for silicon in most rock-forming minerals has been known for a considerable time. It has generally been assumed that these relatively low amounts of B are incorporated through replacements of SiO_4 groups by BO_4 units (e.g., [1]).

Direct evidence of the structural incorporation of boron in nominally boron free minerals (NBFM) of mantle affinity, such as olivine, orthopyroxene and clinopyroxene group minerals, is very scarce. On the basis of chemical and IR-spectroscopic data on natural borian olivine, it has been suggested that the coupled substitution $B(F,OH)Si_{-1}O_{-1}$ operates in the olivine structure and that boron occurs in tetrahedral coordination [2]. However, later studies of B and OH-contents in olivine minerals could not establish a strong correlation between their atomic proportions [3].

With the aim to explore and better understand boron exchange processes and limitations for boron incorporation in NBFMs of mantle affinity we have studied in detail the crystal chemistry and, in particular, boron incorporation mechanisms in synthetic forsterite and clinoenstatite that were produced under dry and boron-saturated conditions. The results of polarised single crystal FTIR-spectroscopy (Fig. 1) in combination with EMP and high-resolution nuclear reaction analyses (NRA) show that relatively high concentrations of boron may be incorporated in these phases and that boron is preferentially occurring in trigonal BO_3-groups that replace SiO_4-groups.

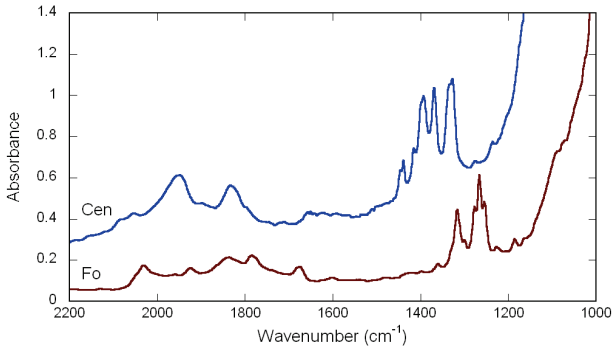

Fig. 1: IR spectra of synthetic clinoenstatite (Cen) polarised in c-direction, and forsterite (Fo) polarised perpendicular to c. Absorption bands in the 1200-1450 cm^{-1} region are assigned to BO_3 vibrations.

The replacement of SiO_4-tetrahedra by trigonal BO_3-groups must involve the breaking of one of the original T-O bonds of the olivine and pyroxene structures. This destabilises the structures and constitutes one important limiting factor for incorporation of higher B-contents in these phases.

[1]. Hervig, R. et al. (2002) *Am. Mineral.*, **87**, 769-774. [2] Sykes, D. et al. (1994) *Am. Mineral.*, **79**, 904-908. [3] Kent, A.J.R. & Rossman, G.R. (2002) *Am. Mineral.*, **87**, 1432-1436.

Geochemical characteristics of Sarmatian volcanic rocks in the Tokaj Mountains, Hungary

Kiss, P.[1*], Molnár, F.[1], Gméling, K.[2] & Pécskay, Z.[3]
[1]Dept. of Mineralogy, Eötvös Loránd University, Budapest, Hungary ([*]geokissp@gmail.com)
[2]Institute of Isotopes, Hungarian Academy of Sciences, Budapest, Hungary
[3]Institute of Nuclear Research of the Hungarian Academy of Sciences, Debrecen, Hungary

The Tokaj Mountains are a part of the Inner Carpathian Volcanic Arc, which formed due to subduction collision and extension processes during the Miocene in the Carpathian-Pannonian Region. In the Tokaj Mountains, intermediate and acidic calc-alkaline volcanic rocks arose during the Middle-Upper Miocene (Badenian-Sarmatian-Pannonian) in a N-S oriented volcanotectonic graben that is underlain by Proterozoic to Mesozoic crystalline rocks. A large number of K/Ar age determinations have been made on the volcanic rocks. [1,2]. Newly collected samples were analysed to make a fully representative sample-set for the whole mountain range. In addition to K/Ar age determinations, major and trace element contents of the volcanic rocks, with an emphasis on B and Cl, were measured to study petrogenetic relationships. Boron is an excellent marker of the fluid circulation in the upper mantle and the lower crust, while chlorine has an important role in ore formation processes of volcanic-hydrothermal systems.

There are differences not only in major [3], but also in trace element geochemistry between the rocks from the northern and the southern part of the Tokaj Mountains. An airborne K anomaly map shows higher K intensity in rhyolite fields from the southern part of the mountains due to the presence of K-feldspar phenocrysts, whereas rhyolite lacks K-feldspar phenocrysts in the northern part. The B content of rocks is increasing from 10.1 to 68.1 µg/kg, which is a typical range for subduction related volcanic rocks [4], with increasing SiO_2 content. There is a positive correlation between the K and B content, while Cl content varies over a greater range in the K-rich rocks, except for perlitic rhyolite, in which Cl-enrichment can be attributed to perlitisation. Nonetheless, there are none of the statistical changes in the B and Cl content of rocks through time or space that is well known from recent subduction zones [5]. Therefore, we can conclude that the volcanism was generated by the decompression melting of an earlier metasomatised mantle rather than by fluid induced melting as other authors had suggested [6,7]. This conclusion is also supported by the trace element data (La/Yb vs. Ba/La, Rb vs. Ba/Rb). Comparison of the B and Ba concentrations in the rocks as a function of either Sm or Zr concentrations helped us to recognize that the fluid which had metasomatised the mantle originated from the altered oceanic crust. The higher Cl content of the high-K rhyolite in the southern Tokaj Mountains appears in agreement with the fact that volcanic centers in this area are laden with shallow zones of low sulphidization-type epithermal systems, whereas the low Cl – low K rhyolites in the northern part of the Tokaj Mountains are either unmineralized or pre-date ore mineralization.

Acknowledgements: supported by OTKA K68153.

[1] Balogh, K. (1985) *ATOMKI Rep.*, **D/1**, 277-288. [2] Pécskay, Z. et al., (1987) *Földt. Közl.*, **117**, 237-253. [3] Liffa, A. (1943) *MÁFI Ann. Rep.*, 359-377. [4] Leemann, W.P. & Sisson, V.P. (1996) *Rev. Mineral.*, **33**, 645-707. [5] Ishikawa, T & Tera, F (1997) *Earth Planet. Sci. Lett.*, **152**, 123-138. [6] Lexa, J. & Konecný, V. 1998 in Rakús, M. (ed.) *Geodynamic development of the Western Carpathians*, 219–240. [7] Harangi, S. (2001) *Act. Geol. Hun.*, **13**, 25-39.

The new microporous lead borate, leucostaurite, $Pb_2[B_5O_9]Cl \cdot 0.5H_2O$, from Atacama Desert

Meisser, N.[1*], Ansermet, S.[1], Brugger, J.[2], Krivovichev, S.[3], Belton, D.[4] & Ryan, C.[4]
[1]Musée Géologique & Inst. de Minéralogie & Géochimie, University of Lausanne, Switzerland ([*]nicolas.meisser@unil.ch)
[2]School of Earth & Environmental Sciences, University of Adelaide, Australia & South Australian Museum, Adelaide, Australia
[3]Dept. of Crystallography, Faculty of Geology, St. Petersburg State University, St. Petersburg, Russia
[4]CSIRO Earth Science and Resource Engineering, Clayton, Australia

The new mineral leucostaurite (IMA 2007-047) was discovered during systematic analytical checking of ore specimens from Mina Asunción, Sierra Gorda. These samples were collected by the consul of Switzerland in Chile, Julius Friedrich Häfliger (1834-1911) and donated by his widow in 1912 to the Natural History Museum of Bern.

Leucostaurite forms thin-tabular {010}, striated // [100], colorless, interpenetrated twinned crystals or sheaf-like aggregates up to 0.8 mm on a paralaurionite and boleite matrix. Other associated minerals are: caracolite, bindheimite, gypsum, penfieldite, challacolloite, schwartzembergite, cesanite and seeligerite.

Chemical analyses were carried out by means of an electron microprobe and by particle-induced gamma-ray emission (PIGE) for boron. The empirical formula is based on Pb+Sr+Ca = 2 *apfu*, with 1 H *pfu* from the structure refinement: $(Pb_{1.967}Sr_{0.026}Ca_{0.007})_{\Sigma 2.000}(B_{5.052}Si_{0.016})_{\Sigma 5.068}(Cl_{1.074}I_{0.004})_{\Sigma 1.078}O_{9.072}\ 0.5H_2O$. Single-crystal X-ray studies were carried with a 4-circle diffractometer and gave the following data: orthorhombic (*a* 11.3757(14) Å; *b* 11.5051(18) Å; *c* 6.5568(7) Å; *V* 858.14(19) Å^3) space group: *Pnn*2 and Z = 4.

The microporous crystal structure of leucostaurite (R_1 = 6.2%). contains a hilgardite-type 3-dimentional framework $Pb_2[B_5O_9]$. Leucostaurite shares the *P*nn2 space group with the synthetic compound $Na_{0.5}Pb_2(B_5O_9)Cl(OH)_{0.5}$ [1]. In this compound, one type of channel contains Cl^- ions, the other is disordered and contains OH^-, Cl^- and Na^+ ions; in leucostaurite these channels are occupied by Cl^- ions and Cl^- ions + H_2O groups, respectively. Upon heating to about 1000°C, the mineral releases HCl and H_2O due to mobility of the channels' content.

Located in central part of Atacama hyperarid desert, the range of Sierra Gorda hills appears as a highly Cu-Pb-Ag-Zn-mineralized area surrounded by lowlands constituted by Neogene and Quaternary salt-encrusted alluvial fans of Andean forarc endhoreic basin. These salts (chlorides, sulphates, borates, iodates, nitrates) are caliche-type salt cements, veins, and crusts within the upper few meters of unconsolidated soil and regolith. They are largely sourced from magmatic volatile compounds, exuded by Andean range volcanism or recycled by hydrothermally driven circulation [2], and in the case of nitrates, by atmospheric condensation [3]. The oxidation of base-metal deposits in the presence of these dispersed salts and/or brines leads to complex and unusual mineral associations. The exotic geochemical signature of these saline species is reflected in some typical minerals from northern and central Atacama deposits like bandylite $Cu_2[B(OH)_4]_2Cl_2$, santarosaite (IMA 2007-013) $(Cu,Pb)B_2O_4$, bellingerite $Cu_3(IO_3)_6 \cdot 2H_2O$, salesite $Cu(IO_3)(OH)$, schwartzembergite $Pb_5IO_6H_2Cl_3$ and seeligerite $Pb_3O(IO_3)Cl_3$.

[1] Belokoneva, E.L. et al. (2000) *Crystallogr. Rep.*, **45**, 744-753. [2] Pueyo, J.J. et al. (2001) *Sedimentology*, **48**, 1411-1431. [3] Böhlke, J.K. et al. (1997) *Chem. Geol.*, **136**, 135-152.

Contrasting compositional trends in tourmaline from intragranitic REL-REE (NYF) euxenite-type pegmatites of the Třebíč Pluton, Czech Republic

Novák, M.[1*], Škoda, R.[1], Macek, I.[1] & Filip, J.[2]
[1]Dept. of Geological Sciences, Masaryk University, Brno, Czech Republic ([*]mnovak@sci.muni.cz)
[2]Centre for Nanomaterial Research, Palacký University, Olomouc, Czech Republic

Tourmalines from granitic pegmatites exhibit compositional trends generally characterized by increasing contents of Al, Li, Mn, F and Fe/(Fe+Mg) ratio but mostly by low Ca and Ti concentrations [1]. Tourmalines in decreasing abundance dravite>schorl>uvite>povondraite from euxenite-type pegmatites of the Třebíč Pluton [2] show several unusual features such as high concentrations of Ca≤0.45 apfu, Ti ≤0.48 apfu, Fe^{3+}/Fe_{tot} = 0.14-0.26 and generally low degree of fractionation with $Fe_{tot}/(Fe_{tot}+Mg)$ = 0.22-0.88 and Al_{tot} = 5.05-6.46 apfu (grey field on Fig. 1). The relative abundances in tourmaline (schorl> foitite>dravite>elbaite>uvite) from the most evolved euxenite-type pegmatite Klučov I [2] is characterized by moderate to high $Fe_{tot}/(Fe_{tot}+Mg)$ = 0.66-0.98, and low to high Al_{tot} = 5.04-7.03 apfu (blank field on Fig. 1). Newly discovered zoned tourmaline from the euxenite-type pegmatite Kožichovice III exhibits very distinct compositional evolution (see black arrow on Fig. 1). The black core is compositionally similar to those from the other euxenite-type pegmatites of the Třebíč Pluton [2] but dark green to dark blue narrow rims resembling rims of Fe-elbaite around schorl from complex (Li) pegmatites tend to Al-enriched dravite (Al_{tot} = 6.06-6.24 apfu, $Fe_{tot}/(Fe_{tot}+Mg)$ = 0.27-0.32) evidently Ti-depleted (≤0.02 apfu) and partly Ca-depleted (≤0.15 apfu). Different mineral assemblages of tourmaline rims: perthitic Kfs + Ab + Qtz at Klučov I and non-perthitic Kfs + Ab + Qtz + Chl at Kožichovice III, suggest distinct processes producing rims of tourmaline crystals although both show very similar textural evolution on the BSE images. Distinct $K_D^{crystal/medium}$ for Mg (at Klučov I medium ~ evolved melt, at Kožichovice III medium ~ hydrothermal fluids) may explain such compositional trends. Rather stable $Fe_{tot}/(Fe_{tot}+Mg)$ values in core and rim also confirm lack of Mg/Fe fractionation in fluids relative to melt at Klučov I (Fig. 1). Lower T and different parental medium at Kožichovice III both indicated by the mineral assemblage very likely controlled this compositional trend including very low Ti- and Ca-contents.

Acknowledgements: This work was supported by the Grant No. P210/10/0743.

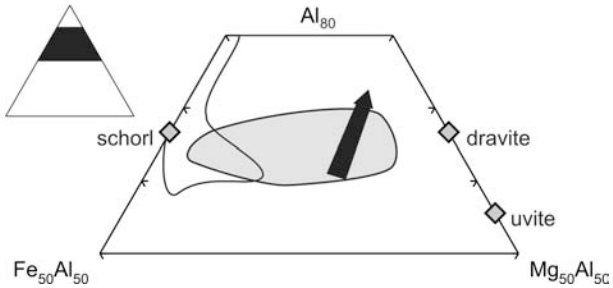

Fig. 1: Chemical compositions of the tourmalines from distinct euxenite-type pegmatites of the Třebíč Pluton (see explanation in the text).

[1] Selway, J.B. et al. (1999) *Eur. J. Mineral.*, **11**, 569-584. [2] Novák, M. et al. (2010) *Can. Mineral.*, submitted.

The influence of mineralization agents to formation of barium borates under hydrothermal conditions

Safronova, E.G.*, Mochenova, N.N. & Dimitrova, O.V.
Lomonosov Moscow State University (MSU), Moscow, Russia
(*safronova-eg@list.ru)

Boron is being reported at almost every stage of the geologic cycle, from magmatic to supergene units, which proves complex migration paths and concentration processes of boron in nature. Their study is only possible on a basis of comprehensive examination of the character of boron in geological systems. Hydrothermal synthesis allows to adjust physicochemical conditions close to the medium-temperature conditions characteristic of borate formation and provides a way to examine the problems of mineral formation and synthetic crystal genesis (including alio- and isovalent isomorphism of anions and cations).

Synthesis parameters have been set by natural borate formation conditions represented by a variety of known minerals. By using halogenides and carbonates of metalloids as additional preparation components it is possible to produce synthetic analogues of minerals in a laboratory environment. Mineralization agents had a dominant role in producing acid-base balance in solutions. Development area of the compounds with the most diverse boron-oxygen complexes, including pentaborates, corresponds to pH values ranging from 5 to 8 [1]. The experiments studied the influence of mineralization agents (Li^+, Na^+, K^+, F^-, Cl^-, Br^-, I^-, CO_3^{2-}) and the amount of B_2O_3 in the load, to generation of the boron-oxygen anion type in compounds at T = 280ºC, P ~ 70 atm. Analysis of the syntheses in a Ba-system proved that cation alkalinity and anion acidity in the mineralization agents composition have an indirect effect on the formation of compounds with a specific boron-oxygen radical, which includes determining acid-base balance of the solution.

The concentration of B_2O_3 in solution helps to adjust the influence of anions and alkaline cations to synthesize pentaborate compounds in multi-component Ba-boron systems. The new compounds and analogues of minerals with pentaborate radicals are received in solutions with BaO/B_2O_3 ratio from 0.5 to 0.3 by weight (Table 1).

Table 1: New chemical compounds synthesized in borate hydrothermal systems [2]

Compound	Related structure type (or fragments of mineral structure)
$Ba_2[B_5O_9]Cl \cdot 0{,}5H_2O$	hilgardite
$Ba[B_5O_8(OH)_2]OH$	(tuslaite)
α-$Ba_2[B_5O_8OH] \cdot H_2O$	biringucite
β- $Ba[B_5O_8(OH)] \cdot H_2O$	
$Ba_5[B_{20}O_{33}(OH)_4] \cdot H_2O$	(gouerite)
$Ba[B_5O_{10}(OH) \cdot B_2O(OH)_3]$	tannelite
$Ba_2[B_5O_8(OH)_2] \cdot (OH)$	

[1] Gorbov, A.F. (1976) *Geochemistry of Boron*. Nedra Publishing, Leningrad. [2] Dimitrova, O.V. (2002) *VMO Notes*, part XXXI, **4**, 107-112.

First description of datolite from Foresudetic Monocline, western Poland

Sokalska, E.T.* & Aagaard, P.
Dept. of Geosciences, University of Oslo, Oslo, Norway
(*e.t.sokalska@geo.uio.no)

Metavolcanic rocks of Foresudetic Monocline (western Poland) are known from numerous drillings. The volcanics are of different chemical composition, from rhyolitic to basaltic and they were formed in different environments. It is possible to recognise subvolcanic dykes, lava flows and ignimbrite layers.

The studied rocks contain a rich assemblage of secondary phases depending on whole-rock chemical composition and metamorphic conditions. The most important phases are pumpellyite, chlorite, mixed layer clays, zeolites, prehnite, epidote, quartz, albite, K-feldspar, Fe-oxides and carbonates. There are also different Ti-phases, actinolite, sulphides and sulphates.

One of studied samples taken from meta-andesite contains small amounts of datolite. This mineral was discovered in 2007 in Bolewice-1 drillcore [1]. It forms amygdule fillings and is intergrown with laumontite and other secondary phases. It was discovered by XRD analysis of amygdule fillings, but was detected in whole rock patterns as well. Unfortunately, B cannot be detected with EDS analysis and the main indicator of datolite presence in amygdule is lack of Al, which is present in Ca-zeolites from the same amygdules.

The datolite-containing rock sample was metamorphosed at temperatures close to 250°C, an estimate based on the secondary phases present. The paragenesis laumontite-datolite fits perfectly to determined metamorphic conditions according to data from Italy [2]. It is the first evidence of B metasomatism in the Foresudetic Monocline. Currently available data suggest that this process happened extremely rarely despite the fact that metamorphic temperatures were usually high enough for datolite formation (higher than 250°C). The most probable source of B for datolite formation was Zechstein brine circulating through the volcanic rocks.

[1] Sokalska, E. T. (2007) *Unpublished Ph.D. Thesis*. [2] Zaccarini, F. et al. (2008) *Chem. Erde*, **68**, 265-277.

Single-crystal X-ray diffraction, Raman, and FT-IR investigations of pyrochlore-supergroup minerals from São João del-Rei, Minas Gerais, Brazil

Andrade, M.B.[1*], Atencio, D.[2], Chukanov, N.V.[3], Ellena, J.[1], Honorato, S.B.[4] & Ayala, A.P.[4]
[1]Depto. de Física e Informática, Instituto de Física de São Carlos, Universidade de São Paulo, Brazil ([*]mabadean@terra.com.br)
[2]Depto. de Mineralogia e Geotectônica, Instituto de Geociências, Universidade de São Paulo, Brazil
[3]Inst of Problems of Chemical Physics, Russian Academy of Science, Moscow, Russia
[4]Dept.o de Física, Universidade Federal do Ceará, Fortaleza, Brazil

Pyrochlore-supergroup minerals have been studied during the last years, due to their economic importance as the major source for Nb, as well as to their exceptional physical and chemical properties. New nomenclature rules are being now introduced by a CNMNC-IMA subcommittee for the pyrochlore supergroup [1]. The investigation of pyrochlore-like materials enabled the development of significant technological applications, such as oxide superconductors, dieletric materials, and nuclear-waste disposals. Pyrochlore-supergroup minerals show $A_2B_2X_6Y$ stoichiometry and crystallize in the cubic space group $Fd\bar{3}m$, $Z = 8$, with $a = 10.4$ to 10.6 Å. A mineral of the microlite group from Volta Grande pegmatite, São João del-Rei, Minas Gerais, Brazil, was studied by electron microprobe, single crystal X-ray diffraction, Raman and FT-IR spectroscopy. Chemical analyses were carried out by means of an electron microprobe (WDS mode). The crystal structure was studied using Mo$K\alpha$ ($\lambda = 0.71073$Å) radiation on an Enraf - Nonius Kappa-CCD diffractometer. The crystal structure has been solved and refined using X-ray reflections [$I_{obs} > 2\sigma(I)$] and compositional constraints from electron microprobe analyses as $[\square_{0.81}(H_2O)_{0.57}Ba_{0.26}Sr_{0.18}U_{0.08}Ca_{0.02}\,Mn_{0.02}Bi_{0.02}\,Nd_{0.02}Ce_{0.01}Pr_{0.01}]_{\Sigma=2.00}\,(Ta_{1.59}Nb_{0.13}Si_{0.15}Sn_{0.10}Ti_{0.02}\,Fe_{0.01})_{\Sigma=2.00}\,[O_{5.21}(OH)_{0.79}]_{\Sigma=6.00}\,[(H_2O)_{0.95}Cs_{0.03}K_{0.02}]_{\sum Y=1.00}$. The occurrence of H_2O (due the cation occupancy of the A site) [2] in the vicinity of the A position (16*d*) and Y position (8*b*) was investigated during the refinement process. The micro-Raman measurements were performed using a T64000 Jobin–Yvon spectrometer equipped with an Olympus microscope and a LN_2-cooled CCD to detect the scattered light, and the infrared spectra was recorded on a Bruker FT-IR VERTEX 70 spectrometer equipped with a Nd:YAG laser (1.064nm excitation line) and a liquid-nitrogen cooled Ge detector. The bands identified, at 1600-1700 cm^{-1} and 3200–3800 cm^{-1}, were assignable to water stretching and bending vibrations. The results from Raman and FT-IR spectra confirm that water plays a significant role in the microlite structure.

Acknowledgements: This research is supported by FAPESP award 2008/04984-7.

[1] Atencio, D. et al. (in preparation). [2] Ercit, T.S. (1994) *Can. Mineral.*, **32**, 415-420.

Peatite-(Y) and ramikite-(Y), two new Li-Na-Y-(±Zr) phosphate-carbonate minerals from Mont Saint-Hilaire, Quebec, Canada

McDonald, A.M.[1*], Back, M.E.[2] & Gault, R.A.[3]
[1]Dept. of Earth Sciences, Laurentian University, Sudbury, Ontario, Canada ([*]amcdonald@laurentian.ca)
[2]Dept. of Natural History, Royal Ontario Museum, Toronto, Ontario, Canada
[3]Research Division, Canadian Museum of Nature, Ottawa, Ontario, Canada

Peatite-(Y), $Li_4Na_{12}(Y,Na,Ca,REE)_{12}(PO_4)_{12}(CO_3)_4(F,OH)_8$ and ramikite-(Y), $Li_4(Na,Ca)_{12}(Y,Ca,REE)_6Zr_6(PO_4)_{12}(CO_3)_4O_4$-$[(OH),F]_4$, are two new minerals discovered in a hydrothermally altered pegmatite (the 'Poudrette pegmatite') at Mont Saint-Hilaire, Rouville Co., Quebec. The two minerals develop in composite (epitaxial?) crystals, consisting of isolated or small clusters of cubes (individuals ranging from 0.1-0.5 mm in size), with ramikite-(Y) occurring as the cores of these crystals (dominant) and peatite-(Y) as very thin rims (< 50 μm in width). Ramikite-(Y) is yellow in color and translucent whereas peatitite-(Y) is pink and transparent. Associated minerals include donnayite-(Y), sabinaite, cryolite, elpidite, rhodochrosite, horváthite-(Y), catapleiite, polylithionite and others. Chemical analyses (EMPA, FTIR, Raman, LA-ICP-MS, single-crystal XRD) were used to confirm the chemistry of the two minerals (including the presence of essential Li, absence of B, Be, *etc*.).

Single-crystal XRD studies confirm that peatite-(Y) is orthorhombic [*P*222, *a* 11.167(2), *b* 11.164(2), *c* 11.162(1) Å] and ramikite-(Y) is triclinic [*P*1, *a* 10.9977(6), *b* 10.9985(6), *c* 10.9966(6) Å, α 90.075(4), β 89.984(4), γ 89.969(4)°]. The structures of both minerals have been solved and refined [R = 0.048 for peatite-(Y), R = 0.036 for ramikite-(Y)]. They both consist of two types of chains that extend along major crystallographic axes (*e.g.*, [001]): 1) alternating (PO_4) tetrahedra and [$YO_6(F,OH)_2$] polyhedra, and 2) alternating (PO_4) tetrahedra, (LiO_6) octahedra and (CO_3) groups. These chains alternate every 45° about each crystallographic axis and are linked together via (LiO_6) octahedra, forming an eight-membered pinwheel-like motif. An open framework of interconnnected eight-membered rings develops via linkages made between (LiO_6) groups and (CO_3) groups. The framework contains numerous channels within which Na and Y or Zr ions are housed in specific configurations: 1) eight-membered rings house Y or Zr in their centres and Na at their peripheries, 2) between respective eight-membered rings, alternating Y or Zr and Na ions, and 3) Y or Zr in the centres of four-membered (CO_3) rings. The crystal structures of the two minerals are intimately related but appear to be unique within the mineralogical realm. Both minerals are late-stage products that developed during the hydrothermal alteration of primary pegmatite minerals (*e.g.*, polylithionite, catapleiite, *etc.*). The interface contact and somewhat distinct chemical compositions of the two suggests early (and predominant) growth of ramkite-(Y) followed by hiatus, then subsequent (and minor) growth of peatite-(Y).

For the times they are a-changin': mineral names, groups, suffixes, the CNMNC and you

Mills, S.J.
Dept. of Earth and Ocean Sciences, University of British Columbia, Vancouver, Canada (smills@eos.ubc.ca)

2010 marks the 50th anniversary of the IMA and mineralogy is experiencing a boom of productivity and output. Recent proposals are changing the way that mineralogy organises itself, and will help move the science forward throughout the 21st Century. Some of the most recent changes are as follows.

The release of new mineral names: new procedures have been put in place to facilitate the dissemination of new mineral names in the public arena. Authors can choose to have the Commission release the new mineral name upon approval of the mineral. The names will appear in the Commission's bimonthly newsletter, which will be published in *Mineralogical Magazine*. This will enable citations to be made using the new mineral name until the full description is published. Authors are also entitled to have the name withheld until final publication, *i.e.*, the *status quo*.

The standardisation of mineral groups: the CNMMNC has recently approved a simplified definition of a mineral group, which is based on the structural and compositional aspects of a mineral. A hierarchical scheme for group nomenclature and mineral classification has been introduced which organises minerals in the following hierarchy.

1. Mineral class
2. Mineral subclass
3. Mineral family
4. Mineral supergroup
5. Mineral group(s)
6. Mineral subgroup or mineral series

A new procedure has also been put in place to facilitate the future proposal and naming of new mineral groups within the IMA–CNMNC framework. This allows for the introduction of new mineral groups as part of a new mineral submission, as part of a CNMNC subcommittee report or as a stand-alone proposal.

The introduction of suffix-based nomenclature schemes: Suffixes remain an issue of continuing debate. They are useful in some instances to simplify nomenclature and to help clarify mineral relationships, as well as to avoid the proliferation of names. However, suffixes should be used with caution, bearing in mind that what is good for one group of minerals might not be good for another and that historical and traditional aspects of mineralogy and nomenclature should always be considered before any changes are made.

Mineralogy of the Cleveland mine, Tasmania, Australia: unusual fluoride minerals in a skarn setting

Birch, W.D.
Geosciences, Museum Victoria, Melbourne, Victoria, Australia (bbirch@museum.vic.gov.au)

The Cleveland mine is situated at Luina in northwestern Tasmania, Australia. The mine exploited tin – copper ore in the form of pyrrhotite – cassiterite – stannite – chalcopyrite mineralisation, occurring as lenses within Cambrian metasediments and mafic volcanics [1]. The mineralisation was emplaced via fluids derived from the underlying Late Devonian Meredith Granite. An early stockwork system of quartz – fluorite – wolframite – molybdenite veins was followed by the sulfide mineralisation during metasomatic replacement of limestone beds. The last stage is represented by veins and vughs filled with quartz, fluorite and carbonates.

During the main period of operations, between 1968 and 1986, attractive specimens of fluorite, quartz and carbonates were collected. A suite of specimens containing assemblages of unusual fluorides and carbonates was also preserved, although where in the deposit they originated is uncertain. Exceptional crystals of rare minerals such as morinite and gearksutite are present, along with K-rich feldspar, bertrandite, siderite and vivianite. The crystal structure of gearksutite was determined using a crystal from this assemblage [2]. Several new minerals have also been characterised. Pseudo-octahedral crystals of a mineral with the stoichiometry of ralstonite, containing significant calcium, were described in the 1990s [3]; with more detailed investigation these have now been identified as a new species, approved by the IMA (CNMNC) in 2009. The new mineral has a crystal structure based on a modified pyrochlore framework that is possibly unique amongst published structures of pyrochlore-like minerals in having 1:3 ordering of Ca and Na in the *A* site and Al and Mg in the *B* site [4]. Another new species (IMA 2009-046), forming silky white dustings, has been shown to be the monoclinic polymorph of a member of the schorl–dravite (tourmaline) series, in which cation ordering of Fe^{2+} and $Mg^{2+}/Li^{+}/Al^{3+}$ cations on the *Y*- site has resulted in lowering of the symmetry.

Fluid inclusion and stable isotope data [1] indicate that these unusual assemblages probably crystallised during the final stage of mineralisation, from hydrothermal fluids that were moderately saline and low in CO_2, at temperatures between 250 and 300°C.

[1] Collins, P.L.F. (1981) *Econ. Geol.*, **76**, 365-392. [2] Marchetti, F. & Perchiazzi, N. (2000) *Am. Mineral.*, **85**, 231-235. [3] Birch, W.D. & Pring, A. (1990) *Mineral. Mag.*, **54**, 599-602. [4] Mumme, W.G. et al. (2010) *Am. Mineral.*, **95**, 736-740.

$Pb_2(S_2O_3)(CO_3)$: the first naturally occurring thiosulphate carbonate and its atomic arrangement

Kolitsch, U.
Mineralogisch-Petrographische Abt., Naturhistorisches Museum, Vienna, Austria (uwe.kolitsch@nhm-wien.ac.at)

A new lead(II) thiosulphate carbonate has been discovered on specimens from two Medieval mine dumps in the Leogang district, Salzburg, Austria. It forms small sprays of colourless to white prismatic crystals (up to 0.4 mm in length, with chisel-like crystal terminations) in thin fissures of massive galena. Further associated species are cerussite, anglesite, rare sulphur and very rare phosgenite.

The crystal structure has been determined using single-crystal X-ray diffraction data (Mo*Kα*, 298 K) which led to the formula $Pb_2(S_2O_3)(CO_3)$, confirmed by chemical analyses (SEM-EDS) and Raman spectroscopy. The new mineral is orthorhombic, space group *Pnma* (no. 62), with a = 16.343(1), b = 8.760(2), c = 4.592(3) Å, V = 657.4(5) Å^3, Z = 2 [$R1(F)$ = 4.2 %]. The structure is built up of an irregular Pb-O polyhedron, a thiosulphate ($S^{6+}O_3S^{2-}$ = S_2O_3) group and a CO_3 group. It has a layered character (Fig. 1), with (100) layers of Pb-O polyhedra and CO_3 groups alternating with layers of distorted $S^{6+}O_3S^{2-}$ tetrahedra. The Pb atom is coordinated by O ligands of the CO_3 groups and $S^{6+}O_3S^{2-}$ tetrahedra; there are only weak interactions between Pb and the anionic S atom.

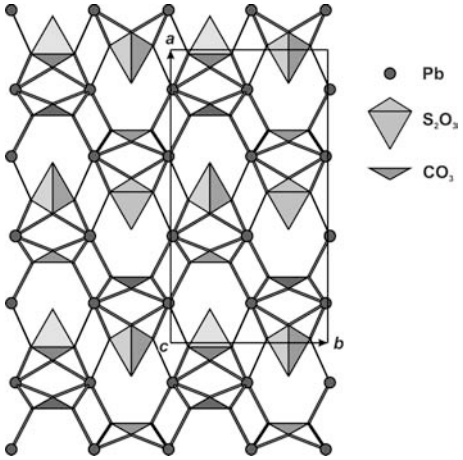

Fig. 1: Crystal structure of $Pb_2(S_2O_3)(CO_3)$, view along [001].

The lone electron pair on the Pb^{2+} cation is stereochemically active. The geometry of the thiosulphate group is in good agreement with literature data (*e.g.*, brief review in [1]). $Pb_2(S_2O_3)(CO_3)$, is a new representative in the very small group of known thiosulphate minerals [viaeneite - $(Fe,Pb)_4S_8O$, sidpietersite - $Pb^{2+}{}_4(S_2O_3)O_2(OH)_2$, steverustite - $Pb^{2+}{}_5(OH)_5(Cu^{1+}(S_2O_3)_3)(H_2O)_2)$] and naturally occurring thiosulphate phases in slags [$Ba(S_2O_3)\cdot H_2O$, $Ba_2F_2(S_2O_3)$].

$Pb_2(S_2O_3)(CO_3)$ is the product of partial oxidation of galena ore, with both S^{2-} and S^{6+} being present. A further occurrence of the new phase at an old mine in the Black Forest, Germany, has been confirmed very recently by a single-crystal structure refinement. These observations confirm previous conclusions ([2] and references therein) that thiosulphate minerals play an underrated role in the mineralogy of ore deposits.

The new species will be submitted for approval to the IMA CNMNC.

[1] Cooper, M.A. & Hawthorne, F.C. (1999) *Can. Mineral.*, **37**, 1275-1282. [2] Kucha, H. et al. (1996) *Eur. J. Mineral.*, **8**, 93-102.

"Galloepidote" – a potential new end-member of the epidote group

Varlamov, D.A.[1*], Soboleva, A.A.[2] & Mayorova, T.P.[2]
[1]Inst. of Experimental Mineralogy, Russian Academy of Sciences, Chernogolovka, Russia ([*]dima@iem.ac.ru)
[2]Institute of Geology, Komi Scientific Centre, RAS Ural Branch, Syktyvkar, Russia

During a mineralogical study of Tykatlova gold-sulfide ore (northern area of the Sub-Polar Urals) a unique complexly zoned ultrahigh gallium (up to 14.5 wt.% of Ga) mineral of the epidote-allanite group was discovered. As far as known, no other gallium silicate mineral has been described.

The Tykatlova ore occurrence is situated in Early Ordovician acid volcanic rocks (rhyolites, rhyodacites) metamorphosed to greenshists facies, and is located in zones of schistosity and secondary silicification with superimposed sulfide mineralization. Ga- bearing phases have been found in sphalerite-pyrite veins with later galena and subordinate quantities of chalcopyrite.

Gallium-bearing phases are represented by minerals of the epidote-allanite group with complexly zoned structure. Usually they are inclusions in sulfides (often in sphalerite, seldom in pyrite), but sometimes are intergrown with sulphides; very rarely, small single grains are associated with gangue minerals.

Sizes of gallium epidote-allanite grains are typically 30-60 and, sometimes up to 100 microns across. Usually they have a complex concentric zoned structure, but in rare cases zones appear as separate homogeneous grains (10-15 microns). The general sequence of zones (from centre to rims) is (a) "galloepidote" (6-20 wt.% Ga_2O_3, REE are almost absent), (b) high-gallium allanite-(Ce) (3-11 Ga_2O_3, 3-20 wt.% REE), (c) allanite-(Ce) (0.0-2.0 Ga_2O_3, 4-19 wt.% REE), (d) epidote-allanite (Ga absent, 0-6 wt.% REE). Calculated formula of the richest Ga-bearing materials are $(Ca_{1.85}Mg_{0.11}Mn_{0.02})_{1.98}(Al_{1.89}Ga_{1.03}Fe^{3+}{}_{0.16})_{3.08}(Si_{2.93}Al_{0.07})_3O_{12}(OH)$ and $(Ca_{1.88}Mg_{0.15}Mn_{0.03})_{2.06}(Al_{1.77}Ga_{0.97}Fe^{3+}{}_{0.26})_{3.00}(Si_{2.91}Al_{0.09})_3O_{12}(OH)$.

Relationships to the epidote group have been drawn in terms of chemical composition and stoichiometry, Raman spectroscopy (measured spectra correlate very well with an epidote reference spectrum), substitution of almost half of the calcium ions by REE (characteristic for the epidote group), and morphologies of grains.

The structure of the mineral is not yet clear, but it is assumed that Ga^{3+} substitutes for Fe^{3+} ions and affect the heterovalent Ca ↔ REE substitution (epidote ↔ allanite). In external zones, lower gallium concentrations allow REE to substitute the epidote structure, as gallium vacates a large octahedral site where bivalent ions (Fe^{2+}, Mg, Mn) can enter for charge compensation for trivalent REE cations.

The richest Ga analyses almost ideally correspond to the formula $Ca_2Al_2Ga[Si_2O_7][SiO_4]O(OH)$, "galloepidote", and other analyses are placed between end-members of the ternary system epidote – "galloepidote" – allanite-(Ce). Thus, we propose that we have found a new end-member of the epidote group, "galloepidote" (a potential future name). The mineral has not yet been submitted for approval to the IMA CNMNC due to absence of the X-ray and another necessary data, but we hope to correct this lack in the near future.

Heteropolymolybdates: structural relationships, nomenclature scheme and new species

Kampf, A.R.[1*], Mills, S.J.[2] & Rumsey, M.S.[3]
[1]Mineral Sciences Dept., Natural History Museum of Los Angeles County, Los Angeles, CA, USA ([*]akampf@nhm.org)
[2]Dept of Earth and Ocean Sciences, University of British Columbia, Vancouver, BC, Canada
[3]Mineralogy Dept., The Natural History Museum, London, England, UK

The molybdoarsenates betpakdalite, natrobetpakdalite and obradovicite and the molybdophosphates mendozavilite, paramendozavilite and melkovite typically occur as coatings of minute, poor-quality and/or complexly twinned crystals. Heretofore, the structure of only betpakdalite had been determined. In this investigation, we examined type material for all of these minerals, as well as similar material from other sources, in an effort to elucidate the interrelationships within this enigmatic family of minerals.

Comparative powder X-ray diffraction proved effective in identifying structurally related phases and obtaining refined cell parameters for those phases for which single-crystal studies could not be conducted. Electron microprobe analyses were performed for all species studied and optimal conditions for analysis were determined. These methods indicated that natrobetpakdalite, mendozavilite and melkovite are isostructural with betpakdalite and suggested that obradovicite has a closely related structure.

Single-crystal investigations yielded several new structure refinements and the solution of the structure of obradovicite. Although crystals of paramendozavilite were inadequate for collection of structure data, cell parameters were for the first time determined. Both the betpakdalite and obradovicite structure types are based upon frameworks containing four-member clusters of edge-sharing MoO_6 octahedra which link by sharing corners with other clusters, with $Fe^{3+}O_6$ octahedra and with PO_4 or AsO_4 tetrahedra. The structures differ with respect to their linkages through the $Fe^{3+}O_6$ octahedra, leading to substantially different, but closely related framework configurations. The cell parameters of paramendozavilite indicate that its structure may be related to those of betpakdalite and obradovicite. We suggest that these minerals be termed "heteropolymolybdates".

Besides the presence of As or P in the tetrahedral site (*T*) of the frameworks, the non-framework cation sites are key to discriminating different species with these structures. One generally smaller cation site (*B*) at a center of symmetry is octahedrally coordinated to H_2O molecules and two or more disordered, partially occupied, generally larger, cation sites (*A*) are coordinated to O atoms in the framework and H_2O molecules. The general formulas for minerals with either the betpakdalite or the obradovicite structure are the same: $[A_2(H_2O)_nB(H_2O)_6][Mo_8T_2Fe^{3+}{}_3O_{30+7}(OH)_{7-x}]$, where: x is the total charge of $A + B$ and n is variable. Dominant cations noted in the *A* sites include K, Na and Ca and in the *B* sites Na, Ca, Mg, Cu and Fe. The various combinations that we identified define at least eight new heteropolymolybdate species.

We believe that a suffix-based nomenclature is most appropriate for the heteropolymolybdates with root names based upon the structure types and the *T* sites cations: betpakdalite (T = As), mendozavilite (T = P) and obradovicite (T = As); followed by two suffixes of the form: *-AB*, corresponding to the dominant cations in the two different types of non-framework cation sites. A new root name would be required for any new obradovicite structure species with T = P.

Our investigation of the paramendozavilite type specimen showed it to contain no paramendozavilite, but rather an apparently closely related new mineral. Another sample of paramendozavilite analyzed showed K > Na.

Qingheiite-(Fe^{2+}), $Na_2Fe^{2+}MgAl(PO_4)_3$, a new member of the wyllieite group

Hatert, F.[1*], Baijot, M.[1] & Philippo, S.[2]
[1]Laboratory of Mineralogy, University of Liège, Belgium ([*]fhatert@ulg.ac.be)
[2]Natural History Museum, Luxembourg

Qingheiite-(Fe^{2+}), ideally $Na_2Fe^{2+}MgAl(PO_4)_3$, is a new mineral species from the Sebastião Cristino pegmatite, Minas Gerais, Brazil [1]. It occurs as rims around frondelite grains, included in a matrix of quartz and albite. The empirical formula is $(\square_{0.65}Na_{0.35})(Na_{0.58}Mn^{2+}_{0.40}Ca_{0.02})$ $(Fe^{2+}_{0.68}Mn^{2+}_{0.32})$ $(Mg_{0.72}Fe^{3+}_{0.23}Fe^{2+}_{0.05})(Al_{0.62}Fe^{3+}_{0.38})[PO_4]_3$, and the single-crystal unit-cell parameters are a = 11.910(2), b = 12.383(3), c = 6.372(1) Å, β = 114.43(3)°, V = 855.6(3) Å^3, space group $P2_1/n$. Qingheiite-(Fe^{2+}) is the Fe^{2+} analogue of qingheiite $[Na_2MnMgAl(PO_4)_3]$, and belongs to the wyllieite group of minerals. The mineral species and its name were approved by the Commission on New Minerals, Nomenclature and Classification of the International Mineralogical Association (CNMNC-IMA) under the number 2009-076.

The crystal structure of qingheiite-(Fe^{2+}) has been refined, based on single-crystal X-ray diffraction data, to R_1 = 2.91 %. The basic structural unit is identical to that of other members of the wyllieite group, and consists of kinked chains of edge-sharing octahedra stacked parallel to {101}. These chains are formed by a succession of M(2a)-M(2b) octahedral pairs, linked by highly distorted M(1) octahedra. Equivalent chains are connected in the *b* direction by the P(1), P(2a) and P(2b) phosphate tetrahedra to form sheets oriented perpendicular to [010]. These interconnected sheets produce channels parallel to *c*, channels that contain the large X sites. The X(1a) site is a distorted octahedron, whereas the X(1b) site can be described as a very distorted cube. The morphology of the X(2) site corresponds to a very distorted gable disphenoid with a [7+1] coordination, similar to the X(2) site of rosemaryite [2] and to the A(2)' site of the alluaudite structure.

The structural features of qingheiite-(Fe^{2+}) are compared to those of other wyllieite-type phosphates: ferrorosemaryite from the Rubindi pegmatite, Rwanda ($\square NaFe^{2+}Fe^{3+}Al(PO_4)_3$, R_1 = 2.43 %, a = 11.838(1), b = 12.347(1), c = 6.2973(6) Å, β = 114.353(6)°) [3], rosemaryite from the Buranga pegmatite, Rwanda ($\square NaMnFe^{3+}Al(PO_4)_3$, R_1 = 4.01 %, a = 12.001(2), b = 12.396(1), c = 6.329(1) Å, β = 114.48(1)°) [2], wyllieite from the Buranga pegmatite ($Na_2MnFe^{2+}Al(PO_4)_3$, R_1 = 2.74 %, a = 11.954(2), b = 12.439(2), c = 6.406(1) Å, β = 114.54(1)°), and qingheiite from the Santa Ana pegmatite, Argentina (R_1 = 2.65 %, a = 11.878(3), b = 12.448(2), c = 6.438(2) Å, β = 114.49(1)°). These new structural data indicate that Al is predominant on the M(2a) site in the investigated samples, not on the M(2b) site as observed in ferrowyllieite [4]. The morphologies of the X(1a), X(1b), and X(2) crystallographic sites are also compared among the different minerals of the wyllieite group.

[1] Hatert, F. et al. (2010) *Eur. J. Mineral.*, **22(3)**, 459-467. [2] Hatert, F. et al. (2006) *Eur. J. Mineral.*, **18**, 775-785. [3] Hatert, F. et al. (2005) *Eur. J. Mineral.*, **17**, 749-759. [4] Moore, P.B. & Molin-Case, J. (1974) *Am. Mineral.*, **59**, 280-290.

New and potentially new garnets from altered xenoliths within ignimbrites of the Upper Chegem caldera, Northern Caucasus

Galuskina, I.O.[1*], Galuskin, E.V.[1], Armbruster, T.[2], Gazeev, V.M.[3], Lazic, B.[2], Dzierżanowski, P.[4], Prusik, K.[5], Pertsev, N.N.[4], Winiarski, A.[6], Kusz, J.[6], Zadov, A.E.[7], Wrzalik, R.[6] & Gurbanov, A.G.[4]

[1]Faculty of Earth Sciences, University of Silesia, Poland ([*]irina.galuskina@us.edu.pl)

[2]Mineralogical Crystallography, Institute of Geological Sciences, University of Bern, Switzerland

[3]Institute of Geology of Ore Deposits, Petrography, Mineralogy and Geochemistry (IGEM), RAS, Moscow, Russia

[4]Institute of Geochemistry, Mineralogy and Petrology, University of Warsaw, Poland

[5]Institute of Materials Science, University of Silesia, Poland

[6]August Chełkowski Institute of Physics, University of Silesia, Poland

[7]OOO Science-Research Center NEOCHEM, Moscow, Russia

New garnets with exotic composition: bitikleite-(SnAl) $Ca_3Sb^{5+}SnAl_3O_{12}$, bitikleite-(ZrFe) $Ca_3Sb^{5+}ZrFe^{3+}{}_3O_{12}$, toturite $Ca_3Sn_2Fe^{3+}{}_2SiO_{12}$, and elbrusite-(Zr) $Ca_3U^{6+}ZrFe^{3+}{}_2Fe^{2+}O_{12}$ [1], were found in the high-temperature skarns developed inside altered carbonate-silicate xenoliths captured by ignimbrites of the Upper Chegem caldera [2]. Primary high-temperature minerals of the ellestadite group, wadalite, rondorfite, lakargiite, srebrodolskite, kimzeyite and its Fe^{3+}-analog (IMA2009-029) are developed in three main skarn zones: I – spurrite, II – Ca-humite (chegemite, kumtyubeite, reinhardbraunsite), III – cuspidine (near-contact zone, formed after primary larnite zone). Bitikleite-(SnAl), bitikleite-(ZrFe) and toturite, and also grossular, andradite and schorlomite are found only in cuspidine zones together with fluorite. Elbrusite-(Zr) was detected both in spurrite and cuspidine zones. Low-temperature minerals are represented by garnets of the katoite-hibschite series, bultfonteinite, ettringite-group minerals, kalumite and numerous calcium hydrosilicates. Composition and structural investigations of high-temperature garnets belonging to the $Ca_3(Zr,Sn,Sb,U,Ti...)_2(Fe,Al,Si,Ti...)_3O_{12}$ solid-solution series and application of the dominant valence rule [3] allowed to distinguish additional new garnet-group minerals: 1) Sn-analog of elbrusite-(Zr) with the end-member formula $Ca_3U^{6+}SnFe^{3+}{}_2Fe^{2+}O_{12}$; 2) garnet of the bitikleite series with formula $Ca_3Sb^{5+}SnFe^{3+}{}_3O_{12}$; 3) Al-analog of toturite $Ca_3Sn_2Al_2SiO_{12}$; 4) Ti-analog of toturite $Ca_3Sn_2Fe^{3+}{}_2TiO_{12}$; 5) Ti-analog of Fe^{3+}-dominant kimzeyite $Ca_3Zr_2Fe^{3+}{}_2TiO_{12}$. Caucasian xenoliths are unique with regard to the number of different garnet-group minerals. To our knowledge, there are 16 garnet species, either new or potentially new minerals. Some of these garnets are non-silicates (ferrites and aluminates) but form a complete solid-solution series with kimzeyite and toturite. Therefore, CNMNC IMA decided to classify them in the garnet group. Such a decision opens the possibility to reorganize the garnet-group classification.

[1] Galuskina, I.O. et al. (2010) *Am. Mineral.*, **95**, 959-967. [2] Gazeev, V.M. et al. (2006) *Vestnik Vladikavkazskogo Nauchnogo Tsentra*, **6**, 18-27. [3] Hatert, F. & Burke, E.A.J. (2008) *Can. Mineral.*, **46**, 717-728.

Chemical classification of tourmalines using the RHA method

Andriyanets-Buyko, A.*, Petrov, T. & Krasnova, N.
Saint-Petersburg State University, St.-Petersburg, Russia
(*a-baa@mail.ru)

A representation of the mineral chemistry for the tourmaline group needs a series of ternary diagrams (up to 16!), any of which, however, can't clearly display the complexity of even one mineral species [1]. We compiled a collection of 788 chemical analyses of natural tourmalines from 33 occurrences. These chemical data were classified using the PETROS program (author S.Moshkin), based on a method developed by T. Petrov [2], and as a result, we obtained the set of ordered RHA data.

R, the rank formula, is a sequence of chemical elements symbols of any analysis ordered on decreasing of their atomic %. En, the information entropy, is the characteristic reflecting complexity of the composition. An, the anentropy, reflects the purity of analysis. The diversity of our tourmalines compositions is represented in uniform hierarchical RHA table, where rank formulae are ordered as in dictionaries according to the number of elements in the Periodic Table. Our RHA-data can be searched in Internet by name: RHA language-method with cited files RHA-Tourmaline-2005.rar, RHA-Tur-Groups-2005.rar and Help_Turm-En on web-site: http://geology.pu.ru/.

Examples of rank formulae (R) for main tourmaline species are shown in Table 1 (elements in brackets can exchange in their rank position):

Table 1: Rank formulas of main tourmaline species

OAlSi(HB)**Li**(**Na**F...)	elbaite
OAlSi(HB**Li**)(**Ca**FNa...)	liddicoatite
O(AlSi)(HB**Mg**)(**NaV**Ca)…	vanadiumdravite
O(AlSi)(HB**MgCr**Na)...	chromdarvite
O(AlSi)(HB)**Mg**(**Na**Fe)…	dravite
OAlSi(HB)(**MnNa**FLi...)	tsilaisite
O(AlSi)(HB**Fe**)(**Na**Mg…)	schorl

In isomorphic rows, the predominance of one element over next in rank formulas can be used for impartial distinguishing of different mineral species. For example: when Mg > Fe – dravites, Fe > Mg – schorls. Combination of bold element symbols point at species inside the tourmaline group. Our suggestions for tourmaline chemical classification in more detail were published in [3].

The RHA-method gives the possibility to allocate the simple and clear-cut groups of the basic mineral species and subspecies; to define them authentically; to search for analogues without preliminary identification of a mineral variety; to estimate the originality of compositions. The RHA-method expands opportunities for improving nomenclature of minerals.

The RHA Database can be integrated in uniform classification of all mineral and rock compositions.

[1] Hawthorne, F.C. & Henry, D.J. (1999) *Eur. J. Mineral.*, **11**, 201-215. [2] Petrov, T.G. (2008) *Otechestvennaya Geologiya*, **4**, 98-105 (in Russian). [3] Andriyanets-Buyko, A.A., et al. (2007) *Zap. Ross. Mineral. Obshchest.*, **136**, 26-41 (in Russian).

Manganoeudialyte, a new mineral from Poços de Caldas, Minas Gerais, Brazil

Atencio, D.[1*], Nomura, S.F.[1], Chukanov, N.V.[2], Rastsvetaeva, R.K.[3], Coutinho, J.M.V.[1] & Karipidis, T.K.[3]
[1]Instituto de Geociências, Universidade de São Paulo, Brazil
(*datencio@usp.br)
[2]Inst. of Problems of Chemical Physics, Moscow Oblast, Russia
[3]Inst. of Crystallography, Russian Academy of Sciences, Moscow, Russia

Manganoeudialyte is a new mineral with ideal formula $Na_{14}Ca_6Mn_3Zr_3[Si_{26}O_{72}(OH)_2]Cl_2 \cdot 4H_2O$, from a khibinite from the northern edge ("Anel Norte") of the alkaline Poços de Caldas massif, Minas Gerais, Brazil. It is concentrated in cm-sized patches interstitial to the main minerals of the rock. Associated minerals are eudialyte, K-feldspar, nepheline, aegirine, analcime, sodalite, rinkite, lamprophyllite, astrophyllite, titanite, fluorite, and cancrinite. Color is pink to purple, streak is white, and luster is vitreous. It is transparent to translucent and is not fluorescent. Mohs hardness is between 5 and 6, tenacity is brittle. Measured density is 2.890 g/cm^3; the calculated density is 2.935 g/cm^3. Manganoeudialyte is uniaxial (+), ω = 1.603(2), ε = 1.608(2) (white light). It is nonpleochroic.

The chemical composition is (by WDS mode electron microprobe data, H_2O content determined by the Penfield method, wt.%): Na_2O 12.01, K_2O 0.59, CaO 10.70, MnO 3.51, SrO 3.00, FeO 2.72, Al_2O_3 0.41, La_2O_3 0.15, Ce_2O_3 0.12, SiO_2 48.70, TiO_2 0.47, ZrO_2 12.08, Nb_2O_5 1.21, HfO_2 0.25, F 0.08, Cl 0.99, H_2O 3.5, -O=(Cl,F) -0.26, total 100.23. The empirical formula based on (Si + Al + Zr + Ti + Hf + Nb) = 29 is: $H_{12.08}Na_{12.05}Sr_{0.90}K_{0.39}La_{0.03}Ce_{0.02}Ca_{5.93}(Mn_{1.54}Fe_{1.18})Zr_{3.03}Nb_{0.28}Al_{0.25}Hf_{0.04}Ti_{0.18}Si_{25.20}O_{79.40}Cl_{0.87}F_{0.13}$.

The crystal structure was solved on a single crystal to R = 0.033. The mineral is trigonal, $R3m$; a = 14.2418(1), c = 30.1143(3) Å, V = 5289.7(1) Å^3, Z = 3. The coordination numbers are 6 for Mn, and 5 for Fe. The distorted octahedron $[MnO_4(H_2O)_2]$ contains two types of H_2O molecules. The crystal chemical formula of manganoeudialyte is: $[Na_{11.93}Sr_{0.81}(H_3O)_{0.70}K_{0.39}Ce_{0.07}]_{\Sigma 13.90}Ca_6]$ $[^{VI}Mn_{1.56}{}^{V}Fe_{1.20}{}^{V}Na_{0.24}]_{\Sigma 3.00}$ $[Zr_3]$ $[^{IV}(Si_{0.38}Al_{0.25})^{VI}(Nb_{0.29}Zr_{0.08})]_{\Sigma 1.00}$ $[^{IV}Si_{0.81}{}^{VI}Ti_{0.19}]_{\Sigma 1.00}$ $[Si_{24}O_{72}]$ $[(OH)_2][(H_2O)_{3.55}Cl_{0.88}(OH)_{0.84}O_{0.40}$ $F_{0.13}]_{\Sigma 5.80}$. The strongest reflection peaks of the powder diffraction pattern [d, Å (I, %) (hkl)] are: 6.421 (37) (104), 4.329 (30) (205), 3.526 (46) (027), 3.218 (100) (208), 3.023 (25) (042), 1.609 (77) (4.1.15), 1.605 (41) (4.0.16). IR spectrum shows that the mineral contains at least two locally different types of water molecules (the bands at 1620 and 1677 cm^{-1}) and the polyhedra $[Fe^{2+}O_5]$ (the band at 529 cm^{-1}). The new mineral species has been approved by the CNMNC (IMA 2009-039).

Classification and potential new minerals in the "mayenite group"

Bailau, R.[1*], Galuskin, E.V.[1], Gazeev, V.M.[2] & Pertsev, N.N.[2]
[1]Faculty of Earth Sciences, University of Silesia, Sosnowiec, Poland (*rbailau@gmail.com)
[2]Institute of Geology of Ore Deposits, Petrography, Mineralogy and Geochemistry (IGEM) RAS, Moscow, Russia

The natural analogue of "Cl-mayenite" ($Ca_{12}Al_{14}O_{32}Cl_2$) and "Fe-wadalite" ($Ca_{12}Fe_8Si_6O_{32}Cl_8$), two new potential minerals, were discovered in the altered calcareous silicate xenoliths in ignimbrites of Upper Chegem caldera, Northern Caucasus, Kabardino-Balkaria, Russia. "Cl-mayenite" was formed from mayenite $^{VIII}Ca_{12}(^{IV}Al_8)^1(^{IV}Al_6)^2O_{33}$ by $O^{2-} = 2Cl^-$ replacement, for example $Ca_{12}[Al_{12.98}Fe^{3+}_{0.81}Si_{0.16}Ti^{4+}_{0.04}S^{6+}_{0.01}]_{14.00}O_{31.98}(OH)_{0.05}Cl_{2.28} \times 3H_2O$ [1]. Further, substitutions of Al^{3+} (Fe^{3+}) $\rightarrow Si^{4+} + Cl^-$, $2Al^{3+}$ (Fe^{3+}) $\rightarrow Si^{4+} + Mg^{2+}$ and $Ca^{2+} + Al^{3+}$ (Fe^{3+}) $\rightarrow Na^+ + Si^{4+}$ generated wadalite, $[Ca_{12.01}Na_{0.14}]_{12.15}[Al_{9.21}Si_{4.07}Mg_{0.15}Fe^{3+}_{0.46}Ti^{4+}_{0.03}Mn_{0.02}]_{13.95}Cl_{5.44}F_{0.03}$ and "Fe-wadalite" $[Ca_{12.10}Na_{0.02}]_{12.12}[Fe^{3+}_{9.07}Si^{4+}_{3.2}Al_{1.55}Ti_{0.06}V^{5+}_{0.01}]_{13.88}Cl_{4.91}$.

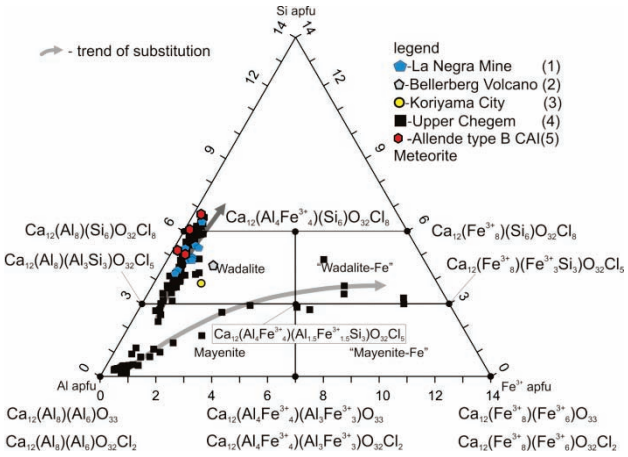

Fig. 1: Classification Si-Al-Fe^{3+}(apfu) diagram of "mayenite group" minerals: (1) wadalite from La Negra mine, Mexico [2]; (2) wadalite from Bellerberg Volcano, Germany [3]; (3) holotype wadalite from Koriyama City, Japan [4]; (4) Minerals of the "mayenite group" from Upper Chegem, Russia; (5) wadalite from Allende type B CAI meteorite [5].

Shorter Al^2-O distances compared with Al^1-O can be related to the prevailing substitution of Si in the Al^2 site [6]. The maximum number of substituted Al atoms by Si in the Al^2 site is 6 apfu [6]. Based on this fact, we propose the boundary between mayenite and wadalite-like minerals at 3 Si pfu. Some wadalite analyses show Si content higher than 6 apfu (Fig. 1), because the small amount of Si goes to the Al^1 site. The Fe^{3+} substitution of Al determines the Fe-rich wadalite and further "Fe-wadalite". The presence of a poorly bonded O atom facilitates its exchange by $2(Cl^-,OH^-)$, giving phases of composition $Ca_{12}Al_{14}O_{32}[O,(OH)_2,Cl_2]$ [7].

[1] Galuskin, E.V. et al. (2009) *Eur. J. Mineral.*, **21**, 1045-1059. [2] Kanazawa, Y. et al. (1997) *Geol. Surv. Japan*, **48**, 413-420. [3] Mihajlović, T. et al. (2004) *N. Jb. Miner. Abh.*, **179**, 265-294. [4] Tsukimura, K. et al. (1993) *Acta Crystallogr.*, **C49**, 205-207. [5] Ishii, H.A. et al. (2010) *Am Mineral.*, **95**, 440-448. [6] Feng, Q.L. et al. (1988) *Acta Crystallogr.*, **C44**, 589-592. [7] Glasser, F.P. (1995) *Acta Crystallogr.*, **C51**, 340.

Kircherite, a new mineral of the cancrinite-sodalite group with a 36-layer stacking sequence: occurrence and crystal structure

Bellatreccia, F.[1*], Cámara, F.[2], Della Ventura, G.[1], Gunter, M.E.[3], Cavallo, A.[4] & Sebastiani, M.[5]
[1]Dipto. di Scienze Geologiche, Università di Roma Tre, Rome, Italy (*bellatre@uniroma3.it)
[2]CNR-Istituto di Geoscienze e Georisorse, UOS Pavia, Italy
[3]Dept. of Geological Sciences, University of Idaho, Moscow, Idaho, USA
[4]Istituto Nazionale di Geofisica e Vulcanologia, Rome, Italy
[5]Dipto. di Ingegneria Meccanica e Industriale, Università di Roma Tre, Rome, Italy

We relate here the occurrence and the crystal structure of kircherite (IMA 2009-084), a new member of the cancrinite-sodalite group of minerals from Valle Biachella, Sacrofano, (Rome), in the Sabatini volcanic complex, Latium, Italy. The mineral occurs within miarolitic cavities of holocrystalline, syenitic, volcanic ejecta, associated with sodalite, biotite, iron oxides, titanite, fluorite, and a pyrochlore group mineral. The groundmass of the ejecta consists essentially of potasium-feldspar, with minor sodalite and brown mica.

Kircherite occurs typically as parallel associations of hexagonal, thin, tabular crystals (2 or 3 mm in diameter and 1 mm in thickness). Single platelets have a thickness that very rarely exceeds 0.5 mm. Crystals are colourless to light gray to white, translucent to opaque in the most altered parts of the crystals; lustre is greasy to silky. Fluorescence is in light pink under LW UV and deep red under SW UV. Hardness is (Mohs): 5.5; micro-indentation VHN load 10 g, mean 648.4 kg mm^{-2}, range ± 208.9 kg mm^{-2}. Cleavage on {001} is good. Density (calc.) is 2.457 g cm^{-3}. Kircherite is non-pleochroic and uniaxial negative with $\omega = 1.510(2)$, $\varepsilon = 1.502(2)$.

Kircherite is trigonal, space group *R*32, with , a = 12.8770(7) Å, c = 95.224(6) Å, V = 13677.2(13) $Å^3$, Z = 1. The empirical chemical formula obtained from EMP analyses is: $(Na_{89.09}Ca_{31.63}K_{18.85}Fe_{0.20}Mn_{0.06}Mg_{0.05}Ti_{0.03})_{\Sigma=139.91}$ $(Si_{108.13}Al_{107.87})_{\Sigma=216.00}O_{430.08}(SO_4)_{32.59}$ $Cl_{2.00}F_{0.53}(CO_3)_{0.09} \cdot 6.86H_2O$, which corresponds to the ideal formula $[Na_{90}Ca_{36}K_{18}]_{\Sigma=144}(Si_{108}Al_{108}O_{432})(SO_4)_{36} \cdot 6H_2O$.

The strongest six reflections in the X-ray powder pattern are [d in Å (I %) (*hkl*)]: 3.72 (100) (300), 2.65 (100) (2.1.28; 0.0.36), 3.23 (65) (2.1.19), 3.58 (60) (1.2.14), 3.60 (53) (1.0.25), 3.80 (52) (1.2.11).

The single-crystal FTIR spectrum rules out OH groups and shows the presence of H_2O and CO_2 molecules in the structural cages of the mineral.

The structure can be described as a stacking sequence of 36 layers of six-membered rings of tetrahedra along the c axis as ACABCABCABCACBCABCABCABCBABCABCABCAB…, where A, B and C represent the positions of the rings within the layers. The structure has 6 cancrinite cages (C), 24 sodalite cages (S) and 6 LOSOD cages (L) within the unit cell, and these account for a maximum of 36 SO_4^{2-} groups and 6 H_2O molecules (or Cl anions). There is a unique sequence of cages, єSSSLSSLSSSє and adjacent sequences are shifted 1/3 along [001]. Kircherite, having 36 layers, is the cancrinite with the longest complex sequence described to date.

The name is for Athanasius Kircher (1602–1680), a German Jesuit who was the founder of the museum of the Collegium Romanum in 1651, hereafter named the Museum Kircherianum.

Ambrinoite $(K,NH_4)_2(As,Sb)_8S_{13}\cdot H_2O$, the first natural (K,NH_4)-hydrated sulfosalt, from Signols (Piedmont, Italy)

Bonaccorsi, E.[1], Biagioni, C.[1], Moëlo, Y.[2], Pasero, M.[1*] & Bersani, D.[3]
[1]Dipto. di Scienze della Terra, Università di Pisa, Italy
([*]pasero@dst.unipi.it)
[2]Institut des Matériaux Jean Rouxel (IMN), Université de Nantes, France
[3]Dipto di Fisica, Università di Parma, Italy

Ambrinoite, ideally $(K,NH_4)_2(As,Sb)_8S_{13}\cdot H_2O$, occurs as a rare mineral species in Triassic evaporitic rocks from Signols, Susa Valley, Piedmont, Italy. It is associated with sulfur and orpiment; in the same occurrence galkhaite was also identified, together with enargite and stibnite. Ambrinoite is red in colour, with a vitreous to resinous lustre. Electron microprobe analyses give (wt.%): K 4.57, Na 0.05, Tl 0.13, N 0.48, As 35.69, Sb 21.69, S 34.69, O 1.52, sum 98.81. With N and O as NH_4 and H_2O, respectively, this gives the following chemical formula: $[K_{1.44}(NH_4)_{0.48}Na_{0.03}Tl_{0.01}][As_{6.00}Sb_{2.00}]S_{13.39}\cdot 1.20H_2O$.

With the data below this gives a calculated density of 3.305 g cm^{-3}. The presence of H_2O and NH_4 was confirmed by micro-Raman spectroscopy (O-H and N-H stretching and bending vibrations).

Ambrinoite is triclinic, space group $P\bar{1}$, with a 9.704(1), b 11.579(1), c 12.102(2) Å, α 112.82(1), β 103.44(1), γ 90.49(1)°, V 1211.6(3) Å^3, Z 2. The strongest X-ray powder diffraction lines [d in Å, (I), (hkl)] are: 10.78 (100) (001), 5.79 (55) (0 $\bar{2}$ 1), 4.23 (35) (102), 5.31 (34) ($\bar{1}$ 02), 5.39 (32) (002).

The crystal structure of ambrinoite was solved by direct methods and refined to R = 0.035 for 2554 reflections with $F_o > 4\sigma(F_o)$. It is based on MS_3 polyhedra (M = As, Sb) sharing corners to form double chains running along [100]; within each chain, trigonal pyramids arranged in M_3S_5 triangular groups alternate with single MS_3 pyramids. (K,NH_4) and H_2O are hosted in channels along [010]; K-S bonds crosslink the double MS_3 chains. H_2O molecules are coordinated to two K ions, but the latter are coordinated only by one H_2O molecule, plus seven or nine S atoms.

According to modular analysis, the crystal structure of ambrinoite corresponds to the stacking along c of two kinds of layer, with common parameters a = 9.7 and b = 11.6 Å, and different widths. The chemical compositions of the two layers are $[(As,Sb)_8S_{13}]^{2-}$ and $[K_2(H_2O)]^{2+}$, respectively. OD theory allowed one to derive two possible MDO polytypes, one triclinic (corresponding to the crystal studied), and the other monoclinic with symmetry $P2_1/c11$.

Ambrinoite belongs to the hutchinsonite merotypic series [1] and is closely related to gillulyite, $Tl_2(As,Sb)_8S_{13}$ [2], and gerstleyite, $Na_2(Sb,As)_8S_{13}\cdot 2H_2O$ [3].

The new mineral has been approved by the IMA CNMNC (2009-071). The name is after Pierluigi Ambrino, a mineral collector.

[1] Makovicky, E. (1997) *EMU Notes Mineral.*, **1**, 237-271. [2] Makovicky, E. & Balić-Žunić, T. (1999) *Am. Mineral.*, **84**, 400-406. [3] Nakai, I. & Appleman, D.E. (1981) *Chem. Letters*, 1327-1330.

Tancaite-(Ce), a new molybdate from Italy

Bonaccorsi, E.[*] & Orlandi, P.
Dipto. di Scienze della Terra, Università di Pisa, Italy
([*]elena@dst.unipi.it)

Tancaite-(Ce), ideally $FeCe(MoO_4)_3\cdot 3H_2O$, is a new mineral species occurring within cavities in the quartz veins which cut the granite at Su Senargiu, Sarroch (CA), Sardinia, Italy. It is a secondary mineral formed in the oxidation zone of a sulphide ore vein. Associated minerals are quartz, muscovite, molybdenite, pyrite and mendozavilite.

Tancaite-(Ce) is red or pale brown in colour, with a vitreous to adamantine lustre. Electron microprobe analyses give (wt.%): SiO_2 0.34, CaO 0.09, Fe_2O_3 11.29, SrO 0.02, La_2O_3 5.04, Ce_2O_3 10.35, Pr_2O_3 1.07, Nd_2O_3 3.66, Sm_2O_3 0.19, ThO_2 2.58, UO_2 0.17, MoO_3 58.62, H_2O 7.43, sum 100.85. It gives the formula: $Fe^{3+}_{1.03}(Ce_{0.46}La_{0.23}Nd_{0.16}Pr_{0.05}Sm_{0.01}U_{0.01}Th_{0.07})_{\Sigma=0.99}(Mo_{2.96}Si_{0.04})_{\Sigma=3.00}O_{12}\cdot 3H_{2.00}O$, which can be simplified as $Fe^{3+}(REE)(MoO_4)_3\cdot 3H_2O$. The calculated density is 3.834 g/cm^3. The presence of H_2O was confirmed by micro-Raman spectrometry (stretching and bending vibrations of O-H).

The X-ray diffraction pattern of tancaite-(Ce) is characterised by a set of strong reflections, which indicate a cubic unit cell, with a = 6.80 Å and space group $Pm\bar{3}m$, plus a set of weaker reflections. By measuring only the strong reflections with a 4-circle diffractometer, it was possible to solve and refine the "average structure" of tancaite (R = 0.032 for 149 unique reflections). The crystal structure consists of FeO_6 octahedra (in violet, Fig. 1a) centred at the origin of the cubic cell and linked together through MoO_4 tetrahedra by corner sharing (Fig. 1b). The molybdate tetrahedra are statistically distributed in four symmetry-related positions, with ¼ occupancy. In the centre of the unit cell the REE cations exhibit 6+3 coordination, bonding six oxygen atoms and three H_2O molecules.

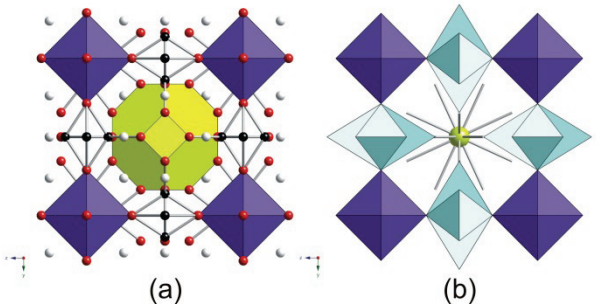

Fig. 1: Crystal structure of tancaite-(Ce) in space group $Pm\bar{3}m$; (a) the REE cation lies within the yellow polyhedron; Fe^{3+}-centred octahedra are indicated in violet; partially occupied Mo, O and H_2O sites are indicated, respectively, by black, red and white spheres; (b) the molybdate groups (light blue tetrahedra) are statistically distributed over four possible and mutually exclusive positions.

The refined structure is clearly an average structure, characterised by statistical disorder which involves the Mo cations, the H_2O molecules and the ligands of the REE cations at the centre of the unit cell. Two intensity data collections were performed in order to measure the weaker reflections and to solve the real crystal structure of tancaite-(Ce). The former was performed at the synchrotron facility Elettra, at the XRD1 beamline; the latter was carried out by means of a CCD-equipped Oxford diffractometer, operating with Mo$K\alpha$ radiation. Both sets of data indicated a larger super-cell with respect to the previous cubic cell with a = 6.80 Å. One of the possible super-cells showed rhombohedral symmetry, with a = 19.2, c = 47.4 Å in the hexagonal setting. The new mineral has been approved by the IMA CNMNC (# 2009-097). The name is after Giuseppe Tanca, mineral collector.

Capranicaite: a new mineral from Capranica, Viterbo, Italy

Callegari, A.M.[1], Boiocchi, M.[2], Bellatreccia, F.[3*], Caprilli, E.[3], Medenbach, O.[4] & Cavallo, A.[5]
[1]Dipto. di Scienze della Terra, Università di Pavia, Italy
[2]Centro Grandi Strumenti, Università di Pavia, Italy
[3]Dipto. di Scienze Geologiche, Università di Roma Tre, Roma, Italy ([*]bellatre@uniroma3.it)
[4]Institute of Geology, Mineralogy and Geophysics, Ruhr-Universität Bochum, Germany
[5]Istituto Nazionale di Geofisica e Vulcanologia, Roma, Italy

Capranicaite, ideally $KCaNaAl_4B_4Si_2O_{18}$, is a new mineral recently approved by the IMA-CNMNC (no. 2009-086), found in the Vico volcanic complex at Capranica, Viterbo, Italy. Capranicaite occurs in miarolitic cavities of a feldspathoid-bearing syenite ejectum, probably formed during late-stage metasomatic processes related to volcanic activity. Capranicaite forms small, tabular crystals no longer than 0.1 mm. Crystals are colourless, with a white streak and a vitreous lustre; they are not fluorescent and have a good {001} cleavage. Capranicaite is biaxial (-) with α = 1.495(1), β = 1.543(1), γ = 1.544(1); 2*V*(obs) = 7.3(2)°. Capranicaite is monoclinic, space group $P2_1/n$, *a* = 4.8507(2), *b* = 16.6156(6), *c* = 20.5445(7) Å, β = 90.245(1)°, *V* = 1655.82(17) Å^3, *Z* = 4. Electron microprobe analysis gives: SiO_2 20.70, Al_2O_3 32.91, B_2O_3 22.90, K_2O 5.36, CaO 11.04, Na_2O 4.08, Cs_2O 2.20, sum 99.19%. Calculated density is 2.41 g cm^{-3}. The formula unit, calculated on the basis of 18 O, is $(K_{0.69}Cs_{0.10})_{\Sigma 0.79}(Ca_{1.19}Na_{0.80})_{\Sigma 1.99}Al_{3.91}B_{3.99}Si_{2.09}O_{18}$.

Capranicaite is a Cs bearing inosilicate with a new topological arrangement of the 2-periodic Si_2O_6 single chains. The crystal structure of capranicaite consists of three overlapping layers of polyhedra (A, B, and C) normal to **c**. The A-layer contains the Si_2O_6 chains that extend along **a**. Respect than pyroxene, in capranicaite the Si-tetrahedra are rotated and the Si_2O_6 groups do not have two apical oxygens pointing towards the same direction. The B-layer is built by isolated AlO_4 tetrahedra and BO_3 triangles connected to form a continuous sheet of six-fold rings (3Al + 3B). Two B-layers are connected to a single sandwiched A-layer to forms a bi-dimensional B-A-B network. The B-A-B networks contain seven fold cavities not completely populated by K and minor Cs. Adjacent B-A-B bi-dimensional networks are linked together *via* the C-layer, constituted by isolated octahedra with a mixed (Ca,Na) population. Along **c** the sequence of layer results C-B-A-B-C-B-A-B-C (Fig. 1).

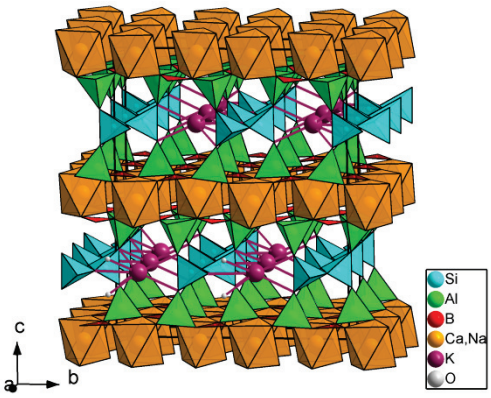

Fig. 1: A simplified sketch of capranicaite structure.

The name is for the locality, Capranica, Latium, Italy, where the holotype was found.

Ni-rich mcguinnessite from Eibenthal, Romania: an intermediate phase toward a new hypothetical rosasite-group end-member

Fehér, B.[1], Szakáll, S.[2*] & Bigi, S.[3]
[1]Dept. of Mineralogy, Herman Ottó Museum, Miskolc, Hungary
[2]Dept. of Mineralogy and Petrology, University of Miskolc, Hungary ([*]askszs@uni-miskolc.hu)
[3]Dept. of Earth Sciences, University of Modena and Reggio Emilia, Modena, Italy

Along the Danube River in the South Banat region (Romania) the gabbro-peridotite massif contains serpentinized dunites. There are some sulphides (*e.g.* chalcopyrite, pentlandite) and secondary minerals (*e.g.* nimite, theophrastite, mcguinnessite, glaukosphaerite) in the fissures of serpentinite.

In the surroundings of Eibenthal rosasite-group minerals occur in great chemical variability, among which the most interesting phase is a Ni-rich mcguinnessite so far. It forms apple green globular aggregates and crusts consisting of 1-2 µm lamellae. It was formed by reaction of primary sulphides and serpentine minerals.

General formula of rosasite-group minerals can be expressed as $M1M2(CO_3)(OH)_2$ where M1 = Cu and M2 = Mg in mcguinnessite. In Eibenthal material considerable amount of Ni substitutes Cu in M1 while M2 = Mg, so it represents an intermediate phase between mcguinnessite and a hypothetical end-member $NiMg(CO_3)(OH)_2$. We performed 15 spot analyses on this material by electron microprobe (see Fig. 1) from which the average composition: NiO 20.18, CuO 23.47, MgO 21.80, CO_2 (calc.) 24.35, H_2O (calc.) 9.97, total 99.77 wt.%. It corresponds to $(Cu_{0.53}\ Ni_{0.47})_{\Sigma=1.00}\ (Mg_{0.98}\ Ni_{0.02})_{\Sigma=1.00}\ (CO_3)\ (OH)_2$.

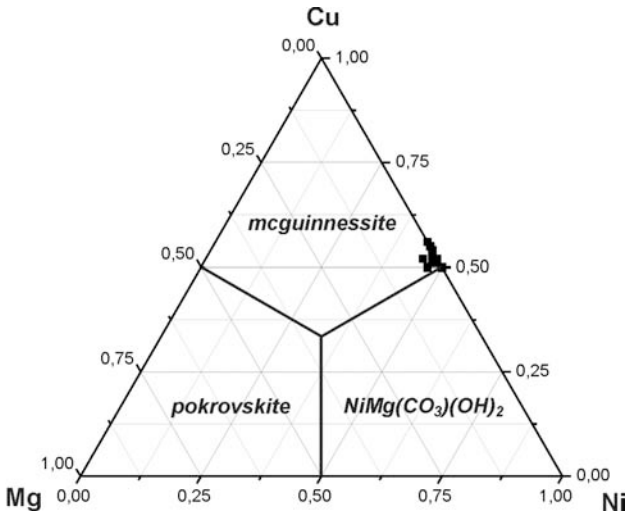

Fig. 1: Ternary diagram of cations in M1 site for Ni-rich mcguinnessite of Eibenthal, where M2 = Mg.

Ni-rich mcguinnessite is monoclinic with space group $P2_1/a$. The refined unit-cell parameters: *a* = 12.98(2), *b* = 9.359(8), *c* = 3.157(3) Å, β = 111.3(2)° are based on 18 reflections in the X-ray powder pattern performed by 114.6 mm Gandolfi camera. It has a cell volume of 357.3(4) Å^3 with *Z* = 4. Calculated density is 3.351 g/cm^3.

Investigated material has been deposited at the mineral collection of Herman Ottó Museum (Miskolc, Hungary) under catalogue number 2009.90.

A new fluorine-rich phase from Eldfell volcano, Iceland

Garavelli, A.[1*], Balić-Žunić, T.[2], Mitolo, D.[1], Acquafredda, P.[1], Leonardsen, E.[3] & Jakobsson, S.P.[4]
[1]Dept. of Geomineralogy, University of Bari, Italy ([*]a.garavelli@geomin.uniba.it)
[2]Dept. of Geography and Geology, University of Copenhagen, Denmark
[3]St. Karlsmindevej, Denmark
[4]Icelandic Institute of Natural History, Reykjavik, Iceland

A new fluorine-rich phase, with ideal formula $CaAlF_5$, was found among fumarolic encrustations collected in 1988 on the Eldfell volcano (Heimaey, Vestmannaeyjar Archipelago, Iceland). The new phase forms a fine-grained mass of 10-50 μm in size (Fig. 1), which was found on 2-3 cm crust on altered scoria of hawaiite [1] deposited after the eruption started on January 23th 1973.

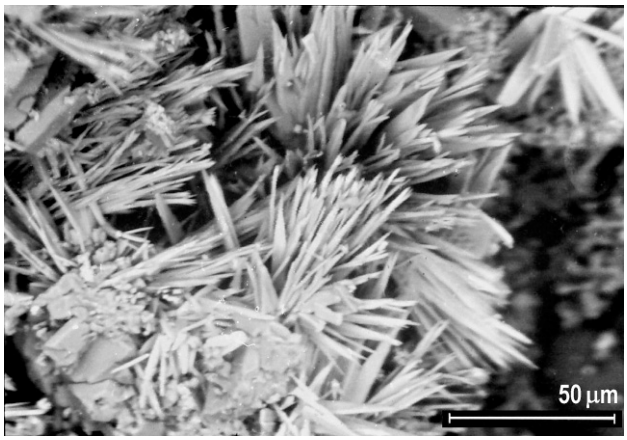

Fig. 1: SEM backscattered image of elongated pointed crystals.

Associated minerals are ralstonite, $Na_xMg_xAl_{2-x}(F,OH)_6 \cdot H_2O$, and another potentially new phase with composition $MgAlF_5 \cdot 1.5H_2O$ [2]. The new phase from Eldfell volcano is colourless to white, transparent, non-fluorescent, has a vitreous lustre and a white streak. The calculated density is 2.79 g/cm^3. SEM-EDS quantitative chemical analysis shows the following range of concentrations (wt.%): Ca 19.15–25.53 (average 21.48), Al 11.42–12.65 (average 11.93), F 52.76–56.30 (average 53.99), O 10.06–14.29 (average 12.24). The empirical chemical formula, calculated on the basis of 7 atoms pfu, is $Ca_{0.84}Al_{0.68}[F_{4.34}(OH)_{1.15}]_{\Sigma=5.49}$. X-ray single-crystal study was prevented by overlapping thin crystals. The X-ray powder diffraction pattern closely resembles that of synthetic α-$CaAlF_5$, which is monoclinic, space group *C*2/*c*. Indexing was performed on the basis of lattice parameters reported for the synthetic analogue (PDF 80-1728). Calculated unit-cell parameters are the following: a = 8.711(5), b = 6.310(4), c = 7.354(6) Å, V = 366.180 Å^3, Z = 4. The strongest reflections in the powder diffraction diagram [d in Å, (I relative to 10)] are: 3.95, (10); 3.17 (9); 3.15, (9); 2.28 (3); 2.01 (1); 1.97, (3); 1.82, (2); 1.77 (2); 1.67 (1).

On the basis of chemical analyses and X-ray data, the new mineral corresponds to the synthetic compound α-$CaAlF_5$ [3] which crystallizes at about 700°C in the system CaF_2-AlF_3 [4].

The new species will be submitted soon for approval to the IMA-CNMNC.

[1] Jakobsson, S.P. et al. (1973) *Lithos*, **6**, 203-214. [2] Feki, M. et al. (1986) *C. R. Acad. Sci. Paris*, **303**, 441-444. [3] Hemon, A. & Courbion, G. (1991) *Acta Crystallogr.*, **C47**, 1302-1303. [4] Holm, J.L. (1965) *Acta Chem. Scandin.*, **19**, 1512-1514.

Drobecite, a novel mineral from the Lavrion, Greece, deposit

Giester, G.[*] & Rieck, B.
Inst. für Mineralogie und Kristallographie, Universität Wien, Vienna, Austria ([*]gerald.giester@univie.ac.at)

Ores of the Manto-Type Cu-Pb-Zn deposits of the Lavrion Mining District [1] are locally enriched in Cd, which leads to a rich suite of Cd-bearing minerals. Primary minerals are greenockite and hawleyite, and secondary minerals niedermayrite [2], otavite, keyite and monteponite have been identified. A detailed study of one such occurrence at the Esperanza Mine revealed the existence of three more species thus far unknown or inadequately described. The mineral with the chemical composition $CdSO_4 \cdot 4H_2O$ has been approved as the new species drobecite (IMA 2002-034), whereas the compounds $CdSO_4 \cdot H_2O$ and $3CdSO_4 \cdot 8H_2O$ have so far been found only in insufficient quantities and qualities to complete their description as new minerals.

The similarity of the powder diffraction pattern of drobecite to that of the rozenite-type members indicated close structural relationships [3]. Isotypy of the crystal structure of drobecite was finally proven by a Rietveld refinement: the crystal structure was refined to R = 0.055 (without hydrogen atoms) with cell-parameters: a = 6.586(5), b = 14.329(5), c = 8.571(5) Å, β = 91.51(4)°, Z = 4 in space group $P2_1/n$.

Drobecite occurs as fibrous, colourless to light blue veinlets < 0.1 mm in the hosting rock and as fibrous aggregates in small cavities containing other Cd-bearing species. Sometimes these aggregates are bent ("rams horn"). The individual grains are not suitable for single crystal determination of the crystal structure with maximum dimensions of 5 × 10 × 500 μm^3.

The chemical composition of drobecite varies between $(Cd_{0.97}Cu_{0.03})SO_4 \cdot 3.92H_2O$ and $(Cd_{0.78}Cu_{0.08}Mg_{0.12}Zn_{0.02})SO_4 \cdot 3.87H_2O$ (normalized to 1 SO_4, H_2O by difference to 100%). It is notable, that all samples contain Cu, whereas the other trace elements often are not present. It is yet unknown, if the always observed Cu content in the naturally occurring material is responsible for the stabilization of the phase.

The density was measured by heavy liquids and found to be 2.23(3) g/cm^3, which agrees well with the calculated density of 2.30(2).

Drobecite is colourless to light blue, depending obviously on the Cu-content. It has a white streak, is lustrous and has a Mohs hardness of 2. The optical parameters determined are α = 1.430(3), β = 1.454(3), γ = 1.470(3), 2V = 70° (77° calc.).

[1] Skarpelis, N. (2007) *N. Jb. Mineral. Abh.*, **183**, 227-249. [2] Giester, G. et al. (1998) *Mineral. Petrol.*, **63**, 19-34. [3] Baur, W.H. (1962) *Acta Crystallogr.*, **15,** 815-826.

Cuproneyite – $Cu_7Pb_{27}Bi_{25}S_{68}$, a new mineral from Băiţa Bihor, Romania

Ilinca, Gh.[1*], Topa, D.[2], Makovicky, E.[3] & Zagler, G.[2]
[1]Dept. of Mineralogy, University of Bucharest, Romania
([*]ilinca@geo.edu.ro)
[2]Dept. of Materials Research and Physics, University of Salzburg, Austria
[3]Dept. of Geology and Geophysics, University of Copenhagen, Denmark

Cuproneyite, with the ideal formula $Cu_7Pb_{27}Bi_{25}S_{68}$, is a new mineral species found in the skarn deposit of Băiţa Bihor, Romania. The mineral occurs in irregular aggregates, nests and veinlets of up to 5 cm, with predominant cosalite, bismuthinite-aikinite derivative $bd_{73\text{-}77}$, and calcite, within the diopside skarn. Cuproneyite is opaque, has a silver-grey color, metallic luster and displays perfect cleavage along crystal elongation. The average Mohs hardness is about 3 (approximated from the average micro-indentation hardness of 222.5 kg/mm^2). Under the microscope, cuproneyite forms irregular or short prismatic grains, 300 μm in length, intergrown with lamellae and irregular patches of cosalite and hammarite-friedrichite. Bireflectance is barely visible in air and moderate in oil immersion, with a grayish white color with faint yellowish tints in the lightest position to grayish white color with faint bluish tints in the darkest position. Between crossed polars, the rotation tints of the most anisotropic grains are dark brownish grey to light brownish grey. Internal reflections are absent. The reflectance data (measured in air) are: 40.4, 47.1 at 470 nm, 39.3, 45.7 at 546 nm, 38.3, 44.3 at 589 nm and 38.1, 43.9 % at 650 nm. The average results of 24 electron-microprobe analyses are Cu 3.36(11), Ag 0.30(3), Pb 40.08(29), Bi 39.55(22), Se 0.12(5), Te 0.12(4), S 16.13(8) wt.%, corresponding to $Cu_{7.1}Ag_{0.38}$-$Pb_{26.03}Bi_{25.47}S_{68}$, calculated on the basis of (S + Se + Te) = 68 atoms per formula unit. The simplified formula (after reconversion of x(Ag + Bi) into 2x Pb) is $Cu_7Pb_{27}Bi_{25}S_{68}$ (Z = 2). It is in agreement with the empirical formula deduced from crystal-structure analysis. The density, 7.14 g/cm^3, was calculated using the structurally derived formula for Z = 1. The unit cell of cuproneyite is monoclinic, with a 37.432(8), b 4.0529(9), c 43.545(9) Å, β 108.803(1)°, V = 6253.62(1) Å^3, space group *C2/m*, and Z = 1. The strongest lines in the calculated X-ray powder pattern (d in Å, (I), *hkl*) are: 3.735, (96), -10.0.3; 3.347, (84), 4.0.10; 2.956, (77), 713; 2.867, (100), 714; 2.027, (81), 020.

Cuproneyite is an isotype of neyite [1]. The defining difference is the fact that the independent Ag position present in neyite is completely occupied by Cu in cuproneyite. Copper has a linear coordination in a flat-octahedral environment, situated in the central portions of the (001) walls of the crystal structure. This site displays a typical Cu-S bond length of 2.239 Å, to be compared with 2.415 Å of the Ag-S bond for silver in this position in neyite. The unit cell dimensions of cuproneyite are reduced against neyite only by 0.1-0.2 Å and the monoclinic angle β is unchanged. The volume of the unit cell is reduced by 65 Å^3. The name of the new mineral reflects this relationship. Both the mineral and its name have been approved by the Commission on New Minerals, Nomenclature and Classification (IMA 2008-053). Neyite has been classified as a typical sulfosalt with a 'box-work' structure (*e.g.*, [1-3]).

[1] Makovicky, E. et al. (2001) *Can. Mineral.*, **39**, 1365-1376. [2] Moëlo, Y. et al. (2008) *Eur. J. Mineral.*, **20**, 7-46. [3] Makovicky, E. & Topa, D. (2009) *Can. Mineral.*, **47**, 3-24.

The crystal-structural and paragenetic classification of minerals revisited (classes of nitrates, iodates and organic minerals)

Kostov, R.I.
Dept. of Mineralogy and Petrography, University of Mining and Geology "St. Ivan Rilski", Sofia, Bulgaria
(rikostov@gmail.com)

A dual crystal-structural and paragenetic principle introduced by Bulgarian mineralogist Ivan Kostov (1913-2004) has been applied to a rational classification of the classes of minerals [1-6]. Main divisions (associations) are based on geochemically allied metals in the composition of these minerals, and subdivisions (axial, planar, pseudoisometric and isometric types) on their overall structural anisometricity. The latter provides both structural similarity and genetic information, as manner of crystal growth in geological setting under different conditions of crystallization. The structural anisometricity may conveniently be presented by the *c/a* ratio of the minerals with high symmetry and by the $2c/(a+b)$, $2b/(a+c)$ and $2a/(b+c)$ ratios for the low symmetry minerals. The respective ratios are less, nearly equal, equal or above 1.00. The unit cell or sub-cell and the corresponding structures are denoted as axial or A-type, pseudo-isometric or (I)-type, isometric or I-type and planar or P-type, notations which correspond to chain-like, framework and sheet-like structures, respectively ino-, tecto- and phyllo-structures. Crystal chemical approach to the classification of minerals has been applied in general mineralogical works [7]. The basic criteria used for classification of minerals are suitably summarized [8-10].

The notations A, (I) and P offered are further enriched by adding as superscript the direction of structural anisometricity for the low symmetry minerals – A^c, A^b and A^a, $(I)^c$, $(I)^b$ and $(I)^a$, and P^c, P^b and P^a. Use is made of the indices (*hkl*) of the crystal habit form and [*uvw*] symbols for elongation added as subscripts. Combinations of both indicate form and elongation. Such type of systematic has been already applied to almost all mineral classes – oxides [11], silicates [12], sulphides [13], phosphates and related minerals [14], sulphates [15], borates [16], and carbonates [17; for review on different classes of minerals see 5, 6].

New examples are given in the last reviewed classes of minerals: nitrates within the Al-Mg-Fe, Na(K)-Ca-Ba and Cu-Pb-Zn associations, iodates within the Na(K)-Ca-Mg and Cu-Pb-Zn associations and organic minerals within the C-H-(O-N), Al-Mg-Fe, Na-Ca-Ba and Cu-Pb-Zn associations.

[1] Kostov, I. (1960) *Zap. Vser. Mineral. Obshchest*., **89**, 1, 90-93 (in Russian). [2] Kostov, I. (1965) *Bull. Inst. Geol.*, **14**, 33-49. [3] Kostov, I. (1968) in *V General Meeting, International Mineralogical Association, Cambridge*, 100-109. [4] Kostov, I. (1977) *Geochem. Mineral. Petrol*., **7**, 3-21. [5] Kostov, I. (1993) *Mineralogy*. Technika, Sofia. [6] Kostov, I. & Kostov, R.I. (1999) *Crystal habits of minerals*. Pensoft, Sofia. [8] Povarennykh, A.S. (1972) *Crystal chemistry classification of minerals*. Plenum Press, New York. [9] Lima-de-Faria, J. (1983) *Garcia de Orta, Ser. Geol.*, **6**, 1-24. [10] Strunz, H. (1984) in *Proc. 27th Int. Geol. Congr.*. Science Press, Utrecht, **10**, 65-112. [11] Kostov, I. (1964) in *Aspects of theoretical mineralogy in the U.S.S.R.* Pergamon Press, New York, 221-224. [12] Kostov, I. (1975) *Geochem. Mineral. Petrol.*, **1**, 5-41. [13] Kostov, I. & Minčeva-Stefanova, J. (1982) *Sulphide minerals.* Schweizerbart'sche, Stuttgart. [14] Kostov, I. (1986) *Geochem. Mineral. Petrol.*, **23**, 3-13. [15] Kostov, I. (2000) *Geochem. Mineral. Petrol*., **37**, 5-11. [16] Kostov, I. & Kostov, R.I. (2002) *Mineral. Zhurnal*, **24**, 1, 5-9. [17] Kostov, I. & Kostov, R.I. (2006) *Ann. Univ. Mining Geology*, **49**, 111-118.

Fluoro-micas from Bayan Obo, Inner Mongolia, China: F-analogues of tetraferriphlogopite and kinoshitalite

Miyawaki, R.[1*], Shimazaki, H.[1,2], Shigeoka, M.[1], Yokoyama, K.[1], Matsubara, S.[1], Yurimoto, H.[3] & Yang, Z.[4]
[1]Dept. of Geology and Paleontology, National Museum of Natural Sciences, Tokyo, Japan ([*]miyawaki@kahaku.go.jp)
[2]University of Tokyo, Japan
[3]Dept. of Natural History Sciences, Hokkaido University, Sapporo, Japan
[4]Inst. of Geology and Geophysics, Chinese Academy of Sciences, Beijing, China

F-analogues of tetraferriphlogopite ($KMg_3Fe^{3+}Si_3O_{10}F_2$) and kinoshitalite ($BaMg_3Al_2Si_2O_{10}F_2$) occur in metamorphosed carbonate rocks from the South ore body of the East Mine, Bayan Obo, Inner Mongolia, China in association with phlogopite, yangzhumingite ($KMg_{2.5}Si_4O_{10}F_2$) [1], bastnäsite-(Ce), cordylite-(Ce), monazite-(Ce), fluorbritholite-(Ce) and huanghoite-(Ce). They formed during a stage of hydrothermal activity or during a metamorphic event.

The F-analogue of tetraferriphlogopite is brown with a white to pale brown streak. It is transparent showing pearly luster and perfect cleavage on {001}. The hardness is 3-4 on the Mohs scale. The calculated density is 2.966 g cm^{-3}. This mineral is optically biaxial (–) with n = 1.576 (min) - 1.582 (max). It shows reverse pleochroism (Z' = colourless, X' = light brown; Fig. 1).

The F-analogue of kinoshitalite is transparent and colourless with a white streak and pearly luster. Cleavage is perfect on {001}. The calculated density is 3.235 g cm^{-3}. Electron microprobe analyses with SIMS for Li gave the empirical formulae (based on 12 anions); $(K_{0.94}Na_{0.02}Ba_{0.01})(Mg_{2.62}Li_{0.15}Fe^{+2}_{0.14}Mn_{0.01})(Si_{3.33}Fe^{3+}_{0.66}Al_{0.01})O_{10}[F_{1.65}(OH)_{0.35}]$ and $(Ba_{0.56}Na_{0.25}K_{0.06})(Mg_{2.76}Fe^{2+}_{0.14}Ti_{0.01})(Si_{2.73}Al_{1.15}Fe^{3+}_{0.12})O_{10}[F_{1.72}(OH)_{0.28}]$ for the F-analogues of tetraferriphlogopite and kinoshitalite, respectively.

XRD data for the minerals obtained with an IP-Gandolfi camera could be indexed by reference to calculated XRD traces based on the single-crystal structures of tetraferriphlogopite [2, 3] and kinoshitalite [4], respectively. Refined lattice parameters, space group $C2/m$, are a = 5.325(3), b = 9.217(5), c = 10.192(7) Å, β = 100.03(5)º, V = 492.6(5) $Å^3$ (F-analogue of tetraferriphlogopite), and a = 5.316(1), b = 9.2082(2), c = 10.044(2) Å, β = 100.16(2)º, V = 483.96(17) $Å^3$ (F-analogue of kinoshitalite).

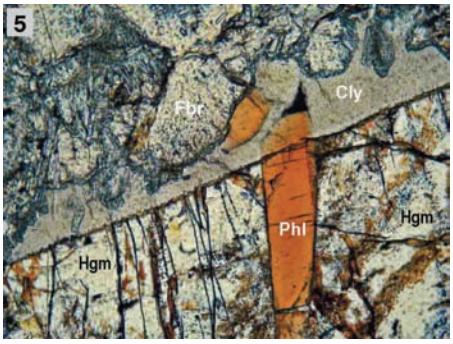

Fig. 1: Photomicrograph of the F-analogue of tetraferriphlogopite with reverse pleochroism taken in plane polarized light. The direction of the polarizer is NS. Width of image is about 1 mm; Phl: F-analogue of tetraferriphlogopite; Fbr: fluorbritholite-(Ce); Hgm: humite-group mineral; Cly: clayey serpentine.

[1] IMA 2009-017. [2] Semenova, T.F. et al. (1977) *Sov. Phys. Crystallogr.*, **22**, 680-683. [3] Brigatti, M.F. et al. (1996) *Clays Clay Miner.*, **44**, 540-545. [4] Gnos, E. & Armbruster, T. (2000) *Am. Mineral.*, **85**, 242-250.

Reinvestigation of orpheite using the type material: is it a valid mineral species?

Mladenova, V.[1*], Kolitsch, U.[2], Kenkman, T.[3], Hecht, L.[3] & Schmitt, R.-T.[3]
[1]Sofia University St. Kliment Ohridski, Sofia, Bulgaria ([*]vassilka@gea.uni-sofia.bg)
[2]Universität Wien Geozentrum, Vienna, Austria
[3]Museum für Naturkunde, Berlin, Germany

Orpheite from the Madzharovo base metal deposit in the Eastern Rhodope Mountains, Bulgaria, was described in 1972. $H_6Pb_{10}Al_{20}(PO_4)_{12}(SO_4)_5(OH)_{40}\cdot 11H_2O$ is an approximate chemical formula [1].

The mineral was approved by the IMA Commission on New Minerals and Mineral Names in 1972. However, in the American Mineralogist abstract of the original description, serious doubts concerning the validity of the species were expressed [2]. Therefore, the species status of orpheite and its chemical formula are noted as being doubtful in many modern data bases. However, orpheite from the Madzharovo deposit has never been reinvestigated and it still retains species status.

In order to obtain new data and to clarify the species status of the mineral, type orpheite and hinsdalite from Madzharovo have been reinvestigated.

The minerals were studied by standard techniques including X-ray diffraction (powders and single crystals), EPMA, SEM-EDS and micro-Raman spectroscopy.

Orpheite and hinsdalite mainly occur as light bluish to colourless, and rarely pale brown, microcrystalline pseudomorphs and perimorphs after hexagonal, prismatic crystals of pyromorphite. Both minerals display simple spindle-like morphology with pointed crystal terminations. Sometimes these terminations are dissolved away, resulting in fibrous forms. Both minerals form the same kinds of penetration twins.

X-ray diffraction studies show close similarities between orpheite and hinsdalite (ICDD-PDF 89-7559), as well as plumbogummite.

Raman spectra of both orpheite and hinsdalite show the same characteristic bands.

BSE analyses reveal strongly zoned crystals of both minerals with widths of different zones varying from less than 1 and up to 10 μm. At the rims of the crystal aggregates an increase in S content and concomitant decrease of P and Al contents is observed, which could be a result of later alteration processes. The highest Pb contents are at contacts with the replaced pyromorphite.

The average chemical formulae of both minerals were calculated on the basis of 2 XO_4, as recommended by Scott for members of the alunite supergroup [3]. For orpheite, the average empirical formula is $Pb_{1.14}Al_{3.00}(PO_4)_{1.91}(SO_4)_{0.09}(H_2O, OH)_6$, and for hinsdalite $Pb_{1.18}Al_{3.22}(PO_4)_{1.87}(SO_4)_{0.13}(H_2O, OH)_6$. Trace amounts of Sr and As (but no Fe) were detected.

According to current nomenclature for the alunite supergroup [3], recalculated microprobe analyses of orpheite and hinsdalite from Madzharovo fit into the plumbogummite field.

Acknowledgements: This study was support by the Synthesys Program (DE-TAF-5203).

[1] Kolkovski, B. (1972) *Ann. Univ. Sofia, Fac. Geol. Geogr.*, **64**, 106-130. [2] Fleischer, M. et al. (1976) *Am. Mineral.*, **61**, 174-186. [3] Scott, K.M. (1987) *Am. Mineral.*, **72**, 178-187.

A new classification scheme for amphibole group minerals: the matrix model

Nikandrov, S.*, Valizer, P. & Nikandrov, A.
Ilmeny State Reserve of the Urals Branch of the Russian Academy of Sciences, Miass, Russia (*nik@ilmeny.ac.ru)

A new classification scheme for amphibole group minerals using a matrix model is suggested. It is based on the charges of cations in the amphibole structure. The matrix model may be presented in various forms. Thus, one format is based on variations of cations at the C and T sites (Fig. 1). Specific cation balances in the basic units (C and T sites) and in the units of the matrix field (A and B sites) were viewed in terms of isomorphous replacement at these sites according to the so-called "50% rule". It is important that at the C site the "50% rule" is applied for cations of various kinds (L and M) and common border conditions of balances of cations at the sites are applied for all amphiboles. The matrix model may be correlated with the 1997 IMA CNMMN amphibole nomenclature [1], but it differs from it in principle. A special system of concepts and appropriate terminology has been elaborated for the matrix model for normal, anomalous, normative, analogues of normative amphiboles, and so on.

	10+ L_5	**11+ L_4M**	**12+ L_3M_2**
C^{VI} →		$Mg_4Al \leftrightarrow Fe^{2+}{}_4Al$	$Mg_3Al_2 \leftrightarrow Fe^{2+}{}_3Al_2$
	$Mg_5 \leftrightarrow Fe^{2+}{}_5$	↕ ↕	↕ ↕
T^{IV} ↓		$Mg_4Fe^{3+} \leftrightarrow Fe^{2+}{}_4Fe^{3+}$	$Mg_3Fe^{3+}{}_2 \leftrightarrow Fe^{2+}{}_3Fe^{3+}{}_2$
32+ **Si_8**	**4+** Tremolites – ferro-actinolites: **□(Ca)$_2$** **Na(CaNa)**: Richterites	**3+** Winchites: **□(CaNa)** **Na(Na)$_2$**: Eckermannites – arfvedsonites	**2+** **□(Na)$_2$**: Glaucophanes – riebeckites
31+ **Si_7Al**	**5+** Edenites: **Na(Ca)$_2$**	**4+** Hornblendes: **□(Ca)$_2$** **Na(CaNa)**: Katophorites	**3+** Barroisites: **□(CaNa)** **Na(Na)$_2$**: Nyböites
30+ **Si_6Al_2**	**6+** Cannilloites: **$CaCa_2$**	**5+** Pargasites – hastingsites: **Na(Ca)$_2$**	**4+** Tschermakites: **□(Ca)$_2$** **Na(CaNa)**: Taramites
29+ **Si_5Al_3**	×××	**6+** !!! **$CaCa_2$**	**5+** Sadanagaites: **Na(Ca)$_2$**

Fig. 1: Matrix model for normative amphiboles (total cationic charge +46).

In comparison with IMA97, the matrix model is stricter and removes a number of logical contradictions. The main feature is the possibility of presenting all minerals of the amphibole group in two-dimensional fields. The problem of dividing total iron from microprobe analyses of amphiboles may be solved by the matrix model with good precision.

The model is convenient for practical use in nomenclature analysis, comparative analysis of different objects, *etc*. [2,3]. Productive application of the model to amphiboles for many years suggests that it represents a real alternative to current nomenclature, including all subsequent corrections and improvements.

The model for amphiboles is described in detail in [2,3].

[1] Leake, B.E. et al. (1997) *Can. Mineral.*, **35**, 219-246. [2] Nikandov, S.N. et al. (2000) *Zap. Vser. Mineral. Obshchest.*, 105-112. [3] Valizer, P.M. et al. (2004) *Amphiboles of the Urals.* IGZ UrO RAN, Miass.

S-rich apatites in sakenites from southern Madagascar

Ohnenstetter, D.[1*] & Giuliani, G.[1,2]
[1]CRPG/CNRS, Vandœuvre-lès-Nancy, France
(*dohnen@crpg.cnrs-nancy.fr)
[2]IRD, Toulouse, France

Sakenites from Sakeny, North of Ihosy (Madagascar) were defined by Lacroix [1,2] as corundum – spinel – sapphirine – anorthite rocks. Their protholiths are either of metasedimentary origin [2,3], argillaceous limestones [3], or more probably metanorthosites [4,5]. They are metamorphosed under high grade granulitic conditions with a peak at 800°C and 6 to 7 kbar followed by metasomatic alteration under less extreme metamorphic conditions, 700-650°C and 6 kbar [3]. The sakenites studied are composed of sappphirine, anorthite, diopside, amphibole, phlogopite, muscovite, spinel, corundum, Cl-apatite, S-rich apatite, xenotime, zircon, monazite, uraninite, titanite, sulfides and sulfates. In new samples, Raith et al. [3] have also reported magnesiotaaffeite, a boron magnesium aluminosilicate. S-rich apatite with SO_3 contents up to 11 wt.% also have high Na content (Table 1).

Table 1: Analytical data for S-rich apatite (wt.%)

SO_3	10.19	S^{6+}	1.269
P_2O_5	32.72	P^{5+}	4.597
SiO_2	0.23	Si^{4+}	0.038
FeO	0.02	Fe^{2+}	0.002
CaO	50.89	Ca^{2+}	9.044
Na_2O	3.56	Na^{+}	1.152
Cl	1.09	Cl^{-}	0.305
H_2O calc.	1.53	OH^{-}	1.695
O=Cl	-0.25		
Total	99.98		

The S-rich apatite could be a new species belonging to a solid solution between ellestadite, $Ca_{10}(SiO_4)_{3-x}(SO_4)_{3-x}(PO_4)_{6-2x}(OH,F,Cl)_2$, and a new end-member $Na_xCa_{10}(SO_4)_x(PO_4)_{6-x}(OH,F,Cl)_2$.

[1] Lacroix, A. (1939) *C. R. Acad. Sci. Paris*, **17**, 609-612. [2] Lacroix, A. (1941) *Ann. Géol. Serv. Mines Tanna*, **11**, 27-36. [3] Raith, M.M. et al. (2008) *J. Metam. Geol.*, **26**, 647-667. [4] Boulanger, J. (1959) *Ann. Géol. Mada*, **26**, 71. [5] Ohnenstetter, D. et al. (2008) *Gac-Mac, Quebec, abstract* 125.

R-dictionary-catalogue of chemical mineral composition

Petrov, T.G. & Krasnova, N.I.*
Saint-Petersburg State University, Russia
(*nataly_krasnova@rambler.ru)

Our *R*-dictionary-catalogue [1,2] contains the information on a chemical composition of minerals as rank formulas that is sequences of elements on decrease in their concentrations. The structure of the catalogue is based on the development of T.G. Petrov RHA-method [3] according to which the rank formulas are ordered linearly unequivocally hierarchically in a column alphabetically – to numbers of elements in the Periodic table of elements. The lexicographic systematisation principle of the dictionary generates the chemical classification of minerals. The rank formula is identical to result of ordering of chemical elements on decrease of the sums of all their coefficients in crystal-chemical formula, without taking into account the valence of elements or their site position. The present *R*-catalogue of chemical compounds of minerals contains over 4800 inputs; the full version of these data displays the file R-Min-Catalogue-2007.rar on web-site: http://geology.pu.ru/.

For the set up of the *R*-catalogue the crystal-chemical formulas of minerals, as resulting in mineralogical databases (http://www.webmineral.com/ and http://www.mindat.org/), were used. For the majority of mineral species of variable composition by results of real chemical analyses 2-5 rank formulas have been designed. The principle of rank formulas ordering is shown in table 1:

Table 1: Principle of rank formulas

Rank formula	Name	Formula
H F N Si	Cryptohalite	$(NH_4)_2SiF_6$
H F= O Al	Rosenbergite	$AlF_3 \cdot 3(H_2O)$
H= S O= Fe= Cu	Orickite	$CuFeS_2 \cdot (H_2O)$
C= Si	Moissanite	SiC
O H C Ca	Caoxite	$Ca(C_2O_4) \cdot 3H_2O$
O H N S	Mascagnite	$(NH_4)_2SO_4$
O Mg Si	Forsterite	Mg_2SiO_4
O Mg= Si Al	Pyrope	$Mg_3Al_2(SiO_4)_3$
O Mg= Si Cr	Knorringite	$Mg_3Cr_2(SiO_4)_3$
O Fe	Magnetite	$Fe^{2+}Fe^{3+}{}_2O_4$

The *R*–catalogue can be used for solution of following tasks. 1. For express identification of minerals by results of chemical analyses. Identification of minerals with the variable contents of H_2O, F, or other elements is not always unequivocal. 2. For minerals of variable composition, in particular, at multielement type of isomorphism, on *R*-indexes it is possible more proved specify the limits between uses of different species names in isomorphic series. 3. The *R*-catalogue can be used for the improvement of mineral nomenclature, it can help to work out the general recommendations at confirmation of names of new minerals, or updating of limits for application of old terms. 4. On the basis of the *R*-catalogue it is possible to create some more detailed chemical classifications for separate groups of minerals, and to predict existence of new species.

[1] Petrov, T.G. & Krasnova, N.I. (2010) R-*dictionary-catalogue of chemical mineral composition.* Nauka, Saint-Petersburg (in Russian). [2] Petrov, T.G. & Krasnova, N.I. (2005) *Mineralogical museums.* Saint-Petersburg. 369-370. [3] Petrov, T.G. (2001) *Scientific-Technical Information, Ser. 2*, **3**, 8-18 (in Russian).

Klajite, a new member of the lindackerite group from Hungary

Szakáll, S.[1*], Fehér, B.[2], Bigi, S.[3] & Mádai, F.[1]
[1]Dept. of Mineralogy and Petrology, University of Miskolc, Hungary (*askszs@uni-miskolc.hu)
[2]Dept. of Mineralogy, Herman Ottó Museum, Miskolc, Hungary
[3]Dept. of Earth Sciences, University of Modena and Reggio Emilia, Modena, Italy

Klajite was found in ore samples collected from the waste dump of the Recsk, Lejtakna ("Inclined adit") area, Lahóca Hill, Mátra Mountains, North Hungary. The ore of the Lejtakna area was discovered in 1969 [1]. It belongs to the Lahóca epithermal high sulfidation Cu-As ore deposit. Primary ore mainly consists of enargite, luzonite and pyrite, with less frequent tennantite, chalcopyrite, galena, and sphalerite [1]. These sulfides usually alter to sulfates, phosphates and arsenates [2].

Klajite occurs in cavities in enargite and quartz, in close association with other secondary minerals including gypsum, jarosite, and an unknown Ca-Cu arsenate which is structurally analogous to the phase Cu-AsO_4-H_2O (3) (ICDD 00-051-1479) described from Jáchymov, Czech Republic [3]. Klajite is a secondary mineral formed by decomposition of enargite and perhaps Mn-rich tennantite.

Klajite forms sheaf-like aggregates made up of lath-like to thin tabular crystals, typically 0.05-0.2 mm in length. Crystals commonly form complex intergrowths. The largest aggregates reach 0.5 mm in diameter. The mineral is translucent, greenish yellow to yellowish green in colour with a white streak and a vitreous lustre. Mohs hardness is 2–3 and the calculated density is 3.213 g cm^{-3}. Klajite has perfect cleavage parallel to {010}, and is very brittle. Its fracture is uneven. Optically klajite is biaxial negative or positive with α = 1.595(30) and γ = 1.665(20). It is weakly pleochroic, colourless to pale green.

The chemical composition of klajite was determined by electron microprobe. After recalculation to 100% the average of seven analyses gave MnO 5.67, CuO 32.03, CaO 0.41, As_2O_5 44.40, H_2O(calc.) 17.49, total 100.00 wt.%. The empirical formula, based on 16 oxygen atoms, is $(Mn_{0.82}Cu_{0.10}Ca_{0.08})_{\Sigma=1.00}$ $Cu_{4.05}As_{3.98}O_{14}(OH)_2 \cdot 9H_2O$, and the simplified formula is $MnCu_4(AsO_4)_2(AsO_3OH)_2 \cdot 9H_2O$.

A powder X-ray diffraction pattern was obtained using Cu*K*α radiation and a Gandolfi camera. The strongest seven lines in the pattern are [d_{hkl} in Å (I_{obs} %, *hkl*)] 10.39 (100, 001), 2.916 (64, 202), 2.708 (29, $\bar{1}$ 13), 3.616 (28, 0 $\bar{2}$ 1), 3.050 (28, 0 $\bar{2}$ 2), 3.956 (27, 020) and 3.110 (24, 122). The mineral is structurally analogous to other lindackerite group minerals; it is triclinic, space group $P\bar{1}$, a = 6.441(3), b = 7.983(4), c = 10.562(3) Å,α = 85.28(4), β = 80.63 (5), γ = 84.80(4)°, V = 532.4(3) Å^3, Z = 1, and $a:b:c$ = 0.807:1:1.323.

Klajite is named after Sándor Klaj (b. 1948), a Hungarian mineral collector. He has found more than 40 mineral species new to Hungary and also provided the samples for this description. The mineral and name have been approved by IMA CNMNC (2010-004). Type material has been deposited at the Herman Ottó Museum, Miskolc, Hungary (catalogue no. 2010.1) and at the Hungarian Natural History Museum, Budapest, Hungary (specimen no. Gyn./1842).

[1] Baksa, C. (1975) *Föld. Közl.*, **105**, 58-74. [2] Szakáll, S. et al. (2005) A magyarországi ásványfajok. Kőország Kiadó, Budapest. [3] Ondruš, P. et al. (1997) *J. Czech Geol. Soc.*, **42**, 77-108.

A Sc-Nb oxide from corundum pegmatites of the Krucze Skały in Karpacz (Karkonosze massif, Lower Silesia, Poland) – a potentially new mineral of the $ScNbO_4$ – $FeWO_4$ series

Szełęg, E.[1*], Galuskina, I.[1] & Prusik, K.[2]
[1]Dept. of Geochemistry, Mineralogy and Petrography, Faculty of Earth Sciences, University of Silesia, Sosnowiec, Poland ([*]eligiusz.szeleg@us.edu.pl)
[2]Inst. of Materials Science, University of Silesia, Katowice, Poland

The Sc-Nb oxide occurs as an accessory mineral in a peraluminous corundum pegmatite of the Krucze Skały in Karpacz–Wilcza Poręba, situated within the Karkonosze massif (Lower Silesia, SW Poland). Orthoclase, biotite, muscovite, albite, chamosite and corundum are the main rock-forming minerals of the pegmatite. Schorl, rutile, ilmenite and ferberite are accessories. The Nb-Sc oxide forms xenomorphic, more rarely idiomorphic, grains up to 30 μm in size (Fig. 1), inside rutile, Nb-bearing rutile and ilmenite grains. Grains showing complex zonation are composed of ferberite cores and Sc-Nb oxide in external parts.

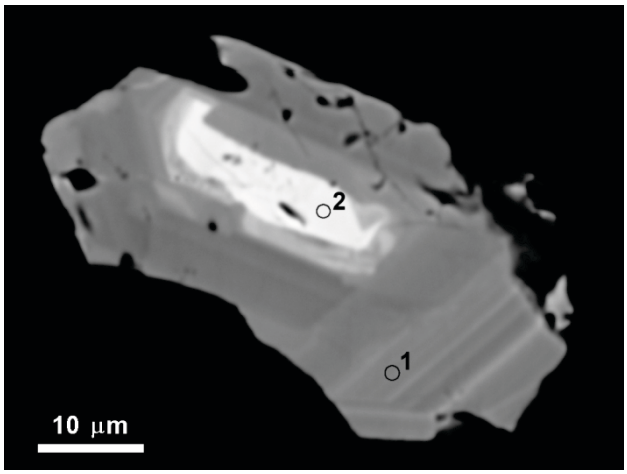

Fig. 1: Idiomorphic zoned grain of Sc-Nb oxides, BSE image; 1 and 2 are analysis sites.

The chemical formula of the zoned external part of a grain (Fig. 1) with maximum concentrations of Sc (1) is $(Sc_{0.55}Fe^{2+}_{0.15}Ti_{0.12}Fe^{3+}_{0.08}Mn_{0.05}Zr_{0.03})_{\Sigma 0.98}(Nb_{0.86}W_{0.07}Sn_{0.06}Ta_{0.03})_{\Sigma 1.02}O_4$. The core (Fig. 1) shows an intermediate composition, belonging to the $ScNbO_4$ – $FeWO_4$ series, with composition (2) $(Fe^{2+}_{0.39}Sc_{0.35}Mn_{0.13}Ti_{0.08}Fe^{3+}_{0.05}Zr_{0.02})_{\Sigma 1.02}(Nb_{0.48}W_{0.47}Ta_{0.01}Sn_{0.01})_{\Sigma 0.97}O_4$. The Sc-Nb oxide has a wolframite-type structure according to EBSD data. All analytical data point to the Sc-Nb oxide being a new mineral species with end-member composition $ScNbO_4$. Recently, the new mineral heftetjernite, $ScTaO_4$, was described [1], and is a Ta-analogue of the mineral from Krucze Skały. After detailed studies the new species will be submitted for approval to the IMA CNMNC.

[1] Kolitsch, U. et al. (2010) *Eur. J. Mineral.*, **22**, 309-316.

Ammineite, $CuCl_2(NH_3)_2$ – the first mineral containing an ammine complex

Walter, F.[1*], Bojar, H.-P.[2], Baumgartner, J.[3] & Färber, G.[4]
[1]Inst. of Earth Sciences (Mineralogy and Petrology), University of Graz, Austria ([*]franz.walter@uni-graz.at)
[2]Dept.of Mineralogy, Universalmuseum Joanneum Graz, Austria
[3]Inst.of Inorganic Chemistry, Technical University of Graz, Austria
[4]Gunnar Färber, Samswegen, Germany

The type locality of ammineite, $CuCl_2(NH_3)_2$, is Caleta Pabellon de Pica, Tarapaca, south of Iquique, Chile. It has been accepted as new mineral by CNMNC (2008-32).

Ammineite occurs as intense sky blue xenomorphic grains up to 4 millimetres in size in solution cavities in halite together with atacamite and darapskite. Ammineite is a reaction product of guano with copper mineralisation.

For ammineite Cu (37.60 wt.%) and Cl (41.67 wt.%) were analysed by EMP, N (16.54 wt.%) and H (3.32 wt.%) by CHNS analyser. O, S and C are below the detection limits. FTIR spectra give exclusively NH_3 frequencies at 3316, 3241, 3160, 1594, 1245, 711, 660 and 480 cm^{-1}.

Ammineite is orthorhombic, space group *Cmcm*, with a = 7.688(1), b = 10.645(2), c = 5.736(1) Å, V = 469.4(2) $Å^3$ and Z = 4. The crystal structure was solved by direct methods and refined with SHELX-97 [1] to R = 0.024 [$F_o > 4\sigma(F_o)$] for 231 unique reflections.

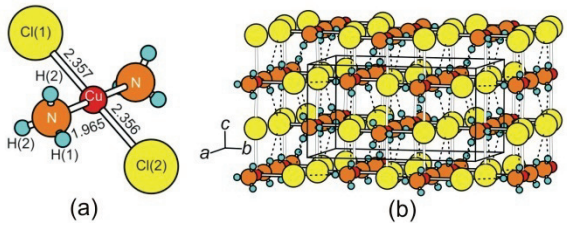

Fig. 1: The crystal structure of ammineite: (a) basic unit, (b) layers of $CuCl_2(NH_3)_2$ parallel (001). Dotted lines indicate hydrogen bonds.

The basic structural unit consists of a central Cu site with *trans* planar coordination of two NH_3 molecules and two Cl ions with Cu-N 1.965(3) Å and Cu-Cl distances of 2.356(2) and 2.357(2) Å (Fig. 1a). In the unit cell the complex forms layers parallel to (001) and oriented by Cl(1)-Cu-Cl(2) parallel to [010] (Fig. 1b). Along [001] Cu is connected to parallel layers nearly perpendicular by two long bonds (Cu-Cl(2) 2.868(1) Å), building orthorhombic dipyramids connected by shared edges to form zigzag chains running along [001]. Some H···Cl distances ranging from 2.69(3) to 2.79(4) Å indicate the presence of weak hydrogen bonds, which connect the complexes within the (001) layers and also from one layer to the next.

X-ray powder data for ammineite and *trans*-diamminedichloro-copper(II), which was synthesized for comparison, are nearly identical. However, calculated powder data using parameters taken from the structure determination of synthetic $Cu(NH_3)_2Cl_2$ reported in [2] are completely different from our data.

[1] Sheldrick, G.M. (1997) *SHELX-97 programs for crystal structure refinement.* University of Göttingen, Germany. [2] Hanic, F. & Cakajdova, I.A. (1958) *Acta Crystallogr.*, **11**, 610-612.

A thermal analysis study of chromium oxyhydroxide nanoplates synthesised under different pH conditions

Frost, R.L.[*] & Yang, J.
Chemistry Discipline, Faculty of Science and Technology, Queensland University of Technology, Brisbane, Australia
([*]r.frost@qut.edu.au)

As a transition metal oxide, chromia (Cr_2O_3) has attracted special attention because of its importance in specific applications, such as in high-temperature resistant materials, solar energy collectors, catalyst, and so on [1]. Chromium oxyhydroxide CrO(OH) is a principal precursor for chromium oxides Cr_2O_3, since the original size and morphology of CrO(OH) precursor can be retained after calcination. Three naturally occurring chromium oxyhydroxides are bracewellite (orthorhombic CrO(OH)), guyanite (orthorhombic CrO(OH)) and grimaldiite (trigonal CrO(OH)) [2]. Nanoscaled grimaldiite material has been successfully synthesised in different pH environments through a simple hydrothermal route. Plate-like CrO(OH) crystals with average diameter of 11 nm were observed from transmission electron microscopy (TEM). Thermogravimetric analysis [3,4] was applied to study the thermal decomposition process for the synthesis CrO(OH) nanomaterials (Table 1). The thermal properties of CrO(OH) nanomaterials and the influence of pH to the crystal growth was deduced from this thermal study.

Table 1: Summary of peaks shown in dTG curves for CrO(OH) nanomaterials synthesised in various pH conditions

CrO(OH)-5.0	*CrO(OH)-5.0*	*CrO(OH)-10.0*
45°C, 84°C, 109°C	45°C, 84°C, 109°C	50°C, 80°C
	276°C	238°C
315°C		318°C
	396°C	
444°C, 463°C	438°C	436°C, 458°C
	643°C	

The thermal gravimetric study indicated that synthesised CrO(OH) nanomaterials decomposed at ~ 450°C (Fig. 1). All products after heated to 1000°C were well crystalline Cr_2O_3 nanomaterials, which were confirmed by X-ray diffraction (XRD).

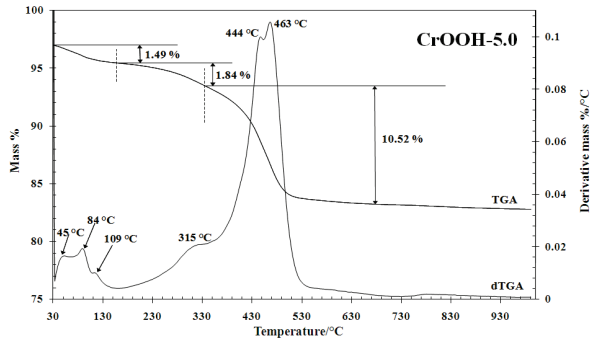

Fig. 1: Thermalgravimetric analysis (TGA) of CrO(OH) nanomaterials synthesised at pH=5.0.

[1] Rotter, H. et al. (2005) *Environ. Sci. Technol.*, **39**, 6845-6850. [2] Shpachenko, A.K. et al. (2006) *Geochem. Int.*, **44**, 681-689. [3] Yang, J. & Frost, R.L. (2008) *Res. Lett. Inorg. Chem.*, 602198. [4] Yang, J. et al. (2009) *Appl. Surf. Sci.*, **255**, 7925-7936.

Cr-rich alunite nodules in acid sulfate alteration zones overlying bentonites at Milos, Greece: evidence for Cr transport by acidic fluids

Gilg, H.A.[1*], Riehl, M.[1], Hattori, K.[2], Takahashi, Y.[3] & Vennemann, T.[4]
[1]Lehrstuhl für Ingenieurgeologie, TUM, Munich, Germany
([*]agilg@tum.de)
[2]Dept. of Earth Sciences, University of Ottawa, Canada
[3]Dept. of Earth and Planetary System Sciences, Hiroshima University, Hiroshima, Japan
[4]Institute of Mineralogy and Geochemistry, University of Lausanne, Switzerland

Nodular alunite concretions occur at the base of acid sulfate alteration zones in Upper Pliocene to Middle Pleistocene pyroclastic rocks overlying bentonites at Siskinos and Aspro Chorio, Milos, Greece. The white concretions with diameters of up to 50 cm consist of euhedral to partly corroded alunite crystals (1-3 µm, 89-99 vol.%) with minor amounts of halloysite, opal-A, and quartz. The alunites at Siskonos, SE Milos, are characterized by intermediate atomic Na/(Na+K) ratios (0.43-0.73) and high Cr (840-1250 ppm), V (240-580 ppm), moderate Sr (520-650 ppm) and Ba (300-730 ppm) and low Zn (<5 ppm) contents. In contrast, an alunite nodule from Aspro Chorio in the NW of Milos has a very low atomic Na/(Na+K) ratio (~ 0.16) and no detectable Cr (<5 ppm), but high Ba (2580 ppm) and Zn content (140 ppm).

Selective leaching experiments using sulfuric acid and ammonia show that Cr in nodules from Siskinos is not adsorbed to clays and not present as discrete chromite, but most probably located in the alunite crystals. EXAFS studies indicate that all Cr is present in a trivalent state. The calculated Cr-O distance is 1.965Å, which is consistent with an octahedral coordination. The Cr in alunites cannot be derived from the andesitic to dacitic protoliths (<20 ppm Cr [1]), but must have been introduced by hydrothermal sulfate-rich fluids. We suggest that Cr was leached by strongly acidic fluids from ultramafic/mafic rocks in the metamorphosed accretionary wedge in the SE part of the island. We note that steam condensates with a pH 1.7 and temperatures of 90°C at Paleochori Bay, SE Milos, contain up to 3.0 µM Cr [2]. The low Cr contents in alunites at Aspro Chorio in the NW part of Milos are probably related to the absence of ultramafic bodies in the basement. The tabular acid-sulfate alteration zones at Siskinos require input of magmatic fluids. Preliminary stable S, O, H, isotope data of alunites are consistent with this interpretation.

[1] Decher, A. (1997) *Aachener Geowiss. Beiträge*, **23**, 1-194. [2] Valsami-Jones, E. et al. (2005) *J. Volc. Geotherm. Res.*, **148**, 130-151.

On the plutonities of the subduction regime (Southern Sinai, Egypt): discrimination and modeling

Ghoneim, M.F.[1*], Lebda, E.M.[2], Abdel-Karim, A.M.[3] & Nasralla, N.[3]
[1]Geological Dept., Faculty of Science, University of Tanta, Egypt ([*]ghoneimf@yahoo.com)
[2]Geological Dept., Faculty of Science, Kafr El-Sheikh University, Kafr El-Sheikh, Egypt
[3]Geological Dept., Faculty of Science, Zagazeg University, Zagazeg, Egypt

Petrological, geochemical and mineralogical characteristics of both calc-alkaline granites and their counterpart gabbros of southern Sinai (Egypt) have been carried out. The rocks are considered to pertain to the island arc regime. The study includes Nesren, Shahera and Minader outcrops as case example.

The granite composition includes diorite, tonalite and granodiorite. The gabbros are pyroxene, pyroxene/hornblende, hornblende gabbros and diorite. Opaque mineral contents are relatively enriched in gabbroid rocks and represented by magnetite, hematite and ilmenite with few sulphides.

From geochemical point of view, the granitic rocks are peraluminous, calc-alkaline and of I-type syncollision volcanic arc. The gabbros exhibit transitional calc-alkaline/tholeiite magma type of island arc setting. Microprobe data of amphiboles indicate that the amphiboles from gabbros are calcic-type and have the composition of actinolite, actinolitic hornblende with subordinate of magnesio-hornblende. They crystallized under medium (Minader and Shahera) to low pressure (Nesren). Amphiboles from the granites have the composition of actinolitic hornblende (Minader), ferroedenite to ferroedenitic hornblende (Nesren). They crystallized under low pressure. Plagioclase from the study rocks varies in composition from oligoclase to andesine. Biotites of the granites are Mg-rich (Minader), Fe-rich (Nesren), and lepidomelane of calc-alkaline and magmatic origin. Plagioclase favours temperature of formation at 1100°C (Minader gabbro), 750 to 850°C (Shahera gabbro) and 900 to 1000°C (granitic rocks) under general pressure of 2 Kbs.

Modeling and thermobarometric calculations elucidate magma generation at a depth of about 30 km for granite and from 15 to 35 km for gabbros. The later rocks have achieved 25% fractional melting of mantle lherzolite.

Origin of rapakivi texture: a case study of the rapakivi-textured granitoids in the Qinling orogen (China)

Wang Xiaoxia[1*] & Wang Tao[2]
[1]Institute of Mineral Resource, Chinese Academy of Geological Sciences, Beijing, China ([*]xiaoxiawang@hotmail.com)
[2]Institute of Geology, Chinese Academy of Geological Sciences, Beijing, China

Rapakivi texture (ovoidal alkali feldspar megacrysts with and/or without plagioclase mantle) is a key marker of rapakivi granitoids. The origin of the rapakivi texture has interested petrologists for more than 100 years. The main models for the origin of the rapakivi texture are (1) hybridization between granitic and more mafic magmas; (2) sub-isothermal decompression of the crystallizing magma; and (3) exsolution of albitic plagioclase from the original alkali feldspar and migration to the grain boundaries. However, each model could not interpret the origin of all rapakivi textures. For instance exsolution model is unable to explain the shape of ovoidal alkali feldspar and oligoclase to andesine mantle. Mixing model is difficult for such huge volumes of homogeneous rapakivi granites in the Wiborg batholith.

The Qinling rapakivi-textured granitoids intruded into the Qinling orogen (central China) at 211–217 Ma. The rapakivi texture is characterized by ovoid or rounded alkali feldspar megacrysts. Some of the megacrysts are surrounded by one or, occasionally, two plagioclase mantles. This study indicates that magma mixing is a major reason for the origin of the texture.

The granitoids contain many mafic to intermediate magmatic enclaves with fine-grained sinuous margins against the granitoids or transitional contacts with the granitoids and disequilibrium textures and mineral assemblage, suggestive of mingling and mixing of mafic and felsic magmas. The *P–T* conditions of crystallization have been determined for early mineral assemblages (inner parts of alkali feldspar megacrysts and their plagioclase, quartz, amphibole and biotite inclusions) and late assemblages (matrix minerals) of the rapakivi-textured granitoids. Al contents in amphibole from the early and late mineral assemblages yield pressures of 1.2–3.0 and 0.7–3.0 kbar, respectively, and indicate only minor pressure change between the crystallization of the early and late assemblages. Amphibole–plagioclase thermometry gives temperatures mainly from 600 to 730°C for both the early and late assemblages indicating nearly isothermal conditions, and it appears that locally the temperature of the late assemblages was even higher. Feldspar thermometers yield lower temperatures. Relative abundances of minerals and their chemical compositions indicate that the late mineral assemblages tend to be richer in MgO, Na_2O and CaO than the early assemblages. Rapakivi texture is interpreted in this case mainly as a result of compositional changes and isothermal temperature related to the hybridization between granitic and more mafic magmas. Another possibility is that a small release of pressure during crystallization of the magma chamber was able to stabilize plagioclase instead of alkali feldspar and produce the rapakivi texture.

LA-ICP-MS measurements on K-feldspar megacrysts of Mórágy granite, Hungary

Király, E.[1*], Chenery, S.[2], Bartha, A.[1], Bertalan, E.[1] & Dobosi, G.[3]
[1]Geological Institute of Hungary, Budapest, Hungary
([*]kiraly@mafi.hu)
[2]British Geological Survey, Keyworth Nottingham, UK
[3]Institute of Geochemical Research, Hungarian Academy of Sciences, Budapest, Hungary

The variscan (~320 Ma) Mórágy Granite (SE–Transdanubia, Hungary) — belonging to Tisza megaunit — is formed by mixing and mingling of a felsic and mafic magma [1]. Microcline megacrysts of both monzogranite and mafic microgranular enclave were analysed by LA-ICP-MS and electron microprobe to characterise trace element (Ba, Rb, Sr, Cs, REE, Pb) profiles in two types of microcline megacrysts for reconstruction of petrogenetic mechanisms. Both types of microcline megacrysts are well ordered, low temperature microcline [2]. There are only very few trace elements built in the lattice. Ba as an index of magma mixing plays the most important role in microcline exchange reaction. In monzogranite the megacryst has some thousands or hundreds ppm of Ba, Sr, Rb and Pb content and only very few ppm of Cs, La and Eu content aside from the main elements of potassium, sodium and calcium. The trace element distributions of the megacryst from monzogranite reveal no systematic zoning however Ba seems to be decreased from zone to zone from core to rim in agreement with the normal magmatic crystallisation. In addition, patchy enrichments in Ca, Sr and Pb couple sometimes with Ba-rich domains however Ba enrichments are commonly independent from the concentrations of the above mentioned trace elements.

In contrast, Ba is clearly enriched at the rim in microcline megacryst of mafic microgranular enclave but the inner part of the megacryst shows more complicated structure. Ba, Sr (compatible elements) and Pb vary together in contrast to the changes in Rb and Cs (incompatible elements) in microcline megacryst.

The linear trends of different trace element substitutions of potassium in microcline suggest similar magma conditions for both megacrysts of the monzogranite and mafic enclave in agreement with the whole rock geochemistry. It means the same source of the microcline formation and close relationship to the two coeval magmas, where the megacrysts developed. Enrichment in Ba at the rim of microcline megacryst from mafic enclave reflects the appearance of the mafic melt during the microcline formation. Ba is enriched in zone, where plenty of plagioclase inclusions are developed illustrating rapakivi-like texture. Both support the granitoid formation by mixing and mingling.

[1] Király, E. (2010) *Magmatic evolution of Mórágy Granite (SE Transdanubia, Hungary)*. Annual report of the Geological Institute of Hungary of 2009 (in press). [2] Buda, Gy. (1974) *Acta Geol. Ac. Sci. Hung*., **18**, 465-480.

New U-Pb and Lu-Hf isotopic constraints on the age and origin of the Mórágy Granite (Mecsek Mountains, South Hungary)

Koroknai, B.[1*], Gerdes, A.[2], Király, E.[1] & Maros, Gy.[1]
[1]Geological Institute of Hungary, Budapest, Hungary
([*]koroknai@mafi.hu)
[2]Institute of Geosciences, Frankfurt am Main, Germany

The Mórágy Granite — located in the south-eastern hilly foreland (Mórágy Hills) of the Mecsek Mts., Hungary — represents the volumetrically most important surface outcrop of the crystalline basement in the northern part of the Tisza mega-unit. The crystallization age of the microcline megacryst-bearing biotite-monzogranites and its mafic enclaves of predominantly monzonitic composition is in dispute. Radiometric dating both by conventional (multi-grain) and single grain U-Pb analyses of zircon yielded controversial results (ages between 339 and 405 Ma, [1–4]). In this study we present new U-Pb and Lu-Hf isotope data obtained on oscillatory zoned domains of zircon grains both from microcline megacryst-bearing monzogranites and its mafic monzonitic enclaves (4 samples, 64 analyses) using the LA-SF-ICPMS (laser ablation-magnetic sector field inductively coupled plasma mass spectrometry) technique.

The results deriving from the monzogranitic rock group imply an age of around 337 Ma for the emplacement and magmatic crystallization of the Mórágy Granite. This result is unambiguously confirmed by the concordia (339±3 Ma) and mean $^{207}Pb/^{206}Pb$ ages (343±9 Ma) of zircons from cogenetic mafic enclaves (monzonite) dated now for the first time. Rarely preserved, internal domains of zircons from monzogranites show U-Pb ages around 355–359 Ma, suggesting also an early stage of zircon crystallisation. On the other hand, no relic, old cores were found in the investigated samples, presumably due to complete resetting of U-Pb isotopic system during the main magmatic event, suggested also by the surprisingly uniform Hf isotopic data of zircons. Eight concordant analyses on single titanites from a hybrid monzonite resulted in a concordia age of 332±3 Ma, which is in accordance with the lower closure temperature of titanite, and indicates moderate cooling of the pluton. The presented ages clearly confirm the assignment of the Mórágy Granite to the Variscan orogeny and exclude a pre-Variscan origin.

Fairly homogeneous Hf isotopic data of zircons both from monzogranite and its mafic enclave suggest considerable equilibration within and between the main rock types of the Mórágy Granite. This is in accordance with the quite uniform main, trace and REE element patterns from the different rock types of the pluton. However, a few internal zircon domains record an earlier event of zircon formation (~357-359 Ma) with distinct, less radiogenic Hf isotope composition. These relics support the idea that the initial isotope heterogeneity was almost completely reset.

Morphology, types and internal zoning of zircon from Mecsek Mountain granitoids resemble very much that of the ultrapotassic durbachites and associated rocks from Bohemian Massif. These rocks most likely formed by melting of metasomatised and enriched lithospheric mantle and all were emplaced shortly after the granulite-facies metamorphic peak in the Bohemian Massif (ca. 340 Ma).

[1] Balogh, K. et al. (1983) *Anu. Inst. Geol. Geofiz.*, **61**, 359-364. [2] Klötzli, U.S. et al. (1999) *Beihefte zur Eur. J. Mineral.*, **11**, 126. [3] Klötzli, U.S. et al. (2004) *Mineral. Petrol.*, **81**, 113-134. [4] Shatagin, K. et al. (2005) *Ann. Rep. Geol. Inst. Hung.*, **2004**, 41-64.

Geochemistry of magnetite from Cu-Mo porphyry + skarn, and Climax Mo deposits in the western United States

Nadoll, P.[1*], Mauk, J.L.[1], LeVeille, R.[2] & Koenig, A.[3]
[1]School of Environment, The University of Auckland, New Zealand ([*]p.nadoll@auckland.ac.nz)
[2]Freeport-McMoRan Copper and Gold Inc., USA
[3]U.S. Geological Survey, Denver, USA

Magnetite (Fe_3O_4) is a common and widespread accessory mineral in many host rocks and mineral deposits. Major- and trace element contents in magnetite are highly susceptible to geologic factors like temperature, oxygen fugacity, silica activity and melt composition. The ability to incorporate a large number of foreign cations in its spinel structure makes magnetite sensitive to hydrothermal processes and therefore an ideal target for geochemical investigations. The ongoing development of analytical techniques such as laser ablation inductively coupled mass spectrometry (LA-ICP-MS) are proven assets in determining even subtle variations in the geochemistry of magnetite from different geological settings. We used electron microprobe (EPMA) and LA-ICP-MS analyses, in combination with petrographic observations and factor analysis, to test whether magnetite from major Cu-Mo porphyry + skarn, and Climax Mo deposits of the western United States has distinct geochemical signatures. Our results show that the large variety of geological settings found in these deposits is reflected in the magnetite geochemistry. For example, in most places, hydrothermal and igneous magnetite can be discriminated by their respective trace element compositions. Furthermore, magnetite from different types of igneous rocks can be distinguished. The best overall discriminators for the trace element geochemistry of magnetite from igneous, porphyry, and skarn deposits are Mg, Al, Ti, V, Co, Mn, Zn, and Ga. These elements commonly occur in magnetite at concentrations above the LA-ICP-MS detection limits, and show characteristic variations across different geological settings. For example, Ti values can range from a few parts per million to several weight percent; higher values typically occur in igneous magnetite. Aluminium and V display a similar trend, although the overlap between hydrothermal and igneous magnetite is more pronounced for these elements. Hydrothermal magnetite hosted in skarn has the highest Mg concentrations, but igneous magnetite typically has higher Mg concentrations than magnetite from porphyry deposits. In contrast, Mn commonly has higher concentrations in hydrothermal magnetite. Factor analysis can help reveal relationships among trace elements that help fingerprint and characterize magnetite from specific geological settings. Although preliminary, our work suggests that three main factors are responsible for most geochemical variation in magnetite from the examined deposits: (1) Mg, Al, Ti, and Ga, reflecting an igneous signature, (2) Mn, Co, and Zn, suggesting hydrothermal control, and (3) V with a negative correlation to Mn. Factor analysis is also helpful for screening the data for analyses that were affected by inclusions. Our research demonstrates that rigorous petrographic examination, EPMA, LA-ICP-MS, and factor analysis can successfully fingerprint magnetite from different geological settings, including plutonic igneous rocks, and porphyry and skarn deposits.

Hungarian Variscan granitoids and their correlation with surrounding granitoids

Buda, Gy.[1*], Koller, F.[2], András, E.[3] & Nagy, G.[4]
[1]Dept. of Mineralogy, Eötvös L. University, Budapest, Hungary ([*]buda@ludens.elte.hu)
[2]Dept. of Lithospheric Research, University of Vienna, Austria
[3]Dept. of Mineralogy, Geochemistry and Petrology, University of Szeged, Hungary
[4]Inst. of Geochemical Research, Hungarian Academy of Science, Budapest, Hungary

The Tisia Composite Terrane (TCT) consists of various high-grade metamorphic series and Variscan granitoids. The TCT forms the basement of South Hungary, NE Croatia, N Serbia and W Transylvania (W Romania), and is surrounded by orogenic belts and faults. In TCT, few Variscan granitoid occurrences are known. The Mecsek granitoids are between the oldest ones (340-354 Ma). They are of I-type, metaluminous, calc-alkaline, high-K and high-Mg, bearing large intrusion with lamprophyre-derived, ultrapotassic, Mg-rich intrusions and/or enclaves (durbachite). The whole intrusion formed in a post-collisional zone. The magma originated from the uplifted and partially melted mantle and continental crust due to extension after the continent-continent collision. The large granitoid intrusion contains microcline megacrysts, zoned plagioclases (An_{60-35}), quartz, actinolitic hornblende, calc-alkaline-type biotite. The basic intrusions/enclaves contain the same mineral assemblages but enriched in Mg-rich amphibole and biotite, the zoned plagioclases are richer in An, and microclines have lower triclinicities. Both contain allanite, apatite, zircon and titanite as accessory minerals, but some of basic enclaves contain chromites. The intrusive bodies belong to the calc-alkaline K-rich monzonitic series. The other intrusions (Papuk, Psunj, Battonya, Muntele Mare [1], Codru) are mostly two micas, peraluminous, monazite-type younger (310-290 Ma) S or S/I-type granitoids. The granitoid melts originated from the partially melted continental crust after collision. The TCT belonged to the Moldanubicum zone of the Variscan orogenic belt. Later the TCT was disconnected by eastward movement of S Alps (Pelso unit) containing peraluminous/peralkaline, S/A-type small intrusions of Permian age (280-275 Ma), indicating the initial rifting.

Acknowledgements: The researches were supported by NRF 67787.

[1] Balintoni, I. et al. (2009) *Geol. Carpath.*, **60(6)**, 495-504.

Archean Lithospheric mantle: its formation, composition and today's remnants

O'Reilly, S.Y.* & Griffin, W.L.
GEMOC, Earth and Planetary Sciences, Macquarie University, Sydney, Australia (*sue.oreilly@mq.edu.au)

Archean subcontinental lithospheric mantle (SCLM) is distinctive in its highly depleted composition, commonly strong stratification, and the presence of rock types absent in younger SCLM. Was the Archean mantle formed in a different way in a distinctive tectonic regime? What is the composition of original Archean mantle and how much persists today?

The "typical" Archean mantle composition used in geochemical/geophysical modelling is depleted garnet lherzolite, derived mainly from peridotite xenoliths in kimberlites from the SW Kaapvaal Craton, and a few from Siberia. However, most such "typical" Archean xenoliths have experienced repeated metasomatism, leading to a progression from dunite/harzburgite through "depleted" lherzolite to "fertile" lherzolite, mirroring the secular evolution of the SCLM. Similar refertilisation processes can be studied *in situ* in peridotite massifs (eg Western Norway, Lherz), showing the lherzolites to be the product of melt infiltration into magnesian dunite/harzburgite protoliths. The most depleted rocks are poorly represented in the published xenolith record; the bias partly reflects the collecting of rocks useful for P-T studies, but also has a geological basis. High-resolution seismic tomography of Archean cratons shows high-Vs volumes surrounded and dissected by zones of lower Vs. The low-Vs parts can be modelled using the "typical" garnet lherzolite compositions, while the higher-Vs volumes require much more depleted rocks. In detail, kimberlites avoid the high-Vs volumes to preferentially follow older zones of fluid passage and metasomatism, hence biasing our "mantle sample" toward the metasomatic products. Seismic tomography suggests that this material still underlies the bulk of Archean cratons to depths of 150-200 km, but is poorly sampled by kimberlites. Relict Archean mantle is also imaged as buoyant high Vp blobs in oceanic regions, a likely source for reported "recycled" geochemical signatures in some ocean island basalts and providing evidence of mechanisms of continental breakup

Hf-isotope data on zircons show that much Proterozoic crust, especially in cratonic areas, has Archean protoliths, suggesting that the underlying SCLM also was originally Archean. Seismic tomography shows high-Vs roots, requiring depleted compositions and low geotherms, under many of these areas; clearly juvenile Proterozoic belts (eg SW Scandinavia) do not have such roots. Re-Os isotopic data for the underlying mantle record similar events, indicating a linked tectonic history. These observations suggest that much of the observed secular evolution in SCLM composition reflects progressive reworking of buoyant Archean SCLM, rather than secular changes in the mechanisms of SCLM production. Seismic tomography suggests that≥50% of existing continental crust is underlain by relict Archean SCLM, modified to varying degrees. This implies a much larger volume of originally Archean crust than currently accepted, and hence very high early crustal growth rates.

Melt-modelling exercises that treat "typical" Archean peridotites as simple residues are invalid, and cannot be used to support "lithosphere stacking" models for SCLM formation. The "primitive" Archean dunites/harzburgites are best modelled as restites/cumulates from high-degree melting at 3-6 GPa, in ascending plumes/mantle overturns. This uniquely Archean regime may have coexisted with a more modern plate-tectonic regime, which produced weakly depleted residues similar to Phanerozoic SCLM. This "modern" SCLM would be inherently unstable, easily recycled and lost to the modern record.

Deformation and melt localization in the subcontinental mantle: a case study from the plagioclase tectonite zone of the Ronda peridotite massif (South Spain)

Hidas, K.[1*], Garrido, C.J.[1], Booth-Rea, G.[2], Gervilla, F.[1], Bodinier, J.-L.[3], Tommasi, A.[3] & Marchesi, C.[3]
[1]Instituto Andaluz de Ciencias de la Tierra, CSIC-UGR, Granada, Spain (*karoly.hidas@gmail.com)
[2]Dept. of Geodynamics, Universidad de Granada, Spain
[3]Geosciences Montpellier, CNRS-Université de Montpellier-2, Montpellier, France

The processes that take place during the transport of melts through the convecting mantle are the least understood and, therefore, state-of-the art problems among a series of processes of formation and evolution of mantle magmas. It is widely accepted that, dunite channels might be pathways by which mantle melts easily pass through the overlying mantle (e.g. [1]). The role of shear strain during the formation of dunite bodies in ophiolites was considered in details by [2]. It was also shown that the stress field can control the melt migration paths marked by dunite bodies occurring oriented regularly relative to the hinge and axial plane of a harzburgite fold [3]. The localization of melt flow and formation of channels under mechanical instability during the formation of dunites is expected to lead to a stronger olivine crystallographic preferred orientation (CPO) in these rocks than in their surroundings. However, accepted models explain formation of dunitic lithology mostly in oceanic environment, but one would face several challenges trying to apply them to the subcontinental lithospheric mantle.

The Ronda massif (southern Spain) is the largest (*ca.* 300km^2) of several orogenic peridotite massifs exposed in the Betic and Rif (northern Morocco) mountain belts in the westernmost part of the Alpine orogen that was tectonically emplaced during early Miocene times. One of the most remarkable features of the Ronda massif is the 'recrystallization front' that represents the transition from the spinel-tectonite to the coarse granular peridotite domain corresponding to a narrow boundary of a partial melting domain caused by thinning and coeval asthenospheric upwelling formed at the expense of former subcontinental lithospheric mantle and associated with melting and kilometer-scale migration of melts by diffuse porous flow through the 'asthenospherized' domain [4, 5, 6]. In the vicinity of the recrystallization front, coarse granular peridotites pass into layered granular peridotites with a typical layered structure composed of plagioclase lherzolites, harzburgites and dunites.

The main scientific goals of this study are to test new mechanism(s) for the formation of dunites and dunite-harzburgite-lherzolite layered bodies in the subcontinental lithospheric mantle on the example of Ronda peridotite massif (Spain), and to introduce new processes that are expected to lead the evolution of the subcontinental lithospheric mantle in extensional settings.

[1] Kelemen, P.B. et al. (1997) *Philos. T. Roy. Soc. A.*, **355**, 283-318. [2] Kelemen, P.B. & Dick, H.J.B. (1995) *J. Geophys. Res.*, **100,** 423-438. [3] Savelieva, G.N. et al. (2008) *Geotectonics,* **42**, 430-447. [4] Van Der Wal, D. & Bodinier, J.L. (1996) *Contrib. Mineral. Petrol.*, **122**, 387-405. [5] Lenoir, X. et al. (2001) *J. Petrol.*, **42**, 141-158. [6] Vauchez, A. & Garrido, C.J. (2001) *Earth Planet.Sci. Lett.*, **192**, 235-249.

Petrogenesis of olivine clinopyroxenites from Sorkhband ultramafic complex, Southern Kerman, Iran: constraints on mineral and whole rock chemistry

Najafzadeh, A.R.[1*], Arvin, M.[2], Pan, Y.[3] & Ahmadipour, H.[2]
[1]Dept. of Geology, Payame Noor University, Kerman, Iran
([*]najafzadeh@pnuk.ac.ir)
[2]Dept. of Geology, Shahid Bahonar University of Kerman, Iran
[3]Dept. of Geological Sciences, University of Saskatchewan, Saskatoon, Canada

The Ordovician Sorkhband ultramafic complex lies in southern Kerman Province of Iran. The wedge shape complex covers an area of more than 100 km^2 and is divided into: lower part, comprises of dunite, largest podiform chromitite deposits in Iran (Faryab mine), massive and dyke like olivine clinopyroxenite, wehrlite and olivine websterite dykes; and an upper part of foliated porphyroclastic diopsidic harzburgite with subordinate lenses and dykes of dunite, massive and dyke like olivine clinopyroxenite and minor orthopyroxenite dykes with no significant chromitite mineralization.

Petrographically the massive and dyke like olivine clinopyroxenites have granular to subgranular textures and modally consist mainly of 80-85% diposidic clinopyroxene ($En_{45}Fs_6Wo_{49}$), 5-20%, olivine (Fo_{90-92}), 1-10% bronzitic orthopyroxene ($En_{81}Fs_{18}Wo_1$), and <0.5% chromite ($Cr^{\#}$=53-87, $Mg^{\#}$=48-67). Clinopyroxenes often exhibit exsolution lamellaes of orthopyroxene with a triple junction boundary.

Mineral chemistry of olivine clinopyroxenites reveals a mantle origin for the Sorkhband ultramafic complex. Moreover, their chondrite normalized rare-earth element (REE) patterns show flat medium REE (MREE) and heavy REE (HREE) patterns, [$(Gd/Yb)_N$~1], and highly light REE (LREE) depletions. Their platinum group element (PGE) patterns also show highly differentiated pattern with a positive slope and high Pd/Ir ratio (0.85-11.49).

The mineral and whole rock chemistry along with REE and transition elements (TE) patterns in Sorkhband olivine clinopyroxenites are quite similar to those reported from pyroxenite of Nan-Uttardite ophiolites in Thailand [1], Leka ophiolites in Norway [2] and San Jorge in Solomon Islands [3]. So, it is most likely that Sorkhband olivine clinopyroxenites have been crystallized from a CaO rich boninitic melt in a supra-subduction zone environment.

[1] Orberger, B. et al. (1995) *Lithos*, **35,** 153-182. [2] Furnes, H. et al. (1992) *Lithos*, **27,** 259-277. [3] Berly, Th.J. et al. (2006) *J. Petrol.*, **47,** 1531-1555.

Textural mapping by SEM in amphiboles and biotites from alkaline rocks: identification of inclusions and implication for Ar-Ar dating

Borges, W.N., Vargas, T. & Geraldes, M.C.[*]
Faculdade de Geologia, Universidade do Estado do Rio de Janeiro, Rio de Janeiro, Brasil ([*]geraldes@uerj.br)

The alkaline complexes which occur in south-southeast of Brazil comprise basically a series of syenitic associations composed of trachyte, tinguaite and nepheline syenite. These rocks yielded K-Ar ages from 80 Ma to 65 Ma. The geodynamic models for the origin of these rocks consider the intrusions lineament of NW-SE direction originated by mantle plume magmatism.

The biotite and amphibole samples obtained from 10 alkaline intrusions (Tinguá, Marapicu, Tanguá, Nova Iguaçu, Itatiaia, Morro de São João, Morro Redondo, Ilha de Cabo Frio, Soarinho and Passa Quatro) were studied by Scanning Electron Microscope (SEM). The sample from Morro Redondo (Fig. 1A) shows apatite intrusion and iron oxide in the biotite. Tanguá sample (Fig. 1B) shows agglomerates of small grains of biotite. In Fig. 1C, the biotite grain has no fractures. In the samples from Morro de São João (Fig. 1D), intrusions of apatites and biotite in the amphybole grains are observed. Locally the amphibole shows a lighter texture, possibly indicating a change to biotite. In Tinguá sample we can see pyrite and amphybole inclusions in the biotite grains (Fig. 1E). In Mendanha sample we notice biotite developed at the borders of amphibole grains. We can also notice a round inclusion of biotite within an amphybole grain (Fig. 1F).

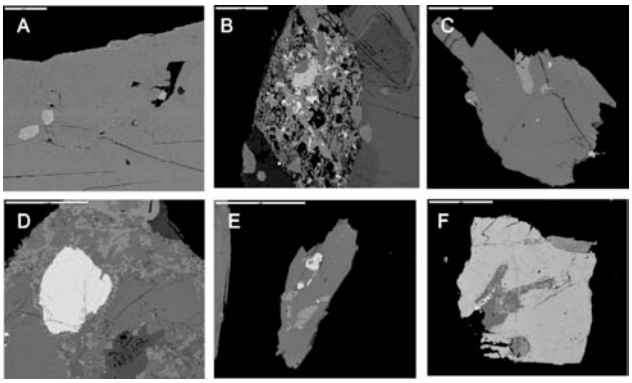

Fig. 1: Images obtained in SEM for biotite and amphibole from alkaline rocks.

The usage of SEM was very useful due practical, economic and accessible procedures. The use of the BSE signal was very useful in the identification of mineral phases, which allows greater accuracy in the interpretations of Ar-Ar age patterns, obtained by step-heating technique. In this sense, the possible age anomalies may be related to solid intrusions not observable in the optic petrography. For these reasons, the use of SEM becomes of fundamental importance to Ar-Ar analysis in mineral grains.

Dilution of a volcanic rare earth element signature in ancient active margin sedimentary basins

Ryan, K.M.[*] & Williams, D.M.
Dept. of Earth & Ocean Sciences, National University of Ireland, Galway, Ireland ([*]kieran.mryan@gmail.com)

The western Ireland Caledonides record the deposition of sediments and tuff bands in a number of depositional settings including: (1) alluvial plain and delta fans [1] and (2) submarine fan environments [2], along an Ordovician active continental margin. The REE profiles from both settings exhibit the typical uniform profile for sandstones [3], however, the medium-coarse grained sandstones in each setting display REE enrichment during post eruption deposition. In the case of the submarine fan sandstones, post-eruption REE concentrations display an average enrichment of 27% compared to the pre-eruption sandstones. The alluvial plain sandstones record a similar profile with 10% post-eruption REE enrichment.

The difference in the level of enrichment between the submarine fan and the alluvial plain sandstones (27% and 10% respectively) can be attributed to two main factors: (a) differences in the mineralogy of the volcanic deposits and (b) differences in surface processes at each setting. In relation to the mineralogy, the volcanism in the alluvial plain setting is represented by rhyodacitic ignimbrites, with embayed quartz and feldspar crystals in a glassy matrix. In contrast, the volcanism in the submarine fan setting is characterised by andesitic-rhyodacitic, coarse-grained, alkali feldspar rich crystal tuffs with glass fragments.

The second factor that may contribute to the difference in the REE enrichment is related to surface processes. The alluvial plain sandstones were deposited rapidly and in close proximity to the source region [1], with limited time for mechanical breakdown and sorting of the sandstone fraction. Therefore, significant chemical differences would not be expected in the pre and post eruption sediments. In contrast the submarine sandstones were deposited as gravity flow sediments in large submarine fans [2], this suggests a greater degree of mechanical reworking to breakdown a less stable volcanic component.

In both environments the erosion of the volcanic deposits results in a short term elevation of the volcanic component in sediment derived from the source region with a return to pre-eruption REE concentrations as sedimentation continued in the basin. The REE profiles from the ancient sedimentary basins support previous studies (e.g. [3]), which identified the difficulty in using the uniform signatures as provenance indicators, but they highlight the potential to use changes in the REE concentrations to indicate volcanic events within sandstone sequences and to decipher localised surface processes.

[1] Williams, D.M. (1984) *Geol. J.*, **19**, 173-186. [2] Archer, B.J. (1977) *Geol. J.*, **12**, 77-98. [3] McLennan, S.M. (1989) in Lipin, B.R. & McKay, G.A. (eds.) *Rev. Mineral.*, **21**, 169-200.

Metamorphic evolution in the Khetri Complex, India

Kaur, P.[1], Zeh, A.[2,3], Okrusch, M.[2*], Gerdes, A.[4] & Chaudhri, N.[1]
[1]Panjab University, Chandigarh, India
[2]Universität Würzburg, Germany ([*]okrusch @würzburg.de)
[3]Freie Universität Berlin, Germany
[4]Universität Frankfurt am Main, Germany

The NE-SW trending Proterozoic Khetri Complex is part of the Aravalli Orogen, an important constituent of the Indian Plate. The northern part of the complex consists predominantly of metasedimentary rocks that were metamorphosed under greenschist to amphibolite facies conditions in Paleoproterozoic times [1]. The metamorphic sequence was intruded at 1.71–1.66 Ga by A-type, alkali feldspar granites [2,3]. These were widely affected, together with their metamorphic country rocks, by a regional sodic metasomatic event leading to albitisation of plagioclase and microcline [4]. Representative mineral assemblages in the metamorphic rocks are:

And–Grt ($Alm_{0.9}Prp_{0.1}$)–Bt (X_{Fe} 0.65)–Chl (X_{Fe} 0.6)

And/Ky–Bt (X_{Fe} 0.5)–Chl (X_{Fe} 0.4)–Ms (Si 3.1 pfu)–Qtz

Grt ($Alm_{0.66}Prp_{0.06}Grs._{0.05}Sps_{0.23}$)–Bt ($X_{Fe}$ 0.4)–Ms (3.1 Si pfu)–Pl (An_{6-12})–Qtz

Ath (X_{Fe}0.55)–Ged (X_{Fe} 0.55)–Bt (X_{Fe} 0.5)–Chl (X_{Fe} 0.5)–Scp (Me_{34-38})–Pl (An_{12-17}),

Ged (X_{Fe} 0.5)–Crd (X_{Fe} 0.3)–Bt (X_{Fe} 0.55)–Chl (X_{Fe} 0.4)–Scp (Me_{26-34}).

From a pseudosection, calculated in the model system KNCMnFMASH for a metapelitic schist, peak P-T conditions at c. 3.5 kbar and 550°C were derived. The timing of regional metamorphism is not well constrained. However, it is bracketed by LA-SF-ICP-MS U-Pb ages of 1.74-1.73 Ga obtained from the youngest detrital zircons grains from a quartzite sample, and the emplacement age of the A-type granites at 1.71 – 1.66 Ga.

[1] Lal, R.K. & Ackermand, D. (1981) *Neues Jb. Miner. Abh.*, **124**, 294-325. [2] Kaur, P. et al. (2006) *Mineral. Petrol*, **87**, 81-122. [3] Kaur, P. et al. (2007) *Geol. Mag*, **144**, 361-378. [4] Kaur, P. et al. (submitted) *J. Petrol*.

Mineralogical and chemical characteristics of chrysotile veins from Semail Ophiolite, Wadi Daftah, United Arab Emirates

Heikal, M.Th.S.[1], Hassan, A.M.[1], El Nashar, E.S.R.[2*] & Lebda, E.M.L.[3]
[1]Geology Dept., Faculty of Science, Tanta University, Tanta, Egypt
[2]Geology Dept., National Research Centre, Dokki, Cairo, Egypt ([*]saidnashar@hotmail.com)
[3]Dept. of Biological and Geological Sciences, Faculty of Education, Kafr El Sheikh University, Kafr El Sheikh, Egypt

Twelve selected sites of chrysotile-hosted serpentinized peridotite in Wadi Daftah across Masafi –Al Fujairah paved road, eastern coast, UAE, have been carefully sampled and collected samples investigated by different techniques of mineralogy and chemistry.

Field data reveal three modes of occurrence and stages of chrysotile; namely: slip-fiber (splintery form), cross-fiber and mass-fiber. Structural control of chrysotile formation is suggested by discontinuous occurrences of the mineral along tight cracks and shear fractures, mostly trending NW and NE.

Petrographically, chrysotile has partly and/or completely replaced olivine and/or pyroxene. On the other hand, the appearance of talc which has subsequently replaced the serpentine and/or pyroxene during retrograde talcification has recorded in few sites.

On the mineralogical basis, differential thermal analysis (DTA) and thermogravimetry (TG) indicate that the process of the thermal decomposition of chrysotile leads to the formation of olivine. The infra-red (IR) absorption technique applied for end products of some selected samples showed that the spectra of the end products are similar and the absorption bands assigned in the range of 1100-800 cm^{-1} and 700-200 cm^{-1} correspond to Si-O and Mg-O vibration modes. The chemical data revealing the similarity in chemical behaviours of chrysotile veins, implies that a close cogenetic relationship among three modes of chrysotile and removal of some major elements occurred during serpentinization; Mg, Fe and Si were removed in solution from the peridotite and precipitated in tension and shear fractures to form fibrous chrysotile and magnetite. The chrysotile serpentinization process is due to metasomatic replacement of peridotite during ocean floor early episode and later due to an episode of ophiolite obduction.

Do the mineralogical and geochemical characteristics of Camlidere Volcanic Rocks (Galatean Volcanic Province), Central Anatolia, Turkey, verify the magma mixing event in its evolution?

Varol, E.[1*], Temel, A.[1] & Gourgaud, A.[2]
[1]Dept. of Geological Engineering, Hacettepe University, Beytepe, Ankara, Turkey ([*]elvarol@hacettepe.edu.tr)
[2]OPGC, UMR-CNRS 6524 'Magmas et Volcans', Blaise Pascal University, Clermont-Ferrand, France

The Camlıdere district, located in Galatean Volcanic Province, NW of Ankara, Turkey, consists mainly of lacustrine sedimentary deposits, pyroclastic deposits, volcanic lava flows, domes and small dikes. The pyroclastic units are rhyolitic fall and flow deposits. The volcanic rocks are rhyolitic, andesitic, trachytic, dacitic and locally basaltic in character from older to younger. All these rocks exhibit hypocrystalline porphyritic textures. The rhyolitic lavas contain plagioclase + biotite + quartz, the andesitic lavas clinopyroxene + orthopyroxene + plagio-clase + amphibole, the trachytic lavas clinopyroxene + orthopyroxene + plagioclase + amphibole + biotite and the dacitic lavas clinopyroxene + orthopyroxene + plagioclase + amphibole + biotite ± quartz. The youngest basaltic rocks crop out as dikes and consist of olivine + clinopyroxene + plagioclase ± orthopyroxene. Oxides occur as accessory minerals or inclusions in the phenocrysts in all type of rocks. The mineralogical characteristics, mineral chemistry and whole-rock geochemistry reveal that magma mixing is an important process on the evolution of these rocks. Some features can be interpreted as evidences of magma mixing process, features such as:

-orthopyroxene surrounded by clinopyroxene,

-normally and reversely zoned, reacted amphiboles,

-coexistence of normally and reversely zoned, sieved and unsieved plagioclase and pyroxene in the same rock,

-having a wide compositional range of An% from core to rim of plagioclase,

-major element modelling using least-square mass balance calculations.

Low-temperature wollastonite: evidence for carbonate reduction around serpentinite

Malvoisin, B.[1], Chopin, C.[1*], Brunet, F.[1], Galvez, M.[1] & Beyssac, O.[2]
[1]Ecole normale supérieure–CNRS, Paris, France
([*]chopin@geologie.ens.fr)
[2]IMPMC, Université P. et M. Curie–CNRS, Paris, France

Siliceous marbles immediately overlying a serpentinite body above Patrimonio, in the Alpine blueschist- to eclogite-facies meta-ophiolitic units of northern Corsica, are remarkable in two respects. i) In a calcite ± quartz matrix, they preserve aragonite inclusions in grossular garnet. The aragonite fibres are oriented perpendicular to the garnet growth surface and impart the garnet porphyroblast a very uncommon, radial to sectoral microtexture [1]. ii) The refolded contact between serpentinite and marble shows a very continuous reaction zone, with a conspicuous, weathering-resistant centimetre-thick selvage of pale 'nephrite' (diopside ± andradite/grossular ± perovskite) on serpentinite side, followed toward the impure marble by a 1 to 5 cm thick, light grey and easily weathered zone of wollastonite (± grossular), followed by a 5 to 20 cm thick, dark zone forming like a dark halo around the serpentinite in the overlying series and consisting essentially of wollastonite + quartz + carbonaceous material (± grossular ± diopside), with no carbonate. The transition to the overlying wollastonite-free, calcite+quartz-bearing layers is sharp.

Considering the stability of calcite + quartz throughout all the regional series, this low-temperature (< 500°C) occurrence of wollastonite is paradoxical. A clue to its origin is the abundance of carbonaceous matter along with wollastonite within a few decimetres of the serpentinite body. We interpret this observation as evidence for local reduction of the carbonate to form carbon and wollastonite (in the presence of quartz), probably by diffusion of/in a highly reducing fluid (< FMQ –1) equilibrated with the serpentinite. The implication is that serpentinite bodies may preserve a reducing redox potential throughout subduction and metamorphism.

[1] Chopin, C. et al. (2008) *Eur. J. Mineral.*, **20**, 857-865.

Preliminary geochemical characteristics of Variscan granitoids from Apuseni Mountains (Romania)

András, E.[1], Pál-Molnár, E.[1*] & Buda, Gy.[2]
[1]Dept. of Mineralogy, Geochemistry and Petrology, University of Szeged, Szeged, Hungary ([*]palm@geo.u-szeged.hu)
[2]Dept. of Mineralogy, University of Eötvös L., Budapest, Hungary

The Tisia Composite Terrane [TCT] is built up from Variscan metamorphic series and granitoids. The TCT forms the basement of South Hungary, NE Croatia, N Serbia and W Romania and it is surrounded by mobile zones and fault lines.

In order of correlation studies between granitoid suits from the Tisia Composite Terrane, an extended field survey is being carried out in the Apuseni Mountains (Romania). The Apuseni Mountains consist of four Alpine tectonic units: the Bihor Unit, the Codru Nappe System, the Biharia Nappe System and the Mureş zone. Its basement is built up from three pre-Alpine Godwanan terranes: Someş, Biharia and Baia de Arieş. These units are built up by metamorphic sequences, most of them contain Variscan granitoid intrusions. The present study focuses on different granitoid occurrences from the Someş Terrane: Şiria granitoid [SG] (presumably the same age as CG), Codru granitoid [CG] (372 Ma), Codru migmatite [CM] (516 Ma), Muntele Mare granitoid [MMG] (both main pluton and satellite branches) (297-291 Ma).

The composition of the suits is more or less heterogenic, many structural and compositional variations are present within a group. The MMG suite contains: equigranular two mica granitoids, biotite granitoids, k-feldspar megacryst bearing granitoids, leucogranites, leucogranites with gneissic texture. The CM suite is mostly metatexite, where both paleosome (~70%) and neosome are present (~30%). The SG and CG are two mica granites with or without feldspar megacrysts.

Petrogenetic and geotectonic interpretations were elaborated based on whole rock geochemical compositions (major and trace elements). Modal and geochemical classifications show granodiorite to monzogranite compositions for MMG, granitic (monzo- and syeno-) for CG and SG, and granodiorite to tonalite for CM.

The studied samples have a calc-alcaline and moderately peraluminous character. The only exceptions are framed by the CM, which are calcic. The samples from MMG, CG and SG show syn-collison and post orogenic origin, while the CM samples are mantle fractionates.

Acknowledgements: Research supported by NRF No. 67787.

Sr-Nd isotope evidence for mixing in the mafic rocks from the Reguengos de Monsaraz Variscan Pluton (Ossa Morena Zone, Portugal)

Antunes, A.[*], Santos, J.F. & Azevedo, M.R.
GeoBioTec, Dep. Geociências, Universidade de Aveiro, Aveiro, Portugal ([*]ana.antunes@ua.pt)

The late-post-kinematic Reguengos de Monsaraz pluton is located in the Ossa Morena Zone, one of the major geotectonic units of the Iberian Variscan Belt. At the presently exposed level, the intrusion is dominated by tonalite-granodiorite rocks, spatially associated with minor bodies of gabbro-diorite composition, particularly in the central part of the area. Field evidence shows that the different intrusive facies define mixing/mingling contact relationships, suggesting a coeval emplacement for mafic and felsic magmas. The Rb-Sr age obtained for the pair amphibole-feldspar in one granodiorite sample (297.5 ± 2.9 Ma, initial $^{87/86}$ Sr = 0.70766 ± 0.00011) provides a minimum estimate for the time of original crystallization [1].

Petrographic and geochemical studies reveal that the different members of the suite have compositions ranging from metaluminous to slightly peraluminous and a distinctive calc-alkaline signature. Furthermore, the occurrence of systematic rectilinear correlations in Harker variation diagrams supports a mixed provenance for this sequence [1].

The εSr_{300}-εNd_{300} co-variation displayed by the least evolved members of the suite indicates that these rocks do no longer represent the mafic mixing end-member. Their relatively low εNd_{300} values [εNd_{300}=-5.1 to -7.8; $^{87}Sr/^{86}Sr_{300}$= 0.70871 to 0.71037] point to a significant interaction with time-integrated LREE-enriched upper crustal source components, comparable to the Late Proterozoic metasediments of the "Série Negra" (Fig. 1).

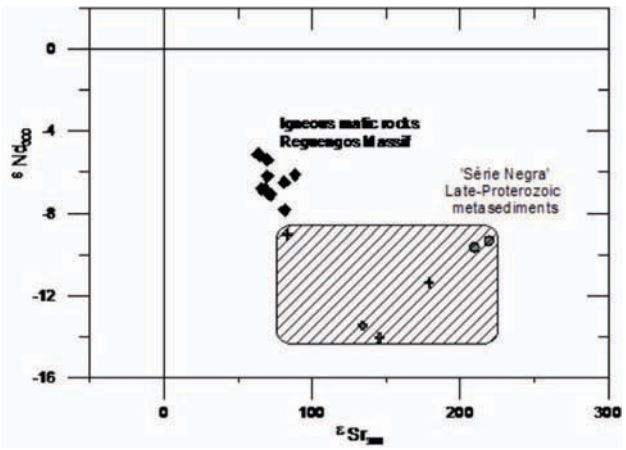

Fig. 1: εSr300-εNd300 diagram for the mafic rocks of the Reguengos de Monsaraz intrusion. Sr-Nd compositions of the "Série Negra" metasediments from Schäfer (1990) [2] and Beetsma (1995) [3].

A scenario where the gabbro-diorite magmas from Reguengos de Monsaraz correspond to contaminated basic liquids is therefore proposed. Further hybridization of mafic magmas with anatectic crustal melts would have generated the entire range of granitoid types present in the massif.

[1] Antunes, A. et al. (2009) *Proc. VII Congreso Ibérico de Geoquímica / X Congreso Nacional de Geoquímica*, Soria, **17**, 788-798. [2] Beetsma, J.J. (1995) *Ph.D. Thesis*, Vrije University, Netherlands. [3] Schäfer, H.J. (1990) *Ph.D. Thesis*, Zurich, Switzerland, EHT Diss., Nº 9246.

Geochemistry of biotite as a petrogenetic indicator for the Castelo Branco granitic pluton, Central Portugal

Antunes, I.M.H.R.[1,2*], Neiva, A.M.R.[3] & Silva, M.M.V.G.[3]
[1]Polytechnic Institute of Castelo Branco, Castelo Branco, Portugal ([*]imantunes@esa.ipcb.pt)
[2]Geoscience Centre, University of Coimbra, Coimbra, Portugal
[3]Department of Earth Sciences, University of Coimbra, Coimbra, Portugal

The reversely zoned pluton of Castelo Branco consists of five concentric late-tectonic Variscan granitic rocks (310 ± 1 Ma), which intruded the Cambrian schist-metagraywacke complex [1]. A muscovite>biotite granite (A) in the pluton's core is surrounded successively by biotite>muscovite granodiorite (B), porphyritic biotite>muscovite granodiorite (C) grading to biotite≈muscovite granite (D) and finally by muscovite>biotite granite (E). The contact between granite A and granodiorite B is sharp, such as the contact between granites D and E. All granitic rocks are peraluminous with A/CNK ratio ≥ 1.1, normative corundum ≥ 2.8 % and of S-type. These granitic rocks are mainly classified as magnesian and alkali-calcic [2]. They contain quartz, microperthitic microcline, plagioclase, biotite, muscovite, tourmaline, monazite, apatite, zircon, ilmenite and rutile. Biotite crystals are euhedral to subhedral, with pleochroism from γ and β – dark reddish brown to α – pale yellow. They are Fe-biotites [3] and have compositions similar to those of biotites from aluminium-potassic rock series [4]. Variation diagrams for major and trace elements and trace/major element ratios of the biotites plotted against whole-rock % total FeO define curvilinear trends between granodorites B and C and granite D. The general increases in Al, Nb, Zn, Sn, Li, Rb, Cs and Ta contents and Rb/K and Li/Mg values and decreases in Mg, Cr, Ni, Co, Sc, Ga and Ba contents and $Mg/(Mg+Fe^{2+})$, Ba/K, Ni/Fe^{2+} and Sc/Fe^{2+} values from biotite of granodiorite B to biotites of granodiorite C and granite D suggest a magmatic differentiation process. The biotites of granites A and E do not fit these trends and are not related, supporting that these granites represent two distinct pulses of granite magma. The granodiorite C and granite D are the products of in situ fractional crystallization of granodiorite magma B by separation of plagioclase, quartz, biotite and ilmenite, which took place outwards in maximum two million years [1].

[1] Antunes, I.M.H.R. et al. (2008) *Lithos*, **103(3/4)**, 445-465. [2] Frost, B.R. et al. (2001) *J. Petrol.*, **42**, 2033-2048. [3] Rieder, M. et al. (1998) *Can. Mineral.*, 36, 905-912. [4] Nachit, H. et al. (2005) *C. R. Geosci.*, **337**, 1415-1420.

Crystal structural characterization of calcite in low-grade metamorphic rocks of the Szendrő Mountains (NE-Hungary)

Bajnóczi, B.[*], Tóth, M. & Árkai, P.
Institute for Geochemical Research, Hungarian Academy of Sciences, Budapest, Hungary ([*]bajnoczi@geochem.hu)

It is well known that the average grain size of carbonate rocks increases with increasing (peak) metamorphic temperature (e.g., [1,2]). However, the grain size is not suitable for a reliable determination of metamorphic grade because there are several factors (e.g., modal composition and textural characteristics of rocks) that control grain growth. The amounts and distributions of associated fine-grained clay minerals and organic matter, strongly related to the original depositional environment and diagenetic history of the rock, display significant influences on the main grain size of metacarbonates (e.g., [3]).

The structural changes in phyllosilicates (mostly illite and chlorite) are well known and widely used empirical indicators for expressing differences in diagenetic and low-T metamorphic (anchi- and epi-) zones. For this purpose the full width at half maximum (FWHM) values of the basal XRD reflection(s) of phyllosilicates is a widely applied method. Changes in average size of submicroscopic crystallites (i.e., in the mean size of domains that scatter coherently the X-ray) of carbonate minerals during metamorphism may provide also a useful empirical tool to differentiate between metamorphic zones.

To test the applicability of FWHM of calcite in metamorphic research, the present study attempts to compare crystal structure characteristics of different metacarbonate rocks originated from a given metamorphic unit. Recrystallized limestones and marbles of the Szendrő Mountains from NE-Hungary were investigated, for which epizonal character based on the FWHM of phyllosilicates is well-known from earlier studies [4, 5]. The studied metacarbonate formations, originated from protoliths from various sedimentary environments, have distinct grain sizes, clay and organic matter contents. In addition to microtextural characterisation, differences among formations were revealed by comparing FWHM values of the maximal intensity X-ray reflection (d_{104} = 3.03 Å) of the bulk (matrix) calcite. In addition single line profile analysis of the maximal intensity reflection was applied to determine mean crystallite size of calcite in each formation.

In the studied formations the average crystallite size correlates fairly well with the grain size. Coarse-grained (0.1 to 0.5 mm), "pure" platform limestone (Rakaca Marble) has lower FWHM and higher crystallite size (0.149 to 0.167 °2theta, 730 to 830 Å) than fine-grained (< 0.05 mm), clayey, basin facies limestone (Verebeshegy Limestone) (0.163 to 0.192 °2theta, 600 to 690 Å). Previously Abod Limestone (metatuffitic, recrystallized limestone rich in phyllosilicates) was regarded as having the highest metamorphic grade (biotite zone) among formations of the Szendrő Mts. The FWHM (0.155 to 0.197 °2theta) and crystallite size (610 to 920 Å) of the Abod Limestone, however, overlaps with that of the Rakaca Marble and the Verebeshegy Limestone in accordance with its medium grain size (0.05 to 0.3 mm).

The FWHM and mean crystallite size of bulk calcite in the Szendrő metacarbonate rocks seem to especially depend on the lithology. To compare the metamorphic grade of different units these parameters can only be evaluated for similar lithological types of carbonate-rich rocks.

[1] Covey-Crump, S.J. & Rutter, E.H. (1989) *Contrib. Mineral. Petrol.*, **101**, 69-86. [2] Tullis, J. & Yund, R.A. (1982) *J. Geol.*, **90**, 301-318. [3] Olgaard, D.L. & Evans, B. (1988) *Contrib. Mineral. Petrol.*, **100**, 246-260. [4] Árkai, P. (1983) *Acta Geol. Hung.*, **26**, 83-101. [5] Árkai, P. (1991) *J. Metamorphic Geol.*, **9**, 723-734.

First report of Mg-rich chloritoid + staurolite assemblage from the Sanbagawa belt, Japan

Banno, Y.
Geological Survey of Japan, National Institute of Advanced Industrial Science and Technology (AIST), Tsukuba, Japan (y-banno@aist.go.jp)

Mg-rich [Mg/(Mg + Fe^{2+}) = 0.37 to 0.49] chloritoid associated with staurolite was found in a corundum-bearing zoisite rock from the Besshi area (N 33°52', E133°24') in the Sanbagawa metamorphic belt, Japan. Chlorotoid is a rare mineral that occurs in the Sanbagawa belt, which is a high-*P*/*T* metamorphic belt [1]. This is the first report of chloritoid + staurolite assemblage from the Sanbagawa belt. The zoisite rock consists mainly of coarse-grained zoisite, corundum, garnet, and pargasite. These minerals are considered to be stable at the peak metamorphic stage under eclogite facies condition. Garnet belongs to the almandine-pyrope series (X_{Alm}: 0.28-0.40, X_{Prp}: 0.38-0.50) and is poor in Mn (X_{Sps}: 0.01) and rich in Ca (X_{Grs}: 0.19-0.24). Corundum was retrogressively replaced by fine-grained secondary chloritoid, zoisite, clinozoisite, chlorite, and paragonite. Staurolite [Mg/(Mg + Fe^{2+}) = 0.27 to 0.35] rarely occurs in aggregates of the secondary phases (chloritoid, chlorite, and paragonite), which occur along the cracks in corundum, and is surrounded by chloritoid (Fig. 1).

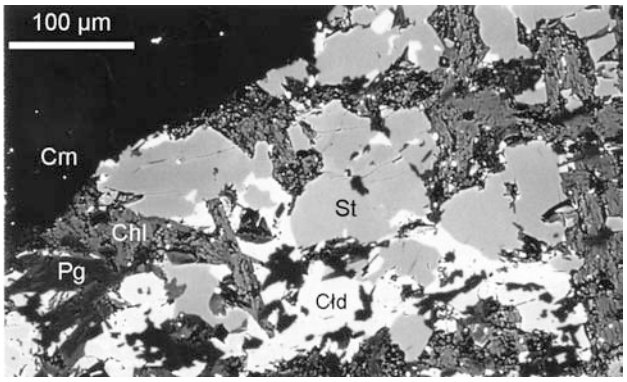

Fig. 1: Backscattered electron image of chloritoid growing into staurolite. Abbreviations: Cld, chloritoid; Crn, corundum; Chl, chlorite; Pg, paragonite; St, staurolite.

This texture indicates that chloritoid was formed by the following retrogressive reaction: 7chlorite + 8corundum + 4staurolite + 15H_2O → 51chloritoid. The *P*-*T* condition during the retrograde stage can be determined using the chloritoid-staurolite-chlorite-corundum assemblage. The mineral equilibrium is calculated using the THERMOCALC program (ver. 3.21) [2] with coexisting compositions of chloritoid, staurolite, and chlorite. The estimated temperature for the above univariant reaction in the MASH system is 637 ± 30 °C at 10 kbar and 744 ± 34 °C at 20 kbar. The temperature obtained from the calculation using the FASH system is approximately 130 °C lower than that obtained from the MASH system at 10-20 kbar. The process of formation of staurolite is not clear. One of the possible reactions for the formation of staurolite at an early stage of retrograde metamorphism is as follows: garnet + corundum + H_2O → staurolite + chlorite. The textural evidence and the estimated temperature suggest that chloritoid formed during the exhumation stage from eclogite to epidote-amphibolite facies conditions.

[1] Zaw Win Ko et al. (2005) *Lithos*, **81**, 79-100. [2] Holland, T.J.B. & Powell, R. (1998) *J. Metamorph. Geol.*, **16**, 309-343.

Geological studies on Pleistocene rubble of Palaeo Danube in Carpathian Basin

Bors, V., Giber, A., Józsa, S., Lévai, E., Micsinai, D.*, Molnár, M., Szabó, Zs., Varga, M. & Vígh, Cs.
Dept. of Petrology and Geochemistry, ELTE, Budapest, Hungary (*dani9@tvnetwork.hu)

At the end of last Glacial the Palaeo Danube stepping out from the Eastern Alps and from the Visegrád-Pilis-Budai Mts. has been depositing its bedload in two large gravel funs: west of Pozsony (Bratislava) on Little Hungarian Plain and south of Budapest on Csepel Plain. These late Pleistocene terraces are mostly covered by thin holocene sediments and consist of gravels with few sporadically embedded angular blocks both containig wide variety of partly exotic rock types. We give summarised petrographic and grain morphologic description of this debris to know more about the environment of the late Pleistocene Palaeo Danube.

1400 pebbles were collected from one gravel pit in Dunavarsány, Csepel Plain to determine rock type distribution and main grain morphological parameters. Beside the dominating quartzite (43%), 40 main rock types were detected. Ostrea bearing conglomerate pebbles and bored limestone pebbles refer about redeposition of some pebbles from miocene marine conglomerate layers. Traces of aeolian erosion were also examined and counted. 64.97% of the whole collection, mainly the hard rock types showed at least partly bright surface. Not so the soft or weathered rock types as andesites and limestones some of which have only special tortoiseshell shape.

Rock type distribution of boulders is similar in the 2 areas, exept miocene andesites occuring only in Dunavarsány. Surface of many blocks have also been formed or/and polished by the wind. Significant group of exotic chrystalline rocks (e.g. granites, granulites, gneises, amphibolites) could be distinguished. Some special rock types were selected for more detailed examinations.

Few blocks of graphic granite with large sheaf shaped muskovite have been found in Dunavarsány. It has macroscopically well visible very special texture.

The andalusite bearing two micas mostly fine grained granite is a very frequent rock type in the whole study area. Short lathy grains of microscopic andalusite often show pale pink pleochroism and surrounded by muskovite. In some of these blocks turmaline and garnet also appear.

Latites and related rocks appear in both areas and form a well distinguishable group. They are dark, very hard, finegrained rocks and contain large (1 cm long) sanidine porphyres, different amount of plagioclase, kinked biotite, finer grained green hornblende and rarely augite.

Felsic granulites from the two main areas were investigated even more detailed. Three main types can be distinguished. Grt-Ky granulites contain HP/HT peak mineral assemblage: garnet-kyanite-ternary feldspar-quartz. In Grt-Sil granulites kyanite is commonly replaced by sillimanite while biotite appears as a stable phase. Some sample show well developed foliation and mylonitic texture. Orthopyroxene-bearing granulite also presents.

The crystalline rock assamblage, the andalusite bearing granites, the latites and the granulite boulders are very similar to those known from certain areas of Bohemian massif. Special textured graphic granite occur on Zerge Hill near Pozsony (Bratislava). Miocene andesites found only south of Budapest have been related to those of Visegrád and Börzsöny Mts.

We suppose as a conclusion that studied boulders were picked up by the Palaeo Danube from the above mentioned areas and transported mainly by pack ice. Before burial most pebbles and boulders of the debris were effected by wind erosion.

Hybridization events in the Tatra Granite, Western Carpathians, Poland

Burda, J.[1*], Gawęda, A.[1] & Klötzli, U.[2]
[1]Faculty of Earth Sciences, University of Silesia, Sosnowiec, Poland ([*]jolanta.burda@.us.edu.pl)
[2]Dept. of Lithospheric Research, University of Vienna, Austria

Mafic magma has long been recognized to play an important role in the granitoid melt generation. The processes of felsic and mafic magma interactions can be observed in different scales: from outcrop scale to micro-chemical and trace by isotopic signatures. The fundamental features that unequivocally prove the presence of mixing – mingling processes are textural ones.

It is currently believed that no single texture can be used to undoubtedly prove the presence of hybridization in granitic rocks, so the term "textural assemblage" was proposed to define the combination of textures, forming together good evidence for mixing – mingling phenomena [1].

In the Variscan Tatra Granite, both in western and eastern parts, the mixing and mingling phenomena can be observed at the contact of mafic precursors of dioritic composition with more felsic granite. The textural assemblage include: 1) plagioclase–K-feldspar–sphene ocella; 2) boxy-cellular plagioclase (An_{20-30}) crystals with spike zonation (An_{40-50}); 3) inversely zoned K-feldspar crystals (Cn_{2-4} in the cores and Cn_{5-9} at rims); 4) mafic cloths, composed of biotite, hornblende, magnetite, zoned allanite, locally pyroxene; 5) poikilitic plagioclases and quartz crystals with micro-inclusions of hornblende, biotite and apatite; 6) mixed apatite morphologies, including prismatic, chemically zoned apatites and unzoned acicular apatites; 7) chemically zoned K-feldspar phenocrysts, with inclusion zones; 8) "hydrogenic" biotite of blade-shape morphology.

The apparent pressure range of the magma hybridization event was calculated at 6.1 kbar to 4.6 kbar, whiles the temperature, calculated by independent methods, is in the range of 810°C -770°C.

U-Pb age data of the hybrid rocks were obtained by in-situ LA-MC-ICP-MS analysis of zircon. Most zircons are characterized by well-developed oscillatory zoning, from fine to broad, displaying variable CL intensities. Some crystals exhibit homogeneous to weakly growth-zoned cores with bright luminescence. Cores are sub-rounded and the contacts with surrounding growth-zoned rims are irregular. Eleven measurements on seven crystals were made. All data points are concordant within the assigned error. Nine analyses from the oscillatory-zoned zircon crystals yield a weighted average age of 368.4 ±7.7 Ma (MSWD= 1.07), interpreted here as the age of igneous crystallization. Two inherited cores give an age of ca. 540 Ma, providing evidence for the assimilation of zircons derived from Ediacaran/Early Cambrian sources.

The occurrence of ages around 368 Ma could be interpreted as an age of magma hybridization and timing of formation of the magmatic precursors for the granitoid magmatism event in the Tatra Mts.

[1] Hibbard, M.J. (1991) in Didier, J. & Barbarin, B. (eds) *Develop. Petrol.*, **13**, 431-444.

Spinel and orthopyroxene exsolution in clinopyroxene from gabbro, southwest Tianshan Mountains: an indicator of fO_2 decrease during cooling in post-collision environment

Chen, J.[1*], Zhu, Y.F.[2] & Christy, A.G.[3]
[1]School of Physics, Peking University, Beijing, China ([*]jchen@pkjchen@pku.edu.cn)
[2]School of Earth and Space Sciences, Peking University, Beijing, China
[3]Research School of Earth Sciences, Australian National University, Canberra, Australia

We report new data for oriented spinel rods and orthopyroxene lamellae exsolved from clinopyroxene in the Haladala gabbro, southwest Tianshan Mountains Xinjiang, NW China. Our study is based on optical, TEM and EDX analyses. Several diffraction patterns of the same microphase were obtained by tilting the sample in the double-tilt stage. The results show that the rods are crystals of a spinel-group mineral. The spinel rods (110) are parallel to their host clinopyroxene $(11\bar{1})$. The TEM images show that the Opx lamellae (010) are strictly parallel to their host clinopyroxene $(11\bar{1})$. The Haladala gabbro intruded into Carboniferous arc segments in the southwest Tianshan mountains. Exsolution of the cation-rich spinel phase from clinopyroxene implies a decrease in fO_2 during cooling, and that the pyroxene started with substantial contents of Fe^{3+}, tetrahedral Al and (Mg,Fe^{2+}) on the M2 site, all consistent with an igneous origin in a relatively oxidized arc environment.

Acknowledgements: This work was sponsored by the National Science Foundation of China (Grant No. 40872048) to Y.F. Zhu and (No. 40872048) to J. Chen.

Textural and mineralogical evidences for magma mixing and mingling: the example of a late-tectonic Variscan granite intrusion from Central Portugal

Costa, M.M.[1*], Neiva, A.M.R.[2] & Azevedo, M.R.[1]
[1]Dept. of Geosciences, University of Aveiro, Aveiro, Portugal ([*]mmcosta@ua.pt)
[2]Dept. of Earth Sciences, University of Coimbra, Coimbra, Portugal

The Touro pluton is a late-kinematic coarse- to medium-grained porphyritic biotite-muscovite granite hosting abundant fine-grained mafic microgranular enclaves from tonalite to granodiorite composition. Both the granite and the mesocratic microgranular enclaves (MME) show a series of textural and mineral assemblages typical of hybrid rocks produced by the interaction of magmas with contrasting compositions. The granite has plagioclase and microcline phenocrysts and its matrix is composed by quartz, microcline, plagioclase, biotite, muscovite, zircon, monazite, apatite, ilmenite and rutile. The MME have higher plagioclase and biotite contents than the host granite. K-feldspar and muscovite are absent in the tonalitic enclave. At the outcrop scale, the MME display round, ellipsoidal and discoid shapes and sizes varying between a few centimeters and one meter long . Their contacts against the host granitoid range from sharp to diffuse suggesting contemporaneous flow and mingling of partly crystalline felsic-mafic magmas. Mechanical transfer from the felsic host to the enclave magma is also documented by the presence of corroded minerals (xenocrysts) within the MME. Petrographic and mineral chemistry studies on both the MME and their host rocks indicate that magma mixing / mingling between granite and evolved mafic melts played a key role during the evolution of the batholith. Disequilibrium textures include: plagioclase crystals with oscillatory zoning, cellular structures (boxy-cellular and/or spongy-cellular), anorthite-rich 'spikes' and resorbed surfaces, acicular apatite with high aspect ratios and quartz *ocelli* rimmed by thin biotite flakes. Plagioclase chemistry is a helpful tool to decipher the complex processes involved in the petrogenesis of these granitoids. As expected from their xenocrystic character, the large plagioclase crystals of the MME exhibit a significant degree of compositional overlap with those of the host granite (An_{20-38} to An_{21-40}). The matrix plagioclase crystals are generally more sodic but tend to define a bimodal distribution pattern, with peaks at An_{15-20} and An_{30-35}, suggesting abrupt changes in the chemistry of the enclave magma. The observed compositional discontinuities appear to reflect variations in the conditions of feldspar nucleation and crystallization during mixing / mingling processes. In contrast, the biotites from the MME and the host granite are compositionally uniform (Fe/Fe+Mg = 0.45 – 0.74) possibly as a consequence of re-equilibration after magma mixing.

The occurrence of tonalite and granodiorite compositions within the MME provides evidence for multiple mixing events involving relatively evolved basic melts, which may themselves correspond to hybrids. Mixing should therefore have occurred under different conditions and at different times in the history of the Touro intrusion. These conclusions are supported by field observations, whole-rock and isotopic geochemistry.

Acknowledgements: This study was supported by the Portuguese Science and Technology Foundation – FCT, through a PhD fellowship awarded to M.M. Costa.

Noble gases in peridotite xenoliths from Tasmania: implications for interaction with the host basalts

Czuppon, Gy.[1*], Matsumoto, T.[2], Matsuda, J.[1], Everard, J.[3] & Sutherland, L.[4]
[1]Dept. of Earth and Space Science, Osaka University, Osaka, Japan ([*]gyorgy.czuppon@univie.ac.at)
[2]Institute for Study of the Earth's Interior, Okayama University, Okayama, Japan
[3]Mineral Resources Tasmania, Rosny Park, Australia
[4]Australian Museum, Sydney, Australia

In order to better understand the evolution of the subcontinental lithospheric mantle (SCLM) beneath Tasmania, spinel peridotite xenoliths were analyzed for elemental and isotopic compositions of noble gases. The noble gas isotopic compositions indicate contributions of radiogenic and MORB-like components to the xenoliths. The typical features of the radiogenic component include (1) lower $^3He/^4He$ ratios than those in MORB (8.75±2.14Ra, [1]); (2) excesses in ^{136}Xe relative to the MORB composition. The MORB-like component is characterized by $^3He/^4He$ ratios between 7-9Ra. The deconvolved argon isotopic ratios also support the presence of these noble gas components. The identified radiogenic component in xenoliths from Tasmania may stem from subduction events, during which the mantle wedge and subcontinental SCLM were metasomatised by U- and Th- rich fluids. As subduction processes have played important role in the evolution of Eastern Australia during the Paleozoic, the radiogenic component is probably associated with this event. The contributions of MORB-like noble gas component to the xenoliths indicate such a component in SCLM beneath Tasmania. This happened in Eastern Australia when extensional rifting in the Late Mesozoic and Cenozoic opened the Tasman Sea. The identified noble gas components are consistent with the geochemical character of the host basalt. This agreement and the petrographic observations indicate that fluids (noble gases, CO_2) most likely propagated from the host basalts to the xenoliths forming fluid inclusions.

[1] Graham, D.W. (2002) in Porcelli, D., Ballentine, C.J. & Wieler, R. (eds.) *Rev. Mineral. Geochem.*, **47**, 247-317.

The petrogenetic meaning of schorl-dravite transition and apatite association in peri-amphibolitic tourmalinites – Northern Portugal

Dias, P.A.* & Leal Gomes, C.
CIG-R – DCT, Universidade do Minho, Braga, Portugal
(*patriciasdias@gmail.com)

In opposite sides of the massif of Serra de Arga, meta-volcanic to meta-sedimentary formations in Monteiro and Verdes include complex suites of amphibolitic rocks with unusual phosphate tourmalinites, mafic and felsic porphyroid proto-tuffs, stratiform tourmalinites, epidotites with graphite levels and phosphate meta-cherts. These rocks are interbedded with regional andalusite phyllitic formations.

The amphibolite lenses are small and have been transported by over-thrusting in structures lately reactivated as strike-slip shear zones. Amphibolite paragenesis holds anorthite, Fe-hornblende, F-rich sphene, fluorite, Cr-rich epidote, F-apatite, scheelite and sulphides. The peri-amphibolitic tourmalinites mainly located at the roof of amphibolite lenses may show distinctive textures and habits of tourmaline aggregates: T1 - massive monomineralic tourmaline and spindle-shaped agglomerations of tourmaline crystals; T2 - cataclastic aggregates with matrix phosphate; and disseminations in the amphibolites matrix and in altered mafic tuffs (Fig. 1). Different generations of tourmaline (schorl compositions and scarce dravite) were identified: G1 - early tourmaline (Fe, Al and□ X richer) affected by micro-displacements; G2 - crystals with oscillatory zoning; G3 - diffuse substitutions of G2 generation; G4 - dravite bands perpendicular to the c axis of G2; G5 - veinlet and micro-fracture remobilizations. F and Ti contents mark well the evolution between early compositions poor in Ti and F till late compositions with oscillatory enrichments.

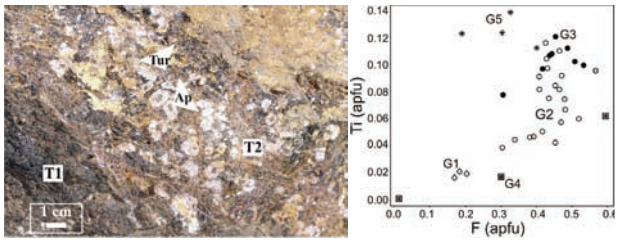

Fig. 1: Tourmaline / apatite textures and Ti/F constituents from T2 tourmalines (crystals G1 to G5).

The amphybolitic facies are interpreted as remnants of alkaline basalt compositions, which could evolve locally to intermediate or felsic end - members. Primary and proto - lithic boron enrichment might be related to proto - exhalitic and/or evaporite activity (compare to [1]), lately remobilized by hydrothermal fluids and contaminated by the various surrounding metassomatized rocks. Hypothetically, a fluid/magma P-saturated phase would be released from the alkaline trend, producing apatite enrichment. Textural relations between tourmaline and apatite seem to be remnants of an ancestral hydraulic breccia of "roof- rock" clasts.

Similarities between tourmaline compositions, here studied, and those occurring in neighbour stratiform tourmalinites, may suggest the introduction of B (± P) in volcanic spots, associated with deep faults, and the spread of metasomatism to adjacent, previously seated, sedimentary sequences.

[1] Byerly, G. & Palmer, M. (1991) *Contrib. Mineral. Petrol.*, **107**, 387-402.

Geothermometry of volcanic rocks from SW Shahrood, N Iran

Ghorbani, G.
School of Earth Sciences, Damghan University of Basic Sciences, Damghan, Iran (ghasemghorbani@yahoo.com)

The study area is located southwest of Shahrood town in Semnan Province (northern Iran). This region is characterized by the presence of a magmatic belt consisting of extrusive and intrusive igneous rocks. Middle Eocene volcanics are the most important rocks of this unit; they are represented by basalt, basalt with olivine, basaltic andesite, andesitic basalt, dacite and equivalent pyroclastic rocks.

Based on their petrographical and geochemical features, these rocks show an alkaline-subalkaline nature. The studied basalts have average Ce/Pb and Nb/U ratios lower than the value for average oceanic basalts (OIB and MORB), but close to the average values of sub-continental lithospheric mantle (SCLM). The chondrite-normalized REE patterns of the basalt samples plot as steep lines, suggesting that the rocks might have been generated via slow melting processes affecting a garnet-enriched peridotitic mantle source.

Amphiboles are present in the rocks cropping out in the northern part of the study area; they are Ca-rich, and show pargasite and ferropargasite compositions**.** Pyroxenes are represented by augite, diopside (as cpx) and enstatite (opx).

Based on previous studies, geobarometry of basaltic andesites located in the northern part of the study area based on the Al-content of hornblende and calculated by using the formula of Schmidt: $P(\pm 0.6Kbar) = -3.01+4.76Al^{tot}$ [1] indicated values ranging from 8.64 to 9.70 and from 3.48 to 4.47 Kbar (at depth of 32-36 and respectively 13–16 km).

Equilibration temperatures of cpx and opx pairs in andesitic basalts rocks were also previously calculated by means of different thermometers; the obtained values range from 709 to 900°C for the rocks in the northern part, while for the southern part they range from 900 to 1100°C.

In the present study, geothermometry information retrieved from olivine and clinopyroxene compositions [2] of basalts suggests that these rocks were crystallized at relatively higher temperatures, ranging from 850 to 1270°C.

[1] Schmidt, M.W. (1992) *Contrib. Mineral. Petrol.*, **110,** 304-310**.** [2] Loucks, R.R. (1996) *Contrib. Mineral. Petrol.*, **125**, 140-150.

Peridotite nodules and xenoliths in the Paleogene alkali basalts from the Muncelu Mare - Muncelu Mic area (Poiana Ruscă Mts., Romania)

Giurgiu, A.M.* & Grindean, R.A.
Dept. of Geology, Babeș-Bolyai University, Cluj Napoca, Romania (*alexa.giurgiu@yahoo.com)

The magmatic activity occurred in the Poiana Ruscă Mountains (the western part of Romania) during late Cretaceous to Paleogene. Mârza & Egri [1] describe the peridotite xenoliths beared by these rocks as autoliths, while Savu et al. [2] describe them as mantle xenoliths. In fact, these igneous rocks contain both nodules and xenoliths.

In the peridotite nodules olivine and pyroxenes are the main participants while the chlorite and magnetite participate as secondary phases. These nodules are consanguine with the basaltic magma, eventually becoming small centers of crystallization in the differentiated magma (Fig. 1).

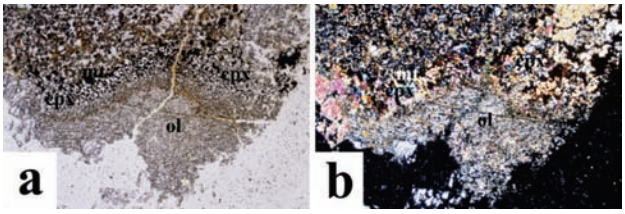

Fig. 1: Granular texture of nodule consisting of coarse grains of clinopyroxene (cpx) and olivine (ol) in alkali basalt (a-1N, b-N+; 35x).

The peridotite xenoliths from the Poiana Ruscă alkali basalts represent unmelted remnants of the primary alkaline magma source [2]. The core of these xenoliths consists of euhedral clinopyroxenes, partially altered to greenish aegirine, and colourless olivine. The matrix is represented by nepheline and alkaline zeolites. Pockets or veinlets of chlorite may support the theory of Na_2O rich melts influx. The rim consists in pyroxenes which are not associated with opaque magnetite minerals (Fig. 2).

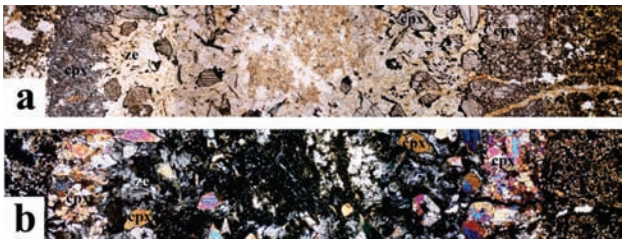

Fig. 2: Microscopic of peridotitic xenolith found in the alkali basalts from Muncelu Mare-Muncelu Mic area (a-1N, b-N+; 35x); cpx-clinopyroxene, ze-zeolite.

Based on the mineralogical and textural differences between the peridotitic terms, and also on the relation of these peridotitic terms to the igneous alkali host rocks, we consider that the alkali basalts from the Muncelu Mare-Muncelu Mic area carry both peridotite nodules − developed from a basaltic magma, and xenoliths − of mantle origin.

[1] Mârza, I. & Egri, E. (1971) *St. Cerc. Geol. Geofiz. Geogr. (Geol.)*, **16(1)**, 95-106. [2] Savu, H., Tiepac, C. & Stoian, M. (1997) *Rev. Roum. Géol.*, **41**, 37-49.

Corundum-quartz, Zn-bearing spinel and staurolite inclusions in garnet, and their implications for metamorphic evolution of the Sor Rondane Mountains, East Antarctica

Hokada, T.[1,2*], Adachi, T.[2,3], Osanai, Y.[3], Nakano, N.[3], Toyoshima, T.[4] & Baba, S.[5]
[1]National Institute of Polar Research, Tokyo, Japan
[2]The Graduate University for Advanced Studies, Tokyo, Japan
(*hokada@nipr.ac.jp)
[3]Kyushu University, Fukuoka, Japan
[4]Niigata University, Niigata, Japan
[5]University of Ryukyus, Okinawa, Japan

Neoproterozoic to Cambrian age magmatic and high-temperature metamorphic terranes comprise the area more than 1000 km along the coast or the inland of Dronning Maud Land in East Antarctica [1]. Among those, the Sor Rondane Mountains consist of greenschist-facies through amphibolite-facies to granulite-facies metamorphic rocks from which quite complicated P-T trajectories including two-stages of heating accompanied by two-stages of decompression have been estimated [2]. The Sor Rondane Mountains can be subdivided into at least two areas - the NE and the SW Terranes [3], and the attempt to unravel the metamorphic records in each area has been made by several authors.

In this paper, we provide some new consideration of metamorphic evolution based on the corundum-quartz, Zn-bearing spinel and staurolite inclusions of garnet in garnet-sillimanite-cordierite and garnet-orthoamphibole-cordierite gneisses from the Austkampane area where is the granulite-facies part of the Sor Rondane Mountains. The metamorphic rocks also suggest the following petrograhical constraints: (1) Garnet in the garnet-sillimanite gneiss commonly includes Zn-bearing spinel (up to 24wt% ZnO) which is commonly associated with sillimanite, cordierite and biotite. Other inclusions in garnet are quartz, biotite, sillimanite, rutile, ilmenite, biotite+rutile, biotite+sillimanite, biotite-staurolite, biotite+quartz and biotite+corundum+quartz aggregates. (2) Porphyroblastic garnet crystals in the garnet-sillimanite-cordierite gneiss are commonly surrounded by cordierite corona with or without quartz and biotite. Cordierite also occurs replacing biotite+sillimanite aggregates. (3) Orthoamphibole (anthophylitic) in garnet-orthoamphibole-cordierite gneiss has Al_2O_3 content commonly less than 4-5 wt% down to 1-2 wt% in the rim.

We will discuss the inferred clockwise P-T trajectory started with the prograde staurolite break down reaction in the sillimanite-stability field followed by the decompression of garnet(+sillimanite) to form cordierite(+quartz+biotite) that are also combined with the corundum-quartz, Zn-bearing spinel and staurolite inclusions in garnet. Metastability of the natural association of corundum and quartz has been discussed by several authors [4]. The mode of occurrence of the corundum and quartz associated with biotite in this study provides some insight for the process to form the natural corundum-quartz metastable association.

[1] Shiraishi, K. et al. (2008) in Satish-Kumar, M. et al. (eds.) *Geol. Soc. London Spec. Publ.*, **308**, 21-67. [2] Asami et al. (1992) in Yoshida, Y. et al. (eds.) *Recent Progress in Antarctic Earth Science*, 7-15. [3] Osanai et al. (1992) in Yoshida, Y. et al. (eds.) *Recent Progress in Antarctic Earth Science*, 17-27. [4] Harlov, D.E. et al. (2008) *Am. Mineral.*, **93**, 608-617.

Geology, petrochemistry of trachyte and rhyolite magmas, Inshiel alkaline volcanics, Southern Sinai Egypt

Imbarak, S.H.[1*], Bilik, I.[2] & Weiszburg, T.G.[3]
[1]Geology Dept., Suez Canal University, Ismailia, Egypt
([*]imbarak25@yahoo.com)
2Dept. of Geochemistry, Eötvös Loránd University, Budapest, Hungary
3Dept. of Mineralogy, Eötvös Loránd University, Budapest, Hungary

The Inshiel Acidic volcanics represented a small volcanic caldera within Kathrina ring dykes (6-7 km diameter). The rocks occur as lavas, ash-flow, welded tuffs and ignimbrites peralkaline quartz trachyte, rhyolite, and high-silica rhyolite.

They tend to be fine-grained, containing small amounts of phenocrysts. Plagioclase (andesine–oligoclase), anorthoclase or occasionally sanidine coexist with some microenclaves minerals such as augite, fayalite, pigeonite, orthopyroxene and magnetite. Quartz phenocrysts are exceedingly rare. Zoning of phenocrysts is limited and the pattern is variable.

They represent the silicic end member of a bimodal suite, between 57 and 62 wt% SiO2); the mafic end member (Rutig volcanics) consists primarily of basic and intermediate lavas.

The rocks classified as dacites, trachytes, low-alkali rhyolites and alkalic rhyolites. Some of the trachytes and alkalic rhyolites are peralkaline

The rocks are relatively Fe-rich and Ca-poor indicating low water pressure in the source. Trace element concentrations follow similar patterns in most central volcanoes. Exceptions are some samples where silicic rocks display a negative correlation of Ba to Th and unusually high Th-contents. The ratios of different high field-strength elements are generally similar within each central volcano or region, which probably reflects different ratios in the source materials. Isotope systematics indicates that the silicic rocks are derived from older basaltic rocks similar to those from the same volcano, and that meteoric water has played a role in the genesis of the silicic rocks.

High-silica rhyolite is not cogenetic with the quartz trachyte-rhyolite suite, and can be best explained as the result of ~5% partial melting of a mafic granulite in the deep crust under the fluxing influence of fluorine. Variation within the high-silica rhyolite is most likely due to fractional crystallization of alkali feldspar, quartz, magnetite, biotite, and monazite. Lavas and tuffs form A-type rhyolite suites, and are broadly similar to rock series described in anorogenic settings both in terms of petrology and petrogenesis.

The caldera is interpreted to have developed in a post-orogenic tectonic setting, or an early stage of continental rifting, and represents the earliest evidence for continental extension in the area.

Neogene quartz andesites from the Oaş-Gutâi Mts. (Romania): new geochemical data

Jurje, M.[1,2*], Ionescu, C.[2] & Hoeck, V.[3,2]
[1]Mineralogical Museum, Baia Mare, Romania
([*]jurjemaria@yahoo.com)
[2]Babeş-Bolyai University, Cluj-Napoca, Romania
[3]Paris Lodron University, Salzburg, Austria

Lava flows, volcaniclastics and subvolcanic bodies of quartz andesites quantitatively represent one of the most important volcanics in the Oaş-Gutâi Mts. This area belongs to the northwesternmost part of the Neogene volcanic chain in the Eastern Carpathians. The volcanics have a calc-alkaline geochemistry and range in principle from basalts and basaltic andesites to dacites and rhyolites. The age of the whole volcanic activity in the Oaş-Gutâi Mts. is Badenian-Pannonian i.e. 15.4 – 7.0 M.a. [1]. Quartz andesites are restricted to Pannonian, i.e. 11.5-10.7 M.a. in the Gutâi Mts., and 10.3-9.5 M.a. in the Oaş Mts. respectively.

Quartz andesites consist of quartz, plagioclase, orthopyroxene, clinopyroxene and amphibole phenocrysts, in a hyalopilitic to intersertal texture or holocrystalline groundmass. From the whole volcanic association, a number of 25 samples were analysed geochemically (ICP-MS) and by Electron Microprobe (EMP).

Geochemically, the volcanics range from andesites to dacites (56 to 65 wt% SiO_2). Major element oxides such as TiO_2, MgO or CaO are negatively, Na_2O and K_2O are positively correlated with SiO_2. The K_2O content classifies andesites as calc-alkaline to high K-calc-alkaline. A significant negative Nb, Ta and TiO_2 anomaly can be observed. The distribution of TiO_2, Zr, Nb and Y argues for crystal fractionation dominated by plagioclase, pyroxene, amphibole and magnetite.

The composition of plagioclases ranges from An_{90} to An_{40} reflecting the partly recurrent zoning from core towards the rim. Ortho- and clinopyroxenes show a wide range of Fe# and Ca-Tschermaks molecule, but little Na, Ti or Cr contents. Amphibole is predominantely magnesiohornblende with a wide range of Al^{IV}. More pargasitic or edenitic compositions are rare. Ilmenite and Ti-magnetite occur as oxides. The Si and K-rich groundmass is glassy or microcrystalline. It contains variable amounts of K-feldspar microliths.

The presence of amphibole as well as An-rich plagioclase argues for a relatively high amount of water present in the melt. The presence of at least two plagioclase generations and their complex zoning suggests magma mixing and an open system with repeated supply of less fractionated magma.

Acknowledgments: Thanks are due for the financial support provided to MJ through the “Human resources development” program, Contract POSDRU 6/1.5/S/3 „Doctoral studies: through science towards society". Partly, the study was financed by ID-2241/2008 project (Romanian Ministry of Education).

[1] Pécskay, Z. et al. (2006) *Geol. Carpath.*, **57(6)**, 511-530.

Ye'elimite and fluorellestadite as new indicators of ultrahigh-temperature–ambient pressure metamorphism

Kokh, S.N.
V.S.Sobolev Institute of Geology and Mineralogy SB RAS, Novosibirsk, Russia (zateeva@uiggm.nsc.ru)

Numerous fossil mud volcanoes (so-called the "Mottled Zone" complexes) cover Upper Cretaceous carbonate strata at the Middle East. Mottled Zone complexes are composed of brecciated sediments of the underlying Cretaceous sequence. Location of high-temperature combustion metamorphic (CM) foci annealed by methane jets ignition was fixed within Nabi Musa fossil mud volcano dome. At the base of the section, CM rocks occur as rounded clasts composed of larnite rocks, spurrite and brownmillerite marble formed at 700 – 900ºC. The foci of the ultrahigh-temperature (T_{min} = 1170 – 1200°C) CM rocks and paralavas are localized within conduits and were related by breccia zones [1]. The uncommon rocks sample depleted in CaO (17.0 wt.%) and enriched by (in wt.%): MgO–14.9, Al_2O_3–9.8, Fe_2O_3–4.5, TiO_2–0.5 and Na_2O–1.6 was found here. It mainly consists of primary minerals such as larnite, fluorellestadite, and brownmillerite with minor ye'elimite, bredigite, Cr-spinel and melilite and accommodated by retrograde spurrite, calcite, aragonite.

Ye'elimite $Ca_4Al_6O_{12}(SO_4)$ occurs as irregular interstitial patches (<300 μm) between melilite, fluorellestadite and bredigite. Ye'elimite is colorless and has specific atypical brownish hues in thin section. Major oxides are in the ranges of 43.03-43.63 Al_2O_3, 35.12-35.35 CaO, 12.46-12.98 SO_3, 4.01–5.82 Fe_2O_3, 0.35-1.86 SiO_2, 0.26-0.70 Na_2O, 0.10-0.28 MgO, 0.07-0.26 K_2O, 0.07-0.20 P_2O_5 (in wt %). The empirical formula is $Ca_{3.910}Al_{5.637}Fe^{3+}_{0.312}Si_{0.036}S_{1.007}O_{16.}$

Bredigite $Ca_7Mg[SiO_4]_4$ forms lath-like crystals (300 μm). Fresh bredigite is colorless in thin section and distinctly pleochroic: X = pale violet; Y = Z = colorless to pale blue, has intense blue fluorescence under the electron beam and contains inclusions of apatite. Bredigite shows little variation in CaO (57.80-58.98), SiO_2 (34.13-35.07), MgO (5.70-5.84), P_2O_5 (0.44-0.62), Na_2O (0.27 – 0.32), Fe_2O_3 (0.23 – 0.26 wt), TiO_2 (0.18-0.25 wt.%). BaO, MnO, SO_3 and K_2O are negligible. Its empirical formula is $Ca_{6.920}Mg_{1.010}Si_{3.946}Al_{0.015}P_{0.032}O_{16}$.

Fluorellestadite $Ca_{10}[(PO_4),(SiO_4),(SO_4)]_6F_2$ occur as <2mm single "pencil-like" crystals, with abundant larnite, spinel, and melt inclusions. Mineral is colorless or grayish and has survived hydrothermal alteration. Fluorellestadite has little variation in CaO (56.91-58.47), P_2O_5 (7.25-9.72), SO_3 (15.81-17.48), and SiO_2 (14.79-15.63 wt.%); F is 3.37-4.19 wt % and Cl is less than < 300 ppm. P, S, Si, and F vary slightly and irregularly from core to rim.

Ye'elimite, together with larnite, fluorapatite, and brownmillerite, were synthesized at 1000-1200ºC and ambient pressure [2], while the upper temperature limit of ye'elimite stability is 1300-1350ºC. The larnite-spurrite-spinel association and the absence of rankinite, imply a minimum of 975°C where $P_{total} = P_{CO2}$ [3]. Bredigite was found to be stable between 979-1381ºC [4]. So, the thermal alteration that produced the assemblage of bredigite, P-bearing larnite, ye'elimite, fluorellestadite, brownmillerite, and spinel with retrograde spurrite, calcite, and aragonite) occurred between 975-1000ºC and 1300-1380ºC.

[1] Sokol, E. et al. (2010) *Basin Res.*, **6**, (in press). [2] Gross, S. (1984) *Geol. Surv. Isr.*, 1984, 1-4. [3] Grapes, R. (2006) *Pyrometamorphism*. Springer, Berlin. [4] Jung, I.H. (2005) *J. Eur. Ceram. Soc.*, **25**, 313-333.

Petrologic and geochemical study on mantle xenoliths and their multi-phased sulfide inclusions from Paleozoic lamprophyre dikes from Tuva (South Siberia, Russia)

Konc, Z.[1,2*], Hidas, K.[1], Szabó, Cs.[2], Sharygin, V.V.[3] & Garrido, C.J.[1]
[1]Instituto Andaluz de Ciencias de la Tierra, CSIC-UGR, Granada, Spain ([*]zoltankonc@ugr.es)
[2]Lithosphere Fluid Research Lab, IGES, Eötvös University Budapest, Budapest, Hungary
[3]Institute of Mineralogy and Petrology, UIGGM, Siberian Branch of the Russian Academy of Science, Novosibirsk, Russia

The main aim of this study is to describe petrographic and geochemical features of upper mantle xenoliths and their sulfide inclusions, hosted in 440-435 million years old lamprophyre dikes in Tuva Region (South Siberia). The study area is located between southern Siberia and northern Mongolia in Central Asia where one of the oldest members of the Calenodines has been exposed due to the tectonic processes from accretion (late Vendian), through collision (Cambrian) to transform faulting (Ordovician). The lamprophyre melts formed and brought up the xenoliths in the last stage of the tectonic period dominated by transform faulting.

The studied xenoliths are frequently poikilitic textures orthopyroxene-rich lherzolites, harzburgites, olivine-websterites and orthopyroxenites which suffered a 10-15% partial melting and their rock forming silicates have common mg# (0.90). The orthopyroxene-rich character of the studied xenoliths can be the result of interaction between subducted slab-derived SiO_2-rich melt and the peridotitic wall rock. The primary sulfide assemblages occur as 1) interstitial phases among mantle silicates (Fig. 1 & 2) enclosed blebs mostly in orthopyroxenes. Both interstitial and enclosed sulfide inclusions have rounded and irregular shape. The size of interstitial sulfide inclusions ranges between 75-300 μm, whereas the enclosed sulfide blebs are generally smaller (30-175 μm). Based on microscopy, X-ray mapping and SEM study, the primary sulfide inclusions consist of maximum four phases. The primary sulfide minerals are pentlandite, chalcopyrite, pyrite and millerite (Fig. 1). Using mass-balance calculation, the bulk composition of the studied sulfide assemblages is mostly plotted in the MSS (monosulfide solid solution) and MSS+$L_{Ni,Cu}$ fields (above 1000°C) in the S-Cu-Fe-Ni systems. The calculated KD_3 values, based on the Fe and Ni content of coexistence sulfides and olivines, suggest equilibrium between the sulfide assemblages and the silicates.

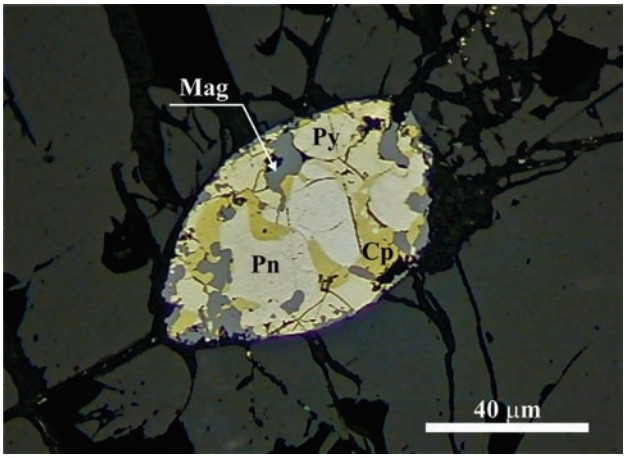

Fig. 1: Microphotograph of a multi-phased interstitial sulfide inclusion among mantle silicates (Cp - chalcopyrite, Pn - pentlandite, Py - pyrite and Mag - magnetite).

Deformation study on upper mantle peridotite xenoliths in relation with their petrographic and geochemical features from SE Iberian Volcanic Province (Spain)

Konc, Z.[1,2*], Garrido, C.J.[1], Tommasi, A.[3], Hidas, K.[1], Szabó, Cs.[2] & Marchesi, C.[3]
[1]Instituto Andaluz de Ciencias de la Tierra, CSIC-UGR, Granada, Spain ([*]zoltankonc@ugr.es)
[2]Lithosphere Fluid Research Lab, IGES, Eötvös University Budapest, Budapest, Hungary
[3]Géosciences Montpellier, Université Montpellier II & CNRS, Montpellier, France

We present here a detailed study on lithospheric mantle beneath SE Iberian Volcanic Province (SEI-VP, Spain) based on petrographic, geochemical and olivine LPO (lattice preferred orientation) analysis of upper mantle xenoliths. The volcanic activity in SEI-VP is the surface expression of magmatism in a complex geodynamic setting during the Cenozoic, which was characterized by a sequence of transpressional and transtensive stages in a "Mediterranean-type" back-arc system. The last stage in this geodynamical evolution was the Neogene alkaline basalt volcanism erupted at 2-3 Ma [1], which sampled the upper mantle beneath SEI-VP providing a unique possibility to study the lithospheric mantle beneath this region.

The studied samples came from the "Cabezo Negro" de Tallante and Los Perez (Murcia). The locality is one of the major xenoliths occurrences within SEI-VP. The xenoliths are spinel peridotites (lherzolite and wehrlite) with textures ranging from fine-grained equigranular to coarse-grained granular. In many samples (~30%) tiny plagioclase and/or amphibole appear mostly interstitially. The LPO of olivine is similar in all samples; it displays a strong [100] maximum, implying dominant activation of high temperature [100] {0kl} slip systems. The strength of the LPO varies in function of the xenolith texture and modal content of clinopyroxene. In coarse-grained peridotites, from lherzolite to wehrlite, the olivine LPO ranges from strong to a weak LPO. The stronger olivine LPO is characterized by alignment of [100] axes close to the lineation and a girdle distribution of [010] with a maximum normal to the foliation. Whereas, the weaker olivine LPO with a [100] maximum is still preserved close to the lineation and [010] one normal to the foliation. Altogether, stronger olivine LPO are observed in the coarse-grained peridotites. Modal enrichment in clinopyroxene and development of fine-grained equigranular texture are both accompanied by a dispersion of the olivine LPO. Based on these results, we suggest that the coarse-grained samples are representative of a primary subcontinental lithospheric mantle that was later affected by re-fertilization reaction that led to dispersion of the LPO, as well as an increase in the clinopyroxene content. This textural evolution may record thermal and chemical erosion of the subcontinental mantle during Cenozoic extension of western Mediterranean region.

[1] Duggen, S. et al. (2005) *J. Petrol.*, **46**, 1155-1201.

Magma mingling and mixing as key processes in the petrogenesis of the Laleaua Albă Neogene composite igneous complex, Gutâi Volcanic Zone, Northern Romania

Kovacs, M.[1*], Fülöp, A.[1], Cook, N.J.[2,3], Kovács-Pálffy, P.[4] & Pécskay, Z.[5]
[1]North University of Baia Mare, Baia Mare, Romania ([*]marinelkovacs@yahoo.com)
[2]University of Adelaide, S.A., Australia
[3]South Australian Museum, Adelaide, S.A., Australia
[4]Hungarian Geological Institute, Budapest, Hungary
[5]Institute of Nuclear Research of the Hungarian Academy of Sciences, Debrecen, Hungary

The Laleaua Albă Neogene igneous complex (8.5-8.0 Ma) was emplaced at the end of volcanic activity in the Gutâi Volcanic Zone, Eastern Carpathian inner volcanic chain. The complex consists of sanidine dacites (hosting abundant mafic microgranular enclaves/MME, of ~50 wt% SiO_2) enveloped by aphyric andesites.

Chemistry and textures of the mineral assemblages from dacites, andesites and MME show constraints on the main magma-mingling and -mixing rock-forming processes. Characteristic features include: disequilibrium textures of the two populations of plagioclase phenocrysts (strongly oscillatory zoned, An_{26-44} and sieve-textured with resorption zones, An_{60-90}); similar high Mg# (79-95) clinopyroxene, mainly chromian diopside (as abundant clusters in dacites and andesites) and high Mg# (71-84) amphibole (Ti-magnesiohastingsite) in the MME, dacites and andesites; clinopyroxene coronas on the quartz phenocrysts exclusively within the andesites; resorption embayments displayed by the large-sized (up to 5 cm) sanidine phenocrysts.

Abundant and evenly distributed MME, disequilibrium phenocryst assemblages and textures of host rocks and enclaves suggest complex open-system processes, mainly magma-mingling and -mixing between a basaltic magma and a silicic one.Geochemical data show a mixing evolution trend from a basaltic composition similar to those of the MME (possible mafic end member) to a silicic composition similar to those of the dacite granophyric groundmass in equilibrium with sodic plagioclase, quartz, biotite and sanidine (possible silicic end member). A multistage magmatic evolution related to multiple replenishment events with hot basaltic magma in a evolved and probably zoned magma chamber, or more likely in a shallow level silicic reservoir, could be invoked in the genesis of the Laleaua Albă magmatic rocks. The andesite envelope represents a hybrid product from a first mingling and mainly mixing stage between the mafic magma corresponding to MME (storage and crystallization at as much as 18-25 km based on Al-in-hornblende and amphibole-plagioclase barometers) and silicic magma. The sanidine dacite formed from a second silicic and more alkalic magma batch during a further mingling stage with MME components.Multistage and complex evolution in the open-magmatic system constrained also by the composition and texture of the MME.

The mineralogical and geochemical similarities between the MME and the Firiza basalts (small basaltic dykes of 8.1-7.0 Ma from the vicinity) suggest the involvement of that basaltic magma as the mafic end member in the multistage magma-mingling and -mixing processes responsible for the genesis of the Laleaua Albă igneous rocks.

Geochemical and isotopic studies of mafic-ultramafic complex, NE Vietnam

Lan, C.Y.[1*], Tri, T.V.[2], Tran, T.A.[3], Usuki, T.[1] & Yang, T.F.[4]
[1]Institute of Earth Sciences, Academia Sinica, Taipei, Taiwan ([*]kyanite@earth.sinica.edu.tw)
[2]Vietnam National Committee for IGCP, Hanoi, Vietnam
[3]Institute of Geological Sciences, Vietnamese Academy of Science and Technology, Hanoi, Vietnam
[4]Dept. of Geosciences, National Taiwan University, Taipei, Taiwan

Mafic-ultramafic complexes outcrop along the Song Lo in NE Vietnam. They occur as blocks in the mélange with groundmass being metamorphosed fine-grained turbidites of lower Paleozoic age. They consist of serpentinite, amphibole gabbro and basalt. The serpentinites show high degree of serpentinization (LOI 11.8-13.8%) and have low SiO_2 (39.8-40.6%), TiO_2 (0.05-0.09%), Al_2O_3 (1.5-2.2%), TFe_2O_3 (7.8-10.5%) and CaO (0.1-1.1%) but high MgO (34.3-37.3%) and $Mg^{\#}$ value (87-9090). Chondrite-normalized REE patterns are U-shaped. They are characterized by high compatible elements of Cr (2439-5781 ppm), Ni (1184-3240 ppm) and Co (120-156 ppm). The amphibole gabbros and basalts are all basaltic in composition with silica contents ranging from 43.3 to 51.1 %. Magnesium content is moderate (6.0-7.8%) and $Mg^{\#}$ value range from 43 to 64. On the discrimination diagrams, basaltic rocks fall in the fields of N-MORB+IAB and WPA in the Zr/Y vs Zr diagram and ternary plots of Ti/100-Zr-3Y and 2Nb-Zr/4-Y. Chondrite-normalized REE patterns are different and show slightly LREE-depleted ($(La/Yb)_N$=0.8-0.9) and LREE-enriched ($(La/Yb)_N$=1.9-11.9), respectively. In the trace-element spidergram, the N-MORB+IAB rocks display slightly negative Nb, Ta and Ti anomalies suggesting the presence of a subduction component. Some WPA basaltic rocks exhibit significantly higher TiO_2 content (2.8-3.4%) when compared with other basaltic rocks (1.1-1.8%). The present εNd and Sr isotopic compositions are +6.2 to +9.1 and 0.70471 to 0.70571 for N-MORB+IAB and -2.9 to +7.5 and 0.70412 to 0.70653 for WPA rocks. The coexistence of serpentinite and N-MORB+IAB and OIB basaltic rocks suggests that the mafic-ultramafic complex represents a remnant of Paleo-Tethys in NE Vietnam.

Granitic pegmatites from the Banabuiú region (Central Ceará Domain, NE Brasil)

Lima, M.N.[1*], Azevedo, M.R.[1], Nogueira Neto, J.A.[2] & Valle Aguado, B.[1]
[1]GeoBioTec, Dept. of Geosciences, University of Aveiro, Aveiro, Portugal ([*]marthageolima@yahoo.com.br)
[2]Dept. of Geology, Federal University of Ceará, Brazil

The Banabuiú pegmatites intrude both a syn-collisional S-type granite pluton emplaced at around 580 Ma and basement rocks of Paleoproterozoic age, extensively transformed into gneisses and migmatites during the Brazilian/Pan-African orogeny (≈ 600 Ma). Most of the pegmatites bodies associated with the granite are barren, homogeneous and occur as fracture-filling dykes and veins, less than 1 m thick. Their main mineralogical assemblage consists of quartz + K-feldspar + albite + muscovite + tourmaline ± garnet.

In contrast, the basement pegmatites range from homogeneous to heterogeneously zoned, show conformable to cross-cutting relationships with the country rocks and vary from barren to transitional (beryl- and beryl-columbite–tantalite-phosphate types) to complex pegmatites (albite + K-feldspar + quartz + muscovite + lepidolite ± columbite – tantalite ± spodumene). Tourmaline is present in all pegmatite types. The development of a zonal sequence from the granite outwards appears to reflect a continuous fractionation trend, extending from the least evolved granite facies to the most geochemically specialized pegmatites.

Petrographic and mineral chemical data for feldspars and muscovites from two heterogeneously zoned pegmatites from the Banabuiú region show that: (1) K-feldspar ($Or_{90}Ab_{10}$ – $Or_{94}Ab_{06}$) is a major rock-forming mineral in these pegmatites, occurring mainly as large, euhedral to subhedral megacrysts in blocky K-feldspar zones. However, much of this phase was converted to sacchroidal albite and cleavelandite by late-stage sodium metasomatism; (2) Plagioclase is present as a fine-grained sacchroidal textured type or as platy to acicular cleavelandite crystals. Both varieties display nearly pure albite compositions ($Ab_{98.2}$ – $Ab_{99.5}$); (3) Muscovite can have primary or secondary origin. The former is light brown to silvery coloured and occurs as coarse books, whereas secondary muscovite is generally associated with albitized zones either after blocky K-feldspar or in beaded quartz texture or as fracture coatings. As seen in the M^{2+}-Al-Si ternary plot of Monier and Robert (1986) [1], they exhibit close to end-member compositions with minor Fe (< 2.3 wt. % FeO) and Na (< 0.3 wt % Na_2O), suggesting high temperature equilibration (≈ 600° C) (Fig. 1).

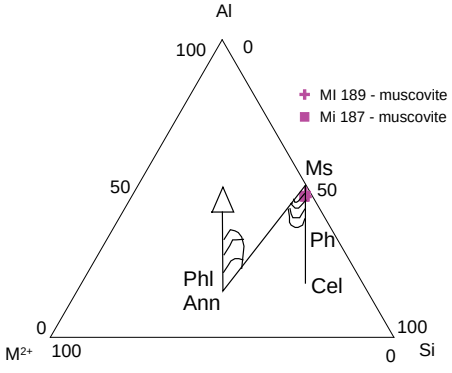

Fig. 1: Electron microprobe muscovite analysis plotted in the ternary diagram of [1]. Cel- celadonite; Ph-phengite; Ms-muscovite; Ann-annite; Phl- phologopite.

[1] Monier, G. & Roberts, J-L. (1986) *Mineral. Mag.*, **50**, 257-266.

Magmatic lithic clasts of ignimbrite as messengers of the magma reservoir: a study from the Bükkalja Volcanic Field (Hungary)

Lukács, R.[1*], Harangi, Sz.[1] & Ntaflos, T.[2]
[1]Dept. of Petrology and Geochemistry, Eötvös University, Budapest, Hungary ([*]lrekuska@freemail.hu)
[2]Inst. of Lithosphere Studies, University of Vienna, Austria

Lithic clasts are accidental or accessory components of pyroclastic flow deposits. They represent rock fragments picked up by the pyroclastic flow accidentally from the surface or they derived from the basement torn down by the uprising magma. Magmatic accessory lithic clasts either derived from the magma reservoir or from the wall rock of the vent area. In the former case the magmatic lithic clasts are messengers of the magma reservoir, and their study can help us to understand the pre-eruptive petrogenetic processes.

In the Bükkalja Volcanic Field, Szomolya locality exhibits a lithic clast rich (up to 15vol %) rhyolitic ignimbrite. 90% of the lithic clasts are magmatic and they are mainly andesites, subordinately rhyolites. The bulk rock geochemistry ($^{87}Sr/^{86}Sr$ isotope, and main and trace element data) of the andesite lithic clasts and pumices of the ignimbrite suggests their genetic relationship. The andesite lithic clasts have fresh or variably devitrified rhyolitic matrix glass. Based on their mineral assemblage at least three lithic types can be recognised. The main mineral phases in each group are plagioclase and orthopyroxene accompanied by clinopyroxene or/and amphibole or/and biotite. Textures of the matrix glass and the phenocrysts suggest rapid quenching of the interstitial melt. The detailed textural investigations combined with in-situ microprobe and La-ICP-MS analyses of the andesite lithic clasts are consistent with a crystal-mush origin, i.e. they represent different parts of the complex crystal-mush zone of the magma reservoir generating the ignimbrite.

The high Mg-orthopyroxenes and high Ca-plagioclases of lithic clasts (Fig. 1) imply the role of mantle derived basaltic magmas in the petrogenesis of the ignimbrite. The mineral geochemical data revealed that the mineral assemblage is not in equilibrium. They were formed from different magmas at different stages of magma evolution. The mineral phases of the andesite lithic clasts are in fact antecrysts and overall they do not represent a true andesitic magma, but rather a mixture of crystals crystallized from basaltic and dacitic/rhyolitic magmas. The distinct origin of the mineral phases suggests that they were mobilised from different parts of the crystal-mush zone probably as a result of an intrusion of fresh magma in the magma reservoir.

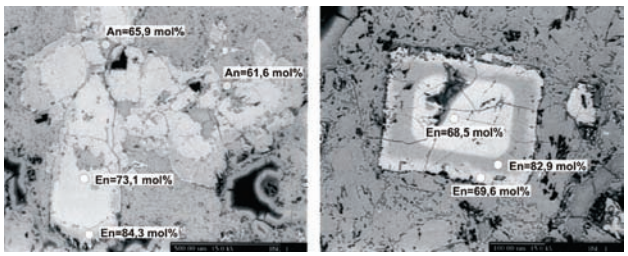

Fig. 1: BSE images of an orthopyroxene-plagioclase cumulate (left) and an oscillatory zoned othopyroxene (right) of an andesite lithic clast. The compositions of different zones are marked with the enstatite (En) or anorthite (An) contents of orthopyroxene and plagioclase, respectively.

The presence of two mutually immiscible melts during the late-stage crystallization of the Kymi topaz granite stock, Finland: evidence from melt and fluid inclusions

Lukkari, S.[1*] & Thomas, R.[2]
[1]Dept. of Geosciences and Geography, University of Helsinki, Finland ([*]sari.lukkari@helsinki.fi)
[2]GeoForschungsZentrum, Potsdam, Germany

The crystallization of the late-stage, F-enriched Kymi topaz granite stock has been investigated by remelting and analyzing crystallized melt inclusions as well as fluid inclusions in quartz and topaz grains from porphyritic and equigranular topaz granites and marginal pegmatite. The melt inclusion compositions show that the topaz granites and the stocksheider pegmatite of the Kymi stock crystallized from very F and H_2O-rich melts (up to 14 wt % F and 29 wt% H_2O), and that Li and B were present in the granitic melt at high concentrations [1].

Previous melt inclusion studies on other granite-pegmatite complexes (Ehrenfriedersdorf, Zinnwald, Königshain) have demonstrated that a late-stage liquid immiscibility and a formation of two separate melt fractions were crucial for the formation of these pegmatites [2]. Although the melt inclusions in this study show only peraluminous compositions, and isolated and preserved peralkaline pegmatite patches are not found in the Kymi stock, the melt and fluid inclusions contain evidences for two mutually immiscible melts, one of these being relatively H_2O- and alkali-poor and the other extremely H_2O- and alkali-rich. Quartz from the granites and pegmatite contains two coexisting melt inclusion types, varying in vapour content. Quartz from the equigranular granite contains also melt inclusions composed of two coexisting silicate glasses, one of which contains chiolithe ($Na_5Al_3F_{14}$) (Fig. 1). The observed chiolithe in the silicate glass nodules of the melt inclusions as well as cryolite (Na_3AlF_6) and $LiAlF_4$ daughter minerals from equigranular granite and zabuyelite (Li_2CO_3) daughter mineral in fluid inclusions in topaz from pegmatite are remnants of the peralkaline character of the melt and mineral-forming fluid.

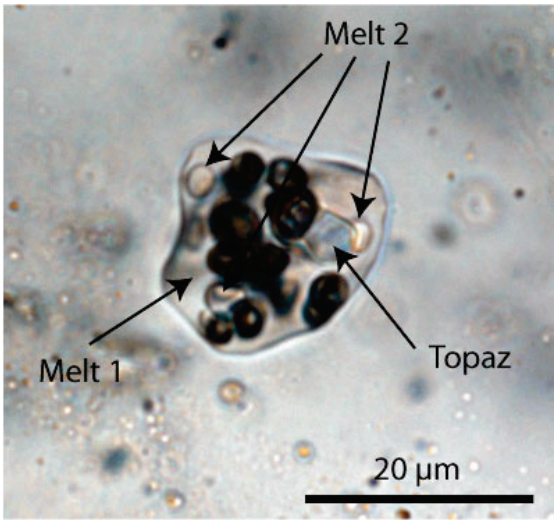

Fig. 1: A melt inclusion in quartz from the equigranular granite composed of two coexisting silicate glasses, topaz daughter crystals and several vapor bubbles after homogenization at 700 °C, 300 MPa and 24 h. The small glass nodules are H_2O-, F- rich silicate glass showing remnants of chiolithe ($Na_5Al_3F_{14}$).

[1] Lukkari, S. et al. (2009) *Can. Mineral.*, **47**, 1359-1374. [2] Thomas, R. et al. (2009) *Contrib. Mineral. Petrol.*, **157**, 505-523.

Metasomatic titanates associated with Cl-rich amphibole and phlogopite in a multiply metasomatized garnet lherzolite from Letseng-la-Terae, Lesotho

Mair, P.[1*], Konzett, J.[1] & Hauzenberger, Ch.[2]
[1]Institute of Mineralogy, University of Innsbruck, Austria
([*]P.Mair@uibk.ac.at)
[2]Institute of Earth Sciences, University of Graz, Austria

The Letseng-la-Terae diamondiferous kimberlite contains a complex suite of upper mantle peridotites and pyroxenites, some of which showing evidence for multi-stage metasomatism [1]. Here we present major and trace element data on a garnet-lherzolite containing an unusually complex suite of Cr-rich oxides consisting of crichtonite + armalcolite + ilmenite + chromite + rutile which have formed by two different metasomatic events. Crichtonite is present as tiny (<10 µm) inclusions in Cr-rich clinopyroxenes which form a narrow vein crosscutting the lherzolite. Unlike almost all crichtonites from other Kaapvaal craton localities [2] which are mostly lindsleyite-mathiasite solid solutions, those from the present study are virtually free of K and Ba but rich in LREE (1.6-1.7 wt% Ce_2O_3, 2.4-3.0 wt% La_2O_3), U, and Th (~0.6 wt% UO_2 and 0.4 wt% ThO_2) indicating significant loveringite and davidite components. The crichtonites are associated with inclusions of Cr-rich spinel and Cr-Zr-rich rutile (0.7-1.6 wt% Cr_2O_3, 0.3-0.4 wt% ZrO_2) calcic amphibole and phlogopite. Both phlogopite and pargasitic calcic amphibole are unusually Cl-rich with up to 0.25 wt% Cl in amphibole und up to 0.4 wt% Cl in phlogopite. Phlogopite and Cr-rich spinel is also present as large matrix grains several hundred microns in diameter. The crichtonite-rutile-amphibole-phlogopite association is thought to have formed by infiltration of a hydrous fluid rich in K-REE-U-Th and Cl. A second metasomatic event most likely involving a hydrous melt caused (1) a partial to complete pseudomorphic replacement of garnet by Al-rich spinel + clinopyroxene + orthopyroxene; (2) replacement of Cl-rich phlogopite-I by F-Ti-Fe-rich and Cl-poor phlogopite-II containing up to 1.0 wt% F and 9.9 wt% TiO_2; (3) modification of the composition of primary clinopyroxene and orthopyroxene along a network of narrow veins to produce Na-Al-poor clinoyproxene and Ca-Al-rich orthopyroxene and (4) formation of Cr-rich armalcolite and ilmenite associated with Na-Al-poor clinoyproxene. The composition of the armalcolite is very similar to that reported from metasomatic xenoliths of the Kimberley area [2]. The application of various geothermobarometers involving major- and trace element exchange between the primary lherzolite phases yields consistent P-T conditions of ~850°C and ~3 GPa. These are significantly lower than conditions of 1100°C and 4.5 GPa reported for other garnet-lherzolites from Letseng affected by multi-stage metasomatism [1] and indicate a considerable depth interval over which metasomatism affected the Kaapvaal lithosphere in the Lesotho area. The xenolith of this study also provides rare evidence for the presence of significant amounts of Cl in hydrous metasomatizing fluids of the shallow Kaapvaal lithosphere.

[1] Simon, N.S.C. et al. (2000) *J. Conf. Abstr.*, **5(2)**, 926. [2] Haggerty, S.E. (1983) *Geochim. Cosmochim. Ac.*, **47**, 1833-1854

Plagioclase phenocrysts and their alteration in rhyodacitic porphyries from Zalas near Cracow (Poland)

Marszałek, M[*] & Czerny, J.
Dept. of Mineralogy, Petrography and Geochemistry, AGH-University of Science and Technology, Krakow, Poland
([*]mmarszal@agh.edu.pl)

The Upper Palaeozoic porphyries of Zalas form a classic laccolith 3-4 km long. These rocks were subjected to complex postmagmatic alterations, expressed mainly in their enrichment in potassium [1,2]. Plagioclase phenocrysts occurring in five colour varieties of the porphyries (black, grey, green, red and white) have been studied. Analyses included SEM, EDS, WDS, XRPD.

The tabular plagioclase phenocrysts with sizes from a fraction of mm to 8 mm make up fifteen or so vol.% of the rocks. They reveal complex, mainly albite and Carlsbad and less frequent pericline twinning; zoning is common. In the smaller crystals zoning is normal, in bigger ones it is recurrent, usually 2-3-fold, with a narrow, inversion outer zone. The chemistry of plagioclases varies from An_{52} to An_{21}, being most often between An_{40} and An_{30}.

The degree of alteration of the plagioclase phenocrysts is variable. In the black variety they are generally fresh, in the grey one only some grains are slightly altered. In the green and red porphyries the phenocrysts are mostly replaced by secondary minerals, and in the white ones only pseudomorphs after plagioclases occur, a few of them with relics of the original feldspar.

The phenocrysts studied were subjected to two types of alterations, usually overlapping. Replacing of plagioclases by secondary minerals is one of them, the other includes leaching of the phenocrysts with subsequent filling empty spaces with the minerals crystallizing from hydrothermal solutions. In metasomatic changes plagioclases are replaced first by albite and next by adular (albitization directly preceded adularization). These alterations are developed along the network of irregular, small veins and concentrate in the form of nests. They are accompanied in places by aggregates of calcite and clays (close to illite). Hydrotherma precipitation has resulted in adular with characteristic rhombohedral habit, rosettes of chlorite overgrown by illite, and occassional quartz. In the white porphyries, pseudomorphs after plagioclases are composed of adular and kaolinite (+/- calcite) with subordinate albite and illite; celadonite instead of chlorite is the clay mineral in the leached out spaces of these phenocrysts.

Acknowledgements: This study was supported by the AGH – University of Science and Technology, project no. 10.10.140.448.

[1] Słaby, E.(1987) *Archiwum Mineralogiczne*, **42(2)**, 69-94. [2] Czerny, J. & Muszyński, M. (2000) *Polskie Towarzystwo Mineralogiczne, Prace Specjalne*, **17**, 91-93.

New insights into the significance of gneisses and tourmalinites in the Nevado-Filabride complex (western Sierra Nevada, Spain), from U-Pb zircon and $^{40}Ar/^{39}Ar$ tourmaline geochronology: geological implications

Martínez-Martínez, J.M.[1], Torres-Ruiz, J.[2], Pesquera, A.[3*] & Gil-Crespo, P.P.[3]
[1]Depto. de Geodinámica e Instituto Andaluz de Ciencias de la Tierra (IACT) , Facultad de Ciencias, Universidad de Granada, Granada, Spain ([*]alfonso.pesquera@ehu.es)
[2]Depto. de Mineralogía y Petrología, Facultad de Ciencias, Universidad de Granada, Granada, Spain
[3]Depto. de Mineralogía y Petrología, Universidad del País Vasco, Bilbao, Spain

The Nevado-Filabride complex, the lowest one in the Betic hinterland, forms a stack of Alpine nappes. The tectonic units consist of metasedimentary sequences whose ages are not well constrained. Gneiss bodies included in the sequences have been one of the few sources of geochronological data in this metamorphic complex. New radiometric data from U-Pb zircon dating on gneisses from the western Sierra Nevada confirm the presence of upper Carboniferous intrusive rocks in the Betic hinterland. These results, combined with available data from the literature and a detailed structural analysis, suggest that the gneisses represent an only late Hercynian magmatic event. Evidence for a close genetic relation between gneisses and tourmalinites is provided by field and petrographic observations, in conjunction with U-Pb zircon (314 ± 7 and 304 ± 23 Ma) and ^{40}Ar-^{39}Ar tourmaline dating (319.85 ± 5.81 and 317.85 ± 3.67 Ma). A pre-upper Carboniferous age for the basal formation of the Nevado-Filabride sequence can be inferred. The gneiss protolith and the graphite schist are considered to be the boron source and the precursor of the tourmalinites, respectively. Superposed tectonically units rather than a continuous Palaeozoic sequence is supported by the occurrence of Palaeozoic rocks at the top of the Nevado-Filabride complex. The nappe tectonics, as evidenced from the contractive character of the unit boundaries and the superposition of more on less metamorphic rocks, is additionally supported by the older on younger rocks superposition.

Olivine and clinopyroxene in tholeiites as indicators of ocean magmas origin

Migdisova, N.A.[*], Sushchevskaya, N.M., Sobolev, A.V. & Kuzmin, D.
Institute for Geochemistry and Analytical Chemistry RAS, Moscow, Russia ([*]nat-mig@yandex.ru)

A study of clinopyroxene and olivine phenocrysts from the basalts of complex geodynamic setting of the Southern Ocean provided insight into the specific conditions of magma formation and origin. The new results on primary melts are reported.

The region of investigation is situated at the western end of the Southwest Indian Ridge (SWIR) near the Bouvet triple junction (BTJ). The Bouvet Triple Junction (BTJ) consists of three main structures of the oceanic floor: Mid Atlantic Ridge (MAR), American Antarctic Ridge (AAR) and Southwest Indian Ridge (SWIR). These three oceanic ridges which constitute the BTJ have been changing their positions in the space and time relatively each other. Clinopyroxene and olivine phenocrysts were separated from the basalts of two SWIR segments: directly opposite Bouvet Island and in the Spiess Ridge, which is the westernmost part of the SWIR. The most abundant basalts of these segments are oceanic tholeiites enriched in lithophile elements and radiogenic isotopes. The basalts of both segments are similar in the character of enrichment. The Spiess Ridge is the largest structure of the Bouvet triple junction. Morphologically it is a large volcanic rise oriented at a low angle to the structures of the Mid-Atlantic Ridge (MAR).

Numerical modeling based on the dependency of clinopyroxene composition on pressure and temperature of crystallization allowed us to estimate the depth of melt fractionation in transitional magma chambers. The pressures of magma fractionating are supposed to be from 1 to 5 kbar defining the level of transit chamber under the ridge.

Ni excess over Mg and Mn deficiency over Fe in olivine phenocrysts suggest the presence of olivine-free pyroxenite lithologies in the sources of primary melts. The lowest amounts of pyroxenite component (X_{PX} Mn/Fe = 0-10%) were recorded for the samples from the station S18-63, located in the MAR valley. The greatest range (X_{PX} Mn/Fe = 0-90% in the single rock) was observed in samples from the station G96-10 situated on the western slope of the Spiess Ridge. Obtained results suggest the participation of recycled crustal component in the generation of primary melts.

BTJ isotopic signatures (Sr, Nd, Pb) and trace element patterns are similar to those in the alkaline basalts of Antarctic Peninsula. These features imply melting of enriched constituent in the mantle source common to the western Antarctica and SWIR. The long-term enrichment of mantle is seen in the more radiogenic Pb and Sr and less radiogenic Nd of basalts. It likely indicates contamination by oceanic crust. Such global mantle heterogeneities could have been formed during various and complicated stages of South Ocean geodynamic evolution.

Mineral chemistry of Kamtal Skarn (Eastern Azarbaijan, NW Iran)

Mokhtari, M.A.A.[1*], Moinvaziri, H.[1], Ghorbani, M.R[1], Mehrpartou, M.[2], Padashi, S.M.[3] & Baburek, J.[4]
[1]School of Science, Tarbiat Modares University, Tehran, Iran
([*]mokhtari1031@gmail.com)
[2]Geosciences Research Center, Geological Survey of Iran, Tehran, Iran
[3]Geological Survey of Iran, Tehran, Iran
[4]Czech Geological Survey, Prague, Czech Republic

Kamtal intrusion is a part of Qaradagh batholith. This batholith with an area more than 1500 km^2, crops out in NW of Iran and republics of Azerbaijan and Armenia. Kamtal intrusion with an area about 25 km^2, is located in southwestern part of Qaradagh batholith in eastern Azarbaijan province, NW of Iran, near the Armenia border.

Compositionally, this intrusion consists of monzogranite, quartz- monzonite and gabbro [1]. Kamtal intrusion is intruded into Cretaceous flysch type rocks. This intrusion leads to formation a wide contact aureole (Kamtal skarn) around the Kamtal body. These rocks characterized by garnet, clinopyroxene and calcite [1]. Epidote, actinolite, quartz and albite are the accessory minerals.

Garnets are the more abundant mineral in these rocks. Many part of skarn aureole have very high concentration of garnet (more than 90%), therefore we can call these rocks as garnetite. Main parts of garnets have grossularitic composition (Ad_{33-35}). Along the fractures, andraditic compositions (Ad_{71-73}) become dominant component. The rims of garnets have intermediate composition between andradite and grossularite ($Ad_{53-55.5}$). Overall, the EPMA data show that the garnets are mainly andraditic–grossularitic (grandite) with negligible amounts of the almandine and spesartine component, varying slightly in composition as follows:

$Na_{(0-0.01)}Ca_{(2.73-3.06)}Mg_{(0.002-0.03)}Fe^{2+}_{(0.05-0.64)}Fe^{3+}_{(0.32-1.57)}Mn_{(0.02-0.1)}Al_{(0.002-0.22)}Ti_{(0.001-0.13)}Si_{(2.78-3)}O_{12}$

Clinopyroxene is common mineral after garnet. Its frequency rarely reaches to 50%. EPMA data from clinopyroxenes indicate that they are mainly salite, and belong compositionally to the hedebergite-diopside series ($Di_{74.5-99.8}$). The rims of clinopyroxenes have more diopsidic component. Johannsenite component have negligible amounts. Overall, clinopyroxenes varying slightly in composition as follows:

$Na_{(0.005-0.024)}Ca_{(0.98-1.03)}Mg_{(0.63-0.9)}Fe^{2+}_{(0.025-0.23)}Fe^{3+}_{(0-0.11)}Mn_{(0.01-0.055)}Al_{(0.002-0.11)}Si_{(1.89-2.04)}O_6$

On the basis of EPMA data, it's concluded that early formed crystals of garnets have high grossularitic component (rich in Ca). This is because of concentration of Ca in marbles. By progressing of metamorphic reactions and consuming of Ca in the structure of early formed garnets, the rim of these crystals and fractures have low grossularitic component (poor in Ca) and high andraditic component (rich in Fe).

[1] Mokhtari, M.A.A. (2009) *Unpublished Ph.D. thesis*, Tarbiat Modares University, Iran.

Discovery of meta-komatiites in the Archaean high-grade polymetamorphic Central Zone of the Limpopo belt, South Africa: remnants of oceanic crust and evidence of cryptic suture?

Mouri, H.[1*], Maier, W.[2], Andreoli, M.[3], Brandl, G.[4] & Rebay, G.[5]
[1]Dept. of Geology, University of Johannesburg, South Africa
([*]hmouri@uj.ac.za)
[2]Dept. of Geology, University of Oulu, Finland
[3]Nuclear Energy Corporation of South Africa, South Africa
[4]Council for Geoscience, Limpopo Unit, Polokwane, South Africa
[5]Dept of Geology, University of Pavia, Italy

Komatiites have been described from many Archaean greenstone belts where they were subjected to greenschist and upper amphibolite facies metamorphic conditions. So far, komatiites have not been reported from high to ultra-high metamorphic grade environments (upper granulite facies conditions). Here we report the discovery of komatiites in the Archaean high to ultra-high grade polymetamorphic terrain of the Central Zone of the Limpopo Belt in South Africa. These rocks have relatively high MgO (26-31%), Cr (2800-3800 ppm) and Ni (1400-1800 ppm), but low SiO_2 (41-46%) and Al_2O_3 (5-7%). These geochemical characteristics, including the unfractionated Rare Earth Element (REE) and the platinum group element (PGE) patterns, are most consistent with late Archaean or Proterozoic aluminum (Al)-undepleted Munro-type komatiites.

Thermodynamic calculations combining classical conventional methods as well as modern techniques such as THERMOCALC, in conjunction with textural relationship and mineral chemistry, indicate that the studied rocks went through upper granulite facies metamorphic conditions reaching a temperature of up to 900°C and an intermediate pressure of up to 10 kbar.

Although the emplacement age of the komatiitic rocks is not yet known, geochemical evidence such as PGE concentrations seem to be consistent with a late Archaean or early Proterozoic age [1].

The discovered rocks might add important insight into our understanding regarding the geological evolution of the Limpopo Belt. According to Light [2] the Kaapvaal and Zimbabwe Cratons may have been separated by a distance of more than 1000 km of oceanic crust before 3350 Ma. This author suggested that the collision between the two cratons was initiated during Palaeo-archaean times (3350Ma) and terminated in the late Neo-archaean (2500Ma). Since komatiites can be potential candidates for Archaean oceanic crust [3], the rocks studied here might represent an ophiolitic remnant of obducted oceanic crust indicating the presence of a hidden suture zone in the Central Zone of the Limpopo Belt.

[1] Maier, W.D. et al. (2009) *Nature*, **460**, 620-623. [2] Light, M.P.R. (1982) *Tectonics*, **1**, 325-342. [3] Arndt, N.T. et al. (2008) *Komatiite*. Cambridge University Press, Cambridge.

Geochemistry and petrology of mantle xenoliths from Poiana Ruscă (W Romania)

Nédli, Zs.[1*], Princivalle, F.[2] & Szabó, Cs.[1]
[1]Lithosphere Fluid Research Lab, Dept. of Petrology and Geochemistry, Eötvös University Budapest, Hungary
([*]nedlizs@yahoo.com)
[2]Dept. of Earth Sciences, University of Trieste, Italy

Recently collected mantle xenoliths from Late Cretaceous - Paleogene alkali basic rocks from the Poiana Ruscă (W Romania) show new petrologic and thermobarometrical aspects of the pre-Neogene subcontinental lithospheric mantle. The xenoliths widely vary among wehrlite, lherzolite and olivine websterite in composition. The most distinctive feature of the modal composition is the high variability in orthopyroxene content (1-45 vol%). Texturally 2 main groups can be distinguished: transitional porphyroclastic-equigranular texture and poikilitic texture xenoliths.

Clinopyroxene has high Al_2O_3 (6-7 wt%) and Na_2O (1.5-2 wt%) content. Spinel is always Al-rich, cr# are low (0.08-0.18). Mg# of pyroxenes varies between 0.89-0.91. The major element chemical composition of minerals shows rather fertile composition and low degree of basaltic melt extraction. Apart from different textures and modal composition, clinopyroxenes generally have enrichment in REE content approx. 10x relative to the chondrite, showing rather flat patterns (Fig. 1). Slight LREE-depletion is typical as a result of basaltic component extraction. Some samples are different with steeply downward REE patterns and in a few samples with notable LREE enrichment.

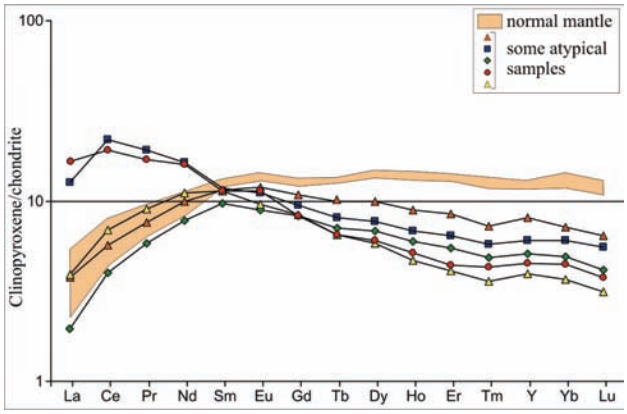

Fig. 1: Chondrite normalized REE diagram for Poiana Ruscă xenolith clinopyroxenes.

Clinopyroxene single crystal X-ray diffraction measurements show low cell (432.9-433.6 $Å^3$) and M1, M2 site volumes. Their structural data are similar to those from garnet-bearing lherzolites worldwide therefore we suggest that they can be equilibrated at high depths near to garnet stability field. Thermometry indicates a homogeneous equilibrium temperature between 950-1010°C.

Chemistry and textural evidences suggest that the mantle might have undergone interaction with a Si-rich melt. Such a metasomatic agent is different from any metasomatism described previously from orthopyroxene-rich xenoliths from the Carpathian-Pannonian Region (e.g. [1]) and from the Dacia block (e.g. [2]) and show a particular metasomatism without significant incompatible element enrichment.

[1] Bali, E. et al. (2007) *Mineral. Petrol.*, **90**, 51-72. [2] Cvetković, V. et al. (2004) *Contrib. Mineral. Petrol.*, **148**, 335-357.

Mineralogical composition of Kamtal intrusion (Eastern Azarbaijan, NW Iran)

Padashi, S.M.[1], Mokhtari, M.A.A.[1,2], Moinvaziri, H.[2], Ghorbani, M.R.[2], Mehrpartou, M.[3], Abedian, N.[1] & Baburek, J.[4]
[1]Geological Survey of Iran, Tehran, Iran
([*]sm_padashi@yahoo.com)
[2]Iran School of Science, Tarbiat Modares University, Tehran, Iran
[3]Geosciences Research center, Geological Survey of Iran, Tehran, Iran
[4]Czech Geological survey, Prague, Czech Republic

Kamtal intrusion is a part of Qaradagh batholith. This batholith with an area more than 1500 km^2, crops out in NW of Iran and republics of Azerbaijan and Armenia. Kamtal intrusion, with an area about 25 km^2, is located in southwestern part of Qaradagh batholith in eastern Azarbaijan province, NW of Iran, near the Iranian-Armenian border.

Compositionally, this intrusion consists of monzogranite, quartz- monzonite and gabbro. Gabbros can be seen as small lenses within the quartz- monzonite. Quartz- monzonites have been intruded by the monzogranite. Both monzogranites and quartz- monzonites are high-K calk alkaline and metaluminous in character and can be classified as I-type granitoids, while the gabbros have tholeiitic nature [1].

Electron-probe micro-analysis (EPMA) was used for determining the composition of some silicate minerals, such as pyroxenes, amphiboles, plagioclases and olivine. These analyses were carried out at Czech geological survey.

Monzogranites outcrop as a small stock. They are microgranular in texture and characterized by quartz, alkali feldspar, plagioclase (An28-30) with some hornblende (magnesio- hornblende) and biotite.

Quartz- monzonites form the main part of the Kamtal intrusion. They are coarse grained and light gray to dark gray in color. They are characterized by alkali feldspar, plagioclase (An29-39), quartz, Hornblende (magnesio- hornblende), biotite (composition between annite and phlogopite) and clinopyroxene (augite). Titanite, apatite, magnetite, rutile and zircon are the accessory phases and epidote, actinolite, chlorite and sericite are the secondary minerals.

Gabbros are coarse grained and dark in color. They have gradational contact with quartz- monzonite. Gabbros characterized by plagioclase (An50-79), clinopyroxene (diopside) and Amphibole (magnesio- hastingsite). Most of the clinopyroxenes have been altered to actinolite. Biotite present as a minor phase in these rocks that mainly altered to chlorite. Olivine present in some samples that has chrysolite composition. Magnetite is a frequent minor phase in these rocks. In some samples, xenomorphic magnetite (wormy shape) can be seen in the groundmass of other minerals. This indicates that magnetite crystallized at end of crystallization. Also, in some samples, wormy shape magnetite aggregation present with small crystals of plagioclase and clinopyroxene. These aggregations may be result of immiscibility.

[1] Mokhtari, M.A.A. (2009) Unpublished Ph.D. thesis, Tarbiat Modares University.

Mineralogy of nepheline syenite dykes from the Ditrău Alkaline Massif, Romania

Pál-Molnár, E.*, Ódri, Á. & Batki, A.
Dept. of Mineralogy, Geochemistry and Petrology, University of Szeged, Szeged, Hungary (*palm@geo.u-szeged.hu)

The Ditrău Alkaline Massif (DAM) is a Mesozoic alkaline igneous complex situated in the S-SW part of the Giurgeu Alps belonging to the Eastern Carpathians (Romania). It outcrops right east of the Neogene-Quaternary Călimani-Gurghiu-Harghita calc-alkali volcanic belt by breaking through the pre-Alpine metamorphic rocks of the Bukovina Nappe. According to our present knowledge, the DAM is an intrusive rock body with an eastern, north eastern tilt, built up by several tectonic blocks providing the massif a complex form. Great number of different rock types appears on the surface (ultrabasites, gabbros, diorites, monzonites, syenites, nepheline syenites, granites, lamprophyres, etc.). Based on K/Ar data [1] originating from various mineral fractions of different rock types has shown that the DAM is the result of a long lasting (Middle Triassic – Lower Cretaceous) two phase magmatic process, which started during the Triassic by the opening up of the Tethys and the detachment of the Getida-Bukovina Microplate from the Eurasian Plate.

Nepheline syenite aplites (tinguaites) are very rare in the DAM, form thin dykes and are in connection with white nepheline syenites which they are also chemically related to [2]. Nepheline syenite dykes chemically belong to the group of foidsyenites however by their texture they are determined as tinguaites [3]. This paper reports new results on the mineralogy of the nepheline syenite dykes which were not discussed yet in former works of the DAM.

Mineral chemistry analyses were determined by Cameca SX-50 elecron microprobe at the Department of Earth Sciences, University of Uppsala, Sweden. Operating conditions were probe current of 15 nA and acceleration voltage of 20 kV.

Nepheline syenite dykes are light grey coloured rocks of small grain size with a porphyric texture. Both groundmass minerals and the phenocrysts are hipidiomorphic to xenomorphic. The phenocrysts of tinguaites are andradite-grossular $[Ca_3Fe^{3+}_{1-1.4}Al_{0.5}(Al_{0.1}Si_{2.9}O_4)_3]$, aluminian sodian ferroan diopside $[Ca_{0.9}Na_{0.1}Mg_{0.5}Fe^{2+}_{0.1}Fe^{3+}_{0.2}(Al_{0.2}Si_{1.8}O_6)]$ and aegirine-augite $[Ca_{0.4}Na_{0.6}Mg_{0.1}Fe^{2+}_{0.3}Fe^{3+}_{0.5}(Al_{0.1}Si_{1.9}O_6)]$. Based on Ti- and Al-content of the pyroxenes the diopsides crystallised under high pressure, while the aegirin-augites formed under low pressure. The groundmass minerals are eckermannite $[Na_{2.8-3.5}Fe^{2+}_{3-3.5}Mg_{0.3-0.7}Al_{0.3-0.4}(Si_8O_{22})(OH)]$, albite ($Ab_{98-99}$), orthoclase and muscovite. Accessories are titanite, zircon and magnetite. Secondary minerals are annite-phlogopite (mg#=0.57-0.76), chlorite, epidote, calcite and sericite.

The mineral composition of nepheline syenite dykes occurring in the DAM confirms their alkali character and largely contributes to the understanding of their petrogenesis.

[1] Pál-Molnár, E. & Árva-Sós, E. (1995) *Ac. Mineral. Petrogr., Szeged*, **36,** 101-116. [2] Streckeisen, A. (1954) *Min. Petr. Mitt.*, **34,** 336-409. [3] Bates, R.L. & Jackson, J.A. (1980) *Glossary of geology.* Am. Geol. Inst., Falls Church, Virginia.

Mineralogy of syenites from the Ditrău Alkaline Massif, Romania

Pál-Molnár, E.[1*], Sogrik, E.[1], Batki, A.[1] & Dobosi, G.[2]
[1]Dept. of Mineralogy, Geochemistry and Petrology, University of Szeged, Szeged, Hungary (*palm@geo.u-szeged.hu)
[2]Institute for Geochemical Research, Hungarian Academy of Sciences, Budapest, Hungary

The Ditrău Alkaline Massif (DAM) is a Mesozoic alkaline igneous complex situated in the S-SW part of the Giurgeu Alps belonging to the Eastern Carpathians (Romania). It outcrops right east of the Neogene-Quaternary Călimani-Gurghiu-Harghita calc-alkali volcanic belt by breaking through the pre-Alpine metamorphic rocks of the Bukovina Nappe. According to our present knowledge, the DAM is an intrusive rock body with an eastern, north eastern tilt, built up by several tectonic blocks providing the massif a complex form. Great number of different rock types appears on the surface (ultrabasites, gabbros, diorites, monzonites, syenites, nepheline syenites, granites, lamprophyres, etc.). Based on K/Ar data [1] originating from various mineral fractions of different rock types has shown that the DAM is the result of a long lasting (Middle Triassic – Lower Cretaceous) two phase magmatic process, which started during the Triassic by the opening up of the Tethys and the detachment of the Getida-Bukovina Microplate from the Eurasian Plate.

The S-SW part of the DAM is formed mainly by syenites. There are several hypotheses on their genesis [2-4] but it is still not complete and clearly understood. We present new results on the mineralogy of the syenites which can contribute to a better understanding of their origin.

Mineral chemistry analyses were determined by JEOL JCXA-733 electron microprobe equipped with WDS and EDS at the Geochemical Research Institute of Hungarian Academy of Sciences, Budapest.

The syenites are holocrystalline, hypidiomorphic and medium-grained (1.9-3.5 mm). The main rock forming minerals are K-feldspar, amphibole, biotite and subordinately plagioclase. The amphiboles are Ca-amphiboles, hastingsite $[Na_{0,7-1,2}K_{0,3-0,4}Ca_{1,6-1,8}Fe^{2+}_{2,1-2,8}Fe^{3+}_{0,2-0,9}Mg_{1,2-2,0}Mn_{0,1-0,2}Al_{0-0,3}(Al_{1,8-2,2}Si_{5,8-6,2}O_{23})]$, pargasite $[Na_{0,8}K_{0,3}Ca_{1,8}Fe^{2+}_{2,1}Fe^{3+}_{0,1}Mg_{2,3}Mn_{0,04}Al_{0,1}(Al_{1,9}Si_{6,1}O_{23})]$ and ferropargasite $[Na_{0,8}K_{0,3}Ca_{1,8}Fe^{2+}_{2,2}Fe^{3+}_{0,1}Mg_{2,0}Mn_{0,1}Al_{0,2}(Al_{1,9}Si_{6,1}O_{23})]$. The biotites are annites (mg# = 0.29-0.48). Perthitic orthoclase and microcline are the dominant feldspar phases, but albite-oligoclase ($An_{0,8-16,5}$) appears as well. Accessories are titanite, apatite, magnetite, rutile and zircon.

The estimated crystallisation pressure based on Al-in-hornblende barometry [5] for hastingsites, pargasites and ferropargasites are approx. 6.9-7.5 kbar which signs the starting of the crystallisation process of syenites. The presence of several secondary minerals such as sericite, chlorite, epidote and calcite assume metasomatic effects on syenites.

[1] Pál-Molnár, E. & Árva-Sós, E. (1995) *Acta Mineral. Petrogr., Szeged*, **36,** 101-116. [2] Streckeisen, A. (1931) *An. Inst. Geol. Roum.*, **16,** 408-413. [3] Streckeisen, A. (1954) *Min. Petr. Mitt.*, **34,** 336-409. [4] Streckeisen, A. & Hunziker, I.C. (1974) *Min. Petr. Mitt.*, **54,** 59-77. [5] Schmidt, M.W. (1992) *Contr. Mineral. Petrol.*, **110,** 304-310.

Mafic plutonic rocks from south of Gorgan (NE Iran) – mineralogical and geochemical data

Rahimi-Chakdel, A.* & Raghimi, M.
Dept. of Geology, Faculty of Science, Golestan University, Gorgan, Iran (*rahimiaz@yahoo.co.uk)

Gorgan schists, exposed as discontinuous outcrops in the southern part of Gorgan town, Eastern Alborz Mountain Ranges, Northern Iran, represent metamorphic relicts of the PaleoTethyan collision in lower Palaeozoic [1]. Consisting of low-grade metamorphic rocks, Gorgan schists are intruded by mafic plutonic rocks, the largest exposed mafic dike having 1 m width and 4 km length.

A total of 7 samples were collected from various locations along the exposed mafic bodies for mineralogical investigations, whole-rock major and trace element analysis.

The mafic dikes are coarse grained and the texture varies from ophitic to intergranular. The mineralogy of the gabbros is dominated by large crystals of clinopyroxene, plagioclase and hornblende. The clinopyroxene displays prominent hornblende coronas in most samples.

The compositional ranges of the major elements are SiO_2 49.75-51.67 wt%, Al_2O_3 11.37-12.65 wt%, Fe_2O_3 10.17-10.65 wt%, MgO 6.66-8.48 wt%, and TiO_2 <2 wt%. All samples show an increase in total Fe_2O_3, K_2O and TiO_2 concentrations with decreasing MgO abundances, whereas Al_2O_3 content decreases with increasing MgO.

Minerals observations and laboratory analysis studies show that these rocks have low to medium K_2O contents, and are of tholeiitic type (Fig. 1). The major and trace element geochemistry suggests that the gabbroic dikes were generated by partial melting of enriched lithospheric mantle with garnet in the residue [2].

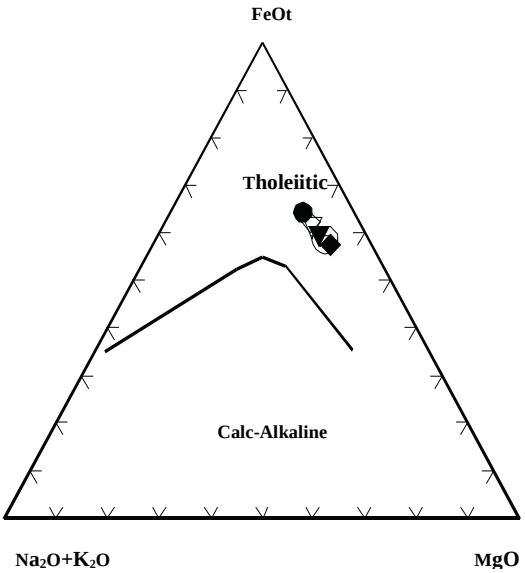

Fig. 1: Samples from the mafic dykes of southern Gorgan, Northern Iran, plotting in the tholeiitic field of AFM diagram.

[1] Allen, M.B. et al. (2003) *J. Struct. Geol.*, **25**, 659-672. [2] Yang, J.H. et al. (2007) *J. Petrol.*, **48**, 1973-1997.

Metamorphic history of late Neoproterozoic Dokhan-type volcanics in the Meknas area, SE Sinai, Egypt

Sadek Ghabrial, D.[1*] & Ren, M.[2]
[1]Geological Dept., National Research Centre, Dokki, Cairo, Egypt (*dghabrial@yahoo.com)
[2]Geological Sciences Dept., University of Texas, USA

The mineralogical and metamorphic features of the Neoproterozoic Meknas volcanics in southeastern Sinai, Egypt, have been studied. These volcanics developed during the late stage of the Pan-African event and occur as successive sheets ranging in composition from andesite to rhyolite. Their mineral assemblages and mineral chemistry indicate these rocks underwent two metamorphic phases; an early contact phase, which is characterized by the assemblage actinolitic hornblende + hornblende + biotite + oligoclase + quartz suggesting amphibolite facies metamorphism, with PT conditions at 550±50°C and <2-3 kbar. This metamorphism was followed by a late hydrothermal phase under the greenschist and sub-greenschist facies conditions as evidenced by formation of actinolite + chlorite + albite in andesite and dacite and chlorite + muscovite in rhyodacite and rhyolite.

Geochemistry of titanomagnetite in rocks and ores of Medvedevskoe deposit, Southern Urals

Shagalov, Ev.S.* & Holodnov, V.V.
Institute of Geology and Geochemistry UB RAS, Ekaterinburg, Russia (*shagalov@igg.uran.ru)

Medvedevsky gabbro massif and associated deposit is attributed to northern abyssal group as a part of Middle-Riphean riftogenic Kusinsko-Kopansky gabbro-granite complex in South Urals [1].

Several genetic types of ore mineralization are revealed in Peredovoy quarry of Medvedevskoe deposit: basic magmatic titanomagnetite (Ti-Mt) ores in stratificated gabbroids and skarn connected with xenolites of host carbonate rocks. Magmatic ores are impregnated and can be rich impregnated in ore melanogabbro; Ti-Mt is an accessory mineral in anorthosites and dyke complex. Solid Ti-Mt-chlorite ores are found in tectonic zone. Second outcrop of solid ores is connected with gabbro and calcareous skarn contact zone of Praskovie-Evgenievskaya mine situated in the central part of the massif [2]. Thickness of layer ores on the contact between gabbroids and skarns is 1-40 cm. Ores are composed of chlorite and magnetite, comprising a great amount of thin (5 μm) ilmenite lamells. Gabbroids in the contact with skarn are dramatically depleted with ore minerals. Magnetite accumulations up to 20 cm in diameter are observed in mine's marbles away from the contact, and on the contact between marble and intrusive diabase dyke Mg-ludwigite is developed [2].

Microelement ICP-MS analysis of basic types of rocks and ores and comprising Ti-Mt was carried out in order to study the chemical composition of sorted out genetic types of Ti-Mt ore mineralization. Titanium content in Ti-Mt is quite consistent in different types of magmatic ores and makes from 6.2 wt% TiO_2 in solid ores up to 8.0 wt% in ore gabbroids (rich impregnated ores). In anorthosites magnetite is depleted with TiO_2 (1.5%). Ti-Mt in near-skarn gabbroids is enriched in TiO_2 up to 14.4%, and magnetite in marbles situated away from contact contains significant amounts of Mn and Mg upon almost total absence of Cu, Eu and Ti. Ti/V ratio in Ti-Mt is also unstable: in solid ores 10, ore gabbros 25-69, anorthosites 10, marbles 0,2-11. Trace elements concentrations in Ti-Mt of basic ore types are irregular. Ores with ∑REE content in Ti-Mt can be divided in two groups: ∑REE less than 2 ppm and more than 4 ppm. All samples are characterized by light prevalence of LREE above HREE and small Eu anomalies of different signs. Besides main components (Ti, V, Mg, Al, Mn and Cr), Li, Sc, Co, Cu, Ni, Zn, Co, As, Sr, Ba, Pb, Nb can be regarded as significant trace elements (n-n*10^2 ppm). Ti-Mt of anorthosites is enriched with almost all elements, especially with chalcophylic, up to ten and hundred times as compared to samples from other rocks. In skarn column (gabbro-ore-skarn-marble) to solid ore on the gabbro contact in Ti-Mt concentration of Sc, V, Co, Ni and Ga is increasing, while Li, Be, Na, and Y decreasing, as well as Zn. Concentrations maximum is slightly shifted to Ti-Mt of gabbroids for Ti, Rb, Sr, Zr, Nb, Mn, Ag, Sn, REE, Hf, Ta and W. Gabbroids itself on the anorhtosite contact have higher REE concentrations (23-52 ppm) with increase to 42-78 ppm in anorthosites, and decrease in the central parts of gabbroid layers (0.8-27 ppm). Ti-Mt of their rocks follows this trend. Differences in Ba and Sr behavior can be noted: gabbroids and comprised ore minerals are enriched in Ba (up to 300 ppm) as compared to anorthosites (less than 80 ppm), the opposite situation is for Sr: in anorthosites peak content of Sr is 700 ppm.

Acknowledgements: The work is supported by ESD RAS programs №2 and №10 (project 09-T-5-1019).

[1] Fershtater, G.B. et al. (2001) *Geol. Ore Dep.*, **2**, 101-117. [2] Shagalov, Ev.S. & Holodnov V.V. (2009) *XIV Readings in memory of A.N. Zavaritzky*. Ekaterinburg: IGG UB RAS, C. 125-127. (in Russian).

Different meanings for cummingtonite-hornblende association in plutonic rocks (Iberian Massif, Portugal)

Solá, A.R.[1,5*], Moita, P.[2], Santos, J.F.[3], Neiva, A.M.R.[4,5] & Ribeiro, M.L.[1,5]
[1]Unidade de Geologia e Cartografia Geológica, LNEG, Lisboa, Portugal (*rita.sola@ineti.pt)
[2]CGE, HERCULES, Dept. Geociências, Universidade de Évora, Portugal
[3]Geobiotec, Dept. Geociências, Universidade de Aveiro, Portugal
[4]Dept. Ciências da Terra, Universidade de Coimbra, Portugal
[5]Centro de Geociências, Universidade de Coimbra, Portugal

Cummingtonite-grunerite series is frequently related to metamorphism or volcanic environments, but rarely described as belonging to a plutonic assemblage [1]. Recently, in the Iberian Massif (Portugal), there have been several references [2-5] of this Fe-Mg amphibole intimately associated with Ca amphiboles (mainly hornblende) in plutonic rocks. Different textural relationships between two amphibole types have been argued for a primary (igneous) or subsolidus metamorphic origin for Fe-Mg amphibole.

Cummingtonite-grunerite (Cum, hereafter all abbreviation from [6]) from gabbros and diorites of the Carrascal Massif (Central Iberian Zone) occurs as tiny exsolution lamellae within a dominant hornblende (Hbl) crystal [3]. This textural occurrence agrees with the subsolidus growth of the Fe-Mg amphibole, reflecting the equation Hbl+Qtz=Cum+An+H_2O [7].

Nevertheless, in the Hospitais tonalite (Ossa-Morena Zone) Cum occurs as euhedral to subhedral cores usually mantled by Hbl [4]. Although Cum is seldom described in literature as a magmatic mineral in plutonic assemblages, its occurrence in the Hospitais tonalite was interpreted as resulting from an early stage of igneous crystallization [4]. As a consequence of the high water content of calc-alkaline magmas, the Fe-Mg amphibole should reflect the equation Opx+H_2O= Cum+Mag+SiO_2+H_2 [8]. The similarity between Mg # on Cum and Hbl from tonalitic rocks suggests an equilibrium crystallizing assemblage, as pointed out by Wones and Gilbert [9] for a hypabyssal igneous suite.

Mineral chemistry data on Cum from the Carrascal gabbro-dorites (Mg#: 0.49-0.64; Al_2O_3: 0.7-2.37%; TiO_2: 0.01-0.37%) and Hospitais tonalite (Mg#: 0.43-0.53; Al_2O_3: 1.22-2.44 %; TiO_2; 0.05-0.27%) exhibit a significant overlap. Therefore, textural relationships should be the main (only?) tool to distinguish between igneous *versus* metamorphic growth. More detailed petrographic studies on plutonic rocks from the Iberian Massif are needed to ascertain the petrogenetic significance of the association Cum-Hbl.

[1] Deer, W.A. et al. (eds.) (1997) *Rock Forming Minerals 2B.* Geol. Soc. London. [2] Antunes, I.M. (2006) *PhD Thesis*. Univ. Coimbra, Portugal. [3] Solá, R. (2007) *PhD Thesis*. Univ. Coimbra, Portugal. [4] Moita, P. (2008) *PhD Thesis.* Univ. Évora, Portugal. [5] Antunes, A. et al. (2010) *Actas do X Congresso de Geoquímica dos Países de Língua Portuguesa/ XVI Semana de Geoquímica*, in press. [6] Kretz, R. (1983), *Am. Mineral.*, **68**, 277-279. [7] Smith, C.G. & Philips, E.R. (2002), *Mineral. Mag.*, **66(2)**, 337-352. [8] Evans, B.W. & Ghiorso, M.S. (1995) *Am. Mineral.*, **80**, 649-663. [9] Wones, D.R. & Gilbert, M.C. (1982) in Veble, D.R. & Ribbe, P.H. (eds.) *Rev. Mineral.*, Mineral. Soc. Am., 355-390.

Crustal sources for the Variscan Danubian granites (South Carpathians, Romania), inferred from oxygen stable isotope and trace elemental data

Stremtan, C.C.[1,2*], Balintoni, I.[2] & Balica, C.[2]
[1]Dept. of Geology, University of South Florida, Tampa, USA ([*]cstremta@mail.usf.edu)
[2]Dept. of Geology, "Babes-Bolyai" University, Cluj-Napoca, Romania

Dynamic processes such as sea-floor spreading, mantle convection, subduction, and continental accretion may be viewed as complex mechanisms of redistribution or recycling of the chemical and isotopic constituents of both crust and mantle. By studying these chemical redistribution processes a more comprehensive understanding of mantle and crustal evolution through geologic time can be achieved. The analysis of oxygen isotopes and trace elemental composition of granitoid rocks has proved to be a powerful tool for tracing the geochemical cycle because of the large difference in oxygen isotopic composition of crustal rocks as compared to rocks derived from mantle material.

The basement of the Danubian domain from South Carpathians of Romania has been intruded by numerous granitoid plutons, majority of them dated as late Variscan (Late Carboniferous to Early Permian in age).

Previous studies have shown that in terms of major elements, the vast majority of the Variscan Danubian granites are calc-alkaline to high-K calc-alkaline, peraluminous to strongly peraluminous but no inference has been made about their possible melt sources. Our preliminary oxygen stable isotope and trace elemental data offer additional information concerning the sources of the melts that eventually generated the Variscan granites. Ten of the Variscan plutons [1] have been sampled and measured for stable isotope and trace elemental composition. Oxygen isotope analyses of the granites reported here were carried out on quartz separates as they are less vulnerable to the effects of post-crystallization re-equilibration. The high $\delta^{18}O$ values measured for the majority of the plutons (highest value of 13.82 and an average of 10.81‰) and the lack of evident subsolidus hydrothermal alteration of the mineral separated support a strong crustal component involved in the production of the melts or their intense contamination with crustal material. The plutons are characteristically Nb depleted, have relatively elevated Rb/Sr, Th/U and low Sm/Nd ratios, consistent with the assertion that the melts had a crustal precursor

However, the presence of magmatic garnet and the REE contents for some of the samples does not preclude the possibility that, at least in some stages, a mantle component was involved as well in the granite generation.

[1] Balica, C. et al. (2007) *Eos. Trans. Am. Geophys. Union*, **88**/**52**, T31B-0476.

P–T–t evolution of granulite from the Namche-Barwa, Eastern Himalayan: new constraints on reaction textures, fluid characteristics and SIMS U-Pb zircon ages

Su, W.[1*], Ye, K.[1], Chen, Y.[1], Zhang, M.[2], Liu, X.[3] & Liu, J.[1]
[1]Institute of Geology and Geophysics, Chinese Academy of Sciences, Beijing, China ([*]suwen@mail.iggcas.ac.cn)
[2]Dept. of Earth Sciences, University of Cambridge, UK
[3]Institute of Tibetan Plateau Research, Chinese Academy of Sciences, Beijing, China

The fluid evolution of continental crust involved in Cenozoic subduction and continent-continent collision processes was investigated by analysis of fluid inclusions, microstructural properties and mineral characteristics, and U-Pb dating (Cameca 1280 SIMS) on granulites from the eastern Himalaya. Four distinct events of fluid influx have been identified and characterised on the basis of petrographic observations and microthermometric measurements. They involve: I. pure CO_2 fluid, present during granulitic metamorphism (S2). II. A low-salinity and low-density aqueous fluid formed at the early retrograde metamorphic stage (S3). The preserved density (0.91 to 0.94 g/cm^3) of trapping in the fluid inclusions gives a tight constraint on the pressure conditions of this stage (0.82 to 0.87 GPa for temperature of 750 °C). III. A low-density and aqueo-carbonic fluid is responsible of the late stage of retrogression (S4), and density of trapping in the fluid inclusions of 0.62 to 0.54 g/cm^3 constrains the pressure of stage S4 at about 0.44-0.35 GPa for a temperature of 700 °C. IV. A late influx of very-low salinity aqueous fluid and the preserved density of trapping is 0.78 to 0.58 g/cm^3, gives a tight constraint on the pressure conditions 0.43 to 0.2 GPa for temperature of 600 °C, which is in equilibrium with greenschist facies-bearing mineral assemblage. Previous U-Pb dating of zircon suggested that peak granulitic metamorphism occurred between *ca*. 50 and 43 Ma [1], in conflict with SHRIMP U-Pb zircon ages, which are younger than 10 Ma for a granulite from the same area [2].

SIMS U-Pb zircon data record three distinct age populations: 1805 Ma (for inherited core), 482–557 Ma (oscillatory inner zone), 22.4–24.9 Ma and 18.2±0.3 Ma (for metamorphic rim). These new high-precision ages in combination with geological field, petrology and microstructure evidence suggest that continental arc rocks including Precambrian basement materials were involved in the granulite-facies metamorphism of the eastern Himalaya. Furthermore the ages of 22.4–24.9 Ma and 18.2 Ma are interpreted as the time of the south Tibetan crust was thickened and then uplifted, respectively.

[1] Ding, Z.L. et al. (2001) *Earth Planet. Sc. Lett.*, **192,** 423-438. [2] Liu, Y. et al. (2007) *Int. Geol. Rev.*, **49,** 861-872.

CO_2 sequestration into hydrothermal system at Ogachi HDR site, Japan

Ueda, A.[1*], Kuroda, Y.[1], Sugiyama, K.[2], Ozawa, A.[2], Kaieda, H.[3], Kaji, Y.[4], Mito, S.[5] & Wakahama, H.[5]
[1]Dept. of Civil Engineering, Kyoto University, Kyoto, Japan
([*]a-ueda@earth.kumst.kyoto-u.ac.jp)
[2]Mitsubishi Materials Techno Corp., Tokyo, Japan
[3]Central Research Institute of the Electric Power Industry, Chiba, Japan
[4]Chuo Kaihatsu Corp., Saitama, Japan
[5]Research Institute of Innovative Technology for the Earth, Kyoto, Japan

In countries with many active volcanic areas such as Japan, one possibility is to sequester CO_2 in hydrothermal regions. The chemical reaction rates between CO_2-saturated water and hot rocks are usually faster than those at room temperature. For example, Reaction 1 can proceed to the right at high temperatures: $CaAl_2Si_2O_8$ (plagioclase) + H^+ + HCO_3^- + H_2O =$CaCO_3$ (calcite) +$Al_2Si_2O_5(OH)_4$ (kaolinite) (1)

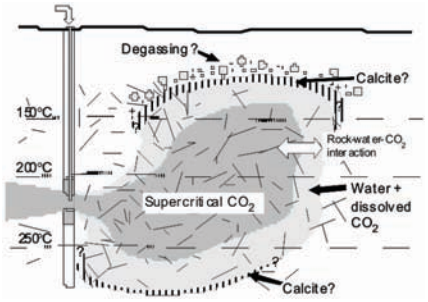

Fig. 1: Outline of CO_2 sequestration into geothermal fields.

Field experiments of CO_2 sequestration into the Ogachi hot dry rock (HDR; the temperature is 200 °C) site were performed to investigate mineralization of a part of CO_2 as carbonates through interaction with rocks (Georeactor; Ca extraction from rocks and carbonate fixation). In 2007, carbonated water (1wt%CO_2; river water with dry ice) with several tracers was directly injected into well OGC-2, Test #1 (from September 2nd to 9th) and Test #2 (from September 11th to 16th). During the Test #2 experiment, additional river water was injected into well OGC-1, 100m apart from well OGC-2, at 2 days after the injection of CO_2 water into well OGC-2 so as to push back carbonated water around this well. Water samples were collected at the depth of ca. 850m by a sampler (500ml in volume) and monitored for their chemical and isotopic compositions. The CO_2 concentrations in fluids collected decreased with duration time and were almost 2/3 of the expected concentration from tracer concentrations. This means that CO_2 injected into well OGC-2 can be removed from fluid by carbonate fixation.

During the field experiments, dissolution or precipitation rates of calcite were determined by using a technique of "in situ observation of crystallization". Calcite crystals covered with Au film were hold in a crystal cell and set in a crystal sonde. The crystal sonde was filled with He gas under a certain pressure and then put into well OGC-2. The fluid at depth of -850m is introduced into the sonde and calcite can start to react with them. After 1 hour, the sonde was recovered to the surface, where the fluid in the sonde is pushed to outside by He gas. The recovered calcite crystal is analyzed for the dissolution or precipitation rates by a newly developed phase shift interferometer. The "in situ analyses" show that calcite precipitation was observed within 2 day after the injection. This probably indicates that the most of CO_2 injected has been fixed as carbonate, supporting our idea that HDR system can be useful for CO_2 sequestration from inland emission sources.

Contribution to the Tertiary Magmatism in Panonian basin (Serbia): REE and HFSE constraints from the volcanics of the Fruška Gora Mt.

Vasković, N.[*], Matović, V., Erić, S. & Arifović, A.
Faculty of Mining and Geology, University of Belgrade, Serbia
([*]nadavask@eunet.rs)

The Eocene/Oligocene-Miocene magmatic rocks in the Pannonian Basin and Tiszia Zone [1] occur in a relatively narrow zone along major faults i.e., Balaton fault - BF, Mid-Hungarian fault – MHF and Sava fault – SF (Fig. 1).

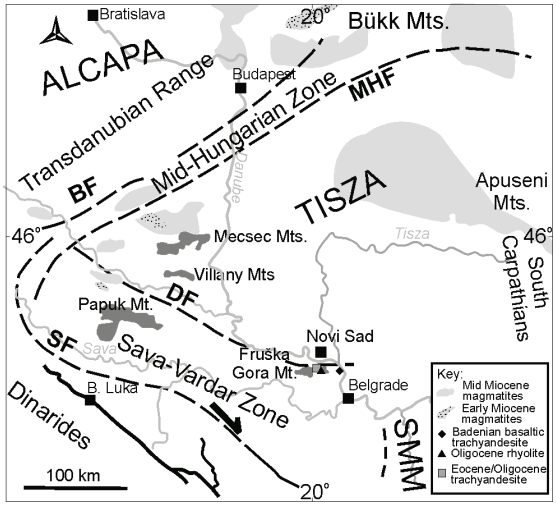

Fig. 1: Major tectonic units and spatial distribution of Paleogene to Mid Miocene magmatic rocks of the Pannonian Basin - [1].

The Eocene/Oligocene (36-31.7 Ma) [2] and Miocene-Badenian shoshonitic to high-K calc-alkaline volcanics from the Mount Fruška Gora are generated in postcollisional settings in the Serbian part of the Pannonian Basin. These rocks exhibit trachyandesitic to rhyolitic (Oligocene) and basaltic trachyandesitic (Badenian) composition (Fig. 2a) as well as the typical geochemical characteristics of subduction-related magmas - elevated LILE, and Pb concentrations, relative depletion in Nb (Fig. 2).

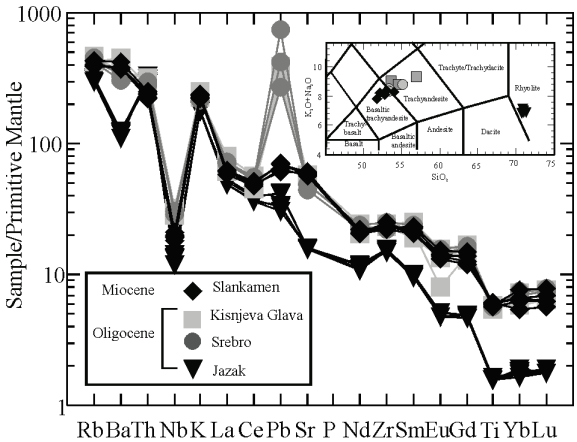

Fig. 2: Primitive mantle–normalized trace-element patterns [3] of Paleogene Eocene/Oligocene and early Miocene volcanic rocks from the Mount Fruška Gora.

[1] Kovács, I. et al. (2007) *Geol. Soc. Am., Sp.. Paper.*, **418**, 93-112. [2] Knežević, V. et. al. (1991) *Proc. Int. Symp.*, 234-235. [3] McDonough, W.F. & Sun, S.-S. (1988) *Chem. Geol.*, **70(1-2)**, 12-12.

Petrographic study of the mylonites in the Druksiai-Polotsk deformation zone in the Lithuania

Vejelyte, I.
Dept. of Hydrogeology and Engineering Geology, Vilnius University, Vilnius, Lithuania (Irma.Vejelyte@gf.vu.lt)

Some E-W crustal-scale deformation zones have been detected in the Proterozoic basement of Lithuania. One of them is Druksiai-Polotsk deformation zone (DPDZ), which is 35-40 km wide, well marked by gravity and magnetic linear anomalies in the North-eastern Lithuania. Microstructural and petrological analyses of granitoids and migmatites, which compose of granitic neosoma and amphibolitic paleosoma show that the DPDZ has a heterogeneous strain profile and both ductile and brittle deformation processes have contributed to the total displacement. Recrystallization microstructures in slightly- to intensely deformed rocks vary in accordance with the degree of strain. The strong shearing localized within the mylonite resulted in the round shape or asymmetrical elongated plagioclase porphyroclasts, amphibole, mica fish, titanite and the generation of fine grained plagioclase, biotite, quartz, amphibole and epidote. Quartz grains are irregular in shape with undulatory extinction, indicating dynamic recrystallization mainly by subgrain rotation. K-feldspar characteristically shows core-mantle structure. Amphibole is long-form, often boudinated. The titanite occurs as subhedral crystals grains and as mantle around opaque minerals, which follows the folation in the host rock. The U–Pb dating of titanite from an augen granitoid mylonite has yielded a concordant age of 1534±9 Ma [1]. The penetrive foliation was obviously formed during retrogression from amphibolite- to epidote-amphibolite facies.

Acknowledgements: This is a contribution to the project "The Precambrian structure of Baltica as a control of its recent environment and evolution" of the Visby Programme supported by the Swedish Institute and the Lithuanian State Science and Studies Foundation.

[1] Vejelyte, I., Bogdanova, S. & Salnikova, J. (2010) *Abstr. Proc. Geol. Soc. Norway* - 29th Nordic Geological Winter Meeting, 205-206.

Granulite boulders from Pleistocene terrace of Danube, Hungary

Vígh, Cs.[1*], Horváth, P.[2,3], Józsa, S.[1] & Nagy, G.[3]
[1]Dept. of Petrology and Geochemistry, Eötvös Loránd University, Budapest, Hungary ([*]geocsaba@gmail.com)
[2]School of Geological Sciences, University of KwaZulu-Natal, Durban, Republic of South Africa
[3]Institute for Geochemical Research, Hungarian Academy of Sciences, Budapest, Hungary

The Pleistocene gravel terrace of the Danube has been mined by several gravel pits SE from Budapest and on the Little Hungarian Plain. Although study of the bench gravel dates back about hundred years, the comprehensive investigation-including petrography of rocks types- have started in recent years. The boulder-bearing gravel is very polymict, contains several rock types with unclear origin (e.g. granulites, high-grade gneisses, migmatites, amphibolites, eclogites, granites, syenites). Our aim was threefold: 1. describe the petrography of the granulites, 2. calculate the pressure-temperature conditions, and 3. identify the possible source area of the pebbles. All studied granulites are felsic, two types were identified:

(1.) Garnet-kyanite granulite contains garnet and/or kyanite porphyroblasts within a quartz+K-feldspar+plagioclase matrix. Relicts of perthitic feldspars can be found as porphyroblast and inclusion in garnets. These garnets contain rutile inclusions as well. A second garnet variety contains Zn-bearing spinel and/or ilmenite inclusions and rimmed by plagioclase corona.

(2.) Garnet-sillimanite granulite: Garnet+sillimanite+K-feldspar+plagioclase+quartz+biotite+ilmenite mineral assemblage is stable, but relics of kyanite grains indicating higher pressure are still present.

The garnets have Ca-poor, Prp-Alm-rich compositions (Alm57-72 Prp25-39 Grs2-12 Sps1-4 And0-1), their Ca content decreases from core to rim while their XFe is influenced by formation of retrograde biotite.

Both granulite types have peraluminious composition, the SiO_2 content varies between 71-75% and the Al_2O_3 is 13-16%. Samples are depleted in Sr and HFSE.

EMPA based Th-U-Pb age dating of monazite revealed Variscan ages (330 Ma) for the peak metamorphism of the studied granulite pebbles.

Ternary feldspar thermometry and phase diagram calculations reflects HT-HP peak metamorphism in the Gt-Ky-Mp-Rt-Qtz-liq field at 900-1000°C and about 18 kbar, and it was followed by a decompressional P-T path.

The nearest occurrences of similar felsic granulites are on the Moldanubian part of the Bohemian massif, so they can be regarded as a potential source region of the investigated granulite boulders.

High geothermal gradient and low uplift rate of Paleoproterozoic granulites from North China craton: implications for Early Precambrian tectonics

Zhai Mingguo
Institute of Geology and Geophysics, Chinese Academy of Sciences, Beijing, China (mgzhai@mail.igcas.ac.cn)

Paleoproterozoic high pressure granulites in the North China craton (NCC) were reported by Zhai et al. [1]. Their high pressure of 10-14 kb attracted attention from researchers, and several continental collisional models have been proposed for early Precambrian tectonic evolution of the NCC. Recent studies show that Paleoproterozoic high-grade metamorphic rocks are extensively distributed in the NCC, and can be subdivided into two groups that are high-temperature and high-pressure granulites (HT-HP) and high-ultrahigh temperature granulites (HT-UHT). The HT-HP granulites are mainly garnet-bearing mafic granulites that are metamorphosed and deformed dykes enclosed in the orthogneisses. The HT-UHT rocks are metamorphosed pelites (khondalites), and sapphirine and spinel in khondalite indicates metamorphic temperatures > 900-1000˚C. This study deals with the occurrences, distribution, metamorphic conditions and history, isotopic ages of the two granulites, and emphasizes the following aspects: 1, the peak metamorphic conditions and *PT* paths with a pressure decrease for the two granulite groups are similar. 2, Their metamorphic ages of the peak and followed decompressional stages are also similar. 3, HT-HP and HT-UHT granulites probably occur in area distribution other than in linear distribution. 4, Some researchers suggested that HP granulites and related rocks represent a typical continent-continent collisional orogen like the Himalayas. However, it is still argued that these rocks have much higher geothermal gradient of ~16ºC/km and much slower uplifting rate of 0.33-0.5 mm/yr than those in Phanerozoic orogenic belts, indicating the rigidities of the old continental crust are significantly different from those of Phanerozoic crust. 5, All these observations suggest that we should rethink geological and tectonic models for the evolution of the North China craton.

[1] Zhai, M.G. et al. (1992) *Science in China (B)*, **12**, 1325-1330.

Metallic mineral deposits related to the style of volcanism in dynamic subduction zone

Watanabe, Y.
Geological Survey of Japan, AIST, Tsukuba, Japan
(y-watanabe@aist.go.jp)

Style and type of hydrothermal metallic deposits are intimately related to the chemistry of source magma and the style of volcanism, which are related to tectonic regime in subduction zones.

In an extreme extensional tectonic regime, rift-related tholeiitic basalt dominates in submarine environment, and massive sulphide base-metal deposits may be associated with the volcanism. In a moderate extensional regime, monogenetic bimodal volcanism of basalt and rhyolite becomes dominant. Large scale calderas are commonly formed in this setting due to the formation of large basaltic magma chambers in the crust. In this regime, kuroko-type massive sulfide deposits form in submarine environment and low-sulfidation epithermal Au deposits form in terrestrial environment. Hydrothermal alteration with low water/rock ratio (sericitic alt.) dominates and normal faults may become the site of mineralization in this regime. A neutral tectonic regime yields a number of polygenetic and composite andesitic volcanoes, which may be associated with precious and base metal epithermal and xenothermal deposits. Hydrothermal alteration with both high and low water/rock ratios is associated with the mineralization. Strike-slip faults may become the site of mineralization. In a slight contraction regime, intrusive activity beneath the polygenetic volcanoes become dominant, and these volcanoes are commonly associated with diatremes and sector collapses. High-sulfidation epithermal Au-Cu and porphyry Cu deposits may form at the apex of the intrusive bodies. Hydrothermal alteration with high water/rock ratio (potassic and advanced argillic alt.) becomes dominant in this regime. In a moderate contraction regime, magmas do not ascend to a shallow crustal level, resulting in lack of volcanic activity and mineralization. These tectonic regimes may change in a couple of million years in the same site, and different volcanic styles and mineral deposits are frequently mixed together in subduction zones.

Main metal species in these mineral deposits reflect the magma chemistry and salinity of hydrothermal fluids. Mantle material rich magmas form the deposits rich in Au, Hg and Cu and crust material rich magmas form the deposits rich in Sn, W, Pb and Zn. Mineral deposits formed in submarine environment are enriched in base metals due to high salinity of the fluids.

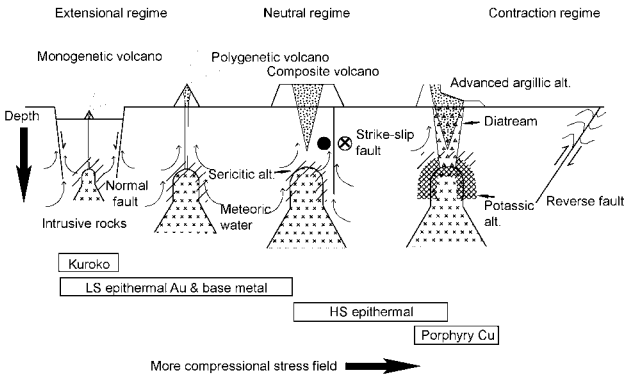

Fig. 1: Schematic figure showing the relationship among the tectonic regime, style of volcanism and associated mineralization.

Magma-sediment-water interaction: a precursor to base metal mineralisation?

Breheny, C.*, Moore, K.R., Costanzo, A. & Feely, M.
Dept. of Earth and Ocean Sciences, National University of Ireland, Galway, Ireland (*c.breheny1@nuigalway.ie)

The Ordovician NE-SW trending volcanic belt, located along the southeast coast of Ireland, is composed of subduction related volcanics and intercalated sediment as a result of Iapetus Ocean closure. Within this belt, the dominantly intermediate composition Bunmahon Formation exhibits a strong island arc tholeiite signature and comprises hyaloclastite, pillow lavas and peperite intercalated with tuff deposits and volcanogenic mudstones. Electron microprobe analysis across sharp to gradational contacts in peperite revealed that magmatic peperite clasts were subject to more extensive alteration than related coherent intrusions, indicating that circulating pore waters within the unconsolidated sediment facilitated the transition to a hydrous chlorite-dominated assemblage. Electron microprobe analysis of mineral compositions showed that chlorite (Fe# = 0.35-0.63) in association with pumpellyite, epidote, pyrite and Fe-oxides formed as a consequence of an iron-rich hydrothermal fluid that interacted with magnesium-rich seawater.

Two distinct types of mineralisation are recognised based on field evidence: (1) stockwork type vein networks composed of quartz and mixed quartz and calcite veins containing sulphides and (2) barren linear veins of quartz or calcite occurring parallel to bedding or fault planes and infilling tension gashes. The role of shallow level intrusions in generating hot mineralising fluids that resulted in vein formation has been investigated using fluid inclusion studies. Fluid inclusions (FIs) hosted in mixed quartz and calcite veins are two phase liquid-rich (liquid + vapour) FIs that homogenise to the liquid phase. Homogenisation temperatures (T_H) range from 100° to 250ºC for both barren and sulphide rich veins. The majority of T_H values observed for both veins occur between 150ºC and 200ºC indicating one fluid population. Isochore modelling based on temperature, composition and salinity show a wide range of temperatures up to a maximum of 375°C true trapping temperature for sulphide-bearing veins. Temperature variations across vein stockworks are consistent with cooling against wall rocks, in which alteration is observed at stockwork zones. Modelled fluid salinities range from 6 to 20 eq. wt% NaCl with a mean of 12.9 eq. wt% NaCl. Two salt systems have been recognised based on phase changes i.e. H_2O-NaCl-KCl and H_2O-NaCl-MgCl. The microthermometry results do not reveal great differences between the stockwork-related and fracture-filling fluids, but coupled with field observations, it is possible that early hydrothermal fluid circulation may have been generated as a result of igneous activity, and these hydrothermal fluids were responsible for the alteration of the host volcanic rocks and concomitant deposition of vein-hosted base metals.

Indium mineralization in magmatic-hydrothermal system

Shimizu, M.[1*], Cook, N.J.[2] & Sundblad, K.L.[3]
[1]Dept. of Earth Sciences, Faculty of Science, University of Toyama, Japan ([*]mshimizu@sci.u-toyama.ac.jp)
[2]Natural History Museum, University of Oslo, Norway
[3]Department of Geology, University of Turku, Finland

Two main primary resources of industrial In are currently from vein and skarn deposits related to felsic magmatism [1] and from massive sulfides [2]. The main In-enriched deposits are subvolcanic and Sn-polymatallic vein types [3]. Tin-bearing, Zn-rich and/or Cu-rich polymetallic vein-type deposits are the primary focus for exploitation of recoverable In as an economically-viable by-product.

The most important mineral is In-bearing sphalerite in Zn-rich polymetallic vein-type deposits. Indium-bearing stannite and cassiterite are generally of lesser importance, whereas minerals with major In content (roquesite, sakuraiite, "zinc-sakuraiite" (Zn analogue of sakuraiite), dzhalindite, etc.) are only minor contributors to the mineralogical balance for In [4],. In Cu-rich deposits, however, roquesite may be the most important, with only minor In contained in stannite, cassiterite, bornite and tennnantite-tetrahedrite, and less in sakuraiite, dzhalindite and so on [5,6].

In situ LA-ICP-MS analysis of In-bearing sphalerite from Toyoha in Japan, Hanes and other deposits in Romania, and deposits in the Svecofennian Domain of the Gennoscandian Shield (some also containing roquesite allows the mechanisms of In mineralization and enrichment of In in sphalerite to be understood. Three In-bearing ore types have so far been recognized in the Fennoscandian Shield: 1) polymetallic (Fe-Zn-Pb-Cu-Sn) skarn at Pitkäranta, 2) polymetallic veins at Korsvik (Cu-As-Sn) and Jungfrubergen (Zn-Pb-Ag), and 3) compact magnetite-sphalerite bodies at Getmossmalmen (Fe-Zn), all related to rapakivi granites.

The physico-chemical environment of In-rich sphalerite can also be compared with that of stannite, stannoidite and roquesite [5]. Sakuraiite and "zinc-sakuraiite" both have high-temperature (cubic, probably isostructural with sphalerite) and low-temperature (tetrahedral) types. Under formation at higher temperatures, partial sphalerite-roquesite solid-solution may be expected, but sphalerite-"zinc-sakuraiite" solid-solution is more preferable. At lower temperatures sphalerite-tetragonal "zinc-sakuraiite" solid-solution is broken down with decreasing of temperature to form roquesite and sphalerite with only residual amounts of In.

Indium-Sn-bearing Zn-rich and/or Cu-rich polymetallic vein-type deposits are generally located in convergent plate margins and orogenic belts with steep geothermal gradients generated by magmatic activity [1]. The Japanese Islands are essentially accretional terrains intruded by various magmas. Back-arc rifts are reasonable tectonic settings for generation of In-rich deposits. In contrast, the highly In-potential rapakivi granites in the Fennoscandian Shield represent an extensional environment within a stable craton.

[1] Schwarz-Schampera, U. & Herzig, M. (2002) *Indium: Geology, Mineralogy, and Economics*. Springer-Verlag Berlin, Heidelberg, New York. [2] Sinclair, W.D. et al. (2006) *Ore Geol. Rev.*, **28**, 123-145. [3] Ishihara, S. et al. (2006) *Res. Geol.*, **56**, 347-364. [4] Cook, N.J. et al. (2009) *Geochim. Cosmochim. Ac.*, **73**, 4761-4791. [5] Shimizu, M. & Kato, A. (1991) *Can. Mineral.*, **29**, 207-215. [6] Shimizu, M. et al. (2007) *Geochim. Cosmochim. Ac.*, **71**, A930.

Submarine volcanism-related hydrothermal alteration in the Darnó- and Szarvaskő Units (NE-Hungary), and in the Dinarides and Hellenides

Kiss, G.[1*], Molnár, F.[1], Bartha, A.[2] & Palinkaš, L.A.[3]
[1]Dept. of Mineralogy, Eötvös Loránd University, Budapest, Hungary ([*]gabriella-kiss@chello.hu)
[2]Laboratory Dept., Geological Institute of Hungary, Budapest, Hungary
[3]Inst. of Mineralogy and Petrology, University of Zagreb, Croatia

Comparative studies on hydrothermal alteration were carried out on submarine basaltic volcanites with different origin. Peperitic basalt occurrences related to the Triassic early rifting of the Neo-Tethys were studied in displaced parts of the Dinarides (Darnó Unit, NE-Hungary) as well as in the Dinarides (Kalnik Mts, Croatia, Vares-Šmreka, Bosnia-Herzegovina) and in the Hellenides (Stragopetra Mts.), while Jurassic basalts formed in an intra-oceanic back-arc-basin of the Neo-Tethys were also studied (Szarvaskő Unit, NE-Hungary).

Within the submarine basaltic lava units 7 volcanological facies were distinguished and these bear different types of hydrothermal alteration. Alteration 1 is characterized by albitization of the rock-forming plagioclase at ~300°C and occurs both in the Triassic and Jurassic rocks. Superimposing alterations (alteration 2) were developed during cooling from 280°C to ~140°C (Jurassic rocks) and ~70°C (Triassic rocks) temperature. During the higher temperature part of these processes chlorite formed in the ground mass, however chlorite and rarely quartz formed in the micro fractures and small amygdales of the Triassic basalts, while chlorite, quartz and prehnite precipitated in the micro fractures of the Jurassic rocks. At lower temperatures calcite formed commonly in the larger amygdales, jig-shaw type veins and as other infillings. Some epidote, pumpellyite, prehnite and laumontite also occur in the Triassic basalts, while datolite is a rare mineral in the Jurassic ones. During this process the system was mainly seawater-dominated because fluid inclusions are characterised by 3.2-7.8 NaCl equ. wt% salinities. Late stage alteration 3 is characterised by argillitization occurring at every studied locality; presence of disordered layer silicate (smectite group) is proven by XRD. Though similar processes happened at the Triassic and Jurassic localities, relatively limited fluid-rock interaction was characteristic to the Jurassic basalts, which resulted in minerals formed at higher temperatures and limited amount of hydrothermal infillings (no amygdales or other infillings occur, only short veins).

On the ground of extended petrochemical study, mobilization of the different elements was followed even in single pillow lava-scale, inside a volcanic facies from fresher to more altered parts and between different facies as well. Mass transfer calculation was made to determine the gains and losses which refer to the (1) and (3) alterations, while results of (2) were mainly eliminated (except ground mass chloritization). Increase of Na_2O (i.e. albitization) is characteristic in a pillow from core to rim, though results of low temperature alteration (decrease in SiO_2, MgO) can also be seen. Examining the processes from fresher to more altered part of a facies the (3) alteration mainly overprint the (1). At distal volcanic facies (such as peperitic basalt and pillow fragmented hyaloclastite breccia) the low temperature alteration and the formation of clay minerals are more dominant, though at the hyaloclastite breccia high grade chloritization is also dominant (increase in MgO). The effect of the basalt on the peperitic limestone is characterized with elevated Cr, Ni, Co, Cu in the sediment, while presence of the limey mud during the cooling of the lava resulted in stronger alteration processes in the contact basalt.

Mineral-forming volcanic gases: the Tolbachik factory (Kamchatka, Russia)

Filatov, S.K.[1*] & Vergasova, L.P.[2]
[1]Dept. of Crystallography, St. Petersburg State University, St. Petersburg, Russia ([*]filatov.stanislav@gmail.com)
[2]Institute of Volcanology and Seismology RAS, Petropavlovsk-Kamchatskiy, Russia

The scoria cones of the Tolbachik Eruption of 1975-76 (Kamchatka, Russia) are still hot and discharge gases with temperatures up to 450°C. The gases are highly oxidized due to a large fraction of the admixed air. The monitoring of these gases during the last three decades reveals a permanent precipitation of minerals directly from the gas phase. A complicated system of fractures and cavities developed at the summits of two Tolbachik cones is desirable for the circulation of gases, precipitation of minerals and alteration of surrounding rocks.

The most spectacular and abundant mineralization was observed on the 2nd Cone where the majority of the discovered 30 new minerals was found. This cone is characterized by a large volume of lava and scoria, and a broad development of concentric and radial fracture zones formed due to the post-eruptive contraction and deformation. The gas vent named "Poisonous" was especially active and productive during two first decades of the monitoring period; it represents shallow chamber of ~ 2 m^3 open to the surface. Such conditions made possible stable mineral-forming processes; hundreds kilograms of mineral aggregates (mainly cupper minerals) were formed inside the chamber demonstrating process of the modern ore-formation.

Mineralogy of the Tolbachik incrustations is very diverse, though their specific is mainly controlled by the high oxidation state of the hot gas + air mixture: sulfates, oxosulfates, chlorides, oxides, selenites, carbonates, fluorides, arsenates, silicates, hydroxides and hydrous chlorides, sulfates, carbonates etc. Seldom grains of native elements (gold) and sulphides (pyrite, realgar, orpiment) were also found.

Fine dispersion and heterophase nature of exhalative products make difficult to separate pure material for investigation by different methods. For this reason natural transport of metals by volcanic gases, mineral formation and precipitation were firstly modeled using method of gas chemical transport reactions in evacuated glass or quartz ampoules. Chlorides, oxochlorides, selenites, oxoselenites and other exhalative minerals from Tolbachik volcano were synthesized and investigated by this way.

The brightest feature of low-temperature period activity of the Tolbachik 1975-76 volcano is the formation of bauxites on the 1st Cone. Broad deposits of new mineral lesukite $Al_2(OH)_5Cl{\cdot}2H_2O$ and gibbsite were found in zones of metasomatic transformations of the erupted material that leads to formation of Al mineralization and probably involves microbiological factors.

Acknowledgements: This research has been supported by Russian Foundation for Basic Research (grant 10-03-00732-a).

Amphibole as a petrological sensor: different points of view

Simakin, A.G., Zakrevskaya, O.Ju.[*] & Salova, T.P.
Institute of Experimental Mineralogy, RAS, Chernogolovka, Russia ([*]zakrev@iem.ac.ru)

Magmatic amphibole composition reflects parameters of the parental melt. Diversity of the crystallo-chemical positions and variable composition make amphibole a potentially powerful PT and fO_2 sensor. This potential is still not fully realized. Measuring and (or) interpretation of the iron oxidation state in amphibole is the critical parameter in developing of the predictive models. Easiness of subsolidus oxidation of amphibole with formation of oxy-amphibole by the scheme $Fe^{2+}(OH^-)> Fe^{3+}(O^{2-})+1/2H_2$ devaluates direct methods of the iron oxidation state analysis. Therefore stoichiometric reconstruction of the Fe^{3+}/Fe^{2+} ratio is the only realistic estimate related to the crystallization conditions. Possibility of such reconstruction is based on the assumption that in a crystallizing magmatic mineral both Fe^{2+} and Fe^{3+} bearing minals of amphibole are composed of hydroxyl (partially substituted by Cl, F) varieties and only Ti^{4+} enters in the oxy-component (accepted at IMA-97). We present experimental data on the amphibole crystallization from the high magnesium andesite (Shiveluch, Kamchatka) at P_{H2O}=2 and 5 kbar and high T=950°C. Analysis of our and published data demonstrates that there is a strong negative correlation between the calculated (model IMA-97) content of octahedral Al and the sum Fe^{3+} and Ti^{4+} in M position. Al^{VI} content (Al^6*) at the extrapolated to zero sum Fe^{3+} + Ti (to eliminate fO_2 influence) reflects its activity in the parental melt. It is well established that the proportion of the octahedral Al in the magmatic melt rises with increase of pressure and water content. At pressure increase aluminium mainly transfers from tetrahedral (network-forming) to 5 and 6 oxygen coordinated state in the melt. Our data combined with the published ones, set up a dependence: Al^{VI}* /approx 0.586+0.583 P(kbar). This dependence is valid for subliquidus high temperature (T=950-1100°C) amphiboles crystallized from andesitic to basaltic-andesitic melts. Parameter Al6*decreases if amphibole crystallizes after other phases even at high T. Our correlations allow to estimate the P and fO_2 in different Shiveluch adakitic rocks (extrusions, lavas, pyroclastics) using amphibole composition. Based on our calibration we interpret maximum pressure of amphibole crystallization in metasomatized spinel peridotite xenoliths from Dish Hill, California [1] to be about 5-6 kbar. This pressure is fairly below the value of 20 kbar estimated by Lamb [2] and close to P=5 kbar predicted with the recent empirical calibration proposed in [3]. This comparison makes questionable the applicability of Popp´s model [4] based on the experimental data on the metastable (single phase of constant composition) oxidation and reducing of amphibole.

[1] McGuire, A.V. et al. (1991) *Contrib. Mineral. Petrol.*, **109**, 252-264. [2] Lamb, W.M. & Popp, R.K. (2009) *Am. Mineral.*, **94**, 41-52. [3] Ridolfi, F. et al. (2010) *Contrib. Mineral. Petrol.*, **160**, 45-66. [4] Popp, R.K. et al. (2006) *Am. Mineral.*, **91**, 54-66.

Formation of chlorine- and sulfur-bearing feldspathoids (sodalite, scapolite, and cancrinite) from silicate-melt and aqueous fluid in alkali-syenite cumulate nodules from the Breccia Museo Formation, Campi Flegrei, southern Italy

Belkin, H.E.[1*], Tarzia, M.[2] & De Vivo, B.[3]
[1]U.S. Geological Survey, Reston, VA, USA
([*]hbelkin@usgs.gov)
[2]Dept. of Materials, Imperial College London, UK
[3]Dip. di Scienze della Terra, Università di Napoli Federico II, Napoli, Italy

Alkali-syenite cumulate nodules from the Breccia Museo Formation, interpreted as fragments of a magma-chamber wall, are especially enriched in Cl and incompatible elements (e.g., U, Zr, Th, and rare-earth elements). Detailed optical petrography, scanning electron microscope imaging, and electron probe microanalysis reveal relatively late-stage precipitation of Cl- and S-bearing feldspathoids among the predominant alkali-feldspar and plagioclase nodule framework. Sodalite, scapolite and cancrinite (the davyne-group) form single crystals and/or complex intergrowths. Sodalite is nearly end-member composition (Cl = 7.1 wt.%) with low concentrations of CaO (0.03 - 0.6 wt.%) and K_2O (~0.11 wt.%). Scapolite is calcian marialite with a limited compositional range; Me ranges from 19 to 21. The scapolite is Cl-rich (~ 4 wt.%) with low SO_3 (< 0.05 wt.%) and a high K_2O content (~ 2 wt.%). The cancrinite chemistry is the most complex. Chlorine varies inversely with SO_3 (r = 0.94); Cl ranges from 5.9 to 10.9 wt.% and SO_3 ranges from 0.1 to 6.7 wt.%. CaO, K_2O, and Na_2O vary from 8.8 to 13.2 wt.%, 2.7 to 11.5 wt.%, and 8.1 to 14.4 wt.%, respectively. Two different groups can be distinguished on the basis of Na_2O and K_2O content; high Na_2O and low K_2O and high K_2O and low Na_2O. The group with K_2O > 8 wt.% are high Cl and low SO_3. These two groups are observed intergrown with anorthite (~An92) and a more Na-rich plagioclase (~An30). No crystallographic determinations were made on any cancrinite phase although the complex textures suggest that such work might yield a mixed analysis. In only one sample was vesiculated glass observed and it coats both sodalite and cancrinite. The glass composition is phonolitic (SiO_2 = 55.5, total alkalis = 15.9 wt.%) with Cl, F, and SO_3 equal to 1.0, 0.8, and 0.04 wt.% respectively; H_2O by difference equals ~ 4 wt.%.

Formation of feldspathoids in the other nodules was from exsolved aqueous brine as suggested by fluid inclusion evidence. The precipitation of the feldspathoids bridges the transition between magmatic and hydrothermal, although a hybrid mixture also could be involved.

Andesites at Mt. Taranaki, New Zealand: assembly of melts and crystals in an arc volcano

Stewart, R.B.[*] & Gruender, K.
INR-CS, Volcanic Risk Solutions, Massey University, Palmerston North, New Zealand ([*]r.b.stewart@massey.ac.nz)

The origin of andesite magmas is a topic that is widely debated. One of the major issues is the widespread disequilibrium between crystals and whole rock compositions in these rocks which makes interpretation of magma processes from whole rock geochemistry difficult. Previous studies of Mt Egmont/Taranaki geochemistry showed that the "phenocrysts" present in the lavas exhibited this typical lack of equilibrium with the whole rock composition of their host. This means they did not crystallise from a melt with the composition of the whole rock, and mineral chemistry showed that the liquid they did crystallise from was more mafic than the host lavas. Further, the matrix glasses present in the lavas and tephras is mostly dacitic to rhyolitic in composition and, in younger lavas, has a high K_2O content. None of the feldspars show an appreciable K_2O component except in some thin rims on larger crystals, consistent with a lack of equilibrium with the glass phase through much of the growth of the feldspar crystals.

Xenoliths of rock types interpreted as lower to mid-crustal in origin are mostly ultramafic pyroxenites to hornblende gabbros, hornblendites and amphibole-bearing gneisses. These xenoliths contain partial melts that are also dacitic to rhyolitic and the xenolith glass major element compositions overlap with those of the matrix glasses in the younger Egmont/Taranaki lavas. One possibility is that the host matrix glass infiltrated along cracks in the xenoliths during entrainment and transport. However, glass is predominantly present in the xenoliths as melt patches enclosed within the xenoliths rather than as crack infill, suggesting a source within the xenolith in most cases. Glass is often found adjacent to amphibole, but also occurs in xenolith lithologies that contain little or no amphibole. Breakdown of aluminospinel to anorthite is also observed. Rare high (80% + SiO_2) glasses were observed as partial melts within quartzofeldspathic sandstones. These exhibit vesicular textures and clearly show melting of the sandstone under hydrous conditions. These glasses have no correlatives within the matrix glass suite.

An alternative view of the Mt Egmont/Taranaki lavas is that they are a mix of crystals from prior fractionation in the subduction "hot zone" that have been remobilised by silicic partial melts of gabbros and ultramafic rocks of the lower crust, possibly significantly driven by amphibole decomposition, and additional inputs from partial melts of other crustal rocks. Although the glass chemistry will be modified by crystallisation and reaction processes in the source rocks, and crystallisation fractionation prior to cooling in the lavas, the lava matrix glass compositions are remarkably similar to the glasses in the xenoliths. The disequilibrium observed between whole rock and mineral chemistry, and between the glass chemistry and minerals, together with the similarities of glass chemistry between xenoliths and lava matrix glasses, is consistent with the mixing hypothesis.

The Goldfield-Superstition Miocene large silicic volcanic province, central Arizona (USA): petrology based on major- and trace-element and mineral compositions

Dombroski, B.A. & Fodor, R.V.*
North Carolina State University, Raleigh, NC, USA
(*rfodor@ncsu.edu)

The Goldfield-Superstition Mountains in central Arizona form a Miocene large silicic volcanic province (LSVP) ~8000 km^2 of peraluminous rhyolite and rhyodacite lavas and pyroclastic flows. Mineral assemblages include plagioclase (An_{50-12}), anorthoclase, sanidine (BaO ≤5 wt%), quartz (mainly resorbed) biotite, amphibole (edenite; Mg#s 66-71), rare clinopyroxene and orthopyroxene (Mg#s 66-70), and accessories that include titanite, zircon, and perrierite (La-Ce-Ti silicate). Important compositional characteristics include negative Nb-Ta and Eu anomalies (wide Eu/Eu* range ~0.95-0.3) in nearly all samples, and moderate LREE-enrichment throughout (La_n ~35-260). Established $^{40}Ar/^{39}Ar$ ages [1] identify initial volcanism as small-scale rhyolite domes, ~20.5 Ma, followed by ~1.5 m.y. of mafic-intermediate magmatism -- and then large-volume eruptions that created the Goldfield-Superstition LSVP ~19-18 Ma.

Petrologic interpretations: Although these silicic rocks are unlikely to be direct partial melts and instead represent at least some fractionation from primary partial melts, we nonetheless propose the following: (i) volcanism began as two types of rhyolite domes. One is undated (Nb-Ta anomaly; no Eu anomaly; mode An_{28-38} only) and has $La/Yb_{(n)}$ ~50, and represents a small percent melt (<5%) of lower crust garnet-bearing amphibolite/pyroxenite. Another dome type, 20.5 Ma (no Nb-Ta anomaly; san_{Or70}+olig+qtz mode; Eu anomaly), has $La/Yb_{(n)}$ ~12, and represents greater melting ~10-30% of the same or similar source (garnet-free, either case). (ii) Melting to produce the domes was provided by heat from the onset of mafic magmatism (SiO_2 ~47 wt%; MgO ~11 wt%). Protracted heat (~1.5 m.y.) from the basaltic magmatism led to (iii) development of the Goldfield-Superstition LSVP. The resulting lavas and pyroclastic flows can largely be modeled as products of various percent melts (10-30%) from lower-crust amphibolite-pyroxenite slightly more incompatible-element enriched than the domes' source(s), and having varying degrees of subduction characteristics (Nb-Ta). These melts experienced differing amounts of crystal fractionation, some magma mixing, and little upper crust contribution (e.g., Eu anomalies; resorbed qtz; spongy-rim plag; Th/Nb <0.5). (iv) The REE accessory perrierite (La_2O_3 11 wt%; Ce_2O_3 20 wt%) had no effect on magma LREE abundances and probably represents REE melt saturation. (v) Application of Al-in-amphibole geobarometry provides ~4 kbar as the highest observed crystallization pressure. (vi) When compared to compositions of other Cenozoic western North American LSVPs, the Goldfield-Superstition province shares most all of their trace element characteristics (e.g., Nb-Ta; varying but some overlapping Th/Nb, Ba/Nb, La/Nb) but remains distinct in details per its source compositions. The Goldfield-Superstition province exemplifies the onset of large-volume silicic volcanism by mantle magmas ponding at or in lower crust for at least 1 m.y.

[1] McIntosh, W.C. & Ferguson, C.A. (1998) *Arizona Geol. Survey Open-File report 98-27.*

The origin of sanidine megacrysts in silicic rocks by coarsening: petrological evidence from the dacites of Taapaca volcano, Chile

Higgins, M.D.
Sciences de la Terre, Université du Québec à Chicoutimi, Chicoutimi, Québec, Canada (mhiggins@uqac.ca)

K-feldspar megacrysts are common in granitoids, but rare in chemically equivalent volcanic rocks, of which the Taapaca dacites are the best known. Sanidine megacrysts up to 10 cm long occur in some of the lavas, and contain abundant chadocrysts of plagioclase, sanidine, amphibole and oxides, as well as glassy magmatic inclusion and voids. Chadocrysts are generally isolated from the host by a thin film of glass. The matrix contains abundant plagioclase crystals, as well as amphiboles and oxides. Both megacrysts and host lavas were imaged using cold-cathode cathodoluminescence. Growth of the megacrysts engulfed plagioclase, sanidine and amphibole crystals. Crystal size distributions (CSD) of sanidine megacrysts are hump-shaped. Large crystals are euhedral and small crystals are rounded. These data show that megacrysts developed from the host magma by coarsening: this was enabled by cycling of the temperature of the magma around the sanidine liquidus temperature in response to injections of more mafic magmas and subsequent magmatic overturns. Chemical zonation of the megacrysts reflects heterogeneity of the host magma and not transfer of crystals from other magmas. Plagioclase crystals enclosed in the megacrysts are small and have straight CSDs, which contrasts with the hump-shaped CSDs of plagioclase in the matrix. This shows that plagioclase was also coarsened, starting at the same time as the growth of the sanidine crystals and continuing afterwards.

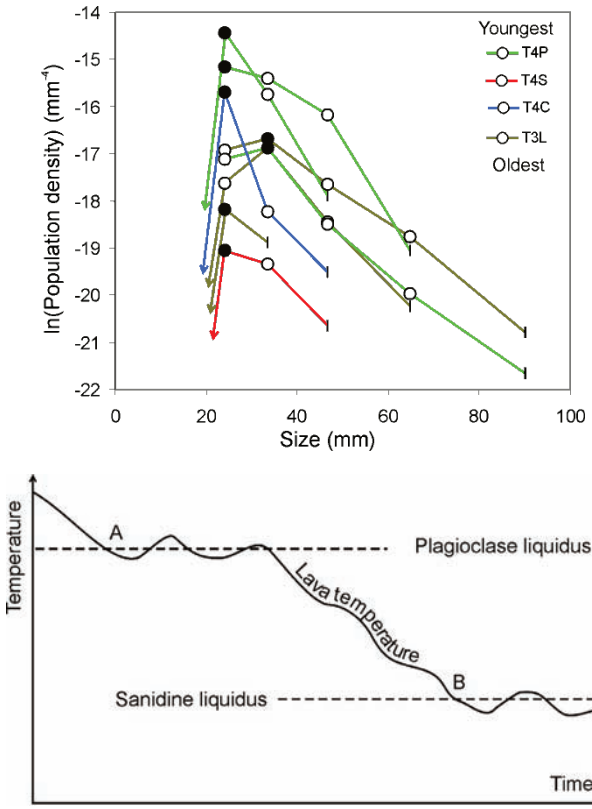

Fig. 1: Eruption of lava between A and B produced plagioclase-phyric rocks. Sanidine megacrysts were only produced if the magma evolved past B.

Combined textural and mineral chemical studies in the reconstruction of magma chamber processes: case studies from the Carpathian-Pannonian region, eastern-central Europe

Harangi, Sz.
Volcanology Group, Dept. of Petrology and Geochemistry, Eötvös University, Budapest, Hungary (szabolcs.harangi@geology.elte.hu)

Reconstruction of magma chamber processes is crucial to evaluate the possible style and as a consequence the potential hazard of volcanic eruptions. Presently there is a change in the paradigm concerning the view of magma chambers or magma reservoirs beneath active volcanoes. There are growing evidences that extended crystal mush zones and multiple open system processes play a major role instead of closed system evolution of magma chambers filled dominantly by silicate liquid. Whole rock composition often reflects the superimposition of several differentiation processes, including crystallization, dissolution, re-equilibration, magma-mixing etc. and thus, the bulk rock geochemical data should be interpreted with caution. Minerals, however, can be strongly sensitive to modifications in the circumstances (e.g., temperature, pressure, volatile content, redox condition) of the magmatic system. Textural and chemical variations of mineral phases could preserve even the complex magmatic processes and therefore, the combined in situ textural and compositional studies have been found to be a powerful tool for understanding the evolution of magmatic systems.

In the Carpathian-Pannonian region, a wide range of volcanic activities, fed by various magmas have occurred for the last 20 Ma. Recently, the members of the Volcanology Group of the Eötvös University have performed integrated textural and compositional investigations in different magmatic systems (basaltic, dacitic and rhyolitic) and could reveal the magma differentiation processes in detail. Here, a couple of key examples are presented to highlight the effectiveness of such research.

During the Miocene (20-12 Ma), repeated eruption of silicic magmas took place resulting in large volume ignimbrites and related fall deposits. Textural and in-situ major and trace element geochemical investigations of the still fresh juvenile glasses and the mineral phases of the ignimbrites and lithic clasts combined with quantitative model calculations revealed open-system magmatic processes, such as remobilization and mixing of crystal mush phases, mixing with variously differentiated melts and particularly the importance of ascent and intrusions of mantle-derived mafic magmas in the silicic magma reservoir.

The in-situ investigation of mineral phases in basaltic rocks formed from 11 to 0.13 Ma provided a new perspective to understand the genesis of mafic magmas. Results of a comprehensive survey on the variation of spinel compositions have shown heterogeneities in the mantle source region in various scales. Furthermore, a major difference could be inferred between the source regions of the mafic magmas in the western and eastern parts of the Pannonian basin.

The last volcanic eruption in this region occurred in the Ciomadul volcano only 30 ka. Complex magma chamber processes have been recognized even in single samples. Remobilization of an almost solidified, possibly granodioritic body by mantle derived mafic magmas, mixing of crystals with various origins and a vertically extended magma chamber has been reconstructed in the genesis of the lava dome rocks.

Acknowledgements: This research is supported by Hungarian Science Foundation OTKA no. 68153.

Compositional sequences in the "Dej Tuff" (Transylvanian Basin, Romania) as recorded by mineral chemistry

Szakács, Al.
Dept. of Environmental Science, Sapientia University, Cluj-Napoca, Romania (szakacs@sapientia.ro)

The rhyolitic Lower Badenian "Dej tuff" is the major (up to 116 m thick) volcaniclastic lithology of the Neogene Transylvanian Basin fill. It basically consists of a complex sequence of diverse lithological entities (coarse volcaniclastics, thick fine to medium-grained tuff beds and alternations of thin tuff and marl layers) mostly resulting from reworking of primarily land-deposited pyroclastic material generated by plinian-type explosive eruptions. Microprobe mineral chemistry of the main rock-forming minerals demonstrates the existence of compositional sequences within the "Dej Tuff" which do not fit the depositional sequences. An% of plagioclase feldspar (Fig. 1), composition and formation temperature of Fe-Ti oxides, along with variation trends in biotite and allanite composition, as well as overall primary mineralogical composition of the rocks themselves, show that the tuff complex records three succeeding and recurrent compositional sequences. Within each of them there is a consistent upward variation trend toward lower An% contents of feldspar and lower formation T of Fe-Ti oxides consistent with the presence of pyroxene and/or amphibole only at the base of the chemical sequences. Slight inter-sequence variation can also be pointed out by shift of the three succeeding sequences towards higher Fe-Ti oxide formation temperatures upward in the lithological sequence. These variation trends in mineral composition likely record varying magma chamber conditions prior to major eruption episodes. Three succeeding explosive eruptions tapped the compositionally and thermally zoned top of the feeding magma chambers hosting differentiated felsic magma derived from a deeper-lying magma of more basic (i.e. calc-alkaline andesitic) composition. It is surprising that the compositional sequences in the tuff complex mimics the right order of magma composition sequences in the magma chamber instead of the expected reverse order. The primarily land-deposited tephra has been reworked in the Transylvanian Basin sea preserving its original compositional zonation pattern, but in the order reproducing the true magma-chamber zonation.

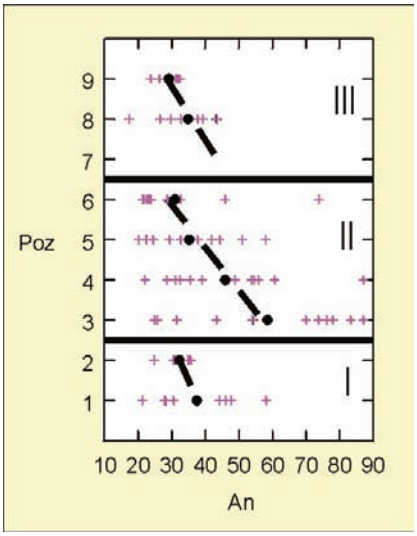

Fig. 1: An% (An) variation in plagioclase with position (Poz, 1 to 9) in the lithological sequence of the "Dej Tuff" at Cepari. Purple crosses are individual microprobe analyses. Black points show average An% for each position, and dashed lines connecting the points show variation trends of An% across tuff levels. I, II and III mark the three compositional sequences pointed out.

The Pleistocene alkali basaltic volcanism at the Perşani Mountains, SE Carpathians, Romania – inferences from olivine phenocrysts and their spinel inclusions

Sági, T.[1*], Harangi, Sz.[1] & Ntaflos, T.[2]
[1]Dept. of Petrology and Geochemistry, Eötvös L. University, Budapest, Hungary ([*]cseregle@gmail.com)
[2]Dept. of Lithospheric Research, University of Vienna, Austria

The Perşani Mountains are situated at the south-eastern part of the Carpathian-Pannonian Region (CPR). At the eastern margin, alkaline basaltic volcanism occurred in the Olt valley. Two active phases were distinguished here, at 1.2-1.4 Ma and 0.5-0.6 Ma, respectively [1]. We collected samples from the effusive products of both phases including also ultramafic xenoliths. Trace element composition of the basalts is fairly similar, although the Racoş basalt from the older phase shows a slight negative Nb-anomaly, whereas in the younger Barc basalt this cannot be observed. The primary magmas could have generated by very low degree of partial melting (about 1-2 %) of spinel-peridotite mantle source. Both basalts are olivine-phyric and the olivines contain commonly Cr-spinel inclusions. In this study we focused on the composition of these minerals to have an inference about the nature of the source regions. For this study the most primitive (Fo>84 mol%) olivine phenochrysts were chosen, in which spinel inclusions appear in the crystal cores. The compositional variation of olivines in the mantle xenoliths was used to estimate the magma ascent rate.

The Cr-spinels have high Al_2O_3- (25-40 wt%), low TiO_2- (<1.5 wt%) and medium Cr_2O_3-content (20-40 wt%). Their cr-number is relatively low (0.2-0.5). Most of the spinels seem to be liquidus phases; therefore their composition could reflect the nature of the residual source region. Their composition resembles the MORB spinels and reflects a MORB-type mantle source. This sharply contrasts what can be observed in the alkali basalts at the western part of the Pannonian basin. Furthermore, a slight change in the source region is inferred between the two eruption phases.

The most primitive olivine phenocrysts have Fo-content close to 90 wt% and they could be in equilibrium with the primitive basaltic melt. Following the calculation scheme proposed by [2], a mantle potential temperature of about 1350°C was calculated, i.e. no thermal anomaly exists beneath this volcanic field. Based on the temperature-dependent diffusion of Ca applied for olivine xenocrysts and olivines in the ultramafic xenoliths, we could estimate the ascending rate of magmas that could be just 1-2 days!

Acknowledgements: This research belongs to the OTKA project No. K68587.

[1] Panaiotu, C. et al. (2004) *Geol. Carpath.*, **55**, 333-339. [2] Herzberg, C. & Asimow, P.D. (2008) *Geochem. Geophy. Geosy.*, **9**, Q09001.

A mineral-scale investigation on the origin of the 2.6 Ma Füzes-tó basalt, Bakony-Balaton Highland Volcanic Field (Pannonian Basin, Hungary)

Jankovics, É.[1*], Harangi, Sz.[1] & Ntaflos, T.[2]
[1]Dept. of Petrology and Geochemistry, Eötvös Loránd University, Budapest, Hungary ([*]jeva182@gmail.com)
[2]Department of Lithospheric Research, University of Vienna, Austria

The Füzes-tó alkaline basalt is the youngest volcanic product of the Bakony-Balaton Highland Volcanic Field (BBHVF; western Pannonian Basin). It was formed by Hawaiian to Strombolian lava fountaining, which built up a scoria cone at 2.6 Ma [1].

The basaltic bombs and massive lava fragments have a unique mineral assemblage, suggesting a complex magma evolution. Approximately the half of the crystals is mantle-derived xenocryst, such as olivine, clinopyroxene, orthopyroxene and spinel. In addition, clinopyroxene and spinel megacrysts can be also found. Peridotite xenoliths are common; they are usually variously altered. The phenocryst assemblage involves olivine and clinopyroxene sitting in a groundmass consisting of clinopyroxene, olivine, plagioclase, Fe-Ti oxides and glass. Clinopyroxene phenocrysts often contain green xenocrystic cores. Thus, the Füzes-tó basalt does not represent a basaltic magma formed in the upper mantle, but a mixture of basaltic melt and mineral phases having various origins.

In spite of the abundance of the mantle-derived xenocrysts, ratios of incompatible trace elements (e.g., Zr/Nb and Nb/Y) could be effectively used to have an inference on the origin of the magma. These suggest that the primary magma was formed in the transitional spinel-garnet stability field, at the uppermost part of the asthenosphere. Spinel inclusions in the olivine phenocrysts provide further information about the nature of the mantle source. Two spinel populations can be distinguished: a dominant Al-rich spinel group (100*Cr/(Cr+Al)<42), which are rare in the alkaline basalts of the Pannonian Basin, and scarce Cr-rich spinels (100*Cr/(Cr+Al)>45). They have Al_2O_3 and TiO_2 content similar to the MORB-spinels (based on the diagram from [2]).

The olivine, orthopyroxene, colourless clinopyroxene and spinel xenocrysts derive from different depths of the subcontinental lithospheric mantle as inferred from their wide range of compositions. The green clinopyroxene cores in the clinopyroxene phenocrysts could represent either high pressure products of crystallization from a more evolved melt than the host magma or they could be derived from mafic lower crustal rocks. The compositions of the olivine and clinopyroxene phenocrysts reflect polybaric crystallization with a final, strongly oxidized stage.

[1] Wijbrans, J. et al. (2007) *J. Volcanol. Geoth. Res.*, **164**, 193-204. [2] Kamenetsky, V.S., Crawford, A.J. & Meffre, S. (2001) *J. Petrol.*, **42(4)**, 655-671.

Inferences for the role of primitive mafic magmas in the genesis of the dacitic magmas of Ciomadul (SE Carpathians, Romania): a mineral-scale study

Kiss, B.[1*], Harangi, Sz.[1], Vinkler, A.P.[1,2] & Ntaflos, T.[3]
[1]Dept. of Petrology and Geochemistry, Eötvös Loránd University, Budapest, Hungary ([*]geobalazs@gmail.com)
[2]University of Milano, Italy
[3]Dept. of Lithospheric Research, University of Vienna, Austria

In the Carpathian-Pannonian region, the last volcanic eruption occurred in the Ciomadul volcano at 30 ka. Considering the long repose time of the volcanic eruptions, the continuation of the volcanic activity cannot be unambiguously excluded in the future [1]. Thus, it is crucial to obtain detailed information about the behaviour of this volcano. The pre-eruptive magma chamber processes and the triggering mechanism could be effectively revealed by combined textural and mineral chemical investigation. Here, we report a unique example, where the role of primitive mafic magmas can be revealed in detail in the genesis of a dacitic volcano.

Two types of mafic mineral aggregates were recognized in one of the lava dome rocks: clinopyroxene (CPX) with FeS inclusions ± olivine (OL1) (hereafter T-1 assemblage) and olivine (OL2) with Cr-spinel (Cr-SP) inclusions (hereafter T-2 assemblage). Olivines have high Fo-content (85-90 mol%) and a CaO content >0.1 wt%. The OL2 contains tiny (10-20μm) euhedral Cr-SPs (Cr-number: 61-68). The clinopyroxenes are also magnesian (mg-number>0.85) and show a complex texture (patchy and/or oscillatory zoning) reflecting both crystallization and resorption. The core to rim analysis of CPX shows significant fluctuation in Cr_2O_3 together with mg-number. Remarkably, the crystal zones with high Cr_2O_3 and mg-number are found in the core and in the outermost rim. The texture, inclusions and composition of the mafic minerals in the dacite demonstrate their magmatic origin, i.e. from a fairly primitive basaltic magma replenished periodically by fresh magma batches. The OL2-type olivines show strong resorbtion in contrast to the OL1 and are surrounded by a breakdown assemblage of orthopyroxene + magnetite and mantled by oscillatory zoned amphibole. The CPX±OL1 assemblages, however, are rarely overgrown by amphiboles as OL2 and never mantled totally. These textural features suggest that the T-1 mafic mineral assemblage could have been incorporated into the silicic magma later than the T-2 mafic mineral assemblage, probably just before the eruption. Intrusion of the T-1-hosted basaltic magma into the dacitic magma chamber could provide the triggering mechanism of the eruption. Composition of spinels in the OL2-type olivines suggests a mantle source region with volcanic arc character.

Acknowledgements: This research belongs to the OTKA project No. K68587. Supported by PRCH Student Science Foundation.

[1] Szakács et al. (2002) *Geol. Carpath.*, **53**, 193-194.

Mineralogy and geochemistry of calcic and/or sodic skarn in the Ulsan Fe-W deposit, Korea

Choi, Seon-Gyu*, Kim, Ji Won & Seo, Jieun
Dept. of Earth and Environmental Sciences, Korea University, Seoul, Republic of Korea (*seongyu@korea.ac.kr)

The Ulsan Fe-W deposit is located within the Cretaceous Gyeongsang volcano-sedimentary basin, Korea. Development of skarn and ore mineralization occurs as a small roof pendant within the Upper Cretaceous sequence along the contact of a Tertiary epizonal granite stock and recrystallized limestone units with serpentinized ultramafic rocks. The deposit represents a unique opportunity to document geochemically the complex evolution of a calcic and/or sodic skarn system which is genetically related to a low sulfidation system. The Fe–W skarn deposit occurs as a nearly vertical ore pipe within recrystallized limestone at the direct contact with the Upper Cretaceous volcanic rocks containing thin layers of pelitic sedimentary rocks.

Calcic skarn is paragenetically characterized by early high-temperature anhydrous mineral assemblages that are dominated by magnetite and late low-temperature hydrous mineral assemblages with scheelite mineralization [1]. Calcic skarn is composed mainly of hedenbergitic clinopyroxene, calcite and andraditic garnet with minor vesuvianite, wollastonite, quartz, Ca amphibole, epidote, chlorite, siderite and ilvite. Albitite has been locally noticed in contact between serpentinite and albitized granite. Based on field relations and geochemical characteristics, the albitite appears to be derived from the Tertiary granite. Sodium enrichment zone in serpentinized ultramafic rocks is characterized by metasomatic textures. The calcic-sodic skarn contains unusual Na-rich clinopyroxene, Na-rich amphiboles (richterite), albite and Sr-bearing plagioclase as accessory phases. Maximum Na_2O concentrations of 6.44 wt.% and 6.53 wt.% are observed in clinopyroxene and amphibole, respectively. Pyroxenes in the sodic skarn show a wide range of variation in composition: diopside-hedenbergite and kosmochlor-acmite solid solutions. Textural evidence indicates that the first stage of skarn was formed as a result of chemical interactions between albitized granites and adjacent ultramafic rocks. The formation of Cr-bearing clinopyroxene and amphibole appears to be related to the release of Cr into the fluid phase by the breakdown of chromite during the prograde skarn stage.

[1] Choi, S.-G. et al. (2000) *Can. Mineral.*, **38**, 567-583.

Common origin of the latites erupted on Lipari and Vulcano islands (Aeolian Arc, Italy) in historical time

Davì, M.*, De Rosa, R. & Donato, R.
Dipto. Scienze della Terra, Università della Calabria, Arcavacata di Rende, Italy (*davi@unical.it)

Southern Lipari and Northern Vulcano (Aeolian Arc, Italy) are considered a single Volcanic Complex over the last 50 ka on the basis of petrography, geochemistry and structural studies [1 and references therein].

This study is focused on the historical activity of Lipari and Vulcano during the which intermediate products (i.e. latites) where erupted together with mafic (Vulcanello- Vulcano, 1100-1600 AD) or rhyolitic (Rocche Rosse - Lipari, 1230±40 AD; Commenda and Palizzi -Vulcano, 1200 AD) rocks. Latites were erupted both effusively, as enclaves in the rhyolitic lavas of Rocche Rosse [2] and Commenda or as unmingled lava flows (Palizzi and Punta del Roveto, Vulcano), and explosively, within Vulcanello III cone [3].

These latites are similar in geochemistry and petrography. The latite bulk rocks show the same major, minor and trace elements signature. Clinopyroxene ($Wo_{43-46}En_{39-44}Fs_{13-15}$, Mg#=0.72-0.76) is the dominant mineral phase followed by amounts of feldspar ($An_{25-60}Or_{12-9}$ and $An_{0-4}Or_{50-70}$) and olivine (Fo_{50-75}). The groundmass is microcrystalline with the same minerals occurring as phenocrysts.

Clinopyroxene ($En_{40}Fs_{13}$) of all latites has a homogeneous trace element composition with superimposed REE patterns (Eu/Eu* ~ 0.65 negatively correlated with Mg#). Plagioclase ($An_{50}Or_{10}$) of Commenda, Palizzi and Vulcanello products shows very similar trace element concentrations with a strong positive anomaly of Sr and very low HFSE contents. LREE patterns are also nearly coincident (Eu/Eu* in the range 6-10). K-feldspar (An_2Or_{65}) of Rocche Rosse and Palizzi products displays strongly similar incompatible trace element contents and coincident LREE patterns while HREE are below the detection limit (Eu/Eu* up to 41). Also olivine (Fo_{70}), investigated only within Rocche Rosse and Vulcanello latites, exhibits similar FME contents.

The microanalytical (LA-ICPMS) study led on the latite mineral phases of historical Lipari and Vulcano allows further investigating similarities between the lithotypes and constraining the historical magmatic systems in the southern sector of the Aeolian Islands. In fact, the trace element content of minerals is strongly related to several pre-euptive parameters (e.g. T, P, water content, magma composition), then the strong similarities among the crystals of different latites suggest a similar, if not the same, primitive magma, which underwent similar magma chamber processes. Geochemical models of major and trace elements suggest that the parental magma could have been the shoshonitic basalt younger than 15 ka found in the olivine melt inclusions within La Fossa cone 1888-1890 products [4].

[1] Gioncada, A. et al. (2003) *J. Volcanol. Geoth. Res.*, **122**, 191-220. [2] Davì. M. et al. (2009a) *J. Volcanol. Geoth. Res.*, **182**, 45-56. [3] Davì, M. et al. (2009b) *Eur. J. Mineral.*, **21**, 1009-1028. [4] Gioncada, A. et al. (1998) *Bull. Volcanol.*, **60**, 286-306.

W-molybdenite in Silurian meta-volcanic rocks of Northern Portugal

Dias, P.A.[1], Leal Gomes, C.[1] & Guimarães, F.[2]
[1]CIG-R – DCT, Universidade do Minho, Braga, Portugal
([*]patriciasdias@gmail.com)
[2]LNEG – S. Mamede de Infesta, Porto, Portugal

In Silurian metavolcanic formations of Serro (Serra de Arga, Minho, Portugal) proto-tuffitic felsic rocks, have disseminated sulphides (with pyrite-pyrrotite predominant), and some rare phases such as W-molybdenite, which occur in small sized crystals (±50 μm), idiomorphic (fig.1), oscillatory zoned (when viewed in EPMA – BSDE) and show a consistent compositional trend from core to rim – border enriched in Mo. W occurs in significant amount.

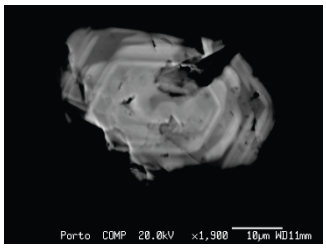

Fig. 1: EPMA - BSDE image of W-molybdenite.

Table 1: Representative core EPMA analysis of molybdenite (Fig. 1)

Fe =	0.17
S =	35.89
W =	14.79
Mo=	46.11
Total=	96.98

The W-molybdenite is considered an exceptionally rare phase formed in association to metasomatic processes: [1] showed experimentally the variability between Mo (molybdenite) and W (tungstenite) end members in the solid solution (Mo W) S_2; [2] observed W-Mo phases as scheelite hosted inclusions in replacement products in Ferbetal paradigmatic deposit; W rich-molybdenite was described by [3] in fenites of the Kola alkaline Complex.

In Serro, the presence of W-molybdenite in felsic meta-volcanics suggests peculiar conditions to the evolution in a primordial hydrothermal stage. According to the experimental data of [2] and [4], W enrichment in molybdenite is correlated with high sulfur activity during early crystallization.

The textural and compositional relationships of the observed crystals - oscillatory zoning, Mo-rich overgrowths and aspects of corrosion - suggest rebalancing with several and repeated fluctuations of oxidation degree (fO2) in the growth medium. According to [4], Mo enrichment to the rim is accompanied by increasing fO2.

The introduction of W in the system possibly accompanied water-interaction, concomitant with the deposition of sulphide mineralization, in a VHMS type model. The evolution to an oxygenated environment would reflect the observed deposition of vein tourmalinites (Cr-rich dravite) in tuffitic protoliths including W-molybdenite, possibly due to exhalitic remobilization. Also, it would facilitate the occurrence of molybdenite, without W content, which is observed in metafelsites, and scheelite, occurring in calcsilicate rocks and amphibolites of the same suites.

[1] Moh, G. & Udubasa, G. (1976) *Chem. Erde*, **35**, 327-335. [2] Holl, R. & Weber-Diefenbach, K. (1973) *Neues Jb. Miner. Monat*, **1**, 27. [3] Barkov, A. et al. (2000) *Can. Mineral.*, **38(6)**, 1377-1385. [4] Hsu, L.C. (1977) *Econ. Geol.*, **72**, 664-670.

Petrography of lava flows in the northern area of Nevado del Ruiz Volcano, Colombia

Forero, J.A.[*] & Zuluaga, C.A.
Dept. of Geosciences, Universidad Nacional, Bogotá, Colombia
([*]jhaforerohe@unal.edu.co)

The Nevado del Ruiz Volcano (NRV), located in the Colombian Central Cordillera, has a high geothermal potential with an important energetic interest. We present a petrographic study of lava flows outcropping in the Northern area of the volcano, between La Plazuela creek and El Gualí river, as part of a geothermal exploration research project in the Nevado del Ruiz Volcano. The study includes petrographic characterization of fresh and altered rock samples of lava flows and their hydrothermal alteration products (about 30 samples).

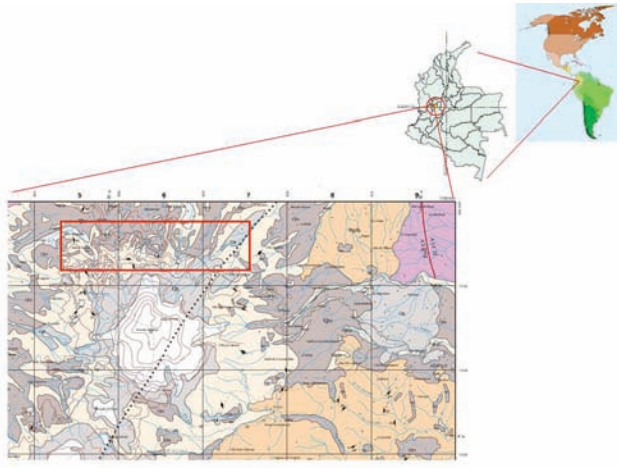

Fig. 1: Sketch geologic map of the study zone, the red rectangle highlight the sampled area.

Several authors [1-4] proposed two different lava suites based in their K content. The lavas with high K content represent almost the 98% of lavas in surface and have been classified as calc-alkaline andesite and dacite. We focus this study in identifying specific petrographic characteristics that allow us to infer the magmatic evolution of the system as well as identify alteration products that have been generated by the active and inactive hydrothermal systems in the study area.

With this study we hope to contribute to the understanding of the evolving volcano and its associated hydrothermal system studies knowing the potential of the system for the exploitation of geothermal energy.

[1] Ayala, L.F. (2009) *BSc thesis*, University of Caldas. [2] Lopez, D.A. (1992) *PhD thesis*, The Louisiana State University, [3] Jaramillo, J.M. (1980) *PhD thesis*, University of Houston. [4] Schaefer, S.J. (1995) *PhD thesis*, Arizona State University.

Crystal chemistry of volcanic allanites indicative of naturally induced oxidation-dehydrogenation

Hoshino, M.[1], Kimata, M.[2], Chesner, C.A.[3], Nishida, N.[4], Shimizu, M.[2] & Akasaka, T.[5]
[1]Mineral Resource Research Group, Institute for Geo-Resources and Environment, Geological Survey of Japan - AIST, Tsukuba, Japan ([*]hoshino-m@aist.go.jp)
[2]Earth Evolution Sciences, University of Tsukuba, Japan
[3]Dept. of Geology and Geography, Eastern Illinois University, Charleston, IL, USA
[4]Chemical Analysis Division, University of Tsukuba, Japan
[5]Center for Tsukuba Advanced Research Alliance, University of Tsukuba, Japan

The crystal chemistry of volcanic allanites from the Youngest Toba Tuff (YTT), Sumatra, Indonesia and SK100 volcanic ash beds (SK100-VAB), Niigata, Japan has been investigated by electron microprobe analysis (EMPA), Fourier-transform infrared spectroscopic analysis (FTIR), and single-crystal structure analysis. In the FTIR study, based on the Diamond ATR accessory, YTT and SK100- VAB allanites were observed to have different OH contents, respectively (Fig. 1): the former has 0.64 wt% H_2O (OH: 0.40 apfu.), while the latter has 1.65 wt% H_2O (OH: 1.00 apfu.).

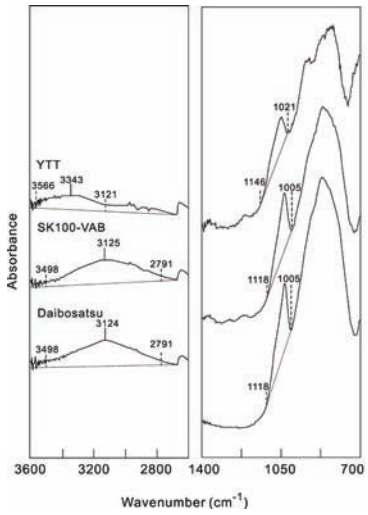

Fig. 1: FTIR-ATR spectra of the powdered allanites from YTT, SK100-VAB and Daibosatsu granitic pegmatite.

The crystal structures of these two allanites were refined to R= 3.64 and 4.25 %, respectively. The OH-poor YTT allanite has the shorter b axis, longer c axis, and larger β value than the relatively OH-rich SK100-VAB one. The bond valence sums of O4 (accepter oxygen for H atom) and O10 (donor oxygen for H atom) are 1.962 and 1.709 v.u. for YTT allanite (valence sum: 3.671 v.u.) and 1.754 and 1.271 v.u. for SK100-VAB one (valence sum: 3.025 v.u.). The difference from the ideal total bond valence value (4.00 v.u.) of O4 and O10 in YTT allanite (0.33 v.u.) is smaller than that in SK100-VAB (0.98 v.u.). These difference values are also broadly consistent with the corresponding differences in OH content between the YTT (OH: 0.40 apfu.) and SK100-VAB allanites (OH: 1.00 apfu.) determined by FTIR- ATR. Therefore, it is concluded that welding of the YTT caused the following post crystallization changes to occur in YTT allanite: oxidation of Fe^{2+} to Fe^{3+}, release of H_2, and the concomitant replacement of OH^- by O^{2-}. These oxidation and dehydrogenation processes advanced during the welding to thereby produce oxyallanite. Oxyallanite had been reported only in laboratory studies where it was produced by heating natural allanite. Our report on natural oxyallanite suggests that it may be present in other welded silicic volcanic rocks as well.

Textural and compositional features of zircons from the Ciomadul dacites (Romania)

Németh, G.[1*], Harangi, Sz.[1], Kiss B.[1] & Ntaflos, T.[2]
[1]Dept. of Petrology and Geochemistry, Eötvös University, Budapest, Hungary ([*]cordelia1987@gmail.com)
[2]Inst. of Lithosphere Studies, University of Vienna, Austria

The last volcanic eruption in the Carpathian-Pannonian region occurred at the Csomád (Ciomadul) volcano in the Eastern Carpathians (Romania), very close to the Vrancea seismic zone. Recent radiocarbon dating suggests that the youngest volcanic rocks were formed 30 ka. In order to evaluate the nature of this volcano, it is essential to understand the pre-eruptive magma chamber processes.

Zircon is a highly resistant mineral phase, durable to chemical and physical influences and particularly useful for geochronological investigations as well as to constrain the physico-chemical condition of the magma evolution. Combined textural and geochemical investigation of individual zircon grains along with the study of the enclosed melt inclusions could help to reconstruct stages of the magma chamber processes.

In this study we examined two samples from the Csomád volcano, one from a dacite lava dome and another one from a younger pyroclastic deposit. The zircon grains display different zoning patterns, such as patchy zoning, oscillatory zoning and unzoned to weakly zoned texture. This difference in texture is associated with a large range of trace and minor element (Hf, Th, U) composition. Variation in the Hf content implies crystallization at different temperature. The fairly high Hf concentration (>10000 ppm) is consistent with a near-solidus condition. In the patchy zoned zircons, we observed Th-U-rich and Hf-poor cores with abundant tiny pores and thorite inclusions. These could have been formed from a crustal magma at relatively high temperature. The oscillatory zoning with the fluctuation of Hf content suggests occasional perturbation of the crystallization temperature possibly due to replenishment of the silicic magma. The low-temperature outer zones and the high silicic rhyolitic melt inclusions indicate that the zircon grains could have been formed in an evolved crystal mush and were subsequently incorporated into the erupted hybrid dacitic magma.

Acknowledgements: This study belongs to the OTKA research work No. K68587.

A study on volcanic tuff deposits of the Outer-Carpathian region, Buzău county, Romania

Popa, R.G.*, Tita, P., Baratu, D.A. & Stochici, R.
Dept. of Mineralogy, University of Bucharest, Bucharest, Romania (*razvangabriel.popa@yahoo.com)

Proofs for volcanism outside the Carpathian Mountains have been looked for since the 1940's [1] but neither of them could confirm the suggested hypothesis. However, traces of activity are visible in the Outer-Carpathian space (east and south-east of the Eastern Carpathians), represented by mineral springs with permanent flow, hydrothermal mineralizations; and by Miocene volcanic tuff deposits which coincide with the volcanic activity of the inner-Carpathian volcanoes.

Our study signals the presence of volcanic tuff deposits within Oligocene formations, documenting them for the first time, and provides their first mineralogical analysis. The studied tuffs are located south of the Carpathians Bend Area, east of Sibiciu Valley, in the close proximity of Colți village, Romania. The area belongs to the External Marginal Carpathian Flysch Formation, more precisely to the Văleni protuberance [2], its main sedimentary characteristic being the Kliwa facies.

The field observations have emphasized extended stratified volcanic tuff outcrops (Fig. 1) in alternation with Kliwa sandstones (Oligocene) and centimetre-thick shale interlayers.

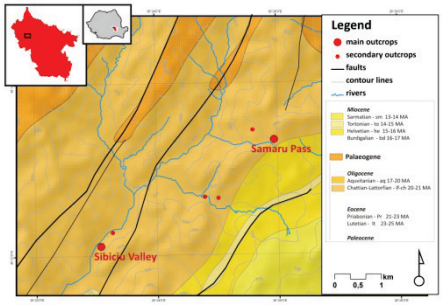

Fig. 1: Geological map of the studied area and location of tuff outcrops, reproduced after 29 L-35-XXI Covasna sheet, scale 1:200.000 (Geological Institute of Romania)

Optical microscopy revealed that these tuffs are dominated by vitroclasts (between 40-70 %) and crystaloclasts (up to 15 %) of which 10% quartz, 4% plagioclase feldspar and 1% biotite, potasic feldspar optically similar to microcline and chlorite pseudomorphosed most probably after pyroxene. Ghoetite is also identified under the same circumstances as chlorite. The remaining mass cannot be identified neither by optical nor by diffractometric means, being most probably composed of fine fragments of shards and crystals. Under diagenetic conditions, pseudomorphs of phyllosilicates have resulted, covering between 5- 50 % of the hyaline mass. Vulcanoclasts measure up to 0.12 mm and show angular, irregular shapes. Taking into consideration the quantitative representation of each mineral phase in contrast with the amount of volcanic glass, it can be stated that these tuffs were most likely related to an acidic, viscous magma that caused an explosive eruption.

In the hyaline mass siliceous diatomic frustules belonging most probably to the Coscinodiscus genre could be identified. In some tuffs frustules are perfectly conserved, while in others they were extensively transformed, crystallizing into quartz. Because of the frustules abundance, the chemical analysis of tuffs is not edifying when defining the original amount of silicon.

[1] Filipescu, M.G. (1944) *Rev. muz. mineralog.-geol. Univ. Cluj*, **VIII**, 1-9. [2] Oncescu, N. (1957) *Geologia Republicii Populare Romîne*. Ed. Tehnică, Bucharest.

Native gold, vanadium and tellurium minerals in sublimates from high-temperature gases of Colima volcano, Mexico

Taran, Y.A.[1*] & Ostroumov M.[2]
[1]Institute of Geophysics, Universidad Nacional Autónoma de México, Mexico City, Mexico (*taran@geofisica.unam.mx)
[2]Universidad Michoacana de San Nicolás de Hidalgo, Morelia, Mexico

Gases, condensates and silica tube precipitates (sublimates) were collected from a 800°C fumarole and hot (~600ºC) steaming ground at Colima volcano, Mexico. We used the silica tube experiments under temperature-controlled conditions for the study of mineral precipitates from volcanic gases. Some results of this study have been already published [1,2].

Here we report new findings and review all the data obtained. The main difference of Colima gas vents from other well studied high-temperature fumarolic fields (Kudryavy, Momotombo, Merapi, Satsuma-Iwojima, Showa-Shinzan) was a very diffuse emission of a hot air-magmatic gas mixture from the whole surface of the former summit dome. Therefore, the mineral set deposited on the inner wall of the silica tube was quite different from minerals of "common", reduced gases. We found in all three silica tube experiments native gold [2], V-sulfates and sulfides [1,3] and Te-sulfates which have never been found inside silica tubes and in natural incrustations before. Native gold was observed in natural incrustations at other volcanoes, but never in silica tubes. The deposited "pneumatolitic" material in silica tubes is close in chemical composition to a rich "high-sulfidation" ore body of precise metals. The observed distribution of metals along temperature gradient is in a good agreement with the modeled distribution using the SOLVGAS computer code with a modified thermodynamic data base. The redox-state and variability of mineral phases is discussed in details, in particular, the cause of the V- and Te- enrichment and the absence of "common" Mo and Cd phases in Colima sublimates. The REE abundances and distribution is also discussed.

[1] Taran, Y.A. et al.(2001), *J. Volcanol. Geoth. Res*, **108**, 245-264. [2] Taran, Y.A. et al. (2000) *Appl. Geochem.*, **15**, 337-346. [3] Ostroumov, M. et al. (2009) *Rev. Mexicana de Ciencias Geologicas*, **26**, 600-608.

Mineralogy, petrography, and geochemistry of the Permian syn-eruptive deposits in the Mecsek Hills, Hungary

Varga, A.[1,2*] & Raucsik, B.[3]
[1]Dept. of Petrology and Geochemistry, Eötvös L. University, Budapest, Hungary
[2]Hortseed Ltd., Mezőkovácsháza, Hungary
([*]andrea.varga.geol@gmail.com)
[3]Dept. of Earth and Environmental Sciences, University of Pannonia, Veszprém, Hungary

The upper Paleozoic succession of the Circum Pannonian Region records the change from the Pangean configuration and compressive regime inherited from the Variscan orogeny to the development of a broad zone of strike-slip and extensional basins [1]. For both tectonic settings intensive synsedimentary volcanism is characteristic and reworked volcanic materials became an integral part of the sedimentary filling sources [1,2].

In southern Transdanubia, SW Hungary, Permian sequences are represented mostly by continental siliciclastic rocks; however, volcaniclastic deposits are also documented [2]. Based on the previous state of knowledge, the upper Permian Cserdi Formation transgressively overlies the eroded surface of the lower Permian Gyűrűfű Rhyolite [1,2]. With respect to the lower part of the Cserdi Formation, however, petrography and geochemistry of the samples previously interpreted as alluvial fan deposits suggest a syn-eruptive volcaniclastic origin (moderately welded ignimbrite). The major goal of this study is to characterize the mineralogical, petrographic, and geochemical features of the Cserdi rocks from different wells (cores D 9015, XIII, and XV) in the western Mecsek Hills.

Based on our petrographic observations, the lower part of the Cserdi Formation consists of welded, poorly sorted fine to coarse tuffs, instead of lithic-feldspathic wacke to litharenite. These rocks are characterized by pumice and/or fiamme fragments with lithic and crystal fragments floating in a fine grained matrix. In the volcaniclastic Cserdi samples, volcanic ash and glass dominantly altered to clay minerals, although chlorite, feldspar and silica minerals are also formed. Other post-depositional processes such as devitrification, albitization, and anhydrite replacement are also common.

X-ray diffraction studies indicate that the mineral assemblage is dominated by quartz and albite. Hematite, illite±muscovite, K-feldspar, dolomite, smectite (S), and chlorite (C) is a minor to trace component. Clay fraction consists of illite (I; 80-90%), kaolinite (0-20%), and mixed-layer I/S or C/S (<10 %). Illite crystallinity (IC) values fall partly in the diagenetic zone (core D 9015, average: IC=0.66), partly in the anchizone to epizone (core XV, IC=0.19-0.39).

Compared with the non-volcaniclastic Cserdi rocks, the volcaniclastic Cserdi samples are enriched in high field strength (Th, Zr, Hf, Nb, Ta) elements, and are significantly depleted in first-row transition elements (V, Cr, Co, Ni, Zn). Therefore, discrimination between these rocks is possible using immobile elements such as Al, Ti, and Zr and first-row transition elements (e.g., $[V+Ni+Cr]/Al_2O_3$ *vs* Zr/TiO_2 diagram).

The mineralogical, petrographic, and chemical composition observed in the volcaniclastic Cserdi samples reveals primary characters and diagenetic modifications, as well as a local metamorphic overprint. These data suggest that combined petrologic and geochemical techniques are required to reconstruct the primary features of rocks and the nature of deposits in the Permian syn-eruptive and subsequent siliciclastic rocks from southern Transdanubia, Hungary.

[1] Vozárová, A. et al. (2009) *Geol. Carpath.*, **60/1**, 71-104. [2] Szederkényi, T. (2001) in Haas, J. (ed.) *Geology of Hungary*, Eötvös Kiadó, Budapest, 148-168.

Manitoba: a "hotspot" of carbonatitic magmatism in the Precambrian

Chakhmouradian, A.R.[1*], Böhm, C.O.[2], Mumin, A.H.[3], Coëslan, C.G.[2], Demény, A.[4], Reguir, E.P.[1], Simonetti, A.[5], Creaser, R.A.[6], Kamenov, G.D.[7], Kressall, R.D.[1] & Lepekhina, E.N.[8]

[1]University of Manitoba, Winnipeg, Manitoba, Canada ([*]chakhmou@cc.umanitoba.ca)
[2]Manitoba Geological Survey, Winnipeg, Manitoba, Canada
[3]Brandon University, Brandon, Manitoba, Canada
[4]Institute for Geochemical Research, Budapest, Hungary
[5]University of Notre Dame, Notre Dame, Indiana, USA
[6]University of Alberta, Edmonton, Alberta, Canada
[7]University of Florida, Gainesville, Florida, USA
[8]Center for Isotopic Research, VSEGEI, St. Petersburg, Russia

Identification of a carbonate rock as carbonatite is not always trivial, particularly in Precambrian settings affected by deformation. In such settings, carbonatite bodies can easily pass unrecognized during routine regional-scale mapping due to their small size, metamorphic fabric and obscured exposure. Carbonatites were not known in Manitoba prior to the discovery of soviet dikes at Eden Lake in the Paleoproterozoic Trans-Hudson orogen in 2002 [1]. The sövite intruded silica-saturated syenitic rocks of shoshonitic affinity, which were transformed into fenites at the contact. These rocks were emplaced after the assembly of the northern part of the orogen ca. 1815 Ma. The most remarkable textural characteristics of the Eden Lake sövite are the presence of microcline and aegirine-augite megacrysts and evidence of post-emplacement ductile flow and remobilization of rare-earth elements (REE). In the southern section of the orogen, beforsite was intersected by drilling in the SW part of Wekusko Lake. Beforsite dikes cross-cut Paleoproterozoic metasedimentary rocks and are not associated with any alkaline rocks. The carbonatite contains abundant phlogopite phenocrysts and diamond-indicator minerals, which explains the initial identification of this rock as kimberlite. This occurrence is much younger (560 Ma) and petrogenetically distinct from the Eden Lake complex. Immediately SE of the Trans-Hudson orogen, deformed Archean gneisses of the Superior craton host modally and texturally diverse calcite and calcite-dolomite carbonatites initially recognized during detailed mapping of the Paint Lake area [2]. These rocks occur as dikes exposed over 21 km of the Superior Boundary Zone. The carbonatites exhibit evidence of modal and cryptic metasomatism along the contact, and contain a variety of REE accessory phases (allanite, titanite, monazite and bastnäsite). Their textural diversity results from post-emplacement tectonic remobilization in the Paleoproterozoic. Further towards the interior of the craton, carbonatites were recognized in association with feldspathoid-syenitic and alkali-granitic rocks at Cinder Lake. The syenites host carbonate ocelli and veinlets, interstitial calcite, and are locally carbonatized and sericitized. The carbonate paragenesis consists of Sr-REE-rich calcite, phlogopite, magnetite, albite, apatite, monazite and britholite. The Cinder Lake complex formed ca. 2700 Ma during the consolidation of the Superior craton.

Our collective work shows that carbonatitic magmatism affected vast areas of the Canadian Shield outside the well-known extensional structures in northwestern Ontario, and spanned at least two billion years. These discoveries have far-reaching implications for the correct interpretation of the tectonic history of the Trans-Hudson orogen and Superior craton, and for mineral exploration in central Canada.

[1] Mumin, A.H. (2002) *Manitoba Geol. Survey, Rep. Activ*. (2002) 187-197. [2] Couëslan, C.G. (2008) *Manitoba Geol. Survey, Rep. Activ*.(2008) 99-108.

Petrology and petrogenesis of carbonatitic rocks in syenites from Central Anatolia, Turkey

Cooper, A.F.[1*], Durmus, B.[2] & Palin, J.M.[1]

[1]Dept. of Geology, University of Otago, Dunedin, New Zealand ([*]alan.cooper@stonebow.otago.ac.nz)
[2]Tunceli University, Tunceli, Turkey

The A-type Karaçayır pluton in Central Anatolia, Turkey, intrudes and entrains xenoliths of Paleozoic limestone. Carbonatitic magmatic rocks within the syenite have been previously interpreted [1] to result from metasomatic alteration and syntectic melting of marble.

Carbonatites and associated calcite-syenites exhibit mineralogical characteristics (Ab-rich plagioclases, Ba-rich K feldspars, low Mg# biotites) that are petrogenetically more evolved than the host syenitic suite. Carbonate-rich magmatic rocks are greatly enriched in Sr, Ba, Th, and REE, and have higher LREE/HREE ratios than either syenites or marbles. Carbonatites have $d^{13}C_{VPDB}$ and $d^{18}O_{VSMOW}$ of -2.1 to -3.5 ‰ and +10.4 to +11.5 ‰ respectively, compared to marble values of +1.5 to +2.7 and +18.9 to +26.3 ‰. Syenites have intermediate values between these two extremes. $^{87}Sr/^{86}Sr$ ratios of calcite-syenite and carbonatite average 0.70749, they are similar to foid syenite (0.70751) and significantly lower than marbles (average 0.70806). Overall, the mineralogical and geochemical characteristics of the carbonatites are incompatible with binary mixing of syenite and marble, but their origin is consistent with derivation of carbonatite from petrogenetically evolved foid syenite. Carbonate-silicate rock types have modal variations compatible with an origin by fractional crystallisation, rather than liquid immiscibility.

[1] Schuiling, R.D. (1961) *Nature*, **192**, 1280.

Carbonatites and associated nephelinites from São Vicente, Cape Verde Islands

De Ignacio, C.[1*], Muñoz, M.[1] & Sagredo, J.[2]
[1]Dept. Petrología y Geoquímica, Fac. Ciencias Geológicas, Universidad Complutense, Madrid, Spain ([*]cris@geo.ucm.es)
[2]Instituto de Geología Económica, CSIC, Universidad Complutense, Madrid, Spain

The island of São Vicente, in the northern part of the Cape Verde archipelago, has been credited for having the most abundant outcrops of carbonatite in those islands [1]. Field survey of its main outcrops has shown that they comprise: extrusive carbonatites forming part of eroded, poorly-exposed but still recognizable volcanic centres; carbonatite dykes; scattered blocks, sometimes resembling bombs, and small apophysis of intrusive carbonatite. These outcrops are occasionally crowned by nephelinite plugs and locally, nephelinite lavas are interspersed with carbonatite lenses, indicating that the same conduits might have been used by both kinds of magmas.

The volcanic carbonatites and dykes show flow texture and modal banding, where carbonate layers alternate with oxide-rich bands. In contrast, the intrusive carbonatite blocks show roughly equigranular, coarse-grained textures, and a wider range of rock-forming minerals including: clinopyroxene (aegirine-augite), iron oxides (magnetite-hematite), fluorapatite, K-feldspar (orthoclase), zircon and mica (phlogopite-biotite).

The three kinds of carbonatites, together with plug nephelinites have been sampled and analysed, for whole-rock geochemistry and mineral composition. Carbonatites define two distinctive geochemical groups. The volcanic ones and dykes are richer in MgO (7-10 wt%), Ba (7000 ppm) and REE (total rare earths = 2000-4000 ppm), also displaying high Sr contents (3000-5000 ppm). They plot close to and within the magnesiocarbonatite field in the classification scheme [2] and could represent more primary compositions. Intrusive carbonatites, however, range from Mg-bearing (5-6 wt% MgO) to Mg-poor (0.5-1 wt% MgO) calciocarbonatites, showing similar Sr contents to those of volcanic carbonatites and dykes, but remarkably lower Ba (300-400 ppm) and total REE (500-900 ppm). The latter seem to be mainly controlled by apatite.

Associated nephelinites contain Ti-rich diopside phenocrysts and small, aegirine-augite crystals in the matrix, together with nepheline, mica, apatite, Fe-oxides, pseudomorphosed olivine and, rhönite. Rhönite is, to our knowledge, described for the first time in the Cape Verde nephelinites. Its occurrence as euhedral, slender prisms with well-defined boundaries indicates that it is a primary phase, which attests for high Ti contents in the nephelinite magma. The rare-earth spectrum of the nephelinite displays the same pattern as the less-enriched, intrusive carbonatites, indicating a possible link between carbonatite and alkaline silicate magmas.

[1] Hoernle, K. et al.(2002) *Contrib. Mineral. Petrol.*, **142**, 520-542. [2] Woolley, A.R. & Kempe, D.R.C. (1989) in Bell, K. (ed.) *Carbonatites: genesis and evolution*. Unwin-Hyman, 1-14.

Graphite-bearing carbonatite of Dolbykha massif, Polar Siberia, Russia

Zaitsev, V.A.[*], Sorokhtina, N.V. & Kogarko, L.N.
GEOKHI RAS, Moscow, Russia ([*]va_zaitsev@inbox.ru)

Dolbykha is a small (~3 km^2) concentrically-zoned alkaline-ultramafic massif, located 75 km south of the Guli massif.

Dolbykha intruded Cambrian dolomitie, which was transformed to dolomitic marbles near the contact. The central part of massif consists of melteigites. These are surrounded by ijolites, and the outer part of massif consists of biotite and biotite-pyroxene carbonatites. Carbonatites of other types form concentric dikes.

This carbonatite is anchimonomineral calcitic rock (sovite) with minor amounts of dolomite, phlogopite, amphibole and K-feldspar. Accessory minerals are apatite, pyrite, graphite, and Nb-bearing rutile.

Graphite forms crusts on the carbonate crystals and intergrowths with phlogopite. G band FWHMs (24-34 cm^{-1}) in Raman spectra of the graphite correspond to temperature 320-500°C [1].

The formation conditions of the mineral association in the Dolbykha carbonatite can be estimated from the reactions:

3 Do +1 H_2O +1Kfs =3 CO_2+3 Cc +1Phl (1)

3 Do +1 H_2O +1 Kfs = 3 Cc +3 Grph +3 O_2 +1 Phl (2)

The reaction (1) allows estimation of the temperature of equilibrium as 400-500°C.

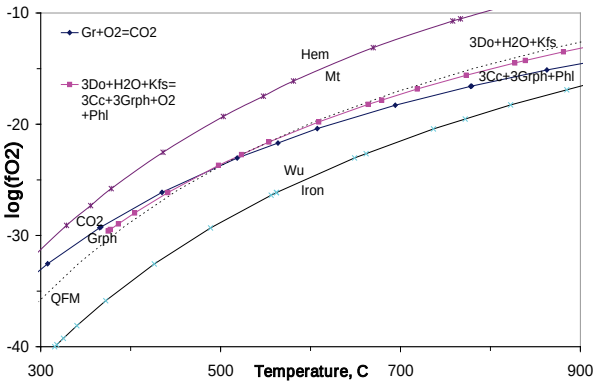

Fig. 1: f(O2)-T conditions for dolomite + K-feldspar + calcite + phlogopite + graphite association estimated by thermochemical calculations with program complex BAYES.

The equilibrium (2) allows estimation of the oxygen fugacity (Fig. 1). The topology of the T-f(O2) diagram (Fig. 1) shows that cooling along the QFM-buffered line results in formation of graphite, calcite and phlogopite after K-feldspar and dolomite at temperatures lower than 500-550°. This means that graphite can be formed as a result of the influence of the fluid, equilibrated with QFM-buffered rock in carbonatite at temperatures lower than 500°C.

Acknowledgements: This work was supported by RFBR grant 09-05-12026

[1] Zaitsev, V.A. et al. (2009) *EGU 2009* (11)-134-3.

Fingerprinting of kimberlite sources by isotope studies of accessory minerals: a mantle tracer

Sarkar, C.[1*], Storey, C.[2], Hawkesworth, C.J.[3], Sparks, S.[1] & Field, M.[4]
[1]Dept of Earth Sciences, University of Bristol, UK ([*]c.sarkar@bristol.ac.uk)
[2]Dept. of Earth and Environmental Sciences, University of Portsmouth, UK
[3]Deputy Principal and Vice-Principal for Research, University of St Andrews, Scotland, UK
[4]DiaKim Consulting Limited, Wookey Hole Wells, UK

Interest in determining the radiogenic isotope and trace element geochemical characteristics of uncontaminated kimberlitic magma has been rekindled by recent studies of accessory groundmass minerals e.g., perovskites, which are strongly resistant to isotope modification [1]. In-situ Sr, Nd, and Hf isotope data along with U-Pb geochronology on perovskites have been preferred over bulk rock studies and they have been interpreted as the primary geochemical signature of kimberlite magma [2,3].

In this study we have analysed several individual groundmass perovskites from different litho-facies of Group I kimberlites of Orapa, Botswana to investigate the trace element and isotope characteristics of the source material and how they vary among different lithofacies. Both in-situ (LA-MC-ICPMS) and solution (MC-ICPMS) analyses have uniform Nd isotopic composition with an average $^{143}Nd/^{144}Nd$ ratio of 0.512742 ± 34. But the initial results show that the $^{87}Sr/^{86}Sr$ ratios of individual grains are heterogeneous and vary from 0.703590 - 0.705407 ± 22. Samples with more radiogenic Sr also correlate with HREE enrichment. In a εNd vs $^{87}Sr/^{86}Sr$ diagram all samples plot within the Group I kimberlite field, defined by whole rock analyses, and they are interpreted to be derived from a primitive mantle source.

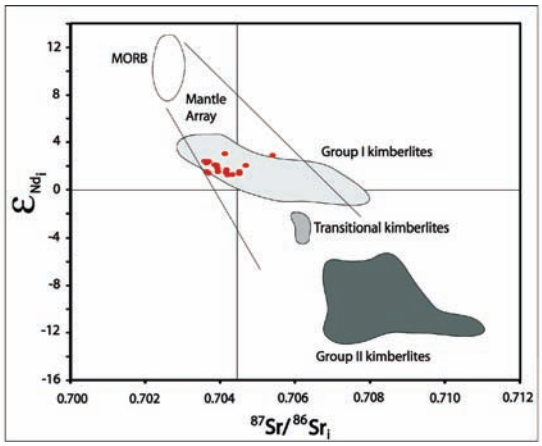

Fig. 1: εNd_i vs $^{87}Sr/^{86}Sr_i$ of perovskites from Orapa along with fields showing group I, group II and transitional kimberlites.

Though the uniformity of the data from perovskites compared to the bulk rock analysis emphasises their reliability over bulk rock geochemistry, some of the variation in Sr isotopes might be a result of post emplacement hydrothermal alteration, which is not always visually recognised. It may be that the perovskites are not as resistant to isotope modification as previously thought and, therefore, more care should be taken while interpreting the geochemical data from perovskites.

[1] Heaman, L.M. (1989) *Earth Planet. Sci. Lett.*, **92**, 323-334. [2] Paton, C. et al. (2008) *Geology*, **35,** 1011-1014. [3] Yang, Y.H. et al. (2009) *Chem. Geol.*, **264,** 24-42

Disclosed data from mantle xenoliths of Angolan kimberlites based on LA-ICP-MS analyses

Robles-Cruz, S.E.[1*], Escayola, M.[2], Melgarejo, J.C.[1], Watangua, M.[3], Galí, S.[1], Gonçalves, O.A.[4] & Jackson, S.[5]
[1]Dept. de Cristal·lografia, Mineralogia i Dipòsits Minerals, Facultat de Geologia, Universitat de Barcelona, Catalonia, Spain ([*]sandra_robles@ub.edu)
[2]National Research Council of Argentina CONICET
[3]ENDIAMA, Luanda, Angola
[4]Depto. de Geologia, Faculdade de Ciências, Universidade Agostinho Neto, Luanda, Angola
[5]Geological Survey of Canada, Ottawa, Canada

The diamondiferous Catoca and Cucumbi-79 kimberlite pipes are located on the Kasai Craton, Angola. Different suites of mantle xenoliths have been characterized by optical petrographic and SEM-BSE studies.

Three types of xenoliths are found in Catoca: eclogites, garnet clinopyroxenites (with G9 [1] garnets and chromian dipside), and garnet lherzolite (with G9 garnets and chromian diopside). Phlogopite is found as a rare accessory in Catoca peridotites. In contrast, the Cucumbi-79 kimberlite contains at least the following types of xenoliths: garnet clinopyroxenites (with G5 garnet, diopside and phlogopite), garnet lherzolites (showing different proportions of G5 or G9 garnets, chromian diopside, enstatite and phlogopite), PIC suite xenoliths (phlogopite, ilmenite, diopside) and glimmerites.

Two main different trends for garnet can be identified in Catoca depending on the REE patterns. Eclogitic garnet has "normal" [2] REE_N patterns, while garnet from lherzolite xenoliths usually has "sinusoidal" [2] REE_N patterns and rarely "normal" REE_N patterns. Eclogitic clinopyroxene is LREE-enriched. Garnet from the lherzolite xenoliths is characterized by a LREE-enrichment, a maximum around the LREE-HREE limit and flat HREE. Unlike in Cucumbi-79, garnet from lherzolite xenoliths presents "normal" patterns with lower REE values. Garnet from phlogopite-rich xenoliths presents "normal" patterns, but their values are significantly (about 10x chondritic value) lower. Only clinopyroxene from phlogopite-rich xenoliths exhibits higher values in LREE than the same xenoliths in Catoca.

Data indicate that the mantle sampled by these two kimberlites might have been under different equilibration conditions and different degrees of metasomatism. Hence, the "normal" pattern exhibited by the Cucumbi-79 garnets might be explained as the result of refertilization of previously depleted peridotite by infiltration of melt [3]. In contrast with garnet patterns in Cucumbi-79, the "sinusoidal" REE_N patterns of garnet from lherzolite xenoliths in Catoca may be the result of different degrees of re-enrichment in incompatible elements.

[1] Grütter, H.S. et al. (2004) *Lithos*, **77**, 841-857. [2] McLean, H. et al. (2007) *Can. Mineral.*, **45**, 1131-1145. [3] Stachel, T. et al. (1998) *Earth. Planet. Sci. Lett.*, **159**, 1-12.

Trace element distribution in carbonatites from Vuorijarvi (Kola Peninsula, Russia)

Smith, B.* & Downes, H.
Dept of Earth and Planetary Sciences, Birkbeck University of London, UK (*barbara.smith28@btopenworld.com)

The Vuorijarvi ultramafic carbonatite complex belongs to the Palaeozoic Kola Alkaline Province. The poorly exposed dyke system at Vuoriyarvi is representative of silica-rich sövites. Geochemical studies were performed on major and trace element distribution in some of the less common minerals in the carbonatites such as monticellite, pyroxene, kimzeyite and phlogopite, as well as the common ones like calcite, apatite and perovskite. Calcite in all the samples exhibits a polygonal recrystallised texture. There are morphological indications of immiscibility between silicate liquid and carbonate or phosphate liquids illustrated by features such as globules and dumbells of calcitic and apatitic composition present in monticellite. Perovskite is very rare, but typically contains numerous apatite and calcite inclusions, giving it an unusual spongy appearance. The rare kimzeyite garnet forms relatively large grains (up to 1mm). The unusual character of kimzeyite lies in its high ZrO_2 content which can be >12 wt%. The striking similarity of perovskite and kimzeyite (Fig. 1) regarding the shape, size, sporadic occurrence and association with apatite suggests that both minerals crystallised in similar condition but probably not in the system which is hosting these phases now.

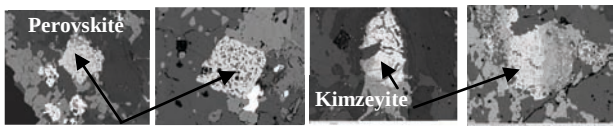

Fig. 1: Perovskite in Vuorijarvi sövite (BR18 left and B218 to the right). Photomicrographs of rare Zr-rich garnet in BA18A and B218A respectively, both intimately associated with apatite.

EPMA analyses show moderately high concentration of Sr in calcite (1-1.5 wt% SrO), typical for a primary carbonate phase. Apatite contains 0.9-1.2 wt% F, classifying this phase as a fluorapatite. The mg# in phlogopite varies from 0.88 to 0.91 but is lower in xenocrystic phlogopite (0.87), suggesting crystallisation from a host liquid slightly depleted in MgO. Rare olivine has high mg# = 0.90, whereas that of monticellite is much lower (0.77-0.79).

Constituent minerals in sövite were analysed for trace elements using LA-ICP-MS (Fig. 2). Perovskite and apatite are strongly enriched in LREEs whereas calcite and phlogopite are 3-4 orders of magnitude lower, with phlogopite displaying anomalously higher MREE concentrations. Monticellite is slightly enriched in HREEs. Most of the analysed minerals are characterised by very high La/Lu ratios (900 for perovskite and 100 for apatite) although La/Lu=40 in calcite and 0.5 in monticellite, suggesting that some phases in carbonatites have taken an important part in the fractionation of the REE.

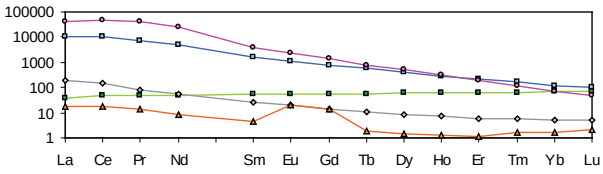

Fig. 2: Average REE distributions pattern in sövite (chondrite-normalised) of the fallowing phases: perovskite (pink), apatite (blue), calcite (grey), monticellite (green), and phlogopite (orange).

Trace element partition coefficients for apatite, calcite and carbonatite melt at crustal pressures and temperatures

Wall, F.[1*], Rosatelli, G.[2] & Jeffries, T.[3]
[1]Camborne School of Mines, University of Exeter, Penryn, UK (*f.wall@exeter.ac.uk)
[2]Dipto. di Scienze della Terra, Universita` G. d'Annunzio, Chieti, Italy
[3]Dept. of Mineralogy, Natural History Museum, London, UK

Partition coefficients are essential for modelling petrogenetic processes. Understanding the fractionation of REE in carbonatitic systems has applications to problems ranging from formation of REE ore deposits to mantle metasomatism. Apatite and calcite are key and almost ubiquitous minerals in carbonatites and thus important controls on REE distribution.

There have been few studies of partition coefficients in carbonate magmas. Apatite-carbonatite melt partition coefficients determined by experiment at 1 GPa, 1250°C, showed that REE are incompatible in apatite [1] and contrasted with coefficients calculated during a trace element study of apatites in various intrusive carbonatites [2].

In this study, we have isolated carbonatite lapilli from calcite carbonatite lapilli tuff at Kaiserstuhl, Germany [3], assumed that these represent a melt composition and analysed them by whole rock ICP-AES and ICP-MS to determine major, minor and trace elements. We have then determined the trace element contents of apatite and calcite (and pyrochlore) by LA-ICP-MS analysis and calculated the partition coefficients.

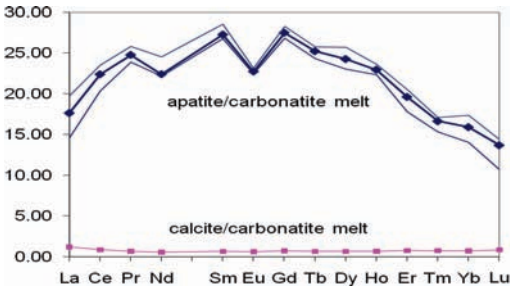

Fig. 1: Partition coefficients for REE in apatite and calcite in calcite carbonatite.

The apatite-carbonatite melt partition coefficients of 14 - 27 calculated here for the REE (Fig. 1) are two orders of magnitude higher than the values calculated from experiment [2]. Results from silicate magmas found that apatite REE partition coefficients are higher in melts with high SiO_2 content and also higher at lower temperature but vary little with pressure [3]. Our K_d values are of similar order to the values calculated using trace element compositions of apatite in intrusive carbonatites [2]. These would have crystallised at lower P and T than used in the experiments [1] and by analogy with silicate melts, the temperature difference in particular could have a large effect on the values. We conclude that the partition coefficients presented here are useful for calculations involving emplacement and crystallisation of carbonatites. The lower apatite coefficients at high P and T, coupled with the low partition coefficients for calcite, even at crustal P and T, could help to explain why deep-seated volcanic carbonatites have low REE.

[1] Klemme, S. & Dalpé, C., (2003). *Am. Mineral.*, **88**, 639-646. [2] Buehn, B. et al. (2001) *Contrib. Mineral. Petrol.*, **141**, 572-591. [3] Keller, J. (1981) *J. Volcanol. Geoth Res*, **9**, 423-431. [4] Watson, E.B. & Green, T.H. (1981) *Earth Planet. Sci. Lett.*, **56**, 405-421.

Hudsonite, an alkali-amphibole-dominant ultramafic rock associated with magnetite deposits in the Hudson Highlands of New York

Martin, R.F.[1*] & Lupulescu, M.V.[2]
[1]Earth & Planetary Sciences, McGill University, Montreal, Canada ([*]robert.martin@mcgill.ca)
[2]New State Museum, Research and Collections, Albany, New York, USA

The Hudson Highlands, in southeastern New York, are the site of a swarm of unusual alkali-rich amphibole-dominant peridotites emplaced in upper-amphibolite- to granulite-facies rocks of Grenvillian (Proterozoic) age. The intrusive rocks are coarse-grained, undeformed, and cut their host rocks with a sharp contact. They are spatially associated with small deposits of magnetite that were exploited 150 years ago. The peridotites do contain magnetite, and may also contain net-textured disseminations of pyrrhotite with pentlandite domains and chalcopyrite. They invariably also contain coarse crystals of phlogopite and, locally, almandine interpreted to be xenocrystic, and also subject to gravitational accumulation. Because of the local presence of interstitial calcite, and of the inferred dominance of CO_2 in the early postmagmatic fluid phase, the olivine is still fresh. The primary rock-forming amphibole is hastingsitic, and rather unusual in being enriched in K and the halogens. Some localities contain a chlorine-dominant K-rich calcic amphibole, whereas elsewhere in the vicinity, fluorine is the dominant halogen. The Greenwood iron mine, in Orange County, is the type locality of fluoro-potassichastingsite, a newly defined end-member [1], ideally $KCa_2(Fe^{2+}{}_4Fe^{3+})Si_6Al_2O_{22}F_2$ (Mg# 0.33, 1.24% Na_2O, 2.93% K_2O, 2.23% F, 0.61% Cl). The amphibole is LREE-enriched. Along with accessory phlogopite, it is the last phase to crystallize, and constitutes the intercumulus phase amidst Cpx + Ol cumulates. It is a property of such amphiboles to approach the bulk composition of a magma of OIB type; for this reason, an unusually coarse grain-size is typical. In view of the variable enrichment in F or Cl, the presence of xenocrystic almandine, the presence of Cpx + Ol cumulates, and saturation in a sulfide melt, the alkaline magmas are considered ultimately of asthenospheric derivation, emplaced at a stage of tectonic relaxation after the culminating Grenville collision in this area, but highly modified by assimilation of granulitic lower crust in which the plagioclase-bearing assemblages had largely been destroyed by alkali metasomatism. How does one classify such ultramafic rocks? The term “cortlandtite” refers to a subalkaline hornblende-dominant peridotite, and thus does not seem relevant; we prefer to revert to the name originally applied to these alkaline peridotites, *hudsonite*.

[1] Lupulescu, M.V. et al. (2009) *Can. Mineral.*, **47**, 909-916.

Mineralogy of carbonatized mantle beneath Antarctica (Oasis Jetty)

Kogarko, L.N.
Vernadsky Institute of Geochemistry and Analytical Chemistry, Moscow, Russia (kogarko@geokhi.ru)

Some mantle-derived East Antarctic rocks have bulk-rock and mineral trace element and isotopic compositions that provide evidence of strong carbonate metasomatism. 46 spinel and garnet peridotite xenoliths from lithospheric mantle beneath Lambert-Amery Rif were studied. Investigated spinel and garnet peridotite xenoliths represent about 80 km thick cross of subcontinental litospheric mantle.

Distinct correlations is observed between contents of MgO and other petrogenetic elements CaO, Al_2O_3, FeO, Na_2O, Co, Ni, V. Comparison of these correlations with estimated trends of batch and fractional melting of initially fertile mantle peridotite [1] demonstrate that Jetty peridotites plot at lower values for SiO_2 and other components.

Garnets are characterized by positive europium anomaly, unusual high LIL element concentrations (Ba/La=4000) and clinopyroxenes from the spinel peridotite suite are highly enriched in LREE [$(La/Yb)_N$ =14] and in HFSE.

The decoupling of major and REE elements and observed mineral assemblages (which include dolomite, calcite, Sr- and LREE-rich apatite,Ti- Ba-rich phlogopite, titanite, perovskite, henrymeierite) indicate that the upper mantle of East Antarctic has been affected by very strong metasomatism.

Henrymeierite was found in mantle material for the first time [2].

Our isotopic data showed complete absence of isotope equilibrium among the rock forming minerals in the xenoliths – Opx, Cpx and Grt. Garnets are characterised by the most radiogenic Sr isotope composition (0.709024-0.714127), whereas Cpx exhibits the lowest $^{87}Sr/^{86}Sr$ ratios (0.702861-0.703711). On the one hand garnets are depleted in terms of Sm-Nd system and on the other hand they are significantly enriched in radiogenic Sr. Such anomalous signature in Antarctic mantle rocks confirm the influx of carbonate metasomatising fluid (or melt) from the source with a time integrated LIL-elements enrichment and more rapid Sr but not Nd diffusion to garnets compare to Cpx.

It is probable that the interaction of primary dolomitic melts-fluids with mantle material according to reactions:
$2Mg_2Si_2O_6+CaMg(CO_3)_2 = 2Mg_2SiO_4+CaMgSi_2O_6+2CO_2$ (1)
$3CaMg(CO_3)_2+CaMgSi_2O_6 = 4CaCO_3+2Mg_2SiO_4+CO_2$ (2)
resulted in wehrlitization and carbonatization. The fluids responsible for this metasomatism were probably derived from the plume that arrived beneath the region at this time.

[1] Niu, Y. (1997) *J. Petrol*., **38**, 1047-1074. [2] Kogarko, L. Kurat, G. & Ntaflos, T. (2007) *Can. Mineral.*, **45(3)**, 497-501.

High-pressure experiments on anhydrous carbonated eclogite at 9-20 GPa – implications for the recycling of carbonate into the mantle

Kiseeva, E.S.[1*], Litasov, K.D.[2], Yaxley, G.M.[1], Ohtani, E.[2] & Kamenetsky, V.S.[3]
[1]Research School of Earth Sciences, Australian National University, Canberra, Australia ([*]kate.kiseeva@anu.edu.au)
[2]Tohoku Univesity, Aramaki Aoba-ku, Sendai, Japan
[3]CODES and School of Earth Sciences, University of Tasmania, Hobart, TAS, Australia

Significant amounts of carbonates may be subducted with the high pressure form of oceanic mafic crust (eclogite) deep into the mantle. However, little experimental work has investigated the fate of subducted carbonated eclogites deeper than about 300 km (>10 GPa). We present the phase relations and solidus temperatures of carbonated eclogite compositions at 9-20 GPa.

Multianvil experiments were conducted using the 3000-ton press at Tohoku University, Sendai at 9, 13, 17, and 20 GPa, and from 1200 to 1800°C. The experimental compositions were GA1 (average MORB) and Volga (GA1-6.5% SiO_2) [1] with the addition of 10% of calcite (10%cc).

The subsolidus mineral assemblages varied with pressure, although garnet (Grt) was the most abundant phase in all runs. At 9 and 13 GPa, clinopyroxene (Cpx), carbonate (Carb) (both calcitic and magnesitic), a high-pressure modified form of rutile (Ru) (only at 9 GPa) and minor stishovite (St) were also observed. No K-rich phase was detected and we infer that K partitions entirely into Cpx (0.3-0.6 wt% K_2O). At 17 GPa Cpx was no longer present; the assemblage consisted of Na-rich majoritic Grt, Carb (both calcitic and magnesitic) and K-hollandite (K-Holl), which contained most of the K. St was observed in most of the runs at 17-20 GPa. At 20 GPa, CAS (in GA1+10%cc) and Ca-perovskite (Ca-Per) (in Volga+10%cc) appeared in addition to Grt and calcitic Carb. K-Holl was also detected at low temperatures. In most GA1+10%cc and few of Volga+10%cc diamonds crystallised, coexisting with crystalline Carb.

Above-solidus runs contained carbonatitic melts in which the amount of alkali elements (Na, K) increased with pressure. None of the runs reached more than about 25% melting and the main melt-contributing phases were Carb, Ru, Cpx in lower pressure runs and K-Holl, CAS, Ca-Per, Carb in high-pressure runs, leaving St and Grt residual phases.

A striking feature of the new data is the relatively flat solidus located between 1200 and 1300°C at all investigated pressures. This may be the result of the relative incompatibility of Na_2O and K_2O with increasing pressure. In the lower pressure runs, Na behaves compatibly due to the high stability of the jadeite component in Cpx. With increasing pressure progressive dissolution of Cpx into majoritic Grt may lead to Na becoming incompatible and it may flux melting at a sodic carbonate solidus. Although being located at lower temperatures relative to other (K-free) carbonated eclogite studies [2] it remains at higher temperatures than the hottest estimated subduction geotherm (e.g. [3]), in good agreement with previous, lower pressure studies [4-6]. Thus, subducting carbonates in eclogite may reach the deep convecting mantle, where they may partially melt to produce carbonate-rich liquids which could have a role in fertilizing the surrounding peridotite mantle and producing enriched magma sources.

[1] Kiseeva, E.S. et al. (2009) *Geochim. Cosmochim. Ac.*, **73**, A663. [2] Litasov, K.D. & Ohtani, E. (2010) *Earth Planet. Sci. Lett.*, submitted. [3] van Keken, P.E. et al. (2002) *Geochem. Geophys. Geosys.*, **3**, 1056. [4] Dasgupta, R. et al. (2004) *Earth Planet. Sci. Lett.*, **227**, 73-85. [5] Hammouda, T. (2003) *Earth Planet. Sci. Lett.*, **214,** 357-368. [6] Yaxley, G.M. & Brey, G.P. (2004) *Contrib. Mineral. Petrol.*, **146**, 606-619.

Alkaline magmas and carbonatites, the ultimate source of granulite fluids

Touret, J.L.R.
Musée de Minéralogie, Mines-Paristech, Paris, France (jacques.touret@ensmp.fr)

Lower crustal granulites, at world scale, have been invaded at peak metamorphic conditions by large volumes of low H_2O-activity (dry) fluids, either high-density, pure CO_2 and/or highly saline aqueous solutions (brines) [1]. Even if it cannot be excluded that some fluids, notably brines, are locally derived, a number of concordant evidences suggest that most of these fluids originate in the mantle, transported into the lower crust by mantle-derived, synmetamorphic intrusives. Fluid inclusions identical to those found in granulites occur also in a number of mantle minerals, including diamond [2]. Regarding CO_2, the case of lake Nyos (Cameroon) illustrates a possible way by which this fluid has been generated at depth [3]. In mantle lherzolitic xenoliths, inclusions occur predominantly, if not exclusively, in clinopyroxenes, whereas neighbouring olivine and, to a lesser extent, orthopyroxene, are virtually inclusion-free. Maximum CO_2-density preserved in inclusions is well above 1.1 g/cc, corresponding to an internal pressure at magmatic temperature of at least 1 GPa (30 km depth). These values are minimal, corresponding to the maximal overpressure that the inclusion host mineral can stand, not too far away of pressure at which carbonatite melts would destabilize during mantle melting (about 2 GPa). The geochemical signature of these xenoliths shows precisely metasomatic contamination by carbonate-rich melts [4]. I consider these melts as the primary source for CO_2, according to a tentative reaction: olivine (or orthopyroxene) + carbonate → clinopyroxene + CO_2.

Brine inclusions are much rarer than CO_2-ones in mantle-derivates, but not absent. Besides diamonds, they have recently been found in amphibolite-bearing peridotite from Ethiopia [5]. The fluid source is assumed to be recycled oceanic lithosphere. Brines as well as CO_2 can thus be generated in the mantle, prior of being transported into the lower crust by synmetamorphic, dominantly alkaline intrusions.

[1] Touret, J.L.R. (2009) *Russ. Geol. Geophys.*, **50**, 1052-1062. [2] Izraeli, E.S., Harris, J.W. & Navon, O. (2001) *Earth Planet. Sci. Lett.*, **187(3-4)**, 323-332. [3] Touret, J.L.R., Grégoire, M. & Teitchou, M.I. (2010) *C.R. Geosci.*, **342**, 19-26. [4] Teitchou M.I. et al. (2010) *Bul. Geol. Soc. Am.*, in press. [5] Frezzotti, M.L. et al. (2010) *Geochim. Cosmochim. Ac.*, **74**, 3023-3039.

The crucial role of lithosphere structure in the generation and release of carbonatites: geological evidence

Woolley, A.R.[1*] & Bailey, D.K.[2]
[1]Dept. of Mineralogy, Natural History Museum, London, UK
([*]a.woolley@nhm.ac.uk)
[2]Dept. of Earth Sciences, University of Bristol, Bristol, UK

In recent years there has been a significant increase in the numbers of known carbonatite localities. The new occurrences have been incorporated into a comprehensive database and world distribution map [1]. They support previous observations of spatial and temporal aspects of these rocks, but also provide new observations that are important for understanding their petrogenesis. The data reveal that there is an overwhelming concentration of carbonatites in Precambrian cratonic areas, most of which are generally elevated topographically. Thus, although approximately two thirds of carbonatites are Phanerozoic in age, at least 86% of all carbonatites are located in the cratons, demonstrating a remarkable tendency for a Precambrian host. This observation is noteworthy as suggesting a link with kimberlites, which are similarly concentrated in cratonic areas, with diamondiferous kimberlites being confined to the Archaean [2]. The collected age data confirm that in many carbonatite-bearing provinces there has been repetition of carbonatite emplacement, with up to five such episodes being separated by hundreds of millions of years. In at least three provinces such activity extends from the late Archaean to relatively recent times and, because of the drift of the plates, this precludes any role for mantle plumes in carbonatite genesis. Instead it underlines the importance of structural control within the continental lithosphere. A model involving lithosphere metasomatism and lithosphere focussing in structurally controlled areas is therefore invoked.

[1] Woolley, A.R. & Kjarsgaard, B.A. (2008) *Carbonatite occurrences of the world: map and database.* Geol. Surv. Canada, Open File **5796**. 1 CD-ROM and 1 map. [2] Janse, A.J.A. (1994) in Meyer, H.O.A. & Leonardos, O.H. (eds.) *Proc. 5th Int. Kimb. Conf., Araxa, Brazil, 1991. 2. Diamonds: characterization, genesis and exploration.* Companhia de Pesquisa de Recurcos Minerais, Brasilia, 215-235.

Deep mantle melting and carbonatitic activity in the mantle beneath central Spain

Humphreys, E.R.[1,2*], Bailey, K.[1], Hawkesworth, C.J.[1,3], Wall, F.[2,4] & Jeffries, T.[2]
[1]Dept. of Earth Sciences, University of Bristol, UK
([*]emma.humphreys@bristol.ac.uk)
[2]Dept. of Mineralogy, Natural History Museum, London, UK
[3]University of St Andrews, UK
[4]Camborne School of Mines, University of Exeter, Penryn, UK

A single crystal of aragonite demonstrates the high-pressure origin of volcanism from Calatrava, Spain. High-pressure and high temperature experimental determinations on the stability of aragonite constrain it to greater than 100km depth, assuming a H_2O+CO_2 bearing mantle lithology. In Calatrava, the lithosphere is estimated to be ~80km thick. Therefore this volcanism may have sampled the sublithospheric mantle and melting is predicted to originate below 100km. Rapid ascension and quenching is required to maintain the aragonite crystal structure. The fine-grained leucitite groundmass and glassy carbonate-silicate melt inclusions also indicate rapid quenching.

The aragonite occurs as an inclusion within olivine (Fo_{87}) from a leucitite lava flow. Olivine is xenocrystic and inclusions of carbonate are common. Carbonate inclusions typically occur as calcite, dolomite or aragonite. Only one example of aragonite has been identified, but many other examples of poly-crystalline calcite with radiating fractures in olivine suggest calcite after aragonite. We observe two distinct groups of inclusions; those with euhedral to subhedral outlines, usually composed of carbonate. The second group have rounded outlines and contain carbonate and coexisting silicate glass or silicate minerals.

LA-ICPMS of individual carbonate inclusions reveal their absolute trace element concentrations and the variation that exists between inclusions. Figure 1 details our results for twenty-three inclusions. Primitive mantle normalised rare earth element concentrations vary over two orders of magnitude, but have similar profiles and are low (<1*Primitive mantle, PM). There is some evidence of light rare earth enrichment, but otherwise the profiles are flat. A negative Ce anomaly is observed in all inclusions, including aragonite (thick blue line, fig. 1).

Petrographically, most inclusions studied show no evidence of interaction with the host magma. Therefore, the trace element profiles of many inclusions may be derived from a carbonated mantle melt. The melt was either trapped by growing olivine phenocrysts, or crystallised, in the case of aragonite, with olivine at high pressures (~3GPa). Our observations suggest that REE contents of high-pressure carbonates are low. Our observations of the REE content of carbonate from the leucitite groundmass show enrichments of LREE up to 100*PM suggesting that REE become more compatible in carbonates at lower pressures.

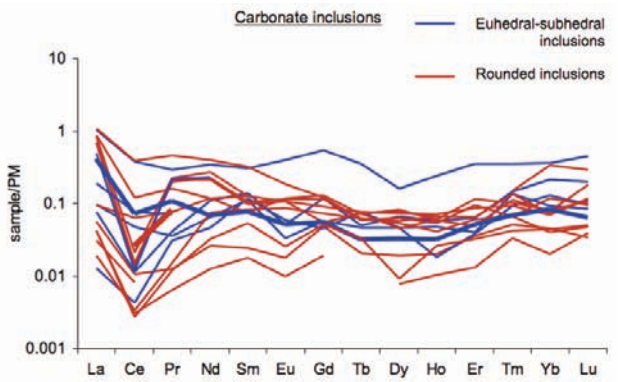

Fig. 1: Rare earth element analyses of carbonate inclusions.

The kinship between lamprophyres and carbonatites: evidence from the south coast of Ireland

Brady, A.* & Moore, K.R.
National University of Ireland Galway, Ireland
(*a.brady9@nuigalway.ie)

Explosive pipes, dykes and sills of phlogopite-bearing lamprophyric and carbonatitic compositions occur in three groups along the coast in County Cork, Ireland (Moore et al, this volume). The lithologies present are summarised in the following groups: xenocryst and xenolith-bearing alkaline ultramafic lamprophyres (Al-UML) of aillikite affinity, xenocryst and xenolith-free alkaline lamprophyres (AL), dolomite-silicocarbonatite, calcite-silicocarbonatite, and subordinate carbohydrothermal calcite-carbonatite. All silicocarbonatite lithologies also contain accidental material. Xenoliths include pargasite-clinopyroxenite.

The Al-UML has high but variable Mg number (59 – 70), and Cr, Ni and V concentrations (up to 419 ppm, 445 ppm and 236 ppm respectively), characteristic of primitive mantle-derived magmas. The alkaline lamprophyres contain higher SiO_2, Al_2O_3 and Na_2O, and lower Mg (27 – 65), Cr and Ni than the Al-UML. However, overlapping major element concentrations and similar concentrations of trace elements suggest that the alkaline lamprophyres are not related to the Al-UML solely by fractionation from a single parent magma, but by progressive overstepping of the solidus in shallower mantle with some subsequent fractionation.

Dolomite-silicocarbonatite contains magnesite and Cr-spinel macrocrysts≤ (40.14 wt.% Cr $_2O_3$), low REE concentrations and exceptionally high Ni and Cr concentrations (up to 971 ppm and 868 ppm respectively). The major element composition and the presence of elevated Ni and Cr content is consistent with both experimental data and the composition of established primary mantle-derived dolomite carbonatites worldwide. Calcite-silicocarbonatite composition contrasts with that of the dolomite-silicocarbonatite in that it contains a lower Mg-number, higher REEs in addition to a pronounced negative Ta anomaly. Phlogopite in calcite-silicocarbonatite contains less titanium than phlogopite that crystallised from the primary magmas, while bulk titanium concentration remains relatively constant. Variations in phlogopite compositions occur due to increasing oxidation of evolving magmas, which promotes the crystallization of Ti-magnetite. Thus, the evolved phlogopite compositions in calcite-silicocarbonatite do not reflect a primary magma from the mantle and the bulk rock geochemistry suggests that the calcite-silicocarbonatite has not fractionated from the dolomite-silicocarbonatite.

The possibility that a continuum between carbonatite and ultramafic lamprophyre exists as a consequence of melting of a carbonated mantle has been experimentally proven [1]. However, observed rock major and incompatible trace element patterns, and xenolith compositions, for the Al-UML, alkaline lamprophyre and dolomite-silicocarbonatite suggest primary derivation by similar fractions of partial melting from a heterogeneous mantle source, accompanied by reaction between magma and wall-rock. Between the Al-UML and calcite-silicocarbonatites, a strong compositional continuum in Si, Ti, Al, Ca, Mn, P, Cr, Ni, Nb and LREE concentrations supports a different genetic relationship. Moderate fractionation of dominantly high Mg-number silicate minerals in the crust accounts for the presence of calcite as the dominant carbonate phase in most carbonatitic intrusions. Supporting evidence for further extensive fractionation is present as the essentially silica-free calcite carbonatite that is considered to be carbohydrothermal residua.

[1] Dalton, J.A. & Presnall, D.C. (1998) *J.Petrol.*, **99**, 1953-1964.

New forms of carbonate volcanism: what to look for and where

Bailey, D.K.
Dept. of Earth Sciences, University of Bristol, U.K.
(ken.bailey@bris.ac.uk)

Volcanoes in the melilitite-nephelinite-leucitite province of Calatrava, central Spain, have erupted carbonate in a variety of forms, notably dominated by maars and cinder cones. Both forms carry mantle debris and megacrysts. Lava flows are rare. Similar volcanism occurs in Limagne province, central France, and in other intra-continental provinces in Europe and Africa, and may be expected in other continents. In Spain there are ~250 vents, with a similar number in France: all examined to date have erupted carbonate, with potentially hundreds of cases.

As the igneous nature of the carbonate had previously passed unrecognised in these areas, it is vital to look more closely at all alkaline mafic-ultramafic provinces, where field geology and petrography will provide the first pointers to carbonate eruptions. Maar rim-breccias and scoria cone deposits have carbonate matrices. Immense quantities of mantle debris have been erupted from maars. Fresh silicate glass is present, with no signs of water driven eruption: maar and scoria deposits pass into carbonate-supported tuff and agglomerate, with carbonate contents > 50%. Sheets of carbonate rich tuffs are spread widely away from the emission centres, and constitute the most abundant effusive carbonate. Carbonate-supported scoria tuffs have the distinctive fabric of black silicate melt clasts in a pale matrix. These pristine silicate glasses, quenched at temperatures >1100°C, contain globules of immiscible carbonate and carbonate phenocrysts, which must be cognate, and intrinsic to the high T melts. Other characteristics are the platy habit of carbonate crystals, and euhedral Ti magnetite spinels with Cr-rich cores.

Pyroclastic eruptions are characteristic of alkaline mafic-ultramafic volcanism but traditionally research has centred on lava flows: there is now a clear need for close examination of fragmental eruptions, especially tuffs with black clasts in a pale matrix. Eruptions composed largely of carbonate are typically lapilli tuffs, and in places show spectacular depositional structures not previously described for igneous carbonates. For any successful search, evidence from the pyroclastic rocks will be vital. As eruptions of carbonate with these compositions have not been witnessed, these eruptive modes may not be in the classic canon of volcanology.

Location of new carbonate volcanism	
(a) Already known cases: **Total, 10:**	**(b) Prime suspect cases (by igneous association)** **Total, 19:**
Europe , 6: Spain, 1 (*Calatrava)*; France, 2 (*Limagne, S. Rhone*); Germany, 1 (*W Eifel*); Italy, 2 (*Veneto, Sicily*). **Africa, 4:** Canary Is.; Cape Verde Is.; Kenya; Zambia	**Europe , 5:** Spain,1; Germany, 2; Czech Republic, 1; Hungary, 1. **Africa, 8:** Morocco; Algeria; Cameroun; NW Kenya; N. Tanzania; S. Tanzania; Uganda; Zaire **Americas, 3:** USA, 1; Brazil, 2. **Australia, 1:** S. Australia. **Antarctica, 1:** Gaussberg. **Oceans, 2:** Kerguelen; Hawaii.

Carbonatite melt inclusions in coexisting magnetite, apatite and monticellite in Kerimasi carbonatite, Tanzania: implications for melt evolution

Guzmics, T.[1*], Mitchell, R.H.[2], Szabó, Cs.[1] & Berkesi, M.[1]
[1]Lithosphere Fluid Research Laboratory, Eötvös University Budapest, Hungary ([*]tibor.guzmics@gmail.com)
[2]Lakehead University, Thunder Bay, Ontario, Canada

Kerimasi calciocarbonatite consists of calcite, apatite, magnetite and monticellite. Carbonatite melt and fluid inclusions can be found in apatite and magnetite, and silicate melt inclusions in magnetite. Calcite contains fluid and S-bearing Na-K-Ca-carbonate inclusions. Our study shows compositional data for quenched S- and P-bearing, Ca-alkali-rich carbonatite melt inclusions in magnetite (Fig. 1) and apatite. Magnetite-hosted silicate melt inclusions have peralkaline composition with normative sodium-metasilicate. Based on our homogenization experiments, apatite-hosted melt inclusions and forsterite-monticellite phase relationships, temperatures of the early stage of magma evolution are estimated to be 900-1000°C. At this time three immiscible liquid phases coexisted: (1) a Ca-rich, P-, S- and alkali-bearing carbonatite melt, (2) a Mg- and Fe-rich, peralkaline silicate melt, and (3) a C-O-H-S-alkali fluid. During the evolution of coexisting carbonatite and silicate melts, the Si/Al and Mg/Fe ratio of the silicate melt decreased with contemporaneous increase in alkalis due to olivine fractionation. In contrast, the alkali content of the carbonatite melt increased with concomitant decrease in CaO resulting from calcite fractionation. Overall peralkalinity of the bulk composition in the immiscible melts increased, causing a decrease in the size of the miscibility gap in the pseudoquaternary system. The studied melt inclusion data indicate the formation of a carbonatite magma that is extremely enriched in alkalis with a composition similar to that of Oldoinyo Lengai natrocarbonatite.

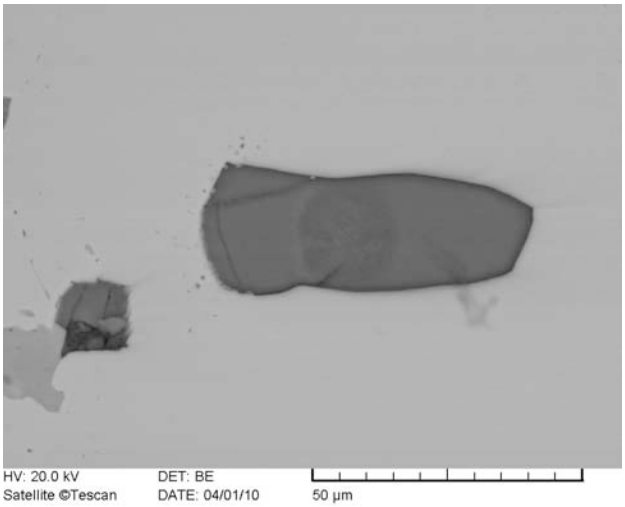

Fig. 1: Magnetite-hosted, quenched carbonatite melt inclusion after heating to 880°C (BSE image).

The compositions of carbonatite melt inclusions are considered as representatives of parental magma composition contrarily to any whole rock that contains negligible amount of alkalis. Consequently, implications for magma composition and evolution using bulk rock carbonatite composition should be reconsidered.

Sadiman volcano, Crater Highlands, Tanzania: does it really contain melilitites and carbonatites or it is just a phonolite-nephelinite volcano?

Zaitsev, A.N.[1*], Wenzel, T.[2], Markl, G.[2], Spratt, J.[3], Petrov, S.V.[1] & Williams, C.T.[3]
[1]Faculty of Geology, St. Petersburg State University, St. Petersburg, Russia ([*]burbankite@gmail.com)
[2]Institut für Geowissenschaften, Universität Tübingen, Germany
[3]Dept. of Mineralogy, Natural History Museum, London, UK

Sadiman is 4.8-4.0 Ma old volcano located in the Crater Highlands area in northern Tanzania [1,2]. Limited published data [2-4] and field observations show that it consists of interlayered phonolitic tuffs and nephelinitic lavas. Rare xenoliths of phonolite and ijolite were observed in the nephelinites. It was suggested that Sadiman volcano contains melilititic and carbonatitic rocks [5]. These also occur as tuffs in the Laetoli area where fossilised footprints from human ancestors are known [6,7] which is why Sadiman is of special interest as a possible source of them.

We found that nephelinites range from phenocryst-poor to phenocryst-rich rocks; the latter seem to be cumulates. Nepheline and diopside are the principal phenocryst minerals; rarely observed are shorlomite, perovskite or wollastonite. Microphenocrysts and groundmass consist of diopside, nepheline, sanidine, titanite, sodalite and apatite in various proportions. Perovskite also occurs as corroded relicts in titanite crystals. Aenigmatite (in grownd mass and as a reaction rim on titanite), magnetite, and pyrrhotite are accessory minerals. Nephelinites are low-magnesium rocks (Mg# = 0.17-0.26) with a peralkaline index ranging between 0.88 and 1.21. On a volatile-free basis these rocks contain 46.3-52.6 wt% SiO_2 and 10.5-15.9 wt% Na_2O+K_2O. Mineralogical and geochemical data suggest that they are highly evolved phonolitic nephelinites.

Phonolites are phenocryst-rich rocks with anorthoclase and nepheline being the principal minerals. Diopside and titanite are minor phases.

Tuffs contain sanidine as a major mineral, as well as highly altered nepheline and diopside. Heavy mineral concentrates from tuffs are enriched in euhedral perovskite crystals.

No evidence was found for the presence of melilite or primary calcite in any of the samples studied. Also, minerals which can be considered as indicators of carbonatitic activity, and known e.g. from the close Kerimasi carbonatitic volcano (nyerereite, pyrochlore or baddeleyite [8]), have not been found at Sadiman. Only secondary calcite, formed during low-temperature (?) alteration of tuffs, occurs as isolated anhedral crystals and forms veinlets.

All available data do not currently support the occurrence of melilitites and carbonatites at Sadiman volcano.

[1] Bagdasaryan, G.P. et al. (1973) *Geochem. Int.*, **10**, 66-71. [2] Mollel, G.F. (2007) *PhD thesis*, Rutgers University. [3] Paslick, C. et al. (1995) *Earth. Planet. Sci. Lett.*, **130**, 109-126. [4] Paslick, C. (1996) *Contrib. Mineral. Petrol.*, **125**, 277-292. [5] Dawson, J.B. (2008) *Geol. Soc., Memoirs*, **33**, 39-77. [6] Hay, R.L. (1978) *Contrib. Mineral. Petrol.*, **67**, 357-367. [7] Hay, R.L. (1986) *Geol. Soc., Sp. Publ.*, **25**, 339-344. [8] Zaitsev, A.N. (2009) *Zapiski RMO*, **5**, 63-77.

Oxygen isotopic composition of garnet, clinopyroxene and zircon megacrysts from kimberlites in Democratic Republic of Congo: insights into their petrogenesis

Pivin, M.[1*], Valley, J.W.[2], Spicuzza, M.J.[2] & Demaiffe, D.[1]
[1]Dept. des Sciences de la Terre et de l'Environnement, Université Libre de Bruxelles, Belgium ([*]mpivin@ulb.ac.be)
[2]Dept. of Geoscience, University of Wisconsin, Madison, WI, USA

Garnet, clinopyroxene (cpx) and zircon megacrysts from the central DRC Mbuji-Mayi diamondiferous kimberlite province (Cretaceous) and garnet megacrysts from the south-eastern DRC diamond-poor Kundelungu kimberlite field (Lower Oligocene) have been analyzed by laser fluorination and mass spectrometry for oxygen isotope compositions at the University of Wisconsin-Madison.

Garnet megacrysts from both localities display similar $\delta^{18}O$ values that match the range of mantle values from garnet peridotites but average ~ 0.2‰ higher than those of garnet megacrysts from other localities worldwide (Fig. 1a,b). The addition of DRC garnet megacrysts (n=51) to the worldwide megacryst population (S. Africa, N. America and Australia, n=121) slightly increases the mean $\delta^{18}O$ value [1] to 5.30±0.42‰ (2SD). The results for cpx are also within the mantle range for peridotites (Fig.1c). Zircon megacrysts show a very narrow $\delta^{18}O$ range, similar to that of other zircon megacrysts worldwide (Fig.1d).

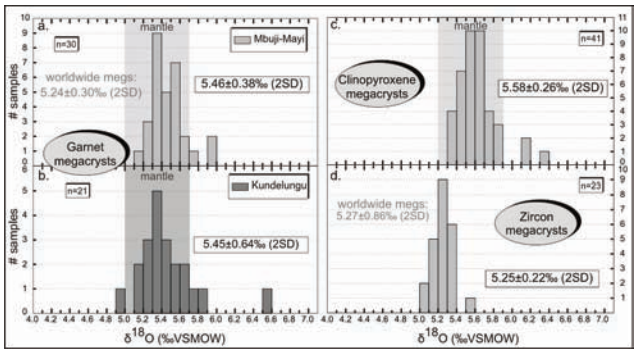

Fig.1: $\delta^{18}O$ distribution histograms for Mbuji-Mayi garnets (a), cpx (c) and zircons (d), and for Kundelungu garnets (b). Also: number of samples analyzed and average of $\delta^{18}O$ compositions. Worldwide megacryst averages: (a) and (b) from [1] and (d) from [2,3]. Mantle $\delta^{18}O$ compositional ranges (a-b-c) from [4].

The homogeneity in zircon megacryst $\delta^{18}O$ values from Mbuji-Mayi confirms the unlikelihood of a metamorphic genesis in a subducted oceanic crust and rather suggests a magmatic/ metasomatic origin [2,3].

DRC garnet and cpx are thought to result from metasomatic transformation of mantle peridotites by a precursor kimberlite fluid which produced a Ti-Fe-K-LREE enrichment [5]. Identical $\delta^{18}O$ averages for Mbuji-Mayi and Kundelungu garnet megacrysts suggest a similar origin. Moreover, the $\delta^{18}O$ ranges of DRC garnet and cpx megacrysts overlap those of mantle peridotites, suggesting a possible genetic relation. DRC garnets display slight but regular $\delta^{18}O$ – major element co-variations that could be explained by the percolation of a metasomatic fluid whose composition gradually changes (open system) through interaction with peridotite wall-rocks.

[1] Schulze, D.J. et al. (2001) *Geochim. Cosmochim. Ac.*, **65**, 4375-4384. [2] Valley, J.W. et al. (1998) *Contrib. Mineral. Petrol.*, **133**, 1-11. [3] Page, F.Z. et al. (2007) *Geochim. Cosmochim. Ac.*, **71**, 3887-3903. [4] Mattey, D. et al. (1994) *Mineral. Mag.*, **58A**, 573-574. [5] Pivin, M. et al. (2009) *Lithos*, **112(2)**, 951-960.

Magma mingling and mantle xenolith transport in the feeder system of diatreme root zones: evidence from the south coast of Ireland

Moore, K.R.[*], Brady, A. & Dempsey, C.
National University of Ireland Galway, Ireland
([*]kathryn.moore@nuigalway.ie)

A suite of late Carboniferous subvolcanic intrusions has cut through the sedimentary sequence of the South Munster Basin in County Cork (Ireland) utilising Caledonian lineaments that were reactivated during the Variscan. Three loci of thermo-hydraulic explosions have been identified. (1) The White Ball Head pipe is a root zone breccia spatially associated with carbonate-bearing lamprophyres. (2) The Cahermore root zone breccia is cut by a silico-carbonatite sill-like pipe that is partly constrained by bedding and jointing in the host rocks. (3) The deep-seated diatreme at Black Ball Head is filled with massive alkaline ultramafic lamprophyre, the inner zone of which contains an anastomosing fluidised fabric rather than a feeder channel (and which is cut by later calcite carbonatite), and the outer zone of which comprises a substantial root zone breccia. The three localities together describe a classic example of the evolution of a diatreme volcano structure by downward propagation of the root zone [1].

Dykes and sills are associated with the three areas of thermo-hydraulic explosions, but the spatial and geochemical associations do not coincide. The centrally-located White Ball Head area includes a dyke and two sills that are found to resemble the Black Ball Head and Cahermore localities in terms of their transported mantle material, geochemistry and mineral assemblages. All three intrusions contain primary mantle carbonate and two of the intrusions contain juvenile magmatic enclaves and schlieren. It is likely that magma mingling occurred shortly before emplacement and caused the evolution of volatiles that may have acted as a trigger for rapid magmatic ascent and entrainment of mantle material. The distribution and constitution of entrained mantle and crust material was examined in order to place some constraints on magma flow rates, which are consistent with previously calculated velocities for Minette dykes [2]. However, the size, abundance and distribution of mantle peridotite xenoliths indicate that, although flow velocity was maintained during ascent and through dykes, it decreased within sills allowing xenolith settling towards the lower half of the intrusion.

Numerous dykes devoid of transported mantle material and evidence of magma mingling have similar trace element signatures to, but not the characteristic chemical markers of, the compositions of explosive root zone intrusions. It is likely that these dykes were feeder dykes for limited duration scoria cone eruptions. In contrast, the xenolith-bearing White Ball Head intrusions are interpreted as a dyke-sill feeder system where magma periodically drained towards the loci of thermo-hydraulic explosions. The initiation of the explosions may be a shallower crustal response to the rapid ascent rates and volatile exsolution caused by magma mingling.

[1] Lorenz, B. & Kurslaukis, S. (2007) *J. Volcanol. Geoth. Res.*, **159**, 4-32. [2] Morin, D. & Corriveau, L. (1996) *Contrib. Mineral. Petrol.*, **125**, 319-331.

Cumulates and crystal mushes: insights into alkaline magma chambers from glass-bearing mafic xenoliths

Downes, H.*, Kelly, J.L. & Beard, A.D.
Dept. of Earth and Planetary Sciences, Birkbeck University of London, UK (*h.downes@ucl.ac.uk)

Cumulate xenoliths consisting of pyroxene and amphibole are common in many regions of mafic alkaline magmatism and represent parts of magma chamber walls. Although most xenoliths were solid when entrained, some contain glass, indicating that melt was still in place when they were brought to the surface. Thus they represent unconsolidated parts of magma chambers which could be described as "crystal mushes". We have investigated such xenoliths from Santo Antao in the Cape Verdes islands, which contain variable proportions of clinopyroxene (diopside) and amphibole (kaersutite to Ti-pargasite), together with accessory apatite, titanite, sodalite-group feldspathoid and Fe-Ti oxides. The interstitial glass, which can reach >20% in some samples, has a broadly tephri-phonolitic composition. The glass compositions are identical to the most evolved lava compositions on Santo Antao [1], indicating that the xenoliths represent fragments of a crystallising magma reservoir beneath the island. In some cases the trapped magma contains vesicles, which are the result of exsolution of volatiles from the magma within the xenolith during eruption.

We have analysed the phases for a wide range of trace elements using LA-ICP-MS (Fig. 2). The interstitial glass has a mantle-normalised incompatible trace element pattern similar to that of evolved lavas from the island. Titanite is the most enriched mineral phase, although it has lower abundances of Rb, Ba, Pb and Sr than the glass. Amphibole and clinopyroxene have similar abundances of most trace elements except for Nb-Ta, Ba and Rb. Haüyne is a significant repository of Sr only. Apatite (only one analysis to date) is strongly LREE-enriched but shows troughs for all the HFS elements (Zr, Hf, Nb, Ta, Ti).

Our results can be used to calculate trace element distribution coefficients for common minerals in equilibrium with phonotephritic magma. The results will be compared to those obtained by Downes et al [2] who investigated similar xenoliths from Germany and Israel that contained basaltic glass.

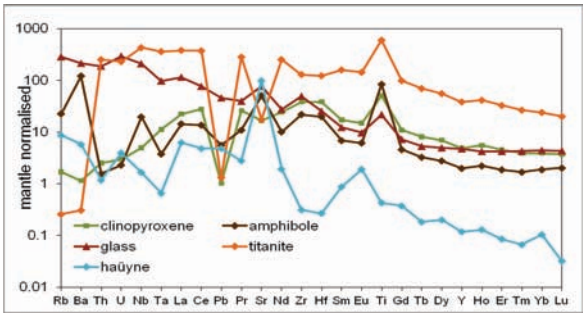

Fig. 1: Average trace element compositions of phases from glassy xenolith CV1.

[1] Holm, P.M. et al. (2006) *J. Petrol.*, **47**, 145-189. [2] Downes, H. et al. (2001) *Lithos*, **75**, 1-17.

Zircons from kimberlites at Lac de Gras, Canada - a section through the continental crust

Nuber, N.[1*], Gerdes, A.[1], Brey, G.[1] & Grütter, H.[2]
[1]Institut für Geowissenschaften, Goethe-Universität Frankfurt, Frankfurt, Germany (*nuber@em.uni-frankfurt.de)
[2]BHP Billiton World Exploration Inc., Vancouver, B.C., Canada

The determination of diamond grain size distribution is an important aspect of the economic assessment of primary deposits. Initial analysis is typically achieved by subjecting 40 to 200 kg samples of kimberlite to caustic fusion in order to quantitatively recover microdiamonds. Only diamonds, zircons, oxide minerals, corundum and occasional rutile survive this intense chemical process. We have analyzed such zircons from six different kimberlites from the Ekati property in the Slave Province, Canada. We consider kimberlite diatremes as drill cores through the continental crust which may provide us with information from the deeper continental crust. The age distribution together with the Hf isotopic composition of the zircons would provide constraints on the time of formation of continental crust. Furthermore, we measured the REE abundances to obtain information about the host rocks.

Three main age groups can be distinguished in 150 LA-ICP-MS analyses we have completed on 100 zircon grains The youngest U-Pb ages are between 54 and 61 Ma (25% of the population) which correspond to the kimberlite emplacement ages at Ekati [1]. However, our zircon REE data is unusual for kimberlite hosts. Typically zircons from kimberlites have low REE abundances and no Eu anomaly [2]. The zircons in this study have high REE contents and a pronounced negative Eu anomaly and thus resemble crustal zircons crystallized from felsic melts. Their εHf scatter from -7.5 to +11.9 indicating that they crystallized from heterogeneous or distinct protoliths.

A second U-Pb age group lies between 93 and 104 Ma (17%), ages so far unknown in this area. Their Hf isotopic composition is highly variable and ranges from juvenile (initial εHf of +11) up to Palaeoproterozoic crustal residence times (T_{DM} ~ 2.0 Ga; initial εHf of -18) of the protoliths.

The third age group forms about 40% of the zircon population and is defined by Archean zircon with U-Pb ages of 2.54 to 2.87 Ga. The majority of them have early Archean depleted mantle model ages (average crustal residence time) of 3.2 to 3.6 Ga, with maxima at 3.3 and 3.5 Ga. Others are more juvenile, pointing to Mesoarchean crust formation of around 2.9 Ga. They arose from several intrusions with variable chemistry from tholeiitic to tonalitic and granodioritic [3].

Paleoarchean crust formation is also support by one grain which yielded an age of 3.3 Ga and a εHf of +1.5.

A minor group of zircons (4%) with ages around 1.8-1.9 Ga suggests Paleoproterozoic recycling of Mesoarchean crust. These could represent recycling in one of several Paleoproterozoic diabase-producing magmatic events. Furthermore, some zircons, with concordant Jurassic to Palaeproterozoic (1.9 Ga) ages and positive εHf, point to very minor addition of juvenile crust during that time.

In summary, the crust of the Ekati-mine district in the Slave province was predominantly formed during Archean times in two phases at Paleoarchean (3.5 – 3.3 Ga) and the Mesoarchean (~ 2.9 Ga) and subsequently recycled during the Neoarchean. In addition, minor amounts of juvenile crust formed through dikes or smaller intrusions sporadically until Eocene.

[1] Creaser, R.A. et al. (2004) *Lithos*, **76**, 399-414. [2] Page, F.Z. et al. (2007) *Geochim. Cosmochim. Act.*, **71**, 3887-3903. [3] Davis, W.J. & Bleeker, W. (1999) *Can. J. Earth Sci.*, **36**, 1169-1187.

Tracing chemical evolution of primary pyrochlore from plutonic to volcanic carbonatites: the role of F

Bambi, A.[1], Melgarejo, J.C.[2*], Costanzo, A.[3] & Gonçalves, O.A.[1]
[1]Dept. de Geologia, Universidade Agostinho Neto, Luanda, Angola
[2]Dept. Cristal·lografia, Mineralogia i Dipòsits Minerals, Universidad de Barcelona, Catalunya, Spain (*joan.carles.melgarejo.draper@ub.edu)
[3]School of Natural Sciences, Earth and Ocean Sciences, National University of Ireland, Galway, Ireland

Three carbonatite outcrops from Angola were selected in order to evaluate change in composition of pyrochlore group minerals during the magmatic evolution in different levels of emplacement: a) Tchivira carbonatites occur in a plutonic complex and are associated with alkaline and basic rocks; b) Bonga carbonatites represent an example of hypabyssal carbonatites and c) Catanda carbonatites consist of volcanic carbonatites, either as lavas or as pyroclastic rocks.

In Tchivira plutonic carbonatites pyrochlores are euhedral and zoning is poorly developed. F fullfill the position for the additional anions, and Na is close to 1 apfu. Zoning may account to substitutions of Nb in the B position, although the content of Ti, Ta and Zr does not reach 0.01 apfu. Contents of REE, U, Th, and LILE are also very low.

Pyrochlores from the hypabyssal Bonga carbonatites are abundant, generally euhedral and vary in grain size up to 1 cm. Oscillatory zoning is also commonly observed. F and Na contents are lower than in Tchivira (~0.8 apfu). In the B position the content of Th, Ti and Ta increases slightly. Accordingly, in the A position the substitutions of Na by Th, U and REE increases, as well as the vacant number. Ca remains approximately constant and close to 1 apfu.

Pyrochlore crystals from Catanda are very small (less than 50 μm), euhedral and display complex internal textures. They generally have a rounded core, relatively corroded and mantled by two or three late generations. Composition of the core is close to that of Bonga pyrochlores. The rims of the crystals are strongly enriched in Zr (up to 0.3 apfu), Ta (up to 0.12 apfu), Th (up to 0.15 apfu), Ce (up to 0.12 apfu) and U (up to 0.17 apfu), but impoverished in F and Na.

Results from this study show that F and Na contents decrease from plutonic to volcanic carbonatites; this trend is also associated to other trends of enrichment such as Th, U and REE in the A position and Ta and Zr in the B position. Zoning in the pyrochlore may be explained by changes in the F fugacity, mainly due to crystallization of fluorite or apatite in the deeper carbonatites, or by degasification in the volcanic carbonatites.

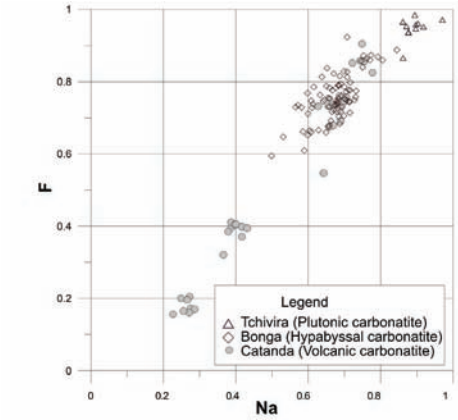

Fig. 1: Plot of Na vs. F contents of pyrochlore in carbonatites from Angola.

A new type of Zr-Nb ore mineralization from the Gremiakha-Vyrmes massif, the Kola Peninsula

Sorokhtina, N.V.[1*], Kogarko, L.N.[1] & Shpachenko, A.K.[2]
[1]Vernadskyernadsky Institute of Geochemistry and Analytical Chemistry RAS, Moscow, Russia (*nat_sor@rambler.ru)
[2]Geological Institute KSC RAS, Apatity, Russia

Gremiakha-Vyrmes is an Early Proterozoic multiphase alkaline-ultrabasic intrusive complex. This massif includes four rock complexes: 1 basic-ultrabasic (gabbro-norites, gabbro-wehrlites, monzodiorite, anorthosites); 2 alkaline-granites, granosyenites and quartz syenites; 3 alkaline rock (melteigites, ijolites, juvites, nepheline syenites, foyaite, foidolites); 4 carbonatites, various albitites, aegirinites which cross-cut ultrabasic and foidolitic rocks [1]. Zr-Nb ore mineralization has been found in albite-microcline and aegirine-albite rocks. Albitites, aegirinites and carbonatites are located in the Aegirine Navolok section in the central zone of the massif and are surrounded by the foidolitic rocks. The rare metal mineralization is represented by zircon and pyrochlore-group minerals. The pyrochlore mineralization is confined to aegirine-biotite albitites, foidolites and syenites.

The following evolutionary sequences of rare metal minerals has been observed: 1 in albitites to gabbro - betafite - uranpyrochlore – thorogummite and coffinite and U-Si-Nb phases – "silicified" pyrochlore; 2 in albitites to foidolites and syenites - pyrochlore – bariopyrochlore or uranpyrochlore or pyrochlore-Sr - "silicified" pyrochlore – deficient hydrated pyrochlore and Fe-Nb, Al-Nb phases.

Extraction and accumulation of rare metals in the rocks of the Gremiakha-Vyrmes massif took place under low temperature hydrothermal conditions at elevated concentrations of Si, Al, Fe sometimes U and Th in solution. Primary pyrochlore is leached, it is hydrated, enriched in Si and deficient hydrated pyrochlore and new phases of Nb, U, Th, Fe-Nb, Al-Nb are formed. This process of transformation of primary Nb minerals is similar to the evolution of rare metal phases in alkaline complexes analogous to Lovozero [2] and in carbonatites.

Isotope data obtained for carbonatites of the Gremiakha-Vyrmes massif, linked to albitites point to a mantle source. Albitites could have formed during the metasomatism triggered by intrusion of carbonatites into the alkakaline complex of the massif.

Acknowledgements: Research covered by RFBR grant 09-05-12026-ofi_m, NSH-3848.2010.5

[1] Vursiy, G.L. (2000) *Vestnik MGTU*, **3**, 285-292. [2] Chakhmouradian, A.R. & Mitchell, R.H. (2002) *Eur. J. Mineral.*, **14**, 821-836.

Recognition of a postcollisional (Oligocene) carbonatitic activity from the Sillai Patti carbonatite complex, Malakand Agency, North West Pakistan: constraints from fission-track dating of apatite

Khattak, N.U[*] & Asif Khan, M.
National Centre of Excellence in Geology, University of Peshawar, Pakistan ([*]nimat_khattak@yahoo.com)

The Sillai Patti carbonatite complex represents the second largest carbonatite complex of the Peshawar Plain Alkaline Igneous Province (PAIP) of northern Pakistan, the first being the Loe-Shilman carbonatite complex. The Sillai Patti is situated about 70 km north of Peshawar and about 20 km west of Malakand, near Sillai Patti village, in Malakand Agency of the North West Frontier Province. This carbonatite body occurs along a thrust fault in the form of a sheet which is striking in the NNE-SSW direction and is roughly dipping to the south. The carbonatite body is about 12 km long and 2-20 m thick. The carbonatite sheet is emplaced either within the metasediments or at the contact of metasediments and granite gneiss.

Emplacement time of the Sillai Patti carbonatite complex has been under considerable dispute since long ago. To resolve the dilemma fission-track dating studies on the crystals of apatite using the external detector method and age standard approach (the ζ method) were carried out. A fission-track age of 29.6 ± 1.5 Ma was obtained for the Sillai Patti carbonatite body. Close resemblance of the fission-track apatite age of this study with the fission-track as well as other high temperature radiometric ages from the same as well as the neighboring carbonatite bodies of the alkaline belt of northern Pakistan strongly suggests that the Sillai Patti carbonatite body was emplaced at high crustal level (shallow burial depths) and cooled there relatively fast to near ambient temperatures (<60°C) required for the complete retention of fission tracks in apatite and that the fission-track age of 29.6 ± 1.5 Ma of this study is the emplacement age of the Sillai Patti carbonatite.

Trace elements and volatile components in silicate and silicate-salt magmas of the Mushugai-Khuduk carbonatite-bearing alkaline complex, southern Mongolia

Andreeva, I.*& Kovalenko, V.
Institute of Geology of Ore Deposits, Petrography, Mineralogy, and Geochemistry, Russian Academy of Sciences, Moscow, Russia (*andreeva@igem.ru)

Inclusions of mineral-forming media were studied using various techniques including X-ray spectral and ion microanalysis. Based on this study, trace elements and volatile components were evaluated in silicate and silicate-salt melts (melt inclusions) from minerals of major rock groups (melanephelinites, shonkinites, phonolites, quartz syenites, and rhyolites) of the Mushugai-Khuduk alkaline carbonatite-bearing complex (Mongolia). The silicate melts form a continuous series from basic to rhyolitic compositions with SiO_2 contents from 47 to 77 wt% [1]. The salt-silicate melts are silicate-phosphate in composition containing up to 10-20 wt% of P_2O_5.

Our data on the trace-element composition of glasses in homogenized silicate melt inclusions in alkaline rocks of the Mushugai-Khuduk complex indicate that all of the melts are characterized by similar trace- element patterns. Glasses in melt inclusions in silicate minerals from the mafic rocks are enriched in REE Th, U, and Li but depleted in Ti and K. Comparing the trace-element and REE patterns of glasses in inclusions in minerals of the mafic rocks (melanephelinites and theralites) and glasses in inclusions in minerals from more evolved derivatives (syenites and rhyolites), one can note that the REE and P_2O_5 patters are similar for all of the inclusions, and the concentrations of these components systematically decrease in inclusions in minerals from more acid rocks, first of all, in apatite, which is the main REE concentrator. The differences in the Ba behavior, which is characterized by positive anomalies in the melanephelinites and theralites and negative ones in the syenites and rhyolites, are likely explained by the fractionation of alkali feldspar, the main Ba concentration of these rocks. Glasses in silicate-salt melt inclusions in apatite from the shonkinites, theralites, and quartz syenites also display similar trace-element patterns. Compared to the silicate melts, they are more strongly enriched in REE, Ba, Th, and U but depleted in Ti, Nb, K, and Zr.

Our data on the trace-element composition of the melts of the alkaline rock series at the Mushugai-Khuduk complex testify that these rocks are genetically interrelated and were likely produced at silicate-salt immiscibility in the magma. The silicate-salt magmas were thereby significantly enriched in certain trace elements and REE compared to the silicate melts. This led us to believe that the genesis of the REE-bearing magnetite-apatite rocks was related to the identified silicate-salt melts. The magma of the mafic rocks of the complex started to crystallize at high temperatures of 1220-1070°C and was poor in water. The water content in the magma of the intermediate and acid alkaline rocks increased in the course of differentiation and reached 4-7.6 wt%.

[1] Andreeva, I.A. & Kovalenko, V.I. (2003) *Per. Mineral*., **72**, Special issue: Eurocarb. P., 95-105.

Pyrochlore from metasomatic rock at Bolshetagninskoe niobium deposit (Eastern Siberia, Russia)

Azarnova, L.A.* & Temnov, A.V.
All-Russian Scientific Research Institute of Mineral Resources Moscow, Russian Federation (*lazarnova@mail.ru)

The Bolshetagninskoe deposit is one of the most important Russia niobium occurrences. It is confined to carbonatite complex of the same name that is situated in the Sayan Mountains, Eastern Siberia. About half of the Bolshetagninskii complex comprises carbonatite the rest consisting of syenite, ijolite and alkaline metasomatic rocks. Pyrochlore is the main economic mineral of niobium at the deposit. It is unique in that the pyrochlore is mostly concentrated in alkaline metasomatic rocks which consist predominantly of microcline and carbonate ("microclinite") or biotite and apatite ("sljudite").

Pyrochlore was analysed in fresh (43 analyses) and weathered (74 analyses) microclinites samples by electron microprobe (fig. 1). Pyrochlore from fresh microclinite has a high A site occupancy of between 1.702-2.009 per 2 B cations. A site is occupied by Na, Ca, Sr (up to 0.080 pfu), U (up to 0.005 pfu). There are sr-bearing pyrochlore nodules in the fresh microclinite pyrochlore. The mineral has low A site occupancy of between 1.399-0.947 and contains Sr 0.116-0.235 pfu.

Secondary pyrochlore occurs throughout weathering metasomatic rocks. The weathering profile of the deposit is represented leaching microclinite in which the major components are microcline, goethite, apatite. The first type of weathered pyrochlore is weakly leaching pyrochlore which has a lower A site occupancy of between 0,849 to 1,771. A site is occupied by major components Na, Ca and minor ones Sr (up to 0,040 pfu) and Ce (up to 0,044 pfu). Another type of weathered pyrochlore is kalipyrochlore. The deposit is the second known locality of kalipyrochlore. The first one is the Lueshe complex, Zaire [1]. Kalipyrochlore has a (Å) 10.54±0.01, very low A site occupancy between of 0.215-0.363 and chemical composition close to kalipyrochlore from Lueshe. The mineral grain is zoning and has A site occupancy 0.267 in central part and 0.281 in outer one (0.201 and 0.190 K, 0.028 and 0.044 Ca, 0.002 and 0.004 Na). Kalipyrochlore grains are zoned with B site cations too: central parts contain (pfu) Nb 1.769, Ti 0.187, Fe 0.044; outer ones contain Nb 1.633, Ti 0.338, Fe 0.030.

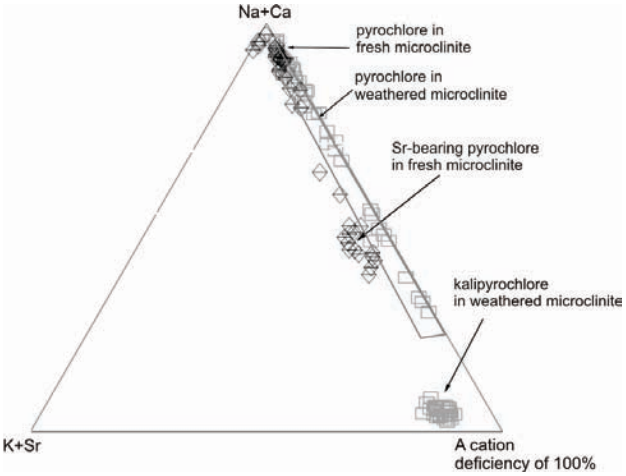

Fig.1: A cation occupancy of pyrochlore of Bolshetagninskoe deposit (calculated per 2 B site cations).

Acknowledgements: The authors thank N.I. Chistjakova and I.S. Naumova (FGUP «VIMS», Moscow) for performing pyrochlore X-Ray and energy-dispersion microprobe analyses.

[1] Wall, F. et al. (1996) *Mineral. Mag.*, **60**, 731-756.

Mineralogy of felsic globular structures of camptonites, Ditrău Alkaline Massif, Romania

Batki, A.* & Pál-Molnár, E.
Dept. of Mineralogy, Geochemistry and Petrology, University of Szeged, Hungary (*batki@geo.u-szeged.hu)

The Ditrău Alkaline Massif (DAM) is a Mesozoic alkaline igneous complex situated in the S-SW part of the Giurgeu Alps belonging to the Eastern Carpathians (Romania). It outcrops right east of the Neogene-Quaternary Călimani-Gurghiu-Harghita calc-alkali volcanic belt by breaking through the pre-Alpine metamorphic rocks of the Bukovina Nappe. According to our present knowledge, the DAM is an intrusive rock body with an eastern, north eastern tilt, built up by several tectonic blocks providing the massif a complex form. Great number of different rock types appears on the surface (ultrabasites, gabbros, diorites, monzonites, syenites, nepheline syenites, granites, lamprophyres, etc.). Based on K/Ar data [1] originating from various mineral fractions of different rock types has shown that the DAM is the result of a long lasting (Middle Triassic – Lower Cretaceous) two phase magmatic process, which started during the Triassic by the opening up of the Tethys and the detachment of the Getida-Bukovina Microplate from the Eurasian Plate.

Camptonites are alkaline lamprophyres with more plagioclase than alkali feldspar, can include Na-foids and containing essential amphibole which dominates over biotite. They are a group of alkali-rich igneous rocks and form subvolcanic dykes, sills, plugs, stocks or vents [2]. This paper reports new results on the mineralogy of felsic globular structures (ocelli) of camptonites which were absolutely not discussed in former works of the DAM.

Mineral compositions were determined by Cameca SX-50 electron microprobe under probe current of 15 nA and acceleration voltage of 20 kV operating conditions at the Department of Earth Sciences, University of Uppsala, Sweden. Cathodluminescence studies were carried out by Reliotron cold cathode luminoscope and Eclipse 600 polarizing microscope at the Institute for Geochemical Research, Hungarian Academy of Sciences, Budapest.

Camptonites occurring in the northern part of the DAM are 20 cm-2 m wide dykes. Based on textural features and mineral composition two types of camptonites can be divided: a pyroxenic and a pyroxene free variety. Pyroxenic camptonites consist of diopside phenocryst, groundmass kaersutite and Mg-biotite, interstitial albite-oligoclase and ocelli filled with euhedral calcite in the core and anhedral plagioclase at the rim. Some of these large calcite crystals can be 2.7 mm in size. The cathodluminescence images of the calcites show homogeneous texture and lighter orange in colour at the rims than in the cores which reflect their variable Fe- and REE-content. The ocelli can contain La-Ce-bearing allanite within plagioclase cores as well which is characteristic at kaersutite-plagioclase intergrowth. Pyroxene free camptonites have groundmass hastingsite–magnesiohastingsite, Fe-Mg-biotite and albite-andesine with the same silica-rich mineral assemblages in the felsic globular structures. In these ocelli the euhedral titanite ($CaTi_{0.89-0.95}Fe_{0.03-0.07}Al_{0.04-0.06}SiO_5$) (up to 550 μm) and apatite are always bigger than the anhedral ones in the groundmass.

The texture and mineral composition of felsic globular structures of the pyroxenic camptonites suggest that they formed by the separation of CO_2-rich volatiles at late-stage of the crystallisation process. The silica-rich ocelli of the pyroxene free camptonites were produced by liquid immiscibility at the final stage as well.

[1] Pál-Molnár, E. & Árva-Sós, E. (1995) *Ac. Mineral. Petrogr., Szeged*, **36,** 101-116. [2] Rock, N.M.S. (1991) *Lamprophyres.* Blackie & Son, Glasgow.

Mineralogical control on the behaviour of Nb-Ta and Zr-Hf pairs in Cenozoic nephelinites and peralkaline phonolites from Saghro (Moroccan Anti-Atlas)

Berger, J.[1*], Ennih, N.[2], Mercier, J.C.C.[3] & Liégeois, J-P.[4]
[1]Université Libre de Bruxelles, Brussels, Belgium (*juberger@ulb.ac.be)
[2]Université Chouaïb Doukkali, El Jadida, Morocco
[3]Université de La Rochelle, La Rochelle, France
[4]Royal Museum for Central Africa, Tervuren, Belgium

Nephelinites and phonolites from Saghro are amongst the most Si-undersaturated and alkali-rich lavas of the Circum-Mediterranean Cenozoic igneous provinces [1,2]. Despite the paucity of lavas with intermediate composition between nephelinites and phonolites, the continuum of clinopyroxene compositions, fractional crystallisation modelling [2] and Sr-Nd-Pb isotopic ratios suggest that the two groups of lavas are linked by a fractional crystallisation process.

Nb concentration does not increase from primitive to evolved nephelinites, whereas Zr content linearly increases with decreasing Mg. This can be explained by early fractionation of perovskite (which can trap up to 2 wt% Nb_2O_3). Phonolites are strongly enriched in the most incompatible elements compared to nephelinites, except for Sr, REE (apatite effect) and Ta. They show high Nb, Zr, Th and U contents (up to 2100 ppm Zr and 600 ppm Nb) with fractionated Nb/Ta and Zr/Hf ratios. Both ratios increase during differentiation (Fig. 1): from 19±1 and 40±10, respectively, in the nephelinites, to 30-69 and 61-82, respectively, in the phonolites; this reflects the more compatible behaviour of Ta compared to Nb and of Hf compared to Zr.

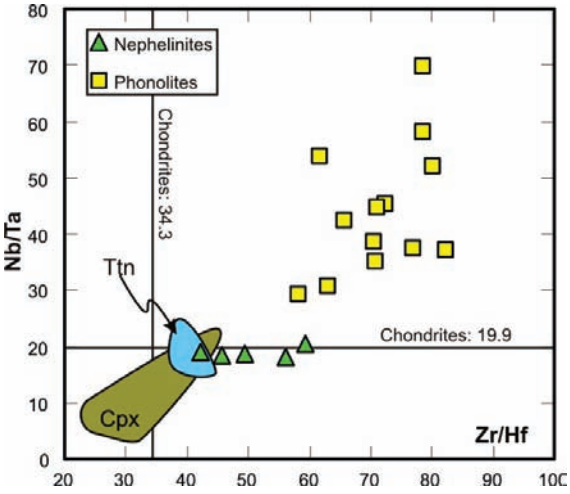

Fig. 1: Nb/Ta and Zr/Hf ratios in Saghro lavas and their minerals.

LA-ICP-MS analyses of the main mineral phases show that both clinopyroxene (cpx) and titanite (ttn) fractionate Nb-Ta and Zr-Hf pairs (Fig.1) with the difference that these elements are incompatible or moderately compatible in the clinopyroxene lattice but strongly compatible in titanite with $D_{Hf}>D_{Zr}$ and $D_{Ta}>D_{Nb}$ (D_{Zr}: 6; D_{Hf}: 9; D_{Nb}: 22, D_{Ta}: 42).

The final steps of crystallisation and differentiation are evidenced by segregations of peralkaline, Zr-, Nb- and volatiles-rich melts that crystallised pure aegirine, apatite, hainite and delhayelite in small microdomains interstitial to the feldspar laths network of phonolites. Brown augite phenocrysts were transformed into green aegirine-augite during reaction with these highly differentiated melts, while titanite reacted into lorenzenite and eudyalite-group minerals.

[1] Lustrino, M. & Wilson, M. (2007) *Earth Sci. Rev.*, **81**, 1-65. [2] Berger, J. et al. (2009) *Mineral. Mag.*, **73**, 59-82.

Geological significance of the Shatingaobao aegirine syenite in Alxa area, Inner Mongolia: constrains from SHRIMP zircon U-Pb geochronology and petrogeochemical characteristics

Cai Jianhui[1*], Yan Guohan[2] & He Guoqi[2]
[1]Institute of Mineral Resources, Chinese Academy of Geological Sciences, Beijing, China ([*]caijh_cags@163.com)
[2]Faculty of Earth and Space Sciences, Peking University, Beijing, China

The Shatingaobao aegirine syenite complex (1.42 km^2) occurs at the Northern margin of Alax League, Inner Mongolia, China, which tectonically belongs to the middle part of the Central Asian Paleozoic orogenic belt. The stock mainly consists of alkali feldspar (65-70%), plagioclase (10-15%) and aegirine. In this paper the SHRIMP U-Pb age (246.4±1.9Ma) of zircons from the Shatingaobao aegirine syenite is reported for the first time, suggesting that its main intrusion is a product of early Triassic alkaline magmatic activity, and there is an early Triassic alkaline intrusion – A-type felsic volcanic rock belt parallel to the suture between the North China – Tarim plate and the Siberian plate, which is composed of the Weiya quartz-syenite (246Ma [1]) in Xinjiang, the Shatingaobao aegirine syenite and the Xilinhaote – Xiwuqi A-type felsic volcanism in Inner Monglia (245Ma, [2]).

According to the contents of major and trace elements (Table 1), the Shatingaobao syenite has low silicon and higher alkalis, with a Rittman index of 5.9-8.3, enriched in Rb, Ba and depleted in Nb, Ta. The contents of REE are high with an average ∑REE of 356×10^{-6}, light REE enriched slightly and a weak negative Eu anomaly. These results have shown that the Shatingaobao syenite is deemed to be both alkaline and an A-type granite, formed in a post-orogenic extensional environment of the Central Asian orogenic belt in the Triassic, the same as the Weiya and the Xilinhaote complexes.

Table 1: The petrogeochemical data of the Shatingaobao aegirine syenites in Alax area, Inner Mongolia

NO.	01ST-1	01ST-2	01ST-3	ST-8	ST-10	NO.	01ST-1	01ST-2	01ST-3	ST-8	ST-10
SiO_2	52.57	51.30	51.66	50.00	49.83	Ga	24.10	22.83	25.40	18.20	22.10
TiO_2	1.00	0.90	1.05	0.96	0.84	Y	27.83	23.74	27.99	20.61	21.67
Al_2O_3	16.97	15.19	16.53	12.87	14.63	Cr				122.0	117.0
Fe_2O_3	6.72	6.56	7.02	6.55	6.63	Ni				76.0	73.0
MnO	0.10	0.12	0.11	0.09	0.08	Co				28.0	24.0
MgO	4.84	4.24	4.22	3.89	4.24	V				139.0	90.0
CaO	4.15	7.40	5.28	5.10	6.34	La	84.09	73.05	86.93	68.79	83.18
Na_2O	2.72	2.31	3.18	2.42	2.68	Ce	178.4	152.0	182.0	126.5	148.5
K_2O	5.05	4.69	5.43	5.19	4.32	Pr	20.21	17.32	21.03	16.48	18.50
P_2O_5	1.21	1.14	1.26	0.90	0.44	Nd	78.23	67.38	81.95	66.87	70.47
LOI	4.60	5.57	4.67			Sm	13.43	11.73	14.08	12.48	12.30
Rb	170.9	166.6	169.2	139.0	169.0	Eu	3.39	3.09	3.51	3.61	3.02
Sr	935	1125	1310	1340	675	Gd	12.08	10.77	12.67	8.82	8.83
Ba	1553	1549	1611	992	1180	Tb	1.34	1.20	1.41	1.14	1.05
Nb	12.93	12.16	14.50	11.83	11.82	Dy	6.04	5.32	6.26	5.06	4.66
Ta	0.90	0.84	0.95			Ho	1.03	0.90	1.05	0.99	0.92
Zr	530	299	463	105	354	Er	2.66	2.28	2.72	2.05	2.01
Hf	11.63	7.17	10.50			Tm	0.35	0.30	0.36	0.31	0.32
U	7.64	8.47	7.67	0.00	4.00	Yb	2.22	1.88	2.30	1.71	1.81
Th	35.98	33.09	34.93	7.00	22.00	Lu	0.32	0.27	0.33	0.28	0.31

The data is analyzed by XRF and ICP-MS (wt% and ppm)

The development of the Central Asian orogenic belt involved three stages: orogenic, post-orogenic and non-orogenic. The post-orogenic stage started at about 320Ma according to previous research. The end time is constrained by the formation age of the early Triassic alkali intrusive – A-type acid volcanic rock belt mentioned above. It is suggested that the post-orogenic stage of the middle part of the Central Asian Palaeozoic orogenic belt is between 320-245Ma.

[1] Zhang, X.H. et al. (2006) *Acta Petr. Sin.*, **22(11)**, 2769-2780. [2] Zhang, Z.Z. et al. (2005) *Acta Geol. Sin.*, **79(4)**, 481-490.

The origin of the tantalum-bearing Upper Fir carbonatite, east-central British Columbia, Canada: preliminary results

Chudy, T.C.[*] & Groat, L.A.
Dept. of Earth and Ocean Sciences, The University of British Columbia, Canada ([*]tchudy@eos.ubc.ca)

The Upper Fir carbonatite is the largest system within a group of carbonatite-alkaline-ultramafic rocks in the Monashee Mountains of British Columbia, Canada. These form sill-like bodies of variable thickness that have been multiply deformed and metamorphosed (upper amphibolite grade) together with the regional miogeoclinal strata. Three compositionally different carbonatite types, an ultramafic rock, a REE-bearing pyroxenite, fenites and various pegmatitic veins have been identified. The most abundant rock type is a magnesio-carbonatite which consists mostly of ferroan-dolomite, fluorapatite, amphibole and minor amounts of zircon, iron oxides and sulfides, and the Nb-Ta minerals pyrochlore and ferrocolumbite. Textures range from fine-grained to porphyritic to coarse-grained carbonatites which also exhibit various degrees of deformation resulting in mylonitized, foliated or cataclastic patterns. Local accumulations of amphiboles or apatites, some of which are also enriched in pyrochlore, underline the compositional heterogeneity. The calcio-carbonatites form inconsistent layers or lenses of variable thickness within the magnesio-carbonatites. Typical flow-like textures result from large, anhedral, ovoid magnetite blobs that mantle apatite and amphibole grains, all suspended or aligned in a very fine-grained calcite matrix. Volumetrically of minor importance are moderately deformed, medium- to coarse-grained mica-magnesio-carbonatites that are composed of biotite, dolomite and apatite. Subordinate rock types are highly altered and heterogranular pyroxenites and undeformed pyroxene-apatite rocks. The latter contain approximately 60 vol.% pyroxene with 30 – 40 vol.% apatite and locally abundant biotite, calcite, monazite, allanite, and pyrochlore. Pegmatitic veins show a wide range of compositions, mostly pyroxene-amphibole-calcite assemblages, and are usually <50 cm thick. Fenites are inconsistently developed at the contact of carbonatites and country rocks.

The Upper Fir carbonatite is a compositionally and texturally heterogeneous system of carbonatites and related rocks, which is also reflected in its Nb-Ta mineralization. Pyrochlore and ferrocolumbite are the major Nb-Ta carriers in this carbonatite and occur as individual grains in the carbonates, as inclusions in other phases, and as composite grains that consist of both phases in variable proportions.

In order to successfully ascertain the petrogenesis of these rare magmatic rocks and the reason for their economically important tantalum enrichment, future work will include (1) detailed petrography of all rock units with emphasis on mineral assemblages, textures, and phase relations; (2) mineral chemistry of rock forming and trace minerals in all identified units; (3) fluid inclusion studies of apatite; and (4) investigations of the isotopic systems of carbon, oxygen, strontium and neodymium (in whole rock and minerals). Results obtained from step (4) will provide important information about any (preserved) magmatic, metasomatic, or metamorphic overprint(s), and contamination, and define the source of the carbonatites. Steps (1) to (3) relate to the magmatic evolution which in general involves the processes of fractional crystallization or liquid immiscibility.

The influence of carbonatite during petrogenesis of nepheline syenites at the Poços de Caldas Complex (Brasil): evidence from geochemistry and fluid inclusions

Costanzo, A.*, Moore, K.R. & Feely, M.
School of Natural Sciences, Earth and Ocean Sciences, National University of Ireland, Galway, Ireland
(*alessandra.costanzo@nuigalway.ie)

The Poços de Caldas caldera complex in São Paulo State, Brazil is almost entirely composed of evolved alkaline rocks. Rock types include phonolites, tinguaites, nepheline-syenites and eudialyte-bearing nepheline-syenites [1]. Intense potassium-rich hydrothermal and metasomatic alteration are responsible for mineralization in the district, which is strongly enhanced by supergene enrichment in some places (e.g., zircon and caldasite occurrences, the U-Zr-Mo ore bodies of the Campo Agostinho and the open pit Osamu Utsumi uranium mine). The Poços de Caldas Alkaline Massif has carbonatite Sr and Ba enrichment, chondrite normalized REE distribution patterns similar to carbonatites, carbonatite-like metasomatism, zirconium mineralization and minor carbonatitic intrusions. These occurrences might imply that carbonatite magma+fluid existed at depths beneath the massif. Geochemistry and fluid inclusion data are used to test the carbonatite influences in the generation of alkaline magmas at Poços de Caldas.

Fluid inclusions (FI) are present throughout the Poços de Caldas rock suite and are hosted most commonly in nepheline. They consist of well-developed, monophase liquid and vapour inclusions, two-phase (liquid-vapour) and three-phase (solid-liquid-vapour) inclusions. Microthermometric data reveal low temperature phase behaviour with temperatures of homogenization below 400°C, but also the occurrence of different populations with higher temperatures (above 400°C). Na^+, K^+ and Cl^- are the dominant phases present in the inclusions. Ca^{2+} and Mg^{2+} are also present in small amounts. Spectra from LRM analyses of solid-rich FIs reveal the presence of burbankite, a rare carbonate mineral previously found as solid inclusions hosted by in carbonatite minerals or silicate minerals in carbonatite complexes. From the fluid inclusion assemblage identified (pyroxene-ilmenite-dolomite), which is similar to the host rock, it is suggested that the solid phases represent trapped solids or trapped melt that crystallized later on. The occurrence of burbankite in the nepheline-hosted inclusions is significant because the mineral assemblage trapped in the inclusions frequently accompanies burbankite in carbonatite. The presence of burbankite crystals in primary FIs in voluminous silicate rocks in addition to carbonatite-like metasomatism, and zirconium mineralization may imply the presence of more extensive carbonatite at depth and earlier in the eruption history of the volcano-plutonic complex. A model for multiple stages of magma generation at the massif will be presented.

[1] Ulbrich, H.H.G.J. & Ulbrich, M.N.C. (2000) *The Poços de Caldas alkaline massif. Post-Congress Field Trip Aft 08 Guidebook*, Int. Geol. Congr., Rio de Janeiro, Brazil, II, 22-44.

Stable carbon and oxygen isotope compositions of carbonatites at Speewah, Kimberley, Australia

Demény, A.[1*] & Gwalani, L.G.[2]
[1]Institute for Geochemical Research, Hungarian Academy of Sciences, Budapest, Hungary (*demeny@geochem.hu)
[2]Speewah Fluorite-Carbonatite Research Project, NiPlats Australia Limited, Perth, Western Australia, Australia

Carbonatites at Speewah in the Kimberley region of Western Australia, about 110 km southwest of Kununurra, form dykes that were emplaced along a north-trending splay from the northeast-trending Greenvale Fault at the western boundary of the Halls Creek Orogen. The carbonatite dykes intrude a thick composite sill of the Palaeoproterozoic Hart Dolerite (~1790 Ma), comprising tholeiitic dolerite and gabbro with its felsic differentiates that form the Yilingbun granophyres and associated granites. The dykes are comprised of massive calcite-carbonatite that hosts very coarse, pegmatitic veins and pods of calcite, and have largely replaced (carbonatitized) and fenitized the country rock Hart Dolerite suite (in a zone up to 150 m wide). Dykes of red-brown siliceous fluidized-breccia and epithermal-textured veins consisting of bladed quartz, adularia and fluorite are closely associated with the carbonatite dykes. Fluorite occurrences (resources currently reported as 6.7 Mt at 24.6% CaF_2) are also thought to be related to carbonatite emplacement. Although the precise age of the carbonatite is not known, it is thought to be post early Cambrian. Carbonatite occurrences from two areas (Yungul and Willmot) have been investigated by means of carbon and oxygen isotope analyses in order to determine the origin of the carbonate. The carbon isotopic compositions have indicated C isotope ranges of about –5.2 to –6.3‰ that support primary, mantle-derived origin for the carbonatites. The C and O isotope compositions show an overall positive correlation that can be attributed to both magmatic and magmatic-hydrothermal processes in their evolution. The Yungul carbonatites show rather wide C and O isotope ranges, whereas the Willmot localities are much more homogeneous, fitting the Yungul compositions. The magmatic C-O isotope trend also indicates crustal contamination and/or low-temperature water/rock exchange.

Microprobe and fluid inclusion evidence for late-stage zirconium, phosphorus, titanium and REE mineralisation in fenite

Dowman, E.[1,2*], Rankin, A.[1], Wall, F.[3], Carter, A.[4] & Jeffries, T.[2]
[1]School of Geography, Geology and the Environment, Kingston University, Kingston upon Thames, Surrey, UK
([*]emma@abdm.co.uk)
[2]Dept. of Mineralogy, Natural History Museum, London, UK
[3]Camborne School of Mines, University of Exeter, Cornwall Campus, Penryn, Cornwall, UK
[4]Dept. of Earth Sciences, UCL, London, UK

Most carbonatite complexes are surrounded by an aureole of metasomatised rocks, known as fenite. These rocks contain high levels of Na and K, with alteration assemblages of aegirine, sodium-rich amphibole and turbid K and Na feldspar. We are studying the mobility of the REE, Nb, P and Zr in well-developed fenite aureoles associated with REE-rich and apatite-magnetite-pyrochlore-bearing carbonatites at Kangankunde and Chilwa Island, Malawi.

Recrystallised quartz in the outer fenite has trapped typical portions of carbonatitic fluids as mostly secondary inclusions (c. 2-20 microns in size). That these traces are closely associated with CO_2-rich and alkali chloride-carbonate-bearing brines is shown by the occurrence of nahcolite ($NaHCO_3$), halite, calcite and the REE-carbonate phase, burbankite, as daughter minerals within fluid inclusions. Trace mineralisation in the form of solid inclusions (30-150 microns) of Nb-bearing rutile, zircon, baryte, strontiantite, fluorite and titanite is present in these outer fenites, together with REE-bearing banded fluorapatite, monazite, bastnäsite, and more rarely, epidote, celestine and plumbopyrochlore. Such assemblages are characteristic of late-stage carbonatitic fluids from mineralised carbonatite complexes. Rutile and fluorapatite are also present as trapped solids within inclusions, and co-eval with the mineralisation.

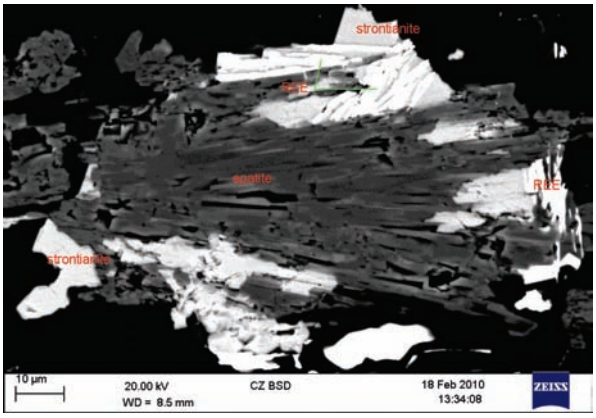

Fig. 1: SEM image of Kangankunde mineral assemblage.

The presence of such late-stage mineralisation derived from carbonatitic fluids in fenitised rock at some distance from carbonatitic intrusive centres supports previous work on the transport capabilities of such fluids [1] and suggests that the fenitising fluid has a direct relationship to the main REE mineralization in the central part of the complex. Fission track dating of apatite confirms a carbonatitic age but zircon from the assemblage dated by LA-ICP-MS gave an older age and may be originally, at least in part, derived from the country rock.

[1] Rankin, A.H. (2005) in Samson, I. & Linnen, R. (eds.) *Rare Element Geochemistry and Ore Deposits.* Mineral. Assoc. Canada Spec. Pub., Short course notes, **17**, 299-314.

The alkaline ring complexes of Egypt, revisited

El-Kaliouby, B.A.[1], Imbarak, S.H.[2*] & Buda, G.[3]
[1]Geology Dept., Ain Shams University, Cairo, Egypt
[2]Geology Dept., Suez Canal University, Ismailia, Egypt
([*]imbarak25@yahoo.com)
[3]Inst. of Geology, Eötvös Loránd University, Budapest, Hungary

The ring complexes of Egypt represent the northward continuation of the chain of ring complexes that associate the East African Rift System. Some fourteen alkaline ring complexes are encountered in the Eastern Desert of Egypt. They were formed during a long period of time extending from the Cambrian to the Upper Cretaceous and are characterized by special geological environments and form a number of characteristic rock associations. The distribution of the ring complexes in Egypt follows certain trends and is restricted to crests of anticlines due to high degree of fracturing along these crests. The largest ring complexes are those formed where two trends intersect. They are circular to elliptical in plain, and include a wide variety of rock types of alkaline affinities, ranging from mafic to felsic and from undersaturated to quartz-bearing syenitic rocks and their volcanic equivalent, all arranged in a concentric fashion.

The presence of nepheline syenite and related feldspathoidal types was described at the central part of Gabal Abu Khrug, Gabal El Kahfa, Gabal Nigrub El Fogani and Gabal El Naga, The presence of some syenite occurrences in connection with the ring complexes at South Eastern Desert is known at Zargat Naam.

There is a distinct change in the degree of alkalinity and silica saturation with age of the complexes. The older complexes are generally silica oversaturated and relatively low in alkalis, whereas the younger complexes are dominated by silica undersaturated rock types and are rich in alkalis

The origin of these complexes is probably due to alkaline melts that have been formed in the asthenosphere by shear heating, caused by changes in plate motion. These melts were emplaced along reactivated Pan-African fractures or pre-existing zones of weakness. The major structural features of the Nubian shield were formed during the Pan-African compression-accretion process (1,000-550 Ma BP) NE-SW and NW-SE zones of weakness. Most of the alkaline complexes of Egypt are associated with these lineaments.

The Egyptian ring complexes are classified into five types on the basis of their magmatic differentiation reflected in the variety of rocks they include, and on the degree of development of the ring nature and complexity of the structure:

(a) **Gabal Abu Khruq type**: These are fully differentiated complexes of a complicated structure containing nepheline syenites.

(b) **Gabal El Gezira type**: These are also highly differentiated complexes but with no nepheline syenite.

(c) **Gabal Mishbeh type**: This type is characterized by the slight differentiation of its rocks, the hardly recognizable ring nature and the rather complicated internal structure. They are formed of a variety of alkaline quartz syenites and some nepheline syenite.

(d) **Gabal Mansouri type**: These are the same as the Mishbeh type but lack any nepheline syenite.

(e) **Gabal Tarbtie type**: These are ring complexes of a simple structure and composition, formed of alkaline quartz syenite (nordmarkite) with relics of the volcanic cone. The dominant structure is a system of ring dykes.

K/Ar ages on mineral separates (biotite and hornblende) from these complexes yielded ages that range from 554 m.y. for Wadi Dib complex to 89 m.y. for Abu Khruq complex, i.e. from the Cambrian to the Upper Cretaceous [1].

[1] Serencsits, M. et al. (1979) *Annals. Geol. Surv.*, **9**, 102-116.

In-situ radiogenic isotope analysis and geochronology of accessory phases in alkaline complexes: Kaiserstuhl-Hegau Complex (Germany) as an example

Ghobadi, M.[1*], Gerdes, A.[1], Brey, G.P.[1], Höfer, H.E.[1] & Keller, J.[2]
[1]Institute of Geosciences, Goethe University, Frankfurt, Germany ([*]M.Ghobadi@em.uni-frankfurt.de)
[2]Institute für Mineralogie-Geochemie, Albert Ludwigs Universität, Freiburg, Germany

The origin and genesis of carbonatites and associated alkaline silicate rocks are since long in the focus of many research studies. Up to now most previous studies on the isotope composition of carbonatites have been based on whole rock analyses. Here we apply in-situ analytical methods to study the elemental and isotopic composition and variability of different accessory phases from the Miocene Kaiserstuhl and Hegau Alkaline Complexes. Our aim is to compare the mineral with whole rock data and to see if we gain additional information about the evolution of alkaline rocks and processes controlling their geochemical variations. Due to high absolute REE and Sr contents in alkaline rocks, the Rb-Sr and Sm-Nd isotope systems are relatively insensitive to crustal contamination and alteration processes.

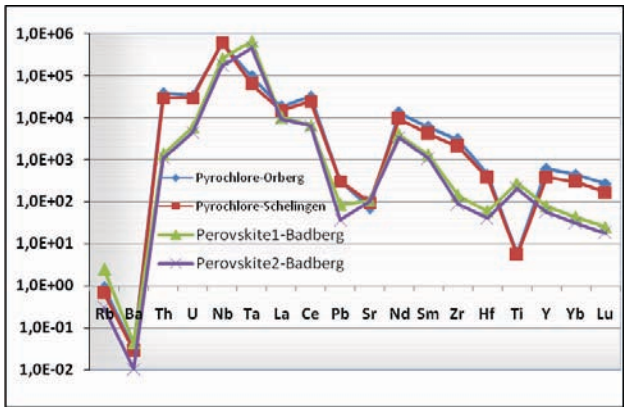

Fig. 1: Primitive Mantle normalized trace element diagram of perovskites and pyrochlores.

Our first results from in-situ LA-SF-ICP-MS Rb-Sr, Sm-Nd, and U-Pb spot analyses of perovskite and pyrochlore agree, in general, well with previous carbonatite whole rock data [1] and K-Ar ages. The εNd for perovskite and pyrochlore show a relatively narrow range from 3.2-4.3 and 3.2-4.4, respectively. This is slightly higher than previous measurements based on whole rock analyses (2.8-4.0) [1]. In the case of Sr isotopes the majority of the pyrochlore analyses ($^{87}Sr/^{86}Sr$: 0.7033-0.7048) overlap with the range known for carbonatites [2]. However, some pyrochlore (0.7052-0.7072) and all perovskite analyses (0.7048-0.7060) yielded considerably higher values. This could suggest either an analytical problem due to incomplete interference correction during isotope analyses or some alteration of the minerals due to interaction with a crustal fluid. The latter process is in line with our $^{206}Pb/^{238}U$ ages of perovskite (14.8 ±0.9 Ma) and pyrochlore (15.5 ± 0.4 Ma), which overlap with the lower range of published K-Ar ages but are significantly younger than the Ar-Ar sandine and phlogopite ages (17.2 and 17.3 Ma, respectively) [3].

[1] Schleicher, H. et al. (1990) *Lithos*, **26**, 21-35. [2] Kogarko, L. et al. (2010) *Mineral. Petrol.*, **98**, 197-208. [3] Kraml, M. et al. (1995) *Beihefte zum Eur. J. Mineral.*, **7**, 142.

REE distribution in clinopyroxenes and amphiboles from Panozero sanukitoid pluton - indication of postcrystallisation autometasomatism

Guseva, N.S.[*] & Skublov, S.G.
Institute of Precambrian Geology and Geochronology RAS, St.-Petersburg, Russia ([*]nadezhda_guseva@mail.ru)

The late Archean Panozero pluton in Central Karelia (Baltic Shield) is a multi-phase high-Mg, high-K intrusion with sanukitoid affinities, emplaced at 2.74 Ga. The magmatic history of the intrusion may be subdivided into three discrete magmatic impulses. The pluton includes rocks ranging from pyroxenites to monzonites. These rocks are products of fractional crystallization of a parental magma in a periodically replenished, periodically erupted magma chamber.

First estimation of the composition of the parental magma shows that it is enriched in LREE, Sr, Ba, Cr, Ni and P [1]. But our study of REE distribution in clinopyroxenes and amphiboles, added to data for the Sm-Nd isotopic system, indicates that there was a stage of LREE enrichments at some stage in the history of the pluton.

Clinopyroxene is the first crystallizing phase of the rocks of first and second impulse, so they in the most part reflected the composition of the parental magma. Clinopyroxenes are unzoned and have Mg# 0.72 –0.75. Amphiboles are calcic and according to the classification [2] are Mg-hornblende, edenite and pargasite (hornblende group) and actinolite-tremolite.

REE in minerals were determined on a CAMECA-IMS-4f ion microprobe. Sm-Nd isotopic system data were adopted from [1].

The results indicate that CPx with nondisturbed Sm-Nd system has moderate LREE enrichment while the CPx with disturbed Sm-Nd system has strong LREE enrichment.

The shape of these REE patterns is unusual for most part of igneous clinopyroxenes, although similar patterns have been noted in clinopyroxenes from some alkaline rocks and metasomatized mantle xenoliths [3].

In the majority amphiboles (in both hornblende and actinolate) the shape of REE distribution is similar to clinopyroxenes that is characteristic for magmatic amphiboles, crystallizing in the conditions close to equilibrium with clinopyroxenes. In some amphiboles the second type of REE distribution, without enrichment by the easy rare earths is observed. Such REE distribution is observed in amphibole from rocks with strong Nd-isotopic system distribution.

REE-distribution patterns in clinopyroxene and amphibole allows us to make the conclusion that the rocks of Panozero pluton have undergone certain process after crystallization which have partially disturbed the Nd-isotopic system in rocks and minerals and led to the REE redistribution between minerals. Such a process may have been capillary metasomatism, caused by the influence of the fluids, which have separated from (parental?) subalkaline magma.

[1] Lobach-Zhuchenko, S.B. et al. (2008) *J. Petrol.*, **49**, 393-420. [2] Leake, B.E. et al. (1997) *Can. Mineral.*, **35**, 219-246. [3] Ionov, D.A. et al. (2002) *J. Petrol.*, **43**, 2219-2259.

Rare element minerals within Ditrău alkaline intrusive complex, East Carpathians, Romania

Hîrtopanu, P.[1*], Andersen, J.[2], Fairhurst, R.[2] & Jakab, G.[3]
[1]Dept. of Mineralogy, University of Bucharest, Romania
([*]paulinahirtopanu@hotmail.com)
[2]Camborne School of Mine, University of Exeter, UK
[3]IG Mineral, Gheorgheni, Romania

The Ditrău alkaline intrusive complex is situated within the crystalline rocks of the inner part of the East Carpathians. It has a distinct ring structure and a succession of magmatic events from gabbroic and dioritic magma to syenitic and various postmagmatic events as well, developed between a Triassic extensional stage and a Jurassic rifting stage. The succession of magmatic events in Ditrău could be completed with carbonatite intrusion, that followed after the alkaline intrusion and used the same pathways of the previous alkaline silicate melt. Its affiliation to anorogenic alkaline magmas explains their general feature Nb>>Ta and the predominance of LREE. The Ditrău carbonatite alkaline intrusive complex represents the end of long lasting fractionation processes in the crust and deep upper mantle, respectively. This explains the modest dimensions of Ditrău intrusion and its enrichment with incompatible elements. The high petrographic complexity of Ditrău massif is doubled by a great diversity of mineral occurrences. In addition to the 85 minerals previously mentioned, approximate 200 were recently identified, many of them being first occurrences in Romania.

The rare element minerals which were determined in Ditrău complex intrusion, belong to the following classes (in the predominant order): I. LREE(Y) carbonates: bastnaesite-(Ce), bastnaesite-(La), parisite-(Ce), parisite-(La), synchysite-(Ce), kainosite-(Y); II. Oxide minerals of Nb, Ta, REE(Y), Ti, Zr, Th, U: 1. Pyrochlore group with two subgroup: A. Pyrochlore subgroup: pyrochlore, yttropyrochlore, thorpyrochlore, ceriopyrochlore, bariopyrochlore, uranpyrochlore; B.Betafite subgroup: betafite, yttrobetafite-(Y); Microlite subgroup, with Ta>Nb is absent; 2. Fergussonite group: fergussonite-(Y); 3. Columbite-Tantalite group: ferrocolumbite, mangancolumbite; 4. Aeschynite group: Aeschynite-(Nd), Aeschynite-(Ce), Aeschynite-(Y); 5. Niobian rutile group; 6. Ilmenorutile group; 7. Baddeleyite group; 8. Secondary Th, Ce, U oxides: thorianite, cerianite-(Ce), uraninite; III. REE(Y), Phosphates: REE-apatite, REE-carbonatfluorapatite, monazite-(Ce), brabantite-huttonite, huttonite-monazite series, cheralite, karnasurtite-(Ce), karnasurtite-(Y), xenotime-(Y); IV. Silicates of REE-(Y), Th, Zr, Pb: allanite-(Ce), thorite, Fe-thorite, Fe-Zr-thorite, Pb-thorite, cerite-(Ce), lessingite-(Ce), cevkinite, zircon, Th-zircon; V. Halides class: Y-fluorite; VI. Tellurides class: Bi-Te (hedleyite) and unnamed Bi,Pb-Te. All these rare element minerals belong to the two different mineralization types, localized in two different areas of the Ditrău massif: Jolotca area, of vein type with rare element minerals rich in LREE, Nb, sulphides (pyrite, sphalerite, molibdenite, galena) linked to calcite- ankerite-, dolomite carbonatite in NV of massif, and Belcina area with Y and Th mineralization, less LREE, less sulphides and rich in Fe-oxides and hydroxides, situated outside the massif (towards SE), in the surrounding metamorphic rocks of Tulgheş Group. The Ta content of pyrochlore group in this area is high, but it maintains lower than Nb (Ta<Nb). The Belcina occurrence could be the last later stage, lower temperature carbonatites.

One can consider the Ditrău carbonatite alkaline intrusive complex as an example of primary magmatic crystallization in the first alkaline stage, followed by a carbonatite magma and then a hydrothermal or carbothermal depositions of largely rare element minerals. On the other hand, some rare element minerals, like Fe-thorite, Pb-thorite, Zr-thorite, Th-zircon, Bi-Pb telluride, etc could be new mineral species.

Morphological and spectroscopic features of microdiamond from Chagatay carbonatites (Uzbekistan)

Isaenko, S.I.[1*], Shumilova, T.G.[1] & Divaev, F.K.[2]
[1]Institute of Geology, Komi SC, UD, RAS, Syktyvkar, Russia
([*]s.i.isaenko@gmail.com)
[2]Central Geological-Geophysical Expedition of Government Geological Committee of Republic Uzbekistan

The new genetic type of diamond connected with carbonatites of Chagatay trachyte-carbonatite complex at the northern slopes of the Southern Nuratau Mts. [1] was discovered at the end of 20th century. By this moment the data about mineralogical particularities of the carbonatitic diamonds are very limited. Here we report for the first time about spectroscopic features of microdiamond enriched from the host rock with the method of thermochemical dissolution. The unique crystal was investigated using optical transparent microscopy, electron scanning microscopy and Raman spectroscopy.

The microdiamond crystal has skeletal habit and size about 50 μm, it is optically transparent and almost colorless with brilliant glance on facets. The crystal has been described with 13th facet variety of octahedron by Shafranovsky I.I. classification.

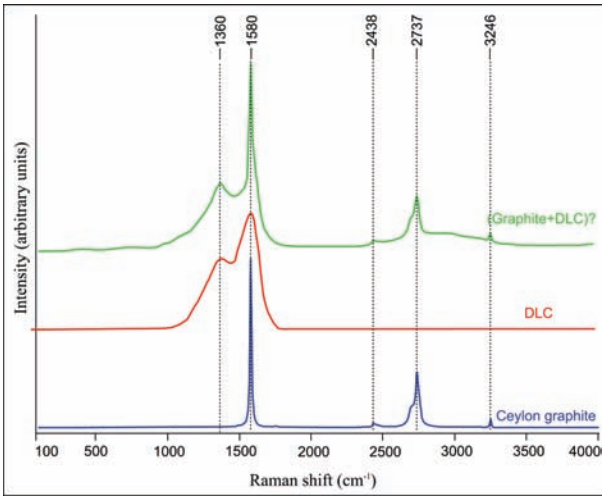

Fig. 1: Raman spectra of the microdiamond and reference standard of DLC and graphite. Raman spectrometer LabRam HR 800 with 488 nm line of external Ar^+ laser was used in this study at room temperature.

Using Raman spectroscopy two main types of spectra were identified. The first type is the spectrum with a peak of 1332 cm^{-1}, which corresponds to the frequency of diamond lattice oscillations at room temperature. The second type of spectrum is additive (Fig. 1, upper) – it consists of overlapping characteristic bands for graphite and DLC (diamond-like carbon). For comparison, reference spectra for the Ceylon graphite and DLC are also shown in the figure.

The received data are very important for understanding of formation mechanism of the new type of origin diamond objects.

[1] Djuraev, A.D. & Divaev, F.K. (1999) in Stanley, C.J. et al. (eds.) *Mineral deposits: Processes to Processing*. Rotterdam, Balkema, 639-642.

Alkaline rocks in the Aris area, central Namibia, Africa

Koller, F.[1*], Palfi, A.G.[2], Szabó, Cs.[3], Niku-Paavola, V.[4] & Popp, F.[1]
[1]University of Vienna, Austria ([*]friedrich.koller@univie.ac.at)
[2]Eximus Technologica Corporation (Pty) Ltd., Windhoeck, Namibia
[3]Lithosphere Fluid Research Lab, Dept. of Petrology and Geochemistry, Inst. of Geography and Earth Sciences, Eötvös University, Budapest, Hungary
[4]Geological Survey, Windhoek, Namibia

In the Aris area, south of Windhoek (Central Namibia) a cluster of Tertiary alkaline volcanic rocks were emplaced on and into the Paleoproterozoic basement gneisses. The alkaline suite consists mainly of highly variable phonolites, formed as subvolcanic or extrusive plugs, nepheline trachytes, extrusive trachytes as pyroclastic rocks and one under-saturated trachybasaltic sill.

The phonolites contain as main minerals nepheline, sodalite, sanidine, albite and aegirine. Blue amphiboles occur extremely rare and were found only at one locality so far. Nepheline and sodalite can be altered to natrolite. Further accessoric minerals are Mn-pectolite and goetzenite and various other unidentified phases. The alkali pyroxene is commonly zoned with a Di+He rich core (acmite >30%) and a Na-rich rim (acmite >90%). The nephelines can be defined by X_{Ks} of 0.15-0.19, sodalite with X_{Cl} values of 0.80-0.85. Both, sanidine and albite are homogenous and rather close to their end members with $Or_{0.90-0.95}Ab_{0.10-0.05}$ and $Ab_{0.97}Or_{0.03}$.

The bulk geochemistry of all phonolites is rather uniform with a Na/K ratio of ~3. In contrast to the homogeneous bulk composition there are strongly varying contents of F (200-12000 ppm) and Cl (50-6200 ppm), further a wide variation in the trace elements. In the phonolites Zr may range in individual complexes from 1300-2600 ppm with a Zr/Y ratio from 50-250. Also Nb show huge differences between the individual phonolite outcrops ranging from 330-1030 ppm. The REE-patterns show highly enriched LREE with La_N/Lu_N ratios are varying in a range of 25-50 and in some cases with a small negative Eu anomaly.

The nepheline bearing trachyte dikes are crosscutting the phonolites and are slightly Mg and Ca richer than the phonolites, but clearly Na poorer with a Na/K ratio around 2. The Zr, Nb, and REE are also slightly lower. The pyroclastic trachytes are K rich and lower in all trace elements.

Peculiarities of garnets from kimberlites of Nakynsky field, Yakutia

Kornilova, V.P., Spetsius, Z.V.[*], Lelukh, M.I. & Gerasimchuk, A.V.
ALROSA Co Ltd, Mirny, Yakutia, Russia,
([*]spetsius@cnigri.alrosa-mir.ru)

The Nakynsky kimberlite field is situated on the east part of Yakutian kimberlite province, about 250 km north–east from the town Mirny. Two diamondiferous kimberlite pipes (Botuobinskaya and Nyurbinskaya) with industrial grade of diamonds have been discovered within the Nakyn field about 10 years ago. Two additional little pipes (Mayskaya and Marxinskaya) were discovered only recently, in 2006. Unlike the other kimberlitic pipes of Yakutian province that belong to group 1, kimberlites of the Nakynsky field are similar to group 2, and are characterized by low K_2O and TiO_2 content, nearly full absence of ilmenite and high diamond grade.

Study of mineral inclusions in diamonds from these kimberlites reveal the presence of unusually large number of orange garnets, indicative of eclogite association. These data are confirmed by a wide distribution of eclogitic garnets in kimberlites of these pipes, which in the whole combine about 50% of garnet population from kimberlitic concentrate (Fig. 1).

Chemistry of garnets from the Nuyrbinskaya and other pipes testify that primary source of kimberlitic magmas of this field was strongly depleted mantle that have been intensively modified by later metasomatose enriched in potassium component.

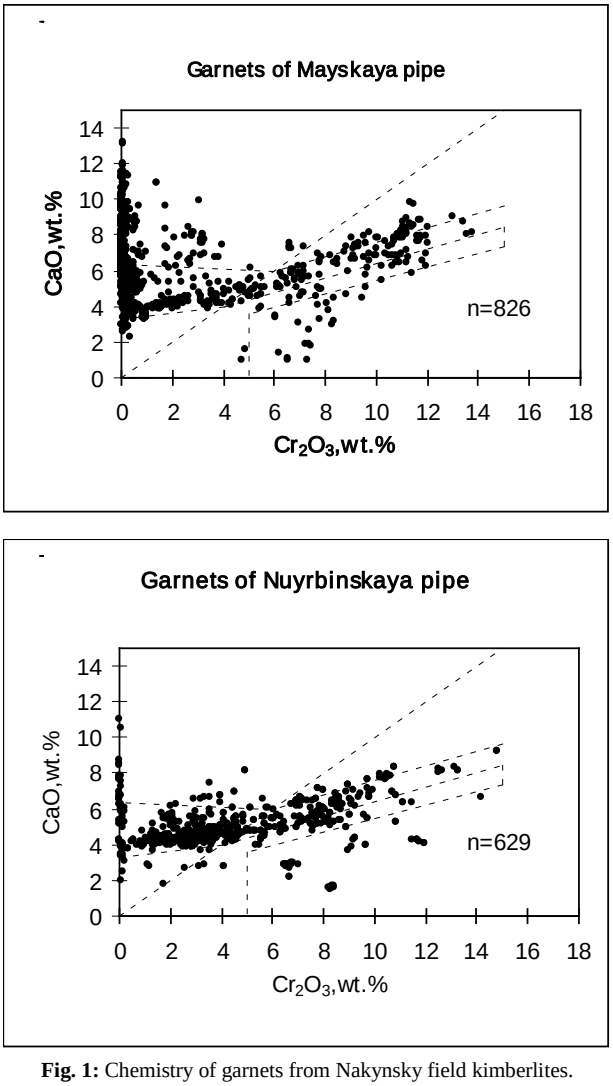

Fig. 1: Chemistry of garnets from Nakynsky field kimberlites.

Rare-earth mineral phases in carbonatites (Timan province, Russia)

Kovalchuk, N.
Institute of Geology, Komi Science Centre of RAS Urals Division, Syktyvkar, Russia (kovalchuk@geo.komisc.ru)

The research object is rare-earth mineral phases in carbonatites from the Kosyu massif (Timan province, Russia). Carbonatite massives are known in various parts of the globe, they are one of the basic sources of rare-earth raw materials. In the world more than 500 carbonatite bodies are known, many of them are commercial deposits. In Russia there are several well studied carbonatite provinces. However the Timan province, despite a number of industrial works in 1970-80s, differs by the least exploration degree. At present problems of phase attributes of rare-earth elements are still badly studied, which is one of the major problems for further estimation of prospects of the given object. The Kosyu carbonatites are characterized by considerable number of rare-earth mineral phases, the most frequent of them were analyzed by V. I. Stepanenko [1]. The modern instruments allows advanced study of substance at microlevel, provides more accurate data on mineral phases.

For the first time for the given object we carried out microprobe investigations of rare-earth mineral phases. In total about 100 analyses of the given type of mineralization have been done, and the phase diagnostics using the database of the museum named after A. E. Fersman and E. I. Semenov's basic monography have been performed. Microprobe studies as well as SEM allowed estimating features of chemical composition of the studied phases and receiving preliminary data on interrelations of rare-earth phases with rock-forming and ore components. In the Kosyu carbonatites the following phases are diagnosed: monazite, bastnaesite, pyrochlore, ancylite, Sr-rare earth carbonate, Nb-containing rutile and also Sr-Ce-La-phase. Rather wide variations of chemical composition of monazite have been determined, its leading geochemical specialization has been defined and its various morphological types of segregations have been determined.

The phase diagnostics has resulted in the considerable extension of data on rare-earth mineral phases in the Kosyu carbonatites, and the given object seems very promising for further investigation.

[1] Kostyukhin, M.N. & Stepanenko, V.I. (1987) *Baikalian magmatism of the Kanin-Timan Region*. Nauka, Leningrad (in Russian).

The RHA mineral classification of rocks exemplified on nepheline syenite family

Krasnova, N.I.*, Petrov, T.G. & Korolev, N.M.
Saint-Petersburg State University, Saint Petersburg, Russia
(*nataly_krasnova@rambler.ru)

A new method of description of mineral composition, which will promote improved nomenclature, is offered. The practical absence of parallel chemical and mineral content analyses of alkaline rocks has compelled the use of their normative composition, calculated by means of the program Norm-4.

The normative compositions for 418 chemical analyses of many alkaline rock varieties taken from different sources have been calculated. The results are represented in volumetric %, that most corresponds to the visual definition of the rock. The full version of data is displayed on the web-site: http://geology.pu.ru/ the file Min comp_alkaline rocks.rar.

The classifications of chemical and mineral composition have been made using the rank-entropy RHA-method [1]. R – the rank formula – is the succession of components in the system ranged according to diminishing content in the analysis. As a result we receive a set of rank formulae (R-Min) – sequences of minerals e.g. of type AbNeOrt… that correspond to decrease of volume fractions (%) of minerals in rock Ab> Ne> Ort>….

The rank formula sets are ordered under a certain "alphabet". The "alphabet" is the sequence of these minerals received in their chemical R-classification (a file R-Min-Catalogue-2007.rar at the same web-site). The principle of mineral rank formulae ordering is shown in the table.

Rank formula mineral				Rock name	An%
Ne	Ort	Ab	Di	khibinite	0
Ne=	Ort	Ab	Di	syenite	0
Ne=	Ort	Di	Ab	syenite Ne	2
Ab	Ne	Ort	Aeg	lujavrite	0
Ab	Ort	Ne	Ol	miaskite	7
Ab	Ort	Ne	Ol	syenite Ne	4
Ab	Ort	Ne	Ol	foyaite	12
Ort	Ne=	Ab	Aeg	khibinite	0
Ort	Ne=	Ab	Aeg	foyaite	0
Ort=	Ne	Ab	Di	syenite Ne	0

Our data illustrate the well-known domination of Ne, Ort and Ab assemblages in the composition of main Ne-syenite types. The RHA-method allows creation of a uniform, unequivocal classification of mineral compositions not only of the nepheline syenite group, but also all sets of rocks. It is necessary to consider the real mineral composition, including micas, amphibole, cancrinite, etc, instead of some virtual components, received sometimes from norm calculation.

Rock classification based on mineral composition using the RHA-method earlier has also been done on an example of phoscorites and carbonatites [2].

[1] Petrov, T.G. & Farafonova, O.I. (2005) *Information-component analysis. RHA method*. Textbook. St.-Petersburg (In Russian). [2] Krasnova, N.I. et al. (2004) in Wall, F. & Zaitsev, A.A. (eds) *Phoscorites and carbonatites from the mantle to mine: the key example of Kola alkaline province.* The Mineral. Soc. Series, 45-74.

Partitioning of trace elements between garnet, clinopyroxene and diamond-forming carbonate-silicate melt at 7 GPa

Kuzyura, A.V.[1*], Wall, F.[2], Jeffries, T.[3] & Litvin, Yu.A.[1]
[1]Institute of Experimental Mineralogy RAS, Chernogolovka, Moscow region, Russia ([*]shu25@rambler.ru)
[2]Camborne School of Mines, University of Exeter, Penryn, UK
[3]Dept. of Mineralogy, Natural History Museum, London, UK

A better understanding of the geochemical behaviour of trace elements at mantle conditions relevant to diamond formation may help to constrain the identity of the mantle medium from which natural diamonds can grow.

Our experimental work studied partitioning of trace elements under high pressure melting of a natural silicocarbonatite, to which representative set of trace elements had been added. Concentrations of trace elements in coexisting garnet, clinopyroxene and completely miscible carbonate-silicate melt were determined using LA-ICP-MS.

Light REE are partitioned favourably into the melt phase, and the rest REE go into garnet (Fig. 1). The Sm and Nd K_D values (for garnet/melt) are near to 1, as usually expected for REE when garnet is present [1]. LILE (Rb, Sr, Ba), Sc, and also Zn, Ta, Pb, Th, U have an affinity for carbonate-silicate melt.

Comparison with published data for garnet, clinopyroxene and carbonatite melt, and garnet, clinopyroxene and silicate melt [2-4] shows that the trace element partitioning is not significantly altered by changes in melt composition, with HREE always concentrated similarly in the garnet (Fig. 1). Carbonate-silicate melt as a diamond-forming medium and carbonatite or silicate melt equilibrated with mantle silicate minerals behave similarly in respect of trace element distribution. This makes it difficult to choose between the two melts as potential diamond-forming media if only the garnet is available for measurement of trace element concentration.

Acknowledgements: This work was supported by INTAS project 05-1000008-7927, the RFBR projects 08-05-00110, 10-05-00654, and grants of the President of Russian Federation 4735.2009.5 and 4754.2009.5

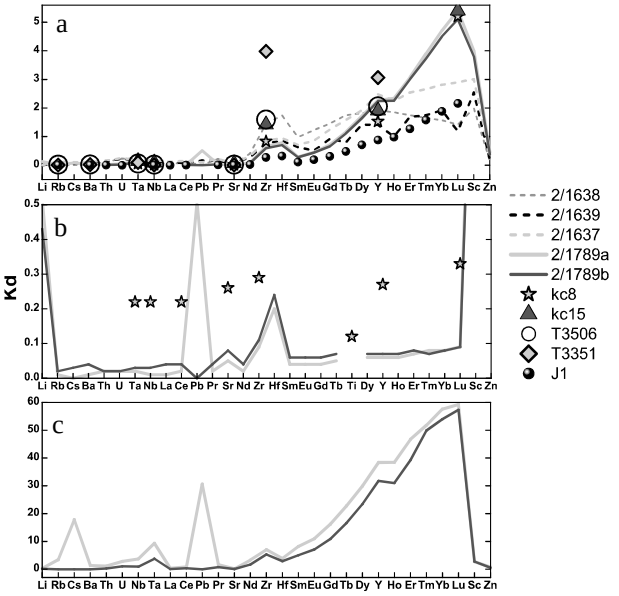

Fig. 1: Partition coefficients: (a) - grt and carbonate-silicate melt; (b) – cpx and carbonate-silicate melt; (c) – grt and cpx.

[1] van Westrenen, W. et al. (1999) *Am. Mineral.*, **84**, 838-847 [2] Sweeney, R.J. et al. (1992) *Earth Planet. Sci. Lett.*, **114**, 1-14. [3] Sweeney, R.J. et al. (1995) *Geochim. Cosmochim. Ac.*, **59**, 3671-3683. [4] Walter, M.J. et al. (2008) *Nature*, **454**, 622-626.

Evolution of rare-earth mineralization in carbonatites of the Lugiin Gol complex, southern Mongolia

Kynicky, J.[1*], Chakhmouradian, A.R.[2], Cheng, Xu.[3], Krmicek, L.[4], Krmickova, M.[5] & Davis, B.[6]
[1]Dept. of Geology and Petrology, Mendel University of Agriculture and Forestry, Brno, Czech Republic ([*]csga@centrum.cz)
[2]Dept. of Geological Sciences, University of Manitoba, Winnipeg, Canada
[3]Laboratory of Materials of the Earth's Interior and Geofluid Processes, Institute of Geochemistry, Chinese Academy of Sciences, Guiyang, China
[4]Institute of Geological Sciences, Masaryk University, Brno, Czech Republic
[5]Dept. of Earth and Environmental Sciences, Karel Englis College, Czech Republic
[6]Geological Survey of Canada, Ottawa, Canada

A large suite of fresh and metasomatically modified carbonatites from the Lugiin Gol (a.k.a. Lugingol'skiy) complex in South Gobi, Mongolia, was examined. The samples chosen represent not only rare carbonatite outcrops, but also drill-core material (down to a depth of 1200 m) that has not been previously studied. The Lugiin Gol carbonatites may have some economic potential due to their overall high content of rare-earth elements (REE). Their chondrite-normalized REE profiles have a steep negative slope and lack any anomalies. In addition, these rocks are characterized by extremely high abundances of Ba and Sr, coupled with low levels of Nb, Ta, Ti, K, Rb and Cs. Their age of emplacement has been determined by U-Pb dating of zircon as Triassic (ca. 240 Ma, i.e. post-orogenic).

The carbonatites are represented predominantly by coarse-grained sövite, consisting of magmatic calcite, minor to accessory Na-Sr-REE-bearing apatite, and a plethora of rare-earth carbonates whose modal content locally reaches several per cent. The latter group is paragenetically diverse and includes both primary carbonates (burbankite–calcioburbankite series and REE fluorocarbonates) and hydrothermally or metasomatically formed phases associated with strontianite, fluorite, barite, celestine and quartz. The primary fluorocarbonates are represented by zoned synchysite-(Ce) crystals (synchysite I) with lamellae of bastnäsite-(Ce), parisite-(Ce) and röntgenite-(Ce).

The primary textures and parageneses are modified and overprinted by such late-stage processes as recrystallization of calcite, alteration of apatite, break-down and replacement of burbankite and other early-crystallized carbonates, followed by precipitation of secondary carbonate parageneses. The primary burbankite is pseudomorphed by an assemblage of synchysite II, calcite and strontianite, and the Na released at this stage is incorporated in khanneshite, carbocernaite and cordylite-(Ce). A careful study of the minerals associated with the REE mineralization and their structural relations shows that most of the carbonatites underwent subsolidus metasomatic processes of two types: (1) high-temperature (max. T ca. 450°C) fluoritization, accompanying the precipitation of REE carbonates and strontianite; and (2) low-temperature ($T \leq 150$°C) precipitation of barite, celestine and quartz.

Our data demonstrate the complexity of magmatic and subsolidus processes involved in the evolution of carbonatites in post-orogenic settings.

Lamprophyres of Middle Timan, Russia

Makeev, A.B.[*] & Bryanchaninova, N.I.
Dept. of Petrography, Institute of Geology of Ore Deposits, Petrography, Mineralogy and Geochemistry RAS, Moscow, Russia ([*]abmakeev@mail.ru)

Subalkaline basic rocks of the dike series are widespread in Timan and belong to the lamprophyre group. These rocks are confined to deep-seated, long-lived faults striking NE, transverse to the general Timan northwestern extension of plicative and disjunctive structures. The host rocks are sandstones and clay shales of the Chetlas and Bystrin groups. In the area of lamprophyres, the sediments of the Chetlas Group form a gently SW-dipping monocline complicated by small gentle folds. Beds commonly dip 10°–20°, becoming steeper near Middle Timan fault zone. The rocks of the Bystrin Group are deformed into simple folds whose limbs dip up to 40°. The lamprophyres comprise hundreds of bodies (predominantly dikes and a few stocks) that show no spatial relation to intrusive magmatism. They form several fields with the area of approximately 1000 km^2 in the southeastern part of the Chetlas Kamen. Postcrystallization transformations of the lamprophyres were caused by autometasomatism (phlogopitization, amphibolization) and hydrothermal processes. Carbonatites spatially related to the lamprophyres and localized in the same fault zones are the younger rocks. Their possible age established by phlogopite K–Ar dating is 600 ± 30 Ma.

Two isochrons were obtained from Rb-Sr dating of the lamprophyres. The first is 819 ± 19 Ma, and the initial Sr ratio $(^{87}Sr/^{86}Sr)_0$= 0.70421 ± 16, definitely indicates the mantle source of the protolith and the absence of post-crystallization alteration. The second isochron hash practically the same age parameter 826 ± 31 Ma but more radiogenic Sr isotopic composition $(^{87}Sr/^{86}Sr)_0$ = 0.70693 ± 24 and is caused by significant crustal contamination of the rock-forming protolith.

It is concluded that the lamprophyres were formed in the Neoproterozoic at 820 Ma, confirming their within-plate (pre-Timanian) origin. Local postcrystallization transformations of lamprophyres took place in the Early Cambrian (530 ± 10 Ma) after the Timanide orogeny.

The sub-alkaline basalts of the dyke series that are widespread in Chetlassky Kamen are typical lamprophyres – they are holocrystalline rocks of porphyritic texture, containing phenocrysts of brown mica, clinopyroxene, amphibole, and a little olivine without any phenocrysts of feldspar at all. Their characteristic structural feature is a fine-grained base made of femic and salic minerals, with roundish, sometimes fused or corroded colored minerals phenocrysts, autoliths and xenoliths. The bodies of Chetlassky Kamen lamprophyres consist of an autonomous row of dikes, not bound to any intrusive massif spatially. According to chemical and mineralogical features the rocks are members of the kersantite – spessartite lamprophyre series. A certain typomorphism is characteristic for the rock-forming and accessory minerals of these rocks. The series of accessory minerals in lamprophyres and metasomatites around them is similar to the accessory minerals in the diamond-bearing Middle Devon conglomerate-breccia of Ichetju that testifies to the genetic closeness of lamprophyres to the rocks of the native source of Timan diamonds.

Rare earth-rich carbonatites at Lofdal, Namibia

Niku-Paavola, V.N.[1], Wall, F.[2*], Ellmies, R.[2,3] & Sitnikova, M.A.[3]
[1]Geological Survey of Namibia, Ministry of Mines and Energy, Windhoek, Namibia
[2]Camborne School of Mines, University of Exeter, Penryn, UK ([*]f.wall@exeter.ac.uk)
[3]BGR, Geozentrum Hannover, Germany

The carbonatites at Lofdal, Namibia are highly unusual in that they contain significant amounts of the the heavy REE mineral, xenotime-(Y). They are under active exploration for REE. The xenotime-(Y) occurs highly oxidised iron-rich calcite carbonatite dykes where it mantles and replaces zircon, forms aggregates in ankerite carbonatite, some of which are associated with hematite, and and forms crystals associated with monazite-(Ce) and synchysite-(Ce). The paragenetic sequence places the xenotime-(Y) at the end of magmatic activity and certainly into the hydrothermal stage [1]. Although the xenotime-(Y) is heavy *REE* enriched, the whole rock compositions are light *REE*-enriched in common with most carbonatites, although they are less enriched in light REE that most other published carbonatite data [1]. The light REE minerals present at Lofdal are also of potential economic interest.

Recent exploration work and mapping at Lofdal has revealed that there is a calcite carbonatite intrusion present in addition to the dyke swarm. This contains apatite and magnetite (but not in high enough quantities to be of economic interest) and is devoid of any significant quantity of rare earth minerals. This is consistent with observations at many carbonatite complexes that REE are concentrated in Fe-rich calcite and dolomite dykes rather than the earlier calcite carbonatite.

[1] Wall, F. et al. (2008) *Can. Mineral.*, **46**, 1251-1267.

Trace-element variations in clinopyroxene from calcite carbonatites

Reguir, E.P.*, Chakhmouradian, A.R., Halden, N.M. & Yang, P.
Dept. of Geological Sciences, University of Manitoba, Winnipeg, Manitoba, Canada (*umreguir@cc.umanitoba.ca)

Clinopyroxene is a common constituent of carbonatitic rocks (sensu lato). Variations in major-element chemistry of clinopyroxenes from carbonatites have been addressed in a number of studies and shown to reflect the changes in temperature, pressure and chemistry of their crystallization environment [1-3]. By contrast, there is virtually no published data on the trace-element composition of these minerals. In this work, we examined the major- and trace-element variations in clinopyroxenes from calcite carbonatites from Murun (Aldan), Prairie Lake (Ontario) and Afrikanda (Kola) using wavelength-dispersive X-ray spectrometry and laser-ablation inductively-coupled-plasma mass-spectrometry.

Strongly zoned clinopyroxene from Murun ranges in composition from $Ae_{64}Di_{14}Hed_{22}$ in the core to $Ae_{78}Di_{11}Hed_{11}$ in the rim. This zoning pattern is accompanied by a decrease in Mn (from 1200 to 5000 ppm), V (from 7000 to 2000 ppm), Zn (from 600 to 160 ppm), Sr (from 350 to 120 ppm), Zr (from 2300 to 100 ppm), Hf and REE (both from 50 to 5 ppm) contents towards the rim. The LREE/HREE ratio also tends to decrease rimward. Clinopyroxene from Afrikanda and Prairie Lake corresponds to Fe-, Al- and Ti-poor diopside (80-86 mol. % and 75-88 mol. % of $CaMgSi_2O_6$, respectively). The zoning pattern of the Afrikanda clinopyroxene (decreasing Mg coupled with increasing Fe content toward the rim), differs from that observed in the Prairie Lake samples. However, the trace-element composition of the Afrikanda and Prairie Lake clinopyroxene shows a similar variation pattern, where the rim is enriched in Mn and REE and, to a much lesser extent, Sc, V and Zr relative to the core (up to 1900 and 4300 ppm Mn, 140 and 130 ppm ΣREE, 145 and 160 ppm Sc, 190 and 220 ppm V, 700 and 600 ppm Zr in the rim, relative to 1100-1400 and 2500-3700 ppm Mn, 25-115 and 35-80 ppm ΣREE, 75-130 and 45-100 ppm Sc, 40-170 and 100-170 ppm V, 110-500 and 85-480 ppm Zr in the core, respectively). The rims of clinopyroxene crystals from Afrikanda and Prairie Lake are characterized by higher LREE/HREE ratios relative to their cores. The observed compositional differences clearly indicate that the clinopyroxene/carbonatite distribution coefficients of Mn, V, Sc, REE and Zr are strongly influenced by the major-element chemistry of clinopyroxene, in particular by its aegirine content.

[1] Kapustin, Yu.L. (1987) *Novye Dannye o Mineralakh*, **34**, 63-70 (in Russ.). [2] Andersen, T. (1988) *Lithos*, **22**, 99-112. [3] Chakhmouradian, A.R. & Zaitsev, A.N. (2002) *Can. Mineral.*, **40**, 1347-1374.

Contrasting trends of trace-element zoning in phlogopite from calcite carbonatites

Reguir, E.P.*, Chakhmouradian, A.R., Halden, N.M. & Yang, P.
Dept. of Geological Sciences, University of Manitoba, Winnipeg, Manitoba, Canada (*umreguir@cc.umanitoba.ca)

Phlogopite is a ubiquitous accessory mineral in carbonatitic rocks and, owing to its large capacity for atomic substitutions and long crystallization span, can be used as a sensitive petrogenetic indicator. In the literature, zoning in phlogopite crystals from carbonatites has been suggested to reflect variations in crystallization conditions (e.g., T and fO_2) in the course of carbonatite evolution. In this work, we examined the major- and trace-element composition of phlogopite in calcite carbonatites from Iron Hill (Colorado), Kovdor (Russia), Prairie Lake and Oka (Canada). The composition of the mineral was determined by wavelength-dispersive X-ray spectrometry and laser-ablation inductively-coupled-plasma mass-spectrometry.

The Iron Hill and Oka samples exhibit similar core-rim evolutionary trends of enrichment in kinoshitalite, $BaMg_3Al_2Si_2O_{10}(OH)_2$, component. The rims also contain higher levels of Sr, Sc, Zr and Nb relative to the cores. The Mn and Rb contents generally decrease rimward, but their variation trend is not as pronounced as the Ba, Sr, Sc, Zr and Nb trend. The Kovdor and Prairie Lake phlogopite shows a strong enrichment in Fe in the rim, and an inverse pattern of Sr, Ba, Mn, Sc and Zr variation relative to that observed in the Iron Hill and Oka samples. There is significant overlap in Rb values in the Kovdor and Prairie Lake phlogopite, although the cores typically contain somewhat higher levels of this element. In common with the Iron Hill and Oka samples, the rims of phlogopite from Prairie Lake are enriched in Nb relative to the cores, whereas the Kovdor material shows an inverse trend. The core-to-rim trend of increasing Co/Ni ratio observed in the Prairie Lake phlogopite contrasts with that of the Kovdor material, whereas crystals from Iron Hill and Oka are Co- and Ni-poor. The V concentrations decrease rimward in the Iron Hill and Kovdor phlogopite, but increase in the Prairie Lake and Oka samples. The ∑REE concentrations do not exceed 14 ppm in any of the samples.

Conclusions. (1) Phlogopite does not contribute significantly to the REE budget of carbonatites, but is the principal host for K, Rb and Cs in feldspar-free carbonatite types. (2) There appears to be no universal pattern of zoning that could be explained by a consistent pattern of trace-element partitioning between phlogopite and carbonatitic magma. (3) Two major trends of trace-element variation can be recognized in zoned phlogopite from calcite carbonatites: (i) kinoshitalite trend, involving a concomitant increase in Sr, Zr, Nb and Sc and a decrease in Mn and Rb; and (ii) Fe-enrichment trend involving a rimward depletion in Ba, Sr, Zr and Sc at an increasing Mn content. (4) Intragranular variations in such trace elements as V, Nb, Ta, Co and Ni lack consistency, which is probably due to competitive

Carbonatitic zircon – geochemical analysis

Savva, E.V.[1], Belyatsky, B.V.[2*] & Antonov, A.V.[3]
[1]IPGG RAS, St.-Petersburg, Russia
[2]VNIIOkeangeologia, St.-Petersburg, Russia
([*]bbelyatsky@mail.ru)
[3]CIR, VSEGEI, St.-Petersburg, Russia

It is well-known that in magmatic systems undersaturated in silica, such as alkali-ultramafic and carbonatite melts, if there is sufficient zirconium, baddeleyite and other zirconium minerals (zirconolite, calzirtite, zirkelite etc) crystallize in preference to zircon, which should be dissolved [1]. However, for many carbonatite–alkali-ultramafic massifs zircon is the prevailing accessory mineral both in silicate and carbonatite rocks. Very often it forms large, up to centimeter, crystals of pseudo-octahedral habit [2]. The following characteristics have been assumed as typical for "carbonatite" zircons basing on restricted data from the Mud Tank carbonatite complex (723 Ma) in Central Australia and the Kovdor complex (380 Ma), Kola Peninsula, Russia: average REE content 600-700 ppm at comparatively flat distribution, (Yb/Sm)n: 3÷30, Th/U up to 100 and more, 2.3<Lu<20.7 ppm, Ta>0.5 ppm, Hf>0.62 % [3]. We tested the plausibility of these characteristics on zircons from carbonatite massifs of different ages and origins, including zircons from the Archean Siilinjärvi massif, Proterozoic Tiksheozero and Elet'ozero massifs, Paleozoic Lovozero and Khibiny massifs and Mesozoic carbonatitic dyke from Antarctica.

We have analyzed more than 100 zircon grains for rare and trace elements. The morphology of the zircons studied repeats the known features of zircons from the other carbonatite massifs [2]. REE patterns of the zircons are characterized by extreme variability – from weakly fractionated flat chondrite-normalised REE distribution with generally low rare elements to fractionated patterns with prominent enrichment in heavy REE and well pronounced negative Eu and positive Ce anomalies, but there are distributions with distinctly increased REE content with positive Eu and weak Ce anomalies: (Sm/La)n: 2÷738, (Lu/Gd)n: 1÷58, Ce/Ce*: 1.2÷194.1, Eu/Eu*: 0.7÷1.78, (La/Gd)n: 0.0005÷0.5, (Pr/Gd)n: 0.01÷1.0, (Gd/Yb)n: 0.03÷0.9. Noteworthy in our case are the wide variations in (Yb/Sm)n: 0.9÷180, Th/U: 0.2÷512; [Hf]: 1020÷8700; [Lu]: 1÷94, [Nb]: 3÷ 2675; [Ta]: 4.7÷68 ppm and only about 45% of the studied zircons could be convincingly classified as carbonatitic according suggested characteristic ratios and element contents [3]. Moreover, variations in zircon composition within the single complex could be compared with general variations and even in some grains there have been observed fluctuations in content of some elements of more than one order of magnitude: [Th] – from 4.7 to 270, [Lu] from 1 to 11, [Y] – from 15 to 430 ppm. Zircons from carbonatitic dykes and veins showed the least variations. Crystallization temperatures of the zircons by Ti geothermometer correspond to a rather narrow interval of 570°–850°C. Surprisingly the elements which are greatly accumulated in carbonatites [4] – REE, HFSE, P, Y, Sr, Ca, vary widely in the zircons and do not demonstrate essential enrichment in comparison with zircons from the other rock types. It is obvious that zircon composition is predominantly determined by evolution of fluid composition due to interaction of carbonate fluids enriched in lithophiles with the matrix minerals. The single geochemical type of "carbonatitic zircon" related to a genetic link with the host carbonatites seems rather ill-founded.

[1] Barker, D.S. (2001) *Contrib. Mineral. Petrol.*, **141**, 704-709. [2] Hanchar, J.M. & Hoskin, P.W.O. (2003) (eds.) *Rev. Mineral. Geochem.*, **53**. [3] Belousova, E.A. et al. (2002) *Contrib. Mineral. Petrol.*, **143**, 602-622. [4] Chakhmouradian, A.R. (2006) *Chem. Geol.*, **235**, 138-160.

Ba-Ti-rich oxymica from olivine nephelinites of the Udokan lava field (Russia)

Sharygin, V.V.
V.S.Sobolev Institute of Geology and Mineralogy SB RAS, Novosibirsk, Russia (sharygin@uiggm.nsc.ru)

Ba-Ti mica was found in olivine nephelinites from oldest (14 Ma) volcanoes of the Udokan field (Ingamakit, Munduzhyak and others). The rocks contain phenocrysts of olivine (Fo_{75-85}), augite (Mg# - 0.95-0.85) and groundmass consisting of olivine (Fo_{70-75}), Ti-rich augite (Mg# - 0.85-0.80), Ti-magnetite (TiO_2 - 12-24 wt.%), fluorapatite, Ba-Ti-mica, nepheline, leucite, rarely ilmenite, K-feldspar or glass. Ba-Ti-mica forms xenomorphic grains in the groundmass and rarely occurs as a daughter phase in olivine-hosted melt inclusions. This mineral is an oxymica (EMPA and SIMS data) and contains low H_2O (0.1-0.3 wt.%), Li (30-50 ppm) and high BaO (6.7-11.5 wt.%), TiO_2 (10-13.3 wt.%), F (to 3 wt.%), Nb (460-920 ppm), Cr (180-420 ppm), Sr (940-1970 ppm), Zr (60-150 ppm) and REE (100-120 ppm) (Table 1). The core-to-rim variations are not significant occasionally showing weak enrichment in K_2O and depletion in BaO. Similar Ba-Ti-rich micas were previously described in olivine nephelinites and related rocks around the world [1-3].

Table 1: Chemical composition (wt.%) of the Udokan Ba-Ti-micas

Sample	Munduzhyak		Ingamakit		Ingamakit	
	core	rim	core	rim	core	rim
SiO_2	30.95	31.19	31.03	32.82	31.93	33.46
TiO_2	13.25	12.96	11.52	11.27	12.75	12.46
Nb_2O_5	0.17		0.21		0.15	
Cr_2O_3	0.11		0.05		0.05	
Al_2O_3	14.55	14.57	13.99	13.65	13.51	13.46
Fe_2O_3	2.11	2.88	0.57	2.09	0.48	3.19
FeO	11.18	10.20	11.15	9.84	11.68	9.67
MnO	0.09	0.08	0.08	0.06	0.07	0.06
MgO	10.67	10.90	12.51	12.42	12.10	12.42
CaO	0.02	0.13	0.01	0.10	0.09	0.11
BaO	9.37	9.14	11.20	8.98	9.83	6.68
SrO	0.23		0.11		0.12	
Na_2O	0.77	0.73	0.57	0.57	0.64	0.53
K_2O	5.33	5.34	5.10	5.63	5.43	6.71
Li_2O	0.01		0.02		0.02	
F	1.28	1.29	1.91	1.80	1.70	1.80
H_2O	0.11		0.29		0.19	
Total	100.22	99.41	100.33	99.23	100.74	100.55

Nb_2O_5, Cr_2O_3, SrO, Li_2O and H_2O were analyzed by SIMS, others - by EMPA. Fe_2O_3 are calculated only as tetrahedral Fe^{3+} in formula.

Oxymica varies from $K_{1.5}Ba_{0.5}(Mg,Fe)_{4.5}Ti_{1.5}[Al_{2.5}Si_{5.5}O_{20}]O_3F$ to $K_{1.25}Ba_{0.75}(Mg,Fe)_{4.5}Ti_{1.5}[Al_3Si_5O_{20}]O_{3.25}F_{0.75}$ and $K_{1.5}Ba_{0.5}(Mg,Fe)_4Fe^{3+}{}_{0.5}Ti_{1.5}[Al_{2.75}Si_{5.25}O_{20}]O_{3.25}F_{0.75}$. It notes that studied micas are related to intermediate members of the theoretical solid solution $K_2(Mg,Fe)_6[Al_2Si_6O_{20}]F_4$ - $KBa(Mg,Fe)_4Ti_2[Al_3Si_5O_{20}]O_4$ via complex isomorphic scheme $K+2(Mg,Fe^{2+})+2Si+4F \rightarrow Ba+2Ti+Al+4O$. In general, the Udokan oxymica strongly resembles oxykinoshitalite $KBa(Mg,Fe)_{3.5}Fe^{3+}Ti_{1.5}[Al_3Si_5O_{20}]O_3F_{0.5}(OH)_{0.5}$ [1] differing in lower Ba, Fe^{3+}, H_2O and higher K and F. Minor substitutions $K+2Si+(Mg,Fe^{2+})+F \leftrightarrow Ba+2Al+Ti+O$ and $K+2Fe^{3+}+O \leftrightarrow Ba+2(Mg,Fe^{2+})+F$ are not excluded in the Udokan micas. All the above schemes do not lead to the appearance of vacancy sites in the structure of these micas.

Low H_2O content in Ba-Ti-mica suggests that the Udokan olivine nephelinite magma and its derivates were essentially "dry". The presence of Fe^{3+} in mica possibly indicates the gradual increasing in fO_2 during nephelinite melt evolution.

[1] Kogarko, L.I. et al. (2005) *Can. Mineral.*, **43**, 1501-1510. [2] Mansker, W.L. et al. (1979) *Am. Mineral.*, **64**, 156-159. [3] Zhang, M. et al. (1993) *Am. Mineral.*, **78**, 1056-1065.

Potassium-rich carbonatite magma: mechanism of formation and mineralogy as a result of examination melt inclusions (eastern Pamir)

Solovova, I.* & Girnis, A.
Institute of Geology of Ore Deposits, Petrography, Mineralogy, and Geochemistry, Russian Academy of Sciences, Moscow, Russia (*solovova@igem.ru)

Almost all known cases of magmatic carbonatites are related to sodium-type alkaline rocks, phonolites and nephelinites. Carbonatites very rarely associate with potassium igneous rock and this makes the carbonatite-bearing potassic basaltoid complex of the Eastern Pamirs especially interesting. The conditions of formation of primary silicate and carbonate melt inclusions in the clinopyroxene of the fergusite of this complex and their chemical and mineralogical compositions has been the object of our study.

At heating melt inclusions the complete dissolution of daughter minerals were observed at 1120–1150°C. The silicate matrix of the inclusions contains carbonatite melt globules and gas bubble (fluid phase). A gas bubble disappeared at 1150–1180°C (the homogenization temperature). The phase boundary between the silicate matrix and carbonatite melt globules did not disappear up to 1210°C; i.e., the initial melt already passed the stage higher-temperature unmixing at the moment of liquidus mineral crystallization (phlogopite, clinopyroxene, apatite). The pressures estimated using fluid inclusions and mineral geobarometers were 0.5–0.7 GPa.

At 1180°C concentration of SiO_2 in the carbonatite melt does not exceed 10 wt%. Note the very high concentration of alkalis (up to 20 %) at K_2O/ Na_2O up to 2.5, which is not typical for natural carbonatites. Chemical compositions of daughter phases and silicate glasses indicate the high contents of volatiles (F, Cl, and S) in the magma. The melts are characterized by high sums of REE and enrichment in Ba, Th, U, Li, and B. According to our research, SiO_2 undersaturated minerals dominated in the crystallized carbonatitic inclusions. Reflecting ultrapotassic nature of melt, the first phases were kalsilite and K-Ba-rich alkali feldspars (up to 9 wt% BaO). The earliest minerals are also Ca-Ti-bearing phases - titanite, perovskite and zoned garnet schorlomite (core is enriched in TiO_2 and rim zones are enriched Fe_2O_3). Among the phase of melt inclusions were determined extremely rare silicate minerals fresnoite and delindeite containing up to 59 and 30 wt% BaO, 13 and 15 wt% TiO_2, respectively. These minerals are characterized by appreciable concentrations of SrO, FeO, CaO, F and H_2O. The carbonate is calcite with up to 0.3 wt % K_2O, 2 wt % SrO, and up to 0.5 wt % FeO, MgO. Ore minerals are mainly K–Cl-bearing sulfide (djerfisherite), typical mineral of lamproites, Fe-sulfide and rare magnitite. Accumulation of volatile components, Ca, Na and Fe in the residual melts leads to crystallization aegirine, scapolite, cuspidine, cancrinite, and H_2O-bearing K-Ba- and Ca-Sr zeolite on the late stages of the magma evolution. Thus, we showed some geochemical and mineralogical sequence of crystallization of high-temperature alkali carbonatite melt in closed conditions: *K+Ba+Si – K+Ba+Ti+Si – K+Fe+Ca+Na+Si - K+Sr+F+Cl+H_2O+S (Si) – Ca+CO_2.*

Amphibole-bearing upper mantle xenoliths from the Perşani Mountains (Transylvania, Romania)

Szabó, Á.[1,2*], Tóth, A.[2,3], Nédli, Zs.[2], Szabó, Cs.[2], Harris, N.[4] & Tindle, A.[4]
[1]Dept. of Mineralogy, Babeş-Bolyai University, Cluj-Napoca, Romania
[2]Lithosphere Fluid Research Lab, Eötvös University, Budapest, Hungary (*sz_abel@yahoo.com)
[3]Dept. of Environmental Sciences, Sapientia University, Cluj-Napoca, Romania
[4]Dept. of Earth & Environmental Sciences, Open University, Milton Keynes, United Kingdom

In the Carpathian–Pannonian Region (CPR) there are five major volcanic areas where basalt volcanoes, active during the Neogene – Quaternary period, brought to the surface large numbers of xenoliths [1]. The easternmost and youngest Plio-Pleistocene alkaline basaltic volcanic field of the CPR developed in the Perşani Mountains (Eastern Transylvanian Basin) where the alkaline basalt contains numerous peridotite and pyroxenite xenoliths, as well as clinopyroxene and amphibole megacrysts. Eight amphibole-bearing xenoliths were selected for this study of mineral chemistry and petrography comprising seven composite xenoliths (six spinel lherzolite/hornblendite and one amphibole-pyroxenite/harzburgite) and one amphibole-clinopyroxenite were classified. All xenoliths have significant amphibole content; in the lherzolite part of the spinel lherzolite/hornblendite composite xenoliths, amphibole is present interstitially to the other silicates, whereas in the hornblendite portion amphibole is a rock-forming mineral.

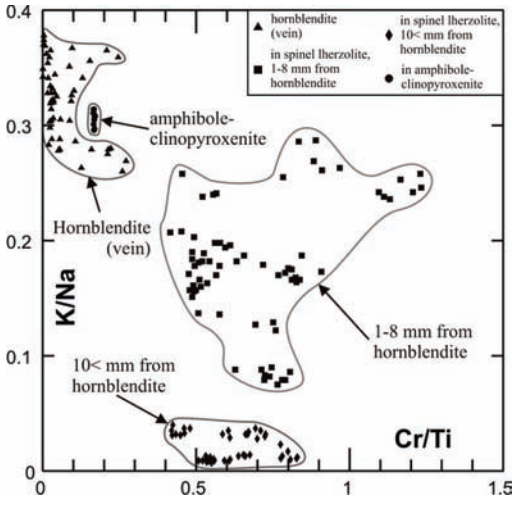

Fig. 1: Cr/Ti vs. K/Na variation diagram for amphibole occurring in different textural position.

Geochemical features of the studied amphiboles show systematic differences relating to their textural position. The interstitial amphiboles are enriched in Na, Cr, Mg, depleted in incompatible trace elements and LREE, whereas amphiboles in hornblendites and amphibole-pyroxenites show elevated K, Ti, Fe, incompatible trace element and LREE content (Fig. 1). The chemical variations of the texturally defined amphiboles indicate a complex history of lithospheric metasomatism at shallow depths beneath the Perşani Mountains. The main aim of this study is to shed light on the details of the general evolution of the lithospheric mantle beneath the studied area by textural and major and trace element geochemical data of amphibole and coexisting clinopyroxene, as well as to constrain metasomatic reactions in the mantle between a suspected mafic melt and peridotitic wall rock.

[1] Szabó, Cs. et al. (2004) *Tectonophysics*, **393**, 119-137.

A mineralogical study of REE minerals from the Higashimatsuura basalt, Kyushu, Japan

Takai, Y.* & Uehara, S.
Dept. of Earth and Planetary Sciences, Faculty of Sciences, Kyushu University, Fukuoka, Japan
(*takai@geo.kyushu-u.ac.jp)

The Higashimatsuura basalt which distributes throughout Higashimatsuura peninsula, Kyushu, Japan is neogene alkali olivine basalt. REE minerals are reported and three new REE minerals are found from this basalt (*e.g.* kimuraite [1]).

Samples were collected from 36 localities and REE minerals are found in 13 localities. Eleven REE minerals are identified; kimuraite, lokkaite, tengerite, lanthanite-(Nd), lanthanite-(La), kozoite-(Nd), kozoite-(La), calcio-ancylite-(Nd), rhabdophane-(La), rhabdophane-(Ce) and rhabdophane-(Nd). Furthermore, three candidates of new minerals are found; "hizenite", "calcio-ancylite-(La)" and "rhabdophane-(Y)".

According to the mineralogical features, crystallization of REE minerals in the Higashimatsuura basalt has four stages.

(1) At the first stage, rhabdophane crystallizes in high temperature condition. Due to the high temperature, difference of ionic radii of REE ions do not affect and rhabdophane can contain larger amount of HREE. Therefore, rhabdophane in this basalt has variety in chemical composition and Y can be predominant REE in some rhabdophane.

(2) Spherical crystal of kozoite crystallizes. This type of kozoite has chemical composition which centers to boundary among kozoite-(Nd), kozoite-(La), calcio-ancylite-(Nd) and calcio-ancylite-(La). In this stage, temperature is lower than the first stage, but it still keeps high temperature on some level. Therefore, spherical crystal of kozoite incorporates higher content of Ca and Y than kozoite which alters after lanthanite.

(3) Tengerite family minerals (tengerite, lokkaite and kimuraite) and lanthanite crystallize in the third stage. In this stage, temperature should be low because these minerals are very weak in heat. Tengerite can keep its crystal structure even in 200°C, however, lanthanite become amorphous in only 80°C. Distribution by ionic radii occurs in this time. LREE incorporates in lanthanite, and HREE incorporates in tengerite family minerals (Fig. 1). Ca^{2+} is contained into tengerite family minerals because lanthanite can not contain Ca^{2+} due to its crystal structure [2].

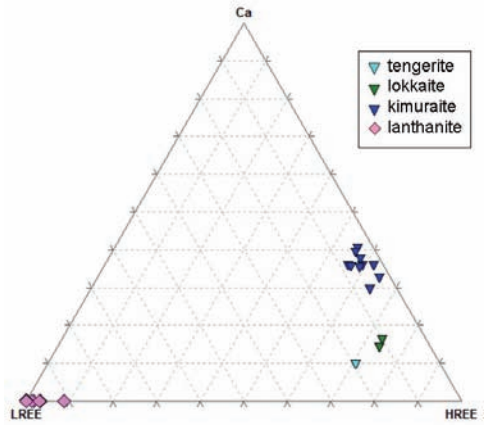

Fig. 1: Miscibility gap between tengerite family minerals and lanthanite.

(4) Some of lanthanite alters to kozoite-(Nd) by heating in the last stage. Because of lower temperature than the second stage, this type of kozoite almost does not contain HREE, and Ca is also contained only a part of aggregate.

[1] Nagashima, K. et al. (1986) *Am. Mineral.*, **71**, 1028-1033.
[2] Dal Negro, A. et al. (1977) *Am. Mineral.*, **62**, 142-146.

Nb and REE minerals from the Virulundo carbonatite (Namibe, Angola)

Torró, L.[1*], Villanova, C.[1], Castillo, M.[1], Campeny, M.[1], Gonçalves, O.A.[2] & Melgarejo, J.C.[1]
[1]Dept. Cristal·lografia, Mineralogia i Dipòsits Minerals, Universitat de Barcelona, Catalunya, Spain
(*lisardtorro@hotmail.com)
[2]Depto. de Geologia, Universidade Agostinho Neto, Luanda, Angola

The Virulundo carbonatite is located in SW Angola, in the Namibe province, and is one of the biggest carbonatite outcrops in the world. It is a Cretaceous subvolcanic plug, which belongs to the Parana-Namibia-Angola alkaline-carbonatitic province. It is found intruding Early Archean granitoids, which are fenitized on the contact.

The structure consists of a central circular body of massive carbonatites, 1.5 km in diameter, surrounded by concentric ring dikes of carbonatitic breccia. The central body is made up of a sequence of calcitic, dolomitic and ankerite intrusions. Finally, some microtrachytic dikes crosscut the ensemble.

Pyrochlore is widespread in all the above mentioned units. It occurs as euhedral crystals, less than a millimetre in size. The crystals show a complex texture with 2 main generations of pyrochlore: a) primary magmatic, displaying concentric zoning, and b) secondary, found in irregular replacements along grain borders, small fractures and other discontinuities. Zoning in primary pyrochlore mainly reflects changes in the F content and the cation filling in the A position (Fig. 1). The secondary pyrochlore is strongly enriched in Ba and Sr, and depleted in F, Ca and Na (Fig. 1). The vacancies also increase in the secondary pyrochlore. Secondary pyrochlore is intimately associated with barite, thus suggesting that the hydrothermal alteration of pyrochlore takes place in oxidizing conditions.

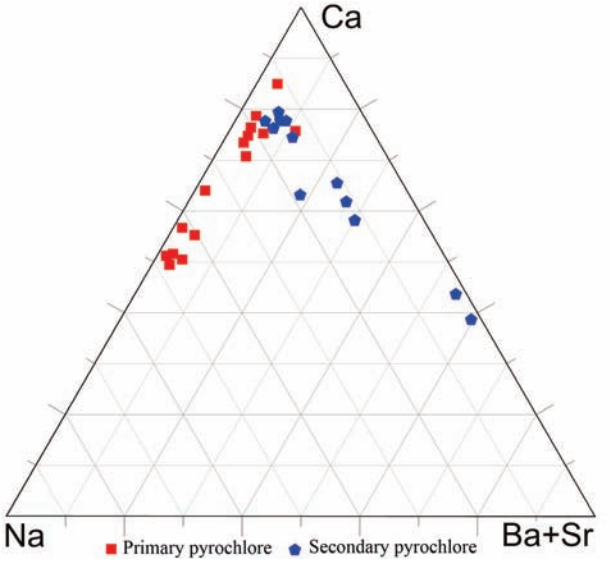

Fig. 1: Distribution of chemical analyses of primary and secondary pyrochlore in the diagram Na-Ca-(Ba+Sr) (a.p.f.u.)

REE minerals are also very common as small crystals and are produced as late replacements of the primary mineral associations, filling porosity in close association with barite. They consist of fluorocarbonates (bastnäsite-(Ce), parisite-(Ce), synchisite-(Ce)) and silicates (britholite-(La), cerite, tritomite-(Ce)).

A fluid-dynamical model of carbonatite-silicate magma interaction

Valentini, L.[1*], Moore, K.R.[2] & Chazot, G.[3]
[1]Dept. of Geosciences, University of Padua, Italy
([*]luca.valentini@nuigalway.ie)
[2]Dept. of Earth and Ocean Sciences, NUI Galway, Ireland
[3]Institut Universitaire Europeén de la Mer, Université de Bretagne Occidentale, Plouzane,France

In a recent work [1] 527 worldwide carbonatite occurrences were catalogued, with approximately 80% of them being associated with silicate rocks. The great majority (~90%) occur in intrusive complexes, where field relations show that emplacement of the carbonatites is generally late with respect to the associated silicate rocks. In contrast, evidence from the 49 extrusive centres [2] reveal that carbonatite and silicate magma extrusion can be contemporaneous, such that interaction processes between the two types of magmas may occur. Nonetheless, the modes of interaction between carbonatite and silicate magmas are still poorly constrained.

In this study, the mechanisms of interaction between a carbonatite magma and a silicate magma are inferred on the basis of the textural, geochemical and rheological features of a carbonate-bearing tuff from the Velay Province (Massif Central, France) characterized by the presence of dolomite globules within a silicate glass matrix.

The results of EPMA transects and elemental maps show that no chemical re-equilibration occurred between the two liquids, although major element compositions rule out the possibility that the two magmas may represent an immiscible equilibrium pair.

In order to explain the observed geochemical and textural features, a two-fluid-dynamical model consisting in the occurrence of an incipient viscous fingering instability, subsequent to the injection of a carbonatite magma into a trachyte magma residing within a chamber, is envisaged. The observed emulsion-like texture resulted from the quasi-instantaneous fragmentation and solidification of the developing fingers. The replenishment event triggered immediate evacuation of the magma chamber such that interaction between the two magmas occurred over a short time scale and large-scale mixing was prevented.

[1] Woolley, A.R. & Kjarsgaard, B.A. (2008) *Carbonatite occurrences in the world: map and database*. Geological Survey of Canada. [2] Woolley, A.R. & Church, A.A. (1989) *Lithos*, **85**, 1-14.

The composition of phlogopites from laprophyric dykes and syenites (South-Eastern Altai)

Vasyukova, E.A.[*] & Sukhorukov, V.P.
IGM SB RAS, Novosibirsk, Russia
([*]helena.yukova@gmail.com)

Lamprophyric dyke complexes are the largest magmatic occurrence from Mesozoic period, in South-Eastern Altai. Lamprophyric magmatism is close to the large ore occurrences in location and age [1]. Two different lamprophyre areas are separated: South-Chuya and Yustyd. The first one is related with Ni-Co-As, U, Cu-Hg-Sb-Ba and hematite mineralization, while in the second area Ag-Sb and Ni-Co-As ore occurrences are located. Tarkhata syenite massive of the same age is placed in the South-Chuya area.

The main rock minerals of lamprophyres are phlogopite (in phenocrysts and in matrix) and K-Na feldspar and carbonate. Some of dykes contain clinopyroxene as phenocrysts. In spite of some differences in petrogenetic elements (for example amount of silica in dykes varies from 40 to 60 wt.%), the character of REE distribution of syenites and dykes are absolutely similar. This chemical resemblance, additional to that of space and time nearness, is evidence of genetic correlations between dykes and syenitic rocks. Changes in composition of phlogopite can be evidence of melt evolution and show us the difference in crystallization conditions in dykes of different area.

The analyses of phlogopites of more then 100 dykes from South-Chuya and Yustyd areas and syenitic massif are carried out. Phlogopites differ in TiO_2 and *f* (*f*=Fe/(Fe+Mg)) (see table 1). Micas of the South-Chuya area contain the lowest *f* (<20%) and TiO2 (<4 wt.%). There is no any correlation between *f* and TiO_2 in syenite micas. Their compositions are located on the *f*-TiO_2 diagram in the area of Yustyd phlogopite. Besides they have the highest Cl and lowest Cr_2O_3 in comparison with dyke phlogopites.

Table 1: Analytical results for phlogopites from studied areas

	South-Chuya lamprophyres	Tarkhata syenites	Yustyd lamprophyres
TiO_2	1-4	3-5.5	3-7
f	<20	20-40	10-50
MnO	<0.2	<0.22	<0.4
Cl	0.05-0.02	~0	~0
Cr_2O_3	0-2.5	<0.5	0-2.5

[1] Obolenskaya, R.V. (1971) *Chuya alkaline basaltoids complex of Gornyi Altai*. Nauka, Novosibirsk (in russian).

Determining depth of lamprophyre magma generation and emplacement: mica thermobarometry revisited

Woodard, J.[1*] & Boettcher, I.[2]
[1]University of Turku, Finland ([*]jdwood@utu.fi)
[2]TU-Clausthal, Clausthal-Zellerfeld, Germany

Lamprophyres are mafic to ultramafic dyke rocks, which commonly contain macrocrystic grains of mica (biotite or phlogopite) together with olivine, clinopyroxene, amphibole or apatite. Rock [1] outlined a six-tier hierarchy of lamprophyre mineralogy from fully cognate groundmass grains to fully xenocrystic grains. Zoned grains are common, representing overgrowth crystallisation from the magma onto xenocrystic or earlier-formed phenocrystic cores. Using the mica thermobarometer developed by Righter and Carmichael [2], systematic analysis of multiple generations of mica from lamprophyres may provide depth estimates for both magma generation and emplacement.

For this study, we have analysed macrocrystic and matrix mica from Palaeoproterozoic shoshonitic lamprophyre dykes in the Fennoscandian Shield. These lamprophyres represent low-volume partial melts derived from an enriched lithospheric mantle. Macrocrysts occur as pseudohexagonal laths, typically around 1 mm but up to 1 cm across. Compositional zoning and castellated textures are common. Many grains contain crystallographically oriented, needle-shaped inclusions of titanite. In some grains, strongly pleochroic inclusion-free rims surround sharply defined inclusion rich cores, while in other cases inclusion-rich rims grade into inclusion free cores. Matrix grains are typically smaller than 0.2 mm, inclusion-free and strongly pleochroic.

Biotite macrocrysts typically exhibit core-to-rim zoning, appearing progressively brighter towards the rims in BSE images. The cores have low Mg# (65-75) and are relatively enriched in Si, K and F. A gradational increase outwards in Mg#, Ti, Al and Ba is observed near the rims. Matrix biotite/phlogopite has similar composition to the inclusion-free outer rims of the macrocrysts, with high Mg# and strong enrichment in both Ti and Ba.

Thermobarometric results from the matrix micas indicate crystallisation at temperatures of 1100-1150°C at 0.2-0.3 GPa, corresponding to an emplacement depth of 7-10 km. This is in accordance with previous depth/exhumation estimates from this area [3]. Thermobarometric results from the macrocrysts form a well-defined trend toward T = 1200°C and P = 2.5 GPa. Still higher values (up to P = 4.5 GPa) were obtained from the core zones of many macrocrysts, however these data become scattered such that a distinct path of decompression is no longer discernable. This uncertainty could reflect a lack of equilibrium between the macrocryst cores and the lamprophyric melt. Another consideration is that the thermobarometer used [2] has not been experimentally calibrated at such high pressures. Nonetheless, source temperatures in excess of 1000°C, the closure temperature of zircon [4], are implied by the presence of mantle zircons [5]. These conditions correspond to pressures >4.5 GPa according to the geotherm of Kukkonen and Peltonen [6], implying that the highest pressures obtained in this study could also be real.

[1] Rock, N.M.S. (1991) *Lamprophyres*. Blackie, Glasgow. [2] Righter, K. & Carmichael, I.S.E. (1996) *Contrib. Mineral. Petrol.*, **123**, 1-21. [3] Niiranen, T. (2000) *Master's Thesis*, University of Turku, Finland. [4] Cherniak, D.J. & Watson, E.B. (2001) *Chem. Geol.*, **172**, 5-24. [5] Woodard, J. et al. (in review) *Lithos*. [6] Kukkonen, I.T. & Peltonen, P. (1999) *Tectonophysics*, **304**, 301-315.

Chrome spinels in ophiolites: from micro-analyses to large-scale plate tectonic interpretations

Pearce, J.A.
School of Earth and Ocean Sciences, Cardiff University, Cardiff UK (pearceja@cf.ac.uk)

Like zircon, chrome spinel [$(Mg,Fe^{II})(Cr,Al,Fe^{III})_2O_4$] is an alteration-resistant accessory phase which carries global tectonic information. Unlike zircon, however, it can be used to investigate mafic–ultramafic rocks and their weathering products (e.g. [1,2]). In ophiolites, chrome spinel in mantle peridotites has proved most informative. Because the divalent (X) site has its closure temperature well below the mantle solidus, the trivalent (Y) site carries the more useful information about petrogenesis and hence tectonic setting which may be obtained by micro-analysis using a combination of EMA and LA-ICPMS. Of the major elements in the Y site, the proportion of Cr, expressed as Cr#, is sensitive to melting history, while Fe^{III} can be used to calculate oxygen fugacity. The plot of oxygen fugacity against Cr# [3-6] remains one of the most effective ways to distinguish mantle protoliths from mid-ocean ridge (MOR), supra-subduction zone ridge (SSZ) and plume-related (P-MOR) ridge settings: SSZ peridotites have high fO_2 and high Cr# resulting from high degrees of wet melting, whereas P-MOR peridotites have low fO_2 and high Cr# resulting from high degrees of dry melting, and MOR peridotites have low fO_2 and relatively low Cr# resulting from lower degrees of dry melting. Of the analysable minor elements in the Y site, Ti and Ga are particularly useful: the incompatibility of Ti makes it particularly sensitive to melt-rock interaction (e.g. [5]); and Ga has the ionic radius of ferric iron but no redox dependency, so providing a way of correcting for the effects of magmatic differentiation on Fe^{III} [6]. Thus the Ti-Ga-FeIII systematics of chrome spinel provide additional tectonic information [6].

Application of these methodologies to ophiolites and their modern analogues demonstrates their chrome spinels may carry a record of more than one setting. For example, many spinels from SSZ ophiolite analogues in the Izu-Bonin forearc have compositions that span the MOR and SSZ fields [3]. Significantly, these follow a vector representing interaction between a MOR peridotite protolith and a SSZ boninite magma. This may be interpreted tectonically in terms of pre-subduction MOR mantle, which reacts with boninite magma following subduction initiation. Interestingly, many SSZ ophiolites follow similar trends (e.g., Semail, Pindos, Zambales), so providing new or supporting evidence of their subduction initiation settings and validating the view that this setting is the one in which most ophiolites form. Chrome spinels from many MOR ophiolite analogues also indicate complex origins, for example the interaction of orogenic peridotites with MOR magma at the Galicia margin during Atlantic opening. Many MOR ophiolites (e.g., Othris) have similar characteristics. On a plate tectonic scale, therefore, chrome spinel micro-analyses indicate that a high proportion of ophiolites form at a time of global tectonic change, specifically during and just after subduction initiation and continental breakup.

[1] Dick, H.J.B. & Bullen, T. (1984) *Contrib. Mineral. Petrol*., **86**, 54-76. [2] Arai, S. (1994) *Chem. Geol.*, **113**, 191-204. [3] Parkinson, I.J. & Pearce, J.A. (1998) *J. Petrol*., **39**, 1577-1618. [4] Parkinson, I.J. et al. (1999) *Chem. Geol*., **160**, 409-423. [5] Pearce, J.A. et al. (2000) *Contrib. Mineral. Petrol*., **139**, 36-53. [6] Dare, S.A.S. et al. (2009) *Chem. Geol*., **261**, 199-216.

Similarity and difference between abyssal and back-arc basin peridotites: inference from xenolith suites from the Sea of Japan

Arai, S.* & Tanaka, C.
Dept. of Earth Sciences, Kanazawa University, Kanazawa, Japan (*ultrasa@kenroku.kanazawa-u.ac.jp)

Petrologic characteristics of the upper mantle peridotite beneath the back-arc basin have not been thoroughly understood because of very limited availability of deep-seated rocks there. We have a few mantle peridotite xenolith localities within or along the Sea of Japan, one of the back-arc basins in the Western Pacific [1].

Peridotite xenoliths captured by alkali basalt dredged from a small seamount (Takeshima Seamount tentatively), ca. 230 km to the north of Oki islands, are possibly representative of the Japan-Sea mantle. They are spinel-bearing lherzolite to harzburgite, which show equigranular to porphyroclastic textures. They can be classified into two types (Type 1 and Type 2) in terms of REE patterns of their Cpx [2]. Type 1 peridotites (Cr# of spinels, 0.4-0.5) are similar in major element chemistry and MREE to HREE concentrations of Cpx to abyssal peridotites. The Cpx in the former shows slight enrichment of LREE. In contrast, Type 2 peridotites have high-REE Cpx with flat to slightly LREE-enriched patterns, and are quite similar to subcontinental peridotites obtained as xenoliths from China. The southern half of the Sea of Japan was formed mainly by thinning and rifting of the continental lithosphere. Type 2 peridotites were derived from a possible remnant of the continental lithospheric mantle.

Harzburgite xenoliths from Oshima-Ôshima volcano in the Sea of Japan off Hokkaido, northern Japan, may represent the upper mantle beneath the Sea of Japan [3]. The Oshima-Ôshima harzburgite (olivine of Fo_{90-91}, spinel Cr# = 0.52) is similar to the Type 1 peridotite from Takeshima Seamount. This type of harzburgite is possibly a residual mantle peridotite of BABB (back-arc basin basalts) of the Sea of Japan because its northern half represents an oceanic basic formed by accretion of BABB through spreading [4].

BABB are very similar in spinel chemistry to MORB, indicating the residual peridotite (or the degree of partial melting) is basically similar between the back-arc basin and mid-ocean ridge. Some of BABB drilled from the Sea of Japan, however, contain high-Cr# (> 0.6 up to 0.8) chromian spinel, indicating the presence of highly refractory peridotite in the mantle. High degree of mantle melting occurs when the spreading rate is high as in the case of the Sea of Japan (up to 60 cm/year) [5]. The high degree of partial melting to produce BABB and Type 1 peridotites may be formed by open-system melting affected by a flux from the downgoing slab.

[1] Tamaki, K. & Honza, E. (1991) *Episodes*, **14**, 224-230. [2] Ninomiya, C., Arai, S. & Ishii, T. (2007) *Japan. Mag. Mineral. Petrol. Sci.*, **36**, 1-14. [3] Ninomiya, A. & Arai, S. (1992) *Bull. Volcanol. Soc. Japan*, **37**, 269-273. [4] Tamaki, K. et al. (1992) *Proc. ODP, Sci. Results*, **127/128**, 1333-1348. [5] Torii, M., Hayashida, A. & Otofuji, Y. (1985) *Kagaku*, **55**, 47-61.

Variable mantle section in Albanian Ophiolites: evidences from mineral and bulk rock composition

Koller, F.[1*], Hoeck, V.[2], Ionescu, C.[3] & Onuzi, K.[4]
[1]University of Vienna, Austria ([*]friedrich.koller@univie.ac.at)
[2]Paris Lodron University, Salzburg, Austria
[3]Babes-Bolyai University Cluj-Napoca, Romania
[4]Instituti i Gjeoshkencave, Universiteti Politeknik i Tiranes, Tirana, Albania

In the classical view, the Albanian Ophiolites were divided in an eastern SSZ and a western MORB belt. This genetic view should be reflected in the mantle section as well, by the predominant occurrence of harzburgites in the eastern and lherzolites in the western belt, respectively. Recent investigations in the western belt revealed a different and more complex picture, with a wide compositional variation of peridotites, at regional scale.

The southern massifs of Voskopoja, Rehove and Morava are dominated by fertile lherzolites and contain, if any, only minor harzburgite bodies. By contrast, the next two massifs further in the north, Devolli and Vallamara, are almost exclusively composed of highly depleted harzburgites.

In turn, the massifs situated in central Albania, such as Shpati, Kuterman and Skenderbeu are built up of almost equal proportions of harzburgites and lherzolites. In all these massifs, harzburgites are dominating in the western parts, while lherzolites are restricted towards the east. The Puka and Gomsique massifs located in the northern part of Albania, are similar to those in the southern part, i.e. dominated by highly fertile lherzolithes. The Krrabi massif, positioned in between the western an the eastern belt, is formed by both harzburgites and lherzolites, thus fitting better into the eastern belt. The latter is more homogeneous and contains only harzburgite- dominated massifs, such for example the Shebenik and the Bitincka.

The Al_2O_3 values in peridotites show accordingly a high variability, ranging from 0.3 to 3.8 wt.%. This is consistent with fertile peridotites on one hand, and extremely depleted peridotites, on the other hand. Likewise, the composition of typical ultramafic minerals such as olivine, chromian spinels and pyroxenes reflect this lithological variability. Both orthopyroxene and clinopyroxene show a wide range of Al_2O_3 content, ranging from 0.5 to 4.5 wt.% and from 0.8 to 5.5 wt.%, respectively. The X_{Mg} values of olivine range from 0.895 in lherzolites to 0.915 in depleted harzburgites. These values are accompanied by Cr# in spinels ranging from 10 to 73, spanning the composition from lherzolites to depleted harzburgites.

A similar wide variation can be found in the Cr# in spinels vs. Cr# of both clinopyroxene and orthopyroxene. The spinels composition range from 11 to 60 wt.% Al_2O_3.

The mantle composition in the Albanian western ophiolite belt, which extends for more than 140 km in N-S direction, changes several times from a lherzolitic composition close to primitive mantle to a highly depleted harzburgite. By contrast, the eastern ophiolite belt seems to have been formed from a more homogeneous harzburgitic mantle.

Spinels in ophiolitic sediments in southern and central Albania: a provenance study

Hoeck, V.[1*], Koller, F.[2], Ionescu, C.[3], Robertson, A.[4] & Onuzi, K.[5]
[1]Paris Lodron University, Salzburg, Austria
([*]volker.hoeck@sbg.ac.at)
[2]University of Vienna, Austria
[3]Babes-Bolyai University, Cluj-Napoca, Romania
[4]Edinburgh University, UK
[5]Polytechnical University Tirana, Albania

The ophiolites in Albania are part of the Dinaric Hellenic ophiolite Belt which extents from Croatia to Greece. In Albania it is built up by two zones, a western MOR-type dominated ophiolites and an eastern SSZ-type. Mantle tectonites form commonly large bodies of lherzolite and/or harzburgite. Crustal sections are mostly restricted to cumulates and gabbros. Sheeted dykes and volcanics are rare in central and southern Albania. Sediment piles on top of the ophiolites are more common and consist of ophiolitic conglomerates and breccias, sandstones with prevailing ophiolite material and calcareous rocks with ophiolitic detritus [1]. The calcareous sediments are most likely Early Cretaceous in age as inferred from the fossil content. Spinels from sediments covering the Luniku, Stravaj, Shpati, and Morava massifs were analysed by EMP. The results were compared with spinel analyses from harzburgites and lherzolites from the ultramafics, cumulates, gabbros and basalts.

Spinels in sediments from the top of the Luniku massif display a wide range of compositions ranging from high to intermediate Cr# (0.85-0.50) and an X_{Mg} between 0.35 and 0.65. These compositions overlap to a certain extent with those of spinels from harzburgites in Shebenik and Shpati massifs, located nearby. Spinels from the sediments higher Cr# could be derived from massive chromite ores. Spinels with lower Cr# and high X_{Mg} common in harzburgites, are missing in the sediments.

The sediments of Stravaj show spinels with a wide variation of the Al_2O_3 content from 5 to 40 wt.%. Low Ti and Al spinels could be associated with a possibly eroded(?) boninitic source, but most spinels are compositionally compatible with those from harzburgites and possibly lherzolites.

Spinels collected from calcareous sediments from the inner part of the Shpati massif show a bimodal distribution. Al and Ti poor spinels with a high Mg# are probably derived from boninites. By contrast, the source of Ti and relatively Al rich spinels are most likely MOR basalts.

The calcareous sediments on top of the Morava Massif in the south of Albania contain at least two spinel populations: one with high Cr# and low Ti content and a second one, with Ti > 0.5 wt.%. The former is indicative for a harzburgitic source, the latter for a MORB source. Harzburgites are rare in Morava, but occur frequently in the massif of Bitinska to the NE of Morava.

Our results imply that in the early Cretaceous mantle and crustal fragments of ophiolites were emplaced onto a shallow marine platform environment where they underwent erosion and mass wasting. These processes delivered the spinels as heavy mineral and, more rarely, as components of mafic and ultramafic clasts into shallow water sediments as recently pointed out by Robertson et al. [1].

[1] Robertson, A. et al. (2010) *Int. J. Earth Sci.* (submitted).

Plagioclase-free harzburgite in equilibrium with MORB from the uppermost mantle of the northern Oman ophiolite

Akizawa, N.[1*], Arai, S.[1] & Tamura, A.[2]
[1]Dept. of Earth Sciences, Kanazawa University, Kanazawa, Japan ([*]nori.plus.x@gmail.com)
[2]Frontier Science Organization, Kanazawa University, Kanazawa, Japan

We have found plagioclase-free harzburgites that are in equilibrium with MORB in terms of clinopyroxene (cpx) and chromian spinel chemistry, which have not been recorded from the current ocean floor, from the uppermost mantle from the northern Oman ophiolite (along Wadi Fizh) (Fig. 1). They are from beneath the wehrlite-dunite layer (= Moho transition zone; MTZ) just under the layered gabbro. The MORB-saturated harzburgites slightly enriched mineralogy (spinels with higher Ti and ferric iron, and cpx with higher Ti), and contain slightly but clearly more abundant in modal cpx (up to 3.5 %) than ordinary Oman depleted harzburgites (with less than 1 % cpx), which are also common as abyssal harzburgite.

The MORB-saturated harzburgite was formed from the ordinary Oman harzburgite in equilibrium with depleted MORB (melt increments by fractional fusion) by impregnation of a MORB-like melt, which has left cpx (not cpx + plagioclase as in plagioclase-impregnated abyssal harzburgite). This may mean that the involved MORB-like melt is not equal to MORB, which precipitates plagioclase after olivine, in that clinopyroxene, instead of plagioclase, is precipitated after olivine. The harzburgites just under the MTZ wehrlite/dunite of Wadi Fizh are highly varied in terms of modification (of cpx) by the MORB-like melt, from the harzburgite only modified in light REE (LREE-enriched) to the MORB-saturated harzburgite via the harzburgite modified in LREE to MREE. Only depleted harzburgites are found in deeper part of the mantle section. This is a result of interaction between the MORB-like melt and depleted harzburgite beneath a spreading center, which is possibly situated not at a mid-ocean ridge but in a back-arc basin.

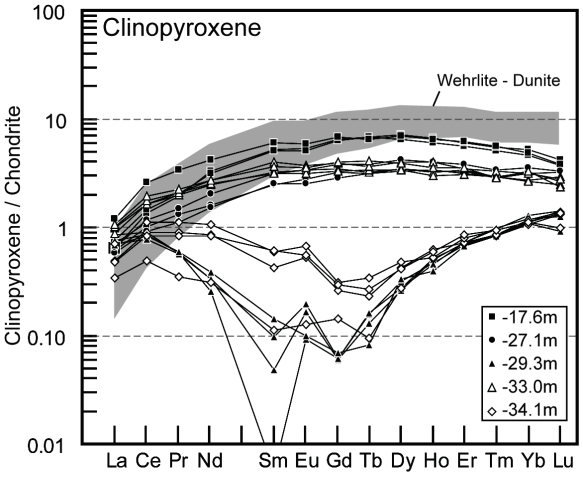

Fig. 1: Chondrite-normalized rare earth element (REE) patterns of clinopyroxenes (cpxs) in wehrlite-dunite (shaded area) and harzburgite. The numbers (in meters) indicate depths of samples from the lower end of the layered gabbro. Note that some of harzburgite cpxs are enriched in M- to HREE, and are possibly in equilibrium with MORB.

Heterogeneity of mantle source for arctic basalts revealed by olivine compositions and isotopic signatures

Sushchevskaya, N.M.[1*], Belyatsky B.V.[2] & Sobolev, A.V.[1]
[1]Vernadsky Institute of Geochemistry, Moscow, Russia ([*]nadyas@geokhi.ru)
[2]Dept. of Antarctic Geology, VNIIOkeangeologia, St.-Petersburg, Russia

Evolution of the Norway-Greenland basin, in general, is connected with Knipovich Ridge formation and the magmatic activity in the Svalbard Archipelago region (about 20 Ma ago), frequently developed in the form of plateau basalts. The process of magmatic activity continued till 10 Ma. In Quaternary time this process caused formation of three volcanoes, alkaline by the main composition of lavas, situated at the northern edge of Breibogen fault.

On the base of the studied Spitsbergen Island basalts and Knipovich ridge lavas it has been shown that in the source of both continental basalts and rift tholeiites there is marked a similar enriched mantle component. Enriched component of Arctic province has high radiogenic isotope signature: $^{207}Pb/^{204}Pb$ – 15.6, $^{206}Pb/^{204}Pb$ – 18.6, $^{208}Pb/^{204}Pb$ – 38.6 and $^{87}Sr/^{86}Sr$ – 0.7048 [1]. Its share in the melts decreases from Neogene trap intrusions via Quaternary alkaline lavas to insignificant admixture in the depleted and weakly enriched magmatism of the Knipovich ridge. On the base of Ni, Mn and Ca olivine contents [2] it was established that this component for Svalbard Archipelago and Knipovich Ridge basalts is approximated to pyroxenite. The amount of this pyroxenite in mantle sources changes from 2% for ridge tholeiites to 80% for Neogene trap of Spitsbergen Island.

Enriched rift basalts were formed during transformation of paleo-Spitsbergen fracture zone into Knipovich ridge. This process is connected with magmatism of west part of Spitsbergen during its separating from the northern Greenland. Enriched melts could be formed as a result of involvement of the lower parts of adjacent continental blocks into the melting process within the spreading zones at the early stage of Norwegian-Greenland Sea opening.

[1] Sushchevskaya, N.M. et al. (2009) *Geochem. Int.*. **10**, 966-978. [2] Sobolev, A.V. et al. (2007) *Science*, **316(5823)**, 412-417.

Petrogenetic and geotectonic significance of Neoproterozoic suprasubduction mantle as revealed by serpentinites from the Wizer ophiolite complex, Central Eastern Desert, Egypt: geochemical and mineralogical constraints

Farahat, E.S.[1*], Hoinkes, G.[2] & Mogessie, A.[2]
[1]Dept. of Geology, Minia University, El-Minia, Egypt
([*]esamfarahat1@yahoo.com)
[2]Institute of Earth Science (Mineralogy and Petrology), Karl-Franzens University, Graz, Austria

Ophiolite complexes, formed in a suprasubduction zone environment during Pan-African orogeny, are widely distributed in the Eastern Desert of Egypt. The mantle sections of these ophiolites provide important information on the origin and paleo-tectonic history of ocean basins these complexes are thought to represent. The geochemistry and mineralogy of the mantle section of the Wizer ophiolite complex, represented by serpentinites after harzburgite containing minor dunite bodies, are presented. The fact that the serpentine minerals are antigorite together with the incipient alteration of chromites and absence of chlorite implies most likely serpentinization in the mantle wedge above subduction zone. Significantly, the Wizer serpentinized mantle has a wide range of chromite compositions. The chromite Cr# [100Cr/(Cr+Al)], decrease gradually from dunite bodies (Cr# = 81-87) and their host highly-depleted harzburgites (Cr# = 67-79) to the less-depleted harzburgites (Cr# = 57-63). Such decrease in mantle refractory character is accompanied by enriched Al and Ti contents in their bulk rock compositions. The estimated parental melt compositions point to an equilibration with melts of boninitic composition for the dunite bodies (TiO_2= ~<0.07 to 0.22 wt.% and Al_2O_3= 9.4 to 10.6 wt.%), boninitic-IAT signature for the highly-depleted harzburgites (TiO_2= <0.09-0.28 wt.% and Al_2O_3= 11.2-14.1wt.%) and more MORB-like affinities for the less-depleted harzburgites (TiO_2= ~<0.38 to 0.51 wt.% and Al_2O_3= 14.5-15.3 wt.%). This is obviously comparable with the overlying volcanic crust, which shows a transitional MORB-island arc geochemical signature with few samples displaying boninitic signature. Comparison with experimentally determined residual spinel composition indicates >45%, 36-43%, and 33-35% equilibrium melting of fertile MORB mantle to form dunite bodies, highly-depleted harzburgites, and less-depleted harzburgites, respectively. Yet, the enrichment of some chromites in TiO_2 and identification of sulfides in these highly-depleted peridotites implies interaction with an impregnating melt. A two-stage partial melting/melt-rock reaction model is advocated. According to this model, melting of a depleted mantle source by reaction with melts of MORB-compositions is followed by a second stage melting by interaction with melts of IAT-boninitic affinities in a suprasubduction zone environment to generate the highly-depleted harzburgites and dunite bodies. The shift from MORB to island arc/boninitic affinities within the mantle lithosphere of the Wizer ophiolite sequence suggests generation in a protoarc-forearc environment. This, together with the systematic lateral (from north to south) change in geochemical character of ophiolites occurring in the Central Eastern Desert (CED) of Egypt from IAT-boninitic affinities to more MORB-like signature, imply that the CED could represent a complete forearc-arc-backarc system above a southeast-dipping subduction zone.

New structural data and ^{40}Ar-^{39}Ar ages from the Danubian ophiolitic sole (SE Europe): implications for the Variscan collision

Plissart, G.[1,2*], Monnier, C.[2], Mărunţiu, M.[3], Neubauer, F.[4], Demaiffe, D.[1] & Diot, H.[2]
[1]GIGC, Université Libre de Bruxelles, Brussels, Belgium & Aspirant du F.R.S – FNRS ([*]gplissar@ulb.ac.be)
[2]LPGN, Université de Nantes, France
[3]Geological Institute of Romania, Bucharest, Romania
[4]Dept. of Geography and Geology, Univ. of Salzburg, Austria

The Danubian ophiolite (~ 500 km^2) crops out in the Southern Carpathians and the Balkans Mountains and consists of four dismembered massifs belonging to the Upper Danubian Alpin unit: Tişoviţa Iuţi in Romania, Deli Jovan and Zaglavak in Serbia and Tcherni Vrah in Bulgaria. Although this ophiolite has been considered as Late Proterozoic [1], the Deli Jovan massif has been recently dated to the Lower Devonian (U-Pb zircon age of 405 ± 2.6 Ma; [2]). The principal feature of the Danubian ophiolite is the occurrence of uncommon metasomatic rocks (Zo + Cal + Cr-Chl + Cr-Ms) developed from metagabbros, under strongly hydrated conditions, at temperatures around 280°C and that could be related to listvenites [3].

This study is focused on deformations observed in the listvenitic gabbros (LG) from Romania and in their adjacent rocks (Corbu Unit - CU). The LG are located in a thin N-S band at the Eastern part of the Tisovita Iuti ophiolite, and present a recurrent mylonitic texture. Similarly, the CU crops out in a 2km N-S wide band, at the Eastern part of the LG, and consists of a mélange of various metamorphic rocks (volcano-sedimentary rocks, margin sediments, acid volcanic rocks and ophiolitic rocks) from low- to high-grade (Gt + St ± And assemblage), and in which the deformation is partitioned between highly deformed mylonites and juxtaposed slightly-deformed rocks.

Foliation planes measured in both LG and CU are oriented North-Southwards and are dipping steeply (Fig. 1a). Also, mylonites from both units are characterized by a strong subhorizontal stretching mineral lineation (Fig. 1b) and isoclinal folds parallel to this lineation. These two fabric elements appear to develop during the same event, giving evidence for components of both simple and pure shear. This implies a deformation phase affecting both LG and CU which probably occurred in a transpressive context.

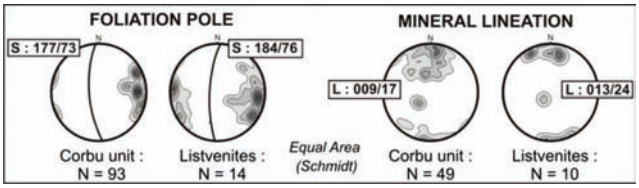

Fig. 1: Density distribution of foliation poles and mineral lineations measured respectively in Corbu Unit (CU) and listvenitic gabbros (LG).

New ^{40}Ar-^{39}Ar ages performed on two LG Cr-micas give plateau ages of 372.6 ± 1.3 Ma and 360.6 ± 1.2 Ma. These ages could represent the period of the listvenitic metasomatism, which occurred in a fluid-rich context certainly facilitating the pervasive deformation observed in the LG.

According to the ^{40}Ar-^{39}Ar results and to the similar deformation type encountered both in the Corbu mélange and in the listvenitic gabbros, we propose that these rocks correspond to the obduction sole of the Danubian ophiolite developed during a Variscan oblique collision.

[1] Haydoutov, I. (1989) *Geology*, **17(10)**, 905-908. [2] Zakariadze, G.S. et al. (2006) *Ofioliti*, **31(2)**, 223-224. [3] Plissart, G. et al. (2009) *Can. Mineral.*, **47**, 81-105.

Geochronology of ophiolites in Turkey: implications for Neotethyan geodynamics in Eastern Mediterranean

Parlak, O.[1,2*], Karaoglan, F.[1], Klötzli, U.[3], Koller, F.[3] & Rizaoglu, T.[4]
[1]Geology Dept., Cukurova University, Adana, Turkey
[2]Technology Faculty, Adiyaman University, Adiyaman, Turkey
([*]oparlak@adiyaman.edu.tr)
[3]Center for Earth Sciences, University of Vienna, Austria,
[4]Geology Dept., Sutcu Imam University, Kahramanmaras, Turkey

The Anatolian segment of the Alpine-Himalayan orogen comprises remnants of the Neotethyan oceanic basins, cropping out along E–W trending tectonic zones, between metamorphic massifs and/or platform carbonates. The remnants of the Neotethys, in a structural descending order, are characterized by ophiolites, metamorphic soles and ophiolitic melanges. These ophiolites and related subduction–accretion units were generated during the closing stages of the Neotethyan oceanic basins in Late Cretaceous. Well-preserved Neotethyan ophiolites in Turkey are of suprasubduction zone (SSZ) type. Late Cretaceous ophiolites in Turkey are mainly located in five zones; these are from north to south: a) Pontide ophiolites, b) Anatolian ophiolite belt, c) Tauride belt ophiolites, d) southeast Anatolian ophiolites and e) the peri-Arabian ophiolites. Important questions about the evolution of the ophiolites along the suture zones include: (i) the crystallization ages of oceanic crusts (ophiolites), (ii) the duration of magmatic activity and (iii) the timing of final emplacement.

The peri-Arabian ophiolites (Kizildag and Antalya), the southeast Anatolian ophiolites (Goksun, Ispendere and Komurhan) and the Tauride belt ophiolites (Mersin, Pozanti-Karsanti, Pinarbasi and Divrigi) were dated by LA-ICP-MS zircon U-Pb. The peri-Arabian ophiolites yielded 92.7±2.9 Ma from the plagiogranites in Kizildag (Hatay) and 86.6±3.2 Ma from the plagiogranites in Antalya. The southeast Anatolian ophiolites yielded 82.2±1.9 Ma from the rhyolitic lavas in Goksun (Kahramanmaras), 89.9±1.6 to 87.2±3.1 Ma from gabbros and 74.6±4.4 Ma from rhyolitic lavas in Komurhan (Elazig). The Tauride belt ophiolites yielded 81.8±4.3 Ma from the gabbros in Mersin, 70.9±3.0 Ma from the gabbros in Pozanti-Karsanti (Adana), 65.4±3.3 Ma from the diabase dikes in Pinarbasi (Kayseri) and 90.6±4.7 Ma from the gabbros in Divrigi (Sivas). The measured ages on different parts of ophiolites along the Tauride belt indicate that the subduction-related magmatic activity started in Turonian and continued until the end of Maastrichtian before their emplacement onto the Tauride platform. Whereas the peri-Arabic belt ophiolites display relatively older ages for the timing of crystallization of the oceanic crust from Cenomanian to Coniacian. The southeast Anatolian ophiolites show crystallization ages of oceanic crust from Turonian to Campanian, that occupies a time span between the peri-Arabic and the Tauride belt ophiolites.

All the data shows that (i) the crystallization ages of the ophiolites are late Cretaceous in general, but display differences from one location to another, (ii) continuous magmatic activities were exist during the closure stages of Neotethyan oceanic basins in SSZ tectonic settings from 92.7±2.9 to 65.4±3.3 Ma, and (iii) emplacement of the ophiolites were in the latest Maastrichtian.

Tracing a fore-arc suture in the Central Eastern Desert of Egypt

Abd El-Rahman, Y.
Geology Dept., Faculty of Science, Cairo University, Giza, Egypt (*yassermedhat@hotmail.com)

The early stages of the evolution of the Eastern Desert of Egypt during the Neoproterozoic are characterized by the formation of intra-oceanic island arc system(s) that was accreted to the Saharan Metacraton. The nature of suture resulted from the accretion/collision between the intra-oceanic arc body and the Saharan Metacraton was obscured by the late Najd fault system-related deformation and post-tectonic magmatism. The present work try to infer the nature of the suture zone in the Central Eastern Desert (CED) based on the new available geochemical data on the Neoproterozoic ophiolitic rocks and the distribution of the major ophiolitic serpentinites masses.

The geochemical data from the Wadi Ghadir and Fawakhir ophiolite complexes, the best preserved Neoproterozoic oceanic crust in the CED, indicate formation in back-arc and fore-arc tectonic settings respectively. Geochemical traverses along the ophiolitic blocks in the mélange of the CED show a systematic variation from a fore-arc geochemical signature towards the west to a back-arc signature towards the east. These geochemical traverses suggest the formation and evolution of the early intra-oceanic arc system above an east-dipping subduction zone. Finally, the island arc system was thrusted and/or collided with the continental margin to the west, which is represented by the Saharan Metacraton.

The ophiolitic serpentinites of the CED represent fore-arc oceanic mantle fragments [1]. The spatial distribution of the large ophiolitic serpentinite masses is in harmony with the distribution of the ophiolitic crust that have an inferred fore-arc affinity. The distribution of the large ophiolitic serpentinite masses in the CED can be traced as a line defining a suture zone at which the fore-arc front of an intra-oceanic arc system was collided with the older continental crust.

[1] Azer, M.K. & Stern, R.J. (2007) *J. Geol.*, **115**, 457-472.

Origin of Neoproterozoic ophiolites of the Arabian-Nubian Shield: evidence from mineral composition in the Eastern Desert of Egypt

Azer, M.K.
Geological Science Dept., National Research Centre, Cairo, Egypt (mokhles72@yahoo.com)

Neoproterozoic ophiolites are common in the central and southern sectors of the Eastern Desert of Egypt, where they occur as tectonized bodies and mélanges. In the complete ophiolitic sequence, the base of most ophiolites consists of ultramafic rocks overlain by gabbros, sheeted dykes and pillow basalt with associated deep-sea sediments at the top. The upper part of the gabbros is isotopic, but the basal part commonly contains cumulate layers. However, because of folding and shearing, the majority of the ophiolites lack one or more of their diagnostic lithologies. In the Egyptian ophiolites, low-grade greenschist facies metamorphism predominates, but in some places the rocks reach amphibolite grade. Alteration resulted in the development of listwaenite, particularly in shear zones. The origin of the Neoproterozoic ophiolites of the Arabian-Nubian Shield exposed in the Eastern Desert of Egypt is still a subject of controversially. Despite deformation and metamorphism, remnant olivine, pyroxene and spinels present and their composition provided important clues to their tectonic environments. The ophiolitic rocks of Egypt were interpreted to have developed mainly at ancient mid-ocean ridges. Now, there is general consensus that the Egyptian ophiolites are formed in the supra-subduction zone setting (fore-arc or back-arc basins). Based on the chemical compositions of primary silicate minerals as well as spinels, the Egyptian ophiolites mostly formed in a forearc during the beginning of subduction. Also, the presence of boninitic affinities of some Eastern Desert ophiolitic rocks supports fore-arc settings.

Clinopyroxene composition as a petrogenetic indicator for the distinction of MORB- and SSZ-affinities in Albanian ophiolites

Beqiraj, A.* & Shallo, M.
Dept. of Earth Sciences, Faculty of Geology and Mining, Polytechnic University of Tirana, Albania
(*ae_beqiraj@yahoo.com)

The Albanian ophiolite complex, that represents a well developed ophiolite unit with a mostly complete and undisturbed ophiolite succession between Pelagonian and Apulian microplates, spread out over a 250km long and 30-40km wide belt with a NNW-SSE strike.

Two different ophiolite belts were distinguished based on their geochemical and petrological features [1,2]: western and eastern-type ophiolite, showing MOR and SSZ signatures, respectively. Clinopyroxene represents one of the most interesting rock-forming minerals because it is present almost in the entire ophiolite section and its composition, that largely depends on the composition of the melt from which crystallizes, shows an extremely wide variation. Compositional differences of clinopyroxene allowed to distinguish cumulate rocks with MOR- and SSZ-affinities within Bulqiza massif [3].

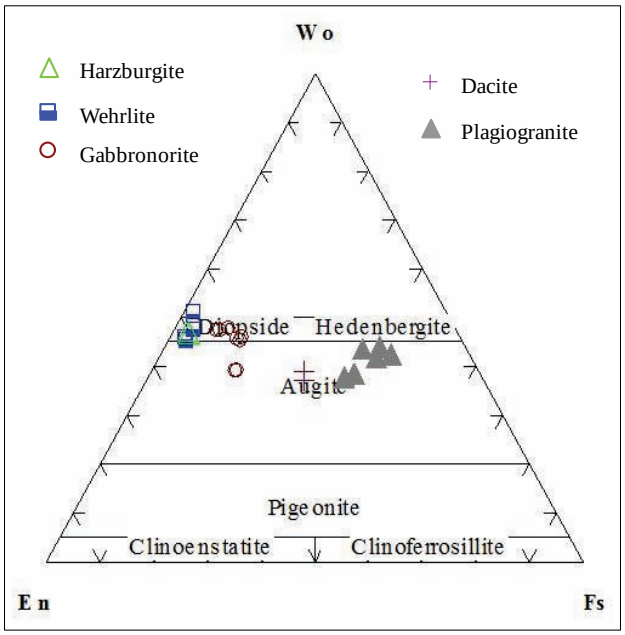

Fig. 1: Pyroxene quadrilateral diagram for the pyroxenes from the Eastern ophiolitic rocks (En-Enstatite; Wo-Wollastonite; Fs-Ferrosilite).

Clinopyroxene from eastern ophiolites shows a wider (Fs=5-45%) (Fig. 1) compositional range than clinopyroxene from western ophiolites (Fs=5-25%) (not shown). The Ti content of clinopyroxene, that ranges from 0.0 to 0.3 %TiO_2 and 0.3-0.9 %TiO_2 for eastern and western ophiolites, suggests their generation in supra-subduction zone (SSZ) and middle oceanic ridge (MOR) environment, respectively [4].

Mantle clinopyroxene is clearly lower in Ti, Fe and Na than magmatic analogue. This later indicates an apparent enrichment trend in iron (mol Fs) from the bottom (wehrlite) to the top (plagiogranite) of the ophiolite plutonic section, but this is not observed for the titanium.

[1] Hoeck, V. et al. (2002) *Lithos*, **65**, 143-164. [2] Shallo, M. & Dilek, Y. (2003) *Geol. S. Am. S.*, **373**, 351-363. [3] Beqiraj, A. & Masi, U. (2006) *Acta Mineral. Petrogr. Conf. Abst.*, **5**, 12. [4] Beccaluva, L. et al. (1989) *Chem. Geol.*, **77**, 165-182.

Ophiolites in the Eastern Cordillera of the central Peruvian Andes

Castroviejo, R.[1*], Rodrigues, J.F.[2], Tassinari, C.[3], Pereira, E.[2] & Acosta, J.[4]
[1]School of Mines, Universidad Politécnica de Madrid, Spain (*ricardo.castroviejo@upm.es)
[2]Fac. Engenharia, Universidade do Porto, Portugal
[3]Institute of Geosciences, Universidade de Sao Paulo, Brasil
[4]INGEMMET, Lima, Perú

A discontinuous NNW-SSE trending belt of scattered ultramafic (UM) and subordinate mafic (M) rocks is exposed along some 250 km in the Eastern Cordillera of the peruvian Andes (Junín and Huánuco Departments, ~9º-12º S). New data question their previously assumed [1,2] intrusive origin. Work in progress shows that the essential geologic and tectonic features are common to most of them, as will be shown on the southernmost occurrences: Tapo and Acobamba (Tarma province). The Tapo massif is the most conspicuous and the only one with chromite mining history. It is a lens-shaped body, 5 km long (NW-SE direction) and 1-2 km wide, lying on detrital sediments of the Lower Carboniferous Ambo Group [3], and comprising extremely tectonised and serpentinised peridotites with subordinate podiform chromitite bodies, meta-gabbros or amphibolites. The Acobamba occurrences comprise serpentinites and subordinate meta-gabbros [4], in contact with phyllites of the Precambrian (?) Huácar Group (Marañón Complex).

In both cases, field work shows a strong shear deformation, with mylonites and phyllonites associated to the basal contact of the UM bodies with the siliciclastic sequences of the basement (either Huácar or Ambo Groups), which show no signs of thermal metamorphism. The interference patterns on the mylonites of these contacts point to a pre-Andean emplacement, followed by late tectonic reworking during the Andean cycle, also evidenced by folding of the basal thrust plane.

The mineralogy is strongly overprinted by metamorphism. The UM rocks are represented by serpentinites (with varying amounts of chromite and magnetite, but only scarce relics or ghosts from pyroxene or olivine) or chlorite-serpentine schists, and by chromitites. Secondary stichtite (Cr-bearing carbonate), kämmererite (Cr-bearing pennine), ilmenite and titanite are seen occasionally. Sulphides (as pyrite, pyrrhotite or millerite) are very scarce. Rodingites, usually grosularia- or andradite-rich rocks with varying amounts of epidote, zoisite, wollastonite or diopside, are present as boudins, and intensively deformed. Altered serpentinites, as listvenites (dolomite or magnesite-talc-antigorite) and birbirites (fine-grained silica), are also found near faults enhancing hydrothermal circulation. The M rocks are metagabros, amphibolites and amphibole-plagioclase mylonites, present in NW-SE trending bands, whose geochemistry strongly suggests an ocean rift or ocean island protolith. Preliminary results from on-going Sm-Nd geochronology point to a Precambrian age for the UM and M protoliths.

All these data preclude an intrusive origin for the UM-M bodies and support their interpretation as dismembered blocks of oceanic lithosphere (ophiolites) thrust on Andean siliciclastic sequences, as is the case for most of the occurrences of the UM belt farther north, thus defining a first example of Peruvian ophiolites (another example of thoroughly dismembered ophiolites along a 250 km belt is known in the Betic Cordillera, SE Spain [5]). Their origin may be related to the break-up of Rodinia and to the evolution of the NW Amazonian margin.

[1] Grandin, G. & Zegarra, J. (1979) *Bol. Soc. Geol. Perú*, **63**, 99-115. [2] Megard et al. (1996) *Bol.* **69 A**. INGEMMET, Lima. [3] Castroviejo, R. et al. (2009) *Proc.10th Biennial SGA Meet.*, Townsville, 927-929. [4] Castroviejo, R. et al. (2009) *Geogaceta*, **46**, 7-10. [5] Puga, E. et al. (2009) *Geoheritage*, **1**, 11-31.

Geochemical fingerprinting of block-in-matrix structures to ophiolitic units in the Western Blue Ridge North Carolina (USA)

Collins, N.C.* & Ryan, J.G.
Dept. of Geology, University of South Florida, Tampa, USA
(*nccollin@mail.usf.edu)

The Blue Ridge province of the southern U.S. Appalachians includes extensive sequences characterized by olistostromal rocks that include blocks of highly metamorphosed mafic, ultramafic, and felsic rocks enclosed in metasedimentary rock matrices. The blocks range in size from a few centimeters across to mappable, >km-scale units, are strongly deformed, and sometimes extensively migmatized. Also, the southern Blue Ridge includes a number of Mafic-ultramafic massifs that, while highly metamorphosed, include lithologic sequences and preserve the geochemical signatures consistent with an oceanic, ophiolitic origin [1-3]. The ophiolitic rocks have been posited to be olistostromal mega-blocks [4-6], and as part of a sequence distinct from the olistostromal units [7]. However, clear petrologic linkages or distinctions between massif mafic units and olistostromal mafic blocks have not been established.

To better understand the connections between Blue Ridge block-in-matrix and ophiolitic units, we are examining the bulk geochemical and mineral chemistry signatures of amphibolitic blocks from parts of the Cullowhee/Cartoogechaye olistostromal terrane for comparison to published data for rocks from the Buck Creek mafic-ultramafic complex [1] and the Carroll Knob Complex [8,2], two of the largest Blue Ridge mafic-ultramafic massifs. Bulk geochemical data is being collected on the ICP-MS at the University of South Florida (USF), using digestion procedures from Kelley et al. 2003 [9]. Thin sections prepared at USF and mineral chemistry was analyzed on the remotely operable JEOL 8900 Superprobe electron microprobe facility at the Florida Center for Analytical Electron Microscopy (FIU).

The olistostromal blocks of the Cullowhee/Cartoogechaye terrane represent rocks with similar chemical trends as the Buck Creek mafic-ultramafic complex and Carroll Knob Complex. Mineral chemistry of amphiboles within the two massif units varies considerably in comparison to the sampled blocks. However, exclusion of high-Mg amphiboles from the massif units reveals chemical signatures within Carroll Knob Complex that are indistinguishable from the olistostromal mafic blocks, as well as areas surrounding the Buck Creek complex. It is our hypothesis that these blocks represent fragments of the upper level of the ophiolitic unit and are working to constrain this through trace and rare earth elemental abundances.

[1] Peterson, V. & Ryan, J.G. (2009) *Geol. Soc. Am. Bull.*, **121**, 615-629. [2] Berger, S. et al. (2001) *SE Geol.*, **40**, 201-212. [3] McElhaney, M.S. & McSween, H.Y. (1983) *Geol. Soc. Am. Bull.*, **94**, 855-874. [4] Raymond, L.A. et al. (1989) *Geol. S. Am. S.*, **228**, 195-215. [5] Laccazette, A.J. & Rast, N. (1989) *Geol. S. Am. S.*, **228**, 217-227. [6] Hatcher, R.D. et al. (2005) *Carolina Geol. Soc. Annual Trip Guidebook*. 1-24. [7] Ryan, J.G. et al. (2005) *Carolina Geol. Soc. Annual Trip Guidebook*. 91-98. [8] Hatcher, R.D. et al. (1984) *Am. J. Sci.*, **284**, 484-506. [9] Kelley, K.A. et al. (2003) *Geochem. Geophy. Geosy.*, **4**, 1-21.

Protolith nature of Baijingsi eclogites from the North Qilian Mountains in NW China and its tectonic significance

Ker Choon-Muar[1*], Yang Huai-Jen[1], Zhang Jian-Xin[2], Tseng Chien-Yuan[1] & Meng Fan-Cong[2]
[1]Dept. of Earth Sciences, National Cheng-Kung University, Tainan, Taiwan (*kcmuar@gmail.com)
[2]Institute of Geology, Chinese Academy of Geological Sciences, Beijing, China

The WNW–ESE trending and ~1000 km long North Qilian suture belt (NQLS) is one of the major suture zones in NW China. It is composed chiefly of blocks of ophiolite mélanges, volcanic rocks and HP/LT metamorphic rocks in sedimentary formations. The protolith nature of these metamorphic rocks and its spatial relationship to the associate ophiolite are basic elements for reconstructing paleo-tectonic environment. In this study, abundances of major and trace element as well as Sr and Nd isotope ratios of 19 eclogite samples from Baijingsi (BJS) area in east part of the NQLS were determined. These data were critically evaluated to infer their protolith characteristics and tectonic significance.

All the analyzed BJS eclogites are of basaltic compositions containing 47–51% SiO_2, 14–20% Al_2O_3, and 6–10% MgO, except for two samples with low MgO contents of 2–4%. Seventeen samples show slight enrichment in LREE over HREE abundances with La/Yb ratio in the range of 1–40. Although consistent with derivation from lavas formed in ocean basins or arcs, such enrichments are not reliable protolith indicators given the mobile behavior of LREE during high-grade metamorphism. The abundances and ratios of relatively immobile Zr, MREE, and HREE are better parameters for deducing the nature of protoliths. The concentrations of these elements in the BJS eclogites are within the ranges for MORB, OIB, and arc lavas, pointing to extrusive, instead of cumulative, igneous precursors. Most significant is the depletions in the abundances of Zr, Hf, Nb, and Ta relative to that of REE with similar compatibility during igneous processes. This feature is the characteristics of lavas generated in arc systems. Collaborating evidence is the Nd isotope ratios. The metamorphic initial Nd isotope ratio, $\varepsilon Nd_{(450\ Ma)}$, of the BJS eclogites varies in the range of 1.5–7 (mostly 4–7), lower than that for MORB and most OIB but consistent with that for lavas formed in convergent zones. If the Nb/Th ratio remained intact during metamorphism, the values of 5–14 for 12 of 19 samples are over the range for North Luzon and Ryukyu arc lavas but within the range for lavas from Lau basin, favoring a back-arc environment. In contrast to the previously proposed MORB and/or OIB protoliths, our new data indicate that BJS eclogites were metamorphosed from lavas in an arc system, most likely back-arc basin lavas.

In developing a tectonic evolution model for NQLS, subduction polarity is a controversial issue. Both northward subduction and southward subduction have been proposed. In such models, a systematic spatial sequence of oceanic ophiolite–arc–back-arc is expected in the north-south direction. The BJS eclogites occur on the north of an oceanic ophiolite belt defined by the Yushiguo and Dongcaohe ophiolites. Consequently, a back-arc protolith for the BJS eclogites is consistent with northward subduction. The development of a back-arc basin also implies that a large ocean basin, instead of a marginal sea, was involved in NQLS subduction system. It is suggested this inferred mature ocean basin is the so-called "Paleo-Qilian Ocean".

Geochemistry and tectonic significance of ophiolites along the Ankara-Erzincan suture zone in northeastern Anatolia

Parlak, O.[1,2*], Colakoglu, A.[3], Donmez, C.[3], Sayak, H.[3], Turkel, A.[3], Yildirim, N.[3], Odabasi, I.[3] & Konak, N.[3]
[1]Adıyaman Üniversitesi, Teknoloji Fakültesi, Adıyaman, Turkey (*oparlak@adiyaman.edu.tr)
[2]Çukurova Üniversitesi, Jeoloji Müh Bölümü, Adana, Turkey
3MTA Genel Müdürlüğü, Ankara, Turkey

The northeastern Anatolia is characterized by two large tectonic units, namely the Eastern Pontides and the Eastern Taurides. These two tectonic units are separated by the Ankara-Erzincan suture zone. The Ankara-Erzincan suture zone includes large bodies of ophiolites and ophiolitic melanges in the northeastern Anatolia. The studied ophiolitic bodies are of (I) Refahiye (Erzincan), (II) Tekman-Pasinler (Erzurum), (III) Karadağ (Erzurum) and (III) Kırdağ (Erzurum). All of these ophiolitic bodies emplaced over the passive margin of the Tauride platform to the south of the suture zone during Late Cretaceous. The ophiolitic units in Refahiye region, except volcanics, are characterized by well-preserved oceanic lithospheric section (mantle tectonites, ultramafic to mafic cumulates, isotropic gabbro, sheeted dikes) and ophiolitic melange (recrystallized limestone, schist, gabbro, serpentinite, spilitic volcanics, sandstone and radiolarite), resting tectonically on the Munzur limestone of the Tauride platform. The ophiolitic units in Tekman-Pasinler region display a well preserved ophiolitic melange, including Triassic to Cenomanian various rock types in which traces of blueschist facies metamorphism were determined and lower part of oceanic lithosphere (peridotite, gabbro and isolated dikes in peridotites) remnants at the top. The Karadağ region displays almost an intact ophiolite succession such as serpentinized harzburgitic tectonites, gabbro, sheeted dike, plagiogranite and volcanics. The Kırdağ region displays a typical features of accretionary melange that includes chaotic mixture of peridotite, gabbro, diabase, limestone blocks, metasandstone, metasiltstone and slices of glaucophane schist. These ophiolitic units in northeast Anatolia are unconformably overlain by Campanian-Maastrichtian sediments that were in turn imbricated with the ophiolitic rocks, suggesting post-emplacement tectonic activity in the region.

Geochemical data for the oceanic crustal rocks along the Erzurum-Kars ophiolite zone (Refahiye, Tekman-Pasinler and Karadağ) display similar geochemical behavior such as (a) tholeiitic in composition (b) depletion of Nb, (c) enrichment in LIL elements, (d) parallel to slightly depleted HFS element patterns compared to N-MORB (e) slightly LREE-depleted to parallel REE patterns and (f) ratios of selected trace elements (Nb/Th, Th/Yb, Ta/Yb). These features suggest that the ophiolitic rocks in the northeastern Anatolia were derived from a island arc tholeiitic magma and formed above an intraoceanic subduction zone. In contrast, the volcanic rocks in the Refahiye ophiolitic mélange show variation in geochemistry (tholeiitic to alkaline nature, depletion & enrichment in REE and HFS elements). These suggest that seamount-type alkaline and subduction-related tholeiitic basaltic rocks were juxtaposed during subduction/accretion.

All the field and geochemical data from the ophiolitic rocks show that they formed along the northern Neotethyan ocean, bounded by the Sakarya Zone (Eastern Pontides) in the north and the Taurides in the south, as a result of north-dipping intraoceanic subduction during the Late Cretaceous. During the closure of the ocean, the rift/passive margin units and the distal edge of the Tauride Carbonate Platform were detached and emplaced together with the over-riding ophiolites. Subduction-accretion units and the leading edge of the northern margin of the Tauride Carbonate Platform were underthrust, deeply buried and metamorphosed under HP–LT conditions.

Petrology and geochemistry of Malakand ophiolitic complex, Pakistan

Sano, S.
Earth Science Laboratory, Faculty of Education, Ehime University, Matsuyama, Japan (sano@ed.ehime-u.ac.jp)

Malakand ophiolitic complex is exposed along suture zone in northern Pakistan [1]. The Malakand complex is a dismembered ophiolite formed with convergence of Neo-Tethyan Ocean by collision of the Indian plate against the Kohistan Arc. The main constituents are harzburgite and dunite, with minor wehrlitic, websteritic and gabbroic dikes. Small-scale chromitite deposits are frequently seen in the dunite zone. Harzburgite displays typical porphyroclastic texture, and clinopyroxene is rarely seen. Porphyroclastic and equigranular textures are observed in dunite. Chrome spinels in dunite and chromitite often include amphibole and clinopyroxene.

Harzburgites contain olivine with $0.906 < X_{Mg} < 0.925$. Olivine in dunites shows much wider X_{Mg} range of 0.911 to 0.943. The variation of Cr# depends on the rock and position of the body. Cr# of spinel in harzburgite ranges 0.50 to 0.75, while that in dunite shows 0.45 - 0.87.

REE concentrations of harzburgite and dunite are extremely low compared with those of mid-oceanic ridge (MOR) peridotites. Chondrite-normalized La, Gd and Lu contents are $(La)_N = 0.0013 – 0.017$, $(Gd)_N = 0.0015 – 0.0079$ and $(Lu)_N = 0.05 – 0.12$, respectively. The harzburgite and dunite display convex-downward REE patterns (Fig. 1). Dunite shows low HREE/MREE ratios, and higher LREE contents. On the other hand, REE patterns of dike rocks of hornblende-gabbro, leucogabbro and olivine-websterite, which intrude into harzburgite and dunite, display wide variety.

Harzburgites and dunites from the Malakand ophiolitic complex probably represent very depleted mantle after large degree of melting. Clinopyroxene-free harzburgite, high X_{Mg} of olivine, high Cr# of spinel and existence of hydrous minerals in chrome spinel indicate that the Malakand complex correspond to uppermost mantle beneath an island arc. Furthermore, it is expected that existence of high Cr# spinel (0.87) engage with a boninitic magma [2].

Very low concentrations of MREE to HREE in the harzburgite and dunite expect that they are residue after multi-stage extended melting at deeper garnet- to shallower spinel-fields [3]. Relative LREE enrichment of the peridotites is possibly resulted in any interaction [4] of circulating melt with harzburgite wall.

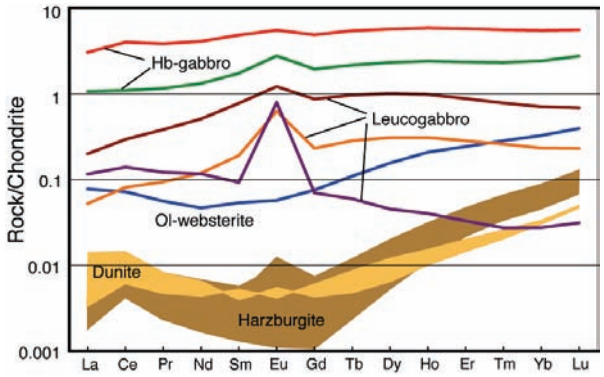

Fig. 1: Chondrite normalized REE patterns of rocks from the Malakand ophiolitic complex, Pakistan.

[1] Asrarullah et al. (1979) in Farah, A. & DeJong, F. (eds.) *Geodynamics of Pakistan*. Geol. Surv. Pakistan, Quetta, 181-192. [2] Bloomer, S.H. & Hawkins, J.W. (1987) *Contrib. Min. Petrol.*, **97**, 361-377. [3] Sano, S. & Kimura, J.-I. (2007) *J. Petrol.*, **48**, 113-139. [4] Takazawa, E. et al. (1992) *Nature*, **359**, 55-58.

Petrology of the Singok ultramafic bodies in Hongseong area, Gyeonggi Massif, South Korea

Seo, J.[1], Rajesh, V.J.[1,2], Choi, S.-G.[1*] & Oh, C.W.[3]
[1]Dept. of Earth and Environmental Sciences, Korea University, Seoul, Republic of Korea ([*]seongyu@korea.ac.kr)
[2]Dept. of Earth and Space Sciences, Indian Institute of Space Science and Technology, Thiruvananthapuram, India
[3]Dept. of Earth and Environmental Sciences, Jeonbuk National University, Jeonju, Republic of Korea

Several isolated lensoidal serpentinized ultramafic bodies occur within the granitic gneiss in the Hongseong area in the western Gyeonggi massif, South Korea. Many of these bodies are highly deformed and metamorphosed under eclogite to greenschist facies conditions. The core compositions of chromian spinel and olivine are used to deduce the petrogenesis and tectonic environments of the Singok ultramafic rocks (one among the representative ultramafic bodies in the Hongseong area). The high Fo content of olivine with moderate to high Cr# (Cr/Cr+Al) of chromian spinel indicate the formation of the ultramafic bodies as mantle residues left after higher degrees of partial melting of a fertile MORB mantle. The data plot in an overlap area of the abyssal and suprasubduction zone peridotite fields in the olivine spinel mantle array (OSMA) diagram. The low TiO_2 content of the chromian spinel along with high Cr# suggest a suprasubduction zone environment. Further, the chromian spinel and olivine compositions are similar to those harzburgites formed in the mature back-arc basin in the Bibong area. We believe that the Singok ultramafic rock was a mantle part of the SSZ ophiolite and formed in the mature back-arc basin tectonic setting by high degrees of partial melting due to the increased supply of fluid or melt from the subducting oceanic crust. This finding substantiates the existence of a collision zone in the Hongseong area of the Gyeonggi massif.

Deciphering a complex geodynamic evolution of an orogen: what is the contribution of the metamorphic petrology?

Bousquet, R.[1*], Oberhänsli, R.[1] & Wiederkehr, M.[2] & Robert, Ch.[3]
[1]Institut für Erd- und Umweltwissenschaften, Universität Potsdam, Germany ([*]bousquet@geo.uni-potsdam.de)
[2]Swisstopo, Wabern, Switzerland
[3]Laboratoire de Géologie, ENS Paris, France

Based on mineralogical works, Ernst [1] was able to use the plate tectonic concept for proposing a first modern model for the evolution of the Alps. In the meantime, [2], as well as [3], started to investigate metamorphism in isochemical systems provided by shales and siliceous carbonates, respectively. This allowed for quantitatively constraining the Cenozoic temperature evolution in the Central Alps. The regional distribution of the Permian and of Cretaceous-Tertiary metamorphic conditions, documented in post-Hercynian rocks across the entire Alpine belt from Corsica-Tuscany in the West to Vienna in the East, will be presented.

Based on metamorphic studies in metasediments, we evidence substantial differences in the metamorphic, and hence the geodynamical evolution along strike the Alpine orogen.

The Western Alps did not reach the mature stage of a head-on colliding belt as is indicated by a continuous metamorphic evolution, representing all the subduction related processes ranging from lower greenschist to UHP conditions. All the metamorphic rocks behind the Pennine frontal thrust were already exhumed to upper crustal level during ongoing oceanic and continental subduction and before collision with the Dauphinois domain from around 32 Ma onwards. Hence, the Western Alps represent a frozen-in subduction zone. Since then only exhumation by erosional processes affected the inner parts of the orogen. The rest of the Alpine orogen later underwent a more important collision process due to the ongoing head-on geometry of subduction and collision. It therefore often but not always shows a bimodal metamorphic evolution with two distinct P and T peaks. The intensity of the thermal overprint relates to the amount of crustal material incorporated to the orogenic wedge. Thermal overprint is primarily related to the amount of crust involved in the subduction and collision processes rather than to processes of shear or viscous heating. The latter mechanism, which suppose high deformation rate will not allow for the preservation of HP-LT assemblages within high-grade rocks. The recorded isotopic data reveal a significant time gap in the order of some 20 Ma between the subduction-related HP/LT event (42-40 Ma) and the later collision-related MP/MT Barrovian overprint (19-18 Ma) supporting the notion of a polymetamorphic evolution in the Centrtal Alps associated with a bimodal P-T path. Amphibolite facies Barrow-type overprint represents a clearly separated heating pulse that post-dates isothermal decompression after the early high-pressure stage. This considerable time interval is in accordance with the interpretation that it is the accretion of vast amounts of European continental crust (forming the present-day Lepontine dome) that provides high radiogenic heat production responsible for amphibolite facies metamorphism, being an entirely conductive and therefore rather slow process.

The relation between the volume of continental crust imbricated and intensity of high-temperature orogenic metamorphism can be generalized over the entire alpine edifice, except for Tuscany where the late thermal overprint is clearly related to lithospheric thinning.

[1] Ernst, W.G. (1971) *Contrib. Miner. Petrol.*, **34**, 43-59. [2] Frey, M. (1969) *Die Metamorphose des Keupers vom Tafeljura bis zum Lukmanier-Gebiet*. Bern [3] Trommsdorff, V. (1966) *Schweiz. Miner. Petrog.*, **46**, 431-460.

Processes of extrusion and extension of the ALCAPA block as mirrored by mafic lower crustal xenoliths from the Bakony-Balaton-Highland basalts (Hungary)

Dégi, J.[1,2*], Török, K.[3], Abart, R.[4] & Belkin, H.E.[5]
[1]Research Institute for Solid State Physics and Optics, Budapest, Hungary ([*]julia.degi@gmail.com)
[2]Lithosphere Fluid Research Lab, Eötvös University, Budapest, Hungary
[3]Eötvös Loránd Geophysical Institute of Hungary, Budapest, Hungary
[4]Dept. of Lithospheric Research, University of Vienna, Austria
[5]U.S. Geological Survey, Reston, Virginia, USA

The Pannonian Basin (PB) is a Mediterranean type back-arc basin with thin crust (25–31 km) in thin lithosphere (60–70 km). The northern part, the ALCAPA block, was part of the Alps in the Upper Cretaceous. This block went through large scale juxtaposition and several drastic changes due to the tectonic processes during the Miocene extension/extrusion of the Pannonian Basin (18–11 Ma). The material of the deep lithosphere has been sampled by post-extensional alkali basaltic volcanism in the Bakony-Balaton Highland Volcanic Field, located in the central region of the Pannonian Basin. We have studied mafic lower crustal granulite xenoliths from this area in order to identify deep lithospheric processes acting associated with the geodynamic evolution.

Peak metamorphic conditions are shown by the granulite facies rock-forming mineral assemblage (clinopyroxene, plagioclase, garnet, ±orthopyroxene ±amphibole ±biotite). In most of the xenoliths, the peak metamorphic mineral assemblage shows equilibrated granoblastic microstructure, while in some samples non-equilibrium poikiloblastic microstructure is present. Petrographic observations and fluid inclusion studies of the latter samples suggest that biotite was destabilized in the presence of CO_2-rich fluids by the reaction Bt + Pl + Qtz = Opx + Grt + melt. Melt was extracted from the rock, and orthopyroxene, garnet and some plagioclase remained as restitic phases. Careful geothermobarometric investigations have shown that the granoblastic xenoliths represent a complete crustal section with equilibrium temperatures and pressures between 750–1070 °C and 1.0–1.6 GPa, which corresponds to 35–60 km depth. This corresponds to the overthickened orogenic root of the Alps, where CO_2-rich fluid input led to the partial melting of the lower crust may be at the beginning of the extension/extrusion of the Pannonian Basin.

According to mineral reactions observable in the rock, peak metamorphic conditions were followed by significant pressure decrease to 0.7–0.8GPa (25–28km), which corresponds to the depth of the present day lower crust. This suggests that the process took place due to significant crustal thinning during the extension/extrusion. Melting of high Ti amphiboles and reactions of rock-forming minerals with melts at lower pressures indicate that partial melting of the lower crust was continuous during the extension. Accessory Fe-Ti-oxides have preserved the traces of interaction of the xenoliths with the host basalt. By the modelling of diffusion profiles in the oxide grains we have estimated that the interaction lasted a few days.

Our results on the metamorphic evolution of lower crustal xenoliths have shown a series of lithospheric processes starting from an overthickened orogenic crust through the extrusion of the ALCAPA block and extension of the Pannonian Basin ending with sampling of the lower crust by late Tertiary basalts, which can be used for refining models of basin formation.

Different metamorphic records in the Western Kaoko Zone (NW Namibia) and their timing

Fuchs, P.[1*], Tajčmanová, L.[1,2], Milke, R.[1] & Konopásek, J.[2]
[1]Institute of Geological Sciences, Free University, Berlin, Germany ([*]parveen.fuchs@fu-berlin.de)
[2]Czech Geological Survey, Prague, Czech Republic

The Kaoko belt is situated in NW Namibia and represents a part of the Neoproterozoic orogenic belt system of western Gondwana developed between the Congo Craton, the Kalahari Craton and the Rio de la Plata Craton in southern Brazil. The metamorphic evolution of the eastern and central part of the Kaoko belt has already been well described by means of thermodynamic modelling [1]. On the contrary, well-constrained data on pressure-temperature (P-T) evolution of the western part of the Kaoko belt are still missing. The westernmost unit of the western Kaoko Zone, the so called Coastal Terrane (CT), is a unit with metamorphic ages of 650-630 Ma and an independent tectonic evolution prior to its collision with the Congo Craton at ~580-550 Ma. The CT consists of migmatitic metasedimentary rocks that are intercalated withfine -grained orthogneisses and amphibolites. Along its eastern margin, the Boundary Igneous Complex (BIC) is exposed and defines the suture between the CT and Congo Craton-related rocks of the Kaoko belt. The BIC is composed of various types of granitoids associated with isolated bodies of pervasively molten metapelites metamorphosed at 580-550 Ma. As the relationship of the CT with the rest of the Kaoko belt and the affinity of granitoids from the BIC is still a matter of debate, we have focused on the key metamorphic lithologies from both units in order to characterize the metamorphic evolution and partial melting in detail. This information combined with already existing geochronological, geochemical and structural data from the two units can help to a better description of the overall tectonic evolution of the area.

In this work, we have particularly focused on metasedimentary rocks from both units because they contain the most suitable assemblages for phase equlibria modelling. All phase equilibria calculations were carried out by using the thermodynamic software set Perple_X. The metasediments from the CT are characterized by a Grt-Bt-Pl-Kfs-Ms-Qtz mineral assemblage. The foliation is defined by biotite and muscovite bands alternating with a quartz-feldspatic matrix. Although the rock was affected by melting, the presence of muscovite documents that temperatures higher than 700°C have never been reached. Samples from the BIC underwent pervasive melting and have a strong stromatitic character. Three different assemblages have been described reflecting the slightly different pressure conditions of equilibration attained during the metamorphic evolution: Grt-Sil-Bt-Pl-Kfs-Qtz; Grt-Crd-Sil-Bt-Pl-Kfs-Qtz and Crd-Sil-Bt-Pl-Kfs-Qtz. Two different generations of garnet occur in the Grt-Sil-Bt samples. The First generation is characterized by medium grained garnets elongated parallel to the foliation and the second generation by undeformed porphyroblasts. This observation serves for more accurate description of the *P-T* path. The temperatures for all three assemblages exceeded 750°C. Regarding the *P-T* results from both units, the two different metamorphic events are characterized by different thermal evolution. The higher temperatures attained during the metamorphic event at 580-550 Ma are interpreted to be connected with an emplacement of a huge amount of granitoids within the BIC.

[1] Will, T.M., Gruner, B.B. & Okrusch, M. (2004) *S. Afr. J. Geol.*, **107**, 431-454.

Island-Arc signature in amphibolites from the boundary between the Ossa Morena Zone and the Central Iberian Zone in Central Portugal

Henriques S.B.A.[1*], Neiva A.M.R.[2], Ribeiro M.L.[1] & Dunning G.R.[3]
[1]Dpt. of Geology, LNEG, Amadora, Portugal ([*]susana.henriques@ineti.pt)
[2]Dept. of Earth Sciences and Geosciences Centre, University of Coimbra, Portugal
[3]Earth Sciences Dept., Memorial University, St. John's, Canada

The Iberian Terrane contains an important tectonic boundary, the Tomar-Badajoz-Cordoba shear zone, between the Ossa Morena Zone and the Central Iberian Zone, where the Cabeço da Moura amphibolites (Pouchão Mafic Complex), crops out close to Abrantes, Central Portugal. It consists of a fine-grained amphibolite that comprises three main mineral assemblages: a) labradorite, magnesiohornblende, augite, diopside, quartz and ilmenite; b) bytownite rimmed by andesine, ferrohornblende, hedenbergite, diopside, epidote, titanite, quartz, magnetite and apatite; c) andesine, magnesiohornblende rimmed by actinolite, diopside, quartz and magnetite. Estimated P-T conditions, based on hornblende Al content [1] and hornblende-plagioclase equilibrium [2], are T=702-724º C, P=4.6-4.9 kb (± 0.6 kb) for the assemblage a); T=703-727º C, P=6.7-7.4 kb (± 0.6 kb) for the assemblage b), showing a progressive metamorphism and T=640-708º C, P=3.8-6.2 kb (± 0.6 kb) for retrograde crystallization evidenced by the formation of actinolite. The analyzed amphiboles have important coupled substitutions such as edenite in all the amphiboles, hastingsite-pargasite in ferrohornblende and magnesiohornblende, titanotschermakite in magnesiohornblende, ferrotschermakite in magnesiohornblende and actinolite and hastingsite in actinolite.

The Cabeço da Moura amphibolites are basic (SiO_2=45.68-50.03 wt %), subalkaline and tholeiitic. The MORB- normalized spider diagram shows enrichment in LILE relatively to HFSE (Rb_N/Y_N=2.67-15.76), a negative Th anomaly and a HFSE pattern (from P_2O_5 to Yb) parallel to MORB, but at a lower level, and in general LILE are enriched above MORB, suggesting an island arc setting. The chondrite normalized REE patterns display enrichments in MREE relatively to HREE (Sm_N/Yb_N=1.07-1.25) and do not show significant negative Eu anomalies (Eu/Eu*=0.92-1.05). The Th-Hf/3-Ta and Zr/4-2Nb-Y diagrams show N- and E-MORB affinities, supported by La_N/Sm_N (0.72-0.91) and La_N/Sm_N (1.29-1.51). Enrichment in LREE relatively to HREE only occurs in E-MORB samples (La_N/Yb_N=1.08 to 1.81), contrasting with N-MORB samples (La_N/Yb_N=0.85-0.87). The ID-TIMS U-Pb age of the metamorphic zircon, that has an equant multi-faceted morphology, is 539 ± 3Ma. These data suggest the presence of a Precambrian island arc that generated magmas from depleted and enriched mantle sources and were metamorphosed in the early Cambrian under amphibolite facies conditions.

Acknowledgements: This study was supported by a PhD grant given to S.B.A. Henriques by the Portuguese Foundation for Science and Technology.

[1]Schmidt, M.W. (1992) *Contrib. Mineral. Petrol.*, **110**, 304-310. [2] Holland, T. & Blundy, J. (1994) *Contrib. Mineral. Petrol.*, **116**, 433-447.

Neoarchaean high-grade metamorphism of pelitic gneisses and ironstones in the Nhlangano area, SW Swaziland

Horváth, P.[1*], Reinhardt, J.[1], Hofmann, A.[1] & Nagy, G.[2]
[1]School of Geological Sciences, University of KwaZulu-Natal, Durban, Republic of South Africa ([*]horvathp@ukzn.ac.za)
[2]Institute for Geochemical Research, Hungarian Academy of Sciences, Budapest, Hungary

Within the broader perspective of an investigation of Archaean geodynamic processes along the southern margin of the Kaapvaal Craton, we quantitatively evaluated pressure and temperature conditions recorded in supracrustal rocks overlying the Kaapvaal basement in southwest Swaziland. The uniqueness of the area is expressed by the occurrence of intensely deformed, high-grade metamorphic rocks of the c. 2900 Ma Pongola Supergroup. Elsewhere, this volcano-sedimentary cover sequence is relatively undisturbed and typically shows no more than low-grade metamorphic overprint.

Metapelitic gneisses of the Nhlangano area have a peak metamorphic assemblage of garnet-cordierite-sillimanite-K-feldspar-plagioclase-quartz-ilmenite. Restitic varieties lack sillimanite, but contain more garnet and cordierite. Silica-undersaturated rocks contain corundum and spinel with garnet, plagioclase, K-feldspar and biotite. These assemblages indicate high-temperature (granulite facies) conditions involving partial melting and, in case of the restitic rocks, melt loss. Meta-ironstones can be divided into two groups, according to petrographic and compositional parameters. The group 1 ironstones contain orthopyroxene with garnet, quartz and magnetite. The group 2 ironstones have no orthopyroxene. Instead, amphiboles are present. Another significant difference between the two groups is the bulk MnO content which is high in the group 2 ironstones. This is reflected in the high MnO content of the major rock-forming minerals (garnet, amphibole). Phase equilibria modelling of metapelites and ironstones indicate metamorphic peak pressure and temperature conditions around 6-8 kbar and 850°C.

Dating of metamorphic monazite in metapelites yielded ages between 2500 and 2700 Ma, suggesting peak (or post-peak) metamorphism during Neoarchaean times.

Distinguishing garnet grains using textural analysis on the pelitic schists of the Sanbagawa metamorphic belts, Shikoku, Japan

Inui, M.
School of Science and Engineering, Kokushikan University, Tokyo, Japan (inui@kokushikan.ac.jp)

The occurrence of garnet grains in the higher grade pelitic schists of the Sanbagawa metamorphic belt (Albite-biotite zone and Oligoclase-biotite zone) exposed along the Asemigawa-river, central Shikoku, Japan, was reexamined for the evidence of disequilibrium and of multiple generation. Those garnet grains play a very important role in constraining the pressure-temperature history of the Sanbagawa metamorphism.

Chemical mapping analysis was carried out on garnet grains in 13 pelitic schist samples to find some grains displaying weak intrasectoral zoning, which was an evidence of disequilibrium. It seemed reasonable to divide the garnet into two groups. Group A grains were porphyroblasts with 0.2 to 1 mm diameter, generally distributed evenly throughout a thin section. They exhibited normal chemical zoning. Group B grains were distinctly smaller and most of them were located in the muscovite-rich layers or included in the albite porphyroblasts. Group B grains often showed intrasectoral chemical zoning.

Group A garnet occurred in the Oligoclase-biotite zone and the upper Albite-biotite zone (the highest grade Oligoclase-biotite zone rocks are sandwiched by the upper and lower Albite-biotite zone rocks). Group B garnet occurred in the Oligoclase-biotite zone and the lower Albite-biotite zone. Group A and B grains were observed in the same thin section of rocks from the lower Oligoclase-biotite zone on the south of the proposed detachment fault [1]. The result of the crystal size distribution analysis supported that they were of two different populations.

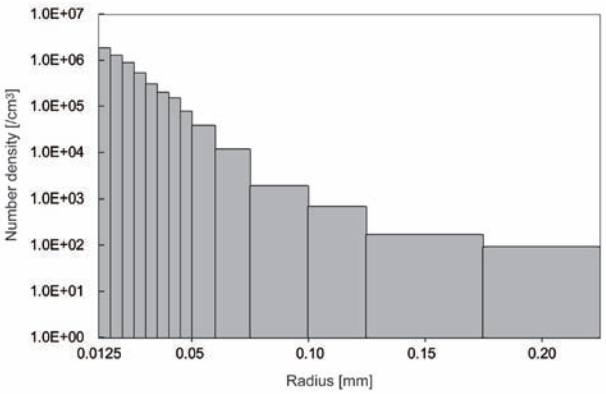

Fig. 1: Crystal size distribution of garnet in sample M19A.

Group A grains included in the albite porphyroblast had the same chemical profile compared to those not included in albite. Group A garnet seemed to have grown during the prograde metamorphism, which predated the formation of the albite porphyroblasts. The group B garnet included in the albite porphyroblasts lacked the rim which the group B grains in the matrix had (middle Oligoclase-biotite zone), or, on the contrary, the rim of the included grains were more preserved compared to the resorbed grains in the matrix (lower Albite-biotite zone). It is indicated that formation of the group B garnet was roughly contemporaneous with that of the albite porphyroblasts, the timing of which is probably after the peak metamorphism. It is possible that garnet grains of post peak generation (group B) are more widely distributed than previously thought.

[1] Osozawa, S. & Pavlis, T. (2007) *J. Struct. Geol.*, **29**, 1131-1147.

Metamorphic *P-T-t* evolution of the Trans-Angarian region, Yenisey Ridge, as a consequence of geodynamic events in the western margin of the Siberian craton

Likhanov, I.I.*, Reverdatto, V.V., Kozlov, P.S. & Popov, N.V.
Sobolev Institute of Geology and Mineralogy, Novosibirsk, Russia (*likh@uiggm.nsc.ru)

We report new isotopic and petrological data on the evolution of polymetamorphic complexes of the Trans-Angarian region, Yenisey Ridge, which allowed us to constrain several major stages in the Riphean geological history of the study area that were controlled by different geodynamic settings.

The first stage was marked by the formation of zoned (LP/HT) metamorphic complexes of the andalusite-sillimanite type over a wide range of temperature and pressure conditions (T=400°C-650°C, P=3.5-5 kbar), suggesting a normal metamorphic field gradient with dT/dP ca. 40°C/km [1]. The inferred relationships between these processes and the Grenville orogeny can be supported by SHRIMP-II U-Pb and ^{39}Ar-^{40}Ar dating of metapelites from the Teya polymetamorphic complex (953-973 Ma) [1]. In the vicinity of thrusts, within the Tatarka deep fault, these rocks underwent medium-pressure metamorphism which resulted in the progressive replacement of andalusite by kyanite and the formation of new mineral assemblages and deformation structures [2]. Some specific features of the kyanite-sillimanite metamorphism include a small thickness of the medium-pressure metamorphic zoning (2.5-7 km) and a gradual increase in pressure from 4.5-5 to 6.5-8 kbar in approaching the thrusts, with a less pronounced temperature zoning, which is indicative of a low metamorphic field gradient with dT/dP ranging from 1-7 to 12°C/km [3]. These specific features are typical of collision-related metamorphism, which can be well substantiated using a model of crustal thickening at high thrusting rates and subsequent rapid exhumation and erosion [4]. Using the calculated exhumation rate (0.368 mm/yr) and the proposed model, we placed age constraints on the five areas and timing of collision-related metamorphism with the peaks at 849-862 and 798-802 Ma. The older metamorphic rocks (Angara, Mayakon, Teya, and Chapa areas) were formed as a result of thrusting of Siberian cratonal blocks onto the Yenisey Ridge that is evidenced by geophysical data and provenance studies. Subsequent collision-related metamorphism was caused by opposite movements of smaller eastward-trending blocks in the zone of higher-order splay faults (Garevka area). On a regional scale, this can be linked to accretion and collision processes when the microcontinent split off the craton at the Early-Middle Riphean boundary and dock onto the Central Asian terrane [5].

[1] Popov, N. et al. (2010) *Dokl. Earth Sci.*, **431**, 418-423. [2] Likhanov, I.I. et al. (2008) *Petrology*, **16**, 136-160. [3] Likhanov, I.I. et al. (2009) *Russ. Geol. Geophys.*, **50**, 1034-1051. [4] Likhanov, I.I. et al. (2004) *J. Metamorph. Geol.*, 22, 743-762. [5] Likhanov, I.I. & Reverdatto, V.V. (2010) *Int. Geol. Rev.*, in press.

Cr-staurolite - bearing rocks from the Valea Someşului Unit (Rodna Mountains, East Carpathians, Romania)

Mosonyi, E.* & Forray, F.L.
Dept. of Mineralogy, Babeş-Bolyai University, Cluj-Napoca, Romania (*emilia.mosonyi@ubbcluj.ro)

Cr- staurolite is described from the Valea Somesului Group gneisses of Alpine Infra-Bucovinian Unit in the Rodna Mountains (East Carpathians). This is a first record of a Cr-staurolite from the polymetamorphic crystalline basement in the East Carpathians. The aim of the study was to characterize a chemically zoned staurolite, the metamorphic evolution of the staurolite- bearing rocks and to compare their evolution with those from overthrusted Sub-Bucovinian Rebra Group gneisses. The Cr- staurolite formed under Barrovian-type metamorphic conditions. As revealed by the microprobe measurements in the staurolite zoning profile three main zones could be delimited, that record three phases in staurolite evolution: two blasthesis phases in prograde, and one resulted during retrogression transformations.

About the Cr origin in these rocks we suppose either a bimodal magmatic event during a cratonic rifting or an accretionary wedge material in convergent plate setting. Using different geothermometers and geobarometers (Ti in biotite [1] and biotite-muscovite geothermometers [2] and phengite geobarometer [3]) it could be outlined that Cr-staurolite-bearing gneisses from Valea Somesului Group/ Bretila Group (BG) a medium pressure metamorphism in amphibolite facies conditions (T_{max}= 580°C, P =5-6.6 kb) suffered during the M_1 (during this collision BG was a part of an upper plate) with two deformation phases (the D_2 phase was associated with some migmatic processes). The Sub-Bucovinian Rebra Group gneisses were metamorphosed in medium pressure amphibolite facies conditions (640ºC, 6kb [4]) in the M_1. During M_2 event in an uplift tectonic setting both groups processed together (parallel, transposed rock fabrics), but in different pressure conditions.

[1] Henry, D.J. et al. (2005) *Am. Mineral.*, **90**, 316-328. [2] Hoisch, T.D. (1989) *Am. Mineral.*, **74**, 565-572. [3] Massonne, H.J. & Schreyer, W. (1987) *Contrib. Mineral. Petrol.*, **96**, 212-224. [4] Mosonyi, E. (1999) *PhD Thesis*, Babeş-Bolyai University Cluj-Napoca, unpublished.

Tertiary eclogites in the lower tectonic unit of East Rhodope (Kechros Complex, NE Greece)

Mposkos, E.* & Baziotis, I.
Section of Geological Sciences, Dept of Mining and Metallurgical Engineering, National Technical University of Athens, Greece (*mposkos@metal.ntua.gr)

The Rhodope Metamorphic Province is one of the major tectonic units in northern Greece. It consists of different tectonometamorphic complexes involved in the Alpine collisional history between the Eurasian and African plates. In eastern Rhodope a Jurassic UHP metamorphism is documented in the uppermost Kimi Complex by the presence of microdiamond inclusions in garnets from pelitic gneisses [1]. Partially or completely amphibolitized eclogites are common recording P-T conditions >1.8 GPa and 750°C for the eclogitic stage [2].

In the underlying Kechros Complex lenses of kyanite eclogites in orthogneisses with Permian ages of their gabbroic protoliths [3] and of common eclogites within metapelites associated with serpentinized peridotites occur.

The mineral assemblage of the kyanite eclogites is Grt + Omp(Jd_{35-55}) + Ky + Tr + Hbl + Zo/Czo + Phg + Qtz + Rt. Garnet shows growth zoning with core composition $Grs_{0.19}Prp_{0.15}Alm_{0.63}Sps_{0.03}$ and rim composition $Grs_{0.20}Prp_{0.27}Alm_{0.52}Sps_{0.01}$. Inclusions in garnet are abundant; they are clinozoisite, kyanite, omphacite (Jd_{45-55}), quartz, actinolite, hornblende and very rare albite and paragonite. Matrix omphacite is in textural equilibrium with kyanite, but commonly it is replaced by Ca-amphibole. A decrease in jadeite component from the core to the rim indicates a re-equilibration tendency during exhumation. Temperatures of 550-600°C and minimum pressure of 1.5 GPa are obtained with Grt-Cpx geothermometry and the jadeite component (Jd_{55}) in omphacite. However, the coexistence of matrix omphacite with kyanite constrains the minimum pressure to 2.1 GPa assuming H_2O activity equal to unity.

In the common eclogites the HP mineral assemblage is Grt + Omp + Rt ± Phg ± Czo ± Gln + Hbl ± Mrg ± Pg. Garnet shows compositional zoning with $Grs_{0.32}Prp_{0.03}Alm_{0.51}Sps_{0.14}$ in the core and $Grs_{0.26}Prp_{0.09}Alm_{0.65}Sps_{0.01}$ at the rim. It contains inclusions of glaucophane, actinolite, clinozoisite, paragonite, oligoclase/albite, omphacite (Jd_{29-41}), titanite and rutile. Glaucophane is present only as inclusions in garnet, omphacite and hornblende and paragonite as inclusions in garnet and hornblende. The paragonite component in margarite ranges from 30-37%. Temperatures of 500-530°C and minimum pressure of 1.4 GPa are obtained with Grt-Cpx geothermometry and the jadeite component in omphacite (Jd_{40}). Maximum pressure is constrained below 2.2 GPa by the presence of margarite and paragonite and the absence of kyanite. In retrogressed samples Ca-amphibole replaces garnet and omphacite. Anorthite-rich plagioclase (An_{55-95}) is formed replacing margarite+zoisite+quartz indicating isothermal decompression from the maximum pressure down to 0.7 GPa.

Ages for the HP metamorphism in the Kechros Complex are not available. A Rb-Sr white mica age of 37 Ma from an orthogneiss records probably a stage of exhumation. The HP event may occurred at the same time with the Eocene HP metamorphism (49-55 Ma) recorded in the Nestos Shear Zone (NSZ) in Central Rhodope [3,4]. The NSZ comprises lithologies of the overlying Sidironero Complex and the underlying Albite-Gneiss Series; the latter represents the westward continuation of the Kechros Complex.

[1] Mposkos, E. & Kostopoulos, D. (2001) *Earth Planet. Sci. Lett.*, **192**, 497-506. [2] Bauer, C. et al. (2007). *Lithos*, **99**, 207-228. [3] Liati, A. (2005) *Contrib. Mineral. Petrol.*, **150**, 608-630. [4] Bosse, V. et al. (2009) *Chem. Geol.*, **261**, 286-302.

Chemical zonation in Ca-amphibole from the Jubrique unit (Betic Cordillera, Spain), and metamorphic *P-T*-t path

Ruiz Cruz, M.D.
Facultad de Ciencias, Malaga University, Málaga, Spain (mdruiz@uma.es)

Zoned Ca-amphibole from metaclastic rocks and veins of the Jubrique area (Alpujárride complex, Betic Cordillera, Spain), and its significance on the metamorphic evolution of these rocks are described for first time. Typical Al-rich metapelites from this area show assemblages consisting of dominant white mica (muscovite and paragonite) and chlorite, with sporadic biotite, kyanite, and chloritoid. Nevertheless, in some Ca-richer phyllites, fine-grained quartzites, and quartz-rich veins, amphibole crystallized with plagioclase and K-feldspar, epidote, titanite, chlorite and quartz. Two main types of amphibole have been identified: Ca-amphibole, the most frequent, and Fe-Mg-amphibole (calcian cummngtonite). Ca-amphibole appears as intergrowths of dominant radial grains and as euhedral crystals. Ca-amphibole displays zonation with actinolite or Si-rich hornblende cores, overgrown by magnesiohornblende (and edenite) and minor tschermakite, indicating growth at increasing metamorphic physical conditions. Retrogressive rims are variably developed in the several lythotypes (Fig. 1 left).

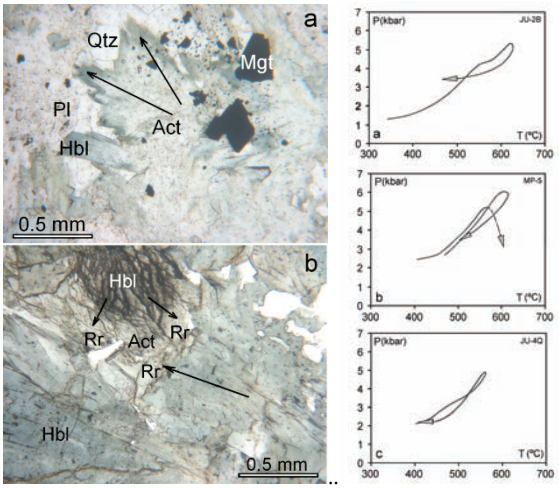

Fig. 1: Left - a) Radial amphibole from quartz-vein with an actinolite core and a narrow rim of hornblende. b) Sub-euhedral dark amphibole from quartzite showing an inverse zonation from hornblende to actinolite. Rr: retrogressive rims. Arrows mark some of the analyzed profiles. **Right** - General *P-T* trends defined by zoned amphiboles from quartz-rich veins (a), phyllites (b) and quartzites (c).

General zonation is well described in terms of the tschermak, the edenite and the $Fe^{3+}Al_{-1}$ and $MgFe^{2+}_{-1}$ exchanges. The Al-in-amphibole thermobarometer [1] provides a range of temperatures between 350ºC and 620ºC (Fig. 1 right), for a pressure range from 0.9 to 6.2 kbar, respectively. Amphiboles define a prograde pressure-temperature path from low pressure-low temperature to medium pressure-medium temperature, typical of Barrovian-type metamorphism.

Acknowledgements: This study has received financial support from the Project CGL 2009-08186 (Ministerio de Ciencia e Innovación) and from the Research Group RNM-199 (Junta de Andalucía).

[1] Zenk, M. & Schulz, B. (2004) *Mineral. Mag.*, **68**, 769-786.

Pumpellyite-bearing assemblages in metapelites and veins from the Federico Units (Internal Zone of the Rif): their application to reconstructing the metamorphic history

Ruiz Cruz, M.D.[1*], Sanz de Galdeano, C.[2], Alvarez-Valero, A.[2], Rodríguez Ruiz, M.D.[1] & Novak, J.[3]

[1]Facultad de Ciencias, Malaga University, Málaga, Spain ([*]mdruiz@uma.es)

[2]Instituto Andaluz de Ciencias de la Tierra, Facultad de Ciencias, CSIC-Universidad de Granada, Granada, Spain

[3]Institute of Geology, Academy of Sciences CR, Prague, Czech Republic

Pumpellyite has been found for the first time in phyllites and synfolial veins of Permo-Triassic units from the Beni Mezala 1 unit (Federico units, Internal Zone of the Rif belt). Two main assemblages were identified in different microdomains: 1) pumpellyite-actinolite-epidote (Fig. 1a & 2) pumpellyite-muscovite-epidote (Fig. 1b). Epidote is Fe-rich; actinolite contains very low Na_2O and Al_2O_3; and white mica has mean Si content of 3.13 *apfu*, all these characteristics being typical of low-*P* conditions.

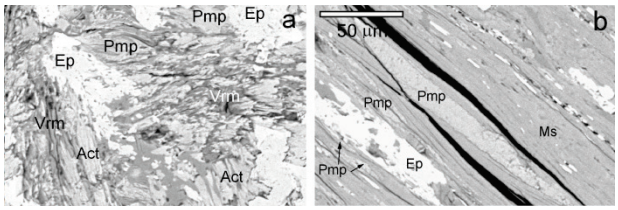

Fig. 1: Back-scattered images of the assemblages pumpellyite-actinolite-epidote (a) and pumpellyite-muscovite-epidote (b).

Assemblages in pumpellyite-bearing rocks indicate *P*≅2 kbar and *T*≅250ºC, in agreement with the estimates deduced from white mica and chlorite from the enclosing phyllites. Nevertheless, peak conditions reached c. 400ºC–5 kbar, as indicated the presence of kyanite-bearing veins (Fig. 2).

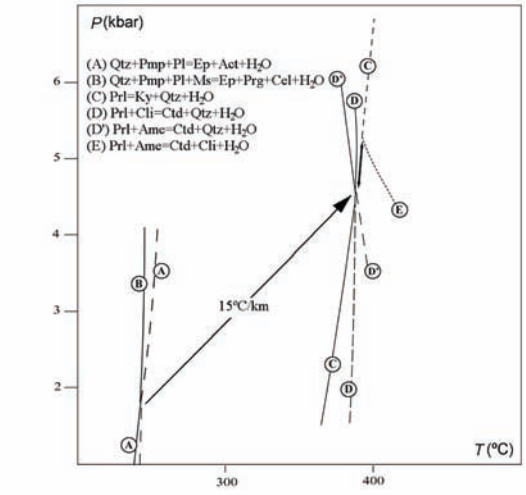

Fig. 2: Schematic *P-T* diagram showing the calculated metamorphic conditions in pumpellyite- and kyanite-bearing parageneses.

The deduced geothermal gradient (15ºC/km) is characteristic of collisional geotectonic settings but the mineral assemblages indicate low-to medium grade metamorphic conditions, which contrasts with previous H*P* estimates.

Acknowledgements: This study has received financial support from the Project CGL 2006-02481 (Ministerio de Educación y Ciencia) and from the Research Group RNM-199 (Junta de Andalucía).

Jadeitites and the subduction factory: progress and questions

Harlow, G.E.[1*] & Sorensen, S.S.[2]
[1]Dept. of Earth & Planetary Sciences, American Museum of Natural History, New York, NY, USA ([*]gharlow@amnh.org)
[2]Dept. of Mineral Sciences, Smithsonian Institution, Washington, DC, USA

Jadeitites are rocks composed principally of jadeitic pyroxene found in serpentinite mélanges with HP/LT tectonic inclusions such as blueschists and eclogites. In recent years it has been increasingly accepted that jadeitites are the product of dehydration fluid interactions in the subduction channel at the boundary or into the hydrating mantle wedge. Lack of protolithic remnants and veinous crystallization textures argue for primary crystallization from the channel fluid. However, some occurrences document encapsulation of eclogite fragments (West Sayan, Syros) by jadeitite or relics of feldspar replacement and inherited zircon (particularly at Mie, Japan) incorporated in jadeitite, indicating a true metasomatic origin. Possibly a spectrum exists between these end members with varying populations in different sources. Mineral assemblages provide poor constraint on crystallization conditions, so presence or absence of quartz has been used with the Jd + Qtz = Ab reaction to constrain *P* and zoisite/lawsonite/pumpellyite (if present) to constrain *T*, yielding brackets from 300-~500ºC and 6 – 20? kbar. However, coexisting Jd-Omph can yield both higher and lower *T* than other assemblages indicate.

Compositions of jadeitite and component minerals indicate large enrichments in the most fluid-mobile elements (Cs, Tl, Rb, Ba, K, Pb, Sn, Li), moderate enrichments of U, Th, Be and LREE and little to no enrichment of HFSE and HREE [1]. Particularly Li concentrations and isotopes argue for jadeitite crystallizing from fluid derived from altered oceanic crust with perhaps 5-15% sediment; variation among different jadeitite point to variation of material entering the subduction zone. Jadeitites appear to record well the transport of trace elements travelling from subduction channel to arc volcanism, now the focus is on light and volatile such as N (as NH_4), Li, S, C, and probably B for which research progress has barely started. The hottest topic in jadeitite research is the origin and dating of zircon. Good arguments for both inheritance (high Th/U ratios, mineral inclusions, zoning) and for primary crystallization from a fluid (low Th/U, mineral and fluid inclusions, zoning), with the latter demanding greater fluid transport of "immobile" elements than expected. The limited number of dates from zircons that are interpreted as crystallized in jadeitite show ages greater than those of related lithologies (e.g., eclogite) by 10-20 Ma with a considerable range. This difference or asynchronism may reflect the growth of jadeitite veins and bodies in the static mantle wedge (or oscillating fragments in the channel) prior to collision and exhumation that metamorphosed downgoing oceanic fragments record.

Jadeitites clearly contain an important record of fluid transport from the subduction channel into the overlying mantle wedge that should help develop a fuller understanding of the subduction factory.

[1] Simons, K.K. et al. (2010) *Geochim. Cosmochim. Ac.*, **74(12)**, 3621-3641.

Understanding of the mineralogy of jadeitites: natural and theoretical studies from a new occurrence of blue jade (Sorkhan area, Iran)

Bousquet, R.[1*], Oberhänsli, R.[1] & Moazzen, M.[2]
[1]Institut für Erd- und Umweltwissenschaften, Universität Potsdam, Germany ([*]bousquet@geo.uni-potsdam.de)
[2]Dept. of Geology, University of Tabriz, Iran

The beauty and wide-ranging expression of jade have held a special attraction for mankind for thou- sands of years. Jade is, strictly speaking, a generic term for two different types of rocks, nephrite or jadeitite, dominated either by amphibole or jadeite, respectively. Nephrites range mainly from medium to dark green or grey-green, but can also be white, yellowish or reddish. Rarer, somewhat harder, and therefore regarded as more precious, jadeitites display hues that include green, but also white or pink, and red, black, brown, violet, lavender and blue. In both rock types, the way the color is distributed varies considerably

Jadeitites, and especially blue jadeitites, are rather uncommon rocks. Generally, they are associated with subduction- related serpentinites along fault zones [1] and generally interpreted as crystallizing from hydrous fluids derived from dehydration of subducted slabs at high P and T [2]. Truly blue and lavender jadeitites are reported from only a few localities around the world. Among the most renowned occurrences, some contain only one clinopyroxene (pure jadeite) as the Olmec blue jade (Quebrada Seca, Guatemala), the blue jade from Ohmi–Kotaki in Japan or the lavender jadeitite from Tavsanli in Western Anatolia, Turkey. Others as the green and bluish jadeites from Burma contain two clinopyroxenes (jadeite and omphacite).

We report here a new locality of clear, sky-blue jadeitite occurring near Sorkhan, in a blueschist belt of southeastern Iran. Jadeitite occur in a vein system along a serpentinite – magnesite contact. The veins are composed of almost pure jadeite, 90 to 99.5 mol.% Jd, contain minor amounts of Ba-bearing K-feldspar, lawsonite and katophoritic amphibole.

The jadeitite veins formed at HP-LT conditions, around 1.6 GPa and 420°C. Thermodynamic studies show that the mineral assemblage within the blue jade is strongly pressure- and temperature-dependent. Jadeitites containing two clinopyroxenes (jadeite and omphacite) are stable at high pressure (0.8 GPa) and low temperature ($\leq$430°C) conditions, whereas blue jade with only one clinopyroxene (jadeite) forms at higher temperature or lower pressure. On the basis of these new calculations, P–T conditions of formation are re-examined for all occurrences of blue jade. From this study, we discuss the composition and the stability of one-and two-pyroxene-bearing jadeitites

[1] Harlow, G.E. (2001) *Eleventh Annual V.M. Goldschmidt Conf.* [2] Johnson, C.A. & Harlow, G.E. (1999) *Geology*, **27**, 629-632.

Jadeitite, omphacite rocks, and albitite as a metasomatic series in a serpentinite melange from the Nishisonogi metamorphic rocks, western Kyushu, Japan

Nishiyama, T.[1*], Shigeno, M.[2] & Mori, Y.[2]
[1]Dept. of Earth & Environmental Sciences, Kumamoto University, Kumamoto, Japan ([*]tadao@sci.kumamoto-u.ac.jp)
[2]Kitakyushu Museum of Natural History and Human History, Kitakyushu, Japan

This contribution presents an overall view of peculiar metasomatic rocks such as jadeitite, omphacite rocks, and albitite which occur as tectonic blocks in a serpentinite melange from the Nishisonogi metamorphic rocks, epidote-blueschist subfacies metamorphic rocks of Cretaceous in age, western Kyushu, Japan. Companion works (Shigeno et al. and Mori et al.) will discuss further details of fluid – rock interaction and mass transfer, and relict igneous zircon in jadeitite as an indicator of the protolith, respectively. There are two localities of jadeitite in this region, Tone and Mie, both of which belong to the same serpentinite melange.

Tone jadeitite [1] is almost a monomineralic rock with small amounts of albite, analcime, muscovite, phlogopite, paragonite, clinozoisite and titanite. Jadeite includes a lot of quartz in its core, of which volume fraction is very close to that produced by the albite breakdown reaction. Thus Tone jadeitite strongly suggests a solid-state transformation from an albite-rich rock. The protolith is estimated to be a plagiogranite by REE pattern of the relict zircon (Mori et al.). The *P-T* condition is estimated to be about 1.5 GPa and 500°C. Mie jadeitite [2] consists mainly of jadeite rimmed by omphacite with small amounts of albite, epidote, muscovite and paragonite. Jadeite rarely includes quartz. Omphacite-bearing metagabbro and monomineralic omphacite rocks also occur in Mie [3]. Such omphacite-bearing rocks consist mainly of omphacite, albite, epidote and actinolite in various amounts. Albite includes a lot of tiny omphacite crystals. Quartz is rarely but jadeite is never found in the rocks. We recognize two metasomatic series, prograde and retrograde series, in these rocks. Various amounts of omphacite in metagabbroic rocks may suggest a series of metasomatic formation of omphacite-bearing rocks from omphacite-poor rocks to nearly monomineralic omphacite rocks, leading to final formation of jadeitite. Retrograde series is represented by zoned omphacite rocks. Some omphacite rocks are enclosed in an albitite with an actinolite-rich selvage between them, which grows towards the omphacite rocks. It clearly shows a metasomatic replacement of the omphacite rocks by albitite during the retrograde stage. Further evidence of the retrograde metasomatic series comes from a zoned jadeitite with the following zonation: jadeitite core, omphacite-albitite, epidote-albitite and the outermost metagabbro (actinolite-albitite). Isocon analysis based on bulk compositions of each zone combined with SVD (singular value decomposition) analysis using mineral compositions show the following characteristics in the metasomatic reactions. SiO_2, Na_2O and K_2O are removed from the jadeitite towards serpentinite, whereas CaO and MgO come from serpentinite to the jadeitite, if the immobility of Al_2O_3 is assumed. Formation of albitite by the process clearly shows that the retrograde metasomatism occurred in the albite stability field. Thus the complicated textures and structures recorded in jadeitite, omphacite rocks and albitite from the Nishisonogi metamorphic rocks are products of prograde and retrograde metasomatic reactions.

[1] Shigeno, M., Mori, Y. & Nishiyama, T. (2005) *J. Mineral. Petrol. Sci.*, **100**, 237-246. [2] Nishiyama, T. (1978) *J. Geol. Soc. Japan*, **84**, 155-156. [3] Nishiyama, T., Uehara, S. & Shinno, I. (1986) *J. Metamorphic Geol.*, **4**, 69-77.

Ba minerals in jadeitites and related rocks: implications for Ba recycling in subduction zones

Shi, G.H.[1*] & Cui, W.Y.[2]
[1]China University of Geosciences, Beijing, China ([*]shiguanghai@263.net.cn)
[2]School of Earth and Space Sciences, Peking University, Beijing, China

Sediment recycling at destructive plate margins is one of the most important issues in the scientific debate on the genesis of arc magmas [1-5]. Recently, attention has been paid to the Ba flux and Ba minerals in high pressure and low temperature (HP/LT) rocks at shallower depth [6-8], for example, in jadeitites [9-11]. Thus, the problem of barium might be better addressed in jadeitites and linked to the international discussion.

Jadeitite is found in serpentinites associated with high-pressure rocks such as eclogite and blueschist and regarded as a marker of subduction zones [9,12-15], occurring at < 15 locations worldwide [4,13,16,17]. Barium minerals identified in clinopyroxene rocks from the Myanmar jadeitite area include celsian, hyalophane, and hydrated barium aluminum silicate (HBAS). The hyalophane and HBAS occur as interstitial phases and sometimes crosscut jadeite crystals. The celsian has two modes of occurrence: i) in association with jadeite in jadeitite; ii) as a single-phase mineral forming part of multi-phase pseudomorphs in chromian omphacite rock (omphacitite). The latter rock type was formed predominantly during the same episode as the jadeitite. The pseudomorphs, with hexagonal form mostly, contain celsian and kaolinite, with or without quartz, graphite and diaspore. The P-T condition constraints on celsian suggest that a precursor phase, probably cymrite, once existed and decomposited into celsian under decreasing pressure [18].

Barium minerals have also been reported at various jadeitite localities [9,10,19,20], appearing that all the well-documented jadeitite localities have Ba silicates. The frequent occurrence of Ba silicates in jadeitites worldwide reflects a Ba-enriched environment for the formation of jadeitite. Therefore, the jadeitite records metasomatism and metamorphism, as well as fluid interactions and phase changes in the BaO-Al_2O_3-SiO_2-H_2O system. Taken together with previous results [21-24], we further suggest that jadeite-forming fluids are derived from the dehydration of the altered oceanic slab containing deep-sea sediments.

[1] Plank, T. (2005) *J. Petrol.*, **46,** 921-944. [2] Guo, Z.F. et al. (2006) *J. Petrol.*, **47,** 1177-1220. [3] Leat, P.T. et al. (2004) *Earth Planet. Sci. Lett.*, **227,** 17-35. [4] Compagnoni, R. et al. (2007) *Per. Mineral.*, **76,** 79-89. [5] Morris, J.D. (1991) *Ann. Rev. Earth Planet Sci Lett.*, **19,** 313-350. [6] Sorensen, S.S. et al. (1997) *J. Petrol.*, **38,** 3-34. [7] Catlos, E.J. & Sorensen, S.S. (2003) *Science*, **299,** 92-95. [8] Bebout, G.E. et al. (2007) *Chem. Geol.*, **239,** 284-304. [9] Harlow, G.E. (1994) *J. Metamorphic. Geol.*, **12,** 49-68. [10] Harlow, G.E. (1995) *Eur. J. Mineral.*, **7,** 775-789. [11] Morishita, T. (2005) *Mineral. Mag.*, **69,** 39-51. [12] Harlow, G.E. et al. (2003) *Ofioliti*, **28,** 115-120. [13] Harlow, G.E. & Sorensen, S.S. (2005) *Int. Geol. Rev.*, **47,** 113-146. [14] Tsujimori, T. (2002) *Int. Geol. Rev.*, **44,** 797-818. [15] Tsujimori, T. et al. (2005) *Int. Geol. Rev.*, **47,** 1048-1057. [16] Sorensen, S.S. et al. (2006) *Am. Mineral.*, **91,** 979-996. [17] Garcia-Casco, A. et al. (2009) *Contrib. Mineral. Petrol.*, **158,** 1-16. [18] Shi, G.H. et al. (2010) *Eur. J. Mineral.*, **22**. 199-214. [19] Coleman, R.G. (1961) *J. Petrol.*, **2,** 209-247. [20] Essene, E.J. (1967) *Am. Mineral.*, **52,** 1885-1890. [21] Shi, G.H. et al. (2003) *Contrib. Mineral. Petrol.*, **145,** 355-376. [22] Shi, G.H. et al. (2005) *Mineral. Mag.*, **69,** 1059-1075. [23] Shi, G.H. et al. (2008) *J. Geol. Soc.*, **165**, 221-234. [24] Shi, G.H. et al. (2009) *Lithos*, **112,** 342-350.

"Jadeitites" of the Escambray Massif, Central Cuba: an evaluation

Maresch, W.V.[1*], Grevel, C.[1,2], Stanek, K.P.[3], Schertl, H.-P.[1] & Carpenter, M.[4]
[1]Institute of Geology, Mineralogy and Geophysics, Ruhr-University Bochum, Germany ([*]walter.maresch@rub.de)
[2]TÜV Rheinland, Cologne, Germany
[3]Institute of Geology, TU Bergakademie Freiberg, Germany
[4]Dept. of Earth Sciences, University of Cambridge, UK

Millán & Somin [1] reported petrographic descriptions of jadeitite as pebbles, cobbles and boulders in isolated fluvial deposits of the Escambray highlands, Cuba. It has been suggested [2] that this is a first but "overlooked" report of jadeitite in Cuba. Although access to the localities is now difficult, we emphasize here that analytical data on samples from these occurrences conforming to the original petrographic descriptions have been available [3-5] for some time.

These macroscopically featureless, massive, dense, grey-green rocks are jadeite-bearing metagabbros of basaltic bulk composition with a "spilite fingerprint" (49 - 54wt% SiO_2; 1 - 1.3wt% TiO_2, ~15wt% Al_2O_3, 8 - 10wt% FeOtot, 6 - 8wt% MgO, 4 - 9wt% CaO, 4 - 6.5wt% Na_2O). Relics of magmatic augite preserving an ophitic texture are common. Completely recrystallized rocks are homogeneous, fine, felty intergrowths of predominantly pale glaucophane and jadeite, the latter with rims and patches of omphacite. Late development of Ca-amphibole, chlorite, epidote and albite is observed. Samples with large (up to 1.5mm) grains of augite show several types of sodic clinopyroxene development, which are well-documented by hot-cathode CL-microscopy. 1) Topotactic replacement of magmatic pyroxene by jadeite and some omphacite. This type of jadeite shows no optical CL. 2) A jadeite + omphacite + pumpellyite + chlorite assemblage dominates in the rock matrix. 3) Jadeite + omphacite + pumpellyite intergrowths occur as lamellae enclosed within and in sharp contact with augite (no diffusion profiles are observed), whereby lamellae and augite clearly mimic an original ophitic texture. 4) Jadeite + omphacite + chlorite assemblages, in which monomineralic jadeite aggregates can occur, fill very thin (500 - 1000 µm) fractures criss-crossing the sample at ~ 2 cm spacing (including type 3 "ophitic augite grains"). CL in types 2 and 3 is similar. Type 4 CL is clearly different; these jadeite grains show features indicative of crystallization from fluid. In all cases omphacite develops irregularly along jadeite rims; however, both may also show straight grain boundaries suggestive of phase equilibration. Late phases are albite, taramite, epidote and additional chlorite.

This unusual occurrence of jadeite in a metabasic rock suggests two contrasting sources. The first, in the rock matrix, is most easily explained as due to local domain equilibration in a rapidly subducted "spilitized" basic rock. The second, in fracture fillings, conforms to an origin as a crystallization product from a pervasive fluid [e.g. 6]. Conceivably, "pooling" of the fluids flowing through the fractures in larger cavities could lead to larger masses of jadeitite. These have not yet been documented in the Escambray Massif.

[1] Millán, G. & Somin, M. (1981) *Litología, estratigrafía, tectónica y metamorfismo del Macizo del Escambray*. Editorial Academia, La Habana, Cuba. [2] García-Casco, A. et al. (2009) *Contrib. Miner. Petrol*., **158**, 1-16. [3] Grevel, C. (2000) Ph.D. Diss. [4] Grevel, C. et al. (1998) *Ber. Dtsch. Min. Ges., Beih. z. Eur. J. Mineral*., **10**, 110. [5] Maresch, W.V. et al. (2007) *Geochim. Cosmochim. Ac.*, **71/15S**, A621. [6] Harlow, G.E. & Sorensen, S. (2005) *Int. Geol. Rev*., **47**, 113-146.

Jadeitite from the Monviso meta-ophiolite, western Alps: occurrence and genesis

Compagnoni, R.[*], Rolfo, F. & Castelli, D.
Dept. of Mineralogical and Petrological Sciences, University of Torino, Italy ([*]roberto.compagnoni@unito.it)

Fine-grained massive jadeitites were known long since by archaeologists because all over western Europe some Neolithic ceremonial stone axes are made of this rock type. However, although at the end of 19th century some alpine geologists suggested that the only possible primary source area should have been the Monviso in the western Alps [1], only recently the first in place occurrence has been reported from this area [2,3]. A further search in the same area allowed a dozen of other jadeitite outcrops to be found, all of them in the westernmost part of the Monviso Basal Serpentinite Unit (cf. [4]), which forms a sheet, a few hundred meters thick, exposed between Val Varaita and Valle Po at the contact with a peculiar banded "smaragditic" (Cr-omphacite bearing) metagabbro. This sheet of sheared antigorite serpentinite, which is characterized by the presence of rounded blocks of different lithologies, including eclogite, metagabbro, omphacitite and jadeitites, has been interpreted as a serpentinite mélange.

The studied jadeitites are fine-grained and typically consist of zoned jadeite and tiny zircons, together with local minor amounts of phlogopite, garnet, Mg-chlorite, allanite, rutile, local retrograde albite, and quartz. A rounded boudin, a few dm across, resulted especially interesting to infer the jadeitite genesis. The boudin consists of a quartz+jadeite+accessory zircon core and a quartz+accessory zircon rim, with gradual transition from core to rim. Both boudin core and rim have been chemically analysed. The core composition matches well with that of a plagiogranite, i.e. the extreme differentiation product of a basaltic magma. Metamorphic plagiogranites of similar composition, interpreted as late-magmatic dikes, have been recently reported from a metamorphic plagiogranite - FeTi-oxide gabbro association exposed in the southern Basal Serpentinite Unit on the northern side of Val Varaita [5], not far from the locations of the jadeitite boudins. Therefore, on the base of geologic, petrologic, and geochemical evidence, it is concluded that the Monviso jadeitite is derived from an original plagiogranite, where the igneous quartz has been totally consumed during serpentinization by reactions altering the original peridotite to serpentinite.

[1] Damour, A. (1881) *Bull. Soc. Minér. France*, **4**, 157-164. [2] Compagnoni, R. & Rolfo, F. (2003) *Geol. Survey of Norway*, Report n° **2003.055**, 37-38. [3] Compagnoni, R. et al. (2007). *Per. Mineral*., **76**, 63-82, Sp. Issue. [4] Blake, M.C., Moore, D.E. & Jayko A.S. (1995) in Coleman, R.G. & Wang, X. (eds.) *Ultrahigh pressure metamorphism*. Cambridge Univ. Press, Cambridge, 182-205. [5] Castelli, D. & Lombardo, B. (2007) *Ofioliti*, **32**, 1-14.

Mineralogy, geochemistry and age of jadeitite and related rocks from the Sierra del Convento subduction mélange (eastern Cuba)

García-Casco, A.[1,2*], Cárdenas Párraga, J.[1], Harlow, G.E.[3], Rojas-Agramonte, Y.[4], Kröner, A.[4], Rodríguez Vega, A.[5], Núñez Cambra, K.[6], Blanco-Quintero, I.F.[1] & Lazaro, C.[1]
[1]Depto. de Mineralogía y Petrología, Universidad de Granada, Spain ([*]agcasco@ugr.es)
[2]Instituto Andaluz de Ciencias de la Tierra (CSIC-UGR), Granada, Spain
[3]Dept. of Earth & Planetary Sciences, American Museum of Natural History, New York, USA
[4]Institut für Geowissenschaften, Universität Mainz, Germany
[5]Depto. de Geología, Instituto Superior Minero-Metalúrgico, Moa, Cuba
[6]Instituto de Geología y Paleontología, La Habana, Cuba

Jadeitite from the subduction mélange of the Sierra del Convento (eastern Cuba) occurs closely associated with albitite, talc, and chlorite rocks and with tectonic blocks of garnet-epidote amphibolite and tonalitic-trondhjemitic epidote gneiss, in a serpentinite matrix. Samples of jadeitite can be classified in two groups according to geochemical and petrographic characteristics. Group A is predominantly composed of jadeite and omphacite with minor to trace amounts of other constituents such as epidote, biotite, albite, sphene and apatite. Group B is impure and mainly consists of jadeite, omphacite, albite and epidote with minor to trace amounts of paragonite, muscovite, sphene and apatite. Textures (including oscillatory zoning) of group A jadeitites show evidence of crystallization from fluids in veins triggered upon episodic infiltration of fluids at >550 ºC. The contents of SiO_2 vary from 58 to 60 wt%, and from 52 to 53.5 wt% in groups A and B, respectively. Group A has lower Al_2O_3, CaO and K_2O contents and higher Na_2O and P_2O_5 contents than group B. In group A, Rb and Ba contents fluctuate between 0.4–1.6 and 7.5–27.7 ppm respectively, being much lower than in group B (1.8–17.5 and 57–764 ppm). Y and Yb contents are slightly higher in group B (<11 and 0.9 ppm, respectively). The higher values of Zr in group A (90 – 180 ppm) compared to group B (<110 ppm) are noteworthy. Both groups display REE abundances similar to those in pegmatites of the Sierra del Convento mélange. These and other geochemical characteristics suggest a genetic link between pegmatitic H_2O-rich melts and jade-forming fluids deep in the subduction channel. The relatively high temperature of formation of jadeitite and the early Cretaceous SHRIMP zircon 206Pb/238U ages of 105-110 Ma from jadeitite, probably corresponding to the isobaric (at ca. 15 kbar) cooling stage of trondhjemitic liquids of the mélange, strengthen this view. We suggest that two types of pegmatite-derived fluids were involved in the formation of jadeitite jade rocks: a fluid rich in K, Ba, and Rb with a strong sedimentary component evolved from K-rich pegmatites (group B), and a depleted fluid with a strong mantle component evolved from K-poor pegmatites (group A), as indicated by Rb/Sr and Sm/Nd isotopes. This new occurrence of jadeite in Cuba opens important perspectives for archaeological studies of pre-Columbian jade artifacts in the Caribbean region.

Geochemistry of Guatemalan HP-LT rocks: jadeitites as proxies for the shallow subduction fluid?

Simons, K.K.[1*], Harlow, G.E.[2] & Sorensen, S.S.[3]
[1]RSMAS, University of Miami, FL, USA
([*]ksimons@rsmas.miami.edu)
[2]American Museum of Natural History, NY, USA
[3]Smithsonian Museum, Washington D.C., USA

High-pressure, low-temperature (HP-LT) rocks occur as tectonic blocks in slivers of serpentinite mélange within and adjacent to the Motagua fault zone in central Guatemala. These blocks (lawsonite eclogite, amphibolite, jadeitite, albitite) are thought to represent a Cretaceous age (~120 Ma) subduction complex exhumed during the collision of the Maya and Chortís continental blocks. Jadeitite and albitite occur as veins and blocks, and are interpreted to be the crystallization products of subduction fluids at relatively shallow depths (< 400°C @ 0.4-1.4 GPa). The extremely low geothermal gradient (~5°C/km), and abundance of hydrous phases and fluid inclusions in the rocks, indicate that metasomatism was likely achieved via an aqueous fluid.

Trace element patterns for these rocks resemble those of arc lavas, with similarities to global subducted sediment (GLOSS). Jadeitites and eclogites lie to the right of the mantle array, indicating fluids sampled had a seawater and/or sediment component. Modelling of $^{143}Nd/^{144}Nd$, $^{87}Sr/^{86}Sr$ and δ^7Li in jadeitites suggests metasomatism by a fluid with up to 10% sediment component [1]. Trace element patterns are thought to be primarily controlled by 1) mineralogy and 2) element concentrations present in the fluid. For example, lawsonite eclogites have the greatest proportion of phengite for the metabasites, and thus have the highest LILE concentrations. Enrichment of Zr and Hf is controlled by the presence of metasomatic zircon, which is best seen in the jadeitites (Fig. 1). LREE and Th enrichment is controlled by the epidote group minerals. Thus the saturation of specific key minerals controls the trace element patterns for these rocks. Increasing the mobility of HFSE like Zr, Hf and Th in aqueous fluids may be facilitated by high water/rock ratios, increased solubilities and increased concentrations of silica, aluminium and alkalis which can act as polymerizing agents [2]. Together these mechanisms serve to dissolve and transport trace elements out of the slab and into the mantle wedge. Because Guatemalan HP-LT rocks were metasomatized close to the interface between the slab and mantle wedge (jadeitites formed the wedge itself), they provide a unique window into the composition of subduction fluids at depth.

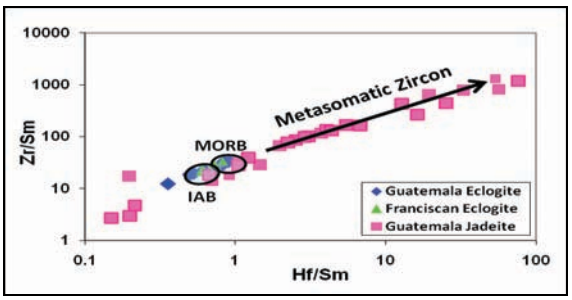

Fig. 1: Enrichments in Zr and Hf relative to Sm demonstrate addition of metasomatic zircon to Guatemalan jadeitites.

[1] Simons, K.K. et al. (in press) *Geochim. Cosmochim. Ac.* [2] Manning, C.E. et al. (2004) *Earth Planet. Sci. Lett.*, **223**, 1-16.

Relict igneous zircon in jadeitite from the Nishisonogi metamorphic rocks, Kyushu, Japan: an indicator of protolith characteristics

Mori, Y.[1*], Orihashi, Y.[2], Miyamoto, T.[3], Shimada, K.[3], Shigeno, M.[1], Gouzu, C.[4], Hyodo, H.[5] & Nishiyama, T.[6]
[1]Kitakyushu Museum of Natural History and Human History, Kitakyushu, Japan ([*]mori@kmnh.jp)
[2]Earthquake Research Institute, University of Tokyo, Japan
[3]Dept. of Earth and Planetary Sciences, Kyushu University, Fukuoka, Japan
[4]Hiruzen Inst. for Geology and Chronology, Okayama, Japan
[5]Research Institute of Natural Sciences, Okayama University of Science, Okayama, Japan
[6]Dept. of Earth and Environmental Sciences, Kumamoto University, Kumamoto, Japan

The Nishisonogi metamorphic rocks (Kyushu, Japan) are a Late Cretaceous subduction complex and include jadeitite as tectonic blocks within serpentinite melange. There are two localities of jadeitite, Mie and Tone. The Tone jadeitite consists mainly of jadeite including a lot of quartz inclusions, suggesting a solid-state transformation from an albite-rich protolith [1]. The aim of this study is to reveal the protolith of the Tone jadeitite based on the U-Pb ages and trace element compositions of relict zircon.

The Tone jadeitite contains euhedral zircon grains, both as inclusions in jadeite and as a matrix mineral. The zircon grains are divided into three types: homogeneous zircon, oscillatory zoned zircon and altered zircon. The homogeneous zircon and the core of zoned zircon yield mean U-Pb ages of 126 ± 7 Ma (± SD, n = 64). This age is clearly older than $^{40}Ar/^{39}Ar$ ages of muscovite in the Tone jadeitite (80-90 Ma). The homogeneous zircon and the core of zoned zircon are considered relicts from the protolith. In contrast, the altered zircon and the rim of zoned zircon show a wide range of U-Pb ages (76-116 Ma). The U-Pb ages of these zircons show a positive correlation with Th/U values (Fig. 1). The y-intercept of this correlation at Th/U = 0 indicates a U-Pb age of 80-90 Ma, consistent with the $^{40}Ar/^{39}Ar$ ages of muscovite in the Tone jadeitite. The altered zircon and the rim of zoned zircon may be the products of recrystallization, resulting in the expulsion of Pb and Th from the lattice.

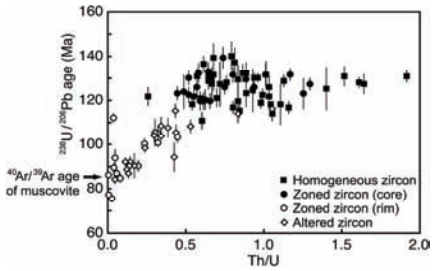

Fig. 1: Relationship between ^{238}U-^{206}Pb ages and Th/U values of zircon grains from the Tone jadeitite. Error bars represent 2SD.

The relict zircons in the Tone jadeitite have high Ti content of 4.89-20.7 ppm, yielding crystallization temperatures of >680°C. These temperatures are higher than the granite solidus and strongly suggest an igneous origin for the relict zircons. The zircon grains contain inclusions of muscovite, biotite, quartz and plagioclase that are likely to have crystallized from melt. The Hf, Y and REE contents of the relict zircons are similar to those of zircon from plagiogranites and indicate light-REE enrichment and no (or minor positive) Eu anomalies in their equilibrium melt. Taken together, the most likely protolith of the Tone jadeitite is plagiogranite with TTG-like REE patterns.

[1] Shigeno, M., Mori, Y. & Nishiyama, T. (2005) *J. Mineral. Petrol. Sci.*, **100**, 237-246.

In-situ jadeitite in blueschist country rocks from the Dominican Republic: mode of occurrence and genesis

Schertl, H.-P.[1*], Maresch, W.V.[1], Stanek, K.-P.[2] & Krebs, M.[1]
[1]Institute of Geology, Mineralogy and Geophysics, Ruhr-University Bochum, Germany ([*]ans-peter.schertl@rub.de)
[2]Institute of Geology, TU Bergakademie Freiberg, Germany

The Rio San Juan Complex (RSJC) of the northern Dominican Republic consists of subduction-related mafic schists cut by diapir-like serpentinite mélanges. These mélanges contain blocks of various metamorphic rock types such as blueschist, eclogite, lawsonite blueschist, jadeitite, cymrite-bearing rock, and orthogneiss.

Comprehensive petrological studies demonstrate a broad diversity of PTt-paths which, however, are closely interrelated: In the early stages of development of the subduction zone, the PTt-paths typically are anticlockwise with shallow ("hot") P/T-gradients. Maximum PT-conditions derived from eclogites are 750°C/28 kbar; the related Lu-Hf-age is 103.9 Ma (Grt-Ep-Amp-Omp-WR isochron). Continuous cooling and steepening of the subduction zone PT-gradient is documented by omphacite blueschists, which experienced peak metamorphic conditions of 500-550°C/16-18 kbar at 80.3 Ma (Rb-Sr on Phe-Amp-WR). Jadeite-blueschists typically are constrained to very steep "cold" P/T-gradients; Rb-Sr-ages (Phe-Amp-WR isochrons) of 62.1 Ma date the peak metamorphic conditions of about 380°C/18 kbar.

Although commonly found as allochthonous blocks, some jadeitite occurrences appear unique and critically important in that they are directly associated with lawsonite blueschists. Two main types of contact relationships can be distinguished. In the first the jaedeitite veins are clearly discordant, whereas the second type is characterized by concordant and intimate, gradational interlayering with the surrounding blueschist.

The jadeitites are fine-grained, whitish-green, and contain jadeite as the main constituent; the amount of jadeite may exceed 90 vol.%. Phengite, omphacite, epidote, Na-amphibole, plagioclase, calcite, lawsonite, pumpellyite, stilpnomelane, garnet and quartz can occur in minor amounts. Titanite, zircon, and rutile are accessories. The homogeneous cores of the jadeite crystals reach 98% jadeitite end-member composition; in some cases these are surrounded by very thin omphacitic rims. In general, the jadeite grains contain numerous microinclusions of quartz and lawsonite (especially within the core regions), leading to a cloudy to dirty appearance. Cathodoluminscence (CL) studies contribute to a better understanding of structural characteristics and genetic relationships. The most important result from these studies is the distinctive oscillatory zoning pattern of the jadeite, which is reminiscent of "magmatic" zonation in zircon. Several jadeites were found to be characterized by a patchy olive-green inner core surrounded by a bluish-red oscillatory mantle and an outermost bright-green luminescent oscillatory rim.

The petrographic character of the jadeitites suggests that many are analogous in both mineralogy and fabric to jadeitites described from the serpentinites of the Motagua Fault Zone in Guatemela. In the light of the two clearly different types of jadeitite contact relationships - discordant versus concordant - the possibility of two different origins is discussed: metamorphism of an appropriate pre-metamorphic protolith vs. formation by fluid-driven mass transfer.

Formation of jadeitite in the Nishisonogi metamorphic rocks, Kyushu, Japan: prograde albite-decomposition and retrograde fluid-jadeitite interaction

Shigeno, M.[1*], Mori, Y.[1], Shimada, K.[2] & Nishiyama, T.[3]
[1]Kitakyushu Museum of Natural History and Human History, Kitakyushu, Japan (*sjfmt461@yahoo.co.jp)
[2]Dept. of Earth and Planetary Sciences, Kyushu University, Fukuoka, Japan
[3]Dept. of Earth and Environmental Sciences, Kumamoto University, Kumamoto, Japan

Current models of jadeitite formation include (1) solid-state transformation from protoliths and (2) direct precipitation from fluids [1]. Although both of the processes may represent possible origins for jadeitite, the jadeitite from the Nishisonogi metamorphic rocks (Kyushu, Japan) supports the former model [2].

The Nishisonogi metamorphic rocks are epidote-blueschist subfacies metamorphic rocks and include jadeitite as tectonic blocks within serpentinite melange. There are two localities of jadeitite, Tone and Mie in Nagasaki City. Primary mineral assemblage of these jadeitite is jadeite/omphacite + paragonite + phlogopite + muscovite ± clinozoisite/epidote. Jadeite grains in the Tone jadeitite have cores including a lot of quartz inclusions and clear rims. Volume fraction of the quartz inclusions within the cores is close to that of quartz produced by isochemical decomposition of albite, suggesting solid-state transformation of the jadeitite from an albite-rich protolith.

The Tone and Mie jadeitites are typically surrounded by reaction zones of albitite and muscovite rock. Mineral assemblage of the albitite is albite + clinozoisite/epidote ± muscovite ± omphacite ± phlogopite ± actinolite ± chlorite, and that of the muscovite rock is muscovite + clinozoisite ± chlorite. The reaction zones represent retrograde products, because albite is stable. Clinozoisite and phlogopite in the reaction zones contain large amounts of Sr and Ba, respectively. Isocon analysis indicates that Sr and Ba have been added to the reaction zones during fluid-jadeitite interaction, which is consistent with the mineralogical observation. Clinozoisite grains in the reaction zones have allanitic cores and exhibit skeletal shapes. REE-rich veinlets emanate from such clinozoisite grains, suggesting REE mobility during the fluid-jadeitite interaction.

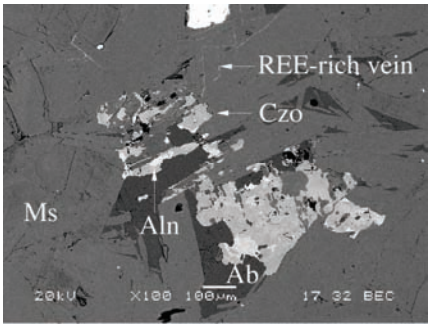

Fig. 1: BSE image from metasomatic reaction zone of Tone jadeitite showing REE mobility during retrograde fluid-jadeitite interaction. Ab, albite; Aln, allanite; Czo, clinozoisite; Ms, muscovite.

Taken together, the jadeitites in the Nishisonogi metamorphic rocks have recorded two stages of formation, prograde albite-decomposition and retrograde fluid-jadeitite interaction.

[1] Harlow, G.E., Sorensen, S.S. & Sisson, V.B. (2007) in Groat, L.A. (ed.) *Geology of gem deposits*. Min. Assoc. Canada, 207-254. [2] Shigeno, M., Mori, Y. & Nishiyama, T. (2005) *J. Mineral. Petrol. Sci.*, **100**, 237-246.

Genesis of jadeitite: a case study from Guatemala

Yui Tzen-Fu[1*], Maki Kenshi[1], Usuki Tadashi[1], Lan Ching-Ying[1], Martens, U.[2], Wu Chao-Ming[3], Wu Tsai-Way[4] & Liou G. Jung[2]
[1]Institute of Earth Sciences, Academia Sinica, Taipei, Taiwan, ROC (*tfyui@earth.sinica.edu.tw)
[2]Dept. of Geological and Environmental Sciences, Stanford University, Stanford, USA
[3]Dept. of Applied Arts, Fu-jen Catholic University, Hsinchuang, Taiwan, ROC
[4]Dept. of Earth Sciences, University of Western Ontario, London, Ontario, Canada

One Guatemala jadeitite sample was collected from north of the Motagua fault, Guatemala, to examine the possible formation mechanisms/conditions. Zircons were also separated for age dating and REE analysis. The sub- to anhedral crystal form, the lack of typical magmatic oscillatory zoning, the presence of fluid and albite/quartz/jadeite inclusions, and the low Th/U ratios (<0.005) clearly demonstrate that zircons in this particular jadeitite sample would have been precipitated from an aqueous solution. It is concluded that, in addition to "metasomatic replacement", "vein precipitation" is a feasible process for jadeitite formation. The U–Pb concordia intercept age of these zircons is 95.1±3.6 Ma.

Both the whole-rock jadeitite and its zircons have very low REE contents, ~1 ppm and 0.5–42 ppm, respectively. The whole-rock jadeitite shows a flat and slightly concave REE pattern and a positive Eu anomaly (Eu/Eu*=1.24). Zircons are enriched in HREE and their REE patterns can be divided into two groups: one with negative Eu anomaly and one with positive Eu anomaly. The latter tends to have smaller positive Ce anomalies. The fluid from which jadeitite formed probably evolved over time, becoming more reducing and more dominated by plagioclase decomposition reactions. Alternatively, trace element compositions of zircons simply demonstrate complicated variations of fluid chemistry during jadeitite formation.

A reducing fluid with high pH values capable of mobilizing Al, Na, Zr and Hf is inferred to be the media during jadeite/zircon formation. If jadeitites are genetically related to serpentinization of ultramafic rocks, as suggested by the common jadeitite–serpentinite association, then three conditions for jadeitite formation under a proper P–T regime in subduction zones must be fulfilled. (1) The ultramafic rocks, whether partially altered, must contain olivine as the major primary phase subjected to serpentinization. Serpentinization of such ultramafic rocks would produce fluids with geochemical characteristics capable of mobilizing Al, Na, Zr and Hf in precipitating/forming jadeite and zircon. (2) A protolith, such as a tectonic block within ultramafic rocks, is needed to provide Al and Na. The block would have escaped earlier alteration reactions (such as rodingitization) and contains feldspars/micas as its major constituents. And (3) the presence of fluid channels and pulses of fluid supply would be the triggers for jadeitite formation reactions. These prerequisites may at least partly, in addition to the possible tectonic controls, explain the worldwide scarcity of jadeitite occurrences in high-P metamorphic belts.

Mineralogy and petrogenesis of the gem-bearing pegmatites of the Shigar valley, Skardu, Northern Pakistan

Agheem, M.H.[1*], Shah, M.T.[2] & Khan, T.[3]
[1]Centre For Pure and Applied Geology, University of Sindh, Jamshoro, Pakistan ([*]mhagheem@yahoo.com)
[2]National Centre of Excellence in Geology, University of Peshawar, Pakistan
[3]Advanced Geosciences Research Laboratories, GSP, Pakistan

Shigar valley is located about 32 km north of Skardu, the head quarter of the Baltistan, and is the gateway for most of the expeditions to the K-2 in the northern areas of Pakistan. This valley has the plenty of pegmatite intrusions, hosting the various types of gemstones, which are being excavated by the local miners for aquamarine, goshenite, topaz, tourmaline and fluorite etc. These gemstones, especially aquamarine, are now marketed internationally.

These pegmatites were mapped and sampled during two field seasons for the sack of their mineralogy, internal structure, and petrogenesis. The field and various analytical techniques have revealed that these pegmatites are not only diverse in their mineralogy, classification, internal structure but on the basis of present data their petrogenetic linkage is also in ambiguity. On the basis of field features and petrographic studies, these pegmatites have been classified into two types as: (1) simple and (2) complex or zoned pegmatites. These pegmatites have further been classified into four sub-classes on the basis of presence or absence of various accessory minerals and gemstones.

Petrogenetic studies of the Shigar valley pegmatites have been carried out on the basis of major, trace and rare earth elements chemistry. These studies suggest that these pegmatites are the separate magmatic pulses generated probably from the metapelites of the Karakoram Metamorphic Complex (KMC) along the axis of the active thrust fault known as the Main Karakoram Thrust (MKT). Although, other post-collisional plutonic units of the Karakoram Batholith such as the Baltoro Plutonic Unit and the Mango Gusar Unit are exposed in the vicinity of the Shigar valley but the aerial extent, field features, and the geochemical data suggest that these pegmatites have no correlation with the off shoots of above-mentioned plutonic units. These pegmatites are of collisional tectonic settings and have been formed after the collision of Indian plate with the Eurasian plate.

Mineralogy and petrography of phosphate minerals from pegmatites of the Conselheiro Pena district, Minas Gerais, Brazil

Baijot, M.[1*], Hatert, F.[1] & Philippo, S.[2]
[1]Laboratory of Mineralogy, University of Liège, Belgium ([*]mbaijot@student.ulg.ac.be)
[2]Section of Mineralogy, National Museum of Natural History of Luxembourg

In Brazil occurs one of the most important pegmatite provinces in the world, the Eastern Brazilian Pegmatite Province (EBPP). This province is located at the Eastern side of the Saõ Francisco craton, mainly in the state of Minas Gerais, as well as the states of Bahia, Espírito Santo and Rio de Janeiro. The Conselheiro Pena district forms part of the EBPP where two intrusions crosscut the basement rocks and its cover: the Galiléia and Urucum magmatic suites which belong to the G1 and G2 supersuites, respectively. In September 2008, we visited several pegmatites located in the Conselheiro Pena district, between Galiléia and Mendes Pimentel, in order to investigate the petrography of phosphate minerals and their relationships with associated silicates. All the pegmatites intrude the garnet-, biotite-, and sillimanite-bearing schists of the São Tomé Formation (Rio Doce group, Late Proterozoïc). Preliminary results obtained from this study will be presented in this paper and allow to better characterize the chemistry and petrography of phosphates and to elaborate the genetic sequence of these minerals.

Phosphate minerals form nodular masses which can reach 2 meters in diameter. Two kinds of phosphate associations occur:

I) Masses showing dendritic or/and skeletic textures involving feldspar and several secondary phosphate minerals.

II) Fresh massive triphylite only altered by vivianite, which give its bluish colour to the phosphate.

Petrographic observations, X-ray diffraction measurements, and electron-microprobe analyses were performed on the phosphates, to confirm their identification, calculate their unit-cell parameters and to characterize their chemistry. The only primary phosphate mineral is triphylite, $Li(Fe^{2+},Mn^{2+})PO_4$, which progressively oxidizes to ferrisicklerite, $Li_{<1}(Fe^{3+},Mn^{2+})PO_4$, and heterosite, $(Fe^{3+},Mn^{3+})PO_4$, following the so-called "Quensel-Mason" sequence. In association I, ferrisicklerite is frequently replaced by several secondary phosphates like barbosalite, tavorite, hureaulite, cyrilovite, leucophosphite, phosphosiderite, minerals of the jahnsite group and minerals of the rockbridgeite-frondelite series. In association II, triphylite is directly replaced by vivianite along cleavage planes. A similar genetic sequence is generally observed in pegmatites of the Conselheiro Pena district, except in the northern part where brazilianite-bearing pegmatites occur. In this area, qingheiite-(Fe^{2+}) (IMA 2009-076), $Na_2Fe^{2+}MgAl(PO_4)_3$, has been described and is produced by reaction between triphylite and albite.

Even if triphylite is the only primary phosphate mineral, it shows interesting chemical variations within the district, with $Fe_{tot}/(Fe_{tot}+Mn)$ ranging from 0.56 to 0.74, and $Fe_{tot}/(Fe_{tot}+Mg)$ ranging from 0.83 to 1.00. A correlation between the chemical composition and the unit-cell parameters of triphylite-type phosphates will also be discussed, with an emphasis on the incorporation of Mg into triphylite from Sapucaia.

Fluid and melt inclusion: windows to hidden pegmatite-forming processes

Thomas, R.[1*] & Davidson, P.[2]
[1]GeoForschungsZentrum Potsdam, Germany
([*]thomas@gfz-potsdam.de)
[2]ARC Centre of Excellence in Ore Deposits, University of Tasmania, Hobart, Australia

For more than 260 years pegmatites have fascinated scientists, amateur mineralogists and artists by their beauty and diversity of minerals, their extraordinary paragenesis and often very strong enrichment of rare elements. We should also remember the thorny path of the discovery of the rare-earth elements, starting in summer of 1787 with the find of an unknown, heavy and black mineral by the Swedish army lieutenant Carl Arrhenius, a student of Berzelius, in an abandoned quarry near Ytterby on the skerry island Resarö in NE of Stockholm. For the REE's journey's end was reached in 1945 by the American chemists Jacob Marinsky, Lawrence Glendenin, and Charles Coryell with the isolation of promethium. The list of pegmatite minerals which have had a profound influence on science is extensive. Here we only review the minerals tantalite and zircon from pegmatites. They were the godparents for the elements Nb, Ta, Zr and Hf. As an example, element number 72 was predicted by Niels Bohr, who advised György von Heversy and Dirk Coster to search for this element in zircon from Norway. They found traces of this element by its characteristic X-ray emission lines in January 1923 in Copenhagen. About 40 years later the mineral hafnon with 72.5 % (g/g) HfO_2 was found in a pegmatite.

The last mentioned element, mostly at low concentration camouflaged in Zr minerals brings us to a central problem of explanation: how is it possible to explain the "inverse" element arrangement in the mineral hafnon, where Hf is the main element and Zr is present only in traces? To understand the appearance of such "abnormal" element enrichment – hafnon is only one example of many, we have to understand much more about the pegmatite-forming media and processes working in nature.

We can not stop with such statements as "Melt solutions in which water is plentiful as an essential volatile component besides large amounts of non-volatile components are called pegmatitic solutions" [1], we have to more accurately constrain the answer based on real facts, directly derived from nature.

An important tool in this intricate task has been developed within the last 150 years, although often simply ignored or underestimated: Fluid and melt inclusions in minerals as media for the deciphering of mineral-forming processes, first on the temperature and pressure and then on the compositions of the long-gone fluids that were actively involved in many environments [2].

Using fluid and melt inclusions is not a simple tool, it requires insight into the processes of trapping, as well as those which modify an inclusion post-trapping, such as recrystallization.

In this presentation we will show important steps in the solution to fundamental questions regarding the pegmatite-forming media and processes, including water concentration in real melts, melt-melt immiscibility, main and trace element distribution in different phases, extreme enrichment of boron and its consequences, and the suggestion that the gel stage may play an important part in pegmatite formation, especially during the formation of the quartz core.

[1] Niggli, P. (1920) *Die leichtflüchtigen Bestandteile im Magma*. B.G. Teubner, Leipzig. [2] Roedder, E. (2003) in De Vivo, B. & Bodnar, R.J. (eds.) *Melt inclusion in volcanic systems: methods, application and problems. Dev. Volcano*., **5**. XV-XVI.

Anomalous, LCT-type, Ta enrichment in NYF-type pegmatites of the Nine Mile pluton in the Wausau syenite complex, Marathon County, Wisconsin, USA

Falster, A.U.[1*], Simmons, W.B.[1] & Buchholz, T.W.[2]
[1]Dept. of Earth and Environmental Sciences, University of New Orleans, LA, USA ([*]afalster@uno.edu)
[2]1140 12th Street North, Wisconsin Rapids, Wisconsin, USA

The anorogenic, NYF-type, Wausau syenite complex is located in central Marathon Co., Wisconsin. The Proterozoic (ca. 1.5 Ga) complex consists of 4 intrusive centers, from oldest and most alkalic to youngest and most silicic: Stettin complex, Wausau pluton, Rib Mountain pluton, and the Nine Mile pluton. The Nine Mile pluton is the best exposed of the 4 intrusives, a result of extensive mining of weathered rocks (grus) for road metal and landscaping. Numerous pegmatite bodies exist throughout the complex. The pegmatites are of modest size, rarely reaching 100 m in maximum dimension. Pegmatites are well-zoned with distinctive wall zones, intermediate zones and core zones. Replacement units (usually albite) occur in some. The mineralogy of the pegmatites is rich in REE-bearing species such as monazite-group minerals, xenotime, bastnaesite-group species and numerous pyrochlore-group minerals. Be minerals occur sporadically, and B minerals are essentially absent, whereas F is widespread as fluorite and other F-bearing minerals. In late-stage primary and secondary miarolitic cavities (left by dissolution of pre-existing quartz or fluorite), a highly-evolved mineral association is seen consisting of tantalite-(Mn), microlite, tantalian rutile, tantalian cassiterite, and tapiolite. In some non-miarolitic pegmatites, Ta-rich minerals (tantalite-(Mn), microlite, tanteuxenite-(Y)) occur embedded in feldspar and quartz mainly along the inner intermediate zone and core margin. Typically, the Ta/Nb ratio steadily increases from the core of the crystals toward the rim, such that significant Ta-dominance is achieved. Sometimes, Ta-rich microlite forms as a late overgrowth on and/or replacement of columbite-group minerals. Zircons found in this assemblage also reflect a similarly high enrichment trend expressed as very low Zr/Hf ratios. The abundance of fluorite suggests that F complexing is the controlling mechanism causing the late enrichment of Ta which produced a late-stage mineral association similar to that seen in highly evolved LCT-type pegmatites.

Geochemical evolution of K-feldspar and muscovite in the pegmatitic field of Giraúl, Namibe (Angola)

Gonçalves, A.O.[1*], Melgarejo, J.C.[2], Alfonso, P.[3], Paniagua, A.[4], Yusta, I.[5] & Velasco, F.[5]
[1]Dept. de Geologia, Universidade Agostinho Neto, Luanda, Angola ([*]tonyolympio72@hotmail.com)
[2]Dept. de Cristal·lografia, Mineralogia, Dipòsits Minerals, Universidad de Barcelona, Spain
[3]Dept. d'Enginyeria Minera i Recursos Minerales, Universidad Politècnica de Catalunya, Manresa, Spain
[4]Dept. de Ciencias de la Tierra, Universidad de Zaragoza, Spain
[5]Dept. Mineralogía y Petrología, Universidad del Pais Vasco, Spain

Diverse pegmatite types crop out in the pegmatitic field of Giraúl (Namibe, Angola). These pegmatites are, from less to more evolved: type I (barren, intrabatholitic and grading to the leucogranite host), type II (barren, peribatholitic); type III (beryl-columbite); type IV (beryl-columbite-phosphate); type V (spodumene).

Two main trends of geochemical fractionation are distinguished in K-feldspar and muscovite: at field scale and at the pegmatite body scale.

At the scale of pegmatitic field, the K/Rb ratio in microcline decreases from type I to type V pegmatites, which have up to 7100 ppm Rb. Cs (2 to 2000 ppm), Ga (7 to 22 ppm), Sn (0.1 to 29 ppm). The P content (450 to 6150 ppm) tends to increase progressively from the more primitive pegmatites to the most evolved ones. Ba, Sr and Pb have opposite evolution trends.

Similar trends are found in muscovite. The next variations are appreciated from type I to V: Rb (263 to 8700 ppm), Li (51 to 4340 ppm), Cs (7.6 to 2000 ppm), Zn (50 to 760), Ga (28 to 183 ppm), Sn (5 to 822 ppm), P (70 to 990 ppm), Nb (33 to 364 ppm), Ta (6 to 170 ppm); inverse correlations are found in Ba (384 to 2 ppm) and Pb (6.4 to 1.3 ppm).

Similar enrichment trends, although not so important, are appreciated in these minerals when comparing their compositions at the scale of the different units of a single pegmatite body. In these cases, fractionation increases from the early-formed zones (border, first and second intermediate zones) to the late replacement units (albite bodies and quartz-muscovite veins).

The concentration of LILE and HFSE elements in the muscovite structure increases at the same time that minerals of these elements start to develop, which suggests that muscovite might have remained saturated in these elements in some stages of crystallization of the pegmatites. Hence, in the late stages of crystallisation of the most evolved pegmatites Cs- and Li-rich muscovite coexists with pollucite, nanpingite, a Cs-rich mica, and with spodumene.

In the same way, the concentration of LILE, HFSE and other incompatible elements increases gradually with the evolution of the pegmatites of the Giraúl field, from the types I and the II (geochemically very similar) up to the types IV and V. This fact suggests that all the pegmatites of the field have a common origin and are linked by a process of magmatic fractionation from the parental leucogranites.

The concentrations of some elements, such as Rb and Cs in muscovite, approach to the economic levels in the most evolved pegmatites, though these values are found only in some of the internal units.

Mn-rich yellow tourmaline: conditions of formation and implications for pegmatite petrogenesis

Simmons, W.B.[1*], Falster, A.U.[1] & Laurs, B.M.[2]
[1]Dept. of Earth and Environmental Sciences, University of New Orleans, LA, USA ([*]wsimmons@uno.edu)
[2]*Gems & Gemology*, Gemological Institute of America (GIA), Carlsbad, CA, USA

Mineralogically, yellow tourmaline is dominantly Mn-rich elbaite and "fluor-elbaite" although very rare yellow rossmanite and "fluor-rossmanite are known. Yellow tourmaline samples from pegmatites (or alluvial deposits inferred to be from pegmatites) in Zambia, Mozambique, Congo, Madagascar, Russia, Nepal, and the United States were analyzed. The composition of these tourmalines from all locations is remarkably similar. Most are elbaite with very low Fe and Mg and with elevated Mn and Ti. A few yellow samples from Mozambique are rossmanite or "fluor-rossmanite". Overall, MnO ranges from 1.50 to 8.90 wt.%, FeO contents are very low (<0.03 wt.%) and TiO_2 contents range from 0.1 to 0.7 wt.%. The yellow coloration is due to Mn^{2+}-Ti^{4+} intervalence charge transfer interaction [1]. Thus, both Mn and Ti are essential for the formation of yellow tourmaline. Analyses reveal that small increases in Fe darken these tourmalines toward brownish colors. The substitution scheme is confirmed to be $2Mn^{+2} = Li^{+1}+Al^{+3}$.

Yellow tourmaline is quite rare because most pegmatites that contain sufficient B to produce tourmaline also contain significant Fe during tourmaline crystallization and most tourmaline-producing pegmatites with low Fe contents don't contain elevated levels of Mn or sufficient Ti. Commonly, in evolved LCT-type pegmatites, Mn is associated with high Li and is incorporated into Li-micas and Li-Mn-phosphates, making the late-stage melts relatively depleted in Mn. Tourmaline forming from these melts will be the more typical colorless, pink, blue or green elbaite, which generally contain less than 2 wt.% MnO. A peraluminous pegmatite melt high in B will preferentially crystallize tourmaline rather than biotite or garnet. Thus, high-B will impede the formation of spessartine and biotite that would remove Mn from the melt. A common sink for Ti is biotite, and with high B contents preventing its formation during the early stages of pegmatite crystallization, Ti will be available to be incorporated into late-stage, low-Fe tourmaline.

Tourmaline is a sensitive recorder of the changing chemical conditions during late-stage crystallization. In pegmatite pockets with color-zoned tourmaline crystals, the chemical conditions of low Fe, high Mn and elevated Ti are achieved only during part of the crystallization history of tourmaline growth, during yellow tourmaline growth. Most zoned crystals in this study were Fe-rich (schorlitic) initially, and as Fe was depleted, the compositions became Mn enriched allowing the formation of yellow zones in the crystal. Subsequently, Mn and Ti typically became somewhat depleted, producing colorless or pink tourmaline or, as is often the case, there was a slight enrichment of Fe giving rise to darker yellow-green to green or blue terminations or rims.

[1] Rossman, G.R. & Mattson, S.M. (1986) *Am. Mineral.*, **71**, 599-602.

Experimental crystallization of Li-B-pegmatites

Sirbescu, M.[1*], Wilke, M.[2], Veksler, I.[2] & Whittington, A.[3]
[1]Dept. of Geology, Central Michigan University, Mt. Pleasant, MI, USA ([*]sirbe1mc@cmich.edu)
[2]GeoForschungsZentrum, Potsdam Germany
[3]Dept. of Geological Sciences, University of Missouri, Columbia, MO, USA

Textural features of pegmatites are thought to be a consequence of the interplay between crystal nucleation and growth rates under conditions of undercooling, which are strongly influenced by water [1,2]. To better understand pegmatite texture in relation to the degree of undercooling and water concentration, we performed dynamic experiments of nucleation and crystallization of synthetic hydrous haplogranite with added 1% Li_2O + 2.3% B_2O_3 (composition C1) and 2% Li_2O + 4.6% B_2O_3 (C2). Time-series isothermal or programmed-cooling runs (from 1 to 30 days) were performed at temperatures ranging from 400 to 700°C at 300 MPa coresponding to variable degrees of undercooling between liquidus and glass transition. Viscosity data at 1 atm indicate that the glass transition of both melts containing 6.5 wt. % is just under 300°C. Moderately fluxed, hydrous melts are sluggish to nucleate. Both melts remained virtually crystal free at 400°C, about 100°C above glass transition, in 14 day-long experiments. At 500° C the incubation times were between 5 and 9 days for C1 and <5 days for C2. The maximum growth rates of ~250 μm/day were produced in composition C2 at 550°C. Reproducible mineral assemblages of alkali-feldspars, muscovite, stuffed β-quartz, petalite, and virgilite nucleated heterogeneously on the capsule wall and crystallized inward. C1 textures resembled fine grained, layered, and graphic outer zones of Li-rich pegmatites (Fig. 1). Hydrous C2 compositions (around or above fluid saturation) had low nucleation density and best resembled the coarse fabric found in highly fractionated inner zones of Li-rich pegmatites.

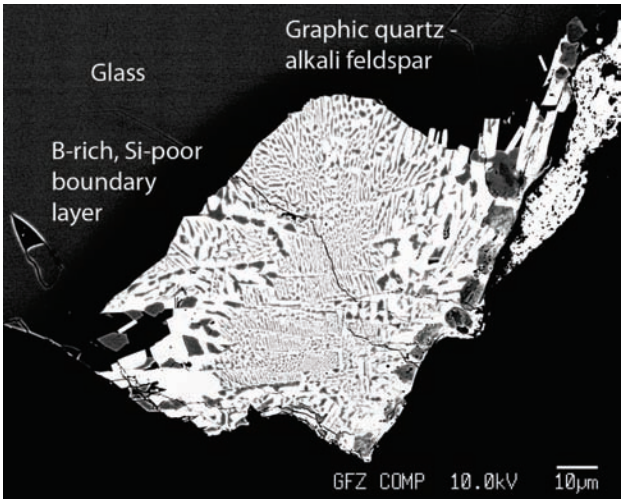

Fig. 1: Graphic intergrowth in composition C1 + 6.6 wt% H_2O, 9 days, programmed-cooling between 750 and 500°C, at 300 MPa.

Water concentrations of several wt. % below saturation lead to extremely high nucleation density, incompatible with typical coarse pegmatitic texture. Within a single charge, local water supersaturation lead to pegmatite texture by reducing nucleation and increasing crystal growth. Gradual textural coarsening by a factor of 3 was observed in areas surrounding large fluid cavities formed in a 200 MPa run similar to textures near "pockets" in shallower myarolitic pegmatites.

[1] London, D. (2008) *Pegmatites*. Can. Mineral., Sp. Publ., **10**.
[2] Nabelek, P. et al. (2009) *Contrib. Mineral. Petrol., Online First* DOI: 10.1007/s00410-009-0479-1.

Production of large crystals in highly undercooled H_2O-rich granite melts

Nabelek, P.I.[1*], Whittington, A.G.[1] & Sirbescu, M.C.[2]
[1]Dept. of Geological Sciences, University of Missouri, Columbia, MO, USA ([*]nabelekp@missouri.edu)
[2]Dept. of Geology, Central Michigan University, Mount Pleasant, MI, USA

Granite pegmatites in the continental crust are characterized by large elongated crystals that often exhibit preferred directions of growth. There has been a shift in viewing pegmatites as products of very slow cooling of granite melts to viewing them as products of crystal growth in undercooled liquids, mostly because thermal considerations require rapid cooling of intrusive sheets. With this change there has been a renewed debate about the role of H_2O in the petrogenesis of pegmatites. On the basis of data on nucleation of minerals and new viscosity models for hydrous granite melts, it is argued that H_2O is an essential component in the petrogenesis of granite pegmatites. H_2O is key to reducing the viscosity of silicate melts, which enhances their transport within the crust. It also dramatically reduces the glass transition temperature, which permits crystallization of melts at hundreds of degrees below the equilibrium solidus. Crystallization of melts below the thermodynamic solidus is demonstrated by trapped fluid and melt inclusions and other features. Recent experimental data show that because H_2O drastically reduces the nucleation rates of silicate minerals, the minerals may not be able to nucleate until the melt is substantially undercooled. In a cooling melt sheet, nucleation starts at its highly undercooled margins, followed by inward crystal growth towards its slower-cooling, hotter core. Delay in nucleation may be caused by competition for crystallization by several minerals in the near-eutectic melts and by the very different structures of minerals and highly hydrated melts. Once a mineral nucleates, however, it may grow rapidly to a size that is determined by the distance between the site of nucleation and the point in the magma at which the temperature is approximately that of the mineral's liquidus, assuming components necessary for mineral growth are available along the growth path. The unidirectional textures and internal zoning that typify many pegmatites are determined by internal temperature gradients.

In contrast to rhyolites that degas prior to or during eruptions, granite pegmatites are apparently able to retain H_2O during most of their crystallization histories within the confinement of their wall rocks. Without retention of H_2O the conditions for pegmatitic textural growth may be difficult to achieve. Loss of H_2O due to decompression and venting leads to microcrystalline texture and potentially to glass during rapid cooling as seen in rhyolites. In contrast, slow cooling within a large magma chamber promotes continuous exsolution of H_2O from crystallizing magma, growth of equant crystals, and final solidification at the thermodynamic solidus. These are the characteristics of normal granites that distinguish them from pegmatites.

Evaluation of the use of fracture minerals for exploration for rare-metal pegmatites

Linnen, R.L.[1*], Galeschuk, C.[1], Halden, N.M.[2] & Lau, L.[1]
[1]Dept. of Earth and Environmental Sciences, University of Waterloo, Canada ([*]rlinnen@uwaterloo.ca)
[2]Dept. of Geological Sciences, University of Manitoba, Canada

Whole rock analyses of Li, Rb and Cs are used to locate hidden rare-metal pegmatite bodies. However, Li-bearing minerals may occur along fractures and cause false positive anomalies. The Dibs pegmatite was selected as a site to evaluate exploration methods because it is a completely buried LCT pegmatite in the Bernic Lake area, near the famous Tanco pegmatite in south eastern Manitoba. In this study, fracture minerals in metabasite around the Dibs pegmatite were analysed and compared to matrix mineral chemistry (both by LA-ICP-MS) and whole rock lithogeochemical data (total digestion ICP).

All three data sets show a progressive dispersion of Li and away from the pegmatite-metabasite contact. There are also less well developed Rb and Cs dispersion halos defined by whole rock and biotite analyses. At the upper pegmatite contact the metabasite contains up to 2954 ppm Li, 176 ppm Rb and 65 ppm Cs, but these values decrease to 28, 17 and 5 ppm, respectively, at a distance of 60 m above the pegmatite. Of the matrix minerals biotite contains the highest concentrations of Li, Rb and Cs. These range from 3264, 1406 and 753 ppm, respectively, at the contact to 150, 212 and 37 ppm, respectively, 60 m above the pegmatite. However it is fracture chlorite that may best reflect dispersion around the Dibs pegmatite. At the pegmatite contact Li values are similar to lithogeochemical and biotite values, at 1000-2000 ppm, but, at 45m above the pegmatite contact fracture chlorite contains approximately 300 ppm Li, which is an order of magnitude higher than whole rock values and 2 to 3 times the values in biotite. Consequently fracture chlorite is demonstrates promise as a recorder of fluid flow around pegmatites and as an exploration tool for rare metal pegmatites.

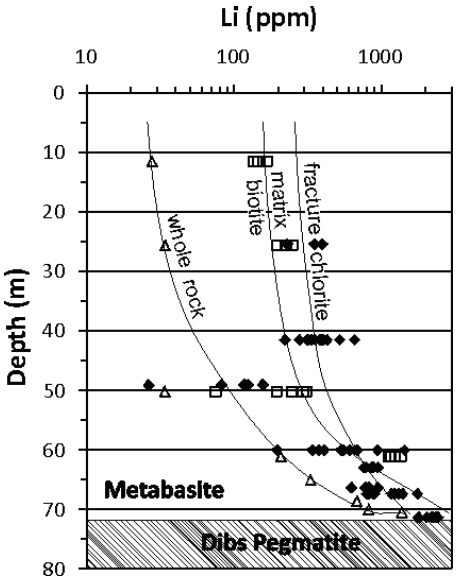

Fig. 1: Dispersion around the Dibs pegmatite. Open triangles represent whole rock lithogeochemistry, open square are matrix biotite and solid diamonds are fracture chlorite analyses.

The role of pegmatites in the Central Alps. Proxies of the exhumation history of the Alpine nappe stack in the Lepontine dome

Guastoni, A.[*], Artioli, G. & Pennacchioni, G.
Dept of Geoscience, University of Padova, Italy
([*]alessandro.guastoni@unipd.it)

The area of this study is located between the town of Domodossola (Western-Central Alps, Italy-Swiss) and the Masino-Bregaglia Oligocene intrusion (Central Alps, Italy). Most of the pegmatitic dikes are hosted by the Southern Steep Belt (SSB), an alpine migmatitic unit, which includes several Lepontine nappes like the Antigorio, the Monte Rosa, the Camughera-Moncucco-Isorno-Orselina and the Adula. Alpine metamorphism in Central Alps is poliphasic and characterized by high temperature greenschist and amphibolitic facies related to Barrovian metamorphism during Oligocene-Miocene age. Barrovian metamorphism is structurally related to D3 phase of backfolding of Alpine nappes in the Central Alps and it forms an asymmetric dome structure named Thermal Lepontine Dome characterized by metamorphic isograds which discordantly crosscut the Pennidic nappes [1-4]. The age determinations of a limited number of aplite-pegmatites dikes injections into the Isorno-Orselina and Monte Rosa nappes on monazite-(Ce) $^{206}Pb/^{238}U$-$^{207}Pb/^{235}U$, xenotime-(Y) $^{206}Pb/^{238}U$-$^{207}Pb/^{235}U$ and zircon $^{206}Pb/^{238}U$-$^{207}Pb/^{235}U$ are between 29-26 m.y [5].

Preliminary field studies based on textural, mineralogical observations and structural relationships of pegmatitic dikes with the hosting rocks which outcrop in the Central Alps allow them to be assigned to different families and classes as reported in the classification of Ćerný & Ercit [6]. Most of pegmatitic dikes (>90%) can be defined as "barren" being composed by K-feldspar and subordinate quartz + muscovite. A minor percentage can be assigned to a population of more "geochemically evolved" pegmatites respectively belonging to the two main LCT (lithium, cesium, tantalum) and NYF (niobium, yttrium, fluorine) families.

The changing from greenschists to amphibolites metamorphic grade in the Central Alps involves a main changing with depth in the fragile/ductile rheology of crustal rocks thrusted during the formation of the Lepontine Alps. Along SSB ductile deformations of pegmatites in amphibolitic facies are overprinted by fragile deformations in greenschists facies. Future studies will focus on:

- isotopic studies to establish relationships between pegmatites and host rocks to define age of crystallizations and rate of coolings of deformed and miarolitic pegmatites, the latter have not been affected by metamorphic overprinting;
- geochemical studies in order to establish whether the pegmatitic field of the Central Alps is genetically related to migmatites terrains of the Alpine Barrovian-type metamorphic belt [3] or related to granitic-tonalitic liquid melts of Masino-Bregaglia intrusion.

[1] Todd, C.S. & Engi, M. (1997) *J. Metamorph. Geol*., **15**, 513-530. [2] Burg, J.P. & Gerya, T.V. (2005) *J. Metamorph. Geol*., **23**, 75-95. [3] Burri, T., Berger, A. & Martin, E. (2005) *Schweiz. Miner. Petrog.*, **85**, 215-232. [4] Maxelon, M. & Mancktelow, N.S. (2005) *Earth Sci. Rev.*, **71**, 171-227. [5] Schärer, U. et al. (1996) *Earth Planet. Sci. Lett*., **123**, 138-158. [6] Ćerný, P. & Ercit, S. (2005) *Can. Mineral*., **43**, 2005-2026.

The rare elements-rich granitic body of Outeiro Mine (Northern Portugal)

Lima, A.[1,2*], Rodrigues, R.[1], Guedes A.[1,2] & Novák, M.[3]
[1]Centre of Geology, University of Porto, Portugal
([*]allima@fc.up.pt)
[2]Dept. of Geosciences, Environment & Territory Management - FCUP, Porto, Portugal
[3]Dept. of Geological Sciences, Masaryk University, Brno, Czech Republic

In Outeiro open-pit (Seixoso area) outcrops a granitic cupola that have been mined in the last decade for the ceramic industry. This structure belongs to the so-called Seixoso-Vieiros pegmatite field that is located in Northern Portugal and contains numerous pegmatite-aplite veins and rare element-rich granites. This field was known in the past for old mining of cassiterite and columbite-tantalite at least from the last century [1]. In Seixoso area the granitic intrusion outcrops as two main apices (Seixoso body and Outeiro body) and numerous, small apices or dike-like bodies. Seixoso and Outeiro granitic bodies are very heterogeneous and characterized by a horizontal magmatic layering, which was accentuated by post-magmatic pervasive albitization and greisenization, this latter being more intensive upwards. They evolved from a biotite-bearing facies at depth, through two-mica or muscovite tourmaline facies into the apex roof. Apical facies (apogranites) are highly evolved and locally (Seixoso granite) poorly mineralized in cassiterite. Biotite bearing facies, apogranites of Seixoso granite or Outeiro granite and the most evolved Seixoso pegmatites are considered to be members of a single differentiation series [2] characterized by a sodalithic-type evolution - a decrease in Si and K is accompanied by increase in Al, Na, Li, F (P, Sn, Ta, Nb, Be). During recent mining the lithium-bearing minerals, such as amblygonite-montebrasite, spodumene, petalite, cookeite became more abundant, although most of them in accessory quantity. They appear together with beryl, chrysoberyl, tourmaline, sekaninaite, eosphorite-childrenite, Th,U-rich monazite-(Y) (9.11 wt.% ThO_2; 7.57 wt.% UO_2), xenotime-(Ce), pretulite, zircon, Nb,Ta,Ti,Sn-oxide minerals - highly heterogeneous niobian rutile (≤3.38 wt.% SnO_2; ≤29.35 wt.% Ta_2O_5; ≤24.14 wt. % Nb_2O_5), Ti,Nb,Ta enriched cassiterite (≤3.67 wt.% TiO_2; ≤2.34 wt.% Ta_2O_5; ≤1.51 wt.% Nb_2O_5), Ti-enriched ferrocolumbite (≤1.66 wt.% TiO_2), ilmenite and ferronigerite and zincnigerite both Ti-enriched (≤5.31 wt.% TiO_2) [3]. This mineral assemblage typically matches the complex petalite or spodumene subtype pegmatites [4]. [5] referred for Seixoso surrounding mined pegmatite-aplite veins, an analogous and extensive list of minerals where also found lepidolite, zinwaldite and topaz.

[1] Maijer, C. (1965) *PhD Thesis*, Rotherdam, Netherlands. [2] Helal, B., Bilal, E. & Pereira, E. (1993) in Fenoll Hach-Ali, P., Torres-Ruiz, J. & Gervilla, F. (eds) *Current Research in Geology Applied to Ore Deposits*, 253-257. [3] Lima, A. et al. (2009) *Estudos Geológicos*, **19(2)**, 182-187. [4] Černý, P. & Ercit, T.S. (2005) *Can. Mineral.*, **43**, 2005-2026. [5] Cruz, A.M.B. (1969) *Memórias e Noticias*, Museu e Laboratório Mineralógico da Universidade de Coimbra e do Centro de Estudos Geológicos, **67,** 1-133.

Age and mineralogy of supergene uranium and manganese minerals - tools to unravel the supergene alteration in pegmatitic and granitic terrains (Bohemian Massif, SE Germany)

Dill, H.G.[1*], Gerdes, A.[2], Hansen, B.[3], Weber, B.[4] & Keck, E.[5]
[1]Bundesanstalt für Geowissenschaften und Rohstoffe, Hannover, Germany ([*]dill@bgr.de)
[2]J.W.Goethe University, Frankfurt, Germany
[3]Georg-August University, Göttingen, Germany
[4]Weiden i.d.OPf., Germany
[5]Etzenricht, Germany

Uranyl phosphates (torbernite, autunite, uranocircite, saleeite) and hydrated uranyl silicates (normal and beta-uranophane) as well as K-bearing manganiferous oxide-hydroxides met at various erosion levels and structures in the Late Variscan granites and pegmatites at the western edge of the Bohemian Massif, Germany, were the target of mineralogical investigations and age dating, using conventional K/Ar methods and more advanced techniques such as Laser-Ablation-Inductive-Coupled-Plasma Mass Spectrometry (LA-ICP-MS). Supergene U minerals have an edge over other rock-forming minerals, because of their inherent “clock” and their swift response to chemical and physical environmental changes on different scales. The azonal duricrusts, involving uraniferous phoscretes and silcretes, can be used to characterize the alkalinity/ acidity of meteoric/ *per descensum* fluids and to constrain the redox conditions during geomorphic processes. Moreover, uraniferous calcretes bearing uranyl vanadates are marker rocks for arid climatic conditions and for a desert depositional environment. This study aimed at deciphering the geomorphological and paleohydraulic history which granitic rocks of the Central European Variscides (Moldanubian and Saxothuringian zones) went through during the Neogene and Quaternary in the foreland of the rising Alpine mobile fold belt. The study provides an amendment to the current subdivision of the regolith by introducing the term “hydraulith” (percolation and infiltration zones) for the supergene alteration zone in granitic terrains. It undercuts the regolith at the brink of the phreatic to vadose hydraulic zones. Based upon the present geomorphological and mineralogical studies a four-stage model is proposed for the evolution of the landscape in a granitic terrain which might also be applicable to other regions of the Saxothuringian and Moldanubian zones of the European Variscides. Stage I (U mineralization in the infiltration zone) is a mirror image of the relic granitic landscape with high-altitude divides and alluvial-fluvial terraces. Its characteristic features are preserved in the uplifted hinterland of a peneplain which is tilted towards a lacustrine basin (or the sea). Stage II (U mineralization in the infiltration zone, regolith and saprock) includes planation and exhumation, resultant in the exposure of inselbergs and quartz reefs in front of the hinterland (stage I). Stages III and IV (U mineralization in percolation zone and saprock) are controlled by the base level lowering in the foreland. Rapid incision caused pinnacle-like tors and large first-order granitic land forms to form, whereas a slow-down of fluvial incision favors its destruction and the development of weathering pits of different kinds. A full blown cycle of planation and incision lasted for approx. 10 Ma, a stage which covers planation and exhumation, resulting in the formation of domal structures lasted for a period of time of as much as 2 Ma. Climate is an important factor but the most crucial factors for the geomorphological processes shaping the granitic landscape in the study area are uplift and erosion. The study area is located within the stress field of an ancient Variscan craton (Mesoeurope) and a highly mobile Alpine fold belt (Neoeurope).

The Na-rich phosphate minerals from Malpensata granitic pegmatite, Piona, Lecco province, Italy

Vignola, P.[1*], Hatert, F.[2], Fransolet, A.-M.[2] & Diella, V.[1]
[1]CNR-Institute for Dynamics of Environmental Processes, Milan, Italy ([*]pietro.vignola@idpa.cnr.it)
[2]Dept. of Geology, University of Liège, Belgium

The Malpensata pegmatitic dike occurs intruded into the high-grade metapelites of the Dervio-Olgiasca Zone (crystalline basement of the Southern Alps). In the field, the Malpensata dike displays an asymmetrical zoned structure composed of different units: 1) a wall zone; 2) an intermediate zone composed of medium-grained white albite and layers of medium grained black tourmaline + garnet + muscovite; 3) a main zone of blocky albite unit (megacryst plagioclase zone) with quartz + tourmaline + garnet graphic textures and many accessory phases as Li-Fe-Mn phosphates, oxides of Nb-Ta-Sn, zircon, uraninite, and many secondary uranium bearing minerals; 4) a roof zone composed of coarse white albite + quartz + muscovite. Masses of phosphates up to 25 cm in diameter were found in the intermediate zone and, mainly, in the blocky albite unit.

Careful investigations of thin sections, EMP chemical analysis and X-ray powder diffraction resulted in the identification of two different phosphates assemblages:

I) Graftonite + sarcopside + triphylite which characterizes the intermediate zone and the marginal part of the blocky albite unit; ferrisicklerite, heterosite, and vivianite are the main secondary phosphates.

II) Graftonite + triphylite + ferrowyllieite + arrojadite + a Na-rich iron phosphate (still under investigation) + sarcopside only observed in the central part of the blocky albite unit; ferrisicklerite, heterosite, Mn-rich vivianite, jahnsite-(CaMnFe), jahnsite-(CaMnMn), metaswitzerite, fairfieldite, rockbridgeite, and mitridatite(?) are the main secondary phosphates.

The usual assemblage I is very simple and Na-free: It is associated with poorly evolved accessory minerals like uraninite, zircon, ferrocolumbite and Th-rich monazite-(Ce). Assemblage II is more complex and particularly rich in Na-bearing phosphates as indicated by the presence of abundant ferrowyllieite, arrojadite, and of this interesting Na-rich iron phosphate. These phosphates are in very close association with highly evolved accessory phases like cassiterite, Sn-bearing zircon, ferrotantalite, ferrotapiolite and three different types of microlite, representing enrichment in Na and U. A Na-free microlite and one with a low Na-content form octahedrons showing an oscillatory zoning, whereas Na- and U-bearing microlite form fracture-fillings. These chemical features of microlite indicate a low temperature of crystallization [2]. We can infer that the primary phosphates belonging to association II crystallized together with the Sn-Ta-Nb-U mineral assemblage at a lower temperature in respect to phosphate association I formed from a fractionated melt strongly enriched in P. As proposed by London et al. [3], the high concentration of P allows the destabilization of albite that we can consider as the sources of Na and Al.

[1] Vignola, P & Diella, V. (2007) in Martin, T. & Vieira, R. (eds.) *Granitic pegmatites: the state of the art. Book of abstracts*. **8**, 102-103. [2] Vignola, P. et al. (2008) *Geophys. Res. Abstr.*, **10**, EGU2008-A-03866. [3] London, D. et al. (1999) *J. Petrol.*, **40**, 215-240.

Paragenetic evolution of Be minerals (silicates and phosphates) from the Nanping No. 31 pegmatite dyke, SE China

Wang RuCheng[*], Rao Can, Zhang WenLan & Wu JinWei
School of Earth Sciences and Engineering, Nanjing University, Nanjing, China ([*]rcwang@nju.edu.cn)

The No. 31 dyke is the most evolved one in the Nanping pegmatite district in southeastern China. It is strongly mineralized in rare elements with crystallizations of cassiterite, columbite-tantalite, microlite, wodginite, spodumene, amblogonite, beryl, pollucite, etc. [1].

Beryllium minerals in the Nanping No. 31 pegmatite dyke exhibit complex parageneses of silicates and phosphates, including beryl, phenakite, herderite, hurlbutite and euclase. Moreover, they show distinct paragenetic features in different internal zones of the pegmatite dyke. In the quartz – albite – muscovite zone (zone I) are found small beryl crystals with fine inclusions of phenakite. These Be silicates are all included in quartz or garnet, or interstitial to albite. Occasionally, vein-like beryl occurs along muscovite cleavages. Be minerals are likely very complex in the saccharoidal albite ± muscovite zone (zone II). Although discrete beryl interstitial to saccharoidal albite can be observed, Be minerals are dominated by beryllosilicate + berryllophosphate + apatite assemblages as cavity-filling among rock-forming minerals, suggestive of a P-saturated environment of crystallization. Large crystals of beryl appear in the quartz – coarse albite – spodumene zone (zone III) and quartz – spodumene – amblygonite zone (zone IV), and chemically are rich in Cs. They exhibit considerably late-generation hydrothermal alteration. Secondary beryl is depleted in Cs, but Cs-dominated muscovite (nanpingite) is closely associated with it.

The study suggests that crystallization of beryllium minerals in the Nanping No. 31 pegmatite dyke followed changes in magma conditions, considerably controlled by P activities on one hand, and by hydrothermal fluids in the late stage on the other.

[1] Rao, C et al. (2009) *Can. Mineral.*, 47, 1195-1212.

Alteration process of a graftonite + sarcopside + triphylite primary phosphate association from Luna pegmatitic dike, Lecco province, Italy

Vignola, P.[1*], Fransolet, A.-M.[2], Diella, V.[1] & Ferrari, E.S.[3]
[1]CNR-Istitute for Dynamics of Environmental Processes, Milan, Italy ([*]pietro.vignola@idpa.cnr.it)
[2]Dept. of Geology, University of Liège, Belgium
[3]Dept. of Earth Sciences, University of Milan, Italy

The mineral assemblage graftonite + sarcopside + triphylite is quite common in phosphate-bearing granitic pegmatites. In contrast to triphylite, graftonite and sarcopside are generally known to be resistant to alteration processes which characterize the crystallization/cooling history of pegmatitic dikes. Brian Mason [1] is the only author who described the alteration of graftonite as an oxidation of Fe^{2+} to Fe^{3+} accompanied by Ca leaching and progressive hydration with a constant Fe/Mn ratio. Nothing is reported in literature about alteration of sarcopside.

In the context of our investigation on phosphate associations of Piona granitic pegmatites, particularly in the Luna dike, phosphate masses consisting of sarcopside lamellae embedded in graftonite with minor triphylite, showing a well-developed alteration rims, have been found. Striking textures observed in thin sections indicate that graftonite + sarcopside underwent an alteration process similar to triphylite (Fig. 1).

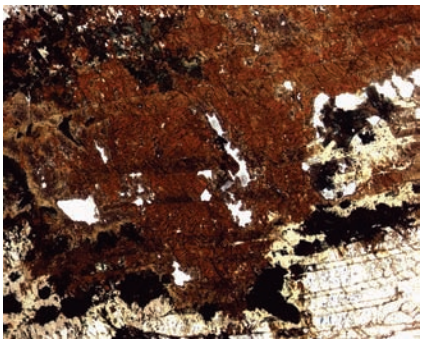

Fig. 1: Replacement of graftonite and sarcopside by brown kryzhanovskite, yellow jahnsite-(CaMnFe) and green-brown rockbridgeite; field of view 3 mm (plane polarized light).

Textural observations, electron microprobe chemical analyses and X-ray diffraction powder method enabled the identification of different alteration products exhibiting complex alteration mechanisms described herein in different steps. The first step, corresponding to the well-known hydrothermal alteration of triphylite, is marked by a progressive lithium leaching and Fe - Mn oxidation to form ferrisicklerite, and heterosite. The second step, involving sarcopside, graftonite, and the alteration products of triphylite, is characterized by a progressive hydration with Ca/Mg leaching in oxidizing conditions with the almost complete preservation of the lamellar texture. This transformation produced two distinct parageneses constituted by phosphoferrite + ferrostrunzite, and by jahnsite-(CaMnFe) + rockbridgeite + lipscombite. In a later alteration stage the auto-oxidation process transformed phosphoferrite-like mineral in kryzanovskite, ferrostrunzite in whitmoreite, and produced a totally oxidized rockbridgeite. It must be pointed out that kryzhanovskite displays two different chemical compositions reflecting those of the primary graftonite and sarcopside, and results as their alteration product.

[1] Mason, B. (1941) *Geol. Fören. Stockholm Förh.*, **63**, 117-175.

Genesis, chemical composition and mineral speciation of tourmalines from the rare-element pegmatite vein with scapolite (Sangilen Highland, Tuva)

Kuznetsova, L.G.[1*], Zolotarev, A.A.[2], Frank-Kamenetskaya, O.V.[2], Rozhdestvenskaya, I.V.[2], Bronzova, Yu.M.[2], Spratt, J.[3] & Ertl, A.[4]
[1]Vinogradov Institute of Geochemistry SB RAS, Irkutsk, Russia ([*]lkuzn@igc.irk.ru)
[2]St. Petersburg State University, St. Petersburg, Russia
[3]Museum of Natural History, London, UK
[4]Institute of Mineralogy and Crystallography, University of Vienna, Austria

Chemical composition and substitution mechanisms of tourmalines with high contents of Ca, Li, Mg, Fe (Li-rich uvites), rarely occurring in granite pegmatites, were examined. They occur in the rare-element pegmatite vein with scapolite in the Solbelder river basin, Sangilen Highland [1]. Petrological study of tourmaline-bearing pegmatite rocks gave the evidence of their magmatic origin in specific P-T environments [2]. Refinement of the crystal structures of these tourmalines was done to determine which mineral species they belong to [3,4].

Most of rare-element granite pegmatites of Solbelder field belong to spodumene type and have typical mineral composition. Some of them are embedded in limestones but have no strong signs of *in situ* contamination. Only one pegmatite vein demonstrates contamination to a particularly high degree. Tourmalines, described in this paper, crystallized in this vein in association with K-feldspar, scapolite (with 73 mol.% Me), quartz, spodumene, pyrochlore, cassiterite and zircon.

Yellow tourmaline from the central zone of the vein has a constant composition, which can be described as a solid solution of 3 components:

(1) $Ca(Mg_2Li)Al_6(Si_6O_{18})(BO_3)_3(OH)_3F$,
(2) $CaMg_3Al_6(Si_6O_{18})(BO_3)_3(OH)_3O$,
(3) $NaMg_3Al_6(Si_6O_{18})(BO_3)_3(OH)_3F$.

Component (1) is dominant and exceeds 50 mol.%, thus yellow tourmaline may be considered as a new mineral species in the tourmaline group.

Zoned grains of tourmaline with a yellow core and green rims from the border zone of the vein reflect strong changes in the chemical regime of pegmatite crystallization. The main changes of their composition from the core to the rim - decrease of Mg and increase of Li, Al, and Fe. Substitution mechanisms are: $Mg^{2+} \leftarrow Fe^{2+}$; $2Mg^{2+} \leftarrow Li^{+} + Al^{3+}$; $Mg^{2+} + OH^{-} \leftarrow Al^{3+} + O^{2-}$. The composition of the yellow core is the same as in tourmaline grains from the centre of the vein. The composition of green rims can be described as a solid solution of 4 components:

(1) $\square(Al_2Li)Al_6(Si_6O_{18})(BO_3)_3(OH)_3(OH)$,
(2) $NaMg_3Al_6(Si_6O_{18})(BO_3)_3(OH)_3(OH)$,
(3) $NaFe_3Al_6(Si_6O_{18})(BO_3)_3(OH)_3(F)$,
(4) $Ca(Al_{1.5}Li_{1.5})Al_6(Si_6O_{18})(BO_3)_3(OH_2O)(F)$.

The dominant component (4) makes up 62 mol.%, thus, green tourmaline also can be represented as a new mineral species.

A unique composition of the studied tourmalines reflects specific environments in which this pegmatite vein was formed.

Acknowledgments: This work was supported by RFBR (grants 09-05-011881-a, 09-05-00769a), SB RAS (IIP N 29).

[1] Kuznetsova, L.G. & Sizykh, Yu.I. (2004) *Dokl. Earth Sci.*, **395(3)**, 406-410. [2] Kuznetsova, L.G. & Prokofiev, V.Yu. (2008) *Proceedings of XIII Intern. Conf. on Thermobarogeochemistry and IV[th] APIFIS Symposium*. IGEM, Moscow, **1**, 102-105. [3] Rozhdestvenskaya, I.V. et al. (2007) *Crystallogr. Rep.*, **52(2)**, 203-207. [4] Rozhdestvenskaya, I.V. et al. (2008) *Crystallogr. Rep.*, **53(2)**, 223-227.

Genesis of spodumene pegmatites related to deep-seated faults in the East Sayan belt, Eastern Siberia, Russia

Makagon, V.M.
Institute of Geochemistry SB RAS, Irkutsk, Russia
(vmak@igc.irk.ru)

The East Sayan pegmatite belt, one of largest in the world, is situated in the south of Eastern Siberia (Russia), confined to the southern mobile marginal part of the Siberian craton. Rare-metal type pegmatite deposits are widely distributed in this belt. Formation of rare-metal pegmatites (LCT family) is divided into spodumene and petalite subformations, differing in the initial pressure of the mineral formation, which was 300-500 MPa, and 200-350 MPa, accordingly [1]. Spodumene rare-metal pegmatites are located in the south-eastern part of belt, occurring in the Urik-Iya graben, which is a rift structure of the southern mobile marginal part of the Siberian platform [2]. The age of the granitoids of the Sayan granitoid complex, with which spodumene pegmatites are connected, is determined by Rb-Sr method to be 1817 Ma and spodumene pegmatites were formed 1692 Ma ago. The Urik-Iya graben is limited by zones of deep fractures departing from a regional Main Sayan fault. The biggest Goltsovoye pegmatite field is controlled by zones of deep faults and is divided into western and eastern blocks. Lithium spodumene pegmatites are typical of the western part, while complex Ta-Cs-Li pegmatites occur in eastern block. On P-T diagram of quartz-saturated stability relations among lithium aluminosilicates in the system $LiAlSiO_4$-SiO_2-H_2O [3] lithium and complex pegmatites of Goltsovoye field crystallize in the field of spodumene stability. The initial pressure of crystallization was 450 MPa and then was lowering. Ta-Sn-Li pegmatites of the Belsk field originally crystallized in the field of spodumene stability, then petalite crystallization occurred, afterwards it was replaced by spodumene-2 and in the end by eucryptite.

Available geochemical data and the presence of large rare-metal pegmatite fields without any clear spatial connection with granitoid massifs do not prove the hypothesis of rare-metal pegmatite formation during differentiation of granite magma which formed these granitoid massifs. The relationship between granitoids and pegmatites is paragenetic. According to the data [2], granite magmatism in the Urik-Iya rift structure is caused by the presence of a deep (mantle) diapir, which was the source of both thermal energy, and fluids. They were transported in the zones of deep faults. Large rare-metal pegmatite fields formed due to a long process of pegmatite melt formation in the deep magmatic chambers under the influence of mantle fluids containing significant amount of SiO_2, alkalies and enriched in Rb, Li, Ta, Nb and other lithophile elements. The possibility of such fluid formation was shown in [4]. Small granodiorite and tonalite intrusions were found in the Urik-Iya graben, their geochemical feature is high Ba and Sr contents, on one hand, and increased Li, Cs and Sn contents, on the other hand. This indicates the possibility of enrichment in rare lithophile metals in the early undifferentiated granodiorite melt portions, which is possible due to the influence of such deep fluids.

Acknowledgements: This work was supported by RFBR (projects 10-05-00964, 10-05-01056) and by SB of RAS (project IIP 29).

[1] Zagorsky, V.E. et al. (1999) *Can. Mineral.*, **37**, 800-802. [2] Shcheglov, A.D. & Moskaleva, V.N. (1998) *Doklady AS SSSR*, **358**, 814-816. [3] London, D. (2008) *Can. Mineral., Sp. Publ.*, **10.** [4] Zharikov, V.A. (1996) *Vestnik MGU, Geologiya*, **4**, 3-12.

The Sosedka gem tourmaline mine, Transbaikalia, Russia: the petrogenetic model of B-rich miarolitic pegmatites

Zagorsky, V.Ye.
Institute of Geochemistry, SB RAS, Irkutsk, Russia
(victzag@igc.irk.ru)

The Sosedka mine is the largest source of gem tourmaline in the Malkhan field of B-rich miarolitic pegmatites, which are confined to the roof pendant between the Bolsherechensk and the Oreshny massifs of porphyritic biotite granites and two-mica leucogranites. Both massifs and the pegmatite field adjoin closely the Chikoy deep-seated fault, along which the Chikoy rift depression was formed in the Lower Cretaceous. The age of the granites and pegmatites is Lower Cretaceous as well, so their formation is related to the rifting. A decrease in pressure, caused by crustal extension and uplift of the northern block of the rift, together with heat and fluid flows within the deep-seated fault zone, induced melting processes and formation of the Malkhan granite-pegmatite system [1]. When the granitic magma transformed into a pegmatitic melt the latter was strongly enriched in B, Cs, and to a lesser degree F, Li, Ta. Because of fluid flow-melt interaction pegmatite melts become heterogeneous, especially relative to alkalis and volatiles [2,3]; as a result, quartz-K-feldspar, quartz-oligoclase and quartz-two feldspar pegmatites are closely linked within the Malkhan field.

The Sosedka ovoid-shaped body (80 x 50 m) has a rather concentric zonal structure. The interrupted external zone, 0-20 m wide, is composed of schorl-rich quartz-oligoclase pegmatite of coarse graphic texture with enclaves of quartz-K-feldspar schorl-free pegmatite and rare lenses of petalite-rubellite-lepidolite-albite composition. The central zone consists of quartz-K-feldspar schorl-free pegmatite of graphic and blocky textures with “inclusions” of quartz-oligoclase pegmatite. Both zones contain abundant miaroles, their size reaching 40 m^3. Based on mineral composition, three types of pockets are recognized: 1) quartz-lepidolite-Li tourmaline (± pollucite, beryl, topaz, hambergite, danburite); 2) quartz-adularia-axinite (± laumontite); 3) quartz-laumontite. Type 1 occurs in the external zone only, mainly near contacts with country rocks. Pockets of types 2 and 3 are typical of the central zone; but sometimes they occur in the external zone, near the central one. Independent pockets of different types often lie 0.5-2 m apart. Pockets are filled with loose material to 80-95% of their volume. Such a quantity of silicate material can not be formed in pockets only due to the fluid released from the melt during crystallization of the pegmatite matrix. Boron-rich melt-like gels are considered to be the mineral-forming medium in pockets [4]. Alkalinity increases from type 1 to type 3 pockets. Adularia, axinite and laumontite indicate unfavourable conditions for gem Li-tourmaline formation.

Primary magmatic genesis of the Sosedka pegmatite is undoubted. All geochemical data and the pattern of distribution of pockets and B-Li-rich mineralization within the body can be explained only by a model of chemically heterogeneous pegmatite magma intrusion [2,3]. The Sosedka’s magma portion included three coexisting melts corresponding to quartz-oligoclase, quartz-K-feldspar and quartz-petalite-rubellite-lepidolite-albite pegmatite varieties with numerous bubbles of a B-rich fluid-gel substance (precursors of future pockets). The heterogeneous state of the pegmatite melts was attained at above-liquidus conditions within the magma chamber.

Acknowledgements: RFBR, grant 10-05-00964.

[1] Zagorsky, V.Ye. & Peretyazhko, I.S. (2010) *Dokl. Earth Sci.*, **430(2)**, 172-175. [2] Zagorsky, V.Ye. (2007) *Mem. Univ. Porto*, **8,** 106-107. [3] Zagorsky, V.Ye. (2009) *Estud. Geológ.*, **19(2),** 365-369. [4] Touret, J.L.R. et al. (2007) *Mem. Univ. Porto*, **8,** 92-93.

Possible mechanisms for the trace elements concentration during the evolution of volatile-saturated granitoid magmas

Badanina, E.V.[1*], Thomas, R.[2] & Syritso, L.F.[1]
[1]Dept. of Geochemistry, State University of St.-Petersburg, Russia ([*]elena_badanina@mail.ru)
[2]GeoResearchCentre of Potsdam, Germany

For the solution to this problem we have investigated the melt (MI) and fluid (FI) inclusions in quartz, topaz and beryl within the fully differentiated massive of the rare-metal granites of Orlovka, Spokojnoje, Etyka, Sherlovaya Gora (Transbaikalia), Voznesenka (Primorje) and the granite-pegmatite systems of Malkhany (Transbaikalia), Voronji Tundry (Kola Peninsula). These studies showed that the traditional process of fractionation is not the only mechanism of rare element concentration. The process of fractionation (ongonite trend) is recorded simultaneously in the rock and melts only to a certain stage of saturation of "typomorphic" elements - F, B, H2O, and Li, after which the melt system becomes heterogenic. Such a process was followed up by us an example of Orlovka massif of Li-F granites [1], where the melt achieved up to 9.9 wt% H2O, 1.8 wt% F, 2.09 wt% B and 2411 ppm Li. By contrast the residual melt concentration of certain associated elements - Al, Na, Li, F, Nb, Ta, REE are reduced which suggests the probable separation of hydrosaline Na-Al-F melt, which in experimental systems are linked the the concentration of rare elements. Liquid immiscibility in pegmatite systems is illustrated by the example of the Voronji Tundry pegmatites, where the separation of Cs-rich melt leads to the formation of unique quartz-pollucite lens [2]. Calculation of distribution coefficients in the systems of melt-mineral (mica, K-, Na-feldspar, quartz) shows a fundamentally different nature of the Li, Rb, Cs, Ta, Nb, REE, F, B behavior in the process of volatile-saturated magma evolution. Thus, at an early stage Li is greatly enriched in the melt, and then concentrated in the micas (equality content in rocks and melt), at later stages it is readily converted into a fluid phase with the formation of the polylithionite in FI [3]. The distribution coefficient for Rb in melt-mineral system is always in favor of the melt, passive during the processes of immiscibility and serves as ideal indicator of fractionation. Cesium is the most incompatible with the aluminosilicates rare alkali elements, which easy removed from the silicate melt. REE - probably moves with the Na-Al-F melt [4], as confirmed experimentally [5]. The absence of columbite-tantalite saturation of the melt and compositional variations of the zonal columbite-tantalite suggest different mechanism for the Ta and Nb concentration: accessory columbite-Fe at an early stage – from local saturation area; the main ore mineralization of the maximum Mn columbite-tantalite from hydrosaline (?) melts; tantalite-Fe in the FI - from saturated fluor-rich fluid. Distribution coefficients in the fluid-melt system are calculated to assess the role of magmatic-hydrothermal transition.

Acknowledgements: This study was supported by the Russian Foundation for Basic Research (grants 08-05-00766-a and 08-05-00771-a) and DAAD (Germany) fellowship.

[1] Badanina, E.V. et al. (2010) *Petrology,* **18**, 131-157. [2] Badanina, E.V. et al. (2007) *ECROFI XIX*, Bern, Switzerland, 196. [3] Thomas, R. et al. (2009) *Mineral. Petrol.*, **96**, 129-140. [4] Badanina, E.V. et al. (2006) *Can. Mineral.*, **44,** 667-692. [5] Veksler, I.V. et al. (2005) *Geochim. Cosmochim. Ac.*, **69**, 2847-2868.

Origin of the Mn-enriched NYF-type pegmatites in the Searchlight granite-pegmatite-aplite District, Clark Co., Nevada, USA

Webber, K.L.[*], Simmons, W.B., Falster, A.U. & Masau, M.
Dept. of Earth and Environmental Sciences, University of New Orleans, Louisiana, USA ([*]kwebber@uno.edu)

Shallowly emplaced mid-Miocene (8-16 Ma) granites exposed near Searchlight in the Newberry Mountains, Clark Co., Nevada are located in the Colorado River extensional corridor in the Basin and Range Province of the western United States. The granites intrude older Proterozoic basement rocks of the Mohave terrane and subsequently, became exposed along several steeply bounded extensional faults. For this study, Newberry granites were divided into three major suites, the Searchlight, Bat Ears and South Ridge, on the basis of petrographic textures and mineralogy. Granites from all three suites host numerous miarolitic pegmatite bodies. Miarolitic cavities in the pegmatites range from microscopic to meter size and they host an assemblage of well-crystallized mineral species including smoky quartz, microcline, albite, annite (high Mg), spessartine, zircon, thorite, titanite, columbite group species, ilmenite-pyrophanite, magnetite, monazite-(Ce), bastnaesite-(Ce), polycrase-(Y) and fluorite.

Geochemically, the mineral assemblage found in the miarolitic cavities indicates enrichment in Mn, Ti, Zr, Nb>Ta, LREE>HREE, Th and F. The observed geochemical signature and mineralogical assemblage is characteristic of the NYF family of granitic pegmatites. Pronounced enrichment in Mn expressed in several mineral species is particularly striking. Annites show a progressive enrichment in both Mn and F from granites to pegmatites. The miarolitic cavities carry a primary assemblage of Ti-,Nb-,Ta-oxide minerals. Compositions of columbite group minerals correspond to manganocolumbite. Garnet in miarolitic cavities is spessartine rich with core and rims averaging $Alm_{13}Sps_{87}$ and $Alm_{17}Sps_{83}$, respectively. Ilmenite is also Mn enriched, with compositions close to pyrophanite. The extreme fractionation of Mn in the Newberry granites and pegmatites is inferred to be the result of high fluorine activity.

Even though the Newberry granites were clearly emplaced during an extensional tectonic event, a low Fe/(Fe+Mg) ratio in annites (compositionally very close to phlogopite), low HFSE and HREE abundances and high Al/Ga are geochemical characteristics that more typically characterize calc-alkaline magmatism or convergent margin tectonic settings. Similar geochemical signatures have been reported for other extension-related rocks in the region of the Colorado River extensional corridor. This suggests a petrogenetic history whereby extension-related, mantle-derived melts are modified by both fractionation and crustal assimilation processes in order to explain the observed geochemical trends in the Newberry granites and related pegmatites along the Colorado River extensional corridor. The differences in the geochemistry and mineralogy of the three Newberry mountain granitic suites and their related pegmatites appear to be the result of differences in magma ascent paths, localized assimilation of Proterozoic basement rocks and fractionation.

Nb-Ta oxide minerals: tracers of complex magmatic to hydrothermal evolution of the Jezuitské Lesy granitic pegmatite, Bratislava Massif, Slovakia

Chudík, P.[1] & Uher, P.[2*]
[1]Dept. of Mineral Deposits, Comenius University, Bratislava, Slovakia
[2]Dept. of Mineralogy and Petrology, Comenius University, Bratislava, Slovakia ([*]puher@fns.uniba.sk)

Nb-Ta phases, especially members of columbite, tapiolite and wodginite groups, represent characteristic accessory minerals of the LCT-family rare-element granitic pegmatites. Detailed BSE and electron-microprobe study of their textural and compositional variations reveal an evolution of parental granitic pegmatites. The Jezuitské Lesy pegmatite exhibits an example of moderately evolved and relatively narrow dike of the beryl-columbite subtype, where several generations of the Nb-Ta minerals portrayed their magmatic to post-magmatic (hydrothermal) evolution.

The pegmatite forms a 1-2 m thick dike in parental Hercynian S-type granodiorites to granites of the Bratislava Massif (SW Slovakia). The dike consists of a coarse-grained quartz-microcline-muscovite zone, locally with gradual transition into blocky microcline, and core quartz zone. Aplitic, fine-grained saccharoidal albite unit (albite >> quartz + muscovite + garnet), rarely platy albite (cleavelandite) extensively replaces the older zones. Accessory beryl, phenakite, bertrandite, almandine-spessartine, gahnite, zircon, fluorapatite, cheralite-huttonite-monazite-(Ce) s.s., uraninite, galena, pyrite, and the Nb-Ta oxide phases were identified.

The first generation of the Nb-Ta minerals comprises ferrotantalite (Ct1), ferrotapiolite (Ft1) and ferrowodginite (Fw1), in the quartz-microcline-muscovite zone. They show Ta,Fe-rich compositions with Ta# [Ta/(Ta+Nb)] = 0.52-0.70 (Ct1), 0.88-0.90 (Ft1) and 0.73-0.86 (Fw1); Mn# [Mn/(Mn+Fe)] = 0.32-0.49 (Ct1), 0.06-0.10 (Ft1) and 0.33-0.41 (Fw1).

The 2nd generation is represented by ferrocolumbite to ferrotantalite (Ct2) in saccharoidal albite, replacement zones of Ct2 in Ct1, and irregular overgrowths of ferrotapiolite (Ft2) and ferrowodginite (Fw2) on Ft1 grains. The minerals of the 2nd generation show decreasing of Ta# in comparison to the 1st group: 0.10-0.60 (Ct2), 0.85-0.87 (Ft2) and 0.73-0.77 (Fw2); Mn# attains 0.30-0.45 (Ct2), 0.06-0.09 (Ft2) and 0.26-0.37 (Fw2).

The 3rd generation includes fissure fillings, overgrowths and replacement zones of manganocolumbite to manganotantalite (Ct3), ferrotapiolite (Ft3) and ferrowodginite (Fw3) on the older Nb-Ta phases (Ct1, Ft1, Fw1, Fw2), in the coarse-grained unit. The 3rd population displays distinct Mn# increasing (Ct3: 0.51-0.69, Ft3: 0.11-0.24, Fw: 0.40-0.41), Ta# values reach 0.16-0.79 (Ct3), 0.88-0.92 (Ft3) and 0.80-0.81 (Fw3).

The latest, 4th generation of the Nb-Ta phases represent irregular veinlets and patches of microlite, replacing Ct1, Ft1, Fw1, Ct2 and Ft3. Microlite is distinctly Ta-rich, the Ta# values are evidently higher in microlite penetrating Ft1 (0.90-0.97) than it associate with Ct1 (0.82-0.85).

The compositional variations of the Nb-Ta phases show a complex evolution trend of the Jezuitské Lesy pegmatite, from initial (1) magmatic crystallization of Ta,Fe-rich assemblage, followed by (2) reversal Ta/Nb fractionation, (3) Mn-enrichment stage, and final (4) hydrothermal overprint.

Phosphates from the albite pegmatites of the Cap de Creus Granite pegmatite field, Eastern Pyrenees, Catalonia, Spain

Alfonso, P.[1], Fontan, F.[2] & Melgarejo, J.C.[3*]
[1]Dept. d'Enginyeria Minera i Recursos Minerale, Universitat Politècnica de Catalunya, Manresa, Spain
[2]Laboratoire de Minéralogie, CNRS-Université Paul Sabatier, Toulouse, France
[3]Dept. de Cristal·lografia, Mineralogia i Dipòsits Minerals, Universitat de Barcelona, Spain
([*]joan.carles.melgarejo.draper@eub.edu)

Albite pegmatites are the most evolved type in the Cap de Creus pegmatite field, and they are the most enriched in accessory phosphates. These pegmatites are internally complex, and the internal structure consists of a fine-grained border zone, two intermediate zones and a quartz core, all of them crosscut by quartz-muscovite lenses and late phosphate veins. The border and intermediate zones are made up by quartz and albite, with minor muscovite and tourmaline; other minor Al-rich silicates are andalusite and sillimanite. Chrysoberyl occurs at the border zones and in quartz-muscovite veins; beryl is common in the intermediate zones. Ta-rich members of the columbite group are found in all the zones, specially in the quart-muscovite veins, accompanied with cassiterite, gahnite, nigerite and Hf-rich zircon. In all the zones columbite minerals are replaced by tanteuxenite, microlite, rynersonite and tapiolite. Metasomatic processes at the exocontact of the pegmatites include replacement of the host biotite schists by apatite, muscovite, graphite and schorl.

Montebrasite is the dominant phosphate in the intermediate zones, with minor amounts of apatite in the border zone. It may be accompanied with Mn-rich members of the graftonite-beusite series, sarcopside and wyillieite. Some Al-rich phosphate nodules consist of intimate intergroths of wyllieite with scorzalite and diaspore, occassionally accompanied with montebrasite. Mn-rich members of the triphylite-lithiophylite are rare, and have been replaced by the typical sequence to sicklerite and purpurite; stanekite replaces the above minerals.

Phosphate veins have a complex mineralogy. The first mineral to be formed is berlinite, which is partly replaced by Al-rich phosphates as wyllieite, trolleite, secondary montebrasite and brazilianite.

Some late phosphates can be produced in supergene conditions and involve replacement of primary phosphates. Crandallite and apatite replace montebrasite.

The occurrence of phosphates in different pegmatite units allowed to analyze the pegmatite evolution in terms of the chemical composition of phosphates, and compare this composition with that of the rest of the field. F content in montebrasite decreases from the earlier stages of the pegmatite evolution, from 2.83% in the first intermediate zone to 0 in the secondary montebrasites. Ca-Fe-Mn-(Li) phosphates are enriched in Mn, and extremely empoverished in Mg. The members of the scorzalite-lazulite series are closer to the scorzalite end-member. The only phosphate rich in Mg from these pegmatites is quingeiite, which can reach up to 4.67 wt % MgO. A new phase similar to triplite, X-phase, was found in these pegmaties. Microprobe analyses reveal high Mn contents. The composition of this mineral is similar than triplite, $(Mn,Fe,Mg,Ca)_2$ $(PO_4)(OH,F)$, but with Cl instead of F.

A high P activity in the corresponding pegmatitic magma determinated not only the development of phosphates in all the pegmatite units, but also a high P content in the pegmatite silicates and an intense apatitization on the pegmatite exocontact. In contrast, a low F activity, as registered in the phosphates, prevented the development of Li silicates.

Evolution of the chemical composition of columbite-tantalite in Li-F granites and pegmatites – a comparative study

Badanina, E.V.[1*], Sitnikova, M.A.[2], Syritso, L.F.[1], Gordienko, V.V.[1] & Abushkevich, V.S.[3]
[1]Dept. of Geochemistry, State University of St.-Petersburg, Russia ([*]elena_badanina@mail.ru)
[2]Federal Institute for Geosciences and Natural Resources, Hannover, Germany
[3]Institute of Geology and Geochronology of Precambrian, St.-Petersburg, Russia

The mineral chemistry of columbite-tantalite from two famous Li-Ta deposits in Russia, the Orlovka and the Kholmozero deposits in Transbaikalia and the Kola Peninsula, respectively, was studied. In the Orlovka massif of Li-F-granites, columbite-tantalite occurs in all five zones of a complex differentiated vertical sequence ranging from protolithionite granites to amazonite granites with lepidolite [1]. In spodumene pegmatites of the Kholmozero deposit, columbite-tantalite is found in four zones of a differentiated pegmatite body. In both deposits, columbite-tantalite is characterised by a zoned internal structure. This zoning mainly reflects Nb/Ta ratios and changes from progressive to oscillatory, overgrowing the old core of the crystals. In late varieties of tantalite from pegmatite, the oscillatory zoning is replaced by irregular spot zoning. Columbite in the pegmatite system develops from Fe-columbite towards pure Mn-tantalite. A columbite group mineral develop only towards Mn-enriched varieties in rare metal granites.

Columbite-tantalite from these two complexes is very different in its trace element contents, especially rare elements and REE. Firstly, columbite-tantalite from Orlovka is characterised by the highest concentrations of REE (up to 12335 ppm) compared to columbite-tantalite in all known pegmatites worldwide. Secondly, columbite-tantalite from Orlovka has high concentrations of Li (up to 106 ppm), Rb (up to 20 ppm), W (up to 1.6 wt%), and Sn (13.8 wt%). Thirdly, no pure Ta-end members of columbite-tantalite are present in the rare metal granites of Orlovka, probably because of the presence of other Ta-oxides like microlite with up to 75 wt% Ta_2O_5.

Columbite-tantalite from the Kholmozero pegmatite is characterised by consistent contents of Rb. The contents of Rb increase from 3.4 to 70.4 ppm from early to late generations. This trend was not observed in columbite-tantalite from the Orlovka Li-F granites.

In general, the behaviour of rare and rare earth elements in columbite-tantalite in Li-F granites indicates a more complex fractionating process compared to pegmatites. The process of fractional crystallisation in small chambers of pegmatite bodies is probably more evolved compared to granites. As a result, "space isolated" parageneses are formed, fixing the time sequence. In rare metal granites, such parageneses are not observed probably because of slower evolution of the granitic melt which leads to an incomplete fractionation process.

Acknowledgements: This study was supported by the Russian Foundation for Basic Research (grants 08-05-00766-a and 08-05-00771-a) and DAAD fellowship.

[1] Badanina, E.V. et al. (2010) *Petrology*, **18**, 131-157.

Epidote populations in contaminated granitic pegmatites from Northern Portugal

Dias, P.A.* & Leal Gomes, C.
CIG-R – DCT, Universidade do Minho, Braga, Portugal
(*patriciasdias@gmail.com)

In Domo de Covas mega-anticline (Serra de Arga, N Portugal) the digestion of metacarbonate host-rocks during pegmatitic intrusion produced Ca saturation and high silica impoverishment, resulting desilicated pegmatite veins with plagioclase, scapolite, and local concentrations of phosphate and epidote.

The following vein-fillings are distinguished:

1. *Hybrid pegmatoids* (π1): include plagioclase (mainly anorthite) ± quartz ± triphylite – lithiophilite. Fluorapatite occurs in border units and mark the transition to π2 veins. Vesuvianite is discordant in exo-contact metasomatic hosts.

2. *Hybrid and fractionated pegmatoids* (π2): occur laterally and are the products of fractionation of π1 pegmatites. They consist mainly of prehnite + pink clinozoisite. The clinozoisite is larger where it has crystallized first and these crystals manifest progressive zoning (Fig. 1). Textures also indicate simultaneous crystallization of zoisite and prehnite. Some latest veins only have prehnite (π2-2).

Oligoclase neosome, with scapolite and epidote, bearing sulphide cavities (chalcopyrite and sphalerite) fall into a more typical primary tendency, directed towards the albite pole in the haplogranite system.

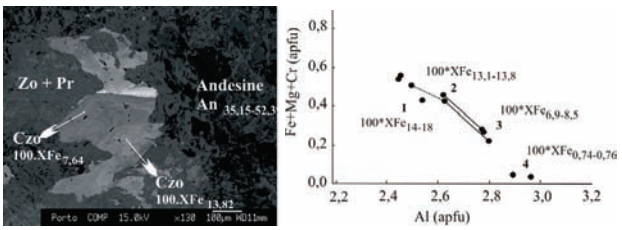

Fig. 1: Mineral intergrowth from veins (π2) – subhedral corroded crystal of clinoizoisite (Czo) in transition to sympletitic zoisite (Zo) and prehnite (Pr) - and compositional fields of epidote from π2 veins.

Epidote and prehnite would come from the earlier crystallization of melts, which composition was modified by desilication. Low Fe content of zoisite (maximum XFe calculated content, 0.76) indicates low P, T conditions. The minimum temperature of crystallization is 440-500ºC (P <5Kbar), deduced from zoisite and clinozoisite compositions, in coexisting crystals, according to [1].

The lowest temperature is accompanied by a zoisite – plagioclase transition, consistent with the final reaction: 3 anorthite + 2 calcite ⇔ 2 zoisite + CO_2. Plagioclase may result from the reaction CO_2 + 2 clinozoisite ⇔ 3 anorthite + calcite + H_2O.

The contamination of Li-rich residual magma by Fe and Mn transfer, gives rise to the emergence of triphylite-lithiophilite concentrations that under normal conditions would not occur. Contamination is also expressed by high Zn concentrations in zircon (maximum content observed, 1.52%) and the deposition of sulphides in oligoclase pegmatoids. The protolith contains exhalite with high contents of Zn and Mn that were remobilized by the intrusion of pegmatite magmas.

[1] Franz, G. & Selverstone, J. (1992) *Am Mineral.*, **77**, 631-642.

Compositional evolution of grossularite from leucotonalitic pegmatite Ruda nad Moravou, Czech Republic; EMPA and LA-ICP-MS study

Gadas, P.* & Novák, M.
Dept. of Geological Sciences, Masaryk University, Brno, Czech Republic (*pgadas@centrum.cz)

The zoned leucotonalitic pegmatite Ruda nad Moravou is characterized by high Ca-contents manifested by an abundance of plagioclase (An_{98-19}), epidote-group minerals including allanite-dissakissite, diopside and grossularite [1]. The latter is present in most textural-paragenetic units from the contact inwards: *G1* is almost monomineral, fine-grained, white zoned grossularite (core - Grs_{97-99} Adr_{1-3}, rim - Grs_{89-90} Adr_{8-9} Sps_{0-1} Prp_{0-1}) from the grossularite subunit, developed along the contact with host serpentinite; *G2* is microscopic, interstitial grossularite (Grs_{77-85} Adr_{11-16} Sps_{0-1} Prp_{0-1} Sch_{0-4}) from leucocratic subunit; *G3* is graphic intergrowths of pale brown grossularite + quartz (Grs_{73-86} Adr_{11-24} Sps_{1-2} Prp_{0-1} Sch_{0-4}) from coarse-grained granitic unit; *G4* is large crystals of colorless grossularite (Grs_{98-100} Adr_{0-1} Prp_{0-1}) at the contact of the blocky unit and quartz core. Grossularite is associated with plagioclase, quartz and epidote-group minerals (*G1*, *G2*). EMPA show compositional evolution from almost pure grossularite (*G1)* through Fe^{3+}-enriched (*G2* and *G3)* to pure grossularite *(G4)*. LA-ICP-MS study of the individual types of grossularite revealed distinct patterns of REE (Fig. 1), which exhibit similar patterns for Fe^{3+}-poor grossularite (*G1+G4*) and Fe^{3+}-enriched grossularite (*G2+G3*), respectively. Similar behavior was obtained also for V, Ni, Cr and Sn. Only concentrations of Ga, Zn and Hf increase during crystallization as well as Zr/Hf ratio.

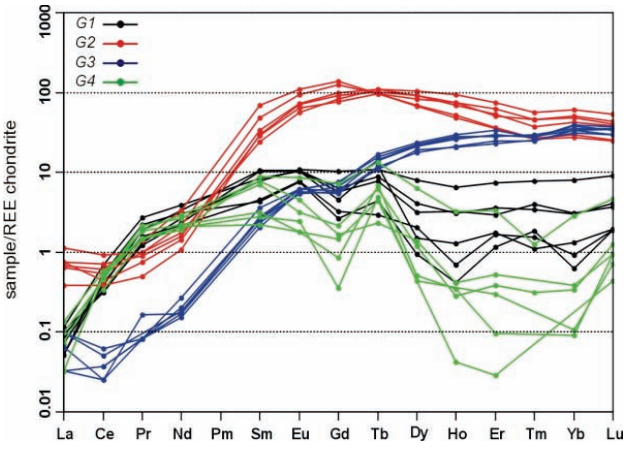

Fig. 1: REE contents of the individual grossularite types compared with chondrite [2].

Incorporation of most trace elements into the grossularite structure is controlled chiefly by crystal structural constraints – entering of Fe^{3+} into the B-site. The role of allanite-dissakissite seems low because *G1*, *G2* show lower La but Ce and LREE are similar or higher relative to *G3* and *G4*. Also the degree of fractionation manifested by evolution of plagioclase from anorthite to oligoclase has only minor importance on concentrations of trace elements except for Ga, Zn, and Ta.

[1] Novák, M. & Gadas, P. (2010) *Can. Mineral.*, submitted. [2] Boynton, W.V. (1984) in Henderson, P. (ed.) *Rare-Earth Element Geochemistry*. Elsevier, Amsterdam, 63-114.

Evolution of phosphates from the pegmatitic field of Giraúl, Namibe (Angola)

Gonçalves, A.O.[1], Fontan, F.[2], Alfonso, P.[3], Melgarejo, J.C.[4*] & Paniagua, A.[5]
[1]Dept. de Geologia, Univ. Agostinho Neto, Luanda, Angola
[2]Laboratoire de Minéralogie, CNRS-Université Paul Sabatier, Toulouse, France
[3]Dept. de Enginyeria Minera i Recursos Minerales, Universidad Politècnica de Catalunya, Manresa, Spain
[4]Dept. de Cristal·lografia, Mineralogia, Dipòsits Minerals, Universidad de Barcelona, Spain
([*]joan.carles.melgarejo.draper@ub.edu)
[5]Depto. Ciencias de la Tierra, Universidad de Zaragoza, Spain

The pegmatitic field of Giraúl (Namibe, Angola) is distributed around a leucogranite intrusion. It comprises 5 types of pegmatites that, from less to more evolved, are: type I (barren, intrabatholitic and grading to the leucogranite host), type II (barren, peribatholitic); type III (beryl-columbite); type IV (beryl-columbite-phosphate); type V (spodumene). With the exception of apatite, phosphates are found only in the 2 last types.

Phosphates in type IV pegmatites occur in all the internal zones. In border and wall zones blue apatite and rare triphylite are found, nearly completely replaced by secondary phosphates. The first intermediate zone contains skelethal triphylite crystals, up to 50 cm in lenght, completely replaced by ferrisicklerite, heterosite and alluaudite, in association with reddish microcline, quartz, albite, muscovite, yellow beryl and minor ferrocolumbite and zircon. However, these phosphates become an important volumetric component in the second intermediate zone, associated with reddish microcline, albite, quartz, muscovite, yellow beryl and ferrocolumbite. Phosphates have nodulous shape and blocky sizes, up to 3 m in diameter. The third intermediate zone is made up by white microcline, quartz, albite, muscovite and white beryl; montebrasite is the only phosphate found therein. Quartz-muscovite-elbaite veins crosscut and replace all the above units, and some montebrasite is formed during this stage.

Phosphates in type V pegmatites have a different mineral association. Blue apatite is found in the earlier zones, and amblygonite is widespread in the third intermediate zone, in asociation with spodumene, petalite, elbaite, beryl, pollucite, manganotantalite and members of the microlite group.

Supergene phosphates are poorly developed, owing to the dry climate from the Giraúl desert. The most common are jahnsite, rockbridgeite, lipscombite and mitridatite. Todorokite and cryptomelane are also produced during the late stages of weathering.

The ratio Fe/Mn is preserved during the triphylite-ferrisicklerite-heterosite replacement. On the other hand, there are no changes in the chemical composition of minerals of the heterosite-purpurite series among the different units in type IV pegmatites. This can suggest that the crystallisation of these phosphates buffers the ratio Fe/Mn during the crystallisation of these zones.

The F content in members of the montebrasite-amblygonite series increases from type IV pegmatites to type V ones. This F increase in phosphates is consistent with the F enrichment in other minerals, especially in members of the tourmaline group, and with the development of spodumene and petalite in the third intermediate zone in type V pegmatites.

On the other hand, a slight enrichment in F is observed from the early to the late units of both type IV and V pegmatites. This enrichment is congruent with the development of elbaite only in the late stages of crystallisation.

Sn-rich thortveitite intergrowth with xenotime-(Y): Y versus Sc fractionation in NYF miarolitic pegmatites at Baveno (Southern Alps, Italy)

Guastoni, A.[*] & Nestola, F.
Dept of Geoscience, University of Padova, Italy
([*]alessandro.guastoni@unipd.it)

The crystal-chemistry of both Sn-rich thortveitite $(Sc,Y)_2Si_2O_7$, and xenotime-(Y) $(Y,HREE)PO_4$ have been investigated by single crystal X-ray diffraction and WDS electron microprobe analysis to assess the activity of scandium and yttrium in NYF miarolitic pockets at Baveno. At this locality the crystallization processes in the pockets are controlled by alkaline supercritical fluids characterized by high contents of H_2O and volatiles elements (B, F, P). Fluoride complexes of scandium, phosphate complexes of yttrium and rare earths are interpreted to be responsible for the transportation and deposition of these incompatible elements once the crystallization of K-feldspar and albite occurred in the cavities. Xenotime-(Y), which forms intergrowth crystals with Sn-rich thortveitite, has crystal faces corroded; Sn-rich thortveitite shows no corrosion, but the core of the crystal is enriched with yttrium and depleted with scandium (Y_2O_3 up to 6.00 wt%, Sc_2O_3 up to 40.50 wt%), the rim depleted with yttrium and enriched with scandium (Y_2O_3 up to 1.6 wt%, Sc_2O_3 up to 44.70 wt%). An early crystallization of xenotime-(Y) is followed by corrosion due to circulation of F-rich fluids. A late crystallization of Sn-rich thortveitite occurs and at the early processes the yttrium enrichment at the core can be related to free Y ions activities liberated by surface corrosion of xenotime-(Y) [1-4].

[1] Flynn, R.T. & Burnham, C.W. (1978) *Geochim. Cosmochim. Ac.*, **42**, 685-701. [2] Gramaccioli, C.M., Diella, V. & Demartin, F. (2000). *Eur. J. Mineral.*, **12**, 795-808. [3] Pezzotta, F., Diella, V. & Guastoni, A. (2005) *Am. Mineral.*, **90**, 1442-1452. [4] Wood, S.A. (1990) *Chem. Geol.*, **88**, 99-125.

Columbite-group minerals in the Cruz del Rayo pegmatite dikes, SW Salamanca, Spain

Llorens, T.* & Moro, Mª.C.
Dept. of Geology, Faculty of Sciences, Salamanca University, Spain (*tllg@usal.es)

The Sn-W Navasfrías district is located in the southwestern part of Salamanca (Spain) and belongs to the Sn and W Variscan Belt of Western Europe. It was mined during the last century for cassiterite and wolframite from a group of intragranitic quartz veins and pegmatite dikes related to the Jálama batholith, a zoned, allochtonous and peraluminous granitic body [1].

There are abundant barren pegmatite dikes hosted by the border leucogranitic and aplitic facies of the Jálama batholith. They contain a scarce tin mineralization but a wide variability of Fe-Mn phosphate minerals depending on the host rock [2,3]. The most evolved granitic pegmatites of the Navasfrías district are hosted by pre-ordovician metamorphic rocks and belong to the Cruz del Rayo pegmatite field. These pegmatites strike N170°E, dip subvertically and have been grouped in two types of pegmatite bodies: on one hand, the pegmatite dikes of granitic composition are essentially constituted of quartz, microcline, albite and muscovite, with accessory apatite, alluaudite and mitridatite; and on the other hand, the greisen-like pegmatite dikes are formed of quartz, muscovite and albite, with abundant beryl and phosphates of the amblygonite-montebrasite series which are especially abundant at the inner zones of the bodies. Both pegmatite types show a more or less complex internal zoning and are affected by a Na-metasomatism which lead to the crystallization of a late albite-rich unit.

Cassiterite and minerals of the columbite group appear disseminated through the dikes, although there are some differences depending on the type of pegmatite bodies. The dikes with granitic-like composition are poorly mineralized, consisting mainly of cassiterite, which commonly includes strongly zoned columbite-(Fe) crystals, and locally tantalite-(Fe). However, the greisen-like pegmatite dikes display a strong mineralization with abundant cassiterite hosting columbite-(Mn) crystals, which display an oscillatory zoning and a Ta- and Mn-rich rim, although sometimes a reverse zoning pattern is present.

The primary minerals of the columbite group evolve from columbite-(Fe) in the granitic-like pegmatite dikes to Mn-rich compositions in the greisen-like bodies, as a consequence of the magmatic differentiation of the pegmatite-forming melts, which increases the F content of the melt. Nevertheless, the secondary assemblage shows a Ta enrichment in both types of dikes, with intermediate amounts of Fe and Mn, which is caused by the late Na-metasomatic replacement processes of the pegmatite dikes.

These fractionation trends and the slight degree of evolution of the columbite-group minerals of the pegmatite dikes, which is shown by a strong Fe enrichment and variable Fe and Mn contents, suggest that they belong to the rare-element class, beryl-columbite-phosphate subtype, in the classification of Černý [4].

[1] Ramírez, J.A. & Grundvig, S. (2000) *Lithos*, **50**, 171-190. [2] Llorens, T. & Moro, Mª.C. (2007) *Granitic Pegmatites: the State of the Art. Memórias*, **8**, 56-57 (abstr.). [3] Llorens, T. & Moro, Mª.C. (2008) *Macla*, **9**, 145-146. [4] Černý, P. (1992) *Appl. Geochem.*, **7**, 393-416.

Nb-Ta-oxide minerals in the LCT granitic pegmatites of La Canalita, SW Salamanca, Spain

Llorens, T.* & Moro, Mª.C.
Dept. of Geology, Faculty of Sciences, Salamanca University, Salamanca, Spain (*tllg@usal.es)

The La Canalita pegmatites in the Navasfrías Sn-W district, in Spain, are a group of Li-rich LCT rare-element pegmatites of the complex type, lepidolite-subtype in the classification of Černý [1], with high phosphorus contents, hosted by low-grade metamorphic rocks of the contact aureole caused by the intrusion of the Cadalso-Casillas de Flores batholith [2]. It consists of several dikes with a constant N130°E to N145°E direction and subvertical dipping of up to 1 m thick, 16 m in length and unknown depth that were mined during the forties and fifties for tin.

The pegmatite dikes of La Canalita show a regular pattern of symmetrical zoning from the outer to the inner parts of the dikes and are mostly composed of quartz, white mica, lepidolite and albite, the latter commonly of the "cleavelandite" habit, and subordinate microcline [3]. Topaz and montebrasite are accessory minerals, although occasionally they can be considered major phases, especially in the outer and intermediate zones of the pegmatite dikes. A fine-grained late unit shows a distinct layering formed of alternating purple bands with dominant lepidolite and quartz and of white albite bands.

The main ore mineral is cassiterite, which is abundant in almost all the zones of the pegmatite dikes but specially hosted by albite aggregates and the late unit. Abundant Nb- and Ta-oxide minerals are found related or not to the cassiterite crystals. A primary assemblage is formed of extremely Mn-rich columbite and tantalite, and microlite, the latter forming the host of columbite-(Mn) exsolution lamellae in the intermediate parts of the dikes.

The influence of metasomatic processes led to the formation of the lepidolite-albite late unit and the crystallization of a secondary assemblage consisting of tantalite-(Fe), tantalite-(Mn) and tapiolite-(Fe). U-rich microlite (up to 6 % wt. UO_2) is present in this assemblage, replacing tantalite.

Subsequently, the possible interaction of residual hydrothermal fluids with metamorphic fluids caused a partial greisen-like alteration of the pegmatite bodies and formed a second generation of microlite replacing tapiolite, with high Ca and Ta and low F contents.

The lack of a chemically suitable protolith in the surrounding metamorphic rocks, combined with the mineralogical paragenesis containing U-rich microlite and the composition of the Sn, Nb and Ta oxide minerals of the pegmatite dikes, suggest that the residual melts of the Cadalso-Casillas de Flores batholith, which migrated through fractures and were probably little influenced by host metamorphic hydrothermal fluids, are the most probable source of the melts forming the La Canalita pegmatite dikes.

[1] Černý, P. (1992) *Appl. Geochem.*, **7**, 393-416. [2] Hassan, A. (1996) *Estudio de los granitos uraníferos del macizo de Cadalso-Casillas de Flores (Salamanca-Cáceres, Spain)*. Universidad Complutense de Madrid. [3] Llorens, T. & Moro, Mª.C. (2010) *Can. Mineral.* (in press).

Trace elements behaviour in tourmaline and mica from the Pinilla de Fermoselle rare-element pegmatite (Zamora, Spain)

Roda-Robles, E.[1*], Gil-Crespo, P.[1], Pesquera, A.[1] & Torres-Ruiz, J.[2]
[1]Dpt. De Mineralogía & Petrología, Universidad del País Vasco (UPV/EHU), Bilbao, Spain ([*]encar.roda@ehu.es)
[2]Dpt. de Mineralogía & Petrología, Univ. de Granada, Spain

The rare-element Pinilla de Fermoselle, (PF) pegmatite, crops out in the apical part of a leucogranite body. It shows a clear non-symmetrical vertical zoning from the contact with the leucogranite to the contact with the metamorphic country-rocks. The pegmatitic facies evolve upwards from (1) the undifferentiated lower border zone (LBZ), with quartz, feldspars, muscovite, biotite and black tourmaline, through (2) the intermediate zone (IZ), with quartz, muscovite, zinnwaldite, black tourmaline and Fe-Mn phosphates, to (3) the highly evolved upper border zone (UBZ), with quartz, albite, lepidolite, Fe-lepidolite, elbaite and beryl.

Trace element analyses of representative samples of mica and tourmaline from the three zones of the pegmatite have been performed by Laser Ablation. In addition, micas from greisenization bodies inside the UBZ and from the associated leucogranites, plus tourmaline associated to hydrothermal veins occurring inside this granite, have been also analyzed for trace elements. Li, Be, Sc and Sr show a similar behaviour for the white and ferro-magnesian micas and tourmaline. Li and Be contents increase from the leucogranite to the most evolved pegmatitic facies (UBZ), whereas Sc and Sr contents decrease upwards. The rest of the trace elements have different behaviour depending on the mineral phase. In the case of the tourmaline, Nb and Ta contents increase upwards, with the increasing evolution degree of the pegmatite facies, whereas Zn contents decrease in this sense and Mn contents increase till intermediate degrees of evolution (IZ), to decrease again in the pinkish elbaite. Rb and Cs show the same trends for white and ferro-magnesian micas, with a gradual increase upwards. Ta and Tl increase from the leucogranite to the UBZ in the white micas, whereas Ga increases till the IZ and later decreases in the UBZ. In the case of the ferro-magnesian micas, Zn, Ga, Nb, Sn, Ta and W show a similar trend, with a gradual increase from the leucogranite to the IZ, and a final decrease in the UBZ. In general, the three mineral phases are depleted in REE. A slight decreasing trend is observed for the HREE in the pegmatitic white micas, whereas for the ferro-magnesian micas the LREE contents decrease with the pegmatitic evolution. White micas are also present in small greisenization bodies occurring in the UBZ. This late mica shows the highest contents in Li, Rb, Cs, Nb, Ta and Tl; and the lowest in Mn, Ga and Sr.

Regarding the distribution of these trace elements among the three mineral phases in the different facies where they occur together (leucogranite, LBZ, IZ and UBZ), Li, Rb, Cs, Mn, Nb, Ta and Tl are mainly partitioned into ferro-magnesian micas. Be, Sc, and W are partitioned into white micas, whereas REE are partitioned into tourmaline. In general, tourmaline is the poorest phase in Li, Rb, Cs, Be, Sc, Sr, Nb, Ta, W, and Tl contents; whereas white mica is the poorest in Mn, Zn and LREE contents. Ferro-magnesian micas are the poorest in Ga and HREE contents.

Chemical variation in micas and tourmaline is consistent with an internal evolution by crystal fractionation processes. Li, Be, Sr and Sc in micas and tourmaline may be indicative of the degree of evolution in the PF pegmatite. Other elements that may be used to establish the degree of evolution in this body are the Rb, and Cs for the micas; and the Nb and Ta for the white-micas and tourmaline. The transition metals Mn and W seem to be a good indicative of fractionation just in the ferro-magnesian micas.

Graftonite-triphylite-sarcopside intergrowths from the Palermo No. 1 pegmatite (New Hampshire, USA): textures and chemistry

Roda-Robles, E.[1*], Nizamoff, J.W.[2], Simmons, W.B.[2], Falster, A.U.[2] & Hatert, F.[3]
[1]Dept. De Mineralogía y Petrología, Universidad del País Vasco (UPV/EHU), Bilbao, Spain ([*]encar.roda@ehu.es)
[2]Dept. of Earth & Environmental Sciences, University of New Orleans, USA
[3]Laboratoire de Minéralogie, Université de Liège, Belgium

The Palermo No. 1 (P1) rare-element pegmatite (North Groton, New Hampshire, USA) belongs to the Grafton pegmatite field, where beryl-columbite-phosphate and beryl-phosphate pegmatites are the most evolved [1]. The P1 pegmatite is hosted by sillimanite-muscovite grade schists of the Devonian Littleton formation. The pegmatite is pod-shaped and mainly concordant with the host rocks. Major minerals in this body are quartz, feldspars, muscovite, phosphates and beryl, with minor schorl.

The core margin and core zones of the P1 pegmatite contain locally abundant phosphate pods (up to 5 m long and 2.5 m across). In these pods, close to 90 different phosphate phases (primary and secondary) have been identified. Triphylite is the most abundant primary phosphate in the pods. Periodically triphylite occurs intergrown with graftonite ± sarcopside. The most common intergrowth is an assemblage of graftonite containing coarse lamellae of triphylite (or ferrisicklerite and/or heterosite). Most lamellae are platy and form a single set that shows a quite uniform optical orientation, enclosed in monocrystalline graftonite, giving rise to a laminated parallel intergrowth. Less commonly graftonite and triphylite show a granular texture, probably as a result of deformation, where the triphylite lamellae are not as regular, and the single crystallographic orientation is lost. In both cases, the triphylite lamellae may in turn host lamellae of sarcopside.

All the phosphates analyzed belong to the Fe-rich end-members, with values for the Fe/(Fe+Mn) ratio in the range 0.57 to 0.73 for graftonite, 0.74 to 0.89 for triphylite, and 0.81 to 0.88 for sarcopside, with a clear correlation among the ratios of the different phases belonging to the same sample. The Ca content in graftonite varies considerably, from 8.64 to 13.23 wt.% CaO. Graftonite intergrown with triphylite + sarcopside is the richest in Ca, whereas no correlation has been found between the Ca contents of graftonite and its Fe/(Fe+Mn) ratio.

In relation to the distribution of Fe, Mn and Mg among coexisting phases, in all the cases, graftonite shows a strong preference for Mn, whereas both triphylite and sarcopside are Fe-rich, with a slight preference of sarcopside over triphylite for this element. Mg is clearly partitioned preferentially into triphylite, with graftonite being the Mg-poorest of the three phases.

Taking into account the textural and chemical features of the graftonite, triphylite and sarcopside from the P1 pegmatite, they all may be considered as primary phases. Exsolution processes from a disordered homogenous precursor most likely could have been responsible for the development of the intergrowths present. In the case of the graftonite-triphylite intergrowths, graftonite exsolved triphylite. In the case of the graftonite-triphylite-sarcopside intergrowths, a Ca-richer graftonite exsolved triphylite, which in turn broke down to triphylite with sarcopside lamellae.

[1] Nizamoff, J. (2006) *The mineralogy, geochemistry & phosphate paragenesis of the Palermo #2 pegmatite, North Groton, New Hampshire*. Master's Thesis, University of New Orleans, USA.

Tourmaline from the rare-element Berry-Havey pegmatite (Oxford County, Maine, USA): paragenesis and petrography

Roda-Robles, E.[1*], Simmons, W.B.[2], Nizamoff, J.W.[2], Pesquera, A.[1], Gil-Crespo, P.[1] & Torres-Ruiz, J.[3]
[1]Dept. de Mineralogía y Petrología, Universidad del País Vasco (UPV/EHU), Bilbao, Spain ([*]encar.roda@ehu.es)
[2]Dept. of Earth & Environmental Sciences, University of New Orleans, USA
[3]Dept. De Mineralogía y Petrología, Univ. of Granada, Spain

The Berry-Havey pegmatite (Poland, Androscoggin County, Maine, USA), belongs to the Oxford pegmatite field, which is proximal to the Sebago granitic batholith. The Berry-Havey is a highly evolved rare-element pegmatite, is enriched in Li, F, B, Be and P, and contains gem-bearing cavities. The pegmatite has a complex internal structure, with five different zones identified: border zone, two intermediate zones, core margin and core zone. Tourmaline is present in all of them, with textural and compositional differences among the different zones.

In the border zone tourmaline is scarce, occurring as very fine-grained prismatic black crystals, together with quartz, feldspars, muscovite, garnet and biotite. The mineralogy of the first intermediate zone is quite similar whereas the average grain size is larger. Graphic intergrowths of quartz and K-feldspar are very common in this zone. Locally, schorl may also be very abundant, appearing as black prismatic crystals up to 6 X 40 cm. In the second intermediate zone the quartz-K-feldspar graphic intergrowths are not so common. In this zone tourmaline is abundant and displays a characteristic texture. Many crystals exhibit a tapered black prism growing perpendicular to the pegmatite contacts, that increases in width in the direction of the core of the pegmatite. The thick end of the crystal is often "crowned" by black ± green tourmaline + quartz ± K-feldspar. The crystals, that show a sharp boundary between the black schorl and the greenish elbaite, are frequently broken, giving rise to a pull-apart structure. The next zone is the core margin, which is the most complex zone, not only because of its mineralogy, but also because of its textures. The main minerals of this zone are quartz, feldspars, micas from the muscovite-lepidolite series and tourmaline. The core margin also contains rounded Fe-Mn phosphate pods, montebrasite, beryl and greenish, fine–to–medium–grained elbaite crystals associated with medium–to–coarse book muscovite crystals. Lepidolite occurs as fine–grained irregular to rounded purple masses, close to the muscovite + green elbaite-containing areas. Small pinkish elbaite crystals have been observed inside the lepidolite masses. Prismatic crystals of watermelon tourmaline have also been observed in this zone, but most are replaced by clay minerals. Moreover, radial prisms of multicoloured tourmaline (elbaite) embedded in feldspars and quartz are also abundant. Finally, the quartz-K-Feldspar core represents the innermost zone of the pegmatite. Along the boundary between the core margin and core, pockets are common and may contain multicoloured gem–quality tourmaline, quartz, hydroxylherderite, cassiterite, cookeite, lepidolite, and beryl, among others.

The textural and chemical variations observed in tourmaline from the pegmatite, from the border zone to the core suggest an inward crystal fractionation model. The development of the quartz-K-feldspar and quartz-tourmaline graphic intergrowths could indicate undercooling of the pegmatite melt. The development of quartz-tourmaline crowns around elongated tourmaline crystals frequently showing pull-apart structures could be related to a sudden change in P conditions. Finally, the pockets located along the core margin and core zone of the pegmatite suggest elevated fluid activity during the last stages of crystallization of this pegmatite.

Hydrothermal synthesis, crystal chemistry, and stability of fillowite-type phosphates in the Na – Mn – Fe^{2+} - Mg – PO_4 system

Rondeux, M.[*] & Hatert, F.
Laboratory of Mineralogy, University of Liège, Belgium
([*]M.Rondeux@ulg.ac.be)

Fillowite [$Na_2CaMn_7(PO_4)_6$], johnsomervilleite [$Na_2Ca(Fe^{2+})_7(PO_4)_6$], and chladniite [$Na_2CaMg_7(PO_4)_6$] are Na-, Mn-, Fe- and Mg-bearing phosphate minerals which occur as primary phases in granitic pegmatites, in metamorphic rocks and in meteorites. Their crystal structure (space group *R*-3, a = 15.28 Å, c = 43.51 Å, Z = 18) is characterized by a hexagonal packing of three types of rods parallel to the c axis [1]. The rods are constituted by an alternation of five- to seven-coordinated sites containing Fe, Mn, and Mg, of six- to nine-coordintaed sites containing Na and Ca, of PO_4 tetrahedra, and of cation vacancies.

In order to understand the stability of fillowite-type phosphates, the $Na(Mn_{1-x}Fe^{2+}{}_x)_4(PO_4)_3$ system (x = 0, 0.25, 0.5, 0.75, 1.0)[2], as well as compounds with the $Na(Mn_{0.33}Fe^{2+}{}_{0.33}Mg_{0.33})_4(PO_4)_3$, $Na(Mn_{0.6}Fe^{2+}{}_{0.2}Mg_{0.2})_4(PO_4)_3$, $Na(Mn_{0.2}Fe^{2+}{}_{0.6}Mg_{0.2})_4(PO_4)_3$, $Na(Mn_{0.2}Fe^{2+}{}_{0.2}Mg_{0.6})_4(PO_4)_3$ starting compositions, were synthesized under hydrothermal conditions, between 400 and 700°C, at 1 kbar. Single-phase fillowite is obtained only for the $NaMn_4(PO_4)_3$ starting composition, between 400 and 700°C. The incorporation of iron and magnesium immediately provokes the crystallization of alluaudite [$Na_2(Mn,Fe^{2+},Mg)_2Fe^{3+}(PO_4)_3$] and of sarcopside [$(Fe^{2+},Mn,Mg)_3(PO_4)_2$], in association with fillowite in the Mn-rich part of the Mn-Mg-Fe diagram. In the Mg-rich part of the system, an assemblage alluaudite + hydrated alluaudite [$\square Na(Fe,Mn)Mg_2(PO_4)(HPO_4)_2$] + $(Mg,Mn,Fe)_2P_2O_7$ occurs at 400 and 500°C, and an assemblage alluaudite + $(Mg,Mn,Fe)_2P_2O_7$ occurs at 600 and 700°C. Finally, in the Fe-rich and central parts of this diagram occurs the alluaudite stability field.

The electron-microprobe analyses of fillowite-type phosphates show an decrease of the $Mg/(Fe_{tot.}+Mn+Mg)$ ratio, from 0.25 at 400°C, to 0.20 at 600°C, followed by an increase to 0.28 at 700°C. At 800°C, the Mg-richest fillowite-type phosphate has been observed, with a composition $Na_{2.14}(Mn_{4.90}Mg_{2.15}Fe^{2+}{}_{0.33}Fe^{3+}{}_{0.37})(PO_4)_6$.

The $Mg/(Fe_{tot.}+Mn+Mg)$ ratio of sarcopside increases from 0.25 at 400°C, to 0.39 at 500°C, and then decreases to 0.14 at 700°C. The composition of the Mg-richest sarcopside is $(Mg_{1.17}Fe^{2+}{}_{1.62}Mn_{0.21})(PO_4)_2$.

At high temperatures, the proportions of alluaudite-type phosphates significantly increase compared to experiments at lower temperatures. This feature probably results in an oxidation of iron, favoured by the increase of hydrogen diffusion through the gold capsule at high temperatures.

[1] Araki, T. & Moore, P.B. (1981) *Am. Mineral.*, **66**, 827-842.
[2] Rondeux, M. & Hatert, F. (2006) *Ber. Dtsch. Min. Ges., Beih. z. Eur. J. Mineral.*, **18(1)**, 111.

Hydrothermal alteration of Y,REE,Nb,Ta,Ti-oxide minerals from the Písek pegmatites, Czech Republic: a low-temperature As enrichment

Škoda, R.[1*], Novák, M.[1], Gadas, P.[1], Cicha, J.[2] & Heroldová, N.[1]
[1]Dept. of Geological Sciences, Masaryk University, Brno, Czech Republic ([*]rskoda@sci.muni.cz)
[2]Prácheň Museum, Písek, Czech Republic

Primary Y,REE,Nb,Ta,Ti-oxide minerals commonly underwent intensive hydrothermal alteration enhanced by their tendency to be metamict [1]. At the Písek pegmatites (beryl-columbite subtype with abundant tourmaline and accessory arsenopyrite and niobian rutile) primary "písekite" (an inadequately described Y,REE,Nb,Ta,Ti-oxide phase [2]) was found as relics, ~ 10-500 μm in size (Fig. 1) of several primary phases compositionally related to polycrase-(Y), samarskite-(Y) and fergusonite-(Y), respectively. These are typically hydrated and altered to a fine-grained mixture of numerous phases with complicated textural relations (Fig. 1). Newly formed monazite-(Ce), xenotime-(Y), zircon, ferrocolumbite, pyrochlore-group minerals, scheelite, uraninite, and pharmacosiderite were tentatively identified by EMP as well as several unidentified phases with unclear stoichiometry, some of them Sc-enriched.

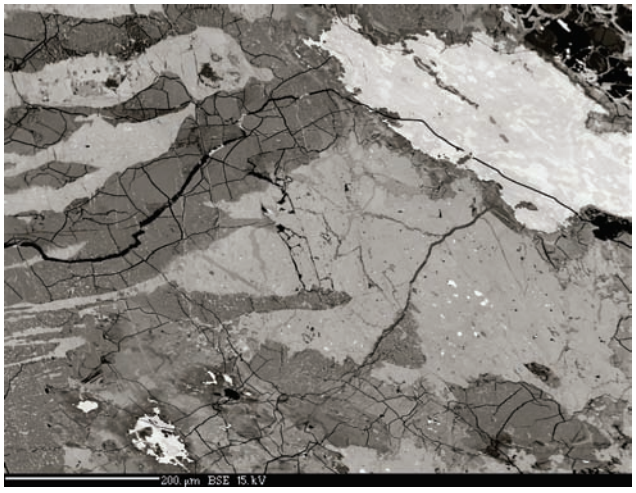

Fig. 1: "Písekite" relic (bright, right upper part) replaced by a mixture of several breakdown products (various shades of grey to bright).

Arsenic was determined as a minor constituent in "písekite" [2]; however, all our examined relics yielded As below the detection limit of EMPA. Elevated contents of As (up to 6.22 wt.% As_2O_5) were found exclusively in highly hydrated outermost portions of "písekite" grains locally associated with other secondary As-rich minerals e.g., metamict zircon and pharmacosiderite. Absence of As in relics of primary Y,REE,Nb,Ta,Ti oxides and its enrichment solely in the outer rims suggest that As was preferentially partitioned to arsenopyrite during the primary (late magmatic to early hydrothermal) stage of pegmatite crystallization. Exclusively during low-temperature hydrothermal alterations of arsenopyrite As appeared to be mobile and entered various metamict Y,REE,Nb,Ta,Ti oxides. Elevated As contents in the outermost parts of "písekite" grains are accompanied by strong depletion of REE and Y and enrichment of Si (up to 7.12 wt.% SiO_2) as well as P (up to 3.72 wt.% P_2O_5**)**.

Acknowledgements: This research was supported by project KJB301630801.

[1] Ewing, R.C. (1975) *Geochim. Cosmochim. Ac.*, **39**, 521-530.
[2] Bouška, V. & Johan, Z. (1972) *Lithos*, **5**, 93-103.

Relationship between clay mineralogy, fluid inclusions and K/Ar ages in the Triassic and Palaeogene hydrothermal alteration zones within the Variscan granite of the Velence Mts. (W-Hungary)

Benkó, Zs.[1*], Molnár, F.[1], Németh, T.[1], Pécskay, Z.[2] & Lespinasse, M.[3]
[1]Dept. of Mineralogy, Eötvös Loránd University, Budapest, Hungary ([*]benko.zsolt@ttmk.nyme.hu)
[2]Institute of Nuclear Research, Hungarian Academy of Sciences (ATOMKI), Debrecen, Hungary
[3]UMR CNRS, Université HP-Nancy 1, Nancy, France

The Variscan (Carboniferous) granite intrusion of the Velence Mountains (W-Hungary) has suffered intense argillic alteration in several zones. To determine the structural, temporal and spatial relationship, as well as the p-T conditions of the hydrothermal systems responsible for alterations, a detailed study of the hydrothermal clay mineral assemblages and mineralogical properties of clay minerals has been completed. The idea was that clay mineral assemblages as well as clay mineral properties (e.g. illite structure, kandite minerals) in hydrothermal alteration zones are useful for temperature estimation. Temperatures were compared with the results of fluid inclusion studies and were used as independent thermometers for pressure estimation. K/Ar radiometric age dating was performed on the illite phase to determine the temporal relationship of the alterations. Comparison of clay mineral assemblages, clay mineralogy, fluid inclusion data and K/Ar radiometric dates suggests that the superimposing hydrothermal alterations can be distributed in three groups:

1) Argillic alteration around the quartz-fluorite-base metal veins is composed of illite-kaolinite and smectite clay mineral assemblage and is regionally characteristic for the granite. Intensity of alteration increases towards to the mineralized NE-SW trending structural zones and towards the quartz-fluorite-base metal veins. Age of this type of alteration and thus of the syngenetic base metal veins is middle-late Triassic according to the results of K/Ar age measurements. Field evidence and mineralogical analysis prove that the clay mineral suites did not form simultaneously. Comparing the fluid inclusion data with the clay mineral thermometer the fluids started to cool down from 220°C at relatively low pressure (1 kbar). Cooling was accompanied by dilution of the hydrothermal fluids.

2) Alteration zones of Palaeogene age in the granite evolved in structurally controlled narrow zones in the eastern part of the granite, in the vicinity of Palaeogene subvolcanic andesite dikes cutting the granite. Alteration can be characterized by well-crystallized illite, thin quartz-stringers and silicification. Structural characteristics of illite indicates temperature of at least 220°C in accordance with the fluid inclusion data, measured on fluid inclusions trapped from a shallow level boiling hydrothermal system. K/Ar ages for illite scatter in a narrow time range between 29 and 32 Ma, indicating early-Oligocene age for the hydrothermal system, as well as for the andesitic magmatism.

3) In the broader vicinity of the illitic alteration zones, but also structurally related Palaeogene andesite dykes, illite and dickite were found. Their assemblage indicates 200-220°C temperature but a characteristic fluid inclusion assemblage cannot be connected to this alteration type. Radiometric ages vary in a very broad range between 200 and 50 Ma, depending on the location and the measured sample. Therefore it is assumed that this assemblage does not represent a third, individual hydrothermal event but can be interpreted as a transitional zone between the Triassic and the Palaeogene alteration zones.

Alpine (Cretaceous) very low- to low-grade metamorphism recorded on illite fraction from South Tisia (eastern Mt. Papuk, Croatia)

Biševac, V.[1*], Balogh, K.[2], Balen, D.[1] & Tibljaš, D.[1]
[1]Institute of Mineralogy and Petrology, Department of Geology, Faculty of Science, University of Zagreb, Croatia ([*]vabisevac@geol.pmf.hr)
[2]Institute of Nuclear Research, Hungarian Academy of Science, Debrecen, Hungary

Alpine very low- to low-grade metamorphism related to Cretaceous orogenesis has been investigated in the Slavonian Mts., Croatia. Samples belonging to the Psunj metamorphic complex (PMC), Radlovac metamorphic complex (RMC) and clastic-carbonate succession of the Late Permian to Early Triassic age i.e. Permian-Triassic sedimentary sequences (PTSS) were studied.

Kübler and Árkai indices of all analysed samples indicate high temperature anchizonal to epizonal conditions of thermal alteration (~300°C). The degree of thermal alteration tends to be constant in all measured samples implying that different complexes passed through and recorded the same event. Measurements of b_0-parametar of samples belonging to the RMC imply transitional low-medium pressure metamorphism. K-Ar ages measured on <2 μm fraction indicate Late Cretaceous very low-grade metamorphism of PTSS as well as Late Cretaceous overprint of older Paleozoic metamorphic rocks (PMC and RMC). No considerable systematic or gradual variation between the K-Ar age of <2 μm fraction and metamorphic indicators of analysed samples, regardless to the stratigraphy, was observed (Fig. 1).

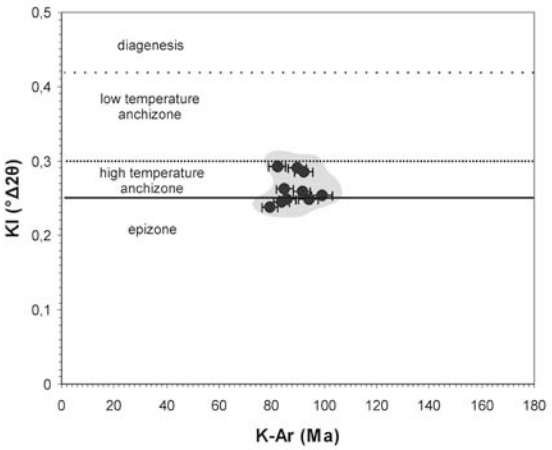

Fig. 1: Plot of KI values vs. K-Ar ages of <2 μm fraction.

All these data together with K-Ar ages measured on <2 μm fraction point to Late Cretaceous very low- to low-grade regional metamorphism related to the Austrian and/or Subhercynian phase of Alpine orogeny that were responsible for the main nappe-forming compressional events in the Pannonian Basin area and the Carpathians [1].

Metamorphic and geochronological evolution of the studied area is in good agreement with similar scenario for the surrounding area of Tisia, but also from ALCAPA (e.g. [2]).

[1] Árkai, P. et al. (1995) *Geol. Rundsch.*, **84**, 334-344. [2] Árkai, P. (2003) *Int. J. Earth Sci.*, **92**, 68-85.

The Arosa zone in Eastern Switzerland, the diagenetic to metamorphic pattern of a tectono-metamorphic mélange

Ferreiro Mählmann, R.[1,3,4*] & Giger, M.[2,3]
[1]Inst. für Angewandte Geowissenschaften, Technische Universität Darmstadt, Germany
([*]ferreiro@geo.tu-darmstadt.de)
[2]Dammweg 27, Thun, Switzerland
[3]Abteilung für Isotopengeologie, University of Bern, Switzerland
[4]Lehrstuhl für Geologie, Geochemie und Lagerstätten der Kohle und des Erdöls, RWTH Aachen, Germany

In the area of Arosa-Davos-Klosters (Eastern Switzerland) the different tectonic elements of the Arosa zone mélange e.g. the Austroalpine fragments, the mafic and ultramafic basement rocks as well as the matrix (oceanic sediments and flysch rocks) show a distinctively different metamorphic history and also a different climax („peak“) of alpine metamorphism. This is proved by a wealth of Kübler Index (KI) - vitrinite reflectance (VR) measurements and kinetic numerical modelling, bituminite reflectance, illitization indices (related to the smectite-illite reaction progress), K-white mica b-cell dimension determinations, index minerals, microprobe data as well as geo-chronological results.

Whereas the matrix sediments of the Arosa zone mélange are overprinted by a low anchizonal to high anchizonal metamorphism Lower Austroalpine fragments in the mélange and the adjacent Lower Austroalpine units (e.g. Tschirpen-Dorfberg nappe) were overprinted by a widespread syn-sedimentary burial and orogenic epizonal metamorphism. High anchizonal rocks are found in the Lower Austroalpine locally. Flysches at the hanging wall of a disconformity in the mélange zone show lower diagenetic thermal conditions.

At least six main metamorphic events can be recognized in the area of Arosa-Davos-Klosters:

i) A pre-orogenic event is recognized in the sediments at the base of the Silvretta nappe, typical for the Upper Austroalpine.

ii) The epizonal oceanic metamorphism observed in the close vicinity of oceanic basement rocks (e.g. pillow-basalts, peridotites of the South Penninic units) of the Arosa zone is another pre-orogenic process.

iii) Based on stratigraphic, tectonic and geo-chronologic considerations the overprint of lower structural Austroalpine fragments in the Arosa zone and the adjacent Lower Austroalpine nappes is attributed to the orogenic metamorphic processes during the Late Cretaceous.

iv) The thermal climax observed in the sediments of the Arosa zone can be bracketed into the time span between the Austroalpine Late Cretaceous (iii) event and the middle Tertiary event in the Middle Penninic (v) as well as the Oligocene "Turba phase". North of Klosters, in the northern part of our study area, the entire tectonic pile from the North Penninic flysches to the Upper Austroalpine is strongly influenced by a late Tertiary event (vi).

In the Arosa zone mélange an individual orogenic metamorphic event is evidenced and gives a new chance to resolve still not understood diagenetic-metamorphic versus deformation relations. By different KI-VR correlations we can distinguish 6 heating episodes in sedimentary rocks and 7 deformation cycles. This is well explained by the propagation of the Alpine deformation front onto the foreland units.

Origin and timing of brittle shear zones in the Mórágy Granite (Hungary): mineralogy and K-Ar geochronology of illite-rich fault gouges

Koroknai, B.[1*], Maros, Gy.[1], Kovács-Pálffy, P.[1], Kónya, P.[1], Viczián, I.[1], Balogh, K.[2] & Pécskay, Z.[2]
[1]Geological Inst. of Hungary, Budapest, Hungary
([*]koroknai@mafi.hu)
[2]Inst. of Nuclear Research, Hungarian Academy of Sciences, Debrecen, Hungary

The Mórágy Granite — exposed in the south-eastern hilly foreland (Mórágy Hills) of the Mecsek Mts. — represents an Early Carboniferous pluton (~340 Ma) in the Variscan crystalline basement (Tisza unit) of the Pannonian Basin. It is mainly composed of microcline megacryst-bearing biotite-monzogranites with mafic enclaves of predominantly monzonitic composition, hybride rocks and leucocratic dykes crosscutting all of these rocks. Following a Variscan regional metamorphism, during cooling associated with the formation of a regional, generally NW-dipping foliation and localized ductile shear zones, the pluton suffered intense brittle deformation in several phases. During these events — beside micro- and macro-scale individual fractures — numerous, map-scale brittle shear zones were also formed which display a remarkably large variety in orientation, width, internal structure as well as in mineralogical composition.

In this study we focus on the so-called core zone(s) of mature shear zones containing well-developed, partly foliated, brittle fault rocks as fault breccias, cataclasites and clay gouges concentrating the deformation into relatively narrow zone(s). Among them, (foliated) clay fault gouges are of special interest, since these represent not only the most intensively deformed brittle fault rocks, but also the products of syntectonic fluid/rock interaction. The analyzed gouge samples contain illite/smectite + chlorite + palygorskite + kaolinite + quartz + K-feldpar + plagioclase + calcite + dolomite + hematite + goethite assemblage with highly various ratios of the individual minerals. Clay minerals and chlorite are clearly new phases, formed at the expense of feldspars and mafic minerals of the original granitoid protolith. According to detailed XRD analyses, the polytypic variety of illite in clay gouges containing illite in considerable amount is almost exclusively 1M, suggesting hydrothermal origin of illite. In some samples minor amounts (<10 wt%) of $1M_d$ and/or $2M_1$ polytypes also occur. The $1M_d$ polytype may represent the low-T alteration product of the 1M hydrothermal illite, whereas the $2M_1$ polytype presumably display inherited component from primary magmatic biotite and/or metamorphic muscovite. The FWHM (full-width-at-half-maximum) values of 1M illite are mostly higher than 0.73 Δº2θ), but another group with significantly lower values (0.51–0.61 Δº2θ) is also present. The higher values of the first group probably reflect the mixed-layer structure (illite/smectite) of the analyzed phases and occasionally additional smectite as well, whereas the second group represents a discrete illite structure. K/Ar dating of illite-rich fine fractions (<10, <2, <1 μm) resulted in strongly scattered Mesozoic ages (Middle/Late Triassic–Late Cretaceous). Considering various mineralogical/structural criteria (amount of I/S, smectite, other, „disturbing” phases, as well as the FWHM values), we conclude that the oldest (Triassic–Early Jurassic) and presumably the youngest (Late Cretaceous) ages seem to represent indeed the time of important brittle tectonic activities accompanied with syntectonic fluid flow. The Middle Jurassic and Early Cretaceous ages might also indicate real tectonic events, if one regards the considerable amounts of illite/smectite and smectite in these samples as cogenetic phases with hydrothermal illite (and not as alteration products of it). However, further detailed investigation is needed to verify this hypothesis.

Two types of illite with different chemical composition in Upper Riphean shale, the Zil'merdak Formation (South Urals)

Zaitseva, T.S.*, Gorokhov, I.M., Kuznetsov, A.B., Melnikov, N.N., Konstantinova, G.V, Turchenko, T.L. & Kutyavin, E.P.
Institute of Precambian Geology and Geochronology, RAS, St.Petersburg, Russia (*tatiana.s.zaitseva@gmail.com)

Precambrian argillaceous rocks often contain mixtures of non-cogenetic illite minerals with different crystallochemical and isotope characteristics. The end-members of these mixtures could be formed at different stages of lithogenesis.

Shale samples were collected from the two sections of the Upper Riphean Zil'merdak Formation (Bakeevo village and Minyar) spaced by 200 km. The <2-μm fractions of these samples were separated into 1-2, 0.6-1, 0.3-0.6, 0.2-0.3 and 0.1-0.2 μm subfractions (SF). SFs were leached with NH_4OAc to remove mobile Sr adsorbed on the surface and located in interlayer positions of clay particles, or incorporated into the soluble accessory minerals such as carbonates and phosphates. SFs were studied by the XRD technique, and concentrations of K, Rb, Sr and the Sr isotope composition were determined in the residues after leaching. All the SFs in both samples are dominated by illite, an admixture of chlorite is no more than 5-10 per cent.

The 0.1-0.2 and 0.2-0.3 μm SFs of the sample from the Bakeevo section contain $1M_d$ illite, the 0.3-0.6 and 0.6-1 μm SFs contain 1M-$1M_d$ illite. A small admixture of $2M_1$ illite occurs only in coarser SFs (0.6-1 and 1-2 μm). The SFs of the sample from Minyar section also consist of illite. $1M_d$ illite is abundant in finer SFs (0.1-0.2 and 0.2-0.3 μm), whereas 1M illite with some amount of $2M_1$ dominates in coarser SFs (0.3-0.6 and 0.6-1 μm). Illites in all the SFs of both samples have high CIS values (Crystallinity Index Standard) and comply with the zone of diagenesis.

Table 1: XRD and chemical data for fine subfractions of the Zil'merdak shale

SF, μm	CIS	I_{002}/I_{001}	K, %	K/Rb	$^{87}Sr/^{86}Sr$	$^{87}Rb/^{86}Sr$
# Bakeevo						
0.1-0.2	1.63	0.46	6.13	254	1.2039	62.26
0.2-0.3	1.57	0.39	6.20	254	1.1491	52.98
0.3-0.6	1.38	0.36	6.11	243	0.9223	21.54
0.6-1	1.17	0.25	5.50	235	0.8506	11.71
1-2	0.95	0.25	5.15	228	0.8282	8.915
# Minyar						
0.1-0.2	0.92	0.40	5.81	225	1.4653	80.29
0.2-0.3	0.80	0.28	5.93	235	1.3615	67.43
0.3-0.6	0.80	0.36	5.56	234	0.8999	17.73
0.6-1	0.74	0.38	4.65	215	0.8397	9.898
1-2	0.60	0.40	4.21	212	0.7854	5.358

These relationships together with the XRD data suggest that the silicate component in SFs includes a mixture of two possibly non-cogenetic illite end-members with different chemical composition. In addition, the linear alignment of the residue data points for the SFs of different size in both the $^{87}Rb/^{86}Sr$ - $^{87}Sr/^{86}Sr$ and the 1/Sr - $^{87}Sr/^{86}Sr$ diagrams provides a convincing proof of the two-component mixing systematics.

Acknowledgements: This study is a contribution to Programme No. 4 of the Earth Sciences Branch of the Russian Academy of Sciences. The financial support of the RFBR (grant 09-05-00877) is acknowledged.

Clay minerals as climatic proxies, possibilities and limitations

Deconinck, J.-F.
Laboratoire Biogéosciences UMR/CNRS 5561, University of Burgundy, Dijon, France
(jean-francois.deconinck@u-bourgogne.fr)

In sedimentary geology, clay minerals have been widely used to reconstruct palaeoclimates as it has been shown that their latitudinal distribution in modern soils depends on climatic conditions. Latitudinal distribution also occurs in marine sediments deposited in oceans, thus allowing clays from old marine sediments to be used for palaeoclimate studies. These include many techniques, the most widely used being the determination of stable isotope ratios measured on carbonates and/or phosphates that give an idea of oceanic temperatures, but few proxies except clay minerals can be used to estimate moisture which is the other main parameter of climate. The combination of stable isotopes and clay mineral studies in very fruitful, as the two main climatic parameters can be associated for the same period.

The interpretation of clay mineral assemblages in terms of climate is possible only if burial diagenesis is negligible, generally when the total burial depth is estimated to be less than 1500m. The occurrence of smectite and/or I/S R0 in the sedimentary successions indicates weak diagenetic influences but additional data on T_{max} measured on organic matter can be very useful to evaluate the diagenetic influences. Practically, in most sedimentary basins it is difficult to identify a reliable climatic signal in sediments older than the Jurassic.

In porous sedimentary rocks (sandstones or dolomites), the occurrence of authigenic clay minerals (kaolinite and chlorite) is common and should be taken into account in the interpretation of clay assemblages. Generally, strong relationships between lithology and clay assemblages reveal the occurrence of authigenic clays.

Palaeoclimatic studies should also be based on many sections originating from different sedimentary basins, because strong differences in clay mineral assemblages are often encountered from one section to another either because of differential settling processes or because of different provenances for clay minerals. Therefore a compilation of clay mineral data originating from coeval sediments is necessary.

Clay minerals must originate from the erosion of weathering profiles contemporaneous to sedimentation. This condition is rarely obtained as clays are often reworked from old sedimentary rocks cropping out on continental areas. Despite all these limitations, we present several examples from Meso-Cenozoic successions showing the possibility of using clay minerals as a palaeoclimatic tool in association with other proxies, but also some examples showing misinterpretations of clay mineral assemblages either because of diagenesis, authigenic processes or reworking from old rocks.

Cretaceous-Paleocene-Eocene sedimentation in Arctic Ocean: results from the clay minerals investigation (IODP-ACEX, 302 data)

Krupskaya, V.[1,2*], Krylov, A.[3], Garshev, A.[2] & Sokolov, V.[2]
[1]Institute of Geology of Ore Deposits, Petrography, Mineralogy and Geochemistry (IGEM RAS), Moscow, Russia ([*]vi.krupskaya@gmail.com)
[2]M.V.Lomonosov Moscow State University, Moscow, Russia
[3]I.S.Gramberg All-Russian Research Institute for Geology and Mineral Resources of the World Ocean (VNIIOkeangeologia), St. Petersburg, Russia

Arctic Ocean's influence on the Earth climate is difficult to underestimate. Evolution of climatic periods of the planet is encrypted in the sedimentary section of the Ocean and can be reconstructed through a detailed study of the sediments composition. Present work is based on the materials obtained from the ACEX-IODP Leg 302 drilling on the Lomonosov Ridge, Central Arctic Ocean. Clay fraction of the Campanian, Paleocene and Eocene sediments sampled from the depths of 200-400 m below sea floor was studied with the following methods: X-ray diffraction of bulk and clay samples, scanning electron microscopy, infrared spectroscopy in the near and medium field, and thermal analysis. Based on these data, as well as published data on paleontology and stratigraphy [1,2], it is possible to study the history of the basin development in the Cretaceous-Paleocene-Eocene time including the Paleocene-Eocene Thermal Maximum (PETM), Early Eocene Climate Optimum (EOCO) and Eocene Thermal Maximum (ETM2). Each of these events, as well as the intervals between them are characterized by various associations of clay minerals and the amount of amorphous silica of different origins and different characteristics of clay minerals structure and morphology, which are interpreted as results of different conditions of weathering and transport. Based on experimental data and published materials [2,3], 7 major stages of sedimentary basin evolution in Cretaceous-Paleocene-Eocene time were distinguished:

1. Around 80 Ma (Campanian) – illite-kaolinite association, transport and deposition of material from the water flow of high density – neritic warm humid conditions. 2. ~55 Ma – PETM – smectite association, traces of transportation of sedimentary material, shallow warm basin. 3. ~ 53 Ma – ETM2 – kaolinite-chlorite-illite association, kaolinitization. 4. ~ 52 Ma – EOCO – illite-smectite association, the content of clay minerals not more than 5-10%, large-scale processes desilication, amorphous silica dominant in sediments – continental (probably soil) conditions in a warm climate. 5. ~ 49 Ma – Azola phase – smectite formation in shallow fresh water channels – continental conditions. 6. ~ 46.5 Ma – Early-Mid Eocene Cooling – smectite-illite association, the content of clay minerals 10-30%, the biogenic silica dominant. 7. ~ 44.5 Ma – high variation of clay minerals, due to drastic changes in the supply of terrigenous clay material under the seasonal ice conditions.

After that surface of Lomonosov Ridge was raised and information about sediments period from 44.5 till 22 Ma was lost.

Acknowledgements: This work was partially supported by grant of Russian Foundation for Basic Research #10-05-01034a.

[1] Backman, J. & Moran, K. (2009) *Cent. Eur. Geosci.*, **1(2)**, 157-175. [2] Sluijs, A. et al. (2006) *Nature*, **441**, 610-613. [3] Brinkhuis, H. et al. (2006) *Nature*, **441**, 606-609.

Clays and authigenic minerals composition on the glacigenic and bedrock contact zone

Lūse, I.[1*], Karpovičs, A.[2], Segliņš, V.[2], Stunda, A.[3] & Randers, M.[2]
[1]Institute of Soil and Plant Sciences, Latvia University of Agriculture, Jelgava, Latvia ([*]Ilze.luse@llu.lv)
[2]Faculty of Geography and Earth Sciences, University of Latvia, Riga, Latvia
[3]Riga Biomaterials Innovation and Development Centre, Riga Technical University, Riga, Latvia

Origin of authigenic minerals in the Pleistocene and modern glacigenic and underlying sediments over the world is known and studied long time. Many scientists (e.g. Lavrushin & Golubiev [1], van der Meer et al. [2]) relate formation of the authigenic minerals in the glacial environment to glacial dynamics, bed material deformations and water implication on the sediments. New formed minerals in these conditions on the sediments contact zones are considered as sensitive paleo-environmental indicators.

Aim of this study was clarify possible authigenic minerals in tills from Latvia for future paleoenvironmental reconstructions. Four geological sections in Latvia were analyzed in details. The study sites are situated on the different last glaciation implication zones – the eastern, western and central parts of Latvia and all selected sites has real and visible recognizable contact zone.

Glacigenic (Weichselian) and underlying illitic clayey (Upper Devonian and Upper Pleistocene glaciolacustrine) sediments were analyzed with x-ray powder diffraction (XRD) method. Clay mineral diagnostic was performed on textured samples with chemical treatment, but untextured samples were used for quantitative analysis applied by Quanto software. Scanning electron microscopy (SEM) was used to verify identified minerals and their morphological studies.

Besides several authigenic minerals like calcite and gypsum in the clay sized fractions were recognised also primary minerals – quartz, hematite, feldspars, and secondary minerals – calcite, dolomite and clay minerals illite, kaolinite, smectite. The authigenic minerals mostly are found in the < 0.4 μm fraction, because the differences in the mineral composition do~~es~~ not indicate only mechanical material mixing as in the fractions < 2 and < 1 μm. Calcite was recognized in all clay fractions in all samples from the contact zones of studied sediments. Amount of calcite increase in the fractions < 1 μm and < 0.4 μm, but in the fraction < 2 μm variety was insignificant. The calcite amount increases until 16% in samples which were taken 15 cm above the sediments contact zone. Gypsum amount increase on the sediments contact zone was recognized in fraction < 0.4 μm in the geological section from the western part of Latvia. Clay mineral composition is different between studied geological sections and those variations at the section are not systematically, just illite quantity decrease with authigenic minerals increase in the < 0.4 μm fraction.

Observed calcite and gypsum amount increase in the clayey bedrocks and till contact zone can be explained with settling in the subglacial conditions or with groundwater activity in the postsedimentation time.

Acknowledgements: This work has been supported by the European Social Fund within the project „Support for the implementation of doctoral studies at Latvia University".

[1] Lavrushin, U.A. & Golubiev, U.K. (1980) *Karbonaty w ocnovnych morenach plejstocenovych materikovych oledeneni. Precesy Kontinentalnovo Litogeneza*. Nauka, Moskva. [2] van der Meer, J., Menzies, J. & Rose, J. (2003) *Quaternary Sci. Rev.*, **22**, 1659-1685.

The influence of allophane and palagonite appearance on the unfrozen water content in the frozen volcanic ashes

Motenko, R.G., Kuznetsova, E.P.*, Vigasina, M.F. & Melchakova, L.V.
Lomonosov Moscow State University, Moscow, Russia
(*geotap@gmail.com)

Kamchatka and Iceland are the subject areas of very few geocryological studies. All the physical and mechanical properties of the frozen grounds and most of geocryological processes in the cryolithozone are predetermined by the unfrozen water content.

Volcanic ashes of different ages and compositions have been collected from the Kluchevskaya volcano group in Kamchatka (№1-8) and in the south of Iceland (№9). Ash samples had different ages (Table 1).

Unfrozen water content (W_w, %) in the Kamchatka ashes (at -5°C) is change from 0 to 11%; and in the Iceland ash it is 3.5 % [1]. Hygroscopic water (W_g, %) is different for all samples too (table 1).

The unfrozen water content in the studied ashes is connected with the transformation of volcanic glass and the appearance of clay minerals that is presumably controlled by the duration of alteration.

The samples were analyzed by IR-spectroscopy (IR-Fourier spectrometer FSM-1201) in order to determine their mineralogical composition [2]. As results, it was found that the sample № 1 was the waterless allophone, the samples № 2, 5, 6, 7 – were opal, № 3, 4, 8 – were allophanes with the various water contents and the sample № 5 – palagonite [3].

The thermal behavior of the allophanes and the palagonite was studied by DTA and TGA techniques on a Q-1500 D derivatograph (Hungary). The thermal study showed that the mass (W_{term}, %) loss depends directly on the ages of the investigated samples (Table 1).

Table 1: The results of water studies in the volcanic ashes

№	W_{term}* %	Age, years	Glass composition	W_g* %	W_w* %
1	0	35	waterless	0	0
3	3.8	1500	allophane	1.24	2
4	6.2	2000	allophane	4.3	10
8	16.8	8500 –9000	allophane	7.3	10
2	0.6	35	opal	0	0
5	3.1	2500	opal	1	1.1
6	4.4	7000	opal	1.32	2
7	6.7	7000	opal	2.52	3
9	11.6	15000-150000	palagonite	4.71	3.5

*Comment: W_{term} – the water amount, mass. %; W_g, W_w – accordingly the gyroscopic humidity and humidity that conform to unfrozen water content (with respect to dry ground mass), %

[1] Motenko, R.G. & Kuznetsova, E.P. (2009) *Proc. of the 8th Internat. Symp. on Permafrost Engineering*, China, 518-521. [2] Kuznetsova, E.P. et al. (2009) *Bull. Sect. Earth Sci. RAS*, **1(27)**, 83. [3] Wenshi, P. (1982) *IR-spectra of minerals.* Science, Beijing.

Geochemistry of the hydrothermal dickite from Jedlina Zdroj (Lower Silesia, Poland): Fe^{3+}

Krstić, N.S., Đorđević, D.M.* & Premović, P.I.
Laboratory for Geochemistry, Cosmochemistry & Astrochemistry, University of Niš, Niš, Serbia
(*dragance73@yahoo.com)

Geochemical analysis for Fe has been made on a representative sample of the dickite-rich hydrothermal clay from Jedlina Zdroj. The mineralogy of the sample is comparatively simple, dickite being the principal component (>90 wt% of total sample), with lesser amounts of goethite and barite. Inductively coupled plasma-optical emission spectrometry (ICP-OES) measurements of the products of subsequent chemical treatments indicate that most of Fe (ca. 97 wt% of total metal) reside in the dickite (Table 1). Electron spin resonance shows that a part of Fe in the dickite structure is in the form of Fe^{3+} ions. A substantial part of these ions (as well as of Fe in the dickite matrix) was probably contained in the original hydrothermal dickite-forming solution.

Table 1: Geochemical concentrations of Fe [ppm][a] in Jedlina Zdroj dickite sample from selective leaching experiments

Fraction	Sediment (±5 wt%)	Fe (ppm)
Acetate buffer	2.0	≤1[b]
Cold-HCl	5.0	3750
Boiling-HCl	2.0	5200
Dickite	91.5	1900
Insoluble residue	0.0	-
Total sample	100.5	2030[c]

[a]Determined by ICP-OES. [b]Detection limit of ICP-OES employed. [c]Obtained by summation of fractional Fe concentrations.

From geochemistry of Fe^{3+}, it is deduced that the oxidation potential (Eh) and H^+ concentration (pH) of the solution during the formation of dickite from the Jedlina Zdroj were approximately >0.45 V (highly oxygenated) and 0-4 (highly acidic), respectively (Fig. 1).

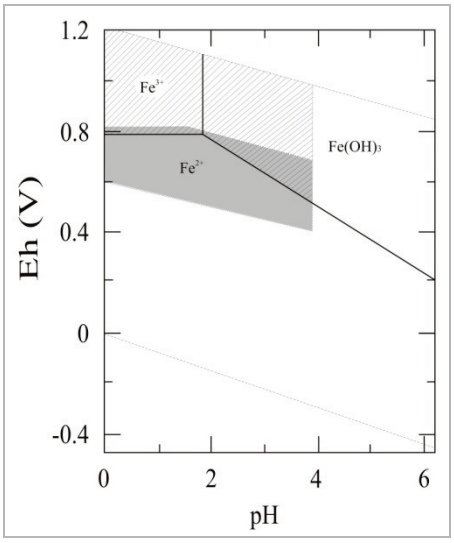

Fig. 1: Eh-pH diagram for iron species in solution at 300 K/l atm. The assumed total Fe concentration is 200 ppm. The shaded area represents Eh/pH region of the hydrothermal waters [1]. Probable physicochemical conditions of the crystallization of dickite from Jedlina Zdroj are represented by the hatched area.

[1] Kraynov, S.R. & Ryzhenko, B.N. (1992) *Geochem. Int*., **29**, 1-8.

Hydrothermal kaolin minerals and smectite occurrences in the Gedikler area (Uşak, western Anatolia, Turkey)

Erkoyun, H.* & Kadir, S.
Dept. of Geological Engineering, Eskişehir Osmangazi University, Eskişehir, Turkey (*herkoyun@ogu.edu.tr)

The Gedikler kaolins and coexisting alteration minerals developed within two Pliocene units: the Ahmetler Formation and Beydağı volcanites. The Ahmetler Formation is made up of the Gedikler member, comprising siltstone, claystone and tuffite that formed in a lacustrine enviroment. The Beydağı volcanites, laid down by volcanic activity in the Pliocene, comprise andesitic lava, tuff and agglomerate, which periodically fed the Ahmetler Formation.

These units have been studied via petrography, reflected-light polished-section microscopy, X-ray diffractometry (XRD), differential thermal analysis-thermal gravimetry (DTA-TG), scanning electron microscopy (SEM-EDX), IR spectroscopy (FT-IR) and geochemical analysis. Plagioclase and K-feldspar are argillized, feldspar is sericitized, biotite and hornblende are opacitized, groundmass is argillized and Fe-oxide/hydroxide phases also developed in the volcanic units.

In Gedikler area, kaolin minerals coexist with illite, smectite, gypsum, barite, quartz, calcite, feldspar, hornblende, dolomite, pyrite and traces of alunite (jarosite locally). Infrared spectral analysis exhibits two peaks at 789 (FeFe-OH) and 430 cm^{-1} (Si-O-Mg), confirming partial substitution of octahedral Al by Fe and by Mg. SEM studies reveal that kaolin occurs as rod-like halloysite and platy kaolinite, and that smectite flakes cover degraded volcanic material. Geochemically, the volcanic rocks plot within the trachyandesite and rhyodacite/dacite fields. SiO_2 contents vary from 43.55 to 66.02%, and Al_2O_3 contents are in the range of 13.12-20.86%. SiO_2/Al_2O_3 ratios decrease from fresh rock samples to pure kaolin samples. High Fe_2O_3 (0.74-14.56%) values indicate alteration and the presence of iron-oxide/hydroxide phases. High K_2O (1.03-5.26%) and lower MgO (0.10-2.28%) values reflect the presence of illite, feldspar and smectite. Na_2O and K_2O, which are highly mobile, are extensively removed from all alteration zones, reflecting plagioclase breakdown. Depletion of Mg suggests the degradation of biotite and hornblende during hydrothermal alteration. All of the samples are enriched in large-ion lithophile elements (LILE) and light rare-earth elements (LREE), and depleted in high-field-strength elements (HFSE) and heavy rare-earth elements (HREE) with respect to primitive mantle and chondrite, and are characterized by distinct negative Eu anomalies. These geochemical signatures reflect fractional crystallization and alteration of feldspar.

Clay mineralogy of the hydrothermal alteration around Sındırgı, Balıkesir, Turkey

Kocabaş, C.[1*], Papoulis, D.[2] & Çolak, M.[1]
[1]Dept. of Geological Engineering, Dokuz Eylül University, İzmir, Turkey (*cumhur.kocabas@deu.edu.tr)
[2]Dept. of Geology, University of Patras, Greece

Hydrothermal alteration hosted by Miocene calc-alkaline volcanism related to extensional tectonic activity is widespread in Western Anatolia. Simav Graben is the latest product of this tectonic regime and includes a wide range of ore deposits and hydrothermal mineralizations.

One hundred samples collected from the surface and cores in the alteration zones of Simav Graben were investigated by XRD, SEM and FTIR. Two types of hydrothermal alteration zones were identified: 1) hydrothermal alteration related to quartz porphyry intrusions and 2) hydrothermal alteration related to epithermal quartz veins. Close to the quartz porphyry intrusion the dominant clay mineral is mixed layer illite/smectite while at a distance of about 20 m dickite is dominant and the mixed layer clay minerals are absent. Secondary quartz and alunite are the non-clay minerals in each zone. The clay mineral sequence from inner to the outer parts of the quartz veins is as follows: kaolinite + illite→ mixed layer illite/smectite + kaolinite→ smectite. Quartz and feldspars of volcanic origin accompany the clay mineral paragenesis.

The presence of quartz-dickite indicates the formation temperature of about 160-200°C, while the transformation of illite/smectite to illite occurs at ~230°C [1,2]. The assemblage kaolinite + illite indicates a temperature of around 200-250°C. It is therefore concluded that the temperature of the hydrothermal fluids was ~200°C in the region.

Hydrothermal alteration is controlled by a fault system, which allows intrusion of quartz porphyry dikes and quartz veins. The presence of alunite and dickite is indicative of an acidic sulfate alteration [3]. On the other hand, alteration around the quartz veins indicates acid to intermediate type of alteration [1].

[1] Reyes, A.G. (1990) *J. Volcanol. Geoth. Res.*, **43**, 279-309. [2] Velde, B. (1995) *Origin and mineralogy of clays*. Springer-Verlag, Heidelberg. [3] Choo, C.O. & Kim, S.J. (2004) *Clay. Clay Miner.*, **52**, 749-759.

Mysterious silver microparticles of the Cretaceous-Paleogene boundary Fish Clay (Stevns Klint, Denmark)

Ilić, B.S.*, Đorđević, N.R. & Premović, P.I.
Laboratory for Geochemistry, Cosmochemistry and Astrochemistry, University of Niš, Serbia
(*bucabule@yahoo.com)

Instrumental neutron activation analysis (INAA) showed the Ag concentration in the Fish Clay is about 1.0 ppm and that its carbonate-free fraction contains about 2 ppm. Alvarez et al. [1] determined the Ag concentrations in the whole Fish Clay (1.2 ppm) and in its carbonate-free fraction (3.5 ppm). In order to evaluate the overall (terrestrial or extraterrestrial) source of Ag in the smectite of the Fish Clay, we compared these data with Ag contents in normal seawater, sediments, soils, igneous rocks (basalts having the highest content), upper continental crust, mantle and chondrites (Table 1). The Ag content of the Fish Clay is much higher than in seawater, sediments, soils, igneous (basaltic) rocks, crust or mantle. Thus, it is likely that none of these sources were capable to supply Ag to the Fish Clay. The concentration of Ag in the Fish Clay is approximately twenty times higher than its average content of chondrites. Consequently, it is likely that most of Ag in the Fish Clay is of the terrestrial origin.

Table 1: Ag content of the Fish Clay and potential suppliers of Ag

Rock	Ag [ppb]
Fish Clay	2×10^{3} (this work)
Seawater	2×10^{-3}
Sediments	120
Soils	700
Igneous (basaltic) rocks	37-110
Upper continental crust	530
Mantle	2.92-19
Chondrites	97-107

We also report here a new find of the occurrence of micrometer-sized silver (Ag) particles in the red layer of the Fish Clay that appear to have been embedded into the biogenic calcite matrix. 100 of these microparticles (AgMPs) were hand-picked under a binocular stereomicroscope. Energy dispersive X-ray analysis (EDS) analysis (Fig. 1A) indicates that these microparticles are composed of pure silver (>99 % of the total weight).

Stereomicroscopy shows that the AgMPs are shiny black or light brown. SEM images show that their shapes are irregular and predominantly rounded with rugged surfaces that often contain a few pits and voids (Fig. 1B). Aggregates of numerous AgMPs are spherical (Fig. 1C), and some of them exhibit dendritic textures (Fig. 1D).

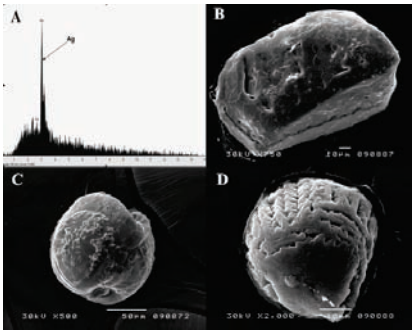

Fig. 1: Ag microparticles from the red layer of the Fish Clay: (A) EDS spectrum; and SEM micrographs of samples: (B) rounded; (C) common spherical; (D) spherical with dendritic surface texture.

[1] Alvarez, L.W. et al. (1980) *Science*, **208**, 1095-1108.

Geochemistry of the Cretaceous-Paleogene boundary (Fish Clay) at Stevns Klint, Denmark: Au in the basal black marl

Krsmanović, M.M.*, Stanković, M.N. & Premović, P.I.
Laboratory for Geochemistry, Cosmochemistry and Astrochemistry, University of Niš, Serbia
(*milena.krsmanovic@yahoo.com)

The Fish Clay (of earliest Danian age) at Højerup belongs to one of the classic Cretaceous-Paleogene boundary deposits at Stevns Klint. This boundary clay constitutes four distinctive layers: the latest Maastrichtian bryozoans-rich chalk, a 2-5 cm thick basal black marl, brown-to-grey marl and grey marl overlain by the lower Danian Cerithium limestone Member. Black and brown-to-grey marls represent the main part of the Fish Clay. The mineralogy of the black marl is comparatively simple, smectite and authigenic (mainly biogenic) calcite being the principal components.

We report here the study of Au in the black marl and in its inorganic (carbonate, smectite, silicate) and kerogen fractions. The selective leaching procedures were used to establish geochemical associations and specific mineralogical residences for Au. The sample was analyzed by instrumental neutron activation analysis (INAA).

Table 1: Geochemical data for Au of basal black marl

Metal		Fraction*				
		Total	Carbonate	Smectite	Silicate	Kerogen
Geochemical concentration						
Au	[ppb]	25	0	35	10	475
Geochemical distribution						
Au	[ppb]	25	0	15	<5	10
	%	100	0	60	6	34

*The percentage of the whole sample: carbonate [52.0 %], smectite [21 %], silicate [25.2 %], kerogen [1.8 %]

The analytical results (Table 1) indicate that most of Au resides in the smectite (60 %) and kerogen (34 %). We suggest that a substantial amount of this metal was probably contained in the detrital smectite (and kerogen) arriving at the site of deposition. Preliminary considerations implied that Au in the black marl could have been both of terrestrial and of meteoritic origin.

Cation exchange capacity (CEC) – a tool for determination of secondary alteration of chlorite from Fore Sudetic Monocline (western Poland)

Sokalska, E.T.[*] & Aagaard, P.
Dept. of Geosciences, University of Oslo, Norway
([*]e.t.sokalska@geo.uio.no)

Chlorites are very common metamorphic and hydrothermal minerals composed of Mg, Fe, Al and Si. They are phases, which can be unstable during retrogressive metamorphism or late stage hydrothermal alteration.

Chlorites from Bolewice-1 borehole (western Poland) were studied using XRD and EMPA methods. Diffraction data indicate that the chlorites are usually altered. The aim of this study was to find a tool suitable for the analysis of spatial differences in the degree of alteration. CEC was applied to determine changes in degree of chlorite alteration in thin section scale. There procedure proposed by [1] using in situ Cs saturation on thin sections and electron microprobe analysis was applied.

There are two factors controlling CEC of partly altered chlorites. First of them is late fluid migration producing vermiculitization of chlorite and the second one is K-metasomatism and celadonite formation which can close the crystal structure to Cs.

The main factor controlling chlorite alteration under retrograde conditions is the contact with migrating fluid. EMPA data collected from samples saturated with Cs indicate that there is strong decrease in CEC in the case of amygdules with good sealing, where secondary fluids couldn't migrate. In these cases CEC can have values less than 3 meq/100 g even if there was no K-metasomatism, whereas clays, which fill pseudomorphs after pyroxene indicate highly differentiated values, usually from 8 to 11 meq/100 g, sometimes even higher than 12 meq/100 g. These values are lower than reported before for mixed layer phases [1], but evidently higher than values proposed for pure chlorite, which should not have any CEC. Moreover, CEC varies between samples from different depths and sometimes indicate values in range 4 – 6 meq/100 g. This is in agreement with XRD data showing different degrees of chlorite alteration.

Celadonitization affected both clays from the amygdules and pseudomorphs and was probably a relatively early process, forming celadonite layers in amygdule fillings. It is connected with the decrease of CEC to values smaller than 5 meq/100 g because K stabilizes crystal structure and does not allow for Cs incorporation into it.

Results of this study indicate that CEC is extremely useful for some type of investigations in clay mineralogy. It allows for discrimination of spatial changes in clay mineral distribution connected with their partial decomposition and alteration, giving us insight into late fluid migration development during hydrothermal metamorphism.

[1] Schiffman, P. & Southard, R.J. (1996) *Clay. Clay Miner.*, **44(5)**, 624-634

Bentonite; its resources and geological settings in Iran

Ghorbani, M.[1,2*] & Tajbakhsh, P.[2]
[1]Dept. of Geology, Faculty of Earth Sciences, Shahid Beheshti University, Tehran, Iran
[2]Pars Geological Research Center – Arian Zamin, Tehran, Iran
([*]arianzamin@arianzamin.com)

Bentonite is a swelling clay rock known to Iranians for ages. Old famous scientists like Avicenna and Ebne Bitare mentioned this material, which was named clay soap (1173), taylorite (1888) and bentonite (1897). Its name is derived from the shaly Benton Formation in the U.S.A. Smectite minerals are the main components of bentonite.

Bentonite often forms in warm and humid environments such as lagoons and shallow coastal areas, which are oxidation zones with basic pH of 8-9. The source rocks of bentonites are acid volcanic rocks ranging from dacite to rhyolite. When these volcanics enter into aforementioned environments they undergo bentonitization process, which may be followed by the burial diagenesis alteration.

So far more than 70 bentonite deposits have been identified in Iran. Most of these deposits formed in the Eocene and Oligocene, i.e. during the time period with intense acid volcanic activities. No bentonite deposit has yet been found in the vicinity of plutonic bodies in Iran. In most cases, the bentonite deposits occur along the contact with acid volcanic rocks. Comparing the distribution map of bentonite deposits with the geological map of Iran, one finds the genetic relationship between these deposits and the volcanic rocks.

The age of the world's bentonite deposits ranges from Jurassic to Pleistocene. There are large reserves of the Cretaceous bentonite in the U.S.A., Europe and Asia. But most of the world's bentonite deposits belong to the Tertiary.

All bentonite deposits in Iran formed after Cretaceous. The absence of large-scale acid volcanism and presence of an exceptional marine environment dominating Iran during the Cretaceous period could explain the formation of bentonite deposits in Iran after Cretaceous. Near 40% of bentonite deposits of Iran formed in the Eocene, and there is almost equal number of the deposits of the Oligocene-Miocene age.

Lower Paleozoic K-bentonites and their application for tectono-stratigraphic correlation in Europe and North America

Huff, W.D.
Dept. of Geology, University of Cincinnati, Ohio, USA
(huffwd@ucmail.uc.edu)

Continuing studies of Ordovician and Silurian K-bentonites in Europe and North America show that many of them are distributed regionally and thus can serve as important marker horizons for stratigraphic correlation. Two examples of projects underway are from the Carnic Alps in Austria and the North American midcontinent. Lower Paleozoic K-bentonites occur in a region of the Carnic Alps that is characterized by a metamorphic overprint ranging from anchizone to epizone. As a consequence of this thermal history, the illite/smectite clay mineralogy that commonly characterizes such beds has been altered to illite and chlorite, similar to the clay minerals found in associated mudrocks. The volcanogenic origin of these beds is confirmed, however, by the presence of primary magmatic phenocrysts of biotite, apatite and zircon. In some samples the zircons show evidence of magmatic resorption. Four horizons fall approximately within the *amorphognathoides* zone at the Oberbuchach section and eight in the Lower Wenlock, which appear to be traceable across the Cellon, Oberbuchach and Nölbling sections. The K-bentonite sampled from the Uggwa section may be of a similar age to those from the Llandovery of Nölbling Graben. Sixteen levels have been recorded from the *vesiculosus* zone and upwards within the Rhuddanian and eleven from the *triangulatus* zone (Aeronian). The abundant presence of these horizons in the Llandovery sequences of the Carnic Alps is similar to those in the British Isles, Sweden, Canada and North America and documents widespread volcanism related to the closing of the Iapetus Ocean and northward drifting of microplates derived from the northern margin of Gondwana. The Osmundsberg K-Bentonite has been recognized throughout NW Europe in the late Llandovery (Telychian) and it is probable that this level may also be identified from the samples taken at this stratigraphic level from the Cellon, Seewarte and Oberbuchach sections (*celloni* zone).

Although Gondwana was tectonically quiescent during the Silurian, Laurentia experienced at least two separate phases of collision. Evidence can be found in the basal Silurian strata of the Appalachian Basin in the form of widespread sheet sands and shale successions, K-bentonites, and zones of soft-sediment deformation. K-bentonites have been positively identified at multiple levels in the Llandovery-Wenlock interval in eastern North America.

For the Silurian rocks of the Cincinnati Arch in Ohio, Kentucky, and Indiana seven depositional sequences are assigned on the basis of through-going unconformities that mirror those already recognized in the early Llandovery to early Ludlow of the northern Appalachian Basin. Revision of the conodont biostratigraphy for the Cincinnati Arch by previous authors has produced results that both agree and disagree with the other lines of data implemented in the sequence stratigraphic depositional model. Biostratigraphic correlations between southern Ohio and the Niagara Falls area are largely in agreement with correlations based on other lines of data, such as K-bentonite evidence, as are correlations between west-central and western Ohio, southeastern Indiana, and northern Kentucky. The integrated analysis suggests a relatively simple history of high-frequency relative sea level fluctuations superimposed on a tectonic signature of long-term basin subsidence and very slow forebulge migration.

Comparative investigation of Sarmatian bentonites in the region of Miskolc (North Hungary)

Papp, I.[1*], Kozák, M.[1], Kovács-Pálffy, P.[2], Püspöki, Z.[1], Vámos M.[1] & McIntosh, R.W.[1]
[1]Dept. of Mineralogy and Geology, University of Debrecen, Hungary ([*]asvanypista@citromail.hu)
[2]Geological Institute of Hungary, Budapest, Hungary

During the complex mapping and investigation of the north-eastern foreland of the Bükk Mountains, our research team noticed an extensive Sarmatian (Upper Miocene) volcanic-sediment series. The Lower and Upper Sarmatian succession showing similar lithological characteristics is subdivided by a widespread extraclastic andesite tuff. The incomplete, eroded sections of these formations occur in numerous locations in the region of Miskolc and Putnok. The thickest and most uniform sediment series is located in Sajóbábony, 5 km to the north of the city of Miskolc. This area was explored at the turn of the millenium with the support of the Széchenyi Program [1,2].

The age of the Sarmatian series was determined on the basis of bivalve fauna and by K/Ar radiometric analyses. Complex analyses were carried out on the material of the bentonitic sequence, including major and trace element analyses and several hundred X-ray diffraction and thermal analyses in order to give a horizontal and vertical, qualitative and quantitative characterisation of the bentonite deposit [3].

Another significant bentonitic sequence is located in the Avas Hill, in the city centre of Miskolc. The underlying extraclastic andesite tuff of the Sajóbábony bentonitic sediment series appears to be the overlying bed of the Avas Hill. The Sarmatian sediment sequence is found under the andesite tuff with a vertical extent of about 80 m. This sequence is composed of alternating bentonite and sandstone layers. On the basis of observations and geodetical measurements of more than a hundred outcrops, the thickness of the bentonite layers varies between 0.5 – 3 m, despite the frequent alternation of layers of different lithology. The characteristics of the bentonite layers in the Avas Hill are very similar to the sediment sequence of the Sajóbábony bentonite deposit. Weathering products of acid tuff in shallow-sea environment were identified in both locations. Both bentonitic sediment deposits contain 30 – 70 % poorly crystalline montmorillonite.

The aim of this presentation is to give a comparative mineralogical and geochemical insight regarding the two sediment sequences, and is to give an overview on the Sarmatian sequence and the processes of the shallow-marine environment from an economic geological and paleoenvironmental point of view.

[1] Kozák, M. & Püspöki, Z. (2003) *Summary final report of the geological exploration of the open air permitted bentonite research called 'Sajóbábony-Sajókeresztúr'*. Archive of Dept. of Mineralogy and Geology, University of Debrecen, Archive of Hungarian the Geological Service, Salgótarján (in Hungarian) [2] Püspöki, Z. et al. (2008) *Clay. Clay Miner.*, **56(1)**, 23-38. [3] Püspöki, Z. et al. (2003) *Földtani Közlöny*, **133(2)**, 191-209 (in Hungarian).

Hydrothermal kaolinite occurrences of the Gediz area (Kütahya, western Anatolia, Turkey)

Kadir, S.*, Erman, H. & Erkoyun, H.
Dept. of Geological Engineering, Eskişehir Osmangazi University, Eskişehir, Turkey (*skadir_esogu@yahoo.com)

The kaolinite occurrences at Akçaalan and Sazak (Gediz area, Kütahya, western Anatolia) formed by hydrothermal alteration of the Civanadağ tuffs and Akdağ volcanites in relation to Miocene volcanism, resulting in the development of a silica cap and iron-oxide/-oxyhydroxide veins, with local precipitation of pyrite. These units were studied via petrography, reflected-light polished-section microscopy, X-ray diffractometry, differential thermal analysis-thermal gravimetry (DTA-TG), scanning electron microscopy (SEM-EDX) and geochemical methods. Petrographically, the volcanites comprise andesite, rhyolite and tuff. Plagioclase and K-feldspar are argillized, biotite and hornblende are opacitized, groundmass is argillized, and Fe-oxide/-hydroxides are widespread in these volcanic units. Mineralogical zonation, such as kaolinite+opal-CT in the inner zone and smectite+illite outward, is observed. Kaolinite, quartz, smectite, illite, opal-CT, feldspar, calcite and dolomite were all determined in these rocks. Micromorphologically, kaolinite is well-crystallized and of vermiform character. SiO_2 of the bulk rocks vary from 52.06 to 70.91%, and Al_2O_3 from 14.71 to 20.77%. Despite increasing SiO_2, Al_2O_3 and Fe_2O_3+TiO_2 decrease laterally, and Fe_2O_3 increases upward. Decreasing Sr values suggest degradation of feldspar at low temperatures. Albitization is compatible with decreasing Rb and K contents. Al was enriched during hydrothermal alteration, in contrast to other elements, which were depleted. All samples are enriched in large-ion lithophile elements (LILE) and light rare-earth elements (LREE), and depleted in high-field-strength elements (HFSE) and heavy rare-earth elements (HREE) with respect to primitive mantle and chondrite. Negative Eu anomalies, relative to chondrite, reflect alteration of feldspar. Field observations along with mineralogical and geochemical determinations reveal that kaolinites of the Gediz area developed by hydrothermal alteration of feldspar, hornblende and volcanic glass within the volcanites.

Mineralogy and environment of the Qarain clay deposits, Riyadh region, Saudi Arabia

Almohandis, A.A.
Dept. of Geology and Geophysics, College of Science, King Saud University, Riyadh, Saudi Arabia (mohandis@ksu.edu.sa)

The Qarain area is about 220 km west of Riyadh city, capital of Saudi Arabia. The Qarain clay deposits lie within the Marrat Formation (Lower Jurassic). They are characterized by the dominance of kaolinite clay mineral. Illite occurs in a lesser amount in the clay fraction. The dominant non-clay mineral is quartz. X ray diffraction analyses were obtained using Ni-filtered K_α radiation from a Philips (PW1050).

It is suggested that the clay deposits were the result of partial laterization of the source rocks, mainly acid igneous rocks of the Arabian shield. Partial laterization occurred under humid tropical conditions. The weathered rocks were transported to the present area and deposited in a shallow and near shore environment of the Toarcian Sea.

The concentration of boron in the 20-2 micron grain size fraction is higher than 50 ppm with an average value of 73 ppm, while the average value of boron is 41 ppm in the finest fraction of 2 micron. It is suggested that the high B contents in the 20-2 micron size fraction largely derived from the source rocks, may indicate a non-marine origin for the Qarain clay deposits.

Stable isotopes in clay minerals from the Northern Alpine Molasse basin as archives for alpine climate and elevation change

Bauer, K.K.[1,2*], Vennemann, T.W.[1], Mulch, A.[2] & Adatte, T.[3]
[1]Institut de Minéralogie et Géochimie, Université de Lausanne, Switzerland ([*]kerstin.bauer@unil.ch)
[2]Institut für Geologie, Leibniz Universität Hannover, Germany
[3]Institut de Géologie et de Paléontologie, Université de Lausanne, Switzerland

The stable isotope composition of oxygen and hydrogen in rain water correlates with the air temperature and with the altitude of precipitation. If meteoric water is taken up into the structure of minerals with a known water-mineral fractionation factor, it is possible to reconstruct its original $\delta^{18}O$ and δD values from the isotopic composition of the host mineral.

Our study aims on reconstructing the oxygen and hydrogen isotopic composition of Miocene water via the analyses of clay minerals from different origins across the European Alps and the north Alpine foreland basin, the so-called Molasse basin. As clay minerals are hydrous, they contain both hydrogen as well as oxygen, allowing the use of both isotope systems to reconstruct the paleoprecipitation. Measurements were carried out on clay mineral separates from Molasse sediments from the northern foreland, covering the deposits from western Switzerland, via southern Germany, the Vienna Basin to the Pannonian Basin, with a sedimentation age from 8.5 to 19.2 Ma. Fossils from the same samples (ostracods, foraminifera, shark teeth, mammal remains) have already been analysed in previous studies for their O and Sr isotope composition [1, 2]. It is the aim of this study to compare the results from both the marine as well as the detrital record in order to address climatic as well as elevation changes in the Alpine region during orogenesis.

Prior to analyses, the material was treated with HCl to remove carbonates and separated to grain size fractions of <2µm, <0.5µm, and <0.2µm by centrifugation based on Stokes' law. XRD measurements were made to determine the mineralogical composition. Smectite and mixed layer minerals, determined with glycol treatment, dominate the clay fractions. SEM analyses of the clays support a detrital origin.

Oxygen isotopes were measured using CO_2 laser fluorination and hydrogen isotopes using high temperature reduction (TC/EA) on dried separates. The values of the <2µm fraction have a range of 14.1‰ to 21.2‰ for $\delta^{18}O$ and –143 to –102 for δD, relative to VSMOW. For hydrogen, a clear grain size dependence was observed, smaller particles have lower δD values down to –164‰, with a non-linear trend. The $\delta^{18}O$ values have no clear relation with grain size. It also appears that there is no overall correlation between the δD and $\delta^{18}O$ values, which indicates that both tectonic and climatic variations may have influenced their isotopic compositions.

An application of the relations proposed by [3] to calculate the $\delta^{18}O$ values of water in equilibrium with the clays and the temperature of clay formation suggests $\delta^{18}O$ values that may be as low as –8 to –9 for the water in the <2µm fraction and temperatures of 10-20°C, both of which are typical for modern precipitation in the circum-alpine region today.

Ongoing research will include sampling more material from the Molasse basin for a better spatial and temporal coverage.

[1] Janz, H. & Vennemann, T. (2005) *Palaeogeogr. Palaeocl.*, **225**, 216-247. [2] Kocsis, L. et al. (2007) *Geology*, **35**, 451-454. [3] Delgado, A & Reyes, D. (1996) *Geochim. Cosmochim. Ac.*, **60**, 4285-4289.

The distribution of late diagenetic illite and kaolinite in Rotliegend aeolian sandstones from the Fore-Sudetic Monocline, SW Poland

Biernacka, J.
Inst. of Geology, University of Poznan, Poland
(julbier@amu.edu.pl)

In terms of hydrocarbon prospecting, Rotliegend aeolian dune sandstones from the Fore-Sudetic Monocline constitute a good target. Their reservoir properties depend primarily on diagenetic clay minerals, which not only are the most abundant among authigenic phases but also dominate the grain surface area. Whereas illite is by far the most ubiquitous diagenetic phase, other clay minerals occur locally. The mutual relationship between late diagenetic illite and kaolinite was studied for the south-eastern part of the Fore-Sudetic Monocline, where these two minerals are common, by a combination of methods (polarising microscopy, XRD, SEM, XRF).

The Rotliegend sandstones are buried at a depth of ca. 2000 m in the area studied, which is the minimal burial after a two-stage Mesozoic inversion. Three distinct sandstone types were observed: (a) kaolinite-rich arenites devoid of detrital feldspars, (b) illite-rich arenites with scarce detrital feldspars, and (c) feldspar-bearing arenites (av. 10 vol% Fsp) containing fibrous illite. Individual types occur in adjacent wells, distant from several hundred meters to 1-2 kilometres. The illite and kaolinite exhibit features of late diagenetic minerals that crystallized after significant compaction and post-dated other diagenetic phases (hematite, dolomite, quartz). The fibrous illite co-occurs with the kaolinite in some wells. Also, the remnants of kaolinite dissolved flakes with illite growing on them were observed under SEM.

A relatively small area studied and one sedimentary facies (aeolian dune) allow assuming similar initial parameters, such as framework grain composition and porosity. Therefore, the crystallization of late diagenetic kaolinite (a) and illite (b) must have been associated with a pore-fluid flow and the alteration of detrital feldspars whereas the fibrous illite (c) crystallized independently at a later stage without feldspar dissolution. A model proposed by Gaupp et al. [1] of acid pore-fluids originated from Carboniferous coal-bearing rocks juxtaposed Permian sandstones along faults is in accord with the case studied. The pore-fluid flow resulted in kaolinite crystallization in the vicinity of faults and illite formation in more distant zones from more neutralized fluids.

[1] Gaupp, R. et al. (1993) *AAPG Bull*., **77**, 1111-1128.

K-Ar ages versus grain size and illite Kübler index: a case study of parametamorphic rocks from eastern Mt. Papuk, Croatia

Biševac, V.[1*], Balogh, K.[2], Tibljaš, D.[1] & Balen, D.[1]
[1]Inst. of Mineralogy and Petrology, Dept. of Geology, Faculty of Science, University of Zagreb, Croatia
([*]vabisevac@geol.pmf.hr)
[2]Inst. of Nuclear Research, Hungarian Academy of Science, Debrecen, Hungary

One of the frequent and most important problems in K-Ar dating is the contamination with detrital materials which can results in hard to interpret mixed ages. The coarse fraction isolated from samples is most often heterogeneous i.e. composed partially of detrital minerals and of more recent authigenic minerals which grew as a result of post-depositional thermal processes. Variable age mostly depends on the proportions of detrital and authigenic phases, both of which are considered to have a fixed K-Ar age. On the contrary, it is generally assumed that small grain-size fractions (e.g. <2 μm fraction) are mostly devoid of the detrital mica, while their K-Ar age represents the "mix age" of different generations of illitic minerals present within it.

A special attention here was paid to the evaluation of the influence of detrital minerals by observation of variation in K-Ar ages and illite Kübler index (KI) obtained on different grain-size fractions. Samples of high temperature anchizonal to epizonal altered parametamorphic rocks, representing various lithologies with different petrographic characteristics and stratigraphic age were used for this purpose.

Some trends can be observed. The decrease of K-Ar ages with decreasing grain-size (Fig. 1) can be attributed to an increase of diffusion of radiogenic ^{40}Ar resulting in increasing reset of the K-Ar system with decreasing grain size and to a reduction of detrital minerals contamination effect which becomes less and less pronounced as grain size decreases. Furthermore, KI of the finer fractions increases with decreasing grain size showing negative correlation with decreasing K-Ar ages. This effect is closely connected with the prolonged formation of illitic minerals and their wide temperature stability.

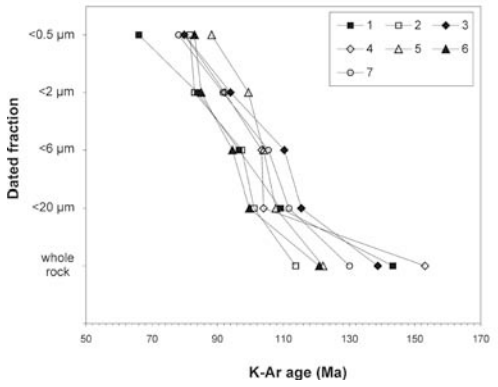

Fig. 1: K-Ar ages determined for different grain size fraction of analysed samples (1- chlorite schist; 2 - chloritoid schist; 3 - metasandstone; 4 - quartzite; 5 - phyllite; 6 - phyllitic metaconglomerate; 7 - quartz metasandstone).

Clay mineralogic evidences for a Mid Paleozoic tectono-thermal event in Zonguldak Terrane, NW Turkey

Bozkaya, O.[1*], Yalcin, H.[1] & Goncuoglu, M.C.[2]
[1]Dept. of Geological Engineering, Cumhuriyet University, Sivas, Turkey ([*]bozkaya@cumhuriyet.edu.tr)
[2]Dept. of Geological Engineering, Middle East Technical University, Ankara, Turkey

The Zonguldak Terrane (ZT), a Gondwana-derived continental microplate [1] along the Black Sea coast in NW Anatolia, was believed to comprise more or less continuous Paleozoic successions. It was considered to be rifted off the northwestern Gondwana-margin in the Early Paleozoic and drifted across the Rheic Ocean during the Mid Paleozoic and successively accreted to Laurasia along the Eastern European Suture during the Variscan Orogeny [2]. Along several cross-sections in ZT, the siliciclastic rocks of Ordovician to Middle Silurian age overlay unconformably a Cadomian basement with orthogneisses, oceanic and island-arc sequences. Late Lower Devonian quartzites unconformably overlay Middle Silurian (Wenlock) graptolitic shales, indicating an important event.

This study aims to investigate whether this unconformity is accompanied by a thermal event, and hence to trace the fingerprints of an orogenic overprint. For this, the diagenetic characteristics of the Paleozoic sedimentary rocks in ZT are investigated by means of petrographic and X-ray diffraction methods. Clay mineralogic associations, Kübler Index value (KI), *b* cell dimension (Å) and polytype of illites are determined throughout Ordovician-Carboniferous units. Siliciclastic and calcareous rocks mainly contain phyllosilicates, quartz, feldspar, calcite, dolomite, hematite and goethite minerals. Phyllosilicates are represented by illite, chlorite, kaolinite, mixed-layered chlorite-vermiculite (C-V), chlorite-smectite (C-S) and illite-chlorite (I-C). Quartz and clay/phyllosilicate minerals are common in all formations, whereas the amounts of feldspar, calcite and dolomite increase in some levels. The main phyllosilicate assemblages of Ordovician-Silurian units are illite + chlorite + I-C ± C-V ± C-S, whereas Devonian-Carboniferous units have illite + kaolinite + chlorite. The appearance of kaolinite and the absence of chloritic mixed-layers in the Devonian units is the main difference in terms of the clay mineral association. KI values of Ordovician-Silurian and Devonian-Carboniferous units (0.58 ± 0.18 and 1.13 ± 0.24 Δ°2θ) reflect late diagenetic and early diagenetic grades, respectively, and show sudden jump from Silurian to Devonian. The *b* cell dimension values of illites of Ordovician-Silurian units (9.011 ± 0.013 Å) are somewhat higher than those of Devonian-Carboniferous units (8.998 ± 0.012 Å). Illites are composed of a mixture of the $2M_1$, $1M$ and $1M_d$ polytypes. Ordovician-Silurian units have $2M_1$ and $1M_d$, whereas Devonian-Carboniferous units include $1M$ polytype in addition to $2M_1$ and $1M_d$ polytypes.

In brief, the new mineralogic data indicate that the pre-Middle Devonian rocks in ZT experienced a tectono-thermal event, prior to the Middle Devonian transgression. This Caledonian-time event is also reported in some Balkan-Moesian terranes but not noticed in the neighboring Istanbul Terrane, supporting a complex terrane distribution [3] at the S margin of Laurasia, prior to the Variscan closure of the Rheic Ocean.

[1] Goncuoglu, M.C. (1997) *Turkish Assoc. Petrol. Spec. Publ.*, **3**, 13-23. [2] Goncuoglu, M.C. (2001) *ESF Europrobe Meeting*, Ankara, 22-23. [3] Yanev, S. et al. (2006) in Robertson, A.H.F. & Mountrakis, H.F. (eds.) *Tectonic Development of the Eastern Mediterranean Region*. Geol. Soc. London, **260**, 51-67.

Clay minerals composition: a significant tool for glacial till studies and paleo reconstruction, with a reference to the glacial history in Drenthe - the Netherlands, North West Germany and the Baltic

Bregman, E.P.H.[1*], Lūse, I.[2], Stunda, A.[3], Karpovičs, A.[4] & Randers, M.[4]
[1]Province of Drenthe & Faculty of Geosciences, Utrecht University, Utrecht, the Netherlands ([*]E.Bregman@drenthe.nl)
[2]Inst. of Soil and Plant Sciences, Latvia University of Agriculture, Jelgava, Latvia
[3]Riga Biomaterials Innovation and Development Centre, Riga Technical University, Riga, Latvia
[4]Faculty of Geography and Earth Sciences, University of Latvia, Riga, Latvia

Till deposits reflect glacial history of landscapes. That is the main reason to have good knowledge about tills for paleo-reconstruction of glaciations and a better understanding of the impact of glacial processes on actual eco(-hydro)logical relationships. For sustainable protection and development of nature- and landscape-values more insights in till deposits are therefore necessary. That is the main conclusion of a recent study in Drenthe, the Netherlands [1].

The aim of our study is to verify a new glacial model. To differentiate glacial tills and sedimentation conditions for (i) glaciations (Saale, Weichsel) in the Netherlands, Germany and the Baltic; (ii) stages within glaciations in Drenthe and (iii) supposed phases within one stage with attention to local conditions.

XRD analyses of clay minerals confirm conclusions of formerly used analyzing techniques (e.g. shear stress-measurements). Clay minerals and their structures are tools to differentiate tills from different stages and phases of surging at a lower level. Contrary to other methods quarries are not needed for sampling. So the method opens more possibilities for sampling and studying tills at more places in areas with a lack of quarries like in Drenthe province.

Our study shows that clay mineral composition in glacigenic sediments indicates significant influence of glacial sedimentation conditions such as sediment transport and postsedimentation changes. Vermiculite is a clay mineral that indicates postsedimentation changes – weathering and soil forming processes. Various mineral compositions may indicate sediment mixing due to surging processes. It was possible to separate different till forming stages.

Our final conclusion is that clay minerals are a useful tool for paleo environmental reconstruction of glacial landscapes of different ages, which give more information about positional, local conditions of formed tills. We showed that in Drenthe, the Netherlands, tills are formed under saltwater conditions whereat indicate authigenic minerals (basanite, halite, syngenite) in fraction < 0.2 µm. The influence of pro- and subglacial processes to surface pressed up deep groundwater changed till composition and weathering products does have also an ecological impact.

[1] Bregman, E.P.H. (2007) *Ph-D research plan.* Internal document.

TEM-AEM study of hydrothermal smectite formation in Fe-Mn-metalliferous sediments: samples from the HMS Challenger expedition (1872-1876)

Cuadros, J.[1], Dekov, V.[2], Arroyo, X.[3*] & Nieto, F.[4]
[1]Dept. of Mineralogy, Natural History Museum, London, UK
[2]Dept. of Geology and Paleontology, University of Sofia, Bulgaria
[3]Depto. de Mineralogía y Petrología, Universidad del País Vasco, Bilbao, Spain ([*]xarroyo001@ikasle.ehu.es)
[4]Depto. de Mineralogía y Petrología and IACT, Universidad de Granada-CSIC, Granada, Spain

The aim of this study is to investigate the formation of smectite in three samples of submarine Fe-Mn-metalliferous sediments of hydrothermal origin, collected by the British HMS Challenger during the first oceanographic expedition (1872-1876). They were collected from the seafloor in the vicinity of the Pacific-Antarctic Ridge and the Chile Ridge. Firstly, the samples were analyzed by means of XRD, chemical analysis, SEM-EDX and IR. After removal of biogenic calcite, the results from the above techniques indicated that they consist mainly of two amorphous or semiamorphous phases intimately mixed: Fe-Mn oxyhydroxides and a Si-Al-Mg-Fe phase of chemical characteristics similar to smectite and with variable proportions of the above elements.

The TEM-AEM study was carried out to complete the previous data. The analysis, obtained from powders dispersed on holey C-coated formvar Au grids, showed the morphological and chemical characteristics of the several components of the sediment. To clearly identify mineral phases, SAED patterns, High-Resolution images and microanalyses were correlated. The appearance of Fe-rich oxyhydroxides, as round-shape particles, is clearly different from that of the other phases. Mn-rich oxides, previously identified by XRD as the δ-MnO_2 phase, related to birnessite, aggregate to form high-contrast clusters with an apparently layered structure. Smectite particles have the typical flaky and wavy morphology of smectite with the particular presence of relative large basal plates. These smectite particles always appear associated to Fe-Mn oxyhydroxides. Smectite composition corresponds in most cases to nontronite, frequently containing a trioctahedral (Mg-rich) component, although there are compositions corresponding to Fe-montmorillonite and Al-montmorillonite. No Mn-rich smectite was detected but Mn abundance is significantly greater than in typical smectites of other geological environments. Electron diffraction patterns confirm the poor crystallinity of both Fe-Mn oxyhydroxides and most smectite particles. These results are interpreted as representing hydrothermal smectite formation from Fe-Mn-rich metalliferous sediments as the Fe-rich gels react with solid particles and dissolved species. Possible sources of Si, Al and Mg are detrital silicate minerals, glass of basaltic origin, silica gel precipitated from hydrothermal fluids and seawater as the main source of Mg.

Acknowledgements: Financial support was supplied by the "Synthesys" program of the European Community and Research Project no. CGL2007-66744-C02-01/BTE of the Spanish MICINN.

Climate recorded by clay minerals from surface sediments of Lake Kusai, the Hoh xil Area, China

Gao Xiang[*], Fang Qinfang, Ma Hongwen & Peng Qiang
National Lab of Mineral Materials, China University of Geosciences, Beijing, China ([*]xiang.gao@sohu.com)

Lake Kusai is selected as research area because it is located in natural safeguard area of the Hoh xil, northern Tibetan Plateau, having too bad natural environment and only weakly influenced by human activity. Present work is aimed at studying the relationship between clay minerals in surface sediments of a lake from high cold region and its climate in recent years.

23 surface sediment samples and their corresponding three oriented aggregates (natural air-dried, glycolated, and heat-treated) of clay minerals were studied by X-ray powder diffraction. The bulk rock results show that major detrital minerals are quartz, feldspar, and calcite, the content of summation is 65%-80%; minor phases are aragonite, gypsum, dolomite, and amphibole. The clay mineral content of the bulk rock samples is 15%-33%. Based on the analysis of oriented specimens, and according to the distribution of illite/smectite mixed-layer (I/S), we plot four districts (Fig. 1).

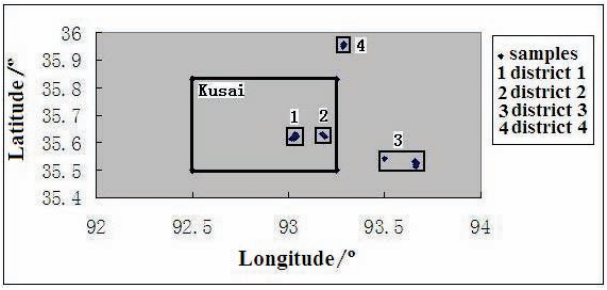

Fig. 1: Samples distributions in Lake Kusai and its nearby.

Clay minerals mainly comprise of illite (65%-82%), chlorite (12%-23%) and kaolinite (5%-7%). 4-15% ordered I/S mixed-layer appears in district 1 and 3 rather than district 2 and 4 (Table 1). Illite and chlorite as major clay minerals indicate that the whole lake area has been dominated by arid and cold climate conditions in recent years. I/S mixed-layer appearing at local areas may indicate the climate had ever undergone alternately arid-humid environment within a short period of time.

Table 1: Qualitative and semi-quantitative clay mineralogical composition, CI and IC values of illite of studied samples

Distribution	Illite	Chlorite	Kaolinite	I/S	CI	ICr	ICa
district 1	66-78%	12-24%	5-7%	5-15%	0.21-0.33	0.41-0.58	0.51
district 2	65-82%	12-25%	5-6%	0	0.27-0.35	0.30-0.46	0.39
district 3	65-77%	12-21%	5-6%	4-12%	0.24-0.33	0.43-0.58	0.48
district 4	70-74%	20-23%	5-6%	0	0.32-0.36	0.34-0.39	0.37

CI-Chemical Index of illite, ICr- IC value range, ICa –IC average value

Five international standard illite samples (provided by Prof. L.N.Warr, Germany) were tested to correct for the experimental conditions, making the data directly comparable to the international standards. The corrected illite crystallinity values (IC) of the samples from district 1and 3 are higher than those from district 2 and 4. Chemical Index (CI) values of illite are less than 0.5 indicating that it is the result of physical weathering, and possesses of Fe-Mg. Therefore, we assume that a weak hydrolysis occurs in our research area, and its intensity in district 1 and 3 is stronger than in district 2 and 4.

In conclusion, we have obtained initial results between clay minerals and the climate, and the formation mechanism of clay minerals in Lake Kusai will be studied later in details.

On spatial-temporal variations of secondary phases formed during mud diagenesis

Hellevang, H.*, Jahren, J., Aagaard, P. & Thyberg, B.
Dept. of Geosciences, University of Oslo, Oslo, Norway
(*helghe@geo.uio.no)

Chemical compaction of soft muds to shales during burial leads to large changes in rock-physical properties like stiffness porosity and permeability. The smectite to illite dissolution presippitation reaction releases surplus silica that is precipitated as fine-grained (1-3µm) pore-filling quartz crystals [1-3]. Surplus magnesium and iron is precipitated in chlorites, or if calcium carbonate is present may be precipitated as ferroan dolomites.

In this study the spatial distribution of secondary phases by varying the effective diffusion coefficient and initial spatial distribution of mineral phases have been explored using the PHAST 3D-reactive transport code. The initial system consisted of a 1 mm cube divided into smectite-rich and smectite-poor domains discretized into 720 cells.

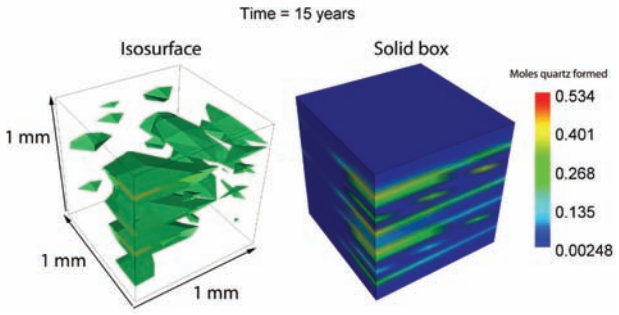

Fig. 1: Spatial distribution of quartz formed at 80ºC. Local quartz formation is dominated in the gradients between the smectite-rich low-diffusivity domains and local K-feldspar. The blue colors denote low/no formation of quartz in smectite-rich domains.

Preliminary simulations suggest that quartz and illite formation is dominated in chemical gradients forming locally between K-feldspar and smectite. As magnesium builds up the transformation slows down and may be locally constrained by the precipitation of the magnesium and iron sink (chlorite or ferroan dolomite, in addition some iron and magnesium is incorporated into illite). Low effective diffusion rates leads to strongly localized illite and quartz precipitation, whereas increasing the effective diffusion coefficient results in more dispersed precipitation. Strongly localized microquartz formation observed in cemented mudstones [1-3] support that low diffusivity and the initial spatial distribution of mineral phases controls the spatial distibution of the secondary phases.

[1] Thyberg, B. et al. (2009) *First Break*, **27**, 27-33. [2] Thyberg, B. et al. (2009) *Mar. Petrol. Geol.* (in press) Doi:10.1016/j.marpetgeo.2009.07.005. [3] Thyberg, B. & Jahren, J. (2010) *AAPG Bull.* (submitted).

Chemical weathering intensity and clay minerals in Plio-Pleistocene red clays (Hungary)

Kovács, J.[1*], Fábián, S.Á.[2] & Varga, G.[2]
[1]Dept. of Geology, University of Pécs, Hungary
(*jones@gamma.ttk.pte.hu)
[2]Dept. of Physical Geography, University of Pécs, Hungary

The Tertiary red clays in the Carpathian Basin of Hungary (Tengelic Red Clay Formation: TRCF; Kerecsend Red Clay Formation: KRCF) are overlain by loess paleosol sequences named Paks Loess Formation (PLF) in S Transdanubia. The thickness of the red clay ranges from 4 to 90 m. The red clay sediments are known from both exposures and boreholes. The age of these formations is ~3.5–1.0 Ma.

Elemental oxide analyses of the red clays were performed by X-ray fluorescence (XRF), and the X-ray powder diffraction (XRD) was used for mineral identification. In this study, we aim to determine the changes of clay minerals due to chemical weathering and age.

As shown in the A–CN–K diagram (Fig. 1), the samples are distributed along the joint A–CN and tend to approach the A-pole, reflecting a process in which K_2O, CaO, and Na_2O are leached out and Al_2O_3 is enriched in the samples, i.e. mineralogically, the dissolution of feldspar minerals and the production of clay minerals (smectite, illite, and kaolinite).

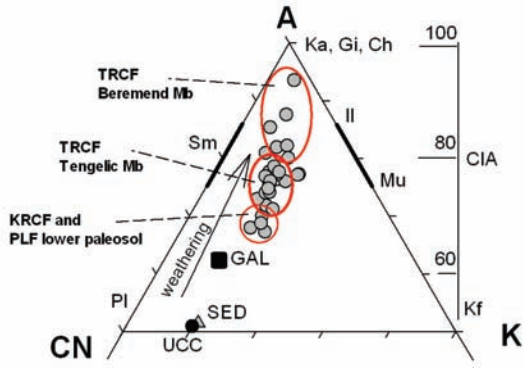

Fig. 1: Basic A–CN–K (Al_2O_3–CaO + Na_2O–K_2O) ternary diagram with CIA values showing the weathering trend of red clays. Note positions of selected mineral compositions (Pl: plagioclase, Kf: K-feldspars, Mu: muscovite, Il: illite, Ka: kaolinite, Gi: gibbsite, Ch: chlorite, Sm: smectite).GAL: global average loess [1]; SED: average sedimentary rock [2]; UCC: upper continental crust [3].

The older type (Beremend Mb) of the TRCF is a red kaolinitic clay containing typically disordered kaolinite, mixed-layer smectite/kaolinite, smectite and little gibbsite. It was formed in a local subaerial weathering crust in warm, humid, subtropical or monsoon climate. The younger member (Tengelic Mb) of the TRCF contains red (or "reddish") clay beds. It contains relatively unaltered material (rich in illite, chlorite), the weathering products are predominantly smectite and goethite formed under warm and temporarily dry climatic conditions of savannah and steppe or forest steppe. The basal red clay layers of the PLF and KRCF contain similar minerals as the underlying red clays belonging to the younger member of the TRCF. The phyllosilicate assemblage (more illite and chlorite, less smectite) indicates a decreased rate of hydrolysis triggered by cooling and/or drying of the climate.

[1] Újvári, G. et al. (2008) *Quaternary Res.*, **69**, 421-437. [2] Ronov, A.B. & Yaroshevsky, A.A. (1976) *Geokhimiya*, **12**, 1761-1795. [3] Rudnick, R.L. & Gao, S. (2003) in Holland, H.D. & Turekian, K.K. (eds.) *Treatise on Geochemistry*. Elsevier–Pergamon, Oxford–London, **3**, 1-64.

Illite crystallinity and intensity ratio in the marine surface sediments around the Korean Peninsula

Moon Dong-Hyeok[1], Cho Hyen Goo[1*] & Yi Hi-Il[2]
[1]Dept. of Earth and Environment Sciences and Research Inst. of Natural Science, Gyeongsang National University, Jinju, Korea ([*]hgcho@gsnu.ac.kr)
[2]Marine Geoenvironment Research Division, Korea Ocean Research and Development Institute (KORDI), Ansan, Korea

Illite is the most abundant clay mineral in the marine surface sediments around the Korean Peninsula. We studied the mineralogical characteristics of illite such as Kübler index (KI) and intensity ratio (IR), using 33 surface sediments which were collected at Northwest Mudbelt deposit (NWMD, 17 samples), South Sea of Korea Mudbelt deposit (SSKMD, 3 samples), Hucksan Mudbelt deposit (HSMD, 2 samples) and Jeju Mudbelt deposit (JJMD, 11 samples).

Illite has very low KI (0.14-0.16) and wide range of IR (1.15-1.90) in the JJMD, medium to high KI (0.32-0.44) and IR (1.46-1.95) in the SSKMD and HSMD, and wide range of KI (0.28-0.58) and IR (1.08-1.70) in the NWMD (Fig. 1).

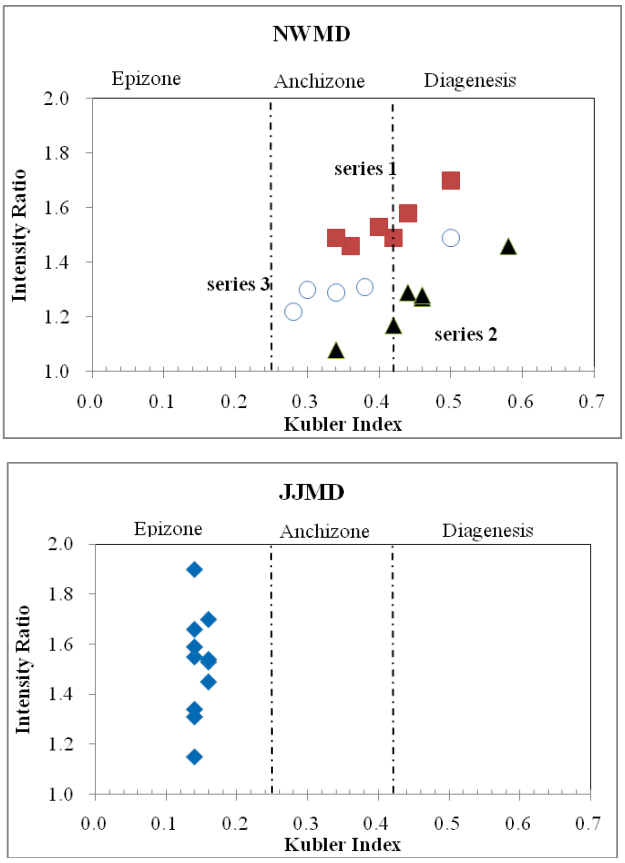

Fig. 1: Relationship between Kubler Index and Intensity Ratio at Northwest Mudbelt deposit (NWMD) and Jeju Mudbelt deposit (JJMD). Dashed lines are boundaries between each metamorphic zone after Kübler [1].

In the NWMD, KI and IR have positive relationship in the NWMD. Generally series 1 is distributed in eastern part, series 2 is in western part, and series 3 is in central part of NWMD. Each series might stand for different sediment provenance.

[1] Kübler, B. (1967) in Wegmann, C.E. (ed.) *Etages tectoniques*. Colloque de Neuchatel, Baconniere, 105-121.

Cretaceous-Paleogene boundary clay (Fish Clay) at Højerup (Stevns Klint, Denmark): Cu and Cr in the smectite concentrate

Stanković, M.N.[1*], Djordjević, M.G.[1], Nikolić, N.D.[1], Todorović, B.Ž.[2] & Premović, P.I.[1]
[1]Laboratory for Geochemistry, Cosmochemistry and Astrochemistry, University of Niš, Niš, Serbia ([*]mpetaric@yahoo.com)
[2]Laboratory for General Chemistry, Faculty of Technology, University of Niš, Leskovac, Serbia

The Fish Clay (of earliest Danian age) at Højerup belongs to one of the classic Cretaceous-Paleogene deposits at Stevns Klint. The main part of this sediment constitutes basal black marl. The mineralogy of the marl is comparatively simple, authigenic (mainly biogenic) calcite and detrital (Cheto-type) Mg-smectite being the principle components.

We report here a geochemical study of trace Cu and Cr in the inorganic (carbonate, smectite, silicate) fractions and in kerogen of the basal black marl. These metals were determined by inductively coupled plasma-optical emission spectroscopy in the whole rock sample, in the inorganic fractions and in kerogen.

Table 1: Geochemical data for Cu and Cr in the basal black marl

	Fraction*				
	Total	**Carbonate**	**Smectite**	**Silicate**	**Kerogen**
Concentration [ppm]					
Cu	80	10	160	15	715
Cr	150	20	350	15	160
Distribution [%]					
Cu	100	6	74	6	13
Cr	100	7	89	<3	<3

* Composition of the whole sample: carbonate [52.0 %], smectite [21 %], silicate [25.2 %], kerogen [1.8 %].

The analytical results show that geochemical concentrations of the Cu and Cr in the smectite concentrate is 160 and 350 ppm, respectively, and most of Cu and Cr reside in this fraction (Table 1). Substantial proportion of Cu is terrestrial and was probably contained in the detrital smectite arriving at the site of deposition. The predominant source of Cr was probably ejecta fallout deposited on the top of nearby coastal soil which was leached by impact-induced, possibly, acid surface waters. Most of Cr was derived from the chondritic component of the fallout. The incorporation of Cr into the smectite took place at the Cretaceous-Paleogene boundary, before the smectite redeposition to the Fish Clay site.

Composition and origin of the Barremian clay-rich sediments from the Mljet Island, Croatia

Tibljaš, D.[1*], Balogh, K.[2], Oros Sršen, A.[3], Molnar, T.[1], Biševac, V.[1], Cvetko Tešović, B.[1] & Gušić, I.[1]
[1]Dept. of Geology, Faculty of Science, University of Zagreb, Croatia ([*]dtibljas@geol.pmf.hr)
[2]Inst. of Nuclear Research, Hungarian Academy of Science, Debrecen, Hungary
[3]Inst. for Quaternary Paleontology and Geology, Croatian Academy of Sciences and Arts, Zagreb, Croatia

Grayish-green clay and marl can be found in several localities on the island of Mljet (Dalmatia, Croatia) within the Lower Cretaceous shallow-water carbonate platform rocks. The clays and marls are usually present as thin irregular layers, couple of centimetres thick, but in some localities they build layers having thickness up to 2 metres. They were analyzed by X-ray diffraction, IR-spectroscopic, chemical and K-Ar dating methods in order to determine their composition and origin. Samples of limestones taken immediately below and above the clay layers were analysed by micropalaeontological and microfacies methods while their insoluble residues were analysed by X-ray diffraction method. This study focuses on major mineralogical observations.

The age of underlying limestones is Barremian, as indicated by their microfossil content (mainly dasycladacean algae). Microfacies analysis of some layers, classified as algal or peloidal-bioclastic wackestone-packstones, indicate shallow sea environment with low to medium energy. Some of them show possible remains of paleosol and mm to cm-sized cracks that could be produced by plant roots (rhizoliths). Limestones above clay layer, deposited in interdital/supratidal environment, classified as mudstone-wackestones, are micritic with cracks and fenestrae showing geopetal infilling and sometimes with stromatolites. The succession of deposits is composed of shallowing-upward cycles and the clays indicate emersion.

Minerals that were determined in the clay are illite, chlorite, kaolinite and calcite. Limestones sampled above the clay layer had 0.4-2.5wt.% of insoluble residue composed of illite, chlorite and kaolinite, which is very similar in composition to the clay samples. In addition some of them contain authigenic potassium feldspar. The mineral composition of insoluble residue, which accounts for 1.6 wt.% of the brecciated limestone underlying the clay layer, is dominated by muscovite, quartz and kaolinite, which is significantly different from that of clay.

The origin of clay cannot be determined unambiguously. Different mineral composition of clay and of the insoluble residue from the underlying limestone indicates that most likely clay is not derived from these limestones. It can be presumed that volcanic dust, possibly transported by wind from very distant areas, can be the source of the clay material, which is a result of volcanic dust weathering and subsequent diagenetic processes.

Interstratified chlorite/smectite minerals from some epithermal Au-Ag vein deposits in Japan, occurrence characteristics and chemical composition

Yoneda, T.[1*], Mokko, T.[2] & Sato, T.[1]
[1]Laboratory of Environmental Geology, Faculty of Engineering, Hokkaido University, Sapporo, Japan
([*]yonet@eng.hokudai.ac.jp)
[2]Graduate School of Engineering, Hokkaido University Sapporo, Japan

Interstratified chlorite/smectite minerals including corrensite occur widely in hydrothermal ore deposits [1]. The occurrence characteristics and mineralogical properties of chlorite/ smectite minerals are important in understanding the formation in hydrothermal environments and the usefulness of hydrothermal indicators in exploration for ores. The occurrence characteristics and chemical composition of the minerals from some Neogene epithermal Au-Ag vein deposits in Japan were investigated by XRD, optical microscopy, SEM, ATEM and EPMA.

The chlorite/smectite minerals are frequently observable as a vein mineral occurring in the ore veins and as an alteration mineral in the host rocks. In the former case it is characteristic that the minerals show microscopically banded or spotted shapes of aggregates in vein quartz, closely assembled with Au-Ag minerals and/or base metal sulphide minerals, and occasionally with manganese minerals. The chlorite/smectite minerals contain Mn in addition to the major octahedral cations (Mg, Fe). The Mn content of the minerals reflects the mineral assemblage, and the minerals assembled with rhodochrosite ($MnCO_3$) show higher Mn content than those without rhodochrosite. It is characteristic that grain by grain ATEM-analysis of the minerals shows a negative correlation of (Mn + Fe) vs. Mg. In addition, Mn/Fe ratios of the chlorite/smectite minerals vary in a wide range and positively correlate with the Mn/Fe ratios of coexisting sphalerite [(Zn, Fe, Mn)S]. As alteration mineral in the host rocks, spatial distribution of the chlorite/smectite minerals exhibits a close relationship with that of the Au-Ag ore veins [2].

These observations suggest that the interstratified chlorite/smectite minerals closely associated with the epithermal Au-Ag vein deposits have formed in and around the ore veins during the Au-Ag ore formation, and that the mineralogical properties of the minerals have been constrained by the hydrothermal conditions of the vein formation.

[1] Yoneda, T. & Watanabe, T. (1989) *Mining Geol.*, **39,**181-190. [2] Murata, K. et al. (2008) *Res. Geol.*, **58**, 111-119.

Geological, mineralogical and chemical characterization of kaolinite from Micaya, La Paz- Bolivia

Zeballos, A.[1*], Weihed, P.[1] & Blanco, M.[2]
[1]Dept. of Chemical Engineering and Geosciences, Technological University of Luleå, Sweden (*arizeb@ltu.se)
[2]Institute of Geology and the Environment, Universidad Mayor de San Andrés, La Paz, Bolivia

The aim of this study is to characterize clay deposits in the Micaya area located between the towns of Totorani and Colquencha, in the North Altiplano, Aroma Province, La Paz in Bolivia. This area was studied in order to enhance the knowledge of the local geology and to characterize kaolinite clay deposits identified within the Vila Vila formation. Geological mapping and chemical and mineralogical analytical techniques such as x-Ray Diffraction (XRD), Differential thermal analysis (DTA), Thermo-gravimetric Analysis (TG) and Induced Couple Plasma (ICP) have been used in this study.

In the Bolivian Altiplano, three main deposits of clays have been discovered, all of them used as construction materials [1]. The clay deposits are widely distributed in the country, and are derived from alteration and weathering of igneous and sedimentary rocks, transported and eventually deposited in the Tertiary and Quaternary sedimentary basins. The geologic mapping was performed in order to identify lithological and geological features, and clay samples from the Vila Vila Formation were collected for analysis and igneous samples for petrographic studies.

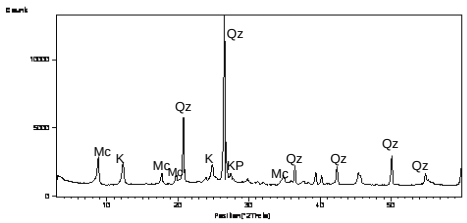

Fig. 1: Representative X-ray powder diffraction pattern of a sample from the Vila Vila Fm., showing the mineral assemblage.

In Figure 1, the XRD pattern of a representative sample from the Vila Vila formation is shown. Quartz is the major constituent showing a strong peak at 26,8° very characteristic of this phase, and is estimated semi-quantitatively as 56 wt.%. Muscovite is represented by a peak at 8,81° and estimated as 21 wt.%, kaolinite shows a peak at 12,3°, characteristic of this mineral phase [2] and corresponding to 18 wt.% and finally potassium feldspar, semi-quantitatively corresponds to 5 wt.%.

ICP analysis result confirms the XRD results with an SiO_2 content of 71wt.% and an Al_2O_3 content of 16,7wt.% for the same samples. DTA and TG analysis show an endothermic peak at 573°C related to the transformation of α-quartz to β-quartz and also an exotherm peak at 989, 1°C due to the phase change of kaolinite, when the hydroxyl (OH) groups are lost during heating.

This initial study shows that kaolinite is a major constituent of the Vila Vila Formation and could constitute a new important source of commercial kaolinite clay in Bolivia.

[1] Escobar-Diaz, A., Bellot-La Torre, J. & Jurado-Aramayo, E. (2000) *Bull. Natl. Serv. Geol. Mining*, **22**, 47-74. [2] Brown, G., & Brindley, G.W. (1980) in Brindley, G.W. & Brown, G. (eds.) Mineral. Soc. Monogr., **5**, 305-359.

Character of chlorite composition in Palaeo-Uplifts of Tarim Basin, China

Zhao, M.[1*], Ji, J.F.[1], Chen, X.M.[1], Wu, C.Z.[1], Chen, Y.Q.[2], Pan, Y.G.[1] & Wu, B.[1]
[1]School of Earth Sciences and Engineering, Nanjing University, Nanjing, China (*zming412@nju.edu.cn)
[2]Survey and Design Institute of Xinjiang Tarim Oilfield, Korla, China

Chlorites are common in mudstones of the Mesozoic Formations in Palaeo-Uplifts of Tarim Basin, China. In order to study the chemical composition of chlorites, the authors collected samples systematically from different depths of bored wells. The rock samples were prepared as probe flakes. The chemical composition of was analyzed by EPMA. The analytical results are listed in Table 1.

Table 1: Results of EPMA measurements on chlorites

depth (m)	2777.4	3586.5	4405.3	5261.2
n	19	13	18	25
Al^{IV}	0.8839	1.0106	0.9880	0.9396
Al^{VI}	1.6384	1.7311	1.5581	1.6376
Si/Al	1.2462	1.0986	1.1906	1.1958
Fe/Fe+Mg	0.4551	0.5049	0.5340	0.5940
Ave.Temp (℃)	249.72	249.73	195.73	144.46

n: number of samples

The results show that in all cases the content of octahedral Al is greater than that of tetrahedral Al (Table 1), which suggests an authigenic origin and typical of what is found in other diagenetic chlorites [1,2]. The excess Al in the octahedral sites is due to the relatively high Si/Al ratio found in these authigenic chlorites (Table 1). The burial depth is strongly correlated with the Fe/Fe+Mg ratio of the chlorite. Using standard methods of geothermometry, for chlorite from the depth of 5261.2 m, a significantly lower crystallization temperature is estimated than for those from the shallower depths (Table 1). Using SEM, chlorite crystals appear together with NaCl grains except of the sample from the depth of 5261.2 m. Considering that other parameters (fO_2 and pH of the solution, coexisting mineral assemblages, and the bulk mineral composition of the host rock etc.) influence chlorite composition [3], an increased salinity indicated by the NaCl grains would be a major parameter influencing the composition of the chlorites in the area. The chemical analysis and the trace element data of rocks also show that the content of Na_2O is only 0.77 wt% in the rocks that does not contain NaCl grains , and the ratio of Sr/Ba is only 0.2; while the content of Na_2O is 1.14-2.29 wt% in the NaCl-rich rocks where the ratio of Sr/Ba is 0.4-5.7. These data can reflect the relative paleosalinity of the rocks. Because the salinities from the depths of 2777.4m and 3586.5m are higher than that of 4405.3m, thus it can be estimated the paleotemperatures are also higher. Furthermore, the paleotemperature from 5261.2m is the lowest since no NaCl grains can be observed at this depth. Therefore, chlorite geothermometry should be used with caution.

Acknowledgements: This work is supported by the National Natural Science Foundation of China (Project number 40772027).

[1] Grigsby, J.D. (2001) *J. Sedim. Res.*, **71**, 27-36. [2] Hillier, S. & Velde, B. (1991) *Clay Miner.*, **26**, 149-168. [3] De Caritat, P., Hutcheon, I. & Walshe, J.L. (1993) *Clay. Clay Miner.*, **41**, 220-239.

Influence of extrinsic factors on granite weathering in a glacier forefield

Wongfun, N.[1*], Brandl, H.[2], Furrer, G.[1] & Plötze, M.[3]
[1]Inst. of Biogeochemistry and Pollutant Dynamics, ETH Zurich, Switzerland ([*]nuttakan.wongfun@env.ethz.ch)
[2]Inst. of Evolutionary Biology and Environmental Studies, University of Zurich, Switzerland
[3]Inst. for Geotechnical Engineering, ETH Zurich, Switzerland

Initial weathering processes and soil formation are of particular interest in alpine postglacial area due to their crucial role on life under harsh conditions [1]. At near-neutral pH under aerobic conditions, the availability of nutrients in fine-grained rock material and soil is usually very low. To overcome this limitation, microorganisms and plants modify their local environment by various exudates including organic ligands, siderophores and also cyanide, which is a very important agent during the initial period of colonization and soil formation.

We study mechanisms of weathering of primary rock-forming minerals in terms of intrinsic (e.g. mineralogy, surface area) and extrinsic weathering factors (e.g. pH, Eh, concentrations of ligands). Rocks and weathered stream sediments were obtained from the Damma glacier area (Central Alps, Switzerland) at approximately 2200 m.a.s.l.

Mineralogical composition determined by X-ray diffraction spectroscopy and Rietveld analysis shows homogeneity throughout the glacier forefield. Grain-size distribution is influenced by hydrological factors such as temporal availability and flow velocity of water. In the grain-size fraction <250 µm, the effect of weathering processes was observed from the loss of feldspar and biotite.

In addition to field observations, weathering of crushed granite is investigated in controlled lab experiments. At 25 °C, the influence of cyanide is studied in batch reactors as function of pH and ligand concentrations. The concentration of cyanide is maintained by a constant partial pressure of hydrogen cyanide through gas bubbling. Thus, the concentration of cyanide anion strictly depends on pH. Preliminary results show that the presence of cyanide leads to an increase in the mobilization of phosphorus and nutrient cations (e.g. calcium and magnesium).

[1] Bernasconi, S.M. et al. (2008) *Mineral Mag.*, **72**, 19-22.

Initial pedogenesis in a recently exposed Alpine proglacial area

Mavris, C.[1*], Egli, M.[1], Plötze, M.[2] & Haeberli, W.[1]
[1]Dept. of Geography, University of Zurich, Switzerland ([*]christian.mavris@geo.uzh.ch)
[2]Institute for Geotechnical Engineering, ETH Zurich, Switzerland

Climate change and glacier melting feed the need for understanding the processes related to weathering of recently exposed areas. Past studies in high Alpine environments show that clay mineral formation rates are higher in younger soils (<1000 yr) than in older soils (>10000 yr). However, investigations of processes that occur in the first decades of soil formation are rare.

In the present study we investigated the clay mineral formation in a recently exposed high Alpine chronosequence. The study was undertaken in the Morteratsch glacier forefield, located in SE Switzerland. The progressively exposed proglacial area offers a full time sequence from 0 to 150 yr old surfaces. The rock basement is the Bernina crystalline unit, a lithostratigraphic formation that is mostly constituted of Variscan granitoid rocks. Previous mineralogical studies carried out in the soils of the proglacial forefield [1] show a decrease of biotite and epidote as a function of time in the fine earth fraction (<2 mm). Mineralogical measurements of the clay fraction (<2 µm) were now carried out using XRD and DRIFT. The X-ray investigations included treatments of the clay fraction (Mg- and K-saturation, ethylene glycol solvation, heating at 335 and 550°C), a hot Na-citrate treatment to determine low-charged 2:1 clay minerals, whose expansion was hindered in the untreated state by interlayered polymers, and a layer charge estimation using alkylammonium (C18). Furthermore, analyses in the d(060) range were carried out. Decreasing content of trioctahedral phases with time in the clay fraction confirm active chemical weathering processes and formation and transformation mechanisms of parent rock mineralogy.

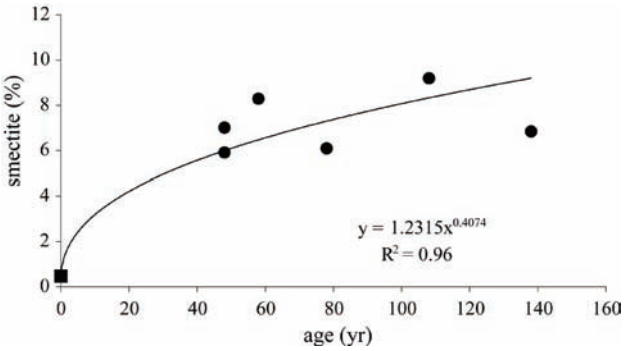

Fig. 1: Smectite formation as a function of time.

Smectite, having a charge of about 0.3 per half formula unit, was detected in a small amount already in the parent material. Along the selected chronosequence, smectite content increased steadily (Fig. 1). Hydroxy-interlayered smectites (HIS) were also present in the very early stages of soil formation and showed a weak increasing tendency with time. The clay mineral formation and transformation processes that are detectable already within a time span of 150 yr, confirm the high reaction rates of young areas in the glacier forefield.

[1] Mavris, C. et al. (2010) *Geoderma*, **155(3-4)**, 359-371.

Weathering and pedogenesis from ultrabasic rocks (dunite-harzburgite complex) in bioclimatic conditions of mountainous tundra, the Polar Urals, Russia

Lesovaya, S.[1*], Krupskaya, V.[2,3], Vigasina, M.[3] & Melchakova, L.[3]
[1]Dept. of Physical Geography and Landscape Planning, St. Petersburg State University, St. Petersburg, Russia ([*]lessovaia@yahoo.com)
[2]Institute of Geology of Ore Deposits, Petrography, Mineralogy and Geochemistry (IGEM RAS), Moscow, Russia
[3]Geological Faculty Moscow State University, Moscow, Russia

Ultrabasic rocks of the Rai-Iz massif, the Polar Urals (Russia) are represented by a dunite - harzburgite complex. Shallow Haplic Cryosols (Reductaquic) [1] are located in mountainous tundra where the permafrost is at a depth of ~ 30cm. Crushed stones and gravels of serpentinous dunites (olivine) are made up by ~ 70% of the total volume in sola. Olivine grains were broken into fragments; in veins, olivine may be replaced by serpentines, talc, and chlorites. Serpentine is also may be replaced by chlorite. Fragments of olivine, amphiboles, chlorites, serpentine, and pyroxenes are frequent in thin sections of soil horizons. Source of pyroxenes are harzburgite.

Mineral identification and swelling properties of minerals were studied in fine size fractions (<1μm and 1-5μm) by a complex of methods: thermal analysis, infrared spectroscopy, scanning electron microscopy, and X-Ray diffraction (XRD) in natural disordered state and oriented mono-cationic forms (Mg, Li, K) - air-dried, ethylene glycol solvated and heated at 550°C during 2 hours.

The studied solum (loamy - clayey loamy) is pH- neutral in the upper and alkaline in the basal horizons keeping by high amounts of exchangeable Mg. In fine size fractions of sola inherited serpentine (chrysotile), talc, and chlorite are identified as well as pedogenic minerals [2]. Pedogenic minerals that are appeared in solum and are absent in rock, are represented by smectite and vermiculite. These minerals are characterised by different distribution in solum. Smectite is present in the bottom (Bgf) horizon as well as in the upper (Ah) where its content decreases. Vermiculite is identified only in the upper horizons of solum. This distribution could be a result of the acidic effect of moss and lichens despite the pH value of bulk samples. The acidic effect is the cause of: (i) selective decomposition of smectite as the most unstable minerals in acid conditions; and (ii) vermiculite appearance as a result of chlorite transformation. The intensity of processes (smectite decomposition and chlorite transformation) increases probably due to permafrost influence leading to pronounced rock disintegration and rise of their dispersion as a consequence of stability of inherited silicates.

Acknowledgements: This work was supported by Russian Foundation for Basic Research, project 09-05-00302 and 10-05-00300.

[1] World Reference Base for Soil Resources (2006) *World Soil Resources Reports*, 103, FAO, Rome. [2] Lessovaia, S.N. & Polekhovsky, Yu.S (2009) *Clays Clay Miner.*, **57**, 476-485.

Clay mineralogy and organo-mineral associations of Carboniferous paleosols (Moscow region, Russia)

Alekseeva, T.V.[*], Zolotareva, B.N., Kabanov, P.B. & Alekseev, A.O.
Institute of Physical, Chemical and Biological Problems of Soil Science, Russian Academy of Sciences, Pushchino, Russia ([*]alekseeva@issp.serpukhov.su)

Lower Carboniferous (Missisipian) and Upper Carboniferous (Pennsylvanian) cyclothems and subaerial unconformities of the Moscow Basin contain abundant paleosols [1]. Here we report the properties of two Lower Carboniferous (334-326 My) and Late Carboniferous (308±2 My) paleosols which were obtained by means of the following methods: XRD, XRF, HCNS, FTIR and solid-state CP/MAS ^{13}C – NMR. Additionally chemical OM fractionation has been done [2].

For Holocene paleosols organic matter (OM) mineralization results in the organic carbon (OC) loss which reaches 50-70% after several hundred years after burial. More ancient paleosols as a rule contain only traces of OC (<1%), which is predominantly concentrated in their clay fraction [3]. OM transformation in paleosols includes not only quantitative but also the compositional changes and the increasing of humic acids and aromatic component is documented

Both Missisipian paleosols were formed under (semi) humid climate. They are smectitic, where beidellite (Profile 1) and saponite (Profile 2) predominate. OC content in their clay fraction is 1.2% and 0.5% respectively. Humic acids dominate in both profiles (C_{HA}/C_{FA} = 1.23-1.53). Humin content is 45% in Profile 1 and 18% in Profile 2. ^{13}C – NMR spectra are very similar and simple with the absolute predominance of aromatic component (60-64%).

Pennsylvanian (semi)arid paleosol is palygorskitic. Its clay fraction contains 1.1 - 1.5% of OC where fulvic acids visibly predominate (C_{HA}/C_{FA} = 0.55). ^{13}C – NMR spectra show the presence of well resolved peaks of alkyl-, aromatic carbon and polysaccharides (30 : 30 : 30%).

Basing on data obtained we suppose that OC content and composition of paleosols depends not only on pedogenesis, age and conditions after burial but also on the mechanisms of OM protection. These mechanisms are determined by the mineralogical composition and interactions between mineral matrix and organic molecules. In case of Pennsylvanian (semi)arid paleosol the labile organic compounds (polysaccharides) were stabilized by palygorskite matrices to a similar extent as humic compounds and both showed the resistance against mineralization for a period more than 300 My. The remarkable preservation of fulvic type of humus is related to formation of organo-mineral derivate where organic molecules are chemically bound to palygorskite lattice [3].

[1] Kabanov, P.B. et al. (2010) *J. Sedim. Res.*, **80** (in press). [2] Ponomareva, V.V. & Plotnikova, T.A. (1980) *Humic Substances and Soil Formation*. Nauka, Leningrad. [3] Alekseeva, T.V. et al. (2009) *Dokl. Biol. Sci.*, **425**, 128-132.

Holocene climate dynamic and biogeochemistry of palaeosols

Alekseev, A.O.*, Alekseeva, T.V., Kalinin, P.I. & Tatianchenko, T.V.
Institute of Physicochemical and Biological Problem in Soil Science, RAS, Pushchino, Russia
(*alekseev@issp.serpukhov.su)

Palaeosols can act as integrative records of past climatic, lithological, geochemical, biological, and hydrological conditions. Kurgans in Russian steppe were constructed at different times from the mid-Holocene onwards; they preserve a range of palaeosols recording past environmental changes through this whole interval. Applying a soil magnetism climofunction, calculated from a modern day soil training set, to each set of buried soils enables quantitative estimation of precipitation at each time step when soil burial occurred [1].

The present study was related to the soil biogeochemical processes in connection with climate variation and duration of weathering. XRF analysis for bulk, clay and course fractions of palaeosols samples were done. Mass balance was used to differentiate between pedogenic processes and sources of elemental additions and losses. Considerable changes in the clay and iron oxide mineralogy, molar chemical ratios of the soils permit us to assess the rates of the mineralogical transformations caused by the climate dynamics in the interval of the last 5000 years. A change in soil mineralogy and as a consequence of the transformation of the chemical composition of the buried soils testifies the primary importance of climate factors in comparison with the total duration of the weathering process.

The relationship of ratio of Rb in humus horizon to the background concentration with climatic changes was observed. In soil, the behavior of Rb is controlled mainly by adsorption on clay minerals and organic matter.

The median Rb content is 60 mg kg^{-1} in subsoil and 80.0 mg kg^{-1} in topsoil; with increase in clay fraction up to 150 mg kg^{-1} in topsoil .The average ratio topsoil/subsoil is 1.45 for bulk samples, and 1.27 for clay fraction. The decrease of the K:Rb in the progressive development of soil observed. Plants use K, whereas Rb is not a biologically important cation, so the difference between the two represents pedogenesis development in our case with variability of climate.

[1] Alekseeva, T. et al. (2007) *Palaeogeogr. Palaeocl. Palaeoec.*, **249**, 103-127.

Clay minerals and humic acids in European paleosoils

Wriessnig, K.* & Ottner, F.
Institute of Applied Geology, University of Natural Resources and Applied Life Sciences, Vienna, Austria
(*karin.wriessnig@boku.ac.at)

Soil characteristics of loess-paleosoil sequences reflect the changes of climate and vegetation during past glacial/interglacial cycles. Clay minerals, soil organic matter and carbonate content are indicators of weathering intensity and pedogenesis [1-3]. In warm periods kaolinite and poorly crystallized expandable minerals like smectite and vermiculite were formed, in cold periods enrichment in better crystallized illites, chlorites and feldspars occurred. The composition and structure of humus substances also reflect the climatic and ecological conditions during the time of their formation [4].

Different loess-paleosoil sequences from Wolkersdorf, Krems and Niederabsdorf (Lower Austria) and Dolni Vestonice (Czech Republic) were studied.

The mineralogical composition (bulk sample and clay fraction <2µm) was determined using X-ray diffraction. Dominating clay minerals in samples from all sites are chlorite, illite, and smectite, in some of the samples considerable amounts of vermiculite were found.

Soil analyses included chemical parameters like pH-value, electrical conductivity, total carbon and nitrogen, C/N-ratio, carbonate content and cation exchange capacity of the fine soil fractions. The CEC of the clay fraction was also determined. Grain size analyses were made by a combination of wet sieving and sedimentation.

Humic acids of the paleosoil samples were extracted using 1M NaOH and characterized using thermogravimetry, differential scanning calorimetry, Fourier transform infrared (FT-IR) spectroscopy and mass spectroscopy.

[1] Bajnóczi, B. et al. (2006) *Geophys. Res. Abst.*, **8**, 05228. [2] Karlstrom, E.T. et al. (2008) *Catena*, **72**, 113-128. [3] Vancampenhout, K. et al. (2008) *Quatern. Res.*, **69**, 145-162. [4] Dergacheva, M. (2003) *Quatern. Int.*, **106-107**, 73-78.

Sorption of copper on the eluviaton and accumulation horizons of a brown forest soil

Balázs, R.[1,2], Németh, T.[2*] & Sipos, P.[2]
[1]Eötvös Lorand University, Budapest, Hungary
[2]Institute for Geochemical Research, Hungarian Academy of Sciences, Budapest, Hungary (*ntibi@geochem.hu)

In this study copper immobilization ability in high ionic strength NaCl solution and at acidic pH is examined by comparing the sorption properties of two distinct soil horizons within one profile. The adsorption experiments were carried out on the well distinguishable eluviation and accumulation horizons of a brown forest soil, one of the dominating soil types in Hungary.

The eluviation (E) and accumulation (B_1) horizons of the studied soil profile differ from each other in their mineral composition and clay mineral characteristics. The clay mineral content of B_1 horizon is 30% larger than that of E horizon. According to the XRD studies two major clay mineral phases were distinguishable in the samples: a swelling interstratified chlorite/vermiculite in the B_1 horizon, and a non-swelling, probably hydroxy-interlayered vermiculite in the E horizon.

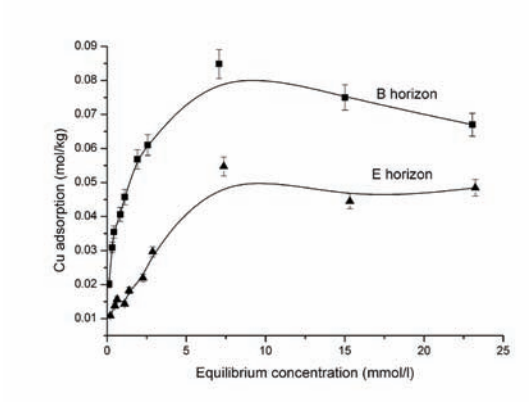

Fig. 1: Cu adsorption isotherms for B and E horizons.

The maximum copper adsorption calculated by Langmuir equation was 0.052 mol/kg Cu (3 304 mg/kg Cu) for the E horizon, and 0.071 mol/kg (4 512 mg/kg) Cu for the B horizon (Fig. 1). The differences arise from the different mineral composition of the distinct horizons. Hydrous iron oxides and swelling chlorite/vermiculite in the accumulation layer increase Cu adsorption capacity, while hydroxy-interlayering in vermiculite, and absence of iron oxides decrease Cu uptake of the eluviated horizon. Based on XRD studies, measurable fraction of Cu was sorbed in the interlayer space of vermiculite by ion exchange mechanism. This sorbed Cu caused the loss of expansion capacity of the vermiculite.

Our study of Cu adsorption on the eluviation and accumulation horizon of a brown forest soil confirmed that the different genetic layers in a soil profile can play different role in the immobilization of heavy metal contaminations.

A K/Ar study of structural and chemical changes of < 2 μm-sized minerals from fertilized soils

Balogh, K.[1*] & Kádár, I.[2]
[1]Institute of Nuclear Research, Debrecen, Hungary
([*]balogh@atomki.hu)
[2]Research Institute for Soil Science and Agricultural Chemistry, Budapest, Hungary

K/Ar dating is based on the measurement of radiogenic ^{40}Ar isotope formed by the radioactive decay of ^{40}K. The K/Ar clock starts (1) at the time of mineral formation, if this happens below the so called „closure temperature", or (2) when it cools below its closure temperature. Diagenesis and low grade metamorphism is dated mostly by K/Ar method using < 2 μm-sized minerals. Difficulties of interpretation of age data have been reviewed recently [1].

During erosion, transportation and deposition clay minerals retain their K/Ar age. The formal age of clay minerals of the Hungarian Plain is mostly Mesozoic. The influence of fertilizers on the structure and chemistry of clay minerals are summarized in [1]. Research of clay mineral transformations in fertilized soils is in progress in Hungary since the 70's [2,3].

During structural change the possible escape of ^{40}Ar(rad) and incorporation of K decrease the K/Ar "age". The samples are taken from soils treated with variable doses of N, P and K fertilizers for 35 years (Table 1). The site of the study is Nagyhörcsök, with calcareous chernozem loamy soil (20-23% clay, 5% $CaCO_3$, 3% humus in the upper 0-30 cm layer). The groundwater table was at a depth of 13-15 m, the water balance of the site was negative. The K-balance was between –2.4 and +4.9 t/ha at the end of the 35 years of the field trial. The NH_4-acetate + EDTA soluble K-content (column 3 in Table 1) showed K-deficiency and high K-supply of the plots.

Table 1: K/Ar ages of clay minerals in NPK treated soils

No.	*N*	*P*	*K*	*(1)*	*(2)*	*(3)*	*(K%)*	*Age±σ My*
1	0	0	0.00	1.88	-1.88	145	2.340	123.6±4.8
2	0	0	2.07	2.48	-0.41	235	2.542	115.1±3.6
3	0	0	4.15	2.67	+1.48	285	2.503	121.0±3.9
4	0	0	6.22	2.78	+3.44	407	2.679	115.7±3.7
5	1	0	2.08	3.47	-1.39	149	2.482	132.4±5.2
6	1	0	4.15	3.80	+0.35	197	2.443	130.9±5.1
7	1	0	6.22	4.22	+2.00	354	2.622	119.5±4.6
8	2	4	0.00	2.44	-2.44	94	2.193	127.4±5.1
9	2	5	0.00	2.00	-2.00	117	2.305	133.0±5.1
10	2	5	7.06	2.15	+4.91	754	2.975	107.5±4.2
11	2	5	7.06	2.35	+4.71	701	2.806	110.2±4.4

Given fertilizers: N0=0, N1=100, N2=200kg/ha/year (N dose); P0=0, P4=50, P5=100 kg/ha/year (P_2O_5 dose); K: t/ha/35years; (1): K uptake by plants in t/ha/35years; (2): K-balance in t/ha/35years; (3) K/soil (mg/kg); K%: in dated mineral

Data in Table 1 show that adding K decreases while N increases the "age". K added by fertilizers and trans-ported by the vegetation change the "age" similarly.

[1] Meunier, A. & Velde, B. (2004) *Illite*. Springer, Berlin-Heidelberg-N.Y. [2] Varjú, E.M. & Stefanovits, P. (1979) In: Mortland, M.M. & Farmer, V.C. (eds.) *Develop. Sedimentol.*, **27,** 349-358. [3] Rózsavölgyi, J., Kádár, I. & Sarkadi, J. (1986) *Növénytermesztés*, **35,** 325-331.

Clay mineralogy of the nickel laterite profiles associated with the Western Vardar ophiolite zone

Bermanec, V.[*], Strmić Palinkaš, S., Palinkaš, L.A., Žigovečki Gobac, Ž. & Kampić, Š.
Institute of Mineralogy and Petrography, Dept. of Geology, University of Zagreb, Croatia ([*]vberman@public.carnet.hr)

Two laterite profiles associated with the Western Vardar ophiolite zone have been investigated in order to estimate the formation conditions of the secondary minerals and the trace element behaviour during tropical weathering of serpentinite from the ophiolitic complex.

Nickel laterite deposit in the village Ba (44.15°N, 20.20°E), Serbia, has been formed by the weathering of serpentinite thrust over the Triassic limestone. The weathering of serpentinite in karstic environment produced a number of nickel-bearing minerals including nickeliferous clay minerals [1]. According to X-ray powder diffraction (XRPD) analysis the principal clay mineral is montmorillonite with cation exchange capacity (CEC) in the range between 70 and 73 mEq/100g. Gibbsite and minor amount of 7Å-halloysite occur as well.

The Ni-laterite weathering crust at Gornje Orešje locality (46.01°N, 16.22°E), Croatia, comprises, from the base up, the bed rocks (serpentinized harzburgite, massive apoharzburgitic serpentinite, apodunitic serpentine and schistose serpentinite); the saprolite zone (highly fractured and oxidized serpentinite) and the clayey zone [2]. Montmorillonite represents the most dominant clay mineral.

The following reaction illustrates the breakdown of serpentine (lizardite) into Mg-montmorillonite:

$$11\ Mg_3Si_2O_5(OH)_4 + 14\ Al^{3+} + 22\ H^+ \leftrightarrow$$
$$6\ [Al_2(Si_{3.67}Al_{0.33})O_{10}(OH)_2]Mg_{0.167} + 32\ Mg^{2+} + 27\ H_2O$$

Logarithmic activity diagram, constructed for standard conditions (p= 1 bar, t =25°C) according to thermodynamic data published by [3] and [4], indicates stability of montmorillonite at $log\ a(Al^{3+})/\ a(H^+)^3$ and $log\ a(Mg^{2+})/\ a(H^+)^2$ above 10 and 0, respectively (Fig. 1). Mobility of aluminium in form of Al^{3+} required decreased pH ($a(Al) = 10^{-6}$; pH < 4.4).

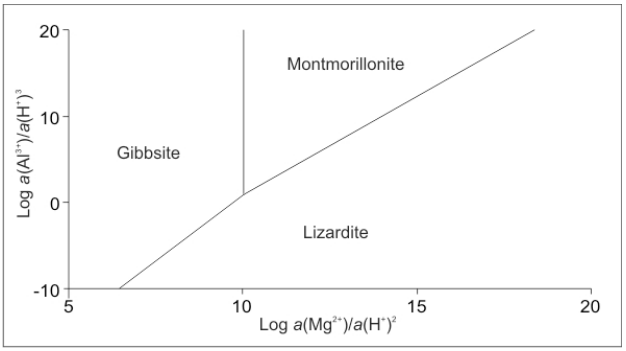

Fig. 1: Stability of Mg-montmorillonite, gibbsite and lizardite (p=1 bar; t=25°C).

[1] Maksimovič, Z. (2004) *Bull. Acad. Serbe Sci. Arts. Classe Sci. Nat. Math., Sci. Nat.*, **42**, 342-361. [2] Palinkaš, L.A. et al. (2006) in Gerzina, N. & Resimić-Šarić, K. (eds.) *Mesozoic Ophiolite Belts of the Northern part of the Balkan Peninsula – Ophiolites.* Faculty of Mining and Geology, Belgrade, 97-101. [3] Woods, T.L. & Garrels, R.M. (1987) *Thermodynamic values at low temperature for natural inorganic materials.* Oxford University Press, New York. [4] Brookins, D.G. (1988) *Eh-pH diagrams for geochemistry*. Springer-Verlag, Berlin.

Clay mineral alterations in a chronosequence of podzols on Alnö Island, Sweden

Bonatotzky, T.[1*], Haslinger, E.[2] & Ottner, F.[1]
[1]Inst. of Applied Geology, University of Natural Resources and Applied Life Sciences, Vienna, Austria
([*]theresa.bonatotzky@boku.ac.at)
[2]Energy Dept., Sustainable Building Technologies, AIT Austrian Institute of Technology, Vienna, Austria

Chronosequences are potent instruments for pedological investigations and testing pedological theories. Chronosequences are especially useful for soils that have developed on surfaces of known age, e. g. moraines, alluvial fans and terraces, lava flows and coastal sand dunes. Since the highest elevation above sea level on Alnö is 128 m at present, it was calculated that the emergence must have taken place between 7400 and 7700 years BP. As this is at the same time the beginning of terrestrial soil formation, the oldest soils on the island are subsequently between 7400 and 7700 years old. By considering the uplift of the land and the development of the shoreline, the age of a soil at a certain elevation above sea level can be determined.

Chronosequences are potent instruments for pedological investigations and testing pedological theories. Chronosequences are especially useful for soils that have developed on surfaces of known age, e. g. moraines, alluvial fans and terraces, lava flows and coastal sand dunes. Since the highest elevation above sea level on Alnö is 128 m at present, it was calculated that the emergence must have taken place between 7400 and 7700 years BP. As this is at the same time the beginning of terrestrial soil formation, the oldest soils on the island are subsequently between 7400 and 7700 years old. By considering the uplift of the land and the development of the shoreline, the age of a soil at a certain elevation above sea level can be determined.

When studying soils, the examination of clay minerals is essential for determining their physical and chemical properties, as clays are often highly reactive. Clay minerals are useful for former and current weathering processes, because the weathering intensity depends on the contact area of the mineral particles and the liquid phase. It has been shown, that the rate of chemical weathering increases with decreasing particle size. The formation of clay minerals depends upon physicochemical conditions, parent material and environmental factors. Clay minerals in podzols are often formed by acidolysis, which occurs when the pH is lower than 5. The dominant clay minerals then are smectites, vermiculites, Al-intergrades and Al-chlorites.

The focus of the project is to elucidate the processes of pedogenesis in the Holocene from a clay mineralogical point of view. As clay minerals are sensitive to changes of their environment, they can be used as indicators for soil development during pedogenesis and, subsequently, as indicators for the soil age. The results of the clay mineralogical analyses and of the assessment regarding the applicability of the clay mineral distribution as relative dating method for soils, will be presented.

The effect of electrolytes on the surface layer formation of a basaltic glass

Dultz, S.[1*], Behrens, H.[1], Cramm, S.[2], Helsch, G.[2] & Deubener, J.[2]
[1]Institute of Mineralogy, Leibniz University of Hannover, Germany ([*]dultz@ifbk.uni-hannover.de)
[2]Institute of Non-Metallic Materials, Clausthal University of Technology,Clausthal-Zellerfeld, and Niedersächsische Technische Hochschule, Germany

Volcanic glasses, produced every year in high amounts by rapid cooling of magma, play an important role in the global and local cycling of numerous elements. The dissolution rates of natural glasses are affected by the composition of the surrounding solution. In presence of aqueous species that lead to the formation of Al-complexes, the dissolution rate of basaltic glass will increase [1]. In this study the zeta potential is used to determine the effect of different anions and cations on the surface layer formation of a basaltic glass.

Experiments were performed with a powder of a synthetic basalt glass with typical MORB composition, which has a mean particle size of 1.9 µm and a specific surface area of 1.7 m^2/g. For determination of electrolyte effects (e.g. NaCl, NaF, $Na_2C_2O_4$, Na_2SO_4, $Ca(NO_3)_2$, $Al(NO_3)_3$) on the zeta potential with time, 100 mg of sample were added to 200 ml of the solutions in the concentration range of 0.0001 to 0.005 mol/L. The zeta potential was determined together with the electrical conductivity of the solution (Zeta PALS, BIC).

The presence of F in the suspension resulted in a decrease of the zeta potential, indicating the adsorption of F on the surface of the basaltic glass (Fig. 1). This trend is strengthened at higher F concentrations indicating more extensive F adsorption. For non adsorbing electrolytes at higher ionic strength an increase of the zeta potential by the compression of the diffuse double layer is observed.

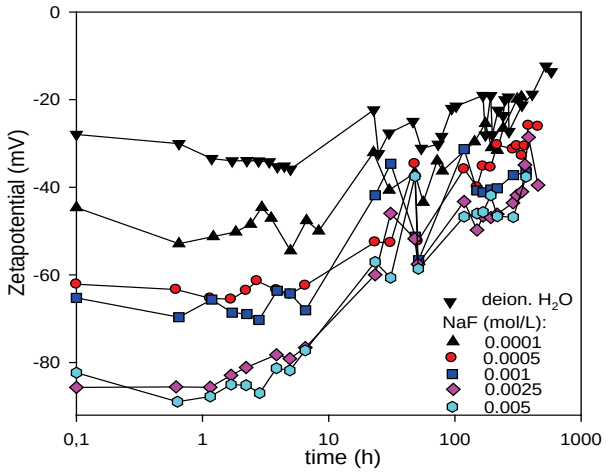

Fig. 1: Effect of NaF on the zeta potential of a basaltic glass in the time period up to 600 h.

With time zeta potential is increasing for all suspensions indicating that most probably Al and Fe in the surface layer are enriched. By the addition of divalent cations together with weakly adsorbing monovalent anions the point of zero charge is reached within the time period of 600 h at slightly acidic pH-values. Here a decrease in the dissolution rate can be assumed which is determined in currently running long term dissolution experiments.

[1] Wolff-Boenisch, D. et al. (2004) *Geochim. Cosmochim. Ac.*, **68**, 4571-4582.

SEM analysis of slickenside surfaces of smectitic soils of Hungary

Fuchs, M.[1] & Nyilas, T.[2*]
[1]Dept. of Soil Science and Agrochemistry, Szent István University, Gödöllö, Hungary
[2]Dept. of Mineralogy, Geochemistry and Petrology, University of Szeged, Hungary ([*]nyilas@gmail.com)

Smectitic soils develop special morphological characteristics under alternate wet-dry conditions determined by swelling pressure, occurring when the swelling clays adsorb water. The dilation of clays during hydration generates an abiotic stress resulting in special morphological features like slickensides [1], and also determines fertility, soil management practises and the success of crop production. These unique smectitic soils are classified as Vertisols according to the modern soil classification systems.

The slickensides, the most characteristic Vertisol phenomena, are polished and shiny ped surfaces, produced by one mass of soil sliding past another to relieve the stress generated by the swelling pressure. Surface characteristics of slickensides from a Vertisol of Kisújszállás, Hungary were studied on fractured, undisturbed blocks with planar orientation by Hitachi S-4700 scanning electron microscope.

The SEM analysis of the slickenside surfaces showed differences from the subjacent micromass of the ped interiors with stronger preferred orientation of clay particles, and increase in micropores. Micro-grooves approximately 4 to 20 µm wide (Fig. 1a) were detected according to the direction of the sliding, developed due to plastic deformation, or sand grains translated parallel to the direction of the shear failure. The stress reoriented clay particles resulted in a "face to face" clay alignment on surfaces of slickensides (Fig. 1b)

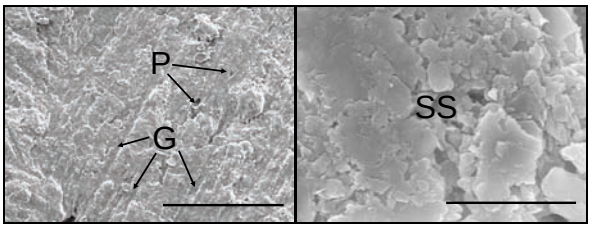

Fig. 1: Scanning electron microphotographs of slickenside surfaces (planar view) of Vertisol of Kisújszállás a) showing grooving (G) and pores (P) (bar length is 300 µm), and b) oriented clay on surface of the slickenside (SS) (bar length is 5 µm).

The presence of an oriented clay layer had direct impact on the orientation and size distribution of pores and cracks also. The presence of stress oriented clay features was resulted in smaller pore size and on slickenside surfaces. Based on the SEM analysis of the slickenside surface of the Kisújszállás Vertisol, the slickenside had pores that were generally less than 7 µm in diameter (Fig. 1a).

These characteristics could make slickensides act as semi-permeable barriers to solute transport, and effect hydrological, and chemical properties of Vertisols, determining agricultural and engineering use also. Thus the knowledge on morphology is essential to be able to make right decisions on suitable management.

[1] Wilding, L.P. & Tessier, D. (1988) in Wilding, L.P. & Puentes, R. (eds.) *Vertisols: Their Distribution, Properties, Classification and Management*. Tech. Mono., **18**, A&M Printing Center, College Station, Texas, 55-79.

Comparison of clay minerals in soils derived from basalts and phonolites under temperate climate of Lower Silesia, Poland

Łobczowski, W.[1*], Weber, J.[1], Tyszka, R.[1] & Kierczak, J.[2]
[1]Institute of Soil Science and Environmental Protection, Wroclaw University of Environmental and Life Sciences, Wroclaw, Poland ([*]wojciech.lobczowski@gmail.com)
[2]Institute of Geological Sciences, University of Wroclaw, Poland

Our study included six soil profiles derived from basalts and phonolites. Each rock was represented by 3 soil profiles. Objects were located in the Sudetes in the Lower Silesia Region, Poland (Fig. 1.). The investigated area lies under temperate climate, with temperatures 7-8.5°C and rainfalls of 650-700 mm. Soil samples were collected in upper parts of the old quarries, at elevation of 250 – 330 m a.s.l. Such approach allowed us to investigate only the effects of parent rock composition on soil properties and weathering products, and to eliminate effects of other soil forming processes. Analyzed soils represent cambisols with shallow profile. Soil samples in this study were collected from the top (A) and parent rock horizons (C) of each profile in order to determine possible differences in clay mineral composition.

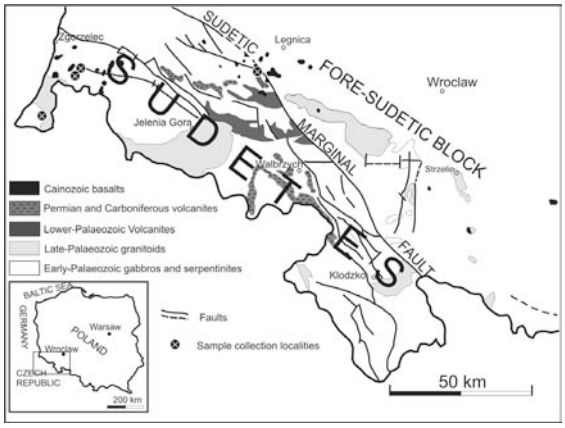

Fig. 1: Sitemap with location of sampling (based on Przybylski [1]).

The clay minerals in each sample were characterized by means of X-ray diffraction patterns and different proportions of clay minerals were observed in phonolites and basalts and also between different basalt types. Kaolinite and illite occur in all studied samples. In soils developed from phonolites kaolinite dominates, illite occurs only in small amounts and vermiculite amount is very low. It is consistent with kaolinite being the main weathering product of K-feldspar and feldspatoids, which are major components of phonolites.

Vermiculite is the dominant clay mineral in two of the investigated basalt derived profiles. Basalt, as a rock rich in Mg- and Fe-, should generally show presence of vermiculite in colloidal fractions in soils under temperate climate. In addition to vermiculite, XRD patterns revealed the presence of kaolinite and illite in the studied samples. In some profiles small amounts of smectites were also observed.

The results of our study showed that, under the temperate climate, weathering products of rocks largely depend on the original mineral composition of the parent rock.

[1] Przybylski, T.A. (2004) *J. Environ. Radioactiv.*, 75, 171-191.

The influence of clay on site characteristics in the Vienna Forest, Austria

Mayrhofer, M.[*], Wriessnig, K. & Ottner, F.
Institute of Applied Geology, University of Natural Resources and Applied Life Sciences, Vienna, Austria
([*]maria.mayrhofer@boku.ac.at)

The Vienna forest is situated in the very east of the Alps, on the western border of the Tertiary Vienna Basin. Covering 1,350 km^2, it is an important local recreation area for Viennese people and also serves as "Green Lung" for the City. In 2005, the Vienna Forest was also designated a Biosphere Reserve by UNESCO.

From Pleistocene till recent days the river Danube is still forming the landscape of the surroundings of Vienna. The following geological classification can be done:

- Gravel and sand from the Danube from Pleistocene till today
- Fine grained sediments like marls from Tertiary time in the Vienna Basin
- Sandstones from the Flysch zone and limestones from the Calcareous Alps
- Red marls – also named "Red Loams" - from the „Klippenzone" of the Ultrahelvetikum

During construction works in the western districts of Vienna (16th, 17th, 18th) extraordinary red loams from the above mentioned "Klippenzone" emerged. In parts of the Vienna forest these red loams are parent material for the pedogenesis.

The term „Red Loam" is generally - and colloquially - used for red soils and comprises Kalkrotlehme and Kalkbraunlehme according to the Austrian Soil Classification System as well as red marls.

Red marls are „Farb-Substratböden". Typical for those types of soil is that the profile of the soil is very much characterized by the colour of the parent material and the genetic differentiation of horizons is hidden. „Kalklehme" are very clayey soils coloured brown to red and developed from the residual material of weathered limestone.

By means of bulk and clay mineral analysis with XRD, STA, FTIR, grain size and further chemical analyses the amount and type of clay minerals in the soils will be characterized. The determined parameters are important for the water and nutrient regime of the forest soils.

The results of bulk and clay mineral analysis done by XRD show unexpected results. The content of clay is very high and reaches from 40 to 60 percent in the investigated samples. Some of them show high amounts of smectite and soil vermiculite and some contain illite and chlorite as well. Although the investigation sites are situated closely to each other, the mineralogical composition of the soils varies and shows different levels of weathering, which is a clear indicator for solifluction processes during the Pleistocene.

Organo - metal and organic matter characteristics of clays from East Maritza Coal Basin (Bulgaria)

Milakovska, Z.I.[1*], Filcheva E.G.[2] & Markova K.I.[3]
[1]Geological Institute, BAS, Sofia, Bulgaria
([*]zlatkam@geology.bas.bg)
[2]ISS "N. Poushkarov" Sofia, Bulgaria
[3]Sofia University "St. Kl. Ochridski", Sofia, Bulgaria

Ten core samples of Miocene black clays from two boreholes (East Maritza Coal Basin, Bulgaria) were characterised by their grain-size distribution, whole rock mineralogy and organic geochemistry. Organic matter composition and type were determined using modified method of Tyurin and Kononova [1,2] based on three extractions with: (1) mixed solution of 0.1 M $Na_4P_2O_7$ and 0.1 N NaOH; (2) 0.1 N NaOH; (3) 0.1 N H_2SO_4. Five fractions were received: 1-pyrophosphate, 2-basic, 3-acidic, i.e. fulvic acids (FA) aggressive fraction, 4-humic acids (HA) total, 5-HA free and/or bound to three valence cations. Humic acids optical characteristics were measured on SPECOL (absorption at λ 465 nm and 665 nm). Zinc and Al content in organo-metal complexes in the extractions were analyzed by means of ICP-OEM.

According to the textural characteristics the clayey sediments are mainly claystones (rarely clayshales) with sandy and silty admixtures up to 30%. Mixed-layered illite/smectite mainly, and kaolinite are the predominant clay minerals. Small amount of quartz and feldspar admixtures were also detected.

The samples studied differ considerably in their total organic carbon (Corg) content (the data fall in the range of 1.21-15.08 %) and do not show any dependence with depth. Non-extracted C_{org} varies from 66.89 to 88.43 %. According to the ratio C_{org} in HA to C_{org} in FA, organic matter is of a humic type in four samples, humic-fulvic - in three, fulvic - in two; and fulvic-humic - in one. In one sample HA were not extracted at all. Humic acids are bound mainly to alkaline earth ions (over 50%) in 7 samples. In two samples only, more than 50% of HA are free and/or bond to three valence cations. Very low content of the aggressive FA fraction (0.1 N H_2SO_4 extract) is characteristic for all samples studied - 0.30-1.61 % of C_{org}. The optical characteristics show that most of the HA are low molecular, low condensed ones, with high values of E_4/E_6 ratio. In three samples E_4/E_6 values vary from 2.16 to 2.74 that probably corresponds to more condensed aromatic cores of their HA.

Aluminium and Zn distribution in all fractions extracted varies irregularly, in a wide range, and independently with the depth. High mean Al values were measured for the pyrophosphate and FA aggressive fraction extracts, and low - for HA free and/or bond to three valence cations. The highest mean Zn values were detected for FA aggressive fractions, and the lowest - for the alkaline fractions. There is one sample (C_{org} - 13.33%) where maximum Al values for pyrophosphate, total and free/or three valences bound HA were measured. In another one (C_{org} - 15.08%) were detected maximum Zn values for basic extracts, HA total, and HA free /or bound to three valence cations.

Based on the result obtained one could suggest that Al in samples studied is bound mainly to HAs whereas Zn is bound mainly to FAs aggressive fraction. It could be also concluded that East Maritza Coal Basin black clays possess presumably low potential for mobile organo-metal complexes generation because the HA are bound mainly to alkaline earth ions.

Acknowledgements: The study is a part of project VU-11/06 financed by NSF, MES, Sofia, Bulgaria.

[1] Kononova, M. (1966) *Soil Organic Matter*. Pergammon Press, London. [2] Filcheva, E. & Tsadilas, C. (2002) *Comm. Soil Sci. Plant Analysis*, **33**, 595-607.

Changes of mineralogical paleoproxy indicators in a Quaternary loess–paleosol section at Beremend, Hungary

Raucsik, B.[1*], Varga, A.[2] & Újvári, G.[3]
[1]Dept. of Earth and Environmental Sciences, University of Pannonia, Veszprém, Hungary
([*]raucsik@almos.uni-pannon.hu)
[2]Hortseed Ltd., Mezőkovácsháza, Hungary
[3]Geodetic and Geophysical Research Institute, Hungarian Academy of Sciences, Sopron, Hungary

Weathering strongly affects mineralogy of sediments including loess deposits with intervening paleosols. A variety of semiquantitative tools has been developed to examine past weathering and pedogenesis, and to reconstruct both paleoenvironmental and paleoclimatic conditions at the time of paleosol formation.

In this study, mineralogical composition was analyzed on loess and paleosol samples from SE Transdanubia, Villány Hills, Hungary. The studied Beremend section represents the Old Loess Series (OLS; ~380–700? ka; Marine Isotope Stage (MIS) 11–17?) and partially the Young Loess Series (YLS; ~130–250? ka; MIS 5–7?) exposing three reddish brown forest soils (Be-S1, Be-S2, Be-S3; OLS) and a brown forest or forest steppe soil (Be-S4; YLS). Unconformities among sediments appear to be common.

The bulk mineral composition of sediments estimated from XRD data indicates that quartz and smectite are the dominant minerals. Interestingly, throughout both the loess and paleosol units, relative proportion of quartz shows no variation. Loess samples contain high amounts of calcite; additionally, dolomite occurs in all loess samples and in the Be-S4 samples. Illitic material together with chlorite is present in all samples but usually in small proportion. Albite, K-feldspar, kaolinite, and goethite are the typical minor components with amorphous material. Aragonite is present only in a single loess sample.

In the clay fraction of the sediments, varying amounts of smectite, illite, chlorite, and kaolinite are present. Paleosol samples can be characterized as smectite-rich compared to loess samples which contain higher amounts of illite. The entire section shows no obvious variation in kaolinite content. Chlorite content is generally low, and slightly decreases upwards.

The quartz-normalized bulk kaolinite content shows systematic variations with lithology, especially in the lower and middle part of the Beremend section (corresponding to OLS). The bulk kaolinite/quartz ratio increases upwards in loess horizons, whereas it decreases in paleosol layers. As a paleoproxy indicator, changes in bulk kaolinite/illite ratio (K/I) show significant differences between the Beremend paleosol ($K/I > 1$) and loess ($K/I < 1$) samples suggesting fluctuations in the intensity of coeval continental hydrolysis. Based on clay mineralogy, the same stratigraphic pattern in the K/I ratio is apparent. In the lower and middle parts of the section (OLS), however, the K/I ratios in paleosols are significantly higher than those of fossil soil Be-S4 (YLS). Synchronous changes in the values of smectite/illite (S/I), smectite/(illite+chlorite) (S/I+C), and smectite/kaolinite (S/K) ratios are also observed.

The relatively higher S/I, S/(I+C), and S/K ratios, observed in paleosols, suggest a strengthened chemical weathering and weak physical erosion. By contrast, lower ratios in loesses, corresponding to glacial periods, indicate intensified physical erosion and weakened chemical weathering. Fluctuation of erosion rate is also supported by variations of bulk kaolinite/quartz ratio. Significantly lower values of mineralogical proxy indicators in the upper part of the Beremend section, corresponding to the YLS, may indicate a climate deterioriation with decreasing rates in continental erosion and chemical weathering from the OLS to YLS in SE Transdanubia.

Origin of aluminium from salt efflorescence on sandstone exposures

Schweigstillová, J.[1*], Bruthans, J.[2] & Mikuš, P.[2]
[1]Institute of Rock Structure and Mechanics of the ASCR, v.v.i., Prague, Czech Republic ([*]finy@seznam.cz)
[2]Charles University in Prague, Faculty of Science, Prague, Czech Republic

Detailed study of salt efflorescence composition in many sandstone castellated rocks in the Middle Europe shows presence of Al-sulphates (alums), mostly on sandstone with clay sandstone matrix.

Isotopic composition confirmed the atmospheric origin of the salt efflorescence [1], but precipitation contains no aluminium [2]. Research in the sandstones of the Northwest Bohemia showed that sandstone vadose water may contain elevated concentrations of Al, Zn, and Cd [3].

Therefore, formation of alums can be explained by the partial dissolution of clay minerals or feldspars present in the sandstone matrix. Release of aluminium from these phases is facilitated by the low pH of the precipitation (pH 4–5) and also locally by organic acids, traces of which were found in the studied efflorescence by the use of infrared spectroscopy [1].

We studied several waters from vadose zone of sandstone and soil waters in one protected landscape area (PLA) from the Northern Bohemia (Czech Republic). Chemical composition of studied waters proved elevated content of aluminium, silica and few other ions compared to precipitation composition normalized to ET enrichment [4].

Study demonstrated that aluminium can be released from clay sandstone matrix (clay minerals or feldspars) or soil cover of sandstone. Presence of alums and other Al containing salt efflorescence is thus valuable indicator of vadose zone acidification, for example in Northern Bohemia.

Acknowledgements: The research was supported by projects no. IAA300130806 and KJB315040801 of the Grant Agency of the Academy of Sciences of the Czech Republic and research project MSM00216220855 (Charles University in Prague) and AV0Z30460519 (Institute of Rock Structure and Mechanics of the ASCR, v.v.i.).

[1] Schweigstillová, J. et al. (2009) *Environ. Geol.*, **58**, 217-225. [2] CHMI - rain water chemistry database: http://www.chmi.cz/uoco/indexe.html. [3] Patzelt, Z. (2007) in Härtel, H. et al. (eds.) *Sandstone Landscapes.* Administration of the Bohemian Switzerland National Park and Academia, Prague, 93-96. [4] Bruthans, J. & Schweigstillová, J. (2009) in Rapantová, N. & Grmela, A. (eds.) *Water – the strategic raw material for the 21th century.* VŠB - Technical University of Ostrava, Ostrava, 43-46 (in Czech).

The study of clay minerals from the granitoids soils developed in a temperate climate

Szadorski, J., Weber, J.[*], Tyszka, R., Dębicka, M. & Kocowicz, A.
Institute of Soil Science and Environmental Protection, Wroclaw University of Environmental and Life Sciences, Wroclaw, Poland ([*]jerzy.weber@up.wroc.pl)

Eight shallow soil profiles developed from different granitoids (leucogranite, granite, granodiorite and tonalite) were investigated, two from each rock type. The soil profiles were located in the Fore-Sudetic Block and the Sudetes, Lower Silesia, Poland (Fig. 1). To investigate only relationships between clay mineral and parent rock composition, and to avoid the effects of other soil forming factors, the profiles were located only on the top parts of hills 169 – 433 m a.s.l. and in similar climatic conditions, including rainfall 600-750 mm and annual average temperature 7.0 – 8.5 oC. The investigated soils were forest and meadow cambisols and leptosols. Two samples were collected from each of the eight profiles (the A and the parent rock horizons) to determine the possible variation in the composition of clay minerals within the profile.

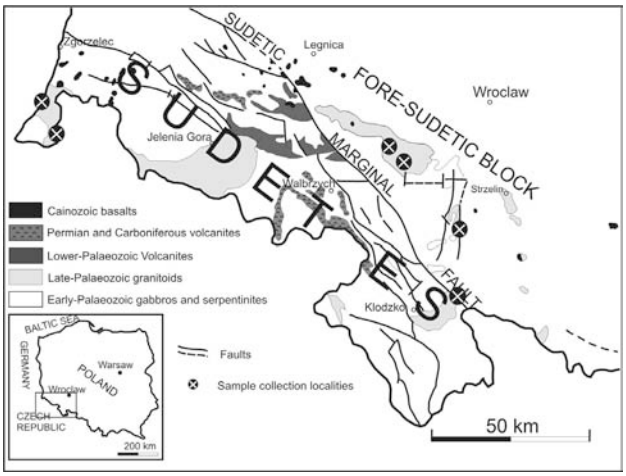

Fig. 1: Sitemap with location of sampling (based on Przybylski [1]).

The study of clay minerals showed that colloidal fraction of soil material – although developed from different granitoids and build up of different feldspars as well as different amounts of mafic minerals – consists of the same minerals. Illite, kaolinite and vermiculite are present in all of the examined profiles, but illite distinctly dominates in soils derived from leucogranite, granite and granodiorite, whereas vermiculite is the main clay mineral in tonalite derived soils, independently of the depth of the soil horizon. On the other hand, soils derived from leucogranite, granite and granodiorite reveal presence of vermiculite in the deeper horizons, while A horizons indicate significant decrease or lack of this mineral. This may suggest the process of transformation of vermiculite into illite, occurring over the time under conditions of temperate climate of Lower Silesia, SW Poland.

There were also differences in clay mineralogical composition between deeper horizons of soils derived from different kinds of granites. Vermiculite was observed in soil material derived from biotite-granite, while there were found only very weak evidence of this mineral in weathered material of two-micas-granite. This confirms that the presence of biotite in rock favours formation of vermiculite during the weathering processes.

[1] Przybylski, T.A. (2004) *J. Environ. Radioactiv.*, **75**, 171-191.

The effect of hydrological conditions and pH on phyllosilicate transformations in pyrite-bearing schist weathering zone in Wieściszowice (Lower Silesia, SW Poland)

Uzarowicz, L.[1], Michalik. M.[2] & Bylina, P.[3*]
[1]Faculty of Geodesy and Cartography, Warsaw University of Technology, Warsaw, Poland
[2]Inst. of Geological Sciences, Jagiellonian University, Cracow, Poland
[3]Inst. of Ceramics and Building Materials, Warsaw, Poland
([*]p.bylina@isic.waw.pl)

Phyllosilicate transformations in acidic environment were investigated in the area of an abandoned pyrite open-pit mine in Wieściszowice (Lower Silesia, SW Poland) using XRD, FTIR, and SEM-EDS methods. The aim of this study was to determine the influence of hydrological conditions and pH of water on phyllosilicate transformations. Dry (well-drained) as well as wet (waterlogged) saprolite samples were investigated.

Parent rock of well-drained saprolites contained exclusively one kind of phyllosilicate: chlorite or mica. Thanks to this opportunity it was easier to determine a chlorite and mica alteration paths in highly acidic conditions (pH 2–3) separately. The chlorite schist consisted of chlorite, quartz, albite, calcite, and pyrite. Saprolite derived after chlorite schist is composed of sulfate minerals, predominantly slavikite (hydrous Mg and Fe sulfate), which it is probably formed at the expense of dissolved chlorite. Clay fraction of chlorite schist saprolite contained major chlorite and minor amounts of mica which could be redeposited from the higher part of the outcrop. Occurrence of chlorite in saprolite, even though its intense dissolution, may be caused by simultaneous physical weathering of parent rock.

Mica schist mainly consisted of dioctahedral micas: muscovite and paragonite, and quartz as well as minor amounts of albite, chlorite and pyrite. Mineral composition of mica schist saprolite is close to the parent rock with the exception of pyrite which completely weathered. Minor amounts of jarosite were also present. Clay fraction of the saprolite is composed of primary micas as well as secondary smectite, which is main component of fine grain fraction (< 0.2 μm). Presumably, smectite formed mostly at the expense of micas.

Wet samples were collected from extremely acidic Purple Pond (pH 2.7) and less acidic Blue Pond (pH 4.6). Purple Pond water contains large amounts of Fe (135 mg/l), Al (68 mg/l), Si (49 mg/l), and SO_4^{2-} ions (1740 mg/l). Content of these components in Blue Pond is significantly lower. Wet saprolites were evolved from the same parent rock – chlorite-mica schist. It consisted of quartz, albite, chlorite, muscovite, paragonite, and pyrite. Bulk mineral composition of the saprolites is similar to the parent rock, except pyrite, which is removed. Clay fraction of Purple Pond sediment contained large amount of smectite, whereas clay fraction from Blue Pond sample contained interstratified swelling mineral probably composed of smectite and vermiculite layers.

Phyllosilicate alterations in the area of Wieściszowice pyrite mine are stronger in dry conditions than in wet ones. This conclusion can be supported by presence of primary phyllosilicates as major components of clay fraction of wet saprolites as well as low amounts of secondary swelling minerals. In dry saprolites chlorite underwent intense dissolution, whereas dioctahedral micas were transformed into swelling clay mineral, mainly smectite. The pH of water is important factor influencing degree of phyllosilicate transformations in studied waterlogged saprolites. Data obtained during this study suggest that phyllosilicate alterations under the influence of extremely acidic waters of Purple Pond are more advanced than in the Blue Pond. Such feature suggests that the scale of phyllosilicate transformations is directly inversely correlated with pH value.

Mineral composition of the clay fraction in soils with a cambic horizon in the Czech Republic

Žigová, A.[1*], Šťastný, M.[2] & Krejčová, J.[3]
[1]Institute of Geology, AS CR, v.v.i., Prague, Czech Republic
([*]zigova@gli.cas.cz)
[2]Institute of Rock Structure and Mechanics, AS CR, v.v.i., Prague, Czech Republic
[3]Crop Research Institute, v.v.i., Prague, Czech Republic

Soils with a cambic horizon are commonly found in many regions of Central Europe. Processes leading to the formation of a subsurface cambic horizon are essentially the same in all climatic zones but the intensities of chemical and biological transformations are different. In the Czech Republic extensive research has been done on gneiss [1], granite and gabbrodiorite [2]. This study presents data about the effect of the parent material on mineral composition and basic properties of soils with the cambic horizon.

The research was conducted in agriculturally utilized areas. Soil profiles with a cambic horizon at the localities of Brodce (Cambic Leptosol on calcareous sandstone, 226 m above sea level, 50°20´ N, 14°52´ E), Humpolec (Haplic Cambisol on paragneiss, 523 m a.s.l., 49°33´ N, 15°21´ E), Náměšť nad Oslavou (Haplic Cambisol on paragneiss, 442 m a.s.l., 49°12´ N, 16°09´ E) and Vysoké nad Jizerou (Haplic Cambisol on orthogneiss, 680 m a.s.l., 50°41´ N, 15°23´ E) were selected for this study. Soil horizons and types were classified according to the World Reference Base for Soil Resources [3].

Samples were collected from excavated pits. Main soil properties from individual horizons, such as the particle size distribution, pH values, cation exchange capacity (CEC), organic carbon and nitrogen were analysed using common pedological methods. XRD tests were obtained on a Philips PW 3710 diffractometer. The analysis of the <1 μm fraction was performed on air-dried oriented samples, and then saturated in ethyleneglycol at 80 °C in a furnace for four hours and finally heated to 550 °C for four hours. Semiquantitative analysis was done basing on the areas of individual mineral basal peaks.

The values of pH are predominantly acid. Cambic Leptosol has a weakly acid pH in the upper part of soil profile and a basic pH further down in horizon Ck. The distribution of cation exchange capacity within the profile corresponds with the particle size distribution and content of organic carbon. Cambic Leptosol has a lower value of CEC than Haplic Cambisols.

Organic carbon content and nitrogen are higher in the upper part parts of the soil profiles. The highest values of organic carbon were documented at the localities of Humpolec and Vysoké nad Jizerou. On the other hand, the lowest organic carbon content was obtained at Brodce.

The analysis of the fraction <1 μm showed that the cambic horizon of Haplic Cambisol is dominated – among clay minerals – by illite and also by kaolinite (Humpolec) and by chlorite (Vysoké nad Jizerou). Cambic horizon of Leptic Cambisol has a higher content of kaolinite.

The results revealed differences in the formation of the cambic horizon. A major role is played not only by the parent material but also by other site-specific conditions.

Acknowledgements: This study was supported by grant project 526/08/0434 from the Czech Science Foundation and the Institutional project AV0Z30130516 of the Institute of Geology AS CR, v.v.i.

[1] Němeček, J. (1974) *Rostl. Vyroba*, **20**, 463-474. [2] Sirový, V. (1974) *Rostl. Vyroba*, **20,** 451-461. [3] IUSS Working Group WRB (2007) *World Reference Base for Soil Resources* 2006, first update 2007. World Soil Resources Reports No. 103. FAO, Rome.

Automated electron Diffraction Tomography (ADT) – a new technique for structure solution of nano-crystalline minerals

Mugnaioli, E.[*], Gorelik, T.E. & Kolb, U.
Institute of Physical Chemistry, Johannes Gutenberg-University, Mainz, Germany ([*]mugnaiol@uni-mainz.de)

Transmission electron microscope (TEM), providing imaging and diffraction information from the same volume, is a powerful tool to investigate nano materials where single crystal or powder X-ray diffraction fail. High resolution TEM can directly visualize structural features at atomic resolution, but demands high electron dose and may cause severe beam damage for frameworked and hydrated inorganic materials (like zeolites). In contrast, electron diffraction needs only a fraction of this electron dose and provides structural data with even higher resolution.

Normally, for a complete structure solution, three-dimensional experimental data are needed. Traditionally, the collection of three-dimensional diffraction data is performed by a tilt of a pre-oriented nano-crystal around a low index crystallographic axis. Diffraction patterns collected in such way are therefore oriented low index zones. This strongly limits the amount of accessible reflections and enhances dynamical effects, hampering the possibility of ab initio structure solution.

In order to reduce these problems and establish an automated routine for electron diffraction data collection and processing, we developed an Automated Diffraction Tomography (ADT) system. The full reciprocal space inside the tilt range limit of the microscope is recorded [1,2]. In order to get diffraction from areas down to 30nm and reduce the beam dose, nano-diffraction mode with mild electron dose settings is used. Crystal is imaged and tracked during the tilt in scanning transmission mode (STEM). Diffraction spots are sampled in non-oriented zones, drastically reducing the dynamical effects. Further improved intensity data come from a combination of ADT with electron beam precession techniques (PED) [3]. Cell parameter determination, three-dimensional reconstruction of reciprocal space and intensity integration are performed automatically with self-developed routines.

In the last two years a number of mineral structures have been solved by ADT. In all these cases, full *ab initio* structure solution was achieved by direct methods. A full kinematical approach was used for structure solution and refinement. The first simple test structure was $BaSO_4$ [4]. Subsequently real challenging cases were investigated. Structure solutions of natural and synthetic zeolites, as well as other large-cell nano-sized minerals, are excellent examples for ADT applications [5]. Synthetic analoga of high-pressure minerals obtained in diamond cell are another interesting area of investigation.

[1] Kolb, U. et al. (2007) *Ultramicroscopy*, **107**, 507-513. [2] Kolb, U. et al. (2008) *Ultramicroscopy*, **108**, 763-772. [3] Vincent, R. & Midgley, P.A. (1994) *Ultramicroscopy*, **53**, 271-282. [4] Mugnaioli, E. et al. (2009) *Ultramicroscopy*, **109**, 758-765. [5] Rozhdestvenskaya, I.V. et al. (2010) *Mineral. Mag.*, **74**, 159-177.

Focused ion beam-SEM and TEM applied to ore minerals: bridging micron- and nanoscales

Ciobanu, C.L.[1,2*], Pring, A.[1,2], Cook, N.J.[1,2] & Green, L.[3]
[1]University of Adelaide, Australia
([*]cristiana.ciobanu@adelaide.edu.au)
[2]South Australian Museum, Adelaide, Australia
[3]Adelaide Microscopy, Adelaide, Australia

Recent advances in electron microscopy techniques, and in particular sample preparation methods, offer an incredible opportunity to address ore-forming processes down to the nanoscale.

Ore minerals record their genetic histories via compositional and structural variations, and, in particular, textures and patterning observable at scales ranging from meters down to nanometers. The practical impasse in going from the micron-scale resolution of the electron microprobe (EPMA) down to the nanometer scale of the transmission electron microscope (TEM) on the same analysis spot has previously hampered attempts to link textures across these scales of observation. The recent breakthrough in TEM sample preparation using the latest generation of Dual Focused Ion and Electron beam (FIB-SEM) instrumentation enables this impasse to be overcome by allowing high-resolution examination of textures, compositions and structures at any chosen location on a sample and in unprecedented detail [1].

We will show results from practice with the Dual Beam FIB-SEM instrumentation at the Australian Microscopy and Microanalysis Research Facility, Adelaide, over the last two years, and in particular, use of the method to prepare FIB-TEM foils. Examples are drawn from the common sulphides (pyrite, sphalerite, Cu-(Fe)-sulphides and molybdenite and from chalcogenides in gold deposits (i.e. Bi-tellurides and sulphosalts).

The types of problems that can be addressed include:

- minor element incorporation,
- grain-scale redistribution of gold and
- recognition of overprinting events (e.g., disequilibrium encoded in stacking sequences of mixed-layer minerals.

The various difficulties that need to be overcome to use FIB-TEM methodology for ore minerals will also be summarised.

[1] Wirth, R. (2009) *Chem Geol*, **261**, 217-229.

Quantitative electron diffraction and electron holography of magnetite at low temperature

Kasama, T.[1*], Harrison, R.J.[2], Church, N.S.[2], Nagao, M.[3], Feinberg, J.M.[4] & Dunin-Borkowski, R.E.[1]
[1]Center for Electron Nanoscopy, Technical University of Denmark, Kongens Lyngby, Denmark ([*]tk@cen.dtu.dk)
[2]Dept. of Earth Sciences, University of Cambridge, UK
[3]Advanced Materials Laboratory, National Institute for Materials Science, Tsukuba, Japan
[4]Institute for Rock Magnetism, Dept. of Geology and Geophysics, University of Minnesota, USA

The Verwey transition in magnetite is associated with an order-of-magnitude increase in magnetocrystalline anisotropy and a change in magnetic easy axis from cubic <111> to monoclinic [001] below ~120 K. Although numerous studies have suggested that magnetic domain walls in magnetite can interact with the ferroelastic twin walls that form at low temperature, no direct evidence for such interactions has been available. Here, we use transmission electron microscopy (TEM) to image both crystallographic features and magnetic microstructure simultaneously at the nanometer scale in synthetic multi-domain magnetite, which was prepared for TEM using conventional Ar ion milling.

We use selected-area electron diffraction and convergent-beam electron diffraction (CBED) to determine crystal symmetry and to identify crystallographic orientations. Energy filtering is used to improve contrast and visibility in CBED disks. The diffraction patterns show that the low-temperature phase has a monoclinic *C*-centered lattice with the *c*-glide plane perpendicular to the *b*-axis and is likely to belong to point group *m*, suggesting that the space group is *Cc*.

We use off-axis electron holography and Lorentz TEM to study the relationships between magnetic domain walls and ferroelastic twin walls in magnetite below the Verwey transition. One of the most striking features is the formation of magnetic domains that are related to "strain-contrast-free" twins. The magnetization direction orients along the monoclinic *c*-axis of each twin domain and changes by close to 90 at each twin boundary. Simulations of the recorded electron holographic phase images [1] are used to interpret the observed magnetic structures quantitatively. The ferroelastic twin walls are observed to resist even the application of a large field of 2T and the magnetic structures at remanence can then be restored. Therefore the twins may have a strong influence on the low temperature magnetic properties of magnetite. Our analysis takes into account the effect of mean inner potential contributions to the phase shift on magnetic induction maps in wedge-shaped TEM specimens.

Acknowledgements: We thank T. Yokosawa and Y. Matsui for valuable discussions.

[1] Beleggia, M. & Zhu, Y. (2003) *Philos. Mag.*, **83**, 1045-1055.

Determination of chemical composition of planar defects in minerals using CEP method

Rečnik, A.[1*], Daneu, N.[1] & Walther, T.[2]
[1]Dept. For Nanostructured Materials, Jožef Stefan Institute, Ljubljana, Slovenia ([*]aleksander.recnik@ijs.si)
[2]University of Sheffield, United Kingdom

Different types of planar defects are present in practically all naturally occurring minerals. These defects form by different mechanisms and may, depending on their formation, contain small amounts of dopant elements. It is not uncommon that the dopant atoms occupy less then one atomic monolayer of the interstitial sites at the boundary. Various other situations, including solid solution (ss) of the dopant in the bulk for example, are possible and thus, chemical analysis of such complex situations is a challenging task. In order to cope with such problems we developed a novel method of analytical electron microscopy using energy-dispersive X-ray spectroscopy (EDS) or electron energy-loss spectroscopy (EELS) in a special geometrical setting. The proposed method is based on acquiring several EDS or/and EELS spectra with parallel electron probes placed concentrically on the analyzed interface. In order to eliminate the effect of specimen thickness the probe centre is maintained concentric for all measurements – concentric electron probe (CEP) method. We demonstrated that the CEP method is approximately 10^2-times more precise (small scatter of the data points) and 10-times more accurate (close to the actual value) than for example the spatial difference technique, allowing determination of down to ±0.1 atoms/nm^2, depending on the type of the solute element that is measured in the interface plane. Because of its high precision we could extend the use of this method not only to accurately measure the amount of the trace element on the interface but also to determine complex solute distribution profiles in the interfacial region. In this contribution we will demonstrate the advantages of the CEP method on three different minerals.

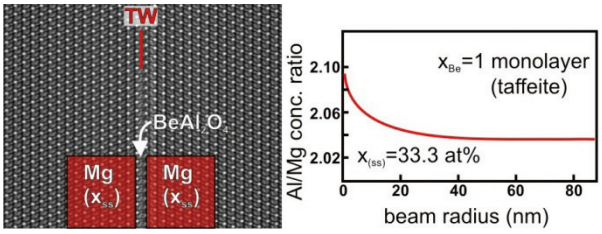

Fig. 1: Case 1 - Be-rich (111) twin boundary in spinel ($MgAl_2O_4$): the solute element (Mg) is present only in bulk, not at the boundary.

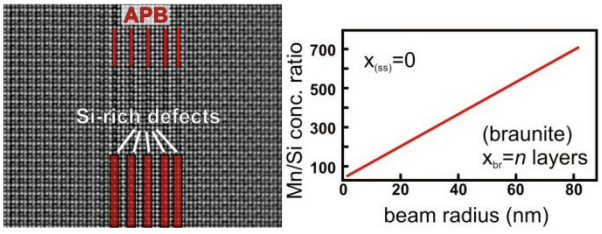

Fig. 2: Case 2 - (100) antiphase boundaries in bixbyite $(Mn, Fe)_2O_3$: the dopant element (Si) is present only at planar defects.

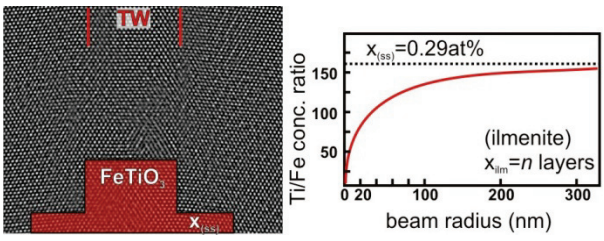

Fig. 3: Case 3 - Fe-rich (301) twin boundary in rutile (TiO_2): the case, where the dopant is present at the boundary and in the bulk (ss).

Direct observation of Th single atoms in thorite by Cs corrected STEM and metamictization process

Akai, J.[1*], Okunishi, E.[2] & Hayashi, H.[1]
[1]Dept. of Geology, Faculty of Science, Niigata University, Niigata, Japan ([*]akai@sc.niigata-u.ac.jp)
[2]JEOL Ltd, Tokio, Japan

In the early days of HRTEM application to material sciences, challenge to observe single atoms were on U and Th atoms in molecules. Recent progress in TEM is new development of Cs corrector-equiped HRTEM. This Cs corrector does not need ultra high accelerating voltage to attain high resolution, reducing spherical aberation (Cs). Using Cs corrected STEM-HAADF (Scanning Transmisson Eectron Microscopy-High Angle Anular Dark Field) images, we tried to observe Th single atoms in metamict thorite, ThSiO4. Furthermore, we examined thermal behaviour of recrystalization of metamict thorite.

STEM-HAADF conditions are as follows: scanning beam is 0.1 nm in diameter and 30 pA; incident beam angle, 25 mrad; receiving angle of diffraction by Anular Detector, 70-250 mrad. ED pattern of the metamict thorite is consisting of almost halo pattern. The halo does not correspond to utterly randomly amorphous state but some diffraction maxima in the halo were found. The diffraction maxima correspond to the positions of strong diffraction spots of thorianite ThO_2. In the HRTEM image, sometimes on the edge, thorianite crystal lattices are found, which may be due to recrystallization by electron beam irradiation. However, mostly amorphous structure is found. Cs-corrected STEM-HAADF image of thorite was taken. The image showed clear spotty patterns (Fig. 1). In STEM-HAADF image, atomic contrast is proportional to Z^2, where Z is atomic number. Thorite consists of Th, Si and O with very small amount of U substituting Th. Thorite composition with metamict state is one of the best sample for STEM-HAADF imaging of single atoms. So, it is reasonably interpreted that every white spots which arrows indicate in the photograph are mostly single Th atoms.

Then, series of STEM images in every 10 seconds were taken. The distribution pattern of the white spots is not the same as before, but changed: this may be due to migration of the Th atoms by electron beam irradiation energy. STEM-HAADF image may be depth sensitive.

Nano domain structures of the thorianite units in the metamict thorite were here suggested and such nano domain structure was dynamically moving if some energey was supplied. Observing newly formed structures and textures in heating experiment, structural changing process was suggested. New application of these textures and structures to geological tool supposing duration of metamictization will be discussed.

This trial of observation of the single atoms in minerals offers wide possibility of new application to mineral science in single atom-scale.

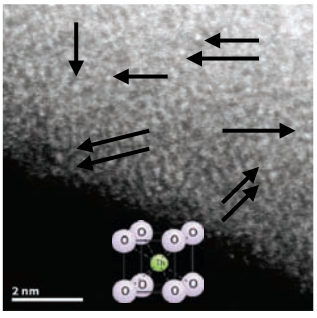

Fig. 1: Th single atoms in metamict thorite by STEM-HAADF.

HRTEM microstructural characterization of pictorial renderings and ground layers in cross section

Báez, M.I.[*], Baldonedo, J.L., Ramírez-Castellanos, J., Vidal, L. & García-Molina, M.J.
Complutense University, Madrid, Spain ([*]mibaez@art.ucm.es)

The intention of this contribution is to show the possibilities offered by high resolution transmission electron microscopy (HRTEM) for the characterization of artistic materials, particularly pigments and fillers, through examination of stratigraphic samples from real pictorial works. This kind of analysis can be applied to any type of painting or polychrome rendering – sculpture, easel painting, mural painting, etc. – and can be used to determine the precise nature of the crystalline species making up the layers.

For a HRTEM study, microsamples are prepared and then ultra-thin sections (50-100 nm) are cut from them; these sections must retain all the particles in the layers intact [1]. Point-to-point EDS microanalyses with HRTEM can be used to locate the elements in each particle; this information is completed by identification of crystalline species by ED. These data are based on a prior study using other microscopic techniques (LM, SEM/EDS). The ultimate objective is to complete a nanostructural characterization using high-resolution transmission electron microscopy (HRTEM).

In the study of pictorial renderings, the characterization of natural coloured earths is especially difficult owing to their peculiar characteristics; the composition of these pigments is highly complex and varied. In general, they are composed of iron oxides associated with various silicates along with other minerals. There are also other loads and products accompanying the material in its original composition, and in many cases there are also substances added by the artist. Many such secondary products are present in tiny quantities and not determined exactly in technical studies.

To demonstrate the possibilities of the technique, this paper presents the results of a study of three pictorial works composed basically of natural earths. Three examples are proposed, each corresponding to a different type of work: (A) red fragment of a mural painting from Mérida Archaeological Site ("Casa del Mitreo"), (B) greenish-brown marble stucco in the Palace of the Congress of Deputies in Madrid and (C) ochre ground layer from oil on canvas by P.P. Rubens (Prado Museum). Table 1 lists some of the representative results from each sample, indicating the principal mineral species characterized by EDS and ED/HRTEM.

Table 1: Mineral species characterized by ED/HRTEM

(A)	(B)	(C)
Calcium carbonate	Gypsum	Calcite (chalk)
Hematite	Calcite	Silica
Cinnabar	Iron oxide hydroxide	Orthoclase
Silica	Glauconite	Biotite
	Hematite	Anatase

These results have made it possible to differentiate the pigments and loads used in all the examples.

Acknowledgements: This work has been carried forward with funding from the Ministry of Science and Technology (Secretaría de Estado para las Universidades), National Plan for Scientific Research and Technological Development Projects (R&D) (Ref.: HUM2006-01847/ARTE).

[1] San Andrés, M., Báez, M.I. & Baldonedo, J.L. (2008) in *MET en el análisis de los Bienes Culturales*, Ministerio de Cultura, Madrid, 81-95.

Application of Patterson-method in electron crystallography

Cora, I.* & Dódony, I.
Dept. of Mineralogy, Eötvös Loránd University, Budapest, Hungary (*corail diko@gmail.com)

Direct methods have become widespread in X-ray crystallography in the last century. A pioneer method for structure determination was developed by Patterson [1,2], that is called Patterson-method. In spite of its simplicity and efficiency it has gone out of interest today. The great advantage of the Patterson-method is that it provides a solid base for phase retrieve. However, resulted Patterson-maps for unit cells with large numbers of atoms still remain unresolved.

We simulated Patterson-maps in Wolfram Mathematica software package [3]. Our software reconstructs Patterson-maps using input data of (1) the measured diffracted intensity values, (2) projected charge density map (PCD) presented in any (text or image) formats and (3) atomic coordinates and unit cell parameters. This software has been converted into public Python language.

We tested the software on [001] projected mica polytypes comparing their experimental electron-diffraction based Patterson-maps to the corresponding simulated ones (Figs. 1–2). A Patterson-map is a reliable method for polytype identification.

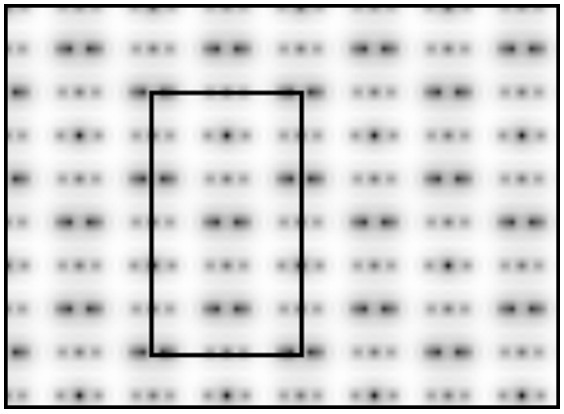

Fig. 1: Projected charge density map of 1M mica polytype (the unit cell is lined out).

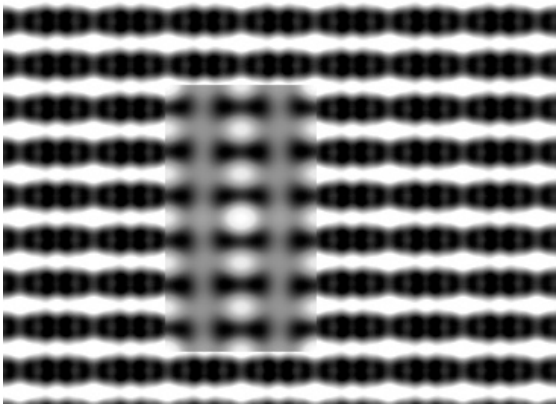

Fig. 2: Crystallographic data based (background) and corresponding experimental Patterson-map of the mica polytype presented above.

[1] Patterson, A.L. (1934) *Phys. Rev.*, **46**, 372-376. [2] Patterson, A.L. (1935) *Z. Krist.*, **90**, 517-542. [3] Wolfram Research, Inc., Mathematica, Version 7.0, Champaign, IL (2008)

Burgers vector determination in deformed materials using the thickness-fringe method

Miyajima, N.* & Walte, N.P.
Bayerisches Geoinstitut, Universitaet Bayreuth, Bayreuth, Germany (*Nobuyoshi.Miyajima@uni-bayreuth.de)

Dislocation is the most important agent in dislocation creep that could become one of dominant deformation mechanisms in the Earth's mantle. Dislocations are line defects and defined by the line direction and the slip vector, Burgers vector, which are identified with these two directions as "screw", "edge" or "mixed" characters. The dislocation line can be visible by selecting diffraction conditions in TEM, but Burgers vector is invisible, to be not directly determined. So we need a proper method to determine it by using a TEM imaging technique

The thickness-fringe method, which was originally proposed by [1], has been performed in deformed materials under high pressure and temperature conditions. The advantage of the method is to enable a complete determination of the character of a dislocation Burgers vector (sign and magnitude) by counting the number of terminating thickness fringes at the extremity of a dislocation from a wedge-shaped thin-foil specimen in weak-beam dark-field (WBDF) TEM images. The visibility criteria, $\boldsymbol{g.b}$ = n ($\boldsymbol{g}$: diffraction vector, $\boldsymbol{b}$: Burgers vector and n: Integral) in TEM images are clearly demonstrated to be superior in unambiguity to conventional invisibility criteria, $\boldsymbol{g.b}$ = 0 [2], which can be comparable with large-angle convergent-beam electron diffraction techniques [3]. Large deviation error (s >> 0) in WBDF images, i.e. pseudo-kinematical diffraction conditions, is also an advantage compared to using $\boldsymbol{g.b}$ = 0 criterion for invisibility of dislocations in elastically anisotropic materials (i.e. almost natural minerals). In addition, the pseudo-parallel beam technique involves only a low-dose illumination of the specimen, which is a critical advantage in applications to sensitive high-pressure minerals to high electron doses.

In this talk, I present some examples of the Burgers vector determination of a perfect dislocation in a post-perovskite structured material [4] as well as partial dislocations in perovskite and olivine structured materials. The different types of dislocations could be distinguished from the dissociation of dislocation lines and the number of terminating thickness fringes in WBDF images (Fig. 1).

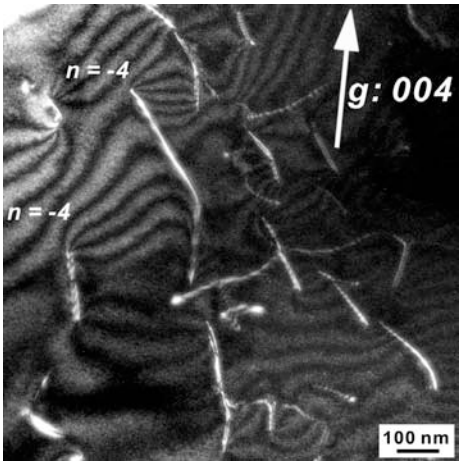

Fig. 1: Weak-beam dark-field TEM micrograph showing partial dislocations in a perovskite structured material.

[1] Ishida, Y. et al. (1980) *Philos. Mag. A*, **42**, 453-462. [2] Hirsch, P. et al. (1977) *Electron Microscopy of Thin Crystals*. Krieger Publishing Company, Malabar, Florida. [3] Cordier, P., Morniroli, J.P. & Cherns, D. (1995) *Philos. Mag.*, **72**, 1421-1430. [4] Miyajima, N. & Walte, N. (2009) *Ultramicroscopy*, **109**, 683-692.

Progress in solving complex mineral structures from electron diffraction data: charoite and denisovite

Mugnaioli, E.[1], Czank, M.[2*], Depmeier, W.[2], Kolb, U.[1] & Rozhdestvenskaya, I.V.[2,3]
[1]Institute of Physical Chemistry, Johannes Gutenberg-University, Mainz, Germany
[2]Dept. of Crystallography, Institute of Geowissenschaften Christian-Albrechts-University, Kiel, Germany
([*]czank@min.uni-kiel.de)
[3]Dept. of Crystallography, Geological Faculty, Saint Petersburg State University, Russia

All earlier attempts to solve the structures of charoite and of denisovite by X-ray methods failed. Several reasons can be addressed for these failures: these minerals have large unit cells (~32x20x7 Å), low symmetries (monoclinic or triclinic) and complex chemical compositions, they consist of intimately intergrown randomly oriented nano-scaled fibres, they are systematically structurally disordered at the scale of few microns. Electron diffraction can provide high resolution structural data from single phase nano-crystals, but it is often biased due to strong dynamic effects and technical difficulties collecting complete data sets by manual tilt. Automated electron diffraction tomography (ADT) [1-3] provides a powerful and quick tool for more reliable, complete and reproducible electron diffraction data collection from single nano-crystals.

ADT is a combination of STEM imaging for crystal tracking and nano electron diffraction, possibly coupled with precession diffraction technique. ADT doesn't require sample alignment and zone-axis orientation, thus reducing significantly the electron dose on the sample and allowing quasi-kinematical intensity collection. The processing software allows full 3D reconstruction of reciprocal space, unambiguous cell parameter determination and automated reflection indexing and intensity integration. With ADT we were able to collect more than 8000 intensities for charoite as well as for denisovite. The quality of the data allowed to solve the structure of charoite [4] *ab initio* in one step by SIR2008 with a fully kinematical approach, namely with the same approach as used for single crystal X-ray data!

Denisovite has diffuse (100) lamellar disorder and probably exists with several polytype structures. The detected cell parameter **b** differs from the value given in the literature [5]. The unit cell of denisovite was found to be very close to that of charoite, but the two minerals differ in chemical composition, symmetry and intensity distribution. Although the structure is not solved yet, one can expect that the various dreier silicate chains and octahedral bands are arranged differently in charoite and denisovite.

Acknowledgements: The authors thank the Deutsche Forschungsgemeinschaft for financial support (DE 412/37-1 and SFB 625).

[1] Kolb, U. et al. (2007) *Ultramicroscopy*, **107**, 507-513. [2] Kolb, U., Gorelik, T. & Otten, M.T. (2008) *Ultramicroscopy*, **108**, 763-772. [3] Mugnaioli, E., Gorelik, T. & Kolb, U. (2009) *Ultramicroscopy*, **109**, 758-765. [4] Rozhdestvenskaya, I.V. et al. (2010) *Mineral. Mag.*, in print. [5] Men'shikov, Yu.P. (1984) *Zapiski Vsesojuznogo Mineralogicheskogo Obshchestva*, **113**, 718-723 (in Russian).

Argon Ion Slicing (*ArIS*) of mineral and rock samples: a novel tool to prepare super large electron transparent thin films for TEM use

Stojic, A.N.[*], Brenker, F.E. & Tkalcec, B.J.
Geosciences Institute, Goethe University, Frankfurt/M., Germany ([*]stojic@em.uni-frankfurt.de)

We report the successful preparation of a 42,500 μm^2 large continuous TEM foil from a carbonaceous chondrite (Fig.1). *ArIS* is a broad ion beam technique similar to argon ion milling: But contrary to the latter *ArIS* benefits from an additional shielding device and therefore provides ultra-large continuous thin foils from polymineralic natural rock sample. *ArIS* was first used in material sciences and has been introduced to Earth and planetary sciences only recently [1,2]. TEM foils produced by *ArIS* do not show any amorphisation or sample distortion. Commonly used preparation techniques, like argon ion milling or ultramicrotomy, yield only small electron transparent areas (<< 500 μm^2) or show a strong mineral-dependent abrasion efficiency.

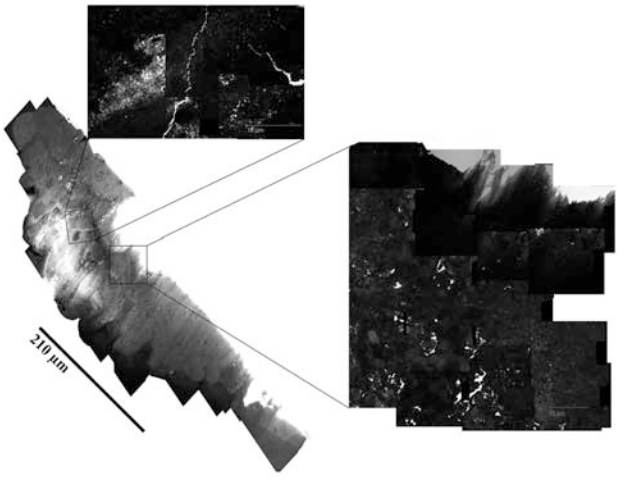

Fig. 1: Murchison (CM 2 carbonaceous chondrite) BF TEM thin film micrographs. To the right, two detailed zoom-ins of electron transparent area. Light grey area to the left is entirely electron transparent.

AriS was successfully applied on various geological samples, namely carbonaceous chondrites, carbonaceous rocks and eclogites.We obtained large (> 20.000 μm^2) continuous electron transparent areas. Based on the quality of the produced thin film and the size of the continuous electron transparent area obtained, *ArIS* is a promising new tool not only in planetary sciences. Next steps will be applying different analytical techniques on ArIS treated samples, such as NanoSIMS, EBSD, microprobe, Synchrotron-XRF and TEM.

[1] Tateno, Sh. et al. (2009) *Rev. Sci. Instrum.*, **80**, 013901. [2] Stojic, A.N. & Brenker, F.E. (2010) *Eur. J. Mineral.*, **22**, 17-21.

Mineral spectroscopy: from gamma rays to microwaves

Rossman, G.R.
Division of Geological and Planetary Sciences, California Institute of Technology, Pasadena, CA, USA (grr@gps.caltech.edu)

Mineral spectroscopy has been a thriving science for the past 50 years. What has been accomplished and what might the future bring? Gamma ray (Mössbauer) spectroscopy has moved from the laboratory to Mars where it has helped to identify the minerals on another planet. High intensity X-ray fluxes from synchrotrons are making great progress probing much of the periodic table at very small dimensions through the use of XANES and EXAFS. The human visual interface with the geological world has been nicely characterized through the study of the atomic causes of the colors of minerals. Gemmological laboratories now use a wide variety of spectroscopic methods to help identify gems, determine their treatments, and to determine origin.

For many years vibrational spectroscopy has contributed to the understanding of the structure and bonding in minerals. With convenient methods such as ATR, it has become a means of rapid and convenient phase identification. Infrared spectroscopy has also played a key role in understanding the role of hydrous components bound in minerals in the deep earth. Raman spectroscopy has become highly convenient and readily available. With the development of extensive libraries of mineral spectra, such as the one produced by the RRUFF project, Raman spectroscopy has become an extraordinarily useful tool for phase identification of minerals even down to sub-micrometer sizes. Future advances in time-resolved Raman spectroscopy that will help remove the interferences that arise from sample fluorescence will greatly increase the utility of the Raman method.

Thermal emission infrared spectroscopy has been widely used for phase identification in planetary exploration. Instruments for infrared and near-infrared spectroscopy are now studying several other bodies in the solar system from both orbit and on the ground.

Far-infrared spectroscopy has played much less of a role in mineral studies, but has proven of value with the increasing availability of high-intensity synchrotron sources, it role will surely increase. Astronomical infrared studies are also moving into the far-infrared with spacecraft orbiting high above the interferences of earth's atmosphere.

Spectroscopy in the microwave region has also played a role in the study of minerals and glasses. NMR spectroscopy has proven useful for establishing details about the local structure of Si in glass structures and the concentration of H in minerals. NMR is also used to examine the dynamic motion of atoms such as Na and H in solids. Electron paramagnetic resonance is exquisitely sensitive for probing low concentrations of paramagnetic ions in crystals. EPR also has played a key role in gathering information about color centers formed in minerals by natural radiation.

In the future spectroscopic tools will only increase in use, in the lab, in the field, and in space. Ever-smaller samples will be studied under ever-more extreme conditions of P and T. And, we will expand our definition of minerals as the spectroscopy of hydrocarbon 'minerals' and ices on other bodies such as Europa and Titan become prime objects of study through spectroscopic methods.

Spectroscopic investigations of alpha-particle haloes in mica- and chlorite-group minerals

Krickl, R.
Institut für Mineralogie und Kristallographie, Universität Wien, Vienna, Austria (robert.krickl@univie.ac.at)

Accumulated alpha-particle doses around radionuclide-bearing inclusions may cause noticeable changes in the physical and chemical properties of host minerals. These so-called radiohaloes have been observed in a number of minerals – the most well known examples being "pleochroic haloes" in sheet silicates. However, little is known on the processes involved in radiohalo formation and modern techniques of investigation were just recently introduced in this topic [1,2]. The presented results are part of a systematic study on natural radiohaloes in muscovite, biotite- and chlorite-minerals, as well as in artificially irradiated samples.

Optical absorption spectra were recorded at different radial distances from the radioactive inclusions, thus giving insight in different stages in radiohalo evolution. Altered absorption colours are mainly caused by a strong shift of the UV absorption edge to lower energies. Changes in the intensity of crystal field *d-d* and metal-metal charge transfer bands indicate radioinduced ionisation of Fe^{2+} to Fe^{3+}. Low to moderate doses cause darkening of the minerals due to intensified absorption in the visible region. Still higher doses result in "colouration reversal", caused by intensity loss of the smaller bands in the visible and near IR.

Polarised spectra of radiohaloes in chlorite (Fig. 1) exhibit an intensified absorption at ~16800 cm^{-1} which is very weak in the unirradiated mineral. This provides new evidence for the existence of this spectral feature (probably a Fe^{2+}-Fe^{3+} charge transfer band), which has hitherto been regarded as doubtful [3].

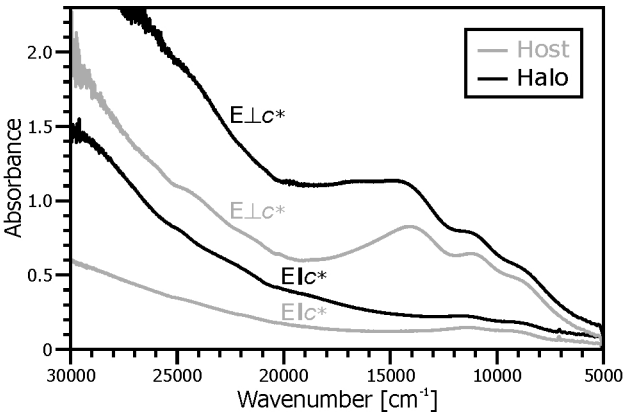

Fig. 1: Polarised optical absorption spectra of a radiohalo in chlorite from Turamdih/India (cf. [2]) in comparison to the unirradiated host (polished thin section, sample thickness 30 µm).

Changes in the structural state were investigated using Raman spectroscopy: Line scans show a very good correlation between the broadening of vibrational bands (interpreted as accumulation of radioinduced point defects) and the radial distance to the radioactive inclusion, corresponding to the modelled point defect density distribution within radiohaloes. Not all bands show a continuous decrease in band intensity with increasing irradiation dose: At low to moderate doses (in "darkened haloes" – see above) Raman bands at ~640 cm^{-1} (chlorite) and ~575 cm^{-1} (muscovite) exhibit a strong increase in intensity. At higher doses, starting with the onset of colouration reversal, they rapidly loose intensity and totally disappear.

[1] Nasdala, L. et al. (2001) *Am. Mineral.*, **86**, 498-512. [2] Nasdala, L. et al. (2006) *Mineral. Petrol.*, **86**, 1-27. [3] Smith, G. (1977) *Can. Mineral.*, **15**, 500-507.

The WURM project – a web-based freely available database of computed physical properties for minerals

Caracas, R.[1*] & Bobocioiu, E.[2]
[1]Laboratoire de Sciences de la Terre, Ecole Normale Superieure de Lyon – CNRS, Lyon, France ([*]razvan.caracas@ens-lyon.fr)
[2]Laboratoire de Sciences de la Terre, Ecole Normale Superieure de Lyon, France

This project aims to build a freely accessible web-based database of computed physical properties for minerals. The database provides for each mineral various physical properties: the crystal structure used in the calculation, the dynamical charges and the dielectric tensors, the refractive index, the Raman spectra with both peak position and intensity and the infrared spectra with peak position. Additional information comprises the parameters of the calculation, to ensure reproducibility of the results.

The vibrational information makes the bulk of the database and constitutes the major computational effort. For each vibrational mode in the zone-center we determine the frequency, the symmetry assignment, the atomic displacement patterns, and the Raman tensors. The Raman spectra are represented in both single crystal and powder with different possible laser polarizations. For the infrared modes we give both the TO and the LO components.

The database is freely available on the web at http://www.wurm.info and is highly interactive. Jmol-powered applets incorporated in the website allow the quick visualization of the crystal structure and of the atomic displacement patters of all vibrational modes.

Further developments include development of a virtual microscope on top of the computed refractive indexes and the analysis of the elastic properties based on the computed elastic constants tensor.

All the results are exclusively obtained from first-principles calculations performed using the local density approximation of density functional theory and density functional perturbation theory in the ABINIT implementation [http://www.abinit.org], based on planewaves and pseudopotentials.

Using Raman spectroscopy to determine the sulphur valance state and $S^{6+}/\Sigma S$ ratio in silicate glasses

Klimm, K.[1*] & Botcharnikov, R.E.[2]
[1]Inst. für Geowissenschaften, Goethe-Universität, Frankfurt, Germany ([*]klimm@em.uni-frankfurt.de)
[2]Inst. für Mineralogie, Leibniz-Universität, Hannover, Germany

Because sulphur (S) has several possible valance states (S^{2-}, S^{4+}, S^{6+}), the total S solubility in silicate melts is a function of fO_2 as the compositional controls on sulphide, sulphate and sulphite incorporation in the glass structure are different. At high fO_2, S^{6+} is dominant and more soluble in silicate melts than S^{2-} which is dominant at low fO_2 [1]. In subduction zones the fO_2 changes from reducing to more oxidising conditions during the rise of volcanic fluids and magmas [2]. Therefore it is crucial to determine the oxidation state of S to understand and model volcanic degassing processes. Until now the S speciation and $S^{6+}/\Sigma S$ in silicate glasses have mostly been determined using SKα wavelength shift measurements on the electron microprobe [1] or using XANES spectroscopy [3]. However, both methods are challenging and difficult to use as standard methods in quantifying accurately the $S^{6+}/\Sigma S$ because of either the low resolution of electron probe spectrometers or the restricted and costly access to synchrotron radiation sources. In addition it has been shown that the sulphur valance state in silicate glasses may change during electron beam exposure [4]. Here we show that Raman spectroscopy can be a cheap and relatively easy alternative method in determining the $S^{6+}/\Sigma S$ in silicate glasses.

Several hydrous sulphur bearing glasses synthesised at fO_2 ranging from QFM-2 to QFM+4 were investigated by Raman spectroscopy ranging from "natural" basaltic, andesitic to rhyodacitic compositions to more "technical" iron-free compositions such as soda-lime glass (SLG) and $K_2Si_4O_9$ (KSG). The presence of sulphate (S^{6+}) is marked in Raman spectra of oxidised synthetic and natural glasses similarly by bands at ~990 and ~1000 cm^{-1}, respectively. The presence of sulphide (S^{2-}) in Raman spectra of the reduced technical SLG and KSG glasses is marked by a band at 2574 cm^{-1} indicating that S^{2-} is present as HS^- in these glasses. Such a band is absent in the Raman spectra of reduced basaltic glass. However, an additional band appears in the Raman spectra of reduced basaltic glass at ~400 cm^{-1} when compared to Raman spectra of sulphur-free reduced basaltic reference glass and the "technical" Fe-free glasses indicating that S^{2-} is present as a metal-complex such as FeS. This is also confirmed by Raman spectra of SLG and KSG glasses that have been doped with Fe showing a band at 400 cm^{-1} besides the band at 2574 cm^{-1}. The band at 400 cm^{-1} systematically increase while the band at 2574 cm^{-1} decrease with decreasing S/Fe from 2 to 0.5 at constant fO_2 indicating that the quantities of dissolved S complexes shift from HS^- to FeS dominated. In all glasses and at intermediate fO_2 both species S^{6+} and S^{2-} can be identified. The intensities of the bands at 990 and 1000 cm^{-1} indicating the presence of S^{6+} increase and the intensities of the bands at 2574 or 400 cm^{-1} indicating S^{2-} decrease systematically with increasing fO_2. The relative abundances of each complex and the $S^{6+}/\Sigma S$ can be quantified by integrating the intensities of each band.

The results shown here demonstrate the potential of Raman spectroscopy in determining and quantifying the sulphur valance state in silicate glasses. In addition the results indicate that S^{2-} is dissolved as completely different complexes when comparing synthetic iron-free and natural iron-bearing silicate glass compositions.

[1] Carroll, M.R. & Rutherford, M.J. (1985) *Am. Mineral.*, **73**, 845-849. [2] Jugo, P.J. (2009) *Geology*, **37**, 415-418. [3] Métrich, N. et al. (2009) *Geochim. Cosmochim. Ac.*, **73**, 2382-2399. [4] Wilke, M. et al. (2008) *Am. Mineral.*, **93**, 235-240.

Mössbauer spectroscopy with a high velocity resolution in the study of iron nickel phosphides extracted from Sikhote-Alin meteorite: an analysis of iron and nickel occupation of the M1, M2 and M3 sites

Oshtrakh, M.I.[1*], Larionov, M.Yu.[1], V.I. Grokhovsky, V.I.[1] & Semionkin, V.A.[1,2]

[1]Faculty of Physical Techniques and Devices for Quality Control, Ural State Technical University – UPI, Ekaterinburg, Russian Federation ([*]oshtrakh@mail.utnet.ru)

[2]Faculty of Experimental Physics, Ural State Technical University – UPI,, Ekaterinburg, Russian Federation

Mössbauer spectroscopy with a high velocity resolution demonstrated new possibilities in the study of various iron bearing minerals in meteorites [1,2]. Therefore, this technique was applied to the study of iron nickel phosphides $(Fe,Ni)_3P$ extracted from Sikhote-Alin iron meteorite. It is well known that artificial Fe_3P and meteoritic $(Fe,Ni)_3P$ have the unit cell with 24 metal atoms in three crystallographically non-equivalent sites M1, M2 and M3, 8 atoms in the each site, which in the case of meteoritic phosphides occupied by Fe and Ni in different way for two different types of phosphides in various meteorites [3].

We studied schreibersite and rhabdites, two types of $(Fe,Ni)_3P$ extracted from Sikhote-Alin meteorite mechanically and electrochemically, respectively. These phosphides were studied using Mössbauer spectroscopy in the temperature range of 295–90 K with automated precision Mössbauer spectrometric system with a high velocity resolution [4]. Measured spectra were different for schreibersite and rhabdites. Nevertheless these spectra fitted on the basis of model [5] using 6 magnetic sextets 3 pairs of which were related to the M1, M2 and M3 sites and paramagnetic doublet. Basing on the relative areas of spectral components related to the each site and the results of chemical analysis of schreibersite and rhabdite we evaluated average numbers of Fe and Ni atoms in the M1, M2 and M3 sites of both schreibersite and rhabdite. These numbers for schreibersite were 8 Fe (M1), 3.8 Fe, 4.2 Ni (M2) and 2.9 Fe, 5.1 Ni (M3) while for rhabdite these numbers were 5.5 Fe, 2.5 Ni (M1) and 3.5 Fe, 4,5 Ni (M2 and M3). Using the structures of schreibersite and rhabdites determined in [6] and average numbers of Fe and Ni atoms in the sites we evaluated nearest environment for the each site in both phosphides. The obtained differences were considered as a reason of different Mössbauer hyperfine parameters for various sites in two phosphides.

[1] Oshtrakh, M.I. et al. (2008) *Meteorit. Planetary Sci*., **43**, 941-958. [2] Grokhovsky, V.I. et al. (2009) *Eur. J. Mineral.*, **21**, 51-63. [3] Geist, V., et al. (2005) *Cryst. Res. Tech*., **40**, 52-64. [4] Semionkin, V.A. (2010) *Bull. Rus. Acad. Sci.: Physics*, **74**, 416-420. [5] Lisher, E.J. et al. (1974) *J. Phys. C: Solid State Phys*., **7**, 1344-1352. [6] Moretzki, O. et al. (2005) *J. Synchrotron Rad*., **12**, 234-240.

The angular dependence of *K* pre-edge in cubic compound: XAS experiments and *ab initio* calculations

Bordage, A.[1,2*], Brouder, Ch.[2], Cabaret, D.[2], Juhin, A.[2], Balan, E.[2] & Glatzel, P.[3]

[1]Laboratoire des Géomatériaux et Environnement, UPEMLV, Marne la Vallée, France ([*]amelie.bordage@impmc.jussieu.fr)

[2]Institut de Minéralogie et de Physique des Milieux Condensés, Univ. Paris 6 et 7, IRD, IPGP, Paris, France

[3]European Synchrotron Radiation Facility, Grenoble, France

The features in *K*-edge X-ray absorption spectra of transition metal cations provide information about their crystallographic environment and electronic structure in minerals. Fine details can be revealed from the pre-edge features, which depend on the valence state and site symmetry of the absorbing atom, by performing measurements for different orientations of a single with respect to the incident beam [1].

Here we present an experimental and theoretical study of the angular dependence of *K* pre-edge in cubic compounds with the case of the V-bearing garnet-grossular $Ca_3Al_2(SiO_4)_3:V^{3+}$. In such a cubic crystal, the angular dependence of the V *K* pre-edge is expected to arise from that of pure electric quadrupole transitions ($1s \rightarrow 3d$) [2,3]. V *K*-edge High Energy Resolution Fluorescence Detection X-ray Absorption Spectroscopy (HERFD-XAS) [4] spectra were recorded on ID26@ESRF for different orientations of a single crystal, in order to reconstruct the complete angular dependence (Fig. 1) and to assess the importance of quadrupolar transitions [5]. Compared with conventional XAS, HERFD-XAS leads to a significant sharpening of the pre-edge features, which facilitates the separation of the pre-edge from the main edge [6].

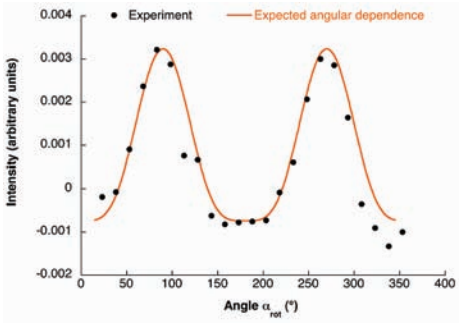

Fig. 1: Experimental (dots) and theoretical (orange line) angular dependence of the V *K* pre-edge in tsavorite.

In parallel, the theoretical X-ray absorption spectrum of V^{3+} in this garnet-grossular was determined by monoelectronic *ab initio* calculations, based on the Density Functional Theory. The comparison between experimental and calculated data makes it possible to obtain accurate information about the crystallographic and electronic structures of V^{3+} in garnet [5]. In particular, it provides quantitative information about the relaxation of the crystal structure around the impurity, a key parameter for understanding the mechanisms controlling the incorporation of colouring trace elements in minerals.

[1] Juhin, A. et al (2008) *Phys. Rev. B*, **78,** 195103. [2] Brouder, Ch. (1990) *J. Phys.: Condens. Mat.*, **2,** 701-738. [3] Cabaret, D. et al. (2010) *Phys. Chem. Chem. Phys.*, **12(21)**, 5619-5633. [4] Glatzel, P. et al. (2009) *Catalysis Today*, **145**, 294-299. [5] Bordage, A. et al. (2010) *Am. Mineral.* (in press). [6] Glatzel, P. & Bergmann, U. (2005) *Coordin. Chem. Rev.*, **249**, 265-295.

EXAFS-derived crystal-chemistry of Zn in di- and trioctahedral phyllosilicates

Juillot, F.[1*], Morin, G.[1], Hazemann, J.L.[2], Proux, O.[2], Belin, S.[3], Briois, V.[3], Brown, G.E.[4] & Robert, J.-L.[1]
[1]Institut de Minéralogie et de Physique des Milieux Condensés (IMPMC), UMR CNRS 7590, & Universités Paris 6/7-IPGP, Paris, France ([*]juillot@impmc.jussieu.fr)
[2]European Synchrotron Radiation Facility (ESRF), Grenoble, France
[3]Synchrotron SOLEIL, Saint Aubin, France
[4]Dept. of Geological & Environmental Sciences, Stanford University, Stanford, USA

Numerous studies have emphasized the importance of M^{2+} (Fe, Zn, Co and Ni) and M^{3+} (Fe, Al) ions incorporation in phyllosilicates in contaminated soils and sediments [1-3 and references therein]. Understanding the behavior of these trace elements in natural impacted systems then strongly depends on our capacity at characterizing the actual crystal-chemistry of these ions in phyllosilicates. For instance, incorporation in di- or trioctahedral species could yield important information on the origin (natural vs. anthropogenic) of the trace element studied. Indeed, the slow kinetics of crystallization of dioctahedral phyllosilicates at room temperature strongly suggests that trace elements incorporated within their octahedral sheets likely derive from anthropogenic sources. At the opposite, occurrence of trace elements within the octahedral sheets of a trioactahedral phyllosilicate in an impacted soil is a strong support for an anthropogenic source for these elements. In addition, the actual distribution of trace elements within the octahedral sheets of phyllosilicates (randomly distributed vs. clusterized) can also yield useful informations on the environmental conditions (temperature, pH) that prevailed during the formation of these mineral species.

The aim of the present study was to collect structural information about the crystal-chemistry of Zn^{2+} ions incorporated at trace levels within the octahedral layers of various natural and synthetic di- and tri-octahedral phyllosilicates (kaolinite, talcs, phlogopite, muscovite). Zn was chosen because this element is the most frequently observed in impacted soils. Due to the low Zn content of the samples investigated (as low as 40 ppm), EXAFS spectroscopy was used to obtain information about the local structural environment of Zn and analysis of these data with *ab initio* FEFF 8 calculations allowed to derive spectroscopic features characteristic of Zn incorporated within the octahedral sheets of phyllosilicates [4]. Changes in these specific features are discussed with respect to Zn concentration and the nature (di- or tri-) of the octahedral sheets. Particular attention was paid to Zn ordering in the trioctahedral sheets in order to try to distinguish between ordered vs. randomly distributed Zn^{2+} ions.

Results indicate that EXAFS spectroscopy is a powerful tool to improve our capacity at deciphering between incorporation of trace elements within di- or tri-octahedral phyllosilicates in impacted soils or sediments and, in turn, to help our understanding of the behavior of these elements in these systems.

[1] Brown et al., (2002) *Rev. Mineral.*, **49**, 1-116. [2] Juillot, F. et al. (2003) *Am. Mineral.*, **88**, 509-526. [3] Manceau, A. et al. (2004) *Geochim. Cosmochim. Ac.*, **68**, 2467-2483. [4] Juillot, F. et al. (2006) *Am. Mineral.*, **91**, 1432-1441.

Health effects of quartz: crystal chemical insights from a multianalytical approach

Di Benedetto, F.[1*], Capacci, F.[2], D'Acapito, F.[3], Fornaciai, G.[1], Montegrossi, G.[4], Innocenti, M.[1], Pardi, L.A.[5] & Romanelli, M.[1]
[1]Dept. of Chemistry, University of Florence, Italy ([*]dibenefr@geo.unifi.it)
[2]Health Agency of Florence, Italy
[3]CNR-IOM-OGG c/o ESRF, Grenoble, France
[4]Inst. for Geosciences and Georesources, CNR, Florence, Italy
[5]Inst. for Physico-Chemical Processes, CNR, Italy

The International Agency for Research on Cancer rated crystalline Silica (inhaled in the form of quartz or cristobalite from occupational sources) as “carcinogenic to humans”, since 1997. There is a general agreement in relate the health effects of crystalline silica to the presence of inorganic radicals, especially if generated during the formation of fresh surfaces. However, effectiveness of biological response to silica exposure can depend on several physical and chemical boundary conditions: among them, the presence and crystal chemistry of heteroions on quartz surface, as e.g. Fe.

This study is aimed to gain a deep insight in crystal chemical features of both inorganic radicals and Fe species in (or associated to) quartz, and to monitor their changes during mechanical and chemical activation performed both under laboratory conditions or during industrial processes. This goal has been pursued through a combined multianalytical spectroscopic approach, including EPR, ESE spectroscopy, XAS and ReflEXAFS a the Fe-K edge, combined with Atomic Force Microscopy.

The results of the present investigation allowed to set up a new method to quantify inorganic radical species having a relevant Zeeman anisotropy. At the same time, a specific interaction between Si-related radical and clay associated phases during the wet ceramic production.

On the other hand, Fe, independently on the valence state, was observed to tend to precipitate forming nanosized oxide particles at the quartz surface, even in concentrations nominally covering just a fraction of a monolayer. Moreover, during the characterisation of mechanically activated samples under laboratory conditions, we faced a singular redox trend: a partial reduction of Fe after mechanical crushing in laboratory. Due to the very low amount of Fe, we tentatively ascribed this aspect to the presence of reducing species in the bulk samples

Formation of the E_1' centre in natural quartz and applications to dating and environmental research

Toyoda, S.[1*], Usami, T.[1], Yamamoto, Y.[1] & Nishido, H.[1]
Okayama University of Science, Okayama, Japan
([*]toyoda@dap.ous.ac.jp)

The E_1' centre in crystalline quartz is one of the fundamental paramagnetic defects in quartz where an unpaired electron is at an oxygen vacancy, detected by electron spin resonance (ESR, same as electron paramagnetic resonance, EPR). Its model for the atomic configuration has been extensively studied [1] since the discovery of the centre, while its formation process in natural quartz has not well been established. Unlike the other paramagnetic defects, the intensity of the E_1' centre increases on heating as was found at the early stage of the studies of this centre [2]. It was suggested to explain this increase that electronic holes in aluminium hole centres (an electronic hole trapped at an aluminium ion replacing silicon) are transferred to oxygen vacancies with two electrons (Si–Si bond) [3].

In the present study, we show detailed experimental results to confirm this electronic process on several natural quartz samples with varying aluminium concentrations. The slices of the samples were irradiated with 4 MeV electrons to create oxygen vacancies in them. After crushing, the samples were measured by ESR spectrometer at liquid nitrogen temperature to obtain the intensity of the aluminium hole centre, $[AlO_4]^0$. The samples were subsequently heated at 300°C for 15 minutes to maximize the intensity of the E_1' centre. The number of the E_1' centres formed in quartz were measured at room temperature. The number of the E_1' centres increased with an increase of the concentration of the aluminium hole centres, while they saturated above a certain amount of the aluminium hole centres where the saturating level is a function of electron dose, as shown in Fig. 1. This saturation level indicates the number of oxygen vacancies, the precursors of the E_1' centres, in quartz [4].

It was already shown that the number of the oxygen vacancies measured as the intensity of the E_1' centre is an indicator useful to discuss the origin of the aeolian dust [5] which is based on the correlation between the number of the oxygen vacancies in quartz and the age of the host granite [6]. The method was applied to loess samples in Japan to find that the source of the aeolian dust coming to the northern part of Japan in MIS2 was different from that in MIS 1 [5]. The results on the deep sea sediments in MIS 1 and 2 in Pacific Ocean will be presented.

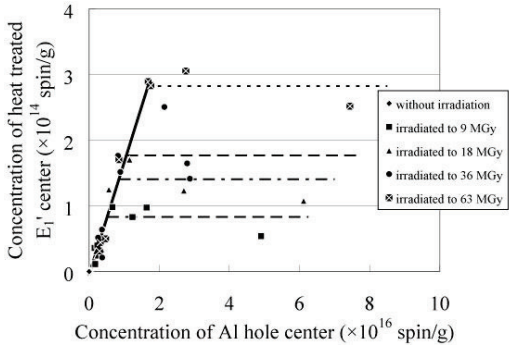

Fig. 1: Correlation between the number of the aluminium centres and that of the E_1' centres after the heat treatment.

[1] Silsbee, R.H. (1961) *J. Appl. Phys.*, **32**, 1459-1462. [2] Weeks, R.A, & Nelson, C.M. (1960) *J. Amer. Ceram. Soc.*, **43**, 399-404. [3] Jani, M.G. et al. (1983) *Phys. Rev. B*, **27**, 2285-2293. [4] Rudra, J.K. & Fowler, W.B. (1987) *Phys. Rev. B*, **35**, 8223-8230. [5] Toyoda, S. & Naruse, T. (2002) *Trans., Jap. Geomorph. Union*, **23**, 811-820. [6] Toyoda, S. & Hattori, M. (2000) *Appl. Radiat. Isot.*, **52**, 1351-1356.

Vibrational spectroscopy of kosnarite-like zirconium and hafnium phosphates with rare-earth elements

Borovikova, E.Yu.[1*], Bykov, D.M.[2] & Kurazhkovskaya, V.S.[1]
[1]Geology Faculty, Moscow State University, Moscow, Russia ([*]amurr@mail.ru)
[2]Dept. of Chemistry, Nizhni Novgorod State University, Nizhni Novgorod, Russia

Double anhydrous orthophosphates of the compositions $R^{III}_{0.33}M_2(PO_4)_3$, where M = Zr, Hf, and R^{III} = La – Lu, Y, belonging to the structure type of kosnarite $KZr_2(PO_4)_3$ (the synthetic analogue is sodium zirconium phosphate $NaZr_2(PO_4)_3$, NZP, Nasicon), have been synthesized in a crystalline state by precipitation method and characterized by Raman and infrared spectroscopy in a mid and far region. These phases are known to possess low coefficients of thermal expansion, ionic conductivity and luminescent properties [1-3]

Most of these compounds crystallize in sp.gr. $P\bar{3}c1$ [4], but the structure of $La_{0.33}Zr_2(PO_4)_3$ has been determined in the sp. gr. $P\bar{3}$ [5]. Factor group analysis has been carried out for space groups $P\bar{3}$ and $P\bar{3}c1$. The assignment of the stretching and bending vibrations of the PO_4 unit has been made. Detailed assignment of the external modes is difficult, because of the greater number of predicted signals compared to the low number of observed bands in the spectra. However, the study of Raman and infrared spectra of corresponding Zr and Hf compounds shows that some bands exhibit an evident Hf - Zr mass effect and can be assigned to M^{IV} translations: 340, 312, 277 cm^{-1} in the Raman spectra and 345, 326, 310, 270 cm^{-1} in the IR spectra. Also two overlapping bands at around 157, 146 cm^{-1} in IR spectra of $La_{1/3-x}Yb_xZr_2(PO_4)_3$ solid solutions show the La-Yb mass effect, so they can be assigned to M^{III} translations.

Despite the similarity of the spectra of $M^{III}_{0.33}Zr_2(PO_4)_3$ with M^{III} = Ce – Yb (sp.gr. $P\bar{3}c1$) and $La_{0.33}Zr_2(PO_4)_3$ (sp.gr. $P\bar{3}$), they have certain distinctions, which become especially visible in the Raman spectra in the regions of stretching and symmetric bending ν_2 vibrations. Another difference in the Raman spectrum of $La_{0.33}Zr_2(PO_4)_3$ is the change in the region corresponding to Zr^{IV} translations and the appearance of an additional band at 106 cm^{-1}, which presumably relates to La^{III} translation in positions with site symmetry C_3 (0.18 of La atoms). The bigger number of overlapping bands in both Raman and IR spectra of $La_{0.33}Zr_2(PO_4)_3$ leads to their lower resolution, compared to spectra of the other compounds.

The morphotropic transition from $P\bar{3}$ to $P\bar{3}c1$ in the series $La_{1/3}Zr_2(PO_4)_3$ - $Yb_{1/3}Zr_2(PO_4)_3$ was shown to appear at the ratio Yb/(La+Yb) of approximately 70-80% (corresponding to $La_{1/18}Yb_{5/18}Zr_2(PO_4)_3$), where the maximum of ionic conductivity has been observed.

[1] Alami Talbi, M. et al (1994) *J. Solid State Chem.*, **110**, 350-355. [2] Bakhous, K. et al. (1999) *J. Solid State Chem.*, **146**, 499-505. [3] Heintz, J.M. et al (1997) *J. Alloy. Compd.*, **250**, 515-519. [4] Bykov, D.M. et al. (2006) J. Solid State Chem., **179**, 3101-3103. [5] Barre, M. et al.(2005) *Chem. Mater.*, **17**. 6605-6610.

Infrared spectroscopy of minerals: modern trends and prospect

Chukanov, N.V.[*] & Dubovitskiy, V.A.
Institute of Problems of Chemical Physics, RAS, Chernogolovka, Russia ([*]chukanov@icp.ac.ru)

Traditionally, the application of IR spectroscopy in mineralogy is reduced to the determination of wavelengths or frequencies of absorption maxima. These values are brought in correspondence with normal vibrations of different chemical bonds or covalently-bonded groups of atoms. Another approach, also based on the use of discrete band maxima, is applied to obtain correlations between vibration frequencies and different characteristics of minerals (hydrogen bond strengths, degree of isomorphous substitutions *etc*.). In particular, correlations of this type have been used by us to determine the degree of condensation of polyhedra in crystal structures of minerals and to identify silanol groups in silicates.

Unlike traditional treatment of infrared spectra (IRS) of minerals as a number of discrete absorption bands, our new approach (full-profile analysis [1]) is based on the consideration of the whole spectral curve within a certain range of frequencies. Spectral curves are considered as elements of a multidimensional vector space. The key point of the method consists of best fitting of analyzed spectrum by nonnegative linear combination of known samples from the base set. This approach is numerically stable due to the application of the concepts of integral error functional and generalized positive solution. Automated data processing is possible with a practically unlimited base set of reference spectra. The application of full-profile IRS analysis makes it possible to avoid the combinatorial stage from the procedure of identification of minerals. On the basis of this approach, an IRS-based quantitative criterion of crystal-chemical similarity (CCS) can be introduced for pairs of minerals to be compared. CCS can be expressed as the normalized square deviation of an analyzed spectrum from a reference spectrum, or from an approximating nonnegative linear combination of reference spectra. Being based on empirical spectroscopic data, this criterion reflects real crystal-chemical relationships: pairs of minerals with similar structure type have the lowest CCS values. Within a given structure type, CCS characterizes compositional relationships.

In order to make full-profile IRS analysis a customary method in mineralogical investigations, during the last 20 years a representative collection of IRS of well-characterized mineral samples was built. It includes about 3000 spectra of more than 2200 mineral species. In the frame of this work, an IRS database was created and more than 100 new minerals have been discovered.

Numerous examples of the application of traditional ("fingerprint"), correlation and full-profile IRS-based approaches to the analysis of fine crystal-chemical features of minerals are given. The latter method is most effective for the identification of mineral species belonging to complex mineral groups (like cancrinite and eudialyte groups), as well as for the quantitative analysis of polymineral mixtures.

Acknowledgments: This work was financially supported by Russian Foundation for Basic Research (grant No. 09-05-12001-ofi_m).

[1] Chukanov, N.V., Dubovitskiy, V.A. & Vozchikova, S.A. (2008) *Geol. Ore Deposits*, **50(8)**, 815-826.

Single-crystal, polarized-light, FTIR spectroscopy of arrojadite

Della Ventura, G.[1*], Bellatreccia, F.[1], Cámara, F.[2], Oberti, R.[2] & Chopin, C.[3]
[1]Dipto. Scienze Geologiche, Univeristy Roma Tre, Italy, ([*]dellaven@uniroma3.it)
[2]CNR-IGG, UOS Pavia, Italy
[3]Laboratoire de Geologie, ENS-CNRS, Paris, France

Arrojadites are extremely complex phosphates which are typically found in granitic pegmatites or hydrothermal veins. Their occurrence in metamorphic rocks [1] suggests wide conditions of formation for these minerals. The crystal structure and crystal chemistry of arrojadite have been debated for several decades, until [2] and [3] re-examined a set of samples from various occurrences and revised the structural model, the formula and the nomenclature of the group. One key aspect in the new crystal-structural model for arrojadite is the presence of three OH-groups [2]: two of these (O-H1 and O-H2) are very similar in local octahedral environment, crystallographic orientation and hydrogen-bond system. In contrast, O-H3 is connected with the apical oxygen of a newly defined tetrahedron in the structure, and is involved in a bifurcated hydrogen bridge with surrounding oxygen atoms. The Raman spectra reported in [2] show two higher-frequency, intense and convoluted bands which were assigned to specific local environments of OH1 and OH2; an additional low-frequency, broad and weak feature in the spectra (Fig. 1, left) could not be assigned with certainty. The FTIR spectra collected in the course of present work on various samples studied in [2], are similar to the Raman spectra in the higher-frequency 3600-3500 cm^{-1} range, with two intense and multi-component bands. In contrast, in the lower-frequency region, FTIR shows a very intense and broad absorption extending from 3500 to 2900 cm^{-1} (Fig. 1, right).

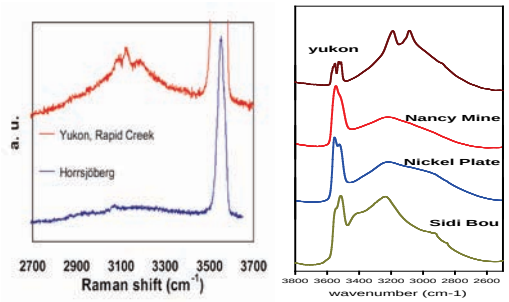

Fig. 1: Raman (left) and FTIR (right) spectra of arrojadites

The FTIR spectrum of arrojadite from Rapid Creek (Yukon) shows also an intense doublet at 3190-3087 cm^{-1} (Fig. 1 right, top) which can be assigned to NH^{4+} groups, as confirmed by EMPA only in this sample. The orientation of the absorber (i.e. the O-H bond) with respect to the crystallographic axis can be determined from polarized-light measurements along the principal optical direction [4]. For the arrojadite studied here, the data are consistent with assignment of the higher-frequency components to the O-H1 and O-H2 groups obtained from the X-ray structure refinements even in the case of partial occupancy, while the assignment of the broad band to the H-O3 group proposed by [2] needs further work. No evidence of molecular water is present in the NIR 4000-6000 cm^{-1} region.

[1] Demartin, F. et al. (1996) *Can. Mineral.*, **34**, 827-834. [2] Cámara, F. et al. (2006) *Am. Mineral.*, **91**, 1249-1259. [3] Chopin, C. et al (2006) *Am. Mineral.*, **91**, 1260-1270. [4] Libowitzky, E. & Rossman, G.R. (1996) *Phys. Chem. Miner.*, **23**, 319-327.

Conservation of Egyptian blue pigments from the Pharaonic and the Gallo-Roman periods

Farges, F.[1,2*] & Etcheverry, M.-P.[3]
[1]LMCM, Muséum National d'Histoire Naturelle, Paris, France ([*]farges@mnhn.fr)
[2]Dept. of Geological and Environmental Sciences, Stanford University, Stanford CA, USA
[3]LRMH, Champs sur Marne, France

Combined µ-XRF and µ-XAFS experiments were performed on four historical Egyptian blue samples. Those two samples illustrates opposite conservation conditions over thousands of years: (1) dry desertic solids with periodic floadings (Nilus river) and (2) constantly wet conditions (Rhône river) since the Gallo-Roman period (France).

The first two samples are coming from the Ancient Egypt: (a) a blue sintered pigment from Karnak (dated 1500 BC) and (b) a copper-rich enamel from a goddess Sekhmet statue (similar age). The two other samples are sintered vitro-ceramics (Gallo-Roman, ca -50AC to +100 BC) from the Lyon area in France: (c) "Rue des Farges" (downtown Lyon), and (d) "St. Romain-en-Gal" (Vienne area).

µ-XRF an µ-XAFS spectra were collected at the Cu K-edge at the Advanced Light Source (Berkeley, UA), operating at 2.4 GeV and 800 mA currents. We used Si(111) double crystal monochromators and KB mirrors. Energetic and lateral resolution are ~1.5 eV and 10 µm, respectively. Samples were polished and set in air while the Kα of Cu was collected using a single-element, solid-state Si detector. µXRF maps were collected (1 second/pixel) while µ-XAFS spectra were collected with 2 sec/point, 0.5 eV steps from 8900 to 9900 eV.

The present report shows that copper is present as cuprorivaïte (samples a, c and d) and as a glassy copper-rich amorphous matrix (samples b, c and d). When polarization effects are accounted for, all XANES for sample (a) are consistent with that of a synthetic cuprorivaïte. In the glassy matrix (samples b, c and d), copper is fully oxidized. This is contrast to the redox of copper in contemporary synthetic glasses prepared under oxidizing conditions (which should show Cu(I) and Cu(II)). Hence, copper has been oxidized in samples b, c and d. In sample d, copper is polymerized as an intergrowth of chrysocolla and tenorite (i.e., $CuOOH/SiO_2$ and CuO). Then, the effect of low temperature weathering of Cu-glasses over thousand of years tends to produced highly enriched domains (spatially highly segregated) in copper. These domains progressively form tenorite crusts as the expense of spertiniite ("chrysocolla") precipitates, which are produced at the rims of weathered domains, themselves enriched in insoluble elements (such as Si and Al).

The binding state of indium and tin in natural sulphides: first results of a comparative study by X-ray absorption spectroscopy at the *L*-edge

Figueiredo, M.O.[1,2] & Silva, T.P.[2,1]
[1]CENIMAT/I3N, Dept of Material. Science, Faculty of Sciences andTechnology, New University of Lisbon, Caparica, Portugal (*ondina.figueiredo@ineti.pt)
[2]Laboratório Nacional de Energia e Geologia I.P. (LNEG), U. Mineral Resources and Geophysics, Alfragide, Portugal

One electron makes the difference between the outer shell of In and Sn, two scarce metals with very distinct crystal chemical behaviour in the Earth's crust: indium is clearly chalcophile, very seldom forming specific minerals and occurring mainly dispersed within excess-metal polymetallic sulphides, while tin is markedly lithophile and currently present as stannic oxide.

Indium is nowadays widely used in many technologic fields (low melting-temperature alloys, solders and various «high-tech» devices like liquid crystal displays (LCD), organic light emitting diodes (OLED), transparent flexible thin-films of ionic amorphous oxide semiconductors (IAOS), photovoltaic cells with increased efficiency based on $Cu(In,Ga)Se_2$ (CIGS). As a consequence, indium consumption is expected to increase in the near future, centring a special interest on the improvement of its exploitation from polymetallic sulphide ores, along with its recycling technology.

Indium recovery stands mostly on zinc extraction from the natural cubic sulphide – sphalerite, the prototype of so-called «tetrahedral structures» where metal ions fill half of the available tetrahedral sites within the cubic closest packing of sulphur anions. Such anionic array is thus particularly suitable to accommodate poly-cations in close edge-sharing tetrahedral sites [1,2], as occurs in excess-metal copper sulphides (e.g., bornite, ideally Cu_5FeS_4), recognized to be relevant In-carrier minerals in many polymetallic sulphide ore deposits. A similar situation holds for the tetrahedral $[Sn_2S_6]$ cluster in special meso-structured semiconductors [3].

X-ray absorption spectroscopy at the *L*-edges (arising from $s,p \rightarrow d$ transitions) is a suitable methodology for probing unoccupied density of states and *s-p* orbital hybridization [4]. Accordingly, a comparative study of In and Sn by X-ray absorption near-edge spectroscopy (XANES) at the L_3-edge was undertaken at the ESRF (European Synchrotron Radiation Facility in Grenoble/France) using the instrumental set-up of beamline ID21.

Beyond two edge shoulders ascribed to $2s \rightarrow 5p$ transitions that were also observed in the In L_3-edge spectra of wurtzite-type indium nitride [5], a third weak white line was noticed at lower energy (3,730 eV) in the XANES spectra collected from a polymetallic ore sample. An identical pattern of pre-edge details was detected in Sn L_3-edge XANES spectra collected at the same irradiated point – an expectable result in view of earlier data [5]. However, a single intense «white line» at 3,730 eV was noticed in a faint In L_3-edge XANES spectra collected at another point of the same ore sample but the impossibility of clearly identifying the nanoscale phase hosting indium has hindered a full interpretation of X-ray absorption data. Further work is in progress focusing on coexisting indium and tin.

Acknowledgements: Work developed through the project PTDC/CTE-GIN/67027/2006 financed by the Portuguese Foundation for Science & Technology (MCTES). Financial support of EU to perform the experiments at the ESRF.

[1] Figueiredo, M.O. et al. (2007) in Andrew, C. et al (eds.) *Proc. 9th Biennal SGA Mtg*., 1355-1357. [2] Figueiredo, M.O. & Silva, T.P. (2009) *ICANS 23* (abstract). [3] Krishnaswarmy, K. et al. (2002) *Nano-Lett.*, **2**, 513-517. [4] Sham, T.K. (1985) *Phys. Rev. B*, **31**, 1888-1902. [5] Thienprasert, T. et al. (2008) *Appl. Phys. Lett.*, **93**, 051903.

Sulfur speciation in silicates: an X-ray absorption spectroscopy study

Göttlicher, J.
Karlsruhe Institute of Technology, Institute for Synchrotron Radiation, Eggenstein-Leopoldshafen, Germany
(joerg.goettlicher@iss.fzk.de)

There is still ambiguity on sulfur speciation in some silicate minerals, especially for minerals that are characterized by cages in its structure (like sodalite group minerals). Several minerals from different localities like

- lazurite ($(Na,Ca)_8[(S,SO_4,Cl_2)|Al_6Si_6O_{24}]$),
- hackmanite ($Na_8[Al_6Si_6O_{24}](Cl_2,S)$,
- afghanite ($(Na,Ca,K)_8[(Cl_2,SO_4,CO_3)_3|Al_6Si_6O_{24}]x0.5H_2O$),
- nosean ($Na_8[SO_4|Al_6Si_6O_{24}]$),
- hauyne ($(Na,Ca)_{4\text{-}8}[Al_6Si_6(O,S)_{24}](SO_4,Cl)_{1\text{-}2}$) and
- davyne ($(Na,K)_6Ca_2[(Cl_2,SO_4)_2|Al_6Si_6O_{24}]$)

have been investigated by x-ray absorption spectroscopy at the sulfur K-edge in order to get information on sulfur valence and moleculare structure.

The measurements have been performed at the X-ray Beamline for Environmental Studies (SUL-X) of the synchrotron radiation source ANKA in Karlsruhe in normal focus and partly in microfocus to separate signals from minerals when they are inter-grown with other sulfur containing phases.

The X-ray absorption near edge structure (XANES) spectra are classified with respect to pre-edge features and edge structures. Hackmanites for example show a sharp pre-edge at the lowest energy so far recognized in S K-edge x-ray absorption spectra [1]. Lazurites are characterized by a sulfate resonance and spectral features that indicate reduced sulfur species. Ultramarine color pigments show two types of spectra, both indicate reduced reduced sulfur species, too.

Besides the above mentioned minerals and color pigments helvine ($Mn_4Be_3[S|(SiO_4)_3]$), vishnevite ($(Na,K)_8[(SO_4,CO_3)|Al_6Si_6O_{24}]x2H_2O$) and other non-tectosilicates like ellestadite ($Ca_5(SiO_4,PO_4,SO_4)_3(F,OH,Cl)$) have been included in the study.

The results will be compared with non-silicate compounds and minerals where sulfur is the main constituent, like elemental sulfur, iron sulfides and different sulfites and sulfates.

A first attempt to gain structural information on sulfur in silicate minerals using S K-edge Extended Fine structure (EXAFS) spectroscopy will also be discussed.

[1] Goettlicher, J. et al. (2010) *Deutsche Tagung für Forschung mit Synchrotronstrahlung, Neutronen und Ionenstrahlen an Großgeräten SNI 2010*. Berlin, Freie Universität.

Long-wavenumber infrared study of tourmalines from tin deposits in Russia

Ivanov, V.V.[1*], Narnov, G.A.[1], Kononov, V.V.[1] & Gorelikova, N.V.[2]
[1]FEGI FEB RAS, Vladivostok, Russia ([*]dom101@mail.ru)
[2]IGEM RAS, Moscow, Russia

Tourmaline is an important petrogenetic indicator of different geological events because it can incorporate by total or partial substitution a great variety of chemical elements depending on the geological setting [1]. The chemical composition of the tourmaline group minerals is represented by the general formula $XY_3Z_6(Si_6O_{18})(BO_3)_3(OH, F)$ [2]. An important method that can be used to explain crystal chemical features of tourmaline is infrared (IR) spectroscopy. We revealed the connection between the cation composition of tourmalines and the features of IR spectra of the mineral group in the long wavenumber range (400-220 cm^{-1}) because this range has not been studied at all for tourmalines.

IR spectra of tourmalines are characterized by clear absorption bands in the studied interval. In spectra of schorls the characteristic absorption bands are the following: 370, 330, 300, 273, 229 cm^{-1}. Besides, a shoulder at 263 cm^{-1} and a poorly defined band at 250 cm^{-1} were found. IR spectra of dravites are dominated by the bands at 373, 329-322, 274, 229 cm^{-1}, and also shoulders at 348, 308, 259 cm^{-1}. Elbaites are characterized in IR spectra by maxima at 372, 354, 226 cm^{-1} and shoulders at 348 and 239 cm^{-1}. IR spectra of intermediate members of schorl-dravite range have characteristic bands at 320, 269 and 224 cm^{-1}. A common feature of all spectra of tourmaline varieties is the presence the major broad band at 340-290 cm^{-1}, including one or two maxima. The absorption band with maximum at 330 cm^{-1} is typical of schorls, 229-222 cm^{-1} is for dravites, 319 cm^{-1} for schorl-dravites. The comparison of IR spectra and the chemical composition of different tourmaline varieties suggest that bands in this range should be conditioned by the variable cation content in the mineral structure.

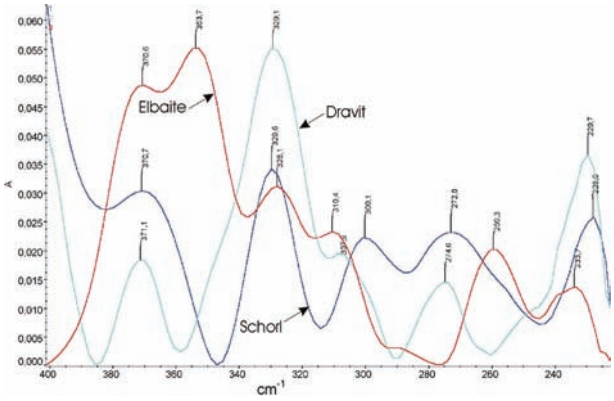

Fig. 1: Typical IR spectra of schorl, dravite and elbaite.

Acknowledgements: This work has been supported by the Russian Foundation for Basic Research of the Russian Academy of Sciences through the project 08-05-00381.

[1] Gorelikova, N.V. (1988) *Parageneses of trace elements in tourmalines from tin formations.* Monograph. Vladivostok. (in Russian). [2] Hawthorne, F.C. & Henry, D.J. (1999) *Eur. J. Mineral.*, **11**, 201-205.

High-pressure Raman spectroscopic studies of ulvöspinel Fe_2TiO_4

Kyono, A.[*], Yamanaka, T., Ahart, M., Mysen, B.O., Mao, H.K. & Hemley, R.J.
Geophysical Laboratory, Carnegie Institution of Washington, Washington D.C., USA ([*]akyono@ciw.edu)

We report in situ Raman spectroscopic studies of ulvöspinel in a diamond-anvil cell under hydrostatic conditions up to 57 GPa at room temperature. There are five first-order Raman active modes ($A_{1g} + E_g + 3F_{2g}$) in the *Fd3m* space group of the spinel structure. Two strong modes at nearby 500 (F_{2g}) and 700 cm^{-1} (A_{1g}) are observed both at ambient and at high pressure conditions (Fig. 1). The remaining three modes could not be observed unambiguously in the measurements. The peak positions and shapes of the Raman spectra agree well with previously published data measured under ambient condition [1].

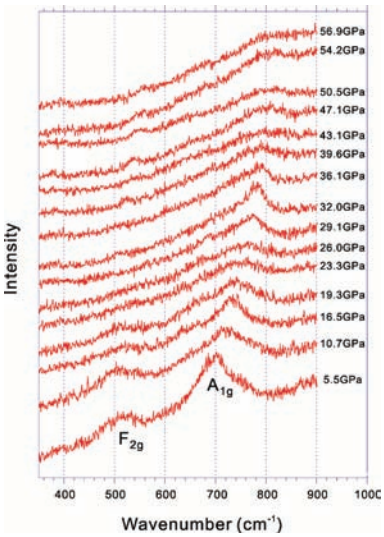

Fig. 1: Pressure dependence of the Raman spectra of ulvöspinel Fe_2TiO_4 under compression up to 54 GPa.

With increasing pressure, the frequencies of the two strong bands A_{1g} and F_{2g} increase continuously up to 13 GPa with pressure derivatives of 2.6 and 1.4 cm^{-1}/GPa, respectively. There is no obvious degradation of crystal symmetry or structural change within this pressure range. These two frequencies gradually decrease with increasing pressure. Above 10 GPa, these peaks broaden and reduce their intensities with pressure. Then, the F_{2g} symmetry mode completely disappears at a pressure of 20 GPa. According to high-pressure X-ray diffraction experiment results [2], the ulvöspinel undergoes a series of transformations: cubic to tetragonal, tetragonal to orthorhombic, and orthorhombic to orthorhombic. At first, the transformation from cubic to tetragonal takes place at 9 GPa. Second, orthorhombic occurred at 13 GPa remains stable up to 48 GPa. New high-pressure phase occurs above 48 GPa. The orthorhombic phase has four Raman active modes ($A_g + B_{1g} + B_{2g} + B_{3g}$). The pressure-induced phase transition from cubic to orthorhombic is accompanied by transformation of the A_{1g} and F_{2g} modes of the cubic into the A_g and $B_{(1,2,3)g}$ modes in the orthorhombic. It seems reasonable to suppose that the remaining peaks above 20 GPa result from the A_g mode in the orthorhombic phase transformed from cubic ulvöspinel.

[1] Wang, A. et al. (2004) *Am. Mineral.*, **89**, 665-680. [2] Yamanaka, T et al. (2009) *Phys. Rev. B*, **80**, 134120

Water speciation in silicate melts: a high temperature Raman spectroscopy study

Le Losq, C.[1], Moretti, R.[2] & Neuville, D.R.[1*]
[1]CNRS-IPGP, Physique des Minéraux et des Magmas, Géochimie et Cosmochimie, Paris, France ([*]neuville@ipgp.jussieu.fr)
[2]Istituto Nazionale di Geofisica e Vulcanologia, sezione di Napoli – Osservatorio Vesuviano

In addition to temperature, pressure and main chemical components, volatiles exert a strong influence on the physical properties of magmas. In particular, water plays a fundamental role in the dynamics and evolution of magmas in the deep interior and during volcano eruption. However, water speciation in silicate melts is not fully understood. Infrared spectroscopy had provided some valuable information about the H_2O/OH^-

SiO_2	Al_2O_3	FeO	MgO	H_2O_{calc}
43.89	2.33	4.18	35.74	13.86

speciation. We know that this speciation is a function of temperature and water contents of melts. It can be very interesting to know it from *in situ* experiments. This can be done using Raman spectroscopy.

Raman spectra are composed of i) a low-wavenumber region which corresponds to vibrations of the silicate network (0-1500 cm^{-1}), and ii) a high-wavenumber region which correspond to the OH^- stretching vibration and H_2O molecular vibration (3100-3750 cm^{-1}). We have performed a first set of *in situ* experiments using a micro-furnace at ambient pressure. We have observed an evolution of the high-wavenumber region as a function of time and temperature. New Raman peaks can be distinguished, particularly near 3650-3700 cm^{-1}. In this communication, we will present our first results on this subject and then discuss them in terms of relation between water and the silicate network.

The polarized spectra (400 – 1600 nm) of antigorite from Aldina Reka (Serbia)

Logar, M.[*], Poharc-Logar, V. & Erić, S.
Dept. of Mineralogy and Crystallography, FMG, University of Belgrade, Serbia ([*]milogar@eunet.rs)

Looking at the available literature [1] it seems that the colour origin of serpentine minerals needs additional study. We couldn't find data on polarized spectra of antigorite. Only one unpolarized spectrum has been published until now [2].

Antigorite from Aldina Reka [3] occurs in the veins as a rod-like aggregate with perfect parting parallel to elongation. Microscopic observations reveal lath-like crystals with apparent pleochroism of a changing green hue (Fig. 1). The chemical analysis (SEM EDX) at the thin-section points where the spectra have been measured are listed in Table 1.

Table 1: Chemical analysis (SEM EDX) of antigorite (wt%)

The spectra of two vibration directions have been measured installing the microscope (Leitz with Nicol prism) in the optical path of the computer controlled monochromator. The chopped signal, synchronized and amplified by lock-in amplifier, was recorded to the computer. Between 400 and 1600 nm 1039 points were measured with the FM tube, Si and InGaAs photo-diodes, using 0.03 mm slit. The spectra have been measured through four different points of the thin-section area (0.5 mm thickness). No significant difference among the four spectra was observed.

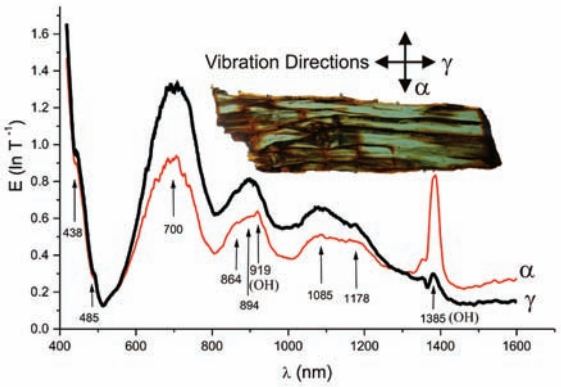

Fig. 1: The polarized spectra of antigorite (green parts).

Absorption peaks found in the spectra can be separated into three groups in accordance with their origin. 1) Polarization-dependent overtones of (OH) stretching vibrations at: 1385 nm (7220 cm^{-1}, $\Delta\upsilon=2$) and 919 nm (10893 cm^{-1}, $\Delta\upsilon=3$). 2) Polarization-independent d-d electron transitions due to octahedral Fe^{2+} calculated for Racah parameters B=750 and C=3250 cm^{-1}: Jahn-Teller separated $^5E(D)$ at 1085 and 894 nm; two spin-forbidden $^3T_1(H)$ at 1178 nm and $^3T_2(H)$ at 867 nm. 3) Polarization-dependent Fe^{2+}- Fe^{3+} charge-transfer band at 700 nm, which produce the pleochroism.

Spin-forbidden Fe^{3+} d-d transitions is not resolved except the shoulder at 438 nm which could be the $^4A_1$,$^4E(^4G)$.

[1] Rossman, G.G. (2010) http://minerals.gps.caltech.edu. [2] Reddy, S.N. et al. (2001) *Neues. Jb. Miner. Mh.*, **6**, 261-270. [3] Logar, M.M. (1999) *Bulletin T. CXIX l'Acad. Serbe Sc. Arts*, Sc. nat., **39**, 205-211.

Matrix-infrared spectroscopy as a tool to monitor admixtures in minerals

Marinova, D.[1*], Wildner, M.[2], Stoilova, D.[1] & Georgiev, M.[3]
[1]Institute of General and Inorganic Chemistry, Bulgarian Academy of Sciences, Sofia, Bulgaria
([*]d.manasieva@gmail.com)
[2]Institut für Mineralogie und Kristallographie, Universität Wien, Vienna, Austria
[3]Dept. of Inorganic Chemistry, University of Chemical Technology and Metallurgy, Sofia, Bulgaria

Matrix-infrared spectroscopy provides important information about the type of the admixtures included in minerals, either as isomorphous (isodimorphous) substitutions or as distinct phase inclusions. The vibrational spectra of distinct phase inclusions are similar to those of the respective neat compounds. However, the vibrational spectra of isomorphously included guest ions are essentially determined by both the site-symmetry, which is assumed to be the same as that of the respective host ions (substitutional type of mixed crystals), and the potential at the lattice sites where the guest ions are located, as shown by the extend of energetic distortion of the matrix-isolated ions.

In the present study, several phases belonging to the large number of natural and synthetic compounds with kröhnkite-type chains have been synthesized as model phases. The crystal structures of $Na_2Me(SeO_4)_2\cdot 2H_2O$ (*Me* = Co, Ni, Zn, Cd) and $K_2Me(CrO_4)_2\cdot 2H_2O$ (*Me* = Zn, Cd) were determined from X-ray single-crystal diffraction data and those of $K_2Me(CrO_4)_2\cdot 2H_2O$ (*Me* = Co, Ni) by X-ray powder diffraction. The structures are build up from $MeO_4(H_2O)_2$ octahedra and XO_4 tetrahedra forming infinite kröhnkite-type octahedral-tetrahedral chains, which are linked by alkali cations to layers and further to a three-dimensional framework via hydrogen bonds. The sodium cobalt, nickel and zinc compounds as well as the potassium cobalt, nickel and cadmium compounds crystallize in the triclinic space group $P\bar{1}$ (type A), the sodium cadmium selenate in the monoclinic space group $P2_1/c$ (type D), and the potassium zinc chromate in the monoclinic space group $C2/c$, thus representing a new structural type (type H).

The vibrational behavior of SO_4^{2-} guest ions included in these chromate and selenate matrices has been studied by infrared spectroscopy. It has been established that the extent of energetic distortion of the SO_4^{2-} guest ions as deduced from the values of $\Delta\nu_{as}$ (site-group splitting) and $\Delta\nu_{max}$ (the difference between the highest and the lowest wavenumbered components of the stretching and bending modes), depends on both the electronic configurations of the Me^{2+} ions and the degree of covalency of the respective Me^{2+}–O bonds. The matrix-isolated SO_4^{2-} guest ions are stronger distorted in the selenates than in the chromates due to the smaller unit-cell volumes of the selenate host compounds as compared to those of the chromate ones and the different ionic radius of the K^+ and Na^+ ions. The smaller Na^+ ions cause a stronger electrostatic field (shorter Na–O bonds), thus leading to remarkably larger values of $\Delta\nu_{as}$ and $\Delta\nu_{max}$ of the guest ions in the sodium compounds.

The temperature stability of quaternary precipitations remanence

Mashukov, A.V.[*], Onufrienok, V.V. & Mashukova, A.E.
Siberian Federal University, Krasnoyarsk, Russia
([*]AVMashukov@)sfu-kras.ru)

The natural remanence, in whose formation a great role is played by iron compounds, is source of information about the value and direction of the ancient magnetic field as well as physicochemical conditions of rock formation.

To reveal the conditions determining the specific character of the quaternary precipitations remanence of the Yenisej river, there were investigated their magnetic and structural properties. The value of the alternating magnetic field, which half reduces the remanence of the samples, makes up 16 kA/m, the coercive force is 30 A/m and the saturation magnetization is more than 800 A/m. In table 1 there are given the values of relative magnetization J/J_0 at different temperatures.

Table 1: Relative magnetization at different temperatures

°C	100	200	300	350	400	450	500	550	595
J/J_0	0.95	0.99	0.95	0.96	0.93	0.93	0.75	0.7	0

To reveal the minerals - magnetization carriers by using a magnetic separation method, there were singled out three fractions by strong-magnetic (1), weak-magnetic (2) and non-magnetic.(3) (Table 2).

Table 2: Parameters of the samples according to the Mossbauer spectroscopy data

Percentage of the samples	Fraction 1	Fraction 2	Fraction 3
Fe_3O_4	87,3±0,2	-	-
Fe_2O_3	0,7±0,7	21,3±0,7	-
FeO	4,7±0,3	36,4±0,1	53,1±0,05
FeOOH	8,0±0,2	42,3±0,2	46,9±0,05

One can see from table 2, that the basic ferruginous mineral in the fraction (1) is magnetite. Hematite is probably located on the surface of magnetite grains. The isomer shifts testify to different surrounding of radiating and absorbing nucleus and to different iron ion valency. The carriers of the fraction (2) magnetization are hematite grains. The compounds FeOOH and FeO do not give any contribution into remanence. The isometric shift and the quadrupole splitting of these compounds are identical with those for the weak-magnetic fraction.

The precipitation with desired deposition conditions in the Earth magnetic field were investigated by using X-ray straight pole figures method for the exploring of the crystallographic ordering effect. The intensity values of the precipitation with magnetic particle size are shown in table 3.

Table 3: Dependence of intensity on particle size

Fraction	1	2	3	4	5
Fe_3O_4 particle size d, mcm	0 ÷ 8	9 ÷ 32	33 ÷ 64	65 ÷100	150 ÷200
Intensity	1,9	1,8	1,4	1,2	1,1

Thus, the Mossbauer spectra make it possible to determine the types of magnetic minerals in complex compounds. Their identification enables to reveal the stability of remanence in geological time scales.

Comparative diffraction and spectroscopic study of the stannite – kesterite – kuramite system

Schorr, S.[1*] & Evstigneeva, T.L.[2]
[1]Institute of Geological Sciences, Free University Berlin, Germany ([*]susan.schorr@fu-berlin.de)
[2] Faculty of Physics, M.V. Lomonosov Moscow State University, Moscow, Russia

The pseudoternary Cu_2FeSnS_4 (stannite) – Cu_2ZnSnS_4 (kesterite) – Cu_3SnS_4 (kuramite) system have been studied by a combination of neutron powder diffraction, EXAFS and Moessbauer spectroscopy.

Stannite and kesterite have structural models derivative of that of chalcopyrite, $CuFeS_2$, the archetype of the extensive family of I-III-VI chalcogenide semiconductors. Chalcopyrite, in turn, has a structural model simply derivative of that of sphalerite, ZnS. The chemical change from ZnS to quaternary chalcogenides is accomplished by successive specialization of cation sites, with a consequent lowering of the overall symmetry of the structure. From $Fm3m$, sphalerite, a tetragonal space group, $I\bar{4}2d$ characterizes chalcopyrite, stannite and kesterite are also tetragonal. Although Fe and Zn have similar chemical behaviour in this materials, crystal chemistry of both ions is significantly different and induces structures in different space groups, $I\bar{4}2m$, stannite and $I\bar{4}$, kesterite. The copper tin sulphide kuramite, $Cu(I)_2Cu(II)SnS_4$, crystallizes in the stannite type structure, where the two Fe and Cu cation sites are occupied just by Cu. A relevant consequence is that Cu(II), necessary in this phase to achieve the charge balance, can not be identified in a single site.

The diffraction and spectroscopic techniques used contribute different aspects to this study: neutron diffraction is mainly devoted to investigate the metal distribution in the cation sites [1]. ^{57}Fe and ^{119}Sn Moessbauer spectroscopy allows to determine the valence state and atom coordination of iron and tin atoms in the structure [2,3]. EXAFS is a X-ray spectroscopy technique which allows the determination of bond distances locally and gives also a hint to the charge state of iron [4].

The presentation will give a comparative discussion of average and local bond distances in the stannite – kesterite – kuramite system, achieved by diffraction and spectroscopy, respectively. Furthermore the valence state of iron, determined by two different spectroscopic techniques, will round the presentation.

[1] Schorr, S., Höbler, H.-J. & Tovar, M. (2007) *Eur. J. Mineral.*, **19**, 65-73 [2] Rusakova, V.S. et al. (2008) *AIP Conf. Proc.*, **1070**, 96-105. [3] Di Benedetto, F. et al. (2005) *Phys. Chem. Minerals*, **31**, 683-690. [4] Zalewski, W. et al. (2010) *J. Alloys Comp.*, **492**, 35-38.

ESR dating of barite in hydrothermal chimneys of deep sea floor

Toyoda, S.[1*], Sato, F.[1], Okumura, T.[1], Ishibashi, J.[2], Nakai, S.[3] & Kumagai, H.[4]
[1]Dept. of Applied Physics, Okayama University of Science, Okayama, Japan ([*]toyoda@dap.ous.ac.jp)
[2]Kyushu University, Fukuoka, Japan
[3]University of Tokyo, Japan
[4]Japan Agency for Marine-Earth Science and Technology, Yokosuka, Japan

Barite ($BaSO_4$), the most common barium mineral, occurs principally as gangue mineral in hydrothermal polymetallic ore deposit. In this study, electron spin resonance (ESR) dating method was applied to marine barite formed in deep sea hydrothermal systems.

We used barite chemically extracted from the portion taken at the basal part of a hydrothermal chimney, consisting of barite, sphalerite and pyrite, at the Archaean site (12°56.4'N, 143°37.9'E) in South Mariana spreading centre. The sample was taken at the time of the dive, YK05-09 cruise by deep-sea submersible vehicle (DSV) Shinkai 6500 performed by the Japan Agency for Marine-Earth Science and Technology (JAMSTEC). ESR spectra were observed using a JEOL PX-2300 at room temperature with a microwave power of 1 mW, the modulation frequency of 100 kHz, and modulation amplitude of 0.1 mT.

The ESR spectrum of marine barite, shown in Fig. 1, is characterized by an electron-type center with g values of 2.0034, 2.0022 and 1.9995 probably attributed to SO_3^- [1]. The signal intensity was enhanced by gamma ray irradiation in the dose range from 110 to 2600 Gy. The accumulated natural dose of 232 Gy was obtained by extrapolating the saturation curve to zero ordinate after fitting a curve to the dose response of the ESR intensity. The ^{226}Ra activity of the barite was measured by gamma ray spectrometry using a low background germanium detector. The Ra concentrations were 7.72 Bq/g, while those of Th series and K_2O were not detected. The natural dose rate was calculated to be 303 mGy/y. The age of the sample was estimated to be 765 years. Barite seems to be a useful mineral for dating hydrothermal activities in the sea floor, however, the age was not consistent with the value obtained by ^{226}Ra-^{210}Pb dating method.

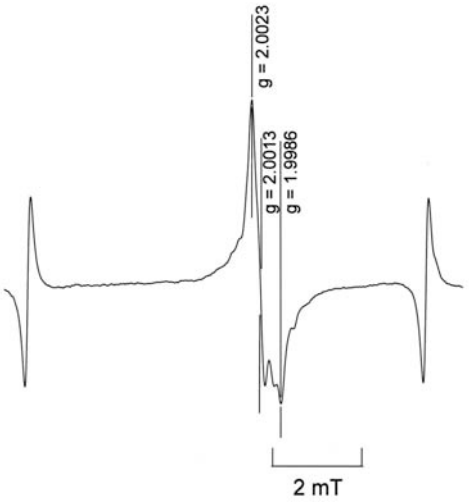

Fig. 1: The ESR signal observed in marine barite. The signal is attributed to SO_3^- radical.

[1] Kasuya, M. et al. (1991) in *Essay in Geology, Prof. Nakagawa Commemorative Volume*, 95-98.

Local structure analysis of tektite by Ti K-edge EXAFS spectroscopy

Wang Ling[1], Yoshiasa Akira[1*], Okube Maki[2], Murai Kei-ichiro[3] & Takeda Takashi[4]
[1]Graduate School of Sciences and Technology, Kumamoto University, Kumamoto, Japan
([*]yoshiasa@sci.kumamoto-u.ac.jp)
[2]Materials and Structure Laboratory, Tokyo Institute of Technology, Yokohama, Japan
[3]Dept. of Advanced Materials, Institute of Technology and Science, the University of Tokushima, Japan
[4]National Institute for Materials Science, Tsukuba, Japan

Local structure of tektite was studied by extended X-ray absorption fine structure (EXAFS) spectroscopy. We have carried out Ti K-edge EXAFS measurements to get information about the local structure and chemical state of Ti in many species with different localities, sizes and colours in tektites of Hainanite, Indochinite, Philippinite, Australite, Bediasite and Moldavite. We have determined the precise local Ti-O bonds in tektite. We also prepared several reference titaniferous minerals.

Tektites have different local structures of Ti. The pattern of XANES spectra has something that looks like high-temperature TiO_2-SiO_2 glass, TiO_2 anatase and $CaTiO_3$ perovskite. All samples show the valence of Ti is 4^+. Based on the local Ti-O distances, coordination numbers and radial structure function determined by EXAFS analyses, we classified the tektites in three types: Type I, Ti occupy 4-fold coordinated tetrahedral site and Ti-O distances are 1.84-1.79 Å; Type II, Ti occupy 5-fold trigonal bi-pyramidal or tetragonal pyramidal site and Ti-O distances are 1.92-1.89 Å; Type III, Ti occupy the 6-fold octahedral site and Ti-O distance is 2.00-1.96 Å. Farges & Brown [1] discussed the coordination number of Ti in tektite according to the pre-edge XANES pattern and concluded all tektites have 4-fold coordination. Though, we have found some tektites with 5- and 6-fold coordinated Ti. Ti occupies the TiO_6 octahedral site in many titanium minerals at ambient conditions. This study indicates that the local structure of Ti should be changed in the impact event and the following stage. Tektites splashed to the space and travelled in several kinds of processes and routes, which lead to different temperature and pressure history. Local structure of Ti should be related with the temperature, pressure, quenching rate, sizes of impact meteorite and size of falling melts. As a result, there are some difference in the bonding structure of Ti atoms and arrangements of neighbouring oxygen.

Table 1: Classification of titanium local structure in tektites based on the local Ti-O distances, coordination numbers determined by EXAFS analyses

	Tektites	Coordination number	Ti-O distance (Å)
Type I	Hainanite	4	1.790(4)
	Indochinite	4	1.812(5)
	Bediasite	4	1.835(3)
Type II	Australite	5	1.890(5)
	Philippinite	5	1.920(5)
Type III	Moldavite	6	2.001(4)

[1] Farges, F. & Brown, G.E. Jr (1997) *Geochim. Cosmochim. Ac.*, **61**, 1863-1870.

IR spectroscopy: quantitative determination of the mineralogy and bulk composition of fluid microinclusions in diamonds

Weiss, Y.[1*], Kiflawi, I.[1,2] & Navon, O.[1]
[1]The Fredy and Nadine Herrmann Institute of Earth Sciences, The Hebrew University of Jerusalem, Jerusalem, Israel
([*]yakov.weiss@mail.huji.ac.il)
[2]Department of Physics, King's College, London, UK

Infrared (IR) spectroscopy is commonly used to determine the concentration and aggregation of nitrogen in diamonds, as well as the presence and concentration of other impurities. In the case of fibrous diamonds, where high density fluids (HDFs) were trapped in myriads of microinclusions, the geometrical arrangement of the inclusions in the diamond is very favorable for IR measurement. The trapped phases are all only a few tens to hundreds of nanometres in size, and are dispersed in the diamond matrix just as mineral powders are dispersed in KBr pellets commonly used in IR measurements. To translate the absorption by the common secondary phases in the microinclusions to their absolute concentration in the diamond or relative abundance in the microinclusions themselves, we determined the absorptivities of 8 minerals (Table1).

Table 1: Mineral IR absorptivity

Mineral	Band [(a)]	ε [(b)]
Garnet	967	1049
Apatite	1049	2590
	605 [(c)]	800
Olivine	894	418
Calcite	1433	739
Dolomite	1442	921
Magnesite	1451	563
Quartz	1084	418
	800 [(c)]	102
Phlogopite	1006	861

[(a)]Main IR band (cm^{-1}); [(b)]Absorptivity (AU·Liter/mole·cm); [(c)]Small IR peak used for the calculations in some of the diamonds.

Using these absortivities we determined the concentrations of the secondary minerals in 13 diamonds that carry carbonatitic to silicic HDFs, as shown by previously EPMA and IR analyses. Normalizing the concentrations to 100% yields the relative concentration of each mineral in the microinclusions, it also annuls the effect of the number-density of microinclusion, which may vary even within a single diamond. Combining the relative abundance with the composition of each mineral in the microinclusions, we calculated the concentration of SiO_2, Al_2O_3, P_2O_5 and MgO+CaO+FeO+BaO+Na_2O (water and CO_3^{-2} free basis) of the bulk HDF and found very good agreement with the EPMA data for the same diamond. These results, together with a +8% corrections to the absorptivity of water [1,2] due to salinity, show that the hydrous solution make up ~10% of the high-Mg carbonatitic HDFs, reach 20-25% in the intermediate ones and, in general, become somewhat drier in the highly silicic compositions.

Although the EPMA adds valuable data on specific oxides and Cl, our results show that IR spectroscopy alone can be used as a semi-quantitative method to determine carbonatitic to silicic HDF compositions in microinclusions-bearing diamonds. Combining EPMA and FTIR a full characterization of the major constituents is achieved, including carbonate and water content.

[1] Thompson, W.K. (1965) *Trans. Farad. Soc.*, **16**, 2635-2640.
[2] Venyaminov, S.Y. & Prendergast, F.G. (1997) *Anal. Biochem.*, **2482**, 234-245.

Synchrotron radiation techniques applied to Earth Sciences samples. Why and how?

Testemale, D.
Institut Néel and FAME beamline at ESRF, Grenoble, France
(denis.testemale@grenoble.cnrs.fr)

Synchrotron radiation techniques have been used more and more widely in the Earth Sciences community: the intensity, energy and size characteristics of this radiation, the development of the detection systems and of the numerical analysis tools are the core of a broad range of applications, particularly suitable for the Earth Sciences samples. Those samples, whether natural or synthetic, are indeed typically heterogeneous and/or at low concentrations and/or of small size, and can be sometimes challenging to analyze.

Through various examples, this presentation will attempt to give an introductory overview of the research areas and problematics where synchrotron radiation techniques are particularly useful, if not mandatory. It will also expose the relevant techniques (X-ray spectroscopy, scattering, tomography, etc.) and the nature of the information retrieved (atomic structure, electronic structure, redox state, elemental concentration, imaging, etc.). Emphasis will be given on recent developments in *in situ* experimentation and on the variety of sample environments available by X-rays experimentation.

Finally, the particular example of metal mobility and fluid/rock interactions at hydrothermal conditions will be presented and also exploited to emphasize the need for complementary numerical techniques.

The oxidation state of vanadium in titanomagnetite determined by HERFD-XAS spectroscopy

Bordage, A.[1,2*], Balan, E.[2], de Villiers, J.P.R.[3], Juhin, A.[2], Glatzel, P.[2] & Brouder, Ch.[2]
[1]Laboratoire des Géomatériaux et Environnement, Univ. Paris-Est Marne la Vallée, Marne la Vallée, France
([*]amelie.bordage@impmc.jussieu.fr)
[2]Institut de Minéralogie et de Physique des Milieux Condensés, Univ. Paris 6 et 7, IRD, IPGP, Paris, France
[3]Dept. of Materials Science and Metallurgical Engineering, University of Pretoria, South Africa
[4]European Synchrotron Radiation Facility, Grenoble, France

Vanadium is an example of multivalent impurities as it occurs in three redox states (+III, +IV and +V) in magmatic systems. It makes it a valuable geochemical probe, providing useful information about redox conditions during natural processes. Vanadium is extracted from titanomagnetite ($Fe_{3-x}Ti_xO_4$), found as massive discrete layers in the Bushveld Complex (South Africa). However, the crystallization process of these layers is still poorly understood. The oxidation state of vanadium may be a potential benchmark to get new information.

K-edge X-ray Absorption Spectroscopy (XAS) is a powerful tool to investigate the electronic structure and crystallographic environment of a transition metal cation occurring at low concentration in minerals. In particular, the energy and relative intensity of pre-edge features depend on the valence state and site symmetry of the absorbing atom [1]. However, in the case of V-bearing titanomagnetite, the high level of titanium (~15wt% TiO_2) compared to that of vanadium (~1.5wt% V_2O_3) hinders the use of conventional XAS measurements: the pre-edge features are masked by a very high background due to the Ti fluorescence [2]. High-Energy Resolution Fluorescence Detected–XAS (HERFD-XAS) [3] overcomes this problem: a single fluorescence line, selected by a high-resolution emission spectrometer, is recorded while scanning the incident energy range [4]. The fluorescence resulting from Ti is thus filtered out and the spectral resolution of the pre-edge and edge features is substantially improved.

We present here a HERFD-XAS study of natural and synthetic samples of V-bearing titanomagnetites. V *K*-edge spectra have been recorded, selecting the V $K\alpha_1$ fluorescence line, on ID26 beamline at the ESRF (Grenoble, France). The pre-edge features indicate the presence of V^{3+} and V^{4+} under various proportions, as observed in a study of V-bearing titanomagnetite from another locality of the Bushveld Complex [5]. The V^{4+}/V^{3+} ratio depends on the oxygen fugacity and its variations are also observed as a function of the stratigraphic height within the Main Magnetite layer of the Bushveld Complex. These variations with depth suggest variations of the redox conditions during the crystallization of the main magnetite layer [2].

[1] Calas, G. & Petiau, E. (1983) *Solid State Commun.*, **48(7)**, 625-629. [2] Bordage, A. (2009) *PhD Thesis*, Univ. Paris 6 (France). [3] Glatzel, P. et al. (2009) *Catalysis Today*, **145**, 294-299. [4] Glatzel, P. & Bergmann, U. (2005) *Coord. Chem. Rev.*, **249**, 265-295. [5] Balan, E. et al (2006) *Am. Mineral.*, **91**, 953-956.

Structural role of Ti and Zr in the nucleation of aluminosilicate glasses by X-ray absorption spectroscopy

Cormier, L.[1*], Dargaud, O.[1,2], Galoisy, L.[1], Calas, G.[1] & Jousseaume, C.[2]
[1]Institut de Mineralogie et Physique des Milieux Condensés, CNRS, Université Pierre et Marie Curie, Université Paris Diderot, IPGP, Paris, France ([*]cormier@impmc.upmc.fr)
[2]Saint-Gobain Recherche, Aubervillier, France

Nucleation plays a central role in the crystallization of igneous and metamorphic rocks and in the making of commercial glass-ceramic materials. The nucleation control is usually achieved by adding nucleating agents, typically ZrO_2 or TiO_2, but their structural role is still poorly understood.

We present an X-ray absorption spectroscopic investigation of the Zr and Ti environment in aluminosilicate glasses and glass-ceramics using Zr K- and L-edges and Ti K-edge. We determine the Zr and Ti environment in MgO-Al_2O_3-SiO_2 glasses, showing their difference with other silicate or aluminosilicate systems. The structural variation around Zr and Ti is followed using both ex situ and in situ experiments in relation with the formation of the first crystalline nanophases. The importance of the initial glassy state is emphasized by our study and the XAS results also allow a better characterization of the primary crystals.

In situ high temperature X-ray absorption investigation at the Na, Ca, Al and Si-edges in melts

Neuville, D.R.[1*], de Ligny, D.[2] & Henderson, G.S.[3]
[1]CNRS-IPGP, Géochimie et Cosmochimie, Paris, France ([*]neuville@ipgp.jussieu.fr)
[2]LPCML, UCBL, Villeurbanne, France
[3]Dept. of Geology, University of Toronto, Canada

Structure of silicate and aluminosilicate melts is not well known at high temperature. X-ray absorption spectroscopy is a very specific and interesting way to probe the network structure and more specifically the Al and Si surrounding. Recent developments on X-ray absorption spectroscopy at light K-edges, made on the LUCIA beamline at the SOLEIL light source, enable to measured XANES spectra at high temperature on the Na, Ca, Al and Si K-edges. We have investigated mineral and melts at different K-edge and different temperature above to the liquidus temperature. The method and first results will be presented. Significant change on the XANES spectra at the Ca K-edge can be observed just after the melting point, where important changes appear in the liquid state. At Al K-edge, we observed also important modifications in the mean resonances. These first measurements are a good illustration of loss of medium range order after melting characterized by the disappearance of structural features in XANES spectra.

Elastic wave velocities and densification of silica glass at high temperatures and high pressures

Matsui, M.[1*], Yokoyama, A.[1], Higo, Y.[2], Kono, Y.[3], Irifune, T.[3] & Funakoshi, K.[2]
[1]School of Science, University of Hyogo, Japan
([*]m.matsui@sci.u-hyogo.ac.jp)
[2]Japan Synchrotron Radiation Research Institute, Hyogo, Japan
[3]Geodynamic Research Center, Ehime University, Matsuyama, Japan

The elastic P and S wave velocities of silica glass at high temperatures and high pressures were measured using a combined use of ultrasonic interferometry, in situ synchrotron X-ray diffraction and radiographic techniques in a large-volume Kawai-type multi-anvil apparatus SPEED1500 at the BL04B1 beam line of SPring-8. Details of the experimental setup were described previously [1,2].

We found no first-order amorphous-amorphous transformation throughout the temperature and pressure conditions up to 5 GPa and 1173 K, contrary to previous studies suggested by MD simulations [3] or those reported using piston cylinder experiments in which the density of silica glass increased discontinuously with pressure by about 20 % at 3.6 GPa and 953 K [4].

For both the 650 and 800 K isothermal runs, the P and S wave velocities of silica glass initially decreased with increasing pressure, reaching minimum values at around 3 – 4 GPa, followed by increases with pressure up to 6 GPa; on successive decompression, both velocities slightly increased irreversibly to ambient pressure due to permanent densification, and no minima were observed in both velocities. Such unusual behavior in the P and S wave velocities associated with densification process at high temperature and high pressure is quite similar to that which occurs in silica glass at room temperature with increasing and decreasing pressures [5,6].

We found that the measured density of recovered silica glass after a second compression-decompression cycle at 800 K, 2.52(1) g/cm^3, agrees within error with that after the first compression-decompression cycle, 2.51(1) g/cm^3, indicating the densified silica glass compressed reversibly (elastically) with decreasing and increasing pressure at 800 K. Using the measured P and S wave velocities in reversible (elastic) compression regions as a function of pressure, we calculated the densities of silica glass up to 6 GPa at three isotherms of 300, 650, and 800 K. We found the density of the glass increases with temperature at high pressures, indicating a negative thermal expansion in the temperature-pressure range studied here; e.g. the densities at 5 GPa are 2.60, 2.70, and 2.74 g/cm^3 at 300, 650, and 800 K, respectively.

[1] Higo, Y. et al. (2008) *Phys. Earth Planet. Int.*, **166**, 167-174. [2] Higo, Y. et al. (2009) *J. Synchrotron Rad.*, **16**, 762-768. [3] Lacks, D.J. (2000) *Phys. Rev. Lett.*, **84**, 4629. [4] Mukherjee, G.D., Vaidya, S.N. & Sugandhi, V. (2001) *Phys. Rev. Lett.* **87,** 195501. [5] Grimsditch, M. (1984) *Phys. Rev. Lett.*, **52**, 2379. [6] Polian, A. & Grimsditch, M. (1993) *Phys. Rev. B*, **47**, 13979.

Structure transition of $Fe_{3-x}Ti_xO_4$ solid solution under pressures

Yamanaka, T.[*], Kyono, A., Kharlamova, S., Ahart, M., Struskin, V., Mysen, B.O., Mao, H.-k. & Hemley, R.J.
Geophysical Laboratory, Carnegie Institution of Washington, Washington DC, USA ([*]t.yamanaka@kce.biglobe.ne.jp)

The solid solutions between Fe_3O_4 and Fe_2TiO_4 are principal magnetic substance for the rock magnetism in the crust. Fe_3O_4 is ferrimagnetic and Fe_2TiO_4 is antiferromagnetic. Several models of the cation distribution in $Fe_{3-x}Ti_xO_4$ solid solutions have been proposed. In the present study electron spin states of these solid solutions under high pressures have been investigated by X-ray powder diffraction, X-ray emission, Raman spectra and Mössbauer studies.

Powder diffraction experiments of $Fe_{3-x}Ti_xO_4$ up to 60GPa using DAC and synchrotron radiation indicates their volumes of the tetrahedral (A) and octahedral site (B) as functions of composition and pressure. High-pressure transition from cubic to orthorhombic structure is found in the whole compositional range. The transition pressure decreases from 27GPa (x=0.0) to 1 GPa (x=1.0). The solid solutions with $0.734 \leq x \leq 1.0$ show the transition from cubic to tetragonal with c/a<1. The transition pressures are 12GPa (x=0.734) and 8 GPa (x=1.0). This transition can be explained by Jahn-Teller effect of Fe^{2+} at the A site or high-low spin transition of Fe^{2+} ion in the A or B site.

Bulk modulus, bond distance and site volume of $Fe_{3-x}Ti_xO_4$ spinels are observed with increasing Ti^{4+} substitution for Fe^{3+} in the octahedral site. The bulk modulus of Fe_2TiO_4 spinel is much larger than that of Fe_3O_4.

X-ray emission study of Fe_2TiO_4 under compression at BL16-IDD APS confirms mixed spin state or intermediate spin of both ions at much lower pressure as 9GPa compared with Fe_3O_4. The ionic radii change by the high-low spin transition may induce the cubic-to-tetragonal transition and bring the first order transition. The emission spectra do not show any other spectra change up to 15GPa even in the orthorhombic phase.

Raman spectra have been observed under high pressures. Four bands were obtained at ambient conditions. These peak positions continuously shift toward the higher energy sides with increasing pressure up to 15GPa.

Boggsite under high pressure: a case of zeolite over-hydration

Quartieri, S.[1], Arletti, R.[2], Vezzalini, G.[2*] & Dmitriev, V.[3]
[1]Dept.of Earth Sciences, University of Messina, Italy
[2]Dept. of Earth Sciences, University of Modena and Reggio Emilia, Modena, Italy ([*]mariagiovanna.vezzalini@unimore.it)
[3]SNBL-ESRF, Grenoble, France

Boggsite is a rare natural zeolite [1-4]. Its crystal structure [2] is characterized by a pentasil framework and an interesting 3D channel system of 10- and 12-rings, which makes this topology potentially very suitable for industrial and environmental applications.

The elastic behavior of boggsite from Terra Victoria Land (Antarctica) is investigated by in-situ H*P* synchrotron X-ray powder diffraction, using both silicon oil (s.o.) (P_{amb}–9.3 GPa) and methanol:ethanol:water (16:3:1) mixture (m.e.w.) (P_{amb}–7.6 GPa), as non penetrating and penetrating *P*-transmitting medium, respectively. Neither X-ray amorphization nor phase transitions are observed up to the highest investigated *P*, and the original unit cell parameters are recovered upon decompression. The following decreases of *a*, *b*, *c*, and *V* are observed: 5.3, 4.2, 4.0 and 13%, in s.o. up to 5.9 GPa; 4.1, 4.1, 3.8 and 11.5%, in m.e.w up to 7.6 GPa.

The Rietveld structural refinements of the powder patterns collected in m.e.w. reveal a significant over-hydration between 0.3 and 2.9 GPa. This occurs with increasing the occupancy of 4 of the 13 extraframework sites already present in boggsite at P_{amb}. In this *P*-range, the compressibility in m.e.w. is lower than in s.o., due to the entering of the additional water molecules, which contribute to make more rigid the structure. At higher *P*, the compressibility is similar for the two media (Fig. 1). The elastic parameters were calculated from P_{amb} to 5.9 GPa for s.o., while for m.e.w. the calculation was performed after the water content stabilization, that is from 2.9 to 7.6 GPa. The following results were obtained: V_0 = 6240(6) Å³, K_0 = 31.1(4) GPa, and V_0 =6405(17) Å³, K_0 = 37(1) GPa, for s.o. and m.e.w., respectively.

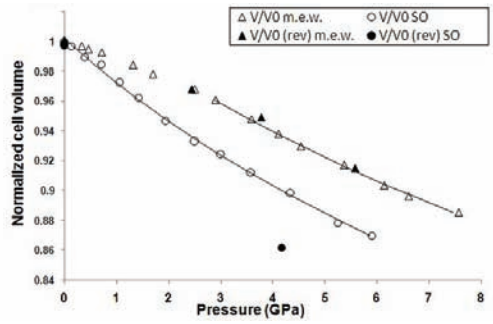

Fig. 1: Plot of ΔV vs. P for boggsite compressed in s.o. and m.e.w. Solid lines represent the EoS fits.

[1] Howard, D.G. et al. (1990) *Am. Mineral.*, **75**, 1200-1204. [2] Pluth, J.J. & Smith, J.V. (1990) *Am.. Mineral.*, **75**, 501-507. [3] Galli, E. et al. (1995) *Eur. J. Mineral.*, **7**, 1029-1032. [4] Alberti, A. et al. (2001*) Stud. Surf. Sci. Catal.*, **135**, 83-91.

Rhombic-shaped nanodomains in columbite driven by contrasting cation ordering

Tarantino, S.C.[1,2*], Zema, M.[1,2], Capitani, G.[3], Scavini, M.[4], Ghigna, P.[5], Brunelli, M.[6] & Carpenter, M.A.[7]
[1]Dipto. di Scienze della Terra, Università di Pavia, Italy
[2]CNR-IGG, Pavia, Italy ([*]tarser06@unipv.it)
[3]Dipto. di Scienze Geologiche e Geotecnologie, Università di Milano-Bicocca, Italy
[4]Dipto. di Chimica Fisica ed Elettrochimica, Università di Milano, Italy
[5]Dipto. di Chimica Fisica "M. Rolla", Università di Pavia, Italy
[6]European Synchrotron Radiation Facility, Grenoble, France
[7]Dept. of Earth Sciences, University of Cambridge, UK

Columbites, having general formula $A^{2+}B^{5+}{}_2O_6$, are well-known for their excellent dielectric properties. Their crystal structure, orthorhombic *Pbcn*, is formed by chains of two different edge-sharing octahedral sites, named A and B, where cations can be hosted. Columbites undergo a convergent cation exchange process which is responsible for a first-order polymeric isomorphic phase transition: when the octahedral sites are randomly occupied, columbite adopts the α-PbO_2-type crystal structure; ordering of divalent cations on A sites and pentavalent cations on B sites gives rise to an …ABBABB… sites sequence along the *a* direction resulting in a tri-α-PbO_2-type structure. It has been suggested that the ordering could have a strong influence on the microwave properties of columbite [1], as also observed in PMN-PSN relaxor ferroelectrics [2].

The mechanism of the intracrystalline cation exchange reaction in a natural columbite from Kragero, with composition $(Mn_{0.85}Fe_{0.15})(Nb_{1.8}Ta_{0.2})O_6$ [3], has been characterised by means of TEM and HR synchrotron-radiation powder diffraction. The natural untreated sample is monophasic and homogeneous as revealed by previous single-crystal diffraction analyses [3] and Rietveld refinement. After few minutes of annealing at 650°C, a highly unusual distribution of ordered rhombic-shaped domains bordered by {310} planes becomes established on a nano-scale within a disordered matrix (Fig. 1).

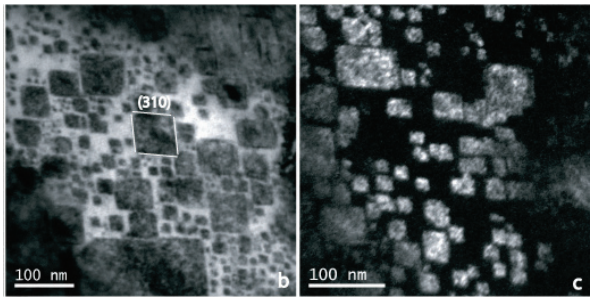

Fig. 1: Diffraction contrast images showing nanosized domains with rhombic shape.

In situ HT powder diffraction clearly evidences the separation into two discrete columbite phases having the same composition but different degrees of order. Biphasic Rietveld refinements of the diffraction patterns show that progressive ordering takes place both within the ordered domains and the disordered matrix but the domains maintain more or less constant shape and distribution over a prolonged time of annealing. In the last stages of annealing, split reflections merge into single peaks and the diffraction pattern is again that of one single columbite phase which is now almost completely ordered.

[1] Kim, D.-W. et al. (2000) *J. Mater. Res.*, **15**, 1331-1335. [2] Farber, L. & Davies, P. (2003) *J. Am. Chem. Soc.*, **86**, 1861-1866. [3] Tarantino, S.C. & Zema, M. (2005) *Am. Mineral.*, **90**, 1291-1299.

ANKA-IR2: a synchrotron infrared center for micro and nanospectroscopy

Gasharova, B., Moss, D. & Mathis Y.-L.*
Karlsruhe Institute of Technology (KIT), ANKA Synchrotron Light Source / Institute for Synchrotron Radiation, PKarlsruhe, Germany (*mathis@kit.edu)

In this presentation we will introduce the infrared (IR) facilities of ANKA, a synchrotron light source at KIT, and we will illustrate the possibilities, which they offer for cutting-edge research in Earth and Planetary sciences.

As the characterization of complex samples on the micro- and even on the nano-scale becomes increasingly important in the geosciences, this research area benefits, in general, from the development of techniques based on synchrotron radiation. Microspectroscopy is traditionally one of the key areas of application for synchrotron IR sources that is of interest for mineralogy and geochemistry. The high brilliance of synchrotron light compared to conventional sources leads to a much higher measurement beam intensity through small sample areas approaching the diffraction limit. Thus IR microscopes coupled to synchrotron beamlines can deliver spectra from a sample spot size of only a few micrometers, with data quality that could only be matched on a benchtop instrument by increasing the spot size to 0.1 mm or more.

Due to the high demand for high spatial resolution infrared equipment ANKA has constructed a second IR beamline, which will be dedicated to IR micro- and nanospectroscopy (Fig. 1).

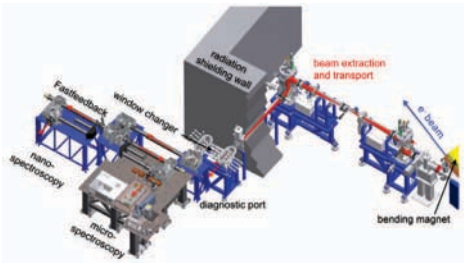

Fig. 1: ANKA-IR2 beamline layout.

Two experimental stations are planned. One is coupled to the IR microscope (formerly at ANKA-IR1), which covers the spectral range from ~100 cm^{-1} up to the NIR. It can be used for transmission, normal-incidence reflection, ATR and grazing-incidence reflection experiments under ambient, HP, HT or LT conditions. Confocal geometry and XYZ-motorized stage allow sample mapping with a micrometric precision. IR images can be taken with a FPA detector. Applications range from cement materials analysis [1,2], biominerals [3], water in nominally anhydrous minerals [4], zeolite nanoparticles [5], FIR study of phylosilicates [6] to fluid inclusions and water in terrestrial materials and meteorites [7,8]. The second station, a Scanning Near-field Infrared Microscope (SNIM) will deliver images at a spatial resolution 100-1000 times better than a conventional IR microscope [9]. The possibility to measure samples at a nano-scale spatial resolution using broadband IR radiation will be further attraction for research in Earth and Planetary sciences.

[1] Garbev, K. et al. (2008) *J. Am. Ceram. Soc.*, **91**, 263-271. [2] Snellings, R. et al. (2010) *Eur. J. Mineral.*, forthcoming paper [3] Klocke, A. et al. (2006) *J. Biomed. Mater. Res. B*, **81B**, 499-507. [4] Sommer, H. et al. (2008) *Miner. Petrol.*, **94**, 1-8. [5] Tosheva, L. et al. (2008) *Angew. Chem. Int. Ed.*, **47**, 8650-8653. [6] Friedrich, F. et al. (2006) *Appl. Spectrosc.*, **60**, 723-728. [7] Moss, D.A. et al. (2008) *Synchrotron Rad. News*, **21**, 51-59. [8] Guilhaumou, N. et al. (2005) *ANKA annual report*, 114-115. [9] http:// ankaweb.fzk.de/ website.php? page=extras_news&id=31.

Application of micro-diffraction to characterise newly formed minerals at interfaces

Dähn, R.[1*], Popov, D.[1], Pattison, P.[2], Mäder, U.[3] & Wieland, E.[1]
[1]Paul Scherrer Institute, Villigen, Switzerland (*rainer.daehn@psi.ch)
[2]ESRF/SNBL, Grenoble, France and EPFL, Lausanne, Switzerland
[3]Institute of Geological Sciences, University of Bern, Bern, Switzerland

Synchrotron-based X-ray micro-diffraction (microXRD) is a potentially powerful method to investigate the inhomogeneity of mineral phases with micro-scale resolution; in particular in combination with micro X-ray fluorescence mappings. However, interpretation of the diffraction patterns from microXRD, which are produced by multi-component samples, is still a challenging task since they are complex images in which many crystal grains from different structures and orientations can contribute. The aim of the present study was to develop microXRD data collection and reduction techniques to study heterogeneous materials with typical features on the micro-meter scale. Exemplarily, synchrotron-based microXRD was employed to characterize the interface between argillaceous rocks and cementitious materials.

Cement-based materials play an important role in multi-barrier concepts developed worldwide for the safe disposal of radioactive waste in deep geological repositories. For example, ~95 wt% of the material of the planned Swiss disposal cavern for low and intermediate level waste consists of cementitious backfill materials. In a deep geological repository very strong chemical gradients control mineral alterations at the interface between the cementitious near field (pH >12.5) and the surrounding claystone formations (pH 7-8) due to the very different chemical conditions encountered in these matrices. While macroscopic reactive transport models are able to capture many essential features of the interaction between cementitious materials and the geosphere, such models consider no information on processes that operate at the relevant pore scale (µm - nm), and at the interface itself.

Two examples will be presented. The first from a multi-year field experiments at the Mt. Terri rock laboratory, where cement mortar was brought into boreholes in the Opalinus clay host rock. MicroXRD was used to study changes in the mineralogy across the cement – host rock interface. The study revealed that predominantly the cementitious zone was altered within two years contact time. In the second example the only known natural hyperalkaline system at Maqarin (Jordan) has been studied. There, high temperature and low pressure conditions led to the formation of clinker, and subsequent re-hydration to the formation of natural cement. U-Th disequilibrium series dating suggested an age of the cement mineralization of ~100000 years. Continuous leaching along fracture-bound groundwater flow-paths formed cementitious in-fills, interfaces to the adjacent bio-micritic and clay-bearing limestone, and diffusion-controlled wall-rock alteration. The interface consists predominatly of small (1 µm) needle-like crystals, which were identified by microXRD as 11Å-tobermorite. The studies demonstrated that crucial information on the mineralogy at interfaces can be obtained by applying synchrotron-based microXRD techniques.

Anomalous X-ray scattering study on chrysocolla

Murao, R. & Sugiyama, K.*
Institute for Materials Research, Tohoku University, Sendai, Japan (*kazumasa@imr.tohoku.ac.jp)

The anomalous X-ray scattering (AXS) technique allows us to obtain environmental structural information around a target element. Recent developement of synchrotron radiation source extensively stimurates the structural analysis of non-crystalline materials using the AXS method. Chrysocolla is a copper silicate mineral with disordered structure and it indicates only diffuse scattering pattern. Therefore, the conventional X-ray powder diffraction analysis serves no useful structural information. The purpose of the present study is to analyze the structure of chrysocolla by the ordinary radial distribution function (RDF) anlysis coupled with the AXS method.

Cu-*K* AXS of chrysocolla from Congo ($Cu_1Si_1O_{4.5}H_{2.6}$) was measured at PF-7C in IMSS, KEK. The present AXS measurement clearly indicates the energy dependence of scattering intensity at the Cu-*K* absorption edge. The observed differential intensity readily leads the environmental RDF around Cu, since only the change in the real part of the anomalous dispersion term of Cu is significant at this energy region. Fig. 1 shows the environmental RDF around Cu and the ordinary RDF of the chrysocolla sample. The Si-O correlation around 1.65 Å in the ordinary RDF indicates the overall presence of SiO_4 tetrahedra. The Cu-O correlation around 2.05 Å corresponds to nearer 4 oxygens out of distorted octahedral coordination around Cu. The Cu-Cu correlation around 3.3 Å is similar to that found in the crystalline $Cu(OH)_2$.

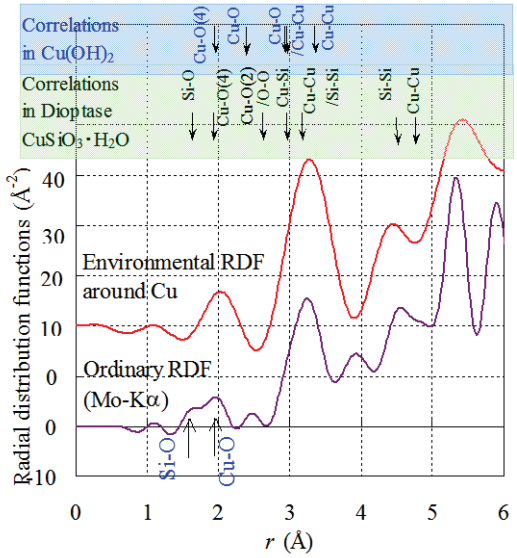

Fig. 1: (*Top*) Environmental RDF around Cu in chrysocolla by the Cu-AXS method. (*Bottom*) Ordinary RDF obtained by Mo-*Kα*. Arrows in upper part indicate correlation distances in related compounds.

Elemental nanoimaging of monazite and zircon using SR XRF

Appel, K.[1*], Appel, P.[2], Martinez-Criado, G.[3], Mocek, B.[4] & Möller, A.[4]
[1]Deutsches-Elektronen Synchrotron DESY, a Research Centre of the Helmholtz Association, Hamburg, Germany (*karen.appel@desy.de)
[2]Institute of Geosciences, CAU Kiel, Germany
[3]European Synchrotron Radiation Facility, Grenoble, France
[4]Dept. of Geology, University of Kansas, Lawrence, KS, USA

Monazite and zircon are among the most important accessory minerals used for U-Th-Pb geochronology of metamorphic and igneous rocks. Additionally, both minerals have a high potential to be used as geothermometers [1-3]. Although widely used in geochronology, the chemical stability and growth mechanisms of monazite and zircon are poorly understood. Using synchrotron radiation induced X-ray fluorescence analysis (SR XRF) at a high spatial resolution below 250 nm, we studied trace element distribution in monazite and zircon from case study localities with the aim to identify and characterize growth domains and their boundaries. This information will be correlated with age information obtained from chemical age dating by the procedure described by [4]. A similar technique is to be developed for chemical age dating of zircon with SR XRF.

Monazite and zircon from polymetamorphic terrains as well as six age reference monazite samples were selected with the Jeol electron microprobe at CAU Kiel, based on cathodoluminescence (zircon) and on back scattered electron images and results obtained from single point chemical ages following the procedure of [5] for monazite. SR XRF measurements were performed at the nano imaging beamline ID22NI at ESRF, Grenoble, with a beam size of 190 nm horizontal and 164 nm vertical. The excitation energy was set to 17.6 keV in order to allow the simultaneous detection of REE and Pb, Th and U via L-shell excitation and elements with Z between 14 and 39 via K-shell excitation, but exclude the excitation of the Zr K-edge. Fluorescence signals were recorded with an energy-dispersive SDD detector in confocal geometry.

It can been shown that the analytical settings and conditions allowed simultaneous detection of K, Mn, Fe, Rb, Ce, Dy, Er, Yb, Lu, Hf, Pb, Th and U in zircon. A correlation could be found between the elements Dy, Er, Hf, Lu, Pb, Th, U and Yb with features revealed by cathodoluminescence in a zircon with an older core and overgrowth rim (Fig. 1). The boundary between the inherited core and the overgrowth was sharp on the 250 nm scale, indicating this to be a true overgrowth with minimal or no recrystallization and scavenging of the core.

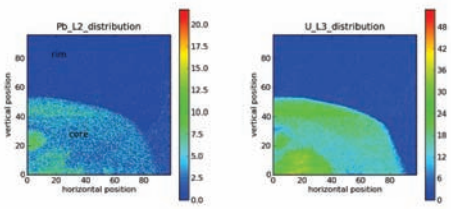

Fig. 1: Lead and U distribution maps of zircon with inherited core and metamorphic rim, axes dimensions in µm. Sample times were 0.4 sec per point, step sizes 0.25 µm in both directions.

[1] Gratz, R. & Heinrich, W. (1998) Eur. J. Mineral., 10, 579-588. [2] Pyle, J.M. et al (2001) J. Petrol., 42, 2083-2107. [3] Watson, E.B. & Harrison, T.M. (2005) Science, 308, 841-844. [4] Schmitz, S. et al. (2009) Eur. J. Mineral., 21, 927-945. [5] Braun, I. & Appel, P. (2006) Eur. J. Mineral., 18, 415-427.

Fast reaction kinetics in the calcium carbonate system: an *in situ* and real-time study

Rodriguez-Blanco, J.D.[1*], Bots, P.[1], Terrill, N.[2], Shaw, S.[1] & Benning, L.G.[1]
[1]School of Earth and Environment, University of Leeds, UK
([*]j.d.rodriguez@see.leeds.ac.uk)
[2]Diamond Light Source Ltd, Chilton, Didcot, UK

Calcium carbonate ($CaCO_3$) polymorphs (vaterite, calcite, aragonite) are found in a wide range of environments (e.g., oceans, lakes, soils) and are a key part of the global carbon cycles. At high supersaturation these phases form via a nanoparticulate, poorly-ordered and metastable precursor, amorphous calcium carbonate (ACC). The formation and transformation of ACC to other calcium carbonate phases can be extremely fast (nucleation in seconds and full transformation in 10s of seconds). In this study we demonstrate the use of an *in situ* time-resolved synchrotron-based Small- and Wide-angle X-ray Scattering approach (SAXS/WAXS) combined with off-line characterization to quantify the fast kinetics and crystallization mechanisms of calcium carbonate formation from ACC.

Experiments were carried out at station I22 at the Diamond Light Source, UK. The precipitation of ACC was induced by mixing equimolar solutions of $CaCl_2$ and Na_2CO_3 at different temperatures (12 to 20°C) and the crystallization was monitored via simultaneous SAXS/WAXS patterns acquisition at 1s time frames. In addition, the effects of common ions in natural aqueous environments (Mg^{2+}, SO_4^{2-} and PO_4^{3-}) on the crystallization reactions were studied, as these ions control the pathways of nucleation, growth and stabilization of carbonates.

WAXS data (Fig. 1) show that the transformation from ACC to Vaterite (Vat) in the pure system occurs within ~100s after a temperature-dependent induction time (60 and 90s at 20 and 12°C, respectively). From the SAXS data an initial radius of gyration for ACC of ~18nm was derived. These ACC nanoparticles transform to Vat nanoparticles (~10nm) via an internal reordering and dehydration process followed by Vat crystal growth via Ostwald ripening. The Vat nanoparticles eventually reach ~50nm in size (after ~3000s) and aggregate to form ~1µm clusters (Fig. 1, bottom right). The sizes for ACC and Vat are in excellent agreement with previous ACC imaging results [1] and complementary SEM observations (Fig 1, at right) from these experiments. Finally, the role and effects of Mg^{2+}, SO_4^{2-} and PO_4^{3-} on the stability of ACC and the tranformation pathways into Vat and Calcite will be discussed [see also 2].

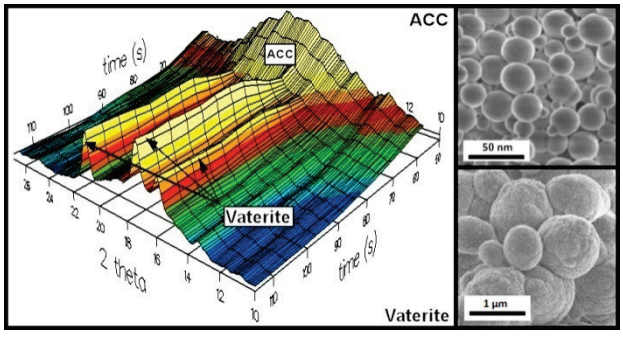

Fig. 1: 3D WAXS and SEM image showing ACC-Vat transformation.

[1] Rodriguez-Blanco, J.D. et al. (2008) *Mineral. Mag.*, **72**, 283-286. [2] Bots, P. et al. (2010) (this volume)

Micro-SR-XRF and micro-PIXE studies for archaeological gold identification – the case of Transylvanian gold

Cristea-Stan, D.[1*], Constantinescu, B.[1], Vasilescu, A.[1], Radtke, M.[2], Reinholz, U.[2], Popescu, Gh.[3], Neacşu, A.[3] & Ceccato, D.[4]
[1]National Institute of Nuclear Physics and Engineering, Bucharest, Romania ([*]daniela_cristea_stan@yahoo.ca)
[2]Federal Institute for Materials Research and Testing (BAM), Berlin, Germany
[3]Dept. of Mineralogy, University of Bucharest, Romania
[4]INFN, Laboratori Nazionali di Legnaro, Italy

Romania was one of Europe's main gold-producing areas since the antiquity, especially through the ore deposits in the "Golden Quadrilateral" of the Apuseni Mountains. The Gold Museum in Brad hosts a collection consisting of about 800 samples of native gold – primary and alluvial. The geochemical investigation of Romanian gold by using micro-nuclear methods (SR-XRF and PIXE) is currently in progress. The goal is to verify if Transylvanian gold was used to manufacture Romanian archaeological objects. This is realized by using information related to trace elements: Sb, Te, Pb – recognized fingerprints for Carpathian Mountains mines and Sn characteristic for the panned river-bed (alluvial) gold. To solve these issues, samples from various Transylvanian mines and rivers and some very small (few milligrams) fragments of archaeological objects are measured. During the experiments, point spectra for 22 natural gold samples from Transylvania and 18 very small (less than 300 microns diameter) samples from Dacian "Koson" – type gold staters were acquired at 34 keV excitation SR energy, using a spatially resolved SR-XRF set-up mounted for analyses at the hard X-ray beam line – BAM-line at BESSY Synchrotron, Berlin.

A summary for the characterization of Transylvanian native gold is the following: (a) high (8 - 30%) Ag and low (0.05 – 0.5%) Cu amounts; (b) placer deposits (Valea Oltului, Stănija, Valea Pianului) contain Sn 150-300ppm – most probably from cassiterite or stanite; (c) primary deposits present Te 200-2000ppm, Sb 150-300ppm; the samples are very inhomogeneous; (d) primary deposit Săcărâmb: Te 0,25%, Sb 500ppm, Sn 200ppm; (e) primary deposit Fizeşti: Pb 1%, Sb 350ppm, Te and Sn traces.

The micro-PIXE experiment was performed using 2 MeV protons at the AN 2000 Van de Graaff accelerator of Laboratori Nazionali di Legnaro - point and map spectra. Two Roşia Montană and Musariu gold polished samples were studied. For Roşia Montană the Au/Ag ratio is very different from a point to another: 53.58/16.30, 34.60/10.78, 13.83/3.75, 34.60/10.53. On the maps a weak presence of Cu in the gold region in comparison with Ag may be observed. Au and Ag are strongly mixed. On the outlying gold grains there are Sb, Te, Zn and also Ag-rich areas. For Musariu sample the Au/Ag/Cu ratio is strongly variable from 3.24/0.42/0.0027, 6.05/1.32/0.0217 to 19.13/4.19/0.0078. In the case of Musariu, Ag and Cu are evidently mixed; a strong presence of Cu is observed. A big amount of Si (quartz) was observed surrounding the gold grains. On the distribution map, Zn-rich areas are observed, beside Au, Sb, and less Ag. There are some metallic Cu-points, Fe-points (pyrite), Pb-points (galena), Mn-points (alabandite) and native As-rich points.

As concerning the "Koson" Dacian coins, the type "with monogram" is made from refined (more than 97%) gold with no Sb, Te or Sn traces (re-melted gold) and the type "without monogram" is clearly made from alluvial gold, partially combined with primary Transylvanian gold (Sn and Sb traces detected). The Greek "Pseudolysimachus" type staters (contemporary with "Kosons") are made from refined re-melted gold (no Sn, Sb, Te presence).

Synchrotron-infrared microspectroscopy

Koch-Müller, M.[1*], Mrosko, M.[1] & Schade, U.[2]
[1]DeutschesGeoforschungsZentrum, Potsdam, Germany
([*]mkoch@gfz-potsdam.de)
[2]Helmholtz-Zentrum Berlin GmbH, Berlin, Germany

Infrared spectroscopy is a sensitive probe for information on the local microscopic structure and bonding in minerals and a powerful tool for quantification of traces of volatiles such as OH, H_2O and CO_2 in ppm range in minerals and glasses. Combined with a high brightness synchrotron source infrared microspectroscopy offers the opportunity to achieve the spatial resolution approaching the diffraction limit of the light. Thus, beside quantification of volatiles in the NIR/MIR region with a spatial resolution down to 8x8 μm, it enables us to investigate pressure-induced structural changes in the THz/FIR region of geomaterials placed in diamond-anvil-cells (DAC). In this contribution we will present two examples of applications of synchrotron IR microspectroscopy on geomaterials:

(1) *Pressure-induced phase transition in Sr-anorthite***:** Anorthite belongs to the group of feldspar minerals, which represents the most common unit within the Earth's crust. The Ca-endmember crystallises with triclinic symmetry in space group $P\bar{1}$. Increasing pressure forces the structure to turn into space group $I\bar{1}$ at 2.6 GPa [1]. Further pressure-induced structural changes take place between 9.6 and 10.3 GPa [2] but are not closer described so far. To investigate these kind of structural modifications in materials we developed a THz/FIR microscope adapted to a Bruker IFS 66/v spectrometer at the BESSY Synchrotron IR-beamline IRIS (Berlin, Adlershof). The microscope was built to conduct in situ pressure depending measurements in diamond anvil cells in the FAR-IR-region. We used the synthetic Sr-anorthite (monoclinic, I 2/c) as analogue material and measured spectra from polycrystalline thin films down to 30 cm^{-1} with pressures exceeding 15 GPa. Between 6 und 7 GPa we observed changes in the compressional behaviour of the FAR-IR-bands, indicating a phase transition. This is confirmed by high pressure XRD-measurements [3] that show a phase transition to $P2_1/c$ at 6.6 GPa.

(2) *Hydrogen zoning in zinc- and lithium-bearing staurolite*: This staurolite occurs as mm-long crystals at the marble footwall of meta-karst-bauxite on eastern Samos. H and Li concentrations were analyzed by secondary ion mass spectrometry (SIMS) with a 15 mm diameter O^{16} beam. In addition OH concentration was quantified by synchrotron-light polarized FTIR spectroscopy on oriented 3-5 mm thin FIB-prepared foils 10 x 20 mm wide and cut closely adjacent to the SIMS traverses. H concentrations are significantly higher in cores (up to 5.97 atoms H pfu) compared to rims (3.9 to 4.5 atoms H pfu). The zonation of H is interpreted as reflecting the P-T history of the growth of the mineral: in a first stage staurolite formed at low T of about 400 - 450°C and high P of > 1.5 GPa and incorporated nearly the maximum amount of H allowed by the staurolite structures. It was subsequently overgrown and marginally replaced during the second growth stage at about the same temperature but much lower pressures (0.2 - 0.4 GPa) resulting in much less hydrous staurolite rims.

[1] Angel, R. (1988) *Am. Mineral.*, **73**, 114-119. [2] Daniel, I. et al. (1995) *Am. Mineral.*, **80**, 645-648. [3] Boffa Ballaran, T. et al. (2008) *BGI annual report.*

Quantification of plagioclase crystals shape and connectivity in synthetic basalt from 3D reconstruction by X-ray CT image

Pupier, E.[1,2*], Nakamura, M.[2], Tsuchiyama, A.[3], Uesugu, M.[3], Uesugi K.[4], Nakano T.[5], Okumura, S.[2] & Duchêne, S.[6]

[1]Dept. Géosciences, Inst. Polytechnique LaSalle Beauvais, France ([*]elsa.ottavi-pupier@lasalle-beauvais.fr)
[2]Dept. of Earth Science, Tohoku University, Sendai, Japan
[3]Dept. of Earth and Space Science, Osaka University, Toyonaka, Japan
[4]Spring-8, Japan Synchrotron Radiation Research Inst., Hyogo, Japan
[5]Geological Survey of Japan, AIST, Tsukuba, Japan
[6]LMTG, Université de Toulouse, Toulouse, France

The three dimensional observation of plagioclase crystal in synthetic basalt by using micro-tomography beam lines at SPring-8 (X-ray CT), is supported by two previous experimental studies realized on the same run charge [1,2]. The overall conclusion of these previous studies is that cooling rate effect on the characteristics of crystal size distribution, "CSD", (namely slope and intercept) is not markedly higher than those of i) coarsening through crystal agglomeration during the crystallization and ii) heterogeneous nucleation controlled by time and temperature spent above the liquidus. Consequently, no precise quantitative use of the CSD of plagioclase as a marker of the cooling history of volcanic rocks will be feasible until the processes of crystal agglomeration and heterogeneous nucleation can be properly understood and quantified. Accordingly, it is here proposed to highlight and to quantify crystal agglomeration during crystallization with help of 3D imaging. Micro-tomography was performed at SPring-8 by ultrahigh-resolution X-ray CT [3]. We got three-dimensional images of the run products in the resolution of 2.74 µm, allowing us to obtain information about the agglomeration of crystals, and in particular to assess connectivity (touching crystals/non touching crystals) and shape of the plagioclase crystals during cooling. Run charges were cooled from above the liquidus (~1175°C) at a rate of 1°C/h. Four samples have been quenched along a ramp with a temperature interval of 20°C. The last run charge contains ~40% crystals at the quenching temperature ~1110°C (Fig. 1).

Size and shape evolution during cooling is clearly visible and especially the lack of acicular plagioclase crystal usually described. The agglomeration process is significant, however, preferential attachment is still difficult to highlight. The connectivity between plagioclase crystals increases very rapidly with the crystallinity from 0.4 in early stages of crystallization (5% plagioclase crystals) to 1 for 20-25 % of plagioclase crystals. This suggests that viscosity of magmas crystallized without magma flow may increase at lower crystallinity than ever estimated in the previous experiments, in which preferred crystal orientation was formed by measurement with a rotational viscometer.

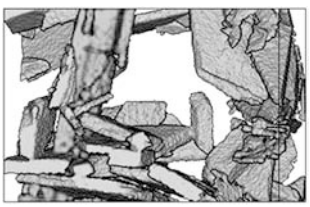

Fig. 1: 3D reconstruction of plagioclase crystals (981x674x537 µm).

[1] Pupier, E. et al. (2008) *Contrib. Mineral. Petrol.*, **155**, 555-570. [2] Duchêne, S. et al. (2008) *Am. Mineral.*, **93**, 893-901. [3] Uesugi, K. et al. (1999) *Proc. Soc. Photo.-Opt. Instrum. Eng.*, **3772**, 214-221.

Zircon and hafnon in H_2O+$Na_2Si_3O_7$±Al_2O_3 fluids to 750 °C, 1 GPa: Zr and Hf solubility and complexation from SR-XRF and XAFS

Schmidt, C.[1*], Wilke, M.[1], Appel, K.[2], Pascarelli, S.[3], Dubrail, J.[1] & Manning, C.E.[4]

[1]GFZ German Research Centre for Geosciences, Potsdam, Germany ([*]hokie@gfz-potsdam.de)
[2]Deutsches Elektronen-Synchrotron DESY, a Research Centre of the Helmholtz Association, Hamburg, Germany
[3]European Synchrotron Radiation Facility, Grenoble, France
[4]Department of Earth and Space Sciences, UC Los Angeles, USA

A key parameter for the mobility of high field strength elements (HFSE) in the lithosphere is the alkali/alumina ratio in fluids and melts, which is determined by the interacting mineral assemblage during equilibration (e.g., [1]). However, there is only fragmentary knowledge on the solubility of HFSE in aqueous alkali silicate fluids at the P -T conditions of the lower crust and upper mantle and the effect of alumina addition to the system, and on the complexation of the HFSE in such fluids.

Using high P-T in-situ techniques, we studied fluids produced by dissolution of known amounts of $Na_2Si_3O_7$ (NS3) or $Na_2Si_3O_7$ + 10 wt% Al_2O_3 (NS3Al10) glass in water, which were equilibrated with zircon or hafnon in hydrothermal diamond-anvil cells at temperatures to 750 °C and pressures to ~1 GPa. The concentrations of Zr and Hf in the fluids were determined by synchrotron radiation micro-XRF analyses at beamline L, HASYLAB. Spectroscopic constraints on the complexation were obtained from dispersive XAFS measurements at the Hf L_3 edge at ID 24, ESRF, along with additional information on the Hf concentration from XRF data.

A consistently observed feature was the substantial decrease in the Zr concentration in the fluid with pressure at constant temperature and NS3 concentration. This indicates pronounced pressure dependent changes in the speciation in aqueous sodium silicate systems and a decreasing Zr mobility with depth in peralkaline fluids, which agrees with observations on natural samples. The Zr concentration in the fluid also showed a strong increase with $Na_2Si_3O_7$ concentration at similar P-T conditions, e.g., by one order of magnitude from 10 to 30 wt% NS3. This signifies that aqueous sodium silicate fluids are efficient means for transport of Zr and other HFSE. Addition of alumina, however, resulted in distinctly lower Zr concentrations in the solutions, e.g., at ~650 °C, ~800 MPa, it was ~200 ppm in H_2O+18 wt% NS3 compared to ~100 ppm in H_2O+20 wt% NS3Al10. Determined Hf concentrations followed similar trends, although they were mostly higher than those of Zr at comparable conditions. On the expense of hafnon, the Hf-analogue of katapleiite formed in a run with H_2O+22 wt% NS3, and probably the Hf-analogue of baddeleyite in a run with H_2O+35 wt% NaOH. In that run, the Hf content in the fluid was much lower than runs with H_2O+28 wt% NS3 or NS3Al10.

This observation, the increase in the Zr and Hf concentrations in the fluid with dissolved Na silicate and the decrease with addition of alumina point to formation of a (Zr,Hf)-O complex involving Na and/or Si. Measured Hf L_3 XANES regions in the fluid were similar for experiments with hafnon and H_2O+NS3, H_2O+NS3Al10 or H_2O+NaOH. Simulation of the XANES using FEFF8.4 for a HfO_6 octahedron at R(Hf-O)=2.07 Å (equal to that of Zr in peralkaline $Na_{3.3}AlSiO_{17}$ glass [2]) approximated these experimental Hf L_3 XANES well. Measured Hf L_3 XANES on H_2O+16 wt% HCl fluids equilibrated with hafnon were significantly different.

[1] Manning, C.E. et al. (2008) *Earth Planet. Sci. Lett.*, **272**, 730-737. [2] Farges, F. et al. (1991) *Geochim. Cosmochim. Ac.*, **55**, 1563-1574.

Determination of Mn speciation in aragonitic freshwater bivalve shells using synchrotron x-ray absorption and emission techniques

Soldati, A.L.[1,2*], Geck, J.[3], Jacob, D.E.[1], Glatzel, P.[4] & Swarbrick, J.C.[4]
[1]Dept. of Geosciences and Earth System Science Research Centre, Johannes Gutenberg-Universität, Mainz, Germany ([*]asoldati@cab.cnea.gov.ar)
[2]CONICET, Grupo Caracterización de Materiales, Centro Atómico Bariloche, S.C. de Bariloche, Argentina
[3]Leibniz Institut für Festkörper-und Werkstoffforschung, Dresden, Germany
[4]European Synchrotron Radiation Facility, Grenoble, France

We investigated shells from seven different freshwater bivalve species by means of spin-resolved x-ray absorption near edge spectroscopy (XANES) and x-ray emission spectroscopy (XES). The shells are composed of aragonite ($CaCO_3$) and less than 5 wt% of organic material. The aim of the experiments was to clarify whether Mn replaces the Ca^{2+} ion in the carbonate structure or if it is associated with the organic molecules in the shells (inter- and intra-crystalline).

Bivalve shells used here comprise specimens of *Hyriopsis cumingii*, *Margaritifera margaritifera*, *Margaritifera falcata*, *Anodonta Cygnea*, *Anodonta Anatina* and *Unio tumidus* as well as modern and archaeological specimens of *Diplodon chilensis patagonicus* from two different Patagonian lakes [1]. All XANES spectra of the different bivalve shells (independent of the bivalve type, provenance, or if modern or archaeological) show the same absorption features with identical positions of the Mn K-edge (6.548 keV), the white line (6.552 keV), as well as of the position (6.540 keV) and intensity of the pre-edge peak [2]. The Mn pre-edge feature is a result of quadrupole 1s→3d transitions and is present at the same energy in all shells as well as in Mn-bearing calcite ($CaCO_3$) and in synthetic and natural rhombohedral $MnCO_3$. In addition, the spin-resolved XANES shows that the electronic configuration of Mn in these materials is largely $3d^5$ corresponding to Mn^{2+}.

Mn-Kβ emission spectra provide detailed information regarding the chemical environment (i.e. the next neighbours). All shells show the same Kβ´ and $K\beta_{1,3}$ main, and $K\beta_{2,5}$ satellite lines. Most importantly, all spectra show the same features as the emission spectra of a Mn-bearing calcite crystal and of $MnCO_3$, while they clearly differ from Mn-bearing aragonites and reference compounds containing other Mn coordination. These data therefore reveal that: (i) Mn in the aragonitic shells resides largely in the mineral part and not in the organic material. (ii) Mn in the orthorhombic shell aragonite is present as Mn^{2+} in a calcite microenvironment with rhombohedral coordination.

[1] Soldati, A.L. et al. (2009) *J. Mollusc. Stud.*, **75**, 75-85; [2] Soldati, A.L. et al. (2010) *J. Synchrotron Rad.*, **17**, 193-201.

Development of a new high-resolution synchrotron Gandolfi camera

Tanaka, M.[1*], Nakamura, T.[2], Noguchi, T.[3], Katsuya, Y.[4] & Matsushita, Y.[1]
[1]NIMS Beamline Station/SPring-8, National Institute for Materials Science, Hyogo, Japan ([*]masahiko@spring8.or.jp)
[2]Dept. of Earth and Planetary Sciences, Faculty of Sciences, Kyushu University, Fukuoka, Japan
[3]Dept. of Materials and Biological Sciences, Ibaraki University, Mito, Ibaraki, Japan
[4]SPring-8 Service, Hyogo, Japan

A new high-resolution Gandolfi camera with a large camera radius of 955 mm has been developed for synchrotron X-ray diffraction experiments.

Gandolfi method [1] is an X-ray diffraction method that enables acquisition of pseudo-powder diffraction patterns from single crystals. Using the Gandolfi method with synchrotron we developed a non-distractive analysis method for mineral phase determination and quantitative mineral-phase analysis [2-3] of micro-amount samples. Applying the multi-phase Rietveld method to the diffraction patterns obtained by the synchrotron Gandolfi method we successfully conducted quantitative mineral-phase analysis [3]. We applied the methods to analysis of micro-amount extraterrestrial samples, but many overlapped peaks were observed in the diffraction patterns. These overlapped peaks decreased the accuracy of the Rietveld analysis. However the new Gandolfi camera can achieve higher angular resolution, which enables separation of the overlapped diffraction peaks, and more accurate quantitative-phase analysis.

The new Gandolfi camera was developed for the diffractometer of BL15XU at SPring-8, the 3rd generation synchrotron radiation facility in Japan. A Gandolfi head of Tenno Co. of Italy, set at the centre of the diffractometer was used to perform the Gandolfi motion and the imaging plate (IP) cassette developed for the Debye-Scherrer powder diffraction camera of the diffractometer [4] was applied to the detector (Fig. 1a). The IP cassette has a cylindrical surface with the radius of 955 mm and the long side of the IP is parallel to the 2θ direction. The minimum step of the 2θ is 0.003 degrees. With the new Gandolfi camera, powder diffraction images were properly collected from the trial samples; NIST-CeO_2 powder and mixtures of some mineral powders fixed in resins (Fig. 1b).

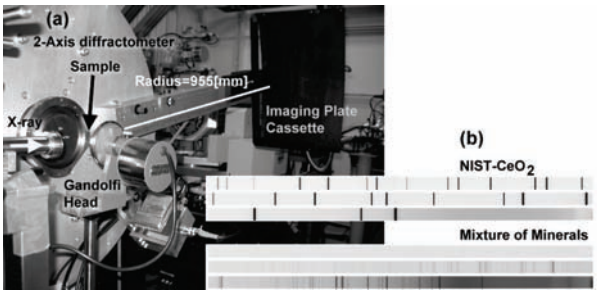

Fig. 1: (a) The photograph of the new high-resolution synchrotron Gandolfi camera. The camera radius is 955 mm and the minimum step of the 2θ angle is 0.003 degrees. (b) The powder diffraction images obtained by the new Gandolfi camera. The imgaes are separated in three sections of lower, middle and higher range of the 2θ.

[1] Gandolfi, G. (1967) *Miner. Petrogr. Acta*, **13**, 64-74. [2] Nakamura, T. et al. (2003) *Earth Planet. Sci. Lett.*, **207**, 83-101. [3] Tanaka, M., Nakamura, T. & Noguchi, T. (2007) in Jae-Young & Tah, S. (eds.) *AIP Conf. Proc.* (Ninth Int. Conf. on Synchr. Rad. Instrum.)**,** 1779-1783. [4] Tanaka, M., Katsuya, Y. & Yamamoto, A. (2008) *Rev. Sci. Instrum.*, **79**, 075106.

Selected advances in neutron techniques for studies of Earth materials

Parise, J.B.[1*] & Tulk, C.A.[2]
[1]Dept. of Geosciences & Chemistry Dept., Stony Brook University, Stony Brook, NY, USA ([*]john.parise@sunysb.edu)
[2]Neutron Scattering Science Div., Oak Ridge National Lab., Oak Ridge, TN, USA

The characteristics of neutrons that make them a unique probe for condensed matter are well known: their electrical neutrality, possession of magnetic moments, polarizability, a scattering cross section (*b*) independent of *Q* and atomic number but dependent on isotope, and the wide range of energy and momentum transfer possible in a scattering experiment. The charge neutrality of neutrons means that they penetrate solids to depths of centimeters, thus enabling studies of bulk phenomena in situ, and ready construction of bulky sample cells capable of high pressures, temperatures and strains. The isotopic dependence and atomic number independence of *b* can be used to study light elements in the presence of heavy elements, study site-occupancies of elements neighbouring in the periodic table, and the concoction of mixed solvents (D_2O/H_2O) that match the scattering contrast of colloid suspended in them. Techniques to produce polarized beams of particles with magnetic moments makes neutrons uniquely sensitive probes of magnetic interactions; the only technique allowing simultaneously determination of arrangements of nuclei and magnetic moments in materials. Neutrons can be readily produced over a wide range of energies ranging from thermal to cold, for investigating the structure and dynamics over length scales from the atomic to the mesoscopic, 1 to 105 Å, and over energy transfers from 10^{-9} to 1 eV. Many developments and applications to Earth Science research, are summarized in a series of presentations (http://neutron.neutron-eu.net/n_nmi3/n_networking_activities/n_nese).

Several examples illustrating new information available from elastic neutron scattering will be presented, including studies of ion exchange in crystalline materials, and nuclear and magnetic structures of crystalline and geonanomaterials. Increasingly researchers seek to carry out these studies under the operating conditions of planetary surfaces and interiors.

Neutron experiments, especially those that seek to study Earth materials *in operando* and as a function of time, are "flux hungry" and this is one driving force behind the development of ever more powerful sources, such as the Spallation Neutron Source (SNS). Additional brightness gains have recently been realized at the Spallation Neutron and Pressure (SNAP) beamline used KB optics. By combining Montel-like nested focusing optics with pressure vessels considerably smaller samples should be accessible at Mantle pressures. Neutron focusing is used to improve spatial resolution and lower detection limits for neutron-based analytical methods. The SNAP beamline is the first fully optimized high pressure beamline at a neutron source, and has several features that allow adaptation of components to fit experiments as varied as studies at extreme conditions for liquids, glasses, nano- and crystalline materials. For example, until very recently, the prospects for high-pressure single crystal studies at anything approaching 50-80 GPa using neutrons seemed remote indeed. The integrated fluxes for neutron sources barely approach that for a laboratory X-ray Source. With the advent of the SNS, large area detectors and novel focusing optics, the SNAP beamline may make routine high-pressure studies on single crystals of a size approaching what is achievable with laboratory-based X-ray investigations. Recent trials suggest this is possible now.

The use of neutron diffraction in studies of planetary ice-rock analogue mixtures

Middleton, C.A.[1,2*], Wood, I.G.[1,2], Grindrod, P.M.[1,2], Fortes, A.D.[1,2], Hunt, S.A.[2], Zhang, S.Y.[3], Covey-Crump, S.J.[4] & Sammonds, P.R.[2]
[1]Centre for Planetary Sciences at UCL/Birkbeck, London, BT, UK ([*]ceri.middleton@ucl.ac.uk)
[2]Dept. of Earth Sciences, UCL, London, UK
[3]ISIS Facility, STFC Rutherford Appleton Laboratory, Harwell Science and Innovation Campus, Chilton, Didcot, UK
[4]School of Earth, Atmospheric and Environmental Sciences, The University of Manchester, UK

We have carried out rheological experiments on planetary ice-rock analogue mixtures in the ENGIN-X beamline at the pulsed neutron source ISIS in Oxfordshire, UK.

Neutron diffraction has previously been used to study the deformation of geologically relevant polyphase materials (e.g. [1]), as it allows the strain in each phase to be determined, and hence (via the elastic constants) the stress partitioning between each phase to be calculated, whereas traditional deformation tests only allow bulk properties of the whole sample to be obtained. We demonstrate for the first time the application of neutron diffraction to the deformation of icy planetary materials at conditions relevant to large icy bodies such as Europa, Ganymede and Titan.

Experiments were conducted on samples with fluorite fraction 0.09 and 0.27, at strain rates of 5×10^{-7} - $5 \times 10^{-6} s^{-1}$, temperatures of 233 and 253K, and confining pressures of 50MPa. This pressure is equivalent to depths of 30-40 km in the largest icy satellites, therefore allowing us to explore the P,T conditions throughout the thickness of Europa's icy crust [2], and much of Titan's outermost ice shell [3], however, strain rates are necessarily faster than planetary rates to allow for results on laboratory timescales.

In order to obtain these conditions, we adapted a previously used pressure vessel design [4] to allow study of cylindrical polycrystalline D_2O ice + fluorite samples of diameter 25mm, length 65mm. This vessel was designed to fit within the beamline cryogenic chamber [5].

Our preliminary results suggest that the ice phase may be experiencing localised melting during higher temperature runs, possibly due to stress increases around the fluorite grains. We suggest that this is due to the angular shape of our rock grains, and would not be seen if our grains were spherical. This would have important ramifications for planetary ice analogue experiments, as using spherical rock particles (e.g. [6]) may not well represent the actual situation in icy bodies, and it may, therefore, be important that interactions between the ice and rock grains are accounted for when considering these polyphase mixtures.

We will present these results, along with further analysis of the strain partitioning between the ice and fluorite phases.

[1] Covey-Crump, S.J., et al. (2006a) *Physica B*, **385-386**, 946-948. [2] Billings, S.E. & Kattenhorn, S.A. (2005) *Icarus*, **177**, 397-412. [3] Grindrod, P.M. et al. (2008) *Icarus* **197**, 137-151. [4] Covey-Crump, S.J. et al. (2006b) *J. Appl. Crystallogr.*, **39**, 222-229. [5] Oliver E. et al. (2008) *Meas. Sci. Technol.*, **19**, 034019. [6] Yasui, M. & Arakawa, M. (2008) *Geophys. Res. Lett.* **35**, L12206.

Evaluation of zirconia anvils for use in high pressure neutron scattering

Komatsu, K.[1*], Sano-Furukawa, A.[2], Abe, J.[2], Hattori, T.[2], Arima, H.[3], Arakawa, M.[1,2] & Kagi, H.[1]
[1]Geochemical Research Center, Graduate School of Science, The University of Tokyo, Japan
([*]kom@eqchem.s.u-tokyo.ac.jp)
[2]Quantum Beam Science Directorate, Japan Atomic Energy Agency, Japan
[3]J-PARC Center, Japan Atomic Energy Agency, Japan

Tungsten carbide(WC) and sintered diamond(SD) are widely used as anvils or pistons in any kind of high pressure apparatus because of their hardness. WC and SD anvils has also been mainly used in opposed type presses like the Paris-Edinburgh cell for neutron scattering as they are somehow transparent for neutron. For example, the attenuation (I/I_0) of WC of 10mm for neutron is 0.2~0.4 depending on the wavelength. Although SD is a bit more transparent than WC, it has strong Bragg edges which may cause a difficulty for intensity correction. Yttria-stabilized zirconia (YSZ), which is also used as anvils for diamond anvil cells [1], was successfully applied for sliding-blocks (anvils) in the mini cubic apparatus for high pressure neutron diffraction [2]. It is quite likely that YSZ has a enough potential to use as opposed anvils in high pressure neutron scattering with the merits of the neutron transparency, low thermal conductivity (for high- or low-temperature experiments) and low cost. In this study, we conducted compression test using YSZ anvils and measured its transparency and neutron diffraction from sample in it in order to evaluate YSZ anvils for use in high pressure neutron scattering experiments.

A pair of YSZ was commercially supplied and machined as single-toroidal anvils for the Paris-Edinburgh cell. A NaCl pellet without pressure medium was put into the anvils as a pressure calibrant. Duralumin (A7075) rings were used as gaskets. Energy dispersive x-ray diffraction from NaCl was obtained at elevated loads at NE7 beamline in PF-AR, Tsukuba, Japan, and each pressure was estimated using Decker's EOS [3]. The obtained load-pressure curve is shown in Fig. 1. Pressure is successfully generated along a slope of 0.1 GPa/ton from 10 to 40 tons. The YSZ anvils survived up to 5.1 GPa, and blowout at 80 tons.

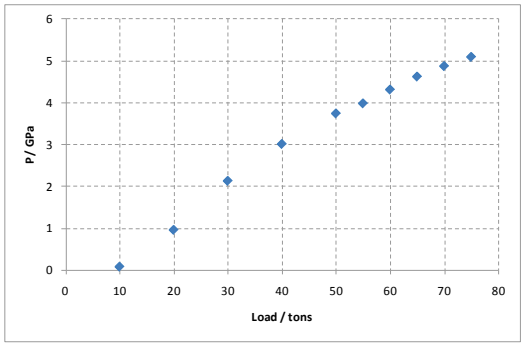

Fig. 1: Load-pressure curve of the single-toroidal zirconia anvil set on the Paris-Edinburgh cell.

Neutron transparency of YSZ as a function of wavelength and neutron diffraction of a lead palette in the YSZ anvils at ambient pressure was measured at an Engineering Materials Diffractometer "TAKUMI" in J-PARC. The results showed that an effective intensity using YSZ anvils is 1.5~6 times more intense than that using the conventional WC anvils.

[1] Xu, J.A. et al. (1996) *High Press. Res.*, **15**, 127-134. [2] Uwatoko, Y. et al. (2008) *Rev. High Press. Sci. Tech.*, **18**, 230-236. [3] Decker, D.L. (1971) *J. Appl. Phys.*, **42**, 3239-3244.

Contrast variation small angle neutron scattering in biomineralization

Schwahn, D.
Institute of Solid State Research of the Helmholtz Research Center Jülich GmbH, Jülich, Germany
(d.schwahn@fz-juelich.de)

Mineralization of calcium carbonate and calcium phosphate in the presence of proteins was explored by small angle neutron scattering (SANS) using the technique of contrast variation. SANS is a rather new experimental technique in biomineralization. It allows full structural characterization of scattering particles of sizes between 10 Å and 1000 Å and delivers detailed information about mineral-protein composites. The last mentioned information is obtained from contrast variation experiments achieved by the exchange of proper isotopes such as from variation of H_2O/D_2O composition in aqueous solutions [1]

Time resolved mineralization of calcium carbonate in the presence of the protein ovalbumin was explored by gas diffusion technique [2]. The mineralization followed Oswald's law by a step-by-step formation from less stable to more stable polymorphs. The formation of the amorphous mineral polymorph occurred in parallel to denaturation and aggregation of the protein. After about 6 h from starting the mineral transformed to the more stable vaterite, and finally after about 10 h to the even more stable aragonite. Calcite as the most stable polymorph was not detected within the experimental time. No complexation of the protein ovalbumin occurs in the presence of $MgCl_2$ and $SrCl_2$.

Another explored protein was fetuin-A which acts as an inhibitor of calcium phosphate mineralization [3]. We found of the order of 1000 Å large mineral-organic particles whose structure was analyzed by contrast variation. We found an octacalcium phosphate core and a dense monolayer of the protein, which protected the mineral from further growth.

[1] Endo, H., Schwahn, D. & Cölfen, H. (2004) *J. Chem. Phys*., **120**, 9410-9423. [2] Pipich, V. et al. (2008) *J. Am. Chem. Soc.*, **130**, 6879-6892. [3] Heiss, A. et al. (2007) *Biointerphases*, **2,** 16-20.

Neutron- and X-ray imaging in archaeology and geosciences in South Africa

De Beer, F.C.[1*] & Masiteng, I.N.[2]
[1]Radiation Science Dept., Necsa, Pretoria, South Africa
([*]Frikkie.debeer@necsa.co.za)
[2]National Cultural History Museum, Pretoria, South Africa

For the past 8 years, the South Africana Neutron Radiography and tomography facility (SANRAD) [1], located at the SAFARI-1 nuclear Research Reactor at Necsa, South Africa, has been exploited successfully in geosciences, palaeosciences and archaeology fields of application [2]. The facility has been also equipped with a 100kV X-ray source for complementary tomography investigations.

The 125 kV X-ray and neutron attenuation coefficients of some metals, which are of high relevance for archaeological investigations, are listed in Table-1 [3].

Table 1: Linear attenuation coefficients of some metals for thermal neutrons and 125 kV X-rays

	Material (cm^{-1})							
Probe	Au	Ag	Cu	Sn	Bronze	Pb	Zn	Fe
Neutrons	6.28	3.99	0.99	0.20	0.87	0.37	0.34	1.20
X-rays	35.9	5.67	1.97	3.98	2.5	22.8	1.64	1.57

It is evident from Table-1 that the high density materials, which are more likely to be found as base material of archaeological artefacts, are more transparent to neutrons as X-rays and therefore is capable to reveal information hidden in precious findings through tomography imaging.

Figure 1 shows a neutron tomogram, revealing the inside structure of an OSIRIS statuette showing the chaplets which indicate that the lost max method were applied during its manufacturing.

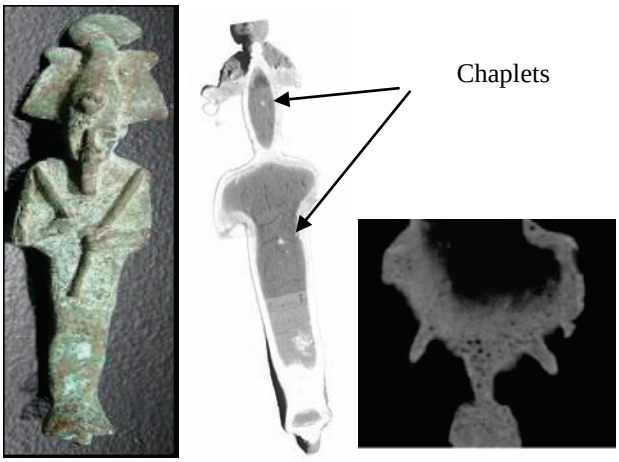

Fig. 1: Photo (left) and thermal neutron tomogram of an OSIRIS bronze artefact sliced from the front (Middle) and an axial cross section of the head area (right)

Sectioning of the neutron tomography in the head area reveals its high porosity and heavily corrosion structure which has storage, curation and conservation implications.

This contribution describes the recent neutron- and X-ray tomography investigations being performed on archaeological and geological samples through collaboration with the national museums and higher educational institutions.

[1] De Beer, F.C. (2005) *Nucl. Instrum. Methods A*, **542**, 1-6. [2] De Beer, F.C. et al. (2009) *Nucl. Instrum. Methods A*, **605**, 167-170. [3] Kardjilov, N. et al., (2006) *J. Neutron Res.*, **14(1)**, 29-36.

H, B, N or Pb, Bi, Cd: the PGAA for multielemental analysis of light and heavy elements in geological samples

Canella, L.[1], Kudejova, P.[2*], Söllradl, S.[3] & Türler, A.[3]
[1]RCM, Technische Universität München, Garching, Germany
[2]FRM II, Technische Universität München, Garching, Germany
([*]petra.kudejova@frm2.tum.de)
[3]Paul Scherrer Institute (PSI), Villigen, Switzerland

Not only when determining light elements in a sample volume non-destructively, the PGAA technique is the method to choose. On one hand, Instrumental Neutron Activation Analysis (INAA) is a well-established method for non-destructive determination of elemental composition of geological samples. However, H, Li, Be, B, C, N, S cannot be determined by INAA and for elements like P, Cd, Gd, Pb – PGAA is a competitive method with regard to the detection limits. The next advantage of PGAA compared to INAA is its rapidity: the irradiation takes max. few hours, the data analysis can be performed on the day of measurement and the sample is not activated for a long time. Depending on the composition, the sample can be given back to the owner within one or more days. This is a great advantage, if another e.g. neutron-based analysis (e.g. rest-strain in material through neutron diffraction) should follow soon or if the researcher wants to have a fast estimation, which elements are to be expected in the object (usually on ppm level). For PGAA, the sample needs no preparation, which also speeds the process of deriving the general composition.

We want to present some of our performed PGAA experiments with the elements named in the title. For example, we have measured hydrogen in clathrates and nitrogen in correlation with sulphur in carbonaceous shales and coals. Next, light elements together with Pb, Cd or Va were measured in air pollution samples. Dynamic range for boron was determined as well as the detection limit and used for measurements of boron in alloys. Distribution of bismuth in lead crystals was determined with very good statistics. Cadmium was analysed also in biological samples for medical research [1,2].

[1] Canella, L. et al. (2009) *Appl. Radiat. Isot.*, **67**, 2070-2074.
[2] Kudejova, P. et al. (2008) *J. Radio. Nucl. Chem.*, **278(3)**, 691-695.

The effect of SEM imaging on the Ar/Ar system in alkali feldspars

Flude, S.[1*], Sherlock, S.C.[1], Lee, M.R.[2] & Kelley, S.P.[1]
[1]Dept. of Earth and Environmental Sciences, Centre for Earth, Planetary, Space & Astronomical Research (CEPSAR), Open University, Milton Keynes, UK ([*]s.flude@open.ac.uk)
[2]Dept. of Geographical & Earth Sciences, University of Glasgow, UK

Alkali feldspars from a range of tectonic environments have been used to reconstruct thermochronological histories by employing the multi domain diffusion (MDD) model of Ar/Ar dating [1]. MDD is based on the notion that, as feldspars cool, they may undergo various processes of exsolution, phase transformation and fluid-mediated recrystallisation that split the crystal into a number of smaller diffusional subgrains However, substantial controversy remains regarding which microtextures and micro structures control Ar-diffusion [2]. A number of studies have addressed these issues using coupled SEM imaging and Ar/Ar UV laser ablation microprobe (UV-LAMP) analysis on the same samples, to enable direct comparison of microtextures with Ar/Ar age data [3].

Here we have tested the idea that SEM work may affect Ar/Ar systematics, leading to inaccurate results in subsequent Ar/Ar analyses. Alkali (Na, K) redistribution due to ionisation and electro-migration during electron microprobe analysis of alkali feldspars is a common problem [4] and radiogenic Ar (^{40}Ar*) is not bonded in the crystal lattice, so is likely to be more mobile than K during electron irradiation. Electron irradiation can also cause hydrocarbon molecules (present on the sample surface or in the sample chamber) to become immobilised on the sample surface [4]. This may be a problem during subsequent Ar-analysis as hydrocarbon fragments can cause mass interferences with Ar isotopes. This is a particular problem for ^{36}Ar, which is used to correct for atmospheric ^{40}Ar by assuming ^{40}Ar/^{36}Ar=295.5, as few mass spectrometers are able to resolve the difference between ^{36}Ar and contaminants. Some SEM techniques require chemical-mechanical polishing with colloidal silica, which may rapidly dissolve some alkali feldspars [5] potentially resulting in differential loss of K and Ar. Similarly, feldspar microtextures may be studied by etching cleavage fragments with HF vapour [6], which again may affect K and Ar within the sample to different degrees.

We are empirically testing the possible effects of these processes on the Ar-system in alkali feldspars. Three feldspars have been selected, with microtextures ranging from simple to complex. The distribution of Ar-isotopes and K (in the form of neutron-induced ^{39}Ar) has been characterised for each sample by UV-LAMP Ar-analysis of thick sections that have not been studied in the SEM. Ar/Ar analysis was carried out using a Nu Instruments Noblesse mass spectrometer, which can distinguish ^{36}Ar from hydrocarbon contaminants. Further thick sections were polished with colloidal silica and imaged in the SEM (60 Pa vacuum, 20 kV and high beam current). Selected areas were irradiated at high magnification for eight minutes to maximise sample damage. UV-LAMP Ar/Ar dating was subsequently carried out on these samples to determine the distribution of Ar-isotopes and K within the sample after SEM imaging. Here two sets of data are compared, facilitating debate on the validity of Ar/Ar ages from alkali feldspars that have been imaged with the SEM.

[1] Richter, F.M. et al. (1991) *Earth Planet. Sci. Lett.*, **105**, 266-278. [2] Parsons, I. et al. (1999) *Contrib. Mineral. Petrol*., **136**, 92-110. [3] Reddy, S.M. et al. (1999) *Geology*, **27**, 363-366. [4] Reed, S.J.B. (2005) *Electron Microprobe and Scanning Electron Microscopy in Geology*. Cambridge. [5] Prior, D.J. et al. (1999) *Am. Mineral*., **84**, 1741-1759. [6] Waldron, K. (1993) *Contrib. Mineral. Petrol*., **116**, 360-364.

Loss of ^{40}Ar(rad) from leucite-bearing basanite at low temperature: implications on K/Ar dating

Balogh, K.[1*], Németh, K.[2], Itaya, T.[3], Molnár, F.[4], Stewart, R.[2], Thanh, N.X.[5], Hyodo, H.[3] & Daróczi, L.[6]
[1]Inst. of Nuclear Research, Hungarian Academy of Science, Debrecen, Hungary ([*]balogh@atomki.hu)
[2]Institute of Natural Resources, Volcanic Risk Solutions, Massey University, Palmerston North, New Zealand
[3]Research Inst. of Natural Sciences, Okayama Univ. of Sciences, Okayama, Japan
[4]Dept. of Mineralogy, Eötvös L. University, Budapest, Hungary
[5]Dept of Geology, Hanoi University of Mining and Geology, Hanoi, Vietnam
[6]Dept. of Solid State Physics, University of Debrecen, Hungary

Ar/Ar ages have been determined [1] on alkali basalts from the Balaton Highland Volcanic Field, Hungary. Some Ar/Ar ages were conflicting with K/Ar data reported earlier [2]. The leucite-bearing basanite of Hegyestű hill has been selected for a detailed study in order to explain why K/Ar ages are too young. It has been found that K/Ar and Ar/Ar ages are similar, if (1) K/Ar dating is performed on samples treated with HCl, or (2) the argon extraction line was baked only at 150°C.

Olivine, augite, plagioclase, magnetite leucite, nepheline and analcime (in one sample) have been identified by XRD investigations. After HCl treatment plagioclase and augite remained in all samples, implying that dissolved minerals are responsible for the loss of ^{40}Ar(rad). Microscopic and EMP investigations have shown that K is concentrated in patches of < 200 μm size. A TEM analysis failed to detect leucite. HCl treatment of 6 samples dissolved 28.0 – 63.5 % of K contents and 4.02 – 6.42 % K have been calculated for the dissolved part of carbonate-free basalts. On the basis of these results leucite is regarded to be responsible for the Ar(rad) loss, but a subordinate role of nepheline can not be excluded. This observation refers only to Hegyestű hill, since it conflicts with the experiences of Ar chronological studies on leucite. Ar may be released at low temperature from (1) very fine-grained leucite without change of the crystalline structure, or (2) due to a change of crystalline structure during baking the argon extraction line.

A set of the same sample has been dated after a stepwise raising of the baking temperature from 55°C to 295°C and the ^{40}Ar(rad) loss and diffusion parameters (D/a^2) have been calculated. In case (1) the diffusion parameters should have arranged along a straight line in the Arrhenius diagram. In contrast, the arrangement of points suggests a structural change in the 145°C–295°C temperature range. XRD investigations did not identify structural change up to now.

K content of the variably altered rocks varies from 2.1 to 0.3 %. The groundmass is not uniform: a coarser- and a finer-grained type can be distinguished, which are well separable in the quarry. Minerals from the basement rock have been recognized: this may influence the K/Ar age too.

[1] Wijbrans, J. et al. (2007) *J. Volcanol. Geoth. Res.*, **164**, 193-204. [2] Balogh, K. et al. (1986) *Acta Miner. Petrogr. Szeged*, **28,** 75-93.

K-Ca ages of authigenic sediments: examples from Paleozoic glauconite and potassium-rich evaporites and applications to low temperature thermochronometry

Cecil, M.R.[1] & Ducea, M.[2*]
[1]Division of Geological and Planetary Sciences, California Institute of Technology, Pasadena, CA, USA
[2]Dept. of Geosciences, University of Arizona, Tucson, AZ, USA ([*]ducea@email.arizona.edu)

K-Ca ages of Cambrian glauconites from the Llano uplift, central Texas, and Permian K-rich evaporites from the Delaware Basin, New Mexico, were determined in order to re-evaluate the ability of the K-Ca system to constrain the timing of deposition of sedimentary packages. All but one of the K-Ca ages presented here were found to be younger than their stratigraphic ages. In addition to being too young, the K-Ca ages are also highly variable, ranging in age from Silurian to Permian in the case of glauconites and from Permian to Cretaceous in the case of the evaporites. The oldest subset of glauconite ages are in agreement with previously published Rb-Sr ages from the same outcrop and provide further evidence for there having been a postdepositional thermal or recrystallization event that reset both the Rb-Sr and K-Ca systems. The range of younger glauconite K-Ca ages are not seen in the Rb-Sr data, but are similar to the distribution of available apatite fission track ages for the Llano basement. K-Ca ages are interpreted as thermochronologic data reflecting partial retention of Ca in thermally fluctuating basin conditions. Estimates of the closure temperature of Ca in glauconite are found to be 75 - 90°C for cooling rates of 0.3 - 1°C/My. Sylvites and langbeinites from the Delaware Basin give K-Ca ages ranging from the timing of primary mineralization (~ 250 Ma) to 100 Ma. The random distribution and wide spread of K-Ca ages is unlike previously published K-Ar and Ar-Ar from the same potash zone, which cluster distinctively and apparently record discrete geologic events. K-Ca ages argue for ongoing recrystallization of the K-salts throughout most of the Mesozoic. The lack of any ages younger than ~ 94 Ma implies that a significant tectonic or paleoenvironmental change occurred at that time, stabilizing the salts and effectively closing even the most sensitive K-Ca system. The K-Ca system is potentially useful as a low temperature thermochronometer with closure temperatures <100°C for glauconite.

The Dej Tuff of Transylvania (Romania): how old, what flavour and where from?

Nicolescu, S.[1,2*] & Mârza, I.[3]
[1]Dept. of Geosciences, University of Arizona, Tucson, USA
[2]*now at*: Peabody Museum of Natural History, Yale University, New Haven, USA ([*]stefan.nicolescu@yale.edu)
[3]36 Bd. 1 Decembrie 1918, Cluj-Napoca, Romania

The Transylvanian Basin of Romania, one of the important sedimentary basins and natural gas producing provinces of SE Europe, belongs to the Central Paratethys stratigraphic domain.

The many kilometres thick basin fill consists of a monotonous, mainly Tertiary, sedimentary sequence of alternating marl, sand/sandstone and clay layers. The only breaks in its stratigraphic monotony are several Miocene to Pleistocene volcanic tuff layers, accounting for about 10 % of the basin fill volume. The most important of these is the Dej Tuff. Because of its regional extent and easily recognisable petrography, the Dej Tuff is an excellent stratigraphic marker. Its biostratigraphic age, based on micro- and nannofossil marker species in adjacent sediments, is Lower Badenian [1]. In spite of repeated radio-isotope and fission track dating attempts, no conclusive eruption age of the tuff has been established so far [2].

Here we present robust zircon (U-Th)/He ages obtained on two zircon populations collected from the Pâglişa (NE Transylvania; 47°00'34.45" N, 23°38'35.41" E; 450 m a.s.l.) Dej Tuff outcrop. The two ages on samples collected about 30 m stratigraphic thickness apart, are identical within error: 14.9 ± 0.7 Ma and 15.6 ± 0.9 Ma respectively. Their weighted average of 15.1 ± 0.5 Ma constrains the eruption of the investigated Dej Tuff occurrence to the Middle Badenian.

Besides the accurate and precise age of the Dej Tuff, other intensely debated points of contention in the literature are its petrographic classification (rhyolite *vs.* rhyodacite/dacite) and eruption source(s). Petrographic classification attempts have been based so far on the rock's major element composition. The problem with this is that the Dej Tuff has undergone pervasive post-deposition alteration and thus its present major element chemistry has changed significantly since emplacement. Therefore, a classification based on "immobile" trace elements, e.g., Zr/TiO_2 *vs.* Nb/Y [3], seems more appropriate. Based on such criteria, the Dej Tuff at Pâglişa falls within the rhyodacite/dacite field.

As already pointed out by many previous studies, identifying the eruption centre(s) of the Dej Tuff is a difficult task. The Transylvanian Basin is bordered to the north, east and west by significant volcanic chains contemporaneous with the Dej Tuff and a systematic study of all possible candidate sources is lacking so far. However, the geotectonic environment of magma generation can be estimated based on trace element abundances. The Rb *vs.* (Y + Nb) discrimination diagram [4] places the Pâglişa occurrence in the volcanic arc post-collision field. When compared to various magma generating environments (MORB/N-MORB, Upper-, Lower- or Average Crust) "the best fit" for the Pâglişa outcrop is with an Upper Crust magmatic source. These data, together with other published geochemical characteristics and combined with its He eruption/cooling age should narrow the field of potential eruption centre candidates of the Dej Tuff.

[1] Mârza, I. & Meszaros, N. (1991) in Mârza, I. (ed.) *The volcanic tuffs from the Transylvanian Basin, Romania*. Univ. Babeş-Bolyai, Cluj-Napoca, 11-21. [2] Szakács, A. (2000) *Unpublished PhD thesis*. University of Bucharest. [3] Winchester, J.A. & Floyd, P.A. (1977) *Chem. Geol.*, **20**, 325-343. [4] Pearce, J.A. (1996) *Episodes*, **19**, 120-125.

U-Pb ages of detrital zircons from Ielova Metamorphic Sequence - constraints on tectonic affiliation within South Carpathians (Romania)

Zaharia, L.[1*] & Jeffries, T.[2]
[1]Dept. of Geology, "Babes Bolyai" University, Cluj Napoca, Romania ([*]luminita.zaharia@ubbcluj.ro)
[2]Dept. of Mineralogy, Natural History Museum, London, UK

The basement of the Romanian Carpathians consists of pre-Variscan metasedimentary and metaigneous units. In the South Carpathians, these units are grouped in two large Alpine domains with different features, namely Getic domain and Danubian domain, and one small domain, Severin, with rift-originated tectonic units.

Situated in south-eastern part of Romania, in Banat area, Ielova Metamorphic Sequence (IMS) is a metasedimentary sequence, with orthogneiss bodies, metamorphosed up to amphibolite facies. It represents a "disputed" area between the two large domains, and more precisely between Sebeş-Lotru (Getic) and Drăgşan (Danubian) terranes, being situated at the tectonic border between the two.

These two terranes have a different paleogeographic origin. Sebeş-Lotru was interpreted as a fragment of the Cadomian Gondwana eastern extension [1,2], while for Drăgşan a northern Gondwanan, Pan-African origin, thus an Avalonian affinity was shown [3,4].

To constrain the tectonic affiliation of IMS to one of the two discussed terranes, based on their different paleotectonic affinities, zircons from four metasedimentary rocks of IMS were extracted and U-Pb izotopic ages were determined by LA-ICP-MS.

Zircon crystals are mostly transparent. Prismatic shapes, with very rounded termination, as well as almost spherical grains were found. Internal structures are complicated. The elongated grains have an internal structure oscillatory-zoned, sometimes with recrystallised areas, or with fine rims due to dissolution. Spherical grains have either no inherited cores and sector zoning, or large inherited cores, represented by irregular fragments of older grains, with narrow dark metamorphic overgrowths.

Most detrital zircon ages are mid-Neoproterozoic-Early Cambrian, specific for the Cadomian interval (650-530 Ma), while older ages are Paleoproterozoic (1.9-2.5 Ga) and Archean (2.5-2.9 Ga). Variscan overprints are also registered. Major age peaks are at 0.55-0.65 Ga, 2.00-2.01 Ga and 2.6-2.7 Ga.

One of the characteristics of IMS detrital ages is the almost complete absence of Mesoproterozoic (Grenvillian) zircons. Only two grains yielded concordant ages of 1.2 and 1.5 Ga. Another feature is the large number of ages falling in the 2.4-1.95 Ga interval. This interval is specific for Cadomian-related terranes, while for the Avalon terrane (sensu lato, [5]) it represent a "minimum zone" with few or no ages.

The IMS detrital age spectrum reveals a strong Cadomian affinity. This supports a tectonic affiliation of IMS at Sebeş-Lotru (Getic) which shows the same affinity. Drăgşan terrane (Danubian) is characterized by an Avalonian inheritance, which cannot be supported by the IMS age.

Acknowledgements: The analytical work was supported by a SYNTHESYS Project (GB-TAF-3596) financed by European Community Research Infrastructure Action under the FP6 "Structuring the European Research".

[1] Balintoni, I. et al. (2009) *Gondwana Res.*, **16**, 119-133. [2] Balintoni, I. et al. (2010) *Gondwana Res.*, **17**, 561-572. [3] Liégeois et al. (1996) *Precambrian Res.*, **80**, 281-301. [4] W Winchester, J.A., Pharaoh, T.C. & Verniers, J. (2002) in Winchester, J.A. et al. (eds.) *Geol. Soc. London Sp. Publ.*, **201**, 1-18. [5] Samson, S.D. et al. (2005) *J. Geol. Soc. London*, **162**, 65-71.

The Annandagstoppane granite, East Antarctica: evidence for Archean intracrustal recycling in the Kaapvaal-Grunehogna Craton from zircon O and Hf isotopes

Marschall, H.R.[1*], Hawkesworth, C.J.[2], Storey, C.D.[3], Dhuime, B.[1] & Leat, Ph.T.[4]
[1]University of Bristol, UK ([*]Horst.Marschall@bristol.ac.uk)
[2]University of St Andrews, UK
[3]University of Portsmouth, UK;
[4]British Antarctic Survey, Cambridge, UK

The Grunehogna Craton (GC, East Antarctica) is interpreted as part of the Archean Kaapvaal Craton of southern Africa prior to Gondwana breakup. The basement of the GC is only exposed within a small area comprising the dominantly leucocratic Annandagstoppane (ADT) granite. The granite (and hence the craton) has been dated previously only by Rb-Sr and Pb-Pb mica and whole-rock methods. Here, the crystallisation age of the granite was determined to 3,068 ± 4 Ma by U-Pb dating of zircon. This age is coeval with granitoids and volcanics in the Swaziland and Witwatersrand blocks of the Kaapvaal Craton.

Inherited grains in the ADT granite were discovered with ages of up to 3,433 ±7 Ma, and are the first evidence of Palaeoarchean basement in Dronning-Maud Land. The age spectrum of the inherited grains reflects well-known tectono-magmatic events in the Kaapvaal Craton and form important pieces of evidence for the connection of the GC to the Kaapvaal Craton for at least three billion years and probably longer. Whole-rock chemistry and zircon O isotopes demonstrate a supracrustal sedimentary source for the granite, and Hf model ages show that at least two or three different crustal sources were contributing to the magma with model ages of ~3.50, ~3.75 and possibly ~3.90 Ga, respectively.

3.1 Ga granites covering ~60 % of the outcrop area of the Kaapvaal-Grunehogna Craton played a major role in the mechanical stabilisation of the continental crust during the establishment of the craton in the Mesoarchean. Combined zircon Hf-O isotope data and the lack of juvenile additions to the crust in the Mesoarchean strongly suggest that crustal melting and granite formation was caused by the deep burial of clastic sediments and subsequent incubational heating of the crust. Intracrustal recycling of this type may be an important process during cratonisation and the long-term stabilisation of continental crust.

Imaging and spectroscopy of ion-beam luminescence (IBL) and X-ray excited optical luminescence (XEOL) of framework silicates

Finch, A.A.*, King, G., Taylor, R.P. & Friis, H.
Division of Earth Sciences, University of St. Andrews, UK
(*Adrian.finch@st-and.ac.uk)

Luminescence contains information about the structural state of metals and defects at ultradilute concentrations. Furthermore, minerals have geological timescales over which to perfect states of defect order, making them ideal materials in which to study luminescence. In principle, light emission is a powerful tool for determining defect structure, but interpreting such data is challenging since we have an incomplete understanding of luminescence in many minerals, and how features such as coordination state and symmetry are encoded within it. Here we present data on two spectroscopic methods in quartz and feldspar. We have measured the light emitted during implantation by ions, known as ion beam luminescence (IBL) or ionoluminescence (IL). We model closely the implantation using Monte-Carlo simulations and, by changing acceleration potential, current and nature of the ions (i.e. H^+, He^+, N^+), we change implantation depth (i.e. bulk vs. surface responses) and the relative proportions of ionisation, vacancy and phonon formation. Comparing ions (H^+) and molecules (H_2^+) contrasts luminescence from excitation of ground states with excitation of excited states, i.e. double excitation. We also monitor the change in luminescence as a function of implantation dose. This allows us to determine whether the changes are consistent with the proposed nature of the luminescence centres. Since most natural minerals have significant radiation damage, we also gain insights into how luminescence of real minerals differs from synthetic mineral analogues.

The development of synchrotrons allows advances in x-ray excited optical luminescence (XEOL, also known as radioluminescence, RL). X-irradiation results in ionisation but not atomic displacements, in contrast to IBL. By comparing IBL and XEOL we deconvolute responses that derive from vacancy formation and atomic recoils. By varying x-ray energy over the absorption edges of particular elements (e.g. Fe), we combine XEOL with x-ray absorption spectroscopy (XAS), used widely to determine local coordination in solids. Initial optically determined (OD-)XAS experiments studies of Fe in feldspar show little variation in light intensity as a function of x-ray energy across the Fe edge. We infer that the long (ms) lifetime of that decay effectively divorces light emission from the XAS and we hypothesise that OD-XAS will be most effective on very fast (e.g. ns) lifetime decays. Experiments to develop time-resolved OD-XAS are underway. Since the spot in XEOL is only a few microns across, there are a whole family of hyperspectral imaging methods which can access structural state within crystals. We briefly review such methods in determining structural state variations in individual crystals.

Advantages of combined cathodoluminescence and Nomarski DIC microscopy in the Earth sciences

Götze, J.
Inst. of Mineralogy, TU Bergakademie Freiberg, Germany
(goetze@mineral.tu-freiberg.de)

Microscopic methods play an important role in modern investigations of minerals and materials. Besides conventional light and electron microscopy, cathodoluminescence (CL) microscopy has developed into a powerful analytical method in the geosciences and materials sciences [1]. The principle of CL is based on the detection of an electron-excited luminescence signal, which is generated by electron transitions at certain point defects within the solid. Accordingly, CL is an excellent method to characterize defects in materials, to distinguish different phases and to reveal information about the chemical composition down to the trace-element level (Fig. 1).

Nomarski interference contrast imaging was developed by G. Nomarski [2] and has routinely been applied especially in reflected light microscopy in metallurgy and materials sciences. Applications in geosciences are rare [3-7]. Nomarski DIC microscopy can visualize different phases and/or surface reliefs in the scale of several nm. The treatment with natural and artificial etching agents can significantly enhance this effect [6]. The method is based on the principle of beam splitting by a double-crystal prism split, resulting in the superposition of laterally shifted wave fronts. Using this effect, micro-textural features can be revealed, which are not discernable using conventional polarizing microscopy (Fig. 1).

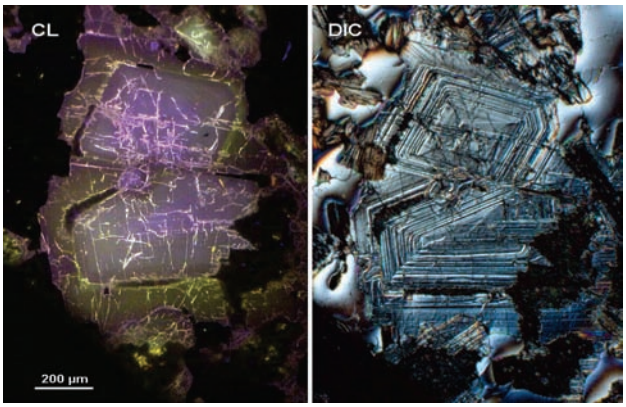

Fig. 1: Altered plagioclase from a granite imaged with CL microscopy (left) and Nomarski DIC (right); CL reveals chemical heterogeneity and cracks, whereas DIC clearly shows oscillatory zoning.

The present study discusses the potential of an integrated application of CL and Nomarski DIC microscopy for the investigation of minerals and rocks in the Earth sciences. By combining these two microscopic techniques, chemical, crystallographic and textural information can be obtained from the same sample area in a polished thin section.

[1] Götze, J. (2000) *Cathodoluminescence microscopy and spectroscopy in applied mineralogy*. Freiberger Forschungsheft C485. [2] Nomarski, G. & Weill, A.R. (1954) *Soc. Francaise Minér. Cristall. Bull.*, **77**, 840-868. [3] Anderson, A.T. (1983) *Am. Mineral.*, **68**, 125-129. [4] Pearce, T.H. et al. (1987) *Am. Mineral.*, **72**, 1131-1143. [5] Pearce, T.H. & Kolisnik, A.M. (1990) *Earth Sci. Rev.*, **29**, 9-26. [6] Wegner, M.W. & Christie, J.M. (1985) *Phys. Chem. Mineral.*, **12**, 90-92. [7] Clark, A.H. & Blyth, D.M. (1993) *Econ. Geol.*, **88**, 1904-1910.

Self-affine pattern of crystal growth from heterogeneous magmas – 3D depiction of LA-ICP-MS data

Słaby, E.[1*], Śmigielski, M.[2] & Domonik, A.[3]
[1]Inst. of Geological Sciences, Polish Academy of Sciences, Research Centre in Warsaw, Poland ([*]e.slaby@twarda.pan.pl)
[2]Inst. of Geology, University of Warsaw, Poland
[3]Inst. of Hydrogeology and Ingineering Geology, University of Warsaw, Poland

Growth textures and the trace element composition of alkali feldspars from the Karkonosze pluton, an igneous body of mixed magma origin have been investigated. Each crystal was analyzed (Ba, Rb, Sr) along several transects, in constant step, from margin to margin. 3D depiction combined with fractal statistics allow us to gain an insight into the mechanism of crystal growth in a system showing non-linear dynamics.

The LA ICP MS spots are located along a traverse (X axis). Each laser ablation pulse (60-120μm in diameter) gives data collected from a 5 μm thick layer of feldspar. About 70-100 impulses were used within one spot; the number of laser impulses and the depth reflects the duration of each LA ICP MS analysis (Y axes). Natural neighbor interpolation [1] was applied to the data. The 3D depiction of the data as a contour map and surface model of element distribution involved the use of Surfer 8.0 (Golden Software), classical izoline maps and 3D models merged with shaded-relief images [2]. Depiction of the three-dimensional models was preceded by a spline smooth procedure without any recalculation of the model. To further improve the resolution of the data depiction and to best display the spatial distribution of an element concentration, the vertical scale on the plots was arbitrarily chosen and usually magnified 2-5 times.

A self-similarity parameter, the Hurst exponent, was used to show the long-range dependence of element behaviour during the growth process. The expected values of H lie between 0 and 1. For H = 0.5, element behaviour shows a random walk and the process produces uncorrelated white noise. For values either higher or lower than 0.5, the system shows non-linear dynamics. H < 0.5 represents anti-persistent (more chaotic) behaviour, whereas H > 0.5 corresponds to increasing persistence (less chaotic).

The magmatic system responsible for the formation of the investigated feldspars shows different, non-linear dynamics. The crystals grew from mixed magmas characterized by different degree of homogenization. Feldspars grown in more chaotic, active regions of mingled magmas are strongly zoned. The Hurst exponent ranges from H=0.06 to H=0.47 reflecting intensive chemical mixing and underlying strong non-linear dynamics of the system. The 3D depiction shows particularly complicated pattern of compositionally heterogeneous domains within each zone, being products of intensive, chaotic magma steering. Feldspars grown from mixed and homogenized magmas are almost homogeneous. Relatively small variation in trace element contents can be still recognized due to 3D depiction. Despite homogenization, the fractal statistics reveal that trace elements were incorporated chaotically into the growing crystals. The anti-persistent, chaotic behaviour of elements during growth of these feldspars is preserved. It appears that 3D depiction combined with fractal statistics is an ideal tool for the identification of the growth mechanism and any subsequent changes occuring due to chaotic processes in on open system.

[1] Sibson, R. (1981) in Barnett V. (ed.) *Interpreting Multivariate Data*. John Wiley and Sons, New York. [2] Yoeli, P. (1965) *Surv. Mapp.*, **25**, 573-579.

From EDS microanalysis towards nanoanalysis: hyperspectral imaging for mineralogical applications using silicon drift detectors (SDD) and EBSD analysis

Salge, T.[*] & Goran, D.
Bruker Nano GmbH, Berlin, Germany
([*]Tobias.Salge@bruker-nano.de)

Within the last decade, SDD systems have become state of the art technology in the field of energy-dispersive spectroscopy (EDS). The main characteristic of the SDDs is their extremely high pulse load capacity of up to 750,000 counts per second at good or reasonable energy resolution (<123 eV Mn-Kα, <46 eV C-Kα at 100,000 counts per seconds). These properties in conjunction with electron backscatter diffraction (EBSD) technique, modern data processing and automated stage control opens a range of innovative analysis options, not only high speed mapping but also hyperspectral imaging techniques.

This paper presents mineralogical applications with the QUANTAX system with EDS SDD and EBSD detector using the options described above: (1) Fast detection and discrimination of minerals within impact-induced accretionary lapilli [1]. (2) Drill core analysis of a Chicxulub impact ejecta sequence from the K/Pg boundary at ODP leg 207 [2] using fast, high resolution element maps. (3) Detection of monazite in granite by the *Maximum Pixel Spectrum* function [3]. (4) Distribution of elements with overlapping peaks by deconvolution at the example of rare earth elements (REE) in zoned monazite. (5) Spectroscopic phase analysis of a sulfate-carbonate-dominated impact matrix at borehole UNAM-7 from the Chicxulub impact crater [1]. (6) Automated baddeleyite particle search within lunar meteorite Dhofar 287 [4] by feature analysis. (7) EBSD studies with examples of iron meteorites and impact-induced, recrystallized carbonate melts [1].

In addition, continuing technological advances require the elemental analysis of increasingly smaller structures in many fields, including mineralogy and nanotechnology in general. It will be demonstrated that using low accelerating voltages, the element distribution of nanometer-sized structures in bulk samples can be displayed in a short time due to optimized signal processing and solid angle. Peaks composed of contributions from several overlapping elements (e.g. Co-L, Ni-L and Fe-L or N-K and Ti-L) can be deconvolved using an improved atomic database with 250 additional L, M and N lines below 4 keV.

Acknowledgements: We thank P. Claeys, P. Schulte, A. Deutsch, ODP, L. Hecht, A. Kearsley, J. Urrutria-Fucugauchi, V.A. Fernandes and O. Tunckan for providing samples.

[1] Salge, T. (2007) *PhD thesis*. Humboldt-Universitaet, Berlin. [2] Schulte, P. et al. (2010) *Science*, **327**, 1214-1218. [3] Bright D.S. & Newbury D.E. (2004) *J. Microsc.*, **216**, 186-193. [4] Fernandes, V.A. et al. (2008) *Geochim. Cosmochim. Ac.*, **72**, A264.

Quantitative estimation of radiation-induced effect on cathodoluminescence of plagioclase

Kayama, M.[1*], Nishido, H.[1], Toyoda, S.[2], Komuro, K.[3] & Ninagawa, K.[2]
[1]Research Institute of Natural Sciences, Okayama University of Science, Okayama, Japan ([*]kayama@rins.ous.ac.jp)
[2]Dept. of Applied Physics, Okayama University of Science, Okayama, Japan
[3]Earth Evolution Sciences, University of Tsukuba, Japan

Cathodoluminescence (CL) halo in quartz caused by alpha-radiation has been investigated for the application to geodosimetry. The halo in feldspar minerals, however, has not been studied from the perspective of CL spectroscopy. In this study, albite, andesine and anorthite implanted by He^+ ion have been characterized by CL spectral analysis to clarify the emission mechanism for the applications to geodosimetry and geochronology.

Single crystals of albite (Or_2Ab_{98}) from Minas Gerais, Brazil, andesine ($Or_2Ab_{51}An_{47}$) from Bekily, Madagascar and anorthite ($Or_0Ab_5An_{95}$) from Yoichi, Hokkaido, Japan were selected for CL measurements. He^+ ion implantation (dose density: $1.23 \times 10^{-4} \sim 7.38 \times 10^{-4}$ C/cm^2) on the samples was performed using a 3M-tandem ion accelerator at 4 MeV corresponding to the energy of alpha-particles from ^{238}U.

CL imaging of the albite shows CL halo on the surface of He^+ ion implanted sample. Approximately 15 μm width of CL halo in the section is consistent with theoretical range of alpha-particles from disintegration of ^{238}U in albite. CL line analysis along the halo section of the albite reveals that an increase in the CL intensity along depth direction substantially corresponds to the Bragg's curve, suggesting an energy loss process of specific ionization along the track of a changed particle. CL intensities of the andesine and anorthite, however, gradually decrease from the implantation surface to approximately 15 micron meters in depth, over which they jump up to the bulk emission level of non-implanted areas.

The spectra of CL halos in albite, andesine and anorthite consist of emission bands at around 400, 580 and 730 nm. Furthermore, a CL emission at around 660 nm is detected in only albite. These emission spectra in energy units can be deconvoluted by Gaussian curves, resulting in four components centred at 3.05, 2.10, 1.86 and 1.56 eV. An integral intensity of the component at 1.86 eV (666 nm) positively correlates with radiation dose of He^+ implantation in the halo area of individual albite. It suggests that the CL emission corresponding to the component at 1.86 eV might be assigned to a radiation-induced defect centre formed by He^+ ion implantation. Therefore, the CL halo of albite caused by alpha-particle radiation can be used to quantitatively estimate the radiation dose of alpha-particles induced on feldspar minerals as an indicator applied for a geodosimeter.

Micro-computed tomography applied to mineralogical samples: towards quantification

Abel, R., Armstrong, R., Hezel, D.C., Elangovan, P. & Williams, C.T.[*]
Dept. of Mineralogy, Natural History Museum, London, UK
([*]t.williams@nhm.ac.uk)

The aim is to present some recent developments in mineralogy using a high-resolution (ca. 5–125 μm) micro-Computed Tomography system (micro-CT Scanner) at the Natural History Museum, London.

The principles of this non-destructive technique will be outlined, and brief (30-second) video clips will illustrate the potential for 3-dimensional representations of mineral specimens, drill core and rock slices. Samples shown will include the 3-D distribution of silicates and metal in meteorite samples; silicates, oxides and sulphides from an ultrabasic sample (rock slice from Rum, Scotland); gold in smectite (drill core from Patagonia), and gold in calcite (Fig. 1, hand specimen from Hope's Nose, UK).

Quantification of 3-D images from multi-phase and variable density materials (i.e. rock and mineral samples) poses significant challenges. We will outline how we are addressing these challenges, and in addition present work in progress on refining the scanning and threshold parameters for different matrices; investigate possible mineralogical applications; establish limitations of the technique and suggest future directions for instrument and software development.

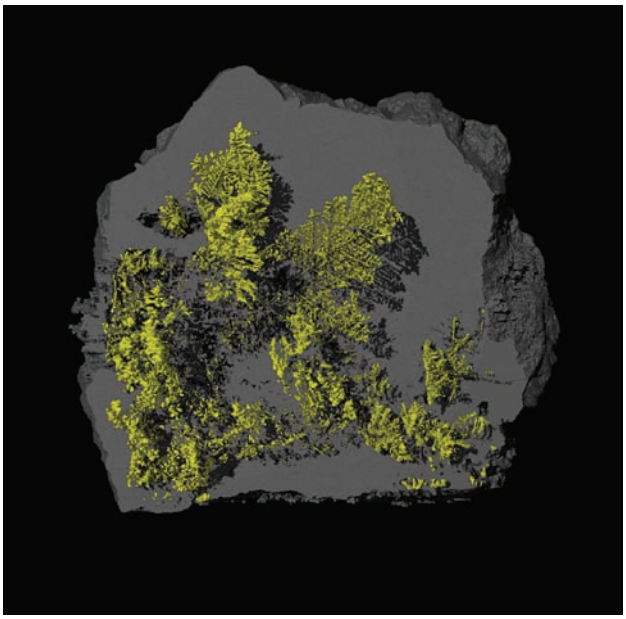

Fig. 1: Perspective rendered cut-away of Au-bearing calcite from Hope's Nose, UK) to reveal frond-like crystals of gold (false-coloured yellow) sitting in calcite matrix (false-coloured grey). Field-of-view approximately 8 cm.

Imaging diamond: using birefringence & infrared to map strain and impurities

Howell, D.[1,2*], Griffin, W.L.[1], O'Reilly, S.Y.[1], O'Neill, C.[1], Wood, I.[2], Dobson, D.[2] & Jones, A.P.[2]
[1]GEMOC, ARC National Key Centre, Macquarie University, Sydney, Australia ([*]dhowell@science.mq.edu.au)
[2]Earth & Planetary Sciences Department, University College London, UK

Birefringence is an anomalous optical property that has commonly been observed in diamond, but until recently has rarely been quantified. With the development of the MetriPol system [1] an automated microscope technique is now available that allows rapid quantitative birefringence analysis of diamond. This technique has some advantages over 2D Raman mapping of diamond's pressure sensitive 1332 cm^{-1} band [2] (Fig. 1). This method of imaging diamond can be used to investigate all of the documented causes of stress and strain within diamond [3].

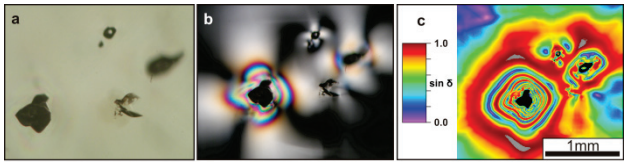

Fig. 1: Series of images of four coesite inclusions in a diamond from Finsch mine (South Africa): (a) plane-polarised transmitted light; (b) cross-polarised light; (c) MetriPol $|\sin(\delta)|$ false colour image.

Since the original classification of diamonds based on their absorption in the one-phonon region of the mid-infrared (IR) range was first introduced, IR analysis has become the principle tool for classifying diamonds based upon the concentration and aggregation state of nitrogen.

Recent technological developments in the field of spectroscopy allow detailed μ-FTIR analysis to be automated and performed rapidly. The Nicolet iN10 microscope allows spectra to be collected with greater efficiency than is possible with conventional μ-FTIR spectrometer-microscope systems. Combining this with a computer controlled *x-y* stage allows the automated measuring of several thousand spectra in only a few hours. IR maps of diamond plates can now be recorded with minimal effort, but this has created the need for an automated technique to process the large datasets of IR spectra and to obtain quantitative data from them. A new computational method achieving this has been accomplished which generates false colour images that can define nitrogen concentrations, aggregation states, as well as hydrogen and platelet defects.

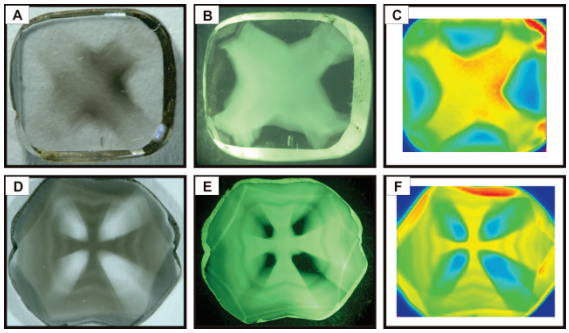

Fig. 2: Images of two diamond crystals showing 'maltese-cross' style growth zonations. Images A and D are under plane-polarised light, B and E are taken under UV, and C and E are false-colour images of the relative intensity of the 3107cm^{-1} (hydrogen) peak taken from IR maps.

[1] Glazer, A.M. et al. (1996) *Proc. R. Soc. London*, **452**, 2751-2765. [2] Howell, D. et al. (2010) *Contrib. Mineral. Petrol.* (in press). [3] Lang, A.R. (1967) *Nature*, **213**, 248-251.

Revealing cryptic alkali feldspar microtextures by SEM charge contrast imaging

Flude, S.[1*], Lee, M.R.[2], Sherlock, S.C.[1] & Kelley, S.P.[1]
[1]Dept. of Earth and Environmental Sciences, Centre for Earth, Planetary, Space & Astronomical Research (CEPSAR), Open University, Milton Keynes, UK ([*]s.flude@open.ac.uk)
[2]Dept. of Geographical & Earth Sciences, University of Glasgow, UK

Understanding the coherency, interconnectivity and microporosity of alkali feldspar microtextures is crucial if their host grains are to be used for Ar/Ar thermochronology, owing to potential of these microtextures to act as fast-diffusion pathways for ^{40}Ar. In this first application of Charge Contrast Imaging (CCI) to alkali feldspars we show that the technique can reveal microtextures that are difficult to image by any other technique but have very important implications for Ar isotope work and determination of geological histories.

CCI work was undertaken on polished but uncoated thin sections using a FEI Quanta 200F SEM operated at ~60 Pa and with water vapour in the chamber. Contrast in CCI comes from differences over grain surfaces in the intensity of secondary electron emission, which relates to the populations of charge traps immediately beneath the surface. CCI enables high contrast and high resolution imaging of crypto- and micro-perthites, but crucially also highlights micrometre-sized patches and veins of deuterically formed 'irregular' microcline within orthoclase. These fine-scale perthites and near-isochemical intergrowths cannot be resolved by Z contrast SEM, but TEM imaging of foils cut from them using the focused ion beam (FIB) technique shows that they are real and not charging artefacts. We speculate that the magnitude and distribution of elastic strain energy within albite exsolution lamellae, and the strained interiors of irregular microcline subgrains, plays a major role in charge trapping and so CCI in feldspars.

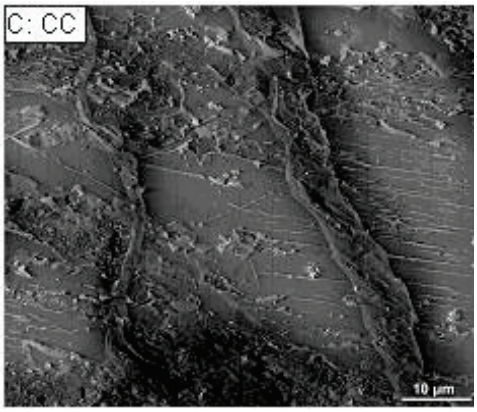

Fig. 1: CCI of alkali feldspar showing veins of irregular microcline.

Using CCI we have examined alkali feldspars from the Dartmoor Granite (UK) and results have provided new insights into its geological evolution. For example, CCI shows that veins of Or-rich feldspar ('irregular microcline') cross-cut orthoclase and are far more abundant than indicated by Z contrast SEM. Importantly this microcline divides volumes of pristine feldspar into tens of micrometre-sized subgrains, which may have a major impact on Ar diffusion rates. As it enhances considerably our ability to characterise and measure microtextures that must be taken into account in Ar isotope work, CCI is thus is of great importance in understanding and refining Ar/Ar thermochronology.

Distribution of bubbles in moldavites

Franz, A., Rantzsch, U.[*] & Kloess, G.
Inst. of Mineralogy, Crystallography and Materials Science, Leipzig University, Leipzig, Germany
([*]rantzsch@uni-leipzig.de**)**

Moldavites occur in several shapes corresponding to their strewn- and sub-strewn fields. Suess [1] published the first extensive work about moldavites. A detailed petrographical and geochemical investigation on Lusatian moldavites was carried out by Lange [2].

Bubbles occur in all tektites. Their origin within moldavites has been studied extensively in previous investigations [3,4]. A correlation of bubble- size, -shape and -alignment has not been done yet.

In the present study 3D µ-CT measurements on moldavites were conducted to gain further information about the bubble shape and their distribution within the samples. The most important advantage of 3D µ-CT measurements is the non destructive process and the higher statistic compared to other methods. Additionally the measurements yield 3D information of the samples and their inclusions.

For interpretation of the data sets the graphic program VGStudio Max 2.0 (Volume Graphics) was used. The 3D µ-CT measurements display significant differences of bubble distribution and elongation within each moldavite (Fig. 1). Different sizes (pore volume) and shapes with spherical or elongated alignment could be determined.

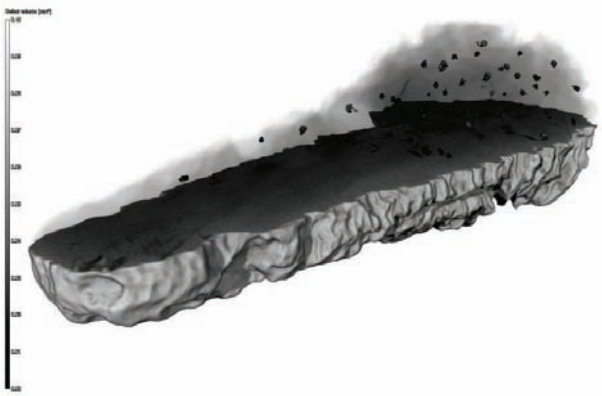

Fig. 1: 3D µ-CT measurement of a moldavite from southern Bohemia with bubble distribution.

Within this study a new method of estimating the pore volume, their shape and distribution will be presented. Especially their alignments indicate findings about the direction of flow of the tektite melts. The non-sphericity is increasing with bubble size. The obtained data will reveal further information about moldavite origin of their aerodynamic morphology.

[1] Suess, F.E. (1900) in: K. u. K. geol. Reichsanstalt Wien, Jahrbuch, **50(2)**, 192-382. [2] Lange, J.-M. (1995) *Lausitzer Moldavite und ihre Fundschichten*. Dissertation, Martin-Luther-Universität Halle-Wittenberg. [3] Barnes, V.E. (1969) *Geochim. Cosmochim. Ac.*, **33**, 1121-1134. [4] Konta, J. & Mráz, L. (1969) *Geochim. Cosmochim. Ac.*, **33**, 1103-1111.

Phase decomposition upon alteration of radiation-damaged monazite–(Ce) from Moss, Østfold, Norway

Nasdala, L.[1*], Ruschel, K.[1], Rhede, D.[2], Wirth, R.[2], Kennedy, A.K.[3], Kinny, P.D.[4], Finger, F.[5] & Groschopf, N.[6]
[1]Inst. für Mineralogie und Kristallographie, Universität Wien, Vienna, Austria ([*]lutz.nasdala@univie.ac.at)
[2]Helmholtz-Zentrum Potsdam, Deutsches GeoForschungsZentrum, Potsdam, Germany
[3]Dept. of Applied Physics, Curtin University of Technology, Perth, Australia
[4]Dept. of Applied Geology, Curtin University of Technology, Perth, Australia
[5]Fachbereich Materialforschung und Physik, Universität Salzburg, Austria
[6]Inst. für Geowissenschaften, Universität Mainz, Germany

Over a century ago there was discussion of whether Th may be present in monazite as a separate Th silicate phase, rather than substituting for Ce^{3+} in the monazite lattice [1]. Our study, addressing chemical alteration textures in large pegmatitic monazite–(Ce) crystals from the Dillingøya island, Moss area, Norway, seems to support, at least partly, the above hypothesis.

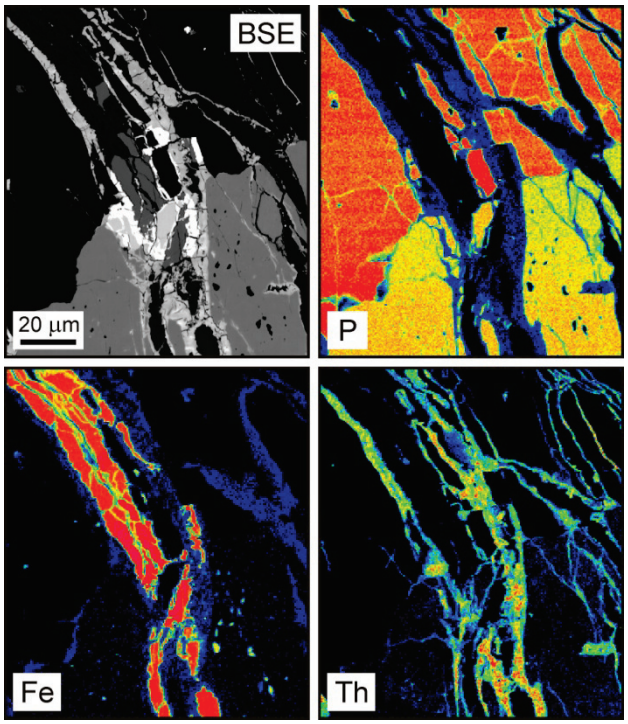

Fig. 1: BSE image and three colour-coded EPMA element distribution maps showing a multitude of Fe sulphide and Th silicate veins pervading apatite (upper left) and monazite–(Ce) (lower right).

The bulk monazite–(Ce), which contains ca. 8 wt% ThO_2, is intergrown with Ca apatite. These two phosphate phases are pervaded by several generations of veins of sulphide phases and thorium silicate (> 50 wt% ThO_2). Both well-crystallised thorite and amorphous $ThSiO_4$ were found in the TEM.

No chemical alteration haloes were observed within the bulk phosphates, emanating from the veins. This suggests that the phosphates cannot represent unaltered remnants of the primary monazite. Rather, the chemical alteration has resulted in virtually complete phase decomposition of the primary crystals, with potentially uncontrolled elemental changes.

[1] Kress, O. & Metzger, F.J. (1909) *J. Am. Chem. Soc.*, **31**, 640-652.

LRGB colour imaging of panchromatic SEM-CL images

Shimobayashi, N.[1*], Takaya, M.[1], Nomoto, T.[1] & Notoya, S.[2]
[1]Dept. of Geology & Mineralogy, Graduate School of Science, Kyoto University, Kyoto, Japan ([*]shimo@kueps.kyoto-u.ac.jp)
[2]Electron Optics Division, JEOL Ltd., Akishima Tokyo, Japan

The SEM-CL system, composed of a detector for cathodoluminescence (CL) attached to a SEM or EPMA, is capable of producing high-resolution digital CL images of luminescent materials. In most conventional SEM-CL, a photomultiplier tube (PMT) is used as a detector for a weak CL signal and then only monochromatic CL images can be obtained directly. In contrast, the colour CL images contain much more valuable information than the monochromatic images. We attempt a colour imaging of the monochromatic SEM-CL images by adopting an LRGB composite technique instead of a traditional RGB method.

The SEM-CL system used is based on an EPMA (JEOL: JXA-8105) and the emitted CL is detected by PMT (Hamamatsu Photonics: R955) through a special light guide. Introduction of a photon-counting method enables us to obtain the high sensitive CL images. Either RGB or LRBG technique requires three monochromatic images, each of which should be obtained by the separate R-G-B component colours. The separate R-G-B images can be obtained by placing bandpass red (R), green (G) and blue (B) filters (Astronomik: LRBG Type-2c) in front of the PMT. Then, these separate R-G-B images are recombined digitally using the conventional photo-retouch software (*e.g.*, Photoshop) to produce a full colour image. The traditional RGB technique, however, has an inconvenience that it takes very long exposure times to acquire the three R-G-B separate images in a high-resolution mode. It takes over three times as long as capturing a monochromatic CL image in the same resolution. The long exposure time is a serious problem for the specimen that is easily irradiation damaged and/or the specimen whose CL emission is short-lived.

In contrast, LRGB combination technique (the "L" referring to "luminance" or "lightness") allows us to shorten the total exposure time. This compositing technique has been developed independently by two amateur astrophotographers, R. Dalby (U.K.) and K. Okano (Japan; plasma physicist). The LRGB technique involves capturing separate R-G-B images to compose the colour as well as the RGB technique, and also a high-quality monochrome image [L image] to act as the luminance (brightness) of the final image. The quality of the final composite image strongly depends on the luminance image. The lower resolution in the colour images does not degrade the final composite. If only the luminance image should be photographed in a fully high resolution mode, the resolution of the three R-G-B colour images produces little effect on a quality of the final composite colour image. The quicker acquisition of the separate R-G-B colour images in a lower resolution makes possible to shorten the total exposure time (Table 1), during which the specimen is exposed by the electron irradiation. Therefore, the introduction of the LRGB technique to the SEM-CL system is useful particularly to the short-lived CL emission or the specimen which is easily subjected to irradiation damage.

Table 1: Comparison of the total exposure times between two composite techniques (*example*)

	(1) RGB	(2) LRGB
L	---	7 min.
R,G,B	12 min. each	2 min. each
Total	36 min.	13 min.

(1) [R,G,B]: 512 x 512 pixels, dwell time: 2 msec/pixel,
(2) [R,G,B]: 128 x 128 pixels, dwell time: 2 msec/pixel,
[L]: 512 x 512 pixels, dwell time: 1 msec/pixel.

Infra-red mapping of defects in diamonds using a focal plane array (FPA) detector

Shiryaev, A.A.[1*], Johner, N.[2] & Zedgenizov, D.A.[3]
[1]Institute of Crystallography, Moscow, Russia
([*]a_shiryaev@mail.ru)
[2]Bruker Optics, Ettlingen, Germany
[3]Institute of Geology and Mineralogy, Novosibirsk, Russia

Nitrogen is the main elemental impurity in diamond. It substitutes carbon in the lattice and forms different defect centres, which determine spectroscopic and some physical properties of diamond crystals. For geosciences nitrogen is an important tracer of growth conditions and of post-growth annealing regime. Infra-red (IR) absorption spectroscopy provides quantitative information about N content of the diamond in almost all cases, since its majority is present as IR-active defects. Hydrogen is another important impurity and its total concentration may be comparable to that of N, but only a fraction of H is IR-active. The models of H-defects are not yet firmly established even for the very common defect manifested as a sharp absorption peak at 3107 cm^{-1}.

Diamonds are notoriously heterogeneous making IR microscopy indispensable in many cases for reliable conclusions. We have studied the N and H spatial distribution in plates cut from natural diamonds from different localities. A FTIR imaging microscope (HYPERION 3000) including modern Focal Plane Array (FPA) detector technology was employed for this study. The used FPA consists of an array of 64×64 elements, allowing simultaneous acquisition of 4096 IR spectra. Using the 15x objective the field of view is 170x170 µm with a pixel resolution of 2.7 µm. To achieve a reasonable signal/noise ratio at very short acquisition times, 4×4 pixel binning was applied. Spectral resolution was 4 cm^{-1}. The OPUS 6.5 software was used for data acquisition and evaluation.

Figure 1 shows the distribution of the A-defect (N pairs), and of the H-related defect (3107 cm^{-1}) in an area of 340x510 μm^2 of a natural diamond from Brazil. For this sample the concentration of the A-defect is a close proxy of the total N content. Positive correlation between these two defects is obvious. Similar trends are observed also for other diamonds with variable concentration and speciation of N-defects.

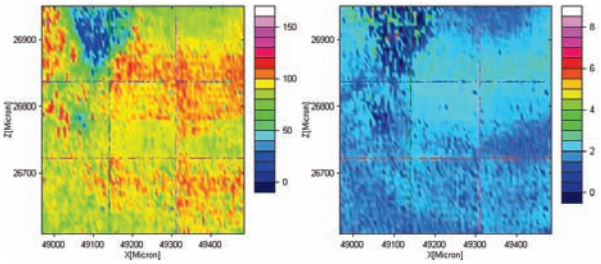

Fig. 1: Spatial distribution of nitrogen (left panel) and of IR-active hydrogen in a natural diamond.

Earlier, the N-H correlation was observed on the basis of IR spectra of individual diamonds. In this work we show that such correlation holds also for individual diamonds and statistics (number of spectra) is substantial. The most likely explanation of the observed behaviour is that nitrogen diffusion during thermal annealing forces redistribution of hydrogen, converting a fraction of it into the IR-active form. Mapping of the spatial distribution of other N-related defects will be also presented.

Acknowledgements: The AAS analysis was partly supported by the Humboldt foundation, via RFBR (09-05-00985) to D.A.Z.

Characterization of wet clays in TEM

Chiou, W.-A.[1*], Ishikawa, A.[2] & Fukushima, K.[3]
[1]NISP Lab, NanoCenter, University of Maryland, College Park, USA ([*]wachiou@umd.edu)
[2]Dept. of Physics, Nihon University, Tokyo, Japan
[3]JEOL Ltd., 3-Chome, Akishima, Tokyo, Japan

Characterization of particle size and shape, including surface morphology, is an important step in clay research. Despite previously reported techniques, the precise measurement of clay particle size remains difficult due to the minuscule size and diversity of shapes, surface activities, and sample preparation methods. The key to successful size analysis lies within the ability to keep the particles well dispersed in their natural (wet or specific liquid) environment. This paper presents novel methods and technologies of studying clay minerals in a fully wet (water) environment using different transmission electron microscopy (TEM) techniques.

Special techniques have been developed to overcome the difficulty of clay specimen preparation in their natural state. The wet environmental-cell TEM (WETEM) technique provides a special wet environment chamber at atmospheric pressure in TEM that allows for examination of individual clay particles at high resolution. The cryo-method involved creates a thin vitrified film of suspensions using a specially designed cryo-plunge device. Two spray methods, EFFA spray system and special atomizer, are also applied to disperse clay particles on carbon coated copper grids for TEM observation. Finally, clay nanocomposite samples are dispersed and embedded in epoxy, and ultra-thin sectioned for TEM study.

Large agglomerates with scattered overlapped clay particles are the typical TEM image obtained from conventional specimen preparation techniques. However, with the fore-mentioned techniques, clay particles can be fully or partially dispersed. The wet environmental-cell TEM technique allows *in-situ* observation of individual particles in wet environment, and thus the size and shape of individual clay particles can be analyzed in high resolution. Clay particles of different shapes (e.g., spherical-like, platy, elongated rod-like, needle, triangular, and polygon) of nano-size are observed in WETEM. The fast quench of clay suspensions in Cryo-TEM is capable of preserving different clay orientation before settling occurs. The spray technique using the atomizer offers relatively good dispersion of clay particles whereas the conventional spray system often produces small aggregates.

Experiments utilizing these techniques demonstrate that the fundamental (the thinnest) individual smectitic clay particles appeared to have a very similar measurement of 5 to 10 nm in thickness, with the majority around 5 nm. This thickness is unique and may be universal. Excellent high resolution characterization of clay particles has also recently been achieved by other techniques such as TEM tomography.

Physical interpretation of Scherrer crystallite size for parallel-layered crystallite aggregate

Wang Chunyun[*] & Xie Xiande
Guangzhou Institute of Geochemistry, Chinese Academy of Sciences, Guangzhou, P. R. China ([*]chunyun@gig.ac.cn)

Scherrer equation was first developed in describing the contribution of the small crystallite size in metallurgy to the peak broadening of X-ray diffraction pattern in the form of full width at half maximum (FWHM) [1], and was hence extensively utilized by chemical physicists, material scientists, applied crystallographers and clay mineralogists to determine the thicknesses of coherently scattering domains (CSD) perpendicular to the diffracting planes for parallel-layer groups of carbon black [1], illite, chlorite [2-6] and other crystallites from the obviously broadened (00l) peak profiles. The Scherrer crystallite size thus derived is called “effective length” [7], “apparent crystallite size” [1,7], “effective crystallite size”[3-4], or “realistic mean thickness” [8], etc., and is simply interpreted as CSD mode of thickness distribution [3,5,6], or as mean weighted by number [4,9-11], by area [12,13] or by volume [14,15], when it is compared with TEM-measured crystallite sizes. Here we show by using interference function for one-dimensional X-ray diffraction [9-11,16] that Scherrer crystallite size as frequently used for parallel-layered crystallite aggregate, in particular clay minerals, is actually the mean thickness weighted by number, rather than by area or by volume, and the Scherrer constant is variable, rather than fixed, with the number of layers in each crystallite.

As the interference function depends on the thickness and the thickness distribution of CSDs, an idealized one-dimensional diffraction pattern from perfectly oriented illite or chlorite clay sample was studied and we found by modeling that Scherrer crystallite size is the average thickness weighted by number perpendicular to the diffraction direction c.

[1] Klug, H.P. & Alexander, L.E. (1974) *X-ray diffraction procedure for polycrystalline and amorphous materials.* John Wiley & Sons, New York. [2] Kubler, B. (1964) *Rev. Inst. Fr. Petrol.*, **19**, 1093-1112. [3] Merriman, R.J., Roberts, B. & Peacor, D.R. (1960) *Contrib. Miner. Petrol.*, **106**, 27-40. [4] Merriman, R.J., et al. (1995) *J. Metamorphic Geol.* **13**, 559-576. [5] Nieto, F. & Sanchez-Navas, A. (1994) *Eur. J. Mineral.*, **6**, 611-621. [6] Dalla Torre, M. et al. (1996) *Contrib. Mineral. Petrol.*, **123**, 390-405. [7] Langford, J.I. & Wilson, A.J.C. (1978) *J. Appl. Cryst.* **11**, 102-113. [8] Eberl, D.D. & Blum, A. (1993) in Reynolds, R.C., Jr. & Walker, J.R. (eds.) *CMS Workshop Lectures, Computer Applications to X-ray Powder Diffraction Analyses of Clay Minerals*, **5**, 124-153. [9] Moore, D.M. & Reynolds, R.C., Jr. (1989) *X-ray diffraction and the identification and analysis of clay minerals.* Oxford University Press, Oxford. [10] Walker, J.R. (1993) in Reynolds, R.C., Jr. & Walker, J.R. (eds.) *CMS Workshop Lectures, Computer Applications to X-ray Powder Diffraction Analyses of Clay Minerals*, **5**, 2-17. [11] Drits, V., Srodon, J. & Eberl, D.D. (1997) *Clay. Clay Miner.*, **45**, 461-475. [12] Warr, L.N. & Nieto, F. (1998) *Can. Mineral.*, **36**, 1453-1474. [13] Li, G. et al. (1998) *Can. Mineral.*, **36**, 1435-1451. [14] Brindley, G.W. (1980) in Brindley, G.W. & Brown, G. (eds.) *Crystal Structures of Clay Minerals and Their X-ray Identification*, 125-195. [15] Jiang, W.-T. et al. (1997) *J. Metamorphic Geol.*, **15**, 267-281. [16] Reynolds, R.C. Jr. (1993) in Reynolds, R.C., Jr. & Walker, J.R. (eds.) *CMS Workshop Lectures, Computer Applications to X-ray Powder Diffraction Analyses of Clay Minerals*, **5**, 44-78.

A new approach to the extraction of illite crystal thickness distribution from XRD data

Szczerba, M.* & Środoń, J.
Institute of Geological Sciences, Polish Academy of Sciences, Kraków, Poland (*ndszczer@cyf-kr.edu.pl)

The classic approach to the calculation of the illite crystal thickness distribution from X-ray diffraction patterns is based on the Bertaut-Warren-Averbach analysis. Before registering the XRD patterns illite and illite-smectite samples are treated with polymer polyvinylpyrrolidone (PVP) in order to split mixed-layer crystals into free fundamental particles. The presence of PVP on the particle surfaces influences XRD patterns. This problem was approximatelly solved by [1].

The alternative approach is based on modeling the structure of PVP on smectite surface and on assumption that the structure of PVP is similar on smectites and on illites [2]. The X-ray diffraction pattern of illite is calculated as a weighted sum of diffraction patterns of illite fundamental particles of particular thicknesses with PVP on their surfaces.

For the purpose of this study a computer program, which employs Genetic Algorithms as the minimization paradigm, was written and tested. It was found that this approach works best if the mean thickness of illite fundamental particles is relatively small.

[1] Eberl, D.D. et al. (1998) *Clays Clay Miner.*, **46**, 89-97. [2] Szczerba, M. et al. (2010) *Appl. Clay Sci.*, **47**, 235-241.

Thermal analysis of synthetic hydrotalcite and bauxite refinery hydrotalcites

Palmer, S.J. & Frost, R.L.*
Chemistry Discipline, Faculty of Science and Technology, Queensland University of Technology, Brisbane, Australia (*r.frost@qut.edu.au)

Hydrotalcites have the useful ability of removing anionic species from solution either by anion exchange or through the initial formation process of the layered double hydroxide structure. This investigation has looked at removing arsenate and vanadate using hydrotalcites prepared in two different ways: 1) co-precipitation and 2) thermal activation. The thermal activation method has been clearly shown to increase the number of anions removed from solution. This increase in effectiveness is due to the increased chemical reactivity of the hydrotalcite structure after dehydration. Hydrotalcites were prepared using synthetic materials, Bayer liquor, and seawater neutralised bauxite refinery residues.

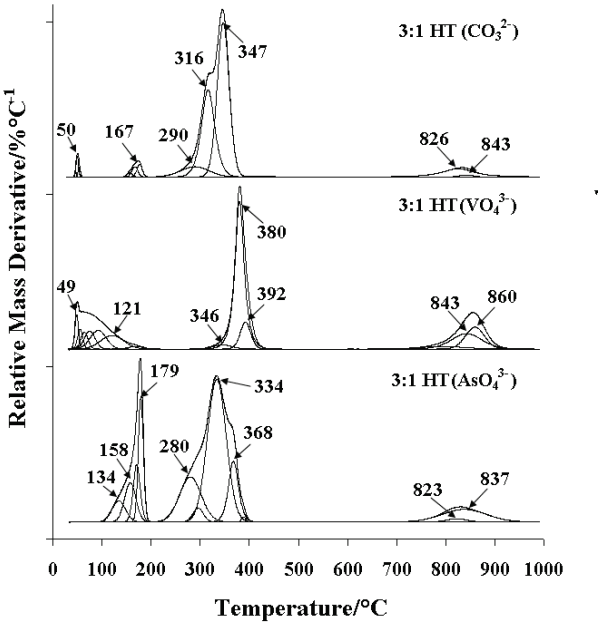

Fig. 1: Thermal analysis patterns of hydrotalcite with intercalated carbonate, vanadate and arsenate.

This work has shown that the intercalation of arsenate and vanadate increases the thermal stability of the hydrotalcite structure compared to carbonate hydrotalcites (Fig. 1). The Mg:Al ratio used for the removal of the toxic anions has been found to be dependent on the method used. For the co-precipitation method the formation of hydrotalcite in solution with a Mg:Al ratio of 3:1 is favoured over the 2:1 and 4:1, whereas for thermally activated hydrotalcites with a Mg:Al ratio of 4:1 is most favourable. Using a variety of techniques the mechanism for the inclusion of arsenate and vanadate has been determined. It has also been established that the removal of toxic anions in highly alkaline solutions is diminished.

This investigation has also shown that Bayer refinery residues may be used for the treatment of solutions containing toxic anions. Thermally activated Bayer hydrotalcite has been shown to be highly effective in the removal of arsenate and vanadate, with 100 % removal being observed. The formation of hydrotalcite during the seawater neutralisation process removes anions via two mechanisms rather than one observed for thermally activated red mud.

Investigation of layered structures using terahertz time-domain spectroscopy

Janek, M.[1,2*], Matejdes, M.[2], Zich, D.[2], Bugár, I.[3], Szöcs, V.[4], Vincze, A.[3], Danielik, V.[5], Velič, D.[2,3] & Darmo, J.[6]
[1]Inst. of Technology, Slovak Academy of Sciences, Bratislava, Slovakia ([*]Marian.Janek@savba.sk)
[2]Dept. of Physical and Theoretical Chemistry, Faculty of Natural Sciences, Comenius University, Bratislava, Slovakia
[3]International Laser Center, Bratislava, Slovakia
[4]Inst. of Chemistry Faculty of Natural Sciences, Comenius University, Bratislava, Slovakia
[5]Dept. of Inorganic Technology, Slovak University of Technology, Bratislava, Slovakia
[6]Inst. of Photonics, Technical University Wien, Vienna, Austria

Model inorganic layered structures based on selected layered minerals from the micas group and boron (aluminium) nitride were investigated in the far infrared region using terahertz time-domain spectroscopy (THz-TDS). This technique allows determination of the complex index of refraction – refractive index and absorption index, including sample thickness determination from single sample and background measurement in the frequency region from 0.1 to ~6.0 THz (3.3 to ~200.0 cm^{-1}). The main advantage for utilization of the THz-TDS is the coherent nature of measured transmitted electric field, providing high sensitivity and resolving phase information [1]. Therefore, this technique is able to deliver frequency dependence of material complex dielectric permittivity related to the refractive properties through Maxwell´s relationships.

The samples were characterised also by X-ray diffraction, Fourier transform infrared spectroscopy and other conventional techniques. Micas were selected in such manner that differed significantly in chemical composition e.g. in structural cations and ratios of interlayer cations. For instance the structural iron content as determined by EDS differed significantly. The results of frequency dependent complex index of refraction ($\tilde{n}_s = n_s - i\kappa_s$) of used layered materials were determined.

Acknowledgements: The financial support of the Slovak Grant Agency for Science VEGA grant No. 1/4457/07 and of the Slovak Research and Development Agency APVV grant APVV-0491-07 and grant VMSP-P-0110-09 is greatly appreciated.

[1] Ferguson, B. & Zhang, X.-Ch. (2002) *Nat. Mater.*, **1**, 26-33.

The benefits of the near-infrared spectroscopy in the characterization of organoclays

Madejová, J.[*], Jankovič, Ľ. & Komadel, P.
Institute of Inorganic Chemistry SAS Bratislava, Slovakia
([*]jana.madejova@savba.sk)

Near infrared (NIR) spectroscopy belongs to spectroscopic methods with dynamic development and spreading into many areas of science and technology, however, its utilization in the organoclays studies is rather rare [1-4]. Detailed analysis of the NIR spectra of montmorillonite-based organoclays was performed to show the advantages of this spectral region in their characterization and in identification of specific bonds "not visible" in the middle infrared (MIR) region. Na-saturated <2 μm fraction of bentonite from Jelšový Potok (Slovakia) was used for organomontmorillonites preparation. Different alkylammonium cations were selected to allow more ways of comparisons of the spectral features within the series. Four samples contained various amounts of octylammonium chains: monooctyl- (1C8), dioctyl- (2C8), trioctyl- (3C8), and tetraoctyl- (4C8) ammonium, while two others had chains of double length, hexadecyl- (1C16) and dihexadecyldimethyl- (2C16) ammonium. Last two cations were of different structure containing aromatic benzene, either without double bonds benzyltrimethylammonium (C10) or with a reactive double bond present in 4-vinylbenzyl-trimethylammonium (C12).

Similar shape of the MIR patterns of CH_3 and CH_2 stretching (3000-2800 cm^{-1}) and bending (1500-1300 cm^{-1}) vibrations was observed within 1C8-4C8 and 1C16-2C16 series. However, the spectra of the samples with 16 C atoms - 2C8 and 1C16, and 32 C atoms - 4C8 and 2C16, were significantly different due to altered ratios of CH_3 and CH_2 groups in the cations. Only weak bands corresponding to stretching NH_3^+ and NH_2^+ vibrations (~3270-3190 cm^{-1}) were resolved in the MIR spectra of 2C8, 3C8 and 1C16, the NH^+ band was overlapped with the CH and/or H_2O vibrations. Only vibrations of trimethylammonium cations were clearly identified in the MIR spectra of C10 and C12, weak bands near 3100 cm^{-1} should correspond to Ar-CH (Ar = aryl). Vibrational modes of Ar-C-C, or H_2C=C (vinyl) group were overlapped with more intense vibrations of aliphatic CH groups.

Based on the vibrations observed in the MIR region the first overtone ($2\nu_{XH}$) and combination $(\nu+\delta)_{XH}$ bands of XH groups (X = O, C, N) were identified in the NIR spectra of organo-montmorillonites. The complex band near 7070 cm^{-1} was assigned to overlapping $2\nu_{OH}$ of the structural OH groups and bound H_2O molecules, the combination modes of H_2O and structural OH groups were found near 5250 cm^{-1} and 4523 cm^{-1} respectively. The intensity and the position of the $(\nu+\delta)_{H2O}$ band was strongly affected by the type of the organic cation used. While the presence of CH_3 and CH_2 groups in 1C8-4C8 and 1C16-2C16 samples was recognized in the 6000-5500 cm^{-1} ($2\nu_{CH}$) and 4450-4100 cm^{-1} $(\nu+\delta)_{CH}$ regions, the overtone and combination bands of Ar-CH (C10 and C12 sample) were clearly shifted to higher wavenumbers. The NIR spectra were found to be extremely useful to identify NH and vinyl groups, which were difficult to recognize in the MIR region. The intensive bands of the first overtone and combination modes of NH_3^+ and NH_2^+ were found in the 6600-6050 cm^{-1} and 5000-4600 cm^{-1} regions, respectively. Though no NH^+ overtone was observed in the NIR spectrum of 3C8, the intensity of the $(\nu+\delta)_{NH+}$ near 4750 cm^{-1} was high enough to unambiguously identify this bond. The characteristic band assigned to $2\nu_{CH2}$ in H_2C=C at 6130 cm^{-1} was detected in the spectrum of C12.

[1] Zhou, Q. et al. (2008) *Spectrochim. Acta A*, **69**, 835-841. [2] Madejová, J. et al. (2009) *Clays Clay Miner.*, **57,** 311-322. [3] Pálková, H. et al. (2010) *Micropor. Mesopor. Mater.*, **127**, 237-224. [4] Lu, L. et al. (2010) *Spectrochim. Acta A*, **75**, 960-963.

FTIR and UV-Vis spectroscopic investigation of illite-smectite minerals from Dolná Ves (Slovakia)

Komadel, P.*, Pentrák, M., Czímerová, A. & Madejová, J.
Institute of Inorganic Chemistry, Slovak Academy of Sciences, Bratislava, Slovakia (*peter.komadel@savba.sk)

Information available from the most common spectroscopies, infrared and UV-Vis, on illite-smectite (I-S) mixed layer minerals is discussed. Figure 1 shows the IR spectra of samples containing a montmorillonite (JP, Jelšový Potok, Slovakia), an I-S (DVS, Dolná Ves, Slovakia) and an illite (Mo, Morris, Illinois, USA). XRD analyses prove 30 and 9 % of swelling interlayers, respectively, in I-S and illite [1]. The IR spectra of JP and DVS suggest similar chemical composition with AlMgOH bending vibrations near 845 cm^{-1}. Higher Al^{IV} for Si substitution in illitic layers generates the Al^{IV}-O (~830 cm^{-1}) and Al^{IV}-O-Si (755 cm^{-1}) vibrations.

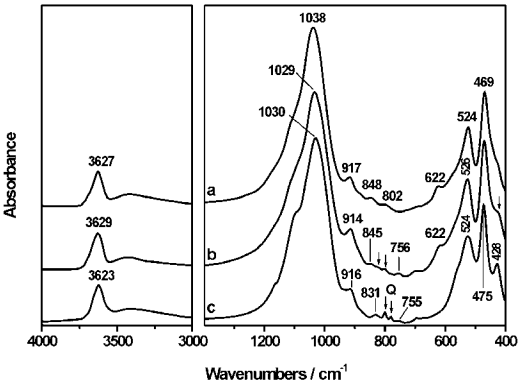

Fig. 1: IR spectra of < 2 μm fractions of a) JP montmorillonite, b) DVS illite-smectite and c) Mo illite; (Q = quartz).

The presence of illitic layers in DVS and Mo modifies the shape of the IR pattern near 620 and 420 cm^{-1}. The well developed band at 622 cm^{-1} in the JP spectrum corresponds to coupled Al^{VI}-O and Si-O vibrations. The intensity of this band is lower for DVS and it is absent from the Mo spectrum. The reverse sequence is found for the Si-O band at 428 cm^{-1}. A well developed band appears for Mo, a shoulder for DVS, and no absorption for JP. A similar dependence was found for a set of DVS samples with different expendability. These IR features may help to differentiate illitic layers in clay samples but not to distinguish between a mixture of individual minerals and an I-S.

Cationic dyes, such as methylene blue or Rhodamine 6G (R6G), form molecular aggregates on clay surface and change their colour. Dye cation agglomeration is a good tool for testing layer charge density on smectites which affects the distance between the dye species. Formation of aggregates results in creation of different forms of the dye, absorbing visible light at different wavelengths. Second-derivative of UV-Vis spectra (SDS) of a series of I-S from DVS deposit with R6G show a direct relationship between the SDS amplitude for the band assigned to the H-aggregates and the expandability. I-S interact with R6G more intensely than do smectites [2].

[1] Pentrák, M., Madejová, J. & Komadel, P. (2010) *Philos. Mag.*, **90**, 2387-2397. [2] Šucha, V., Czímerová, A. & Bujdák, J. (2009) *Clay. Clay Miner.*, **57**, 361-370.

Structure elucidation of organoclay-polymer composites by instrumental techniques

Horváth, E.[1], Khunová, V.[2], Kristóf, J.[1*] & Makó, É.[3]
[1]Institute of Environmental Engineering, University of Pannonia, Veszprém, Hungary (*kristof@almos.vein.hu)
[2]Dept. of Plastics and Rubber, Faculty of Chemical and Food Technology, The Slovak University of Technology, Bratislava, Slovak Republic
[3]Institute of Materials Engineering, University of Pannonia, Veszprém, Hungary

The industrial application of layer-structured minerals depends on their surface reactivity. In addition to the common applications (e.g. paper, plastics, rubber, pharmaceutical and ceramic industries) they can improve the physical and/or chemical properties of polymers as additives in an amount of 2-5 %. The requested properties can be achieved by the addition of highly dispersed (micro- or nanoscaled) minerals (kaolinite, halloysite and montmorillonite) embedded in the polymer (e.g. polypropylene, polyethylene and polycaprolactone) matrix. The use of reactive modifiers is also necessary to ensure compatibility between the mineral particles and the polymer.

Organoclay nanocomposites can be obtained either by ion exchange (in the case of montmorillonites) or by intercalation (in the case of halloysites and kaolinites in solution or with mechanochemical treatment). Since property improvement is proportional with increased dispersity and reduced particle size of the mineral additive, delamination and the formation of nanotubes is the main goal of this research. The structure of the nanocomplexes formed and that of the clay-polymer composites prepared can be investigated by instrumental techniques such as FTIR (DRIFT) spectroscopy, Raman microscopy, thermal analysis combined with mass spectroscopy, XRD, etc.

Delamination of different kaolinites and halloysites was made by multiple intercalation using urea and triethanol amine. With an electrophilic agent tetraalkyl ammonium cations have been synthetized between the layers reacting with a polyacryl sodium salt added to the system.

Polymer nanocomposites have been prepared by melt mixing in a twin-screw extruder at temperatures of 130 (PCL), 200 (PP) and 250°C (PA).

The addition of 1,3-phenylenedimaleimide (BMI) as reactive modifier further increased the expansion of montmorillonite and improved all of the end-use properties of the polymer. The most significant effect (some 80%) was the improvement in gas permeability. Dissimilarly to montmorillonite-based nanocomposites, no further expansion was observed with 1:1 type minerals with the addition of BMI. In this case improvement in mechanical properties was due to BMI forming an interphase between the clay particles and the polymer matrix.

[1] Letalief, S. & Detellier, C. (2009) *Langmuir*, **25(18)** 10975-10979. [2] Horváth, E., Kristóf, J. & Frost, R.L. (2010) *Appl. Spectroscop. Rev*, **45**, 130-147.

The effect of dry grinding on the structure of sepiolite from Turkey

Dikmen, S.[1*], Özçelik, H.[1], Yılmaz, G.[2] & Yörükoğulları, E.[1]
[1]Physics Dept., Science Faculty, Anadolu University, Eskisehir, Turkey ([*]sdikmen@anadolu.edu.tr)
[2]Porsuk Vocational School, Anadolu University, Eskisehir, Turkey

The effects of grinding on clay minerals are investigated with great interest because this process produces changes in the textural and structural properties of powdered material.

Sepiolite is a fibrous hydrated magnesium silicate and a natural clay with a unit cell formula $(Si_{12})(Mg_8)(O_{30})(OH)_4(OH)_2 \cdot 8H_2O$ [1]. This mineral is 2:1 layer silicate, which means that the octahedral layer is bound above and below by a silica tetrahedral sheet. The tetrahedral sheets are linked infinitely in two dimensions. It is structurally different from other clay minerals in that the octahedral sheets extend in only one dimension and the tetrahedral sheets are divided into ribbons by a periodic inversion of rows of tetrahedrons [2].

The sepiolite powder sample supplied from Element Mining Co., Eskişehir. The raw mineral was subjected to dry grinding by ball milling, for periods ranging from 0 (smaller than 40 μm) to 120 min, using a planetary ball mill (Fritsch Pulverisette 6).

The physico-chemical and structural alterations are determined by particle size distribution (PSD), specific surface area (BET method), density, porosity, color (L, a, b), X-ray diffraction (XRD), scanning electron microscopy (SEM), FT-IR analyses were carried out. According to the mineralogical and chemical analysis results, the raw mineral can be accepted pure sepiolite ore (Table 1). With grinding, the rate of size reduction decreases with time, but reduction continues up to about 30 min. At this time of grinding, particle size reduction decreases with time, but reduction continues up to about 30 min. Grinding of sepiolite produces an increase of the starting BET surface area value progressively up to a maximum of 364 m^2g^{-1} at 30 min. A subsequent decrease of surface area with increasing grinding time was observed. A breakdown of the initial particles due to grinding effect observed more rounded particles, aggregates and agglomerates, as proved SEM images.

Table 1. Chemical, mineralogical composition and some physical properties sepiolite

Chemical analysis	**Unit**	**Value**
SiO_2	wt%	51.76
MgO	wt%	21.42
CaO	wt%	0.73
Al_2O_3	wt%	4.43
Fe_2O_3	wt%	1.83
K_2O	wt%	0.46
Na_2O	wt%	0.13
TiO_2	wt%	0.24
MnO	wt%	0.09
LOI*	wt%	18.9
Total	wt%	**99.99**
Mineralogical analysis		
Sepiolite	wt%	%85.7
Dolomite	wt%	10.4
Quartz	wt%	3.9
Physical Properties		
Density	g/cc	2.34
Specific surface area	m^2/g	265.12

*LOI: Loss on ignition

[1] Grim, R.E. (1968) *Clay Mineralogy*. McGraw Hill, New York. [2] Murray, H.H. & Zhou, H. (2006) in Kagel, J.E. et al. (eds.) *Industrial Minerals & Rocks*. SME, 401-406.

AFM study of vermiculite particles

Barabaszová, K.* & Valášková, M.
Nanotechnology Centre, VŠB-TU of Ostrava, Czech Republic
(*karla.barabaszova@vsb.cz)

Atomic force microscopy (AFM) has been evolved as a promising device to explore the mineral surface, determine morphology, visualize the sorption of organic substances, measure size and thickness of clay-size particles and also measure growth, dissolution, heterogenous nucleation and redox processes [1]. AFM is a powerful technique for the characterization of particles with the size ranging from 1 nm to 10 μm and therefore it can be used for exploration of clay minerals [2,3].

Vermiculite small particles were prepared using two milling procedures. Each sample was milled for 15 minutes in jet mill (Sturtevant Micronizer®) parallel with 15 min of milling in planetary ball mill (wolfram carbide mill chamber and balls). Jet milling was realized with the pressure of compressed air (as the grinding energy) 350 kPa and constant feed rate of grinding material (1.5 g/min) to obtain particles of size approximately 2 μm. Both vermiculite powder fractions showed uniform mean particles size of 3 μm, as it was determined using the laser method (Fritsch Particle Sizer Analysette 22). Morphology of vermiculite particles was examined using the scanning electron microscope (SEM).

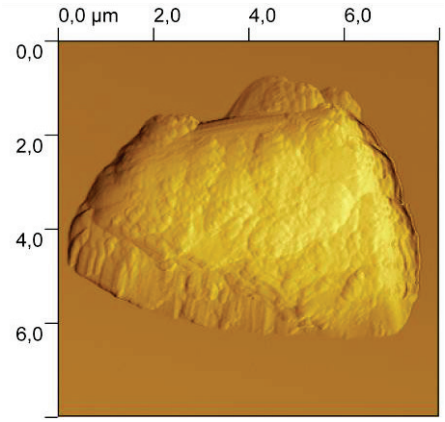

Fig. 1: The 2D AFM image of jet milled vermiculite particle.

In comparison to the traditional technique (SEM), AFM can give 3D and 2D images with Z information through color intensity, providing the opportunity to obtain quantitative measurements of particles using GWYDDION software.

The morphology of the milled vermiculite particles was studied with atomic force microscopy AFM-Explorer™. The suspension of the vermiculite powder in anhydrous ethanol was placed on mica plate and then dried at 60°C for 10 minutes. The AFM scanning was performed with the silicon probe 1650-00 in non-contact mode with 8 μm Z-linearized dry scanner.

The particle size distribution, orientation and the aspect ratio of vermiculite particles after different mechanical disintegration procedures were by the help of AFM with non-contact mode successfully studied.

Acknowledgements: This work was supported by the Grant Agency of Czech Republic GAČR grant no: 205/09/0352.

[1] Sachan, A. & Mehrotra, V. (2008) *Current Sci.*, **95(12)**, 1699-1706. [2] Sachan, A. & Penumadu, D.J. (2007) *Geotechn. Geoenviron. Eng.*, **133(3)**, 306-318. [3] Zbik, M. & Smart R.St.C. (1998) *Clays Clay Miner.*, **46(2)**, 153-160.

Gas barrier properties of natural rubber/mechanochemical treatment coal bearing strata kaolinite nanocomposites prepared by melt blending

Frost, R.L.* & Cheng, H.
Chemistry Discipline, Faculty of Science and Technology, Queensland University of Technology, Brisbane, Australia
(*r.frost@qut.edu.au)

Nanocomposites materials are two-phase systems that consist of a polymeric matrix and dispersed inorganic particles of nanometer scale [1]. The use of organic clays as precursors to nanocomposite formation have been extended into various polymer systems including epoxys, polyurethanes, nitrile rubber, styrene-butadiene rubber, isobutylene–isoprene rubber and ethylene propylene diene monomer [2,3]. Kaolinite-rich rocks are very abundant in the Permo-Carboniferous coal-bearing strata of North China and are widely used [4]. Thereafter, coal bearing strata has been applied to incorporate the layered silicates in polymer hosts by in situ polymerization, solution intercalation or simple melt mixing. Recently, much of the work clay application in the rubber has been done to improve the barrier performance of rubbery materials with organic montmorillonite particles [5], and there are relatively few reports on organic kaolinite in this application.

The X-ray diffraction pattern at room temperature indicated that the intercalation of potassium acetate into kaolinite causes an increase of the basal spacing from 0.718 to 1.42 nm, and with the particle size reduction, the surface area increased sharply with the intercalation and exfoliation by ball-milling. the particulates have high aspect ratio according SEM images.

It is also shown coal bearing strata kaolinite layers are finely dispersed into the natural rubber matrix and orientationally arranged in parallel. These highly filled natural rubber/mechanochemical coal bearing strata kaolinite (NR/MCBK) nanocomposites exhibit outstanding mechanical properties, excellent gas barrier properties and much higher thermal stability compared to the pure natural rubber. The significant improvements in the mechanical properties (Table1), thermal stability and gas barrier properties may be attributed to the restriction of the parallel kaolinite platelets to the free movement of rubber molecule chains and the retardation of the impermeable kaolinite layers to the progress of gas molecules through the rubber composites.

Table 1: Mechanical properties of NR composites filled with various MCBK loadings

MCBK content /phr	Hardness (HA)	Stress /MPa		Tensile strength /MPa	Elongation at break /%	Permanent set /%
		300%	500%			
0	37	1.89	5.49	23.2	745	25
70	55	4.35	14.2	25.2	663	68

[1] Choudalakis, G. & Gotsis, A.D. (2009) *Eur. Polymer J.*, **45**, 967-984. [2] Takahashi, S. et al. (2006) *Polymer*, **47**, 3083-3093. [3] Liu, Q. et al. (2008) *Appl. Clay Sci.*, **42**, 232-237. [4] Liu, Q. et al. (2001) *Appl. Clay Sci.*, **19**, 89-94. [5] Zulfiqar, S. et al. (2008) *Appl. Surf. Sci.*, **255**, 2080-2086.

Thermal analysis of China kaolin –kaolinite, coal-bearing strata kaolinite and halloysite

Frost, R.L.* & Cheng, H.
Chemistry Discipline, Faculty of Science and Technology, Queensland University of Technology, Brisbane, Australia (*r.frost@qut.edu.au)

Kaolinite and its polytype, halloysite have a wide variety of applications in industry [1]. These applications include their use in the fabrication of paper, paints and inks, rubber and plastic, ceramic raw material, medicines, etc. [2-4]. Most of the industrial kaolin in china which generally contain a certain amount of organic carbon need to be calcined to improve whiteness [5]. Thermal stability and whiteness are very important properties of calcined kaolin particularly for industrial applications [6]. Therefore, the thermal analysis of kaolin also gives new insights not only about improvement of the properties but also protection of the environment.

Comparing the temperature of dehydroxyl, it is established that kaolinite with lower Hinckley crystallinity index dehydroxylates easilier than those whoes Hincley index are high. The comparison of kaolinite and hallosite is shown that the thermal decomposition of kaolin is determined by different factors, such as degree of the structural ordering, mineral impurities and adsorbed and substituted ions. The mass gain in the MS curves corresponds precisely with the mass loss in the TG curves.

The thermal decomposition of kaolin occurs in main three main steps (a) desorption of water blow 100 °C, (b) dehydration at about 225°C, (c) well defined dehydroxylation at around 450°C (Fig. 1).

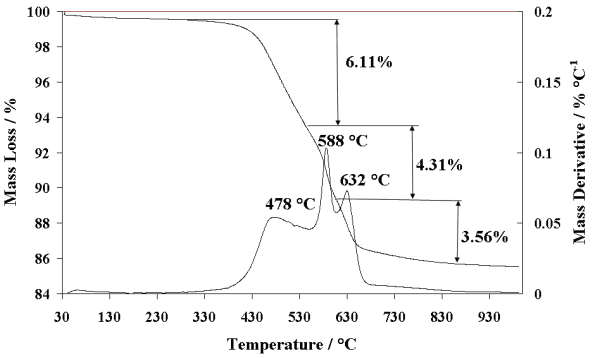

Fig. 1: TG and DTG curves of coal bearing strata kaolinite.

The temperature of dehydroxylation of kaolinite is found to be influenced by the degree of disorder of the kaolinite structure and the gases evolved in the decomposition process can be various because of the different amount and kind of impurities. It is evident by the mass spectra that the interlayer carbonate from impurity of calcite is released as CO_2 around 225, 350 and 710°C in the kaolin samples. TGA-MS show the coal bearing kaolinite released CO_2 about 450°C. Thus for geosequestration decarbonization and purification before industry application of kaolin is necessary.

[1] Murray, H.H. (2000) *Appl. Clay Sci.*, **17**, 207-221. [2] Franco, F. et al. (2004) *J. Colloid Interface Sci.*, **274**, 107-117. [3] Mako, E. et al. (2009) *J. Colloid Interface Sci.*, **330**, 367-373. [4] Liu, Q. et al. (2001) *Appl. Clay Sci.*, **19**, 89-94. [5] Ding, S.-l. et al. (2009) *Proc. Earth Planet. Sci.*, **1**, 1024-1028. [6] Murray, H.H. & Wilson, I. (2007) *Clays Clay Miner*. **55**, 644-645.

Characterization of bleaching phenomena in German red bed sediments by directly coupled evolved gas analysis (DEGAS).

Hilse, U.*, Goepel, A., Pudlo, D., Heide, K. & Gaupp, R.
Institute of Earth Sciences, Friedrich-Schiller-University Jena, Germany (*ulrike.hilse@uni-jena.de)

In this study varied coloured Buntsandstein sandstones in Central Germany (Thuringian Vorderrhön) were investigated by a thermo-gravimetric/pyrolytic method (DEGAS – directly coupled evolved gas analysis) to analyse the degassing behaviour of red bed sediments and their bleached modifications. Often such bleaching of primary red bed sandstones is contributed to fluid-rock interactions. Therefore the investigations were focused on geochemical/mineralogical features of such sediments to validate the causes of such bleaching processes. The pyrolytic experiments were performed using a commercial, slightly modified NETZSCH TG-MS system (thermobalance coupled directly to quadrupole mass spectro meter). All gaseous species were analysed in multiple ion detection mode and correlated with the total pressure change in the sample chamber during heating (temperature range: from room temperature (22°C) to 1200°C and 1450°C, respectively) [1]. The ion current for different mass/charge ratios (e.g. m/z 18, 44 & 78, Tab. 1) was recorded as a function of time. Depending on the amount of volatiles in the sample about 10 mg of sample material were used. The samples were taken from core plugs and carefully prepared without using cooling additives to avoid any contamination.

Table 1: Detected element species during MS analysis

Mass number	Fragment ions	Geogene source
1	H^+	sheet silicates,
2	H_2^+, D^+	hydroxides,
17	OH^+, NH_3^+	hydrates
18	H_2O^+	& organic material
28	N_2^+, $C_2H_4^+$, CO^+	carbonates
44	CO_2^+, $C_3H_8^+$, N_2O^+	& organic material
78	$C_6H_6^+$	organic material

Degassing patterns of sample M44 indicate a preferential breakdown of sheet silicates, hydroxides, hydrates and carbonates [2]. Its two red subsamples M44-R1 and -R2 are dominated by the release of H_2O and CO_2, whereas in the two bleached subsamples M44-B1 and -B2 an additionally H^+ source without any correlation with m/z 17 and 18 occurred, probably due to the presence of hydrocarbon species. Another Buntsandstein sample M49 was separated into 12 subsamples representing a profile from unbleached to bleached rock portions. The increase of m/z 44 in subsamples M49-1, -3 and -9 are attributed to small carbonate domains in the sample. A prominent signal of m/z 78 in the transition zone between bleached and unbleached areas implies the presence of a further hydrocarbon species.

The performed mass spectrometric gas analysis sustain geochemical differences in red and bleached sandstone rock composition, sometimes only weakly maintained by conventional geochemical methods (XRF, ICP). The results constrain that DEGAS might serve as an efficient and complementary analytical tool in sedimentary research in evaluating the involvement of specific gaseous species during fluid-rock processes.

[1] Heide, K. & Schmidt, C. M. (2003) *J. Non-Cryst. Solids*, **323**, 97-103. [2] Hilse, U. (2009) *Dipl. thesis* (unpubl., in German), Friedrich-Schiller-University of Jena.

X-Ray Diffraction and lithologico-mineralogical studying of Kazakhstan clay minerals

Kudaikulova, G.A.* & Aitugulova, B.A.
Geology Prospecting Inst., Kazakh National Technical University, Almaty, Kazakhstan (*kgulzhanabd@mail.ru)

Among all existing methods of studying the mineral structure of clay minerals, the X-Ray method is the most authentic. More over, the X-Ray method can state a quantitative estimation whereas other methods are qualitative. From X-Ray methods it is most effective diffractometrical.

In the present work, roentgenograms of clay minerals have been obtained on X-Ray Diffraction type DRON – 3 with CuK_α – radiation, monochromatized by graphite monochroma-tor installed in the front of the counter. Interpretation of diffractograms has been carried out with the help of the ASTM Powder diffraction card file datas and diffractograms purefied from impurities of minerals. The Kazakhstan samples of clays Taukentsky, Akkalkinsky (2 samples) and Akzharsky deposits have been investigated.

Results of X-ray and also lithologico – mineralogical analyses have shown that Taukentsky clay concerns clays of hydromicas-mont-morillonite group with prevalence of montmorillonite component of alkaline-earth calcium–magnesian form. In the investigated sample crystallites of blended-layer formations are formed which decrease exchange capacity of a clay. Estimated content of a hydromicaceous component is 10–15 % and montmorillonite component – 60 – 65 %. The total content of a clay component is approximately 80 %.

An assay of Akkalkinsky clay (the sample № 1) consists of 79.4 % of pelite fractions (<0.01 mm); 15.8 % of aleurite fractions (0.01–0.1 mm); 4.8 % of sandy fraction (> 0,1мм). The sample № 2 of Akkalkinsky clay consists of 91. 0 % pelite fractions, 8.8 % aleurite fractions and 0.2 % – sandy. By the prevalence of montmorillonite clay (both samples) concerns to bentonite type.

By the results of the mineralogical analysis Akzharsky clay concerns to adjournment bottom Eocene and is combined bentonite clays of is light – grey to dark – grey colour, fat, high-plastic, as soap with the raised maintenances montmorillonite. On the figure diffractogram of Akzharsky clay is shown.

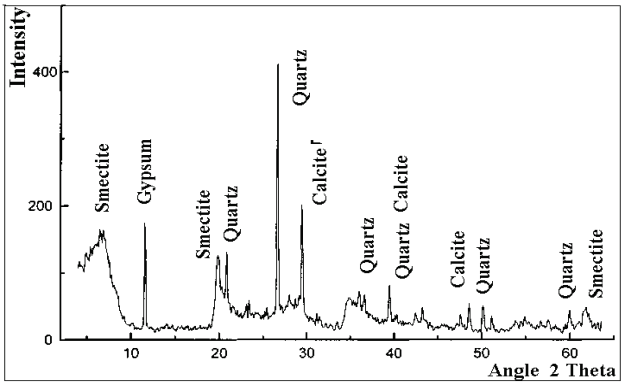

Fig. 1: Diffractogram of Akzharsky clay.

Thus, X-Ray diffraction and lithologo-mineralogical studying of clay minerals of the Kazakhstan deposits has allowed to draw a conclusion that montmorillonite component of the studied minerals allow successfully use them as raw materials for preparation drilling muds in geology-prospecting and oil-gas industries.

Study of dispersions and thin films based on montmorillonite and fluorescent dyes

Matejdes, M.[1*]& Janek, M.[1,2]
[1]Dept. of Physical and Theoretical Chemistry, Faculty of Natural Sciences, Comenius University, Bratislava, Slovak Republic (*matejdes@fns.uniba.sk)
[2]Institute of Technology, Slovak Academy of Sciences, Bratislava, Slovak Republic

Preparation of novel organic-inorganic nanocomposites reflects their significant potential for its possible utilization as novel materials e.g. shown in the recent years in combinations with polymers and semiconducting polymers [1] with electroluminiscent properties. These nanocomposites are forward-looking not only for improved mechanical properties, but in the case of luminiscent materials, they could also provide broadening of spectral field compared with conventional semiconductors. Properties of these nanocomposites are dependent not only on the properties of individual components, but also on their morphological properties, the character of the phase interface, charge characteristics of clay lamellas, etc.

In our study we are trying to shed more light on the preparation conditions of the fluorescent dyes based nanocomposites, while the functional skeleton is based on the organized structure of the sodium montmorillonite particles. The sense of its preparation rests on the fact that this material may be used as narrow frequency response on the exciting radiation, polarisation component in optical devices, or as a part of the solar panels or devices, where the energy transfer with high effectiveness is necessary.

In most studies related to the nanocomposite materials preparation based on clay minerals with negative layer charge and organic cation molecules, the production of the aggregates of organic molecules [2] occurs on the surface of clay mineral. The disadvantage of the production of the aggregates is that their optical and other properties are different from the properties of their monomer form. In the report related to this issue, we assume that the arised problem can be solved by additing the appropriate spacer (β-cyclodextrin), which is able to interact with one organic molecule for purpose of the supramolecular complex formation. The outcome is that we suppose the prevention of the molecular aggregates creation.

Acknowledgements: This work was financially supported by grants from Slovak Ministry of Education VEGA 1/4457/07, Comenius University UK/143/2009 and APVV-0491-07.

[1] Lebaron, P.C., Wang, Z. & Pinnavaia, T.J. (1999) *Appl. Clay Sci*., **15**, 11-29. [2] Bujdák, J., Czímerová, A. & Iyi, N. (2008) *Thin Solid Films*, **517**, 793-799.

Preparation of nano-spherical smectite particles by hybrid atomization

Minagawa, K.[1*], Yamada, H.[1], Tamura, K.[1], Morimoto, K.[1] & Watanabe, Y.[2]
[1]National Institute for Materials Science, Tsukuba, Japan (MINAGAWA.Kazumi@nims.go.jp)
[2]Kanazawa Institute of Technology, Hakusan, Japan

Nano-particles of smectites have various applications related to catalysis, catalytic support, adsorption and development of new functional nanomaterials. We present a novel process called hybrid atomization in the production of nano-spherical particles of smectites. Hybrid atomization is new technique that combines gas atomization with centrifugal atomization [1,2]. Such process has been successfully applied in the production of fine, spherical metal powders at lower costs. The average sizes of the powders are 20 μm in diameter with a homogenous size distribution.

In its use for molten metals, the melt is broken into several tens to several hundreds μm droplets by gas atomization and subsequently sprayed on a high speed rotating disk. A thin film of liquid less than 10μm is formed on the disk and the fine droplets are scattered from the edge of the disk. For the case of aqueous suspensions and organic solvents, the atomization modes can be used to control a homogenous size distribution and a desired shape for nano-particles of smectites. The products were characterized by XRD, SEM and TEM. The results will be compared further with those from conventional methods such as spin-coating and spray-dry methods.

These results confirmed that the nano-spherical particles with narrow size distribution from smectites were formed following the same atomization mode, that is, ligament formation in the case of the aqueous solutions and organic solvent. A new process, hybrid atomization method, would effectively produce the inorganic nano-spherical particle for any chemical compositional system.

[1] Minagawa, K. et al. (2003) *JSME Int. J. A Solid Mech. Mat. Eng.*, **46(3)**, 260-264. [2] Minagawa, K. et al. (2004) *Trans. Mat. Res. Soc. Japan*, **29(5)**, 2145-2148.

Short Wavelength InfraRed petrology: a new laboratory and remote sensing method in low to very low-grade pelites

Potel, S.[1*], Doublier, M.P.[2] & Roache, T.[3]
[1]Dépt. Géosciences, Institut Polytechnique LaSalle Beauvais, Beauvais, France ([*]sebastien.potel@lasalle-beauvais.fr)
[2]Geological Survey of Western Australia, Kalgoorlie, Australia
[3]CSIRO, Earth Science and Resource Engineering Perth, Australia

Since Kübler (1967) [1], X-ray diffraction has become a standard method to characterize the metamorphic grade of metapelites metamorphosed under very low- and low temperature conditions. This method is based on the full width measurement of the first illite/muscovite peak at middle height (FWHM).

The few attempts that have been made to quantitatively apply spectroscopy methods to K-white mica in the field of very low-grade petrology focused on the infrared wavelength area ('Flehmig index' [2]) and have gained little application [3].

The new illite spectral maturity (ISM) method uses Short Wavelength InfraRed Reflectance spectroscopy (SWIR) to measure K-white mica mineral physicochemistry within very low grade metamorphic pelites. The three ISM measures used in this study parameterize the absorption features at 1900 nm and 2200 nm in terms of their area, depth and asymmetry. Through comparison with the powder XRD-derived Kübler index it is demonstrated that ISM allows the differentiation of anchizonal from diagenetic domains in very low-grade pelites (Fig. 1).

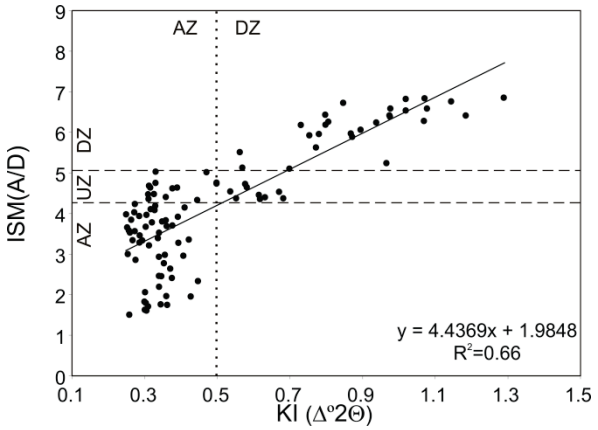

Fig. 1: Correlation between KI (in Δ°2Θ) and ISM measures determined by SWIR. The black dotted line corresponds to the anchizone/diagenetic zone boundary after Kisch et al. (2004), and the stippled lines define the 'unassignable zone' (UZ) for the ISM measures based on that boundary. AZ – anchizone; DZ – diagenetic zone.

The wavelength of the 2200 nm absorption feature provides a measure of the celadonite substitution. It shows a linear correlation (R^2=0.85) with K-white mica *b* cell dimension (powder XRD), and can be used to differentiate the metamorphic pressure facies and related geothermal gradients in pelites of greenschist facies and anchizonal metamorphic grade. The boundaries between LP/MP and MP/HP facies series can be defined at 2204 and 2220 nm, respectively.

[1] Kübler, B. (1967) in Schaer, J.P. (ed.) *Étages tectoniques*. Colloque de Neuchâtel 1966, 105-122. [2] Flehmig, W. (1973) *Neues Jb. Miner. Monat.*, **7/8**, 351-361. [3] Hunziker, J.C. et al. (1986) *Contrib. Mineral. Petrol.*, **92**, 157-180.

Magnesium sulfate trihydrate: an elusive mineral on Earth and Mars?

Fortes, A.D.[1,2*], Lemée-Cailleau, M.-H.[3], Knight, K.S.[4,5] & Jura, M.[4]
[1]Centre for Planetary Sciences at UCL/Birkbeck, London, UK
([*]andrew.fortes@ucl.ac.uk)
[2]Dept. of Earth Sciences, University College London, UK
[3]Institut Laue-Langevin, Grenoble, France
[4]ISIS Facility, STFC Rutherford Appleton Laboratory, Harwell Science and Innovation Campus, Chilton, Didcot, Oxfordshire, UK
[5]The Natural History Museum, London, UK

Magnesium sulfate trihydrate was, hitherto, one of the last $MgSO_4$ hydrates with an unknown structure. Amongst the $M^{2+}SO_4$ hydrates, only two other trihydrates are known, the mineral bonattite ($CuSO_4{\cdot}3H_2O$) and $CrSO_4{\cdot}3H_2O$, which are isostructural in space-group Cc. We have grown large (order 1 mm^3) single crystals, with a flat bladed morphology [forms {100}, {010}, {102}], which are comparatively stable in air at room temperature for periods of at least several days. Our synthesis method suggests to us that $MgSO_4$-trihydrate may be formed commonly in low-T hydrothermal systems, but will transform over time to pseudomorphs composed of hexahydrite ($MgSO_4{\cdot}6H_2O$) and/or epsomite ($MgSO_4{\cdot}7H_2O$). However, on Mars, the hydration process may be inhibited by the low atmospheric water abundance and the low temperatures.

We report the crystal structure of $MgSO_4{\cdot}3D_2O$, determined from neutron single-crystal diffraction measurements made using the VIVALDI diffractometer at the Institut Laue Langevin, and X-ray single-crystal measurements. We also report complementary measurements of the thermal expansion of $MgSO_4{\cdot}3D_2O$ powder in the range $8 < T < 295$ K made using the High Resolution Powder Diffractometer (HRPD) at the ISIS neutron spallation source, as well as C_p and TGA data. $MgSO_4{\cdot}3D_2O$ undergoes a first-order phase transition at 245 K from the high-T Pbca structure to a low-T monoclinic structure ($P2_1/c$ after permutation of the axes into a standard monoclinic setting); the transition is apparently caused by orientational ordering of the disordered hydrogen bonds in the structure. Unit-cell dimensions are a = 8.1925(2) Å, b = 10.9210(2) Å, c = 12.3866(4) Å at 295 K, and a = 12.3616(5) Å, b = 8.1414(3) Å, c = 10.8324(2) Å, β = 91.131(3)° at 8 K.

The axial thermal expansion is highly anisotropic, being largest along the b-axis (the direction perpendicular to the plane of the h-bonded sheets in the structure) and smallest along the c-axis. The volume thermal expansion at room temperature is comparable to that of hexahydrite, and much larger than that of epsomite, suggesting that $MgSO_4$-trihydrate may exert large (i.e., damaging) pore pressures in natural or manmade materials wherever hot aqueous fluids are able to precipitate.

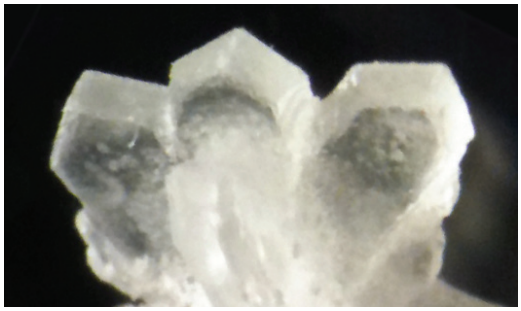

Fig. 1: Synthetic $MgSO_4{\cdot}3D_2O$ typically forms small clusters of blades (each shown here is ~ 1mm across the 010 face). These may occur in nature as hexahydrite or epsomite pseudomorphs.

Structure, thermodynamics and redox flexibility of Fe^{II-III} oxyhydroxycarbonate green rust homologous to fougerite mineral in gleysols as monitored by Mössbauer spectroscopy

Génin, J.-M.R.[1*], Morin, G.[2], Ona-Nguema, G.[2] & Ruby, C.[1]
[1]Institut Jean Barriol, CNRS-Université Henri Poincaré, Vandoeuvre-lès-Nancy, France
([*]jean-marie-genin@esstin.uhp-nancy.fr)
[2]Institut de Minéralogie et de Physique des Milieux Condensés Université Paris 6 et 7, Paris, France

Speciation of iron was monitored by Mössbauer spectroscopy during corrosion of iron. Intermediate compounds belonging to the layered double hydroxide family have been observed, where cations were Fe^{II} and Fe^{III}. Commonly called green rusts, many GRs have been synthesized and their structure determined by XRD and Mössbauer spectroscopy revealing long range order for Fe and anions, e.g. Cl^-, SO_4^{2-}, CO_3^{2-}, $HCOO^-$, $C_2O_4^{2-}$, SeO_4^{2-}.

GRs get usually oxidized by dissolving before precipitating into several types of orange ferric oxyhydroxides FeOOH rusts, such as ferrihydrite, lepidocrocite, goethite or even akaganeite depending upon the dissolved anion species and pH of aqueous solution. But, *in situ* oxidation may also occur by deprotonation of OH^- ions within the GR without any structural change as shown by Mössbauer spectroscopy, XRD and TEM. For CO_3^{2-} ions, $[Fe^{II}_4Fe^{III}_2(OH)_{12}]^{2+} \bullet [CO_3^{2-} \bullet 3H_2O]^{2-}$, the Fe^{II-III} hydroxy-carbonate GR(CO_3^{2-}), becomes Fe^{II-III} oxyhydroxycarbonate GR*(x), $[Fe^{II}_{6(1-x)}Fe^{III}_{6x}O_{12}H_{2(7-3x)}]^{2+} \bullet [CO_3^{2-} \bullet 3H_2O]^{2-}$ where ferric molar ratio $x = [Fe^{III}/Fe_{total}]$ belongs to the [0, 1] interval. It ends into ferric green rust, $[Fe^{III}_6O_{12}H_8]^{2+} \bullet [CO_3^{2-} \bullet 3H_2O]^{2-}$, GR($CO_3^{2-}$)*, which is in fact orange. Mössbauer spectra of GR and GR*(x) display a continuous change *in situ* when x varies as prepared by adding a controlled amount of H_2O_2 to the initial GR precipitate.

The major interest of this type of oxidation process concerns an outstanding redox flexibility of GR(CO_3^{2-})* which is the chemical compound equivalent to the "fougerite" mineral (IMA 2003-057) found in waterlogged areas [1] and responsible for the bluish-green color of gley sols This identification was confirmed by XRD patterns of samples found in ground water at Bornholm and Äspo where d_{003} distances in $R\bar{3}m$ space group structure were measured at 7.594 and 7.605 Å [2] in excellent agreement with those of synthetic samples (Table 1).

Table 1: Interplanar distances d_{hkl} and cell parameters of $R\bar{3}m$ space group GR*(x) computed from XRD data versus $x = [Fe^{III}/Fe_{total}]$

x	0.33	0.50	0.67	0.83	1
d_{003} (Å)	7.632	7.569	7.565	7.54	~ 7.34
d_{012} (Å)	2.679	2.669	2.672	-	-
c (Å)	22.896	22.707	22.695		
a (Å)	3.182	3.169	3.173		

Detailed structure of GR*(x) was obtained from XRD patterns and Mössbauer results that led to magnetic ordering based on the structure of GR(CO_3^{2-}). Occurrences of fougerite mineral are limited for values of x in the [0.33, 0.67] interval. *E*-pH diagram of GR(x)* is drawn from chemical potential data with parallel lines for reduction: $GR^*(x)+dx\ H^+ + dx\ e^- \rightarrow GR^*(x)$.

Simulation of GR(CO_3^{2-})* formation by bacterial reduction of ferric oxyhydroxides explained the existence of fougerite in anoxic zones of groundwater [3]. Then, evidences showing the reduction of pollutants such as nitrates by GR(CO_3^{2-})* and consequently fougerite will be presented. A friendly process for water purification simulating natural conditions is developed.

[1] Génin, J.-M.R. et al. (1998) *Environ. Sci. Technol.*, **32**, 1058-1068. [2] Christiansen, B.C. et al. (2009) *Environ. Sci. Technol.*, **43**, 3436-3441. [3] Ona-Nguema, G. et al. (2002) *Environ. Sci. Technol.*, **36,** 16-20.

Crystallographic orientation relationship between SFCA and hematite

Monkawa, A.[1*], Mikouchi, T.[2] & Sugiyama, K.[3]
[1]Tokyo Metropolitan Industrial Technology Research Institute, Tokio, Japan ([*]monkawa.akira@iri-tokyo.jp)
[2]Dept. of Earth and Planetary Science, Graduate School of Science, University of Tokyo, Japan
[3]Inst. for Materials Research, Tohoku University, Sendai, Japan

The quality of iron ore sinter has effects on blast furnace performance. It is well known that the iron ore with higher amount of alumina decreases the strength of sinter. The main phases of the sinter are hematite, magnetite, silica-ferrite of calcium and aluminum (SFCA) and silicates. SFCA is the most voluminously produced mineral in fluxed iron-ore sintering and has long been regarded as an important bounding phase industrial sinters. The strength of sinter is closely related to the boundary structure between SFCA and other minerals. The SFCA is iso-structural with aenigmatite-rhönite group [1]. Rhönite, which belongs to aenigmatite-rhönite group, was found among natural amphibole reaction rim together with ilmenite, Ti-augite, and olivine. Fig 1 shows SEM image for the amphibole reaction rim. It must be helped very much to understand the boundary structure between SFCA and other minerals if the crystallographic orientation relationship between rhönite and other minerals can be clarified. Electron backscatter diffraction (EBSD) pattern (Kikuchi diffraction pattern) analysis is used to provide crystallographic and phase information on micro sized crystalline materials with little or no difficult sample preparation [2]. In this study, the crystallographic orientation relationship between rhönite and other minerals was clarified by EBSD analysis. EBSD analysis shows that all rhönite minerals in the reaction rim possess the same crystallographic orientation. The crystal structure of rhönite is well demonstrated by an alternating stacking of the tetrahedral and octahedral layers. The octahedral layer of rhönite is parallel with that of pyroxene based on the crystallographic analysis of EBSD pattern. This result suggest that the crystallographic orientation relationship exists between SFCA and the mineral having octahedral layers. The hematite in iron ore sinter is composed of gibbsite-type octahedral layers stacked six-high normal to the c-axis. Therefore, it can be assumed that the crystallographic orientation relationship exists between SFCA and hematite in the same manner as the relationship between rhönite and pyroxene. The crystallographic orientation relationship was investigated in sinter samples prepared by a solid state reaction technique. The sinter sample mainly contains un-reacted hematite nuclei in a matrix consisting of SFCA. This study adopted EBSD analysis to clarify the crystallographic orientation relationship between hematite nuclei and SFCA.

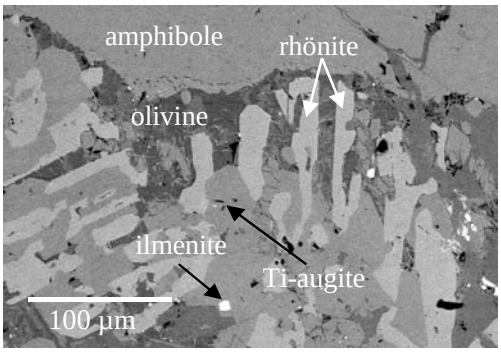

Fig. 1: SEM image for amphibole reaction rim.

[1] Sugiyama, K. et al. (2005) *ISIJ Intern.*, **4**, 560-568. [2] Goehner, R.P. & Michael, J.R. (1996) *J. Res. Natl. Insr. Stand. Technol*, **101**, 301-308.

What really determines coordination numbers in mineral structures - can a two-radius model for atoms help?

Christy, A.G.
Research School of Earth Sciences, Australian National University, Canberra, Australia ([*]andrew.christy@anu.edu.au)

Compatibility of trace element in minerals, as well as the extent of solid solution of major components and the activity models appropriate for describing thermodynamics of mixing, are all determined by the preferences of specific cations for specific coordination environments. The majority of textbooks still rationalise coordination behaviour in terms of radius ratios of "billiard ball" ions, despite the fact that this model gives wrong predictions more than 50% of the time for even simple classes of chemical compound such as the alkali halides. Much more success in understanding and predicting structures and their stability has been achieved over the last 30 years through a combination of the bond valence model for bond length-bond strength relationships (cf. [1] and references therein) and a Lewis acid/base strength model generating preferred bond valences between specific species, which has demonstrated considerable ability to explain the polymerisation, stoichiometry and water content of hydrated oxysalt minerals [2].

The Lewis acid/base strength paradigm, with species showing innate preference for a particular range of bond valences, can be understood as a consequence of nonlinear bond valence-bond energy relationships. However, it is likely that this is a strong controlling factor on bond valence and coordination number in only a few cases. In general, Madelung energies show that it is energetically feasible to maximise coordination number in so far as this is not counteracted by crowding of ligands. Hence, the major determinant of coordination number is actually a ratio of distances, but these are not "ionic radii"; they are the centre-ligand bonded distance and the ligand-ligand nonbonded distance. A model is proposed for predicting coordination numbers, and hence broad structure types, using these two distance parameters. Observed distances are consistent with the idea that to a first approximation, atoms in a structure have a "bonded radius" and a "nonbonded radius" which are approximately additive, subject to corrections for bond valence, and maybe bond polarity and topology. The concept of a well-defined non-bonded radius is not new [3] but has seen little exploration since its introduction.

Consideration of nearest-neighbour bonded and next-nearest neighbour nonbonded distances around both cations and anions rationalises observed structure types far better than other approaches, and can distinguish between stability fields of some topologically different structures with the same coordination numbers. The effects of pressure and temperature on coordination number depend on the relative sensitivity of these lengths to the state variables. For instance, the usually assumed increase in coordination with pressure arises since the nonbonded polyhedra edges are more compressible than the bonded centre-ligand distances. Scenarios can be predicted where the converse would be true.

[1] Brown, I.D. (2009) *Chem. Rev.*, **109**, 6858-6919. [2] Hawthorne, F.C. & Schindler, M. (2008). *Z. Kristallogr.*, **223**, 41-68. [3] O'Keeffe, M. & Hyde, B.G. (1981) in O'Keeffe, M. & Navrotsky, A. (eds.) *Structure and Bonding in Crystals*. Academic Press, New York, 227-254.

Optimization of site occupancies in mineral structure analysis: a call for user input

Wright, S.E.[1*], Hughes, J.M.[2] & Foley, J.A.[1]
[1]Miami University, Oxford, USA ([*]wrightse@muohio.edu)
[2]University of Vermont, Burlington, USA

The crystal structure analysis of minerals is unique because of the multiple components that occupy sites in minerals. Mineralogists face unique challenges in analyzing the atomic arrangement of natural phases: substituents must be assigned to particular sites to best fit the observed site scattering, site bond valence, bond lengths and chemical analysis. However, the assignments are rarely made with mathematical rigor.

Wright et al. [1] proffered a quadratic programming methodology to optimize the occupants of each site on the basis of site scattering, chemical analysis, and bond-valence sums, with an additional option for bond lengths. The methodology was implemented as a program, *OCCQP*, in the *MATLAB* numerical computing environment. *OCCQP* has proven very effective in assigning occupants to various crystallographic sites and provides crystallographers with a mathematically robust starting point for the determination of site occupancies.

However, use of *OCCQP* has not been as widespread as anticipated or desired, reportedly because of the inertia of using the *MATLAB* environment, which is not widely used in mineralogy, and because of the lack of seamless creation of input files. We thus are preparing to make the optimization method compatible and seamless with the most commonly used refinement program, and independent of the *MATLAB* computing environment. We seek input from mineral structure analysts for their desired attributes of input and output. Examples of the power of the optimization method will be given.

[1] Wright, S.E., Foley, J.A. & Hughes, J.M. (2000) *Am. Mineral.*, **85**, 524-531.

Structural and electronic transformations in transition-metal sesquioxides and sesquisulfides at high pressures and temperatures

Prewitt, C.T.
Dept. of Geosciences, University of Arizona, Tucson, Arizona, USA (prewitt@email.arizona.edu)

When studied as a group of related structures, the sesquioxides and sesquisulfides present many different crystal-chemical features that are of interest to mineralogy and mineral physics. Although most of these phases are not considered to be major constituents of Earth's mantle, knowing their high-pressure behavior is important for understanding overall mantle character and, in particular, its oxidation state. In addition, recent developments in x-ray emission spectroscopy that provide a powerful new tool in detecting spin crossover in iron-containing materials at high pressure have created wide interest in phase transitions in Fe-containing sesquioxides. Also, there is much to be learned from high-pressure experiments on other compositions having a range of different structures under varying conditions, i.e., Al_2O_3, Sc_2O_3, Ti_2O_3, V_2O_3, Cr_2O_3, Mn_2O_3, Fe_2O_3, Co_2O_3, Ga_2O_3, In_2O_3, Tl_2O_3 and Rh_2O_3.

Sesquisulfides have become of interest recently because the structure of U_2S_3 is proposed to be closely-related to that of a possible post-postperovskite structure of Al_2O_3 [1]. Sleight and Prewitt [2] explored the crystal chemistry of rare-earth sesquisulfides a number of years ago and this work is being reviewed here to explore other possible analogies with phase transitions in sesquioxides at high pressures.

[1] Umemoto, K. & Wentzcovitch, R.M. (2008) *Proc Natl Acad Sci USA*, **105**, 6526-6530. [2] Sleight, A.W. & Prewitt, C.T. (1968) *Inorg Chem*, **7**, 2282-2288.

Full analysis of feldspar texture and crystal structure by combined X-ray and electron techniques

Balic-Zunic, T.[1*], Piazolo, S.[2], Katerinopoulou, A.[1] & Schmith, J.H.[1]
[1]Natural History Museum, University of Copenhagen, Denmark ([*]tonci@geo.ku.dk)
[2]Dept. of Geology and Geochemistry, Stockholm University, Stockholm, Sweden

Feldspar crystals typically show a range of exsolution and polysynthetic twinning textures which can present problems for their full characterization, but at the same time give important information about the history of geological processes. Recent improvements in the instrumentation and calculation procedures in diffraction methods allow a full and direct characterization of finely intergrown feldspars. An integrated procedure was applied to the analysis of perthitic intergrowths in large pegmatite feldspar grains from the Larvik plutonic complex in the southern part of the Oslo region, Norway. X-ray powder diffraction was used for a preliminary identification of the mineral components and determination of their crystal lattice parameters. Electron Microprobe analysis was used to bracket the chemical compositions of the constituents. Electron Back-Scatter Diffraction was used to reveal the textural characteristics of the samples and spatial distribution and crystallographic orientation of the homogeneous crystal domains. Single-grain X-ray diffraction recorded by an area detector was applied for a simultaneous integration of reflection intensities for all orientationally different constituents. Based on this, their crystal structures were simultaneously refined using the program JANA2006. Finally, a Rietveld refinement of the powder diffraction data based on the determined crystal structure parameters was applied for the quantitative determination of phase proportions in perthites and the calculation of the chemical composition of the equivalent high-temperature homogeneous alkaline feldspar. The results show that the samples from two different pegmatites have similar global compositions, but different cooling histories, with closing temperatures differing by about 200K.

The combination of methods presented here is widely applicable in mineralogy. Its advantage is in the mutual support which makes each analysis simpler and more accurate, providing in the end reliable and full information of complex mineral intergrowths.

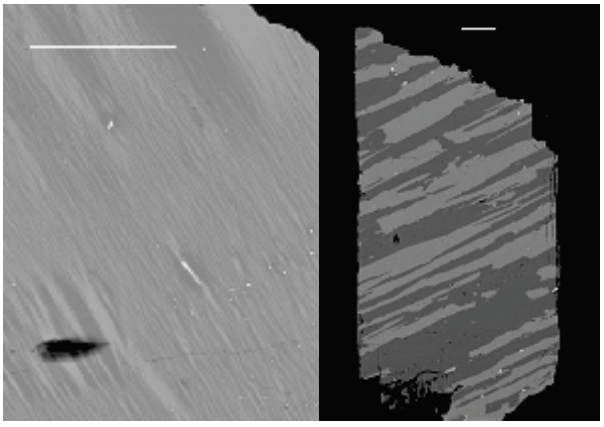

Fig. 1: Back-scatter electron images of the two investigated samples. Lighter regions belong to K-feldspar, darker to Na-feldspar. Horizontal bars in each case correspond to 100 μm.

Principles of feldspar thermal expansion

Hovis, G.[*], Medford, A., Conlon, M., Romanoski, A. & Tether, A.
Dept. of Geology and Environmental Geosciences, Lafayette College, Easton, PA, USA ([*]hovisguy@lafayette.edu)

Following the recent thermal expansion work of Hovis et al. [1] on $AlSi_3$ feldspars, we have investigated the thermal expansion of plagioclase, Ba-K, and Ca-K feldspar crystalline solutions [2]. X-ray powder diffraction data were collected between room temperature and 925°C on six natural plagioclase specimens ranging in composition from anorthite to oligoclase (and as well on their K-exchanged equivalents) and five synthetic Ba-K feldspars with compositions from 25 to 99 mol% $BaAl_2Si_2O_8$. The resulting thermal expansion coefficients for volume (α_V) have been combined with earlier results for end-member Na- and K-feldspars. Unlike $AlSi_3$ feldspars, Al_2Si_2 feldspars, including anorthite and celsian from the present study plus Sr- and Pb-feldspar from other workers [3,4], show essentially constant, and relatively limited, thermal expansion. In the context of structures where the Lowenstein rule requires Al and Si to alternate among tetrahedra, the proximity of bridging Al-O-Si oxygen atoms to divalent neighbours (ranging from 0 to 2) results in Ca-O (or Ba-O) bonds that are especially short. It is suggested that short bonds such as these have a partly covalent character resulting from the requirement for local charge balance. This in turn stiffens the structure. For feldspar series with coupled substitution, the change away from a purely divalent M-site occupant gives the substituting (less strongly bonded) monovalent cations increasingly greater influence on thermal expansion. Overall, thermal expansion in the feldspar system is well represented on a plot (Fig. 1) of α_V against room-temperature volume (V_{RT}), where one sees a quadrilateral bounded by data for (a) $AlSi_3$ feldspars whose expansion behaviour is governed largely by the size of the monovalent alkali-site occupant, (b) Al_2Si_2 feldspars whose expansion is uniformly limited by divalent cations having stronger, partially-covalent, bonds to bridging Al-O-Si oxygens, and (c,d) plagioclase and Ba-K feldspars where expansion behaviour across the series transitions from one control to the other. Overall, the coefficient of thermal expansion in any binary feldspar series is a linear function of V_{RT} between the pertinent end members. This makes it possible to predict the thermal expansion behaviour of any feldspar simply from knowledge of its chemical system and room-temperature volume.

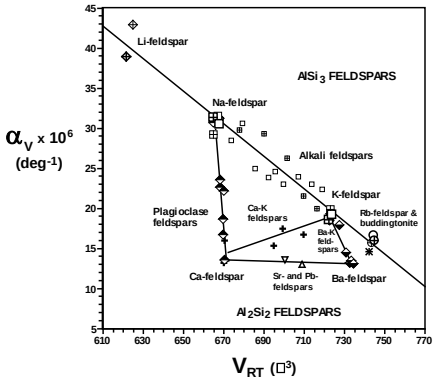

Fig. 1: Coefficient of thermal expansion (α_V) plotted against room-temperature unit-cell volume (V_{RT}) for members of the feldspar system.

[1] Hovis, G.L. et al. (2008) *Am. Mineral.*, **93**, 1568-1573. [2] Hovis, G.L. et al. (2010) *Am. Mineral.*, **95**, 1060-1068. [3] Henderson, C.M.B. (1984) in Henderson, C.M.B. (ed.) *N.E.R.C. Report 6*, 78-83. [4] Benna, P., Tribaudino, M. & Bruno, E. (1999) *Am. Mineral.*, **84**, 120-129.

Ardennite, tiragalloite and medaite: structural control of (As^{5+}, V^{5+}, Si^{4+})O_4 tetrahedra in silicates

Nagashima, M.[1,2*] & Armbruster, T.[1]
[1]Mineralogical Crystallography, Institute of Geological Sciences, University of Bern, Switzerland
[2]Dept. of Earth Science, Graduate School of Science and Engineering, Yamaguchi University, Yamaguchi, Japan
([*]piemontite@gmail.com)

Several silicate-minerals have (V^{5+}, As^{5+}, P^{5+})O_4-tetrahedra, such as ardennite ($Mn^{2+}{}_4MgAl_5[Si_5(As^{5+}, V^{5+})O_{22}](OH)_6$, Z = 2), tiragalloite ($Mn^{2+}{}_4[Si_3As^{5+}O_{12}(OH)]$, Z = 4), and medaite ($Mn^{2+}{}_6[Si_5(V^{5+}, As^{5+})O_{18}(OH)]$, Z = 4). Using electron-microprobe analysis (EMPA) and single-crystal X-ray diffraction methods, the crystal chemistry of ardennite (Salam-Château, Belgium and the Vernetto mine, Italy), tiragalloite (Gambatesa mine, Italy), and medaite (the Molinello mine, Italy and the Fianel mine, Switzerland), were studied.

Structure refinements converged to R_1 values of 2.10-5.67 %. According to chemical analysis, Σ(As + V + P) content increases with decreasing Si content. Thus, Si replaces pentavalent cations in tetrahedral coordination. The (As^{5+}, V^{5+}, P^{5+}, Si^{4+})O_4-tetrahedra are categorized by their connections to SiO_4 tetrahedra. The (As^{5+}, V^{5+}, P^{5+}, Si^{4+})O_4-tetrahedron of ardennite is isolated (0-bridging) and those of tiragalloite and medaite terminate a tetrahedral chain (1-bridging) (Fig. 1)

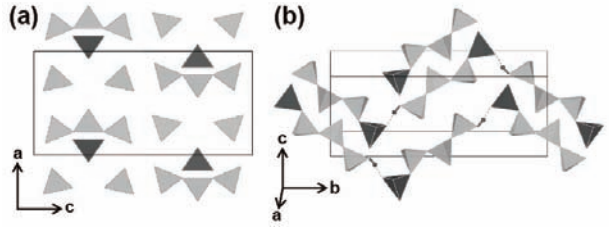

Fig. 1: Topology of tetrahedra in ardennite (a) and tiragalloite (b). (As, V)O_4-tetrahedra are represented as dark gray.

<T-O> of the isolated (As, V, P, Si)O_4-tetrahedron shows a positive correlation versus mean ionic-radius (Fig. 2). For (As, V, P, Si)O_4-tetrahedra with one T-O-T link, <T-O> and mean ionic-radius are also correlated. In addition, the longest bridging T-O bond occurs between (As, V, P, Si)O_4 and the adjacent SiO_4-tetrahedron. The bridging O atom is over-bonded to satisfy the charge requirement of Σ(As + V + Si).

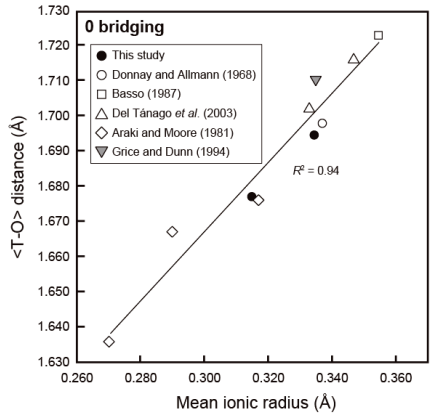

Fig. 2: Variation of <T–O> distances for 0-bridging (As^{5+}, V^{5+}, P^{5+}, Si^{4+})O_4-tetrahedra (Å).

Boron occupation of aluminium site in spinel- and olivine-related structures under high-pressure

Yoshiasa, A.[1*], Sakai, S.[2], Sugiyama, K.[2], Okube, M.[3], Wang, L.[1] & Nakatsuka, A.[4]
[1]Graduate School of Sciences and Technology, Kumamoto University, Kumamoto, Japan
([*]yoshiasa@sci.kumamoto-u.ac.jp)
[2]Inst. for Materials Research, Tohoku University, Sendai, Japan
[3]Materials and Structure Laboratory, Tokyo Institute of Technology, Yokohama, Japan
[4]Dept. of Advanced Materials Science and Engineering, Yamaguchi University, Ube, Japan

It is important to know pressure effect on solubility of boron in materials as solid solutions and crystal chemical behaviour of boron in the Earth's interior. Boron is the same group element as Al and its ionic radius is considerably small. The phase equilibrium and boron occupation of Al-site in spinel- and olivine-related structures in the Mg-Al-B-O system has been studied under high-pressure and high-temperature. Crystals of spinel- and olivine-related structure were synthesized under pressure of ~15 GPa at 1900 K using large volume multi-anvil-type apparatus. To determine the site occupancy of Mg, Al and B in crystal phases, the structure refinements of single-crystal diffraction method were carried out using a laboratory diffractometer with a imaging plate detector and using a four-circle diffractometer with synchrotron radiation at Photon Factory, Japan.

The olivine-type $MgAlBO_4$ sinhalite transforms to pseudosinhalite at 8.2 GPa and 1900 K. Pseudosinhalite is stable even at 12.0 GPa 1900 K. $MgAl_2O_4$ spinel decomposed to MgO and Al_2O_3 under the pressure of 14.5 GPa at 1273 K. Detailed structure of sinhalite and pseudosinhalite determined under pressure and temperature. B^{3+} ion can not occupy the octahedral Al site and it occupies only tetrahedral B site in sinhalite and pseudosinhalite. The B-Al substitution could not detect even at high pressure and high temperature. Site preferences of ions in olivine-type $MgAlBO_4$ sinhalite and pseudo-sinhalite obey the Pauling's first principle. $MgAl_2O_4$ spinel would prefer inverse spinel, if we considered Pauling's first principle. On the other hands, it is well known that $MgAl_2O_4$ spinel has a normal spinel and a peculiar site preference with higher symmetry, i.e. the octahedral sites are preferred by smaller Al ion than larger Mg ion.

The $MgAl_2O_4$ spinel can solve the much amount of boron. The maximum content of boron in $MgAl_{2-x}B_xO_4$ ($0<x<1$) spinel was about x=0.13 at 1273K and 11GPa. The small B ions do not occupy the small tetrahedral site and interstitial sites, but it occupies largely the octahedral site in $MgAl_2O_4$ spinel crystal [1]. We have estimated the cation distribution of each site from the reproduction of the observed average distance using the observed local bond distances for Mg-O and Al-O [2] and the normal B-O distance. The chemical formula of B-bearing spinel is estimated such as $(Mg_{0.50},Al_{0.50})[Al_{1.37},Mg_{0.50},B_{0.13}]O_4$. These spinel solid-solutions are largely disordered crystals and the inversion parameter grow up to 0.5 in the tetrahedral site. The site preference of boron depends greatly on the structure of host crystal. More ever, the smallest B^{3+} ion gives priority to the octahedral Al site most in Mg-Al-B spinel structure. The B^{3+} ions can replace considerably bigger Al^{3+} ion under pressure.

[1] Yoshiasa, A. et al. (2010) *Z. Anorg. Allg. Chem.*, in press.
[2] Ito, T. et al. (2000) *Z. Anorg. Allg. Chem.*, **626**, 42-49.

Crystal chemistry and the nomenclature of chromium-bearing tourmalines

Vereshchagin, O.S.*, Rozhdestvenskaya, I.V. Frank-Kamenetskaya, O.V. & Zolotarev, A.A.
Saint-Petersburg State University, Saint-Petersburg, Russia
(*oleg-vereschagin@yandex.ru)

Some aspects of crystal chemistry and nomenclature of chromium-bearing tourmalines on the basis of the original and published crystal structural refinements (Table 1) are considered.

All examined tourmalines were found in ultramafic and basic rocks. They belong to oksydravite - chromdravite series. The degree of the order of the Cr^{3+} cation distribution between Y and Z octahedral sites is distinguished.

Table 1: Characteristic of examined samples

Sub-group	Cr_2O_3 (wt. %)	Site population (apfu)		Deposit	Ref.
		Y	Z		
Order	1.48-5.90	0.19	0	Silver Knob, California, USA	[1]
		0.75	0	Middle Ural, Russia	Our data
		0.54 - 0.75	0	Middle Ural, Russia	
Dis-order	9,8-35.6	1.17	0.12	Outokumpu, Finland*	[2]
		1.29	0.89	Nausahi, India	[3]
		1.74 - 2.30	0.97 - 2.20	Sludyanka, Russia	[4]
		1.80	3.35	Onegsky progib, Centralnaya Kareliya, Russia	Our data
		1.56	3.60		[5]

Note: Cr^{+3} distribution was determined from the unit cell parameters and element composition [6].

Order subgroup. Cr^{3+}-ions occupy the Y-site. The compensating for an arising charge disbalance occurs according to the scheme: $^{Y}Cr^{3+}+^{W}O^{2-}\rightarrow{}^{Y}Mg^{2+}+^{W}OH^{-}$. Simultaneously the redistribution of Mg^{2+} and Al^{3+} ions begins: $^{Y}Mg^{2+}+^{Z}Al^{3+}\rightarrow{}^{Z}Mg^{2+}+^{Y}Al^{3+}$. The difference between <Y-O> and <Z-O> decreases from 0.116 (dravite [7]) to 0.065 Å (Cr-dravite); between the cation charge in Z and Y sites - from 0.9 to 0.4 ē, accordingly.

Disorder subgroup. Chrome ions occupy the Y and Z-sites. The incorporation of Cr^{3+} ions in Z- octahedra begins in the interval of 5.90-9.80 of Cr_2O_3 (wt. %). As a result of the $^{Z}Cr^{3+}\rightarrow{}^{Z}Al^{3+}$ substitution the <Z-O> bond distance increase; the difference between the <Y-O> and <Z-O> and the cation charges in Y and Z site decrease. In Al-free chromdravite from Kareliya with statistical distribution Cr^{3+} ions over octahedral sites this difference is 0.013 Å only. The cation charge Y site is more then Z site for 0.02 ē. Approved earlier the formula of chromdravite [8] demands revision. We suggest the ideal formula of this species $Na(Cr_2Mg)(Cr_4Mg_2)(BO_3)_3(Si_6O_{18})(OH)_4$. The increase of Cr^{3+} - ion content in tourmaline structure results in commensuraty of Y and Z octahedra.

Acknowledgements: This work was supported by FRBR grant 09-05-00769.

[1] Foit, F.F. Jr. & Rosenberg, P.E. (1979) *Am. Mineral.*, **64**, 788-798. [2] Peltola, E et al. (1968) *Geol. Soc. Finland Bull.*, **40**, 35-38. [3] Nuber, B. & Schmetzer, K. (1979) *N. Jb. Min. Abh.*, **137**, 184-197. [4] Bosi, F et al. (2004) *Eur. J. Mineral.*, **16**, 345-352. [5] Gorskaya, M.G et al (1984) *Sov. Phys. Crystallogr.*, **27**, 63-66. [6] Frank-Kamenetskaya O.V. & Rozhdestvenskaya, I.V. (2004) *Atomic defects and crystal structure of minerals*. Yanus, St.Petersburg. [7] Buerger, M.J. et al. (1962) *Acta Crystallogr.*, **15(4)**, 583-590. [8] Rumyantseva, E.V. (1983) *P. Russ. Mineral. Soc.*, **112**, 222-225 (in russian).

The relationships of bulk structure, surface structure, chemistry, and physical properties of mineral phases with six- and eight-membered silicate rings

Elmi, C.[1*], Brigatti, M.F.[1], Pasquali, L.[2,3], Montecchi, M.[2,3], Nannarone, S.[2,3], Laurora, A.[1] & Malferrari, D.[1]
[1]Dipto. di Scienze della Terra, Università di Modena e Reggio Emilia, Modena, Italy (*chiara.elmi@unimore.it)
[2]Dipto. di Ingegneria dei Materiali e dell'Ambiente, Università di Modena e Reggio Emilia, Modena, Italy
[3]TASC INFM-CNR Area Science Park, Basovizza (TS), Italy

The goal of this research is to better understand the relationship between chemical composition and atomic structure (both bulk and surface structure) of minerals having six-membered silicate rings, such as osumilite and eight-membered silicate rings, such as vesuvianite. Osumilite under investigation occurs in thin fissures within a rhyolite from the volcanic massif of Mt. Arci, Sardinia (Italy). Vesuvianite sample is from skarns of Somma-Vesuvius volcano (Italy) instead.

The osumilite and vesuvianite bulk structures were refined via single crystal X-ray diffraction. Osumilite sample is hexagonal, with symmetry *P*6/*mcc* and unit cell parameters a = 10.1550(6) c = 14.306(1) (Å). The structural formula is $(K_{0.729})_C(Na_{0.029})_{B'}(Si_{10.498}\ Al_{1.502})_{T1}(Al_{2.706}\ Fe^{2+}_{0.219}\ Mg_{0.075})_{T2}(Mg_{0.660}\ Mn_{0.091}\ Fe^{2+}_{1.258})_A O_{30}$. When compared to literature data [1], osumilite sample from Mt. Arci is characterized by a significantly high Fe^{2+} content (1.478 apfu) [2].

X-ray photoelectron spectroscopy (XPS) enabled the crystal chemical characterization of osumilite surface, where iron was still observed in its divalent state, thus confirming a similarity in osumilite surface and bulk chemical composition [2]. A further evidence of Fe oxidation state at osumilite surface is provided from X-ray absorption spectroscopy (XAS) at Fe-$L_{2,3}$ edge.

Vesuvianite is a complex tetragonal silicate. Vesuvianite ideal formula is $Ca_{19}(Al,Mg)_{13}(B, Si)_{18}O_{68}(OH, O, F)_{10}$ and crystallizes, generally, in the space group *P*4/*nnc* [3]. Vesuvianite presents in nature two different structural type: a high temperature type (at about 1000°C) and a low temperature type (at about 900°C) [3]. To recognize which type of vesuvianite our sample belongs to, we studied its thermal decomposition via X-ray powder diffraction method by using a Philips X'Pert PRO diffractometer equipped with X'Celerator area detector. Finally we could assure that our sample is a high temperature vesuvianite with high symmetry *P*4/*nnc*.

Unlike osumilite, vesuvianite surface is very complex to study because of its roughness on given faces of the crystal. However we could obtain preliminary information on the chemical composition of the surface via XPS and subsequently compare these data to bulk chemical composition. Moreover, unlike osumilite sample, vesuvianite presents Fe in octahedral site both in divalent and trivalent state, as confirmed by XAS experiments performed at the $L_{2,3}$ edge of iron [2,4].

[1] Armbruster, T & Oberhaesnsli, R. (1988) *Am. Mineral.*, **73**, 585-594. [2] Elmi, C. et al. (2010) *Phys. Chem. Miner.*, in press, available on line, DOI 10.1007/s00269-010-0357-4. [3] Groat, L.A. et al. (1992) *Can. Mineral.*, **30**, 19-48. [4] Zabiński, W. et al. (1996) *J. Therm. Anal.*, **46**, 1437-1447. [5] Van Aken P.A. et al. (1998) *Phys. Chem. Miner.*, **25**, 323-327.

Crystallochemical aspects of potassium-calcium silicates

Arroyabe, E.* & Kahlenberg, V.
Institute of Mineralogy and Petrography, University of Innsbruck, Austria (*Erik.Arroyabe@uibk.ac.at)

Although the phase relationships among main group element silicates are of fundamental importance for geosciences and materials engineering, it is a simple matter of fact that in a large number of binary and ternary systems there are still many fundamental problems to be solved. In this respect, the system K_2O-CaO-SiO_2 can serve as an excellent example. To be precise, the only comprehensive study, focussing on the more SiO_2-rich part of the system dates back to 1930 [1]. The authors explored the melting relations and reported the existence of seven different potassium calcium silicates. Only few more subsequent surveys dealt with the phases of the system. All these investigations were restricted to the presentation of basic crystallographic data. This general lack in structural knowledge is surprising since the ternary system is of definite interest for several technologically seminal processes that are related to applied mineralogy including, for example, production of inorganic membrane filters, adsorbents or concrete additives.

The presented results are part of an ongoing investigation on compound formation, sub-solidus equilibria and crystal chemistry of the ternary phases in the system K_2O-CaO-SiO_2. Before its start, there has been only one detailed structural consideration of a potassium calcium silicate [2]. In the meantime several "white spots" on the crystal structure map could be charted. The aim of this contribution is to give a systematic outline of the achieved findings and to discuss them on the basis of crystallochemical considerations.

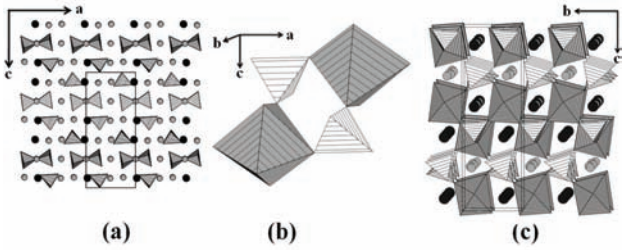

Fig. 1: Possible considerations of $K_2Ca_6Si_4O_{15}$ [3]: the compound can be described solely as **(a)** a mixed anion silicate, built of $[SiO_4]$ as well as $[Si_2O_7]$-units or as **(c)** a mixed polyhedral framework with Kroehnkite-type basic building chains **(b)**.

[1] Morey, G.W., Kracek, F.C. & Bowen, N.L. (1930) *J. Soc. Glass Technol.*, **14**, 149-187. [2] Kahlenberg, V., Kaindl, R. & Többens, D.M. (2006) *J. Solid State Chem.*, **179**, 1948-1956. [3] Arroyabe, E. et al. (2009) *J. Solid State Chem.*, **182**, 3254-3261.

Outstanding structural complexity of layered Pb oxyhalides induced by the presence of stereochemically active lone-electron pairs

Siidra, O.I.* & Krivovichev, S.V.
Dept. of Crystallography, Saint-Petersburg State University, Saint-Petersburg, Russia (*siidra@mail.ru)

In the course of our ongoing research in Pb(Il) oxyhalide structural chemistry [1], new layered lead oxyhalides have been prepared by different technique [2]. The crystal structures of synthetic compounds and minerals [3] were solved by direct methods. In all studied layered Pb(II) oxyhalides with so-called "additional" O atoms, lone electron pairs on the Pb^{2+} cations are stereochemical active. All of the studied crystal structures are based upon OPb_4 oxocentered tetrahedra.

Natural and synthetic layered lead oxyhalides are important phases that occur under variety of natural and technological conditions. They were found as secondary minerals in oxidation zones of mineral deposits: kombatite, sahlinite, parkinsonite, symesite, blixite, schwartzembergite etc.

All known layers of OPb_4 tetrahedra can be derived from the [OPb] tetrahedral layer that has been observed in the structure of litharge, PbO. To transform the [OPb] layer into any layer type observed in OPb_4 inorganic compounds and minerals, one has to excise certain blocks of OPb_4 tetrahedra from the former. Lead oxychlorides with layered PbO-derived blocks have first been described as synthetic compounds by Aurivillius [4]. Structural investigations revealed that the structures of these phases consist of PbO-like blocks [3] alternating with tetragonal sheets of halide ions. Recently investigated crystal structure of mereheadite $Pb_{47}O_{24}(OH)_{13}Cl_{25}(BO_3)_2(CO_3)$ [3] is another example of layered lead oxyhalides consisting of PbO blocks. Generally, there are three basic mechanisms associated with transition of the crystal structure from idealized version (ideal PbO blocks alternating with tetragonal sheets of halogen atoms): 1.replacement of PbO_4 groups by coordination groups of highly-charged cations, 2.$O^{2-} \leftrightarrow OH^-$ substitution, 3. insertion of additional Pb^{2+} cations into the halogen sheet.

A method of square lattices for the description of topologies of PbO-derivative layered structures is proposed [5]. The method is based upon reconstruction of an abstract model of 2D layer with black and white squares symbolizing tetrahedral positions and vacancies respectively.

[1] Siidra, O.I. et al. (2008) *Z. Kristallogr.*, **223**, 114-125. [2] Krivovichev, S.V. et al. (2006) *Inorg. Chem.*, **45**, 3846-3848. [3] Aurivillius, B. (1982) *Chemica Scripta*, **19**, 97-107. [4] Krivovichev, S.V. et al. (2009) *Mineral. Mag.*, **73**, 103-117. [5] Siidra, O.I. et al. (2006) *Vestn. S.-Peterb. Univ.*, **3**, 18-26.

Lead-gold inclusions together with gold and platinum traces within olivine: evidences from a TEM-AEM study

Ferraris, C.* & Lorand, J.P.
Laboratoire de Minéralogie et Cosmochimie, Muséum National d'Histoire Naturelle and CNRS (UMR 7202) Paris, France
(*ferraris@mnhn.fr)

Precious metals commonly form their own, discrete phases in mantle-derived rocks [1]. Although of sub-micrometric size, these phases may account for a non-trivial percentage of the whole-rock budget for gold. How do these gold micro-phases occur is not fully understood. Transmission and Analytical Electron Microscopy (TEM-AEM) analyses show the presence of sparse inclusions of a both a lead-gold intermetallic compound and evidences of gold traces within the plastic deformation microstructure of olivine crystals matrix from a lherzolite (Lherz massif - Eastern French Pyrenees). Otherwise, SEM investigation of the polished thin section of this lherzolite revealed one tiny native gold inclusion, 1 micrometer across, inside a serpentinized grain boundary.

The lead-gold phase appears as isolated platy crystals few hundred nano meters in length. Crystals appear generally irregularly shaped and less commonly as rectangular flat inclusions. AEM analyses clearly show that, besides signals coming from the surrounding olivine matrix, the inclusions are precipitates of Pb and Au in about 2:1 ratio. Selected Area Electron Diffraction (SAED) attempts on the biggest crystals indicated that very likely the Pb-Au intermetallic compound has crystallographic characteristic identifying it as possible anyuiite (Tetragonal, s.g. *I4*/*mcm*, a = 7.338 Å, c = 5.658).

More difficult, and at the moment without any specific evidence, is the almost constant presence of the Au chemical signal in AEM analyses from apparently pure olivine matrix. The signal is not homogeneously distributed excluding any kind of instrumental artefacts; the Au amount is within the range of 0.1 up to 0.5 wt%. SAED investigations give no evidences about the presence of nano inclusions and/or precipitates or exsolutions of a gold phase. In correspondence of volumes where the gold signal is stronger, low magnification TEM images show the presence of randomly distributed rectangular shaped areas about 100 nm long and 20 nm width. These areas are characterized by an extremely ordered alternation of dark and bright bands about 5 nm widths. TEM high resolution images show that in correspondence of such band alternations the olivine crystal structure is affected by extremely regular waved deformation, but again no evidences of Au are referable.

In our opinion, the coincidence of high Au signal within olivine showing the described deformation, are strong evidences about the presence of gold precipitates within the olivine plastic deformation microstructures. In which form and/or geometry the gold is present is not yet clear. Hopefully, ongoing investigations using high angular annular dark field (HAADF) detectors will allow discover of such isolated gold clusters within the olivine structure as it was the case for Ir-bearing rutile exsolutions within a Cr-rich spinel from a harzburgite from the same Pyrenean peridotite occurrence [2].

[1] Lorand, J.P. et al. (2010) *Earth Planet. Sci. Lett.*, **289**, 298-310. [2] Ferraris, C. & Lorand, J.P. (2008) *Earth Planet. Sci. Lett.*, **276**, 167-174.

X-ray and neutron Rietveld study of synthetic $Ca_2Al_{3-p}Mn^{3+}{}_pSi_3O_{12}(OD)$-piemontite

Akasaka, M.[1*], Nagashima, M.[2], Hamada, M.[1], Sano, A.[3] & Ejima, T.[1]
[1]Dept. of Geoscience, Shimane University, Matsue, Japan
([*]akasaka@riko.shimane-u.ac.jp)
[2]Dept. of Geosphere Sciences, Yamaguchi University, Yamaguchi, Japan
[3]Japan Atomic Energy Agency, Japan

Crystal structures of synthetic $Ca_2Al_{3-p}Mn^{3+}{}_pSi_3O_{12}(OD)$-piemontites were refined using X-ray and neutron powder diffraction method for the determination of hydrogen positions in epidote structure. The starting materials (s.m.s) of oxide mixture of stoichiometric compositions with p = 0.75, 1.0 and 1.1 and D_2O were used for hydrothermal synthesis experiments at 0.3-0.4 GPa and 500 ˚C. The products from s.m.s of p = 0.75 (0.3 GPa), 1.0 (0.3 GPa), 1.1 (0.3 GPa) and 1.1 (0.4 GPa) were piemontite (Pm) + anorthite + bixbyite (Bx), Pm + Bx + parawollastonite (Pwo) (Pm>>Bx,Pwo), Pm, and Pm + Bx + Wo (Pm>>Bx,Pwo), respectively. Average Al:Fe-ratio of piemontite synthesized from the p = 1.1 s.m. at 0.4 GPa was 2.12:0.83 (EPMA data), indicating decrease of Mn contents by crystallization of bixbyite.

The crystal structures of piemontite synthesized from p = 1.0 and 1.1 s.m.s at pressures of 0.3 and 0.4 GPa, respectively, and temperature of 500 ˚C, were refined using X-ray powder diffraction data, and the structure of the former was also refined using a neutron powder diffraction data. The X-ray and neutron diffraction data were obtained using an X-ray powder diffractometer with Cu$K\alpha$-radiation and JRR3-HRPD, respectively. The crystal structures were refined using RIETAN-FP program [1].

The R-factors for X-ray powder diffraction data of the piemontite from p = 1.0 s.m. were R_{wp} = 9.75, R_e = 6.01, and S = 1.62; the unit-cell parameters were given as a 8.8455(5), b 5.6676(2), c 10.1483(7) Å, and β 115.499(4)°; the site occupancies at M1 and M3 were refined as Al0.86Mn0.14(1) and Al0.55Mn0.45(1), respectively; thus, total Mn was 0.59 atoms per formula unit (apfu). The results of the refinements of the piemontite from p = 1.1 s.m. were R_{wp} = 10.66, R_e = 5.23, and S = 2.03; a 8.9154(7), b 5.7063(3), c 10.2285(9) Å, and β 115.543(5)°; the site occupancies at M1 and M3 of Al0.88Mn0.12(1) and Al0.30Mn0.70(1), respectively; total Mn was 0.82 atoms per formula unit (apfu) which is consistent with EPMA data. The refined unit-cell parameters, site occupancies and atomic positions are consistent with those after [2]. The structure refinement of the piemontite from p = 1.0 starting material using the neutron diffraction data resulted in the unit-cell parameters of a 8.854(2), b 5.6751(4), c 10.159(2) Å, and β 115.54(1)°, where the site occupancies at M1 and M3 were fixed to those refined using X-ray diffraction data. The O10-D distance derived from the refined positions of O10 and D without any constraint is 0.31 Å is considerably shorter than the published values.

[1] Izumi, F. & Ikeda, T. (2000) *Mater. Sci. Forum*, **321/324**, 198-203. [2] Nagashima, M. & Akasaka, M. (2004) *Am. Mineral.*, **89**, 1119-1129,

Scheelite- and molybdenite-bearing andradite skarn from Mraconia Valley, Romania

Anason, A.[*], Marincea, Ş., Ghineţ, C. & Iancu, A.
Geological Institute of Romania, Bucharest, Romania
([*]angela.anason@yahoo.com)

This contribution aims to provide new X-ray powder and scanning electron microscopy data on the main minerals from the skarn in the upper basin of Mraconia Valley, Almăj Mountains, Romania, as well as on the associated mineralization. The skarn develops at the very contact between crystalline limestones of the Neamţu Series and a porphyric granodiorite of unknown age, probably Triassic.

The skarn is mainly andraditic, but, beside andradite, plagioclase, potassic feldspar, feroactinolite, magnetite, epidote, apatite, vesuvianite and wollastonite can occur in significant proportions. Four stages of mineralization overprint the primary skarn: (1) a first stage, of high temperature, consists in the deposition of scheelite as impregnations in the mass of the andradite-bearing skarn; (2) a new hydrothermal stage overprints the first event, conducing to deposition of pyrite, chalcopyrite and calcite on the cracks and to impregnations of pyrite and chalcopyrite in the skarn mass; (3) a third hydrothermal stage conduced to massive deposits of chalcopyrite, pyrite, sphalerite, galena, scarce pyrrhotite and tertahedrite, which forms veins and lenses in the skarn mass; (4) a low temperature hydrothermal stage yields the formation of bornite and covellite on chalcopyrite but also of hematite (specularite) on magnetite.

Andradite is the main skarn mineral, accounting for up to 80% of the rock volume. The mineral is generally isotropic, but optically anomalous garnet can occur; both sectorial and lamellar "twinning" was described by Marincea [1]. The X-ray powder data recorded for six representative samples were used for the least-squares refinement of the unit-cell parameters. The obtained values [a = 12.006(4) Å – 12.066(3) Å] compare well with the values reported by [1] *i.e.* a = 11.984(3) Å – 12.041(3) Å, being indicative for andradite.

Scheelite is the mean exponent of the high-temperature hydrothermal phase, occurring as isolated crystals or clusters of crystals, generally included in the andradite mass. The individual crystals are up to 2 mm in length and up to 1 mm thick, and have a prismatic-bipiramidal, tetragonal habit. All the samples fluoresce in short wave UV light (λ = 254 nm). As observed by Marincea [1] the UV response colour is characteristic for two different generations of scheelite, as follows: (1) a first generation, with yellow fluorescence, characteristic for a Mo-bearing scheelite, associates only with andradite, and (2) a second generation, that fluoresces in blue-violet tints, contains minor powellite and associates with sulphides, pistacite, quartz and calcite. The cell parameters obtained as mean of those obtained for 4 scheelite samples, as refined by least-squares analysis of the X-ray powder data, are: a = 5.242(3) Å, c = 11.370(7) Å and V = 312.5(4) Å^3.

Molybdenite is widespread in the association from Mraconia. The mineral occurs on fissures affecting the granodiorite mass, near the contact, where it associates with quartz, pyrite and chalcopyrite, and as impregnations in the andradite-bearing skarn. Individual crystals, up to 1 mm across, have lamellar hexagonal habit and generally form sheave-like, rosette-like or scaly aggregates. The unit-cell parameters, obtained by least-squares refinement of the X-ray powder datasets obtained for eight representative samples are a = 3.151(6) Å, c = 12.292(9) Å and V = 105.7(2) Å^3.

[1] Marincea, Ş. (1992) *Rom. J. Miner Dep.*, **75**, 45-53.

Chabournéite from Monte Arsiccio mine (Apuan Alps, Tuscany, Italy): occurrence and crystal structure

Bonaccorsi, E.[1*], Biagioni, C.[1], Moëlo, Y.[2] & Orlandi, P.[1]
[1]Dipto. di Scienze della Terra, Università di Pisa, Italy
([*]elena@dst.unipi.it)
[2]Institut des Matériaux Jean Rouxel (IMN), Université de Nantes, France

Chabournéite is a very rare Tl-Pb-Sb sulfosalt found only in the hydrothermal deposit of Jas Roux (Hautes-Alpes, France) [1], at the Toya-Takarada mine (Okkaido, Japan) [2], and as an unnamed mineral at Hemlo gold mine [3]. The crystal structure of a Pb-rich chabournéite was determined by [4]. The As-rich isotype of chabournéite, dalnegroite, was discovered recently [5]. The new finding of chabournéite at the baryte-pyrite-iron oxides deposit of Monte Arsiccio allowed a new crystallographic study. At this locality, chabournéite is associated with baryte, pyrite, realgar, sphalerite, stibnite, and zinkenite.

Electron microprobe analyses collected on two different grains give (wt.%): Tl 16.81(27), Pb 10.65(17), Sb 41.75(17), As 6.59(4), S 23.43(11), total 99.24(36) and Tl 15.05(26), Pb 13.04(32), Sb 45.49(29), As 3.07(4), S 22.77(14), total 99.42(39). On the basis of Σ*Me* = 26 *apfu*, the formula of the chabournéite grains are $Tl_{3.79}Pb_{2.37}Sb_{15.79}As_{4.05}S_{33.65}$ and $Tl_{3.47}Pb_{2.97}Sb_{17.63}As_{1.93}S_{33.50}$, in agreement with the structural formula $Tl_{5-x}Pb_{2x}(Sb,As)_{21-x}S_{34}$. Crystal structure determination shows that this chabournéite is triclinic, space group *P*–1, with unit cell parameters *a* 8.150(2), *b* 8.716(2), *c* 21.579(4) Å, α 85.18(1)°, β 96.94(1)°, γ 88.60(1)°, *V* = 1515(1) Å^3. Due to the very small crystal size, intensity data were collected at the XRD beamline of the Elettra synchrotron facility (Basovizza, Trieste, Italy). The crystal structure was solved by direct methods and refined to $R = 0.048$ for all 3392 reflections with $F_o > 4\sigma(F_o)$.

The new crystal structure solution confirms the general features given by [4], but on the basis of a simpler, more symmetric unit cell, without any visible superstructure. While in [4] all cation positions correspond to pure sites (Tl, Pb, Sb or As), the new structure presents mixed (Tl,Pb), (Pb,Sb) and (Sb,As) sites, together with pure Tl, Pb and Sb sites. According to [6], it is built up on the basis of two kinds of layer. The first one, derived from the SnS archetype, is closely related to sartorite [7] and parapierrotite [8], and is here enriched with As, while the second one, of the PbS archetype, is As-poor. Weak bonding in the middle plane of this last layer may act as a cleavage plane.

The high Sb/As ratio of chabournéite from Monte Arsiccio appears as the main factor precluding the 2*a* superstructure visible in As-rich chabournéite from Jas Roux as well as in dalnegroite.

[1] Johan, Z. et al. (1981) *Bull. Minéral.*, **104**, 10-15. [2] Shimizu, M. et al. (1999) *Res. Geol.*, **20**, 31-37. [3] Harris, D. (1989) *Geol. Surv. Canada*, Econ. Geol. Report. [4] Nagl, A. (1979) *Z. Kristall.*, **150**, 85-106. [5] Nestola, F. et al. (2009) *Mineral. Mag.*, **73**, 1027-1032. [6] Makovicky, E. (1985) *Fortschr. Miner.*, **63**, 45-89. [7] Berlepsch et al. (2003) *Am. Mineral.*, **88**, 450-461. [8] Engel, P. (1980) *Z. Kristall.*, **151**, 203-216.

Occurrence of a new oxy-hydroxy iron(III) sulphate from Fornovolasco (Apuan Alps, Italy)

Bonaccorsi, E.[*], Biagioni, C. & Orlandi, P.
Dipto. di Scienze della Terra, Università di Pisa, Italy
([*]elena@dst.unipi.it)

A new oxy-hydroxy iron(III) sulphate from the small magnetite-pyrite ore body at Fornovolasco (Apuan Alps, Tuscany, Italy) was identified. The origin of this mineral is related to the action of strongly acid solutions derived from the alteration of pyrite in the old tunnels of Fornovolasco mines. It is strictly associated with other sulphates, like alum-(K), copiapite, halotrichite, melanterite, römerite, and voltaite. The new mineral occurs as bladed crystals, elongated on [010], up to 50 μm long and less than 5 μm across.

XRPD showed that this mineral is the natural analogous of the synthetic compound $Fe_4(SO_4)(OH)_{10}$. This new sulphate is monoclinic, with cell parameters *a* 16.085(2), *b* 3.054(1), *c* 10.929(2) Å, β 93.78(1)°, space group *C*2/*m*. Electron microprobe analyses give Fe_2O_3 63.33, SO_3 14.07, H_2O 17.18, sum 94.58. The sum of the wt% of oxides is low even after the addition of the calculated water content. This may be a consequence of the very small crystal size, which have a thickness of less than 5 μm.

Owing to the very small size, intensity data were collected at the XRD beamline of the Elettra synchrotron facility (Basovizza, Trieste, Italy). The crystal structure was solved and refined to $R = 0.078$ for all 259 reflections with $F_o > 4\sigma(F_o)$. Figure 1 shows the crystal structure of this oxy-hydroxy iron(III) sulphate.

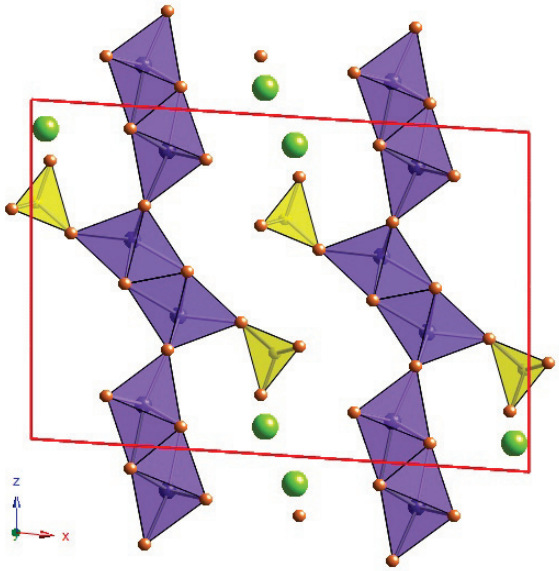

Fig. 1: crystal structure of the new mineral seen along [010].

The crystal structure is composed by ribbons of edge-sharing Fe-octahedra running along [010], linked together by corner-sharing to form wavy layers. As it is not possible to locate two $[SO_4]$ groups at distance of only 3 Å, it is probable that a regular alternation of $[SO_4]$ groups and H_2O molecules takes place along the **b** direction. Such ordered sequence should double the *b* parameter, with the occurrence of additional superstructure reflections. Actually, only continuous streaks were detected in the diffraction patterns.

According to the structural refinement and the bond-valence balance, the chemical formula of this new oxy-hydroxy iron(III) sulphate is $Fe^{3+}_4(SO_4)O_2(OH)_6{\cdot}2H_2O$.

Li-bearing pegmatites from Conţu, Romania

Călin, N.[*], Dumitraş, D.G. & Marincea, Ş.
Geological Institute of Romania, Bucharest, Romania
([*]nicolae_cln@yahoo.com)

Pegmatites from Conţu are hosted by micaschists and gneisses related to the Sebeş-Lotru Series (Southern Carpathians, Romania) [1]. Their mineralogical composition closely matches to that of the granitic Li-bearing pegmatites. The mineral composition is largely dominated by K-feldspar, spodumene, quartz, plagioclase, Li-bearing muscovite, but the accessory minerals include phosphates in the triphylite - lithiophilite heterosite – purpurite, and sicklerite – ferrisicklerite series, fluorapatite, cassiterite, tantalite, magnocolumbite, scarce schorl, beryl, uraninite, topaz and spessartine.

Spodumene is the main Li-bearing mineral, accounting for up to 20 % from the pegmatite volume. It occurs as large crystals of up to 20 cm in length, randomly distributed in the pegmatite mass and generally surrounded by feldspar and quartz. The color is greenish-white, which turns in bluish-green due to the alteration into kaolinite + cookeite. The cell parameters averaged for 17 spodumene samples, as refined by least-squares analysis of the X-ray powder data, are: a = 9.476(13) Å, b = 8.403(7) Å, c = 5.227(5) Å, β = 110.12(12)°, V = 390.8(7) Å^3.

Phosphates in the triphylite - lithiophilite series ($LiFePO_4$ - $LiMnPO_4$) generally occur as nests in the spodumene and feldspar mass. They form granular masses of greenish-gray color that turns locally into dark brown or black, due to the weathering. The mean unit-cell parameters, obtained as average of those refined by least-squares from the X-ray powder datasets obtained for two representative samples are: a = 4.713(7) Å, b = 10.378(3) Å and c = 6.043(6) Å.

Feldspar is the second phase as abundance in the pegmatites from Conţu, accounting for up to 25 % of the rock volume. Both primary and metasomatic phases were identified; chemical analysis and XRD revealed the presence of albite (cleavelandite), anorthite, oligoclase and microcline.

Muscovite is widespread in the pegmatite mass. Two types of muscovite could be distinguished: (1) a greenish Li-richer muscovite associated with spodumene, albite and quartz, resulted as secondary product of the rock metasomatism; and (2) a yellowish white Li-poor muscovite associated with quartz and K feldspar probably of primary origin. The cell parameters averaged for 23 muscovite samples, as refined by least-squares from the X-ray powder data, are a = 5.17(3) Å, b = 9.02(4) Å, c = 20.06(8) Å, β = 95,0(5)°, V = 931.6(48) Å^3.

Phosphates in the purpurite – heterosite series ($MnPO_4$ - $FePO_4$) occur as reddish-brown crusts, generally disposed on triphylite - lithiophilite. The unit-cell parameters taken as mean of those refined for four representative samples are: a = 5.83(2) Å, b = 9.77(3) Å, c = 4.776(5) Å.

Fluorapatite occurs as prismatic hexagonal crystals of up to 5 mm across and 8 mm in length, of white-greenish color. The unit cell parameters, determined as mean of 6 sets of individual values refined by least squares on the basis of X-ray powder data are a = 9.366(2) Å, c = 6.8833(7) Å and V = 522.81(2) Å^3. The Fourier-transform infrared spectrum recorded for a selected sample shows the presence of the OH and F stretching at 3570 cm^{-1}, of the OH libration at 634 cm^{-1} and of bands attributable to the PO_4 stretching motions (ν_3 antisymmetric stretching at 1033 cm^{-1}, ν_1 symmetric stretching at 971 cm^{-1}).

[1] Săbău, G., Apostoloiu, A. & Urcan, T. (1989) *D.S. Inst. Geol. Geophys.*, **74/1**, 259-262.

In situ high-temperature powder X-ray diffraction study of the synthetic $Ca_2Sb_2O_7$ weberite-type compound

Chelazzi, L.[1*], Boffa Ballaran, T.[2], Bindi, L.[3] & Bonazzi, P.[1]
[1]Dipto di Scienze della Terra, Università degli Studi di Firenze, Italy ([*]laura.chelazzi@unifi.it)
[2]Bayerisches Geoinstitut, Universität Bayreuth, Germany
[3]Museo di Storia Naturale, Università di Firenze, Italy

An *in situ* high-temperature powder X-ray diffraction study has been carried out from room temperature up to 1000°C on a sample of $Ca_2Sb_2O_7$ synthesised by direct reaction of the component oxides in a platinum crucible. The $Ca_2Sb_2O_7$ compound adopts an orthorhombic weberite structure (space group *Imma*) when synthesised under ambient pressure conditions, whereas the cubic pyrochlore structure is favoured with pressure higher than 6 GPa [1]. Most of the natural and synthetic $A_2B_2O_7$ oxides ($A=M^{2+}$; $B=M^{5+}$) adopt a zirconolite-polytype (commonly pyrochlore-like) or a weberite-polytype structure, depending on the kind of cations (ionic radius, electronegativity, etc.), as well as the pressure and/or temperature of crystallization. Therefore, investigation of their thermodynamics properties (e.g. thermal expansion and compressibility) is crucial in determining their stability fields.

In the range of temperature investigated in this study, the unit-cell parameters show a gradual increase with the increase of temperature and no phase transition has been observed. The bulk thermal expansion coefficient is $\alpha_V = 27.0 \times 10^{-6}$ K^{-1} and the cofficients of thermal expansion along various axes are: $\alpha_a = 9.52 \times 10^{-6}$ K^{-1}, $\alpha_b = 10.2 \times 10^{-6}$ K^{-1}, $\alpha_c = 7.51 \times 10^{-6}$ K^{-1}, showing an anisotropic behavior with increasing temperature.

The structure of the $Ca_2Sb_2O_7$ can be described as a sequence of pairs of polyhedral layers (*M* and *N*) stacked along [011]. As far as the cation sites are concerned, *M* and *N* layers have general formula AB_3 and A_3B respectively, where B are octahedral sites (B1 and B2) which accommodate Sb^{5+}. The octahedral framework gives rise to two types of larger cavities (A1 and A2) hosting Ca. With increasing temperature, the structure expands along the directions parallel to the layers more markedly than along the stacking axis, where the A1-O2 bonds are aligned. Indeed, being O2 oxygen the most underbonded of the structure, the A1-O2 bonds act as a constraint to the expansion in their direction. Due to the large uncertainties of the structural data, it is difficutl to constrain accurately the evolution of the polyhedral volumes with *T*. As general feature, the increase of temperature favours a regularization of the structure similar to that for the synthetic $Ca_2Os_2O_7$ [2].

[1] Knop, O. et al. (1980) *Can. J. Chem.* **58**, 2221-2224. [2] Reading, J. et al. (2002) *J. Mat. Chem.*, **12**, 2376-2382.

Crystal chemistry of a new CaMnMn-dominant member of the whiteite group

Chernyatieva, A.P.[1*], Krivovichev, S.V.[1], Yakovenchuk, V.N.[2] & Pakhomovsky, Y.A.[2]
[1]Dept of Crystallography, St.Petersburg State University, St. Petersburg, Russia (*nastya250@mail.ru)
[2]Geological Institute, Kola Science Center, Russian Academy of Sciences, Apatity, Russia

According to Moore and Ito [1], minerals of the whiteite group have the general formula $XM(1)M(2)_2M(3)_2(PO_4)_4(OH)_2\ 8H_2O$, where M(3) = Fe^{+3} for the jahnsite series, and Al^{3+} for the whiteite series. During investigations of secondary pegmatite phosphates from Hagendorf, we have located a whiteite-group mineral with X =Ca, M(1) = Mn, and M(2) = Mn. This composition has not been observed in the whiteite series so far. The X-ray diffraction data were collected using both STOE IPDS II and Bruker Smart APEX II diffractometers. Crystal structure determination indicated that the mineral is monoclinic, space grope *P*2/*a*, a = 15.020(5), b = 6.959(2), c = 10.137(3) Å, β = 111.740(4)°, Z = 2, D_{calc} = 2.677 g/cm^3. The crystal studied was microscopically twinned on (100) (which is usual for whiteite group [2]) with partial overlap of the diffraction spots from two twin components. The program HKLF5 [3] was employed in order to account for the effects of twinning. Examination of diffraction space using STOE images demonstrated that, in reciprocal space, diffuse streaks parallel to the **a*** axis are present, indicative for strong layer stacking disorder along the [100] direction. The structure was refined to $R1$ = 0.068 on the basis of CCD data.

Electron microprobe data provided the empirical formula $(Ca_{0.57}Zn_{0.24}Na_{0.14})_{0.95}(Mn_{0.80}Fe_{0.20})_{1.00}(Mn_{1.24}Fe_{0.58}Mg_{0.19})_{2.01}Al_{2.03}(PO_4)_4(OH)_2x8H_2O$, ideally $CaMnMnAl_2(PO_4)_4(OH)_2x\ 8H_2O$. This formula is in general agreement with the results of crystal-structure refinement, which provides site occupancies for the X site as $Ca_{0.55}Zn_{0.30}Na_{0.15}$, for the M(1) site as $Mn_{0.80}Fe_{0.20}$ and for the M(2) site as $(Mn_{1.24}Fe_{0.58}Mg_{0.19})$. These data support our suggestion that the mineral studied is a new CaMnMn-dominant member of the whiteite series of the whiteite group.

Acknowledgements: This work was supported by the Russian Ministry of Science and Education.

[1] Krivovichev, S.V. (2009) *Structural Crystallography of Inorganic Oxysalts*. Oxford Univ. Press, Oxford. [2] Mackay, A. (1976) *Phys. Bull*., **27**, 495. [3] Hawthorne, F.C. (1994) *Acta Cryst*., **B50**, 481-510. [4] Yushkin, N.P. (1982) *Zapiski VMO*, **111**, 432-442. [5] Hazen, R.M. et al. (2008) *Amer. Mineral*. **93**, 1693-1720. [6] Hopcroft, J.E. et al. (2001) *Introduction to Automata Theory, Languages, and Computation*, Addisson-Wesley, Boston. [7] Krivovichev, S. (2004) *Acta Cryst.*, **A60**, 257-262.

Mineral-like *M*1–*M*2–H-arsenates ($M1^{2+}$ = Sr, Ba, Cd; $M2^{2+}$ = Mg, Co, Ni, Cu, Zn): crystal structure of $Cd_{0.74}Mg_{2.76}(AsO_4)(HAsO_4)_2$

Đorđević, T.[1*], Stojanović, J.[2] & Karanović, Lj.[3]
[1]Institut für Mineralogie und Kristallographie, Universität Wien, Vienna, Austria (*tamara.djordjevic@univie.ac.at)
[2]Applied Mineralogy Unit, Institute for Technology of Nuclear and Other Mineral Raw Materials, Belgrade, Serbia
[3]Laboratory for Crystallography, Faculty of Mining and Geology, University of Belgrade, Serbia

An ongoing comprehensive study on hydrothermal synthesis, and crystallographic properties of arsenate(V) compounds in the insufficiently known system *M*1O–*M*2O–As_2O_5–H_2O yielded a large number of new *M*1–*M*2–H-arsenates that are characterized structurally, and, in part, by spectroscopic techniques. Among them are a few mineral-like compounds (Table 1).

Table 1: Mineral-like *M*1–*M*2–H arsenates

Chemical formula	Mineral-group	Ref.
$SrCo_2(AsO_4)(AsO_3OH)(OH)(H_2O)$	tsumcorite	[1]
$SrCo(OH)(AsO_4)$	descloizite-adelite	[2]
$CdCo(OH)(AsO_4)$	descloizite-adelite	[2]
$CdCu(OH)(AsO_4)$	descloizite-adelite	[3]
$BaZn_2(AsO_4)_2(H_2O)$	paracelsian	[4]
$Cd_{0.74}Mg_{2.76}(AsO_4)(HAsO_4)$	alluaudite	new

The crystal structure of the novel, hydrothermally synthesized Cd0.74Mg2.76(AsO4)(HAsO4) (Teflon-lined steel autoclave, 493 K, 8 days, Cd(OH)2 + MgO + 3As2O5·5H2O) was determined by single-crystal X-ray diffraction data. The compound is monoclinic, space group C2 with a = 11.992(2), b = 12.429(3), c = 6.7462(13) Å, β = 112.92(3)°, V = 926.2(3) Å³, Z = 4. The refinement yielded R1(F) = 0.031, wR2(F2) = 0.072 for 1895 unique reflections; for 1781 'observed reflections' with Fo2 ≥ 4σ(Fo2) R1(F) is 0.028. The crystal structure was solved from a racemic twin (twin ratio = 0.42(2):0.58(2)). All H atoms were found in a difference Fourier map and successfully refined as riding atoms, with restraints on the O–H bond distances of 0.82(2) Å. Uiso(H) values were fixed at 1.5 Ueq(O).

$Cd_{0.74}Mg_{2.76}(AsO_4)(HAsO_4)$ is related to the alluaudite-like compounds. They adopt general formula $A1A2M1M2_2(X1O_4)(HX2O_4)_2$. In minerals, *A*-position is mostly occupied with Na, Ca, Mn, *M*-position with Mn, Fe, Al, Mg, and *X* with P. Synthetic members show much broader chemical variability. Alluaudites crystallize monoclinic, and the most common space group is *C*2/*c*. The crystal structure consists of kinked chains of edge-sharing *M*1 and *M*2 octahedra that are stacked parallel to [101] and are connected by the *X*1 and *X*2 tetrahedra in the *b*-direction. These interconnected chains produce channels parallel to *c*-axis, where the large *A*1 and *A*2 cations are located.

The new compound represents previously unknown structure variant among alluaudites. The symmetry reduction from *C*2/*c* to *C*2 is probably the consequence of the cation type and quantity. In the $Cd_{0.74}Mg_{2.76}(AsO_4)(HAsO_4)$ *A*1 site is empty. In the *A*2 site are situated Cd atoms. The *M*1 site is shared between Mg and Cd, and the *M*2 site is filled with Mg.

Acknowledgements: Financial support of the Austrian Science Foundation (FWF) (Grant T 300-N19) and the Ministry for Science and Technological Development of the Republic of Serbia (Project Nos. 142030 and 19002) are gratefully acknowledged.

[1] Mihajlović, T. & Effenberger, H. (2004) *Mineral. Mag*., **68**, 757-767. [2] Đorđević, T. (2007) Mitt. Österr. Min. Gesellschaft, **153**, Meran, Italy, 40. [3] Effenbereger, H. (2002) *Z. Kristallogr., Suppl. Issue*, **19**, 85. [4] Đorđević, T. & Tillmanns, E. (2008) *Abstract Vol. Frontiers in Mineral Sci.*, Cambridge, UK, 99.

The Fe-Nb-S system

Drabek, M.[1*], Hybler, J.[2] & Rieder, M.[1,3]
[1]Czech Geological Survey, Prague, Czech Republic, ([*]milan.drabek@alumni.uni-heidelberg.de)
[2]Institute of Physics of the ASCR,v.v.i., Prague, Czech Republic
[3]CPIT, VŠB-TU Ostrava, Ostrava-Poruba, Czech Republic

Due to niobium's high affinity to oxygen, practically all of its minerals are oxides [1]. However, an iron niobium sulphide, edgarite ($FeNb_3S_6$), has been found in nature [2]. To better understand the phase relations of edgarite, we carried out experiments in the Fe-Nb-S system. The experiments were performed using the evacuated silica glass tubes technique, in the temperature interval 1000 – 400ºC. Because of unfavourable kinetics, some runs were performed in salt fluxes (in NaCl, KCl or KI) or in the presence of a small amount of iodine [3]. The central portion of the system is dominated by a broad solid solution Fe_xNbS_2 where 0.5>x>0 (14.2 - 0 at.% Fe). This Fe_xNbS_2 solid solution includes the composition of edgarite. Our experiments indicate that at T >742°C, the following univariant assemblages are stable: Fe_xNbS_2ss + $Fe_{1-x}S$ + S, Fe_xNbS_2ss + Nb_3S_4 + NbS, Fe_xNbS_2ss + $Fe_{1-x}S$ + Fe and Fe_xNbS_2ss + Fe + NbS. Below 742°C, pyrite comes into play, and the assemblage Fe_xNbS_2ss + $Fe_{1-x}S$ + S disappears in favour of assemblages, FeS_2 + Fe_xNbS_2ss + S and FeS_2 + Fe_xNbS_2ss + $Fe_{1-x}S$. Crystal structures of two phases were refined: 1) $Fe_{0.27-0.32}NbS_2$ (edgarite), space group *P*6322, *a*=5.7609(3) Å, *c*=12.1370(8) Å; 2) $Fe_{0.48}NbS_2$ ("Fe-rich phase"), space group *P*63/*mmc*, a=3.3322(2) Å, *c*=12.3533 Å. The experiments performed show that the Fe_xNbS_2 solid solution includes the composition of edgarite and participate in stable assemblages with iron sulphides. Under conditions prevailing in nature, Nb prefers oxides, but in order to bind with sulphur, apparently very specific sulphur/oxygen ratios are needed. So, the presence of edgarite probably indicates a low oxygen fugacity during its formation.

[1] Černý, P. & Ercit, T.S. (1989) in Möller et al. (eds.) *Lantahanides, Tantalum and Niobium*. Springer-Verlag, Berlin, 27-79. [2] Barkov, A.Y. et al. (2000) *Contrib. Mineral. Petrol.*, **138**, 229-236. [3] Hinode, H. et al. (1987) *J. Cryst. Growth*, **84**, 413-418.

Andorite VI and owyheeite from the El Zancudo deposit, Colombia: chemistry and structure

Gallego, A.N.[1*], Akasaka, M.[1] & Nakamuta, Y.[2]
[1]Dept. of Geosciences, Shimane University, Matsue, Japan ([*]albanurygh@yahoo.com)
[2]Kyushu University Museum, Kyushu University, Fukuoka, Japan

The El Zancudo Pb-Sb-Ag-bearing sulfosalts have been regarded as members of the andorite series, $Ag_xPb_{3-2x}Sb_{2+x}S_6$ (And_n: $n = 100x$), and the owyheeite solid solution, $Ag_{3+x}Pb_{10-2x}Sb_{11+x}S_{28}$ ($-0.13 < x < 0.20$). These two sulfosalts occur as aggregates in interstices between quartz and carbonates, along with Pb-Cu-Ag-sulfosalts, Ag-rich tetrahedrite, arsenopyrite, sphalerite, pyrite, galena and electrum [1]. The purpose of this study is to describe the occurrence of Pb-Sb-Ag sulfosalts from the El Zancudo deposit based on both chemistry and structural data.

Andorite and owyheeite occur as acicular crystals up to 1 mm long and less than 0.05 mm wide. They are opaque, brittle, and light gray in reflected light. Andorites with compositions ranging from $Ag_{0.96-1.00}Pb_{0.93-1.11}Sb_{2.96-3.31}S_6$ (And_{100}) were found in ores from the Albertos, Povenir and Manuela veins (Fig. 1). Andorite with compositions of $Ag_{0.78}Pb_{1.28}Sb_{2.79}S_6$ (And_{87}) and $Ag_{0.75}Pb_{1.73}Sb_{2.84}S_6$ (And_{74}) were also found in ores from Albertos and Manuela veins, respectively. The chemical formulae of owyheeite in ores from the Albertos, Colombiana and Castano veins are $Ag_{2.62}Pb_{8.79}Sb_{10.44}S_{28}$, $Ag_{2.95}Pb_{9.35}Sb_{10.70}S_{28}$, and $Ag_{3.04}Pb_{11.95}Sb_{12.96}S_{28}$ respectively. Although the Ag, Pb and Sb contents are somewhat variable, Ag:Pb:Sb-ratios are 1:3.33-3.93:3.62-4.26, which are similar to an ideal value of 1:3.33:3.67.

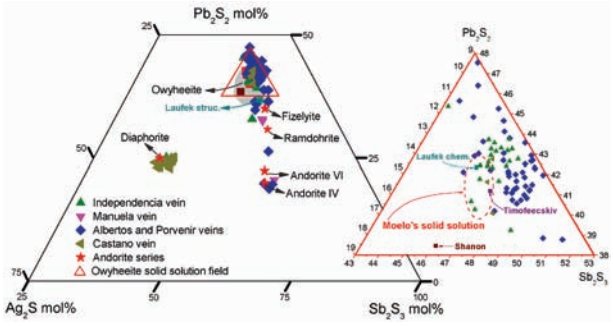

Fig. 1: Pb-Sb-Ag system showing the compositional variation of andorite and owyheeite from several veins in the El Zancudo deposit.

X-ray diffraction data of an aggregate (0.1×0.1×0.05mm) of $Ag_{1.0}Pb_{0.98}Sb_{2.96}S_6$ (And_{100})-andorite crystals from the Porvenir vein were collected using a Gandolfi camera and Imaging Plate system to reveal their structural properties. CuK_α radiation was generated using a rotating anode X-ray tube operated at 41 kV and 38 mA. The crystal structure was refined to that of andorite VI (a = 12.9864(5), b = 19.154(2), c = 25.6648(9) Å, V = 6383.9(6) Å^3 in space group $Pna2_1$) with R_{wp} = 6.89, R_e = 2.95 and S = 2.34. The unit-cell parameters are consistent with those of Sawada et al. [2]. The result that the andorite in this vein is andorite VI is consistent with the fact that And_{100} has the 6C type structure [2].

Although And100 was identified as andorite VI, andorite with calculated compositions of And87 and And74 cannot be identified as andorite IV (And93.75), ramdohrite (And68.75), or fizelyite (And62.5). Owyheeite also shows wide compositional variations, possibly due to the presence of very fine intergrowths of Pb-Sb-Ag sulfosalts.

[1] Gallego, A.N. & Akasaka, M. (2007) *Resource Geol.*, **57(4)**, 386-399. [2] Sawada, H. et al. (1987) *Z. Kristallogr.*, **180**, 141-150.

Gehlenite-bearing high-temperature skarns from Oraviţa, Romania

Ghineţ, C.*, Marincea, Ş., Anason, A. & Iancu, A.
Geological Institute of Romania, Bucharest, Romania
(*ghinet.cristina@yahoo.com)

Beside the similar occurrences at Cornet Hill, Măgureaua Vaţei, Ciclova – Tiganilor Brook, the Oraviţa – Crişenilor Brook gehlenite-bearing high-temperature skarns are quite exotic: fewer then forty such occurrences were reported so far in the world. These four occurrences circumscribe the Banatitic Magmatic and Metallogenetic Belt from Romania, and occur at the very contact between dioritic or monzodioritic bodies of Upper Cretaceous age and carbonaceous sequences of Mesozoic age.

At Oraviţa, apart from the sporadic occurrence of brown dark skarn mainly composed of well-crystallized late-stage andradite associated with Cu, W and Bi mineralization, most of the skarns are barren, with a striking predominance of yellow-geen vesuvianite on the inner exoskarn zone and of some coarse grained wollastonite-2*M* on the outer exoskarn.

The most conspicuous exception to the general schema just described is a small occurrence on Crişenilor Brook, first reported by Constantinescu et al. [1]. The inner skarn zone has a massive metasomatic texture and is mainly composed by medium to coarse gehlenite (up to 98% from the volume of the rock), which associates with monticellite, grandites, hydroxylellestadite and scarce spurrite. Late-stage metasomatic replacement of gehlenite by vesuvianite and clintonite is common, as well as its replacement by hibschite, thomsonite, 11 Å tobermorite and allophane as a result of late hydrothermal and weathering processes.

Gehlenite forms euhedral, rarely subhedral, grains, 0.3 mm to nearly 1 cm across. Individual crystals show a short prismatic to tabular habit; they seem to consist of tetragonal prisms {100} simply terminated with {001} pinacoids. Macroscopically, gehlenite has a color that varies from dark gray to bluish gray. In thin section, the mineral is colourless to pale yellow.

The solid solutions toward åkermanite + Fe-åkermanite varies from Ak 34.10 to Ak 51.18 (mean Ak 41.18), wheareas at Măgureaua Vaţei and Cornet Hill the composition varies from Ak 30.36 to Ak 42.88 (mean Ak 38.29) and from Ak 24.31 to Ak 41.73 (mean Ak 32.94), respectively. The content in Na-melilite is low (up to 3.60 mol.%). The cell parameters are highly variable: for the analyzed samples, *a* ranges from 7.679(3) to 7.734(3) Å whereas *c* varies from 5.043(3) to 5.065(3) Å. In the analyzed samples, the cell parameter remains practically constant within experimental errors, in spite of the advancing åkermanite-for-gehlenite substitution, due to the opposite influence of Na-melilite component. The åkermanite substitution prevails over the opposite influence of Na-melilite in increasing the cell volume and sums with the influence of Na-melilite in decreasing the *c* cell parameter. The record in the infrared-absorption spectra of a couple of bands located at ~ 855 cm^{-1} and ~670 cm^{-1} respectively, that may be tentatively assigned to Al-O-Al stretchings, is indicative for the presence of gehlenite instead åkermanite.

[1] Constantinescu, E., Ilinca Gh. & Ilinca, A. (1988) *D.S. Inst. Geol. Geofiz.*, **72-73/2**, 27-45.

Crystal chemistry of chromian pumpellyite from Osayama, Okayama Prefecture, Japan

Hamada, M.[1*], Akasaka, M.[1], Seto, S.[2] & Makino, K.[3]
[1]Dept. of Geoscience, Graduate School of Science and Engineering, Shimane University, Matsue, Japan
(*cr_pumpellyite@yahoo.co.jp)
[2]International Technical and Training Center EO Technical Division, EO Training andApplication Group, JEOL DATUM LTD., Akishima, Tokyo, Japan
[3]Dept. of Geology, Faculty of Science, Shinshu University, Matsumoto, Japan

The crystal structure and crystal chemistry of chromian pumpellyite from basic schist block in the Osayama ultramafic body, Okayama, Japan, were investigated to determine the distribution of chromium between two independent octahedral sites and structural changes caused by ionic substitutions in pumpellyite, $^{VII}W_8{}^{VI}X_4{}^{VI}Y_8{}^{IV}Z_{12}O_{56-n}(OH)_n$ (Z=1). The samples were collected from domains consisting of chromian pumpellyite, chromian phengite, chromian chlorite and chromite in a basic schist block [1,2]. Chromian pumpellyite is reddish gray to the naked eye, colorless in thin section, anhedral in form, and exhibits twinning. Grain size varies from 0.05 to 0.3 mm. Five pumpellyite crys-tals (ocp1211, ocp0604, ocp1028, ocp1013 and ocp1016) with 0.52, 1.65, 1.26, 1.94 and 1.43 Cr atoms per formula unit (EPMA data), respectively, were picked from a hand specimen for X-ray diffraction analysis. The reflection statistics and systematic absences were consistent with space groups *C*2/*m*. In the refinements including the H atoms for all samples, the *R*1 indices and *S*-values (goodness-of-fit) were converged to the smallest values of 4.08 % and 1.088 for ocp1211, 5.02 % and 0.954 for ocp0604, 6.32 % and 1.039 for ocp1028, 6.92 % and 1.564 for ocp1013 and 7.88 % and 1.583 for ocp1016. The resulting site populations at the *X* and *Y* sites are ocp1211: $(Mg_{1.88}Al_{1.51}Fe^{2+}_{0.38}Cr_{0.16}Mn^{2+}_{0.05}Ni_{0.02})^X(Al_{7.90}Ti_{0.07}V_{0.03})^Y$; ocp0604: $(Mg_{1.81}Al_{1.53}Cr_{0.42}Fe^{2+}_{0.18}Mn^{2+}_{0.04}Ni_{0.01})^X(Al_{7.34}Cr_{0.65}V_{0.01})^Y$; ocp1028: $(Al_{1.62}Mg_{1.60}Cr_{0.61}Fe^{2+}_{0.13}Mn^{2+}_{0.03}Ni_{0.01})^X(Al_{7.36}Cr_{0.61}V_{0.03})^Y$; ocp1013: $(Mg_{1.79}Al_{1.33}Cr_{0.47}Fe^{2+}_{0.33}Mn^{2+}_{0.08})^X(Al_{6.66}\ Cr_{1.31}V_{0.03})^Y$; ocp1016: $(Mg_{1.94}Al_{1.23}Cr_{0.38}Fe^{2+}_{0.37}Mn^{2+}_{0.08})^X(Al_{6.72}Cr_{1.25}V_{0.03})^Y$. Cr^{3+} ions in ocp1211 are distributed only in the *X* site. Cr/Al-ratio at the *X* site increases rapidly with the increase of total Cr content in contrast to the linear increase of Cr/Al-ratio at the *Y* site. The distribution coefficient of Cr and Al between the *X* and *Y* sites, defined as $(Cr/Al)^X/(Cr/Al)^Y$, is 1.66, 1.79, 3.09 and 4.54 for ocp1016, ocp1013, ocp0604 and ocp1028, respectively, indicating a stronger preference of Cr for the *X* site than the *Y* site as well as the result on the Sarany chromian pumpellyite [3]. The *a* and *b* axes increase with increasing Cr content, whereas the *c* axis is almost constant. The mean *Y*-O distances increase linearly with increased Cr^{3+} in the *Y* site. However, the mean *X*-O distances do not depend on the substitution of Cr^{3+} for Al^{3+} at the *X* site.

The bond valence sums and the difference Fourier synthesis indicate that hydroxyl groups are located at the O5, O7, O10 and O11 positions. FTIR spectrum shows main absorption bands at ca. 2911, 3220, 3397 and 3512cm^{-1} of OH stretching vibrations, indicating the presence of OH···O hydrogen bonds.

These results on the site populations of cations at the *X* and *Y* sites are significant not only for construction of a general rule on the behavior of transition elements in pumpellyite, but also for nomenclature.

[1] Sakamoto, S. (1997) *Mem. Fac. Sci. Eng. Shimane Univ. A*, **31**, 217-241. [2] Hamada, M. et al. (2008) *J. Miner. Petrol. Sci.*, **103**, 390-399. [3] Nagashima, M. & Akasaka, M. (2007) *Can. Mineral.*, **45**, 837-846.

An Al-Si order and composition model for scapolite solid solutions with conformation from HRPXRD data

Hassan, I.[1] & Antao, S.M.[2*]
[1]Dept. of Chemistry, University of the West Indies, Mona, Kingston, Jamaica
[2]Dept. of Geoscience, University of Calgary, Calgary, Alberta, Canada ([*]antao@ucalgary.ca)

An Al-Si order-disorder and compositional model is proposed for the scapolite solid solution. The model predicts the Al-Si order and average <T-O> distances from Me_0 to Me_{100}. This model is based on the observed order of clusters and on two solid solutions that meet at Me_{75} coupled with predicted composition and <T-O> distances. The $[Na_4{\cdot}Cl]^{3+}$ and $[NaCa_3{\cdot}CO_3]^{5+}$ clusters are ordered from $Me_{0\text{-}75}$, whereas the clusters $[NaCa_3{\cdot}CO_3]^{5+}$ and $[Ca_4{\cdot}CO_3]^{6+}$ are disordered from $Me_{75\text{-}100}$. To confirm the structural model, the structure of scapolite samples between $Me_{6\text{-}93}$ has been obtained by using synchrotron high-resolution powder X-ray diffraction (HRPXRD) data and Rietveld structure refinement. The structures were refined in space group $P4_2/n$. The <T-O> distances indicate that the T1 (= Si), T2 (= Al), and T3 (= Si) sites are fully ordered at $Me_{37.5}$, where complete cluster order occurs and gives rise to antiphase domain boundaries (APBs) based on Cl-CO_3 order instead of Al-Si order. From $Me_{37.5}$, the Al-Si order changes in a regular and predictable manner toward the end members, Me_0 and Me_{100}. For the first time, the observed cell parameters and several structural parameters show a discontinuity at Me_{75}, where the series is divided into two. There is no structural evidence to support any other transition. The T1 site contains only Si from Me_0 to $Me_{37.5}$; from $Me_{37.5}$ to Me_{100}, Al atoms enter the T1 site and the <T1-O> distance increases linearly to Me_{100}.

Brushite and gypsum in phosphogypsum deposits from Turnu Măgurele and Valea Călugărească (Romania)

Iancu, A.M.[*], Dumitraş, D.G. & Marincea, Ş.
Geological Institute of Romania, Bucharest, Romania
([*]aurash83@yahoo.com)

Phosphogypsum is a technogenic product remaining after the extraction of phosphoric acid from raw phosphate, mainly apatite [ideally $Ca_5(PO_4)_3(F,OH,Cl)$]. The technology of extraction consists normally in sulfuric leaching of apatite, which is the case in all the Romanian deposits. Huge quantities of phosphatic rock, of both sedimentary and magmatic origin were imported by Romania from Morocco, Jordan, Tunisia Syria, and Russia, respectively. This importation increases the volume of phosphogypsum wastes, which represent about 50 % in volume and 60 % in surface of the hazardous industrial wastes in the country. The major waste dumps are located at Valea Călugărească (56 ha of phosphogypsum stacks), and Turnu Măgurele (64 ha of phosphogypsum stacks).

This paper aims to give new data on the mineralogy and geochemistry of Romanian phosphogypsum, based on X-ray powder data (XRD), and scanning electron microscopy (SEM). XRD analyses of phosphogypsum from the four occurrences, corroborated with Fourier-transform infrared absorption spectra, showed that the main crystallized phases in this kind of material are gypsum ($CaSO_4{\cdot}2H_2O$), and bassanite ($CaSO_4{\cdot}0.5H_2O$), reaching up to 90 wt.% and 5 wt.% from the mass, respectively. A phosphate-bearing phase identified as ardealite or brushite is common. Impurities consist of quartz, calcite (probably resulted from the treatment of the plants with CaO, in order to reduce their acidity) and minor clay minerals. The SEM study shows that the masses macroscopically perceived as powder crusts are composed of randomly oriented or compact radiating aggregates of platy crystals Two kinds of aggregates were identified: (1) aggregates of randomly oriented interlocking or subparallel platy crystals, having locally rosette-like nuclei and (2) rosette-like aggregates of spherical shape, resembling to the gypsum "sand roses". These aggregates are sometimes composed by fully idiomorphic crystals issued by recent precipitation from acidic solutions, but normally they are composed by "broken" aggregates of parallel grown crystals sometimes reduced to cauliflower-like concretions.

The unit-cell parameters were refined by least squares, on the basis of the lines in the X-ray powder patterns recorded for "n" samples, indexed on an *I* 2/a monoclinic cell.

Table 1: Unit-cell parameters of gypsum from the Romanian phosphogypsum deposits

Cell parameter	Turnu Măgurele	Valea Călugărească
n	6	14
a (Å)	5.664 – 5.680	5.662 – 5.683
b (Å)	15.183 – 15.209	15.139 – 15.190
c (Å)	6.514 – 6.526	6.499 – 6.516
β (°)	118.35 – 118.46	118.08 – 118.47
V (Å^3)	493.0 – 495.8	491.3 – 493.9

The infrared absorption spectra of representative phosphogypsum samples from the two occurrences show vibrations which could be assumed to gypsum or bassanite, quartz and rarely calcite. The bands assumable to molecular water (the H-OH stretching vibrations at about 3610, 3550, 3405 and 3240 cm^{-1}, the corresponding bending vibrations at ~1685 and 1620 cm^{-1} and the composed modes at 2220 and 2130 cm^{-1}) are particularly well developed, suggesting a high level of hydration of the samples.

Structure refinement of high-pressure K- and Na- hexagonal aluminous phases

Kojitani, H.*, Iwabuchi, T., Kobayashi, M. & Akaogi, M.
Dept. of Chemistry, Gakushuin University, Tokyo, Japan
(*hiroshi.kojitani@gakushuin.ac.jp)

Hexagonal aluminous phase is one of Al-rich phases observed in high-pressure phases of the mid-ocean ridge basalt under lower mantle conditions. The general chemical formula of the hexagonal aluminous phase is $[M3][M2]_2[M1]_6O_{12}$ where the small-, middle-, and large-sized cations occupy the M1, M2, and M3 sites, respectively. Large size cations like K, Na and Ca can be accommodated in the M3 site. It was found that the hexagonal aluminous phase has relatively high K abundance [1]. It is also well known that ^{40}K is one of major heat sources in the Earth's history. Therefore, structure and properties of the hexagonal aluminous phase are of interest as a host phase of Al and K in the deep mantle. In this study, we tried to synthesize a hexagonal aluminous phase in the $KAlSiO_4$-$MgAl_2O_4$ system, described hereafter as K-hexagonal aluminous phase. Also, Rietveld analyses of K-hexagonal aluminous phase and a hexagonal aluminous phase in the $NaAlSiO_4$-$MgAl_2O_4$ system (Na-hexagonal aluminous phase) were performed to examine detailed crystal structures.

K-hexagonal aluminous phases was synthesized by heating a gel with $KMg_2Al_5SiO_{12}$ composition at 20 GPa, 1500 °C for one hour using a Kawai-type high-pressure apparatus. Similarly, Na-hexagonal aluminous phase was synthesized by keeping a mixture of high carnegieite-type $NaAlSiO_4$ and $MgAl_2O_4$ spinel ($NaAlSiO_4$:$MgAl_2O_4$ = 2:3 in mole ratio) at 22 GPa, 1500 °C for two hours. Compositions of recovered samples were analysed by SEM-EDS. Their XRD profiles for the Rietveld analysis were obtained by a powder X-ray diffractometer (Rigaku RINT2500V, 45 kV, 250 mA, Cr Kα). Crystal structures of the K- and Na-hexagonal aluminous phases were refined by the RIETAN-2000 program using a crystal structure model based on $CaMg_2Al_6O_{12}$ hexagonal aluminous phase [2].

Measured compositions of K- and Na-hexagonal aluminous phases were $K_{1.01(3)}Mg_{2.01(1)}Al_{4.81(2)}Si_{1.13(2)}O_{12}$ and $Na_{1.04(2)}Mg_{1.88(2)}Al_{4.64(2)}Si_{1.32(2)}O_{12}$, respectively. This is the first report of the synthesis of K-hexagonal aluminous phase in which half of the M3 sites are occupied by only K. The results of the Rietveld refinement indicate that the average sizes of all cation sites in both the K- and Na-hexagonal aluminous phases are consistent with those expected from ionic radii of accommodated cations. Size and shape of $M1O_6$ octahedra are changed by the substitution of Si for Al in the M1 site. It is suggested that this change in the M1 site may make possible to adjust the size of the M3 and M2 sites. Furthermore, it was found that average size of $(Al, Si)O_6$ octahedra in a crystal structure consisting of double chains of $(Al, Si)O_6$ octahedra decrease linearly with increasing Si content by combining our results with those of calcium ferrite-type $MgAl_2O_4$ and $NaAlSiO_4$, and hollandite-type $KAlSi_3O_8$. In the $NaAlSiO_4$-$MgAl_2O_4$ join, Na-hexagonal aluminous phase is formed in the relatively wide compositional range from 50 to 70 mol% in $NaAlSiO_4$ at pressure above about 18 GPa [3]. The fact can be explained by possible exchange of Mg^{2+} for Na^+ in the M2 site and by shrinkage and deformation of $M1O_6$ octahedra with the coupled substitution: $^{M1}Mg^{2+} + {}^{M1}Al^{3+} \rightarrow {}^{M2}Na^+ + {}^{M1}Si^{4+}$.

[1] Miyajima, N. et al. (2001) *Am. Mineral.*, **86**, 740-746. [2] Miura, H. et al. (2000) *Am. Mineral.*, **85**, 1799-1803. [3] Ono, A. et al. (2009) *Phys. Earth Planet. Int.*, **174**, 39-49.

The ternary skutterudites – ordered or disordered? The case of $FeSb_2Te$ and $IrGe_{1.5}Se_{1.5}$

Laufek, F.[1*] & Navrátil, J.[2]
[1]Czech Geological Survey, Prague, Czech Republic
(*frantisek.laufek@geology.cz)
[2]Joint Laboratory of Solid State Chemistry of IMC ČR and University of Pardubice, Pardubice, Czech Republic

The compounds with the skutterudite structure (general formula MX_3 where M = Co, Rh or Ir; X = P, As or Sb; $Im\bar{3}$ symmetry) have become of interest in materials science in last two decades because these compounds posses attractive transport properties for thermoelectric applications. Ternary skutterudites are phases isoelectronic to the binary skutterudites and can be obtained by isoelectronic substitution on the anion site, X (e.g. $CoGe_{1.5}Te_{1.5}$ [1]) or on the cation site M (e.g. $Fe_{0.5}Ni_{0.5}Sb_3$ [2]).

The ternary skutterudites $FeSb_2Te$ and $IrGe_{1.5}Se_{1.5}$ were synthesised from individual elements by high-temperature solid-state reactions using silica glass tube technique. Their crystal structures were characterized by powder X-ray diffraction.

The crystal structure of $IrGe_{1.5}Se_{1.5}$ compound ($R\bar{3}$, a = 12.09 Å, c = 14.88 Å) can be derived from simple cubic skutterudite structure, where Ge and Se atoms show long-range ordering in planes perpendicular to the [111] of the original cubic cell. This ordering lowers the symmetry from cubic to trigonal ($R\bar{3}$). Nevertheless, the $a^+a^+a^+$ tilt system of octahedra of the parent skutterudite structure MX_3 is preserved. This compound is isostructural with $CoGe_{1.5}Te_{1.5}$ [1] synthetic phase and both compounds can be considered as anion-ordered ternary skutterudites.

Contrary to that, the $FeSb_2Te$ phase shows simple cubic skutterudite structure with cubic symmetry ($Im\bar{3}$, a = 9.10 Å). No indication of ordering of Sb and Te atoms was observed. Hence this phase can also be viewed as a ternary skutterudite, however with a disordered crystal structure.

[1] Vaqueiro, P. et al. (2006) *J. Solid. State Chem.*, **181**, 768-776. [2] Kjekshus, A. et al. (1976) *Acta Chem. Scand.*, **A28**, 99-103.

New features in VESTA: a three-dimensional visualization system

Momma, K.[1*], Izumi, F.[1,2] & Ida, T.[2]
[1]Quantum Beam Center, National Institute for Materials Science, Tsukuba, Japan ([*]MOMMA.Koichi@nims.go.jp)
[2]Ceramics Research Laboratory, Nagoya Institute of Technology, Nagoya, Japan

VESTA is a crystallographic tool for visualization and investigation of crystal structures and volumetric data such as electron and nuclear densities, Patterson functions, electrostatic potentials, wave functions, *etc*. [1]. Recently, we have added a new feature of drawing the external morphology (faces) of crystals to VESTA. All the symmetrically equivalent faces are automatically generated from indices input by users according to point-group symmetry. Faces inconsistent with point-group symmetry may also be added for ease of modelling crystal habits. Crystal faces can be overlapped with a structural model (Fig. 1) and isosurfaces of volumetric data. Multiple lattice planes, which serve to show orientation of cleavages, can be inserted as well.

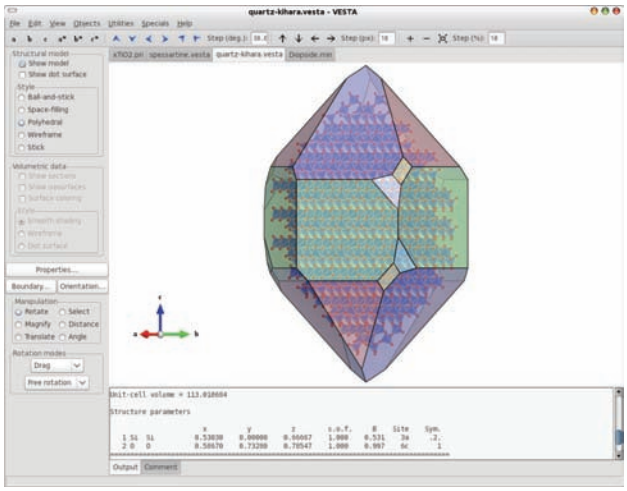

Fig. 1: A composite image of coordination polyhedra and external morphology for quartz.

For close investigation of volumetric data, we implemented another new feature of their integration by Voronoi tessellation. Integration of electron densities or densities of coherent scattering lengths, b_c, allows us to calculate site occupancies and assign chemical species to sites during structure refinement because the resulting values of integral are little affected by thermal motion of target atoms. Table 1 exemplifies an application of Voronoi tessellation to electron densities determined for rutile from X-ray powder diffraction data by a maximum entropy method.

Table 1: Voronoi tessellation for electron densities in rutile

	Peak density ($Å^{-3}$)	Number of electrons	Voronoi volume ($Å^3$)
Ti	303	20.0	7.7
O	57	9.0	11.8

Other new features added to VESTA include (a) overlaying multiple structures, (b) calculation of electron and nuclear densities from structure parameters, (c) extended bond-search algorithm to allow more sophisticated search for complex molecules and cage-like structures, (d) support for custom symmetry operations input by users, and (e) improved support for various file formats.

[1] Momma, K. & Izumi, F. (2008) *J. Appl. Cryst.*, **41**, 653-658.

X-ray Rietveld and ^{57}Fe Mössbauer studies of epidote and piemontite on the join $Ca_2Al_2Fe^{3+}Si_3O_{12}(OH)$ – $Ca_2Al_2Mn^{3+}Si_3O_{12}(OH)$ formed by hydrothermal synthesis

Nagashima, M.[1,2*] & Akasaka, M.[1]
[1]Dept. of Geoscience, Faculty of Science and Engineering, Shimane University, Matsue, Japan
[2]Dept. of Earth Science, Graduate school of Science and Engineering, Yamaguchi University, Yamaguchi, Japan
([*]piemontite@gmail.com)

Fe^{3+} and Mn^{3+} distributions on octahedral M1, M2 and M3 sites in synthetic epidote/piemontite from $Ca_2Al_2Fe^{3+}{}_qMn^{3+}{}_{1-q}Si_3O_{12.5}$ starting material and their effects on the crystal structure were investigated using X-ray Rietveld and ^{57}Fe Mössbauer methods. Epidote and piemontite were crystallized as almost single phases from q = 1.0, 0.75, 0.5 and 0.25 starting materials at P_{fluid} of 200–400 MPa and a temperatures of 500°C, using standard cold-seal pressure vessels. The Mn_2O_3-MnO_2 buffer was used to produce fO_2 adequate to maintain Fe^{3+} and Mn^{3+}. The Rietveld refinements converged to goodness-of-fit ranges from 1.21 to 1.60 (Fig. 1).

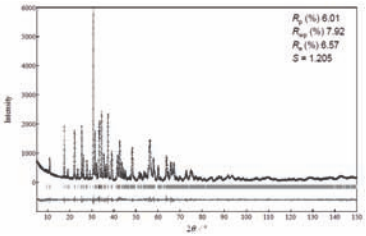

Fig. 1: Rietveld refinement plot for the product from q = 0.25 starting material at 370 MPa and 500°C (Run No. 30).

At this temperature, site preferences of $\Sigma(Fe^{3+} + Mn^{3+})$ for octahedral sites are M3 > M1 (>> M2) (Fig. 2). K_D-values of $\Sigma(Fe^{3+} + Mn^{3+})$, where $K_D = [(Fe^{3+} + Mn^{3+})/Al]^{M1}/[(Fe^{3+} + Mn^{3+})/Al]^{M3}$, (0.05–0.13) are similar to those of individual Mn^{3+} and Fe^{3+} versus Al^{3+}, respectively. However, the K_D-values of Fe^{3+} and Mn^{3+} for M1 and M3, where $K_D = (Fe^{3+}/Mn^{3+})^{M1}/(Fe^{3+}/Mn^{3+})^{M3}$, vary with $Fe^{3+}{}_{Total}$: $Mn^{3+}{}_{Total}$-ratios. In epidote with Fe^{3+} content larger than 0.4 atoms per formula unit (apfu) and Mn^{3+} less than 0.6 apfu, Fe^{3+} has a stronger preference for M1 than Mn^{3+}. In piemontite with 0.12 Fe^{3+} and 0.73-0.78 Mn^{3+} apfu, the preference of Mn^{3+} for M1 is greater than that of Fe^{3+}. The site occupancies of individual Mn^{3+} and Fe^{3+} are governed by the individual K_D values and the Mn^{3+} and Fe^{3+} concentrations in corresponding epidote and piemontite. Variations of the unit-cell parameters indicate the combined result of linear variation due to Al ↔ Fe^{3+} substitution and nonlinear variation due to Al ↔ Mn^{3+} substitution.

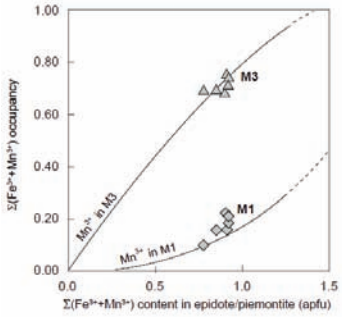

Fig. 2: Variations of the $\Sigma(Fe^{3+} + Mn^{3+})$ occupancies at M1 and M3 against $\Sigma(Fe^{3+} + Mn^{3+})$ contents in synthetic epidote/piemontite.

Re-investigation of structure of vanadinite, $Pb_5(VO_4)_3Cl$: libration of VO_4 tetrahedron and anisotropic ADPs of Cl

Niinou, M. & Okudera, H.*
Dept. of Earth Sciences, Kanazawa University, Kanazawa, Japan (*okudera@kenroku.kanazawa-u.ac.jp)

Vanadinite, $Pb_5(VO_4)_3Cl$, is one of Pb-bearing chlorapatites. Its structure has been known [1,2], and its structure had not been refined with anisotropic displacements of oxide ions in precision.

Crystals we employed (from Mibladen, Morocco) were nearly perfect: Impurity was undetectable with JEOL 8800 EPMA, and X-ray photographs showed no sign of superstructure in any direction.

Conventional single-crystal X-ray diffraction experiments (a Rigaku AFC-5S, Mo-Kα radiation, 2θ up to 70°, 12664 Bragg points) on nearly spherical vanadinite ($r \approx 0.08$ mm) yielded reasonable results. Least-squares calculation converged at $R_{(F)}$ = 3.76% for 40 parameters with 610 averaged F_{obs}s. Anisotropy in ADPs at oxide ion sites and smaller ADPs at V site than those at Pb sites indicate librational motion of the VO_4 tetrahedron. These observations indicate VO_4 tetrahedron behaving as a rigid body in the structure.

Thermal vibration ellipsoid at the Cl site is elongated along [001], while that in pyromorphite was nearly isotropic [3]. In $A_5(PO_4)_3Cl$ chlorapatites, the amplitude along [001] of the thermal vibration ellipsoid at the Cl site becomes larger with decreasing $rA(2)^{2+}$ [3,4].

Similar consideration can be made among $A_5(BO_4)_3Cl$ compounds: The larger the void in the $A(2)_3$ regular triangle (at z = 1/4) the larger the u_{33} (vibrational amplitude along [001], Å^2) at the Cl site. The size of the void (approximated as a sphere) and u_{33} were r = 1.337 Å and 0.013 Å^2 for pyromorphite, r = 1.346 Å and 0.022 Å^2 for $Sr_5(PO_4)_3Cl$, and r = 1.389 Å and 0.023 Å^2 for vanadinite. Similarly, the larger the void in the $A(2)_6$ octahedron the larger the u_{11} (amplitudes in directions normal to [001], Å^2). As a result, anisotropy in ADPs (= u_{33}/u_{11}) is larger in vanadinite than in pyromorphite, while not as highly anisotropic as in $Sr_5(PO_4)_3Cl$.

Crystallographic data: space group $P6_3/m$, $a = b$ = 10.317(1) Å, c = 7.336(1) Å.

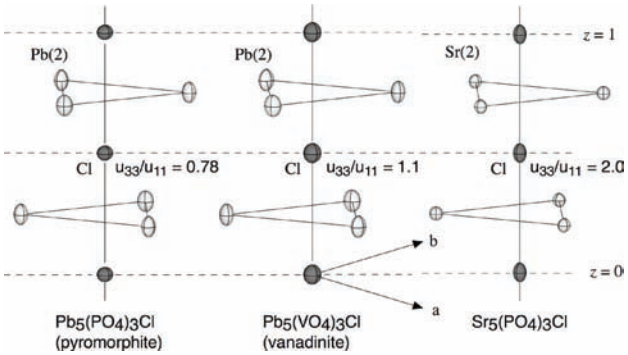

Fig. 1: ORTEP diagrams (70% probability) of anion channel along the c axis of some chlorapatites. $Sr_5(PO_4)_3Cl$ from ref. [4].

[1] Dai, Y.S. & Hughes, J.M (1989) *Can. Mineral.*, **27**, 189-192. [2] Laufek, F., et al. (2006) *J. Czech Geol. Soc*., **57**, 271-275. [3] Hashimoto, H. & Matsumoto, T. (1998) *Z. Kristallogr*., **213**, 585-590. [4] Sudarsanan, K. & Young, R.A. (1974) *Acta Crystallogr*., **B30**, 1381-1386.

The structural deformations of three $Ca_2(Ge_x, Si_{1-x})O_4$ olivines

Nishi, F.[1*] & Miyawaki, R.[2]
[1]Saitama Institute of Technology Fukaya, Saitama, Japan (*nishi@sit.ac.jp)
[2]National Museum of Nature and Science, Tokyo, Japan

Three kinds of structures of olivine whose compositions were Ca_2SiO_4, $Ca_2Si_{1/2}Ge_{1/2}O_4$ and Ca_2GeO_4 were synthesized. The average bond lengths of the M1 octahedron among three structures were not significantly different. Moreover, those of the M2 octahedron among three were not significantly different, too. We paid attention to the O-M-O bond angles of M1 and M2 octahedra. In case of the olivine structures, the oxygen atoms are almost arranged in the scheme of the hexagonal closest packing. Although the ideal bond angles of the O-M-O of the ortho-octahedra are just 90°, those values of this study derived from the structure analysis showed the values between 80° and 100° widely. As an indicator of the structural deformation of the real octahedra, we noticed of the differences between each O-M-O bond angle and 90° (the ideal bond angle). Those differences are 12 values per a octahedron and they were summed up after being made the absolute values. The indicators were calculated about the M1 and the M2 octahedra in three structures (Fig. 1).

As the result, the indicators of the M1 octahedra are 135.1(3), 125.2(3) and 119.0(6) degrees for Ca_2SiO_4, $Ca_2Si_{1/2}Ge_{1/2}O_4$ and Ca_2GeO_4 respectively. Those of the M2 octahedra are 108.2(3), 97.4(3) and 88.4(6) degrees for Ca_2SiO_4, $Ca_2Si_{1/2}Ge_{1/2}O_4$ and Ca_2GeO_4. It may be said that the more those indicators increase, the more the structure is unstable. We may conclude that Ca_2GeO_4 is most stable but Ca_2SiO_4 is most unstable among three structures, judging from this geometrical consideration.

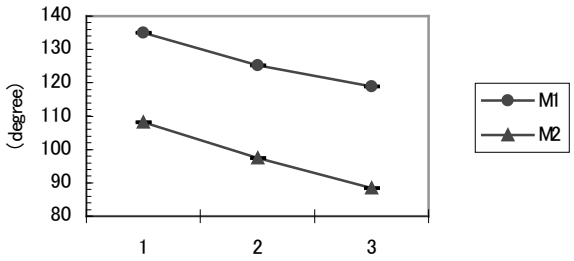

Fig. 1: Variations of the indicators for three olivines (1=Ca_2SiO_4, 2=$Ca_2Si_{1/2}Ge_{1/2}O_4$, 3=Ca_2GeO_4).

As seeing the crystal structure of olivine, we can realize that the deformations are caused by the shared edges of the octahedra and the tetrahedra. The lengths of the shared edges are increasing in accordance with increasing the Ge amounts at the (Si, Ge)-tetrahedral site where Si and Ge atoms are disordered. The lengths of the more shared edges become closer to the lengths of the edges of the ideal ortho-octahedron. As the results, the octahedra which have the longer shared edges have the less structural deformations. In other words, they are more stable. This conclusion supports our conclusion.

Crystal-chemistry of synthetic Mn-bearing clinoamphiboles and phyllosilicates

Papin, A. & Robert, J.-L.*
Institut de Minéralogie et de Physique des Milieux Condensés, Université Pierre et Marie Curie, Paris, France
(*jean-louis.robert@impmc.upmc.fr)

The behaviour of Mn in rock-forming minerals strongly depends on its valence state, i.e. of oxygen fugacity. The crystal-chemistry of Mn in series of synthetic clinoamphiboles (richterite - $^{[M4]}$Mn-richterite, richterite - $^{[M4]}$Mn-cummingtonite and tremolite - $^{[M4]}$Mn-cummingtonite) and phyllosilicates (talc and phlogopite) prepared by hydrothermal synthesis at 700°C for amphiboles and 600°C for phyllosilicates, under different fO_2 conditions has been investigated mainly by XRD and FTIR spectroscopy. Mn^{2+} is a quite large cation (0.83 Å) intermediate in size between Mg^{2+} and Ca^{2+}. Therefore, it is supposed to be able to occupy different sites in the clinoamphibole structure, replacing Ca^{2+} at M4 sites and/or Mg^{2+} at M(1,2,3). The $Ca^{2+} \rightarrow Mn^{2+}$ substitution is observed along the join richterite $Na(NaCa)Mg_5Si_8O_{22}(OH)_2$ - $^{[M4]}$Mn-richterite $Na(NaMn)Mg_5Si_8O_{22}(OH)_2$, under NNO buffering conditions. Mn^{2+} completely replaces Ca^{2+} and partially Na^+ at M4, the charge imbalance is compensated by the loss of Na^+ at the A-site. The composition shifts towards $^{[M4]}$Mn-cummingtonite $\square Mn_2Mg_5Si_8O_{22}(OH)_2$. The is no evidence for $Mg^{2+} \rightarrow Mn^{2+}$ substitution at M(1,2,3) sites in this case. Along the tremolite $\square Ca_2Mg_5Si_8O_{22}(OH)_2$ - $^{[M4]}$Mn-cummingtonite join, the situation is different. Mn^{2+} also replaces Ca^{2+} at M4, but also Mg^{2+} at M(1,2,3) and some Mg^{2+} shifts to M4. All M-sites incorporate Mn^{2+} in this case. The introduction of Mn at M(1,2,3) sites in clinoamphiboles is observed along the richterite - $^{[M(1,2,3]}$Mn - richterite, nominally $Na(NaCa)Mn_5Si_8O_{22}(OH)_2$. The behaviour of Mn depends on fO_2 conditions. The larger solid solution extent is reached under MW and NNO conditions, with a maximum value of X_{Mn} = Mn/(Mg + Mn) = 0.5, without accessory phases. For higher X_{Mn} values, additional phases appear, mainly serandite. In no case, the X_{Mn} value is larger than 0.7. Under oxidizing conditions (HM buffer), the solid solution range is much restricted and accessory phases (diopside and quartz) are present for X_{Mn} > 0.3. The same is observed with amphiboles along the tremolite - $^{[M(1,2,3]}$Mn-tremolite join, where no single phase amphibole is obtained, whatever X_{Mn}, under HM buffering conditions. The analysis of OH-stretching band intensities with increasing X_{Mn}, under oxidizing conditions, clearly indicates a progressive deprotonation of the amphibole. It is related to the presence of Mn^{3+}, confirmed by optical spectrometry.

In talc, the Mg→ Mn substitution is limited to X_{Mn} = 0.2 under reducing conditions, probably for dimensional reasons. In phlogopite, maximum X_{Mn} values are 0.3 with MW buffer, 0.4 with NNO and 0.6 with HM. Clearly, under oxidizing conditions, Mn^{3+} enters the structure and the excess of charge is balanced by a deprotonation, like in clinoamphiboles.

Dimensional misfits between the I-beam and the double chains of tetrahedra, in amphiboles, and between tetrahedral and octahedral layers, in phyllosilicates, generated by the incorporation of the large Mn^{2+} explain these limited solid solution extends.

Crystal chemistry of synthetic amphiboles along the richterite - ferro-richterite join

Robert, J.-L.[1*], Della Ventura, G.[2], Redhammer, G.J.[3], Iezzi, G.[4], Bellatreccia, F.[2] & Sergent, J.[1]
[1]Institut de Minéralogie et de Physique des Milieux Condensés, Université Pierre et Marie Curie, Paris, France
(*jean-louis.robert@impmc.upmc.fr)
[2]Università di Roma Tre, Rome, Italy
[3]Rheinisch-Westfälische Technische Hochschule, Aachen, Germany
[4]Dipartimento di Scienze della Terra, Università G. D'Annunzio, Chieti Scalo, Italy

In this work we relate the synthesis and crystal-chemical study of amphiboles along the join richterite - ferrorichterite [nominally $Na(NaCa)(Mg_{5-x}Fe^{2+}_x)Si_8O_{22}(OH)_2$], at 700°C, 1 kbar, under redox conditions imposed by a MW solid buffer. XRPD shows essentially single-phase run products at both end-member compositions, with minor (10-15%) pyroxene and quartz for intermediate compositions. Interestingly, there is a significant evolution of the amphibole morphology across the solid-solution series: Mg end-member richterite is extremely acicular (length up to 15 μm, diameter up to 1 μm) whereas for increasing Fe in the system the amphibole becomes increasingly stubby, with a length:diameter ratio≈ 3:1 for the Fe -rich end-member. Notably, the refined cell parameters show linear variations across the series, suggesting a complete Mg-Fe^{2+} solid-solution along the join. The OH-stretching FTIR spectra show complex patterns for intermediate compositions with up to eight bands which can be assigned to the various configurations involving Mg/Fe^{2+} at M(1,3), locally associated with both full and empty A-sites. Combination of Mössbauer and FTIR spectroscopy however shows that the composition of the amphibole is much more complex than expected just from XRPD data: Fe^{2+} is in fact disordered among all M-sites, and, despite the strongly reducing conditions during syntheses, there is significant Fe^{3+} in the amphibole; it is fully ordered at M(2). For increasing Fe in the system, the amount of Fe_{tot} in the amphibole is systematically lower than expected as is Fe^{2+} at the M(1-3) octahedra, while $^{M(2)}Fe^{3+}$ increases toward more iron-rich compositions (Fig. 1). These results definitively stress the need for a proper characterization of the experimental run products because these may depart from the expected stoichiometry in a significant way.

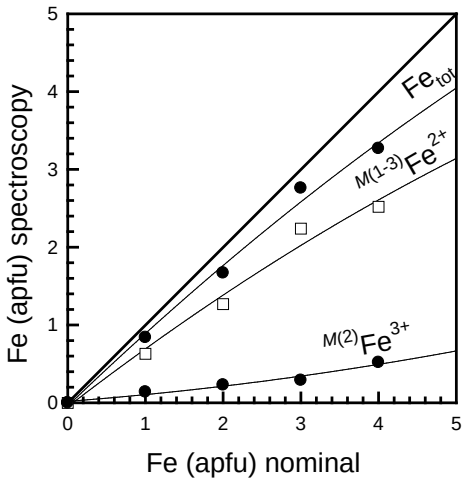

Fig. 1: The Fe^{2+}/Fe^{3+} distribution in synthetic richterites as a function of the nominal Fe in the system.

Direct EMP or single-crystal X-ray refinement is highly desirable, however spectroscopic methods may provide a valuable alternative, particularly when the Fe^{3+} *vs.* Fe^{2+} composition is needed.

Reappraisal of the crystal structure of Tinaksite from Murun massif (Russia): cation partition and structural disorder

Scordari, F.[1], Mesto, E.[1*], Vladykin, N.[2] & Koneva A.[2]
[1]Dipto Geomineralogico, Università degli Studi di Bari, Italy
([*]mesto@geomin.uniba.it)
[2]Institute of Geochemistry, Irkutsk, Russia

Tinaksite is a widespread mineral in the rocks of charoite complex of the Murun massif (Russia). The structure of tinaksite was reported for the first time in 1971 by Petranunia [1]. Until now, it is the only one silicate known based on a hybrid anion. According to Libeau [2], the latter can be described briefly by {**hB**, 2^1_∞}[$^3Si_6O_{17}(SiO_2)$], which represents the joint of an unbranched dreier single chain with a loop-branched dreier single chain. In 1980 von Bissert [3] confirmed the general structure architecture of tinaksite proposed by Petranunia [1], but found a more regular tetrahedral conformation. According to von Bissert [3], tinaksite is triclinic with the following chemical composition: $NaK_2Ca_2Ti[^3Si_7O_{19}]OH$. The compound here investigated has been solved in P1, *a*=7.0565(1) Å, *b*=10.3750(1) Å, *c*=12.1885(2) Å, α=92.802(1)°, β=90.763(1)° , γ=99.241(1)°, but differently from those studied by Petranunia [1] and von Bissert [3], it shows a more complex chemistry ($(Na_{0.855}K_{1.993}Ca_{2.008}Ti_{0.792}Mg_{0.082}Fe^{3+}_{0.142}Mn_{0.100}Ba_{0.006}Sr_{0.006}Zr_{0.007}Zn_{0.004}Ni_{0.003}Cr_{0.002})[^3Si_7O_{19}]OH$) and a more interesting structural details.

In this work, the cation partition, derived by means of SCXRD and EMPA measurements, is presented. The structure has been anisotropically refined to a R(F) = 0.025 (for 5238 observed reflections with $F_o > 3\sigma(F_o)$). The highest peak in the Fourier difference map seems due to some structural disorder inside the Ti octahedron. This disorder likely is related to the entrance of the large K in place of six-fold coordinated Na atom. The replacing of Na by K seems to change the coordination number of the polyhedron from 6 to 7, so perturbing the neighbouring Ti atom position.

Another point of interest concerns the K1 and K2 potassium atom located inside the system of one-dimensional channels of the structure, formed by double chains of silicate. According to von Bissert [3], the higher K1 thermal parameters with respect to the K2 one indicates the disorder on K1 site. The structural refinement shows that in the first case K occupies at least three different positions. A charge distribution analysis, performed by means of the Chardi-It software [4], has returned an ECON number [5] of 11 and 9 for the K1 and K2 site respectively. The bond distances for the three K atoms concerning K1 show these atoms are not always bonded to the same oxygens. In fact, K can move inside a cage formed by 14 oxygen atoms with a volume of about 90 Å^3. This volume results to be much larger than of one assigned to K atom.

[1] Petrunina, A.A., Ilyukhin, V.V. & Belov, N.V. (1971) *Sov. Phys Dokl.*, **16**, 338-340. [2] Libeau, F. (1985) *Structural Chemistry of Silicates: Structure, Bonding and Classification.* Springer-Verlag. [3] von Bissert, G. (1980) *Acta Crystallogr.*, **B36**, 259-263. [4] Nespolo, M. et al. (2001) *Acta Crystallogr.*, **B57**, 652-664. [5] Hoppe, R. (1979) *Z. Kristallogr.*, **150**, 23-52.

Rietveld refinement of stibnite crystal structure

Şeclăman, A.C.
Dept. of Mineralogy, University of Bucharest, Bucharest, Romania (seclaman_alexandra@yahoo.com)

The stibnite samples used in this study are from Băiuţ mine, Maramureş, Romania. The powders were prepared from large crystals, through fine grinding.

The data collection was done using a PANalytical X'Pert Pro MPD diffractometer fitted with an X'Celerator detector, which allows for very short acquisition times. Several measurement settings were used in an effort to find highest quality data possible. The final data collection was set with the following parameters: 2θ range: 5 - 90°, 0.01° steps and 30 seconds acquisition time per step. The scan was continuous and a standard Cu X-ray source was used.

For the Rietveld refinement the parameters and atomic coordinates described by Lundegaard et al. [1] – at normal values of temperature and pressure – were used. The Rietveld refinement was performed with the help of General Structure Analysis Software. After approximately 300 refinement cycles, the residual value R has reached a minimum of 0.1387 beyond which no further improvements could be done.

Table 1: The refined unit-cell parameters (*Pnma*)

	a	b	c
Å	11.197438	3.799043	11.121890

The newly refined unit-cell parameters are shown in Table 1. The unit cell volume is 473.1201 Å^3. The atomic fractional coordinates are presented in Table 2.

Table 2: The atomic fractional coordinates

Atom	x	y	z
Sb_1	0.9707 (04)	0.25	0.1730(05)
Sb_2	0.6487 (06)	0.25	0.9646 (05)
S_1	0.7958 (18)	0.25	0.3099 (20)
S_2	0.4324 (22)	0.25	0.8787 (21)
S_3	0.6307 (17)	0.25	0.5558 (15)

The standard deviations for each atomic coordinate did not exceed 0.0022. The *y* parameters correspond to special positions and remained unchanged through the refinement. The results of this Rietveld refinement are not ideal, because of the data acquisition procedure. The results can further be improved through longer acquisition times.

Acknowledgements: I would like to thank Gh. Ilinca and B. Soare for their support in apprehending the basic operating techniques of the X-ray powder diffraction device and for assistance during refinement.

[1] Lundegaard, L.F. et al. (2003) *Phys. Chem. Miner.*, **30**, 463-468.

Compositional trends in hakite, possible discrepancies from ideal structure

Škácha, P.[1*], Vlček, V.[1], Sejkora, J.[2], Plášil, J.[2] & Goliáš, V.[1]
[1]Inst. of Geochemistry, Mineralogy and Mineral Resources, Charles University, Prague, Czech Republic
([*]skachap@seznam.cz)
[2]Dept. of Mineralogy and Petrology, National Museum, Prague, Czech Republic

Stoichiometry and site occupancies of minerals of the tetrahedrite group was suggested by simplified general formula [1] – $^{[III]}A_6{}^{[IV]}(B,C)_6{}^{[III]}X_4{}^{[IV]}Y_{12}{}^{[VI]}Z$, where *A* = Cu, Ag; *B* = Cu, Ag and *C* is generally divalent metal (typically Fe, Zn but also Hg, Mn, Cd etc.) in the same coordination as *B*; *X* = Sb, As, Bi, Te; *Y* and *Z* = S and Se. Hakite is Se – dominant member of tetrahedrite group. Since the experimental determination of the hakite structure is lacking the structure model based on the crystal structure of tetrahedrite with fully substituted *Y* and *Z* sites was adopted. Studied samples of hakite were found in a rich paragenesis of Ag, Hg, Pb, Cu, Sb, Cd, Tl selenides and other minerals containing As, Te, Sb, and U at the new occurrence in Příbram (uranium-base metals ore district, Czech Republic). Amount of 69 microprobe (WDS) analyses on 11 individual samples were performed. Based on different substituents detected by the microprobe study, several types of hakite were determined. *A* position is represented by Ag and Cu contents. At the *B* site Cu and at the *C* site Hg, Zn and lower amounts of Fe and Cd occur (Table 1). *X* site was occupied by Sb, minor contents of As and trace amounts of Te were detected. S-Se substitution was ascertained according to the abundant association of sulphides.

Table 1: Content of elements in Příbram hakite based on 29 apfu

	B	**C**			
	Cu	*Cd*	*Zn*	*Hg*	*Fe*
	3,41-4,85	0-1,05	0,01-1,82	0,01-1,95	0-0,73
mean	4,31	0,16	0,60	1,19	0,06
	A		**X**		
	Cu	*Ag*	*Sb*	*As*	*Te*
	5,71	0,03-1,20	3,36 - 4,18	0 - 0,67	0-0,52
mean	5,71	0,29	3,90	0,15	0,07
	Y, Z				
	S	*Se*	sum of anions		
	0,01 - 4,52	8,00 - 12,75	12,28-13,19		
mean	1,35	11,20	12,55		

According to the Table 1, it is obvious that the sum of anions is deficient compared to the ideal structure model of tetrahedrite. Mean of anions sum of 17 wds analyses on coexisted tetrahedrite gave 12,89 apfu. In spite of the rarity and small grain size of hakite, several samples were prepared for the X-ray powder diffraction study. Compared to the theoretical diffraction patterns calculated from the crystal-structure data the observed patterns of the hakite samples exhibited few additional reflections probably of the superstructure character.

Based on the chemistry and XRD results, we suppose presence of structural disorder and distortions of the hakite lattice with respect to the idealized structure adopted from tetrahedrite.

[1] Moëlo, Y. et al. (2008) *Eur. J. Mineral.*, **20**, 7-46.

Structure of nagelschmidtite $Ca_7Si_2P_2O_{16}$

Sugiyama, K.[1*], Kato, Y.[1] & Mikouchi, T.[2]
[1]Institute for Materials Research, Tohoku University, Sendai, Japan ([*]kazumasa@imr.tohoku.ac.jp)
[2]Dept. of Earth and Planetary Science, University of Tokyo, Hongo, Japan

The metallugical properties of steelmaking slags are influenced by the formation of silicophosphates in the binary $2CaO{\cdot}SiO_2$ (C2S) - $3CaO{\cdot}P_2O_5$ (C3P) system. Silicophosphates with high concentration of phosphate in the slag are important as lime- and phosphorus-containing fertilizer. Several phase diagrams for the C2S-C3P system are found in the literatures and a wide stability region of α-C2S and $\bar{\alpha}$-C3P solid-solutions was confirmed at high temperatures above 1450°C [1,2]. In this context, nagelschmidtite [$Ca_7Si_2P_2O_{16}$] is generally inferred to be structurally similar to α-C2S [3]. Nevertheless, structural details of nagelschmidtite have not been revealed yet.

The single crystals of nagelschmidtite were prepared from a sintered pellet with the chemical composition $CaO:SiO_2:P_2O_5:Fe_2O_3$=49.2: 25.7: 12.0: 13.1mass%). The sintered sample was first melted at 1600°C and cooled down to 1400°C at a rate of 10°C/h. Almost colourless crystal ($P6_1$; a=10.82≈2*5.4Å, c=21.46≈7.1*3Å) could be selected and the structure was analyzed by the single crystal X-ray diffraction. The structure was solved by a combination of direct-methods and difference Fourier syntheses and Fig. 1 shows the obtained structural model. The structure is constructed by Ca layer and Ca-T layer similar to that of α-C_2S. Ca vacant site due to the substitution of PO_4 for SiO_4 is ordered in the Ca-T layer. The arrangement of TO_4 units (T=Si and P) is similar to that found in α–, α'$_H$-, α'$_L$- and β-C_2S structures.

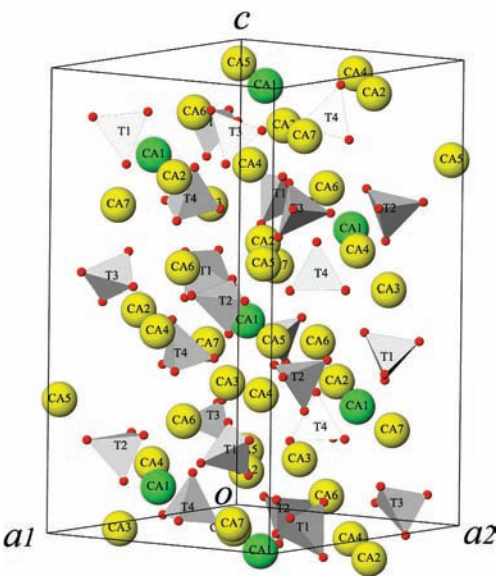

Fig. 1: Structure of nagelschmidtite [$Ca_7Si_2P_2O_{16}$].

[1] Nurse, R.W. et al. (1959) *J. Chem. Soc.*, **220**, 1077-1083. [2] Fix, W. et al. (1969) *J. Am.Ceram. Soc.*, **52**, 346-347. [3] Mumme, W.G. et al. (1996) *N. Jb. Miner. Abh.*, **170**, 171-188.

The crystal structure of esperite, with a revised chemical formula, $PbCa_2(ZnSiO_4)_3$, isostructural with beryllonite

Tait, K.T.[1*], Yang, H.[2], Downs, R.T.[2], Li, C.[2] & Pinch, W.W.[3]
[1]Dept. of Natural History, Royal Ontario Museum, Toronto, Ontario, Canada ([*]ktait@rom.on.ca)
[2]Dept. of Geosciences, University of Arizona, Tucson, Arizona USA
[3]19 Stonebridge Lane, Pittsford, New York, USA

Esperite from Franklin, New Jersey was first described as monoclinic with a well-developed "superlattice" a = 2 × 8.814(2) Å, b = 8.270(3) Å, c = 2 × 15.26(1) Å, $\beta \approx 90°$, space group $P2_1/n$ (subcell), and a chemical formula $PbCa_3(ZnSiO_4)_4$ [1]. They attributed "superlattice" reflections to the ordered distributions of Pb and Ca cations over four beryllonite-type subcells for esperite with the Ca:Pb ratio greater than 2:1.

A fragment of esperite from the holotype sample (CMNMC 56855), Parker Shaft, Franklin, Sussex Co., New Jersey, U.S.A. was obtained for this study. We examined two esperite fragments from this sample using single-crystal X-ray diffraction, electron microprobe analysis, and Raman spectroscopy.

Although both fragments have Ca:Pb ≈ 1.8, one exhibits the "superlattice" reflections as observed in previous studies [1], whereas the other does not. The sample without "superlattice" reflections has unit-cell parameters a = 8.7889(2), b = 8.2685(2), c = 15.254(3) Å, β = 90.050(1)°, V = 1108.49(4) Å^3 and the chemical composition $Pb_{1.00}(Ca_{1.86}Fe^{2+}_{0.07}Mn_{0.04}Cr^{3+}_{0.02})_{\Sigma=1.99}(Zn_{1.00}Si_{1.00}O_4)_3$. Its crystal structure was solved in space group $P2_1/n$ (R_1 = 0.022). Esperite is isostructural with beryllonite, $NaBePO_4$, and its ideal chemical formula should, therefore, be revised to $PbCa_2(ZnSiO_4)_3$, Z = 4. The ZnO_4 and SiO_4 tetrahedra in esperite share corners to form an ordered framework, with Pb^{2+} occupying the nine-coordinated site in the large channels and Ca^{2+} occupying the two distinct octahedral sites in the small channels. The so-called "superlattice" reflections are attributed to triple twins, a twilling of ~60° rotational twinning around the b-axis, similar to those observed in many other beryllonite-type materials. A phase transformation from a high-temperature polymorph to the esperite structure is proposed to be responsible for the twinning formation.

[1] Moore, P.B. & Ribbe, P.H. (1965) *Am. Mineral.*, **50**, 1170-1178.

A new acentric silicate: $K_{2.9}Rb_{0.1}ErSi_3O_9$

Wierzbicka-Wieczorek, M.[1,2*], Kolitsch, U.[2] & Tillmanns, E.[1]
[1]Institute for Mineralogy and Crystallography, University of Vienna, Austria ([*]maria.wierzbicka@univie.ac.at)
[2]Dept. of Mineralogy and Petrography, Natural History Museum, Vienna, Austria
[3]*present address*: Institute for Geosciences, Friedrich-Schiller University Jena, Germany

In a comprehensive study we had focused on the preparation, structural characterisation and classification of novel microporous and small-pore mixed-framework silicates containing seven specific octahedrally coordinated M^{3+}-cations (M = Sc, V, Cr, Fe, In, Y, Yb) [1] and, in a subsequent step, syntheses of representatives with REE^{3+} cations (REE = Eu, Gd, Tb, Ho and Er). The latter work yielded thirteen new REE-silicates, including colourless crystals of $K_{2.9}Rb_{0.1}ErSi_3O_9$, one of four new Er silicates. All compounds were grown with a high-temperature flux-growth technique in air (MoO_3–based flux mixtures in Pt crucibles; T_{max} = 1150°C, cooling rate 2 K/h, T_{min} = 900°C).

The crystal structure was determined from single-crystal X-ray intensity data (Mo$K\alpha$, 293 K) in space group $P\bar{1}$ (no. 1), with a = 6.672(1), b = 6.719(1), c = 6.725(1) Å, α = 108.87(3), β = 106.72(3), γ = 107.61(3)°, V = 245.82(6) Å^3, Z = 1, $R(F)$ = 2.81 %, Flack parameter 0.062(9).

The title compound represents a novel, pseudorhombohedral structure type. It is characterised by a mixed octahedral-tetrahedral framework, in which each corner of the isolated ErO_6 octahedra (<Er-O> = 2.26 Å) is linked to infinite $[Si_3O_9]$ chains extending approximately along [111] (Fig. 1). Narrow channels host three non-equivalent K sites, one of which is partially substituted by Rb. The unusual space group symmetry is mainly caused by the alkali sites that violate $R\bar{3}$ symmetry.

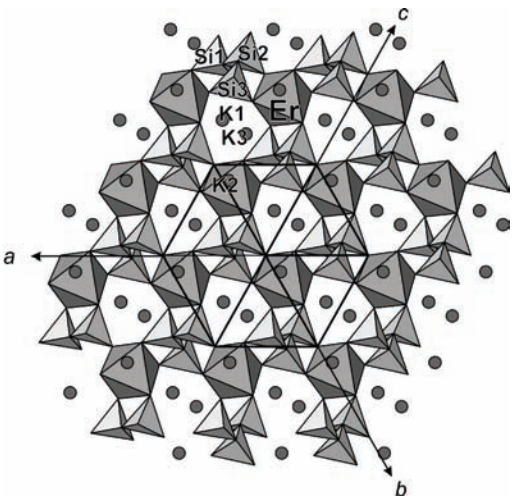

Fig. 1: View of $K_{2.9}Rb_{0.1}ErSi_3O_9$ along [111].

The geometry of the chain in $K_{2.9}Rb_{0.1}ErSi_3O_9$ is similar to that in pectolite, $NaCa_2[HSi_3O_9]$ [2]. The structural relation to further natural or synthetic chain $[Si_3O_9]$ silicates is less pronounced.

Acknowledgements: Financial support by the Austrian Science Foundation (FWF) (Grant P17623-N10) is gratefully acknowledged.

[1] Wierzbicka-Wieczorek, M. (2007) *Ph.D. Thesis*, University of Vienna. [2] Takeuchi, Y. et al. (1976) *Am. Mineral.*, **61**, 229-237.

Crystal structure of (REE, Fe)-rich rengeite (saimaite) from Saima alkalic complex, NE China

Yang, Z.[1*], Giester, G.[2], Ding, K.[1] & Tillmanns, E.[2]
[1]Key Laboratory of Engineering Geomechanics, Institute of Geology and Geophysics, Chinese Academy of Sciences, Beijing, China ([*]yangzhm@mail.igcas.ac.cn)
[2]Institut für Mineralogie und Kristallographie, Universität Wien, Vienna, Austria

Saimaite was first described as a new mineral from Saima alkalic complex in Liaoning Province, NE China, and is an unconfirmed mineral. Previous single crystal and powder X-ray study gave monoclinic symmetry, space group *C*2/*m*, a = 13.8934, b = 5.6703, c = 11.9120 Å, β = 114.083°, V = 856.73 Å^3. Electron microprobe analyses indicate a general formula $(Sr,REE)_4Fe(Ti,Zr)_2Ti_2Si_4O_{22}$, where Fe is dominant in the B site [1]. Saimaite was also suggested to be the equivalent of strontio-chevkinite [2].

The present single crystal X-ray study on the type material was performed on a Nonius KappaCCD diffractometer. The structure was solved and refined in space group *C*2/*m*, with a = 13.973(3), b = 5.6984(11), c = 11.988(2) Å, β = 114.10(3)°, V = 871.3(3) Å^3, to R1 = 0.037, wR2 = 0.098. The formula of saimaite is $(Sr, Ce)_4Zr(Ti, Fe)_2(Ti, Fe)_2(Si_2O_7)_2O_8$ with Z = 2 according to the crystal structure refinement.

Saimaite is basically isostructural with rengeite (Fig. 1). According to the structural refinement strontium and rare earths were assigned into Sr sites. Zirconium occupies preferentially one of three octahedral sites. Iron shares the other two octahedral sites with Ti. Based on the study of Mössbauer spectroscopy, Fe^{3+} occupies two octahedral sites and Fe^{2+} occupies only one octahedral site. On the basis of cation radii Ca preferentially was assigned into the 8-coordinated Sr sites, then into Zr octahedral site. The formula of saimaite can be expressed as: $(Sr_{2.39}\,REE_{1.21}\,Ca_{0.35}\,Na_{0.09})_{\Sigma 4.04}\,(Zr_{0.80}\,Ca_{0.16}\,Hf_{0.02}\,Nb_{0.02}Th_{0.02}U_{0.01})_{\Sigma 0.99}\,(Ti_{1.44}Fe^{2+}_{0.32}Fe^{3+}_{0.20}Mg_{0.03}\,Mn_{0.02})_{\Sigma 2.01}\,(Ti_{1.80}\,Fe^{3+}_{0.20})_{\Sigma 2.00}\,(Si_{3.94}\,Al_{0.03})_{\Sigma 3.98}\,O_{22}$, where Zr is dominant in the B site. Compared with rengeite, saimaite is rich in rare earths, iron and calcium.

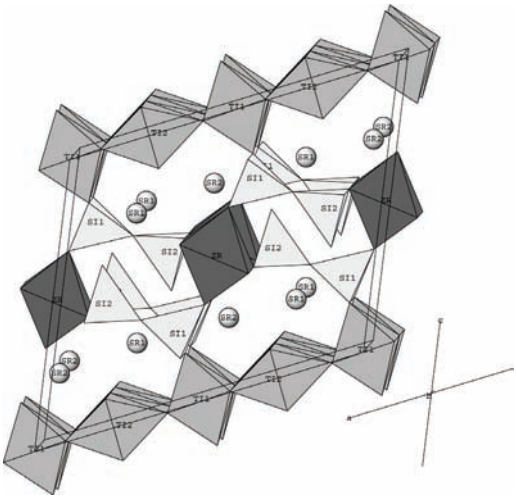

Fig. 1: Crystal structure of (REE, Fe)-rich rengeite (saimaite).

The crystal structure of saimaite was refined in space group *C*2/*m*, while the true space group of rengeite is $P2_1/a$. Although there are no significant differences in both refinements for rengeite[3], saimaite may be considered as a (REE, Fe)-rich polymorph of rengeite.

[1] Ding, K. et al. (1984) *Chinese Sci. Bull.*, **28(11)**, 678-681. [2] Jambor, J. L. et al. (2000) *Am. Mineral.*, **85**, 1843-1847. [3] Miyawaki, R. et al. (2002). *J. Miner. Petrol. Sci.*, **97**, 7-12.

Hemimorphic wulfenite crystals from lead-zinc ore deposit Mežica, Slovenia

Zavašnik, J.[1*], Rečnik, A.[1], Samardžija, Z.[1], Meden, A.[2] & Dódony, I.[3]
[1]Jožef Stefan Institute, Ljubljana, Slovenia
([*]janez.zavasnik@ijs.si)
[2]FKKT, University of Ljubljana, Slovenia
[3]Eötvös L. University, Budapest, Hungary

Mežica lead-zinc ore field is located in the Northern Karavanke geotectonic unit, which belongs to Eastern Alps. The ore bodies span over a 64 sq. km wide area in the upper Meža valley. The ore is emplaced mostly in Triassic carbonate rocks. In addition to primary sulphides galena and sphalerite, the major oxidation product is lead molybdate ($PbMoO_4$) wulfenite that crystallized in economic quantities along shattered fault zones permeable for descending meteoric waters. While being abundant, Mežica wulfenites possess some peculiar morphological features, which are not observed on wulfenites from other localities. In addition to regular crystals with I4/m symmetry (tetragonal bipyramidal) we frequently encounter hemimorphic crystals with lower I4 symmetry (tetragonal pyramidal) with one of basal terminations flat, and the other pyramidal. In first reports on hemimorphism of Mežica wulfenites lower symmetry was proved by etching and piezoelectricity [1]. As a consequence of this low symmetry two different twinning laws have been described based on the macroscopic morphological characteristics of the crystals [2]. With the availability of modern analytical methods this problem was assessed by single crystal X-ray spectroscopy, transmission electron microscopy using high-resolution phase contrast and electron micro-diffraction techniques [3]. Our preliminary WDS analysis showed that wulfenites from Mežica are stoichiometric with Pb/Mo atomic ratio of 1:1 containing up to 0.30 at% of V replacing Mo in tetrahedral sites. Other impurity elements may be present below the detection limit. Micro-diffraction analysis showed a slight difference in intensity of **+g** and **-g** Friedel pairs of reflections related to the polar *c*-axis. Similar asymmetry is observed in the fine contrast features on high-resolution phase contrast images (below). Full structural analysis of the Mežica wulfenite and related planar defects; (001) basal plane inversion boundaries and interpenetration (110) twins is in progress.

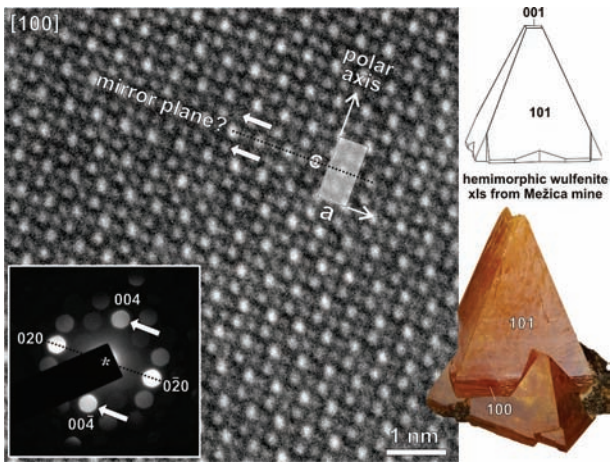

Fig. 1: HRTEM image with superimposed micro-diffraction pattern from hemimorphic Mežica wulfenite imply possible non-centrosymmetricity along the *c*-axis. The breakdown of Friedel's law is visible by difference in intensity of reflection pairs and by differences in image contrast.

[1] Hurlbut, C.S. (1955) *Am. Mineral.*, **40**, 857-860. [2] Rečnik, A., et al. (2009) *Mineralien Welt,* **20(4)**, 40-83. [3] Mader, W. & Rečnik, A. (1998) *Phys. Status Solidi A*, **166**, 381-395.

Crystal structure of dumortierite from Lower Silesia, Poland

Zelek, S.M.[1*], Pieczka, A.[2] & Stadnicka, K.M.[1]
[1]Faculty of Chemistry, Jagiellonian University, Krakow, Poland
([*]zelek@chemia.uj.edu.pl)
[2]Faculty of Geology, Geophysics and Environment Protection, AGH University of Science and Technology, Krakow, Poland

X-ray structure analysis was used to investigate single crystals of dumortierite $(Al,Fe,Ti,\square)_7[O_3|BO_3|(SiO_4)_3]$ from Krucze Rocks, Karpacz, where this boro-silicate is an accessory mineral of Karkonosze pegmatites (Fig. 1). The mineral was found as grey-violet aggregates, up to 1 cm in size, formed by violet blades up to 1 mm long.

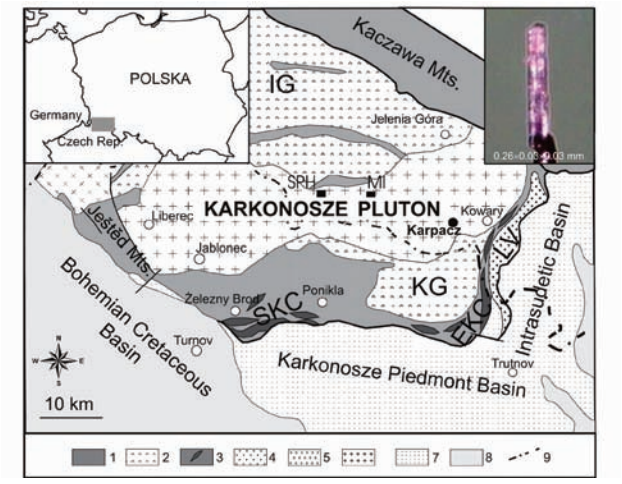

Fig. 1: Sketch map of Karkonosze-Izera massif (after [1]) with the view of dumortierite crystal from Krucze Rocks, Karpacz, inserted in the right-top corner.
1: Low-grade metasediments with subordinate metavolcanics, 2: Medium-grade metasediments and metagranitoids, 3: Low-grade metamorphosed volcano-sedimentary sequences with abundant bimodal metavolcanics, 4: Low- and medium-grade metamorphosed volcano-sedimentary sequances dominated by mafic rocks, 5: Late Proterozoic and Cambria/Ordovican granitoids, 6: Variscan granitoids, 7: Carboniferous and Permian syn- and post-orogeic deposits, 8: Mesozoic platform deposits, 9: Polish - Czech border, IG: Izera gneisses with mica schist belts, EKC: East Karkonosze Complex, LV: Leszczyniec unit, SKC: South Karkonosze Complex; SHP: Szklarska Poręba Hute, MI: Michałowice quarries.

Lattice cell parameters of the dumortierite from Poland are shown in Table 1 with respect to those of dumortierite of different origin.

Table 1: Comparison of the lattice cell parameters (Å) for dumortierite minerals of different origine. Space group setting: Pnma

	[2]: Saharina, Madagascar	[3]: Dora-Maira, Western Alps	[4]: Gföhl, Lower Austria	[4]: Weißenkirchen in der Wachau, Lower Austria	This work: Krucze Rocks, Karpacz
a	4.7001(5)	4.730(2)	4.6900(3)	4.6948(2)	4.6935(1)
b	11.828(1)	11.91(3)	11.7875(6)	11.8037(5)	11.7894(3)
c	20.243(3)	20.40(3)	20.1823(11)	20.2106(8)	20.2197(6)

The violet colour of the dumortierite from Krucze Rocks may suggest, according to [5], the existence of two types of Fe-Ti dimers: [-□-Fe^{2+}-Ti^{4+}-□-] and [-M-Fe^{2+}-Ti^{4+}-□-], with some disorder in the M(1) chains including the voids.

[1] Słaby, E. et al. (2002) *Acta Geol. Polonica*, **52**, 501-519. [2] Moore, P.B. & Araki, T. (1978) *Neues. Jb. Miner. Abh.*, **132**, 231-241. [3] Ferraris, G. et al. (1995) *Eur. J. Mineral.*, **7**, 167-174. [4] Fuchs, Y. et al. (2005) *Eur. J. Mineral.*, **17**, 173-183. [5] Platonov, A.N. et al. (2000) *Eur. J. Mineral.*, **12**, 521-528.

Crystal structure of NO_3 – bearing haüyne from Oldoinyo Lengai volcano, Northern Tanzania

Zolotarev, A.A. Jr.[1*], Krivovichev, S.V.[1], Zaitsev, A.N.[1,2] & Keller J.[3]
[1]Saint-Petersburg State University, Saint-Petersburg, Russia
([*]aazolotarev@gmail.com)
[2]Dept. of Mineralogy, Natural History Museum, London, UK
[3]Institute of Geoscience Mineralogy - Geochemistry, Freiburg University, Freiburg, Germany

We have studied crystal structure of sample of gem-quality haüyne from alkaline plutonic rock of the active Oldoinyo Lengai volcano in northern Tanzania [1]. Single crystal experiment (Stoe IPDS II, MoKα radiation) provided space group *P*-43*n*, a = 9.0319(9) Å, V = 736.8(1) $Å^3$. Final refinement converged to agreement indices (R_1) 0.0525 for 332 unique observed reflections. Crystal chemical formula calculated on the basis of chemical analysis [1] is in accord with the results of crystal-structure refinement: $(Na_{6.75}Ca_{0.87}K_{0.37})_{\Sigma 7.99}(Al_{5.97}Fe^{3+}_{0.03}Si_{6.00}O_{24})[(SO_4)_{0.89}(OH)_{0.54}(NO_3)_{0.23}Cl_{0.20}(CO_3)_{0.12}]_{\Sigma 1.98}$.

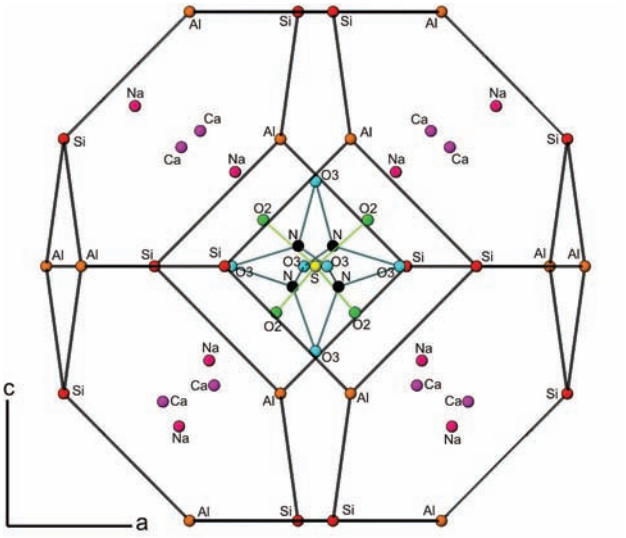

Fig. 1: The content of NO_3 – bearing haüyne cage.

The Al-Si ordered tetrahedral framework of our mineral is typical for sodalite-group minerals. The content of haüyne cages (Fig. 1) is highly disordered [2-4]. Our mineral is the first naturally occurring NO_3-bearing species from the sodalite group [1].

Acknowledgements: Russian Ministry of Science and Education (state contract 02.740.11.0326), Grant of President of Russia for young scientists (MK-1783.2010.5).

[1] Zaitsev, A.N. et al. (2009) *Gems Gemol.*, **45**, 200-203. [2] Hassan, I. & Grundy, H.D. (1991) *Can. Mineral.*, **29**, 123-130. [3] Ballirano, P. & Maras, A. (2005) *Eur. J. Mineral.*, **17**, 805-812.

Is the oxygen really involved in the β-As_4S_4 – pararealgar transformation?

Zoppi, M.[1*] & Pratesi, G.[1,2].
[1]Museo di Storia Naturale – Sezione di Mineralogia, Università di Firenze, Florence, Italy ([*]matteo.zoppi@unifi.it)
[2]Dipto. di Scienze della Terra, Università di Firenze, Florence, Italy

The mineral realgar (As_4S_4) and its polymorphs have often attracted the attention of mineralogists and chemists for their peculiar alteration process induced by light. Realgar, along with orpiment (As_2S_3), have been employed as orange and yellow pigments, respectively, by artists through different ages, from the ancient Egypt to the Middle Age and the Renaissance. During the alteration, the orange colour of realgar turns yellow; such process is highly interesting both from the structural point of view and owing to the implications regarding the study and conservation of antique paintings. The process of light-induced alteration of the high temperature polymorph of realgar, β-As_4S_4, has been studied through X-ray powder diffraction applying the Rietveld method, thus giving a structural interpretation of the χ-phase, a precursor of pararealgar already recognized as playing an important role in the alteration process. Synchrotron radiation has been employed to use the highest X-ray intensities and counting statistics in a case where the material undergoes strong degradation and reorganization of its structure. The light-induced alteration carried out on the β-As_4S_4 crystalline powder, encapsulated in kapton tape, brought to the full transformation to pararealgar with the remarkable result that any presence of arsenolite was detected. The alteration causes an anisotropic increase of the unit-cell volume of the β- As_4S_4, with the decreasing of the a and β parameters, and the increasing of b and c. The process takes place through different stages that have been described using a different structural model with respect to that previously proposed. Initially the structure of β- As_4S_4 begins changing because of the transformation of its molecules into those typical of pararealgar, still maintaining the same packing. The alteration proceeds until about half of the As_4S_4 molecular units are replaced, then this phase progressively disappears transforming into pararealgar which still retains a certain amount of molecules of the β- As_4S_4 in its lattice. The last part of the process shows a contraction of the unit-cell volume of pararealgar, performed through a decreasing of the a, b and c parameters and an increasing of the β angle. The χ-phase is here described as a disordered molecular mixing of different units, those of the β- As_4S_4 and pararealgar. The formation of arsenolite, observed in many cases, might be rather an effect of the rupture of the realgar-type molecule in the presence of oxygen and the only creation of As-O bonds.

The topologies of nano-scale uranium clusters

Burns, P.C.[*], Ling, J., Sigmon, G.E., Unruh, D.K. & Forbes, T.Z.
Dept. of Civil Engineering and Geological Sciences, University of Notre Dame, Notre Dame, IN, USA
([*]pburns@nd.edu)

The topological details of approximately 30 nano-scale uranium oxide clusters will be examined. These clusters form through the edge-sharing of uranyl hexagonal bipyramids. Some are fullerene topologies containing 12 pentagons and an even number of hexagons, whereas others also containing squares, leading to considerable topological diversity.

Novel crystal-chemical relations in layered Ti silicates

Cámara, F.[1*] & Sokolova, E.[2]
[1]CNR-IGG, UOS Pavia, Italy ([*]camara@crystal.unipv.it)
[2]Dept. of Geological Sciences, University of Manitoba, Winnipeg, MB, Canada

We consider structure topology for a group of Ti disilicates based on our single-crystal X-ray structure work on four Ti-disilicate minerals, jinshajiangite, cámaraite, bornemanite and nechelyustovite, and two possible new mineral species with preliminary ideal formulae $Na_4BaTi_2Nb(Si_2O_7)_2O_3(OH)(H_2O)_2$ (mineral A) and $Na_3KBaTi_2Nb(Si_2O_7)_2O_3(OH)(H_2O)_6$ (mineral B). These minerals belong to a group of Ti silicates with a TS (titanium silicate) block [1-4]. Structure types of cámaraite, bornemanite, nechelyustovite and minerals A and B are new.

The general formula of the TS block is $A^P{}_2B^P{}_2M^H{}_2M^O{}_4(Si_2O_7)_2X_{4+n}$, where $M^H{}_2$ and $M^O{}_4$ are cations of the H and O sheets; M^H = Ti, Nb, Zr, Mn^{2+}, Ca; M^O = Ti, Zr, Fe^{2+}, Mn^{2+}, Ca, Na; A^P and B^P = cations at the peripheral (*P*) sites = Na, Ca, Ba, K; X = O, OH, F; n = 0,2,4 [4]. The TS block is composed of a central trioctahedral (O) sheet and two adjacent (H) sheets of [5-7]-coordinated polyhedra and (Si_2O_7) groups. All structures consist of a TS block and an **I** (intermediate) block that comprises atoms between two TS blocks. The **I** block consists of alkali and alkaline-earth cations, (H_2O) groups and the oxyanions (PO_4), (SO_4) and (CO_3). Structures of Ti disilicate minerals have been divided into four groups, each characterized by different linkage, content and stereochemistry of Ti (= Ti+Nb) in the TS block. In Groups I, II, III and IV, Ti = 1, 2, 3 and 4 *apfu*, respectively [4]

In jinshajiangite and cámaraite, Ti = 2 *apfu* and the TS block exhibits the stereochemistry of Group II. In bornemanite, nechelyustovite, minerals A and B, Ti = 3 *apfu*, the TS block is as in Group III. Jinshajiangite contains one type of **I** block (as in perraultite); cámaraite, bornemanite and minerals A and B, two types of **I** block; nechelyustovite, three topologically and chemically different **I** blocks. The structures of nechelyustovite and mineral B contain a new (for TS-block minerals) type of **I** block, an array of H_2O groups of ideal composition $(H_2O)_5$. Structures with a new type of TS block (more than one **I** block and more than one type of self-linkage of TS blocks) are related to structures of other minerals from the same Group: cámaraite, to bafertisite and jinshajiangite (Group II); bornemanite, to vuonnemite and barytolamprophyllite (Group III); nechelyustovite, to epistolite, barytolamprophyllite and a yet unknown structure (Group III); mineral A, to epistolite and barytolamprophyllite (Group III); mineral B, to barytolamprophyllite and a yet unknown structure. Minerals with a new type of TS-block structure and related minerals occur in the same environment and often form intimate intrgrowths. Discovery of five minerals with a new type of a TS-block structure (a) confirms that the chemical composition of the **I** block dictates the type of self-linkage of TS blocks [5]; (b) emphasizes the role of Ba↔Na exchange which results in changes in the topology of the **I** block and subsequently self-linkage of TS blocks (e.g. the bafertisite-cámaraite-jinshgagiangite series); (c) enlarges the number of transformation-mineral series [6] due to Na-depletion, bornemanite → nechelyustovite, Group III.

[1] Belov, N.V. (1976) *Essays on Structural Mineralogy*. Nedra, Moscow. [2] Pyatenko, Yu. A. et al. (1976) *Mineralogical crystal chemistry of titanium.* Nauka, Moscow. [3] Egorov-Tismenko, Yu.K. & Sokolova, E.V. (1990) *Mineral. Zh*., **12(4),** 40-49 (in Russian). [4] Sokolova, E. (2006). *Can. Mineral.*, **44**, 1273-1330. [5] Christiansen, C.C. et al. (1999) *Neues Jb. Miner. Abh*., **175**, 153-189. [6] Khomyakov, A.P. (1995) *Mineralogy of hyperagpaitic alkaline rocks*. Clarendon Press, UK.

From chemical composition to structure topology in Ti silicates

Sokolova, E.[1*] & Cámara, F.[2]
[1]Dept. of Geological Sciences, University of Manitoba, Winnipeg, Canada ([*]elena_sokolova@umanitoba.ca)
[2]CNR-Istituto di Geoscienze e Georisorse, Unità di Pavia, Italy

Sokolova [1] developed general structural principles and established the relation between structure topology and chemical composition for 24 Ti disilicate minerals containing the TS (titanium-silicate) block. The TS block is composed of a central trioctahedral (O) sheet and two adjacent (H) sheets of [5-7]-coordinated polyhedra and (Si_2O_7) groups. The general formula of the TS block is $A^P{}_2B^P{}_2M^H{}_2M^O{}_4(Si_2O_7)_2X_{4+n}$, where $M^H{}_2$ and $M^O{}_4$ are cations of the H and O sheets; M^H = Ti (= Ti + Nb), Zr, Mn^{2+}, Ca; M^O = Ti, Zr, Fe^{2+}, Mn^{2+}, Ca, Na; A^P and B^P = cations at the peripheral (*P*) sites = Na, Ca, Ba, K; X = anions = O, OH, F; n = 0, 2, 4. All structures consist of a TS block and an **I** (intermediate) block that comprises atoms between two TS blocks. Usually, the **I** block consists of alkali and alkaline-earth cations, (H_2O) groups and the oxyanions $(PO_4)^{3-}$, $(SO_4)^{2-}$ and $(CO_3)^{2-}$. Structures of Ti disilicate minerals naturally fall into four groups, each characterized by the topology and stereochemistry of the TS block. In Groups I, II, III and IV, Ti = 1, 2, 3 and 4 *apfu*, respectively. General structural principles of Sokolova [1] have been developed for structures that contain one type of a TS block, one type of an **I** block and exhibit one type of self-linkage of TS blocks. We define them as ***basic*** structures.

Here we consider 32 Ti disilicates. Of those 24 minerals [1], structure refinement was done for rinkite, barytolamprophyllite, nabalamprophyllite, murmanite and lomonosovite. *Basic* structures have been reported for mosandrite [2], nacareniobsite-(Ce) and jinshajiangite. Our recent work on 5 titanium disilicates, bornemanite, nechelyustovite and cámaraite, and two possible new mineral species, with preliminary ideal formulae $Na_4Ba\ Ti_2Nb\ (Si_2O_7)_2\ O_3\ (OH)\ (H_2O)_2$ (mineral A) and $Na_3KBa\ Ti_2Nb\ (Si_2O_7)_2\ O_3\ (OH)\ (H_2O)_6$ (mineral B), has resulted in discovery of a new type of TS-block structure. These new structures have more than one type of **I** block and one or more types of self-linkage of TS blocks. We define them as ***derivative*** structures. A *derivative* structure is usually related to two *basic* structures of the same Group, and all three structures have the same topology of the TS block and content of Ti. All derivative structures occur in Groups II and III (Ti = 2 and 3 *apfu*) and contain Ba in at least one **I** block. Discovery of *derivative* structures allows us to predict possible new structure topologies for Groups II and III. Those structure models will be developed in our talk.

Here, we also address another problem: different topologies for Ti and Fe^{3+} disilicates. The crystal structure of orthoericssonite, ideally $BaMn_2Fe^{3+}(Si_2O_7)O(OH)$, does not obey the general topological principles for Ti disilicates with the TS block. The substitution $Ti^{4+} \rightarrow Fe^{3+}$ is quite common because of the similar size of the cations: 0.58 Å for $^{[5]}Fe^{3+}$ and 0.51 Å for $^{[5]}Ti^{4+}$. The O sheet of the HOH block in orthoericssonite is identical to the O sheet in the structures of Group-II Ti disilicates: $M^O = Fe^{2+}$, Mn^{2+}, but the topology of the HOH block is different from the structures of Group II. We explain how bond-valence requirements of anions shared by the O and H sheets dictate different topologies for Ti and Fe^{3+} disilicates.

Based on new structural information, revised structural principles for Ti disilicates are outlined.

[1] Sokolova, E. (2006) *Can. Mineral.*, **44**, 1273-1330. [2] Bellezza, M. et al. (2009) *Can. Mineral.*, **47**, 897-908.

The role of Be in the formation of beryllosilicate crystal structures

Grice, J.D.
Research Division, Canadian Museum of Nature, Ottawa, Ontario, Canada (jgrice@mus-nature.ca)

Topological diagrams, based on the primary building units (PBU), the tetrahedral coordination sites, were constructed for all layered [1] and framework [2] beryllium silicates. These diagrams are used to calculate topological density (TD), identify secondary building units (SBU) and to extract vertex symbols (VS) and coordination sequences (CS). The SBU's, are used to create a structural classification and hierarchy among beryllosilicates. The VS's facilitate identification of the most common ring formations; 4-, 5- and 8-fold rings in layered structures and 3-, 4-, and 6-fold rings in framework structures. CS's give insight into relationships between crystal structures of widely varying chemical composition. CS's may be used to calculate the cluster population (CP) for any shell volume within the structure. In beryllosilicates the FD and CP are highly correlated (R^2 = 0.94). Using the CP has some advantages over the CP for determining crystal structures versus chemical composition correlations as it is independent of the tetrahedral cation size.

The effect of the Be content on CP or FP is of great interest as it can be used in the design parameters of a framework. Si alone cannot form 3-fold rings in framework silicates. The addition of Be increases the number 3-fold rings. A Be proportion of up to 30% of the tetrahedral sites decreases FD but further addition of Be rapidly increases FD. Zeolite formation, which requires a low FD, can be adjusted with the Be content.

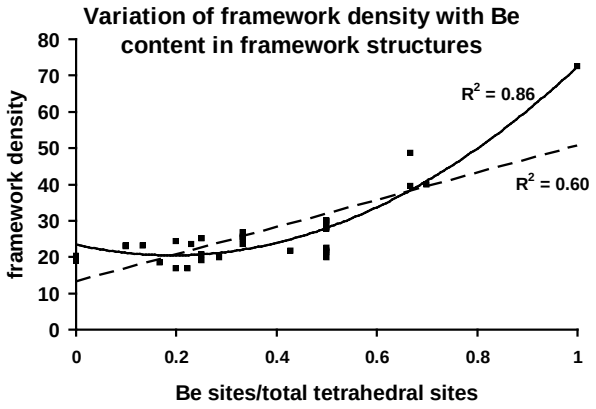

Fig. 1: Variation of framework density with Be content in framework structures.

[1] Grice, J.D. et al. (2009) *Can. Mineral.*, **47**, 193-204. [2] Grice, J.D., Raade, G. & Cooper, M.A. (2010) *Can. Mineral.*, **48(2)**, 255-266.

Some topological aspects of the crystal chemistry of actinide borates

Alekseev, E.V.[1*], Wang, S.[2], Albrecht-Schmitt, T.E.[2] & Depmeier, W.[1]
[1]Dept. of Crystallography, University of Kiel, Germany
([*]ea@min.uni-kiel.de)
[2]Dept. of Civil Engineering and Geological Sciences and Dept. of Chemistry and Biochemistry, University of Notre Dame, Notre Dame, Indiana, USA

The methods of nuclear fuel vitrification in borate or boroaluminate glasses are very common in nuclear industry. The glasses contain actinides and the products of their decay. For a long time this type of storage of very dangerous components has been considered as very safe because of the high kinetic and chemical stability of the borate glasses. The study of the products (actinyl borates) of the potential re-crystallization of the corresponding glass-blocks is very important in view of understanding their stability on geological time scales (thousands and million years).

Recently, we have found a very easy and efficient method for the synthesis of actinide borates. Using a H_3BO_3 flux, we have synthesized several actinyl borates (24 uranyl borates, 4 neptunyl borates, 1 plutonyl and 1 thorium borate) [1-4]. These phases were characterized by X-ray diffraction, spectroscopic and other methods. Several synthesized phases possess unique structural properties, both in actinide chemistry and in chemistry in general. For example, in the structure of Np-borates we have found three different oxidation states (+4, +5 and +6) and three different coordination polyhedra of Np (coordination numbers 6, 7 and 8). The thorium borate (NDTB-1) has a unique supertetrahedral cationic framework with large open channels and pores. This structure allows fast anionic exchange of MnO_4^-, CrO_4^{2-}, $Cr_2O_7^{2-}$. The most important particularity of NDTB-1 is that it exchanges TcO_4^-. The results are very promising as NDTB-1 removed 72% of Tc from solution in 36 hours. Many of the synthesized uranyl borates are non-centrosymmetric and demonstrate non-linear optical properties.

Many of these properties appear because of the special topologies of oxo-borate sheets and clusters which is passed on to the resulting layered or framework structures. Nine different types of oxo-borate sheet topology have been observed by now in uranyl, neptunyl and plutonyl compounds. Only one of these structures has oxo-borate chains as a structural fragment. Some of the topologies are enantiomorphic, while others are not. The centro-symmetric and non-centrosymmetric structures achieved in the uranyl borates depend on the type of the oxo-borate sheets, their alteration and orientation within the crystal structures. A classification of the crystal structures and oxo-borate sheets based on their topological aspects is proposed.

[1] Wang, S. et al. (2010) *Chem. Mater.*, **22**, 2155-2163. [2] Wang S. et al. (2010) *Inorg. Chem.*, **49**, 2948-2953. [3] Wang, S. et al. (2010) *Angew. Chem.*, **122**, 1075-1078; *Angew. Chem. Int. Ed.*, **49**, 1057-1060. [4] Wang, S. et al. (2010) *Angew. Chem.*, **122**, 1285-1288; *Angew. Chem. Int. Ed.*, **49**, 1263-1266.

Finite automata, formal languages and bond topologies in mineral and inorganic structures

Krivovichev, S.V.
Dept. of Crystallography, St. Petersburg State University, St. Petersburg, Russia (skrivovi@mail.ru)

The basic property of crystalline matter that makes possible their investigation by means of X-ray diffraction is its periodicity, which means that topological graph of chemical bonds in the structure is always periodic. In turn, this means that the structure is the result of periodic process, i.e. its construction involves a finite number of local chemical interactions that repeats over and over during structure growth. The process of growth of periodic mathematical structure that symbolizes a real chemical structure (e.g., graph, tiling [1]) may be modeled using theory of finite automata.

A finite automaton (FA) is defined as consisting of finite number of states (each equivalent to a certain chemical configuration) and finite number of transition rules that describe transformation of chemical configurations during growth process. Deterministic FA (=DFA) produces completely ordered structures, whereas non-deterministic FA (=NDFA) may generate structures with a certain degree of chemical or configurational disorder. In some sense, crystals are results of performance of computer programs, which were identified by A. Mackay [2] as 'inorganic genes'. Since structures of many minerals and inorganic compounds are known and their formal topological classifications are elaborated [3], it is an interesting task to classify their programs or 'genes' (the last term makes a perfect sense from the viewpoint of mineral evolution [4,5]), and to see how these genes evolve over micro or macro geological history.

Another interesting aspect of application of FA to crystal structures is that, in computer science, FA are put in direct correspondence to formal languages [6], and the formal structure (state diagram) of FA is associated with rules that govern formation of words from a finite set of symbols (production rules). From this viewpoint, FAs generating related bond topologies may be grouped into families of languages that may be derived from one superlanguage or pra-language.

It should be noted that formal language is a highly abstract construction. Its construction may be represented by FA, and the projection of the FA into topological space produces a graph, which, in turn, projects into real chemical space to produce a bond topology. How many different pra-languages are behind mineral structures? Do these pra-languages mix? How languages are related to chemical properties of ions, coordination polyhedra or fundamental building blocks? Questions of this type are highly provocative but are absolutely justified from the viewpoint of automata and formal language theory of mineral structures.

A special class of DFA is cellular automata that are used as models of discrete dynamic systems in different branches of science and can be used to model structures of minerals and inorganic materials [7].

Acknowledgements: This work was supported by the Russian Ministry of Science and Education.

[1] Krivovichev, S.V. (2009) *Structural Crystallography of Inorganic Oxysalts*. Oxford, OUP. [2] Mackay, A. (1976) *Phys. Bull*., **27**, 495. [3] Hawthorne, F.C. (1994) *Acta Cryst*., **B50**, 481-510. [4] Yushkin, N.P. (1982) *Zapiski VMO*, **111**, 432-442. [5] Hazen, R.M. et al. (2008) *Amer. Mineral*., **93**, 1693-1720. [6] Hopcroft, J.E. et al. (2001) *Introduction to Automata Theory, Languages, and Computation*, Boston, Addisson-Wesley. [7] Krivovichev, S. (2004) *Acta Crystallogr*., **A60**, 257-262.

Generating functions for structure and chemical composition

Hawthorne, F.C.
Dept. of Geological Sciences, University of Manitoba, Winnipeg, Canada (frank_hawthorne@umanitoba.ca)

Any crystal structure may be represented by a weighted chromatic digraph, the vertex set of which represents atoms and the edge set of which represents chemical bonds. We may write tetrahedrally coordinated cations and their associated anions as $\{T_{2n}\Theta_m\}$. For $\{T_{2n}\Theta_m\}$ to be a chain or ribbon, $5n < m \leq 6n$, and we may write m as 5n + N, where N is an integer. Within the $\{T_{2n}\Theta_{(5n+N)}\}$ unit, we may recognize three types of anion vertices: (1) bridging anions, Θ^{br}, that are bonded to two T cations; (2) apical anions, Θ^{ap}, that are involved in linkage to other cations out of the plane of the bridging anions; and (3) linking anions, Θ^{l}, that link to non-T cations in the plane of the bridging anions. We can incorporate the connectivity of the cations our algebraic representation of the chain as follows: $\{T_{2n}\Theta^{br}{}_a\Theta^{nbr}{}_b\Theta^{ap}{}_c\}$ where a + b + c = 5n + N. The apical anions of the T-layer map onto a 6^3 net which, in turn, maps onto the 3^6 net of anions of the O-layer. We may use the handshaking dilemma of graph theory to examine the interaction between the two types of layers, and write a *Structure-Generating Function*, $S_{\mathbf{n}}$, that gives both the stoichiometry and aspects of the bond topology of the structures. Where N = 1, the T component is $\{T_{2n}\Theta_{5n+1}\} = \{T_{2n}\Theta^{br}{}_{3n-1}\Theta^{ap}{}_{2n}\Theta^{l}{}_2\}$. Each T-$\Theta^{br}$-T linkage spans an octahedron, and hence there are 3n-1 octahedrally coordinated cations between opposing $\{T_{2n}\Theta^{br}{}_{3n-1}\Theta^{ap}{}_{2n}\Theta^{l}{}_2\}$ ribbons. In the biopyribole series, the $\{T_{2n}\Theta^{br}{}_{3n-1}\Theta^{ap}{}_{2n}\Theta^{l}{}_2\}$ ribbon is unbranched and contains (n-1) loops. Each loop must correspond to one additional anion (denoted φ) that is bonded to the M cations and not bonded to a T cation. We may thus write the structure-generating function, $S_{\mathbf{n}}$, for the biopyribole structures as follows: $S_n = [M_{(3n-1)}\Psi_{2(n-1)}\{T_{2n}\Theta^{br}{}_{(3n-1}\Theta^{ap}{}_{2n}\Theta^{l}{}_2\}_2]$; note that the anion notations Θ^{br}, Θ^{ap} and Θ^{l} carry information on the structural linkage that the chemical formula does not. Interstitial sites are occupied by $X_{\mathbf{I}}$ cations so as to (1) achieve electroneutrality, and (2) satisfy the local-sum rule of bond-valence theory. For n = 1, $S_1 = X_{\mathbf{I}}[M_2\Psi_0\{T_2\Theta_6\}_2]$, the pyroxenes. For n = 2, $S_2 = X_{\mathbf{I}}[M_5\Psi_2\{T_4\Theta_{11}\}_2]$, the amphiboles. For n = 3, $S_3 = X_{\mathbf{I}}[M_8\Psi_4\{T_6\Theta_{16}\}_2]$, the triple-chain pyriboles. For n = 4, $S_4 = X_{\mathbf{I}}[M_{11}\Psi_6\{T_8\Theta_{21}\}_2]$; no structure of this formula has yet been found. For $n = \infty$, $S_\infty = X_{\mathbf{I}}[M_{(3n-1)/n}\Psi_{2(n-1)/n}\{T_2\Theta_{(5n+1)/n}\}_2 = X_{\mathbf{I}}[M_{(3-1/n)}\Psi_{2-2/n}\{T_2\Theta_{5+1/n}\}_2] = X_{\mathbf{I}}[M_3\Psi_2\{T_2\Theta_5\}_2]$ (*e.g.*, phlogopite). Where N = 2, the general form of the T component is $\{T_{2n}\Theta_{5n+2}\}$ which corresponds to the T component of H-layers in the polysomatic H-O-H series in which the ribbons are linked laterally by [5]- or [6]-coordinated cations, D, which have the coordination $(D\Theta^{l}{}_4\Phi^{\mathbf{ap}}\Phi^{\mathbf{t}}_{\mathbf{0\text{-}1}})$. The general formula for an H layer is $[D\Phi^{\mathbf{ap}}\{T_{2n}\Theta^{br}{}_{3n-2}\Theta^{ap}{}_{2n}\Theta^{l}{}_4\}\Phi^{\mathbf{t}}_{\mathbf{0\text{-}1}}]$, where $\Phi^{\mathbf{t}}$ after the T component occurs on the outside of the H-layer and is involved in linkage between adjacent H-O-H sheets. The H-layer links via its apical anions to the O-layer, giving the general formula of an H-O-H sheet as $[M_{3n+1}(D\Phi^{\mathbf{ap}}\Psi_n\{T_{2n}\Theta_{5n+2}\}\Phi^{\mathbf{t}})_2]$. These H-O-H sheets can link directly through the $\Phi^{\mathbf{t}}$ anions of the $(D\Theta^{l}{}_4\Phi^{\mathbf{ap}}\Phi^{\mathbf{t}}_{\mathbf{0\text{-}1}})$ octahedra, giving $S_{\mathbf{n}} = X_{\mathbf{I}}[M_{(3n+1)}\Psi_{2n}(D_2\Phi_2\{T_{2n}\Theta_{5n+2}\}_2)\Phi_{0\text{-}2}]$. For n = 1, $S_1 = X_{\mathbf{I}}[\{M_4\Psi_2(D_2\Phi_2\{T_2\Theta_7\}_2)\Phi_{0\text{-}2}]$, the group-1 TS-block structures (*e.g.*, seidozerite: $Na_2[Na_2MnTiO_2(Zr_2\{Si_2O_7\}_2)F_2]$). For n = 2, $S_2 = X_{\mathbf{I}}[M_7\Psi_4(D_2\Phi_2\{T_4\Theta_{12}\}_2)\Phi_{0\text{-}2}]$, the astrophyllite-group structures (*e.g.*, $K_2Na[Fe^{2+}{}_7O_2(OH)_2F(Ti_2\{Si_4O_{12}\}_2)(OH)_2]$). For n = 3, $S_3 = X_{\mathbf{I}}[M_{10}\Psi_6(D_2\Phi_2\{T_6\Theta_{17}\}_2)\Phi_{0\text{-}2}]$, *e.g.*, nafertisite: ideally $Na_2[Fe^{2+}{}_{10}O_2(OH)_6(Ti_2\{Si_{12}O_{34}\})](H_2O)_{0\text{-}2}$. For n = 4, $S_4 = X_{\mathbf{I}}[M_{13}\Psi_8(D_2\Phi_2\{T_8O_{22}\}_2)\Phi_{0\text{-}2}]$, *e.g.*, $Na_2[Fe^{2+}{}_{13}O_2(OH)_8(Ti_2\{Si_{16}O_{44}\})(OH)_2]$; no structure of this formula has yet been found. For $n = \infty$, $S_\infty = X_{\mathbf{I}}[M_{(3n+1)/n}\Psi_{2n/n}(D_{2/n}\Phi_{2/n}\{T_2\Theta_{(5n+1)/n}\}_2)\Phi_{2/n}] = X_{\mathbf{I}}[M_{(3-1/n)}\Psi_2(D_{2/n}\Phi_{2/n}\{T_2\Theta_{(5+1/n}\}_2)\Phi_{2/n}] = X_{\mathbf{I}}[M_3\Psi_2\{T_2\Theta_5\}_2]$ (e.g., phlogopite , $K[Mg_3(OH)_2\{AlSi_3O_{10}\}]$).

Crystal structure of $Na_3Fe(SO_4)_3$, a high temperature product of thermal decomposition of sideronatrite, $Na_2Fe(SO_4)_2(OH)3H_2O$

Scordari, F.[1], Ventruti, G.[1*], Gualtieri, A.F.[2] & Lausi, A.[3]
[1]Dipto. Geomineralogico, Università degli Studi di Bari, Italy
([*]ventruti@geomin.uniba.it)
[2]Dipto. di Scienze della Terra, Università degli Studi di Modena e Reggio Emilia, Modena, Italy
[3]Sincrotrone Trieste, Basovizza(TS), Italy

The iron sulphate $Na_3Fe(SO_4)_3$ studied here has been obtained as a high temperature (HT) product (~400°C) of the thermal decomposition of a hydrated sulphate of sodium and ferric iron, sideronatrite ($Na_2Fe(SO_4)_2(OH)\cdot 3H_2O$), from Sierra Gorda, Chile [1]. Its structure has been determined and refined using high resolution powder diffraction data collected at the MCX beamline at ELETTRA synchrotron source (Trieste, Italy). The $Na_3Fe(SO_4)_3$ compound is trigonal, space group: R-3 with a = 13.6452(1), c = 9.0842(2) Å, V = 1464.80(2) $Å^3$ and Z = 6. Building blocks of the structure are FeO_6 octahedra linked by corner-sharing $(SO_4)^{2-}$ tetrahedra to form infinite columns $[Fe(SO_4)_3]^-$ running along the c axis. These columns occur around three-fold axes and are linked to each other by interstitial Na.

The characteristic topology of this compound is also present in the mineral ferrinatrite, $Na_3(H_2O)_3Fe(SO_4)_3$ [2], where adjacent chains are linked both by interstitial Na atoms and hydrogen bonds belonging to H_2O coordinated by Na cations. The structure of the $Na_3Fe(SO_4)_3$ HT phase can be described as the 'imploded' version of ferrinatrite. The structure of a new mineral pyracmonite, $(NH_4)_3Fe(SO_4)_3$, has been recently solved by Demartin et al [3]. Like our compound, it is based on infinite $[Fe(SO_4)_3]_\infty$ chains but, differently from it, interchain linkages involve only hydrogen bonds from the ammonium ions. Recently a further new mineral having the same composition $Na_3Fe(SO_4)_3$, was found among fumarolic encrustations at Eldfell volcano, Heimaey Island, Iceland [4]. It occurs in association with eldfellite, ralstonite, anhydrite, gypsum, bassanite, hematite, opal and tamarugite. The mineral is hygroscopic and unstable in the open air. Synthetic $Na_3Fe(SO_4)_3$ played an important role in several high temperature solid state reactions in the industrial processes of pigments, catalysis and magnetic materials.

[1] Scordari, F. & Ventruti, G. (2009) *Am. Mineral.*, **94**, 1679-1686. [2] Scordari, F. (1977) *Mineral. Mag.*, **41**, 375-383. [3] Demartin, F., Gramaccioli, C.M. & Campostrini, I. (2010) *Can. Mineral.*, in press, private communication. [4] Balić-Žunić, T. et al. (2009) *Mineral. Mag.*, **73**, 51-57.

Between modular and modulated: composite layer structures of complex sulfosalts

Makovicky, E.
Dept. of Geography and Geology, University of Copenhagen, Denmark (emilm@geol.ku.dk)

Complex sulfides of Pb, Sn, Sb, Bi or As, often with minor Cu, Ag and/or Fe, contain structural families with a modular or modulated character. Modularity and modulation occur in different proportions, types and combinations in the new/recently refined structures of sulfosalts with a composite layer character shown here.

Cylindrite, exemplified here by its synthetic representative, $Sn_{31.5}Sb_{6.2}Fe_{3.1}Se_{59.1}$ [1], is composed of alternating pseudotetragonal (Q) layers Me_2Se_2, two atomic planes thick, and pseudohexagonal (H) layers MeS_2. The composite structure is noncommensurate in two dimensions and sinusoidally modulated in one of them, with OD phenomena in layer stacking. It is an accretional homologue N = 1, whereas N = 2 homologue is *franckeite*, $Pb_{4.6}Ag_{0.2}Sn_{2.5}Sb_2Fe_{0.8}S_{12.6}$, with a newly determined crystal structure in which the Q layers are of double thickness (four atomic planes thick), with a central gap accommodating lone electron pairs of cations in an SnS-like manner. Orientation of the Q layers in this family of Pb-Sn^{2+}-Sn^{4+} structures differs from the following Pb-Bi sulfosalts.

Cannizzarite is a modulated, 1D-incommensurate composite structure in which the M_2S_3 H-layer has double thickness. The hypothetical sectioning of cannizzarite layers into ideally commensurate moduli by [2] has been substantiated when we found one of these component moduli as an independent structure. The accretional *proudite-felbertalite* homologous series of Cu-Pb-Bi sulfosalts [3] is based on pseudohexagonal double-octahedron H-layers alternating with Q layers. Its accretional character (interface modulation) is demonstrated by the variable width of straight layer portions between copper-bearing step-like offsets. This series, however is the N =2 homologue in the thickness of H layers; the N =1 variety is *junoite*, $CuPb_3Bi_7(S,Se)_{14}$.

A new family of structures has Q layers that are three atomic planes thick and H layers only one atom thick. They are composite *lock-in* structures with a simple ratio of subperiodicities of the two layer types. The Q layer contains linear-coordinated Ag or Cu whereas the H layer has triangular-to-tetrahedral Cu or Ag. *Berryite*, $Cu_3Ag_2Pb_3Bi_7S_{16}$ [4], is composed of two alternating types of Q moduli whereas the two new isotypic structures, Cu-based *watkinsonite*, $Cu_2PbBi_4Se_8$, and the Ag-based *litochlebite*, $Ag_2PbBi_4Se_8$, have only one type.

Acknowledgements: This invited talk is based on the results of a research group in which participated Drs. D. Topa, V. Petříček, M. Dušek, J. Sejkora, H. Dittrich, W.G.Mumme and E.M. Support of FNU (Denmark) and Czech and Austrian funding agencies is gratefully acknowledged.

[1] Makovicky, E. et al. (2008) *Am. Mineral.*, **93,** 1787-1798. [2] Matzat, E. (1979) *Acta Crystallogr.*, **B35**, 133-136. [3] Mumme, W.G. et al. (2009) *Can. Mineral.*, **47**, 25-38. [4] Topa, D. et al. (2006) *Can. Mineral.*, **44,** 465-480.

Disordered structures and polytypism – the OD approach

Merlino, S.
Dipto. di Scienze della Terra, Università di Pisa, Italy (merlino@dst.unipi.it)

The OD approach in dealing with polytypic structures, one-dimensional disorder and twinning (mainly polysynthetic twinning) has been introduced more than fifty years ago [1]. Notwithstanding the theory is firmly built and a number of practical tools for its utilization are available [2], it is still far from constituting a 'normal' professional equipment for mineralogists, and crystal chemists and crystallographers as well.

The main reasons for that are probably the assumption that OD structures are relatively few in number and that their arrangements may be solved and described without the introduction of OD theory and its apparently abstruse terminology.

On the contrary, it may be pointed that the number of substances which display OD features is very large, especially among inorganic compounds, both synthetic and natural. Moreover, sometimes it is just through an OD approach that the 'real' structure of some compounds may be understood. It is the case of the various members of tobermorite group; their real structures, which for long time eluded the efforts of mineralogists and cement chemists, could be effectively modelled and refined just through the application of the OD procedures.

In any case, the OD approach gives a deeper insight into the structural problem, suggesting interesting relations and pointing to possible new natural or synthetic compounds.

In this contribution, after a short presentation of the basic aspects of the OD approach, few examples of complex mineral structures will be presented (charoite, molybdophyllite and fukalite) where OD theory is extraordinarily helpful in dealing with their polytypic features and disorder.

[1] Dornberger-Schiff, K. (1956) *Acta Cryst.*, **9**, 593-601. [2] Ferraris, G., Makovicky, E. & Merlino, S. (2008) *Crystallography of modular materials.* Oxford University Press.

Polysomatic defects in astrophyllite

Grobéty, B.
Dept. of Geosciences, University of Fribourg, Switzerland
(bernard.grobety@unifr.ch)

Astrophyllite belongs to the heterophyllosilicate mineral group [1], which can be represented as a polysomatic series based on beam modules taken from the endmembers bafertisite (B module) and mica (M module). The group can also be described as T'OT' sheet silicates with modified tetrahedral layers i.e. the T'-layers contain cations with non-tetrahedral coordination. Different members of the series may be derived by variation in the module sequence and orientation in two directions. Stacking errors may, therefore, occur also in two directions i.e along the heterophyllosilicate sheet (basal plane, *b*-direction) and in the stacking direction of the latter (along [001]). A set of astrophyllite samples has been analyzed by high resolution electron microscopy (HRTEM). The most common faults consist of module multiplicity faults i.e presence of additional bafertisite or mica modules along *b* changing the normal astrophyllite sequence from ..MBMB.. to .. MBMBBMB.. or ..MBMMBMB.. These multiplicity faults propagate usually through the entire crystal. Stacking disorder along [001] (=polytypic stacking faults) are much rarer. The faults are most likely growth defects. There is no indication of solid state reaction which may change the module sequence as it is observed in the biopyribole polysomatic series.

[1] Ferraris, G. et al. (1996) *Eur. J. Mineral.*, **8**, 241-249.

Polytypic and polysomatic structures based on hydromagnesite layers

Mills, S.J.[1*], Christy, A.G.[2], Wilson, S.A.[3], Dipple, G.M.[1], Whitfield, P.S.[4] & Raudsepp, M.[1]
[1]Dept. of Earth and Ocean Sciences, University of British Columbia, Vancouver, Canada ([*]smills@eos.ubc.ca)
[2]Research School of Earth Sciences, Australian National University, Canberra, Australia
[3]Dept. of Geological Sciences, Indiana University, Bloomington, USA
[4]Institute for Chemical Process and Environmental Technology, National Research Council of Canada, Ottawa, Canada

Hydromagnesite, $Mg_5(CO_3)_4(OH)_2{\cdot}4H_2O$, is a secondary carbonate mineral that commonly occurs in weathered ultramafic rocks (particularly serpentinites), in low temperature hydrothermally altered dolostones and in cave assemblages. Hydromagnesite and carbonate assemblages are of great interest for their ability to sequester greenhouse gasses directly from the atmosphere. Dypingite, $Mg_5(CO_3)_4(OH)_2{\cdot}{\sim}5H_2O$, is an environmentally benign, metastable carbonate mineral that also acts as a host for greenhouse gases. Dypingite is more easily precipitated than the more stable hydromagnesite under conditions at the Earth's surface. Given time and temperature, it decomposes to the better ordered hydromagnesite structure. Hydromagnesite is known to further decompose to magnesite, which is among the most stable mineral traps for CO_2.

The hydromagnesite structure is based on a three-dimensional corrugated framework of corner-connected MgO_6 octahedra and carbonate triangles. The hydrogen atoms and water molecules form hydrogen-bonded crankshaft chains running parallel to **c**. The structure is strongly pseudo-orthorhombic (*Bbcm*), but in the standard monoclinic $P2_1/c$ setting, a = 10.105, b = 8.954, c = 8.378 Å, β = 114.44º and Z = 4. Infinite superstructures of the *Bbcm* average structure can be produced by ordering polarities of the H-bonded chains in different ways, producing stacking of layers along **b**, each of width $(b/2)_{hydromag}$. Because alternate layers have opposite point directions along **a**, there must be an even number 2n of layers in a unit cell, which then has a *B*-centred cell with a = 18.399 Å, b = 8.954 × n Å, c = 8.378 Å, β = 90º and Z = 4n.

The maximum-degree-of-order arrangements of H-bonded changes both have n = 2, but with space groups *Bbc*2 for *ferro* ordering, $B12_1/c1$ for the *antiferro* structure of hydromagnesite. The only possible space groups (with multiplicity > 2) for longer periodicities are these two for n = odd, or $B112/b$ for n = even. The number of different polytypes grows rapidly with n, even for these maximal-symmetry cases. There are 3 possible $B12_1/c1$ and 3 *Bbc*2 structures for n = 5, and 7 of each for n = 7, both of which periodicities have been observed in nature and in synthetic compounds. The cases with even n have not been observed, possibly due to greater resistance to monoclinic lattice strain on (001) as opposed to (010).

Dypingite and widgiemoolthalite, $Ni_5(CO_3)_4(OH)_2{\cdot}{\sim}4H_2O$, both have **b** repeats ca. 7× that of hydromagnesite. In widgiemoolthalite, minor relaxations of the layers are present, while for dypingite, **b** is expanded significantly to accommodate extra water, which can be modelled by replacing some hydromagnesite layers by a second type of structural module. Thus, the system shows polytypic and polysomatic variability. Other minerals such as giorgiosite are also likely to be based on the hydromagnesite parent structure.

Modular structures as modulated crystals

Perez-Mato, J.M.[*] & Elcoro, L.
Dept. Fisica de la Materia Condensada, Fac. Ciencia y Tecnologia, Universidad del Pais Vasco, Bilbao, Spain
([*]jm.perez-mato@ehu.es)

The use of the superspace formalism has been recently extended to the description and refinement of homologous series of modular structures. Ideal modules can be quantitatively described as modulated configurations with step-like atomic occupation modulations and sawtooth displacive modulation functions (see Fig. 1 and [1]). A single superspace symmetry for the whole series can be defined, and an idealized model for any member of the series can automatically be obtained by choosing the width of the occupation domains and the modulation wave vector. Different orientations of the same module can be introduced by means of large zigzag modulation functions.

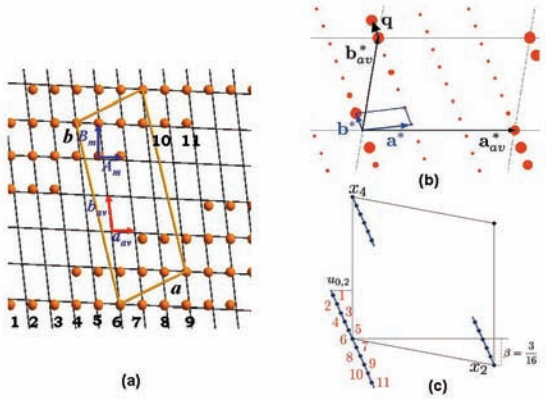

Fig. 1: Superspace description of an ideal module as a modulation. (a) average, module and superstructure unit cell, (b) Fourier spectrum with the choice of modulation wave vector, (c) superspace unit cell on the x_2x_4 plane with sawtooth occupation and displacive modulation.

The deviations of the atomic positions from the idealized modules are given by additional small displacive modulations. If the size of the modules is large, they can be refined using less parameters than in a conventional approach. These additional modulations show hidden fustrated competitions between different length scales for the interatomic distances (see Fig. 2).

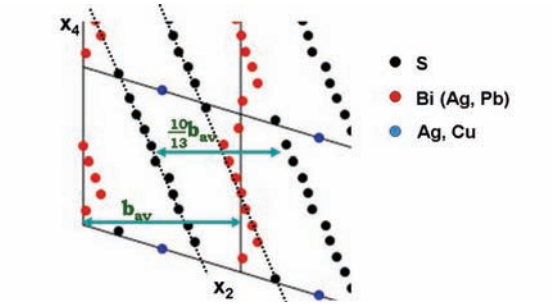

Fig. 2: Superspace embedding on the x_2x_4 plane of the experimental structure of benjaminite ($Cu_{0.5}Ag_{2.3}Pb_{0.4}Bi_{6.8}S_{12}$ [2]) of the pavonite series showing competing average interatomic distances.

After a brief introduction to the superspace description of modulated structures, its application in the field of modular structures, outlined above, will be reviewed by means of a few examples.

[1] Elcoro, L. et al. (2008) *Acta Cryst. B*, **64**, 684-701. [2] Makovicky, E. & Mumme, W.G. (1979) *Can. Mineral.*, **17**, 607-618.

Superspace description of modulated wagnerite polytypes

Lazic, B.[1*], Armbruster T.[1], Chopin, C.[2], Grew, E.S.[3], Baronnet, A.[4] & Palatinus, L.[5]
[1]Institute of Geological Sciences, University of Bern, Switzerland ([*]biljana.lazic@krist.unibe.ch)
[2]Ecole Normale Supérieure, CNRS, Paris, France
[3]Dept. of Earth Sciences, University of Maine, Orono, Maine, USA
[4]CRMCN-CNRS, Marseille, France
[5]Institute of Physics, Academy of Sciences of the Czech Republic, Prague, Czech Republic

More than 40 wagnerite samples $(Mg,Fe,Mn)(PO_4)(F,OH)$ from diverse geological environments have been investigated by EMP, X-ray single-crystal diffraction, and HRTEM analysis. Results suggested a major role for compositional control in determining modulation periodicity: 2*b*, 3*b*, 5*b*, 7*b*, and 9*b* [1]. All modulated structures share the same topological arrangement of cations and oxygen atoms, but differ mainly in positional modulation of F, (OH). In wagnerite F, (OH) occupies one of two positions, leading to two distinct arc configurations along *a*: arc up (U) or arc down (D). Different periodicities of U and D sequences lead to multiplication of the structural periodicity along *b* and hence various polytypes (five are known to date).

In this study, a unified superspace model [2] is constructed for ordered stacking sequences of four polytypes 3*b*, 5*b*, 7*b*, and 9*b* based on the average triplite structure model with a ≈ 12.8 Å, b ≈ 6.4 Å, c ≈ 9.6 Å, β ≈ 117 º and the (3+1)-dimensional superspace group $C2/c(0b0)s0$. Modulation vectors are $\mathbf{q} = \beta\mathbf{b}^*$, where $\beta = 0.3460(3) \approx 1/3$; $\beta = 0.4106(4) \approx 2/5$; $\beta = 0.4275(4) \approx 3/7$ and $\beta = 0.4466(3) \approx 4/9$ for 3*b*, 5*b*, 7*b*, and 9*b* structures, respectively. As the β components of the **q** vectors are close to commensurate values, it is not surprising that refinements using superstructure models also give reasonable results [3]. However, **q**-vector refinements show small but significant deviations from commensurate values.

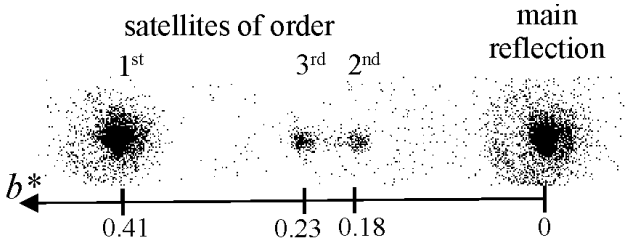

Fig. 1: Position of satellite reflections for a 5*b* wagnerite polytype: Splitting of 2nd and 3rd order reflections from a position at 1/5 = 0.2 proves the incommensurate nature of the structure.

In the four studied polytypes incommensurate models are converging to better agreement factors. In addition to the better refinements, the superspace approach provides a unified model with a common space group, and simplifies description of positional and occupational modulation of Mg/Fe and F/OH in wagnerite polytypes.

[1] Armbruster, T. et al. (2009) *Geochim. Cosmochim. Ac.*, **73(1)**, A32. [2] van Smaalen, S. (2007) *Incommensurate Crystallography*. Oxford University Press Inc., NewYork. [3] Ren, L. et al. (2003) *Can. Mineral.*, **41**, 393-411.

Rational *ab initio* modeling for low energy hydrogen-bonded phyllosilicate polytypes

Mercier, P.H.J.* **& Le Page, Y.**
Institute for Chemical Process and Environmental Technology, National Research Council of Canada, Ottawa, Ontario, Canada
(*patrick.mercier@nrc-cnrc.gc.ca)

This abundantly illustrated talk details the very simple concepts subtending an ongoing recent series of papers [1-3] that has so far rationalized the disparate known facts about the kaolin system at ambient and low pressures [1], correctly predicted the existence at high pressure of two new translations (-**a**/3 and (**a**+**b**)/3) allowing 5-fold coordination for Si [2], correctly predicted [1,2] two newly and independently observed [4] kaolinite polytypes (kaolinite II and III), predicted the existence of a still unobserved (SU) kaolinite IV phase at a pressure no higher than 60 GPa [3], and predicted the SU transformation of dickite II [5] into dickite III around 10 GPa [3] as well as that of nacrite at similar pressure into SU nacrite II. Optimized crystal structures for the most likely low enthalpy polytypes are printed [3], allowing simplification of their identification when they will be observed, as they did in [4] for kaolinite II and III.

The concept of energy independence of non-neighbouring hydrogen-bonded phyllosilicate layers is shown to imply that low energy models derive from an initial undistorted ideal layer for the phyllosilicate through repetition of either (a) a same [**R**,**T**]= operation or (b) the succession [**R**,**T**]=[**R***,**T***]= where **R*** denotes the enantiomorph of rotation **R**, and **T*** that of translation **T**, while the = symbol indicates hydrogen bonding between layers enclosed within brackets [ ]. Combination of the application of this most simple concept with total energy *ab initio* DFT calculations has allowed derivation of the above wealth of scientific results.

Whereas the new kaolin phases taking place under compression can occur because they only involve translations by at most a couple Å between adjacent layers, we argue that no solid-state transformations between kaolinite, dickite and nacrite can occur at any pressure without dissolution and recrystallization, even under conditions where any one of those phases would have lower enthalpy. Indeed, as such polytype transformations would involve rotation between adjacent kaolin layers, they require macroscopic atom displacements that cannot occur in the solid state, but just at crystallization time. Interpretation of polytype abundances in sedimentary rocks, particularly the evolution of kaolinite-to-dickite ratios observed as function of burial depths will be discussed.

Our goal in this research effort has been to print inexpensive theoretical results that can be verified/falsified with a single powder pattern, thus pointing directions for exploratory experimental studies in an experimentally difficult system as well as exposing the complementarity of theory and experiment. While waiting for literature results of discriminative structural, thermochemical, or hydrothermal experiments in the kaolin system, we are currently extending the above concepts to the high pressure phases of additional hydrogen-bonded phyllosilicate families where observed phase transitions in the literature are awaiting polytype identification and thermodynamical interpretation. In all our studies, all DFT calculations were performed with *VASP* [6] while all structure modeling as well as VASP file preparation and interpretation was performed with *Materials Toolkit* [7].

[1-2] Mercier, P.H.J. & Le Page, Y. (2008) *Acta Cryst. B*, **64**, 131-143 & (2009) *Mater. Sci. Tech.*, **25**, 437-442. [3] Mercier, P.H.J. et al. (2010) *Am. Mineral.*, **95**, 1117-1120. [4] Welch, M.D. & Crichton, W.A. (2010) *Am. Mineral.*, **95**, 651-654. [5] Dera, P. et al. (2003) *Am. Mineral.*, **88**, 1429-1435. [6] Kresse, G. & Hafner, J. (1993) *Phys. Rev. B*, **48**, 13115-13118. [7] Le Page, Y. & Rodgers, J. (2005) *J. Appl. Cryst.*, **38**, 697-705.

Self-organisation in the modulated structure of pyrrhotite: direct observations by TEM

Harries, D.*, Pollok, K. & Langenhorst, F.
Bayerisches Geoinstitut, University of Bayreuth, Germany
(*dennis.harries@uni-bayreuth.de)

Pyrrhotite is a layered iron sulfide of the general non-stoichiometric composition $Fe_{1-x}S$ ($x < 0.125$) and is one of the most abundant iron sulfides in the Earth's crust. Due to variable Fe deficiency large numbers of possible structural variants arise from the ordering of Fe vacancies within the NiAs-based structure. The resulting superstructures show very different physicochemical and magnetic properties bearing on pyrrhotite's contribution to rock magnetisation and the paleomagnetic record, as well as on many issues in geochemistry, petrology, and technical mineral processing.

In ferrimagnetic monoclinic 4*c*-pyrrhotite ($Fe_{0.875}S$) vacancies are ordered into every second Fe layer of the NiAs substructure, alternating along the *c*-axis with fully occupied Fe layers. In (pseudo-)hexagonal N*c*-pyrrhotites ($Fe_{0.875}S$ to ~$Fe_{0.92}S$) Fe deficiency and ordering sequences of vacant and filled Fe layers are different and commonly lead to vanishing net magnetic moments at ambient temperatures. TEM-SAED observations on such samples frequently show them to be of a structure variant in which the superstructure periodicity relates in a non-integral manner to the substructure periodicity. As N*c*-pyrrhotites are generally richer in Fe compared to the 4*c* variety, structural models suggest that Fe enrichment is accomplished by insertion of additional fully occupied Fe layers, forming double layers in which all lattice positions are filled by Fe. We suggest that the variably ordered periodic or aperiodic arrangements of such double layers, being equivalent to non-conservative anti-phase domain boundaries of the 4*c* Fe sublattice, result in translation interface modulated structures.

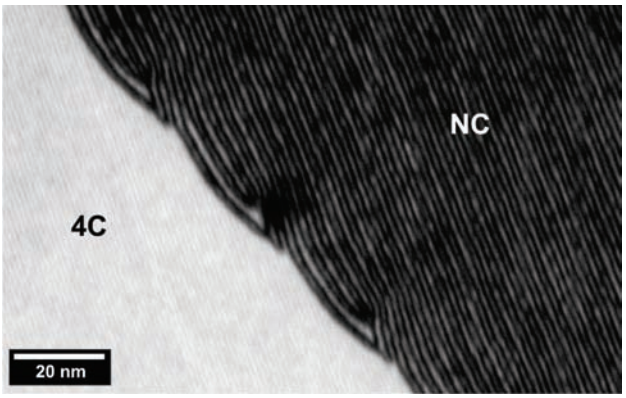

Fig. 1: TEM-SDF image of the interface between 4*c*- and N*c*-pyrrhotite.

We illustrate the usefulness of TEM to decipher microstructural complexity in pyrrhotite by obtaining dark field images from superstructure reflections (TEM-SDF). This imaging technique allows direct observation of double Fe layers and their complex behaviours at internal phase boundaries formed from exsolution of 4*c*-pyrrhotite lamellae in the host N*c*-pyrrhotite. In different samples from various geological settings we found large (tens of nm) and very similar node structures in which double layers annihilate (Fig. 1), pointing to a common mechanism of self-organisation. The driving forces of such structure formation and the consequences for physicochemical and magnetic properties are matter of current research and may have important implications for the geophysical and geochemical understanding of pyrrhotite in nature.

The crystal structure of a 4-layer pyrrhotite and a comparison of the vacancy distribution in 4-layer pyrrhotites

de Villiers, J.P.R.[1*], Becker, M.[1] & Liles, D.C.[2]
[1]Dept. of Materials Science and Metallurgical Engineering, University of Pretoria, South Africa
([*]johan.devilliers@up.ac.za)
[2]Dept. of Chemistry, University of Pretoria, South Africa

The crystal structure of a novel 4-layer pyrrhotite was determined from single crystal measurements on a crystal from the Impala platinum mine in South Africa. The crystal is monoclinic, with cell dimensions a = 11.890(4) Å, b = 6.872(2) Å, c = 22.786(8) Å, and β = 90.124(5)°, with space group $C2$. The cell dimensions are very similar to those of the 4-layer pyrrhotite described by Tokonami et al. [1] in the $F2/d$ setting, and the structure differs from the latter in that there is only one cation layer containing cation vacancies. All the other layers are characterized by layers containing fully occupied cation sites, alternating with layers containing partially occupied sites. This is contrasted with the structure described by Tokonami et al. [1] where layers containing fully occupied sites alternate with layers containing vacant sites. The two structures are however, very similar and this can be seen in the detailed cation arrangements of the two structures (Fig. 1).

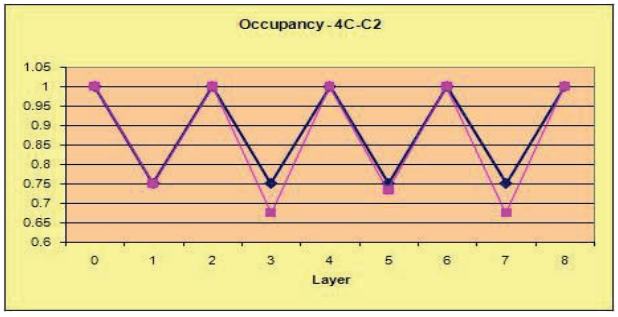

Fig. 1: Occupancy of iron atoms in the layers of 4-layer pyrrhotite in this structure (purple) as compared with that of the structure described by [1] (An occupancy of 1 denotes a fully occupied layer).

The structure described here is postulated to be the most cation deficient of all the pyrrhotites,($Fe_{6.83}S_8$), and this is allowed by the structure, whereas the Tokonami structure is stoichiometric Fe_7S_8 and does not accommodate any other non-stoichiometric composition.

[1] Tokonami, M., Nishiguchi, K. & Morimoto, N. (1972). *Am. Mineral.*, **57**, 1066-1080.

HT-study on fettelite, $[Ag_6As_2S_7][Ag_{10}HgAs_2S_8]$: ionic phase transition indicating the possible existence of different polytypes

Bindi, L.[1] & Menchetti, S.[2*]
[1]Museo di Storia Naturale, Università di Firenze, Italy
[2]Dipto. di Scienze della Terra, Università di Firenze, Italy
([*]crystal@unifi.it)

The crystal structure of fettelite, $[Ag_6As_2S_7][Ag_{10}HgAs_2S_8]$, a rare silver sulfosalt, was recently solved and described by Bindi et al. [1] from a twinned crystal from Chañarcillo, Copiapó Province, Chile. The structure consists of the stacking of two module layers along [001]: an *A* module layer with composition $[Ag_6As_2S_7]^{2-}$ and a *B* module layer with composition $[Ag_{10}HgAs_2S_8]^{2+}$. The As atoms form isolated AsS_3 pyramids typical of sulfosalts, Hg links two sulfur atoms in a linear coordination, and Ag occupies sites with coordination ranging from quasi linear to almost tetrahedral. The *A* module layer found for fettelite is identical to that described for the minerals belonging to the pearceite-polybasite group [2]. Differential Scanning Calorimetry experiments were carried out on the sample from Chañarcillo on 25 mg of powders sealed in aluminium pans using a Mettler DSC 30 instrument from 218K to 423K. The experiments did indicate a phase transition occurring at about 380K. To analyze the HT-structural behaviour by means of X-ray diffraction, a crystal was mounted on a CCD-single-crystal diffractometer equipped with a N_2-heating device. Unfortunately, the highest temperature allowed by the nitrogen device we used (i.e., 350K) was not sufficient to explore the eventual phase transition in fettelite, but the structural results we obtained clearly point toward a structural phase transition likely due to the increase of ionic conductivity with the increase of temperature. The structural data we collected seem indicate a halving of cell along the **a** and **b**-directions and an increase of structural disorder in the *B* module layer. This does mean that at least two polytypes could exist for fettelite. The ordered, monoclinic structure (with unit-cell parameters: a = 26.0388(10), b = 15.0651(8), c = 15.5361(8) Å, β = 90.48(1)° and space group $C2$ – [1]), and a fast ion conducting, disordered HT-form with a and b parameters halved. The two unit-cell types (corresponding to two different polytypes) could be also found in nature. This would account for the different unit-cell types observed for different fettelite samples coming from different localities (e.g., Odenwald, Chañarcillo, Imiter). In addition, slightly different chemical compositions for different fettelite samples (e.g., different Ag/Hg ratios) could play a crucial role as driving forces for different unit-cell stabilizations.

[1] Bindi, L. et al. (2009) *Am. Mineral.*, **94**, 609-615. [2] Bindi, L. et al. (2007) *Am. Mineral.*, **92**, 918-925.

Structural study of members of the polysomatic series epidote-törnebohmite from Stetind pegmatite, northern Norway

Bonazzi, P.[1*], Bindi, L.[2], Chopin C.[3], Husdal, T.A. [4] & Lepore, G.O.[1]
[1]Dipto. di Scienze della Terra, Università di Firenze, Italy
([*]paola.bonazzi@unifi.it)
[2]Museo di Storia Naturale, Università di Firenze, Italy
[3]Ecole normale supérieure–CNRS, Paris, France
[4]T. A. Husdal, Høglia 81, Bodø, Norway

Modules (*E*) of epidote-type structure were found to match easily with those (*T*) of törnebohmite, $(REE)_2Al[SiO4]_2(OH)$, to form a polysomatic series (*E*, *ET*, *T*). In particular, the presence of REE being essential to form *T* modules, *E* modules of epidote members belonging to the allanite or dollaseite subgroups are expected to form *ET* polysomes. Up to now, two minerals – gatelite-Ce [1] and västmanlandite-(Ce) [2] – were found which can be regarded as a regular alternation of (001) slabs of epidote-type structure and (-102) slabs of törnebohmite-type structure. They differ in unit-cell, space-group symmetry and in composition of the epidote-type module, which is of dissakisite-(Ce) composition in gatelite-(Ce) and of dollaseite-(Ce) composition in västmanlandite-(Ce).

This work reports the results of a structural study on crystals resembling gatelite-(Ce) found by one of the author (T.A.H) in the yttrian fluorite masses within the Stetind pegmatite of the Tysfjord granite, northern Norway. The Stetind pegmatite is a granitic REE-pegmatite enriched in niobium, yttrium and fluorine (NYF family) and hosts a large number of different REE- and Y-bearing silicates, REE-bearing carbonates and niobian oxides [3].

The unit-cell dimensions of the examined crystals are in the range a = 8.907-8.933.0, b = 5.639-5.699, c = 17.525-17.600 Å, β =116.3-116.6 °, without any evidence of doubling of the translation unit along the **a**-axis observed in gatelite-(Ce). Although all the crystals were examined with long exposure times on a CCD-equipped diffractometer (Oxford Xcalibur™ 2), neither superstructure reflections such as in gatelite-(Ce) nor the weak, continuous streaking as in västmanlandite-(Ce) were detected. Thus, like in the case of västmanlandite-(Ce), the average structure was refined in the $P2_1/m$ instead of $P2_1/a$ space group, disregarding the slight distortion away from the mirror plane normal to the **b**-axis. However, whereas the continuous streaking in västmanlandite-(Ce) is due to the offset from the (010) mirror plane of two sites (A3 and O15, occupied by REE and oxygen, respectively), in the crystals here studied only O15 exhibits an offset from the mirror plane; therefore, continuous streaking at $a^*/2$ due to short-range order, if any, would be here even weaker than in västmanlandite-(Ce).

Semiquantitative SEM-EDS analyses together with structural data point toward a mineral related to gatelite-(Ce) having the *E* module approaching that of allanite-(Ce).

[1] Bonazzi, P. et al. (2003) *Am. Mineral.*, **88**, 223-228. [2] Holtstam, D. et al. (2005) *Eur. J. Mineral.*, **17**, 129-141. [3] Husdal, T.H. (2008) *Kongsberg Mineralsymposium*, 5-28.

Atomic structure of {110} interpenetration twin boundary in pyrite from St. Katarina (Slovenia)

Daneu, N. & Rečnik, A.*
Dept. for Nanostructured Materials, Jožef Stefan Institute, Ljubljana, Slovenia (*aleksander.recnik@ijs.si)

Pyrite crystals from St. Katarina (Slovenia) are found in yellow to greenish marls concordant with the Upper Permian micritic dolomite. Most of the crystals have well-developed pentagon-dodecahedral {210} faces, modified by accessory cube {100} facets. Their morphology varies with the depth of the marl. Iron-cross pyrite twins are only found in a thin layer of pink-coloured marl on the Tehovec locality. The twinned pyrites are at least twice as large (3-5 mm) as the untwinned crystals in this layer. Morphologically, the twinned crystals are composed of two interpenetrating pentagon dodecahedrons rotated by 180° about the [110] twin axis. While crystallographically the twinning law is well understood, the real cause of twinning in pyrite at the atomic scale has not been properly explained.

For our study, the twinned pyrite crystals were cut parallel to the (001) plane near the centre of the crystal. We found that the boundaries between two interpenetrating twin domains follow {110}, as well as {100} planes. The primary {110} twin (type-A) can be split into secondary {100} twins (type-B), following a simple crystallographic relation: (110) → a·(100) + b·(010), where a=b in an idealised interpenetration twin, while a≠b in the case of realistic twins. The two types of twin boundaries (TB) can also be distinguished by their chemical composition. While the type-A TB comprise a significant amount of Cu, type-B TB appear to be devoid of any dopant element. The amount of Cu at the type-A TB was measured by collecting several EDS spectra at the TB using the concentric electron probe (CEP) method. The arbitrary width of Cu atoms present on the twin boundary is 0.18±0.03 nm, which would correspond to one octahedral layer of Cu, or about two monolayers of tetrahedrally coordinated Fe and Cu, as found in chalcopyrite. Based on our results we may conclude that the primary twin boundaries of type-A are growth boundaries, while the secondary type-B twin boundaries form after impingement of the growth twin domains.

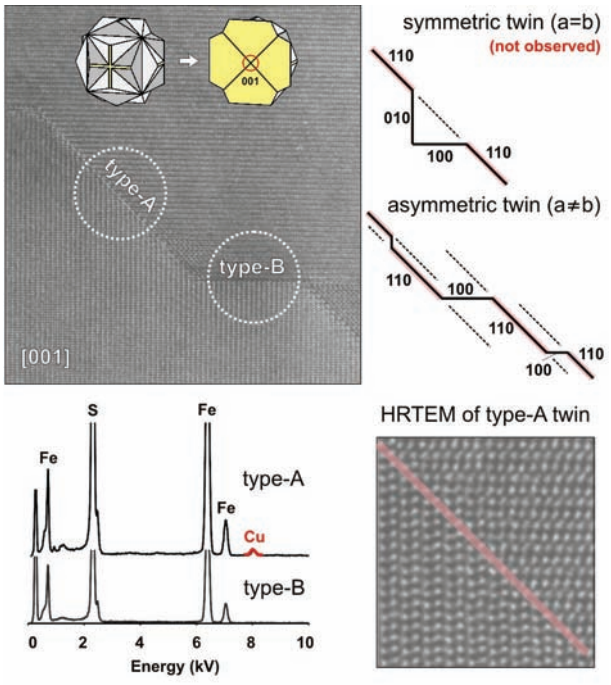

Fig. 1: TEM image of two types of TBs in pyrite twins from Katarina. The EDS analyses show Cu-enrichment at the type-A twin boundary.

First finding of a 94-layer long-period mica nano-polytype by HRTEM

Fregola, R.A.* & Scandale, E.
Dipto. Geomineralogico, Università di Bari "Aldo Moro", Bari, Italy (*r.fregola@geomin.uniba.it)

The stacking sequences of long-period mica polytypes can be unambiguously determined using high resolution transmission electron microscopy (HRTEM) images recorded down two zone axes rotated 30° apart about **c*** (*e.g.* [010] and [-110]). Up to now, the longest ordered stacking sequence in micas was a 36-layer found in a crystal of oxybiotite from the Ruiz Peak rhyodacite rocks [1].

A longer periodicity 94-layer mica nano-polytype was observed by transmission electron microscopy for the first time in this work. It was found in a fragment (γ1a) of the same Mg-rich annite crystal (Bt9568a) from dacite rocks of Džep, Serbia, of a previous study [2]. The prefix "nano" accounts for the sub-micrometer-sized extension along **c*** (about 800 nm) of the crystal region containing the 94-layer polytype. One-dimensional lattice fringe images obtained by bright-field (BF) illumination along the [-110] zone axis showed a high number of stacking faults repeating in the same periodic sequence eight consecutive times along **c***. The c_0 period of this sequence is 95.9214 nm. The 94-layer nano-polytype is bordered by a cleavage surface on one side, whilst on the other side no physical discontinuity occurs and it turns into a different sequence of non-periodic stacking faults. The eight consecutive repetitions of the 94-layer period contain just a single localized planar defect (D). The atomic structure of D was observed by HR images. It is made-up of atomic extra-sheets whose total extension along **c*** is less than that of a mica unit layer (10.2044 Å in this case). D does not alter the regular repetition of the 94-layer stacking sequence.

Selected area electron diffraction (SAED) and HRTEM images taken along the [010] zone axis showed that the observed polytypic stacking sequence belongs to the subfamily-*A* of mica polytypes. SAED patterns and HR images viewed down the [-110] zone axis allowed to identify the inhomogeneous stacking sequence belonging to the $2M_1$ structural series. The otherwise ordered $2M_1$ (2-2) stacking sequence is broken-up by an ordered sequence of two kinds of stacking faults: -22 and 20-2. The Ross-Takeda-Wones (RTW) symbol [3] of the whole 94-layer stacking sequence is: [(2-2)$_3$20-2(2-2)$_3$-22(2-2)$_2$-22(2-2)$_3$-22(2-2)20-2(2-2)-22(2-2)$_3$-22(2-2)$_2$-22(2-2)$_4$–22(2-2)$_2$-22(2-2)$_3$-22(2-2)$_4$-22(2-2)$_2$-22].

Using the planar defect D as reference position, the fringe contrasts of the BF images were correlated to the 94-layer stacking sequence determined by HR images. Specific fringe contrasts had been associated to each type of stacking fault (-22 and 20-2) recurring in the sequence as well as to the $2M_1$ (2-2) unit layer. This correlation allowed to verify that the same 94-layer stacking sequence occurred for eight consecutive times. It also confirms the usefulness of one-dimensional lattice fringe images for a simple and immediate evidence of mica stacking "disorder" [4], especially when such disorder turns into ordered stacking arrays as it is the case of mica very long-period inhomogeneous polytypes. In fact, the one-dimensional lattice fringe images show the modulation due to the superstructure having longer periodicity than that of the unit layer. However, the analysis of HR images is needed to accurately associate the fringe contrasts to the correct stacking sequence.

[1] Kogure, T. & Nespolo, M. (1999) *Acta Cryst.*, **B55**, 507-516. [2] Fregola, R.A. et al. (2009) *Am. Mineral.*, **94**, 334-344. [3] Ross, M. et al. (1966) *Science*, **151**, 191-193. [4] Iijima, S. & Buseck, P.R. (1978) *Acta Cryst.*, **A34**, 709-719.

Crystal structure of a new member of the polysomatic series törnebohmite-epidote from carbonatites of Eastern Siberia

Gurzhiy, V.V.[1*], Karimova, O.V.[2], Kartashov, P.M.[2] & Krivovichev, S.V.[1]
[1]Dept. of Crystallography, Faculty of Geology, St. Petersburg State University, St. Petersburg, Russia ([*]vladgeo17@mail.ru)
[2]Laboratory of Crystal Chemistry of Minerals, Institute of Geology of Ore Deposits RAS, Moscow, Russia

A new member of the polysomatic series törnebohmite-epidote was found in three carbonate veins that crosscut surrounding fenitized gneisses at Biraya REE-Fe ore occurrence (Vitim highland, Russia). One of the veins, a törnebohmite vein, is enriched with a new mineral species, which constitutes a metasomatic zone up to 2 cm thick. The vein has the following zonation from margin to center: compact ferriallanite rim, ferriallanite-calcite zone, strontianite-calcite, törnebohmite-carbonate and axial carbonate zones with biraite-(Ce)-bastnäsite-(Ce) segregations. Therefore three zones marked out by REE-silicates are present in the vein: outer ortho-diortho-silicate, intermediate orthosilicate and inner diorthosilicate. The new mineral being mixture of ferriallanite-(Ce) and törnebohmite modules in ratio 1:1, formed along the boundary of the ferriallanite-(Ce)-törnebohmite zones as a metastable relict phase.

A crystal was mounted on a STOE IPDS II diffractometer equipped with an Image Plate area detector. The unit cell parameters were determined by the least squares method. It is monoclinic, $P2_1/m$, a = 8.955(1), b = 5.7335(5), c = 15.856(2) Å, β = 94.33(1)°, V = 811.8(2) Å^3. The crystal structure was solved by direct methods and refined to R_1 = 0.059 (wR_2 = 0.137) for 1703 reflections with $|F_o| \geq 4\sigma_F$.

The structure consists of chains of edge sharing Fe, Mg and Al octahedra running along the *b* axis and cross-linked by SiO_4 and Si_2O_7 groups to form layers. Cavities within the layer are occupied by Ca atoms. Channels between the layers are occupied by Ce atoms. Using modular approach, the structure can be described as sequence of epidote and törnebohmite-(Ce) layers parallel to the (001) plane.

The mineral formula according to the results of the structure analysis is $Ce_3(Ca_{0.94}Ce_{0.06})(Fe^{II}_{0.54}Mg_{0.46})(Fe^{II}_{0.91}Mg_{0.09})(Al_{1.90}Fe^{III}_{0.10})$ $Si_5O_{19}(OH)_2(O,OH)$. Thus the new mineral species is a Fe-rich and F-deficient analogue of västmanlandite-(Ce).

Acknowledgements: This work was supported for VVG and SVK by the Russian Ministry of Science and Education (State contract # 02.740.11.0326).

Redetermination of crystal structure of semseyite, $Pb_9Sb_8S_{21}$

Matsushita, Y.
Beamline BL15XU, SPring-8, NIMS-branch office, Sayo-cho, Hyogo, Japan (MATSUSHITA.Yoshitaka@nims.go.jp)

Sulfosalt-mineral semseyite $Pb_9Sb_8S_{21}$ belongs to the plagionite series ($Pb_{3+2n}Sb_8S_{15+2n}$, $\boldsymbol{n}$ = 0, 1, 2, 3) [1]. All of minerals in this series have same space group (C2/c) with similar lengths of $\boldsymbol{a}$ and $\boldsymbol{b}$ axes. On the other hand, $\boldsymbol{c}$ axes are systematically changed varying with $\boldsymbol{n}$ number, and the $\boldsymbol{\beta}$ angles are alternatively changed with odd number or even number of $\boldsymbol{n}$. [2] The crystal structure of semseyite had been reported by Kohatsu and Wuensch [3] and Matsushita, Nishi and Takéuchi [4]. The results suggest that the structure has PbS-like substructure elongating to two different directions, parallel to (112) layer and (-112) layer. Each of substructures to form the semseyite structure is alternatively connected by the (112) layer and by the (-11-2) layer, and they are related by the twofold axes. The {112} planes correspond to the cleavage plane of the series minerals. However, previous refinement levels are relatively low (R = ~10 % and ~7 %) to discuss with details of the structure. Therefore, we re-examined single-crystal diffraction work.

A crystal of semseyite for this work was found in the sample labelled as plagionite ($Pb_5Sb_8S_{17}$, Wolfsberg, Germany). From the EPMA analysis, the chemical composition of the crystal is $Pb_{9.05(3)}Sb_{8.01(3)}S_{21.05(3)}$. The crystallographic checks and the intensity collections were carried out on a CCD area detector (Bruker SMART APEX) and graphite-monochromatized MoKα radiation (λ = 0.71069 Å) at room temperature. The crystal belongs to space-group C2/c with a = 13.6267(10) Å b = 11.9742(9) Å, c = 24.5891(18) Å, β = 105.997(3) °, V = 3856.8(5) Å^3, Z = 4, Dc = 4.400 g/cm^3, and R1 = 4.71 %. The crystallochemical details will be presented.

[1] Anthony, J. W. et al. (1990) *"Handbook of Mineralogy, Vol. 1, Elements, Sulfides, Sulfosalts"*. Mineral. Soc. Am. [2] Kohatsu, J.J. &d Wuensch, B.J. (1974) *Acta Cryst.*, **30**, 2935-2937. [3] Kohatsu, J.J. & Wuensch, B.J. (1974) *Am. Mineral.*, **59**, 1127. [4] Matsushita, Y., Nishi, F. & Takéuchi, Y. (1997) in Takéuchi, Y. (ed.) *"Tropochemical cell-twinning. A structure-building mechanism in crystalline solids"*. Material Science of Minerals and Rocks, Terra Scientific Publishing Comp., Tokyo.

Structural refinement and OD character of a 4-layer ferrophlogopite

Pignatelli, I.* & Nespolo, M.
CRM^2 UMR-CNRS 7036, Institut Jean Barriol, Nancy-Université, Mancy, France
(*Isabella.Pignatelli@crm2.uhp-nancy.fr)

In this study we analysed a new non-MDO 4–layer polytype from the Ruiz Peak ferrophlogopite [1], with cell parameters: a = 5.3312(7), b = 9.2237(8), c = 39.978(6), β = 92.48(1)°. The space group $C2/c$ has been obtained by the stacking sequence calculated from the PID analysis [2] and expressed by the OD symbols 2040 in the homo-octahedral approximation [3]. The initial model was obtained from the atomic positions of the 1M polytype [4] by applying the stacking sequence. Refinement was performed in $C2/c$ with Jana2006 [5] and converged to about 6%. The structure of this polytype is characterized by two kinds of mica layers (M layers) in the asymmetric unit. The first has layer symmetry $C12/m(1)$: the $M1$ (trans) site is in special position (site-symmetry group $\bar{1}$, Wyckoff position 4c), whereas the $M2$ (cis) site is in general position, like the two independent tetrahedral sites. The second layer, instead, has layer symmetry $C12(1)$; the octahedral sites are all independent and in special position (on a twofold axis, Wyckoff position 4e). The analysis of the peaks in the experimental Fourier map suggests a non-homogeneous distribution of the cations in the octahedral sites. The peaks corresponding to the $M1$ sites are significantly different from those in the $M2$ sites; for the second layer, the peaks in the sites $M2$ and $M3$ are close. Both layers are therefore meso-octahedral. The origin of a meso-ochtahedral sheet is chosen on the site with different occupancy [6], *i.e.* in the *trans* site ($M1$) of both our layers. This type of layer is called the M1-layer to distinguish it from that whose origin is in a *cis* site, called the M2-layer [7]. The meso-octahedral OD symbol is:

5	. 5	3	. 3	1	. 1	5	. 5
2	*	0	*	4	*	0	*

Being the first occurrence of a polytype with layers of different symmetry, we checked whether this difference could be an artefact of the model, by repeating the refinement in all the *translationengleiche* subgroups of $C2/c$ (Cc, $C2$, $C\bar{1}$ and $C1$). No improvement in the refinement results was obtained, while a number of correlations appeared, clearly indicating that the true symmetry of this structure is indeed $C2/c$.

[1] Ross, M., Takeda, H. & Wones, D.R. (1966) *Science*, **151**, 191-193. [2] Takeda, H. (1967) *Acta Cryst.*, **22**, 845-853. [3] Ďurovic, S. (2004) *International Table for Crystallography*, Vol **C**, section 9.2.2. [4] Otha, T., Takeda, H. & Takéuchi, Y. (1982) *Am. Mineral.*, **67**, 298-310. [5] Petricek, V., Dusek, M. & Palatinus, L. (2006) *Jana2006. The crystallographic computing system*. Institute of Physics, Praha, Czech Republic. [6] Dornberger-Shiff, K., Backhaus, K.O.& Ďurovic, S. (1982) *Clay. Clay Min.*, **30(5)**, 364-374. [7] Nespolo, M., Takeda, H. & Kogure, T. (1999) *Acta Cryst.*, **55**, 659-676.

Coexistence of 1M and 2M_1 polytypes in Ti-phlogopite from the Central Fields volcanics of the Southwest Uganda

Scordari, F., Schingaro, E., Mesto, E.* & Lacalamita, M.
Dipto. Geomineralogico, University of Bari, Italy.
(*mesto@geomin.uniba.it)

In the present work, the crystal chemistry of natural Ti-phlogopites from alkali-rich igneous rocks from the Central Fields of Bunyaruguru and Katwe-kikorongo (Southwest Uganda) has been investigated. The host rocks are characterized by olivine – melilitite and olivine – kalsilite – nepheline – clinopyroxene assemblages [1]. The phlogopites from the former rock are labelled BU (specifically, BU1, BU3 and BU4) whereas those from the latter are labelled KK (in detail, KK8 and KK13). All samples underwent chemical (Electron Micro Probe Analysis, EMPA), structural (Single Crystal X-ray Diffraction, SCXRD) and spectroscopic (FTIR) investigation.

EMPA yielded the following ranges: MgO (17.87-21.48 wt%), FeO_{tot} (5.40-9.22 wt%) and TiO_2 (4.59-7.05 wt%) for BU samples whereas MgO (17.98-18.51 wt%), FeO_{tot} (8.17-8.86 wt%) and TiO_2 (6.02-6.49 wt%) for KK crystals.

SCXRD analyses showed the coexistence of both the 1M and the 2M_1 polytypes within the same sample. The BU3 mica is an exception because, to date, only crystals belonging to the 2M_1 polytype have been found. Average cell parameters are a = 5.33, b = 9.22, c = 10.22 Å and β = 100.06° for the 1M whereas a = 5.33, b = 9.23, c = 20.22 Å and β = 95.08° for the 2M_1 phlogopites. Structure refinements using anisotropic displacement parameters were performed in space group $C2/m$ for 1M and $C2/c$ for 2M_1 samples and converged at $1.63 \leq R \leq 4.64$ %, $1.96 \leq R_w \leq 5.45$ % and $2.46 \leq R \leq 4.00$ %, $1.37 \leq R_w \leq 4.41$ % for the two polytypes, respectively.

Micro-FTIR provides insightful informations about octahedral cationic environments, the substitution mechanisms trough which cations enter the mica structure and the hydrogen orientation [2-4]. The samples so far analyzed display, to different extent, fine structure in the OH^- stretching region.

In terms of substitution mechanisms this implies that the samples contain different combination of M^{3+}-Tschermak, M^{3+}-oxy substitutions, whereas they are not affected by M^{3+}-vacancy substitutions. Indeed the bands at about 3620 and 3535 cm^{-1}, which correspond to $Al^{3+}Al^{3+}$-OH and $Fe^{3+}Fe^{3+}$-OH local configurations [5] are missing.

[1] Lloyd, F.E.et al. (1991) in Kampunzu, A.B. & Lubala, R.T. (eds.) *Magmatism in extensional structural settings, the Phanerozoic African Plate*. Springer-Verlag, New York, 23-72. [2] Scordari, F. et al. (2006) *Eur. J. Mineral.*, **18**, 379-391. [3] Scordari, F. et al. (2008) *Phys. Chem. Mineral.*, **35**, 163-174. [4] Lacalamita, M. (2009) *PhD Thesis*, University of Bari. [5] Libowitzky, E. & Beran, A. (2004) in Beran, A. & Libowitzky, E. (eds.) *Spectroscopic methods in mineralogy*. EMU notes in mineralogy, Eötvös University Press, Budapest, 227-279.

Marcasite lamellae defects in pyrite framboids

Zhang, M.[1,2], Konishi, H.[2], Sun, X.[1,3*], Xu, H.[2], Lu, Y.[1] & Xu, L.[3]

[1]Dept. of Earth Sciences, Sun Yat-sen University, Guangzhou, China

[2]Dept. of Geoscience, University of Wisconsin-Madison, USA

[3]School of Marine Sciences, Sun Yat-sen University, Guangzhou, China ([*]sxm158@hotmail.com)

Authigenic pyrite is a common mineral in the sediments on continental slopes and is thought to form by reaction of dissolved sulfide (produced by microbial sulfate reduction) with detrital iron-bearing minerals [1]. Pyrite dominantly occurs as framboids in modern anoxic environments. Its ubiquity and remarkable physical appearance has attracted many researchers. However, the mechanism controlling formation of pyrite framboids is not known.

The two polymorphs of FeS_2 are pyrite and marcasite. Fe atoms are octahedrally coordinated in both minerals.

We studied pyrite rods in seafloor core sediments near Dongsha Island in the South China Sea using scanning electron microscopy and high resolution transmission electron microscopy (HRTEM). The water depth of sampling area is about 3000m. Most pyrite is formed of spherical and pyritohedron aggregates of submicron pyrite microcrystals, which occur as framboids and have later pyrite overgrowths. HRTEM and select area electron diffraction analyses show pyrite has planar faults parallel to (001). As described by Dódony et al. [2], marcasite is found in the faults, and single (101) layers of marcasite disrupt the regular sequence of (002) layers in pyrite. Marcasite layers in pyrite might limit the growth of the pyrite crystal and be responsible for the characteristic framboid morphology of the pyrite spherules [2].

Butler and Rickard [3] propose that the framboidal texture forms by rapid nucleation in an aqueous environment strongly supersaturated with respect to pyrite. Marcasite forms in acidic aqueous solutions (pH<5) at low temperatures (T<240°C) [2,4]. The samples in this study were collected from an area with the potential for gas hydrates [5]. Both methane and sulfate are needed for anaerobic oxidation of methane to produce sulfide and dissolved inorganic carbon. The existence of marcasite layers in pyrite restricts the pH condition and the concentration of Fe^{2+} and H_2S in the aqueous solution. According to the hypothesis offered by Valentine and Reeburg [6], $2CH_4+2H_2O \rightarrow CH_3COOH + 4H_2$ and acetate and hydrogen are both consumed by sulfate reducing bacteria to produce S^{2-} and H_2S: $SO_4^{2-} +4H_2 \rightarrow S^{2-}+4H_2O$ and $SO_4^{2-} +CH_3COOH \rightarrow H_2S+2HCO_3^-$. When the supply of methane is continuous and the rate of acetate and H_2 production is higher than SO_4^{2-} consumption, the aqueous solution becomes acidic and marcasite can form. Therefore, the occurrence of marcasite lamellae in framboidal pyrite shows there is an almost inexhaustible supply of methane under the site.

Acknowledgements: This work was jointly supported by the Project of Key Laboratory of Marginal Sea Geology, Guangzhou Institute of Geochemistry and South China Sea Institute of Oceanology, CAS (Nos. MSGL08-01, MSGL08-05, MSGLCAS03-4), Specialized Research Fund for the Doctoral Program of Higher Education (No.20090171120019), International Program of Project 985, Sun Yat-Sen University.

[1] Berner, R.A. (1984) *Geochim. Cosmochim. Ac.*, **48**, 605-615. [2] Dódony, I., Pósfai, M. & Buseck, P.R. (1996) *Am. Mineral.*, **81**, 119-125. [3] Butler, I.B. & Rickard, D. (2000) *Geochim. Cosmochim. Ac.*, **64**, 2665-2672. [4] Schoonen, M.A.A. & Barnes, H.L. (1991) *Geochim. Cosmochim. Ac.*, **55**, 1495-1504. [5] Guo, T.M. et al. (2004) *J. Petroleum Sci. Engin.*, **41**, 11-20. [6] Valentine, D.L. (2000) *Arch. Microbiol.*, **174**, 415-421.

Quantification and identification of illite/smectite interstratifications at nanometric scale: association of TEM/EDS/SAED

Fernandez, J.-B.[1*], Kohler, E.[1], Gay, A.-S.[2] & Jullien, M.[3]
[1]Geology-Geochemistry-Geophysics Division, IFP, Rueil-Malmaison, France ([*]jean-baptiste.fernandez@ifp.fr)
[2]Physics and Analysis Division, IFP, Solaize, France
[3]Nuclear Energy Direction, CEA, St Paul lez Durance, France

In the context of CO_2 sequestration, studies aimed at characterizing the sealing capacity of the argillaceous barriers and at constraining their evolution. In that case, clayey cap-rocks play a key role on confining function supported by their petrophysical properties. The illites-smectites are one of the main components of the CO_2 storage cap-rock in the studied area, the Paris basin. A study [1] points out an illitization of the initial matrix upon micrometric reactive fronts when samples are subjected to supercritical CO_2 in laboratory conditions (with mix of CO_2/H_2O from pure water to pure CO_2). For a good enough safety assessment, the numerical modellings must take into account the geochemical interactions at the reaction's scale: identification of initial/new crystallized minerals and their evolution along the I:S ratio. Such characterizations can be performed by a few precise and routinely practical methods [2]. The technical difficulties of characterization are related to the clays crystals small size and their apparent chemical composition heterogeneity due to the deposition and burial history through diagenesis transformations. A method has been developed that combine both crystallographic data obtained from selected area electron diffraction (SAED) and chemical analyses obtained by energy dispersive spectrometry (EDS) using a transmission electron microscope (TEM). This association allows to determine the ratio I:S and their chemical composition at nanometric scale of the same I/S crystal. Natural references and synthetic I/S, which have been characterized by X-Ray Diffraction (XRD) are used to test the method. The natural I/S are constitued of both ISCz-1 which is a Clay Mineral Society standard and samples from Saint Martin de Bossenay (Paris Basin, France). The synthetic I/S result from an illitization process of synthetic smectites. The advantage of these synthetic materials is the strict control of the chemical composition and the mixed-layering level. The results of SAED patterns along c* obtained from specific preparation (resin exchange, preferential orientation, ultrathin cut) allow the discrimination between illite, smectite and illite/smectite. The chemical analyses confirm an illitization process and ratios.

[1] Kohler, E. et al. (2009) *Clay. Clay Miner.*, **57**, 616-637. [2] Murakami, T. et al. (2005) *Clay. Clay Miner.*, **53**, 440-451.

Comparison of approaches for modelling disorder of clay structures in Rietveld phase analysis

Kleeberg, R.[1*], Ufer, K.[1], Bergmann, J.[2] & Dohrmann, R.[3]
[1]Institut für Mineralogie, TU Bergakademie Freiberg, Germany ([*]kleeberg@mineral.tu-freiberg.de)
[2]Ludwig-Renn-Allee 14, Dresden, Germany
[3]BGR/LBEG, Hannover, Germany

The complicated and variable disorder of the common clay minerals hampers the adequate modelling of the diffraction profiles as necessary for correct structure and phase analysis by the Rietveld method. Various types of stacking faults occur solely and mixed in natural layer silicates, e.g. well-defined translations and rotations of adjacent identical layers, turbostratic stacking, and mixed-layering of different layer types. Consequently, a number of approaches have been introduced to fit the experimental diffraction patterns. Typically, the anisotropic line broadening by well-defined stacking faults is described by any *hkl*-dependent line broadening model, e.g. [1,2], based on an ideal mean structure. Turbostratic disorder can be approximated by the single-layer approach [3]. Mixed-layering may be modelled by introducing the recursive calculation [4] in a supercell structure model [5]. However, in practice the true type of disorder may be unknown, or a complex disorder model in recursive description needs overmuch computing time for routine purposes. In such cases, an empirical approximation based on manually modified *hkl*-lists [6] may be useful. Such *hkl*-lists can be used together with all other types of structural models.

The presentation discusses the advantages and limitations of the different approaches, focusing on their application in quantitative phase analysis using the Rietveld method. The problem is demonstrated for 1:1 and 2:1 dioctahedral minerals with different types of disorder (pure phases and mixtures). Typically, *hkl*-dependent line broadening models can be applied just to a certain degree of disorder, but may fail when applied to minor components. Flexible but complicated models tend to yield overestimation of phase abundances in mixtures if phases with similar structures are present. Recursive calculation may approximate real patterns very well, but even an extensive fixing and constraining of parameters does not always prohibit tedious computation time. The application of *hkl*-lists [6] may help to speed up routine work to obtain reliable mineral quantification, but does not allow structural investigations of those phases described with the proposed *hkl*-lists.

[1] Bergmann, J. & Kleeberg, R. (1998) *Mat. Sci. Forum*, **278-281(1)**, 300-305. [2] Popa, N.C. (1998) *J. Appl. Cryst.*, **31**, 176-180. [3] Ufer, K. et al. (2004) *Z. Kristallogr.*, **219**, 519-527. [4] Treacy, M.M.J., Newsam, J.M. & Deem, M.W. (1991) *Proc. R. Soc. London*, **A433**, 499-520. [5] Ufer, K. et al. (2008) *Z. Kristallogr. Suppl.*, **27**, 151-158. [6] Taylor, J.C. & Matulis, C.E. (1994) *Powder Diffr.*, **9**, 119-123.

Globular layer silicates of the illite-glauconite series, the Upper Proterozoic, northern Siberia, Russia

Ivanovskaya, T.A.
Geological Institute RAS, Moscow, Russia
(ivanovskaya@ginras.ru)

A representative collection of globular dioctahedral 2:1 layer silicates from marine deposits (predominantly silicoclastic, rarely, glauconitites, limestones, dolomites, clayey rocks) of the Lower and Middle Riphean (Osorchayata and Arymass, Debengda, Khaipakh Formation, respectively) and the Vendian (Maastakh Formation) of the Olenek Uplift and of the Lower (Ust'-Il'ya Formation) and the Lower-Middle Riphean (Ysmastakh Formation) of the Anabar Uplift (Northern Siberia, Russia) has been studied. The mineralogical studies were performed by a complex of modern chemical and physical methods (X-ray diffraction, oblique-texture electron diffraction, scanning electron microscopy, classical chemical and micro-probe analyses, Mössbauer spectroscopy etc.), which allowed determining structural and crystal-chemical varieties of the minerals. Best-preserved grains were used for isotope dating.

The glauconite grains have globular, irregular and platy shapes. In the diagenesis zone glauconite globules seem to have been formed by synthesis from colloidal solution, and platy glauconite, by transformation of terrigenous Fe-mica (biotite). Glauconite was mainly formed with the active influence of microorganisms.

Among the studied layer silicates continuous series of solid solutions from illite ($^{VI}Al/^{VI}Al+ {}^{VI}Fe^{3+} \geq 0.6$) via Al-glauconite (Fe-illite) to glauconite ($^{VI}Al/^{VI}Al+ {}^{VI}Fe^{3+} \leq 0.5$) has been observed. Some samples consist entirely or partly of proper glauconite of the Middle Riphean (Debengda Formation) and the Lower Riphean (Ust'-Il'ya Formation). Illite (rarely, Al-glauconite) have been revealed in the Lower and Middle Riphean (Osorchayata and Arymass, Debengda, Khaipakh, respectively) and the Vendian (Maastakh Formation).

Structural varieties from mica to mixed-layer phyllosilicates (≤10 and >10% smectite layers respectively) have been determined. Mixed-layer silicates with a trend to ordering in the alternation of mica and smectite layers (short-range order factor S>1) have been found in Debengda and Khaipakh Formations. The transition from Al-species to Fe-species is accompanied by a variation of the unit cell *b* parameter from 9.00 to 9.08Å.

Mg-rich Al-glauconite has been found in dolomites of the Ysmastakh Formation. This mineral is characterized by unique structural and crystal-chemical peculiarities caused by non-equilibium conditions in reduction zone of shallow dolomite deposits.

Among the studied samples there are globules consisting of two mica (glauconite, illite) phases (Ust'-Il'ya Formation) (b=9.00−9.08Å). The compositional division in biphase globules occurred at the level of individual microcrystals (0.5−5μm) of micaceous minerals. These minerals form an isomorphic series from Al to Fe-varieties within a single globule.

The studied rocks containing globular glauconite-illite minerals are altered by deep diagenesis. Globular and platy grains of illite (Osorchayata Formation) show the same rejuvenated ages. The isotopic ages of globular glauconite-illite minerals of other studied formations correspond to their stratigraphic positions.

Deposition of layered double hydroxides on alumina support

Kovanda, F.[1*], Jirátová, K.[2] & Koloušek, D.[1]
[1]Dept. of Solid State Chemistry, Institute of Chemical Technology, Prague, Czech Republic
([*]Frantisek.Kovanda@vscht.cz)
[2]Institute of Chemical Process Fundamentals of the ASCR, v.v.i., Prague, Czech Republic

Layered double hydroxides (LDHs) are often used as precursors for preparation of mixed oxide catalysts. A deposition of LDHs on supports would be advantageous due to a better utilization of usually expensive active components. In this work, a formation of LDHs on anodized aluminum foil is studied; the hydrothermal reaction in aqueous solutions containing divalent metal nitrates [1,2] was adopted to obtain supported LDH and mixed oxide layers. The composition and molar ratios of metal cations in used solutions were adjusted as follows: Ni-Mn (2:1), Co-Mn (2:1), Ni-Co-Mn, Ni-Cu-Mn and Co-Cu-Mn (all 1:1:1); total metal ion concentration of 0.1 mol l^{-1} and pH of 6.8 and 8.5 were applied and the deposition was carried out under hydrothermal conditions at 140°C for 65 h.

Powder XRD patterns of the samples obtained after hydrothermal reaction showed well-crystallized hydrotalcite-like phases. A formation of M^{II}-Al and M^{II}-Cu-Al LDHs (M^{II} = Ni and/or Co) with only a slight Mn content can be expected. An increasing pH in the solutions enhanced the LDH deposition and facilitated incorporation of Co and Mn in the solid; on the other hand, products with lower Cu content were obtained. It can be explained by a difference in the pH, at which various divalent metal hydroxides are precipitated. The products obtained at higher pH showed an increased lattice parameter *a*; it also indicates a higher concentration of Mn cations in the formed LDHs.

Relatively homogeneous layers consisting of thin curved platelets oriented nearly perpendicularly to the support were observed in SEM images. The same morphology of the deposited products was found also in the samples calcined at 500°C (Fig. 1). NiO-like and spinel-like mixed oxides were formed during calcination of Ni- and Co-containing samples, respectively, but no distinct Cu-containing phases were detected by XRD in the obtained M^{II}-Cu-(Mn)-Al oxides. The LDH-related mixed oxides deposited on Al_2O_3/Al support exhibited a worse reducibility in comparison with those obtained by calcination of coprecipitated precursors; it could be explained by a high structure ordering of the formed oxide phases. The deposited mixed oxides containing Cu showed reduction peaks at relatively low temperatures (250 – 300°C) and consequently also a reasonable catalytic activity in total oxidation of ethanol.

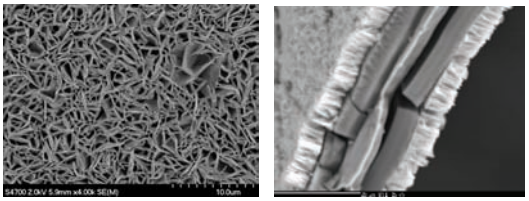

Fig. 1: SEM images of the deposited Co-(Mn)-Al LDH layer (left) and profile of the calcined sample (right).

Acknowledgements: This work was supported by the Czech Science Foundation (P106/10/1762 and 106/09/1664) and by the Ministry of Education, Youth and Sports of the Czech Republic (MSM 6046137302).

[1] Chen, H. et al. (2006) *Adv. Mater.*, **18**, 3089-3093. [2] Kovanda, F. et al. (2009) *Clays Clay Miner.*, **57**, 425-432.

Hydrothermal synthesis of Al-Fe^{3+} smectites: a crystal chemistry study

Andrieux, P.[1*], Petit, S.[1], Gates, W.[2], Marichal, C.[3] & Grauby, O.[4]
[1]Laboratoire HydrASA, Université de Poitiers, France ([*]pauline.andrieux@univ-poitiers.fr)
[2]Dept. of Civil Engineering, Monash University, Clayton, Australia
[3]Equipe Matériaux à Porosité Contrôlée, Institut de Science des Matériaux de Mulhouse, France
[4]Laboratoire CRMCN, Université de Marseille, France

Synthesis in laboratory allows control of the chemical makeup and the conditions for crystallization of clay minerals. Clay synthesis is then a useful approach for understanding natural clay minerals formation. Well defined samples having distinct chemical composition in series can be synthesized which are well suited for spectroscopic interpretations.

A series of Al-Fe^{3+} smectites with a wide range of chemical compositions have been synthesized for the first time. These smectites were synthesized by hydrothermal treatments from coprecipitated gels. The hydrothermal syntheses were performed at different temperatures and pHs. For Fe^{3+}-rich smectites, low temperature and relatively basic pH conditions are suitable whereas for Al-rich smectites, higher temperatures and more acidic pHs are appropriate [1].

These smectites have been analyzed by X-Ray Diffraction (XRD), infrared (IR in the near and the middle region, respectively NIR and MIR), Extended X-ray Absorption Fine Structure (EXAFS at the Fe K-edge and Fe L-edge) and Nuclear Magnetic Resonance (NMR) spectroscopies. Chemical analyses of the smectite particles have been performed using Transmission Electron Microscopy (TEM) equipped with an EDX (Energy Dispersive X-ray) system.

The smectitic nature of the synthesized samples is confirmed by their swelling behavior after ethylene-glycol treatment measured by XRD on oriented deposits. MIR and NIR spectra reveal variations of the relative intensities of the $Fe^{3+}{}_2OH$, $AlFe^{3+}OH$ and Al_2OH bands all along the chemical series indicating the crystal-chemical changes in these smectites in response to composition. Fe K-edge spectra reveal the presence of Fe in tetrahedral sites in the Fe-rich smectites. Fe L-edge spectra were fitted using ferrite spectrum as Fe(III) tetrahedral reference and NAu-1 nontronite as Fe(III) octahedral reference to obtain the percentage of Fe(III) in the different sites. The percentage of tetrahedral Fe(III) in these samples globally decreases with increasing Al in the structure.

^{27}Al MAS NMR spectra were recorded even for smectites very rich in iron providing information on at least some of the site occupancies (Al(4)/Al(6)) depending on the synthesis conditions.

[1] Andrieux, P. & Petit, S. (2010) *Appl. Clay Sci.*, **48**, 5-17.

"Mauritzite": a ferro/ferri-saponite transforming by immediate in-situ oxidation in dacite cavities, Erdőbénye, Hungary

Weiszburg, T.G.[1*], Pekker, P.[2], Jánosi, M.[1], Tóth, E.[3] & Kuzmann, E.[4]
[1]Dept. of Mineralogy, Eötvös Loránd University, Budapest, Hungary ([*]weiszburg@ludens.elte.hu)
[2]BAY-NANO Institute for Nanotechnology, Miskolc, Hungary
[3]Eötvös Museum of Natural History, Eötvös Loránd University, Budapest, Hungary
[4]Laboratory of Nuclear Chemistry, Chemical Research Center, Hungarian Academy of Science – Eötvös Loránd University, Budapest, Hungary

The pyroxene dacite laccolith of Mulató Hill (Erdőbénye, Tokaj Hills, NE-Hungary) formed as part of the Neogene Inner-Carpathian volcanic chain. Quarried since 1925, the laccolith is well-known for its hydrothermal cavity-filling mineral assemblage [1]. Amygdules host among others siderite, tridymite, chalcedony and an iron-rich saponite. Saponite is a cavity-lining, mostly vermicular phase forming few-mm-long fibres of ca. 0.1 mm diameter. It is mid-blue when the host cavity is opened (i.e., when first gets into contact with air), but rapidly (few ten minutes) darkens and finally turns bluish black due to in-situ oxidation.

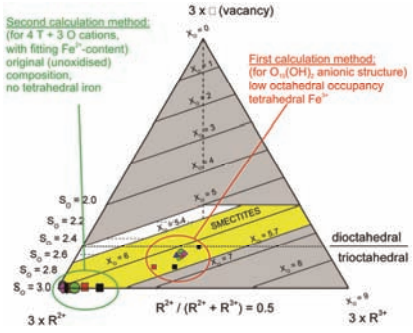

Fig. 1: Ternary diagram showing the composition of the octahedral sheet of the studied smectite. S_O = octahedral site occupancy; X_O = octahedral cation charge; R^{2+}, R^{3+} = octahedral cations.

The subhedral crystallites are up to 500 nm wide and a few nm thick, and exhibit the typical ring-like diffraction pattern of smectites. Mössbauer spectroscopy revealed that 90% of the iron content is Fe^{3+}. Tetrahedral Fe^{3+} was excluded. Calculating the crystal chemical formula from TEM-EDX data and 10% Fe^{2+}, for $O_{10}(OH)_2$ anionic structure, octahedral occupancy was found to be low (2.6 *a.p.f.u.*) and the tetrahedral sites had 0.2 *a.p.f.u.* Fe^{3+}, contradicting Mössbauer data. If modelling the original, unoxidised state of the mineral, calculating the formula for 4 tetrahedral + 3 octahedral cations, fitting iron oxidation state to retrieve an electrostatically neutral formula, 90-97% of Fe is Fe^{2+}, and there is no iron in the tetrahedral positions. It is suggested that the iron-rich trioctahedral smectite has originally around 90% of its iron content in the divalent form, which is mostly oxidised to Fe^{3+} in contact with air, accompanied by the deprotonation of the OH groups. The original (unoxidised) formula is approximately $Ca_{0.15}K_{0.04}(Mg_{1.5}Fe^{3+}{}_{0.14}Fe^{2+}{}_{1.37}Al_{0.1})[Si_{3.5}Al_{0.5}O_{10}](OH)_2$, while the oxidised one is approximated as $Ca_{0.15}K_{0.04}(Mg_{1.5}Fe^{3+}{}_{1.37}Fe^{2+}{}_{0.14}Al_{0.1})[Si_{3.5}Al_{0.5}O_{10}]O_{1.23}(OH)_{0.77}$. Based on the calculated chemical formula, the oxidised form and partly the unoxidised form (where Fe^{2+} > Mg) can be regarded as new smectite species.

[1] Papp, G. et al. (1993) (eds.) *Topographia Mineralogica Hungariae,* **1,** 1-89.

Structure modeling and its application to the analysis of crystal-chemical variations in dioctahedral micas

Zviagina, B.B[*] & Drits, V.A.
Geological Institute RAS, Moscow, Russia
([*]zviagina@ginras.ru)

An improved structure modeling procedure has been elaborated for the calculation of atomic coordinates in dioctahedral micas from the experimental data on cation composition and unit-cell parameters. The algorithm is based on regression equations relating the structural features and chemical composition of dioctahedral micas that were obtained from the analysis of published data on refined structures of micas of various compositions. The new technique follows the general approach [1], but in order to account for new high-precision refined structural data on dioctahedral $2M_1$ micas published since 1993 the majority of regression equations were modified. In addition, changes were made in the calculation algorithm.

The empirical relationships used in the algorithm accurately describe the observed structural distortions in dioctahedral micas, such as tetrahedral tilt and rotation, tetrahedral elongation, octahedral flattening; hydroxyl depression *etc.*, and include the following dependences:

mean tetrahedral and octahedral bond lengths, d_T and d(M-O,OH) *vs* tetrahedral and octahedral cation composition, respectively;

differences between non-bridging and bridging tetrahedral bond lengths, d_{nbr} and d_{br} *vs* cation composition;

differences between distances from the octahedral cation to hydroxyl and non-hydroxyl oxygen anions, d(M-O) and d(M-OH), *vs* cation composition;

tetrahedral sheet basal surface corrugation, ΔZ, *vs* d(M-O) and b;

tetrahedral sheet thickness calculated over non-depressed basal O anions, $h_{T,\,max}$, *vs* ΔZ;

tetrahedral mean basal edge length, l_b, *vs* tetrahedral and interlayer cation composition;

tetrahedral elongated basal edge length, l_{bl}, *vs* octahedral cation composition;

tetrahedral ditrigonal rotation angle, α_T, *vs* l_b and b;

mean octahedral sheet thickness, $<h_{oct}>$, *vs* octahedral cation composition and b;

hydroxyl depression, Δ_{OH}, *vs* octahedral cation composition;

octahedral cation shift in dioctahedral $2M_1$ micas *vs* octahedral cation composition.

The estimated standard deviations are 0.002-0.007 Å for distance parameters and 0.5° for α_T

Structure modeling was used to deduce atomic coordinates for several low-temperature 1*M* dioctahedral micaceous minerals from solid solutions (Mg, Fe)-free illite-aluminoceladonite via Mg-rich illite and Fe^{3+}-rich glauconite-celadonite, for which structure studies are problematic because of fine dispersion and low structural order. The application of the structure modeling procedure to these samples was based on the assumption that the structural features of the 2:1 layer in 1*M* micas should be similar to those in $2M_1$, so that the structural data modeled for the 1*M* mica structures should have similar reliability. Analysis of the modeled structures revealed the basic factors responsible for crystal-chemical variations in the two sample series.

[1] Smoliar-Zviagina, B.B. (1993) *Clay Miner.*, **28**, 603-624.

Excess protons and tetrahedrally coordinated Ni^{2+} in triocta-dioctahedral micas

Robert, J.-L.[1*] & Abs-Wurmbach, I.[2]
[1]Institut de Minéralogie et de Physique des Milieux Condensés, Université Pierre et Marie Curie, Paris, France
([*]jean-louis.robert@impmc.upmc.fr)
[2]Technische Universität, Berlin, Germany

Series of Ni-micas have been prepared by hydrothermal synthesis at 500°C, 1 kbar PH_2O, in the K_2O-NiO-SiO_2-H_2O system. A complete mica solid solution has been obtained under the chosen experimental conditions, between two end-members with the nominal compositions $K(Ni_{2.5}\square_{0.5})Si_4O_{10}(OH)_2$ [A] and $KNi_3(Si_{3.5}Ni_{0.5})O_{10}(OH)_2$ [B]. The [A] phase is a triocta-dioctahedral mica, with 50% OH groups bonded to three Ni^{2+} and 50% bonded to two Ni^{2+} and adjacent to an octahedral vacancy. At the [B] end-member, Ni^{2+} is present in both [6] and [4] coordination numbers, which is an uncommon situation. Along the join, the mica color reflects the evolution of the composition, from pale green for [A], which contains only $[6]Ni^{2+}$, to sky blue for [B].

Both UV-vis and FTIR spectroscopies confirm the presence of $^{[4]}Ni^{2+}$ besides $^{[6]}Ni^{2+}$. In UV-vis, the first transition ν_1(t): $^3T_1$ (F) → $^3T_2$ (F) is outside the observable range. ν_2(t): → 3A2 (F) is at 9078 cm^{-1} and ν_3(t): $^3T_1$ (P) includes two bands at 15280 and 17120 cm^{-1}. CFSE Δ_t and Bt were calculated as 4910 cm^{-1} and 887 cm^{-1}, respectively. From these data, ν_1(t) was derived as 4160 cm^{-1}. FTIR spectroscopy in the antisymmetric T-O-T region, around 1000 cm^{-1}, also demonstrates the presence of $^{[4]}Ni^{2+}$. The [A] end-member shows two bands in this region, a high intensity band at low wavenumber, 970 cm^{-1}, due to the antisymmetric Si-O-Si motion, and a low intensity one, at 1120 cm^{-1}, assigned to the Si-O ⊥ vibration. Towards [B], a second doublet appears, at 1020 and 1080 cm^{-1}, also assigned to T-O-T and Si-O ⊥ vibrations but involving SiO_4 adjacent to NiO_4 tetrahedra.

Along the [A]-[B] join, vacant octahedral sites and NiO_4 tetrahedra, both generating local charge imbalances, are expected to be as far as possible from each other. On the contrary, they are systematically associated which provokes a strong charge imbalance on the apical oxygens of NiO_4 tetrahedra. These local defects are compensated by the incorporation of additional protons, very strongly bonded to the structure. FTIR spectroscopy in the OH stretching region confirms the presence of $^{[4]}Ni^{2+}$ and excess protons. The spectrum of the [A] mica mainly shows two bands, at 3677 and 3543 cm^{-1}, due to OH-groups in trioctahedral (Ni_3) and dioctahedral ($Ni_2\square$) environments, respectively. Along the [A]-[B] join, the IR spectra become more and more complicated in this region, and up to six bands are observed, from 3664 cm^{-1} to 3507 cm^{-1}, corresponding to the different combinations Ni_3-OH, $Ni_2\square$-OH in the octahedral layer plus Si-O-Si and Si-O-Ni in the tetrahedra. This very low wavenumber band is assigned to remaining dioctahedral OH-groups bonded to $2^{[6]}Ni^{2+}$ pointing towards $^{[4]}$Si-O-$^{[4]}$Ni tetrahedral associations. A broad grows at high wavenumber, 3635 cm^{-1}, as $^{[4]}Ni^{2+}$ content increases in the solid solution. It is assigned to the additional OH-groups.

Finally, a clear 1:1 correlation is observed between $^{[4]}Ni^{2+}$ and the additional H^+ content, measured by thermogravimetric analysis. We conclude that the [B] mica is off-composition. The structural formula of the corresponding compound can be written $K(Ni_{2.75}\square_{0.25})(Si_{3.5}Ni_{0.5})O_{9.5}(OH)_{2.5}$.

Characterization of the interlayer space of synthetic micas by far infrared spectroscopy

Robert, J.-L.[1*], Diaz, M.[2], Laperche, V.[3] & Prost, R.[2]
[1]Institut de Minéralogie et de Physique des Milieux Condensés, Université Pierre et Marie Curie, Paris, France ([*]jean-louis.robert@impmc.upmc.fr)
[2]INRA, Unité de Sciences du Sol, Versailles, France
[3]BRGM, Service EPI, Orléans, France

Series of synthetic mica solid solutions, related to phlogopites, have been characterized by far infrared absorption spectroscopy in order to derive the influence of octahedral, coupled tetra- and octahedral, and anionic substitutions on the properties of the interlayer site and specially on the interactions between the compensating cation and the basal oxygens of the tetrahedral layers.

In the far infrared region (wavenumbers < 200cm^{-1}), three main groups of bands can be observed: (1) a band at ν > 150 cm^{-1}, frequently broad with several shoulders, and sometimes well resolved, like in talc with a doublet at 177 and 166 cm^{-1}. The wavenumber of this band, or doublet, is sensitive to the nature of the octahedral cation and its assignment is beyond the scope of this work. (2) a plus or minus broad band, in the range 140-130 cm^{-1} and (3) a low-wavenumber band, with ν < 110 cm^{-1}. The last two bands evidently involve the interlayer cation C, first because they are absent in talc and second because they shift as a function of the nature of this cation (mass and charge effect). Previous measurements on oriented single crystals led to assign the first band(s) to out-of-plane C-O motions, roughly along the c* direction, and the low-wavenumber band(s) to in-plane C-O vibrations.

The micas investigated belong to the joins phlogopite $KMg_3(Si_3Al)O_{10}(OH)_2$ - $KM^{2+}{}_3(Si_3Al)O_{10}(OH)_2$, with M^{2+} = Fe^{2+} , Co^{2+} and Ni^{2+}, phlogopite - eastonite $K(Mg_{2.5}Al_{0.5})(Si_{2.5}Al_{1.5})O_{10}(OH)_2$, phlogopite - tetrasilicic Mg mica (TMM) $K(Mg_{2.5}\square_{0.5})Si_4O_{10}(OH)_2$, and their OH^- - F^- substituted equivalents, plus trioctahedral Na-micas along the join aspidolite $NaMg_3(Si_3Al)O_{10}(OH)_2$ - preiswerkite $Na(Mg_2Al)(Si_2Al_2)O_{10}(OH)_2$.

The low-wavenumber band (in the range 110 - 80 cm^{-1}) is particularly sensitive to variations of crystal-chemical features. A systematic correlation is observed between the geometry of the interlayer site and the position of this band. The main factor is the ditrigonal distorsion of the tetrahedral layer, measured by the α angle. This distortion is required to compensate the misfit between tetrahedral and octahedral layers and can be measured by XRD. It depends on the tetrahedral and octahedral occupancies: $^{[4]}$(Si,Al) proportion and ionic radius of the $^{[6]}$M cation(s) and varies from ≈ 1° in annite (the Fe^{2+} equivalent of phlogopite), to 20° in preiswerkite. In all series, the wavenumber of the in-plane C - O vibration increases with α, indicating higher C - O bond strengths, and a better retention of the interlayer cation.

The evolution of out-of-plane vibration(s) with composition is less clear. Generally the trend is in the reverse way, and frequently this band overlaps with the higher wavenumber ones, see (1). Nevertheless their evolution also reflects crystal-chemical modifications in the interlayer space.

Application of XANES experimental and theoretical studies to high-coordination cations. The case of potassium in micas

Xu Wei[1], Cibin, G.[2], Mottana, A.[3,4], Marcelli, A.[4*], Wu Ziyu[5,1], Chen Dongliang[1], Chu Wangsheng[1] & Brigatti, M.F.[6]
[1]BSRF, Institute of High Energy Physics, Beijing, P.R. China
[2]Diamond Light Source, Rutherford Appleton Laboratory, Chilton, Didcot, Oxfordshire, UK
[3]Dipto. di Scienze Geologiche, Università degli Studi Roma Tre, Rome, Italy
[4]Istituto Nazionale di Fisica Nucleare, Laboratori Nazionali di Frascati, Italy ([*]marcelli@lnf.infn.it)
[5]NSRL, University of Science and Technology of China, Hefei, P.R. China
[6]Dipto. di Scienze della Terra, Università di Modena e Reggio Emilia, Modena, Italy

Polarized synchrotron radiation allows recording angle-dependent XANES (AXANES) spectra of layered minerals, such as trioctahedral 1*M*-micas [1,2]. The experimental spectra can be evaluated for both their in-plane and out-of-plane component fractions of the electric dipole contribution, so that the related multiple-scattering pathways can be extracted. Most contributions arise from multiple-scattering interactions of the photoelectron ejected from the absorber (K in the interlayer *I*) colliding with other coplanar K and/or alkali atoms, and also with facing oxygen atoms that lie on the basal planes of the tetrahedral *T* sheets [3]. By contrast, the out-of-plane component fractions arise from multiple-scattering pathways that cross the energetic and structural barrier represented by the *T* sheets and reach the *W* anions that are located on the upper level of the octahedral *M* sheets and also the metal cations centering the *M* sheet itself. *Ab initio* calculations help to further interpolate experimental angle-dependent XANES work and to deduce from it the related physical/chemical effects. Calculations show that there are unexpected, large distortions in the mica local structure around the K atoms of the interlayer *I*. Such structural distortions are highly correlated with the compositional disordering that arises from electronic interactions between anions and cations, and extend far away *I* entering deep into the nearby *T* and *M* sheets [4].

[1] Marcelli, A. et al. (2006) *Rad. Phys. Chem.*, **75**, 1596-1607. [2] Cibin, G. et al. (2006) *Amer. Mineral.*, **91**, 1150-1162. [3] Brigatti, M.F. et al. (2008) *Amer. Mineral.*, **93**, 821-830. [4] Xu, W. et al. (2010) submitted.

Kaolinite and dickite behaviour after deformation by compaction and shear

Aparicio, P.[1*], Johnston, C.[2] & Valdrè, G.[3]
[1]Dpto. Cristalografía, Mineralogía y Q. Agrícola, University of Seville, Spain (*paparicio@us.es)
[2]Crop, Soil and Environmental Sciences, Purdue University, West Lafayette, USA
[3]Dept. of Earth and Geo-Environmental Sciences, University of Bologna, Italy

The structural changes produced on commercial powdered kaolin deformed by compaction and shear was investigated by X-ray diffraction (XRD), low temperature FTIR, differential thermal analysis and thermogravimetry (DTA/TG). Kaolin is composed by 40% of well orderered kaolinite, 18% of dickite and 42% of quartz. The deformation was induced through a specifically built planetary ball milling working in a controlled thermodynamic environment at room temperature and at a vacuum of 0.13 Pa (10^{-3} Torr). In this controlled environment the mechanical apparatus induces simultaneous compaction and shear stress to the material as described in detail by [1]. Kaolin samples were milled for 1, 5, 10 and 20 hours.

The deformation treatment produces a kaolinite structural order decrease, from a low-defect kaolinite to a high-defect kaolinite according to the AGFI index determined by XRD [2]. An index to evaluate the changes produced on dickite was determined following the fitting procedure described in [2]. The results indicated that dickite is apparently less affected by the deformation than kaolinite. A structural order was defined by FTIR and the results were correlated with AGFI results.

Low-temperature FTIR spectral analysis of kaolin group minerals provides a sensitive method for detecting the presence of kaolinite, dickite and nacrite [3]. Using this technique it was confirmed that dickite is more resistant to the deformation process than kaolinite. This technique indicates also that the deformation process produces a hydrous phase which increases with the time of the treatment and, at the same time, that kaolin minerals decrease (Fig.1). The presence of this hydrous phase was also confirmed by DTA/TG, which indicates that its percentage increases especially after 5 hours of treatment.

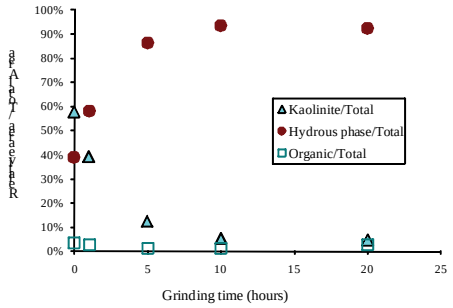

Fig. 1: Evolution of kaolinite and hydrous phase, determined by low temperature FTIR, versus time of deformation process.

In summary our peculiar milling induced a structural change to the octahedral sheets of kaolinite and subsequently to the tetrahedral ones. A progressive reduction of the stacking layer coherence is observed, although the complete amorphisation was not induced even after prolonged milling for 20 hours. Dickite remains after the deformation treatment by compaction and shear even for long times.

[1] Dellisanti, F. & Valdrè, G. (2005) *Appl. Clay Sci.*, **28**, 233-244. [2] Aparicio, P. et al. (2006) *Clay Miner.*, **41**, 811-817. [3] Johnston, C. et al. (2008) *Clay. Clay Miner.*, **56**, 470-485.

Synthesis and degradation mechanism of a swelling fluoromica

Cota, A.[1*], Alba, M.D.[2], Castro, M.A.[2], Pavon, E.[2], Naranjo, M.[2], Orta, M.M.[2] & Pazos, M.C.[2]
[1]Laboratorio de Rayos-X, CITIUS, Universidad de Sevilla, Seville, Spain (*acota@us.es)
[2]Instituto Ciencia de los Materiales de Sevilla, CSIC-Universidad de Sevilla, Seville, Spain

Na-2-mica, a synthetic swelling fluoromica, has recently attracted much attention for its unique combination of high charge (2 charges per unit cell) and its capacity to expand and exchange cations from the interlayer space. A variety of studies regarding the exchange and retention properties of those fluoromicas have been published, as well as their applications in the decontamination of soils [1,2]. However, few studies have been devoted so far to clarify key aspects such as the formation mechanism, the local order of the tetrahedral cations and the arrangement of interlayer species [3-5].

It is well-known that the distribution of aluminum in the framework, and thus the local framework negative charge, would have a dramatic effect on the properties of aluminosilicates [6,7]. If Al distribution in synthetic aluminosilicates could be adjusted, it would offer a way to control their properties. To achieve an exhaustive control of Al distribution through the conditions of synthesis, an experimental method for the determination or, at least, for indirect estimation of the distribution of aluminum in the aluminosilicate framework should be available.

The objectives of this research were to synthesize fluoromica at variable reaction times between 0 and 600 hours. That could enable us to determine the optimum reaction time for the process and identify the appearance of intermediate species which inform of the reaction mechanism. At the same time, the local order changes accompanying the synthesis process, which influence the final physico-chemical properties of the product, could be analyzed.

With the combined use of techniques that inform of both the long and short range structural order, we have shed a light on the synthesis mechanism of high-charge swelling mica and its stability range. The precursors are rapidly transformed into intermediate phases such as tectosilicates and 2:1 phyllosilicate. The precursors are transformed into fluoromica which remains stable for a period of time. Finally, the fluoromica starts to decompose and only the firing products are present.

[1] Kodama, T. et al (1999) *J. Mat. Chem*., **9**, 2475-2479. [2] Komarneni, S. et al. (1991) *New Development in Ion Exchange. Proc. Int. Conf. Ion Exchange*. Tokyo. [3] Kodama, T. et al. (2001) *J. Mat. Chem*., **11**, 2072-2077. [4] Kodama, T. et al. (1999) *J. Mat. Chem.*, **9**, 533-539. [5] Mukherjee, P.K. et al. (2006) *Phys. Rev. B*, **73**, 035414. [6] Armor, J.N. (2001) *Catalysis by Unique Metal Ion Structures in Solid Matrices. Science to Application*, NATO Science Series II, Kluwer Academic Publishers. Dordrecht. [7] Yang, J.H. (2001) *J. Mater. Chem*., **11**, 1305-1312

Surface structure of natural muscovite

Elmi, C.[1*], Brigatti, M.F.[1], Malferrari, D.[1], Castro, G.R.[2] & Ferrer Escorihuela, P.[2]
[1]Dipt. di Scienze della Terra, Università di Modena e Reggio Emilia, Modena, Italy ([*]chiara.elmi@unimore.it)
[2]SpLine at European Synchrotron Radiation Facility, Grenoble, France

The aim of this project is to study the atomic surface structure of a natural muscovite crystal by means of the synchrotron radiation light and the grazing incidence X-ray diffraction (GIXRD).

The muscovite studied [$(K_{0.92}Na_{0.08})$ $(Al_{1.86}Fe^{3+}_{0.01}Mg_{0.07}$ $Fe^{2+}_{0.06}Ti_{0.02})$ $(Si_{3.03}Al_{0.97})$ O_{10} $F_{0.09}$ $(OH)_{1.91}$] is monoclinic, $2M_1$ polytype, with space group $C2/c$ and unit cell parameters: a = 5.19690(10), b = 9.0138(3), c = 20.0835(7) Å, β = 95.763(2)°.

The muscovite structure was refined by single crystal X-ray diffraction and the final refinement yielded the agreement factor R = 0.0299. The difference Fourier map shows a significant residual electron density (2.2 e^-) close to the position related to the M1 site, thus indicating that the excess of octahedral cations is located at M1. The <M1-O> mean bond distance is 2.247(9) and the <M2-O> distance is 1.929 Å.

Grazing incidence X-ray diffraction (GIXRD) was recently performed at SpLine at the European Synchrotron Radiation Facility (ESRF). This type of analysis is very useful to identify typical structural features of the surface, such as possible imperfections, relaxations or reconstructions [1]. Usually, the atoms on surfaces, and sometimes those as deep as several layers down, assume positions different from their equilibrium positions in the bulk. Generally mineral surfaces will not be reconstructed unless they have been heated to temperature higher than 100°C [2]. In our case, the muscovite surface has been exposed to a delay of the first layer in order to study a freshly cleaned surface and data collected by GIXRD confirm that on muscovite surface only a relaxation occurs from an equivalent plane in the bulk. This is a common case for minerals with a low-symmetry structure, e.g. for feldspar [3].

[1] Brown, G.E. et al. (2008) in Nilsson, A. et al. (eds) *Chemical bonding at surfaces and interfaces*. Elsevier, 457-504. [2] Hochella, M.F. Jr. (1995) in Vaughan, D.J. and Pattrick, R.A.D. (eds) *Mineral surfaces*. Chapman & Hall, 17-60. [3] Hochella., M.F. Jr. et al. (1990) *Am. Mineral.*, **75**, 723-30.

Preparation of homoionic exchanged smectites in bentonites: influence of cation valence and soluble minerals on the success of exchange

Emmerich, K.[*] & Steudel, A.
Karlsruhe Institute of Technology (KIT), Competence Center for Material Moisture (CMM) c/o Institute for Functional Interfaces (IFG), Eggenstein-Leopoldshafen, Germany ([*]katja.emmerich@kit.edu)

The interlayers of natural smectites are commonly occupied by a mixture of Na^+ and/or Ca^{2+} and Mg^{2+}, respectively, and to less extent by K^+. Many chemical, mechanical and thermal properties of smectites and smectite-rich materials depend on the interlayer cations. Therefore, homoionic exchanged materials are prepared to investigate reaction mechanism as function of the interlayer cation or as function of the layer structure with uniform interlayer occupation. 54 publications from different journals from 1950 to 2009 were reviewed with respect to the applied homoionic exchange procedure. Only 6 papers [1-6] reported on the success of homoionic exchange. Up to now there exists no general instruction to prepare homoionic exchanged smectites in dependency of layer charge, cation exchange capacity (CEC) and the obtained level of homoionic interlayers. The aim of the present study was to create a general instruction based on smectite properties, overall phase content and experimental conditions.

For the research three natural bentonites were applied, which differ in content of calcite, dolomite, and gypsum and whose smectites differ in layer charge, CEC and interlayer composition. The homoionic exchange was achieved by repeated reactions of air dry clay aliquots with suspensions of readily soluble chlorides of different cations (Na, Li, K, Mg, Ca, and Cu). The concentration of the chloride solutions was equal to 1x CEC, 5x CEC, 10x CEC and 20x CEC of each material. The solid-liquid ratio averaged 4.4%. The success of homoionic exchange was monitored by exchange of interlayer cations with Cu-Trien and subsequent analysis of the cations in the supernatant exchange solution by ICP-OES.

As expected from charge, size and hydration properties of the cations the homoionic exchange with bivalent cations (Mg, Ca, and Cu) was more effective compared to that with monovalent cations (Na, Li, and K). In addition the exchange of monovalent cations was strongly inhibited or even prevented during exchange experiments with low salt concentrations (1-5x CEC) by present carbonates and sulfates that were dissolved during the exchange reactions. The released Ca or Mg replaced the monovalent cations in the interlayer, thus, the amount of Ca and Mg increased compared to the starting material.

The homoionic exchange was regarded successful if more than 95% of the interlayer consists of a single type of cation. To reach this occupancy rate, 20x CEC (three times exchange) was necessary for monovalent cations and 5x CEC (three times exchange) for bivalent cations. Purification improved the uptake of monovalent cations (reduced concentration of exchange solution, e.g. 5x CEC for K).

Our results briefly indicate that the following information: layer charge, CEC, solid-liquid ratio, concentration of salt solution, type of salt, reaction time, repetitions, and success of exchange should be reported as exchange procedure differs for materials in dependence of material properties, pretreatment and experimental conditions to enable comparison of different studies.

[1] Berend, I. et al. (1995) *Clay Clay Min.*, **43**, 324-336. [2] Cases, J.-M. et al. (1997) *Clay Clay Min.*, **45**, 8-22. [3] Emmerich, K. et al. (1999) *Clay Clay Min.*, **47**, 591-604. [4] Mosser, C. et al. (1997) *Clay Clay Min.*, **45**, 789-802. [5] Rutherford, D.W. et al. (1997) *Clay Clay Min.*, **45**, 534-543. [6] Steudel, A. et al. (2009) *Clay Clay Min.*, **57**, 486-493.

Structural and crystallochemical characterization of sepiolites

González, N.[1], Cuevas, J.[2] & Ruiz, A.I.[2*]
[1]RTL Laboratorio DRX Policristal, Universidad Autónoma de Madrid, Spain
[2]Dept. de Geología y Geoquímica, Universidad Autónoma de Madrid, Spain ([*]anai.ruiz@uam.es)

Sepiolite is a hydrous Mg-rich silicate clay mineral with fibrous morphology that typically occurs as fine-grained, poorly crystalline masses. It is an important industrial mineral with more than 100 commercial uses today in the pharmaceutical, fertilizer, and pesticide industries [1].

In this study, we report the structural and crystallochemical characterization of two sepiolite locations in the same geological context. This is in order to establish structure-properties relations of these clays. The materials came from a lacustrine environment in the Intermediate Unit of Miocene sediments of the Madrid basin (Spain), specifically located in the East of Madrid, Barajas - Vicálvaro.

The crystal structure of four samples of sepiolite was analysed using X-ray diffraction technique and the Rietveld structural refinement method. Sepiolites from Barajas show dolomite and quartz as accessory minerals. Crystal parameters obtained by Rietveld refinement are different depending on the origin, Barajas or Vicálvaro and are attributed to different hydration states.

Structural formulae of sepiolite samples calculated from the results of the chemical analysis, corrected by using the quantification of secondary mineral phases by Rietveld refinement, were close to the ideal formula based on the literature [2].

On the other hand, the X-ray thermodiffraction study revealed zeolitic H_2O is lost during heating from 25 to 200ºC; bound H_2O molecules are released completely at 750ºC; and hydroxyl groups are lost above 850ºC. However, the more ideal sepiolite composition is related to significant better thermal properties characterized by the maintenance of the dehydrated sepiolite structure unchanged up to 350ºC. Above this T a similar evolution can be followed for the several sepiolites, ending with a phase transformation to enstatite mineral.

[1] Jones, B.F. & Galán, E. (1988) in Bailey, S.W (ed.) *Rev. Mineral.*, **19**, 631-674. [2] Galán, E. & Carretero, I. (1999). *Clay. Clay Min.*, **47**, 4, 399-409.

Characterization of clay material from chalk reservoirs in Denmark

Hem, C.[1*], Skovbjerg L.L.[1], Andersson, M.P.[1], Balogh, Z.[1], Makovicky, E.[2] & Stipp, S.L.S.[1]
[1]Nano-Science Center, Dept. of Chemistry, University of Copenhagen, Denmark ([*]hem@nano.ku.dk)
[2]Dept. of Geography and Geology, University of Copenhagen, Denmark

The presence of clay in reservoir chalk has an effect on calcite recrystallization [1]. It has been suggested that a high clay content enhances chalk dissolution and hence calcite recrystallization [2,3]. Clay could also inhibit recrystallization when it nucleates and grows over the chalk particles. Therefore, although chalk might only contain a few percent of clay, its mineral composition, morphology, size and structure can play an important role in the properties and behaviour of the reservoir. In this study, we examined Maastrichtian age samples from the Aalborg Portland pit (Jutland, Denmark) and from a shallow borehole at Klintholm (Fyn) as well as from the North Sea basin.

Clay was separated from the chalk and analyzed using X-ray diffraction (XRD), X-ray photoelectron spectroscopy (XPS), scanning electron microscopy (SEM), atomic force microscopy (AFM) and infrared spectroscopy (IR). The clay types varies from sample to sample, but there is little variation among samples from the same location. SEM and AFM show that there are two distinctly different morphologies of clay. By volume, the major part consists of detrital larger grain smectite or mixed layer smectite/illite but we also find smaller particles of clay, sometimes single layers, which have grown in pore spaces and on the surface of other chalk particles.

[1] Baker, P.A. et al. (1980) *Mar. Geol.*, **38**, 185-203. [2] Fabricius, I.L. (2007) *Sedimentology*, **54**, 183-205. [3] Hardman, R.F.P. (1982) *Bull. Geol. Soc. Denmark*, **30**, 119-137.

Crystal chemistry and thermodynamic properties of kerolite-stevensite mixed-layer minerals

Krupskaya, V.V.[1,2*], Vigasina, M.F.[2], Melchakova, L.V.[2], Ogorodova, L.P.[2] & Kiseleva, I.A.[2]
[1]Institute of Geology of Ore Deposits, Petrography, Mineralogy and Geochemistry, Moscow, Russia
[2]Dept.of Mineralogy, Geological Faculty, M.V. Lomonosov Moscow State University, Moscow, Russia (*vi_kru@bk.ru)

Two kerolite-stevensite mixed-layer minerals from residual soils of serpentinized ultra basic rocks (Ural, Russia) are studied by X-ray diffraction (XRD), infrared spectroscopy (FTIR), differential thermal (DTA), thermogravimetric (TG, DTG), electron microprobe, and thermochemical analyses. The FTIR-spectra of both air-dried samples indicate that these belong to kerolite-pimelite-trioctahedral smectite minerals with different levels of Ni for Mg substitution [1-3]. This is confirmed by XRD modeling, which additionally shows a mixed layer structure with ca. 30-40% expandable layers. Both samples in air-dried state exhibit the 001 reflection at 11.6 Å shifting to 9.7 Å upon heating at 550-600°C. The corresponding patterns of the ethylene-glycolated samples depend on Ni content (25.0, 13.0, 9.3, 5.3 Å and 24.0, 17.0, 9.0, 5.3 Å for the Ni-poor and Ni-rich samples, respectively).

The TDA and TG curves of both samples are similar and show three steps of water loss: 100-200°C – adsorption water (7.5 and 7.7%) with t_{max} = 100°C, 200-780°C – structural water (2.8 and 3.5%) with $t_{max} \approx 380^oC$, and 780-1050°C – dehydroxylation (4.3 and 3.8%) with t_{max} = 850°C, for the Ni-poor and Ni-rich samples, respectively. Chemical formulas calculated on the basis of a +22 total cation charge were:

$[(Mg_{2.91}Ni_{0.02}Fe_{0.02}Al_{0.01})Si_4O_{10}(OH)_2][Na_{0.02}Ca_{0.02}] \cdot 0.7H_2O$ (I), $[(Mg_{2.07}Ni_{0.87}Fe_{0.08}Al_{0.04})\ (Si_{3.76}Al_{0.24})\ O_{10}\ (OH)_2]\ [Na_{0.02}Ca_{0.03}]\cdot 0.9H_2O$ (II).

Thermochemical investigations by "transposed temperature drop solution calorimetry" are performed in molten $2PbO\cdot B_2O_3$ at T=973 K with a Tian-Calvet high-temperature heat-flux calorimeter. The calibration of the calorimeter was performed by dropping pieces of platinum wire with known enthalpy increments, and the sum of the heat of solution and the heat content of the sample was measured: $\Delta H = [H^o(973\ K) - H^o(298.15\ K) + \Delta H_{sol.}973\ K)]$. The enthalpies of formation from the elements of the kerolite-stevensite mixed-layer minerals were determined after corrections for adsorbed water and by employing reference data for the constituent oxides according to the equation: $\Delta_f H^o_{el}(298.15\ K)_{min.} = \sum \nu_i \Delta H_{oxi} - \Delta H_{min.} + \sum \nu_i \Delta_f H^o_{el}(298.15\ K)_{oxi}$, where ν_i are the stoichiometric coefficients in the reaction of mineral formation from the oxides. The resulting $\Delta_f H^o_{el}$(298.15 K) values are -6018.4±8.5 kJ·mol^{-1} for the Ni-poor sample (I) and -5823±14kJ·mol^{-1} for the Ni-rich sample (II). These values suggest that the Mg-rich members of the kerolite-stevensite mixed-layer minerals are more stable than their N-rich analogs.

Acknowledgements: This work was supported by Russian Foundation for Basic Research (Grant № 09-05-00302). Authors wish to acknowledge G. Chryssikos and V. Gionis of the Theoretical and Physical Chemistry Institute, NHRF (Athens, Greece) for advices.

[1] Brindley, G.W. et al. (1977) *Mineral. Mag.*, **41**, 443-452. [2] Brindley, G.W. et al. (1979) *Am. Mineral.*, **64,** 615-625. [3] Dekov, V.M. et al. (2008) *Chem. Geol.*, **247**, 171-194.

Crystallization of natural montmorillonite applying very-high pressure and temperature

Nakazawa, H.* & Taniguchi, T.
National Institute for Materials Science, Tsukuba, Japan
(*nakazawa.hiromoto@nims.go.jp)

Clay minerals of the smectite group are inorganic materials with ability to react with organic compounds. For this reason, they attract particular attention for their application as nanohosts for organic guest molecules. However, smectite occurs usually as a poorly crystallized fine powder. Their characterization and application have been hindered by a lack of large single crystals.

An entropy consideration suggests that a 3D-ordered smectite, if it would exist, might be stable under higher pressure than smectite with a turbostratically disordered structure. Previously, one of the authors has been successful in synthesis of smectite crystals using a silica-alumina glass as starting material by applying 5.5 GPa and 1600°C [1]. However, their crystal sizes were still insufficient for an X-ray structure analysis and nothing was known about their stability relations at very high pressures and temperatures.

In this contribution, similar pressures and temperatures were applied to natural montmorillonite and a highly purified bentonite from Yamagata, Japan, as starting materials. The purification procedures and characterization have been reported in detail elsewhere [2].

The montmorillonite was placed in 100% of humidity for 24 h before the experiment and was encapsulated in a Pt tube with water of about 15 wt.%. Very high pressures and temperatures were applied to the sample by using a belt-type apparatus, e.g. 5.5 GPa and 1500°C for 1 hr [3]. A series of runs under 5.5 GPa were carried out at different temperatures in the range from 1700 to 1000 °C and for durations from 1 to 25 h.

The high pressure product was lightly crushed, mounted on a glass slide, observed by optical microscope and studied by X-ray diffraction for identification. The sample was then exposed to ethylene glycol vapour for one night and investigated again for confirmation of characteristic expansion of smectite. Its morphology was observed by electron microprobe analyzer (JEOL, JXA-8500F) and transmission electron microscope (JEOL, JEM 2000EX).

X-ray diffraction (XRD) study showed that the products consist mostly of montmorillonite with small admixture of kyanite. All the XRD peaks of montmorillonite were extremely sharp. Morphologies of particles revealed in the SEM and TEM images corresponded to long euhedral laths and rare hexagonal thin plates.

Because the starting montmorillonite was extremely fine nanometer-scale powder and completely disordered from structural viewpoint, the euhedral morphology of the high pressure montmorillonite and its size of some tens of micron meter indicate that they were surely grown under high pressure and temperature, probably by the Ostwald ripening mechanism. This suggests that there may be a stable phase of 3D-montmorillonite at very high pressure and temperature around 5.5 GPa and 1700°C. The synthesis of large single crystals of montmorillonite is therefore not entirely impossible and seems to be rather realistic.

[1] Nakazawa, H., Yamada, H. & Fujita, T. (1992) *Appl. Clay Sci.*, **6**, 395-401. [2] Suzuki, K., et al. (2007) *Nenndo Kagaku* (*J. Clay Sci. Soc. Japan*), **46**, 147-155. [3] Taniguchi, T. & Yamaoka, S. (2001) *J. Cryst. Growth*, **222**, 549-557.

How to calculate mineral formula for 3-members mixed layers from EDX-analysis by Transmission Electron Microscopy: example – kaolinite-smectite-vermiculite mixed layers in Friedland Clay (Germany)

Nguyen, T.L.[1*], Kasbohm, J.[2] & Hoang, T.M.T.[3]
[1]Inst. of Geography and Geology, University of Greifswald, Greifswald, Germany (*thanhlangeo@googlemail.com)
[2]GeoENcon Ltd., Greifswald, Germany
[3]Fac. of Geology, Hanoi University of Science, Hanoi, Vietnam

Transmission electron microscopy (TEM) is a very sensitive tool to recognize alteration processes of montmorillonite or other clay mineral phases. The variability of chemical composition of interlayer space, octahedral as well as tetrahedral sheets of each TEM-EDX investigated particle is mirroring this process of alteration.

The contribution offers a methodology to calculate the mineral formula also from particles, which represents e.g. irregular interstratified mixed layer structures with three end members composed by kaolinite, smectite and dioctahedral vermiculite (KSV-ml).

For the calculation of a model mineral formula of KSV-ml it was developed a series of equations to convert the TEM-EDX-analysis of each particle. This conversion is controlled by three parameters: (i) total charge (22 ... 28 per $(OH)_n$ O_{10}), (ii) Si-amount in tetrahedral sheet and (iii) numbers of atoms in octahedral sheet (2 ... 4 per $(OH)_n$ O_{10}).

The contribution contains also an approach of this methodology for the German Friedland clay. Friedland clay is composed mainly by Fe-rich illite-smectite mixed layer (IS-ml), kaolinite (15 wt.%), mica, quartz. KS-ml or KSV-ml could be not detected there before by XRD. After deconvolution of XRD-traces (oriented mounts: air dried, ethylene-glycol saturation) by BGMN-Rietveld technique X-ray diffraction of Friedland clay confirms now also the occurrence for KSV-ml.
Applying presenting TEM-EDX-methodology following different compositions of KSV-ml were calculated in three different samples of Friedland clay. Each analysed sample of Friedland clay is representing a different geological history.

KSV-ml in Friedland Clay 1 *(%K 60%, %S 25%, %V 15%)*
$Mg_{0.01}Ca_{0.02}Na_{0.05}K_{0.08}Al_{2.96}Fe^{3+}{}_{0.13}Mg_{0.08}Ti_{<0.01}(OH)_{5.54}$
$Si_{3.90}Al_{0.10}O_{10}]$
KSV-ml in Friedland Clay 2 *(%K 45%, %S 40%, %V 15%)*
$Mg_{0.03}Ca_{0.01}Na_{0.03}K_{0.06}Al_{2.76}Fe^{3+}{}_{0.11}Mg_{0.03}Ti_{<0.01}[(OH)_{4.72}$
$Si_{3.88}$ $Al_{0.12}O_{10}]$
KSV-ml in Friedland Clay 3 *(%K 50%, %S 35%, %V 15%)*
$Mg_{0.02}Ca_{0.02}Na_{0.00}K_{0.06}Al_{2.64}Fe^{3+}{}_{0.24}Mg_{0.03}Ti_{<0.01}[(OH)_{4.79}$
$Si_{3.89}Al_{0.11}O_{10}]$

Friedland Clay 1 represents the original composition located in the core of ore body. Friedland Clay 2 shows alterations by interaction with glacial water in a closed system. Friedland Clay 3 mirrors the effect of rain to the clay mineral matter (Clay 2) at the surface of open cast mine (= open system).

The differences between Clay (1) and (2) are comparable with smectitization. The differences between Clay (2) and (3) are pronounced by higher octahedral Fe3+ in substitution of octahedral Al. The origin of Fe is the result of degradation processes of Fe-rich IS-ml phases and oxidation of pyrite.

KSV-ml structures in Friedland Clay undergo similar processes of alteration in closed and open systems like described for smectite by Herbert et al. (2008) [1] from batch experiments with bentonites.

[1] Herbert, H.-J. et al. (2008) *Phys. Chem. Earth*, **33(1)**, S327-S342.

The kaolinite-dickite relation by thermodynamic data

Ogorodova, L.P.[1*], Vigasina, M.F.[1], Melchakova, L.V.[1], Kiseleva, I.A.[1], Krupskaya, V.V.[1,2], Luse, I.V.[3] & Randers, M.A.[3]
[1]Dept. of Mineralogy, Geological Faculty, M.V. Lomonosov Moscow State University, Moscow, Russia
(*logor@geol.msu.ru)
[2]Institute of Geology of Ore Deposits, Petrography, Mineralogy and Geochemistry, Moscow, Russia
[3]Dept. of Applied Geology, Faculty of Geography and Earth Sciences, University of Latvia, Riga, Latvia

The thermodynamic properties of the kaolinite $Al_2Si_2O_5(OH)_4$ and its polymorph dickite were studied on natural samples of kaolinite from the Glukhovetskoye (Ukraine) and dickite from Tibskoye deposits (Russia). Samples were characterized by optical microscopy, X-ray diffraction, electron probe microanalysis, infrared spectroscopy (FTIR) and differential thermal and thermogravimetric analyses. The XRD data refined by Rietveld method with QUANTO software [1] showed rather purity of both studied samples (kaolinite – more 96%, dickite – more 92%). They were well-crystallized, the IR-absorbance spectra and the thermal curves correspond to pure minerals. All thermodynamic investigations were performed with a Tian-Calvet high-temperature heat-flux calorimeter ("Setaram", France). The enthalpies of formation from the elements were determined by "transposed temperature drop solution calorimetry" in molten $2PbO{\cdot}B_2O_3$ at T=973 K. The sum of the heat of solution and the heat content of the sample was measured:

$$\Delta H = H^o(973\ K) - H^o(298.15\ K) + \Delta H^o_{solution}(973\ K).$$

Before experiments, all samples were heated at 200°C for 1.5 hours to remove minor amount of low-temperature water. Calibration of the calorimeter was performed by dropping pieces of platinum wire with known enthalpy increments [2]. With the calorimetric data obtained and needed thermochemical [3, 4] and reference [2] data for pyrophyllite, corundum and quartz the standard enthalpies of formation of natural minerals of kaolinite group from the elements were calculated on the basis of reaction:

$$2Al_2Si_4O_{10}(OH)_2 = Al_2Si_2O_5(OH)_4 + Al_2O_3 + 6SiO_2.$$

For the calculation the following equation was used:

$$\Delta_f H^o_{el}(298.15\ K)_{mineral} = 2\Delta H_{pyrophyllite} - \Delta H_{mineral} - \Delta H_{corundum} - 6\Delta H_{quartz} + 2\Delta_f H^o_{el}(298.15\ K)_{pyrophyllite} - \Delta_f H^o_{el}(298.15\ K)_{corundum} - 6\Delta_f H^o_{el}(298.15\ K)_{quartz},$$

where ΔH – calorimetric data for all constituent minerals. The resulting values of $\Delta_f H^o_{el}(298.15\ K)$ are -4118±10 kJ mol^{-1} for kaolinite and -4127±10 kJ mol^{-1} for dickite. Taking into account the reference data on their entropies [2] the Gibbs energies of formation from the elements were calculated: -3796±10 kJ mol^{-1} and -3805±10 kJ mol^{-1}, respectively. These results show that kaolinite is metastable relative to dickite and agrees with data from [5]. The more widespread natural occurance of kaolinite vs. dickite is due to kinetic factors rather than thermodynamics.

Acknowledgements: This work was supported by Russian Foundation for Basic Research (Grant № 09-05-00302), EU Social Fund (Grant № 2009 / 0138 / 1DP / 1.1.2.1.2 / 09 / IPIA / VIAA / 004).

[1] Altomare, A. et al. (2001) *J. Appl. Cryst.*, **34**, 392-397. [2] Robie, R.A. & Hemingway, B.S. (1995) *Thermodynamic Properties of Minerals and Related Substances at 298.15 K and 1 Bar (10^5 Pascals) Pressure and at Higher temperatures.* U.S. Geol. Surv. Bull., **2131**, Washington. [3] Ogorodova, L.P. et al. (2003) *Thermochim. Ac.*, **403**, 251-256. [4] Kiseleva, I.A. et al. (1979) *Geokhimiya*, **12,** 1811-1825. [5] Zotov, A. et al. (1998) *Am. Mineral.*, **83**, 516-524.

Theoretical study of one-layered kaolinite polytypes

Orbán, R.[*] & Dódony,I.
Dept. of Mineralogy, Eötvös Loránd University, Budapest, Hungary ([*]orban.richard@gmail.com)

The stacking of adjacent kaolinite-type structural layers with one-layer periodicity is studied using **R** vector and „+", „–" notation introduced by Dódony [1] for trioctahedral TO phyllosilicates. In this notation, **R** is the projection of the **c** axis onto the **ab** plane and „+" or „–" signs the slant of octahedral sheet. The length of **R** can be 0, **a**/3 and **b**/3, with directions of <100>, <110> for **a**/3 shifts and <010>, <310> for **b**/3 shifts, relating subsequent layers.

In the present work, all the twenty crystallographically different one-layer kaolinite polytypes allowed by H-bonding are derived as a result of possible combinations of **R** and slant of octahedral sheet („+", „–"). The number of polytypes, which is 20 (including 8 enantiomorph modifications), is in disagreement with previosuly reported 6 one-layered polytypes [2,3].

Each polytype is characterized by simulated X-ray powder diffraction pattern, [001] selected area electron diffraction (SAED) pattern and [001] projected charge density map. All simulations were calculated for the chemical composition of $Al_2Si_2O_5(OH)_4$, and with the structural dimensions of a = 5.023 Å, b = 8.700 Å, the *layer thickness* ($d_{(001)}$) = 7.000 Å and γ = 90°.

Patterns of the [001] projected charge density map of non-enantiomorph polytypes (12) differ from each other, because they are crystallographically different. By comparison of simulated data, every non-enantiomorph polytype can be identified by combination of intensity distributions and geometry of XRD and [001] SAED patterns.

[1] Dódony, I. (1997) in Merlino, S. (ed.) *Modular Aspects of Minerals*, EMU Notes in Mineralogy, **1**, 57-80. [2] Newnham, R.E. (1962) *Mineral. Mag.*, **32**, 683-704. [3] Zvyagin, B.B. (1962) *Kristallografiya*, **7**, 51-65.

Molecular simulations of layered double hydroxides (LDHs) by various porphyrine molecules

Pospíšil, M.[1*], Kovář, P.[1], Kovanda, F.[2], Káfuňková, E.[3] & Lang, K.[3]
[1]Faculty of Mathematics and Physics, Charles University in Prague, Czech Republic ([*]pospisil@karlov.mff.cuni.cz)
[2]Dept. of Solid State Chemistry, Inst. of Chemical Technology, Prague, Czech Republic
[3]Inst. of Inorganic Chemistry, v.v.i., Academy of Sciences, Řež, Czech Republic

Molecular simulations were applied for structure analysis of Mg_2Al LDH (original nitrate form) intercalated with [5,10,15,20-tetrakis(4-sulfonatophenyl) porphyrin (TPPS)] [1] and Pd-TPPS. LDH was prepared with an Mg/Al molar ratio of 2. The results are supported by experimental methods like powder X-ray diffraction (XRD) analysis, infrared (IR) spectroscopy and thermogravimetry.

In the case of TPPS, three different types of structures were modelled. The experimental XRD patterns of LDH intercalated with TPPS show 70–80% loading with respect to the theoretical anion exchange capacity (AEC). Type 1 model represent single-phase systems with a 100% TPPS loading in the interlayer space, type 2 show the coexistence of two separate phases, the first phase has interlayer saturated with TPPS anions and the second phase has interlayer fully occupied with NO_3^- anions. Total loading of TPPS in type 2 models was in the interval of 75 – 92 %. Type 3 model represent a structure with the coexistence of both TPPS and NO_3- anions in the same interlayer space. The agreement between experimental and calculated X-ray diffraction patterns and energy characteristic of models show type 2 as most probable.

In the case of Pd-TPPS two models with various loadings (10% and 100%) were investigated. Geometry of Pd-TPPS was optimized by *ab initio* calculations. Optimized geometry of this molecule was inserted into interlayer space from parallel to nearly perpendicular arrangement. The resultant position of Pd-TPPS in the interlayer depends on the degree of intercalation and is related to AEC.

Acknowledgements: This work was supported by the Ministry of Education, Youth and Sports of the Czech R. (MSM 0021620835, MSM 6046137302), the Czech Science Foundation (203/06/1244, 202/05/H003, 205/08/0869), the Grant Agency of the Academy of Sciences of the Czech R. (KAN 100500651).

[1] Kovář, P. et al. (2010) *J. Mol. Model.*, **16**, 223-233.

Sonication induced reduction reactions of the Ojén (Andalucía, Spain) vermiculite

Poyato, J.[1*], Pérez-Rodríguez, J.L.[1], Lerf, A.[2] & Wagner, F.E.[3]
[1]Instituto de Ciencia de Materiales de Sevilla, Consejo Superior de Investigaciones Científicas, Universidad de Sevilla, Spain ([*]jpoyato@us.es)

[2]Walther-Meissner-Institut, Bayerische Akademie der Wissenschaften, Garching, Germany
[3]Physik-Department, Technische Universität München, Germany

Sonication produces a delamination and a reduction of the particle size without the significant destruction of the vermiculite structure that is caused by grinding [1]. The extent of particle size reduction and the closely related increase of the surface areas (S_{BET}) are almost independent of the choice of the transfer medium (water or a water/H_2O_2 mixture) [2]. However, chemical analysis, Mössbauer spectroscopy and infrared (IR) spectroscopy show clearly that the choice of the transfer medium can affect the structure of a particular material on a more local scale [2].

More puzzling than the oxidation in presence of hydrogen peroxide was the reduction of the Ojén vermiculite observed during sonication in pure water. Water itself does not reduce the Ojén vermiculite. Interlayer water does not play a role in the reduction of the Ojén vermiculite, since the extent of reduction is roughly the same when the potassium-exchanged Ojén vermiculite, where K^+ is almost unhydrated, is sonicated in water.

Possible reducing agents could be the $H^\bullet$ or the $HO_2^\bullet$ which are formed as an intermediate product in the sonication of (aerated) water or subsequent reactions products like H_2. Especially interesting is the $HO_2^\bullet$ radical because solid surfaces can trigger its formation [3]. Furthermore, it is well documented that these hydroperoxyl radicals react in Fenton systems even in the presence of hydrogen peroxide as a reducing agent [4,5].

To get more insight in the reduction mechanism we carried out sonication in water under air and under nitrogen. By means of Mössbauer spectroscopy we observed a significant difference: the Fe^{3+}/Fe^{2+} + Fe^{3+} ratio amounts to 0.59 under nitrogen and to 0.39 under air (cf. for untreated vermiculite it is 0.73). Though under air the influence of oxygen and, thus, the contribution of $HO_2^\bullet$ cannot be neglected. Under exclusion of oxygen gaseous hydrogen cannot be the reducing agent because it does not react with the Ojén vermiculite at temperatures below 400 °C. The only other choice is the $H^\bullet$. For this radical to act on the clays as reducing agents the cavitation bubbles must be closely attached to the vermiculite surface and they have to reduce the structural iron ions prior to the recombination/decomposition to H_2 or H_2O (together with $OH^\bullet$).

[1] Pérez-Maqueda, L.A. et al. (2001) *Phys. Chem. Miner*., **28**, 61-66. [2] Poyato, J. (2009) *Ultrasonics Sonochem*., **16**, 570-576. [3] Kitajima., N. et al. (1978) *J. Phys. Chem*. **82**, 1505-1509. [4] Lin, S.-S. & Gurol, M.D. (1998) *Environ. Sci. Technol*., **32**, 1417-1423. [5] Watts, R.J. et al. (1999) *Environ. Sci. Technol*., **33**, 3432-3437.

Influence of interlayer charge and water mobility on ^{29}Si NMR chemical shift of 2:1 phyllosilicates

Sanz, J.[1], Sobrados, I.[1] & Robert, J.-L.[2*]
[1]Instituto de Ciencia de Materiales de Madrid, CSIC, Madrid, Spain
[2]Institut de Minéralogie et de Physique des Milieux Condensés, Université Pierre et Marie Curie, Paris, France ([*]jean-louis.robert@impmc.upmc.fr)

A series of synthetic sodium-rich saponites $Na_xMg_3(Si_{4-x}Al_x)O_{10}(OH)_2.nH_2O$, with $0.33 \leq x \leq 1$ and trioctahedral Na-micas $Na(Mg_{3-y}Al_y)(Si_{3-y}Al_{1+y})O_{10}(OH)_2.nH_2O$, with $0 \leq y \leq 1$ have been investigated by ^{29}Si magic angle spinning nuclear magnetic resonance (MAS-NMR) spectroscopy. The salient result is the major effect of the interlayer charge on ^{29}Si chemical shift of four detected NMR components ascribed to Si_3, Si_2Al, $SiAl_2$ and Al_3 environments. The contribution of the interlayer charge is much more important than the previously reported contribution of the ditrigonal distortion of tetrahedral layers, generated by the misfit between tetrahedral and octahedral layers. This observation derives from the peculiar disposition of tetrehedra in phyllosilicates, with three out of four oxygen atoms exposed to the interlamellar space. In saponites with $x < 1$, ^{29}Si MAS-NMR spectra change considerably with the amount and mobility of adsorbed water, indicating that for a given tetrahedra, chemical shift depends on the proximity and amount of interlayer charge seen by this tetrahedron. In dehydrated saponites, where Na^+ cations are disposed in ditrigonal cavities, NMR components split as a consequence of the partial occupancy of three neighbouring cavities. In hydrated saponites, chemical shifts of splitted components are averaged as a consequence of interlayer water and cation mobility. In this analysis, the effect of the increasing octahedral charge of micas is considerably lower than that of interlayer charge. In micas, chemical shift discontinuities detected near $y = 0.5$ are discussed in terms of distortions and relative disposition of contiguous layers.

Computational study of TMA^+ fluorohectorite intercalate

Scholtzová, E.
Institute of Inorganic Chemistry, Slovak Academy of Sciences, Bratislava, Slovak Republic (uacheva@savba.sk)

The structural data of TMA^+ fluorohectorite intercalate (TMA-H) into 2:1 layer silicates suggest two possible orientations of TMA^+ cations with low occupancy (~0.9) [1]. The TMA^+ atoms could only appear in any of the positions constrained in the original space group (*C*2/*m*) to the 8*j* Wyckoff position. In the triclinic space group *P*1, TMA^+ cations are free to translate and rotate, though all the movements are restricted by the potential field generated by surrounding atoms. The 64 computational models of mutual orientation of TMA^+ cations were based on this assumption. The primary aim of this study is to find the energetically most favorable arrangement of the TMA^+ cations in fluorohectorite interlayer space. The second task is to identify whether a particular configuration can be detected using X-ray powder diffraction and/or vibration spectroscopy. The main tool in this study is a density functional (DFT) method as applied for the solid state in the VASP program [2]. The analysis of total energies of the models shows that approximately 70% of models fall to the region with very close energies. Hence it is very difficult if ever possible to distinguish the mutual orientation of the TMA^+ cations in these models. The calculated powder diffraction patterns for model with the lowest (BEST) and with the highest (WORST) energy confirm this result. The differences in the intensities of both patterns are almost negligible. The analysis of the calculated vibrational modes for BEST, COMMON (representing group of models with close energies) and WORST models were done in details (Fig. 1). The minimal changes in the position of the C-H stretching modes are caused by changes, formation and/or interruption of the weak C-H…O hydrogen bonds according to mutual orientation of TMA^+ cations in the models.

It can be concluded that experimental distinguishing of mutual orientations of TMA^+ cations in the fluorohectorite interlayer space by the methods discussed above is not possible.

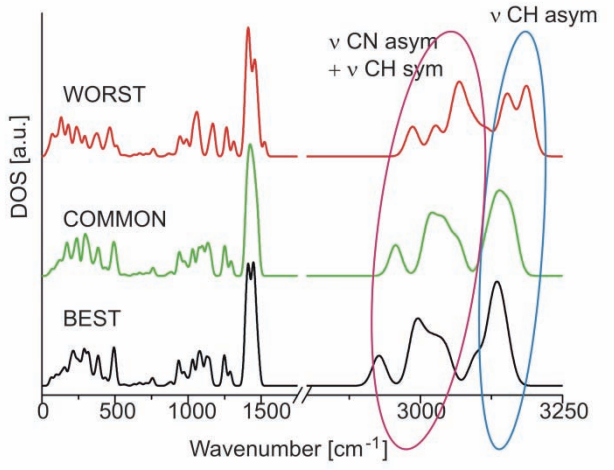

Fig. 1: The calculated vibrational density of states for selected models.

Acknowledgements: Financial support from the Slovak Grant Agency (grant VEGA 2/0150/09) is gratefully acknowledged.

[1] Seidl, W. & Breu, J. (2005) *Kristallogr.*, **220,** 169-176. [2] Kresse, G. & Hafner, J. (1993) *Phys. Rev.*, **B48**, 13115-13118.

Occlusion of sulphate salts into the Mg-Al-SO_4 hydrotalcite

Stanimirova, Ts.
Sofia University "St. Kliment Ohridski", Sofia, Bulgaria (stanimirova@gea.uni-sofia.bg)

Occlusion of the different salts or molecules into the layered minerals (clays, mica), zeolites, etc. is a well known phenomenon [1]. However, there are only a few papers describing an occlusion of sulphate salts in the natural layered double hydroxides, which are also known as anionic clays or hydrotalcite-like minerals (HTs) [2-4].

This contribution presents the results of experimental investigations of occlusion (possibilities, conditions and peculiarities) of sulphate salts in the interlayer space of Mg-Al-SO_4 hydrotalcite.

Occlusion was obtained by two main ways:

1) During syntheses of the Mg-Al-SO_4 hydrotalcites (Mg:Al =2:1) by co-precipitation of mixed acid solution ($MgCl_2$ and $AlCl_3$) with mixed alkali solution (NaOH and Na_2SO_4 or K_2SO_4 in 5-fold excess). 2) Through post-synthetic reactions (sulphate solution treatment and anion exchange) of dried samples (Mg-Al-SO_4, Mg-Al-NO_3 and Mg-Al-$B_4O_5(OH)_4$ HTs) dispersed in water solutions of Na_2SO_4, K_2SO_4 or $MgSO_4$ with 5-fold excess of SO_4^{2-} anions. All obtained samples were characterized by X-ray powder diffraction (XRD) and Fourier-transform infrared spectroscopy (FTIR).

According to the literature data, lattice parameters of natural and synthetic Mg-Al-SO_4 (Mg:Al=2:1) HTs are a = 0.3044 nm and c = 2.667 nm. Table 1 lists values of the d_{003} and d_{110} reflections, which correspond to the lattice parameters $c = 3 \cdot d_{003}$ and $a = 2 \cdot d_{110}$, respectively.

Table 1: Chemical composition and cell parameters of the materials

Sample	Chemical formula	d_{003}, nm	d_{110}, nm
Occlusion during syntheses and post-synthetic treatment			
Extra Na_2SO_4	$Mg_4Al_2(OH)_{12}SO_4.mNa_2SO_4.nH_2O$	1.122	0.1522
-add. washing	$Mg_4Al_2(OH)_{12}SO_4.3H_2O$	0.889	0.1522
-above + $MgSO_4$	$Mg_4Al_2(OH)_{12}SO_4.mMgSO_4.nH_2O$	1.092	0.1525
Extra K_2SO_4	$Mg_4Al_2(OH)_{12}SO_4.mK_2SO_4.nH_2O$	1.121	0.1523
-add. washing	$Mg_4Al_2(OH)_{12}SO_4.3H_2O$	0.888	0.1523
-above + Na_2SO_4	$Mg_4Al_2(OH)_{12}SO_4.mNa_2SO_4.nH_2O$	1.121	0.1523
Occlusion through anion exchange reactions			
NO_3-HT	$Mg_4Al_2(OH)_{12}(NO_3)_2.1.5H_2O$	0.883	0.1522
-above + Na_2SO_4	$Mg_4Al_2(OH)_{12}SO_4.mNa_2SO_4.nH_2O$	1.122	0.1522
$B_3O_3(OH)_4$-HT	$Mg_4Al_2(OH)_{12}(NO_3)_2.1.5H_2O$	1.072	0.1521
-above + K_2SO_4	$Mg_4Al_2(OH)_{12}SO_4.mK_2SO_4.nH_2O$	1.122	0.1521

In the XRD patterns of the products obtained by all three types of occlusion of Na and K sulphate, the MgAl-SO_4 HTs with d_{003} = 1.12 nm were registered. These values are in agreement with previously published d_{003} values of natural MgAl-SO_4 HTs with high content of interlayer water molecules and occluded Na_2SO_4 [3]. However, after additional washing of the occluded samples, in the XRD patterns the phase with d_{003} = 0.889 nm only was observed. It can be concluded that the occlusion and extraction of the sodium and potassium sulphate salts are reversible processes and depend on the concentration of sulphate salts in the solutions and on the washing process.

In the case of occlusion of the sulphate salts of divalent cations (Mg, Ni, Zn, Co, Cd, Mn etc.) it should be taken into account the order of selectivity of divalent cations in the hydrotalcite: Mg<Mn<Cd<Co≈Ni<Zn, because the occluded cations may affect the composition of the host structure [5].

[1] Barrer, R.M (1982) *Hydrothermal chemistry of zeolites.* Academic Press, London. [2] Bish, D.L. & Livingstone, A. (1981) *Mineral. Mag.*, **44**, 339-343. [4] Drits, V.A. et al. (1986) *Clay. Clay Miner.*, **35**, 401-417. [4] Lisitzina, N.A. & Drits, V.A. (1985) *Litol. Polez. Isop.*, **6**, 20-39. [5] Stanimirova, Ts. & Kirov, G. (2003) *Appl. Clay Sci.*, **22**, 295-301

Thermal transformation of chrysotile asbestos

Uehara, S.[1*], Takai, Y.[1] & Mashima, H.[2]
[1]Dept. of Earth and Planetary Sciences, Faculty of Sciences, Kyushu University, Fukuoka, Japan
([*]uehara@geo.kyushu-u.ac.jp)
[2]New Material Research Institute Co. Ltd, Tokyo, Japan

Chrysotile is a fibrous form of serpentine. Thermal reactions of chrysotile have been extensively investigated (see, e.g. [1]), and thermal treatment is a possible method of converting the material into less hazardous form [2].

Differential thermal (DTA) and thermogravimetric (TGA) analyses were made simultaneously on a SII NanoTechnology SSC/5200 thermal analyzer using 20 mg samples. A JEOL JEM-3200FSK instrument was used for transmission electron microscopy (TEM), scanning electron microscopy (STEM) and electron diffraction analysis. Thermal transformation of chrysotile from Thetford Mines-Black Lake, LAB Chrysotile Mine, Quebec, Canada, were heated to 1000ºC in dry conditions (N_2) at a rate of 10 º/min for DTA/TG analysis was studied by TEM, STEM with EDS and selected area electron diffraction (SAED).

Morphological changes of many fibrils were observed (Fig. 1). The dehydration products have generally irregular to granular shape and a few other grains show fibrous morphology. Chemical analysis of the thermal products show intermediate compositions of forsterite and enstatite, which means that very tiny grains of enstatite were formed together with forsterite (Fig. 2). The SAED pattern is complex due to the coexistence of forsterite, enstatite, and amorphous areas.

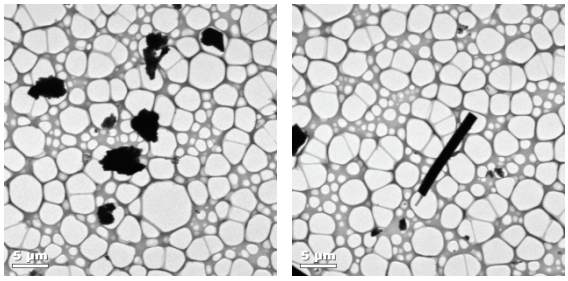

Fig. 1: TEM images of chrysotile asbestos after DTA/TG analysis. (a) granular shape grains. (b) fibrous morphology.

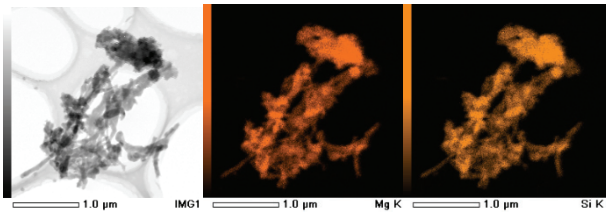

Fig. 2: STEM image (a) of chrysotile asbestos after DTA/TG analysis up 1000ºC and X-ray mapping images for Mg*K*α (b) and Si*K*α (c).

[1] Souza Santos, H.D. & Yada, K. (1979) *Clay. Clay Miner.*, **27**, 161-174. [2] Gualtieri, A.F. et al. (2008) *J. Hazard. Mater.*, **152**, 563-570.

Globular phyllosilicates of the Lower Riphean Ust'-Il'ya Formation, Anabar Uplift, Northern Siberia – crystallochemical and isotope data

Zaitseva, T.S.[1*], Gorokhov, I.M.[1], Ivanovskaya, T.A.[2] & Melnikov, N.N.[1]
[1]Institute of Precambrian Geology and Geochronology, RAS, St. Petersburg, Russia ([*]tatiana.s.zaitseva@gmail.com)
[2]Geological Institute, RAS, Moscow, Russia

Geological interpretation of K-Ar and Rb-Sr dates for globular phyllosilicates has been an important task since the 1950s, when these minerals have received wide acceptance as isotopic geochronometers. In many cases, the results agreed well with biostratigraphic data or with the ages of associated igneous rocks. But along with such data, there were overestimated or "rejuvenated" age values, and it was necessary to explain them and find criteria assuring suitability of globular phyllosilicates for dating. The structural simulation together with the Mössbauer data for globular phyllosilicates enables to estimate, whether the cation distribution in their crystal lattice is primary or resulted from post-diagenetic transformation of the mineral structure. The efficiency of such approach has been demonstrated by the examples of globular phyllosilicates of the Lower Riphean Ust'-Il'ya Formation, Anabar Uplift.

The modeling is based upon the following concept of glauconite formation. It is supposed [1,2], that an unordered distribution of the octahedral cations is typical for the newly formed glauconite. At this point atoms of the ^{40}Ar and ^{87}Sr inherited from a mineral-precursor do not leave glauconite structure yet. Only at the final stages of glauconite formation involving significant increase of the K content, the cation ordering occurs in the octahedral layer. The ordered distribution appears to result from a layer-by-layer dissolution-precipitation process. The redistribution of the cations in all glauconite layers should result in expulsion of radiogenic ^{40}Ar and ^{87}Sr alien to the mineral structure and in startup of the "radioactive clock", based on the decay of ^{40}K and ^{87}Rb. If such a glauconite is free from secondary alteration, its isotope date should correspond to the timing of early diagenesis, i.e. should be close to the stratigraphic age.

Globular phyllosilicates of the Ust'-Il'ya Formation are characterized by the ordered cation distribution in the structure formed at the stage of early diagenesis of the sediments. This means that the Ust'-Il'ya globular phyllosilicates appeared to undergo no important chemical and structural transformations which could result in loss of radiogenic ^{87}Sr and ^{40}Ar. The Rb-Sr isochron age (1483±5 Ma) and K-Ar dates (1459±10 Ma) of these minerals [3] do correspond to the Lower Riphean. An agreement between the stratigraphic position of glauconites and their isotope ages suggests that the Rb-Sr and K-Ar systems of minerals were not seriously distorted since the early diagenesis.

Acknowledgments: This study is a contribution to Programme No. 4 of the Earth Sciences Branch of the Russian Academy of Sciences. The financial support of the RFBR (grant 09-05-00877) is acknowledged.

[1] Gorokhov, I.M. et al. (1995) *Lithol. Miner. Resour.*, **30(6)**, 556-571. [2] Clauer, N. et al. (1992) *C. R. Acad. Sci. Paris, Ser. II*, **315,** 321-327. [3] Gorokhov, I. et al. (1991) *Int. Geol. Rev.*, **33(8)**, 807-821.

Historical minerals from the Evje-Iveland pegmatites at the Natural History Museum in London

Müller, A.[1*], Rumsey, M.[2] & Ihlen, P.[1]
[1]Geological Survey of Norway, Trondheim, Norway
([*]Axel.Muller@ngu.no)
[2]Natural History Museum, London, UK

The granitic pegmatites of Evje-Iveland in southern Norway have attracted the attention of mineralogists for more than a century due to the large number and extraordinary crystal size of rare metal-containing minerals. Many of these, such as the scandium-bearing mineral thortveitite, were first discovered and described from localities in this district. Mineral collectors became fascinated by exotic minerals, such as thortveitite and the local farmers, who mined the pegmatites for feldspar, soon realised an opportunity to improve their income by selling specimens. Through farmers and then more professional mineral dealers, it was not long before these rare minerals began to appear in both public and private mineral collections worldwide. As part of the EU Synthesys project GB-TAF-5516 – a collaboration project between the Geological Survey of Norway and the Natural History Museum (NHM) in London – the mineral specimens from Evje-Iveland in the NHM collection and their history were studied. About one hundred high quality mineral specimens from the Evje-Iveland pegmatite district are registered in the collection, including specimens of beryl (n=15), thortveitite (12), aeschynite-(Y) (12), gadolinite (8), ilmenorutile (8), monazite (7), euxenite (4), columbite (3) and tveitite-(Y) (2) and other more common minerals.

The oldest mineral specimen from Evje-Iveland is a giant topaz crystal that weighs about 60 kg and is ca. 48 x 33 x 20 cm in size. It was purchased from Christiania Bergbureau of Norway in 1901 for 27 pounds 11 shillings and 11 pence, which was a considerable amount of money at the time. It is remarkable that even before the first scientific description of the Evje-Iveland minerals by Brøgger [1], the NHM collection had already obtained a beautiful topaz specimen from the region.

Besides interesting early Evje-Iveland specimens, the NHM collection also contains some important scientific specimens, including sample BM 1908,74 registered as an ilmenorutile which was described and analysed by W.C. Brøgger in 1906 [1]. In his article, Brøgger used the specimen to determine that ilmenorutile was distinct from rutile and at that time should be considered a separate species. Since this time, there has been much controversy over the classification of ilmenorutile which was eventually concluded in its discreditation as a mineral species in 2006.

One of the most famous minerals of the region is thortveitite, which is one of only three terrestrial minerals known to contain a large quantity of scandium (>20%). It was first described by Jacob Schetelig in 1911 [2] from the Ljosland mine in Iveland and is named after the Norwegian feldspar trader Olaus Thortveit who operated this pegmatite mine. The first two thortveitite specimens obtained by the NHM were purchased in 1914. It should be noticed that only three years after the first description of thortveitite, two high quality specimens had already been purchased by the museum in London.

These and other examples illustrate the historical and scientific importance of the rare minerals from Evje-Iveland pegmatite district.

[1] Brøgger, W.C. (1906) *Videnskaps-Selskapet i Christiania*, **1/6**, 1-162. [2] Schetelig, J. (1911) *Centralblatt für Mineralogie, Geologie und Palaeontologie*, 721-726.

Early 19th century scientific networking – a study in Jacob Berzelius' mineral collection

Langhof, J.
Dept. of Mineralogy, Swedish Museum of Natural History, Stockholm, Sweden (jorgen.langhof@nrm.se)

Jacob Berzelius (1779-1848), one of the most renown chemists of all times, is credited, among others, for the discovery of four new elements (Ce, Se, Th, and Si), establishing the today-used chemical symbols system, and coining chemical terms such as catalysis, protein, isomerism etc. But not to forget, he is also the founder of modern systematic mineralogy, introducing a chemical classification of minerals in 1814.

From the early 1800's up to his last year of life, he accumulated a mineral collection of nearly 2,400 specimens from all over the world. His mineral collection was donated to the Swedish Museum of Natural History (SMNH) in 1848, then a part of the Royal Swedish Academy of Sciences in Stockholm, were he acted as Secretary for 30 years. This is today part of the museums' vast systematic mineral collection and it is kept with the original hand written labels of Berzelius. His collection contains the holotypes of acmite, aeschynite-(Ce), thorite (and hence of the element thorium!), and the "proto-holotype" of xenotime-(Y). Also many of his original published mineral analyses are based on specimens from his own collection.

Berzelius was a prolific correspondent and wrote and received thousands of letters from several hundreds of scientists, industrialists, physicians, politicians etc. Many of the important correspondences have been published over the years (for example with Wöhler, Berthollet, Goethe, Davy, and Rammelsberg). Berzelius field-collected himself and received mineral specimens as gifts or in exchange; he usually documented from whom, on the labels.

During the digitalization of the catalogues at the Department of Mineralogy at the SMNH, a detailed survey on donations of collections has been performed. And by a more thorough study of Berzelius' original labels, we have been able to establish many of his sources for mineral specimens, not always traceable in the preserved letters from archives. Many famous names known from the mineral realm have been thus revealed: Cordier, Zinken, Stromeyer, Haüy, Brewster etc. The work on the important Berzelius mineral collection will continue; we plan to publish the final results in the near future.

The scientific heritage and biography of Friedrich Martin Berwerth (* 16.11.1850, Sighişoara, Romania – † 22.9.1918, Vienna, Austria)

Hammer, V.M.F.[1*], Pertlik, F.[2] & Seidl, J.[3]
[1]Dept. of Mineralogy and Petrography, Museum of Natural History, Vienna, Austria ([*]vera.hammer@nhm-wien.ac.at)
[2]Institute of Mineralogy and Crystallography University of Vienna, Geozentrum, Vienna, Austria
[3]Archive of the University of Vienna, Austria

F. M. Berwerth was born on the 16th of November in 1850 in Sighişoara (former Hung.: Segesvár, Germ.: Schäßburg), Romania, as the son of the pharmacist F. Berwerth. There he visited the protestantic secondary school. In 1869, already one year before school leaving examination, he was graduated an adjunct in pharmacy. Since then he matriculated at the University of Vienna and later on in Graz, where he finished pharmacy in 1872. For postgraduate studies he went to Heidelberg, where he obtained his PhD in chemistry within one year only. His teacher was Robert W. Bunsen (1811–1899).

His scientific career started in 1874, when he became employee of G. Tschermak-Seysenegg (1836–1927) at the University of Vienna and in the same year he became an assistant at the Imperial Mineralogical Cabinet. The following years he chiefly worked as analyst of minerals together with E. Ludwig (1842–1915).

In 1884 he married E. Frankel (1860–1936), a niece of the geologist E. Suess (1831–1914). They raised three children.

The transfer of the mineral collection from the Imperial Royal Mineralogical Court Cabinet – originally hosted by the Imperial Palace to the new Imperial Museum of Natural History building situated on the Viennese "Ringstrasse" – was mainly performed by F. M. Berwerth together with director M. A. Brezina (1848–1909). F. M. Berwerth oversaw the revision and re-numbering of more than 108,000 mineral specimens. In 1888 F. M. Berwerth was nominated as curator I. class and in this function he was the man in charge of the new scientific presentation of the mineral-, the rock- and the meteorite collection. Since 1896 he was the head of the Mineralogical-Petrographical Department of the Imperial Museum but he was designated as the director around the year 1904.

F. M. Berwerth´s research interests changed from mineral chemistry to petrography and geology, followed by the classification of meteorites. His scientific work is reflected in more than 150 scientific papers about regional petrography, geology and about meteorites, as one of the main fields of his personal interest. In this context, he was author of "Fortschritte in der Meteoritenkunde" and "Mikroskopische Strukturbilder der Massengesteine", a benchmark for students.

With the petrographic description of the rocks from Jan Mayen Island collected during the Austrian Polar Expedition he got the postdoctoral lecture qualification for Petrography at the University of Vienna in 1888 and became professor in 1907.

F. M. Berwerth did a lot of collecting field trips; among others he started the geological mapping of the Hohe Tauern in Austria in 1892 while the construction of the Tauern-Railway was in progress.

F. M. Berwerth was honoured by the Austrian Emperor, as well as by the king of Spain and he became elected member of the "Imperial Academy of Science". Berwerth was a founder of the Austrian (former Viennese) Mineralogical Society as well as an originator of the German Mineralogical Society.

F.M. Berwerth died in 1918 shortly after his retirement.

[1] Hammer, V.M.F et al. (2009) *Berichte der Geologischen Bundesanstalt*, **45**, 16-17.

Rock samples from World War I in the collections of the Prussian Geological Survey (PGLA)

Ehling, A.
Federal Institute for Geosciences and Natural Resources, Berlin, Germany (angela.ehling@bgr.de)

When preparing the digital documentation of the non-displayed collection at the German Geological Survey in Berlin, Germany, we came across a sizeable suite of samples (more than 700 pieces) from the Balkan region, which had been collected between 1914 and 1918 by the staff of the Prussian Geological Survey.

This discovery represented the starting point of a study on whether and how these samples reflect the events of World War I (WWI), specifically the activities of German geologists during this historical period.

Some of Germany's objectives during the WWI were the conquest of ore-rich regions of France and Luxembourg, as well as military, political and economic control over Belgium, which would have provided access to its mineral-rich colonies in Africa. At the beginning of WWI, Germany founded a "War Raw Material Department". Its original task was to establish an inventory of mineral deposits in Germany, later on expanded to industrial mineral deposits from regions conquered for war economic purposes, such as phosphate, graphite, fluorite and asbestos.

From the collection of about 700 samples that was under investigation, about one third of the samples originated from abroad: France (Alsace-Lorraine), Belgium, Serbia, Ukraine, Turkey and Congo. These samples partly reflect the period's exploration efforts, including reports documenting the 'usable' deposits in Belgium [1] and Serbia [2], especially coal, phosphor and iron.

This material apparently was of great importance to the military at the time. A new name, *i.e.* "War geology" was thus born, and "War geologists" took part, after the war, to the negotiations from Brest-Litowsk [3] (with the purpose to obtain mineral ores, coal and oil from Ukraine) aimed to establish the damage produced by the German army during the war in mining regions of France [4].

[1] Krusch, D.P. (1916) *Die nutzbaren Lagerstätten Belgiens, ihre geologische Position und wirtschaftliche Bedeutung*. Essen. [2] Krusch, D.P. (1917) *Die nutzbaren Lagerstätten Serbiens und ihre wirtschaftliche Bedeutung für die Zentralmächte*. Metall und Erz, XIII (N.F.IV.), 4, Sonderdruck, Halle. [3] Stensland, H. (2009) *Der Anschnitt*, **61**, 255-273. [4] Udluft, H. (1968) *Beih. Geol. Jb*., **78,** 1-170.

The concept of mineral evolution in Russian mineralogical literature (1979–2008)

Krivovichev, S.V.
Dept. of Crystallography, St.Petersburg State University, St. Petersburg, Russia (skrivovi@mail.ru)

A recent paper on mineral evolution [1] and the subsequent series of papers in the February 2010 issue of 'Elements' [2] attracted considerable attention on this subject from both professional and popular scientific circles.

However, for the sake of historical truth, it is worthy to indicate that the very idea of mineral evolution was under consideration in Russian mineralogical literature as early as 1979 [3], when the late A.G. Zhabin considered different aspects of mineral evolution and subdivided three major periods of this development: "meteoritic", "basaltic" and "corous". He also emphasized the importance of this concept in the elaboration of evolutionary mineralogy of our planet, "…which will be the source of new ideas and predictions in the study of mineralogy of other planets of the Sun System". Later, N.P. Yushkin, D.V. Rundqvist, D.P. Grigoriev and others [4-6, etc.] suggested distinguishing between phylogeny and ontogeny of the mineral world with the note that "ontogeny is a brief repetition of phylogeny". A highly original but rather controversial paper [7], investigated the evolution of minerals from the viewpoint of the evolution of their structure types. A.P. Khomyakov and N.P. Yushkin formulated basic principles of inheritance (or heredity) in the mineral world [8]. Later, N.P. Yushkin (2004-2008) emphasized the importance of coevolution of the biosphere and the mineral world.

It is thus obvious that the concept of mineral evolution did not start in 2008 [1] as announced in the February 2010 issue of "Elements", but was under serious consideration at least 30 years prior to its publication in the Western literature.

[1] Hazen, R.M. et al. (2008) *Am. Mineral*., **93**, 1693-1720. [2] Hazen, R.M., (2010) (ed.) *Elements*, **6**, 9-46. [3] Zhabin, A.G. (1979) *Dokl. AN SSSR*, **247**, 199-202 [Engl. Translation in: *Dokl. Earth Sci. Sect.*, **247**. Am. Geol. Inst.]. [4] Yushkin, N.P. (1982) *Zapiski VMO*, **111**, 432-442. [5] Yushkin, N.P. (1990) *The XVth Gen. Meeting of the IMA*. Beijing, 1990, **1**, 127-129. [6] Rundqvist, D.V. & Marin, Yu.B. (1985) (eds.) *Minerals, Rocks and Mineral Deposits in Geological History*. Leningrad, Nauka (in Russian). [7] Smirnova, N.L. & Belov, N.V. (1979) in: *History and Methodology of Natural Sciences*. Moscow, 94-102. [8] Khomyakov, A.P. & Yushkin, N.P. (1981) *Dokl. AN SSSR*, **256**, 1229-1233 [Engl. Translation in *Dokl. Earth Sci. Sect.*, **256**, Am. Geol. Inst.].

Jean-Pierre Alibert (1820–1905): when science becomes art

Touret, L.
Musée de Minéralogie, Mines-ParisTech, Paris, France (lydie.touret@mines-paristech.fr)

In the early XIXth century, a French fur merchant at the court of the Russian tars, Jean-Pierre Alibert (1820–1905) was given the permission to prospect for new mines in Siberia. He was first looking for gold, with significant results, but found in 1840 traces of graphite. He was already aware of the fact that Cumberland mines, since 1550 the only producer of quality graphite for art pencils, were close to exhaustion. He then engaged all his strength, as well as a considerable amount of money, for finding the graphite source. After several frustrating years, excavating thousands of cubic meters of hard rock, he finally discovered an incredible graphite seam occurring in alkaline syenite on the top of the remote Mount Botogol, roughly 500 km west of Irkutsk. With the help of the local Saïoute people, he opened a mine, "Siberian graphite" becoming soon a reference for the rest of the world. He also found nearby huge boulders of nephrite, this being the first discovery of this jade variety outside of China.

Alibert left abruptly Siberia in 1865, having secretly sold his mine and related rights to the German Faber who, together with few other competitors, notably Hardtmuth from Austria, became the best specialists in quality pencils. Botogol was at this time very close from the Chinese border, and names like Koh-I-Noor, or pencils painted in yellow, as Hardtmuth did in 1889, were clear references to the "Siberian (or Chinese) graphite". Still to-day, 80% of all pencils sold in the USA are yellow.

Alibert took to Paris the best pieces of graphite, carefully selected during the 10 years of his mine management, together with a number of minerals or animals, all representative for Siberia. Being an admirer of Napoleon III and Alexandre II, he produced in their honour elaborate, very artistic trophies, mainly made of exquisitely carved graphite. These trophies were exhibited (and awarded) at several World Exhibitions, then presented to the most famous educational institutions: in Paris, to Conservatoire des Arts et Métiers, Museum d'Histoire Naturelle, Sorbonne university and, finally, Ecole des Mines. He left behind also a unique book, "Souvenir de Sibérie", containing 146 aquarelles depicting all the stages of his travel between Saint-Petersburg and Mount Botogol, and the most spectacular aspects of Siberian life style.

Incidentally, the Botogol deposit has proven to be not only of best quality ever, but also to contain a number of interesting trace elements (germanium, silicon). Former Soviet authorities did classify this deposit as having strategic importance; its location and existence were thus almost forgotten, but not the name of Alibert by local people, who, hoping on his return, maintained the Botogol village until the beginning of the XXth century. Alibert is now considered as a national hero in the newly independent Bouriatian republic, being also rediscovered in his own home country after a long period of oblivion.

CSI mineralogy: fakes, frauds and shoddy science

Kampf, A.R.
Mineral Sciences Dept., Natural History Museum of Los Angeles County, Los Angeles, California, USA (akampf@nhm.org)

Minerals are, by definition, naturally formed. Their distinctive properties, appearances and modes of occurrence have made them objects of both wonder and scientific interest. As collectables, they formed an important component of the cabinets of curiosities of Renaissance Europe that eventually morphed into today's natural history museums. It is the fascination with the natural beauty of minerals that has ironically tempted some to use unnatural means to enhance that beauty.

The fakery of mineral specimens, including attaching crystals to matrix, cutting and polishing faces, adding color, bending and shaping wires, synthesizing crystals, and ascribing incorrect locality information has been going on for hundreds of years and there is certainly not a major mineral collection in the world that contains no fakes. Of course, there are a variety of motives for faking specimens, some perfectly ethical, but when the motive is to deceive, especially for personal gain, the practice becomes fraud.

Mineralogical fraud is most dangerous when it directly enters the scientific arena, where it is manifest as manufactured minerals and manufactured or intentionally mishandled data. An important rationale for requiring the deposition of type specimens in institutional collections is that they allow others to corroborate the physical existence, natural occurrence and described properties of the minerals. Unfortunately, it is sometimes the case that researchers are not meticulous in their designations of type specimens and deposit specimens that they merely sight-identified and, in the worst case, that don't even contain the described minerals.

Natural history museums are, first and foremost, repositories for natural objects. It is the responsibility of museum curators to uncover mineral fakery, fraud and shoddy scientific practice in order to maintain the integrity, authenticity and scientific reliability of their collections.

Winestone, limestone and rhinestone – examples of low-budget educational museum projects

Schumacher, R.
Mineralogisches Museum, Steinmann-Institut, University of Bonn, Germany (R.Schumacher@uni-bonn.de)

The following are examples of museum projects that were carried out on a minimal budget and – at the same time were meant to educate lay people about and fascinate them with geoscientific topics. The two most common winestone crystals, potassium hydrogen tartrate ($KHC_4H_4O_6$) and calcium tartrate tetrahydrate ($CaC_4H_4O_6 \cdot 4H_2O$) are well-known to the wine connoisseur: they appear like small pieces of broken glass in the "last drops" of a bottle of good quality wine. This project combined crystallographic research [1] with a museum exhibit, thus using an object encountered in daily life to introduce mineralogical themes like crystal structures and chemical reactions.

In a project within the German network "Steine-in-der Stadt" ("Rocks in the city") [2], the building stones of the cathedral of Bonn were presented to the public on the nationwide "Day of the building stone". On demand, tours were offered from a booth in front of the cathedral. Participants learned about traditional regional building stones and their geological history. One of these building stones is a limestone; the quarried material used to be deposited in a Roman aqueduct leading from the northern Eifel to Cologne. Among other rocks, this local limestone was used in the project to build a "bridge" between geology and local history.

A rhinestone is a simulated diamond made of quartz, glass or plastic. Rhinestone is also known as strass, named after the Alsatian jeweler Georg F. Strass, who imitated diamonds by coating the lower side of glass with metal powder. In an exhibit on "Real or fake" presented on the Gem and Mineral shows in Denver, Colorado and Tucson, Arizona, a replica of the Bavarian crown (Fig. 1) with rhinestones and other imitations of gemstones was the center piece of an exhibit with various real gemstones and their "fake" equivalents and helped to explain imitations of gemstones and artificial/synthetic products.

Fig. 1: Replica of the Bavarian Crown.

[1] Barbier, B. & Euler, H (2000) *Powder Diffr.*, **15**, 175-179.
[2] http://www.geo.tu-berlin.de/steine-in-der-stadt/

The Teck Suite of Galleries: Earth's Treasures at the Royal Ontario Museum, Toronto, Canada

Tait, K.T.
Dept. of Natural History, Royal Ontario Museum, Toronto, Canada (ktait@rom.on.ca)

The Royal Ontario Museum (ROM) opened in 1914 and is located in Toronto, Ontario, Canada. It is Canada's largest museum of world culture and natural history objects, with over 6 million objects and over 40 galleries. Showcasing exceptional mineral, gem, rock and meteorite specimens, the Teck Suite of Galleries: Earth's Treasures is one of the ROM's newest galleries. The 2,100 m^2 combined gallery space is divided into the Vale Inco Limited Gallery of Minerals, the Canadian Mining Hall of Fame Gallery and the Gallery of Gems and Gold.

The Vale Inco Limited Gallery of Minerals**,** the largest gallery in the Teck Suite of Galleries, presents the ROM's exceptional specimens of minerals, meteorites and rocks, exploring such areas as the classification of minerals, their physical and scientific properties, causes of mineral colour and the geological environments necessary for mineral growth. This gallery features the ROM's renowned meteorite collection, including one of the biggest lunar meteorites on display in the world, as well as the Tagish Lake meteorite, a rare carbonaceous meteorite that fell in Canada in 2000.

This gallery employs a new interactive touch-screen labeling system in lieu of conventional printed specimen labels. Each case is flanked by computer kiosks, 42 stations in total, containing high resolution images of the minerals and detailed information about the items displayed in the case or elsewhere in the gallery. This sophisticated labeling technology allows visitors to pinpoint where specimens are located within each case as well as in the gallery. The label script can also be enlarged for ease of reading and is in French and English. The high resolution photography of each of the minerals, combined with the zoom-in feature of the system, allow visitors to appreciate each item's intricate details. This kiosk system also allows us to present different layers of information to the visitor. The casual visitor who is only interested in the aesthetics of the minerals, can casually walk through the gallery, taking in the beauty of minerals without being bombarded with information. Whereas the more inquisitive visitor can spend time on each mineral, learning such information as the locality where it was discovered, its chemical formula, crystal structure and any other information and quick facts we would like to highlight.

The Gallery of Gems and Gold is a 245 m^2 room specially-designed to highlight gems, crystals and precious metals. Highlighted in the gallery is the 898-carat "Light of the Desert", the largest faceted cerussite gem in the world.

The Canadian Mining Hall of Fame Gallery showcases the importance of the mining industry in our everyday lives and highlights the exceptional contributions of Canadians to this industry. A 4.5 x 1.8 m fully bilingual, interactive video wall controlled by two computer kiosks located in front, dominates this area. Divided into two sections, the left side portrays the biographies and personal stories of the Canadian Mining Hall of Fame inductees. On the right of the screen, a presentation explains how mining touches every part of our lives and short videos explore a variety of minerals such as silver, titanium and zinc.

A new Romanian meteorite, from a museological perspective

Pop, D.[1*], Benedix, G.[2], Ionescu C.[3], Har, N.[3] & Benea, M.[3]
[1]Museum of Mineralogy, Babeş-Bolyai University, Cluj-Napoca, Romania ([*]dana.pop@ubbcluj.ro)
[2]Dept. of Mineralogy, Natural History Museum, London, UK
[3]Dept. of Mineralogy, Babeş-Bolyai University, Cluj-Napoca, Romania

On June 12, 2008 (21:45 hrs local time), a bolide was observed by eye witnesses crossing the skies of 6 counties (spanning along 325 km distance) in south Romania. Locally, the event was accompanied by sonic booms [1]. The fireball was white-green and very brilliant; it had a W-E trajectory, at an angular height of 35–40º above the horizon (report on "Urbi et Orbi" homepage, by V. Ghincolov). A fragment of 6.913 kg landed in a private garden in Pleşcoi village (Buzău County, Romania), at 12-15 m distance from an eye-whiteness. In November 2008, the complete sample was sent by the finder (M. Popescu) to the Museum of Mineralogy at Babeş-Bolyai University. On December 2008, the new fall was announced in specialized circles by the Romanian meteorite collector A. Răzvan.

The specimen shows a dull, black, fusion crust patched by a thin network of cracks. The flat, basal surface exhibits some lighter-coloured strips and parallel thread-like lines marked by drops of melt (Fig. 1). The first investigations on the new meteorite used nondestructive methods, only, *i.e.* tomography and X-ray fluorescence measurements, and additional 3d-modelling techniques. In January 2010, the material was investigated further at the Natural History Museum in London by means of optical microscopy and electron microprobe (EMP), among other thechniques.

Fig. 1: Surface features on the flat base of Pleşcoi meteorite.

These studies showed that chondrule outlines are obscure under the optical microscope, but more discernable in back-scattered electron (BSE) images. Recognizable chondrule types include barred olivine and radiating pyroxene. The fusion crust is up to 2 mm thick; it is enriched in opaque minerals, displayed along fissures and cleavage planes within silicates. The matrix is fully recrystallized; brecciation is not obvious. Fe,Ni metal and troilite (FeS) grains are relatively fresh, sometimes with thin weathering rims. Olivine exhibits undulatory extinction, but no shock veins. The main non-metallic minerals, identified by EMP, are olivine ($Fa_{25.5\pm0.3}$), low-Ca pyroxene ($Fs_{21.4\pm0.1}$; $Wo_{1.3\pm0.2}$), and chromite (Cr/Cr+Al=0.85; Fe/Fe+Mg=0.86). Based on these features, the "Pleşcoi" meteorite, has been classified as an ordinary chondrite (L5-6), with S2 shock stage and W1 weathering grade.

On May 15, on the occasion of the Night of Museums 2010, a new exhibition will be inaugurated, having the Pleşcoi meteorite and its fall and research history as main focus.

Acknowledgements: This research received support from the SYNTHESYS Project http://www.synthesys.info/ which is financed by European Community Research Infrastructure Action under the FP7 Integrating Activities Programme.

[1] Pop D. (2008) in Bucur, I.I. & Filipescu, S. (eds.) *Contrib. Ann. Sci. Sess. "Ion Popescu Voiteşti"*. Cluj-Napoca. Cluj University Press, 53-56.

Study on digital technology applied to minerals and museums

Yang Liang-Feng
The Geological Museum of China, Beijing, China
(yanglf@mail.gmc.org.cn)

Minerals and museums are two traditional topics of interest; their combination gave birth to mineral museum. As in the case of other similar institutions, mineral museums acquire, preserve, study, communicate and exhibit the tangible and intangible mineralogical heritage of humanity and its environment for purposes of education, study and enjoyment. Digital technology transfers these functions of mineral museums from reality into the immense virtual space. Thus, it brings vitality and intensity of expression to museums, and establishes another type of museums, *i.e.* the digital museum, which exists in the virtual world on the web. Many organizations or museums have been constructing and developing such digital museums, for example the Virtual Heritage Network (USA), the European Cultural Heritage Network, the Globe Digital Museum (Japan), the Platform of Modern Distance Learning (China), the National Infrastructural Natural Resource (China), the China Digital Science and Technology Museum, the National Digital Museum (China), the National Digital Archives Program (China, Taiwan) etc.

For mineral museums, in the real as well as in the virtual world, mineral specimens and knowledge on their mineralogy represents the core of the displays. In a real museum, it is a fact that some minerals might be destroyed due to physical changes triggered by the lightning conditions of the display; some minerals are difficult to display because of their very small sizes; while too many minerals never have a chance to be on display because of the limitations of the display space. Virtual reality technology provides potential powerful solutions to rebuild the appearance and shape of natural specimens in the virtual world, as virtual minerals; thus, these virtual minerals could be displayed with no limits. Nevertheless, because mineral usually are composed of many crystals and one single crystal shows many crystal faces with different orientations, image capture and shape reconstruction may be difficult procedures. The capture manner and the reconstruction technology, as well as the light used for capture are important factors which should be taken into consideration.

Like in the case of museums in the real world, the attractivity of digital museums arises from their content and display manner. The content of a digital mineral museum should be represented by scholarly information data as well as by more practical information for non-specialists. Scholarly information may relate to databases of scholarly knowledge, research results and specimen images. Non-expert information may link to databases of basic professional information on specimens, publicly-intelligible science illustrations, and multimedia courseware. The first data type supplies professionals with systematic mineralogy knowledge in order to assist mineralogical teaching, research and mineral mining, as assistant tools. The language used in this case should be learned, precise and unadorned. The second type of information provides the society with easily-understandable mineralogical knowledge; this should be acquired *via* interactive display systems that allow scientific knowledge to be communicated to the public in an interactive way. In this case, the language has to be popular, accessible, artistic, as well as joyful and playful. These two kinds of information can be transferred by implementing up-to-date information technology which is currently rapidly-developing.

Lorenz Oken and his mineralogical activities in Jena, Germany

Kreher-Hartmann, B.
Mineralogical Collection, Dept. of Geoscience, Friedrich-Schiller-University of Jena, Germany (cbk@uni-jena.de)

Lorenz Okenfuß (1779-1851), known as Lorenz Oken, was notorious as physician and philosopher, member of the Leopoldina and first principal of the University of Zürich, Switzerland. He edited the journal “Isis” between 1817 and 1822, which was one of the most significant journals for natural science in the early 19th century. But not much was written about his mineralogical activities, although von Kobell named a mineral - O(c)kenite - after him.

Oken spent in Jena 17 years in total, with the main focus on mineralogy at that time. During the first period, from 1807 to 1819, he had been appointed the position of honorary professor for Medicine and Pharmacy. Due to his scientific work in the field, he was acknowledged as ordinary professor for Natural Science in 1812. He held his lectures in the zoological cabinet because of some dissents with J.G. Lenz, who had been the professor for mineralogy in Jena at that time. The main dissagreement concerned the arrangement and system of minerals. Oken preferred a system of five groups, oriented more on the philosophical side. He considered mineralogy as “Irdlehre” (eng. „understanding of the Earth), while Lenz had been an autodidact, non-critical scholar of the theories of A.G. Werner in Freiberg, Saxony. Oken published only a few books. One was entitled „The natural system of the ores”, another one was dedicated to explaining the concept of Natural Science. He used this concept as the basis for his lectures. As opposed to Lenz, he tried to combine new chemical knowledge with the tradititional describing parts of mineralogy.

But not only mineralogy filled his time. He got involved with the uprising of the students and attended the „Wartburgfest”. Together with his political work, his activities had been no longer tolerated and he had been released in 1819. This was decided by J.W. von Goethe, who acted as a minister at that time and was in response to the request of the University of Jena.

After three years of absence, in 1822 Oken came back to Jena as a private scholar and worked with his system of philosophical aspects on mineralogy. He tried to rename minerals and physical characteristics of minerals based on his views, but in the end he failed. Thus, after another five years, he left Jena for ever.

The rediscovery of the "French Blue" diamond

Farges, F.[1,2*] & Sucher, S.[3]
[1]LMCM, Muséum national d'Histoire naturelle, Paris, France
([*]farges@mnhn.fr)
[2]Dept. of Geology and Environmental Sciences, Stanford University, Stanford, CA, USA
[3]The Stonecutter, Tijeras, NM, USA

Within the collections of the Muséum national d'Histoire naturelle, Paris, an unknown lead cast of the "French Blue" diamond (FB), the mythic-, 69 carats-, deep-blue diamond of the French crown jewels [1] was identified. FB was stolen in 1792, and then set in an amazing jewel, the Golden Fleece. Both had never reappeared.

The lead cast was laser-scanned, in order to reveal details in the precious stone's cut. Based on this 3D information, we have assumed for the first time that FB was subsequently recut into the "Hope" diamond. This lead cast was probably donated around 1815 to Haüy by "Mr Achard", the highest authority in gems from Paris at that time. Achard wrote that "Mr Hoppe of London" possessed the original diamond, i.e., the FB. Would it have been possible that Achard and/or Haüy, the founders of scientific gemmology, had confused the FB with the "Hope" diamond? This second discovery suggested instead unsuspected connections of H.-P. Hope with the FB. This is consistent with historical reports suggesting that one of the 1792 thieves, Cadet Guillot, brought the Golden Fleece to London in 1796, when H.-P. Hope started to inherit his parent's immense fortune. But between 1808–1813 H.-P. Hope had severe financial problems, thus the diamond has most likely been pawned to D. Eliason, a London jeweller, who had it recut in 1812. Nevertheless, the recut diamond reappeared within Hope's collection near 1830 when his fortune was back.

Optical spectroscopy for the "Hope" diamond, kindly provided by J. Post (Smithsonian) was used to virtually recreate the FB, based on its 3D laser data. Remarkably, the brilliance of the FB is accurate at ± 5°. The FB shows a bright "7-fold rose" on its pavilion. This unsuspected, spectacular and complex design was clearly intended to symbolize King Louis XIV [1], the "sun-king", with its "7 planets in the deep-blue universe". FB has been cut in 1673, following the constraints of the "Tavernier Blue" (TB) diamond [2] but not only. The diamond shows intriguing ratios of integers for its dimensions, asymmetry of opposite sides and joint diagonals in front of the culet. These constraints follow the "canon of proportions", defined by architects Vitruvius (Antiquity) and Palladio (Renaissance). Thus, the FB fits Da Vinci's "Vitruvian man", where its "membro virile" points to the FB's culet, i.e., the centre of the square representing "the cosmic world", features which make FB a harmonic allegory of the sun-king of divine rights. Additionally, the natural crystal from which the TB was cut has been predicted based on TB's crystallography [2] and refined using the Bravais–Friedel, and Donney–Harker theories [3]. The refined hypothetical crystal, a rhombicuboctahedron, was so thick that its colour was almost black. Cleavages along (111) were thus required to make thinner "slices" within the crystal to reveal its greyish-blue colour. This suggests that two other roughs for this diamond must have existed.

The first recreation of the Golden Fleece of King Louis XV, by using the FB, a 107 ct spinel and 490 other diamonds, conducted by Herbert Horovitz, jeweller in Geneva make the subject of a 90 min. documentary that will be broadcasted by the end of 2010 on National Geographic and Arte channels, among others.

[1] Farges, F. et al. (2009) *Gems Gemol.*, **Sp09**, 4-19. [2] Sucher, S. (2009) *Gems Gemol.*, **F09**, 178-185. [3] Kaminsky. W. (2007) *Appl. Crystallogr.*, **40**, 382-385.

Some tools to adapt mineralogical museums to new trends: the example of the UPMC-La Sorbonne collection

Boulliard, J.-C.
Institut de Minéralogie et de Physique des Milieux Condensés (IMPMC), Université Pierre et Marie Curie (UPMC), Paris France (jean-claude.boulliard@impmc.upmc.fr)

In 1983, Paul Desautel (a former curator of the Smithsonian) stated that: "the mineral museums are deathly sick… science has moved off and left them." This terrible diagnosis appears to have ended an era, in which institutional collections were, above all, places of science and research.

Since that time, a tremendous interest in minerals has raised from the public. In addition to research and teaching, the mineral museums have to respond to this public demand. The museum of the Université Pierre et Marie Curie de Paris (UPMC) has developed the following tools which will be presented at the conference:

- a CD, edited in 2006, that tries to be a virtual visit of the collection. It contains 450 pictures of specimens. They have been selected among the most beautiful and important (for science and/or industry) specimens on display. One chapter deals with the history of the collection. Other chapters contain answers to the most frequent questions asked by the public;
- an audioguide (to the knowledge of the author the first one for a mineral museum) tells the story of the collection and describes the contents of the show cases;
- a luxurious book, published in November 2010, presents 150 (mainly large) specimens at 1/1 scale. The photographer offers a new, more artistic vision on mineral photography. Short texts describe the minerals and their classification. Longer texts are more epistemological and museological. They are devoted to the history of the UPMC collection, the general history of the mineral collections and criteria that make a specimen a highlight of the legacy of nature.

18th century collections, 21st century audiences

Chambers, S.* & Mitchell, L.
Royal Cornwall Museum, Truro, Cornwall, UK
(*sara.chambers@royalcornwallmuseum.org.uk)

The Royal Institution of Cornwall's (RIC's) collection of South West of England mineralogy is one of the finest in the world. It is housed and managed by the Royal Cornwall Museum (RCM), the main vehicle by which the RIC's extensive collections are made accessible to the public. Our challenge is to re-present this collection to 21st century audiences.

The mineral collection comprises some 15,000 specimens. At its core is the outstanding early collection of Philip Rashleigh (1729-1811); the most famous of Cornish mineral collectors, who lived near Fowey, Cornwall. Rashleigh collected over 3,000 mineral specimens not only from Cornwall but also from around the world, corresponding with dealers and exchanging with collectors throughout Europe.

Years of under-funding and insufficient human resources resulted in the progressive dormancy of the mineral collection. By the end of the 20th century it was in a state of some disorder and had effectively ceased to function as a learning resource and existed only as a group of display items.

Since then much collection recovery work has been undertaken and behind the scenes, these benefits are already apparent. However, the public face of this collection is still seen via a traditional, pseudo-systematic, gallery display, based on creating knowledge through the development and research of collections and disseminating it through formal, passive, displays. Not only is the gallery physically inaccessible to many of its key audiences; it is intellectually impenetrable to all but the most knowledgeable subject specialists.

Learning is at the heart of the RCM, but we need to redefine our role, not only as a result of pressure from government and current funding streams but also in recognition that we have a bigger role to play in society.

The way in which we present collections to the public has shifted; we have recognised the need to see ourselves no longer as simply collections-focussed but audience-centred. This shift is critical when thinking about how we re-present our collections to the discerning, 21st century, visitor. We face challenging times, competing for funding as well as people's leisure time. What is needed is an understanding of audiences and an outward-looking agenda. Visitor expectations have risen dramatically, and so must ours.

Our evidence suggests that the mineral collection's audience appeal is broad in range - including audience groups that might at first appear mutually exclusive: subject specialists and family or younger visitors. As the largest museum in Cornwall, strategically placed within the region, we have a key role to play in helping tell the story of Cornwall and to promote a deeper knowledge and appreciation of its unique landscape and mining heritage. Our world class collection of minerals can help communicate these narratives: effective interpretation strategies can unlock the scientific understanding of the collection as well as revealing the human stories behind how this collection came to be.

Armed with an understanding of interpretation and how this can be used to present and layer information, as well as specialists from all disciplines (curatorial, learning, interpretation and exhibition), the challenge now is to ensure we have the processes in place, as well as the intellectual flexibility, to make these changes.

The 70 years-old mineralogical collection of Comenius University in Bratislava (Slovak Republic)

Ozdín, D.
Dept. of Mineralogy and Petrology, Comenius University, Bratislava, Slovak Republic (ozdin@fns.uniba.sk)

The Faculty of Natural Sciences was established in 1940, as the fourth faculty of the Comenius University in Bratislava. Complicated war conditions and revolutionary changes in 1948 marked the beginning of a 20-year consolidation process of individual institutes and departments, through periodic organizational changes. The collection of the Mineralogical-Petrographical Institute of the Slovak University in Bratislava was established in 1940–1942. Its founder was Prof. R. Lukáč, the head of the institute, but in the same time the curator (May 1939–August 1940) of the Slovak Mining Museum (former Dionyz Štúr Museum) in Banská Štiavnica, as well as the manager of the Mineralogical-Petrographical Institute of the Faculty of Chemical technological engineering of the Slovak Technical University.

For almost 40 years, R. Lukáč has built the basis of the most distinguished academic mineralogical and petrological collections in Slovak Republic. Besides specimens from Slovak and Czech localities, significant collections were represented by minerals from Krantz Company in Bonn, Peschl collection, the collection of Ronge from Broumov, specimens from Freiberg Mining Academy (Mineralien Niederlage), as well as samples originally belonging to the Slovak Mining Museum in Banská Štiavnica. Later on, the collection was enriched through donations, field-collected specimens and acquisitions resulted from scientific research of the faculty staff.

In the following 20 years, the collection was enriched mostly with samples from active Slovakian deposits (*e.g.* Banská Štiavnica, Rudňany). A big expansion of the collection was recorded after 2000, when new collections were established: gemmological collection, collection of meteorites and tektites, and, of special significance, systematic and topographical collections of minerals from Slovakia. At that time, the largest and most complete, still unparalleled, Slovak systematic collection was opened. Several private collectors contributed with many specimens to this exhibition. Additionally, the Department of Mineralogy and Petrology preserves a rich petrographical collection, one of the largest in European Universities.

Inauspiciously, in the last decades a few hundreds specimens were stolen. However, the worst year for the collection was 2006, when the department's storage place, hosting thousands of specimens mostly from Slovakia and Czech Republic was destroyed.

Traditionally, the department had one or two curators as members of the staff: Prof. Rudolf Lukáč (1940–1977), Vlasta Judinová (1961–1982), Daniela Briatková (1979–1989), Ivan Friedl (1989–1991), Viktória Fejdiová (1991–1997), Miroslav Horal (1997–2000) and Daniel Ozdín, PhD. (2000–).

The department is currently dominated by three main exhibitions: the Mineralogical System of Slovakia, the World Mineralogical System and the Petrographical collection. Smaller displays on ore textures, genesis of minerals, gemmology, SiO_2 phases and historical scientific instruments (as the technical museum of the department) have been opened in 2010.

Thus, we consider our exhibition as one of the best among university mineralogical collection in Central Europe.

Between tradition and innovation: the new Mineralogical Section of the Natural History Museum of the University of Firenze (Italy)

Pratesi, G.[1,2*], Bindi, L.[1], Poggi, L.[1], Fantoni, L.[1], Andreani, M.C.[1] & Scali, G.[1]
[1]Natural History Museum, University of Firenze, Italy
[2]Dept. of Earth Sciences, University of Firenze, Italy
([*]g.pratesi@unifi.it)

The Natural History Museum of the University of Firenze was founded, in 1775, by Grand Duke Pietro Leopoldo Lorena. It was located in Torrigiani Palace, near the Pitti Palace, in order to create an ideal connection between art and science. Nevertheless, the earliest collections date back to the 15th century, namely from the times of Lorenzo de' Medici. The Museum has adsorbed, during its long history, many other collections: it is worthy mentioning that Niels Stensen's specimens – as well as the collections of Targioni Tozzetti, Foresi, Roster, Capacci, Ciampi, Ponis, Brizzi – are preserved in this institution. In 1880, the collections moved near the Botanical Garden (named Giardino dei Semplici) and San Marco church where they have remained until now. The mineral collection of the Museum – containing over 50,000 specimens – ranks among the world's finest due to its very broad representation, wealth of rare species and large number of specimens first described in the scientific literature - namely holotypes, the Island of Elba collection, pegmatite minerals from Brazil etc.

In order to allow a greater public visibility to the about 800 mineral specimens on display, the Mineralogical Section deserved a new exhibition which has been projected by architect Piero Roberto Papi and which was recently opened.

Fig. 1: The new entrance of the Mineralogical Section of the Natural History Museum of Firenze.

A cursory review of the exhibited collections reveals world-class specimens of covellite, elbaite, topaz, beryl, sulphur, celestine and dozens of other minerals. At the entrance, the visitors are welcomed by an amazing view of the best specimens from the Ponis collection and an exciting display of back-lighted thin slices of agate and liddicoatite. Showcases on meteorites, lithology, crystal growth, polymorphism, crystal chemistry, crystallography, physical properties, mineral deposits and use of minerals and rocks add to the educational and visual experience. Finally, the systematic display gathers over 200 beautiful specimens from all over the world, grouped according to their chemical classification.

Mineral collections and museums in Germany: past, present, future

Simon, G.[1*] & Schumacher, R.[2]
[1]Museum Mensch und Natur, Staatliche Naturwissenschaftliche Sammlungen Bayerns, München, Germany
([*]simon@musmn.de)
[2]Mineralogisches Museum am Steinmann-Institut, Bonn, Germany

In Germany, minerals' curation has a long tradition, a fact that immediately becomes evident from the history of classical collections, their establishment and the people in charge. University collections like those of the Humboldt University of Berlin (founded 1781), Bonn (1818), Freiberg (1765), Jena (1779), and Marburg (1790), as well as museums like the State Museum of Mineralogy and Geology in Dresden (1587), the Hessian State Museum Darmstadt (1774), the Senckenberg Natural History Museum in Frankfurt (1817) and the Bavarian State Collection of Mineralogy (1803), are only a few among such well-known historical institutions. The people in charge were internationally-known authorities, for instance A. Breithaupt, B. Cotta, V.M. Goldschmidt, P. v. Groth, A. v. Humboldt, F. Mohs, J.J. Nöggerath, H. Rosenbusch, H. Schneiderhöhn, F.A. Walchner and A.G. Werner.

At present, the general situation of mineralogical collections in Germany has become very problematic, financial support and staff having been reduced. In addition, new duties have been imposed upon curators of mineralogical collections. Storing minerals is only one of the activities. Modern collections have to grow, all samples have to be documented in detail, and, finally, the collections have to represent an area of public information and scientific research. Apart from physical geography, geosciences are not taught in German schools. Thus, one of the main tasks of curators in museums and in universities is also to attract school classes and the general public to geosciences.

Curators of German mineral collections are organized in the "Mineralogical Museums and Collections" working group within the German Mineralogical Association (DMG). The working group periodically organizes meetings to encourage communication and cooperation, to initiate and coordinate joint projects, and to arrange mutual support. Actual activities are represented by this contribution, "Mineralogical Collections and Museums in Germany", as poster at IMA2010, an email network, the "Type Specimen Catalogue Germany" and a joint website (http://www.mineralogische-sammlungen-dmg.de).

The poster presents an overview of the most important mineral and rock collections in Germany, together with their major fields of research and interest.

The tradition of Theophrastus' "On Stones" during the early stages of modern mineral science

Mottana, A.
Dipto. di Scienze Geologiche, Università Roma Tre, Rome, Italy (mottana@uniroma3.it)

Theophrastus' περι λιθων (*De lapidibus* = On Stones) reached western Europe *c*. 1413-27, as one of the many Opuscula then being transferred from Byzantium to Italy. Possibly, the original source was a copy of *Vaticanus graecus 1302*, a codex written in Byzantium c. 1300-30 [1]. However, περι λιθων entered the European Latin-speaking learned community only in the second half of the 15th century, via a number of copies carried out in Italy by Greek expatriates after the taking of Byzantium by the Turks (1453). In particular, it was studied by Hermolaus Barbarus (*c*. 1490) while preparing the first corrected edition of Pliny's *Naturalis Historia*, and it was first printed by Aldus Manutius [2]. Aldus' editorial decision of printing only the Greek text hindered the diffusion of Theophrastus' ideas on the formation of stones and also on the names and properties of the 60-odd minerals contained in his book, thus no real progress for the new science of Mineralogy occurred till a selection of περι λιθων was translated to Latin by Georgius Agricola and incorporated into his *Bermannus* (1530). This is the first innovative treatise on mines and ores published in Europe after Albertus Magnus' *De mineralibus* (*c*. 1265). Agricola added more quotations later, in his *De ortu et causis subterraneorum* and *De natura fossilium* (1546), which contain his theoretical resp. descriptive knowledge on stones. Little else he added into *De re metallica* (1555), which is devoted to mining. Two full Italian translations of Agricola's *corpus* (1550, 1556) helped diffusing Theophrastus' work among scientists much more than could two emended printings of the Greek text (1541, 1577) or one Latin full translation of it (1578), all being of interest only to philologists.

A translation of περι λιθων into Italian was carried out by F. Imperato (1599) and introduced by him into *Dell'Historia Naturale* [3]. His translation is the first one ever made into a modern language, but it is partial, as it covers only 48 sections of Theophrastus' text. Imperato's translation did not help spreading Theophrastus' ideas because: a) his book was printed privately in a small number of copies and circulated only among a selected group of colleagues, albeit of high reputation; b) Italian was already fading out as a widely-known international language, particularly among scientists in the protestant country, where science was advancing rapidly.

Theophrastus' name kept being well known among scientists, but not his ideas. These had no impact onto the "scientific revolution" and remained substantially out of reach for most mineralogists till the English complete translation by J. Hill [4] made περι λιθων known at a level beyond superficiality. The translations into French and German that followed immediately afterwards were carried out from Hill's English text and contributed to farther spreading, as well as to accelerate the "industrial revolution". They created the fame of Theophrastus as the "grandfather" of Mineralogy, much as Agricola gained his fame of "father" of Mineralogy. This outcome took place at the same time when Crystallography overcame Mining as the leading branch of the science of minerals by the efforts of J.-B. Romé de l'Isle and R.-J. Haüy and the separation of Mineralogy from Oryktology (= Petrography) due to A.G. Werner.

[1] Burnikel, W. (1974) *Palingenesia VIII*. Steiner, Wiesbaden. [2] *Aristotelis et Theophrasti opera volumen II*, 254-261 (1497). Aldina, Venetiis. [3] Mottana, A. (2010) *Rend. Fis. Acc. Lincei*, s. 9, **21**, 1-22. [4] Hill, J. (1746) *Theophrastus's History of Stones*. Davis, London.

Sir James Hall's visit in Schemnitz

Rózsa, P.
Dept. of Mineralogy and Geology, University of Debrecen, Hungary (rozsap@puma.unideb.hu)

Sir James Hall of Dunglass (1761–1832) (Fig. 1) is regarded to be the founder of experimental geology. In these experiments he proved that cooling rate affects the texture of molten rocks [1]; demonstrated the stability of limestone under high pressure and temperature [2]; and performed scale models of folding under compression [3].

Fig. 1: Portrait of the young Hall by Angelica Kauffmann (Scottish National Portrait Gallery).

He attended Christ's College, Cambridge, and the University of Edinburgh, where he studied chemistry and natural history under Joseph Black (1728–1799) and John Walker (1730–1803), respectively; however, he obtained no graduation. In 1783–1786 he went on a 'Grand Tour', which was a flourishing custom of the upper-class British young men. He travelled through France, Germany, Austria, Switzerland and Italy. Although he never published any account on this tour, his handwritten diary survived [4]. Thereafter, he lived in Dunglass and Edinburgh, where he became acquainted with James Hutton (1726–1797) and John Playfair (1748–1819); their excursion to Siccar Point, which proved to be a turning point in history of geology, started from Sir James Hall's house in Dunglass.

During his 'grand tour', in the spring of 1784 he made a three-week-trip from Vienna to Hungary. His main aim was to visit the mining-metallurgical region near Schemnitz (Selmecbánya, now Banská Štiavnica, Slovakia). In his diary he gives a detailed description on hydraulic mining machines and metallurgical processes. He visited several times the chemical laboratory of the 'Bergakademie', and met Anton Ruprecht (1748–1814?), who was the professor of chemistry in the Academy. The excellent chemical-metallurgical laboratory developed by Ruprecht as well as his training method, i.e. the student could make experiments by their own, had a deep impact on the young Hall.

This eminent scientist's account also proves that the Begakademie in Schemnitz, and particularly the chemical-metallurgical training belonged to the European forefront in the last decades of the 18th century.

[1] Hall, J. (1805) *Trans. R. Soc. Edin.*, **5**, 43-75. [2] Hall, J. (1812) *Trans. R. Soc. Edin.*, **6**, 71-185. [3] Hall, J. (1815) *Trans. R. Soc. Edin*., **7**, 79-108. [4] Eyles, V.A. (1963) *Ann. Sci.*, **19(3)** 153-182.

Letters of German naturalists to Domokos Teleki, the first president of the Jena Mineralogical Society

Viczián, I.
Hungarian Institute of Geology, Budapest, Hungary
(viczian@mafi.hu)

Count Domokos Teleki (1773-1798), a young Hungarian aristocrat studied in Vienna University (1789-1793), later he lived in his native district in Transylvania but occasionally he returned to Vienna. He owned a valuable collection of minerals. On a journey in 1795 he visited the Saxonian principalities in Germany. After returning home he received many letters from Germany. Shortly after his visit, in 1797 the Jena Mineralogical Society was founded, probably the first scientific society in mineralogy ever existed. As a result of his visit and correspondence he was elected for first president of the society.

Ten letters of this correspondence addressed to Domokos Teleki were preserved in the archives of the Teleki Library in Marosvásárhely (Târgu Mureş, Romania). They are so far unpublished. Letters sent in the opposite direction by Teleki and other Hungarian members of the Society are preserved mainly in the archives of the Jena University and have been partly published [1,2].

Teleki received letters in the period 1796-1798 from the following persons:

- J. F. Freiherr zu Racknitz, a high standing official and collector of minerals, Dresden,
- August J. G. K. Batsch (1761-1802), professor of botany and founder of the Society of Natural History (1793) in Jena,
- Johann Georg Lenz (1745-1832), professor of mineralogy and founder of the Mineralogical Society (1797) in Jena,
- prince Ernst of Saxony-Coburg (1784-1844), later ruler of the principality as Ernst I (1806-1844),
- prince Ferdinand of Saxony-Coburg (1785-1851), later incorporated into the Hungarian nobility (1827) after marrying the Hungarian duchess Maria-Antonia Koháry (1816).

The letters are dealing with donation and exchange of precious mineral samples, mainly various gold ores and precious opals of Hungarian origin. Another theme is the Jena Mineralogical Society itself, its organisation, members and activity in the first year after the foundation. Persons like Werner, Klaproth, Goethe, Herder, the Hungarian secretary Bredeczky etc. are mentioned. In this respect the letters represent a valuable source of data concerning the contemporary specimens, collections and scientific studies of minerals.

The letters indicate that mineralogy was widely accepted in high social classes and among leading literary persons in Germany around the end of the 18th century.

[1] Viczián, I. & Deé Nagy, A. (1997) *Acta Min.-Petr. Szeged*, **38**, 165-173. [2] Viczián, I. (1998) *Múzeumi Füzetek. Az Erdélyi Múzeum-Egyesület Természettud. és Mat. Szakoszt. Közl. Új sorozat*, **7**, 3-19. Kolozsvár.

Minerals from Carpathians Mountains and Transylvania donated by emperor Josef II (1785) to the Museum of Collegio Nazareno, Rome

Mussino, A.[1], Nasti, V.[1] & Mottana, A.[1,2*]
[1]Gruppo Mineralogico Romano, Rome, Italy
Dipartimento di Scienze Geologiche, Università Roma Tre, Rome, Italy ([*]mottana@uniroma3.it)

The mineralogical museum of Collegio Nazareno, the teaching institution of the "Order of Poor Clerks Regular of the Mother of God of the Pious Schools", in short: "Piarists", was founded, *c*. 1760, by Gian Vincenzo Petrini (Lucca, 1725-1814). It included minerals from all over Europe, and also gifts received by various popes. Minerals from Vesuvius and the Latium volcanoes implemented the collection thanks to Petrini himself and Scipione Breislak [1].

On March 24, 1769 the museum was visited by Josef II, emperor and king of Hungary, who was in Rome as an incognito tourist, but, in fact, had been sent by Maria Theresia to organize the election of a pope who would abolish the Jesuit order. Several years later (June 14, 1785), the museum received a large gift from the emperor, which consisted in eight boxes of minerals, mostly from Transylvania, all carefully classified according provenance and morphological characters. This gift is described extensively in the book, in two volumes, written by Petrini [2] to clarify the find of the new mineral species described by foreign scientists visiting the surroundings of Rome (cf. [3]).

Volume 2 (1791) contains, in addition, the description of the Au-bearing minerals of "Beseraw" and "Boiza" mines, in Transylvania, and of specimens of "gold mixed with iron and copper sulphides and manganese" coming from the "rich mine of Nagyag … which produced so much on behalf of the house of Austria". Petrini further states that the imperial collection had been arranged by the "celebrated Baron of Born" (= Ignaz edler von Born: Alba Iulia, 1742-Vienna, 1791), who had also made the description of the specimens (mostly in Latin). Among them, two were considered by Petrini to be especially valuable samples of *gelfertz* (= auriferous and/or argentiferous chalcopyritic viz. pyritic ore: [4] p. 29): one is from Sankta Barbara mine near Fuszerchs (= Füzzérádvany) and the second one from Sankt Anton quarry in the Boiza valley.

The mineralogical museum of Collegio Nazareno has survived and, in particular, most (unfortunately not all) imperial gift is carefully preserved by Gruppo Mineralogico Romano, an association of mineral amateurs and collectors that helps scientists in studying the minerals of this internationally-known volcanic region. The imperial collection in the museum represents a rare set of samples arrived unchanged to us from 18th century Europe. They are organized according to Agricola's principles, i.e., on the basis of his idea of ore mining, slightly modified on a chemical basis. Thus, its organization shows the state of Mineralogy before the change of paradigm induced by J.-B. Romé de l'Isle's and R.-J. Haüy's crystallographic approaches (*c*. 1780-1790).

[1] Ruali, P.M. & Nasti, V. (1997) *Il Cercapietre*, **n. sp.**, 23-26. [2] Petrini, G.V. (1791-92) *Gabinetto Mineralogico del Collegio Nazareno descritto secondo i caratteri esterni e distribuito a norma de' principj costitutivi*. Roma, Lazzarini. [3] Mottana, A., Bellatreccia, F. & Della Ventura, G. (2008) *Mem. Descr. Carta geol. Italia*, **80**, 247-271. [4] Papp, G. (2004) *History of minerals, rocks and fossil resins discovered in the Carpathian Region*. Budapest, Hungarian Natural History Museum.

Some central European geoscientists of the 18th century and their influence on Mozart's music

Whittaker, A.[1] & Tillmanns, E.[2*]
[1]British Geological Survey, Kingsley Dunham Centre, Keyworth, Nottingham, UK
[2]Institut für Mineralogie und Kristallographie, Universität Wien, Vienna, Austria ([*]ekkehart.tillmanns@univie.ac.at)

The lives and contributions of several central European geoscientists of the 18th century, Rudolph Erich Raspe (1736-1794), Ignaz von Born (1742-1791), Karl Ludwig Giesecke (1761-1833), Karl Haidinger (1756-1797), Nicolaus Joseph von Jaquin (1727-1817), Johann Anton Scopoli (1723-1788), Franz Joseph Müller von Reichenstein (1740-1825), Johann Gottlob Lehmann (1719-1767), Anton Ruprecht (1748-1814) are discussed, many of whom had close contact with composer and musician Wolfgang Amadeus Mozart (1756-1791) by contributing either directly or indirectly to some of his musical works, especially "Die Zauberflöte" (The Magic Flute) as well as making significant contributions to various aspects of geoscience and related technology which are still important today. Mozart's "Kantate auf den hochwürdigen Bruder Born" für Solo, Chor und Orchester (KV 471), also known as „Die Maurerfreude" (Masonic Joy), was composed on the occasion of Born's introduction of the amalgamation process in the Habsburg dominions which was a big social event at the time. It seems certain that Mozart used Giesecke to provide the words of this cantata. Born took an active part in the Vienna musical scene, attending Mozart's concerts and recitals. Especially close was Mozart's connection to the Jaquin family after N. J. von Jaquin returned from his professorship at the Mining Academy in Selmecbánya (Banska Štiavnica, Schemnitz) to Vienna as professor of botany and chemistry. Mozart took an active part in the Jaquin family's musical life and in their musical evenings and dedicated several of his works to Jaquin's sons Joseph Franz and Emilian Gottfried. Jaquin's daughter Franziska studied the piano with Mozart who wrote the piano part of the Kegelstatt-Trio (KV 498) for her.

It seems worthwhile to mention that in 1991, 200 years after his death a new mineral $CaMn^{3+}[OH/SiO_4]$ was detected by Italian mineralogists [1] in the Cerchiara manganese mine, near Faggiona, Val di Vara, Liguria, Italy and was named after him, Mozartite.

Also discussed is the connection of these individuals to other European scientists of the time like John Hawkins (1761-1841), Johann Jakob Ferber (1743-1790), Matthew Boulton (1728-1809), Johann Friederich Blumenbach (1752-1840), Abraham Gottlob Werner (1749-1817), Martin H. Klaproth (1743-1817), Robert Townson (1762-1827), Nicolaus Poda (1723-1798), Friedrich Wilhelm Heinrich von Trebra (1740-1819), Johann Friedrich Wilhelm von Charpentier (1735-1805) and the establishment of the Selmecbánya (Banska Štiavnica, Schemnitz) Mining Academy and its important contributions to geoscience and relation to technical mining matters and its particular importance at the time of the Industrial Revolution. Influential in connection with the scientists mentioned were the North American Benjamin Franklin (1706-1790) and the Spanish mineralogist Fausto d'Elhuyar (1755-1833), founder of Mining Academies in Madrid and Mexico.

The discovery of the element tellurium and the relevance of the Academy to major scientific arguments of the day such as the position and status of alchemical theories and the phlogiston theory are also briefly discussed.

[1] Basso, R. et al. (1993) *Can. Mineral.*, **31**, 331-336.

On the formation of giant crystals of gypsum: the science behind beauty

Garcia-Ruiz, J.M.[1*], Canals, A.[2], Villasuso, R.[3], Van Driessche, A.E.S.[1] & Otálora, F.[1]
[1]Laboratorio de Estudios Cristalograficos, CSIC-Universidad de Granada, Spain (*jmgruiz@ugr.es)
[2]Universidad de Barcelona, Spain
[3]Unidad Naica, Compañia Peñoles, Mexico

Giant crystals of gypsum are fascinating masterpieces of Nature. Until the development of flat glass technology, they were used as sophisticated building materials as reported by Pliny the Elder who described the existence of large crystals of gypsum -*lapis specularis*- in Segobriga (Spain) renowned for their transparency and size.

Fig. 1: a) Cave of crystals in Naica's mine (Chihuahua, Mexico) Note man on the left for scale;b) Gypsum crystal from Naica showing the non-singular faces {1k0};c) AFM picture of the {010} face showing void formation.

Other localities with even larger crystals were reported during the last century such as the unique Geode of Pulpí (Spain), the giant crystals of El Teniente mine in Chile and the spectacular caves and caverns in the range of Naica (Mexico) [1,2]. Among them, the so-called Cave of Crystals in the Naica mine is one of the most amazing displays of mineral beauty ever created by Nature. In addition to the colossal crystals, which reach up to eleven meters in length and exceed one meter in thickness, the scenery developed by the individual crystalline beams going through the darkness of the cave, from the floor to the ceiling, is a unique example of harmony based on crystal symmetry. But at the same time, deciphering the mechanism of formation of these crystals is a fascinating scientific challenge. We will discuss in this lecture the scientific basis of this remarkable phenomenon of mineralization. The study is supported by data obtained with a number of techniques including fluid inclusions analysis, confocal differential interference contrast microscopy, atomic force microscopy, stable isotopic analysis, as well as experimental and theoretical nucleation and crystal growth studies of calcium sulfate. Our explanation is based on a solution mediated anhydrite-gypsum phase transition occurring in a slow and smooth cooling scenario. Our fundamental studies have also revealed the importance of kinetics of that mineral transition under natural conditions. Finally, we will also offer an explanation for gypsum properties based on their peculiar growth features.

[1] Garcia-Ruiz, J.M. et al. (2007) *Geology*, **35**, 327-330. [2] Garcia-Ruiz, J.M. et al. (2008) *Mcgraw-Hill Yearbook of Science &Technology*. Mcgraw-Hill, New York, 154-156.

Genesis of amethyst geodes at Ametista do Sul, Rio Grande do Sul, Brazil

Gilg, H.A.[1*], Krüger, Y.[2], Taubald, H.[3], Morteani, G.[4] & Frenz, M.[2]
[1]Lehrstuhl für Ingenieurgeologie, TUM, Munich, Germany (*agilg@tum.de)
[2]Institute of Applied Physics, University of Bern, Switzerland
[3]Lehrstuhl für Geochemie, University of Tübingen, Germany
[4]Gmain No.1, Isen, Germany

Amethyst-bearing geodes in the Ametista do Sul area, RS, Brazil, are hosted by 40 to 50 thick lava flows of the Lower Cretaceous Paraná Continental Flood Basalt province [1]. They show characteristic hydrodynamic shapes, thus the cavities formed by ascending accumulations of magmatic gas bubbles. Geode infill starts with celadonite, pyrite, and chalcedony, followed inwards by colorless quartz, amethyst with goethite and anhydrite inclusions, and locally rare barite and late gypsum. Calcite crystallized throughout the paragenetic sequence. Mineralized fractures and breccia textures indicate repeated tectonic activity before, during, and after geode infill.

New H, O, and S isotope data and microthermometry on monophase aqueous liquid inclusions reveal novel insights into amethyst mineralization. The fluid inclusion measurements were performed after nucleation of a vapor bubble in the metastable inclusions induced by single femto-second laser pulses [2]. The $\delta^{34}S_{VCDT}$ values of pyrite associated to early celadonite and chalcedony range from -25 to -32‰ indicating bacterial sulfate reduction and temperatures of less than 80°C during initial geode infill related to a maximum burial of about 2 km. Monophase pseudo-secondary aqueous fluid inclusion in amethyst have homogenization temperatures of up to 130°C and three distinct salinity modes of 0.7, 3.4, and 5.9 wt.% NaCl-equiv. Formation temperatures of late calcite and gypsum are below 50°C. The sulfur isotope values of sulfates decrease from 9.6‰ (anhydrite) to 5.6‰ (gypsum). The δD values of amethyst-hosted fluid inclusions range between -59 and -51‰. These values are significantly lower than local meteoric waters [3], but within the range of values reported from the Guaraní aquifer [4]. Oxygen isotope values of amethyst scatter between 28 and 34‰. The isotope composition of waters in equilibrium with gypsum water is intermediate between local meteoric waters and waters in equilibrium with amethyst at temperatures of 50 to 130°C.

These new data suggest that meteoric fluids from the artesian Guaraní aquifer underlying the flood basalts were not the sole mineralizing source [1,5], but repeated injection of hot brines from deep parts of the sedimentary basin into a relatively cool wall rock probably during Andean tectonic phases played a significant role in amethyst formation.

[1] Gilg, H.A. et al. (2003) *Miner. Deposita*, **38**, 1009-1025. [2] Krüger, Y. et al. (2007) *Eur. J. Mineral.*, **19**, 693-706. [3] Matsui, E. et al. (1974) *Geol. Soc. Amer. Bull.*, **85**, 577-580. [4] Silva, R. B. G. (1983) *PhD thesis*, Uni. São Paulo, Brazil. [5] Morteani, G. et al. (2010) *Int. J. Earth Sci.* (in press).

Emerald gastropod fossils from the Mantecanã mine (Gachalà district, Colombia): a record of the recipe for Colombian emerald formation

Giuliani, G.[1,2]
[1]IRD, Toulouse, France (giuliani@crpg.cnrs-nancy.fr)
[2]CRPG/CNRS, Vandœuvre-lès-Nancy, France

Colombian emeralds are famous for their colour, clarity and carat value. They continue to set worldwide standards for emerald and still the finest and most spectacular crystals unearthed. Forming in cavities, emerald crystals developed prism and basal faces and reached spectacular size with zoned and clear prisms up to 15 cm long. Some gems from the Gachalá district are unique in the world: El Monstro, 16020-carats; the Emilia, 7025-carats; the Gachalá emerald, 858-ct; the 75-carats square cut Gachalá stone in the Hooker brooch of the Smithsonian collection. The presence of fluid circulation in an extensional vein-system under an impermeable seal is thus the clue for the free-standing crystal growth of Colombian emeralds. In this mine, a remarkable set of fossilized gastropods shells replaced by emerald were discovered in 1994. In 1998, the tunnel collapsed and "mining" of the fossils ceased.

Twenty-four fossils have been studied and three forms of gastropods identified (*Ataphrus, Pseudomelania and Ampullospira*). All are from the mineralized Guavio formation of Berriasian age (135-130 Ma). The gastropod shells were epigenised by emerald following the usual processes of dissolution-substitution. Such processes are well-known for pyrite, carbonates or opal substitution but have never been described for precious gems. After the burial of gastropods at Berriasian time and dissolution of the aragonitic test, the voids corresponding to the shelly test were filled at about 65 Ma by emerald which perfectly replicated the original form of the shells.

In Mantecaña, the emerald-bearing zone now corresponds to a stratiform brecciated level formed of disrupted blocks of albitites, black shales and limestones from the Guavio formation. The emerald-bearing structures (breccia and veins) are on the hanging-wall of the brecciated level which is also mineralized. The brecciated level is an evaporite dissolution residue which acted as a local detachment. The mineralizing fluids expulsed by evaporite dissolution by basinal brines, flowed in the well-developed set of extensional fractures, simultaneously percolating the gastropod-bearing formation. Emerald deposited both in vugs within carbonate veins but also in voids by impregnation of the gastropod shells.

This unique record of emerald in fossils is the combination of different factors: the development of breccias and extensional vein set at the bottom of a fossil-bearing horizon; the presence of highly reactive salty brines resulting from evaporite dissolution; the high permeability of mechanically-induced (breccia) or chemically-induced (voids by dissolution of shells), and the rapid sealing of the structures due to the competent black shales. All of these factors, combined with the particular expulsion of 300°C fluids and the high concentration in beryllium in the brines resulted in this unique occurrence of emerald fossilizing gastropods and the finest and spectacular emerald crystals yet found on the planet.

Is the V/Cr ratio a fingerprint of the geographical origin of 'tsavorite' in the Mozambique Belt?

Feneyrol, J.[1*], **Giuliani, G.**[2,1], **Ohnenstetter, D.**[1], **Galoisy, L.**[3] **& Pardieu, V.**[4]
[1]CRPG/CNRS, Vandœuvre-lès-Nancy, France
([*]feneyrol@crpg.cnrs-nancy.fr)
[2]IRD, Toulouse, France
[3]IMPMC, Paris, France
[4]GIA, Bangkok, Thailand

The green colour of 'tsavorite', a grossular [$Ca_3Al_2(SiO_4)_3$] garnet variety, is due to the presence of vanadium (V) and chromium (Cr) in the garnet structure [1,2]. Vanadium and Cr contents of 'tsavorites' from several deposits in the metamorphic Mozambique Belt (MB) in Tanzania, Kenya, Madagascar and Pakistan are reported in Table 1.

Table 1: Mean range of V and Cr contents (in wt%) in 'tsavorites' from Tanzania (1), Kenya (2), Madagascar (3) and Pakistan (4)

	(1)	(2)	(3)	(4)
Number of deposits/analyses	7/582	6/310	2/210	1/45
V_2O_3 (wt%)	0.08-2.48	0.07-2.69	1.12-4.02	2.74-6.51
Cr_2O_3 (wt%)	0.04-0.35	0.35-1.42	0.17-0.64	0.54-0.82
V/Cr	0.7-10.1	0.2-4.4	5.1-6.7	5.1-7.9

Detection limits of EPMA: V=14 ppm and Cr=14 ppm.

All 'tsavorites' contain V and Cr, but their concentrations in Kenyan 'tsavorites' differ from that in other deposits in the MB (Fig. 1).

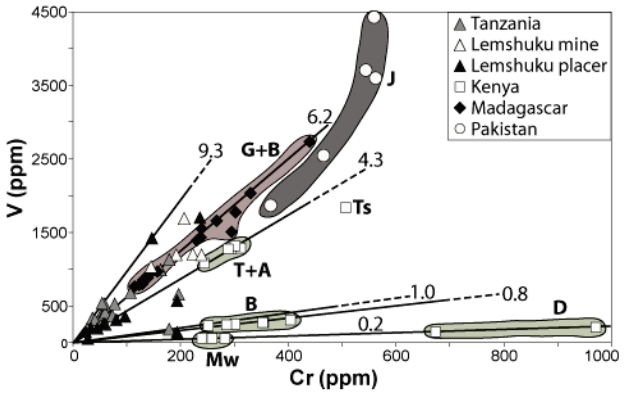

Fig. 1: V vs Cr diagram for the 'tsavorites' of the Mozambique Belt.

Kenyan 'tsavorites' contain more than 240 ppm of Cr and V/Cr is ≤ 4.3. The Baraka (B), Mwatate (Mw) and Dicka (D) deposits can be distinguished by their very low V/Cr ratios. Other Kenyan 'tsavorites' have V/Cr ratios close to 4.3: Tsavo (Ts), Tsavolite and Aqua mines (T+A). 'Tsavorites' from Madagascar and Pakistan display V/Cr ratios higher than 4.3. In Madagascar, the Gogogogo and Behara (G+B) 'tsavorites' contain more than 750 ppm of V and 110 ppm of Cr. Jambil (J) 'tsavorites' from Pakistan have the highest V contents, up to 4500 ppm. Tanzanian 'tsavorites' contain less than 1800 ppm of V and 240 ppm of Cr. Most of them have V/Cr ratios between 4.3 and 9.3. The 'tsavorites' from the Lemshuku placer show a large variability of the V/Cr ratio suggesting: (i) highly variable concentrations of V and Cr in the host-rock, *i.e.* the graphitic gneiss; (ii) variations of the intensity of fluid-rock interactions. In conclusion, the V/Cr ratio can be used to distinguish the geographic origin of most 'tsavorites' from the MB.

[1] Switzer, G.S. (1974) *Gems Gemol.*, **14**, 296-297. [2] Gübelin, E.J. & Weibel, M. (1975) *Lapidary J.*, **29**, 402-426.

Tektites and microtektites Fe oxidation state and water content

Giuli, G.[1*], Eeckhout, S.G.[2], Cicconi, M.R.[1], Koeberl, C.[3], Glass, B.P.[4], Pratesi, G.[5], Cestelli-Guidi, M.[6], Marcelli, A.[6], Carroll, M.R.[1] & Paris, E.[1]

[1]Dip. Scienze della Terra, Universita' di Camerino, Italy ([*]gabriele.giuli@unicam.it)

[2]European Synchrotron Radiation Facility (ESRF), Grenoble, France

[3]Dept. of Lithospheric Research, University of Vienna, Austria

[4]Dept. of Geology, University of Delaware, Newark, USA

[5]Dip. Scienze della Terra, Universita' di Firenze, Italy

[6]LNF-INFN, Frascati, Italy

Asteroid or cometary impacts onto the Earth surface are known to have played an important role in modifying the composition of the earth crust. Impact glasses, resulting from the rapid cooling of the molten target rock, are clues of the complex melting and metamorphic processes taking place during an impact. Tektites and micro-tektites are a sub class of impact glasses formed during the very first stages of the cratering process by high temperature melting of the target rock. They usually display rounded shapes and can be found over wide areas called strewn fields. As Fe oxidation state could be a useful probe to obtain information on the formation conditions of tektites, it has been the focus of many studies. However, the difficulties in analysing samples with small dimensions and high Fe dilution have so far hindered the possibility to systematically study the Fe oxidation state in these glasses.

To this aim, XANES is an ideal technique as it allows to determine the Fe oxidation state also in small samples even at very high dilution without deteriorating the error in the $Fe^{3+}/(Fe^{2+}+Fe^{3+})$ ratio. Fe K-edge XANES spectra have been collected in fluorescence mode at the ID26 beamline of ESRF using a Si (311) monochromator focusing the X-ray beam down to about 50 x 200 μm. The excellent energy reproducibility (±0.03 eV) allowed to obtain a small error in the determination of the Fe oxidation state. Micro-IR data have been collected in transmission mode at the LNF (Frascati, Italy). Areal analyses (50 x 50 μm) have been collected for 16 moldavites, 7 North American tektites and 5 microtektites.

Tektite glasses display $Fe^{3+}/(Fe^{2+}+Fe^{3+})$ ratios close to 0.05 (±0.03). With few exceptions (moldavites from the Moravian area), no significant variations have been found in the Fe oxidation state of tektite samples according to impact age or target rock composition [1]. Even for very large impacts events, where the target rock presumably displayed a wide range of Fe oxidation states, tektites have been homogeneously reduced to almost exclusively Fe^{2+} [2]. Similar behaviour has been observed in molten rock from the first atomic bomb test (Alamogordo, USA) [3]. Contrary to tektites, North American microtektites show a wide variation in the Fe oxidation state raising the issue of a possible difference with the formation mechanism of tektites [4].

Water content of all the tektites and microtektites are in the range of already published tektite water content data and display no correlation with the Fe oxidation state. The low water content of North American microtektites studied suggests that there has been no sea-water induced alteration in these samples, thus strongly suggesting that the variation of the Fe oxidation state in the North American microtektite samples studied here is not due to secondary alteration. We maintain that the mechanism responsible for NA microtektite oxidation is not sea-water alteration, nor oxidation in air.

[1] Giuli, G. et al. (2002) *Geochim. Cosmochim. Ac.*, **66**, 4347-4353. [2] Giuli, G. et al. (in press) *Geol. S. Am. S.* [3] Giuli, G. et al. (in press) *Geol. S. Am. S.* [4] Giuli, G. et al. (in prep).

Buddha from space – an ancient object of art made of a Chinga iron meteorite fragment

Buchner, E.[1,2*], Schmieder, M.[1], Kurat, G.[3], Kramar, U.[4], Kröchert, J.[1] & Ntaflos, Th.[5]

[1]Institut für Planetologie, Universität Stuttgart, Germany ([*]elmar.buchner@geologie.uni-stuttgart.de)

[2]HNU Neu-Ulm University, Germany

[3]Formerly: Museum of Natural History, Vienna, Austria

[4]University of Karlsruhe, Germany

[5]University of Vienna, Austria

In memoriam Gero Kurat († 27.11.2009)

Meteorites have been regarded as devotional and ritual objects by multitudinous cultures since prehistoric times. Objects of art made of meteoritic iron were found in old Egyptian king tombs and in Mesopotamian sanctuaries. In the Buddhist art in the Middle and Far East (e.g., [1]), meteoritic iron used to be carved but that tradition died out a long time ago, and only ancient artifacts are known. Figurative illustrations or religious sculptures of gods carved in meteorites are not reported in the literature. We here present a sculpture made of an iron meteorite that displays a unique particularity in religious art.

Origin and age of the sculpture, carved from one piece of iron meteorite (now ~10.6 kg and about 24 x 13 x 10 cm) [2,3], is still a matter of speculation. The Swastika on the cuirass of the statue is a minimum 3000 years old Indian sun symbol and is used as an allegory of fortune to date; the scale armor was originally gilded. The sculpture possibly portrays the Buddhist god Vaiśravana (also called Jambhala or Namthöse in Tibet, or Hindu Kubera), either a God of fortune and wealthiness or a God of war (e.g., [4]). The provenance of the meteorite sculpture strongly points to Central Asia.

A plate (~1cm thick, ~500 g) was cut from the base of the sculpture. The texture of the metal is that of a Ni-rich ataxite with streight and curved schlieren bands visible at the etched surface. It fits in detail that of the Chinga (IRUNGR) meteorite. The metal consists of a very fine-grained intergrowth of kamacite and taenite (16 wt% Ni, 0.6 wt% Co), which includes a few daubreelite ($FeCr_2S_4$) crystals of varying size (<1-10 mm) and small (<1 mm) kamacite spindles (5 wt% Ni, 0.6 wt% Co), both rimmed by clear taenite. Clear taenite also forms very long (>10 mm), thin bands, one of which grades into a fissure that contains brecciated taenite, metal, and silicates set in rust.

Detailed geochemical analyses of the iron meteorite revealed mean values for Fe: 84.3 wt% (Chinga: 83.6 wt%), Ni: 15.7 wt% (Chinga: 16.4 wt%), Co: 0.6 wt% (Chinga: 0.57 wt%), and Cr: 897 ppm (Chinga: 810 ppm), as well as a sigificant enrichment of the platinum group elements (PGE) [5-7]. Most of the trace element values analysed (i.e., the PGEs) perfectly fit the geochemical composition of the Chinga iron meteorite. As an exception, the Ge content is significantly higher compared to Chinga. The discrepancy may be caused by analytical imprecision and/or material inhomogeneities.

The data as a whole strongly suggest that the "meteorite man" is the third largest piece from the Chinga strewn field discovered in the border region of Siberia and Mongolia in 1912. One can speculate whether this specimen was discovered earlier as a single find. A part of the cut socket plate is stored at the Museum of Natural Sciences, Vienna. Further geochemical studies are under way.

[1] Kotowiecki, A. (2004) *Meteoritics Planet. Sci.*, **39**, 151-156. [2] Buchner, E. et al. (2009) *72nd MetSoc*, abstr. #**5074**. [3] *National Geographic* Germany 12/2009. [4] Fisher, E.J. (1997) *Art of Tibet*. Thames & Hudson, New York. [5] Kramar, U. et al. (2001) *Planetary Space Sci.*, **49**, 831-837. [6] Schaudy, R. et al. (1972) *Icarus*, **17**, 174-192. [7] Buchwald, V.F. (1977) *Philos. T. Roy. Soc. A*, **286**, 453-454.

Origin of strong staining of olivine in the Martian meteorite Northwest Africa 2737

Bläß, U.W.[1*], Langenhorst, F.[2] & McCammon, C.A.[2]
[1]Institut für Geowissenschaften, Friedrich-Schiller Universität Jena, Germany ([*]Ulrich.Blaess@uni-jena.de)
[2]Bayerisches Geoinstitut, Universität Bayreuth, Germany

Intense brown staining of olivine from meteorites is attributed since a long time to shock damage (e.g. [1]). However, the origin of the staining is still not well understood and has been assigned either to shock-induced reduction or oxidation processes. The recently recovered Martian achondrite Northwest Africa 2737 (NWA 2737), which represents the second chassignite ever found, raises these questions again, because it exhibits distinct shock-related features compared to Chassigny, while its mineralogical composition is quite similar [2]. These features comprise essentially the dark appearance of the rock due to an intense olivine staining embedding rectangular sets of bright lamellae [2], a completely different noble gas content similar to shergottites [3] and the exsolution of metallic iron nanoparticles as first published by [4].

In order to gain a better understanding for the physical processes responsible for the formation of these unique shock-induced features and resulting implications to the shock-history of this meteorite, we have investigated in detail the microstructural features of NWA 2737 olivines using transmission electron microscopy (TEM). The trivalent iron fraction has been on average determined by Mössbauer milliprobe spectroscopy and locally by electron energy loss spectroscopy (EELS).

The results reveal that all strongly stained olivine regions are microstructurally characterised by the occurrence of metallic iron nanoparticles and a fine mottled contrast in TEM bright field images, which is due to an extremely high density of polygonised dislocations with Burgers vector [001]. The quantification of EELS-spectra of these regions resulted locally in a high trivalent iron fraction of up to 16 %. In contrast, the bright lamellae contain nearly no metallic nanoparticles, a sufficiently lower trivalent iron fraction and at least one order of magnitude lower density of individual dislocations.

Model calculations confirmed our hypothesis that a sufficient amount of trivalent iron can be incorporated as a laihunite-component into the dislocation core of polygonised dislocations and could therefore be responsible for the intense brown staining. Iron metallic nanoparticles would represent residual disproportionation products and darken the olivine additionally. Resulting spectra are consistent with spectroscopic observations described by [5]. Since the polygonisation of dislocations and the exsolution of metallic iron are both diffusion controlled processes, the meteorite must have remained sufficient time at elevated temperatures. For typical diffusion length of < 10 nm in this meteorite we calculated an annealing time of several days at ~ 500°C or < 1 hour at 800°C.

The different microstructural characteristics of the bright lamellae comprise considerable implications for the shock history of the meteorite. The lamellae are interpreted as regions, which re-crystallised simultaneously during the annealing process. Therefore implemented individual dislocations argue for the occurrence of a second impact event, which likely caused to the ejection of this unique meteorite from Mars.

[1] Stöffler, D. et al. (1991) *Geochim Cosmochim Ac.*, **55**, 3845-3867. [2] Beck, P. et al. (2006) *Geochim Cosmochim Ac.*, **70**, 2127-2139. [3] Marty, B. et al. (2006) *Meteorit. Planet. Sci.*, **41**, 739-748. [4] Van de Moortèle, B. et al. (2007) *Earth Planet. Sci. Lett.*, **262**, 37-49. [5] Pieters, C.M. et al. (2008) *J. Geophys. Res.*, **113**, E06004.

On the darkening of olivine in Martian meteorites

Mikouchi, T.[*] & Kurihara, T.
Dept. of Earth and Planetary Science, University of Tokyo, Japan ([*]mikouchi@eps.s.u-tokyo.ac.jp)

Olivine is one of the major minerals in Martian meteorites, but their color is sometimes darkened unlike other extraterrestrial olivines. Recent TEM studies on the NWA2737 chassignite revealed that Fe-Ni metal nano-particles in olivine were responsible for the dark color of olivine. Color change of olivine is important to properly understand the remote sensing data and their magnetic signatures. Since similar dark olivine is fairly common among Martian meteorites, especially in shergottites, Fe-Ni metal nano-particles may be widely present in these olivine grains. Here we report TEM observations of olivine in several Martian meteorites and discuss their formation by using the results of shock experiments on olivine.

We found nano-particles in all samples we studied whose sizes range 5-20 nm in diameter. Their abundance appears related to the degree of darkening. ALH77005 and Y000097 contain Fe-Ni metal nano-particles similar to NWA2737. However, magnetite nano-particles were found (5-20 nm) in LEW88516, NWA1950, Dhofar 019, and LAR06319 (Fig. 1). The presence of magnetite nano-particles would be also responsible for the darkening of olivine similar to the case of Fe-Ni metal nano-particles.

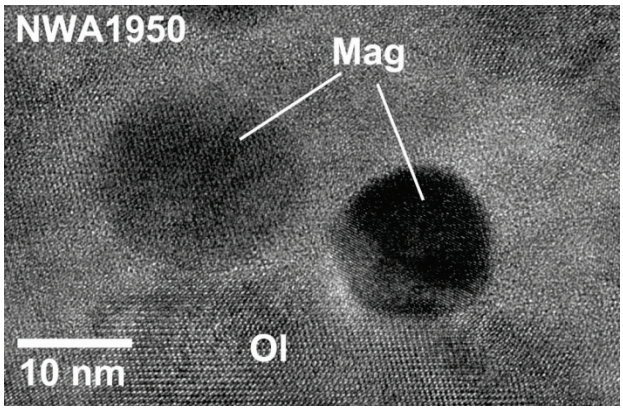

Fig. 1: High resolution TEM image of magnetite nano-particles in olivine from the NWA1950 lherzolitic shergottite.

There has been suggested that Fe-Ni nano-particles have formed by reduction of Fe^{2+} in olivine during heavy shock. Although the formation of magnetite requires oxidation of Fe^{2+}, similar shock metamorphism should be responsible for the formation of magnetite nano-particles. In order to demonstrate the possibility of the nano-particle formation in olivine, we performed shock experiments on San Carlos olivine (Fo_{90}) at 20, 30, 40, and 46 GPa. We found that shock pressure higher than 30 GPa produced magnetite nano-particles in olivine. These shock degrees are consistent with the observation that only highly-shocked Martian meteorites contain dark olivine. It is interesting that both Fe-Ni metal and magnetite coexist in different shergottite samples. The formation of different Fe-rich nano-particles would be explained by the different redox state during shock on (or near) the Martian surface. However, it is unlikely to suppose drastic change of redox state among Martian meteorites because they crystallized under similar conditions (e.g., fO_2, burial depth, crystallization age). Then, temperature difference during shock could be another possible factor. When temperature increase was significant, Fe-Ni nano-particles would be formed rather than magnetite. In fact, we could produce Fe-Ni metal nano-particles instead of magnetite for the preheated (400 and 800°C) San Carlos olivine at 40 GPa.

Soil components in heterogeneous impact glass in Martian meteorite EETA79001

Schrader, C.M.[1*], Cohen, B.A.[2], Donovan, J.J.[3] & Vicenzi, E.P.[4]
[1]NASA-ORAU, Marshall Space Flight Center, Huntsville AL, USA ([*]Christian.M.Schrader@nasa.gov)
[2]NASA, Marshall Space Flight Center, Huntsville AL, USA
[3]Dept. of Chemistry, Univ. of Oregon, Eugene OR, USA
[4]Smithsonian Inst., Museum Conservation Inst., Washington DC, USA

Martian soil composition can illuminate past and ongoing near-surface processes such as impact gardening [2] and hydrothermal and volcanic activity [3,4]. Though the Mars Exploration Rovers (MER) have analyzed the major-element composition of Martian soils, no soil samples have been returned to Earth for detailed chemical analysis. Rao et al. [1] suggested that Martian meteorite EETA79001 contains melted Martian soil in its impact glass (Lithology C) based on sulfur enrichment of Lithology C relative to the meteorite's basaltic lithologies (A and B) [1,2]. If true, it may be possible to extract detailed soil chemical analyses using this meteoritic sample.

We conducted high-resolution (~0.3 µm/pixel) element mapping of Lithology C in thin section EETA79001,18 by energy dispersive spectrometry (EDS). We use these data for principal component analysis (PCA).

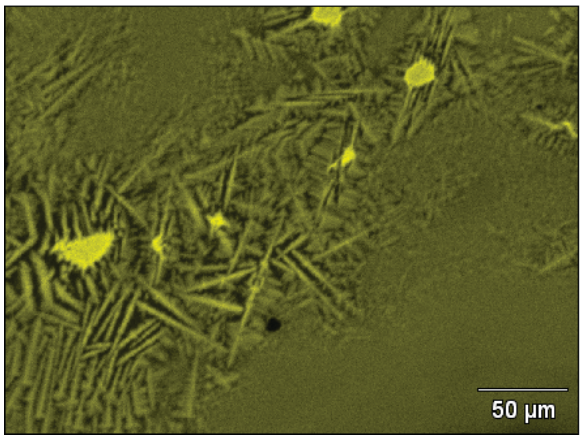

Fig. 1: Magnesium map of EETA79001 Lithology C. Brighter yellow colors correspond to higher Mg contents of pixel. Yellow, sub-angular relict olivine and elongate quench crystals are set in a glassy matrix.

Though visually glassy, EETA79001 Lithology C is heterogeneous. PCA identifies several significant components that may originate either in the basalt or in the soil, but one component with strongly positive eigenvectors for K and Cl likely represents a soluble soil component originating by hydrothermal or evaporitic processes.

We are conducting quantitative beam analysis of the glass to determine minor and trace elements, including halogens. We will compare these to compositions of EETA79001 basalt [5,6] and to MER rock and soil compositions [7,8,9] to constrain the origin of components in EETA79001 Lithology C.

[1] Rao, M.N. et al. (1999) *Geophys. Res. Lett.*, **26**, 3265-3268. [2] Rao, M.N., & McKay, D.S. (2002) *65th Ann. Meeting of the Met. Soc.*, # **5042**. [3] Newsom, H.E. and Haggerty (1999) *J. Goephys. Res.*, **104**, 8717-8728. [4] Sutton, S.R. et al. (2002) LPSC XXXIII, #**1278**. [5] Mellin, M.J. et al. (2007) LPSC XXXVIII, #**2324**. [6] Mellin, M.J. et al. (2008) LPSC XXXIX, #**2150**. [7] McSween, H.Y. et al. (2004) *Science*, **305**, 842-845. [8] Gellert, R. et al. (2004) *Science*, **305**, 829-832. [9] Rieder, R. et al. (2004) *Science*, **306**, 1746-1749.

Occurrences and mineral chemistry of chromite and xieite in the shocked Suizhou L6 chondrite

Xie Xiande[*], Chen Ming, Wang Deqiang & Wang Chunyun
Guangzhou Institute of Geochemistry, Chinese Academy of Sciences, Guangzhou, China (*xdxie@gzb.ac.cn)

Three types of occurrences for chromite were observed in the Suizhou L6 chondrite: coarse chromite, cluster of tiny chromite fragments in molten plagioclase, and exsolution chromite in olivine. All the chromite grains of the first two types are remarkably similar in chemical compositions, no matter how fine the chromite fragments are in molten plagioclase, but the composition of exsolution chromite is variable in Al_2O_3, MgO, Cr_2O_3 and not so homogeneous.

Xieite is a post-spinel CT-phase of chromite firstly found in the Suizhou meteorite [1-3]. Three types of occurrences of xieite have also been revealed in this meteorite: coarse xieite grains, complex three-zone- grains consisting of the inner xieite, the intermediate lamellae-like CF-phase and the outer chromite phase, and two-phase-grains consisting of xieite and one of the high-pressure silicate minerals lingunite, ringwoodite or majorite. The curved boundary between xieite and the silicate half in two-phase grains is indicative of some partial or even full melting of the silicate phase.

EPMA results show that the compositions of xieite inside/contacting the veins are also identical to that of chromite outside the veins. However, some element diffusion appeared in between the xieite and the silicate halves in the two-phase grains. For the xieite + lingunite grains, xieite contains higher content of Al_2O_3 (6.19 *vs* 5.45 wt %) and lower content of Cr_2O_3 (56.48 *vs* 57.98 wt %) than its precursor chromite. On the other hand, the lingunite contains higher contents of Cr_2O_3 (0.32 *vs* 0.03 wt %) and FeO (1.97 *vs* 0.41 wt %), and lower contents of Al_2O_3 (19.98 *vs* 21.73 wt %) than its precursor plagioclase. For the xieite + ringwoodite grains, some of Fe^{2+} from ringwoodite migrated to xieite, and some of Cr^{3+} migrated from xieite to ringwoodite. Majorite garnet in two-phase grains is fully molten and shows remarkable decrease of SiO_2 and MgO, and notable increase of Al_2O_3, CaO and Cr_2O_3. The complexity in mineral chemistry of these two-phase grains can be explained by the much higher shock peak temperature in melt veins (1800-2000°C) than in unmelted chondritic rock (~1000°C)[4], and by the much higher density of xieite (5.63 g/cm^3) than the silicates (<3.80 g/cm^3). Being a refractory and a high-impedance material, xieite is chemically more stable and easier to reflect shock wave into the silicate halves and to cause the partial or even full melting of silicate phases, upon which some diffusion or exchanges of elements between the two phases themselves, or even mixing of molten majorite garnet and the surrounding silicate melt took place.

[1] Chen, M. et al. (2002) *Geochim. Cosmochim. Ac.*, **67**, 3937-3942. [2] Chen, M. et al. (2003) *Proc. Natl. Acad. Sci. USA*, **100**, 14651-14654. [3] Chen et al. (2003) *Chinese Science. Bull.*, **53**, 3341-3345. [4] Xie, X. et al. (2001) *Eur. J. Mineral.*, **13**, 1177-1190.

Carbonate spherules as Chicxulub ejecta in the K-Pg event deposit: detailed characteristics as revealed by micro-chemical and EBSD

Deutsch, A.[1*], Schulte, P.[2] & Salge, T.[3]
[1]Institut für Planetologie, Universität Münster, Germany
([*]deutsca@uni-muenster.de)
[2]GeoZentrum Nordbayern, Universität Erlangen, Germany
[3]Bruker Nano GmbH, Berlin, Germany

New petrographic observations suggest that considerable amounts of carbonate melt were generated and ejected by the Chicxulub impact, and deposited in the Gulf of Mexico region [1]. The amount of carbonate ejecta frequently exceeds that one of silicic melt lithologies in K-Pg event beds. Carbonate and silicic melts were dispersed concurrent but as distinct melt batches that, in part, were mixed as evidenced by emulsion-like bubbly textures and Cc spherules with thin shells of silicic melt.

Carbonate spherules in the Chicxulub ejecta deposits addressed by previous authors [e.g. 2-4] as alteration product of silicic melt droplets display very complicated textures that cannot be understood in terms of pseudomorphic replacement.

Currently we are evaluating the criteria necessary to distinguish primary textures from those grown during alteration and diagenesis using microchemical, cathodoluminescence, and electron back-scatter diffractions techniques.

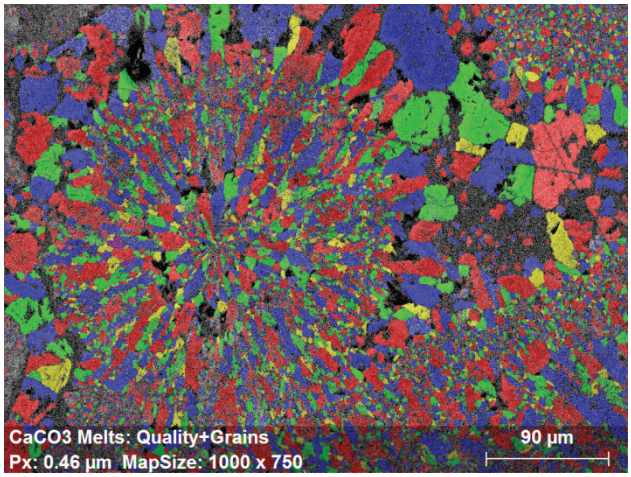

Fig. 1: EBSB micrograph of a carbonate spherule from El Guayal, S. Mexico with radially grown Cc crystals. SEM: ZEISS Supra 55, beam current ~11 nA, HV: 15kV.

[1] Deutsch, A. & Schulte, P. (2010) *41 Lunar Planet. Sci. Conf.*, abstract **1596**. [2] King Jr., D.T. & Petruny, L.W. (2008) *Geol. S. Am. S.*, **437**, 178-187. [3] Pitakpaivan K. et al. (1994) *Earth Planet. Sci. Lett.*, **124**, 49-56. [4] Bohor, B.F. & Glass, B.P. (1995) *Meteoritics*, **30**, 182-198.

Shock-metamorphic effects in chert: evidence from the Jebel Waqf as Suwwan impact structure, Jordan

Schmieder, M.[1*], Buchner, E.[2,1], Reimold, W.U.[3], Khirfan, M.[4], Salameh, E.[4] & Khoury, H.[4]
[1]Institut für Planetologie, Universität Stuttgart, Germany
([*]martin.schmieder@geologie.uni-stuttgart.de)
[2]HNU Neu-Ulm University, Germany
[3]Museum for Natural History, Berlin, Germany
[4]University of Jordan, Amman, Jordan

The petrographic study of a chert nodule recovered from the central uplift of the recently discovered ~6 km Jebel Waqf as Suwwan impact structure, Jordan [1,2], revealed - in addition to some well-established shock-metamorphic effects in quartz [3,4] - new potential shock features in crypto- to microcrystalline varieties of silica. The microcrystalline chert groundmass exhibits a dendritic and a superimposed orthogonal fracture pattern at the cm- to mm-scale, commonly associated with microscopic quartz 'recrystallization bands' that intersect the primary diagenetic chert fabric. Aggregates of spherulitic microfibrous silica (first-generation chalcedony *sensu stricto* and second-generation quartzine [5]) in veins are locally of shattered appearance. Quartzine shows conspicuous sets of 'curved fractures' (Fig. 1A) that run perpendicular to the fiber direction (c-axis) and commonly trend subparallel to planar fractures (PF) in neighbouring coarser-crystalline shocked quartz. Quartz exhibits PF, sometimes combined with feather features (FF) [6] (Fig. 1B), and mainly single sets of planar deformation features (PDF) parallel to the basal plane (0001) (Brazil twins) with rare additional PDF in the {10-13} direction.

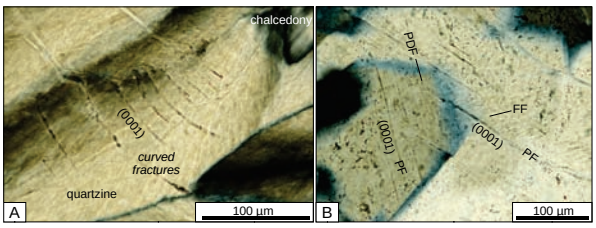

Fig. 1: Microdeformation features in chert from Jebel Waqf as Suwwan, Jordan; **A**: 'curved fractures' in microfibrous spherulitic quartzine; **B**: shocked quartz exhibiting planar deformation features (PDF), planar fractures (PF), and feather features (FF) (A and B cross-polarized light).

Shock petrography indicates shock pressures of ≥10 GPa and high shock-induced differential stresses [4,7] that affected the chert nodule as a whole. The internal crosscutting relationships between primary diagenetic and deformational features suggest that the dendritic-orthogonal fractures in the chert groundmass are post-diagenetic and most likely related to impact-induced shear deformation. Curved fractures in spherulitic quartzine (as possible microstructural equivalents to planar fractures parallel to the basal plane in quartz) might represent particular low- to medium-pressure shock effects in cryptocrystalline fibrous silica, unless noted in rocks not affected by shock metamorphism. Recrystallization bands probably represent healed fractures and cannot be linked with either shock or shear deformation. A systematic comparative study of deformation features in cherts from various terrestrial impact structures and cherts deformed by diagenesis and tectonism is planned.

[1] Salameh, E. et al. (2008) *Meteoritics Planet. Sci.*, **43**, 1681-1690. [2] Kenkmann, T. et al. (2010) *Geol. S. Am S.* (in press). [3] Stöffler, D. & Langenhorst, F. (1994) *Meteoritics*, **29**, 155-181. [4] French, B.M. (1998) *Traces of Catastrophe*. LPI Contrib., 954. [5] Hesse, R. (1989) *Earth Sci. Rev.*, **26**, 253-284. [6] Poelchau, M.H. & Kenkmann, T. (2010) *LPSC* XLI, #1987. [7] Trepmann, C.A. (2008) *Earth Planet. Sci. Lett.*, **267**, 322-332.

Feather features as a new low shock pressure feature in quartz

Poelchau, M.H.* & Kenkmann, T.
Museum für Naturkunde, Berlin, Germany
(*michael.poelchau@mfn-berlin.de)

In impact cratering research, the recognition of planar deformation features, (PDFs; sets of 2-3 µm wide, amorphous lamellae), in quartz and other minerals is generally accepted as one of the strongest unequivocal indicators for shock metamorphism, and thus is commonly used to determine if a geological structure is an impact feature. Experimental research has shown that the onset of PDF formation is at >10 GPa. To date, very little systematic research has been done in the shock pressure regime from ~3 to 10 GPa. The recognition of the lowest possible pressures at which unequivocal shock features are induced requires further experimental work and the comparison to natural samples. Feather features (FFs), a recently discovered planar microstructure found in shocked quartz, have the potential to become a standard low-shock pressure indicator.

In the current study, feather features in samples from the Nördlinger Ries (Germany) and the Matt Wilson (Australia) impact structure were microscopically analyzed and crystallographically indexed. FFs occur as short, parallel to subparallel lamellae with a similar spacing as, or sometimes even narrower than, planar deformation features, and are always found in combination with a planar fracture (PF). FFs are crystallographically controlled to a certain degree, with the majority of lamellae oriented parallel to rational low index crystallographic planes. FFs are typically straight and parallel close to their base at the PF and become increasingly curved with progressing length, sometimes even intersecting each other. Angles measured between PFs and sets of FFs average at 50-60°.

Microscopic analysis of quartz grains with feather features show that their formation is linked to shearing along the associated PFs during shock deformation. When the sense of shearing can be determined, FFs are always oriented in the same direction according to the sense of shear. The formation of FFs along sheared PFs implies that high deviatoric stresses in the order of ~5 GPa are necessary, along with elevated confining pressures found in low-pressure shock waves that have progressed further away from the point of impact.

Quartz grains in one thin section of an unoriented sample, MW7, a coarse-grained sandstone, were measured with a U-stage and plotted in stereoplots. PFs in the thin section can be divided into two groups oriented 90° to each other, representing a conjugate set of shear fractures. The majority of sets FFs were all parallel to each other ±~20°. The orientation of PFs and FFs in rock samples is suggested to be controlled by loading along the principle axis of stress in the shock wave, with sheared PFs at ~45° angles to the axis and feather features aligned ±parallel to the axis.

Controlled plane wave shock recovery experiments were performed at the Ernst Mach Institute in Weil am Rhein, Germany, on cylindrical samples of single crystal quartz. Shear fractures with FFs were generated in the pressure range of ~7-10 GPa, thus confirming that FFs are microstructures that can be induced by low-pressure shock waves.

Experiments and FFs found in natural samples that lack PDFs show that FFs can be defined as microstructures that have a lower formation limit at shock levels <10 GPa. Based on their appearance in shocked quartz grains in an increasing number of impact craters (25 so far) and the current lack of reports of these features in endogenically deformed crustal rocks, their uniqueness as a new type of impact-induced planar microstructure alongside PDFs and PFs is proposed.

Geochemical characterization of a large collection of moldavites by neutron, photon, and prompt gamma activation analyses

Mizera, J.[1*], Řanda, Z.[1], Tomandl, I.[1], Skála, R.[2] & Žák, K.[2]
[1]Nuclear Physics Inst., Academy of Sciences of the Czech Republic, Řež, Czech Republic (*mizera@ujf.cas.cz)
[2]Institute of Geology, Academy of Sciences of the Czech Republic, Praha, Czech Republic

The study presents geochemical characterization of a large collection of more than one hundred moldavites based on determination of about fifty major and trace elements using various modes of instrumental neutron activation analysis, supplemented by instrumental photon activation analysis and prompt gamma activation analysis (INAA, IPAA, and PGAA, respectively). The collection includes moldavites from the major parts of the Central European tektite strewn field: Southern Bohemia (59 samples including 4 samples from Radomilice area), Cheb Basin (30 samples), Moravia (13 samples), and Lusatia (1 sample). The study provides information on detailed chemical composition of well documented (by site location, size, colour, etc.) samples, unbiased with interlaboratory systematic errors. Information on contents of some elements, as fluorine and boron determined at the ten ppm level by IPAA and PGAA, respectively, has so far been unavailable. Correlation/cluster analysis was applied to the obtained geochemical data and the results have been discussed in view of parent materials and processes involved in formation and subsequent geographical distribution of moldavites.

In agreement with previously published data, the analysis enabled quite clear distinction of the sample sets associated with individual moldavite substrewn fields, and assigning their parent materials based on the generally accepted concept of three main components of the moldavite parent materials - quartz sands, clay and clayey soil, and carbonates of Ca and Mg. From this standpoint, the Moravian moldavites (and the only available sample from Lusatia) represent samples with the most pronounced imprint of the clay component, expressed mainly by higher aluminium content and its perfect correlation with contents of the elements associated with the phyllosilicate minerals. The widespread elemental pattern of the largest group of the South Bohemian moldavites points to mixing of the three components in various ratios. Moldavites from the latest discovered substrewn field, the Cheb Basin, or at least their substantial fraction, have elemental patterns quite different from the other groups, which can be hardly satisfactorily interpreted by the present three-component system. Significant positive correlations between K, Ca, Mg and Mn, and the enrichment in these elements observed in the Cheb Basin moldavites, as well as other facts, as high K/Na and K/Rb ratios, extremely high Zn and Ba levels, etc., may be attributed to source materials originated from the uppermost soil layers, with possible contribution of the ash produced by burning of vegetation present in the pre-impact Ries area under the extreme thermal and pressure condition of the meteoritic impact.

Formation of pseudotachylitic breccias from the Vredefort Dome, South Africa

Mohr-Westheide, T.[1*], Reimold, W.U.[1], Gibson, R.L.[2], Mader, D.[3] & Koeberl, C.[3]
[1]Museum für Naturkunde, Leibniz Institute at Humboldt University Berlin, Germany ([*]Tanja.Mohr@mfn-Berlin.de)
[2]School of Geosciences, University of the Witwatersrand, Johannesburg, RSA
[3]Dept. of Lithospheric Research, University of Vienna, Austria

"Pseudotachylite" is friction melt formed along faults or shear zones. It is produced by frictional heating, which generally requires sliding velocities consistent with seismic slip. The distinction between "impact" and "tectonic" "pseudotachylite" plays an important role in impact settings, as melt breccias in impact structures often closely resemble tectonic friction melt but may have been formed by different processes: (1) shearing (friction melting); (2) shock compression melting (with or without a shear component); (3) decompression melting immediately after shock propagation through the target / related to rapid uplift; (4) combinations of these processes; (5) intrusion of allochthonous impact melt. Resolving this problem requires detailed multidisciplinary analysis in order to comprehensively characterize the nature of these breccias and to identify the exact melt-forming process(es). In order to distinguish between bona fide "pseudotachylite" and breccias of similar appearance in impact structures of still debated origin we refer in the latter case to "pseudotachylitic breccia" (PTB).

PTB are the most prominent impact-induced deformation in the central uplift of the Vredefort Impact Structure [1,2]; similar breccias occur in abundance also at Sudbury, Canada (e.g., [3,4]). We present chemical data for small-scale (1 mm – 3 cm) PTB from mafic (dioritic) and granitic host rocks and compare with the chemical compositions of their respective host rocks.

Electron microprobe analysis of PTB groundmass in comparison to XRF bulk chemical analysis of pseudotachylitic breccias and their host rocks revealed that PTB generally displays a close chemical relationship to the adjacent host rock. This confirms that melt was formed from material of the same composition and for mm to cm wide breccia veinlets is of local origin. In granitic environments, the refractory behavior of quartz seems to be the main reason for the slight chemical differences between PTB and host rock. Our first chemical investigations of PTBs in mafic host rocks revealed that the elements associated with plagioclase and/or hydrous ferromagnesian minerals are enriched in PTB veins. PTB seemingly occur preferentially in amphibole-rich host rock portions – an observation that confirms the macroscopic observations of [5,6]. Thus, PTB genesis in mafic host rock seems to be controlled by the mineralogical composition of the target rock. A further factor is likely the melting temperature of minerals involved that determines the ratio at which feldspar and mafic minerals are melted.

None of the analyzed veinlets has yielded any textural evidence supporting a significant influence from shearing /faulting. Our PTB's of up to 1 m width all contain clast populations that represent local lithologies only, with distinct differences between clast population and host rock mineral abundances likely the result of different mechanical behavior and different melting temperatures of the various minerals.

[1] Dressler, B.O. & Reimold, W.U. (2004) *Earth Sci. Rev.*, **67**, 1-60. [2] Reimold, W.U. & Gibson, R.L. (2006) *Geol. S. Am S.*, **405**, 233-253. [3] Dressler, B.O. (1984) *Ontario Geol. Surv.*, **1**, 97-284. [4] Lafrance, B. et al. (2008) *Precambrian Res.*, **165**, 107-119. [5] Reimold, W.U. & Colliston, W.P. (1994) *Geol. S. Am S.*, **293**, 177-196. [6] Reimold, W.U. (1991) *Neues. Jb. Miner.*, **161**, 151-184.

Teaching evolution of a chondritic asteroidal body using the Antarctic Meteorite Educational Thin Section Set of the National Institute of Polar Research, Tokyo, Japan

Bérczi, Sz.[1*], Józsa, S.[2], Szakmány, Gy.[2], Gucsik, A.[3], Nagy, Sz.[1], Gyollai, I.[1], Ninagawa, K.[4] & Nishido, H.[4]
[1]Cosmic Materials Space Research Group, Eötvös University, Budapest, Hungary ([*]bercziszani@ludens.elte.hu)
[2]Dept. of Petrology and Geochemistry, Eötvös University, Budapest, Hungary
[3]Max Planck Institute for Chemistry, Mainz, Germany
[4]Okayama University of Science, Okayama, Japan

A set of Antarctic Meteorites (30 polished thin sections) supplied by the National Institute of Polar Research (NIPR), Tokyo, Japan, was lent to Eötvös University 15 years ago. This availability has promoted our synthesis of an evolutionary path of regions (belts) in the chondritic parent body arranging the chondritic set members according to the degree of thermal metamorphism. We deduced crust and core region set members after the differentiation of the parent body. Metamorphism stages can be demonstrated for the H, L and LL chondritic types in the NIPR set [2]. Later stage differentiation after the primitive achondritic stage (represented by the primitive achondrite itself and by the ureilite sample) can be shown by various layers in the gradually differentiating body. A pallasite sample corresponds to the boundary region between the iron core and the outer olivine rich mantle. Mesosiderite is a representative of the region where partial melting of iron and iron-sulfide components began. Second stage partial melts are characteristic of the HED meteorites which moved to the surface. HED meteorites are both in igneous and brecciated forms in the set.

The NIPR set also contains two lunar and one Martian meteorite sample. Parallel use of the NASA Lunar Meteorite Set allows comparisons between in situ collected and impact delivered lunar samples. The main difference is in the shock stage between the two sources. Impact ejected samples always contain maskelynite. Shock effects also affect several chondrites. For example, L6 specimens frequently contain shock-transformed high pressure minerals.

The NIPR set has basic importance in space science and cosmomineralogical education. This collection involves thermal metamorphism, partial melting of components, and the shock events that occurred on the surface of the asteroids.. Mineralogical studies on the processes responsible for the chondritic assemblages were also closely related to other terrestrial and even industrial technological processes (in steel industry, ceramics) - broadening the perspective of the students in the course of cosmic material studies [3].

Acknowledgments: We thank the National Institute of Polar Research for the loan of the Antarctic Meteorite Educational Thin Section Set to Eötvös University.

[1] Yanai, K. & Kojima, H. (1987) *Photographic Catalog of the Antarctic Meteorites.* NIPR. Tokyo. [2] Lukács, B. et al. (2005) *36th Lunar Planet. Sci. Conf.*, #**1300**. LPI, Houston. [3] Bérczi, Sz. et al. (2008) *Meteorit. Planet. Sci.*, **43(7)**, A23.

Cathodoluminescence characterization of forsterite in Kaba meteorite

Endo, T.[1], Nakazato, T.[1], Kayama, M.[1], Nishido, H.[1*], Ninagawa, K.[1], Gucsik, A.[2,3], Bérczi, Sz.[4], Rózsa, P.[5], Posta, J.[5] & Nagy, M.[6]
[1]Okayama University of Science, Okayama, Japan ([*]nishido@rins.ous.ac.jp)
[2]Max Planck Institute for Chemistry, Mainz, Germany
[3]Savaria University Center, Szombathely, Hungary
[4]Eötvös University, Budapest, Hungary
[5]Debrecen University, Debrecen, Hungary
[6]Reform College, Debrecen, Hungary

Kaba carbonaceous chondrite is the most primitive unshocked CVoxB fall collected nearby the Kaba village, East Hungary. It contains many types of chondrules associated with porphyritic, granular, radial and barred olivine, which have a variety of composition including almost end members of forsterite and fayalite occasionally with normal or reversed zoning. Cathodoluminescence (CL) has been used to characterize meteoritic minerals such as olivine and feldspar for the investigation of thermal history and shock pressure effect due to high detection sensitivities of structural defects and activator elements with high spatial resolution. In this study CL imaging and spectroscopy have been conducted to clarify formation mechanism of luminescent forsterite characteristic of Kaba meteorite stored at Debrecen University.

CL color imaging was carried out using Luminoscope (ELM-3R). CL scanning images at high magnification were recorded by a Mini-CL detector (Gatan) installed in a SEM. CL spectroscopy was made by a SEM-CL system, which is comprised of SEM (JEOL: JSM-5410) combined with a grating monochromator (OXFORD: Mono CL2).

Highly forsteric olivine (Fo: 99.2-99.7) emits bright CL, whereas the olivine containing fayalitic composition, even if only slightly, shows no luminescence due to quenching effect of divalent Fe ions. Red luminescent forsterite is predominant, and occasionally zoned forsterite shows blue in the core and red in the rim. CL spectra of red luminescent forsterite have two broad bands at approximately 630 nm in red region and over 700 nm in the IR region. The former band can be assigned to impurity centers of divalent Mn ions as an activator. The latter one shows a magnificent red emission in a wide range of wavelength responsible for trivalent Cr ions, which possess two components caused by Cr activator and structural defect related to interstitial Cr ions. CL spectra from blue luminescent area in the core of forsterite give a characteristic broad band emission at approximately 400 nm, also associated with minor red emissions related to Mn and Cr ions. This blue emission is attributed to intrinsic structural defect because it can be detected in pure synthetic forsterite. EPMA analysis of the forsterite reveals that minor elements of Mn (0.01-0.08 wt%), Cr (0.11-0.34 wt%) and Fe (0.22-0.86 wt%) are concentrated in red luminescent rim, but Ca (0.60-0.88 wt%) and Al (0.19-0.46 wt%) in blue luminescent core. In this case, the quenching effect of divalent Fe ions on CL might be slight and homogeneous over a forsterite grain due to low and unvaried concentration of Fe. Therefore, CL color variation observed in Kaba forsterite should be attributed to intrinsic structural defect, of which distribution cannot be detected by any other methods. It implies that aqueous alteration on the forsterite might eliminate intrinsic structural defects progressively from the rim of the grain to the core, accompanied by the migration of diffusible ions of Mn, Cr and Fe to the rim where Ca and Al ions might still lie in the core. This process could proceed at low temperatures (<300°C) over a short reaction time.

Review study of shock metamorphism on specimens of the Antarctic Meteorite Educational Thin Section Set of the National Institute of Polar Research, Tokyo, Japan

Gyollai, I.[1*], Bérczi, Sz.[1], Józsa, S.[1], Nagy, Sz.[1] & Gucsik, A.[2]
[1]Cosmic Materials Sp. R. Gr., Eötvös University, Budapest, Hungary ([*]gyildi@gmail.com)
[2]Max Planck Institute for Chemistry, Mainz, Germany

In studies on shock metamorphism of impact craters of Earth, quartz is an important index mineral. Several measuring techniques are based on shock features in quartz. Additionally, in meteorites shock features are present also in olivines, pyroxenes, and feldspars. On the basis of shock features presented by these 3 minerals, Stöffler et al (1991) [1] has elaborated a sequence of shock metamorphic stages, going from **S1** (unshocked) to **S2 (**very weakly shocked), **S3 (**weakly shocked), **S4 (**moderately shocked), **S5 (**strongly shocked) and finally to **S6 (**very strongly shocked).

For defining their degree of shock metamorphism, olivines, pyroxenes and feldspars have been studied petrographically in thin sections, as well as by means of infrared spectroscopy (for feldspar), and micro-Raman spectrometry in Antarctic meteorite specimens from the National Institute of Polar Research (NIPR) collection. A brief description follows.

Y-691 - EH3 chondrite: The sample is built up of microchondrules in an iron oxide-rich matrix. Most chondrules show poikilitic and granular texture realized by pyroxene and olivine. Pyroxenes show mechanical twins.

ALH-77257 – Ureilite is built up of olivine and pyroxene. As a rule, olivines show carbon- ontaining veins and aggregates at crystal boundaries. Pyroxenes show exsolution (augite-pigeonite) features and differently spaced mechanical twins.

Asuka-881757 - Lunar gabbro meteorite has coarse-grained texture and consists of olivine and pyroxene phenocrysts. One of the pyroxenes shows abundant mechanical twin lamallae and strong mosaicism. In the proximity of the pyroxene, the olivine with strong mosaicism shows short PDFs perpendicular to the exsolution (miscibility) lamellae.

ALH- 77005 – Shergottite has a coarse grained texture; it contains olivine and pyroxenes rich in fractures and veins. Features of shock metamorphism (*e.g.* PFs, PDFs) can be observed in olivine. There is a melt pocket in the sample, which contains glass and olivine needles and larger subgrained olivines. Some olivines consist of subgrains aggregates, pointing to solid state recrystallization.

Y-86032 - Lunar breccia contains a number of shocked minerals. Fractured feldspar, olivine and feldspar with strong mosaicism were noticed. PFs and PDFs are present in the olivine showing strong mosaicsm. The shock metamorphism can be both progressive and retrograde. A melt pocket is also incuded, where the glassy material started to recrystallize into feldspar needles.

Shock metamorphic features occur locally in some minerals but not in the whole rock samples. For the studied metorites, the following shock stages (according to Stöffler's scale, [1]) were defined: Y-691 (EH3) S3, ALH-77257 (ureilite) S2-S3, Asuka-881757 (lunar gabbro) S3-S5, ALH- 77005 (shergottite) S2-S6, and Y-86032 (lunar breccia) S4-S6.

[1] Stöffler, D., Keil, K. & Scott, E.R.D. (1991) *Geochim. Cosmochim. Ac.*, **55**, 3845-3867.

Cathodoluminescence spectroscopy on shock metamorphosed alkali feldspar

Kayama, M.[1*], Nishido, H.[1], Sekine, T.[2], Nakazato, T.[1] & Ninagawa, K.[3]
[1]Research Institute of Natural Sciences, Okayama University of Science, Okayama, Japan ([*]kayama@rins.ous.ac.jp)
[2]National Institute for Materials Science, Tsukuba, Japan
[3]Dept. of Applied Physics, Okayama University of Science, Okayama, Japan

Shock pressure induced on meteorites and impactites has been estimated based on refractive indices of plagioclase-maskelynite, which has been not available for weakly shocked materials below 15 GPa and micro-size samples. Cathodoluminescence (CL) spectroscopy provides useful information on the existence and distribution of defects and trace elements with high spatial resolution. This technique could be applied to clarify shock pressure effect on the feldspar in meteorites and impactites. In this study, CL spectral analyses of experimentally shocked sanidines and alkali feldspars in Martian meteorites have been conducted to characterize their emission mechanisms related to shock metamorphism.

Single crystal of sanidine from Eifel, Germany was selected as a starting material for shock recovery experiments at pressure of 10 to 40 GPa by a propellant gun. Alkali feldspars inducing diaplectic glasses in shergotty of Dhofar 019 ($Or_{49}Ab_{42}An_9$), Shergotty ($Or_{71}Ab_{22}An_7$), Zagami ($Or_{67}Ab_{26}An_7$) and NWA 2975 ($Or_{69}Ab_{28}An_3$), and in nakhlite of Yamato 000749 ($Or_{70}Ab_{27}An_3$) were employed for CL spectral measurements. CL spectra were obtained by SEM-CL system, which is comprised of SEM (JEOL: JSM-5410) combined with a grating monochromator (OXFORD: Mono CL2).

CL spectrum of unshocked sanidines has an emission band at 430 nm in UV-blue region. Shocked sanidine above 20 GPa have UV-blue CL emissions at 380 and 330 nm of which intensities increase with an increase in shock pressure. The shocked samples above 30 GPa and alkali feldspars in shergottite have emission bands at 380 and 330 nm. It indicates that these emission bands might be characteristic of CL signals derived from diaplectic glass. Spectral deconvolution of the CL in energy unit can successfully separate the emission bands into four Gaussian components at 2.82, 2.95, 3.26 and 3.88 eV. The integral intensities of these components closely relate to shock pressure on the sanidine, suggesting CL emissions derived from shock-induced defect centers. The deconvoluted CL spectra of all alkali feldspars in shergottite and nakhlite have a component at 2.95 eV. This correlationship could be employed for the calibration to estimate shock pressure on Martian meteorites. Furthermore, CL component at 2.95 eV is detected in other shocked alkali feldspar such as microcline with different structural order. Therefore, CL spectral deconvolution method allows us a new indicator for an evaluation of shock pressure in a wide range below 40 GPa for the micron-size alkali feldspar in meteorites and impactites. Quantitative estimation of shock pressure on the Martian meteorites using CL spectroscopy will be discussed here in detail.

CL characterization of shock-induced effects on the rock-forming minerals from Ries meteorite crater

Kayama, M.[1*], Nishido, H.[1], Endo, Y.[1], Gucsik, A.[2] & Ninagawa, K.[3]
[1]Research Institute of Natural Sciences, Okayama University of Science, Okayama, Japan ([*]kayama@rins.ous.ac.jp)
[2]Max Planck Institute for Chemistry, Mainz, Germany
[3]Dept. of Applied Physics, Okayama University of Science, Okayama, Japan

Cathodoluminescence (CL) spectroscopy and microscopy provide important information on the existence and distribution of defects and trace elements in materials, which are related to shock metamorphism. CL of silica minerals and feldspars in impactites and meteorites has been applied to examine the textures formed due to the shock metamorphism such as Planar Deformation Features (PDFs) containing amorphous lamellae system and to clarify high-pressure minerals (e.g., maskelynite). Only a few CL studies on rock-forming minerals in impactites, however, have been reported so far. In this study, the CL of quartz and alkali feldspar from the Ries Crater has been measured to characterize their CL features related to shock metamorphism.

Quartz and alkali feldspar ($Or_{84-91}Ab_{9-15}An_{0-1}$) in the drilling core samples between 601 and 602 m depth from the surface in the Ries Crater wasselected for the CL measurements. CL spectroscopy were carried out in the range from 300 to 800 nm using a SEM-CL system, which is comprised of a secondary electron microscope (JEOL: JSM-5410) combined with a grating monochromator (OXFORD: Mono CL2). CL images were collected with a MiniCL (Gatan) equipped with a SEM-CL. Operating conditions of SEM-CL and MiniCL imaging system were set at 15 kV (accelerating voltage) and 1.0 nA (beam current).

CL spectra of quartz exhibit emission bands at around 390 and 650 nm in blue and red region. Blue CL emission is related to Ti^{4+} or $[AlO_4/M^+]^0$ (M^+: H^+, Li^+, Na^+ and K^+) defect center. An emission band at 650 nm is attributed to oxygen vacancy center. CL images of quartz at room temperature show a homogeneous distribution of intensity, whereas those at liquid nitrogen temperature indicate thin dark lines superimposed on more brightly luminescent background. Decreasing temperature leads to a drastic enhancement of CL intensity in quartz due to the temperature quenching effect, which might allow an observation of easily visible line texture at low temperatures. These textures correspond to PDFs by impact-shocked metamorphism observed under an optical microscope. Interference shock wave with high pressure might cause structural destruction with parallel array along wave front, resulting in non-luminescence in PDFs. This fact indicates that CL imaging at low temperature can be used to detect PDFs in shocked quartz.

Most of the alkali feldspar has CL emissions at around 430 and 720 nm. These blue and red-IR CL emissions are attributed to $Al–O^-–Al$ defect and Fe^{3+} impurity center, respectively. CL spectra of only isotropic alkali feldspar under optical microscope (crossed nicol) consist of an emission band at around 380 nm. Similar UV-blue emission has been reported in CL spectra of maskelynite. Therefore, this emission band of the isotropic alkali feldspar might be responsible for shock-induced defect center.

Paleomagnetism and new magnetic mineralogical investigations from Maâdna (Talemzane) impact structure (Algeria)

Lamali, A.[1*], Merabet, N.[1], Rochette, P.[2], Gattacecca, J.[2], Maouche, S.[1], Abtout, A.[1] & Ayache, M.[1]
[1]CRAAG, Algiers, Algeria ([*]lamani_atmane@yahoo.fr)
[2]CEREGE, CNRS/University of Aix-Marseille, France

The Maâdna (Talemzane, Algeria) simple impact structure is located on the Sahara Platform and occurs within sedimentary (limestones) rocks initially lying horizontally and ranging from Senonian to Eocene in age. It is located approximately 400 km south of Algiers, at 33°19' N, 4°19' E. The structure is circular, about 1.75 km in diameter, and 70 m deep. The age of this structure is not yet precisely known and several aspects of the cratering formation process and shock metamorphism phenomena remain poorly constrained. Previous studies have shown some petrographic evidence of shock metamorphism, which were reported in the form of poorly developed PDFs (planar deformation features) in a few quartz clasts [1]. A recent multidisciplinary research program, led by CRAAG with French collaboration (CEREGE), has initiated geological and geophysical surveys with mineralogical and paleomagnetic sampling to investigate the age of this structure. Other objectives are the investigation of the petrological and geochemical characteristics of the rocks at the various sites with a special emphasis toward determining the possible presence of a meteoritic component.

The processing of the geophysical data collected during the first measurement campaign suggest a magnetized body in the central zone of the crater that possibly relates to the presence of some magnetic rocks, maybe a melt component [2]. This geophysical signature (magnetic anomaly) will be further investigated by studying the magnetic properties of the collected samples, paleomagnetic data, and the effect of shock on the natural remanent magnetization [3-6]. We will present and discuss the rock magnetic and magnetic mineralogy data of the sampled target lithologies at the Maâdna impact structure. We also discuss the methods used to identify the impact effect on the intrinsic magnetic properties of sampled breccias and basement rocks inside and outside of the crater. Such data contribute to the understanding the mechanisms creating and modifying magnetic properties during impact cratering processes.

We will attempt to deduce the paleomagnetic age of the Maâdna impact structure by using the magnetostratigraphic data and Apparent Polar Wander Paths (APWP) for Africa (scale 10-100 My; [8,9]). Consequently, dating Algerian impacts is particularly interesting because of the rapid drift of Africa since the past 300 My.

[1] Lambert, P. et al. (1980) *Meteoritics*, **15**, 157-179. [2] Lamali, A. et al. (2009) *First AICAC Conference*. [3] Lamali, A. et al. (2005) *Eos Trans. AGU*, **86(52)**, Fall Meet Suppl., #GP43A-0883. [4] Gattacceca, J. et al. (2006) *Geology*, **34**, 333-336. [5] Gattacceca, J. et al. (2007) *Phys. Earth Planet. In.*, **162**, 85-98. [6] Lamali, A. et al. (2007) *Publs. Inst. Geophys. Pol. Acad. Sc.*, C-99 (398). [7] Cogné, J.P. (2003) *Geochem. Geophys. Geosyst.*, **4**, 1007. [8] Pesonen, L.J. et al. (1992) *Tectonophysics*, **216(1-2)**, 123-142. [9] Hargraves, R.B. & Perkins, W.E. (1969) *J. Geophys. Res.*, **74**, 2576-2589.

Diagnostic shock features of the Serra da Cangalha impact structure, northeastern Brazil: preliminary analysis

Vasconcelos, M.A.R.[1*], Crósta, A.P.[1], Reimold, W.U.[2] & Kenkmann, T.[3]
[1]Institute of Geosciences, University of Campinas, Campinas, SP, Brazil ([*]vasconcelos@ige.unicamp.br)
[2]Museum für Naturkunde, Leibniz Institute at Humboldt University of Berlin, Germany
[3]Institut für Geowissenschaften, Albert-Ludwigs-Universität Freiburg, Germany.

The Serra da Cangalha (SdC) structure, located in Tocantins state, northeastern Brazil, is presumably a complex impact structure of 13.7 km in diameter with a central uplift of 5.8 km in diameter [1]. It was formed in ressentially undisturbed Phanerozoic sedimentary rocks of the Parnaíba Basin. Strata at the center were uplifted by ~ 0.6 km [2] which, in combination with erosional processes, resulted in a strong contrast in the local relief. Impact features, such as shatter cones and PDFs, were described in the 1980s in SdC rocks [3, unpublished]. Only the presence of diagnostic shock-metamorphic effects, such as shatter cones and PDF, besides chemical traces of the projectile, is generally accepted as unambiguous evidence for an impact origin [4]. Recent fieldwork conducted by the authors at SdC resulted in the discovery of some diagnostic macroscopic and microscopic impact features. In the collar of the central uplift the strongly folded strata are variably upturned or overturned [1]. Monomict and polymict breccias were found in the central uplift, as well as shatter cones. Both, breccias and shatter cones were found within the inner depression of the central uplift, wich corresponds to the area of occurrence of the lowermost stratigraphic unit, the Longá Formation. A small outcrop of sandstone with several cm sized shatter cones was found. Preliminarly analysis of some thin sections from the central uplift samples shows that sandstones and shales exhibit intense cataclasis of quartz and feldspar grains. Usually, the breccias show intense fracturing with distinctive planar features (PF), with up to three sets of different orientations in quartz grains. PF are also frequent in sandstone samples from the collar around the uplift, and also in quartz of shales from drill cores through the Longá Fm. (the core came from shallow boreholes drilled into the center in the early 1970s). Thin section analysis of these lithologies show the presence of feather features with planar fractures mostly parallel to (0001) in quartz. Furthermore, we found intersecting sets of PDF in quartz. The occurrence of these features allows to conclude beyond doubt that Serra da Cangalha was formed by a meteorite impact event.

[1] Kenkmann, T. Et al. (2010) *41st Lunar Planet. Sci. Conf.*, #1237. [2] Vasconcelos, M.A.R. et al. (2010) *41st Lunar Planet. Sci. Conf.*, # 1868 [3] McHone, J.F. Jr. (1986) *PhD thesis*. University of Illinois at Urbana-Champaign. [4] French, B.M. & Koeberl, C. (2010) *Earth Sci. Rev.*, **98**, 123-170.

Lithophile elements in iron meteorites

Palme, H.[1*], Vogel, I.[2], Spettel, B.[3] & Pack, A.[4]
[1]Sektion Meteoritenforschung Forschungsinstitut und Naturmuseum Senckenberg, Frankfurt, Germany ([*]herbert.palme@uni-koeln.de)
[2]Universität zu Köln, Germany
[3]Max-Planck-Institut für Chemie Mainz, Germany
[4]Geowissenschaftliches Zentrum, Universität Göttingen, Germany

Some of the major groups of iron meteorites are widely believed to have formed by fractional crystallisation of a molten mass of FeNi with some S, P and C. It is further assumed that metal segregated by melting of a chondritic mineral assemblage. This leads to equilibration of liquid metal and, partly or completely, molten silicate liquid. During this process a small fraction of typical lithophile elements will partition into the metal. The concentrations of lithophile elements in the metallic FeNi phase are sensitive indicators for the conditions of metal formation. Lithophile element concentrations in metal depend on the nature of the lithophile element, its compatibility of the metal species with FeNi (e.g. the activity coefficient), the oxygen fugacity during metal-silicate equilibration and the temperature. We have calculated the distribution of Si and Cr during metal-silicate equilibration by using experimentally determined activity coefficients of Si and Cr in FeNi-metal and we have measured the concentrations of Si (by SIMS) and Cr (by INAA) in iron meteorites [1,2].

The activity coefficients of Si in FeNi metal are, between 10^{-3} and 10^{-4} and they further decrease with increasing Ni contents. There is also a weak temperature dependence. The Cr activity coefficients are between 1 and 2, depending on temperature [1].

The concentrations of Si in iron meteorites as determined by SIMS are very low, between 0.1 and 0.3 ppm, independent of the type of iron meteorite and there is no difference between kamacite and taenite in a given meteorite. The Cr contents of iron meteorites are mostly below 100 ppm many are below 5 ppm [1,3]. Metal grains in chondrules of CR-chondrites representing metal-silicate equilibrium at magmatic temperatures have several hundred ppm Si and several thousand ppm Cr [4]. Although calculations show that concentrations of both elements decrease with decreasing temperature of metal-silicate equilibration, lower temperatures are not sufficient to explain the low observed concentrations of Si and Cr in iron meteorites. The only possibility is metal-silicate equilibration at low temperatures, below the solidus and/or metal-silicate equilibration at oxidizing conditions. The second effect is limited by the Ni contents of iron meteorites. Core formation at oxidizing conditions leads to high FeO in silicate and Ni-rich metals, not frequently observed in iron meteorites. Sub-solidus, low temperature equilibrations seems inescapable.

[1] Vogel, I. et al. (2006) *Lunar Planet. Sci.*, **XXXVII**, #2150. [2] Vogel, I. et al. (2010) submitt. [3] Pack, A. et al. (2010) submitt. [4] Schoenbeck, T.W. & Palme, H. (2004) *Lunar Planet. Sci.*, **XXXV**, #1706.

Do calcite veins in Antarctic CM2 carbonaceous chondrites indicate asteroidal fluid flow?

Sofe, M., Lindgren, P. & Lee, M.R.[*]
Dept. of Geographical and Earth Sciences, University of Glasgow, Scotland, UK ([*]Martin.Lee@ges.gla.ac.uk)

The CM2 carbonaceous chondrites contain minerals including phyllosilicates and carbonates that provide good evidence for the former presence of aqueous fluids within their parent body. A consistent problem in understanding the mechanism of aqueous alteration has been the paucity of petrographic indicators for fluid movement through parent body interiors. This is especially problematic as thermal modelling indicates that vigorous fluid convection should have taken place [1,2].

Using transmitted light and backscattered electron imaging, together with electron backscatter diffraction (EBSD) mapping, we have found Ca(Mg)-carbonate veins in two Antarctic CM2 finds, LON94101 and QUE93005. The millimetre sized vein in LON94101 is composed of twinned calcite crystals, some of which have detached from their host vein (Fig. 1). Small equant calcite grains that are typical of the CM2s are concentrated in one part of the thin section, with the vein lying at the edge of this carbonate-rich area. The veins in QUE93005 are smaller, they cross-cut the fine-grained rims around chondrules, and contain calcite, dolomite and pentlandite.

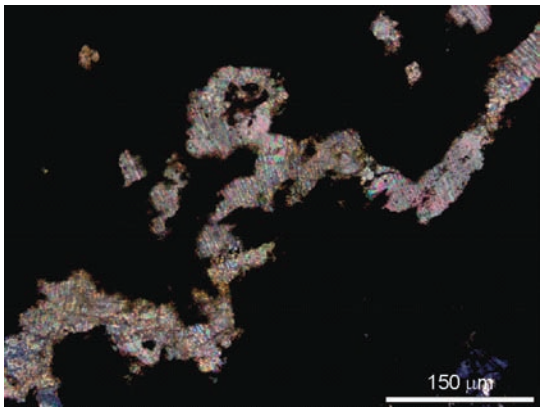

Fig. 1: Part of a twinned and fragmented calcite vein within LON94101. Transmitted light image between crossed polarisers.

The paucity of previous evidence for carbonate veins in the CM2, CM1 or CI1 meteorites could suggest that the veins described here are products of terrestrial weathering. However, we suggest that they formed within the parent body because: (i) it is very hard to imagine how the pressures required to twin and fragment the LON9410 calcite vein could have been attained whilst the meteorite was lying in the Antarctic ice, (ii) dolomite and pentlandite are very unlikely to form by weathering, and (iii) the fusion crust on QUE93005 is cut by abundant fine fractures, none of which contain carbonates. If water for calcite precipitation had been derived from outside of the meteorite, there should be some evidence for its movement through the fusion crust to the meteorite interior.

We conclude that veins in LON94101 and QUE93005 provide good evidence for fluid movement along open fractures within the CM parent body during aqueous alteration. The twinning and fragmentation of LON9410 calcite also suggests that it experienced >10 MPa pressures, probably during impact-related regolith gardening. These results beg the question of why carbonate veins are absent from other carbonaceous chondrites.

Acknowledgements: We are grateful to NASA for the loan of the samples used in this study.

[1] Young, E.D. et al. (1999) *Science*, **286**, 1331-1335. [2] Young, E.D. et al. (2003) *Earth Planet. Sci. Lett.*, **213**, 249-259.

Heterogeneous condensation of Mg-silicate and metallic iron: implication for cosmochemical fractionation in the early solar nebula

Nagahara, H.* & Ozawa, K.
Dept. of Earth and Planetary Science, The University of Tokyo, Japan (*hiroko@eps.s.u-tokyo.ac.jp)

The solar system, at least its inner portion, was once vaporized to gas in its early stage of evolution and then cooled to condense Al- and Ca-rich oxides and silicates, Mg-silicates, and metallic iron as the major components in the decreasing order of temperature. Cosmochemical fractionation of elements basically controlled by volatility (e.g., [1]) is one of the most convincing evidence for the evaporation. The fractionation is, however, not fully explained solely by volatility of elements but it requires phase control. Though chemical equilibrium gives reference information about mineral formation, actual process should have proceeded in a kinetic condition and the phases appeared and the appearance temperature should have been different from estimation from chemical equilibrium.

We have developed a new kinetic condensation model, which describes heterogeneous condensation of minerals as a function of cooling time of the gas (τ) and critical dust separation size (R) in an open system. Heterogeneous condensation is evident in recent meteorite studies (e.g., [2]). A basic equation is the nucleation and growth of minerals derived from kinetic theory of gas molecules that includes condensation coefficients (α) and critical super saturation ratio (σ) for heterogeneous condensation as kinetic parameters. Another basic equation is the mass conservation. The system is assumed to consist of H-He-C-N-O-Mg-Al-Si-Fe and phases applied are corundum, forsterite, enstatite, SiO_2 and metallic iron. The total pressure of the system is fixed to be 10^{-5} bar. For α and σ, we used the values obtained by condensation experiments by our group. We have calculated size distribution, structure, and number density of grains and bulk composition of condensed dust and remaining gas.

The results show that chemical fractionation in the solar nebula was possible in a limited range in the space of τ and R. Cosmochemical fractionation among ordinary chondrites are explained by large supersaturation for forsterite condensation onto corundum and small supersaturation for Fe on forsterite, which suggests surface atomistic kinetics plays a key role than the scale of surface tension. Applying the grain size of corundum observed in primitive chondrites [3], plausible cooling time of the gas at the time of corundum condensation ranged from 10^2 to 10^3 year in order, which suggests advective transport of dust from gas.

The obtained condensation conditions were achieved in two disc models. One is condensation and large dust separation during inward movement of gas and dust, where the condensation of corundum should have started at the high temperature region of the surface layer of the disc followed by forsterite and Fe condensation at the lower temperature region in the lower portion of the disc. In this model, H, L, and LL chondrites were located in the inward order in the disc. Another model is more dynamic, where dust moves outward along the midplane of the disc. Condensation of corundum took place in the inner edge of the disc, which was followed by forsterite and metal at the farther region from the sun. H, L, and LL chondrite was located in this order from inner to outer regions.

[1] Palme, H. et al. (1988) in *Meteorite and the Early Solar System*. Univ. Arizona Press, Arizona, 436-461. [2] Krot, A.N. et al. (2004) *Geochim. Cosmochim. Ac.*, **68**, 1923-1941. [3] Nakamura, T.M. et al. (2007) *Meteorit. Planet. Sci.*, **42**, 1043-1463.

Evaporation experiments for studying the interaction between air and cosmic Fe,Ni metals

Pack, A.[1*], Albrecht, N.[1] & Hezel, D.C.[2]
[1]Geowissenschaftliches Zentrum, Georg-August-Universität Göttingen, Germany (*apack@uni-goettingen.de)
[2]Mineralogy Dept., Natural History Museum, London, UK

Iron meteorites and I-type micrometeorites are frictionally heated to high temperatures when passing through the atmosphere. I-type micrometeorites consist of Fe,Ni-oxides and most probably formed by aerial oxidation of cosmic Fe,Ni metal [1]. They are enriched in heavy isotopes [2,3]. The metal isotope enrichment is related to evaporation during atmospheric entry [3]. For oxygen isotopes, exchange with ^{18}O-rich stratospheric oxygen [2] or evaporation [3] was suggested. Iron meteorite fusion crusts are moderately enriched in $\delta^{18}O$ with values around +13.5 ‰ [2] and no fractionation in metal isotopes [4].

We attempted to simulate the atmospheric entry using an aerodynamic levitation device in combination with infrared laser heating [5] in order to test if fusion crust and I-type micrometeorites can be used as probe for the isotope composition of oxygen at different heights [2].

We used Fe,Ni-oxides with approximately chondritic element ratios (4.8 mol% Ni) as starting material. Samples were fused and evaporated while floating on a vertical air gas stream for up to several hours. The mass loss was determined by measuring the mass of the sample before and after the experiment in combination. The Fe and O isotope composition of starting materials and run products was determined by solution MC-ICPMS (Imperial College, London) and by laser fluorination (Göttingen), respectively.

The mass loss varied between 39 and 80 %. The $\delta^{18}O$ ($\Delta^{17}O$) of the starting oxide mixture was –4.7 ‰ (–0.07 ‰) and changed to +12.3±0.2 ‰ (–0.17±0.02 ‰) after evaporation. No relation between mass loss and $\delta^{18}O$ is observed. The $\delta^{56}Fe$ of the starting material was +0.4 ‰. After evaporation $\delta^{56}Fe$ varied between +1.4 and +6.0 ‰. The $\delta^{56}Fe$ systematically increased with mass loss. Modeling all data with a Rayleigh process gives $\alpha_{liquid\text{-}gas} \approx 1.00458$.

The oxygen isotope composition is likely to be caused by *equilibration* of the molten oxides with air O_2 ($\delta^{18}O$ = +23.9 ‰, $\Delta^{17}O$ = –0.384 ‰, [6]). Kinetic fractionation should vary with time and with degree of evaporation; none of both/neither of them are observed. The fractionation in $\delta^{18}O$ is –11.4 ‰ and the 3-isotope exponent for the fractionation is $\beta = 0.5063$. Our results explain the $\delta^{18}O$ = +13.4 ‰ and $\Delta^{17}O$ = –0.17 ‰ in iron meteorite fusion crusts [2] by equilibration with air O_2. The variability of $\delta^{18}O$ in I-type micrometeorites, however, may indicate that some fractionation during evaporation occurs [3].

The Fe isotope fractionation is smaller as expected from Rayleigh-type evaporation of Fe or FeO. The α-value suggests evaporation of a species with a molar mass exceeding that of magnetite. One explanation would be evaporation in form of molecule clusters that have molar masses of ~270. Alternatively, evaporated material back-reacts with the liquid. We suggest that the difference between our results and the α-value (57/54) of 1.0274 from vacuum evaporation of wüstite [7] is related to the 1 bar atmosphere in which our experiments have been conducted.

[1] Genge, M.J. et al. (2008) *MAPS*, **43**, 497-515. [2] Clayton, R.N. et al. (1986) *Earth Planet. Sci. Lett.*, **79**, 235-240. [3] Engrand, C. et al. (2005) *Geochim. Cosmochim. Ac.*, **69**, 5365-5385. [4] Xue, S. et al. (1993) *Meteoritics*, **28**, 462. [5] Pack, A. et al. *Geochem. Trans.*, in review. [6] Barkan, E. & Luz, B. (2005) *Rap. Comm. Mass Spectr.*, **19**, 3737-3742. [7] Wang, J. et al. (1994) *LPSC*, Houston.

Calcium-aluminum-rich inclusions in CK3/4 carbonaceous chondrites

Chaumard, N.[1*], Devouard, B.[1], Devidal, J.-L.[1] & Zanda, B.[2]
[1]LMV, Univ. Blaise Pascal - CNRS, Clermont-Ferrand, France
([*]n.chaumard@opgc.univ-bpclermont.fr)
[2]Muséum National d'Histoire Naturelle - CNRS, Paris, France

Dated at 4568.5 ± 0.5 Ma [1] calcium-aluminum-rich inclusions (CAIs) are the first solids in the solar nebula. They mainly occur in CV and CO carbonaceous chondrites [2]. CK chondrites, which comprise the only metamorphic series (petrological types 3 to 6) among carbonaceous groups [3], were initially described as CAI-poor objects. However, at least some CKs have CAI abundances similar to those of CVs [4]. We studied CAIs in CK chondrites at the 3 to 4 transition to characterize their modification by parent-body processes.

This study was carried out on DAG 431 (CK3-An.), NWA 1559 (CK3), NWA 4724 (CK3.8), NWA 4425 (CK3.8), NWA 4423 (CK3.9), NWA 4422 (CK4), NWA 2519 (CK4), TNZ 057 (CK4), Karoonda (CK4), and Maralinga (CK4). CAIs were recognized by visual identification on polished slabs or/and SEM-BSE imaging, depending on the sample size.

No CAIs were recognized in Karoonda, Maralinga, and NWA 2519. All other CKs display CAIs with abundances from 1.4 to 16.4%. Abundances obtained from small sections should be considered as poorly representative. Samples for which pluri-centimetric surfaces were available (NWA 4425, 20 cm^2, and TNZ 057, 865 cm^2) give CAI abundances of 10.3 and 8.9%, respectively.

Fine-grained CAIs, irregularly shaped, mm to cm-sized, are ubiquitous in most CKs. They are composed of Ca-rich pyroxene and plagioclase (An_{15-97}), with minor low-Ca pyroxene and olivine. Coarse-grained CAIs up to ca. 2 cm, often surrounded by a fine-grained Ca-pyroxene-plagioclase rim, were observed in NWA 1559, DAG 431, NWA 4425, and TNZ 057. Two coarse-grained CAI were analysed in TNZ 057 and DAG 431. They display a primary spinel-fassaite-anorthite assemblage and secondary grossular, forsterite and Ca-pyroxene. The replacement of primary phases by grossular is interpreted as evidence for parent-body alteration. All CAIs in CK chondrites were enriched in Fe during parent body metamorphism. Fe diffuses from matrix to CAI phases and causes chemical zonations, mainly in spinel and fassaite. Fassaite is locally destabilized to Ca-pyroxene and Ti-rich oxydes. In CK4s, the fine-grained CAIs are chemically equilibrated with the matrix and recrystallized as irregular assemblages of plagioclase + Ca-rich pyroxene +/- olivine +/- Ca-poor pyroxene.

We analysed several CAIs in TNZ 057 by LA-ICP-MS. In some fine-gained CAIs, rare earth element (REE) patterns in Ca-rich pyroxene are similar to those of group II CAIs [5] and of CV bulks [6]: light REE (LREE) enriched compared to heavy REE (HREE), with a positive anomaly of Tm. In other CAIs, REE in Ca-rich pyroxene are enriched (ca. 20×CI) with patterns similar to those reported in fassaite. These reequilibrated CAIs thus retained a pristine signature in spite of thermal metamorphism.

[1] Bouvier, A. et al. (2007) *Geochim. Cosmochim. Ac.*, **71**, 1583-1604. [2] Scott, E.R.D. et al. (1996) in Hewins R.H. et al. (eds.) *Chondrules and the Protoplanetary Disk.* Cambridge Univ. Press, 87-96. [3] Kallemeyn, G.W. et al. (1991) *Geochim. Cosmochim. Ac.*, **55**, 881-892. [4] Chaumard, N. et al. (2009) *MAPS. Suppl.*, abstr. #5206. [5] MacPherson, G.J. et al. (1988) in Kerridge, J.F. & Matthews, M.S. (eds.) *Meteorites and the Early Solar System.* Univ. of Arizona Press, 746-807. [6] Shinotsuka, K. & Ebihara, M. (2001) *32th LPSC*, abstr. #1771.

Silicate mineral inclusions in the Muonionalusta iron meteorite

Fujimaki, H.[1*] & Fuyuya, K.[1,2]
[1]Dept. of Earth and Planetary Material Science, Graduate School of Science, Tohoku University, Sendai, Japan
([*]h-fujimaki@m.tains.tohoku.ac.jp)
[2]Dept. of Earth Planetary Sciences, Graduate School of Science, Kobe University, Kobe, Japan

Mineralogical and geochemical investigation has been carried out on a magmatic iron meteorite. Although many magmatic iron meteorites have been investigated so far, only four IVA irons contain silicate inclusions. Two IVA irons contain a few number of tridymite crystals, and two others contain up to 50 percent silicates in volume; they are mostly pyroxene and tridymite mixed with metal; some of them reach to centimeter size. Muonionalusta iron meteorite (IVA) has been investigated and the results are reported in this presentation. Previous investigation has found stishovite that was presumably trydimite before impact. In contrast, I found many other different kinds of silicate and oxide minerals in the iron meteorite. Alkali feldspars, plagioclase, olivine, zircon, garnet, micas and hornblendes were recognized for the first time not only in the Muonionalusta iron meteorite but in the entire iron meteorites. I identified those minerals using Raman micro spectroscopy, and their compositions were analyzed by energy-dispersive micro probe spectroscopy. Especially the occurrence of hornblende in iron meteorites is unusual. It occurs as a rectangular grain up to 0.8 mm long surrounded by hematite matrix. Its composition is close to magnesio-hornblende, and the texture indicates that it formed as a primary (pre-terrestrial) mineral. Such mineral assemblages imply that these silicates might have crystallized from felsic magma generated by partial melting of the parent body. We now may see the fragments of the planet that once had crust like Earth. On the other hand, it is impossible to deny the possibility as follows: the iron meteorite was partially molten and included terrestrial minerals at the impact. However, no similar occurrence has been reported. In the latter case we may have to consider new physical model of impact. Possibility and the origin of such magma on the parent body should be discussed in feature. We may have unconsciously disregarded such minerals and mineral assemblages in meteorites.

Structural parameters of chromites from H6 Kernouvè chondrite and detrital extraterrestrial L-chondrites

Lenaz, D.[1*], Schmitz, B.[2] & Princivalle, F.[1]
[1]Dept. of Geosciences, University of Trieste, Italy
([*]lenaz@units.it)
[2]Dept. of Geology, University of Lund, Sweden

Chromite is a minor but regular constituent of ordinary chondrites and its chemistry in meteorites have been studied since the 60es. Besides the main components FeO and Cr_2O_3, it contains minor amounts of MgO and Al_2O_3. It has been noticed that Fe and Mg content of chromites is related to that of the olivines in the H, L and LL groups of equilibrated chondrites.

The here studied chromites are from the Kernouvè H6 chondrite and from ~ 470 Ma old fossil micrometeorites, found in Ordovician limestone at Kinnekulle in Sweden and derived from the disruption of the L-chondrite parent body [1].

Despite the fact that their chemistry has been studied since about 40 years, to our knowledge no single crystal diffraction studies have been performed on extraterrestrial chromites. The cell edge in H6 chondrite ranges from 8.3480 (2) to 8.3501 (1) Å, while in L-chondrite it varies from 8.3347 (3) to 8.3463 (3). The oxygen positional parameter is comprised between 0.2627 (2) and 0.26291 (7) in H6 and between 0.2625 (1) and 0.26267 (9) in L. These values show that there are some little differences between the two chondritic typologies. By comparison with the structural parameters of chromites from terrestrial occcurrences, in an oxygen positional parameter vs. cell edge diagram (Fig. 1) the extraterrestrial chromites fall in a proper field close to those of chromites from komatiites [2], kimberlites and included in diamonds [3].

Because meteoritic material on the Earth surface is rapidly altered or weathered away with the exception of chromite, different methologies have been recently developed to recognise the extraterrestrial detrital chromitic material [1, 4]. This work demonstrates that a structural study can, as well, identify extraterrestrial from terrestrial material and also that different chondritic origin can be recognised.

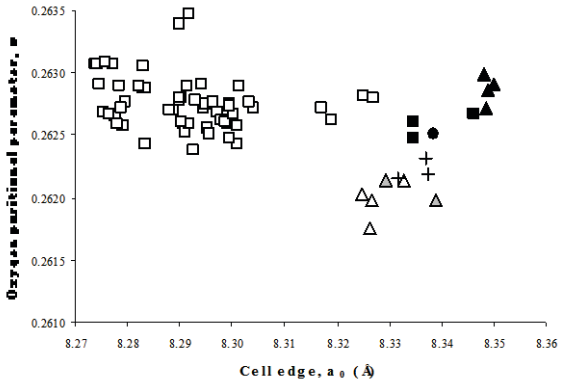

Fig. 1: Oxygen positional parameter vs. cell edge. Full triangle: H6 chondrite; Full square: L-chondrite. Full circle: Acapulco meteorite; Open square: layered intrusions; Open triangle: diamond inclusions; Grey triangle: kimberlites; Crosses: komatiites.

[1] Heck, P.R. et al. (2010) *Geochim. Cosmochim. Ac.*, **74**, 497-509. [2] Lenaz, D. et al. (2004) *Mineral. Petrol.*, **80**, 45-47. [3] Lenaz, D. et al. (2008) *Geochim. Cosmochim. Ac.*, **72**, 475-479. [4] Alwmark, C. & Schmitz, B. (2009) *Geochim. Cosmochim. Ac.*, **73**, 1472-1486.

Dust in protoplanetary disks

Henning, T.K.
Max Planck Institute for Astronomy, Heidelberg, Germany
(henning@mpia.de)

Circumstellar disks around young stellar objects are the birthplaces where planetary systems form. Small solid particles and molecular gas in these protoplanetary disks are the building blocks for planets. Space-based infrared spectroscopy with the "Spitzer" and "Herschel" observatories and infrared data from the gound constrain the nature of protoplanetary dust. This talk will summarize the main properties of the small particles, including their mineralogy. In addition, the various formation and evolution processes of the dust grains will be discussed.

The mineralogy of circumstellar silicates preserved in cometary dust

Keller, L.P.* & Messenger, S.
Code KR, NASA Johnson Space Center, Houston, TX, USA
(*Lindsay.P.Keller@nasa.gov)

Interplanetary dust particles (IDPs) contain a record of the building blocks of the solar system including presolar grains, molecular cloud material, and materials formed in the early solar nebula [1]. Cometary IDPs have remained relatively unaltered since their accretion because of the lack of parent body thermal and aqueous alteration. We are using coordinated transmission electron microscope (TEM) and ion microprobe studies to establish the origins of the various components within cometary IDPs. Of particular interest is the nature and abundance of presolar silicates in these particles because astronomical observations suggest that crystalline and amorphous silicates are the dominant grain types produced in young main sequence stars and evolved O-rich stars (e.g. [2]).

Five circumstellar grains have been identified including three amorphous silicate grains and two polycrystalline aggregates. All of these grains are between 0.2 and 0.5 μm in size. The isotopic compositions of all five presolar silicate grains fall within the range of presolar oxides and silicates [3], having large ^{17}O-enrichments and normal ^{18}O/^{16}O ratios (Group 1 grains from AGB and RG stars). The amorphous silicates are chemically heterogeneous and contain nanophase FeNi metal and FeS grains in a Mg-silicate matrix. Two of the amorphous silicate grains are aggregates with subgrains showing variable Mg/Si ratios in chemical maps. The polycrystalline grains show annealed textures (equilibrium grains boundaries, uniform Mg/Fe ratios, [4,5]) and consist of 50-100 nm enstatite and pyrrhotite grains with lesser forsterite. One of the polycrystalline aggregates contains a subgrain of diopside. The polycrystalline aggregates form by subsolidus annealing of amorphous precursors [4].

The bulk compositions of the five grains span a wide range in Mg/Si ratios from 0.4 to 1.2 (avg. 0.86). The average Fe/Si (0.40) and S/Si (0.21) ratios show a much narrower range of values and are ~50% of their solar abundances. The latter observation may indicate a decoupling of the silicate and sulfide components in grains that condense in stellar outflows.

The amorphous silicate grains described here were not extensively affected by irradiation, sputtering, or thermal processing and may represent relatively pristine circumstellar grains. They are strong candidates for the "dirty silicates" in astronomical observations of circumstellar dust shells. The polycrystalline grains were originally amorphous silicate grains that were likely annealed in the early solar nebula [5] but the processing was not sufficient to erase their anomalous oxygen isotopic compositions.

[1] Messenger, S. et al. (2006) *MESS*, 187. [2] Molster, F. & Waters, L.B.F.M. (2003) in Henning, T.K. (ed.) *Astromineralogy*, *Lect. Notes Phys.*, **609**, 121-170. [3] Nittler, L.R. et al. (1997) *Astrophys. J.*, **483**, 475-495. [4] Keller, L.P. & Messenger, S. (2009) *LPSC*, **XXXX**, 2121. [5] Messenger, S. & Keller, L.P. (2010) *LPSC*, **XXXXI**, 2483.

Mixing and thermal processing of pre-planetary materials in protoplanetary disks

Apai, D.
Space Telescope Science Institute, Baltimore, USA
(apai@stsci.edu)

Protoplanetary disks are the both the site and the raw material for the formation of planets. With the rapidly increasing number of exoplanets and the wealth of high-quality observations of protoplanetary disks it is compelling to place the formation of the Solar System in the broader context of planet formation in the Galaxy.

A key question in this endeavour is how the bulk composition of planets is influenced by their formation process; and, in particular, what is the extent and role of the thermal and chemical processing of preplanetary components.

Primitive meteoritic materials reveal abundant evidence for thorough processing and mixing of solids in the proto-Solar nebula. Chondrules, Ca-Al-rich inclusions, interplanetary dust particles, or chondritic matrix all suggest that at least 80% of the solids in the inner Solar System underwent powerful heating and melting, often under high pressures. Recently, the Spitzer Space Telescope revealed widespread evidence for crystalline silicates in a broad variety of protoplanetary disks. The presence of crystalline silicates evidence thermal processing in the disks; but, surprisingly, the strongest crystalline features were observed around the coolest stars and brown dwarfs (e.g. [1,2]).

In this talk I will review the presence and properties of crystalline silicates in disks. I will connect these observations to evidence for thermal processing in the proto-solar nebula and discuss the constraints they provide on the mixing of solids in protoplanetary disks. I will also briefly describe a large, coordinated effort by astronomers and cosmochemiststs to develop a consistent framework for the formation and evolution of the proto-solar nebula and protoplanetary disks around other stars [3].

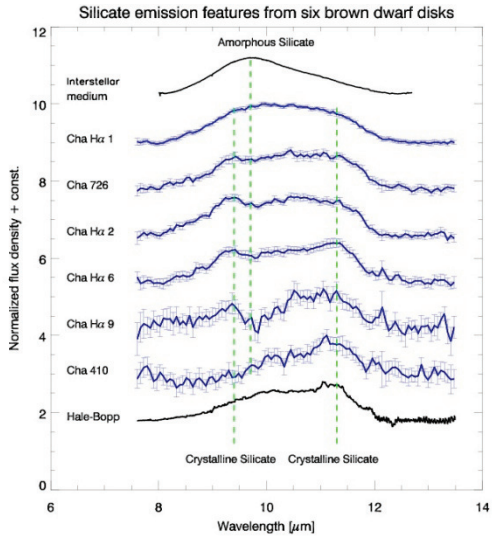

Fig. 1: The prominent crystalline silicate peaks reveal powerful thermal processing of the solids in protoplanetary disks, a surprising finding around very cool stars. From [1].

[1] Apai, D. et al. (2005) *Science*, **310**, 834-837. [2] Pascucci, I. et al. (2009) *Astrophys. J.*, **696**, 143. [3] Apai, D. & Lauretta D.S (eds.) (2010) *Protoplanetary Dust: Astrophysical and Cosmochemical Perspectives*. Cambridge University Press

Formation and transport of forsterite crystals in the disk of EX Lup

Juhasz, A.[1*], Abraham, P.[2], Bouwman, J.[3], Dullemond, C.P.[3], van Boekel, R.[3], Henning, Th.[3], Kospal, A.[1], Sicilia-Aguilar, A.[3], Moor, A.[2], Acosta-Pulido, J.[4], Mosoni, L.[2], Regaly, Zs.[2], Szokoly, Gy.[5] & Sipos, N.[2]
[1]Leiden Observatory, Leiden, The Netherlands
([*]juhasz@strw.leidenuniv.nl)
[2]Konkoly Observatory, Budapest, Hungary
[3]Max-Planck-Institute for Astronomy, Heidelberg, Germany
[4]Instituto de Astrofisica de Canarias, La Laguna, Spain
[5]Eotvos Lorand University, Budapest, Hungary

Crystalline silicates are known to be missing from the interstellar medium, but they are frequently observed in protoplanetary disks as well as Solar System comets. Although there were indirect evidences for the formation of crystalline silicates in protoplanetary disks the process itself was not yet observed.

Here, we report on the first direct observation of on-going crystal formation in the disk of EX Lup, the prototype of the EXor class of young eruptive stars. These stars are known to show repetitive outbursts at optical wavelengths, which are thought to be related to runaway accretion onto the central star.

EX Lup went into its most recent outburst at the beginning of 2008 and returned to the quiescent phase in Sep. 2008. We observed the source with the Infrared Spectrograph (IRS) onboard the Spitzer Space telescope in Apr. 2008 and compared it to that from the pre-outburst phase from the Spitzer archive. The pre-outburst spectrum shows the typical triangular-shaped 10 micron feature of amorphous silicates, signatures of crystals are not present in the spectrum. The outburst spectrum, however, shows new peaks at 10, 16 micrometer and a shoulder at 11.3 micrometer, which are the characteristic band positions of crystalline forsterite. Our analysis shows that the only possible explanation for the 'new' features is the in-situ formation of forsterite crystals in hot inner disk of EX Lup.

Spitzer IRS spectra were taken also in the post-outburst phase (Oct. 2008 and Apr. 2009). These spectra show forsterite bands also at 24 and 28 micrometer. Our modeling shows that the most likely explanation for the strength of these forsterite bands is the fast radial transport of crystals in the disk. The freshly produced crystals must have been transported by about 30-40km/s. Such high velocities require some kind of stellar/disk wind driven radial transport mechanism [2].

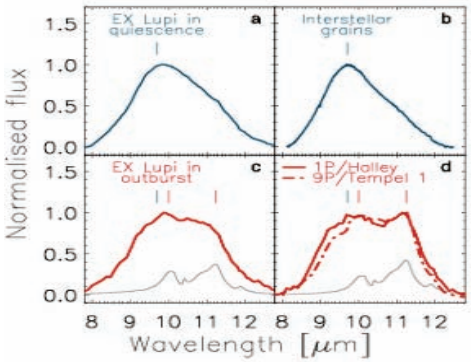

Fig. 1: 10 μm silicate feature of EX Lup in the pre-outburst phase (a) and in the outburst (c). For comparison the silicate feature of the interstellar dust grains (b) and comet Halley and 9P/Tempel 1 (c) are also shown. The grey line in the bottom panel shows the emissivity of sub-micron sized forsterite grains at 1250K (c) and 300K (d).

[1] Abraham, P. et al (2009) *Nature*, **459**, 224-226. [2] Juhasz, A. et al. (2010) *Astrophys. J.*, submitted.

Experimental demonstration of a forsterite cycle from evolved stars to the solar system

Kimura, Y.[1*] & Nuth, J.A. III[2]
[1]Dept. of Earth and Planetary Materials Science, Tohoku University, Sendai, Japan ([*]ykimura@m.tains.tohoku.ac.jp)
[2]Astrochemistry Laboratory, Code 691, NASA's Goddard Space Flight Center, Greenbelt MD, USA

Magnesium rich silicate minerals are widely and abundantly distributed in the solar system and also in many other astrophysical objects. During the formation of silicate dust particles in the outflows of AGB stars, whether a silicate grain becomes crystalline or amorphous depends sensitively on its' temperature history. The presence of both amorphous and crystalline silicates around AGB stars suggests that the formation conditions, such as cooling rate or the temperature at which grain nucleation begins in such objects may vary or that the crystalline silicates are a result of annealing previously formed amorphous silicates.

In our solar system, several comets show 10 μm emission features characteristic of a mixture of amorphous and crystalline silicates. In addition, mixtures of amorphous and crystalline silicates are observed in stratospherically collected IDPs (e.g. [1]) and their IR spectra are coincident with that of comets [2]. Crystalline silicates have also been identified in comet Wild-2 (Stardust) samples [3]. Since most interstellar silicates are in an amorphous state, it has been proposed that the amorphous silicates gradually crystallized via thermal annealing in the hot inner solar nebula over time.

In the scenario to get crystalline silicates by annealing, there are difficulties. For examples, thermal annealing will not produce forsterite unless the chemical composition of the precursor particles is of olivine composition. In addition, the oxygen isotopic compositions of crystalline silicates (200 – 1,000 nm) in IDPs and Wild-2/Stardust samples is indistinguishable from solar [4,5]. The abundant presolar crystalline silicates, determined from oxygen isotopic anomalies, are much less abundant than presolar amorphous silicates, which are thought to be GEMS [6]. Therefore, it is possible that solar silicates are the result of condensation, and not of annealing of interstellar amorphous particles. One experiment achieved the direct formation of crystalline silicate (forsterite) via homogeneous nucleation so far [7]. The smoke particles showed various degrees of crystallinity of forsterite. This result suggested that the crystallinity depends on the interval time of reactions. Recently, Kimura and Nuth (2009) [8] suggested another possible origin of solar forsterite by oxidation of magnesium silicide. There are several possible formation processes, annealing of presolar grains, direct condensation of crystalline grains, condensation of amorphous grains followed by annealing and oxidation of metallic precursors such as Mg_2Si. Solar system silicates may be a result of all of these processes, i.e., degree of contribution should be elucidated. Recent laboratory studies have given us more complex results. In this study, we will show the selective formation of amorphous and crystalline silicates in hydrogen absent or dominant gas atmosphere and alteration by thermal annealing using differential scanning calorimetry (DSC).

[1] Bradley J.P. et al. (1988) in Kerridge, J.F. & Matthews, M.S. (eds.) *Meteorites and the early solar system*. Tucson, AZ, Univ. Arizona Press, 861-895. [2] Sandford, S.A. & Walker, R.M. (1985) *Astrophys. J.*, **291,** 838-851. [3] Brownlee, D. et al. (2006) *Science*, **314,** 1711-1716. [4] Messenger, S. & Keller L.P. (2005) *LPI Contrib*. No. 1278, 9024. [5] McKeegan, K.D. et al. (2006) *Science*, **314**, 1724-1728. [6] Matzel, J. et al. (2008) *39th Lunar and Planetary Science Conference*, 2525. [7] Kimura, Y. et al. (2008) *Astrophys. J.*, **684**, 1496-1501. [8] Kimura, Y. & Nuth, J.A. III (2009) *Astrophys. J.*, **697**, L10-13.

Comparison of the mineralogy of comet Wild 2 coma grains to other astromaterials

Frank, D.[1*] & Zolensky, M.[2]
[1]ESCG/Hamilton Sundstrand, NASA Johnson Space Center, Houston, TX, USA ([*]david.r.frank@nasa.gov)
[2]ARES, NASA Johnson Space Center, Houston, TX, USA

We propose that Kuiper Belt samples (in this case comet coma grains from the Jupiter family comet Wild 2) are recognizably different from the bulk of materials in outer belt asteroids, because of their different formation positions and times in the early solar system. We believe this despite similarities found between some Wild 2 grains and components of carbonaceous chondrites (i.e. some CAI and chondrules). Kuiper Belt samples must preserve measurable mineralogical and compositional evidence of formation at unique positions and times in the early solar nebula, and these formational differences must have imparted recognizable special characteristics. We hypothesize that these characteristics include: (1) Unique major element compositional ranges of common astromaterial minerals, especially olivine and pyroxene; (2) Unique minor element compositions of major silicate phases, especially olivine and low-Ca pyroxene; (3) Degree and effects of radiation processing – including amorphous rims, metal coatings, and Glass with Embedded Metal and Sulfides (GEMS) [1-3]; (4) Presence of abundant presolar silicate grains as recognized by anomalous oxygen in silicates [1,3,4]; (5) Oxidation state of the mineral assemblage [5].

We will work our way through all available Wild 2 samples as they are allocated to us, selecting 1-2 non-consecutive viable TEM grids from each possible extracted Wild 2 grain. We especially prefer TEM grids from grains for which complete mineralogical details have not been published (which is to say the majority of the extracted grains). We are performing a basic mineralogic survey by E-beam techniques, to establish the essential features of the extracted Wild 2 grains. We are making a particular effort to carefully and accurately measure minor elements of olivine and pyroxene, as these minerals are widespread in astromaterials, and comparisons of their compositions will serve to place the Wild 2 silicates in contact with asteroids, meteorites and chondritic interplanetary dust particles processing [1-6]. We are also making a special effort to search for mineralogical products of aqueous alteration, since their presence would reveal that Wild 2 was once internally heated, a result with dramatic implications for models of early solar system primitive bodies. Thus far carbonates are the only potential evidence for aqueous alteration for Wild 2.

[1] Bradley, J.P. (1994) *Science*, **265**, 925-929. [2] Chi, M. et al. (2007) *Lunar Planet. Sci.*, **XXXVIII**, #2010. [3] Nakamura-Messenger, K. et al. (2008) *MAPS*, **43**, #5247. [4] McKeegan et al. (2006) *Science*, **314**, 1724-1728. [5] Westphal, L.J. et al. (2008) *Lunar Planet. Sci.*, **XXXIX**, #1457. [6] Zolensky, M. et al. (2006) *Science*, **314**, 1735-1740.

The discovery of new warm debris disks around F-type stars: implications for recent collisions

Moór, A.[1*], Apai, D.[2], Pascucci, I.[2], Ábrahám, P.[1], Grady, C.[3], Henning, Th.[4], Juhász, A.[4], Kiss, Cs.[1] & Kóspál, Á.[5]
[1]Konkoly Observatory of the Hungarian Academy of Sciences, Budapest, Hungary ([*]moor@konkoly.hu)
[2]Space Telescope Science Institute, Baltimore, MD, USA
[3]NASA Goddard Space Flight Center, Code 667, Greenbelt, MD, USA
[4]Max-Planck-Institut für Astronomie, Heidelberg, Germany
[5]Leiden Observatory, Leiden University, The Netherlands

We report on the results of a Spitzer program devoted to studying debris disks around F-type stars. The motivation of the program was to outline disk evolution effects in a constrained stellar mass range, and also to make the bridge between the major Spitzer surveys of debris disks around A-type and G,K-type stars. We observed 86 F-type stars with IRS and MIPS instruments, many of them with previous indications for infrared excess from IRAS or ISO. The observed debris disk population shows a large variety in dust temperatures. In this contribution we report the discovery of four warm debris disks, which significantly increases the number of such systems known. Based on the fractional luminosity and age, three out of the four warm debris systems are consistent with a steady state disk evolution picture. The oldest source, HD 169666, displays a dust fractional luminosity too high to be in a steady state and we suggest that this system recently underwent a transient event of dust production. In addition, two spectra of this star separated by approximately three years show silicate emission features, indicative of submicron- to micron-sized grains. We argue that such small grains would be rapidly depleted and their presence in both spectra suggests that the production of small dust is continuous over a timescale of at least a few years. We predict that systems showing variable mid-infrared spectra, if they exist, will provide valuable help in distinguishing the possible scenarios proposed for dust replenishment.

Erosion rate determination of Allchar region (Macedonia) with cosmogenic radioactive (^{10}Be, ^{26}Al, ^{53}Mn) and stable (^{3}He, ^{21}Ne) nuclides

Pavićević, M.K.[1], Vermeesch, P.[2], Niedermann, S.[3], Amthauer, G.[1*], Boev, B.[4], Jelenković, R.[5] & Pejović, V.[6]
[1]Dept. of Materials Engineering and Physics, University of Salzburg, Austria ([*]georg.amthauer@sbg.ac.at)
[2]School of Earth Sciences, Birkbeck University of London, Great Britain
[3]Deutsches GeoForschungsZentrum GFZ, Potsdam, Germany
[4]Faculty of Mining and Geology, University of Štip, FYR Macedonia
[5]Faculty of Mining and Geology, University of Belgrade, Serbia
[6]Faculty of Physics, University of Belgrade, Serbia

Allchar is a Sb-As-Tl-Au deposit located at the north - western margin of the Kozuf Mountains in Macedonia, close to the Greek border. The mine contains the world's largest known concentration of thallium-bearing minerals, especially lorandite ($TlAsS_{2)}$. LOREX, the acronym for LORandite EXperiment, is the only geochemical solar neutrino experiment still actively pursued. It addresses the determination of the long-term average of the solar neutrino flux, based on the neutrino-capture reaction $^{205}Tl + \nu_e \rightarrow {}^{205}Pb + e^-$ occurring in the lorandite of the Allchar mine. The final step of LOREX will be the extraction of the lorandite and the quantitative determination of the ^{205}Pb / ^{205}Tl ratio, thus providing the product of solar neutrino flux and neutrino-capture cross section, integrated over the lorandite age of $4.31 \cdot 10^6$ yr. Based on the present-day solar luminosity, it is expected that about 23 atoms of ^{205}Pb of solar neutrino origin will be found per gram of lorandite. In contrast with the production of ^{205}Pb by solar neutrinos, which is independent of depth, cosmogenic ^{205}Pb produced from fast muons of cosmic ray origin is strongly depth-dependent and very sensitive to the long-term erosion history of the field area. For erosion rate determination, we have so far applied three independent series of measurements of cosmogenic ^{26}Al, ^{10}Be and ^{53}Mn. First, the ^{26}Al concentration in quartz was determined using the AMS system at VERA (**V**ienna **E**nvironmental **R**esearch **A**ccelerator). Second, a series of measurements of the ^{10}Be and ^{26}Al contents was performed at the AMS of PRIME Lab, Purdue University, and finally AMS measurements at the Tandem facility of the TU Munich provided concentration of ^{53}Mn in pyrite (FeS_2). For the two ore bodies containing lorandite, we derived lower limits of the erosion rate of ~33 m/Myr at Crven Dol (NW part of Allchar deposit) and 67 m/Myr in the central part (SE part of Allchar deposit), in fair agreement with quantitative geomorphologic studies. In addition, mass spectrometric determinations of comogenic ^{3}He and ^{21}Ne concentrations in diopside, quartz and sanidine from three different Allchar locations (near to Central part) are currently underway at GFZ Potsdam. The combination of various cosmogenic nuclides will enable us to accurately decipher the erosion history of the Allchar deposit, including any period of intermediate cover, e.g. by ice or sediments. Such knowledge is critical in order to assess the production of cosmogenic ^{205}Pb, which interferes with that produced by solar neutrino and cosmic ray interaction.

Colours of stardust: absorption properties of selected oxides and silicates in their transparency regimes

Zeidler, S.[1], Mutschke, H.[1*], Posch, T.[2], Richter, H.[2] & Wehrhan, O.[3]
[1]Astrophysikalisches Institut, Jena, Germany
([*]mutschke@astro.uni-jena.de)
[2]Institut für Astronomie, Vienna, Austria
[3]Institut für Optik und Quantenelektronik, Jena, Germany

Several astrophysically relevant solid oxides and silicates have extremely small values of the imaginary part k of their complex indices of refraction in the visual and near-infrared spectral ranges. Datasets for the absorption index k are hardly available in these cases, but very important for thermal and dynamical properties of stardust grains. With increasing absorbance the equilibrium temperature of grains in circumstellar shells increases.

We aimed at closing the 'gaps' in the sets of optical constants particularly characterizing spinels and olivines with different contents of Cr and Fe. For that, two principal methods have been used: preparing small sections of natural minerals and synthesizing melt droplets under the electric arc furnace. In both cases, the absorption properties of the samples were measured by transmission and scattering spectroscopy. From these data the optical constants have been derived.

For the synthesized Cr doped spinels ($MgAl_{2-x}Cr_xO_4$), we investigated the strength of the absorption features, which arose by successive exchange of Aluminum with Chromium(III)Ions. On the other hand we used a natural spinel from Burma to compare the influence of both Chromium and Iron with the pure stoichiometric and only Chromium doped spinels.

For the investigations on the olivines, two natural crystals with different Fe content have been used: one from San Carlos and another one from Sri Lanka. We studied the influence of Iron on the absorption spectra of olivine for both polarized and unpolarized light in the near infrared to the UV.

Presolar nanodiamonds in meteorites: properties and origins

Ott, U.
Dept. of Biogeochemistry, Max-Planck-Institute for Chemistry, Mainz, Germany (uli.ott@mpic.de)

Primitive meteorites contain grains of stardust, i.e. "pre-solar" grains that formed in the outflows or ejecta of stars [1]. Among these are nanodiamonds with a mean size of ~2.6 nm and a nominal abundance reaching up to ~0.15 % by weight [2]. The identification of a presolar origin rests on the observation of trace elements within them, notably the noble gas xenon, with an unusual isotopic composition. However, since the isotopic analysis of single diamonds (some 1000 carbon atoms on average) is not feasible, and "bulk" analysis of large numbers (millions or so) of diamonds results in a C isotopic composition in the range of normal solar-system carbon, it is presently unclear what fraction of the nanodiamonds really is pre-solar.

The isotopic composition of "HL"-xenon is characterized by excesses of both the heaviest and the lightest isotopes, which is reminiscent of the p- and r-processes of nucleosynthesis that are thought to occur during supernova explosions [3]. There are differences in detail, however, which may indicate some unconventional types of element synthesis in stars [4] or modification by secondary processes [3]. Recoil loss from nanometer-sized grains during decay of unstable precursor nuclides has been suggested as an explanation, but experiments we have performed do not support this idea [5].

Astronomical observations indicate the presence of diamonds around young stars, but have not unambiguously identified them in the interstellar medium or around evolved stars. Raman spectroscopy of nanodiamonds from the Allende meteorite has revealed a shift of the 1332 cm^{-1} diamond peak downward to ~1326 cm^{-1}, but it is not clear whether this is due to origin by shock or a feature caused by small grain size [6]. The small size leads also to quantum confinement effects observable in their x-ray absorption fine structure [7]. TEM observations are more in line with a CVD origin [8].

Gases within the diamonds were probably trapped by ion implantation [9] and occupy two different types of sites characterized by different release temperatures [10]. Excesses of ^{21}Ne and ^{3}He are probably due to cosmic ray effects, partly from recoil implantation and possibly also from cosmic ray ^{3}He trapped as such [11]. The latter may offer a possibility to extract information about the diamonds' residence time in the molecular cloud from which the solar system formed.

[1] Hoppe, P. (2008) *Space Sci. Rev.*, **138**, 43-57. [2] Ott, U. *Space Sci. Rev.*, **130**, 87-95. [3] Ott, U. (1996) *Astrophys. J.*, **463**, 344-348. [4] Meyer, B.S. et al. (2000) *Astrophys. J. Lett.*, **540**, L49-L52. [5] Marositts, E. & Ott, U. (2006) *Meteorit. Planet. Sci.*, **41**, A113. [6] Gucsik, A. et al. (2008) *Proc. IAU Symp. 251 "Organic Matter in Space"*, 335-339. [7] Berg, T. et al. (2008) *J. Appl. Phys.*, **104**, 064303. [8] Daulton, T.L. et al. (1996) *Geochim. Cosmochim. Ac.*, **60**, 4853-4872. [9] Koscheev, A.P. et al. (2001) *Nature*, **412**, 615-617. [10] Koshcheev, A.P. et al. (2008) *Russ. J. Phys. Chem.*, **82**, 1908-1914. [11] Huss, G.R. et al. (2008) *Meteorit. Planet. Sci.*, **43**, 1811-1826.

Challenges of identifying diamond polytypes of natural nanodiamonds

Németh, P.[1*], Garvie, L.[2] & Buseck, P.R.[3]
[1]Institute of Nanochemistry and Catalysis, CRC-HAS, Budapest, Hungary ([*]peter.nemeth@chemres.hu)
[2]Center for Meteorite Studies, Arizona State University, Tempe, Arizona, USA
[3]School of Earth and Space Exploration, Arizona State University, Tempe, Arizona, USA

Nanodiamonds (Fig. 1) with sizes down to 1 nanometer are abundant in meteorites, impact craters, and as globally dispersed products caused by extraterrrestrial impacts. Their morphology, polymorphic modifications, and lattice defects can provide information regarding formation conditions (e.g., [1]).

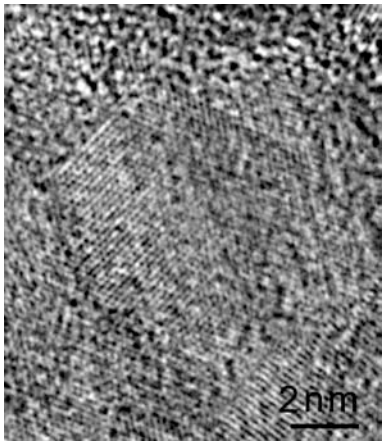

Fig. 1: Nanodiamond from the Gujba meteorite.

The last decade has revealed numerous new carbon allotropes with cell parameters and space groups that differ from those of Fd-3m diamond. In particular, large numbers of new carbon modifications have been described from synthetic materials, but the structures and properties of many of these have only been incompletely characterized.

The transmission electron microscope (TEM) is the most powerful tool to identify different diamond allotropes, but challenges exist because of both the small sizes and the subtle differences of the carbon phases. Moreover, dynamic effects such as multiple scattering arising from thickness variations make the identification of given modifications difficult. To link such allotropes as direct indicators of a specific geological phenomenon is problematic.

In our presentation we examine carbonaceous materials from the Gujba and Canyon Diablo meteorites and illustrate the atomic-scale structural complexity of nanodiamonds. Furthermore, we draw attention to the difficulties and challenges occurring during the identifications of diamond polytypes.

[1] Daulton, T.L. et al. (1996) *Geochim. Cosmochim. Ac.*, **60**, 4853-4872.

Study of impurities in nanodiamonds from meteorites by spectroscopic methods: implications for their formation

Shiryaev, A.A.[1*], Fisenko, A.V.[2], Vlasov, I.[3] & Semjonova, L.[2]
[1]Institute of Physical Chemistry, Moscow, Russia
([*]a_shiryaev@mail.ru)
[2]Vernadsky Institute of Geochemistry, Moscow, Russia
[3]General Physics Institute, Moscow, Russia

Meteoritic nanodiamonds (MND) are the most abundant protoplanetary Solar System relic phases in comparison with other compounds (graphite, SiC etc.). Nanodiamonds contain isotopically anomalous Xe, presumably originated in r- and p-processes of type II supernovae explosion. Mass-spectrometry shows that H and N are the main chemical impurities in MND. The N content of some of the grains (up to 4 %) exceeds significantly not only the average (0.04 %), but also the maximal (0.3 %) N content reported for terrestrial natural and synthetic (nano)diamond. Therefore, models of MND formation must explain high impurity content.

Speciation of N in MND is unknown and up to now no reliable spectroscopic evidence of N-related defects in MND has been reported. We will present results of our extensive spectroscopic comparative investigation of meteoritic nanodiamonds from Efremovka CV3 and Orgueil CI chondrites with synthetic nanodiamonds produced by very different methods: CVD, detonation (DND), Physical Vapour Deposition (PVD). The samples were analysed using luminescence and Raman spectroscopies, EELS, and NEXAFS at C and N absorption edges. The structure and size distribution of the grains was analysed using X-ray diffraction and scattering.

XRD and PEEM show that the phase composition of the MND and UDD are similar. This observation may indicate similarities of their structures in the sense that they presumably consist of diamond core surrounded by (semi)amorphous and graphite-like carbon. EELS and XANES analysis of the nanodiamond grains with high spatial resolution showed that both MND and UDD contain high amount of nitrogen located almost exclusively in twin lamellae and other similar imperfections. This N does not have obvious spectroscopic manifestations. Such localisation of nitrogen is also encountered in some nanocrystalline diamond films. No unambiguous manifestations of radiation defects are observed.

This work has direct implications for the origin of meteoritic nanodiamonds: high concentration of nitrogen in nanodiamonds could be achieved only if their growth (or, at least, nucleation) is extremely fast and proceeds on the time scale of 1-5 microseconds. In case of quasi-equilibrium growth when impurity trapping is determined by kinetics of absorption-desorption, the impurity content is invariably much smaller, than that encountered in meteoritic nanodiamonds. The grains enriched in nitrogen, most likely, were formed in a fast process, probably from a C-N-rich plasma.

For the first time the silicon-vacancy complex (the “silicon” defect) is observed in meteoritic nanodiamond by photoluminescence spectroscopy. Moreover, this is the first observation of this defect in dispersed nanodiamond of any origin. The current study suggests a new isotopic system in studies of the meteoritic nanodiamond – silicon, which is potentially capable to improve understanding of the astrophysical environment of its formation.

Fluid-induced dislocation pipe diffusion along olivine low-angle subgrain boundaries

Plümper, O.* & Austrheim, H.
Physics of Geological Processes, University of Oslo, Norway
(*oliver.pluemper@fys.uio.no)

Low-angle subgrain boundaries are a common microstructure in olivine that is a result of dislocation alignment into planar arrays due to crystal-plastic deformation. These dislocation arrays can act as fast pathways for diffusing atoms and dissociated water molecules. This phenomenon, known as pipe diffusion [1], is thought to originate from the disordered core region that lowers the activation energy for diffusion [2]. Recent in-situ transmission electron microscopy (TEM) experiments on a single dislocation line observed enhanced diffusivity along the dislocation cores of up to three orders of magnitude difference when compared to bulk diffusion [3]. However, most investigations have observed these phenomena in metals and ceramics only. Here we present new observations supporting dislocation pipe diffusion in olivine from the hydrated upper mantle section of the Leka Ophiolite Complex, Nord-Trøndelag, Norway.

Intragranular striped chemical zoning in olivine grains was observed using optical microscopy and back-scattered electron imaging. The zoning is parallel to the typical olivine kink bands and the optical undulose extinction that is caused by intragranular misorientation. Two types of chemical zoning were found; (1) Fe-enriched and (2) Fe-depleted zoning. Both types of zoning had distinct, parallel spacing across the olivine grains. The most pronounced zoning was found to spread out from serpentine needles that transect into the olivine. Focused ion beam sample preparation technique combined with transmission electron microscopy revealed that the observed striped zoning is in direct spatial relationship with low-angle (100)ol subgrain boundaries composed of (010)[100] edge dislocations. The edge dislocation cores in the (010)[100] system are parallel to the c (i.e. [001]) direction. Scanning TEM, utilizing high-angle annular dark field imaging coupled with energy-dispersive X-ray spectrum profiling, revealed that the striped chemical zoning (Fe-enriched & Fe-depleted) is located at the subgrain boundary on the nanometer scale.

Nanometer-sized serpentine clusters and fluid inclusions (100-200 nm in size) were found at subgrain boundaries associated with the Fe-depleted zoning. High-resolution TEM revealed serpentine nuclei, several unit cells large, in direct relationship with the subgrain boundaries. However, subgrain boundaries associated with Fe-enriched zoning showed no evidence for olivine replacement by serpentine.

From the striped chemical zoning and serpentine replacement we infer that (100)ol subgrain boundaries, the locus of edge dislocation piling, potentially channels fluid entry. We suggest that this channeled entry causes highly anisotropic diffusion and physico-chemical alteration due to pipe diffusion along edge dislocation cores within the subgrain boundaries. Pipe diffusion could lead to a dislocation core instability at Fe-depleted subgrain boundaries which potentially could trap water, resulting in the transformation of olivine to serpentine via dissolution and reprecipitation.

This could dramatically weaken the olivine grains and have overall implications for the rheology of the hydrated upper mantle. Furthermore, this could have an important influence on the homogeneity of fluid infiltration and hence the hydration of olivine to form serpentine.

[1] Love, G.R. (1964) *Acta Metall.*, **12**, 731-737. [2] Rabier, J. & Puls, M.P. (1989) *Philos. Mag.*, **59**, 533-546. [3] Legros, M. et al. (2008) *Science*, **319**, 1646-1649.

Atomic structures and energies of grain boundaries in Mg_2SiO_4 forsterite from atomistic modelling

Adjaoud, O.* & Jahn, S.
Deutsches GeoForschungsZentrum GFZ, Section 3.3, Potsdam, Germany (*adjaoud@gfz-potsdam.de)

Most real materials are not single crystals but consist of crystalline grains of various sizes, misorientated with respect to each other. The grain boundaries influence many of the material properties. For example, when considering mantle rocks these boundaries become important since they provide a means for creep and ion migration, likely causes of mantle rheology. Olivine is a major component of the Earth's upper mantle and therefore it is of considerable importance to study its physical and thermodynamic properties.

The structure of grain boundaries can be investigated using high-resolution transmission electron microscopy (HRTEM) [1]. Atomistic simulations are not only useful to provide the structural model needed for the interpretation of the HRTEM images, but they are also a unique tool to link structure and physical or thermodynamic properties of grain boundaries. In the present study, we report the results on the atomic structure, the respective energies and excess volumes of symmetric tilt grain boundaries in Mg_2SiO_4 forsterite with different tilt angles. We construct [100] symmetrical grain boundaries with tilt angle α by aligning a chosen crystallography plane (0kl) parallel to the tilt axis [100] and misoriented with $\alpha/2$ to the (010) plane. One-half crystal (grain) is rotated by a 180° rotation relative to the other about the normal [0kl]. Since we use periodic boundary conditions, our simulations have large cells containing a few thousand atoms. The interactions between the atoms are described by an advanced ionic potential model [2] that accounts for polarization and deformation of the ions. In order to find stable grain boundary structures, we first perform molecular dynamics simulations to relax atomic positions. Then, we apply a combination of molecular dynamics and metadynamics method [3] to map the free energy surface and to search for other low energy grain boundary structures. We have found that the energies and excess volumes of the grain boundaries in Mg_2SiO_4 forsterite depend significantly on the misorientation angle of the grain boundary. We compare our results with HRTEM observations and relate them to previous studies of grain boundaries in ionic materials and in metals.

[1] Heinemann, S. et al. (2005) *Phys. Chem. Minerals*, **32**, 229-240. [2] Jahn, S. & Madden, P.A. (2007) *Phys. Earth Planet. Int.*, **162**, 129-139. [3] Laio, A. & Gervasio, F.L. (2008) *Rep. Prog. Phys.*, **71**, 126601.

Mineral replacement: modeling, phenomena, and mechanisms in terms of crystallogenesis

Glikin, A.E.
Dept. of Crystallography, St.Petersburg State University, St.Petersburg, Russia (glikin@ag2460.spb.edu)

Crystallogenesis is the principal basis for interpretations of mineral origin. It introduces fundamental concepts of layer and normal growth mechanisms, faceting, capturing impurities and inclusions, etc. Classical concepts concern crystal formation in unary and binary systems (quantitative and qualitative approaches, respectively). On the contrary, minerals form in a strongly complicated way while natural systems are of a multi-component/multiphase character. The main complication is a chemical reaction between different crystal compounds, which accompanies any crystal formation. The interaction consists of coordinated dissolution and growth processes and causes various forms of mineral replacement.

Modeling of replacement processes was carried out as interaction of a crystal with a foreign aqueous solution using more than 200 systems at room temperature. The systems included couples of soluble salts of either fixed or isomorphic compositions. Special devices enabled the microscopic in-situ observation of morphological and kinetic phenomena. The results were interpreted in terms of crystallogenesis based on traditional and modified concentration phase diagrams.

Metasomatic substitution of crystals occurs itself under isothermal conditions as interrelated synchronous dissolution and growth. The product shape is either inherited from the protocrystal (pseudomorphs) or different from that (automorphs) depending on the kinetic properties of the system. The product pattern (remaining monocrystalline or becoming polycrystalline) and volume effect are determined by the phase equilibria and can be resulted from the concentration phase diagram. A temperature change results in additional growth or dissolution and can cause negative (hollow) products. Joint growth of several phases under a finite supercooling includes an urgent metasomatic stage which effects on the kinetics and causes a profound case of a temporary metastable dissolution of a phase. A mutual influence of the phase compounds on their solubility causes a nonmonotonic effect of supercooling on the growth kinetics including conversion to dissolution. Recrystallization of two-phase aggregates consists in a complex combination of the metasomatic substitution, growth and dissolving of individuals. Temperature oscillations or gradients cause it. Temperature oscillation in salting-in-systems results in a redistribution of matter in a two-phase aggregate of stationary mineral-granulometric composition, and a monomineral aggregate. Recrystallization does not undergo in salting-out-systems. Temperature gradients result in a cavity near the maximum temperature and layered rearrangement of matter around the cavity. Mixed crystal formation is characterized by unordinary phenomena. Monocrystal substitution is accompanied either by inclusion implantation (volume deficit) or inhomogeneous crystal extension (volume excess) with a specific face relief. The substitution is reduced at a supercooling down to halting corresponded to the metastable heterogeneous crystal-solution equilibrium. Spontaneous precipitation results in a multi-modal distribution of crystals in composition. The mechanisms are controlled by the isomorphic miscibility of the substances and interpreted with help of modified concentration diagrams.

The considerations give novel crystallogenetic approaches and adequate mineralogical models.

Acknowledgements: The investigation is supported by RFBR (10-02-01303).

[1] Glikin, A.E. (2009) *Polymineral - Metasomatic Crystallogenesis*. Springer-Verlag, New York.

Potassium diffusion in alkali feldspar – an experimental study

Neusser, G.[1*], Norberg, N.[2], Abart, R.[3] & Harlov, D.[2]
[1]Inst. für Geologische Wissenschaften, Freie Universität Berlin, Germany ([*]neusser@zedat.fu-berlin.de)
[2]Helmoltz Zentrum Potsdam, Germany
[3]Dept. For Lithospheric Research, Universität Wien, Vienna, Austria

Cation exchange experiments were conducted using alkali feldspars and KCl rich salt melts. A gem quality sanidine (Or85Ab14Cs1) from the Eifel (Germany) was used as starting material. To obtain defined sample geometries 3 mm long cylinders with a diameter of 2 mm were milled out of a homogeneous feldspar crystal of about 6 cm size. The long axis of the cylinders coincides with the a axis of the feldspar, the cross section contains the b and the c* axis. All experiments were carried out at 850°C and room pressure in sealed quartz glass tubes. To establish a quasi infinite salt reservoir 30 moles salt per one mole of feldspar were used. Three different salt compositions with the molar KCl/NaCl ratios of 0.8, 0.9 and 1 were used for a time series with run durations of 1, 2, 4, 8 and 16 days. Because of the hygroscopic nature of the salt the ion exchange reaction is assumed to take place under anhydrous conditions.

At 850°C the salt mixture is completely molten and reacts with the feldspar cylinders inducing an exchange reaction during which the initial feldspar is progressively transformed and a rim of almost pure sanidine forms. The newly-formed rim is chemically homogeneous and separated from the pristine core by a relatively well defined exchange front. The width of this front and the composition gradients within it seem to be primarily controlled by the salt composition. After reaction with pure KCl the exchange front is less than 10 µm wide, whereas, if salt mixtures with $K_{0.9}Na_{0.1}Cl$ and $K_{0.8}Na_{0.2}Cl$ are used, the front width increases up to more than 20 µm. In contrast, the run duration does not seem to have a significant effect on the sharpness and the shape of the exchange front. Both seem to remain largely unchanged until the feldspar grain is completely exchanged. The propagation of the exchange front into the pristine crystal seems to be linear with $\sqrt{t}$, which indicates a diffusion-controlled mechanism. The reaction is driven by chemical potential gradients between the initial feldspar and the K-rich salt melts. Potassium is favored to enter the monoclinic sanidine structure, which results in an ion exchange of K^+ ions from the salt melt for Na^+ ions from the feldspar lattice. WDX mappings show that tetrahedrally incorporated trace elements such as Fe are not involved in this reaction. They remain homogeneously distributed within the feldspar crystal. Therefore alkali diffusion occurs within an inert tetrahedral framework. The assumed water-free environment in combination with the immobility of trace elements and the lack of secondary porosity indicates a strictly diffusion-controlled mechanism. However, a chemically homogeneous rim combined with a rather sharp reaction front as observed in this study is not characteristic for a simple diffusion setting, where a smooth diffusion profile from the crystal surface towards the interior is expected. Therefore, secondary effects such as elastic strain within the exchange front may also play an important role during the exchange process. During the exchange of larger K ions for Na the molar volume of the feldspar increases up to 0.74%. Since HR-TEM measurements show that the feldspar lattice remains coherent across the reaction front, the change in volume induces elastic strain. This strain-build up seems to have a large effect on the shape of the chemical profile across the reaction front.

Reaction kinetics and akali diffusion during replacement of K-rich alkali feldspars in (Na,K)Cl solutions

Norberg, N.[1*], Neusser, G.[2], Harlov, D.[1] & Abart, R.[3]
[1]Helmoltz Zentrum Potsdam, Germany
([*]nicholas@gfz-potsdam.de)
[2]Inst. Für Geologische Wissenschaften, Freie Universität Berlin, Germany
[3]Dept. For Lithospheric Research, Universität Wien, Vienna, Austria

The kinetics of the feldspar replacement reaction $K_{1-x}Na_xAlSi_3O_8+Na^+/K^+ \rightarrow Na_{1-y}K_yAlSi_3O_8+K^+/Na^+$ were studied experimentally between 500°C and 750°C at 200 MPa. Fragments and cylinders of gem-quality sanidine (Eifel, Germany, Or85Ab14Cs1) and orthoclase (Madagascar, Or95Ab5) were reacted in aqueous (Na,K)Cl solutions with molar Na/K ratios of 1, 0.8 and 0.75 in order to initiate different molar volume changes between initial and product phase. A 20 molar excess of salt was used to provide a quasi-infinite cation reservoir. The dominant replacement process was identified as dissolution-reprecipitation showing all characteristic textural features (e.g. [1]). In the early stages of replacement when the initial reaction interface coincides with the grain surface, the replacement proceeds linearly with time indicating interface-reaction control. After the reaction rim reaches a critical thickness the mechanism changes and the reaction seems to become increasingly transport-controlled. In this regime the rate of replacement depends on the mass flux from the fluid reservoir to the reaction front through already replaced areas. The overall reaction rate as well as the transition from an interface- to transport-controlled mechanism significantly depends on temperature, the difference in molar volume ΔV (causing porosity) and the chemical potential gradients between the initial feldspar and the fluid.

In general fluid-aided replacement reactions produce extremely sharp interfaces, characterized by abrupt chemical and microstructural changes within less than 10 nm. However, at hypersolvus temperatues (750°C) these initially sharp boundaries are blurred by volume diffusion of Na and K across the moving reaction front with time. At lower temperatures as well as during the interface-reaction controlled stage of the replacement at high temperatures, the progress of the fluid-driven reaction front into the parent crystal exceeds the velocity of the Na/K interdiffusion across the interface. Consequently the resulting front is chemically sharp. However, due to the significantly increased diffusivities of Na and K at 750°C, volume diffusion of alkalis becomes dominant after the fluid-assisted replacement becomes transport-controlled and the front propagation decreases relatively to the mobilities of Na and K. For example, in the case of pure NaCl solutions this results in diffusive Na and K distributions with profile widths of >10 µm after 4 days, superimposed on a sharp interface caused by dissolution-reprecipitation.

The position of this interface is represented by an abrupt change in the concentrations of tetrahedrally incorporated Fe and Al indicating a complete breakdown of the initial feldspar framework during dissolution-reprecipitation. This transition remains chemically sharp independent of run duration due to the much lower diffusivities of Fe and Al at these conditions. With regard to structural characteristics of the reaction interface, HR-TEM revealed that despite the complete reorganization of the Si/Al framework it seems that the reaction front is not characterized by a total break in lattice coherency. Hence, molar volume differences of up to 7.6%, although partly compensated by nano-porosity, defects or twinning, induce elastic strain along the interface, which results in reaction-induced fracturing.

[1] Putnis, A. (2009) *Rev. Mineral. Geochem.*, **70**, 87-124.

Replacement of plagioclase by cordierite in hydrothermal experiments

Hövelmann, J.[1*], Austrheim, H.[1] & Putnis, A.[2]
[1]Physics of Geological Processes, University of Oslo, Norway
([*]j.e.hovelmann@fys.uio.no)
[2]Institut für Mineralogie, University of Münster, Germany

Commonly, Al-rich minerals such as corundum, sillimanite, cordierite and sapphirine are considered indicators for a sedimentary origin of a metamorphic rock. However, the presence of sapphirine and corundum has recently been reported in gabbroic rocks from the Bamble sector, South Norway [1]. The formation of the Al-rich minerals in these rocks is interpreted to be a result of pervasive Mg-metasomatism. Based on this interpretation a metasomatic origin has also been suggested for the orthoamphibole-cordierite schists that occur in the same area.

We have performed hydrothermal experiments (T: 600-700°C, P: 2 kbar) on the interactions between calcic plagioclase ($Na_{0.4}Ca_{0.6}Al_{1.6}Si_{2.4}O_8$) and Mg-rich aqueous solutions in order to investigate the possibility of a metasomatic origin of Al-rich minerals. Back scattered scanning electron microscope images of cross sections of the reacted crystals reveal that the original plagioclase has been partly replaced by cordierite ($Mg_2Al_4Si_5O_{18}$), indicating that Mg from the fluid has been consumed, while Ca and Na from the plagioclase have been released during the reaction. The Al that was released from plagioclase dissolution has been consumed by subsequent cordierite precipitation. The cordierite product forms rims, up to 200 µm thick, around relicts of the original plagioclase commonly occurring as several isolated islands within the "cordierite matrix". Optical microscopy demonstrates that these islands have the same crystallographic orientation indicating that they were originally part of one single crystal. The cordierite is orthorhombic with a high degree of Al,Si ordering ($Q_{od} \approx 0.97$), as indicated by Raman spectroscopy, and shows sector-like twinning with opposite sectors having the same crystallographic orientation. Previously, sector twinning in cordierite has been attributed to the transformation from the hexagonal to the orthorhombic form during annealing [2,3]. However, the sector-like twinning in the cordierite from our experiments possibly formed directly during growth.

Our study may have implications for both the origin of sector twinning in cordierite and the origin of Al-rich minerals in metamorphic rocks. The experimental results confirm that Al-rich minerals may be formed by metasomatic processes and, in particular, also support the hypothesis of a metasomatic origin of the orthoamphibole-cordierite rocks in the Bamble sector.

[1] Engvik, A.E. & Austrheim, H. (2010) *Terra Nova*, **00**, 1-6. [2] Zeck, H.P. (1972) *J. Petrol.*, **13**, 367-380. [3] Putnis, A. & Holland, T.J.B. (1986) *Contrib. Mineral. Petrol.*, **93**, 265-272.

Growth mechanisms for decompression plagioclase rims around metastable kyanite from high-pressure felsic granulites (Bohemian Massif)

Tajčmanová, L.[1*], Abart, R.[2], Rhede, D.[3] & Wirth, R.[3]
[1]Institute of Geological Sciences, Free University, Berlin, Germany ([*]lucataj@gmail.com)
[2]Dept. of Lithosphere Research, University of Vienna, Austria
[3]Helmholtzzentrum Potsdam, Deutsches GFZ, Potsdam, Germany

We investigate two different textural settings for decompression plagioclase rim growth in high-grade metamorphic rocks. The studied samples are felsic granulites from the Bohemian Massif (Variscan belt of Central Europe) characterized by a Grt-Ky/Sil-Bt-Pl-Kfs-Qtz mineral assemblage. These rocks show well developed plagioclase reaction rims around metastable kyanite grains which are either randomly distributed in the polycrystalline matrix or enclosed within large perthitic K-feldspars. Kyanite is regarded as a relic of an earlier high-pressure metamorphic assemblage, which became metastable during low pressure overprint.

Growth of the plagioclase rims around the metastable kyanite crystals requires transfer of CaO and Na_2O components from the surrounding matrix or host K-feldspar. Through the plagioclase rim, the kyanite grains are successively isolated from the quartz- and K-feldspar-bearing matrix. Mass balance considerations show that only a small amount of kyanite was consumed to provide the Al_2O_3–component for the growing plagioclase. In majority, Al_2O_3 and SiO_2 were supplied together with CaO and Na_2O from the surrounding matrix material. Plagioclase rims from both microstructural settings show continuous changes in composition from An_{25} at the contact to kyanite to An_{19} at the contact to the K-feldspar or to the matrix. Plagioclase rims developed around kyanite inclusions within large K-feldspar blasts have a radial thickness of up to 50 µm. In contrast, the radial thickness of plagioclase rims around kyanites in the polycrystalline matrix is significantly larger, up to 200 µm. Another peculiarity for both microstructures is the crystallographic character. The plagioclase rims around kyanite in the matrix are polycrystalline, whereas the plagioclase rims around kyanite inclusions in perthitic hosts are single crystals of plagioclase. This difference has a profound effect on mass transfer across the growing plagioclase rim and explains the systematic difference in rim thickness for the two microstructural settings. Assuming that the cation availability in the source (either host alkali feldspar or rock matrix) was the same in both settings, it is hypothesized that the comparatively large thickness of the plagioclase rims grown around kyanite in the matrix is due to the contemporaneous operation of grain-boundary and volume diffusion. On the other hand, in the large K-feldspar grain only volume diffusion was efficient, which only allowed for comparatively slow volume diffusion across the plagioclase rims.

Electron beam microanalytical techniques combined with high spatial resolution (FEG-EMS, FEG-SEM, TEM) and FIB sample preparation technique were used to directly observe the traces of intergranular diffusion both, within the alkali feldspar or matrix and across the plagioclase rims. Using these techniques and comparing single crystal and polycrystal reaction rim growth from the two different microstructural settings, the relative contributions of volume and grain boundary diffusion are assessed in a semi-quantitative manner. This offers new insights into the kinetic processes, which controlled the microstructural and chemical evolution during the decompression of felsic high grade rocks.

How reliable are microstructural criteria defining a “metamorphic event”?

Putnis, A.[1*] & Austrheim, H.[2]
[1]Institut für Mineralogie, University of Münster, Germany ([*]putnis@uni-muenster.de)
[2]Physics of Geological Processes, University of Oslo, Norway

A metamorphic event is defined in terms of a sequence of metamorphic reactions in P,T space. However, the distinction between reactions driven by changes in P,T and those driven by compositional changes due to infiltration of fluid (i.e. metasomatic reactions) is not always clear [1]. Metamorphism and metasomatism both involve material transport but on different length scales, so every metamorphic reaction is metasomatic on a local scale. Fluids provide a transport mechanism which is orders of magnitude faster than solid state diffusion and induce reequilibration through dissolution of parent phases and reprecipitation of products. Albitisation is used as an example to describe the coupling between dissolution and precipitation. Albitisation of feldspars in nature and in experiments is a pseudomorphic replacement which generates porosity in the albite [2,3]. Porosity generation associated with interface-coupled dissolution-precipitation allows rapid material transport and together with fluid induced fracturing, is the mechanism of pervasive fluid flow through reacting crystals.

Examples of metamorphic reactions in granulite-eclogite rocks illustrate the role of fluids in inducing chemical changes along fluid pathways. Microstructural criteria for a metamorphic event are critically reviewed by describing the corona formed by reaction between kyanite and garnet, as well as partial replacement textures. We conclude that both corona structures and partial replacement textures are as indicative of a metasomatic reaction as they may be of a metamorphic reaction. This raises the question of the extent to which fluids play not only a catalytic role, but also a thermodynamic role in determining the course of a metamorphic reaction [4].

[1] Vernon, R. et al. (2008) *J. Metam. Geol*., **26**, 437-449. [2] Engvik, A.K. et al. (2008) *Can. Mineral.*, **46**, 1401-1415. [3] Hövelmann, J. et al. (2010) *Contrib. Mineral. Petrol.*, **159**, 43-59. [4] Putnis, A. & Austrheim, H. (2010) *Geofluids*, in press.

Kelyphite and symplectite after garnet: the microstructure, formation processes and reaction kinetics

Obata, M.[1*], Ozawa, K.[2] & Spengler, D.[3]
[1]Dept. of Geology and Mineralogy, Graduate School of Science, Kyoto University, Kyoto, Japan ([*]obata@kueps.kyoto-u.ac.jp)
[2]Dept. of Earth and Planetary Sciences, Graduate School of Science, University of Tokyo, Japan
[3]Geodynamics Research Center, Ehime University, Ehime, Japan

Kelyphite is a fine grained, fibrous and radially-oriented mineral assembly typically surrounding garnet. Texturally it appears to represent a replacement of garnet, although not isochemical to garnet, suggesting that the replacement reaction is a chemically open-system phenomenon involving material transfer across the reaction zone. We made a comparative study of kelyphites developed in mantle-derived garnet peridotites from various localities (including Czech Moldanubian, western Norway), using optical microscopy, electron probe microanalyzer and EBSD analysis for consideration of the reaction mechanism.

In garnet peridotites, fine-grained kelyphite (Opx+Cpx+Sp with or without accessory Amp) is typically surrounded by a thin (ca. a few hundreds of micron) rim of coarse Opx, which separates the kelyphite from the matrix olivine. Optical microscopy shows that kelyphite consists of several domains of Opx. EBSD studies show that each domain represents a single crystal of Opx, which includes small patches of Cpx, and both pyroxenes contain thin (sub-micron size) lamellae of spinel, forming a spinel-pyroxene symplectite. Each kelyphite domain has an internal coherent structure of lineation defined by the spinel lamellae. The kelyphite Opx is optically and crystallographically continuous to the adjacent coarse rim-Opx, forming a larger domain of a single crystal. We refer to this domain covering the fine-grained kelyphite and the adjacent Opx rim as a 'cell' and consider it as a growth unit. EBSD analyses revealed that each domain (cell) has a topotaxic relationship between Opx and Cpx by sharing (100) and (010) and [001]. Two kinds of cells are recognized according to the topotaxic relationships between spinel and pyroxene: (1) topotaxic cell, in which one of spinel {111} coincides with pyroxene (100) and one of spinel {110} coincides with pyroxene (010); (2) non-topotaxic cell, in which topotaxic relationships between spinel and pyroxene are incomplete or absent. The topotaxic relationship may be understood in terms of the oxygen close-packed structure of crystals. It appears that kelyphite that formed at relatively high-temperatures (e.g. Czech Mohelno garnet peridotite [1]) contains topotaxic cells whereas kelphite of lower-temperature origin, such as western Norway, dominantly consists of non-topotaxic cells. The spinel-pyroxene symplectite from the Horoman spinel peridotite is regarded to represent a topotaxic cell that was formed after garnet at highest temperatures (>1000 degree C) [2]. From these observations we hypothesize that a topotaxic relationship may form when spinel nucleates at the initial stage of kelyphitization and the initial crystallographic relationship may be inherited during subsequent growth of the cell in the kelyphite. At relatively low temperatures, such topotaxic relationships may fail to form probably because of the large degree of supersaturation of the reaction.

[1] Kamei, A. et al. (2010) *J. Petrol.*, **51**, 101-123. [2] Odajima, N. et al. (2008) *J. Mineral. Petrol. Sci.*, **103**, 1-14.

Textural development and fluid flow during mineral vein formation

Okamoto, A.[*], Saishu, H. & Tsuchiya, N.
Graduate School of Environmental Studies, Tohoku University, Sendai, Japan ([*]okamoto@mail.kankyo.tohoku.ac.jp)

Ubiquitous occurrences of quartz veins indicate that precipitation of silica minerals is of special importance for spatial and temporal variations of rock permeability and rock strength at shallower crustal levels. However, the physico-chemical conditions during quartz vein formation (fluid compositions, flow rate, fracture geometry etc.) have been poorly constrained. In this study, we conducted hydrothermal flow-through experiments at 430°C and 31 MPa on silica precipitation to understand the controlling factor for textural development of quartz veins. Then, implications to the formation of natural veins are discussed.

In the reaction vessel (internal diameter = 10.8 mm, length = 550 mm), eighteen granite blocks (6.5x6.5x30 mm) are placed along the flow path. Two types of Si- saturated solutions were used: a pure Si solution created by dissolution of quartz sand and a multi-component solution created by dissolution of garniate sand. We found that the mineralogy and textures of silica precipitates systematically changes depending on the degree of supersaturation ($\Omega = C_{Si}/C_{Si,eq,Qtz}$), presence of additive ions (Al, Na, K with several ppm) in the solution and substrate type. In the case of the low degree of supersaturation ($\Omega < 1.5$), silica precipitation occurred only as overgrowth on the substrate quartz. On the other hand, the precipitation mechanism from solutions with higher Si content ($\Omega > 1.5$) was more complex due to nucleation. From the pure Si solutions, amorphous silica and/or opal-C predominantly formed and partly translated into quartz. From the impure solutions with additive ions, quartz nucleated directly from the solutions. Our experimental results suggest that vein textures are good indicators of Si concentration during vein formation.

The textures observed in the hydrothermal experiments are comparable to those of the natural quartz veins that (1) epitaxial growth from quartz grains within the wall rocks (elongate-blocky, fibrous textures), and (2) filling of equant grains (blocky textures) [1,2]. The mineral veins hosted in the pelitic schists in the Sanbagawa metamorphic belt, Japan, are divided into two types [1]: Qtz-Ab-Kfs-Chl veins are characterized by quartz and albite crystals grown from the wall and bridge to the opposite side (stretched crystal textures), and show the mineral distribution depending on the compositional banding of the host rocks. Qtz-Ab-Cal veins are filled by double-terminated euhedral quartz and albite crystals (blocky texture), and mineral distribution is homogeneous along the vein length. Both veins formed at the same stage of the exhumation of the Sanbagawa belt (200-400˚C, 0.2-0.4 GPa), but show contrasting vein width; the former is much thinner than the latter. These observations suggest that the materials were transported by molecular diffusion from the adjacent host rock for the stretched crystal veins, whereas by advective fluid flow from distant sites for the blocky veins. Okamoto & Tscuhiya [2] suggest that high flow ascent rate (0.01-0.1 m/s) is required for the formation of the blocky veins, based on the analyses of crystal size distributions and crystal settling theory. Such a high fluid flow rate realized the high degree of supersaturation that enabled the nucleation of quartz in fluids as observed in the experiments. In contrast, in the case of stretched crystal veins, fluid was static, the rate limiting process was diffusion, and thus epitaxial growth preferentially occurred in solutions with a low degree of supersaturation.

[1] Okamoto, A. et al. (2008) *Contrib. Mineral. Petrol.*, **156**, 323-336. [2] Okamoto, A. & Tsuchiya, N. (2009) *Geology*, **37**, 563-566.

Retention of colloids at rough limestone surfaces

Fischer, C.[1,3*], Darbha, G.K.[1], Michler, A.[1], Schäfer, T.[2] & Lüttge, A.[3]
[1]Georg-August University, Göttingen, Germany
([*]cornelius@rice.edu)
[2]INE, KIT, Karlsruhe, Germany
[3]Rice University, Houston, TX, USA

Colloid-aided mobilization and immobilization of contaminants is an important environmental process. Deposition of colloids on mineral and rock surfaces is predominantly caused by attractive electrostatic forces. However, close to the point of zero charge (PZC) of minerals or mineral aggregates as well as during conditions of electrostatic repulsion, the importance of surface roughness for deposition of colloids is increased. According to a previous study [1], at PZC of calcite, a positive correlation between the number of adsorbed particles and the surface roughness of the crystal surface with etch pits was found. The range of root mean square roughness *Rq* was about 10 to 40 nm, particle size was 499 nm and 903 nm.

Here we expand the investigation of particle adsorption at rough calcite surfaces to fine-grained, micritic limestone. Grain-size of the dense limestone investigated here is 5-10 µm according to thin-section analysis. Polished limestone samples were etched at pH = 4.7 for 60', 120', 180', and 240' in a fluid cell to obtain a rough surface similar to those in nature. For reaction periods > 60' the limestone surface areas show a constant maximum root mean square roughness (*Rq* ~ 400 nm). Surface topography was characterized and quantified using vertical scanning interferometry (VSI). The resulting three-dimensional data sets were used for roughness parameter calculation [2].

Particle adsorption experiments were carried out using negatively charged polystyrene latex colloids (d = 1 µm). Deposition experiments were conducted at PZC of calcite. First results based on VSI data show a pattern of high-density particle adsorption sections at the micrite surface. Such sections have a diameter of about 20 µm. The density of adsorbed particles of such sections is approx. 20 times higher compared to adjacent surface sections. First results also indicate that enhanced particle adsorption occurred preferentially at surface sections where *Rq* is relatively low (*Rq* ~ 200 nm).

In the environment, e.g., in karstic regions, adsorption of clay minerals as well as iron and manganese oxides at limestone surfaces modifies fundamentally the original fluid-rock interface. As a consequence, dissolution as well as adsorption kinetics are altered. With the results of our experimental approach we try to provide quantitative constraints to predict the evolution of fluid-rock interfaces due to particle adsorption.

[1] Darbha, G.K. et al. (2010) *Langmuir*, **26(7)**, 4743-4752. [2] Fischer, C. & Lüttge, A. (2007) *Am. J. Sci.*, **307(7)**, 955-973.

The influence of mineral replacement reactions on rock deformation and shear zone development

Brouwer, J.* & Putnis, A.
Institut für Mineralogie, University of Münster, Germany
(*J.Brouwer@uni-muenster.de)

Natural shear zones show that reaction and deformation are often spatially interrelated. Study of these reactions shows that often fluids are involved (e.g. [1]). Fluid–assisted mineral replacement is generally not isovolumetric [2] and may therefore lead to an increase in permeability through the formation of pores or cracks. Subsequent fluid infiltration can lead to further progress of the replacement process and reaction weakening of the rock.

When the rock is stressed, the combination of physical and chemical driving forces may trigger simultaneous reaction and deformation, where the rates of both processes may be significantly higher than if they would be operating separately. The combination of localized, reaction-induced permeability leading to further fluid-infiltration may thus lead to a localization of deformation. This is possibly a key issue in shear-zone development.

We have performed compaction experiments using a set-up as described by [3] that show the effects of volume change during deformation and how mineral reaction influences pressure solution rates and vice versa. Using chemical systems with a limited number of reactants and products, they form a starting point in our understanding of the complex interplay between reaction and deformation in natural rocks.

[1] Austrheim, A. (1987) *Earth Planet. Sci. Lett.*, **81**, 221-232. [2] Putnis, A. (2009) *Rev. Mineral. Geochem.*, **70**, 87-124. [3] de Meer, S. & Spiers, C.J. (1997) *J. Geophys. Res.*, **102**, 875-891.

Symplectite formation during decompression induced garnet breakdown in lower crustal mafic granulite xenoliths: mechanisms and rates

Dégi, J.[1,2*], Abart, R.[3], Török, K.[4], Bali, E.[5], Wirth, R.[6] & Rhede, D.[6]
[1]Research Institute for Solid State Physics and Optics, Budapest, Hungary (*julia.degi@gmail.com)
[2]Lithosphere Fluid Research Lab, Eötvös University, Budapest, Hungary
[3]Dept. of Lithospheric Research, University of Vienna, Austria
[4]Eötvös Loránd Geophysical Institute of Hungary, Budapest, Hungary
[5]Bayerisches Geoinstitut, University of Bayreuth, Germany
[6]GFZ German Research Centre for Geosciences, Helmholtz Centre Potsdam, Germany

The complex microstructure of kelyphitic rims around garnet in lower crustal garnet granulite xenoliths from the Bakony–Balaton Highland Volcanic Field, Central Pannonian Basin has been studied in order to identify controls on garnet breakdown. Symplectites comprised of a vermicular intergrowth of submicron sized anorthite, orthopyroxene and spinel replace garnet at a sharp reaction front. Based on element distribution maps the transformation of garnet to symplectite is isochemical. Phase diagram calculations indicate this reaction was induced by a pressure decrease and/or a temperature increase.

In site-specific TEM foils prepared by FIB technique and oriented parallel and perpendicular to the reaction front 200 nm wide rods of anorthite and 20 nm wide rods of spinel are identified. The rods are oriented approximately perpendicular to the replacement front and are embedded in an orthopyroxene matrix. The regular spacing of the symplectite phases along the reaction front suggests that their growth is controlled by diffusion. The kinetics of symplectite formation has been modelled based on irreversible thermodynamics.

During interaction of the xenolith with the host basalt the microstructure and chemistry of the An–Opx–Spl symplectite was significantly modified and it was partially replaced by an olivine bearing symplectite. In contrast to primary symplectite formation, these processes were metasomatic in nature including addition of sodium, titanium and some trace elements from the basaltic melt and can clearly be discerned from the garnet breakdown. Based on these observations it is inferred that symplectite formation took place within the deep crust during the extension of the Pannonian Basin between 15–30 km depth at high temperature (850–1050°C) prior to the volcanic transport to the surface.

Unidirectional solidification texture (UST) and garnet layering textures from the Y-enriched garnet-bearing aplite-pegmatites, western part of the Cadomian Brno Batholith, Czech Republic

Hönig, S., Leichmann, J.* & Novák, M.
Dept. of Geological Sciences, Masaryk University, Brno, Czech Republic (*leichman@sci.muni.cz)

Felsic layered garnet-bearing aplite-pegmatite dykes of the Hlína granitic suite, ~2 to 50 m thick and up to ~200 m long with general NW–SE orientation and dip 40-80° into ESE or WSW, cut granodiorites to granites at the SW part of the Brno Batholith, Brunovistulicum. Aplite-pegmatite bodies are characterized by alternation of two main textural units: (i) a fine-grained aplite unit and (ii) a coarse-grained pegmatite with comb-like UST unit both developed in zones with the thickness varying from several cm to ~ 1-2 m for the aplite unit, and ~ 10 cm for the UST unit. In this paper, we use the term "UST" (unidirectional solidification texture) which describes rock layer composed of crystals oriented perpendicularly to the plain of layering.

All rock types are characterized by high contents of SiO_2 (74.6 – 75.7 wt. %), K_2O (4.61 – 4.94 wt.%), Na_2O (3.82 – 4.21 wt.%), moderate concentrations of CaO (0.94 – 1.11 wt. %), and low to very low concentrations of Fe_2O_3 (0.62 – 0.93 wt.%), MgO (0.02 – 0.03 wt. %), and TiO_2 (≤ 0.03 wt. %). Low K/Rb (212–241), high K/Ba ratios (1034 – 2303) and deep Eu anomalies indicate a high degree of fractionation. Both textural units consist of perthitic microcline, plagioclase An_{15-8} and quartz. The total amount of accessory minerals is typically very low, commonly < ~ 1 vol.% in the aplite unit, in the UST unit they are almost absent. Accessory minerals include relatively common Y-rich garnet Sps_{42-38} Alm_{32-28} And_{15-7} Grs_{21-15} Prp_{2-1} (1.10 wt.% Y_2O_3 - 0.06 apfu, 0.53 wt.% Yb_2O_3 and 0.20 wt.% Er_2O_3) with oscillatory and sector zoning. Other minerals commonly closely associated with garnet are extremely rare: magnetite, chloritized biotite, muscovite, Ta-rich titanite I, Al,F-rich titanite II, and ilmenite. Primary zircon, xenotime-(Y), monazite-(Nd), fersmite, ferrocolumbite, REE,Y-rich pyrochlore are strongly altered. Geochemical and mineralogical features of the Hlína aplite-pegmatites characterized by (i) metaluminous to slightly peraluminous A-type (NYF) affinity indicated by elevated concentration of Y, REE (especially HREE), Zr, U, Th, (ii) specific accessory minerals including Y-rich garnet, Nb>>Ta, HREE>>LREE, (iii) almost entire absence of micas and other minerals with volatiles (B, F, P and also H_2O) are remarkable. They differ from all other granitic rocks with UST textures described to date typically characterized by high activity of volatiles and peraluminous signature. Magmatic layering of garnet is explained by the formation of a boundary chemical front bordered margin of the coarse-grained UST unit.

Modelling of nonlinear inter-granular diffusion under local equilibrium with a mineral: an example in the system muscovite – quartz – H_2O

Nishiyama, T.
Dept. of Earth & Environmental Sciences, Kumamoto University, Kunamoto, Japan (tadao@sci.kumamoto-u.ac.jp)

Diffusion through an inter-granular fluid plays an important role in texture formation of the metamorphic rocks such as reaction zones and metamorphic layering. The nature of the diffusion is, however, not well understood. This paper will discuss the situation such that a fluid species diffuses down its chemical potential gradient under the constraint of local equilibrium with a co-existing mineral. The constraint will cause a coupling of diffusive fluxes, which is described by nonlinear diffusion equations. The aim of this paper is to evaluate the effect of the coupling which possibly contributes to the texture formation in metamorphic rocks.

Suppose a metamorphic rock in the system muscovite – quartz – H_2O, which consists of a muscovite – rich layer and a quartz – rich layer. At an initial pressure - temperature condition, the system is in an equilibrium, namely, muscovite, quartz and H_2O (an inter-granular fluid) are in equilibrium with each other in both layers. The system will destabilize according to a pressure – temperature change. If temperature is raised, the solubility of minerals increases. The muscovite – rich layer will reach the muscovite saturation condition before arriving at the new quartz – muscovite equilibrium condition, because the amount of dissolved species is proportional to the total surface area of the mineral and hence the concentration of dissolved Al species is higher than that at the new quartz – muscovite equilibrium condition. Similarly, the quartz – rich layer reaches the quartz saturation condition before arriving at the new quartz – muscovite equilibrium condition. Then spontaneous diffusion will take place between the two layers. The diffusion is assumed to occur under local equilibrium with muscovite. The local equilibrium condition with quartz is not introduced, because it does not drive diffusion of Si species. We will discuss only diffusion of Al and Si species, assuming that diffusion of K is much faster than that. The model nonlinear diffusion equations become coupled PDEs. By Boltzmann transformation, the coupled PDEs are transformed into coupled ODEs. Perturbation expansion decomposes the coupled ODEs into uncoupled ODEs. Finally the uncoupled ODEs are solved numerically with MATLAB. Essential features of the nonlinear diffusion can be summarized as the following. (1) The coupling of diffusive fluxes causes advection in Al concentration profiles. (2) The case of smaller D_{SiSi}/D_{AlAl} shows larger advection effects in Al. (3) The coupling causes suppression in Si concentration profiles. (4) The case of smaller D_{SiSi}/D_{AlAl} shows uphill diffusion of Si in a muscovite – rich layer. This study is a first step to clarify the effect of nonlinear diffusion on the development of texture in metamorphic rocks.

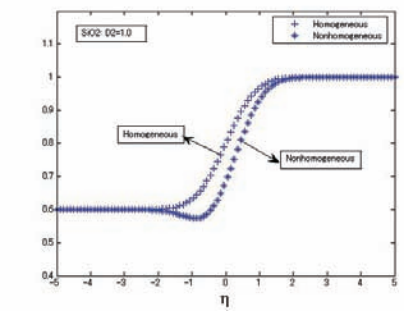

Fig. 1: Comparison of Si profiles between normal and nonlinear diffusion. Nonlinear diffusion shows uphill diffusion near the boundary.

New calorimetric data on feldspars: implications for modelling the ternary mixing behaviour

Benisek, A.[1*], Dachs, E.[1] & Kroll, H.[2]
[1]Materialforschung und Physik, Universität Salzburg, Austria
([*]artur.benisek@sbg.ac.at)
[2]Institut für Mineralogie, Universität Münster, Germany

New calorimetric work [1-3] on feldspars in the $NaAlSi_3O_8$-$KAlSi_3O_8$-$CaAl_2Si_2O_8$ system enabled the formulation of a mixing model, which is based exclusively on calorimetric and volumetric data [4]. When compared to models based on phase equilibrium experiments distinct differences are revealed. The calorimetry based model shows less solubility for both K in Ca-rich plagioclase and Ca in K-rich alkali feldspar. On the other hand, the stability field of Na-rich feldspars is broadened.

The two approaches are tested on natural feldspar assemblages from different rocks. One of these rocks is the Klokken syenogabbro, South Greenland, which was thoroughly investigated by Parsons and Brown [5]. The rock contains two perthites whose bulk compositions should lie on the ~970°C/1kbar isotherm derived from melting experiments and petrologic reasoning [5]. The figure below compares this isotherm calculated from different mixing models. The calorimetry based model far better agrees with the petrologic expectation than do the phase equilibrium based models.

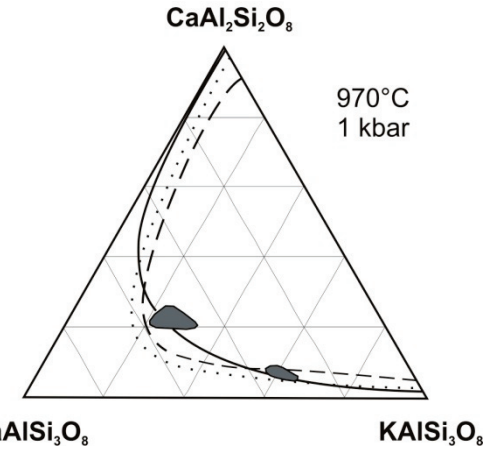

Fig. 1: Compositions of the feldspars from the Klokken syenogabbro, South Greenland [5]. The 970°C/1kbar isotherm of this study (*solid line*) is compared to those resulting from phase equilibrium experiments [6] - *dashed line*; [7] - *dotted line*.

[1] Benisek, A. et al. (2009) *Am. Mineral.*, **94**, 1153-1161. [2] Benisek, A. et al. (2010) *Phys. Chem. Minerals*, **37(4)**, 209-218. [3] Benisek, A. et al. (2010) *Eur. J. Mineral.*, in press [4] Benisek, A. et al. (2010) *Contrib. Mineral. Petrol.*, DOI 10.1007/s 00410-009-0480-8. [5] Parsons, I. & Brown, W.L. (1983) *Contrib. Mineral. Petrol.*, **82**, 1-12. [6] Fuhrman, M.L. & Lindsley, D.L. (1988) *Am. Mineral.*, **73**, 544-559. [7] Elkins, L.T. & Grove, T.L. (1990) *Am. Mineral.*, **75**, 544-559.

Spessartine garnet: a calorimetric and thermodynamic study

Dachs, E.[1], Geiger, C.A.[1*], Withers, A.C.[2] & Essene, E.J.[3]
[1]Universität Salzburg, Austria ([*]chg@min.uni-kiel.de)
[2]University of Minnesota, Minneapolis, USA
[3]University of Michigan, Ann Arbor, USA

Garnet is an important rock-forming mineral and a detrmination of its thermodynamic properties is imperative in order to undertake various Earth science investigations [1]. Many thermodynamic studies on aluminosilicate garnet have been made. However, there are still gaps of knowledge concerning the various thermodynamic functions for even the garnet end-members. This is the case for spessartine.

The heat capacity of two different synthetic spessartine samples was measured on 20-30 mg-size samples in the temperature range 2 to 864 K by heat-pulse calorimetry (HPC) and differential scanning calorimetry (DSC). Samples were synthesized in two different laboratories and characterized by X-ray powder diffraction and electron-microprobe analysis. The heat capacity data show a prominent lambda transition with a peak at 6.2 K, which is interpreted to be the result of a paramagnetic-antiferromagnetic phase transition. The calorimetric standard entropy for the two samples is S^o = 334.6 ± 2.7 J/mol/K and 336.0 ± 2.7 J/mol·K. The preferred standard third-law entropy for spessartine is S^o = 335.3 ± 3.8 J/mol/K. The DSC data around ambient T agree well with the HPC data and can be represented by the C_p polynomial at T > 250 K as:
C_p(J/mole/K) = 610 - 3060 $\cdot T^{-0.5}$ -1.45 $\cdot 10^7 \cdot T^{-2}$ + 1.82 $\cdot 10^9 \cdot T^{-3}$.

The vibrational heat capacity was analyzed giving $S_{vib}^{298.15}$ = 297.7 J/mol/K at 298.15 K. The magnetic heat capacity and entropy of spessartine, S_{mag}, were also calculated. S_{mag} is 38.0 J/mol/K, which is 85% of the maximum possible magnetic entropy given by the Boltzmann relation (i.e. 3Rln6 = 44.7 J/mol/K).

Published model-dependent lattice-dynamic calculations of $S_{vib}^{298.15\ K}$ are analyzed and compared to the experimental data. An analysis shows that there is no need to include a S^{conf} term to give the third-law entropy of spessartine. The large entropy value for aluminosilicate garnets is related to the large amplitude, low-frequency vibrational behavior of the E-site cation.

Using these new calorimetric data, together with high P-T experimental phase equlibrium data on Mn-Mg partitioning between garnet and olivine, allows calculation of the standard enthalpy of formation of spessartine. This gives $\Delta H^o_{f,Sps}$ = -5693.6 ± 1.4 kJ/mol, a value that is nearly 50 kJ more negative than published estimates. The Gibbs free energy of spessartine was also calculated as $\Delta G^o_{f,Sps}$ = -5364.3 kJ/mol at 298.15 K.

[1] Geiger, C.A. (2008) *Am. Mineral.*, 93, 360-372.

Internally consistent thermodynamic data for divalent sulfate hydrates

Grevel, K.-D.[1,2*] & Majzlan, J.[1]
[1]Institute of Geosciences, Friedrich-Schiller University, Jena, Germany
[2]Institute for Geology, Mineralogy and Geophysics, Ruhr-University, Bochum, Germany ([*]Klaus-Dieter.Grevel@rub.de)

Divalent metal sulfate hydrates (general formula $M^{2+}SO_4 \cdot nH_2O$) are a diverse group of minerals and are characteristic for the surface environments of the Earth. They play an important role in the storage and transport of metals released upon weathering of metallic ore deposits or mine wastes. [1] In numerous reversal experiments, it was shown that they will change their hydration state in response to the local temperature and humidity conditions. Commonly, *n* decreases as the relative humidity is decreased or temperature is increased [2-7].

Quite often, the results of these experiments are in poor agreement with calculations based on thermodynamic properties of the respective substances taken from the literature. Here, using mathematical programming (MAP) techniques [cf. 8], standard thermodynamic values consistent both with calorimetric data taken from the literature and reversal experiments could be derived (Table 1).

Table 1: Thermodynamic properties of selected sulfate hydrates

Phase	Formula	$\Delta_f H^0_{298}$ [kJmol^{-1}]	S^0_{298} [JK^{-1}mol^{-1}]
Rozenite	$FeSO_4 \cdot 4H_2O$	–2128.89	281.52
Melanterite	$FeSO_4 \cdot 7H_2O$	–3014.39	409.29
Bianchite	$ZnSO_4 \cdot 6H_2O$	–2777.42	363.41
Goslarite	$ZnSO_4 \cdot 7H_2O$	–3077.54	388.87
Retgersite	$NiSO_4 \cdot 6H_2O$	–2683.10	334.40
Morenosite	$NiSO_4 \cdot 7H_2O$	–2976.77	378.99
Moorhouseite	$CoSO_4 \cdot 6H_2O$	–2683.43	367.31
Bieberite	$CoSO_4 \cdot 7H_2O$	–2979.32	406.36
Bonattite	$CuSO_4 \cdot 3H_2O$	–1684.53	221.40
Chalcanthite	$CuSO_4 \cdot 5H_2O$	–2279.54	301.20

[1] Jambor, J.L. et al. (2000) *Rev. Mineral. Geochem.*, **40**, 303-350. [2] Chou, I.M. et al. (2002) *Am. Mineral.*, **87**, 108-114. [3] Chou, I.M. & Seal, R.R. (2003a) *Am. Mineral.*, **88**, 1943-1948. [4] Chou, I.M. & Seal, R.R. (2003b) *Astrobiology*, **3**, 619-630. [5] Chou, I.M. & Seal, R.R. (2005a) *Am. Mineral.*, **90**, 912-917. [6] Chou, I.M. & Seal, R.R. (2005b) *Chem. Geol.*, **215**, 517-523. [7] Chou, I.M. & Seal, R.R. (2007) *J. Geophys. Res. Planet.*, **112**, E11004. [8] Grevel, K.-D. & Majzlan, J. (2009) *Geochim. Cosmochim. Ac.*, **73**, 6805-6815.

Enthalpies and entropies of mixing in alkali-bearing aluminosilicate mineral and glass solutions

Hovis, G.L.
Dept. of Geology and Environmental Geosciences, Lafayette College, Easton, PA, USA (hovisguy@lafayette.edu)

Over the years this laboratory has investigated the thermodynamic mixing properties of numerous solid-solution series. Enthalpies of solution have been measured at 50°C in 20.1 wt% HF under isoperibolic conditions for four alkali feldspar series having different Al-Si ordering states [1], three nepheline-kalsilite series having various Al:Si ratios [2-4], Rb- and Cs-leucite-analcime analogue series [5], multiple hydrated alkali aluminosilicate glasses [6,7], anhydrous Qz-Or-Ab glasses [8], and sodium silicate glasses [9]. In systems that show substantial thermodynamic nonideality, e.g., feldspars and feldspathoids, enthalpies of mixing can be correlated well with immiscibility [4,10,11] that is reflected by experimentally determined solvi (e.g., the nepheline-kalsilite system shown above [4]) as well as exsolution in natural samples. It becomes clear, however, that the overall Gibbs free energies of mixing cannot be explained solely by the non-ideal behaviour of enthalpy [4,12]. Nor does consideration of configurational entropy completely account for the differences. This leaves excess vibrational entropies to account for the connection between the enthalpy data and the Gibbs free energies of mixing. Such entropies, based on low-temperature heat-capacity measurements for multiple samples across solid-solution series, are available for relatively few systems (e.g., [12-15]). It is important that such data be collected, not only to fully characterize and understand thermodynamic mixing behaviour in mineral and glass systems, but also so that phase equilibria can be calculated for intermediate members of solid-solution series.

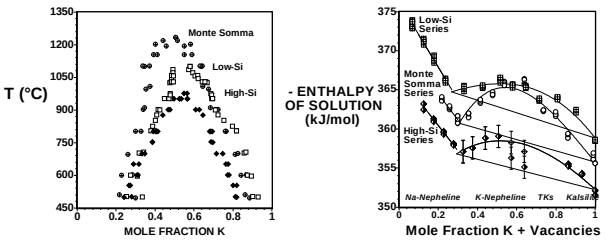

Fig. 1: (left): Directly-determined nepheline-kalsilite solvi, based on reversed phase equilibria, for solutions with various Al:Si ratios [4]. (right): Negative enthalpies of solution for the same three nepheline-kalsilite series shown on the left [4].

[1] Hovis, G.L. (1988) *J. Petrol.*, **29**, 731-763. [2] Hovis, G.L. & Roux, J. (1993) *Am. J. Sci.*, **293**, 1108-1127. [3] Hovis, G.L.& Roux, J. (1999) *Eur. J. Mineral.*, **11**, 815-827. [4] Hovis, G.L., Mott, A.V. & Roux, J. (2009) *Am. J. Sci.*, **309**, 397-419. [5] Hovis, G.L., Roux, J. & Rodrigues, E. (2002) *Am. Mineral.*, **87**, 523-532. [6] Richet, P. et al. (2004) *Geochim. Cosmochim. Ac.*, **68**, 5151-5158. [7] Richet, P., Hovis, G.L. & Whittington, A. (2006) *Earth Planet. Sci. Lett.*, **241**, 972-977. [8] Hovis, G.L. (1984) *Geochim. Cosmochim. Ac.*, **48**, 523-525. [9] Hovis, G.L., Toplis, M.J. & Richet, P. (2004) *Chem. Geol.*, **213**, 173-186. [10] Hovis, G.L. & Crelling, J.A. (2000) *Am. J. Sci.*, **300**, 238-249. [11] Hovis, G.L., Delbove, F. & Roll, M. (1991) *Am. Mineral.*, **76**, 913-927. [12] Haselton, H.T. Jr. et al. (1983) *Am. Mineral.*, **68**, 398-413. [13] Dachs, E. & Geiger, C.A. (2006) *Am. Mineral.*, **91**, 894-906. [14] Dachs, E. & Geiger, C.A. (2007) *Am. Mineral.*, **92**, 699-702. [15] Benisek, A., Dachs, E. & Kroll, H. (2009) *Am. Mineral.*, **94**, 1153-1161.

Heat capacity, entropy, and magnetic properties of jarosite-group compounds

Majzlan, J.[1*], Glasnák, P.[2], Fisher, R.A.[3], White, M.A.[4], Johnson, M.B.[4], Woodfield, B.[5] & Boerio-Goates, J.[5]
[1]Inst. of Geosciences, Friedrich-Schiller University, Jena, Germany ([*]Juraj.Majzlan@uni-jena.de)
[2]Inst. of Geosciences, University of Freiburg, Germany
[3]MSD, Lawrence Berkeley National Laboratory, Berkeley, CA, USA
[4]Dept. of Chemistry, Dalhousie University, Halifax, Nova Scotia, Canada
[5]Dept. of Chemistry and Biochemistry, Brigham Young University, Provo, USA

Jarosite phases are common minerals in acidic, sulfate-rich environments. In addition to being the flagship minerals in acid mine drainage, they are notable for their unusual magnetic properties, namely frustrated magnetism and spin-glass character of some of them. We studied samples close to the nominal composition $A Fe_3(SO_4)_2(OH)_6$, where A = K, Na, Rb, and NH_4. One of the samples has a significant number of defects on the Fe sites and is called the defect jarosite; others are referred to as A-jarosite. The measured heat capacities (C_p) of the jarosite phases were fitted with a set of appropriate polynomials and the integration of C_p/T from 0 to 298.15 K gave the entropies (all values in $J \cdot mol^{-1} \cdot K^{-1}$) of K-jarosite of 427.4, Na-jarosite 436.4, Rb-jarosite 411.9, NH_4-jarosite 447.2, and defect jarosite 412.7. There are additional configurational entropies of 13.14 and 8.23 $J \cdot mol^{-1} \cdot K^{-1}$ in defect and NH_4-jarosite, respectively. A detailed analysis of the synchrotron X-ray diffraction patterns showed a large anisotropic peak broadening for defect and NH_4-jarosite. The fits to the low-temperature (< ~12 K) C_p data showed that our samples can be divided into two groups. The first group is populated by the K-, Na-, Rb-, and NH_4-jarosite samples, antiferromagnetic at low temperatures. The second group contains the H_3O-jarosite (studied previously) and the defect jarosite. H_3O- and defect jarosite are spin glasses and their low-T C_p was fit with the expression $C_p = \gamma T + \Sigma B_j T^j$, where j = (3,5,7,9). The linear term is typical for spin glasses and the sum represents the lattice contribution to C_p. Surprisingly, the C_p of the K-, Na-, Rb-, and NH_4-jarosite samples, which are usually considered to be antiferromagnetic at low temperatures, also contains a large linear term. This finding suggests that even these phases do not order completely but have a partial spin-glass character below their Néel transition temperature.

Lattice dynamics and theoretical spectroscopy at high pressure

Caracas, R.
CNRS, ENS de Lyon, Laboratoire de Sciences de la Terre, Lyon, France (razvan.caracas@ens-lyon.fr)

We present some of the latest applications of the density-functional perturbation theory in the characterization of solids under extreme thermodynamic conditions. We determine stability fields and compute thermodynamic properties of different structures, we build phase diagrams and we compute elastic constants tensors and accurate Raman spectra (with both peak position and intensity) of various solids under pressure.

We find that the analysis of the phonons can reveal even fine effects associated to weak structural distortions, like in the case of the pressure-induced spin transitions in Fe-bearing $MgSiO_3$ perovskite. These compounds are major constituents of the Earth lower mantle and thus benefit of a special attention from the geoscientific community. Lattice dynamical analysis shows that unstable phonon modes develop for structures with low-spin configurations. The atomic displacements associated to these phonons break the local symmetry and induce high-spin to low-spin transitions. The phase transition sequence can then be deciphered from the accurate analysis of the phonon instabilities.

At least as spectacular, we show that the stability field of ice X, the high-pressure ionic form of water ice is delimited by a disordered structure below 114GPa and by an orthorhombic pseudo-hexagonal structure beyond 430GPa. Both transitions are obtained and explained based on the analysis of the unstable phonon modes. An alternative phase to ice VIII can be deduced and analyzed from lattice dynamics. The transition regimes and our new structures give excellent explanations to previously unexplained experimental and computational results.

We determine Raman spectra of materials under pressure as a diagnosis tool. The Raman spectra depend on the frequency of the incident laser, on the temperature, on the active-mode frequency (which comes straightforward from calculations) and on the Raman tensor. This latter factor is obtained today from the derivative of the dielectric tensor with respect to the atomic displacements that correspond to the vibrational pattern of the mode. Formerly, these derivatives were computed from finite differences. The calculations of the Raman spectra are very encouraging, given the extreme requirements for convergence and accuracy of dielectric properties, usually hard to obtain. The agreement to experiment is excellent for both peak position and intensity.

A new dense phase of silica initiating silicates breakdown in giant terrestrial planets

Tsuchiya, T.[1*], Tsuchiya, J.[2], Metsue, A.[1] & Ishikawa, T.[1]
[1]Geodynamics Research Center, Ehime University, Matsuyama Ehime, Japan ([*]takut@sci.ehime-u.ac.jp)
[2]Senior Research Fellow Center, Ehime University, Matsuyama Ehime, Japan

Silica (SiO_2) is one of the most common, most fundamental and also most important materials from several research fields of solid-state physics and chemistry, materials science and geoscience. It has been known that silica shows a sequential phase evolution from quartz, coesite, stishovite, $CaCl_2$, α-PbO_2 and pyrite (modified fluorite) with elevating pressure [1-3]. However, further denser phases are still underdetermined, although studies on some low-pressure analogs such as ZrO_2 and HfO_2 [4], TiO_2 [5], MgF_2 [6] and most recently SnO_2 [7] have suggested an orthorhombic cotunnite phase as the final high-pressure phase.

In order to elucidate the post-pyrite phase of silica, we performed structure search based on the *ab initio* density functional computation method. After examining several dense structure types with AX_2 compound, we successfully discovered a new phase transformation of pyrite type SiO_2 at multi-megabar condition to an unexpected phase (New-HP), which possesses quite high nine-fold coordinated Si and eclipses the cotunnite stability field in the entire pressure range up to 1500 GPa (Fig. 1). We subsequently investigated high-pressure stabilities of some important silicate compounds ($MgSiO_3$ and $CaSiO_3$) and found that the new phase change in silica could initiate breakdown of these silicates to oxide mixtures in the conditions relevant to the interior of super-Earths and exoplanets, which would lead to various complexities in their internal structures. High-*P*,*T* phase boundaries, changes in density, elasticity and also electronic property associated with the new phase transitions, which are the most fundamental information to understand the structure and dynamics of giant terrestrial planets, will be presented.

Acknowledgements: Research supported by JSPS Grant-in-Aid for Scientific Research Grants 20001005 and 21740379 and the Ehime Univ G-COE program "Deep Earth Mineralogy".

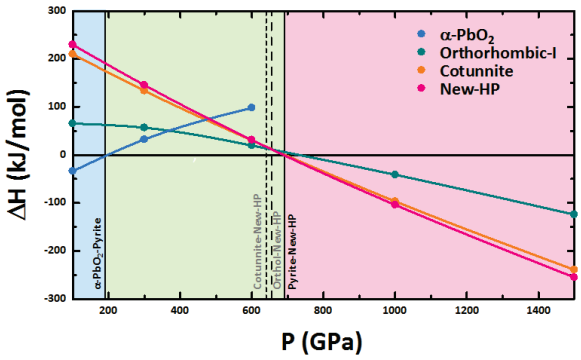

Fig. 1: Calculated static enthalpy differences of some SiO_2 polymorphs relative to the pyrite phase. Pyrite-to-New-HP transition is found to occur at 690 GPa prior to the transitions to Orthorhombic-I and also cotunnite expected in previous studies.

[1] Teter, D.M. et al. (1998) *Phys. Rev. Lett.*, **80**, 2145-2148. [2] Tsuchiya, T. et al. (2004) *Geophys. Res. Lett.*, **31**, L11610. [3] Kuwayama, Y. et al. (2005) *Science*, **309**, 923-925. [4] Haines, J. et al. (1997) *J. Am. Ceram. Soc.*, **80**, 1910-1914. [5] Dubrovinskaia, N.A. et al. (2001) *Phys. Rev. Lett.*, **87**, 275501. [6] Haines, J. et al. (2001) *Phys. Rev. B*, **64**, 134110. [7] Shieh, S.R. et al. (2006) *Phys. Rev. B*, **73**, 014105.

Fe^{3+} incorporation in Mg-rich garnet

Woodland, A.B.
Institut für Geowissenschaften, Universität Frankfurt, Germany
(woodland@em.uni-frankfurt.de)

Equilibria involving Fe^{3+}-bearing components in garnet can be used to estimate the prevailing oxygen fugacity within the garnet peridotite facies of the Earth's mantle (e.g. [1,2]). Since mantle garnets are generally pyrope-rich, it is important to understand how Fe^{3+} substitution occurs in Mg-bearing garnets. To this end, the joins $Mg_3Al_2Si_3O_{12}$–$Ca_3Fe_2Si_3O_{12}$ (pyrope-andradite) and $Mg_3Al_2Si_3O_{12}$–$Fe_3Fe_2Si_3O_{12}$ (pyrope -"skiagite") have been investigated experimentally and by EMPA, XRD and Mössbauer spectroscopy.

Synthesis of pyrope-andradite garnets was unsuccessful, even at 6 GPa. Partial reduction of Fe^{3+} to Fe^{2+} occurred even in the presence of PtO_2 as an O_2 source. A significant $Ca_3Al_2Si_3O_{12}$ component was also found by EMPA. The additional presence of Fe^{3+}-rich spinel or Fe_2O_3–Al_2O_3 solid solutions indicates Fe^{3+}-saturation in the garnets, with maximum Fe^{3+} contents increasing with increasing Ca. A significant miscibility gap must exist between pyrope and andradite at least up to 6 GPa.

Pyrope-"skiagite" synthesis at 9 GPa was more successful, although minor reduction produced an additional $Fe_3Al_2Si_3O_{12}$ component. Unit-cell parameters calculated assuming ideal mixing in ternary garnets are smaller than those measured.

Hyperfine parameters from Mössbauer spectra reveal: 1) the electronic environment of 8-fold Fe^{2+} is similar in all solid solutions involving "skiagite" or almandine components, 2) Fe^{3+} in pyrope-"skiagite" garnets has the same parameters as the "skiagite" endmember. Thus, octahedral cation substitutions have little effect on the electronic environment of Fe^{3+} occupying this site. Mg-Fe^{2+} substitution on the adjacent 8-fold site has likewise only a minor effect on the hyperfine parameters of Fe^{3+}. This behaviour contrasts with the stronger effects observed for Ca-Fe^{2+} substitution in andradite-"skiagite" garnets [3].

Determining $Fe^{3+}/\sum Fe$ in garnets requires consideration of differing recoil-free fractions for Fe^{2+} and Fe^{3+}. Simple correction factors for spectra measured at room T and 80 K were reported by [3], based upon spectra from a series of almandine-"skiagite" and andradite-"skiagite" solid solutions. Comparison of ratios determined at room T and 80 K for the pyrope-"skiagite" garnets reveal a slight systematic difference in this correction factor, although this difference lies well within the uncertainties. Thus, it is concluded that the correction factors to account for the differing recoil-free fractions for Fe^{2+} and Fe^{3+} reported by [3] are generally applicable to silicate garnets, including those that are Mg-rich.

[1] Gudmundsson, & Wood, B.J. (1995) *Contrib. Mineral. Petrol.*, **199**, 56-67. [2] Woodland, A.B. & Koch, M. (2003) *Earth Planet Sci. Lett.*, **214**, 295-310 [3] Woodland, A.B. & Ross, C.R. II (1994) *Phys. Chem. Minerals*, **21**, 117-132.

Single-crystal H*T* X-ray diffraction study of anthophyllite

Cámara, F.[1*], Welch, M.D.[2] & Oberti, R.[1]
[1]CNR-IGG, UOS Pavia, Italy ([*]camara@crystal.unipv.it)
[2]The Natural History Museum, London, UK

The crystal chemistry of amphiboles is now well understood. However, very little is known about their physical properties, such as compressibility and thermal expansivity [1], both of which are fundamental to mineral stability. Of the few published expansivity data, all are for monoclinic amphiboles, including cummingtonite, tremolite and richterite and recently also pargasite [2]. There are no data for orthorhombic amphiboles. Furthermore, rapid disordering of divalent cations between *M*(1,2,3,4) sites in monoclinic amphiboles on heating has been observed *in situ* to occur within 2–4 hours at $T \sim 300 – 700$°C [3,4]. Beyond 600°C, dehydrogenation has been also observed [2]. The absence of thermal expansivity data for orthorhombic amphiboles and the possibility of *in situ* disordering of cations led us to undertake a high-temperature diffraction experiment on anthophyllite. A gem-quality Mg-rich crystal of anthophyllite coming from American Museum of Natural History (AMNH 34856) with composition $^{A}Na_{0.05}{}^{B}(Mg_{1.34}Mn_{0.56}Ca_{0.09})\ ^{C}(Mg_{4.98}Fe_{0.02})\ ^{T}(Si_{7.97}\ Al_{0.03})\ O_{22}(OH_{1.99}F_{0.01})$ was studied by single-crystal XRD. Data were collected *in situ* using a micro furnace. Lattice parameters were refined at intervals of 25 K in the *T* range 298-1073 K; intensity data were collected at 298, 473, 673, 873, 973 and 1073 K. Above 973 K a homogeneous contraction in volume is observed which is related to dehydrogenation accompanied by a increase in mosaicity indicating the decomposition of the crystal. Thermal expansivities for *V*, *a*, *b*, *c* were obtained by fitting the equation $V(T) = V_T e^{[\alpha\ (T-Tr)]}$: $\alpha_V = 3.668(3) \times 10^{-5}$ K^{-1}, $\alpha_a = 1.49(1) \times 10^{-5}$ K^{-1}, $\alpha_b = 0.969(2) \times 10^{-5}$ K^{-1}, $\alpha_c = 1.206(9) \times 10^{-5}$ K^{-1}. These values are the highest observed so far for amphibole. Thermal expansion is thus anisotropic with $\alpha_a{:}\alpha_b{:}\alpha_c$ = 1.53:1:1.24, with a larger expansion in the (010) plane, essentially along [100]. This behaviour contrasts with the chemically similar but monoclinic manganoan cummingtonite [2] which shows a lower α_c, although α_b values are almost the same in both monoclinic and orthorhombic structures. Structure refinements show that, after correcting for thermal motion, while tetrahedra behave as rigid units up to 1073 K, C-group octahedra expand at the same rate within experimental error ($\alpha_{M1,2,3} = 5(2) \times 10^{-5}$ K^{-1}), whereas *M*(4) expands more ($\alpha_{M4} = 7.8(3.1) \times 10^{-5}$ K^{-1}).

A change in rate is observed in the *c* parameter which starts around 700 K and coincides with disordering of Mn from the B to the C sites in agreement to previous observations in manganocummingtonite [3]. However, on disordering at high-*T* in anthophyllite, the Mn^{2+} site preference is *M*(1,2) > *M*(3), in contrast with *M*(2) > *M*(1,3) reported by [3] in manganoan cumingtonite and also with $M(1,3) \geq M(2)$ found in richterite [4]. This result indicates that the composition of *M*(4) is more constraining than topology in determining the thermal behaviour of amphibole.

[1] Welch, M.D. et al. (2007) *Rev. Mineral. Geochem.*, **67**, 223-260. [2] Oberti, R. et al. (2009) *ECM25*, Abstracts, **176**. [3] Reece, J.J. et al. (2000) *Mineral. Mag.*, **64(2)**, 255-266. [4] Welch, M.D. et al. (2008) *Mineral. Mag.*, **72(4)**, 877-886.

Experiments to determine thermodynamic controls for the transition from garnet-biotite to garnet-talc in metapelites and metagreywackes

Chmielowski, R.M.*, Fumagalli, P. & Poli, S.
Dipto. Scienze della Terra, Università degli Studi, Milan, Italy
(*reia.chmielowski@unimi.it)

The thermodynamic controls which govern the transition from garnet-biotite to garnet-talc assemblages during the metamorphism of mica-dominated sediments are not yet well understood. Investigations on synthetic compositions in the model system CaO-K_2O-FeO-MgO-Al_2O_3-SiO_2-H_2O are carried out in a piston cylinder apparatus at pressures and temperatures from 2 to 3 GPa and to 600-700°C. Experiments are buffered with graphite, and are generally run under fluid saturated conditions.

The experiments are run using bulk compositions representative of both metapelites (NM and H) and metagreywackes (NP and L). Variations in the bulk compositions studied were chosen to bracket the almandine-chlorite tie line in the Al_2O_3-Annite-Phlogopite plane and the annite-aluminosilciate and annite-almendine tie lines in the Al_2O_3-K_2O-(Mg,Fe)O plane (Fig. 1) to provide greater control of the compositional effects on the reactions.

The preliminary results of this study are presented (Fig. 2).

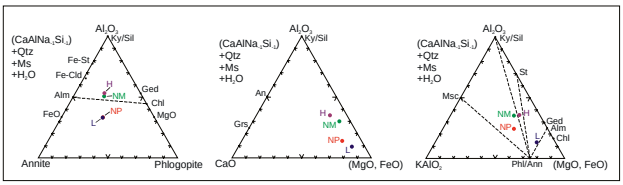

Fig. 1: (a) Projection from Ms, Qtz, H_2O and exchange vector CaAlNa-1Si-1 in the Al_2O_3-Annite-Phlogopite plane (note that H and NM plot above the almandine-chlorite join, L and NP below); **(b)** projection from Ms, Qtz, H_2O and the exchange vector CaAlNa^1Si^1 in the Al_2O3-K_2O-(Mg,Fe)O plane; H and L plot on the right-hand side of the join connecting Ky/Sil to Phl/Ann (i.e. lower $KAlO_2$ than NM and NP); **(c)** projection from Ms, Qtz, H_2O and the exchange vector CaAlNa-1Si-1 in the Al_2O_3-CaO-(Mg,FeO) plane.

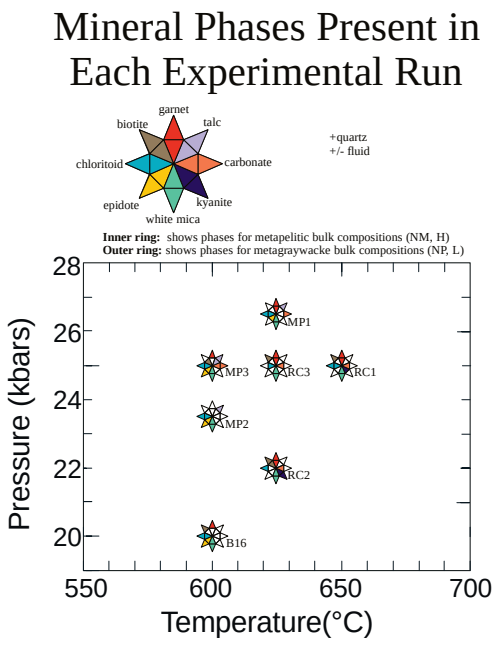

Fig. 2: The phases present in each experimental run are indicated.

Crystal chemistry of fluor-chlorapatite solid solutions

Gottschalk, M.[1*], Schettler, G.[2] & Harlov, D.E.[1]
[1]Dept. of Chemistry and Physics of Earth Materials, GFZ, Potsdam, Germany (*gottschalk@gfz-potsdam.de)
[2]Dept. of Climate Dynamics and Landscape Evolution, GFZ, Potsdam, Germany

A series of synthetic apatite crystals along the fluorapatite-chlorapatite $Ca_5(PO_4)_3(F, Cl)$ join have been synthesized at 1220 to 1375 °C from $Ca_3(PO_4)_2$ dissolved in a CaF_2-$CaCl_2$ melt. The solid solutions have then been characterized both chemically and structurally. The apatite solid solutions were characterized by IR spectroscopy, X-ray powder diffraction using Rietveld refinements (XRD), and single crystal diffraction (SCXRD) structure determinations. IR-spectra indicate no or only a very minor OH-apatite component in the solid solutions. Lattice parameters of the apatite solid solutions vary systematically with composition. IR-spectra indicate no or only a very minor OH-apatite component in the solid solutions. Lattice parameters of the apatite solid solutions vary systematically with composition. The *a*-lattice parameter varies linearly.

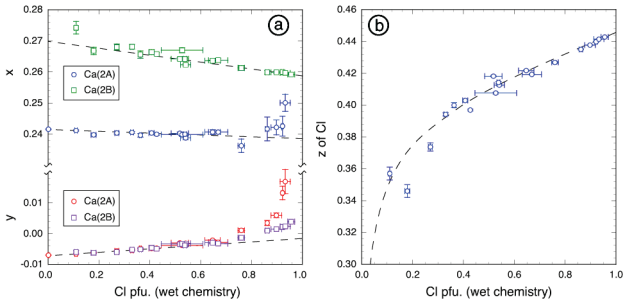

Fig. 1: a) The x- and y-position of the Ca(2A) and Ca(2B)-site and b) the *z*-position of Cl as a function of chlorine-content.

In contrast to F^-, which occupies a special position at (0,0,1/4) in the unit cell, because of the larger ionic radius of Cl^-, this position is split for Cl^- with *z*-coordinates ranging from 0.346(4) to 0.4428(2). Single crystal structure determinations reveal that the Ca(2)-site is also split into Ca(2A)- and Ca(2B)-sites for F^- and Cl^- as nearest neighbors, respectively. In comparison to the Ca(2A)-F^- arrangements, the larger Cl^- ion presses the triangular arrangement of Ca-ions outward to facilitate an energetic more favorable constellation to form Ca(2B)-Cl^- arrangements.

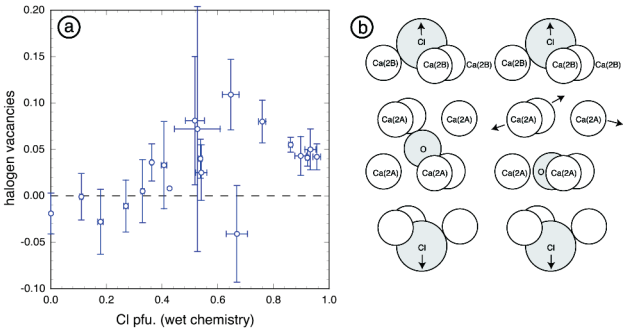

Fig. 2: a) Halogen deficiency as a function of chlorine-content. b) Avoiding symmetry reduction by the insertion of O^{2-} for charge balance.

Apatites rich in Cl (x_{Cl} > 0.5) show a deficiency in halogens, which is charge balanced by oxygen forming an oxyapatite component. The oxyapatite component prevents F-absent apatites from crystallizing in the monoclinic modification and stabilizes the hexagonal modification.

The melting curve of ice re-examined - anomalous high pressure behaviour of H_2O

Mirwald, P.W.
Inst. of Mineralogy & Petrography, University of Innsbruck, Austria (peter.mirwald@uibk.ac.at)

A compression study of water combined with determinations of the dehydration boundary of gypsum ($CaSO_4$*$2H_2O$) to bassanite and anhydrite respectively led to the conclusion that H_2O is characterised by a complex system of high pressure anomalies [1,2]. These experiments were conducted in a piston cylinder apparatus using pressure change and related piston displacement as monitoring parameters (Differential Pressure Analysis). Based on this DPA-technique, a detailed re-examination of the melting curve of the ice polymorphs I, III, V and VI was a further step to elucidate this phenomenon. The data obtained reveal several anomalies in the dP/dT course of the melting line: ice I at 27 MPa, Ice III: 290 MPa, Ice VI: 780 and 1180 MPa. In addition, compression anomalies were found in ice clearly to be related to the other data. Fig. 1 gives a synoptic P-T overview of the the data obtained so far.

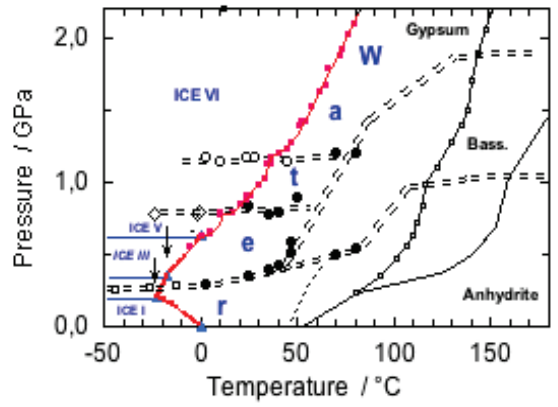

Fig. 1: Synoptic diagram of anomalous PVT behaviour of H_2O documented by the dehydration boundary system of gypsum-bassanite-anhydrite, the ice melting curve and H_2O compression anomalies (dashed double lines).

The new data augment the picture lined out previously [1,2] and strongly support the concept of anomalous PVT behaviour of H_2O. Apart from the anomalous compression behaviour of H_2O, the anomalies are indicated by a specific dP/dT behaviour of dehydration boundaries, e.g. of gypsum and bassanite as well as by the ice melting curve: in each case the dP/dT boundary slope shows a distinct increase below the anomaly followed by a break at the anomaly which then leads to a shallower dP/dT-course towards higher pressure. In accordance with the Clausius Clapeyron and Ehrenfest relation this aprupt slope change may be related to a drastically increased change of entropy or of the thermal expansion. First results of a QM/MM molecular dynamic simulation of water compression (Randolf, Mirwald, Rode; unpublished data) suggest that these anomalies may be related to changes of the coordination assemblages of the H_2O-molecules.

[1] Mirwald, P.W. (2005) *J. Chem. Phys.*, **123**, 124715. [2] Mirwald, P.W. (2008) *J. Chem. Phys.*, **128**, 074502.

Stability field of the high-temperature orthorhombic phase in $Mg_2Si_2O_6$-$CaMgSi_2O_6$ system

Ohi, S.[1,2*], Miyake, A.[2] & Yashima, M.[3]
[1]Dept. of Interdisciplinary Enviroment, Graduate School of Human and Environmental Syudies, Kyoto University, Kyoto, Japan ([*]shugo-ohi@kueps.kyoto-u.ac.jp)
[2]Dept. of Geology and Mineralogy, Division of Earth and Planetary Sciences, Graduate School of Science, Kyoto University, Kyoto, Japan
[3]Dept. of Materials Science and Engineering, Interdisciplinary Graduate School of Science and Engineering, Tokyo Institute of Technology, Yokohama, Japan

In the system $Mg_2Si_2O_6$-$CaMgSi_2O_6$, there had been the controversy about the appearance and stability of the orthopyroxene (Opx) phase near 1400°C other than protoenstatite (Pen) since the discovery by Foster [1]. In recent years, Ohi et al. [2] observed the phase transition between low-temperature Opx (LT-Opx) and high-temoperature Opx (HT-Opx) for the composition of $(Ca_{0.06}Mg_{1.94})Si_2O_6$ at 1170°C. They concluded that Opx the phase near 1400°C was HT-Opx. In previous studies, phase diagrams for $Mg_2Si_2O_6$ and the En–Di system at high pressure were drawn without taking account of HT-Opx. The purpose of our study was to reconsider the phase diagrams for $Mg_2Si_2O_6$ and the En–Di system and to calculate the stability field of HT-Opx at high pressure.

First, we performed differential scanning calorimetry (DSC) experiments to obtain the transition enthalpy (ΔH) between LT-Opx and HT-Opx and then calculated the dP/dT line along the LT-Opx = HT-Opx boundary. Furthermore, to estimate the transition temperature (Tc) toward Ca-composition, we examined Ca-free orthoenstatite (Oen) with HT-XRD.

The transition enthalpy, transition temperature, volume change, and transition slope for the composition of $(Ca_{0.06}Mg_{1.94})Si_2O_6$ were estimated to be 6.2 kJ/mol, 1170°C, 10.25 Å^3/unit cell, and 0.0056 GPa/°C, respectively, and the phase boundary between LT- and HT-Opx was defined as P (GPa) = 0.0056T (°C) – 6.55. The transition temperature of Ca-free LT-Oen to HT-Oen was estimated to be 1120°C, which was lower than that of Ca-poor LT-Opx to HT-Opx (about 1170°C); hence, dTc/dX_{Di} (X_{Di} = 2Ca/(Ca+Mg) × 100) has a positive slope. This slope shows that, at the same temperature, LT-Opx is a more Ca-rich phase than HT-Opx.

The phase boundary between LT- and HT-Opx defined as P (GPa) = 0.0056T (°C) – 6.55 shows that the invariant point of four-phase equilibria for Pen + HT-Opx + pigeonite + diopside is at around 1240–1280°C and 0.1–0.2 GPa, rather than the equivalent system involving LT-Opx as described in previous studies. We developed phase diagrams for $Mg_2Si_2O_6$ and the $Mg_2Si_2O_6$–$CaMgSi_2O_6$ system taking into account the results of previous synthetic experiments and the phase boundary that we determined between LT-Opx and HT-Opx.

Our phase diagrams for $Mg_2Si_2O_6$ showed that HT-Oen is more stable than Pen at pressure above ~0.8 GPa, and that the boundary between HT-Oen and Pen has a gently negative slope. As pressure rises from 1 atm to about 0.2 GPa, the lower temperature limit of stability of HT-Opx decreases from ~1370°C to ~1200°C. Above 0.9 GPa, the stability field of Pen disappears and Ca-free HT-Oen becomes stable. On the basis of our results, we suggest that further high-resolution analyses of the thermodynamics of the $Mg_2Si_2O_6$-$CaMgSi_2O_6$ system at high temperatures and high pressures are required.

[1] Foster, W.R. & Lin, H.C. (1975) *EOS*, **56**, 470. [2] Ohi, S. et al. (2008) *Am. Mineral.*, **93**, 1682-1685.

A thermodynamic model for titanium and ferric iron solution in biotite

Tajčmanová, L.[1*], Connolly, J.A.D.[2] & Cesare, B.[3]
[1]Institute of Geological Sciences, Free University, Berlin, Germany ([*]lucataj@gmail.com)
[2]Dept. of Earth Sciences, Swiss Federal Institute of Technology, Zürich, Switzerland
[3]Dept. of Geosciences, University of Padova, Italy

Recent crystallographic data indicate that in biotite Ti and Fe^{3+} order preferentially onto the M2 octahedral site rather than onto the M1 site as assumed in previous solution models for K2O–FeO–MgO–Al_2O_3–SiO_2–H_2O–TiO_2–O_2 (KFMASHTO) biotite. In view of these data, we reformulate and reparameterize the former biotite solution model. Our reparameterization takes into account Fe-Mg order-disorder and ferric iron contents of natural biotites as well as both natural and experimental observations on biotite Ti-content over a wide range of physicochemical conditions. In comparison to previous biotite models, the new model reproduces the Ti-content and stability field of biotite as constrained by experiments with significantly better accuracy. The predictive power of the model is tested by comparison with petrologically well-characterized natural samples of SiO_2-saturated and SiO_2-undersaturated rocks that were not used in the parameterization. In all of these tests, the reformulated model performs well.

The crystal structure of δ-Al(OH)$_3$ at high pressures

Matsui, M.[1*], Ikeda, E.[1] & Komatsu, K.[2]
[1]School of Science, University of Hyogo, Japan
([*]m.matsui@sci.u-hyogo.ac.jp)
[2]Geochemical Research Center, The University of Tokyo, Japan

A high pressure phase of Al(OD)$_3$, called δ, was synthesized at 18 GPa and 973 K using a Kawai-type multi-anvil apparatus [1]. Based on powder X-ray diffraction at ambient conditions, Komatsu et al. [1] showed that δ-Al(OD)$_3$ is isostructural with δ-Al(OH)$_3$ with space group *Pnam*, previously synthesized at high temperatures and high pressures [2]. Using the Rietveld method and the difference-Fourier analysis, Komatsu et al. [1] reported a structural model for δ-Al(OD)$_3$, in which positional disorders of the D atoms were proposed in their hydrogen bonds. However, successive neutron diffraction measurements at ambient conditions [3] revealed that the real space group of δ-Al(OD)$_3$ is $P2_12_12_1$, but not *Pnam* as reported by X-ray diffraction experiments [1]. Komatsu et al.[3] suggested that the positions of D atoms may be in ordered in hydrogen bonds in the $P2_12_12_1$ structure. Here we use first-principle calculations to study structural and enegetic properties of δ-Al(OH)$_3$ in more detail.

All calculations were performed with the Vienna Ab Initio Simulation Package VASP [4]. The projector-augmented wave (PAW) method [5] was used in the generalized-gradient approximation (GGA) for the exchange-correlation functional [6]. Atomic positions were relaxed with observed crystal-symmetry constraints. In order to check the reliability and applicability of the computations, we first calculated the structures and energies of the three known Al(OH)$_3$ polymorphs, gibbsite, bayerite, and η-Al(OH)$_3$, with the results that the calculated values reproduce the observed ones accurately.

There exist 7 independent atoms, including one Al, three O and three H atoms, in the asymmetric unit in the $P2_12_12_1$ δ-Al(OH)$_3$ structure. The initial lattice parameters and atomic positions of both Al and O were taken from previous X-ray data for the *Pnam* structure [1], while the H atom positions were taken to be in ordered configurations and were selected from either one of the two disordered sites in the hydrogen bonds in the *Pnam* structure [1]. We tested several structural models, and finally found an energy-minimized model that 1) reproduces the measured lattice parameters of δ-Al(OH)$_3$ accurately, 2) gives reasonable Al-O, O-H, and hydrogen bond distances, and 3) shows reasonable energetic relations between the Al(OH)$_3$ polymorphs; namely gibbsite is stable at ambient pressure, the δ phase has the lowest enthalpy at pressures greater than about 1 GPa, while both bayerite and the η phase are metastable over the whole pressure range. We further confirmed that the calculated powder neutron diffraction intensities based on the present δ-Al(OH)$_3$ structural model reproduces well the observed data [3]. In addition we found the $P2_12_12_1$ δ phase transforms to another high pressure form with space group *Pnam* and with symmetrical hydrogen bonds at around 80 GPa.

[1] Komatsu, K. et al. (2007) *Z. Kristallogr.*, **222**, 13. [2] Dachille, F. & Gigl, P. (1983) *High Temp. High Press.*, 15, 657-675. [3] Komatsu, K. et al. (2007) *ILL Experim. Rep.*, 5-24-285. [4] Kresse, G. & Furthmüller, J. (1996) *Phys. Rev. B*, **54**, 11169 [5] Blöchl, P.E. (1994) *Phys. Rev. B*, **50**, 17953 [6] Perdew, J.P. et al. (1996) Phys. Rev. Lett., **77**, 3865.

Order-disorder phase boundary in ice VII-VIII investigated by first principles

Umemoto, K.[1*], Wentzcovitch, R.[2], de Gironcoli, S.[3] & Baroni, S.[3]
[1]Dept. of Geology and Geophysics, University of Minnesota, Minneapolis, MN, USA ([*]umemoto@cems.umn.edu))
[2]Dept. of Chemical Engineering and Materials Science, University of Minnesota, Minneapolis, MN, USA
[3]SISSA & INFM-DEMOCRITOS National Simulation Center, Trieste, Italy

Phase boundaries amond the various forms of ice are difficult to be determined experimentally because of large hysteresis involved at low temperatures. Theoretically, there are also great challenges, including the order-disorder transition. The ice VII-VIII boundary is a typical order-disorder phase boundary, which has been well constrained experimentally over a wide pressure range, and is a good target to be studied theoretically. We present a first-principles study consisting in the complete statistical sampling of molecular orientations within a 16-molecule supercell. Vibrational effects are included within quasi-harmonic theory. Our calculation accounts well for several important aspects: equation of state of ice VII, negative Clapeyron slope, and isotope effect. We will discuss also some factors to be improved, including XC functionals.

Acknowledgements: Research was supported by NSF grants EAR-0757903, EAR-0635990, and ATM-0428774 (Vlab). Computations were performed at the Minnesota Supercomputing Institute.

The spin transition in Fe-bearing perovskite and its consequences for the lower mantle

Caracas, R.[1*], Mainprice, D.[2] & Thomas, C.[3]
[1]Laboratoire de Sciences de la Terre, CNRS, ENS de Lyon, France ([*]razvan.caracas@ens-lyon.fr)
[2]CNRS, Géosciences Montpellier, Université Montpellier, France
[3]Institut für Geophysik, Westfälische Wilhelms Universität Münster, Germany

In the last years more and more evidence emerged, from both experimental and theoretical sides, that points to a magnetic phase transition in Fe2+-bearing perovskite and post-perovskite at high-pressure [1-3]. Experimentally it was observed that the ferrous iron in perovskite and post-perovskite undergoes a high-spin to intermediate-spin to low-spin transition. First-principles calculations based on density functional theory suggest that Fe-bearing $MgSiO_3$ perovskite undergoes a spin transition from high-spin state to low-spin state. This high-spin to low-spin transition has been found first by applying random displacements on the atomic positions in the Pbnm orthorhombic parent structure. These displacements create enough energy in the system that it was able to break the potential barriers corresponding to the spin transition. Non-randomized structures are uniquely obtained by the replacement of Mg by Fe in the Pbnm structure, leading to much higher transition pressures [4].

Using a novel approach we are able to disentangle a part of the complex phase diagram and spin behavior of the $FeSiO_3$ perovskite. To to this we investigated the dynamic stability of Pbnm $FeSiO_3$ perovskite and show the existence of unstable phonon modes. We tracked the eigen-displacements of the phonons modes to find the low-spin and the intermediate spin states. On solid state physical basis we explored, a set of hypothetical structures with various spin configurations and considerably lower enthalpy than the parent orthorhombic Pbnm structure. At mega-bar pressures we studied various stable monoclinic and triclinic configurations with intermediate spin state and a triclinic low-spin structure.

Our results demonstrate that distorted perovskite with intermediate spin state can exist in the Earth as an independent phase or can coexist with domains in a high-spin configuration. Changes due to chemistry or temperature or both can easily shift the equilibrium from one spin configuration to the other; this would in turn affect the thermal and electrical conductivities, the seismic properties, the rheology and the chemical behavior of the mantle and thus could be at the origin of small-scale mantle heterogeneities and enhance chaotic convection.

Then we determine the elasticity of Fe-bearing perovskite for various spin configurations using density-functional theory calculations. The elastic moduli and the bulk seismic wave velocities are weakly affected by the spin transition. However, we show that the intrinsic differences in seismic anisotropy between the high-spin and low-spin phases of Fe-bearing perovskite coupled with lattice preferred orientation that can develop during mantle flow leads to distinct seismic signatures between the top and the bottom of the lower mantle. These signatures should be detectable by seismic observations and they need to be taken into account in tomographic studies of the Earth's lower mantle.

[1] Badro, J. et al. (2004) *Science*, **305**, 383-386. [2] McCammon, C. et al. (2008) *Nat. Geosci.*, 1, 684-687. [3] Lin, J.F. et al. (2008) *Nat. Geosci.*, **1**, 688-691 [4] Caracas, R. and Cohen, R.E. (2005) *Geophys. Res. Lett.*, **32**, L16310.

Physico-chemical features of aluminium hydroxides as modelled with hybrid B3LYP functional and localized basis functions

Demichelis, R.[1*], Noel, Y.[2], Ugliengo, P.[1], Zicovich-Wilson, C.M.[3] & Dovesi, R.[1]
[1]Dipto. di Chimica IFM, Università di Torino and NIS – Nanostructured Interfaces and Surfaces – Centre of excellence Torino, Italy ([*]raffaella.demichelis@unito.it)
[2]Institut des Sciences de la Terre de Paris (UMR 7193 UPMC-CNRS), UPMC - Paris Universitas, France
[3]Facultad de Ciencias, Universidad Autónoma del Estado de Morelos, Cuernavaca, Morelos, Mexico

Aluminium hydroxides are a family of seven compounds (akdalaite, boehmite, diaspore, bayerite, doyleite, gibbsite, nordstrandite) covering an important role as row materials in the aluminium industry, which involves various technological fields. An extremely large variety of experiments and simuations were performed in the last 50 years on this class of materials. However, many of their properties still remain a matter of investigation and debate. Moreover, a unitary and comparative overview of the full family is still lacking.

Some of the open questions related to their structure (space group definition, H order-desorder), energetics (relative stability with respect to each other and to the dehydrated phase) and vibrational spectrum (broad bands in the OH stretching region: large differences in the interpretation of the experimental IR and Raman spectra by the various authors) are here tackled with a quantum mechanical *ab initio* approach, using the CRYSTAL09 periodic code, a rich all-electron Gaussian type basis set and the hybrid B3LYP functional (comparison to results obtained with other DFT functionals are also provided). [1-7]

Calculated properties are compared to experimental data when available. H positions were optimised, so that it is possible to attribute a space group to boehmite, akdalaite and doyleite, and propose a unit cell for nordstrandite. The thermodynamic and vibrational analyses of Al hydroxides here presented are shown to be extremely helpful for the interpretation of the experimental results.

This work represents the first complete, systematic and homogeneous (same method, computational parameters, basis set and Hamiltonian) analysis of the crystal structure, energetics and vibrational spectra of this family of compounds, showing how important can be the contribution of simulation to the field.

[1] Demichelis, R. et al. (2007) *J. Phys. Chem. B*, **111**, 9337-9346. [2] Noel, Y. et al. (2009) *Phys. Chem. Miner.*, **36**, 47-59. [3] Demichelis, R. et al. (2008) *J. Phys. Conf. Ser.*, **117**, 012013. [4] Demichelis, R. et al. (2008) *Chem. Phys. Lett.*, **465**, 220-225. [5] Demichelis, R. et al. (2009) *J. Phys. Chem. C*, **113**, 6785-6791. [6] Demichelis, R. et al. (2010) review in preparation. [7] Demichelis, R. et al. (2010) *Int. J. Quantum Chem.* (in press).

Calculated and experimental Raman spectra of the polymorphic forms of $Y_2Si_2O_7$

Kaindl, R.*, Többens, D.M. & Kahlenberg, V.
Institute of Mineralogy and Petrography, University Innsbruck, Austria (*reinhard.kaindl@uibk.ac.at)

Crystalline material with the chemical composition $Y_2Si_2O_7$ shows not only promising properties in the fields of laser materials, high-energy phosphors or advanced ceramics, but also a complex polymorphism, which at present reports about seven different modifications [1]. Principally, Raman spectroscopy can provide structural information, but the interpretation of the spectra is challenging and frequently prone to error. This contribution presents experimental spectra of the different polymorphic forms of $Y_2Si_2O_7$, and compares them with calculated data obtained from density functional theory (DFT) approximations implemented in the CRYSTAL 06 program [2,3].

Experimental Raman spectra were recorded for six modifications, whereas the computations were performed for five polymorphs of $Y_2Si_2O_7$. Various functionals were evaluated. The results of the Dirac-Slater (LDA) exchange in combination with the Vosko-Wilk-Nusair (VWN) correlation, for example, agreed within 1% for the lattice parameters and within 2% for interatomic distances with the respective experimental values. The average and maximum deviation between observed bands and computed modes was ± 8 cm^{-1} and 20 cm^{-1}, respectively. Structurally, the different polymorphs can be divided into three main groups: Two forms are composed of $[Si_2O_7]$ dimers in antiparallel, three with parallel orientation and two forms can be classified as mixed anion silicates, containing both trimers and monohedra. Specific spectral features can be used to gain information about the degree of condensation of the $[SiO_4]$ tetrahedra. For example, a characteristic band around 660 cm^{-1}, which is assigned to O-Si-O bending mode appears in all forms composed of $[Si_2O_7]$-units whereas it is absent in the structures containing $[Si_3O_{10}]$-trimers.

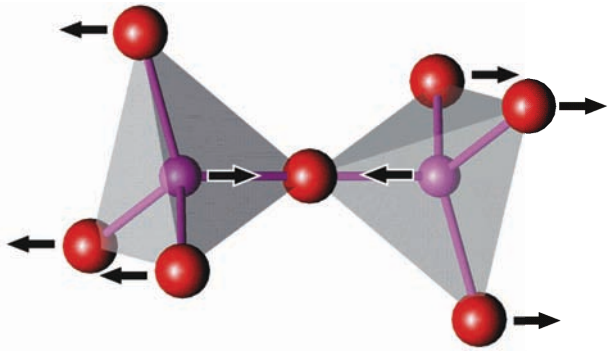

Fig. 1: O-Si-O bending mode at 660 cm^{-1}, appearing in all $Y_2Si_2O_7$ forms composed of double tetrahedra.

The relations between the highly variable structures and Raman spectra of the polymorphs of $Y_2Si_2O_7$ could be derived and most bands assigned to certain vibrational modes. Combining experimental and computational data allowed conclusions on structural details such as tetrahedral configurations.

[1] Kahlenberg, V. et al. (2008) *Z. Anorg. Allg. Chemie*, **634**, 1166-1172. [2] Dovesi, R. et al. (2006) *CRYSTAL06 - A computational tool for solid state chemistry and physics*. University of Turin. [3] Kaindl, R. et al. (in press) *J. Raman Spectrosc*.

Dissolution morphology of galena and sphalerite crystals from the Madan Pb-Zn deposits, Bulgaria

Atanassova, R.
Geological Institute, Bulgarian Academy of Sciences, Sofia, Bulgaria (radi@geology.bas.bg)

Polyhedral sulphide crystals and aggregates with diverse morphology are well known from the Madan ore district. The economically important Pb-Zn hydrothermal deposits include both veins and metasomatic ore bodies and are enclosed in the metamorphic rocks of the Rhodope massif. The mineralization consists of: -early skarns mainly of Mn-pyroxene and pyroxenoide composition, replacing marbles; -main sulphide ores of galena, sphalerite, pyrite and chalcopyrite and others; and -late quartz and carbonates [1].

Sometimes, sulphide crystals are affected by selective natural hydrothermal dissolution [2-4]. The dissolution morphological features of large galena and sphalerite crystals and their various local differences are described. Several types of anisotropic dissolution morphology are revealed by SEM studies. Dissolution patterns inheriting the growth features are specific along the different crystallographic direction on a given crystal face. In the study of surface dissolution topography the orientation relation in respect to the outline of the crystallographic faces, presented in the different habits, are taken into account, thus distinguished are dissolution patterns on galena along <100>, <111> and <110> (Fig. 1).

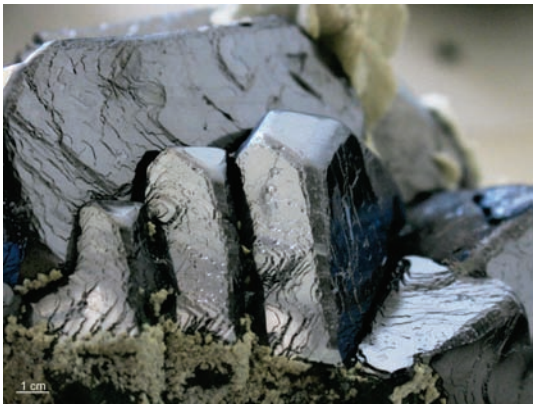

Fig. 1: Large galena cubo-octahedral crystals with dissolution macro patterns on (100) // <111>, Yuzhna Petrovitsa.

The dissolution features, formed under the control of defects result in characteristic morphological elements of the corroded galena and sphalerite surfaces. Such are: separated etch pits, dissolution grooves developed along sub grain or preferential etching at the galena twin (111) boundaries, triangular or square pyramidal hillocks, 3D channels and oval internal cavities after former fluid inclusions, etc.

The dissolution forms depend mainly from the undersaturation of the solutions, which is driving force of the process [5] and can be grouped as follows. At low undersaturation fine-layered, oval and rounded forms arise, starting from the original crystal edges and corners. Whereas at larger undersaturation single etch pits, grooves along grain and twin boundaries, pores, channels, bulges, etc. are predominant, formed under the control of the main surface defects [3].

Acknowledgements: This work is supported by the Bulgarian National Science Fund (DO1-904/MON).

[1] Vassileva, R.D. (2009) *XX ECROFI meeting*, Granada, 271-272. [2] Bonev, I.K. & Rice, C.M. (1997) *Mineral. Mag*., **61**, 377-386. [3] Bonev, I.K. (2007) *Proceed. Geosciences*, 50-51. [4] Atanassova, R. (2009) *Mitt. Österr. Miner. Ges*. 155, 24. [5] Sunagawa, I. (2005) *Crystals.* Cambridge University Press.

X-ray study and molecular dynamics computer simulation on melanophlogite

Ida, A.[1*], Kihara, K.[1], Okudera, H.[1] & Fujinami, S.[2]
[1]Graduate School of Natural Sciences and Technology, Kanazawa University, Kanazawa, Japan
([*]akihiro-ida@earth.s.kanazawa-u.ac.jp)
[2]School of Chemistry, College of Science and Engineering, Kanazawa University, Kanazawa, Japan

Melanophlogite (MEP), $23SiO_2 \cdot M^{12} \cdot 3M^{14}$ (Z = 8 and 2 for low- high-temperature phases, respectively), is one of silica clathrate minerals. MEP can accommodate small gas molecules (CO_2, CH_4, N_2, etc.) in two kinds of cages M^{12} and M^{14}. These guest molecules are held in the cages via van der Waals contact with the framework atoms.

Single crystals of guest-free MEP (GF-MEP) were prepared by heating natural ones from Mt. Hamilton, USA, and the structures at -50, 23, 100, 200 and 400°C were refined with X-ray single-crystal diffraction method together with that of guest-bearing one at 23 and 84°C. Space group *Pm*-3*n* gave the most satisfactory results and there was no sign of phase transitions in our experiments over the range of the temperatures.

The unit cell volume was slightly expanded *c.a.* 0.9% with removing guest molecules. In spite of this change, the original framework structure was retained with nominal Si-O bond length. Since the cell expanded, Si-O-Si bond angles should be changed to enlarge the cages. This change could be seen, though not large.

Difference-Fourier calculations revealed some guest molecules remained in these cages. Less than a half of M^{12} and more than a half of M^{14} were still occupied by unidentified guest molecules. Molecular dynamics (MD) calculations with different occupancy states at constant pressure and temperatures indicated that a model, CO_2-filled M^{14} and empty M^{12}, could represent experimental structure. M^{12} was expanded ≈ 1% by removing CH_4 from the cage. The volume of SiO_4 tetrahedron was constant even in these MD calculations. Presence of guest molecule, and interaction between the guest molecule and the host framework, is strong enough to change the volume of cage and thus the unit cell.

Car Parrinello molecular dynamics study of Fe-bearing smectites

Liu Xiandong[1,2*], Meijer, E.J.[2], Lu Xiancai[1] & Wang Rucheng[1]
[1]State Key Laboratory for Mineral Deposit Research, School of Earth Sciences and Engineering, Nanjing University, Nanjing, P. R. China ([*]xiandongliu@nju.edu.cn)
[2]Van't Hoff Institute for Molecular Sciences and Amsterdam Center for Multiscale Modeling, University of Amsterdam, The Netherlands

In order to identify the influences imposed by iron substitution, density functional theory-based Car-Parrinello molecular dynamics simulations are performed to study both oxidized and reduced Fe-bearing smectites. The following fundamental properties are investigated: local structures in the structural layer, hydroxyl orientations, and the vibration dynamics of hydrogen and silicon. Structural analyses indicate that the average Fe-O bond lengths are about 2.08 Å and 2.02 Å in the reduced and oxidized models respectively, and both Fe substitutions do not affect the coordination structures of the Al-O and Si-O polyhedrons. For hydroxyl orientations, Fe(III) substitution has no obvious influences but Fe(II) makes the coordinated hydroxyls present another high-angle distribution (Fig. 1).

The present work proves that both substitutions can red-shift the hydroxyl in-plane bending mode. The analyses also reveal Fe(III) substitution has no effect on the Si-O stretching, while Fe reduction causes a blue-shift of the out-of-plane stretching mode. These results provide quantitative constraints and clues for future research.

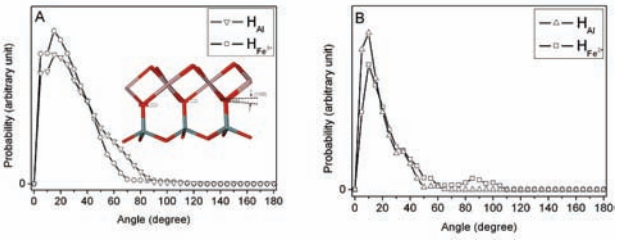

Fig. 1: Hydroxyl orientations in the (A) oxidized and (B) reduced models. Here H_{Fe} means the H from the hydroxyls coordinating with the Fe atom and H_{Al} denotes the other H atoms. The OH orientations are characterized by the distributions of the angle denoted on the stick model shown in panel A.

[1] Car, R. & Parrinello, M. (1985) *Phys. Rev. Lett.*, **55**, 2471-2474. [2] Stucki, J.W. (2006) in Bergaya, F., Theng, B.G.K. & Lagaly, G. (eds.) *Handbook of Clay Science*. Elsevier, Amsterdam, 423-476.

High-temperature molecular dynamics simulation of aragonite

Miyake, A.[1*] & Kawano, J.[2]
[1]Dept. of Earth and Planetary Science, Graduate school of Science, Kyoto University, Kyoto, Japan ([*]miya@kueps.kyoto-u.ac.jp)
[2]Research Institute for Applied Mechanics, Kyusyu University, Fukuoka, Japan

Calcium carbonate ($CaCO_3$) has various polymorphs, such as calcite and aragonite, and is important both in the earth science, as rock-forming minerals, and in chemical technology, as raw materials for industrial processes. Although calcite undergoes various structural phase transitions involving rotation of CO_3 groups or slight differences in the position of Ca^{2+} ions, structural transitions such as these have not been reported for aragonite. In a molecular dynamics (MD) simulation, Bearchell and Heyes [1] obtained a structure in which CO_3 groups were rotated through an angle of 30° around a three-fold axis from their positions in aragonite. However, they did not analyze the structure in detail. To extend this previous work, we used MD simulations using the aragonite structure as the initial state, to investigate the possible existence of a new polymorph related to aragonite.

MD calculations were carried out using the MXDTRICL [2] program with the two-body central force interatomic potential function, which includes terms for the Coulombic interaction between two point charges, short-range repulsion, van der Waals attraction, and Morse potential. The parameter set was empirically derived to reproduce aragonite structure at 300 K and 1 atm, which was based from our previous studies [3, 4] for calcite. We used the Verlet method for integration of equations of atomic motion and the Ewald method for summation of electrostatic interactions. Temperature and pressure were controlled by scaling atomic velocities and simulation of cell parameters, respectively. The time step was 0.5 fs throughout our simulations. Periodic boundary conditions for aragonite were imposed with a basic MD cell of 144 crystallographic units containing 2880 atoms.

The cell parameters changed with increasing temperature. From 300 to 500 K, each of these parameters gradually increased with temperature. Around 510 K, however, *a* and density decreased, whereas *b* and *c* increased. Above 510 K, b was about 1.73 times *a*. The coordination number changed from 9 to 6 at around 510 K. These abrupt changes of unit-cell parameters, density, and coordination number indicate that a first-order phase transition from aragonite to a high-temperature phase occurred at around 510 K, which occurs metastably within the stable region of calcite and the dT/dP slope of the phase boundary between them was about 1.25×10^3 K GPa-1. The point group and space group of the high-temperature phase were determined uniquely as 622 and $P6_322$, respectively (hexagonal aragonite). In the hexagonal aragonite structure, CO_3 groups were rotated by 30° around the c-axis and move up and down along the c-axis from their position in aragonite, and Ca ions were 6-coordinated as they are in calcite. The CaO_6 octahedron of hexagonal aragonite was strongly distorted, whereas in the calcite structure it is an almost ideal octahedron. The transition between hexagonal and orthorhombic aragonite involves only small movements of CO_3 groups. Therefore, it is possible that hexagonal aragonite plays an important part in the metastable formation of aragonite within the stability field of calcite and in the development of sector trilling in aragonite.

[1] Bearchell, C.A. & Heyes, D.M. (2002) *Molecular Simulation*, **28**, 517-538. [2] Kawamura (1997-2009) *JCPE*, #77. [3] Kawano, J. et al. (2009) *J. Phys. Condens. Matter.*, **21**, 095406. [4] Kawano, J. et al. (2009) *J. Phys. Condens. Matter.*, **21**, 275403.

Bct C_4: a new viable sp^3-carbon allotrope

Umemoto, K.[1*], Wentzcovitch, R.[2], Saito, S.[3] & Miyake, T.[4]
[1]Dept. of Geology and Geophysics, University of Minnesota, Minneapolis, USA ([*]umemoto@cems.umn.edu)
[2]Dept. of Chemical Engineering and Materials Science, University of Minnesota, Minneapolis, USA
[3]Dept. of Physics, Tokyo Institute of Technology, Tokyo, Japan
[4]Research Institute for Computational Sciences, AIST, Tsukuba, Japan

We have investigated by first principles the viability of a new form of sp^3 crystalline carbon recently found in tight-binding molecular dynamics simulations of carbon nanotubes (CNT) under pressure [1]. It consists of unique 4-membered rings and has body-centered-tetragonal structure (henceforth bct-C_4). It is also a polymerized form of (2,2) CNT, the smallest CNT. This phase is dynamically stable at zero pressure and is more stable than graphite beyond 18.6 GPa. At zero pressure it is also more stable than fcc C_{60} and (7,0) and (8,0) CNTs. Inspection of this transparent polymorph shows a peculiar relationship with hexagonal diamond, which suggests that this phase might be an intermediate phase along the graphite to hexagonal diamond transformation path. This possibility appears to be supported by the good agreement between simulated x-ray diffraction pattern of bct-C_4 and that of an intermediate transparent and hard phase of carbon produced by cold compression of graphite [2].

[1] Omata, Y. et al. (2005) *Physica E*, **29**, 454-468. [2] Mao, W.L. et al. (2003) *Science* **302**, 425-427.

Ab-initio study of dolomite cation disordering. Preliminary results

Zucchini, A.[1*], Prencipe, M.[2], Comodi, P.[1] & Frondini, F.[1]
[1]Earth Sciences Dept., University of Perugia, Italy ([*]azzizuc@libero.it)
[2]Mineralogical and Petrological Sciences Dept., University of Turin, Italy

Disordering of Ca/Mg cations can strongly affects thermodynamic and kinetic properties of dissolution of dolomite [$CaMg(CO_3)_2$] which may have important implications on several fields, i.e. the capability of dolomite horizons as geological reservoirs, strongly depends on dedolomitization processes. By *in-situ* heating experiments it is well known that disordering on Ca/Mg positions first appears at a temperature of about 1200K and it increases up to a temperature of about 1400K where it is complete [1]. By *ex-situ* studies of synthetic and natural dolomite samples it is not possible to reach high degree of disorder, probably due to a very rapid reordering rates occurring during the quench [2].

To improve our knowledge on cation disordering in dolomite structure, and to study thermodynamic stability of different disordered dolomite structures (Fig. 1), first-principle calculations, at the hybrid Hartree-Fock/Density Functional Theory (HF/DFT) level [3,4], have been carried out in this work, by using a development version of the CRYSTAL program [5]. *Ab-initio* calculations were computed by using the WC1LYP Hamiltonian which includes a non local exact Hartree-Fock exchange contribution.

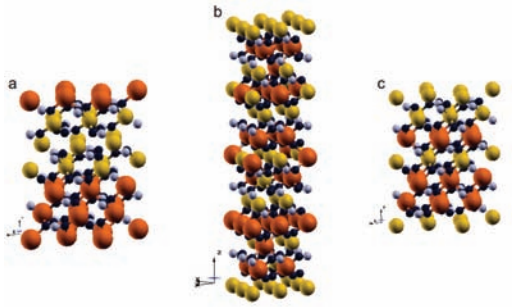

Fig. 1: Examples of *Ab-initio* simulated cation distribution of a stoichiometric dolomite in non-conventional supercell 2x2x2 (b) and conventional cell (a, c). (C-gray, O-black, Ca-red, Mg-yellow).

Total-energy calculations have shown that all of the disordered structures are, on average, about 15 KJ/mol energetically less stable than the ordered one. Moreover, we developed thermodynamic data processing in order to trace the characteristic disordering temperatures (T_{cd}). Analyzing the results we noticed that calculated the T_{cd} are quite in agreement with experimental values [1,6]. However, the calculated temperature disordering range (between about 800 K to 2000 K) resulted larger than the experimental one.

The results allowed us to conclude that highly disordered dolomites are energetically stable only at relatively high temperature conditions. The effect of pressure on cationic disordering will be investigated to better understand the natural environmental disordering conditions.

Further and thorough data will be presented in the extended work.

[1] Parise, J.B. et al. (2005) *Powder Diffr.*, **20**, **2**, 80-86. [2] Reeder, R.J. & Wenk, H. R. (1983) *Am. Mineral.*, **68**, 769-776. [3] Hohenberg, P & Kohn, W. (1964) *Phys. Rev. B: Condens. Matter*, **136**, 864-871. [4] Kohn, W. & Sham, L.J. (1965) *Phys. Rev. A: At. Mol. Opt. Phys.*, **140**, 1133-1138. [5] Dovesi, R. et al. (2005) *Z. Kristallogr.*, **220**, 571-573. [6] Antao, S.M. et al. (2004) *Am. Mineral.*, **89**, 1142-1147.

Characterisation of the structural bonding of selenium in pyrite by XAFS and XPS analysis

Diener, A.* & Neumann, T.
Institut für Mineralogie und Geochemie, Karlsruher Institut für Technologie, Karlsruhe, Germany (*alexander.diener@kit.edu)

The Se-79 radionuclide is highly mobile and has a long lifetime. Hence, it´s geochemical behaviour has to be considered for the assessment of a high-level nuclear waste repository. Pyrite itself is considered as one important host phase for radionuclides in high level nuclear waste disposal sites. Therefore, our investigations focus on selenium in pyrite as solid solution phase for acidic and anoxic conditions predicted for a nuclear waste repository. A main topic is the stability of Se fixture due to its type of bonding in the crystal structure.

The preparation of Se-doted Fe-sulfide grains were accomplished under argon atmosphere in a glove box from solutions with different constant acidic pH- and Eh-levels, containing Se-concentrations (–II, IV) between 10-3–10-6 M.

Results via XRD and SEM analysis reveal a synthesis of pure spheroidal pyrite grains with a mean diameter of 1-2 µm and Se contents up to 2 mol-%. XANES measurements determine the k-edges of Se at an energy of 12656.5 – 12657, typically for Se(-I,-II). Independant of the chosen Se-concentration and pH value, all XANES-spectra are very similar.

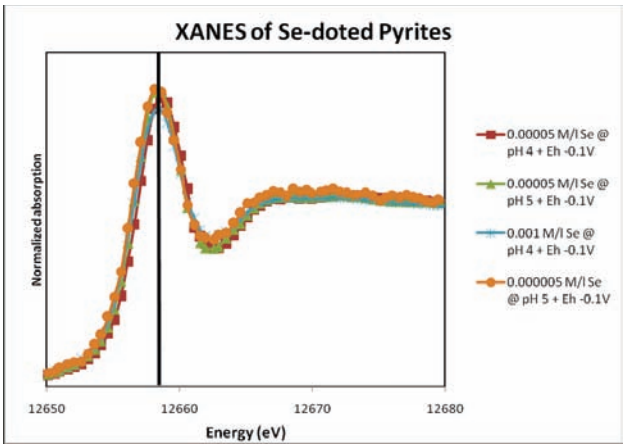

Fig. 1: XANES-spectra of Se-doted pyrite.

Based on the EXAFS results, the distance of Se to the atomic neighbours will be presented and experimental results will be compared with calculated stability diagrams. First XPS measurements complement the XANES results indicating a reduced valence state of the structural substitution of sulfide by selenide.

Crystal truncation rod studies of the pyrite (001) surface

Gilbert, B.[1*], Eng, P.J.[2], Banfield, J.F.[3] & Waychunas, G.A.[1]
[1]Earth Sciences Division, Lawrence Berkeley National Laboratory, Berkeley, USA (*bgilbert@lbl.gov)
[2]University of Chicago, USA
[3]Dept. of Earth & Planetary Science and Dept. of Environmental Science, Policy and Management, University of California – Berkeley, USA

Pyrite, FeS_2, is a common sulfide mineral that can exert a huge environmental impact when it is oxidized following exposure to air. Oxidation leads to the formation of acid mine drainage (AMD), low pH waters that typically contain elevated levels of heavy metal contaminants. The chemical pathway of pyrite oxidation has been studied by numerous researchers. The information obtained from these studies are limited since they use surface analysis techniques that require ultra-high vacuum conditions, provide only indirect structural information or require large amount of oxidation products.

Crystal truncation rod (CTR) analysis is a synchrotron-based scattering technique that is capable of determining the atomic-scale structure of hydrated interfaces. We are employing CTR to solve the structure of the water - pyrite (001) interface and to determine how oxidants such as ferric iron interact with the surface. This effort is a foundation for subsequent studies that will seek to capture changes in the surface structure that accompany the first steps in the oxidation process.

The preparation of high-quality pyrite surfaces for CTR is challenging because it lacks natural cleavage planes and because it is susceptible to oxidation under ambient conditions. We have developed an anaerobic chemical – mechanical polishing method that creates low-roughness pyrite (001) surface shown by atomic force microscopy (AFM) to be dominated by irregularly shaped (001) terraces (Fig. 1).

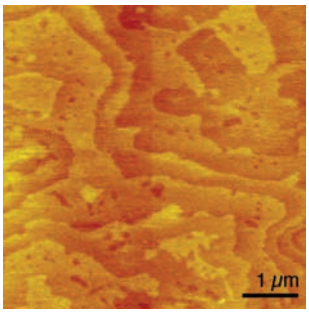

Fig. 1: Atomic force microscope image of a pyrite (001) surface prepared by anaerobic polishing method.

CTR studies of two pyrite (001) surfaces under a helium atmosphere confirm that a reproducible surface structure is obtained in this way. We are combining CTR data with surface electronic and vibrational spectroscopy in order to derive a detailed model for the pristine surface.

A first principles study of the structure and stability of iron-sulfides and their surfaces

Spagnoli, D.*, Wright, K. & Gale, J.D.
Nanochemistry Research Institute, Dept. of Chemistry, Curtin University of Technology, Perth, Australia (*dino@ivec.org)

Iron sulfide minerals are an intrinsic and essential part of the global biogeochemical sulfur cycle [1] and have also been proposed as possible candidates for the catalytic reactions involved in the origins of life [2]. As yet there are very few computational studies which examine the structure and stability of iron-sulfide surfaces that are thought to be important in the iron-sulfur-world.

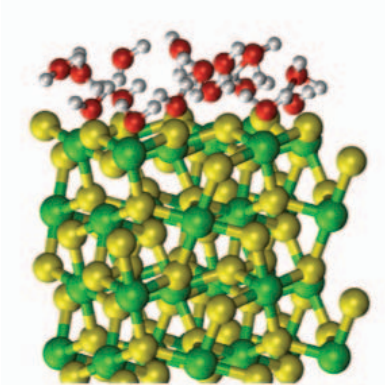

Fig. 1: Simulation of water at the pyrite (001) surface.

Using first principles quantum mechanical methods we preformed a study of the bulk phases of pyrite, marcasite, troilite, and pyrrhotite. Good agreement of the lattice parameters and spin states was found between experimental and simulation data. From these bulk minerals we are able to construct surfaces and begin to explore the structure and stability of solvated iron-sulfide surfaces. Based on this, it is possible to begin to explore both the thermodynamics and activation energies for plausible reaction pathways that control the kinetics for the formation of the precursors of life as catalysed by iron sulfides.

[1] Rickard, D. & Luther, G.W. (2007) *Chem. Rev.*, **107,** 514-562. [2] Wachtershauser, G. (1988) *Microbiol. Rev.*, **52,** 452-484.

Incorporation of trivalent actinides and lanthanides into Ca-carbonates: process understanding on a molecular level

Stumpf, T.
Karlsruher Institut für Technologie KIT, Institut für Nukleare Entsorgung INE, Karlsruhe, Germany
(Thorsten.Stumpf@kit.edu)

Demonstrating the geochemical aspects of the long term safety of a nuclear waste repository can significantly be improved by a molecular level understanding of the actinides behavior in the geosphere. In particular the interaction of radionuclides with minerals (adsorption, structural incorporation) strongly affects their mobility and retardation. In this presentation we will focus on the interaction of trivalent actinides and lanthanides with Ca-carbonates, with special focus on the structural incorporation.

Carbonates are omnipresent minerals in many rocks which are discussed as potential host for a nuclear waste repository. Furthermore, many waste repository designs include cement based components. Calcite is one of the major secondary alteration products formed during the degradation of cement over geological timescales. Actinide and lanthanide partition data derived from co-precipitation experiments indicate a high sorption affinity of these elements to calcite but a comprehensive understanding of actinide and REE uptake by calcite is not yet available. From a geochemical perspective the molecular level substitution mechanism is of key interest. Trivalent actinides and lanthanides have a similar ionic radius compared to Ca(II), the charge compensation mechanism upon substitution is unclear despite various recent studies.

We have studied synthetically Cm and Eu doped calcite, aragonite and vaterite crystals with Time Resolved Laser Fluorescence Spectroscopy (TRLFS). Particularly the Cm(III) fluorescence spectroscopy provides speciation information at very low concentrations (10^{-12} mol/L). In that sense, Cm(III) has been used here as a molecular probe to study the structural incorporation of trivalent 4f and 5f elements into Ca-carbonates. Site-selective TRLFS measurements at temperatures < 20 K show the presence of various incorporated molecular species and indicate clearly the charge-compensating role of Na^+ during the incorporation of Cm^{3+} and Eu^{3+} into Ca-carbonates.

Ra-barite solid solution formation during recrystallization in aqueous solutions

Curti, E.[1*], Fujiwara, K.[2], Iijima, K.[2], Tits, J.[1], Cuesta, C.[1], Kitamura, A.[2], Glaus, M.[1] & Müller, W.[1]
[1]Laboratory for Waste Management, Paul Scherrer Institute, Villigen, Switzerland ([*]enzo.curti@psi.ch)
[2]Geological Isolation Research Unit, Geological Isolation Research and Development Directorate, Japan Atomic Energy Agency, Tokai-Mura, Japan

High-purity synthetic barite was added to pure water or aqueous solutions containing soluble salts ($BaCl_2$, Na_2SO_4, NaCl and $NaHCO_3$) at 23 ± 2 °C. After a short pre-equilibration time (4 h), the suspensions were spiked either with ^{133}Ba or ^{226}Ra. The isotopic exchange between solid and aqueous phase was then monitored by radiometric analysis over a period of 120-406 days. The data consistently showed a continuous, slow decrease of radiotracer activity in the aqueous phase, both for ^{133}Ba and ^{226}Ra.

Mass balance calculations indicated that the removal of ^{133}Ba from solution cannot be explained by surface adsorption only, as it largely exceeded the 100% monolayer coverage limit. This was a strong argument in favor of recrystallization as the main uptake mechanism. Since complete isotopic equilibration between aqueous solution and solid was approached or even reached in all experiments, we concluded that substantial fractions of the barite initially added to the aqueous solutions had recrystallized during the experiments.

The ^{133}Ba data could be successfully fitted assuming constant recrystallization rates and homogeneous incorporation of the tracer into newly formed barite. An alternative model based on partial equilibrium of ^{133}Ba with the mineral surface (without internal isotopic equilibration of the solid) could not reproduce the measured activity data. Calculated recrystallization rates for the solutions with soluble salts ranged from 2.4 to 16 μmol m^{-2} d^{-1}, with no specific trend related to solution composition. For barite suspended in pure water, significantly higher rates (49 ± 22 μmol m^{-2} d^{-1}) were determined.

Radium uptake was determined by monitoring the decrease of ^{226}Ra activity in the aqueous solution with alpha spectrometry, after filtration of the suspensions and sintering. The Ra uptake results, in conjunction with the recrystallization data, consistently indicated formation of non-ideal solid solutions, with moderately high Margules parameters (W_{AB} =3720-6200 J/mol). These parameters are significantly larger than an estimated value from the literature (W_{AB} =1240 J/mol) [1].

Regardless of the unexpected non-ideal mixing behaviour, our results indicate that radium forms solid solutions with barite at fast kinetic rates and in complete thermodynamic equilibrium with the aqueous solutions. Moreover, this study provides essential quantitative data that can be used for the calculation of radium concentrations in environmentally relevant systems, such as radioactive waste repositories and uranium mill tailings.

[1] Zhu, Ch. (2004) *Geochim. Cosmochim. Ac.*, **68**, 3327-3337.

Precipitation of rhabdophane ($REEPO_4 \cdot nH_2O$) from supersaturated aqueous solutions: implications for the fate of Rare Earth Elements in natural waters

Roncal-Herrero, T.[1,2*], Rodríguez-Blanco, J.D.[2], Oelkers, E.H.[1] & Benning, L.G.[2]
[1]Géochimie-Biologie Experimentale -LMTG-Université de Toulouse-CNRS-OMP, Toulouse, France ([*]roncal@lmtg.obs-mip.fr)
[2]School of Earth and Environment, University of Leeds, UK

The concentration and distribution of Rare Earth Elements (REE) in aquatic systems is strongly influenced by the dissolution/precipitation of REE bearing phosphate minerals [1]. The goal of this study was to illuminate the role of Rhabdophane (Rha) on the behavior of REE in natural waters.

Aqueous solutions supersaturated with respect to La and Nd Rha were obtained at 5, 25, 50, and 100°C and pH ~1.9 by mixing two solutions containing KH_2PO_4 and $REE(NO_3)_3 \cdot 9H_2O$ (where REE stands for La or Nd). During the experiments, the change in aqueous PO_4 and REE concentrations were followed by ICP-MS and UV-Vis spectrophotometry, while the resulting solids were characterized via powder XRD, SEM, TEM and FTIR.

The formation of Rha occurs via:

$$REE^{3+} + PO_4^{3-} + nH_2O \leftrightarrow REEPO_4 \cdot nH_2O$$

The logarithm of the ion activity product (Log (IAP)) of the reactive fluids with respect to Rha decreased rapidly after mixing tending towards equilibrium. The steady state Log(IAP) in these experiments was found to be ~$10^{-23.0}$ and ~$10^{-21.1}$ at 25°C, for La and Nd Rha respectively [Fig. 1 inset]. Analyses of the solids confirmed that crystalline La and Nd Rha nanoparticles precipitated immediately after mixing. Their initial sizes depended on temperature and REE identity, while growth in both cases was time and temperature dependent (Fig. 1). For example, over 168 h of reaction the La-Rha average particle size increased from 44 to 54 nm at 5ºC and from 54 and 105 nm at 100°C.

The initially rapid equilibration of Rha supersaturated aqueous solutions and the progressive Rha crystal growth observed in our experiments suggests that the REE concentrations of many natural waters may be buffered by Rha phases precipitating from supersaturated natural waters.

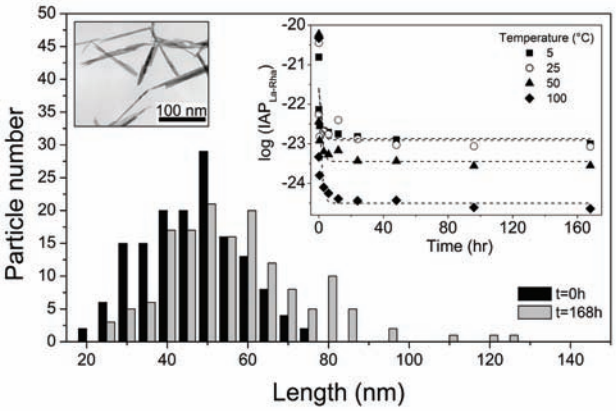

Fig. 1: La-Rha particle length distribution synthesized at T=5 ºC for times t=0 and t=168 hr. The insets show a TEM photomicrograph at T=100 ºC and t=0 hr and the evolution of Log (IAP) for La-Rha as a function of time and temperature.

[1] Köhler, S.J. et al. (2005) *Chem. Geol.*, **222**, 168-182.

Sorption and precipitation of phosphate on calcite surfaces

Stelling, J.[1*], Neumann T.[1] & Fischer, U.[2]
[1]Institut of Mineralogy & Geochemistry, KIT - Karlsruhe Institute of Technology, Karlsruhe, Germany
([*]stelling@kit.edu)
[2]Rheinkalk Akdolit GmbH & Co. KG, Pelm, Germany

Calcite is a major constituent of sedimentary rocks on the Earth surface [1] and its crystal growth mechanisms have been studied in detail in the past [2]. Moreover, the ability of calcite to adsorb phosphate from raw, sea and artificial water [3,4] has been investigated intensively to recover P as a valuable nutrient [5]. To date, understanding atomic-level processes that govern the kinetics of calcite growth with respect to foreign ions is still incomplete.

As part of the RECAWA joint project (www.recawa.de, Reactivity of Calcite/Water Interfaces,), we investigate the sorption and co-precipitation processes of phosphate on calcite surfaces from (super)saturated calcite solutions. Solutions were prepared from p.a. grade chemicals ($CaCl_2$, $NaHCO_3$) in MilliQ water (18.2 MΩ·cm), phosphate was added as H_3PO_4 or $Na_3PO_4{\cdot}6H_2O$ (50 to 500 µM/L), pH was adjusted to 8.0, ionic strength to 0.1 M (NaCl). 100 mg of precipitated calcium carbonate (PCC, SSA = 37.45 m^2/g), limestone powder (1.76 m^2/g), Iceland spar (1.6 m^2/g) or Merck $CaCO_3$ p.a. (0.2 m^2/g) powders were added as seed crystals to 20 mL calcite solution and shaken for 24 h. Afterwards, solutions were filtered and HCO_3^-, Ca^{2+}, P concentrations and pH was analysed. Relative to the starting value, the pH of the batch solution remained stable (± 0.15) during the experiments.

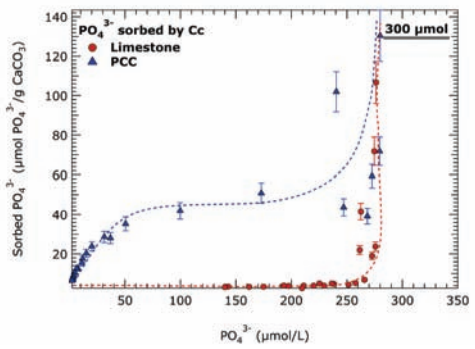

Fig. 1: Phosphate sorption isotherms of limestone (blue) and PCC (red), initial PO_4^{3-} concentration in solution 300 µmol/L.

Preliminary experimental results show that phosphate uptake is much more effective on PCC surfaces than on limestone powder surfaces. Overall decrease of phosphate ranges from 2 % to 100 % depending on the calcite powders. In contrast to limestone experimental series of, phosphate was eliminated from the batch solution of the PCC series completely. Adding high amounts to the batch solution (~25 g/L) results in a complete phosphate elimination, whereas limestone powder decreases the PO_4^{3-} concentration by max. 59% (Fig. 1). Fixation occurs not only due to pure adsorption processes. Multiple mechanisms such as precipitation and (trans)formation into stable Ca-P-compounds are involved in sorption and precipitation processes [6].

Upcoming analytical work of the experimental calcite powders includes the identification of different P fixation mechanisms for which ESEM, XRD and XAFS spectroscopy (XANES/EXAFS) is strongly required.

[1] Morse, J.W. et al. (2007) *Chem. Rev.*, **107**, 342-381. [2] Larsen, K. et al. (2010) *Geochim. Cosmochim. Ac.*, **74**, 2099-2109. [3] Babin, J. et al. (1994) *Lake Reserv. Manage.*, **8**, 131-142. [4] Song, Y. et al. (2006) *Chemosphere*, **63**, 236-243. [5] Gilbert, N. (2009) *Nature*, **461**, 716-718.

Nanoscale observations of calcium oxalate overgrowth onto calcite

Ruiz-Agudo, E.[*], Putnis, C.V. & Putnis, A.
Institut für Mineralogie, Universitat Münster, Germany
([*]eruiz_01@uni-muenster.de)

Calcium oxalates have attracted a significant amount of research due to their presence in kidney stones, scale deposits on sugar mill evaporators or natural patinas on calcitic stones in buildings. This has lead to the existence of a voluminous literature dealing with Ca-oxalates formation and dissolution.

An aspect that comparatively has received less attention is the precipitation of oxalates on Ca-bearing phases. In particular, very little is known about the mechanism of calcium carbonate to calcium oxalate transformation. This transformation is of particular relevance for kidney stone formation [1] or oxalate patinas development in building stones [2]. Experimental observations suggest that the growth of oxalates onto calcite follows the typical pattern of a replacement reaction (i.e. coupled dissolution-reprecipitation) where the parent calcite phase acts as a template for nucleation of the new phase. Geider et al. [1] suggested that calcium oxalate grows epitaxially onto calcite on the basis of lattice fit calculations and the observation of the regular orientation of oxalate crystals on calcite crystals. However, no details on the epitaxial relationship between the parent crystal and the overgrowth are given. The exact microscopic mechanism for this transformation remains essentially unexplored.

The present work provides a systematic in situ Atomic Force Microscopy (AFM) study of calcium oxalate growth onto calcite on changing solution composition. Whewellite ($CaC_2O_4{\cdot}H_2O$) crystals precipitated onto Iceland Spar crystals with their {100} and {010} planes parallel to {10.4} calcite faces. Growth of whewellite occurs mainly through formation and propagation of three-dimensional nuclei (Fig. 1). These observations point toward a “Volmer-Weber” mechanism of epitaxial growth, which is characteristic of weak adhesion between substrate and overgrowth. The effect of organics on this transformation has been also studied.

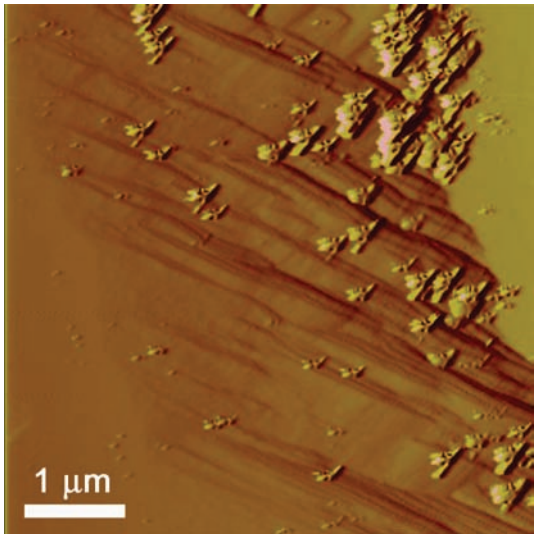

Fig. 1: Calcium oxalate overgrowth on calcite cleavage surfaces.

[1] Geider, S. et al. (1996) *Calcif. Tissue Int.*, **59,** 33-37. [2] Del Monte, M. & Sabbioni, C. (1983) *Environ. Sci. Technol.*, **17**, 518-522.

Structure and reactivity of the calcite - water interface

Heberling, F.[1,2*], Lützenkirchen, J.[1], Denecke, M.A.[1] & Bosbach, D.[2,3]
[1]Institute for Nuclear Waste Disposal, Forschungszentrum Karlsruhe, Germany ([*]Frank.Heberling@kit.edu)
[2]Helmholtz Virtual Institute, Advanced Solid –Aqueous RadioGeochemistry
[3]Institut for Energy Research 6, Forschungszentrum Jülich, Jülich, Germany

In this experimental study the calcite surface properties are characterized over a wide range of pH and p(CO_2) conditions using electrophoretic zetapotential and streaming potential measurements. In situ surface diffraction measurements at the calcite(104)-water interface are used to search for structural changes associated with the changes in the composition of the contact solution.

The zetapotential is found to be mainly determined by the calcium and carbonate ion concentration. pH plays only a minor role. The part of the 3D structure of the calcite - water interface surface diffraction measurements are mainly sensitive to does, however, not change significantly, even upon extreme changes in the composition of the contact solution. At all conditions the surface ions relax only slightly from their bulk positions, and two layers of water are observed above the surface. Water molecules of the first layer are located 2.35 ± 0.05 Å above the surface calcium ions, those of the second layer are located 3.24 ± 0.06Å above the surface, associated with the surface carbonate ions. No indications for calcium or carbonate inner-sphere complexes at flat terraces on the calcite(104) face are observed.

Based on these observations a new Basic-Stern surface complexation model for calcite is developed that describes the measured zetapotentials exclusively by outer-sphere ion adsorption.

The effect of sulphate and magnesium on the formation and stability of vaterite

Bots, P.[*], Rodriguez-Blanco, J.D., Shaw, S. & Benning, L.G.
School of Earth and Environment, University of Leeds, United Kingdom ([*]p.bots@see.leeds.ac.uk)

Vaterite (μ-$CaCO_3$) rarely forms in natural systems, as it is thermodynamically unstable with respect to calcite and aragonite [1] and it rapidly transforms in solution to the more stable phases. However, it has been shown that vaterite can be stabilized by certain inorganic (e.g. SO_4^{2-}) [2] and organic additives [3], yet a quantification of these processes is still lacking. The aim of this study was to quantify the effect of inorganic additives on the nucleation, formation and stability of vaterite.

The effect of SO_4^{2-} and Mg^{2+} on the crystallisation pathways of vaterite from amorphous calcium carbonate (ACC) was studied using synchrotron-based time resolved (seconds /frame) Small – and Wide Angle X-ray Scattering (SAXS/WAXS) on station I22 at Diamond Light Source. The reaction was quantified by mixing $CaCl_2$ and Na_2CO_3 at SO_4/CO_3 = 0 and 0.1. Equivalent off line experiments with varying SO_4/CO_3 were also carried out. Furthermore, vaterite, crystallized from a solution with SO_4/CO_3 = 25, was aged with increasing SO_4^{2-} concentrations for up to 24h. Finally, the effects of these additives on vaterite formation and its stability were studied by performing 48h long constant addition experiments.

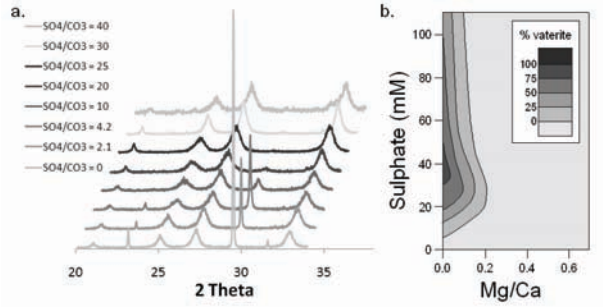

Fig. 1: a. XRD patterns from off line experiments as a function of SO_4/CO_3; b. fraction of precipitated vaterite from the constant addition experiments as a function of Mg/Ca and SO_4^{2-}.

The synchrotron SAXS/WAXS data showed that pure ACC transformed to vaterite within 10s of seconds [4]. Increasing SO_4/CO_3 to 0.1 in the initial solutions delayed the transformation of ACC to vaterite by about 25%. However, increasing Mg/Ca to 0.1 completely inhibited vaterite nucleation and promoted the nucleation of calcite. The off line crystallization data (Fig. 1a) showed that with increasing SO_4/CO_3, vaterite stability increased. Vaterite precipitated at SO_4/CO_3 = 25 (structural SO_4/CO_3 = 0.04), was stable up to 24h in a solution with SO_4^{2-} concentrations higher than 30mM. Data from the constant addition experiments (Fig. 1b) also confirmed that SO_4^{2-} promoted both the formation and stability of vaterite. Its stabilization likely occurred by the incorporation of SO_4^{2-} [2]. However, increasing Mg/Ca to 0.2 (Mg/Ca in seawater is 5.4) completely inhibited vaterite formation (Fig. 1b), which was comparable to the SAXS/WAXS results. These results show that SO_4^{2-} has a clear stabilizing effect on vaterite, while Mg^{2+} prevents its formation.

Our results show how vaterite can be formed and stabilized inorganically and give clues on calcium carbonate mineralogy in multiple environmental settings and industrial processes.

[1] Plummer, L.N. & Busenberg, E. (1982) *Geochim. Cosmochim. Ac.*, **46**, 1011-1040. [2] Fernández-Díaz, L. et al. (2009) *Geochim. Cosmochim. Ac.*, **73**, A367. [3] Wang, L.L. et al. (2008) *Polymer*, **49**, 1199-1210. [4] Rodriguez-Blanco, J.D. et al. (2010) *this issue.*

Influence of sulfate groups on the polymorphism of $CaCO_3$

Fernández-González, Á.[1*], Fernández-Díaz, L.[2] & Prieto, M.[1]
[1]Depto. de Geología, Universidad de Oviedo, Spain
([*]mafernan@geol.uniovi.es)
[2]Depto. de Cristalografía y Mineralogía, Universidad Complutense de Madrid, Spain

Calcium carbonate minerals often form in evaporitic environments. In this type of environments, the concentration of dissolved sulfate is high and calcium carbonate minerals incorporate this anion in their structures during growth. There are evidences that the presence of sulfate in the crystallization medium affects the calcium carbonate polymorph selection, promoting the formation of metastable vaterite and inhibiting the transformation of this phase into the more stable calcite [1,2]. With the aim of understanding this influence we conducted (1) precipitation and maturing experiments of $CaCO_3$ from aqueous solutions containing different SO_4^{2-}-CO_3^{2-} ratios and (2) a molecular simulation study of the effect that the isomorphic substitution of a small amount of carbonate by sulfate has on the relative energies of vaterite, aragonite and calcite.

The X-ray diffraction analyse of the precipitates sampled after different reaction times showed that, when the reaction time is short (≤ 1 hour), these precipitates always consist of a mixture of calcite and vaterite, irrespective the initial SO_4^{2-}-CO_3^{2-} ratio in the aqueous solution. However, the relative abundance of vaterite increases with the amount of sulfate in the solution. After reaction times longer than 24 hours, vaterite has totally transformed into calcite when the SO_4^{2-}-CO_3^{2-} ratio is low (≤ 1) but persists as a major phase component of the precipitate when the SO_4^{2-}-CO_3^{2-} ratio is higher. Moreover, the reaction time required for the total transformation of vaterite into calcite also increases with the sulfate content in the solution.

The computational modeling of the substitution of small percentages of CO_3^{2-} groups by SO_4^{2-} in the structures of calcite, aragonite and vaterite shows that this substitution introduces an important distortion in calcite and aragonite structures but very limited in vaterite structure. Moreover, it is energetically favorable in the case of vaterite, but unfavorable in calcite and aragonite structures.

The progressively more sluggish kinetics of the transformation of varite into calcite as the content of sulfate in the aqueous solution increases can be related to changes in the relative solubility of these two polymorphs due to the incorporation of sulfate groups in their structures. These changes are consistent with the results of our computational modeling.

Acknowledgments: Financial support through the Spanish Ministry of Science and Innovation (Project CGL2007-65523-C02-01 and -02) is gratefully acknowledged.

[1] Lippmann, F. (1973) *Sedimentary Carbonate Minerals*. Springer-Verlag. [2] Grasby, S.E. (2003) *Geochim. Cosmochim. Ac.*, **67**, 1659-1666**.**

Computational study of the calcium carbonate-water interface

Raiteri, P.[*] & Gale, J.D.
NRI and Dept. of Chemistry, Curtin University of Technology, Perth WA, Australia ([*]paolo@ivec.org)

Calcium carbonate is important in many fields of geology, chemistry and biology for its role in geo-sequestration of carbon dioxide and bio-mineralization. Despite its importance, the atomic mechanisms underlying the nucleation and growth of $CaCO_3$ crystals are not fully understood, either from the experimental or theoretical standpoints. In particular, the role of speciation and of hydration of the growing nucleus in the early stages of growth is completely unknown.

To gain a better insight into these processes we have developed a new force field which accurately reproduces the thermodynamics of hydration of ions and molecules as well as the dissolution enthalpies of the solid phases [1]. Molecular dynamics simulations of the aqueous interface of virtually infinite calcite layers and of nanoparticles (Fig. 1) have then been performed to study the molecular processes underpinning the calcium carbonate interfacial properties. Moreover, to address the role of bicarbonate, different approaches to simulate the proton reactivity within our classical force field framework have been explored and compared against large scale density functional theory calculations. The performance of all reactive approaches will be analysed in terms of their computational efficiency and the reliability of their description of the properties of the mineral-water interface.

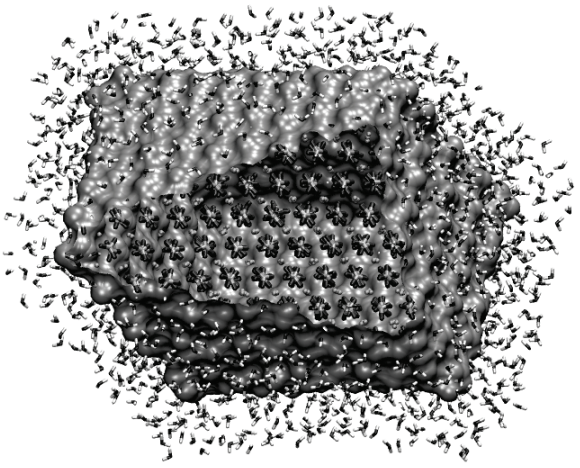

Fig. 1: Calcite nanoparticle in water.

[1] Raiteri, P. et al. (2010) *J. Phys. Chem. C*, **114(13)**, 5997-6010.

Uptake of heavy metals by abiogenic calcite and aragonite from freshwater and seawater

Carneiro, J.F.*, Stoll, H.M. & Prieto, M.
Depto. de Geología, Universidad de Oviedo, Spain
(*joana@geol.uniovi.es)

In the last decades, continental anthropogenic inputs have increased the concentration of heavy metals in many estuarine and coastal areas, enhancing the potential harmful effects for organisms. One example of coastal contamination is found in the southwestern coast of Spain, where the Tinto and Odiel rivers release metals from the Iberian Pyrite Belt into the Gulf of Cadiz [1]. Several geochemical studies have focused on the sorption of divalent metals on calcite from freshwater (e.g. [2]), but few have considered the removal of metals by aragonite (with the exception of [3] and [4]). Likewise, the inorganic uptake of metals from seawater by calcite and aragonite has not been extensively studied.

The aim of this study is to compare the removal of the metals Cd, Co, Ni, and Zn from both freshwater and seawater, by sorption on abiogenic calcite and aragonite. To evaluate the significance that this uptake could have on a reduction of metal concentrations in aqueous solutions, we ran several series of batch interaction experiments. These experiments were carried out in continuously stirred reactors at ambient conditions. For each series, mineral particles (either calcite or aragonite) reacted with a metal-bearing aqueous-solution (either calcite-saturated deionised water or artificial seawater). The aqueous solutions used were enriched with 1 ppm of Cd, Co, Ni, or Zn. Aqueous samples were collected at different reaction times, for 7 to 15 days. The metal concentrations in the samples were determined by inductively coupled plasma atomic emission spectrometry (ICP-AES).

Fig. 1 shows a decrease in the concentration of Cd in solution from about 1000 ppb, at the onset of the experiment, to nearly 550 ppb, after 2 weeks of interaction. These results suggest that Cd can be effectively taken up from artificial seawater by calcite, under the experimental conditions.

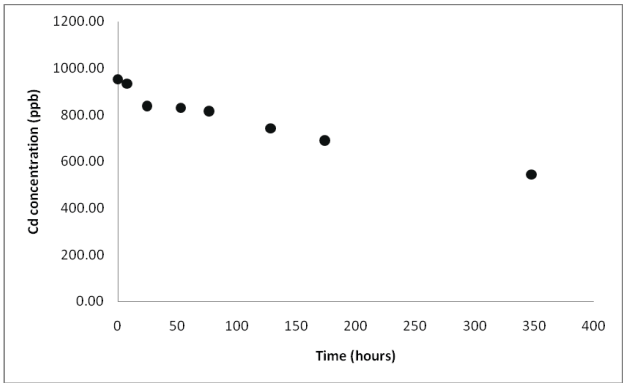

Fig. 1: Concentration of Cd in artificial seawater for different reaction times.

[1] van Geen, A. et al. (1997) *Geology*, **25**, 291-294. [2] Zachara, J.M. et al. (1991) *Geochim. Cosmochim. Ac.*, **55**, 1549-1562. [3] Kornicker, W.A. et al. (1985) *Chem. Geol.*, **53**, 229-236. [4] Prieto, M. et al. (2003) *Geochim. Cosmochim. Ac.*, **67**, 3859-3869.

An experimental study of monazite dissolution in low-temperature (150 and 200°C) as a function of fluid chemistry

Čopjaková, R.[1*] & Škoda, R.[2]
[1]Czech Geological Survey, Brno, Czech Republic
(*copjakova@sci.muni.cz)
[2]Dept. of Geological Sciences, Masaryk University, Brno, Czech Republic

Low temperature (150 and 200°C) experiments concerning hydrothermal alteration of natural monazite were carried out. Monazites were treated in steel pressure vessels with PFTE liner using fluids of different compositions: distilled water, 2M solutions of $CaCl_2$, NaF+KF and NaOH in H_2O during 100 days. Quartz, plagioclase and biotite were added into the vessels to simulate natural siliciclastic sedimentary basin.

Monazite dissolution increases with increasing temperature and in relation to fluid chemistry in following order: distilled water < Cl^- fluids < OH^- fluids < F^- fluids; well documented by different degree of surface corrosion (corrosive furrows and etch pits). Newly-formed REE phases (fluorides and silicates) were observed only in experiments with F^- and OH^- fluids. F-rich fluids at 200°C caused almost total monazite destruction accompanied by growth a variety of secondary REE phases.

The newly-formed REE phases ($REEF_3$-CaF_2 s.s.) in the experiment with F^- fluids at 150°C show REE patterns similar to parent monazite. In 200°C experiments (where several secondary REE phases precipitated) was observed a conspicuous evolution in REE distribution from inner to outer zone of the newly-formed REE mineral aggregates: from steep LREE enriched chondrite normalized REE-patterns with positive Ce anomaly to relatively flatter ones often with negative Ce anomaly. This trend is probably resulted by greater HREE solubility in hydrothermal fluids ; strange behaviour of Ce can be attributed to partial oxidization of Ce^{3+} to Ce^{4+}, but only in F-rich fluids the oxidization of Ce is clearly confirmed by precipitation of Ce^{4+} rich phase, corresponding to Ce^{4+} analogue of umbite ($K_2CeSi_3O_9{\cdot}H_2O$).

The outermost part of monazite relicts overgrown by newly-formed phases leached in F^- fluids shows significant depletion of P, Th, U and Pb and enrichment in F, Ca, K and Na compared with fresh monazite. It suggests selective removal of some elements from altered monazite prior to the total monazite dissolution. Low contents of U and Pb in all newly-formed phases and altered parts of natural monazite and high contents of U in fluids (especially in OH- and F-rich fluids) confirm preferential release of Pb and U from monazite into the solution and their higher solubility in OH- and F-rich fluids.

The REE contents in solutions are quite similar for all types of fluids, the most typically 1-8 μg/l for Sm, Gd, Dy, Er and 8-25 μg/l for La, Pr, Nd and Y, except OH-rich fluids at 200°C, with the solubility of REE 10-200 times higher. Cerium contents are relatively low, the most typically < 15 μg/l, except the F^- and OH^- fluids at 200°C (120 and 3111 μg/l, respectively). The solubility of REE in fluids increases in this order: distilled water ~ F^- fluids < Cl^- fluids < OH^- fluids. All type of fluids show flat chondrite normalized REE patterns predominantly with negative Ce anomalies. Only F^- and OH^- solutions from 200°C experiments show steeper LREE enriched pattern without negative Ce anomaly. This supports nonstoichiometric monazite dissolution with preferential leaching of HREE and the highest stability of Ce in the monazite in the experiments where no secondary phases precipitated.

Acknowledgements: Financial support from the grant GAČR No. 205/07/474 is gratefully acknowledged.

Molecular simulation of the aragonite-calcite polymorphic transformation induced by sulphate substitutional impurities

Fernández-González, A.[1*], Fernández-Seivane, L.[2,3], Fernández-Díaz, L.[4], Ferrer, J.[2,3] & Prieto, M.[1]
[1]Depto de Geología, Universidad de Oviedo, Oviedo, Spain
([*]mafernan@geol.uniovi.es)
[2]Depto. de Física, Universidad de Oviedo, Oviedo, Spain
[3]Centro de Investigación en Nanomateriales y Nanotecnología (CINN) (CSIC-UO-Principado de Asturias), Edificio Fundación ITMA, Llanera, Spain
[4]Depto. de Cristalografía y Mineralogía, Universidad Complutense de Madrid, Spain

It is well known that when calcium carbonate precipitates from aqueous solutions, the presence of dissolved foreign ions in the fluid can favour the formation of metastable $CaCO_3$ polymorphs. For example, it has been stated that small concentrations of Mg^{2+} or Sr^{2+} in the growth medium promote the precipitation of aragonite instead of the more stable calcite, whereas high Mg:Ca ratios favours the precipitation of amorphous calcium carbonate (ACC). The presence of dissolved foreign anions has also been related to the formation metastable phases, like the hydrated $CaCO_3$ ikaite ($CaCO_3.6H_2O$), in the case of significant concentrations of phosphate. Moreover, SO_4^{2-}:CO_3^{2-} ratios in the fluid seem to stabilize vaterite [1]. Although the effect of some of these foreign ions on the polymorph selection of $CaCO_3$ can be attributed to specific surface effects, it can not be ruled out that the incorporation of these impurities in the crystalline structure of the precipitated calcium carbonate could also have a significant influence both on the formation of metastable phases and on subsequent polymorphic transformations of the metastable precursors. Molecular simulations methods arise as useful tools to evaluate this influence, since they can provide accurate information at the atomic scale on the possible mechanisms involved in the development of impurity-induced polymorphic transformations. In the particular case of $CaCO_3$, molecular simulation methods can unfold into a deeper understanding of the energetic and the nanoscopic phenomena affecting the aragonite-calcite limit.

In this work, the aragonite-calcite transformation induced by the SO42+-CO32+ substitution has been simulated both by first principles (DFT) and empirical potential methods [2,3]. The relaxation of the aragonite structure doped with a certain proportion of sulphate anions readily converges to a calcite-type structure. The evolution of the corresponding powder diffraction diagrams has also been simulated by Rietveld analysis techniques. The distortion of the local environment around sulphate anions occupying carbonate positions in a aragonite-like crystal structure is relaxed through structural changes, which eventually lead to the global transformation into a calcite-like structure. The application of this approach to other mineral polymorphic transformations is likely to provide a better understanding of the behaviour of key rock-forming mineral systems.

Acknowledgments: Financial support through the Spanish Ministry of Science and Innovation (Project CGL2007-65523-C02-01 and -02) is gratefully acknowledged. Some of the simulations have been done in the supercomputer MareNostrum at Barcelona Supercomputing Center (The Spanish National Supercomputing Center).

[1] Fernández-Díaz, L. et al. (2010) *Geochim. Cosmochim. Ac.*, submitted. [2] Soler, J.M. et al. (2002) *J. Phys. Condens. Matter*, **14**, 2745-2779. [3] Gale, J.D. & Rohl, A.L. (2003) *Mol. Simulat.*, **29**, 291-341.

Investigating the link between topography and reactivity of mineral surfaces in solution

Godinho, J.[*] & Piazolo, S.
Dept. of Geological Sciences, Stockholm University, Stockholm, Sweden
([*]jose.godhino@geo.su.se)

In this study the reactivity of mineral surfaces in aqueous solution is investigated by analysing the changes in topography.

By studying the surface at the nano scale with confocal profilometry and SEM, as well as the composition of the liquid phase by ICP, through time, it is possible to relate the reaction rate to the presence of high energy sites on the surface (i.e. grain boundaries). The combination of these techniques allows the observation of topographic changes and the determination of its influence on the reaction rates.

A batch reactor is used, with and without stirring. The solution is kept far from equilibrium and in a range of pH from 2 to 4.

Here, we present first results of such experiments from a variety of minerals: natural and sintered fluorite, natural olivine and sintered ceria (used as an analogue for uranium dioxide i.e. nuclear waste pellets).

Crystallisation of $Ca_6Al_2O_6(SO_4,SeO_4)_3{\cdot}26H_2O$ solid solution

Jiménez, A.* & Prieto, M.
Dept. de Geología, Universidad de Oviedo, Spain
(*amjimenez@uniovi.es)

Ettringite ($Ca_6Al_2O_6(SO_4)_3{\cdot}26H_2O$) is a phase formed during the early hydration of Portland cements when sulphate is present in alkaline environments. The crystal structure of ettringite accepts numerous oxyanions, some of them radioactive and toxic. For instance, selenate (the form of selenium in alkaline medium surroundings) can be placed in the crystalline structure of ettringite by substituting sulphate groups [1]. However, the extent of selenium substitution in ettringite phase remains poorly understood. The aim of this work is to crystallise different members of $Ca_6Al_2O_6(SO_4,SeO_4)_3{\cdot}26H_2O$ solid solution and to determine its composition by X-ray diffraction.

Crystallization experiments were performed by mixing CaO (24 mmol) and stoichiometric amounts of $Al_2(SO_4)_3$, Al_2O_3, Na_2SeO_4 (Table 1) in ultrapure water in a nitrogen glove-box to minimise the CO_2 contamination. The mixture was stirred at 300 rpm during 48 hours and then it was maintained statically during two weeks at room temperature in nitrogen atmosphere. The precipitates formed during these experiments were filtered using 0.45 μm filters and analysed by powder X-ray diffraction (XRD). Two reference diffractograms of $Ca_6Al_2O_6(SO_4)_3{\cdot}26H_2O$ (41-1451) and $Ca_6Al_2O_6(SeO_4)_3{\cdot}26H_2O$ (42-224) were used to identify the pure end members as well as to calculate the structural data of the intermediate member of the solid solution.

Table 1: Parent solutions (mmol), composition and cell parameters

	$Al_2(SO_4)_3$	Na_2SeO_4	Al_2O_3	X	a	c
SSe1	4	0	0	0	11.234	21.371
SSe2	3	3	1	0.38	11.292	21.979
SSe3	2.5	4.5	1.5	0.53	11.317	21.878
SSe4	2	6	2	0.59	11.320	21.469
SSe5	1	9	3	-	11.309	22.077
SSe6	0	12	4	1	11.391	22.238

The main reflections (100, 110, 104, 114, etc.) present in the standard diffractograms have been identified in all precipitates. These reflections exhibit a continuous shift towards lower 2θ angles from the sulphate end member (SSe1) to the selenate end member (SSe6). These results confirm that different members of the solid solution have been crystallised. Table 1 shows the dimensions of the unit cell parameters (hexagonal setting) calculated using the computer program X'Pert Plus. An estimation of the solid-phase composition can be obtained from the unit cell parameter *a* (assuming Vegard's law), as shown in Table 1. As can be observed, in the case of SSe5, the value of *a* does not continue the linear trend. These results indicate that even though selenate anions can substitutes for sulphate in ettringite crystal structure, a compositional gap between $0.59 < X(SeO_4) < 1$ can not be discarded.

[1] Baur, I. & Johnson, C.A. (2003) *Cement Concrete Res.*, **33**, 1741-1748.

Stability of selenites and arsenates in oxidizing environments: Eh–pH diagrams of the systems $Me–Se–H_2O$ and $Me–As–H_2O$ (Me=Co, Ni, Fe, Cu, Zn, Pb) at 298 K

Krivovichev, V.G.[1], Charykova, M.V.[1], Yakovenko, O.S.[1*] & Depmeier, W.[2]
[1]Saint-Petersburg University, Saint-Petersburg, Russia
(*ojakovenka@gmail.com)
[2]Institut für Geowissenschaften, Universität Kiel, Germany

Since the discoveries of toxic properties of selenium and arsenic, there has been continual study of the geologic occurrence and geochemistry of these elements in oxygenated aqueous environments. Drainage from mineralized and mined areas may have high dissolved selenium and arsenic concentrations, and of major interest as the natural sources of Se and As in waters, soils and plants are likely to be the low-temperature oxidizing environments in the vicinity of ore bodies which contain Se- and As-bearing sulfides, arsenides and selenides [1].

The most selenites and arsenates were formed at chemical weathering of ores by oxygenated waters establishes conditions of increased Eh and low or neutral pH (at seasonal fluctuations of temperatures and atmospheric pressure). The interpretations are summarized on the Eh-pH diagrams, synthesized from equilibrium calculations, and reported geologic occurrences. The most recent thermodynamic data available [2] were used for the construction of diagrams from reactions which are balanced equations of Eh-pH relationships among species which are thermodynamically stable within the ranges of oxidation potential and pH considered for each reaction.

The estimation of activity of the components in natural waters which are formed out of zones natural and anthropogenous pollution by selenium and arsenic ($a_{\Sigma Se} = 10^{-9}$, $a_{\Sigma As} = 3{\cdot}10^{-8}$, $a_{\Sigma Fe} = 10^{-5}$, $a_{\Sigma Cu} = 10^{-7}$, $a_{\Sigma Zn} = 5{\cdot}10^{-7}$, $a_{\Sigma Co} = {\cdot}10^{-8}$, $a_{\Sigma Ni} = 6{\cdot}10^{-8}$, $a_{\Sigma Pb} = 10^{-8}$) and waters which are formed in an oxidation zone ($a_{\Sigma Se} = 10^{-5}–10^{-4}$, $a_{\Sigma As} = 10^{-3}$, $a_{\Sigma Fe} = 10^{-2}$, $a_{\Sigma Cu} = 10^{-2}$, $a_{\Sigma Zn} = 10^{-2}$, $a_{\Sigma Co} = 10^{-3}$, $a_{\Sigma Ni} = 10^{-2}$, $a_{\Sigma Pb} = 10^{-4}$) was done. Calculation and construction of diagrams Eh–pH was spent by means of software package Geochemist's Workbench (GMB 7.0). The used databank includes thermodynamic characteristics for 46 elements, 47 basic species, 48 redox couples, 551 aqueous species, 624 solid phases, 10 gases. Eh–pH diagrams of systems $Me–Se–H_2O$ (Me=Co, Ni, Fe, Cu, Zn, Pb) have been constructed for the average content of these elements in underground waters and for their contents in acidic waters of the oxidation zones of sulphide deposits. The formation of selenites and arsenates of Co, Ni, Fe, Cu, Zn, Pb in near-surface conditions are discussed. For the geologic purposes of this work, ionic concentrations have been considered equivalent to ionic activities.

Eh-pH stability relationships have been determined for selenites and arsenites (chalcomenite, cobaltomenite, alpheldite, mandarinoite, molibdomenite, and adamine, annabergite, symplesite, scorodite, schultenite, erythrite) and in order to interpret conditions of formation of these minerals and to compare their geologic stabilities of ore deposits.

These parameters define migration of selenium and arsenic, and their precipitation in the form of various solid phases. The understanding of mechanisms of their behavior in the near-surface conditions is one of actual problems of modern mineralogy and geochemistry and it is very important for the solving of some environmental problems.

Acknowledgements: The work is supported by grants of «Russian Foundation for Basic Research» (08-05-00253-a, 09-05-00567-a).

[1] Lollar, B.S. (2004) (ed.) *Treatise Geochem.*, **9**. [2] Charykova, M.V. et al (2009) *P.. Rus. Min. Soc.*, **138**, 105-117.

Epitaxial growth of brushite ($CaHPO_4{\cdot}2H_2O$) on gypsum cleavage surfaces: an AFM study

Pinto, A.J.[1,3*], Ruiz-Agudo, E.[2], Putnis, C.V.[2], Putnis, A.[2], Jiménez, A.[3] & Prieto, M.[3]
[1]CREMINER, Dept. of Geology, University of Lisbon, Portugal ([*]afipinto@fc.ul.pt)
[2]Inst. of Mineralogy, University of Münster, Germany
[3]Dept. of Geology, University of Oviedo, Spain

Brushite ($CaHPO_4{\cdot}2H_2O$) can grow epitaxially on gypsum ($CaSO_4{\cdot}2H_2O$) cleavage surfaces as a result of the interaction between slightly acidic, phosphate-bearing aqueous solutions and gypsum [1]. The present study investigates the phenomenon of mutual orientation at the nanoscale, by means of Atomic Force Microscopy (AFM). The experiments consisted of placing freshly cleaved gypsum fragments in contact with slightly acidic phosphate-bearing solutions, in an AFM fluid-cell. This allowed *in situ* observation of micro and nano-topographical features on gypsum cleavage surfaces as the interaction process evolved.

The structural relationships between gypsum (space group *A2/a*) and brushite (space group *Aa*) give rise to several crystallographic peculiarities such as the induced 2-fold twining, habit polarity and topographic effects due to the coalescence of equally oriented individuals (Fig. 1).

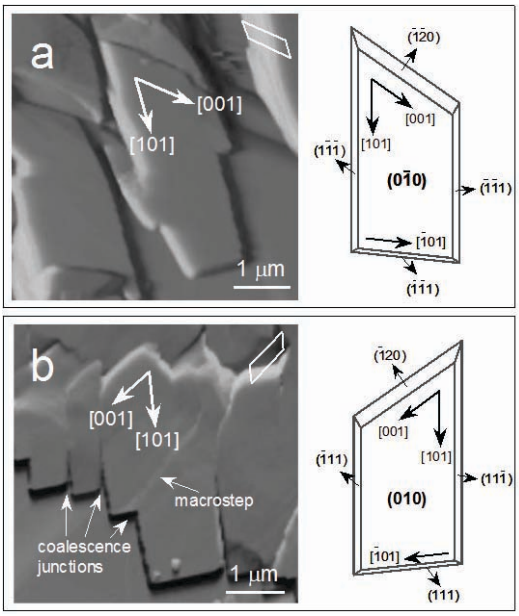

Fig. 1: AFM images of the epitaxial growth of brushite on **a)** gypsum's (0 $\bar{1}$ 0) and **b)** (010) cleavage surfaces.

The observed brushite growth is strongly anisotropic, involving a growth rate relationship of [101]>[$\bar{1}$ 01]>[010] (*Aa* space group), which leads to tabular morphologies elongated on [101]. The coupling between growth and dissolution is reflected by growth rate fluctuations due to changes in the saturation state of the solution with respect to both brushite and gypsum.

[1] Pinto, A. et al. (2009) *Am. Mineral.*, **94**, 313-322.

Modelling of rare earth elements adsorption onto hydrous manganese oxide using a diffuse double-layer surface complexation model

Pourret, O.[1*] & Davranche, M.[2]
[1]Dépt. Géosciences, Institut Polytechnique LaSalle-Beauvais, Beauvais, France ([*]olivier.pourret@lasalle-beauvais.fr)
[2]Géosciences Rennes, Université Rennes 1, Rennes, France

Manganese oxides are important scavengers of trace metals and especially rare earth elements (REE) in the hydrosystems. In order to better understand REE behavior, which are geochemically important tracers, modeling REE adsorption onto manganese oxide should be considered. The inclusion of Mn oxides in speciation models suffered from a lack of comprehensive set of sorption reactions consistent with a given surface complexation model (SCM). In consequence there are large discrepancies between published sorption data and predictions performed with available models. The compilation established by Tonkin et al. [1] was selected to describe surface complexation reactions for synthetic hydrous Mn oxide (HMO) using a two surface site and the diffuse double layer SCM model. The same specific surface area (i.e., 746 m^2/g), surface side density (i.e., 2.1 mmol/g) and pH_{IEP} (i.e., 2.2) were selected. Two sites (≡XOH and ≡YOH) were used with pK_{a2} of 2.35 (≡XOH) and 6.06 (≡YOH). The fraction of high affinity sites was fixed at 0.36.

Published data of REE sorption onto Mn oxides [2,3] were used to determine equilibrium surface complexation constants for lanthanide. They were modelled using the computer programs PHREEQC [4] and PhreePlot [5]. Both programs used the Nagra/PSI data base [6], which was modified to include well-accepted infinite-dilution (at 25 °C) of inorganic species.

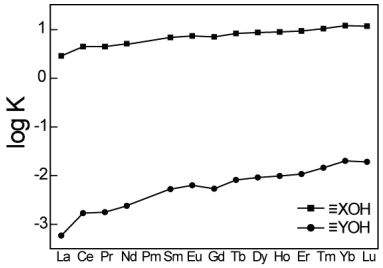

Fig. 1: REE patterns for log K (≡XOH-REE) and log K (≡YOH-REE).

The influence of pH, ionic strength and metal loading were combined and log K determined are displayed in Fig. 1. As illustrated on Fig. 1, log K globally increase from light REE to heavy REE and more specifically display a convex tetrad effect. At low metal loading, ≡YOH site type strongly express their affinity towards REE whereas at higher metal loading ≡XOH site type does. This study evidences thus heterogeneity in the distribution of the Mn oxide binding sites among REE. Eventually, as redox was not considered, Ce behavior was not correctly predicted. Indeed, Ce(III) may oxidize to Ce(IV) by oxidation scavenging with Mn oxide and such process should be further modeled.

[1] Tonkin, J.W. et al. (2004) *Appl. Geochem.*, **19**, 29-53. [2] DeCarlo et al. (1998) *Aquat. Geochem.*, **3**, 357-389. [3] Ohta, A. & Kawabe, I. (2001) *Geochim. Cosmochim. Ac.*, **65**, 695-703. [4] Kinniburgh, D.G. & Cooper, D.M. (2009) PhreePlot: Creating graphical output with PHREEQC. [5] Parkhurst, D.L. & Appelo, C.A.J. (1999) User's guide to PHREEQC (Version 2) - A computer program for speciation, batch-reaction, one-dimensional transport, and inverse geochemical calculations. [6] Hummel, W. et al. (2002) Nagra/PSI Chemical Thermodynamic Data Base 01/01. Universal Publishers, Parkland.

The role of the surface fluid layer in the control of crystal growth

Putnis, C.V.[*] & Ruiz-Agudo, E.
Institut für Mineralogie, University of Münster, Germany
([*]putnisc@uni-muenster.de)

Atomic force microscopy (AFM) experiments have shown that growth on mineral surfaces can occur from solutions when the bulk composition is undersaturated with respect to the precipitating phase. As growth can only take place from supersaturated solutions, the implication is that the composition of the solution in the fluid boundary layer in contact with the surface must become supersaturated with the new phase growing at the mineral surface. This has been observed in a number of systems, including the growth of new phases on calcite cleavage surfaces, such as Ca phosphonates, and on gypsum surfaces, such as Ca phosphates, where the partial dissolution of the substrate provides ions included in the new phase. The precipitation of calcite from pure water flowing over a stressed calcite surface is a clear example of a boundary layer becoming supersaturated with the precipitating phase when the bulk fluid contains no ions included in the new phase. This can be explained in terms of the increased solubility of stressed calcite allowing the boundary layer to become supersaturated with an unstressed calcite phase which then precipitates. The thickness of the boundary layer can be deduced from the solution composition and the reacting surface area.

The concept of a boundary layer becoming supersaturated with respect to another phase, which then precipitates, is essential to the understanding of coupled dissolution-precipitation as a mechanism of mineral replacement [1]. Real-time phase-shift interferometry has been used to show the steep compositional gradient at the surface of a crystal of KBr being pseudomorphically replaced by KCl [2] and this has been used as a model system for more complex earth systems during such processes as metasomatism, metamorphism and weathering.

[1] Putnis, A. & Putnis, C.V. (2007) *J. Solid State Chem.*, **180**, 1783-1786. [2] Putnis, C.V., Tsukamoto K. & Nishimura, Y. (2005) *Am. Mineral.*, **90**, 1909-1912.

Dissymmetrization and sectoral-twinning in Ni-rich tourmaline

Rakovan, J.[1*], Hughes, J.M.[2], Ertl, A.[3], Rossman, G.R.[4], Baksheev, I.[5] & Bernhardt, H.-J.[6]
[1]Dept. of Geology, Miami University, Oxford, Ohio, USA
([*]Rakovajf@muohio.edu)
[2]Dept. of Geology, University of Vermont, Burlington, USA
[3]Institut für Mineralogie und Kristallographie, Geozentrum, Universität Wien, Vienna, Austria
[4]Division of Geological and Planetary Sciences, California Institute of Technology, Pasadena, California, USA
[5]Geology Dept., Lomonosov Moscow State University, Moscow, Russia
[6]Institut für Geologie, Mineralogie und Geophysik, Ruhr-Universität, Bochum, Germany

Ni-bearing tourmaline crystals from the Berezovskoe gold deposit, Middle Urals, Russia, are optically anomalous and show a heterogeneous biaxial optical character [1]. Domains of different optical orientation and 2*V* (from 4 to >10 degrees) correspond directly to trigonal prism |100|, |010| and pedion |001| sectors, indicating sector twinning or optical sectoral zoning. Irregular domains of different optical orientation and undulatory extinction are observed within some sectors and are attributed to strain. Crystal structure refinement was done using single crystal X-ray diffraction (R = 4.41%), with a triply primitive pseudo-hexagonal cell to mimic the hexagonal tourmaline cell [a 15.903(1) b 15.9118(8) c 7.2304(4), α 90.063(2) β 89.793(2) γ 119.742(3) V 1588.57(18)].

Compositional sectoral and concentric zoning are also observed within the crystals. The distribution of Ni, Cr and Fe in the prism sectors shows clear indication of concentric zoning. The distribution of Na and Mg is different from that of Ni, Cr and Fe. There is no obvious concentric zoning within the prism sectors, nor is there an observable difference in concentration between nonequivalent prism sectors. There is, however, a distinct concentration difference of Na and Mg between the prism sectors and the pedion sector.

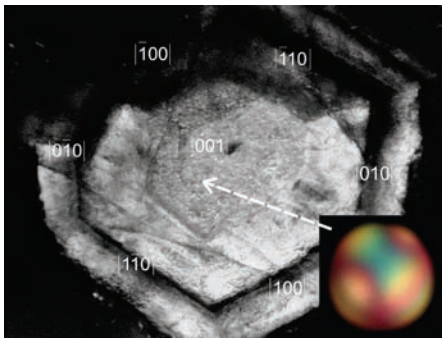

Fig. 1: A (001) section of Ni-rich tourmaline under crossed polars. The section is roughly 500 μm across. The |0-10| and |1-1 0| sectors are close to extinction while other sectors are not. Inset in lower right corner is an interference figure taken within the |001| sector.

In contrast to previous studies, the observed dissymmetrization occurs as a result of inequalities of both the hexagonal *Y* and *Z* tourmaline sites. The ordered arrangement of cations on the *Y* and *Z* sites and the correlation of optical orientation with specific sectors indicate that dissymmetrization occurred by differential incorporation of constituent elements at structurally different atomic sites at the surface of the crystal during growth.

[1] Hughes, J.M. et al. (in review) *Can. Mineral.*

Dissolution kinetics of tremolite in natural and biological conditions. Effect of citrate

Rozalén, M.[1*], Fiore, S.[2], Gervilla, F.[1] & Huertas, F.J.[1]
[1]Instituto Andaluz Ciencias Tierra, CSIC-UGR, Granada, Spain ([*]mrozalen@eez.csic.es)
[2]Environmental and Medical Mineralogy and Geochemistry – IMAA- CNR, Tito Scalo (PZ), Italy

The study of the degradation mechanism of asbestos under natural and biological conditions is essential to understand the clearance mechanisms of particles inhaled in the human body and the development of diseases as lung cancer or mesothelioma. The aim of this study is to evaluate tremolite dissolution rates by using soil and human-body conditions, including citrate as a proxy for organic acids in alveolar fluids.

Tremolite from Sierra Nevada (Granada, Spain) was used as a starting material. The effect of pH under Earth surface conditions was investigated using batch reactors at 25°C and buffered solutions (pH 1-8) with 0.01 M KNO_3 as background electrolyte. Aliquots of the suspension were filtered and analyzed for dissolved Si along time in order to calculate overall dissolution rates. The results show that log rate decreases linearly from -12.28 to -13.32 mol/gs when pH increases from 1 up to 5.6. The empirical rate law obtained correspond with a proton promoted dissolution mechanism:

$$\log Rate_{Si}(mol/gs) = -12.07 - 0.21pH$$

The effect of citrate on the dissolution rate was measured at 37ºC (corporal temperature) in stirred flow-through reactors by using modified Gamble's solutions at pH 4 (macrophages) and 7.4 (interstitial fluids) containing 0, 0.15, 1.5 and 15 mM of citrate. The dissolution rates calculated from Si concentration in the output solutions showed a little effect of temperature between 25 and 37°C. The results obtained point out that citrate enhances dissolution rates at both pH 4 and 7.4, although in a different grade: At pH 4 and 15 mM concentration, citrate increases almost 6 times tremolite dissolution rates with respect to citrate free solutions. At pH 7.4 the effect of similar citrate concentration is slighter, increasing 3 times dissolution rates with respect to citrate free solutions.

The overall dissolution rate has been expressed as the contribution of proton and ligand promoted dissolution mechanism and the concentration dependence can be expressed as follows:

$$\log Rate_{Si}(mol/gs) = -11.52 - 0.22\log[Cit] \text{ at pH 4}$$

$$\log Rate_{Si}(mol/gs) = -12.62 - 0.17\log[Cit] \text{ at pH 7.4}$$

These results suggest that the mechanism promoted by ligands needs to be considered in order to quantify asbestos dissolution in both soils and biological conditions. More studies are necessary to evaluate the species in solution, their interact with the mineral surface and their role in the dissolution process(es).

In-situ and ex-situ evaluations of calcite growths in laboratory and natural field experiments

Satoh, H.[1,2*], Tsukamoto, K.[2] & Ueda, A.[3]
[1]Mistubishi Materials Co., Naka, Japan ([*]hsatoh@mmc.co.jp)
[2]Tohoku University, Sendai, Japan
[3]Kyoto University, Kyoto, Japan

Recent study of growth kinetics of calcite is highly focused on underground storages of carbon dioxide. In Japan, utilization of geothermal field is considered to be a potential site for the CO_2 sequestration, because of faster dissolution and precipitation reaction than that at normal aquifers. In order to estimate the CO_2 capturable budget and its feasibility, we conducted three experiments: (1) laboratory experiment by in-situ interferometry; (2) field experiments at the surface monitoring station of the Ogachi geothermal research laboratory, Japan; (3) field experiment of on-site reacted samples recovered from GL-1000 m deep hydrothermal.

Laboratory experiment using a PSI-M (phase-shift interference microscope [1]) was performed at 22-200°C, 0.1-3.5 MPa. Normal pressure runs at 0.1 MPa were performed to determined spiral growth kinetics. Results showed growth curves of hillock as a function of supersaturation (Q/K_{sp}, e.g., [2,3]). Their growth rates showed dependency on temperature from 22 to 100°C [3], which enables estimation of spiral growth at higher temperature. Calcite growth at higher temperature showed significant enhancement of 2D nucleation.

Ex-situ runs at the surface was conducted using flow-through chambers which is connected to the recycling system comprised of CO_2-enriched groundwater (~600 ppm) and hot dry rock (~200°C) beneath Ogachi geothermal field. During 60 min, prepared hillocks of calcite showed successive growth in normal velocity of 6.5E-3 nm/s and steeper slopes than initials.

Another ex-situ runs were employed with a newly developed equipment named "Crystal Growth Sonde (CGS)" dived into deep underground hydrothermal system. After CO_2 injection (~600 ppm of CO_2), calcite formed etch-pits with a dissolution velocity of 0.17 nm/s, but after 1 day, calcite turned to grow with 2D nucleation with a velocity of 0.18 nm/s. This fast growth velocity can be recognized to be a benchmark data for CO_2-capturing at the Ogachi geothermal site. Based on the previous kinetic data [3], the Q/K_{sp} of this system could be ~1.8.

According to a recent study [4], spiral growth of calcite is inhibited in the Si-rich solution but 2D nucleation is promoted. Our in-situ PSI measurement confirmed growth inhibition in Si-rich solution (0.8 mM) at 35 °C (Fig. 1). The solution recovered by CGS at GL-1000 m was analyzed to be Si-enriched as ~4 mM. It is inferred that the calcite-precipitation could initially be initiated as spiral growth slowly due to Si-inhibition by enriched silica molecules or colloids, but lately be enhanced as 2D or 3D-nucleation growth. These growth behaviours in natural geothermal system such as CO_2-sequestration site need to be considered for better evaluation of the storage.

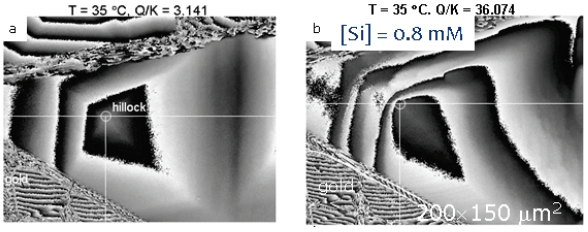

Fig. 1: Growth hillock of calcite with (a) and without silica (b).

[1] Satoh, H. et al. (2007) *Am. Mineral.*, **92**, 503-509. [2] Teng, H.H. et al. (2000) *Geochim. Cosmochim. Ac.*, **64**, 2255-2266. [3] Shiraki, R. & Brantley, S.L. (1995) *Geochim. Cosmochim. Ac.*, **59**, 1457-1571. [4] Pina, C.M. et al. (2009) *Cryst. Growth Des.*, **9**, 4084-4090.

Insights into the dehydroxylation kinetics of lizardite and chrysotile

Trittschack, R.* & Grobéty, B.
Dept. of Geosciences, University of Fribourg, Switzerland
(*roy.trittschack@unifr.ch)

Lizardite and chrysotile represent two prominent trioctahedral 1:1 phyllosilicates of the serpentine mineral group. Lizardite ($Mg_3Si_2O_5(OH)_4$) has a conventional sheet silicate structure, whereas in chrysotile the same TO-layers are rolled to cylinders. The chrysotile structure has thus not a classical 3D-symmetry, but only rotational and no radial symmetry. Physical properties are, therefore, expected to reflect also this non-conventional symmetry.

The aim of this study is to understand the influence of special symmetry of chrysotile on the mechanism and the rate determining steps of the dehydroxylation reaction. The dehydroxylation kinetics of lizardite serves, thereby, as reference. Theoretical deprotonation and water forming schemes were compared with results of in-situ High-Temperature X-ray diffraction, in-situ IR-spectroscopy, FTIR and Differential Thermogravimetry experiments on well characterized chrysotile and lizardite samples. In-situ IR and HT-XRD experiments under ambient pressure gave starting temperatures for the dehydroxylation of lizadite between 500°C and 550°C which lies in the range of former investigations [1]. Chrysotile dehydroxylation depend on structural features like the inner and outer tube diameter which itself dictate the physical properties. The dehydroxylation starts at the outermost layers at around 450°C and 500°C, whereas innermost layers breakdown about 600°C [2]. The initial dehydroxylation product of both polymorphs is X-ray amorphous, but crystallizes after a certain time to forsterite. These phase transformations were also followed by FTIR analyses, which offer a detailed insight into the structural recombination during the dehydroxylation.

Kinetic data were calculated from two independent methods, in-situ High-Temperature X-ray diffraction and Differential Thermogravimetry techniques for different atmospheres (N_2, O_2, air, etc.). Assuming proportionality between the integral intensity of diffraction peaks and the amount of serpentine present, the reaction rate can be extracted from the rate of intensity decrease. Data from isothermal runs have been treated with the conventional Avrami method as well as the "time to a given fraction" (TGF) method. Latter one offers the possibility to discover changes in the activation energy E_a during the course of dehydroxylation [3]. The same reaction progress dependency of E_a can also be obtained by the isoconversional Friedman analysis from a series of dynamic DTG data.

Isothermal HT-XRD experiments on lizardite yielded E_a of around 340kJ mol^{-1} (Avrami method). Data treated with the TGF method showed a progressive increase of the E_a with the fraction transformed from around 200kJ mol^{-1} (α=0.1) to 340kJ mol^{-1} (α=0.9). Non-isothermal DTG analyses on lizardite with different heating rates and under a controlled nitrogen atmosphere confirmed the TGF results and enabled a much more detailed resolution of the E_a during the dehydration progress. A preliminary mechanistic interpretation of these results will be given.

[1] Frank, M.R. et al. (2005) *GSA Annual Meeting Abst.*, **37**, 271. [2] Metraux, C. et al. (2002) *J. Mater. Res.*, **17**, 1129-1135. [3] Putnis, A. (1992) *Introduction to Mineral Sciences.* Cambridge University Press.

Application of FM-AFM to the study of calcite-aragonite transition in atomic level

Araki, Y.[1], Tsukamoto, K.[1*], Miyashita, T.[2], Oyabu, N.[3] & Yamada, H.[3]
[1]Tohoku University, Sendai, Japan
(*ktsuka@m.tains.tohoku.ac.jp)
[2]Kinki University, Wakayama, Japan
[3]Kyoto University, Kyoto, Japan

Some bivalve shells contain calcite and aragonite simultaneously although aragonite is metastable at normal temperature and pressure. Previous studies showed that organic matrices in shells control polymorphs of $CaCO_3$, though it was not clear whether magnesium ions were responsible for the aragonite formation. Frequency Modulation AFM (FM-AFM) has been employed for the first time for the direct study of calcite-aragonite phase transition in the presence or absence of peptides (50μg/ml) and magnesium ions (0.05M).

A cleaved calcite surface has been grown in $CaCO_3$ solution containing polypeptide, followed by the FM-AFM observation to see the change of atomic arrangement of the surface. This AFM has a capability to resolve the arrangement of atoms during crystal growth. The images are Fourier transformed to see the symmetry of atomic arrangement of the topmost surface.

The following results were obtained:

(1) Both calcite and aragonite surface at atomic level was obtained by FM-AFM.

(2) Addition of peptide to the solution is not enough to get aragonite configuration (Fig. 1).

(3) Both peptide and magnesium ions are needed to change calcite structure to aragonite structure (Fig. 2).

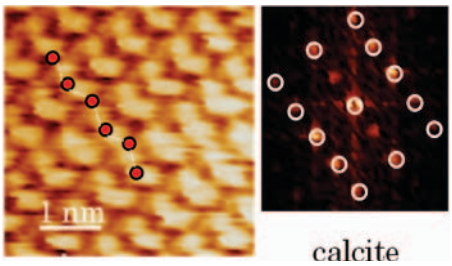

Fig. 1: Calcite surface grown from $CaCO_3$ solution containing the synthetic polypeptide without magnesium and the corresponding Fourier transformed image (right).

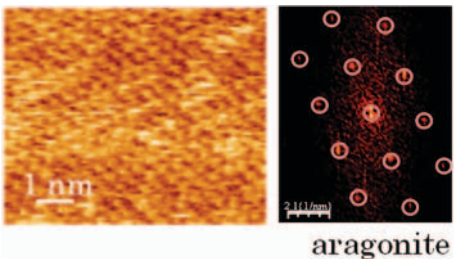

Fig. 2: The aragonite surface grown in the presence of both peptides and magnesium ions (left) and the corresponding Fourier transformed image (right).

Confocal differential interference contrast microscopy applied to studying mineral growth: the gypsum case

Van Driessche, A.E.S.[1*], Garcia-Ruiz, J.M.[1], Delgado, J.M.[1] & Sazaki, G.[1,2]
[1]Laboratorio de Estudios Cristalograficos, IACT, CSIC-University of Granada, Spain ([*]sander@lec.csic.es)
[2]The Institute of Low Temperature Science, Hokkaido University, Sapporo, Japan

The combination of confocal differential interference contrast microscopy and atomic force microscopy is a powerful method for studying mesoscopic and microscopic step dynamics on a mineral surface. To demonstrate the usefulness of this method we studied the kinetics of gypsum crystals growing from aqueous solution as a function of temperature and supersaturation.

We found that 2D nucleation is the main step generation mechanism, even at low supersaturation. The crystallographic direction of stable steps on the (010) face are [001] and [102]. Due to the elongated morphology of the 2D islands along the *c*-axis and the frequent nucleation of multilayer 2D islands a "hills and valley" topography is formed on {010} faces.

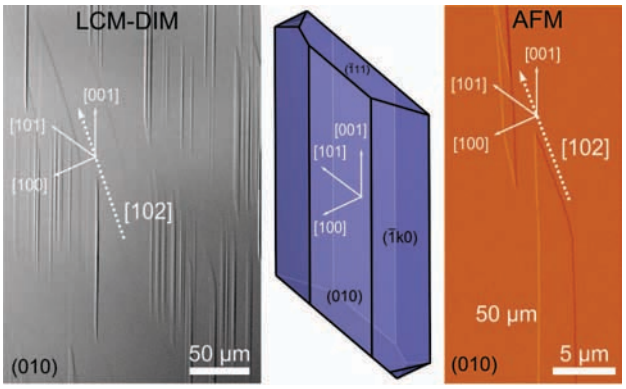

Fig. 1: Schematic representation of the structure of gypsum and the {010} face (middle image). LCM-DIM image at high supersaturation (left image) and AFM image at low supersaturation (right image) showing the crystallographic directions of steps found on the {010} face of gypsum.

The step kinetic coefficient, β_{st}, was determined in the temperature range 20-80ºC and a steep increment in the kinetic coefficient is found with increasing temperature. From these data we were able to calculate the activation energy barrier for incorporation of molecules in the crystal lattice. We found that gypsum crystals grow at low temperature in a mixed regime while at higher temperatures growth is controlled by diffusion. This is explained due to the increment of the kinetic coefficient with temperature. Overall, our results suggest that temperature govern the growth regime controlling gypsum crystallization and that measurement of the microscopic and mesoscopic step dynamics is decisive for explaining the morphology of gypsum crystals.

Simulation of the nucleation and growth of clay particles: the code Nanokin

Fritz, B.[1*], Clément, A.[1] & Noguera, C.[2]
[1]Laboratoire d'Hydrologie et de Géochimie de Strasbourg, Université de Strasbourg/EOST, CNRS, Strasbourg, France ([*]bfritz@unistra.fr)
[2]CNRS, Institut des Nanosciences de Paris, UMR 7588, Paris, France

In water-rock interaction processes, the formation of secondary phases from aqueous solutions is obviously a kinetically controlled phenomenon. Solutions producing clay phases must be oversaturated enough to favour the nucleation of new particles. This nucleation phase has a strong feed-back effect on the aqueous solution: created particles may grow or disappear as a function of the evolution of their oversaturation state in the aqueous solution.

In our attempt to model these processes we have developed a theoretical approach [1,2] combining nucleation, growth and re-dissolution of particles, embedded in a code, called Nanokin. It allows predicting the formation of populations of clay particles along a water-rock interaction process: classes of particles are described in sizes and abundances as a function of time, and the crystal size distribution can be followed.

The model has been applied to various systems [3,4] where the oversaturation state of the aqueous solution with respect to clay minerals is either due to: (1) the initial chemical composition of the aqueous solution as would be done in a laboratory approach or (2) to the alteration of a natural rock like in a geological environment. The competitive formation of simple clay phases like kaolinite and halloysite has been obtained first in both cases of oversaturation, the halloysite being generally formed on short term as a precursor of kaolinite for long term precipitation.

The effect of a temperature increase on these processes has been tested considering: (1) the simulated weathering process at 25°C of a granitic rock producing first competing halloysite and kaolinite and later Ca-montmorillonite, and (2) the hydrothermal alteration of a granitic rock at 150°C producing kaolinite and later illite [3,4]. This temperature effect was also tested in a diagenetic process: the interaction between sandstone–type sediments and sea water lead to the formation of an illitic clay together with the possible formation of albite as often described in diagenetic processes.

The model is now ready for application in systems where the formation and evolution of clay phases may play a key-role in the long-term evolution. This is particularly interesting for the simulation of weathering processes in watersheds, leading to the formation of soils, or in the prediction of long term stability of clay barriers in nuclear waste storages [6].

Acknowledgements: Support of the French ANR-PNANO 2006 program (project "SIMINOX" 0039) is acknowledged.

[1] Noguera, C. et al. (2006a) *J. Crystal Growth*, **297**, 180-186. [2] Noguera, C.et al. (2006b) *J. Crystal Growth*, **297**, 187-198. [3] Fritz, B. et al. (2009) *Geochim. Cosmochim. Ac.*, **73,** 1340-1358. [4] Fritz, B. & Noguera, C. (2009) in Oelkers, E. & Schott, J. (eds.) *Rev. Mineral. Geochem.*, **70**, 371-410. [5] Noguera, C. et al. (2010) *Chem Geol*., **269,** 89-99. [6] Marty N. et al. (2010) *Appl. Clay Sci*., **47**, 82-90.

Crystallization and transformation of iron sulphates on polished and fractured colloform pyrite surfaces

Dimitrova, D.[1*], Mladenova, V.[2] & Hecht, L.[3]
[1]Geological Institute, Bulgarian Academy of Sciences, Sofia, Bulgaria ([*]didi@geology.bas.bg)
[2]Sofia University "St. Kliment Ohridski", Sofia, Bulgaria
[3]Natural History Museum, Berlin, Germany

The phenomenon of sulphate formation on samples that contain colloform or spherulitic pyrite as a result of pyrite oxidation during their laboratory storage, gives us an extraordinary opportunity to study these minerals, which are highly unstable in natural conditions.

Two types of specimens containing colloform pyrite from the low-temperature Fe-Hg mineralization of the Ag-Pb Chiprovtsi deposit in NW Bulgaria have been studied: 1) colloform pyrite with quartz; and 2) colloform pyrite, cinnabar, quartz, calcite, quartz, barite, fluorite, ± ankerite and kutnohorite. Colloform pyrite contains variable amounts of As (0.66-4.77 wt.%), as well as Sb, Co, Ni and trace amounts of Tl, Ag and Au [1]. Sulphates have been formed on both types of specimens, on polished and fractured surfaces, but more abundant on the second type.

SEM study of sulphates formed on fractured surface of colloform pyrite revealed that tiny hexagonal-shaped platy crystals (coquimbite?) with slightly rounded edges start growing directly on the fine striated and cracked surface of the fibres within the spherulite. In open cracks at least two mineral phases crystallize simultaneously (szomolnokite and halotrichite or szomolnokite and coquimbite). Crystallization in cracks contributes toward their opening and further fracturing of the samples, thus increasing the surface area for oxidation, which in colloform, spherulitic and framboidal pyrite is very high. Evidences of partial dissolution like small pits (sometimes triangular-shaped) orientated along weak sites on crystal surfaces and rounded crystal edges and faces, are often observed on the newly form crystals. Transformation of one into another mineral phase occurs when the conditions change (temperature and air humidity mainly). Through partial oxidation szomolnokite may be converted to hydroxysulphate as copiapite.

The following hydrous sulphates were identified using XRD and SEM-EDS: szomolnokite ($Fe^{2+}SO_4.H_2O$), aluminocopiapite ($Al_{2/3}Fe^{3+}_4(SO_4)_6O(OH)_2.20H_2O$), coquimbite ($Fe^{3+}_2(SO_4)_3.9H_2O$), halotrichite ($Fe^{2+}Al_2(SO_4)_4.22H_2O$) and voltaite ($K_2Fe^{2+}_5Fe^{3+}_3Al(SO_4)_{12}.18H_2O$). All of them occur as well formed nano- to micro-sized crystals and aggregates: fibres (halotrichite), cubic and combinative forms (voltaite), prismatic (szomolnokite), platy and platy-sheet hexagonal (aluminocopiapite and coquimbite, respectively), rounded (effects of partial dissolution).

Pyrite oxidation in air is explained as electrochemical process requiring electron transfers to and from surface distinct cathodic and anodic sites where dissociation of the sorbed O_2 and H_2O occur as a precursor to formation of SO_4^{2-} and H^+ [2,3]. The small amounts of calcite and ankerite in the samples act as buffer neutralizing the reaction and resulting in formation of iron sulphates and gypsum as well. Arsenic from the colloform pyrite is incorporated in coquimbite, szomolnokite and halotrichite. This fact supports the idea that arsenic from As-bearing pyrite is easily released to the environment through formation of water soluble minerals. Unlike pyrite, cinnabar does not show apparent indications of oxidation.

[1] Dimitrova, D. & Mladenova, V. (2009) *Mitt. Österr. Miner. Ges.*, **155**, 50. [2] Rosso, K.M. et al. (1999) *Am. Mineral*, **84**, 1549-1561. [3] Todd, E.C. et al. (2003) *Geochim. Cosmochim. Ac.*, **67**, 881-893.

In-situ observation by interferometer during condensation of smoke particles

Kimura, Y.[1*], Tsukamoto, K.[1] & Maki, T.[2]
[1]Dept. of Earth and Planetary Materials Science, Tohoku University, Sendai, Japan ([*]ykimura@m.tains.tohoku.ac.jp)
[2]Product Development Dept. 1, Micro-Imaging Systems Division, Olympus Corporation, Tokyo, Japan

When nanoparticles are formed directly from gas phase in homogeneously, they should be condensed under supercooling with nonequilibrium state. This situation should be common for the formation of cosmic dust particles in ejecta gas of evolved stars and possibly in a plume after energetic shock in primitive solar nebula. Therefore, nucleation and growth conditions and processes of nanoparticles must be understood to model the growth and evolution of cosmic dust particles, which are actually nanometer order. In fact, however, there is very limited quantitative data concerning a homogeneous condensation from a gas phase.

One of the best methods of producing nanoparticles in gas phase is the smoke experiment, which is termed the gas evaporation method. The gas evaporation method was developed in Japan (1963) after stimulation by investigation of Kubo, which has been known as the Kubo effect, in the field of solid-state physics [1]. When an evaporant is initiated in an inert gas, rising smoke from the evaporation source can be observed. The evaporated vapor subsequently cools and condenses homogeneously in the gas atmosphere, i.e., solid particles are obtained directly from the gas cloud. So far, only temperature distribution around a hot source in an argon gas atmosphere has been measured by thermocouple without smokes and expected the condensation and terminal growth temperature of nanoparticles under the similar experimental condition except evaporant [2]. Here, we will show a first achievement of in-situ visualization of nucleation and growth environments of smoke nanoparticles using Mach-Zehnder interferometer and attempt to determine the homogeneous condensation temperature and supersaturation of several kinds of materials in gas phase.

Figure 1 shows an example of our first smoke produced in newly constructed smoke chamber. The smoke was produced by heating of a tungsten wire with 0.2 mmϕ and 70 mm depth in a mixture gas of Ar (9×10^3 Pa) and O_2 (1×10^3 Pa). Tungsten has been evaporated as oxide at the source temperature ~1200 K, which measured by pyrometer. Evaporated oxide molecules are subsequently cooled following the convection current produced by hot source and WO_3 particles have been condensed and formed the smoke. Since there is no heterogeneous nucleation cite, solid grains were obtained homogeneously from the gas cloud. The evaporated tungsten oxide vapour is concentrated at the interface between interior WO_3 vapor rich atmosphere and outer mixture gas. Their condensation temperature can be determined from the interferogram. We analyzed the produced smoke particles using TEM and recognized the formation of WO_3 single crystal nanoparticles with 20-200 nm in diameter.

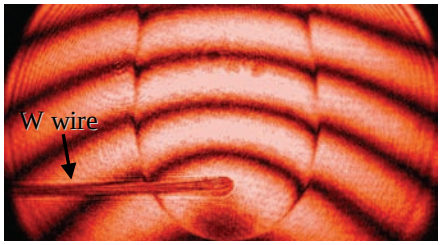

Fig. 1: Typical interferometric image of smoke particles.

[1] Kubo, R. (1962) *J. Phys. Soc. Jpn.*, **17**, 975. [2] Kaito, C. et al. (1976) *J. Appl. Phys.*, **47**, 5161-5166.

Account of chemical variability and cationic exchange in the nucleation and growth of minerals in aqueous solutions

Noguera, C.[1*], Clément, A.[2] & Fritz, B.[2]
[1]INSP, CNRS-UPMC, Paris, France ([*]noguera@insp.jussieu.fr)
[2]LHYGES, CNRS-UDS, Strasbourg, France

Chemical variability and ion exchange in mineral phases are very important geochemical processes which take place in many natural systems and are related to societal questions such as contamination of soils and ground-waters, global element cycles, hydrothermal ore-forming processes, etc. They concern both major and minor ions present in most of the natural solutions in contact with mineral phases. However the full simulation of nucleation and growth of solid-solutions in aqueous media (SS/AS), including kinetic effects in the first steps of their formation and later during their evolution, still remains a challenge.

As an extension of our previous studies of the precipitation of minerals of fixed composition [1-4], we present here a formalism which describes the precipitation for SS of the $A_{1-x}B_xC$ type, with variable composition x. It is based on the classical nucleation theory, on a size-dependent (algebraic) growth law allowing growth, resorption and ripening of particles simultaneously, and on conservation laws akin to a thermodynamically closed system [5]. At all times, one obtains a full characterization of the size and composition of the population of particles, and of the AS composition as a feed-back effect. A similar formalism applies to the description of cationic exchange in particles of clay minerals during their formation as secondary minerals. However, from the simulation point of view, the challenge is to include, in the same simulation tool, several kinetic processes with largely different time scales for mineral formation and evolution: quasi-instantaneous cationic exchange near equilibrium and longer term mineral precipitation or re-dissolution.

These approaches have been embedded in the geochemical code Nanokin that we have elaborated [3-4]. We will present results for the precipitation of solid-solutions whose end-members have either similar or very different solubilities, thus allowing distinct ion partitionings and composition profiles. We will also present some first applications for Na/Ca and K/Ca exchange in montmorillonites and illites during their precipitation.

Acknowledgements: Support of the French ANR-PNANO 2006 (project "SIMINOX" 0039) is acknowledged.

[1] Noguera, C. et al. (2006) *J. Cryst. Growth*, **297**, 180-186. [2] Noguera, C. et al. (2006) *J. Cryst. Growth*, **297**, 187-198. [3] Fritz, B. et al. (2009) *Geochim. Cosmochim. Ac.*, **73**, 1340-1358. [4] Fritz, B. & Noguera, C. (2009) in Oelkers, E. & Schott, J. (eds.) *Rev. Mineral. Geochem.*, **70**, 371-410. [5] Noguera, C, Fritz, B. & Clément, A. (2010) *Chem. Geol.*, **269**, 89-99.

Kinetics of anisotropic evaporation of forsterite

Ozawa, K.[1*], Nagahara, H.[1], Morioka, M.[2] & Matsumoto, N.[1]
[1]Dept. of Earth & Planetary Science, University of Tokyo, Japan ([*]ozawa@eps.s.u-tokyo.ac.jp)
[2]Radioisotope Center, University of Tokyo, Japan

Congruent evaporation of a condensed substance in vacuum is one of the extreme reactions where backward reactions and transport processes in the reactant can be neglected, in which only surface processes and intrinsic nature of the substance control the reaction. We have conducted a series of evaporation experiments in vacuum for crystallographically oriented forsterite, which is one of the most important constituents of the terrestrial planets, meteorites, and interstellar dusts.

The overall evaporation rate (retreat rate of averaged surface) shows anisotropy; the rate is largest for (001), intermediate for (100), and smallest for (010) with maximum difference by a factor of four between 1500 and 1750 °C. The activation energy of overall evaporation rate below 1750°C is smallest for (010) (~620 kJ/mole), intermediate for (001) (~650 kJ/mole), and largest for (100) (~680 kJ/mole). The large activation energy for overall rate from (100) comes from the comparable evaporation rates for (100) and (001) at ~1750°C and for (100) and (010) at ~1500°C. In addition to this, a high apparent activation energy for (010) above ~1750°C diminish the anisotropy in the overall evaporation rate to within a factor of 1.5.

The intrinsic evaporation rate, which is defined to be the evaporation rate from dislocation-free surface, was estimated by analysis of time-dependence of evaporation rate and by evaluating contribution of preferential evaporation around dislocations. The intrinsic rates are smaller than the overall rates for (100) particularly above ~1700°C and for (010) above ~1600°C. The difference is attributed to preferential evaporation around dislocation, which is consistent with abrupt increase in pit density for (010) above ~1750°C and gradual increase in pit density for (100) above ~1600°C. as well as that of (100) and (010). The activation energy of intrinsic rate for (010) (~610 kJ/mol) is much lower than that for (100) (~740 kJ/mol). The intrinsic evaporation rates for (001) are better fitted by higher activation energy above ~1700°C (790 kJ/mol) and lower one below ~1600°C (680 kJ/mol).

The presence of steps with height of nanometer order and variously bunched steps on (100) and (010) at all experimental temperatures and other morphological information indicate that evaporation from the two surface takes place by lateral motion of steps (layer-by-layer mechanism). The absence of steps with nanometer-scale height on (001) above ~1650°C indicate change of evaporation mechanism from layer-by-layer to detachment of evaporation units from rough surface at ~1650°C.

We infer that rough-smooth transitioin takes place at this temperature. The temperature shows good correspondence to that of change in activation energy of intrinsic rate for (001). The temperature of rough-smooth transition is inferred to be higher than ~1800°C or not realized below melting temperature of forsterite for (100) and (010).

The lower roughening transition for (100) than for (100) is in contradiction with the prediction based on the anisotropy in attachment energy. The discrepancy is attributed to a surface kinetic process, probably selective evaporation of Mg from M1 site forming SiO_4 chains along [001], which is then broken to complete evaporation (kinetic roughening).

The structure of the feldspar-feldspathoid intergrowths in the rocks of Khibiny massif

Ageeva, O.A.*, Borutzky, B.Ye. & Karimova, O.V.
Institute of Ore Geology, Petrography, Mineralogy, and Geochemistry (IGEM) RAS, Moscow (*agolga7@yandex.ru)

We used the 4-Axis Universal Stage for study of the structure of the feldspar-feldspathoid intergrowths (often concerned as pseudoleucite) which are widespread in potassic rocks of Khibiny alkaline massif (Kola Peninsula, Russia). These intergrowths are composed of parallel or differently directed lamellas of feldspathoids (kalsilite, more rare nepheline) in giant poikilocrysts of potassium feldspar (OR). The lamellas are well formed, complanate by c-axis, and extremely elongated along plane (0001). The intergrowths often contain central isometric nepheline grains (NE) with veinlet, frontal rims or unformed kalsilite inclusions (Fig. 1a). The study showed that the optical orientation of the kalsilite (kls) of both morphological types was not accidental. In most cases it was related with orientation of the intergrowing feldspar. It could be caused by some crystal structure features of these minerals.

An examination of the crystal structures minerals drew our attention to two details: 1) An existence of channels, running through their Si,Al framework: along all axes in both the feldspathoids and along directions [001], [010], [100], [101], [110], [112], [310] in feldspar. In most examined samples the c-axis (only accessible for optical detection) of kalsilite was oriented exactly along these directions in the feldspar. One case of such orientation coincidences is demonstrated (Fig. 1b). 2) A similarity of some features of their elementary cells: the angle of monoclinicity of feldspar β=116° in plane (010) is close to the angle of feldspathoid hexagonal cell γ=120° in plane (0001). The most frequent coincidence directions in the examined samples (c-axis of feldspathoid is parallel to b-axis of feldspar) reflects parallel disposition of these planes in the intergrowths. Thus, the minerals locations in these intergrowths are related by common orientation of their crystal structure elements. A structure state of the feldspar changes from low sanidine to orthoclase and microcline. Often all these modifications are found in limits of single poikilocrysts. It was noticed a tendency to fall of structure ordering in areas the kls-lamellas concentration and near the nepheline central grains.

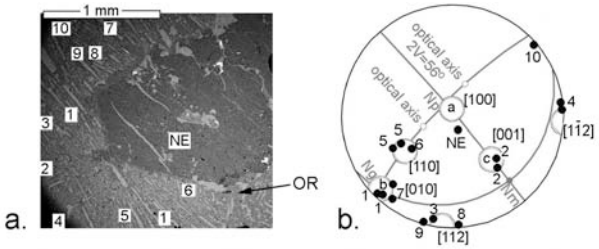

Fig. 1: a) back-scattered electron imaging: numerals mark feldspathoids of different orientations; b) their projection on the Wulff net (black points mark position of c-axis of feldspathoids), and projection of intergrowing feldspar (the circles mark the directions of its structure)

We suppose an action of ion-changing reactions through the structure channels, which results a divide into two mineral phases and an appearance of phase borders crossing the directions of their spread. It may explain the complanate (by c-axis) form of kalsilite alternating with regularly oriented feldspar. A more profound study of their growth mechanism needs to use of additional methods, including X-ray structure observations. Coming studies are directed on a detection of primary mineral (probably nepheline), stages of formation of these intergrowths in metastable feldsparization or other processes, a following collecting recrystallization, and an examination of epitaxy of the intergrowing minerals.

Superficial energy and structure of crystal-forming media

Askhabov, A.M.
Institute of Geology, Komi Science Centre, Ural Branch, RAS Syktyvkar, Russia (xmin@geo.komisc.ru)

In this work we suggest a simple way of estimation of the first amendment to superficial tension on curvature of interphase boundary.

For dependence of specific superficial energy σ from radius r of a particle the following formula is suggested:

$$\sigma = \sigma_o(1-\frac{n_S}{n}) = \sigma_o(1-\frac{2\delta}{r}),$$

where σ - specific superficial energy for flat boundary of the section. Parameter δ is treated as diameter of cluster-forming atoms, molecules or other structural units of medium, n_S - number of such units on cluster surface, n - total number of particles.

This formula in form is close to the formulas received before by Tolman within the frames of the thermodynamic capillarity theory and H.Reiss within the frames of the theory of scale units.

Accordingly, for specific superficial energy of the condensed liquid medium in which the formation of clusters (clusters of "hidden" phase or quatarons) takes place, we obtained the following expression:

$$\sigma_o^L = \frac{5.847 * 10^{-16} T}{\delta^2}, \text{ (erg/cm}^2\text{)}$$

Calculations under this formula give close to experimental values. Here from follows an interesting conclusion that knowing σ_0^L, it is possible to define diameter of cluster-forming particles (structural units). For example, for water σ_0^L = 75, 62 erg/cm^2, accordingly δ = 0,46 nanometers that corresponds to the second maximum on function of radial distribution for water. From this it follows that structural cluster-forming water unit includes 13 molecules. The optimum structure built of such quantity of molecules, is icosahedron. Similar estimations of structure give following values: for lead melt - 4, aluminum - 6, copper - 7, silver - 8, gold - 6, sodium - 9. If to interpret corresponding cluster formations in terms of polyhedrons then these are simple geometrical figures - a tetrahedron (n = 4), an octahedron (n = 6), an aligned octahedron (n = 7), a hexahedron (n = 8) etc. Actually quatarons are not steady geometrically and energetically optimized structures. These are the dynamic and usually hollow structures constantly changing their form.

Acknowledgements: This work is supported by RFBR (08-05-00346-a) and Programs of RAS Presidium and Earth Sciences Dept.

Anorthoclase twins of Mount Erebus (Antarctica)

Boulliard, J.-C.
Collection des Minéraux, Institut de Minéralogie et de Physique des Milieux Condensés, Université Pierre et Marie Curie (UPMC), Paris, France (jean-claude.boulliard@impmc.upmc.fr)

Mount Erebus volcano is well known for its anorthoclase "giant" crystals (megacrysts) and twins. So far, the albite, X-Carlsbad and Mannebach twins have been recognized. Thanks to a set of more than 400 specimens, we have improved the knowledge about the twins of this locality. Several well-known twins, not yet mentioned in this locality, have been determined. The status of the X-Carlsbad has been revisited. Two new twins have been discovered. The first one (Tazieff twin), which possesses some features of the Emfola twin, was theoretically predicted but never found. There is no mention of the second twin (Erebus twin). Statistics about the appearance of different twins have been recorded. Moreover, the study of anorthoclase twin and group habits gives rise to the opportunity to get information about several mechanisms, like the re-entrant corner effect or the oriented attachment mechanism.

Mechano-chemical effect of brucite powder in the wet super-fine grind process

Du Gao-xiang[1,2*], Xue Qiang[1], Liao Li-bing[1], Ding Hao[1] & Guo Wei-juan[1]
[1]School of Materials Science and Engineering, China University of Geosciences, Beijing, China ([*]dgx@cugb.edu.cn)
[2]Hebei Yingdu Composite Materials Co. Ltd, Xingtai, China

The mechanochemistry of brucite during wet grinding in a ball-stirred mill was studied. Raw brucite and ground brucite were characterized by XRD and FTIR. The particle size of raw brucite and ground brucite were measured. The solutions of the slurry during grinding were sampled and their Mg^{2+} contents were tested by chemical analysis. The change of Mg^{2+} content in the solution of the slurry shown that the solubility of brucite in water was increasing at the initial grinding stage, and stabilized in about 30min. The (110) peak intensity in the XRD pattern of the ground brucite decreased initially and then increased with grinding time, which was probably resulted from the recrystallization of brucite during the grinding. The FTIR absorption band of Mg-O bond for the ground brucite splits compared to that for the raw brucite, which may indicate the activation of brucite and is related to the forming of new type of Mg-O bond. Particle size measurement indicated that the mean particle size of brucite decreased and tended to be even gradually in the process of grinding.

Acknowledgements: Supported by the China postdoctoral science foundation special program (grant No.200902128) and the National Key Technology R&D Program (Grant No. 2008BAE60B06)

Trace elements in titanite: chemical (ICP-MS) studies and implications for fractional crystallization

Geraldes, M.C.[1*], Janasi, V.A[2] & Tupinambá, M.[1]
[1]Faculdade de Geologia, Universidade do Estado do Rio de Janeiro, Rio de Janeiro (RJ), Brazil
([*]geraldes@uerj.br)
[2]Instituto de Geociências, Universidade de São Paulo, São Paulo, Brazil

The present study reports a titanite grains REE compositions investigation as a function of magnetic susceptibility. This study was possible due to the ICP-MS low limit of detection for trace elements, allowing for the characterization of chemical composition in titanite magnetic fractions. With exception of Nb, all trace elements and REE have increasing content from titanite fraction M(4) to fraction M(12) (see Fig 1). Variations are: Y values range from 574 ppm to 1331 ppm. U amounts increase from 75 ppm to 243 ppm. Th amounts increase from 67 ppm to 173 ppm. Pb amounts encrease from 5 ppm to 73 ppm.

LREE (La, Ce, Pr, Nd, Sm, Eu, Gd and Tb) amounts have larger enrichment than HREE (Dy, Ho, Er, Tm, Yb and Lu) from fraction M(4) to fraction M(12). Consequently LREE have the behavior similar to compatible elements, which variations are: La from 35 ppm to 594 ppm; Ce from 136 ppm to 1969 ppm; Pr from 19 ppm to 349 ppm; Nd from 70 ppm to 1259 ppm; Sm from 22 ppm to 258 ppm; EU from 11 ppm to 76 ppm; Gd from 29 ppm to 214 ppm; and Tb from 9 ppm to 44 ppm.

HREE presented smaller variation (from 49% to 342%) than LREE. The HREE content variations are: Dy from 70 ppm to 240 ppm; Ho from 20 ppm to 51 ppm; Er from 60 ppm to 128 ppm; Tm from 13 ppm to 24 ppm; Yb from 94 ppm to 147 ppm; Lu from 14 ppm to 21 ppm.

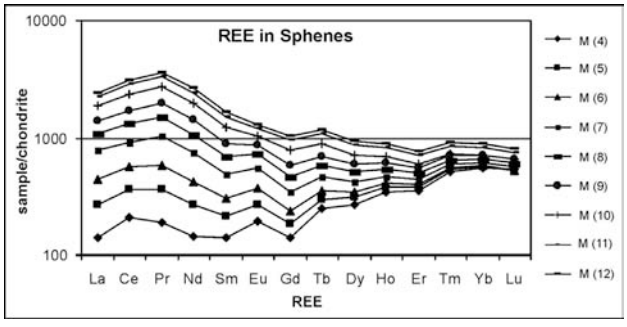

Fig. 1: Rare Earth Element patterns of titanite grains.

These results show that variations of trace elements in each titanite fractions are probably correlated to increasing amounts of these elements in the melt phase during fractional crystallization. Trace element content variations may represent part of the history of magma crystallization at the hand-sample scale, with accessory minerals playing important role in concentrating incompatible elements. As consequence, the whole rock REE pattern should be regarded as integration of a significant number of phase parameters, a fact to be taken into consideration when interpreting REE patterns in magma crystallization processes.

On the growth habit of precipitates in minerals: the normal-to-delta g principle for optimum interphase boundaries

Hwang Shyh-Lung[1*], Shen Pouyan[2], Yui Tzen-Fu[3] & Chu, Hao-Tsu[4]
[1]Dept. of Materials Science and Engineering, National Dong Hwa University, Hualien, Taiwan, ROC
([*]slhwang@mail.ndhu.edu.tw)
[2]Dept. of Materials and Optoelectronic Science, National Sun Yat-sen University, Kaohsiung, Taiwan, ROC
[3]Inst. of Earth Sciences, Academia Sinica, Taipei, Taiwan, ROC
[4]Central Geological Survey, Taipei, Taiwan, ROC

Minimization of interfacial energy is the dominant factor governing the equilibrium habit, *i.e.* orientation and morphology, of a precipitate in the parent crystal. The existing models on optimum interphase boundaries have established criteria, which minimize the lattice misfit and/or the strain energy, by comparison of the dimensions of two interpenetrating lattices. Based on a detailed analytical transmission electron microscopy study of two precipitate-matrix systems with different degrees of structural similarity in oxygen sublattices, *i.e.* hematite in rutile of an eclogite from the ultrahigh-pressure (UHP) Kokchetav terrane and magnetite in clinopyroxene of a garnet-clinopyroxenite from the UHP Sulu terrane, here we report that the optimum interphase boundary and the equilibrium habit of a precipitate in these structurally complex systems can be defined from the special geometry characteristics of diffraction patterns along specific zone axes. AEM results show that the precipitate in a parent crystal, either with or without a similar oxygen framework, always poses a specific crystallographic relationship with the differences of **g**-vector pairs (Δ**g**s), *i.e.* misfits of diffraction-spot pairs, of two structures aligned in the same direction, and that the precipitate would exhibit a growth habit plane normal to the Δ**g**s. This new insight into the interfacial energetics controlled mineral growth can be understood by the coherency of lattice planes in the interphase boundary, and rationalized by the normal-to-Δ**g**s principle originally developed for structural transformations in alloys with simple close-packed structures [1, 2]. The normal-to-Δ**g**s principle is formulated to calculate the optimum interphase boundaries in several mineral systems and gives results comparable to other models, yet in a more straightforward manner. This alternative approach can be readily applied in interphase boundary modeling of minerals and sheds light on the growth habit of mineral precipitates as a potential geothermobarometer of metamorphic rocks.

[1] Khachaturyan, A.G. (1983) *Theory of Structural Transformations in Solids.* John Wiley & Sons, New York. [2] Zhang, W.-Z. & Purdy, G. R. (1993) *Philos. Mag.*, **A68**, 291-303.

Genesis of a unique stalactite formed in a tunnel under the River Danube (Budapest, Hungary)

Kármán, K.[1,2*], Fórizs, I.[1], Tóth, M.[1], Németh, T.[1] & Szabó, Cs.[2]
[1]Institute for Geochemical Research, Hungarian Academy of Science, Budapest, Hungary ([*]anitszirk@hotmail.com)
[2]Lithosphere Research Lab, Eötvös University, Budapest, Hungary

Carbonate minerals were measured growing on the concrete tunnel under the Danube River. The examined tunnel is made of ferroconcrete. It crosses the river in the depth of 10-12 m below the bottom of the Danube at Budapest (Hungary). Inside of the tunnel two pipes carry the drinking water towards the capitol. The tunnel consists of cylinder shaped concrete elements. On several localities there are white, yellow or amber coloured dripstone formations. In these locations the water is leaking and forms stalactite or rarely stalagmite.

Five stalactite, one stalagmite and one concrete samples have been taken for X-ray diffractometric, stable C and O isotopic and optical microscopic analyses. We would have liked to know the origin of these formations.

The mineralogy of the concrete: quartz >> plagioclase, K-feldspar, calcite > phyllosilicate, gypsum. The stalactites proved to be almost pure calcite (with sporadic gypsum in tiny amount). The stalactites are very porous and brittle formations. Their stable C and O isotopic compositions ($\delta^{13}C$, $\delta^{18}O$) show very significant differences between the samples (Fig. 1), which is uncharacteristic for natural dripstones formed in one cave. The $\delta^{13}C$ (-19.2 to -30.7 ‰ vs. VPDB) and the $\delta^{18}O$ (+4.7 to +14.0 ‰ vs. VSMOW) values show exceptional depletion comparing to natural dripstones in Hungary ($\delta^{13}C$ = -4 to -11 $[‰]_{VPDB}$; $\delta^{18}O$ = (+19.5 to +25.5 $[‰]_{VSMOW}$; [1]), but they are highly similar to those of carbonate growths on concrete structures [2,3]. This observation indicates that the studied stalactites cannot be deposited from the regionally ascending old groundwater of high TDS. There is a very good linear correlation between the $\delta^{13}C$ and $\delta^{18}O$ values (see Fig. 1), which may suggest a strong kinetic isotope fractionation. Although the details of processes forming carbonate growth on concrete structures significantly depleted in ^{13}C and ^{18}O are not clearly understood, our observations indicate that the interaction between the water and concrete material plays an important role in the formation of the studied stalactites, which may shorten the life-time of the tunnel.

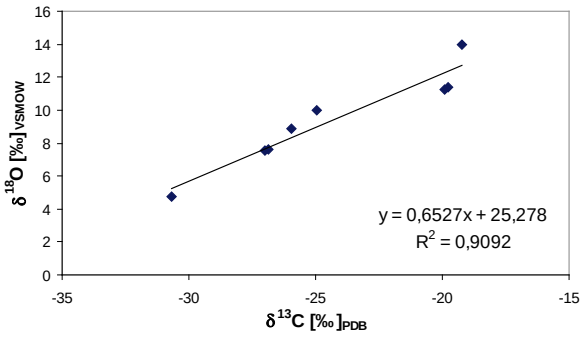

Fig. 1: $\delta^{13}C$ and $\delta^{18}O$ values in the stalactites. The good linear correlation may indicate a strong kinetic isotope fractionation.

[1] Demény, A. et al. (2010) in Bondár, M. & Raczky, P. (eds.) *Pytheas*, Budapest, 437-447. [2] Krishnamurthy, R.V. et al. (2003) *Appl. Geochem.*, **18**, 435-444. [3] Macload, G. et al. (1991) *Chem. Geol.*, **86**, 335-343.

Surface specific growth on olivine in acidic saline solutions

King, H.E.[1*], Satoh, H.[2,3], Tsukamoto, K.[2] & Putnis, A.[1]
[1]Institut für Mineralogie, University of Münster, Germany ([*]hking_01@uni-muenster.de)
[2]Dept. of The Earth and Planetary Science, Tohoku University, Sendai, Japan
[3]Mitsubishi Materials Corporation, Japan

Understanding the dissolution of olivine has important implications for a variety of areas including weathering and predicting the rate of in-situ carbon dioxide sequestration in peridotites. There are large discrepancies between laboratory determined and natural dissolution rates, which are attributed to the formation of secondary phases that armour the reactive surface. For olivine, phases such as amorphous silica [1] and hematite [2] have been previously observed during experiments at temperatures above 90°C. The majority of dissolution experiments are stirred to prevent the formation of such phases, however, the use of powdered olivine creates more reactive surfaces than would be expected in nature. The presence of parting in natural peridotites can expose specific surfaces to fluids and thus control olivine dissolution [3]. To study the rate of dissolution at different surfaces we have used real-time phase-shift interferometry (PSI, [4]). Solutions were based on a 0.1 M NaCl solution which was acidified using 0.1 M HCl to pHs between 4.7 and 1. Flow rate through the sample cell was 40 µL/min (105 µm/s). Surfaces formed when olivine crystals are broken result from conchoidal fracturing and thus are not suitable for PSI measurements due to the high surface curvature. Therefore, surfaces used in our experiments were cut from natural euhedral forsteritic olivine crystals with well defined faces from the Sapat region, Pakistan and chemically polished using hydrofluoric acid.

We observed that the dissolution increased with decreasing pH in agreement with previous dissolution studies [5]. Dissolution rates showed minimal variation with surface orientation with the exception of dissolution at pH 3 and 1 on the (021) surface. On this surface we also observed the growth of a new phase. The precipitates are a maximum size of 0.3 µm in width and present everywhere on the surface, including at etch pit sites. Thermodynamic calculations performed using PHREEQC show that the super saturated phases in the system were amorphous silica, sepiolite or talc. Raman spectroscopy was conducted to identify the precipitate. The dominance of olivine peaks could mask additional precipitate peaks. However, the spectra have some peaks which are not associated with olivine or other phases commonly associated with olivine as accessory minerals. These peaks do not correlate with those of talc or the broad peaks which are characteristic of sepiolite. Experiments of Mg-silicate growth at low temperatures typically precipitated an amorphous Mg-rich phase rather than sepiolite or talc at low pH [6]. Therefore, the phase is expected to be an amorphous hydrated Mg-silicate phase that forms from the dissolution of olivine and nucleation of the new phase at the olivine surface. The presence of the new phase appears to have limited passivating effect on the overall dissolution of olivine.

[1] Bearat H. et al. (2006) *Environ. Sci. Technol.*, **40**, 4802-4808. [2] Giammar, D.E., Bruant, R.G. & Peters, C.A. (2005) *Chem. Geol.*, **217**, 257-276. [3] Boudier, F., Baronnet, A. & Mainprice, D. (2010) *J. Petrol.*, **51**, 495-512. [4] Satoh, H., Nishimura, Y. & Tsukamoto, K. (2007) *Am. Mineral.*, **92**, 503-509. [5] Pokrovsky, O.S. & Schott, J. (2000) *Geochim. Cosmochim. Ac.*, **64**, 3313-3325. [6] Packter, A. (1986) *Cryst. Res. Technol.*, **21**, 575-585.

Mixed crystal formation by direct growth and isomorphic replacement in aqua solutions

Kryuchkova, L.Y.* & Glikin, A.E.
Dept. of Crystallography, St.Petersburg State University, St.Petersburg, Russia (*2106@list.ru)

Mixed crystal formation is featured by a permanent exchange of isomorphic components between the crystal and solution that is the universal mechanism for an inherent regulation of a crystal composition. [1,2]. The exchange proceeds either in itself or in a combination with growth (or dissolution). It is realized by simultaneous acts of epitaxial growth and dissolution distributed along the surface chaotically in a form of spontaneously alternating micro-spots, which sizes vary in the range of orders 0.1–100 micrometers. The spots walk randomly (including appearance and disappearance) all along the surface. The boundary solution acquires an inhomogeneity of a corresponding distribution and change. Overgrowths cover these surface mosaics protecting them from a homogenization. In their turn, the covers undergo the same micro-processes, and new covers bury them in a non-homogenized state, etc. As a fundamental result, mixed crystals consist of coherent blocks, which compositions vary in wide ranges gravitating to discrete values determined by specific metastable equilibria.

Mass precipitates show similar picture of crystal distribution in isomorphic composition. The distributions are characterized by a bimodality, which corresponds with a bimodality of crystal sizes [2]. The absence of intermediate fractions emphasizes size bimodality in some cases. Crystals of the smallest and biggest fractions (<10 and >100 microns respectively) are of a similar composition enriched by one of the components (which can be either more soluble or less soluble in different systems) while their abundances are brought together in intermediate fractions. Supercooling change causes a displacement of the distribution maxima without an influence on the general picture of distribution and more remarkable on the total composition of the precipitate. Thus the ratio between isomorphic compounds does not depend of growth rate immediately. Such a discrete distribution can be also interpreted in terms of composition gravitating to specific metastable equilibria.

Metastable equilibria were established between solid solutions and liquid solutions supersaturated by isomorphic substances and determined as a characteristic feature of such systems. Supercooling stops crystal dissolution causing stoppage of salting-out and growth of crystal substance with other composition. Crystals of two kinds of the isomorphic ratio can be in the equilibrium that is the reason of the compositional distribution peculiarities. Those spots on the monocrystal surface and individuals of precipitates, disposed randomly within suitable liquid portions, survive while the others dissolve.

Acknowledgements: The investigation is supported by RFBR (10-02-01303).

[1] Glikin, A.E. (2009) *Polymineral - Metasomatic Crystallogenesis.* Springer-Verlag, New York. [2] Glikin, A.E. et al. (2007) *Zapiski RMO*. Sp. iss., **7**, 7-35.

Redox-controlled element migration during subsolidus syntheses of Fe-Ti oxide samples

Langner, R.[1,2] & Lattard, D.[1*]
[1]Institut für Geowissenschaften, Universität Heidelberg, Germany (*Dominique.Lattard@geow.uni-heidelberg.de)
[2]Institut für Geologie, Mineralogie und Geophysik, Ruhr-Universität Bochum, Germany

Synthetic Fe-Ti oxide samples are useful to study the physico-chemical properties and phase relations of titanomagnetite (Tmt_{ss}), ilmenite-hematite (Ilm_{ss}) and pseudobrookite (Psb_{ss}). In most cases such samples have been synthesised at 1 bar and sub-solidus temperatures in gas mixing furnaces. The run products are polycrystalline aggregates, either single or multi-phased. Ideally, each phase should have a constant composition within each crystal as well as over the whole sample, and in multi-phased run products the crystals should be equally repartitioned over the sample. In fact, chemical and textural heterogeneities frequently occur, especially near the surface of the sample. The present study aims at identifying the processes controlling these heterogeneities.

The starting materials were mixtures of TiO_2 and either Fe° or Fe_2O_3 or both. The reagents were weighted, ground and homogenized in an agate mortar and pressed to cylindrical pellets of a few mm in diameter and height. They were fired at 1300°C at $fO_2 = 10^{-6.9}$ (ΔNNO = -0.2; established by a CO/CO_2 mixture) for various, short run durations (0.25 to 20 h). The runs were terminated by drop-quench into water. Three different bulk compositions were chosen, with Ti/(Ti+Fe) of 20, 33 or 53 atom%, which, at equilibrium, yield single phase Tmt, Tmt_{ss} + Ilm_{ss} and Ilm_{ss} + Psb_{ss}, respectively.

When the starting materials are made up of TiO_2 and Fe° (Type III), i.e. are strongly reduced, the run products display at least 3 concentric shells. The outermost shell (100 to a few hundred µm thick) consists only of Fe-rich oxides (magnetite or Tmt ± wüstite), in the other shells the bulk Fe/Ti steadily decreases towards the pellet centre. The outer shell is dense; the inner shells are more porous. These concentric shells appear already after short run durations (0.25 h), whereby the innermost shell consists of Fe°+Psb_{ss}+Rutile, i.e. is still in a reduced state. This implies that Fe must have migrated over hundreds of µm towards the surface at the very beginning of the high-temperature experiment, before fO_2 was equilibrated throughout the pellet.

When the starting materials are mixtures of TiO_2 and Fe_2O_3 (Type II), i.e. strongly oxidized, the run products display a monomineralic Ti-rich, porous outer shell that directly surrounds the central part of the pellet with the equilibrium assemblage. Since this concentric structure pattern also appears in short runs, it points to inward migration of Fe at the beginning of the experiments. It is not clear whether Ti may have also migrated in the opposite direction.

With both types of starting materials, the concentric structures remain, even after long run durations. With starting material Type II, the phase compositions re-equilibrate according to the fO_2 of the gas mixture throughout the whole pellet. With starting material Type III, however, disequilibrium assemblages persist in core regions over long run durations.

With mixtures of TiO_2, Fe° and Fe_2O_3 as starting materials (Type I) the formation of concentric shell is generally avoided, provided the original oxidation state is close to that established by the gas mixture. Already after 1 h run duration the phases have the desired chemical compositions in all parts of the pellet.

Our results show that redox-controlled element migration over hundreds of µm rapidly takes place (within a few minutes) in solid state, high-temperature reaction processes. It induces compositional gradients within the synthetic samples, which persist even if the phase compositions re-equilibrate later on.

Tracing nucleation and growth of forsterite from amorphous thin films

Oehm, B.[1], Lattard, D.[1*], Burchard, M.[1], Dohmen, R.[2], Chakraborty, S.[3] & Langenhorst,F.[4]
[1]Institut für Geowissenschaften, Universität Heidelberg, Germany ([*]Dominique.Lattard@geow.uni-heidelberg.de)
[2]Dept of Earth Sciences, University of Bristol, UK
[3]Institut für Geologie, Mineralogie und Geophysik, Ruhr Universität Bochum, Germany
[4]Bayerisches Geoinstitut, Universität Bayreuth, Germany

Observations of accretion disks of Young Stellar Objects have revealed dust of crystalline Mg-silicates, in particular of forsterite (Fo), which is assumed to result from high temperature annealing of amorphous cosmic dust particles. We are performing annealing experiments to obtain kinetic parameters of the crystallization that are necessary for the numerical modeling of accretion disks.

We use thin films obtained by Pulsed Laser Deposition (PLD) on Si (111) wafers. The thin films are completely amorphous, chemically homogeneous (on the Mg_2SiO_4 composition) and with a continuous and flat surface. They are annealed for 1 to 260 h at temperatures in the range 973-1073K in a vertical quench furnace and drop-quenched on a copper block. To monitor the progress of crystallization, the samples are characterized by AFM, SEM and TEM imaging, and IR spectroscopy.

After short annealing times (e.g. 2.5 h at 1073 K) AFM images reveal elliptical features, approx. 1 µm in diameter, with a central elevation and surrounded by a lowering of the surface. TEM images show that these features represent nucleation sites in an amorphous matrix. The IR spectra still show the broad bands of Si-O stretching modes typical of the amorphous, unprocessed silicate thin film

After e.g. 6 h of annealing at 1073 K, AFM and SEM images show circular and square features both with a central elevation. IR spectra show a few weak bands that can be assigned to crystalline Fo (bending and stretching of tetrahedra).

With increasing annealing duration planar faces appear in the former pyramidal features and the surrounding matrix evolves into domains with spherolitic appearance. IR spectra of these samples display typical bands of crystalline Fo. After longer annealing, AFM images picture the further growth of the planar faces towards idiomorphic crystals and SEM imaging shows increasing surface roughening.

The quantitative evaluation of the surface roughness of AFM images point to three evolutionary stages during annealing. The quantitative evaluation of IR spectra reveals that the Fo peaks continuously grow with increasing annealing time up to a certain duration (e.g. 64 h at 1073 K) but that no significant change appears for longer run durations.

AFM imaging proves to be a sensitive tool to detect the very first signs of crystallization and to trace its further evolution.

Experimental screening of the morphology of gypsum crystals

Ossorio, M., Van Driessche, A.E.S.[*], Garcia-Ruiz, J.M.
Laboratorio de Estudios Cristalográficos, IACT, CSIC-University of Granada, Spain ([*]sander@lec.csic.es)

Gypsum (calcium sulfate dihydrate, $CaSO_4.2H_2O$) is the most abundant sulfate mineral throughout natural earth systems and is also present in a wide range of industrial processes (e.g. construction material, fertilizer) where the morphology and size of the crystals determines the final characteristics of the product. But despites its importance in natural and artificial processes neither the growth nor equilibrium morphology of gypsum crystals are properly understood. Therefore we are currently working on identifying the factors that influence the mechanisms of nucleation, growth and, finally, the morphology of calcium sulfate in both natural and laboratory environments.

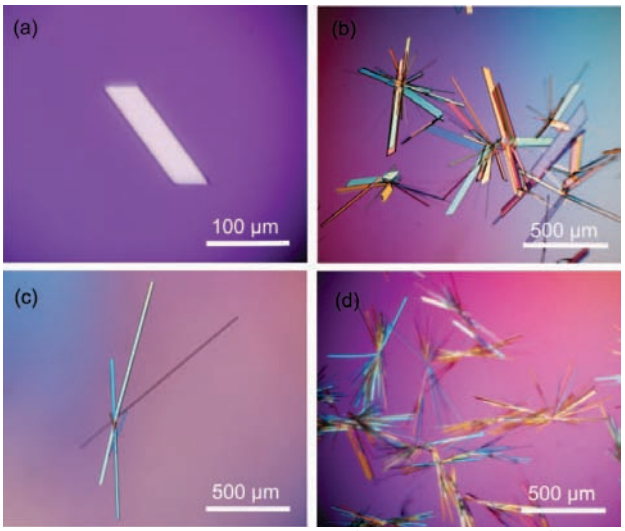

Fig. 1: Representative morphologies of gypsum crystals at different temperatures and initial supersaturation, a) 4ºC, b) 20ºC, c) 40ºC, d) 60ºC.

A series of crystallization experiments were conducted to identify the key parameters that control the growth morphology of gypsum crystals. It was found that both temperature and supersaturation have the most significant effect on the growth morphology of gypsum. This influence is explained in terms of changing growth kinetics and mass transport with varying temperature and increased nucleation at higher supersaturation.

Reactivity of iron oxide nanoparticles

Erbs, J.J.[1], Burrows, N.D.[1], Yuwono, V.M.[1], Berquo, T.[1], Banerjee, S.K.[1], Lowry, G.V.[2], Reinsch, B.C.[2], Gilbert, B. & Penn, R.L.[1*]
[1]University of Minnesota, Minneapolis, USA
([*]rleepenn@umn.edu)
[2]Carnegie Mellon University, Pittsburgh, Pennsylvania, USA
[3]Lawrence Berkeley National Laboratory, Berkeley, CA, USA

Iron oxide nanoparticles are a major source of reactive surface in many natural systems. These nanoparticles are dynamic from the perspectives of size, phase, morphology, reactivity, aggregation-state, and available reactive surface area. We quantify the kinetics of reactions between iron bearing nanoparticles and model pollutant molecules (e.g., carbon tetrachloride and 4-chloronitrobenzene) in order to elucidate the link between the physical and chemical properties of the nanoparticles with their reactivity in aqueous systems. Furthermore, we employ low temperature magnetic susceptibility, which provides a sensitive tool for detecting aggregation state for particles (prepared with and without organic coatings) in the dry state. Finally, using cryogenic transmission electron microscopy (cryo-TEM), the nanoparticles can be directly characterized in their aqueous environment, enabling in situ characterization of aggregative state. Results enable comparisons of reactivity with varying particle size, aggregation, composition, and other properties.

Following electron transfer pathways and products in iron oxide nanoparticles

Gilbert, B.[1*], Katz, J.E.[1,4], Zhang, X.[2], Attenkofer, K.[2], Zhang, H.-Z.[4], Rosso, K.M.[3], Banfield, J.F.[4], Falcone, R.[5] & Waychunas, G.A.[1]
[1]Lawrence Berkeley National Lab., Berkeley, CA, USA
([*]bgilbert@lbl.gov)
[2]Argonne National Lab., Argonne, IL, USA
[3]Pacific Northwest National Lab., Richland, WA, USA
[4]Dept. Earth & Planetary Science, UC – Berkeley, CA, USA
[5]Dept. Physics, UC – Berkeley, CA, USA

Iron oxide and oxyhydroxide nanoparticles are high-surface area minerals that are widespread in the environment. Because of the ferric/ferrous iron redox couple, these nanophases are important participants in natural redox cycles. In particular, when reducing conditions develop in soils and sediments containing iron oxide nanoparticles, the consequent changes in geochemistry and mineralogy are tightly coupled to the fate of electrons transferred to the nanophase minerals. Electron transfer and iron reduction can cause a diverse range of consequences including nanoparticle dissolution or phase change as well as secondary transformations of species such as adsorbed contaminants. Figure 1 depicts a general scheme for the fate of electrons transferred to an iron oxide nanoparticle.

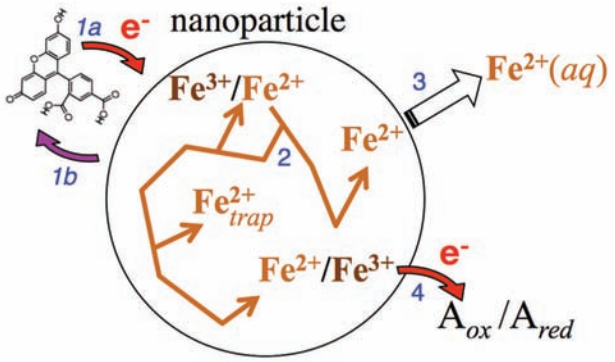

Fig. 1: Scheme depicting possible fates of an electron transferred to an iron oxide nanoparticle from a surface-adsorbed electron donor. **1a** and **1b** = forward and back electron transfer, respectively; **2** = electron mobility within nanoparticle; **3** = dissolution of ferrous iron; **4** = reduction of adsorbed electron acceptor, **A**.

The reaction products depicted in Fig. 1 are amenable to straightforward identification and quantification but transient intermediate species such as structural ferrous iron sites within the nanoparticle are inaccessible to conventional observation. The identification of transient species and measurement of their lifetimes is an important step in determining mechanisms that control the rates and yields of competing processes

We are studying the fate of ferrous iron sites created by electron transfer to ferric iron oxide nanoparticle surfaces. By adsorbing photoactive electron donor molecules to the nanoparticle surfaces, iron redox dynamics can be followed at the nanosecond timescale using X-ray spectroscopy. Our spectroscopic measurements of the chemical state and lifetime of transient ferrous iron species may be interpreted by aid of classical molecular dynamics predictions of local structure changes and *ab initio* simulations of electron mobility within iron oxides. Because nanoparticles contain a diversity of structural sites and defects, our ability to derive accurate molecular–scale models of electron transfer will be aided by complementary studies of ferric-iron containing cluster compounds.

Reactive ferrous iron in titanomagnetite ($Fe_{3-x}Ti_xO_4$) nanomaterials

Pearce, C.I.[1*], Qafoku, O.[1], Liu, J.[1], Arenholz, E.[2], Heald, S.M.[3], Felmy, A.R.[1], Ilton, E.S.[1], Droubay, T.[1], Henderson, C.M.B.[4] & Rosso, K.M.[1]

[1]Chemical and Materials Sciences Division, Pacific Northwest National Laboratory, Richland, WA, USA ([*]Carolyn.Pearce@pnl.gov)

[2]Advanced Light Source, Lawrence Berkeley National Laboratory, Berkeley, CA, USA

[3]Argonne National Laboratory, Argonne, IL, USA

[4]Daresbury Laboratory, Warrington, UK

Magnetite is a key ferrous-iron-containing mineral phase present in contaminated sediments, including at the Hanford nuclear processing site, WA, USA [1]. Magnetite can contain isostructural multivalent metal impurities and Ti(IV) is a common substituent. The resulting titanomagnetites ($Fe_{3-x}Ti_xO_4$) form a magnetite (x=0) to ulvöspinel (x=1) solid-solution series. Ti(IV) substitution is charge compensated by increasing Fe(II), and this 'tunable' Fe(II)/Fe(III) ratio affects redox reactivity with respect to the reduction of polyvalent metal contaminants such as Tc(VII).

Compositionally controlled $Fe_{3-x}Ti_xO_4$ materials were synthesized as model systems to investigate rate controlling factors in heterogeneous reduction, such as surface passivation and Fe(II) resupply: (i) thin films were deposited by pulsed laser deposition to produce crystallographically oriented, defined surfaces; (ii) bulk powders were synthesized at 900°C; and (iii) aqueous nanoparticle suspensions were synthesized under ambient conditions to produce high surface area material for batch studies. Fe(II), total Fe and total Ti content were measured by acid digestion and ferrozine/ICP-MS. *In situ* XRD, Mössbauer spectroscopy, XANES/EXAFS, and *ex situ* TEM, XPS and XMCD were also used to determine Fe(II)/Fe(III) ratios in the bulk and at the surface. Information on local coordination, bond distances and magnetic ordering allowed discrimination of different reactive ferrous iron pools, including Fe(II) in octahedral and tetrahedral sites and sorbed Fe(II). Bond lengths and charge and spin distributions calculated from first principles were used to aid interpretation. XAS confirmed that Ti(IV) entered octahedral sites in bulk titanomagnetite powders, up to x=0.94. Fe(II) increased with Ti-content, but only entered tetrahedral site when $x \geq 0.4$. XMCD showed the sensitivity of the micron-sized bulk particle surfaces to redox conditions [2]. Nanoparticle titanomagnetite accepted Ti(IV) into octahedral sites with concomitant increase in lattice Fe(II) up to x=0.35; higher x values yielded amorphous Fe(II)/Ti(IV) phases on the surface. Fe(II) release from the nanoparticles into solution increased systematically with Ti-content. At pH 8, Fe(II) release kinetics were initially fast, followed by slower apparent reabsorption of Fe(II) for $x \leq 0.35$. Reaction with Tc(VII) yielded exponentially decaying reduction kinetics with rates increasing with Ti-content. In preliminary studies, x=0 films, but not x=1 films, reduced Tc(VII) due to more facile passivation of the latter by pre-oxidation.

These collective results suggest a condition-sensitive dynamic exchange of reducing equivalents between highly interactive surface-associated Fe(II) and less accessible bulk lattice Fe(II), the relative proportions of which relate to the structural disorder and electron density redistribution caused by Ti(IV) substitution. Contaminant reduction kinetics are found to strongly depend on the availability and relative proportions of these different Fe(II) pools.

[1] Horton, D.G. et al. (2001) *Pacific Northwest National Laboratory Technical Report PNNL*-13653. [2] Pearce, C.I. et al. (2010) *Am. Mineral.*, **95**, 425-439.

Zero-field and in-field ^{57}Fe Mössbauer spectroscopy applied for study of iron oxide phases

Tuček, J.[1,2*] & Zbořil, R.[1,3]

[1]Nanomaterials Research Centre, Faculty of Science, Palacky University, Olomouc, Czech Republic ([*]jiri.tucek@upol.cz)

[2]Dept. of Experimental Physics, Faculty of Science, Palacky University, Olomouc, Czech Republic

[3]Dept. of Physical Chemistry, Faculty of Science, Palacky University, Olomouc, Czech Republic

^{57}Fe Mössbauer spectroscopy is a very sensitive experimental technique which allows monitoring the changes in the local environment of the iron atoms in the crystal lattice. Hyperfine parameters acquired from the spectral line positions, such as the isomer shift, δ, the quadrupole splitting, ΔE_Q, and the hyperfine magnetic field, B_{hf}, provide important information on the electronic density, its symmetry and magnetic properties at the ^{57}Fe Mössbauer probe nucleus. The method also yields valuable material characteristics from the widths of the spectral lines, their relative intensities, asymmetry of the spectrum, and temperature dependence of the hyperfine parameters. The valence and spin states of iron, quantification of non-equivalent iron sites in the crystal lattice, co-ordination of iron in its individual positions, level of ordering and stoichiometry, type of the magnetic ordering, orientation of the magnetic moments in external magnetic fields (*i.e.*, spin canting, spin frustration, spin nonlinearities), magnetic anisotropy, and magnetic transition temperature can be derived from the temperature-dependent zero-field and in-field Mössbauer spectra.

In this contribution, we present how Mössbauer spectroscopy is a powerful tool to study various physico-chemical properties of iron oxides and to distinguish between different crystalline polymorphs of iron oxides [1]. In particular, we show its advantages when investigating and explaining various magnetism-related physical phenomena occurring in the nanosized iron oxide materials [2,3]. A stress is devoted to in-field Mössbauer spectroscopy which brings light in some questionable areas concerning physical phenomena occurring in nanosized iron oxides and enables more precise determination of quantitative phase composition of the mixture samples based on different magnetic response of different iron oxide polymorphs when exposed under an external magnetic field. In this context, a particular attention is, for example, focused on the stoichiometry issue of magnetite and maghemite and possibilities of distinguishing between maghemite, hematite and amorphous Fe_2O_3. Some future perspectives of Mössbauer spectroscopy in the area of iron oxides are also discussed with regard to our recent research results.

[1] Zboril, R., Mashlan, M. & Petridis, D. (2002) *Chem. Mater.*, **14**, 969-982. [2] Tucek, J., Zboril, R. & Petridis, D. (2007) *J. Nanosci. Nanotechnol.*, **6**, 926-947. [3] L. Machala, L., Zboril, R. & Gedanken, A. (2007) *J. Phys. Chem. B*, **111**, 4003-4018.

Novel methods for the synthesis of magnetite nanoparticles with special morphologies and textured assemblages

Nyirő-Kósa, I.[1*], Rečnik, A.[2] & Pósfai, M.[1]
[1]Dept. of Earth and Environmental Sciences, University of Pannonia, Veszprém, Hungary ([*]kosaili@gmail.com)
[2]Jožef Stefan Institute, Ljubljana, Slovenia

Controlling the sizes, shapes and compositions of magnetite nanoparticles have become an important issue because of the technological applications that require magnetic nanoparticles with specific material properties. There are several methods for synthesising octahedral or irregularly shaped magnetite nanoparticles with sizes from ~5 to ~120 nm. In a previous study we investigated the influence of various inorganic co-precipitation processes on the sizes and shapes of nano-sized magnetite particles [1]. In the present study we synthesized magnetite crystals at low temperature by using organic compounds, including Fe(II) oxalate, ethylene glycol (EG) and tetraethylene glycol (TEG), in order to investigate their effects on the physical and chemical properties of the crystals. In all synthesis routes the magnetite crystals formed from precursor materials (sulfate or oxalate green rust) that have special morphological and textural features. The intermediate and the final products were studied using transmission electron microscopy (TEM), selected-area electron diffraction and X-ray powder diffraction.

TEM images show that magnetite nanoparticles produced under different synthesis conditions have different shapes and sizes. Crystals precipitated from Fe(II) oxalate have regular octahedral shapes. The mean particle size is 100 nm. In a synthesis route that used $FeSO_4$ as the starting material and TEG as an additive, the crystals are rod-shaped and elongated along [110]. The crystals are arranged in hexagonal-shaped clusters that have straight edges, indicating that the shape of the precursor crystal (sulfate green rust) has been conserved. Using a different amount of TEG, large rounded polycrystals of magnetite formed with irregular edges, heterogeneous contrast and a porous structure. Particles synthesized with the addition of EG instead of TEG have similar morphologies but show homogeneous contrast, suggesting that no pores are present and the particles have approximately constant thickness. The 270 nm-sized particles consist of few nm-sized crystals that attach to one another in the same crystallographic orientation, producing a diffraction pattern characteristic of a single crystal.

Our results indicate that octahedral magnetite crystals can be produced from Fe(II) oxalate in a simple co-precipitation process at low temperature. By using different kinds and amounts of polyols, various types of particle morphologies and nanocrystal textures can be produced, including hexagonal-shaped clusters of elongated crystals and porous and solid, rounded polycrystalline aggregates. Some of these products could find technological applications, for example, porous magnetite grains could be used as drug carriers.

[1] Nyirő-Kósa, I. et al. (2009) *Eur. J. Mineral.*, **21,** 293-302.

High-temperature transformation of nanocrystalline Fe- and O-based minerals

Filip, J.[*], Blechta, V., Janata, M. & Zboril, R.
Centre for Nanomaterial Research, Palacký University, Olomouc, Czech Republic ([*]jan.filip@upol.cz)

Iron oxides (hematite α-Fe_2O_3, maghemite γ-Fe_2O_3, magnetite Fe_3O_4), hydroxides ($Fe(OH)_3$), oxyhydroxides (goethite α-FeOOH, akaganéite β-FeOOH, lepidocrocite γ-FeOOH), hydrated oxide-hydroxides (ferrihydrite $5Fe_2O_3 \cdot 9H_2O$) and oxyhydroxysulfates (schwertmannite $Fe_{16}O_{16}(SO_4)_2(OH)_{12} \cdot nH_2O$) commonly forms micro- to nano-sized crystals. Aside from their unique magnetic, physico-chemical (e.g., sorption of various metals, [1]) and catalytic properties [2], they could easily be transformed into nanoparticles with specific properties [3]. We report on results of controlled and well reproducible thermally-induced solid-state transformation of all abovementioned synthetic and natural minerals under reducing atmosphere (hydrogen/forming gas) and compare it with transformations performed in air and inert atmosphere. For in-situ monitoring of high-temperature transformation we employed X-ray reaction chamber XRK900 (Anton Paar, GmbH) installed on conventional X-ray powder diffractometer. Raw and transformed material was further characterized with Mössbauer spectroscopy, BET surface area analyzer, scanning and transmission electron microscopy and SQUID magnetometer.

Generally, the HT reductive transformation of Fe(III) oxides/hydroxides/oxyhydroxides proceed towards more stable Fe(III) oxides, further to Fe(II) or mixed Fe(II)-and-(III) oxides and subsequently ends with formation of metallic α-Fe (bcc structure) nanoparticles (Fig. 1). Employing isothermal treatment we could easily control the particle-size of all particular phases formed as a result of HT transformation of any precursor.

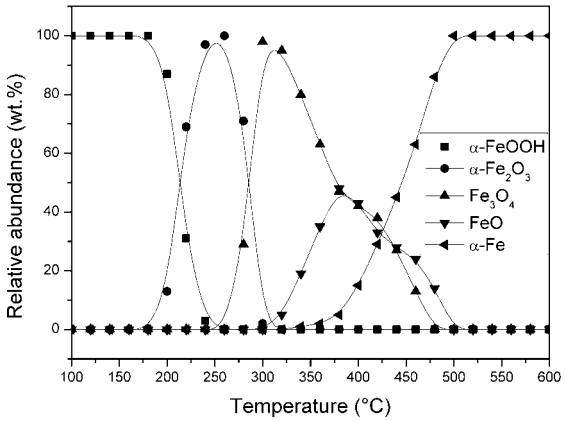

Fig. 1: Reductive transformation of goethite under hydrogen atmosphere.

Morphological study of transformed material demonstrates that the newly-formed nanoparticles or aggregates remain in the form of precursor material. Moreover, the surface properties could be modified using of controlled air-intake procedure (i.e., passivation [3]) and/or utilizing suitable surfactants and polymers [4]. The resulting nanomaterials were tested as potential catalyst for decomposition of hydrogen peroxide and as suitable agents for surface and/or ground water treatment.

[1] Cornell, R.M. & Schwertmann, U. (2003) *The iron oxides*. WILLEY-VCH Verlag GmbH & Co. KGaA, Weinheim [2] Hermanek, M. et al. (2007) *J. Am. Chem. Soc*., **35**, 10929-10936. [3] Filip, J. et al. (2007) *Environ. Sci. Technol*., **41**, 4367-4374. [4] Kvitek, L. et al. (2008) *J. Phys. Chem. C*., 15, 5825-5834.

TiO_2 nanoparticles: structure, properties, reactivity

Ponaryadov, A.
Institute of Geology of Komi SC UB RAS, Syktyvkar Russia
(alex401@rambler.ru)

Titanium minerals are interesting due to their structure and properties and the most important source of titanium, a strategic metal in modern industry. The structure, composition, and properties of nanodisperse structures of these minerals are of great interest. However several studies showed that synthetic analogues of natural oxide forms had fundamentally new structural features and physical-chemical properties. The structuring of nanodisperse forms of titanium minerals occurred due to many various geological processes that determined their genesis.

At the same time, nanosize implies isolation of the laws of formation of structures and properties of titanium minerals as compared with macrohomologs. The study of special conditions of surface reactions with the participation of organic molecules on the nanostructured titanium minerals draws attention due to potential programming of the form, dimension, texture, and even crystalline structure during crystal growth.

We have successfully synthesized TiO_2 nanoparticles with tubular structure using soft chemical treatment of commercially available anatase with sodium hydroxide solution [1]. The obtained samples have been characterized by nitrogen adsorption isotherms, XRD, TEM, UV and IR spectroscopy. Also fractal surface dimension (FSD) has been calculated. Chemical reactivity of surfaces of nanostructured systems has been studied with several test reactions including preferential CO oxidation.

According to XRD nanostructured samples do not show the crystal structure of initial material. Noticeable widening of peaks is present due to formation of nanosize particles. On TEM images titanium dioxide nanotubes of spiral type are clearly observed.

The specific surface area calculated by BET method from nitrogen adsorption isotherms enlarged from 87, for initial anatase powder, to 221 m^2/g for TiO_2 nanotubes [2]. According to obtained FSD values the surface of nanstructured samples became smoother.

CO conversion on nano-TiO_2 was studied in temperature region 323–673 K by IR spectroscopy using Nicolet Impact 400 spectrometer. Self-supporting wafers of the samples were heated up to 673 K in situ in IR cell for 1 hour at He, cooled to room temperature and diffusion reflectance spectra of the wafer were determined in the presence of 1.8%O2/3.29%CO/He flow.

The reaction of CO oxidation on active surface sites was studied. We obtained more than 60 % CO conversion instead of 11 % on regular form of titanium dioxide [2].

Thus, nanostructured titanium dioxide is considered to be a specific substance form, which physical and chemical characteristics differ from regular anatase. New geotechologies could be based on these unique properties.

[1] Ponaryadov, A. & Kotova, O. (2009) *Dokl. Earth Sci.*, **425A(3)**, 664-667. [2] Kotova, O. & Ponaryadov, A. (2009) *J. Mining Sci.*, **45(1)**, 93-98.

An efficient, selective and low cost method for the adsorption and separation of Lanthanum Rare Earth Metal Ion using Iron (II) sulfide coated on magnetite nanoparticles

Bagheryan, S.
Islamic Azad University - Aligudarz Branch, Aligudarz, I.R.Iran (syamak.bagheryan@gmail.com)

A novel iron sulphide adsorbent using magnetite embedded with nanosized Fe_3O_4 was prepared and applied to separate lanthanum (III) from aqueous solution. This adsorbent combines the advantages of magnetic nanoparticle with magnetic separability and high affinity toward rare earth metals, which provides distinctive merits including easy preparation, high adsorption capacity, and easy isolation from sample solutions by the application of an external magnetic field. The effect of pH, contents of loaded iron sulphide nanoparticles, ionic strength, contact time, and temperature on adsorption capacity of the magnetic beads was investigated. Complexation, ion exchange and electrostatic interaction were all believed to play a role in lanthanum adsorption on magnetic beads. We hope that this procedure will be applicable for mineral processing and economically mineralization.

Synthesis and aging of nanocrystalline FeS

Csákberényi-Nagy, D.[1*], Maróti, B.[1], Rečnik, A.[2], Samardžija, Z.[2] & Pósfai, M.[1]
[1]Dept. of Earth and Environmental Sciences, University of Pannonia, Veszprém, Hungary ([*]dorottka@gmail.com)
[2]Jožef Štefan Institute, Ljubljana, Slovenia

Nanocrystalline iron sulfides typically form in anoxic marine sediments. The iron sulfide initially forms as disordered mackinawite (FeS) that converts to greigite (Fe_3S_4) [1], which, in turn, converts to pyrite (FeS_2) [2]. In order to better understand the structural, morphological and compositional changes associated with these transitions, we studied synthetic iron sulfides that were precipitated from hydrous solutions at room temperature. The products were studied using scanning and transmission electron microscopy, selected-area electron diffraction and X-ray powder diffraction.

Freshly precipitated iron sulfide is typically poorly crystalline, and forms aggregates of disordered, curved sheets (Fig. 1a). The sheets consist of 3-6 layers that are structurally likely similar to the tetrahedral iron sulfide layers that occur parallel to (001) in mackinawite. However, their spacings are significantly larger (5.4 to 5.5 Å) than d(001) in crystalline mackinawite (5.03 Å). As the material is aged in solution, the spacing between the individual layers decreases and the particles adopt a distinctly crystalline, platy shape (Fig. 1b). After ten months aging, the structure of the platy crystals is consistent with that of greigite. In the course of transition from poorly crystalline FeS to greigite, ordered mackinawite was never observed. Samples that were cured in an autoclave at 200°C transformed to greigite within a few hours, but the mechanism of transformation appeared to differ from that in the aged samples, since the products included both larger greigite crystals and sheets of poorly crystalline iron sulfide.

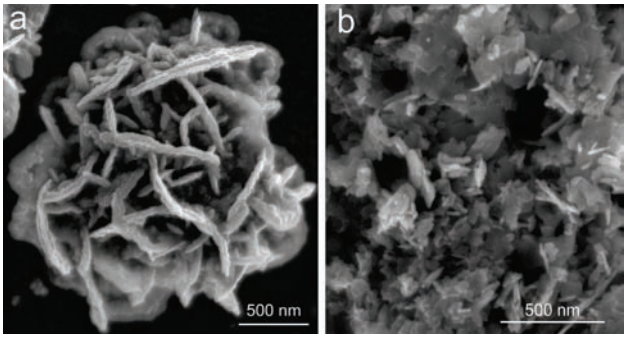

Fig. 1: Scanning electron microscope images of nanocrystalline iron sulfides (a) immediately after precipitation, and (b) after aging in solution for 10 months.

Our results indicate that while the crystallinity of iron sulfide increases during aging, the transformation from poorly ordered sheets to greigite platelets results in a reduction of the sizes of distinct morphological units. Iron sulfides can act as sinks for trace metals either by coprecipitation or adsorption both in marine sediments and in contaminated environments; however, our results suggest that the incorporation or adsorption of metals may vary with the age of the precipitate because of the complex structural and morphological changes during aging. Further studies are in progress on the incorporation of trace elements in iron sulfides.

[1] Hunger, S. & Benning, L.G. (2007) *Geochem. Trans.*, **8,** 1-20. [2] Lennie, A.R. et al. (1997) *Am. Mineral.*, **82,** 302-309.

Chrysotile and imogolite: Quantum mechanical *ab initio* study of structure and energetics

Demichelis, R.[1*], Noel, Y.[2], D'Arco, P.[2] & Dovesi, R.[1]
[1]Dipto. di Chimica IFM, Università di Torino and NIS – Nanostructured Interfaces and Surfaces – Centre of excellence Torino, Italy ([*]raffaela.demichelis@unito.it)
[2]Institut des Sciences de la Terre de Paris (UMR 7193 UPMC-CNRS), UPMC - Paris Universitas, Paris, France

A recent implementation in the CRYSTAL code of the helical symmetry exploitation in quantum mechanical simulation of nanotubular systems allows the investigation of inorganic nanotubes at the *ab initio* level, using rich Gaussian Type basis set and hybrid functionals, with a relatively reduced computational cost [1-4].

Single-walled chrysotile ($Mg_3Si_2O_5(OH)_4$) and imogolite ($Al_2(OH)_3SiO_3OH$) nanotubes with different radius and chirality were studied with hybrid B3LYP functionals and Gaussian-type basis sets (6-31G* for chrysotile, larger VDZ-type for imogolite). Details regarding the calculation costs and the efficacy of the adopted strategy are presented (see Table 1).

Table 1: Effect of the point symmetry exploitation in the simulation of chrysotile [2]

	Radius, Å	N_A	N_{AO}	N_R	t_{SCF}, s	t_{GRAD}, s
[001] slab	∞	18	236	1	1033	9801
chrysotile	35.13	864	11328	48	1901	12025

N_A, N_{AO}, N_R: number of atoms, atomic orbitals, helical operators in the unit cell; t_{SCF}, t_{GRAD}: cost of a single SCF step and of the gradient calculation. (1CPU - Intel Xeon, 1.86GHz, RAM 8Gb - B3LYP).

The stability with respect to the ideal 2D-layers (lizardite mono-layer for chrysotile, hypothetical structure containing a gibbsite-like hexagonal layer linked to asilanolic unit for imogolite) is investigated and the role of hydrogen bonding (HB) and Si-O bonds in the stabilization of imogolite tubes is discussed.

Different rolling polarities (chrysotile) and directions (imogolite) are explored. Chrysotile results less stable than the flat layer for all the radii within the range 20-35 Å, whereas all the considered imogolite tubes are more stable than the flat reference structure. Both the explored rolling directions of imogolite (zigzag and armchair) present a minimum energy structure, which seems to be the result of three main factors: SiO_4 rigidity, HB setting (zigzag only), and electrostatic repulsion among apical oxygen atoms (inner wall of the tubes).

HBs and orientation of the silanolic group inside the tube play an important role in stabilising imogolite. The zigzag minimum energy structure (10,0) is 10.6 kJ/mol per formula unit more stable than the armchair one (8,8), the difference being due, at least partially, to the formation of hydrogen bonds in the inner wall of the tube. Two curves are observed in the zigzag case, whose minima, both at n=10, are separated by 2.01 kJ/mol per formula unit. These two structures are extremely similar, the main difference being the orientation of the OH unit pointing inside the tube.

[1] Noel, Y. et al. (2010) *J. Comp. Chem.*, **31**, 855-862. [2] D'Arco, P. et al. (2009) *J. Chem. Phys.*, **131**, 204701 [3] Demichelis, R. et al (2010) submitted. [4] Noel, Y. & Demichelis, R. (2010) "Nanotube systems", www.crystal.unito.it/tutorial/nanotube

The influence of synthesis condition on the supermolecular structures of silica. Mechanism of self-assembly of the structural units of opal-like materials

Kamashev, D.V.
Komi SC UB RAS, Institute of Geology, Syktyvkar, Russia (kamashev@geo.komisc.ru)

The problems of silica supermolecular matrix synthesis arouse recently a certain interest. It is connected, on the hand, with the fact that such structures can be used in the synthesis of noble opal analogues, on the other hand they are the most convenient examples for modeling the processes of supermolecular crystallization. The problems of study of supermolecular structures generation arouse a certain interest, since recently they find a more broad application in different spheres of chemistry, physics, including their application as matrices for nanocomposite materials. The available data on the mechanism of formation of supermolecular structures and their components is insufficient which connected with certain difficulties of their analysis.

In the present work, on the basis of experimental data, we considered the influence of different physical and chemical conditions of supermolecular structures synthesis on the sizes and morphology of resulting silica particles, and also the features of their precipitation into well-ordered structure. On the basis of the obtained results we suggested the model of spherical particle structure.

The formation of monodisperse silica spheres was based on Stober-Fink method [1], which we improved [2]. Three series of experiments were conducted. The first series was conducted under 18°C, all the preparation of tetraethyl ortosilicate came to its preliminary purification through distillation. The second series was conducted like the first one but under 8°C. The third series was conducted using TEOS processed with combined method [2], in concentration interval (0.04÷4.75) mole/dm^3 for NH_3 and (1.5÷31.8) mole/dm^3 for H_2O, with the constant concentration of tetraethyl ortosilicate of 0.28 mole/dm^3 and of the temperature at 18ºC. Just in this series we were able to obtain monodisperse silica spheres in the wide ratio of the system components: (0.2÷0.8) mole/dm^3 for NH_3 and (2.75÷6.4) mole/dm^3 for H_2O and hence in the wide size range of 235-765 nm. At lower temperatures and also beyond, the suggested concentration interval the disturbance of both monodisperses and of spherical form of particles occurred.

The oscillation of dependence of particle sizes on the concentration of the system components: TEOS-C_2H_5OH-NH_3-H_2O along with the discreteness of sizes of resulting particles let us suppose the following mechanism of spherical particle structure. According to concepts of cluster self-organization of matter at nanolevel [3], ultradisperse particles of the size, typical for opal balls, are composed of much smaller particles than mentioned above 10 nm. The sizes of these particles depend on the satiety of solution and in amorphous state can reach about 2.4 nm. Accordingly all the compact amorphous formations can be formed resulting from hierarchical aggregation. In the first case, when clusters are located around the central one, cluster aggregation of the 1st hierarchical level is formed. In the same way the cluster of the 2nd level is formed, etc. Thus, we interpret the formation of silica spheres as the process of hierarchical self-organization of matter at nanolevel.

Acknowledgements: The work has been completed with the partial support of RFBR (grant № 08-05-00346a) and Program of Presidium RAS №27 (09-П-5-1028).

[1] Stober W., Fink A. & Bohn E. (1968) *J. Coll. Interface Sci.*, **26**, 62-69. [2] Kamashev D.V. & Askhabov A.M. (2000) *Vestnik Inst. Geol.- Syktyvkar*, **12**, 7-9. [3] Askhabov A.M. & Ryazanov M.A. (1998) *Dokl. Russ. Acad. Sci.*, **362(5)**, 630-633.

Response of clays on their long-term thermal treatment in open and closed systems

Valter, M.* & Plötze, M.
Institute for Geotechnical Engineering, ClayLab
ETH Zurich, Switzerland (*martin.valter@igt.baug.ethz.ch)

Clays are used in various applications. In many of them it is necessary to preserve their unique properties for long periods of time, e.g. in radioactive waste disposal. The presented work is focused on time dependent changes in different properties of various clays during long-term thermal treatment under near field relevant conditions. The clays under investigation are: Na-bentonite MX-80, Ca-bentonite Calcigel, Na-smectite Cloisite, vermiculite, illite and kaolinite. The clays are stored at temperatures between 50 °C and 200 °C. One group of samples is treated in an open system and the other group in closed containers with different water saturation states. Changes are expected in such parameters like cation exchange capacity and layer charge but also in related properties. Furthermore, physical parameters will be analyzed, e.g. the surface area, swelling behaviour and the thermal conductivity.

First results for MX-80, Calcigel and Cloisite show different responses on thermal treatment. The CEC of MX-80 and of Calcigel decreases during the first 4 - 32 weeks of heating. However, with longer heating the CEC gains back even at higher temperatures (Fig. 1). Cloisite, on the other hand, shows a weak but opposite tendency. The MLC of the smectites changes insignificantly and without obvious trends even after more than one year of heating.

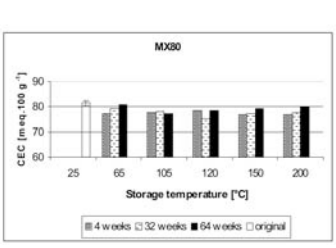

Sample	MLC
MX80 original	0,29
Week 4_Temp. 65°C	0,28
_T105°C	0,28
_T120°C	0,28
_T150°C	0,27
_T200°C	0,27
Week 32_Temp. 65°C	0,29
_T105°C	0,28
_T120°C	0,28
_T150°C	0,28
_T200°C	0,28
Week 64_Temp. 65°C	0,28
_T105°C	0,27
_T120°C	0,27
_T150°C	0,27
_T200°C	0,27

Fig. 1: Evolution of CEC and mean layer charge of MX-80 during thermal treatment (open system).

The development of CEC cannot be explained (only) by changes in MLC. Presumably, cations in the interlayer/ ditrigonal cavities in the tetrahedral sheet are stronger bound thus preventing their exchange. Beside possible edge effects, a further process can be the formation of interlayers which are no longer accessible for the exchanging Cu-complex solution, e.g. due to occurring cementations or clay mineral transformations, i.e. formation of hydroxy-interlayered clay minerals. The evolution of water vapour adsorption is the same for all investigated clays: the adsorption ability decreases with increasing temperature but independent from heating time. XRD and FTIR investigations, the study of water uptake and swelling behaviour will give further insight to explain this phenomenon.

Thermal stability and phase transition of natural Na- and Ca-montmorillonites from China, an *in-situ* XRD study under non-ambient condition

Wang Heijing[1*], Zhou Jian[2], Li Ting[1], Wang Mingzhen[1] & Fan Erping[1]
[1]School of Earth and Space Sciences, Peking University, Beijing, P. R. China (*hjwang@pku.edu.cn)
[2]Chinese Academy of Geological Sciences, Beijing, P. R. China

Two natural specimens of Na- and Ca-montmorillonite (Mnt hereafter) were collected from NW and central China [1] for physical properties research [2]. SEM and EDS analyses reveal flake-like habits of both Na- and Ca-Mnts with formulae of $K_{0.1}Na_{0.40}Ca_{0.08}(Mg_{0.54}Al_{1.44})_{1.98}(Al_{0.19}Si_{3.81})_4O_{10}(OH)_2$-$xH_2O$ and $Ca_{0.20}(Fe_{0.13}Mg_{0.72}Al_{1.40})_{2.25}(Al_{0.40}Si_{3.60})_4O_{10}(OH)_2$-$xH_2O$, respectively. The *in-situ* XRD technique was used to investigate the thermal stability and phase transition of these two typical specimens under non-ambient conditions. From room-temperature to 900°C the XRD patterns were measured at 5, 10 and 25°C intervals depending upon the gaps of phase transitions. Deconvolution technique was used to quantitatively measure the ratio of 6-water Mnt to 4-water Mnt and that of 4-water Mnt to paragonite- and margarite-like micas.

With increasing temperature from room condition to 900°C, both Na- and Ca-Mnts dehydrate and change into 9.6-9.7Å mica and finally collapse into glass. Na-Mnt dehydrates from 6-water Mnt into 4-water one in a range of 90-135°C and from 4-water Mnt into paragonite-like mica in range 175-240ºC, whilst Ca-Mnt dehydrates from 6-water Mnt into 4-water one in range 40-85°C and from 4-water Mnt into margarite-like mica in 150-350°C respectively. At a little bit higher than 875°C, both paragonite- and margarite-like micas entirely collapse into black glass and yellow glass, respectively.

There exists a "step" relation between the position of "first basal reflection" of Mnts and corresponding temperature, in which there are three plateaus and two slopes. The first plateau is the stable section of 6-water Mnt, the second plateau renders that of 4-water Mnt and the third one is that of 9.6-9.7Å mica respectively, whilst the first slope indicates the transition from 6-water Mnt into 4-water one and the second slope describes the transition of 4-water Mnt into 9.6-9.7Å mica, respectively. With the help of regression analysis four equations were derived for the two slopes as:

$$d_{6/4\text{water-Na-Mnt}}(Å) = -0.461\ T(ºC) + 66.77 \quad (1)$$
$$d_{4\text{water-Na-Mnt/mica}}(Å) = -0.269\ T(ºC) + 64.958 \quad (2)$$
$$d_{6/4\text{water-Ca-Mnt}}(Å) = -0.197\ T(ºC) + 26.259 \quad (3)$$
$$d_{4\text{water-Ca-Mnt/mica}}(Å) = -0.028\ T(ºC) + 18.385 \quad (4)$$

There exist a series of correlations between the amount (integrated intensity percentage) of 6-water specimen in total Mnts, amount of 4-water specimen in the mixture of Mnt and 9.6-9.7Å mica and corresponding temperature:

$$T(°C) = 134.36 - 0.435M_{6/4\text{water-Na-Mnt}}(\%) \quad (5)$$
$$T(°C) = 83.84 - 0.477M_{6/4\text{water-Ca-Mnt}}(\%) \quad (6)$$
$$T(°C) = 239.98 - 0.661M_{4\text{water-Na-Mnt/mica}}(\%) \quad (7)$$
$$T(°C) = 153.85 - 0.384M_{4\text{water-Ca-Mnt/mica}}(\%) \quad (8)$$

Assuming that the situation of natural Mnts in air-dried condition could represent their thermal stability of formation, the Na-Mnt from NW China and the Ca-Mnt from central China would originate in a temperature range of 135-175°C and 85-150°C respectively.

[1] Xu, G.Q. et al. (1994) in Xu, G.Q. et al. (ed.) *Selected bentonite deposits in China*. Nuclear Industry Press, Beijing, 186-190. [2] Balek, V. et al. (2002) *Appl. Clay Sci.*, **21**, 295-302.

De-hydroxylation of kaolinite to metakaolin – a molecular dynamics study

Sperinck, S.*, Raiteri, P., Marks, N. & Wright, K.
Nanochemistry Research Institute, Dept. of Chemistry, Curtin University of Technology, Perth, Australia
(*shani.sperinck@postgrad.curtin.edu.au)

Kaolinite, $Al_4[Si_4O_{10}](OH)_8$, is a 1:1 dioctahedral phyllosilicate material and is the main component of the kaolin group of minerals. Calcining kaolinite at temperatures between 450ºC and 750ºC produces metakaolin – a 2-dimensionaly ordered, highly pozzolanic state that is used in the food-processing industry, oil shale processing, and ceramics and as a feedstock for geopolymer cement. The transformation is characterized by a complete de-hydration of the structure, loss of crystallinity and a concomitant change in aluminium coordination from octahedral to tetrahedral.

This transformation of kaolinite to metakaolin has been investigated using molecular dynamics (MD) simulations with an empirical force field that accurately produces the experimental kaolinite structure. Starting from the kaolinite structure (Fig. 1) we performed a series of NPT runs with increasing levels of de-hydroxylation to understand the effects on the structure of kaolinite and the change in aluminium coordination. Our study shows, for the first time, the atomic mechanisms underpinning the loss of crystallinity, which occurs during the de-hydroxylation of kaolin to metakaolin (Fig. 2).

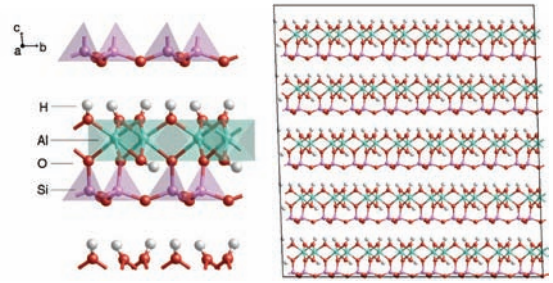

Fig. 1: Layered structure of kaolinite (left) and the initial simulation cell prior to de-hydroxylation (right).

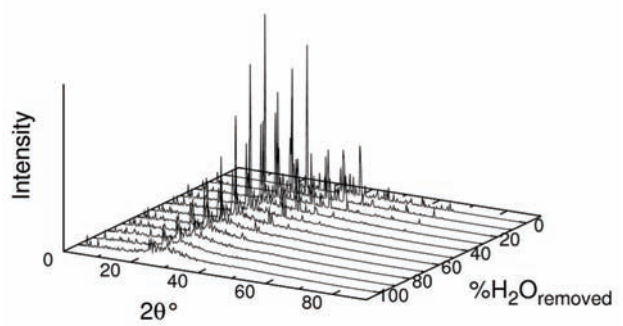

Fig. 2: Simulated x-ray diffraction data showing the loss of crystallinity.

Intercalation and dynamics of hydrated Fe^{2+} in the vermiculites from Santa Olalla and Ojén (Spain)

Lerf, A.[1*], Wagner, F.E.[2], Poyato, J.[3] & Pérez-Rodríguez, J.L.[3]
[1]Walther-Meissner-Institut, Bayerische Akademie der Wissenschaften, Garching, Germany
(*anton.lerf@wmi.badw.de)
[2]Physik-Department, Technische Universität München, Garching, Germany
[3]Instituto de Ciencia de Materiales de Sevilla, Consejo Superior de Investigaciones Científicas-Universidad de Sevilla, Spain

Whereas the uptake of Fe^{3+} into vermiculites and smectites via ion exchange is notoriously difficult and accompanied by the deposition of iron oxyhydroxides on the external surfaces of the phyllosilicate particles [1], the insertion of Fe^{2+} is much easier. To reduce the tendency towards oxidation one can carry out the ion exchange under nitrogen or one can use Fe^{2+} salts (e.g. gluconate) which are less sensitive to oxygen. The vermiculites were treated twice for one hour with freshly prepared Fe^{2+} solutions. Afterwards the solid was washed at least five times with deaerated water and dried. The samples so obtained were stable against oxidation for months when stored in closed vessels (no special protection against air).

The Mössbauer spectrum at room temperature (Fig. 1) looks like the typical spectrum of a vermiculite. Just the peak at ~2.5 mm/s belonging to the quadrupole doublet of the Fe^{2+} site gets slightly broader towards higher quadrupole splitting and increases in intensity slightly.

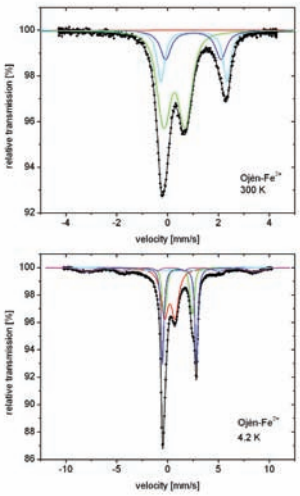

Fig. 1: Mössbauer spectra of the Fe^{2+} intercalated Ojén vermiculite at room temperature (top) and at 4 K (bottom). Dots are the data points, the solid lines marks the individual components as obtained from the fit to the data points.

At 4 K the right of the peak at 2.5 mm/s (Fig. 1) increases dramatically in intensity and the quadrupole splitting of this new site (~3.3 mm/s) can be assigned to the hydrated Fe2+ ions. The dramatic increase in intensity as a function of temperature is mainly due to a strong rise of the Mössbauer-Lamb factor at low temperature, indicating that the Fe2+ ions, which are highly mobile at room temperature, are frozen in definite lattice sites at low temperature. We will discuss also the temperature dependence of the rise of the Mössbauer-Lamb factor with increasing temperature.

[1] Ramírez-Valle, V. et al. (2008) *Clay Miner.*, **43**, 487-499.

High-pressure phase transitions in serpentines

Bezacier, L.*, Caracas, R. & Reynard, B.
ENS Lyon, CNRS, Lyon, France (*lucile.bezacier@ens-lyon.fr)

Serpentines are formed by interaction of water with basic to ultrabasic rocks under conditions that range from shallow (<10 km) ocean floor hydrothermal systems to intermediate depths (150-200 km) of subduction zones. Several Raman and X-ray diffraction data on various serpentine varieties at pressures up to 10 GPa [1-3] suggested phase transformations that were recently confirmed by single-crystal X-ray diffraction on antigorite [4]. DFT calculations on lizardite [5] suggested phase transformation at higher pressures.

We performed first-principles calculations on lizardite using the generalized gradient approximation (GGA) of the density functional theory as implemented in the ABINIT package based on plane waves and pseudopotentials. We compute the lattice dynamical properties, the phonon frequencies and the atomic displacement pattern of the vibrational modes within the density functional perturbation theory.

Results of DFT calculations are compared with former and new high-pressure Raman spectroscopic data and with X-ray diffraction data. They show good agreement on phase transitions observed below 10 GPa. Consequences for serpentine seismic properties and detection in subduction zones are discussed.

[1] Auzende, A.L. et al. (2004) *Phys. Chem. Mineral.*, **31**, 269-277. [2] Hilairet, N. et al. (2006a) *Geophys. Res. Lett.*, **33**, L02302. [3] Hilairet. N. et al. (2006b) *Phys. Chem. Mineral.*, **33**, 629-637. [4] Nestola, F. et al. (2010) *Contrib. Mineral. Petrol.*, **60(1)**, 33-43. [5] Mookherjee. M. & Stixrude, L. (2009) *Earth Planet. Sci. Lett.*, **279**, 11-19.

High-pressure transformations in kaolinite

Welch, M.D.[1*] & Crichton, W.A.[2]
[1]The Natural History Museum, London, UK
(*mdw@nhm.ac.uk)
[2]European Synchrotron Radiation Facility, Grenoble, France

Polytypic transformations are a key aspect of the crystallography and stability of sheet silicates. However, their physical significance in natural systems at high *P* is largely unexplored.

Kaolinite, $Al_2Si_2O_5(OH)_4$, is a hydrous sheet-silicate of considerable geological, industrial and technological importance. While numerous studies of its ambient and near-ambient stability and geochemistry have been made, almost nothing is known about its *P* response. Recent modelling of kaolinite stability by *ab initio* methods [1,2] has predicted a sequence of polytype stability as a function of *P*: kaolinite ("kaolinite-I", polytype 11a of [1])→ "kaolinite -II" (polytype 5a or 7a of [1])→ "kaolinite -III" (polytype 18 of [2]). Unlike kaolinites I and II, kaolinite–III has trifurcated interlayer H-bonds that arise from the operation of an unusual layer stacking vector and the production of a new kind of polytype.

We have studied the behaviour of Keokuk kaolinite (space group *C*1) to 8 GPa at 298 K using synchrotron X-ray powder diffraction and a diamond-anvil cell [3]. Two transformations were encountered: kaolinite-I → kaolinite -II at 3.7 GPa and kaolinite-II → kaolinite -III at 7 GPa. The two high-*P* phases were identified from calculated diffraction patterns based on the model polytype structures listed by [1,2]: kaolinite-II is the 5a polytype of [1], and kaolinite-III is the one-layer model 18 polytype of [2]. Thus, experiment has confirmed the predictions of *ab initio* modelling.

Both transformations involve layer translation without rotation. Kaolinite I↦II involves the removal of unfavourable vertical cross-interlayer Al-Si superpositions, and so is analogous to the 2.7 GPa transformation in dickite [4]. Kaolinite II→III involves the formation of a new kind of polytype, which has a very different hydrogen-bonding topology and layer stacking from kaolinites I and II. Kaolinite-III can be quenched to ambient conditions from 7.8 GPa. Its ambient density of 2.77 g/cm^3 is 6% higher than those of kaolinite-I, dickite and nacrite; thus, it is a significantly collapsed structure.

Bulk and linear moduli for kaolinites I and III were obtained from compression curves of the EoS study. Unit-cell parameters were obtained by refinement of powder diffraction patterns and fitted to a 2nd-order Birch-Murnaghan EoS (K' = 4).

Kaolinite-I: K_0 = 59.7(0.7)GPa, K_a = 88.6(3.5)GPa, K_b = 85.4(2.8)GPa, K_{001} = 34.6(0.5)GPa.

Kaolinite-III: K_0 = 50.2(1.5)GPa, K_a = 63.3(4.1)GPa, K_b = 54.8(1.6)GPa, K_{001} = 38.2(1.2)GPa.

The higher compressibility (lower K_0) of kaolinite-III is due to softening parallel to the polyhedral sheets.

[1] Mercier, P.H.J. & Le Page, Y. (2008) *Acta Cryst.*, **B64**, 131-143. [2] Mercier, P.H.J. & Le Page, Y. (2009) *Mat. Sci. Tech.*, **25**, 437-442. [3] Welch, M.D. & Crichton, W.A. (2010) *Am. Mineral.*, **95**, 651-654. [4] Dera, P. et al. (2003) *Am. Mineral.*, **88**, 1428-1435.

Trioctahedral micas: relationships between crystal chemistry and magnetic behaviour

Affronte, M[1], Brigatti, M.F.[2], Malferrari, D.[2*], Marcelli, A.[3] & Pini, S.[2]
[1]Dipto. di Fisica, Università di Modena e Reggio Emilia, Modena, Italy
[2]Dipto. di Scienze della Terra, Università di Modena e Reggio Emilia, Modena, Italy ([*]dmalf@unimore.it)
[3]Istituto Nazionale di Fisica Nucleare, Laboratori Nazionali di Frascati, Italy

This study is aimed at verifying the factors affecting magnetic susceptibility χ variation in micas in relation to: I) Fe content; ii) Fe^{2+}/Fe^{3+} ratio; iii) occurrence of Fe in tetrahedral and octahedral sites, outlining possible ordering effects.

Other aspects considered in our study will involve: i) eventually observed variation in magnetic properties for samples showing similar chemical composition, but occurring from different areas and different crystallization environments; ii) possible influence of strong magnetic anomalies over magnetic properties of samples therein occurring.

All these aspects were thus addressed by characterizing samples belonging to phlogopite – annite, tetra-ferri-phlogopite – tetra-ferri-annite and polylithionite – siderophyllite series. Some samples, representative of the whole sample set, were then selected for magnetic susceptibility characterization. Some of them also required calorimetric analyses, in order to better describe and understand their behaviour.

Other experimental methods used in this investigation include: electron microprobe, structure resolution by X-ray single crystal methods, X-ray absorption spectroscopy, with a particular attention to the understanding of the XANES region.

Main results demonstrate that: i) magnetic phenomena associated with maxima of magnetic susceptibility could be observed at low temperature (T<10 K) and weak magnetic field (10 Oe); ii) magnetic properties depend not only on the total Fe content. Samples where Fe is mostly in octahedral coordination are predominantly ferromagnetic, strongly depending on the $[6]Fe^{2+}/([6]Fe^{2+}+[6]Fe^{3+})$ ratio, which was observed to increase with Curie-Weiss θ constant (ranging from 13 to 24 K and from 4.4 and 5.2 K for samples showing higher and lower $[6]Fe^{2+}/([6]Fe^{2+}+[6]Fe^{3+})$ ratio, respectively). In tetra-ferri-phlogopite, dominant interactions were observed to be anti-ferromagnetic, as shown by a negative Curie-Weiss θ constant value (-25 K). Furthermore Curie-Weiss constant (θ) and the temperature value giving the maximum in the magnetic susceptibility (Tm) seem to be dependent not only on the mean number of Fe atoms in octahedral coordination (Z) per unit cell, but also on its ordering. Tm linearly depends on several structural parameters as well, e.g., the tetrahedral rotation angle α.

Effect of temperature on Hg-cysteine complexes in vermiculite and montmorillonite

Malferrari, D.[1*], Brigatti, M.F.[1], Marcelli, A.[2], Chu, W.[3] & Wu, Z.[2,3]
[1]Dipto. di Scienze della Terra, Università di Modena e Reggio Emilia, Modena, Italy ([*]dmalf@unimore.it)
[2]Istituto Nazionale di Fisica Nucleare, Laboratori Nazionali di Frascati, Italy
[3]Beijing Synchrotron Radiation Facility (BSRF), Institute of High Energy Physics, Chinese Academy of Sciences, Beijing, P.R. China

This work describes the influence of temperature on two Hg(II)-cysteine modified clay minerals with different layer charge (*i.e.*, vermiculite and montmorillonite) by using chemical analyses, thermal analyses coupled with evolved gas mass spectrometry (TGA-MSEGA), synchrotron-based X-ray absorption spectroscopy (XAS), and X-ray powder diffraction (XRPD) techniques. These two latter techniques were applied on samples heated "*in situ*" up to 900°C. Hg binds cysteine by the thiol group with Hg–SH bond lengths similar in both clay minerals, thus suggesting their independence from layer charge. On the contrary, the thermal behaviour of the adsorbed organometallic complexes is strictly layer charge dependent, as evidenced by decomposition temperatures, which are commonly lower in montmorillonite than in vermiculite. Results from X-ray absorption near edge structure (XANES) spectroscopy evidence a nearly completely Hg removal in montmorillonite at temperature values ranging from 600 to 700°C, unlike in vermiculite where Hg is still present at these temperatures.

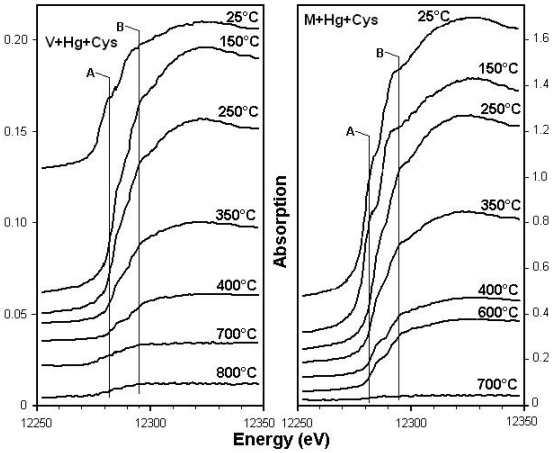

Fig. 1: XANES spectra of Hg-Cysteine treated vermiculite (left side) and montmorillonite (right side) vs. temperature.

Kinetics of Zn-Al hydrotalcite structure reconstruction process

Zimowska, M.*, Napruszewska, B.D., Dula, R., Mucha, D. & Serwicka, E.M.
Institute of Catalysis and Surface Chemistry, Polish Academy of Sciences, Krakow, Poland (*nczimows@cyf-kr.edu.pl)

The unique ability of anionic clays known as „memory effect" allows for the reconstruction of the layered structure of calcined hydrotalcite-like samples. In view of this, our intention was to investigate the kinetics of structure reconstruction of the zinc-aluminum hydrotalcite type samples calcined at 450 °C for 3 hours. Hydrotalcite-like samples (Htl) with atomic ratio of Zn:Al = 3:1, synthesized by standard co-precipitation method at a constant pH=7, using either Na_2CO_3 and NaOH, or $(NH_4)_2CO_3$ and NH_3 (aq) for precipitation and control of pH. The precipitates were calcined at a desired temperature and subsequently exposed to humid air at room temperature.

XRD analysis of the starting materials confirmed that the synthesized samples possessed Htl structure, mainly with carbonates as compensating anions. The presence of some nitrate anions was evidenced with the EGA and FTIR results. Nitrate contribution was, at least in part, associated with $Zn_3(OH)_4(NO_3)_2$ phase whose traces were observed in both samples (especially in the solid synthesized with Na_2CO_3 and NaOH). XRD patterns of calcined samples showed strongly amorphous materials, with poorly crystalline ZnO as the only identifiable phase. The reconstruction process was carried out at controlled humidity (94%) and temperature (295K) conditions.

Already after 10 days in all calcined samples strong reflections originating from recovered Htl structure were observed. The progress of reconstruction was investigated over a period of up to 150 days. In all samples, independently of the applied preparation method, the position of d_{003} reflection was constant and appeared at 0.755 nm, which shows that, as expected, a carbonate form of Htl was formed upon reconstruction. Even after the longest applied treatment (150 days), not all of the ZnO phase was consumed. Analysis of the XRD patterns suggests that in the first place reconstruction occurs at the expense of the finest ZnO grains. Apparently, their high surface energy is responsible for facile rebuilding of the Htl lattice at the beginning of experiment.

Noteworthy, crystallinity of the reconstructed phase was better than that of the starting Htl. This is also illustrated by SEM images, which show the changes in grain morphology at different stages of the reconstruction experiment.

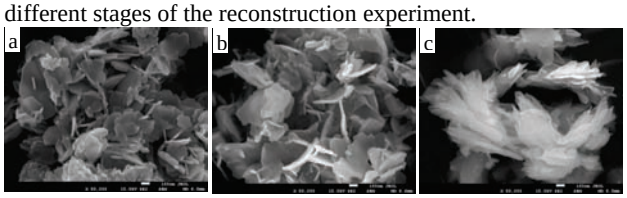

Fig. 1: SEM images of a) fresh Zn-Al Htl precipitated with Na_2CO_3 and NaOH, b) calcined at 450°C, c) after the reconstruction.

Acknowledgements: This work was financed in part by NoE IDECAT and the National Centre for Research and Development within the project KB/69/13848/IT1-B/U/08.

Deformation and lattice preferred orientations of antigorite serpentine

Reynard, B.[1*], Bezacier, L.[1], Van de Moortèle, B.[1] & Hilairet, N.[2]
[1]ENS Lyon, CNRS, Lyon, France ([*]bruno.reynard@ens-lyon.fr)
[2]GSECARS APS, University of Chicago, Chicago, IL, USA

Antigorite is the major component of serpentinites in subduction zone context. Its presence and deformability likely control the downdip extent of the seismogenic zone and exhumation processes. Lattice preferred orientations (LPO) of serpentines induce a strong anisotropy of various properties in serpentine bearing-rocks. For example, seismic anisotropy is potentially extreme in serpentinites and may allow their seismic detection as well as the determination of the deformation pattern at the plate interface and in the mantle wedge. LPO of antigorite had so far been obtained only by X-ray diffraction techniques. We have applied EBSD to the measurement of the LPO of antigorite in a naturally deformed high-pressure serpentinite. This technique is very sensitive to sample preparation that can lead to surface amorphization in the case of serpentine. A polishing procedure is described that avoids amorphization and allows accurate EBSD measurements with optimized experimental conditions in a variable pressure SEM. Results indicates that deformation leads to LPO characterized by extremely strong c-axis clustering perpendicular to the foliation, as expected for a layered silicate. In the foliation plane, a significant clustering of the a-axis is observed and tentatively attributed to intracrystalline deformation mechanisms. These data suggest that antigorite deforms mostly by gliding along the basal plane of the layered phyllosilicate structure, but that gliding may occur along directions favoring a-axis alignment. EBSD appears to be a reliable method for determining phyllosilicate LPO in deformed rocks, with potential applications for determining anisotropy of properties like seismic velocities or thermal and electrical conductivities. Applications concerning seismic anisotropy are shown. Comparison with deformation in experimentally deformed antigorite is in progress and will be presented.

Influence of clay microfabrics on petrophysical properties of clay stones and bentonites

Klinkenberg, M.[1,2,3*], Dohrmann, R.[2], Kaufhold, S.[2] & Siegesmund, S.[3]
[1]present address: Institute of Energy Research (IEF-6), Research Centre Jülich GmbH, Jülich, Germany ([*]m.klinkenberg@fz-juelich.de)
[2]Technical Mineralogy, Sedimentology, BGR/LBEG, Hannover, Germany
[3]Geowissenschaftliches Zentrum der Universität Göttingen, Germany

Claystones and bentonites are currently being investigated as potential host rock and geotechnical barrier, respectively, for radioactive waste disposal. For this application, the hydraulic conductivity, swelling properties, water uptake, rheological and mechanical properties are important. The Opalinus Clay (Mont-Terri, Switzerland) and the Callovo-Oxfordian clay stone (France) are the most frequently studied clay stones. One goal is to develop a numerical model being able to predict the mechanical behaviour of clay stones under repository-like conditions.

The results of this study show that Opalinus Clay and Callovo-Oxfordian clay stone behave different with respect to the dependence of mechanical strengths on the carbonate content. The failure strength of Opalinus Clay decreases with increasing carbonate content, while it increases for Callovo-Oxfordian clay stone [1]. For the investigation of the microfabrics, scanning electron microscopy of polished sections and image analysis were used. Opalinus Clay shows large elongated carbonate grains of shell fragments, whereas Callovo-Oxfordium clay stones show a homogeneous distribution of fine-grained and more isometric carbonates. The most important result of this study is that not only the carbonate content, but also the microstructure (grain size distribution, shape, spatial distribution, and intergrowth of carbonates) affects the mechanical behaviour of the claystones. The microscopy and image analysis techniques proved to be an excellent tool, which can be employed in model development.

Furthermore, the microfabric of 38 bentonites was investigated. During genesis bentonites undergo continuous maturation from glass to smectite. Almost all bentonites show glass relict structures. The microfabric of the bentonites, particularly the intergrowth with relict volcanic glass may have an additional influence on relevant geotechnical properties. Based on the optical characterisation, a model of maturation was developed, containing five alteration-classes. The following petrophysical properties of bentonites were determined and compared to the microstructural characteristics namely density, porosity, BET-surfaces, abrasivity of bentonite suspensions [2], electrical conductivity, and water uptake capacity [3]. The results show that all these properties are affected by the microfabric.

[1] Klinkenberg, M. et al. (2009) *Eng. Geol.*, **107**, 42-54. [2] Klinkenberg, M. et al. (2009) *Appl. Clay Sci.*, **46**, 37-42. [3] Kaufhold, S. et al. (2010) *Clay Clay Miner.*, **58(1)**, 37-43.

Relationship between morphological preferred orientations and landslides

Bortolotti, D., Brigatti, M.F., Elmi, C., Malferrari, D.* & Pattuzzi, E.
Dipto. di Scienze della Terra, Università di Modena e Reggio Emilia, Modena, Italy (*dmalf@unimore.it)

Crystals orientation in polycrystalline natural compounds may be either completely random or else follow preferred directions, which reflect physical processes in which the materials have been involved during the solidification and / or after the solid state had been reached.

The preferred orientation can be divided into two main groups: i) preferred orientation of the crystal lattice (LPO, lattice preferred orientation) and ii) grains preferred orientation (i.e., morphological preferred orientations, MPO). Frequently there is a close relationship between these two groups. Geological processes that determine the formation of LPO are, for example, tectonic (regional) compressive movements; on the other hand MPO can be induced also by local stress (i.e., gravitational movements). While tectonic (regional) compressive movements may produce LPO even on already lithified rocks, usually, MPO are induced only on not-lithified and incoherent rocks.

The preferred orientation cab be observed: i) macroscopically (the rock structures) ii) microscopically, grains orientation and morphological textures of the rock according to the classic concept of optical microscopy, iii) with diffraction methods (i.e., X-rays and neutrons diffraction), to study both LPO and MPO when, this last, cannot be studied via optical methods because, for example, of a very small grain size.

This research will investigate MPO via X-ray diffraction only. We collected, and kept oriented, samples in several landslide areas. In particular samples were collected both in the active crumbling area and at the landslide margin. Samples were analyzed for texture using X-ray diffractometer equipped with a phi-chi Eulerian cradle. We analyzed the preferred orientation of the hkl reflections: i) (001) and (060) in smectiti and illite; ii) (001) and (100) in caolinite; iii) (24-1) in plagioclase.

Preliminary investigation demonstrated a direct correlation between the number of MPO and the amount of clay minerals. Texture measurements on samples collected in the crumbling area agree with other morphological field measurements, providing, in addition to the main direction of the landslide, also the vertical module, thus probably defining the preferential path for interstitial fluids migration. Only in one case we could observe preferred orientation in a sample coming from a margin of a landslide, data which could testify a past movement (paleo-landslide) or else a quiescent landslide.

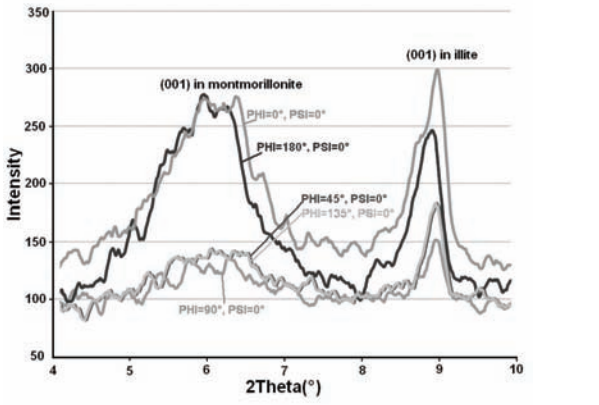

Fig. 1: Intensity variation of (001) in montmorillonite and illite varying sample orientation.

The influence of scaly fabric on the illitization reaction in faulted claystones

Dellisanti, F., Pini, G.A. & Valdrè, G.*
Dept. of Earth and Geo-Environmental Sciences, University of Bologna, Italy (*giovanni.valdre@unibo.it)

A closely-spaced fabric, related to the interlacing of striated and polished shear planes, is commonly defined as scaly fabric in the geological literature. A tens-of-meters-wide belt characterized by pervasive scaly fabric occurs in claystones of the Northern Apennines foothills, south of the town of Bologna, in a shallow-level fault zone. The shear planes are arranged in different oriented sets defined hereafter as R, P, R' and D planes, following the terminology after Tchalenko (1968) [1].

Microscopical observations (SEM) show a significant increase of parallel orientation of the clay platelets ("face to face" arrangement) on the surfaces and in the proximity of shear planes, leading to development of clavage domains and porosity decrease. Despite, far from the shear planes in the undeformed domains (microlithons), the clay particles show a more open texture with a "edge to face" disposition, due to a more disordered arrangement of the clay particles.

A systematic mineralogical study performed by XRD on the less than 2 micron grain-size fraction has evidenced a progressive illitization of smectites and mixed layer illite/smectites (I/S) along shear planes and cleavage domain associated. The progressive change from smectites-rich I/S into illite-rich I/S was also confirmed by microchemical EDS data, which showed an enrichment in K^+.

The studied claystones were sampled in absence of significant mechanical compaction and clay mineral diagenesis and the alignment of clay platelets and illitization occurred in shallow burial conditions and very low thermal maturity (< 60°C) [2]. Moreover, the illitization reaction in the scaly cleavage domain is isothermal and probably driven only by K^+-rich fluid circulation.

The progressive transition from smectite-rich I/S to illite-rich I/S is due to enhanced fluid migration, which is preferred within the scaly cleavage domains because enriched in oriented phyllosilicates (P-domains), whereas the circulation is inhibited in microlithon cores because of disordered arrangement of clay particles. The anisotropic fabric is caused by tectonic strain, which produces flattening and extension of clayey rocks leading to a volume decrease and consequent fluid expulsion. This tectonic dewatering mechanism involves chemical changes within the microstructural domains favouring progressive illitization of clay particles.

[1] Tchalencko, J.S. (1968) *Tectonophysics*, **6**, 159-174. [2] Dellisanti, F. et al. (2008) *Int. J. Earth Sci.*, **97**, 601-616 .

Experimental shear test of montmorillonite: the role of water on geomechanical behaviour of smectite

Dellisanti, F., Pini, G.A. & Valdrè, G.*
Dept. of Earth and Geo-Environmental Sciences, University of Bologna, Italy (*giovanni.valdre@unibo.it)

In order to investigate the role of the interlayer water molecule of Ca-montmorillonite on the geomechanical behaviour, a cycle of controlled experimental shear deformations on natural and structurally modified Ca-montmorillonites have been performed and correlated to structural and morphological analysis. Experimental shear tests were performed on five types samples: (1) a natural Ca-montmorillonite; (2) the same montmorillonite after heating for three hours at 80°C; (3) at 250°C; (4) at 335°C, and (5) after inducing defects in the tetrahedral and octahedral sheets. The five samples have been shear-tested by a specifically built shear box apparatus under 19.6 MPa condition of normal pressure. All samples, before and after the shear deformation, have been analysed by SEM and XRD.

The shear-deformed samples were cohesive and presented striated and polished shear planes along the displacement surfaces imposed by the experimental apparatus. The shear planes were arranged in sets disposed at low angle with respect to the principal shear surface, which correspond to R, P and D planes, [1,2]. The disposition of planes and the lustrous aspect of the surfaces are quite similar to the ones observed in natural examples. In our experiments striations are not related to ploughing by coarse grains or asperities because we have deliberately used montmorillonite with homogeneous composition and granulometry. XRD and SEM analyses indicated that in the vicinity of the shear planes the clay platelets appear preferentially orientated and with a “face to face” arrangement, whereas in zones far from the shear planes the platelets present a lower degree of orientation and an “edge-face” disposition. The shear strain also produced a reduction of structural ordering and an increase of both lattice defects and microstrain in the mineral. Moreover, natural montmorillonite presented a typical strain softening behaviour and the geotechnical parameters (cohesion and internal friction angle) of overconsolidated clayey rocks

The cohesion and compaction of the material are essentially related to the capability to release what is called “absorption water”, whereas the development of striated shear planes has to be attributed to the role of interlayer water. The last hypothesis is supported from the experiments carried on the same material heated up to 80°C (to desorb completely the water), which showed only scaly cleavage and striations. Samples heated up to 250 and 335°C, which have almost completely lost the interlayer water molecules, did not show neither development of scaly cleavage nor striations on the principal shear surface. However, they showed a very moderate strain hardening behaviour. Defective montmorillonite with disorder in the tetrahedral and octahedral sheets (hindering absorption and release of water, as described by [3], presented, as expected, a strain hardening behaviour without any striations and scaly cleavage. The general strain softening behaviour of natural montmorillonite can be explained by the presence both absorption and interlayer water that allow the sliding of clay platelets along the TOT layers. However, the montmorillonite, which contains defects and disorder is hindered to a deformation by a sliding mechanism and therefore does not develop shear planes and alignment of clay platelets.

[1] Skempton, A.W. (1966) Proc. *Int. Soc. Rock Mechanics Congress*, **6**, 329-335. [2] Tchalencko, J.S. (1968). *Tectonophysics*, **6**, 159-174. [3] Dellisanti, F. & Valdrè, G. (2005) *Appl. Clay Sci.*, **28**, 233-244.

Adsorption properties of clays in teaching of Environmental Chemistry

del Hoyo Martínez, C.[1*] & Queiruga Dios, A.[2]
[1]Dept. of Inorganic Chemistry, University of Salamanca, Spain ([*]hoyo@usal.es)
[2]Dept. of Applied Mathematics, University of Salamanca, Spain

In the last fifty years, environmental issues has required the study of air pollution, water and soil to prevent and remedy the adverse effects of waste originating from anthropogenic activity and the development of new energies and new materials. The teaching of this discipline has been marked by lectures on general lines, materials, disciplines, who explained biased objects of reality, but often forgot the task of reconstruction and integration of such visions. Moving from that model, otherwise quite static, to a dynamic relational model, would in our view, a real revolution in education. This means taking a systematic approach to complex both in interpreting reality and in favor when learning. Children relationships are as important or more than single objects, and it is to discover fundamental organizational principles of phenomena we seek to interpret or in other words, find the pattern that connects. Thus, we must work on relationships and also take into account the relation between the observer and the observed. Educate about relationships means that studies should always be considered within a framework of probabilities, not absolute certainties.

This model of systemic thinking, dealing with complexity, is a possibility to bring coherence to our educational work, because the complexity is not taught, complexity is live, so that complex thinking is extended (and fed) in a form educate complex. It is the task of teaching to help people move from level to level of decision reviews. This means that systems thinking should be extended in a local action, action that engages the individual and the environment. So we must work with our students helping them to understand, in this case, environmental problems from their daily reality, where the real subject of study.

Environmental Chemistry has emerged as a discipline of free choice for pupils attending chemical engineering which has been assigned 4.5 credits theorists. The chemical engineer's professional profile within the current framework is defined as a professional knowledge as a specialization technical / functional, working in a learning organization and the formation of which enables him to continuous improvement and innovation.

There are different materials used in the adsorption and immobilization of chemical contaminants, most of which remain under patent, so they do not know the procedures and products used, but in all cases the safety and / or biodegradability of materials used is an important issue in their choice for environmental applications. Regarding the materials, safe and low cost, clays and clay minerals must be mentioned, because their colloidal properties, ease of generating structural changes, abundance in nature and low cost make them very suitable for absorption of chemical contaminants. We proposed to use these materials to show the different aspects for the study of the Enviromental Chemistry.

Minerals in context: the Earth, rocks, and society

Dutrow, B.L.
Dept. Geology & Geophysics, Louisiana State University, Baton Rouge, LA, USA (dutrow@lsu.edu)

Minerals are the fundamental building block of our Planet and are the heart of a geoscience education. Yet, there is an increasing perception that a foundation in mineral sciences is no longer relevant, nor critically necessary for a comprehensive geosciences education. Teaching *"minerals in context"* provides a powerful approach for engaging students in the exciting, important and socially relevant field of mineralogy.

At Louisiana State University, U.S.A., this is accomplished in three different classes ranging from the required mineralogy course through elective advanced courses. For our first core curriculum course in mineralogy, the context of minerals is Planet Earth and the approach focuses on teaching minerals from the core to the crust. Systematic mineralogy is introduced via elements in the core and proceeds outward increasing in mineral complexity as one proceeds to the crust. With this emphasis, crystallographic concepts are woven into the discussion of minerals as they are encountered. For example, mantle minerals provide a backdrop for teaching polymorphic phase transitions in context of their environment in the transition zone. Further, relevance can be given by connecting to deep-focus earthquakes. Crystal chemical concepts are reiterated once crustal minerals are described. This approach sets the stage for the multitude of complexity found in crustal minerals both in terms of environment, chemistry, and structure. Here, numerous connections are made with reference to minerals in our lives as well as minerals as key indicators of environmental conditions. Such an approach emphasizes the central focus of mineralogy and its linkage to other disciplines.

For the advanced level, two approaches continue to focus on teaching minerals in context: minerals as fingerprints of geologic conditions (in the course Petrologic Mineralogy) and minerals in our lives (course: Earth Materials and the Environment-EME). Petrologic mineralogy continues to explore the crystal chemistry and structure of minerals in the context of deciphering tectonic evolution; that is, minerals as geochronometers, geothermobarometers and/or as provenance indicators. In this course, students complete a semester-long research project where they chemically analyze minerals in order to determine derivative information such as P-T, age, or source. In contrast, for the EME course, minerals are explored as both problems and solutions in the context of societally relevant issues. These range from various health effects (e.g. asbestosis, silicosis), to solutions for global warming (e.g. carbon capture and sequestration) and nuclear waste (e.g. material templates for encasement, geologic barriers), to requirements for our standard of living (e.g. metals, rare earth elements, PGEs). Such a context not only raises awareness of the critical nature of our science and its importance to government policy but also provides opportunities for improving critical thinking skills as related to the development of public policy dealing with these issues. In both cases, students appear to engage more fully in the material because it relates to their lives and opens their eyes to potential career goals and their everyday lives.

Volcanic petrology in six weeks

Nicholls, J.
Dept. of Geoscience, University of Calgary, Alberta, Canada
(nichollj@ucalgary.ca)

At the University of Calgary students have to learn igneous petrology in six weeks. I've heard of similar reductions in time allocated to mineralogical science courses at other universities. Responses to the reductions included: provide an overview, teach everything anyway, or teach through special projects. An overview provides little depth. Covering everything leaves students frustrated and feeling inadequate. Projects are great but students don't reach an appreciation of the many different faces of igneous petrology.

Several decades ago, the goal of a geology program was a student who could work at a professional level in any geologic setting. Today, many students specialize; they expect to work at the professional level in the energy industry, on problems of climate change, or on problems of environmental remediation, to name but a few popular career fields. Prospective employers often share their expectations. Most students graduating with geoscience degrees will never look at an igneous rock as a professional geoscientist. Why then, do they need to learn about igneous rocks? This is the first of three important questions that geoscience educators must answer if they expect to keep igneous petrology in geoscience curricula.

Igneous petrology is integral to geoscience. Igneous events sporadically intrude themselves into our lives, often with a vengence. Those who graduate with a degree in geoscience will be expected to assess the events for themselves, their families, and their communities. If they cannot, their reputations will suffer along with the reputations of the departments granting their degrees and along with the reputations of the faculty in those departments.

Second question: supposing these arguments convince the powers that be to keep igneous petrology in the curriculum, what should be included in a six-week course? At a minimum, geoscience graduates should be able to assess articles on igneous phenomena in popular science magazines such as *National Geographic*, *Scientific American*, *American Scientist*, *Elements*, and *Earth*. I recently reviewed several issues of these magazines and compared their contents to the material I had taught in igneous petrology a decade ago. Two features stood out: (1) Articles were almost always about volcanic, not plutonic, events and products; (2) The articles were devoid of rock names, textural descriptions, rock compositions, and theoretical petrology, for example thermodynamics and phase diagrams. The articles focused on the effects eruptions had or could have on society and civilization. I would leave out plutonic rocks and theoretical petrology. Six weeks is not enough time to do justice to all three aspects. Geologic context, texture, mafic index, silica activity, alumina activity, and chemical composition would be emphasized. If students know something about these features for any particular volcanic rock they will know a lot about its nature and can infer much about the processes that formed it.

Third question: how can a six-week course in volcanic petrology enhance the degree of an undergraduate who plans a specialized professional career?

Graduating students should be able to discover the geologic context of a volcanic rock, describe its textural features, identify the critical minerals it contains, and become familiar with its chemistry. With this background, they should be able to read and assess mass media accounts of volcanic activity, take part in geoscience outreach programs where they could talk about volcanic phenomena with confidence and without misconceptions, and they should be able to write accounts of volcanic phenomena suitable for popular science magazines.

Teaching mineralogy for geology students at the Eötvös L. University, Budapest, Hungary

Buda, Gy.
Dept. of Mineralogy, Eötvös L. University, Budapest, Hungary
(buda@ludens.elte.hu)

Teaching mineralogy at the Eötvös L. University began in 1774. The separate Department of Mineralogy was established in 1849. From this time several text-books were available based on Dana's Mineralogy or Klockmann and Ramdhor text-books. After World War II., geology training started and students of geology received detailed and specialised mineralogy during the first and second semester. Due to the demand of students of geology several university notebooks and textbooks were published. The last one was the textbook of Koch S and Sztrókay K. I (first published 1955, last one in 1986 in two volumes). These lectures and text-books, besides the well known general mineralogy (crystallography, X-ray crystallography, crystal chemistry, physical properties of minerals etc.), dealt with systematic mineralogy. The systematic mineralogy part, written by Sztrókay, differs from the previous text-books. It is based on crystal chemistry and the sequence of mineral classes reflects Sztrókay's concept [1].

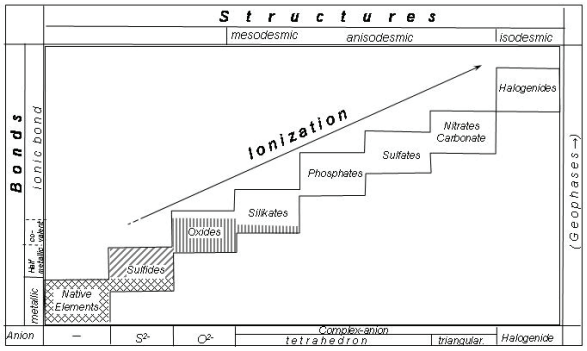

Fig. 1: Sequence of mineral classes by K. Sztrókay (1982).

He started with metallic (native metals and sulphides), followed by covalent (oxides) and more and more ionic bonds (silicates, phosphates, sulphates, borates, carbonates, nitrates, halogenides) and finished with the molecular structures of organic minerals. When describing the individual mineral species, Sztrókay included crystal structure, lattice parameters etc., but also emphasized the diagnostic features and gave information on genetics and localities needed for geologists. Unfortunately the two levels (BSc, MSc) of the new Bologna-system radically decreased number of the lectures of mineralogy. Basic knowledge of natural sciences by secondary school students is becoming poor and consequently there is now little chance to make them understand principles of mineralogy. There is a greater chance that mineralogy as one of the main subjects for students of geology shall disappear from the geology curriculum in Hungary.

[1] Sztrókay, K.I. (1962) *Über die Grundprinzipien einer zeitemässen Systematik des Mineralreichs*. I. Teil. Ann. Univ. Scien. Bp. de R. Eötvös Nom. Sec. Geol. Budapest, **5**, 139-149.

Teaching of crystallography and gemmology at the "Museum of Unique Crystals", Sofia, Bulgaria

Kostov, R.I.
Dept. of Mineralogy and Petrography, University of Mining and Geology "St. Ivan Rilski", Sofia, Bulgaria
(rikostov@gmail.com)

The newest mineralogical museum in Bulgaria is devoted to the famous collector and donator of Bulgarian origin – Mr. Ilia Deleff, who in the past decades worked for preservation of the mineral heritage on the planet. Mr. Deleff (Brazilian citizen, born 1921 in Bulgaria) is a well known collector of phenomenal giant and rare minerals. In 1983 Mr. Deleff exhibited for the first time in the world his collection with giant crystals in the National Museum of Natural History in Paris. In 1987 in Sofia was opened to the public the "Earth and Man" National Museum, where the main and central part constitutes the remarkable collection of Mr. Deleff of unique giant quartz crystals and other minerals from Brazil [1]. In Bulgaria Mr. Deleff made also several donations with minerals from Brazil to the University of Mining and Geology "St. Ivan Rilski" in Sofia, which can be seen in the newest mineralogical museum – Museum of Unique Crystals "Ilia Deleff". In the museum are exhibited rare crystals and minerals from Brazil in the following sections: crystal flowers of nature; parade of phenomenal crystals; treasures of Minas Gerais; gem pegmatite minerals; mineral wealth of Brazil; world of agates; the noble amethyst; the quartz palette; rock crystal fairy; nature and art. Special ascents at the museum are the "Amethyst Room" and the "Rock Crystal Cave".

The Museum of Unique Crystals (MUC) at the Rectorate is open to the public and for social events as the most representative museum among the other academic museums (geological and paleontological; mineralogical and petrographical) at the university. Since its opening in November 2007 the MUC serves also as a place for lectures and education in mineralogy and crystallography for the bachelor degree [2] and in gemmology for the bachelor and master degrees [3]. Impact in the teaching process is made on the richness of crystal habits of minerals [4], mainly quartz varieties of different size, perfection and colour, as well as some gem minerals as topaz, beryl, tourmaline, kunzite and feldspar. As Bulgaria is not so rich of gem and decorative minerals [5] compared to Brazil, the exhibit allows a broad enrichment of the knowledge of different common and rare mineral species. The main hall is used for presentations and scientific films, including for scientific conferences. Students and other visitors of the museum are assisted in their mineralogical research also by a gem and mineral shop.

[1] Deleff, I. (2004) *Phenomenal Crystals*. Pensoft, Sofia-Moscow. [2] Kostov, R.I. (2000) *Fundamentals of Mineralogy*. Pensoft, Sofia-Moscow (in Bulgarian). [3] Kostov, R.I. (2003) *Precious Minerals: Testing, Distribution, Cutting, History and Application (Gemmology)*. Pensoft, Sofia-Moscow (in Bulgarian). [4] Kostov, I. & Kostov, R.I. (1999) *Crystal Habits of Minerals*. Bulgarian Academic Monographs, 1. Co-published by Pensoft Publishers and Prof. Marin Drinov Academic Publishing House, Sofia. [5] Petrussenko, S.I. & Kostov, R.I. (1992) *The Precious and Decorative Minerals in Bulgaria*. Publishing House of the Bulgarian Academy of Sciences, Sofia (in Bulgarian with a Russian and English abstract)

Interactive Wolfram Mathematica demonstrations and physical models for studying crystal structures

Kabai, S.
Uniconstant Co., Budapest, Hungary (unico@t-online.hu)

From Version 6 on (launched on May 1, 2007) the computer software Wolfram Mathematica is capable of showing interactive graphics, which can be used preferably to study crystal shapes and structures. In this paper selected demonstrations are shown that are related to crystal structures (Fig. 1-3). In the last part the modeling with polystyrene blocks is introduced. The blocks are cut out with the proprietary machine of the author, and then sticked together (Fig. 4) (http://demonstrations.wolfram.com/search.html?query=kabai).

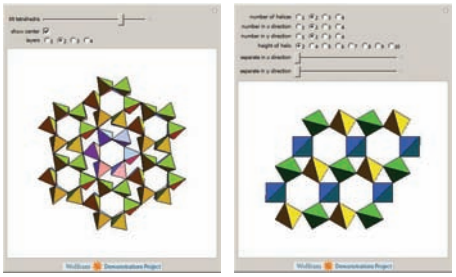

Fig. 1: (left): Expanding Tetrahedral Network - Tetrahedra are attached at their vertices in groups of six. **(right):** Helices of Tetrahedra - Tetrahedra are arranged along helices connected at vertices.

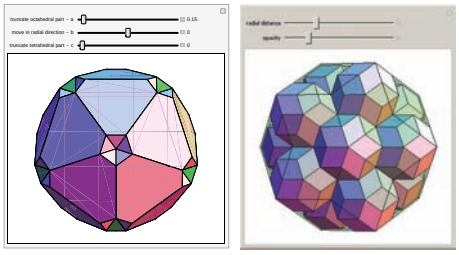

Fig. 2: (left): Boron suboxide - (chemical formula B60) is a solid compound of boron and oxygen. **(right):** Twelve rhombic triacontahedra are placed at the vertices of an icosahedron. Occur in quasicrystals

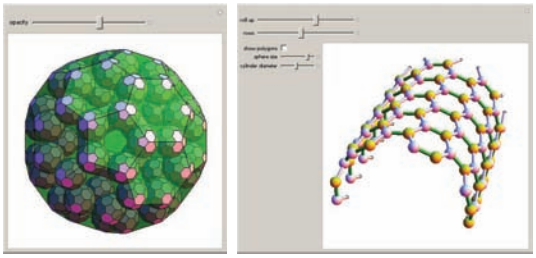

Fig. 3: (left): Buckyball of buckyballs. **(right):** Graphene. A planar hexagonal lattice is rolled up into a cylinder.

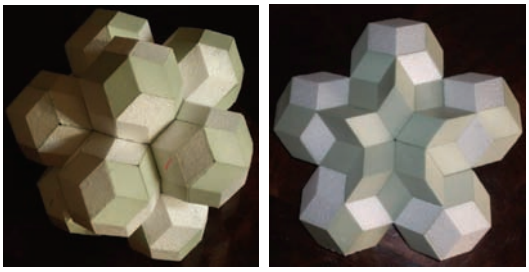

Fig. 4: Solid models.

IMACS: an international Master programme entirely devoted to clays

Patrier Mas, P.[1], Petit, S.[1*], Christidis, G.[2], Ferreira da Silva[3], G., Rocha, F.[3], Blanchette, C.[4], Detellier, C.[4] & Mexias, A.[5]
[1]Université de Poitiers, UMR 6269 CNRS HydrASA, Poitiers, France ([*]sabine.petit@univ-poitiers.fr)
[2]Technical University of Crete, Chania, Greece
[3]University of Aveiro, Portugal
[4]University of Ottawa, Canada
[5]Federal University of Rio Grande Do Sul, Porto Alegre, Brazil

Most existing Masters Courses dealing with clays focus on a single discipline or domain in which Clay Science does not necessarily constitute the main part of the course (Earth Sciences, Civil and Geotechnical Engineering, Materials Science, Environmental and Life Science, Chemistry and Chemical Engineering). However, Clay Science is a multidisciplinary endeavour, combining geology, mineralogy, crystallography, with physics, geotechnology, and soil mechanics together with inorganic, organic, physical and colloid chemistry and biochemistry. The IMACS (International Master in Advanced Clay Science) is the first multi-disciplinary programme that brings together the widely-distributed knowledge of clay science.

IMACS is an integrated 2 years master programme developed by five universities: the University of Poitiers (France), the Technical University of Crete (Chania - Greece), the University of Aveiro (Portugal), the University of Ottawa (Canada) and the Federal University of Rio Grande Do Sul (Porto Alegre – Brazil). AIPEA is an associated member of this consortium. The French Clay Group (GFA) also supports IMACS.

The teaching language is English. During the first year, basic knowledge on clays is provided, followed by a four month master project, which completes the first year programme. The second year incorporates two elective specialization options in the following fields: 1) Environment, soil and geological systems, 2) Geomaterials and civil engineering – Assessment and processing, 3) Advanced clay – nanomaterials, and 4) Healing minerals. The master thesis (6 months) completes this second year and can be carried out at any of the partner research laboratories. The completion of the curriculum is rewarded by a multiple Master Degree.

The IMACS programme was approved by the European Commission under a very competitive application scheme as an Erasmus Mundus Joint Master programme in July 2009 and it will open in September 2010. Erasmus Mundus is a cooperation and mobility programme in the field of higher education supported by the European Commission. This programme offers financial support for high-quality joint master courses, attractive scholarships/fellowships for both Non European and European student candidates and short-term scholarships for Non European and European academics to carry out research or teaching assignments as part of the joint masters project. Free language training in the local languages is offered by the five higher education institutions. Moreover, the programme makes available a range of services and facilities (e.g. visa request, accommodation, insurance, bank account opening, social and cultural activities among many others…) to the students.

This Masters Course is open to students holding a BSc (or a degree equivalent to 180 ECTS) or an academic equivalence based on professional experience, and a fluent understanding of the English language.

IMACS website: http://www.master-imacs.org

Education and Culture DG
ERASMUS MUNDUS

Teaching clay science and technology within a Geological Engineering Master program: Bologna Process implications

Rocha, F.
Geosciences Dept., Geobiotec Unit, University of Aveiro, Portugal (tavares.rocha@ua.pt)

Aveiro University (AU) was created in the mid-70's, establishing a Geosciences Department, the first in Portugal of its kind with the purpose of integrating the various areas regarding Sciences of the Earth, including the Engineering Science as well as the Geophysical Science. Teaching of clays and clay minerals deserve, since the beginning, particular attention in the Geological Engineering graduation program. Clay-related matters were teached within disciplines like Industrial Minerals, Ceramic Raw Materials and Crystallochemistry and Diffraction, but two very important steps were fulfilled first in 1986 with the inclusion, on the Geological Engineering graduation program, of a new discipline called Clays, entirely focused on clay science and technology, then in 1994 with the creation of the master degree in Industrial Minerals and Rocks (1994), offering clay formation within disciplines, such as Geology of Industrial Minerals, Exploration and Exploitation, Industrial Applications, Technologies, Mineral Economy.

The implementation of the Bologna process caused significant changes in the courses offered at AU. In the scope of Master Degrees, apart from the recreation of a master degree in Geological Engineering, the Department of Geosciences of the AU launched in conjunction with the Department of Geology of the Science Faculty of the University of Porto, a master degree in Geomaterials and Geological Resources, both offering several clay-related disciplines.

Recently, some advanced training courses (ATC), in which the Geosciences Department will play an important role, were put forward: (1) Strategies for the Protection of Lands, (2) Strategies for the Evaluation of contamination, (3) Rehabilitation of Lands; (4) Hydrogeophysics. The first three are strongly articulated among them and involve formation on clay science and technology. They are all related to fields of study aimed at an audience with a wide range of training in scientific and technological areas. The ATC does not confer degrees, but the approval in this type of training can be credited in other post-graduate, including doctoral programs.

ERASMUS IP: a simple and effective way for European teaching co-operations, the example of the ADVANCECLAY IP series (2008–2010)

Tóth, E.[1*], Weiszburg, T.G.[2], Pop, D.[3], Raucsik, B.[4] & Tombácz, E.[5]
[1]Eötvös Museum of Natural History, Eötvös Loránd University, Budapest, Hungary ([*]zsike@abyss.elte.hu)
[2]Dept. of Mineralogy, Eötvös Loránd University, Budapest, Hungary
[3]Mineralogical Museum, Babeş-Bolyai University, Cluj-Napoca, Romania
[4]Dept. of Earth and Environmental Sciences, University of Pannonia, Veszprém, Hungary
[5]Dept. of Physical Chemistry and Materials Science, University of Szeged, Szeged, Hungary

The Eötvös Loránd University (Budapest) has a long tradition in coordinating and hosting LLL ERASMUS Intensive Programmes (IPs) in the field of mineral sciences. The first IP took place in 2000 in Budapest, and since then, each year a 10-day international summer course was organized. Originally, the application and funding was coordinated from Brussels, but recently, applications have to be submitted in the host country of the IP. The application and the financial administration procedures of the ERASMUS IPs are relatively simple and they are really effective in enhancing international co-operations. In such training- and instrumentation-demanding fields like mineral sciences, IPs can further the usage of well equipped laboratories and fill up the gaps in university teaching programmes that originate from the lack of instrumentation.

We present our experience in the new, host country application system, through the ADVANCECLAY IP series, running in the years 2008–2010, in the hope to raise interest in organising similar events in other countries in the future. A specialty of the Hungarian IPs is that it is not only a tutorial event with lectures, practicals and labs, but students can present their results in the poster session and thus in a friendly environment they can experience how professional conferences work and how one shall prepare, and present a poster.

The ADVANCECLAY 1 IP took place in 18–29 July, 2008 in Budapest, on the topic "Dioctahedral Clay-Related Layer Silicates", with the participation of 23 teachers and 38 students, from 9 partner universities. It was the most classical summer school, with lectures, some practicals and a field trip.

The ADVANCECLAY 2 IP was held in 23 August – 2 September, 2009, in Budapest and Pécs (South Hungary), on the topic "Economic and Environmental Importance of Clays", with the participation of 13 teachers and 54 students, involving 6 partner universities. Here the emphasis was more laid on field activities: mine, factory and industrial plant visits.

The ADVANCECLAY 3 IP is scheduled for 27 August – 7 September, 2010, in Szeged, at the University of Szeged. The topic of the school is "Colloid Properties of Clays and Environmental Applications", with the participation of 63 students and 15 teachers, involving 11 partner universities. The main goal of the school is to amalgamate the mineralogical and chemical theoretical background of clay studies, with a large number of lab practicals.

Educational projects in Earth Sciences at University of Miskolc (Hungary)

Hartai, É.[*] & Földessy, J.
Institute of Mineralogy and Geology, Faculty of Earth Sciences & Engineering, University of Miskolc, Hungary
([*]foldshe@uni-miskolc.hu)

The Institute of Mineralogy and Geology, Faculty of Earth Science & Engineering has been coordinating several EU-co-funded educational projects. At the moment the Institute runs three projects of this kind.

The "EURO-AGES" (European Accredited Geological Study Programs) project aims at developing a qualification framework for geology, based on learning outcomes rather than input factors on the European level, thereby increasing transparency of the Earth Sciences qualifications and ultimately facilitating academic and professional mobility across Europe. The coordinator of the project is the ASIIN Consult GmbH Germany, the partners are from Belgium, Hungary, Spain and Sweden. The project moreover will provide important reference points for quality assurance and related recognition issues focused on learning outcomes. In this sense the project will add value to the implementation of the 2005 Directive on Recognition of Qualifications.

The project titled "Telkibánya Field Training Park" is being implemented in Hungarian-Slovakian cross-border cooperation. Telkibánya is a significant ancient mining town with outstanding medieval monuments of industrial history. In the frame of the project the partners create a joint field education centre in the area of the explored epithermal gold-silver mineralization. Besides setting up the infrastructural background, new teaching materials in English are worked out for field programs in geology, geophysics, mineralogy, geochemistry, ore exploration, mining, geotechnics and environmental engineering. Demo-courses for Hungarian and Slovakian participants at different levels (students at BSc, MSc, PhD, teachers of geography and environmental sciences, civil participants) are also organized as a part of the project. The training park is also offered as a scene for field programs for other universities as well.

The third project focuses on the development of teaching materials for the BSc program in Earth Science Engineering. The main aim is that beside the traditional contact hours, using multimedia tools, new, practice-oriented teaching materials are created for 16 courses in Hungarian and in English, which will be modern, on-line accessible and interactive. As the results of the project, the BSc in Earth Science Engineering program will be harmonized with the similar programs at other European universities, the international education facilities will be widened and the foreign job opportunities will be more favourable.

New approach in mineralogy and crystallography education by application of complex symmetry structures in old Eurasian ethnomathematics of Scythian, Xiongnu and Chinese archaeological finds of Ukraine, Russia, Mongolia and China

Bérczi, Sz.
Institute of Physics, Eötvös University, Budapest, Hungary
(bercziszani@ludens.elte.hu)

The crystallographic structure of minerals can be described by the symmetries of the crystal lattice. Complex structures contain more than one space symmetry group for the arrangement of different atoms in their positions in the unit cell. For example in the garnet structure (pyrope) the AlO_6 octahedral and the SiO_4 tetrahedral units form a subsystem, and the position of the Mg atoms also can be given well visible in a coloured subsystem.

Over the classical group theoretical approaches there are other methods to help forming the spatial view and visuality of the students. Some technological structures triggered development of 2D complex crystallographic structures, which were discovered even in the 2500 years old Eurasian ornamental arts. Within this work, we collected several of them from the complex structures found on archaeological finds in royal tombs of Scythians (Kul Oba, Ukraine; Pazyryk, Russia), Xiongnu Huns (Noin Ula, Mongolia;) and Chinese (Urumchi and Mawangdui, China) (These studies are also called ethnomathematics).

This educational course uses both symmetry and cellular automata principles in forming the operations of complex patterns and structures (From symmetry to cellular automata). From friezes double friezes, woven 2D symmetry patterns and the two types of complex (composite) plane symmetry patterns are generated. Complex patterns of Coxeter-type [1], and Curie-type [2,3] are shown in archaeological finds. Coxeter-type colored groups of cm/pm and cmm/pmg occur at Pazyryk. The multilayered structures of Scythians (Kul Oba, cmm//pmm//cm) and Xiongnu Huns (Noin Ula, p4m//cm//p1) and Chinese (cmm//cm, Ürümchi) are the Curie-type variants. Even Curie-type multilayered structures with complex unification of four different patterns were found among the later steppe structures (Afrasiab, today Samarkand, Uzbeghistan) with p4m//cm//pm//pg structure.

Complex symmetry patterns help the spatial imagination and make more complete and vivid the rigid mathematical background, and also demonstrate that ancient masters of technologies were rich enough in intuitive structural knowledge to give ideas even for the recent time crystallographers.

[1] Coxeter, H.S.M. (1985) *Int. J. Quantum Chem.*, **31**, 455-461. [2] Curie, P. (1894) *J. Physique*, **3**, 393-415. [3] Bérczi, Sz. (2004) *Forma*, **19(3)**, 265-277, Tokyo.

Formal and non-formal learning about minerals and mineralogy. A case study

Gomes, C.S.R.[1,3*], Gomes, E.M.C.[2,3] & Rola, A.S.[3]
[1]Centre for Geophysics (CG), University of Coimbra, Portugal,
[2]Geosciences Centre (GC), University of Coimbra, Portugal,
[3]Earth Sciences Dept., University of Coimbra, Portugal
([*]romualdo@dct.uc.pt)

Minerals have been precious materials for the development of civilizations and societies since the Prehistoric Times. First, the naturalists and the collectors, and then the Museums of Natural History have played an important role in the advancement and dissemination of Mineralogy. Moreover Museums have also been important as learning environments of Mineralogy. The purpose of this study is to present two examples of the teaching and learning of Mineralogy, considering the Mineralogy teaching experience at the Mineralogical and Geological Museum and at the Earth Sciences Department of the University of Coimbra in a non-formal and formal way respectively. A greater interest in minerals has been shown by teachers of Secondary Schools in the last decade. They often come to the Museum with their students. This interest may be related to the inclusion of the geological issues in the national curricula. Moreover, some scholars in the Department of Earth Sciences and in the Mineralogical and Geological Museum have developed some practical activities for the learning of minerals in a perspective of Education for sustainability in a non-formal way. These activities have been made to enable an active learning by participants, for example, by solving exercises and by handling minerals and rocks samples and everyday objects made from minerals. The participants, especially young boys and girls, aged 10 to 14, sometimes with their parents or their teachers, also have an opportunity to learn about minerals, as far as their classification, composition, diversity, occurrence, and use as a geological resource is concerned. Some activities also included the microscopic observation of minerals. Very often, the participants had a poor initial knowledge on these issues, but they developed good performances during activities and, ultimately, they evaluated them as important to very important [1]. Similar activities have also been developed within the framework of master courses for training teachers of Secondary Schools. In this case, materials for teaching minerals are being developed by master students who are attending the specific curricular units such as, Observation and Experimentation in Geosciences and Didactics of Geosciences II. In the last two years, 22 master students have made didactic materials to teach minerals in various perspectives, including the study of minerals as an important resource and the importance of minerals in the urban dust composition. At the end, these activities are significant not only because they contribute to the teacher training but also because they constitute potential activities to be developed in secondary schools in a classroom context or in the lab. Besides, school visits to the Museum are also an excellent opportunity to use these didactic materials. These two cases are examples of activities to promote learning about minerals and about their importance at different levels of education. We emphasize the learning and teaching minerals in a perspective of a *Sustainable Development.* These activities have been a success and they contribute to competence development of the participants, especially as far as the knowledge of mineralogy, geological resources and their uses and environmental implications is concerned. The promotion of these competences leads to a better understanding of minerals and to a greater discussion and participation performances.

[1] Gomes, C.R et al. (2009) *Enseñanza de las Ciencias*, Número Extra VIII Congreso Internacional sobre Investigación en Didáctica de las Ciencias, Barcelona, 2626-2629.

Joint European educational programs in mining, environmental and mineral sciences - Hungarian aspects

Mádai, F.*, Ormos, T. & Hartai, É.
University of Miskolc, Faculty of Earth Sciences & Engineering, Miskolc, Hungary (*askmf@uni-miskolc.hu)

The safe, sustainable and cost-efficient supply of primary and secondary raw materials is an indispensable base of a prosperous society. Against this background the European Geotechnical and Environmental Course (EGEC) as a part of the Erasmus Mundus Minerals and Environmental Programme (EMMEP) is a two-year MSc course to educate future managers and leaders in the European and worldwide mineral extractive industry. Other two coursef of the EMMEP are the European Mining Course (EMC) and the European Mineral Engineering Course (EMEC). The whole program is implemented by a consortium of six European universities with strong engineering background: TU Delft, University of Exeter (Camborne School of Mines), TU Helsinki, TU Wroclaw, University of Miskolc, and RWTH Aachen. The Erasmus mundus program leads to a double MSc degree in Minerals and Environmental Engineering. Students who complete the program have the advantage of excellent international employment opportunities.

The course is a two-year 120 ECTS programme in English. The consortium offers a unique curriculum with mineral resource and environmental courses in a combination which is not available at a single European institution. Entry requires a Bachelors' degree in natural resource engineering, or an equivalent discipline. The study plan comprises four semesters. Two semesters are reserved for an 8 months joint curriculum at 4 universities. The remaining two semesters are spent at the two universities awarding the double degree. Non-European candidates have the opportunity to get a scholarship from EU, which covers all their expenses during the four semesters.

The Faculty of Earth Science and Engineering, University of Miskolc takes part in the EGEC program. In 2010-2011 the following courses are offered: Environmental Risk Assessment, Environmental Bioprocessing, Environmental Geology and Environmental Geophysics (two month, 4 ETCS each). In the 3rd semester the students can study Groundwater Flow, Geotechnical Engineering, Engineering/Mining Geophysics, Mine Waste Geochemistry, Mineral Processing Tailings Management and Utilization, Numerical Methods in Geotechnics (four months, 5 ETCS each). In the last semester students have to take part in project works, and they should complete their thesis works.

Last year, in the frame of EGEC program there were participants from China, Chile, Namibia, Sierra Leone, Ethiopia, India, Pakistan, Iran, Nepal, and from a number of European countries, together with Hungarian students. In June 2010 the University of Miskolc and the Delft University of Technology awarded the master double degree in Miskolc for absolvents from Pakistan and Namibia.

The program is strongly supported by the industry (near 50 multinational firms, including the worldwide leading mining companies). The participating universities and the additional institutions and companies are in co-operation in the FEMP (Federation of European Mineral Programs). This has proven to be one of the most important factors of its success. A choice of internships and job opportunities are offered to participating EU and non-EU students. Further information is available at www.emmep.org

MINSPEC – the first Marie Curie Chair of Excellence in mineralogy (2006–2009)

Nasdala, L.* & Tillmanns, E.
Institut für Mineralogie und Kristallographie, Universität Wien, Vienna, Austria (*lutz.nasdala@univie.ac.at)

This contribution summarises the activities and impact of the Marie Curie Chair of Excellence for Mineral Spectroscopy (project no. MEXC–CT–2005–024878; acronym MINSPEC). It has made an outstanding contribution to the advanced-level teaching and training of mineralogy students, both in Vienna and on a European scale. This chair was established at the Institut für Mineralogie und Kristallographie, Universität Wien, Austria, for a three-year time period (April, 2006 – March, 2009). MINSPEC was the third Marie Curie Chair at all awarded to a host organisation in the country of Austria, and it was the first Europe-wide in the field of mineralogy.

In the framework of its Human Resources and Mobility (HRM) Activity, the European Commission funds, among others, a limited number (ca. 15/year) of temporary university chairs. The establishment of Marie Curie Chairs, part of the Marie Curie Excellence Promotion and Recognition program, aims at improving the university education in disciplines where the needs of an emerging research are not met by the existing, limited training opportunities. MINSPEC's main focus were mineralogical micro-spectroscopy techniques, in particular those that use light for sample excitation (i.e., Raman, infrared absorption, optical absorption, and photoluminescence).

The project's objectives have been accomplished convincingly. The host institute has strengthened its position as one of the internationally leading places for competent training in mineralogical light spectroscopy; an enormous amount of international recognition was gained. The dissemination of spectroscopy-related knowledge and data was improved, and it is being centralised by the chair's www pages (especially the "Spectroscopy Links"). The establishment of a European Centre for Mineral Spectroscopy at the host institute was initiated.

Activities included the training of graduates, Ph.D. students, and researchers; both at the host institute and at other institutions. One diploma and three Ph.D. projects were supervised by the chair-holder, and three more Ph.D. students from other countries were co-supervised during four-month periods which they spent at the host institute. On-site spectroscopy training was also provided to 28 short-term visitors (graduates, Ph.D. students, and researchers) from institutions in 13 countries. At the Universität Wien, the chair-holder taught 19 classes plus one field trip. In addition, three one-week short courses held at the host institute were organized, which overall gathered 94 participants (coming from 19 European countries, Russia, Israel, the U.S.A., Thailand, and Australia) and 15 invited international lecturers. External teaching and training was provided through lectures at universities in Germany, Slovakia, Slovenia, the United Kingdom, France, Spain, Greece, Norway, Russia, Thailand, and Australia; and a two-day short-course in Ljubljana, Slovenia, which was attended by 36 participants.

Associated was the research project "Micro-spectroscopy of radiation-damaged minerals". This and a broad range of additional research topics was dealt with, motivated by the goal to involve the supervised Ph.D. students in a large variety of analytical problems. Results led to important contributions to the understanding of radiation effects in minerals. Scientific co-operation with 51 institutions worldwide was conducted. Research results were presented in 20 papers in peer-reviewed journals (8 more were submitted by the time of the end of the project) and 34 conference presentations, five of which were invited. The Universität Wien has finally decided to maintain the chair beyond the temporary EU funding period, as permanent full professorship for mineralogy and spectroscopy.

Using in-situ produced cosmogenic ^{10}Be in quartz to constrain deglaciation histories of Romania

Gheorghiu, D.[1*], Fabel, D.[1] & Xu, Sh.[2]
[1]Dept. of Geographical and Earth Sciences, University of Glasgow, Scotland, UK ([*]Delia.Gheorghiu@ges.gla.ac.uk)
[2]Scottish Universities Environmental Research Center (SUERC) – AMS, Glasgow, Scotland, UK

Detailed knowledge of the climatic and environmental development during the Late Devensian and Holocene stems mainly from investigations in western and northern Europe, with only fragmentary evidence from regions situated in eastern and/or southeastern Europe. To fully address the temporal and spatial variability of Late Glacial climate fluctuations, and their impact on the environment, more palaeoenvironmental data are needed from different latitudes and altitudes.

The Rodna Mountains were glaciated in the past; however, there are no constraints on the timing, extent and dynamics of this glaciation in the northern part of Romania. The former ice extent of two major glacial advances (Late Devensian and Younger Dryas) was reconstructed based on mapping and surveying of glacial features. The morphostratigraphy of the area suggests two episodes of glaciation: an older one during the Late Devensian, and a subsequent smaller glaciation. Field evidence suggests that during the Devensian glaciation, ice reached lower elevations (~ 750 m) in Rodna Mountains than previously suggested. The relative chronology was supplemented with surface exposure dating using the *in situ* produced cosmogenic nuclide ^{10}Be in quartz, which provides a preliminary chronology for ice retreat. Two boulders were abandoned about 36.8 ± 1.0 ka at an elevation of ~ 850 m. Glacial erratics and bedrock samples (n = 27) provide a good chronology for deglaciation during the Late Glacial, suggesting that ice retreated into the corries between 18.1 – 13.2 ka (1100 – 1800 m altitude). Final deglaciation took place in the corries at about 12.5 - 11.2 ka (n = 8).

Continuing field and laboratory analysis will further constrain spatial and temporal limits of glaciation allowing ice masses and palaeoenvironmental conditions to be reconstructed within the Rodna Mountains. Comparison with the other glaciated areas in NW Europe (Scotland) will provide new insights into the past climatic gradient across Europe.

Nanomineralogy – modern challenges and perspectives

Koneev, R.I.
Dept. of Mineralogy and Geochemistry, Faculty of Geology, National University of Uzbekistan, Tashkent, Uzbekistan (rkoneev@yahoo.com)

The swift development of nanosciences and nanotechnologies in XXI century caused an appearance of new scientific directions – nanomineralogy, nanogeochemistry and others. The nature has been used nanotechnological methods in different geological processes long before the human. All minerals passed the stage of nanostate (during crystallization or destruction) and modern methods of research allow determining those signs: fullerenes of schungite, opal nanostructures, "invisible" gold in sulfides and etc. Study of ores from different deposits by sound methods had shown that the majority of elements with *n*ppm – *n*ppb clarks and industrial content (Au, Bi, Te, etc.) form nanoassemblages withing the matrix of macrominerals. Nanominerals form during the processes of natural nanotechnologies "upwards" – from the atom to nanocrystal or on "gel-sol" technology. Weathering, dispersion in fault zones and other processes form nanoparticles of minerals in the "upwards" technologies.

There are very difficult questions for nanomineralogy:

- Are lows of nanotechnologies of artificial materials applied to the processes of natural nanotechnologies?
- Are the sizes of nanominerals limited by 1-100 nm interval or their size might be bigger?
- Could be nanominerals of fullerenes type with symmetry axes of the 5 order considered as crystals?
- How size effects affect on stoichiometry, physical and other properties of nanominerals?
- Is it necessary to differentiate the lows and rules of mineral formation in macrosystems from the processes with participating of nanoparticles and nanominerals?

The possibilities of nanominerals and nanoparticles formation in the nature are various: anthropogenic, explogenic and other processes; the crystallization from heterogenic, colloid systems; decay and separation of admixture from heavy solutions, diffusion and localization of elements in the defects of structure, decay of unstable isotopes and unstable compounds, weathering and so on. The problem of the development of new terminology and methods of research became actual one.

The decision of listed and other problems opens new perspectives of the decision of theoretical and practical questions of ore formation. For example why are hydrothermal deposits confined to the fault zones, different breccias, black shales? Is it possible that the explanation of it is that powdered, carbonaceous nanomaterial initiates different chemical reactions and sorbs elements from the solutions, creating industrial concentrations during non optimal thermodynamic parameters due to high surface energy. The analysis of nanoassemblages creates new basis for the search, typification, evaluation of perspectives and technological properties of noble and rare metals deposits.

Definition of bio-minerals

Miura, Y.
Yamaguchi University, Yamaguchi, Japan
(dfb30@yamaguchi-u.ac.jp)

Defining bio-minerals related with both astrobiology and life activity is required for the following factors: 1) Combined mixture of life-materials between inorganic (minerals) and organic compounds (used both as INOG). 2) Material state changes of gas-liquid-solid (VLS) phases by continuous dynamic reaction, where solid includes minerals. 3) Space and time (ST) factors, significant for dynamic processes of water from Earth planet [1-5].

Almost all life materials are combined with the following two materials: 1) Inorganic (IN) materials of mineral crystals with carbonates, phosphates and oxides in composition, with cyclic materials (called as "fossil" as some state IN with relatively long cyclic system), where carbon (C), hydrogen (H) and phosphorous (P) together with minor elements (Fe, Ni, Mg, S, Cl, Mn, Cr, Co, Cu, and Zn [2]) found in bone and shell etc. are richer in carbonaceous meteorite than in terrestrial rocks as the cosmic abundances based on silicon (10_6) [5-7]. 2) Organic (OG) materials with carbon-bearing organic materials in composition, with cyclic materials (some state OG with relatively short cyclic system), where carbon-based organic compositions of RNA and DNA found in the life cell and blood are characteristic for active reactions with short periods in life, which is changed to solid-state (to minerals). In this sense, life materials are considered to be "combined materials of inorganics (minerals) and organics (used as INOG)", which differ in composition and activity (with short (IN) and long (OG) periods of "inorganic fossil" [6,7]).

There are two processes on material changes of life activity as follows: 1) *VLS State changes:* Life activity (in human, animal and plants etc.) shows cyclic system of the following three VLS states: a) Vapor state V (like gases of oxygen and carbon dioxides). b) Liquid state L (like liquids of cell and blood etc.). c) Solid state S (like solids or minerals of bone and shell etc.). 2) *State changes for cyclic system:* Life activity (in human, animal and plants etc.) is required dynamic changes of materials by the VLS state change for overall cyclic system of the following phenomena: a) Birth and death (used as BD in life activity). b) Formation and destroy (used as FD in inorganic fossil, any minerals and rocks). In this sense, life materials reveals "dynamic VLS activity with carbon, hydrogen, oxygen and nitrogen (CHON), which produces "dynamic mini-cycle materials" on "the water-air-planet of the Earth with the VLS".

Astro-life materials are largely required to be considered to be dimensions of space and time (ST) as follows: 1) In close space and short time (to the Earth of the Solar system): a) Time: short period (from second to year). b) Space: localized space (from nm to km). 2) In deep space and long time (in the cosmic space): a) Time: long period (from year to light-year). b) Space: localized space (from km, a.u. to lightyear distance). In this sense, life materials can be "discovered" not only in the Earth Planet (of the solar system), but also in deep space if there are similar dynamic and cyclic systems of three states.

[1] Miura, Y. and Fukuyama, S. (1998) *Rev. High Press. Sci. Tech.*, **7**, 1306-1308. [2] Miura, Y. (2006) *LPI Contrib.*, **1331**, #7001. [3] Miura, Y. (2006) *LPI Contrib*., **1335**, #4051. [4] Miura, Y. (2008) *LPI Contrib.*, **1439**, #3001; **1446**, #4047 & #4051. [5] Univ. Sheffield (2009) *Periodic table web-elements*, http://www.webelement.com. [6] Miura, Y. (2009) *6th AOGS*, #PS09-15-A012. [7] McKay, D.S. et al. (1996) *Science*, **273**, 924-930.

MINCALC-V5 a non EXCEL based computer program for general electron-microprobe mineral analyses data processing

Bernhardt, H.-J.
Ruhr Universitaet, Bochum, Germany
(heinz-juergen.bernhardt@rub.de)

The electron-microprobe today is a routine instrument for quantitative analyses in the micrometer scale applied in many fields of science among these Geology and Mineralogy. Besides tabular or graphical presentation of the analyses, structural formula and end-member calculations are needed to complete analyses evaluation. This may include the calculation of not measurable elements like H or Li and the separation of e.g. Fe^{2+} and Fe^{3+}. Mineral specific programs [1] or EXCEL sheets [2] are normally used for this purpose. Only few more general programs [3] exist, which are not really flexible and easy to modify and adapt to specific problems.

MINCALC-V5 combines the following features: **a)** Input filters for various probe output files are implemented in order to convert them to MINCALC-files for further use. The original files remain untouched. **b)** Long time storage and fast retrieval of analyses data as needed in a multiuser microprobe laboratory. **c)** Analyses files normally contain the results of several mineral species, therefore simple and very versatile analyses selection options are provided as numerical filters, analyses similarities, definable keys (e.g. mineral or sample name), plots and manual selection. **d)** Complex structural formula and end-member calculations using a simple programming language inside the program is possible (e.g. *Al_t= FILL Si with Al to 3;* meaning: if Si is less than 3, then fill the position of Si with Al up to 3 or less if not enough Al is present; then store the result as Al_t). Programs may be stored for further use. **e)** Plots of all measured and computed variables can be made in terms of histograms, line plots, X-Y-plots and triangular plots. It may be requested to show additionally all variables linked with the plot point specified using the mouse curser. **f)** The program user is completely free to define the output sequence of tables. All results may be printed, stored or transferred to the clipboard. Thus, also communication with other programs can be managed. **g)** A formula data base is available to simplify mineral identification; the user may search for any element combination also with exclusion of defined elements. **h)** To compare measured analyses with theoretical values, the weight-% of end-members or end-member combinations are calculable. **i)** MINCALC files may be merged to very long files (tested with 12000 analyses composed of more than 300 single files). Applying the above mentioned keys it easy to select e.g. a certain mineral species from a certain sample or from several samples and use a predefined program to compute required parameters. The advantage is to minimize the number of needed files. **j)** When two reference points are defined, the x-y-microprobe coordinates of measured points may be transformed to optical- or scanning-microscope coordinates.

[1] Pesquera, A. et al. (2008) *Min. Mag.*, **72(5)**, 1021-1034. [2] Locock, A.J. (2008) *Comput. Geosci.*, **34**, 1769-1780. [3] Brandelik, A. (2009) *Comput. Geosci.*, **35**, 1540-1551.

Radium isotopes in the hot-spring sediments, Karlovy Vary (Carlsbad, Czech Republic)

Goliáš, V.[1*], Řanda, Z.[2], Tříškala, Z.[1], Vylita, T.[3], Strnad, L.[4], Šebek, O.[4] & Supiňková, T.[1]
[1]Inst. of Geochemistry, Mineralogy and Mineral Resources, Faculty of Science, Charles University in Prague, Czech Republic ([*]wiki@natur.cuni.cz)
[2]Nuclear Physics Inst., Academy of Sciences of the Czech Republic, Řež, Czech Republic
[3]Mineral Water Bureau of Karlovy Vary, Czech Republic
[4]Laboratories of Geological Inst., Faculty of Science, Charles University in Prague, Czech Republic

The curative thermomineral waters in Carlsbad are Glauber-type ($Na\text{-}HCO_3\text{-}SO_4\text{-}Cl$), highly gaseous ($CO_2$) with TSD about 6.4 g l^{-1} and up to 73°C hot. Its outflow is 30 l s^{-1} of water and 100 l s^{-1} of gaseous phase.

In all hydrothermal system is strong sinter precipitation, mainly caused by the *Cyanobacteria* life cycle metabolites [1]. Calcite and aragonite are both present. The Hot-spring sediments are a big problem for the spas thermal water supply system (Fig. 1).

Fig. 1: The historical pipeline (1920-1935) filed up by aragonite sinter.

Due to the highly radioactive host rock (Carlsbad granite) also the water and its precipitates (sinters) have increased radioactivity caused mainly by radium isotopes. The recent types contains up to 3.29 Bq g^{-1} ^{226}Ra and 0.87 Bq g^{-1} ^{228}Ra. The sinter type that is in full contact with gaseous phase reach specific activities up to 26.03 Bq g^{-1} of ^{210}Pb as the radon long-term deposit. The autoradiography shows a quite homogenous distribution of radioactivity sources. The radioactivity of the fossil Hot-spring sediments is very low due to radium decay.

The both of aragonite and calcite types have an increased content of Be, Ba, Fe, Mg, Pb and Sr (ICP-MS and ICP-OES results).

The radium content in carbonate sinters is not bond with sulphate phase (radiobarite) as in the other cases [2]. As the results of the sequential leaching is the main portion of radium in HCl-leachable fraction in both of aragonite and calcite types. We suppose that the radium and also ^{210}Pb are present as a substituent in the structure of the aragonite–witherite-cerrusite phases, and it can be also incorporate in the calcite structure [3] in the case of calcite-type sinters.

[1] Lisá, L., Hladil, J. & Vylita, T. (2007) *Vesmír*, **86**, 137, 420-425. [2] Řanda, Z. et al. (2010) *J. Radioanal. Nucl. Chem.*, **283**, 89-94. [3] Yoshida, Y., Yoshikawa, H. & Nakanishi, T. (2008) *Geochem. J.*, **42(3)**, 295-304.

A census of mineral species – 2010

Higgins, M.D.[1*] & Smith, D.G.W.[2]
[1]Sciences de la Terre, Université du Québec à Chicoutimi, Québec, Canada ([*]mhiggins@uqac.ca)
[2]Dept. of Earth & Atmospheric Sciences, University of Alberta, Edmonton, Alberta, Canada

This census of minerals is a 'snapshot' of the state of the population of named and valid unnamed species – how it is growing and the characteristics of its members. This study is based on the very substantial MinIdent-Win mineral properties database. The availability of such data compilations put us in a position to see a broad view of mineral properties, and their variations, much more easily and more accurately than at any time in the past. Using histograms and graphs we can show the variations in such parameters as symmetry, density, indices of refraction, birefringence, reflectance, hardness, as well as the population of the major mineral divisions. Additionally, it is possible to explore in detail similar variations within major mineral groups such as the amphiboles. This poster will explore a substantial range of such variations and present the results in a series of simple diagrams. The following are examples of the results of this compilation.

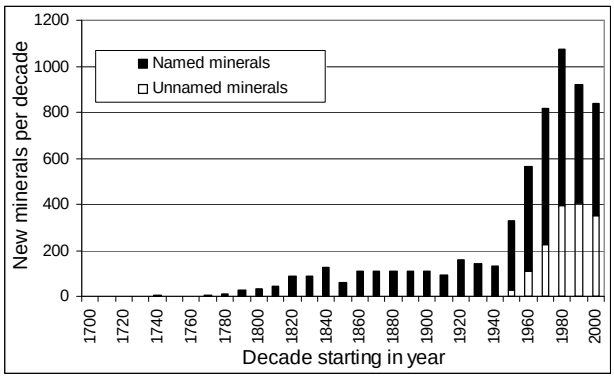

The number of new minerals described per decade increased fairly steadily to ~150 until the 1950s, when it accelerated to peak at over 1000 in the 1980s. The decrease since then may reflect maturity in the subject, or stricter controls on new mineral naming. Unnamed minerals make up 23% of the total, but ~40% of new minerals defined since 1980.

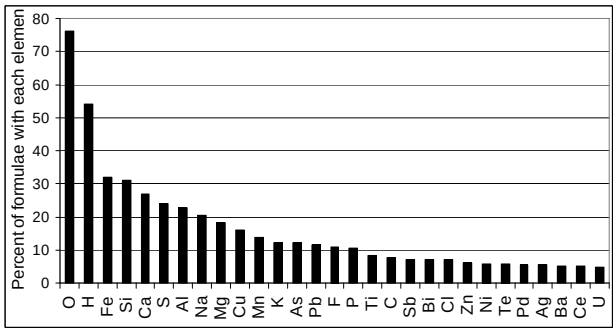

The formulae of minerals reflect their major element compositions and mineral major divisions. O is the most common element, in 76% of formulae, followed by H (53%). Although other elements abundant in the crust are well-represented in mineral formulae, there are minor or trace elements that are over-represented amongst minerals, such as As, Pb, Sb, Bi, Te, Pd, Ce, U, *etc*.

Ca-rich plagioclase formed with hot CO_2 gas

Miura, Y.
Yamaguchi University, Yamaguchi, Japan
(dfb30@yamaguchi-u.ac.jp)

Anorthite, the Ca-rich plagioclase, is considered to be formed by continuous silicate crystallization at magmatic high-temperature condition. Recently, carbon-bearing anorthite mineral has been found separately in cavities of basaltic rocks from Shimonoseki, Yamaguchi, Japan [1,2].The main purpose of the paper is to elucidate the conditions of anorthite formation by hot carbon dioxides (CO_2) -rich condition by mixing with carbon-bearing calcite during dynamic explosion processes of volcanic process.

Significant amounts of carbon are found in Ca-rich plagioclase minerals, which occur only on phlogopite plates (as shown in Fig. 1), from some cavities in volcanic basalts from Shimonoseki, Yamaguchi, Japan [1,2].

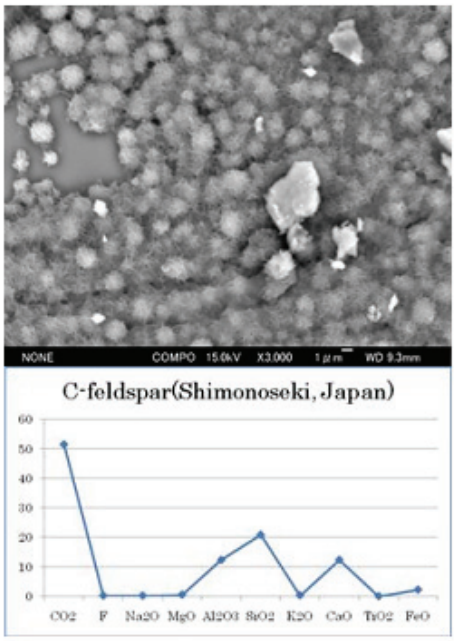

Fig. 1: Electron micrograph (FE-ASEM) of fine carbon-bearing anorthite minerals found on phlogopite plates in cavities from Shimonoseki, Yamaguchi, Japan [1,2]. Bar is 1μm in size.

Carbon is considered to be transported from the buried limestone which is broken by normal magmatic melting of basalt with few Na and K elements. The present results are similar with those found by studying anorthite formation at various volcanic rocks on the Earth (Nagahama-Hamada, Mishima-Hagi, Miyake-Jima and Sakura-Jima, Japan) and at impact breccias of the lunar anorthites on the Moon [3].

The present study is summarized as follows: 1) Ca-rich plagioclase can be formed separately from Ca-rich limestone and silicate-rich wall rocks with carbon dioxides condition at explosive magmatic intrusion. 2) Fine carbon-rich anorthite plagioclases are found in the smaller basaltic intrusion with buried limestone at Shimonoseki-Yamaguchi, Hamada-Shimane and Mishima-Hagi, Japan, whereas large carbon-bearing anorthites with hot carbon dioxides are found in active volcanoes of Miyake-Jima in Japan. 3) The present results will be applied for studyind carbon-bearing impact breccias on the Moon and Mars.

[1] Miura, Y. (2009) *Eos Trans. AGU*, 90(22), Jt. Assem. Suppl., V13C-01. [2] Miura, Y. (2008) *EOS-Trans, AGU*, 89(53), MR33B-1861 (SG). [3] Haruyama, J. et al. (2009) *Geophys. Res. Lett.*, **36**, L21206.

Advanced Mineralogy in Mexico: results and future research

Ostrooumov, M.
Dept. of Geology and Mineralogy, University of Michoacan, Morelia, Mexico (ostroum@umich.mx)

Nature endowed Mexico with enormous metallic and non-metallic mineral resources. This has been proven many times as a result of the immense field of study that mineralogists have undertaken in the country. However, in spite of the extensive research, at the end of the XX century scientists paradoxically have still not appropriately explored the Mexican territory from the mineralogical point of view [1,2].

In the last few years, European specialists have implemented an approach that may be called Advanced Mineralogy [3]. This approach may be defined as new ideas and concepts based on recent mineral studies. Ten years ago the fundamental task for Mexican mineralogists was rise to an agreed level of development of Advanced Mineralogy as occur in other countries.

During the last 10 years (2000-2009) the Mexican mineralogists have worked to improve the situation in Mexican mineralogical science. The aim of this paper is to report the results of the recent investigations in Mexico from different areas of Advanced Mineralogy: physics and crystal chemical features of minerals, environmental mineralogy, applied mineralogy to the prospecting of mineral deposits, and mineral discovery of new species and deposits [4-11]. As a result of all these research, Mexico is now on the map of the Advanced Mineralogy and in WEB publications [12,13]

The author emphasizes the importance of the creation of the Mexican mineral catalogue with its base in the modern crystal chemical classification that signifies the first scientific and systematic inventory of mineralogy of the country. The intention of this inventory was to analyze not only the present mineralogical catalogue from a scientific point of view, but also from the practical point of view, characterizing in detail those mineral species that can be used as an important guide in the exploration of the mineral deposits as well as in the mining and benefit of the ores.

The organization and realization of the systematic mineralogical research of the Mexican subsoil has great importance. As a result of this study, mineralogists will establish laws that will guide the exploitation and concentration of the economic minerals to allow the creation of the scientific bases of metallogeny and the mineralogical prospecting of new mineral deposits. Mineralogists must develop new areas of Advanced Mineralogy in Mexico to continue to study the different mineral formations: the mineral genesis in volcanoes, oceanic bottom, historical monuments, and mining wastes. The contemporary arsenal of analytical methods permits to analyze minerals together without influencing or modifying original properties; therefore complete and necessary information is obtained as a result which can be used towards the successful solution of pending or future mineralogical problems in Mexico.

[1] Victoria, A. (1998) *Bol. Min.*, **12**, 84. [2] Ostrooumov, M. (2001) *Bol. Min.*, **15**, 7-16. [3] Marfunin, A. (ed.) (1994-1998) *Advanced Mineralogy*. New York: Springer-Verlag. [4] Ostrooumov, M. et al. (1999) *Eur. J. Mineral*., **11**, 899-908. [5] Ostrooumov, M. et al. (2002) *Comp. Rend. Acad. Sci*., **334**, 21-26. [6] Ostrooumov, M. et al. (2003) *Rev. Mex. Sci. Geol.*, **20**, 223-232. [7] Ostrooumov, M. et al. (2004) *Can. Mineral*., **334**, 21-26. [8] Ostrooumov, M. (2007) *Spectrochim. Acta*, **68**, 1070-1076. [9] Ostrooumov, M. (2009) *Spectrochim. Acta*, **73**, 498-504. [10] Ostrooumov, M. et al. (2009) *Rev. Mex. Sci. Geol.*, **26**, 600-608. [11] Ostrooumov, M. (2009) *Geoarchaeol.*, **24**, 619-637. [12] http://www.iim.umich.mx/smexmineralogia [13] http://www.mineralog.net.

Paleoenvironmental controls on clay mineralogy of Carnian sections from the Transdanubian Central Range, Hungary

Rostási, Á.* & Raucsik, B.
Dept. of Earth and Environmental Sciences,
University of Pannonia, Veszprém, Hungary
(*rostasi.agnes@almos.uni-pannon.hu)

Clay mineralogy is considered to be a powerful tool for interpretation of weathering conditions and paleoclimate in the source area. In general, illite and chlorite have been considered to be less sensitive to chemical weathering and may be used as internal standards or comparators, hence the kaolinite/illite and/or smectite/illite ratios are used by many authors as paleoclimate proxies. The abundance of kaolinite is especially a good indicator of landmasses with hot and humid (subtropical to tropical) climate supported by high water/rock ratio and steep slopes with good drainage. Smectite is generally suggested to form during weathering in seasonally wet and dry climates with low water/rock ratio and lower slopes, and low relief with poor drainage.

The Upper Triassic sediments both in NW Europe and in the Mediterranean show evidences for a generally arid climate regime. However, in the Carnian, a biotic crisis, extinction event, oceanographic changes, increased rainfall and an anomalous siliciclastic input to the oceanic basins occurred contemporaneously at this time, which interrupted the warm and arid climatic conditions. The paleoclimatic and paleo-environmental interpretation of the changes recorded by Carnian successions in Europe remain controversial.

The Carnian marine succession of Veszprém Marl and Sándorhegy Formations from the Transdanubian Central Range (Hungary) shows significant change in sedimentation: pelagic carbonate deposition was replaced by formation of fine-grained marly sediments. The clay mineralogical composition of 240 samples four boreholes (Bszü-1, Bfü-1, Met-1, and Zs-14) was determined by XRD analysis in order to model the paleoenvironment.

The clay fraction of the samples includes variable proportions of illite, illite/smectite mixed-layer minerals (IS), chlorite, and kaolinite. High degree of expandability (50–70%) and poorly ordered character (S=0) of the IS resulted from relatively low degree of diagenetic overprint. Therefore, the clay mineralogical composition seems to be an original signal applicable to reconstruct the paleoenvironment. The relatively large amount of detrital illite (~40–60%) and chlorite (~10–30%) associated with kaolinite (~10–20%) reflects strong erosion of high relief areas and increased rate of continental weathering. The IS (up to ~60%) can be formed from smectite via burial diagenesis and the originally smectitic material could be derived from altered volcanogenic rocks. Carbonate-rich intervals are enriched in IS whereas marl-dominated intervals are richer in illite which was caused either by fluctuations of terrigenous input or sea-level fluctuations. Based on these results, mixed carbonate-siliciclastic basinal sediments representing the 'Carnian Pluvial Event' in the Transdanubian Central Range could be a superimposed product of climatic change, sea-level variation and tectonism.

AUTHORS' INDEX

Page numbers in ***bold italics*** refer to papers presented by the given author
Note: blank pages are not included in the pdf file

Aagaard, P. 486, 628, 635
Abart, R. 591, 800, 801, 802, 805
Abd El-Rahman, Y. ***586***
Abdel-Karim, A.M. 505
Abdioğlu, E. 97
Abdu, Y. 415
Abe, J. 680
Abedian, N. 528
Abel, R. 689
Ábrahám, P. 792, 794
Abreu, M.M. 338
Abs-Wurmbach, I. 750
Abtout, A. 785
Abushkevich, V.S. 419, 614
Acarlıoğlu, S. 97
Ackermann, S. 342
Acosta, J. 587
Acosta-Pulido, J. 792
Acosta-Vigil, A. 191
Acquafredda, P. 496
Adachi, T. 519
Adamcova, R. ***135***
Adatte, T. 631
Adjaoud, O. ***799***
Adriano, P. 123
Afanasiev, V. 141, 184
Affronte, M. 852
Ageeva, O.A. ***837***
Agheem, M.H. ***603***
Aguiar, P.M. 415
Aguzzi, C. 397, 412
Ahart, M. 663, 671
Ahmadipour, H. 509
Ahuja, R. 165
Aimoz, L. ***353***
Aitugulova, B.A. 702
Akai, J. ***380***, 651
Akaogi, M. ***150***, 154, 158, 720
Akasaka, M. 285, 415, ***713***, 717, ***718***, 721
Akasaka, T. 450, 547
Akhmedshanova, G.M. 363
Akizawa, N. ***583***
Alba, M.D. ***397***, 405, ***412***, 752
Albrecht, N. 788
Albrecht-Schmitt, T.E. 362, 733
Aldabsheh, I. 402
Alekseev, A.O. 640, ***641***
Alekseev, E.V. ***733***
Alekseeva, T.V. ***640***, 641
Alessi, D.S. 383
Alexa, I.F. 54, ***411***
Alfenin, R. 122
Alfonso, P 605, 614, 616
Alicu, D. 114
Allard, T. 104, ***361***, 364
Almohandis, A.A. ***631***
Alonso Mori, R. 37
Alonso, F.J. 129
Alvarez de Buergo, M. 128
Álvarez-Lloret, P. 4, 19, 137, ***371***
Alvarez-Valero, A. 596
Al-Zoubi, A.S.Cr. 328
Amaya Perea, Z. 223
Ambrosi, J.P. 337
Amplieva, E.E. ***419***
Amthauer, G. 11, ***795***
An, Fang 292
Anason, A. ***713***, ***718***
Andaloro, E. ***112***
Andersen, J.C. ***279***, 570
Andersson, M.P. 754
Ando, J. ***420***
Ando, R. 40
Andrade, M.B. ***487***
András, E. 507, 513
Andreani, M.C. 769
Andreeva, I. ***564***
Andrejkovičová, S. ***135***
Andreoli, M. 527
Andreozzi, G.B. ***320***
Andrieux, P. ***749***
Andriyanets-Buyko, A. ***492***
Angeli, N. ***268***
Angelini, I. 105, ***110***
Anikina, E. ***420***, ***421***, 424
Anjos, C. 338
Anraku, S. ***354***, 357
Ansermet, S. 485
Antao, S.M. 719
Antonov, A.V. 445, 576
Antunes, A. ***513***
Antunes, I.M.H.R. 233, ***514***
Antunes, R. 341
Aoki, T. 183
Apai, D. ***792***, 794
Aparicio, C. *9*
Aparicio, P. 752
Apostolaki, Ch. ***68***
Appel, K. ***674***, 677
Appel, P. 674
Ara, D. 467
Arai, S. 190, 205, ***581***, 583
Arakawa, M. 680
Arakawa, Y. 433
Araki, Y. 833
Arana, L. 293
Araujo, R. 112
Ardia, P. 40, 44
Arehart, G.B. 228
Arenholz, E. 844
Arifović, A. 533
Arima, H. 680
Arizzi, A. 118
Árkai, P. 514
Arletti, R. 47, 53, ***103***, 672
Armbruster, T. 11, 26, 55, 479, 491, 709, 739
Armstrong, R. 291, 689
Arribas, A. 236
Arroyabe, E. ***711***
Arroyo, X. ***634***
Arslan, M. 97
Arteeva, T.A. 330
Artioli, G. 65, ***69***, ***104***, 105, 110, 607
Arvidson, R.S. 1, 73
Arvin, M. 509
Asfora,V.K. 112
Ashchepkov, I. ***141***, ***184***
Asif Khan, M. 563
Askhabov, A.M. ***837***
Aslanian, S. 380
Atanassova, R. 437, ***818***
Atencio, D. 487, ***492***
Atichat, W. 23
Atlas, Z.D. 471
Attenkofer, K. 843
Audetat, A. 195
Auge, T. 263
Austrheim, H. 61, 799, 801, 802
Avril, C. 386, 391
Axisa, D. 332
Ayache, M. 785
Ayala, A.P. 487
Azarnova, L.A. ***564***
Azbej, T. ***197***, 201
Azer, M.K. ***586***
Azevedo, M.R. 513, 517, 523
Azim Zadeh, A.M. ***270***
Azzali, E. 341, 346

Baba, S. 519
Babcsán, N.B. 411
Baburek, J. 527, 528
Bacak, G. ***100***
Bachmaf, S. ***75***
Bačík, P. 448, ***477***
Back, M.E. 487
Bačo, P. 296

Badanina, E.V. ***419***, ***612***, ***614***
Badino, G. 465
Badmaeva, S.V. ***91***
Báez, M.I. ***651***
Baeza, N. 132
Baggio, H. 351
Bagheryan, S. ***421***, ***847***
Bahranowski, K. 88
Bai, Wenji 155, 157
Baijot, M. 490, ***603***
Bailau, R. ***493***
Bailey, D.K. 557, ***558***
Bajda, T. 399
Bajnóczi, B. ***113***, 116, 289, ***514***
Bakacsi, Zs. 405
Bakallbash, J. 239
Bakker, R.J. ***172***, ***193***, 264, 480
Bakos, F. 296
Baksheev, I.A. 27, 831
Bakun-Czubarow, N. ***208***, ***452***
Balan, E. 657, 669
Balassone, G. 275, 279
Balázs, R. 642
Baldonedo, J.L. 651
Balek, V. 83
Balen, D. 124, ***451***, 462, ***481***, 621, 632
Bali, E. ***195***, 805
Balica, C. 532
Balić-Žunić, T. 155, 496, ***708***
Balintoni, I. 532
Balogh, K. 231, 621, 622, 632, 637, ***642***, ***683***
Balogh, Z. 754
Bambi, A. 562
Banerjee, S.K. 843
Banfield, J.F. 821, 843
Banks, D. 24
Banno, Y. ***515***
Barabaszová, K. 100, 394, ***700***
Baratu, D.A. 548
Barbanson, L. 288
Bardelli, F. 356
Bargar, J.R. 383
Baricza, Á. ***322***
Barker, S.L.L. 60
Baroni, S. 815
Baronnet, A. 739
Barra, F. 260
Barreto, S.B. ***28***, ***112***
Bartha, A. 506, 538
Bartoli, O. 191, 480
Bartucz, D. 204
Bass, J.D. 144, ***159***
Batanova, A.M. 36
Batki, A. 529, ***565***
Bauer, K.K. ***631***
Bauer, M. ***340***
Baumgartner, J. 501
Baur, W.H 50
Baziotis, I. 595
Bazylinski, D.A. 382
Beal, K. ***454***
Beard, A.D. 561
Beaudoin, G. ***250***
Beaufort, D. 361
Becker, M. ***4***, 741
Becker, U. 358
Behrens, H. ***172***, 644
Beinlich, A. ***61***
Belete, K.H. 264
Belin, S. 658
Beljavskis, P. 482
Belkin, H.E. ***540***, 591
Bellatreccia, F. ***493***, ***495***, 661, 723
Bellini, A. 409
Belmonte, D. 35, ***143***
Below, M. ***80***
Belton, D. 485
Belviso, C. 50
Belyatsky, B.V. ***445***, ***576***, 583
Ben Haj Amara, A. 16
Ben Rhaiem, H. 16
Benea, M. 114, 116, 121, 765
Benedix, G. 765
Benisek, A. ***807***
Benkó, Zs. ***224***, 289, ***621***
Benning, L.G. ***385***, 675, 823, 825
Bente, K. 114
Benvenuti, M. 356
Benzerara, K. 383
Beqiraj, A. ***587***
Beran, A. 175
Bérczi, Sz. 375, 783, ***783***, 784, ***864***
Berger, J. ***303***, ***565***
Bergmann, J. 747
Berkenbosch, H.A. ***252***
Berkesi, M. ***189***, 559
Bermanec, V. 16, 99, 325, 359, 399, ***423***, 424, 437, 439, ***643***
Bernardini, F. ***111***, ***113***
Bernhardt, H.-J. 281, 831, ***869***
Bernier-Latmani, R. ***383***
Berquo, T. 843
Bersani, D. 249, 494
Berta, M. 62
Bertalan, É. 308, 506
Bertier, P. 58
Bertka, C.M. 154
Bertoni, E. 103
Berzina, A.N. ***454***
Berzina-Cimdina, L. 17
Beurlen, H. ***477***
Beyssac, O. 512
Bezacier, L. 144, 851, 855
Bezerra, U.T. ***418***
Biagioni, C. 494, 714
Bicocchi, G. 59
Bidny, A.S. ***27***
Bielańska, E. 88
Bieniok, A. ***467***
Biernacka, J. ***632***
Bigi, S. 436, 495, 500
Bilik, I. 520
Billard, P. 384, 389
Billström, K. 224, 254
Bina, C.R. 176
Bindi, L. 153, 715, 742, 769
Bingen, B. 455
Birch, W.D. ***488***
Birkenmajer, K. 483
Biró, T.K. 108, 110, 111, 136
Biroň, A. 289, 296
Biševac, V. ***621***, ***632***, 637
Bismayer, U. 367
Bjondahl, F. 1
Blamey, N.J.F. 22
Blanc, P. 407
Blanchette, C. 862
Blanco, M. 638
Blanco-Quintero, I.F. 600
Bläß, U.W. ***778***
Blechta, V. 845
Blyth, R. 37
Bobocioiu, E. 656
Bobrov, A. ***148***, 153, 179
Bodinier, J.-L. 508
Bodnar, R.J. 193, 194, 200
Bodor, B. ***197***
Boerio-Goates, J. 809
Boettcher, I. 580
Boev, B. 795
Boffa Ballaran, T. 143, 147, 158, 715
Bogdanov, K.B. ***270***
Bogrash, A. 310
Böhm, C.O. 551
Böhmová, V. 344, ***461***
Boiocchi, M. 495
Bojar, H.-P. 501
Bolanz, R.M. ***321***, ***342***
Bolormaa, O. 77
Bonaccorsi, E. 494, ***494***, ***714***
Bonatotzky, T. ***643***
Bonazzi, P. 715, ***742***
Bonferoni, C. 412
Boni, M. 275, 279, ***301***
Bonilla Pérez, A. 223
Bonneville, S. 385
Bónová, K. 453
Boon, R.G.J. 339
Booth-Rea, G. 508
Bordage, A. ***28***, 44, ***657***, ***669***
Borensztajn, S. 386
Borg, G. 106
Borges, W.N. ***509***
Borisover, M. ***87***
Borodajenko, N. 17
Borojević Šoštarić, S. ***292***
Boros, Á. 326
Borovikova, E.Yu. ***660***
Borowiec, W. 321
Borrini D. 11
Bors, V. 515
Bortnikov, N.S. ***91***, 248, 260, 419, 420

Bortolotti, D. 856
Borutzky, B.Ye. 837
Bosbach, D. 825
Bosi, F. ***476***
Botan, A. ***57***
Botcharnikov, R.E. 656
Bots, P. 675, ***825***
Botz, R. 302
Boulliard, J.-C. ***422***, ***768***, ***838***
Bourgoin, V. 422
Bousquet, R. ***591***, ***597***
Boussafir, M. 92
Bousta, F. 115
Bouwman, J. 792
Bovet, N. 365, ***369***
Bożęcki, P. ***342***
Bozkaya, G. ***293***
Bozkaya, O. ***633***
Bozsó, G. ***322***
Bradshaw, D.J. 4
Brady, A. ***558***, 560
Braga, R. 191
Brandl, G. 527
Brandl, H. 639
Brandtstaetter, F. 457
Brathwaite, R.L. 252
Bray, A.W. 385
Brea, C. 281
Bregman, E.P.H. ***633***
Breheny, C. ***537***
Brendel, U. 467
Brenker, F.E. ***196***, 653
Bressel, L. 41
Brey, G.P. 561, 569
Brey, M. ***229***
Brigatti, M.F. 14, 710, 751, 753, 852, ***852***, 856
Bril, H. 350
Briois, V. 658
Broekaert, J.A.C. 367
Broman, C. 254
Bronzova, Yu.M. 610
Broska, I. 451, ***453***, 460
Brouder, Ch. 657, 669
Brouwer, J. ***805***
Brown, G.E. 658
Brown, G.E., Jr. 337, 383
Brtáňová, A. ***397***
Brugger, J. 485
Brügmann, G. 25
Bruintjes, R. 332
Bruneel, O. 345
Brunelli, M. 672
Brunet, F. 386, 512
Bruno, E. 147
Brusnitsyn, A.I. 229
Bruthans, J. 468, 647
Bryanchaninova, N.I. 152, 574
Bryzgalov, I.A. 416
Bubnova, R.S. ***9***, 479
Buchholz, T.W. 604
Buchner, E. ***777***, 780
Buda, Gy. ***507***, 513, 568, ***860***
Buday, T. 375
Budzyn, B. 447
Bugár, I. 697
Bugoi, R. 107
Bujdák, J. 80, ***394***
Bujdáková, H. 394
Bukhanovsky, N. 87
Bunnag, N. 33
Burchard, M. 842
Burda, J. ***449***, ***516***
Burg, J.-P. 458
Burgassi, P. 59
Burlinson, K. ***255***
Burns, P.C. ***364***, 366, ***731***
Burrows, N.D. 843
Buseck, P.R. ***v***, 332, 797
Butenko, E. ***88***, ***398***
Butterfield, D.A. 252
Bykov, D.M. 660
Bylina, P. ***648***
Bytchkov, A. 44
Bzowska, G. 340, 343, 423

Cabaret, D. 657
Cabral Pinto, M.M.S. ***323***
Cabral, A.R. 274
Cabri, L.J. 266
Caddeo, G.A. 468
Cadoni, M. 48
Cai, Jianhui ***566***
Cai, Y.Q 151
Cai, Yuanfeng 329, ***422***
Calaforra, J.M. 465
Calas, G. ***38***, 345, 363, 364, 670
Calia, A. ***134***
Călin, N. ***715***
Callegari, A.M. 495
Calligaro, T. 107
Calvot, G. 173
Cama, J. 66, 232
Cámara, F. 31, 493, 661, ***731***, 732, ***811***
Campbell, A.J. ***161***, 164
Campeny, M. ***230***, 230, 242, 578
Camprubí, A. ***221***, ***293***, ***294***
Canals, A. 775
Candeias, A.E. 69, 122, 123, 341
Canella, L. 3, 682
Canet, C. 293, 294
Capacci, F. 658
Capitani, G. 672
Čaplovičová, M. 310
Caprilli, E. 495
Caracas, R. ***191***, ***656***, ***809***, ***816***, 851
Carbone, C. 346
Cardell, C. 19, 137
Cárdenas Párraga, J. 600
Carelse, C. 279
Carletti, C. 1
Carneiro, J.F. ***827***
Carpenter, M.A. 599, 672
Carroll, M.R. 777
Carter, A. 568
Carvalho, P.C.S. ***256***
Casas, D. 63
Cassiot, C. 345
Castelli, D. 599
Castillo, M. 230, ***230***, 242, 578
Castro, G.R. 753
Castro, M.A. 405, 752
Castro-Mora, J. 294
Castroviejo, R. 276, ***281***, ***587***
Catalina, J.C. 281
Catalli, K. ***152***, 442
Catchpole, H. ***285***
Catillon, G. 104
Čavajda, V. ***310***
Cavalcante, F. 50
Cavalcanti, J.A.D. 483
Cavallo, A. 493, 495
Cavarretta, E. 374
Cazzaniga, A. 272
Cebulak, S. 340
Ceccato, D. 107, 676
Cecil, M.R. 684
Čejka, J. 349
Celik, S. 293
Celis, R. 85
Cempírek, J. 456, ***478***
Cerezo, P. 397, 412
Cesare, B. ***191***, 814
Cestelli-Guidi, M. 777
Chabangu, N. 266
Chakhmouradian, A.R. ***443***, ***445***, ***551***, 573, 575
Chakraborty, S. 842
Chambers, S. ***768***
Chareev, D.A. 263
Charlet, L. 356
Charykova, M.V. 829
Chaudhri, N. 510
Chaumard, N. 789
Chauvet, A. 288
Chazot, G. 579
Checa, A.G. 371
Chelazzi, L. ***715***
Chen, Dongliang 751
Chen, Fanrong 362
Chen, Haiyan 222
Chen, Huei-Fen 432
Chen, J. ***516***
Chen, Jiawei 13, 18
Chen, Jun 451
Chen, L.H. 192
Chen, Ming 779
Chen, Xiaoming 422, 638
Chen, Y.Q. 638
Chen, Yi 215, ***216***, 532
Chenery, S. 506
Cheng, H. ***215***, 700, 701
Cheng, Xu. 573
Cherata, I. ***114***
Chernyatieva, A.P. ***716***
Chesalov, Yu.A. 77, 396
Chesner, C.A. 547

Chetty, D. ***278***
Chevrel, O. 39
Chiou, W.-A. ***695***
Chirikure, S. 105
Chmielowski, R.M. ***812***
Cho, Hyen Goo ***636***
Choi, Bu Kap 231
Choi, Chang Seong ***295***
Choi, J. ***323***
Choi, S.Y. 328
Choi, Seon-Gyu ***231***, ***545***, ***590***
Chon, H.T. ***324***
Choo, Ko Yeon ***10***
Chopin, C. 512, 661, 739, 742
Chovan, M. ***231***, 327, 335
Christenson, B.W. 252
Christiansen, B.C. 365
Christidis, G.E. ***307***, 862
Christy, A.G. 516, ***706***, 738
Chryssikos, G.D. 311
Chu, H.X. 204
Chu, Hao-Tsu 839
Chu, Wangsheng 751, 852
Chudík, P. 613
Chudy, T.C. ***566***
Chukanov, N.V. 487, 492, ***660***
Chumakov, A. 442
Chung, E.H. 324
Church, N.S. 650
Chust, T. 381
Cibin, G. 751
Cicconi, M.R. 37, 42, 777
Cicha, J. 620
Ciesielczuk, J. ***340***, ***343***, ***423***
Çina, A. ***269***
Ciobanu, C.L. 277, ***649***
Císařová, I. 351
Civalleri, B. 143
Cleaves, H.J. 370
Clément, A. 834, 836
Cnudde, V. 132
Čobić, A. 423, ***424***, 437, 439
Cochain, B. 41
Cocić, M. 10
Cocker, H.A. ***280***
Cody, G.D. 370
Coëslan, C.G. 551
Cohen, B.A. 779
Cohen, R.E. 191
Çolak, M. 626
Colakoglu, A. 589
Collins, N.C. 470, ***588***
Combes, R. 390, 391
Comodi, P. ***153***, 346, 820
Compagnoni, R. ***599***
Condamine, P. 173
Conlon, M. 708
Connolly, J.A.D. 814
Constantinescu, B. ***107***, 676
Contrell, E. 162
Cook, N.J. ***277***, 649, 522, 538
Cooke, R. 449
Cooper, A.F. ***551***
Čopjaková, R. ***827***
Coppola, D. 120
Cora, I. ***652***
Cordier, P. 181
Cormier, L. 38, 363, ***670***
Cornejo, J. ***75***, ***85***
Cornell, D. 259
Corzo, A. 388
Costa, M.M. ***517***
Costagliola, P. 356
Costanzo, A. ***22***, ***19***, 537, 562, ***567***
Cota, A. 405, ***752***
Cottignoli, V. 374
Courtin-Nomade, A. 350
Coutinho, J.M.V. 492
Covey-Crump, S.J. 679
Cramer, T. 223
Cramm, S. 644
Craw, D. ***250***
Creaser, R.A. 551
Creţescu, I. 54
Crichton, W.A. 851
Cristea-Stan, D. ***676***
Crossingham, A. ***184***
Crósta, A.P. 786
Cruciani, G. 69
Cruz, T. 123
Csákberényi-Nagy, D. ***847***
Csempesz, F. 81
Csengeri, P. 108
Csillag, G. 333
Csoma, A.É. 465
Cuadros, J. 634
Cuesta, C. 823
Cuevas Castell, J.M. 132
Cuevas, J. 754
Cui, Q. xi
Cui, W.Y. 598
Cultrone, G. 137, 138
Curti, E. 353, ***823***
Curutchet, G. 396
Cusack, M. ***369***
Cuthbert, S.J. ***207***
Cvetko Tešović, B. 637
Cvetković, L. 294
Cvetković, Ž. ***324***
Czank, M. ***653***
Czerny, J. 525
Czímerová, A. ***80***, 83, 393, 698
Czuppon, Gy. ***517***

D'Agostino, L.Z. 482
D'Acapito, F. 658
Dachs, E ***51***, 807
Dähn, R. 353, 673
Daigneault, R. 259
Dal Santo, M. 341
Dalbeck, P. 369
Dalconi, M.C. 69
Dalla Vecchia, E. 383
Damrat, M. 321
Daneu, N. 650, 743
Dang, Zhi 329, 332
Daniel, F. 124
Danielik, V. 697
Danyushevsky, L.V. 277
Dararutana, P. 126
Darbha, G.K. 82, 804
D'Arco, P. 848
Dargaud, O. 38, 670
Darmo, J. 697
Daróczi, L. 683
Dashinamzhilova, E.Ts. 410
da Silva, M.R.R. 477
Davì, M. ***545***
Davidson, P. 604
Davis, B. 573
Davranche, M. 830
de Beer, F.C. ***681***
De Capitani, L. 341, 358
De Francesco, A.M. 112
de Gironcoli, S. 815
de Hoog, J.C.M. ***208***
de Ignacio, C. ***552***
de la Boisse, H. 125
de Ligny, D. 41, 670
de los Ríos, A. 128
De Min, A. 111, 113
de Nolf, W. 196
de Parseval, Ph. ***455***
de Putter, Th. 301
de Ronde, C.E.J. 252, ***252***
De Rosa, R. 545
de Vaux, D. 275
de Villiers, J.P.R. 4, 669, ***741***
De Vivo, B. 540
De Waele, J. ***467***, ***468***
Deacon, J. 302
Dębicka, M. 647
Deconinck, J.-F. ***623***
Decrée, S. ***301***
Deda, T. 239
Dediu, V.A. 372
Dégi, J. 169, 202, ***591***, ***805***
Dékány, I. 87
Dekov, V. 634
del Hoyo Martínez, C. ***6***, ***859***
del Villar, L.P. 59
Delangle, C. 271
Delaye, J.-M. 363
Delgado, J.M. 339, 834
Della Ventura, G. 493, ***661***, 723
Dellisanti, F. 856, 857
Demaiffe, D. 560, 584
Demény, A. 19, 551, ***567***
Demichelis, R. ***816***, ***848***
Demir, Y. 268
Dempsey, C. 560
Denecke, M.A. 825
Deng, Y. 84, 334
Depiné, M. 248, ***256***
Depmeier, W. 479, 653, 733, 829
Derevska, K.I. 298
Derr, J. 47

Derré, C. 388
Deshenenkov, I.S. ***315***
Desobry, S. 384, 389
Detellier, C. 862
Deubener, J. 644
Deutsch, A. ***780***
Devidal, J.-L. 22, 789
Devouard, B. ***22***, ***789***
Dewaele, S. 301
Dewanckele, J. 132
Dhuime, B. 685
Di Benedetto, F. ***11***, ***356***, ***658***
Di Renzo, F. 53
Dianiška, I. 448
Dias, A.C. 338, 393
Dias, P.A ***518***, ***546***, ***615***
Diaz, M. 751
Diella, V. 609, 610
Diener, A. ***821***
Dikmen, S. 76, ***81***, ***699***
Dikmen, Z. 76, 81, ***98***
Dill, H.G. ***221***, ***302***, ***608***
Dimitrova, D. ***835***
Dimitrova, O.V. 486
Ding, Hao 838
Ding, Hongrui ***386***
Ding, K. 727
Ding, Ning 95
Dingwell, D. ***39***, 42
Dini, A. 474
Dinis, P.A. 323
Diot, H. 303, 584
Dipple, G.M. 26, 60, 738
Distler, V.V. ***271***
Ditchburn, R.G. 252
Dittrich, H. 11
Divaev, F.K. 570
Djordjević, M.G. 636
Dmitriev, V. 672
Doan, D.H. 328
Dobosi, G. ***185***, 506, 529
Dobrzhinetskaya, L. 208, 210, ***210***, ***218***
Dobson, D. 690
Dobson, P. 369
Dódony, I. 395, 652, 727, 757
Dohmen, R. 842
Dohrmann, R. 302, 308, 747, 855
Dolejš, D. ***166***, ***194***, 217, 218
Dombroski, B.A. 541
Domonik, A. 688
Donato, R. 545
Dong, D. 37
Dong, Guochen ***222***, ***455***
Dongbao, F. 276
Donmez, C. 589
Donovan, J.J. 779
Đorđević, D.M. 625
Đorđević, N.R. 627
Đorđević, T. ***716***
Dormán, J. ***313***
Dorofeev, S.A. 349
dos Muchangos, A. ***304***
Doublier, M.P. 703
Douglas, N.K. 368
Doušová, B. ***77***, 82
Dovesi, R. 816, 848
Dowman, E. 568
Downes, H. 554, ***561***
Downs, R.T. 726
Drábek, M. 263, 274, ***717***
Drahota, P. ***343***, 344
Drits, V.A. 750
Droubay, T. 844
Drouin, S. 92
Du, Gao-xiang ***838***
Dubessy, J. 189
Dubois, M. ***124***, ***125***, ***288***, 348, 356
Dubovitskiy, V.A. 660
Dubrail, J. ***153***, 677
Dubrovinskaia, N. 162
Dubrovinsky, L. ***162***, 442
Ducea, M. ***684***
Duchêne, S. 677
DuFrane, S.A. 142
Dula, R. 853
Dullemond, C.P. 792
Dultz, S. 80, 85, ***644***
Dumitraş, D.G. 433, 715, 719
Dunin-Borkowski, R.E. x, 650
Dunkley, D. 447
Dunning, G.R. 592
Duong Anh Tuan 27
Duran, A. 385
Duran, C. 455
Durmus, B. 551
Dušek, M. 349
Duthie, L. ***127***
Dutrow, B.L. 475, ***859***
Dymshits, A. 148
Dynes, J.J. 379
Dyulgerova, E. 376
Dziak, R.P. 252
Dzierżanowski, P. 444, 491
Dzikowski, T.J. ***26***

Eeckhout, S.G. 37, 777
Effenberger, H.S. 470
Egal, M. 345
Egli, M. 639
Ehling, A. ***136***, ***762***
Ehser, A. ***106***
Eichert, D. 111
Eichhubl, P. 193
Eilu, P. ***254***
Ejima, T. ***415***, 713
Eklund, O. 1
El Amawy, M. 305
El Nashar, E.S.R. ***511***
Elangovan, P. 689
Elcoro, L. 739
El-Kaliouby, B.A. 568
Ellena, J. 487
Ellmies, R. 574
Elmi, C. ***710***, ***753***, 856
Elsen, J. ***106***
Emmerich, K. ***753***
Emmerling, F. 67
Emsbo, P. 248, ***249***
Endo, T. 783
Endo, Y. 785
Eng, P.J. 821
Ennaciri, A. 288
Ennih, N. 565
Enzmann F. 23, 178
Epossi Ntah, Z.L. ***114***
Eppelbaum, L.V. ***103***
Erbs, J.J. 843
Ercit, T.S. 473
Eremyashev, V. 46
Erić, S. 324, 533, 664
Erickson, K. 59
Erkoyun, H. ***626***, 630
Erman, H. 630
Erőss, A. 465
Ertel-Ingrisch, W. 42
Ertl, A. ***476***, 610, 831
Esaifan, M. 402
Escayola, M. 553
Espí, J.A. 276
Essene, E.J. 807
Etcheverry, M.-P. 661
Evans, R.J. 473, ***481***
Everard, J. 517
Evstigneeva, T.L. ***265***, ***267***, 306, 666
Ewing, R.C. ***ix***, 358
Ezhov, A.K. ***316***

Fabbri, B. ***115***
Fabel, D. 867
Fábián, S.Á. 391, 635
Fairhurst, R. 570
Faivre, D. x
Falagán, C. 63
Falcon, I. ***339***
Falcone, R. 843
Fall, A. ***193***
Fallick, A.E. 24, 289, 296, 426
Fallon, S.J. 60
Falster, A.U. ***604***, 605, 612, 618
Falus, Gy. 62, 169, 174
Fan, Erping 849
Fan, Hong-Rui 257, ***257***
Fandeur, D. 337
Fang, Jian-Neng 432
Fang, Qinfang 634
Fang, Qingsong 155, 157
Fantoni, L. 769
Farahat, E.S. ***584***
Färber, G. 501
Farges, F. 104, ***661***, ***767***
Farkas, I.M. ***337***, 418
Faryad, S.W. ***209***, ***217***, 218
Favreau, G. 422
Fayek, M. ***361***, 364
Fazekas, P. ***81***

Fedortchouk, Y. 149
Feely, M. 22, 198, 537, 567
Fehér, B. 430, 436, 446, ***495***, 500
Fei, Y. 162
Feinberg, J.M. 650
Felmy, A.R. 844
Féménias, O. 303
Feneyrol, J. 24, ***776***
Fenyvesi, É. 81
Ferlat, G. 38
Fernandez Martinez, A. 356
Fernandez, J.-B. ***747***
Fernández, M. 398
Fernández, R. ***49***
Fernández-Díaz, L. 826, 828
Fernández-González, Á. ***826***, ***828***
Fernández-Seivane, L. 828
Ferrand, J. 104, 115
Ferrari, E.S. 610
Ferraris, C. ***712***
Ferraris, G. ***48***
Ferraz, E. 135
Ferreira da Silva, E.F. 338, 393
Ferreira da Silva, G. 862
Ferreiro Mählmann, R. ***622***
Ferrer Escorihuela, P. 753
Ferrer, J. 828
Ferrero, S. 191
Fialips, Cl. 407
Field, M. 553
Figueiredo, M.O. ***662***
Figuła, A. ***399***
Fiket, Ž. ***399***
Filatov, S.K. 9, 479, ***539***
Filcheva, E.G. 646
Filip, J. 9, 460, 485, ***845***
Filipescu, R. ***116***
Filippi, M. 343, ***344***, ***468***
Filippov, V.N. 330
Finch, A.A. 21, ***687***
Finger, F. ***447***, 448, ***449***, 459, ***462***, 692
Fintor, K. ***198***
Fio, K. ***325***
Fiore, S. ***50***, 832
Fisch, M. ***11***, 55
Fischer, C. ***71***, 82, ***804***
Fischer, J. 149
Fischer, R.A. 161, ***164***
Fischer, R.X. 47, ***50***
Fischer, U. 824
Fisenko, A.V. 798
Fisher, R.A. 809
Fittschen, U.E.A. 367
Fletcher, I. 449
Florian, P. 43
Flude, S. ***683***, ***691***
Fodor, R.V. ***541***
Fodorpataki, L. 347
Földessy, J. ***225***, ***308***, 417, 863
Földvári, M. 19
Foley, J.A. 707
Fomina, M. 384
Fontan, F. 614, 616
Fontboté, L. 285, ***287***
Forbes, M. 291
Forbes, T.Z. 364, 731
Forero, J.A ***546***
Foresti, M.L. 11
Fórizs, I. 840
Fornaciai, G. 11, 658
Fornós, J.J. 469
Forray, F.L. 121, 341, 347, 594
Fort, R. 119, 127
Fortes, A.D. 679, ***705***
Forti, P. ***465***, ***466***
Fossum, J.O. 78
Fouquet, Y. 419
Fournier, J. 320
Fourrier, S. 124
Franco Victoria, J.A. 223
Franco, S.I. 293
François, P. 306
Frank, D. ***794***
Frank-Kamenetskaya, O.V. 139, 373, 610, 710
Fransolet, A.-M. 433, 609, ***610***
Franz, A. 691
Frau, F. 468
Freemantle, G.G. 303
Freer, A. 369
Fregola, R.A. ***743***
Freney, E. 332
Frenz, M. 775
Fricker, M. 249
Friedel, O. 110
Friedl, G. 449
Friis, H. 52, 317, 687
Frimmel, H.E. 247, 256, ***248***
Fritsch, E. 22, 337
Fritz, B. ***834***, 836
Frondini, F. 346, 820
Fröhlich, F. 124
Fröschl, H. 109
Frost, D.J. 143, 158
Frost, R.L. ***503***, ***696***, ***700***, ***701***
Fuchs, M. 644
Fuchs, P. 296, ***592***
Fuchs, S. ***232***, 302
Fuchs, Y. 28, 351
Fujimaki, H. ***789***
Fujinami, S. 818
Fujino, K. 148, ***151***
Fujisawa, A. 428
Fujiwara, K. 823
Fukushi, K. 355
Fukushima, K. 695
Fülöp, A. 522
Fumagalli, P. 812
Fumo, S.M. 304
Funakoshi, K. 40, 141, 671
Furrer, G. 639
Fuyuya, K. 789
Fyfe, C.A. 481
Gaboreau, S. 407
Gaboury, D. 259
Gadas, P. 460, ***615***, 620
Gadd, G.M. ***384***
Gadegaard, N. 369
Gagnon, J. 336, 352
Gaidzik, K 423
Gailhanou, H. 407
Gajović, A. 437
Gál, Á. ***295***, 341
Gál, B. ***265***
Gale, J.D. 822, 826
Galeschuk, C. 607
Galí, S ***232***, 242, 240, 553
Gallardo, T. 240
Gallego, A.N. ***285***, ***717***
Galli, E. 467
Galoisy, L. 38, ***363***, 364
Galuskin, E.V. ***444***, ***482***, 491, 493
Galuskina, I.O. 444, ***491***, 501
Galvez, M. 512
Gamyanin, G.N. 421, ***424***, ***425***
Ganguly, J. 143
Ganzel, J. 71
Gao, Xiang ***634***
Gao, Xiaoying 349
Garavelli, A. ***496***
García Robledo, E. 388
García-Casco, A. ***600***
García-Molina, M.J. 651
García-Romero, E. ***307***
Garcia-Ruiz, J.M. ***775***, 834, 842
García-Talegón, J. ***131***
Garda, G.M. ***482***, ***483***
Garofalo, P.S. ***249***, 465
Garrido, C.J. 508, 521, 522
Garshev, A. 624
Garuti, G. 264, 266, 268, 270, 480
Garvie, L. 797
Gasharova, B. 673
Gassen, N. 340
Gates, W. 749
Gattacecca, J. 785
Gauert, C.D.K. 232, ***239***, ***302***
Gault, R.A. 487
Gaupp, R. 701
Gauthier, A. ***348***, ***356***, 391
Gautron, L. 153
Gawęda, A. 516
Gaweł, A. 88
Gay, A.-S. 747
Gazeev, V.M. 444, 491, 493
Gazze, A.S. ***387***
Geck, J. 678
Geiger, C.A. 51, ***61***, ***807***
Gemmell, J.B. 252
Gemmi, M. 149
Génin, J.-M.R. ***705***
Georgiev, M. 665
Georgieva, M. 218
Geraldes, M.C. 509, ***839***

Gerasimchuk, A.V. 571
Gerasimova, E.I ***473***
Gerdes, A. 449, 462, 506, 510, 561, 569, 608
Gerges, A. 225
Gergulova, R. 376
Gervilla, F. ***227***, 508, 832
Gerzabek, M.H. 95
Ghaleb, D. 363
Ghany, N.A.A. 72
Gheorghiu, D. ***867***
Gherdán, K. ***136***
Ghergari, L. 109
Ghigna, P. 672
Ghineț, C. 713, 718
Ghobadi, M. ***569***
Ghoneim, M.F. ***505***
Ghorbani, G. ***518***
Ghorbani, M. ***628***
Ghorbani, M.R 527, 528
Giannini, M. 5
Giannossi, M.L. 372
Giber, A. 515
Gibson, J.L. 249
Gibson, R.L. 782
Gieré, R. ***320***
Giester, G. 34, ***496***, 727
Giesting, P. ***58***
Giger, M. 622
Gilbert, B. ***821***, 843, ***843***
Gilbert, S. 277
Gil-Crespo, P.P. ***425***, 526, 618, 619
Gilg, H.A. ***503***, ***775***
Gin, S. 363
Ginés, A. 469
Ginés, J. 469
Gionis V. 311
Girardi Jurkić, V. 124
Girnis, A. 577
Giuli, G. ***37***, 39, ***42***, ***777***
Giuliani, G. ***24***, 499, 776, ***776***
Giunti, I. ***105***
Giurgiu, A.M. ***519***
Gjoka, F. 12
Glasnák, P. 809
Glass, B.P. 777
Glatzel, P. 37, 657, 669, 678
Glaus, M. 823
Glazyrin, K. 442
Gleeson, S.A. 301
Glikin, A.E. 13, ***800***, 841
Gliozzo, E. 121
Głogowska, M. 423
Gméling, K. ***483***, 484
Gobi, R. 462
Godinho, J. ***828***
Goepel, A. 701
Goga Beqiraj, E. ***12***
Goliáš, V. 725, ***869***
Golovin, A.V. 443
Gomes, C.S.R. ***325***, 326, ***864***
Gomes, E.M.C. 325, ***326***, 864
Gomes, M.E.P ***233***
Gomez, S. ***315***
Gomez-Heras, M. ***127***
Gómez-Villalba, L.S. 119, 127
Gomi, H. ***164***
Gonçalves, A.O. 230, 242, 553, 562, 578, ***605***, 616
Goncuoglu, M.C. 633
Gonzaga, R.S.G. 28
Gonzales-Romero, M. 385
González, N. 754
González-Jiménez, J.M. 227
González-López, N. 63
González-Muñoz, M.T. ***140***
González-Partida, E. 293, 294
Goran, D. 688
Goranov, V.A. ***372***
Gordienko, V.V 614
Gorelik, T.E. 649
Gorelikova, N.V. 429, 663
Gorodnov, A.V. 315
Gorokhov, I.M. 623, 760
Goryachev, N.A. 421, 425
Göttlicher, J. 321, 335, 341, ***662***
Gottschalk, M. ***812***
Götze, J. ***687***
Gourgaud, A. 511
Gouzu, C. 601
Göz, E. 97
Grady, C. 794
Graham, I.J. 252
Gramenitskiy, E.N. 36
Grangeon, S. 319
Grant, K. 177
Grauby, O. 749
Greau, Y. 213
Gréaux, S. 153
Green, D.H. 156
Green, H.W. 210, 218,
Green, L. 649
Gregor, M. 289, ***426***
Grémillet, J.P. 271
Grevel, C. 599
Grevel, K.-D. ***808***
Grew, E.S. 473, ***479***, 481, 739
Grice, J.D. ***732***
Grieco, G. 233, 272, 305, 341, 358
Griesser, U.J. 6
Griffin, W.L. ***vi***, 177, 180, 181, 213, 508, 690
Grigoryeva, A.A. ***51***
Grindean, R.A. 519
Grindrod, P.M. 679
Grist, B. 275
Grizelj, A. ***404***
Groat, L.A. 26, ***473***, 481, 566
Grobéty, B. ***738***, 833
Grocholski, B. ***141***, 442, ***443***
Grokhovsky, V.I. 657
Groppo, C. 191
Grosch, M. ***326***
Groschopf, N. 692
Gruber, M. 125
Gruender, K. 540
Grütter, H. 561
Grybos, M. ***384***, 389
Grygar, T. 77, 343, 400
Gu, J.-D. ***319***
Gualtieri, A.F 734
Gualtieri, S. 115
Guan, Y. 169
Guastoni, A. 31, ***607***, ***616***
Gucsik, A. 375, 783, 784, 785
Guedes A. 608
Guggenheim, S. ***58***, 58
Guillem López, C. 132
Guillong, M. 236, 285
Guillot, B. ***35***
Guimarães, F. 546
Gumbert, J. 47
Gunter, M.E. 493
Günther, D. 249
Guo, Shun ***215***, 216
Guo, Wei-juan 838
Gurbanov, A.G. 444, 491
Gürel, A. 97
Gurzhiy, V.V. 373, ***744***
Guseva, N.S. ***569***
Gušić, I. 637
Gutzmer, J. 278, 330
Guyot, F. 386
Guzmics, T. ***559***
Guzzo, P.L. 28
Gwalani, L.G. 567
Gygi, F. 191
Gyollai, I. 783, 784

Hadnagy, A. ***426***
Haeberli, W. 639
Häger, T. 25, ***27***, 378
Hahn, T. 331
Hainschwang, T. ***24***
Halden, N.M. 575, 607
Hålenius, U. ***484***
Hallberg, A. 234
Hamada, M. 713, 718
Hamane, D. 151
Hammer, V.M.F. 34, ***762***
Hammerschmidt, K. 71
Han, X. 319
Han, Xiaodong 345
Hanes, R. 296
Hannibal, J. ***130***
Hannington, M.D. 252
Hansen, B. 608
Har, N. 765
Haraguchi, M. 150
Haranava, Y.A. 372
Harangi, Sz. 483, 524, ***542***, 543, 544, 547
Harfouche, M. 44
Harlov, D.E. ***447***, 459, 800, 801, 812
Harlow, G.E. ***597***, 600
Harries, D. 381, ***740***

Harris, C. 256
Harris, J.W. 21, 149, 187, 196
Harris, N. 577
Harrison, R.J. 650
Hartai, É. ***863***, ***865***
Harte, B. 210
Hartinger, S. 109
Hasan, O. 117
Haslinger, E. 643
Hassan, A.M. 511
Hassan, I. ***719***
Hassan, M.S. ***304***
Hatert, F. ***490***, 603, 609, 618, 619
Hatta, T. 96, 407
Hattori, K.H. 208, ***263***, ***331***, 503
Hattori, T. 680
Hauck, S.A. 228
Hautojärvi, A. 66
Hauzenberger, C.A. 212, 525
Havancsák, I. ***116***
Hawkesworth, C.J. 553, 557, 685
Hawthorne, F.C. ***vii***, 415, ***734***
Hayashi, H. 651
Hazemann, J.L. 658
Hazen, R.M. ***v***, ***154***, ***370***
He, Guoqi 566
He, Hongping 14, ***79***
Heald, S.M. 844
Heberling, F. ***825***
Hecht, L. 498, 835
Hećimović, I. 404
Hedenquist, J.W. ***287***
Heide, K. 61, ***701***
Heikal, M.Th.S. 511
Heimann, R.B. ***105***
Hein, J.R. 331
Heinrich, C.A. 285
Heinrich, W. 459
Heiss, A. 376
Hellevang, H. ***635***
Helsch, G. 644
Hem, C. ***754***
Hemley, R.J. 154, 663, 671
Henderson, C.M.B. 844
Henderson, G.S. ***37***, 670
Hennet, L. 44
Henning, T.K. ***791***, 792, 794
Henriques, S.B.A. ***592***
Henry, D.J. ***475***
Hermann, J. 156, 169
Hermosín, M.C. 85
Hernandez, R. 323
Heroldová, N. 620
Herrero Fernández, H. 131
Herrington, R.J. 280, 291
Herzogová, L. 77, ***400***, 401, 403
Hetherington, C. 447
Hezel, D.C. 689, 788
Hidalgo, A. 68
Hidas, K. 169, 174, ***508***, 521, 522
Higgins, M.D. ***541***, ***870***
Higo, Y. 141, 671
Hilairet, N. 855
Hilse, U. 701
Hirai, H. ***62***
Hirao, N. 163
Hiraoka, N. 151
Hirose, K. 161, 164, 166, ***441***
Hîrtopanu, P. ***570***
Hloušek, J. 351
Hoang, T.M.T. 756
Hochella, M.F. 381
Hoeck, V. 109, 520, 582, ***582***
Höfer, H.E. 569
Hofmann, A. 306, 593
Hofmeister, W. 25, 27, 378
Högdahl, K. 234
Hohmann, M. 84
Hoinkes, G. 211, ***212***, 584
Hokada, T. ***519***
Holawe, F. 109
Holeček, M. 368
Holodnov, V.V. 531
Honda, M. 62
Honfi, K. ***87***
Hong, H.T. 53
Hönig, S. 806
Honorato, S.B. 487
Hopf, J. 381
Horn, A.H. 28, 351
Horváth, Á. 330, 405, 406
Horváth, E. 93, ***117***, 698
Horváth, P. 534, ***593***
Hoshino, M. ***450***, ***547***
Hourani, M.K. 402
Houzar, S. 429, ***456***
Hövelmann, J. 61, ***801***
Hovis, G. ***708***, ***808***
Howell, D. ***177***, ***690***
Hrazdil, V. 456
Hu, Fang-Fang 257, ***257***
Hu, X. 329, 422
Huang, E. 53
Huang, J-x. ***213***
Huang, Ko-Chun ***456***
Huang, Xiaoling 89, 408
Huang, Z. 329
Huberty, J.M. 207
Hudson-Edwards, K.A. ***335***
Huertas, F.J. 50, 68, 832
Huff, W.D. ***629***
Hughes, J.M. 476, ***707***, 831
Huijsmans, J.P.P. 479
Huizenga, J.M. 184
Humphreys, E.R. ***557***
Hundáková, M. ***92***
Hunt, G.A. ***469***
Hunt, S.A. 679
Hunter, H.M.A. ***280***
Hurai, V. 214, 231
Hurlbut, J.F. ***29***
Husdal, T.A. 742
Hwang, Shyh-Lung 839
Hybler, J. 717
Hyodo, H. 601, 683
Hyslop, E. 127

Iancu, A. 713, 718, ***719***
Iancu, O.G. ***457***
Iannuccelli, V. 409
Ida, A. ***818***
Ida, T. 721
Iezzi, G. 723
Ihlen, P. ***761***
Ii, Hiroyuki ***427***
Iijima, K. 823
Iizuka, Y. 53
Ikeda, E. 815
Ilić, B.S. ***627***
Ilicheva O.M. ***15***
Ilijanić, N. ***117***
Ilinca, Gh. ***497***
Ilton, E.S. 844
Imai, A. 288
Imbarak, S.H. ***520***, ***568***
Inácio, M. 323
Ingrin, J. 169, ***173***, 455
Iñigo, A.C. 131
Innocenti, M. 11, 658
Inoue, T. 36, ***171***
Inui, M. ***593***
Ioannou, I. 133
Ionescu, C. ***109***, 121, 347, ***520***, 582, 765
Ionov, D. 141, 184
Iregui Ramírez, I. 223
Irifune, T. ***141***, 151, 182, ***182***, 671
Isaenko, S.I. ***570***
Ishibashi, H. 178
Ishibashi, J. 252, 666
Ishido, T. 148
Ishii, H. 151
Ishii, T. ***154***
Ishikawa, A. 695
Ishikawa, T. ***165***, 810
Ishimaru, S. ***190***
Ismail, A.I.M. ***72***
Isobe, F. 182
Itaya, T. 683
Ito, K. 355
Ivanic, T. 187
Ivanov, V.V. ***234***, ***663***
Ivanovskaya, T.A. ***748***, 760
Iwabuchi, T. 720
Iwahori, K. 390
Izatulina, A.R. ***373***
Izumi, F. 721

Jablonovska, K. ***400***
Jackson, S. 553
Jacob, D.E. ***25***, ***178***, 378, ***678***
Jacobsen, J.K. 112
Jacobsen, S.D. 176
Jadrijević, A. 359
Jahn, B.-M. 207
Jahn, S. 799

Jahnen-Dechent, W. 376
Jahren, J. 635
Jakab, G. 570
Jakobsson, S.P. 496
Jakubíková, B. 77, 400, ***401***, 403
Janák, M. 208, ***214***
Janasi, V.A 839
Janata, M. 845
Janek, M. 86, ***697***, 702
Jankovič, Ľ. 78, 80, ***401***, 697
Jankovics, É. ***543***
Jánosi, M. ***327***, ***418***, 749
Janoušek, V. 474
Janssens, K. 196
Järvinen, L.J. ***1***
Jäsberg, J. 1
Javadi, M.S. 369
Jayananda, M. 388
Jean-Soro, L. 390
Jeffries, T. 554, 557, 568, 573, 685
Jelenković, R. 795
Jelínek, E. 209
Jeong, Heon Do 10
Jercinovic, M. 447
Jerzykowska, I. 427
Ji, B. 369
Ji, J.F. 638
Ji, W.H. 323
Jiang, Wei-Teh 2, 456
Jimenez Arias, J.L. 388
Jiménez, A. ***829***, 830
Jiménez-Lopez, C. ***382***
Jirátová, K. 748
Jiřičková, M. 93
Johansson, B. 165
Johner, N. 693
Johnson, C.A. 249
Johnson, M.B. 809
Johnson, S. 217
Johnston, C. 752
Jollivet, P. 363
Jones, A.P. 185, 690
Jonsson, E. ***234***
Jordi, B. 59
Jörg Bowitz, J. 136
Jousseaume, C. 670
Józsa, S. 525, 534, 783, 784
Jroundi, F. 140
Juhász, A. ***792***, 794
Juhin, A. 657, 669
Juillot, F. ***337***, 345, ***658***
Jukov, A.V. 243, 258
Jullien, M. 747
Juncosa, R. 339
Jung, Haemyeong 208, ***211***, 216
Jung, S.Y. 235
Jung, Sejin 211
Jung, Yeon Ho 231
Jura, M. 705
Jurečeková, J. 394
Jurje, M. 520
Jurkovič, L. 321
Kabai, S. ***861***
Kabanov, P.B. 640
Kacandes, H.G. 89
Kádár, I. 642
Kádas, K. ***165***
Kadir, S. ***97***, 626, ***630***
Káfuňková, E. 757
Kagi, H. ***178***, 680
Kahlenberg, V. ***6***, 155, 711, 817
Kaieda, H. 533
Kaindl, R. ***817***
Kajdas, B. ***427***
Kaji, Y. 533
Kákay-Szabó, O. 333
Káldos, R. ***199***
Kalinin, P.I. 641
Kamada, S. 163
Kamashev, D.V. ***848***
Kamenetsky, M.B. 190
Kamenetsky, V.S. 177, 190, 192, 252, 443, 446, 556
Kamenov, G.D. 551
Kamilli, R. 200
Kaminsky, F. ***180***
Kampf, A.R. ***490***, ***764***
Kampić, Š. 99, 359, 643
Kaneda, H. 428
Kang, Heung Seok 231
Kang, S.A. 235
Kantor, I. 442
Kantsou, P. 307
Kappler, A. 383
Kaps, Ch. 84
Kapustin, A. 88, 398
Kara, J. 1
Karabtzov, A.A. 429
Karampatsou, G. 120
Karampelas, S. ***23***
Karanović, Lj. 716
Karaoglan, F. 585
Kargaltsev, A.A. 46
Karimova, O.V. 744, 837
Karipidis, T.K. 492
Kármán, K. ***840***
Karpovičs, A. 309, 624, 633
Kartashov, P.M. 744
Kasama, T. x, ***650***
Kasbohm, J. 756
Kasina, M. ***7***, ***12***
Kasztovszky, Zs. 110
Katayama, Ikuo 219
Katerinopoulou, A. ***155***, 708
Kato, T. 141
Kato, Y. 725
Katsuda, M. 171
Katsuki, H. 89
Katsuya, Y. 678
Katz, J.E. 843
Kaufhold, S. 855
Kaur, P. 510
Kawakatsu, K. 298
Kawamoto, T. 190
Kawamura, T. 62
Kawano, J. 819
Kawano, S. 375
Kayama, M. ***689***, 783, ***784***, ***785***
Kaza, Gj. 239
Kazerouni, A.M. 52, ***317***
Kearns, B.J. 470, 471
Keck, E. 608
Kelemen, É. 118
Keller, J. 569, 728
Keller, L.P. ***791***
Kelley, S.P. 683, 691
Kelly, J.L. 561
Kelly, N.M. ***x***, ***457***
Kenkmann, T. 498, 781, 786
Kennedy, A.K. 692
Kennedy, C. 127
Keppler, H. 195
Ker C.-M. ***588***
Kerestedjian, T. 227
Kersten, M. 342
Khalmatov, E.A. 235, 258
Khan, T. 603
Khankhasaeva, S.Ts. 91, ***410***
Kharlamova, S. 671
Khattak, N.U. ***563***
Khirfan, M. 780
Kholmogorov, A. 424
Khoury, H.J. 28, 112, 780
Khoury, H.N. ***328***, ***402***
Khunová, V. 698
Kierczak, J. 645
Kiflawi, I. 667
Kihara, K. 818
Kikegawa, T. 36
Kilár, A. 94
Kilár, F. 87, 94
Killick, D. 105
Kim, Chang Seong 295
Kim, J.W. 545
Kim, Tae Hyung 231
Kim, Tae Hwan 10
Kim, W.J. 291
Kim, Y.J. 235
Kimata, M. 433, 450, 547
Kimura, Y. ***793***, ***835***
King, G. 687
King, H.E. ***840***
King, J.J. ***254***
Kingston, D.M. 276
Kinnaird, J.A. ***303***
Kinny, P.D. 692
Kinoshita, Y. 141
Király, Cs. ***62***
Király, E. 506, ***506***
Kirste, J. ***42***
Kirwin, D.J. ***291***
Kiseeva, E.S. ***556***
Kiseleva, D.V. ***373***
Kiseleva, G.D. ***428***
Kiseleva, I.A. 755, 756
Kiss, B. ***544***, 547
Kiss, Cs. 794
Kiss, G. ***538***

Kiss, P. ***484***
Kitamura, A. 823
Klápová, H. 209, 218
Kłapyta, Z. 96
Klasa, J. ix, ***374***
Kleeberg, R. ***747***
Klika, Z. 94
Klimko, T. ***327***, 335
Klimm, K. ***656***
Klimova, E.V. ***99***
Klinkenberg, M. ***855***
Klochko, K. 370
Klocke, A. 367
Kloess, G. 42, 691
Klötzli, U. 449, 516, 585
Klumpp, E. 87, 94
Klysubun, W. 30
Kniewald, G. 16, 399
Knight, K.S. 705
Knop, E. 447
Knoper, M.K. 272
Knoper, M.W. 273
Kobayashi, M. 720
Kobayashi, S. ***428***
Kocabaş, C. ***626***
Koch-Müller, M. 147, ***170***, 676
Kocourková, E. 344
Kocowicz, A. 647
Koděra, P. ***289***, ***296***, 426
Koeberl, C. 777, 782
Koenig, A.E. 248, 507
Kogarko, L.N. 144, 552, ***555***, 562
Koglin, N. ***247***, 248
Kohler, E. 747
Kojitani, H. 150, 154, 158, ***720***
Kokh, S.N. ***521***
Kokubo, T. ***367***
Kolb, U. 149, 649, 653
Kolitsch, U. 48, ***489***, 498, 726
Koller, F. 202, 507, ***571***, 582, ***582***, 585
Koloušek, D. 77, 82, 400, 748
Komadel, P. 83, 397, 697, ***698***
Komarneni, S. 89
Komatsu, K. ***680***, 815
Komlóssy, Gy. ***223***
Komuro K. 689
Konak, N. 589
Konc, Z. ***521***, ***522***
Konečný, P. 452, 453, 460
Koneev, R.I. ***226***, ***235***, 258, ***867***
Koneva, A. 724
Konishi, H. 746
Kono, Y. 141, 671
Kononkova, N.N. 473
Kononov, V.V. 663
Konopásek, J. 592
Konstantinov, L. 376
Konstantinova, G.V 623
Kónya, P. ***52***, 308, 333, 622
Konzett, J. 212, 525
Koo, Minho 231, 295
Koprubasi, N. 268
Korbelová, Z. 461
Kořistková, T. ***328***
Korkanç, M. ***129***
Kornilova, V.P. ***571***
Koroknai, B. ***506*** ,***622***
Korolev, N.M. 572
Korostelev, P.G. ***429***
Koshenskaya, T.O. 27
Koskinen, W.C. 85
Košler, J. 258
Kóspál, Á. 792, 794
Koster van Groos, A.F. 58
Kostopoulos, D.K. 458
Kostov, R.I. ***497***, ***861***
Kotelnikov, A.R. 199, 363
Kotelnikova, Z. ***199***
Kóthay, K. ***200***
Kotlyar, L.S. 276
Kotova, O.B. ***241***, 282, 311
Kountcheva, D.R. ***365***
Koutsopoulou, E. ***402***
Kouzmanov, K. 285
Kovács Kis, V. 334
Kovács, A. 93
Kovács, I. ***156***, ***169***, ***174***, 189
Kovács, J. ***391***, ***635***
Kovacs, M. ***522***
Kovács-Pálffy, P. 308, 522, 622, 629
Kovalchuk, N. ***572***
Kovalenker, V.A. ***225***, 290, 428
Kovalenko, V. 564
Kovalskii, A.M. ***363***
Kovanda, F. ***93***, ***748***, 757
Kovář, O. 429
Kovář, P. 757
Kozák, M. 629
Kozák, O. ***403***
Kozlov, P.S 594
Kozyreva, I.V. ***458***
Kramar, U. 777
Krasnova, N.I. 492, ***500***, ***572***
Kraus, I. 289, 412
Krebs, M. 601
Kreher-Hartmann, B. ***766***
Krejčová, J. 648
Krejčová, S. 77, 400, 401, ***403***
Krenn, E. ***448***, ***459***
Krenn, K. 211, 212
Kressall, R.D. 551
Kresta, J. 276
Krickl, R. 655
Krishnamurti, G.S.R. 354, 359
Krist, G. 125
Kristály, F. ***2***, 101, ***118***, 225, 295, ***417***, 430, 436, 446
Kristavchuk, A.V. 263
Kristiansson, P. 484
Kristóf, J. 93, ***698***
Krivovichev, S.V. 485, 711, 716, 728, ***733***, 744, ***763***
Krivovichev, V.G. 829
Krmicek, L. 573
Krmickova, M. 573
Kröchert, J. 777
Kroeker, S. 415
Krogh Ravna, E. 214
Kroll, H. 807
Kröner, A. 600
Kronz, A. 178, 291
Krsmanović, M.M. ***627***
Krstić, N.S. ***625***
Krüger, H. 155
Kruger, R.A. 5
Krüger, Y. 775
Krupnov, I. 310
Krupskaya, V.V. 310, 311, ***624***, 640, ***755***, ***756***
Kryazhev, A.A. ***430***
Krylov, A. 624
Kryuchkova, L.Y. ***841***
Krzhizhanovskaya, M.G. ***479***
Ksenofontov, D.A. 416
Kucha, H. 251, 381
Kucherinenko, Ya. 45
Kudaikulova, G.A. ***702***
Kudejova, P. 3, 682
Kudlacz, K. ***118***
Külah, T. 97
Kuligin, S. 141, 184
Kulkov, A. ***13***
Kulkova, M.A. ***119***
Kullerud, K. 214
Kulyapin, P.S. ***314***
Kumagai, H. 666
Kung, J. 276
Kunimoto, T. 182
Kupi, L. 225, ***430***
Kurat, G. 144, 185, 777
Kurazhkovskaya, V.S. 660
Kurihara, T. 778
Kurio, A. 182
Kurnosov, A. 158
Kuroda, Y. 533
Kusiak, M.A. 452
Kusy, D. 208, 452
Kusz, J. 25, 482, 491
Kutyavin, E.P. 623
Kuzmann, E. 749
Kuzmin, D. 526
Kuznetsov, A.B. 623
Kuznetsova, E.P. ***625***
Kuznetsova, L.G. ***610***
Kuzyura, A.V. 573
Kynicky, J. ***573***
Kyono, A. 663, 671

Labanowski, J. 386, 390, 391
Labat, F. 22
Labrador, M. 240
Lacalamita, M. 745
Lalinská, B. 327, ***335***
Lam, A.E. 481
Lamali, A. ***785***
Lampronti, G.I. 65

Lan, C.Y. ***523***, 602
Landi, E. 372
Lang, Bao 13
Lang, K. 93, 757
Langenhorst, F. 143, 381, 740, 778, 842
Langhof, J. 761
Langner, R. 841
Lanson, B. ***319***
Laperche, V. 751
Lapides, I. 87
Large, R.R. ***245***
Larionov, M.Yu. 657
Lattanzi, P.F. 356
Lattard, D. ***841***, ***842***
Lau, L. 607
Laubach, S.E. 193
Laufek, F. 263, 720
Laurora, A. 14, 710
Laurs, B.M. 605
Lausi, A. 735
Lavalle, H. 112
Lavin, P. 22
Lawrence, J.R. 379
Lawver, D.R. 368
Lazaro, C. 600
Lazarovici, Gh. 109
Lazarovici, M. 109
Lazic, B. 55, 479, 491, ***739***
Lazutkina, E.N. 316
Le Losq, C. 43, 664
Le Page, Y. 276, 740
Le, Thi-Thu Huong 27
Leal Gomes, C. 478, 518, 546, 615
Leal-Mejía, H. ***258***
Leat, Ph.T. 685
Lebda, E.M.L. 505, 511
Lecumberri Sanchez, P. ***200***
Lee, H.E. 328
Lee, J.S. 324
Lee, J.Y. 323, 328
Lee, Jae Seok 211, ***216***
Lee, M.R. 127, 370, 683, 691, ***787***
Lee, N. 370
Lee, Sangbong 231
Lee, Y.J. ***235***, ***328***
Lee, Yu Chen ***2***, 18
Leelawattanasuk, T. 23
Lehbib, S. ***236***
Lehmann, B. 274
Lehrl, M. 34
Leichmann, J. ***17***, 328, ***806***
Leiro, J.A. 1
Leiss, B. 136
Lelong, G. 38
Lelukh, M.I. 571
Lemée-Cailleau, M.-H. 705
Lempp, Ch. 59
Lenart, A. ***29***
Lenaz, D. ***431***, 435, ***790***
Lengauer, C.L. ***48***
Leno, V. 108
Lenti, F. ***201***
Lentz, D.R. 454
Leonardsen, E. 496
Leoni, F. 238
Lepekhina, E.N. 445, 551
Lepore, G.O. 742
Lerf, A. 758, ***850***
Leroux, F. 353
Leroux, H. 181
Lesovaya, S. ***640***
Lespinasse, M. 224, 621
Lettieri, M. 134
Lévai, E. 515
LeVeille, R. 507
Lewis, J.F. 232, 240
Lexa, J. ***286***, 289, 296, ***297***, 426
Leydier, M. 44
Lezama-Pacheco, J.S. 383
Lezzerini, M. 120
Lhotka, M. 77, ***82***, 400
Li, C. 726
Li, Guowu ***155***, 157
Li, Jia 408
Li, Jinhong 18
Li, Juan 345
Li, Q.L. 215
Li, Shengrong 222, ***222***
Li, Ting 849
Li, Xiang ***329***, 422
Li, Xuefen 95
Li, Xuejun ***13***
Li, Y.L. 319
Li, Yan 377, 382, 385, 386, ***387***, 392
Li, Yuanyuan 18
Li, Yu-Ho ***432***
Liao, Libing 8, 838
Licha, T. 128
Liégeois, J-P. 565
Likhanov, I.I. ***594***
Liles, D.C. 741
Lim, H.S. 324
Lima, A. ***608***
Lima, M.N. ***523***
Lima, S.S.M. ***459***
Lin, L.H. 204
Lin, Ming Fong 18
Linares-López, C. 294
Lindgren, P. 787
Ling, J. 364, 731
Linnen, R.L. ***607***
Liou, J.G. 207, 602
Lischka, H. 95
Litasov, K.D. 148, 556
Litvin, Yu.A. 148, 179, ***179***, ***573***
Litvinov, N.D. 416
Liu, Dong 14
Liu, Hongmei 14
Liu, J. 532, 844
Liu, J.Q. 192
Liu, Jianying 377
Liu, Jingbo 215, 216
Liu, Qian 146
Liu, T.C. ***53***
Liu, X. 532
Liu, Xiandong 317, ***819***
Liu, Yun ***329***
Llorens, T. ***617***
Lloyd, J.R. ***vii***, 365
Lo, K. 303
Łobczowski, W. ***645***
Logar, M. ***10***, 324, ***664***
Loges, N. 378
Lograsso, J. 291
Logvinova, A. 141, 184, 431
Loidl, G.C. ***277***
Loisel, C. 115
Longo, F. 240
Longo, M. 149
Lopes, M.C. 122
López-Aguayo, F. 63
López–Arce, P. ***119***
López-Buendía, A.M. ***130***, ***132***
López-Galindo, A. 19
López-Hernández, A. 293
Lorand, J.P. 181, 712
Lorenzi, R. 115
Losos, Z. ***175***, ***429***
Loun, J. ***344***
Lovas, Gy. 81
Lowell, R.P. 194
Lowry, G.V. 843
Lu, Anhuai 377, 382, ***385***, 386, 387, 392
Lu, Jianjun ***345***, 451
Lu, Xiancai ***317***, 345, 819
Lu, Y. 746
Lucchetti, G. 346
Lüders, V. 231
Lührs, H. ***47***
Lukács, R. ***524***
Lukanin, O.A. 46
Lukkari, S. ***524***
Lukoczki, G. 201
Luna, L. 352
Lupton, J.E. 252
Lupulescu, M.V. 555
Luque, A. ***137***, 138
Lūse, I.V. 309, ***624***, 633, 756
Lussier, A.J. ***415***
Luttge, A. ***1***, 71, ***73***, 82, 804
Lützenkirchen, J. 825
Lygina, T.Z. 15
Lykova, I.S. 416
Lynch, E.P. 2
Lysyuk, A. ***43***
Lysyuk, G. ***432***

Ma, Hongwen 634
Ma, Junhong 13, 18
Ma, Yuehong 79
Ma, Zhesheng 155, 157
Macek, I. 485
Machado, J. 397
Machida, S. 62

Machovič, V. 77, 82, 344
Maciejowska, A. 72
MacKenzie, D.J. 250
Mádai, F. ***347***, 500, 865
Madala, F. 266
Madejová J. 78, 83, 310, 393, 697, 698
Mader, D. 782
Mäder, U. 353, 673
Madjer, K. 44
Mádl-Szőnyi, J. 465
Magalhães, M.C.F. ***338***
Maggetti, M. ***108***
Maier, W. 527
Maillot, F. ***345***
Mainprice, D. 816
Mair, P. ***525***
Majoros, P. 225
Majzlan, J. 229, 321, 335, 342, 808, ***809***
Makagon, V.M. ***611***
Makeev, A.B. ***152***, ***185***, ***574***
Makhaniok, A.A. 372
Maki, K. 207, 602
Maki, T. 835
Makino, K. 718
Makó, É. ***93***, 698
Makovicky, E. 497, ***737***, 754
Makri, P. 307
Malavergne, V. 44, 386, 391
Malfait, W.J. ***40***, ***44***, ***45***
Malferrari, D. ***14***, 710, 753, 852, ***852***, ***856***
Mali, H. 264
Malsy, A.K. ***26***
Malvoisin, B. ***512***
Malý, P. 94
Malyshev, M.E. 396
Mamontov, E. 39
Manceau, A. 319
Manghnani, M.H. 149
Manning, C.E. 677
Mao, H.K. 663, 671
Maouche, S. 785
Mapani, B.S. ***217***
Maqueda, C. 83, 406
Maras, A. ***374***
Marbler, H. ***59***
Marcacci, M. 372
Marcelli, A. ***751***, 777, 852
Marchel, C. ***318***
Marchesi, C. 508, 522
Marchetto, P. 14
Maresch, W.V. ***599***, 601
Marescotti, P. ***341***, ***346***
Márialigeti, K. 327
Marichal, C. 749
Marincea, Ş. ***433***, 713, 715, ***718***, 719
Marinova, D. ***665***
Mariotti, M.G. 346
Maritan, L. 65
Markl, G. 559
Markó, A. 136
Markopoulos, Th. 68, 120, 133
Markova K.I. 646
Marks, N. 850
Maros, Gy. 506, 622
Maróti, B. 847
Marques, A.F.A. ***236***
Marques, R. 323
Marrese, G. ***120***
Marry, V. 57
Marschall, H.R. ***213***, ***474***, ***685***
Marschall, P. 65
Marshall, D. 26
Marszałek, M. ***525***
Martens, U. 602
Martín Romero, F. 294
Martin, R.F. ***555***
Martínez de Yuso, M.V. 138
Martínez, J. 63
Martinez-Criado, G. 674
Martínez-Martínez, J.M. 526
Martins, M. 186
Martinsson, O. 254
Márton, E. 334
Márton, I. ***246***
Martos, R. 63
Mărunțiu, M. 584
Mârza, I. 684
Marzoli, A. 149
Masau, M. 612
Mashima, H. 760
Mashlan, M. 9
Mashukov, A.V. ***665***
Mashukova, A.E. 665
Masieri, M. 134
Masiteng, I.N. 681
Maslennikov, V.V. 237
Maslennikova, S.P. 237
Massault, M. 388
Massiot, D. 43
Massoth, G.J. 252
Mata, M.P. ***63***, ***388***
Matejdes, M. 697, ***702***
Matějka, D. 32
Mathis Y.-L. 673
Matović, B. 10
Matović, V. 533
Matrenichev, V.A. 99
Matskova, N.V. ***310***, 311
Matsubara, S. 498
Matsuda, J. 517
Matsueda, H. 299
Matsui, M. ***671***, ***815***
Matsui, T. ***433***
Matsumoto, N. 836
Matsumoto, T. 517
Matsushita, Y. 678, ***744***
Matusik, J. ***88***
Mauk, J.F. ***253***
Mavris, C. ***639***
Mayet, F. 122
Mayorova, T.P. ***330***, 489
Mayrhofer, M. ***645***
Mazeran, F. 125
Mazzoli, C. 65
McCammon, C. ***162***, 218, ***442***, 778
McCracken, T. 276
McDonald, A.M. ***266***, ***487***
McFarlane, C. 454
McIntosh, R.W. 629
McMaster, T.J. 387
McNaughton, N.J. 449
McNeill, A.W. 252
Meccheri, M. 121
Médard, E. 40
Meden, A. 727
Medenbach, O. 479, 495
Mederer, J. ***246***
Medford, A. 708
Mees, F. 301
Meftah, M. 16
Megharaj, M. 354, 359
Mehrpartou, M. 527, 528
Meibom, A. 181
Meijer, E.J. 819
Meisser, N. ***485***
Meisztérics, A. 15
Mel'gunov, M.S. 396
Melchakova, L.V. 625, 640, 755, 756
Meleshyn, A. 90
Melgarejo, J.C. 230, 236, 242, 258, 553, ***562***, 578, 605, ***614***, ***616***
Meli, S. 191
Melichová, Z. 397
Melnikov, N.N. 623, 760
Menchetti, S. ***742***
Meneghini, C. 356
Menezes, P. 69
Meng F.-C. 588
Mengoli, D. 103
Menguy, N. 364
Menyhárt, A. ***434***
Merabet, N. 785
Mercier, J.C.C. 565
Mercier, P.H.J. ***276***, ***740***
Merino, A. 469
Merkel, B.J. 75
Merli, M. 157
Merlini, A. 233, ***272***, ***305***
Merlini, M. ***149***
Merlino, S. ***737***
Mernagh, T.P. 156
Mertens, G. 106, 114
Mesiarkinová, M. ***434***
Messenger, S. 791
Mesto, E. ***724***, ***745***
Metsue, A. 810
Mexias, A. 862
Meyer, A. 39
Michaelis, V.K. 415
Michalik, M. 7, 12, ***72***, 321, 427, 648
Michel, J. 23

Michler, A. ***82***, 804
Michňová, J. ***237***
Michot, L. 389
Micsinai, D. ***515***
Middleton, C.A. ***679***
Migdisova, N.A. ***526***
Mihăilă, A. ***138***
Mihailova, B. ***367***
Mihaljevič, M. 343
Mikami, M. 357, ***357***
Mikhail, S. 185
Miklin, Ž. 404
Miko, S. 117
Mikouchi, T. 706, 725, ***778***
Míková, J. 475
Mikulčić Pavlaković, S. 423
Mikuš, P. 647
Milakovska, Z.I. ***646***
Milke, R. ***71***, 592
Miller, D.E. 266
Miller, N.A. 161
Mills, S.J. ***488***, 490, ***738***
Minagawa, K. ***703***
Minato, H. ***7***
Minder, P. ***76***
Mindszenty, A. 465
Minter, W.E.L. 248
Miot, J. 383
Miranda, M.R. 28
Mirao, J. ***69***, ***122***, ***123***, ***341***
Mirmohammadi, M. 270
Mironova-Ulmane, N. 17
Mirtič, B. 29
Mirwald, P.W. ***813***
Mitchell, L. 768
Mitchell, L.D. 63
Mitchell, R.H. ***441***, 445, 559
Mito, S 533
Mitolo, D. 496
Mitterlehner, C. 109
Mityukhin, S. 141, 184
Miura, Y. ***30***, ***868***, ***870***
Miyajima, N. ***652***
Miyake, A. 813, ***819***
Miyake, T. 820
Miyamoto, T. 601
Miyashita, T. 833
Miyata, N. 319, 390
Miyawaki, R. ***498***, 722
Mizera, J. ***781***
Mizukami, T. 190
Mladenova, V. ***498***, 835
Mladenovič, A. 359
Mo, Xuanxue 222, 455
Moayyed, M. 270
Moazzen, M. 597
Mocek, B. 674
Mochenova, N.N. 486
Mockovčiaková, A. 404, 412
Moëlo, Y. 714
Mogessie, A. ***264***, 265, 584
Mogoru, T.J. 5
Mohr-Westheide, T. ***782***
Moinvaziri, H. 527, 528
Moiseenko, A.S. 314
Moita, P. 69, 531
Mokhov, A.V. 428
Mokhtari, M.A.A. ***527***, ***528***
Mokko, T. 637
Molenda, J. xi
Möller, A. 457, 674
Molnár, F. 224, ***228***, 265, 286, ***289***, 290, 295, 296, ***296***, 297, 465, 484, 538, 621, 683
Molnár, L. ***296***
Molnár, M. 515
Molnar, T. 637
Momma, K. ***721***
Monarumit, N. ***30***
Mondal, S.K. 227
Mondillo, N. ***275***
Mondlane, S., Jr. 304
Monkawa, A. ***706***
Monnier, C. 584
Montagna, G. 47, 53
Montagnac, G. 388
Montagnari Kokelj, E. 111, 113
Montecchi, M. 710
Montegrossi, G. ***59***,465, 484, 538, 621, 683
Montorsi, M. ***409***
Montouillout, V. 43
Moon, Dong-Hyeok 636
Moór, A. 792, ***794***
Moore, K.R. 198, 537, 558, ***560***, 567, ***579***
Moore-Shay, L.J. 366
Morales, I. 352
Morales, N. 291
Moretti, R. 664
Morgado, P. 107
Morgan, D. 385
Morgan, R. 306
Mori, Y. 598, ***601***, 602
Morichon, E. 361
Móricz, F. 347
Morillo, E. 406
Morimoto, K. 97, 354, ***395***, 407, 703
Morimoto, T. 7
Morin, G. 337, 345, 364, 383, 422, 658, 705
Morioka, M. 836
Morishita, T. 190
Morishita, Y. 226
Moritz, R. 246, ***247***, 260
Moro, M.C. 617
Moroni, M. ***238***, 272
Morrison, J.M. ***366***
Morteani, G. 775
Mosenfelder, J.L. 169
Mosoni, L. 792
Mosonyi, E. ***594***
Moss, D. 673
Mosselmans, J.F.W. 21
Mosyagin, A.V. ***139***
Motenko, R.G. 625
Mottana, A. 751, ***771***, ***772***
Moulas, E. ***458***
Mouri, H. ***527***
Mposkos, E. ***595***
Mrosko, M. 147, 676
Mucha, D. 853
Mueller, U. 67
Mugnaioli, E. 149, ***649***, 653
Mukherjee, R. ***227***
Mulch, A. 631
Müller, A. ***291***, 331, ***761***
Müller, M. 326
Müller, P. 333
Müller, W. 823
Mumin, A.H. 551
Mun, Yu.S. ***238***
Muñoz, M. 115, 552
Murai, Kei-ichiro 667
Murakami, M. ***150***
Murakami, T. ***417***
Murao, R. 674
Murphy, W.L. xi
Mussino, A. 772
Mustin, C. 389
Mutschke, H. 795
Mysen, B.O. 663, 671

Nabelek, P.I. ***606***
Nadoll, P. ***507***
Nagahara, H. ***788***, 836
Nagai, T. ***148***, 151
Nagao, M. 650
Nagao, T. 415
Nagashima, M. ***709***, 713, ***721***
Nagy, G. 113, 507, 534, 593
Nagy, H.É. ***330***, 333
Nagy, M. 783
Nagy, Sz. 783, 784
Nagy-Korodi, I. ***347***
Nahodilová, R. 217
Naidu, R. 354, 359
Najafzadeh, A.R. ***509***
Nakai, S. 666
Nakamura, E. 215
Nakamura, M. 677
Nakamura, T. 678
Nakamuta, Y. ***183***, 717
Nakano, T. 677
Nakano, N. 519
Nakatsuka, A. 709
Nakazato, T. 783, 784
Nakazawa, H. ***755***
Nannarone, S. 710
Napruszewska, B.D. 853
Naranjo, M. 405, 752
Narjisse, A.M. 63
Narnov, G.A. 663
Narygina, O. 162, 442
Nasdala, L. ***692***, ***865***
Nasralla, N. 505
Nasti, V. 772
Naumkina N.I. 15

Navon, O. 180, 667
Navrátil, J. 720
Nazzareni, S. 153, ***171***
Neacşu, A. 676
Nedel, S. ***365***
Nédli, Zs. 197, ***528***, 577
Nee, P. 210
Negishi, R. 141
Négyesi, L. 327
Neiva, A.M.R. 233, 256, 459, ***478***, 514, 517, 531, 592
Németh, B. 201, ***202***, 204,
Németh, G. ***547***
Németh, K. ***41***, 683
Németh, N. 225, 417
Németh, P. ***797***
Németh, T. 331, 334, ***395***, 621, ***542***, 840
Németi, J. 116
Nespolo, M. 745
Nestola, F. 31, 147, ***149***, 616
Netzkár, A. 94
Neu, T.R. 379
Neubauer, F. 292, 584
Neumann, T. 821, 824
Neusser, G. ***800***, 801
Neuville, D.R. ***41***, ***43***, ***664***, ***670***
Nex, P.A.M. 303
Ng, S. 276
Ngaruye, J.C. 239
Nguyen, Ngoc Khoi 27
Nguyen, T.L. ***756***
Ni, P. ***192***
Nicholls, J. ***860***
Nicolescu, S. ***684***
Niedermann, S. 795
Niemetz, W. 34
Nieto, F. 634
Niewa, R. 3
Niinou, M. 722
Niiranen, T. 254
Nikandrov, A. 499, ***499***
Nikolić, N.D. 636
Nikolopoulou, A. ***89***
Niku-Paavola, V.N. 571, 574
Nimis, P. 105, 149
Ninagawa, K. ***375***, 689, 783, 784, 785
Nishi, F. ***722***
Nishida, N. 450, 547
Nishido, H. 375, 659, 689, 783, ***783***, 784, 785
Nishio-Hamane, D. 146
Nishiyama, N. 141
Nishiyama, T. ***598***, 601, 602, ***806***
Niu, L. 331
Niwa, K. 146
Nizamoff, J.W. 618, 619
Noel, Y. 816, 848
Noetinger, B. 57
Noguchi, T. 678
Nogueira Neto, J.A. 523
Noguera, C. 834, ***836***
Nomoto, T. 692
Nomura, R. 375
Nomura, S.F. 492
Norberg, N. 800, ***801***
Noret, A. 388
Notoya, S. 692
Novák, J.K. 461, 596
Novák, M. 344, 349, ***460***, ***475***, 478 ***485***, 608, 615, 620, 806
Novikov, V.M. 91
Ntaflos, T. 141, 144, 184, 524, 543, 544, 547, 777
Nuber, N. ***561***
Núñez Cambra, K. 600
Nuth, J.A.III 793
Nyilas, T. ***644***
Nyirő-Kósa, I. ***845***

O'Day, P.A. ***353***
O'Driscoll, B. 431
O'Neill, C. 177, 690
O'Reilly, S.Y. vi, 177, 213, ***508***, 690
O'Reilly, S.Y.
Obata, M. ***803***
Oberhänsli, R. 591, 597
Oberti, R. ***145***, 661, 811
Obst, M. 379, 383
Odabasi, I. 589
Ódri, Á. 529
Odúlio, J.M.M. 99
Oehm, B. 842
Oelkers, E.H. ix, 823
Ogorodova, L.P. 755, 756
Ogushi, N. 7
Oh, C.W. 590
Oh, S.G. 328
Ohara, S. 370
Ohfuji, H. 178, 182, ***182***, 420
Ohi, S. ***813***
Ohishi, Y. 161, 163, 166
Ohnenstetter, D. 24, 271, ***499***, 776
Ohnenstetter, M. ***271***
Ohshiro, M. 146
Ohta, K. 164, 441
Ohtani, E. 40, 148. ***163***, 163, 556
Ojala, V.J. 254
Okada, T. 146
Okamoto, A. ***803***
Okimoto, S. 182
Okoemova, V. 179
Okrugin, A. 181
Okrusch, M. ***510***
Okube, M. 667, 709
Okudera, H. ***722***, 818
Okumura, S. 677
Okumura, T. 666
Okunishi, E. 651
Olivelli, M. 396
Omana Sanz, B. 348
Onac, B.P 469, ***469***, ***470***, 471, ***471***
Ona-Nguema, G. 705
Ondrejka, M. 448, 453
Onufrienok, V.V. 665
Onuzi, K. ***239***, 582
Oota, S. 357, ***357***
Orbán, R. ***757***
Orberger, B. ***306***, ***388***
Orekhov, A.A. 429
Orhun, O. ***76***, 81, 98
Ori, G. 409
Orial, G. 115
Origlia, F. 121
Orihashi, Y. 601
Orlandi, P. 494, 714
Ormos, T. 865
Orolínová, Z. ***404***, 412
Oros Sršen, A. 637
Oršulić, D. 359
Orta, M.M. 405, 752
Osacký, M. 393
Osadchi, E.G. 263
Osanai, Y. 519
Oshtrakh, M.I. ***657***
Ossorio, M., 842
Osterrieth, M. ***389***
Ostroumov, M. 548, ***871***
Otálora, F. 775
Othmane, G. ***364***
Ott, U. ***797***
Ottner, F. ***109***, 641, 643, 645
Ottonello, G. ***35***, 143
Oueslati, W. ***16***
Oulkadi, D. ***389***
Ounorn, P. 33
Oxley, A. 280
Oyabu, N. 833
Ozawa, A. 533
Ozawa, H. ***166***
Ozawa, K. 788, 803, ***836***
Ozdín, D. 237, ***240***, 434, 477, ***769***
Özçelik, H. 699
Ozhogina, E.G. 32, 311
Özdamar, S. 100

Paar, W.H. 259
Pacella, A. 320
Pačevski, A. ***294***, ***297***
Pack, A. 787, ***788***
Padashi, S.M. 527, 528
Padya, A.B. 280
Páger, Cs. 94
Paikaray, S ***348***
Pakhomovsky, Y.A. 716
Paktunc, D. ***336***
Palatinus, L 468, 739
Palessky, V. 141
Palfi, A.G. 571
Pálfy, J. 101
Palin, J.M. 551
Palinkaš, L.A. 99, 290, 292, 538, 643
Pálková, H. ***78***

Palme, H. ***787***
Palmer, S.J. 696
Pál-Molnár, E. 322, ***513***, ***529***, 565
Pan, Hui 408
Pan, Y. 509
Pan, Y.G. 638
Pan, Yuguan 422
Panagiotaras, D. 89
Panchenko, V.N. 77, 396
Pandolfo, F. ***31***, ***147***
Paniagua, A. 605, 616
Panne, U. 67
Panseri, S. 372
Panther, C. 291
Pap, L. 375
Papin, A. 723
Papoulis, D. 89, 402, 626,
Papp, G. ***435***
Papp, I. 1, ***375***, ***629***
Papp, I.P. ***411***
Paquette, J. 416
Pardi, L.A. 11, 658
Pardieu, V. 776
Pareschi, R. 341
Paris, E. 37, 42, 777
Parisatto, M. 69
Parise, J.B. ***63***, ***679***
Parisi, F. 157, ***435***
Park, Munjae 211
Park, Y.T. 323
Parker, S.C. 90
Parlak, O. ***585***, ***589***
Parsons, I. ***370***
Partal, P. 406
Pašalić, H. 95
Pasarín, I.S. 369
Pašava, J. ***258***
Pascarelli, S. 677
Pascua, C.S. 407
Pascucci, I. 794
Pasero, M. ***494***
Pasquali, L. 710
Păstrăvanu, C. ***54***, 411
Pásztor, L. 405
Pataki, A. 322
Patarachao, B. 276
Patinha, C.A. 323, 338, 393,
Patrier Mas, P. 862
Pattarawarin, P. 33
Pattison, P. 673
Pattrick, R.A.D.P. 365
Pattuzzi, E. 856
Pavićević, M.K. 795
Pavón, E. ***405***, 752
Pazdziora, E. 92
Pazos, M.C. 405, 752
Pearce, C.I. ***844***
Pearce, J.A. ***581***
Pearson, N. 177
Pécskay, Z. 224, 289, 297, 483, 484, 522, 621, 622
Pedrotti, M. ***233***
Peiffer, S. 340, 348
Pejović, V. 795
Pekker, P. 101, 395, 446, 749
Pekov, E.I. 473
Pekov, I.V. 51, 55, ***416***, 438
Peng, Qiang 634
Penn, R.L. ***843***
Pennacchioni, G. 607
Pentrák, M. ***83***, 698
Perchuk, A.L. ***212***
Perdikatsis, V. 68
Pereira, A. 325, 587
Peresson, M. 125
Pérez-Barnuevo, L. ***276***, 281
Perez-Gonzalez, T. 382
Pérez-Huerta, A. 369
Perez-Mato, J.M. ***739***
Perez-Outeiral, F.J. 388
Pérez-Rodríguez, J.L. 83, 758, 850
Pérez-Sayago, M. 406
Pernicka, E. 106
Pernyeszi, T. 87, ***94***
Perşoiu, A. 471
Persson Nilsson, K. 234
Persson, P. 383
Pertlik, F. 762
Pertsev, N.N. 444, 482, 491, 493
Perucchi, A. 189
Pesquera, A. 425, ***526***, 618
Péterdi, B. 136
Peterson, D. 265, 288
Pethe, M. 334
Petit, S. 749, ***862***
Petrakov, A.P. 430
Petrík, I. ***460***
Petrík, P. 453
Petrinec, R. 135
Petrinec, Z. 451, 481
Petrov, A.N. ***316***
Petrov, O. 376
Petrov, S.V. 559
Petrov, T.G. 492, 500, 572
Petrovsky, V.A. 186
Pezzotta, F. ***474***
Philander, C. 279
Philippo, S. 490, 603
Philokyprou, M. 133
Phoenix, V. 127, ***379***
Pi, T. 293
Piazolo, S. 708, 828
Pich, B. ***355***
Pichon, L. 107
Pieczka, A. 473, 728
Pignatelli, I. ***745***
Pileri, D. 233
Piloyan, G.O. 91
Pinch, W.W. 726
Pini, G.A. 856, 857
Pini, S. 852
Pintér, F. 19
Pintér, Zs. ***202***
Pinto, A.J. ***830***
Pipich, V. 376
Pirard, E. 281
Pironon, T. 22
Pisutha-Arnond, V. 33
Pivin, M. ***560***
Plachá, D. ***394***
Plášil, J. ***349***, 351, 725
Plevová, E. 100
Plimer, I.R. 277
Plissart, G. ***584***
Plotinskaya, O.Yu. 225, ***290***
Plötze, M. 76, 135, 639, 849
Plümper, O. 61, ***799***
Poelchau, M.H. ***781***
Pogaridou, E. 307
Poggi, L. 769
Poharc-Logar, V. 664
Pokhienko, L. 141, 184
Pokhienko, N. 184
Pokidko, B.V. 310, 311
Polgári, M. ***331***
Poli, S 149, 812
Pöllmann, H. 59
Pollok, K. ***381***, 740
Polyak, V.J. 469
Pompilio, M. 171
Ponaryadov, A. ***846***
Pongkrapan, S. ***31***, 126
Pont, S. 104
Pop, D. 107, ***121***, ***765***, 863
Popa, R.G. ***548***
Popescu, Gh. 676
Popov, D. 673
Popov, M.P. 27
Popov, N.V. 594
Popova, S. 424
Popovici, E. 54, 411
Popp, F. 571
Poros, Zs. ***465***
Porro, S.L. 341, ***358***
Posch, T. 795
Posern, K. 84
Pósfai, M. ***x***, 332, 845, 847
Posilović, H. ***16***, 117, 325
Pospíšil, M. ***757***
Posta, J. 783
Posukhova, T.V. ***156***, ***349***
Potapov, I.L. 267
Potel, S. ***703***
Potuzak, M. 39
Poulson, S. 228
Pourret, O. ***830***
Power, I.M. 60
Poyato, J. ***758***, 850
Prakapenka, V. 141, 442, 443
Pratesi, G. 729, ***769***, 777
Praus, P. 403
Prechtel, F. ***170***
Precup, C. 109
Preisinger, A. ***380***
Premović, P.I. 625, 627, 636
Prencipe, M. 820
Prewitt, C.T. ***707***

Přichystal, A. 123
Prieto, M. 826, 827, 828, 829, 830
Přikryl, J. 460
Přikryl, R. 133, ***140***
Princivalle, F. 157, 431, 435, 528, 790
Pring, A. 649
Prochaska, W. 231
Proenza, J.A. 230, 232, ***240***, 266, 268
Prohászka, A. 289
Prokofyev, V.Yu. ***248***, 249
Prol-Ledesma, R.M. 293, 294
Prost, R. 751
Proux, O. 658
Provencio, P. 469
Proyer, A. ***211***
Pršek, J. 448
Prudêncio, M.I. 323
Prusik, K. 444, 491, 501
Pudlo, D. 701
Punin, Yu.O. 373
Pupier, E. ***677***
Puşcaş, C.M. ***471***
Pushcharovsky, D.Yu 51
Püspöki, Z. 629
Pustková, P. ***94***
Putnis, A. 13, 801, ***802***, 824, 830, 840
Putnis, C.V. 824, 830, ***831***
Pystin, A.M. ***241***, ***267***
Pystina, Yu.I. 267, 267

Qafoku, O. 844
Qin, Shan 166
Qing, Yanhong 79
Qu, Kai 222
Quarta, G. 134
Quartieri, S. ***47***, 672
Queiruga Dios, A. 6, 859
Quirico, E. 388
Quirt, D. 361

Rabadjieva, D. 376
Radtke, M. 107, 676
Raghimi, M. 530
Ragnarsdottir, K.V. 387
Ragozin, A.L. 186
Rahier, H. 402
Rahimi-Chakdel, A. ***530***
Rahmoun, N.S. 61, 479
Railsback, L.B. 468
Raiteri, P. ***826***, 850
Raith, J.G. ***251***, ***259***, ***381***
Rajesh, H.M. 272
Rajesh, V.J. 590
Rak, Zs. ***358***
Rakotoarisoa, O. ***350***
Rakovan, J. ***831***
Ramdohr, R. ***306***
Ramírez-Castellanos, J. 651
Rammlmair, D. 339, ***350***
Ramos, J.M.F. 459
Řanda, Z. 781, 869
Randers, M. ***309***, 624 ,633, 756
Rankin, A. 568
Rantzsch, U. ***691***
Rao, Can 609
Rastsvetaeva, R.K. 492
Raucsik, B. 549, ***646***, 863, 872
Raudsepp, M. 60, 738
Raynaud, S. 125
Razafitianamaharavo, A. 390
Rebay, G. 527
Rečnik, A. ***650***, 727, ***743***, 845, 847
Redhammer, G.J. 723
Redwan, M. 350
Regaly, Zs. 792
Regier, T. 37
Reguer, S. 44
Reguir, E.P. 443, 551, ***575***
Reich, T.Y. 342
Reichar, P. 176
Reimold, W.U. 780, 782, 786
Reinhardt, J. 593
Reinholz, U. 676
Reinsch, B.C. 843
Reis, P.A. 323, 338, 393
Relvas, J.M.R.S. 236
Ren, M. 530
René, M. ***450***, ***461***
Rentsch, D. ***11***
Repouskou, E. ***120***
Reverdatto, V.V. 594
Reynard, B. ***144***, ***851***, ***855***
Rhede, D. 692, 802, 805
Ribeiro, E. 351
Ribeiro, M.L. 531, 592
Richardson, S.H. 187
Richter, H. 795
Ridley, J.R. 249
Rieck, B. 496
Rieder, M. 717
Riehl, M. 503
Rimstidt, J.D. 194
Rini, M. 362
Rizaoglu, T. 585
Roache, T. 703
Robert, Ch. 591
Robert, J.-L. ***92***, 658, ***723***, ***750***, ***751***, ***758***
Roberts, J. 278
Robertson, A. 582
Robles-Cruz, S.E. ***553***
Robu, I.N. 457
Roccotielo, E. 346
Rocha, A.F. 325
Rocha, F. 107, 135, 323, ***338***, ***393***, 862, ***862***
Rochette, P. 785
Roda-Robles, E. ***618***, ***619***
Rodrigues, J.F. 587
Rodrigues, R. 608
Rodríguez Ruiz, M.D. 596
Rodríguez Vega, A. 600
Rodriguez-Blanco, J.D. ***675***, 823, 825
Rodriguez-Guanter, M.J. 130
Rodriguez-Navarro, A. B. ***4***, 19, 118, 371, ***371***
Rodríguez-Navarro, C. 118, 139, 140
Rogers, H. 280
Rogoz, A. 122
Röhling, S. 308
Röhrs, S. 107
Rojas-Agramonte, Y. 600
Rola, A.S. 864
Rolfo, F. 599
Rollet, Ph. 104
Rollinson, G.K. 279
Romanek, C.S. 382
Romanelli, M. 11, 356, 658
Romano, C. 39
Romanoski, A. 708
Romero Martín, F. 352
Romero Sanchez, S. 391
Romero-Guadarrama, J.A. 294
Roncal-Herrero, T. ***823***
Ronchi, P. 465
Rondeau, B. 181
Rondeux, M. ***619***
Roque, J. 240
Rosa, A.D. ***145***
Rosa, C. 236
Rosado, L. 122
Rosana, M.F. ***286***, 299
Rosatelli, G. 554
Rose, D.H. ***272***
Rosenthal, A. 156
Roser, B.P. 285
Rosière, C.A. 306
Ross, J. 63
Rossano, S. 28, ***44***, ***104***, ***115***, ***351***, ***386***, ***390***, ***391***
Rossi, A. 467
Rossman, G.R. ***169***, ***655***, 831
Rosso, K.M. 843, 844
Rosta, L. 15
Rostási, Á. ***872***
Rotenberg, B. 57
Rouchon, V. 388
Rovillos, P. 291
Rozalén, M. 68, ***832***
Rozendaal, A. ***279***
Rozhdestvenskaya, I.V. 610, 653, 710
Rózsa, P. 118, ***771***, 783
Rozynek, Z. ***78***
Ruby, C. 705
Rudashevsky, N.S. 266
Rudenko, K.V. ***298***
Rueedi, J. 65
Ruggieri, G. 59
Ruiz Cruz, M.D. ***595***, ***596***
Ruiz, A.I. ***754***
Ruiz-Agudo, E. 118, 139, 830, 831, ***824***

Rumsey, M.S. 490, 761
Rusakov, V.S. 46
Ruschel, K. 692
Ruskov, T. 218
Russo, A. 372
Ryabchikov, I.D. ***144***
Ryan, C. 485
Ryan, J.G. 588
Ryan, K.M. ***510***
Ryan, P.C. 331
Ryden, N. 72
Rygał, J. 423
Rzepa, G. 342

Sabino, N. 69
Saccone, L. 387
Sachan, H.K. 197
Sadek Ghabrial, D. ***530***
Sadykova, N.O. 373
Safonov, O. 186, ***203***
Safronov, P.P. 429
Safronova, E.G. ***486***
Sager, M. 324
Sági, T. ***543***
Sagredo, J. 552
Sahai, N. ***xi***
Saikia, A. 145
Saishu, H. 803
Saito, S. 820
Saja, D.B. 130
Sakai, S. 709
Sakai, T. ***163***, 163
Sakamaki, T. 40
Sakurai, H. 178
Salameh, E. 780
Salas, E.C. 73
Salcedo, I. 397, 412
Salge, T. ***688***, 780
Salomon, J. 107
Salova, T.P. 45, 539
Salvador, L. 374
Salvioli-Mariani, E. 191
Samardžija, Z. 727, 847
Sammonds, P.R. 679
Samper, J. 281
Sánchez Escribano, V. 6
Sanchez, R. 397, 412
Sánchez-Bellón, A. 63
Sanchez-Navas, A. 371
Sanchez-Valle, C. 40, 44, 144, 145, 147
Sánchez-Vargas, L.I. 294
Sand, K.K. 369
Sandri, G. 412
Sandri, M. 372
Sanehira, T 182
Sanna, L. 465, 467
Sano, A. 713
Sano, S. ***589***
Sano-Furukawa, A. 680
Santos Silva, A. 69, 123
Santos, J.F. 513, 531
Sanz de Galdeano, C. 596
Sanz, J. 758
Saragoça, C.S. 326
Šarić, K. 297
Sarkar, B. ***354***, ***359***
Sarkar, C. ***553***
Sata, N. 151, 161, 163, 166
Satitkune, S. 23, ***25***
Sato, F. 666
Sato, T. 89, 354, 355, ***355***, 357, 637
Satoh, H. ***832***, 840
Sator, N. 35
Sautter, V. ***181***
Savva, E.V. 576
Sawlowicz, Z. ***122***, ***224***
Sayak, H. 589
Sazaki, G. 834
Scacchetti, M. 480
Scaillet, B. 37
Scali, G. 769
Scandale, E. 743
Scavini, M. 672
Schade, U. 676
Schäfer, T. 82, 804
Schalkwyk, C. 278
Schaller, K. 136
Schertl, H.-P. 599, ***601***
Schettler, G. 812
Schiavon, N. 122
Schingaro, E. 745
Schiro, M. ***139***
Schlegel, M. ***67***
Schlöglová, K. ***218***
Schmalenberger, A. 385
Schmidt, C. 195, ***677***
Schmidt, M. 59
Schmieder, M. 777, ***780***
Schmith, J.H. 708
Schmitt, R.-T. 498
Schmitz, B. 790
Schmitz, M. ***308***
Schmitz, S. 196
Schollenbruch, K. 143
Scholtzová, E. ***759***
Scholz, R. 424, 439
Schorr, S. 11, ***666***
Schouwstra, R.P. ***275***, 278
Schrader, C.M. ***779***
Schubert, F. 198, 201
Schüler, D. x
Schulte, P. 780
Schulze, N. 42
Schumacher, R. ***764***, 770
Schwahn, D. ***376***, ***680***
Schwarz, J.-O. 23
Schweigstillová, J. ***647***
Schwyn, B. 65
Sciascia, L. ***157***
Scordari, F. 724, 735, 745
Scott, S.D. 236
Seagle, C.T. ***162***
Sebastián, E. 137, ***138***
Sebastiani, M. 493
Šebek, O. 869
Secco, M. ***65***
Şeclăman, A.C. ***724***
Seftel, E.M. 54, 411
Seghedi, I. 199
Segliņš, V. 624
Segundo, F. 281
Seidl, J. 762
Seiffarth, T. ***84***
Sejkora, J. 349, 351, 725
Sekine, T. 784
Seltmann, R. 290, 291
Semenyak, B.I. 429
Semionkin, V.A. 657
Semjonova, L. 798
Sennit, C.M. 291
Seo, Jieun 231, 545, 590
Sergeev, S.A. 445
Sergeeva, Hadjiev, A. 227
Sergent, J. 723
Sergueev, I. 442
Serwicka, E.M. 853
Šesták, J. ***368***
Seto, A. 718
Seto, Y. 146, 151
Seyama, H. ***390***
Seydoux-Guillaume, AM. 455
Shagalov, E.S. ***531***
Shah, M.T. 603
Shallo, M. 587
Shan, L.H. 204
Shapley, T. 90
Sharygin, V.V. ***190***, 200, 443, ***444***, ***446***, 521, ***576***
Shatskiy, A. 148
Shau, Yen Hong 18
Shaw, S. 675, 825
Shaybekov, R. ***273***
Shchapova, Yu.V. 373
Shen, Junfeng ***146***
Shen, Pouyan 839
Shen, Xuhui 146
Sherlock, S.C. 683, 691
Sherwood, J. 427
Shi, G.H. ***598***
Shi, Nicheng 155, ***157***
Shigeno, M. 598, 601, ***602***
Shigeoka, M. 498
Shim, S.-H. 141, 152, ***442***, 443
Shimada, K. 601, 602
Shimazaki, H. 498
Shimizu, M. 450, ***538***, 547
Shimizu, T. ***226***
Shimobayashi, N. ***436***, ***692***
Shin, J.K. 235
Shinmei, T. 141, 151, 182
Shiryaev, A.A. ***181***, ***186***, ***693***, ***798***
Shmakov, A.N. 396
Shpachenko, A.K. 562
Shtukenberg, A.G. 373
Shu, Xiao-Hua 329, 332
Shumilova, T.G. 570

Shumlyanskyy, V.O. 298
Shushkov, D. ***54***
Shvetsova, I.V. 458
Shchekina, T.I. ***36***
Sicard, D 173
Sicilia-Aguilar, A. 792
Šída, P. 113
Siegesmund, S. 128, 137, 855
Sierra, S. 1
Sigmarsson, O. ***vi***
Sigmon, G.E. 364, 731
Siidra, O.I. ***711***
Silaev, V.I. 186
Siligardi, C. 409
Silva, E.A.F. 323
Silva, M.M.V.G. 256, 323, 514
Silva, T.P. 662
Simakin, A.G. 45, 539
Simard, M. ***259***
Simha Martynková, G. 394
Šimić-Kanaet, Z. 124
Simmons, W.B. 604, ***605***, 61, 618, 619
Simon, G. ***770***
Simon, K. 128
Simon, S. 109
Simonetti, A. 362, 551
Simonov, V.A. 237, 419
Simons, K.K. ***600***
Simpson, E.T. x
Sinkó, K. ***15***
Sinmyo, R. 441
Sipos, N. 792
Sipos, P. 334, 642
Sirbescu, M.C. 606, ***606***
Sitnikova, M.A. 574, 614
Škácha, P. ***725***
Skála, R. 32, 461, 781
Skartsila, K. ix
Skiba, M. 96
Škoda, R. 175, 349, 456, 485, ***620***, 827
Skogby, H. 171, 175, 431, 484
Skovbjerg, L.L. 365, 754
Skublov, S.G. 569
Słaby, E. ***688***
Slaty, F. 402
Slobodník, M. ***123***
Sluzhenikin, S.F. 265
Śmigielski, M. 688
Smirnov, N.G. 373
Smirnov, S.Z. ***192***
Smirnova, D.A. 479
Smith, A.J.B. ***278***
Smith, B. ***554***
Smith, D.G.W. 870
Smith, V.C. ***416***
Smolárik, M. 310
Soares, D.R. 477
Sobolev, A.V. 526, 583
Sobolev, N.V. 431
Soboleva, A.A. 489
Soboleva, S.V. 91
Sobott, R. 114
Sobrados, I. 758
Soda, Y. 420
Sofe, M. 787
Sogrik, E. 529
Sokalska, E.T. ***486***, ***628***
Sokolov, V. 624
Sokolova, E. 731, ***732***
Solá, A.R. ***531***
Šolc, R. 95
Soldati, A.L. 25, 378, 678
Soler, J.M. ***66***, 66, 232
Söllradl, S. ***3***, ***682***
Solovova, I. ***577***
Somboon, C. 23
Somers, J. 362
Somoza, L. 63
Sorensen, S.S. 597, 600
Sorokhtina, N.V. 552, ***562***
Sorokina, E.S. ***32***
Soumar, J. ***32***
Southam, G. 60, 381
Spadafora, M.J. 291
Spagnoli, D. ***822***
Spandler, C.S. 156
Spangenberg, J. 121
Sparks, B.D. 276
Sparks, S. 553
Spengler, D. 803
Sperinck, S. ***850***
Spetsius, Z.V. ***177***, 571
Spettel, B. 787
Spicuzza, M.J. 560
Spirov, I. 218
Spratt, J. 559, 610
Sreenivas, B. 417
Sremac, J. 325
Srikantappa, C. ***203***, ***462***
Środoń, J. ***313***, 696
Stachel, T. ***21***, 196
Stadnicka, K.M. 728
Stalder, R. 147, 170, ***174***
Stanek, K.P. 599, 601
Staněk, T. 3, 17
Stanimirova, Ts. ***759***
Stanjek, H. ***57***
Stanković, M.N. 627, ***636***
Stanley, C.J. 266, 435
Starijaš, B. 462
Starikova, A.E. 482
Starnini, E. ***110***
Šťastná, A. ***140***
Šťastný, M. 648
Stavrova, O.O. 419
Steele-MacInnis, M.J. ***194***
Stein, H. 259
Steininger, R. 335, 341
Steinle-Neumann, G. 166
Stelling, J. ***824***
Stenina, N.G. 291
Steudel, A. 753
Stewart, R.B 41, ***540***, 683
Stickland, R.J. 279
Stipp, S.L.S 365, 369, 754
Stochici, R. 548
Stoilova, D 665
Stojanović, J. 716
Stojic, A.N. ***653***
Stoll, H.M. 827
Storey, C. 553, 685
Strelchenko, V.V. 314
Stremtan, C.C. ***532***
Striček, I. 393
Strmić Palinkaš, S. ***99***, ***290***, 643
Strnad, J. 368
Strnad, L. 869
Strnad, Z. 368
Struskin, V. 671
Stumpf, T. ***822***
Stunda, A. ***17***, 309, 624, 633
Sturhahn, W. 152, 442
Šturm, S. 29
Štyriak, I. 412
Štyriaková, I. 400, ***412***
Su, Haiquan ***89***, ***95***, ***408***
Su, Tung Hsin ***18***
Su, W. ***532***
Suárez, M. 307
Subetto, D.A. 119
Subrt, J. 83
Šucha, V. ***393***
Sucher, S. 767
Sugiyama, K. 533, ***674***, 706, ***725***
Sukharev, A.E. ***186***
Sukhorukov, V.P. ***463***, 579
Sulovský, P. ***3***, 17
Sumiya, H. 182
Summa, V. ***372***
Sun, Xiaoming 245, 746
Sundblad, K.L. 538
Sundvall, R. ***175***
Sung, Y.H. 328
Supiňková, T. 869
Sushchevskaya, N.M. 526, ***583***
Sutherland, L. 517
Sutthirat, C. 33
Suvorova, E.I. 383
Suvorova, V.A. 363
Suzuki, A. ***40***
Svendsen, J.B. 52, 317
Sverjensky, D.A. 370
Swarbrick, J.C. 678
Syritso, L.F. 419, 612, 614
Szabó, Á. ***577***
Szabó, Cs. 62, 174, 189, 197, 199, 200, 201, 202, 204, 205, 322, 326, 330, 333, 405, 406, 521, 522, 528, 559, 571, 577, 840
Szabó, J. 405
Szabó, K.Zs. 322, ***405***
Szabó, Zs. 326, ***406***, 515
Szadorski, J. 647
Szakács, A. 286, 295, 341, ***542***
Szakáll, S. 52, 417, 430, 434, ***436***, 446, 495, ***500***

Szakmány, Gy. 108, ***110***, 111, 783
Szappanosné Vágó, E. ***260***
Szczerba, M. ***84***, ***96***, ***696***
Székely, E. 62
Szekszárdi, A. ***111***
Szełęg, E. ***501***
Szilágyi, V. ***108***, 110
Szöcs, V. 697
Szokoly, Gy. 792

Tabara, T. 375
Tacker, R.C. ***368***
Tait, K.T. ***726***, ***765***
Tajbakhsh, P 628
Tajčmanová, L. 592, ***802***, ***814***
Takada, M. 355
Takahashi, T. 263
Takahashi, Y. 331, 503
Takai, Y. ***578***, 760
Takaya, M. 692
Takeda, T. 667
Talla, D. 175
Tămaş, C. 121
Tămaş, T. 471
Tampieri, A. 372
Tamura, A. 190, 583
Tamura, K. ***96***, 395, 407, 703
Tan, Daoyong 14
Tanaka, C. 581
Tanaka, M. 678
Tanaka, T. 62, ***288***
Tange, Y. 141
Tani, Y. 319, 390
Taniguchi, M. 427
Taniguchi, T. 755
Taran, Yu.A. 287, ***548***
Tarantino, S.C. 5, ***672***
Tarrida, M. 390
Tarzia, M. 540
Tassi, F. 59
Tassinari, C. 587
Tateno, S. ***161***, 166
Tatianchenko, T.V. 641
Taubald, H. 108, 775
Tauler, E. 230, 232, 240
Tavares, D. 122
Taviot-Guého, C. 353
Taylor, R.P. ***21***, 687
Tchouankoue, J.P. 202
Teixeira, R.J.S. 233
Tembo, F. 217
Temel, A. 511
Temnov, A.V. 564
Tene Djoukam, J.F. 202
Tepavitcharova, St. 376
Terasaki, H. 40, 163
Terata, S. ***158***
Terracciano, R. 301
Terrill, N. 675
Terroso, D. 338, 393
Testemale, D. ***669***
Tether, A. 708
Thalhammer, O.A.R. 264, 268, 277
Thamó-Bozsó, E. ***333***
Thanh, N.X. 683
Thawornmongkolkij, M. 126
Theodoridou, G. 307
Theodoridou, M. ***131***, ***133***
Thomas, C. 816
Thomas, R. 176, 524, ***604***, 612
Thomas, S.-M. ***176***
Thomas, V.G. 192
Thöni, M. 259
Thyberg, B. 635
Tibljaš, D. ***124***, 404, 462, 621, 632, ***637***
Tiboni, Ch. 238
Tillmanns, E. 48, 476, 726, 727, ***773***, 865
Timofeeva, M.N. ***77***, ***396***
Tindle, A. 577
Tippelt, G. 347
Tita, P. 548
Titorenkova, R. ***376***
Tits, J. 823
Tkalcec, B.J. 653
Többens, D.M. 817
Tobler, D.J. 379
Todorović, B.Ž. 636
Toh, S. 183
Toll, F. 276
Tomandl, I. 781
Tomašić, N. ***437***
Tombácz, E. 411, 863
Tommasi, A. 508, 522
Tompa, É. ***332***
Tomshin, M.D. 181
Tonarini, S. 474
Tončić, T. 294
Topa, D. 497
Török, Á. ***128***, 131
Török, K. 202, 591, 805
Torres Sanchez, R.M. ***396***, ***398***
Torres-Ruiz, J. 425, 526, 618, 619
Torró, L. 230, 242, ***578***
Tóth, A. 577
Tóth, E. 749, ***863***
Tóth, J. ***314***
Tóth, M. 108, 113, 116, 514, 840
Tóth, T.M. 198
Touret, J.L.R. 189, ***556***
Touret, L. ***763***
Toyoda, S. ***659***, ***666***, 689
Toyoshima, T 519
Tran, T.A. 523
Trapote, A. ***66***
Travin, S. 141
Trcera, N. 390
Tredoux, M. ***266***
Tretiakova, L. ***33***
Tri, T.V. 523
Triantafyllou, G. ***133***
Trigo, C. 85
Trindade, W.M. 351
Třískala, Z. 869
Trittschack, R. ***833***
Troll, V.R. 234
Trønnes, R.G. 155
Tropnikov, E. ***282***
Trots, D.M. ***158***
Trubkin, N.V. 267
Trumbull, R.B. 482, 483
Try, E. 288
Tseng, C.-Y. 588
Tsintsov, Z.L. 270
Tsolis-Katagas, P. 89, 402
Tsuchiya, J. ***165***, 219, 810
Tsuchiya, N. 803
Tsuchiya, T. 165, 219, ***810***
Tsuchiyama, A. 677
Tsuei, K.D. 151
Tsukamoto, K 832, ***833***, 835, 840
Tsukamoto, S. 150
Tsybulya, S.V. 77
Tu, Bowen 345
Tucci, P. 120
Tuček, J. ***844***
Tuduri, J. 288
Tuğrul, A. 129
Tulk, C.A. 679
Tunega, D. ***90***, ***95***
Tuniz, C. 111, 113
Tupinambá, M. 839
Turbanti Memmi, I. ***121***
Turchenko, T.L. 623
Turchkova, A.G. 51, ***55***
Turkel, A. 589
Turkina, O.M. 452
Türler, A. 3, 682
Turq, P. 57
Tyrała, L. 321
Tyszka, R. 645, 647

Udvardi, B. 405
Ueda, A. ***533***, 832
Uehara, S. 578, ***760***
Uesugi, K. 677
Uesugu, M. 677
Ufer, K. 747
Ugliengo, P. 816
Uher, P. ***448***, 477, ***613***
Uhlík, P. 289, 310, 393
Uhlir, C. 136
Újvári, G. 646
Ulmer, P. 42
Ulrych, J. 461
Umemoto, K ***142***, ***815***, ***820***
Undabeytia, T. ***406***
Unruh, D.K. 364, 761
Unruh, T. 39
Upton, P. 250
Uram, J. 334
Urata, Y. 420
Urmantseva, L.N. ***452***, 463
Urquiola, M.M. 130

Usami, T. 659
Uster, B. 383
Usui, Y. 219
Usuki T. 523, 602
Uysal, I. ***268***, 270
Uz, B. 100
Uzarowicz, L. 648

Vaccari, L. 189
Váczi, T. 446
Vainio, U. 15
Vajna, B. 327
Vakhrushev, A.V. 241, ***311***
Valášková, M. 92, ***100***, 394, 700
Valdrè, G. ***409***, ***752***, ***856***, ***857***
Valenti, P. 39
Valentini, F. 372
Valentini, L. 69, 579
Valenzano, L. 356
Valero Juan, M. 6
Valfrè, C. 374
Valizer, P. 499
Valle Aguado, B 523
Valley, J.W. 560
Valsami-Jones, E. ***ix***, 374
Valter, M. 135, ***849***
Valverde Tercedor, C. 382
Vámos, M. 629
van Boekel, R. 792
Van de Moortèle, B. 144, 855
Van der Merwe, F. ***273***
Van Driessche, A.E.S. 775, ***834***, ***842***
van Hinsberg, V.J. 254
van Hullebusch, E. 115, 351, 386, 390, 391
van Roermund, H. 209
Vance, Z.R. 368
Vandevoorde, D. ***132***
Varga, A. ***549***, 646
Varga, G. 391, 635
Varga, M. 515
Vargas, T. 509
Varlamov, D.A. ***489***
Varol, E. ***511***
Vasconcelos, K.K.F. 418
Vasconcelos, M.A.R. ***786***
Vaselli, O. 59
Vasilescu, A. 107, 676
Vasiliev, P. ***179***
Vasković, N. ***533***
Vasserman, D.V. 15
Vassileva, R.D. ***437***, ***438***
Vasyukova, E.A. ***579***
Vaughan, D.J. 365
Vázquez, P. ***129***
Vazquez-Calvo, C. ***128***
Veiga, R. 123
Vejelyte, I. ***534***
Vekemans, B. 196
Veksler, I. 606
Velasco, F. 605
Velič, D. 697
Velić, I. 325
Velosa, A. 135
Velušček, A. 111, 113
Vempere, D. 17
Vennemann, T.W. 503, 631
Ventalon, S. 124, 125
Ventruti, G ***735***
Verchovsky, S. 185
Vercouter, T. 364
Verel, R. 44
Vereş, D. 471
Vereshchagin, O.S. ***710***
Vergasova, L.P. 539
Verhaeven, E. 132
Vermeesch, P. 795
Verryn, S.M.C. ***5***
Vervoort, J.D. 215
Vespa, M. 353, ***362***
Vetlényi, E. 204
Vető, I. 19
Vetuschi Zuccolini, M. 35, 143
Vezzalini, G. ***47***, 53, ***103***, ***672***
Vicente Navarro, J. 140
Vicenzi, E.P. 779
Victoria, J. 339
Viczián, I. ***98***, 622, ***772***
Vidal, L. 651
Vieillard, P. ***407***
Vigasina, M.F. 625, 640, 755, 756
Vígh, Cs. 515, ***534***
Vigh, T. 331
Vigil de la Villa, R. 49
Vignola, P. ***609***, 610
Vikentev, I.V. ***253***
Vikenteva, O.V. ***260***
Viljoen, K.S. 184, ***187***, 272, 273, 278
Villa, I.M. 105
Villanova, C. 230, ***242***, 578
Villanueva-Estrada, R.E. 293
Villasenor-Cabral, M.G. ***352***
Villasuso, R. 775
Villaverde, J. 406
Vincze, A. 697
Vincze, L. 196
Vinkler, A.P. 544
Viseras, C. 397, 412
Vitos, L. 165
Vladykin, N. 141, 724
Vlahović, I. 325
Vlasov, D.Yu. 139
Vlasov, I. 798
Vlassopoulos, D. 353
Vlček, V. 725
Vogel, I. 787
Völgyesi, P. ***333***
Voloshin, V. 310
Volovetsky, M.V. ***46***
von Seckendorff, V. 256
Voronin, M.V. 263
Votyakov, S.L. 373
Vrabec, M. 208, 214
Všianský, D. 9
Vuorio, M. 66
Vylita, T. 869
Vymazalová, A. 258, ***263***, ***274***

Wadoski, E. ***55***
Wagner, C. 388
Wagner, F.E. 758, 850
Wagner, G. 42
Wakahama, H. 533
Walder, I.F. ***339***, 347
Walder, P. 339
Wall, F. ***554***, 557, ***568***, 573, ***574***
Walsch, J. 80, ***85***
Walsh, L. 268
Walte, N.P. 652
Walter, F. ***501***
Walther, T. 650
Wang, B. 78
Wang, Changqiu ***377***, 382, 385, 386, 387, 392
Wang, Chunyun ***695***, 779
Wang, Deqiang 779
Wang, Hejing ***377***, ***849***
Wang, J.Y. 145, ***147***
Wang, Lijuan 13, ***18***
Wang, Ling ***667***, 709
Wang, Mingzhen 849
Wang, RuCheng ***451***, ***609***, 819
Wang, S. 733
Wang, Tao 505
Wang, X. 367
Wang, Xiaoli 89
Wang, Xiaoxia ***505***
Wang, Xin ***382***
Wang, Y. 345
Wang, Zh. 452
Wanhainen, C. 254
Wanthanachaisaeng, B. ***33***
Wastiels, J. 402
Watanabe, J. 390
Watanabe, K. 288
Watanabe, Y. ***537***, 703
Watangua, M. 553
Watenphul, A. ***195***
Wathanakul, P. ***23***, 30, 31, ***126***
Waychunas, G.A. ***xi***, 821, 843
Webber, K.L. ***612***
Weber, B. 608
Weber, J. 645, ***647***
Weber, P.A. 336, 352
Wegner, R.R. 99, 423, 418
Wehrhan, O. 795
Wehrmeister, U. 25, ***378***
Wei, Huixiao ***245***
Wei, X.F. 204
Weibel, R. 52
Weihed, P. 254, 638
Weisener, C.G. ***336***, ***352***
Weiss, W. 302
Weiss, Y. ***180***, ***667***
Weiszburg, T.G. 295, 327, 337, 418, 520, ***749***, 863

Welch, M.D. 145, 811, ***851***
Wentzcovitch, R 815, 820
Wenzel, T. 559
Wernisch, J. 380
White, M.A. 809
Whitehead, K. 187
Whitfield, P.S. 63, 738
Whittaker, A. 773
Whittington, A.G. 606
Wiedenbeck, M. 482, 483
Wiederkehr, M. 591
Wieland, E. 673
Wierzbicka-Wieczorek, M. ***726***
Wieser, B. 259
Wilczyńska-Michalik, W. 72, ***321***
Wildau, A. 266
Wildner, M. ***34***, 665
Wilke, M. ***viii***, 44, 153, 606, 677
Williams, C.T. 320, 559, ***689***
Williams, D.M. 510
Williams, M. 447
Williams-Jones, A.E. 254
Wilson, S.A. ***60***, 738
Wimmer-Frey, I. ***125***
Winiarski, A. 491
Wirth, R. 71, 178, 180, ***210***, 388, 692, 802, 805
Wisła-Walsh, E. 88
Withers, A.C. 807
Wongfun, N. ***639***
Wongkokua, W. 31
Won-in, K. 126
Wood, I.G. 690, 679
Woodard, J. ***580***
Woodfield, B. 809
Woodland, A.B ***143***, ***810***
Woods, J.R. 276
Woollett, A. 275
Woolley, A.R. ***557***
Wriessnig, K. ***641***, 645
Wright, K. 822, 850
Wright, S.E. 707
Wrzalik, R. 491
Wu, B. 638
Wu, C.M. 602
Wu, C.Z. 638
Wu, JinWei 451, 609
Wu, Shijun ***362***
Wu, T.W. 602
Wu, X. ***166***, 442
Wu, Z. 751, 852
Wunder, B. 459

Xavier, R.P. 483
Xi, Y. 354, 359
Xie, Lei 451
Xie, Xiande 695, ***779***
Xiong, Ming 155, 157
Xu, D. 452
Xu, H.F. 207, 746
Xu, Hong ***334***
Xu, J.H. ***204***
Xu, L. 746
Xu, Sh. 867
Xu, Wei 751
Xue, Qiang 838
Xue, X.Y. 45

Yagi, T. 62, ***146***
Yakovenchuk, V.N. 716
Yakovenko, O.S. ***829***
Yakovleva, O.S. ***438***
Yalcin, H. 633
Yamada, A. ***36***
Yamada, H. 96, 395, ***407***, 703, 833
Yamaguchi, Y. ***298***, 375
Yamamoto, J. 190
Yamamoto, S. 218
Yamamoto, Y. 62, 659
Yamanaka, T. 663, ***671***
Yan, Guohan 566
Yan, Yunhua ***392***
Yanagisawa, N. ***299***
Yang, Chen 332
Yang, F. 39
Yang, H. 726
Yang, H.-J. 18, 588
Yang, J. 503
Yang, J.S. 323
Yang, K. 204, ***205***
Yang, Kui-Feng 257
Yang, Liang-Feng ***766***
Yang, M. 369
Yang, P. 575
Yang, Ruochen 377
Yang, T.F. 523
Yang, Y. xi
Yang, Zhuming 498, ***727***
Yapaskurt, V.O. 55
Yariv, S. 87
Yashima, M. 813
Yates, M.G. 479
Yaxley, G.M. 156, 556
Ye, K. ***215***, ***216***, 532
Yebra-Rodríguez, Á. ***19***, 371
Yemel'yanov, M.V. 190
Yi, Hi-Il 636
Yi, Jianzhou 245
Yi, Xiao-Yun 332
Yildirim, N. 589
Yılmaz, G. 699
Yin, H. 369
Yin, S. 89
Yokoyama, A. 671
Yokoyama, K. 498
Yoneda, T. 354, 355, 357, ***637***
Yoo, In Kol 231
Yörükoğulları, E. 699
Yoshiasa, A. 667, ***709***
Youlton, B.J. 303
Yuan, Peng ***14***, 79
Yudovskaya, M.A. 271
Yui, T.F. ***602***, ***839***
Yuningsih, E.T. ***299***
Yurimoto, H. 171, 498
Yushkin, N.P. ***413***
Yushkova, M.A. 119
Yusta, I. 605
Yuwono, V.M. 843

Żaba, J. 423
Zaccarini, F. 264, ***264***, 266, 268, 270, ***480***
Zachariáš, J. ***251***
Zacher, T. ***86***
Zadov, A.E. 444, 491
Zagler, G. 467, 497
Zagorsky, V.Ye. ***611***
Zaharia, L. ***685***
Zaitsev, A.N. 190, 443, ***559***, 728
Zaitsev, V.A. ***269***, ***552***
Zaitseva, T. ***623***, ***760***
Zajzon, N. ***19***, ***101***, 225, ***334***, 417, 430, ***446***
Žák, K. 781
Zakrevskaya, O.Yu. ***45***, ***539***
Zakusin, S.V. 310, ***311***
Zanazzi, P.F. 171
Zanda, B. 789
Zarasvandi, A. ***242***
Zavarzina, M.S. ***243***
Zavašnik, J. ***727***
Zbořil, R. 844, 845
Zeballos, A. ***638***
Zebec, V. 423, 424, ***439***
Zedgenizov, D.A. 693
Zeh, A. 247, 510
Zeidler, S. ***795***
Zelek, S.M. ***728***
Zelenskaya, M.S. 139
Zellmer, G.F. 252
Zema, M. ***5***, 145, 672
Zeman, J. 429
Zeng, Cuiping ***392***
Zeng, Shanghong 95
Zhai ,Wei 245
Zhai, M.G. ***535***
Zhang, Bingbing 89, 95, 408
Zhang, Bo 377
Zhang, Cong ***209***
Zhang, H.-Z. 843
Zhang, J. 159
Zhang, J.-X. 588
Zhang, Jing 334
Zhang, Lifei 209
Zhang, Lihu 317
Zhang, M. 532, ***746***
Zhang, N. xi
Zhang, P. 89
Zhang, R.Y. 207
Zhang, S.Y. 679
Zhang, WenLan 609
Zhang, X. 843
Zhang, Xiaohong 95
Zhang, Xiubao 222
Zhao, Changchun 8
Zhao, M. ***638***

Zhao, S.T. 210
Zhao, Wenwen 377
Zhao, Xingqing 345
Zhao, Zhidan 455
Zheng-Cui, M. 23
Zhou, Feng 245
Zhou, Jian 377, 849
Zhou, Qing 317
Zhou, Yuefei 345
Zhou, Z.Y. 215
Zhu, Dicheng 455
Zhu, Jianxi 14, 79
Zhu, R. ***90***
Zhu, Yongfeng ***261***, ***292***, 516
Zhukov, I.G. ***229***, ***237***
Ziberna, P. 149
Zich, D. 697
Zicovich-Wilson, C.M. 816
Žigová, A. ***648***
Žigovečki-Gobac, Ž. 16, 99, ***359***, ***439***, 643
Zimowska, M. 78, ***853***
Zippel, B. ***379***
Žitňan, P. 296
Zoheir, B. ***305***
Zöldföldi, J. 108
Zolensky, M. 794
Zolotarev, A.A. 610
Zolotarev, A.A., Jr. 710, ***728***
Zolotareva, B.N. 640
Zoppi, M. ***729***
Zotti, M. 346
Zubaj, R. 448
Zubko, M. 25
Zubkova, N.V. 51, 473
Zucali, M. 238
Zucchini, A. ***820***
Zuluaga, C.A. 546
Zviagina, B.B. ***750***
Zyryanova, L.A. 416

Type localities corresponding to the numbers on front cover picture

(CZE: Czech Republic, HUN: Hungary, POL: Poland, ROM: Romania, SVK: Slovakia, UKR: Ukraine)

1: Ornak Mt.; POL
2: Žeravice; CZE
3: Pernek; SVK
4: Bratislava; SVK
5: Župkov; SVK
6: Banská Hodruša; SVK
7: Banská Belá; SVK
8: Banská Štiavnica; SVK
9: Sklené Teplice; SVK
10: Kalinka; SVK
11: Pinciná; SVK
12: Kremnica; SVK
13: Špania Dolina; SVK
14: Ľubietová; SVK
15: Dúbrava; SVK
16: Slanická Osada; SVK
17: Dobšiná; SVK
18: Spišská Nová Ves; SVK
19: Revúca; SVK
20: Železník; SVK
21: Rudňany; SVK
22: Smolník; SVK
23: Gelnica; SVK
24: Lenartov; SVK
25: Červenica; SVK
26: Poruba pod Vihorlatom; SVK
27: Remetské Hámre; SVK
28: Pécs-Vasas; HUN
29: Bakonya; HUN
30: Bazsi; HUN
31: Zalahaláp; HUN
32: Ajka; HUN
33: Jásd; HUN
34: Mány; HUN
35: Dorog; HUN
36: Nagybörzsöny; HUN
37: Dunabogdány; HUN
38: Leányfalu; HUN
39: Budapest-Újlak; HUN
40: Gyöngyös-Mátraháza; HUN
41: Gyöngyösoroszi; HUN
42: Recsk; HUN
43: Szarvaskő; HUN
44: Miskolc-Hámor; HUN
45: Perkupa; HUN
46: Tállya; HUN
47: Erdőbénye; HUN
48: Tolcsva; HUN
49: Füzérradvány; HUN
50: Telkibánya; HUN
51: Kaba; HUN
52: Muzhiyevo; UKR
53: Uzhhorod; UKR
54: Olen'ovo; UKR
55: Boryslav; UKR
56: Skole; UKR
57: Kalush; UKR
58: Delyatyn; UKR
59: Oaş depression; ROM
60: Ilba; ROM
61: Baia Mare; ROM
62: Baia Sprie; ROM
63: Chiuzbaia; ROM
64: Herja; ROM
65: Trestia; ROM
66: Cavnic; ROM
67: Vama; ROM
68: Şaru Dornei; ROM
69: Broşteni; ROM
70: Borca; ROM
71: Almaş valley; ROM
72: Piatra Neamţ; ROM
73: Slănic-Moldova; ROM
74: Vălenii de Munte; ROM
75: Bădeni; ROM
76: Şinca Nouă; ROM
77: Sebeşu de Jos; ROM
78: Olăneşti; ROM
79: Obârşia Lotrului; ROM
80: Pianu de Sus; ROM
81: Săsciori; ROM
82: Cioclovina Seacă cave; ROM
83: Vaidei; ROM
84: Baia de Aramă; ROM
85: Moldova Nouă; ROM
86: Sasca Montană; ROM
87: Ciclova Montană; ROM
88: Oraviţa Montană; ROM
89: Comarnic cave; ROM
90: Dognecea; ROM
91: Ocna de Fier; ROM
92: Caransebeş; ROM
93: Gladna Română; ROM
94: Uroi; ROM
95: Săcărâmb; ROM
96: Vaţa de Sus; ROM
97: Brad; ROM
98: Boteş hill; ROM
99: Faţa Băii; ROM
100: Baia de Arieş; ROM
101: Băiţa [Bihor]; ROM
102: Bolhac (Ungurului Mare) cave; ROM
103: Mădăraş; ROM
104: Ditrău; ROM
105: Jolotca; ROM

INSTRUCTIONS FOR AUTHORS

General

Acta Mineralogica-Petrographica (AMP) publishes articles (papers longer than 4 printed pages but shorter than 16 pages, including figures and tables), notes (not longer than 4 pages, including figures and tables), and short communications (book reviews, short scientific notices, current research projects, comments on formerly published papers, and necrologies of 1 printed page) dealing with crystallography, mineralogy, ore deposits, petrology, volcanology, geochemistry and other applied topics related to the environment and archaeometry. Articles longer than the given extent can be published only with the prior agreement of the editorial board.

In the form of two subseries, AMP publishes materials of conferences (AMP Abstract Series) and field guides (AMP Field Guide Series), or, occasionally supplement issues related to other scientific events.

The journal accepts papers that represent new and original scientific results, which have not appeared elsewhere before, and are not in press either.

All articles and notes submitted to AMP are reviewed by two referees (short communications will be reviewed only by one referee) and are normally published in the order of acceptance, however, higher priority may be given to Hungarian researches and results coming from the Alpine-Carpathian-Dinaric region. Of course, the editorial board does accept papers dealing with other regions as well, let they be compiled either by Hungarian or foreign authors.

The manuscripts (prepared in harmony of the instructions below) must be submitted to the Editorial Office in triplicate. All pages must carry the author's name, and must be numbered. At this stage (revision), original illustrations and photographs are not required, though, quality copies are needed. It is favourable, if printable manuscripts are sent on disk, as well. In these cases the use of Microsoft Word or any other IBM compatible editing programmes is suggested.

Language

The language of AMP is English.

Preparation of the Manuscript

The different parts of the manuscript need to meet the instructions below:

Title

The title has to be short and informative. No subtitles if possible. If the main title is too long, an additional shortened title is needed for the running head.

Author

The front page has to carry (under the main title) the full name(s) (forename, surname), affiliation(s), current address(es), e-mail address(es) of the author(s).

Abstract and keywords

The abstract is required to be brief (max. 250 words), and has to highlight the aims and the results of the article. The abstracts of notes are alike (but max. 120 words). As far as possible, citations have to be avoided.

The abstract has to be followed by 4 to 10 keywords.

Text and citations

The format of the manuscripts is required to be: double-spacing (same for the abstract), text only on one side of the page, size 12 Times New Roman fonts. Margin width is 2.5 cm, except the left margin, which has to be 3.5 cm wide. Underlines and highlights ought not be used. Please avoid the use of foot and end notes. Accents of Romanian, Slovakian, Czech, Croatian etc. characters must be marked on the manuscript clearly.

When compiling the paper an Introduction – Geological setting – Materials and Methods – Results – Conlclusions structure is suggested.

The form of citations is: the author's surname followed by the date of publication e.g. (Szederkényi, 1996). In case of two authors: (Rosso and Bodnar, 1995) If there are more than two authors, after the first name the co-authors must be denoted as "et al.", e.g. (Roser et al., 1980).

References

The reference list can only consist of published papers, M.Sc., Ph.D. and D.Sc. theses, and papers in press.

Only works cited previously in the text can be put in the reference list. Examples:

Best, M.G., Christiansen, E.H. (eds.) (2001): Igneous petrology. Blackwell, Edinburgh, 458p.

Upton, B.G.J., Emeleus, C.H. (1987): Mid-Proterozoic alkaline magmatism in southern Greenland: the Gardar province. In: Fitton, J.G., Upton, B.G.J. (eds.): Alkaline Igneous Rocks. Blackwell, Edinburgh, 449–472.

Rosso, K.M., Bodnar, R.J. (1995): Microthermometric and Raman spectroscopic detection limits of CO_2 in fluid inclusions and the Raman spectroscopic characterization of CO_2. Geochimica et Cosmochimica Acta, **59**, 3961-3975.

Szederkényi, T. (1996): Metamorphic formations and their correlation in the Hungarian part of Tisia Megaunit (Tisia Megaunit Terrane). Acta Mineralogica-Petrographica, **37**, 143-160.

Bakker, R.J. (2002): http://www.unileoben.ac.at/~buero62/minpet/Ronald/Programs/Computer.html. Accessed: June 15, 2003.

The full titles of journals ought to be given. In case more works of the same author are published in the same year, then these has to be differentiated by using a, b, etc. after the date.

Illustrations

Finally, each figure, map, photograph, drawing, table has to be attached in three copies, they must be numbered and carry the name of the author on their reverse. All the illustrations ought to be printed on separate sheets, captions as well if possible. Foldout tables and maps are not accepted. In case an illustration is not presented in digital form then one of the copies has to be submitted as glossy photographic print suitable for direct reproduction. Photographs must be clear and sharp. The other two copies of the illustrations can be quality reproductions. Coloured figure, map or photograph can only be published at the expense of the author(s).

The width of the illustrations can be 56, 87, 118, or 180 mm. The maximum height is 240 mm (with caption).

All figures, maps, photographs and tables are placed in the text, hence, it is favourable if in case of whole page illustrations enough space is left on the bottom for inserting captions. In the final form the size of the fonts on the illustrations must be at least 1,5 mm, their outline must be 0,1 mm wide. Digital documents should be submitted in JPG-format. The resolution of line-drawings must be 400 dpi, while that of photographs must be 600 dpi. The use of Corel Draw for preparing figures is highly appreciated, and in this case please submit the .CDR file, as well.

Proofs and offprints

After revision the author(s) receive only the page-proof. The accepted and revised manuscripts need to be returned to the Editors either on disc, CD or as an e-mail attachment. Proofreading must be limited to the correction of typographical errors. If an illustration cannot be presented in digital form, it must be submitted as a high quality camera-ready print.

The author(s) will receive 25 free offprints. On payment of the full price, further offprints can be ordered when the corrected proofs are sent back.

Manuscripts for publication in the AMP should be submitted to:

Dr. Pál-Molnár Elemér
E-mail: palm@geo.u-szeged.hu
Dr. Batki Anikó
E-mail: batki@geo.u-szeged.hu
Phone: 00-36-62-544-683, Fax: 00-36-62-426-479
Department of Mineralogy, Geochemistry and Petrology University of Szeged
P.O. Box 651
H-6701 Szeged, Hungary

Distributed by the Department of Mineralogy, Geochemistry and Petrology, University of Szeged, Szeged, Hungary.

established in 1922

ACTA MINERALOGICA-PETROGRAPHICA ABSTRACT SERIES

VOLUME 6 2010

HU ISSN 0324-6523
HU ISSN 1589-4835

Printed in Hungary by mondAt Ltd.